

# HANDBOOK OF METAL FORMING

# HANDBOOK OF METAL FORMING

EDITOR  
**KURT LANGE**  
Professor Emeritus, University of Stuttgart

COEDITORS  
**KLAUS PÖHLANDT**  
**RAGU S. RAGHUPATHI**  
**JOHN D. SANITER**  
**WOLFGANG J. SAUER**  
**JOHN A. SCHEY**  
**KLAUS J. WEINMANN**  
**G.E.O. WIDERA**



**Society of Manufacturing Engineers**  
One SME Drive, P.O. Box 930  
Dearborn, Michigan 48121, U.S.A.

Copyright<sup>©</sup> 1985 by Kurt Lange  
All rights reserved. This book, or parts thereof, may not be reproduced  
in any form without permission of the copyright owner.

First Edition  
98765432

Published by Society of Manufacturing Engineers. The publisher does not, by publication of data in this book, ensure anyone using such data against liability of any kind, including infringement of any patent. Publication of any data in this book does not constitute a recommendation of any product. The Society of Manufacturing Engineers, as well as all contributors of information in this book, disclaim any and all responsibility for use of the information contained herein by readers and users of this book.

English language edition first published by McGraw-Hill, Inc., 1985.

Originally published in German under the title *Lehrbuch der Umformtechnik*, Bd. 1, 2, and 3. Copyright<sup>©</sup> 1972 and 1975 by Springer-Verlag, Berlin/Heidelberg. All rights reserved.

Library of Congress Catalog Card Number: 83-19897

International Standard Book Number: 0-87263-457-4

Additional copies may be obtained by contacting:  
Society of Manufacturing Engineers  
One SME Drive, P.O. Box 930  
Dearborn, Michigan 48121  
313-271-1500, 800-733-4763

Cover photo courtesy of Matra Datavision. New-generation simulation software predicts forming results prior to tool design. A thickness distribution performed on a car floor following a forming simulation indicates in violet where areas are too thin.

Printed in the United States of America

# CONTENTS

*How This Book Was Prepared* vii

*About the Original Book* ix

*Preface* xi

## **PART ONE FUNDAMENTALS OF METAL FORMING** 1.1

Chapter 1 General Terms and Symbols	1.3
Chapter 2 Metal-Forming Processes as a System	2.1
Chapter 3 Fundamentals of Metallurgy	3.1
Chapter 4 Flow Curves	4.1
Chapter 5 Fundamentals of Technical Plasticity Theory	5.1
Chapter 6 Tribology	6.1
Chapter 7 Measurement of Process Parameters	7.1
Chapter 8 Machine Tools for Metal Forming	8.1
Chapter 9 Dimensional Accuracy and Surface Quality	9.1

## **PART TWO BULK-METAL FORMING** 10.1

Chapter 10 Upsetting	10.3
Chapter 11 Forging	11.1
Chapter 12 Rolling	12.1
Chapter 13 Fundamentals of Extrusion and Drawing	13.1
Chapter 14 Drawing and Ironing	14.1

Chapter 15	Cold and Warm Extrusion	15.1
Chapter 16	Hot Extrusion	16.1
Chapter 17	Indentation Processes	17.1

### **PART THREE SHEET-METAL FORMING**

Chapter 18	Sheet-Metal Properties and Testing Methods	18.3
Chapter 19	Bending	19.1
Chapter 20	Deep Drawing	20.1
Chapter 21	Metal Spinning	21.1
Chapter 22	Collar Drawing	22.1
Chapter 23	Stretch Forming, Expanding, and Other Tensile Forming Processes	23.1

### **PART FOUR BLANKING, PIERCING, SLUG PRODUCTION**

Chapter 24	Blanking and Piercing	24.3
Chapter 25	Slug Production	25.1
Chapter 26	Heat and Surface Treatment	26.1

### **PART FIVE METAL FORMING UNDER SPECIAL CONDITIONS**

Chapter 27	High-Energy-Rate Forming	27.3
Chapter 28	Forming under Hydrostatic Pressure	28.1
Chapter 29	Forming with Superimposed Vibrations	29.1
Chapter 30	Forming by Exploiting Special Material Properties	30.1

### **PART SIX TOOLS FOR METAL FORMING**

Chapter 31	Dies for Metal Forming, Separating, and Joining Processes	31.3
Chapter 32	Die Manufacture	32.1
Chapter 33	Process Combinations for Die Manufacture and Die-Manufacturing Costs	33.1

### **APPENDIXES**

Appendix A	Comparative Designations for Steels	A.1
Appendix B	Comparative Designations for Nonferrous Metals	B.1
Appendix C	Chemical Composition of Steels	C.1
Appendix D	Chemical Composition of Nonferrous Metals	D.1
Appendix E	General References	E.1
Appendix F	Abbreviations Used in This Book	F.1

Index	I.1
-------	-----

## HOW THIS BOOK WAS PREPARED

The contents of this handbook are based mainly on the German *Lehrbuch der Umformtechnik*, edited by Prof. Dr.-Ing. Kurt Lange and published by Springer-Verlag, Berlin/Heidelberg/New York, in three volumes from 1972 to 1975. Great effort was expended by the editor and the coeditors to update and extend the information contained in the original version. This includes the introduction of recent developments in processes, materials, tools, and equipment, as well as the adaptation to U.S. terminology, standards, and units. The handbook represents a joint effort by eight editor-writer-translators, who contributed as indicated below:

Name	Chapter
<b>Dr.-Ing. Dr.h.c. Kurt Lange</b> , Professor Emeritus, Institut für Umformtechnik, University of Stuttgart, Stuttgart, Germany	1, 27, 28, 29
<b>Dr.-Ing. habil. Klaus Pöhlandt</b> , Apl. Professor, Institut für Umformtechnik, University of Stuttgart, Stuttgart, Germany	3, 4
<b>Dr.-Ing. Ragu S. Raghupathi</b> , Manager, Robert Bosch Corporation, Farmington Hills, Michigan, U.S.A.	7, 8, 9, 12, 13, 14, 15, 18, 24
<b>John D. Saniter</b> , B.Sc., C.Eng., Innovation Consultant, Ingenieurbüro Saniter, Bopfingen, Germany	2, 11, 16, 25, 26, 31, 32, 33
<b>Dr. Wolfgang J. Sauer</b> , Associate Professor, University of Southern Colorado, Pueblo, Colorado, U.S.A.	20, 21, 22, 23
<b>Dr. John A. Schey</b> , Distinguished Professor Emeritus, University of Waterloo, Waterloo, Ontario, Canada	6
<b>Dr. Klaus J. Weinmann</b> , Professor, Michigan Technological University, Houghton, Michigan, U.S.A.	10, 17, 19, 30
<b>Dr. G.E.O. Widera</b> , Professor and Chairman of Mechanical and Industrial Engineering, Marquette University, Milwaukee, Wisconsin, U.S.A.	5

## ABOUT THE ORIGINAL BOOK

The *Lehrbuch der Umformtechnik*, 3 vols., Springer-Verlag, Berlin/Heidelberg/New York, 1972–1975, was prepared in German by the following authors:

Dalheimer, Rolf, Prof. Dr.-Ing., *President, Fachhochschule Hamburg, Germany*  
Dannenmann, Eckart, Dipl.-Ing., *Institut für Umformtechnik, Universität Stuttgart, Germany*  
Dieterle, Klaus, Dr.-Ing., *BASF AG, Ludwigshafen, Germany*  
Geiger, Manfred, Prof. Dr.-Ing., *Universität Erlangen-Nürnberg, Erlangen, Germany*  
Geiger, Rolf, Dr.-Ing., *PRESTA Press- & Stanzwerk AG, Eschen, Liechtenstein*  
Gieselberg, Klaus, Dr.-Ing., *BASF AG, Ludwigshafen, Germany*  
Höneß, Hartmut, Dr.-Ing., *Jenaer Glaswerk Schott & Gen., Mainz, Germany*  
Kaiser, Hartmut, Dr.-Ing., *Dornier System GmbH, Friedrichshafen, Germany*  
Kast, Dieter, Dr.-Ing., *DEGUSSA AG, Hanau-Wolfgang, Germany*  
Kilp, Karl-Heinz, Dipl.-Ing., *Bundesministerium für Forschung und Technologie, Bonn, Germany*  
Krämer, Wilfried, Dr.-Ing., *Richard Neumayer, Gesellschaft für Umformtechnik mbH, Haussach, Germany*  
Lange, Kurt, Prof. Dr.-Ing., *Institut für Umformtechnik, Universität Stuttgart, Germany*  
Müller, Herbert, Dr.-Ing., *Danfoss-Flensburg GmbH, Flensburg, Germany*  
Noack, Peter, Dr.-Ing., *Flohr-Otis, Stadthagen, Germany*  
Pohl, Walther, Dr.-Ing., *Mathematischer Beratungs- und Programmierungsdienst GmbH, Fildesstadt, Germany*  
Schacher, Hans-Dieter, Dr.-Ing., *Daimler-Benz AG, Stuttgart, Germany*

## X ABOUT THE ORIGINAL BOOK

Schelosky, Hans U., Dr.-Ing., *Mannheimer Versorgungs- und Verkehrsgesellschaft mbH, Mannheim, Germany*

Schlosser, Dieter S., Dr.-Ing., *Josef Vögele AG, Mannheim, Germany*

Schmidt, Volker, Dr.-Ing., *Institut für Umformtechnik, Universität Stuttgart, Germany*

Schmitt, Gerhard, Dr.-Ing., *Marketing Consulting Dr. G. Schmitt, Ludwigsburg, Germany*

Schröder, Günther, Dr.-Ing., *Brown, Bovary & Cie., Baden-Dättwil, Switzerland*

Steck, Elmar, Prof. Dr.-Ing., *Lehrstuhl B für Mechanik, Technische Universität Braunschweig, Germany*

Warlimont, Hans, Prof. Dr. rer. nat., *Vacuumschmelze GmbH, Hanau, Germany*

Wilhelm, Hans, Dr.-Ing., *Motoren und Turbinenunion GmbH, München, Germany*

Zeller, Rolf, Dr.-Ing., *Robert Bosch GmbH, Stuttgart, Germany*

## ABOUT THE EDITOR

Kurt Lange is Professor Emeritus at the University of Stuttgart. He was Professor for Metal Forming Technique and Director of the Research Institute from 1963 to 1988. A professional in the metal forming field since 1949, he has held responsible positions at the Die-forging Research Institute, Technical University of Hannover, and with Daimler-Benz AG, Stuttgart-Untertürkheim. He is also an internationally successful consultant, and was a member of the editorial committees of various scientific-technical journals. He published an extended version of the *Handbook of Metal Forming* as a four volume edition in German, entitled *Metal Forming Technique - Handbook for Science and Industry* from 1984 to 1993. In 1986 he received the SME Gold Medal; in 1987 he was appointed Doctor honoris causa by the Technical University of Budapest, Hungary; in 1988 he was elected to the National Academy of Engineering, Washington, DC, as Foreign Associate; and in 1990 he became an Honorary Member of the Japan Society for Technology of Plasticity, Tokyo. He is also an Honorary Member of the International Institution for Production Engineering Research CIRP, for which he served as president in 1985/86.

## PREFACE

This book is intended to be a broad general introduction to the fundamentals of metal-forming technology. Included are the relevant aspects of metallurgy, tribology, technical theory of plasticity, material properties, and process data determination. Also dealt with are production methods, tools, machine tools, and other equipment, as well as tool-manufacturing methods and problems of production economy. Much of the detailed information is presented with a view toward easy application in the solution of practical problems. In its entirety, the material is selected so as to represent a comprehensive handbook of metal forming.

The book is divided into six parts and thirty-three chapters. Part 1 concentrates on the fundamentals of metallurgy, material properties, plasticity theory, tribology, and machine tools. In addition, it gives a systematic presentation of all known metal-forming processes following the German DIN standards 8582 to 8587. As is seen in Chapter 2, this system is based on stress state, process kinematics, and tool or workpiece geometry. As such it effectively contributes to an easier understanding of the differences between forming processes as well as the general influence of the stress state on forming limits, tool loading, and so on. Other aspects, however, such as process temperature and sheet or bulk forming, are not accounted for in some parts of this system. As these parameters will have a great influence on the selection of tools, machines, and other equipment, the presentation of forming and separating processes is divided in Parts 2 to 5 into the following topics: bulk-metal forming; sheet-metal forming; piercing, blanking, and slug preparation; and metal forming under special conditions. Within these four central parts of the book, not only the particular technology and its specific theory but also workpiece materials, tools, and equipment are covered in great detail. Some processes, such as rolling, upsetting, and heading, are treated in a somewhat concise manner because there is already much excellent literature available on these topics. The same applies to the discussion of metallurgy, technical theory of plasticity, and tribology in Part 1. The concluding Part 6 deals with tools for metal forming, their classification, special design features, material selection, and manufacture in general.

Besides the chapters dealing with some of the fundamentals of metal forming, Part 1 also contains two additional chapters. One is devoted to machine tools in general: basic design features, characteristics, and performance of hammers, screw presses, mechanical presses, and hydraulic presses. The other presents the interrelation between processes, tools, and machine tools with

regard to workpiece accuracy and includes information on typical dimensional accuracy values for a variety of processes.

In Part 2 the most important processes of bulk-metal forming are dealt with. The term *bulk-metal forming* signifies that, during deformation, substantial changes of cross sections, wall thickness, and so on, take place: the material will be displaced in three dimensions. The starting material will be in the form of bars, billets, slugs, or (for larger parts) even ingots. Bulk-metal forming plays an important role in the production of semifinished products by rolling, extrusion, and forging. Although all these processes, as well as drawing, ironing, and indentation processes like hobbing, are discussed, the emphasis of this book is more on secondary processes, namely, those used for the production of workpieces from semifinished products, such as bar stock. Consequently forging and especially hot-die forging, drawing, ironing, and cold, warm, and hot extrusion are treated in detail, while rolling, upsetting, and indentation processes are presented in a less comprehensive manner. In the chapter on rolling, however, is found a discussion of some important processes for the production of finished workpieces (such as roll forging, surface rolling, thread rolling, rolling of spline shafts and gears, and flow turning), together with an introduction to the theory of strip rolling.

Part 3 deals with the important processes of *sheet-metal forming*. The latter is characterized by the formation of hollow parts with more or less uniform wall thickness from flat-rolled material; except for some processes, such as stretch forming, the wall thickness is not changed significantly. Extensive thinning must be avoided because process limits are often revealed by necking with subsequent ductile fracture. In general the permissible range of deformation is much smaller in sheet-metal forming than in bulk-metal forming. As the success of sheet-metal forming depends to a large extent on the metallurgical and mechanical properties of the parent materials, one chapter of Part 3 is devoted to sheet-metal properties and the corresponding test methods. The process groups dealt with in the five other chapters are bending, deep drawing, spinning and flow turning, flanging, stretch forming, and expanding.

In Part 4 peripheral processes of metal forming, such as piercing and blanking (mainly with regard to sheet metal), slug preparation, and heat and surface treatment for various processes (primarily for cold forging), are presented. These chapters contain many details taken from industrial practice.

Part 5, devoted to metal forming under special conditions, contains chapters on high-energy-rate forming, forming under hydrostatic pressure, forming with superimposed vibrations, forming while the material is in a special state (e.g., superplastic forming), and thermomechanical forming (e.g., ausforming). These processes are important and applicable in special cases, where conventional methods fail to produce parts of very complex geometry, where the material is very difficult to form, or often where parts are to be made from expensive materials in small quantities. The processes presented here belong partly to bulk-forming and partly to sheet-forming techniques, but the salient features of these processes made it preferable to combine them in a separate part of this book.

It should be mentioned here that for the last two decades the computer has strongly influenced the technique of metal forming, for example: (1) by opening the field of numerical analysis to processes, (2) by improving data processing in the experimental investigation of such areas as tribology and materials behavior, and (3) by allowing detailed analysis of the stress and strain states in tools, machine tools, and other equipment under mechanical and thermal loading. In fact many data presented in this book were obtained by computer work. On the other hand, in spite of a significant increase in capacity combined with a sharp drop in prices, the use of computers is still in its infancy for tasks such as process design and optimization, work preparation (including cost estimation), computer-aided design and machining of tools, or process design for numerically controlled forging. This is mostly due to the lack of applicable software. There is no doubt, however, that there will be fast and broad progress, which may revolutionize wide fields of metal forming technique before the end of this century.

## ACKNOWLEDGMENTS

Dr. Taylan Altan, Battelle Columbus Laboratories, Research Leader\*, and Prof. John A. Schey, University of Waterloo, Ontario, supported the project by reading various chapters and by suggesting improvements.

Prof. B.F. von Turkovich, University of Vermont, Burlington, encouraged the editor to start the project and made valuable suggestions.

The editor wishes to thank Brigitte Wand, Institut für Umformtechnik der Universität Stuttgart, for her engaged and careful assistance during the preparation of the manuscript and during proofreading. He also wishes to thank the publisher, especially Harold B. Crawford and Susan Thomas, for the excellent cooperation and for the substantial support during the preparation and production of the handbook. Finally he wishes to express his deep gratitude and devotion to his family who accepted his absence from home for many evening and weekend hours over several years so that this book could appear.

---

\*Now Professor and Head, Engineering Research Center for Net Shape Manufacturing, Ohio State University, Columbus, Ohio, U.S.A.

#### **PREFACE FOR THE SECOND PRINTING, 1994**

Since 1985, the *Handbook of Metal Forming* has been used by many thousands of students and engineers in the U.S. and in many other countries. An official and an unofficial reprint in two southeast Asian countries also seem to be good indicators for the usefulness of this type of handbook, which offers solid, experimentally backed up data and other information for a large variety of processes both in the SI system and in the U.S. customary system. On the other hand, the book is a very comprehensive and systematic introduction to the broad field of metal forming technologies, their fundamentals, materials, tribology, and tool technology for beginners and engineers from other fields.

In the preface for the first printing, it was mentioned that the introduction of the computer, which became increasingly effective for metal forming since approximately 1970, would influence process and tool design and their optimization, numerical process control, and product quality dramatically before the end of the 20th century. This has been confirmed by the very fast development of powerful and economical computer hardware and software and their increasing application. This development is still in full flow and will without doubt contribute significantly to the near net shape or net shape production of many complex components by forming technologies. A large variety of books, many publications in conference proceedings and transactions, as well as information from software companies provide information about this important and fascinating field.

However, discussions show very clearly that the well trained and experienced expert will be needed even more in the future for the successful time and money saving realization of a scientifically based and application oriented modern metal forming technique. The editors of the *Handbook of Metal Forming* are convinced that this volume will contribute significantly to this aim for many years to come.

#### **PUBLISHING NOTE**

The Society of Manufacturing Engineers has served metalworking professionals since its beginnings in 1932. It is with a sense of responsibility to these members and associates that we issue this second printing of the *Handbook of Metal Forming*, which otherwise might have gone out of print. For this opportunity to serve manufacturing, we are grateful to Professor Kurt Lange, Dr. Markus Knoerr, and Dr. Taylan Altan at the Engineering Research Center for Net Shape Manufacturing at Ohio State University; Ms. Caroline Davis at Springer-Verlag; Ms. Bonnie Beacher and Mr. Harold B. Crawford at McGraw-Hill; and all the editors, reviewers, and contributors to the *Handbook of Metal Forming*.

Dearborn, Michigan, 1994

1

**FUNDAMENTALS OF METAL FORMING**

---

---

## GENERAL TERMS AND SYMBOLS

---

---

The aim of this book is to present, in a systematic and unified way, the principles, techniques, and technology of metal forming, including tools, machine tools, and other equipment. Therefore the general use of a unified terminology and of unified symbols is essential. Although during the past decade international standards such as the SI system (ISO R31/1), the ISO recommendations for quantities and units R31/III (mechanics), R31/IV (heat), and R31/V (electricity and magnetism), and others have been issued and were introduced into practice in many countries, the process of conversion is still going on in some countries for both traditional and economic reasons. Thus some compromises had to be made in this book to take account of this situation.

Furthermore, over the past 30 years, some remarkable developments have taken place in the field of plasticity theory. On the one hand, the elementary or slab theory that dominated the field before the introduction of the computer has been improved steadily. It still remains a powerful tool for the analysis of metal-forming processes and the calculation of stresses, load, and energy requirements. On the other hand, the von Mises theory of plasticity has taken advantage of the introduction of the computer, which permits the fast and easy application of numerical methods to the solution of complex partial differential equation systems. While the slab theory considers the deformations of whole bodies or larger portions of such bodies assuming homogeneous deformation, the von Mises theory is based on the incremental strain and stress state in a given specimen. Traditionally different symbols (e.g., for strains and strain rates) have been used in each of the theories. This tradition, which is also followed by the International Institution for Production Engineering Research, Paris (CIRP) in their "Recommended Symbols in Forming Technology," will be adhered to in this book. The slab theory will be utilized in most instances because the equations for strains, stresses, load, and energy requirements describe the influence of the governing process parameters in an easily understandable manner and in general with sufficient accuracy. When necessary, applications of the von Mises theory, such as the upper bound method, will be included.

Table 1.1 contains the symbols used throughout the book together with their definitions based on ISO R31/III, IV, and V and on CIRP "Recommended Symbols in Forming Technology" (1976).

as well as symbols that were selected freely. Additional or different symbols are listed at the beginning of each chapter.

Symbols used for material properties in material testing are mainly based on the *ASME Metals Handbook* (9th edition, 1978) rather than on ISO R82 or ISO/TC17 N 1093. These symbols and their definitions are listed in Table 1.2.

As for units, both SI units and U.S. customary units are used throughout the book. Normally the latter are given in parentheses. Temperatures, for example, are given in °C and °F, mechanical stresses in N/mm<sup>2</sup> (following a resolution of the ISO Committee TC17 of June 1970, confirmed September 1973 and June 1979) and psi, while pneumatic and fluid pressures are expressed in terms of MPa and psi. Hardness values HB and HV are expressed in the customary units of kgf/mm<sup>2</sup>, but the units are not mentioned specifically. Consequently these hardness values as well as those of HRC or HRB are given only as numbers.

For the convenience of the reader, a condensed list of units and conversion factors from SI to U.S. customary units or vice versa is included in Table 1.3.

For dimensional accuracy, values of the International Tolerance (IT) Grade according to ISO Recommendation R 286-1962 ("ISO System for Tolerances and Fits") will be used. This metric system comprises 18 tolerance grades for the range of longitudinal dimensions (including diameters) between 1 and 500 mm. Tolerances in the range between 3 and 500 mm and for the tolerance grades IT 5 to 16 are given as multiples of the basic tolerance factors

$$i = 0.45 \sqrt[3]{D + 0.001D}$$

where  $D$  = dimension in mm

$i$  = dimension in  $\mu\text{m}$

For instance IT6 =  $10i$ , IT 7 =  $16i$ , IT 8 =  $25i$ , IT 11 =  $100i$ , IT 16 =  $1000i$ ; this means that the tolerances grow with the factor 1.6 from one tolerance grade to the next. For smaller dimensions and for other tolerance grades, some slightly different regulations apply. For practical application, ISO tolerances are presented in tables for certain ranges of dimensions.

**Table 1.1** Symbols and Definitions

**Remark:** In the case where symbols are used with various definitions, detailed explanations are given in the appropriate chapters or sections.

Symbol	Definition
$a$	acceleration
$A$	area
$b$	width
$c$	specific heat
$C$	spring constant; material constant; etc.
$d$	diameter
$E$	energy; modulus of elasticity
$f$	frequency; linear elastic deformation
$F$	force; load
$g$	acceleration due to gravity
$G$	weight; shear modulus
$h$	height; bottom thickness; stroke (instantaneous value)
$H$	total stroke
$k$	shear flow stress (flow stress in shear according to the von Mises criterion)
$k_s$	shearing; blanking resistance
$K$	compression modulus
$l$	length
$m$	mass; friction shear factor
$M$	moment

**Table 1.1 (Continued)**

Symbol	Definition
$n$	number of revolutions (strokes) per time unit (e.g., r/min); strain-hardening exponent
$p$	impulse; pressure
$P$	power
$Q$	heat content
$r$	radius; anisotropy factor
$R$	radius; plastic strain ratio (e.g., extrusion ratio)
$R_t$	peak-to-valley height
$R_a$	average roughness deviation from mean surface
$R_p$	smoothing depth
$s$	thickness; deformation travel; upsetting ratio
$t$	time
$T$	temperature; torque
$u$	clearance
$v$	velocity
$V$	volume
$W$	work (dissipated energy)
$\alpha$	angle; coefficient of linear thermal expansion; heat transfer coefficient
$\beta$	angle; deep-drawing ratio
$\gamma$	angle; infinitesimal shear strain
$\dot{\gamma}$	shear strain rate
$\epsilon$	engineering strain
$\epsilon$	infinitesimal strain (von Mises theory of plasticity)
$\dot{\epsilon}$	strain rate (von Mises theory of plasticity)
$\ddot{\epsilon}$	strain-rate tensor
$\bar{\epsilon}, \dot{\bar{\epsilon}}$	equivalent strain, strain rate
$\eta$	efficiency
$\lambda$	thermal conductivity
$\mu$	(Coulomb's) coefficient of friction
$\nu$	Poisson ratio
$\sigma$	normal stress
$\sigma$	stress tensor
$\sigma_f$	flow stress
$\bar{\sigma}$	equivalent stress
$\sigma'$	deviatoric stress
$\sigma'$	stress deviator
$\tau$	shear stress
$\varphi$	natural or true strain (log deformation ratio) (slab theory)
$\dot{\varphi}$	strain rate (slab theory)
$\bar{\varphi}, \dot{\bar{\varphi}}$	equivalent strain, strain rate (slab theory)
Subscripts	
a	axial
b	bottom
B	bending
C	contact; compressive
D	die; drawing
def	deformation
e	electric
eff	effective

**Table 1.1 (Continued)**

Symbol	Definition
Subscripts	
el	elastic
FR	frictional
h	height
i, I	inner
id	ideal
l	longitudinal; lower
L	losses (lost)
m	mean
max	maximum
min	minimum
M	machine
n	normal
N	nominal
o, O	outer
opt	optimum
p	pressurized
P	punch
pl	plastic
r	radial
rel	relative
S	shearing; blanking
Sh	shear
t	tangential; torsion
T	tool; tensile
tot	total
u	ultimate; upper; uniform
U	useful
W	workpiece
$\vartheta$	tangential
Examples	
$A_p$	area under pressure
$d_i$	inner diameter of workpiece
$d_{D,i}, d_{D,o}$	inner diameter of die
$F_{sh}$	shear force
$F_S$	shearing force, blanking force
$h_{B,2}$	bottom thickness after second step of deformation
$h_N$	stroke portion corresponding to nominal (maximum) press force
$p_{p,max}$	maximum punch pressure
$t_C$	contact time
$u_s$	clearance between punch and die in shearing, blanking
$u_p$	clearance between punch and die in (deep) drawing
$v_p, v_T$	punch velocity, tool velocity
$W_{eff}, W_U$	effective work, useful work
$W_{id}$	ideal work, homogeneous work (work for homogeneous deformation)
$\epsilon_l = \Delta l / l_0$	relative change in length (engineering strains)
$\epsilon_A = \Delta A / A_0$	relative change in area (engineering strains)
$\epsilon_r, \epsilon_\theta, \epsilon_z$	strains in $r, \epsilon_\theta, z$ coordinate system (infinitesimal strains)
$\eta_{def}$	efficiency of deformation
$\tau_{FR}$	friction shear stress
$\varphi_1, \varphi_2, \varphi_3$	principal strains

**Table 1.2** Symbols for Material Properties

Symbol	Material properties
CVN	Charpy V-notch energy
$d_0$	diameter of a test piece of circular cross section
$e_t$	percentage elongation at fracture (total elongation)
$e_u$	percentage elongation before necking (uniform elongation)
HB	Brinell hardness
HRC	Rockwell C hardness
HV	Vickers hardness
$L$	gauge length
RA	percentage reduction of area at fracture
$S_B$	bending strength
$S_C$	compressive strength
$S_u$	ultimate tensile strength
$S_Y$	yield strength
$S_{0.2}$	yield strength at 0.2% nonproportional elongation
$S_{y,h}$	upper yield point
$S_{y,l}$	lower yield point
$\Delta A_{rel}$	percentage reduction of area

**Table 1.3a** Units

	SI	USCS
Length	$\mu\text{m}$ , mm, m	$\mu\text{in}$ , mil, in, ft
Area	$\mu\text{m}^2$ , mm <sup>2</sup> , m <sup>2</sup>	in <sup>2</sup> , ft <sup>2</sup>
Volume	mm <sup>3</sup> , m <sup>3</sup>	in <sup>3</sup> , ft <sup>3</sup>
Time	ms, s, min, h	s, min, h
Frequency ( $f = 1/T$ )	Hz	Hz
Circular frequency	$\text{s}^{-1}$	$\text{s}^{-1}$
Number of revolutions per time unit	$\text{s}^{-1}$ , min <sup>-1</sup>	$\text{s}^{-1}$ , min <sup>-1</sup>
Velocity	mm/s, m/s	in/s, ft/s, in/min, ft/min
Acceleration	$\text{m/s}^2$	ft/ $\text{s}^2$
Volume flow	$\text{m}^3/\text{s}$	in <sup>3</sup> /s, ft <sup>3</sup> /s, in <sup>3</sup> /min, ft <sup>3</sup> /min,
Mass	kg, t	lb, ton (short)
Density	kg/m <sup>3</sup>	lb/in <sup>3</sup>
Specific volume	$\text{m}^3/\text{kg}$	in <sup>3</sup> /lb
Moment of inertia	$\text{kg}\cdot\text{m}^2$	lb·in <sup>2</sup> , lb·ft <sup>2</sup>
Force, load	N, kN, MN	lbf, ton (short)
Moment (e.g., bending)	N·m, N·mm	lbf·in, lbf·ft
Impulse	kg·m/s	lb·in/s
Mechanical stress <sup>a</sup>	N/mm <sup>2</sup>	psi, ksi
Fluid or gaseous pressure	kPa, MPa	psi, ksi
Modulus of elasticity	N/mm <sup>2</sup>	lbf/in <sup>2</sup>
Dynamic viscosity	Pa·s	lbf·s/in <sup>2</sup>
Kinematic viscosity	$\text{m}^2/\text{s}$	ft <sup>2</sup> /s
Area moment, first grade	$\text{m}^3$	ft <sup>3</sup> , in <sup>3</sup>
Area moment, second grade	$\text{m}^4$	ft <sup>4</sup> , in <sup>4</sup>
Energy	J, kJ, MJ	ft·lbf
Work	J, kJ, MJ	ft·lbf
Power	W, kW	W, kW, ft·lbf/s
Temperature	°C	°F

<sup>a</sup>1 N/mm<sup>2</sup> = 1 MPa

**Table 1.3b** Conversion Factors

	USCS	to	SI	SI	to	USCS
Length	1 <i>μ</i> in	=	0.0254 <i>μ</i> m	1 <i>μ</i> m	=	39.37 <i>μ</i> in
	1 mil	=	0.00254 mm	1 mm	=	0.03937 mil
	1 in	=	25.4 mm	1 m	=	0.03937 in
	1 ft	=	0.3048 m	1 m	=	3.281 ft
Area	1 in <sup>2</sup>	=	645.16 mm <sup>2</sup>	1 mm <sup>2</sup>	=	0.00155 in <sup>2</sup>
	1 ft <sup>2</sup>	=	0.0929 m <sup>2</sup>	1 m <sup>2</sup>	=	10.7643 ft <sup>2</sup>
Volume	1 in <sup>3</sup>	=	16387 mm <sup>3</sup>	1 mm <sup>3</sup>	=	61.02 × 10 <sup>-6</sup> in <sup>3</sup>
	1 ft <sup>3</sup>	=	0.02832 m <sup>3</sup>	1 m <sup>3</sup>	=	35.315 ft <sup>3</sup>
Velocity	1 in/s	=	25.4 mm/s	1 mm/s	=	0.03937 in/s
	1 ft/s	=	0.3048 m/s	1 m/s	=	0.00328 ft/s
	1 in/min	=	304.8 mm/s	1 mm/min	=	3.2808 ft/s
	1 ft/min	=	25.4 mm/min	1 m/min	=	0.039 in/min
Acceleration	1 ft/s <sup>2</sup>	=	0.3048 m/s <sup>2</sup>	1 m/s <sup>2</sup>	=	3.281 ft/s <sup>2</sup>
	1 in/s	=	16387 mm/s	1 mm/s	=	61.02 × 10 <sup>-6</sup> in/s
Volume flow	1 ft <sup>3</sup> /s	=	0.02832 m <sup>3</sup> /s	1 m <sup>3</sup> /s	=	35.32 ft <sup>3</sup> /s
	1 lb	=	0.4536 kg	1 kg	=	2.205 lb
Mass	1 ton (short)	=	907.2 kg	1 t	=	1.102 ton (short)
	1 lb/in <sup>3</sup>	=	27.68 × 10 <sup>3</sup> kg/m <sup>3</sup>	1 kg/m <sup>3</sup>	=	36.127 × 10 <sup>-6</sup> lb/in <sup>3</sup>
Density	1 lb/in <sup>3</sup>	=	27.68 × 10 <sup>-3</sup> kg/cm <sup>3</sup>	1 kg/cm <sup>3</sup>	=	36.127 lb/in <sup>3</sup>
	1 lb·in <sup>2</sup>	=	0.2927 × 10 <sup>-3</sup> kg·m <sup>2</sup>	1 kg·m <sup>2</sup>	=	3417.47 lb·in <sup>2</sup>
Moment of inertia	1 lb·ft <sup>2</sup>	=	0.04214 kg·m <sup>2</sup>	1 lb·ft <sup>2</sup>	=	23.725 lb·ft <sup>2</sup>

Force, load	$1 \text{ lbf}$ $1 \text{ ton (short)}$	$=$ $=$	$4,448 \text{ N}$ $8,897 \text{ kN}$	$=$ $=$	$1 \text{ N}$ $1 \text{ kN}$	$=$ $=$	$0.225 \text{ lbf}$ $225 \text{ lbf}$	$=$ $=$
Moment	$1 \text{ lbf}\cdot\text{in}$ $1 \text{ lbf}\cdot\text{ft}$	$=$ $=$	$0.113 \text{ N}\cdot\text{m}$ $1.356 \text{ N}\cdot\text{m}$	$=$ $=$	$1 \text{ MN}$ $1 \text{ N}\cdot\text{m}$	$=$ $=$	$0.1125 \text{ ton (short)}$ $112.5 \text{ ton}$	$=$ $=$
Impulse	$1 \text{ lb}\cdot\text{in}/\text{s}$	$=$	$0.0115 \text{ kg}\cdot\text{m}/\text{s}$	$=$	$1 \text{ kg}\cdot\text{m}/\text{s}$	$=$	$0.7376 \text{ lbf}\cdot\text{ft}$	$=$
Mechanical stress	$1 \text{ psi}$ $1 \text{ ksi}$	$=$ $=$	$0.0069 \text{ N/mm}^2$ $6.9 \text{ N/mm}^2$	$=$ $=$	$1 \text{ N/mm}^2$	$=$	$86.96 \text{ lb-in/s}$ $145 \text{ psi}$	$=$ $=$
Pressure	$1 \text{ psi}$	$=$	$6,8947 \text{ kPa}$	$=$	$1 \text{ kPa}$	$=$	$0.145 \text{ psi}$	$=$
			$0.0689 \text{ bar}$	$=$	$1 \text{ MPa}$	$=$	$145 \text{ psi}$	$=$
				$=$	$1 \text{ bar}^a$	$=$	$0.145 \text{ ksi}$	$=$
				$=$	$6,895 \text{ MPa}$	$=$	$0.0145 \text{ ksi}$	$=$
Absolute viscosity	$1 \text{ psi}\cdot\text{s}$	$=$	$0.0069 \text{ Pa}\cdot\text{s}$	$=$	$1 \text{ Pa}\cdot\text{s}$	$=$	$145 \text{ psi}\cdot\text{s}$	$=$
Kinematic viscosity	$1 \text{ ft}^2/\text{s}$	$=$	$0.0929 \text{ m}^2/\text{s}$	$=$	$1 \text{ m}^2/\text{s}$	$=$	$10,764 \text{ ft}^2/\text{s}$	$=$
Energy, work	$1 \text{ ft-lbf}$ $1 \text{ ft-ton}$	$=$ $=$	$1.356 \text{ J}$ $2,712 \text{ kJ}$	$=$ $=$	$1 \text{ J}$ $1 \text{ kJ}$	$=$ $=$	$0.738 \text{ ft-lbf}$ $0.3888 \text{ ft-ton}$	$=$ $=$
Power	$1 \text{ ft-lbf/s}$	$=$	$1,353 \text{ W}$	$=$	$1 \text{ W}$	$=$	$0.738 \text{ ft-lbf/s}$	$=$
				$=$	$1 \text{ kW}$	$=$	$737.9 \text{ ft-lbf/s}$	$=$
Temperature	$1^\circ \text{ F}$ $\text{Temp } ^\circ \text{F}$	$=$ $=$	$745.7 \text{ W}$ $(\% \times \text{Temp } ^\circ \text{C}) + 32$	$=$ $=$	$1^\circ \text{ C}$ $\text{Temp } ^\circ \text{C}$	$=$ $=$	$1.325 \text{ hp}$ $\% \text{ (Temp } ^\circ \text{F} - 32)$	$=$ $=$

<sup>a</sup>1 bar =  $10^5 \text{ Pa} = 0.1 \text{ MPa}$   
1 Pa =  $10^{-5} \text{ bar}$   
1 MPa = 10 bar



## METAL-FORMING PROCESSES AS A SYSTEM

The term *metal forming* refers to a group of manufacturing methods by which the given shape of a workpiece (a solid body) is converted to another shape without change in the mass or composition of the material of the workpiece.

**Classification of manufacturing processes:** Metal forming is used synonymously with *deformation* or *deforming* and comprises the methods in group II of the manufacturing process classification shown in Fig. 2.1. The manufacturing processes are divided into six main groups:

**Group I—Primary forming:** Original creation of a shape from the molten or gaseous state or from solid particles of undefined shape, that is, creating cohesion between particles of the material.

**Group II—Deforming:** Converting a given shape of a solid body to another shape without change in mass or material composition, that is, maintaining cohesion.

**Group III—Separating:** Machining or removal of material, that is, destroying cohesion.

**Group IV—Joining:** Uniting of individual workpieces to form subassemblies, filling and impregnating of workpieces, and so on, that is, increasing cohesion between several workpieces.

**Group V—Coating:** Application of thin layers to a workpiece, for example, galvanizing, painting, coating with plastic foils, that is, creating cohesion between substrate and coating.

**Group VI—Changing the material properties:** Deliberately changing the properties of the workpiece in order to achieve optimum characteristics at a particular point in the manufacturing process. These methods include changing the orientation of microparticles as well as their introduction and removal, such as by diffusion, that is, rearranging, adding, or removing particles.

## 2.2 FUNDAMENTALS OF METAL FORMING

Creation of cohesion	Maintenance of cohesion	Destruction of cohesion	Increase of cohesion
<i>Shape modification</i>			
	II Deforming	III Separating	IV Joining
I Primary forming		VI Changing the material properties <i>a</i> Addition of <i>b</i> Removal of particles <i>c</i> Rearrangement of particles	V Coating

FIG. 2.1 Classification of manufacturing processes. (After [2.1].)

In manufacturing technology, particularly in groups I to IV, we are continually faced with the problem of how to manufacture most economically a particular technical product with specific tolerance requirements, surface structure, and material properties. Disregarding the influence of production conditions and quantities at this stage, Fig. 2.2 illustrates that workpieces such as a simple bolt can be produced by a number of methods from each of the first four groups.

**Characteristics of deformation methods:** In contrast to the very large group of methods of shaping parts by means of separation (group III), metal-forming methods have the following characteristics:

- 1 The loads and stresses required for deformation are very high. The stresses vary between 50 and 2500 N/mm<sup>2</sup> (7–360 ksi), depending on the method and material concerned. Since usually the entire workpiece, or at least a major part of it, is to be deformed, the loads can also be very high. In forging presses, for example, they may reach 750 MN (85 kilotons). By comparison, a heavy planing machine produces only a few kilonewtons of cutting force, a small horizontal shaping machine about 20 kN (2.3 ton), and a large twin-column shaping machine about 200 kN (23 ton).

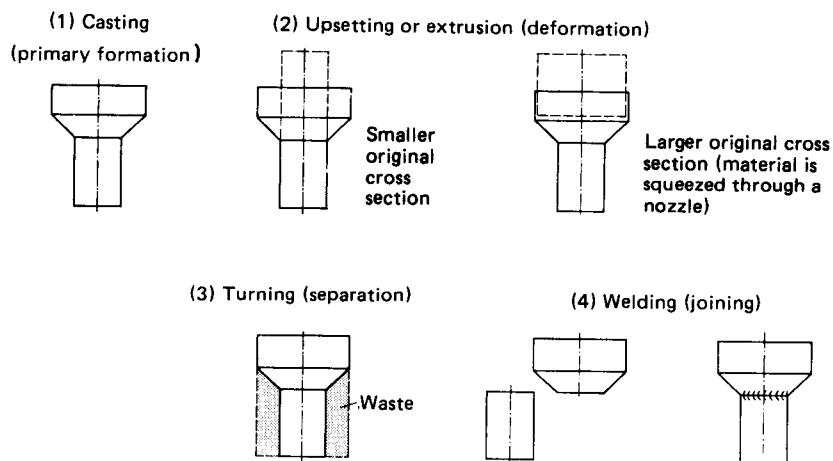


FIG. 2.2 Methods of manufacturing a bolt. (1) Primary formation. (2) Deformation. (3) Separation. (4) (Separation +) joining.

- 2 The majority of the parts are completely deformed. Because of the high loads involved, the tools are generally very large, heavy, and correspondingly expensive. The manufacture of metal-forming tools requires well-equipped workshops and highly skilled workers since the tolerances required approach those of precision engineering and gauge making. Thus metal-forming technology is closely associated with machining through the manufacture of metal-forming tools. However, only small batches, or even a single set, are the rule.
- 3 Because of the high costs of machinery and tools, certain minimum quantities are a prerequisite for production to become economical. When minimum quantities are assured, the advantages of the deformation methods are (a) high productivity and short production times, (b) high accuracy, within particular tolerances, with regard to dimension and shape, and (c) good mechanical properties of the manufactured component.

## 2.1 TECHNICAL AND ECONOMIC SIGNIFICANCE OF METAL FORMING

The following list outlines the most important areas of application of workpieces produced by deformation, underlining their technical significance:

- 1 Components for automobiles and machine tools as well as for industrial plants and equipment. Here metal forming is a vital link in the development of modern design in light alloys.
- 2 Hand tools, such as hammers, pliers, screwdrivers, and surgical instruments.
- 3 Fasteners, such as screws, nuts, bolts, and rivets.
- 4 Containers, such as metal boxes, cans, and canisters.
- 5 Construction elements used in tunnelling, mining, and quarrying (roofing and walling elements, pit props, etc.).
- 6 Fittings used in the building industry, such as for doors and windows.

With regard to the variety of materials to be deformed, the 1970s brought about continued diversification, corresponding to higher demands for strength, and resistant to fatigue, heat, and corrosion by the users of such workpieces. Besides steel (carbon and alloy steels, including stainless and heat-resistant steels), nonferrous light and heavy alloys, such as aluminum, zinc, and copper and their alloys, may be shaped by deformation. Furthermore, metals such as titanium and its alloys are in increasing demand, as are heat-resistant nickel-based materials and metals such as tungsten, molybdenum, and zirconium and their alloys, as well as other similar materials. Strong impetus for the development of the latter materials has come from the fields of aerospace and reactor technology.

The great economic significance of metal forming to modern industrial states can be only briefly outlined here. Both ferrous and nonferrous metals—unless cast directly in their final shapes—pass through either rolling mills or extrusion presses. This creates a so-called “semifinished” product. In the subsequent step from semifinished to finished product, the significance of sheet-metal working has tended to increase proportionally with the improvement in the standards of living. If one accepts that from 20 to over 40% of all rolled steel production (depending on the standard of living) is in the form of sheets and coils, it is clear that many millions of tons of steel go on to be worked by metal-forming processes. In the manufacture of bulk-metal components, hot forging of steel and nonferrous materials—as used for high-strength temperature-resistant workpieces for aircraft and engine components—as well as cold extrusion and upsetting in conjunction with other processes are of major importance for the manufacture of shaped components and fixtures. The advantages of cold bulk-metal forming, namely, the low weight and high strength of the product, have led in the United States to a steel consumption of approximately 1.3 million t (1.43 million tons) for cold-formed parts in 1980. More specifically, in a medium-size automobile between 50 and 70 kg (110–155 lb) of steel is used for cold-formed parts as well as for standard and special-purpose fasteners and fixtures.

In machine-tool manufacture in the United States as well as in West Germany metal-forming machine tools have accounted for one-third of the total output in value for many years. As a rule,

these machines have a considerably higher productivity than metal-cutting machine tools and thus represent an even larger share of the total production capacity.

## **2.2 METHODS USED IN METAL FORMING**

The following classification of the deformation methods into five groups is based mainly on the important differences in effective stresses. No simple descriptions of stress states are possible since, depending on the kind of operation, different stress states may occur simultaneously, or they may change during the course of the deforming operation. Therefore the predominant stresses are chosen as the classification criteria. The five groups of metal-forming processes may then be defined as follows:

- 1 Compressive forming** (forming under compressive stresses [2.3]): German standard DIN 8583 covers the deformation of a solid body in which the plastic state is achieved mainly by uni- or multiaxial compressive loading.
- 2 Combined tensile and compressive forming** (forming under combined tensile and compressive stresses [2.4]): DIN 8584 covers the deformation of a solid body in which the plastic state is achieved mainly by combined uni- or multiaxial tensile and compressive loading.
- 3 Tensile forming** (forming under tensile stresses [2.5]): DIN 8585 covers the deformation of a solid body in which the plastic state is achieved mainly through uni- or multiaxial tensile stresses.
- 4 Forming by bending** (forming by means of bending stresses [2.6]): DIN 8586 covers the deformation of a solid body in which the plastic state is achieved mainly by means of a bending load.
- 5 Forming by shearing** (forming under shearing stresses [2.7]): DIN 8587 covers the deformation of a solid body in which the plastic state is achieved mainly by means of a shearing load.

Within these groups, further subdivision is possible on the basis of kinematic considerations (a relative movement between tool and workpiece), of tool geometry and workpiece geometry, as well as of the relationship between the two. However, these aspects are not necessarily of the same importance in the different groups.

In order to facilitate any subsequent inclusion of new methods, the classification of the individual methods is completely free of references to the manufacturing processes employed, as, for example, in particular branches of the industry.

For any particular field, such as open-die forging or sheet-metal working, the processes used may be selected from the five groups listed above, as well as from the main groups illustrated in Fig. 2.1 (separating, joining, coating, and changing the material properties). They may also be rearranged according to the particular structure of the industrial branch or company. The classification of metal-forming methods intentionally leaves open the question of whether a process is carried out without preheating, that is, at room temperature, or after heating to a higher temperature. Up to now, the recrystallization temperature has been taken by metallurgists as the boundary between cold and hot forming. However, although this undoubtedly influences the behavior of the workpiece material during forming, it is widely recognized today that spontaneous recovery plays a far greater role in rapid forming operations. In addition, this terminology leads to a confusing situation with the wide variety of materials now in use. For example, the deformation of lead at room temperature should be termed "hot forming" while that of molybdenum at 800°C (1472°F) would be "cold forming." For this reason DIN 8582 [2.2] makes a distinction between deformation performed at room temperature and deformation performed on a workpiece heated above room temperature. Apart from this, account must be taken of whether a permanent change occurs while the operation is taking place. With the aid of these two criteria, metal-forming methods may be divided as follows:

- 1 Forming after heating = hot forming
- 2 Forming without heating = cold forming

Both divisions can be further subdivided as follows:

- a Forming without change in mechanical properties
- b Forming with temporary change in mechanical properties
- c Forming with permanent change in mechanical properties

Forming operations whose main purpose is to bring about a change of shape are also very often used to perform a deliberate, controlled change in material properties, usually to obtain improved strength and ductility. Forming processes whose main aim is to change the material properties (e.g., surface rolling) will, where the shape of the workpiece is not noticeably altered, be allocated to group VI of Fig. 2.1.

The classification system chosen has the great advantage that each process appears only once. It permits, at least in groups 1 to 3 of the metal-forming methods, to draw qualitative conclusions as to what changes in shape may be aimed at by means of the methods belonging to these groups. It is well known that formability (a measure of the shape change that a workpiece can withstand) decreases until external or internal damage occurs. This happens when the stress state in the deformation zone changes from multiaxial pressure through combined tensile and compressive stresses to tri-, bi-, or uniaxial tension. Examples of this are extrusion, upsetting, deep drawing, and stretch forming (Fig. 2.3). The process boundary, that is, the degree of deformation attainable, depends either on the load that the tool will withstand (as in cold extrusion) or on the loading of the workpiece (as in stretch forming).

A summary showing how the five groups of metal-forming methods may further be divided into 18 subgroups is given in Fig. 2.4. These subgroups comprise a total of about 230 basic methods of which special applications exist, in particular where rolling is concerned. Furthermore, innumerable combinations of these methods are used in industry [2.8] to [2.15].

### 2.2.1 Compressive Forming

Group 1 of the metal-forming processes, DIN 8583, is divided into rolling, free or open-die forming, closed-die forming, indenting, and pushing through an orifice. The rolling processes are subdivided on the basis of kinematic considerations into longitudinal, cross, and lateral rolling; on the basis of roll geometry into flat and contour rolling; and on the basis of workpiece geometry into solid and hollow section rolling (Fig. 2.5). In addition to processes used to make semifinished and finished rolling mill products, they also include processes performing a wide variety of jobs in today's manufacturing industry, such as thread rolling, which is cross-contour rolling (plunge method) or inclined contour rolling (run-through method), splined shaft rolling, and surface rolling.

The compressive forming methods, such as flow turning, are also included in this subgroup under the headings "flat lateral rolling" or "profile lateral rolling" (Figs. 2.6 to 2.8).

The open-die and drop-forging processes embrace metal-forming processes with opposed movement of tools. Either the tool's shape does not reflect or barely reflects the shape of the workpiece (free or open-die forming, Fig. 2.9a), or it corresponds completely or to a large degree to the shape of the workpiece (closed-die forming, Fig. 2.9b). Open-die forging includes such important processes as drawing out, swaging, upsetting, heading, rotary forging, and so on, underlining once again that we are dealing with a generic term (Fig. 2.10). In die forging the situation is similar, the most important processes being die forging with and without flash and heading in a die. A number of other bulk- and sheet-metal-forming methods are also included in the die-forging group, based on the definition given above (Fig. 2.11).

The term *indenting* is used to describe those methods in which a tool is pressed into the workpiece, whereby a relative movement along the surface between tool and workpiece may also

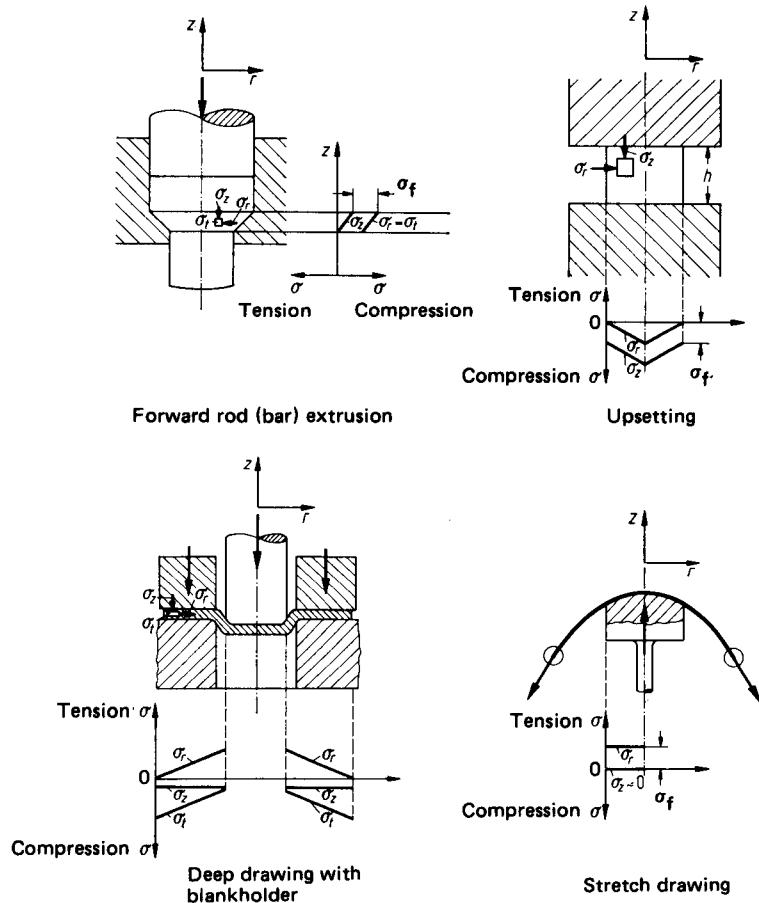


**FIG. 2.3** Stress condition in the deformation zone for different deformation methods (according to elementary theory of plasticity).

occur. Examples are punching, die sinking by indentation, embossing of sheet metal using notched tools (without relative movement), and thread tapping (with relative movement) (Fig. 2.12).

Among the processes based on pushing material through a shape-giving tool aperture (Fig. 2.13), hot and cold extrusion are the most important, apart from free extrusion and open-die extrusion (i.e., the generation of small cross-sectional changes in solid and hollow bodies). Both are very similar in their deformation mechanism, but they differ with regard to the tools and equipment used as well as the products manufactured. While hot extrusion is used mainly for the production of solid and hollow extrusions (rods, tubes, and profile sections) and semifinished products, cold extrusion is used to manufacture individual workpieces. Today the cold extrusion of steel is well established. Included in this development is its combination with other techniques to give *cold forging* and *cold die forging*. The same holds true for the cold extrusion of cups, cans, and tubes in aluminum, zinc, and so on. The basic processes are subdivided into forward and backward extrusion of solid and hollow bars and cups on the basis of kinematic considerations and the final shape of the workpiece (Fig. 2.14).

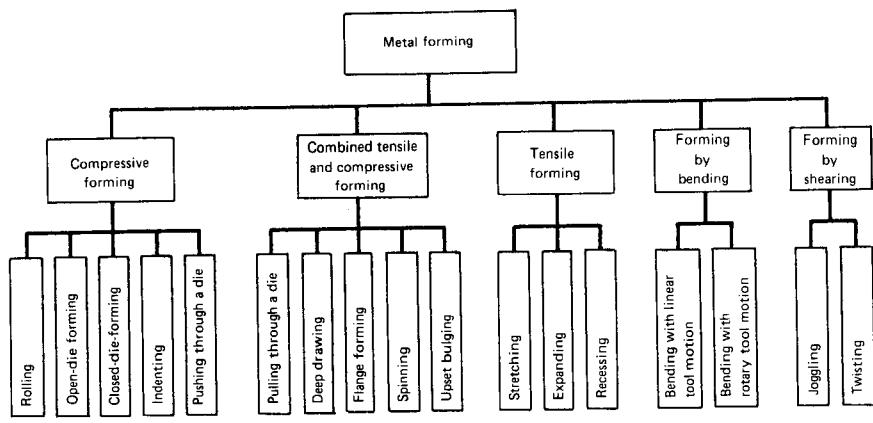


**FIG. 2.4** Classification of metal-forming methods by subgroups. (After [2.2].)

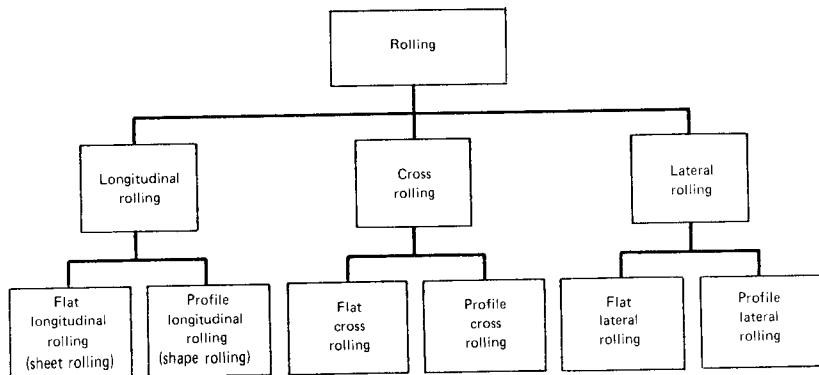


**FIG. 2.5** Classification of rolling processes. (After [2.3].)

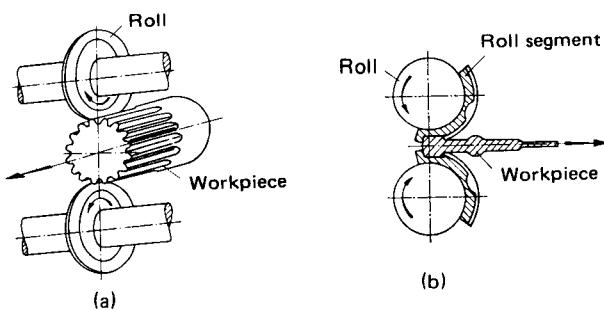


**FIG. 2.6** Examples of longitudinal rolling. (a) Rolling of a splined shaft. (b) Roll forging. (After [2.3].)

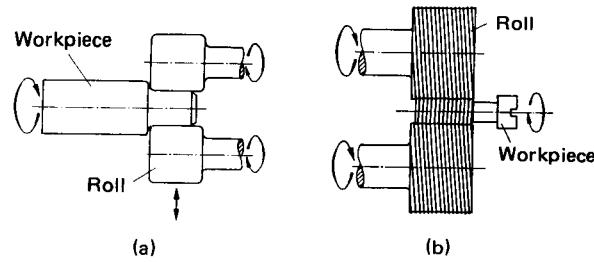


**FIG. 2.7** Examples of cross rolling. (a) Surface burnishing by the plunge method. (b) Thread rolling by the plunge method. (After [2.3].)

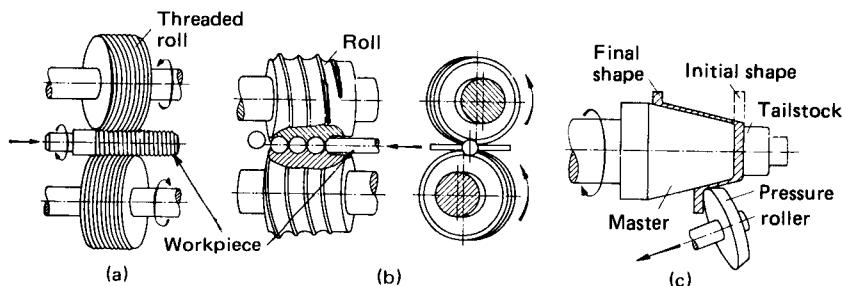


**FIG. 2.8** Examples of lateral rolling. (a) Thread rolling by the run-through method. (b) Lateral rolling of spheres. (c) Flow turning. (After [2.3].)

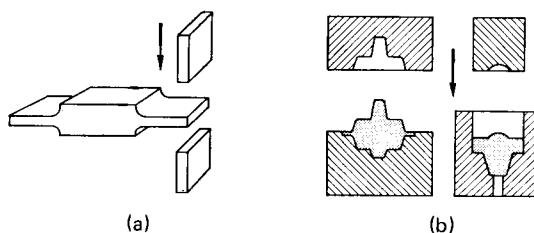


**FIG. 2.9** (a) Free or open-die forming. (b) Closed-die forming.

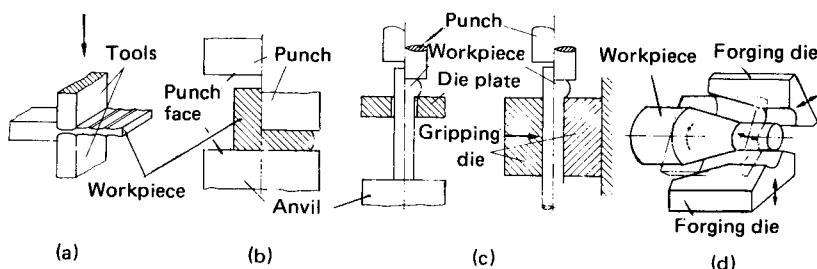


**FIG. 2.10** Examples of open-die-forming processes. (a) Drawing out a solid body. (b) Upsetting. (c) Heading. (d) Rotary or radial forging with axial feed. (After [2.3].)

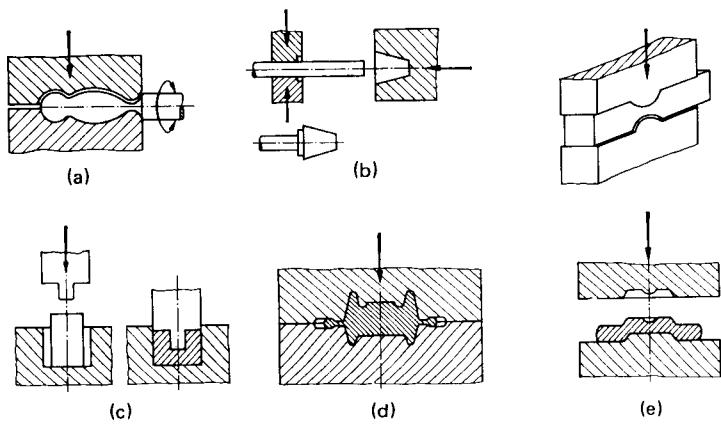


**FIG. 2.11** Examples of die-forming processes. (a) Fullering. (b) Heading in a die. (c) Closed die forging without flash. (d) Closed impression die forging (with flash). (e) Upsetting in a die. (After [2.3].)

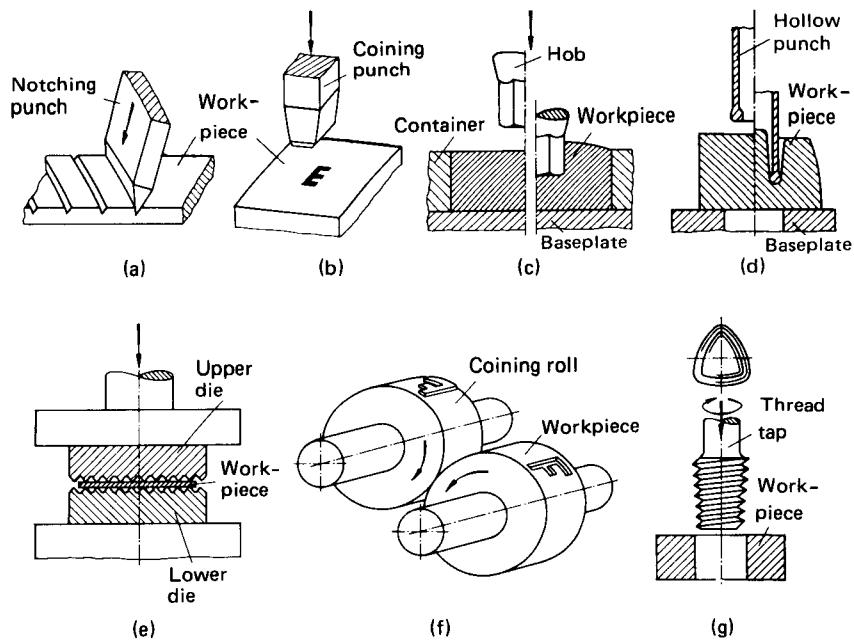


**FIG. 2.12** Examples of indenting processes. (a) Notching. (b) Punching. (c) Die hobbing. (d) Piercing with a hollow punch. (e) Planishing. (f) Roller embossing. (g) Thread tapping. (After [2.3].)

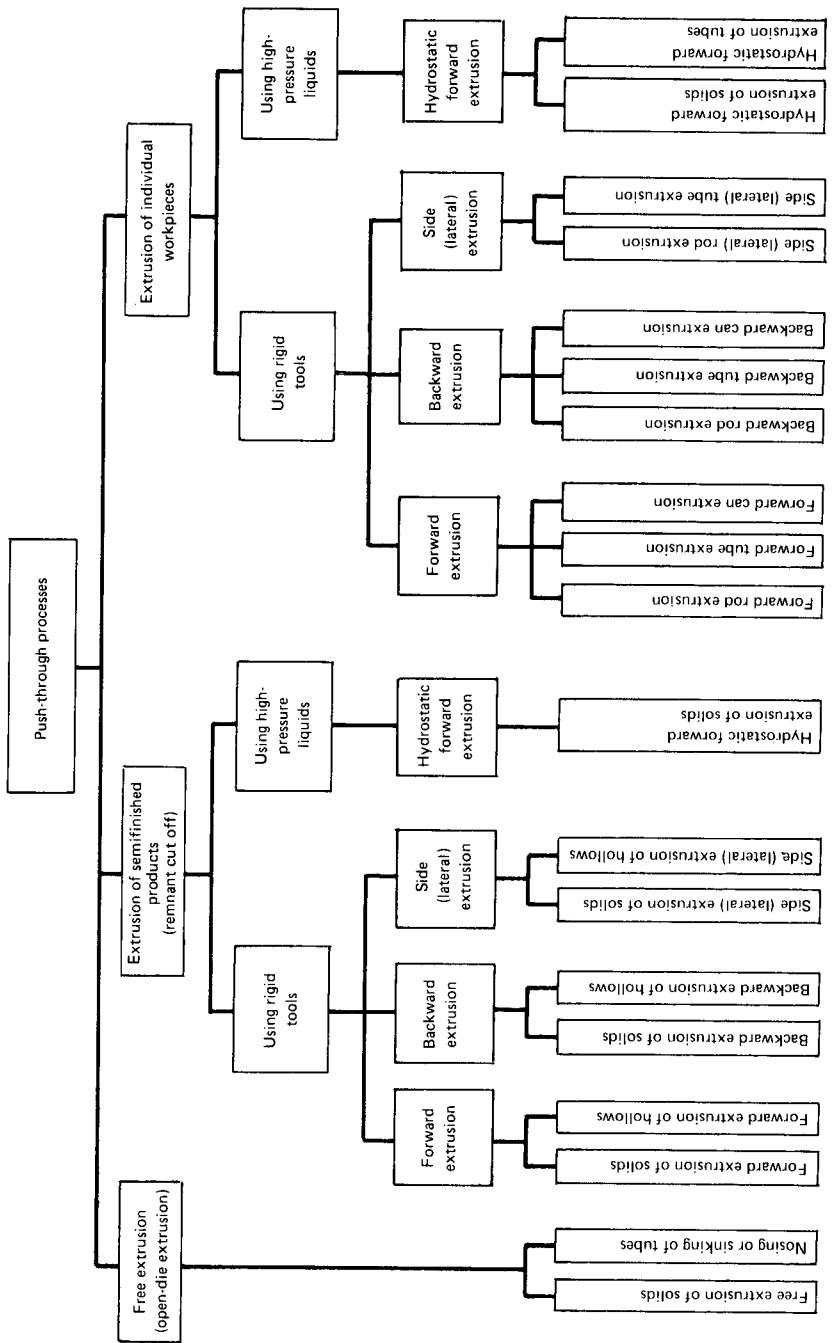


**FIG. 2.13** Classification of the push-through processes. (After [2.3].)

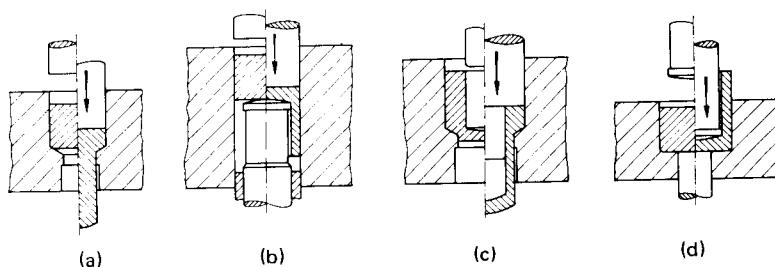


**FIG. 2.14** Basic extrusion processes. (a) Forward extrusion of solids. (b) Forward can extrusion. (c) Forward extrusion of tubes. (d) Backward can extrusion. (After [2.3].)

### 2.2.2 Combined Tensile and Compressive Forming

Group 2 of the metal-forming processes, DIN 8584, encompasses a large number of bulk- and sheet-metal-forming techniques characterized by the widely differing tensile and compressive stresses induced to produce the plastic condition in the deformation zone. The group is divided into five subgroups:

- Pulling through a die
- Deep drawing
- Spinning
- Flange forming
- Upset bulging

The subgroup *pulling through* embraces the well-known processes of bar, rod, wire, tube, and profile drawing with dies or by rolls (Fig. 2.15). In some cases one may detect a certain overlap with the rolling processes used for manufacturing semifinished products, but this is inevitable since the ways in which the different "pure" processes may be combined are almost unlimited. Mention should be made here of ironing (the reduction in wall thickness of hollow bodies), often used in combination with deep drawing, which likewise is a pulling-through process.

*Deep drawing*, which is very important in sheet-metal working, is defined as the combined tensile and compressive deformation of a sheet (or foil, plate, blank, etc.) to form a hollow body, or of a hollow body to form a hollow body of smaller size, without intentional change in sheet thickness. The inclusion of all deep-drawing processes, even those using liquid pressure, shock waves, magnetic fields, and so on, calls for the division of the subgroup into three categories:

- Deep drawing using dies
- Deep drawing using a working medium
- Deep drawing by energy activation

The dies used in the first category may be rigid or pliable (e.g., an elastic cushion or punch), with the former being more common in practice.

The deep drawing of a blank to form a can or cup is referred to as *first draw*, while the subsequent deformation to create a hollow body of smaller diameter is termed *redraw*. Marginal cases are *flanging* and *dishing* in first drawing. An important application of redrawing is *reverse drawing* (Fig. 2.16).

With the methods using elastic tools, a further subdivision was deliberately limited to "deep drawing with an elastic punch" and "deep drawing with an elastic cushion" (Fig. 2.17). Thus it is possible to avoid mentioning the many methods bearing proprietary names, which anyhow say nothing about the processes themselves.

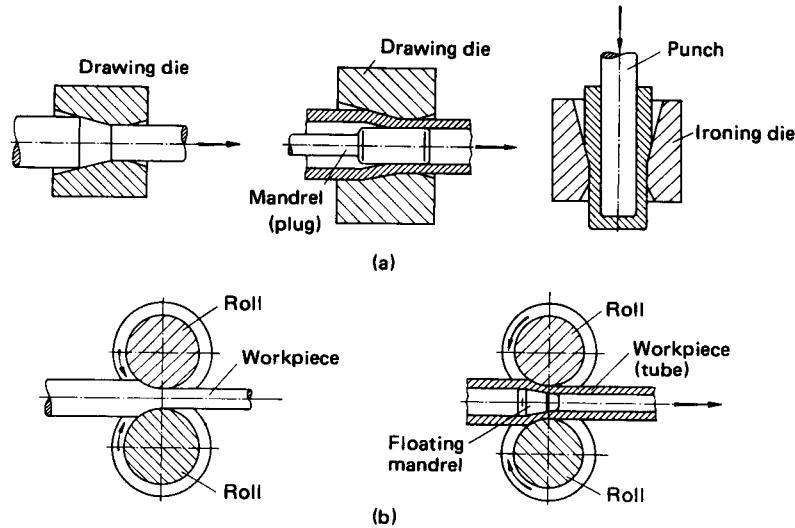


**FIG. 2.15** Basic drawing processes. (a) Drawing through a die (rod drawing, drawing over a fixed mandrel, ironing). (b) Drawing through rolls (wire drawing, drawing over a floating mandrel). (After [2.4].)

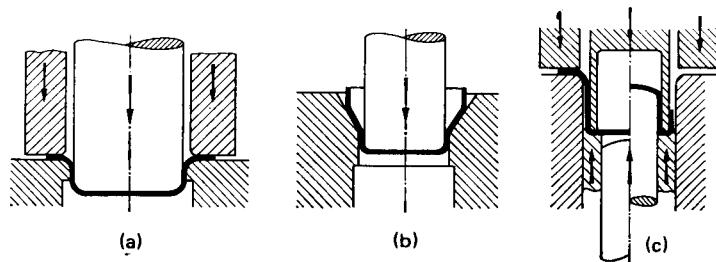


**FIG. 2.16** Basic deep-drawing processes with rigid tools. (a) First draw with blankholder. (b) Redraw without blankholder. (c) Reverse drawing. (After [2.4].)

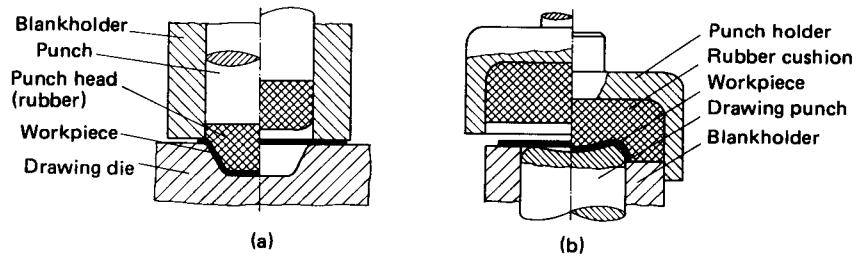


**FIG. 2.17** Basic deep-drawing processes with elastic tools. (a) Deep drawing with a rubber punch. (b) Rubber-pad forming. (After [2.4].)

The pressure media used in deep drawing may be solid particles of undefined shape, liquids, or gases, liquids being the most common in practice. They may transmit either static forces, as with deep drawing using a water bag, membrane, and so on, or kinetic energy (Fig. 2.18).

The pressure wave created by the sudden release of energy may be achieved by detonation of explosives, ignition of a gas mixture, spark discharge, or a sudden release of highly compressed gases. In practice here, too, liquids are used in most cases as the pressure medium, such as for explosive forming of large workpieces in a water tank or for electrohydraulic forming in closed dies.

Finally, deep drawing by means of activating energy may be carried out using a quick-acting electromagnetic field (Fig. 2.19).

The subgroup *spinning* is split up into spinning of hollow bodies (i.e., the deformation of a flat disk to form a hollow body), expanding by spinning, and necking by spinning (Fig. 2.20).

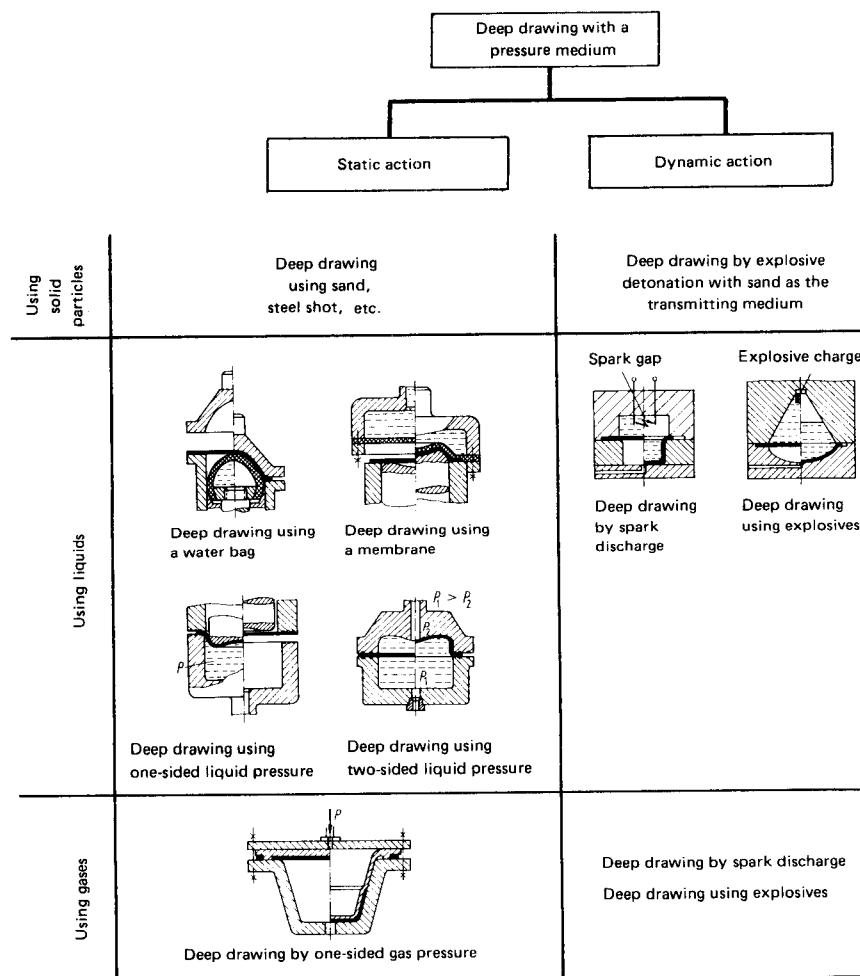
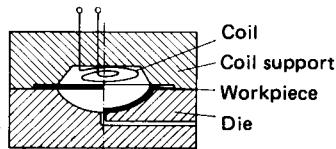
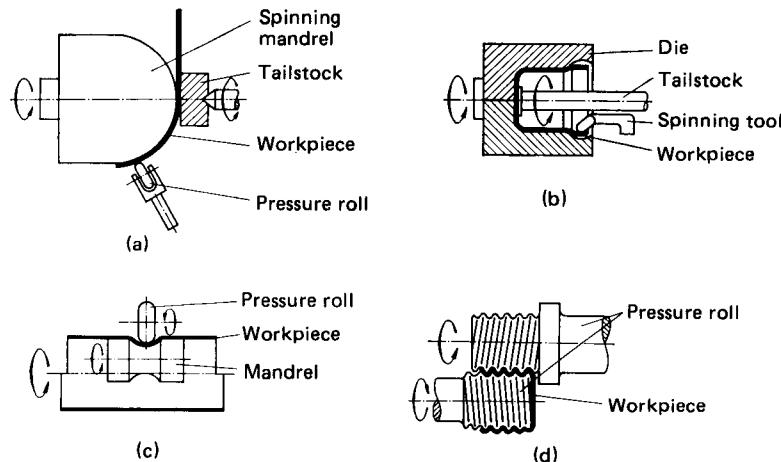


FIG. 2.18 Deep drawing by means of a pressure medium. (After [2.4].)



**FIG. 2.19** Deep drawing by means of energy activation (e.g., electromagnetic field).



**FIG. 2.20** Spinning processes. (a) Spinning of hollow bodies starting from a blank. (b) Expanding by spinning. (c) Necking by spinning. (d) Thread forming by spinning. (After [2.4].)

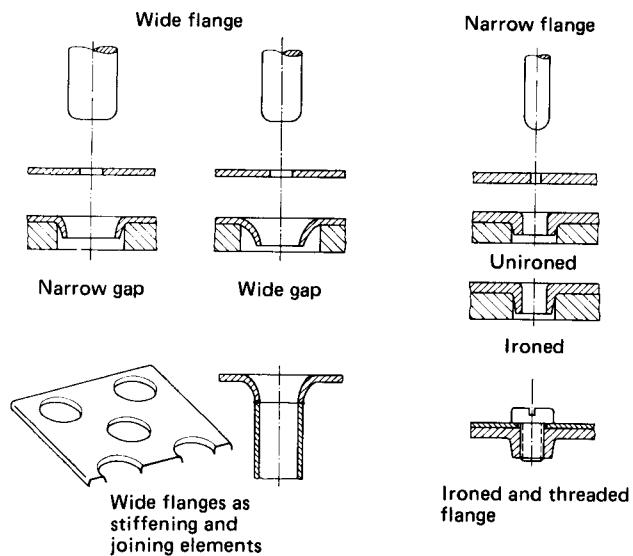


**FIG. 2.21** Flange-forming methods.

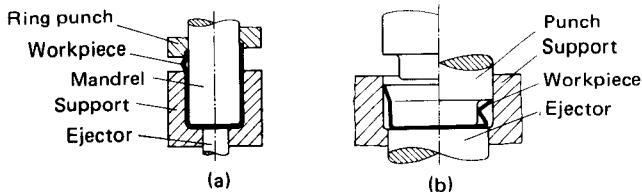


FIG. 2.22 Upset-bulging processes. (a) Outward. (b) Inward. (After [2.4].)

Here again, no change of sheet thickness is intended. With these processes the boundaries between *combined tensile* and *compressive loading* and *tensile loading* or *compressive loading* are often indistinct. Since, however, at some stage in the process (even in the cases of expanding and necking) a combined tensile and compressive loading condition may occur, the spinning processes have been grouped together in one subgroup as shown. The flow-turning processes, on the other hand, with an intentional change in wall thickness, are grouped with the rolling processes, as already mentioned (Fig. 2.8).

The subgroups *flange forming* and *upset bulging* were created because here the combination of tensile and compressive loading stresses is quite different from either pulling through a die or deep drawing. Whereas in those cases there is either radial compression and axial tension or radial tension and tangential compression, in flange forming tangential tensile and radial compressive stresses govern the process, which may be applied either on flat or curved sheets (e.g., tubes), sometimes in combination with piercing and ironing (Fig. 2.21). In upset bulging (e.g., upsetting of a tube), however, there are axial compressive and tangential tensile stresses. The two basic upset-bulging processes are shown in Fig. 2.22.

### 2.2.3 Tensile Forming

Group 3 of the metal-forming processes, DIN 8585, is comprised of three subgroups: stretching, expanding, and recessing.

*Stretching*, characterized by a tensile load in the direction of the longitudinal axis of the workpiece, is mainly used for stretch straightening to remove curvature and twist in rods, tubes, and profile sections as well as unevenness in sheets. The tensile test is an extreme example of this method.

The term *expanding* is used to denote the increase in circumference of a hollow body by means of tangential loading. The processes in this category may be performed by rigid or elastic tools, activating media, or activating energy. Their classification is analogous to that of deep drawing (Fig. 2.23).

The same is true of *recessing*, used to form shallow depressions in flat or curved sheet-metal components by means of tensile loading, the surface area being increased through a reduction in wall thickness (Fig. 2.24). In the category "recessing with a rigid tool" two important processes are *stretch drawing*, where a rigid punch is forced into a sheet-metal blank clamped at the edges, an extreme example of this being the Erichsen test, and *embossing* or deepening with a rigid or elastic punch in an opposed die or tool, where the deepening is small in comparison with the size of the workpiece.

When considering the deep-drawing and recessing processes, one finds that a particular process may be classified as either *tensile and compressive forming* or just plain *tensile forming*, depending on the shape of the workpiece. With irregularly shaped components, different parts of the workpiece will often be stressed differently; for example, they will be subjected to tension, tension and compression, bending, and/or compression. Elements of deep drawing, recessing, bending, embossing, and so on, combine in influencing the design of the tooling. Examples of this are the drawing of auto-body parts or the manufacture in general of hollow bodies from thin sheet. Since in most cases tools are in the form of dies, the combination of the different processes described above should be termed *drawing in a die* or *die forming*.

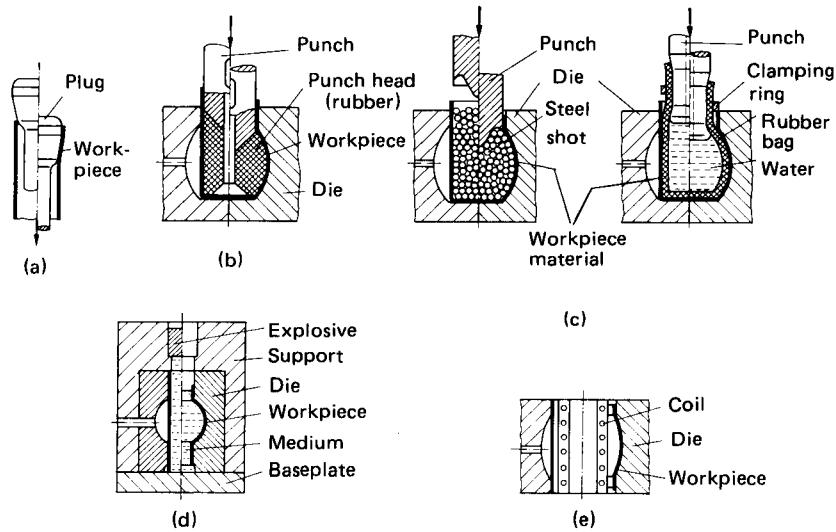


**FIG. 2.23** Expanding (bulging) processes. (a) Expanding with a rigid tool. (b) Expanding with an elastic tool. (c) Expanding by means of a pressure medium (static action) (e.g., steel shot, water bag). (d) Expanding by means of a pressure medium (dynamic action) (e.g., explosive detonation). (e) Expanding by means of energy activation (e.g., electromagnetic field). (After [2.5].)

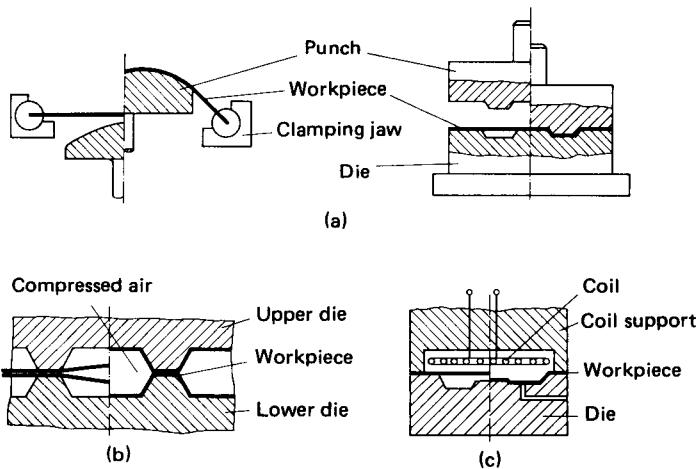


**FIG. 2.24** Shallow and deep recessing processes. (a) Recessing with a rigid tool (e.g., stretch drawing, embossing). (b) Recessing by means of a pressure medium (static action). (c) Recessing by means of energy activation (e.g., electromagnetic field). (After [2.5].)

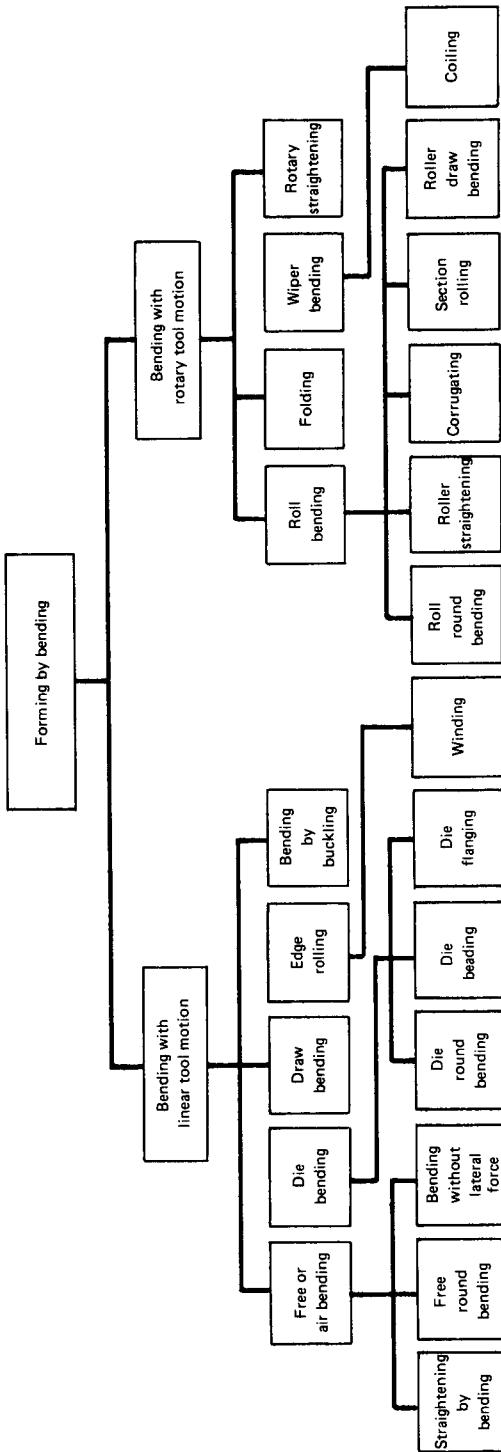


**FIG. 2.25** Classification of bending processes. (After [2.6].)

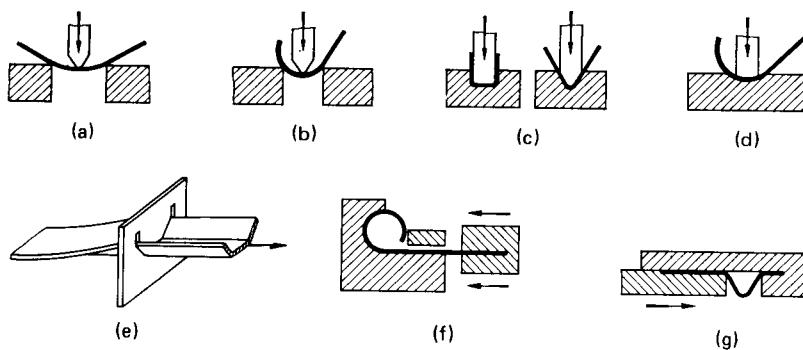


**FIG. 2.26** Examples of formation by bending with linear tool motion. (a) Free or air bending. (b) Free round bending. (c) Die bending. (d) Die round bending. (e) Draw bending. (f) Edge rolling. (g) Bending by buckling. (After [2.6].)

#### 2.2.4 Forming by Bending

This group, DIN 8586, is comprised of the two subgroups *bending with linear tool motion* and *bending with rotary tool motion* (Figs. 2.25 to 2.27). Wherever possible, the word “bending” has been incorporated in the name of the process in question. In some cases the amount of deformation involved may determine which category is most appropriate. For instance, *wiper bending* is termed *coiling* when deformation is over more than  $360^\circ$ . With the systematic approach chosen, intermediate groupings have also had to be defined, such as *roll bending* for the group comprised of *roll round bending*, *roller straightening*, *corrugating*, *section rolling*, and *roll draw bending* (Fig. 2.25).

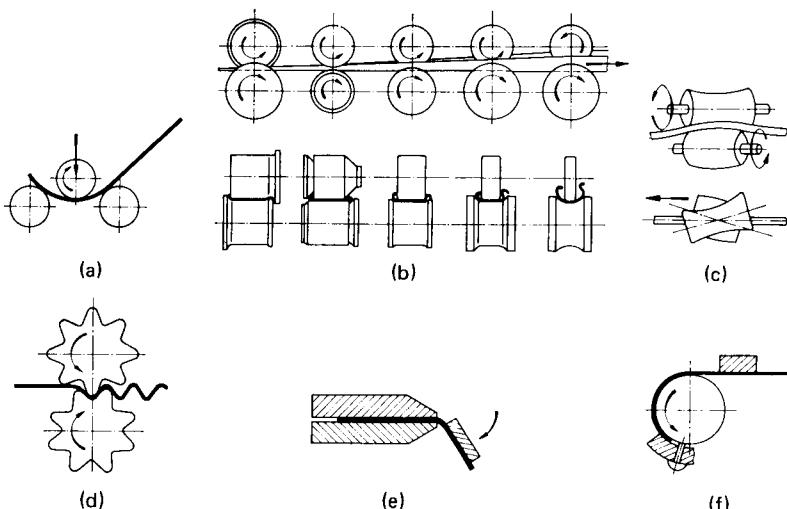


**FIG. 2.27** Examples of formation by bending with rotary tool motion. (a) Roll bending. (b) Section rolling. (c) Roller straightening. (d) Corrugation. (e) Folding. (f) Wiper bending. (After [2.7].)

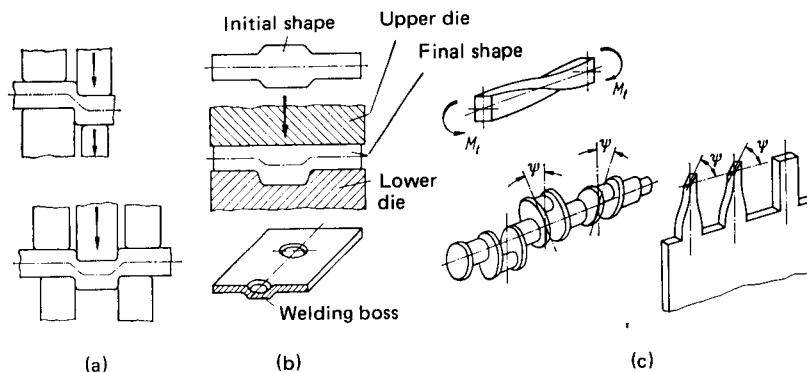


**FIG. 2.28** Shearing deformation processes. (a) Lateral displacement. (b) Embossing. (c) Twisting. (After [2.7].)

### 2.2.5 Forming by Shearing

This last group, DIN 8587, comprises only a small number of processes under the headings *joggling* and *twisting*. In the joggling processes (free and constrained lateral displacement) neighboring cross sections of the workpiece are moved relative to each other in a direction parallel to the applied load, while in the twisting processes (e.g., wrenching) they are rotated relative to each other. Deformation by constrained lateral displacement is used, for example, to form bosses for welding purposes and to locate lugs in sheet-metal components (Fig. 2.28).

The manufacturing process classification system described and the terminology chosen should above all:

- 1 Facilitate education at colleges, universities, and industrial training establishments
- 2 Make a positive contribution to the speed and reliability of both written and oral communications
- 3 Form a firm basis for meaningful discussion with people whose mother tongue is not English
- 4 Provide those involved in process planning in factories with a precise vocabulary from which they can choose appropriate terminology, thus assuring that engineers, technicians, supervisors, and skilled workers speak the same language

## 2.3 BULK FORMING AND SHEET FORMING

In industrial practice relating to metal forming, a distinction is made between the two groups of bulk or massive forming and sheet forming, independent of the classification described in DIN 8582. These terms say nothing more than that in the processes concerned with bulk forming of bars and castings (Fig. 2.29), the material of the workpiece is displaced in all spatial directions, often with very large changes in cross section and hence wall thickness. On the other hand, in sheet-forming processes, blanks are used to make hollow parts with near constant wall thickness, close to the thickness of the original blank. Bulk-deformation processes are characterized principally by multiaxial compressive loading, and the forces involved are in general considerably greater than in sheet forming. As a result, bulk-deformation machines need to be more rigid and generally of sturdier construction than machines used for sheet forming. The same is true for the design of the tools and of the tool materials.

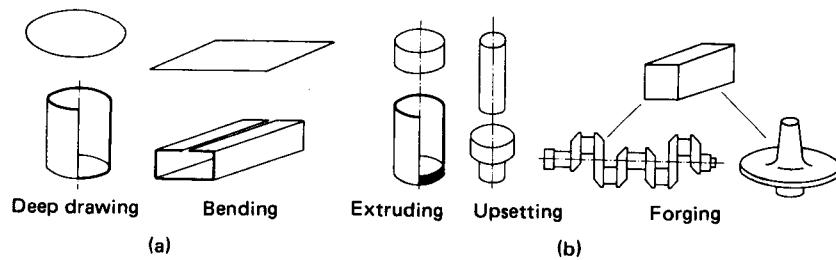


**FIG. 2.29** (a) Sheet forming; (b) bulk or massive deformation. (After [2.16].)

From an historical point of view, bulk deformation is very much older than sheet forming. It can be traced back about 6000 years to the end of the Neolithic Age. In those times the base metal was worked by forging and hammering. With the advent of wrought iron, hot forging became the dominant metal-forming process. It occupied this position for over 2000 years, right up to this century. Only toward the end of the 18th century did it gradually cease to be a predominantly manual process. Producing the raw material for sheet forming, that is, the sheet itself, is one of the most important bulk-deformation processes. While the size limits of sheets produced by forging were roughly 600 by 600 mm (2 by 2 ft) with a thickness of approximately 1 mm (0.04 in), today's rolled sheet is wider, much longer, often very much thinner, and, above all, of more constant thickness. The beginning of modern sheet forming can be traced back to the last third of the 19th century. Besides the ability to make sheet of sufficiently accurate thickness for the important basic process of deep drawing, two further innovations about this time were decisive: the availability of cast steel (a material with better isotropy than puddle steel) and the invention of the double-acting press.

Since then, sheet-working technology has undergone a tremendous development, not the least because of the intense demands of the automobile industry. Today it is not unusual to find that both bulk- and sheet-forming techniques are used in the manufacture of a particular workpiece. In many cases, the results are high workpiece accuracy and low production cost (Fig. 2.30).

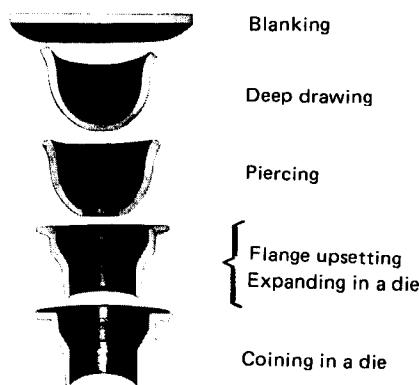


**FIG. 2.30** Example of combined bulk- and sheet-metal forming of a workpiece (production of a flange). (Courtesy of Daimler Benz.)

## 2.4 SYSTEMATIC APPROACH TO METAL-FORMING PROCESSES

A systematic approach developed by W. H. Backofen, E. Gebhardt, O. Kienzle, J. H. Schey, and K. Lange can be used to describe fully all the processes arising in metal forming. It divides the encountered problems into eight areas, ranging from plasticity theory and metallurgical considerations to production questions [2.17], [2.18]. As may be seen from Fig. 2.31, the system is primarily concerned with those points (1 to 6) that are closely linked to the central process. A consideration of many, often very different, processes has shown, however, that the problem areas described by the six points basically remain unchanged. The sketches outlining the process principles, as shown in Fig. 2.32, may thus be interchanged without alteration to the system as a whole. Points 7 and 8 represent the framework within which the production process in question is carried out.

Area 1, the *plastic zone*, concerns the determination of the material behavior in the plastic state. Using plasticity theory and initially assuming an idealized, isotropic material, the stresses, strains, and material flow may be determined. Based on these, the temperature distributions may be found at different locations and for different points in time. Metallurgy allows a description of the behavior of the material on a microscopic scale (anisotropy, textures, etc.).

Area 2 deals with the *characteristics of the workpiece before deformation*. These affect more or less the behavior of the material in the deformation zone and the characteristics of the resulting workpiece. Besides the chemical composition, mechanical properties play an important role here as well as the crystal structure, texture and microstructure (such as grain size, amount, and type of second-phase particles). Apart from the chemical composition, all of the properties mentioned can be changed to a greater or lesser degree by heat treatment. Further, the surface properties and the surface treatment prior to the forming process are also of significance.

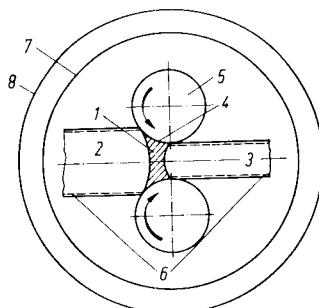


**FIG. 2.31** System of approach to metal-forming problems (example: rolling). (After Backofen, Gebhardt, Kienzle, Lange, and Schey.)

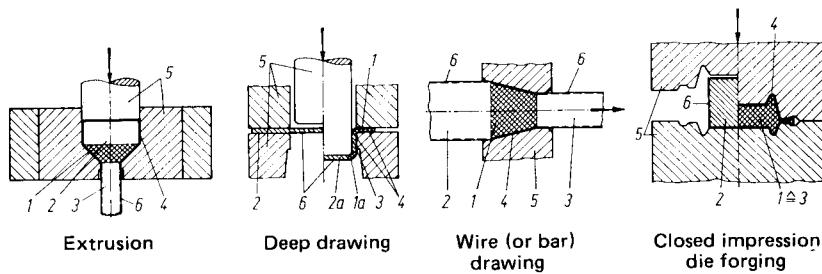


**FIG. 2.32** Sketches illustrating the system of approach to metal-forming problems.

Area 3 concerns the *workpiece characteristics*. These are primarily the mechanical properties, surface properties, and workpiece accuracy *after deformation*. The workpiece characteristics after the forming process largely determine how the component will behave in service (e.g., work hardening in fastener production).

Area 4 considers the *boundary area* between the partly elastic (rigid), partly plastic *workpiece* and the elastic *tool* (= *gap*) and concerns all the questions connected with friction, lubrication, and wear. The interaction of the workpiece and the tool materials plays an important role here. Further, in this area considerable changes in the original workpiece surface may sometimes occur.

A metal-forming operation cannot be regarded in isolation from the *forming tool*. For this reason, area 5 deals with the many-sided problems connected with tool layout and tool materials. Appropriate design (e.g., to achieve the required stiffness of the machine and for guiding moving tool parts with respect to each other) directly influences workpiece accuracy (area 3).

In area 6, which is outside the zone of tool–workpiece interaction, *surface reactions* can take place between the workpiece and the surrounding atmosphere, such as formation of oxides during hot forming or gas absorption when forming exotic metals. On the one hand these operations may considerably affect the resulting surface properties, and on the other hand they may also influence the workpiece characteristics in the same area, for example, with exotic metals through the absorption of small amounts of gases.

The tool–workpiece system (problem areas 1 to 6) is always incorporated in a *machine tool* (e.g., forging hammer, mechanical or hydraulic press, or rolling mill). The machine tool is symbolized by the inner circle, area 7. It must provide the necessary forces for the different operations at each stage of the process and assure sufficiently accurate guiding of the different parts of the tool with respect to each other. This calls for appropriate dimensioning of the tooling and, where necessary, of the workpiece-handling equipment for the application concerned (e.g., bulk forming or sheet forming). Finally, important factors affecting productivity are the stroke rate, setup time, and so on.

Beyond this, area 8 is concerned with the integration of the metal-forming process itself into the production system as a whole. It covers all auxiliary equipment and functions (e.g., heat treating, cleaning, handling, and automation) on the shop floor as well as factory organization (e.g., work preparation, production control, and cost estimation).

The system described is well adapted to aid in the understanding of problems of basic research, applied research, product development, and production, not only in the scientific context but also from the production point of view.

In research and development, a systematic approach appears particularly necessary because on the one hand, the eight problem areas described interact directly and thus cannot be entirely separated from each other; on the other hand, experience gained with different processes may be transferred to other processes in a more or less modified form. In this way, one may hope to establish scientific elements systematically, which, for known conditions, may also be valid for other operations, thereby reducing the time required for research and development of the entire area of forming processes.

## REFERENCES

- 2.1 DIN 8580: "Begriffe der Fertigungsverfahren, Einteilung (Manufacturing Process Terms, Classification)," 1st ed., Oct. 1963.
- 2.2 DIN 8582: "Fertigungsverfahren Umformen (Manufacturing Process: Metal Forming)," 1st ed., 1971.
- 2.3 DIN 8583: "Fertigungsverfahren Druckumformen (Manufacturing Process: Compressive Forming)," sheets 1 and 6, 1st ed., 1969; sheets 2–5, 1st ed., 1970.
- 2.4 DIN 8584: "Fertigungsverfahren Zugdruckumformen (Manufacturing Process: Combined Tensile and Compressive Forming)," 1st ed., 1970.
- 2.5 DIN 8585: "Fertigungsverfahren Zugumformen (Manufacturing Process: Tensile Forming)," sheets 1 and 2, 1st ed., 1970; sheets 3 and 4, 1st ed., 1971.

- 2.6 DIN 8586: "Fertigungsverfahren Biegeumformen (Manufacturing Process: Forming by Bending)," 1st ed., 1970.
- 2.7 DIN 8587: "Fertigungsverfahren Schubumformen (Manufacturing Process: Forming by Shearing)," 1st ed., 1969.
- 2.8 Kienzle, O.: "Terms and Nomenclature of the Manufacturing Processes" (*in German*), *Werkstattstechnik*, **56**, 1966, pp. 169–173.
- 2.9 Lange, K.: "Nomenclature and the Definition of Terms in the Field of Metal Forming" (*in German*), *Ind.-Anz.*, **86**, 1964, pp. 84–85.
- 2.10 Pawelski, O.: "Work on the Standardization of the Terms Concerning Rolling" (*in German*), *Tech. u. Forsch.*, **43**, 1965, pp. 816–820.
- 2.11 Feldmann, H.-D.: "Terms and Nomenclature in Metal Forming" (*in German*), *Werkstatt u. Betr.*, **99**, 1966, pp. 260–262.
- 2.12 Feldmann, H.-D.: "Terms and Nomenclature in Metal Forming" (*in German*), *Draht*, **17**, 1966, pp. 301–304; **18**, 1967, pp. 33–38.
- 2.13 Lange, K.: "Terms and Nomenclature in Metal Forming" (*in German*), *Ind.-Anz.*, **87**, 1965, pp. 1573–1578.
- 2.14 Rechlin, B.: "Terms and Nomenclature for Metal Forming" (*in German*), *Kleipzig Fachber.*, **73**, 1965, pp. 493–496.
- 2.15 Rechlin, B.: "Terms and Nomenclature for the Processes of Forming by Bending and Shearing" (*in German*), *Werkstattstechnik*, **56**, 1966, pp. 173–175.
- 2.16 Lange, K.: "Development Stages of Metal Forming" (*in German*), *Ind.-Anz.*, **87**, 1965, pp. 967–970.
- 2.17 Lange, K.: "Teaching and Research at the Institute of Metal Forming at Stuttgart University" (*in German*), *Ind.-Anz.*, **91**, 1969, pp. 669–670.
- 2.18 Lange, K.: "A System for the Investigation of Metal Forming Processes," in *Proceedings of the 10th International MTDR Conference*, Oxford, Pergamon, 1970.



## FUNDAMENTALS OF METALLURGICAL METAL FORMING

---

---

### List of Special Symbols

---

$a$	atomic distance
$b$	magnitude of Burgers vector
$\mathbf{b}$	Burgers vector
$2c$	crack length
$d$	grain diameter
$d_{sk}$	subgrain diameter
$e$	unit vector perpendicular to slip plane
$g$	unit vector in slip direction
$(hkl)$	Miller indices
$H_1, H_2, H$	half-planes caused by step dislocations
$l_\alpha, l_\beta_1, l_\alpha_2, l_\beta_2$	cosines of direction
$r_0, r_{90}$	$r$ -value (vertical anisotropy); subscripts: angle between testing and rolling direction
$s_1$	slip plane
$S_{y0.01}$	0.01 proof stress
$t$	dislocation line
$T_R$	recrystallization temperature [K]
$T_M$	melting temperature [K]
$u, v, w$	coordinates of lattice points
$[uvw]$	directional indices
$\gamma$	specific surface energy

### 3.2 FUNDAMENTALS OF METAL FORMING

$\lambda, \lambda_1$	angle between stress vector and slip direction
$\mu$	factor of orientation
$\rho$	dislocation density
$\sigma$	stress related to initial cross section
$\sigma'$	stress related to corresponding cross section
$\tau_0$	critical shear stress
$\chi, \chi_1$	angle between stress vector and slip plane
$\top, \perp$	symbols for positive and negative step dislocations
$\odot$	symbol for screw dislocation

The application of metal-forming processes presupposes certain material properties. Under an acting stress caused by external forces, the material must deform like plastic without undergoing a loss in cohesion.

Among the materials having plastic properties, metals occupy the most important position in production engineering. The plastic behavior of metals can be observed in tensile tests. In the tensile test the sample is slowly and continuously extended until it finally breaks. Thereby force is plotted versus extension.

It is usual in materials testing to define stress as the acting force  $F$  per initial cross section  $A_0$ :

$$\sigma = \frac{F}{A_0} \quad (3.1)$$

Correspondingly, strain is defined as the extension  $\Delta l$  divided by initial length:

$$\epsilon = \frac{\Delta l}{l_0} \quad (3.2)$$

The stress  $\sigma$  versus strain  $\epsilon$  gives the stress-strain diagram, as shown in Fig. 3.1. There are two regions of different behavior of materials.

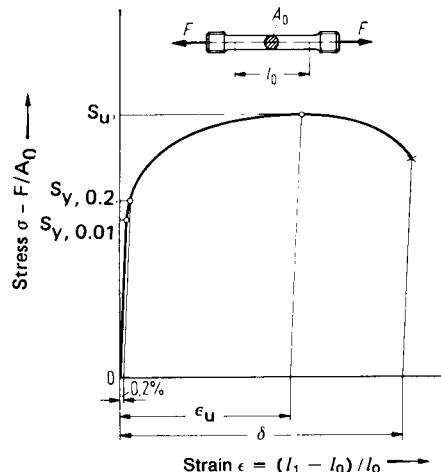


FIG. 3.1 Schematic stress-strain curve of a metal without upper yield stress in tensile test.

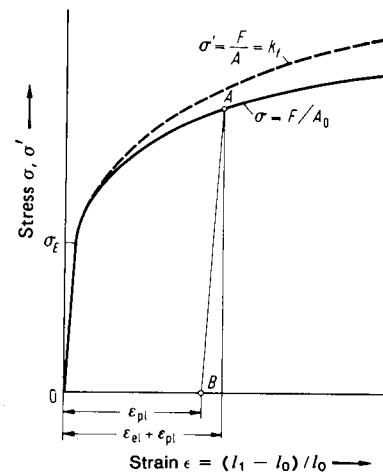


FIG. 3.2 First part of stress-strain diagram.

**Elastic range:** By definition, no permanent deformations are achieved in the elastic range. For metallic materials there is a linear relationship between stress and strain:

$$\sigma = E\epsilon \quad (\text{Hooke's law}) \quad (3.3)$$

The modulus of elasticity  $E$  determines the behavior of a material under normal stresses. The elastic range is limited by the elastic limit  $\sigma_E$  (Fig. 3.2).

**Elastoplastic range:** If the test piece is subjected to stress beyond its elastic limit, the material begins to "flow" like plastic. The sample shows permanent nonproportional elongation even after stress is removed. The term *proof stress* was introduced as a measure of the beginning of the plastic range. Proof stress gives the magnitude of force per initial cross section by which a given permanent nonproportional elongation is obtained. Technically the 0.01 proof stress  $S_{y,0.01}$  (nonproportional elongation of 0.01%), which is also called *technical elastic limit*, together with the 0.2 proof stress  $S_{y,0.2}$  (nonproportional elongation of 0.2%) are important (Fig. 3.1).

For some metallic materials there appears an unsteadiness at the beginning of plastic flow. In this case it is possible to determine a (natural) yield point (see Sec. 3.5). For materials with steady force–elongation curves the 0.2 proof stress is considered the yield point.

Beyond the elastic limit, the total extension under stress is given by the sum of the elastic elongation  $\epsilon_{el}$  and the plastic elongation  $\epsilon_{pl}$ . After release of stress, the plastic elongation  $\epsilon_{pl}$  remains. Fig. 3.2 illustrates this relationship for load applied from 0 to A and the subsequent release of load from A to B.

Metal-forming processes take place in the elastoplastic range. In addition to required permanent deformations, there appears also elastic resilience. Though elastic deformations normally are rather small, their effects must be taken into consideration (e.g., resilience in bending).

In order to achieve true stresses in the longitudinal direction, the force  $F$  must be divided by the instantaneous cross section A:

$$\sigma' = \frac{F}{A} \quad (3.4)$$

For comparison, the stress  $\sigma' = f(\epsilon)$  is plotted in Fig. 3.2. In tensile tests in the range of uniform extension  $\epsilon_u$ , that is, before necking, there is a uniaxial stress state. In this range the stress  $\sigma' = F/A$  in the plastic range corresponds to the yield stress  $\sigma_f$  (see Chap. 4). The stress  $\sigma' = F/A$  increases until fracture. With increasing elongation, the stress required for further deformation also increases: the material hardens (see Sec. 3.4.3).

The above described behavior of a metal is based upon atomistic processes in structure. These processes are examined by methods of metal physics and metallurgy. It is possible, starting from elementary processes, to interpret the observed macroscopic phenomena and to calculate certain characteristic properties.

### 3.1 CRYSTAL STRUCTURE AND TEXTURE OF METALS

Pure metals are chemical elements which are technically used only in special cases (e.g., in electrical engineering, pure copper is used as conductive material). Most metallic materials are alloys of two or more metals. The mechanical properties can be altered through alloying.

A metal consists of a large number of single grains which are separated by grain boundaries. The grains have a crystalline structure and are called *crystallites*. Depending on pretreatment and composition, the grain size can vary in broad ranges (approximately from  $10^{-4}$  mm to 10 mm [ $4 \cdot 10^{-6}$  to 0.4 in]). The orientation of grains, including grain boundaries and structural defects, is termed *texture*.

In a crystal the atoms are arranged in such a manner that their distances are repeated periodically in all directions. This regular atomic arrangement is called *crystal lattice*. The atomic arrangement of each crystal lattice can be described by the concept of an elementary cell (Fig. 3.3). The atoms are in equilibrium at their lattice positions due to forces of attraction and repulsion caused by electrons and nuclei. Crystal structures can be investigated by x-ray diffraction.

### 3.4 FUNDAMENTALS OF METAL FORMING

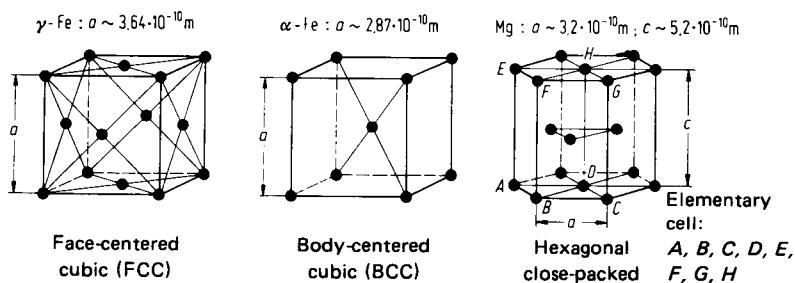


FIG. 3.3 Elementary cells of important crystal systems.

For technically important metals and alloys the three most common crystal structures are:

- 1 Body-centered cubic lattice
- 2 Face-centered cubic lattice
- 3 Hexagonal lattice

The structures of some important metals are given in Table 3.1. A number of metals have different crystal structures at different temperatures. The change of a given structure into another one is termed *phase transformation*. These types of phase transformations occur more often in alloys than in pure metals and are used in some cases to obtain certain material properties. Apart from defects which are explained below, the crystal lattice inside a grain is of regular structure.

The structure and orientation of the lattice (with respect to a coordinate system fixed to the sample) as well as the shapes of grains depend on the prehistory of the metal. The crystal orientation of grains can be statistically random. In general, however, there are certain preferred orientations.

Table 3.1 Crystal Structures of Important Metals.

Crystal structure	Metals having only one structure	Metals having several structures and their temperature ranges
Face-centered cubic (FCC)	Aluminum (Al) Nickel (Ni) Copper (Cu) Silver (Ag) Platinum (Pt) Gold (Au) Lead (Pb)	Iron (Fe) Cobalt (Co) 911–1392°C (1672–2538°F) >1120°C (2048°F)
Body-centered cubic (BCC)	Vanadium (V) Chromium (Cr) Niobium (Nb) Molybdenum (Mo) Tantalum (Ta) Tungsten (W)	Iron (Fe) except 911–1392°C (1672–2538°F) Titanium (Ti) >882°C (1620°F) Zirconium (Zr) >852°C (1566°F) Hafnium (Hf) >1975°C (3587°F)
Hexagonal	Beryllium (Be) Magnesium (Mg) Zinc (Zn)	Titanium (Ti) <882°C (1620°F) Cobalt (Co) <1120°C (2048°F) Zirconium (Zr) <852°C (1566°F) Hafnium (Hf) <1975°C (3587°F)

### 3.2 ELASTIC AND PLASTIC DEFORMATION OF SINGLE CRYSTALS OR PERFECT CRYSTALS

Shape changes of metallic materials by metal forming result from the combined effects of elementary processes within each grain. For an understanding of the mechanisms of plastic deformation, it is useful to neglect at first the interaction between grains and the influence of grain boundaries. For this purpose, single crystals are examined, which in their initial state have no grain boundaries and only a low density of other lattice defects. There are different methods to produce big single crystals which can be used for tensile or upsetting tests. Schmid and Boas [3.9] give a comprehensive overview of single-crystal investigations.

#### 3.2.1 Elastic Deformation

Similarly to Hooke's law for tensile or compressive stresses, there exists a linear relationship between shear stress  $\tau$  and the resulting displacement  $\gamma$ :

$$\tau = G\gamma \quad (3.5)$$

The shape changes are based on translations of atoms in the crystal lattice. This can be explained with the help of a cubic-primitive lattice, where the atoms are positioned at the corners of cubes. Fig. 3.4 demonstrates how an angular change in a perfect crystal is related to the movement of atoms out of their equilibrium positions. In elastic distortion the displacement of atoms is so small that they return to their equilibrium positions after removal of the stress.

#### 3.2.2 Plastic Deformation

There are two basic mechanisms which result in the plastic deformation of metals. Deformed single crystals show gradations on their surfaces which can be explained through the fact that parts of the crystal slip over one another. This leads to the assumption of a coupled atomic displacement (slipping) along a lattice plane (Fig. 3.5). Slipping takes place preferably along certain planes and directions of the crystal lattice (see Fig. 3.6). In general, total slipping amounts to a multiple of the atomic distances in the slip direction. The slip system is formed by a slip plane together with a slip direction lying therein. Theoretical and experimental investigations have found that mostly slip planes are crystallographically closest packed planes, and slip directions are closest packed lattice directions. The number of slip systems has an effect on the plastic behavior of metals. For example, due to a restricted number of slip systems, metals having a hexagonal crystal structure normally can only be deformed in a restricted manner.

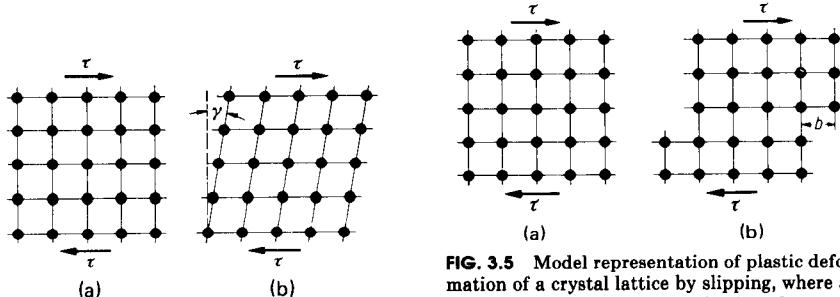


**FIG. 3.4** Elastic distortion of a crystal lattice.  
(a) Initial state, undistorted. (b) Distorted.

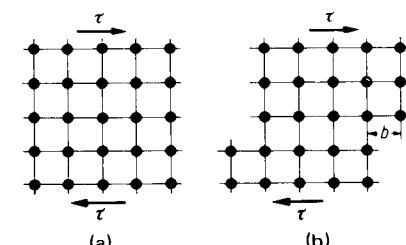


**FIG. 3.5** Model representation of plastic deformation of a crystal lattice by slipping, where all atoms on both sides of the lattice planes are moved at the same time. (a) Initial state. (b) After slipping.

Structure, metals	Slip systems	Number of			Slip systems	Slip planes	Slip directions	Number of Slip systems
		Slip planes	Slip directions	Slip systems				
FCC: Cu, Al, Ni, Pb, Au, Ag, $\gamma$ -Fe		4	3	12		1	3	3
BCC: $\alpha$ -Fe, W, Mo $\beta$ -brass		6	2	12		3	1	3
		12	1	12				
		24	1	24				

Slip plane  Slip direction

**FIG. 3.6** Most important slip systems of some metals. FCC—face-centered cubic crystals; BCC—body-centered cubic crystals.

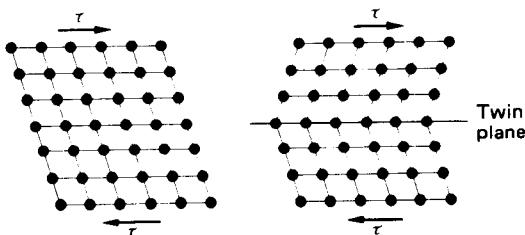


**FIG. 3.7** Scheme of twin formation in crystal lattice.

Investigations on single crystals have led to the result that, in a slip system, plastic deformation through slipping begins when a critical shear stress is reached. For a given stress state, that slip system will be activated first for which the effective shear stress first equals the critical shear stress. According to Schmid's law, the relationship between the stress acting in the axial direction of a single crystal and the shear stress in the slip direction is given by

$$\tau = \sigma_0 \sin \chi \cos \lambda \quad (3.6)$$

Hence the acting stress  $\tau$  in a slip system can be calculated from the magnitude and direction of stress  $\sigma_0$ . Conversely, if the critical shear stress  $\tau_0$  and the orientation  $\chi, \lambda$  of a slip system are known, the normal stress required for slipping to begin is given by

$$\sigma_0 = \frac{\tau_0}{\sin \chi \cos \lambda} \quad (3.7)$$

Another process which leads to plastic deformation is mechanical twinning (see Fig. 3.7). By shear stresses of sufficient magnitude, a part of the crystal lattice is transformed to a twinned position. The plane of symmetry is called *twin plane*.

Contrary to slipping, where the orientation remains unchanged above and below the slip plane, twin formation leads to a change in orientation above the twin plane. The importance of twin formation lies mainly in the fact that a new slip-off is possible following the change in orientation. The stress necessary for twin formation is higher compared to that for slipping. Hence twin formation occurs mainly when slip processes are hindered, such as for face-centered cubic metals at low temperatures or high strain rates. For hexagonal metals the small number of slip systems results in high yield stresses for certain directions and, consequently, in enhanced twin formation.

### 3.3 LATTICE DEFECTS

#### 3.3.1 Types of Lattice Defects

The crystal structure of metallic materials is disturbed by various types of defects. Lattice defects can be subdivided according to their dimensions:

- 1 Zero-dimensional defects (e.g., vacancies, interstitial atoms)
- 2 One-dimensional defects (dislocations)
- 3 Two-dimensional defects (e.g., grain boundaries, twin boundaries, phase boundaries)

Crystals having lattice defects are called *real crystals*. The importance of lattice defects for many properties should not obscure the fact that they occur in relatively low concentration.

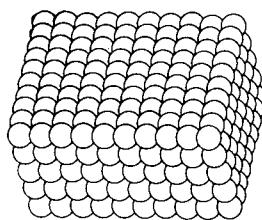


**FIG. 3.8** Sphere model of a perfect crystal in primitive cubic lattice form. (After [3.11].)

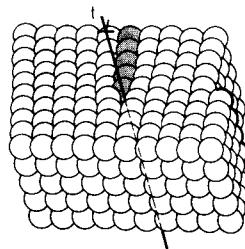


**FIG. 3.9** Crystal with step dislocation.  $t$ —dislocation line. (After [3.11].)

### 3.3.2 Dislocations

G. J. Taylor, E. Orowan, and M. Polanyi submitted theoretically that plastic deformation is caused by the movement of one-dimensional lattice defects (dislocations). In 1952 F. C. Frank succeeded in showing dislocations on the surfaces of crystals by means of an electron microscope. In 1956 P. V. Hirsch and co-workers succeeded in showing dislocations inside crystals [3.10]. For the description of dislocations and their behavior there are essentially two possibilities:

- 1 **Atomistic viewpoint:** Dislocations are considered as defects of crystal lattices built up of atoms.
- 2 **Continuum theory:** Since dislocations distort the crystal lattice in their vicinity, they cause elementary stresses which can be treated by the methods of continuum mechanics.

#### *Types of Dislocations*

The basic types of dislocations can be explained with the help of the primitive cubic lattice in which the atoms are represented by spheres (Figs. 3.8 to 3.10). Fig. 3.8 shows the structure of a perfect crystal. A *step dislocation* (short sign  $\perp$ ) is characterized by a plane ending in the crystal lattice (shaded spheres in Fig. 3.9). The boundary line of this crystal plane is termed the dislocation line  $t$ , which corresponds to the center of maximum distortion of the lattice. Fig. 3.10 represents another basic type, called *screw dislocation* (short sign  $\odot$ ). Here the lattice planes spiral the dislocation line as the axis.

#### *Burgers Circuit and Burgers Vector*

The Burgers vector and the orientation of the dislocation line in the lattice describe the dislocations quantitatively. The *Burgers vector* expresses the distortion of the lattice by dislocations. It can be calculated with the help of the *Burgers circuit*.

Initially, in a perfect crystal, a closed atom-to-atom progressing path is defined (Fig. 3.11a), where the starting point  $O$  and end point  $E$  coincide. Fig. 3.11b represents a corresponding path for a crystal with the step dislocation having a half-plane  $H$ . In this case the path is not closed. The vector connecting the starting and end points is the *Burgers vector* of dislocation.

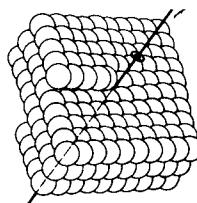


**FIG. 3.10** Crystal with screw dislocation.  $t$ —dislocation line. (After [3.11].)

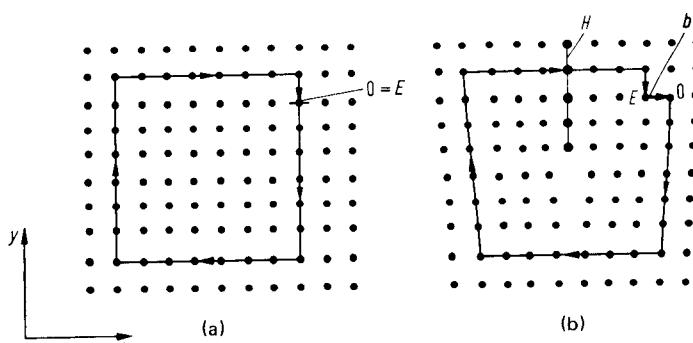


**FIG. 3.11** Burgers circuit. (a) Undistorted crystal. (b) Crystal with step dislocation.

### 3.3.3 Other Types of Lattice Defects

#### Zero-Dimensional Lattice Defects

The most important point defects are vacancies (Fig. 3.12a) and interstitial atoms, which are atoms arranged between exact lattice positions (Fig. 3.12b). These lattice defects have only atomic dimensions in all directions. Vacancies are created and annihilated at kinks and also at grain boundaries. Vacancies are most important for the movement of dislocations and the consequent plastic deformation, because at higher temperatures, step dislocations overcome obstacles by climbing.

#### Two-Dimensional Lattice Defects

Grain boundaries and phase boundaries are the most important two-dimensional lattice defects. A possible subdivision of the grain boundaries is based on the difference of the lattice orientations at the boundaries. Deviations in orientation of up to  $5^\circ$  are called *small-angle* grain boundaries (Fig. 3.13); greater deviations cause *large-angle* grain boundaries [3.8]. Small-angle grain boundaries are built up by dislocations. They are often generated by crystal recovery processes (see Sec. 3.6.2).

During the solidification of melts, nuclei of crystallization are formed which grow until they contact one another. The grains are bound together tightly at their contact planes (large-angle

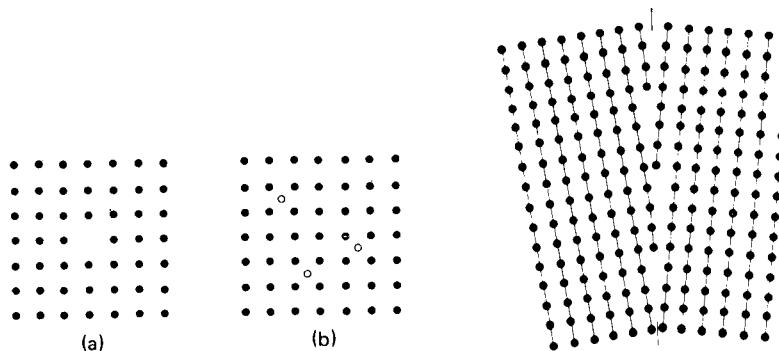


**FIG. 3.12** Scheme of crystal with point defects. (a) Vacancy. (b) Interstitial atoms.

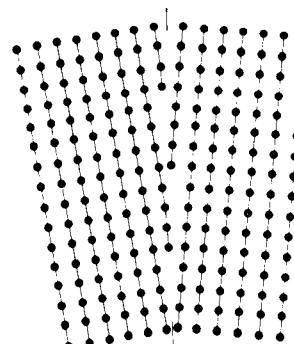


**FIG. 3.13** Scheme of small-angle grain boundary built up by dislocations.

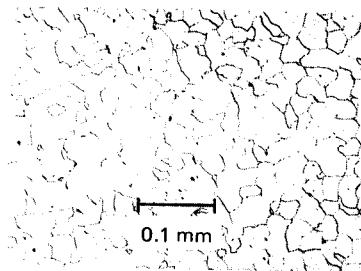


**FIG. 3.14** Structure of low-carbon steel, C10 annealed;  $0.1 \text{ mm} = 3.94 \text{ mil}$ .

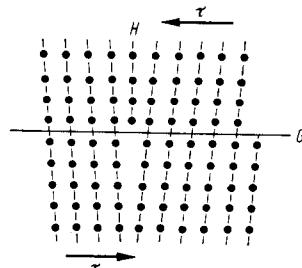


**FIG. 3.15** Crystal lattice with step dislocation.  $H$ —half-plane caused by step dislocations;  $G$ —slip plane.

grain boundaries). Fig. 3.14 demonstrates the grain boundaries of a polycrystalline steel. The boundaries between crystals of the same phase are termed *grain boundaries* in the narrow sense, whereas *phase boundaries* separate grains of different types of crystals.

In large-angle grain boundaries the crystal lattices are undistorted right up to the grain boundaries. The thickness of the grain boundaries, namely, the breadth of the disturbed crystal zone, is 2 to 5 atomic distances at the most.

A special type of grain boundary are the so-called “twin boundaries.” In this case the crystal parts on both sides of the boundary show an orientation relationship (the twin relationship), whereas in all other grain boundaries the orientation relationship can be arbitrary. Grains often consist of subgrains with small orientation differences in the crystal lattice. They are separated by small-angle grain boundaries. At lower temperatures grain boundaries generally have high tensile strength and do not weaken the basic metal. Hence in forced fracture, cracks in deformed metals and alloys appear across the grains at lower temperatures (transcrystalline cleavage). With increasing temperature and slow strain rates, the tensile strength of the grain boundaries decreases more than that of the crystals. In this case cracks grow along the grain boundaries (intercrystalline cleavage). Besides the forming temperature, other factors such as the slip behavior of the lattice, the nonhomogeneous distribution of different atoms, precipitations, and surface effects can determine the crack path.

### 3.4 DISLOCATIONS AND MATERIAL PROPERTIES

#### 3.4.1 Plastic Deformation by Dislocation Movement

Movement of the dislocations is the basic mechanism of plastic deformation. The external forces cause stress fields which are superimposed on those of the dislocations. If the stresses of the resulting stress fields reach a certain magnitude, the dislocations begin to move. To understand the process of dislocation movement, let us consider a step dislocation. Fig. 3.15 is a top view of the crystal with step dislocation illustrated in Fig. 3.9. The half-plane  $H$  traverses fully from the front to the back across the crystal. It ends in the slip plane  $G$ . The movement of the dislocation under shear stress  $\tau$  can be explained by the fact that vertical atom arrays below the slip plane glide against the atoms lying above by one atomic distance to the right. Fig. 3.16a shows a crystal with a step dislocation. Atoms on the plane  $Y$  move to the right due to the acting shear stress. Atom  $A$  takes position  $A'$ , and so on, as shown in Fig. 3.16b. Now plane  $X$  traverses continuously from top to bottom, while plane  $Y$  ends in the slip plane. So the dislocation line has moved by 1 atomic distance to the right. The movement of a dislocation consists of gliding of atoms above and below the slip plane, the dislocation line being the boundary between the sheared and unsheared crystal parts. Fig. 3.16c shows the crystal after completion of the dislocation movement. The upper half of the crystal has sheared by 1 atomic distance along the slip plane against the lower half. Since during the dislocation movement the atoms of a plane do not slip simultaneously but step by step, the force required is much smaller than that for a simultaneous movement.

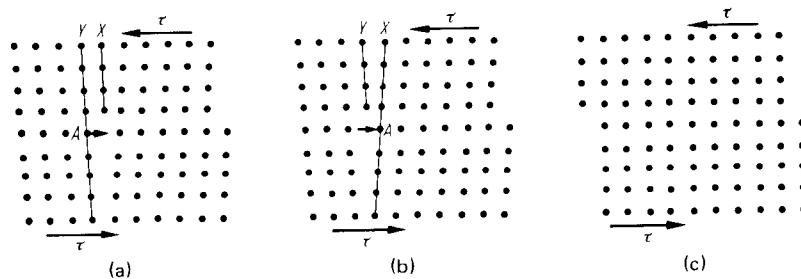


**FIG. 3.16** Slipping by movement of step dislocation. (a) Initial state according to Fig. 3.15. (b) Dislocation having moved to the left for 1 atomic distance. (c) Dislocation having passed through crystal. (After [3.6].)

### 3.4.2 Production of Dislocations and Dislocation Sources

Dislocations are generated during the growth of crystals out of melts. The total slip of a crystal can be estimated from the dislocation density, the length of the dislocation paths, and the amount of the Burgers vectors [3.12].

A typical value of the dislocation density for soft-annealed metals is approximately  $10^7$  dislocations per square centimeter. Estimation of the dislocation density from a measured slip as well as its direct determination under an electron microscope showed that during deformation, multiplication of the dislocations must have occurred. After large deformations, dislocation densities of nearly  $10^{12}$  dislocations per square centimeter were observed under an electron microscope. Dislocations are produced both at grain boundaries and inside grains.

#### Frank-Read Mechanism

According to the Frank-Read mechanism, closed dislocation loops can be produced under shear stress acting in a slip system. Let points *A* and *B* be the knots of a dislocation network on which the dislocation line *AB* is pinned (Fig. 3.17). The line  $\overline{AB}$  lies on a slip plane and bends under the influence of an external stress  $\tau$ . When the dislocation line forms a semicircle, it expands further without additional increase in stress. The dislocation line takes forms 1 to 7 because the force acting on an element of the dislocation line acts vertically to the tangent of this element [3.11]. The segments at points  $C_1$  and  $C_2$  in stage 5 are screw dislocations with opposite signs. Their stress fields evoke attracting forces on the dislocation loops. Finally, dislocations with opposite signs

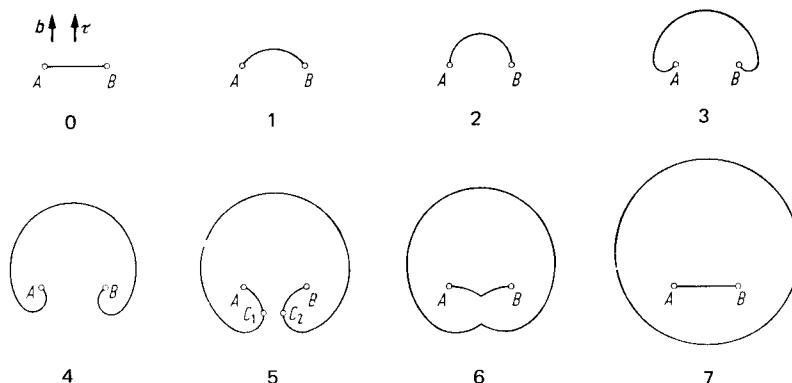


**FIG. 3.17** Different stages of dislocation formation; scheme of Frank-Read source.

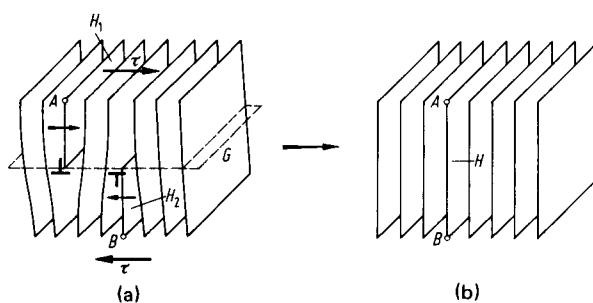


**FIG. 3.18** Annihilation of two step dislocations having opposite signs.

contact one another and annihilate screw. A closed dislocation ring and a new dislocation line  $\overline{AB}$  have emerged, which may now form another dislocation ring (Fig. 3.17, stages 6 and 7). Annihilation of dislocations with opposite signs shall be explained with an example of step dislocation. Fig. 3.18a shows a crystal with a positive step dislocation (short sign  $T$  half-plane  $H_1$ ) and a negative step dislocation (short sign  $T$ , half-plane  $H_2$ ). The crystal lattice is indicated by a group of planes. Both step dislocations move toward each other under the effect of shear stress  $\tau$ . A complete lattice plane  $H$  is formed by both half-planes  $H_1$  and  $H_2$  if they meet. The dislocations are annihilated, and the lattice is now undisturbed (Fig. 3.18b).

A dislocation source cannot produce an unlimited number of dislocations because the produced dislocations are stopped at obstacles, and act back toward the source through their stress fields. Obstacles may consist of stationary dislocations, precipitations, or grain boundaries. The loops of dislocation rings that are lying in the same direction starting from the source have the same sign and repel one another. Thus the dislocations emanating from the source are backing up (Fig. 3.19), resulting in an increase in the stress field so that subsequent dislocations come to a standstill. Finally, the source ceases to function when the effective shear stress is compensated by the stress field of the backed-up dislocations.

The Frank-Read source is only one possibility for the formation of new dislocations under stress. Grain boundaries or boundary planes between crystals of different structures can also act as sources.

### 3.4.3 Strain Hardening

Strain hardening is a phenomenon whereby, during the deformation of metals at lower temperatures, the yield stress increases with increasing strain (see Fig. 4.2). This applies to forming temperatures that are so low that thermally activated processes play no significant role (Sec. 3.6). Strain hardening results in higher forming force and forming work, thus enhancing the load stresses acting on the tool. As a result of strain hardening, in many cases a heat treatment must

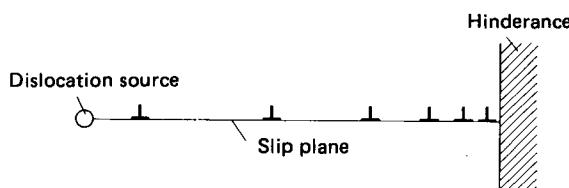


**FIG. 3.19** Congested dislocations between a dislocation source and an obstacle.

take place after each forming operation to increase the formability for obtaining the required deformation. Another possibility is metal forming at elevated temperatures. However, in this case the accuracy and the surface quality of the product are lower than after cold forming.

Besides these undesirable side effects of strain hardening, there is an increase in the strength values of the finished components through forming which is very desirable. Strain hardening can be used for practically all metals and alloys to increase hardness and tensile strength. The increase in yield point and tensile strength permits the use of materials with lower initial strength compared to components produced by machining. Moreover, in many cases heat treatment becomes unnecessary because of strain hardening. However, with increased strain hardening, ductility is reduced.

### *Causes of Strain Hardening*

During metal forming the dislocation density increases by several orders of magnitude. By this, zones of higher dislocation density emerge, which represent a hindrance for moving dislocations (Figs. 3.20 and 3.21). Therefore the dislocations can only pass by or cut across one another at an increased stress. The inner stresses also cause the dislocation sources to be activated again only at higher stresses. The stress fields of the dislocations, which act against the emergence and movement of further dislocations, must be considered as the main cause of strain hardening. In polycrystalline metals, grain boundaries and the difference in orientation of the slip planes between grains act as additional obstacles for the dislocation movement. Fig. 3.22 shows the congestion of dislocations at a grain boundary.

### **3.5 UPPER AND LOWER YIELD POINTS, STRAIN AGING, AND BLUE BRITTLENESS**

A peculiarity of various alloys, particularly of those with interstitial solid solution, is the occurrence of a sharp yield point during the tensile test (Fig. 3.23). Plastic deformation takes place if the stress exceeds the upper yield point  $S_{y,h}$ , from which it drops to the lower yield point  $S_{y,l}$ . The stress only rises again when the strain is further increased by up to several percentage points (Fig. 3.23). Usually the upper yield point is determined by tensile tests. Yield-point values which are given in material standards refer to the upper yield point.

After reaching the upper yield point, deformation in the tensile test specimen does not occur homogeneously, but rather in the form of narrow bands which spread over the specimen. These are called *Lüders' lines*. They can be seen clearly on the polished surfaces of the test specimen. During the sheet-metal-forming processes the inhomogeneous deformation within the yield-point

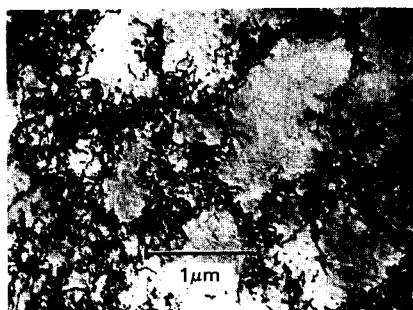


**FIG. 3.20** Structure of dislocation of a weakly deformed metal. Copper rolled; relative height reduction 8%; 1  $\mu\text{m}$  = 40  $\mu\text{in}$ . (After Warlimont.)



**FIG. 3.21** Structure of dislocation of a strongly deformed metal. Copper rolled; relative height reduction 16.6%; 1  $\mu\text{m}$  = 40  $\mu\text{in}$ . (After Warlimont.)

zone can lead to rough surfaces, especially in deep-drawing components which thus become unsuitable for usage. Examples of metals with sharp yield points are steels with low carbon content and aluminum-magnesium alloys.

A theoretical explanation of the sharp yield point has been put forward by Cottrell. Atoms which lie on interstitials (e.g., carbon and nitrogen in most body-centered cubic metals) cause a lattice expansion. For energetic reasons they tend to occupy preferential positions, for example, in tensile stress regions of step dislocations (Fig. 3.24). This leads to a lower lattice distortion and therefore is a state of lower energy compared to the arrangement on undisturbed interstitial positions.

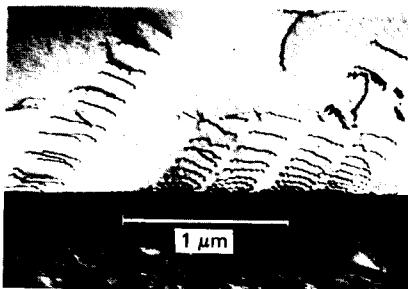


**FIG. 3.22** Congested dislocations at a grain boundary.  $1 \mu\text{m} = 40 \mu\text{in}$ . (After Warlimont.)

and nitrogen atoms move within the crystal because of diffusion, even at room temperature. Increased dislocation densities due to metal forming can accelerate the movement of carbon and nitrogen atoms toward the dislocations. The dislocations are blocked anew, and the yield point rises. Fig. 3.25 illustrates the course of stepped tensile tests. Here curve II indicates the course during faster reloading and curve III during loading after aging has taken place. Apart from the increase in yield point mentioned above, the aging of steels also causes embrittlement. The elongation values are reduced and the ductile-brittle transition temperature of notch toughness is raised. In the case of components under load, this effect must be considered carefully.

The rate of diffusion rises with increasing temperature. In Cottrell's view there should be a temperature range where the rate of diffusion of carbon and nitrogen atoms matches the rate of the dislocation movement. In this temperature range we encounter a higher yield stress since the dragged atoms hinder dislocation movement considerably. In fact, steels with low carbon content show an increase in yield stress of between about 400 and 750 K [3.15]. Due to a simultaneous drop of the elongation values, this process is also called *blue brittleness*.

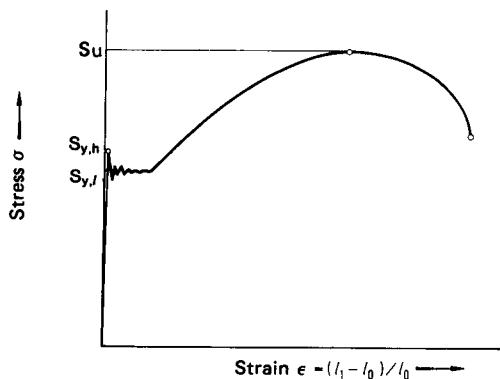


**FIG. 3.23** Stress-strain curve of a metal with sharp yield point.

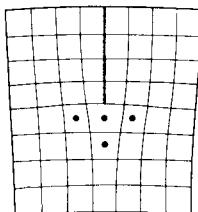


**FIG. 3.24** Interstitials of detached atoms near a step dislocation.

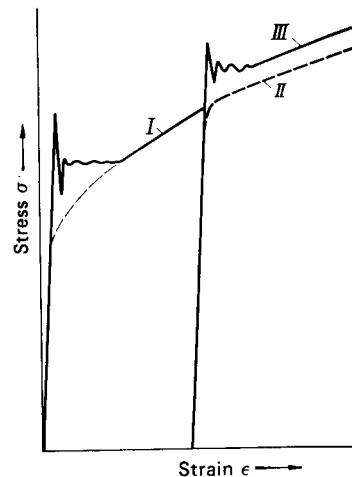


**FIG. 3.25** Effect of age hardening on result of interrupted tensile test. Curve III obtained after age hardening.

## 3.6 THERMALLY ACTIVATED PROCESSES

### 3.6.1 Review

When the temperature is increased, the strength values (yield stress, proof stress, tensile strength) fall and the metal becomes "softer" (Fig. 3.26). Besides, the possible degree of deformation at higher temperatures is, as a rule, greater and the metal becomes more ductile. This change of properties at rising temperatures is widely used for metal forming.

It is desirable in all forming processes to keep the required force and work as small as possible. A further requirement is that the material permit large deformations without loss in its cohesion. This is possible for nearly all metals by choosing a sufficiently high temperature. The disadvantages of hot forming are a higher rate of oxidation, increased gaseous solubility of many metals, and a lower precision of the produced workpieces.

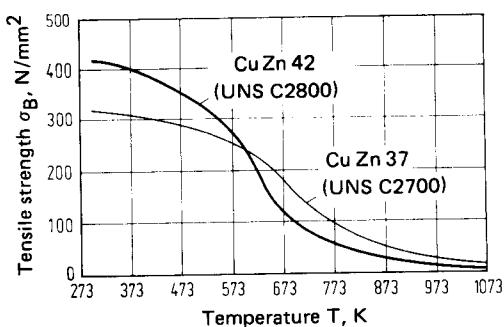


**FIG. 3.26** High-temperature strength of brass. Cu Zn 42, Cu Zn 37; short-time test. (After [3.19].)

Oxidation of the upper surface lowers the surface quality and may cause surface defects. Gas absorption can lead to embrittlement of the material. To avoid this, heating and forming should take place in a protective environment. Another method is forming in the so-called "warm forming range" at intermediate temperatures, which results in a lower rate of oxidation. The temperature range in which thermally activated processes, which lead to changes of the mechanical properties cited, occur to a significant degree, depends on the material, and in particular on its melting temperature. A precise limit cannot be given, since apart from temperature, the time and the degree of deformation appear as effective factors.

DIN 8582 defines the practical procedure of hot forming as forming after addition of heat and cold forming as forming without addition of heat. Since room temperature is selected as the limiting temperature, the definitions of the terms *hot forming* and *cold forming* lose their relationship to metallurgical processes.

An increase in temperature means an increment of energy. At higher temperatures the atom jumps, and movements of the lattice defects are thermally activated, resulting in higher mobility. Therefore small yield stresses suffice to cause deformations. Along with the fact that metals become softer by heating, another decisive factor is that by heating there occurs little or no strain hardening during the forming process. This is due to processes which act against an increase of the dislocation density during forming, that is, it is mainly due to recovery and recrystallization. The effects of recovery and recrystallization on the mechanical properties are similar in many respects [3.16].

According to a more recent definition, all processes belonging to recrystallization are connected to the emergence and shifting of large-angle grain boundaries [3.18]. This is how to distinguish between recrystallization and recovery processes.

Besides in hot forming, where the recovery and recrystallization processes take place simultaneously with deformation, these processes are also used during heat treatment after deformation or between several steps of deformation in order to lower strain hardening and to permit more steps of deformation.

Since thermally activated processes take place at finite rates, the yield stress becomes strongly dependent on the strain rate.

### 3.6.2 Recovery

The plastic behavior of metals is determined by the arrangement and movement of dislocations. Therefore, any changes in properties by heating must be explained by changes of the structure of dislocations or of the dislocation density. The dislocation density rises during deformation at lower temperature. That is why strain hardening takes place (see also Chaps. 4, 5, and 6). This strain hardening can be reduced by changing either the dislocation density or the arrangement of the dislocations.

During lowering of the dislocation density by recovery, dislocations of opposite signs annihilate each other. The remaining dislocations rearrange themselves very often and form subgrain

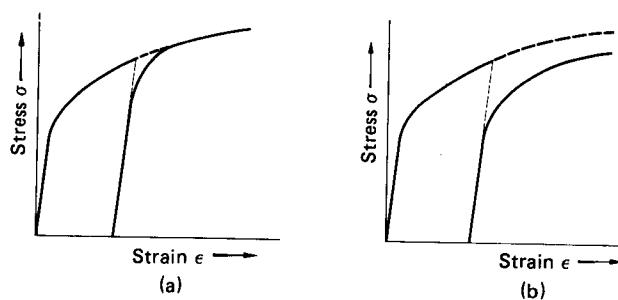


**FIG. 3.27** Effect of recovery annealing on stress-strain diagram.  
(After [3.1].)

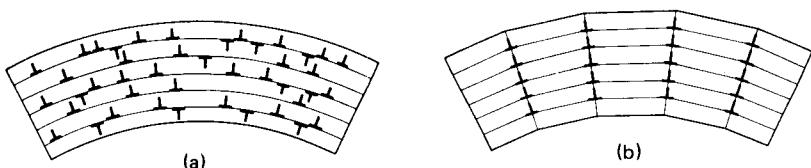


**FIG. 3.28** Scheme of polygonization in a bent crystal. (a) Arrangement of dislocations in bent crystal. (b) Arrangement of dislocations after polygonization.

boundaries. The climbing of step dislocations during the rearrangement of dislocations is viewed as a significant procedure [3.17].

Vacancies are necessary for the climbing of step dislocations. During a forming process they appear in higher concentrations since they are produced continuously through dislocation reactions. As a result, during hot forming, recovery processes can take place much faster than during subsequent annealing [3.17]. For a long time great importance was accorded to recrystallization during hot forming. However, Stüwe [3.14], [3.17] showed that the rate of recrystallization is often too small compared to the rate of deformation in order to form new grains during forming. Thus in many cases the metal does not recrystallize during forming, but rather afterward.

Recovery processes depend strongly on temperature. This can be seen during step tensile tests (Fig. 3.27). Initially the yield point is merely lowered, whereas the yield stress remains nearly constant at higher strain (meta recovery, Fig. 3.27a). The yield stress is reduced at temperatures  $T \gtrsim 0.5 T_M$  (orthorecovery, Fig. 3.27b). The rearrangement and reactions of dislocations during recovery cause changes in structure which can be seen in an electron microscope.

Recovery causes an energetically preferable arrangement of dislocations compared to the "dislocation forest" after deformation. Here dislocations with opposite signs annihilate each other. The remaining dislocations with equal signs arrange themselves to form small-angle grain boundaries (subgrain boundaries). This process of polygonization can be illustrated nicely by bent crystals (Fig. 3.28).

During recovery in deformed metals, subgrains with lower dislocation density emerge, which are separated by small-angle grain boundaries of higher dislocation density (Fig. 3.29).

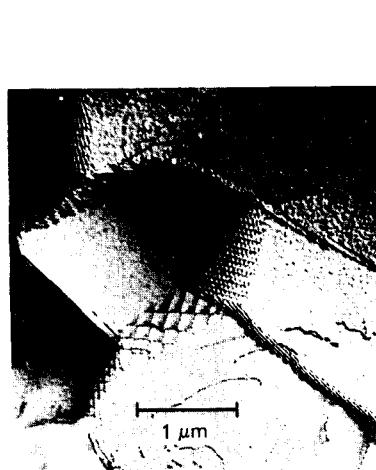


**FIG. 3.29** Subgrain formation during polygonization. Fe - 11.7 Al; 1  $\mu\text{m}$  = 40  $\mu\text{in}$ . (After Warlimont.)

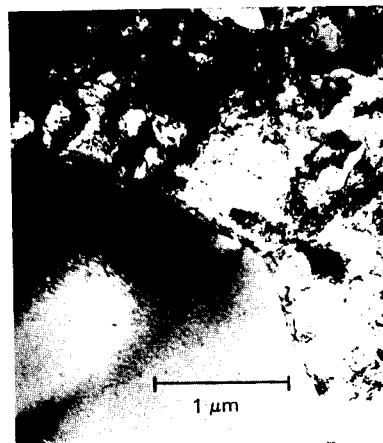


**FIG. 3.30** Recrystallized grain grows in an area of higher dislocation density. Cu<sub>2</sub>Au, cold deformed, annealed at 653 K (380°C); 1  $\mu\text{m}$  = 40  $\mu\text{in}$ . (After Warlimont.)

### 3.6.3 Recrystallization and Grain Growth

Recrystallization takes place at higher temperatures than recovery. It consists of processes which lead to the emergence and shifting of large-angle grain boundaries (Fig. 3.30).

In the beginning a new formation of grains takes place in the deformed structure. This process is called *primary recrystallization*. In primary recrystallized metals further recrystallization processes may take place: secondary recrystallization and grain growth.

#### Primary Recrystallization

During primary recrystallization there is a dependence of the new formation of grains and grain growth on strain, temperature, and annealing time. The following relationships can be summed up qualitatively [3.1]:

- 1 Recrystallization occurs only if a certain minimum dislocation density is available. To attain that, a certain degree of deformation must be exceeded.
- 2 The higher the previous deformation, the smaller is the temperature at which recrystallization occurs.
- 3 Through an increase of annealing time, recrystallization can be achieved at lower temperatures.
- 4 After recrystallization the grain size will be larger, the smaller the deformation (more than the minimum value mentioned under point 1) and the higher the annealing temperature has been.

In pure metals even small impurities can increase the temperature of recrystallization considerably.

From the preceding it is evident that the temperature at which recrystallization takes place does not only depend on the metal alone, but on a whole number of variables. Besides, no unified definition is used for the temperature of recrystallization. According to Reed-Hill [3.6] the recrystallization temperature is the temperature at which a metal by means of a certain cold-forming method within a limited time interval (normally 1 h) recrystallizes completely. For technically pure metals at high strain, a rough estimate is given by

$$T_R \geq (0.4-0.5)T_M \text{ [K]} \quad (3.8)$$

The relationship between grain size, temperature of recrystallization, and strain is often illustrated in three-dimensional diagrams (Fig. 3.31).

In cases of small strain the dislocation density as well as the number of growing grains are small. The result is the formation of coarse grains at low strains and high temperatures. The formation of coarse grains is especially undesirable in sheet-metal forming if, after recrystallization annealing, further forming processes are carried out which roughen the surface.

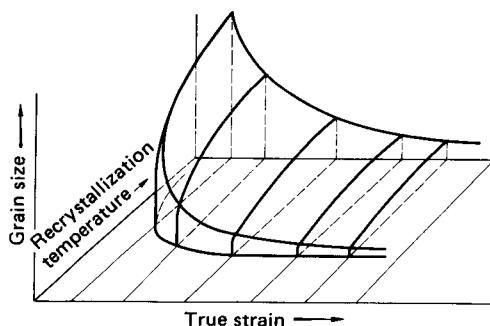


**FIG. 3.31** Scheme of recrystallization diagram.  
(After [3.3].)

Recrystallization can be strongly affected by precipitation processes which can occur earlier or simultaneously. Depending on their sizes and shapes, the precipitations can strongly hinder the formation and the movement of grain boundaries. These relationships are used to achieve the desired size, form, and orientation of grains during recrystallization.

### **Secondary Recrystallization and Grain Growth**

The primary recrystallized structure is not yet in thermodynamic equilibrium. The grain boundaries possess an energy similar to the surface energy of a soap bubble having the same surface stress. At high temperatures and long annealing times, further grain growth processes take place in the primary recrystallized structure. The driving force is thereby the energy gain due to a lowering of the ratio of the grain boundary area to the enclosed volume [3.1].

Two processes are distinguished during grain growth: secondary recrystallization and grain growth. In secondary recrystallization only individual grains grow preferentially. Hence during this process, very large grains are present near the primarily recrystallized grains. The structure may finally consist of very large individual grains.

Contrary to secondary recrystallization, there is an increase in the average grain diameters during grain growth. In general, secondary recrystallization and grain growth cause a deterioration of the mechanical properties. The decrease in the elongation values is particularly unfavorable. In addition, due to the large grain sizes, a rough surface with large average grain diameters is obtained during deep drawing, stretch forming, and bending.

#### **3.6.4 Static and Dynamic Changes of Structure during Hot Forming**

Recrystallization and recovery not only occur during annealing of cold-formed metals, they also determine the forming behavior and structure adjustment during hot forming.

It is usual to speak of dynamic recrystallization and dynamic crystal recovery if these processes take place within the forming zone, namely, during plastic deformation at corresponding stresses and strain rates. New dislocations and vacancies are thereby produced continuously. A new state of equilibrium may be achieved through dynamic recovery and recrystallization. The rates of crystal recovery and recrystallization are enhanced considerably by the high concentration of vacancies during deformation as compared to the static case. Contrary to this, recrystallization and crystal recovery during annealing, heating, or cooling are termed *static* since, in this case, there is a change in a given structure. During hot forming (e.g., extruding, hot rolling, or forging), the initial structure changes itself within the deforming zone through dynamic recrystallization and undergoes, as a rule, a further change during cooling through subsequent static processes (Fig. 3.32). The volume fraction of material which undergoes dynamic recovery and recrystallization in the forming zone is determined by the material (stacking fault energy) and by the forming conditions, particularly strain.

From the standpoint of material, stacking fault energy is the parameter (see Chap. 4) that determines the structure of dislocations and, therefore, the behavior of recrystallization and recovery. Dynamic and static recovery are strongly encouraged in metals with high stacking fault energy (aluminum,  $\alpha$ -Fe, ferritic alloys).

The partial dislocations are close to each other at high stacking fault energy. Therefore climb and cross-slip processes of dislocations, which cause crystal recovery, can easily take place [3.19].

As shown in Fig. 3.32, the processes in the forming zone and the structure of formed work-pieces depend on the following parameters:

- Initial structure
- Material (stacking fault energy)
- Strain rate (dynamic)
- Strain (static)
- Temperature

کتابخانه تخصصی و مرکز استناد  
دانش و پژوهشکده شهید باکری

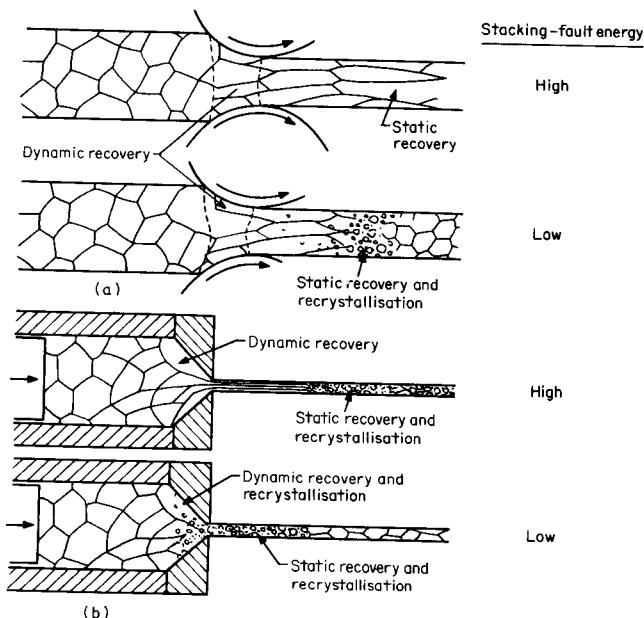


**FIG. 3.32** Static and dynamic structure deformations during hot forming. (a) Hot rolling with small reduction in thickness (e.g.  $E_h = 50\%$ ). (b) Extrusion with large reduction in cross section (e.g.,  $E_a = 99\%$ ). (After [3.27].)

During hot forming, it is possible to control the final structure by forming conditions and a cooling-heating treatment. Examples of such thermomechanical treatments are nickel-based dispersion alloys and drop forging of steels which are chilled and tempered.

Dynamic recovery and recrystallization processes affect the course of the flow curves (see Chap. 4) in a typical manner. Hot flow curves with constant or slightly falling yield stress are typical for dynamic recovery (Fig. 3.33a). On the contrary, the flow curves during dynamic recrystallization (after initial hardening) show a sudden decrease in yield stress which then adopts a constant or slightly falling course (Fig. 3.33b).

### ***Dynamic Recovery***

The course of dynamic recovery can be observed on the flow curves (Fig. 3.33a). A considerable increase of dislocation density occurs during the hardening phase, phase I. The dislocations are enmeshed and form a cell structure within the grains.

As the flow curves reach the stationary phase, phase II, subgrains form themselves [3.19]. Their size, uniformity, and orientation depend on the metal, the strain rate, and the temperature. The main parameters of the subgrains, namely, the dislocation density between the dislocation walls, their average distances, and the mutual differences in orientation, do not change during phase II of the flow curves. The yield stress  $\sigma_f$  is, to a good approximation, inversely proportional to the subgrain size  $d_{sk}$  (Fig. 3.34):

$$\sigma_f \sim d_{sk}^{-1} \quad (3.9)$$

Even at large strains the subgrains remain unstretched compared to the grains which distort themselves in proportion to the deformation [3.19].

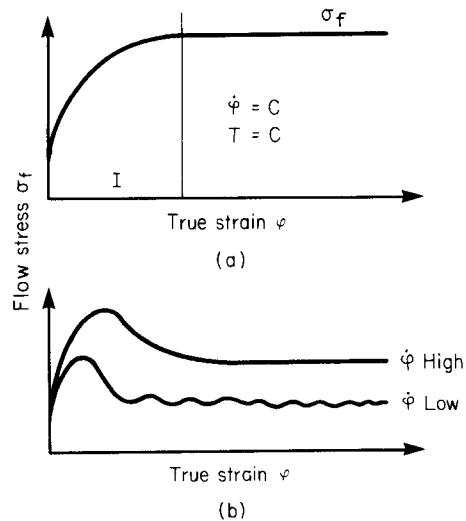


**FIG. 3.33** Schematic form of hot flow curves by dynamic softening. (a) Dynamic recovery alone. (b) Both dynamic recovery and recrystallization.

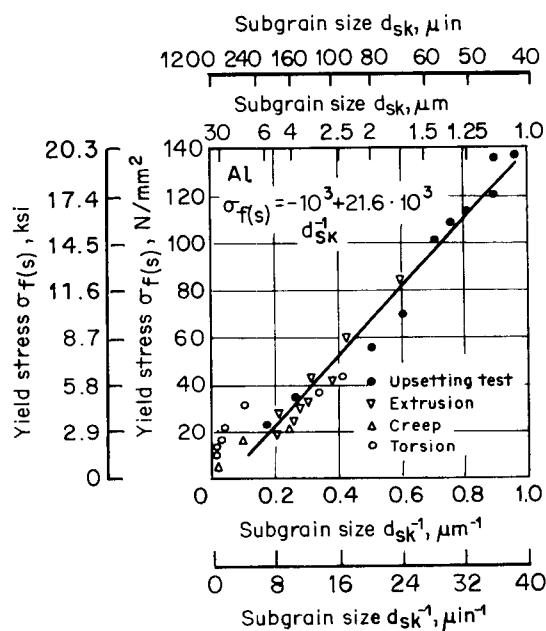


**FIG. 3.34** Relationship between yield stress  $\sigma$  in stationary zone of hot flow curve and subgrain diameter  $d_{sk}$  for technically pure aluminum. (After [3.27].)

There exists a dynamic equilibrium between the formation of dislocations and annihilation, which leads to a constant dislocation density and constant yield stress. As shown in Fig. 3.34, the relationship between subgrain size and yield stress is also of significance for subsequent static recrystallization since the grain size of the recrystallized structure is influenced by it. The rate of formation of dislocations depends on the effective stress and the strain rate. On the other hand, the rate of decrease of the dislocations through recovery is a function of the dislocation density as well as of the conditions for climbing and cross slip, especially the concentration of vacancies and the stacking fault energy. Hence it is understood that dynamic recovery occurs more easily in metals with higher stacking fault energy where the small gap between partial dislocations facilitates combination, climbing, and cross slip [3.19], [3.26]. In face-centered cubic metals, which have relatively high stacking fault energies (aluminum,  $\alpha$ -Fe, ferritic steels), dynamic recovery always takes place [3.26]. Similar conditions apply for hexagonal metals (zinc, zirconium), where dynamic recovery occurs in the same way [3.19], [3.26].

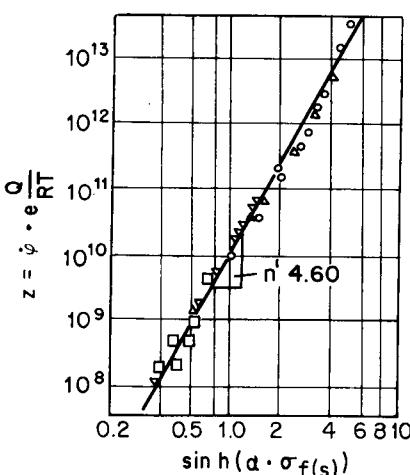


FIG. 3.35 Relationship between temperature-compensated strain rate  $Z = e^{-Qrt}$  and stationary yield stress  $\sigma_f$ . (After [3.26].)

which in turn favors dynamic recrystallization. The yield stress of metals in which dynamic recovery determines the stationary part,  $\sigma_f = f(\dot{\phi}T)$ , can be described by the following equation [3.26]:

$$\sigma_f = f(\dot{\phi} e^{Q/RT}) = f(Z) \quad (3.10)$$

where  $Q$  = activating energy (self-diffusion, creep, hot forming)

$R$  = gas constant

$T$  = absolute temperature [K]

$Z$  = temperature-compensated strain rate

Fig. 3.35 shows that this functional relationship can be represented in a double logarithmic plot by a straight line of the form

$$Z = \dot{\phi} e^{Q/RT} = A (\sinh \alpha \cdot \sigma_f)^{n'} \quad (3.11)$$

where  $A, \alpha$  = constants

$n'$  = exponent of the slope

Eqs. 3.10 and 3.11 prove that diffusion-regulated processes play an important role during dynamic recovery, such as climbing of dislocations. Eq. 3.11 permits a simple representation of the relationship  $\sigma_f = f(\dot{\phi}, T)$  for the stationary range of hot flow curves during dynamic recovery (see also Chap. 4).

### Dynamic Recrystallization

The occurrence of dynamic recrystallization changes the flow curve in a characteristic manner (Fig. 3.33b). In most forming processes that have relatively high strain rates, a decrease in yield

stress occurs after the hot flow curve has reached a maximum and a subsequent transition in a plateau. This is the result of continuous fast and dynamic recrystallization. At lower strain rates, waves are often observed in the flow curves. These waves are due to repeated dynamic recrystallization.

Regions of nearly constant yield stress are also obtained during dynamic recrystallization (Fig. 3.33b). In this case there is a dynamic equilibrium between dislocation formation and annihilation. This also leads to a constant grain size for this state of equilibrium. At the start of dynamic recrystallization there is a critical strain which is about 20% lower than the strain at which the maximum of the flow curve is obtained. The yield stresses associated with dynamic recrystallization are lower (for the stationary region) than when only dynamic recovery takes place.

The first prerequisite for dynamic recrystallization is that deformation exceed the critical value  $\epsilon_c$ . However, as a rule, dynamic recrystallization in metals and alloys occurs mainly if they show only little dynamic recovery. These are predominantly metals and alloys with lower stacking fault energy, such as copper and copper alloys, nickel and nickel alloys, and austenitic steels. It must, however, be emphasized that dynamic recovery always precedes dynamic recrystallization or runs in parallel. It is hardly a question of whether one process or the other takes place, but rather of how much a part each process plays in softening (Fig. 3.32). Dynamic recovery occurs exclusively at smaller strains below the maximum of the flow curve (e.g., small reductions of thickness during rolling). It is facilitated by a stacking fault energy which favors the climbing of dislocations.

At high strains (e.g., extruding) and difficult climbing of dislocations (low stacking fault energy), dynamic recrystallization is predominant.

### 3.7 ANISOTROPY

In many forming processes it is possible to start with the conception that a polycrystalline metallic material behaves like an isotropic one and has equal properties in all directions. A refined method of observation must take into consideration the influence of direction on the material properties. A well-known example of the effect of anisotropy is the earing of metal sheets during deep drawing. During deep drawing the limit drawing ratio of metal sheets depends also on normal anisotropy. In bulk forming the anisotropy of plastic properties affects material flow and the properties of the workpiece (Fig. 3.36).

From the standpoint of forming technology, elastic and plastic anisotropy as well as anisotropic strain hardening are of importance. The causes of mechanical anisotropy lie in crystal anisotropy combined with texture and in structure anisotropy, which is produced by the alignment of certain structure elements like grain boundaries or phases.

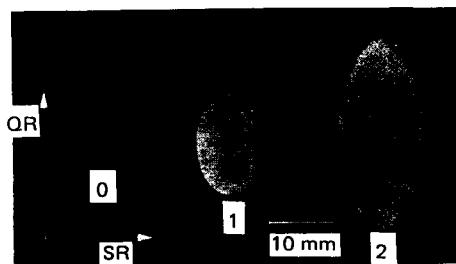


**FIG. 3.36** Change in the end face form of an initial circular cylindrical sample during upsetting. SR = extrusion direction; QR = cross direction; 10 mm = 0.4 in. (After [3.20].)

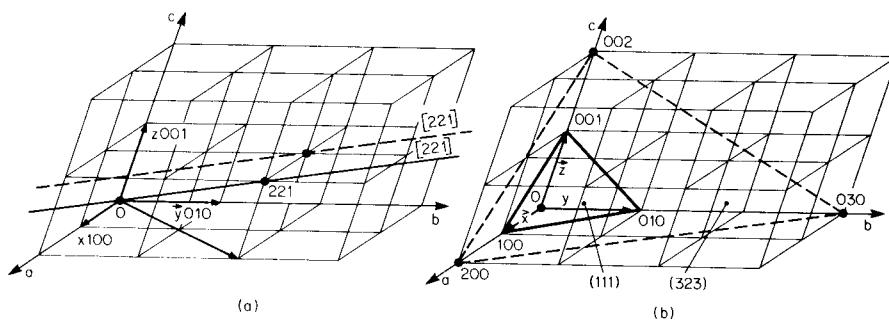


FIG. 3.37 Indexes of (a) lattice directions and (b) lattice planes.

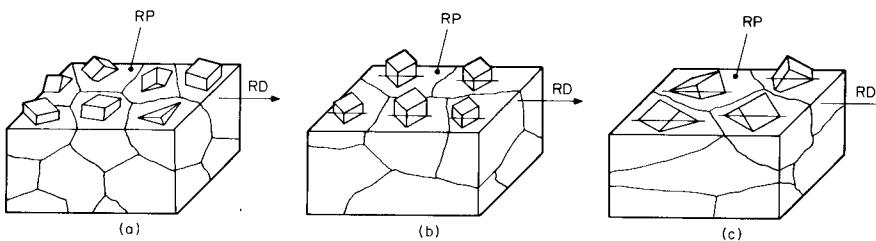
### 3.7.1 Crystal Anisotropy and Structure Anisotropy

An analytical description of the space lattice is a prerequisite for a clear understanding. Each of the lattice points can be represented by a vector. To mark a lattice line, a straight line is drawn through the zero point in the desired direction, and the coordinates of a point are determined on it (Fig. 3.37a). The smallest whole-number triple of coordinates is taken as the index of the direction and is put in square brackets. The indexes of direction are generally shown in the form  $[uvw]$ . A lattice plane is uniquely defined by the coordinates on three axial intercepts (Fig. 3.37b). To avoid large numbers and to achieve the same indexes for parallel planes, the reciprocal axial intercepts are utilized. The smallest integers proportional to the inverse axial intercepts are united in a triple and written in parentheses. The indexes shown in the form  $(hkl)$  are called *Miller indexes* [3.1], [3.20]. Here the minus sign is not put in front of, but above the number concerned, such as  $(12\bar{3})$ .

In polycrystalline materials, crystal anisotropy is only noticeable if there is a preferred orientation, that is, a texture. If this texture is sharply pronounced, it can be marked with the help of an "ideal position" [3.1], which means the orientation of a large part of crystallites in relation to a characteristic direction of the workpiece. During metal sheet forming the texture is often, to a nearest approximation, described by  $(hkl)$  and  $[uvw]$ , where  $(hkl)$  is the slip plane parallel to the rolling plane and  $[uvw]$  is in the rolling direction (Fig. 3.38). In face-centered cubic metals a  $(12\bar{3})$   $[41\bar{2}]$  or a  $(011)$   $[21\bar{1}]$  texture develops through rolling, whereas body-centered cubic metals produce a  $(100)$   $[011]$  texture (Fig. 3.38b). After stretch forming, sheet metals frequently possess a fiber texture (Fig. 3.38c).

Fiber textures are always present in drawn wires and extruded bars. To characterize them it is often sufficient to give the data of the direction parallel to the wire axis since the distribution perpendicular to it is mostly at random (Fig. 3.39). With the help of so-called "pole figures" it is possible to describe it quantitatively by x-ray photography [3.16].

If we assume all the grains to be at the center of a sphere and draw perpendiculars on a certain crystallographic plane of different grains, it is possible to characterize the position of the surfaces by the piercing points of the perpendiculars on the positioned sphere (Fig. 3.40a). The stereo-

FIG. 3.38 Sheet-metal textures. (a) Quasi-isotropic. (b)  $(100)$   $[011]$  texture. (c)  $[111]$  fiber texture.

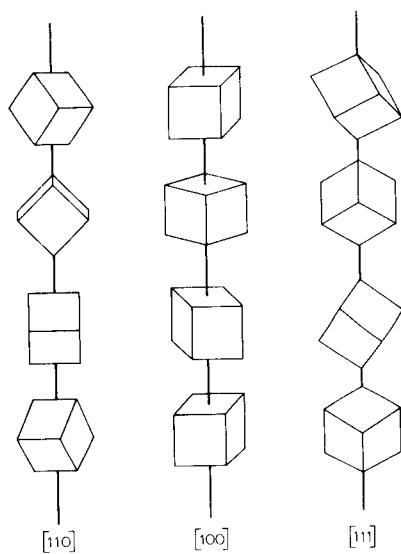


**FIG. 3.39** Fiber textures.

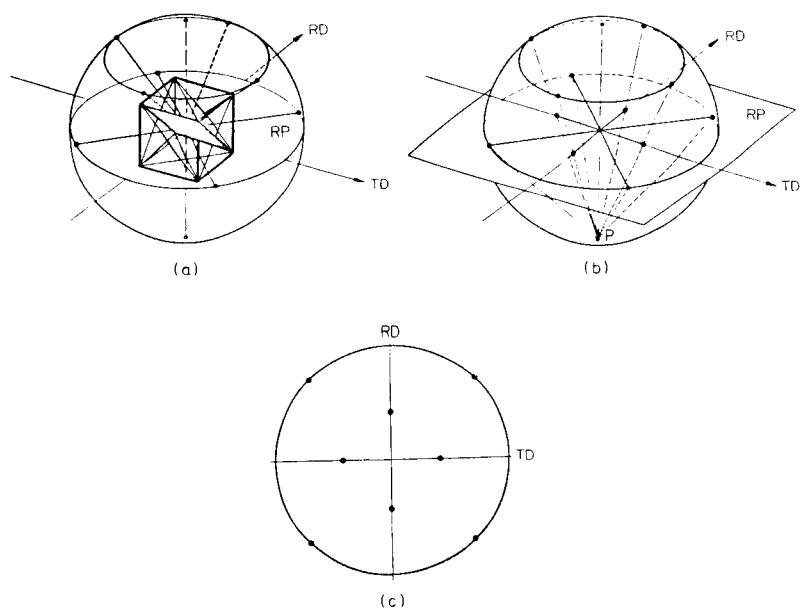


**FIG. 3.40** Emergence of a (110) pole figure. (a) Relation between crystal areas and surface poles. (b) Relation between surface poles and points of projections. RD—rolling direction; TD—transverse direction; RP—rolling-plane. (c) (110) pole figure.

### 3.26 FUNDAMENTALS OF METAL FORMING

graphic projection of the piercing points on the equator plane, with  $p$  as the center of projection, is termed *pole figure* (Fig. 3.40b). It indicates the orientation of the lattice planes or their normal directions with respect to the initially fixed coordinate system. Further, it also gives an idea of the orientation distribution function. For random orientation the piercing points are distributed evenly (loading density = 1). In the case of a texture they pile up at some places. Regions of equal loading density are marked by curves (Fig. 3.41).

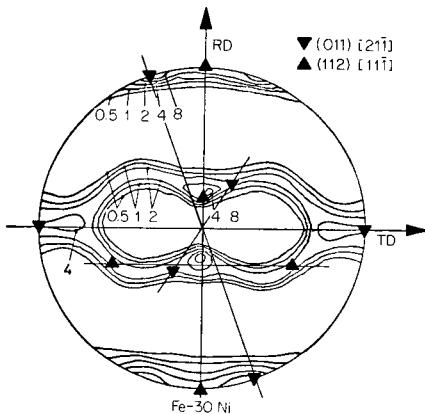


**FIG. 3.41** (111) pole figure of rolling texture of an Fe - 30 Ni alloy (After [3.28].)

A directional relationship can also be caused by grain sizes, the distribution of granular forms, and the arrangement in texture. A typical example of the influence of the granular form is the secondary texture of a pure steel metal sheet which shows a stretched grain (pancake texture, Fig. 3.42a).

From the nonmetallic inclusions the influence of manganese sulfide on the texture anisotropy in steel is strongest since these sulfides stretch during hot forming and can form inclusion lines of various lengths, depending on the form of the product (Fig. 3.42b). Along with the orientation relative to the rolling direction, a crystallographic orientation of segregated particles may occur as shown in Fig. 3.42c for the  $\theta$ -phase in an aluminum-copper alloy.

#### 3.7.2 Elastic and Plastic Anisotropy

In general, the changes in properties develop symmetrically to certain planes. If there are three planes lying vertically to one another, such a material is termed *orthotropic*. Rolled metal sheets with their reflection planes perpendicular to the rolling, transverse, and normal directions can be taken as an example.

If in a plane the properties are independent of direction, this is a special case of orthotropy. Such materials are called *normal anisotropic*. Metal sheets with fiber texture and wire are examples. We begin the treatment of mechanical anisotropy with an orthotropic material.

The elastic behavior and, thus, elastic anisotropy is of interest only if natural stresses are to be considered or if the deformed zone is to be plasticized only in part. It also plays a certain role in all plastic kinking processes, such as fold formation during deep drawing. In general, the elastic modulus of a crystal depends on direction since the elastic behavior is associated with atomic forces [3.21]. In polycrystals, in addition to the effect of orientation distribution, texture anisotropy is of importance (Fig. 3.43). In the tensile test a plastic deformation occurs if the tensile stress equals the yield stress  $\sigma_f$ . For an anisotropic material the usual dependence of the yield stress  $\sigma_f$

$$\sigma_f = f(\text{material}, \varphi, \dot{\varphi}, T) \quad (3.12)$$

becomes

$$\sigma_f = f(\text{material}, \varphi, \dot{\varphi}, T, \text{direction}) \quad (3.13)$$

Plastic anisotropy can be determined by finding the yield stresses in the main directions and measuring the deformations. Usually plastic anisotropy is measured by  $r$ -values, that is, the  $r_0$ -value and the  $r_{90}$ -value in the tensile test according to the formulas

$$r_0 = -\frac{\varphi_2}{\varphi_2 + \varphi_1} \quad (3.14)$$

$$r_{90} = \frac{\varphi_1}{\varphi_2 + \varphi_1} \quad (3.15)$$

where  $\varphi_1$  and  $\varphi_2$  are the strains in the longitudinal and transversal directions and the subscripts 0 and 90 refer to the angle between specimen axis and rolling direction. Since the  $r$ -value gives a yield stress ratio, it can be used to interpret the forming and the strain-hardening behavior as well as to find the force involved. An example of the effect of anisotropy in metal forming is earing during deep drawing.

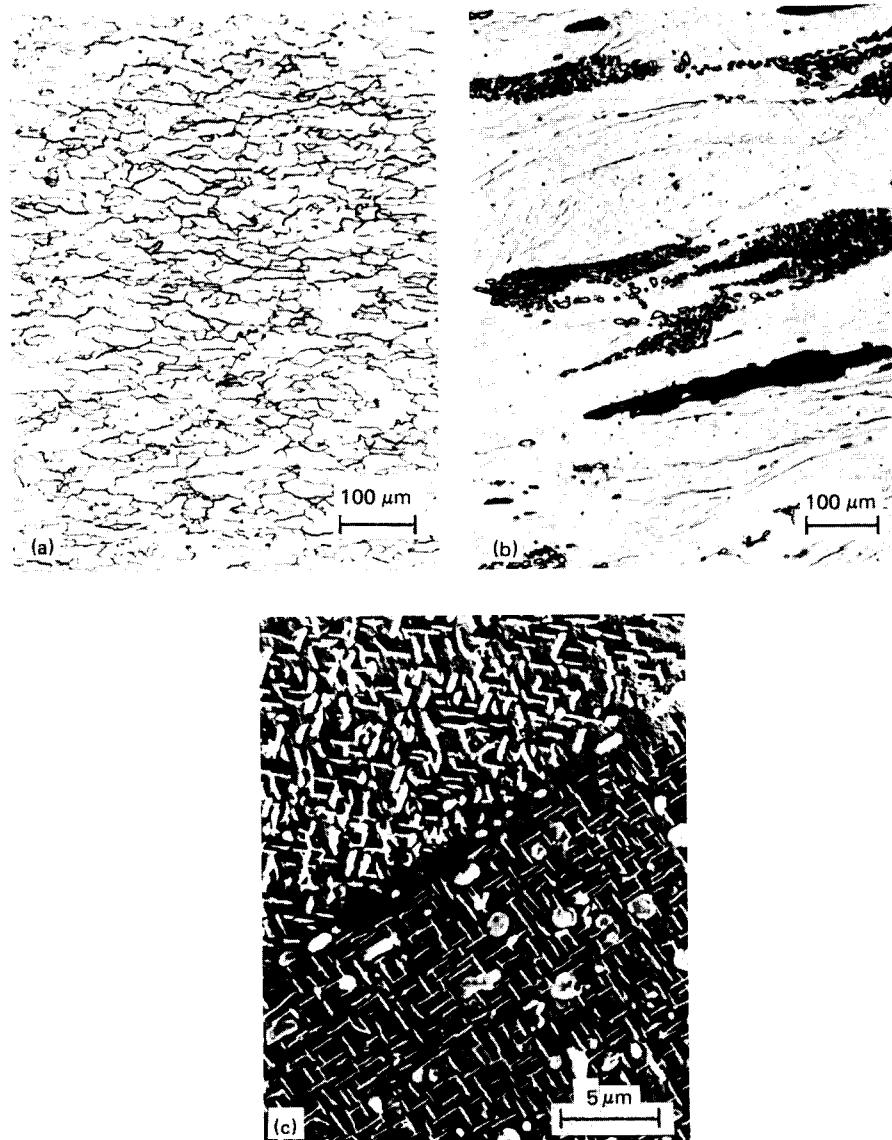


**FIG. 3.42** Texture anisotropy. (a) Grain shape.  $100 \mu\text{m} = 4000 \mu\text{in}$ . (b) MnS inclusions (black), ferrite, and cementite in 9 SMn 28 machining steel extruded at room temperature. Scale 500:1. (c) Oriented precipitated particles.  $5 \mu\text{m} = 200 \mu\text{in}$ .

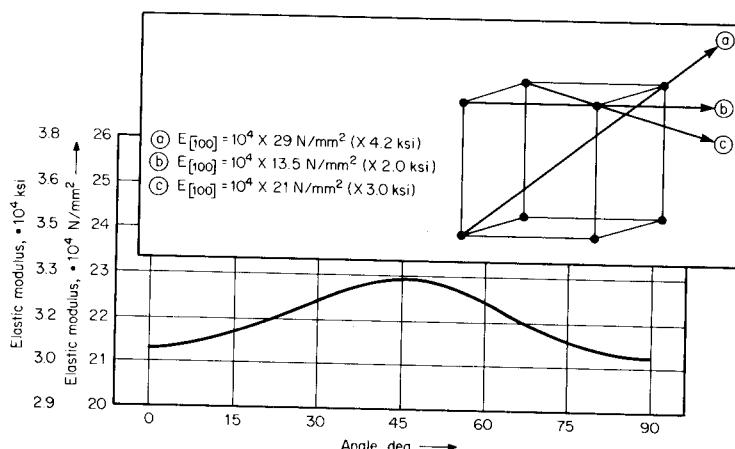


FIG. 3.43 Directional dependence of elastic modulus of a textured metal sheet.

Since there are no shear stresses in a purely hydrostatic stress state, the flow behavior is not affected by it. Therefore it is possible to represent the beginning of yield without loss of generality in the plane  $\sigma_{11}-\sigma_{22}$  by the equation

$$\tau_0 = l_{\alpha_1} l_{\beta_1} \sigma_{11} + l_{\alpha_2} l_{\beta_2} \sigma_{22} \quad (3.16)$$

where

$\alpha$  = slip plane

$\beta$  = slip direction

1, 2 = external main directions (1 = rolling direction, 2 = transverse direction)

$l_{\alpha_1}, l_{\beta_2}$  = directional cosines of slip plane normals and slip direction related to external main directions

Plastic yield starts when the critical value  $\tau_0$  in a slip system  $\sigma_{\alpha\beta}$  is reached.

As a geometrical solution, straight-line equations are obtained which give the yield locus curve in the  $\sigma_{11}-\sigma_{22}$  coordinate system. Further, the main stresses are denoted by  $\sigma_1$ ,  $\sigma_2$ , and  $\sigma_3$ . Yield locus curves are the geometrical sites for all  $\sigma_1-\sigma_2$  combinations at which plastic flow sets in. For a polycrystal, where the grains are to remain in mutual contact in order to hinder the formation of holes, five independent slip systems must be used (Taylor model [3.22] to [3.24]). The selection of the actual slip system is made according to the principle of the minimum deformation work. Here it is supposed that the critical shear stress has the same value in each slip system.

The slip type  $(hkl)$  [111], also called *pencil glide*, does not possess any definite slip plane but only a slip direction. Of course, the  $r$ -value is defined if the yield locus curve is known.

It should be kept in mind that by this model, plastic flow takes place only due to dislocation slips, while grain forms as well as metallic and nonmetallic secondary phases are not taken into account.

Isotropic hardening is a prerequisite for an arithmetic comprehension of the forming processes. It is the case when the yield locus curve, through rising deformation under constant stretch conditions of the axes, expands continuously.

Because of the directional dependence of deformation-induced martensite, anisotropic hardening occurs in metastable austenitic steels [3.25]. In hexagonal metals, anisotropy is very prevalent.

## REFERENCES

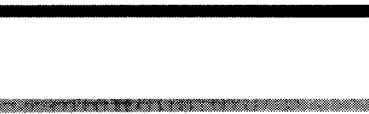
- 3.1 Böhm, H.: "Introduction into Metals Science" (*in German*), in *B. I. Hochschultaschenbuch* 196/196a, Mannheim/Zürich, Bibliographisches Institut, 1968.
- 3.2 Barrett, C. S., and Massalski, T. B.: *Structure of Metals*, 3d ed., New York, McGraw-Hill, 1966.
- 3.3 Eisenkolb, F.: *Introduction into Materials Science* (*in German*), 9th ed., vol. I–V, Berlin, VEB Verlag Technik, 1966.
- 3.4 Flügge, S.: *Handbook of Physics* (*in German*), vol. VII, "Crystal Physics I and II," Berlin/Göttingen/Heidelberg, Springer, 1955–1958.
- 3.5 Hornbogen, E., and Warlimont, H.: *Metals Science* (*in German*), Berlin/Heidelberg/New York, Springer, 1967.
- 3.6 Reed-Hill, R. E.: *Physical Metallurgy Principles*, 4th ed., Toronto/Princeton, N.J./London, van Norstrand, 1967.
- 3.7 Schulze, G. E. R.: *Metal Physics* (*in German*), Berlin, Akademie-Verlag, 1967.
- 3.8 Schumann, H.: *Metallography* (*in German*), 7th ed., Leipzig, VEB Verlag für Grundstoffindustrie, 1969.
- 3.9 Schmid, E., and Boas, W.: *Crystal Plasticity* (*in German*), Berlin, Springer, 1935.
- 3.10 Dehlinger, U.: "Lattice Defects and Technical Strength" (*in German*), Umschau, 1968, pp. 432–437.
- 3.11 Kröner, E.: *Continuum Theory of Dislocations and Residual Stresses* (*in German*), Berlin/Göttingen/Heidelberg, Springer, 1958.
- 3.12 Kochendörfer, A.: "Physical Fundamentals of Flow Stress of Metals," Supplement 1966 (*in German*), Düsseldorf, Verlag Stahleisen, 1967.
- 3.13 Macherauch, E.: "Structure Mechanical Fundamentals of Cold Forming" (*in German*), Z. Metallk., **61**, (1970), pp. 617–628.
- 3.14 Stüwe, H.-P.: "Flow Curves of Polycrystalline Metals and Their Application in the Theory of Plasticity" (*in German*), Z. Metallk., **56**, 1965, pp. 633–642.
- 3.15 Schack, J.: "The Behavior of Flow Stress of Iron-Manganese-Carbon Alloys in the Range of Blue Brittleness" (*in German*), Dr.-Ing. thesis, Technical University Hannover, 1965.
- 3.16 Byrne, J. G.: *Recovery, Recrystallization and Grain Growth*, New York/London, Macmillan, 1965.
- 3.17 Stüwe, H.-P., and Drube, B.: "Metallurgical Fundamentals of Hot Forming" (*in German*), Z. Metallk., **58**, 1967, pp. 499–506.
- 3.18 Wassermann, G.: "Recrystallization processes" (*in German*), Z. Metallk., **57**, 1966, pp. 493–499.
- 3.19 *The Wieland Book of Heavy Metals* (*in German*), Ulm, Wieland-Werke AG, 1964.
- 3.20 Schröder, G.: "Influence of Anisotropy in Upsetting of Extruded Zinc" (*in German*), Ind.-Anz., **91**, 1969, pp. 13–16, 53–57.
- 3.21 Wassermann, G., and Grewen, J.: *Textures of Metallic Materials* (*in German*), 2d ed., Berlin/Göttingen/Heidelberg, Springer, 1962.
- 3.22 Taylor, G. I.: "Plastic Strain in Metals," J. Inst. Met., **62**, 1938, p. 307ff.
- 3.23 Bunge, H. J. Schulze, M., Greszik, D.: "Calculation of the Yield Locus of Polycrystalline Material according to the Taylor Theory," *Salzgitter-Berichte*, to be published.
- 3.24 Reissner, J.: "The Role of Yield Locus for Sheet-Metal Forming" (*in German*), Bleche Röhre Profile, to be published.
- 3.25 Reissner, J.: "Flow Curves of Austenitic Steels and Their Representation by Empirical Functions" (*in German*), Maschinemarkt, **84**, 1978, p. 552.

### **3.30 FUNDAMENTALS OF METAL FORMING**

- 3.26 Jonas, J. J., Sellars, C. M., Tegart, W. J. MCG.: "Strength and Structure under Hot-Working Conditions," *Int. Metallurg. Rev.*, **14**, 1969, pp. 1-24.
- 3.27 McQueen, H. J., Jonas, J. J.: "Recovery and Recrystallisation during High-Temperature Deformation," in *Treatise on Materials Science and Technology*, vol. 6, San Francisco, Academic Press, 1975.
- 3.28 Grewen, J.: "Emergence of Deformation Textures"(in German), in Stüwe, H.-P. (ed.): *Mechanical Anisotropy*", Wien, Springer-Verlag, 1974, pp. 73-103.

## CHAP. 4

### FLOW CURVES



© 1999 John Wiley & Sons, Inc. All rights reserved. Printed in the United States of America.

#### List of Special Symbols

---

$a$	radius of torsion test piece
$a, b$	dimensions of plane strain upsetting test piece
$C$	constant in Eq. 4.12
$d$	average grain diameter
$F$	upsetting force
$k$	constant in the Hall-Petch equation 4.7
$k_R$	resistance to deformation
$l$	length of torsion test piece
$l_0$	initial length of tensile test specimen
$m$	strain-rate sensitivity index
$M$	torque
$n$	strain-hardening coefficient
$r^*$	critical radius in torsion test piece
$s$	height reduction of upset specimen
$\gamma_t$	shear strain in torsion test
$\gamma_a$	shear strain at circumference
$\gamma^o$	shear strain at critical radius
$\rho$	radius of necking in tensile test
$\sigma_{f,1}$	constant in Eq. 4.8
$\sigma_k$	grain-size-independent part of yield stress according to Eq. 4.7

## 4.2 FUNDAMENTALS OF METAL FORMING

$\tau^*$	shear stress at critical radius
$\varphi_u$	strain at uniform elongation in tensile test
$\psi$	twisting angle in torsion test

To calculate the forces required for metal-forming processes, it is necessary to know the flow curves of the metals to be formed. The flow curve is given by the flow stress as a function of strain, where stress is defined by

$$\sigma_f = \frac{F}{A} \quad (4.1)$$

$F$  being the actual force and  $A$  the actual cross section of a uniaxially deformed tensile test specimen. The natural strain (true strain) is given by

$$\varphi = \ln \left( 1 + \frac{\Delta l}{l_0} \right) \quad (4.2)$$

where  $l_0$  is the initial length of the test piece and  $\Delta l$  the elongation. Assuming constant volume, the actual cross section  $A$  in Eq. 4.1 is given by

$$A = \frac{\pi r_0^2 l_0}{l_0 + \Delta l} \quad (4.3)$$

The function

$$\sigma_f = \sigma_f(\varphi) \quad (4.4)$$

is called the *flow curve*, which gives the stress required for plastic deformation to occur under a uniaxial state of stress. The relation between this stress and the stress in a multiaxial state of stress is given by the concepts of equivalent stress  $\bar{\sigma}$  and equivalent strain  $\bar{\epsilon}$  (see Chap. 5). For the uniaxial tensile test, however, strain and equivalent strain are equal, that is,

$$\bar{\epsilon} = \varphi \quad (4.5)$$

In this chapter, for simplicity, the symbol  $\varphi$  shall be used if it does not cause any misunderstanding.

Stress does not only depend on strain but also on strain rate, temperature, and, in general, on directional effects caused by anisotropy. Furthermore there is a weak dependence on hydrostatic stress [4.2], [4.3].

If the flow curve is known, the ideal work required for metal forming per unit volume can be calculated, that is,

$$\frac{W_{id}}{V} = \int_0^\varphi \sigma_f(\varphi') d\varphi' \quad (4.6)$$

where the prime indicates variable of integration so that it is not confused with the limit of integration. The shapes of flow curves which have been obtained from experiments can be explained qualitatively by the theory of dislocations (see Chap. 3).

The flow curves of polycrystals deviate from those of monocrystals because the individual grains cannot be deformed independently of the grains in their vicinity. Therefore several "glide systems" (see Chap. 3) have to be activated in each grain. In many cases the yield point of a polycrystal as a function of grain size can be described by the *Hall-Petch* equation

$$\sigma = \sigma_k + \frac{k}{\sqrt{d}} \quad (4.7)$$

This equation is satisfied for many metals (Fig. 4.1). In the range of high strains, however, the effect of grain size on flow stress is more complex.

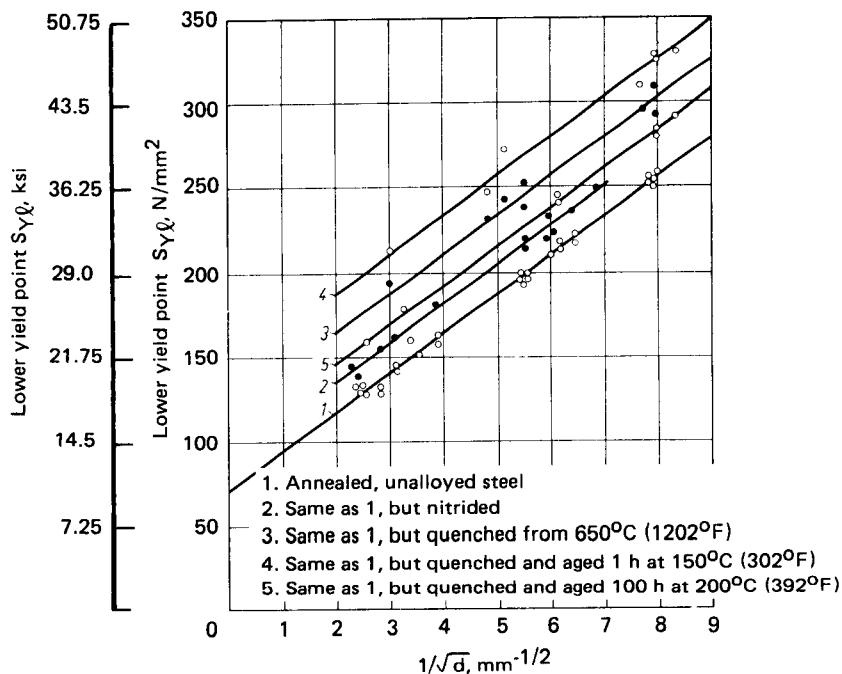


FIG. 4.1 Lower yield point versus average grain size. (After [4.4].)

From the viewpoint of metal physics, the room temperature is of no importance with respect to the elementary processes of plastic deformation. However, for practical reasons, cold and hot forming are defined as deformation at room temperature and deformation at elevated temperatures, respectively. Fig. 4.2 shows the flow curves of some metals which at room temperature are not affected by thermally activated processes. In such cases the flow stress increases monotonically with growing strain, the slope  $d\sigma_f/d\varphi$  of the curve being highest at low strains. At elevated tem-

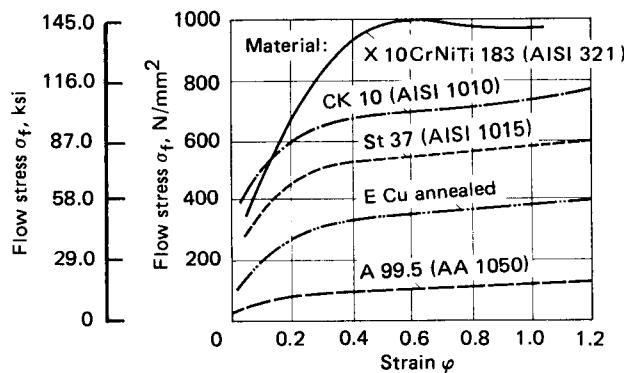
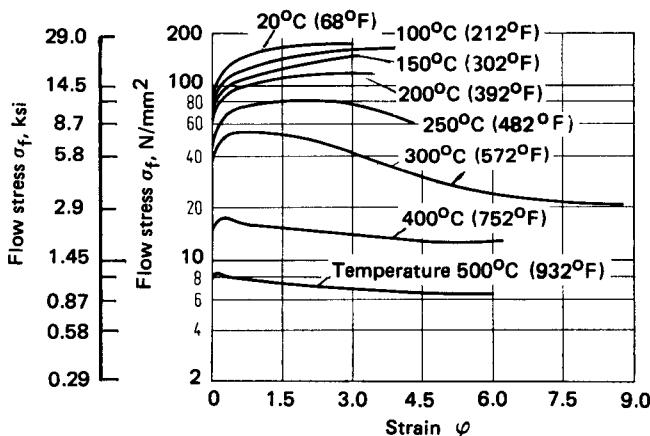


FIG. 4.2 Flow curves of some metals at room temperature. (After [4.5].)



**FIG. 4.3** Flow stress of aluminum (technical purity) as a function of strain at different temperatures. (After [4.1].)

peratures, when recovery and recrystallization take place, the flow curves depend strongly on temperature and strain rate (see Chap. 3). The flow curves in Fig. 4.3 exhibit a maximum stress at about 220°C (428°F). Their shapes can be explained qualitatively by the “climbing” of dislocations, which takes place at elevated temperatures (see Chap. 3).

Since both recovery and recrystallization take place at a finite temperature-dependent rate, flow stress depends strongly on the strain rate. At a given temperature the effect of the strain rate on flow stress can be approximated by the relation

$$\sigma_f \approx \sigma_{f,1} \left( \frac{\dot{\varphi}}{\dot{\varphi}_1} \right)^m \quad (4.8)$$

where  $\sigma_{f,1}$  is the flow stress at the strain rate  $\dot{\varphi}_1$ . For steels typical values of the exponent  $m$  range from  $-0.02$  to  $+0.05$  at  $20$ – $450^\circ\text{C}$  ( $68$ – $845^\circ\text{F}$ ) and from  $0.1$  to  $0.2$  at temperatures above  $880^\circ\text{C}$  ( $1616^\circ\text{F}$ ). Fig. 4.4 shows the flow curve of C15 steel at different strain rates.

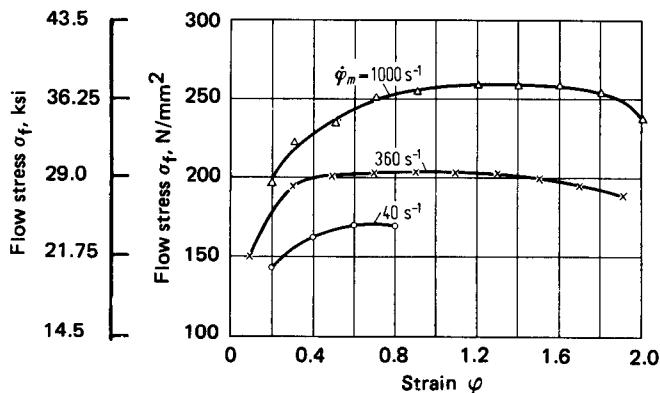


**FIG. 4.4** Effect of strain rate on flow stress of C 15 steel at  $1100^\circ\text{C}$  ( $2012^\circ\text{F}$ ). (After [4.6].)

## 4.1 DETERMINATION OF FLOW CURVES

### 4.1.1 Tensile Test

In general, flow curves are determined by experiments, the most important of which are the tensile test, the upsetting test, and the torsion test [4.5], [4.7], [4.8]. There is no "best" experiment since each has a special field of application. The proper choice of testing method depends on the metal-forming process to be simulated. For this reason the size of the test pieces cannot be chosen freely. If the flow curve is only to be determined for low strains, the tensile test is normally preferred because of its simplicity and also because for this experiment the conditions of testing have been well defined by standards. The tensile test will also be preferred if the flow curve that has been determined for low strains can be extrapolated toward higher strains. For the range of uniform deformation it is usually assumed that stress is constant over the cross section of the specimen. Hence the flow stress is given by Eq. 4.1, where the cross section  $A$  is given by Eq. 4.3. The range of uniform deformation is limited by the elongation  $e_u$  for which the maximum force is obtained. Beyond this elongation, deformation begins to become unstable because of necking. The major disadvantage of the tensile test is that necking occurs at rather low strains. For many metals Eq. 4.9 holds:

$$\varphi_u = \ln(1 + e_u) \approx 0.2-0.3 \quad (4.9)$$

According to Siebel and Schwaigerer [4.9] the flow curve for the region of necking can also be determined by means of the equation (Fig. 4.5)

$$\sigma_f = \frac{F}{A_{\min}(1 + r/4\rho)} \quad (4.10)$$

where  $A_{\min}$  is the minimum cross section in the necking zone at a given force. The corresponding equivalent strain is given by

$$\varphi = \ln \left( \frac{A}{A_{\min}} \right) \quad (4.11)$$

By this method the flow curve can be determined for strains up to the order of unity ( $\varphi \approx 1$ ).

A simplified determination of the flow curve is possible for unalloyed and low-alloyed steels at room temperature up to a strain  $\varphi \approx 1$ . In these cases the flow curves satisfy the equation

$$\sigma_f(\varphi) = C\varphi^n \quad (4.12)$$

where  $C$  and  $n$  are specific constants of the material ( $n$  is the strain-hardening coefficient). Eq. 4.12 shall be referred to as the Ludwik equation [4.10], although it was first proposed by Hollomon [4.11]. If Eq. 4.12 can be assumed, only the constants  $C$  and  $n$  have to be determined. For this purpose, according to Reihle [4.12], use is made of the relations

$$n = \varphi_u \quad (4.13)$$

$$C = S_u \left( \frac{e}{n} \right)^n \quad (4.14)$$

Thus only the strain  $\varphi_u$  at uniform elongation and ultimate tensile strength has to be known.

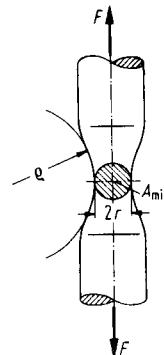


**FIG. 4.5** Necking of tensile test piece (schematic).

## 4.6 FUNDAMENTALS OF METAL FORMING

The determination of uniform elongation can be carried out in different ways. The most accurate way consists of deforming the specimen beyond the initiation of necking, and measuring the elongation of a section outside the region of necking.

An approximate method consists in calculating uniform elongation from the equation

$$e_u = e_{10} - e_5 \quad (4.15)$$

where  $e_{10}$  and  $e_5$  are the elongations to fracture which have been obtained from test pieces of initial length-to-diameter ratios of 10 and 5, respectively. (Eq. 4.15 is based on the assumption that the length of the necking zone is equal in both types of test pieces.)

From uniform elongation the hardening coefficient can be calculated easily by the equation

$$n = \ln(1 + e_u) \quad (4.16)$$

A disadvantage of this method is that the test pieces have to be machined very accurately, the diameter having a tolerance of only 0.02 mm ( $\approx 0.001$  in).

### 4.1.2 Upsetting Cylindrical Test Pieces

Normally the formability of metals is lowest at tensile hydrostatic stress [4.13], [4.14]. Therefore higher strains are obtained with upsetting tests than with tensile tests. If a cylindrical test piece is compressed between parallel dies (Fig. 4.6), the equivalent strain according to the Tresca criterion (see Chapter 5) is given by the equation

$$\bar{\epsilon}(F) \approx \ln\left(\frac{h(F)}{h_0}\right) < 0 \quad (4.17)$$

where  $h(F)$  is the specimen height at a force  $F$ . During the test the height reduction, that is,

$$s(F) = h_0 - h(F) \quad (4.18)$$

is registered. From Eq. 4.17 it follows that

$$h(\bar{\epsilon}) = h_0 e^{-|\bar{\epsilon}|} \quad (4.19)$$

where equivalent strain  $\bar{\epsilon}$  is negative by definition (see Eq. 4.17). Usually it is assumed that the effect of hydrostatic stress on flow stress can be neglected so that

$$\sigma_f(\bar{\epsilon}) = \sigma_f(-\bar{\epsilon}) \quad (4.20)$$

For the determination of flow stress from experimental data we can write, as a first approximation,

$$\sigma_f(F) \approx \frac{F[h_0 - s(F)]}{\pi r_0^2 h_0} \quad (4.21)$$

Using Eqs. 4.17, 4.18, and 4.21, strain and stress can be calculated from the measured curve  $F(s)$ . In this calculation the error of force only propagates into stress while the error of height reduction propagates into both stress and strain. Thus it can be expected that the experimental error of  $s$  is more important than that of force  $F$ .

#### Friction

Friction between the test piece and the dies requires an additional force for obtaining a given strain. Eq. 4.21 has to be replaced by

$$\frac{F(\bar{\epsilon})}{\pi r^2(\bar{\epsilon})} \approx \sigma_f(\bar{\epsilon}) \left[ 1 + \frac{2\mu r(\bar{\epsilon})}{3h(\bar{\epsilon})} \right] \quad (4.22)$$

where  $\mu$  is the coefficient of friction. The left-hand side of Eq. 4.22 is the resistance to deformation denoted by  $k_R$ :

$$\frac{F(\bar{\epsilon})}{\pi r^2(\bar{\epsilon})} = k_R(\bar{\epsilon}) \quad (4.23)$$

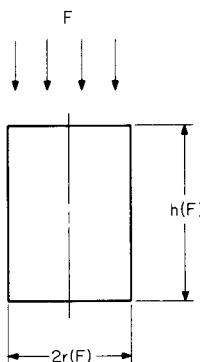


**FIG. 4.6** Scheme of upsetting test on cylindrical test pieces.

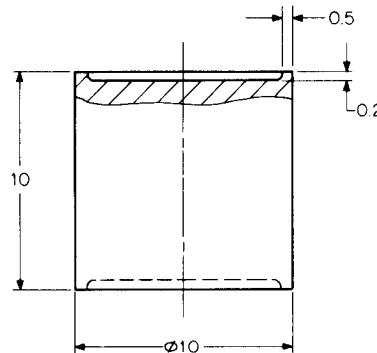


**FIG. 4.7** Upsetting test piece according to Rastegaev. Dimensions in mm. (After [4.23].)

Due to friction the specimen does not remain cylindrical. The contour of barrelling of the specimen must be measured for a correction of the test results. This causes an additional error which propagates into the calculated flow curve.

In the literature several modifications of the upsetting test have been described by which friction is either suppressed or eliminated when calculating the flow curve from the experimental results [4.15] to [4.28]. The simplest way of reducing friction is to use a proper lubricant (polytetrafluoroethylene,  $\text{MoS}_2$ ). Improved lubrication is obtained by using specimens according to Rastegaev [4.19] to [4.28]. In this case paraffin is filled into the end recesses of the test piece as a lubricant (for experiments at room temperature).

Experiments described in [4.26] showed that the resistances to deformation obtained from Rastegaev specimens of different slenderness ratios were equal within the limits of error.

From Eq. 4.23 it follows that within the limits of error the coefficient of friction was zero. Hence,

$$\sigma_f(\bar{\epsilon}) \approx k_R(\bar{\epsilon}) \quad (4.24)$$

By a more rigorous treatment of the Rastegaev test, however, a finite contribution of friction is obtained [4.20]. Fig. 4.8 shows that Rastegaev specimens retain a cylindrical shape up to high strains. Unfortunately for these specimens, the reduction of height is measured with increasing error compared with conventional specimens since the end faces do not remain plane [4.19]. From this, an error for both stress and strain results, which increases exponentially with increasing strain. Therefore it makes no sense to continue the Rastegaev test to strains higher than  $|\varphi| = 1.2\text{--}1.5$ . This error cannot be reduced by using test pieces of increased slenderness ratio, since due to perfect lubrication, the Rastegaev specimens would skew laterally.

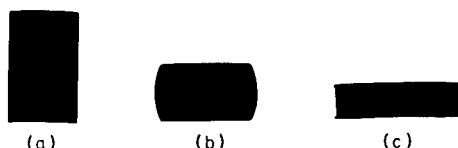


**FIG. 4.8** Cylindrical upsetting specimens ( $h_0 = 16$  mm,  $r_0 = 5$  mm) with and without end recesses according to Rastegaev. (a) Before test. (b) Without lubrication,  $\varphi \approx 0.7$ . (c) Rastegaev test piece,  $\varphi \approx 1.3$ . (After [4.26].)

Thus the following condition must be fulfilled:

$$\frac{h_0}{2r_0} \leq 1.5 \quad (4.25)$$

On the other hand, it must be kept in mind that there is a considerable measurement error of the height reduction in upsetting tests on cylindrical test pieces of any kind, since the specimen cross section grows with increasing strain, causing increasing elastic deformation of the upsetting device.

#### 4.1.3 Plane Strain Upsetting Test

This experiment is described in [4.29] to [4.31]. Two adjacent rectangular dies are pressed into a strip specimen (Fig. 4.9). To obtain plane strain conditions, the ratio  $b/h$  should exceed 6. The theory of the experiment has been described in [4.29]. Here only some important characteristics of the test shall be pointed out:

The area under load remains constant during the test. Therefore an experimental error of the height reduction does not propagate into stress but only into strain since the following relation holds:

$$\sigma_t(F) = \frac{F}{ab} \quad (4.26)$$

The dies must be kept exactly centric since otherwise the area under load would be reduced.

The stress concentration along the edges of the dies causes initiation of fracture at a lower strain than would be the case for pure uniaxial deformation.

#### 4.1.4 Upsetting Tests at Elevated Temperatures

At elevated temperatures stress is strongly strain-rate-dependent. Therefore the strain rate should be kept constant during deformation. However, for upsetting tests at a constant speed of movement of the dies it follows from Eqs. 4.17 and 4.18 that

$$\dot{\epsilon} = \frac{s}{h_0} e^{(\bar{t})} \quad (4.27)$$

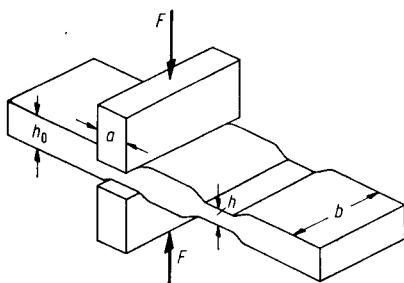


FIG. 4.9 Scheme of plane strain upsetting test.

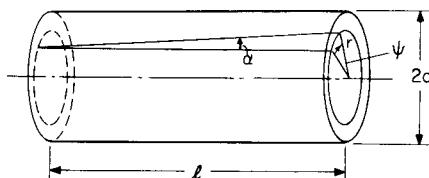


FIG. 4.10 Scheme of torsion test.

Thus at a constant speed  $s$  of the die the strain rate increases exponentially with strain. To obtain a constant strain rate,  $s$  must be reduced continuously during the test in such a way that

$$\dot{s} = \dot{s}(\epsilon) = s_0 e^{-\bar{\epsilon}} \quad (4.28)$$

This condition can be fulfilled by using a "plastometer" [4.31].

Since the simulation of technical hot-forming processes requires a high absolute strain rate, the increase of temperature of the specimen due to *adiabatic* heating must be discussed. Obtaining an *isothermal* flow curve is only possible by interrupting the experiment at certain intervals. However, this may cause some other errors. The temperature increase of the test piece is calculated in [4.32].

#### 4.1.5 Torsion Test

In the torsion test a cylindrical specimen is twisted by a torque acting around its axis (Fig. 4.10). Stress  $\sigma_f$  has to be calculated from the measured torque  $M$ , and strain from the twisting angle  $\psi$ .

Since the specimen geometry remains almost unchanged during deformation, the strain rate can be kept constant more easily than in tensile or upsetting tests by simply keeping the number of revolutions constant. Therefore the torsion test is especially useful for studying deformation at elevated temperatures.

The determination of the stress-strain curve from the test data is described in detail in [4.33] to [4.35].

The shear strain at a distance  $r$  from the axis of a long test piece at a twisting angle  $\psi$  is given by [4.33]

$$\gamma_r(\psi) = \tan \alpha = \frac{r\psi}{l} \quad 0 \leq r \leq a \quad (4.29)$$

Here it has been assumed that the material is homogeneous, isotropic, and incompressible, and that the length of the specimen remains constant during deformation.

Conventionally strain and stress are calculated for the circumference of the test piece ( $r = a$ ). For this radial distance Eq. 4.29 becomes

$$\gamma_a(\psi) = \frac{a\psi}{l} \quad (4.30)$$

The corresponding shear strain rate is given by

$$\dot{\gamma}_a = \frac{a\dot{\psi}}{l} \quad (4.31)$$

The local shear stress can be shown to be given by Eq. 4.32,

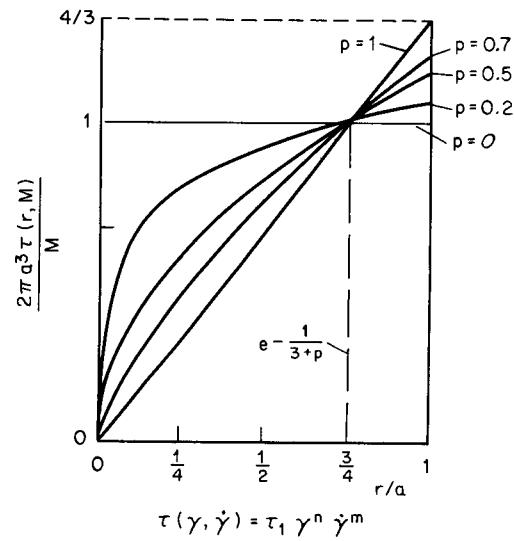
$$\tau(\gamma_a, \dot{\gamma}_a) = \frac{3M(a, \gamma_a, \dot{\gamma}_a)}{2\pi a^3} \left\{ 1 + \frac{1}{3M} \left[ \gamma_a \frac{\partial M}{\partial \gamma_a} + \dot{\gamma}_a \frac{\partial M}{\partial \dot{\gamma}_a} \right] \right\} \quad (4.32)$$

This calculation of the local strain and stress for the surface of the test piece is mathematically correct. However, stress and strain are determined for a position where they are strongly distorted due to machining, oxidation, and so on. For these reasons methods are described in [4.34] and [4.35] for calculating strain and stress for a radial distance inside the test piece (below the surface). It is shown that a critical radius  $r^*$  exists for which the stress is almost independent of the shape of the flow curve as long as the following equation is satisfied (compare Eqs. 4.8 and 4.12):

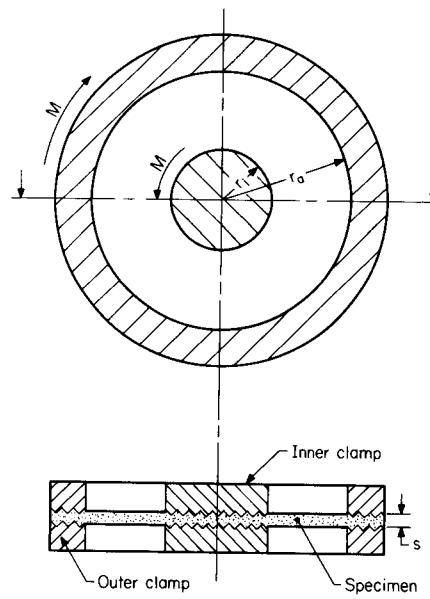
$$\sigma_f(\epsilon, \dot{\epsilon}) = \sigma_{f,1}\epsilon^n \dot{\epsilon}^m \quad (4.33)$$

Fig. 4.11 demonstrates that the curves for shear stress, for a given torque, at different values of  $n$  and  $m$  intersect almost exactly at the same point. The critical radius is given by

$$r^* = \%a \quad (4.34)$$



**FIG. 4.11** Shear stress in a torsion test piece for different values of  $p = n + m$  (assuming Eq. 4.33 for the flow curve). (After [4.35].)



**FIG. 4.12** Scheme of plane torsion test on thin sheet.

Using Eq. 4.30, the strain is obtained:

$$\gamma^* = \% \gamma_a \quad (4.35)$$

The corresponding shear stress can be shown to be [4.35]

$$\tau^* = \frac{3M}{2\pi a^3} \quad (4.36)$$

From the curve  $\tau^*(\gamma^*)$ , the flow curve has to be calculated using either the von Mises or the Tresca yield criterion. In any case the equivalent strain  $\epsilon$  is proportional to the shear strain  $\gamma^*$ . (The nonlinear relation given in [4.36] should not be used for calculating flow curves.) The difference between the von Mises and the Tresca yield criteria results mainly in a difference of the absolute amount of the flow stress, while the relative course of the flow curve and its strain-rate sensitivity are not strongly affected by the choice of the yield criterion. It must be emphasized, however, that both yield criteria mentioned are based on simplifying assumptions concerning the material, and the assumption of isotropy can cause an essential error [4.37], [4.38]. Both criteria are also based on the assumption of strain-rate-independent flow stress. Since the torsion test is used preferably for testing strain-rate-sensitive materials only, this means a fundamental contradiction. However, until now no yield criterion seems to be known which takes into account the strain-rate sensitivity and is nevertheless simple enough for practical applications.

Simulation of hot forming requires high strain rates, which can be obtained by using specimens of high radius-to-length ratios [4.31], [4.39] to [4.42]. For such test pieces the concept of *effective length* must be used for calculating the strain. The effective length of a specimen can be determined either experimentally or semiempirically. The notch effect, which is of importance at the circumference of a short test piece, can almost be neglected when calculating stress and strain for the critical radius  $r^*$  [4.35].

## 4.2 SPECIAL METHODS OF TESTING THIN SHEETS

This section is mainly concerned with sheets of less than 3-mm (0.12-in) thickness. In this case tensile test pieces normally are stamped out of the sheet without further machining so that they do not have a circular cross section. Since for such specimens the region of necking cannot be measured with sufficient accuracy, the tensile test can only be carried out up to uniform elongation. Thus the flow curve is only determined in the range

$$\varphi \leq \varphi_u \approx n \quad (4.37)$$

In spite of this, the tensile test is carried out on thin sheets more often than any other testing method since in the tensile test the  $r$ -value of anisotropy can be determined simultaneously with the flow curve. In the hydraulic bulge test [4.43] to [4.46] strains up to the order of  $\varphi \approx \ln 2 \approx 0.7$  can be obtained [4.44]. However, in many cases the flow curve obtained from this experiment deviates considerably from that obtained by tensile tests. This deviation may be caused by the normal anisotropy of the sheet [4.45].

Recently the plane torsion test has been described [4.47] to [4.49] (Fig. 4.12) by which flow curves of thin sheets can be determined up to high strains. Experimental details of the test are given in [4.49].

## 4.3 FLOW CURVES OF SOME IMPORTANT METALS

The Ludwik equation 4.12 can be derived from Eq. 4.33 by setting  $m = 0$ , that is, for room temperature when the strain-rate sensitivity can be neglected. Table 4.1 lists the constants  $C$  and  $n$  for some important metals. (See also [4.50].)

**Table 4.1** Values of Constants  $C$  and  $n$  in Eqs. 4.13 and 4.14.

Material <sup>a</sup> [DIN]	$C, \text{N/mm}^2 (\text{ksi})$	$n$	$\dot{\varphi}, \text{s}^{-1}$	Range of strain $\varphi$
St38	730 (106)	0.10		
St42	850 (123)	0.23		
St60	890 (129)	0.15		
C10	800 (116)	0.24		
Ck10	730 (106)	0.22		
Ck35	960 (139)	0.15		
15Cr3	850 (123)	0.09	16	0.1–0.7
16MnCr5	810 (117)	0.09	1.6	0.1–0.7
20MnCr5	950 (138)	0.15		
100Cr6	1160 (168)	0.18		
Al99.5	110 (16)	0.24		
AlMg3	390 (57)	0.19	$10^{-3}$	0.2–1.0
CuZn40	800 (776)	0.33	$10^{-3}$	0.2–1.0

<sup>a</sup>For chemical composition and the corresponding U.S. designations see Appendixes A to D.

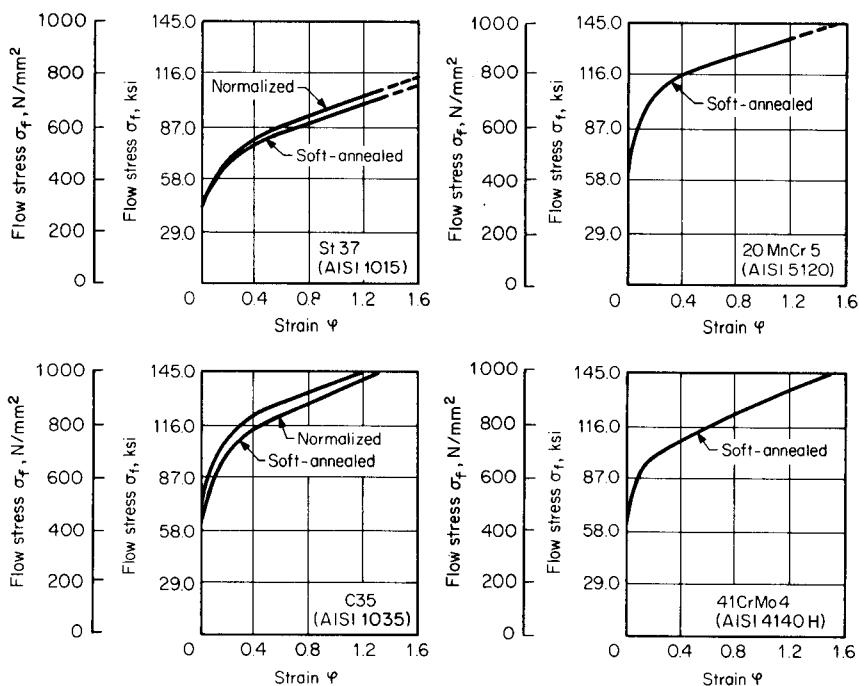


**FIG. 4.13** Flow curves of some common steels. (After [4.51].)

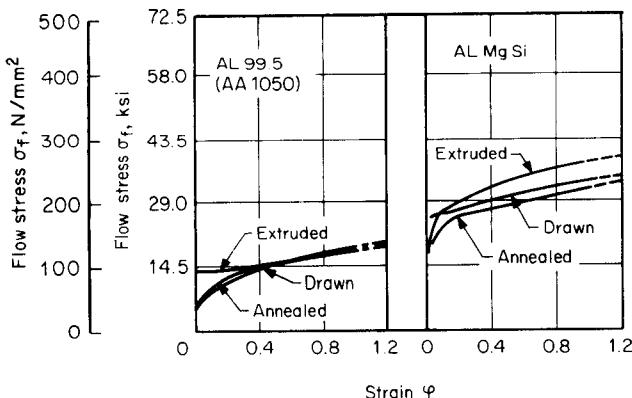


FIG. 4.14 Flow curves of some aluminum alloys. (After [4.51].)

In the more general case the hardening coefficient cannot be assumed to be constant, that is,

$$n = n(\varphi) \quad (4.38)$$

Flow curves of steels are given in [4.51] and [4.52], and flow curves of nonferrous metals in [4.53]. Some examples shown in Figs. 4.2, 4.13, and 4.14. Examples of flow curves at elevated temperatures are shown in Figs. 4.3, 4.15, and 4.16.

At elevated temperatures the strain rate is often much stronger than the strain dependence of

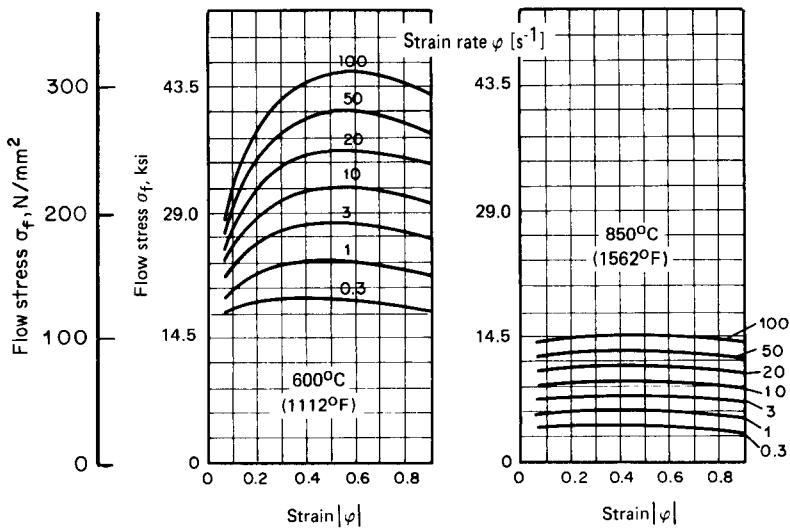
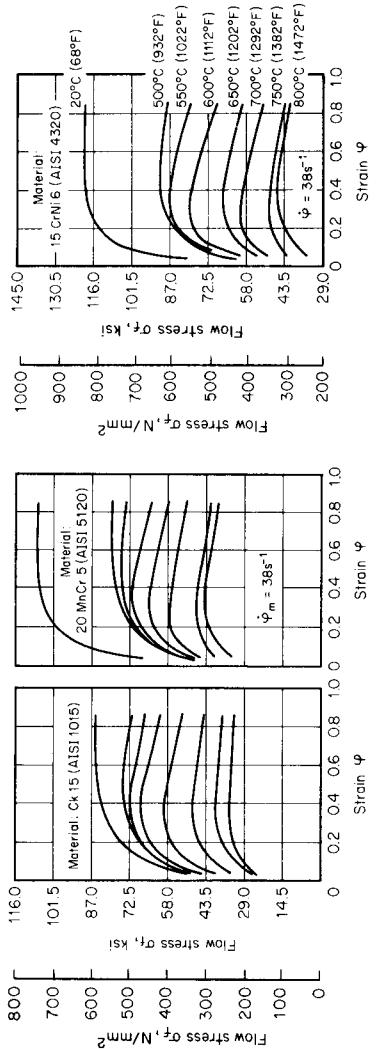
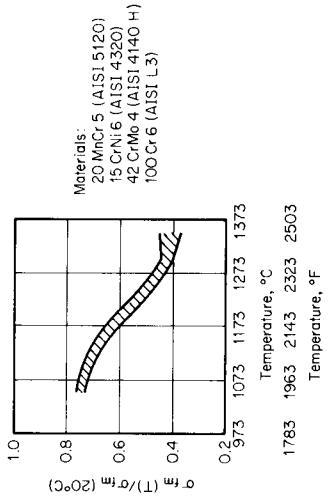


FIG. 4.15 Flow curves of Cu Zn 28 (After [4.54].)

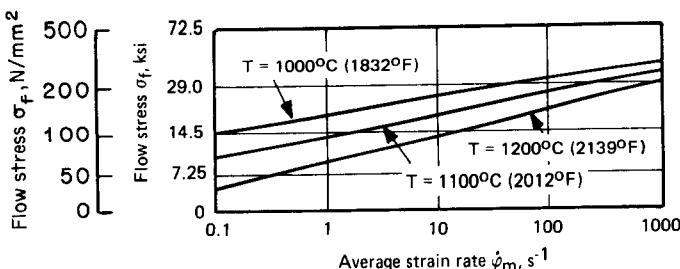


(a)



(b)

**FIG. 4.16** (a) Flow curves of some steels in the temperature range of warm forming. (b) Dependence of flow stress on temperature (After [4.5]).

FIG. 4.17 Flow stress versus strain rate for C 15 steel,  $\varphi = 0.5$ . (After [4.56].)

flow stress. In this case, as an approximation, Eq. 4.8 can be derived from Eq. 4.33 with  $n = 0$ . Eq. 4.8 is proved by the curves shown in Fig. 4.17. These curves can be used for a variety of metals by means of the values given in Table 4.2. Finally it shall be mentioned that for some unalloyed and alloyed steels the flow curve can be calculated from their chemical analyses and their mechanical properties [4.57] to [4.59].

**Table 4.2** Conversion Factors for Flow Stress of Several Metals Compared to Flow Stress of C15 (1015) Steel, Accuracy of 5–20%.

Material <sup>a</sup> [DIN]	Ratio of flow stress $\sigma_f/\sigma_{f,C15}$		
	1100°C (2012°F)	1000°C (1832°F)	900°C (1652°F)
C15	1	1	1
16MnCr5	1.05	1.09	1.12
20MnCr5	1.05	1.10	1.13
C35	1.06	1.10	1.16
C45	1.02	1.12	1.27
C60	1.11	1.19	1.38
26CrV7	1.05	1.09	1.27
37MnV7	1.10	1.13	1.22
42MnV7	1.14	1.18	1.27
37MnSi5	1.21	1.28	1.36
100Cr6	1.16	1.28	1.51

<sup>a</sup>For chemical composition and the corresponding U.S. designations see Appendixes A to D.

Source: After [4.56].

## REFERENCES

- 4.1 Stüwe, H.-P.: "Flow Curves of Polycrystalline Metals and Their Application in the Theory of Plasticity" (in German), *Z. Metallkd.*, **56**, 1965, pp. 633–642.
- 4.2 Herbertz, R., and Wiegels, H.: "The Difference between Tensile and Upsetting Flow Curves as Explained by the Effect of Hydrostatic Stress" (in German), *Arch. Eisenhüttenwes.*, **51**, 1980, pp. 413–416.
- 4.3 Bridgeman, P. W.: *Studies in Large Plastic Flow and Fracture*, New York, McGraw-Hill, 1952.

- 4.4 Siebel, E., and Pomp, A.: "Further Development of the Compression Test" (*in German*), *Mitt. Kaiser-Wilhelm-Inst. Eisenforsch.*, **10**, 1928, pp. 55–62.
- 4.5 Krause, U.: "Comparison of Different Methods for Determining Flow Stress in Cold Metal Forming" (*in German*), Dr.-Ing. thesis, Technical University, Hannover, 1962.
- 4.6 Bühler, H., and Vollmer, J.: "Flow Curves of Metallic Materials at Large Strains and Strain Rates" (*in German*), *Ind.-Anz.*, **91**, 1969, pp. 2021–2023.
- 4.7 Rao, K. P., et al.: "Flow Curves and Deformation of Materials at Different Temperatures and Strain Rates," *J. Mech. Work. Technol.*, **6**, 1982, pp. 63–88.
- 4.8 Bauer, D.: "Basic Experiments of Metal Forming" (*in German*), *Metall*, **32**, 1978, pp. 778–781.
- 4.9 Siebel, E., and Schwaigerer, S.: "Mechanics of Tensile Test" (*in German*), *Arch. Eisenhüttenwes.*, **19**, 1948, pp. 145–152.
- 4.10 Ludwik, P.: *Elements of Technological Mechanics* (*in German*), Berlin, Springer, 1909.
- 4.11 Hollomon, J. H.: "Tensile Deformation," *Trans. AIME*, **162**, 1945, pp. 268–290.
- 4.12 Reihle, M.: "A Simple Method of Determining Flow Curves of Steel at Room Temperature" (*in German*), *Arch. Eisenhüttenwes.*, **32**, 1961, pp. 331–336.
- 4.13 Stenger, H.: "On the Dependence of the Formability of Metallic Materials on the Stress State" (*in German*), Dr.-Ing. thesis, Technical University Aachen, 1965.
- 4.14 Vater, M., and Lienhart, A.: "Dependence of the Formability of Metallic Materials on the Stress State at Different Temperatures and Strain Rates" (*in German*), *Bänder Bleche Röhre*, **13**, 1972, pp. 387–395.
- 4.15 Pawelski, O.: "Comparison of Methods for Testing the Hot Formability of Metals" (*in German*), in *Hot Forming and Hot Strength Symposium* (Bad Nauheim, 1975), Oberursel, DGM, 1976.
- 4.16 Sachs, G.: *Z. Metallkd.*, **16**, 1924, p. 55.
- 4.17 Cooke, M., and Larke, C.: "Resistance of Copper Alloys to Homogeneous Deformation in Compression," *J. Inst. Met.*, **71**, 1945, pp. 371–390.
- 4.18 Sato, Y., and Takaeyama, H.: "An Extrapolation Method for Obtaining Stress-Strain Curves at High Rates of Strain in Uniaxial Compression," *Tech. Rep. Tohoku Univ.*, **44**, 1980, pp. 287–302.
- 4.19 Nester, W., and Pöhlandt, K.: "Determination of Flow Curves in Different Modifications of the Upsetting Test" (*in German*), *Rheol. Acta*, **21**, 1982, pp. 409–412.
- 4.20 Suyarov, D. I., et al.: "Determination of the Flow Stress of Metals" (*in Russian*), *Zavod Lab.*, **21**, 1955, pp. 97–99.
- 4.21 Wiegels, H., and Herbertz, R.: "Upsetting Test on Cylindrical Test Pieces with High Friction for the Determination of Flow Stress" (*in German*), *Stahl u. Eisen*, **99**, 1979, pp. 1380–1390.
- 4.22 Pöhlandt, K., and Nester, W.: "The Determination of Stress-Strain Curves by the Compression Test, pts. I and II," *Wire*, **32**, 1982, pp. 62–68, 150–153.
- 4.23 Rastegaev, M. V.: "New Method of Homogeneous Upsetting of Specimens for the Determination of Flow Stress and the Coefficient of Internal Friction" (*in Russian*), *Zavod Lab.*, **1940**, p. 354.
- 4.24 Turno, A.: "Determination of Strain-Hardening Curves Using Specimens with End Recesses" (*in Polish*), *Obrobka Plast. (Poznań)*, **11**, 1972, pp. 123–127.
- 4.25 Krokha, V. A.: "A Method of Determining the Flow Stress in Compression to High Degrees of Plastic Deformation," *Ind. Lab.*, **40**, 1974, pp. 754–758.
- 4.26 Pöhlandt, K.: "Upsetting Test for Determining Flow Curves According to Rastegaev" (*in German*), *Ind.-Anz.*, **101**, 1979, no. 48, pp. 28–29 (HGF 79/26.)
- 4.27 Rafalski, Z., and Misiolek, Z.: "Estimation of Plastic Properties of Cold Formed Metals" (*in German*), *Bänder Bleche Röhre*, **21**, 1980, pp. 459–463.

- 4.28 Chang, T., and Shü, U.: "The Stress-Strain Relationship of Metals under Homogeneous Compression," *Sci. Sin.*, **10**, 1961, pp. 377-385.
- 4.29 Lippmann, H., and Mahrenholtz, O.: *Theory of Plasticity of Metal Forming (in German)*, vol. 1, Berlin, Springer, 1967.
- 4.30 Watts, A. B., and Ford, H.: "On the Basic Yield Stress Curve for a Metal," *Proc. Inst. Mech. Eng.*, **169**, 1955, pp. 1141-1150.
- 4.31 Kaspar, R., and Pawelski, O.: "A Computer-Controlled Simulation of Hot Work by Flat Compression on a High Speed Servo-Hydraulic Testing Machine," in Davies, B. J. (ed.): *Proceedings of the 19th MTDR Conference* (Manchester, Sept. 13-15, 1978), London, Macmillan, 1979.
- 4.32 Lahoti, G. D., and Altan, T.: "Prediction of Temperature Distributions in Axisymmetric Compression and Torsion," *Trans. ASME, J. Eng. Mater. Technol.*, **96**, 1974, pp. 1-8.
- 4.33 Stüwe, H.-P., and Turck, H.: "On the Determination of Flow Curves in the Torsion Test" (in German), *Z. Metallkd.*, **55**, 1964, pp. 699-703.
- 4.34 Barracough, D. R.: "Effect of Specimen Geometry on Hot Torsion Test Results for Solid and Tubular Specimens," *J. Test. Eval. (JTEVA)*, **1**, 1973, pp. 220-227.
- 4.35 Lach, E., and Pöhlandt, K.: "Testing the Plastic Behavior of Metallic Materials in Torsion Tests" (in German), *Draht*, **33**, 1982, pp. 689-693.
- 4.36 Nadai, A.: *Theory of the Flow and Fracture of Solids*, New York, McGraw-Hill, 1950.
- 4.37 Pöhlandt, K.: "On the Optimization of Specimen Shape and the Evaluation of Data from the Torsion Test" (in German), Dr.-Ing. thesis, Technical University Braunschweig, 1977.
- 4.38 Witzel, W.: "Inhomogeneous Deformation Due to Changes of Texture" (in German), *Z. Metallkd.*, **69**, 1978, pp. 337-343.
- 4.39 Pöhlandt, K.: "Testing Strain-Rate Sensitive Materials in the Torsion Test," *Materialprüfung*, **22**, 1980, pp. 399-406.
- 4.40 Ithara, M., *Rep. Tohoku Univ.*, **11**, 1935, pp. 489-528, cited in Siebel, E.: *Handbook of Materials Testing*, vol. 2, Berlin, Springer, 1939.
- 4.41 Horiuchi, M. R., et al.: "The Characteristics of the Torsion Test for Assessing Hot Workability of Aluminum Alloys," Institute for Space and Aeronautical Science, University of Tokyo, Rep. 443, 1970.
- 4.42 Weiss, H., et al.: "A Torsion Machine for Programmed Simulation of Hot Working," *J. Phys. E. Sci. Instrum.*, **6**, 1973, pp. 710-714.
- 4.43 Panknin, W.: "Determination of Flow Curve and Formability of Sheet Metal by Hydraulic Bulge Test" (in German), *Ind.-Anz.*, **86**, 1964, pp. 915-918.
- 4.44 Gologranc, F.: "Investigation of the Hydraulic Bulge Test for the Determination of Flow Curves" (in German), *Ind.-Anz.*, **90**, 1968, pp. 775-779.
- 4.45 Schott, H. K.: "Plastic Deformation and Stability in Hydraulic Bulge Tests" (in German), Dr.-Ing. thesis, Technical University Braunschweig, 1973.
- 4.46 Sawada, T.: "Error Estimates during Stress-Strain Diagram Measured with the Hydraulic Bulge Test," Department of Mechanical Engineering, Tokyo University of Agriculture and Technology, Priv. Rep., 1981.
- 4.47 Marciniak, Z., and Koloziejski, J.: "Assessment of Sheet Metal Failure Sensitivity by Method of Torsioning the Rings," *Proceedings of the 7th Biannual Congress of the IDDRG* (Amsterdam, 1972), pp. 61-64.
- 4.48 Tekkaya, A. E., and Pöhlandt, K.: "Determining Stress-Strain Curves of Sheet Metal in the Plane Torsion Test," *Ann. CIRP*, **31**, 1982, pp. 171-174.
- 4.49 Pöhlandt, K., and Tekkaya, A. E.: "Determining Flow Curves of Thin Sheets by the Plane Torsion Test" (in German), *Arch. Eisenhüttenwes.*, **53**, 1982, pp. 421-426.
- 4.50 Hensel, A., and Spittel, Th.: *Force and Work Requirement of Metal Forming Processes (in German)*, Leipzig, VEB Deutscher Verlag für Grundstoffindustrie, 1976.

#### 4.18 FUNDAMENTALS OF METAL FORMING

- 4.51 "Flow Curves of Metallic Materials" (*in German*), VDI Data Sheets 3200 to 3202, Oct. 1978.
- 4.52 Dahl, W., and Rees, H.: *The Stress-Strain Curve of Steel* (*in German*), Düsseldorf, Verlag Stahleisen, 1976.
- 4.53 Deutsche Gesellschaft für Metallkunde (DGM): "Atlas of Hot Formability of Nonferrous Metals" (*in German*), vol. 1: "Aluminum and Its Alloys," vol. 2: "Copper and Its Alloys," Oberursel, DGM, 1978.
- 4.54 Heinemann, H. H.: "Flow Stress of Different Aluminum and Copper Alloys at High Strain Rates and Temperatures" (*in German*), Dr.-Ing. thesis, Technical University Aachen, 1961.
- 4.55 Diether, U.: "Determining Flow Curves at Elevated Temperatures in the Upsetting Test" (*in German*), *Ind.-Anz.*, **102**, 1979, pp. 67-68 (HGF 79/87).
- 4.56 Neuberger, F., et al.: "Testing Common Forging Metals by Upsetting Tests" (*in German*), *Maschinenbau-Technik*, **7**, 1958, pp. 249-254.
- 4.57 Leykamm, H.: "Calculation of Flow Curves and of Strength, Elongation to Fracture and Fracture Necking of Cold Formed Parts of Extrusion Steels from Chemical Analysis According to Wagenbach" (*in German*), *Draht*, **29**, 1978, pp. 648-651.
- 4.58 Jonck, R., et al.: "Effect of Alloy Constituents on Cold Forming Behavior," *ZwF*, **69**, 1974, pp. 419-424.
- 4.59 Mathon, M. P.: "Influence of the Impurities of Steels on Cold Formability" (*in French*), *Formage et Matériaux* **1**, 1969, pp. 15-19.

## FUNDAMENTALS OF TECHNICAL PLASTICITY THEORY

---

---

---

Plasticity theory is the foundation for the numerical treatment of metal-forming processes. The use of its fundamental equations, though, often results in mathematical difficulties when applied to practical problems. This led to the development of solution techniques which today collectively carry the name of *elementary plasticity theory*. In this theory, the mathematical difficulties are circumvented by making simplifying assumptions regarding the deformation and stress states occurring in the workpiece. As a result, one obtains an approximate quantitative description of a metal-forming process. The various solution techniques associated with the elementary and the more general technical theory of plasticity are given in Fig. 5.1.

In this chapter, the basic concepts and equations of elementary plasticity theory are presented in detail. A brief account of the von Mises plasticity theory and its principal solution techniques is also given. Both theories are illustrated by example problems. Further examples can be found in subsequent chapters that deal with individual metal-forming processes.

### 5.1 FUNDAMENTALS OF ELEMENTARY PLASTICITY THEORY

#### 5.1.1 Plasticity, Yield Strength, and Strain Hardening

Materials science and metallurgy can explain the origins of the plastic state of metallic bodies and its dependence on various parameters, such as process speed, prior history, temperature, and so on. The essentially older *plasticity theory* deals with the calculation of stresses, forces, and deformation. Its formulation does not directly incorporate the body of metallurgical knowledge, even though the accuracy of the description of metals undergoing plastic flow could thereby be increased.

Plasticity theory is rather based on macroscopically observed phenomena; in other words, on the properties of materials which can be observed and measured directly in deformation processes,

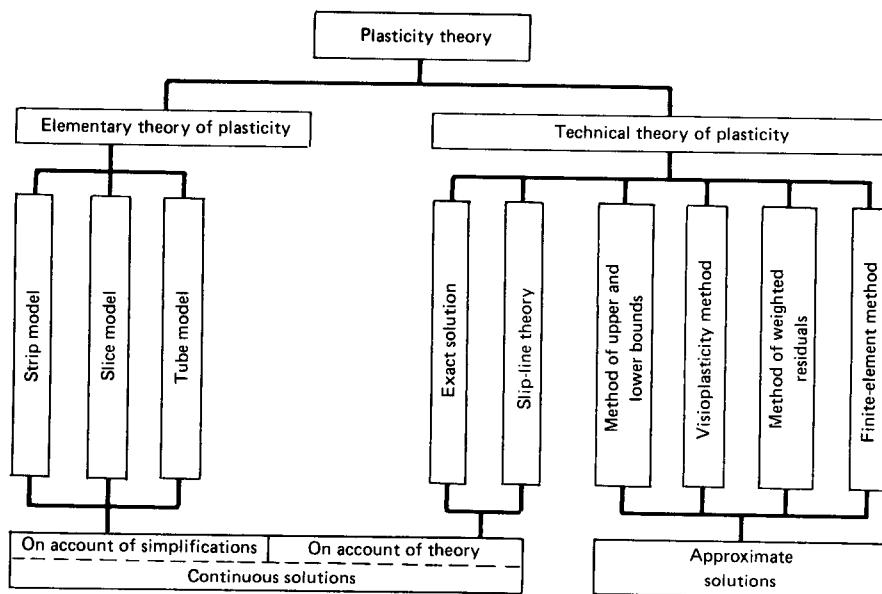


**FIG. 5.1** Theoretical solution techniques for metal-forming problems. (After [5.48].)

such as the tension and compression tests. This leads to the following simple description of the plastic state.

Plasticity is the capacity of a material to change its shape permanently under the action of forces when the corresponding stress state reaches a material-dependent critical magnitude called *yield strength* or *initial flow stress* (see Fig. 4.1). As seen from the results of the tension test, when the stress is below the yield strength, the deformation disappears upon unloading: the material behaves elastically. If the stress exceeds the yield strength, permanent deformation results. Upon unloading, the workpiece has a form that is different from its initial one. It is then said to have been plastically or permanently deformed, or, if a definite final shape was sought, it has been (trans)formed. Materials which behave in an elastic-plastic manner can, after having been permanently deformed, again be loaded until the flow stress is reached (it now has a magnitude larger than the initial one) without additional permanent deformation setting in. This increase in the flow stress as a result of prior deformation is called *strain hardening*.

### 5.1.2 Displacement

The foundation of the global description of a metal-forming process is the description of stresses and strains and their relation when referenced to a volume element of the material. The displacement of these volume elements can be represented in terms of a *velocity field*. This field determines the instantaneous velocity of the elements, both direction and magnitude (Figs. 5.2 and 5.3).

As *streamlines* of the velocity field one designates those lines which have the velocity vector as tangents. The actual paths undergone by the elements during the process are called *path lines* or *flow lines*.

If the displacement, that is, the velocity field, changes during the process, then the latter is called *nonsteady-state*. If, on the other hand, the velocity field does not change, the process is *steady-state*. (A steady-state velocity field is in reality only present for portions of a particular process.) For steady-state processes the stream- and path lines coincide, for a nonsteady-state one

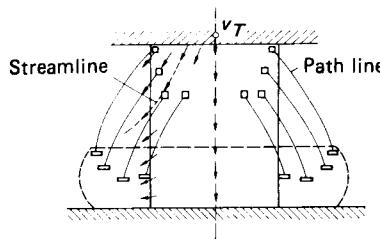


**FIG. 5.2** Motion in a nonsteady-state metal-forming process (upsetting).

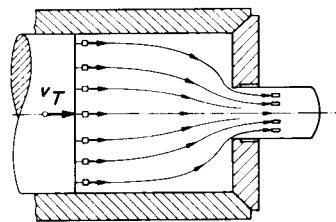


**FIG. 5.3** Motion in a steady-state metal-forming process (extrusion).

they do not. Thus it is easily seen that for a steady-state displacement, the other process-related quantities, especially stresses and forces, do not change with time.

The flow of the material can be portrayed by sectioning the workpiece and then inscribing a network of lines which get deformed (Fig. 5.4), or it can be illustrated by model experiments.

### 5.1.3 Strain and Strain Rate

If one examines the displacement of small portions of material (the so-called material elements) between a definite time  $t$  of the process and an interval  $\Delta t$ , one notices that the elements will have changed their shape; deformation is said to have occurred (Fig. 5.5).

The total deformation can generally be expressed in terms of two different types of strains: normal strain and shear strain.

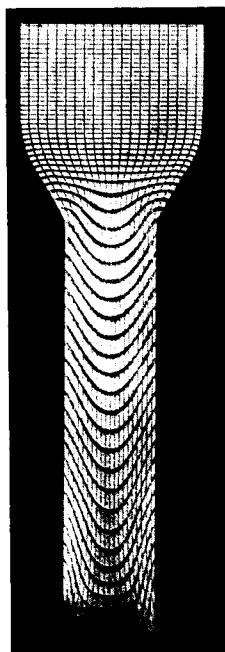


**FIG. 5.4** Experimental determination of displacement by use of a grid pattern.

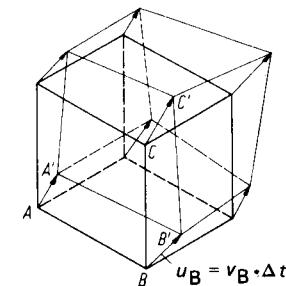


**FIG. 5.5** Deformation of a material element during time  $\Delta t$ .  $u_B$  is displacement of point B.

sequently the new length  $\overline{A'B'}$  can be taken to be equal to its projection on the  $x$ -axis. One thus obtains

$$\overline{A'B'} = \Delta x - u_x^{(A)} + u_x^{(B)} = \Delta x + \Delta u_x \quad (5.1)$$

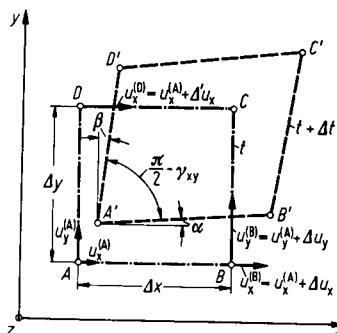


**FIG. 5.6** Deformation of the surface of an element parallel to  $xy$  plane.  $u_x^{(A)}, u_y^{(A)}, u_z^{(A)}$ —displacements of point  $A$  in  $x$ -,  $y$ -, and  $z$ -directions, respectively.

where  $u_x$  is the displacement of a point in the  $x$ -direction. The average normal strain is determined by

$$\epsilon_x = \frac{\Delta x + \Delta u_x - \Delta x}{\Delta x} = \frac{\Delta u_x}{\Delta x} \quad (5.2)$$

In the limit as  $\Delta t$  and  $\Delta x$  approach zero,

$$\epsilon_x = \frac{\partial u_x}{\partial x} \quad (5.3a)$$

Similarly,

$$\epsilon_y = \frac{\partial u_y}{\partial y} \quad (5.3b)$$

$$\epsilon_z = \frac{\partial u_z}{\partial z} \quad (5.3c)$$

### Shear Strain

Shear strains are determined by considering the change in the original right angles of the volume element. The change in the angle  $DAB$  is thus

$$\gamma_{xy} = \alpha + \beta \quad (5.4)$$

$$= \frac{\partial u_x}{\partial y} + \frac{\partial u_y}{\partial x} \quad (5.3d)$$

The above holds because  $\alpha$  and  $\beta$  are very small angles, and in their determination one can assume  $\overline{A'B'} = AB$  and  $\overline{A'D'} = AD$ . The other shear strains can be obtained similarly,

$$\gamma_{xz} = \frac{\partial u_z}{\partial x} + \frac{\partial u_x}{\partial z} \quad (5.3e)$$

$$\gamma_{yz} = \frac{\partial u_z}{\partial y} + \frac{\partial u_y}{\partial z} \quad (5.3f)$$

In metal-forming processes, strain rates as well as strains are of importance. Let the velocity of an element in the  $x$ -direction be given by

$$v_x = \frac{\partial u_x}{\partial t} \quad (5.5a)$$

and correspondingly,

$$v_y = \frac{\partial u_y}{\partial t} \quad (5.5b)$$

$$v_z = \frac{\partial u_z}{\partial t} \quad (5.5c)$$

Then the normal and shear strain rates are

$$\dot{\epsilon}_x = \frac{\partial \epsilon_x}{\partial t} = \frac{\partial}{\partial t} \frac{\partial}{\partial x} (u_x) = \frac{\partial}{\partial x} \left( \frac{\partial u_x}{\partial t} \right) = \frac{\partial v_x}{\partial x} \quad (5.6a)$$

$$\dot{\gamma}_{xy} = \frac{\partial v_x}{\partial y} + \frac{\partial v_y}{\partial x} \quad (5.6b)$$

Having defined strain and strain rate as above, one can now describe the deformation state and its change with time for a small volume element. This state can change from point to point in the workpiece and is also dependent on the orientation of the element.

Once the deformation state has been determined for a particular system of axes, say,  $x-y-z$ , the state of strain for a rotated system of axes  $x'-y'-z'$  through the same point can be determined if the angle of rotation is given [5.1].

It is possible to orient an element at each point in a body stressed below the yield strength in such a way that it experiences only normal strains and no shear strains. The perpendicular directions given by the corners of such an element are known as principal strain directions, or principal axes of the strain state.

In metal-forming processes, the plastic or permanent strains are as a rule very much larger than the elastic ones. Because of this, the elastic strains are generally neglected. Experiments have shown that the plastic strains correspond to no change in volume of the material. This leads to the fundamental rule employed for all metal-forming processes:

The volume remains constant during forming.

This statement can be expressed as either

$$\epsilon_x + \epsilon_y + \epsilon_z = 0 \quad (5.7a)$$

or

$$\dot{\epsilon}_x + \dot{\epsilon}_y + \dot{\epsilon}_z = 0 \quad (5.7b)$$

### 5.1.4 Homogeneous Deformation, Natural Strain

The change in the dimensions of a workpiece during forming generally yields only qualitative information about what is happening on the inside. Different strain states can yield very similar overall changes. However, one can visualize forming processes and then assume that they represent actual ones, a stepwise approximation in which at each point of the workpiece the same straining takes place, that is, the process is *homogeneous*.

It is easily seen that only such homogeneous processes lend themselves to an experimental determination of mechanical properties. In these experiments, the change in external dimensions due to applied loads is measured. Conclusions can only be made, however, regarding the material's stress-strain behavior if the observed external change is representative of the change for each volume element.

The tension test satisfies this condition to good approximation as long as the phenomenon of necking has not taken place as yet. Another example of a homogeneous process is friction-free upsetting between parallel platens. While this forming process is difficult to carry out in reality, it does, however, possess importance for theoretical considerations.

If a specimen of rectangular cross section is upset between frictionless parallel platens (Fig. 5.7), then it can be shown that the velocities are linear functions of the coordinates. They are given by

$$v_x = \frac{v_T}{2h} x \quad (5.8a)$$

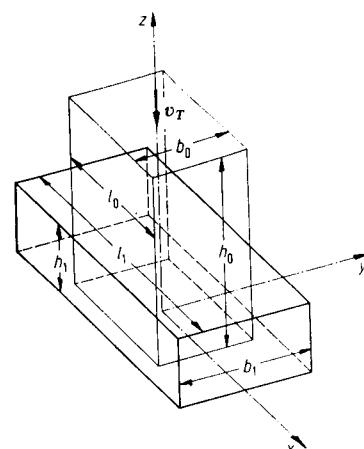


FIG. 5.7 Homogeneous deformation of a rectangular solid.  $v_T$ —velocity of moving upper surface.

## 5.6 FUNDAMENTALS OF METAL FORMING

$$v_y = \frac{v_T}{2h} y \quad (5.8b)$$

$$v_z = -\frac{v_T}{h} z \quad (5.8c)$$

With these, the normal strain rates become

$$\dot{\epsilon}_x = \frac{v_T}{2h} = \dot{\varphi}_l \quad (5.9a)$$

$$\dot{\epsilon}_y = \frac{v_T}{2h} = \dot{\varphi}_b \quad (5.9b)$$

$$\dot{\epsilon}_z = -\frac{v_T}{h} = \dot{\varphi}_h \quad (5.9c)$$

These expressions satisfy the volume constancy condition. All shear strain rates are identically zero. The  $x$ -,  $y$ -, and  $z$ -directions are in this case the principal directions for each volume element of the specimen, and the normal strain rates have the same value at each point.

In metal forming, one designates the principal normal strain rates which arise during homogeneous deformation as strain rate  $\dot{\varphi}$ . For each element, they are determined from  $v_T$  and  $h$ .

The strains which each element experiences during the interval  $t_1-t_0$  can also be expressed in terms of these parameters. For example, the natural strain in the  $z$ -direction is given by

$$\varphi_h = \int_{t_0}^{t_1} \dot{\varphi}_h dt = \int_{t_0}^{t_1} \left( -\frac{v_T}{h} \right) dt \quad (5.10)$$

If  $h_0$  is the height of the specimen at time  $t_0$  and  $h_1$  that at  $t_1$ , then with

$$dh = -v_T dt$$

we have

$$\varphi_h = \int_{h_0}^{h_1} \frac{dh}{h} = \ln h_1 - \ln h_0 = \ln \frac{h_1}{h_0} \quad (5.11a)$$

Similarly,

$$\varphi_l = \ln \frac{l_1}{l_0} \quad (5.11b)$$

$$\varphi_b = \ln \frac{b_1}{b_0} \quad (5.11c)$$

The quantity  $\varphi$  is known as *natural* or *true strain*. Eqs. 5.11 for the determination of the  $\varphi$ 's hold not only for one-dimensional stress states, but also for multiaxial ones. It must be assumed, however, that the deformation state remains homogeneous because only for this assumption does  $\varphi$  represent a measure of the local deformation. For nonhomogeneous deformation states it makes no sense to speak of a natural strain  $\varphi$ . It is then only a geometric quantity, which is, however, often used in metal forming.

The natural strains in different directions can be related to each other via the volume constancy condition. From

$$V = h_0 b_0 l_0 = h_1 b_1 l_1$$

there results

$$\frac{h_1 b_1 l_1}{h_0 b_0 l_0} = 1$$

which in turn becomes

$$\ln \frac{h_1}{h_0} + \ln \frac{b_1}{b_0} + \ln \frac{l_1}{l_0} = \varphi_h + \varphi_b + \varphi_l = 0 \quad (5.7c)$$

This equation is a special case of Eq. 5.7a for the case of homogeneous deformation.

If the specimen possesses a circular cross section rather than a rectangular one, then one speaks of homogeneous deformation if the normal strain rates in the radial, circumferential, and longitudinal directions remain the same at each point of the workpiece. The latter is the case when upsetting or pulling rotationally symmetric specimens.

For the strain in the axial direction, one then obtains

$$\varphi_l = \ln \frac{l_1}{l_0}$$

and for the radial and circumferential directions,

$$\varphi_r = \varphi_t = \ln \frac{r_1}{r_0}$$

### 5.1.5 Yield Criteria and Stress–Strain Relations

In the one-dimensional tension–compression test, yielding (flow) takes place when the stress  $\sigma = F/A$  reaches the value  $\sigma_f$ . This condition can be considered to be a yield criterion,

$$\left| \frac{F}{A} \right| = \sigma_f \quad (5.12)$$

For multiaxial stress states, the onset of yielding is not dependent on a single stress (for example, the largest tensile or compressive stress), but on a combination of all stresses. From the many yield criteria which have been proposed, two have shown good agreement with experimental results. These are:

- 1 Maximum shear stress criterion (Tresca, Mohr) [5.2]
- 2 Distortion energy criterion (von Mises, Hencky) [5.3]

They have served as the basis for most of the work in the field of plasticity. Both contain the one-dimensional criterion, Eq. 5.12, as a special case.

The *maximum shear-stress criterion* states that the material at a point in the workpiece receives permanent deformation when the largest of the shear stresses at this point reaches a critical value. It can be expressed as

$$|\tau_{\max}| = k \quad (5.13)$$

Here  $k$  is the material-dependent shear yield strength which, for example, can be determined from a torsion test. It is to be recalled that the stress state like the deformation state possesses principal axes. These axes, which are mutually perpendicular, represent the directions of the *principal stresses*  $\sigma_1$ ,  $\sigma_2$ , and  $\sigma_3$ .

A planar state of stress with principal stresses  $\sigma_1$  (the largest) and  $\sigma_3$  (the smallest) can be represented by *Mohr's circle*, as shown in Fig. 5.8 [5.4]. This circle, which represents the stress states at a point in the material for any rotation of the axes, has for its radius the maximum shear stress  $\tau_{\max}$ . The latter can be expressed as (Fig. 5.8):

$$\tau_{\max} = \frac{\sigma_1 - \sigma_3}{2} \quad (5.14)$$

Stress states which induce permanent deformation in the material are thus represented by Mohr's circle of radius  $k$ .

In the uniaxial tension test ( $\sigma_2 = \sigma_3 = 0$ ), one has, at the moment of yielding (Fig. 5.9),

$$\sigma_1 = \frac{F}{A} = \sigma_f = 2k$$

This yields

$$k = \frac{\sigma_f}{2} \quad (5.15)$$

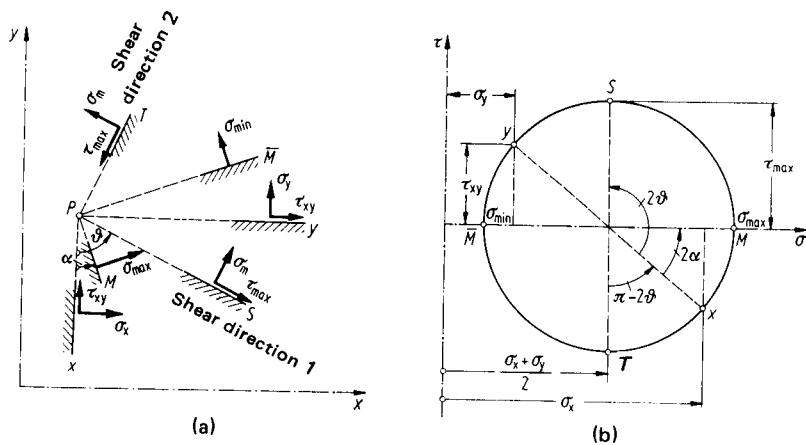


**FIG. 5.8** Representation of plane state of stress by Mohr's circle. (a) Physical space. (b) Stress space.

The maximum shear-stress criterion, as a result, can be written as

$$\sigma_1 - \sigma_3 = \sigma_f \quad (5.16)$$

An examination of Fig. 5.8 furthermore indicates that the position of the circle, or rather that of its center, in  $\sigma$ - $\tau$  space has no influence on the onset of yielding. The mean normal stress

$$\sigma_m = \frac{\sigma_1 + \sigma_2 + \sigma_3}{2} \quad (5.17)$$

whose negative value

$$p = -\sigma_m \quad (5.18)$$

is known as the hydrostatic pressure, therefore, does not influence yielding. This agrees with the experimental observation that when a workpiece is subjected to a uniform pressure, creating a hydrostatic stress state everywhere,

$$\sigma_1 = \sigma_2 = \sigma_3 = -p$$

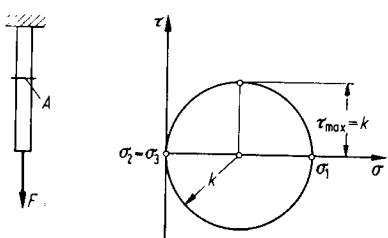
then no permanent deformation results.

In determining whether or not a particular stress state has caused flow to occur, the maximum shear-stress criterion takes into account only a part of the stress state (for example, the largest and smallest principal stresses). In comparison, the *criterion of von Mises*, which involves the *energy of distortion*, considers the entire stress state. It can be stated in the following way. The onset of flow must depend on a combination of normal and shear stresses whose magnitude does not change with a change in coordinate system. The latter is so because a coordinate system, and thereby the orientation of a material element, should have no influence on the yielding process.

**FIG. 5.9** Mohr's circle for uniaxial tension.

On the basis of these considerations, von Mises postulated a yield criterion which, when expressed in terms of principal stresses, takes the form

$$\sqrt{\frac{1}{2}[(\sigma_1 - \sigma_2)^2 + (\sigma_2 - \sigma_3)^2 + (\sigma_1 - \sigma_3)^2]} = \sigma_f \quad (5.19)$$



This criterion can also be written as

$$\sqrt{\frac{1}{2}[(\sigma_1 - \sigma_m)^2 + (\sigma_2 - \sigma_m)^2 + (\sigma_3 - \sigma_m)^2]} = \sigma_f \quad (5.20)$$

when use is made of the definition of mean stress.

This criterion also contains as a special case the yield criterion for one-dimensional tension or compression (Fig. 5.9). For with

$$\sigma_1 = \frac{F}{A} \quad \sigma_2 = \sigma_3 = 0$$

the von Mises criterion becomes

$$\sqrt{\frac{1}{2} \cdot 2\sigma_1^2} = \sigma_f$$

Both criteria also yield the same expression for the maximum shear stress at the onset of yielding,

$$\tau_{max} = \frac{1}{2}\sigma_1 = 0.5\sigma_f$$

For other states of stress, the distortion energy criterion produces larger maximum shear stresses than the *Tresca criterion*. The largest difference between them occurs for the case of pure shear (Fig. 5.10). Here

$$\sigma_3 = -\sigma_1 \quad \sigma_2 = 0$$

According to the shear-stress criterion, one obtains

$$\tau_{max} = \sigma_1 = 0.5\sigma_f$$

while the von Mises criterion yields

$$\tau_{max} = \sigma_1 = \frac{\sigma_f}{\sqrt{3}} = 0.577\sigma_f$$

The differences in the maximum shear-stress prediction are thus seen to lie between 0 and 15%. Experiments [5.5] have confirmed the fact that the von Mises criterion is able to describe the actual conditions more accurately.

After the yield strength is reached, the material starts to flow under the influence of the stress state. In the plastic regime there exists no one-to-one correspondence between stress and strain as there is for elastic behavior. Rather, the same deformation can result from different stress states and vice versa. The following, however, is true in all cases:

- 1 If the material starts to flow at a particular point of the workpiece, then the stress state there must have reached the yield strength.
- 2 The manner of flow is dependent on the character of the stress state.
- 3 Normal strains cannot be directly related to the stresses.

The relation between the strain rates and the stress state is known as the *flow rule*. Expressed in terms of principal directions and incorporating the von Mises yield criterion, it can be written as

$$\varphi_1 = \lambda(\sigma_1 - \sigma_m) \quad (5.21a)$$

$$\varphi_2 = \lambda(\sigma_2 - \sigma_m) \quad (5.21b)$$

$$\varphi_3 = \lambda(\sigma_3 - \sigma_m) \quad (5.21c)$$

These relations express the fact that the principal strain rates are proportional to the difference between the corresponding principal stress and the mean stress. The right-hand side of these equations incorporates the fact that under hydrostatic pressure no deformation takes place. The quantity  $\lambda$  is isotropic and can be assumed to depend on the material, temperature, strain, and strain rate.

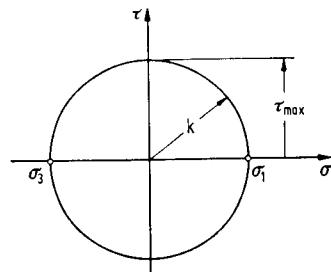


FIG. 5.10 Mohr's circle for pure shear.

### 5.1.6 Forming Limit

Forming is only possible until a particular magnitude of the deformation is reached. If, for example, a definite normal strain is exceeded in the tension test, then rupture takes place. One then speaks of the fact that the deformation capacity of the material is exhausted.

Rupture theories, which predict either a critical strain or a stress state, are not yet fully enough developed to be able to deliver quantitative results. One is forced, therefore, to employ qualitative results based on experiments. The *forming limit* is mainly influenced by three quantities: the type of stress state, the temperature profile of the process, and the strain rates.

In general, tensile stresses cause rupture earlier than compression stresses. Thus if the stress state is influenced in such a manner that the resulting stresses lie in the compression region, then the forming limit is increased. The mean stress can be taken as a measure of how far a particular stress state lies in the compression region (Fig. 5.11).

With increasing temperature, the forming limit is also increased. This is due, among other things, to the crystal-recovery and recrystallization processes which now take place during forming.

**FIG. 5.11** Dependence of forming limit on mean normal stress  $\sigma_m$ .

The favorable influence of both compressive stress and increased temperature on the rupture capacity of materials is employed in numerous metal-forming processes to produce large deformations.

An increasing strain rate brings about an increase in the tendency for brittle fracture. As a rule, the forming limit decreases in this case.

### 5.1.7 Power and Work

Forming processes are irreversible processes. For the most part, the mechanical work expended to cause deformation is converted into thermal energy. This work, in contrast with the energy stored during elastic deformation, cannot be recovered.

Consider the *homogeneous* deformation of a rectangular volume element (Fig. 5.12). Let us designate the velocity with which the lengths of the edges  $AB$ ,  $BC$ , and  $BD$  increase by  $v_h$ ,  $v_b$ , and  $v_l$ . Because of

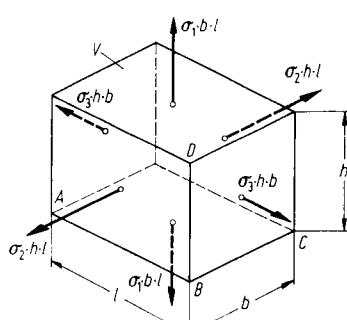


**FIG. 5.12** Homogeneous deformation of a rectangular solid.

$$\varphi_h = \varphi_1 = \ln \frac{h}{h_0}$$

one has

$$\dot{\varphi}_1 = \frac{d}{dt} \left( \ln \frac{h}{h_0} \right) = \frac{h_0}{h} \frac{1}{h_0} \frac{dh}{dt} = \frac{v_h}{h}$$

$$\text{Also, } \varphi_b = \varphi_2 = \ln \frac{b}{b_0} \quad \dot{\varphi}_2 = \frac{v_b}{b}$$

$$\varphi_l = \varphi_3 = \ln \frac{l}{l_0} \quad \dot{\varphi}_3 = \frac{v_l}{l}$$

The expression for the instantaneous power (force times velocity) is

$$P = \sigma_1 b l v_h + \sigma_2 h l v_b + \sigma_3 h b v_l$$

or, using the above expressions

$$P = (\sigma_1\dot{\varphi}_1 + \sigma_2\dot{\varphi}_2 + \sigma_3\dot{\varphi}_3)V \quad (5.22)$$

The power density is in turn given by

$$p = \frac{P}{V} = \sigma_1\dot{\varphi}_1 + \sigma_2\dot{\varphi}_2 + \sigma_3\dot{\varphi}_3 \quad (5.23)$$

which, because of homogeneous deformation, has the same value for each arbitrary volume element.

If the power is integrated over the time interval  $t_1 - t_0$ , then the *deformation work*  $W$  expended during this interval is

$$W = V \int_{t_0}^{t_1} (\sigma_1\dot{\varphi}_1 + \sigma_2\dot{\varphi}_2 + \sigma_3\dot{\varphi}_3) dt \quad (5.24)$$

If the stresses are dependent on the natural strains (as is the case in cold forming with strain hardening) rather than the velocities, then  $\dot{\varphi} dt = d\varphi$  and

$$W = V \left( \int_0^{\varphi_1} \sigma_1 d\varphi_1 + \int_0^{\varphi_2} \sigma_2 d\varphi_2 + \int_0^{\varphi_3} \sigma_3 d\varphi_3 \right) \quad (5.25)$$

Here  $\varphi_1$ ,  $\varphi_2$ , and  $\varphi_3$  represent the amount of forming during the given time interval.

The conversion of mechanical energy into thermal energy leads to heating of the workpiece. Forming processes are in general not homogeneous. Therefore at different points of the workpiece, different amounts of heat are liberated. Furthermore, as this heat is given to the tooling and the surrounding air, one finds it difficult to determine the temperature distribution during forming.

### 5.1.8 Equivalent Strain and Strain Rate

The behavior of a material, that is, the dependence of the flow stress as a function of  $\varphi$ ,  $\dot{\varphi}$ , and  $T$ , is generally determined from a one-dimensional test and illustrated by a flow curve. In order to apply the values thus obtained to metal-forming processes having multiaxial stress states, one has to introduce the concept of the equivalence of processes.

The most important parameter which is measured in a uniaxial test, and which must be incorporated in the consideration of more general processes, is the measure of the strain hardening which a material experiences. In this regard, it is assumed on the basis of sufficient agreement with experiments that the strain hardening for a particular material depends on the work per unit volume which has been expended.

Let the work done be calculated for a particular element of the workpiece which was deformed under the multiaxial stress state. Then this element, according to the above considerations, possesses the same flow stress as an element in a uniaxial tension or compression test made of the same material and expending the same amount of work.

If we orient the element so that its edges are parallel to the principal stress directions, then the increment of work during a time period  $dt$  for small deformation  $d\varphi_1$ ,  $d\varphi_2$ , and  $d\varphi_3$  is given by

$$dW = (\sigma_1 d\varphi_1 + \sigma_2 d\varphi_2 + \sigma_3 d\varphi_3)V \quad (5.26)$$

If this is divided by time  $dt$ , one obtains an expression for the instantaneous power,

$$P = \frac{dW}{dt} = (\sigma_1\dot{\varphi}_1 + \sigma_2\dot{\varphi}_2 + \sigma_3\dot{\varphi}_3)V \quad (5.27)$$

The natural strain in the direction of the external force in a uniaxial test is designated as the equivalent strain  $\bar{\varphi}$ . Since the stress has a magnitude of  $\sigma_f$ , the increment of work during a time interval  $dt$  is given by

$$dW' = \sigma_f d\bar{\varphi} V' \quad (5.28)$$

where  $V'$  is the volume of the specimen. From this we obtain for the power

$$P' = \sigma_{ff} \dot{\varphi} V' \quad (5.29)$$

If in a particular time interval the given material element and the material in a uniaxial test possess the same flow resistance, then the strain hardening during the following time period  $dt$  is the same if

$$\frac{dW}{V} = \frac{dW'}{V'} \quad \text{or} \quad \frac{P}{V} = \frac{P'}{V'} \quad (5.30)$$

holds. From this it follows that

$$\sigma_{ff} \dot{\varphi} = \sigma_1 \dot{\varphi}_1 + \sigma_2 \dot{\varphi}_2 + \sigma_3 \dot{\varphi}_3 \quad (5.31)$$

The stresses  $\sigma_1$ ,  $\sigma_2$ , and  $\sigma_3$ , on the basis of the von Mises theory, must satisfy the yield criterion and the flow rule, and thus the stresses can be eliminated from Eq. 5.31. One then obtains a relation between the strain rates  $\dot{\varphi}$  and  $\dot{\varphi}_1$ ,  $\dot{\varphi}_2$ , and  $\dot{\varphi}_3$ ,

$$\dot{\varphi} = \sqrt{\frac{2}{3}(\dot{\varphi}_1^2 + \dot{\varphi}_2^2 + \dot{\varphi}_3^2)} \quad (5.32)$$

If the variation of time of the deformation process is known for the element (i.e., the strain rates are given as a function of time), then the equivalent natural strain

$$\bar{\varphi} = \int_{t_0}^{t_1} \dot{\varphi} dt \quad (5.33)$$

can be calculated. This determines the strain in the direction of the stress in a uniaxial test which yields the same strain hardening as that which the element received as a consequence of its deformation.

The application of the Tresca yield criterion yields the following expression for the equivalent strain rate [5.4]:

$$\dot{\varphi} = \dot{\varphi}_{\max} \quad (5.34)$$

$$\text{and thus } \bar{\varphi} = \varphi_{\max} \quad (5.35)$$

For a more detailed discussion of the deformation resulting from the application of the Tresca criterion, one should consult [5.14].

## 5.2 METHODS OF SOLUTION FOR ELEMENTARY PLASTICITY THEORY

The foundations of these solution techniques were developed in 1924 and 1925 by Siebel [5.6] and von Karman [5.7] in connection with the rolling process. Subsequent investigators examined the drawing [5.8] and forging processes [5.9]. The solution procedure employed for each of these forming processes was different because of the different assumptions which were employed. For processes which result in a plane deformation state, all these methods have been lumped together today under the name *strip* or *slab theory*. Their extension to axisymmetric processes has led to the development of *disk* and *tube* theories. A detailed description of the elementary theory, including the influence of inertia forces, can be found in [5.10].

### 5.2.1 Strip or Slab Theory

In the following, the method of elementary plasticity theory is illustrated by use of the strip theory, that is, for processes for which a plane deformation state can be assumed. It is assumed that:

- 1 Tooling possesses symmetry.
- 2 Weight and inertia forces can be neglected.

3 Coulomb-type friction with constant coefficient exists between workpiece and tooling.

4 Flow stress  $\sigma_f$  is given as a function of  $\varphi$ ,  $\dot{\varphi}$ , and  $T$ .

The principal starting point of elementary plasticity theory is a simplified assumption regarding the displacement field. Fig. 5.13 shows a basic model useful for the description of the theory.

It is assumed that the velocity  $v_x$  is the same at each point of a cross section  $x = \text{constant}$ . This implies that the sections  $x = \text{constant}$  and thus the boundaries remain plane during the whole process.

If the velocity  $v_x^*$  is known for a particular section  $x = x^*$ , then the velocity for any other arbitrary section can be calculated. This is due to the volume constancy of the material.

For a tool which is at rest,  $v_T = 0$ , the same amount of material crosses section  $x^*$  and enters the volume defined by sections  $x^*$  and  $x$  as in turn exists over section  $x$ . From this it follows that if the forming zone has a width  $b$  perpendicular to the plane of the figure, then

$$h^* v_x^* b = h v_x b \quad (5.36)$$

or

$$v_x = v_x^* \frac{h^*}{h} \quad (5.37)$$

If the halves of the tool move relative to each other, then the volume enclosed by sections  $x^*$  and  $x$  at time  $t$  is given by

$$V = b \int_{x^*}^x h dx$$

and at time  $t + dt$  by

$$V + dV = b \int_{x^*}^x (h + v_T dt) dx$$

This is so because the height of all strips lying between  $x^*$  and  $x$  has been changed by  $v_T dt$ . The rate of change of volume  $V$  with time is given by

$$\begin{aligned} \dot{V} &= \frac{dV}{dt} = \frac{b \int_{x^*}^x (h + v_T dt) dx - b \int_{x^*}^x h dx}{dt} \\ &= b \int_{x^*}^x v_T dx = bv_T(x - x^*) \end{aligned} \quad (5.38)$$

Employing the volume constancy assumption yields

$$h^* v_x^* b - h v_x b = bv_T(x - x^*) \quad (5.39)$$

or

$$v_x = \frac{1}{h} [h^* v_x^* - v_T(x - x^*)] \quad (5.40)$$

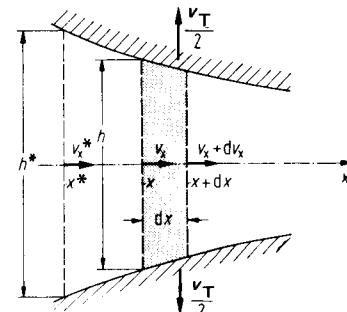


FIG. 5.13 Strip or slap model.

The rate of change of the height with time  $\dot{h}$  of a strip is determined partially by the velocity with which the upper and lower boundaries approach one another. It also depends on the slope of the tool at the contact point with the strip and the velocity with which the strip moves in the  $x$ -direction.

For a stationary tool, one has

$$\dot{h} = \frac{\partial h}{\partial t} = \frac{\partial h}{\partial x} v_x \quad (5.41)$$

For a movable tool, one obtains

$$\dot{h} = \frac{\partial h}{\partial x} v_x + v_T \quad (5.42)$$

The assumed motion leads to a homogeneous deformation of each strip. Thus the natural strain in the  $y$ -direction is

$$\varphi_h = \ln \frac{h}{h_0} \quad (5.43)$$

and

$$\dot{\varphi}_h = \frac{\partial \varphi_h}{\partial t} = \frac{\dot{h}}{h} \quad (5.44)$$

Upon differentiating Eq. 5.40 with respect to  $x$ , one obtains

$$\frac{\partial v_x}{\partial x} = -\frac{1}{h} \left( \frac{\partial h}{\partial x} v_x + v_T \right) = -\frac{\dot{h}}{h}$$

The following relationship is thus seen to exist between  $v_x$  and  $\dot{\varphi}_h$ :

$$\frac{\partial v_x}{\partial x} = -\dot{\varphi}_h \quad (5.45)$$

The principal axis of the homogeneous deformation field is parallel to the  $x$ - and  $y$ -axes. On planes  $x = \text{constant}$ , no shear stress exists and the normal stress  $\sigma_x$  is uniformly distributed (Fig. 5.14a).

Acting normal to the strip are the forces  $\sigma_x b h$  at  $x$  and  $\sigma_x b h + d(\sigma_x b h)$  at  $x + dx$ . The tool exerts on the strip the normal force  $\sigma_n b ds$ , which in turn leads to the friction force  $\mu \sigma_n b ds$ . If the strip moves in the positive  $x$ -direction, then the friction force is taken as positive in the direction shown. If the motion is opposite, then  $\mu$  must be replaced by  $-\mu$ .

Summation of forces in the  $x$ - and  $y$ -directions leads to (Fig. 5.14b)

$$dF_y = -\sigma_y b dx = \sigma_n b ds \cos \alpha - \mu \sigma_n b ds \sin \alpha \quad (5.46)$$

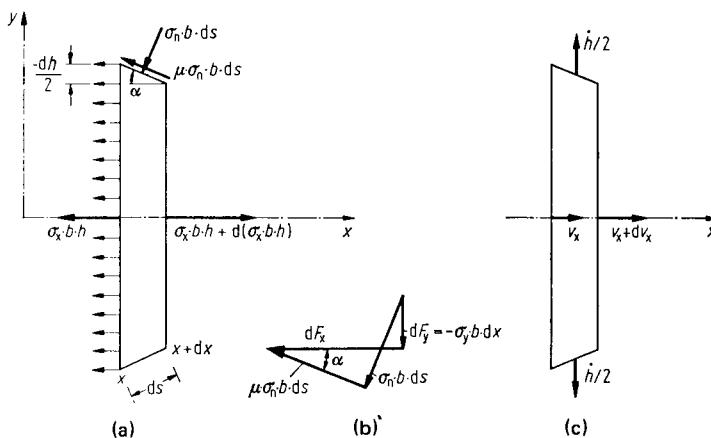


**FIG. 5.14** (a) Stresses on strip. (b) Determination of forces in  $x$ - and  $y$ -directions. (c) Movement of strip.

$$dF_x = \sigma_n b ds \sin \alpha + \mu \sigma_n b ds \cos \alpha \quad (5.47)$$

As

$$ds = \frac{dx}{\cos \alpha}$$

one obtains

$$\sigma_y = -\sigma_n(1 - \mu \tan \alpha)$$

$$dF_x = \sigma_n b dx (\tan \alpha + \mu) = -\sigma_y b dx \frac{\tan \alpha + \mu}{1 - \mu \tan \alpha}$$

If one substitutes for the coefficient of friction

$$\mu = \tan \rho \quad (5.48)$$

then

$$dF_x = -\sigma_y b dx \tan(\rho + \alpha) \quad (5.49)$$

since

$$\tan(\beta + \gamma) = \frac{\tan \beta + \tan \gamma}{1 - \tan \beta \tan \gamma}$$

These forces, along with the velocities shown in Fig. 5.14c, produce the power needed at each instant of the deformation process. This power must be compared with that calculated for a uniaxial test.

In elementary plasticity theory, the Tresca yield criterion is always employed. The equivalent strain rate is thus given by

$$\dot{\varphi} = \dot{\varphi}_{\max} = \frac{\dot{h}}{h} \quad (5.50)$$

The power expended in deforming the strip is

$$P = -(\sigma_x b h)v_x + [\sigma_x b h + d(\sigma_x b h)](v_x + dv_x) - 2dF_x v_x + h\sigma_y b dx \quad (5.51)$$

For the uniaxially deformed strip one obtains

$$P' = \mp \frac{\dot{h}}{h} hb dx \sigma_f \quad (5.52)$$

where the upper sign on the right-hand side holds for the case when the strip is compressed since then  $\dot{\varphi} = \dot{h}/h$  is negative. The resulting power is then positive.

In order to compare uniaxial and multiaxial processes, one must, according to Eq. 5.30, compare the powers for the same volume. Thus neglecting products of differentials, one obtains

$$v_x = \left[ \frac{d(\sigma_x h)}{dx} + 2\sigma_y \tan(\rho + \alpha) \right] + h[\pm \sigma_f + \sigma_y - \sigma_x] = 0 \quad (5.53)$$

Using the Tresca yield criterion, which for the strip takes on the form

$$\sigma_x - \sigma_y = \pm \sigma_f \quad (5.54)$$

(for the compressed strip  $\sigma_x$  is the algebraically largest principal stress), one has from the above

$$\frac{d(\sigma_x h)}{dx} + 2\sigma_y \tan(\rho + \alpha) = 0 \quad (5.55)$$

Use of the relation

$$\frac{dh}{dx} = -2 \tan \alpha$$

yields the following differential equation for the determination of  $\sigma_x$ :

$$\frac{d\sigma_x}{dx} + f(x)\sigma_x + g(x) = 0 \quad (5.56)$$

$$\text{where } f(x) = \frac{2}{h} [\tan(\rho + \alpha) - \tan \alpha] \sigma_x$$

$$g(x) = \mp \frac{2}{h} \sigma_t \tan(\rho + \alpha)$$

The general solution can be shown to be

$$\sigma_x(x) = e^{-\int_x^{x'} f dx} \left[ \sigma'_x - \int_{x'}^x (g e^{\int_x^{x'} f dx}) dx \right] \quad (5.57)$$

Here  $\sigma'_x$  is the known  $\sigma_x$  stress at some point  $x = x'$ .

This general solution, however, is only useful if a closed-form evaluation of the integrals can be carried out. If this is not possible, as is often the case, then one must treat Eq. 5.57 numerically (see Problem 2 in Sec. 5.2.3). Once  $\sigma_x$  has been obtained, then  $\sigma_y$  can be determined without difficulty from eq. 5.54.

### 5.2.2 Axisymmetric Forming

Axisymmetric forming processes can be described by use of the so-called disk theory. This theory is the counterpart of the development given in the previous section (Fig. 5.15). As generally there is no tool velocity in these processes, the velocity in the  $x$ -direction is given by

$$v_x = \frac{A^*}{A} v_x^* \quad (5.58)$$

where  $v_x^*$  is the assumed known velocity at section  $x^*$ . The equivalent strain rate is

$$\dot{\varphi} = 2 \frac{\dot{r}}{r} = - \frac{\partial v_x}{\partial x} \quad (5.59a)$$

and the equivalent natural strain is

$$\bar{\varphi} = 2 \ln \frac{r}{r_0} \quad (5.59b)$$

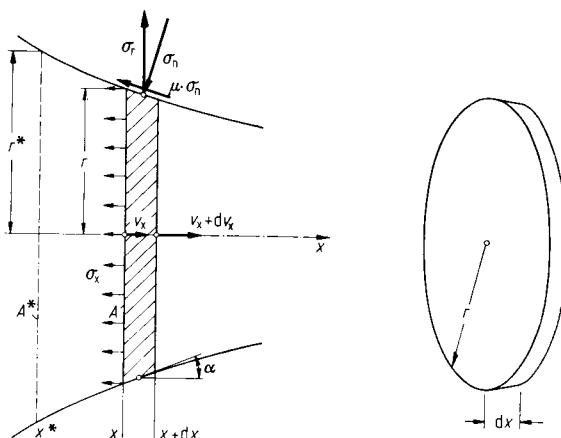


FIG. 5.15 Disk model.

If one again assumes the normal stress  $\sigma_x$  to be uniform over the section and lets the radial pressure from the tool on the workpiece be  $-\sigma_r$ , then

$$\sigma_x - \sigma_r = \pm \sigma_t \quad (5.60)$$

with

$$\sigma_r = \sigma_\theta$$

The upper sign in Eq. 5.60 holds if the radii become smaller during forming. For the determination of  $\sigma_x$ , one has the equation

$$\frac{d\sigma_x}{dx} + \frac{2}{r} [\tan(\rho + \alpha) - \tan \alpha] \sigma_x \mp \frac{2}{r} \sigma_t \tan(\rho + \alpha) = 0 \quad (5.61)$$

The solution of this equation proceeds similarly to that for Eq. 5.56.

With reference to the shape of the tool, use of the disk theory only requires that the flow of the material be axisymmetric. In contrast, the applicability of the tube theory is severely restricted. In its strict sense, this theory can be applied to the upsetting of solid cylinders between plane platens. The reason is that only for this process can a uniaxial comparison case be found [5.10]. As an approximation it can be applied to such other cases for which

$$|2 \frac{x}{h} \tan \alpha| \ll 1$$

holds.

In those cases where tube theory is applicable, Eqs. 5.54 and 5.56 hold for the stresses shown in Fig. 5.16. In these equations one needs to replace  $x$  by  $r$ ,  $\sigma_x$  by  $\sigma_r$ , and  $\sigma_y$  by  $\sigma_z$ .

### 5.2.3 Example Applications

The application of elementary plasticity theory is now illustrated by considering two problems.

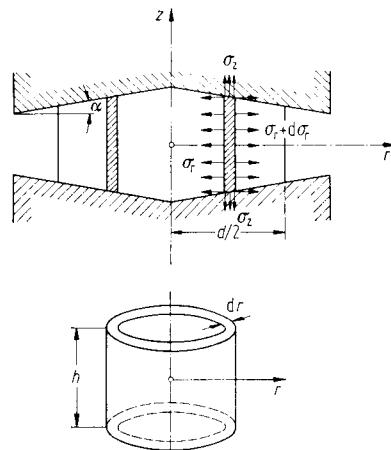


FIG. 5.16 Tube model.

#### Problem 1 (Fig. 5.17)

A crank press of  $h = 200$ -mm (7.87-in) stroke and operating at 30 strokes per minute is used to upset a cylindrical specimen made of AISI 1015 steel with initial dimensions  $h_0 = 30$  mm (1.18 in) and  $d_0 = 40$  mm (1.47 in). The final height is  $h_1 = 20$  mm (0.79 in) (Fig. 5.17a). The process temperature is  $1100^\circ\text{C}$  ( $2011^\circ\text{F}$ ). Friction exists between tool and workpiece, with the coefficient of friction  $\mu = 0.3$ .

The upsetting force is to be determined as a function of the instantaneous height  $h$ . In the calculation the strain-rate dependence of  $\sigma_t$  is to be considered.

For determining the stresses  $\sigma_r$  and  $\sigma_z$ , use is made of Eqs. 5.54 and 5.57. With  $\alpha = 0$  and  $\tan \rho = \mu$ , one obtains

$$f = \frac{2\mu}{h} \quad g = -\frac{2\mu}{h} \sigma_t$$

At

$$r = \frac{d}{2}$$

one has

$$\sigma_r = 0$$

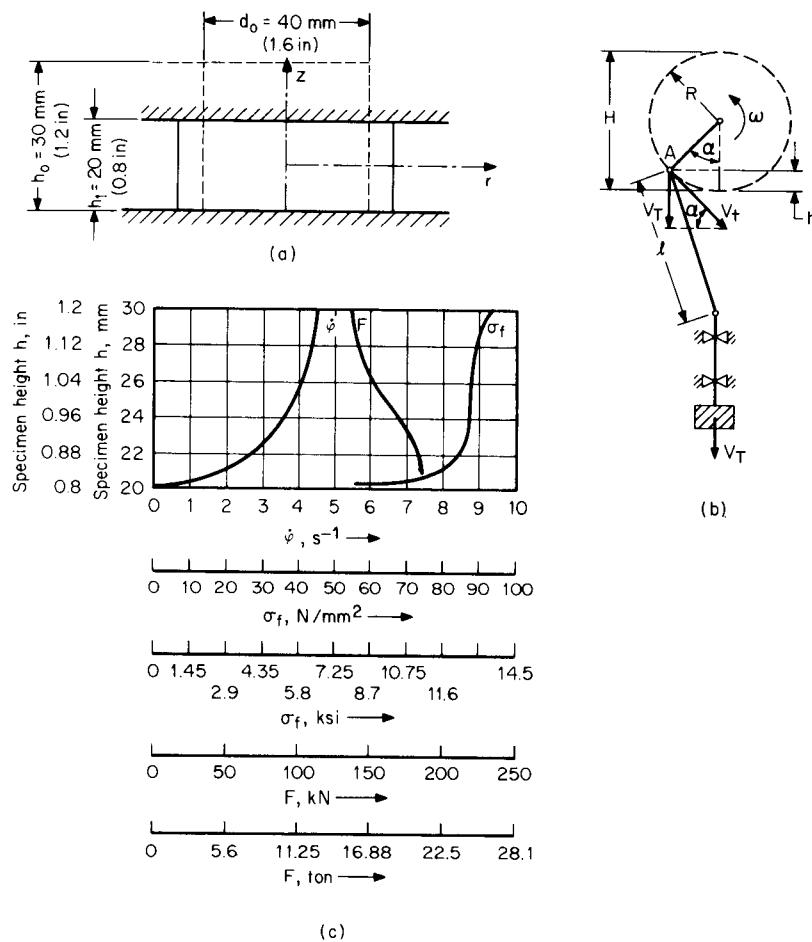


**FIG. 5.17** (a) Initial and final heights of cylindrical specimen. (b) Assumed kinematics of press. (c) Variation of  $\dot{\varphi}$ ,  $\sigma_f$ , and  $F$  during upsetting.

One thus obtains

$$r' = \frac{d}{2} \quad \sigma'_r = 0$$

with

$$d = d_0 \sqrt{\frac{h_0}{h}}$$

With the above,  $\sigma_r$  can be expressed as

$$\sigma_r = \sigma_f [1 - e^{(2\mu/h)(d/2 - r)}]$$

while  $\sigma_z$  becomes

$$\sigma_z = -\sigma_f e^{(2\mu/h)(d/2-r)}$$

When  $-\sigma_z$  is summed over the contact surface between workpiece and tool, one obtains the following expression for the upsetting force  $F$ :

$$F = 2\pi\sigma_f \int_0^{d/2} e^{2(\mu/h)(d/2-r)} r dr = 2\pi\sigma_f \left[ \frac{h^2}{4\mu^2} (e^{\mu d/h - 1}) - \frac{hd}{4\mu} \right] \quad (5.62)$$

Through the kinematics of the press, the instantaneous height of the specimen is related to the tool velocity  $v_T(h)$  (Fig. 5.17b). It is assumed that the dimensions of the press are such that  $v_T$  can be taken as the vertical component of the tangential velocity  $v_t$  of point A. This is equivalent to assuming that the length of the connecting rod is large compared to the stroke, and the elasticity of the press is negligibly small.

At the final height  $h_1$ ,  $\alpha$  should be zero. The following then hold:

$$v_T = v_t \sin \alpha = v_t \sqrt{1 - \sin^2 \alpha}$$

$$h = h_1 + h' = h_1 + R(1 - \cos \alpha)$$

$$\cos \alpha = 1 - \frac{h - h_1}{R}$$

$$v_T = v_t \sqrt{1 - \left(1 - \frac{h - h_1}{R}\right)^2}$$

$$\varphi = \ln \frac{h}{h_0}$$

$$\dot{\varphi} = \frac{d [\ln(h/h_0)]}{dt} = \frac{1}{h} \frac{dh}{dt} = \frac{v_T}{h}$$

As

one obtains

$$\dot{\varphi} = \frac{v_T}{h} \sqrt{1 - \left(1 - \frac{h - h_1}{R}\right)^2} \quad (5.63)$$

The dependence of flow stress on the strain rate is taken as

$$\sigma_f = 74 \cdot \dot{\varphi}^{0.125}$$

The strain rate and upsetting force as functions of  $h$  can now be determined from Eqs. 5.62 and 5.63. They are illustrated in Fig. 5.17c as functions of  $h$ .

### Problem 2 (Fig. 5.18)

The case of axisymmetric extrusion is now examined. Forming takes place at room temperature. AISI 1010 steel is chosen as the material, and the variation of its flow stress with natural strain  $\varphi$  is shown in Fig. 5.19. To be found is the radial pressure on the die and the extrusion force  $F$  for constant punch velocity (steady-state process).

The use of Eq. 5.57 for this problem would lead to complicated integrals if strain hardening is taken into account. In this case, therefore, one is better off to start with Eq. 5.61 and then to integrate numerically.

One of the techniques to accomplish this is the method of finite differences. The deformation zone is thereby split into  $n$  equal intervals of width  $B = L/n$ . The derivative  $d\sigma_x/dx$  in Eq. 5.61 is replaced by

$$\frac{\Delta\sigma_x}{\Delta x} = \frac{\sigma_{x_{i+1}} - \sigma_{x_i}}{x_{i+1} - x_i} = \frac{\sigma_{x_{i+1}} - \sigma_{x_i}}{B}$$

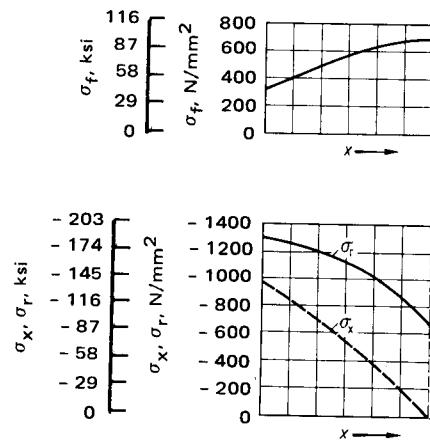
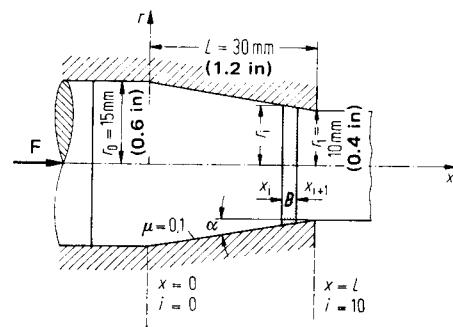


FIG. 5.18 Sketch of cold-extrusion process and variation of  $\sigma_t$ ,  $\sigma_x$ , and  $\sigma_y$  in deformation.

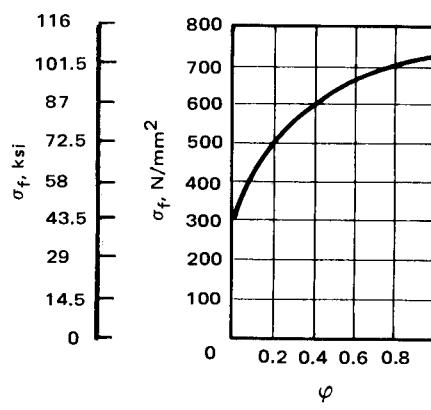


FIG. 5.19 Flow curve for steel C10 (AISI1010).

**Table 5.1** Procedure for the Calculation of the Extrusion Force

<i>i</i>	$x_i$ , mm	$r_i$ , mm	$\frac{r_0}{r_i}$	$ \varphi_i $	$\sigma_{f,i}$ , N/mm <sup>2</sup>	$\frac{2B}{r_i}$	$C_i$	$C_i - 1$	$D_i$ , N/mm <sup>2</sup>	$\sigma_{x_i}$ , N/mm <sup>2</sup>	$\sigma_{r_i}$ , N/mm <sup>2</sup>
10	30	10.0	1.500	0.810	697					—	697
9	27	10.5	1.429	0.712	694	0.571	0.0594	-0.9406	107.39	-114.2	— 808
8	24	11.0	1.364	0.620	679	0.545	0.0567	-0.9433	100.28	-227.3	— 906
7	21	11.5	1.304	0.530	656	0.521	0.0542	-0.9458	92.62	-338.3	— 994
6	18	12.0	1.250	0.446	625	0.500	0.0520	-0.9480	84.69	-446.2	— 1071
5	15	12.5	1.200	0.364	587	0.480	0.0500	-0.9500	76.36	-550.0	— 1137
4	12	13.0	1.154	0.286	542	0.461	0.0480	-0.9520	67.71	648.9	— 1191
3	9	13.5	1.111	0.192	479	0.444	0.0462	-0.9538	57.64	-740.8	— 1220
2	6	14.0	1.071	0.138	438	0.428	0.0445	-0.9555	50.80	-828.4	— 1266
1	3	14.5	1.034	0.066	378	0.414	0.0430	-0.9570	42.41	-910.0	— 1288
0	0	15.0	1.000	0.000	317	0.400	0.0416	-0.9584	34.36	-985.3	— 1302

$$n = 10; B = x_{i+1} - x_i = L/10 = 3 \text{ mm (0.12 in)}; C_i = \frac{2B}{r_i} [\tan(\rho + \alpha_i) - \tan \alpha_i]; D_i = \frac{2B}{r_i} \sigma_{f,i} \tan(\rho + \alpha_i); \tan \alpha_i = \tan \alpha = 5/30 = 0.167, \alpha = 9.5^\circ; \tan \rho = 0.100, \rho = 5.7^\circ; \tan(\rho + \alpha) = 0.271.$$

Here  $\sigma_{x_i}$  represents the normal stress in the  $x$ -direction at  $x = x_i$ . Because of the boundary condition  $\sigma_x = 0$  at  $x = L$ ,  $\sigma_{x_i}$  can be determined from Eq. 5.61.

$$\sigma_{x_i} = \frac{(2B/r_i)\sigma_{f,i} \tan(\rho + \alpha) - \sigma_{x_{i+1}}}{(2B/r_i)[\tan(\rho + \alpha_i) - \tan \alpha_i] - 1}$$

The radial stress can then be obtained from Eq. 5.60 and the extrusion force  $F$  from

$$F_p = \pi r_0^2 |\sigma_x(x=0)|$$

Here,  $\sigma_{f,i}$  is determined from the flow stress curve, using

$$|\varphi_i| = 2 \ln \frac{r_0}{r_i}$$

$$r_i = r_0 - \frac{r_0 - r_1}{L} x_i$$

A typical calculation is shown in Table 5.1.

The value of the extrusion force determined in this manner is

$$F_p = 696.1 \text{ kN}$$

### 5.3 FUNDAMENTALS AND APPLICATIONS OF VON MISES PLASTICITY THEORY

In the previous sections, fundamental equations governing the description of a plastic material were developed with reference to principal axes of stress and strain. If one departs from the assumption of homogeneous deformation inherent in elementary plasticity theory, then the use of specialized coordinates is no longer necessary.

Forming processes are nonhomogeneous by nature. That implies, for example, that the principal axes of the deformation and stress states have different directions at each point of the work-piece. If one wanted to use relations which are formulated for principal axes, then one should know these at the outset. This knowledge can, however, first be obtained from the solution of the problem. It is therefore necessary to formulate the fundamental equations in such a way that they are independent of the orientation of the coordinate system. This departure from the simplified

description of the flow field leads to increased mathematical difficulties in the treatment of practical problems. In order to minimize these difficulties, one makes use of a simplified description of the material behavior.

### 5.3.1 Material Models

The principal properties of a material which behaves plastically are the presence of a yield strength and the appearance of permanent deformations when the stresses reach the yield strength.

The simplest material models which contain these characteristics are *elastic-perfectly plastic* and *rigid-perfectly plastic* models. Their one-dimensional stress-strain behavior is shown in Fig. 5.20.

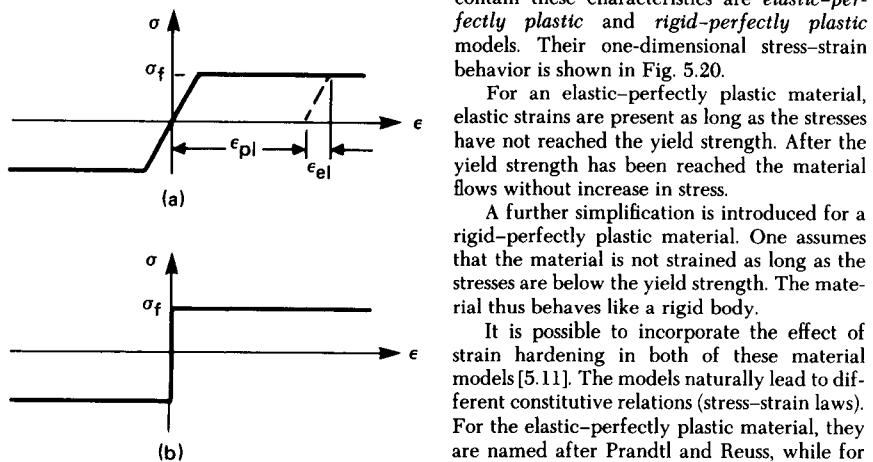


**FIG. 5.20** Stress-strain diagrams. (a) Elastic-perfectly plastic material. (b) Rigid-perfectly plastic material.

siders the elastic portion of the deformation, yields more complicated constitutive relations than the von Mises theory. As a consequence it also leads to greater mathematical difficulties in practical applications. It must be used for those processes in which the elastic and plastic strains are of the same order. This is the case in structural engineering or for bending and blanking or piercing operations.

In most metal-forming operations, the permanent strains are much larger than the elastic ones. One therefore incurs no great error by assuming the material to behave as a rigid body prior to yielding. It is for this reason that one mainly employs the rigid-perfectly plastic material idealization. In the von Mises theory the magnitude of the tool velocity has no influence on the stresses. Thus the stresses at the end of a deformation process are independent of the time it took to carry out the operation. They depend only on the geometric changes which took place. The rigid-perfectly plastic material shows no viscosity.

The general development of the governing equations for a rigid-perfectly plastic material are not gone into in the following. The material is thought to be too complex for a book of this type, and the interested reader can, for example, consult [5.10] to [5.12] for details. Rather, we will present the governing equations for a particular coordinate system and discuss some of the solution techniques which have been employed using the von Mises plasticity theory.

### 5.3.2 Fundamental Equations

Stated here are some of the basic equations of the von Mises plasticity theory. They are given with reference to a cylindrical coordinate system, one in which the behavior is axisymmetric (Fig.

For an elastic-perfectly plastic material, elastic strains are present as long as the stresses have not reached the yield strength. After the yield strength has been reached the material flows without increase in stress.

A further simplification is introduced for a rigid-perfectly plastic material. One assumes that the material is not strained as long as the stresses are below the yield strength. The material thus behaves like a rigid body.

It is possible to incorporate the effect of strain hardening in both of these material models [5.11]. The models naturally lead to different constitutive relations (stress-strain laws). For the elastic-perfectly plastic material, they are named after Prandtl and Reuss, while for the rigid-perfectly plastic material they carry the name of von Mises. One thus speaks of the *Prandtl-Reuss* theory and the *von Mises* theory.

The Prandtl-Reuss theory, because it con-

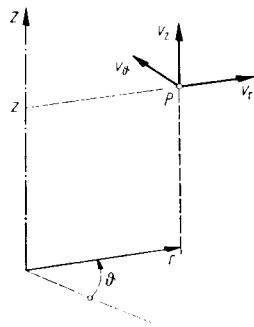


FIG. 5.21 Cylindrical coordinates.

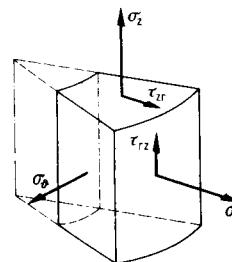


FIG. 5.22 Stresses on a material element for axisymmetric processes.

5.21). In these coordinates the constitutive equation (*Levy-von Mises* equations) are (Fig. 5.22)

$$\begin{aligned}\dot{\epsilon}_r &= \lambda(\sigma_r - \sigma_m) \\ \dot{\epsilon}_\theta &= \lambda(\sigma_\theta - \sigma_m) \\ \dot{\epsilon}_z &= \lambda(\sigma_z - \sigma_m) \\ \dot{\gamma}_{rz} &= \lambda\tau_{rz}\end{aligned}\quad (5.64)$$

Here  $\sigma_m$  is the mean stress,

$$\sigma_m = \frac{1}{3}(\sigma_r + \sigma_\theta + \sigma_z) \quad (5.65)$$

and  $\lambda$  given by

$$\lambda = \frac{\sqrt{I_2}}{k} \quad (5.66)$$

where  $I_2$  represents the second invariant of the strain-rate tensor and  $k$  is the shear flow stress,

$$I_2 = -(\dot{\epsilon}_r\dot{\epsilon}_\theta + \dot{\epsilon}_\theta\dot{\epsilon}_z + \dot{\epsilon}_z\dot{\epsilon}_r) + \dot{\gamma}_{rz}^2 \quad (5.67)$$

The strain rates are determined from the velocities by the relations

$$\begin{aligned}\dot{\epsilon}_r &= \frac{\partial v_r}{\partial r} \\ \dot{\epsilon}_\theta &= \frac{v_r}{r} \\ \dot{\epsilon}_z &= \frac{\partial v_z}{\partial z} \\ \dot{\gamma}_{rz} &= \frac{\partial v_r}{\partial z} + \frac{\partial v_z}{\partial r}\end{aligned}\quad (5.68)$$

The assumption of incompressibility leads to the following form of the continuity equation:

$$\dot{\epsilon}_r + \dot{\epsilon}_\theta + \dot{\epsilon}_z = 0 \quad (5.69)$$

The stresses must satisfy the condition of equilibrium at each point in the material. These equations are given by

$$\begin{aligned}\frac{\partial \sigma_r}{\partial r} + \frac{\partial \tau_{rz}}{\partial z} + \frac{\sigma_r - \sigma_\theta}{r} &= 0 \\ \frac{\partial \tau_{rz}}{\partial r} + \frac{\partial \sigma_z}{\partial z} + \frac{\tau_{rz}}{r} &= 0\end{aligned}\quad (5.70)$$

## 5.4 METHODS OF SOLUTION FOR VON MISES PLASTICITY THEORY

Exact solutions of the von Mises plasticity theory equations (equilibrium equations, continuity equations, yield criterion, and constitutive relations) which satisfy the given boundary conditions can only be found for special and simple problems. One is therefore generally forced to employ approximation techniques. In the following some techniques which can be employed in the solution of practical problems are discussed. These approximation techniques are methods which do not involve a further simplification of the given problem. (Recall that elementary plasticity theory assumes a homogeneous deformation state.) The concern in the remainder of this chapter will be with the determination of the stresses and strains which satisfy the von Mises theory with sufficient accuracy.

### 5.4.1 Exact Solutions

Exact solutions, as previously mentioned, can be determined only in special cases. In these cases one deals with problems in which the geometry of the process *a priori* determines a portion of the stress and strain magnitudes. Here the case of plane deformation is of special importance since numerous solutions have been obtained by use of *slip-line theory*.

Examples of operations for which an exact solution can be obtained are given, for example, in [5.12].

### 5.4.2 Slip-Line Theory

Slip-line theory has at this time lost some of its former importance due to the development of newer numerical methods for solving three-dimensional problems. It does yield, often with the need for time-consuming graphic representation, solutions for a few cases of plane plastic flow. A detailed discussion of slip-line theory and its application can be found in [5.11] to [5.15].

For plain-strain plastic deformation, slip lines indicate the directions of the maximum shear stresses (see Fig. 5.28) and, according to the von Mises flow rule, also the directions of maximum shear-strain rates. The normal stresses are everywhere equal to the hydrostatic pressure. Along slip lines, therefore, the normal strain rates are equal to zero. In addition to information about stresses, the slip-line field is thus seen to yield also conditions for the velocity field.

For particular problems, subject to boundary conditions on stress and velocity, slip-line fields describing the stresses can be constructed using the *Hencky* equations [5.16], while the corresponding velocity field is determined from the *Geiringer* equations [5.17]. A suitable example of such an analysis can be shown to be backward extrusion [5.4]. The resulting slip-line field is shown in Fig. 5.23. Note that in carrying out the analysis, one finds it convenient to assume the die to be stationary while the container and billet move with unit velocity. The estimate for the extrusion pressure obtained in this case is

$$p_e = 2.58k$$

In the newer work the attempt is made to extend slip-line theory for processes with axial symmetry [5.4]. Also, new slip-line fields have been proposed which consider more realistic interface friction conditions [5.18].

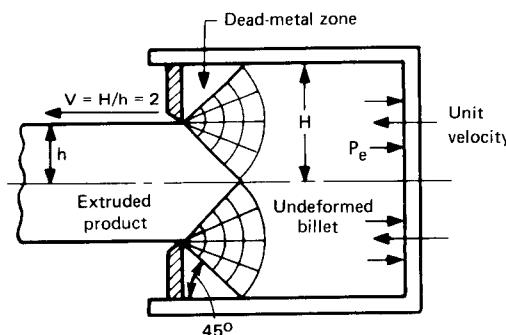


**FIG. 5.23** Slip-line field for backward extrusion with unlubricated die.

#### 5.4.3 Bound Theorems

The extremum principles of the von Mises plasticity theory are employed in metal forming mainly to obtain upper and lower bounds on the external forces needed to carry out the operation. With the help of assumed, admissible stress and velocity fields, one can determine the value of the forming force, which one knows will be neither higher nor lower than the actually needed value.

A word statement of the two bound theorems is as follows [5.12]:

- 1 **Lower-bound theorem:** The rate of work done by the actual surface tractions with prescribed velocities is greater than or equal to the rate of work done by the surface tractions corresponding to any other statically admissible stress field. A stress field is statically admissible if it satisfies the equilibrium equations, the prescribed stress boundary conditions, and nowhere violates the yield criterion.
- 2 **Upper bound theorem:** The rate of work done by the actual surface tractions with prescribed velocities is less than or equal to the rate of work done by the surface tractions corresponding to any other kinematically admissible velocity field. A velocity field is kinematically admissible if it satisfies the prescribed velocity boundary conditions and the requirement of the incompressibility of the material.

In solving practical problems, one would like to be able to find the forming force by closely separated upper and lower bounds. This, however, leads to difficulties which arise from the setting up of statically admissible stress fields. As a result, one often does not determine the lower bound and satisfies oneself with the much easier determination of the upper bound. This bound represents an approximation for the forming force, which is valuable for the initial sizing of the tooling and the machine because it will in all possibility not be exceeded by the actually occurring force.

As an example of the application of the upper-bound theorem, consider the case of axisymmetric backward extrusion. The deformation zone consists of two parts (Fig. 5.24): a cylindrical region I and a ringlike region II.

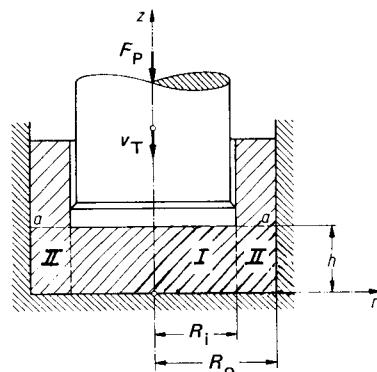


**FIG. 5.24** Division of deformation zone for backward extrusion.

The material above line  $a-a$  is assumed to be rigid. The velocity field

$$v_{r,I} = \frac{1}{2} \frac{v_T}{h} r \quad v_{r,II} = \frac{v_T}{2h} \frac{R_i^2}{R_a^2 - R_i^2} \left( \frac{R_a^2}{r} - r \right)$$

$$v_{z,I} = - \frac{v_T}{h} z \quad v_{z,II} = \frac{v_T}{h} \frac{R_i^2}{R_a^2 - R_i^2} z$$

satisfies the boundary and interface conditions, as well as the continuity equation. It is therefore kinematically admissible. Use of this velocity field in the upper-bound theorem yields the following estimate for the forming force [5.19]:

$$F = \frac{1}{v_T} (P_{U,I} + P_{U,II} + P_{FR} + P_S)$$

where

$$P_{U,I} = \sigma_f \pi v_T R_i^2$$

$$P_{U,II} = \frac{1}{\sqrt{3}} \pi v_T \sigma_f \frac{R_i^2}{R_a^2 - R_i^2} \left[ R_a^2/2 - \ln \sqrt{3} \right.$$

$$\left. - R_i^2 \left( \sqrt{\left(\frac{R_a}{R_i}\right)^4 + 3} - \ln \frac{(R_a/R_i)^2 + \sqrt{(R_a/R_i)^4 + 3}}{\sqrt{3}} \right) \right]$$

$$P_{FR} = \frac{\mu \sigma_f v_T \pi}{3h} \left[ 2R_i^3 + \frac{R_i^2}{R_a + R_i} (2R_a^2 - R_i R_a - R_i^2) + \frac{3h^2 R_i^2 R_a}{R_a^2 - R_i^2} \right]$$

$$P_S = \frac{\sigma_f v_T \pi}{\sqrt{3}} \left[ \frac{h R_a^2 R_i}{R_a^2 - R_i^2} + \left( \frac{1}{3h} \right) \frac{R_i^2}{R_a + R_i} (2R_a^2 - R_i R_a - R_i^2) \right]$$

Other examples of the application of bound theorems can be found in [5.20] to [5.25].

#### 5.4.4 Method of Weighted Residuals

For some problems which are not amenable to an exact solution treatment, use of the bound theorems yields acceptable expressions for the forces necessary to perform the forming operation. In general, however, they do not yield any definite information about the stresses and strains in the workpiece. A method is now presented which even for complex forming processes can yield an acceptable approximation of the stress and strain states. This technique belongs to the methods of weighted residuals [5.26], which has found many applications in science and engineering.

To explain the weighted residual technique, let us consider its application to axisymmetric problems. The continuity (volume constancy) condition as well as the equilibrium equations will be identically satisfied if one introduces a stream function which describes the velocity and two stress functions which describe the stresses. One then expresses each of the stream and stress functions in terms of a series of functions (polynomial expressions have proved useful) with arbitrary parameters. These parameters are then determined by the method of least squares. According to this method, the parameters are determined in such a way that the error, in not identically satisfying the constitutive equations and those boundary conditions not already satisfied by the chosen functions, is made as small as possible.

From the method of weighted residuals it is seen that increasing the polynomial series can only decrease the error and not increase it, and that one could, by use of an infinite series, approach with sufficient accuracy the exact solution. In the solution of problems, this consideration is offset by the size of the thus resulting system of equations, the amount of computer time, and the round-off errors which occur.

The proper choice of functions is one of the principal questions arising in the application of the method of weighted residuals. Even though one cannot set up hard and fast rules, one can

say, however, that the functions should be chosen in such a way that they satisfy as many of the boundary and subsidiary conditions as possible and still remain relatively simple.

Consider as an example the determination of the stresses and material flow in axisymmetric upsetting (Fig. 5.25) between two parallel platens. The following boundary and symmetry conditions are established:

- 1 The axial velocity  $v_z$  must be zero along the  $r$ -axis.
- 2 The radial velocity  $v_r$  must be zero along the  $z$ -axis.
- 3 The axial velocity must be equal to the platen velocity at the interface.
- 4 The shear stress  $\tau_{rz}$  must be zero along the  $r$ - and  $z$ -axes because of symmetry.
- 5 The radial stress  $\sigma_r$  must be zero on the cylindrical surface.
- 6 The shear stress must vanish on the cylindrical surface.
- 7 The shear stress and the radial velocity are related at the interface by

$$\tau_{rz} = cv_r, \quad -1 < c < 0$$

With this condition, the friction between platen and workpiece is taken into consideration.

Even though upsetting is a nonsteady-state process, calculations can be carried out by assuming quasistatic behavior in a step-by-step fashion. This can be done as follows. Once the velocity field has been determined for the initial state, the displacement of points in the cylinder during a time interval  $\Delta t$  is determined from

$$u_r = v_r \Delta t$$

$$u_z = v_z \Delta t$$

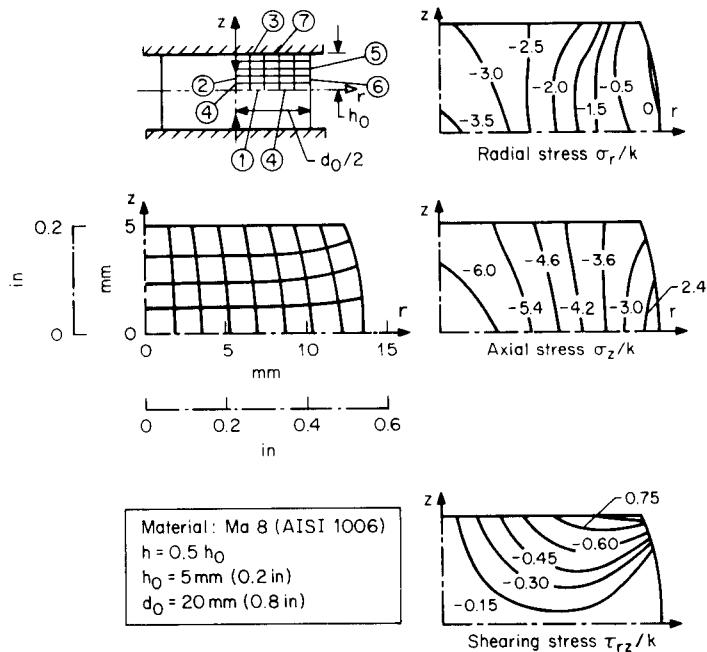
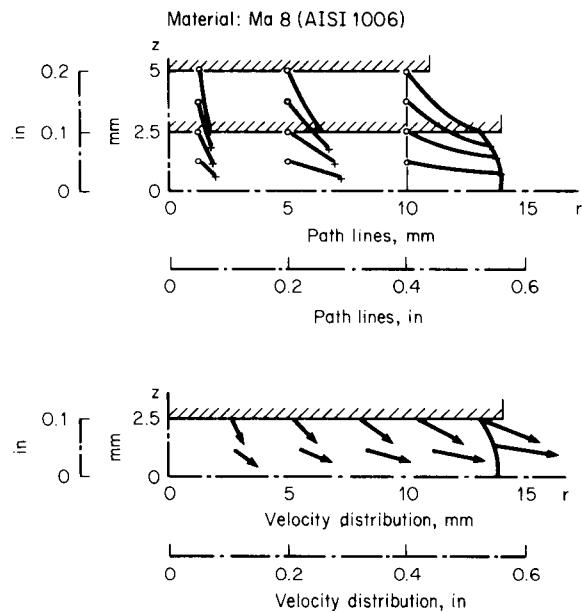


FIG. 5.25 Stresses in axisymmetric upsetting.(After [5.48].)



**FIG. 5.26** Path lines and velocity distribution in upsetting. (After [5.48].)

The integration over time is thus replaced by a summation. It must be noted that the larger the  $\Delta t$  chosen, the less precise are the calculations.

Shown in Fig. 5.25 are the results for the stress state for a reduction in height of 50%. The effect of strain hardening has been incorporated in the material behavior. Fig. 5.26 shows the corresponding path lines and the velocity field.

The method of weighted residuals can be applied easily to simple deformation processes, but difficulties arise for complex ones. One way of overcoming these problems is with the use of macroelements. For example, an extrusion process could be modeled by a proper superposition of three elements:

- 1 Element describing upsetting
- 2 Element describing extrusion
- 3 Element describing a rigid area

These elements are linked to each other by appropriate boundary conditions. Other complex processes could be modeled similarly.

Other applications of the method of weighted residuals in technical plasticity theory can be found in [5.27] to [5.31].

#### 5.4.5 Viscoplasticity

In many forming processes it is possible to determine the velocity field approximately by a parting of the workpiece and then inscribing a network of lines (grid pattern) which deforms during the operation on the parted surfaces (Fig. 5.27).

Consider a nonsteady-state process. In this case instantaneous photographs of the grid pattern

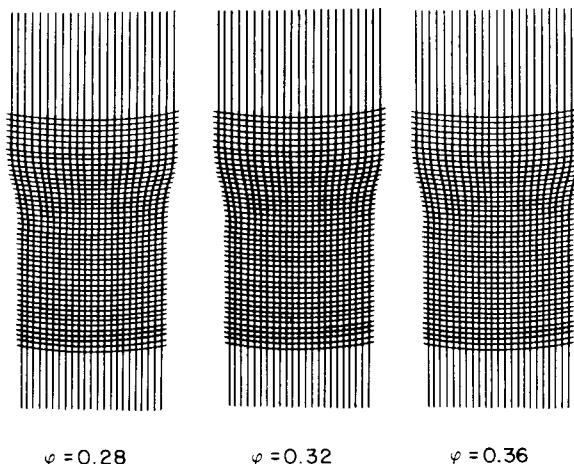


**FIG. 5.27** Parted specimen with grid pattern. Material—Ma8 (AISI 1006). (After [5.32].)

during deformation must be obtained, and the grid distortions must be analyzed as functions of time. From the two consecutive grid patterns, the instantaneous velocity components can be determined assuming that a previous grid point moves to its new position with an average velocity during an incremental deformation step. The relative displacements of grid points between each consecutive step are calculated from the measurements of the coordinates of the grid points. The instantaneous strain-rate components can be calculated from the known velocity components. The instantaneous stress components at any point in the deformation zone can now be determined from the strain rates by considering the equilibrium and plasticity equations as well as the mechanical properties of the material.

Difficulties can arise when calculating the stress field. These are due to the following facts:

- 1 The equilibrium equations are no longer identically satisfied.
- 2 The stresses are determined not at arbitrary points, but only at grid points in the deformation zone. Thus the distance between grid points has a great influence on stress calculations. In general it is impossible to obtain a mesh size smaller than 1 mm (0.039 in). This size may be too coarse to obtain the proper stress gradient in a complex deformation zone.

The method, though, does serve as a useful input for upper-bound applications [5.32].

The viscoplasticity method was developed by Thomsen and co-workers [5.33], [5.34].

#### 5.4.6 Finite-Element Method

The finite-element method has been used extensively for elastic problems [5.35], [5.36]. The method is a powerful one and is reserved for problems that can be programmed and solved by computer techniques. The literature over the last 20 years abounds with references to finite-element development and application, and many all-purpose finite-element codes are now commercially available [5.37].

As the name implies, the basic building block is an element of finite dimensions. The object to be analyzed is divided into a number of these small elements. These elements are joined at corners, and it is usually assumed that the stress is uniform throughout the element. The element distortions are computed by conventional theory. The total behavior of the structure depends on the integrated effects of each of the parts. Thus since a part is usually divided into a multitude of

elements, a solution is possible with the help of a computer. The accuracy of the finite-element method depends on both the type of problem and the number and type of elements selected.

In the late 1960s the success of the finite-element problems stimulated the work of extending the application of the method to the area of plastic deformation [5.38], [5.39]. It was originally applied to elastic-plastic problems, ones in which the plastic strain is of the order of the elastic one. Here the strain is separated into an elastic part and a plastic part. The elastic part is governed by Hooke's law, while the plastic part used the Prandtl-Reuss equations. The nonlinearity in the constitutive equations is satisfied iteratively. This can be accomplished by either the initial-strain method or the initial-stress method. Of these two methods, the initial-stress method has found increased favor [5.40]. The reason is that one can show that except for the case of an ideally plastic structure, the initial-stress method never diverges. With this method, the deformation zone can be very accurately determined. Fig. 5.28 shows the spreading of the plastic zone by plane and axisymmetric upsetting. The problem was calculated using different elements, and good agreement was reached. Fig. 5.29 shows a comparison of finite-element calculations with results obtained by use of elementary theory and the method of weighted residuals. Again, good agreement is indicated.

It needs to be pointed out that in contrast to, say, the method of weighted residuals, the finite-element method is not geometry-dependent. Rather, with this technique one can analyze arbitrary geometrically complicated structures.

For large deformations it is generally not necessary to consider elastic deformations. In fact, in the analysis of most metal-forming operations, as a rule one can neglect them and employ the rigid-plastic material model. An exception to this rule is that it is generally mandatory to utilize

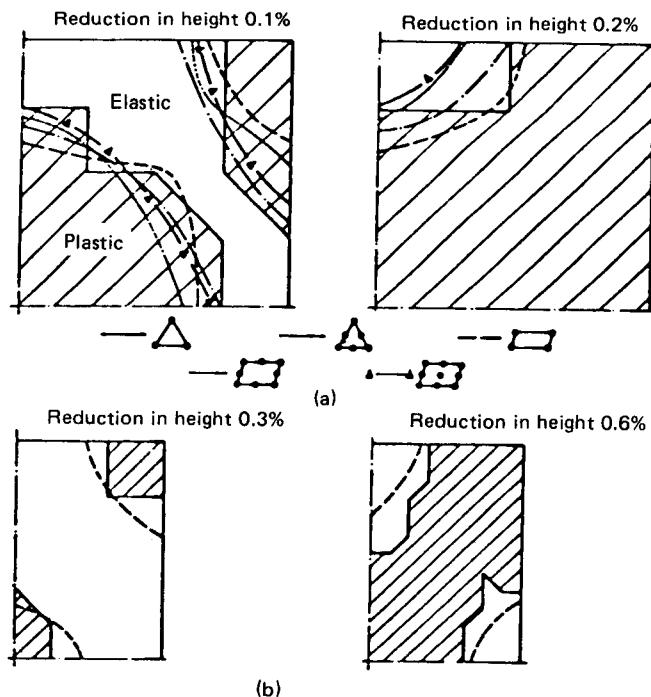
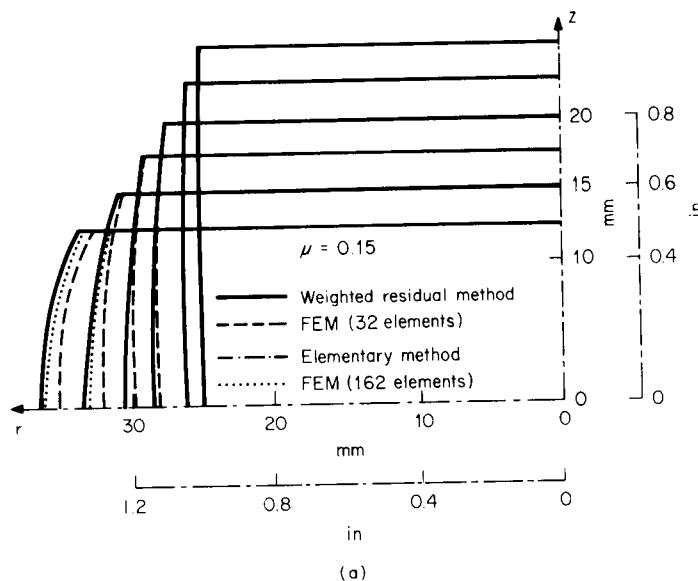
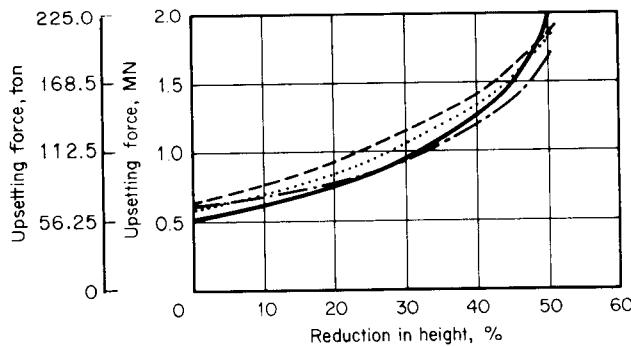


**FIG. 5.28** Growth of plastic zones. (a) Plane strain.  $\square$ — $50 \times 50$  mm (2 × 2 in). (b) Axisymmetric.  $d_0 = 20$  mm (0.8 in);  $h_0 = 30$  mm (1.2 in). (After [5.49].)



(a)



(b)

**FIG. 5.29** Axisymmetric upsetting of cylinder. (a) Computed bulge profiles. (b) Force reduction in height curves. (After [5.49].)

elastic-plastic analysis in order to be able to predict forming defects. Defects comprise the initiation and growth of internal or surface cracks in the deforming metal or the localization of deformation through plastic instability, which could impair the dimensional accuracy of the finished workpiece. Similarly, residual stresses in the unloaded workpiece cannot be evaluated using a rigid-plastic model [5.41].

The rigid-plastic finite-element formulation makes use of a modified upper-bound theorem, one in which the restriction of incompressibility has been removed by means of a Lagrangian parameter. As was the case for the elastic-plastic material, nonlinear constitutive equations must be handled iteratively. This leads to a large amount of computer time which in turn restricts the

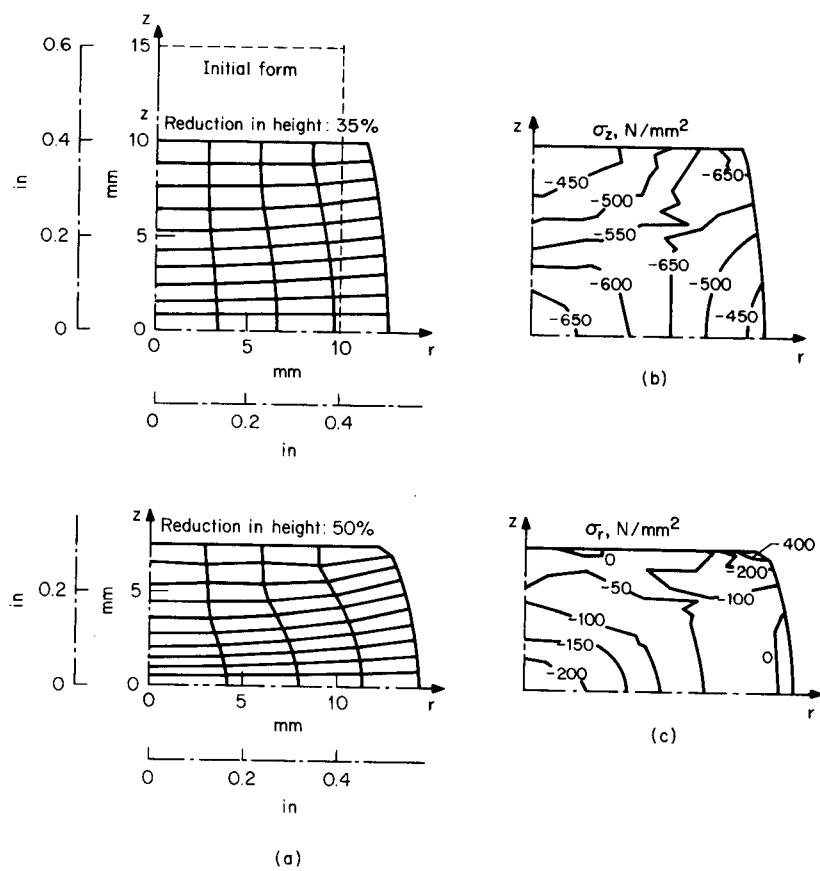


**FIG. 5.30** Axisymmetric upsetting. (a) Grid distortion for various reductions in height. (b)  $\sigma_z$  ( $N/mm^2$ ) contour lines. (c)  $\sigma_r$  ( $N/mm^2$ ) contour lines. (After [5.49].)

number of elements to be used in the model. Computations show that the simplest elements lead to the best results. This is also true for elastic-plastic material.

The rigid-plastic finite-element approach can be employed for both steady-state and non-steady-state processes [5.42] to [5.49]. In the latter case the time integration is replaced by a simple summation. Thus one has to be careful not to make the time step too large since this can lead to convergence problems and sometimes to nonsensical results. Fig. 5.30 shows an example of a non-steady-state process, the upsetting of a cylindrical workpiece. The coefficient of friction was taken as  $\mu = 0.15$ .

## REFERENCES

- 5.1 Beer, F. P., and Johnston, E. R.: *Mechanics of Materials*, New York, McGraw-Hill, 1981.
- 5.2 Tresca, H.: "Sur l'écoulement des corps solides soumis à des fortes pressions," *C. R. Acad. Sci. Paris*, **59**, 1864, pp. 754, 764; **62**, 1867, p. 809.
- 5.3 von Mises, R.: "Mechanics of Solid Bodies in a Plastic State" (in German), *Gött. Nachr. Math. Phys. Kl.*, 1913, pp. 582–592.

- 5.4 Slater, R. A. C.: *Engineering Plasticity*, New York, Halsted, 1977.
- 5.5 Taylor, G. E., and Quinney, H.: "The Plastic Distortion of Metals," *Trans. R. Soc. London (A)*, **230**, 1931, pp. 323–362.
- 5.6 Siebel, E.: "Forces and Material Flow in Plastic Deformation" (in German), *Stahl u. Eisen*, **45**, 1925, pp. 1563–1566.
- 5.7 von Karman, Th.: "Contribution to the Theory of Rolling" (in German), *Z. angew. Math. Mech.*, **5**, 1925, pp. 139–141.
- 5.8 Sachs, G.: "On the Theory of the Tension Test" (in German), *Z. angew. Math. Mech.*, **7**, 1927, pp. 235–236.
- 5.9 Siebel, E., and Pomp, A.: "On the Further Development of the Compression Test" (in German), *Mitt. Kaiser-Wilhelm-Inst. Eisenforsch.*, **10**, 1928, pp. 55–62.
- 5.10 Lippmann, H., and Mahrenholz, O.: *Plastomechanics of the Forming of Metallic Materials* (in German), Berlin, Springer, 1967.
- 5.11 Hill, R.: *The Mathematical Theory of Plasticity*, Oxford, Clarendon, 1950.
- 5.12 Prager, W., and Hodge, P. G.: *Theory of Perfectly Plastic Solids*, New York, Wiley, 1941.
- 5.13 Johnson, W., Sowerby, R., and Haddow, J. B.: *Plane Strain Slip-Line Fields*, New York, American Elsevier, 1970.
- 5.14 Ewing, D. J. F.: "A Series Method for Constructing Plastic Slipline Fields," *J. Mech. Phys. Solids*, **15**, 1967, pp. 105–114.
- 5.15 Thomsen, E. G., Yang, C. T., and Kobayashi, S.: *Mechanics of Plastic Deformation in Metal Processing*, New York, Macmillian, 1965.
- 5.16 Hencky, H.: "On Some Statically Determinate Cases of Equilibrium in Plastic Bodies" (in German), *Z. angew. Math. Mech.*, **3**, 1923, pp. 241–251.
- 5.17 Geiringer, H.: "Contribution to the Complete Plane Plasticity Problem" (in German), in *Proceedings of the 3d International Congress of Applied Mechanics*, vol. 2, 1930, pp. 185–190.
- 5.18 Wilson, W. R. D.: "Slipline Solutions for Strip Drawing with Arbitrary Friction Conditions," in *Proceedings of the 5th NAMRC SME*, 1977, pp. 80–86.
- 5.19 Steck, E.: "Load Determination in Metalforming by Use of Upper Bound Theorem" (in German), *Werkstattstechnik*, **57**, 1967, pp. 273–279.
- 5.20 Johnson, W.: "Estimation of Upper-Bound Loads for Extrusion and Coining," *Int. J. Mech. Sci.*, **1**, 1960, pp. 57–83, 229–252, 366–368.
- 5.21 Kobayashi, S., and Thomsen, E. G.: "Upper and Lower Bound Solutions to Axisymmetric Compression and Extrusion Problems," *Int. J. Mech. Sci.*, **7**, 1965, pp. 127–143.
- 5.22 Baraya, G. L., and Johnson, W.: "Flat Bar Forging," in *Advances in Machine Tool Design and Research Conference*, London/New York, Pergamon, 1965.
- 5.23 Avitzur, B.: "Flow through Dies with Hydrodynamic Lubrication Treated as an Adiabatic Process," in *Proceedings of the 17th International Machine Tool Design and Research Conference*, 1976, pp. 445–451.
- 5.24 Nagpal, V., Lahoti, G. D., and Altan, T.: "A Numerical Method for Simultaneous Prediction of Metal Flow and Temperature in Upset Forging of Rings," *Trans. ASME, Jo. Eng. Ind.*, **100**, 1978, pp. 413–42.
- 5.25 Johnson, W.: "Continuous Mechanics and Deformation Processing," in *Advances in Deformation Processing*, New York, Plenum, 1978, pp. 1–49.
- 5.26 Finlayson, B. A., and Scriven, L. E.: "The Method of Weighted Residuals—A Review," *Appl. Mech. Rev.*, **19**, 1966, pp. 743–748.
- 5.27 Adler, G.: "A Technique for the Approximate Determination of Stress and Strain States in the Flow of Rigid-Plastic Materials" (in German), in *Berichte aus dem Institut für Umformtechnik, Universität Stuttgart*, vol. 12, Essen, Girardet, 1969.

## 5.34 FUNDAMENTALS OF METAL FORMING

- 5.28 Steck, E.: "A Technique for the Approximate Determination of Stress and Strain States in Metal Forming" (*in German*), *Ann. CIRP*, 17, 1969, pp. 251-258.
- 5.29 Pohl, W.: "A Method for the Approximate Determination of Heat Flow and Temperature Distribution in Cold Forming of Metals" (*in German*), in *Berichte aus dem Institut für Umformtechnik, Universität Stuttgart*, vol. 23, Essen, Giradet, 1972.
- 5.30 Dahlheimer, R.: "Contribution to the Question of Stresses, Strains and Temperatures in Axisymmetric Extrusion" (*in German*), in *Berichte aus dem Institut für Umformtechnik, Universität Stuttgart*, vol. 20, Essen, Giradet, 1970.
- 5.31 Gelin, J. C., Oudin, J., and Ravalard, Y.: "Plastic Flow, Instability and Ductile Fracture in Upsetting of Solid Cylinders," *Ann. CIRP*, 30, 1981, pp. 193-197.
- 5.32 Binder, H.: "Investigations into the Nosing of Rods" (*in German*), *Berichte aus dem Institut für Umformtechnik, Universität Stuttgart*, vol. 58, Berlin, Springer, 1980.
- 5.33 Thomsen, E. G., Yang, C. T., and Bierbower, J. B.: *An Experimental Investigation of the Mechanics of Plastic Deformation in Metals*, Berkeley, University of California Press, 1954.
- 5.34 Shabaik, A. H., and Kobayashi, S.: "Computer Application to the Visioplasticity Method," *Trans. ASME, J. Eng. Ind.*, 89, 1967, pp. 339-346.
- 5.35 Zienkiewicz, O. C.: *The Finite Element Method in Engineering Science*, London: McGraw-Hill, 1971.
- 5.36 Gallagher, R. H.: *Finite Element Analysis*, Englewood Cliffs, NJ, Prentice-Hall, 1975.
- 5.37 Perrone, N., and Pilkey, W.: *Structural Mechanics Software Series*, vol. 2, Charlottesville, University of Virginia Press, 1978.
- 5.38 Yamada, Y., Yoshimura, H., and Sakurai, T.: "Plastic Stress-Strain Matrix and Its Application for Solution of the Elastic-Plastic Problem by the Finite Element Method," *Int. J. Mech. Sci.*, 10, 1968, pp. 343-354.
- 5.39 McMeeking, R. M., and Rice, J. R.: "Finite Element Formulation for Problems of Large Elastic-Plastic Deformation," *Int. J. Solids Struct.*, 11, 1975, pp. 601-606.
- 5.40 Zienkiewicz, O. C., Valliappan, S., and King, P. I.: "Elasto-Plastic Solutions of Engineering Problems. Initial Stress, Finite Element Approach," *Int. J. Numer. Methods Eng.*, 1, 1969, pp. 75-100.
- 5.41 Lee, E. H., Mallett, R. L., and McMeeking, R. M.: "Stress and Deformation Analysis of Metal Forming Processes," *ASME Spec. Publ. PVP-PB-025*, 1977, pp. 19-34.
- 5.42 Lee, C. H., and Kobayashi, S.: "New Solutions to Rigid-Plastic Deformation Problems Using a Matrix Method," *ASME Trans., J. Eng. Ind.*, 95, 1973, pp. 865-873.
- 5.43 Lung, M., and Mahrenholz, O.: "A Finite Element Procedure for Analysis of Metal Forming Processes," *CSME Trans.*, 2, 1973-1974, pp. 31-36.
- 5.44 Dieterle, K.: "Folding as a Process Limit in Upsetting of Hollow Cylinders" (*in German*), in *Berichte aus dem Institut für Umformtechnik, Universität Stuttgart*, vol. 30, Essen, Giradet, 1975.
- 5.45 Kobayashi, S.: "Rigid-Plastic Finite Element Analysis of Axisymmetric Metal Forming Processes in Numerical Modeling of Manufacturing Processes," *ASME Spec. Publ. PVP-PB-025*, 1977, pp. 49-65.
- 5.46 Osakada, K., Tawasaki, N., and Mori, K.: "A Method of Determining Flow Stress under Forming Conditions," *Ann. CIRP*, 30, 1981, pp. 135-138.
- 5.47 Li, G.-J., and Kobayashi, S.: "Rigid Plastic Finite Element Analysis of Plane Strain Rolling," *ASME 81-WA/Prod-13*, 1982, pp. 1-9.
- 5.48 Lange, K., Rebholz, M., and Roll, K.: "An Approximation Method for the Calculation of Forming Operations," in *1978 Manufacturing Engineering Transactions*, 6th NAMRC, pp. 142-150.
- 5.49 Roll, K.: "Calculation of Metal Forming Processes by Finite Element Methods," in *Application of Numerical Methods to Forming Processes*, ASME AMD, 1978, vol. 28, pp. 67-79.

## CHAP. 6

### TRIBOLOGY

#### List of Special Symbols

---

$a$	proportion of pressure-welded surface area
$b$	proportion of boundary-lubricated surface area
$c$	proportion of surface area covered with contaminant
$h$	proportion of hydrodynamically lubricated surface area
$h_0$	film thickness at entry of deformation zone
$R_a$	average roughness deviation from mean surface
$R_p$	smoothing depth
$R_t$	peak-to-valley height
$s_f$	forward slip in rolling
$\alpha$	temperature coefficient of viscosity; pressure-sensitivity coefficient for polymer shear strength
$\beta$	angle of entry
$\gamma$	pressure coefficient of viscosity
$\eta$	kinematic viscosity
$\mu_B$	coefficient of friction in boundary-lubricated zone
$\mu_H$	coefficient of friction in hydrodynamic pockets
$\mu_{\text{mix}}$	average coefficient of friction in mixed-film lubrication
$\tau_B$	shear strength of boundary film
$\tau_c$	shear strength of contaminant film
$\tau_{fp}$	shear strength of polymer film

## 6.2 FUNDAMENTALS OF METAL FORMING

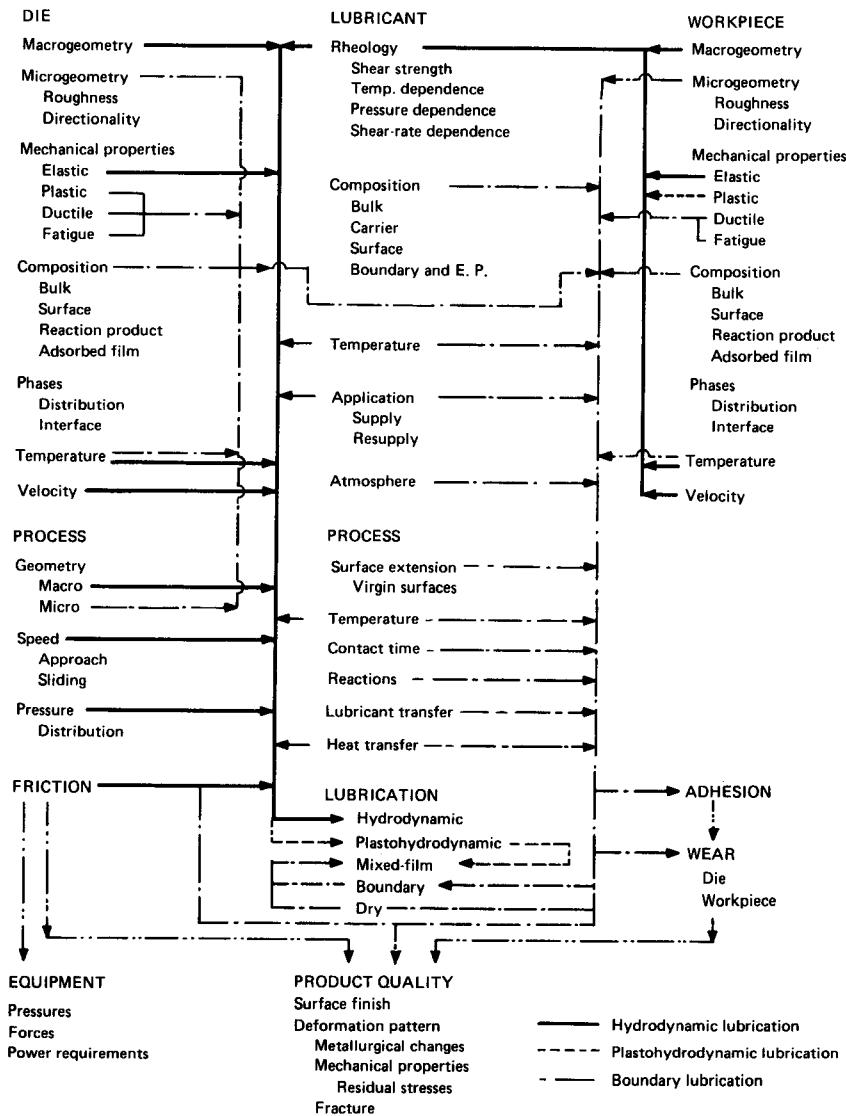


FIG. 6.1 Elements of a metalworking lubrication system. (After [6.2].)

In the vast majority of metalworking processes the workpiece is deformed by means of a contacting die. The pressure required for deformation generates a normal stress to the die surface, and movement of the workpiece relative to the die surface generates a shear stress at the interface. Thus a classical tribological situation arises, with friction at the die-workpiece interface, and with potential for wear of both die and workpiece materials. Mitigation of these effects then calls for the introduction of a lubricant. In contrast to nonmetalworking situations, deformation of the

workpiece results in a sometimes very substantial enlargement of surface areas. Thus new, fresh metal surfaces are exposed, and the lubricant must protect not only the old but also the new surfaces. The success or failure of such lubrication has important consequences on the quality of the issuing product, and also on pressures, forces, energy requirements, and often the very possibility of plastic deformation itself. For these reasons, the field of friction, lubrication, and wear (tribology) in metalworking has been the subject of many investigations [6.1] to [6.7].

Factors entering the tribology of metalworking are numerous, and their interactions are exceedingly complex. A simplified presentation of the inputs, system variables, and outputs (Fig. 6.1) gives at least a sense of the complexities, and indicates the interdisciplinary nature of the problem; that is, in addition to mechanical considerations, chemical and metallurgical effects must also be taken into account.

## 6.1 FRICTION IN DEFORMATION PROCESSES

Friction is the resistance to motion encountered when one body slides over another. In metalworking processes it arises from sliding of the workpiece against the die.

### 6.1.1 The Die–Workpiece Interface

In the first approximation, the interface has a well-defined macrogeometry, as given by the die and workpiece geometries (Fig. 6.2a). In the cold working of technically important metals the die temperature  $T_D$  and the workpiece temperature  $T_W$  are close to room temperature, although the work of deformation is transformed into heat and this, together with the work of friction, may cause a temperature rise of several hundred degrees Celsius. In hot working  $T_W$  is at some temperature below the melting point of the alloy:  $T_D = T_W$  in isothermal working, but much more frequently,  $T_D \ll T_W$  in conventional hot working. The normal pressure  $p$  on the die may be a small fraction of the flow strength  $\sigma_f$  of the material in sheet-metal working, but frequently reaches a multiple of  $\sigma_f$  in bulk deformation processes.

Deformation usually proceeds with relative motion between workpiece and die. This movement may originate in imposed velocity differences (as in wire drawing), or it may develop as a consequence of the deformation process itself (as in the upsetting of a cylinder), or it may result from a combination of both (as in the rolling of a strip). Relative motion is opposed by friction, which can be simply (and accurately) described by assigning an average frictional shear strength  $\tau_{FR}$  to the interface. When this value reaches the shear flow strength of the workpiece material  $k$ ,

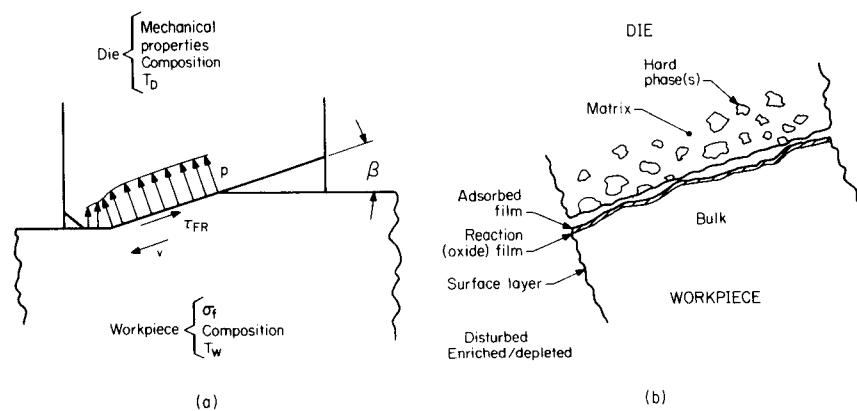


FIG. 6.2 Die–workpiece interface. (a) On the macro scale. (b) On the micro scale.

it is energetically more favorable for deformation to take place by internal shearing in the body of the workpiece. Movement at the interface ceases and the condition called *sticking friction* is attained (although no actual sticking or adhesion between die and workpiece needs to take place).

This simplified macroscopic view is totally inadequate if the sources of friction and the mechanisms of lubrication are to be understood. On the microscopic scale both die and workpiece show minute peaks, asperities, and valleys (Fig. 6.2b). Both the magnitude and the directionality of this microgeometry play an important part in creating friction and also in establishing and sustaining lubricant films designed to mitigate friction. Metallurgical factors become important too (Fig. 6.1). The die and workpiece are usually described by their composition. However, more important may be the kind and distribution of phases. The composition of the surfaces may differ from that of the bulk, either because of intentional surface treatment or because of diffusion effects in the materials (Fig. 6.2b). Pure metal surfaces (in the language of tribology, *virgin* surfaces) seldom exist. Instead, surfaces are covered with reaction products formed through exposure to air, humidity, or lubricants. Often films resulting from different reactions are superimposed. For example, a naturally formed oxide film may be impregnated with a lubricant film, which may also enter into chemical reactions with the oxide and/or substrate.

### 6.1.2 Mathematical Representation of Friction

For purposes of predicting interface pressures, deforming forces, and energy requirements, the magnitude of  $\tau_{\text{FR}}$  must be known. However, analysis is usually made simpler if the effect of friction is expressed by some nondimensional parameter. To date, two such parameters have found wide acceptance.

Following Coulomb's classical definition, the coefficient of friction  $\mu$  is simply the ratio of frictional force to normal force, or of frictional stress to normal stress (die pressure),

$$\mu = \frac{F_{\text{FR}}}{F_n} = \frac{\tau_{\text{FR}}}{p} \quad (6.1)$$

It is possible that  $\tau_{\text{FR}}$  increases linearly with  $p$ , and then  $\mu$  may reach any constant value (Fig. 6.3a). This is the case, for example, in the blankholder zone of a deep-drawing operation. However,  $\mu$  cannot rise indefinitely [6.8] because sticking friction sets in when  $\mu p \geq k$ . In many bulk deformation processes  $p \gg k$ , and because  $k$  remains constant, the calculated  $\mu$  actually drops (Fig. 6.3b). Since  $k \approx 0.5\sigma_f$  (or  $0.557\sigma_f$  according to von Mises), it is sometimes said that  $\mu_{\text{max}} = 0.5$ , but this is true only when  $p = \sigma_f$ . It is much more accurate to say that the coefficient of

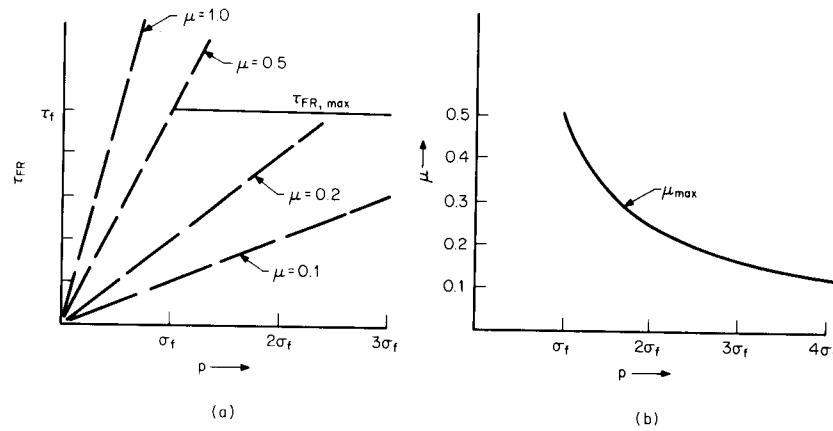


**FIG. 6.3** (a) Variation of interface shear strength and (b) variation of maximum coefficient of friction with pressure.

friction becomes meaningless when  $\mu p \geq k$  since there is no relative sliding at the interface. The possible misinterpretation of  $\mu$  has led to the introduction of the frictional shear factor  $m$  defined as

$$\tau_{\text{FR}} = mk \quad (6.2)$$

Since  $\tau_{\text{FR}}$  is now linked to a workpiece material property  $k$  which is a priori known (rather than to  $p$  which must be calculated), the use of  $m$  greatly simplifies calculations, especially those based on upper-bound theory or numerical techniques.

Whether  $\mu$  or  $m$  is a better descriptor of interface properties has been a matter of debate, and not even a preliminary judgment can be made until the properties of real interfaces are examined [6.9].

### 6.1.3 Adhesion

The sources of frictional restraint are manifold [6.10]. In the simplest view, asperities must be deformed elastically and/or plastically for sliding to take place. Asperities of the harder die material may also plow into the workpiece material. Because of the intimate contact established in metal deformation, atoms of die and workpiece approach closely enough for interatomic forces to develop. In the absence of contaminant or lubricating films, these forces may become measurable when die and workpiece are separated after sliding under pressure. This is described as adhesion.

Adhesion is exploited in such processes as cold pressure welding, friction welding, and the roll cladding of metals. It is, however, undesirable at the interface, and one of the basic requirements of a die material would be low adhesion to the workpiece material.

Unfortunately factors that govern adhesion are poorly understood. Diffusion is certainly a factor. Therefore solid solubility at the temperature of contact and prolonged duration of contact promote adhesion. For a given material pair, adhesion becomes more pronounced at hot-working temperatures characterized by high atomic mobility. Mechanical properties also contribute, with a high elastic modulus usually allowing separation without adhesion. This accounts for differences in adhesion between materials of different crystallographic structure or orientation. The surface energy of adhesion may also play a role.

Because dies usually owe their desirable properties to a multiphase structure in which hard intermetallics are embedded in a metallic matrix, their resistance to adhesion to various workpiece materials is not predictable at this time. It is known, however, that differences do exist, and that adhesion can be reduced by coating the surface with a hard film (for example, by chrome plating). In general it is desirable that surface films be intimately bonded to the substrate. Therefore diffusion coatings of chrome and boron are generally more successful. However, coating may interfere with beneficial reactions between die and lubricant and, even though adhesion may be reduced, the efficiency of the lubricant system may also be impaired [6.11]. Sometimes die hardness is sacrificed and greater die wear accepted in return for protecting the workpiece from surface damage (as in the use of heat-treatable aluminum bronze dies in working stainless steels [6.12]).

In some instances, particularly in hot working, ceramic surfaces give better performance, although it is not clear whether the improvement should be attributed to reduced adhesion or to greater heat resistance alone.

## 6.2 LUBRICATING MECHANISMS

Friction is sometimes helpful. For example, high friction on the punch surface helps increase reductions in deep drawing and ironing. In a few instances it has to have at least some small value, as in rolling where it assures entry of the workpiece into the roll gap and helps maintain rolling without skidding of the workpiece. However, in most instances friction is preferably reduced to zero by the introduction of a lubricant. We have seen that interface conditions range very widely and they may change even within the deformation zone itself. Lubricants respond to these conditions in different ways, leading to a variety of lubricating mechanisms.

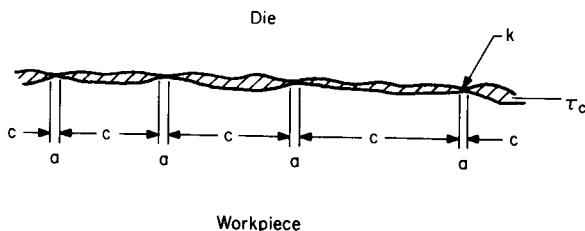


**FIG. 6.4** A dry interface.  $a$ —proportion of surface area that has been pressure welded;  $c$ —proportion of surface covered with contaminant film of  $\tau_c$  shear strength.

### 6.2.1 Dry Interfaces

Even in the absence of an intentionally applied lubricant, technical surfaces (Fig. 6.2b) are protected by adsorbed films and reaction products. However, in the course of deformation the surface expands, and virgin surfaces are exposed. Adhesion between die and workpiece will then govern the events. If adhesion is high, cold welding takes place. On further sliding, a piece of the weaker workpiece material may be torn out to remain welded to the die surface. Such pickup leads to scoring of subsequently contacted workpiece surfaces, and pickup formation proceeds at an increasing rate. The properties of such an interface (Fig. 6.4) can be described by

$$\tau_{FR} = ak + cr_c \quad (6.3)$$

where  $a$  is the relative proportion of the surface area that has been pressure-welded and  $c$  is the proportion of the surface covered with a contaminant film of shear strength of  $\tau_c$ . The interface shear factor is then

$$m = \frac{\tau_{FR}}{k} = a + c \frac{\tau_c}{k} \quad (6.4)$$

and the coefficient of friction is

$$\mu = \frac{\tau_{FR}}{p} = a \frac{k}{p} + c \frac{\tau_c}{p} \quad (6.5)$$

Obviously neither  $m$  nor  $\mu$  can be constant if  $a$  is not constant, and mathematical modelling of this situation becomes exceedingly difficult. A constant coefficient of friction has often been found in unlubricated hot rolling of steel and some other metals. However, these are really examples of rolling with a solid-film lubricant.

### 6.2.2 Solid-Film Lubrication

A continuous solid film, thick enough to separate die and workpiece surfaces at all points (Fig. 6.5), can act as a lubricant if  $\tau_c < k$ . (Even if  $\tau_c > k$ , such a film would be useful in preventing die-workpiece contact, but it is then usually called a *separator* rather than a lubricant.)

For an oxide film to work as a lubricant, it must be softer than the metal and must be capable of following the surface extension of the workpiece without rupture. Few, if any, oxides satisfy these conditions, but the situation improves if the oxide can reform between successive engagements of the die with the workpiece. Thus lubrication depends not only on the nature of the oxide, but also on the process itself. For example, steel is adequately protected by its oxide in hot rolling, but it needs additional lubricants in hot extrusion; copper and brass are borderline in hot rolling, whereas aluminum with its brittle and hard oxide needs other protection in all deformation processes.

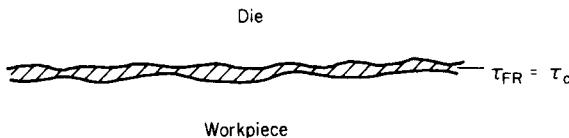


**FIG. 6.5** Solid-lubricated interface.

The interface can be described as in Eq. 6.3 except that  $a$  is, hopefully, zero. It is not known whether  $\tau_c$  is a function of normal pressure, although it does change with temperature. If the metallic contact area  $a$  is negligible, any pressure dependence of  $\tau_c$  would make  $\mu$  a suitable descriptor. As  $\tau_c$  has nothing to do with  $k$ ,  $m$  is unsuitable.

Coatings of a soft, ductile metal deposited on the workpiece surface are among the most effective solid lubricants. The shear strength of the interface  $\tau_{FR}$  is simply the shear flow strength of the coating metal  $\tau_f$ . For most metals  $\tau_f$  is insensitive to imposed hydrostatic pressure (Fig. 6.6). Therefore  $\mu$  decreases with increasing  $p$  and can be misleading. The value of  $m$  can remain constant only if strain hardening and strain-rate sensitivity are the same in the coating as in the workpiece material, assuming that both undergo the same deformation. None of these conditions are likely to be satisfied, and one cannot expect a constant  $m$  either.

Instead of a soft metal film, a polymer layer can be interposed, either as a separate film or as a deposit on the die and/or workpiece surface. The shear strength of many polymers is a function of hydrostatic pressure. Therefore their shear strength can be described as

$$\tau_{fp} = \tau_0 + \alpha p \quad (6.6)$$

where  $\tau_0$  is shear strength at zero pressure, and  $\alpha$  is a pressure-sensitivity coefficient. At high interface pressures  $\tau_0$  becomes negligible, and then

$$\tau_{fp} = \alpha p \quad (6.7)$$

and  $\alpha$  is identical to  $\mu$ . Obviously no relationship with the shear flow strength of the workpiece material exists, and  $m$  is quite inappropriate.

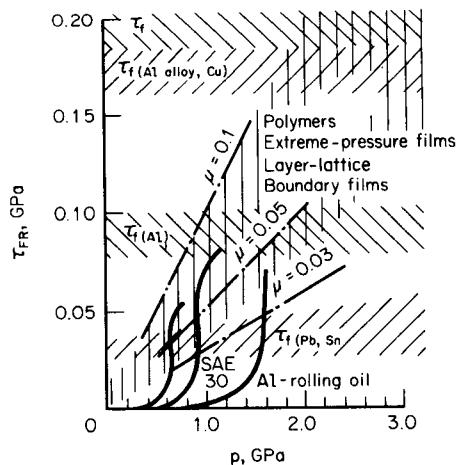


**FIG. 6.6** Effect of hydrostatic (normal) pressure on the shear strength of various substances. (After [6.9].)

Layer-lattice compounds such as graphite and  $\text{MoS}_2$  can be very effective lubricants provided they form a truly continuous film. Film formation is a mechanical process, aided by appropriate deposition techniques, by rubbing to create physical alignment of layers on surfaces, and by reactions between lubricant and substrate (die and/or workpiece surfaces). Most importantly, a reacted film resists destruction on sliding contact and is much more durable than a purely physically formed film [6.11]. This accounts for the greater effectiveness of  $\text{MoS}_2$  on copper and iron than on aluminum or titanium. Similarly, reactions are suspected between graphite and steel surfaces. The shear strength of these films is sensitive to imposed pressure, and can be described approximately by  $\mu = 0.05$  (Fig. 6.6).

### 6.2.3 Extreme Pressure and Boundary Lubrication

As the name implies, lubrication is performed by thin films which remain intact even when asperity–asperity contact takes place. There are two possible mechanisms.

In *extreme pressure (EP) lubrication*, the surface film is formed by reaction of the metal with an organic compound containing phosphorus, sulfur, and/or chlorine. The reaction product has a low shear strength, and because it grew by reaction with the substrate, it is also firmly attached. As with all chemical reactions, EP reactions are time-dependent and need fairly high temperatures to take place at a reasonable rate. Rubbing and exposure of new surfaces in metalworking are helpful by increasing the activity of the surface, but reaction times are usually too short to form a film on the workpiece. The repeated contact characteristic of many processes can, however, be helpful for reactions with the die surface. Nothing is known about the pressure dependence of the shear strength of reacted films, and one can only surmise that these organometallic films behave similarly to  $\text{MoS}_2$ .

*Boundary lubricants* are organic substances composed of unbalanced (polar) molecules. They attach themselves practically instantaneously to the surface of the metal or its oxide, and, if possible, they also enter into chemical reactions. This is typical of fatty acids, which form a well-aligned surface layer on nonreactive metals and a soap film of higher melting point on reactive ones. The melting point of fatty acids and of the reacted soap products increases with chain length. Thus longer-chain acids can be used for more severe operations. When the melting point of the acid or soap is reached, the adsorbed film becomes disoriented and ceases to be effective. Pressure raises the melting point. Many boundary agents that are liquids at room temperature and atmospheric pressure solidify at high pressure. From the rather scanty evidence available [6.13] it appears that the shear strength of boundary films depends on hydrostatic pressure as in Eq. 6.7. Thus a constant  $\mu$  can be used for modelling (Fig. 6.6).

The continued exposure of lubricants to shear strain and temperature may lead to the formation of a so-called “friction polymer.” The freshly formed surfaces act as catalysts in decomposing the lubricant, the fragments of which recombine to form a polymer of low shear strength.

Both EP and boundary additives rely on chemical reactions for developing their full potential, and the compositions of the die and workpiece surfaces are critical [6.11].

### 6.2.4 Hydrodynamic Lubrication

When the geometry of the deformation process is favorable, and the relative approach or sliding velocities are high enough, a viscous lubricant can form a continuous film (sometimes described as full-fluid film) that separates the die and workpiece surfaces even at asperities.

Only the bulk properties of the lubricant matter, unless there is a layer of lubricant at the surfaces which has a higher viscosity because of alignment of base or boundary-additive molecules (a proposition that is still controversial). This regime can usually be analyzed by treating the inlet zone from classical hydrodynamic theory, with due allowance for the plastic deformation of the workpiece [6.14], [6.15]. Film thickness  $h_0$  at the entry to the deformation zone is

$$h_0 \propto \frac{\eta v}{\beta \sigma_f} \quad (6.8)$$

where  $\eta$  is the viscosity,  $v$  the workpiece (or strip plus roll) velocity, and  $\beta$  the angle of entry (bite) (Fig. 6.2a). Pressure builds up gradually to satisfy the yield criterion at the point of entry. In the deformation zone the film thins with the expanding surface, while pressure sufficient to maintain plastic deformation is supported. In the outlet zone pressure drops back to ambient.

Pressure  $p$  increases and temperature  $T$  decreases the viscosity  $\eta$  of most oils exponentially,

$$\eta = \eta_s \exp [\gamma p - \alpha(T - T_s)] \quad (6.9)$$

where  $\eta_s$  is the viscosity at zero pressure,  $T_s$  is the surface temperature, and  $\gamma$  and  $\alpha$  are the pressure and temperature coefficients of viscosity, respectively.

Calculated film thicknesses first rise with increasing speed as indicated above, but frictional heating causes a thinning above some critical speed. Thus a full-fluid film can exist only under ideal conditions. In most metal-working situations some asperity contact is unavoidable: sliding speeds may be too low, heating of the lubricant film and interface pressures too high.

Under practical operating conditions full-fluid film lubrication can be obtained [6.2] by intentionally augmenting the lubricant film, as by specially designed or double dies in wire drawing and by pressure-lubricated deep drawing. Full-fluid lubrication may be undesirable. For example, it leads to periodic thickness variations in extrusion and to skidding and lack of control in rolling.

### 6.2.5 Mixed-Film Lubrication

Many metalworking lubricants are liquid or are dissolved or dispersed in a liquid carrier for a variety of reasons. Heat of deformation and friction may have to be removed; boundary, EP, or solid lubricants may have to be carried into the interface; the ability of liquids to develop at least partial hydrodynamic or squeeze films may have to be exploited. There will therefore be substantial entrapment of liquids, and the limited compressibility of such liquids results in the formation of hydrodynamic (hydrostatic) pockets in the surface of the deforming workpiece, while the rest of the workpiece will be in boundary contact with the die.

Qualitatively the most important factors in such mixed-film lubrication are not difficult to perceive (Fig. 6.7). For a given process geometry and interface pressure, the quantity of fluid carried into the interface increases with viscosity and velocity, as in Eq. 6.8; thus more of the surface lifts off. Lubrication gradually shifts from predominantly boundary to predominantly hydrodynamic (Fig. 6.8). The mean  $\tau_{FF}$  (and, for a constant interface pressure, the average  $\mu$ ) drops, and the surface of the deformed product roughens. Increasing interface pressure causes a shift back toward boundary conditions (Fig. 6.8, right-hand side).

A complete analysis of this most important lubricating mechanism is not yet available. As is seen from Fig. 6.1, mixed-film lubrication embodies all the complexities of both plastohydrodynamic and boundary lubrication and, for this reason, metallurgical and chemical factors, and the dynamics of film formation and breakdown must be considered.

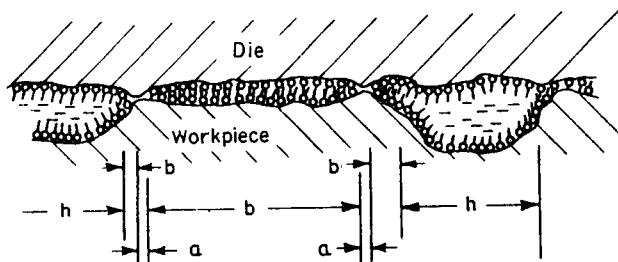
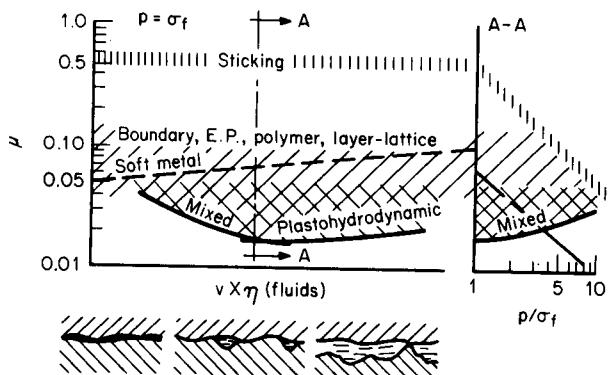


FIG. 6.7 Mixed-film lubrication at die-workpiece interface. (After [6.2].)



**FIG. 6.8** Regimes of lubricating mechanisms at a normal pressure of  $p = \sigma_f$  and at higher interface pressures. (After [6.9].)

If a  $b$  fraction of the surface is in boundary contact (Fig. 6.7) and the boundary film exhibits a pressure-sensitive shear strength  $\tau_B$  such that  $\tau_B = \mu_B p$ , then an average coefficient of friction  $\mu_{\text{mix}}$  may be defined [6.16] as

$$\mu_{\text{mix}} = (1 - b)\mu_H + b\mu_B \quad (6.10)$$

where  $\mu_H$  is the coefficient in the hydrostatic pockets.

As  $\tau_B$  is of the order of 0.05 to 0.1 for most boundary-type lubricants (Fig. 6.6), and  $\mu_H$  is less than one-tenth of this for a hydrodynamic film,  $\mu_{\text{mix}}$  is governed mostly by  $\mu_B$ , unless  $b$  is very small. In many practical situations there is also a small  $a$  fraction of area in direct metallic contact (Fig. 6.7),

$$\mu_{\text{mix}} = h\mu_H + b\mu_B + a\left(\frac{k}{p}\right) \quad (6.11)$$

Even though  $a$  may be small, its contribution can be quite significant, especially at low  $p$ . This may well account for rather high  $\mu_{\text{mix}}$  often measured under relatively mild interface conditions.

Hydrodynamic (or static) pockets are filled with a liquid yet fully compressed lubricant, which carries substantial load in proportion to the  $h$  fraction of contact. Yet its contribution to friction is small, and in a first approximation can be neglected relative to the boundary and metallic contributions (Eq. 6.11). Thus friction in mixed-film lubrication depends greatly on the micro-geometry of the interface.

### 6.2.6 Effects of Surface Roughness

It was already mentioned that real surfaces are not perfectly smooth, but are covered with asperities and valleys (Fig. 6.2b). The magnitude, distribution, and directionality of these roughness features are important in establishing a lubricant film and are, on the workpiece surface, subject to change as a result of surface deformation in the presence of lubricants. Thus the surface of the issuing product will bear evidence of its original condition and of changes superimposed during deformation. Many finished products must have a controlled roughness. Therefore, an understanding of variables is of greatest importance.

#### Characterization of Surface

A workpiece or die cannot conform perfectly to its nominal dimensions and shape, even on a macro scale, but these large-scale deviations seldom enter into lubrication considerations. Much more important is that, on the finer scale, the surface exhibits waviness and roughness. Both can

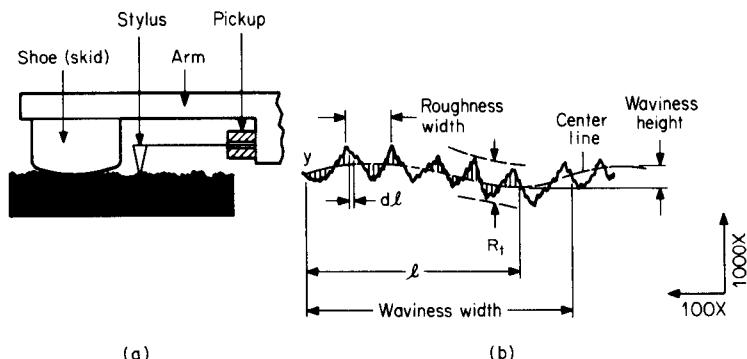


**FIG. 6.9** Surface roughness. (a) Measurement. (b) Characteristic dimensions. (After [6.18].)

be measured quantitatively by various techniques, of which measurement by a stylus instrument is the most widespread. An arm with a reference rest is drawn across the surface, while a stylus follows the finer surface details (Fig. 6.9). The surface profile can then be recorded after suitable amplification, usually distorted (with a larger gain on the vertical axis), or the signal may be processed electronically to give numbers that characterize the surface.

A line, drawn in the profile in such a way that the area filled with material equals the area of unfilled portions, defines the centerline. The average deviation from this mean surface is called the *centerline average* (CLA) or arithmetical average (AA), denoted also by  $R_a$ ,

$$R_a = \frac{1}{l} \int_0^l |y| \, dl \quad (6.12)$$

The root mean square (rms) value is often preferred,

$$\text{rms} = \left( \frac{1}{l} \int_0^l y^2 \, dl \right)^{1/2} \quad (6.13)$$

The peak-to-valley height  $R_t$  is often of more interest, especially if there are localized asperities or valleys that fail to show up in the averages, yet may pierce through the lubricant film. Sometimes a number of  $R_t$  values (say, five or ten) are averaged.

From a tribological point of view, the fullness of the profile is important [6.17]. For this, a reference profile must be established, essentially by taking the path the shoe surface travels in the course of measuring the surface roughness (Fig. 6.9). The mean distance of the actual surface from this reference surface then defines the smoothing depth  $R_p$  (Fig. 6.10), which is widely used in Europe,

$$R_p = \frac{1}{l} \int_0^l h_i \, dl \quad (6.14)$$

Of the horizontal dimensions (Fig. 6.9), waviness is less important because it disappears on plastic deformation. Roughness width is most significant though because it determines, together with depth dimensions, the fullness of the profile, which in turn depends on the manufacturing method used to make the part.

Full characterization of the surface takes more than just roughness depth and width dimensions. For identical widths and depths, profiles may show wide variations in fullness (Fig. 6.11b) and, more importantly for lubricant entrapment, in free space. When a line is drawn at a distance  $c$  from the reference surface, a *load-bearing area* can be determined. Evidently, a surface with rounded asperities has a much larger load-bearing area than one with sharp peaks (Fig. 6.11a).

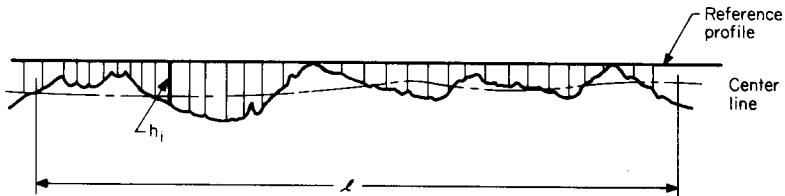
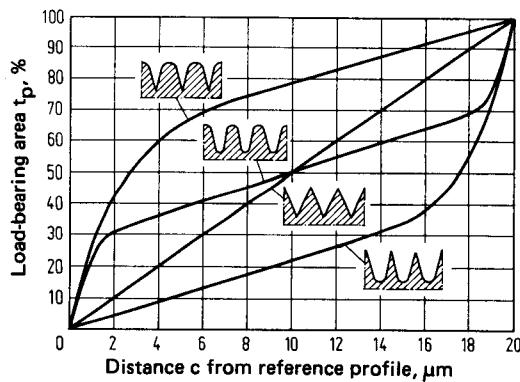


**FIG. 6.10** Dimensions needed for defining the fullness of a surface profile.



(a)

Idealized surface profile	Roughness measures, $\mu\text{m}$			Fullness $k = (R_t - R_p)/R_t$	Free space $\lambda = R_p/R_t$	Form factor $\delta = R_a/R_p$
	$R_t$	$R_a$	$R_s$			
	20	5	10	0.5	0.5	0.5
	20	6.3	10	0.5	0.5	0.63
	20	3.65	15.7	0.215	0.785	0.23
	20	3.65	4.3	0.785	0.215	0.85

(b)

**FIG. 6.11** Differences in load-bearing area for roughness profiles of identical peak-to-valley dimensions. (After [6.17].)

For an identical peak-to-valley roughness, the profile may be highly variable depending on the manufacturing technique [6.18], and consequently, it may also have very differing degrees of lubricant-retention ability.

From a tribological point of view, the directionality of surface roughness is also of great importance. Some finishes have a unidirectional lay, such as those produced by grinding, turning, side milling, or rolling with ground rolls. Others may have a two-directional lay, such as those produced by Blanchard grinding or face milling. Yet others are random, such as those produced by lapping, shot blasting, EDM machining, or rolling on shot-blast rolls. Cast and forged surfaces are usually random, but tend to have a more uneven asperity distribution than machined surfaces.

### ***Deformation of Free Surfaces***

In some metalworking processes one or more of the workpiece surfaces deform without contacting a tool. Changes in roughness then depend on the deformation mode [6.19]. In tension (stretching), initially smooth (say,  $R_t = 1 \mu\text{m}$ ) surfaces roughen because individual grains deform differently depending on their crystallographic orientation; roughening is greater for larger strain and for coarser-grain material. Initially rough (say,  $R_t = 65 \mu\text{m}$ ) surfaces get somewhat smoother because the surface features are stretched out. In contrast, in upsetting a cylinder, the free surface roughens irrespective of initial roughness, because surface features are pushed closer and become deeper. In other processes a combination of the two phenomena may occur. Thus in bending a sheet, the outer surface changes as in tension, whereas the inner, compressed surface changes as in upsetting.

### ***Deformation of Constrained Surfaces***

Workpiece surfaces in contact with a die surface also undergo changes which are greatly influenced by the absence or presence of a lubricant.

When the interface is dry, contact is made only at asperities, and the deforming force must be transmitted through them. Asperities of the workpiece surface, such as those produced by machining, can be more heavily strain-hardened than the bulk. More importantly, they are initially prevented from free deformation by the restraint of the underlying elastically stressed material. The situation is similar to that of indentation, and it takes a pressure of about  $p = 3\sigma_t$  to deform an asperity. Thus the pressure required for initiating bulk plastic flow can be transmitted through a relatively small real contact area. When the minor surface features superimposed on the larger asperities are taken into account, it can be shown that the real area of contact reaches 88% or more of the apparent area of contact when sliding takes place [6.20].

If sufficient quantities of lubricants are present to fill the surface profile, surface roughness changes as a function of the lubricating mechanism. An initially smooth workpiece surface becomes rougher in the presence of a thick lubricant film for two reasons. First, the lubricant cushion transmits pressures like a hydraulic medium. Surface oxide films are penetrated, and then individual grains of polycrystalline material begin to yield to differing degrees, depending on orientation and constraint. Coarser-grained material becomes rougher for otherwise identical conditions. Second, entrapped lubricant behaves as an incompressible reservoir of fluid, indenting the workpiece. This is true of solid lubricants capable of plastic flow, such as polymers, waxes, and soaps (Fig. 6.12), and also of full-fluid films. Thus all variables that encourage hydrodynamic lubrication, such as a converging gap, large approach or sliding speed, or high viscosity and low pressure, also contribute to roughening.

A shift toward mixed-film lubrication results in an increasing proportion of boundary contacts (Fig. 6.8). Thick films exist only locally, in the form of hydrodynamic or hydrostatic pockets. Consequently an originally rough surface becomes smoother, whereas a smooth surface roughens (Fig. 6.12) [6.21]. It is possible to calculate an average film thickness, but it is really much more important to define the boundary contact area ( $b$  in Fig. 6.7 and in Eq. 6.11). The contact area  $b$  can be measured by various light-reflection techniques [6.22], but theoretical prediction is difficult. Some beginnings have been made. Starting from plasticity theory, it has been shown [6.20] that the bulk modulus of the lubricant is the dominant factor, while asperity slope and frictional shear factor  $m$  are of secondary importance. Starting from plastohydrodynamic theory, a mean lubricant film thickness can be calculated by postulating a thick-film mechanism and a given rough-

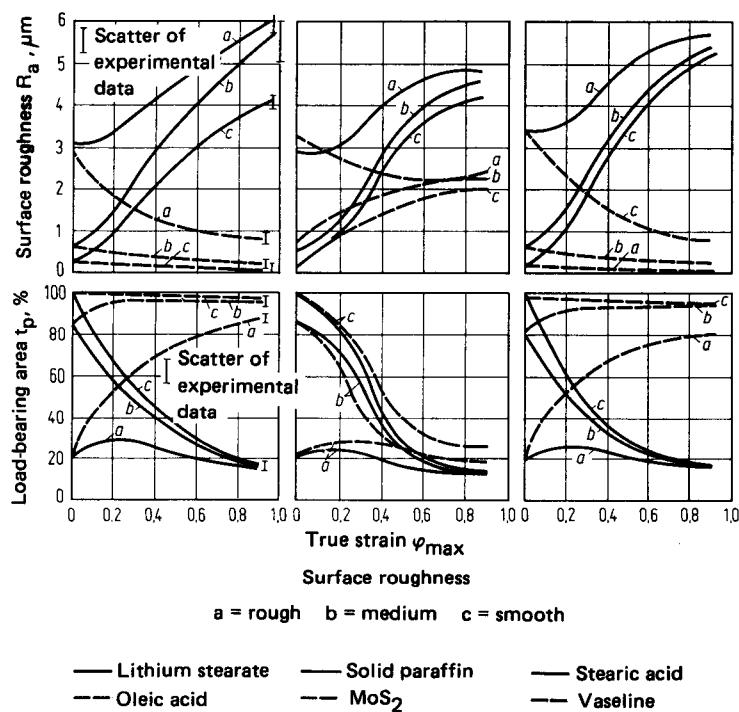


**FIG. 6.12** Effects of initial surface roughness and lubricant on the surface configuration of the end face of cylinder specimens upset to varying strains. (After [6.21].)

ness-height distribution [6.23], or it may be assumed that the mean film thickness is equal to the combined roughness of surfaces [6.14]. From thick-film theory the pressure carried in the lubricant pockets is then calculated, and from a knowledge of the required pressure to be supported, the *b* fraction can be found.

### **Effect of Workpiece and Die Surface Roughness**

It is evident from the above considerations that any factor capable of increasing lubricant input into the deformation zone also helps to reduce *b* and thus friction.

Moderate workpiece surface roughness (say, of the order of 0.5 to 2.0  $\mu\text{m AA}$ ) is helpful if it is properly oriented. Asperities aligned in the direction of relative sliding between die and workpiece would break through the lubricant film and can be counterproductive with low-viscosity lubricants. However, roughness with a lay perpendicular to the relative motion helps in carrying lubricant into the deformation zone. In many processes the sliding direction changes during deformation, and then a random finish, such as produced by shot blasting or by rolling a sheet on shot-blast rolls, is most helpful. Similarly, roughening due to deformation prior to entry into the die-workpiece zone is also helpful.

Die surface roughness is conventionally regarded to be harmful, and this is indeed true for the mixed-film regime. However, moderate roughness (on the order of 0.5  $\mu\text{m AA}$ ) can be beneficial for solidlike fats, waxes, and polymers, and for layer-lattice compounds. These are entrapped in surface troughs to be fed out to asperity tips in the course of deformation (Fig. 6.13). The lay must be perpendicular to the sliding direction, or in multidirectional sliding, it must be random

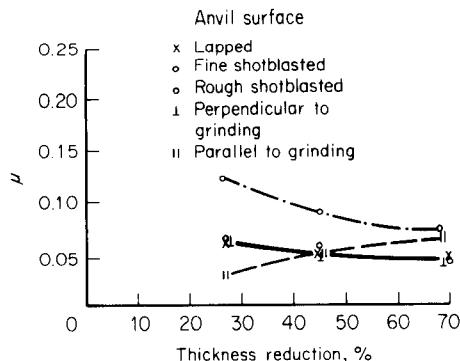


**FIG. 6.13** Effect of roughness and roughness orientation on the coefficient of friction measured in ring upsetting of AA 6061 aluminum alloy with sprayed-on PTFE film. (After [6.11].)

[6.11]. In the mixed and boundary lubrication regime, die asperities would pierce through the lubricant film. Therefore, the surface should be as smooth as technically possible, and any residual roughness should have a lay oriented parallel to the relative sliding direction.

### 6.3 WEAR

When the die and workpiece surfaces are fully separated by a thick lubricant film, wear is theoretically absent. However, such thick film is not only difficult to maintain, but it may also be undesirable because of the surface roughening it causes. Therefore in most practical metalworking operations some asperity contact is normally encountered, and relative motion of the surfaces may then result in a loss of die and/or workpiece material through various wear processes.

As indicated earlier, adhesion results in die pickup. The heavily worked junction is usually stronger than the workpiece material. Therefore a fragment becomes detached from the workpiece on further sliding, resulting in the formation of wear debris. Occasionally some part of the die may be ripped out too. Wear volume increases with normal pressure and sliding distance; it decreases with die hardness.

The presence of hard particles (such as oxides or wear debris) accelerates wear by abrasion. Thus removal of scale formed during heating (for example, by high-pressure water or mechanical descaling of the workpiece) becomes important in hot forging and rolling of steel, and filtration is a must in all recirculating lubricant-coolant systems. For a given abrasive size and population, a rougher workpiece surface and a thicker lubricant film can accommodate particles without damage more readily than a very smooth surface.

Chemical corrosion effects may combine with other wear mechanisms to produce accelerated corrosion wear. This happens when an aggressive chemically active additive is incorporated into the lubricant. It may attack not only the workpiece but also the die.

Thermal cycling typical of many hot-working operations imposes additional stresses on the die material and induces surface fatigue. In combination with adhesive and corrosive mechanisms, this may lead to very rapid die wear.

### 6.4 LUBRICANTS

Despite the extremely wide range of conditions under which lubricants must function, some systematic approach to selection can be made. Final selection is almost always a matter of compromise, but there are some fairly general, desirable attributes [6.1]:

## 6.16 FUNDAMENTALS OF METAL FORMING

- 1 *Separation of die and workpiece surfaces.* This is always desirable for reduced wear. A continuous film need not be of the same thickness everywhere, but should protect even asperities. If wear particles are formed, they should not be abrasive.
- 2 *Controlled friction.* The lowest possible  $\tau_{\text{FR}}$  is desirable in many instances, but some minimum value is required in processes that rely on traction to assure metal movement (as in rolling) or support (as on the punch in deep drawing or ironing).
- 3 *Prevention of cold welding (pressure welding).* Even when continuity of the low-shear-strength film is lost, there should be sufficient surface contamination left to limit adhesion between die and workpiece material.
- 4 *Controlled surface finish.* This may range from a bright finish of high specular reflectivity (as produced with very thin or boundary lubricant films) to relatively dull, rough finish (as results from hydrodynamic pockets). In all instances the finish should be uniform over the entire workpiece surface.
- 5 *Control of surface temperatures.* In hot working, retention of workpiece temperature calls for a lubricant of good heat-insulating properties. In contrast, lubricants in cold working (and sometimes in hot working) are often required to provide also a cooling function.
- 6 *Reactivity with workpiece and/or die surface.* A high rate of reaction is usually desirable, particularly if the reaction is to occur on the workpiece during its passage through the deformation zone. If the workpiece is basically nonreactive, the die material should form protective reaction layers. Any damage to the film should heal quickly. The lubricant should, however, not be corrosive to the dies, equipment, or finished product.
- 7 *Controlled stability.* The lubricant should remain unchanged during storage and, if possible, during use. Some changes may be desirable but should be controlled.
- 8 *Easy application and removal.* Any residues left should be harmless or possibly beneficial from the point of view of subsequent operations such as annealing, welding, or painting.
- 9 *Easy handling, safety, and low cost.* The lubricant should not cause skin irritation, not contain toxic substances, nor generate toxic or objectionable gases. Disposal should not present insurmountable problems. Finally, the cost should be commensurate with the benefits.

### 6.4.1 Oil-Base Lubricants

Mineral oils obtained from the distillation of crude oils (or their synthetic equivalents) provide the base for many well-established industrial lubricants. Their viscosity is usually chosen to assure predominantly hydrodynamic lubrication at the existing velocities, pressures, temperatures, and process geometries. Temperatures increase during plastic deformation even in cold working, and this leads to a reduction in their viscosity, counterbalanced by the usually exponential increase in viscosity with pressure (Eq. 6.9). Above some critical pressure oils become solids and behave as a polymer film would (Fig. 6.6).

Because in cold working lubrication is mostly of the mixed-film type, additives are almost invariably incorporated to protect against direct metal-to-metal contact at asperities. The type of additive depends on the workpiece and die compositions and on the severity of operation. Boundary additives, such as fatty acids, alcohols, or amines, are most effective with reactive metals such as aluminum, and to a lesser extent with copper and iron. Even esters, such as butyl stearate, may suffice for relatively mild duties in the cold rolling of aluminum when freedom from staining on annealing is most important.

EP additives can be effective only when contact time and temperature combinations are sufficient to initiate reaction. This condition can be satisfied only on repeated contact. Thus, sulfur and chlorine are added to cold-heading oils for steel and chlorine to oils for stainless steels. Often both boundary and EP additives are incorporated to provide protection over a wide temperature and pressure range.

Natural oils, fats, and waxes of animal or vegetable origin offer a wide range of viscosities, relatively low solidification pressures, and usually also contain some free boundary agents. Thus

they can be used as complete lubricants on their own. When their viscosity is too high, they may be deposited from a volatile solvent, as is done with lanolin in the coating of aluminum slugs for cold extrusion.

Some practical lubricant formulations contain further additives, such as solid lubricants and inert fillers, to prevent metal-to-metal contact when conditions are unfavorable for thick-film formation.

All oils ignite at their flash point and while the residue may lubricate, especially if the oil contains additives, the resulting pollution is objectionable and has led to a diminishing use of oil-base lubricants for hot-working processes.

#### **6.4.2 Aqueous Lubricants**

Water is the best coolant, but its viscosity is too low for lubrication. With chemicals added for corrosion protection, it is still used for its cooling qualities in the hot rolling of steel where iron oxide acts as the lubricant. However, hot rolling of nonferrous metals and all cold-working operations are conducted with emulsions in which water serves as the carrier for an oily phase, dispersed with the aid of emulsifiers. It is believed that the oily phase separates, "plates out" on the workpiece once it arrives at the interface, and then behaves somewhat like a similarly formulated oil-base lubricant would.

Technical, economic, and ecological considerations demand that aqueous (and, if used in quantities, also oil-base) lubricants be circulated in a system that comprises filters for the removal of wear debris, holding tanks, heaters, coolers, and provisions for lubricant makeup.

#### **6.4.3 Soaps and Greases**

Soaps are the reaction products of a metal hydroxide with a fatty acid. With the exception of alkali metal soaps, they are water-insoluble. At high pressures and shear rates they behave as non-Newtonian substances<sup>\*</sup> and are capable of forming thick lubricant films, as in the dry drawing of steel wire. Their apparent viscosity decreases with temperature. Thus friction first decreases, but after reaching a minimum at around 200°C (400°F), it increases because of increasing boundary contact [6.24].

Greases too are non-Newtonian fluids, with their properties derived from the presence of a thickening or jelling agent in a liquid lubricant. Many greases are based on soaps in a petroleum oil, and contain boundary, EP, and lamellar additives. They are used when process conditions are not favorable for establishing a thick enough lubricant film with an oil or emulsion.

#### **6.4.4 Solid Films**

Soft metal films are still used when the base metal cannot be effectively lubricated. The coating is chosen for its low shear strength, high ductility, good adhesion to the base, reduced adhesion to the die, and improved reactivity with the lubricant. Current examples are copper on stainless steel or steel wire and tin on steel cans.

Molten glass films may act simply as low-shear-strength films (as in the hot forging of titanium), as gradually melting films (as in hot extrusion of steel and titanium- and nickel-base alloys), or as hydrodynamic agents (as in hot extrusion with predeposited films).

Layer-lattice compounds are the only alternatives to glass in hot working when emulsions prove inadequate, as in hot forging and hot wire drawing. Graphite is a crystalline material of hexagonal structure in which bonding between adjacent basal planes is relatively weak but must

\*The shear strength of a Newtonian fluid is simply its viscosity multiplied by the shear strain rate; non-Newtonian substances deviate from this linear response to strain rate.

be further weakened with the adsorption of condensable vapors, such as gases, water, or oils. Individual covalently bonded lamellae of  $\text{MoS}_2$  are bonded by weak forces to each other, and easy shearing is assured even in vacuum. The major problem with both graphite and  $\text{MoS}_2$  is the difficulty of depositing a uniform and continuous film. They have no spreading ability, thus deposition from a carrier (water, oil, or air) is required. Ecological considerations favor water. Then wetting of the die or workpiece surface (at an often quite high temperature) is aided by wetting agents and polymeric binders. Oxidation of  $\text{MoS}_2$  at temperatures in excess of  $400^\circ\text{C}$  ( $670^\circ\text{F}$ ) limits its use, but graphite can be used to  $800^\circ\text{C}$  ( $1470^\circ\text{F}$ ) [6.24].

Polymer films [polyethylene, polytetrafluoroethylene (PTFE), methyl methacrylate] are used occasionally, although their inability to self-repair film damage can create problems.

#### 6.4.5 Lubricant Carriers and Conversion Coatings

One of the greatest problems of metalworking lubrication is to assure that the lubricant actually gets into the deformation zone and, once there, is not displaced or punctured.

Controlled surface roughness can be helpful as outlined in Sec. 6.2.6. Under more severe conditions, as presented by high interface pressures, extensive sliding, unfavorable process geometry, and large surface extensions, further aids are needed. These usually take the form of a carrier that firmly adheres to the workpiece surface and also offers a suitable microscopic surface configuration to facilitate lubricant entrapment.

For conditions of medium severity, such as exist in wire drawing, a lime or borax coating on steel is adequate in conjunction with a dry soap lubricant. For severe cold extrusion, a conversion coating must be formed chemically. Zinc iron phosphate formed on steel has high adhesion by virtue of its formation from the substrate, and possesses a microscopic channel structure that helps to entrap and hold the lubricant, usually a soap. The soap may be reacted with the phosphate, or for heaviest duties, an  $\text{MoS}_2$  film may be superimposed on the phosphate-soap system by tumbling the parts in  $\text{MoS}_2$  powder. Appropriate conversion coatings are available also for aluminum, titanium, and nickel alloys (see Chap. 26).

#### 6.4.6 Lubricant Application

In principle the minimum quantity of lubricant that will fulfill its intended function is supplied, although large excesses may have to be provided when the lubricant is to serve other functions, such as cooling. Proper application is just as important as the choice of the right lubricant.

An excess of lubricant is usually applied to processes where the die-workpiece geometry itself controls the thickness of the lubricant film. This is true of rolling, drawing of wire, bar, and tube, and many cold-heading applications. A carefully measured amount of the lubricant is applied when lubricant excess could lead to problems, such as filling of the die cavity and unfilled workpieces in forging, or periodic variation of the lubricant film and thus extruded workpiece diameter in extrusion.

Some of the more generally used lubricants are given in Tables 6.1 and 6.2 [6.1].

### 6.5 MEASUREMENT OF FRICTION

The magnitude of friction needs to be known for two reasons. First, pressures, forces, and energy requirements can be calculated only if interface conditions can be described by  $\tau_{\text{FR}}$ ,  $\mu$ , or  $m$ . For this, a numerical value must be established. Second, reduced friction is often the main criterion in choosing a lubricant. For this, comparative values are often sufficient. The ultimate choice of the lubricant may have to be based on full-scale operating experience, but such tests can be disruptive and prohibitively expensive. Therefore at least a preliminary evaluation is usually conducted in simulating tests or small-scale laboratory versions of actual metalworking processes. Whenever possible, they are chosen to give additional information, such as tendency to lubricant breakdown, pickup formation, and wear.

**Table 6.1** Typical Lubricants Used in Hot Working and Representative Coefficients of Friction

Process	Steel	$\mu$	Stainless steel, nickel-base	$\mu$	Titanium	$\mu$	Copper, brass	$\mu$	Aluminum, magnesium, $\mu$
Rolling	None	ST <sup>a</sup>	As steel		As steel		MO-FA-EM <sup>b</sup>	0.2	MO-FA-EM 0.2
	(GR suspension) <sup>c</sup> (MO-FA-EM)	0.2 0.2							
Extrusion <sup>d</sup>	GL	0.02	GL	0.02	GL	0.02	None (GR) (GL)	ST 0.2 0.02	None ST
	(GR)	0.2							
Forging	None	ST	GR	0.2	GL	0.05	GR	0.1-0.2	GR 0.1-0.2
	GR	0.2			MoS <sub>2</sub>	0.1			MoS <sub>2</sub> 0.1-0.2

<sup>a</sup>The symbol ST indicates sticking friction.<sup>b</sup>Hyphenation indicates that several components are used in the lubricant.<sup>c</sup>Less frequent lubricant usage is shown in parentheses.<sup>d</sup>Interface pressures can be very high, and sticking may occur even if  $\mu$  is low.

EM—emulsion; the listed lubricants are emulsified and 1–5% is dispersed in water.

FA—fatty acids, alcohols, amines, esters.

GL—glass (sometimes in conjunction with GR on the die).

GR—graphite.

MO—mineral oil.

Source: Compiled from [6.1].

**Table 6.2** Typical Lubricants Used in Cold Working and Representative Coefficients of Friction

Process	Steel	$\mu$	Stainless steel <sup>a</sup> nickel base <sup>c</sup>	$\mu$	Titanium <sup>b</sup>	$\mu$	Copper, brass	$\mu$	Aluminum, magnesium <sup>d</sup>	$\mu$
Rolling	FO	0.03	CL-MO <sup>e</sup>	0.07	FO-MO	0.1	FO-MO(10-50)	0.03	1-5% FA-MO	0.03
	FO-EM	0.07	CL-FO-EM	0.1	MO on oxidized surface	0.1	FO-MO-EM	0.07	(5-20) (or synthetic MO)	
	(FO-MO)	0.05			SP	0.1				
Extrusion <sup>f</sup>	EP-MO	0.1	CL-MO	0.1	SP or GR grease on fluoride-PH	0.05	FO-MO	0.1	Lanolin	0.05
	SP on PH	0.05	SP on oxalate	0.05			GR-FO	0.05	Zn stearate	0.05
	MoS <sub>2</sub> +SP on PH	0.05					GR-grease	0.05	SP on PH	0.05
Forging, light	EP-MO	0.1	EP-MO	0.1	As extrusion		FO	0.05	FO	0.05
	SP on PH	0.05	CL-MO	0.1			SP	0.05	Lanolin	0.05
			SP on oxalate	0.05						
Wire drawing, light	SP-FO-EM	0.1	CL-MO	0.1	As extrusion		SP-FO-EM	0.1	FO-MO(20-40)	0.03
	SP on lime or borax	0.05	SP on oxalate	0.05			FO-MO(20-80)	0.05	FO-MO(100-400)	0.05
			PC or CL-MO	0.05			SP-FO-EM	0.1	FO-MO-EM	0.1

Process	Steel μ	Stainless steel, <sup>a</sup> nickel base <sup>c</sup> μ	Titanium <sup>b</sup> μ	Copper, <sup>c</sup> brass μ	Aluminum, magnesium <sup>d</sup> μ
Bar drawing	EP-FO-MO on lime or PH grease or GR grease	0.1 CL-EP-MO 0.1	As extrusion, or PC	FO-MO SP	0.1 SP 0.05 FO-MO(50-400)
Tube drawing	EP-FO-MO SP on PH	0.1 SP on oxalate PC 0.05	0.05 as bar	as bar	0.1 as bar
Light pressing	MO, SP-EM	0.05 EP-MO EP-MO-EM 0.1	MoS <sub>2</sub> -MO 0.1	MO-EM 0.07	FA-MO 0.1 0.05
Heavy sheet drawing	FO; FO-EP-MO SP; SP on PH Pigmented FO-SP	0.1 SP 0.05 CL-MO 0.05	0.1 GR-grease <sup>e</sup> 0.1	FO-MO Pigmented FO-SP 0.07 0.05	FO 0.07 FO 0.05
Heavy ironing	EP-GR-grease SP on PH	0.1 SP on oxalate 0.05	GR-grease <sup>e</sup> GL + GR 0.05	FO 0.1 SP 0.05	0.1 Lanolin 0.1 0.05

<sup>a</sup>Chlorine is the most effective EP agent on stainless steel.

<sup>b</sup>Chlorine is avoided for titanium.

<sup>c</sup>Sulfur is avoided for nickel because of reaction and for copper because of staining.

<sup>d</sup>Magnesium alloys are usually worked warm (above 200°C).

<sup>e</sup>Hypniation indicates that several components are used in lubricant.

<sup>f</sup>Interface pressures can be very high, and sticking may occur even if  $\mu$  is low.

<sup>g</sup>Usually conducted hot.

CL—chlorinated paraffin.

EM—emulsion; the listed lubricants are emulsified and 1-20% is dispersed in water.

EP—"extreme pressure" compounds (containing S, Cl, and/or P).

FA—fatty acids, alcohols, amines, esters.

FO—fats and fatty oils, such as palm oil, synthetic palm oil.

GR—graphite.

MO—mineral oil [viscosity in units of centistoke ( $= \text{mm}^2/\text{s}$ ) at 40°C].

PH—phosphate surface conversion.

PC—polymer coating.

SP—soap (powder, or dried aqueous solution, or as a component of an EM).

Source: Compiled from [6,1].

### 6.5.1 Simulating Tests

Ideally one would like to use a simple bench-type test that would simulate all process variables. A consideration of Fig. 6.1 will show that this is impossible. Therefore all simulating tests represent compromises. There are, however, minimum criteria that must be satisfied. Thus one of the sliding partners must be typical of the die and the other of the workpiece material. The temperatures must be the same as in the process to be simulated. The surface finish of the die and workpiece, relative sliding directions, and approach and sliding velocities should be the same too, although compromises may have to be made. Simulating tests fall into several categories.

Commercial oil-laboratory test equipment can be modified by changing the rubbing partners to be representative of the die and workpiece materials. The contact geometry may be a point, as in sliding a hemispherical pin against a flat surface, or a ball against three clamped balls (Shell test) or crossed cylinders. Line contact is obtained when the outer surface of a ring is slid against a flat (Timken), two disks against each other (Amsler), or a bar against a split bushing (Almen) or against v-blocks (Falex). Even though surface finishes, sliding speeds, and process geometry are very different from most metalworking operations, surprisingly good agreement has occasionally been reported. It is likely though that such agreement is fortuitous and should not be relied upon.

Flat-on-flat geometry has the advantage that  $\tau_{FR}$  or  $\mu$  can be determined directly. Flat-ended pins sliding on a flat surface (Fig. 6.14a) have been used in general tribological studies, but proved less successful in metalworking. In twist compression (Fig. 6.14b) the preapplied lubricant film is exposed to prolonged rotation under pressure, and its resistance to breakdown and potential for die pickup are evaluated. The test has shown surprisingly good agreement with processes such as cold extrusion where fresh lubricant cannot be supplied to the deformation zone. Pressures are, however, limited to the flow stress of the hollow specimen, and this limitation has been overcome by rotating a punch against a confined workpiece (Fig. 6.14c). Much lower pressures are applied in drawing a sheet between parallel flat dies (Fig. 6.14d), thus simulating conditions existing in the blankholder zone of deep drawing.

All the above tests suffer from the absence of bulk deformation, even though rubbing under high pressure serves to break through the surface oxide films. There are various tests that generate new surfaces while sliding under high normal pressure. In one group of tests the specimen is upset (Fig. 6.15a and b) while slid against the die surface [6.26], in another group the specimen is pushed (Fig. 6.15c) [6.27] or drawn (Fig. 6.15d) [6.28] through a converging die gap. Frictional and normal forces can be measured separately and thus  $\tau_{FR}$  or  $\mu$  determined directly. In the third group of tests the new surface is generated by indenting the workpiece (Fig. 6.16). By changing the geometry of the indenter tool, virgin surface generation can range from almost zero to 90% of the contact surface [6.29]. Severe wear conditions are created when the tool indents (scratches) the workpiece [6.30], or when repeated contact is made by rotating a castellated disk against the cylindrical surface of a punch [6.31].

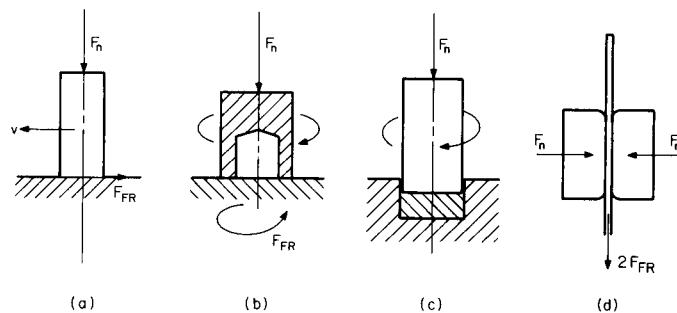


**FIG. 6.14** Simulating tests with flat-on-flat geometry. (a) Pin on flat. (b) Twist compression. (c) Twist compression with confined workpiece. (d) Strip drawing.

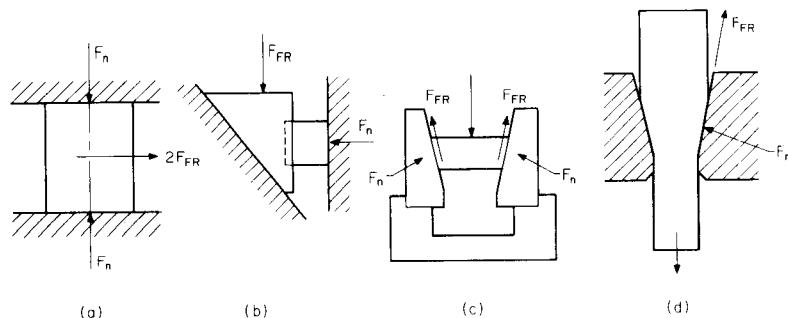


**FIG. 6.15** Simulating tests with bulk deformation: (a) and (b) Upsetting with sliding. (c) Pushing through. (d) Flat bar drawing.

There are some metalworking processes which are uniquely suited for lubricant evaluation because the magnitude of interface friction can be judged without resorting to instrumentation. In the so-called cigar test a thin, long rectangular slab is upset between overhanging platens, and the increase in length (which is greater for low friction) is measured (Fig. 6.17a). The test is very sensitive at low friction values. A wider range of friction is covered by the ring-compression test. When a ring is compressed with zero friction, it expands as though it would be part of a solid

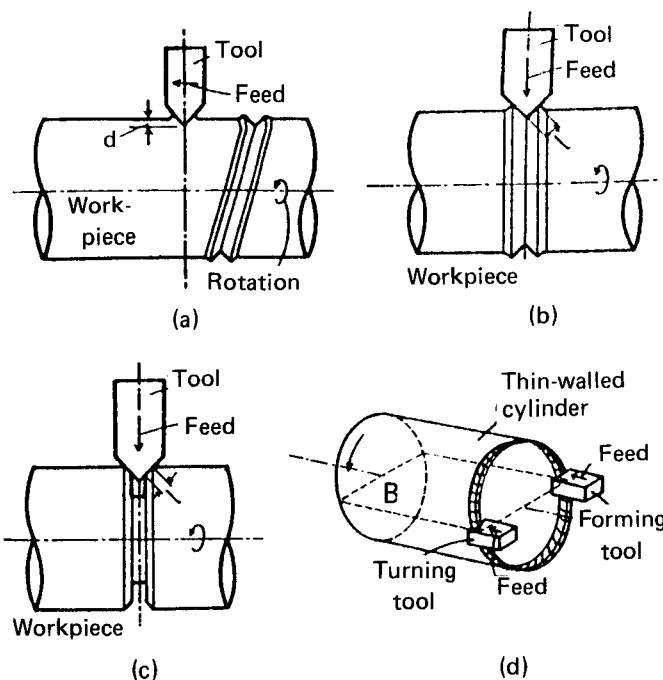


**FIG. 6.16** Simulating test with varying degrees of new surface generation. (a) Indenting in helical path. (b) Indenting in single groove. (c) Indenting along premachined groove. (d) Forming fresh surface by machining. (After [6.29].)

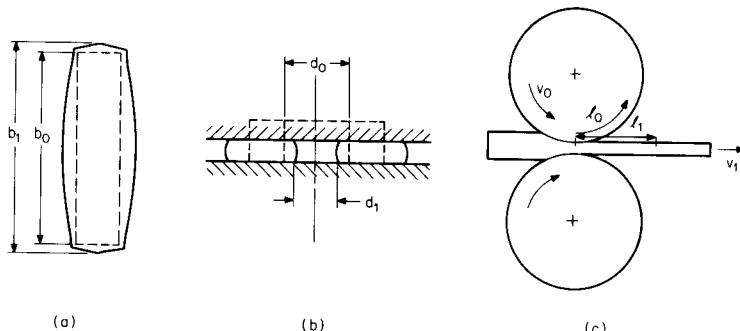


**FIG. 6.17** Methods for determining friction from deformation. (a) Cigar test. (b) Ring compression. (c) Forward slip.

cylinder. Increasing friction presents increasing resistance to free expansion, and the hole grows to a lesser extent. At yet higher friction a neutral circle develops from which material flows both outward and also toward the center, resulting in a decrease of the ring internal diameter (Fig. 6.17b). Thus lubricants can be ranked simply by measuring the change in internal diameter. The situation is similar to that in rolling (Fig. 6.17c). Here frictional balance in the roll gap determines the position of the neutral point, where the strip moves with the roll at speed  $v_0$ . The strip emerges at a higher speed  $v_1$  from the roll gap. The speed difference, called forward slip  $s_f$ , increases with increasing friction. Lubricants can be ranked by measuring forward slip with the aid of lines scribed on the roll surface at a distance  $l_0$  from each other; their imprint on the strip is  $l_1$ . The forward slip from simple dimensional measurement is given by

$$s_f = \frac{v_1 - v_0}{v_0} = \frac{l_1 - l_0}{l_0} \quad (6.15)$$

Because the above tests are so easy to perform, repeated attempts have been made to use them for simulating other metalworking processes. However, the cigar and ring-compression tests are limited to processes with normal tool-workpiece approach, and rolling simulates just rolling. Direct transfer of results to other processes is extremely difficult if not impossible because neither the process geometry nor the sliding conditions can be changed without affecting the lubricating mechanism and thus the results. It is possible though to generalize the results if effects of process conditions on lubricating mechanisms are understood.

### 6.5.2 Friction Measurement in Metalworking Processes

Most experimental and much production equipment is equipped with force-measuring instrumentation, and the efficiency of a lubricant and the magnitude of friction can then be judged by comparing forces. It should be noted though that friction contributes often less than 5% to the total deforming force, and comparisons are valid only if the workpiece material flow stress is very closely reproducible. Trends are often more important than absolute forces. Thus recordings of force versus stroke (or time) can reveal a tendency toward lubricant breakdown, such as is indicated by erratic force variations in drawing or deep drawing, or by a rising force toward the end of the stroke in extrusion. Frequently a large number of tests must be performed to establish resistance to pickup or to measure wear rates [6.32], [6.33].

Sometimes a  $\mu$  or  $m$  value is calculated from measured forces with the aid of a suitable theory. However, variations in the flow stress of the material may make the calculated values unreliable.

The value of  $\tau_{FR}$  or  $\mu$  can be determined without resorting to theory and without the need of knowing the flow stress of the material by suitable instrumentation. Thus in drawing a strip the

die can be instrumented to give both frictional and normal force readings (as in Fig. 6.15d), and similar provisions can be made, often with the aid of ingenious die design and instrumentation, in some other processes. Even more detailed information may be gained by building pins that bear on small load cells into the die surface. A pin oriented normal to the surface gives the normal stresses, and an obliquely embedded pin the shear component. The technique is laborious and subject to errors, but it is still one of the few that can give detailed information on the distribution of normal and shear stresses along the die surface.

It is obvious that the universal friction test has not been and will never be found. In view of the very great variety of process conditions that a lubricant may have to contend with, there is thus some merit in evaluating lubricants by a number of techniques. Because of their simplicity, ring compression and wire (bar) or sheet drawing are usually chosen, supplemented by plain-strain and twist compression or deep drawing and back extrusion, depending on the intended range of applications.

A further problem with all laboratory tests is that scaling up to production can be difficult. Even if the process geometry is appropriately scaled and surface finishes are representative of full-scale operation, production speeds and temperatures are sometimes difficult to maintain. The resulting change in lubricating mechanisms then makes the results questionable. Nevertheless, if a systematic correlation is established between laboratory behavior and plant performance, valid lubricant evaluation becomes possible.

## REFERENCES

- 6.1 Schey, J. A.: *Tribology in Metalworking: Friction, Lubrication and Wear*, Metals Park, OH, American Society for Metals, 1983.
- 6.2 Schey, J. A.: "Tribology in Metal Forming Processes," in *Proceedings 4th International Conference on Production Engineering*, Tokyo, 1980, pp. 102-115.
- 6.3 Kalpakjian, S., and Jain, S. C., eds.: *Metalworking Lubrication*, New York, ASME, 1980.
- 6.4 *Friction and Lubrication in Metal Processing*, New York, ASME, 1966.
- 6.5 *Tribology in Iron and Steel Works*, London, Iron and Steel Institute Publ. 125, 1969.
- 6.6 *Proceedings of the 1st International Conference on Lubrication Challenges in Metalworking and Processing*, Chicago, IIT Research Institute, 1978. (2d Conference, 1979.)
- 6.7 *Tribology in Metal Working—New Developments*, London, Metals Society, 1980.
- 6.8 Shaw, M. C., Ber, A., and Mamin, P. A.: "Friction Characteristics of Sliding Surfaces Undergoing Subsurface Plastic Flow," *Trans. ASME, J. Basic Eng.*, **82**, 1960, pp. 342-346.
- 6.9 Schey, J. A.: "Modelling of the Tool-Workpiece Interface," in *Metal Forming Plasticity*, Lippmann, H., ed., Berlin, Springer, 1979, pp. 336-348.
- 6.10 Bowden, F. P., and Tabor, D.: *Friction*, London, Heinemann, 1974.
- 6.11 Schey, J. A.: "Material Aspects of Friction and Wear in Manufacturing Processes," *J. Met.* **32**, no. 1, 1980, pp. 28-33.
- 6.12 Krämer, W.: "Investigation of Lubricants for Deep Drawing" (in German), *Ind.-Anz.*, **86**, 1964, pp. 2164, pp. 2167-2170.
- 6.13 Amazu, J. K. A., Briscoe, B. J., and Tabor, D.: "Friction and Shear Strength of Polymers," *ASLE Trans.*, **20**, 1977, pp. 354-358.
- 6.14 Wilson, W. R. D.: "Friction and Lubrication in Bulk Metal Forming Processes," *J. Appl. Metalwork.*, **1**, 1979, pp. 7-19.
- 6.15 Dowson, D., Parsons, B., and Lidgitt, P. J., "An Elasto-Plasto-Hydrodynamic Lubrication Analysis of the Wire Drawing Process," in *Elastohydrodynamic Lubrication: 1972 Symposium*, London, Institution of Mechanical Engineers, 1972, pp. 97-106.
- 6.16 Vogelpohl, G.: "Hydrodynamic Theory and Semi-Fluid Friction," *Öl und Kohle vereinigt mit Erdöl und Teer* (in German), **12**, no. 42, Nov. 1936, pp. 943-947.

- 6.17 Hansen, N.: "The Characterization of Machined and Deformed Surfaces by the Load Carrying Area" (*in German*), *Werkstattstechnik*, **57**, 1967, pp. 379–383.
- 6.18 Schey, J. A.: *Introduction to Manufacturing Processes*, New York, McGraw Hill, 1977.
- 6.19 Kienzle, O., and Mietzner, K.: *Atlas umgeformter metallischer Oberflächen* (*in German*), Berlin, Springer, 1967.
- 6.20 Wanheim, T., and Bay, N.: "A Model for Friction in Metal Forming Processes," *Ann. CIRP*, **27**, 1978, pp. 189–194.
- 6.21 Wiegand, H., and Kloos, K. H.: "Cold Upsetting as a Simulting Test for Friction and Surface Phenomena" (*in German*), *Werkstattstechnik*, **56**, 1966, pp. 129–137.
- 6.22 Kudo, H., Tanaka, S., Immamura, K., and Suzuki, K.: "Investigation of Cold Forming Friction and Lubrication with a Sheet Drawing Test," *Ann. CIRP*, **25**, 1976, pp. 179–184.
- 6.23 Tsao, Y. H., and Sargent, L. B., Jr.: "A Mixed Lubrication Model for Cold Rolling of Metals," *ASLE Trans.*, **20**, 1977, pp. 55–63; **21**, 1978, pp. 20–24.
- 6.24 Pawelski, O.: "The Effects of Lubrication and Deformation Conditions on Friction in the Deformation of Steel" (*in German*), *Schmiertechnik*, **15**, 1968, pp. 129–138.
- 6.25 Schey, J. A.: "Metal Processing-Deformation," in *CRC Handbook of Lubrication*, Booser, E. S., ed., vol. 2, Boca Raton, FL, ASLE-CRC Press, 1983, pp. 317–333.
- 6.26 Nittel, J.: "A New Method of Lubricant Evaluation for Deformation Processes by Measuring Friction" (*in German*), *Fertigungstech. u. Betr.*, **18**, 1968, pp. 301–304.
- 6.27 Doege, E., Melching, R., and Kowallick, G.: "Investigations into the Behaviour of Lubricants and the Wear Resistance of Die Materials in Hot and Warm Forging," *J. Mech. Work. Tech.*, **2**, 1978, pp. 129–143.
- 6.28 Pawelski, O.: "A New Device for Measuring Friction in Plastic Deformation" (*in German*), *Stahl u. Eisen*, **84**, 1964, pp. 1233–1243.
- 6.29 Oyane, M., Shima, S., and Nakayama, T.: "Universal Testing for Workpiece Material, Tool Material, and Lubricant in Metal Forming," in *Metalworking Lubrication*, Kalpakjian, S., and Jain, S. C., eds., New York, ASME, 1980, pp. 13–21.
- 6.30 Kudo, H., Tsubouchi, M., Fukuhara, Y., and Ito, Y.: "Determination of Friction and Wear Characteristics of Some Lubricants and Tool Materials for Cold Forging with the Simulation Testing Machine," *Ann. CIRP*, **28**, 1979, pp. 159–163.
- 6.31 Becker, H.: "Simplified Model for Lubricant Selection" (*in German*), *Bänder Bleche Rohre*, **19**, 1978, pp. 362–366.
- 6.32 Geiger, R., and Stefanakis, J.: "Ring Upsetting and Back Extrusion of Cans as Lubricant Test Methods for Bulk Deformation" (*in German*), *Ind.-Anz.*, **96**, 1974, pp. 2245–2246.
- 6.33 Schlosser, D.: "Die Materials for the Deformation of Austenitic Stainless Steel Sheet" (*in German*), *Bänder Bleche Rohre*, **17**, 1976, pp. 97–102.

## CHAP. 7

# MEASUREMENT OF PROCESS PARAMETERS

A metal-forming machine tool can be defined as a piece of working equipment which uses a tool to deform plastically a workpiece with controlled guidance and which provides the forces, moments, and energy required for the deformation process at every instant (refer also to Chap. 8). By this definition there exists a very close relationship between the deformation process and the metal-forming machine tool. The special requirements of the deformation process on the machine and the characteristics of the machine can be described by machine data [7.1]. A matching of these requirements is possible with proper selection of the machine parameters. The values required for such comparisons are termed the *characteristic values* for the metal-forming machine tool.

In addition to the characteristic values, other parameters that are typical for a particular process from the standpoints of both workpiece and material should also be considered since these workpiece and material parameters permit a comparison with other metal-forming processes.

When measuring process parameters, the distinction must be made whether the parameters are measured in the actual process or with model material, whether in scaled-down models or by model processes. All these methods are basically aimed at determining the characteristic parameters of the deformation process. The approach in this chapter will be toward illustrating the general methods of determining the process parameters and not toward establishing the individual characteristics of the various metal-forming processes. Judgment of the usefulness of the process parameters and any decision with regard to their application must be postponed since several boundary conditions affect the individual processes.

### 7.1 PROCESS PARAMETERS

#### 7.1.1 Force, Travel, and Energy

The most important process parameter in any deformation process is the force requirement on the machine to carry out the process successfully. In general, in many metal-forming processes

## 7.2 FUNDAMENTALS OF METAL FORMING

the deformation force is nearly constant throughout the deformation period. The maximum force necessary for deformation must therefore be considered as a characteristic process parameter. The force is transmitted from a tool to the workpiece, causing a reaction force in the mating tool. To measure the force it is therefore necessary to identify the force flow in the system machine–tool–workpiece. This is important so that the actual force in the system is measured. The measuring unit must be placed in the force-flow system.

The deformation stroke or travel is a practical characteristic parameter in processes with linear tool movement only. The deformation stroke is the distance covered by the force-transmitting tool during the actual deformation process. Individual workpiece elements of the deformed workpiece may travel longer or shorter distances during the process. The deformation travel can generally not be measured at the point of contact of the tool with the workpiece; it is measured as a relative movement of the top tool with respect to the bottom tool or the machine bed or bolster. It should be remembered that the elastic deformations of the tool and the machine will affect the measured travel (Fig. 7.1).

The deformation time or period is the time required for the deformation travel to be completed. An average velocity for the tool during the process can be calculated using the deformation time. Yet this average velocity is not a characteristic parameter for the process. The tool velocity at the instance of contact with the workpiece may, however, be important in some cases.

Another characteristic of a deformation process is the force–travel diagram, which is the representation of the force over the distance traveled. Every deformation process has a typical force–travel diagram (Fig. 7.2). The maximum punch force occurs at different points in time during the deformation stroke for various processes. This particular characteristic is important for the selection of the appropriate metal-forming machine tool since the force variation along the machine stroke and the maximum available force at any given time of the stroke are machine-dependent. The force–travel diagram can be plotted on  $x$ - $y$  recorders by simultaneous measurement of force and travel. If the force is plotted against travel, the curve closes down on the travel axis. The measured force–travel diagram must be corrected for the elastic deformation work of the machine–tool system to obtain the actual force–travel diagram. Fig. 7.1 shows the principle of such corrections. The area enclosed by the curve is the deformation work necessary for the process; it can then be compared with the work capacity of the machine.

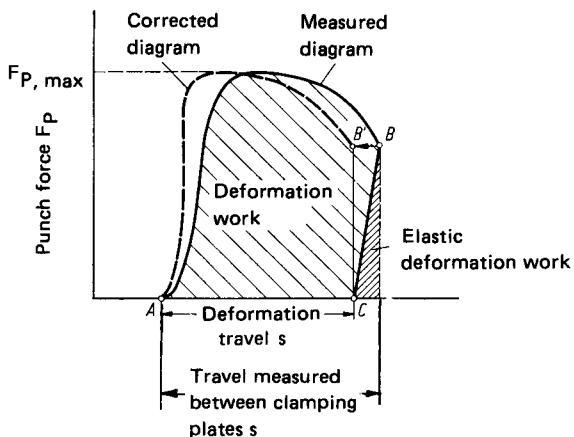


**FIG. 7.1** Example of a force–travel diagram (backward can extrusion). *A*—start of deformation process; *B*—end of deformation process and return travel of ram; *C*—lifting of punch tip from workpiece.

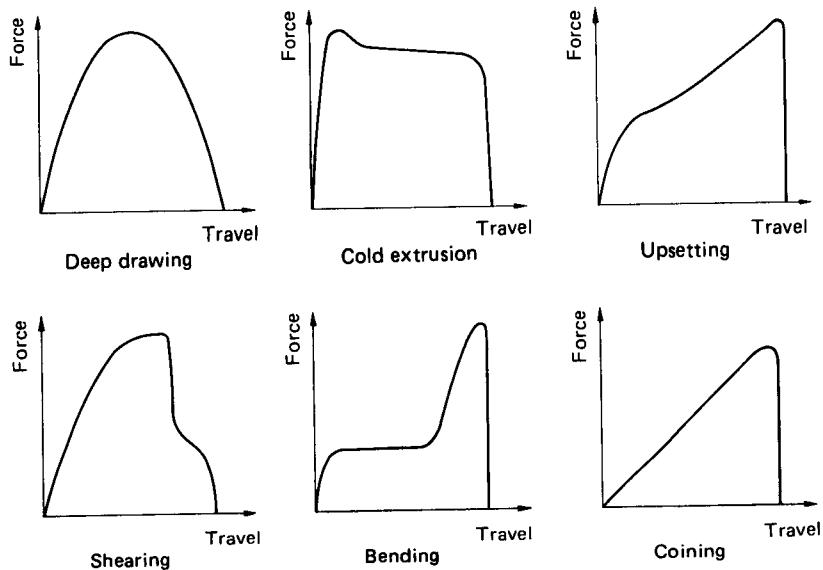


FIG. 7.2 Force-travel diagrams of different metal-forming processes.

### 7.1.2 Measurement Methods

The various characteristic parameters discussed above are measured electrically and converted to mechanical values. A detailed description of the various measurement methods can be obtained from published literature [7.2] to [7.6]. Travel measurement devices are:

- Resistance transducer (linear and rotary potentiometers)
- Inductive transducer (LVDT)
- Capacitive transducer
- Optical and laser length-measuring systems
- Digital meter

Velocities are generally derived from travel measurements or measured directly based on the induction principle.

**Force transducer:** The elastic deformation of force dynamometers is measured either by travel measurement techniques or with strain gauges. Furthermore, piezoelectric transducers can be used or the force can be measured from pressure measurements on a fluid.

**Pressure transducer:** The pressure can be measured either by piezoelectric transducers or through a membrane by means of travel measurements.

**Temperature measurement:** Temperatures are measured with either thermocouples or resistance thermometers.

The various devices mentioned require always amplifying or rectifying instruments to amplify or rectify the measured signals so that they can be recorded. These additional instruments are very often available as a package with the measurement transducers.

Recording instruments either register several measuring signals with respect to time or plot one or several values against others in an  $x-y$  recorder. Quasistationary values can also be recorded

digitally by using appropriate printers. Increasingly, measured values are directly transferred to computers by analog-to-digital converters for on-line conversion and plotting of desired variables.

## 7.2 MEASUREMENT OF DEFORMATION CHARACTERISTICS

The magnitude of deformation can be represented by the geometric features of the workpiece (such as length, height, or area of cross section) before and after deformation and expressed either as ratios relevant to the deformation process (such as upsetting ratio or drawing ratio) or as change of initial conditions (such as change of cross section). These parameters do not, however, permit a direct comparison of different processes.

The strain rates and the natural strain (deformation ratio) were defined in Chap. 5 using the elemental particle velocities in the workpiece. As a basis for such definitions, a process of homogeneous deformation was selected; that is, it was assumed that at every point in the workpiece the strains are the same. In reality, however, these strains can be very different at various locations in the workpiece. Hence the strain distribution, for example, along a longitudinal or a lateral section of the workpiece, is a characteristic of the deformation process. The material flow is influenced by the strain distribution and the differential strain-hardening effects coupled with it. Other important factors affecting the material flow are (1) the geometry of the tooling (radii, tapers), (2) the friction conditions between workpiece and tool, and (3) the metallurgy of the workpiece (microstructure, texture). The material flow is therefore another characteristic encompassing a multitude of variables.

The stress state in the workpiece during the deformation process determines the achievable deformation limits. For such an assessment the presence and the direction of action of tensile or compressive stresses are important. The stress distribution must be known at least approximately in three directions inside the deformation zone of the workpiece so that the above cited predictions can be made. In simple or elementary plasticity theory, the stresses at the beginning and at the end of deformation are assumed based on externally acting forces and flow criteria. In the region of the deformation zone the stresses are interpolated linearly. Advanced plasticity theory can be used to determine the stresses in the deformation zone from local strains obtained from material movement (visioplasticity, see Chap. 5). The material flow pattern for such an analysis should be obtained from experiments. As is explained in Sec. 7.2.1, the local strains can be determined only at discrete points.

Another important parameter describing the behavior of the workpiece material to be deformed is the flow stress  $\sigma_f$ . The flow stress is not really a process characteristic since it affects the process only indirectly. The flow stress and its importance are covered in detail in Chap. 4.

The characteristic parameters describing a deformation process are based, with a few exceptions, on mechanical length or linear measurements.

### 7.2.1 Visioplasticity

Visioplasticity is a method of obtaining information on material flow by using experimentally determined displacement or velocity fields. Rectangular or mostly square grids composed of line nets are used. In bulk forming these grids are used on longitudinally cut sections, and in sheet-metal working the grids are inscribed on the sheet surface. The grids can be circular in shape in sheets to determine the direction of action of the principal stresses. The grid mesh can be inscribed on the material by either mechanical means or etching [7.7] or by photographic methods [7.8] or pressing. The grid mesh (inscribed by either photographic or offset printing methods) should not split off, and the nodal points should not spread, which would make the measurements difficult. The grid lines must also be thin and sharp. For sheet-metal parts the offset printing method has been used successfully (Fig. 7.3) [7.9].

The material flow can be determined by comparing undeformed and deformed grids (Fig. 7.4). This method has been known for several years [7.10], but has gained greater importance in the past decade because of quantitative measurements of nodal-point displacements in stepwise deformation, thereby describing the metal flow pattern. In Fig. 7.5 point A is a particular work-

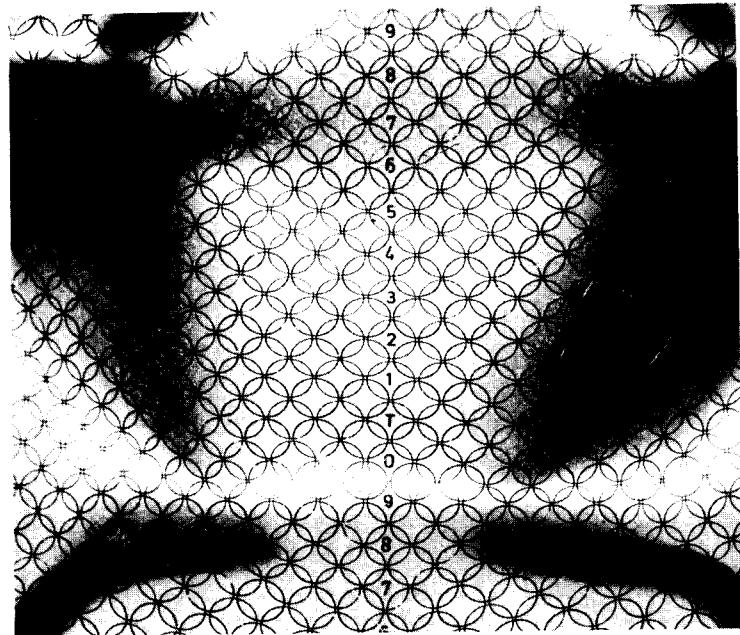


FIG. 7.3 Grid mesh on a sheet-metal part. (After [7.24].)

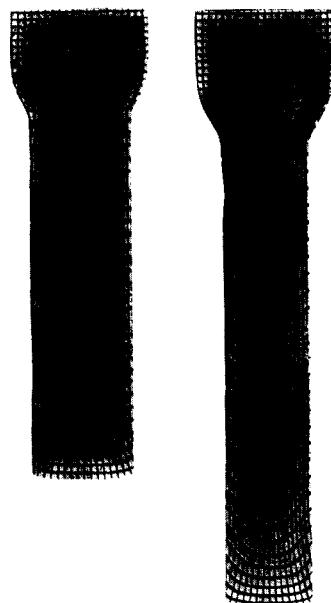
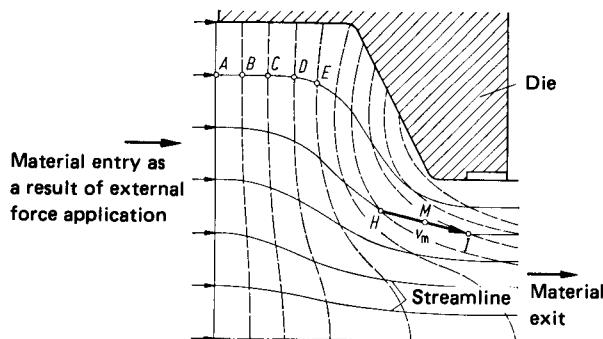


FIG. 7.4 Grids after deformation (rod extrusion).



**FIG. 7.5** Determination of the velocity field from deformed grids.  
(After [7.11].)

piece element before deformation. Point *A* moves to *B* during deformation and follows a path called the motion line. (In this case the motion line is also the streamline because of the quasi-stationary material flow.) If the deformation step is relatively small, the line joining the start and end points, namely, *H* and *I*, is also a measure of the magnitude and the direction of the velocities at points *H* and *I*. However, in reality the deformation step cannot be made infinitely small. The velocity therefore changes between one point and the next on the same streamline. An average velocity  $v_m$  is therefore assumed between the points *H* and *I*. If this procedure is carried out at all points in the grid mesh, an approximate velocity field for the process can be determined. Measurements are made on measuring or coordinate measurement microscopes. From the velocity field the strain rates and the stresses can be computed using plasticity equations.

The above process, though permitting the determination of the magnitude and the distribution of the strains in the deformed workpiece, is highly experimental and calculation-intensive. It has therefore been attempted to use simpler methods to predict strains. A definite relation between the Vickers hardness and the deformation undergone by the workpiece material has been established from experiments [7.11]. It is possible to determine the magnitude and the distribution of local strains from hardness measurements.

### 7.2.2 Local Stresses

In addition to using the method of visioplasticity, it is also possible to measure the stresses on the material surface in contact with the tool surface as loads acting on the tool. Fig. 7.6 shows the measurement of axial stresses on a hot-extrusion die. The measuring principles of such experiments are described in Sec. 7.1.2.

Small hollow cylinders have been used instead of strain-gauge load cells to measure stresses [7.13]. The elastic compression of the hollow cylinders is measured by inductive transducers. It must be remembered that this method gives valid values only if there is no material flow along the tool surface (that is, perpendicular to the load cell). Radial stresses have also been measured based on similar principles [7.14] and were used to determine the stress and strain distribution in upsetting [7.15]. The measuring rods were positioned inclined to the surface to consider also the force effects on the flat tool surfaces. The measurement transducers can be inserted slightly below the die surface to determine the bending effects of the remaining material using membrane theory [7.16]. The advantage of this process is the unchanged tool surface, assuming unhindered flow of material along the surface. Other techniques have been used to measure normal stresses of tools in recent experimental work on closed-die forging [7.17].

No methods are yet known to measure local stresses in the interior of the workpiece. The basic problem is that the measurement transducer, however small, distorts the material composition and the stress distribution when used inside the workpiece material.

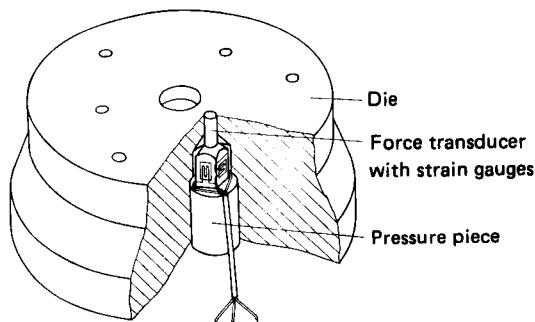


**FIG. 7.6** Schematic illustrating the measurement of axial stresses. (After [7.12].)

### 7.2.3 Model Technique

The term "model technique" covers all methods used to determine process parameters without conducting the actual deformation process. In other areas of technology (fluid mechanics, heat transfer, chemical processes) model experiments are very common as the model mainly represents a reduction of the geometry based on similarity laws. These model experiments can also be carried out with other materials and processes if the physical similarity of such a model with the actual deformation process is satisfied. Similarity laws are used to ensure the proper transfer of the model test results to the actual test conditions. The basic principles for such transfers have been detailed in the literature [7.18], [7.19].

For metal-forming processes the aim of using model studies is to obtain working information, based on similarity laws, on stresses, strains, and material flow and to extend these to deduce forces and energy. New materials in aerospace technology and very large components increase the advantage of obtaining reliable information on material behavior and technology from such model experiments.

#### *Model Materials*

The model tests can be carried out with materials that are different from the materials used in actual tests or production. This will permit conducting the tests either with smaller force requirements or at room temperature instead of at elevated temperatures. For such cases it is essential to select materials that behave in a way that is similar to that of the actual material under actual working conditions. Especially the flow-curve behavior  $\sigma_t = f(\varphi, \dot{\varphi}, T)$  must be similar for both the model and the actual materials.

Model materials permit experimenting with simpler and cheaper tools (such as wood). If the force requirements for the model test are small, one portion of the tool can be made of glass or transparent plastics so that the material flow can be observed during the tests. Several published sources are available on the application of model materials [7.20], [7.21].

In warm forming of steel above the recrystallization range, the flow stress does not vary appreciably with deformation strain. One should therefore select a model material that exhibits similar behavior even at room temperature. Lead and sodium satisfy the above requirement. Plasticene is used in model tests where the most important factor to be investigated is the material flow. This can be used, for example, to study the filling of a forging die (Fig. 7.7). Friction coefficients in model tests must be the same as under actual conditions. A qualitative analysis of the process can be made with model tests compared with quantitative results obtainable from viscoplastic studies.

Model materials for cold-forming processes must have suitable work-hardening characteristics. For this purpose materials with smaller strength values can be used. In some investigations, commercially pure aluminum was used as a model material for steel, and reasonably accurate results were obtained for material flow and force requirements [7.22]. Special wax mixes have also been

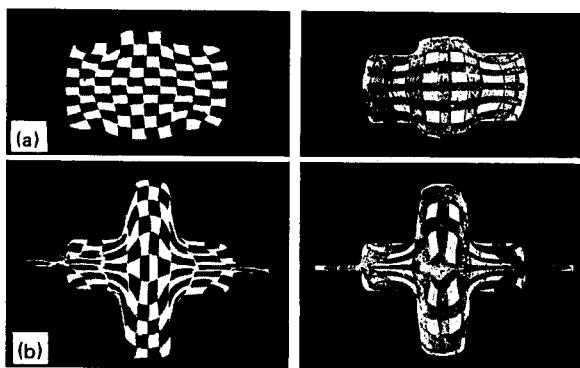


FIG. 7.7 Visible material flow in model tests. (After [7.21].)

developed as model materials [7.23]. Suitable mixing ratios of waxes can be used to obtain flow stresses in the range of  $0\text{--}200 \text{ N/mm}^2$  ( $0\text{--}29 \text{ ksi}$ ) with strain-hardening coefficients between 0 and 0.3.

### Model Processes

Model processes are generally simplified methods to determine some required values and do not relate directly to the actual deformation process with regard to both geometric scaling and the model material.

Some classic examples of model processes are the tension, compression, and torsion tests from which the material parameters such as yield point are obtained. Tensile tests help determine some critical characteristic parameters relating to the workpiece material, though the state of stress in such tests is uniaxial compared with the three-dimensional state of stress in the majority of the deformation processes.

A few typical model tests have been used widely to test the technological behavior of materials, thereby determining special process parameters. The well-known Erichsen cupping test stresses the sheet in a similar way as in metal-forming processes where at least partial thickness reductions are encountered (stretch forming, panel drawing for automobile bodies). The small cup-drawing test can be seen as a model test for the deep-drawing process. Both model tests mentioned give sufficient results to determine material behavior in actual process conditions. Other model tests used in sheet-metal working are the folding test, the to and fro bending test, and the expansion test. In bulk forming the simple upsetting test is important to determine strain limits qualitatively, and it has a special importance for heading and flanging processes (fastener production). Processes of shearing and backward can extrusion can be modelled on the penetration of a wedge or a conical tool in a block. The strain and stress distribution at the wedge tip can be determined as a function of the penetration depth.

### REFERENCES

- 7.1 Kienzle, O.: "Characteristic Parameters of Presses and Hammers" (in German), *Werkstatts- tech. u. Maschinenbau*, 43, 1953, pp. 1–5.
- 7.2 Pflier, P. M.: *Electrical Measurement of Mechanical Variables* (in German), Berlin/Göttingen/Heidelberg, Springer, 1956.
- 7.3 Merz, L.: *Basic Course on Measurements* (in German), vol. 2, "Electrical Measurement of Nonelectrical Variables," München/Wien, Oldenbourg, 1968.

- 7.4 Nelting, H., and Thiele, G.: *Electronic Measurement of Nonelectrical Variables (in German)*, Eindhoven, The Netherlands, Philips Technical Library, 1966.
- 7.5 Fink, K., and Rohrbach, Chr.: *Handbook of Stress and Strain Measurements (in German)*, Düsseldorf, VDI-Verlag, 1958.
- 7.6 Friedrich, K.-H.: "Contribution to the Measurement of Block Surface Temperatures in Hot Extrusion" (in German), *Berichte aus dem Institut für Umformtechnik, Universität Stuttgart*, no. 33, Essen, Girardet, 1975.
- 7.7 Pearce, R., and Drinkwater, I. C.: "Some Aspects of Electrochemical Marking," *Sheet Metal Ind.*, 45, 1968, pp. 751-755.
- 7.8 Müschenborn, W.: "Investigations of Strains on Two Drawn Pieces Using a Photochemically Etched Grid Mesh" (in German), *Thyssenforschung*, 1, 1969, pp. 109-115.
- 7.9 Häsek, V.: "On the Strain and Stress Analysis in the Drawing of Large Irregular Sheet Metal Parts" (in German), *Berichte aus dem Institut für Umformtechnik, Universität Stuttgart*, no. 25, Essen, Girardet, 1973.
- 7.10 Eisbein, W., and Sachs, G.: "Force Requirement and Flow Process in Hot Extrusion" (in German), *Mitt. dtsch. Mater.-Prüfungsanst.*, Sonderheft 16, 1931, pp. 67-96.
- 7.11 Wilhelm, H.: "Investigations on the Relation between Vickers Hardness and Equivalent Strain in Cold Deformation Processes" (in German), *Berichte aus dem Institut für Umformtechnik, Universität Stuttgart*, no. 9, Essen, Girardet, 1969.
- 7.12 Dalheimer, R., and Erbslöh, J. C.: "Measurement of Axial Stress Distribution on the Surface Area of Flat Dies in Axisymmetrical Hot Extrusion" (in German), *Ind.-Anz.*, 91, 1969, pp. 1575-1580.
- 7.13 Dohmann, F.: "Measurement of Mechanical Contact Stresses in the Contact Zone between Workpiece and Tool in Metal-Forming Processes" (in German), *Berichte aus dem Institut für Umformtechnik, Universität Stuttgart*, no. 27, Essen, Girardet, 1974.
- 7.14 Vater, M., and Rathjen, C.: "Investigations on the Magnitude of the Punch Force and Inner Pressure in the Die Assembly in Hot Extrusion of Metals" (in German), *Untersuchungsberichte, VDI-Z.*, ser. 2, no. 9, Düsseldorf, VDI-Verlag, 1966.
- 7.15 Vater, M., and Nebe, G.: "On the Stress and Strain Distribution in Upsetting" (in German), *Untersuchungsberichte, VDI-Z.*, ser. 2, no. 5, Düsseldorf, VDI-Verlag, 1965.
- 7.16 Pawelski, O., and Armstroff, O.: "Measurement of Pressure Distribution in Tube and Rod Drawing" (in German), *Arch. Eisenhüttenw.*, 38, 1967, pp. 527-534.
- 7.17 Hoang-Vu, Kh.: "Possibilities of Application and Limitations of Closed-Die Forging of Steel and Aluminum Alloys at Room Temperature (Cold Closed-Die Forging)" (in German), *Berichte aus dem Institut für Umformtechnik, Universität Stuttgart*, no. 65, Berlin/Heidelberg/New York, Springer, 1982.
- 7.18 Weber, M.: "The General Similarity Principle of Physics and Its Relation with the Dimensional Analysis and Model Technique" (in German), *Jahrb. Schiffbautech. Ges.*, 31, 1930, pp. 274-354.
- 7.19 Wallot, J.: *Magnitude Equalities, Units and Dimensions (in German)*, 2d ed., Leipzig, Barth, 1957.
- 7.20 Heuer, P. J.: "Model Processes for Metal Forming," in *Flow Processes, Material Constants, Deformation Parameters (in German)*, VDI-Forschungsheft 493, Düsseldorf, VDI-Verlag, 1962.
- 7.21 Brill, K.: "Application of Model Materials to Determine Geometrical and Dynamic Test Values in Die Forming" (in German), *Werkstattstechnik*, 53, 1963, pp. 537-542.
- 7.22 Kast, D.: "Model Laws in Backward Extrusion of Geometrically Similar Cups" (in German), *Berichte aus dem Institut für Umformtechnik, Universität Stuttgart*, no. 18, Essen, Girardet, 1969.

## 7.10 FUNDAMENTALS OF METAL FORMING

- 7.23 Wanheim, T., et al.: "Model Technique and Its Application in the Investigation of Bulk Forming Processes" (*in German*), *Proceedings of Seminar Neuere Entwicklungen in der Massivumformung*, Forschungsinstitut Umformtechnik der Ingest Stuttgart, 1977.
- 7.24 Håsek, V.: "Forming Limit Diagram and Its Applications to Deep Drawing and Stretch Forming" (*in German*), *wt.-Z. ind. Fertig.*, **70**, 1980, pp. 575–580.

**MACHINE TOOLS FOR  
METAL FORMING**

**List of Special Symbols**

---

<i>a</i>	guidance play	<i>u</i>	velocity
<i>C</i>	spring constant	<i>V</i>	rate of flow
<i>e</i>	eccentricity; loss ratio	<i>z</i>	potential height
<i>f</i>	elastic deflection	$\alpha$	crank rotation angle; angle
<i>F</i>	force	$\beta$	angle
<i>H</i>	fall height; total stroke	$\delta$	angular offset
<i>k</i>	impact velocity ratio	$\eta$	efficiency
<i>K</i>	bulk modulus	$\lambda$	radius-to-length ratio
<i>n</i>	revolutions per minute; number	$\rho$	density
<i>Q</i> <sup>°</sup>	mass ratio	$\omega$	angular velocity
<i>R</i>	crank length		

**Subscripts**

---

<i>A</i>	anvil	<i>F</i>	frame
<i>B</i>	bottom; blow	<i>FR,G</i>	friction in guides
<i>C</i>	crank; continuous	<i>FR,S</i>	friction in screw
<i>CR</i>	connecting rod	<i>G</i>	guide
<i>D</i>	drive	<i>L</i>	longitudinal
<i>DTD</i>	die-to-die	<i>L</i>	left; loss
<i>el,l</i>	longitudinal elastic work	<i>N</i>	nominal
<i>el,t</i>	torsional elastic work	<i>p</i>	prestressing

## 8.2 FUNDAMENTALS OF METAL FORMING

R	right; ram	TR	tie rod
S	single stroke; stroke, sleeve	U	upper
T	tool; tup (ram)	$\alpha$	angular

In metal-forming processes workpieces are generally fully or nearly fully formed by using two-piece tools. A metal-forming machine tool is used to bring the two tool pieces together to form the workpiece. The machine also provides the necessary forces, energy, and torque for the process to be completed successfully, ensuring guidance of the two tool halves.

Based on the type of relative movement between the tools or the tool parts, the metal-forming machine tools can be classified mainly into two groups (Fig. 8.1):

- 1 Machines with linear relative tool movement (Fig. 8.2)
- 2 Machines with nonlinear relative tool movement (Fig. 8.3)

Machines in which the relative tool movements cannot be classified into either of the two groups are called special-purpose machines. The machines belonging to this category are those operating on working media and working energy.

In series production, pressure-exerting machine tools (such as hammers and presses of various types) are used more frequently than other types of metal-forming tools. The detailed discussion in this chapter pertains only to this group of machines.

### 8.1 CHARACTERISTICS OF PRESSURE-EXERTING MACHINE TOOLS

The requirements of a metal-forming process with regard to the metal-forming machine should be matched with the characteristics of the machine [8.1]. These are generally described by the characteristic parameters of a machine. Hence a successful matching of the machine with the process is possible only after a thorough understanding of these characteristic parameters or values.

In presses and hammers, three groups of characteristic parameters must be thoroughly understood [8.2]:

- 1 Energy and force characteristics
- 2 Time-dependent characteristics
- 3 Accuracy characteristics under no load and load

In addition to these characteristic parameters, the geometric features of the machine tool such as the stroke in a press or hammer and the dimensions and features of the tool-mounting space (shut height), are also important. Other important values are the general machine data, space requirements, weight, and the associated power requirements.

#### 8.1.1 Force and Energy Characteristic Values

In every metal-forming process a definite force is transmitted at a given time by the tool onto the workpiece. This requires a particular amount of energy, depending upon the deformation work performed. The force requirement as a function of the travel is different for the various deformation processes, and hence the force-travel variation is also a characteristic parameter. It is therefore obvious that a metal-forming process can be carried out in a metal-forming machine tool only when the machine can deliver at a given time the necessary force, which is at least equal to or greater than the deformation force, and when the energy available from the machine for the deformation period is sufficient to cover the deformation work. If  $F_M$  is the available force in the machine,  $E_M$  the work capacity of the machine,  $F$  the deformation force necessary, and  $W$

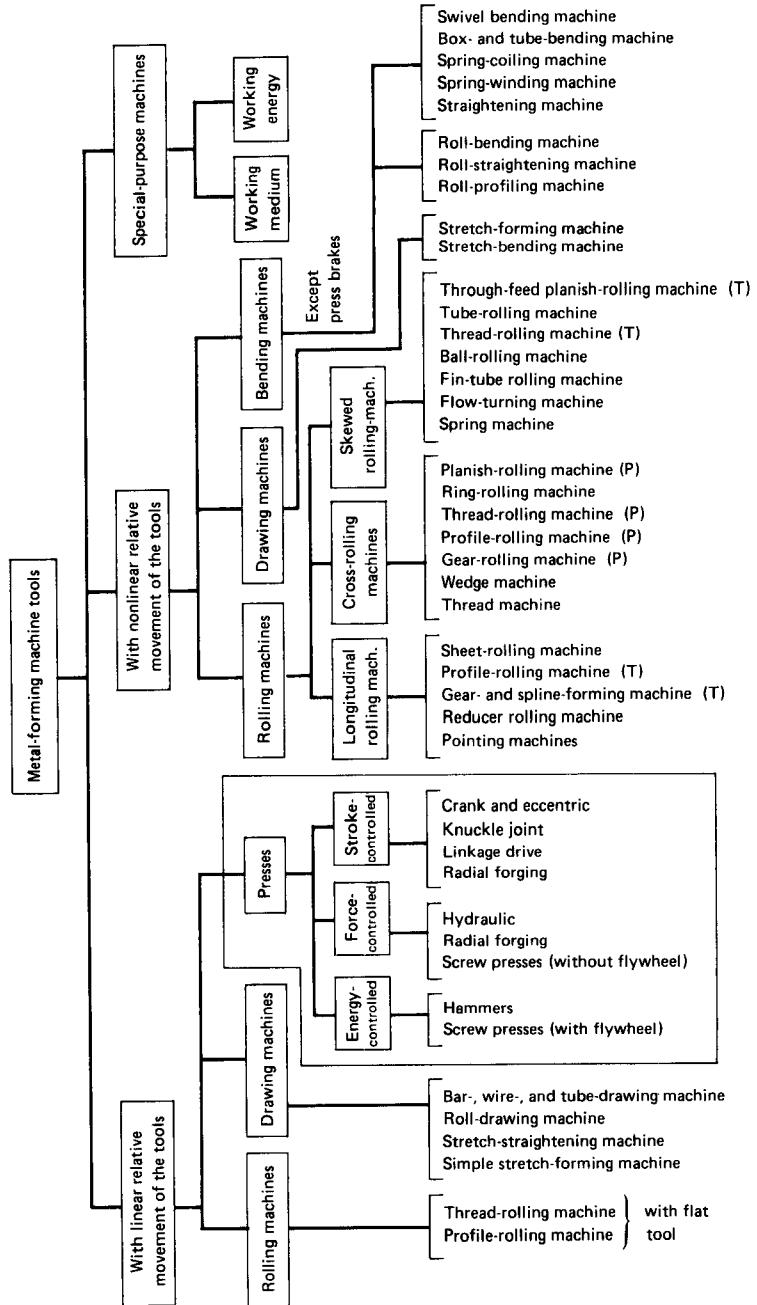


**FIG. 8.1** Classification of metal-forming machine tools. T—through feed; P—plunge feed.

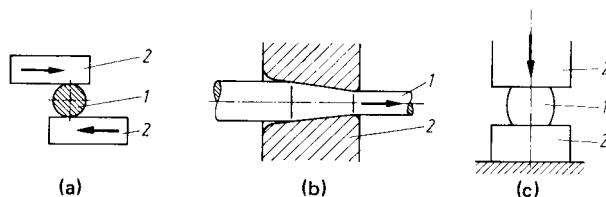


**FIG. 8.2** Metal-forming machine tools with linear relative tool movement. (a) Rolling machine. (b) Drawing machine. (c) Press. 1—workpiece; 2—tool.

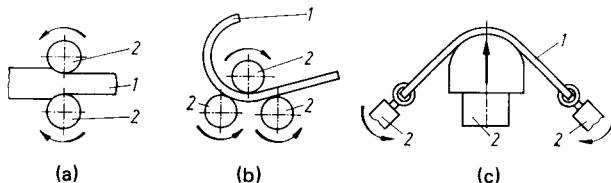


**FIG. 8.3** Metal-forming machine tools with nonlinear relative tool movement. 1—workpiece; 2—tool. (a) Rolling machine. (b) Roll-bending machine. (c) Stretch-forming (tangential) machine.

the deformation work, the following equalities are valid:

$$F_M \geq F \quad (8.1a)$$

$$E_M \geq W \quad (8.1b)$$

In simple terms, the characteristic values of the metal-forming process should be available from the machine during the deformation process.

In the selection of the metal-forming machine tool, the force and energy available from the machine should be only slightly larger than the process requirements of force and energy from the point of view of economy. An optimum solution is an exact matching of the machine characteristics with the process requirements ( $F_M = F$  and  $E_M = W$ ) [8.1] to [8.3].

Such an optimum selection will be possible only in exceptional cases, since there are errors involved in determining the deformation force and work, and their variations during a production run require a certain reserve in the machine values.

Other force and energy values to be considered are the requirements of auxiliary units, such as die cushions, blankholders, and ejectors.

Another very important factor is the elastic deformation work  $W_{el}$ , which must also be supplied by the machine, especially in machine tools controlled by force or travel (presses) and by work capacity (screw presses). If the deformation force on the tool-workpiece system rises from zero to  $F$ , the system deforms elastically by  $f_{tot}$  after compensating for the bearing or tool clearance (Fig. 8.4). The elastic deformation work is then

$$W_{el} = \frac{1}{2} F f_{tot} \quad (8.2)$$

which is stored as potential energy in the tool-machine system. Since the elastic deformation varies linearly with the force (Fig. 8.4), the spring constant is

$$C_{tot} = \frac{F}{f_{tot}} \quad (8.3)$$

which can be substituted in Eq. 8.2 to obtain the elastic work,

$$W_{el} = \frac{1}{2} \frac{F^2}{C_{tot}} \quad (8.4)$$

The potential energy stored in the tool-machine system can be recovered for use later in the process under special conditions. This is explained by means of Figs. 8.5 and 8.6.

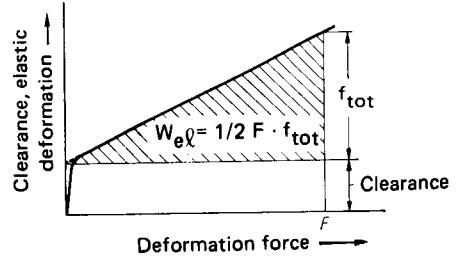


**FIG. 8.4** Schematic representation of elastic work in a press.

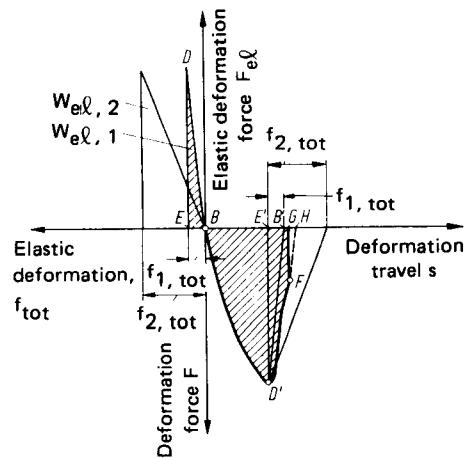


**FIG. 8.5** Elastic work in blanking process. (After [8.1].)

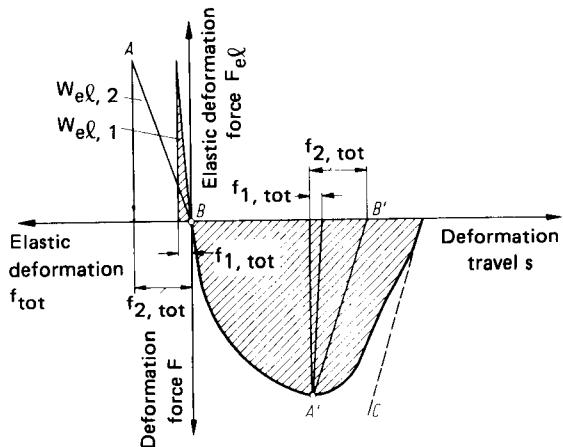


**FIG. 8.6** Elastic work in deep-drawing process. (After [8.1].)

## 8.6 FUNDAMENTALS OF METAL FORMING

The force-travel diagrams of two processes blanking (Fig. 8.5) and deep drawing (Fig. 8.6), are shown in the right halves of these figures. The left-hand sides show the elastic deformation work  $W_{el,1}$  and  $W_{el,2}$  for the maximum forming force of two tool-machine systems with different elastic deflections  $f_{1,tot}$  and  $f_{2,tot}$ . When the forming force decreases after having attained its maximum value, the elastic deformation of the tool-machine system also decreases. The elastic energy thus released is again made available to the process. Recovery of the elastic work is only possible when, during reduction of the forming force, at every point on the force-travel curve the deformation travel is equal to or greater than the elastic deformation of the tool-machine system [8.1]. This yields, with  $dF/ds < dF/df_{tot}$  and with Eq. 8.3,

$$C_{tot} > \frac{dF}{ds} \quad (8.5)$$

For the deep-drawing process in Fig. 8.6 the condition of recovery is fulfilled for both the stiff ( $f_{1,tot}$ ) and the weak ( $f_{2,tot}$ ) presses. However, in the case of the blanking process, the elastic work recovery is possible only with the stiff press, and only up to point  $F$  on the force-travel curve. The remaining elastic work, as given by the area  $FGH$ , gets lost, as does the entire elastic work of a weak tool-machine system. The unused elastic work is absorbed by the drive and the frame of the press and leads to vibrations.

From the point of view of energy requirements, it is therefore desirable to have a stiff tool-machine system because of the following two reasons: (1) it may be possible to recover the elastic work in certain cases (Eq. 8.5), and (2) if it is not possible to recover the elastic work (in processes where the deformation force falls very rapidly after having attained its maximum value, as in die forging, coining, or extrusion), there is only a minimum of energy lost (Eq. 8.4).

Depending upon the method of making the force and the energy available for the process, there are three types of pressure-exerting machine tools (Fig. 8.1):

- 1 Presses controlled by work capacity (energy)
- 2 Presses controlled by force
- 3 Presses controlled by travel (stroke)

**Presses and hammers controlled by work capacity or energy:** Machines in this category have a definite energy or work capacity, which is used completely in a working stroke. Any process carried out in such a machine comes to a stop as soon as the energy of the machine is expended. If the work capacity required for the process is greater than the energy available per stroke in such a press, then the process can be completed by successive strokes (Fig. 8.7). The decisive characteristic parameter of this metal-forming machine tool group is the nominal work capacity or energy  $E_N$ . Hammer and screw presses with flywheel belong to this category. In screw presses the drive and the frame should be able to sustain the deformation forces as reaction forces.

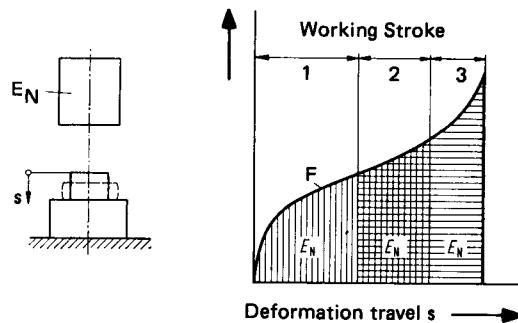


**FIG. 8.7** Machine controlled by work capacity or energy. Schematic of drop hammer. The forging process is split up into three working strokes.

Hence for screw presses the value of the force that can be applied with the designed drive and frame is another important characteristic parameter. This force is the nominal force  $F_N$ .

**Presses controlled by force:** These presses are capable of supplying a force at any ram position. The magnitude of such a force at any ram position and its greatest value, denoted by the nominal force  $F_N$ , are dependent on the machine design. This is the deciding characteristic parameter of this machine group since normally the nominal force cannot be exceeded in a forming process.

Hydraulic presses, which belong to this category, are classified as direct-driven and accumulator-driven presses (Fig. 8.8). While in the case of direct-driven presses the work capacity or

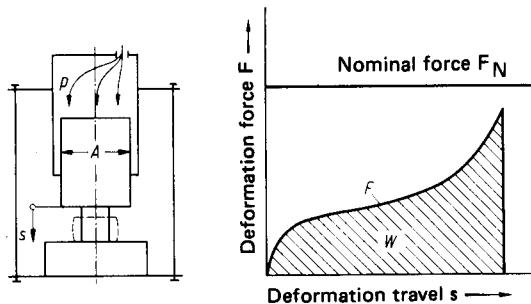


FIG. 8.8 Machine controlled by force. Schematic representation and force limits of hydraulic press.

energy plays a minor role (the required energy is supplied by the drive motor), it plays a very important role in the case of accumulator-type presses, where the work capacity is determined by the capacity of the accumulator.

**Presses controlled by stroke:** In these presses the ram travels in a path as determined by the kinematics of the main drive. The magnitude of the ram force  $F_R$  is dependent on the ram position or travel (Fig. 8.9). At the final position the ram force can theoretically become infinite. Since in these presses the drive and the frame lie also in the force flow of the reaction forces and the tool forces, the ram force should not exceed the nominal force  $F_N$  determined by the design of drive and frame. The important parameters are hence the ram force,  $F_R = F_R(h)$ , and the

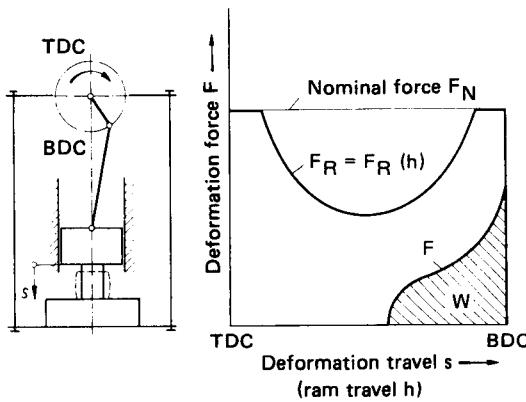


FIG. 8.9 Machine controlled by stroke (path). Schematic representation and force limits of crank press.

nominal force  $F_N$ . Presses in this category generally have a flywheel drive. The design of the flywheel determines the work capacity or energy available in a working stroke. Hence the work capacity of these presses is also an important characteristic parameter. Important presses belonging to this category are crank-driven presses (eccentric, crank, knuckle joint, link, and double crank) and cam-driven presses.

### 8.1.2 Time-Related Characteristics

The time-related characteristics of a metal-forming machine tool describe the machine-dependent process time and velocities. Such time-dependent values are stroke time in presses and hammers and contact time in presses. The stroke time is dependent solely on the drive or the drive with its control, whereas the contact time is also dependent on the total stiffness of the machine tool in relation to the process. Another important time-related characteristic is the tool velocity.

**Characteristic time-related values:** One of the basic factors in manufacturing technology is productivity [8.4]. In the case of presses, the productivity is given either by the time per stroke or the number of strokes per minute or by the useful number of strokes. For a drop hammer the blow period is dependent on the height of drop and hence is related to gravity. In power drop hammers the blows can be increased with shorter strokes by accelerating the ram with pressure. In hydraulic presses the useful stroking period is a function of the selected stroke length, which can be divided into rapid traverse and working stroke, and the achievable ram velocity in the above two regions. The time necessary for a working stroke in presses controlled by stroke is determined by the number of rotations of the crank or the main drive. The number of rotations of the crank is smaller under load than at idle speed. In single-stroke operation the stop-start operation reduces the available number of strokes per minute still further.

The contact time between the tool and the workpiece under pressure is an important time-dependent characteristic in warm and hot forming. The heat transfer rates during this period are much larger than without contact pressure [8.5]. Long contact times lead to large tool wear, and the cooling of the workpiece results in higher force requirements due to increased flow stresses. Typical contact times under pressure in bulk-forming processes are given below:

Hammers	$10^{-3}$ to $10^{-2}$ s
Screw presses (with flywheel)	$10^{-2}$ to $10^{-1}$ s
Presses controlled by stroke	$10^{-1}$ to $5 \times 10^{-1}$ s
Hydraulic presses	$10^{-1}$ to $> 1$ s

The contact time under pressure in presses controlled by stroke depends on the total stiffness. The contact time is larger for smaller spring constants (weaker press) (Fig. 8.10).

**Velocities:** As described earlier, the tool velocity is an important time-related characteristic. For forming processes the velocity at the instant of touching the workpiece and the variation of the tool velocity during the process are important. The forming strain rate  $\dot{\phi}$  at any instant is given by

$$\dot{\phi} = \frac{v_T}{h} \quad (8.6)$$

where  $v_T$  is the tool velocity at that particular instant and  $h$  is the instantaneous height.

The tool velocity during the forming process in hammers is dependent on the process, and in presses controlled by stroke it is dependent on the press kinematics. The forming strain rate as defined by Eq. 8.6 can therefore also increase during a working stroke (Fig. 8.11b). The change of strain rate is especially large in machines controlled by energy. This results in force variations in hot forming due to the dependence of the flow stress on deformation temperature and strain rate (refer also to Chap. 4).

The elastic behavior of presses controlled by stroke makes the relation described above more complicated since the actual tool velocity can deviate considerably from the theoretical velocity shown in Fig. 8.11a. The foregoing explanation is also valid in a limited sense for hydraulic

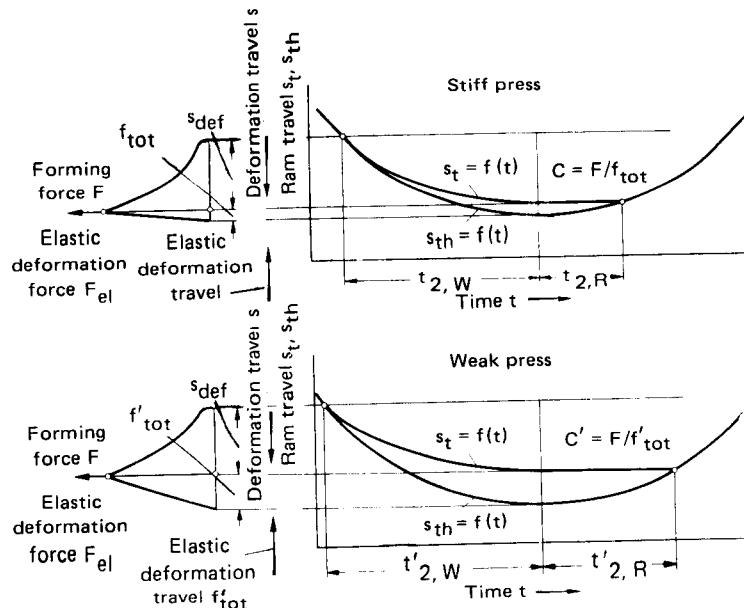


FIG. 8.10 Contact time under pressure in presses controlled by stroke (path) and with different spring constants.  $t_{2,W}, t'_{2,W}$ —contact times during working stroke;  $t_{2,R}, t'_{2,R}$ —contact times during return stroke;  $s_{th} = f(t)$ —theoretical stroke curve;  $s_t = f(t)$ —actual travel-time curve of ram. (After [8.3].)

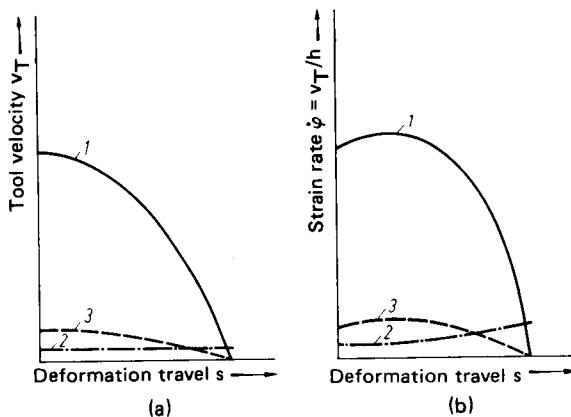


FIG. 8.11 (a) Tool velocity and (b) strain rate as a function of deformation travel in upsetting. 1—drop hammer (screw presses with flywheel); 2—hydraulic press; 3—crank press.

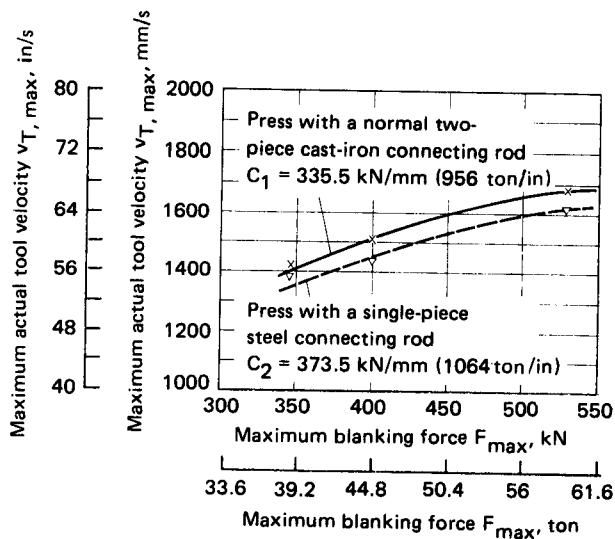


FIG. 8.12 Maximum actual tool velocity as a function of blanking force and spring constant. Eccentric press  $F_N = 500 \text{ kN}$  (56 ton);  $n = 50$  strokes/min. (After [8.6].)

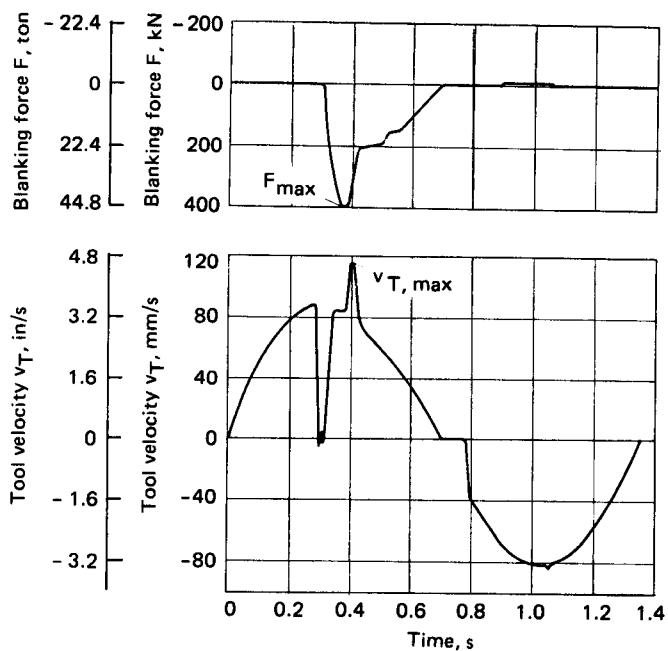


FIG. 8.13 Variation of actual tool velocity and force in blanking. Eccentric press  $F_N = 500 \text{ kN}$  (56 ton);  $n = 50$  strokes/min. (After [8.6].)

presses. For processes requiring smaller strokes (such as coining or blanking), carried out in presses controlled by stroke, the difference between theoretical and actual tool velocities decreases with an increasing spring constant of the press (Fig. 8.12). An example of blanking is shown in Fig. 8.13. The effect of the spring constant is smaller for processes requiring longer strokes (such as deep drawing, bending, and ironing); that is, the machines can be less stiff.

The energy stored in the fluid medium in hydraulic presses causes the press ram to accelerate once the blanking process is completed, resulting in very large velocities (80–100 times the value obtained during the process).

### 8.1.3 Characteristics Related to Accuracy

These characteristics relate to achievable accuracy values in forming processes. The metal-forming machine tool must guide the tooling onto the workpiece accurately. Deviations from accurate machine guidance cause positional errors on the tool parts, resulting in errors in the workpiece.

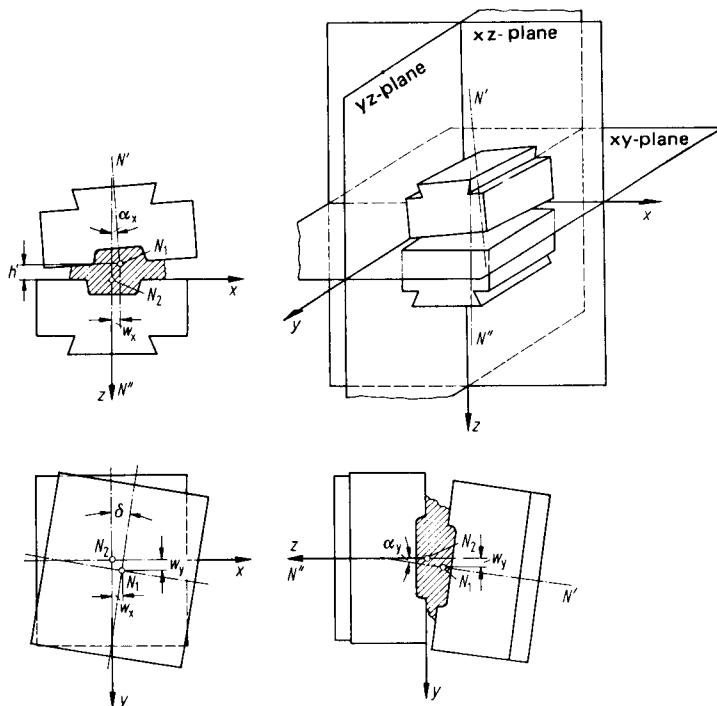


**FIG. 8.14** Workpiece errors as a result of positional errors of tools in hammers and presses. (After [8.7].)

There are two types of positional errors, those at contact and those due to drifting. The positional error due to initial contact is due to geometric inaccuracies of the machine in the unloaded state. During loading the elastic deformation of the machine causes the tooling to drift, resulting in additional positional errors. Hence it must be distinguished between the accuracy characteristics of a metal-forming machine tool in the loaded and in the unloaded states.

The accuracy characteristics in the loaded state are, however, more important for the workpiece accuracy. The following errors can occur due to inaccuracies in machine guidance [8.7] (Fig. 8.14):

1. **Parallelism errors:** Angle between die axes  $N'$  and  $N''$  in the  $x$ - and  $y$ -directions.
2. **Offset  $w_x, w_y$ :** Displacement of points  $N_1$  and  $N_2$  in the  $x$ - and/or  $y$ -directions. The points lie on the tool contact surface and on the die axes  $N'$  and  $N''$ .
3. **Angular offset  $\delta$ :** Angle of the die halves about the  $z$ -axis.
4. **Errors in height  $h'$ :** Incorrect distance between points  $N_1$  and  $N_2$  in the  $z$ -direction.

The positional errors due to contact and tool drifting are included in the above four errors, and the total spring constant has an effect on the error in height as well.

The most important accuracy characteristics for unloaded machines are the parallelism between bed face and ram face and the perpendicularity of the ram movement to the bed face.

These values can be measured using specified methods. Standards and recommendations have been published for metal-forming machine tools controlled by stroke [8.9] to [8.11]. The spring constant can also be used to obtain the relative displacement in the loaded state with respect to the unloaded state.

Errors due to parallelism are caused (1) always in nonsymmetrical press frames (C-frame), even with symmetrical loading (Fig. 8.15a) and with an angular spring constant  $C_\alpha$ , and (2) in symmetrical press frames when the resultant forming force is offset from the axis of the press (Fig. 8.15b).

Angular deflection causes a portion of the offset (Fig. 8.14), in addition to parallelism errors. The rest of the offset is due to the drifting of the ram parallel to the bed plane.

Angular offset, which is the rotation of the tool halves with respect to each other, is dependent on the geometry of guidance, the guidance play, and the lateral stiffness of the frame.

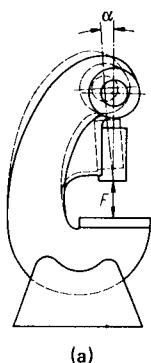


**FIG. 8.15** Tilting of ram. (a) Central loading on nonsymmetrical frame (C-frame). (b) Eccentric loading of closed frame. (After [8.7] and 8.8].)

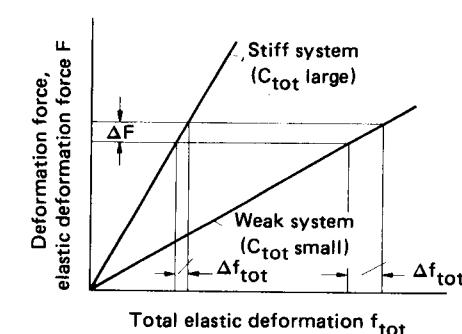


**FIG. 8.16** Stiffness and elastic deformation of presses for a given force fluctuation.

Errors in the height of the workpiece are caused by the overall spring constant in presses controlled by stroke. Fig. 8.16 shows that for the same force fluctuation  $\Delta F$  in a process, the height variation  $\Delta f_{tot}$  is smaller for larger overall spring constants  $C_{tot}$ .

The overall spring constant  $C_{tot}$  for the machine-tool-tool system is given by [8.12]

$$C_{tot} = \frac{C_{tot,P} C_T}{C_{tot,P} + C_T} \quad (8.7)$$

Hence a large overall spring constant  $C_{tot}$  can only be achieved with large spring constants for the press ( $C_{tot,P}$ ) and the tool  $C_T$ .

Fig. 8.17 shows the various spring constants as measured in a backward extrusion process. The stiffness values are higher at larger nominal forces.

There are no guidelines available for the quantification of displacement errors due to drifting, and so far no definite method of testing has been postulated.

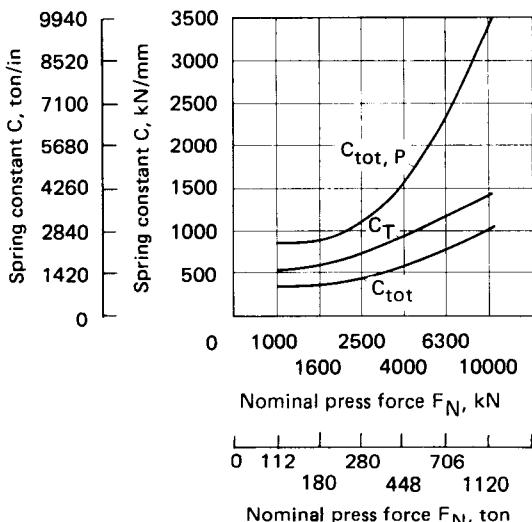


**FIG. 8.17** Spring constants of presses ( $C_{\text{tot},P}$ ), tool ( $C_T$ ), and press–tool system ( $C_{\text{tot}}$ ) as a function of nominal press force in backward can extrusion. (After [8.12].)

#### 8.1.4 Summary of Important Characteristic Parameters for Presses and Hammers

A summary of the important characteristics for presses and hammers is given in Table 8.1. This can be further expanded depending on specific applications and operating methods of the machines. Examples of such areas are the clamping force in horizontal forging machines for hot die forging, the blankholder pressure in deep-drawing presses, and the ejector force in cold forming.

## 8.2 HAMMERS

Hammers are the cheapest metal-forming machines from the point of view of generating a large force and transmitting a definite energy, as long as the high contact velocities, which are normally between 3 and 8 m/s (118–315 in/s), do not cause damage to the workpiece. The design features of hammers are relatively simple, and the forces resulting from forming need not be transmitted through the drive and frame system as is the case with mechanical presses. Therefore the hammer cannot be overloaded. Hammers are flexible; that is, for increased energy requirements one or more additional blows can be used.

Hammers still occupy a leading position in hot forging in spite of increased press applications in this area in recent times. Major areas of application of hammers are open-die forging and die forging. In special cases, hammers are also used for coining, hot extrusion, and sheet forming.

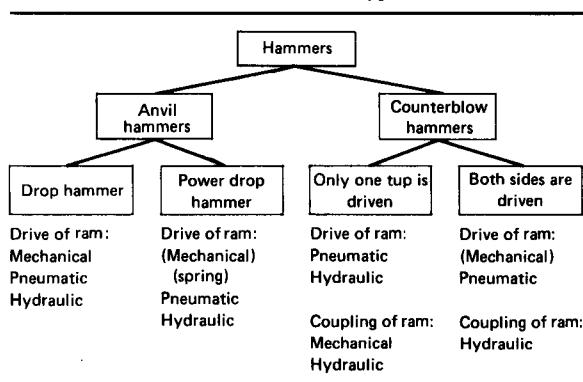
### 8.2.1 Types of Hammers

A rough classification of hammers is given in Table 8.2. The acceleration of the tup (ram) in the direction of the blow is larger than the acceleration due to gravity for all types of hammers except the gravity-drop hammers. In general anvil-type hammers the tup with mass  $m_T$  and velocity  $v_T$  hits the anvil which is stationary ( $m_A = v_A = 0$ ). In counterblow hammers both tups move toward each other, and hence the foundation will not experience any shock (Figs. 8.18 and 8.19).

**Table 8.1** Summary of Important Characteristic Values of Presses.

	Machines controlled by work capacity/energy		Machines controlled by force		Machines controlled by stroke (path)
	Hammer	Screw presses with flywheel drive	Direct driven hydraulic presses	Accumulator type hydraulic presses	Crank presses, eccentric presses, knuckle-joint presses, etc.
Energy and force					
Work capacity	×	×		×	×
Nominal force		×	×	×	×
Ram force (variation)					×
Time					
Stroking	×	×	×	×	×
Contact under pressure		×	×	×	×
Initial contact velocity	×	×	×	×	×
Accuracy					
Unloaded state					
Parallelism of tool clamping surfaces	×	×	×	×	×
Perpendicularity of ram movement to bed surface	×	×	×	×	×
Under load					
Spring constant		×	(×)	(×)	×
Dynamic ram tilting	×	×			

Source: After [8.2].

**Table 8.2** Classification of Hammer Types.

Drop hammers with anvils are used in hot forging and sheet-metal forming. For a fall of  $H = 1\text{--}2 \text{ m}$  (39.4–78.7 in) the tup velocity is 4.5–6 m/s (177–236 in/s). The number of strokes  $n_s$  for  $H = 1 \text{ m}$  (39.4 in) can be between 50 and 60 min $^{-1}$ . Fig. 8.20 shows the common types of anvil hammers. In belt and board drop hammers the tup is lifted to its fall height by means of friction rolls acting between the belt or board and the drive roll. Both drive systems have simple design features and require very little capital investment and maintenance. However, the major disadvantage is the wear of the belt or board. The amount of blow can be controlled somewhat better in belt drop hammers than in board drop hammers since the stroke starts automatically

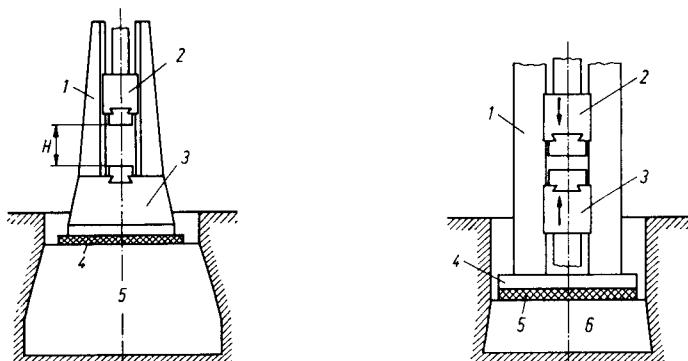


**FIG. 8.18** Schematic of anvil hammer. 1—frame; 2—tup; 3—anvil; 4—base plate; 5—foundation.

**FIG. 8.19** Schematic of counterblow hammer. 1—frame; 2—top tup; 3—bottom tup; 4—base plate; 5—intermediate plate; 6—foundation.

Features	a	b	c	d	e	f
Energy	$m \cdot g \cdot H$	$m \cdot g \cdot H$	$m \cdot g \cdot H$	$m \cdot g \cdot H$	$m \cdot g \cdot H$	$\frac{1}{2} m v^2$
Coupling	Clutch band	Belt and pressure roll	Friction disc	Board and pressure roll	Piston	
Lifting device	Textile belt		Chain	Board	Piston rod	
Pushing device	—	—	—	—	Piston rod	
Storage	Flywheel				Pressure medium	

**FIG. 8.20** Types of anvil hammers. (a) Belt drop hammer (wind drive). (b) Belt drop hammer (slip drive). (c) Chain drop hammer (wind drive). (d) Board drop hammer (slip drive). (e) Drop hammer with piston rod (air lift hammer). (f) Double-acting hammer (steam drop hammer). Pressure media in e and f are steam, air, or oil.

from a preset height. In the British design of a belt drop hammer belt and clutch are separate (Fig. 8.20a). This is also true for the chain drop hammer (Fig. 8.20c). Tups in drop hammers with piston rod (lifting type) (Fig. 8.20e) are lifted either pneumatically for large piston cross sections or hydraulically (oil) for smaller piston cross sections. The trend in Europe is toward the latter design, whereas in the United States it is toward the former. Both designs avoid the disadvantage of belt and board drop hammers, namely, wear. Even the most modern drop hammers face very stiff competition from small and fast-stroking pneumatically or hydraulically (oil) driven power drop hammers.

In power drop hammers with anvils the anvil is either fixed to or separated from the hammer frame, depending on the area of application (hot die forging and sheet-metal forming or open-die forging). Both designs have either a single-frame structure for light energy levels [ $E_N \leq 5000 \text{ N} \cdot \text{m}$  (3680 ft-lbf)] (Fig. 8.21) or the more common double-frame structure (Fig. 8.22). The double-frame structure for open-die forging hammers has a large gap between the columns so that

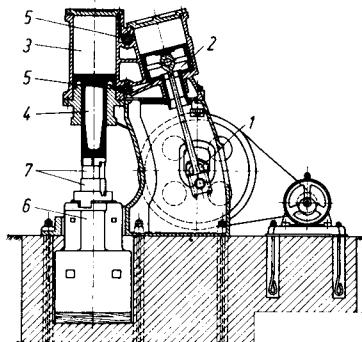


**FIG. 8.21** Single-frame pneumatic hammer.  
1—drive shaft; 2—compressor piston; 3—tup cylinder; 4—tup; 5—rotary valve for overflow; 6—anvil; 7—forging dies. (Courtesy of Eumuco.)

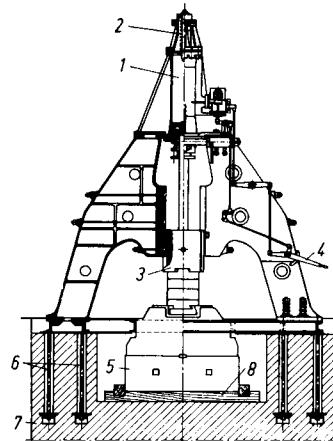


**FIG. 8.22** Double-frame power drop hammer for open-die forging with single-stroke control.  
1—cylinder; 2—spring buffer; 3—tup with fixed piston rod; 4—hand control level; 5—anvil; 6—anchor bolts; 7—foundation; 8—wooden padding. (Courtesy of Eumuco.)

large workpieces can be rotated easily in all directions and the tools can be easily set (Fig. 8.22). The gap between columns is smaller for hot die forging because of large forging pressures [ $1000 \leq p_m \leq 1400 \text{ N/mm}^2$  (145–203 ksi)] and to ensure good guidance (parallel) of the tup (a height-to-width ratio  $\geq 1$  is desirable). The hammer is driven with either compressed air or steam of 6–7 MPa (85–100 psi), either from the general compressor pipeline in forge shops or with separately driven compressors [up to 2 MPa (28 psi)]. In the latter case the tup moves up and down with the alternating air supply to the lower and upper ports. A control adjusts only the energy in the blow (Fig. 8.21).

In power drop hammers (the working principle is illustrated in Fig. 8.20f) the tup velocity and thus the energy are not dependent on the height of fall (or travel) but on the pressure on the piston. The larger the ratio of piston force to tup weight, the greater will be the acceleration. The tup stroke for a given final velocity can therefore be made smaller, which leads to a compact and stiff design. A power drop hammer based on a conventional American concept with a large stroke and a medium-size piston (air- or steam-driven) is shown in Fig. 8.23. The short stroke hammer has a much larger piston cross section to obtain the same tup velocity for the same operating

pressure (Fig. 8.24). The latest development uses oil as the working medium with a very small piston size (Fig. 8.25).

Counterblow hammers (Fig. 8.26) weigh only 35% of the anvil-type hammers having the same energy or work capacity. They have replaced pressure drop anvil-type hammers for  $E_N \geq 100,000 \text{ N}\cdot\text{m}$  (73600 ft·lbf), especially in West Germany and elsewhere in Europe, and are used mainly in batch-type forging [workpiece mass up to 4000 kg (8800 lb)]. In traditional counterblow

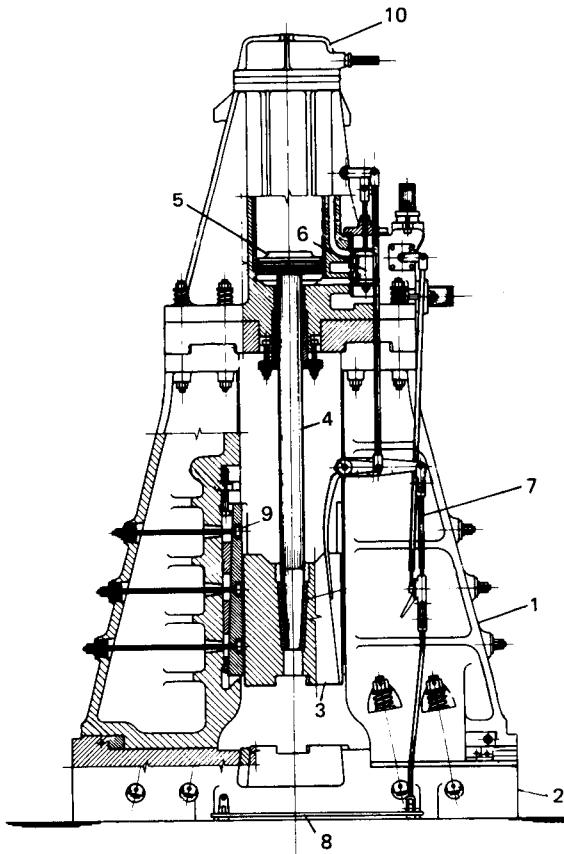


**FIG. 8.23** Double-frame steam drop hammer for die forging. 1—frame; 2—anvil; 3—tup; 4—piston rod; 5—cylinder; 6—control; 7—control rod with sabre; 8—foot pedal; 9—guide pads; 10—safety cushion for head. (Courtesy of Erie Press Systems.)

hammers the drive is as in power drop hammers, and the coupling of the top and bottom tups is either by a steel band (Fig. 8.26a) or by a hydraulic system (Fig. 8.26b) for the tups to have the same velocity. The lower tup is about 2–5% heavier than the top tup so that (1) the tups remain in their initial positions, and (2) the coupling medium is relieved of its load during forging. In the horizontal counterblow hammer both tups are actuated by compressed air (Fig. 8.26c). Feeding of the workpiece into the forging area can be achieved in the above case independent of the tup motions.

High-velocity hammers are generally of the counterblow type. Both masses—tup and frame or upper and lower tups—are accelerated by high-pressure air or nitrogen (in special cases also oil). The frame or the lower tup has a much larger mass than the upper tup and travels only a small distance (Fig. 8.26d and e).

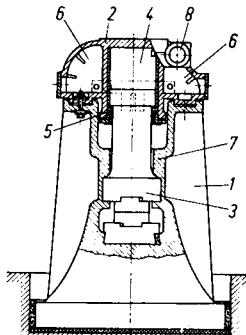


**FIG. 8.24** Short-stroke hammer, 10–100 kN·m (7376–73,760 lbf·ft). 1—frame (cast anvil); 2—crown with cylinder; 3—tup and piston rod (single piece); 4—space on top of cylinder; 5—space on bottom of cylinder; 6—equalizing area; 7—guide; 8—entry for air. (Courtesy of Béché and Grohs.)

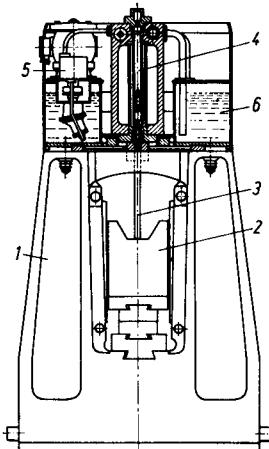


**FIG. 8.25** Oil-hydraulic power drop hammer. 1—anvil and frame (cast single piece); 2—tup; 3—piston rod; 4—cylinder; 5—drive motor with oil pump; 6—oil reservoir. (Courtesy of Eumuco.)

## 8.2.2 Characteristics of Hammers

The most important characteristic of a hammer is its work capacity  $E$ , which is the energy available at the beginning of the forming process. During the actual forming energy losses occur; only the remainder is transformed into useful work. The blow efficiency  $\eta_B$  is the ratio of the useful work  $W_U$  to the available energy  $E$ . The efficiency of the hammer  $\eta_H$  is the ratio of the available energy  $E$  to the input energy  $E_I$ . Other important characteristics are the striking velocity  $v$  and the number of blows per minute  $n_B$  or its reciprocal value, namely, the blow time  $t_B$ .

**Anvil-type hammers:** The work capacity of an anvil-type hammer is obtained from the tup (ram) mass and its velocity,

$$E = \frac{1}{2} m_T v^2 \quad (8.8)$$

For gravity drop hammers with a drop height  $H$ , neglecting energy losses,

$$E = m_T g H \quad (8.9)$$

In practice the available energy is only 70–90% of the above value. For power drop hammers,

$$E = (m_T g + p_m A) H \quad (8.10)$$

where  $A$  is the piston area and  $p_m$  is the indicated steam, oil, or air pressure on the piston.

Table 8.3 gives some typical characteristic values for anvil-type hammers.

**Counterblow hammers:** The work capacity for conventional counterblow hammers is obtained from the top and bottom tup (rams) masses  $m_{TU}$  and  $m_{TB}$  and their velocities  $v_{TU}$  and  $v_{TB}$  as

$$E = \frac{1}{2} (m_{TU} v_{TU}^2 + m_{TB} v_{TB}^2) \quad (8.11)$$

Features	(a)	(b)	(c)	(d)	(e)
Energy	$(m_1 + m_2) \frac{v^2}{2} \approx mv^2$	$(m_1 + m_2) \frac{v^2}{2} \approx mv^2$	$(m_1 + m_2) \frac{v^2}{2} = mv^2$	$(m_1 \frac{v_1^2}{2} + m_2 \frac{v_2^2}{2})$	$(m_1 \frac{v_1^2}{2} + m_2 \frac{v_2^2}{2})$
Number of pistons	1	1	2	2	1
Ram coupling	Steel bands	Fluid medium	Fluid medium	—	Air
Mass ratio of rams, upper/lower	$\approx 1$	$\approx 1$	1	$> 1$	$\gg 1$
Pressure medium	Air/steam	Air/steam/oil	Air	Nitrogen	Nitrogen (air)

**FIG. 8.26** Types of counterblow hammers. (a) With mechanical coupling. (Courtesy of Béché.) (b) With hydraulic coupling (Courtesy of Béché.) (c) Horizontal with hydraulic coupling (IMPACTER, courtesy of Chambersburg.) (d) High-energy-rate hammer without coupling (CEFF, courtesy of Weingarten.) (e) High-energy-rate hammer without rigid coupling (DYNAPAK, courtesy of General Dynamics).

**Table 8.3** Characteristic Values of Anvil-Type Hammers.

	$E$ , kN·m (ft·lbf)	$\eta_B$	$v_T$ , m/s (ft/s)	$n_B$ , min <sup>-1</sup>	$\eta_H$
<b>Drop hammer</b>					
Belt	40 (29,440)	0.3–0.6	4–5 (13–16.4)	40	0.2–0.3
Board	16 (11,780)	0.3–0.6	4–5 (13–16.4)	35	0.2–0.3
Chain	100 (73,600)	0.3–0.6	4–5 (13–16.4)	55	0.5
Piston	63 (46,370)	0.3–0.6	4–5 (13–16.4)	60	0.5
<b>Power drop hammer</b>					
Pneumatic	50 (36,800)	0.8–0.9	5–8 (16.4–26.3)	80–250	0.45–0.55
Open-die, single-frame	40 (29,440)	0.8–0.9	5–8 (16.4–26.3)	450	0.45–0.55
Open-die, double-frame	250 (184,000)	0.8–0.9	5–8 (16.4–26.3)	55–240	0.5
Die forging	100 (73,600)	0.3–0.6	5–8 (16.4–26.3)	55–240	0.5

**Table 8.4** Characteristic Values of Counterblow Hammers.

	$E$ , kN·m (ft·lb)	$\eta_B$	$v_{rel}$ , m/s (ft/s)	$n_B$ , min <sup>-1</sup>	$\eta_H$
Pneumatic drive with band coupling	400 (294,400)		6 (19.7)	40–60	0.5
Pneumatic drive with hydraulic coupling	1250–1500 (920,000–1,104,000)	Similar to pressure drop anvil hammers	6 (19.7)	30–60	0.5
Hydraulic drive with hydraulic coupling	125 (92,000)		8 or 14 (26.3 or 45.9)	120	
CEEF (Weingarten)	550 (404,800)	—	20 (65.6)	7.5–12	
DYNAPAK (General Dynamics)	760 (559,380), horizontal 2070 (1,523,580), vertical		20 (65.6)	Up to 12	
IMPACTER (Chambersburg)	630 (463,700)		4–12 (13.1–39.4)		0.5

and for horizontal-type hammers with only one side with additional pressure,

$$E = (m_{TL}g + p_{m,L}A_L)H_L - m_{TR}gH_R \quad (8.12)$$

where  $m_{TL}$  and  $m_{TR}$  are the masses of the left and right tups,  $p_{m,L}$  is the indicated average pressure on the left piston, and  $H_L$  and  $H_R$  are the travals of the left and right tups, respectively. For hammers where the travals of the left and the right tups are the same, and when both are operated with the same operating pressure  $p_m$ , the work capacity is given by

$$E = 2p_mAH \quad (8.13)$$

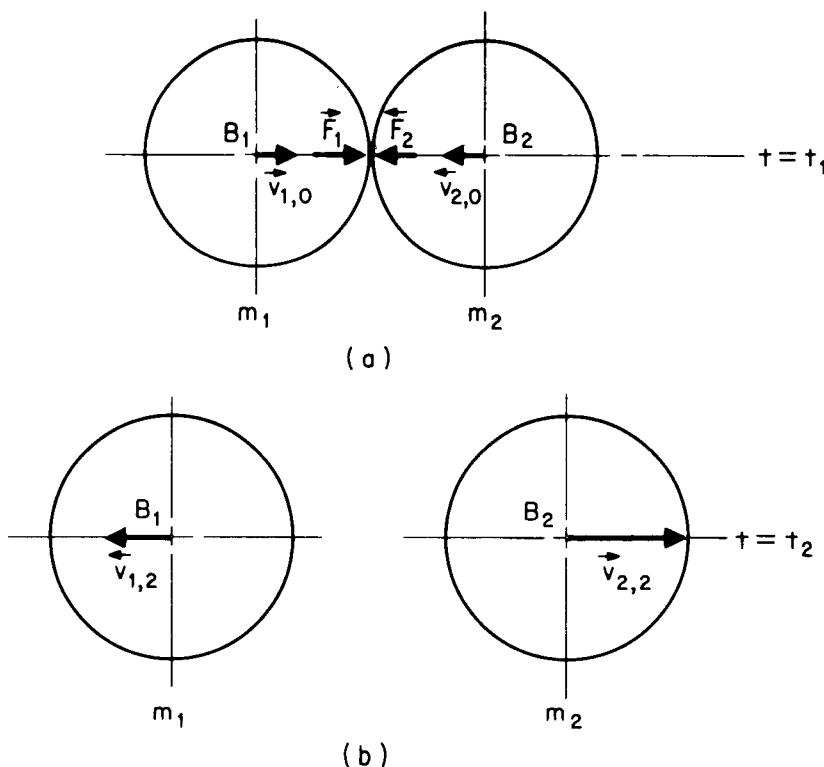
Although no anvil losses are present in counterblow hammers, a small portion of the energy is still transmitted to the floor due to frictional losses on tup guidances.

Table 8.4 gives some characteristic values of a few typical counterblow hammers. A detailed discussion of blow and machine efficiency is presented in the following section.

### 8.2.3 Operating Efficiency of Hammers

For a complete understanding of the dynamic behavior of the hammer tup, frame, and anvil, an understanding of the impact theory is necessary. The operating efficiency of the hammer can be obtained from such an analysis.

When two bodies with masses  $m_1$  and  $m_2$  (Fig. 8.27a) impact each other with velocities  $v_{1,0}$  and  $v_{2,0}$ , the impact process can be divided into two stages [8.13]. In the first stage ( $t_0 \leq t \leq t_1$ ) the



**FIG. 8.27** Impact process in hammer forging.  $B_1, B_2$ —bodies 1 and 2. (a) First stage of impact. (b) Second stage of impact.

**Table 8.5** Values for Impact Factor  $k$ .

$v$ , m/s (ft/s)	$k$	Type of blow
2–3 (6.6–9.8)	0.55	Hard blow
6–8 (19.7–26.3)	0.85	Hard blow
	0.05–0.1	Soft blow (free forming)
	0.4–0.6	Medium blow (die forging)

two bodies approach each other. At time  $t = t_1$  both bodies are at their nearest points. The bodies deform due to the resulting impact force. At the end of this stage the deformations are at their maximum. At the end of the first stage,  $t_1$ , the bodies have the same velocity,

$$v_{11} = v_{21} = u \quad (8.14)$$

The velocity  $u$  can be calculated from the impact law as

$$u = \frac{m_1 v_{10} + m_2 v_{20}}{m_1 + m_2} \quad (8.15)$$

In the second stage of the impact process ( $t_1 \leq t \leq t_2$ ) the deformations are partly permanent (actual blow) and partly elastic. The end of the second stage is characterized by the two bodies no longer having contact with each other. The corresponding velocities of the bodies are then  $v_{12}$  and  $v_{22}$ . The impact factor  $k$  characterizes the amount of plastic blow or the elastic portion as follows:

$$k = \frac{v_{12} - v_{22}}{v_{20} - v_{10}} \quad (8.16)$$

The factor  $k$  can have a value between 0 (plastic blow) and 1 (elastic blow); Table 8.5 gives some characteristic values. It is obvious that for metal-forming processes a lower value of  $k$  is desired.

For an anvil-type hammer the above equations can be applied to obtain useful information. Considering the various tup and anvil parameters given in Fig. 8.28, the tup with mass  $m_T$  travels with velocity  $v_T$ , and the equivalent anvil mass  $m_A^*$  with velocity  $v_A$ .

The equivalent anvil mass  $m_A^*$  is a combination of the actual anvil mass  $m_A$  and the foundation mass  $m_F$ . (Typical ratios are  $m_F/m_T = 16–20$ ,  $m_F/m_A = 60–80$ . For weak systems  $m_A^* = m_A$ , and for stiff systems  $m_A^* = m_A + m_F$ .) The various relevant equations to obtain the operational efficiency are

$$u = \frac{m_T v_T}{m_T + m_A^*} \quad (8.17)$$

$$k = \frac{v_{A,2} - v_{T,2}}{v_T} \quad v_A = 0 \quad (8.18)$$

$$v_{T,2} = u + k(u - v_T) \quad (8.19)$$

$$v_{A,2} = u(k + 1) \quad (8.20)$$

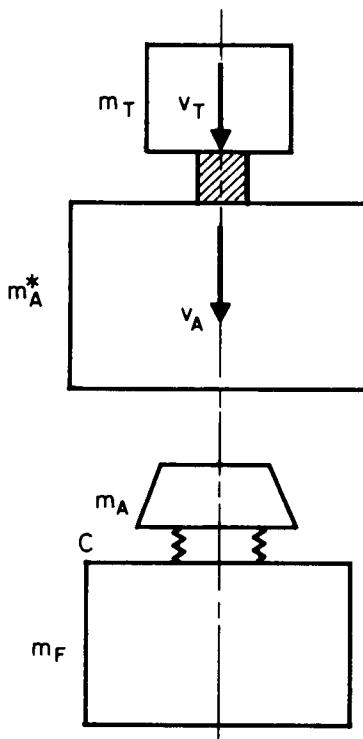


**FIG. 8.28** Schematic of impact phenomenon in anvil-type hammers.

Similar equations for the conventional counterblow hammer are, with  $m_T \approx m_A^* = m$  and based on symmetry,  $v_{TU,0} \approx -v_{TL,0} \approx v_0$  and  $v_{TU,2} \approx v_{TL,2} = v_2$ ,

$$u = 0 \quad (8.21)$$

and

$$v_2 = kv_0 \quad (8.22)$$

**Blow efficiency:** The blow efficiency of a hammer can be obtained by computing the energy balance,

$$E = W_U + W_L \quad (8.23)$$

where  $E$  is the total energy,  $W_U$  the useful work, and  $W_L$  the lost work or energy.

The energy balance equations at  $t = t_1$  and  $t = t_2$  are given, respectively, by

$$E = W_U + W_{A,1} + W_{T,1} + W_{el,T} + W_{BL,1} \quad (8.24)$$

and

$$E = W_U + W_{A,2} + W_{T,2} + W_{BL,2} \quad (8.25)$$

The kinetic energy of the equivalent anvil mass  $m_A^*$  at  $t_1$  is

$$W_{A,1} = \frac{m_A^*}{2} u^2 \quad (8.26)$$

The kinetic energy of the tup  $W_{T,1}$  at  $t_1$  is

$$W_{T,1} = \frac{m_T}{2} u^2 \quad (8.27)$$

The elastic deformation work in the tool  $W_{el,T}$  at  $t_1$  is recovered in the second period. The losses in the tup due to the blow have been represented as  $W_{BL,1}$  and  $W_{BL,2}$  at the two impact periods. At  $t = t_2$ , the kinetic energy of the equivalent anvil mass  $W_{A,2}$  is given by

$$W_{A,2} = \frac{m_A^*}{2} v_{A,2}^2 \quad (8.28)$$

Similarly the kinetic energy of the tup at  $t = t_2$  is

$$W_{T,2} = \frac{m_T}{2} v_{T,2}^2 \quad (8.29)$$

The blow efficiency is defined as

$$\eta_B = \frac{W_U}{E} \quad (8.30)$$

This blow efficiency should be the same for both periods, that is, at  $t = t_1$  and  $t = t_2$ .

Applying the above principles to an anvil-type hammer, with the initial anvil velocity  $v_{A,0} = 0$ , the following equations are valid:

1 Tup and anvil losses at  $t = t_1$ ,

$$e_{A,1} + e_{T,1} = \frac{W_{A,1} + W_{T,1}}{E} = \frac{1}{1 + Q^*} \quad (8.31)$$

where  $Q^* = m_A^*/m_T$ , the mass ratio.

2 Anvil loss at  $t = t_2$ ,

$$e_{A,2} = \frac{W_{A,2}}{E} = Q^* \left( \frac{k+1}{1+Q^*} \right)^2 \quad (8.32)$$

3 Tup loss at  $t = t_2$ ,

$$e_{T,2} = \frac{W_{T,2}}{E} = \left( \frac{1-kQ^*}{1+Q^*} \right)^2 \quad (8.33)$$

4 Elastic deformation work at  $t = t_1$ ,

$$e_{el,T} = \frac{W_{el,T}}{E} = \frac{F_1^2}{2C_T E} \quad (8.34)$$

where  $F_1$  is the final forming force and  $C_T$  the spring constant of the tool.

5 Blow losses at  $t = t_1$ ,

$$W_{BL,1}$$

In order to consider this portion of the energy losses, the factor  $k$  is introduced,

$$k = \frac{W_{BL,1}}{W_L} \quad (8.35)$$

where  $W_L$  is the sum of the losses. The factor  $k$  depends on the spring constant  $C_T$  of the tool and on the tool setting on the tup as well as on the anvil. The final expression for the blow efficiency is [8.14]

$$\eta_B = 1 - \frac{1}{1-k} \left[ \frac{1}{1+Q^*} + \frac{F_1^2}{2C_T E} \right] \quad (8.36)$$

The value of  $k$  has been measured to be between 0.15 and 0.45, the smaller value being for a less stiff die and loose clamping and the larger value for stiffer tooling and tight clamping.

The blow efficiency  $\eta_B$  for various  $k$  values as a function of the mass ratio  $Q^*$  is shown in Fig. 8.29. For the same work capacity or energy the blow efficiency decreases with increasing  $k$  and forming force  $F_1$ ; the blow efficiency increases with increasing tool spring constant  $C_T$  and mass ratio  $Q^*$ .

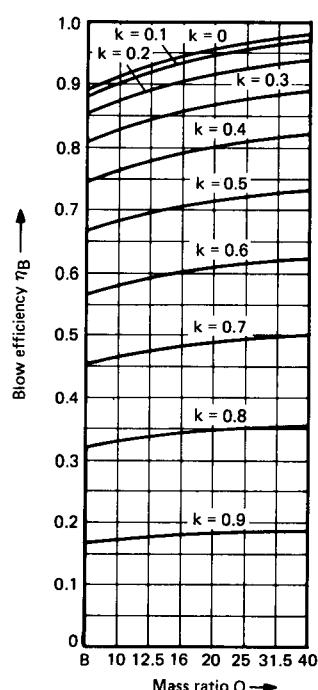


FIG. 8.29 Blow efficiency as a function of mass ratio.

For counterblow hammers with  $v_{TU,0}$

$$\eta_B = 1 - k^2 - e_{BL,2} \quad (8.37)$$

where  $e_{BL,2} = W_{BL,2}/E$ . Assumptions similar to those for anvil-type hammers should be made to obtain  $e_{BL,2}$  to determine the blow efficiency of counterblow hammers. Tables 8.3 and 8.4 contain typical values for the blow efficiency of anvil-type and counterblow hammers. The application ranges of the various hammers discussed in this chapter are shown in Fig. 8.30.

### 8.3 SCREW PRESSES

Screw presses are generally built as double-column presses (Fig. 8.31). The frame can be of either a single-piece (welded steel construction) or multipiece (cast steel with tie rods and bolts) design.

The major characteristic of these presses is the drive. The motor drives a flywheel which is either directly connected or can be connected as necessary to the screw spindle. The screw spindle transmits the rotary motion through the threads (multiple start), which have pitch angles between 13 and 17°, to a linear movement of the main ram. On contact with the workpiece the complete kinetic energy of the flywheel and the ram is transformed into useful work and losses (elastic deformation work and

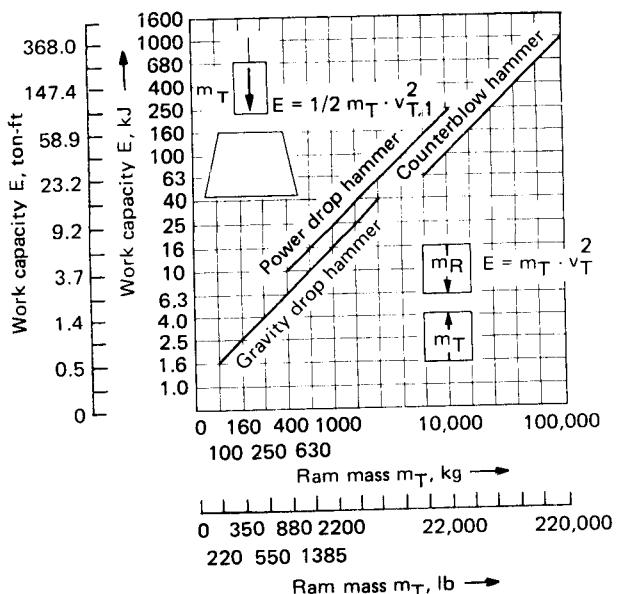


FIG. 8.30 Application ranges for various types of hammers in die forging. Tup (ram) mass  $m_T$  is for a 1-ram counterblow hammer.

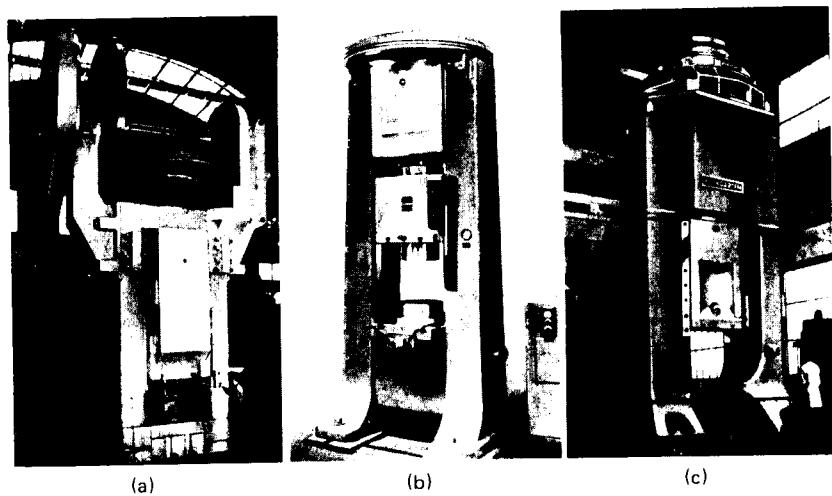
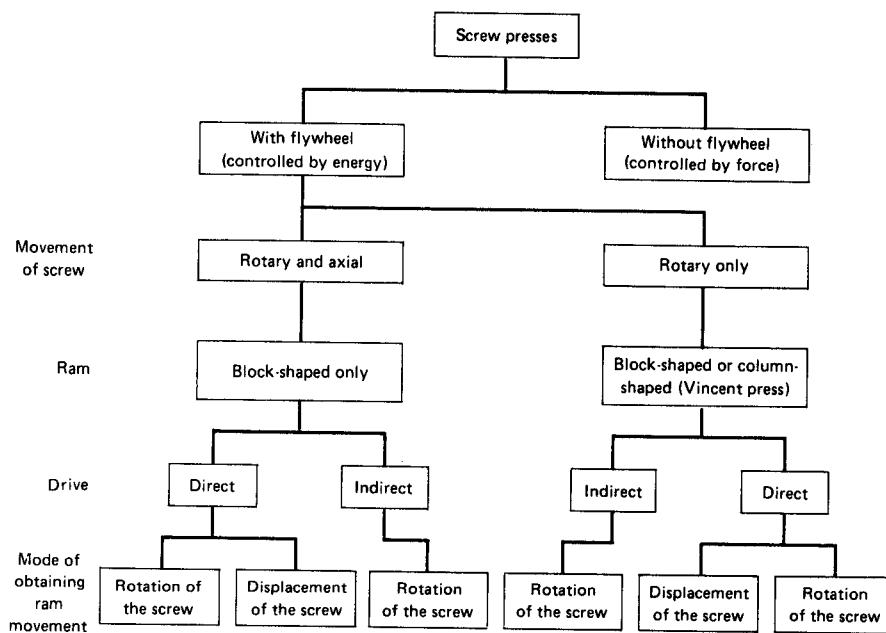


FIG. 8.31 Types of screw presses. (a) Four-disk drive: screw turns and moves axially; friction-drive. (Courtesy of Hasenclever.) (b) Single-disk drive: screw only turns; friction drive, single-piece frame. (Courtesy of Weingarten.) (c) Single-disk drive: screw only turns; direct electric drive, multipiece frame. (Courtesy of Weingarten.)

**FIG. 8.32** Classification of screw presses.

frictional). The elastic deformation work results in a reaction force in all the press parts lying in the force transmission path. The elastic deformation force stored in the frame and the drive causes a reverse acceleration of the flywheel. By proper reversal of the drive control, the ram is brought back to its initial position. This forms the complete cycle of a working stroke.

Screw presses are generally single-acting. Using hydraulic, pneumatic, or mechanical devices, a second action can be obtained (for example, an ejection unit).

A classification of the different screw presses is shown in Fig. 8.32. The most important characteristic parameter for distinguishing between the various types of screw presses is the mode of screw movement. (The screw presses without flywheel are not considered here.) The screw can be fixed in position either in the frame (rotary movement only) or in the ram (rotary and longitudinal movements).

### 8.3.1 Type of Drives and Ram Travel Characteristics

The traditional drive for screw presses is through friction disks. Fig. 8.33 shows a few typical ram travel characteristics of different drive systems.

In the case of a rotary-disk-driven press (Fig. 8.33a) the continuously rotating driving disks are moved axially so that one of the two disks activates the motion by friction—one for the working stroke and the other for the return stroke. The force transmission at the friction point is achieved through a lining of either special leather material or plastic on the circumference of the flywheel. At the starting position of the ram stroke, the flywheel is also at the top point so that the frictional contact starts at the smallest circumferential velocity of the driving disks and the ram is then accelerated. During the return stroke, the frictional contact takes place with the other drive disk at the point of its maximum circumferential velocity, and the acceleration decreases continuously until the ram comes to a stop at the starting point. The change in the number of revolutions per minute of the flywheel and the driving disks clearly demonstrates the above effects, as shown in Fig. 8.33a.

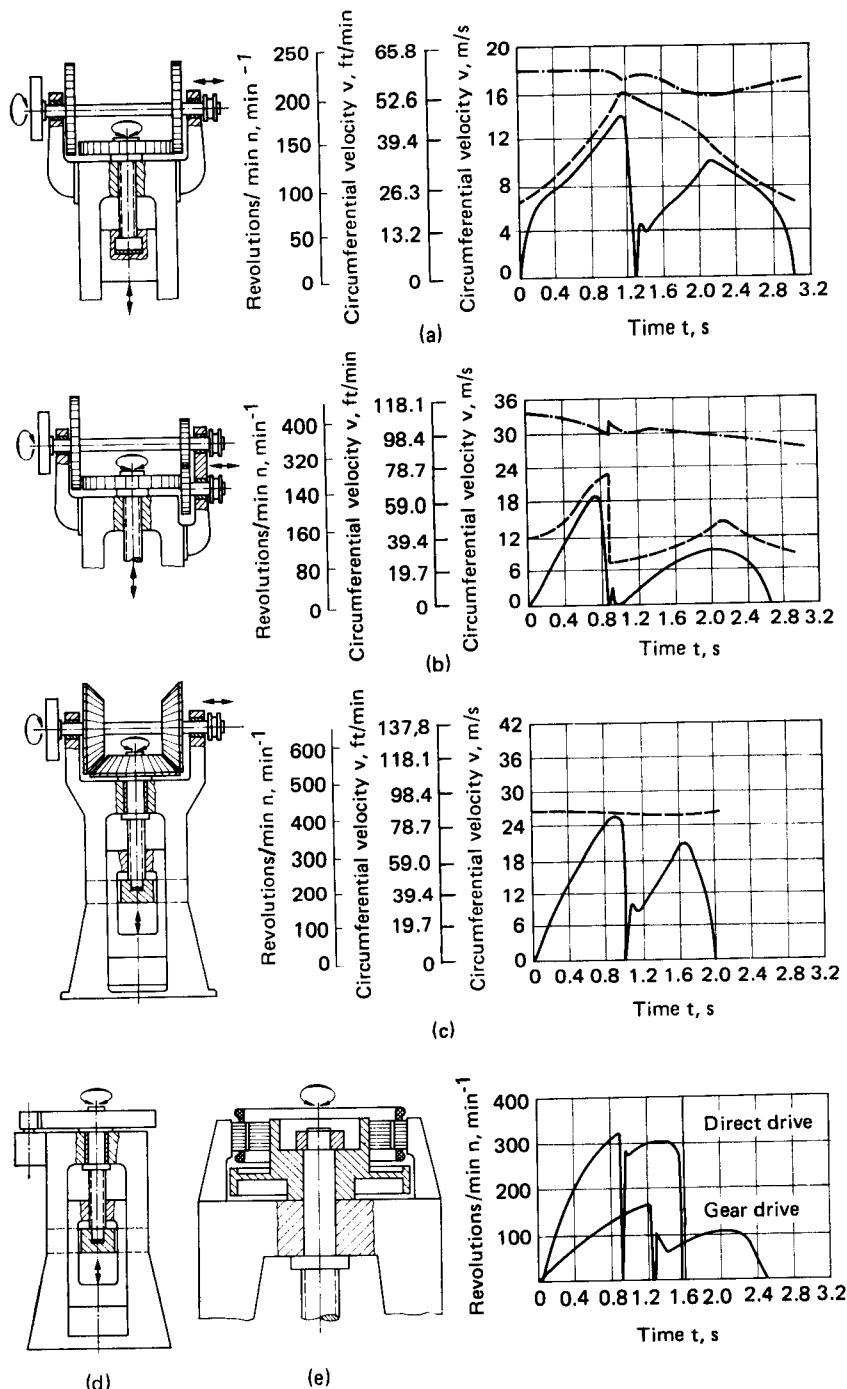


**FIG. 8.33** Displacement diagrams of flywheel and driving disk for various screw presses. (a) Rotating-disk drive: screw with axial movement. (b) Four-disk drive: screw with axial movement. (c) Vincent press: stationary screw. (d) Percussion type with gear drive, electric or hydraulic motor: stationary screw. (e) Percussion press with direct electric drive: stationary screw. (After [8.15] and [8.16]). — Flywheel rpm. --- Flywheel of drive disk. — Velocity of drive disk at point of contact.

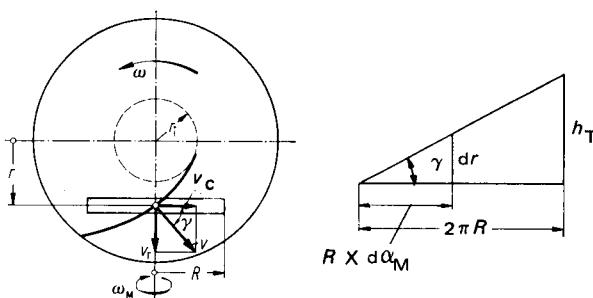


**FIG. 8.34** Symbols and definitions for the drive of rotary-disk-drive screw press.  $R$ —radius of middle disk (flywheel);  $\omega_M$ —angular velocity of middle disk;  $\omega$ —angular velocity of driving disk;  $v_c$ —circumferential velocity of middle disk;  $v_r$ —axial velocity of middle disk;  $v$ —velocity of contact point;  $\alpha_M$ —angle of rotation of middle disk;  $r$ —distance of contact point from driving-disk axis;  $r_i$ —smallest distance of contact point from driving-disk axis;  $h_T$ —pitch of screw thread.

Assuming that there is no slippage, the motion of the flywheel can be calculated. Using the symbols used in Fig. 8.34, we have

$$v_c = r\omega = R\omega_M = R \frac{d\alpha_M}{dt} \quad (8.38)$$

and

$$\frac{d\alpha_M}{dt} = \frac{2\pi}{h_T} \quad (8.39)$$

Using Eqs. 8.38 and 8.39, we get

$$v_c = \frac{2\pi R}{h_T} \frac{dr}{dt} = \frac{2\pi R}{h_T} v_r \quad (8.40)$$

$$\frac{v_r}{v_c} = \tan \nu = \frac{h_T}{2\pi R} \quad (8.41)$$

where  $\tan \nu$  is a characteristic value for screw presses. With  $\omega = \omega_0 = \text{constant}$  it follows from Eq. 8.41 that

$$v_r = \tan \nu r\omega_0 = \frac{dr}{dt} \quad (8.42)$$

or

$$\int_{r_i}^r \frac{dr}{r} = \tan \nu \omega_0 \int_0^t dt \quad (8.43)$$

Integration of Eq. 8.43 yields

$$r = r_i e^{\omega_0 t \tan \nu} \quad (8.44)$$

Eq. 8.44 describes the path of movement of the contact point on the side disk and represents a logarithmic spiral.

Correspondingly the velocities are given by

$$v_r = \frac{dr}{dt} = r_i \omega_0 \tan \nu e^{\omega_0 t \tan \nu} \quad (8.45)$$

$$v_c = \frac{v_r}{\tan \nu} = r_i \omega_0 e^{\omega_0 t \tan \nu} \quad (8.46)$$

The acceleration is

$$a = \frac{dv_c}{dt} = r_i \omega_0^2 \tan \nu e^{\omega_0 t \tan \nu} = r \omega_0^2 \tan \nu \quad (8.47)$$

The acceleration is linearly proportional to the radius so that the energy transmission takes place without any slippage. Furthermore the torque and the pressing force must be made proportional to the acceleration. However, the velocity curve will get distorted due to slipping (compare with Fig. 8.33a). Slipping causes both an energy loss and wear of the friction lining.

In the case of the four-disk drive of Fig. 8.33b, the slippage during the return stroke is not as high as in the previous case.

In the Vincent-type screw press (Fig. 8.33c) the flywheel and the screw are fixed in space so that the frictional contact always takes place at the point of the largest circumferential velocity of the drive disks. The disks also have a cone shape for better transmission of the force. The box-shaped ram is a distinguishing feature of Vincent-type screw presses. The frame will not be subject to the deformation force in this type of press. The loading of the various parts of this press is shown in Fig. 8.35.

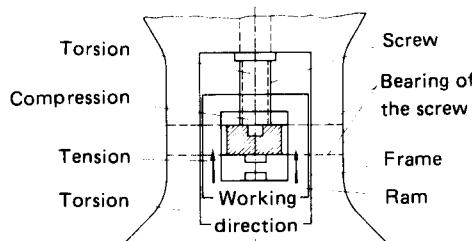


**FIG. 8.35** Loading of the various parts in a Vincent-type screw press.

The flywheel and the screw are also fixed in space in the single-disk screw press (Fig. 8.33d). The force is transmitted through a friction roll, which is directly fixed on the shaft of the main motor. The pressing force on the friction roll is achieved by the spring-loaded motor positioning. Wedge profiles in both the flywheel and the friction roll help in better force transmission. For the return stroke the direction of rotation of the drive motor must be changed. Such frequent changes in the direction of rotation of the motor require the use of special motors (reversible). The losses due to slippage can be reduced if the gear drive can be used to transmit the motion from the motor to the flywheel.

In direct-driven screw presses (Fig. 8.33e) the flywheel and the motor shaft are one unit, and hence no mechanical transmission of force is necessary between the motor and the flywheel. The slip losses in the electric motor are, however, very high in this case. The heat generated due to such high slip losses in the special motor must be transferred by additional special fans.

For the purpose of safety, the flywheel and/or the screw are held in a standstill position by brakes, since the ram starts moving down due to its own weight as soon as the force coupling with the drive motor is cut off. The stop brake can also be used as a working brake in single-disk presses.

Recently several designs using hydraulic drive systems have been developed to reduce

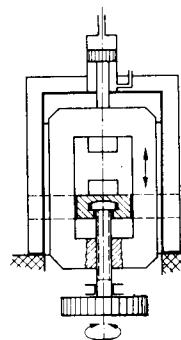


**FIG. 8.36** Vincent-type screw press with flywheel at the bottom. Drive is by hydraulic medium.

or eliminate the frictional losses in the traditional drives. Since this is an ongoing development, only some essential features of these designs are mentioned here:

- 1 A pinion is fixed on top of the flywheel and moved by a rack. The rack is actually the piston rod of two hydraulic cylinders positioned opposite each other. These cylinders move the rack forth and back.
- 2 The ram is pushed downwards hydraulically. Its longitudinal movement is transformed to a rotary movement of the flywheel through the screw and a nut. An example is shown in Fig. 8.36.
- 3 A special motor is positioned directly on the screw which is capable of both rotary and longitudinal movements.

### 8.3.2 Energy Conversion and Efficiency

The ram with the top tool deforms the workpiece placed on the bottom tool. The forming force resulting from the above operation depends on the deformation resistance of the workpiece. The forming force causes elastic deformation of the press frame and other press parts lying in the force flow. Two examples of the force-travel diagram,  $F = f(s)$ , are shown in Figs. 8.37 and 8.38. The maximum force  $F_{\max}$  is normally reached when the total energy stored in the flywheel is expended. As a rule  $F_{\max}$  should not exceed the nominal force  $F_N$  of the press (Fig. 8.37). In general screw presses are designed to take up only a particular portion of the flywheel energy transformed to elastic deformation work. If the energy required for the process is too small, then a larger portion of the expended flywheel energy must be transformed into the elastic deformation work, resulting in a very large force (Fig. 8.38). In the so-called "die-to-die blow" the total flywheel energy is transformed into elastic and friction work, which may cause cracking of some press parts if such blows are repeated frequently.

From an economic viewpoint, screw presses for hot bulk forming (die forging) cannot be designed to be totally safe against die-to-die blows because of the large requirement of deformation energy.

When a large workpiece is to be deformed, several working strokes may be necessary to complete the forming process if the deformation energy required cannot be obtained in a single stroke of the press. In such an operation the deformation travel becomes successively smaller and the maximum force increases, resulting in the danger of die-to-die blows.

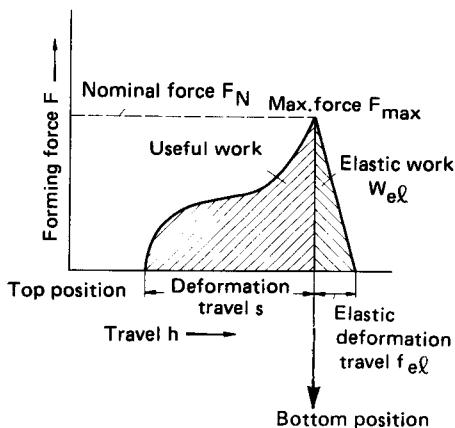


**FIG. 8.37** Ideal energy conversion in screw press.  
Work capacity and nominal force are used fully.

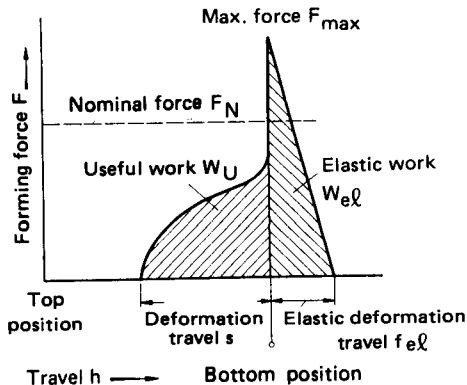


**FIG. 8.38** Overloading of screw press. Work capacity is not fully used, and nominal force is exceeded.

When used for coining processes (such as sizing), which require small deformation travel, the work capacity available per stroke must be regulated by a proper selection of the flywheel dimensions or speed so that the die-to-die blows do not load the press excessively. Furthermore the presses must be provided with overload safety devices (shear pins, slip clutch) to limit the torque transmitted from the flywheel to the screw (refer to Sec. 8.6).

Neglecting the torsional springback of the screw and the frictional losses, the maximum force  $F_{\max}$  for a given deformation process can be calculated from the work capacity  $E$ , the longitudinal spring constant  $C_l$ , and the deformation travel  $s$  as [8.15]

$$E = W_N + W_{el} \quad (8.48)$$

where

$$W_N = \int_0^h F \, ds = F_m s \quad (8.49)$$

and

$$W_{el} = \frac{1}{2} F_{\max} f_l = \frac{1}{2} \frac{F_{\max}^2}{C_l} \quad (8.50)$$

and where  $F_m$  is the average force during the deformation travel  $s$  and  $f_l$  is the elastic deformation.

Introducing a force correction factor  $m$  as defined by

$$m = \frac{F_m}{F_{\max}} = \frac{1}{sF_{\max}} \int_0^h F \, ds \quad (8.51)$$

Eq. 8.48 is written as

$$E = mF_{\max}s + \frac{1}{2} \frac{F_{\max}^2}{C_l} \quad (8.52)$$

The force correction factor  $m$  takes characteristic values depending on the type of process (such as upsetting or deep drawing).

The maximum force  $F_{\max}$  is obtained from Eq. 8.52,

$$F_{\max} = C_l \left[ \sqrt{\frac{2E}{C_l}} + (ms)^2 - ms \right] \quad (8.53)$$

Since the machine has been designed for a definite maximum permissible force  $F_{\max,p}$ , there is a minimum deformation travel required. This is obtained from Eq. 8.53,

$$s_{\min} = \frac{1}{m} \left[ \frac{E}{F_{\max}} - \frac{F_{\max}}{2C_1} \right] \leq s_{\text{req}} \quad (8.54)$$

where  $s_{\text{req}}$  is the required deformation travel. The maximum permissible force  $F_{\max,p}$  is generally the same as the nominal force  $F_N$ ; in some cases it can be larger. In the case of die-to-die blows  $W_N = 0$ , and the force on the press is

$$F_{\text{DTD}} = \sqrt{2C_1 E} \quad (8.55)$$

The frictional losses in the driving elements and the sliding area must also be considered for determining the economy of using screw presses in industrial practice. A schematic representation (Fig. 8.39) shows the various losses in a screw press for a working stroke.

The contact velocities of the tool with the workpiece are relatively high in screw presses. Even for this case the term "blow" can be used to characterize the working operation, although the velocities in drop hammers are four to six times greater than those in a screw press. The blow efficiency can therefore also be defined for screw presses as the ratio between the useful work and the work capacity,

$$\eta_B = \frac{W_U}{E} = 1 - \frac{W_L}{E} \quad (8.56)$$

or  $\eta_B = 1 - \frac{1}{E} (W_{\text{FR,G}} + W_{\text{FR,S}} + W_{\text{el,l}} + W_{\text{el,t}}) \quad (8.57)$

The blow efficiency consists of a constant term and a variable term that depend on the final forming force. The elastic deformation work losses  $W_{\text{el,l}}$  and  $W_{\text{el,t}}$  increase with increasing force. Furthermore the blow efficiency depends on the screw friction coefficient  $\mu$  (Fig. 8.40) [8.14].

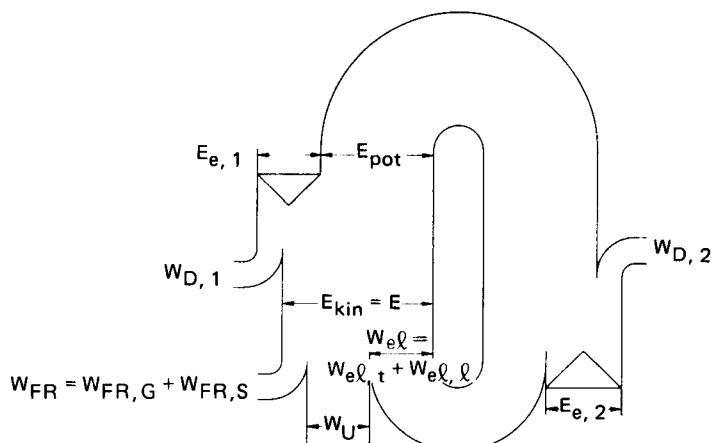


**FIG. 8.39** Schematic of losses in working stroke of a screw press.  $E_{e,1}$ —supplied electric energy during process;  $E_{\text{pot}}$ —potential energy of ram, flywheel, and screw at start of the working stroke;  $W_{D,1}$ —losses in drive (including guide and screw friction) in downward travel;  $E_{\text{kin}} = E$ —kinetic energy (work capacity) before actual deformation process;  $W_L$ —total lost work;  $W_U$ —useful work;  $W_{\text{FR}}$ —frictional energy losses;  $W_{\text{FR,G}}$ —frictional losses in guides during deformation process;  $W_{\text{FR,S}}$ —frictional losses in screw during deformation process;  $W_{\text{el,l}}$ —elastic deformation work in longitudinal direction;  $W_{\text{el,t}}$ —elastic deformation work due to torsional effects;  $W_{D,2}$ —losses in drive during return stroke. Energy balance equation— $E_{e,1} + E_{e,2} = W_{D,1} + W_U + W_{D,2}$ .

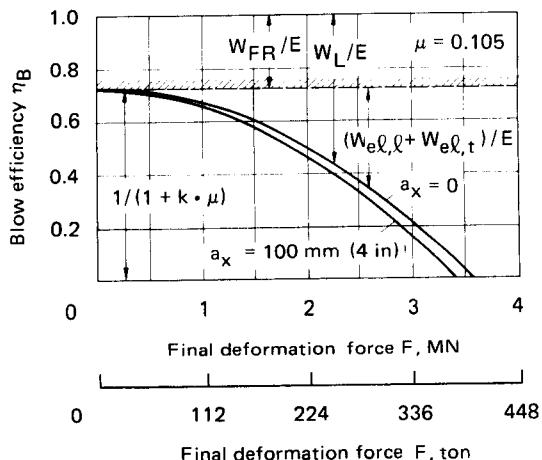


**FIG. 8.40** Blow efficiency of screw press. Friction coefficient  $\mu = 0.105$ ;  $a_x$ —distance of force offset in eccentric loading. (After [8.14].)

### 8.3.3 Controls

The drive motor in single-disk presses can only be switched on if (1) the cooling fan is already running and (2) the solenoid disconnects the band brake. For activation of the return stroke (reversing of the motor) the limit switches are actuated by control cams just before the ram touches the bottom workpiece. These control cams are located on the ram of the screw press. The top stopping point for the ram can again be controlled by another limit switch and a control cam. This limit switch switches off the drive motor and applies the brake on the flywheel. An adjustment of both the control cam and the limit switch allows for an accurate setting of the stroke. Additional controls can be used to obtain different blowing sequences based on a definite program.

In the case of multidisk screw presses the flywheels are axially movable and are pressed against the center disk using a servo motor and a pressure medium. The revolutions of the center disk are transformed into a proportional voltage by a dynamo, and this voltage is amplified to switch on an adjustable relay for stroke setting. When the set voltage is reached, the control unit switches off the servo motor through a solenoid and the flywheel is pushed to its median position, breaking the frictional contact with the center disk. The velocity of the return stroke can be controlled in the same way. Since the square of the revolutions per minute of the flywheel is proportional to the work capacity, it can also be set accurately. Furthermore several setting values can be preselected according to a required sequence of blows.

### 8.3.4 Application and Capacities of Screw Presses

Screw presses are used in hot bulk forming (die forging of steel and nonferrous metals) and in cold bulk forming (cutlery manufacture, coin manufacture, and sizing). They compete in these areas with mechanical presses controlled by stroke, hydraulic presses, and hammers.

An advantage of the screw press is that the total energy of the center disk is transformed to work energy in every stroke of the press. If the required work capacity is high, the screw press for such an operation will be smaller and cheaper than an equivalent crank press. A simple comparison of the same work capacity of a screw press ( $E \approx \frac{1}{2} \theta_M \omega_M^2$ ) and a drop hammer ( $E = m_T g H$ ) shows that the tup mass in the hammer must be six times that of the flywheel mass (assuming reasonable drop heights, flywheel diameter, and revolutions per minute). Compared with ham-

mers, the screw presses have a higher working accuracy since the acceleration distance is relatively small and large ram guidances can be used. The contact time of the tool with the workpiece is smaller in screw presses than in crank presses as the ram velocity is the highest [0.5–1 m/s (1.64–3.28 ft/s)] at the time of contact of the top and bottom tools (refer also to Fig. 8.33).

A major disadvantage of the screw presses is the lower number of strokes per minute. For hot forming it yields about 20 pieces per minute and in the automated cold-forming production it can be as high as 30 pieces per minute. In the friction screw press the wear of the lining is rather high.

The nominal force of three- and four-disk presses available in the market is as high as  $F_N = 31.5 \text{ MN}$  (3540 tons), and the work capacities are up to 630 kJ (464,300 ft·lb). The single-disk presses with hydraulic drive are available with nearly four times the nominal force of the above presses, and the work capacity is nearly double that of the above.

#### 8.4 HYDRAULIC PRESSES

The possibility of generating large forces with high-pressure fluids was recognized very early (Pascal, 1662). A patent in the year 1795 by the Englishman Bramah was given for a hydraulic press with hand pump drive. In 1860 Haswell, also from England, built a water hydraulic open-die forging press which was put to use in Austria.

Force generation and the movements in hydraulic presses are achieved using fluids under pressure.

The following equation is valid for the stationary flow of a frictionless incompressible fluid along a streamline:

$$\frac{v^2}{2g} + \frac{p}{\rho g} + z = \text{constant} \quad (\text{D. Bernoulli}) \quad (8.58)$$

The three terms are represented by pressure heads, where  $v^2/2g$  is the head due to the velocity of flow,  $p/\rho g$  is the head due to the pressure of the fluid, and  $z$  is the head due to the position.

The essence of Bernoulli's equation is that the sum of the velocity, potential, and pressure heads is a constant and has a characteristic value along a streamline in a stationary flow of an ideal fluid.

A simplified schematic representation of a hydraulic press is shown in Fig. 8.41. The relevant details can be derived from this figure. Pump 1 driven by the motor M transforms the mechanical energy of the fluid medium to hydraulic energy. The fluid flows through the pipes and the valves of hydraulic cylinder 2, where the hydraulic energy is again transformed to mechanical energy. The fluid medium can be assumed to be incompressible for the following analysis.

$$A_1 v_1 = A_2 v_2 = \dot{V} \quad (8.59)$$

where  $\dot{V}$  is the rate of flow from pump 1. The velocity of the piston is given by

$$v_2 = \frac{A_1}{A_2} v_1 = \frac{\dot{V}}{A_2} \quad (8.60)$$

Considering the fluid friction (viscosity), a general form of the Bernoulli equation can be written for the hydraulic press shown in Fig. 8.41,

$$\frac{v_1^2}{2g} + \frac{p_1}{\rho g} + z_1 = \frac{v_2^2}{2g} + \frac{p_2}{\rho g} + z_2 + h_{L,1,2} \quad (8.61)$$

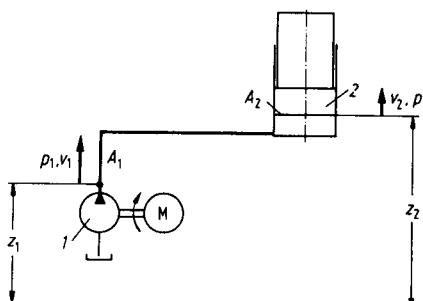


**FIG. 8.41** Schematic of a hydraulic press. 1—pump; 2—hydraulic cylinder.

The losses represented by head  $h_{L,1,2}$  include the frictional losses of the flowing fluid in pipes, valves, and cylinders.

The hydrostatic pressure  $p_2$  acting on piston 2 can be obtained from Eq. 8.61 as

$$p_2 = p_1 + \rho g(z_1 - z_2) + \frac{\rho}{2}(v_1^2 - v_2^2) - \rho g h_{L,1,2} \quad (8.62)$$

In hydraulic presses the terms  $\rho g(z_1 - z_2)$  and  $(\rho/2)(v_1^2 - v_2^2)$  are relatively small compared to the hydrostatic pressure  $p_1$ . Hence from Eq. 8.62,

$$p_2 = p_1 - \rho g h_{L,1,2} \quad (8.63)$$

The hydraulic presses therefore operate based on the principle of hydrostatic pressure.

While in hydraulic turbines the kinetic energy of the flowing fluid is used, the flow in hydraulic presses is used mainly for obtaining the various movements and also for force generation.

The flow losses  $h_{L,1,2}$  in the valves, lines, and so on, can be determined by using the well-known principle of hydrodynamics, and the final velocity obtainable is important for understanding the various movements of the press.

The hydrostatic pressure acts perpendicular to the surface of the piston generating a force. The force along the axis of the piston is

$$F = pA \quad (8.64)$$

where  $A$  is the projected area of the piston in the piston axis (Fig. 8.42).

Combining Eqs. 8.63 and 8.64, the force on piston 2 in Fig. 8.41 is

$$F_2 = p_2 A_2 = (p_1 - \rho g h_{L,1,2}) A_2 \quad (8.65)$$

and neglecting  $h_{L,1,2}$ ,

$$F_2 = p_1 A_2 \quad (8.66)$$

By choosing the pressure and the piston area properly, different forces can be obtained easily.

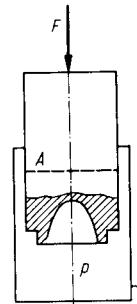


**FIG. 8.42** Force in axial direction of a piston of arbitrary shape subjected to hydrostatic pressure.

#### 8.4.1 Fluid Media

The operational efficiency of a hydraulic press depends, among other factors, to a great extent on the selection of a suitable fluid and its properties. In hydraulic presses, hydraulic oil or water (with the addition of some oil) are mainly used as fluid media.

#### Functions of Fluid Media

The main function of the fluid medium is the transmission of energy from the point of its generation (pump) to the point of its use (for example, hydraulic cylinder). Most of the fluid media also serve as a lubricant for the moving parts of the press in contact with the fluid. Other functions of the fluid media are flushing of dirt particles, corrosion protection of the inner portions of the units, and heat transfer (cooling) [8.16].

#### Important Characteristics of Fluid Media

A force  $F$  is necessary to overcome the inner friction of the fluid in order to move a flat plate of area  $A$  with constant velocity  $v$  parallel to the wall at a small distance  $h$  from the wall (Fig. 8.43). Using Newton's law of flow, we get

$$F = \eta A \frac{dv}{dz} \quad (8.67)$$

The dynamic viscosity  $\eta$  is a measure of the inner friction of the fluid. The unit for  $\eta$  in the SI system is Pa·s (pascal-seconds) = N·s/m<sup>2</sup>. In fluid mechanics, the term "kinematic viscosity  $\nu$ " is often used,

$$\nu = \frac{\eta}{\rho} \quad (8.68)$$

The unit for  $\nu$  in the SI system is m<sup>2</sup>/s. The practical unit of measuring viscosity using a viscometer is °E (degrees Engler).

Selection of the proper viscosity for a fluid requires a compromise. At lower viscosities the flow losses are small; the pump performance, the loading on the hydraulic aggregate, and the effect of lubrication at low loadings are also good. However, leaking tendencies (losses) are higher at lower viscosities. For hydraulic presses, mineral oils with a viscosity of 5°E at 50°C (112°F) are recommended [8.17]. The viscosity of fluids decreases with increasing temperature. The fluid media in hydraulic presses are subjected to considerable temperature variations, and hence the temperature dependence of the viscosity of the oil chosen should be small to limit the differences in the working performance of the press.

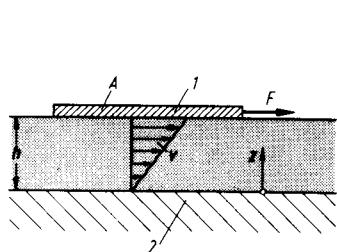


**FIG. 8.43** Velocity distribution in a viscous fluid while moving plate 1 parallel to wall 2.

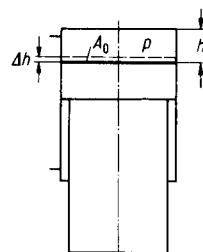


**FIG. 8.44** Elastic deformation  $\Delta h$  due to compression of the fluid medium in a hydraulic cylinder.

Fluid media can be compressed very little. This affects the spring constant of the machine and hence its dynamic behavior.

For a volume reduction  $dV$  (compressed) with a pressure increase  $dp$  we get

$$dV = \frac{1}{K} V_0 dp \quad (8.69)$$

where  $K$  is the bulk modulus, and

$$\frac{1}{K} \approx 7 \times 10^{-5} \text{ bar}^{-1} (4.77 \times 10^{-3} \text{ ksi}^{-1}) \quad \text{for airfree oil}$$

$$\frac{1}{K} \approx 5 \times 10^{-5} \text{ bar}^{-1} (3.4 \times 10^{-3} \text{ ksi}^{-1}) \quad \text{for water}$$

The spring constant of the press cylinder resulting from the compressibility of the fluid medium can therefore be obtained (Fig. 8.44) using Eq. 8.69,

$$C_F = \frac{dF}{dh} = \frac{KA_0}{h} = \frac{KF}{hp} \quad (8.70)$$

For a hydraulic press with a nominal force  $F_N$ , stroke  $H$ , and pressure  $p$ , the spring constant at the bottom of the stroke for the nominal force is

$$C_F = \frac{KF_N}{Hp} \quad (8.71)$$

As an example, if  $F_N = 6300$  kN (708 tons),  $H = 800$  mm (31.5 in),  $p = 31.5$  MPa (4481 psi), and  $1/K = 7 \times 10^{-6}$  MPa $^{-1}$  ( $9.95 \times 10^{-3}$  ksi $^{-1}$ ),

$$C_F = 357 \text{ kN/mm (1017 ton/in)}$$

The elastic deformation travel is

$$h = \frac{F_N}{C_F} = 17.6 \text{ mm (0.693 in)}$$

The forming velocities can therefore change appreciably compared to the theoretical values during loading because of the compressibility of the fluid medium and the elastic deformation of the press parts. Thus especially in blanking (shearing) processes, problems may be caused by the expansion of the fluid medium during the steep force drop.

The fluid medium ages due to reaction with atmospheric oxygen. This results in the formation of oxides and polymers that are not soluble in oil. Advanced aging can be recognized from the dark color of the oil and an increase in its viscosity. The process of aging is increased by the catalytic action of various metals (such as copper and bronze) as well as by dirt, water, and rust.

The aging rate increases very rapidly at temperatures over 70°C (158°F) [8.16]. Protection against corrosion of the hydraulic aggregates is very important for the life of the unit, and this can be achieved by some special additives.

The fluid media must have sufficient sticking and lubricating properties to avoid mixed friction conditions at very high pressures because of mixtures.

There should be no reaction (chemical) between the fluid medium and the seals, since this would lead to the breaking of the seals, sticking to the metal, and dirtying of the fluid medium.

If there is improper filling or sealing, air can get trapped in the oil. This increases the compressibility of the fluid, and froth formation can occur during removal of the air. Antifroth compounds can be used to prevent air entrapment and froth formation.

If water gets into the hydraulic system because of condensation and leaky seals, the danger of corrosion is increased and the lubrication effect is reduced. Furthermore the water can react chemically with the fluid, forming alcoholic or acidic compounds. The fluid should be checked regularly and changed periodically.

### ***Fluids that Are Difficult to Burn***

In hydraulic presses used for hot forming there exists a danger of sparking a fire in the hydraulic oil in the event of leaks. In order to reduce the danger of fire, special fluids that do not ignite easily have been developed. Even those fluids will catch fire for a short period of time when coming into contact with a fire source. While the mineral oil sparks and continues to burn when brought into contact with hot pieces, fluids that are difficult to burn form gases which put out the flame.

Fire-resistant fluid media are [8.16]:

- 1 Fluids containing water
  - a. Emulsions: oil in water, water in oil
  - b. Solutions: water glycol
- 2 Water-free synthetic fluids
  - a. Chlorinated carbohydrates
  - b. Pure phosphoric acid
  - c. Chlorinated phosphoric acid
  - d. Silicone
  - e. Fluorocarbohydrates

Many of the fluids that are difficult to burn have a higher specific heat and a smaller lubricity than mineral oil. The problems of seals (material) for these types of oils have not yet been solved successfully.

#### 8.4.2 Drive Systems

Fluids are pumped with high pressure into one or more cylinders in hydraulic presses to convert the hydraulic energy to mechanical work. Based on the type of energy source for the fluid, hydraulic flow in forming machines can be classified into two groups [8.18]:

- 1 Hydraulic circuit with flow source
- 2 Hydraulic circuit with pressure source

An ideal flow source supplies the hydraulic cylinders with a constant fluid flow whose magnitude is independent of the system. Correspondingly the ideal pressure source has a constant pressure which is independent of the flow extracted from the pressure source. The systems in the hydraulic presses are in practice only approximately ideal sources.

##### *Presses with Flow Source (Direct Pump Drive)*

The fluid flow from the high-pressure pump is supplied to the hydraulic cylinder through pipelines and control valves. Oil is used as the fluid medium. A simplified representation of a hydraulic press with a direct pump drive is shown in Fig. 8.45.

The pump delivers a definite amount of fluid. The pressure in the hydraulic system develops as a result of the external force and of the resistance to the flow in the system. The efficiency of

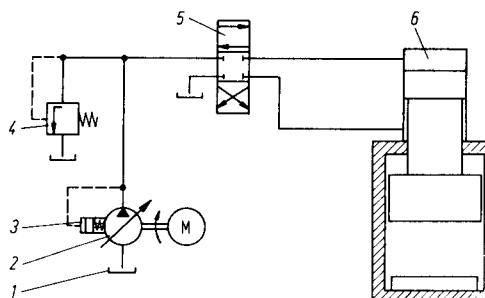


**FIG. 8.45** Schematic of direct-pump-driven hydraulic press. 1—reservoir; 2—adjustable pump; 3—governor; 4—pressure value; 5—4/3 hydraulic valve; 6—hydraulic press cylinder. (After [8.18].)

the drive system is therefore good, even for processes requiring less than the nominal force of the press, since the pump has to meet only the demands of the specific process. The drive can be designed so that the revolutions of the pump and thus the flow rate depend only to a small extent on the pressure in the hydraulic circuit. Hence with direct-pump-driven hydraulic presses the required velocity can be obtained even in processes with large variations in force requirements. This may become extremely important in processes like hot extrusion of materials that are difficult to extrude.

The speed of the press can be varied infinitely by regulating the flow from the pump. These types of presses are therefore especially suitable for automated press lines used in production lines.

Due to design limits on the flow and performance of high-pressure pumps, several pumps with different flow rates are used for large presses. By combining the appropriate pumps, the working velocity can be varied in discrete steps. The pumps not required for a particular combination are

either switched off or run idle. Furthermore by combining several pumps with the same flow in very large units with a pump with adjustable flow, the velocity can be varied infinitely [8.19].

An important characteristic of the direct-driven hydraulic presses is that the power requirement of the pump and the drive motor be designed for the maximum power requirement of the press [8.20]. The power requirement of the pump is

$$P_p = \frac{1}{\eta_H} F_N v_{\max} \quad (8.72)$$

Large pumps are necessary for large nominal forces and/or velocities. This will require very high input power requirements from the supply line.

#### **Presses with Pressure Source (Accumulator Drive)**

The fluid is delivered to the hydraulic cylinders from the accumulator through the pipelines and valves. A schematic representation of an accumulator-driven hydraulic press is shown in Fig. 8.46. As the fluid medium, water with 1–3% oil addition is used [8.19]. The modern accumulators are high-pressure units in which the fluid medium is under pneumatic pressure. The pressure of air decreases due to expansion when the fluid is removed from the accumulator. The pressure drop should be kept within limits, usually about 10–15%. The accumulator delivers the fluid at a given hydrostatic pressure. The quantity of fluid flow and thus the velocity of the press are determined by the resistance in the system, which in turn is dependent on the forming force and losses due to flow and friction. The velocity of the press can further be controlled by the regulating valve. The excess hydraulic energy is thereby converted into heat energy.

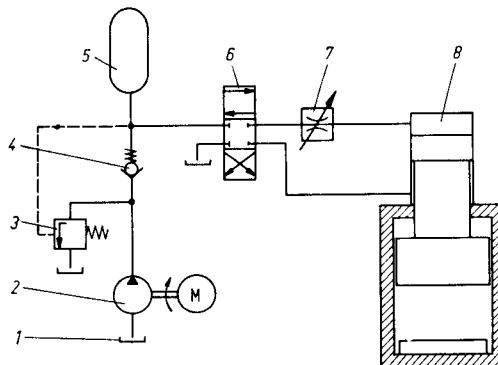


**FIG. 8.46** Schematic of a hydraulic circuit for an accumulator-driven hydraulic press. 1—reservoir; 2—pump with motor; 3—pressure valve; 4—reverse-flow control valve; 5—accumulator; 6—4/3 hydraulic valve; 7—flow control valve (adjustable); 8—hydraulic press cylinder. (After [8.18].)

An advantage of the accumulator-type hydraulic presses is that the pumps and the driving motors have to be designed to an average power of the press only, unlike for the direct-pump-driven presses. In this case the pumps deliver to the accumulator over a longer period of time, and the accumulator takes care of the short peaks in power requirements. A disadvantage, however, is that the pump always has to deliver against the full working pressure in the accumulator, although the nominal force of the press may not be used all the time [8.19].

#### **Areas of Application of Drive Systems**

Recent trends indicate an increasing application of direct-driven-presses. The limit is set by the maximum capacity of the available pump. The direct drive is used for small- and medium-size

presses and for large presses with small working velocities. The limit for forging presses is at present about 20,000–30,000 kN (2240–3360 tons). Infinitely variable working velocities and dependable and quick control using solenoid valves (especially when oil is the fluid medium) have been instrumental in increasing the application range of the direct-driven hydraulic presses in mass production. Hydraulic presses used in sheet-metal working and cold forging are also generally direct-driven.

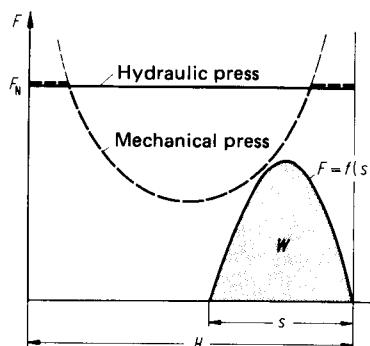


**FIG. 8.47** Comparison of a hydraulic press and a mechanical press with reference to force–travel diagram.  $F = f(s)$  of a forming process.

For presses with very large nominal forces and/or large working velocities, accumulator-type hydraulic presses are preferred. Several presses can be supplied from one accumulator if the working strokes are at different periods for these presses. However, the trend toward the use of direct-driven hydraulic presses continues to increase since the handling times are decreasing with the use of manipulators, resulting in a higher number of useful strokes of the press. In such cases the time available for maintaining the pressure in the accumulator also becomes shorter, and the required pump capacities approach those for direct-driven presses [8.19].

#### 8.4.3 Characteristics of Hydraulic Presses

The available force during the ram stroke is not a constant in a mechanical press and depends on the type of drive (crank, knuckle joint, etc.), as shown in Fig. 8.47. In a hydraulic press, however, the entire force is available throughout the course of travel. Yet this force cannot be exceeded (presses controlled by force).

For loading the press, the force–travel diagram of the process is important:

$$F = F(s) \quad W = \int_0^s F \, ds \quad (8.73)$$

Neglecting friction and inertia, the following relations are valid for hydraulic presses:

$$\text{Press force as per Eq. 8.66} \quad F \approx pA \quad (8.74)$$

$$\text{Theoretical tool velocity} \quad v = \frac{\dot{V}}{A} \quad (8.75)$$

$$\text{Work done} \quad W = \int_0^s pA \, ds \quad (8.76)$$

For the design of hydraulic presses the pressure  $p$  and the flow rate  $\dot{V}$  are the most important parameters.

#### 8.4.4 Designs of Hydraulic Presses

Hydraulic presses are used in all areas of metal forming where linear tool movement is necessary. Correspondingly there are several designs and sizes of hydraulic presses available.

Depending on the type of drive, hydraulic presses are classified as (1) direct-driven presses and (2) accumulator-type presses.

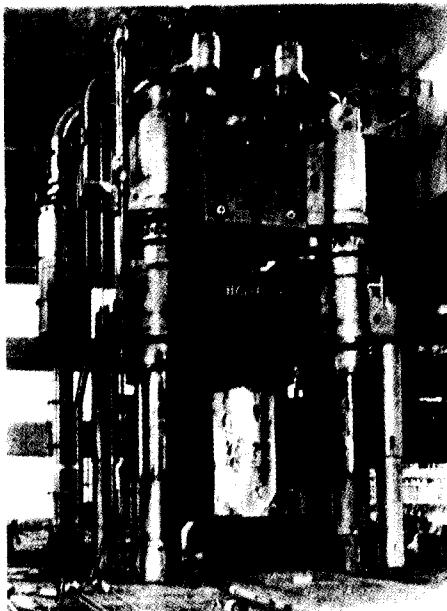


**FIG. 8.48** Three-stage hydraulic open-die forging press in four-column design. Nominal force 60,000 kN (6720 ton); force steps 20,000/40,000/60,000 kN (2240/4480/6720 ton); accumulator drive  $p = 200$  bar (2940 psi). (*Courtesy of Hydraulik.*)

Hydraulic presses can be further classified according to the purpose for which they are used: sheet-metal presses and bulk-forming presses.

A common method of classifying hydraulic presses is based on the process for which they are used. Examples are open-die forging press, hot-extrusion press, drawing press, and so on.

The frame designs for the hydraulic presses follow the same rules as for mechanical presses and depend on their applications (cold forming, sheet forming, etc.). Special designs have also been developed for specific applications. Figs. 8.48 and 8.49 show hydraulic presses used in various forming processes.

## 8.5 MECHANICAL PRESSES

The machines listed in Sec. 8.1.1, which belong to the category of presses controlled by stroke, are generally called mechanical presses.

This group of presses is probably the one used most frequently in batch forming. Based on the application requirements, several designs are available. A classification according to the type of drive will provide useful information on the working of presses belonging to this category.

Two major groups of mechanical presses are:

- 1 Presses with crank drive
- 2 Presses with cam drive (Fig. 8.50)

Crank presses may have either simple or extended crank drives. Conventional crank presses (the total stroke cannot be varied) and eccentric presses (the total stroke is variable) belong to the

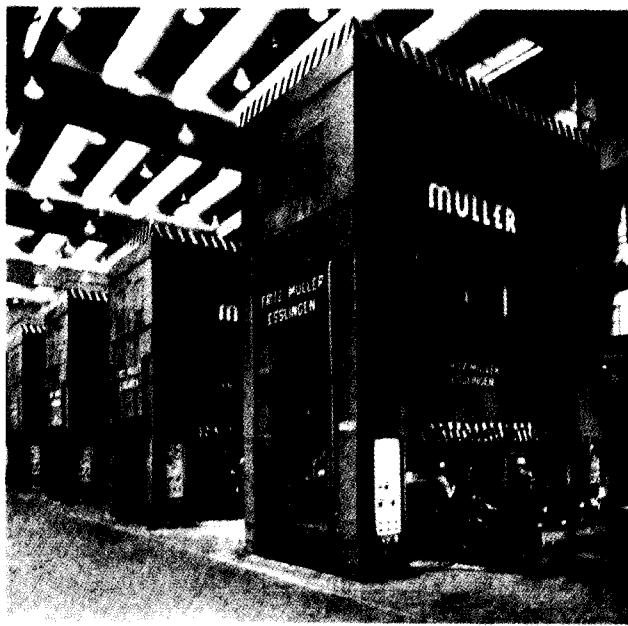


**FIG. 8.49** Press line for manufacturing automobile panels. (Courtesy of Müller-Weingarten.)

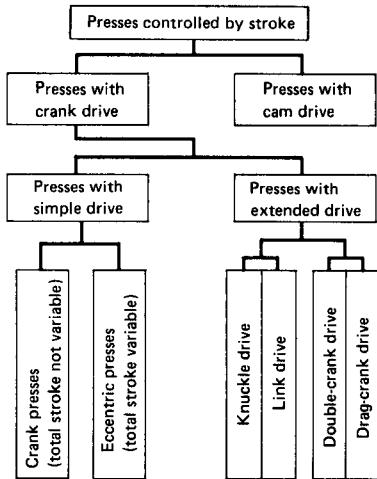


**FIG. 8.50** Classification of presses controlled by stroke, based on main drive.

simple drives. If either a knuckle or a lever is used to extend the crank drive, the designs are called knuckle joint or link drive presses. Multipoint presses are those in which two or more cranks are used to drive the same ram.

Other methods of classification are:

Frame type: C or closed frame

Number of useful motions: Single or more

Location of drive: Top drive (connecting rod subjected to compression) and bottom drive (connecting rod subjected to tension)

Positioning of drive shaft: Longitudinal or cross shaft

Number of connecting rods: One-, two-, or four-point drive

Some of the above drives are identified in the schematic representation of the various crank drives in Fig. 8.51.

### **8.5.1 Kinetics and Kinematics of Mechanical Presses**

The kinetic and kinematic behavior of mechanical presses, especially the force obtainable from the ram and its travel cycle, are determined from the type and design of the main drive. The most common drives are shown schematically in Fig. 8.52. For the various drives, the areas of application are as follows:

- 1 Simple crank drives, generally with compressive loading on the connecting rod, are the most common ones. A detailed analysis of these types of drives is presented in the next subsection.
- 2 Extended or modified crank drives are especially suitable for processes which require a smaller velocity in the working range than that obtainable in simple crank drives, or where large ram forces are required for relatively small ram travels. The link and multicrank drives are suitable for the former operation, and the knuckle-joint drive is suitable for the latter. The knuckle-joint crank drive is analyzed in detail in a later subsection.
- 3 Cam drives allow any arbitrary travel pattern for the ram. Their applications are, however, limited to presses of smaller tonnage.

#### ***Direct (Simple) Crank-Drive Mechanical Presses***

**Forces and moments:** The torque  $M_C$  (Fig. 8.53) on the crankshaft causes a tangential force  $F_t$  in the direction of motion of the crank end, a radial force  $F_r$  perpendicular to the movement of the crank end, and a force  $F_{CR}$  on the connecting rod (Fig. 8.54a). Neglecting friction, the above forces can be calculated as

$$\text{Tangential force} \quad F_t = \frac{M_C}{r} \quad (8.77)$$

$$\begin{aligned} \text{Connecting-rod force} \quad F_{CR} &= \frac{F_t}{\sin(\alpha + \beta)} \\ &= \frac{M_C}{r \cdot \sin(\alpha + \beta)} \end{aligned} \quad (8.78)$$

$$\begin{aligned} \text{Radial force} \quad F_r &= F_{CR} \cos(\alpha + \beta) \\ &= \frac{M_C}{r \cdot \tan(\alpha + \beta)} \end{aligned} \quad (8.79)$$

The reaction force due to the radial force must be supported by the crankshaft bearings.

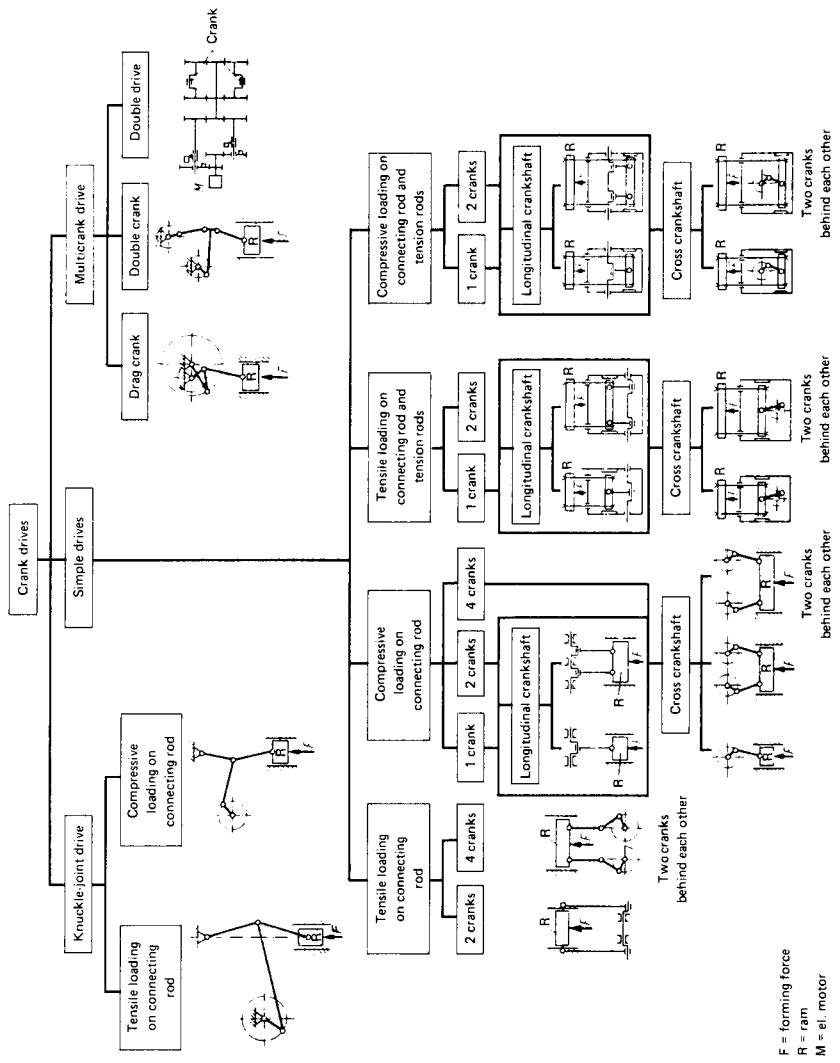
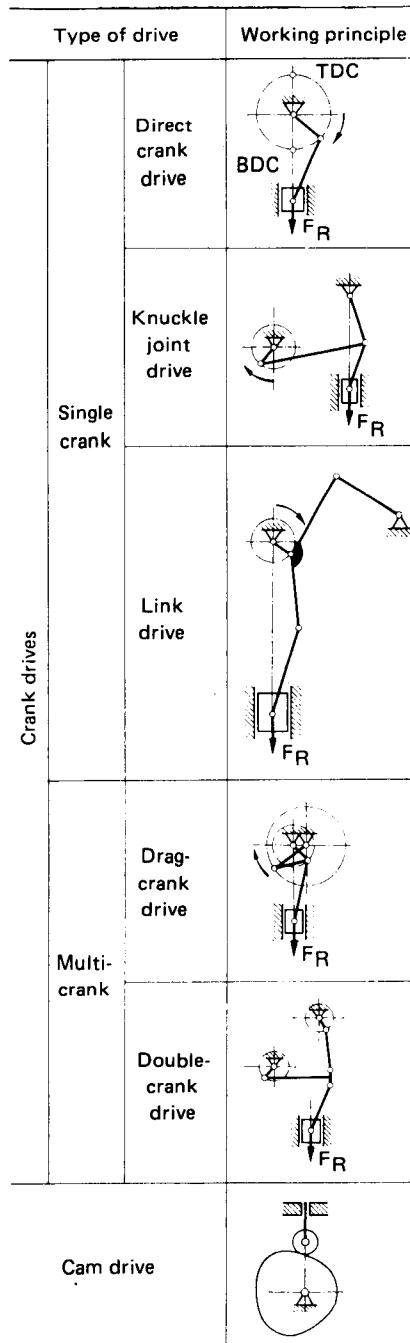
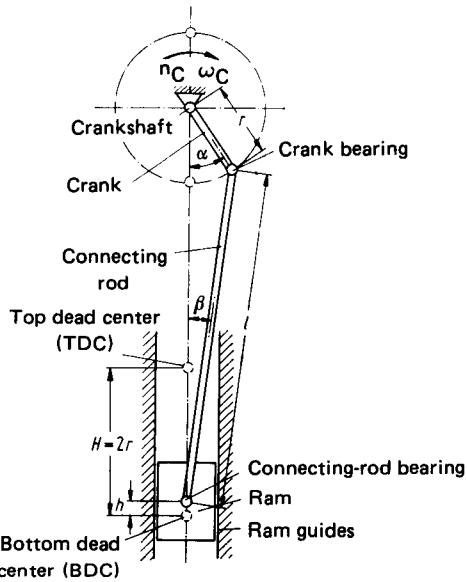


FIG. 8.51 Types of crank drives in mechanical presses. (After [8.21].)



$F_R$  = ram force

**FIG. 8.52** Schematics of various drives. TDC—top dead center; BDC—bottom dead center. (After [8.21].)



**FIG. 8.53** Symbols and definitions for simple direct crank drive.  $r$ —length of crank;  $l$ —length of connecting rod;  $\lambda = \frac{r}{l}$ —length ratio;  $\alpha$ —crank angle;  $\beta$ —angle of connecting rod corresponding to  $\alpha$ ;  $H = 2r$ —total stroke;  $h$ —ram travel to bottom dead center.

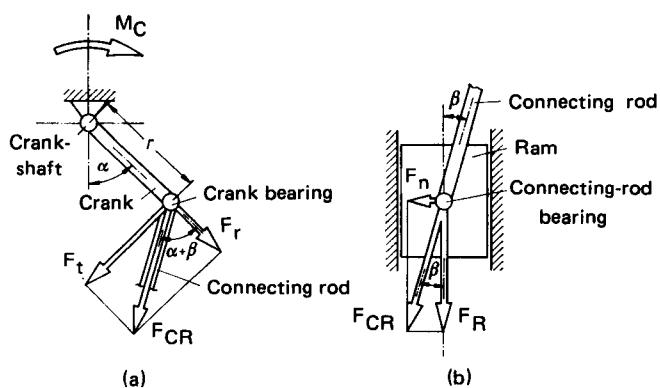


**FIG. 8.54** Forces in simple crank drive. (a) Crank load. (b) Connecting-rod load.

The connecting-rod force  $F_{CR}$  causes the ram force  $F_R$  and a force  $F_n$  perpendicular to it. The following equations are valid for these forces:

$$\begin{aligned} \text{Ram force } F_R &= F_{CR} \cos \beta \\ &= \frac{M_C}{r} \frac{\cos \beta}{\sin(\alpha + \beta)} \end{aligned} \quad (8.80)$$

$$\begin{aligned} \text{Normal force } F_n &= F_{CR} \sin \beta \\ &= \frac{M_C}{r} \frac{\sin \beta}{\sin(\alpha + \beta)} \\ &= F_R \tan \beta \end{aligned} \quad (8.81a) \quad (8.81b)$$

The reaction force  $F_n$  will be supported by the guides.

The length  $l$  of the connecting rod is generally much larger than the crank length  $r$  in simple-drive crank presses. The value  $\lambda = r/l$  lies between  $\frac{1}{4}$  and  $\frac{1}{5}$ , and on the average  $\lambda = \frac{1}{4}$ . This leads to the angle  $\beta$  becoming small. (For  $\lambda = 0.1$ , for example,  $\sin \beta = \lambda \sin \alpha$ , and  $\beta$  will have a maximum angle of  $6^\circ$ .) Hence Eq. 8.80 can be simplified with  $\cos \beta = 1$  and  $\sin(\alpha + \beta) = \sin \alpha$ ,

$$F_R = \frac{M_C}{r} \frac{1}{\sin \alpha} \quad (8.82)$$

The ram force is therefore a function of the crank torque, its radius  $r$ , and the crank angle  $\alpha$ .

The turning moment or torque  $M_C$  is determined for a mechanical press by specifying a definite force  $F_N$  corresponding to a particular crank angle  $\alpha_N$ . This angle is the useful or nominal angle, and the force is the rated or nominal force  $F_N$ . The necessary torque required for generating this force is

$$M_C = F_N r \sin \alpha_N \quad (8.83)$$

The ram force at any crank angle will therefore be using Eqs. 8.82 and 8.83,

$$F_R = F_N \frac{\sin \alpha_N}{\sin \alpha} \quad (8.84)$$

Some standards specify that the nominal force for eccentric and crank presses must be achievable at a stroke corresponding to a  $30^\circ$  crank angle from the bottom dead center.

For a general design with  $\alpha_N = 30^\circ$ , the turning moment is

$$M_C = F_N r \sin 30^\circ = F_N \frac{r}{2} \quad (8.85)$$

and the ram force is

$$F_R = F_N \frac{\sin 30^\circ}{\sin \alpha} = \frac{F_N}{2} \frac{1}{\sin \alpha} \quad (8.86)$$

The ratio  $F_R/F_N$  is plotted in Fig. 8.55 against the crank angle. For the forming region of  $90^\circ \leq \alpha \leq 0^\circ$  the following observations can be made:

- 1 For  $\alpha > 30^\circ$  the available ram force decreases with increasing crank angle and reaches a minimum value  $F_{R,\min}$  which is half the nominal force (at a crank angle  $\alpha = 90^\circ$ ). If the ram force increases (at any point of the crank rotation) more than the available force as given by Eq. 8.86, a higher torque will be required from the crankshaft, which may lead to overloading of the drive. In the region  $90^\circ \leq \alpha \leq 30^\circ$  the permissible ram force is either smaller or, at most, equal to the available ram force.
- 2 For angles  $\alpha < 30^\circ$ , the ram force increases very rapidly with decreasing crank angle and theoretically has an infinite force at the bottom dead center ( $\alpha = 0^\circ$ ). Since the nonrotating

parts in a press are designed to withstand the nominal force  $F_N$  of the press only, the permissible ram force in the region  $30^\circ \leq \alpha \leq 0^\circ$  is either smaller or, at most, equal to the nominal force of the press.

The area of application of mechanical presses is determined by the variation of the ram force with the ram travel  $h$  rather than by its variation with the crank angle  $\alpha$ . Using the same designations as in Fig. 8.53, the ram travel  $h$  is given by

$$h = r(1 - \cos \alpha) + l(1 - \cos \beta) \quad (8.87)$$

and for  $\lambda \leq 0.4$ , Eq. 8.87 changes to

$$h = r[(1 - \cos \alpha) + \frac{1}{2} \lambda \sin^2 \alpha] \quad (8.88)$$

The variation of the ram travel as a function of the crank angle for a value of  $\lambda = 0.1$  is plotted in Fig. 8.56. For a simple crank drive the ram force variation with ram travel is shown in Fig. 8.57. It is seen that the ram can make the nominal force available only during a relatively

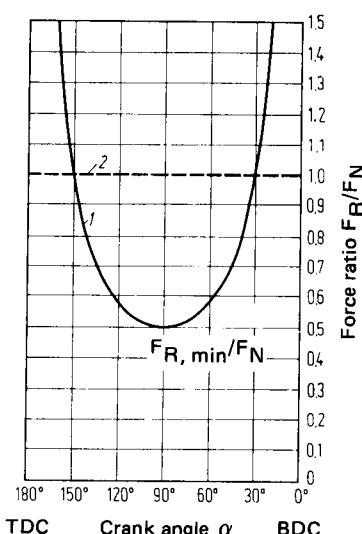


**FIG. 8.55** Limits of ram force in normal crank drive. 1—force limit for rotating parts; 2—force limit for nonrotating parts.

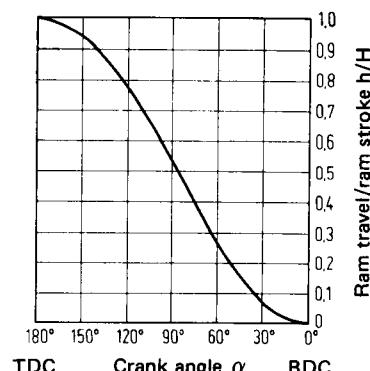


**FIG. 8.56** Relation between ram travel and crank angle in simple crank drive.  $\lambda = 0.1$ .

short ram travel ( $h_N = 0.073H$ ). The ram force decreases very rapidly with increasing stroke and reaches its minimum value at half the total stroke. This results in the nominal force not being fully utilized in processes requiring long forming travel (deep drawing) and where a force peak occurs at the beginning of the process (cold extrusion). The usable travel may not be fully utilized, on the other hand, in processes requiring a short stroke (blanking) and where the force peak occurs at the end of the process (die forging). It is therefore a practice to design the crank drive according to the process for which the press is to be used so that the nominal force is made available at required useful crank angles. Based on Eq. 8.83, the crankshaft torque changes with the useful crank angle  $\alpha_N$ , and the ram force  $F_R$  changes accordingly (Eq. 8.84). Table 8.6 gives the design data for presses used for specific processes [8.22]. The variation of the permissible ram force as a function of ram travel for various useful crank angles is shown in Fig. 8.58.

It is easier and more economical to design a press to suit a particular deformation process by selecting the proper useful crank angle than to match the machine with a specific stroke value. This will be explained in the following example.

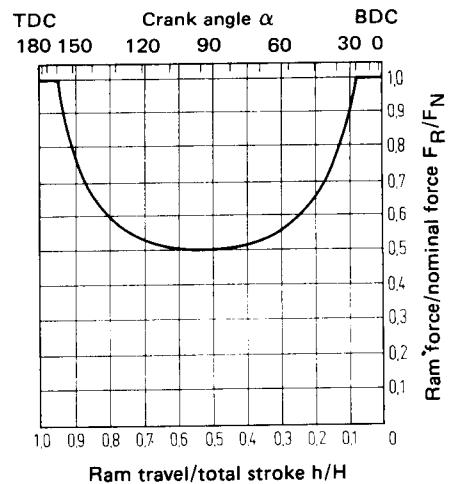


**FIG. 8.57** Variation of ram force as a function of ram travel for simple crank drive.  $\lambda = 0.1$ .

**Table 8.6** Summary of Important Design Data for Various Crank Presses Depending on Useful Crank Angle.

Application	Design $\alpha_N$	$h_N/H$	$F_{R,\min}/F_N$	$M_C/M_{C30}$
Hot forging	10°	0.008	0.17	0.35
Blanking	20°	0.033	0.34	0.68
Average design	30°	0.073	0.50	1.00
Cold extrusion	45°	0.158	0.71	1.41
Deep drawing (utensils)	75°	0.398	0.97	1.93

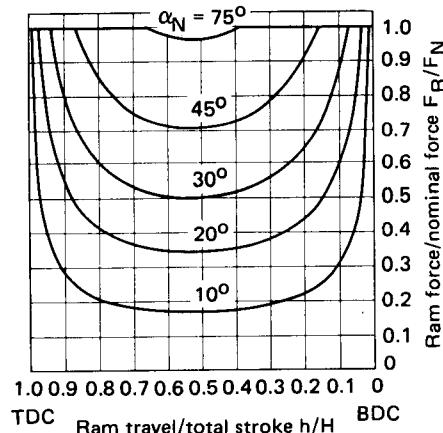


**FIG. 8.58** Variation of ram force with ram travel for several useful crank angles.  $\lambda = 0.1$ .

In a simple crank drive the available nominal force is in the range of  $0 \leq h \leq h_N (= 0.073H)$ . An increase of this range of the nominal force (for example, doubling it) can be achieved either by increasing the total stroke to double its value or by changing the useful crank angle from  $\alpha_N = 30^\circ$  to  $\alpha_N = 45^\circ$  (with  $h_N = 0.158H$ ). The required turning moment on the crankshaft is also doubled if the total stroke value is doubled (Eq. 8.83), whereas for an increased useful crank angle to achieve the same effect, the turning moment is increased only by a factor of 1.41. (See also Table 8.6.)

The work capacity  $E_C$  of a normal crank-driven press with continuous stroking is equal to the product of the nominal force  $F_N$  and the corresponding ram travel  $h_N$ ,

$$E_C = F_N h_N \quad (8.89)$$

The work capacity of a press according to Eq. 8.89 is represented by the shaded area in Fig. 8.59, which shows the variations of ram force with ram travel for different types of press operation. The shaded rectangular portion can be considered as the work done in a deformation process requiring a deformation force  $F (= F_N)$  and a travel of  $h (= h_N)$ .

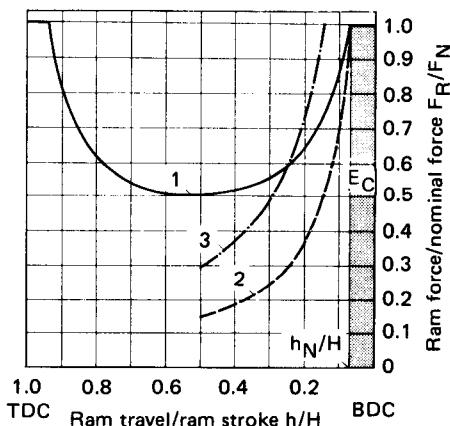


**FIG. 8.59** Ram-force-ram-travel diagram. 1—limiting curve for normal design; 2—limiting curve for processes whose force-travel diagrams can be approximated to be rectangles: continuous stroking ( $E_M = E_C$ ); 3—limiting curve for processes whose force-travel diagrams can be approximated to be rectangles: single-stroke operation ( $E_M = E_S = 2E_C$ ).

For processes whose force-travel diagrams can be approximated by rectangles (such as cold extrusion) with deformation travel  $s > h_N$ , a limit  $F$  is automatically set on the forming force with regard to the available energy from the press. The work performed is

$$W = Fs \quad (8.90)$$

From the condition  $E_C \leq W$  (Eq. 8.1b) it follows that the forming force should not exceed

$$F \leq \frac{F_N h_N}{s} \quad (8.91)$$

Based on the above equation, limiting curves for various press operations are plotted in Fig. 8.59. It is clear that for processes requiring a deformation travel  $s > h_N$ , only a part of the available ram force can be used. In order to utilize the press capacity fully from the points of view of both force and energy, some deviations may have to be made from Eq. 8.89 with regard to the available work capacity of the machine.

It is also relevant to point out at this stage that the work capacity available from the press for a single-stroke operation  $E_S$  can be twice that for a continuous operation ( $E_S = 2E_C$ ) [8.22]. This leads to a higher available ram force for single-stroke operation (Fig. 8.59). Since the productivity is lower in single-stroke presses, a compromise must be made between higher productivity (continuous operation) and larger work capacity (single-stroke operation).

**Ram velocity:** The ram velocity is an important time-related characteristic. Assuming a constant circumferential velocity of the crank end, the ram velocity is

$$\begin{aligned} v_R &= r\omega \frac{\sin(\alpha + \beta)}{\cos \beta} \\ &= r \frac{\pi n_C}{30} \left( \sin \alpha + \frac{1}{2} \lambda \sin 2\alpha \right) \end{aligned} \quad (8.92)$$

The ram velocity according to Eq. 8.92 has been plotted as a function of crank angle in Fig. 8.60 and as a function of ram travel in Fig. 8.61 for a total stroke  $H = 2r = 1 \text{ mm}$  (0.040 in), crank revolutions  $n_C = 1 \text{ min}^{-1}$ , and with  $\lambda = 0.1$ .

The ram velocity of any other press system for which the total stroke and the crank revolutions are known can be obtained by using these figures in conjunction with Eq. 8.92.

The ram velocity attains its maximum value around half the total stroke and decreases to zero at the end positions of the ram.

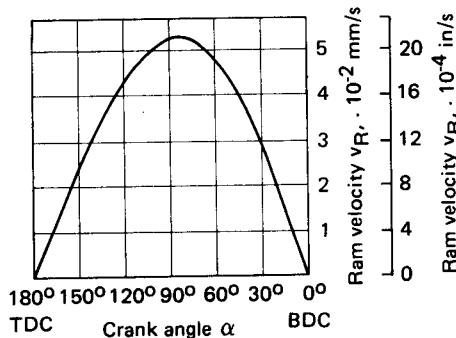


FIG. 8.60 Ram velocity as a function of crank angle.  
 $H = 1 \text{ mm}$  (0.040 in);  $n_C = 1 \text{ min}^{-1}$ ;  $\lambda = 0.1$ .

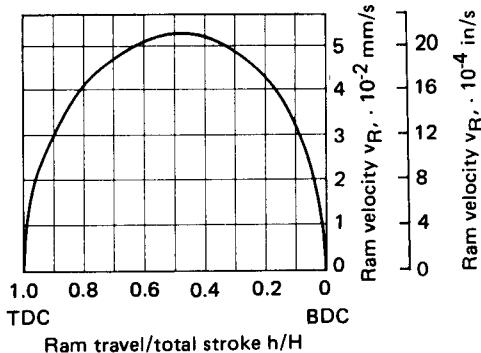


FIG. 8.61 Ram velocity as a function of ram travel.  $H = 1 \text{ mm}$  (0.040 in);  $n_C = 1 \text{ min}^{-1}$ ;  $\lambda = 0.1$ .

For many forming processes, such as automobile frame drawing and cold extrusion, a small ram velocity at the time of contact is desirable. The total stroke of the press has the maximum effect on the ram velocity. Hence for forming processes requiring longer deformation travel, presses with small strokes should be used.

### Eccentric Presses

**Stroke adjustment:** The stroke settings in some small- and medium-size presses can be changed. The principle of stroke adjustment is shown in Fig. 8.62.

The center  $O_S$  of the eccentric shaft  $S$  is offset with respect to the eccentric hub  $E$  with its center at  $O_H$  by  $e_1$  ( $e_1 = O_H - O_S$ ). The bushing  $B$  on the bore can be rotated. The bore is

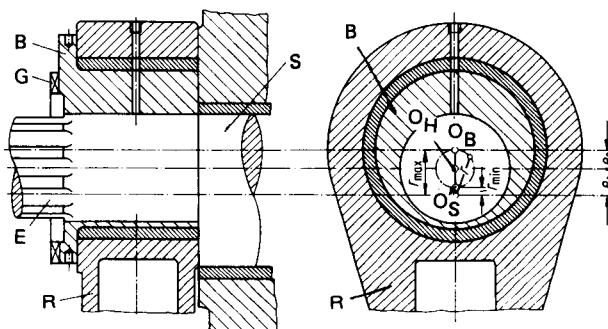


FIG. 8.62 Principle of stroke adjustment. (After [8.15].)

eccentric with the eccentric hub by  $e_2 = O_B - O_H$ . The connecting rod  $R$  is mounted on the bushing  $B$ . Rotation of the bushing  $B$  on the hub changes the distance  $O_S O_B$ , which corresponds to the effective crank radius  $r = H/2$ . The center  $O_B$  of the bushing traverses the path as shown in the right-hand side of Fig. 8.62. The bushing can be fixed at any discrete position on the hub by means of a ring (not shown in the figure) whose inner teeth mesh with the outer teeth of the bushing and which is located on the wedge profile of the hub. The ring cannot rotate, but it can be moved axially. The change of stroke is possible only in discrete steps based on the module of the gear  $G$ .

Between the eccentricities  $e_1$  and  $e_2$  and the maximum and minimum number of total strokes, the following equations are valid:

$$\text{Maximum total stroke } H_{\max} = 2(e_1 + e_2) \quad (8.93)$$

$$\text{Minimum total stroke } H_{\min} = 2(e_1 - e_2) \quad (8.94)$$

It follows from Eqs. 8.93 and 8.94 that the stroke range can be varied by

$$\begin{aligned} \Delta H &= H_{\max} - H_{\min} \\ &= 4e_2 \end{aligned} \quad (8.95)$$

The range of stroke change is, however, limited from the point of view of design considerations. For presses with medium capacities, a ratio of  $H_{\max}/H_{\min} \leq 10$  can be achieved.

**Effects of stroke adjustment:** A change of stroke leads to a change of the useful nominal force and of the ram velocity, whereas the work capacity of the press is not affected. Generally the drive of an eccentric press is designed for the largest stroke so that the nominal force of the press is available at  $\alpha_N = 30^\circ$ . The variation of the ram force with crank angle and ram travel is as shown in Figs. 8.55 and 8.57.

Assuming that the value of the turning moment on the eccentric shaft for the maximum total

stroke (Eq. 8.85) does not change with the change of stroke, the permissible ram force for any stroke  $H (= 2r)$  can be obtained from Eq. 8.82 as

$$\begin{aligned} F_R &= \frac{M_C}{r \sin \alpha} \frac{1}{r} \\ &= \frac{F_N}{2} \frac{r_{\max}}{r} \frac{1}{\sin \alpha} \\ &= \frac{F_N}{2} \frac{H_{\max}}{H} \frac{1}{\sin \alpha} \end{aligned} \quad (8.96)$$

The permissible ram force as given by Eq. 8.96 is plotted for  $0.4H_{\max} \leq H \leq H_{\max}$  against the crank angle in Fig. 8.63. It is seen from this figure that a decrease of the total stroke increases the useful crank angle. An increase in the useful crank angle pushes the minimum ram force to higher values (for  $H = H_{\max}/2$ ,  $F_{R,\min} = F_N$ ) and increases the range of ram travel over which the nominal force of the press is available (Fig. 8.64) (for  $H \leq H_{\max}/2$ ,  $F_R = \text{constant} = F$ , and also  $h_N = H$ ).

The last mentioned feature is especially advantageous if the characteristics of the press are to be matched with the requirements of the forming process (Fig. 8.64). The force–travel diagram of a blanking process is shown in that figure for a maximum force  $F_{\max} = F_N$  and the completed work  $W = E_C$ . As can be seen, the process cannot be carried out at the maximum ram stroke, since at the beginning of the process  $F > F_R$ . By reducing the ram stroke to  $H = 0.6H_{\max}$ , the limiting curve is displaced toward a higher ram force minimum, and at the beginning of the process  $F \leq F_R$ .

The ram velocity also changes with the change of stroke (Eq. 8.92). However, the basic variation of the ram velocity with the ram stroke remains the same as in the crank press.

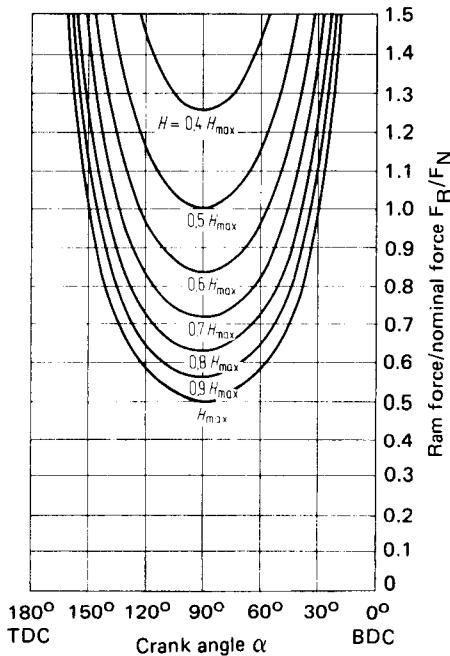


**FIG. 8.63** Effect of stroke adjustment on the controlling ram force. Normal design is  $H = H_{\max}$ .

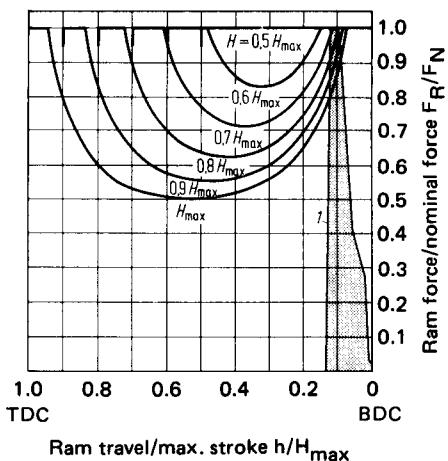


**FIG. 8.64** Ram force limits as a function of ram travel. Normal design is  $H = H_{\max}$ . 1—force-travel diagram of a blanking operation.

### Knuckle-Joint Presses

The knuckle-joint presses are widely used among the presses with extended crank drives.

**Design:** The knuckle-joint system consists of a crank-drive system connected to the rod activating the ram through a knuckle joint pivoted through an oscillating lever. The two common systems of knuckle-joint drives are shown in Fig. 8.65, where the connecting rod is either under tension (Fig. 8.65a) or under compression (Fig. 8.65b). In special under-floor-driven knuckle-joint presses the connecting rod is under tension [8.23]. The ram force is a maximum when the transmitting angle  $\psi_{\max} = 90^\circ$ , that is, when the connecting rod is at a right angle to the stretched knuckle system [8.24]. In order to ensure that the ram does not get locked at the bottom dead center, the knuckle-joint system has a slight inclination toward its pivoting point at the bottom dead center.

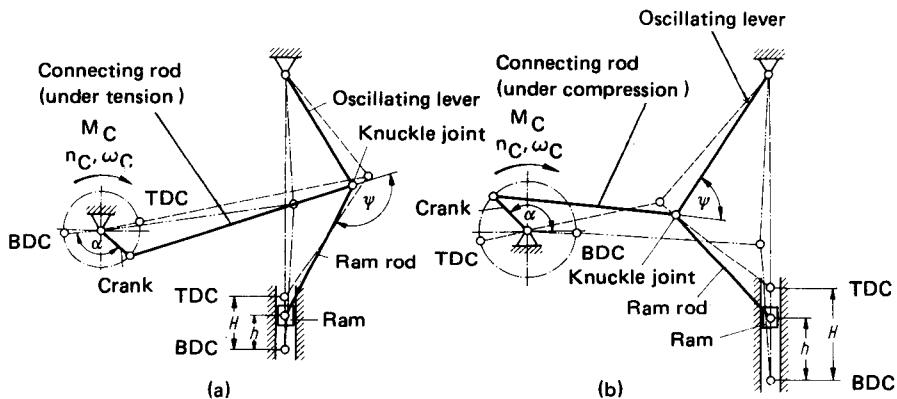


**FIG. 8.65** Schematic and major components of knuckle-joint drive systems. (a) Connecting rod under tension. (b) Connecting rod under compression.

**Ram force and work capacity:** An analytical determination of the forces and moments requires considerable effort. Graphic methods may be used to obtain the ram force variation at different crank angles (Fig. 8.66). For a given constant crankshaft torque, which is measured at the instant when the ram force is equal to the nominal force (at a useful crank angle of  $\alpha_N = 30^\circ$ ), the ram force variation at different crank angles is shown in Fig. 8.67 for a knuckle-joint drive with the connecting rod under tensile load. The variation of the ram force in a crank press is also plotted on the same figure. The ram force increases to infinity at the lower positions of the ram in knuckle-joint presses also. The minimum ram force occurs at an angle  $\alpha = 130^\circ$  before the bottom dead center. The value  $F_{R,\min} = 0.05F_N$  is very much lower than the minimum ram force available in a crank press ( $F_{\min} = 0.5F_N$ ).

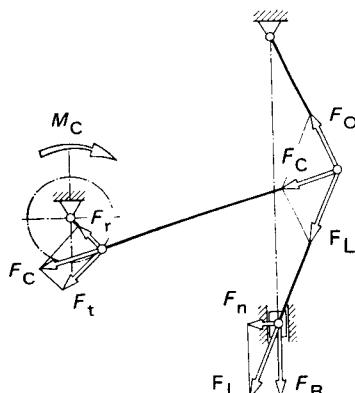


FIG. 8.66 Forces in the linkages of a knuckle-joint drive.  $F_C$ —connecting rod force;  $F_O$ —oscillating level force;  $F_L$ —connecting level force;  $F_R$ —ram force;  $F_n$ —normal force;  $F_r$ —radial force;  $F_t$ —tangential force.

As in crank presses, for knuckle-joint presses the following are valid: in the region  $0^\circ \leq \alpha \leq \alpha_N$  the permissible ram force is equal to or smaller than the nominal press force, and for  $\alpha > \alpha_N$  the permissible ram force is equal to or smaller than the force available from the crankshaft torque.

The ram-travel–crank-angle variation of a knuckle-joint drive and, for comparison, the ram-travel–crank-angle curve of a crank drive are shown in Fig. 8.68. The ram movement from top-dead center to bottom dead center requires more than half of a crankshaft rotation in a knuckle-joint press. In this region half of the stroke is achieved within  $60^\circ$  of the crankshaft rotation whereas the remaining portion requires a larger crankshaft rotation. Near the bottom dead center a crankshaft rotation of  $60^\circ$  results in a ram travel of only  $0.05H$ .

From the force–travel diagram drawn in Fig. 8.69 it is clear that in a knuckle-joint press designed to deliver the nominal force at a crank angle  $\alpha_N = 30^\circ$  the nominal force is available only through a small stroke ( $h_N \approx 0.005H$ ). This proportion corresponds to a crank press with a useful crank angle  $\alpha_N = 7^\circ 30'$ .

If it is desired to have in a knuckle-joint press a similar ram-force–travel variation as in a normal crank press, the knuckle-joint drive must be designed with a useful crank angle  $\alpha_N = 67^\circ$

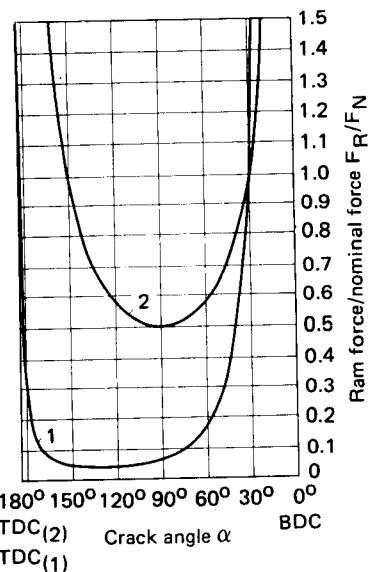


FIG. 8.67 Ram force crank angle variations. 1—knuckle-joint drive,  $\alpha_N = 30^\circ$ ; 2—crank drive.

(Fig. 8.69). However, the minimum available ram force is very much lower here than for the corresponding crank press. Based on the force-travel curve, knuckle-joint presses are suitable for processes with small deformation travels and where the maximum force occurs at the end of the process (such as coining or tube extrusion).

The design features of the various knuckle-joint drives vary so considerably that the force-travel and the travel-crank-angle curves differ greatly from each other. It is therefore a standard practice to indicate the availability of the nominal force at a definite ram travel  $h_N$  instead of the traditional crank-angle position  $\alpha_N$ .

The magnitude of the work capacity of knuckle-joint presses is  $E_C = F_N h_N$ , as in crank presses.

**Ram velocity:** The ram velocity in knuckle-joint presses is shown in Fig. 8.70 as a function of ram travel. The variation is similar to that of the ram velocity in crank presses (which is also plotted on the same figure). In the region of larger ram travels the ram velocity is higher in knuckle-joint presses than in a comparable crank press (total stroke and crankshaft revolutions). In the working region the ram velocity is smaller in knuckle-joint presses.

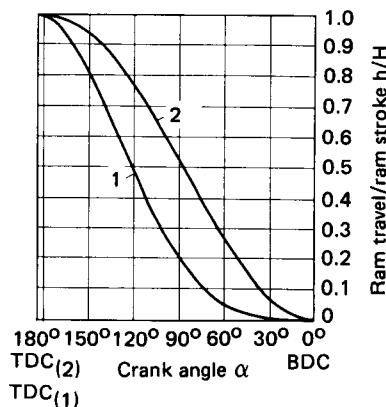


**FIG. 8.68** Relation between crank angle and ram travel. 1—knuckle-joint drive of Fig. 8.66; 2—crank drive,  $\lambda = 0.1$ .

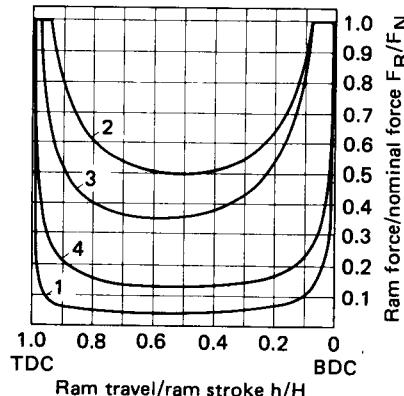


**FIG. 8.69** Force-travel curve for knuckle-joint drives of different designs. 1—knuckle-joint drive of Fig. 8.66,  $\alpha_N = 30^\circ$ ; 2—simple crank drive,  $\alpha_N = 30^\circ$ ; 3—knuckle-joint drive of Fig. 8.66,  $\alpha_N = 67^\circ$ ; 4—simple crank drive,  $\alpha_N = 7^\circ 30'$ .

### 8.5.2 Accuracy Characteristics of Mechanical Presses

The accuracy of presses is important under both unloaded and loaded conditions.

**Accuracy in the unloaded state:** The manufacturing accuracy of the press influences the accuracy of press operation in the unloaded state. The geometry of the tool-mounting space and the accuracy of the ram movement are two important characteristics in the unloaded state [8.24]. Important factors for machine accuracy are:

- 1 Parallelism of the bed with respect to the ram face
- 2 Perpendicularity of the ram movement with respect to the bed
- 3 Parallelism of ram bore and ram movement, especially when the top tool is clamped onto the ram bore by a spigot

Guidance values for permissible deviations from the geometrically ideal conditions have been standardized for single-column and double-column eccentric presses [8.9], [8.10]. These values more or less correspond to the values in [8.11]. The permissible play in the ram guidance has,

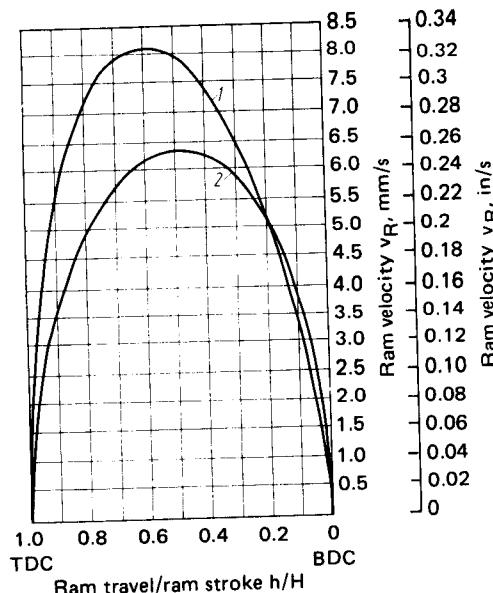


FIG. 8.70 Ram velocity as a function of ram travel. 1—knuckle-joint drive of Fig. 8.66; 2—crank drive ( $\lambda = 0.1$ ) with same total stroke [ $H = 120 \text{ mm (4.72 in)}$ ] and crank revolutions ( $n_C = 1 \text{ min}^{-1}$ ).

however, not been mentioned in the above standards, but the perpendicularity of the ram movement with respect to the ram bed is influenced by the play in the ram guidance.

**Accuracy in the loaded state:** The displacements of the tool-bearing areas of the loaded machine, as compared to the unloaded state, are obtained by means of spring constants. For non-symmetrical presses three spring constants are necessary to describe the elastic deflections [8.8]:

- 1 The spring constant in the  $z$ -direction  $C_{z,\text{tot}}$  (direction of ram movement, Fig. 8.71),

$$C_{z,\text{tot}} = \frac{F}{f_{z,\text{tot}}} \quad (8.97)$$

where  $f_{z,\text{tot}}$  is the elastic deflection in the  $z$ -direction corresponding to a force  $F$ .

- 2 The spring constant in the  $y$ -direction  $C_y$ , which is obtained from the elastic deformation  $f_{y,\text{tot}}$  of the ram bottom front edge,

$$C_y = \frac{F}{f_y} \quad (8.98)$$

- 3 The angular spring constant, which is obtained from the angle  $\alpha$  (elastic) between the ram guide and the ram axis of the unloaded machine,

$$C_\alpha = \frac{F}{\alpha} \quad (8.99)$$

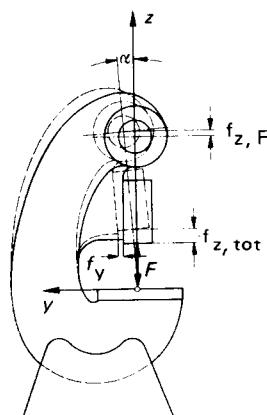


FIG. 8.71 Elastic deformations for a C-frame press under load. (After [8.8].)

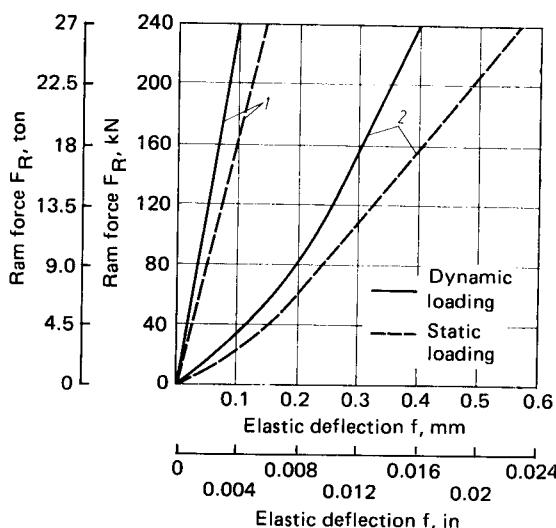


FIG. 8.72 Spring characteristics of cold-forging automatic machine. 1—frame deflection; 2—total deflection. (After [8.26].)

The units of the linear spring constants are kN/mm (ton/in), and for the angular spring constants they are  $\text{kN}/\mu\text{m} \cdot \text{m}$  (ton/ $\mu\text{in} \cdot \text{in}$ ).

For symmetrical presses, only one spring constant, namely,  $C_{z,\text{tot}}$ , need be known to determine press behavior under loading.

The static spring constant  $C_{z,\text{tot,stat}}$ , obtained under quasistationary loading, and the dynamic spring constant  $C_{z,\text{tot,dyn}}$  can differ greatly from each other [8.25]. The dynamic spring constant has been determined in exceptional cases only. Some measured spring constants for a cold-forging automat are shown in Fig. 8.72 [8.26]; these results cannot be transferred to other types of machines.

The overall spring constant of a press is the combined effect of the frame spring constant  $C_F$  and the drive spring constant  $C_D$ ,

$$C_{z,\text{tot}} = \frac{C_D C_F}{C_D + C_F} \quad (8.100)$$

The drive spring constant is the smaller of the two values. The following ratios are generally valid for the two values [8.24]:

For C-frame presses  $C_F/C_D = 1.5-3$

For closed-frame presses  $C_F/C_D = 3-12$

Given the above proportions, any substantial increase in the overall spring constant can be achieved only by increasing the drive spring constant (Fig. 8.73).

An empirical relation can be used to obtain the total elastic deflection as a function of the nominal force of the press,

$$C_{z,\text{tot}} = K \sqrt{F_N} \quad (8.101)$$

The constant  $K$  is a factor representing the elastic behavioral quality of mechanical presses. Its values are in the following ranges:

For C-frame presses  $K = 9-25 \text{ kN}^{1/2}/\text{mm}$  ( $25.6-71.2 \text{ ton}^{1/2}/\text{in}$ )

For closed-frame presses  $K = 25-50 \text{ kN}^{1/2}/\text{mm}$  ( $71.2-142.4 \text{ ton}^{1/2}/\text{in}$ )

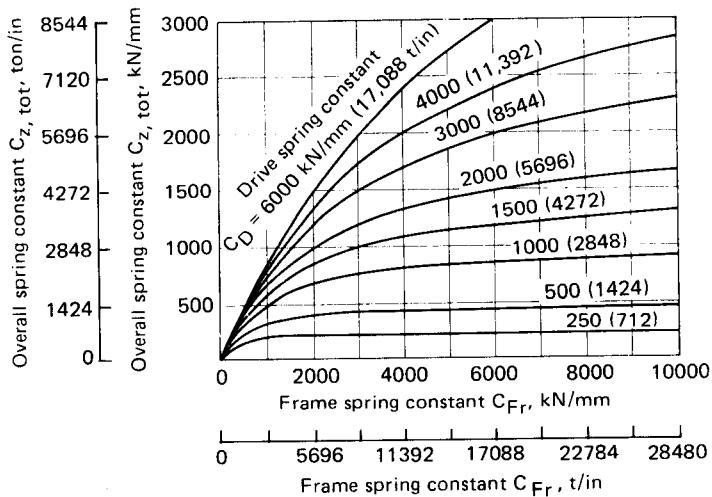


**FIG. 8.73** Relation between frame spring constant  $C_{Fr}$ , drive spring constant  $C_D$ , and overall spring constant  $C_{z,\text{tot}}$ . (After [8.27].)

Errors in height due to force variations can be determined from the spring constant  $C_{z,\text{tot}}$ .

The angular deflection in C-frame presses leads to errors in parallelism and can be determined from the force  $F$  and the angular spring constant  $C_\alpha$ . It has been determined from experiments that the spring constant  $C_\alpha$  is dependent on the nominal force in C-frame presses [8.8]. The variation of the angular spring constant is linear with the nominal force of the press (Fig. 8.74).

Angular deflection and deflection in the  $y$ -direction  $f_y$  of the front edge of the guide cause an offset  $\Delta T$  in the tool plane  $TT$  (see Eq. 8.102), which can be obtained from Fig. 8.75.

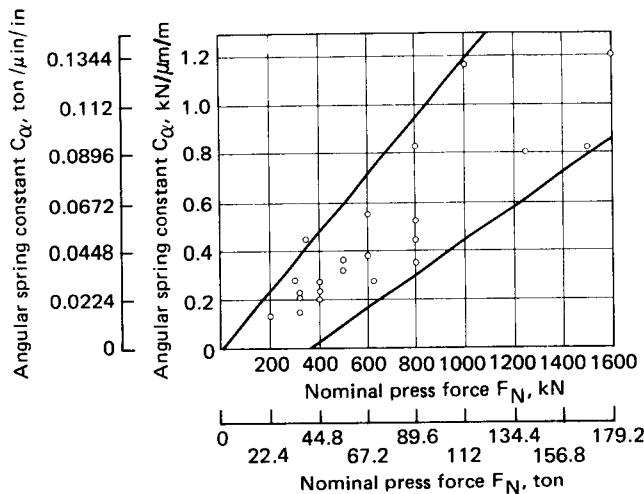


**FIG. 8.74** Dependence of angular spring constant on nominal force in a C-frame press. (After [8.8].)

$$\Delta T = f_y - \alpha(z_G - z_T) \quad (8.102)$$

Off-center loading on the ram, irrespective of the type of frame, leads to ram tilting within the limits of the guidance play, or in some extreme cases to elastic deflection of the guide plates (Fig. 8.76). This in turn causes errors in parallelism and offset, which show up in the corresponding elastic deflection of the frame.

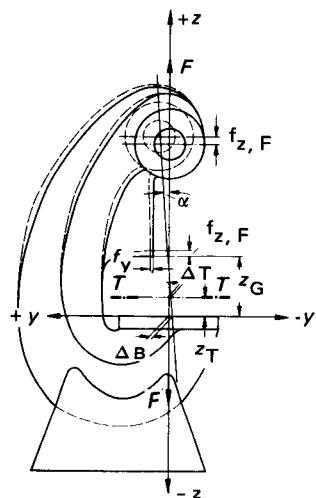


**FIG. 8.75** Elastic deformation of a C-frame for press under forming load. (After [8.8].)

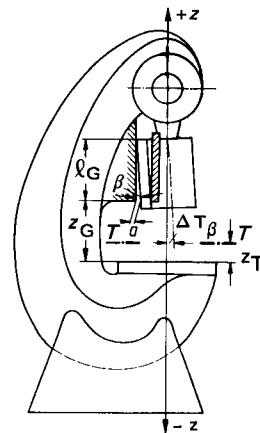


**FIG. 8.76** Tilting of ram and offset in tool plane as a result of guidance play (After [8.8].)

The angle  $\beta$  between the ram axis and the ram guide  $y$ , caused by the ram tilt, is given by

$$\beta = \frac{a}{l_G} \quad (8.103)$$

where  $a$  is the guidance play plus the elastic deflection of the guide plate, and  $l_G$  is the effective guide length.

The offset on the tool plane caused by ram tilting is given by

$$\Delta T_\beta = a \pm (z_G - z_T)\beta \quad (8.104)$$

Very few published results are available on the total offset in the tool plane of C-frame presses and the magnitude of parallelism errors caused by ram tilting [8.24], [8.28]. Some typical values are shown in Fig. 8.77.

### 8.5.3 Frames of Mechanical Presses

The frames of mechanical presses can be classified into two types (Fig. 8.78):

- 1 C-frames (open frame)
- 2 O-frames (closed frame)

C-frames are used generally for smaller- and medium-capacity presses. They are further divided into single- and double-column presses (Fig. 8.78).

The main part in a single-column press is the vertical column, which is made up of sections resistant to bending. The drive is positioned on the middle and upper portions of the frame. The

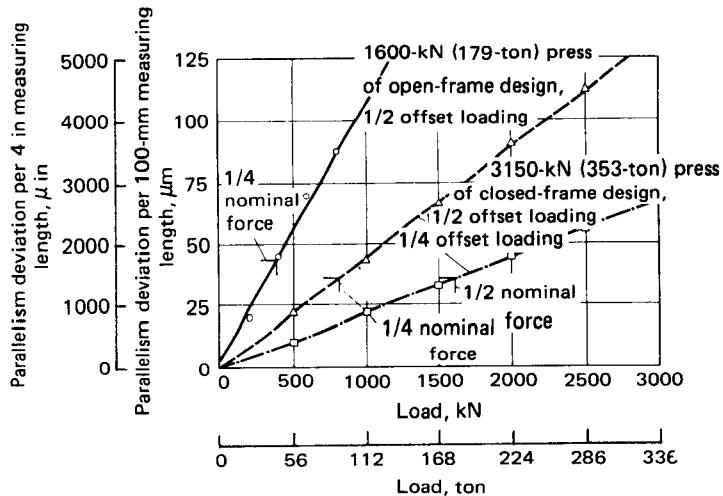


**FIG. 8.77** Parallelism errors between ram force and bed for eccentric load. (After [8.8].)

crank or the eccentric shaft are perpendicular to the front of the press (cross shaft drive). The press bed is either fixed rigidly to the bottom of the frame or adjustable for height. The single-frame design is either vertical or inclined.

The double-column frame is built with two vertical columns, which are connected at both the crown and the bed. The main drive lies parallel to the frame front (longitudinal shaft drive). Several variations of the double-column C-frame presses are shown in Fig. 8.79.

Important dimensions of C-frames such as the size and quality of the bed surface, the bed height, the height adjustment of the bed, and the largest inclination angle of the frame have all been standardized. (Refer to the additional references at the end of this chapter.)

C-frame presses have the advantage of easy access for tool mounting from three sides in the case of single-column design and from four sides in double-column design. The disadvantage, however, is the bending of the frame under load, which leads to errors in parallelism and offset in the workpieces (refer also to Sec. 8.5.2). The disadvantage can be offset by providing tension tie rods on the front of the press—the frame becomes closed (Fig. 8.80). If the spring constant of

C-frame		O-frame	
Single-column design	Double-column design	Double-column design	Pillar-guide design

**FIG. 8.78** Frame and design variations for mechanical presses. (After [8.21].)

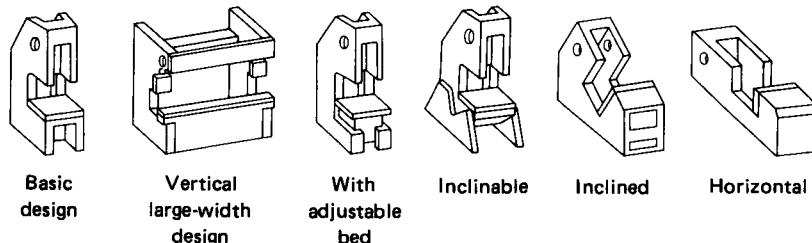


FIG. 8.79 Designs of double-column frames. (After [8.21].)

the rod is  $C_{TR}$  and assuming that the tie rod is at the level of the ram axis, the spring constant in the vertical ( $z$ ) direction is given by

$$C_{z(F,TR)} = C_F + C_{TR} \quad (8.105)$$

Hence the use of the tie rod increases the total spring constant and reduces the elastic deformation of the frame (Fig. 8.81a).

The tie rod will, however, make mounting the tools more difficult. Furthermore the frame must absorb the additional forces in the tie rod during unloading. The energy released from the frame and the tie rod during the dropping of load has to be absorbed by the frame alone once the ram reaches its starting position. This results in increased springback as compared to the elastic deformation under load.

The above disadvantage can be overcome by using a prestressed sleeve over the tie rod. The effects of using the sleeve can be explained with reference to Fig. 8.81b. The prestressing force  $F_p$  stretches the frame and the tie rod, based on their spring constants, by  $f_{p,F(F,TR)}$ . The corresponding compression on the sleeve is  $f_{p,S}$ . Subjecting this system to a ram force  $F$ , the load on the frame and the tie rod is increased to  $F_p + F_{(F,TR)}$ , and the corresponding reduced load on the sleeve is  $F_p - F_S$ . The frame and the tie rod stretch by  $f_{z(F,TR,S)}$ , and the sleeve also elongates by the same amount. The spring constant of the above prestressed system under the ram force  $F$  is

$$C_{z(F,TR,S)} = \frac{F}{f_{z(F,TR,S)}} \quad (8.106)$$

With  $F = F_{(F,TR)} + F_S$  (Fig. 8.81b), Eq. 8.106 changes to

$$C_{z(F,TR,S)} = \frac{F_{(F,TR)}}{f_{z(F,TR,S)}} + \frac{F_S}{f_{z(F,TR,S)}} \quad (8.107)$$

In terms of the spring constants, Eq. 8.107 can be rewritten as

$$C_{z(F,TR,S)} = C_{z(F,TR)} + C_S \quad (8.108)$$

Hence the use of a prestressed sleeve not only reduces the amount of springback, but it also increases the stiffness in the  $z$ -direction.

O-frames can be classified into double-column and pillar-guide designs. The latter design is used only very rarely (Fig. 8.78).

Double-column presses for smaller and medium capacities are of a single-piece design. Larger-capacity presses are made from joining the bed, side frames, and crown. Tie rods are used to hold the pieces together.

In those presses the tool mounting space can be accessed only from the front and the back. Openings on the side columns are generally made for feeding and transport of the workpieces. The behavior of the closed-frame presses with tie rods can be explained using Fig. 8.82. The

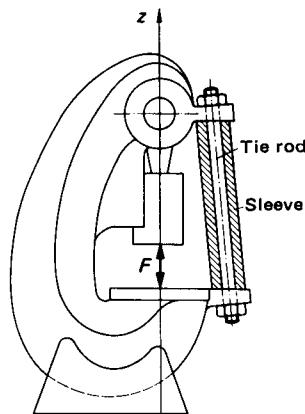
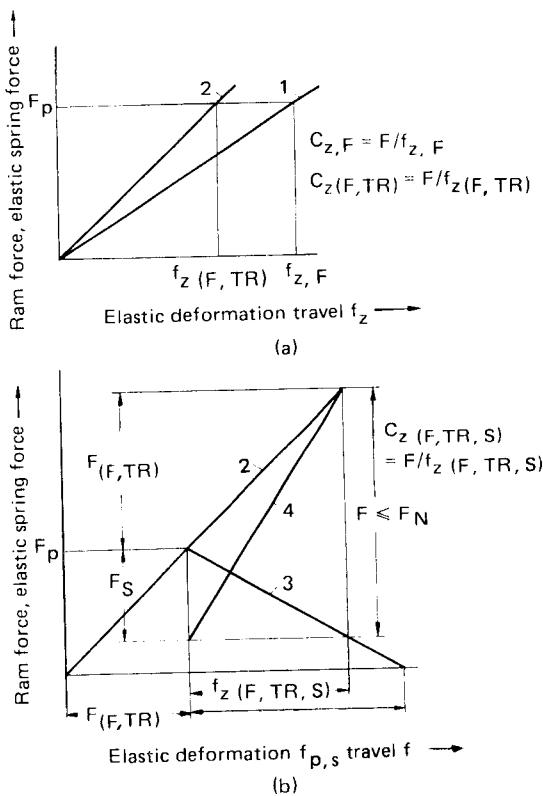
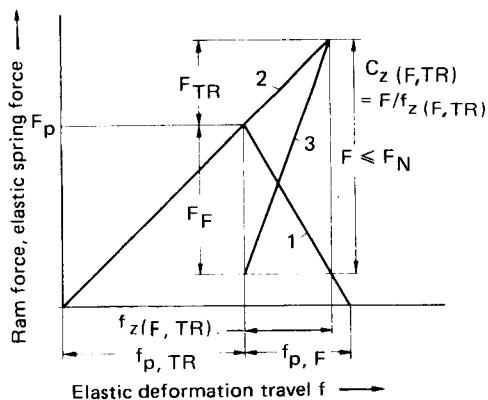


FIG. 8.80 Increasing the stiffness of C-frames by means of a tie rod and sleeve. (After [8.8].)



**FIG. 8.81** Elastic characteristics of C-frames. 1—frame; 2—frame with tie rod; 3—sleeve; 4—frame with tie rod and sleeve.  
(a) Without and with tie rod. (b) With tie rod and sleeve.



**FIG. 8.82** Loading diagram of a two-column frame with prestressed tie rod. 1—frame; 2—tie rod; 3—frame with tie rod.

prestressing force  $F_p$  causes a compression  $f_{p,F}$  in the frame and an elongation  $f_{p,TR}$  in the tie rod based on their respective spring constants. The ram force  $F$  increases the loading on the tie rod to  $F_p + F_{TR}$ , and the force on the column becomes  $F_p - F_F$ . In order that contact surfaces of the column with the bed and the crown do not separate under load, the prestressing force  $F_p$  must be selected to be greater than the residual force, namely,  $F_p - F_F > 0$ . The working force causes an additional elongation  $f_{z(F,TR)}$  on the tie rod, and the unloaded frame also experiences the same elongation. Similar to C-frame presses, the total spring constant of the press in the  $z$ -direction is

$$\begin{aligned} C_{z(F,TR)} &= \frac{F}{f_{z(F,TR)}} \\ &= C_F + C_{TR} \end{aligned} \quad (8.109)$$

Present press-building practice increasingly uses welded-steel-plate construction instead of cast-iron frames for presses with smaller nominal forces (mainly C-frame presses). Large-capacity presses are made almost exclusively of welded-steel-plate construction. Welded construction can be built with maximum possible stiffness using a minimum amount of material, and they have a

larger elastic modulus than cast construction. The compromise on such welded-steel designs is the smaller damping capacity of the steel frames compared with cast-iron frames.

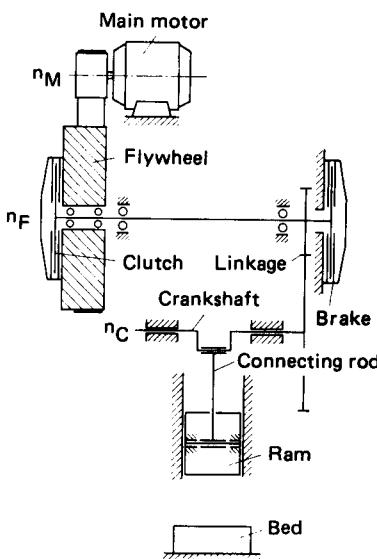
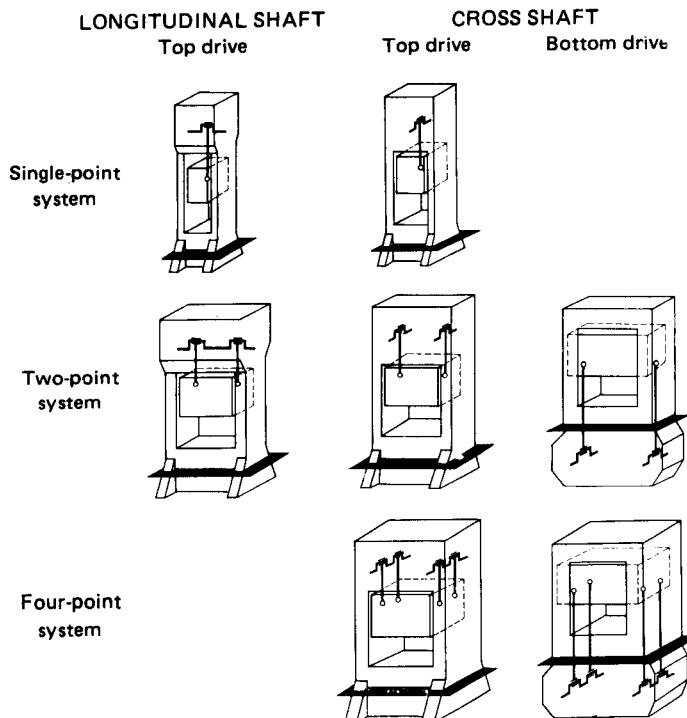


FIG. 8.83 Schematic of crank press drive.

the above time period. It is therefore uneconomical to design the main motor for peak energy requirements during the forming process. The drives of mechanical presses are in general equipped with energy-storing media such as flywheels. The energy is removed from these elements during the forming process, and this energy is restored to the element in the time period before the start of the next forming process. The main motor can therefore be designed to deliver an average energy throughout the stroke. The flywheel speed drop or increase is a function of the energy given out or absorbed.

The permissible drop in speed of the flywheel (slip) as well as the slip efficiency for the various types of operation are given below.

	Permissible slip	Degree of slip efficiency
Single stroke	0.29	0.50
Continuous stroke	0.13	0.25



**FIG. 8.84** Various types of main drive systems for double-column crank presses. (After [8.21].)

As was pointed out in Sec. 8.5.1, it can be observed from the slip efficiency values given above that the work capacity of mechanical presses in single-stroke operation is about twice that of machines with continuous operation.

For rams of small widths and depths the force can be transmitted to the ram through a single connecting rod (single-point drive). Rams with larger widths require two connecting rods (two-point drive) and very large rams require four connecting rods (four-point drive). The main drive shaft can be either parallel or perpendicular to the machine front (longitudinal or cross shaft) for single-point and two-point drives. The drive system for four-point drives is generally of the cross-shaft type (Fig. 8.84). The normal forces on the connecting rods cancel each other in these drives since the shafts rotate in directions opposite to one another (Fig. 8.85).

Counterbalancing arrangements are provided in medium- and large-capacity presses to balance the weight of the ram and the tool. This leads to quiet operation of the press by minimizing the effect of bearing play.

## 8.6 SAFETY AGAINST OVERLOADING

Presses must have safety devices to (1) protect the operators and (2) prevent overloading on important press components. The former safety function is generally overseen by operational safety requirements existing in the various parts of the world. We therefore attempt to discuss the latter portion of safety only, which is incorporated into all quality presses.

Overloading of presses can lead to enormous downtime due to repair, and hence affect production. This is especially detrimental when the press under repair is coupled with other working

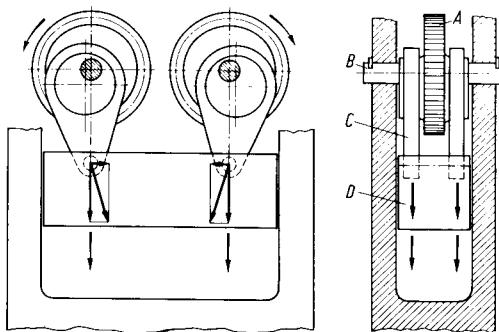


**FIG. 8.85** Schematic of drive system in a four-point drive.  
A—gear with stroke control disks; B—shaft (fixed); C—connecting rod; D—ram. (After [8.29].)

presses in a production line. Safety precautions must hence be taken to guard the presses against overloading.

#### 8.6.1 Safety Devices for Mechanical Presses in the Region of Useful Stroke

The characteristics of the crank drive make it extremely susceptible to overloading, especially near the bottom dead center, when two pieces are on the die.

The force increase in a fast-stroking blanking press takes place within 0.1 or 0.25 s, and it is not possible to apply the brakes within this short time span to avoid overloading. Hence an effective safety device must be installed in the force flow in the form of a machine element that gives way under overloading. Such an element also prevents locking of the press at the bottom dead center by making one-tenth to one-fifteenth of the stroke available.

The safety devices that reduce the effective connecting-rod length are

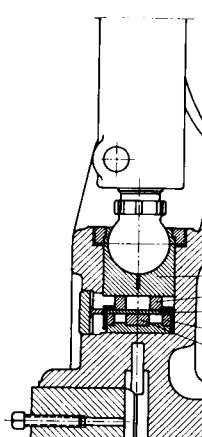


**FIG. 8.86** Shear plate overload safety device.  
1—shear plate; 2, 3, 4—shear rings; 5—pitman ball. (Courtesy of Schuler.)

- 1 Shear plate
- 2 Hydraulic cushion
- 3 Knuckle lever

The shear plate overload safety device consists of a die and a shear ring or punch (Fig. 8.86) between which the shear plate is positioned. The shear plate is made from brittle material, such as cast iron or hardened steel. The shear strength must be close to the tearing strength so that entry of the punch into the shear plate causes shearing. Measurements under static and dynamic loading have shown that by using shear plates with close tolerances, the breaking force in continuous stroking can be as high as 1.3 times the nominal force when the press is delivering the nominal force [8.30].

The principle of operation of an overload safety device using a hydraulic cushion is shown in Fig. 8.87. The hydraulic oil is pushed into an auxiliary hydraulic cylinder by means

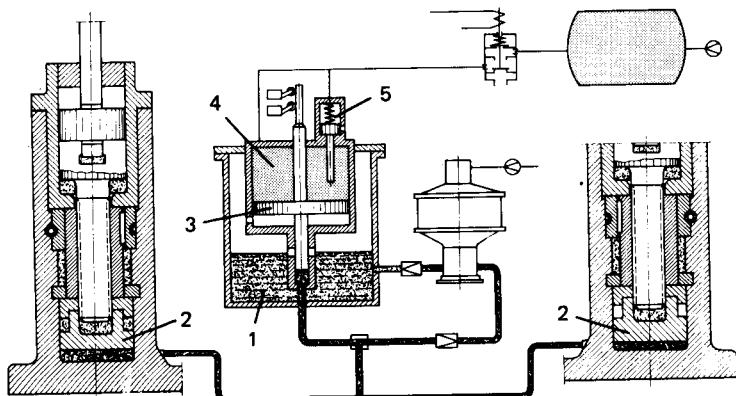


**FIG. 8.87** Hydraulic-cushion overload safety device. (Courtesy of Weingarten.) 1—oil reservoir; 2—ram piston; 3—double-action piston; 4—compressed air; 5—overload safety pressure valve.

of the piston built into the ram. This hydraulic cylinder has a double-piston rod assembly on one side of which air pressure is acting. The air pressure can be controlled to activate the overload pressure valve at any desired ram pressure. Once the set pressure is reached, the air escapes, freeing the double piston. This pushes more oil into the hydraulic cylinder, which results in a free travel of the ram without load. As in the previous case, depending on the switching velocity and the pressure-limiting ratio of the safety valve, the ram force can reach 1.5 times the nominal force before the safety valve operates.

It may be possible to use a partial overload position system by using a spring element in the force flow. This spring element will absorb part of the overload energy so that the available energy is reduced when overloading occurs. These spring elements can either be a stack of springs (Fig. 8.88) or ring-shaped springs with wedge-shaped contact surfaces which are located below the connecting rod in the ram assembly. The disadvantage is that a large space may be required to accommodate the springs for larger press forces. Further the free travel that can be achieved on overloading is also limited due to the permissible spring compression, and this may not be sufficient for the ram to return past the bottom dead center. The overall spring constant of the press is also reduced considerably in these designs.

Instruments used on the machine to indicate the force can also be useful as partial prevention devices. They will not be able to prevent unforeseen overloading, but can switch off the press and apply the brakes to prevent overloading in the subsequent stroke. In order for this to happen, it is necessary to measure a strain corresponding to the overload. This can be done, for example, by measuring the compression of the connecting rod or the elongation of the columns or tie rods in split constructions of the frame. Using a calibration curve, the press force can hence be determined. On exceeding the permissible press load, a limit switch is actuated, which stops the drive of the press. Simultaneously the electric

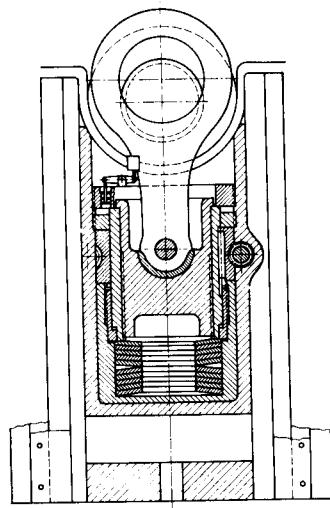


**FIG. 8.88** Plate-spring overload safety device.

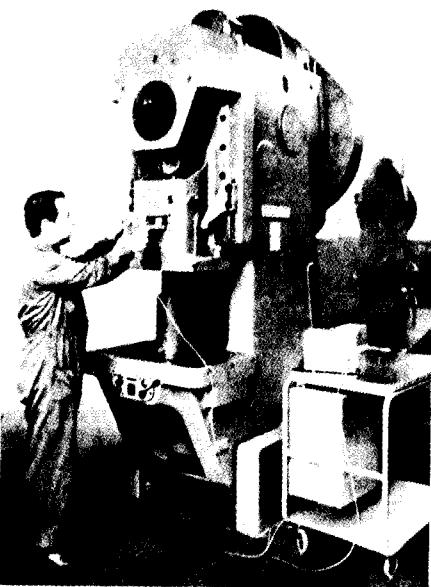


**FIG. 8.89** Load measurement using strain-gauge dynamometer inserts. (*Courtesy of Erichsen.*)

circuit for the operation of the subsequent stroke is broken. The devices made for such controls are generally robust in design, and hence their accuracies are low. Since the response times of these indicators are relatively long, such devices can be used only in slow-stroking presses or in processes requiring long deformation travel.

Another possibility is to paste strain gauges at suitable points on the press and measure the strains in these gauges after amplification by means of force indicators. This method opens up a wide range of application possibilities for different end uses.

Inserts with strain gauges pasted on them can be used to measure the press force if they are introduced in the area of the shear plate assembly in a press (Fig. 8.89). This procedure can be used to determine the forces at the time of testing the presses.

#### 8.6.2 Safety Devices for Mechanical Presses In the Entire Stroke Range

The drive of the press is designed based on the useful stroke. The designed nominal torque will generally be required after the forming process starts. The lever arm of the crank is reduced at this point, and the velocity of the ram had already reached its maximum before this period. If the ram encounters an obstacle ahead of the above region of the working stroke, the danger of overloading is due to excessive torque rather than force. Hence a safety device must be built in between the drive motor with the flywheel and the drive system.

In mechanical presses overload safety can be provided in the clutch and brake system. In the case of friction clutches, the holding force on the friction areas can be limited in such a way that slipping occurs when the permissible torque is exceeded, and the excess energy is converted to heat energy.

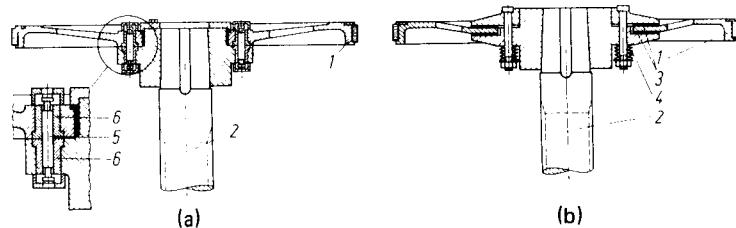


**FIG. 8.90** Overload safety devices in screw presses. 1—flywheel; 2—screw; 3—friction pad on slip clutch; 4—plate washers for prestressing clutch; 5—shear pin; 6—shear housing. (a) Shear pin between flywheel and screw. (b) Slip clutch in flywheel. (After Georg and Huydts.)

### 8.6.3 Safety Devices in Screw Presses

Recent developments in controls have made it possible to regulate the energy availability per stroke. Regulation of energy is the best method of overload safety protection in screw presses.

Overloading results in great danger to the weakest part in the force-flow train, namely, the screw. Fracture can occur easily.

If the work capacity of the screw press is large, so that different workpieces may be accommodated, a safety device must be used between the flywheel and the screw to protect the screw when the press is used for smaller energy requirements. The shearing pin method (Fig. 8.90a) was popular in older machines. The major disadvantage is the time required to replace the pin. Furthermore the shear housing can also get damaged, resulting in considerable downtime of the press for repair.

The newer machines have a slip clutch arrangement (Fig. 8.90b). The moment to be transmitted is limited to a preset moment. The flywheel starts to slip once that preset moment is exceeded. For very large requirements, a double safety device is necessary to protect the gear teeth on the flywheel (Fig. 8.91). This requires intricate design considerations and hence is used only in high-capacity screw presses.

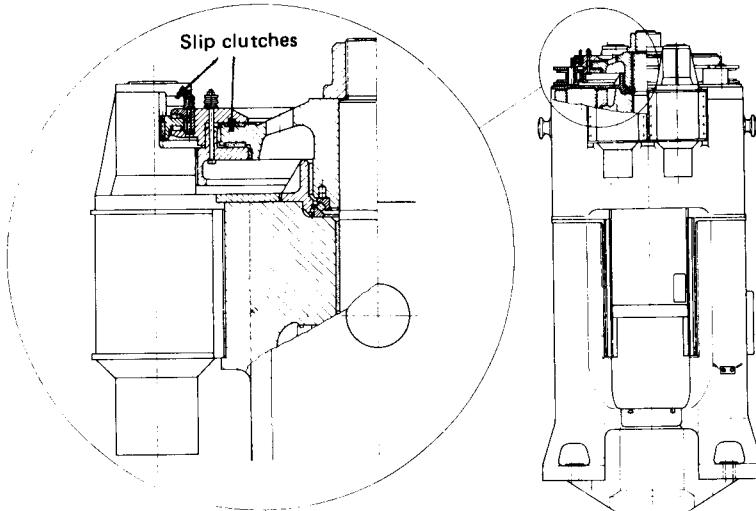


**FIG. 8.91** Double overload safety in a large screw press. (Courtesy of Weingarten.)

## REFERENCES

- 8.1 Kienzle, O.: "Characteristic Values of Presses and Hammers" (in German), *Werkstattstech. u. Maschinenbau*, 43, 1953, pp. 1–5.
- 8.2 Kienzle, O.: "Characteristic Parameters of Metal-Forming Machine Tools for Die Forging" (in German), *Schmiedetechnische Mitteilungen*, no. 5, Sonderteil zu *Werkstatttechnik*, 55, 1965, pp. 509–514.
- 8.3 Kienzle, O.: "Development Trends in Metal-Forming Machine Tools" (in German), *Werkstatttechnik*, 49, 1959, pp. 479–489.
- 8.4 Kienzle, O.: "The Basic Pillars of Manufacturing Technology" (in German), *Werkstattstech. u. Maschinenbau*, 46, 1956, pp. 204–209.
- 8.5 Beck, G.: "Temperature Loading of Tool Steels in Hot Upsetting and Forging in Dies" (in German), *Stahl u. Eisen*, 78, 1958, pp. 1556–1563.
- 8.6 Doderer, A. W.: "The Actual Tool Velocity Variation in Blanking Presses" (in German), *Mitt. Forsch. Blechverarb.*, 1958, pp. 149–152.
- 8.7 Watermann, H. D.: "Working Accuracy of Hammers and Screw Presses with Flywheel Drive under Eccentric Loading" (in German), *Werkstatttechnik*, 53, 1963, pp. 413–421.
- 8.8 Münnich, H.: "Elastic Deformation on Loaded Presses" (in German), *Werkstattstech. u. Maschinenbau*, 44, 1954, pp. 502–509.
- 8.9 DIN 8650: "Acceptance Conditions for Machine Tools—Single-Frame Eccentric Presses" (in German), June 1942.
- 8.10 DIN 8651: "Acceptance Conditions for Machine Tools—Double-Frame Eccentric Presses" (in German), June 1942.
- 8.11 Schlesinger, G.: *Testing Procedures for Machine Tools* (in German), 7th ed., Middelburg, de Boer, 1962.
- 8.12 Podrabinnik, I. M., and Rodov, E. M.: "On the Stiffness of Mechanical Presses for Cold Extrusion and the Accuracy of Extruded Workpieces" (in German), *Draht*, 18, 1967, pp. 208–212.
- 8.13 Szabo, I.: *Introduction to Engineering Mechanics* (in German), Berlin/Göttingen/Heidelberg, Springer, 1959.
- 8.14 Watermann, H. D.: "Blow Efficiency of Hammers and Screw Presses with Flywheels" (in German), *Ind.-Anz.*, 85, 1963, pp. 1727–1738.
- 8.15 Mäkelt, H.: *Mechanical Presses* (in German), München, Hanser, 1961.
- 8.16 Vorberg, K.: "Fluid Medias in Hydraulic Plants" (in German), *Maschinenmarkt*, 75, 1969, pp. 834–838.
- 8.17 Oehler, G.: *Hydraulic Presses* (in German), München, Hanser, 1962.
- 8.18 Zymak, V.: "Simplified Method of Designing Hydraulic Flow in Forming Machines" (in German), *Ölhydraulik u. Pneumatik*, 12, 1968, pp. 429–438.
- 8.19 Dohrn, W.: "Economy of Different Drives in Hydraulic Presses" (in German), *Werkstattstech. u. Maschinenbau*, 45, 1955, pp. 515–520.
- 8.20 Müller, E.: *Hydraulic Presses and Fluid Medium Units* (in German), Berlin/Göttingen/Heidelberg, Springer, vol. 1, "Forging Presses," 3d ed., 1962; vol. 2, "Presses for the Manufacturing and Forming of Tubes, Hollow Bodies, Plates and Sheets Made from Steel," 1955; vol. 3, "Presses for the Manufacture of Tubes, Solid and Hollow Profiled Rods, Wires, as well as Cables Made from Nonferrous Metals," 1959.
- 8.21 Engineer's Handbook (in German), vol. 1/2, Leipzig, VEB Fachbuchverlag, 1965.
- 8.22 Miller, S.: "Calculation of Knuckle-Joint Drives" (in German), *Maschinenbautechnik*, 15, 1966, pp. 411–414.
- 8.23 May, O.: "Presses for Slow Plastic Flow" (in German), *Werkstattstech. u. Maschinenbau*, 46, 1956, pp. 20–21.

- 8.24 Schwer, W., and Hoppe, H.: "On the Accuracy of Mechanical Presses" (in German), *Mitt. dtsch. Forschungsges. Blechbearb. u. Oberflächenbehandl.*, **19**, 1968, pp. 90–95.
- 8.25 Foucher, J.: "Effect of Rapid Force Increase in Loaded Presses" (in German), *Forschungsberichte d. Landes Nordrhein-Westfalen*, no. 1612, Köln/Opladen, Westdeutscher Verlag, 1967.
- 8.26 Najuch, H.: "Testing of the Rigidity of Cold Upsetting Machines" (in German), *Maschinenaufbau*, **13**, 1964, pp. 358–361.
- 8.27 Kienzle, O., and Neumann, H.: "Methods of Determining the Elastic Behavior of Presses of Arbitrary Width" (in German), *Forschungsberichte d. Landes Nordrhein-Westfalen*, no. 1696, Köln/Opladen, Westdeutscher Verlag, 1966.
- 8.28 Olivo, G.: "Testing of Static Rigidity of Eccentric and Crank Presses" (in German), *Maschinenaufbau*, **13**, 1964, pp. 345–352.
- 8.29 Akademischer Verein Hütte, Ed.: *Handbook for Engineers (Betriebshütte)* (in German), vol. 2, 6th ed., Berlin/München, Ernst, 1964.
- 8.30 Kilp, K. H.: "Computations and Investigations on Eccentric Presses with C-Frame under Static and Dynamic Loads" (in German), *Bänder Bleche Rohre*, **11**, 1970, pp. 10–20.

### Additional References

- 8.31 Keilholz, F.: "Investigations on a Few Hammer Frames" (in German), *Werkstattstechnik*, **53**, 1963, pp. 421–427.
- 8.32 Widera, O. E.: "Comparison of the Dynamic Behavior and Single and Multipiece Anvils in Upsetting" (in German), *Ind.-Anz.*, **91**, 1969, pp. 659–663.
- 8.33 Hammersen, H.: "Comparative Investigations on the Behavior of Different Screw Presses" (in German), *Werkstattstechnik*, **48**, 1958, pp. 237–243.
- 8.34 Pahnke, H. J.: "Acceptance and Maintenance of High Speed Forging Presses with Oil Hydraulic Drive" (in German), *Stahl u. Eisen*, **87**, 1967, pp. 993–1003.
- 8.35 Blechschmidt, A.: "Comparison of Hydraulic and Mechanical Presses" (in German), *Blech*, **3**, 1968, pp. 138–141.
- 8.36 Rose, J.: "Mechanical Presses—A Dying Breed?" *Sheet Met. Ind.*, 1982, pp. 630–634.
- 8.37 Doege, E.: "Static and Dynamic Stiffness of Presses and Some Effects on the Accuracy of Workpieces" (in German), *Ann. CIRP*, **29**, 1980, pp. 167–171.
- 8.38 Linden, H.: "Design of Flywheel Drives for Metal-Forming Machine Tools" (in German), *Werkstatt u. Betr.*, **89**, 1956, pp. 661–664.
- 8.39 Panknin, W.: "Requirements in the Design of C-Frame Eccentric Presses for Forming" (in German), *VDI-Z.*, **100**, 1958, pp. 1287–1293.
- 8.40 Tauber, H.: "Fundamentals of Testing and Acceptance of Forming and Blanking Machines" (in German), *Maschinenaufbau*, **13**, 1964, pp. 337–344.
- 8.41 Lange, K.: "Automation Aspects in Metal Forming" (in German), in Pentzlin Kienzle: *Automation in Manufacturing*, Berlin/Heidelberg/New York, Springer, 1969.
- 8.42 Kienzle, O.: "Steps to Automation in Metal Forming" (in German), *Werkstattstechnik*, **47**, 1957, pp. 393–402.
- 8.43 Lange, K.: "Automation and Forming Machines" (in German), *VDI-Berichte*, no. 123, Düsseldorf, 1968, pp. 115–124.
- 8.44 Dolezalek, C. M.: "Technical Fundamentals for Automation in Manufacturing" (in German), *Ann. CIRP*, **11**, 1962/63, pp. 15–24.
- 8.45 Kralowetz, B.: "Recent Developments in Automating Open-Die and Die Forging Operations" (in German), *VDI-Berichte*, no. 123, Düsseldorf, 1968, pp. 131–135.

## **8.72 FUNDAMENTALS OF METAL FORMING**

- 8.46 Böhringer, H., and Kilp, K. H.: "Development of Screw Forging Presses" (*in German*), *Werkstattstechnik*, **55**, 1965, pp. 28–30.
- 8.47 Lange, K., Noller, H., and Schmidt, V.: "Contribution of Numerical Control (NC) to the Development of Metal Forming Processes" (*in German*), *Ann. CIRP*, **31**, 1982.
- 8.48 "Presses and Hammers for Metal Forming" (*in German*), in Dubbel, *Taschenbuch für den Maschinenbau*, 15th ed., Berlin/Heidelberg/New York, Springer, 1983.

**DIMENSIONAL  
ACCURACY  
AND SURFACE QUALITY**

---

---

**List of Special Symbols**

---

$A_s$	end stop area
$C_s$	spring constant of end stop
$d$	average grain size (diameter)
$\Delta f_s$	elastic deformation change of end stop
$H_s$	height of end stop
$i$	international tolerance unit
$r_u$	radius of unstretched fiber in bending
$R_a$	average roughness deviation from mean surface
$R_p$	smoothing depth
$R_t$	peak-to-valley height
$R_z$	overall average roughness
$T_T$	tool temperature
$T_w$	workpiece temperature
$u$	clearance between punch and die
$\alpha$	coefficient of linear expansion
$\lambda$	shrinkage allowance
$\psi$	slope of wear curve

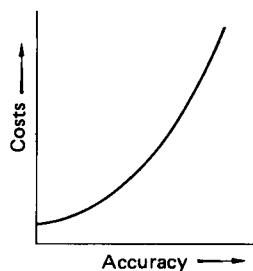


**FIG. 9.1** Schematic representation of the relationship between cost and accuracy.

achievable without having to take any extra care during the process. Better accuracies naturally require higher involvement, thereby also increasing the costs of obtaining higher accuracies (Fig. 9.1). Hence in any manufacturing process, economy and accuracy have to be kept in proper perspective.

The term *accuracy* can be defined as the degree to which the desired result is approached [9.2]. As a measure for accuracy one always uses the inaccuracy, that is, the deviation between the actual and the nominal or desired values.

## 9.1 ERRORS

### 9.1.1 Systematic and Random Errors

In every manufacturing process both systematic and random errors occur.

*Systematic errors* are errors that show a particular trend during the manufacturing process, such as an increase of the diameter of turned shafts due to tool wear, an increase of upset heads due to frictional wear and tool deformation, or thickness reduction due to tool deformation in die forging (Fig. 9.2).

*Random errors* are errors that do not show any particular trend from workpiece to workpiece. These are caused by various cumulative and annulling factors, such as temperature changes, changes in sections as well as material volume, deviations in material composition and microstructure, elastic deformation fluctuations of the tool-machine system due to variations in forces, and other factors. The random errors also follow statistical rules; that is, with enough observed and measured values, typical normal distribution curves can be obtained (Fig. 9.3).

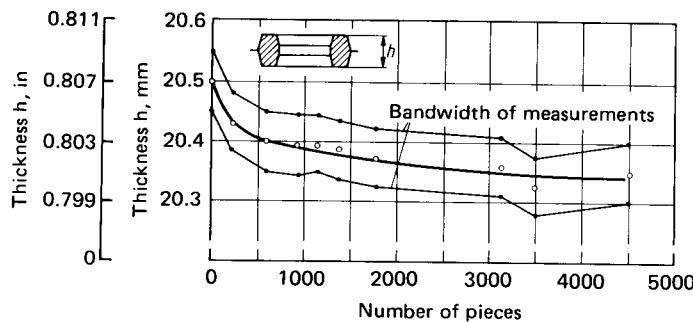


**FIG. 9.2** Effect of tool deformation on the thickness of a die-forged workpiece.  
(After [9.3].)

The four cornerstones of manufacturing technology are [9.1]: (1) principal geometrical features, (2) control of defects and errors, (3) productivity, and (4) working environment. The second cornerstone, namely, control of defects and errors, is concerned with mastering the unavoidable deviations of a workpiece from the nominal or desired values, caused by various factors.

The major factors affecting the unavoidable deviations are process, workpiece material, tool, machine, and process layout. The more intricate the shape of the workpiece, the greater are the deviations. Furthermore every process has an associated accuracy, which is

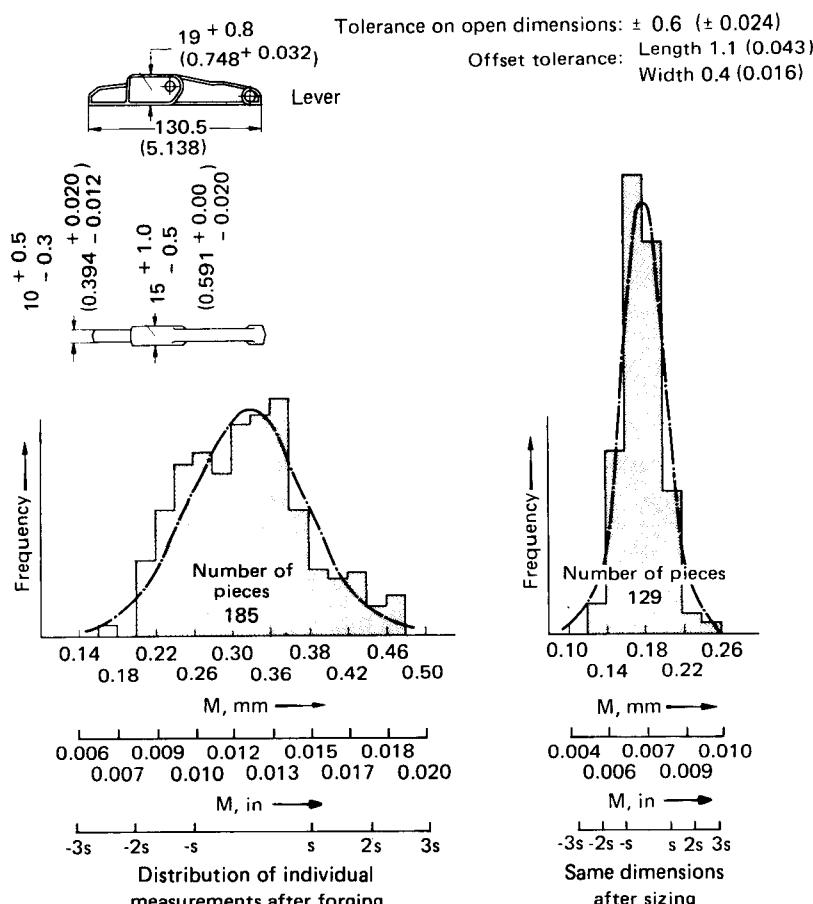


**FIG. 9.3** Frequency distribution of thickness in die-forged workpieces (measurement  $15 \pm 1.0$  mm [ $0.591 \pm 0.039$  in] of the forging). M—measurement; s—limits; y—mean values of dimensional deviations. Dimensions are in mm (in). (After [9.4].)

### 9.1.2 Workpiece Errors

The following errors may occur on a workpiece (Fig. 9.4):

**Dimensional error:** Deviations of the actual value from the desired or nominal value

**Positional error:** Deviation of two axes in a body from their desired position, for example, parallelism

**Form error:** Deviation of the macrogeometrical ideal shape of a body, for example, errors in cylindricity, flatness, parallelism of bottom and flange areas, ovalness

**Surface error:** Deviation of the microgeometrical ideal shape of a body [in terms of micrometers (microinches)]

**Material properties error:** Caused, for example, by incorrect heat treatment

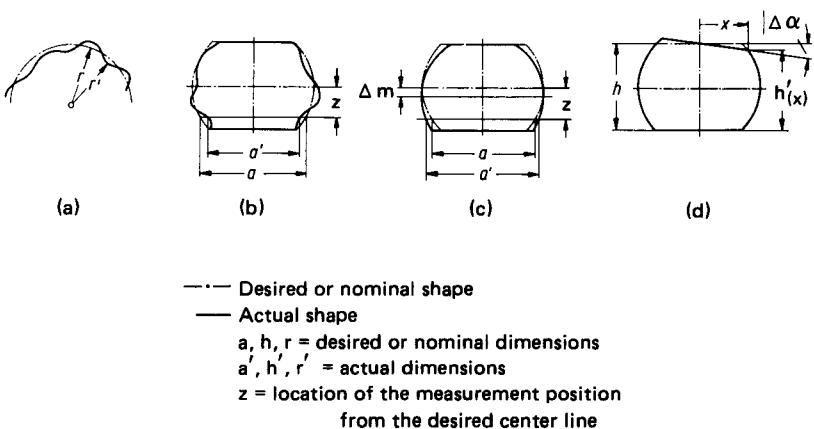


**FIG. 9.4** Examples of form, dimensional, and positional errors on technical bodies. (a) Form error of an area  $r' \geq r$ . (b) Form and dimensional errors of an element as a result of form error of an area. (c) Form and dimensional errors of an element as a result of an error in relative position  $\Delta m$  of an area. (d) Form and dimensional errors of an element as a result of an error in inclination  $\Delta\alpha$  of an area. (After [9.4].)

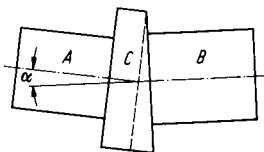


**FIG. 9.5** Position error caused by form errors.

A unique description of the errors in a workpiece is not always possible. For example, in Fig. 9.5, the positional error of cylinders A and B is caused by the form error (axial runout) in cylinder C.

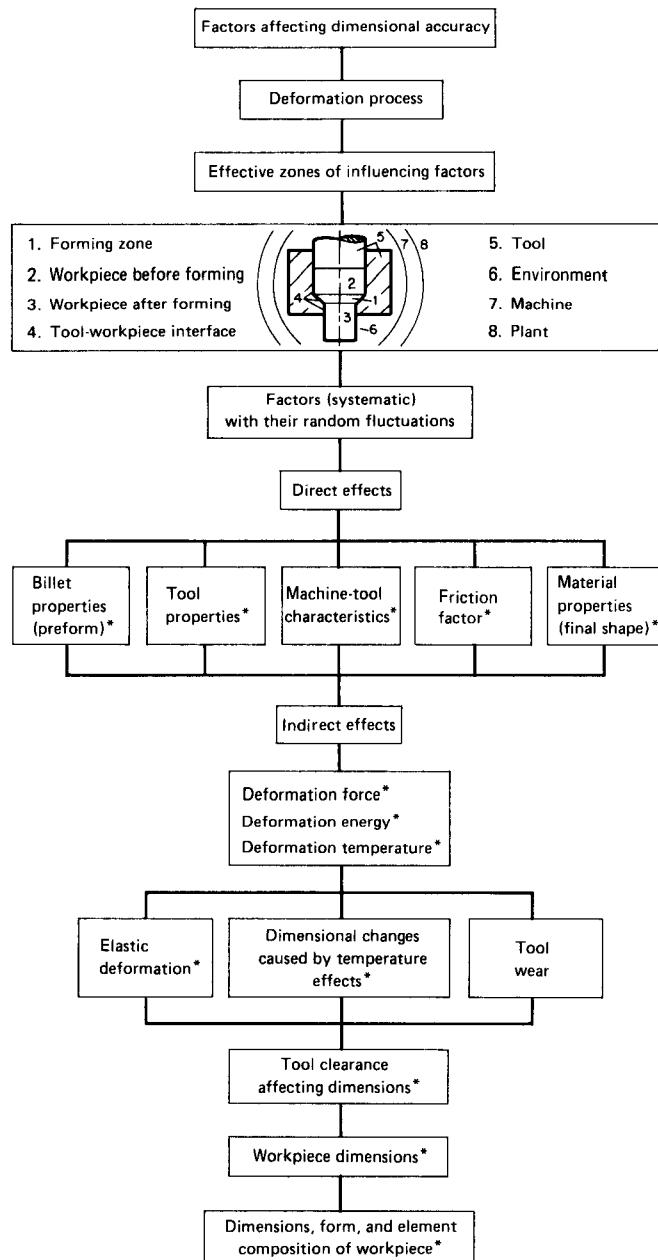
The following geometrical errors may occur in the workpiece after cold and warm bulk forming with two-piece tooling [9.5] (refer also to Figs. 8.14, 9.10, and 9.15 to 9.18): (1) parallelism, (2) offset, (3) radial runout, and (4) errors in height.

The first three errors are caused by inaccuracies in the machine and by defective tool setting. One systematic error that occurs due to such inaccuracies is drifting of the tools, that is, the displacement of one part of the tool with respect to the other in a definite direction. Random errors occur when the tool drifts in the direction of action of the force within the limits allowed by guidance play.

Errors in height are the result of dimensional, strength, and temperature fluctuations of the billet, the force or energy available from the machine (random error), and the tool wear (systematic error) (Fig. 9.6).

## 9.2 FACTORS AFFECTING ACCURACY IN FORMING

Factors affecting dimensions, form, surface, position, strength, and weight due to process, material, tool, machine, and process layout are numerous, and hence a thorough analysis is not possible. The schematic representation in Fig. 9.6 gives several interacting factors with regard to workpiece accuracy.



\*Factors and values aimed at with natural deviations.

**FIG. 9.6** Schematic of factors affecting dimensional accuracy in deformation processes. (After [9.6].)

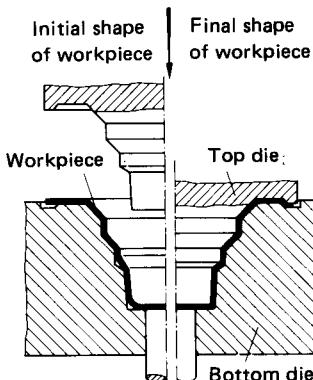


**FIG. 9.7** Sheet thickness variation and workpiece clearance effects in form pressing (coining in die).

and springback. Springback is especially undesirable in bent pieces with a large bending radius. Variations in the forming forces affect the elastic deformation of the tool and the machine directly, and hence the dimensional accuracy (such as bottom and flange thickness). Dimensional accuracy can generally be improved through (1) careful heat treatment of the billet, preform, or interstage; (2) favorable lubricant conditions; and (3) more rigid tooling.

**Dimensional fluctuations in starting material:** The tolerances in sheet thicknesses have a considerable effect on the dimensional accuracy in sheet-metal working:

**Bending:** Effect on springback,  $= f(r_u/s_0)$ .

**Folding:** Errors in thickness are cumulative.

**Deep drawing:** Drawing clearance  $u$  must be sufficiently large ( $>s_0$ ); otherwise ironing will take place.

**Die forming (also drawing of shapes):** Thickness effects are cumulative (coining in die) (Fig. 9.7).

[Based on DIN 1541, the variations in sheet thickness are between 13 and 16% on thicknesses of 0.5–2.0 mm (0.02–0.08 in).]

These disadvantages can be partly overcome by increasing the accuracy of the sheet in the preceding stage, that is, in the rolling mill.

Inaccuracies in the preform or interstage are also disadvantageous in bulk forming. Volume fluctuations in the parting of bars are a result of variations in the cross sections. [The roll mill tolerance for a 20-mm (0.8-in) bar is  $\pm 0.5$  mm ( $\pm 0.02$  in), a variation in the cross section of  $\approx 10\%$ .] In addition, variations in the parted-off lengths (caused by the process) also affect the volume accuracy.

Volume variations in forming with closed dies result in force fluctuations with changing elastic deformations of the tool and the machine. The danger of overloading also exists when the used volume  $V$  becomes larger than permissible. For open-die operations  $V_{min}$  must be large enough to fill the cavity. The result is therefore a higher material requirement. In most cases a higher material requirement is probably more economical than increased accuracy in rolling, shearing, or sawing. The excess material flow must be either trimmed (hot forging) or machined (cold extrusion). Cylindricity errors on thin-walled hollow workpieces are caused by the material elastic springback and the resulting residual stress condition in the workpiece [9.6].

## 9.2.1 Material

**Fluctuations in material properties and microstructure:** Important parameters are  $R_m$ ,  $R_p$ ,  $\delta$ , and  $\sigma_f = f(\varphi, \dot{\varphi}, T)$ , which describe the work-hardening characteristic (for example,  $n$ ).

In *hot forming*, if the forces are to remain the same from piece to piece, the deformation temperature  $T$  and the strain rate  $\dot{\varphi}$  must be controlled within very close limits. Fluctuations in  $T$  affect either the accuracy of the workpiece directly [shrinkage allowance  $\lambda = f(T_w)$ ] or in  $T$  and  $\dot{\varphi}$  indirectly (elastic deformation changes of tool and machine as a result of force fluctuations).

In *cold forming*, fluctuations in the chemical composition, microstructure, and grain size of the workpiece material affect the flow curve.

The result is a spread of the deformation forces

## 9.2.2 Tools

The accuracy of tools is very important for the accuracy of deformed workpieces since forming is in a way copying in which the tool can be considered as analog storage for the dimensions and

shape. Deviations from the desired values in the tools show up as systematic errors in the workpiece.

Requirements on the tools are (1) high accuracy in their manufacture and (2) small dimensional changes during manufacturing through wear. For high performance the tool quality should be 3 to 5 ISO qualities better than the desired accuracy. This necessitates the following tool accuracy requirements:

Forging dies	IT 7/8 to 12
Upsetting and extrusion tools	IT 5/6 to 9
Shrink rings for extrusion dies	IT 3/4 to 7 (accuracy of gages)

In many cases it is very difficult to obtain these values by available tool manufacturing methods (see Chaps. 32 and 33).

In the case of hot working tools, shrinkage must also be considered; that is, the tool dimensions will be larger. The correction for shrinkage can be calculated as

$$\Delta l = \alpha l(T_w - T_t) \quad (9.1)$$

Some values for  $\alpha$  may be found in Table 9.1.

For an accurate workpiece, the tool should be heated and maintained at a definite temperature.

In production the dimensions of the tool change because of wear and deformation. The wear due to sliding friction is smaller when there are smaller sliding movements during deformation. If sliding cannot be avoided, the wear can be reduced by using wear-resistant tools and good lubrication, such as phosphating plus soap, graphite, MoS<sub>2</sub>, mineral oil with the addition of fatty acid, pure mineral oil, and emulsions. (See also Chap. 6.) When the wear behavior under production conditions is known, it will be possible to change or rework the tooling after a known number of workpieces have been produced within a given tolerance level. In such cases sample control will be useful. As a general rule, in tools subject to very high normal pressures there is a large region of linear wear pattern after an initial plastic deformation [9.3], [9.7]. The slope  $\psi$  of this region can be considered as a measure of wear (Fig. 9.8). Failure of the tool starts at the end of the linear region. Production tools must be changed before reaching this stage.

The tool deformation can be plastic or elastic. Plastic deformation occurs generally at the beginning of production, when the stresses are greater than  $S_y$ . The plastic deformation continues until the tool material gets sufficiently work-hardened. (Examples are loading surfaces in forging dies and extrusion punches.)

The elastic deformation of the tool is affected by the deformation forces. A large Young's modulus  $E$  of the tool material is desirable [if necessary, carbides,  $E = 44-63 \times 10^4 \text{ N/mm}^2$  (63,660-91,150 ksi)]. For sheet-metal forming tools, steels [ $E = 21 \times 10^4 \text{ N/mm}^2$  (30,385 ksi)] can be used instead of cast iron [ $E = 10 \times 10^4 \text{ N/mm}^2$  (14,470 ksi)]. Thus variations in forces result in deviations of dimensions. Rigid tooling has a higher spring constant (with smaller elastic deformations) for a given loading condition.

**Table 9.1** Selected Values for Mean Coefficient of Linear Thermal Expansion  $\alpha$ , m/m · °C

Material	DIN	AISI	Mean coefficient of linear thermal expansion between room temperature and:				
			800°C (1472°F)	900°C (1652°F)	1000°C (1832°F)	1100°C (2012°F)	1200°C (2192°F)
C45	1045		$11 \times 10^{-6}$	$12 \times 10^{-6}$	$13 \times 10^{-6}$	$14 \times 10^{-6}$	$15 \times 10^{-6}$
C90	1090		$15.5 \times 10^{-6}$	$16.5 \times 10^{-6}$	$17.5 \times 10^{-6}$	$18.5 \times 10^{-6}$	$19.2 \times 10^{-6}$
X12CrNi188	302		$18.8 \times 10^{-6}$	$19.2 \times 10^{-6}$	$19.7 \times 10^{-6}$	$20 \times 10^{-6}$	$20.3 \times 10^{-6}$
X15CrNiSi2520	314		$16.8 \times 10^{-6}$	$17.3 \times 10^{-6}$	$17.7 \times 10^{-6}$	$18 \times 10^{-6}$	$18.3 \times 10^{-6}$

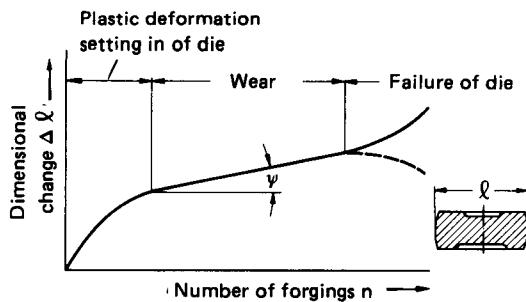


**FIG. 9.8** Schematic representation of dimensional change in dies with large inner pressure.

### 9.2.3 Machine Tools

Factors that affect the production accuracy from the point of view of machine tools are ram or hammer guidance, stiffness behavior in machines controlled by travel and force, and fluctuations in the work capacity of machines controlled by energy.

**Guidance:** Since the forming tool is generally made of two parts, a proper guidance of the ram in the frame is important for good positional accuracy (offset, difference in wall thickness, eccentricity).

The positional error of a tool is the sum of [9.5]:

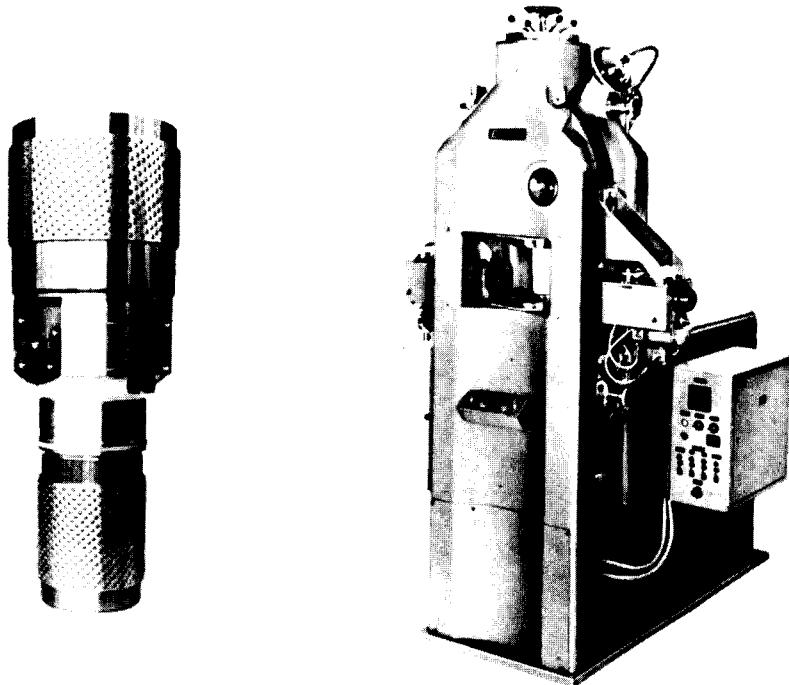


**FIG. 9.9** Roller guidance for ram, and fine-blanking press in which such a system is used.  
(Courtesy of ESSA.)

- 1 Positional error during contact (without load)
- 2 Positional error due to drifting (under central and eccentric loading), resulting in ram tilt

Causes for these positional errors from the machine design point of view are (1) guidance clearance of the unloaded press, (2) local elastic deformation on the guides, and (3) sideward tilt of the ram. For example, the positional error for mechanical presses under load is at least four times the value under no load [9.8].

As a guidance value for the accuracy of the ram movement under no load (as measured by the perpendicularity of the ram guides to the ram surface as well as by the clearance of the guides), a tolerance value of  $40 \mu\text{m}$  for a stroke of 100 mm (0.0016 in for 4 in) is normal. Closer tolerances are not economical.

As a rule, the accuracy of guidance is not as good in presses as in chip-forming machine tools. [In lathes it is, for example,  $15\text{--}30 \mu\text{m}/\text{m}$  ( $15\text{--}30 \mu\text{in/in}$ ).] Hence tools with pillar guides (roller-bearing sleeve guides) are used to improve the accuracy of guidance. A disadvantage in such guidance systems is unnecessary overdesign (two guidance systems).

Several improvements have been made in recent times on the accuracy of ram guidance. With roller guides on the ram, nearly playless guidance has been achieved. An example of such guidance is shown (Fig. 9.9) for a fine-blanking press; the clearance is on the order of a few micrometers (microinches). Such roller guides are also being used increasingly for high-speed blanking presses with lower drive as well as for regular presses.

**Elastic deformation:** An absolutely rigid press does not exist. The frame and drive system components deform depending on their elastic spring constants  $C_F$  and  $C_D$ , respectively. As it was shown in Chap. 8, the overall spring constant  $C_T$  of the press is more or less determined from the drive system deformation. A noticeable increase in the total stiffness  $C_T$  is only possible by increasing the drive system stiffness  $C_D$  (refer also to Fig. 8.73). For variations in the force transmitted because of changes in volume, lubricant, material properties, and so on, fluctuations in elastic deflections of the press will be smaller in a more rigid press.

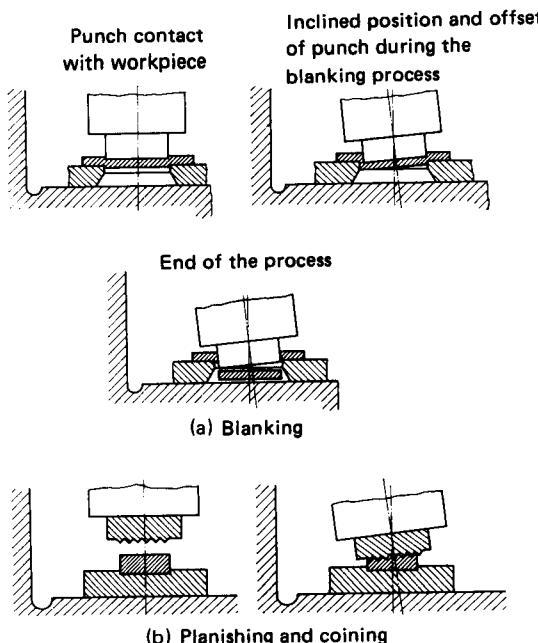


FIG. 9.10 Effect of elastic deflection on processes in loaded presses.

It is therefore necessary to use more rigid presses in processes such as die forging and coining in order to obtain close dimensional tolerances on thickness in the force direction. Close-framed presses are preferable for such processes [including shearing (blanking)] to C-frame presses (Fig. 9.10; refer also to Chap. 8).

The larger the stiffness of the press, the shorter is the contact time between the tool and the workpiece under load (refer to Fig. 8.10). This results in reduced thermal loading on the tool in hot forging, leading to longer tool life. In this respect the stiffness also influences indirectly the maintenance of production accuracy.

Less rigid mechanical presses (crank) are, however, advantageous for springback control in bending. Thickness variations in bent sheets require only very small changes in the coining force (force at the end), and the contact times are not increased substantially with changes in the coining force. The average springback reduces with increasing force [9.9]. In less rigid presses, a contact time increase raises the coining impulse  $\int F dt$ , thereby reducing the spread of springback.

**Work capacity:** Fluctuations in the work capacity of hammers and screw presses (for a given mass and changes in drop height  $H$  and velocity  $v$ ) affect the thickness dimensions of the workpieces. The available work capacity  $E$  should therefore be maintained constant for increased requirements on accuracy.

The control of drop hammers by means of end relays and that of pneumatic hammers by air flow (difficult) are some possibilities to control the availability of energy.

In the case of screw presses either a stroke-limiting procedure or control of the screw speed (better method) can be used to control the work capacity.

#### 9.2.4 Process Design and Layout

The dimensional accuracy is greatly affected by the complete manufacturing cycle. The various factors of manufacturing that contribute toward achieving the desired accuracy are material, annealing, descaling, lubrication, heating in warm and hot forming, tool lubrication, tool temperature, interstage design, and finishing process. By proper design of the initial billet shape, the interstage, and the finish form, more can be achieved as far as accuracy is concerned than by a single machine finish forming. Engineers have a special job in this area, the design of process sequences to achieve the necessary quality level without large investments. Statistical methods are used to study the quality levels and to implement the appropriate suggestions [9.10]. Fig. 9.11 shows the dimensional changes observed in a production run of hot forging, and Fig. 9.12 shows a normal distribution of workpiece dimensions to illustrate the statistical nature of dimensions obtained in production. From the point of view of optimum tool utilization, it is advisable to make the allowable tool wear and deformation as large as possible. This can be achieved by reducing the spread of values (damping of random errors).

Investigations on the regular production of cold-extruded workpieces show that the working condition of the tools, especially the working temperature (caused by heat conduction from the workpiece) [80–150°C (175–300°F)] affect the spread of the maximum forming force [9.11]. At the beginning the spread was 12–15% for the largest workpiece and 5% for the smallest workpiece. The spread reduces after the tool temperature has attained a steady value. Changes in the lubricant effect caused variations of up to 20% in the average force, while the thickness of the phosphate coating in the case of steel had no appreciable effect.

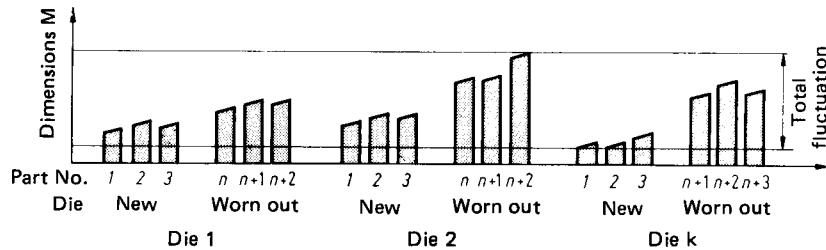
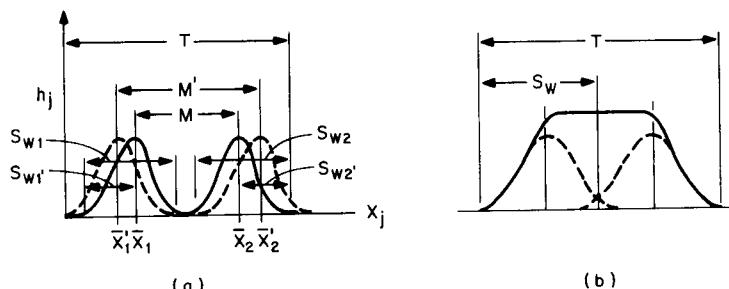


FIG. 9.11 Dimensional variations in production where several tools are used. (After [9.4].)



**FIG. 9.12** Distribution of workpiece dimensions in hot-die forging production. (a) Distribution of dimensional deviations  $h_j$ . (b) Total distribution of dimensional deviations.  $h_j$ —relative frequency;  $S_w$ —distribution range of dimensional deviations in successive workpieces ( $S_{w,1}$ ,  $S_{w,2}$ )—at beginning and end of forging with one die;  $S_w$ ,  $S_w'$ —large and small distribution ranges of  $X$ );  $\bar{X}$ ,  $\bar{X}'$ —mean values of dimensional deviations with large and small distribution ranges;  $T$ —total dimensional tolerance;  $M$ ,  $M'$ —usable amount of  $T$  for dimensional change of die (die wear) during die life. (After [9.4].)

### 9.3 ACCURACY OF VARIOUS PROCESSES

#### 9.3.1 Hot and Cold Forming

Hot (or warm) forming (forming after heating the workpiece) and cold forming have been discussed earlier as far as the material behavior (flow curve, formability) is concerned. From the viewpoint of dimensional accuracy, warm (hot) forming is less accurate than cold forming because of (1) differential shrinkage effects and (2) oxidation of surfaces coupled with material loss.

Warm- (hot-) formed workpieces are therefore a few ISO qualities less accurate than cold-formed workpieces. By a combination of warm- and cold-forming processes the advantages of both processes can be used optimally—lower forces and energy as well as larger formability in the heated condition and better accuracy and surface quality at room temperature.

#### 9.3.2 Hot-Die Forging

The process sequence in hot-die forging calls for a larger number of stages from the point of view of accuracy. This is especially true for large quantities and complicated geometries. The factors (both direct and indirect) affecting the dimensions, form, positional accuracy, and surface quality in hot-die forged workpieces can be described quantitatively based on detailed available investigations. The most important factors in hot-die forging are die temperature, die accuracy, control of energy expended, and machine and tool guidance. For uniform heating of large quantities, continuous ovens and inductive heating systems are used. Scaling can only be completely avoided by heating in electrical ovens under a protective atmosphere.

Examples of precision-forged workpieces are gas turbine blades with a thickness tolerance of  $\leq 0.2\text{--}0.25 \text{ mm}$  ( $0.008\text{--}0.01 \text{ in}$ ), sewing and office typewriter parts with  $0.25\text{--}0.4 \text{ mm}$  ( $0.01\text{--}0.016 \text{ in}$ ), ready-to-assemble gears (bevel, spur) of quality levels 7 to 8 (DIN 3961) [9.12], cold-coined to level 6. The process of precision forging is closely controlled: heating under atmosphere in a close range of temperatures, dies whose major elements are a part of the die itself (avoiding unnecessary parting-line errors), and careful control of the deformation energy (Fig. 9.13) [9.13], [9.14].

A systematic investigation of the effects of various factors on the accuracy of drop-forged workpieces has resulted in a usable tolerance system for steel and nonferrous metals [9.4], [9.15] to [9.19]. The widely used industrial process combination of hot-die forging followed by cold forming increases the accuracy either locally or in the entire workpiece.

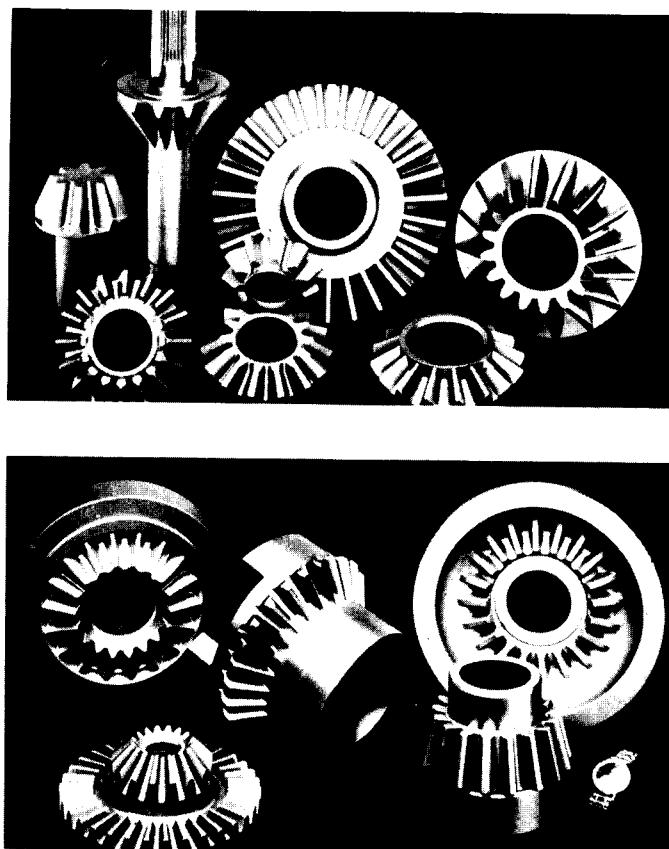


FIG. 9.13 Precision-forged gears. (Courtesy of BLW, Munich.)

### 9.3.3 Coining (Sizing)

Coining (or sizing) can be used to improve the dimensional accuracy on thicknesses of hot-die forged workpieces, bent specimens, and other pieces [9.20], [9.21]. This process can also be used to improve the surface quality. The process of such coining operations can be described as the upsetting at room temperature between two parallel tools with small thickness reductions.

The effect of a nonuniform normal stress distribution should be kept to a minimum in order to avoid an error due to tool bulging at the center (Fig. 9.14). This is because of the differential springback of the workpiece at various points along the surface of contact. (Refer to the schematic representation of  $\sigma_z$  over  $h$  in Fig. 9.15.) The bulging effect can be minimized by taking the following measures:

- 1 Small thickness reduction  $\epsilon_h$  (between 0.03 and 0.05) (hence small  $\sigma_f$  variation for work-hardening materials)
- 2 Good lubrication of coined surfaces
- 3 Tool inserts with large Young's modulus (Fig. 9.16, carbides)
- 4 Removal of material in the center (Fig. 9.17) if permitted from the design point of view
- 5 Small diameter-to-thickness ratios

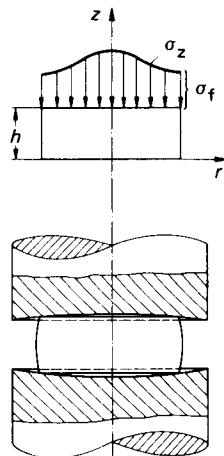


**FIG. 9.14** Normal stress distribution and tool-workpiece deformation in coining.

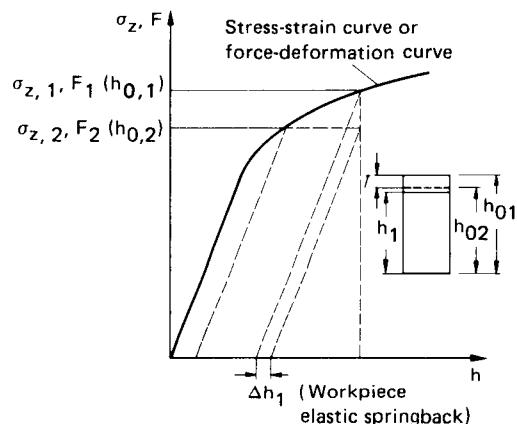


**FIG. 9.15** Schematic representation of variations of elastic springback in coining.

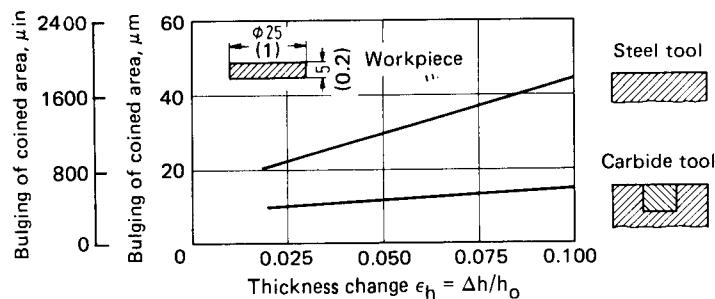


**FIG. 9.16** Tool material and tool bulging in coining. Dimensions are in mm (in). (After [9.20].)

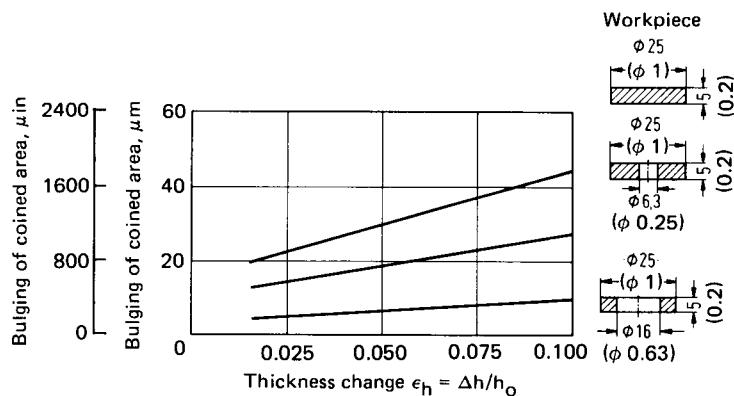


FIG. 9.17 Material removal at the center and bulging in coining. Dimensions are in mm (in). (After [9.20].)

The inaccuracies in the initial shape (forged workpiece, sheet-metal piece) are perpetuated until the final shape, since the force fluctuations between workpieces [ $f(A, \sigma_f(\varphi_h))$ ] cause different deformations on the machine, and the tool and the workpieces spring back differently from each other.

The total spread of dimensional variations after coining in presses controlled by stroke (Fig. 9.18a) is

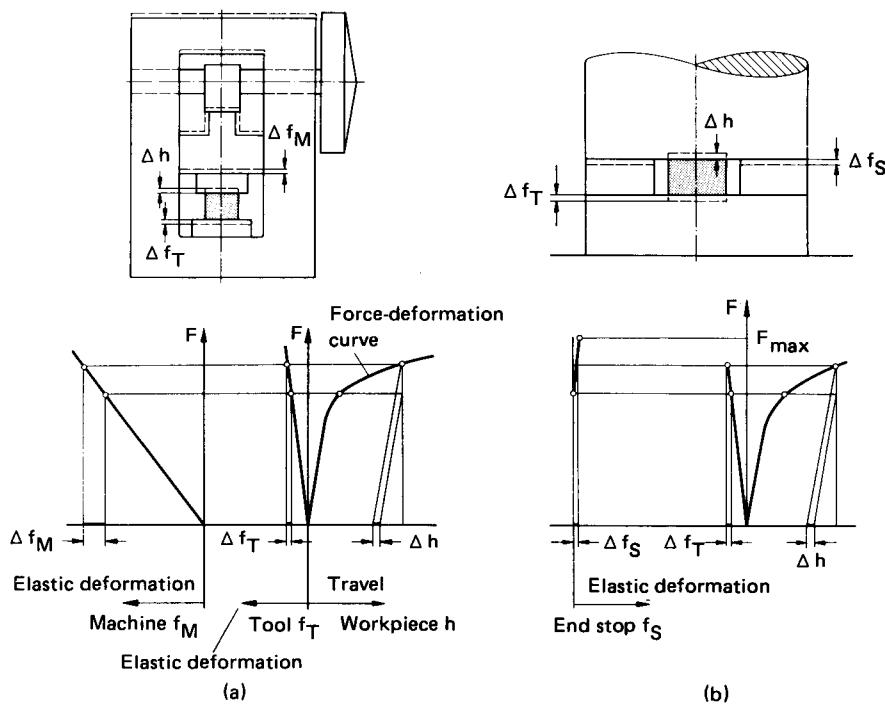


FIG. 9.18 Behavior of presses controlled by stroke and energy during coining process. (After [9.20].)

$$S_1 = h_{1,\max} - h_{1,\min} = \Delta h + \Delta f_T + \Delta f_M \quad (9.2)$$

Since the machine frames are relatively soft, the use of end stops in presses controlled by force and energy will increase the accuracy (Fig. 9.18b). In this case

$$S_1 = \Delta h + \Delta f_T + \Delta f_S \quad (9.3)$$

The stops are stiffer with increasing area  $A$  and smaller heights since

$$C_S = \frac{EA_S}{H_S} \quad (9.4)$$

Achievable quality levels in coining are given in Table 9.2.

#### **9.3.4 Cold Extrusion**

The following factors affect the dimensional accuracy in cold-extruded workpieces [9.6], [9.22]:

- 1 Material differences, property variations
- 2 Dimensional, volume (mass), and geometrical (form) variations of the billet (sheared, sawed)
- 3 Irregular pattern of heat and surface treatments
- 4 Tool dimensions and fluctuations in tool elastic deformations

Free flow (for excess material) and dimensional variations are a result of the volume control of the billet. An exact volume (mass) estimate and control will help in limiting such dimensional variations. Variations in the forming forces, caused by fluctuation in the flow stresses (material, heat treatment) and variations in the frictional conditions (surface treatment), are the cause of variations in bottom thickness (cans) and flanges. By working against stops in hydraulic presses, a better accuracy of the thicknesses of can bottoms and flanges can be obtained than with mechanical presses.

The cold-extruded workpieces are affected by form and positional errors rather than by dimensional errors. Offset of can thicknesses (positional error) can be caused with long and not very rigid punches—drifting of the punch. Further, if the billet does not have clean parallel surfaces, punch drifting can take place. In such cases a sizing operation may be necessary. To achieve better accuracies, the following improvements can be made:

- 1 Accurate tool setting (floating axis punch-die)
- 2 Good punch and ram guidance
- 3 Parallel billet surfaces with small clearance in the die cavity

The error in the cylindricity of workpieces is caused by variations in die elastic deformation (due to radial pressure variation along the die wall) and the resulting residual stress condition in the material. If an accurate dimension is required, processes with a constant radial pressure must be chosen, such as ironing or open-die extrusion. By controlling all the process parameters (includ-

**Table 9.2** Achievable Dimensional Accuracy in Coining

Type of workpiece	Material	Starting accuracy	Coined accuracy
Hot-die forged workpiece			
Circular cross-section	Steel	IT 12-14	IT 9-11
Hollow ring sections	Steel	IT 12-14	IT 8-10
Sheet metal parts			
Circular sections	Steel	IT 12-15	IT 10-12
Circular sections	Pure aluminum	IT 12-15	IT 9-11

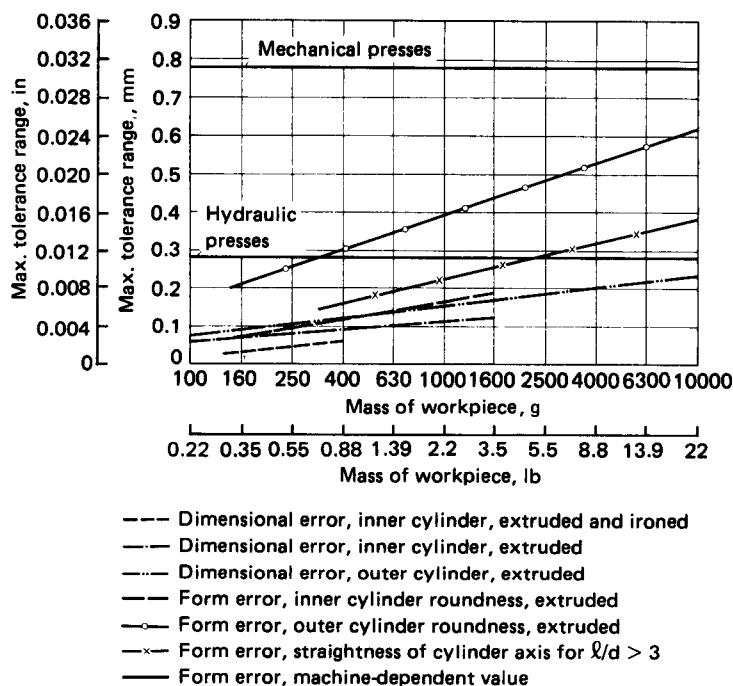


FIG. 9.19 Relation between mass of workpiece and various dimensional and form errors in cold impact extrusion with different machine types. (After [9.22].)

ing steady tool temperature), the dimensional errors can be controlled to between 0.25 and 0.6% of the desired diameter, depending on the deformation ratio. This order of magnitude of error corresponds to an ISO quality of between 4 and 9. As a general rule, the following accuracies can be achieved in cold extrusion with normal efforts:

Inner dimensions IT 8 to 12

Outer dimensions IT 10 to 13

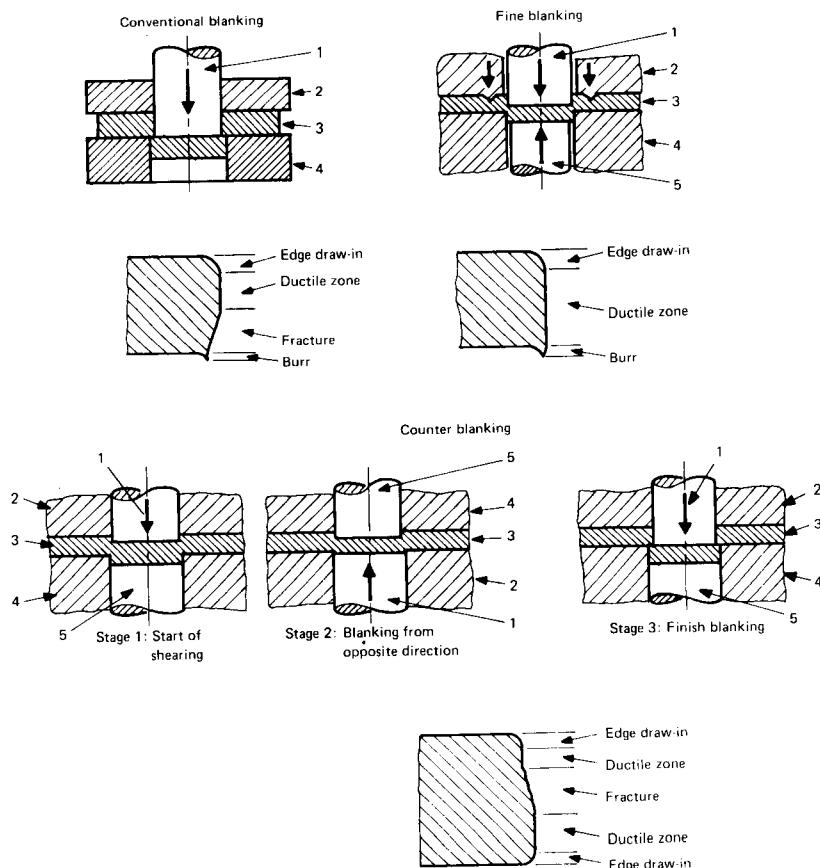
In general all functional surfaces need no further finishing operation in cold extrusion, as long as they can be manufactured by the process.

Fig. 9.19 shows the achievable range of tolerances for steel workpieces established by statistical methods based on innumerable measurements on production parts. This illustration may provide sufficient guidelines for determining accuracies in production.

### 9.3.5 Shearing and Blanking

Depending upon the type of shearing or blanking process, the deformed zone has different proportions of edge draw-in, ductile fracture zone, and brittle fracture zone (Fig. 9.20). The dimensional accuracy of shearing or blanking measured in the sheared zone lies between the quality levels of IT 9 and IT 14.

If the entire sheared surface is to be smooth (ductile fracture), the process of fine blanking can be used. The use of a ring indenter in the fine-blanking process superimposes compressive stresses in the deformation zone, thus preventing the formation of cracks.



**FIG. 9.20** Surfaces obtained in different blanking processes. 1—punch; 2—blank holder; 3—workpiece material; 4—die; 5—counterpunch.

In the conventional blanking or piercing process the outer dimensions are related to the die dimensions and the inner dimensions to the punch dimensions. Deviations from the desired or nominal dimensions are the result of material flow during the process and elastic springback of the workpiece after the process. Fine-blanked pieces exhibit two common errors: the surface is not exactly cylindrical (barrel-shaped) and pierced diameters show deviations.

## 9.4 DIMENSIONAL TOLERANCES

### 9.4.1 Tolerance Ranges

It is not possible to manufacture any workpiece with absolutely correct dimensions—hence tolerances are established for the dimensions. The tolerances must be so chosen that they ensure the functional requirement of the workpiece. They need not be smaller than required, thereby making the production process uneconomical.

The dimension obtained in production must be between the maximum permissible dimension

$M_x$  and the minimum dimension  $M_n$ . The tolerance lies between the values of  $M_x$  and  $M_n$ . Related to the nominal dimension  $N$ , the tolerance  $T$  is divided into upper part  $U$  and lower part  $L$ . Hence

$$U = N - M_n \quad L = M_x - N$$

$N$  can be chosen as either  $M_x$  or  $M_n$ . An example of a dimension with tolerance is

$$28^{+0.12}_{-0.15} \text{ mm } (1.100^{+0.005}_{-0.006} \text{ in})$$

The various values are  $N = 28$  mm (1.1 in),  $U = 0.12$  mm (0.005 in),  $L = 0.15$  mm (0.006 in), and  $T = U + L = 0.27$  mm (0.011 in).

Fig. 9.21 shows the various tolerance ranges for blanking and piercing, considering dimensional variations in tool manufacture.

#### 9.4.2 ISO Tolerances

The basic tolerance factor in the ISO tolerance system for round and parallel flat portions of the workpiece is

$$i = 0.45 \sqrt[3]{d} + 0.001d$$

where  $i$  is in micrometers for a given dimension  $d$  in millimeters.

ISO tolerances have been introduced for the nominal dimension range of 1–500 mm (0.04–20 in). Every part dimension can be given a dimensional tolerance in 16 (18) tolerance grades (designated as IT). The magnitude of the tolerance for every quality level is fixed by a definite multiple of the basic tolerance factor  $i$ . The grades from IT 6 ( $= 10i$ ) are geometrical series with a factor of 1.6 (preferred number). Tolerance grades below IT 6 are partly geometric and partly linear. Table 9.3 gives an example of the ISO tolerances.

Fig. 9.22 shows the achievable accuracy for diameters, thickness, and so on, for different processes (some of which were discussed earlier in this chapter). Some machining processes have also been included. The values given in the figure must be considered as guidance values only.

## 9.5 SURFACE QUALITY

Manufacturing technology must ensure the production of workpieces with the desired characteristics, which, apart from the geometry (shape and dimensions) and the mechanical properties, also include the surface quality. The economics of the metal-forming processes, for example, material savings, can be used to advantage only when the manufactured workpieces are functionally suitable without any major finishing operations. In other words, it must be possible to achieve the workpiece shape, dimensions, and surface quality with the selected metal-forming process. An essential prerequisite for manufacturing workpieces with the desired surface quality is the knowledge of the effect of the production conditions (process, type) on the surface topographical changes.

The surface layers in a metal-forming process generally remain at the surface, although they

Table 9.3 ISO Tolerances

Tolerance grade <sup>a</sup>	IT 5	IT 6	IT 7
Tolerance magnitude	$7i$	$10i$	$16i$
Dimensional range			
6–10 mm	6	9	15 $\mu\text{m}$
30–50 mm	11	16	25 $\mu\text{m}$
120–180 mm	18	25	40 $\mu\text{m}$

<sup>a</sup>The ISO tolerance grades are in the geometric proportion of 1.6; e.g., IT 5  $\rightarrow 7i$ , IT 6  $\rightarrow 7i \times 1.6 \rightarrow 10i$ , IT 7  $\rightarrow$  IT 6  $\times 1.6 \rightarrow 10i \times 1.6 \rightarrow 16i$ .

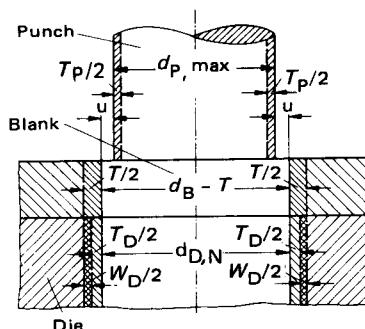


**FIG. 9.21** Tolerance ranges, maximum and minimum dimensions, in blanking and piercing.  
 $d_{p,\max}$ —maximum punch dimension;  $d_{D,N}$ —nominal dimension of die;  $W_D$ —wear of die;  
 $d_B$ —nominal blank diameter;  $T_p$ —manufacturing tolerance of punch;  $T_D$ —manufacturing tolerance of die;  $T$ —tolerance of blank;  $u$ —nominal clearance. The nominal die diameter is chosen as the minimum blank dimension.

$$\text{maximum dimension } d_D = (d_B - T) + T_D + W_D$$

$$d_p = (d_B - T) - \frac{2u}{2u}$$

$$\text{nominal dimension } d_{D,N} = d_B - T$$

Process \ ISO quality	5	6	7	8	9	10	11	12	13	14	15	16
Die forging												
Precision die forging												
Cold extrusion												
Rolling (thickness)												
Finish rolling (thickness)												
Finish coining (thickness)												
Deep drawing												
Ironing												
Tube and wire drawing												
Shearing/blanking												
Fine blanking												
Turning												
Cylindrical grinding												

**FIG. 9.22** Guidance values for achievable accuracies in various processes.

are subject to physical, chemical, and micro- and macrogeometrical changes during the process. This phenomenon is in contrast to machining and other metal-removal processes, where a new surface layer is formed after every working cycle. The quality of a deformed surface in the final stage is therefore determined from the initial surface quality and the history of the various forming processes undergone by the surface [9.23].

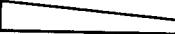
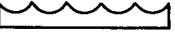
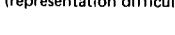
### 9.5.1 Surface Quality Parameters

The description of the surface through various parameters has been well established in different standards. Surface texture is the result of repetitive or random deviations from the nominal surface, which form the pattern on the surface. The surface texture includes waves, grooves, marks, scratches, and microstructure effects, and it forms part of the deviation of the workpiece from its desired shape as shown in Fig. 9.23. The shape deviations of the second to the fifth order form the surface texture as described in this chapter.

In the discussion of surface texture, especially waviness and roughness, a profile section (Fig. 9.24) is considered. Some of the important values describing the surface texture are:

- 1 The peak-to-valley height  $R_t$  is the distance between the base profile and the nominal or reference profile.
- 2 The centerline or average profile is an imaginary line such that the sums of the areas contained between it and those parts of the profile which lie on either side of it are equal.
- 3 The smoothing depth (peak-to-mean line height)  $R_p$  is the distance between the centerline (average profile) and the nominal profile,

$$R_p = \frac{1}{l} \int_{x=0}^{x=1} y_t dx \quad (9.5)$$

Geometrical deviations (schematic)	Examples	Causes
Type 1: Form deviations 	Flatness Roundness	Errors in the guides of machines Bending of machine or the workpiece Wrong clamping of the workpiece Wear
Type 2: Waviness 	Waves	Eccentric clamping or form error of a cutter Vibrations of a machine tool or the tooling
Type 3: 	Grooves	Shape of cutting edge Feed or adjustment of the tool
Type 4: 	Marks Scratches Indentations	Chip formation process Material deformation in sandblasting Improper galvanizing
Type 5: (representation difficult) 	Micro-structure	Recrystallization process Pickling Corrosion
Type 6: (representation difficult) 	Material crystal structure	Physical and chemical processes in the material formation Stresses and slip planes in crystal structure
		

Types 1 through 4 overlap each other to form a profile surface.

FIG. 9.23 Geometrical deviations with examples.

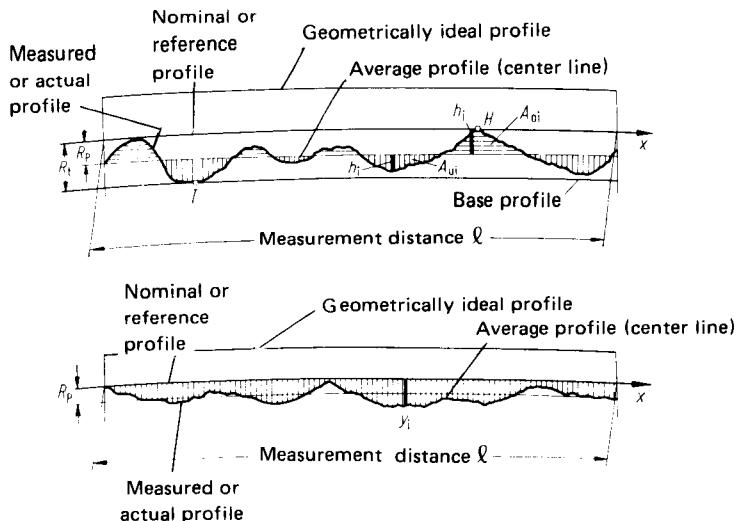


FIG. 9.24 Representation of various characteristics of surface texture.

- 4 The average roughness (arithmetical average height)  $R_a$  is the arithmetic average of the absolute values of the distances  $h_i$  of the nominal profile from the average profile (centerline),

$$R_a = \frac{1}{l} \int_{x=0}^{x=1} |h_i| dx \quad (9.6)$$

- 5 The overall roughness  $R_z$  is the average of five successive roughness heights, measured with electrical measuring equipment, and  $R_{\max}$  is the maximum of the five roughness depths.

The method of description illustrated is also the international method of representing roughness values. In the American system, a typical roughness description is as follows:

$$a = \sqrt{\frac{b - c}{d}} \quad (9.7)$$

where the various parameters are:

$a$  = roughness height (arithmetic average, same as  $R_a$ )

$b$  = waviness height (same as peak-to-valley height  $R_t$ )

$c$  = waviness width (distance between successive wave peaks)

$d$  = roughness width cutoff (greatest spacing of repetitive surface error)

$e$  = direction of the predominant surface pattern, ordinarily determined by the production method used

$f$  = roughness width (distance between successive peaks or ridges)

Typically, in the SI system roughness values as defined above are expressed in micrometers and in the American system in microinches.

### 9.5.2 Changes in Surface Texture Caused by Hot and Cold Forming

In hot-forming operations, oxidation (scaling in steel workpieces) affects the surface texture. The oxide layers must be removed by processes like pickling, tumbling, and blasting. The surface

texture obtained by such treatments is not generally suitable for functional surfaces without finishing operations such as machining, cold coining, or finish rolling. The surface texture of hot-formed workpieces is not the final surface the workpieces will normally have following finishing operations. However, precision hot-forming processes are an exception to this rule.

To understand surface textures obtained by cold-forming processes, free and constrained forming conditions must be considered. In the case of free forming conditions, the surface areas (macrogeometrical) are increased or decreased without coming into contact with tool surfaces. (Examples are tensile, compressive, and torsion tests.) In constrained metal forming, the tool directly imparts compressive and shear forces on the workpiece. All the technical metal-forming processes, especially the finish-forming processes, belong to the class of constrained forming processes, where it is aimed at producing workpieces with the desired shape and dimensions. It has, however, been determined that a combination of both free and constrained forming takes place in almost all the production forming processes. In various areas of the workpiece the free and the constrained flow can take place simultaneously, or the free flow is followed by constrained forming. In the example of upsetting between flat tools, the free surface is the cylindrical shell line and the top and bottom surfaces are constrained.

### 9.5.3 Surface Texture in Free Forming

It has been shown that a linear relationship can be observed (in both tension and compression) between the increase of roughness of a relatively smooth surface [ $R_{t,0} = 0.5\text{--}2 \mu\text{m}$  ( $20\text{--}80 \mu\text{in}$ )] and the magnitude of the local strain (Fig. 9.25) [9.24], [9.25]. For relatively smaller initial roughness [ $1$  and  $16 \mu\text{m}$  ( $40$  and  $640 \mu\text{in}$ )] in the figure, the roughness increases with straining for both upsetting and stretching, with the increase being slightly larger in upsetting. However, at larger initial roughness, the roughness increases with strain in upsetting but decreases in stretching. Two mechanisms are responsible for the change of roughness with straining—deformation of individual grains and the slip phenomenon [9.25]. The individual grain size determines the amount of change of the surface; the larger the initial grain size, the higher is the increase of roughness with deformation (Fig. 9.26). In a uniaxial compression or tensile test the relation between the thickness strain  $\varphi_s$  and the longitudinal strain  $\varphi_l$  is given by

$$-\varphi_s = \frac{\varphi_l}{2} \quad (9.8)$$

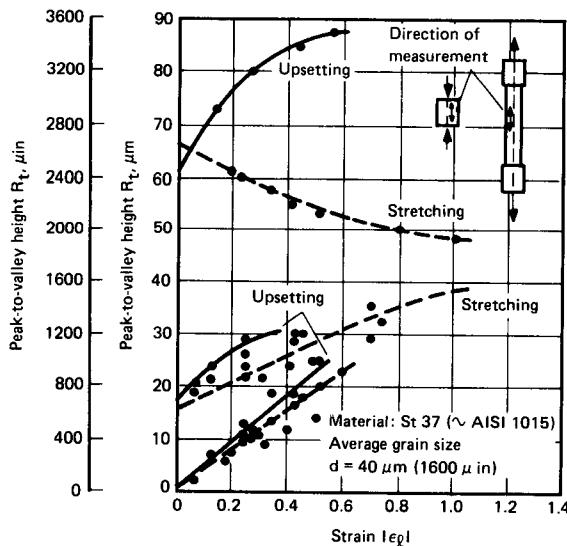
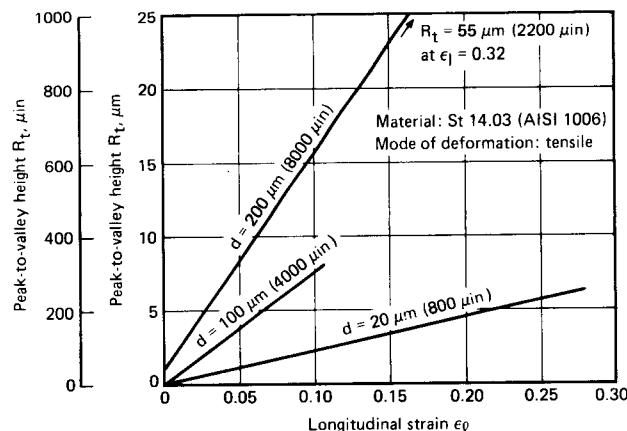


FIG. 9.25 Change of surface roughness in free forming.



**FIG. 9.26** Effect of grain size on roughness change in free forming.

Hence drawn against engineering strain, upset specimens tend to show a higher roughness increase than stretched specimens. However, on a scale of true strain, the roughness changes are the same for both upsetting and stretching (Fig. 9.27). The compressed layer in Fig. 9.27 (bending) has a larger roughness since the true strain of the layer on the compressive boundary is more than the tensile boundary layer (the engineering strains are, however, the same).

#### 9.5.4 Surface Texture In Constrained Forming

In constrained forming, the free deformation of the corners is hindered by the normal stresses on the workpiece from the tool. The surface texture of the workpiece is therefore dependent on the macro- and microgeometrical shape of the tool and the relative movement between them. Propositions similar to those used in explaining the surface texture in free forming are not yet postulated for constrained forming operations. However, the friction and lubrication conditions in the

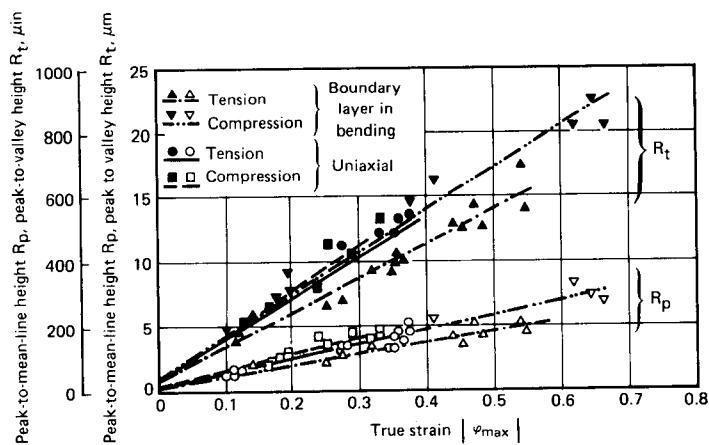


**FIG. 9.27** Change of surface roughness in free forming as a function of true strain  $|\varphi_{\max}|$ .

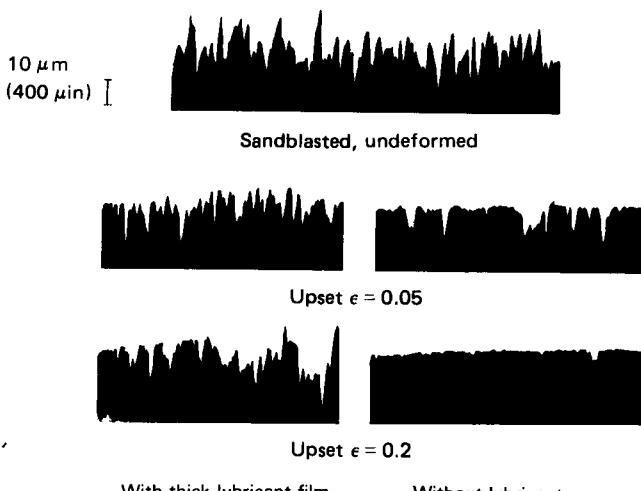


**FIG. 9.28** Surface roughness changes in cold coining with and without lubricant. (After [9.25].)

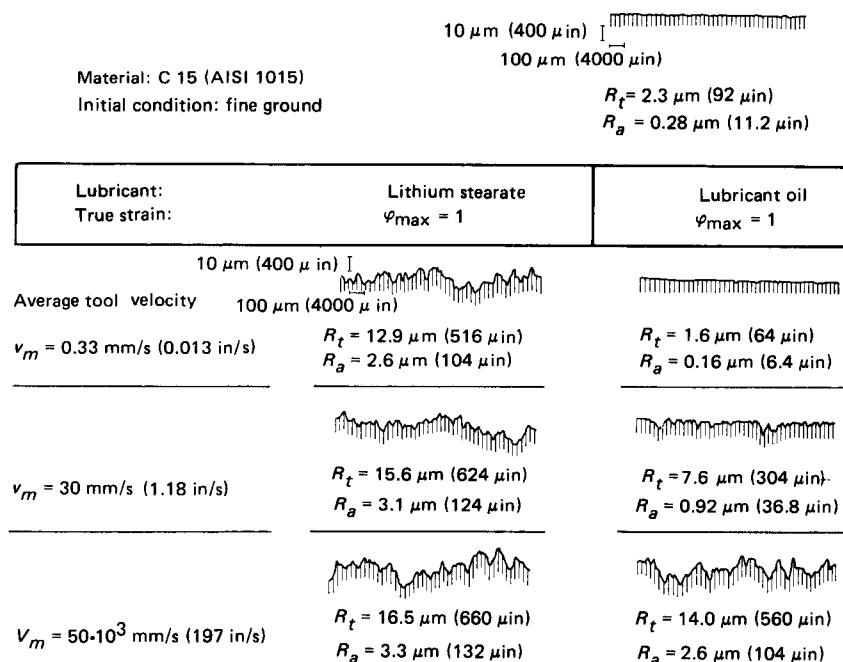


**FIG. 9.29** Effect of lubricant and tool velocity on surface texture of top surface of upset specimens. (After [9.26].)

contact zone between the workpiece and the tool are important to be considered for understanding surface texture changes in constrained forming processes. (See also Chap. 6.)

The possible friction conditions are:

**Dry friction ( $\mu > 0.3$ ):** Direct contact exists between two metallic surfaces with no lubricant.

**Boundary friction ( $\mu = 0.1\text{--}0.3$ ):** Friction exists between the outer layers of the two surfaces separated by a very thin layer of lubricant.

**Hydrodynamic friction ( $\mu < 0.03$ ):** The surfaces are separated by a definite layer of lubricant film capable of withstanding the normal pressures.

**Mixed friction ( $\mu = 0.03\text{--}0.1$ ):** This is a common friction condition in metal-forming processes—a mixture of hydrodynamic and boundary friction.

Sticking friction may occur under dry friction conditions and sometimes also under extreme boundary friction conditions, while sliding friction is significant for hydrodynamic and mixed friction conditions.

Mixed friction and the boundary friction conditions are more favorable than hydrodynamic lubrication for obtaining smoother surface textures. In other words, mixed friction and boundary friction are better for obtaining smoother surfaces than a perfectly lubricated condition. In boundary or dry friction conditions, highly smooth surfaces can be obtained with (highly) polished tools. These facts are illustrated in Fig. 9.28.

The tool velocity also affects the surface texture in combination with lubrication. At low tool velocities, a fluid lubricant in upsetting can lead to more favorable surface textures (compared with the initial surface texture) than a solid lubricant (Fig. 9.29). At higher velocities the fluid lubricant behaves the same way as a solid lubricant at low tool velocities. The lubricant stays on the surface without allowing for further smoothening [9.26].

### 9.5.5 Surface Quality in Various Processes

Fig. 9.31 (next page) shows the surface roughness obtainable in some metal-forming and machining processes. The dotted lines on the left-hand side are the limits that can be obtained with extra efforts in manufacturing—better surface finish on tools in forming, for example. When properly selected and used, some forming processes can impart the same or better surface quality than the competing machining process.

A process that is commonly used to improve surface finish is burnishing, an upsetting process with small deformations. In a burnishing process without lubricant it has been observed that the peak-to-mean line height  $R_p$  is lower on the surface near the boundary than at the center (Fig. 9.30), although the normal stresses are higher at the center. In this case sliding friction on the outer layers has a more pronounced effect on the surface texture than the larger normal pressures at the center.

If lubricants are to be used for such processes, they should be thin. Lubricants such as graphite in oil form small aggregates and leave impressions on the burnished workpiece, thereby imparting a poor surface texture.

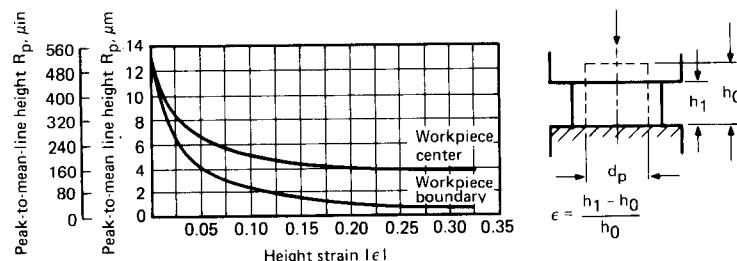


FIG. 9.30 Effect of burnishing on surface texture. Material—C15 (AISI 1015);  $h_0/d_0 = 1.0$ .

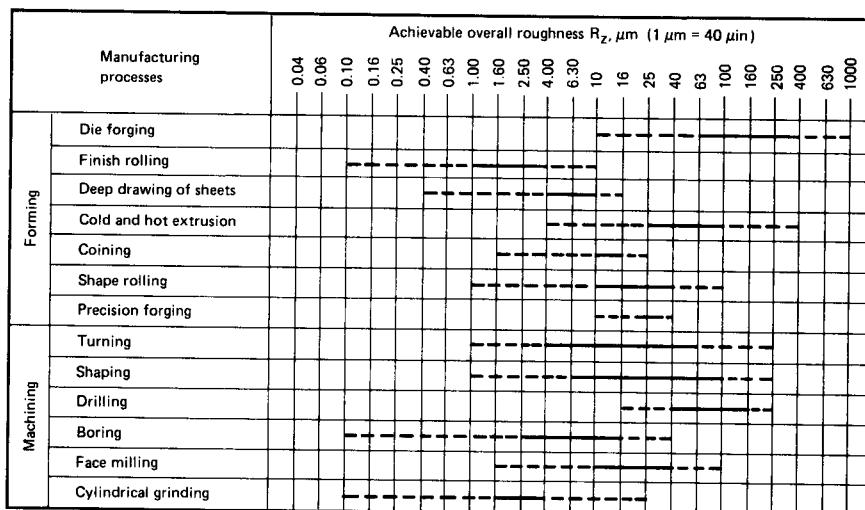


FIG. 9.31 Achievable overall roughness in selected manufacturing processes.

## REFERENCES

- 9.1 Kienzle, O.: "The Corner Stones of Manufacturing Technology" (in German), *Werkstattstechn. u. Maschinenbau*, 46, 1956, pp. 204–209.
- 9.2 Ickert, J.: *The Subject of Accuracy in Technical Standards* (in German), Berlin/Göttingen/Heidelberg, Springer, 1955.
- 9.3 Lange, K.: "Accuracy in Die Forging with Hammers" (in German), Dr.-Ing. thesis, Technical University, Hannover, 1953; *Forschungsberichte des Wirtschafts- und Verkehrsministeriums Nordrhein-Westfalen*, no. 98, Köln/Opladen, Westdeutscher Verlag, 1954.
- 9.4 Huwendiek, D. J.: "Analysis of Manufacturing Tolerances Using Statistical Methods as Applied to Die Forging of Steel" (in German), Dr.-Ing. thesis, Technical University, Hannover, 1963.
- 9.5 Watermann, H. D.: "Dimensional Accuracies of Hammers and Screw Presses in Eccentric Loading" (in German), *Werkstattstechnik*, 53, 1963, pp. 413–421.
- 9.6 Leykamm, H.: "Studies on the Dimensional Accuracy of Cold Bulk Forming" (in German), *Berichte aus dem Institut für Umformtechnik, Universität Stuttgart*, no. 57, Berlin/Heidelberg/New York, Springer, 1980.
- 9.7 Lange, K.: *Die Forging of Steel* (in German), Berlin/Göttingen/Heidelberg, Springer, 1958.
- 9.8 Schweer, W., and Hoppe, H.: "On the Accuracy of Mechanical Presses" (in German), *Mitt. dtsch. Forschungsges. Blechverarb. u. Oberflächenbehandl.*, 19, 1968, pp. 90–95.
- 9.9 Tafel, K.: "Investigation of the Contact Time Effects on the Spread of Springback in Bent Specimens" (in German), *Berichte aus dem Institut für Umformtechnik, Technische Hochschule Stuttgart*, no. 1, Essen, Girardet, 1964.
- 9.10 Soom, E.: *Statistical and Mathematical Methods in Manufacture* (in German), vols. 1 and 2, Blaue TR-Reihe, no. 72 and 82, Bern, Verlag Technische Rundschau.
- 9.11 Witte, H. D.: "Investigation on the Spread of Forces and Energy in Cold Extrusion in Production and the Effect of the Phosphate Coating Thickness and the Lubricant" (in German), *Berichte aus dem Institut für Umformtechnik, Universität Stuttgart*, Essen, Girardet, 1967.

- 9.12 DIN 3961: "Toleranzen für Stirnradverzahnungen, Grundlagen (Accuracy of Cylindrical Gears, Basics)," 1974.
- 9.13 Schorp, G.: "Forming of Gears" (*in German*), *VDI-Berichte*, no. 47, Düsseldorf, VDI-Verlag, 1961.
- 9.14 Mages, W. J.: "Precision Die Forging" (*in German*), *Wt.-Z. Ind. Fertigung*, **69**, 1979, pp. 541–548.
- 9.15 DIN 7526: "Toleranzen und zulässige Abweichungen für Gesenkschmiedestücke aus Stahl (Tolerances and Permissible Deviations for Die-Forged Workpieces Made of Steel)," 1969.
- 9.16 Kienzle, O.: "Dimensional Tolerances on Deformed Workpieces, Example: Hot-Die Forging of Steel" (*in German*), *Werkstattstechnik*, **59**, 1969, pp. 257–265.
- 9.17 DIN 1749: "Gesenkschmiedestücke aus Aluminium (Hot-Die Forged Aluminum Workpieces)," 1963.
- 9.18 DIN 9005: "Gesenkschmiedestücke aus Magnesium (Hot-Die Forged Magnesium Workpieces)," 1963.
- 9.19 DIN 17673: "Gesenkschmiedestücke aus Kupfer und Kupferknetlegierungen (Hot-Die Forged Copper and Wrought Copper Alloys)," 1963.
- 9.20 VDI-Richtlinie 3172: "Flachprägen (Coining)," Düsseldorf, VDI-Verlag, 1961.
- 9.21 Kienzle, O. and Meier, R.: "Achievable Dimensional Accuracy and Surface Quality of Hot-Die Forged Workpieces" (*in German*), *Werkstattstechnik*, **51**, 1961, pp. 545–551.
- 9.22 Wagener, H. W., and Leykamm, H.: "Dimensional Tolerances of Cold Extruded Steel Workpieces" (*in German*), *Ind.-Anz.*, **90**, 1968, pp. 45–52.
- 9.23 Kienzle, O.: "On the Various Types of Deformed Metallic Surfaces" (*in German*), *Microtechnic*, **14**, 1960, pp. 134–140.
- 9.24 Kienzle, O., and Mietzner, K.: "Microgeometrical Changes of the Surface Texture in Cold-Forming Processes" (*in German*), *Forschungsberichte des Landes Nordrhein-Westfalen*, no. 812, Köln/Opladen, Westdeutscher Verlag, 1960.
- 9.25 Dannenmann, E.: "Surface and Boundary Layer Effects in Blanking" (*in German*), *Tech. Mitt.*, **73**, 1980, pp. 893–901.
- 9.26 Wiegand, H., and Kloos, K. H.: "Cold Upset Test as a Model Process to Understand Frictional and Surface Characteristics" (*in German*), *Werkstattstechnik*, **56**, 1966, pp. 129–137.



**2**

**BULK-METAL FORMING**

---

---



## CHAP. 10

### UPSETTING

Upsetting is defined as “free forming, by which a workpiece segment is reduced in dimension between usually plane, parallel platens,” according to DIN 8583, sheet 3 [10, 1]. It also includes coining and heading. Closed-die forming (DIN 8583, sheet 4 [10, 1]), shape upsetting, or die heading involve tools which contain the intended shape wholly or in part.

Upsetting is of interest for theoretical studies as a model process. Among the processes of metal forming it represents a basic process which can be varied in many ways. A large segment of industry depends primarily on the predominant application of upsetting processes. Parts produced are screws, nuts, rivets, nails, and bolts.

A very extensive bibliography of publications dealing with problems of cold upsetting is contained in [10.2].

#### 10.1 FUNDAMENTALS OF UPSETTING

Although upsetting has great significance for metal forming, research remains to be done with regard to stresses and deformation which occur during the process. This is due to significant difficulties which result from the transient nature of the process and the difficulty of defining friction conditions between tool and workpiece.

##### 10.1.1 Material Flow, Friction, and Lubrication

Upsetting is a transient forming process, that is, streamlines and flow lines do not coincide during forming (see Chap. 5). Material flow, characterized by streamlines and flow lines, can be made visible through grid lines or photos of light dots (Fig. 10.1). According to [10.3], both the state of motion and the deformation distribution are affected more profoundly by friction than by tem-

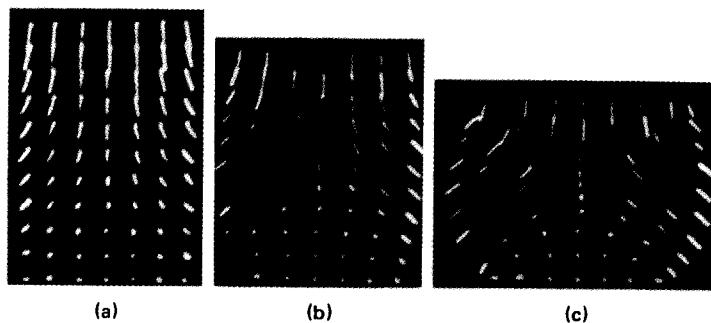


**Fig. 10.1** Velocity fields in upsetting. (a) Original shape. (b) Intermediate shape. (c) Final shape.

perature and strain rate. The severity of friction increases for large reductions and for workpieces with initially high diameter-to-thickness ratios. For such cases good lubrication becomes especially important.

Deformation distribution can be determined by microhardness scanning. According to [10.4] a distribution is obtained which had previously been provided qualitatively by Siebel: deformation is concentrated on an area, which extends diagonally outward from the center of the sample. In hot upsetting, the distribution of local deformation becomes more uniform with increasing tool contact speed [ $0.4 \text{ m/s} \leq v \leq 45 \text{ m/s}$  ( $1.3 \text{ ft/s} \leq v \leq 148 \text{ ft/s}$ )]. This is indicated by diminishing bulging of the peripheral surface [10.5]. According to [10.6], however, cold upsetting with high tool contact velocities [ $0.14 \text{ m/s} \leq v \leq 45 \text{ m/s}$  ( $0.46 \text{ ft/s} \leq v \leq 148 \text{ ft/s}$ )] results in a deformation distribution which is less uniform in the upset direction, but more uniform perpendicular to it (see Chap. 4).

The contact areas expand by both sliding and fold-over of parts of the free surface onto the die face [10.7]. By choosing the inclination of the platens sliding can be influenced, resulting in a change of the relative amounts of sliding and fold-over. In hot upsetting the increase in tool-workpiece contact area of cylindrical samples is greatly dependent upon work material (AISI 430, 302, and 1015 steels were tested), tooling, initial diameter-to-length ratio  $d_0/l_0$ , and strain  $\phi = \ln(l_1/l_0)$ . If the ratio  $d_0/l_0 > 1$ , sliding increases with increased compression when hot upsetting between plane platens, while for  $d_0/l_0 < 1$  sticking occurs at the interfaces. Regions of impeded deformation, which can be determined by metallography or hardness testing, become smaller with increasing  $d_0/l_0$ . In cold upsetting of nonlubricated, slender, axisymmetric samples, a region of impeded or even prevented radial motion is also observed in the middle of the interface areas [10.4], [10.6]. For very slender samples a sticking region is formed. It was, however, not observed for lubricated samples.

### 10.1.2 Elementary Plasticity Theory (Slab Method)

Based on elementary plasticity theory (see Chap. 5), upsetting forces can be determined approximately. To do so, the distribution of the normal stress at the tool-workpiece interface is required. The rectangular slab technique is used for plane-strain deformation, and the tubular slab technique for axisymmetric problems (Fig. 10.2).

Axisymmetric upsetting with Coulomb friction yields force equilibrium in the radial direction (Fig. 10.3):

$$\sigma_r r l d\varphi - (\sigma_r + d\sigma_r)(r + dr) l d\varphi + 2\sigma_t \sin\left(\frac{d\varphi}{2}\right) l dr - 2\mu\sigma_z r d\varphi dr = 0 \quad (10.1)$$

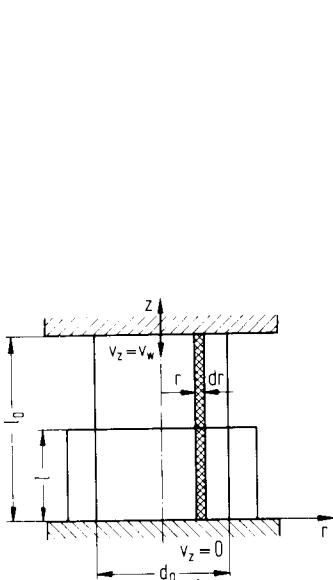


Fig. 10.2 Sketch of upsetting process.

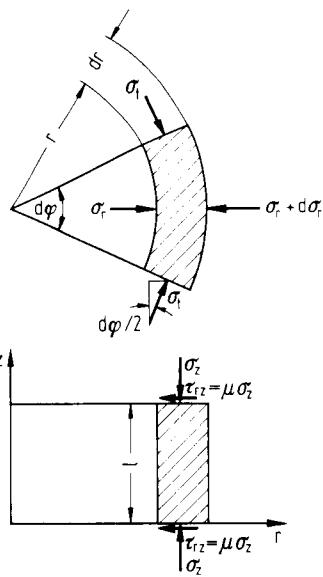


Fig. 10.3 Forces acting on an annular volume element, axisymmetric forming.

It is assumed that  $\sigma_t = \sigma_r$ , and that second-order differential terms can be neglected. Since  $\sin \alpha \approx \alpha$  for small angles, Eq. 10.1 reduces to

$$\frac{d\sigma_r}{dr} + \frac{2\mu}{l} \sigma_z = 0 \quad (10.2)$$

Substitution of the Tresca yield criterion

$$\sigma_r - \sigma_z = \sigma_f \quad (10.3)$$

yields

$$\frac{d\sigma_r}{dr} + \frac{2\mu}{l} \sigma_r = \frac{2\mu}{l} \sigma_f \quad (10.4)$$

The solution of this inhomogeneous linear differential equation of the first order is

$$\sigma_r = \exp\left(-\frac{2\mu r}{l}\right) \left[ \sigma_f \exp\left(\frac{2\mu r}{l}\right) + C \right] \quad (10.5)$$

for the boundary condition

$$\sigma_r = 0 \quad \text{when} \quad r = \frac{d}{2} \quad (10.6)$$

the constant for the integration is

$$C = -\sigma_f \exp\left(\frac{\mu}{l} d\right) \quad (10.7)$$

## 10.6 BULK-METAL FORMING

Thus the radial stress is

$$\sigma_r = -\sigma_f \left\{ \exp \left[ \frac{2\mu}{l} \left( \frac{d}{2} - r \right) \right] - 1 \right\} \quad (10.8)$$

With the help of the Tresca criterion (Eq. 10.3) the interface pressure is

$$\sigma_z = -\sigma_f \exp \left[ \frac{2\mu}{l} \left( \frac{d}{2} - r \right) \right] \quad (10.9)$$

The first two terms of the series expansion of the exponential function provide the expression by Siebel [10.8] for the pressure distribution,

$$\sigma_z = -\sigma_f \left[ 1 + \frac{2\mu}{l} \left( \frac{d}{2} - r \right) \right] \quad (10.10)$$

For the frictionless upsetting Eq. 10.2 reduces to

$$\frac{d\sigma_r}{dr} = 0 \quad (10.11)$$

and  $\sigma_r = \text{constant}$ . With boundary condition 10.6 and yield condition 10.3

$$\sigma_z = \sigma_r - \sigma_f = -\sigma_f \quad (10.12)$$

is obtained. This agrees with the result obtained by substitution of  $\mu = 0$  into Eq. 10.10. Fig. 10.4 shows the interface pressure distributions provided by Eqs. 10.9, 10.10, and 10.12.

The forming force is obtained by integration of the pressure over the contact area  $A$ ,

$$F_z = \int_A \sigma_z dA \quad (10.13)$$

For the axisymmetric case considered (Eq. 10.10),

$$F_z = -A\sigma_f \left( 1 + \frac{1}{3}\mu \frac{d}{l} \right) \quad (10.14)$$

The friction coefficient  $\mu$  is a function of lubrication, tool-workpiece material pairing, and temperature. For cold upsetting of steel  $0.05 \leq \mu \leq 0.15$  is generally expected under lubricated conditions, while for hot upsetting of steel  $0.25 \leq \mu \leq 0.5$ . Experimentally determined friction coefficients are contained in Chap. 6.

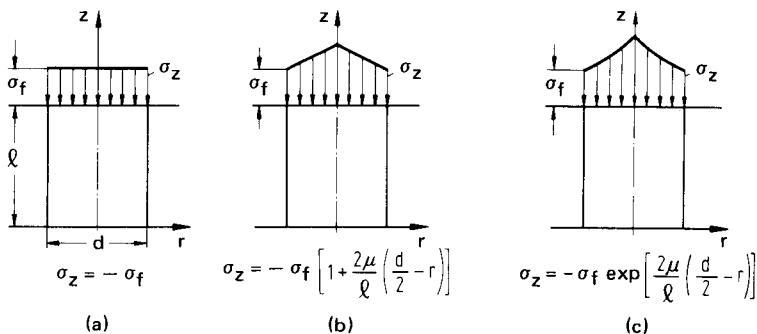


**Fig. 10.4** Normal stress distribution  $\sigma_z$  at the interfaces of axisymmetric upset cylinders, elementary theory of plasticity. (a) Frictionless upsetting. (b) Upsetting with friction, series expansion. (c) Upsetting with friction, exponential distribution.

The energy of deformation is obtained from

$$W = \int_{s=0}^{s=l_0-l_1} F_z ds \quad (10.15)$$

Most of this energy is dissipated as heat. Since in general deformation is inhomogeneous, different temperatures occur in the workpiece. If as a first approximation a homogeneous and adiabatic process is assumed, a mean temperature increase is obtained:

$$\Delta T_m = \frac{W}{cpV} \quad (10.16)$$

A detailed treatment of elementary plasticity theory for upsetting is provided in [10.9].

### 10.1.3 Deformation and Stress States

The normal stress distribution at the interfaces is dependent upon workpiece geometry and friction condition. A bell-shaped pressure distribution was measured in cold upsetting of nonlubricated axisymmetric samples of aluminum, copper, brass, and steel, with a ratio of initial diameter to initial length  $d_0/l_0 > 3$  [10.4]. This was observed for all lubricated samples [10.4], and also in hot upsetting of an Al-Mg-Si alloy ( $d_0/l_0 = 1.0$ ), according to [10.10].

For ratios  $0.5 \leq d_0/l_0 \leq 2.0$  a normal pressure distribution, with stress peaks both at the edge and in the center of the workpiece, was determined for cold upsetting of nonlubricated samples (Fig. 10.5) [10.4]. In hot upsetting of steel ( $d_0/l_0 = 0.67$ ) a parabolic pressure distribution is obtained with its minimum at the center of the workpiece [10.10]. With increasing compression this pressure distribution reverses, the edge stresses decrease, and the stresses at the center increase (Fig. 10.6). The maximum value of stress at the edge for lower deformations is attributed to elastic effects of workpiece and tool or to cooling effects [10.4], [10.10].

The principle of least power of deformation (upper bound, see Chap. 5) was applied to upsetting in [10.11] to [10.13]. While in [10.11] and [10.12] only the state of motion and the force of deformation were analyzed, in [10.13] the tool-workpiece interface pressure distribution was also determined from the velocity field. The experimentally determined radius of the sticking friction region was used to indicate the friction condition rather than an estimated value for the friction coefficient. Good agreement is demonstrated between analysis and experiment (Fig. 10.7).

The shear stress distribution at the workpiece-platen interface was calculated from the velocity field [10.13]. At the center of the interface the shear stress  $\tau$  vanishes since it changes direction there. It increases in value as it approaches the edge. The same holds true for the friction coefficient  $\mu = \tau/\sigma_z$  (see Chap. 6). This distribution is borne out qualitatively by experiment [10.4] (see Fig. 10.5).

Dynamic effects upon the states of stress and deformation are treated specifically in [10.6], [10.14], and [10.15]. Slip-line fields are known for both plane upsetting [10.16] and axisymmetric upsetting [10.17].

## 10.2 CHARACTERISTIC PARAMETERS AND PROCESS LIMITS

Successful upsetting depends upon three process limitations:

### 1 Upset strain

$$\varphi = \ln \left( \frac{l_0}{l_1} \right) \quad (10.17)$$

as the forming limit of the work material

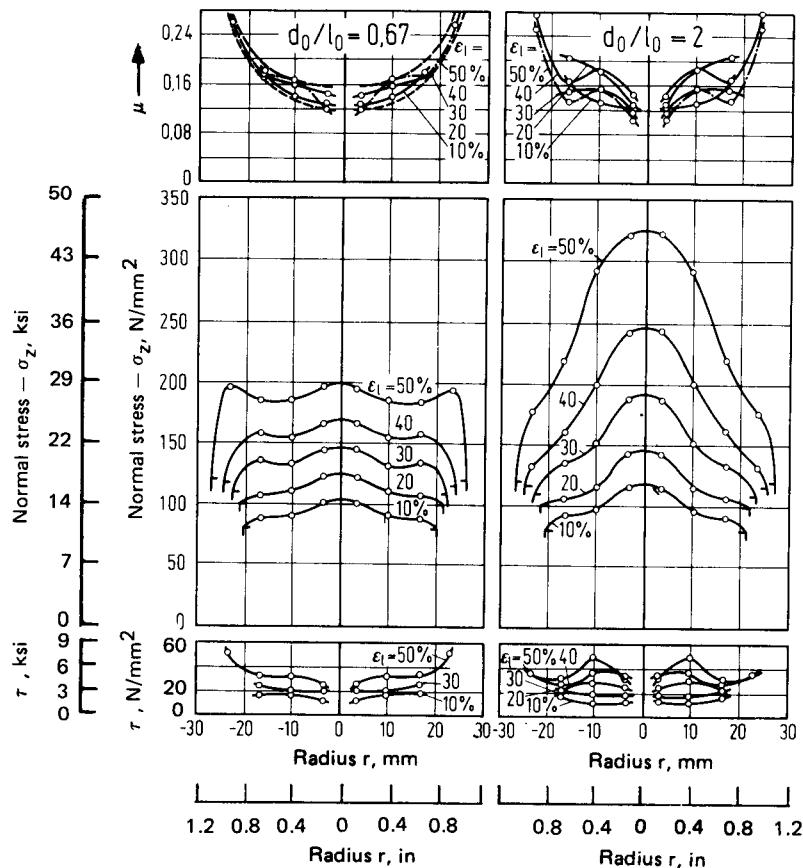


**Fig. 10.5** Distribution of friction coefficient  $\mu$ , normal stress  $-\sigma_z$ , and shear stress  $\tau$  at the interfaces of nonlubricated axisymmetric samples of commercial-purity aluminum.  $d_0 = 40$  mm (1.57 in);  $T = 20^\circ\text{C}$  ( $68^\circ\text{F}$ ). (After [10.4].)

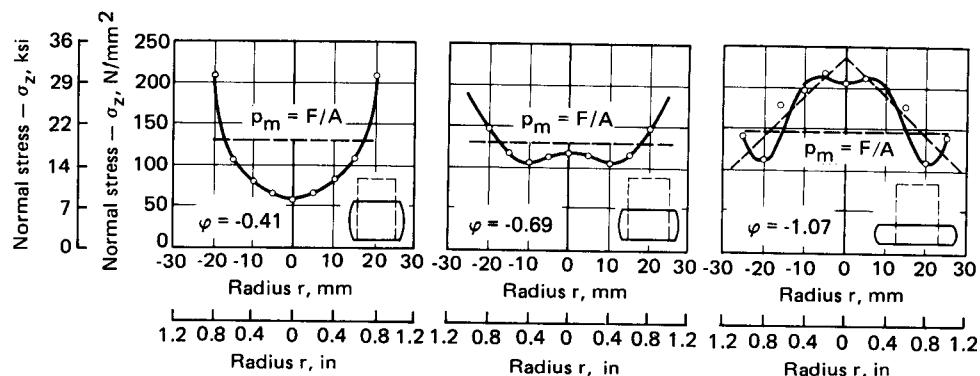


**Fig. 10.6** Distribution of normal stress  $-\sigma_z$  at the interfaces of axisymmetric samples. Steel with 0.091% C;  $T = 1050^\circ\text{C}$  ( $1922^\circ\text{F}$ );  $h_0 = 60$  mm (1.97 in);  $d_0/h_0 = 0.67$ . (After [10.10].)

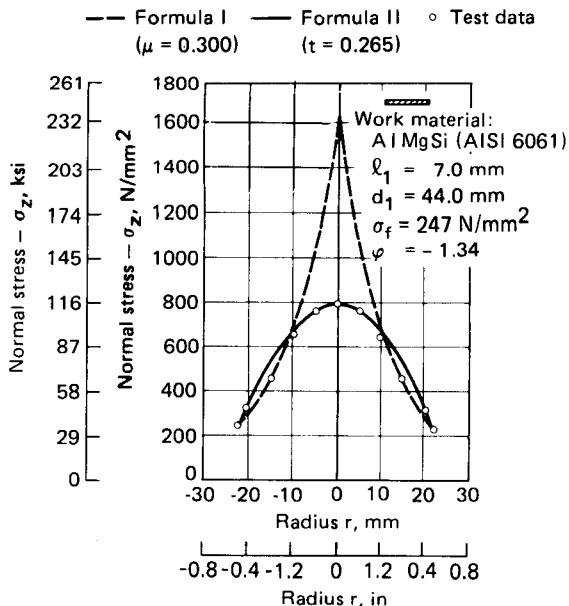


**Fig. 10.7** Distribution of normal stress  $-\sigma_z$  at the interfaces of axisymmetric samples.  $T = 20^\circ\text{C}$  ( $68^\circ\text{F}$ ); eq. I—elementary theory of plasticity; eq. II—upper bound. (After [10.13].)

## 2 Upset ratio

$$s = \frac{l_0}{d_0} \quad (10.18)$$

as the limit to buckling of the workpiece

## 3 Specific change in length

$$\epsilon_l = \frac{l_1 - l_0}{l_0} \quad (10.19)$$

as the limit to increased tool loading

Fig. 10.8 provides permissible values for cold upsetting of steel, with all three process limits taken into account.

For heading with shape dies these additional considerations are important:

- 4 Proper filling of the die
- 5 Minimum flash formation

### 10.2.1 Forming Limit

In cold upsetting of axisymmetric steel objects a maximum strain  $\phi_{\max} = 1.6$  can be achieved, which is independent of the number of forming stages. For greater deformations the danger of peripheral crack formation exists.

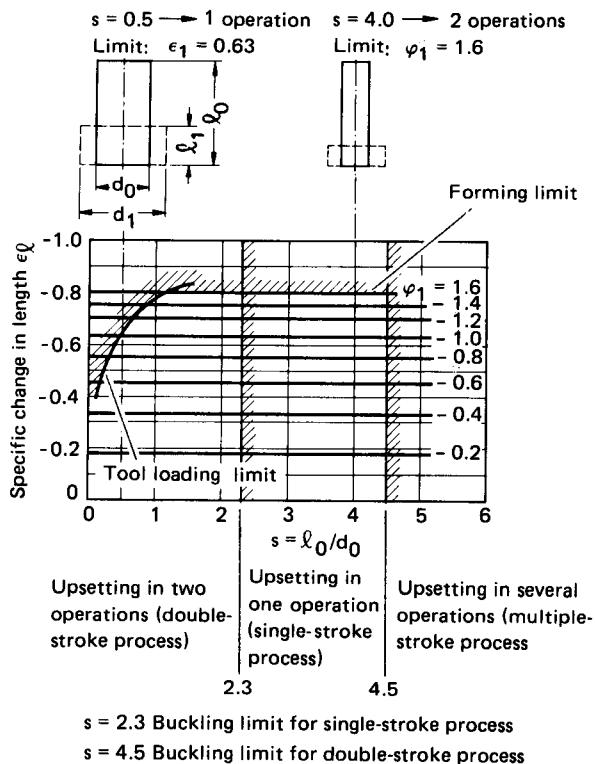


Fig. 10.8 Process limits in cold upsetting of steel.

For head shapes which are not axisymmetric, upset strain is not meaningful as a measure of deformation, since local transverse strains depend upon the shape of the head. According to [10.18], the head diameter should not be greater than  $2.2d_0$ .

The forming limit can be increased by measures that counteract strain hardening (intermediate annealing, hot upsetting), or by a more favorable head shape which creates an additional radial pressure, thus shifting the mean normal stress  $\sigma_m$  to arithmetically smaller values.

### 10.2.2 Limiting Upset Ratio

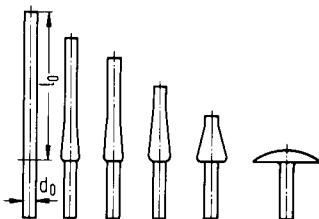


Fig. 10.9 Production of an upset part with large head. (After [10.20].)

The upset ratio  $s = l_0/d_0$  is limited by the possibility of buckling. It has nothing to do with deformation as such, but can assume different values for the same upset strain  $\phi$ . The contact faces of the tools and the workpiece should be as plane as possible and be perpendicular to the longitudinal axis of the workpiece to avoid buckling. In addition, both the surface condition and the shape of the upsetting tool as well as the lubricant used affect the ratio limit. It is virtually independent of the work material [10.19].

### Cold Upsetting

In cold upsetting a ratio of  $s = l_0/d_0 \leq 2.3$  can be achieved in one hit if deformation occurs over part of the length of the workpiece. The fibers do not display any evidence of buckling under these conditions. Larger values of  $s$  require several deformation stages (Fig. 10.9). In this case a length  $l' \leq 2.0d_0$  is upset per blow.

The following values for  $s$  are recommended:

One operation (single-stroke process)	$s \leq 2.3$
Two operations (two-stroke process)	$s \leq 4.5$
Three operations (three-stroke process)	$s \leq 8.0$
More than three operations (multistroke process)	
With whole die	$s \leq 10.0$
With split die	$s \leq 20.0$

For whole dies  $s$  is limited by difficulties arising during ejection.

### Hot Upsetting

Hot upsetting can be carried out in a single operation with  $s \leq 2.3$  [10.19]. The limiting upset ratio is dependent upon the ratio of final diameter to initial diameter  $d_1/d_0$  (Fig. 10.10) for cylindrical shapes, while for conical shapes the determining ratios are that of smallest cone diameter to initial diameter  $d_{1,\min}/d_0$ , and that of largest cone diameter to initial diameter  $d_{1,\max}/d_0$  (Fig. 10.11). Die heading of conical shapes permits greater upset ratios than die heading of cylindrical shapes.

For cylindrical shapes the ratio  $d_1/d_0$  should not exceed the value of 1.3 significantly (Fig. 10.10). Although workpieces having  $d_1/d_0 > 1.3$  may show no exterior defect, an unfavorable fiber structure is likely (Fig. 10.12). This is generally deemed acceptable, however. If a flawless fiber structure is important, the limits for cold upsetting should be observed [10.20].

A greater upset ratio  $s$  can also be achieved with electropunching (Fig. 10.13). The bar is conduction-heated between the movable platen (anvil electrode) and the fixed-clamping electrode

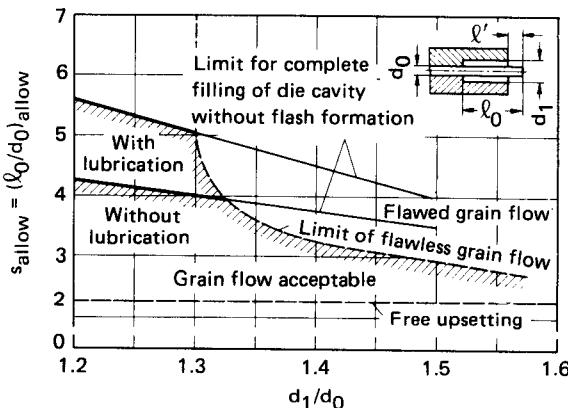
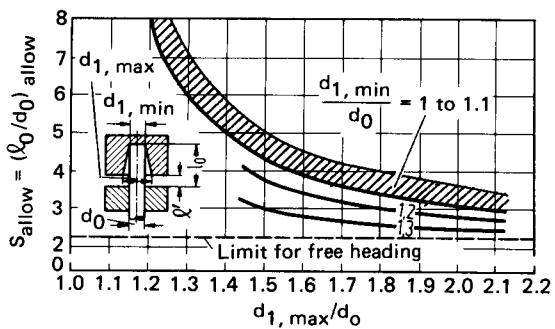


Fig. 10.10 Limiting upset ratio in die heading of cylinders.  $d_0 = 10 \text{ mm (0.4 in)}$ ; flash gap thickness =  $0.3 \text{ mm (0.01 in)}$ ;  $T = 1140^\circ\text{C}$  ( $2084^\circ\text{F}$ ). (After [10.19].)



**Fig. 10.11** Limiting upset ratio in die heading of cones.  $d_0 = 10$  mm (0.4 in). (After [10.19].)

only. Through a controlled feed rate of the bar, different upset shapes can be produced (Fig. 10.14). The achievable upset ratio is limited by the stroke of the platen. As a result of limited scale formation and exact temperature control, induction upsetting is suitable for forging with increased precision. It is used primarily for the production of preforms of engine valves, flanged shafts, and so on (Fig. 10.15).

### 10.2.3 Permissible Tool Stresses

The force required for upsetting rises steeply toward the end of the stroke. According to [10.21], this force increase is especially pronounced in cold upsetting of smaller head thicknesses (Fig. 10.16). Extreme tool wear is therefore to be expected in this domain. The force versus tool travel curve is dependent upon the workpiece geometry: with increasing  $d_0/l_0$  ratios the steep rise in force is shifted to smaller values of the change in length  $\epsilon_l$  (Fig. 10.16).

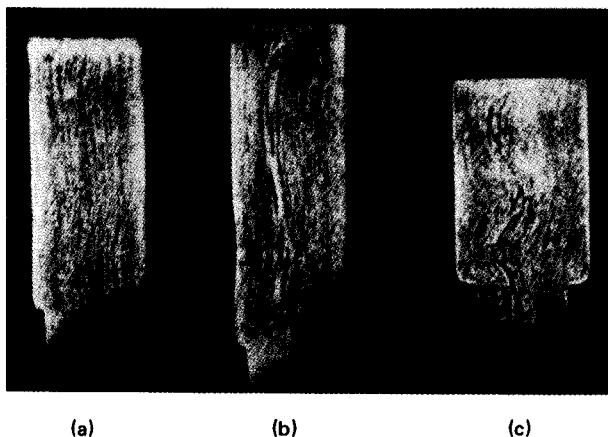


**Fig. 10.12** Grain flow in cylindrical upset samples. (a)  $s = 5.2$ , lubricated. (b)  $s = 6.3$ , lubricated. (c)  $s = 3.7$ , nonlubricated. (After [10.19].)

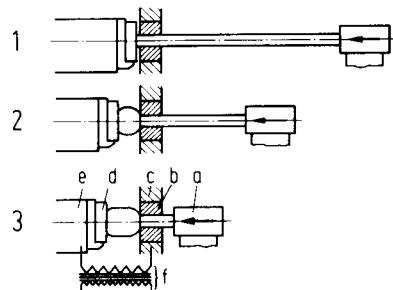


**Fig. 10.13** Schematic of upset process in elec-trousetting. 1—initial geometry; 2—intermediate stage; 3—final shape. *a*—upsetting punch; *b*—clamping jaw; *c*—guiding electrode; *d*—wear plate; *e*—anvil electrode; *f*—transformer. (After [10.20].)

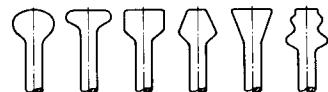


**Fig. 10.14** Head shapes obtainable with elec-trousetting. (After [10.20].)

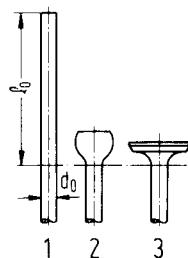
### 10.3 PREFORM HEADER

When forming in several stages, the design of the heading preforms is decisive for a favorable fiber structure of the final shape. The heading preforms are to be shaped such that:

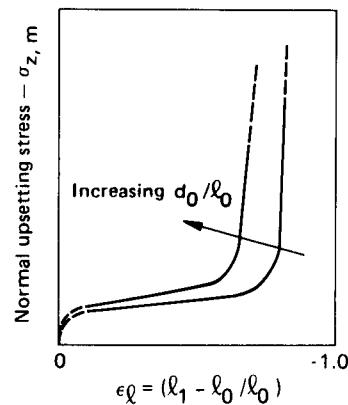
- 1 The workpiece is guided correctly (reducing the danger of buckling)
- 2 No fold-type defect formation occurs

#### 10.3.1 Solid Preform Header

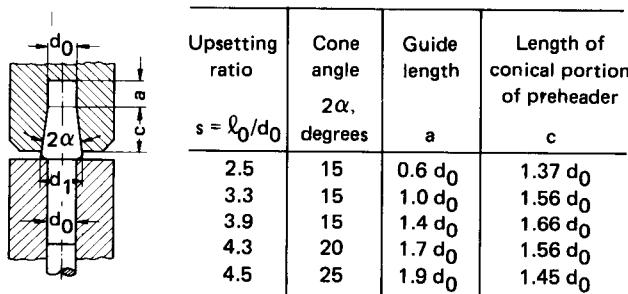
A preform header shape that proved useful is shown in Fig. 10.17. It is simple, hence inexpensive to produce and apply. It does, however, require close tolerances of wire and barstock. The allowable upsetting ratio is dependent upon the cone angle and can reach  $s = 4.5$  for the two-stroke



**Fig. 10.15** Production steps of disk valve. 1—initial workpiece; 2—intermediate shape (elec-trousetting); 3—final shape (screw press). (After [10.20].)



**Fig. 10.16** Fundamental development of the specific upset force  $-\sigma_{z,m}$ . (After [10.21].)

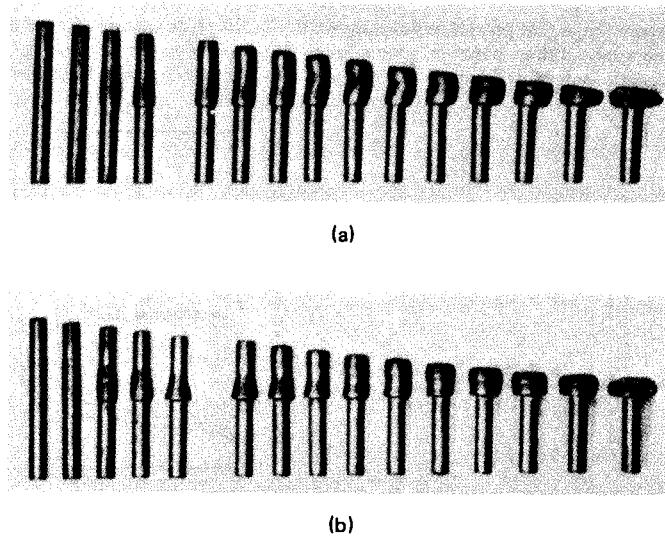
**Fig. 10.17** Solid preform header. (After [10.22].)

process (Fig. 10.17). The most favorable range for the cone angle is  $15^\circ \leq 2\alpha_{\text{opt}} \leq 25^\circ$ , while the free heading length should always be  $l' \leq 2.0d_0$ .

The choice of cone angle is dictated by two limiting cases. For a cone angle chosen too small, buckling is likely to occur for the free end in the subsequent forming stage (Fig. 10.18a). Too liberal a cone angle, on the other hand, tends to lead to the formation of a peripheral fold-type defect during finish heading (Fig. 10.18b).

### 10.3.2 Spring-Loaded Preform Header

An upset ratio  $s < 4.5$  can be obtained in the two-stroke process with a spring-loaded preform header. It is therefore popular for cold heading, even though it is more elaborate to produce, more difficult to apply, and hence more expensive than the solid header. In contrast to the solid

**Fig. 10.18** Defects in preform heading. (a) Formation of buckling fold during finish heading. (b) Formation of annular fold during finish heading. (After [10.20].)

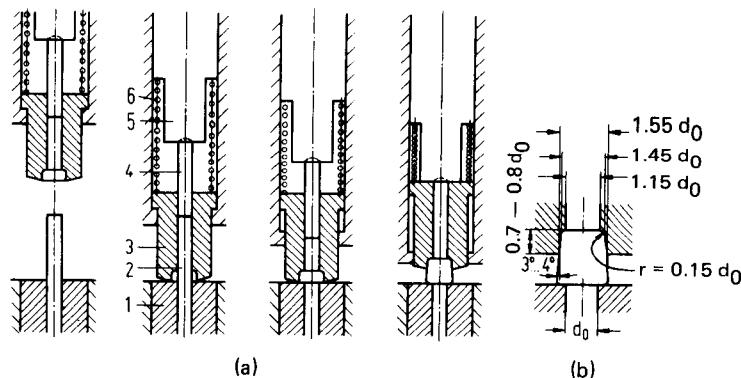


**Fig. 10.19** Spring-loaded preform header. (a) Operating scheme. 1—die, 2—work-piece; 3—preform header; 4—heading pin; 5—ram; 6—helical compression spring. (b) Guidelines for dimensioning. (After [10.20].)

header it is useful for different volumes. The heading process proceeds as follows (Fig. 10.19). The preform heading punch retracts against a coil spring, thus making room for the work material being formed. Since the free upsetting length  $l'$  is small, there exists no danger of buckling. As a result, the tolerances can be larger for the original work material than for the solid preform header.

#### 10.4 UPSETTING PROCESSES

For the selection of an upsetting process the following parameters are significant: dimensions of the workpiece, its strength, its formability, the required upset ratio, the desired accuracy and surface quality, as well as economic considerations.

For trouble-free and economic production the workpiece material must be of uniform quality (chemical composition, mechanical properties, and surface finish).

##### 10.4.1 Cold Heading

###### Work Materials

Steels and nonferrous metals with substantial formability (low-carbon steels, copper, aluminum) are suited for cold heading. Occasionally steels with higher carbon content, alloy steels, and special alloys are formed as well. These are the same work materials as those normally used for extrusion (see Chap. 15). Wire, bar, and billet sections that are produced by cropping or sawing are processed. Information regarding the production and prior treatment of slugs is available in Chaps. 25 and 26.

Customarily hot-rolled stock is used as the starting material. Due to the coarse tolerances, the first heading operation is often preceded by a sizing or preforming process during which the slug receives its exact intended shape. In some cases the use of drawn material is preferred, since variations in volume are reduced.

Smaller parts are cold-formed due to the small forming forces. Heating of such parts is not very advantageous, since rapid cooling results from the unfavorable surface-to-volume ratio. Production volume is high, and the increase in strength due to work hardening can be utilized constructively. On the other hand, formability is limited. This disadvantage can be dealt with by warm or hot forming.

### Processes of Cold Heading

For cold heading, that is, at room temperature, both the single-stroke process (one punch, one die) and the two-stroke process (two punches, one die) are of primary importance. In addition, major use is made of the multiple-stroke-process, in which each die operates with its own punch.

The single-stroke process (Fig. 10.20) is only applicable for upset ratios  $s \leq 2.3$ . The workpiece is finish-headed in one blow. The production volume corresponds to the stroke frequency of the machine. For upset ratios  $2.3 \leq s \leq 4.5$  the two-stroke process (Fig. 10.21) is applied. The punch holder, which performs an additional oscillating motion, holds two punches: a preform-heading punch and the finish-heading punch. During the first blow, the head is formed with the preform-heading punch; the part is then finished in the same die during the second blow. The output equals one-half of the stroke frequency of the machine. A distinction is made between two methods: heading with closed die (Fig. 10.21b) and heading with split (open) die (Fig. 10.21a). Whenever the shaft length exceeds  $8-10d_0$ , difficulties can arise during ejection of the workpiece. They are avoided with the split die.

For upset ratios  $s > 4.5$  the multiple-stroke technique is employed (Fig. 10.22). The number of strokes equals the number of punches or dies. Workpiece transfer is accomplished by a system of grippers. Every working stroke yields a finished part. The output corresponds to the stroke frequency of the machine.

There exist different variations of these basic processes, some of which can be combined with other forming processes (Fig. 10.22) (e.g., extrusion). The mechanical properties of the workpiece are dependent upon the deformation steps performed (Fig. 10.23).

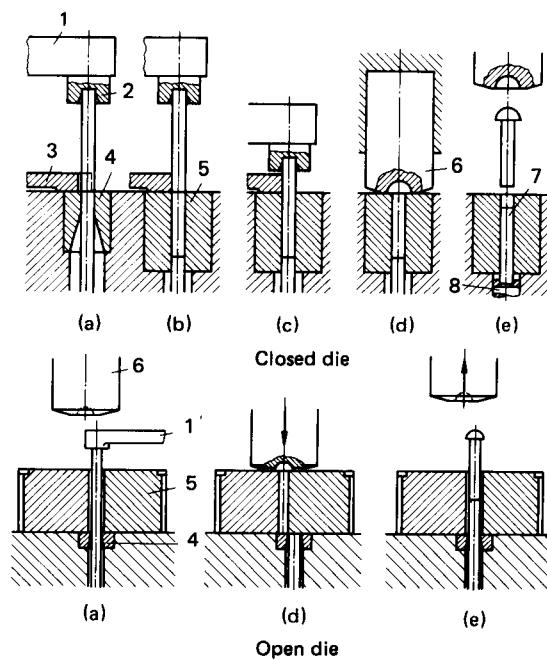


**Fig. 10.20** Single-stroke process. (a) Insertion of work material and shearing. (b) Transfer of slug to die. (c) Insertion of slug into die. (d) Heading. (e) Ejection. 1—stop; 2—workpiece insertion pusher; 3—shearing blade; 4—upsetting die; 5—upsetting die; 6—heading punch; 7—ejector pin; 8—ejector. (After [10.22].)

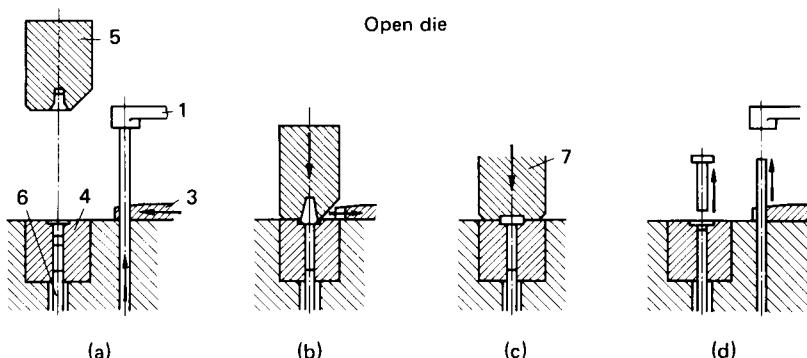
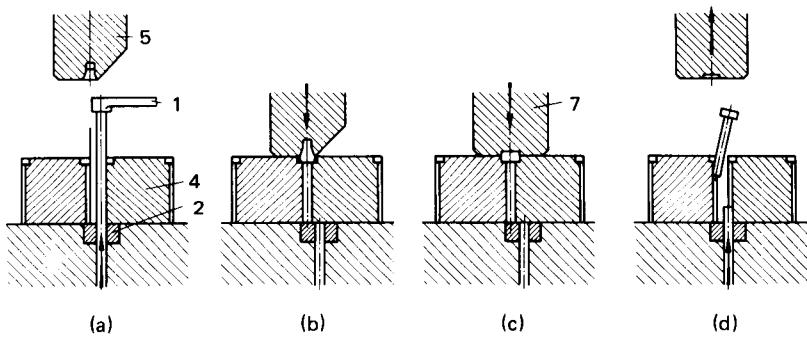


**Fig. 10.21** Two-stroke process. (a) Insertion of work material and shearing. (b) Preform heading. (c) Finish heading. (d) Ejection. 1—stop; 2—shearing blade; 3—upsetting die; 5—preform header; 6—ejector; 7—heading punch. (After [10.22].)

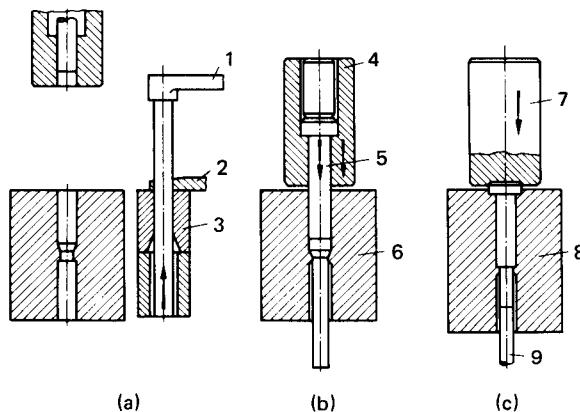


**Fig. 10.22** Multiple-stroke process (production of a screw blank). (a) Shearing. (b) Extrusion of shaft. (c) Reduction of thread portion and formation of head. 1—swing stop; 2—shear blade; 3—shearing die; 4—punch holder; 5—extrusion punch; 6—extrusion die; 7—heading punch; 8—reduction die. (After [10.22].)

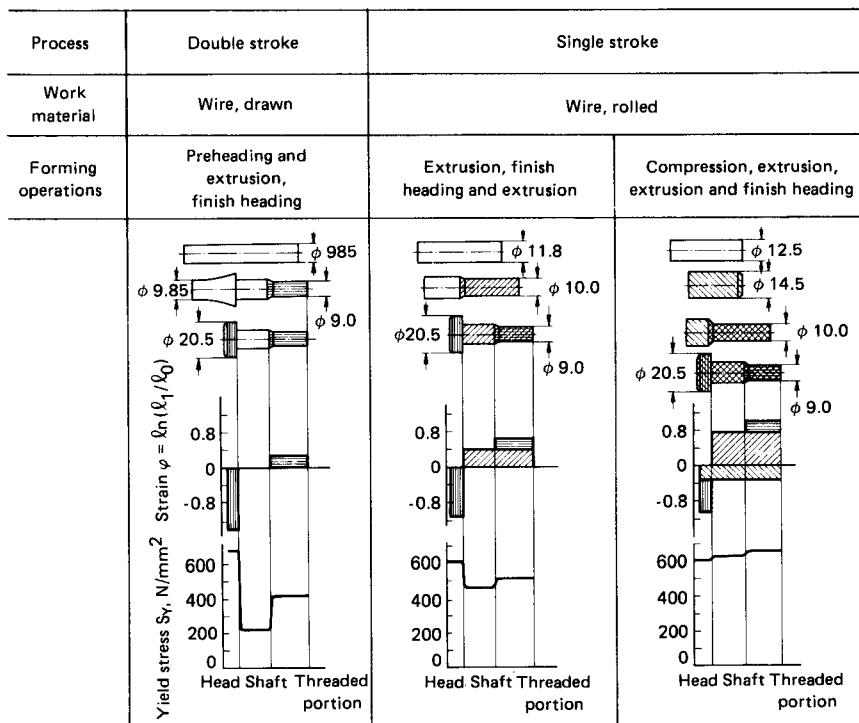


**Fig. 10.23** Variation in yield strength  $S_y$  in a hexagonal head screw as a function of the forming process. Work material—AISI 1008 (DIN UQSt 36-2) steel. Dimensions are in mm. (After [10.22].)

#### 10.4.2 Coining

Coining is a special application of cold upsetting [10.23]. It is used as smooth coining and as calibration coining. The objective of smooth coining is an extremely high surface quality, while calibration coining is to result in exceedingly close thickness tolerances. Incremental strains are  $0.025 < |\epsilon_i| < 0.05$  for sizing and  $0.1 < |\epsilon_i| < 0.2$  for smooth coining (Fig. 10.24) [10.24]. The improved surface quality in smooth coining is obtained through larger sliding distances between workpiece and tool. A more detailed treatment of sizing is found in Chap. 9.

#### 10.4.3 Hot Heading

Shapes which are large and difficult to form are usually formed at temperatures above room temperature in order to hold down forming forces. Both surface quality and dimensional accuracy are not as good as in cold heading. However, surface quality and accuracy can often be improved at critical locations through a subsequent coining step (see Chap. 9). Economic heating is a precondition for hot heading. The choice between batch and pusher furnaces and between electric resistance and induction heating (see Chap. 11) depends on the requirements. Hot upsetting is almost always a part of a forging process. This problem will receive further treatment in the next chapter. Work materials frequently selected for hot upsetting are found in Tables 11.4 to 11.10.

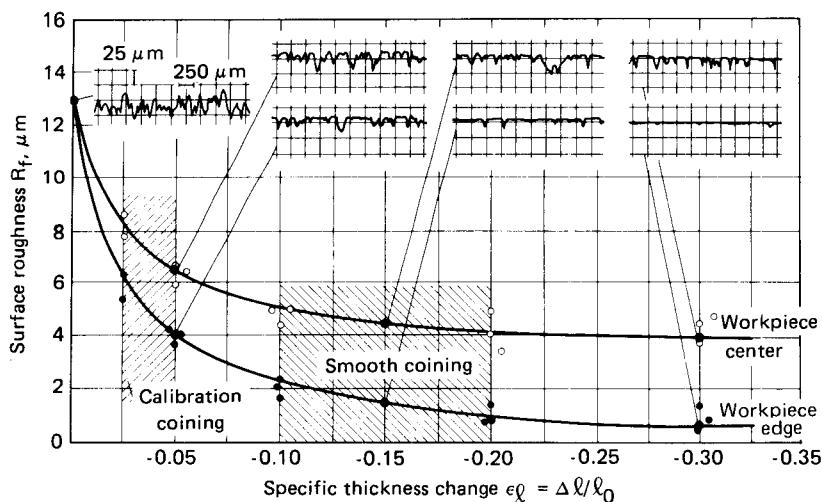


**Fig. 10.24** Dependence of surface roughness upon incremental thickness change  $\epsilon_\ell$  in cold coining. Work material—AISI 1015 (DIN Cq 15) steel;  $d_0/l_0 = 1$ ;  $d_0 = 25 \text{ mm}$  (1 in); sandblasted. (After [10.24].)

## 10.5 MACHINE TOOLS

Basically all types of hammers and presses can be used for upsetting. For special requirements of various upsetting processes and the production of certain parts specialized machines have been developed.

Path-dependent presses (see Chap. 8) are particularly suited for upsetting, since a force peak occurs at the end of the process. Through fixing of the energy capacity the point of full utilization can be reached (utilization of available energy and allowable peak force). With hydraulic presses (see Chap. 8) only the force can be utilized, but not the energy.

### 10.5.1 Machine Tools for Cold Heading

A multitude of specialized machines have been developed for cold heading, which are intended for the production of nails, pins, rivets, bolts, screws and so on (Fig. 10.25). Some representatives of these machines are wire pin, bolt, nut, and rivet presses. In addition, there exist single-purpose machines for the production of balls, hollow rivets, rollers, and rolls. Based on the method of operation, one distinguishes between single-stroke (one die), two-stroke (one die), three-stroke (two dies), and multiple-stroke presses (with transfer unit) (Figs. 10.26 to 10.28).

The principle of operation is the same for all automatic cold headers. The work material is generally fed in as wire or bar stock, drawn in by a multiroll straightener (Fig. 10.29), straightened, and subsequently sheared to length.

The workpiece is formed in one or several operations and subsequently ejected. Machines of horizontal construction with horizontal workpiece transfer are encountered most frequently. Smaller, fast rotating presses generally have a crank drive, while larger machines may also have knuckle-joint drives.

Due to the large output, considerable value is placed on uninterrupted and exact workpiece transfer. In single- and two-stroke presses the workpiece is customarily clamped between the

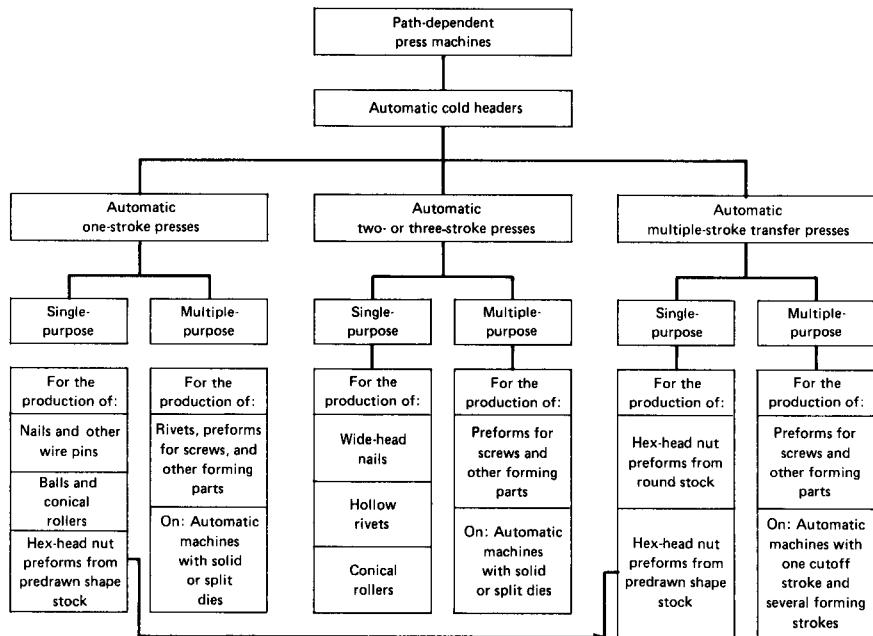


**Fig. 10.25** Classification of automatic cold headers. (After [10.25].)

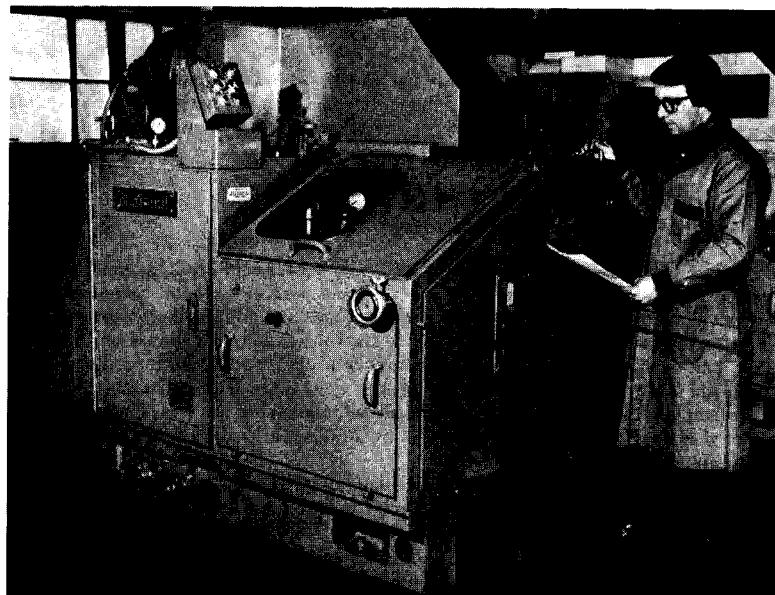


**Fig. 10.26** Single-stroke press. Ballheader; wire diameter 6–8 mm (0.2–0.3 in); output 710 min<sup>-1</sup>. (Courtesy of National Machinery Co.)

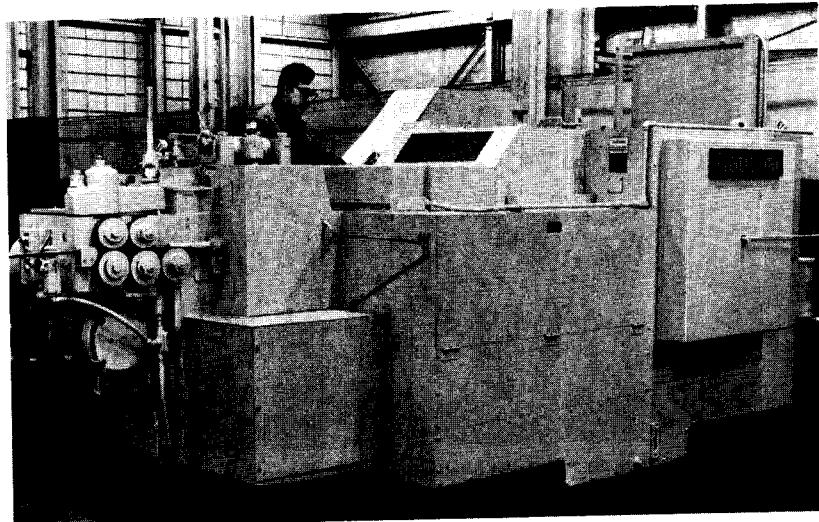


**Fig. 10.27** Two-stroke press. Roller header; wire diameter 19 mm (0.75 in); output 90–95 min<sup>-1</sup>. (Courtesy of National Machinery Co.)

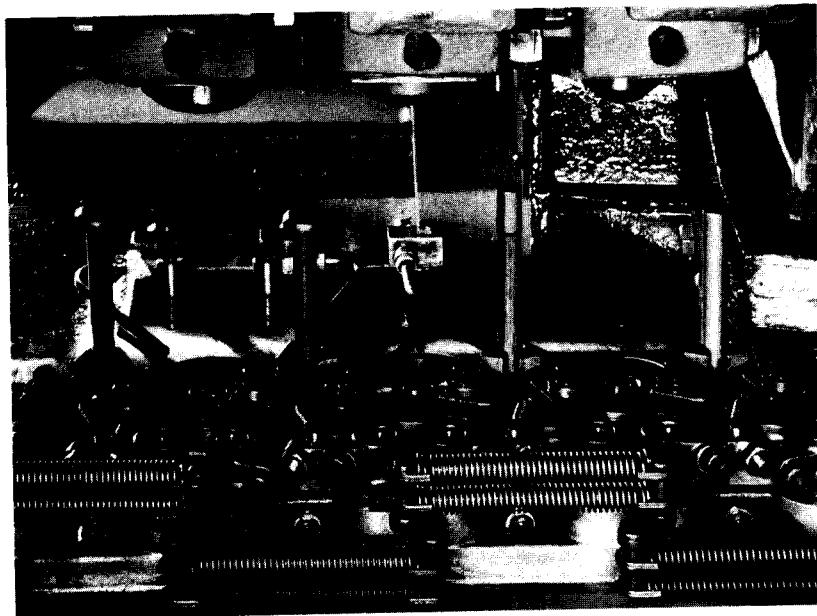


**Fig. 10.28** Tool box of multiple-stroke press with gripper transfer. Long parts like these bolt blanks are transferred straight across the face of the dies during forming. The transfer fingers open to let the punches (bottom) push the part into the dies for forming and close tightly on the shanks as the parts eject from the dies after forming. Finger opening and closing are cam-controlled, and spring pressure enhances finger gripping and part control. (Courtesy of National Machinery Co.)

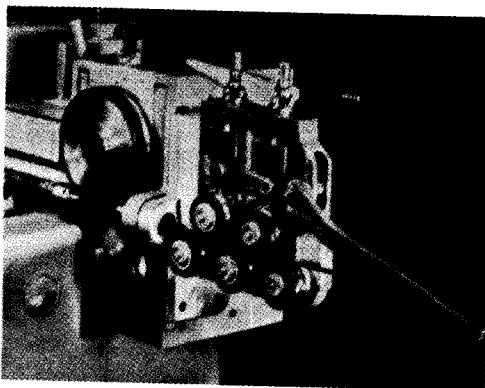


**Fig. 10.29** Roller leveller and intake rolls of a multiple-stroke press. (Courtesy of Hatebur.)

shearing blade and a holder, and taken to the die Fig. 10.30a and b). A different design (Fig. 10.30c) employs a gripper. The workpiece insertion pusher (Fig. 10.20) has also proved useful.

In multiple-stroke presses workpiece transfer is handled by gripping units, which at times are equipped with turning fingers (Fig. 10.31). A capability for end-for-end part turnaround between two forming stages increases the forming possibilities significantly. Additional possibilities are pro-

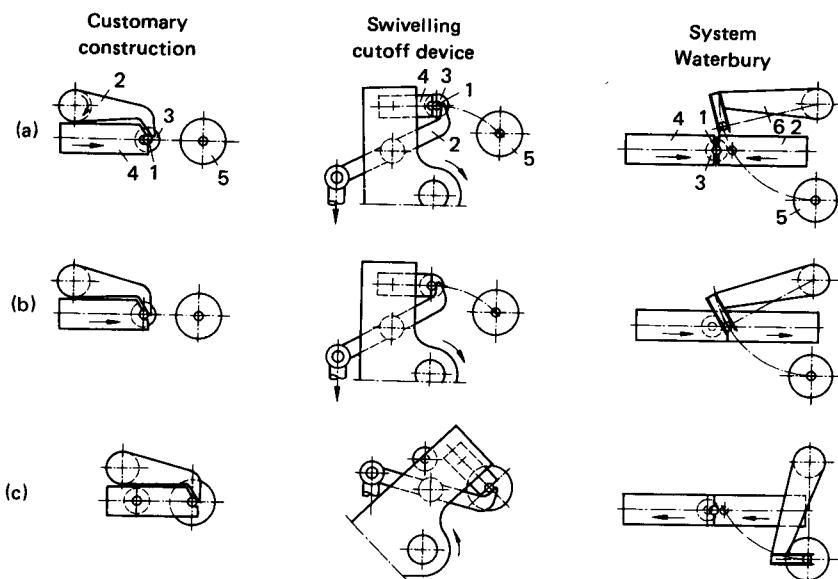
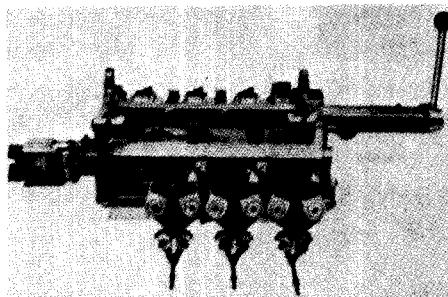
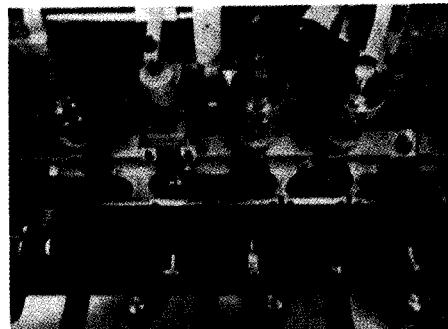


**Fig. 10.30** Wire cutoff devices and workpiece transfer. (a) Advancement of wire. (b) Shearing of wire. (c) Transfer of slug to heading die. 1—wire; 2—wire clamping device; 3—cutoff die; 4—shearing blade; 5—heading die; 6—gripper. (After [10.20].)



(a)



(b)

**Fig. 10.31** Transfer gripping units. (a) Customary design. (*Courtesy of Hatebur.*) (b) End-for-end part turnaround fingers. (*Courtesy of Malmedie.*)

vided by a combination of different processes (e.g., upsetting and extrusion) in a multiple-stage press. The tools are usually arranged horizontally, but sometimes also vertically (Fig. 10.28).

A transfer unit permitting part rotation by 90° has also been introduced [10.26]. This capability permits work at a right angle to the longitudinal axis of the part.

The design of the ejector is important. Ejectors are always provided on the die side, but are also found on the punch side of multiple-stage units. The ejectors, which can be adjusted separately for each forming stage, are generally controlled by cams (Fig. 10.32).

For parts requiring high accuracy the machine frame must be as rigid as possible in order to keep elastic deformation within narrow limits. A unit cast-steel frame is best suited for this purpose (Fig. 10.33). A rigid design of the heading slide has also proved successful. Guides should be dimensioned liberally so that punch displacement remains small for eccentrically applied punch forces. The punches can be adjusted independently of one another (Fig. 10.34).

The shape of the slug has also considerable influence upon the results of the effort. Workpieces should have contact faces that are as flat as possible, and which are perpendicular to their centerlines. The centerline itself should be straight. Variations in volume should be held as small as possible. For rolled wire this can be achieved by a drawing stage ahead of the shearing step.

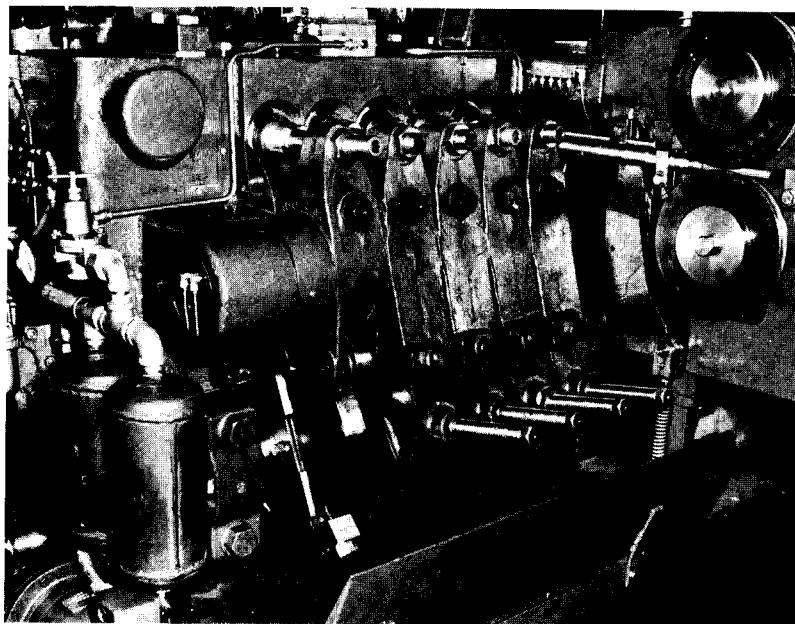


**Fig. 10.32** Ejector control. Cast steel levers are driven by precisely generated cams (bottom) to move kickout rods (top). (*Courtesy of National Machinery Co.*)

### 10.5.2 Machine Tools for Hot Upsetting

In addition to the customary crank presses, eccentric and screw presses, hammers, and horizontal upsetters (Fig. 10.35) are employed. The latter is used mostly for die heading. It has a crank drive, and in addition to the punch motion it has a second degree of freedom for clamping the workpiece in the split heading die. This second movement, which is either derived from the main drive or independent from it, can also be utilized for forming. Workpiece transfer takes place horizontally or vertically. (See also the corresponding figures in Chap. 11.)

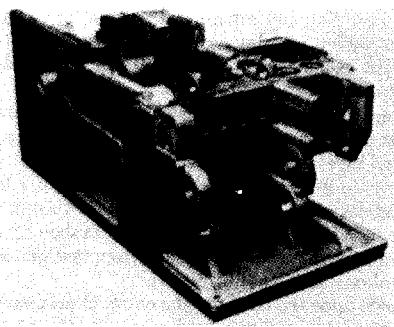


**Fig. 10.33** Body of a multiple-stage press, cast steel. (*Courtesy of Hatebur.*)

## 10.6 TOOL DESIGN AND MATERIALS

Upsetting tools are stressed primarily by pressure and friction rather than by bending. They must therefore be designed to withstand fracture and wear. They should also display little tendency toward cold welding. Tensile loading can occur in punches with die cavities (e.g. the hexagonal head of a screw). Information regarding the magnitude and distribution of such loading as well as recommendations regarding the design of possibly necessary shrink-fit assemblies are contained in Chap. 15.

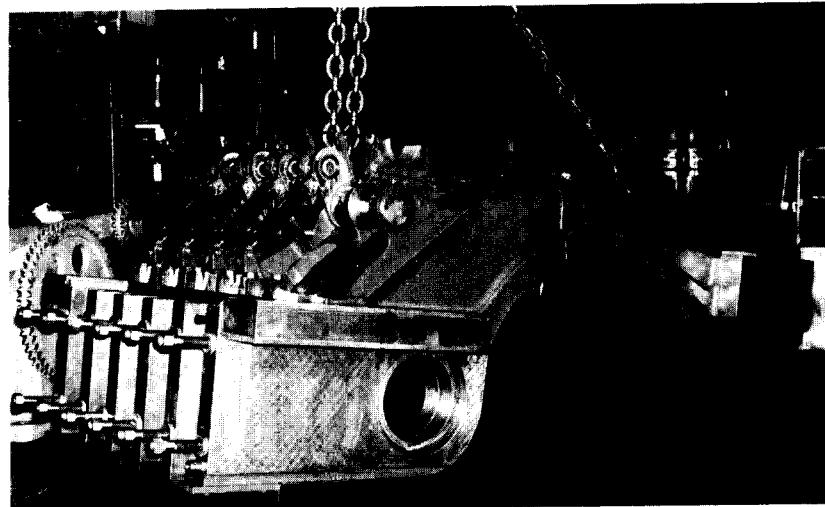


**Fig. 10.34** Heading slide for multiple-stroke cold former, made of cast steel alloy. Lubricated hand-scraped bronze liners reduce friction during operation and help ensure accurate alignment for close-tolerance part forming. (Courtesy of National Machinery Co.)

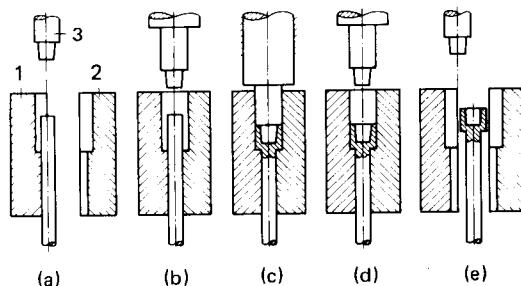


**Fig. 10.35** Stages of forming process in a horizontal header.  
(a) Insertion of slug in open jaws. (b) Closing of jaws. (c) Heading. (d) Ejection. 1—fixed clamping jaw; 2—movable clamping jaw; 3—heading punch. (After [10.20].)

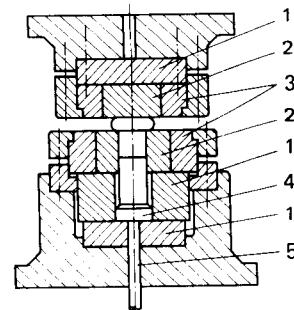


**Fig. 10.36** Characteristic design of an upsetting tool. 1—pressure plate; 2—upsetting platen; 3—shrink ring; 4—counterpunch; 5—ejector. (After [10.27].)

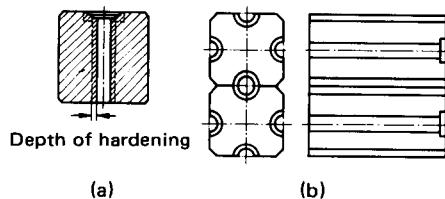


**Fig. 10.37** Heading dies. (a) Closed die with smooth bore. (b) Split die. (After [10.22].)

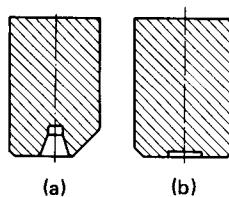


**Fig. 10.38** Heading punches. (a) Preform heading punch. (b) Finish heading punch. (After [10.22].)

**Table 10.1** Steels for Composite Upsetting Platens and Unit Punches<sup>a</sup>

Trend of main properties					
Wear resistance and compressive strength	Toughness	Steel designation			
		AISI	DIN	Hardened to HRC	Remarks
Decreasing	Increasing	M4 M2 D3 D2	S6-5-3 S6-5-2 X210CrV12 X165CrMoV12	62-64 62-64 60-62 60-62	Preferred

<sup>a</sup>After [10.27].

**Table 10.2** Cemented Carbides for Composite Upsetting Platens and Unit Punches.<sup>a,b,c</sup>

Trend of main properties		Carbide type		
Wear resistance	Toughness	Cobalt by %wt	Density, g/cm <sup>3</sup>	Vickers hardness
Decreasing	Increasing	15-18	14.0-13.7	1200-1100
		19-24	13.6-13.2	1050-950
		25-30	13.1-12.5	950-750

<sup>a</sup>After [10.27]

<sup>b</sup>Tungsten carbides with cobalt binder are considered only.

<sup>c</sup>Refer also to Table 14.4

For upsetting processes requiring large forces, a tool assembly is recommended, which is related to the tooling for extrusion (Fig. 10.36; see also Chap. 15). When small forces are involved, it is possible to omit the pressure plates.

Two types of upsetting dies are encountered in multiple-stage presses. Solid dies are used when the parts produced are to meet high requirements with regard to surface quality and dimensional accuracy (Fig. 10.37a). Ejecting the piece can become difficult when the shaft length  $l > 8-10d_0$ . In this case the bore is made slightly conical. Split dies are better, as shown in Fig. 10.37b. Slight flash formation must be accepted in this case, however. The addition of several die shapes to every die half, as shown in Fig. 10.37b, conserves die material. Frequently used shapes for preform heading and finishing punches are depicted in Fig. 10.38. Tool materials for cold upsetting are listed in Table 10.1 (steels) and 10.2 (cemented carbides). In addition, the tool materials named for extrusion tooling apply (see Chap. 15). For hot upsetting, materials used in forging dies are recommended (see Chap. 11).

## REFERENCES

- 10.1 DIN 8583: "Fertigungsverfahren Druckumformen (Manufacturing Processes—Compressive Forming)," sheets 3 and 4, 1970.
- 10.2 Gentzsch, G.: *Cold Upsetting, Extrusion, Bulk Coining (in German)*, Düsseldorf; VDI-Verlag, 1968.
- 10.3 Brill, K.: "Modelling Materials for Bulk Deformation of Metals" (in German), Dr.-Ing. thesis, Technical University, Hannover, 1963.
- 10.4 Vater, M., and Nebe, G.: "On Stress and Strain Distribution in Upsetting" (in German), *VDI-Z. Progress Rep. ser. 2, no. 5*, Düsseldorf, VDI-Verlag, 1965.
- 10.5 Bühler, H., and Bobbert, D.: "On Strain Distribution in Upsetting" (in German), *Ind.-Anz.*, 88, 1966, pp. 2175-2178.
- 10.6 Metzler, H. J.: *On the Effect of Tool Velocity upon the Upsetting Process (in German)*, *Berichte aus dem Institut für Umformtechnik, Universität Stuttgart*, no. 21, Essen, Girardet, 1970.
- 10.7 Honke, M.: "Processes Occurring in the Boundary Layer in Warm Upsetting of Metal Cylinders" (in German), Dr.-Ing. thesis, Technical University, Aachen, 1964.
- 10.8 Siebel, E.: *Forming in the Plastic State (in German)*, Düsseldorf, Verlag Stahleisen, 1932.
- 10.9 Lippmann, H., and Mahrenholz, O.: *Plastomechanics of Forming of Metallic Materials (in German)*, vol. 1, Berlin/Heidelberg/New York, Springer, 1967.
- 10.10 Stöter, H.-J.: *Investigation of the Forging Process in Hammer and Press, Especially with Regard to Die Filling (in German)*, *Untersuchungsbericht des Landes Nordrhein-Westfalen*, no. 848, Köln/Opladen, Westdeutscher Verlag, 1960.
- 10.11 Steck, E., and Schmidt, K.: "The Application of the Principle of Least Forming Energy to Upset and Forging Processes" (in German), *Ind.-Anz.*, 87, 1965, pp. 1751-1755.
- 10.12 Andresen, K.: "Characteristics and Limit Analysis in the Theory of the Plastic Layer (in German)", Dr.-Ing. thesis, Technical University, Braunschweig, 1970.
- 10.13 Burgdorf, M.: *Investigation of Upsetting and Extrusion Forming (in German)*, *Berichte aus dem Institut für Umformtechnik, Technische Hochschule Stuttgart*, no. 5, Essen, Girardet, 1966.
- 10.14 Ruppin, D.: "Investigation of the Heading of Enlarged Sections of Long Structural Shapes Using Explosives" (in German), *VDI-Z. Progress Rep. ser. 2, no. 8*, Düsseldorf, VDI-Verlag, 1966.
- 10.15 Behrens, A.: "Contribution to the Theory of High-Speed Forging" (in German), Dr.-Ing. thesis, Technical University, Braunschweig, 1968.
- 10.16 Hill, R.: *The Mathematical Theory of Plasticity*, London, Oxford University Press, 1960.

- 10.17 Besdo, D.: "Principal and Slip-Line Method for Axisymmetric Rigid-Plastic Deformation" (*in German*), Dr.-Ing. thesis, Technical University, Braunschweig, 1969.
- 10.18 Auerswald, H.: "Cold Upsetting and Its Machines" (*in German*), *Maschinenbautechnik*, 8, 1959, pp. 192-202.
- 10.19 Meyer, H.: *Investigation of the Forming Process in Horizontal Upsetters (in German)*, *Untersuchungsbericht des Landes Nordrhein-Westfalen*, no. 890, Köln/Opladen, Westdeutscher Verlag, 1960.
- 10.20 Billigmann, J., and Feldmann, D.: *Upsetting and Pressing (in German)*, München, Hanser, 1973.
- 10.21 Tholander, E.: "Forging Displacement Measurements in Drop Hammers with Lead as Test Material" (*in Swedish*), *Tek. Medd. (Sveriges Mekanförbund, Stockholm)* 12, 1961, pp. 12-30.
- 10.22 VDI-Richtlinie 3171: "Stauchen und Formpressen (Upsetting and Preforming)," Berlin/Köln, Beuth-Verlag, 1981.
- 10.23 VDI-Richtlinie 3172: "Flachprägen (Coining)," Düsseldorf, VDI-Verlag, 1961.
- 10.24 Meier, R.: "The Accuracy of Cold Sizing of Metallic Workpieces" (*in German*), Dr.-Ing. thesis, Technical University, Hannover, 1961.
- 10.25 Auerswald, H., and Zschokelt, H.: "Automatic Cold Headers", (*in German*) *Die Technik*, 14, 1959, pp. 147-150.
- 10.26 Dallas, D. B.: "New Innovations in Cold Forming," *Manuf. Eng.*, 85, 1980, pp. 96-99.
- 10.27 ICFG data sheet 4/70: "General Aspects of Tool Design and Tool Materials for Cold Forging of Steel," London, Institute for Sheet Metal Engineering, 1970.

#### Further Reading

- Schey, J. A.: *Introduction to Manufacturing Processes*, New York, McGraw-Hill, 1977.  
*Metals Handbook*, vol. 4, "Forming," Metals Park, OH, American Society for Metals, 1969.

## CHAP. 11

### FORGING

© 2002 The McGraw-Hill Companies, Inc. All Rights Reserved.

#### List of Special Symbols

---

$a$	distance between opposite outer edges of flash or die land
$\bar{a}, \bar{b}, \bar{c}$	unfilled portions of die cavity in die forging without flash
$A_f$	local cross-sectional area of finished die-forged part
$A_{F1}$	local cross-sectional area of flash
$A_{p,F1}$	area of flash or die land projected in the plane of parting
$A_{p,pt}$	area of die-forged part projected in the plane of parting
$A_{p,tot}$	total area of forged material projected in the plane of parting
$A_p$	cross-sectional area of punch
$b$	width of flash or die land
$b^*$	momentary width of flash
$b_c$	width of die cavity
$B$	block width
$c$	mean specific heat
$C_{tot}$	total spring constant
$d_o$	outer diameter of part
$d_c$	diameter of die cavity
$F_{0,1,2}$	force at time 0,1,2
$F_{def}$	deformation force
$F_f$	force at end of forging operation
$F_{FR}$	friction force
$F_N$	nominal force rating
$F_S$	shearing force
$h$	height; forging stroke
$\bar{h}_f$	mean height of finished shape or part

## 11.2 BULK-METAL FORMING

$h_{F1}$	height of flash at end face
$h_i$	initial height
$h_p$	punch stroke
$h_{p'}$	punch stroke during forging
$h_u$	stressed height
$h_z$	web height
$H$	block height
$k_R$	deformation resistance
$L$	block length
$m_{env}$	mass of smallest regularly shaped solid body capable of enveloping the largest dimensions of a formed part
$m_f$	mass of finished shape or part
$m_i$	mass of initial materials
$p_m$	mean pressure; punch pressure
$P_{def}$	power required for deformation
$P_{FR}$	power required to overcome forging friction
$P_s$	power required for shearing
$Q_{eff}$	useful heat
$Q_s$	supplied heat
$r_h$	mean radial distance of the highest section of a part from the part center
$R$	deformation ratio $A_0/A$
$R_t$	surface roughness (peak-to-valley height)
$R_u$	upsetting ratio $A_1/A_0$
$s$	flash gap thickness
$s^*$	momentary thickness of flash
$s_f$	Feed stroke during forging
$t_c$	pressure contact time
$T_{0,1,2}$	temperature at time 0,1,2
$T_{D,i}$	temperature of die prior to contact with workpiece
$T_{D,m}$	mean temperature of die over a given period of time
$\bar{T}_{F1}$	mean flash temperature over a given period of time
$\bar{T}_{F1'}$	mean flash temperature at a particular moment in time
$T_m$	melting temperature
$T_{Pt,i}$	temperature of part immediately prior to forging
$T_{Pt,F1}$	temperature of part at start of flash formation
$T_T$	temperature of tool
$u$	shearing gap
$v$	sliding speed
$v_R$	ram speed
$v_T$	tool speed
$v_{Tup}$	tup speed
$V$	volume
$V_C$	volume of die cavity
$V_f$	volume of finished shape or part
$V_{in}$	volume of smallest regularly shaped body capable of enveloping the largest dimensions of a formed part
$W_N$	nominal work rating
$\alpha$	coefficient of thermal expansion; heat flux
$\beta$	angle of inclination of die-land opening to the normal direction of flash flow
$\Delta m$	difference between initial and final material mass
$\Delta T_{FR}$	temperature increase due to friction
$\Delta T_w$	temperature increase due to forging

$\eta_{\text{def}}$	deformation efficiency
$\rho$	density
$\sigma_{f,\text{lead}}$	flow stress of lead
$\sigma_{f,\text{steel}}$	flow stress of steel
$\sigma_{r,m}$	mean radial stress
$\sigma_{z,C}$	normal compressive stress in die cavity
$\sigma_{z,F1}$	normal compressive stress in flash
$\tau_{\text{FR}}$	sliding friction stress

Forging consists of a group of manufacturing processes which are mainly *deformation processes*. These are augmented by *parting* (separating) and *joining* processes, the latter being used where large or complicated workpieces are made up of individual parts. The individual processes are defined in the following DIN standards:

DIN 8583	Compressive forming [11.1]	Open-die forging, closed-die forging, indenting, piercing, (rolling)
DIN 8586	Forming by bending [11.2]	Bending with linear tool motion
DIN 8587	Shear forging [11.3]	Twisting, spiral twisting
DIN 8588	Sectioning [11.4]	Shear cutting, wedge cutting
DIN 8593	Joining [11.5]	Joining by force, material bonding

Forging is divided into two main groups, open-die forging and closed-die forging, on the basis of whether material is allowed to flow freely (as in open-die forging) or whether flow is constrained (as in closed-die forging).<sup>\*</sup> In order to reduce stresses and forces and to increase deformability, forging is usually carried out after heating to a temperature range at which recovery and recrystallization operations occur. Some metals and alloys need to be forged within a narrow temperature range in order to avoid undesirable phase changes. Many nonferrous metals and even steels can nowadays also be deformed at room temperature. This is termed cold forging or cold-die forging. However, this chapter is mainly concerned with *hot forging*. The processes most commonly used in open- and closed-die forging are shown in Fig. 11.1. The most important processes of the two main groups separating and forming are described below.

## 11.1 BASIC FORGING PROCESSES

In accordance with Fig. 11.1, forging may be defined as “manufacture by means of deformation in conjunction with heating, separating, (and joining) of a workpiece without permanent work hardening.” While in open-die forging “simple tools are used whose shape is not closely related to the desired shape of the workpiece,” in closed-die forging, “tools are used whose shape is closely related to the desired shape of the finished part.” In order to produce the desired material distribution and bending required for subsequent closed-die forging processes (i.e., closed-die forging with and without flash as well as upset forging in a die), it is necessary to use open-die forging processes.

### 11.1.1 Processes for Changing Cross Sections

These are the most fundamental forging processes. According to the law of constant volume, changes in cross-sectional area produce corresponding changes in length. Changes in cross-sec-

\*See Chap. 2, Figs. 2.9 and 2.11.

## 11.4 BULK-METAL FORMING

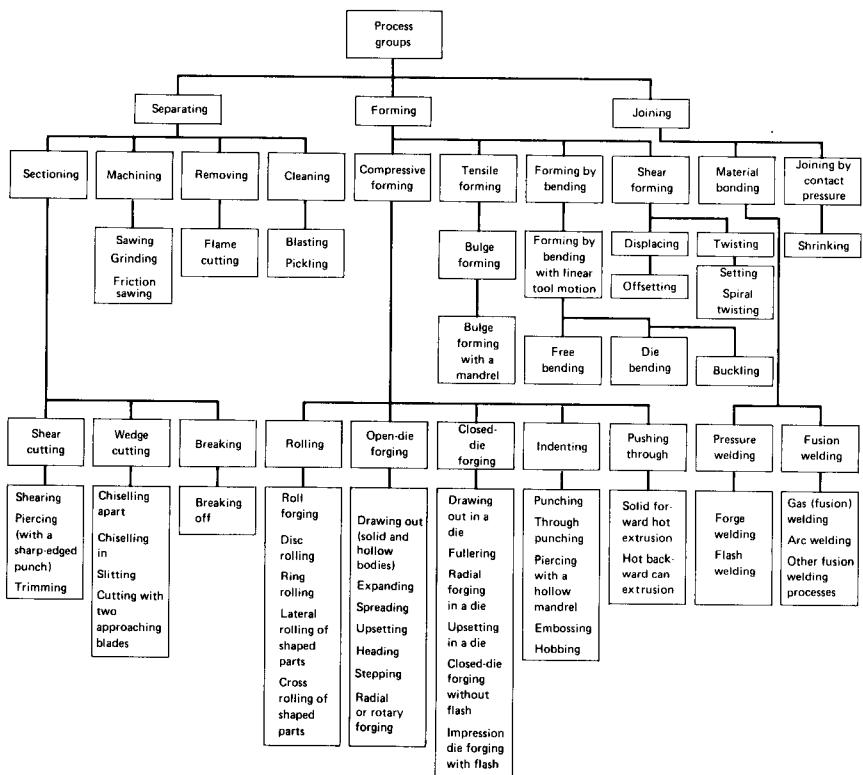


**FIG. 11.1** Processes used in forging plants. (After [11.6].)

tional area may be achieved by decreasing or increasing a cross section, whereby the cross-section-decreasing processes are the more common (Fig. 11.2). In these latter processes, the forged work-piece is subjected to triaxial compressive stresses, with the exception of its free faces. Here the compressive stress may be either dissipated in one direction or transformed into a tensile stress. The almost unbounded deformability of common steels is then limited only by the danger of localized cracking. The following values can be taken as guidelines for the cross-sectional ratios that can be achieved:

$$\text{Drawing out, spreading} \quad A_0/A_1 \gg 4-5$$

$$\text{Solid extrusion, can extrusion} \quad A_0/A_1 < 4-5$$

$$\text{Upsetting, heading} \quad A_1/A_0 < 3-5$$

Traditional drawing-out processes are very time-consuming and, with the exception of automated operations such as rotary swaging, require skilled personnel. Nowadays for small- and medium-sized parts they are increasingly being replaced by upsetting and, more recently, by extrusion. In open-die forging of large parts, on the other hand, drawing out will continue to remain the most important forging process.

Drawing out (including rotary swaging and extrusion) and upsetting can produce different grain flows, starting from the same rolled material. By suitable choice of the forging process, or of the sequence of processes, the grain flow may be chosen so that it is best suited to a specific

Open-die forming		Closed-die forming	Pushing through	Rolling
1	Saddle Mandrel	7 Die saddle Workpiece	13 Solid forward hot extrusion	15 Backward cup hot extrusion Stretch rolling
2	Drawing out over a mandrel	8 Draw	14 Solid side extrusion	16 Ring rolling
3	Wide saddle	9 Forging jaw Workpiece	17 Cross rolling	
4	Radial forging	10 Upsetting in a die		
5	Spreading	11 Radial forging in a die		
6	Upsetting	12 Upset die forging		
Material displacement		Combined material concentration and displacement		
Upsetting		10 Heading in a die	11 Heading in a horizontal upsetting machine	
Upsetting		12 Upset die forging		
Upsetting		13 Upset die forging		

FIG. 11.2 Forging processes for changing cross-sectional area.

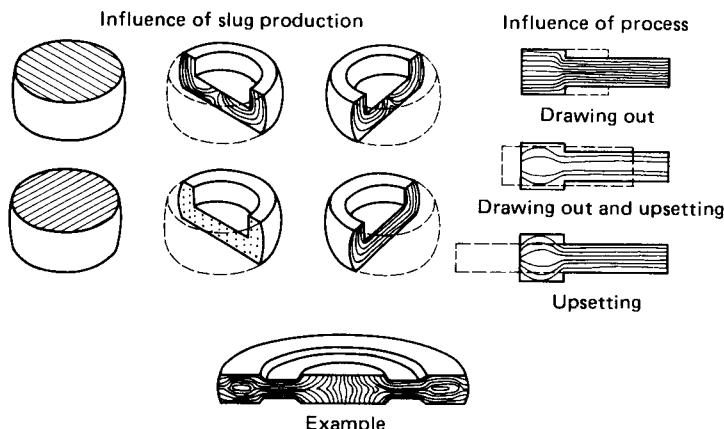


**FIG. 11.3** Choice of blank, process, and grain structure for forged parts. (After [11.7].)

application. While  $S_y$ ,  $e_t$ , and  $\Delta A_{rel}$  do not differ substantially, in the direction of and at a right angle to the grain fiber, larger differences occur in the notched-bar impact test and in fatigue strength. In some cases the initial material must be produced in such a way (e.g., by cutting off from bars or cutting out of slabs) as to take into account the stressing of the finished component (Fig. 11.3). Correctly designed and produced forgings are well suited for dynamically highly stressed components.

On the basis of the slip-line theory, compression of a workpiece between small identical punches, as in drawing out, leads to the slip-line fields shown in Fig. 11.4a, which delineates the different forming zones [11.8]. The smaller the ratio  $b/h$ , that is, the thicker the parts to be forged, the higher must be the tool pressure  $F/A = R_m$  in order to deform the material in the core of the workpiece. This phenomenon is discussed in more detail in Sec. 11.2.1. In drawing out, to ensure that the workpiece is forged through to the core, the feed rate  $s_f$  must be kept very small for ratios  $b/h \leq 1$  (Fig. 11.4b). For  $b/h > 1$  a feed rate  $s_f \approx b/2$  is suitable, and this is commonly used in finish forging. The conditions existing at the beginning of a localized upsetting operation become more favorable as the operation progresses since the zones of plastic deformation impinge on one another, and thus the area of penetration in the core becomes wider.

For the desired mechanical properties of workpieces forged from cast ingots, an extensive and homogeneous transformation of the coarse crystalline grain structure into a fine-grained forgeable structure is necessary. It has been shown that a relationship exists between changes in cross section and mechanical properties ( $S_y$ ,  $e_t$ ,  $\Delta A_{rel}$ , notch strength). In particular the notch strength, the elongation  $e_t$ , and the reduction in area after fracture  $\Delta A_{rel}$  improve with an increasing deformation ratio  $R = A_0/A_1$  as a result of drawing out. On the other hand, upsetting in general does not bring any measurable improvements in the properties of the forged part over the entire cross section. (Here the analogous term upset ratio  $R_u = A_1/A_0$  is used.) For production purposes it may, however, sometimes be necessary to combine drawing out and upsetting, for example, to ensure a sufficient degree of forging where there is little difference in the cross-sectional areas of the ingot and the forged part. Here it is usually best to begin with drawing out the workpiece somewhat, then upset it, and finally finish drawing it out [11.9]. The following degrees of deformation can be defined, as shown in Fig. 11.5:

$$\begin{aligned} \text{For cross section } A_3: \quad & R_1 + R_{u,2} + R_3 \\ \text{For cross section } A_4: \quad & R_1 + R_{u,2} + R_4 \end{aligned}$$

It has been shown, however, that the deformation ratios  $R_3^* = A_0/A_3$  and  $R_4^* = A_0/A_4$  are more closely related to the desired values of tensile and notch strength. For unalloyed and low-alloyed

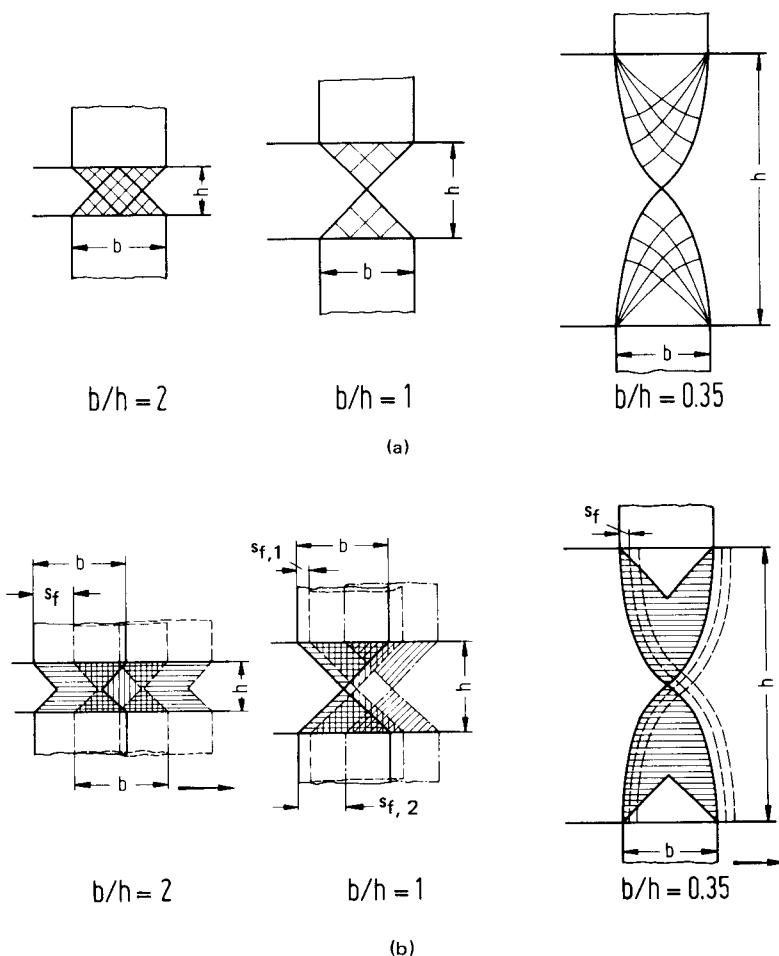


FIG. 11.4 Forging by drawing out. (a) Slip-line-field plastic zones for different  $b/h$  ratios. (After [11.8].) (b) Spreading of plastic zones depending on feed.

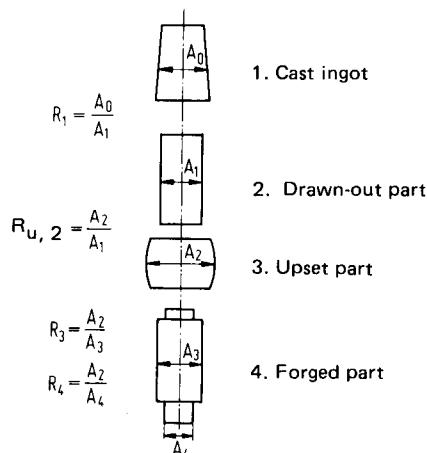
steels, a deformation ratio of  $2 < R < 3$  due to drawing out is sufficient to achieve the required values.

### 11.1.2 Bending in Twisting Processes

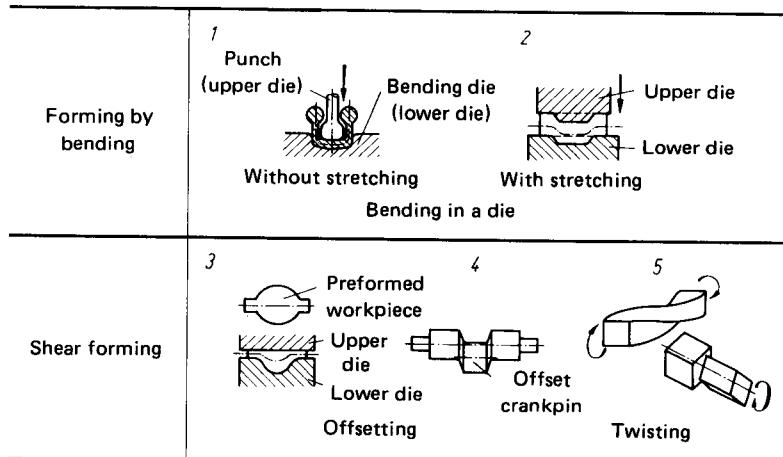
This group includes bending processes—free bending and die bending—and shear-forming processes. The fundamental principles of bending are discussed in Chap. 19. In die bending operations, as illustrated in Fig. 11.6, example 2, the material is not able to fill the bending die without stretching because of resistance due to friction. As a result of stretching, local changes in cross section are unavoidable. They occur the more frequently, the smaller the bending radius.

The shear-forming process of offsetting consists of the displacement of a specific mass of material away from a given axis. In the plane of displacement, the shear stress  $\tau_{\max} = k$ . A similar

## 11.8 BULK-METAL FORMING



**FIG. 11.5** Degrees of forging in combined drawing-out and upsetting operations.

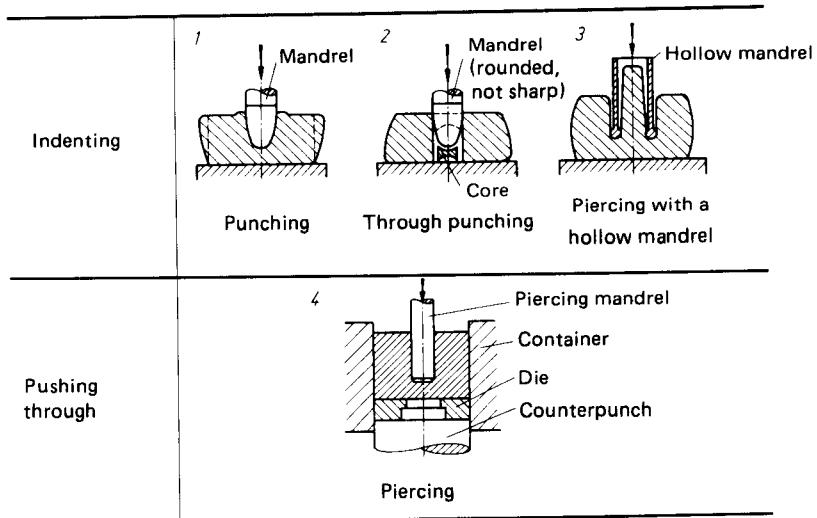


**FIG. 11.6** Direction-changing processes.

stress condition exists in twisting (pure shearing). Offsetting and twisting are used in particular for manufacturing large open-die forged parts, such as crankshafts.

### 11.1.3 Processes for the Formation of Cavities

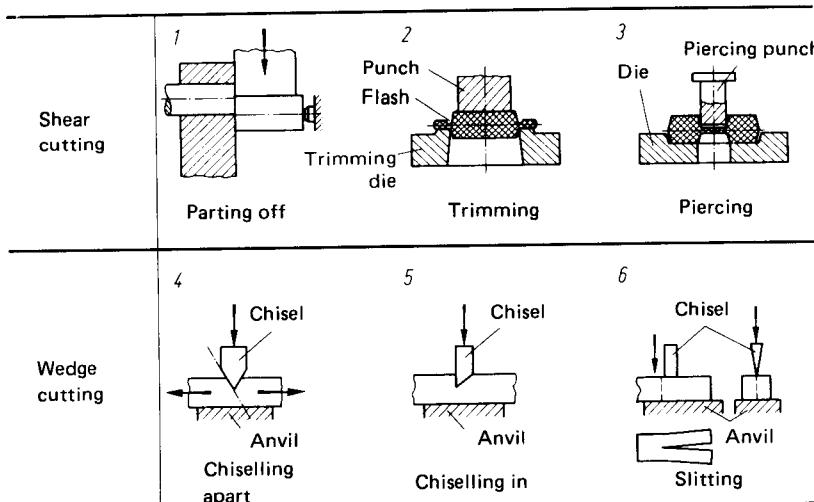
Cavities are formed by indenting and pushing-through processes (Fig. 11.7). In indenting processes, a rounded solid or hollow mandrel is pressed into the workpiece. The workpiece material is constrained to flow sideward (solid mandrels) or simultaneously sideward and into the mandrel cavity (hollow mandrels). Solid mandrels (examples 1 and 2 in Fig. 11.7) are used to make closed and open-ended cavities. For the latter it is necessary to turn the workpiece over. Piercing with a hollow mandrel is used almost exclusively for producing open-ended holes in large forgings from one side only. However, here material waste is greater.

**FIG. 11.7** Processes for creating holes.

Piercing (example 4 in Fig. 11.7)—without the holing plate, also known as the Ehrhardt process—is a boundary case of backward can extrusion with a relatively small reduction in cross-sectional area. It is mainly used for long hollow bodies, especially where these require subsequent forging operations.

#### 11.1.4 Parting Processes

The parting or separating processes most commonly used in forming are shown in Fig. 11.8. Shear-forming processes with an open cutting line are used for cutting the starting material of a given

**FIG. 11.8** Parting processes.

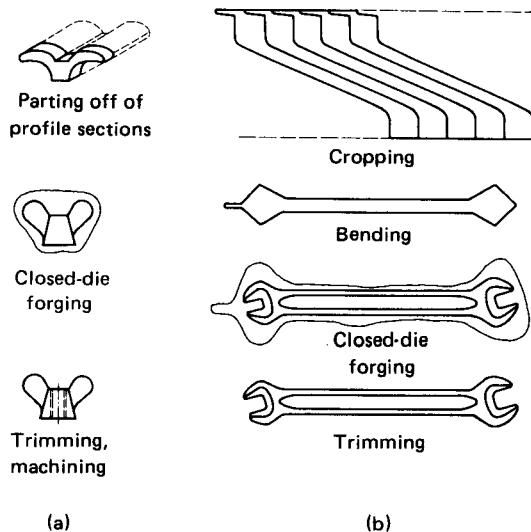


**FIG. 11.9** Particular examples of parting-off processes. (a) Shearing off from a profile section bar for the production of wing nuts. (b) Cropping of shaped blanks for forging into spanners. (After [11.10].)

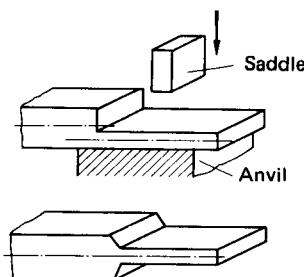


**FIG. 11.10** Thickness reduction by chiselling and drawing out.

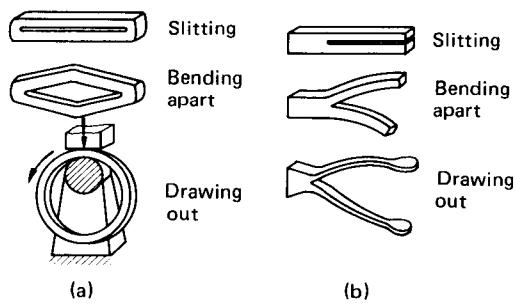


**FIG. 11.11** Uses of slitting for open-die forged parts. (a) Forging of rings. (b) Forging of fork-shaped parts.

cross section to a specific length or volume without waste. This is also the aim in parting off from profile bars in order to save intermediate operations in closed-die forging (Fig. 11.9a). A special case is the shape cropping [11.10] of blanks for closed-die forging (Fig. 11.9b). Here the intermediate form for material distribution is produced simultaneously and without waste (see Chap. 24). Shear cutting with a closed cutting line is used for cutting out blanks that are round or of different shapes. It is also used extensively for trimming and for making holes in closed-die forging (Fig. 11.8, examples 2 and 3).

Chiselling off, one of the wedge-cutting processes (Fig. 11.8, example 4), is used to remove excess material in open-die forging. Nowadays, with the advent of large open-die forgings it is being replaced by other processes, such as grinding and sawing, which are carried out away from the capital-intensive forging equipment. Chiselling in is used in conjunction with drawing out to produce sharp changes in cross section which cannot be produced otherwise because of material flow (Fig. 11.10). This procedure is termed *stepping*. Finally, slitting is used with a closed cutting line as a preparatory operation in the forging of rings and similar parts and with an open cutting line in the production of forgings with forks or end limbs (Fig. 11.11).

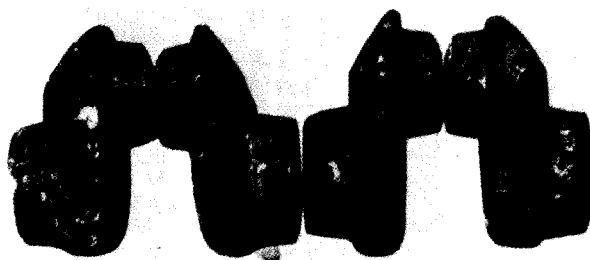


FIG. 11.12 Die-forged crank webs with half a main journal and half a pin journal per part. (After [11.11].)

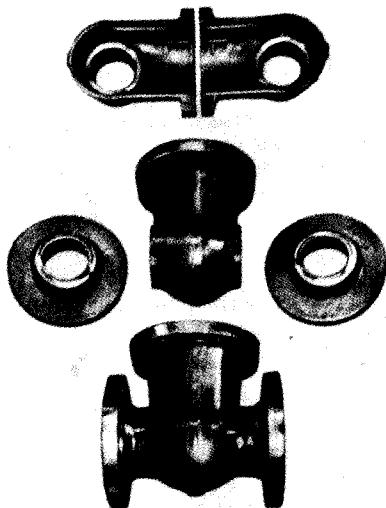


FIG. 11.13 Production of a high-pressure valve body by die forging and joining (flash-butt and fusion welding). (After [11.12].)

### 11.1.5 Joining Processes

Joining processes are used to connect different elements of large or complicated forgings (Fig. 11.12). Forgings are even sometimes joined to cast steel components (as with very large marine diesel crankshafts) or rolled profile sections (as with driving rods for locomotives).

The most important joining processes are shrinking and welding. In shrinking, the heated outer part is made to fit snugly on the slightly oversized inner part. In welding, the traditional method of forge welding has largely been replaced by the more modern fusion and butt welding processes (Fig. 11.13). These have been augmented more recently by electron-beam welding on highly stressed components for aerospace applications. In the same area, new diffusion bonding processes are currently being developed.

### 11.1.6 Die-Forging Processes

Fig. 11.14 shows the different types of closed-die forging processes whose sole aim is the production of a specific workpiece geometry with the best possible dimensional and volumetric accuracy. The processes concerned are heading, closed-die forging without flash, and closed-die forging with flash. The process most commonly used in industry is closed-die forging with flash, since in mass production it is difficult to part off an exact amount of material by means of sawing, shearing, or breaking, so that forging could be carried out without flash. For closed-die forging with flash, dies with precision-designed die land or flash gap are used.

While in open-die forging the material moves or "flows" at a right angle to the direction of tool motion (the motion may be hindered by frictional forces), in closed-die forging material is constrained to move in particular directions, that is, both in the direction of tool motion and at a right angle to it. This may be termed *constrained displacement* of the material. Fig. 11.15 illustrates three basic operations of which usually at least two occur during any given operation. In practice there are no sharp divisions between the individual categories.

- 1 **Upsetting:** Reduction in initial height without extensive spreading and without substantial flow along the tool surface. Material flow is essentially parallel to the tool motion.
- 2 **Spreading:** Lateral outward displacement of material—often toward the end of upsetting operations—with long flow paths under high normal compression. Material flow is mainly at a right angle to the tool motion.
- 3 **Rising:** Filling of deep die cavities by localized increases in the initial height, often associated with long flow paths and high normal pressures after entry of material into the flash gap.

Closed-die forging with flash always starts and ends with upsetting. In the latter stage, after the die cavities have been completely filled, the excess material is forced out into the flash gap. The design of the flash gap (or die land) affects the stress conditions both in the flash gap itself and in the die cavity.

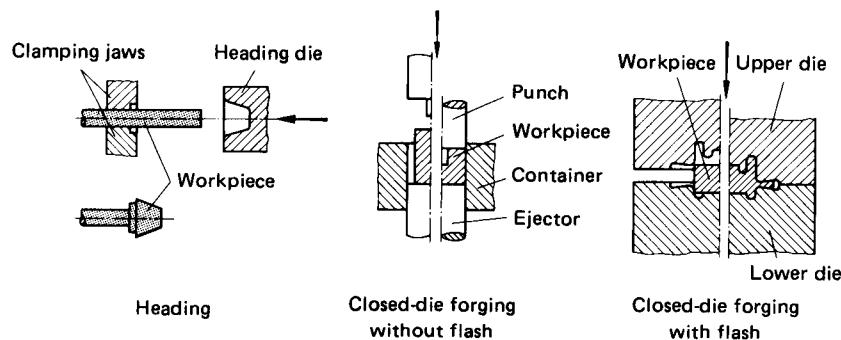
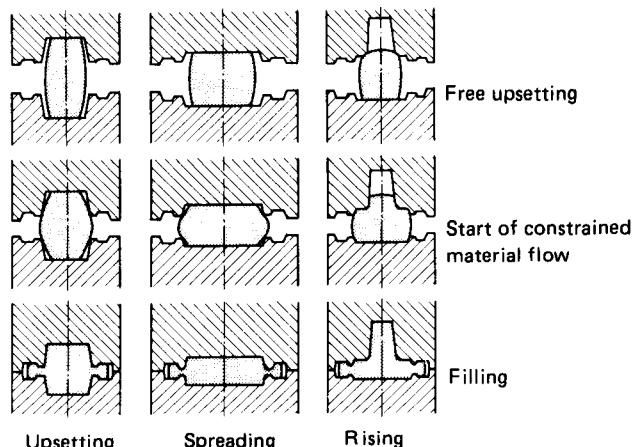


FIG. 11.14 Closed-die forging processes.



**FIG. 11.15** Basic types of material flow for filling die cavities.

## 11.2 FUNDAMENTAL PRINCIPLES

Forging operations are nonstationary processes occurring as a result of indirect pressure, generally under conditions of three-dimensional stress and deformation. Furthermore, due to friction and the constraints of the die geometry, deformation is not homogeneous. The coefficients of friction are of the order of  $\mu \approx 0.2\text{--}0.25$  and above. Sticking friction occurs in many cases during upsetting operations. These coefficients of friction are considerably higher than those customary in cold forming with good lubrication. This explains why the relevant deformation stresses and forces are higher than one would otherwise expect. In the case of carbon steel, for example, when heated to forging temperature, the flow stress  $\sigma_f$  falls to between 10 and 15% of its value at room temperature. The effect of a higher coefficient of friction increases with the ratio of surface area to volume of the workpiece, and thus is particularly significant in the case of small parts of complex geometry. Here pressures of  $1000\text{--}1500\text{ N/mm}^2$  (145–217.5 ksi) are not exceptional, whereas by comparison, in drawing out and upsetting of large open-die steel forgings, pressures of about  $50\text{ N/mm}^2$  (7.25 ksi) are typical.

### 11.2.1 Open-Die Forging

#### *Material Flow and Changes in Shape*

The laws governing upset forging (Chap. 10) also apply by analogy to the processes for changing the cross-sectional area. Local deformation largely depends on the conditions of friction and on the rate of deformation. Investigations with upset specimens have shown that cross-sectional deformation of upset test pieces becomes less and less homogeneous the higher the coefficients of friction ( $0.2 < \mu < 0.577$ ) (Fig. 11.16). The same tendency is also observed (Fig. 11.17) when the tool speed at the start of the operation is increased, in this case from  $0.14$  to  $45\text{ m/s}$  ( $0.5$  to  $150\text{ ft/s}$ ). This inhomogeneous deformation also affects the consistency of the material properties after hot forging.\*

A study of the end faces of upset test pieces (circular, square, and rectangular) shows a change

\*In other investigations into distortion during hot upsetting of soldered laminar steel test pieces, increasingly consistent shape changes have been observed for increasing tool speeds from  $0.4$  to  $43.5\text{ m/s}$  ( $1.3$  to  $145\text{ ft/s}$ ). Here the significance of the intermediate layer of solder has yet to be explained [11.15].

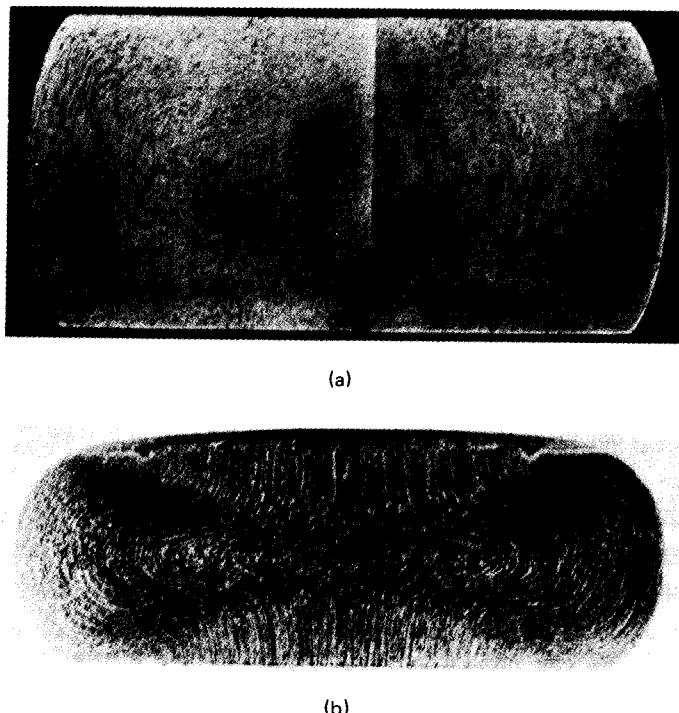


**FIG. 11.16** Effect of the coefficient of friction on deformation during upsetting. (a) CuZn 37 (UNS C27000);  $v_{T,0} = 0.14 \text{ m/s}$  (0.46 ft/s);  $\varphi = 0.73$ ;  $d_0 = 18 \text{ mm}$  (0.71 in);  $h_0 = 27 \text{ mm}$  (1.06 in), at room temperature  $\mu \approx 0.2$ . (After [11.13].) (b) Cq 45 (AISI 1045);  $\varphi = 1.17$ ;  $d_0 = 53 \text{ mm}$  (2.09 in);  $h_0 = 106 \text{ mm}$  (4.17 in);  $T = 1197^\circ\text{C}$  (2187°F); sticking friction. (After [11.14].)

in shape (at  $\mu \neq 0$ ) and size with increased upsetting. Circular faces remain circular, while square and rectangular faces tend to become increasingly circular. This is used in practice when lengths cut from cheap square billets—rolled material  $> 50 \text{ mm}$  (2 in) in side length—are upset in a single stroke to form disk-shaped blanks for die forgings of shape categories 1 and 2 (see Fig. 11.70). The “flow” of material at a right angle to the direction of tool motion is explained by the different frictional shear stresses which individual particles in contact with the tool surface have to overcome; they try to reach the boundary by the path of least resistance. According to the material flow hypotheses of Preussler [11.16] and Falk [11.17], this is also the shortest path. However, Lange [11.18] found that the material particles flow radially in all directions along paths whose curvatures and directions depend increasingly on the ratio  $d/h$  and on the conditions of friction the further the upsetting operation progresses. The direction of flow is given by the tangential angle  $\beta$ , as shown in Fig. 11.18a. Experiments confirmed by Eder [11.19] both experimentally and theoretically showed that the particles try to attain a final direction of flow at a right angle to the circumference of the material (Fig. 11.19). At the center of the workpiece a zone is created where, under suitable conditions of friction, the material particles remain comparatively stationary relative to the tool. According to Schey [11.14], it only starts to flow when  $h/d < 0.25$ , regardless of the initial ratio  $h_0/d_0$ .

In drawing out and spreading, use is made of the differing rates of material flow to achieve the desired deformation of the workpiece. The drawing-out saddle (Fig. 11.2, example 1) is applied in such a way that its longitudinal axis is at a right angle to the main axis of the bar. The

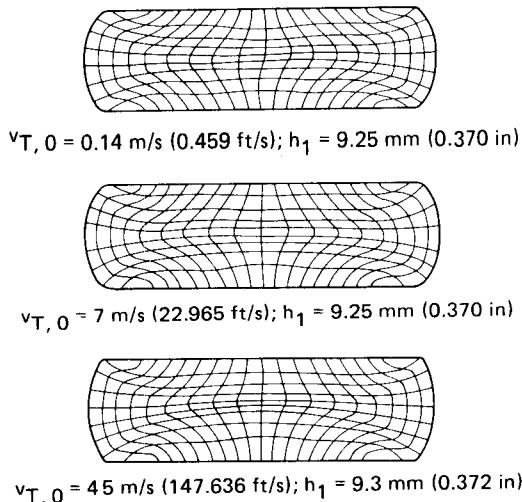


**FIG. 11.17** Effect of forging rate on deformation during upsetting. Material—E-Cu (UNS C11000);  $h_0 = 27$  mm (1.06 in);  $d_0 = 18$  mm (0.71 in). [After 11.13.]

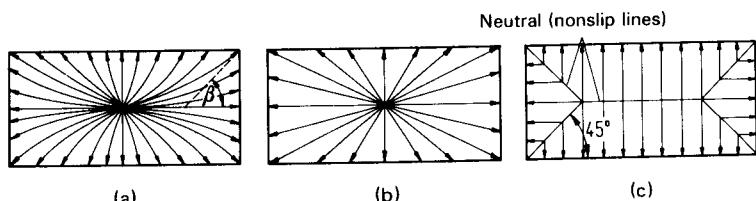


**FIG. 11.18** Material-flow hypotheses for the end faces of upset rectangular sections.  
 (a) After H. Lange [11.18]. (b) After A. Falk [11.17]. (c) After H. Preussler [11.16].

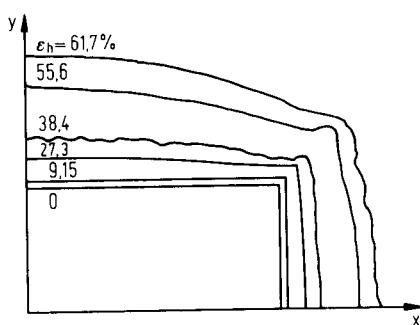


**FIG. 11.19** Deformation of a rectangular test piece in five stages. Material—AlMgSi 1 F28 (AA 6061-H);  $l_0 = 19.4$  mm (0.76 in);  $b_0 = 9.5$  mm (0.37 in);  $h_0 = 8.2$  mm (0.32 in). (After [11.19].)

## 11.16 BULK-METAL FORMING

material then flows predominantly in the direction of least frictional resistance, that is, mainly in the longitudinal direction (stretching) and only to a lesser extent at a right angle to it (spreading). The spreading is "forged back" after a  $90^\circ$  rotation of the bar about its main axis. This results in loss of energy and time. In modern drawing-out forging machines with three or four forging tools (Fig. 11.2, example 4), spreading is largely avoided by the simultaneous action of tools approaching from different directions—material is practically forged back as soon as it is displaced. There is, however, no real energy saving since the mean stress  $\sigma_m$  in the workpiece is definitely greater. Where material flow at a right angle to the main bar axis is desired, that is, spreading, identical rectangular saddles are used with their longer sides parallel to the main axis of the workpiece, as shown in Fig. 11.2, example 3. Where the geometry of the forging demands both drawing out and spreading, for example, in the case of bar sections with  $b/h > 2.5$ , drawing out is performed first, followed by spreading, since otherwise the relatively flat workpiece might buckle during forging back of the displaced material [11.20].

### Stresses, Forces, and Work

The elementary equations of plasticity theory given in Sec. 10.1 may be applied to upsetting operations. By analogy, they also apply to drawing out and spreading, although here the "rigid" material adjacent to the deformation zone leads to increases in stress. When these operations are considered to approximate plane deformation, it is possible to draw the following conclusions for the slip-line fields shown in Fig. 11.4 (according to [11.8]). For  $b/h = 1$  and all other ratios of  $b/h = n$ , where  $n$  represents the range of positive integers, the mean punch pressure  $p_m = 2k = \sigma_f$ , that is, a compressive force  $F = A_p \sigma_f$  must be applied in order to produce plastic deformation of the material in the area of the slip-line fields. For  $b/h < 1$  the punch pressure required  $p_m/\sigma_f$  increases to a theoretical maximum of approximately 2.5 at  $b/h \leq 0.12$ ; at  $b/h = 0.35$  the punch pressure  $p_m/\sigma_f \approx 1.4$ .\*

It is most important—as in all force calculations concerned with forging—to know the flow stress  $\sigma_f = f(T, \varphi, \dot{\varphi})$  as exactly as possible. Here the effect of true strain is negligible during deformation in the recrystallization range, that is, above  $T_m/2$ . The effect of the deformation rate on  $\sigma_f$  and on the deformation resistance  $k_R$ , on the other hand, increases with temperature [11.12], [11.22], [11.23], although the effect of temperature itself is by far the greatest (Fig. 11.20). For limited ranges, empirical equations of the form

$$k_R = A \cdot B^T \cdot \dot{\varphi}_m^{(C \cdot T - D)} \times 10 \quad \text{N/mm}^2 \quad (11.1)$$

can be derived for calculating the deformation resistance during upsetting with low surface friction ( $\mu < 0.1$ ). Here  $T$  represents the temperature in degrees Celsius. Table 11.1 lists the constants  $A$ ,  $B$ ,  $C$ , and  $D$  determined for various steels. Their use is limited to the temperature range specified.

As Table 11.2 shows, the mechanical properties of metals at room temperature bear no relation to the flow stress at forging temperature. Accordingly, the force and work required to forge light alloys is sometimes greater than that required to forge mild steels [11.12], [11.20], [11.25]. Table 11.2 also contains typical values for the *mean* temperature increase in the deformation zone. Specific values in the slip planes (Fig. 11.21), in the area of the flow lines (Fig. 11.4) in which most of the deformation occurs, may be several times higher. It is particularly important to take this into consideration in the case of temperature-sensitive materials. The existence of higher temperatures in the slip planes is made apparent by differences in temper color. Johnson calls these planes of increased temperature *heat lines*, which he investigated for steel by means of color film [11.26].

In practice the ability to calculate forces in drawing out, spreading, and upsetting is mainly used to determine a few typical values as guidelines, taking into account the forging stroke and the work done. Experience has led to certain rules for the allocation of different sized forgings to particular forging machines, as shown in the table on p. 11.20.

\*According to Siebel, the force required for drawing out is given by  $F = A_p \sigma_f (1 + \frac{1}{2} \mu \ell/h + \frac{1}{2} h/\ell)$ . Here  $A_p = b\ell$ ,  $\ell$  being the punch or saddle length [11.21].

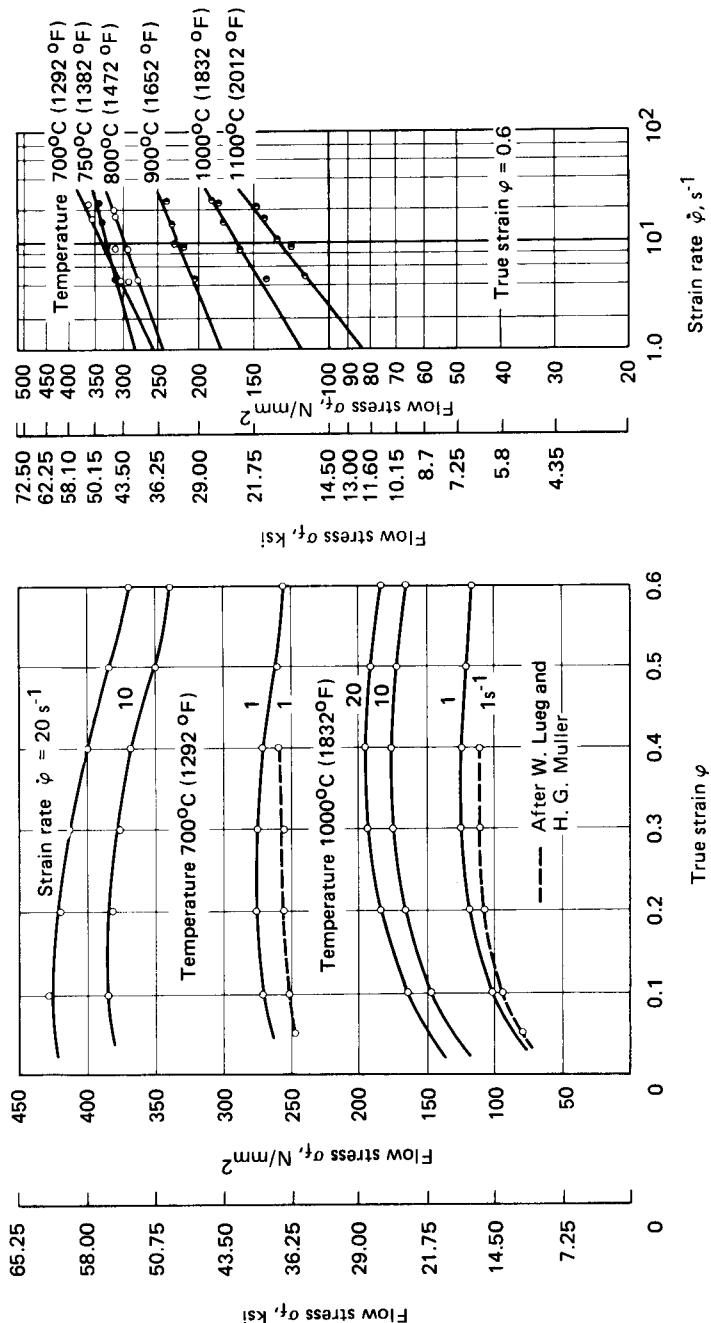


FIG. 11.20 Effect of strain rate on the flow stress  $\sigma_f$  for C 45 (AISI 1045). (a)  $\sigma_f = f(\varphi, T)$ . (b)  $\sigma_f = f(\dot{\varphi}, T)$ .  
(After [11.23].)

**Table 11.1** Values of the Constants Required to Calculate Flow Stress According to Eq. 11.1<sup>a</sup>

DIN	Steel designation	Composition, wt%						Constants					
		AISI	C	Mn	Si	Cr	Ni	Mo	V	A	B	C	D
With phase transformation: Valid for the temperature range 850°C (1562°F) < T < 1150°C (2102°F)													
C.35	C1035	0.35	0.57	0.26	1.49	4.29	0.38	0.16	190	0.9969	0.000229	0.048	
30 NiCrMoV 16	P21	0.34	0.47	0.36	0.37	15.80			780	0.9958	0.000357	0.210	
25 Cr 60	—	0.26	0.35	0.37	0.70	12.60			310	0.9970	0.000320	0.170	
200 Cr 50	D3	2.00	0.32	0.70					4000	0.9943	0.000600	0.402	
Without phase transformation: Valid for the temperature range 600°C (1112°F) < T < 1150°C (2102°F)													
X10 CrNiMo 22.8	—	0.12	0.62	21.70	8.05	3.20			480	0.9966	0.000265	0.111	
X10 CrNiMo 17.12	316	0.12	0.78	16.90	12.60	2.90			300	0.9968	0.000294	0.104	
X8 Cr 17	430	0.07	0.32	17.50					265	0.9958	0.000382	0.107	
X110 Mn 14	—	1.09	13.70						550	0.9961	0.000335	0.131	

<sup>a</sup>Valid for 0.25 < φ < 1; 0.05 < φ<sub>m</sub> < 160 [s<sup>-1</sup>]; φ<sub>m</sub> ≈ φ<sub>0</sub> for hammers and mechanical presses.

Source: Compiled from [11.22].

**Table 11.2** Strength, Forging Temperature, Flow Stress, Specific Heat, and Temperature Increase during Forging of Various Materials

Material	Strength $S_{ut}$ , N/mm <sup>2</sup> (ksi)	Soft annealed, HB	Forging temperature, °C (°F)	Flow stress (deformation resistance) at $\dot{\varphi} \approx 1\text{s}^{-1}$ , N/mm <sup>2</sup> (ksi)	Density $\rho$ , kg/m <sup>3</sup> (lb/in. <sup>3</sup> )	Mean specific heat, J/kg·°C (J/lb·°F)	Temperature increase $\Delta T$ at $\dot{\varphi} \approx 1$ , °C (°F)
C-steel (0.25% C)	350 (51) 220 (32) 410 (59)	130 18 47	950–1200 (1742–2192) 730–900 (1346–1652) 650–730 (1202–1346)	80–50 (12–7) 80–40 (12–6) 45–25 (7–4)	7800 (0.28) 8900 (0.32) 8400 (0.30)	428 (17) 376 (94) 376 (94)	20–10 (36–18) 40–12 (72–22) 15.8 (27–14)
Copper							
Brass (58% Cu)							
Pure aluminum	50 (7) 330 (48)	14 80	450–550 (842–1022) 380–500 (716–832)	25–10 (4–1) 90–50 (13–7)	2700 (0.10) 2800 (0.10)	920 (230) 920 (230)	10–4 (18–7) 35–15 (63–27)
Al-Mg alloy							
Mg alloy							
Ti–6Al–4V/(TiAl6V4)	1020 (148)	381	850–950 (1562–1742)	60–30 (9–4) 300–150 (43–22)	1800 (0.07) 4400 (0.16)	1003 (251) 580 (145)	35–15 (63–27) 50–25 (90–45)

Source: Compiled from [11.12], [11.24].

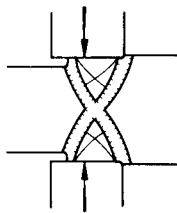


**FIG. 11.21** Slip bands during drawing out. (After [11.20].)

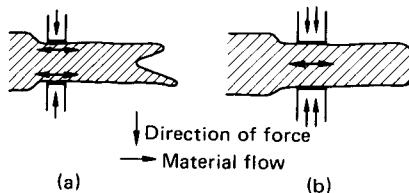


**FIG. 11.22** Effect of tool size, magnitude of compressive force, and heating through on the material flow during hot drawing out. (a) Tools too small, compressive force too low, and core temperature too cold. (b) Sufficiently wide tools, relatively high compressive force, even temperature throughout cross section. (After [11.20].)

These data are valid for carbon steels and light to medium alloy steels. It can be seen by observation of the surface material flow whether the forging plant and the tool have been chosen appropriately for a particular open-die forging operation. Too small saddles, too little pressure  $p_m$  on the contact surface, and insufficient heating of the workpiece to be forged lead to distortion of the surface layers (Fig. 11.22). With wide tools, higher compressive stresses  $p_m$ , as well as sufficient and even heating, the desired deformation is achieved over the entire cross section of the workpiece.

Dimensions, mm (in)	Shapes	Machine criteria
Up to 150 (6)	Round or square	500 kg (0.55 ton), hammer
Up to 200 (8)	Round or square	1000 kg (1.1 ton), hammer
Up to 300 (12)	Round or square	2000 kg (2.2 ton), hammer
Up to 450 (18)	Round or square	3000 kg (3.3 ton), hammer 5000 kN (563 ton), press
Up to 550 (22)	Octagonal	10,000 kg (11 ton), hammer 10 MN (1125 ton), press
Up to 650 (26)	Octagonal	15 MN (1688 ton), press
Up to 2200 (87)	Octagonal	40 MN (4500 ton), press

Source: Ref. [11.20].

### 11.2.2 Closed-Die Forging

#### Material Flow and Deformation

As with open-die forging, closed-die forging operations are nonstationary processes. Material flow and deformation are largely determined by the shape of the tools.

The rules for upsetting described in Sec. 11.2 also apply to heading in a die (Fig. 11.14, left). Material contacts the die wall without appreciable slip motion. The formation of folds and overlaps can be avoided by good tool support. Uneven grain flow is reduced by optimal centering, good lubrication, and accurate preparation of the end faces at a right angle to the main bar axis (Figs. 10.8, 10.10, and 10.11) [10.22]. Conical shapes are basically preferable to cylindrical ones since material is concentrated where it is required for finish forming (see Sec. 11.5.2). With conical shapes, complete filling, even of deeper areas of the die cavity, causes little difficulty, and undesirable flash formation can be avoided more easily.

**Closed-die forging without flash (Fig. 11.14b):** Recent investigations have shown that, apart from the need to control fluctuations in volume, complete filling of the corners of the die cavity can only be achieved by using very high forging pressures [11.27]. The sharp bend in the force-

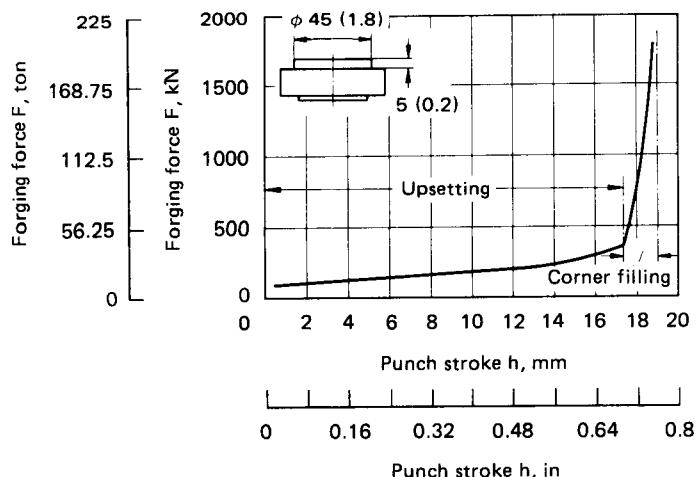


**FIG. 11.23** Force-stroke curve for closed-die forging without flash. Material—C 15 (AISI 1015); forging temperature 1197°C (2187°F), oil/graphite lubrication. Dimensions in mm (in). (After [11.27].)

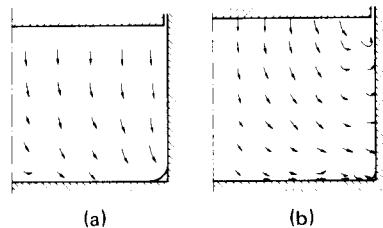


**FIG. 11.24** Flow pattern for filling of corners during closed-die forging without flash. (a) Rising. (b) Spreading. (After [11.28].)

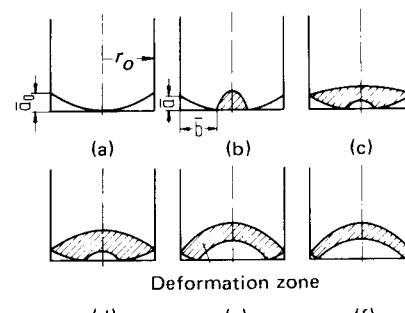


**FIG. 11.25** Shape of the deformation zones in die filling of deep cavities (rising) during closed-die forging without flash.  $a$ —height of unfilled edge in the direction of force;  $b$ —width of unfilled edge at a right angle to the direction of force;  $h_C > 0.5 d_C$ . (After [11.28].)

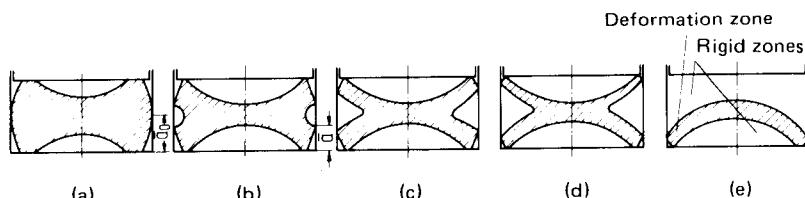


**FIG. 11.26** Shape of the deformation zones in spreading during closed-die forging without flash.  $d_C/h_C = 0.5$ ,  $d_C = 60$  mm (2.36 in);  $a$ —as in Fig. 11.25. (After [11.28].)

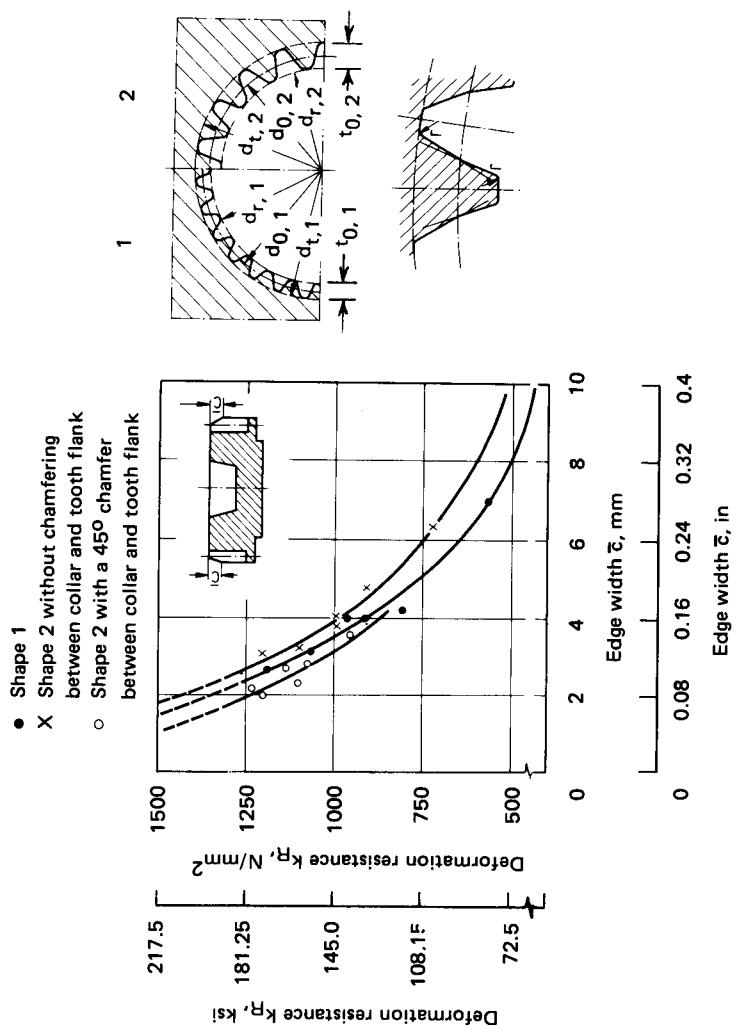


**FIG. 11.27** Deformation resistance  $k_R$  during die forging of spur gears without flash. Material—C 15 (AISI 1015); forging temperature 1197°C (2187°F); oil/graphite lubrication. (a)  $\bar{c}$ —edge width (of nonfilled area). (b) Tooth shapes: 1— $m_1 = 2$  mm (0.08 in),  $t_{0,1} = 2$ ,  $d_{t,1} = 56$  mm (2.20 in),  $d_{r,1} = 60$  mm (2.36 in),  $d_{r,2} = 54$  mm (2.05 in),  $Z_1 = 28$ ,  $r = 0.5$  mm (0.02 in); 2— $m_2 = 3$  mm (0.12 in),  $t_{0,2} = 3$ ,  $d_{t,2} = 48$  mm (1.89 in),  $Z_2 = 18$ ,  $r = 1.0$  mm (0.04 in),  $d_{r,2} = 60$  mm (2.36 in),  $d_{t,2} = 48$  mm (1.89 in),  $Z_2 = 18$ ,  $r = 1.0$  mm (0.04 in).  $Z$  = number of teeth (After [11.28].)

stroke curve in Fig. 11.23 shows the magnitude of the force increase required for corner filling. Fig. 11.24 shows the lines of motion of material particles entering the corner of a die cavity during rising and spreading. The deformation zones of these two basic operations exhibit considerable differences. In rising, that is, with the upward displacement of material into deep hollow cavities ( $h < d/2$ ), the advancing core is upset at the start of the forging-out operation (Fig. 11.25a and b). As the end face is further flattened, starting from  $b/r_0 = 0.8$ , an increasingly large friction zone is created (Fig. 11.25c to f). At the same time the deformation zone becomes increasingly arched, until at about  $b/r_0 = 0.35$  it again begins to flatten out (Fig. 11.25f). When spreading an upset barrel-shaped body in die, the arched shape of the deformation shown in Fig. 11.26 first occurs toward the end of the forging-out operation (Fig. 11.26e). Prior to this, the total volume lying in the deformation zone decreases progressively (Fig. 11.26a to d) [11.28]. The permissible variation in volume depends mainly on the initial geometry of the workpiece, assuming a deformation resistance  $k_R$  or a forging pressure  $\leq 1000\text{N/mm}^2$  ( $\leq 145$  ksi), a maximum side length  $a \leq 2$  mm (0.08 in), and a thickness tolerance  $P$  according to DIN 7526 [11.29], for a given elastic constant for the press-tool system of  $C \approx 1800 \text{ N/mm}$  (261 ksi). Experiments have shown that with relatively flat initial shapes ( $d_i/h_i = 4$ ), variations in volume of 7–11% are permissible, while with thinner workpieces ( $d_i/h_i = 2$ ) variations in volume of only 1–4% are acceptable. Too much material causes end flash and exceeding of the permissible tool load  $k_R$ . End flash is easier to avoid at somewhat reduced temperatures of approximately  $1000^\circ\text{C}$  ( $1832^\circ\text{F}$ ), but the tool load then increases because of the unavoidable increase in  $k_R$  [11.27].

In closed-die forging without flash of nonrotationally symmetrical workpieces, the conditions described above are often completely altered by secondary shape elements. Particular concentrations of material may lead to one-sided material shortages, and thus to uneven loading of the die. Localized formation of end flash may occur due to differing compressive stresses [11.30]. Experiments have shown that in forging out, the degree of filling of the corners is the main parameter. In forging gear teeth, variations in the corner dimensions on the order of  $1 \leq c \leq 3$  mm (0.12 in), for example, can only be achieved at very high values of deformation resistance, such as 1200  $\leq k_R \leq 1600 \text{ N/mm}^2$  ( $174 \leq k_R \leq 232$  ksi) (Fig. 11.27). Where forgings have asymmetrical protrusions on one particular side, additional material must be provided in order to assure complete filling of the die cavity. In general, even in the case of more than one protrusion, material first flows into the deeper parts of the cavity where there is less resistance (Fig. 11.28), and only thereafter it fills the remaining areas of the cavity at a greatly increased value of  $k_R$ . Forgings with deep areas, on the other hand, cause little difficulty with regard to deformation resistance during closed-die forging without flash. Material flow around protrusions in the cavity, however, can lead to forging defects (Fig. 11.29), and thus it is necessary to distribute the material carefully before final forging.

**Closed-die forging with flash:** Material flow proceeds in principle as illustrated in Fig. 11.15. Depending on the particular process involved, the forging sequence starts either with contacting or with sliding (Fig. 11.30). However, sliding predominates at the end of the operation, and is characterized by a lateral displacement of material in the direction of the flash gap. The

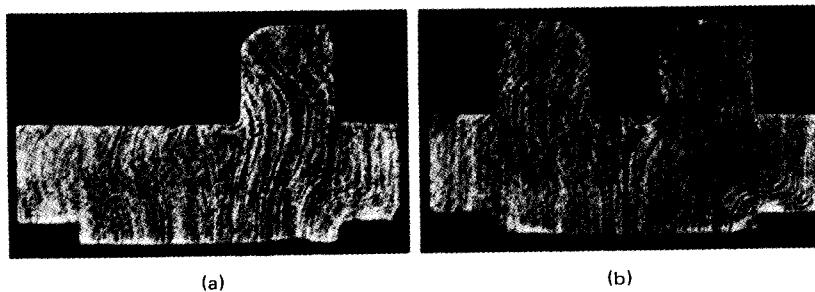


**FIG. 11.28** Material flow (grain structure) of forged parts with local shape elements formed by closed-die forging without flash. (a) One shape element, out-of-center projection. (After [11.30]). (b) Two symmetrically out-of-center located shape elements. (After [11.28].)



**FIG. 11.29** Material flow (grain structure) of a forged part with local indentation formed by closed-die forging without flash. Note the material separation at corner A. (After [11.28].)

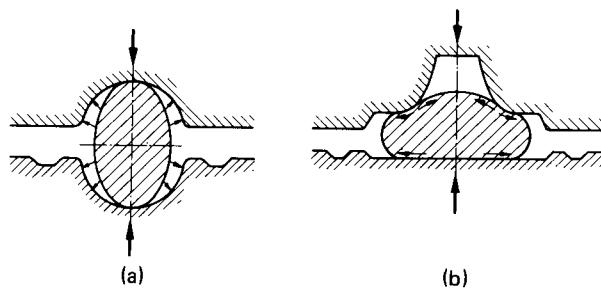


**FIG. 11.30** Material flow in a die. (a) Contacting (without sliding). (b) Sliding. (After [11.31].)

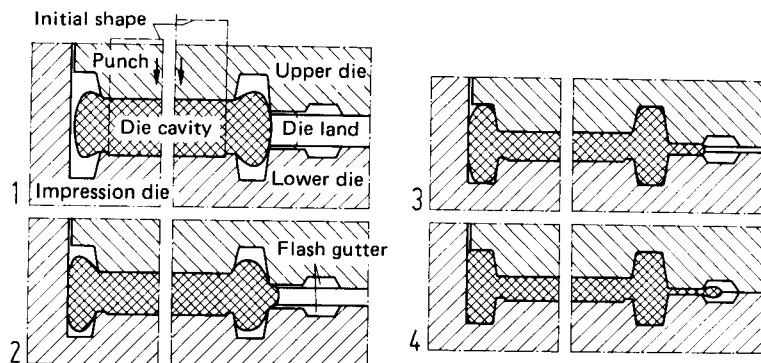


**FIG. 11.31** Schematic representation of the filling of a closed die without flash (left) and of a die with flash gutter (right). (After [11.28].)

difference in filling a cavity of H-shaped cross section with and without flash is shown in Fig. 11.31. If the tool geometry is not carefully designed to suit the given conditions (material, temperature, workpiece size, main dimensions), especially with regard to the transition radii, forging defects (material separation) may occur (Fig. 11.32). Where material flows from relatively deep impressions in the upper or lower dies into the flash gap, discontinuities may occur in the grain (fiber) structure, which with certain materials may lead to a reduction in fatigue strength, although the strength and fracture strain values remain unchanged [11.32]. In spreading of thin-walled forgings, where no increase in cross section occurs in the transition area between the outer

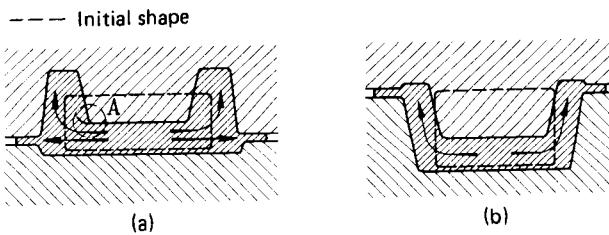


**FIG. 11.32** Material flow during rising and spreading. (a) Rising. (b) Spreading. Material separation may occur at corner A. (After [11.12].)

edge of the parts and the flash (see, for example, Fig. 11.13), discontinuities of this kind are largely avoided. The rate of flow  $v$  during such operations (Fig. 11.32b) may be several times higher than the tool speed  $v_T$ . In experiments with plasticine at reduced scale, for example, speed ratios in the range of  $4 < v/v_T < 8.5$  were found [11.12]. In hammer forging, with  $v_{Top} \approx 6 \text{ m/s}$  (18 ft/s), this would correspond to a rate of flow of between about 25 and 50 m/s (75 and 150 ft/s). In the flash gap itself even higher rates of flow are likely to occur.

As already mentioned in Sec. 11.1.6, in closed-die forging with flash, dies with exactly defined flash-gap geometry are used. The die land is characterized by its width  $b$  and by the gap thickness  $s$ . Additional characteristics are the instantaneous flash width  $b^*$  and flash thickness  $s^*$  prior to completion of the forging operation. Even though qualitative and quantitative methods of calculating the normal and tangential friction stresses as a function of the geometry of the die land have been known for a long time and have been used with success [11.21], [11.33], [11.34], new investigations have only more recently provided quantitative data on the relationship between excess flash-gap geometry and filling of the die cavity [11.35], [11.36]. As Fig. 11.33 shows, the excess material  $\Delta m$  required to fill the die cavity during rising decreases considerably when the gap thickness  $s$  is reduced or the ratio  $b/s$  is increased. How far this increases the normal pressure  $p_m$  in the die land and in the die is discussed in the next section.

### Stresses, Forces, and Work Required

Fundamental to the consideration of likely stresses and forces is the clear distinction between closed-die forging *without* flash and closed-die forging *with* flash. The group to which *heading in a die* belongs depends on whether the operation is performed with or without flash. In general one tries to carry out heading without flash.

**Closed-die forging without flash:** The normal compressive stresses  $p_m$  acting on the workpiece and the deformation resistance  $k_R$  are of about the same order as in closed-die forging with the flash, that is, in some cases considerably above  $1000 \text{ N/mm}^2$  (145 ksi), in particular when the volumes of the initial material and the die cavity are similar. For small parts, where  $d \approx 50\text{--}60 \text{ mm}$  (2.0–2.4 in), the pressures required for closed-die forging without flash are lower than those for closed-die forging with flash. Such observations are explained by the increase in flow stress in the flash as a result of the more rapid cooling of small volumes [11.37]. As described in the preceding section, the mean normal pressure in the die cavity  $p_m$  and the resistance to deformation  $k_R = F/A_p$  depend closely on the degree of filling of the least accessible corners of the cavity (see Fig. 11.27). Calculations and measurements by Johne have led to good agreement in this area for a range of differently shaped forgings [11.28], [11.30], [11.38]. Basically, similarly sized unfilled corners lead to higher deformation resistances in rising than in spreading. Figs. 11.34 and 11.35 show examples in which  $k_R$  is limited to  $1000 \text{ N/mm}^2$  (145 ksi) as described in Sec. 11.2.2.

The radial stresses  $\sigma_r$  at the die surface increase with increasing degrees of filling. Fig. 11.36 shows the radial stresses occurring during rising and spreading of commercial lead; the relationship between mean radial stress (at depth  $h$ )  $\sigma_{r,m}$  and  $k_R$  is shown in Fig. 11.37. The axial stress  $\sigma_z$  depends largely on the workpiece geometry  $d/h$ , as shown for closed cylindrical cavities in Fig. 11.38 for lead.

The above information, even though incomplete, should give an idea of the kinds of stresses and forces that exist in practice. The data shown in Fig. 11.39 may be used for the conversion of

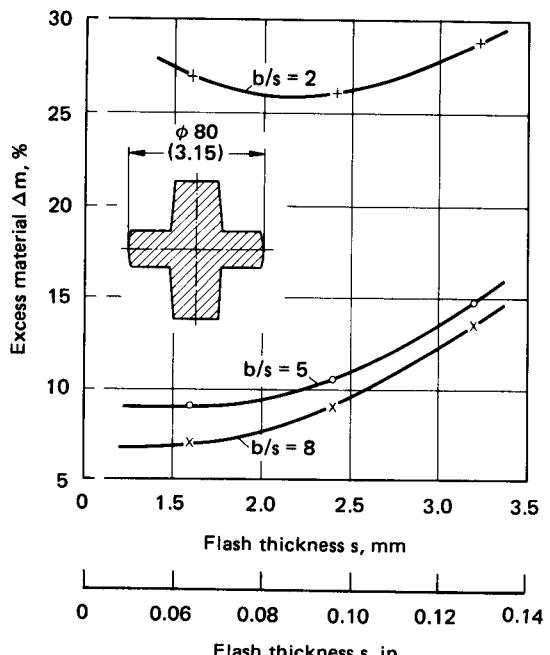


FIG. 11.33 Effect of flash-gap thickness on the amount of excess material required to ensure filling of die cavity. Dimensions are in mm (in). (After [11.36].)

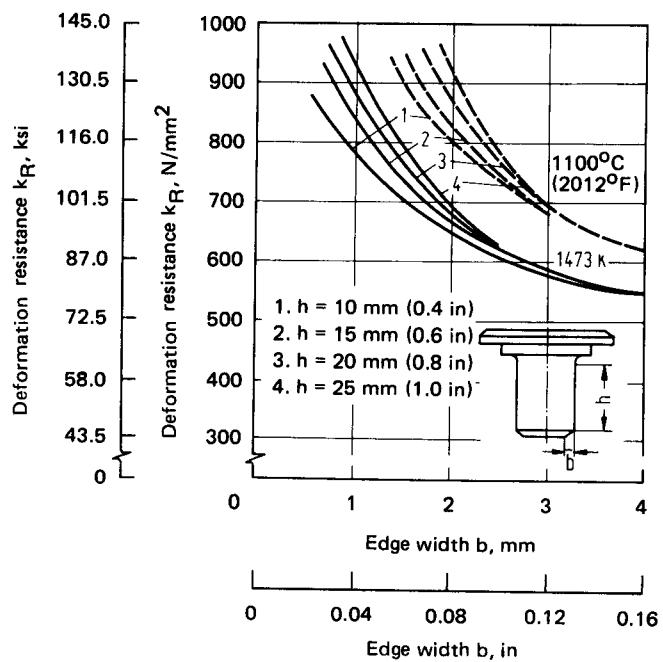
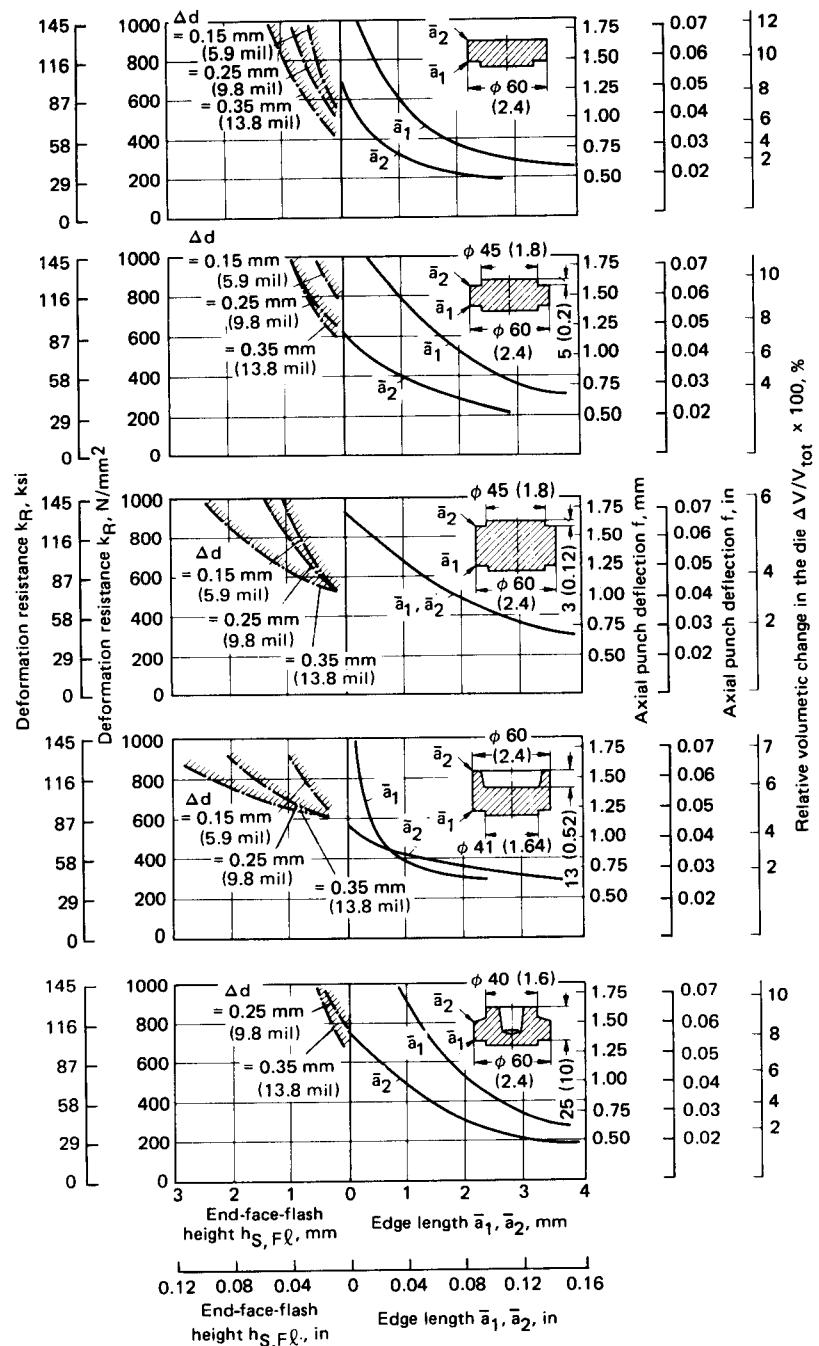
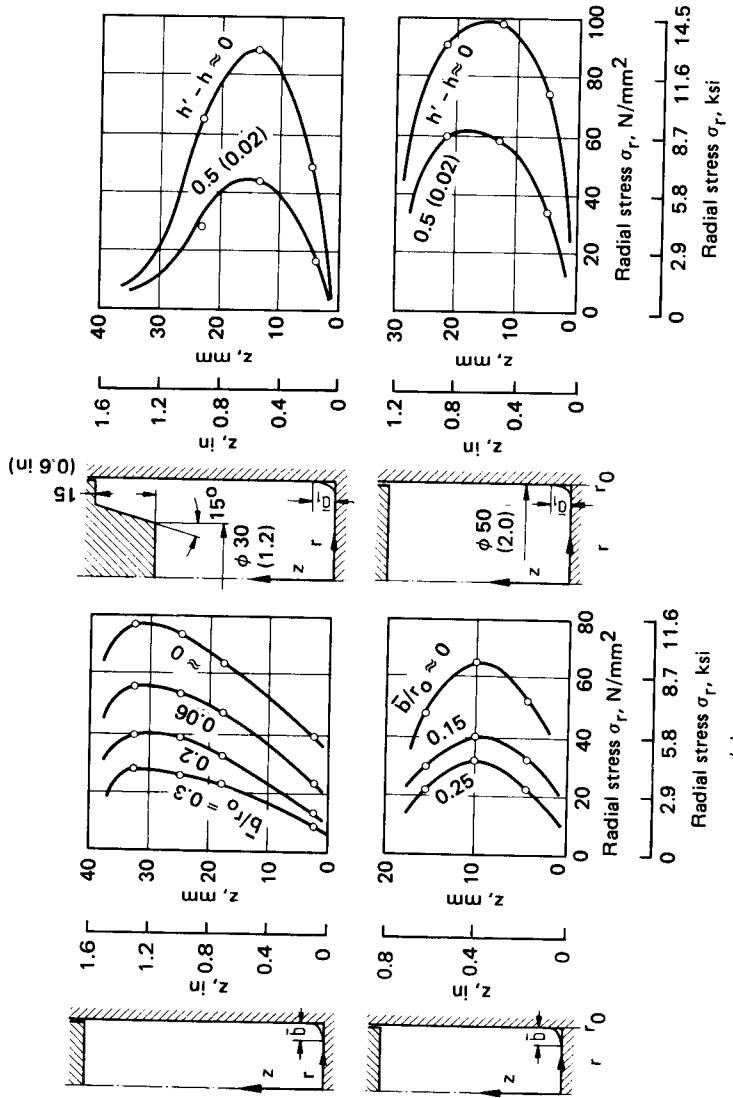


FIG. 11.34 Deformation resistance  $k_R$  during rising closed-die forging without flash; measured values. Material—C 15 (AISI 1015); no lubrication;  $T = 1100$  and  $1200^\circ\text{C}$  (2012 and  $2192^\circ\text{F}$ ). (After [11.28].)



**FIG. 11.35** Deformation resistance  $k_R$  during spreading closed-die forging without flash for differently shaped forged parts; measured values. Material—C 15 (AISI 1015); oil/graphite lubrication;  $T = 1200^\circ\text{C}$  ( $2192^\circ\text{F}$ ),  $\Delta d = d_{P_t} - d_D$ . Dimensions are in mm (in). (After [11.28].)



**FIG. 11.36** Radial stress distribution in the lower die during closed-die forging without flash. Material—commercially pure lead (99.9%), room temperature; no lubrication;  $h'$ —punch travel;  $h'$ —punch travel during forging. Dimensions are in mm (in). (a) Spreading. (b) Rising. (c) Spreading. (d) Rising. (After [11.28]).

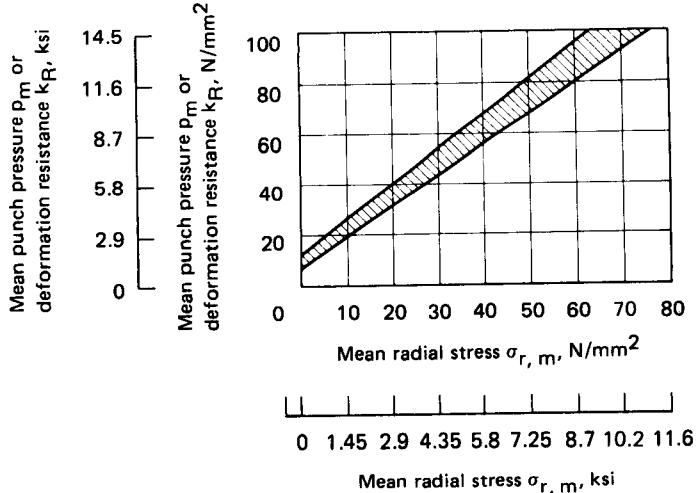


**FIG. 11.37** Relationship between deformation resistance  $k_R$  (mean punch pressure  $p_m$ ) and radial stress  $\sigma_{r,m}$  during closed-die forging without flash. Upper limit corresponds to flatter parts. Material—commercially pure lead (99.9%); room temperature. (After [11.28].)

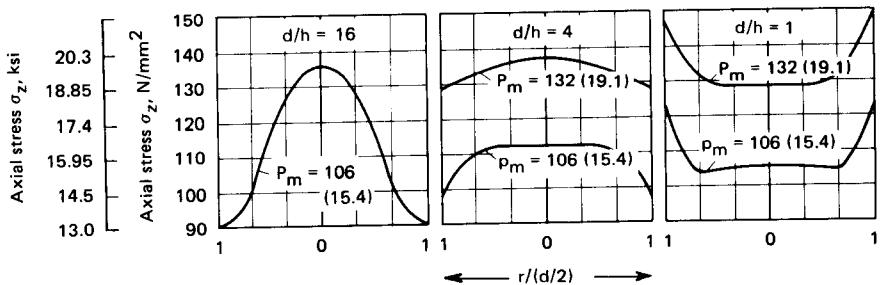


**FIG. 11.38** Axial stress distribution  $\sigma_z$  for differently shaped parts during closed-die forging without flash. Material—commercially pure lead (99.9%), room temperature. Normal compressive stress  $p_m$  is shown in N/mm $^2$  (ksi). (After [11.39].)

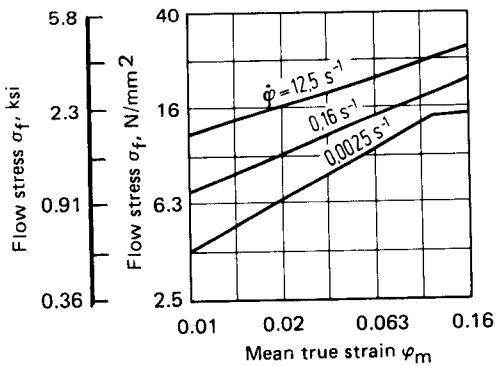


**FIG. 11.39** Flow stress  $\sigma_f$  of commercially pure lead (99.9%). (After [11.40].)

experimental values obtained with commercial lead. Disregarding the different conditions of friction, the following equation applies:

$$k_{R, \text{steel}} \approx k_{R, \text{lead}} \frac{\sigma_{f, \text{steel}}}{\sigma_{f, \text{lead}}} \quad (11.2)$$

$\sigma_z$  and  $\sigma_r$  may be calculated in the same way. Here it is very important to determine  $\sigma_{f, \text{steel}} = f(T, \varphi, \dot{\varphi})$  as accurately as possible, following the recommendations made on page 11.40.

**Closed-die forging with flash:** It is possible, via the geometry of the flash gap, to influence not only the amount of excess material required but also the stresses in both the die land and the main die cavity (Fig. 11.40). The following rule applies: high normal pressure in the die land leads to increased stresses in the tool, but also, often, to considerable reductions in the amount of material required. Between these two constraints the optimal solution must be found (Fig. 11.41). For die land I, with flash width  $b_2$  the ordinate values of excess material required and of normal compressive stress in the flash are indicated by the two arrows. When for the same flash thickness  $s$  the flash width is increased to  $b_3$ , this leads to further rise in flash pressure (corresponding to II), but is accompanied by a reduction in excess material. Conversely, if the flash width  $b_2$  is held constant and the flash thickness  $s$  is increased (corresponding to III),  $\sigma_{z, \text{fl}, \text{max}}$  falls and  $\Delta m$  rises. According to Vieregge, however, increasing  $b/s$  above a value of about 5 or 6 does not lead to any further appreciable decrease in  $\Delta m$  (Fig. 11.42). On the other hand, the flash pressure, forging force, and work required continue to rise. Increasing  $b/s$  above the value mentioned does, however, have the advantage of improving the height attainable in rising, although tool loading is also correspondingly high (Fig. 11.43).

A number of different methods of calculation are available for determining the optimal size

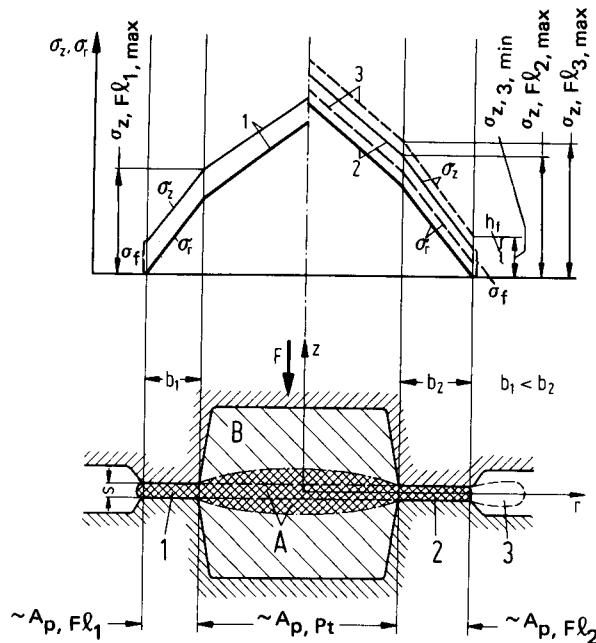
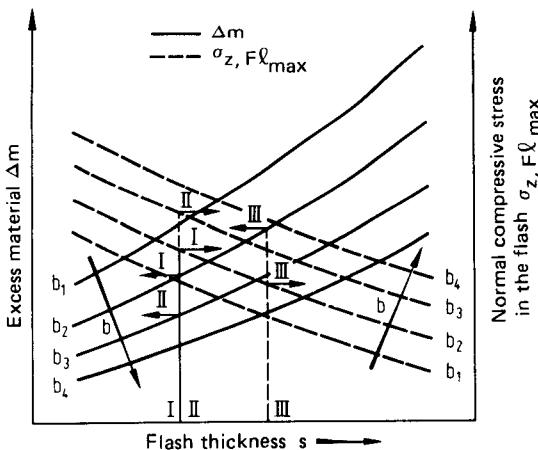


FIG. 11.40 Qualitative distribution of radial and normal stresses in closed-die forging with flash. 1—Narrow die land; 2—wide die land; 3—flash extending into flash gutter; A—deformation zone; B—rigid zone. (After [11.36].)



**FIG. 11.41** Effect of die-land gap thickness on excess material and on normal pressure in the die-land  $\sigma_{z,F\ell,\max}$ . (After [11.36].)

of the die land. Bruchanow and Rebelski [11.41] propose that the following equation be used for flash thickness  $s$ :

$$s = 0.015 \sqrt{A_{p,pt}} \quad (11.3)$$

The ratio  $b/s$  depends on the geometry of the die cavity and lies between 1.5 and 13. Voigtländer [11.42] suggests the following relationship based on statistical evidence:

$$s = 0.016 d_o \quad (11.4a)$$

$$\frac{b}{s} = \frac{63}{\sqrt{d_o}} \quad (11.4b)$$

where  $d_o$  is the workpiece outer diameter in millimeters.

Neuberger and Möckel [11.34] have shown, also based on statistical evidence, that  $s$  and  $b/s$  are dependent on the mass of the forged part (Fig. 11.44). Vieregge [11.35], [11.43] proposes a method for calculating the size of the die land, taking into account the size and geometry of the workpiece:

$$s = 0.017 d_o + \frac{1}{\sqrt{d_o + 5}} \quad (11.5a)$$

where  $s$  and  $d_o$  are in millimeters, and

$$\frac{b}{s} = \frac{30}{\sqrt[3]{d_o[1 + 2d_o^2/h(2r_h + d_o)]}} \quad (11.5b)$$

where  $d_o$ ,  $h$ , and  $r_h$  are in millimeters.

These empirical equations and those of the other authors do not claim to be exact in the mathematical sense. With noncylindrical parts the width of the cross section concerned should be substituted for  $d_o$ . Fig. 11.45 shows various values of  $b/s$  and  $s$  as a function of  $d_o$  for three differently shaped parts.

It is appropriate to mention here briefly the effects of lubrication, which are discussed in more detail in Sec. 11.2.3. Lubricants affect both the coefficient of friction and the transfer of heat between workpiece and tool [11.44]. Although the large variety of different lubricants and parameters make any generally valid statements impossible, experiments have shown that the use of solid lubricants ( $\text{MoS}_2$ ) results in lower flash pressures, leading to worse die filling than in forging

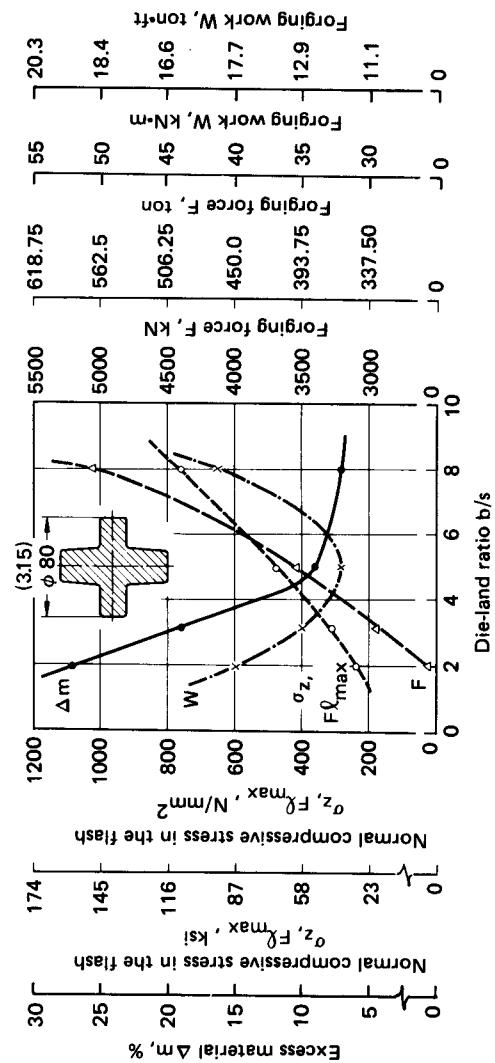


FIG. 11.42 Effect of die-land ratio on excess material, flash pressure, deformation force, forging force, and work done during forging. Material—C 15 (AISI 1015);  $T = 1100^\circ\text{C}$  ( $2012^\circ\text{F}$ );  $s = 1.6 \text{ mm}$  ( $0.06 \text{ in}$ ). (After [11.36].)

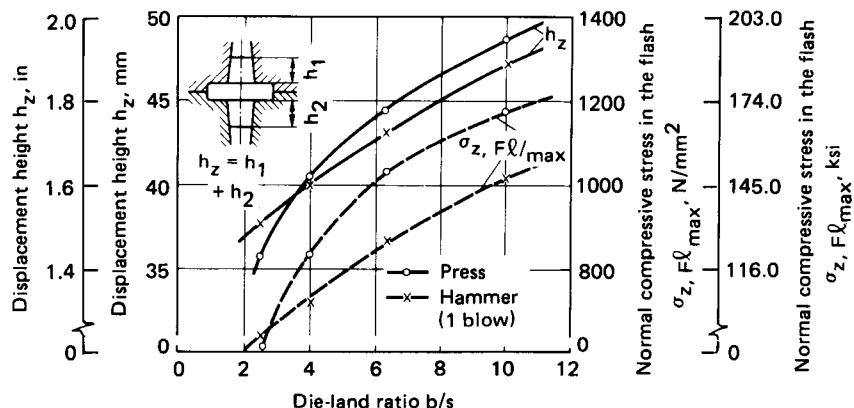


FIG. 11.43 Effect of die-land ratio on rising height and flash pressure during closed-die forging with flash using a hammer and a crank press. Material—C 15 (AISI 1015);  $T = 1100^\circ\text{C}$  ( $2012^\circ\text{F}$ ). (After [11.36].)

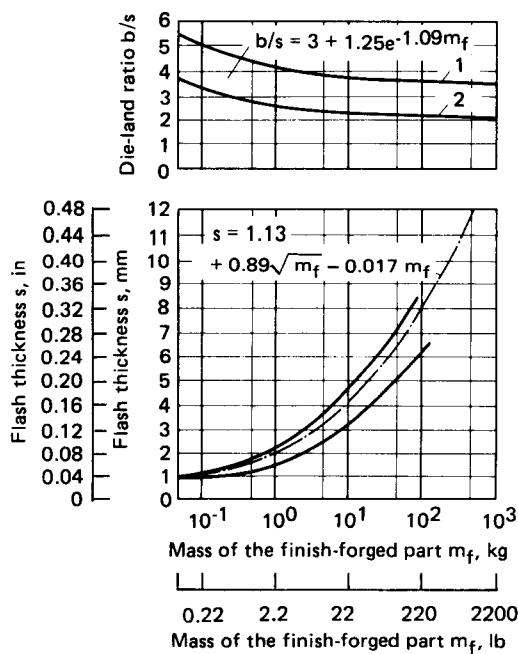


FIG. 11.44 Typical values of flash thickness and die-land ratio for common forging steels. 1—difficult shapes; 2—simple shapes. (After [11.34].)

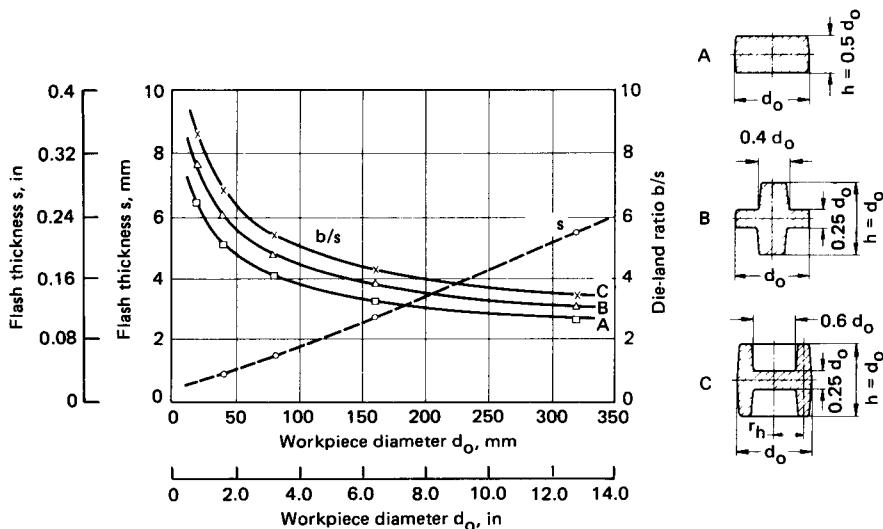


FIG. 11.45 Calculated flash dimensions as a function of part shape and size. (After [11.43].)

without lubrication. Thus where lubrication is used, the die-land ratio  $b/s$  should also be increased, for instance by increasing the flash width  $b$  by up to 10–15%.

Graphs of the normal compressive stress  $\sigma_z$  and the radial compressive stress  $\sigma_r$  are shown in Fig. 11.40. Applying the Tresca flow criterion (see Sec. 5.1.5), those stresses, which differ by an amount equal to the flow stress  $\sigma_f$ , increase uniformly from the outer flash edge to its inner edge, that is, to the edge of the die cavity. This increase and the maximum value of the normal compressive stress in the flash  $\sigma_{z,\max}$ , which is important in assessing the suitability of the operation, are a function of the die-land geometry, the coefficient of friction, and the flow stress. It has been adequately shown that Siebel's equation for normal and radial stress distribution during horizontal upsetting [11.45],

$$\sigma_z = -\sigma_f \left( 1 + 2\mu \frac{x}{h} \right) \quad (11.6)$$

where  $x$  is the distance from the edge and  $h$  the momentary height, can be used with reasonable accuracy to calculate  $\sigma_{z,\max}$  in the form

$$\sigma_{z,\max} = -\sigma_f \left( 1 + 2\mu \frac{b}{s} \right) \quad (11.7)$$

Since aside from determining  $\sigma_f$ , problems arise mainly in the choice of a suitable value for the coefficient of friction, Stöter [11.33] has derived the equation

$$\sigma_{z,\max} = -\sigma_f \left( 1 + 0.92 \frac{b}{s} \right) \quad (11.8)$$

This equation has been indirectly confirmed by the work of Voelkner who used the slip-line theory. There is excellent agreement between the elementary Siebel equation (Eq. 11.7) and the slip-line theory for the relationship of  $\sigma_z/\sigma_f$  to  $b/s$  for coefficients of friction of 0.25 and 0.5 [11.46]. In this connection it should be pointed out that the excess of material displaced from the die land into a flash gutter increases the stresses  $\sigma_r$  and  $\sigma_z$  by superposition of radial compressive stress caused by cooling down and shrinking of the flash. For the cases shown in Fig. 11.46b and c Voelkner gives  $\sigma_{z,\min} = 1.28\sigma_f$  and  $2.85\sigma_f$ , respectively. These values are for plain-strain deformation only. However, in the cases illustrated in Fig. 11.46 b and c which predominate in prac-

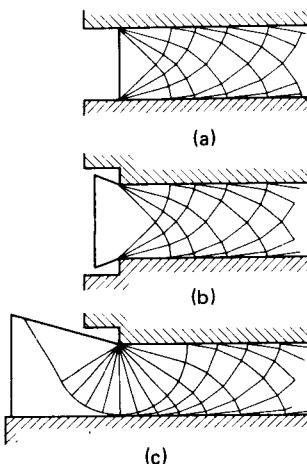


**FIG. 11.46** Slip-line fields for different shapes of flash. Shear stress due to friction  $\tau_{FR}$  equals shear flow stress  $k$ . (a) Die without flash gutter. (b) Die with two-sided flash gutter. (c) Die with one-sided flash gutter. (After [11.46].)

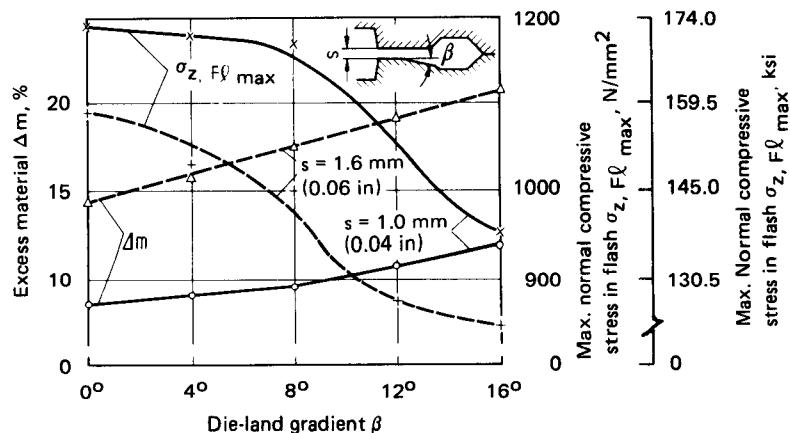


**FIG. 11.47** Excess material  $\Delta m$  and maximum normal compressive stress in the flash for different wedge-shaped flash gutters of angle of inclination  $\beta$  (After [11.36].)

tice, values of  $\sigma_{r,\min} > 0$  and  $\sigma_{z,\min} > \sigma_f$  may occur at the outer edges, which is also shown by example 3 of Fig. 11.40.

According to Vieregge [11.36], these stresses in the part of the flash no longer contained in the flash gap are often reduced by upward bending of the flash ring or by radial cracking. However, no quantitative evidence is given. On the other hand, the same author states that for nonparallel (e.g., wedge-shaped) die land increasing outward in size,  $\sigma_{z,\max}$  decreases, but at the same time the amount of excess material required  $\Delta m$  increases [Fig. 11.47].

By forging a test part with a flange and one-sided protrusion, Stöter has demonstrated that the

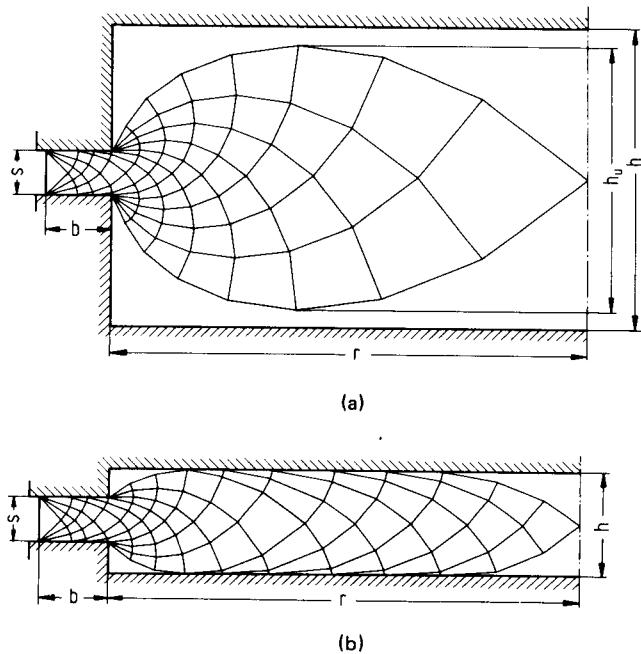


**FIG. 11.48** Slip-line fields in closed-die forging with flash (symmetrical middle flash).  $\tau_{\text{FR}} = k$ ;  $\mu = \mu_{\text{max}}$ . (After [11.46].)

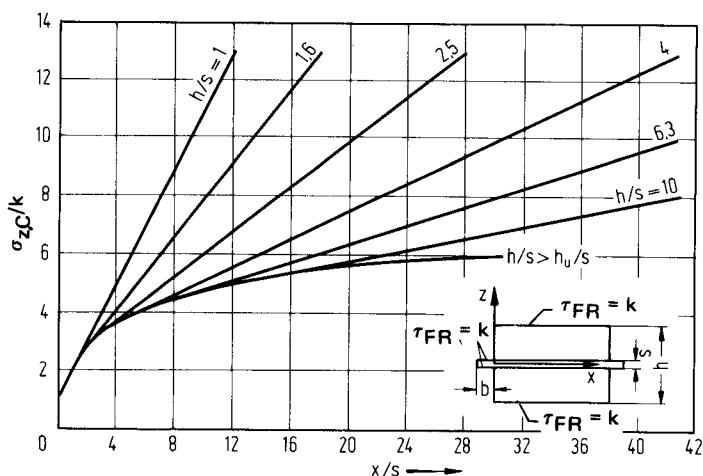


**FIG. 11.49** Normal stresses in forging die cavities under axisymmetrical forging conditions as a function of the relative dimensions of the cavity  $x/s$  and  $h/s$ .  $\tau_{\text{FR}} = k$ ;  $\mu = \mu_{\text{max}}$ . (After [11.46].)

normal stresses  $\sigma_z$  in the die cavity cannot be less than the highest values measured in the die land [11.33]. Quantitative data on the compressive stresses in the die cavity during filling are not available. Since here free areas occur, which are sometimes increasing and sometimes decreasing and on which no normal stresses can impinge (see Figs. 11.30b and 11.31, right side), the compressive stresses are also of secondary importance [11.47]. The situation changes in the last stage of the operation, after the die cavity has been filled with material. At this stage the aim is to achieve the desired height by displacing the remaining excess material into the flash. Visioplastic investigations have shown that the flow of material in closed dies with sufficiently deep cavities occurs either radially in a layer of constant thickness equivalent to or slightly greater than the thickness of the flash, or in a lens-shaped zone (Fig. 11.40); the remaining volume may be considered rigid [11.48] to [11.51]. Slip-line theory also considers large portions of the material filling the die cavity as rigid (Fig. 11.48). Fig. 11.49 shows the normal stresses in the die cavity acting horizontally in the plane of the parting line during axisymmetric deformation. In theory, they are little affected by the amount of friction in the flash. The stresses in the flash  $\sigma_{z,\max}$  must be added to the stress values given in Fig. 11.49 to obtain the total stress  $\sigma_{z,\text{tot}}$  [11.46]:

$$\sigma_{z,\text{tot}} = \sigma_{z,\max} + \sigma_{z,C} \quad (11.9)$$

The effect of temperature and forging rate on the coefficient of friction  $\mu$  and the flow stress  $\sigma_f$  was long neglected. According to Stöter [11.33], one of the most important factors here is the pressure time  $t_C$ , that is, the time during which contact between the die and the forging is maintained under the force of deformation. The following are typical values for  $t_C$ :

Forging tool and speed	Pressure time $t_p$ , ms
High-speed hammers, $v_{\text{Top}} \approx 16 \text{ m/s}$ (48 ft/s)	0.5–5
Drop-forging hammer, $v_{\text{Top}} \approx 6 \text{ m/s}$ (18 ft/s)	1–10
Crank presses	20–100
Friction screw presses, $v_R \approx 0.5 \text{ m/s}$ (1.5 ft/s)	50–150
Hydraulic presses, $v_R \approx 0.1 \text{ m/s}$ (0.3 ft/s)	250–500

During the pressure contact time  $t_C$  the flash cools down at a rate increasing with the time  $t_C$  and the ratio  $b/s$  or the absolute values of  $b$  and  $s$ . During this time heat is supplied to the flash as a result of friction and forging work. Thus the mean flash temperature is given by

$$\bar{T}_{\text{FI}} = \bar{T}_{\text{FI}}^* + \Delta T_w + \Delta T_{\text{FR}} \quad (11.10)$$

According to Altan and Nagpal [11.47], the mean flash temperature  $\bar{T}_{\text{FI}}^*$  due to cooling at the surfaces in contact with the die may be calculated for any given moment by the equation

$$\bar{T}_{\text{FI}}^* = T_D + (T_{\text{FI}0} - T_D) \exp \left( -\frac{2\alpha t_C b}{c\rho b^* s^*} \right) \quad (11.11a)$$

where  $\alpha$  is the coefficient of heat transfer,  $c$  the mean specific heat, and  $\rho$  the density. For carbon steels at temperatures of 1000 and 1100°C (1832 and 2012°F) in contact with hot-working tool steels, the coefficients of heat transfer during  $t_C$  have been determined experimentally as follows:  $\alpha \geq 17$  and  $14 \text{ kW/m}^2 \cdot ^\circ\text{C}$  (14.6 and  $12 \text{ ft-lbf/s} \cdot \text{in}^2 \cdot ^\circ\text{F}$ ) respectively, at  $p = 55\text{--}80 \text{ N/mm}^2$  ( $8.0\text{--}11.6 \text{ ksi}$ ) [11.52]; and at  $p = 120\text{--}400 \text{ N/mm}^2$  ( $17.4\text{--}58.0 \text{ ksi}$ ),  $\alpha = 5.6\text{--}6.8 \text{ kW/m}^2 \cdot ^\circ\text{C}$  ( $4.82\text{--}5.85 \text{ ft-lbf/s} \cdot \text{in}^2 \cdot ^\circ\text{F}$ ) [11.53].\* At the end of the forging operation  $s^* = s$ . It follows that

\*The differences can be explained partly by the fact that in [11.52] the contact time  $t_C$  under pressure was taken into account, while in [11.53] it was not. Also the real contact area will increase by microplastic deformation of the tool surface, which may lead to an increased heat flow  $\alpha$ . On the other hand, above 1000–1100°C (1832–2012°F) the insulation effect of increasing oxide layers decreases the heat flux. As a result, for  $T = 1200^\circ\text{C}$  (2192°F) the heat flux between carbon steel and hot-working tool steel will tend to  $8 \leq \alpha \leq 20 \text{ kW/m}^2 \cdot ^\circ\text{C}$  ( $6.9 \leq \alpha \leq 17.2 \text{ ft-lbf/s} \cdot \text{in}^2 \cdot ^\circ\text{F}$ ) for  $t_C$  between 20 and 170 ms. This shows the strong influence of surface microstructure. For the heat flux between AlMgSi (AA6061) and hot-working tool steel, however, good coincidence between the two authors [11.53] and [11.54] was found with  $6.7 \leq \alpha \leq 7.9 \text{ kW/m}^2 \cdot ^\circ\text{C}$  ( $5.8 \leq \alpha \leq 6.8 \text{ ft-lbf/s} \cdot \text{in}^2 \cdot ^\circ\text{F}$ ) and  $2.8 \leq \alpha \leq 8 \text{ kW/m}^2 \cdot ^\circ\text{C}$  ( $2.4 \leq \alpha \leq 6.9 \text{ ft-lbf/s} \cdot \text{in}^2 \cdot ^\circ\text{F}$ ) for dry surfaces with peak-to-valley heights of between 10 and 80  $\mu\text{m}$  (390 and 3180  $\mu\text{in}$ ).

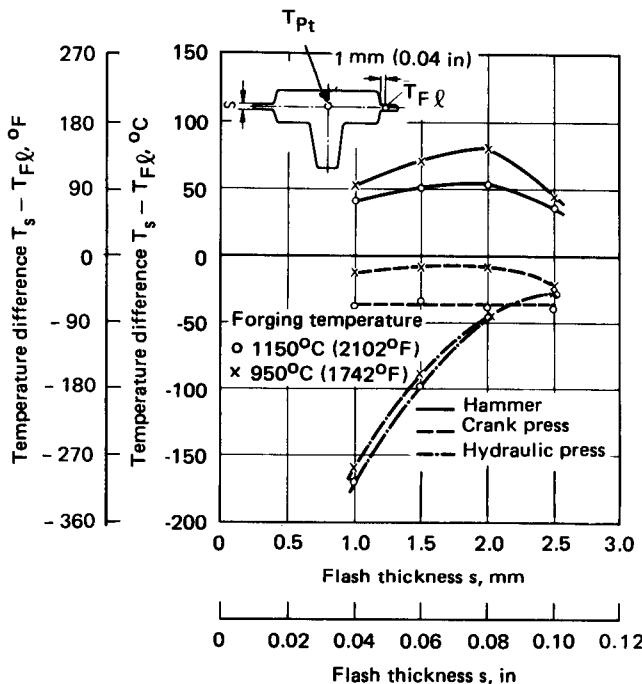


FIG. 11.50 Difference between the temperature of the forged part  $T_{Pt}$  and the mean temperature of the flash  $\bar{T}_{Fl}$ . (After [11.52].)

$$\bar{T}_{Fl}^{\circ} = T_D + (T_{Fl0} - T_D) \exp\left(-\frac{2\alpha t_C b}{cpb^* s}\right) \quad (11.11b)$$

$\bar{T}_{Fl}$  can be calculated when  $\Delta T_w$  and  $\Delta T_{Fr}$  are known. Here the following equations may be used:

$$\Delta T_w = \frac{\sigma_{f,m}\varphi}{cp} \quad (11.12)$$

$$\Delta T_{Fr} = \frac{\tau_{Fr} r A_{p,Fr} t_C}{Vcp} \quad (11.13)$$

Since the results are relatively uncertain, in part because of insufficient knowledge of material and process data, it is expedient to make use of experimental data. Fig. 11.50 contains information concerning the temperature difference  $T_{Pt} - \bar{T}_{Fl}$ . The effect of flash thickness and pressure contact time is clearly evident; the actual forging temperature is of little significance over the ranges considered. Only for very large values of  $t_C$  (as with hydraulic presses) and for very small thicknesses  $s$  does the flash cool down considerably. Otherwise its mean temperature remains roughly constant or may even increase. Individual temperatures in the flash, of course, may vary from the calculated or measured values depending on the specific values of  $\epsilon$ ,  $\epsilon$ ,  $\mu$ , and  $\sigma_z$  [since  $\alpha = f(\sigma_z)$ ].

When calculating  $\sigma_{z,max}$  in the die land, the effect of temperature may be taken into account by choosing the appropriate flow stress  $\sigma_f$  corresponding to  $\bar{T}_{Fl}$  on the flow curve. The best approach is described later in this section. Information about the effect of temperature on the coefficient of friction  $\mu$  is still very patchy.

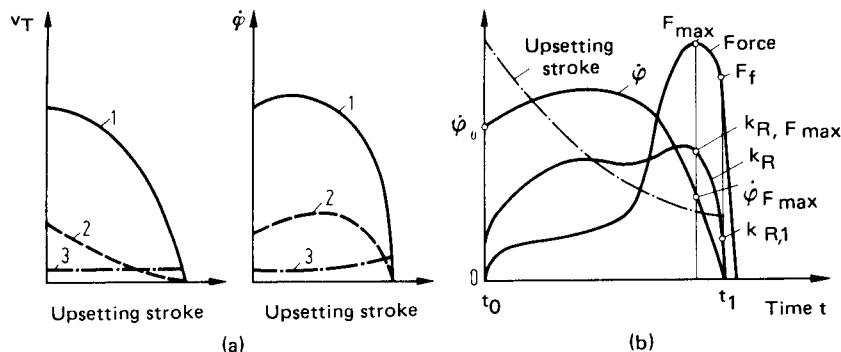


FIG. 11.51 Effect of tool speed on strain rate, deformation force, and deformation resistance. (a) Tool speed  $v_T$  and strain rate  $\dot{\phi}$  of a hammer (1), a crank press (2), and a hydraulic press (3). (b) Upsetting operation in a horizontal upsetting machine. (After [11.57].)

For steel workpiece material the coefficient of friction seems to increase with temperature. This, however, has only been proved for the case of workpieces forged at different temperatures  $T_{p,i}$  and is probably due to oxidation being a function of temperature (according to [11.55]). Circular upsetting experiments carried out in an inert atmosphere and using different lubricants, with the initial part temperature ranging between room temperature and  $830^\circ\text{C}$  ( $1526^\circ\text{F}$ ), have shown that the coefficient of friction depends closely on the mean lubricant gap temperature of  $47$ – $74^\circ\text{C}$  ( $117$ – $133^\circ\text{F}$ ) [11.56]. Whether the coefficient of friction also varies with  $\bar{T}_{f1}$  during the operation, after material has already entered the die land, is still an open question. At least in the case of hammers and fixed-stroke mechanical presses,  $\mu$  should not vary appreciably since the temperature varies little, and thus Eq. 11.8 remains valid.

According to Meyer [11.57], stresses and forces in general do not increase with falling temperature to the same extent as the theoretical increase in flow stress  $\sigma_f$  would lead one to expect. The reason for this is the strong decrease in the strain rate  $\dot{\phi}$  near the end of the operation; at this stage  $\dot{\phi}$  approaches zero (Fig. 11.51). These conditions are valid for open-die forging and do not necessarily apply to closed-die forging. The amount of cooling is affected by the size of the workpiece, its shape, and by the temperature of the tool, all of which should be taken into account when making comparisons. Thus in model experiments the relationships valid for cold forming, namely, that forces are proportional to areas and work is proportional to volume, no longer apply for warm working [11.58].

The estimation or calculation of the forces occurring in closed-die forging with flash may be performed in several different ways, all based on the determination of the maximum values. Fig. 11.52 shows the considerable increase in force toward the end of the operation due to cooling of the workpiece, increasing amounts of flash, and thus the increasing size of the compressed surface. The simplest empirical relationship for calculating the force at the end of the forging operation is shown in the following equation.

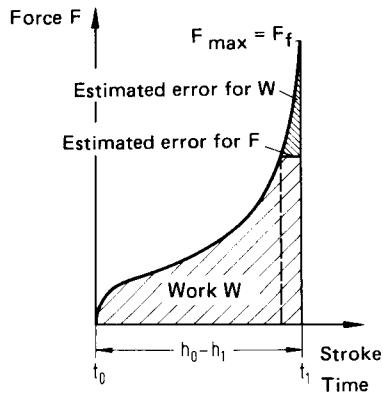


FIG. 11.52 Force-stroke diagram for closed-die forging with flash. (After [11.59].)

$$F_f \approx F_{\max} = A_p k_{R,1} \quad (11.14)$$

$A_p = A_R + A_{p,F}$  is at a right angle to the direction of action of the force, as shown in Fig. 11.40, and  $k_{R,1}$  is the deformation resistance (i.e., the mean normal stress  $\sigma_{z,m}$  over the entire area of die cavity and land) at the end of the operation. It is several times higher than  $\sigma_{f,0}$  (the flow stress at the beginning of the operation).  $k_{R,1}$  can be determined for particular part shapes and forging machines. Fig. 11.53a shows the results of such experiments where  $k_{R,1} \approx k_{R,F,\max}$ , based on the mean final height of the forged part

$$\bar{h}_f = \frac{m}{A_p \rho} \quad (11.15)$$

(According to Fig. 11.51b small variations may occur.)

The shape of the part corresponds to category 2 or 3 of the Spies shape classification [11.61]. The effect of shape complexity is demonstrated by the two boundary curves shown in Fig. 11.53a [11.62].

Another approximate method of calculating  $F_f$  that is much used in practice is based on the formula for determining the change in normal stress in the die land (Eqs. 11.7 and 11.8). Here  $\sigma_{z,\max}$  is determined as in Fig. 11.40, and this value is then taken to be the normal compressive stress acting evenly over the entire area  $A_p$ . Thus

$$F_f \approx F_{\max} = A_p \sigma_{z,\max} \quad (11.16)$$

The error due to neglecting the higher normal pressure in the die cavity (see Fig. 11.49) is counteracted in part by the fact that  $\sigma_{z,\max}$  is considered to act up to the edge of the die land [11.59]. The main problem here is how to determine the "correct" value of  $\sigma_f = \sigma_{f,1}$ , which cannot be estimated exactly. The following approach is recommended:

- 1 Estimate the temperature of the flash material near the end of forging based on Eqs. 11.10–11.13 and Fig. 11.50.
- 2 Determine  $\sigma_f$  for this temperature, taking into account the maximum strain rate  $\dot{\varphi}_{F,\max}$  (Fig. 11.51).
- 3 Calculate  $\sigma_{z,\max}$  using Eq. 11.8 after selection of the die-land ration  $b/s$ .

Step 1 causes the greatest difficulties. It is also not easy to determine  $\sigma_f$  in step 2, although  $\dot{\varphi}_{F,\max}$  certainly lies below  $\dot{\varphi}_0$ . With hammers  $\dot{\varphi}_{F,\max} \leq \dot{\varphi}_0/2$ ; with crank presses  $\dot{\varphi}_{F,\max} \leq \dot{\varphi}_0/3$ . As is well known,  $\dot{\varphi}_0$  can be determined quite accurately from the tool speed at contact  $v_{T,0}$  and the initial height  $h_0$ . On the whole, an estimate of  $\sigma_{f,1}$  to within about 15% may be considered good.

Another very promising way of calculating the forces in closed-die forging is the upper-bound method [11.50], [11.59] (see also Chap. 5). Here one assumes, for example, that material motion takes place in one "disk" of flash thickness  $s$ . Between this disk and the neighboring rigid material shearing exists, that is,  $\tau = k$ , while in the flash gap either sliding ( $\tau_{FR} < k$ ) or likewise shearing (sticking friction,  $\tau_{FR} = k$ ) is assumed. Thus three components exist (Fig. 11.54):

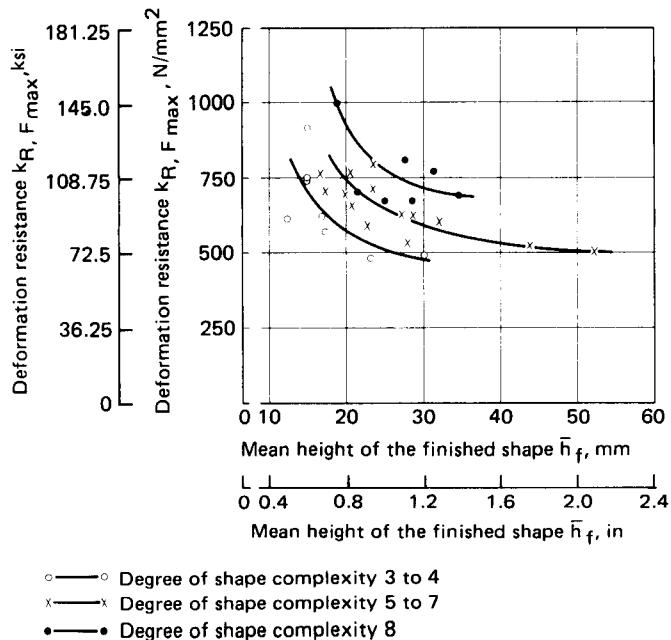
Deformation power  $P_{\text{def}}$  in area 1     $asl$  or  $a^2 s \pi / 4$

Shear power  $P_S$  in area 2                  Boundary surfaces  $BB'$  and  $CC'$

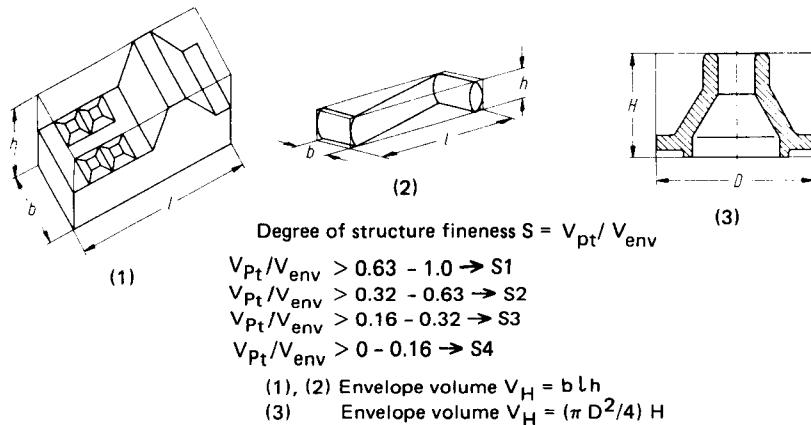
Friction power  $P_{\text{FR}}$  in area 3                  Friction surfaces  $AB$ ,  $A'B'$  and  $CD$ ,  $C'D'$

In calculating the final force, the shape of the die cavity is of minor significance. More important are the width of the die cavity  $b_C$  or its diameter  $d_C$ , the flash thickness  $s$ , and the distance  $a$  between the outer edges of the flash or die land. For the plane-strain state, with length of cavity  $l$  and uniform cavity cross section  $\gg b_C$ , the following relationship is given in [11.50] using the von Mises flow criterion,

$$F_{\max} = \sigma_{f,1} l \left[ \frac{2}{\sqrt{3}} \alpha + \frac{b_C^2}{2\sqrt{3}s} + \frac{\mu}{2s} (a^2 - b_C^2) \right] \quad (11.17a)$$



(a)



(b)

**FIG. 11.53** Effect of the mean height of the final shape  $h_{mf}$  on the resistance to deformation  $k_{R,F_{\max}}$  for unalloyed steels at about 1100°C. (Fig. 11.53a.) The degree of difficulty posed by a particular shape is given by the assessment numbers for complexity  $S$  (see Fig. 11.53b) and shape. (See classification in Fig. 11.70.) Complexity S1—1 point; S2—2 points; etc.; shapes 101–104, 211–213—1 point; 214–224, 311–312, 321—2 points; 225, 313–315—3 points; 322–325, 331–335—4 points. ≤ 4 points—few difficulties; 5–7 points—moderately difficult; 8 points—very difficult. (After [11.60].)

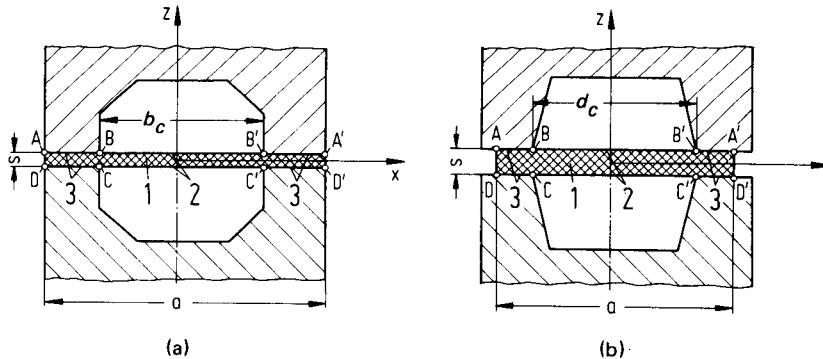


**FIG. 11.54** Assumed cross sections of die cavity for calculations based on the upper-bound method.

or using the Tresca flow criterion,

$$F_{\max} = \sigma_{f,1} l \left[ a + \frac{b_c^2}{4s} + \frac{\mu}{2s} (a^2 - b_c^2) \right] \quad (11.17b)$$

For rotational symmetry the final force  $F_{\max}$ , also according to [11.50], is given by the von Mises flow criterion as

$$F_{\max} = \sigma_{f,1} \pi \left[ \frac{a^2}{4} + \frac{d_c^3}{12\sqrt{3}s} + \frac{2}{3} \mu (a^3 - d_c^3)/8s \right] \quad (11.18a)$$

and by the Tresca flow criterion\* (see also [11.59]) as

$$F_{\max} = \sigma_{f,1} \pi \left[ \frac{a^2}{4} + \frac{d_c^3}{24s} + \frac{\mu(a^3 - d_c^3)}{12s} \right] \quad (11.18b)$$

Besides the difficulty of estimating the correct value of  $\sigma_f$ , the choice of the coefficient of friction  $\mu$  also presents problems. It lies in the range of  $0.3 < \mu < 0.5$  (or 0.577).† Comparisons of calculated results and measurements of known flow stresses have shown very good agreement. Conditions are more complicated in the case of nonrotational and simple flat parts. In the case of simple geometries it is possible, according to Steck and Schmid [11.50], to determine, with a reasonable amount of calculation, not only the maximum force  $F_{\max}$  but also the progression of the total force  $F_{\text{tot}} = F_{\text{def}} + F_S + F_{\text{FR}}$  and its component forces over the entire forging stroke.

The tool speed may affect not only the material flow but also the work done and the forces in both the die cavity and the die land. According to Wallace and Schey [11.63], by increasing the tool speed from  $v_T = 12.5 \text{ mm/s}$  (0.5 in/s) (with presses) to  $8 \text{ m/s}$  (320 in/s) (with hammers) the total force  $F_{\text{tot}}$  increases by 25%. The flash force, however, does not increase, but in fact decreases slightly. Thus the rise in the overall force requirement is due to increased forging work in the die cavity. These considerations may in some cases affect the results calculated by the upper-bound method. For the sake of completeness it should also be mentioned that in the case of very rapid deceleration, inertial forces which according to experiments by Ecker [11.64] are undetectable in the axial direction at  $a \approx -60 \times 10^3 \text{ g}$  ( $g$  being the acceleration due to gravity) can also affect material flow and forging force. Radial inertial forces may, for example, impede rising.

The well-known methods of calculating forging work  $W$  during closed-die forging with flash are all based on Siebel's equation

\*To calculate the sliding friction stress  $\tau_{\text{FR}}$  it is assumed that the normal stress acting on the surfaces of the flash is  $\sigma_z = \sigma_f$ . This is certainly too low because of the increase away from the edge. The error can in part be compensated for by choosing a relatively high value for the coefficient of friction.

†According to selected yield criterion.

$$W = V \varphi_{\max} k_{R,m} \quad (11.19)$$

where the mean deformation resistance  $k_{R,m} = F/A$  (averaged over the operation) is determined from  $\sigma_{f,m}/\eta_{def}$ . Here both  $\varphi_{\max}$  and  $k_{R,m}$  are difficult to estimate because of workpiece geometry. In upsetting operations with nonplane tools a first approximation for  $\varphi_{\max}$  is given by

$$\varphi_{\max} = \ln \frac{\bar{h}_t}{h_i} = \ln \left( \frac{\text{mean height of final shape}}{\text{initial height of slug}} \right) \quad (11.20)$$

and because of constant mass,

$$\varphi_{\max} = \ln \left( \frac{m}{A_t \rho h_i} \right) \quad (11.21)$$

where  $m = \bar{h}_t A_t \rho$ ,  $k_{R,m}$  and  $\eta_{def}$  can be estimated both on the basis of experimental results and empirically. Thus, for example, in upsetting a simple rectangular section in a die without flash  $\eta_{def} \approx 0.75$ . In die forging a horizontal H cross section (also without flash), however,  $\eta_{def}$  is only 0.4. In closed-die forging with flash  $\eta_{def}$  lies between 0.4 and 0.25 and lower in some cases. Figs.

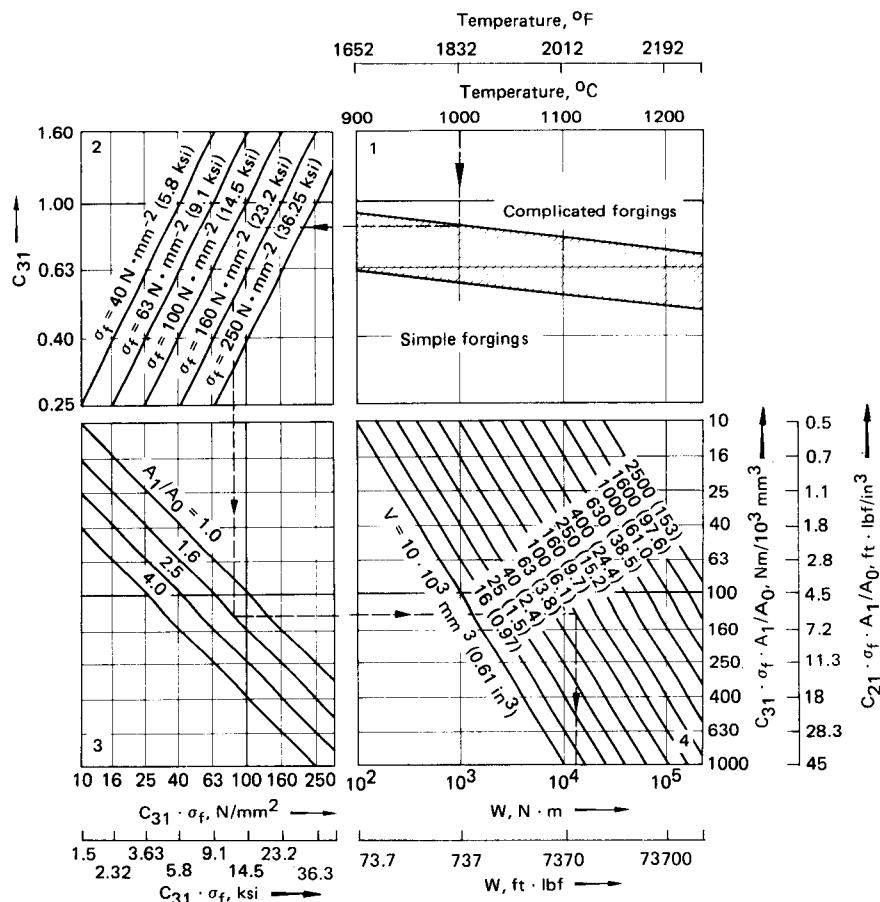


FIG. 11.55 Nomogram for calculating the work  $W$  required for closed-die forging of oblong parts with flash. (Shape category 31 in Fig. 11.70.) Material—carbon and low-alloy steels. (After [11.65].)

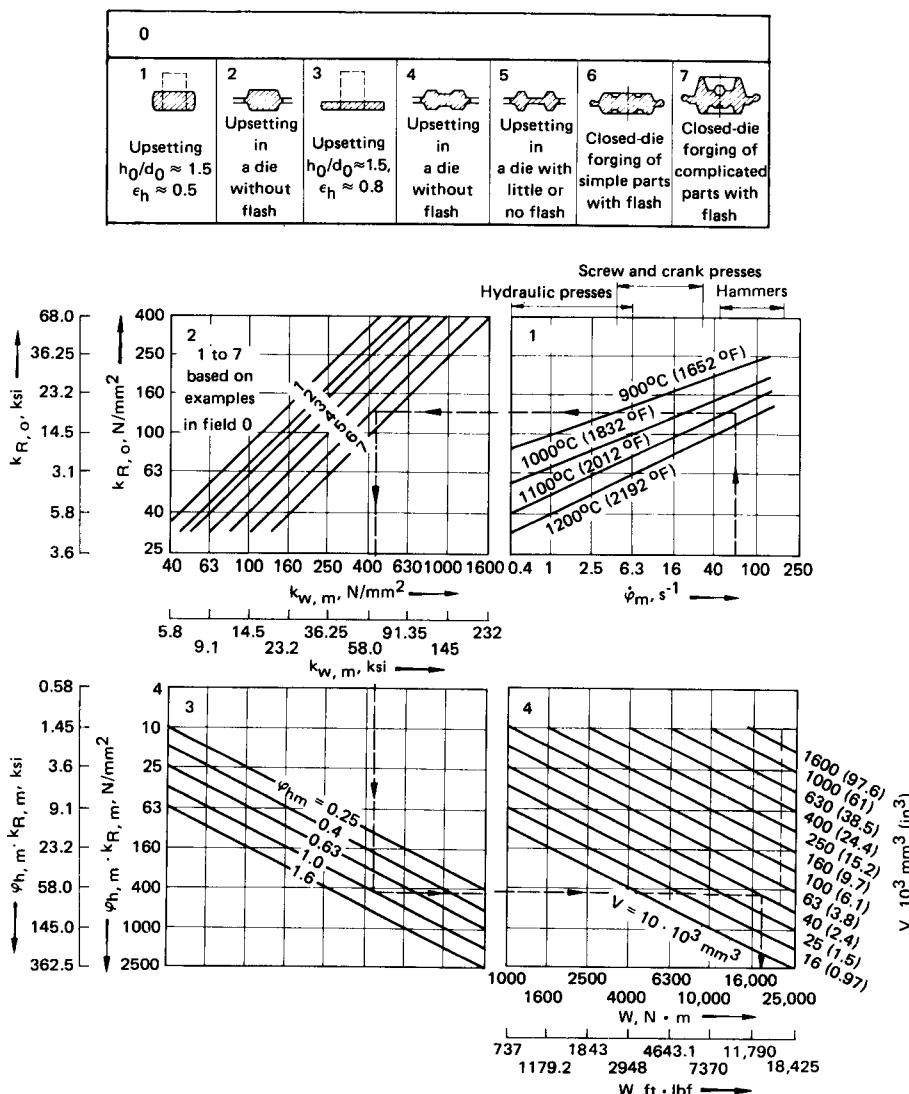


FIG. 11.56 Nomogram for calculating the work  $W$  required for closed-die forging of small circular parts. Material—carbon and low-alloy steels. (After [11.12].)

11.55 and 11.56 present nomograms for calculating the forging work based on the factors outlined above. Fig. 11.55 is valid for long forgings corresponding to class 3 of the Spies shape classification (see Fig. 11.70); Fig. 11.56 applies for the predominantly rotational parts shown.\* Basically it is easier to estimate the forging work  $W$  precisely than to determine the final force  $F_f \approx F_{\max}$ , as may be seen from Fig. 11.52. An error of 30% in the force calculation corresponds to an error of

\*Recent investigations [11.60] have shown the values for forging work given in this diagram to be too high for simple compact parts. However, good concurrence was found for complex shapes in the range  $200 < k_{R,m} < 400 \text{ N/mm}^2$  ( $29 < k_{R,m} < 58 \text{ ksi}$ ).

only 5–10% in the forging work [11.59]. A nomogram for calculating the forces and work during upsetting in horizontal upsetting machines has been published in [11.66].

The reader may find several publications [11.52], [11.53], [11.67], [11.68] helpful in choosing the material and process parameters for use in the equations discussed earlier in this section, in particular with regard to temperature estimation.

### 11.2.3 Surface Finish and Lubrication

Closed-die forged parts exhibit considerable variations in surface structure. This is due to the following factors:

- Surface structure of the tool
- Oxide formation during heating and after forging
- Choice of lubricant
- Localized stresses (normal compressive stress  $\sigma_n$  and friction stress  $\tau_{FR}$ )
- Relative flow rates in the material

The extent to which the *structure of the tool surface* affects the surface of the forged part depends on the other four factors. Smooth tool surfaces are in principle preferable. However, oxidation, frictional wear, and plastic deformation modify the initial surface condition, thus making machining to  $R_t < 5\text{--}10 \mu\text{m}$  (0.2–0.4 mil) uneconomical [11.69]. Three different zones can be identified based on localized conditions (Fig. 11.57):

**Sticking friction zone:** High normal compressive stress  $\sigma_n$ , sticking friction ( $\mu = 0.5$  or  $0.577$ ,  $\tau_{FR} = k$ ), no relative motion between tool and workpiece; “orange-skin”-grained surface

**Sliding friction zone:** Lower normal compressive stress  $\sigma_n$ ,  $\mu \approx 0.3$  (for steel), in some cases high relative speed between tool and workpiece (see Sec. 11.2.2); scored, unidirectional surface structure

**Shear-pressure zone:** Transition zone, between above zones, limited in area, mean normal compressive stress  $\sigma_n$ ,  $\mu$  approaching  $\mu_{max}$ ,  $\tau_{FR}$  less than  $k$ , little relative motion between tool and workpiece; scaly surface with cracks at a right angle to the material motion in the die surface

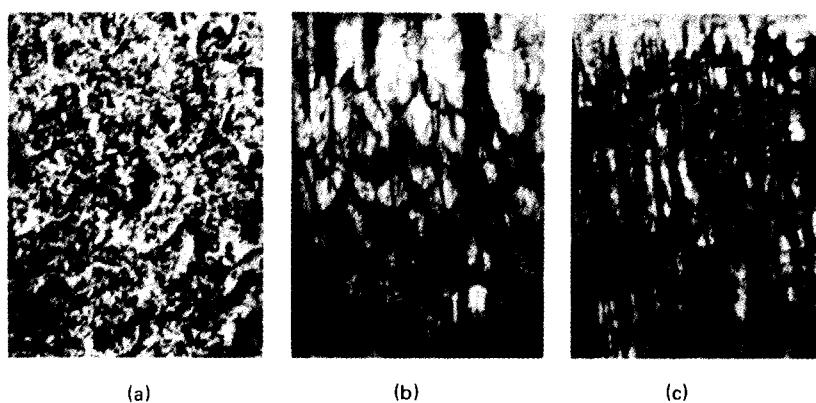


**FIG. 11.57** Surface structure of a forging die cavity used for die pressing of steel with flash at temperatures of 930–1230°C (1706–2246°F). (a) Pressure zone. (b) Shearing pressure zone. (c) Sliding friction zone.

Networklike cracking of the die material caused by thermal loading leads to completely different surface structures (Fig. 11.58). Oxide (scale in the case of steel), lubricant particles, and transition products (e.g., ash) can fill up the smaller cracks and so produce a certain smoothing effect [11.70]. Thin layers of scale on the forging can have a positive effect as a separating layer. Thick layers of scale (e.g., residual primary scale from heating), however, may damage both tool and workpiece surfaces.

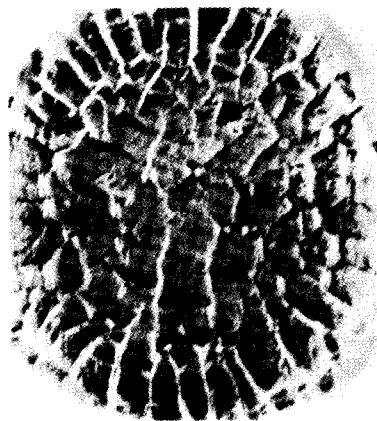


**FIG. 11.58** Surface of a press die for radiator caps after forging 2000 parts. Material—56 NiCrMoV7 ( $\approx$  AISI 6F3);  $S_u \approx 1600 \text{ N/mm}^2$  (232 ksi) (hardened and tempered); part temperature  $1030\text{--}1080^\circ\text{C}$  (1886–1976°F);  $t_C = 120 \text{ ms}$ , cycle time between parts 20 s, die temperature  $\approx 190^\circ\text{C}$  (374°F). (After [11.69].)

Chap. 6) precludes any generally valid conclusions. Furthermore, the high temperatures that accompany chemical and physical reactions often add to the difficulty in interpreting experimental results [11.13].

Most of the experiments have been carried out on cylinders and, to a lesser extent, on rings and flat specimens. Further experimental results concern forging in simple circular dies in which, by measuring the force or the rising height, knowledge has been gained about the effect of lubricants on the coefficient of friction during sliding and, by measuring the ejection force, about their effect on the coefficient of friction during adhesion [11.72], [11.73]. Several hundred lubricants were investigated during the course of this work. Surprisingly a suspension of graphite in water, oil, or grease proved most effective for many materials. Table 11.3 shows the results of studies by Tolkien [11.72] on several common lubricants, including saw dust which is traditionally used in die-forging plants. Lubricants were assessed with respect to their effect on the sliding friction, sticking friction, gas pressure (due to combustion and gasification products), and frictional wear (changes in dimensions due to the abrasion of material particles). Table 11.3 shows that colloidal graphite in water is suitable where problems of forging removal from deep die cavities do not arise. When using graphite, attention must be paid to the effect of ash formation on die wear. On combustion, flaked graphite produces 5–10% ash, which acts like sand paper, whereas amorphous graphite produces 15–40% ash [11.13]. The particle size is also significant. In some cases very small particles are preferable; in others, such as with light alloys, larger particles are preferred. It has also been shown that oxidation layers do not absorb large particles as easily as colloidal graphite.

With graphite as lubricant, for example, with light alloys in the temperature range of 20–600°C (68–1112°F), the coefficient of friction  $\mu$  varies between 0.06 and 0.13, with a maximum value of 0.15 at 300°C (572°F). Other observations during upsetting of flat cylindrical disks with different graphite-based lubricants resulted in coefficients of friction of between 0.06 and 0.16 at die temperatures of 267°C (513°F) and workpiece temperatures of 437°C (819°F). In experi-

ments in the forging surface that are much greater than 20–30  $\mu\text{m}$  (0.8–1.2 mil) may be caused by thick pieces of scale being forced into the surface. They are easily visible after the rest of the scale has been removed, and in the case of machined surfaces they may lead to parts being scrapped. Where a layer of scale has been removed from the metal surface, the latter has an average roughness  $R_t$  of about 15- $\mu\text{m}$  (0.6-mil) peak-to-valley height, measured on the scale that has been removed [11.71]. Furthermore, the surface finish is a function of the mass of the workpiece: larger masses correspond to higher values of surface roughness, that is, for  $m < 0.2 \text{ kg}$  (0.4 lb),  $\rightarrow R_t = 10\text{--}65 \mu\text{m}$  (0.4–2.6 mil); for  $1 \text{ kg}$  (2.2 lb)  $< m < 2 \text{ kg}$  (4.4 lb),  $\rightarrow R_t = 17\text{--}170 \mu\text{m}$  (0.7–6.8 mil). However, the structure and finish of any surfaces formed by heating, forging, and secondary scale formation during cooling are completely transformed by the common mechanical descaling processes (e.g., shot blasting) and tumbling (Fig. 11.59).

Undoubtedly lubricants have a considerable effect on the resulting surface finish in the operations described, especially through their effect on  $\mu$  and  $\tau_{\text{PR}}$ . The highly complex interaction between tool and workpiece (see also

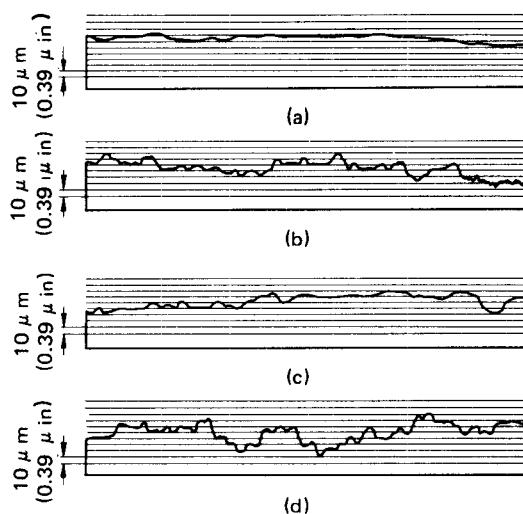


**FIG. 11.59** Surface finishes of die-forged parts. (a) Die. (b) Forged part after removal of scale. (c) Forged part after tumbling. (d) Forged part after blasting with medium-sized shot. (After [11.71].)

ments without lubricants, a coefficient of friction  $\mu = 0.48$  was measured. When brass was lubricated with a graphite emulsion, the coefficient of friction  $\mu \approx 0.06\text{--}0.07$  was measured, as compared with dry friction values  $\mu \approx 0.25\text{--}0.30$  at  $447^\circ\text{C}$  ( $837^\circ\text{F}$ ). Unlubricated titanium and titanium alloys have a coefficient of friction  $\mu = 0.5$  or  $0.577$  over a temperature range of  $280\text{--}980^\circ\text{C}$  ( $536\text{--}1796^\circ\text{F}$ ). Up to about  $730^\circ\text{C}$  ( $1346^\circ\text{F}$ ), graphite and molybdenum disulfide have the effect of reducing these values by  $\Delta\mu = 0.20$  when applied to the tools. In the case of carbon and alloy steels at  $930\text{--}1080^\circ\text{C}$  ( $1796\text{--}1976^\circ\text{F}$ ), the coefficient of sliding friction was  $\mu \approx 0.35\text{--}0.38$ . This was reduced by  $\Delta\mu = 0.12$  when lubricants containing graphite were used [11.13]. Measurements of the coefficient of friction using the ring upsetting test with Ck 45 (AISI 1045) and 16 MnCr5 (AISI 5117) in the mean lubricant gap temperature range of  $20\text{--}750^\circ\text{C}$  ( $68\text{--}1382^\circ\text{F}$ ) [initial test-piece temperature  $\approx 120\text{--}1150^\circ\text{C}$  ( $248\text{--}2102^\circ\text{F}$ )], at  $p_{\max} = 1000 \text{ N/mm}^2$  (145 ksi) in the gap, showed that lubricants containing graphite led to the lowest coefficients of friction (of

**Table 11.3** Effects of Different Lubricants Used in Closed-Die Forging of Steel

Lubricant	Effect on			
	Sliding friction	Static (sticking) friction	Gas pressure	Die wear
Sawdust	4 <sup>a</sup>	4	1	1
3.6% colloidal graphite in water	1	1	5	3
4% colloidal graphite in light oil	3	3	2	2
17% $\text{Na}_2\text{CO}_3$ in water	2	2	3	5

<sup>a</sup>The numbers represent a range from most desirable effect (1) to least desirable effect (5).  
Source: Compiled from [11.72].

the order of  $\mu < 0.05$  over a wide range of temperatures). But for lubricant gap temperatures greater than 550–750°C (1022–1382°F)  $\mu$  often increases rapidly. However, the lubricants continue to act as separating layers. A watery MoS<sub>2</sub>-based lubricant led to higher coefficients of friction [ $\mu_{\min} \approx 0.08$  at about 430°C (806°F)] than a watery graphite emulsion in the same temperature range [11.74]. Mean coefficients of friction  $\mu$  between 0.12 and 0.14 were measured for both graphite and graphite-based pastes at  $p_{\max} = 10\text{--}60 \text{ N/mm}^2$  (1.45–8.7 ksi) [11.52].

In the case of unlubricated stainless steels over the temperature range of 0–1000°C (32–1832°F) coefficients of sticking friction  $\mu = 0.5\text{--}0.577$  exist. The best filling of the die cavity was obtained by using a mixture of sodium-based grease and extra-fine flaked graphite at forging temperatures of 1277°C (2331°F) and die temperatures of 340–600°C (644–1112°F). The value of  $\mu$  was not given [11.13].

### 11.3 FORGING MATERIALS

The materials used for making forged parts are steels (unalloyed, low-alloyed, high-alloyed), nonferrous light metals (aluminum and magnesium and their alloys), nonferrous heavy metals (copper and its alloys, nickel, cobalt, molybdenum, and tungsten and their alloys), titanium and its alloys, beryllium, and other special metals. In addition to metals obtained by smelting, use is also made of sintered metals for smaller workpieces. This latter technique is developing rapidly (see Sec. 11.9). Tables 11.4 to 11.10 list some important examples of materials chosen from the groups mentioned above, mainly on the basis of their practical significance. The tables contain data about composition, areas of application, and forging temperature ranges. Further information may be obtained from the appropriate standards, material sheets, data made available by the metal-producing industry, and from specialist publications [11.24], [11.75] to [11.82]. In particular, the standards of the following U.S. societies may be found useful:

AA	Aluminum Association
AISI	American Iron and Steel Institute
ASM	American Society for Metals
ASTM	American Society for Testing and Materials
CDA	Copper Development Association
SAE	Society of Automotive Engineers

The following DIN standards are also relevant:

DIN 17006	Iron and steel, systematic nomenclature
DIN 17100	General construction steels, quality specifications
DIN 17200	Heat-treatable steels, properties
DIN 17210	Case-hardening steels, quality specifications
DIN 17240	Heat-resistant steels for nuts and bolts, quality specifications
DIN 17440	Stainless steels, quality specifications
DIN 1749	Die-forged parts made of aluminum, strength properties
DIN 9005	Die-forged parts made of magnesium, technical specifications
DIN 17673	Die-forged parts made of copper and copper alloys, strength properties
DIN 17864	Die-forged parts made of titanium (open- and closed-die forged parts)

As a guideline to whether a material is easy or difficult to forge the term *forgeability* is used. Its main function is to give a guide to the amount of deformation that can be tolerated before cracking occurs (see also Chaps. 3, 5, 16, and 28), as well as to flow stresses and temperatures. In the list on p. 11.60, the materials are arranged qualitatively in their order of formability [11.24].

**Table 11.4** Steel Used for Forged Parts

No.	Material designation		Composition, wt%							Typical applications				Forging temperatures, °C / °F)
	DIN	AISI	C	P	S	N	Si	Mn	Cr	Ni	Mo	V	W	
<b>1 General construction steels</b>														
1	UPS37-2	1015	0.22	0.063	0.063	0.009	—	—	—	—	—	—	—	850–1150 (1562–2102)
2	FSt50-2	1015 1031	0.19 0.30	0.055 0.055	0.055 0.008	—	—	—	—	—	—	—	—	850–1100 (1562–2012)
<b>2 Unalloyed tempering steels</b>														
3	C35	1035	0.32–0.40	0.045	0.045	—	0.15–0.35	0.4–0.7	—	—	—	—	—	Housings, hubs, bearing caps, flanges, levers, tie rods, Crankshafts, camshafts, stub axles, steering knuckles, connecting rods, gear wheels, bolts, flywheels
4	C45	1045	0.42–0.5	0.045	0.045	—	0.15–0.35	0.5–0.8	—	—	—	—	—	850–1100 (1562–2012)
<b>2.1 High-grade steels</b>														
5	Ck35	1034	0.32–0.4	0.035	0.035	—	0.15–0.35	0.4–0.7	—	—	—	—	—	As for 3 and 4, but where higher demands exist as to consistency, surface finish, and defects due to inclusions
6	Ck45	1045	0.42–0.5	0.035	0.035	—	0.15–0.35	0.5–0.8	—	—	—	—	—	850–1100 (1562–2012)
<b>2.2 Special steels</b>														
7	34Cr4	5132	0.3–0.37	0.035	0.035	—	0.15–0.35	0.5–0.8	0.9–1.2	—	—	—	—	850–1050 (1562–1922)
8	41Cr4	5135	0.38–0.44	0.035	0.035	—	0.15–0.35	0.5–0.8	0.9–1.2	—	—	—	—	850–1050 (1562–1922)
9	42CrMo4	4140	0.38–0.45	0.035	0.035	—	0.15–0.35	0.5–0.8	0.9–1.2	—	0.15–0.25	—	—	850–1050 (1562–1922)
<b>3 Alloyed tempering steels, special steels</b>														
7	34Cr4	5132	0.3–0.37	0.035	0.035	—	0.15–0.35	0.5–0.8	0.9–1.2	—	—	—	—	850–1050 (1562–1922)
8	41Cr4	5135	0.38–0.44	0.035	0.035	—	0.15–0.35	0.5–0.8	0.9–1.2	—	—	—	—	850–1050 (1562–1922)
9	42CrMo4	4140	0.38–0.45	0.035	0.035	—	0.15–0.35	0.5–0.8	0.9–1.2	—	0.15–0.25	—	—	850–1050 (1562–1922)

**Table 11.4** Steel Used for Forged Parts (Continued)

No.	Material designation	Composition, wt%								Typical applications	Forging temperatures, °C (°F)				
		DIN	ANSI	C	P	S	N	Si	Mn	Cr	Ni	Mo	V	W	
<b>4 Unalloyed case hardening steels</b>															
<b>4.1 High-grade steels</b>															
10	Ck15	1015	0.12–0.18	0.045	0.045	—	0.15–0.35	0.035	0.25–0.5	—	—	—	—	Parts for case hardening, camshafts, steering shafts, gauges, hubs, cams, levers, rollers	850–1150 (1562–2102)
<b>4.2 Special steels</b>															
11	Ck15	1015	0.12–0.18	0.035	0.035	—	0.15–0.35	0.035	0.25–0.5	—	—	—	—	As for 7, but where higher demands exist as to consistency, surface finish, and defects due to inclusions	850–1150 (1562–2102)
<b>5 Alloyed case hardening steels, special steels</b>															
12	15Cr3	5015	0.12–0.18	0.035	0.035	—	0.15–0.35	0.035	0.4–0.6	0.5–0.8	—	—	—	Case-hardened components with high demands on core strength and toughness	850–1150 (1562–2102)
13	16MnCr5	5117	0.14–0.19	0.035	0.035	—	0.25–0.35	0.035	1.0–1.3	0.8–1.1	—	—	—	Gears, gauges, camshafts, drive shafts, connecting rods, steering shafts	850–1100 (1562–2012)
14	15CrNi16	4320	0.12–0.17	0.035	0.035	—	0.15–0.35	0.035	0.4–0.6	1.4–1.7	1.4–1.7	—	—	Highly stressed small gear wheels and shafts	850–1100 (1562–2012)
<b>6 Steels for specific applications</b>															
<b>6.1 Creep-resistant steel</b>															
15	34CrNiMo6	4340	0.3–0.38	0.035	0.035	—	0.15–0.35	0.04–0.7	1.4–1.7	1.4–1.7	0.15–0.25	—	Components requiring high thermal resistance, such as flanges, welded parts	850–1050 (1562–1822)	
16	24CrMoV55	—	0.2–0.28	0.035	0.035	—	0.15–0.35	0.3–0.6	1.2–1.5	0.6	0.5–0.6	0.15–0.25	—	Bolts for superheaters, flanges, turbine blades	850–1050 (1562–1822)

**6.2 Valve steels (mean chemical analysis)**

17	X45SiCr4	—	0.45	0.03	0.03	—	4.0	0.45	2.65	—	—	—	Highly stressed inlet and outlet valves for diesel and gasoline engines	900–1050 (1652–1922)
18	X45CrSi9	MnV3	0.45	0.03	0.03	—	3.0	0.45	9.0	—	—	—	Highly stressed outlet valves	900–1050 (1652–1922)

**6.3 Heat-resistant steels (mean chemical analysis)**

19	X10CrAl13	Type 405	0.12	—	—	—	1.2	0.06	13.0	—	A1: 1.0	—	Support and conveyor parts, heat resistant components for boilers and process plant	850–1100 (1562–2012)
----	-----------	----------	------	---	---	---	-----	------	------	---	---------	---	---	----------------------

**6.4 Stainless steels**

20	X15Cr13	410	0.12–0.17	—	—	—	1.0	1.0	12.0–14.0	—	—	—	Structural components of all kinds, turbine blades, and impellers	750–1150 (1382–2102)
21	X12CrNi18.8	302	0.12	—	—	—	1.0	2.0	17–19	8–10	—	—	Equipment for the food industry, surgical instruments	750–1150 (1382–2102)

**6.5 Martensitic steels (mean chemical analysis)**

22	15Ni7.0Mo Grade 250	—	0.026	max 0.01	—	max 0.1	max 0.1	—	18.5	4.5	C: 0.70	Ti: 0.4	Housings for rocket engines, aircraft, and undercarriage components, gun barrels	1092–1262 (1998–204)
----	------------------------	---	-------	----------	---	---------	---------	---	------	-----	---------	---------	--	----------------------

**Table 11.5** Aluminum Alloys Used for Forged Parts (After DIN 1712, Sheet 3, and DIN 1725, Sheet 1)

No.	DIN	AA	Composition, wt %			Typical applications	Minimum, °C (°F)	Optimum, °C (°F)
			Alloying elements, %	Permissible additional elements, %				
1	Al99.5	1050 0		Si: 0.30 Fe: 0.40 Ti: 0.05 Cu: 0.05 Zn: 0.07 Others: 0.03 each	0.5 in total	Forged components for electrical engineering applications	350 (662)	480–550 (896–1022)
2	AlMg3	5754	Mg: 2.6–3.4 Mn: 0–0.5 Cr: 0–0.3 Remainder: Al	Si: 0.40 Fe: 0.40 Cu: 0.05 Zn: 0.20 Ti: 0.10 Others: 0.05 each	0.15 in total	Forged components for aerospace-industry, pressure vessels	320 (608)	350–420 (662–788)
3	AlMgSi1	6061	Mg: 0.6–1.2 Si: 0.75–1.3 Mn: 0.4–1.0	Fe: 0.50 Cu: 0.10 Zn: 0.20		Forged components for automobile industry	400 (752)	460–520 (860–968)

4	<b>AlCuMg1</b>	2017	Cr: 0-0.3 Al: 3.5-4.5 Mg: 0.4-1.0 Mn: 0.3-1.0 Al: 0.20	Ti: 0.10 Others: 0.05 each Si: 0.60 Fe: 0.50 Cr: 0.10 Zn: 0.50 Ti: 0.20 Others: 0.05 each	Forged components for automobile aerospace industries	360 (680)	400-450 (752-842)
5	<b>AlCuSiMn</b>	2014	Cu: 3.9-5.0 Si: 0.5-1.2 Mn: 0.4-1.2 Mg: 0.2-0.8 Al: 0.20	Fe: 0.70 Cr: 0.10 Zn: 0.25 Ti: 0.15 Others: 0.05 each	General highly stressed forged components, propeller blades	372-482 (702-900)	
6	<b>AlZnMg1</b>	7020	Zn: 4.0-5.0 Mg: 1.0-1.4 Mn: 0.1-0.5 Cr: 0.1-0.25 Ti: 0.01-0.2 Al: 0.20	Si: 0.50 Fe: 0.50 Cr: 0.10 Others: 0.05 each 0.15 in total Al: 0.20	Highly stressed aircraft components, forged components for military applications	500-510 (932-950)	

**Table 11.6** Magnesium Alloys Used for Forged Parts (After DIN 1729, Sheet 1)

No.	Material designation		Composition, wt%		Typical applications	Minimum, °C (°F)	Optimum, °C (°F)	Forging temperature
	DIN	UNS	Alloying elements, %	Permissible additional elements, %				
1	Mg Al3Zn	M11311	Al: 2.5–3.5 Zn: 05–1.5 Mn: 0.15–0.4 Remainder: Mg	Si: 0.1 Ca: 0.1 Fe: 0.03 Ni: 0.005 Cd: 0.04 Others: 0.1 in total	Medium mechanically stressed components with still good chemical resistance	250 (482)	270–350 (518–662)	
2	Mg Al6Zn	M11610	Al: 5.5–7.0 Zn: 0.5–1.5 Mn: 0.15–0.4 Remainder: Mg	Si: 0.1 Cu: 0.1 0.1 Fe: 0.03 Ni: 0.005 Others: 0.1 in total	Medium to high mechanically stressed components	250 (482)	270–350 (518–662)	
3	Mg Al8Zn	M11800	Al: 7.8–9.2 Zn: 0.2–0.8 Mn: 0.12–0.3 Remainder: Mg	Si: 0.1 Cu: 0.05 Fe: 0.005 Others: 0.3 in total 0.3 in total	High mechanically stressed components	—	287–412 (549–774)	
4	Mg Zn6Zr	M16600	Zn: 4.8–6.2 Zr: 0.45–0.8 Remainder: Mg	Others: 0.3 in total 0.3 in total	High mechanically stressed components	—	317–400 (603–752)	

**Table 11.7** Copper Alloys Used for Forged Parts (After DIN 1787, 17660, 17664, 17665, 17666)

No.	Material designation DIN	UNS	Composition, wt %			Typical applications	Minimum, °C (°F)	Optimum, °C (°F)
			Alloying elements, %	Permissible additional elements, %				
1	SF Cu	C12200	Cu: 99.90 at least			Forged parts for electrical engineering industry, components used in plant engineering Fittings and fixtures	500 (932)	800–900 (1472–1652)
2	CuZn 40	C28000	Cu: 59.5–61.5 Remainder: Zn	Al: Fe: Mn: Ni: Pb: Sb: Sn:	0.05 0.3 0.1 0.3 0.5 0.01 0.2		500 (932)	700–800 (1292–1472)
3	CuZn40Ni	—	Cu: 56.0–58.0 Ni: 1.0–2.0 Mn: 0.5–1.0 Remainder: Zn	Others: 0.2 in total Fe: Sn: Al: Pb: Si:	0–1.0 0–0.5 0.1 0.5 0.1	Ship building, general plant engineering, especially refrigerating plant	—	—
4	CuAl9Mn	—	Cu: 86.5–90.0 Al: 7.7–9.7 Mn: 1.5–3.0	Others: 0.5 in total Fe: Ni: Pb: Si: Sn: Zn:	0–1.0 0–0.8 0.02 0.2 0.2 0.5	Highly stressed bearing components, gears and worm wheels, valve seats	—	—
5	CuAl11Ni	C63200	Cu: 74.0–78.5 Al: 10.5–12.5 Ni: 5.0–7.5 Fe: 4.8–7.3	Mn: Pb: Si: Sn: Zn: Others: 0.3 in total	0–1.5 0.05 0.2 0.2 0.5 Others: 0.3 in total	High-strength construction parts, highly stressed bearing components, valves, valve seats, components subject to wear	—	—

**Table 11.8** Titanium Alloys Used for Forged Parts (After DIN 17850, 17851)

No.	Material designation		Composition, wt. %		Typical applications	Forging temperature, °C (°F)	
	DIN	US	Alloying elements, %	Permissible additional elements, %			
1	Titanium	Unalloyed	Remainder: Ti	Fe: 0.2–max 0.35 C: 0.08–max 0.10 N: 0.05–max 0.07 O: 0.10–max 0.30 H: max 0.013	Corrosion-resistant fittings, container cladding, pump manufacture	Intermediate shapes Final shapes Max. finish-forging temperature, depending on degree of purity	850–900 (1562–1652) 700–800 (1292–1472)
2	Ti Al5Sn2 α-alloy	Ti–5Al–25Sn	Al: 4.0–6.0 Sn: 2.0–3.0 Remainder: Ti	Fe: 0.50 C: 0.08 N: 0.05 O: 0.20 H: 0.013	Propulsion units, air frames, rocket and space applications, fittings and plants	Intermediate shapes Final shapes Max. finish-forging temperature	785–850 (1445–1562) 842–1037 (1548–1899) 817–1022 (1503–1872)
3	Ti Al8Mo1V1 α-alloy	Ti–8Al–1Mo–1V	Al: 7.5–8.5 Mo: 0.75–1.25 V: 0.75–1.25 Remainder: Ti	Fe: 0.30 C: 0.08 N: 0.05 O: 0.12 H: 0.013	Aircraft and propulsion unit manufacture	Intermediate shapes Final shapes Max. finish-forging temperature	927–1012 (1700–1854) 927–982 (1700–1800)
4	Ti Al6Sn2Zr4Mo2 α-alloy	Ti–6Al–2Sn–4Zr–2Mo	Al: 5.5–6.5 Sn: 1.8–2.2	Fe: 0.25 C: 0.05	Propulsion unit manufacture, creep-	Intermediate shapes Max. finish-forging	913–968 (1675–1774) 1010 (1850)

		Zr: 3.6-4.4 Mo: 1.8-2.2 Remainder: Ti	N: 0.05 O: 0.12 H: 0.013	resistant components, highest-temperature- resistant titanium alloy	temperature	952 (1746)	
5	TiAl6V4 $\alpha + \beta$ alloy	Ti-6Al-4V	Al: 5.5-6.75 V: 3.5-4.5 Remainder: Ti	Fe: 0.30 C: 0.08 N: 0.05 O: 0.20 H: 0.013	Much used titanium alloy, creep-resistant forged components for aerospace, instrumentation, and measurement	Intermediate shapes Final shapes Max. finish-forging temperature	950-1000 (1742-1832) 750-900 (1382-1652) 970 (1778)
6	TiAl7Mo4 $\alpha + \beta$ alloy	Ti-7Al-4Mo	Al: 6.5-7.3 Mo: 3.5-4.5 Remainder: Ti	Fe: 0.25 C: 0.08 N: 0.05 (O: 0.30) H: 0.0125	Fittings and fixtures Aerospace, instrumentation, and measurement applications, fittings	Intermediate shapes Final shapes Max. finish-forging temperature	842-952 (1548-1746) 817-927 (1503-1700) 985 (1805)
7	TiAl6V6Sn2 $\alpha + \beta$ alloy	Ti-6Al-6V- 2Sn	Al: 5.0-6.0 V: 5.0-6.0 Sn: 1.5-2.5 Cu: 0.35-1.0 Remainder: Ti	Fe: 0.35-1.0 C: 0.05 N: 0.04 (O: 0.20) H: 0.013	Aerospace, instrumentation, and measurement applications, fittings	Intermediate shapes Max. finish-forging temperature	880-950 (1616-1742) 887 (1647)
8	TiV13Cr11Al3 $\beta$ -alloy	Ti-3Al-13V- 11Cr	V: 12.5-14.5 Cr: 10.0-11.0 Al: 2.5-3.5 Remainder: Ti	C: 0.05 N: 0.08 (O: 0.20) H: 0.025	Rocket technology	Intermediate shapes Max. finish-forging temperature	871-982 (1600-1800) 1012 (1854)

**Table 11.9** Heat-Resistant Superalloys Used for Forging of Iron-, Nickel-, and Cobalt-Based Parts

No.	Material designation	Composition, wt%										Typical applications	Forging temperature Minimum, °C (°F)	Optimum, °C (°F)	
		C	Mn	Si	Cr	Ni	Mo	Ti	Al	B	V				
<b>Iron-based (Fe-Ni)</b>															
1	AISI 660	0.08	1.35	0.95	15.0	26.0	1.25	2.15	0.20	0.003	0.30	—	52.7	—	1062–1122 (1945–2052)
2	AISI 651	0.32	1.15	0.55	18.5	9.00	1.40	0.25	—	—	—	1.35 Cb + Ta: 0.4 Cu: 0.15	66.9	—	—
<b>Nickel-based</b>															
3	Monel K	0.06	0.01	0.02	—	55.0	—	—	0.02	—	—	S: 0.005 Cu: 44.0	0.05	950 (1742)	1050–11150 (1922–2102)
4	Hastelloy Alloy B	0.05	1.00	1.00	61.2	28.0	—	—	—	0.30	—	Co: 2.50	5.0	—	—
5	Inconel Alloy 718	0.04	0.20	0.20	19.0	52.5	3.00	0.80	0.60	—	—	Cb + Ta: 5.2	18.0	—	1072–1204 (1982–2199)
<b>Cobalt-based</b>															
6	Haynes Alloy 25	0.10	1.50	1.00	20.0	10.0	—	—	—	—	—	Co: 49.4	3.0	High thermally stressed components for gas turbines	—
														1072–1250 (1982–2300)	

**Table 11.10** Molybdenum and Tungsten Alloys Used for Forged Parts

No.	Material Designation	Composition, wt %				Typical applications	Forging temperature, °C (°F)
		Mo	Ti	Zr	W		
Molybdenum alloys							
1	Unalloyed molybdenum	—	—	—	—	Missile and rocket parts, components for rocket propulsion Gas turbine blades. Material in general use in the aerospace industry	1032–1315 (1890–2400)
2	Mo–Ti–Zr (TZM alloy)	99.4	0.50	0.10	—	—	1204–1482 (2200–2700)
Tungsten alloys							
3	Unalloyed tungsten	—	—	—	—	Same as for molybdenum alloys	1204–1649 (2200–3000)
4	W–15Mo alloy	15.0	—	—	85.0	—	1093–1371 (2000–2500)
5	W–2ThO <sub>2</sub> alloy	—	—	—	98.0	2.0	1315–1371 (2400–2500)

- 1 Aluminum alloys
- 2 Magnesium alloys
- 3 Copper alloys
- 4 Carbon steels and alloyed steels
- 5 Maraging steels
- 6 Austenitic stainless steels
- 7 Nickel alloys
- 8 Titanium alloys
- 9 Iron-based superalloys
- 10 Cobalt-based superalloys
- 11 Molybdenum alloys
- 12 Nickel-based superalloys
- 13 Tungsten alloys
- 14 Beryllium

Each material needs to be forged within a specific temperature range (see Tables 11.4 to 11.10). The lower boundary must be at least as high as the recrystallization temperature. Taking into account the transformations in the crystal lattice [e.g.,  $\alpha$ - $\gamma$ -transformation in steel, 721–906°C (1330–1663°F), depending on the carbon content in hypoeutectoid steels)], the lower boundary is usually chosen somewhat higher. The upper boundary is determined by excess oxidation, coarse grain formation, or again by phase transformation. The flow stress  $\sigma_f$  may vary considerably within the forging temperature range. In order to keep the stresses and forces as low as possible, hot forging is usually started at the highest permissible temperature since cooling due to the temperature difference between workpiece and tool is unavoidable. Care must be taken that the temperature is as even as possible over the entire cross section of the slug. This becomes increasingly difficult with large cross sections and where the thermal conductivity is poor. Carbon steels generally pose no special problems. Chrome, nickel, and manganese steels, on the other hand, exhibit poor thermal conductivity accompanied by high creep resistance. Thus thorough heating to the core is a slow process. This is especially true for large open-die forgings where heating may last several days [11.20] in order to avoid damage to the material due to thermal stresses. Fig. 11.60 illustrates how the type of material, smelting, chemical analysis, degree of purity, ingot shape, heating, workpiece shape, and heat treatment after forging may affect the strength and toughness of open-die forgings made of steel. While the forging process itself is very important, it is not the only important factor. Fig. 11.60 also applies to other forging materials with minor modifications. The significance of grain flow and its effect on the ability of components to withstand dynamic stresses has already been discussed in Sec. 11.1.1. For highly stressed ferrous and nonferrous forgings requiring isotropic mechanical properties, vacuum-melted or remelted material is used.

Metals expand on heating; after forging they contract, or they shrink during cooling. The degree of shrinkage used to quantify this behavior can be calculated from the coefficient of thermal expansion  $\alpha$  (average value between room temperature and the temperature  $T_1$  at the end of forging) and the difference between  $T_1$  and the tool temperature  $T_T$ :

$$\lambda = \alpha(T_1 - T_T) \times 100 \quad [\%] \quad (11.22)$$

Depending on material and temperature,  $\lambda = 0.5\text{--}2\%$ ; for certain materials it may be even higher.

## 11.4 HEATING

The heating of a metal workpiece reduces the flow stress and thus leads to a corresponding decrease in the force and work required for deformation. The heat energy supplied to the workpiece, however, far exceeds the deformation work, and thus hot forging offers no advantage from the point of view of energy efficiency. Cold upsetting of a cylinder made of soft carbon steel with  $d_o = 50$  mm (2 in) from  $h_o = 65$  mm (2.6 in) to  $h_i = 20$  mm (0.8 in) requires, for example,

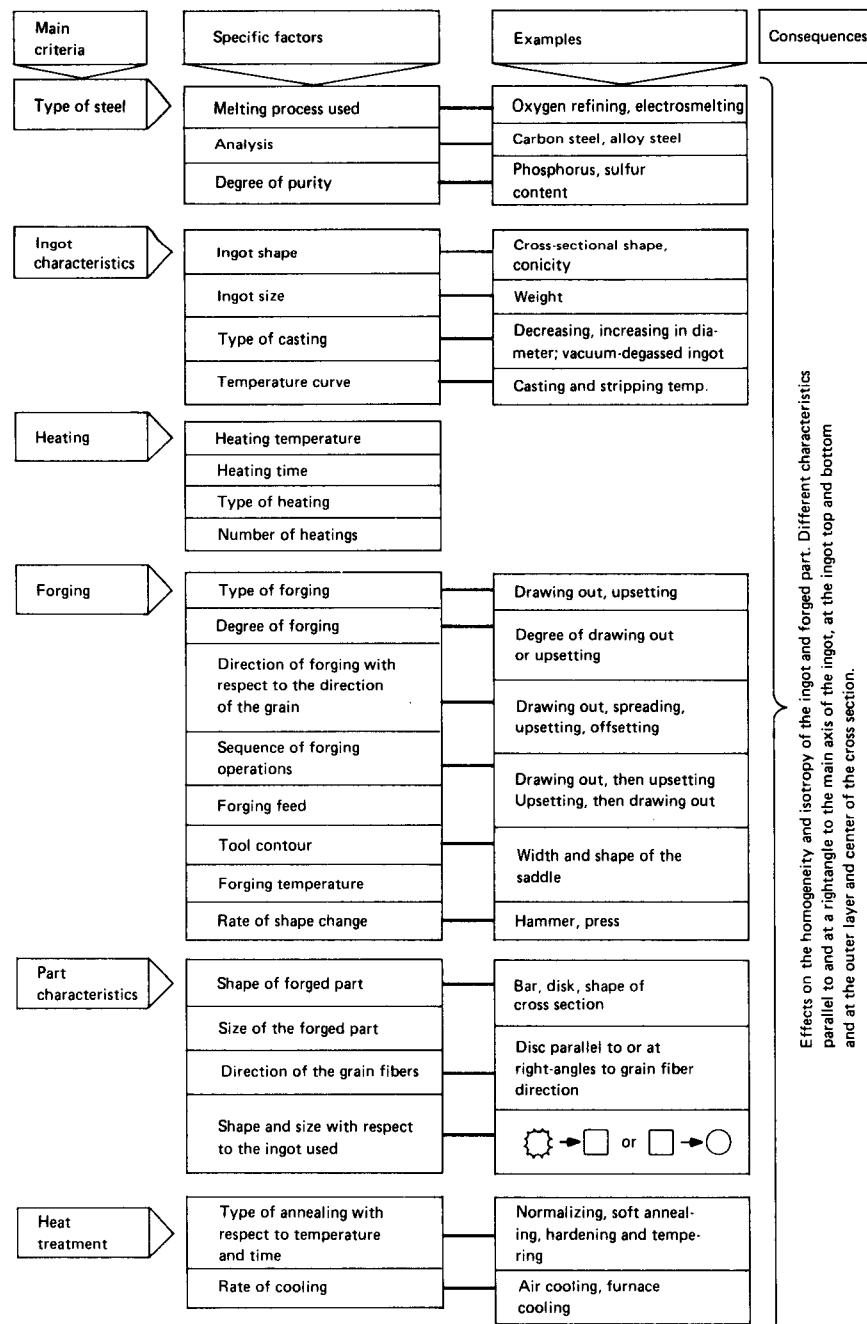


**FIG. 11.60** Outline of main factors affecting the strength and toughness of hot hammer forging made of steel. (After [11.9].)

about 50 kJ (18.4 ft·ton) work; hot upsetting at 1200°C (2192°F), on the other hand, requires  $\approx$  6300 J (2.3 ft·ton) for upsetting and 3400 kJ (1253 ft·ton) for heating at a thermal efficiency of 25% [1 kg (2.2 lb) carbon steel contains approximately 850 kJ (313 ft·ton) at 1200°C (2192°F).] Thus hot upsetting requires in this case about 17 times as much energy as cold upsetting [11.12].

The following methods may be used to heat a workpiece to forging temperature:

**Heating in a furnace:** Heat is largely transmitted to the surface of the workpiece by means of convection and radiation. Heat is generated by burning gas (town gas, natural gas, generator gas) and oil (light and heavy mineral oils). Electrically heated furnaces are also used. The ratio of convection to radiation depends on furnace design and operating conditions; electrically heated furnaces give off radiant heat only.

**Induction heating:** Heat is generated in the surface layer of varying thickness by means of eddy currents. The factors affecting the depth of penetration are frequency, conductivity, and permeability. Economic areas of application for high ( $f \geq 10,000$  Hz), medium ( $1000 < f < 10,000$  Hz), and low frequency depend on material, size, and shape.

**Conduction heating (resistance heating):** Heat is generated directly in the workpiece. Low resistance is required in the transition zones between the electrodes and the workpiece (in the secondary winding of a transformer at line frequency with  $\approx 2\text{--}6$  V).

**Furnace heating:** Fig. 11.61 illustrates the increase in temperature of two different sized test pieces during heating in a furnace. This shows that there is always a temperature difference between the outer layers and the core zone, which can only be minimized by "holding" at the desired temperature for a longer period of time. The heating speed thus depends on the cross-sectional area and on the tendency of the material to form cracks (see Sec. 11.3). Large forgings are heated in four stages:

- 1 Heating to 650°C (1197°F)
- 2 Holding at 650°C (1197°F)
- 3 Heating from 650°C (1197°F) to forging temperature
- 4 Soaking (holding at a given temperature for a longer period of time)

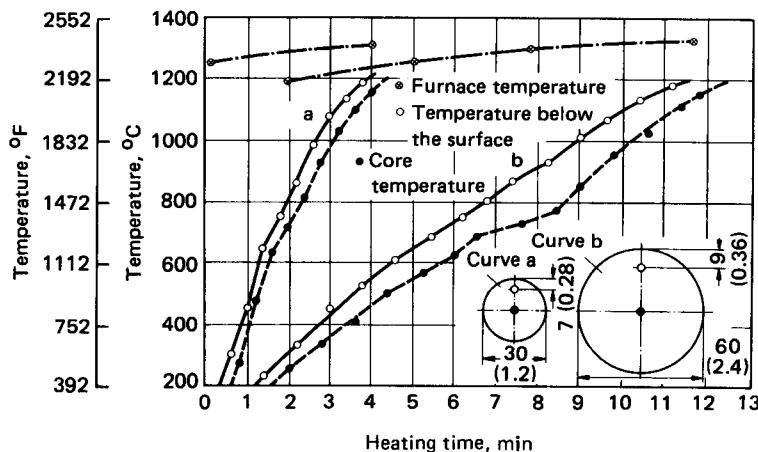


FIG. 11.61 Temperatures of cylindrical steel parts, made of C45 (AISI 1045), during heating in a chamber furnace. Dimensions are in mm (in). (After [11.12].)

The initial heating of smaller sized workpieces,  $d < 200$  mm (7.9 in), made of carbon steels (up to 0.35% C) is performed at a rate of 30–250°C/h (54–450°F/h). Larger workpieces made of medium-hard steels are heated at a rate of 10–30°C/h (18–54°F/h). Hard and very hard alloyed steels, liable to brittle cracking, are heated at a rate of 2–20°C/h (3.6–36°F/h). Heating above 650°C (1197°F) can be performed much more quickly. Thorough warming of larger workpieces, after the surface layers have reached the forging temperature, requires at least several hours. An exact heating sequence is usually specified for large open-die forgings.

The following types of furnaces are being used in forging shops [11.12]:

- |   |   |
|---|---|
| <b>1 Large forging furnaces [<math>&gt; 4\text{-m}^2</math> (144-ft<sup>2</sup>) hearth area]</b> |   |
| <i>a</i> Bogie hearth furnaces  | Large open-die forgings                         |
| <i>b</i> Continuous or pusher-type furnaces   | Large open-die forgings                         |
| <i>c</i> Chamber or batch furnaces  | Open- and closed-die forgings                   |
| <b>2 Small forging furnaces [<math>\leq 4\text{-m}^2</math> (144-ft<sup>2</sup>) hearth area]</b> |   |
| <i>a</i> Chamber or batch furnaces  | Closed-die forgings                             |
| <i>b</i> Chamber or batch furnaces for bar heating and bolt heating furnaces                      | Die forging and upset workpieces                |
| <i>c</i> Small continuous or pusher-type furnaces   | Small open-die forgings and closed-die forgings |
| <i>d</i> Continuous discharge furnaces (fixed cycle time)   | Closed-die forgings                             |
| <i>e</i> Rotating hearth furnaces   | Closed-die forgings                             |

Of the energy  $Q_s$  supplied to the furnace in the form of chemical energy bound to the combustion material only a small proportion  $Q_{eff}$  is actually used to heat the forging material. The proportion of useful heat  $Q_{eff}/Q_s$  depends on the proportion of  $Q_s$  that is released by the hot gases inside the furnace as well as on the heat transferred to the forging material and thus on the output of the hearth area (e.g., in  $\text{kg/m}^2 \cdot \text{h}$ ). Table 11.11 shows some typical values of  $Q_{eff}/Q_s$  for different types of furnaces used in closed-die forging [11.12].

**Table 11.11** Ratio of Useful Heat  $Q_{eff}$  to Supplied Heat  $Q_s$  for Different Types of Furnaces Used in Die Forging of Steel at  $T \approx 1200^\circ\text{C}$  (2192°F)

Type of furnace	Heat efficiency $Q_{eff}/Q_s, \%$
Gas-fired chamber furnaces without preheating of the air	6–12
Chamber furnaces for heating billet with air preheating	18–25
Pusher-type furnaces	25–30
Fixed-cycle furnaces (continuous throughput furnaces)	35–45

**Induction heating:** Fig. 11.62 shows isothermal curves set up during induction heating of a 100-mm (3.94-in) diameter workpiece over a period of 10 min [11.83]. The figure, which is based on results obtained with two different frequencies, shows clearly the greater effect of the eddy currents in the outer layers and the increase in temperature over time. Naturally the temperature increase also depends on the energy concentration (e.g., in  $\text{W/cm}^2$ ) at the surface. Economic diameter sizes for induction heating of steel are  $d < 150$  mm (5.9 in) at  $f = 50$  Hz;  $d = 30$ –120 mm (1.18–4.72 in) at  $f = 2000$  Hz;  $d = 20$ –85 mm (0.79–3.35 in) at  $f = 5000$  Hz;  $d = 14$ –60 mm (0.55–2.36 in) at  $f = 10,000$  Hz. To heat steel up to  $1200^\circ\text{C}$  (2192°F), 0.35–0.60 kWh/kg (0.16–0.27 kWh/lb) is required; to heat brass and copper up to  $830^\circ\text{C}$  (1526°F), 0.25–0.40 kWh/

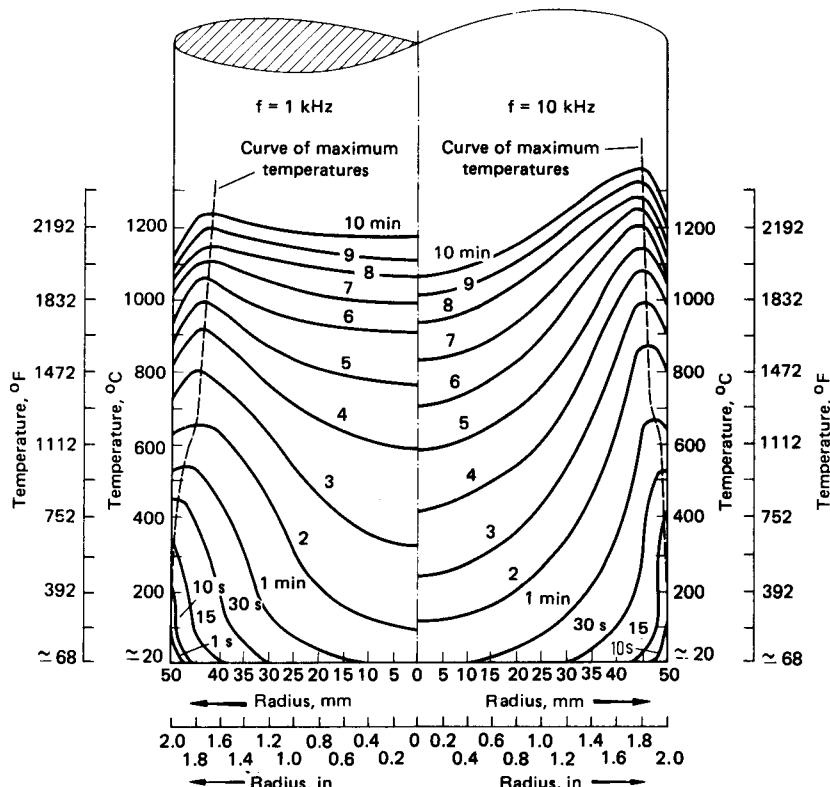


**FIG. 11.62** Temperatures as a function of frequency and time during induction heating of a cylindrical part made of carbon steel. (After [11.83].)

kg (0.11–0.18 kWh/lb) is needed; and to heat aluminum and its alloys to 550°C (1022°F), 0.35–0.50 kWh/kg (0.16–0.23 kWh/lb) is needed [11.84]. For steel the ratio of useful heat to supplied heat  $Q_{\text{eff}}/Q_s$  lies in the range of 0.45–0.65.

**Conduction heating (resistance heating):** When magnetic steels are heated from room temperature up to the Curie point [approximately 767°C (1413°F)], the current flows in a layer below the surface because of the skin effect. This layer is thus warmer than the core, which is heated by thermal conduction. Above 767°C (1413°F), current flow is evenly distributed over the entire cross section. With increasing radiation losses, the heat flow is reversed, since the surface is cooler than the core. With a 60-mm (2.36-in) square billet, temperature differences of about 50°C (90°F) were recorded for a surface temperature of approximately 1100°C (2012°F) [11.85].

The energy required to heat steel up to 1200°C (2192°F) is about 0.28–0.35 kWh/kg (0.13–0.16 kWh/lb). This corresponds to a ratio of useful heat to supplied heat of 0.65–0.80. In practice it is difficult to achieve good surface contact between the workpiece and the electrode after shear cutting. Thus electric resistance heating is still largely limited to bolt and rivet heating equipment and electropressetting machines, whereas induction heating is widely used, despite higher investment costs. One important factor here is the reduction in oxide formation. The oxide that forms is also chemically different. Whereas in furnace heating the reaction of iron with H<sub>2</sub>, H<sub>2</sub>O, CO, and CO<sub>2</sub> in the furnace atmosphere provides the foundation for scale formation, in induction and electroresistance heating it mainly reacts with the oxygen in the surrounding air. The time available for reaction is generally shorter than with furnace heating because of the reduced heating

time as a result of higher energy concentration. Above 727°C (1341°F) it is particularly important for steel to be heated quickly since from here on the amount of oxide formed in a given time increases rapidly with temperature. With all electrical heating methods oxide formation can be avoided almost completely if protective gas atmospheres are used (i.e., incompletely burned gas mixtures with O<sub>2</sub> and CO<sub>2</sub> removed or inert gases). By taking appropriate steps in the design stage of the furnace (it is important to ensure a shortage of air during combustion), it is possible to achieve low scale formation, if not completely scale-free heating. Such furnaces, however, require precise control, monitoring, and maintenance [11.86]. With steel, short heating times and the use of low-oxygen, neutral, or inert protective gases also have a positive effect on surface decarburization, which otherwise may reach depths of 1 mm (0.04 in) or more after only a few minutes of heating [11.87]. Even deeper decarburization occurs as a result of longer periods of heating.

## 11.5 PROCESS SEQUENCE

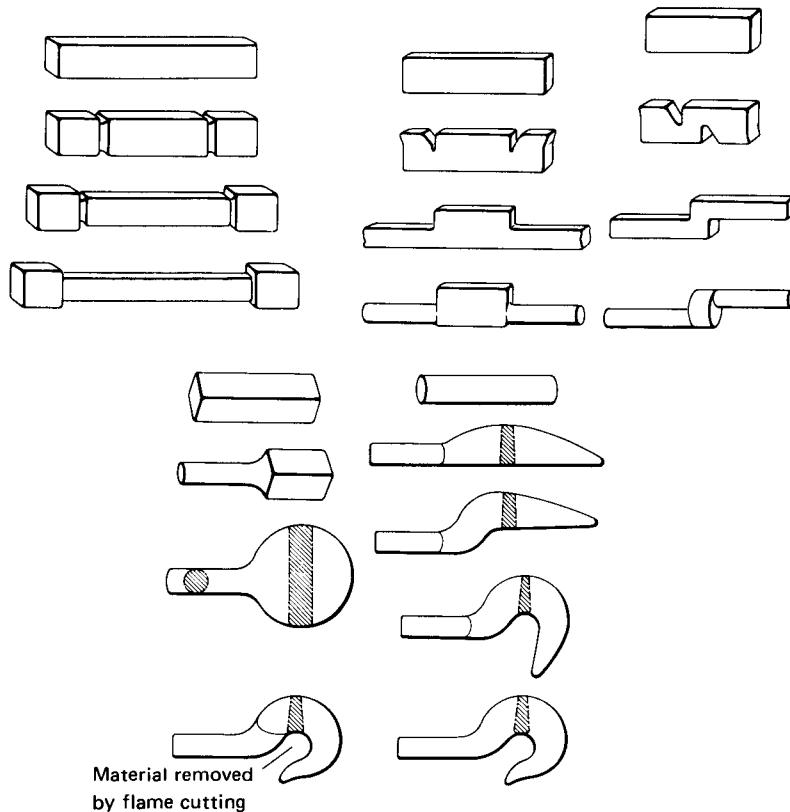
The preceding sections have shown that the sequence of operations differs widely in open- and closed-die forging. Open-die forging is mainly concerned with single-item or small-batch production of workpieces between 1 kg (2.2 lb) and 350 t (386 ton), while the main emphasis in closed-die forging of steel is on medium- and large-batch production of parts between 50 g (0.11 lb) and 1.5 t (1.65 ton). Open-die forged parts tend to require a considerable amount of mechanical machining. The larger their size, the greater is the effect of the material properties on the work sequence. Closed-die forgings are often only partly machined. In some cases they can be finish-forged ready for assembly (e.g., gear wheels). An optimal manufacturing sequence, aided by mechanization and automation where appropriate, together with accurate geometric size and shape and good surface finish, are as important as the properties of the material itself.

### 11.5.1 Open-Die Forging

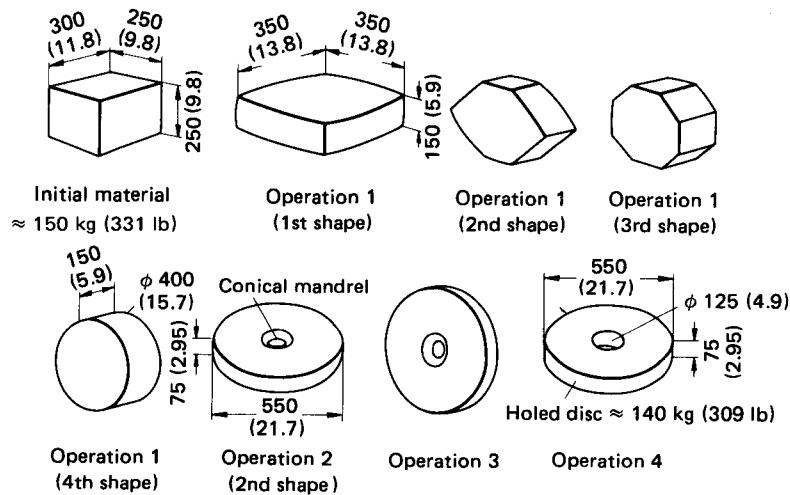
The work sequences of open-die forged products, such as forged semifinished products (ingots, billets, slabs, bars), standard products (disks, punched disks, rings, liners), die blocks, and large open-die forgings (crankshafts, hollow bodies, pressure vessels, rotors, turbine wheels, machine and equipment components), need to take into account the dependence of the mechanical properties on the rolled grain structure. Some typical work sequences, including drawing out, spreading, bending, chiselling in, and stepping, are shown in Fig. 11.63. The work sequence shown in Fig. 11.64 for open-die forging of a punched disk is divided into two parts. In the first, a length of square bar is forged in three stages to form a 400-mm (15.75-in) diameter disk; in the second, the diameter is increased to 550 mm (21.65 in), the thickness reduced to 75 mm (2.95 in) by upsetting, and the central hole preforged using a conical mandrel. The circumference is then flattened, finish-forged, and finally punched out from the back with a sharp-edged mandrel. Blanks for forged rings are produced in a similar manner. The workpiece in this case is finished by forging over a mandrel, which is supported on one or both sides, the diameter being increased and the cross section reduced during the course of the operation. Undesired spreading in the form of bulging of the sidewalls may have to be corrected by one or several upsetting operations [11.89].

Fig. 11.65 illustrates the open-die forging of a large crank throw for a crankshaft to be made by joining together premachined parts. The work sequence shows clearly how the process has been carefully designed to ensure thorough forging and optimal grain flow with regard to the subsequent stressing of the part. In this example the finished part, which weighs 15.7 t (17.3 ton), was made from 29.4-t (32.4-ton) ingot. Fig. 11.66 shows an example of a heavy four-throw crankshaft forged in one piece, with the crankpins forged in their correct positions. In many cases the procedure followed is not to forge the crankpins in position, but to offset them, possibly after machining (e.g., recessing of the pin diameter), and to position them later in a twisting operation under localized heating. To forge a turbine rotor from vacuum-degassed steel with 3.5% Ni, having an ingot weight of 190 t (209 ton) and a mean diameter of 2.55 m (7.77 ft), 12 heatings\* were

\*One heating denotes an individual heating or reheating in the furnace.



**FIG. 11.63** Examples of basic open-die forging operations shown in the order used for forging steel hooks. (After [11.88].)



**FIG. 11.64** Work sequence used in forging a ring starting from a length of square steel bar. Dimensions are in mm (in). (After [11.88].)

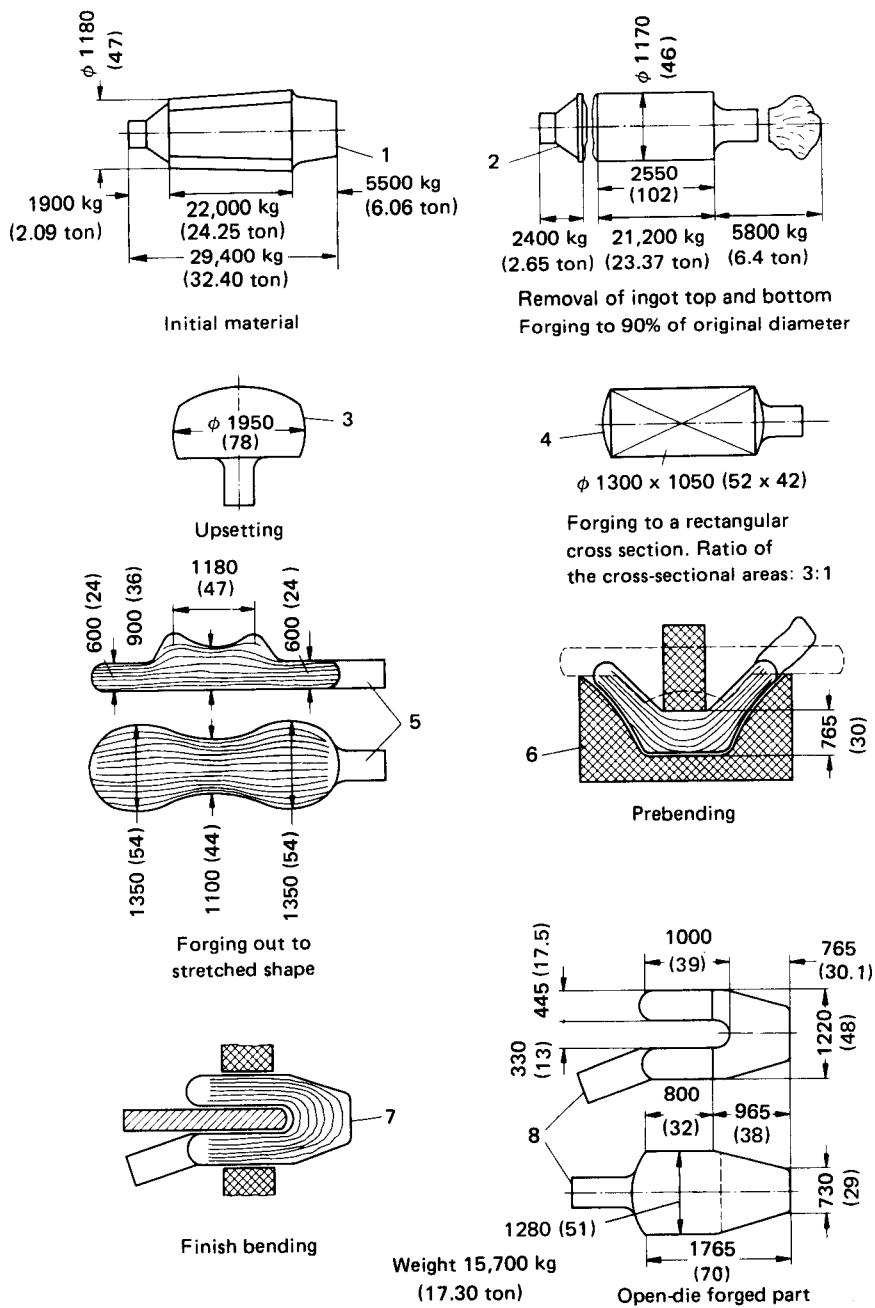


**FIG. 11.65** Schematic of the method used to forge a crank throw (Sulzer RD 90). Material—steel (0.35% C, 0.70% Mn, 0.25% Si, 0.14% V); equipment—50-MN (5625-ton) hydraulic forging press. Unlabelled dimensions are in mm (in). (After [11.90].)

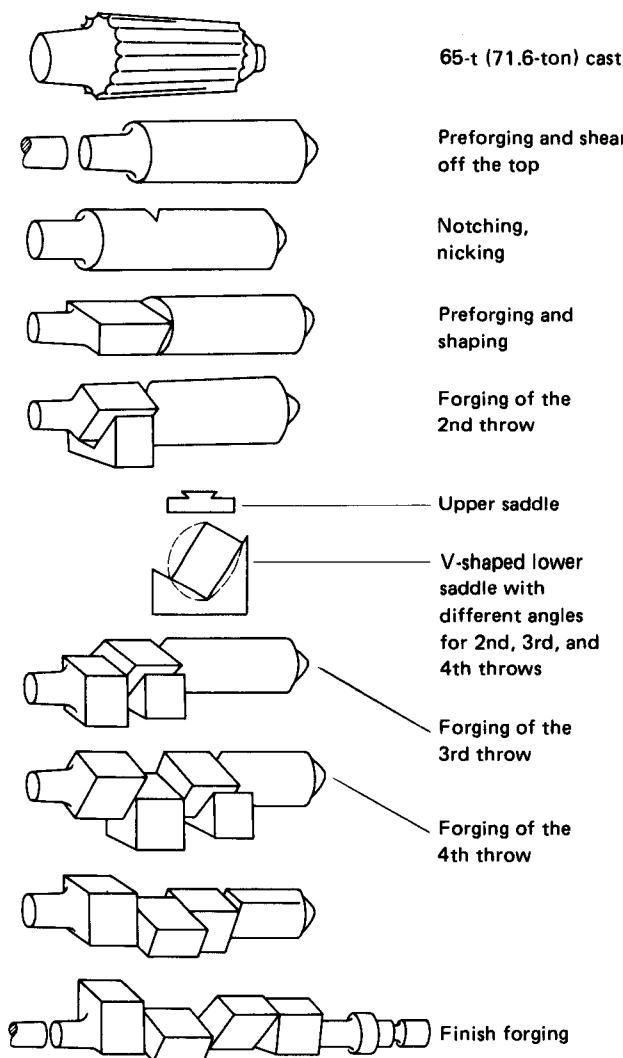


**FIG. 11.66** Sequence of operations used to forge a four-throw crankshaft from a 65-t (71.5-ton) ingot. Material—steel (0.21% C, 0.32% Si, 0.75% Mn). (After [11.90].)

required (with several operations per heating). The total heating time for the 12 heatings was 205 h, the transport time 7 h, and the time required for work under the 75-MN (8438-ton) hydraulic forging press was also 7 h [11.91].

Through mechanization and, where appropriate, automation of the forging process, the overall forging time and the total number of operations required may be reduced since with faster forging several previously separate operations can be carried out in the same heating period. To gain time, manipulators are used, which often are controlled centrally from the press. Twin-column underfloor presses of 10MN (1125 tonf) up to several times this amount have proved particularly suitable because of their good accessibility (Fig. 11.67). However, manipulators of both the free-

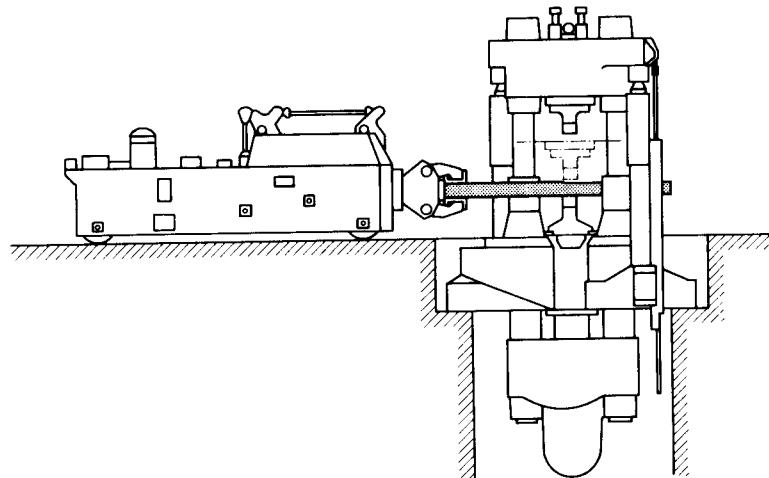


**FIG. 11.67** Two-column underfloor press working in conjunction with a manipulator.  
(Courtesy of SMS Hasenclever, Düsseldorf.)

moving and the rail-running types are also used with the more common four-column presses as well as with single-pillar presses and hammers [11.92].

Since 1945 several specialized processes have been developed for particular shapes, such as for crankshafts with 300–600-mm (11.8–23.6-in) stroke and weighing 2–10 t (2.2–11 ton), permitting throw-by-throw forging in closed dies. An example is shown in Fig. 11.68. The operations are performed in three heatings, calling for tool movements in two directions. This type of crankshaft manufacture is characterized by continuous grain flow, exact shaping, and thus less subsequent machining. It represents an intermediate technique between open- and closed-die forging.

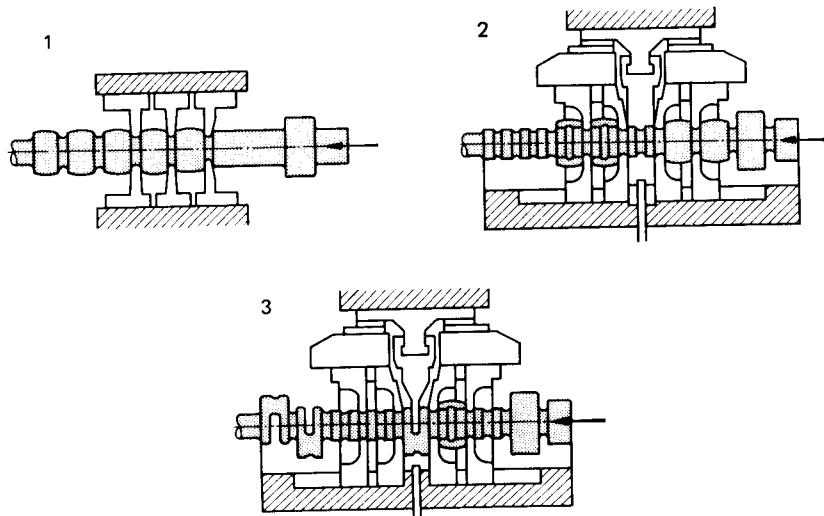


**FIG. 11.68** Crankshaft forging process. Work sequence: 1—pressing of main and pin journals; 2—preforging of webs in desired angular position; 3—offsetting of crankpins in desired angular position and finish-forging of webs. (Courtesy of SMS Hasenclever, Düsseldorf.)

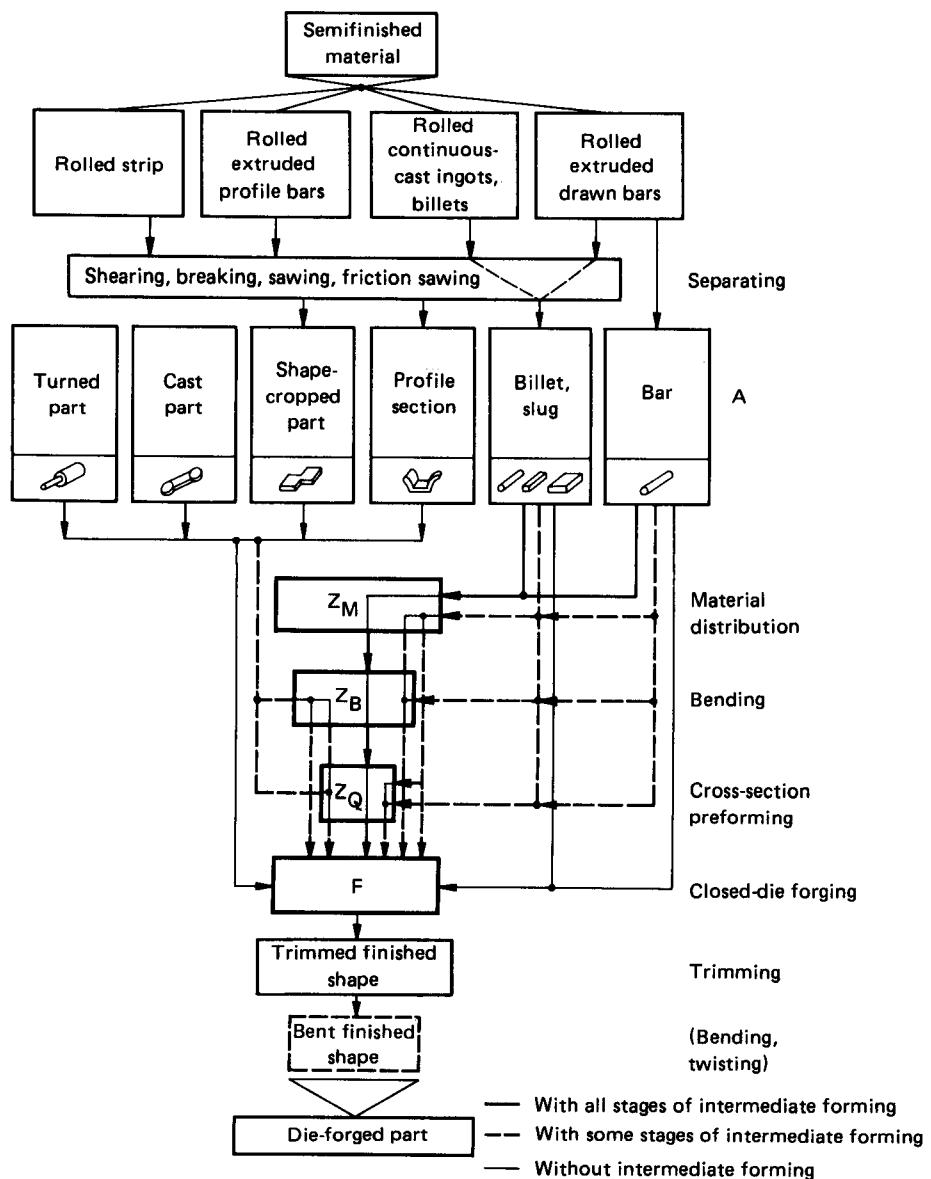


FIG. 11.69 Work sequence used in closed-die forging. **A**—initial shape;  $Z_M$ —intermediate shape producing desired material distribution;  $Z_B$ —intermediate shape to give required bending;  $Z_Q$ —intermediate shape to preform required cross section; **F**—final shape.

### 11.5.2 Closed-Die Forging

Closed-die forging is used to produce (1) components for machines and equipment as well as for land, sea, and air vehicles; (2) nuts, bolts, rivets, and screws; (3) tools such as hammers, pliers, screwdrivers, hoes, and forks; (4) surgical and cutting instruments (knives and shears); and (5) hot-forged thick-walled components made of sheet metal. The most common starting materials are rolled, continuously cast, or extruded bars, billets, slabs, profile and flat products, drawn profile sections, cast lengths, and, in some cases, machined (mainly turned) blanks.

This is true for practically all materials, although for certain groups of materials particular semifinished production processes predominate for economical or technical reasons (Fig. 11.69) [11.93]. The required amount of material is either parted off just prior to forging (by shearing, breaking, sawing, or grinding) or remains on the rolled bar. In certain cases the initial forging material is in the form of small ingots, billet lengths, profile section lengths, or cropped slugs. These have to progress through a certain number of intermediate stages (material distribution, bending, preforming of the cross section) before attaining their final shapes. The following may serve as a guideline. Simple, compact forgings, corresponding to categories 1 and 2 of the Spies shape classification [11.61] (Fig. 11.70), can be finish-forged in a die without intermediate shaping operations. The same is true for more complex forgings with several limbs, corresponding to shape category 3, where the shape of the initial material is closely adapted to that of the finished forging by splitting, casting, extrusion, or rolling. With very small workpieces of category 3 this approach is also sometimes adopted when the intermediate shaping costs surpass the cost savings in material, provided there is no risk of forging defects (cracks and overlaps). In all other cases, especially in category 3, the number of intermediate forming stages increases with the complexity of the workpiece geometry, with decreasing deformability, and with the increasing number of parts to be produced.

Shape category 1: Compact shapes  Spherical and cubical parts	Subgroup:	101 Without secondary shape elements 	102 With secondary shape elements on one side 	103 With circumferential secondary shape elements 	104 With circumferential and one-sided secondary shape elements 
Shape category 2: Disc shapes  Parts of circular, square, and similar circumferences. Cross-shaped parts with short limbs. Upset heads or longitudinal shapes (e.g., flanges, valve heads, etc.)	Subgroup: Shape group: ↓	Without secondary shape elements 	With hub 	With hub and hole 	With edges 
21 Disc shape with secondary shape elements on one side	211 Disc shape with secondary shape elements on one side				
22 Disc shape with secondary shape elements on two sides	222 Disc shape with secondary shape elements on two sides				
Shape category 3: Longitudinal shapes 	Subgroup: Shape group: ↓	Without secondary shape elements 	With secondary shape elements symmetrical to the axis of the main shape 	With Open or closed fork 	With secondary shape elements nonsymmetrical to the axis of the main shape 
Parts with pronounced longitudinal axes: Longitudinal groups: 1. Short parts $l < 3b$ 2. Medium-length parts $3 < l \leq 8b$ 3. Long parts $l > 8b$ 4. Very long parts $l < 16b$ (Numbers indicating the longitudinal group can be added after a diagonal line: e.g., 334/4)	31 Main shape element with straight longitudinal axis				
	32 Longitudinal axis of the main shape element bent in one plane				
	33 Longitudinal axis of the main shape element bent in more than one plane				

FIG. 11.70 Classification of forged parts according to shape. (After [11.61].)

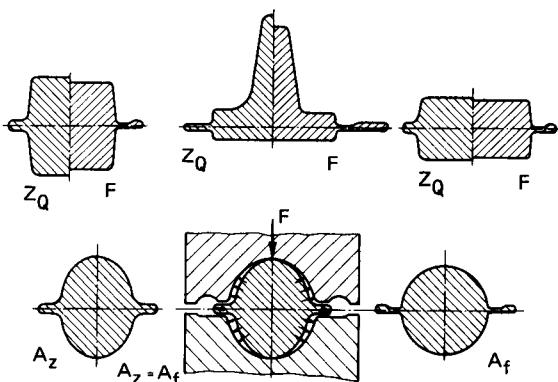


**FIG. 11.71** Formation of desired cross section in die forging.  $Z_Q$ —intermediate shape to give required cross section;  $F$ —final shape;  $A_z$ —cross-sectional area of intermediate shape;  $A_f$ —cross-sectional area of final shape. (After [11.94].)

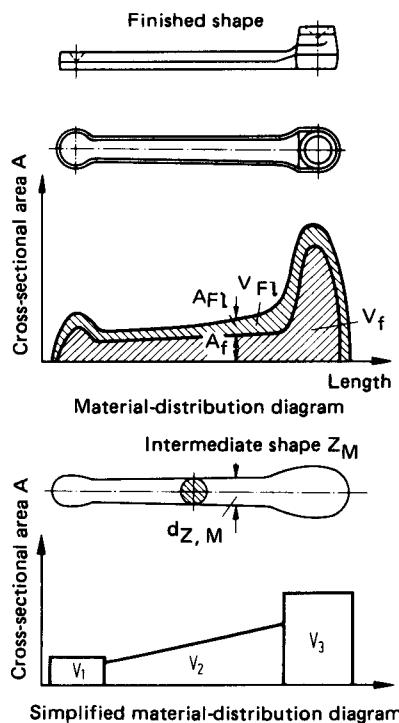


**FIG. 11.72** Development of material distribution diagram for forging an oblong part. (After [11.94], [11.95].)

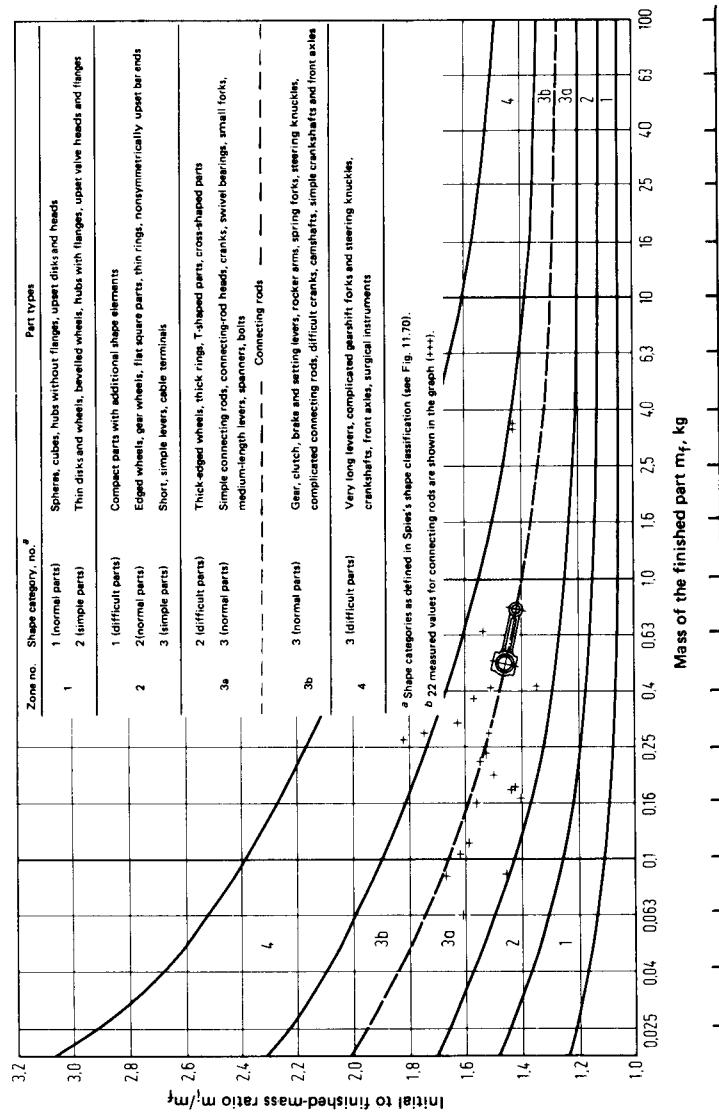


**FIG. 11.73** Chart for determining the amount of excess material required for flash as a function of the finished weight of the die-forged part. Material—steel. (After [11.95].)

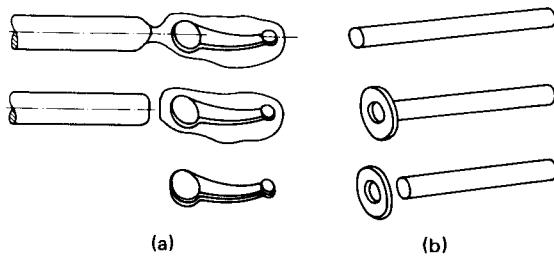


**FIG. 11.74** Direct forging of steel bar without intermediate forging steps. (a) Using hammers. (b) Using horizontal forging machines.

The methods used for intermediate forming are shown in Figs. 11.2, 11.6, and 11.71. The purpose of preforming (Fig. 11.71) is to impart a higher and narrower shape to the intermediate cross section prior to finish forging of the workpiece in closed dies with thick flash. The material then contacts the walls of the die cavity without sliding along them, and thus die wear is reduced considerably [11.12].

Calculation of the intermediate shape required for material distribution is performed as follows according to [11.41], [11.94], and [11.95]. The surface areas of the various cross sections of the final shape, obtained from the part drawings or from a master, are projected at a right angle to the main longitudinal axis and above it (Fig. 11.72). To these, the areas of the required flash cross section are added. Thus the mass distribution shape is obtained with symmetrical material distribution about the main axis and simplified cross sections (rounds, squares, and ovals), or the simplified material distribution diagram. The first diagram represents the geometry of the intermediate shape needed for material distribution (drawn-out parts, rolled parts, etc.). The second diagram is particularly useful for determining the best work sequence when there are large variations in the cross section. Here the changes in cross section that can be achieved with the production equipment available are taken into account (as described in Sec. 11.1.1). For the purposes

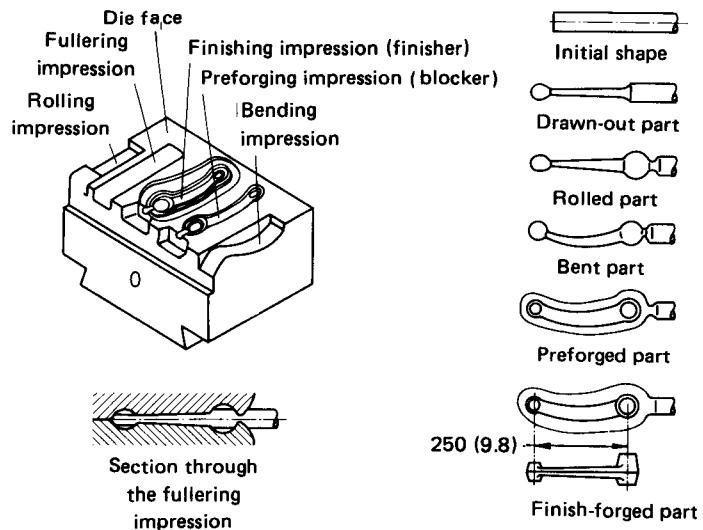


**FIG. 11.75** Closed-die forging of a lever showing all the intermediate forging operations performed with a multistage hammer die. (After [11.41].)

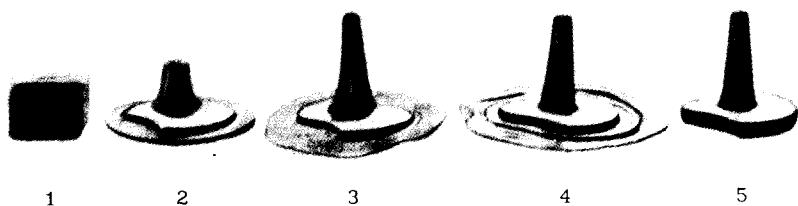


**FIG. 11.76** Closed-die forging of small combustion engine half-crank shafts. 1—initial material; 2—first die, first blow; 3—first die, second blow; 4—second die, final shape; 5—trimmed part.

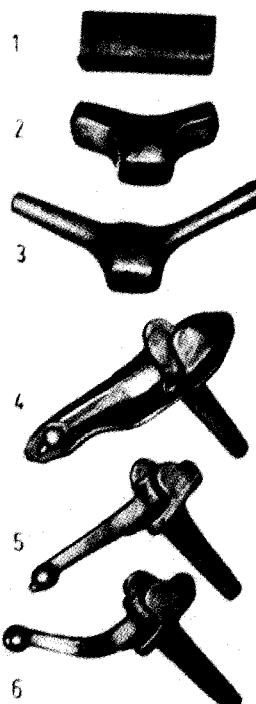


**FIG. 11.77** Work sequence used in forging steering knuckles. 1—initial material; 2—material distribution by a combined process of offsetting, upsetting, and bending in a press die; 3—forging out the projecting limbs; 4—closed-die forging under a hammer; 5—trimming; 6—bending to final shape.

of the material distribution diagram, workpieces with bent main axis are best drawn as if they had been straightened out. The amount of additional material required for flash, which largely depends on the size and shape of the workpiece, is shown in Fig. 11.73 for carbon and low-alloy steels. The weight loss due to oxidation varies between 0.5% of the final weight of the forging (for electric heating and for rapid single-stage heating in oil- and gas-fired furnaces) and 3% (for grad-

ual heating over longer periods of time in strongly oxidizing atmospheres and for multistage heating).

In the following, typical examples of different work sequences are given. Fig. 11.74 illustrates forging from stock, without intermediate forming, using a hammer and a horizontal forging machine. By contrast, Fig. 11.75 shows an example of hammer forging with all the intermediate forming stages. Two examples of die forging using preformed starting material (profile lengths, split lengths) have already been given in Fig. 11.9. Fig. 11.76 shows the work sequence during die forging of part of a motorcycle crankshaft. The preforming and finish-forming of the cross section are performed by closed-die forging with flash under a hammer using several blows at each stage. Finish-forging, which requires the highest forces, should always take place in the middle of the die block so that the resulting deformation force is as near as possible to the main axis of the hammer or press. In multistage dies (as illustrated in Fig. 11.75) the work sequence should start at the outer edge of the die and work inward. The material distribution in the case of the work sequence for a steering knuckle shown in Fig. 11.77 starts with a combination of offsetting, localized upsetting, and bending. After subsequent drawing out, the final part shape is obtained by closed-die forging with flash, using several hammer blows. This operation is followed by trimming and bending of one of the limbs. The foot-brake linkage forged in six steps shown in Fig. 11.78 is first upset twice in a horizontal forging machine before being bent and then finish-forged in a die using a hammer. The wide scope of horizontal forging machines is illustrated by the shape

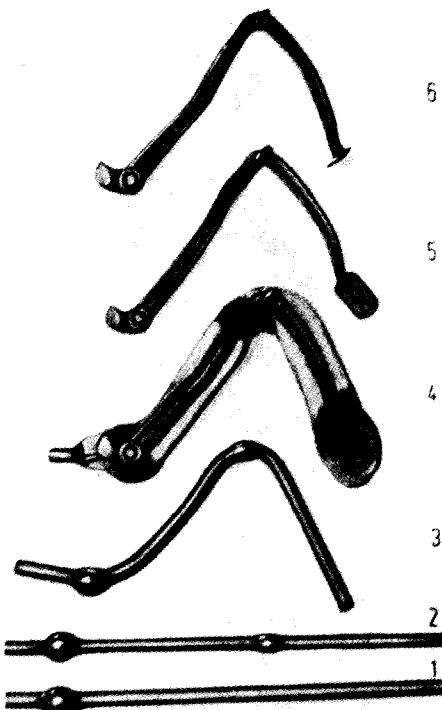


**FIG. 11.78** Work sequence used in forging foot-brake linkages. 1, 2—upsetting on a horizontal upsetting machine; 3—bending in single plane; 4—closed-die forging under a hammer with bending in second plane; 5—trimming; 6—bending foot pedal into final position.

Systematic outline			Examples		
Classification criteria		Shape groups	Solid bodies (upsetting)	Hollow bodies with closed- ended holes	Hollow bodies with open- ended holes
Basic shapes	Type	Solid bodies   Hollow bodies With open- ended holes   With blind holes			
	$d_1/h_1$	$< 1$ $= 1$ $> 1$			
	$d_1/d_0$	$< 2$ $= 2$ $> 2$			
	$d_2/d_1$	$> 0.5$ $= 0.5$ $< 0.5$			
	Direction of forging	Axial (main punch)   Lateral (Clamping jaws)			
	Symmetry	Symmetrical   Nonsymmetrical to the longitudinal axis			
Number of forged zones	One				
	Several				
Length of the shaft	$1 = 0$ $L = \text{small}$ $L = \text{large}$				

FIG. 11.79 Classification of part shapes with special reference to horizontal forging machines. (After [11.96].)

classification shown in Fig. 11.79. Apart from closed-die forging without and with flash, upsetting, piercing, and through-punching are the most important processes that can be carried out on horizontal forging machines, which act in two directions. In these processes, as with forging with fixed-stroke presses, only one stroke can be performed per tool, the work sequence being determined by tool design down to the last detail.

Fig. 11.80 shows typical work sequences for die-forging presses. Die-forging presses are fur-

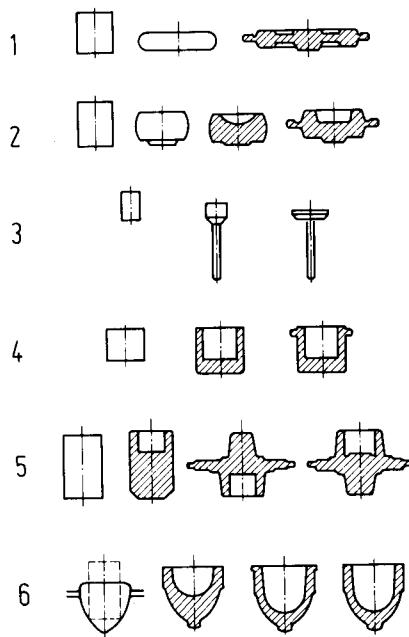


**FIG. 11.80** Example of forging operations carried out with a die-forging crank press. 1, 2—upsetting and spreading without and with cavities; 3—solid forward extrusion; 4—backward can extrusion and closed-die forging with flash; 5—combined extrusion, upsetting and spreading, closed-die forging with flash; 6—upsetting in a die, opening out, and closed-die forging with flash. (After [11.41].)

ther used to finish-form numerous other parts of different geometric shapes, such as crankshafts and connecting rods.

Newly developed impact-forging presses represent an economic synthesis of the extrusion and the die-forging processes. When operating in the hammer mode, the deformation force  $F_f$  over a small displacement may be several times as high as the largest deformation force when operating as a press (Fig. 11.81) [11.97]. Die forging with high-speed hammers is limited for both economical and technical reasons (very high deceleration forces during forging) to workpieces made from high-temperature-resistance materials with high deformation and small wall thicknesses at a right angle to the direction of forging. The main advantages of such machines, which act on the workpiece with an initial contact speed of 15–20 m/s (45–60 ft/s), namely, small moving masses and compact design, are of most use where high energy is required to provide a high finish-forging force (Fig. 11.82) [11.98].

## 11.6 DESIGN OF DIE FORGINGS

The following factors must be taken into account in the design of die forgings: material flow, tool design, dimensional accuracy, and ease of subsequent machining [11.99].

### 11.6.1 Design for Material Flow and Die Layout

The main consideration is to reduce the deformation resistance  $k_R$  by avoiding sharp edges, abrupt changes in cross section, and thin webs and fins (corresponding to deep, narrow cavities in the die), thus lessening the chance of forging defects (cracks and overlaps; see Fig. 11.32). Bases and sidewalls should be as thick as possible in order to avoid rapid cooling. The initial slug or preform and the finished forging should correspond to each other closely enough to ensure desirable grain flow in the finished part (see Sec. 11.1.1, Fig. 11.3). Guidelines concerning minimal wall thickness, suitable radii, and angular draft of the sidewalls, which are necessary for easy removal of the

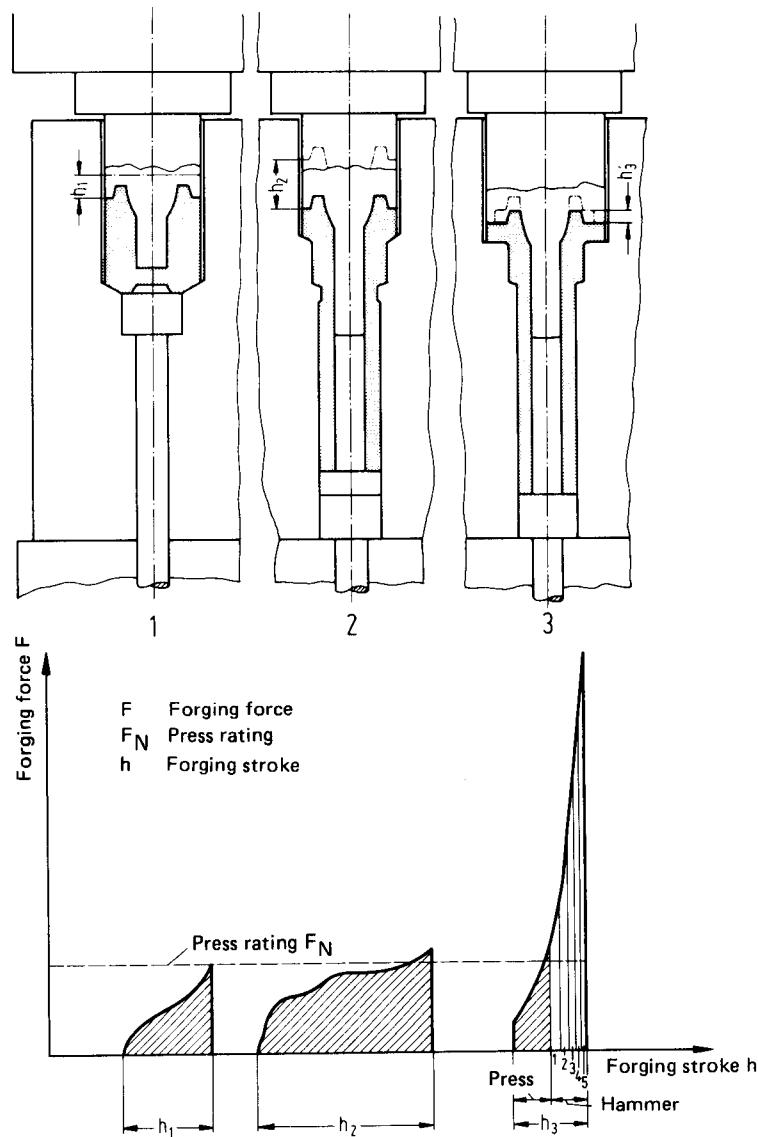


**FIG. 11.81** Work sequence for producing flanged hollow shafts on electrohydraulic impact-forging presses (Lasco). 1—preforming (indenting); 2—hollow forward extrusion of shaft; 3—closed-die forging of flange without flash.

forging from the die, are contained in Table 11.12. Consideration of the desirable draft and transition radii lead to the recommended cross-sectional shapes for ease of material flow shown in Fig. 11.83. These shapes also take die-related factors into account.

In closed-die forging the workpiece shape must be divided between at least two tools (dies) (see Fig. 11.87). Correct positioning of the dividing line is extremely important and requires great

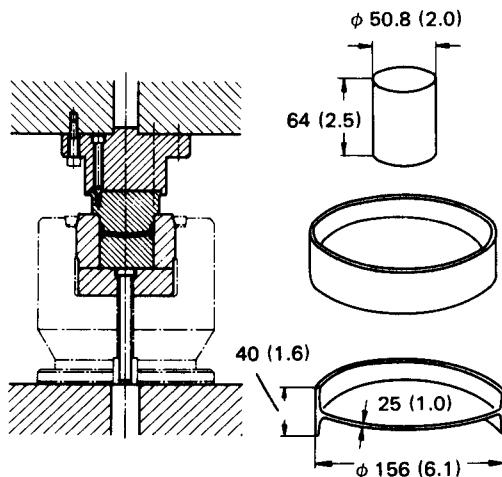


**FIG. 11.82** Closed-die forging with high-energy forming hammer in a single blow (Weingarten). Material—steel (0.45% C, 0.75% Mn, 0.55% Ni, 1.0% Cr); forging temperature—1175°C (2147°F). Dimensions are in mm (in).

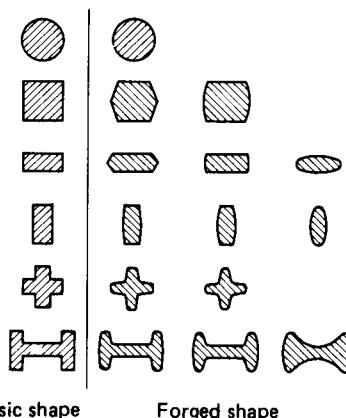


**FIG. 11.83** Cross-sectional shapes of die-forged parts for optimal material flow and conditions in die.

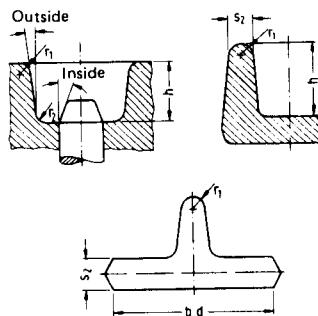
experience, especially for parts of complex geometry. Four basic rules must be observed (Fig. 11.84):

- 1 The parting line (flash line) should divide the forging—in all sections if possible—into two halves of equal depth. The material requirement for a given angular draft is then minimized. The flash should not be placed at the edge of the forging, since this increases the difficulties encountered during trimming and makes checking for correct alignment more difficult.
- 2 The parting line should be in one plane wherever possible. This corresponds to the smallest height of the die block and facilitates machining of the inner and outer tool surfaces.

**Table 11.12** Typical Values for Draft, Transition Radius, and Minimum Wall Thickness for Forged Parts Made of Steel, Light Alloys, Copper, and Copper Alloys

Draft			Transition radius, minimum values		
Material	Outward	Inward	<i>h</i> , mm (in)	<i>r</i> <sub>1</sub> , mm (in)	<i>r</i> <sub>2</sub> , mm (in)
<b>Steel</b>			<b>Forged parts made of steel</b>		
Hammer	1:10	1:6	<25 (<1.0)	2 (0.08)	4 (0.16)
Press	1:20	1:10	25-40 (1.0-1.6)	3 (0.12)	6 (0.24)
Horizontal forging machine	1:50	1:20	40-63 (1.6-2.5)	4 (1.16)	10 (0.40)
Al and Al alloys			63-100 (2.5-4.0)	6 (0.24)	16 (0.64)
Without ejector		1:20	100-160 (4.0-6.4)	8 (0.32)	25 (1.0)
With ejector		1:60	160-250 (6.4-10)	10 (0.40)	40 (1.6)
Cu and Cu alloys	$\approx 1:115$	$\approx 1:60$	250-400 (10-16)	16 (0.64)	63 (2.52)
<b>Minimum wall thickness</b>			<b>Forged parts made of light alloys</b>		
Cross section at 90° to the direction of forging					
<i>b</i> or <i>d</i> , mm (in)		<i>s</i> <sub>1,min</sub> , mm (in)			
<b>Forged parts made of steel</b>					
<25 (<1.0)		2-3 (0.08-0.12)			
40-63 (1.6-2.52)		5-6 (0.20-0.24)			
63-100 (2.52-4.0)		6-8 (0.24-0.32)			
160-250 (6.4-10)		12-16 (0.48-0.64)			
<i>A</i> , mm <sup>2</sup> (in <sup>2</sup> )		<i>s</i> <sub>1,min</sub> , mm (in)			
<b>Forged parts made of light alloy</b>					
2500-5000 (100-200)		3.5 (0.14)			
10000-20000 (400-800)		5.5 (0.22)			
40000-80000 (1600-3200)		8.0 (0.32)			
<b>Minimum wall thickness</b>			<b>Cross section in the direction of forging</b>		
<i>h</i> , mm (in)	<i>r</i> <sub>1,min</sub> , mm (in)	<i>s</i> <sub>2,min</sub> , mm (in)			
<b>Forged parts made of steel</b>					
<10 (<0.4)		3 (0.12)			
10-16 (0.4-0.64)	2 (0.08)	4 (0.16)			
16-25 (0.64-1.0)	2 (0.08)	5 (0.20)			
25-40 (1.0-1.6)	3 (0.12)	8 (0.32)			
40-63 (1.6-2.52)	4 (0.16)	12 (0.48)			
63-100 (2.52-4.0)	6 (0.24)	20 (0.80)			
<i>h</i> , mm (in)	<i>r</i> <sub>1,min</sub> , mm (in)	<i>s</i> <sub>3,min</sub> , mm (in)			
<b>Forged parts made of light alloy</b>			<b>Fin Sidewall</b>		
6-10 (0.24-0.40)	1.0 (0.04)	3.5 (0.14)			
10-16 (0.40-0.64)	1.5 (0.06)	4.5 (0.18)	3 (0.12)		
16-25 (0.64-1.00)	2.0 (0.08)	6.0 (0.24)	4 (1.06)		
25-40 (1.00-1.60)	2.5 (0.10)	7.5 (0.30)	5 (0.20)		

*A* is the circular area in the case of round parts, the area of the surrounding square in the case of differently shaped parts.



Source: Compiled from [11.93] to [11.103].

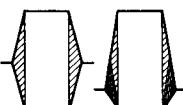
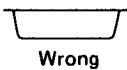
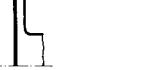
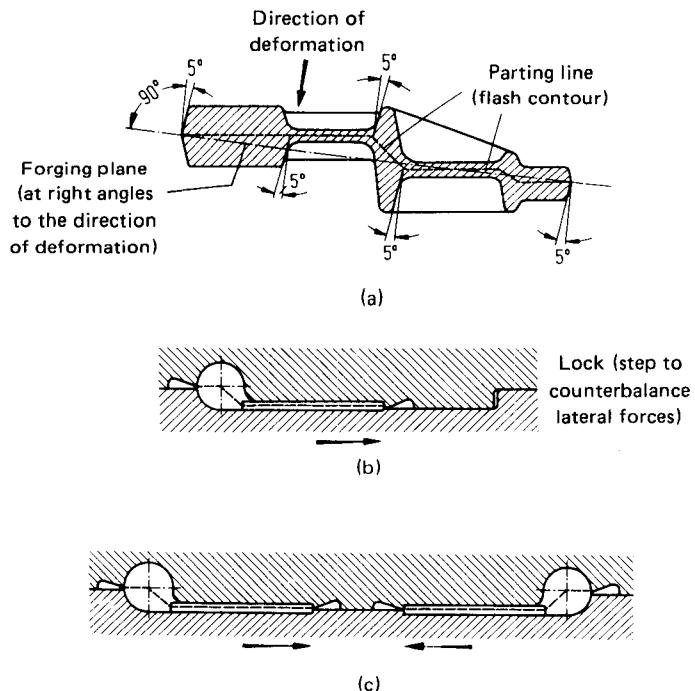
Design criteria	Principles	Examples
1 Symmetrical parting line		
Flash line not at the edge of the part	Right      Wrong 	 
2 Flat parting line		 
3 Parting line chosen to facilitate material flow	Desirable  Undesirable  "Stepped" often facilitates flow	
4 Parting line chosen to facilitate machining	Few surfaces with draft  Adequate clamping surfaces   	

FIG. 11.84 Basic rules for choosing the position of the parting line.

- 3 The parting line (flash line) should be positioned such as to facilitate material flow and reduce possible forging defects. In this respect, a broken parting line may be more suitable than a flat one, such as in the case of U-shaped sections and angles. With circular, pierced, and punched-through forgings with internal and external flash, a broken parting line is always preferable.
- 4 The parting line (flash line) should be positioned such as to facilitate clamping and material removal during subsequent machining. Surfaces to be machined and those used for clamping



**FIG. 11.85** Part position in die with stepped parting lines. (a) Sloping sides and parting line contour. (After [11.104].) (b) Lock (restraining ridge). (c) Forging in pairs.

as well as protruding surfaces should, where possible, not be in the sloping sides and should be kept free of flash.

Where a broken parting line exists, such as with nonaxisymmetrical forgings, components of the deformation force try to push the different parts of the die sideways with respect to each other. To prevent this, the impression must be cut in the die block in such a way that the parting line terminates at the same height and in the same plane as the forging plane, at a right angle to the direction of deformation. Where necessary, the angular draft must take into account local differences in slope angle between the parting line and the forging plane (Fig. 11.85a). Force compensation can also be achieved by providing a retaining ridge or by forging in pairs in order to achieve symmetry (Fig. 11.85b and c).

### 11.6.2 Design for Dimensional Accuracy

Variations in size due to shrinkage and changes in the dies must be taken into account by providing suitable tolerances. Standards for closed-die forgings made of steel are contained in DIN 7526 [11.29] which concerns the effect of dimensions, die parting, workpiece material, and geometry. The reader is also referred to Chap. 9 on dimensional accuracy. Dimensional tolerances for die forgings made of aluminum, magnesium, copper, and copper alloys are standardized in DIN 1749 [11.101, sheet 4], DIN 9005 [11.102, sheet 3], and DIN 17673 [11.103, sheet 4]. An improvement in the dimensional accuracy of individual dimensions may be achieved by sizing (Sec. 9.3.3).

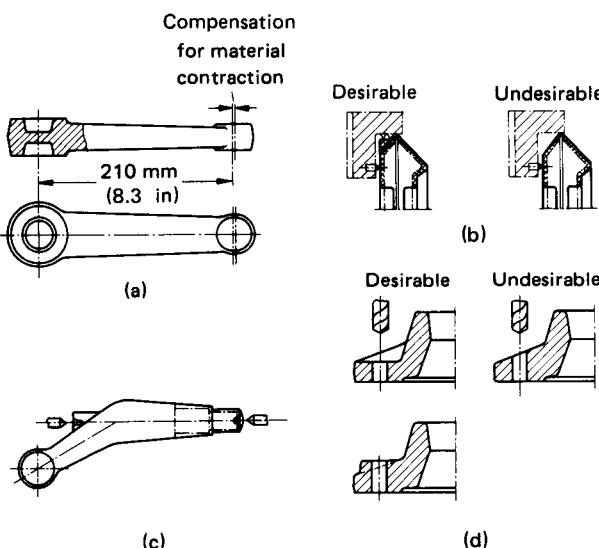


**FIG. 11.86** Design of die-forged parts to facilitate machining. (a) Design of lugs, eyes, etc. (b) Clamping of thin-walled parts. (c) Centering projection on bent lever. (d) Design to facilitate drilling.

### 11.6.3 Design for Ease of Machining

Machining allowances depend less on the surface finish of a die forging (see Sec. 11.2.3) than on surface decarburization and on surface cracks (in the case of difficult materials). With steel, a minimum machining allowance of 1.5 mm (0.06 in) is recommended. With long forgings, the circular lugs, journals, and cams are often forged oval in shape in order to counteract shrinkage. The surfaces most suitable for use as locating and clamping surfaces during the first machining operation are those where the tools are least subject to wear and permanent deformation. Surfaces to be drilled should be at a right angle to the direction of drilling (Fig. 11.86) [11.105] [11.106].

## 11.7 CLOSED-DIE FORGING TOOLS

### 11.7.1 Dies

An overview of the most important types of closed-die forging dies is given in Fig. 11.87. Dies with several impressions are termed *multipart* dies when the same operation is performed simultaneously on a number of different workpieces. *Multistage* dies, on the other hand, contain several impressions in the same tool for carrying out a sequence of *different* operations. Combined multipart, multistage dies also exist for certain small forgings. The use of die inserts can lead to savings in expensive tool materials, for example, in press forging of high-temperature steels. Inserts may be either clamped in position or held in place by the forging force itself [11.108], [11.109], [11.12]. Their main advantages are that they can often be produced economically in small batches and they require relatively little storage space.

Fig. 11.88 shows the important features of a hammer-forging die. The minimum block dimensions required for a given impression depth  $h$ , namely, the width, height, and length of the die block, can be determined easily by reference to Fig. 11.88 and Table 11.13. Different types of locating surfaces, as shown in Fig. 11.89, are provided to assure accurate positioning of the two halves of the die with respect to each other and to facilitate setup [11.110]. This necessitates addi-

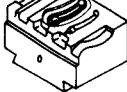
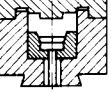
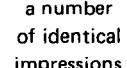
Die with flash gutters			Closed die	Die with several parting lines
Single-part die 	Multipart die: 	Multistage die 		Multistage die Workpiece Upset mandrel Holing punch Punch holder Die inserts Clamping die
Solid die 	Insert with a number of identical impressions 			

FIG. 11.87 Different types of forging dies. (After [11.107].)

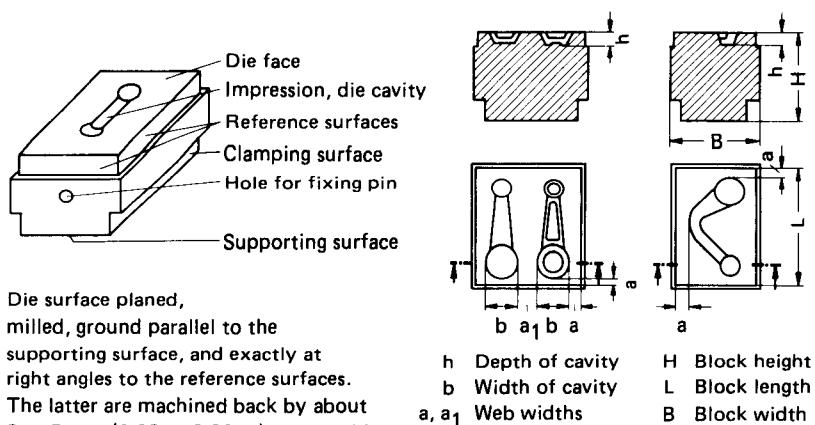
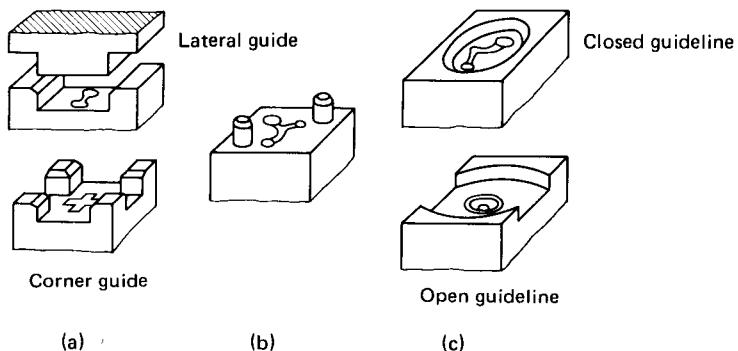


FIG. 11.88 Important parts of a forging die.

Table 11.13 Typical Dimensions of Die Blocks

<i>h</i> , mm (in)	<i>a</i> , mm (in)	<i>a</i> <sub>1</sub> , mm (in)	<i>H</i> , <sup>a</sup> mm (in)
6 (0.24)	12 (0.47)	10 (0.39)	100 (3.94)
10 (0.39)	32 (1.26)	25 (0.98)	125 (4.92)
40 (1.57)	56 (2.20)	40 (1.57)	200 (7.87)
100 (3.94)	110 (4.33)	80 (3.15)	315 (12.40)

<sup>a</sup>Add 10–25 mm (0.4–1.0) in the case of resinking.



**FIG. 11.89** Guiding of forging dies. (a) Flat guideway faces. (b) Guide pins dowels. (c) Cylindrical guideways.

tional material and a good deal of extra machining and thus should be avoided where possible. The same result can often be achieved by providing appropriately designed, correctly aligned, and well-maintained guideways on the forging equipment itself in conjunction with accurate and reliable clamping of the tools. Hammer dies are secured by tapered keys, that is, rammed keys and, more recently, tapered bolts [11.111; 11.112]. Press dies are normally bolted in place [11.113].

Forging dies are subjected to high mechanical and thermal stresses:

- 1 Deformation forces varying from 0 to 800–1000 N/mm<sup>2</sup> (116–145 ksi) and occasionally above
- 2 Frictional wear as a result of material particles sliding across the die surface under pressure at speeds up to 50 m/s (165 ft/s)
- 3 Shear stressing in the surface layers in the transition zone between sliding and sticking (leading to shear crack formation)
- 4 Rapid heating of the surface of the die cavity due to contact with the forging material under pressure; the die temperature increases from 100–200°C (212–392°F) (mean temperature of the die block during forging) to a maximum of 650–700°C (1202–1292°F) in the case of hammer forging of steel [temperature gradient 1000–3000°C/s (1832–5432°F/s)] (Fig. 11.90)
- 5 Higher heat penetration in the case of press dies, ranging from 330°C (626°F) to over 580°C (1076°F)
- 6 Localized annealing of the tempered die material as a result of forgings “sticking” to the die surface [above 730–830°C (1346–1526°F) in the case of steel]

The demands made on the die material are met to a greater or lesser extent by a range of different materials the use of which depends on the size, geometry, and material of the forging as well as on the batch size. Carbon steels with 0.7–0.85% C are appropriate for small tools and flat impressions, medium-alloyed tool steels for hammer dies, and high-alloyed steels for high-temperature-resistant dies used in presses and horizontal forging machines (Table 11.14). For cast dies and die inserts, such as those produced by the Shaw process, steels of similar composition are used [11.115], [11.116].

The dimensions of the die cavity (created by casting, cold hobbing, hot hobbing, turning, milling, spark erosion, and chemical removal processes; see Chaps. 31 to 33) should be 3–5 ISO qualities (minimum 1 ISO quality; see Sec. 9.4) better than the accuracy required of the work-piece. These dimensions change during forging due to wear and permanent deformation as a result of the stressing mentioned above. Cushion faces (impact surfaces) on hammer dies should be large enough to prevent deformation. According to [11.41] they should be  $15-18 \times 10^3$  mm<sup>2</sup>/t (21.1–25.3 in<sup>2</sup>/ton) of tup weight at  $v_T \approx 5$  m/s (15.2 ft/s) and  $25-30 \times 10^3$  mm<sup>2</sup>/t (35.2–42.2 in<sup>2</sup>/ton) at  $v_T \approx 7$  m/s (21.3 ft/s). Fig. 11.91 shows which parts of the die impression are most liable to permanent deformation and wear resulting from mechanical and thermal fatigue.

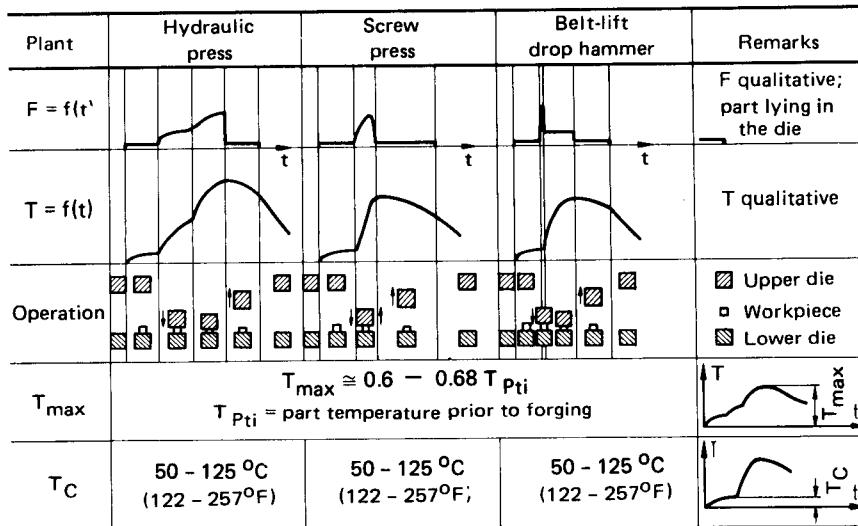


FIG. 11.90 Force and temperature at die surface during upsetting with different forging plants. (After [11.114].)

Wear depends not only on the shape of the forging and on the die material (Fig. 11.92), but also on how the workpiece is heated and on the heat treatment and coating of the die surface. For the latter, nitriding and chromium plating are being used (Fig. 11.93). In recent years boriding [11.120] has also been introduced with considerable success. Investigations [11.118], [11.119] have shown that the tensile strength of the die material, the die temperature, and the alloying elements have an approximately equal effect on the wear of Cr-W-Mo-V-alloyed die steels. It is recommended to harden and temper dies to the highest strength possible. The "operating tem-

Table 11.14 Common Steels Used for Forging Dies<sup>a</sup>

Forging material	Steel		Copper and copper alloys		Light alloys	
	DIN	AISI	DIN	AISI	DIN	AISI
Forging dies	C70W2	—	X30WCrV53	H21	X30WCrV53	—
	C85W2	—	X38CrMoV51	H11	X38CrMoV51	H11
	60MnSi4	—	X32CrMoV33	H10	55NiCrMoV6	6F2
	40CrMnMo7	—	57NiCrMoV77	—	56NiCrMoV7	6F3
	55NiCrMoV6	6F2	—	57NiCrMoV77	—	—
Die inserts	56NiCrMoV7	6F3	—	—	—	—
	57NiCrMoV77	—	—	—	—	—
	35NiCrMo16	—	—	—	—	—
	X38CrMoV51	H11	X30WCrV93	H21	X38CrMoV51	H11
	X32CrMoV33	H10	X32CrMoV33	H10	X32CrMoV33	H10
	X30WCrV53	—	X30WCrV53	—	X30WCrV53	—
	X37CrMoW51	H12	—	—	—	—

<sup>a</sup>See App. C.

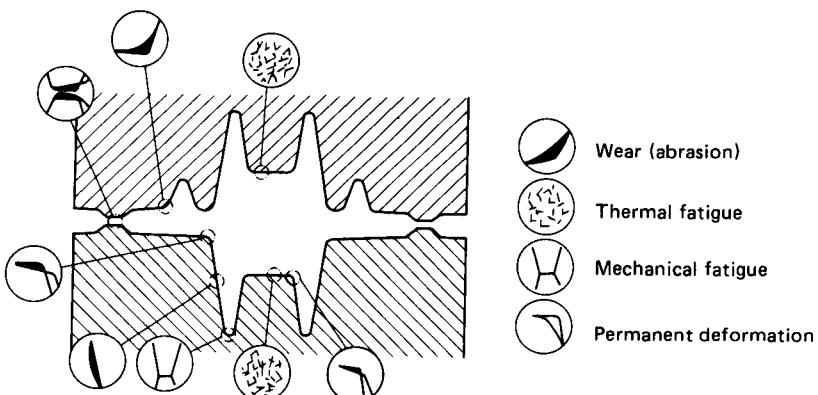


FIG. 11.91 Different types of die failure. (After [11.117].)

perature," which is a function of forging temperature and time, should not exceed the annealing temperature. The improvement in wear resistance obtained by the addition of chromium, tungsten, molybdenum, and vanadium is due to the tendency of these elements to form carbides.

### 11.7.2 Trimming Tools

Fig. 11.94 shows the principal types of trimming tools. Trimming and punching of forgings whose flash is not at the edge of the workpiece are performed with a large clearance gap  $u > 0.5$  mm (0.02 in). The shearing operation is already over by the time the punch enters the clipping bed.

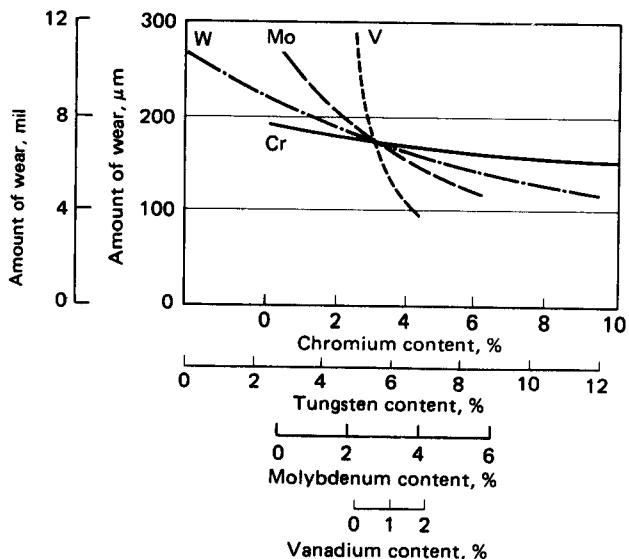
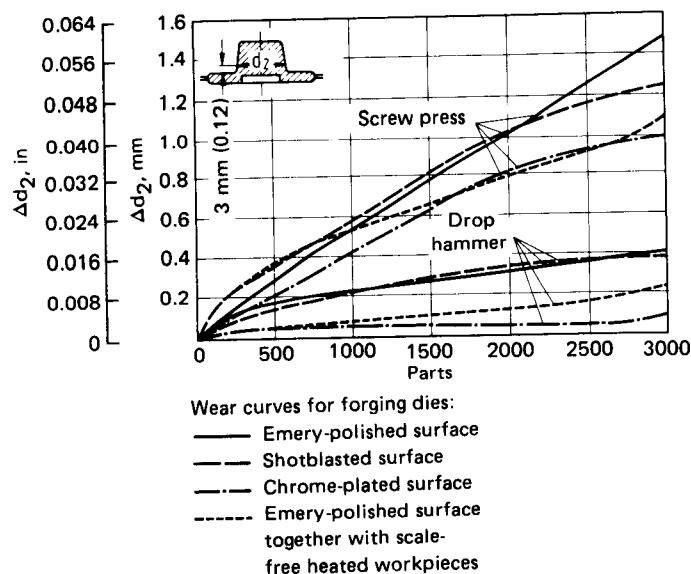


FIG. 11.92 Degree of wear as a function of the presence of the alloying elements Cr, W, Mo, and V. Mean die temperature  $T_0 = 275^\circ\text{C}$  ( $527^\circ\text{F}$ );  $S_u = 1600 \text{ N/mm}^2$  (232 ksi). (After [11.118], [11.119].)



**FIG. 11.93** Frictional wear of forging dies. Influence of the equipment used, the type of surface finish of the die, and the type of heating of the part. (After [11.69].)

When the flash runs along one edge, similar conditions exist as those occurring in shearing of sheet metal. A clearance gap  $u \approx 0.3$  mm (0.01 in) is needed to obtain a clean cut. When an external and an internal flash has to be removed from the same workpiece, this can be performed either in sequence or simultaneously using combination tools. Such tools can also carry out additional operations such as straightening.

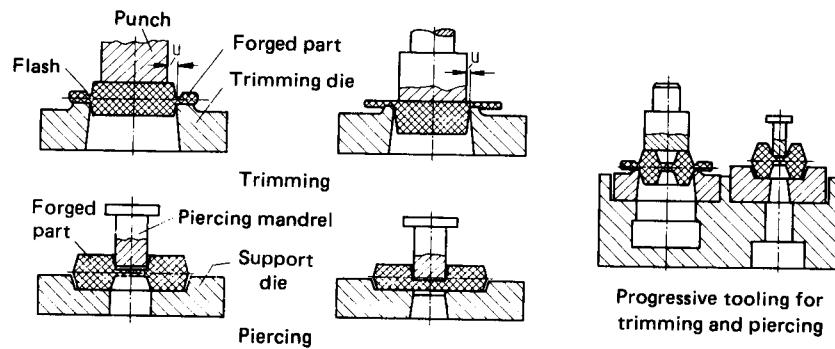
The choice of which material to use for trimming tools depends on temperature, flash thickness, flash length, and the resistance of the forging material to shearing. Table 11.15 contains some steels commonly used for trimming tools. As with dies, highly stressed trimming tools can be “armorplated” at the cutting edges through localized disposition of special metals\* by welding. The main materials used in conjunction with hot-trimming beds are C35, C45, and C60; for hard facing by built-up welding special materials such as X30WCrV53 (AISI H21) are used.

## 11.8 FORGING EQUIPMENT

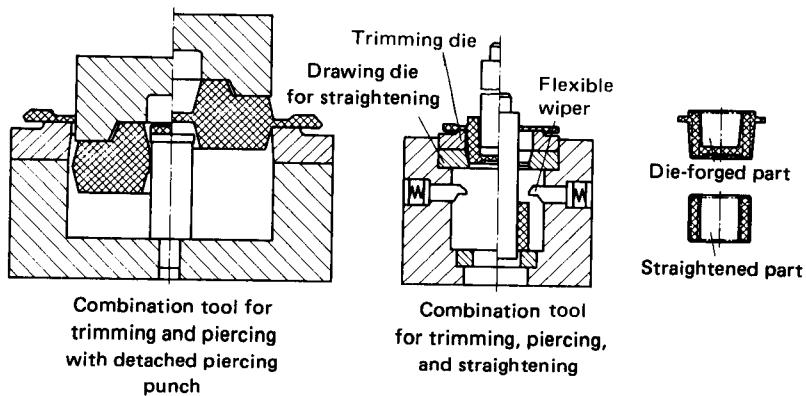
Forging is performed by means of hammers (drop hammers, double-acting anvil hammers, counterblow hammers, high-speed hammers) and presses (screw presses, crank or eccentric presses, hydraulic presses). For certain categories of forged parts, horizontal forging machines, multistage presses, and ring rolling machines are suitable. Rotary forging machines, electropressetting machines, and forging rolls (for section rolling and cross rolling), as illustrated in Fig. 11.2, are used mainly for preforming (material distribution). Trimming and piercing as well as straightening or bending after closed-die forging are carried out on crank and hydraulic presses.

Selection of the most appropriate forging machine depends on the operation to be performed, the workpiece (geometry, size, material), the number of parts required, the degree of automation,

\*Hard-facing materials for dies (also used for die repairs) are low-alloy ferrous metals, high-alloy ferrous metals, nickel-based and cobalt-based alloys, and carbides according to alloy groups 1 to 5 in [11.78, pp. 563–567], as well as cobalt-based alloys, such as stellite 6B or 6K and Haynes 25, according to [11.78, pp. 589–590].



(a)



(b)

**FIG. 11.94** Trimming tools for forged parts. (a) Basic design. (b) Particular examples.**Table 11.15** Steels Used for Trimming Tools<sup>a</sup>

Trimming tool	Material designation	
	DIN	US
Hot trimming	C67W3	SAE C1070
	40CrMnMo7	—
	45WCrV7	AISI S1
	60MnSi4	—
	55NiCrMoV6	AISI 6F2
	56NiCrMoV7	AISI 6F3
Cold trimming	C70W2	—
	C85W2	—
	60WCrV7	AISI S1
	X210CrW12	AISI D6

<sup>a</sup>See App. C.

**Table 11.16** Types of Forging Equipment<sup>a</sup>

Type of equipment	Capacity kJ (ft · ton)	Automation	Personnel	Vibration noise	Applications	
					Open-die forging	Closed-die forging
Hammers						
Arvil hammers						
Belt-type drop hammers	1.6–40 (0.6–14.7)	Difficult	Skilled			All forged parts, especially those requiring large forces with respect to their size or weight. (Thin parts of large surface area; parts with abrupt changes of crosssection or pronounced ribs.)
Pneumatic lift hammers	6.3–80 (2.3–29.5)	Difficult	Skilled			
Hydraulic lift hammers		Difficult	Skilled			
Board drop hammers	1.6–50 (0.6–18.4)	Difficult	Skilled			
Pneumatic hammers	1.6–50 (0.6–18.4)	Difficult	Skilled			
Double-acting hammers	5–100 (1.8–36.8)	Difficult	Skilled			
Counterblow hammers						
Vertical, equal masses	80–1250 (29.5–460)	Difficult	Skilled			High-energy forming of high- strength material
Vertical, unequal masses		Difficult	Skilled			requiring high finish-forging forces. Forging in
horizontal, equal masses	6.3–63 (2.3–23.2)	Given	Semiskilled			a single blow.
High-speed hammers (counterblow principle usually with unequal masses)	60–2270 (22.1–836)	Difficult	Skilled			

**Table 11.16** Types of Forging Equipment<sup>a</sup> (*Continued*)

Type of equipment	Capacity	Automation	Personnel	Vibration noise	Applications	
					Open-die forging	Closed-die forging
Presses	MN (ton)					
Mechanical presses						
Screw presses	0.63–63 (70.9–7090)	Possible	Semiskilled	Little vibration, medium noise levels	Upsetting and piercing	Smooth-surfaced parts with a single main shape. Parts mainly requiring upsetting or extruding.
Crank (eccentric presses)	3.15–100 (354–11,250)	Possible	Semiskilled			Variations in temperature and initial weight of material cannot be excluded.
Hydraulic presses	5–750 (562–84,400)	Possible	Skilled	No vibrations, medium to low noise levels	Bar forging, bending, etc. up to $\approx$ 10 MN (1125 ton) For large forgings up to 150 MN (16875 ton)	Trimming, upsetting of large steel workpieces up to $\approx$ 15 MN (1690 ton). Isothermal forging of light alloys up to 750 MN (84,400 ton).

Special-purpose finish-forming machines	MN (ton)		
Horizontal forging machines	Possible	Semiskilled	Disk-shaped parts, with or without shafts, pierced workpieces, rings.
(Hot) multistage presses	Given	Skilled	Disk-shaped parts without shafts, rings.
Ring rolling machines	Possible	Skilled	Rings.
Special-purpose material-distributing machines (finish forming of simple parts possible)			
Stretch rolling machines	Possible	Semiskilled	Bar-shaped parts of varying cross sections.
Cross rolling machines	Possible	Semiskilled	Circular parts of cross-sectional ratio $A_0/A_n \approx 4$ .
Electropunchsetting machines	Possible	Semiskilled	Upsetting of large volumes of material.
Rotary forging machines	Possible	Semiskilled	Stepped and tapered shafts.

<sup>a</sup>See also Chap. 8, Tables 8.3 and 8.4.

Source: Compiled from [11,107].

the skill of the operating personnel, and on other factors, such as permissible vibration and noise levels. Another important factor is the optimal size of each type of machine.

A forging operation is described by its force-displacement curve, the temperature of workpiece and tool, and the time taken to carry it out. Material distribution operations, such as drawing out and upsetting, in general have a gradually increasing force-displacement curve, whereas in piercing with a mandrel, the force remains more or less constant over the entire forging stroke. In bending, the maximum force arises at between 30 and 70% of the forging stroke. By contrast, closed-die forging with and without flash is characterized by a rapid increase in the deformation force just before the end of the forging operation (see Fig. 11.52). Thus it is possible to use crank presses with small angles of action ( $\alpha \approx 10^\circ$ ), relatively low work capacities, large numbers of strokes, and correspondingly short contact times for the closed-die forging of steel. Light alloys permit isothermal forging in heated dies, without exceeding the annealing temperature of the die. Thus considerably more powerful hydraulic presses can be used with  $F_{N,\max}$  up to 750 MN (84,400 ton) (in the United States up to 50,000 ton), while crank presses are only built to  $F_{N,\max} \approx 100$  MN (12,000 ton). With hydraulic presses both force and speed can be controlled easily so that they have now largely superseded hammers for open-die forging where smaller forces are required. Hammers, for their part, have the advantage of ease of adaptability to changing conditions. They are the cheapest machines for generating large forces, but have the disadvantage that they are very noisy and often cause vibrations. Table 11.16 (p. 11.90) is based on the consideration of these and other important factors. Guidelines for the allocation of closed-die steel forgings to hammers and presses based on their weight are given in Fig. 11.95. The allocation of open-die forgings to hammers and presses was discussed in Sec. 11.2.1.

The fundamental principles of forging hammers and presses were described in Chap. 8. That chapter also contains numerous examples of such equipment to which the reader is referred. Thus this section only contains additional information to illustrate how forging operations and forging equipment interact with one another. Material, deformation speed, forging temperature, work-

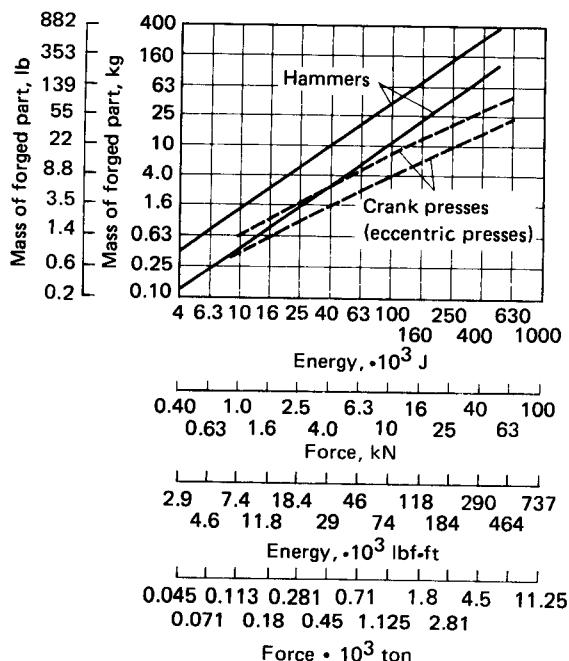


FIG. 11.95 Choice of hammers and crank (eccentric) presses for forging parts of different weights. After [11.107].)

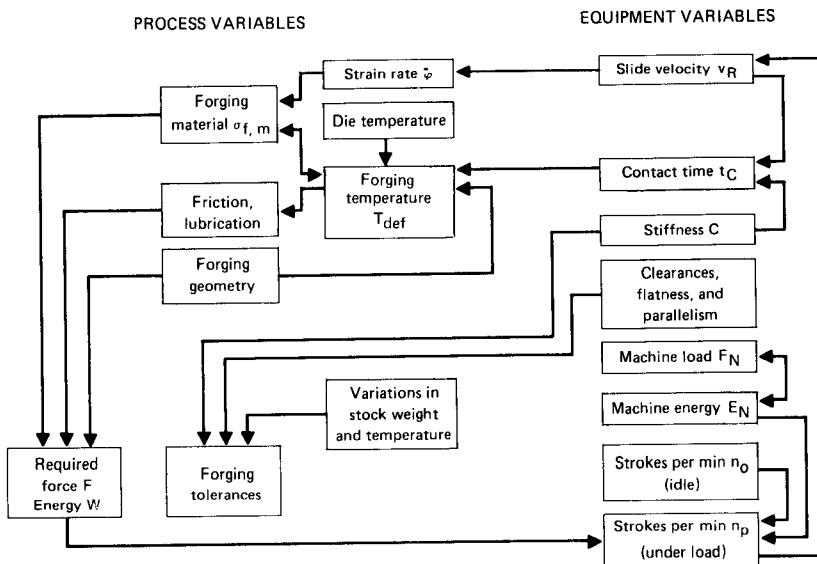


FIG. 11.96 Relationships between process and equipment variables in closed-die forging with a screw press. (After [11.46].)

piece geometry, slug shape, friction, and lubrication all affect the force and work requirements and the working accuracy (see Chap. 9). The interrelationship between these factors is shown in Fig. 11.96 based on the example of closed-die forging with a screw press. The figure represents a preliminary step toward a flow diagram and opens up the way to numerical systems analysis. By varying input values the effects on the equipment and the forging can be assessed quantitatively. Optimal conditions can be determined by means of simulation [11.47].

### 11.8.1 Equipment for Open-Die Forging

Both single- and twin-column hammers are used for open-die forging. In all types of hammers, the emphasis is placed on easy accessibility to the work area to facilitate workpiece manipulation. The anvil sits on a foundation and is not joined directly to the hammer frame itself. The driving force is provided by compressed air or steam at pressures of 6–7 bar (87–102 psi). Control independent of the tup motion permits setting and “sticking” blows. Modern hammers are often valve-controlled. Single-column power hammers are built to capacities of about 40 kJ (14.7 ft·ton), which corresponds to a tup weight of 2 t (2.2 ton).

Small rapid-blow hammers for drawing out high-grade steel bars [ $E_N = 1.6\text{--}1.7 \text{ kJ}$  (0.6–0.62 ft·ton)], with tup weights of 100–400 kg (220–882 lb)] reach rates of between 200 and 400 blows per minute. The twin-column power hammers shown in Fig. 8.22 are used for forging shaped components. They are built to capacities of  $E_N = 250 \text{ kJ}$  (92.1 ft·ton), although in practice they seldom go beyond  $E_N \approx 100 \text{ kJ}$  (36.8 ft·ton). More recently they have largely been superseded by hydraulic presses. Besides hammers whose energy is sup-

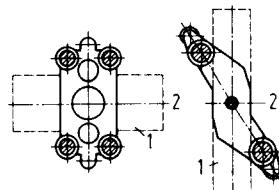
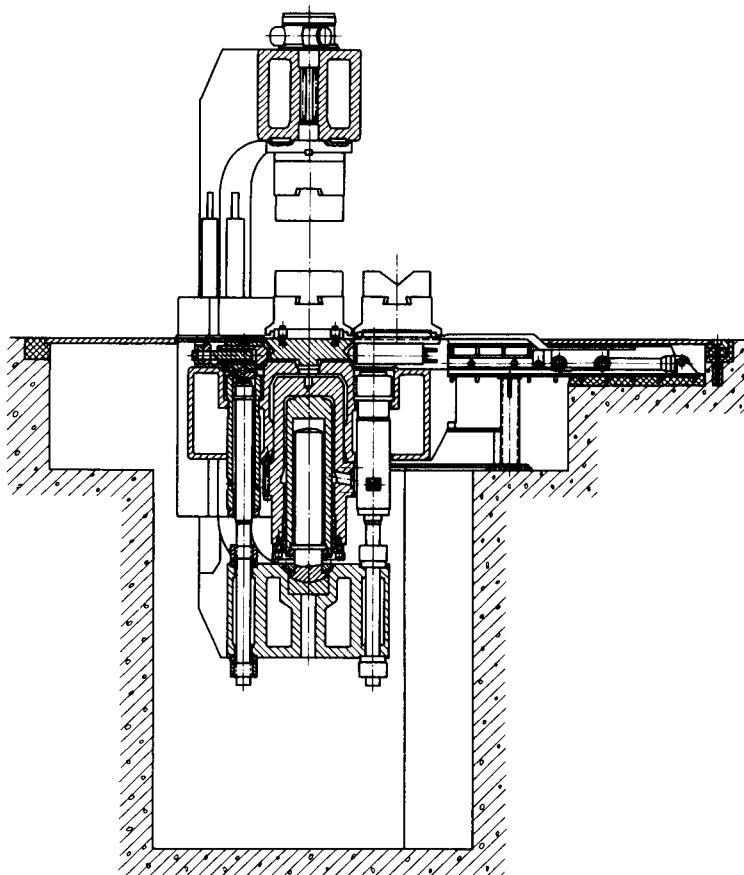


FIG. 11.97 Location of columns in two- and four-column presses. 1—space for tooling; 2—operating position.

plied by a centralized supply system, so-called air hammers (see Fig. 8.21) are widely used for forging bars and shaped components. Their range extends to 50 kJ (18.4 ft·ton) with between 80 and 250 blows per minute.

Forging presses are of the single-frame and the two- and four-column types (Fig. 11.97). Single-frame presses have the advantage of providing unimpeded access from three sides. However, undesirable stressing in the C-shaped frame limits their use to  $F_N \leq 12 \text{ MN}$  ( $1.35 \times 10^3 \text{ ton}$ ). Twin-column diagonal-frame presses with underfloor drives have found wide acceptance up to  $F_N \approx 20 \text{ MN}$  ( $2.25 \times 10^3 \text{ ton}$ ). They are used in particular in automated forging processes with manipulators and similar handling aids (see Fig. 11.67). Fig. 11.98 shows a section through such a press. The rectangular cross section of the frame exhibits good resistance to deflection during off-center loading. Four-column presses for open die forging are available (as a rule with several force ranges) for up to  $F_N \approx 150 \text{ MN}$  ( $1.69 \times 10^4 \text{ ton}$ ). The largest presses are capable of forging ingots up to and sometimes exceeding 350 t (386 ton). Fig. 11.99 shows a section through a 16/25/41-MN (1800/2812/4612-ton) forging press (see also Fig. 8.48). Hydraulic pressures lie between 250 and 315 bar (3.63 and 4.57 ksi). While steam presses have lost their former significance, purely hydraulic presses up to  $F_N \approx 20 \text{ MN}$  ( $2.25 \times 10^3 \text{ ton}$ ), with storage vessel and water as the hydraulic medium, are gaining importance, as well as presses with direct pump drive, which use oil as the hydraulic medium. For bar forging a particularly rapid sequence control is



**FIG. 11.98** Section of a diagonal-frame underfloor hydraulic press. (Courtesy of Sack.)

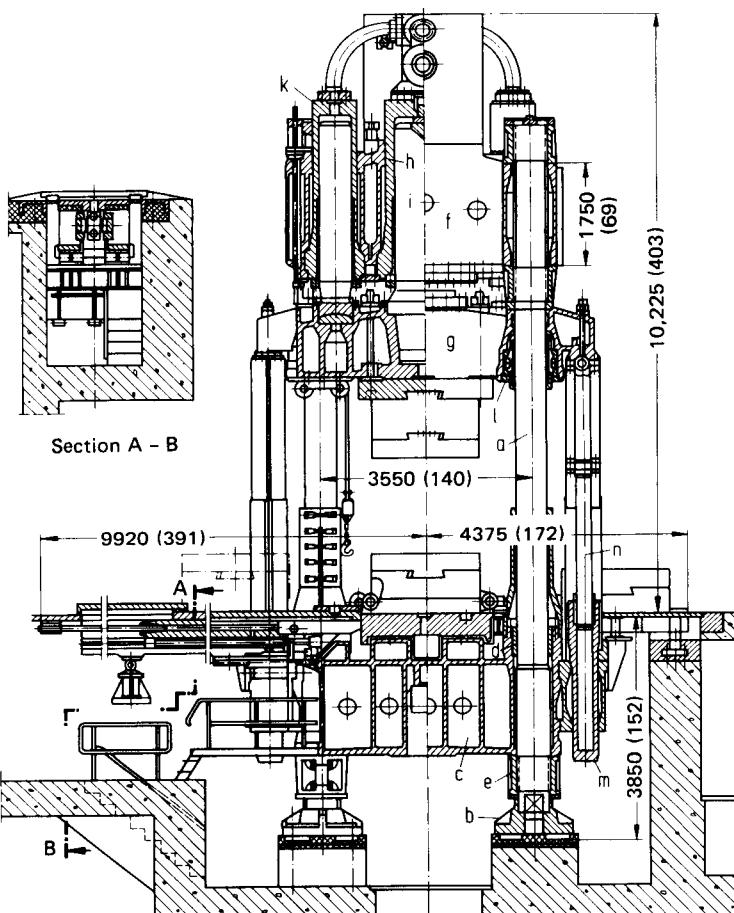


**FIG. 11.99** Hydraulic four-column open-die forging press. Forging force 16/25/41 MN (1800/2813/4613 ton), hydraulic pressure 315 bar. *a*—columns; *b*—column feet; *c*—lower holm; *d,e*—sleeves; *f*—cylinder holm; *g*—moving holm; *h*—main cylinder; *i*—piston; *k*—side cylinder; *l*—guide bearings; *m*—retracting cylinders; *n*—plunger. Dimensions are in mm (in). (Courtesy of SMS Hasenclever, Düsseldorf.)

needed. For example, at  $F_N = 15 \text{ MN}$  ( $1.69 \times 10^3 \text{ ton}$ ), 40–60 preforging strokes and 100–150 finish-forging strokes of 20–30 mm (0.79–1.18 in) are required per minute. Finally, a special-purpose drive for bar forging is provided by crank-driven equipment with a corresponding constant press stroke, where the stroke position is varied by the supply and withdrawal of pressurized water.

### 11.8.2 Equipment for Closed-Die Forging

#### *Equipment for Finish-Forging and Preforming*

For information on the most commonly used forging hammers the reader should refer to Secs. 8.1 and 8.2.1. Likewise, Sec. 8.2.2 contains detailed information with regard to screw presses,

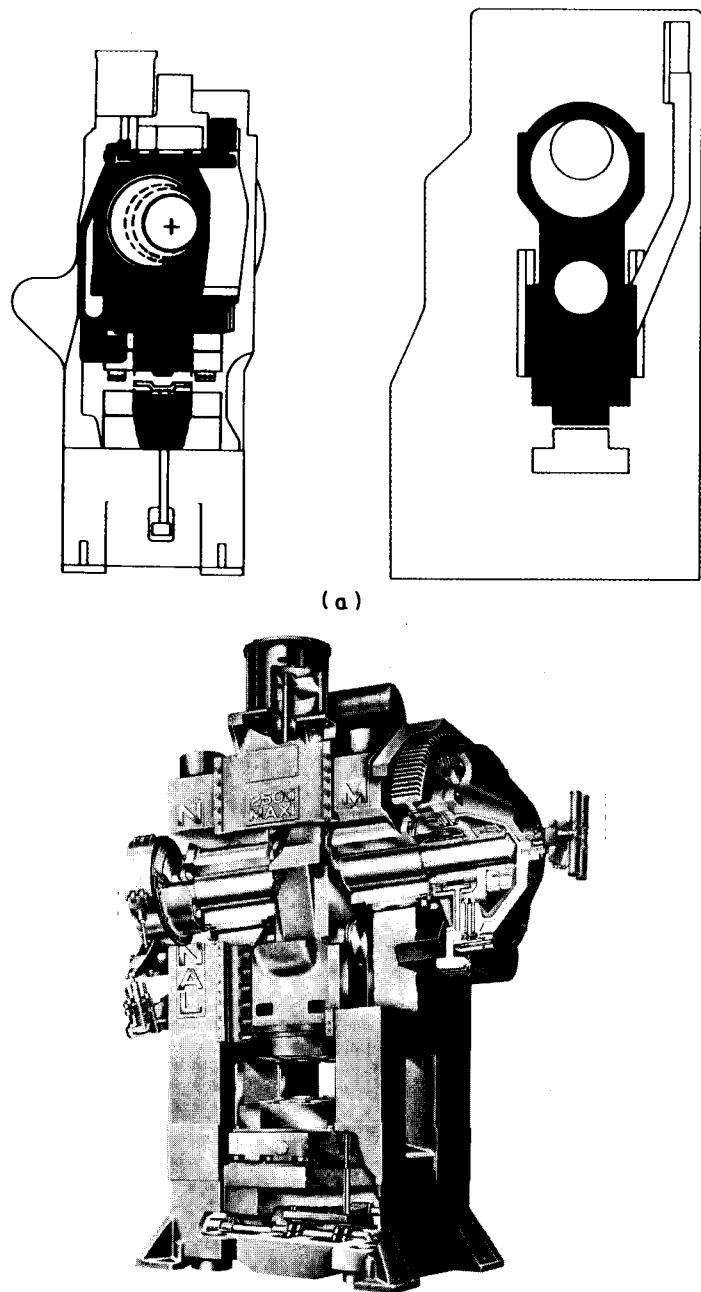


**FIG. 11.100** Mechanical forging presses with eccentric drive. Force 25,000 kN (2755 ton); stroke 355 mm (14 in); strokes per minute 55; table dimensions 1208 × 1372 mm (48.3 × 54 in). (a) Drive systems—Scotch yoke drive (left), Pitman arm design (right). (Courtesy of ERIE Press Systems.) (b) 2500-ton Maxipress with optional hydraulic wedge ram wear plate and two-point lower kickout. (Courtesy of National Machinery.)

which have the advantage over hammers of greater working capacities for equal amounts of moving weight.

Mechanical fixed-stroke vertical crank presses for closed-die forging, similar to the one shown in Fig. 11.100, have been built for force ratings up to  $F_N \approx 100$  MN (12,000 ton). Such presses are characterized by very small crank angles  $\alpha_N$ , rigid construction, and high stroke rates. Recent development in Germany [11.121] has concentrated on wedge-type presses with the drive away from the main line of the acting force (Fig. 11.101). This arrangement permits even higher longitudinal spring constants and counteracts the tendency of the ram toward tilting due to eccentric loading, which is common with multistage dies. As a result of a wedge ratio of about 2:1, both the crankshaft and the pressure bar are subjected to only about one-half the total compressive load. At present wedge-type die-forging presses ranging up to 120 MN (135 ton) are being planned. All types of mechanical fixed-stroke die-forging presses are highly suitable for automation.

Hydraulic presses for closed-die forging of the four- and multicolumn types as well as frame constructions are generally driven overhead. The various types of drives are the same as for open-die forging presses. In the few presses rated above 200 MN (22,500 ton) [in West Germany 300 MN (33,800 ton), in the United States 450 MN (50,600 ton), and in the USSR 750 MN (84,400 ton)] hydraulic pressures of more than 315 bar (4.57 ksi) are used in order to keep down the size or the number of the required cylinders. The very large presses as well as most of the smaller ones use water as the hydraulic medium in conjunction with storage vessels.

### *Special-Purpose Equipment for Finish-Forging*

The most commonly used special-purpose machines for finished-forging are horizontal upsetting machines, multiple-die presses, and ring rolling mills.

Horizontal upsetting machines, often referred to as horizontal forging machines, are effectively double-acting crank or eccentric presses lying on their sides [11.122]. Split tools or "clamping dies" are driven via a clamping drive. They grip the workpiece tightly during forging by means of a punch fixed to the ram. (The tools are shown in Fig. 11.87, suitable workpieces in Fig. 11.79.) Various designs exist, which differ in the position of the parting line (horizontal or vertical), the type of drive, and the shape of the frame. Fig. 11.102 shows a widely used design with a vertical parting line, while Fig. 11.103 shows one with a horizontal parting line. The latter arrangement facilitates automation in the multistage forging process. All types of horizontal forging machines are constructed in such a way that the clamping force is equal to the rated value of the main ram. The clamping jaws or ram can take between two and six tools, depending on size.

Automatic hot multiple-die presses are used for the mass production of small [10 g to > 2 kg

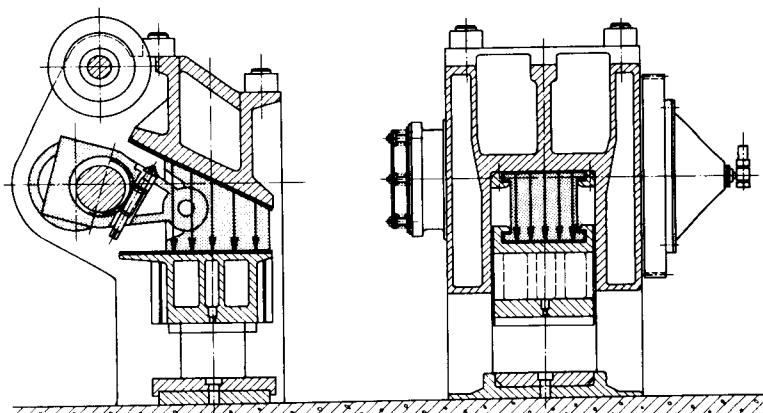
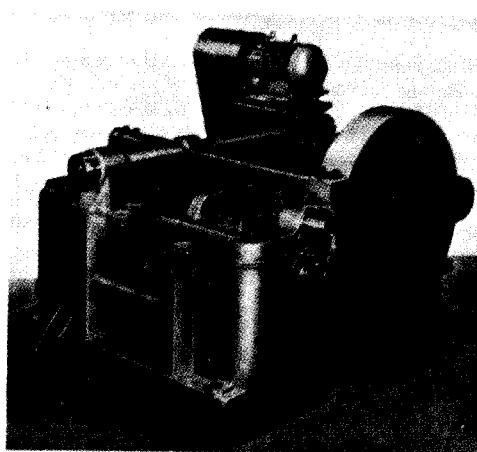


FIG. 11.101 Wedge-type die-forging press. (Courtesy of Eumuco.)



**FIG. 11.102** Horizontal forging machine (upsetter) with vertical clamping dies. (*Courtesy of Kieserling/Ajax.*)

(0.02 to  $> 4.4$  lb)], mostly disk-shaped workpieces for gear blanks, nuts, and rings. They are high-performance machines and work in conjunction with integral heating and handling equipment.

Ring rolling mills, operating on the principle shown in Fig. 11.2, are used to roll rings to precise diameter, wall-thickness, and height tolerances. Blanks are in the form of upset and pierced disks. Rolling out is performed in several stages with automatic handling of the workpiece between steps. Four-stage rolling mills with a vertically driven central roll are the most common type [11.12].

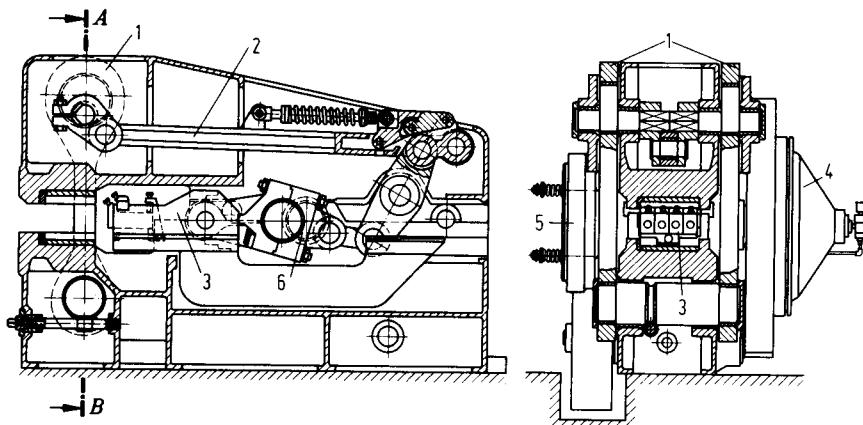


**FIG. 11.103** Horizontal forging machine (upsetter) with horizontal clamping dies and jaw clamping system. 1—connecting rods for clamping; 2—safety pressure bar of clamping drive; 3—ram (upsetting slide) with tool holder; 4—electropneumatic clutch; 5—electropneumatic brake; 6—crankshaft. (*Courtesy of Eumuco.*)

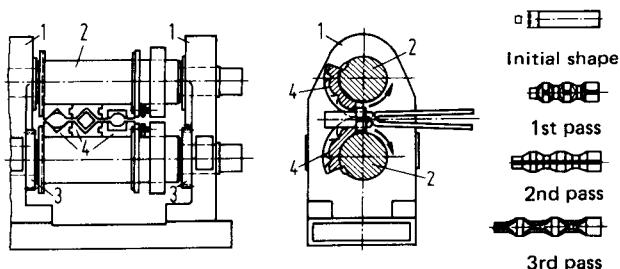


**FIG. 11.104** Forging roll. 1—frame (drive on left not shown); 2—rolls; 3—drive for setting rolling gap; 4—roll segments. (Courtesy of Eumuco.)

### Special-Purpose Machines for Preforging (Material Distribution)

Preforging rolling mills are longitudinal profile rolling machines used to modify workpiece cross sections. The tools are in the form of roll segments which can be changed easily. Roll forging is usually a reversing process; that is, the workpiece returns to its starting position after one rotation. Continuous throughput processes also exist. Workpiece handling can be automated. Fig. 11.104 shows the operating principle of a roll-forging mill. The distance between rolls can be varied by adjusting the eccentrically mounted journals. The rolls are linked electropneumatically to the drive. The characterizing parameters are work capacity, torque, power, and roll size. Preforging rolling mills have roll segment diameters of 240–800 mm (9.45–31.5 in), drives of 10–40 kW (13.4–53.6 hp), and rotational speeds of 140–50 r/min. Typical bar sizes lie between 25 and 150 mm (1.0 and 5.9 in) in diameter.

Cross-rolling mills (which operate on the principle shown in Fig. 11.105) are more productive than section-rolling mills, but have a narrow field of application. Workpieces are finish-rolled in one revolution. Cross-rolling mills are used for preforging to obtain desired material distributions and also to produce blanks for machining on automatic lathes and plunge-type grinding machines.

Electropunching machines are used to achieve localized concentrations of large quantities of material. Further information is given in Sec. 10.2.2.

Rotary forging or swaging machines, which are usually of the horizontal type for automatic forging of round and different-shaped bars, may be used for forging stepped bars of varying cross-sectional areas. They work on a feeding-through or plunging-in basis, as shown in principle in

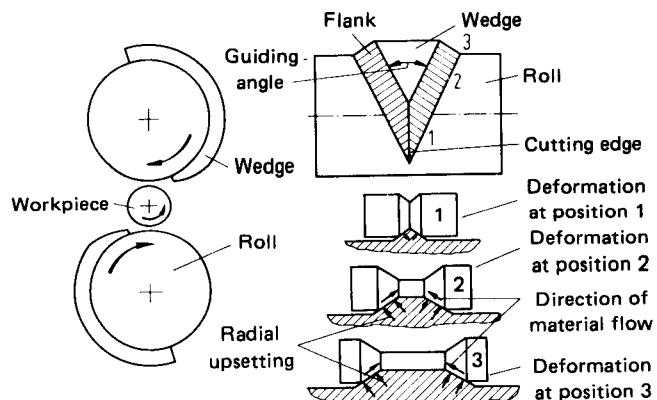
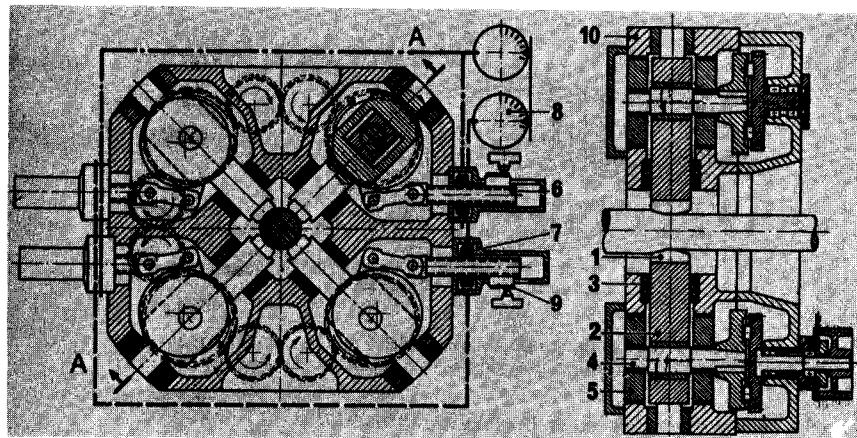
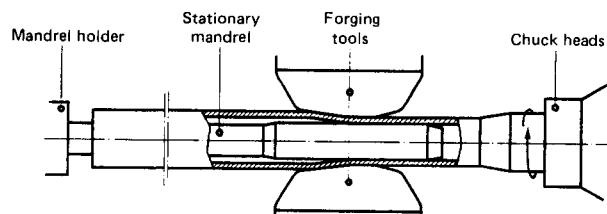


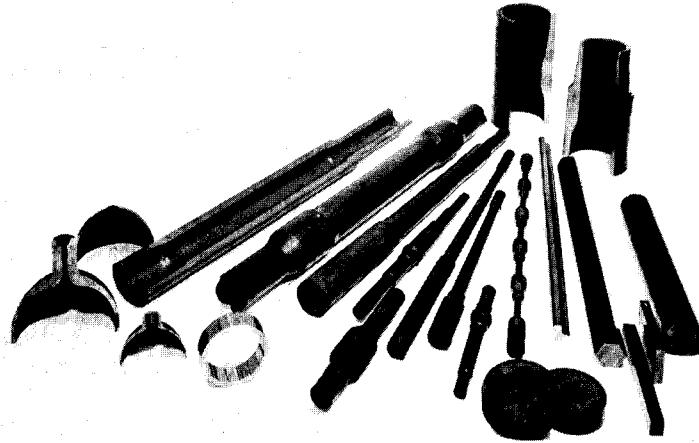
**FIG. 11.105** Method of operation of a transverse or cross rolling machine. (Courtesy of WMW.)



(a)



(b)



(c)

**FIG. 11.106** Precision-forging machine with eccentric drive. (a) Forging box with chuck head component feed. 1—forging tool; 2—connecting rod; 3—straight guide; 4—eccentric; 5—adjustment housing; 6—adjusting screw; 7—worm drive; 8—setting scale; 9—adjustable cams; 10—forging box. (b) Calibrating a tube on stationary mandrel with horizontal workpiece axis. (c) Samples of precision forgings. (Courtesy of GFM.)

Fig. 11.2. The workpiece is either rotated and moved forward or simply rotated. Due to scale formation, only rotary forging machines with crank drive and three or four radially positioned rams working toward each other are suitable for hot forging, the stroke of the rams being varied by means of eccentric journals (Fig. 11.106). Axial and rotational feed of the workpiece is via a moving headstock. Rotary forging machines are most economical for small- and medium-batch production of stepped shafts. Control is either analog by means of cams and dogs, or digital by means of numerical control.

## 11.9 FORGING DEFECTS

Defects in forgings resulting from the forging process itself may be divided into the following categories [11.82]:

- 1 Surface marks or cracks, usually caused by mistakes during formation of the initial or intermediate shapes.
  - a Marks on the finished forging due to defects in the surface of the initial or intermediate shapes, for example, caused by cropping or intermediate trimming operations.
  - b Overlaps resulting from bending of intermediate flash, usually caused by excessive spreading, for example, during swaging or stretch rolling (Fig. 11.107).
  - c Crack formation as a result of (1) Sharp edges combined with inappropriate dimensioning of the intermediate shape of the forging during rising. The workpiece material first loses contact with the die while flowing over the edge. The resulting cavity closes up later on (Fig. 11.108). (2) Sharp corners and edges on bent intermediate shapes because the material in the area between the two limbs of the forging is not joined together properly (Fig. 11.109). Folds of this kind often extend right into the core of the forging. They can be avoided by designing a web in the critical area (Fig. 11.110). (3) Too much material. When the die cavity is already full before the finishing point has been reached, material is forced outward from the core through the flange cross section (Fig. 11.108c). Here a possible solution is to change the position of the flash.
  - d Marks due to cracks in the dies.
- 2 Inadequately filled forgings due to an insufficient volume of material, unsuitable intermediate shapes, inexact positioning, incorrect dimensioning of the die land, or high lubricant gas pressures.
- 3 Mistakes in the material structure, such as defects in the grain flow.

Shape and dimensional errors are discussed in Chap. 9. Further sources of error are impure starting material and incorrect heat treatment. Where the defects are removed by subsequent machining, they do not lead to rejection of the forging.

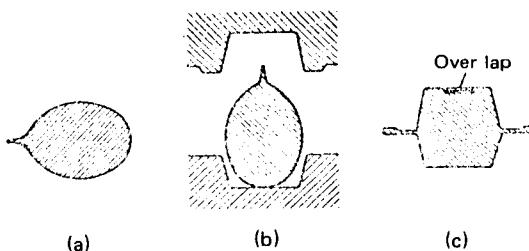


**FIG. 11.107** Overlap formation. (a) Rolled intermediate shape with one-sided flash. (b) Position in finishing dies. (c) Defective forging.

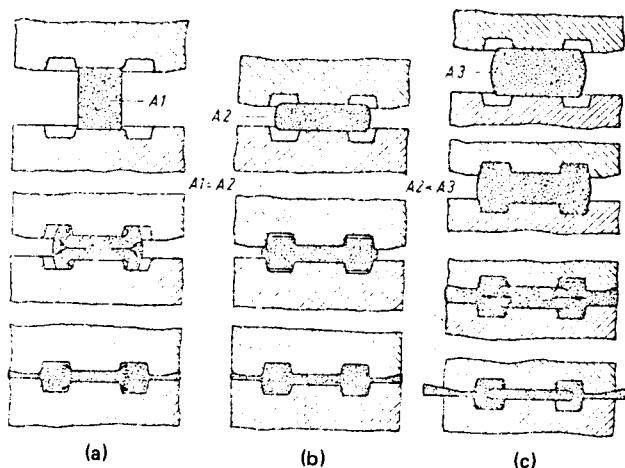


**FIG. 11.108** Forging of H sections from starting materials of different shapes and sizes. (a) Wrong. (b) Right. (c) Wrong. (After [11.95].)

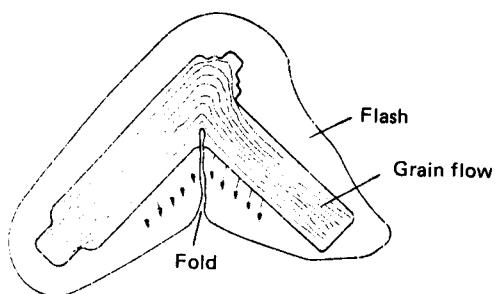


**FIG. 11.109** Fold resulting from inhibited flash flow. (After [11.123].)

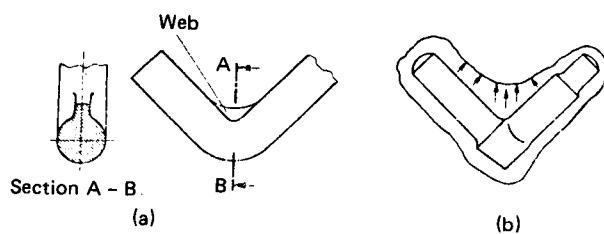


**FIG. 11.110** Intermediate bent shape with web to avoid fold formation. (a) Bent shape. (b) Finished shape. (After [11.124].)

## 11.10 ADVANCED FORGING TECHNIQUES

The term *advanced forging techniques* is used here to describe processes which either produce a much more accurate surface finish or aim at achieving special mechanical properties. In many cases the processes discussed aim at making improvements in both of these directions. Particular impetus for the development of advanced techniques and processes in the areas of primary forming and forging has come from the aerospace industry and its rapid development over the past 40 years. The need to manufacture highly stressed airframe and engine components led very rapidly to the combination of specific primary forming and forging processes. In particular, spectacular advances have been made through the combination of powder metallurgy and forging processes. Exactly how many "new techniques" have been created in this way is difficult to estimate, but it is true to say that more and more applications are now being found in other fields too, such as in automobile and machine tool manufacture, as a result of the increasing pressure to save time, material, and energy.

### 11.10.1 Precision and High-Precision Forging

The term *precision forging* is used to describe closed-die forging processes in which manufacturing accuracy with regard to shape and dimensional tolerances as well as surface finish exceeds the normal standards by such an amount that at least one finish-machining operation can be saved.

The requirements of narrow tolerances close to those of the finished shape and of good surface finish occur both individually and together. The work sequence in precision forging does not differ in principle from that of closed-die forging. However, greater care is needed at all stages of the process in order to avoid the errors listed in Table 11.17 [11.125]. Closer approximation of the forging to the finished component—through reduced thickness of the base, thinner ribs, smaller transition radii, and so on—results, for example, in higher tool loads. Thus often both the work sequence and the tools need to be modified accordingly. Additional intermediate-shaping, trimming, or heating operations are introduced to ensure more accurate dosage or flow of the workpiece material.

The precision forging, without side draft, shown in Fig. 11.111 is part of an aircraft door of honeycomb design made of aluminum alloy. With conventional forging, the sloping sides require full machining because both the outer and the inner faces of the flange are used for fixing. Elimination of side draft means that the only machining still required is the drilling and reaming of the fixing holes.

Precision forgings differ from conventional forgings in the following respects: the draft angle is  $0^\circ$  or close to this value, tolerances are narrower, length and width tolerances including offsetting are typically only half those of conventional forging, and thickness tolerances are reduced to about two-thirds of their former values.

The manufacturing processes used in conventional and precision forging are similar in principle. Precision forging may be considered as an intermediate stage between closed-die forging with and without flash. With the component shown in Fig. 11.111, in order to reduce the die load, provision has been made for flash on the web, although the flash thickness must be kept to a minimum. This may be achieved by accurately controlling the weight of the intermediate forging. The flash is subsequently removed by sawing.

The precision forging without side draft shown in Fig. 11.112 is a part of an aircraft window made of aluminum alloy. The component is subjected to a complex system of tensile and torque stresses corresponding closely to the stresses in the fuselage shells of the aircraft. A conventional forging requires almost complete machining on all sides. Value analysis showed the great economic savings of using a precision forging which eliminates all the machining required except for the machining of the fixing holes. Furthermore the elimination of surface machining improves the mechanical properties of the component with respect to fatigue and stress corrosion since the grain flow is not interrupted. Draft on precision forgings according to Fig. 11.112 is reduced from  $5$  to  $1.5^\circ$ , the minimum web thickness being  $3.05$  instead of  $6.35$  mm ( $0.12$  instead of  $0.25$  in), and the transition radii and part thicknesses are also smaller. The length and width tolerances, on the other hand, are the same as with conventional forging, although offsetting is reduced and the demands on flatness are higher. A further consideration is the need for exact and even trimming, since no residual flash is permissible either on the outside or on the inside of the part.

**Table 11.17** Measures for Improving the Accuracy of Closed-Die Forged Parts

	Initial material parting off	Heating	Process	Tools	Machine
1. Dimensional tolerances					
1.1 Die-dependent dimensions ( $l, b, d$ )	Constant-temperature furnace control, constant cycle time	Constant final temperature, constant cycle time, intermediate reheating, calibration of preform		Production accuracy, low wear	
1.2 Machine-tool-dependent dimensions	Dosage of material, narrow tolerances, premachined (e.g., peeled) starting material, accurate shearing	Constant-temperature furnace control, constant cycle time	As above, but with trimming instead of calibration		Increased rigidity
1.3 Offsetting				Accurate locating, fixing	Reduced free play in guideways

		Calibration of preform	
2.	Differences: finished forging, finished part	Dosage of material, narrow tolerances, premachined (e.g., peeled) starting material, accurate shearing	
2.1	Small wall thickness		
2.2	Thin ribs	Calibration of preform	Lubricating
2.3	Small radii		Low edge wear
2.4	Little draft		Ejector
3.	Surface defects	Scale-free (low-scale) heating	Cleaning of die cavity, low wear of die cavity
		Descaling	

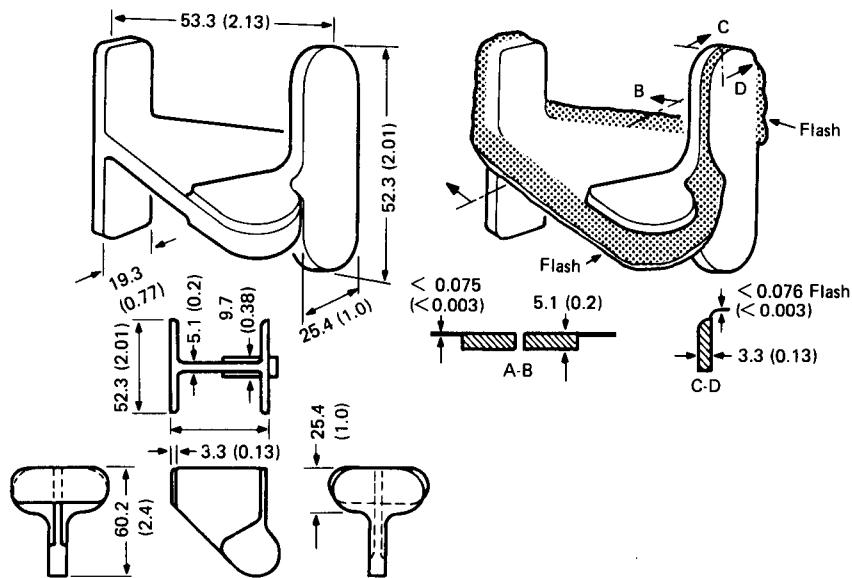


**FIG. 11.111** Closed-die forging without side draft made of aluminum alloy. Dimensions are in mm (in). (After [11.126].)

The work sequences of conventional and precision forging are very similar in this case. Material distribution is performed by means of upset forging of an ingot. Punching out the core and ring rolling are then used to create the desired grain flow. In the initial ingot the grain is parallel to the main axis, after upsetting it lies in the radial direction, and finally after rolling it runs in a tangential direction. Ring rolling is followed by the main forging operations, namely, preforming of the cross-section, finish-forging, and trimming. No further changes are required other than the necessary modifications to the tools, more exact material distribution (in order to avoid overlap-

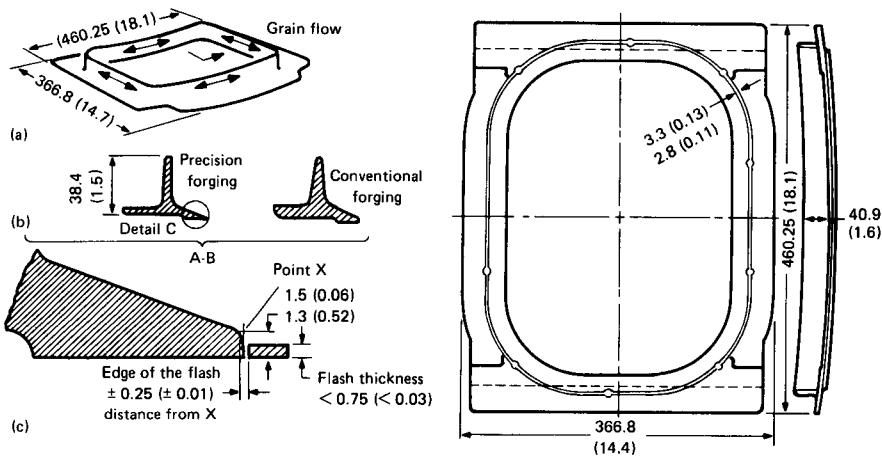


**FIG. 11.112** Precision forging made of aluminum alloy. Dimensions are in mm (in). (After [11.126].)

ping in the transition zones), and more powerful forging equipment [80 instead of 50 MN (9000 instead of 5625 ton)] because of the greater reductions in part thickness to be achieved.

*High precision forging* may be considered a special case of precision forging. Through high-precision forging components can be produced ready for assembly to an accuracy normally only achieved by machining. High demands are made not only on dimensional and shape accuracy, but also on surface finish, and this not just with respect to individual dimensions or surfaces, but with regard to the entire workpiece or a major part of it, as in the case of turbine blades. Thus it is possible to make a distinction between precision and high-precision forging, even though the boundary is blurred. The dimensional tolerances that can be achieved are given for some examples in Table 11.18.

In high-precision forging the conditions laid down in Table 11.17 must be respected even more closely than with precision forging. In particular, the following points must be observed:

- 1 High-quality finish of the die cavity, corresponding at least to ISO quality IT 8.
- 2 Reduction of tool wear through suitable choice of die material. Avoidance of scale formation through rapid heating of the workpiece, heating in an inert atmosphere, or forging in the warm condition (i.e., at reduced temperature). Attention must be paid to good agreement between intermediate and final shapes.
- 3 Precise control of both die and workpiece temperatures.
- 4 Precise control of the volume of the starting material. In addition, the material should be clean and free of surface defects. In some cases this may necessitate machining prior to forging.

It is necessary to avoid oxidation and decarburization as far as possible during heating, forging, and heat treatment. In order to improve surface finish after forging and heat-treatment operations, parts are usually pickled and then polished [11.127], [11.128].

### 11.10.2 Closed-Die Forging without Flash

In closed-die forging without flash the workpiece is forged in tools from which no material can escape (Fig. 11.113). It is thus one of the most effective processes for economizing on material. The process is mainly used for the production of disk-shaped parts, such as for ball races, gear blanks, and wheel hubs (Fig. 11.114), in particular in conjunction with multistage presses. Larger forgings produced by this method are generally forged on crank presses.

In closed-die forging without flash the following conditions should be fulfilled:

- 1 Equal volumes of the starting material, the intermediate shapes (where appropriate), and the finishing die. This may be achieved, for example, by weighing during parting off or by intermediate trimming. Where this is not practicable, compensation areas should be provided in the finishing die (Figs. 11.115 and 11.116). Where no provision is made in the die for accepting excess material, the permissible variation in weight is of the order of 0.5–2.0%.
- 2 Equal areas of corresponding cross sections of the intermediate forging and the finishing dies in the case of elongated parts whose main axis lies at a right angle to the direction of forging, that is, *localized* excesses or deficiencies of material are *not* permissible. This stipulation calls for accurate material distribution.
- 3 Exact positioning of the material to be forged in the finishing die so that the axes of the intermediate and the finished forgings correspond closely with each other. In some cases it may be necessary to provide locating surfaces to achieve this. Angular differences in the direction of the main axes of the intermediate and finished forgings are also unacceptable (Fig. 11.117).
- 4 Regulation of material flow so that by means of suitable intermediate shaping, flash at the end face, for example, can be avoided (Fig. 11.116a). Where tools have been designed to accommodate excess material, the latter should not enter the compensating areas until after the main cavity has been completely filled.

**Table 11.18** Examples of Typical Hot-Forging Tolerances

*Source:* Compiled from [11,127].

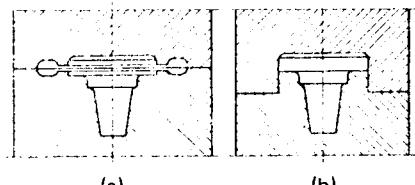


**FIG. 11.113** Closed-die forging. (a) With flash.  
(b) Without flash. Dimensions are in mm (in).

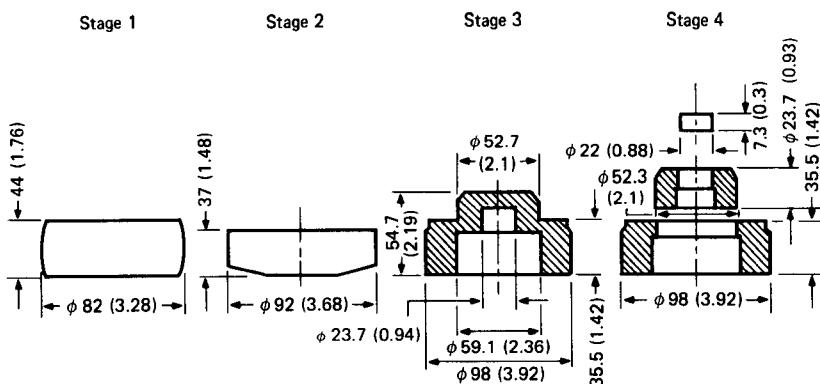


**FIG. 11.114** Manufacture of a ball hub and joint socket from a single blank using a multistage press. ( $d_o = 55 \pm 0.4$  mm (2.17  $\pm$  0.02 in); narrow tolerances of initial material. Dimensions are in mm (in). (After [11.129].)

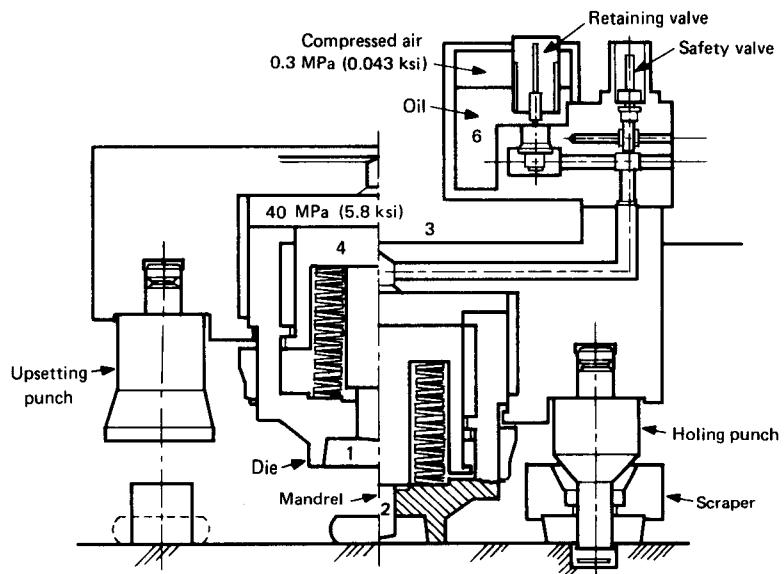


**FIG. 11.115** Dies for flashless forging with volume compensation. (After [11.130].)

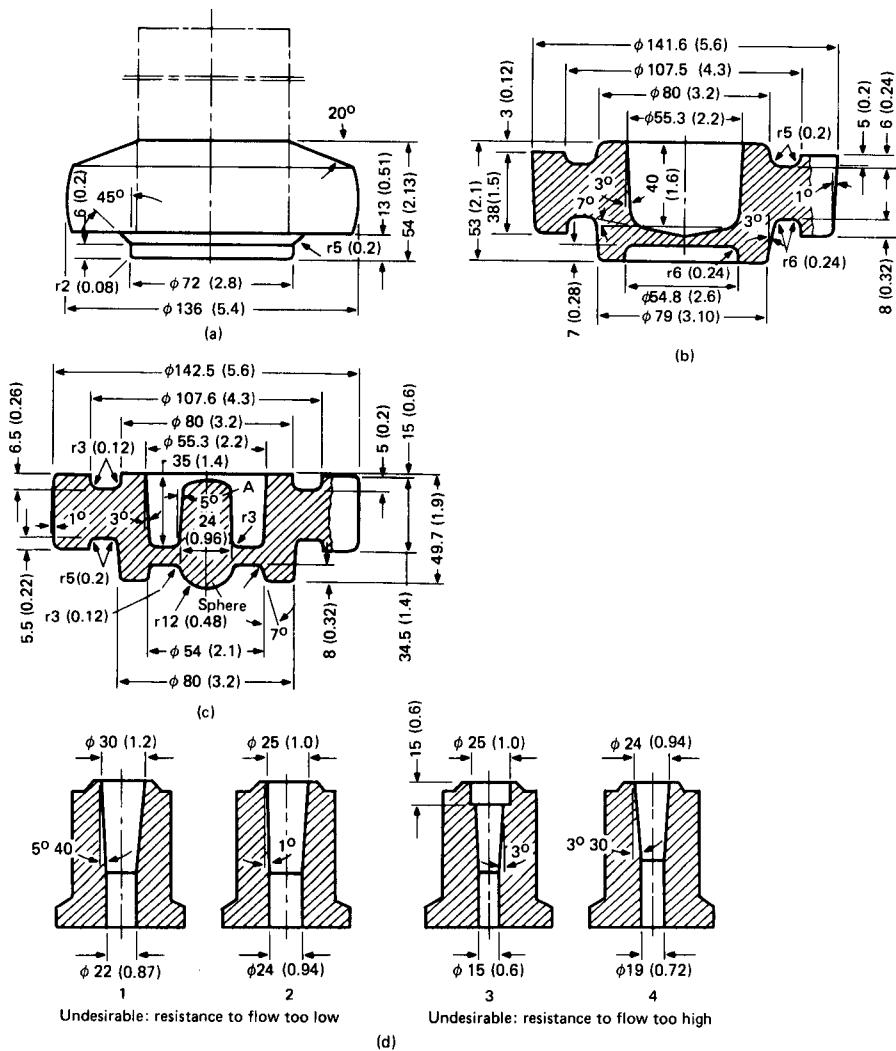


**FIG. 11.116** Intermediate shapes formed during die forging of a gear blank without flash. (a) Shape after upsetting. (b) Shape after preforming the cross section. (c) Finished shape. (d) Tool inserts used to take up excess material. Dimensions are in mm (in). (After [11.131].)

The saving in material compared to closed-die forging with flash is counterbalanced by the increased expense involved in the more accurate production of initial and intermediate workpieces. In die forging with flash, variations in weight of the initial slugs are overcome by trimming at the finish-forging stage, whereas in die forging without flash such variations are either minimized by more accurate parting off or else corrected during intermediate forming. In most cases swaging and stretch rolling are not sufficiently accurate to produce intermediate forgings for elongated workpieces. Sintered powder-metal slugs or preforms, on the other hand, are very suitable

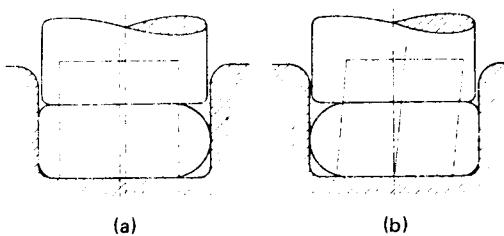
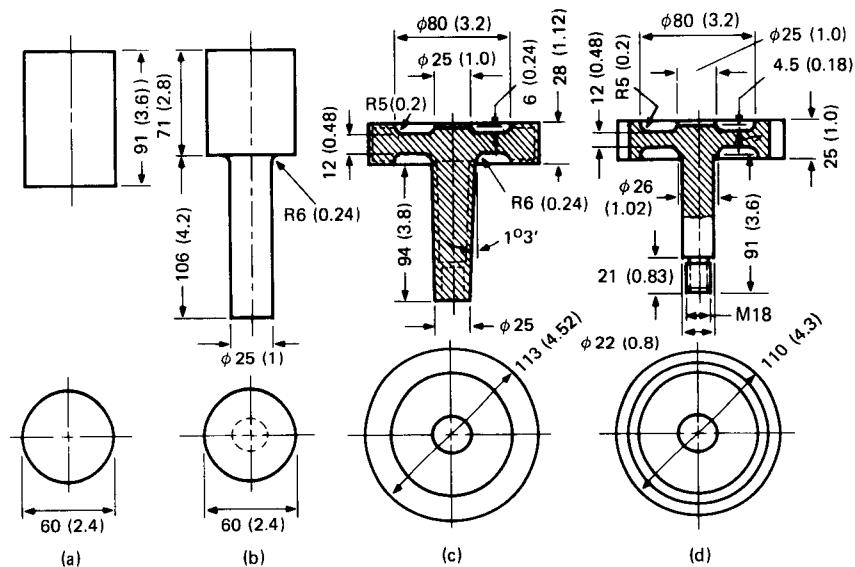


**FIG. 11.117** Positioning errors in closed-die forging without flash. (a) Off-center positioning of initial material. (b) Sideways leaning of material axis.



Forging	
With flash (hammer)	Without flash (crank press)
$m_A$	3.6 kg (7.9 lb)
$m_S$	2.6 kg (5.7 lb)
$m_F$	1.6 kg (3.5 lb)
F	25 MN (2813 ton)
	6 MN (675 ton)

**FIG. 11.118** Manufacture of a pinion by means of press forging without flash, compared to die forging with flash. (a) Initial shape. (b) Extruded shape. (c) Finished forging. (d) Finished component.  $m_A$ —mass of slag (a);  $m_S$ —mass of extrusion (b);  $m_F$ —mass of forged part (c); F—forging force. Dimensions are in mm (in). (After [11.132].)

because of their precise weights. The following advantages and disadvantages of closed-die forging without flash can be mentioned:

**Advantages:**

Savings of 10–30% or more in the weight of material used (see example in Fig. 11.118)

No trimming required

Lower deformation forces, especially in the case of smaller forgings where the ratio of the area of the die land to that of the die itself is large

Better mechanical properties through the elimination of residual flash

**Disadvantages:**

Precise volume of material required

Careful distribution of material required

Workpiece requires very exact positioning in the die cavity

Tendency toward end-face flash formation

Variations in wall thickness

Closed-die forging without flash is also used in conjunction with closed-die forging with flash by either preforging the cross section without flash followed by finish-forging with flash to obtain consistent wall thickness, or preforging with flash followed by trimming and finish-forging without flash. In the first case the excess material is initially taken up in the direction of thickness and then displaced as flash; in the second case an intermediate shape of precise volume is produced.

### 11.10.3 Hot Impact Extrusion

Hot impact extrusion is a bulk-forming process in which the heated material to be deformed is forced to flow out under load, essentially in one direction, through a specific opening in the forming die [11.133]. Although hot impact extrusion is similar in principle to cold or warm extrusion, the two processes bear little resemblance to each other in practice. The high temperature of the material to be formed [1150–1200°C (2102–2152°F) in the case of steel] leads to very different technological conditions. The tools are not only subjected to high compressive loading, but also to extremely high thermal stresses. An advantage of hot impact extrusion is that far larger workpieces can be produced than are economical with cold forming.

The work sequence in hot impact extrusion depends on the desired shape of the finished part. The latter should be designed taking the production process into account. For instance, in hot impact extrusion the length tolerance of the billet directly affects the length of the forged part. The normal procedure is thus to start with the shape of the finished forging and work backward to find out how much initial material is required to produce it. In this way it is possible to determine the most suitable shape of the workpiece at each intermediate stage in the process and to select the amount of material required accordingly.

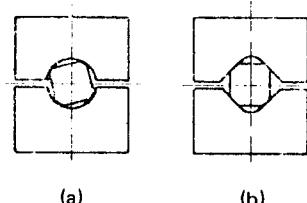


FIG. 11.119 Rounding off the corners of square billets. (a) With semicircular dies. (b) With straight-sided dies.

For economic reasons the most common starting materials used in hot impact extrusion are rolled or continuously cast square billets. However, for a particular volume, such billets are longer than equivalent round bars. This situation may be improved through rounding off the corners by forging between semicircular dies (Fig. 11.119a). Straight-sided dies can also be used (Fig. 11.119b), although these have the disadvantage of necessitating accurate positioning of the workpiece. As an alternative to fixed dies, the material may be passed between suitable moving rolls. A useful side effect of

rounding off the corners is that end-face scale is often removed in the process. An important economic factor affecting hot impact extrusion is tool life. Not only the replacement costs of worn tools must be taken into consideration, but also the effects of downtime required for tool changing. In order to keep tool wear to a minimum, it is essential that only descaled billets enter the tools.

Upset forging of a billet by about 10–15% of its initial length is one of the cheapest and most effective ways of descaling. By placing disks of appropriate thickness on the upsetting bed, it is possible to adjust the amount of upsetting so that the cross section of the upset billet is slightly smaller than the diameter of the tool, thus reducing sideward flow of the material during extrusion to a minimum.

The shape of the starting material should be chosen such that the ratio of the overall length of the billet to its side length  $l/b \leq 2$ . When this value is exceeded, the upset workpiece, instead of becoming barrel-shaped, will tend to buckle (Fig. 11.120).

With *solid* forged parts, the starting material is usually a long square billet which has been descaled by water jets. The diagonal of the billet cross section is chosen slightly less than the diameter of the die (Fig. 11.121a). The cross section of the punch should not be smaller than the area to be filled between the die diameter and the slug.

In the production of *hollow* parts the main aim is to form a body that can be transformed into a tube-shaped forging by punching out the center. Descaling is best performed by upsetting (Fig. 11.121b).

*Solid forward hot impact extrusion* is used to manufacture flanged shafts, stub axles, drive pinions, all kinds of flanges, and valve cones with long shafts. The square billet starting material is first descaled by upset forging. Because of the differences in size of the flange and shaft shown in Fig. 11.122, chamfering of the billet corners is unnecessary. However, with small flanges, rounding of the corners is essential.

*Closed hollow forward extrusion* is used to make hollow bodies which are closed at one end. Here, too, the billet first has to be descaled by upsetting. When the ratio of the size of the mandrel to the die is sufficiently large, rounding of the corners is not required. The only intermediate forging operation which may sometimes be necessary is backward extrusion. Fig. 11.123 shows an example of a gas cylinder made by this procedure. Because of the length of the cylinder and the thinness of its wall, the formation of a certain amount of flash during intermediate forging of the diameter is unavoidable.

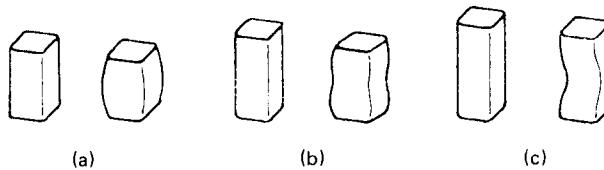
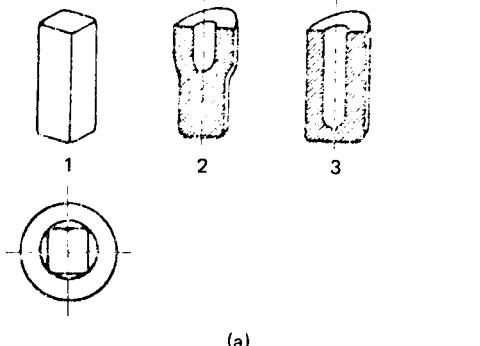


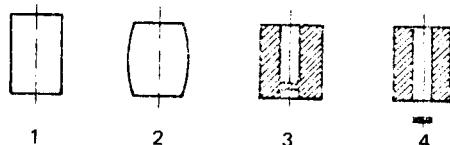
FIG. 11.120 Descaling a square billet by upset forging. (a) Barrel-shaped upset forging. The consequences are (b) bending and (c) buckling. (After [11.133].)

#### 11.10.4 Warm Forging

The aim of warm forging is to capitalize on the advantages of both hot and cold forging. The forging temperature affects both the behavior of the material during deformation and the properties of the finished part (Fig. 11.124). In comparison to hot forging, warm forging requires higher forces because of the greater flow stress, thus making increased demands on the forging tools and equipment. On the other hand, greater part accuracy in terms of both dimensions and surface finish can be achieved. The optimal temperature for a particular warm-forging operation always represents a compromise: its lower limit is set by the force which can be produced by the forging press and by the forgeability of the material; the upper limit is determined by the amount of oxidation—and thus the amount of scale—which can be tolerated. The temperature range for warm forging of steel is limited for these reasons to 450–900°C (842–1652°F) [11.134], [11.135].

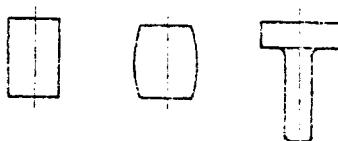


(a)



(b)

**FIG. 11.121** Work sequences used in backward extrusion to produce an intermediate forging. (a) Solid parts: 1—billet length; 2—prepiercing with a mandrel; 3—finish-piercing. (b) Hollow parts: 1—billet length; 2—upsetting; 3—piercing from both sides; 4—punching out the center. (*After [11.133]*.)



(a)

(b)

(c)

**FIG. 11.122** Work sequence in solid forward extrusion. (a) Billet length. (b) Upset forging. (c) Extrusion. *After [11.133]*.

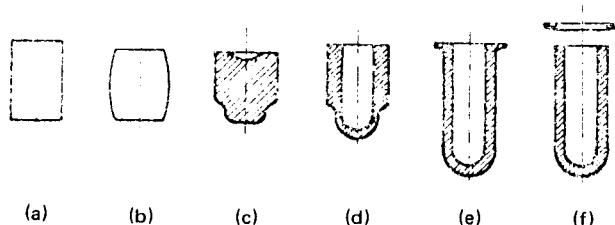


**FIG. 11.123** Work sequence in hollow forward extrusion of a hollow body closed at one end (e.g., a gas cylinder) (a) Billet length. (b) Upset forging. (c) Sizing and preforming. (d) Rising backward can extrusion. (e) Hollow forward extrusion. (f) Trimming. (*After [11.133]*.)

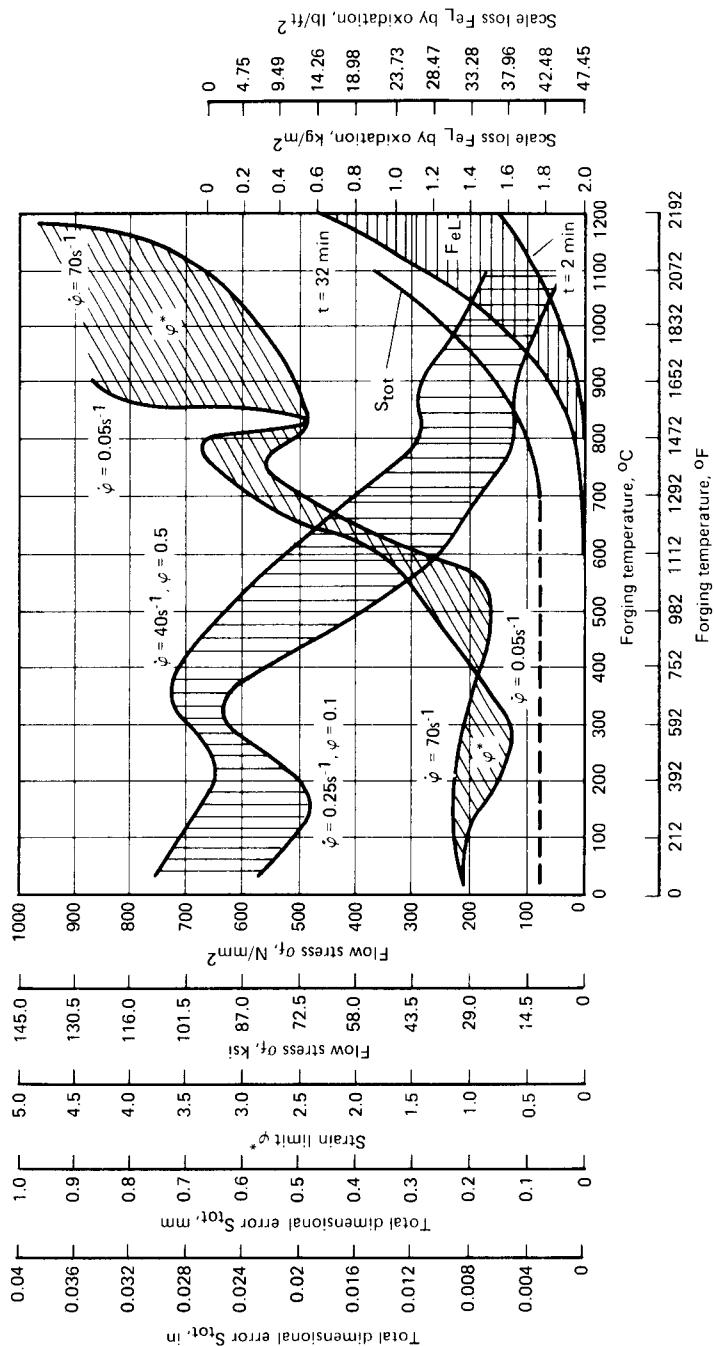


**FIG. 11.124** Effect of forging temperature on forgeability and material properties. Material—Ck 15 (AISI 1015). (After [11.134].)

Phosphate coating of the slug to be forged, as in cold extrusion of steel, is not required at these temperatures. Lubricants used in warm forging are characterized by low coefficients of friction, good wetting properties, good adhesion to the surface, and a disinclination to decompose. Graphite-based lubricants have proved particularly suitable [11.136]. Graphite oxidizes above 500°C (932°F) and thus lubricants are normally applied onto the tool surface since it rarely reaches such temperatures. If it does, it is usually only for brief periods, under exclusion of air, during the forging operation. Low coefficients of friction and good wear resistance are also exhibited by lead monoxide (PbO) based lubricants [11.137], although these present a serious health hazard. Recent investigations have shown that similar results can be obtained with lubricants made from molybdenum disulfide ( $\text{MoS}_2$ ) or graphite and boric oxide ( $\text{B}_2\text{O}_3$ ), or from borax ( $\text{Na}_2\text{B}_4\text{O}_7$ ), as the cheaper basic constituent, mixed with bismuth trioxide ( $\text{Bi}_2\text{O}_3$ ) [11.137].

Suitable materials for warm-forging tools are S6-5-2 (AISI M3-2) for punches, 5% CrMoV steels for dies, and 56NiCrMoV7 (AISI 6F2) for armor plating. Tool materials should contain no inclusions and should have an even carbide distribution. They should be tempered several times and machined without score marks. Stress concentrations should be avoided by the design of large transition radii and small angles of taper. The required rigidity of the forging equipment and the accuracy of the guideways are as in cold extrusion.

The mechanical properties of warm-forged parts depend on the degree of deformation, the forging temperature, and the rates of deformation and cooling. Tolerances are of the order of 0.2–0.3 mm (0.007–0.012 in) for diameters of 50 mm (2 in) and 0.4–0.8-mm (0.015–0.031-in) thickness. Surface roughness depends on the lubricant used and is generally in the range of 10–60  $\mu\text{m}$  (0.4–2.4 mil). Tensile strength and yield strength are 1.1–1.5 times as great as for normally annealed materials. In practice, warm forging has up to now been limited almost exclusively to extrusion and upsetting operations.

The work sequence compacting–sintering–warm forging offers the possibility of producing workpieces with a relative density of  $\approx 1$  from powder-metal blanks [11.145]. In this process, which is still in the experimental stage [11.146], the metal powder is first compressed and then sintered. When the shape of the compact is suitable, sintering of the preforms may be carried out by induction heating. Forging of the sintered workpiece in the temperature range of 600–900°C (1112–1652°F) not only leads to an improvement in the static and dynamic strengths of the part compared with that of the unforged starting material, but it also produces a considerable improvement in ductility. Notch impact test results are similar to those obtained with smelted materials. Dimensional accuracy and surface finish, too, are comparable to those of warm-forged smelted material.

#### 11.10.5 Hot-Die Forging of Powder-Metal Preforms

Three main process variations are used in die forging of powder-metal materials [11.139] (Fig. 11.125): (1) hot pressing following compacting, (2) high-precision forging of powder-metal preforms without flash, and (3) closed-die forging with flash. The latter is the least significant since it bears the closest resemblance to conventional forging and thus does not make full use of the advantages of powder-metal technology. The work sequence is usually as follows: compacting of the powder, (sintering), storage, heating, forging, (finishing).

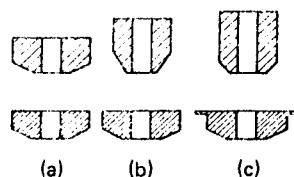


**FIG. 11.125** Sinter forging processes. (a) Warm secondary pressing. (b) High-precision forging. (c) Closed-die forging with flash. (After [11.139].)

Where the workpiece is hot-compressed or high-precision forged just prior to reaching the sinter temperature, one may speak of *powder forging*; otherwise the more general term *sinter forging* applies. The preforms have a porosity of 15–25% and either they are designed to correspond closely to the desired final shape, as in the first process variation mentioned, or a not insignificant amount of material flow is required to take place during the forging operation, as in the second and third variations. The porosity of the finished part is on the order of 0.5–5%, or in some cases even 0–1%. Preheating temperatures lie in the range of 800–1200°C (1472–2192°F) (for iron

powders). Besides the quality of the powder itself, the precise shaping operation, performed under high hydrostatic pressure, is of particular importance. This, in conjunction with the shearing forces which are set up, leads to intensive welding of the material particles. The material structure of sinter-forged parts is very fine-grained and homogeneous. The mechanical properties are thus largely isotropic, which in some cases has a positive effect on the fatigue strength of sinter-forged parts, making them superior to conventionally forged components. Sinter forging is used in industry for the manufacture of connecting rods, crown wheels, gear and coupling components, and synchronizing rings. Typical dimensional tolerances lie in the range of ISO qualities IT 8–10, and surface finishes are of the order of 5–30  $\mu\text{m}$  (0.2–1.2 mil).

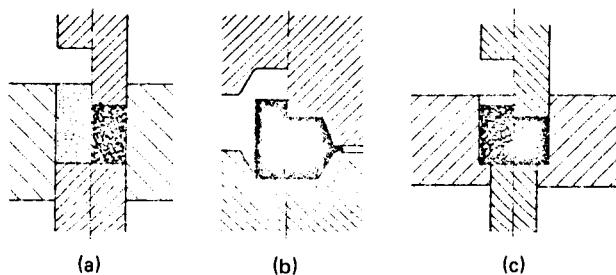
### Tool Design

Fig. 11.126 shows, in very simplified form, a powder-compacting die, a conventional forging die, and a powder-forging die [11.140]. The main characteristics of the powder-forging die are clearly visible despite the simplified representation. It bears a much closer resemblance to the compacting die than to the conventional forging die. The forged part is removed from the die by means of an ejector. Since the material is forged from a relative density of about 80% to a density of nearly 100% in a completely enclosed die cavity, it is essential to ensure exact dosage of the starting material corresponding to the weight of the finished component. Exceeding the amount by as little as 1% can lead to overloading and possibly fracture of the powder-forging die. This also applies to the density distribution in the preform. The density of powder in the different sections of the preform often varies considerably.

Since in the majority of cases very little sideways flow of material takes place during powder forging, it is not possible—or only possible to a very limited extent—for excess material to flow from one section to another. Thus the geometry of the preform must be modified with respect to the shape of the finished part in such a way that despite variations in density, no localized overloading of the forging dies occurs. Having once determined the required geometry, care must be taken to ensure that the required densities are actually achieved in the different sections of the preform. In this respect, the production of such preforms is more difficult than the manufacture of conventionally sintered parts. Preconditions for success here are consistent quality of the initial powder and accurate adjustment of the powder press.

### Properties and Use of Powder-Metal Components

The isotropic structure, that is, nondirectional grain flow, in powder-forged materials is the reason for the isotropic properties of such components. This is illustrated in Fig. 11.127, based on the example of fatigue strength. While the fatigue strength of conventionally forged steel differs by about 100% in the longitudinal and transversal directions, the corresponding values for powder-forged steel are the same in whatever direction they are measured. This isotropic property is a great advantage in many components. Noteworthy examples are the increased fatigue strength of powder-forged connecting rods [11.141] and the reduction in the tendency of teeth to fail in fatigue tests on powder-forged gear wheels [11.142].



**FIG. 11.126** Schematic sections of tools used in various forging processes. (a) Conventional powder compacting. (b) Closed-die forging. (c) Powder forging.

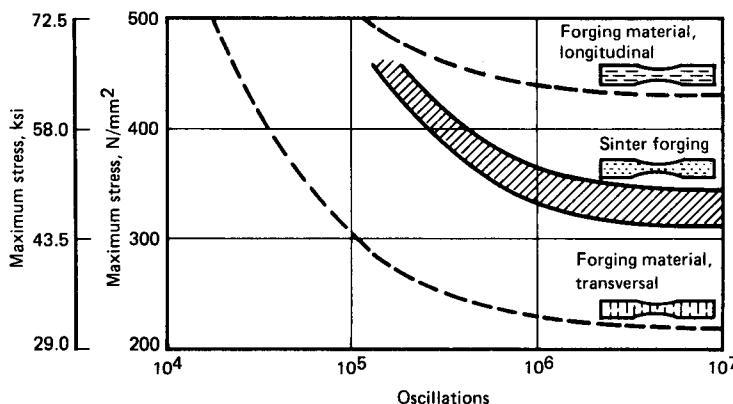


**FIG. 11.127** Comparison of the fatigue strengths of powder-forged and conventional die-forged steels. (After [11.141].)

Connecting rods and gear wheels are just two examples of part families for which powder forging offers advantages over traditional methods, particularly in the case of components which have to withstand high dynamic stresses. Where, in addition to such stresses, the design of the part poses problems of material distribution, powder forging is almost unrivalled. The only alternative methods of manufacture are either expensive mechanical machining or casting techniques, whereby in the latter case the parts are seldom able to withstand very high dynamic stresses. This may be illustrated by the following two examples, which through reference to the critical zones and dimensional tolerances to be respected, give also an indication of the current stage of development of powder-forging batch production. Fig. 11.128a shows a powder-forged sprocket wheel. Two such wheels are mounted together on a shaft (Fig. 11.128b) in order to assure the force transmission of a 50-kN (5.6-ton) crane. The components are case-hardened to reduce wear caused by the motion of the chain in the wheel pockets. The high stress in the tips of the teeth is evident

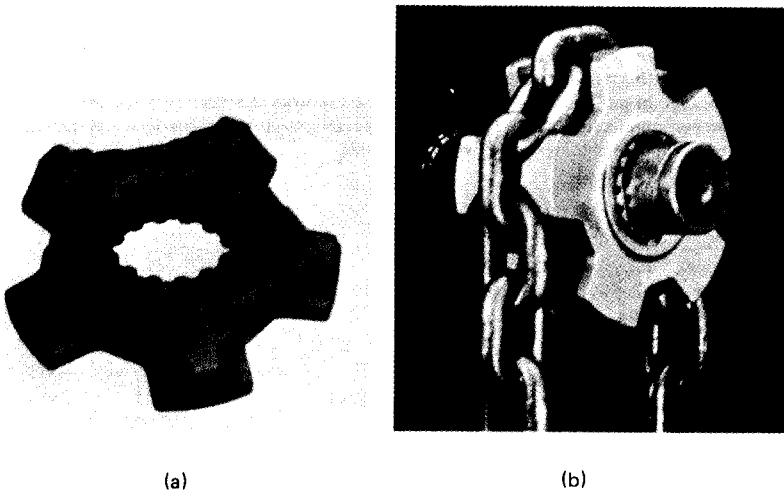


**FIG. 11.128** Sprocket wheel.

in Fig. 11.128b. It can happen that for brief periods of time the total load of the crane has to be carried by just two opposing gear teeth, which a short while later are then completely relieved of the load.

The requirement that the components withstand high dynamic stresses is accompanied by tight dimensional tolerances. The distance between the tips of neighboring teeth is required to be accurate to within  $\pm 0.05$  mm (2.0 mil). Compared with the former die-forged components, which needed extensive machining, cost savings of just under 50% have been achieved. Other manufacturing techniques are less advantageous than powder forging because of extreme variations in material distribution.

Fig. 11.129 shows a powder-forged brake shoe for an automobile hand brake. Its asymmetric shape precludes manufacture by other forming processes. The characteristics of the comparable cast component are not as good as those achieved by powder forging. The powder-forged part is subsequently hardened and tempered. The greatest stress occurs in the transition zone between the fixing flange and the stop faces. For this reason this critical safety component is inspected using an oscillating testing machine. The brake shoe is bolted by the flange to the machine and then subjected on one side to a cylindrical load of 35 kN (3.9 ton). The component is required to withstand 1200 load cycles without fracture. The most critical tolerances are the parallelism of the side faces of the protrusion and the distance separating the fixing holes, namely,  $58 \pm 0.1$  mm ( $2.283 \pm 0.004$  in.).

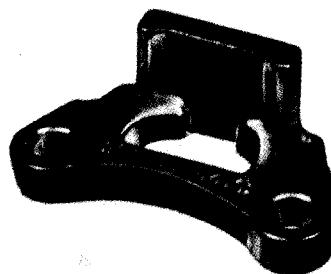


FIG. 11.129 Brake shoe.

#### 11.10.6 Hot-Die, Isothermal, and Superplastic Forging

##### *Hot-Die Forging*

In contrast to conventional die forging, where the differences in temperature between workpiece and die may be up to  $1000^{\circ}\text{C}$  ( $1800^{\circ}\text{F}$ ) and more, in the hot-die process the temperature of the die is only about  $200^{\circ}\text{C}$  ( $360^{\circ}\text{F}$ ) less than that of the forging. Hot-die forging was developed in

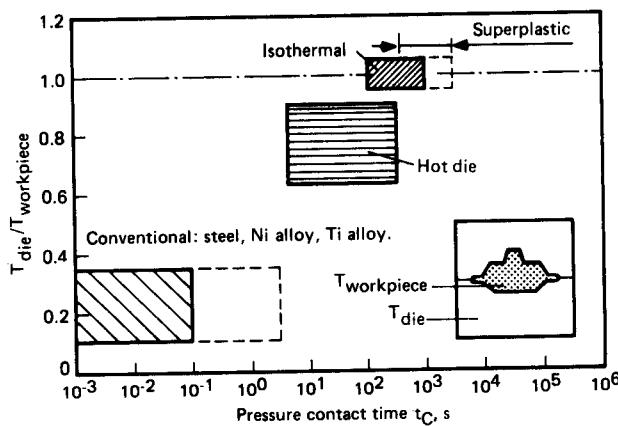


FIG. 11.130 Different forging processes according to die temperature and pressure contact time. (After [11.143].)

order to be able to use nickel-based materials for die manufacture [11.143]. At operating temperatures of 750–850°C (1382–1562°F) these alloys require no vacuum or inert gas atmosphere. Titanium alloys are forged at temperatures of about 950°C (1742°F). The process may be seen as a compromise between isothermal and conventional forging, although in fact it is more closely related to isothermal forging. The boundaries between the various forging processes mentioned are illustrated in Fig. 11.130.

### *Isothermal Forging*

Isothermal forging may be considered as a further development of the hot-die forging process and is characterized by the fact that, using suitable heating equipment, the workpiece and the die are kept at approximately the same temperature (Fig. 11.131). The main area of application of isothermal forging is for mechanically and thermally highly stressed components used in the aerospace industry [11.144]. The materials most used are titanium and high-temperature-resistant nickel-based alloys, which because of their high flow stress, are very difficult to forge. The mechanical properties of the materials remain unchanged or are minimally improved by the use of isothermal forging. However, the amount of finish-machining is often drastically reduced compared with conventional die forging. In isothermal forging the deformation force is generally about one-quarter to one-fifth of that required for conventional forging of the same material because of considerably reduced rates of deformation. These permit forging of much more complicated workpieces than is possible with adiabatic forging. Reductions in cross section of up to 80% can be achieved in a single operation, thus facilitating the forging of parts with thin fins and ridges. The die material most commonly used for forging titanium alloys (generally without a surrounding inert gas atmosphere) is the nickel-based alloy IN 100. Titanium alloys are generally forged at about 950°C (1742°F). When higher temperatures are required, such as for components made of nickel-based alloys, molybdenum-based die materials are needed. Since molybdenum

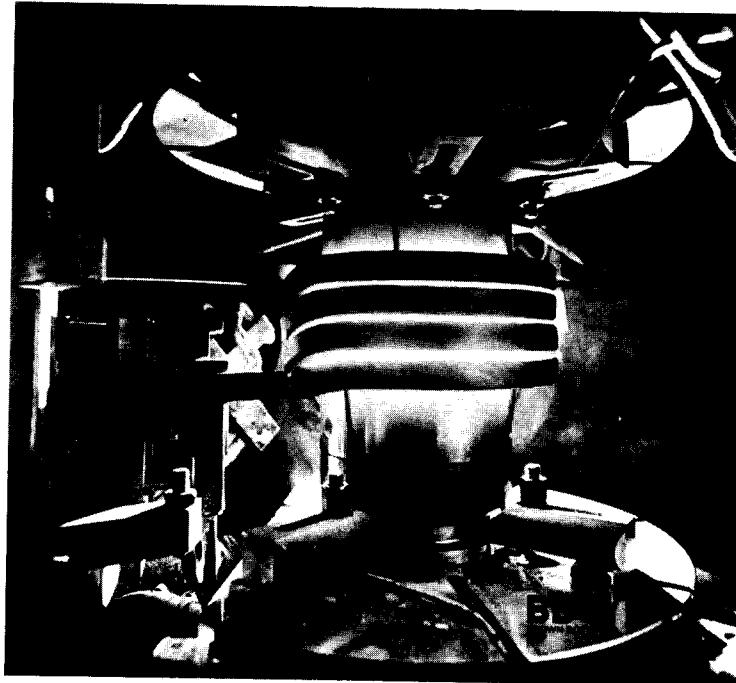
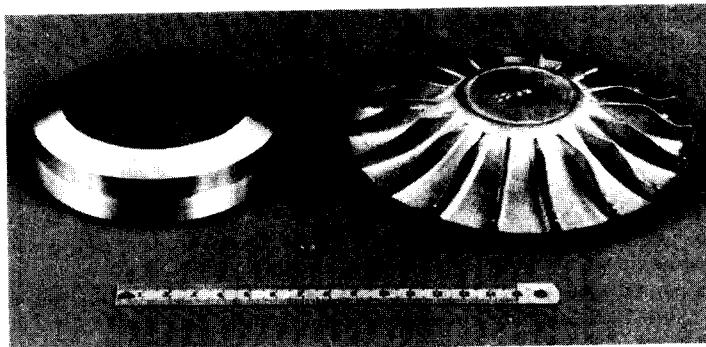


FIG. 11.131 Tools used in isothermal forging. (Courtesy of Brown Boveri.)



**FIG. 11.132** Superplastic isothermally forged impeller wheels made of TiAl6V4 (Ti-6Al-4V). (Courtesy of Brown Boveri.)

reacts strongly with oxygen at high temperatures, it is necessary to protect the dies from the surrounding air by either an inert atmosphere or a vacuum, otherwise they would be oxidized to pieces in just a few minutes. The process can be used economically for batch sizes of between 100 and 1000 parts [11.143].

### *Superplastic Forging*

The boundary between isothermal forging and superplastic forging is a fairly fluid one (Fig. 11.130). The latter process is carried out at even lower strain rates than isothermal forging. This is accompanied by an increase in the pressure contact time and a further reduction in the deformation force. The preconditions for superplastic behavior of a material are:

Very fine structure with grain sizes of just a few micrometers. Changes in structure due to grain growth during forging are not permissible.

The forging temperatures must lie above  $T_m/2$ , where  $T_m$  is the melting point of the material in K (degrees kelvin).

Strain rates must be very small ( $\dot{\phi} = 10^{-1}\text{--}10^{-5} \text{ s}^{-1}$ ).

Superplasticity occurs in principle with all pure metals. However, preference is generally given to eutectic or eutectoid alloys since they also usually fulfil the first precondition, namely, that of a fine grain structure. The temperatures required for superplastic forging of high-temperature-resistant nickel- and titanium-based alloys lie between 800 and 1150°C (1472 and 2102°F). In this range, due to high thermal and long-term stresses, it is necessary to make the dies from molybdenum-based alloys. Superplastic forging is mainly used to manufacture high-temperature-resistant engine components made of IN 100, René95, Waspaloy, and Astroloy. An example of a superplastically forged radial impeller is shown in Fig. 11.132.

### REFERENCES

- 11.1 DIN 8583: "Fertigungsverfahren Druckumformen (Deformation Processes—Compressive Forming)," 1st ed., 1969.
- 11.2 DIN 8586: "Fertigungsverfahren Biegeumformen (Deformation Processes—Forming by Bending)," 1st ed., 1970.
- 11.3 DIN 8587: "Fertigungsverfahren Schubumformen (Deformation Processes—Shear Forming)," 1st ed., 1969.

## 11.124 BULK-METAL FORMING

- 11.4 DIN 8588: "Fertigungsverfahren Zerteilen. Einordnung, Unterteilung, Begriffe (Manufacturing Process Separating. Main Divisions, Subdivisions, Terms)," Aug. 1966.
- 11.5 DIN 8593: "Fertigungsverfahren Fügen. Einordnung, Unterteilung, Begriffe (Manufacturing Process Joining. Main divisions, Subdivisions, Terms)," Dec. 1967.
- 11.6 Lange, K.: "Nomenclature and Definitions of Terms Used in Forging" (*in German*), *Ind.-Anz.*, 86, 1964, pp. 84–85.
- 11.7 Lange, K.: "Die-Forged Parts for Machining" (*in German*), *Ind.-Anz.*, 84, 1962, pp. 1726–1731.
- 11.8 Krause, U.: "Deformation Resistance of Cold-Forging Materials" (*in German*), in *Principles of Metal Deformation*, Düsseldorf, Verlag Stahleisen, 1966.
- 11.9 Vater, M., Nebe, G., and Heil, H.-P.: "Changes in the Mechanical Properties of Open-Die Forged Parts Caused by Drawing Out and Upsetting" (*in German*), *Stahl u. Eisen*, 86, 1966, pp. 892–905.
- 11.10 Voigtländer, O.: "Splitting Forge Steel Flats" (*in German*), *Werkstattstech. u. Maschinenbau*, 42, 1952, pp. 139–140.
- 11.11 Wuppermann, Th.: "Electric Butt Welding and Its Use for the Manufacture of Complicated Forgings," in *Freiformschmieden* (Proceedings of the International Forging Conference, 1965), Düsseldorf, Verlag Stahleisen, 1966.
- 11.12 Lange, K.: *Closed-Die Forging of Steel*, Berlin/Göttingen/Heidelberg, Springer, 1958.
- 11.13 Metzler, H. J.: "On the Effects of Tool Speed on Upset Forging" (*in German*), *Berichte aus dem Institut für Umformtechnik, Universität Stuttgart*, no. 21, Essen, Girardet, 1970.
- 11.14 Schey, J. A.: *Metal Deformation Processes. Friction and Lubrication*, New York, Dekker, 1970.
- 11.15 Bühler, H., and Bobbert, D.: "On Material Displacement during Upset Forging" (*in German*), *Ind.-Anz.*, 88, 1966, pp. 309–312.
- 11.16 Preussler, H.: "On Questions Concerning Shape-Changing Processes" (*in German*), *Stahl u. Eisen*, 45, 1925, pp. 1422–1428.
- 11.17 Falk, A.: "Theory of Material Transformation during Rolling and Forging" (*in German*), *Stahl u. Eisen*, 32, 1912, pp. 816–822, 863–867, 1269–1272.
- 11.18 Lange, H.: "Material Displacement in the Outer Layers of Metal Bodies during Cold Upset Forging" (*in German*), *Ind.-Anz.*, 86, 1964, pp. 86–92.
- 11.19 Eder, E.: "Material Flow and Specific Normal Force in the Outer Layers of Plastically Deformable Bodies during Open-Die Upsetting between Parallel Surfaces" (*in German*), *Arch. Eisenhüttenw.*, 38, 1967, pp. 821–829.
- 11.20 Duesing, F. W., and Stodt, A.: *Open-Die Forging* (*in German*), pt. I, 4th ed, Werkstattbücher no. 11, Berlin/Göttingen/Heidelberg, Springer, 1954.
- 11.21 Geiger, M., and Geiger, R.: "Elementary Plasticity Theory: Ways of Estimating Forces during Forging Operations after Siebel et al." (*in German*), *Ind.-Anz.*, 95, 1973, pp. 385–389.
- 11.22 Valorinta, V.: "Investigations into the Effect of Temperature and Deformation Rate on Deformation Resistance" (*in German*), *Werkstattstech. u. Maschinenbau*, 48, 1958, pp. 452–456.
- 11.23 Lueg, W., and Krause, U.: "Deformation Resistance of C45 (AISI 1043) Steel during Hot Upset Forging at Medium Forging Speeds" (*in German*), *Stahl u. Eisen*, 80, 1960, pp. 1061–1067.
- 11.24 Jenson, J. E.: *Forging Industry Handbook*, Cleveland, OH, Forging Industry Association, 1966.
- 11.25 Siebel, E.: "State of the Art of Hot Forming and Forging" (*in German*), *Stahl u. Eisen*, 76, 1956, pp. 393–397.

- 11.26 W. Johnson, Ridge Hall, Chapel-en-le-Frith, United Kingdom, personal communication.
- 11.27 Johne, P.: "Investigation of the Permissible Variations in the Amounts of Material Used in Closed-Die Forging without Flash" (*in German*), *Ind.-Anz.*, **92**, 1970, pp. 259–263.
- 11.28 Johne, P.: "Closed-Die Forging without Flash in Dies without Compensation Spaces" (*in German*), Dr.-Ing. thesis, Technische Universität Hannover, 1969.
- 11.29 DIN 7526: "Toleranzen und zulässige Abweichungen für Gesenkschmiedestücke aus Stahl (Tolerances and Permissible Variations in Closed-Die Forged Parts Made of Steel)," 1969.
- 11.30 Johne, P.: "Filling of Nonrotationally-Symmetrical Die Cavities" (*in German*), *Ind.-Anz.*, **92**, 1970, pp. 650–652.
- 11.31 Lange, K.: *Aspects of Closed-Die Forging and Its Further Scientific Development (in German)*, Berlin/Göttingen/Heidelberg, Springer, 1957.
- 11.32 Lange, K.: "Report on a Study Tour through the United States 1968" (*in German*), Stuttgart, Institut für Umformtechnik, 1969.
- 11.33 Stöter, J.: "Investigation of the Hammer and Press Forging Operations with Special Reference to Rising" (*in German*), *Forschungsbericht des Landes Nordrhein-Westfalen*, no. 848, Köln/Opladen, Westdeutscher Verlag, 1960; see also *Werkstatttechnik*, **49**, 1959, pp. 223–230.
- 11.34 Neuberger, F., and Möckel, L.: "Guidelines for Determining Flash Thickness and Die-Land Ratio in Closed-Die Forging of Steel" (*in German*), *Fertigungstechn. u. Betr.*, **11**, 1961, pp. 492–495.
- 11.35 Vieregge, K.: "Concerning the Design of Die Land in the Closed-Die Forging of Steel" (*in German*), Dr.-Ing. thesis, Technische Universität, Hannover, 1969.
- 11.36 Vieregge, K.: "Effect of Flash Gap in Closed-Die Forging" (*in German*), *Ind.-Anz.*, **92**, 1970, pp. 1119–1121.
- 11.37 Meyer-Nolkemper, H.: "Forging in Closed Dies—An Evaluation of the Relevant Literature" (*in German*), *Werkstatttechnik*, **55**, 1965, pp. 398–404.
- 11.38 Bühler, H., and Johne, P.: "Forging in Dies without Draft" (*in German*), *Forschungsbericht des Landes Nordrhein-Westfalen*, no. 2032, Köln/Opladen, Westdeutscher Verlag, 1969.
- 11.39 Ochromenko, J. M., and Kopiskij, B. D.: "Investigation of Internal Pressure during Upsetting in Closed Dies" (*in Russian*), *Kusn.-Stamp.Proizvod.*, **3**, no. 9, 1961, pp. 7–11.
- 11.40 Meyer-Nolkemper, H.: "Flow Lines in Commercial Lead" (*in German*), unpublished.
- 11.41 Bruchanow, A. N., and Rebelski, A. V.: *Die Forging and Hot Pressing (in German)*, Berlin, Verlag Technik, 1955.
- 11.42 Voigtländer, O.: Concerning Lange [11.31] (*in German*), *Werkstatttechnik*, **49**, 1959, pp. 775–776.
- 11.43 Vieregge, K.: "Design of Forging Flash Gap" (*in German*), *Ind.-Anz.*, **92**, 1970, pp. 1561–1564.
- 11.44 Teterin, G. P., and Tarnovskij, I. J.: "Calculation of the Flash Produced in Hammer Forging of Disk-Shaped Parts" (*in Russian*), *Kusn.-Stamp. Proizvod.*, **10**, no. 5, 1968, pp. 6–11.
- 11.45 Siebel, E.: *Shape Transformation in the Plastic State (in German)*, Düsseldorf, Verlag Stahleisen, 1972.
- 11.46 Voelkner, W.: "On Theoretical Stress Determination in Closed-Die Forging with Flash" (*in German*), *Wiss. Z. Technische Universität, Dresden*, **17**, 1968, pp. 1273–1281.
- 11.47 Altan, T., and Nagpal, V.: "Impression and Closed-Die Forging," *Int. Met. Rev.*, Dec. 1977, pp. 322–341.
- 11.48 Geleji, A.: *Forming of Metals—Calculations and Experiments (in German)*, Berlin, Verlag Technik, 1960.

- 11.49 Kobayashi, S., and Thomsen, G.: "Approximate Solutions to a Problem of Press Forging," *Trans. ASME, J. Eng. Ind.*, **81B**, 1959, pp. 217-227.
- 11.50 Steck, E., and Schmid, K.: "Application of the Principle of Minimum Forging Work to Upsetting and Forging Operations" (*in German*), *Ind.-Anz.*, **87**, 1965, pp. 1751-1755.
- 11.51 Semjenow, E. I.: "Investigation of the Stress and Deformation Conditions in Die Forging and Forward Extrusion" (*in German*), *Fertigungstechn. u. Betr.*, **19**, 1969, pp. 685-687.
- 11.52 Klafs, U.: "On the Determination of Temperature Distribution in the Tool and the Workpiece during Hot Forging" (*in German*), Dr.-Ing. thesis, Technische Universität, Hannover, 1969.
- 11.53 Beck, G.: "Temperature Occurring in the Material Flow Lines and in the Dies during Upset Forging of Cylindrical Test Pieces Made of Steel and Pantal" (*in German*), *Werkstattstechn. u. Maschinenbau*, **48**, 1958, pp. 561-567.
- 11.54 Dahlheimer, R.: "Concerning the Stresses, Strains, and Temperatures Occurring during Hot Extrusion" (*in German*), *Berichte aus dem Institut für Umformtechnik, Universität Stuttgart*, no. 20, Essen, Girardet, 1970.
- 11.55 Löwen, J.: "On the Determination of Friction Conditions during Closed-Die Forging" (*in German*), Dr.-Ing. thesis, Technische Universität, Hannover, 1971.
- 11.56 Geiger, R.: "Investigation of Lubricants for Warm Forging of Steel" (*in German*), *Ind.-Anz.*, **92**, 1970, pp. 623-629.
- 11.57 Meyer, H.: "Comparative Investigations into Flow Stress and Deformation Resistance in Closed-Die Forging" (*in German*), *Werkstattstechnik*, **51**, 1961, pp. 435-437.
- 11.58 Valorinta, V.: "Investigation into the Transposition of Common Deformation Resistances to Geometrically Similar Parts" (*in German*), *Werkstattstechnik*, **51**, 1961, pp. 723-725.
- 11.59 Lange, K., Steck, E., and Adler, G.: "Principles of Closed-Die Forging" (*in German*), in *Principles of Metal Deformation*, Düsseldorf, Verlag Stahleisen, 1966.
- 11.60 Geck-Müller, Th.: "Forging Force and Forging Work during Closed-Die Forging Using Hammers and Presses" (*in German*), unpublished, Closed-Die Forging Group, Technische Universität Hannover.
- 11.61 Spies, K.: "A Classification System of Forged Parts" (*in German*), *Werkstattstechn. u. Maschinenbau*, **47**, 1957, pp. 201-205.
- 11.62 Neuberger, F., and Pannasch, S.: "Determination of Deformation Forces and Work Done in Closed-Die Forging Using a Crank Press" (*in German*), *Fertigungstechn. u. Betr.*, **12**, 1962, pp. 775-779.
- 11.63 Wallace, P. W., and Schey, J. A.: "Speed Effects in Hot Closed-Die Forging," in *Proceedings of the 10th International M.T.D.R. Conference*, Oxford/New York, Pergamon, 1970, pp. 525-535.
- 11.64 Ecker, W.: "The Effect of Inertia Forces on Rising in an Impression-Forging Die with Flash Gap" (*in German*), *Ind.-Anz.*, **92**, 1970, pp. 257-259.
- 11.65 Neuberger, F., Möckel, L., and Schmidt, W.: "Calculating the Work Requirement in Advance of Closed-Die Forging" (*in German*), *Fertigungstechn. u. Betr.*, **10**, 1960, pp. 17-23.
- 11.66 Meyer, H.: "Deformation Forces and Work Done during Hot Upset Forging in Horizontal Forging Machines" (*in German*), *Werkstattstechnik*, **50**, 1960, pp. 450-453.
- 11.67 Lange, K.: "Theory and Principles of Closed-Die Forging" (*in German*), *Ind.-Anz.*, **85**, 1963, pp. 1393-1400, 1549-1555, 1739-1742; *Metal Treatment and Drop Forging*, 1965, pp. 184-185, 210-220, 230, 264-270.
- 11.68 Stöter, J.: "Measuring the Contact Time in Die Forging" (*in German*), *Werkstattstechn. u. Maschinenbau*, **49**, 1959, pp. 143-144.
- 11.69 Lange, K., and Meinert, H.: "Effect of Surface Finish on the Wear of Forging Dies" (*in German*), *Werkstattstechn. u. Maschinenbau*, **46**, 1956, pp. 313-319.

- 11.70 Mühlenweg, H.: "Effect of Scale on the Surface Roughness of Forged Parts" (*in German*), *Werkstattstech. u. Maschinenbau*, **48**, 1958, pp. 140–142.
- 11.71 Lange, K., and Hammersen, H.: "Surface Finish of Die-Forged Parts" (*in German*), *Werkstattstech. u. Maschinenbau*, **44**, 1954, pp. 647–649.
- 11.72 Tolkien, H.: "Lubrication Effects in Forging Dies" (*in German*), *Werkstattstechnik*, **51**, 1961, pp. 102–105.
- 11.73 Shaw, H. L., Boulger, F. W., and Lorig, C. H.: "Developments of Die Lubrication for Forging and Extruding Ferrous and Nonferrous Materials," Battelle Memorial Institute, Columbus, OH, no. AF33(600).26272, 1955.
- 11.74 Geiger, R.: "Investigation of Lubricants for Hot Forging of Steel" (*in German*), *Ind.-Anz.*, **92**, 1970, pp. 623–629.
- 11.75 *1982 Annual Book of ASTM Standards*, pts. 1, 3, 4, 5, 6, 8, American Society for Testing and Materials, 1982.
- 11.76 *Metals Handbook*, 9th ed., vol. 1, "Properties and Selection: Irons and Steels," Metals Park, OH, American Society for Metals, 1978.
- 11.77 *Metals Handbook*, 9th ed., vol. 2, "Properties and Selection: Nonferrous Alloys and Pure Metals," Metals Park, OH, American Society for Metals, 1979.
- 11.78 *Metals Handbook*, 9th ed., vol. 3, "Properties and Selection: Stainless Steels, Tool Materials, and Special-Purpose Metals," Metals Park, OH, American Society for Metals, 1980.
- 11.79 Hufnagel, W.: *Key to Aluminum Alloys—Standard Designations, Compositions, Trade Names of Aluminum Materials*, Düsseldorf, Aluminium Verlag, 1982.
- 11.80 *Handbook of Comparative World Steel Standards*, Tokyo, Japan, International Technical Information Institute, 1980.
- 11.81 Unterweiss, P. M.: *ASM Engineering Handbook—Worldwide Guide to Equivalent Irons and Steels*, Metals Park, OH, American Society for Metals, 1979.
- 11.82 Lange, K., and Meyer-Nolkemper, H.: *Closed-Die Forging* (*in German*), 2d ed., Berlin/Heidelberg/New York, Springer, 1982.
- 11.83 Seulen, G. W.: "Principles of Induction Heating and Practical Areas of Application" (*in German*), Essen, 1953.
- 11.84 VDI-Richtlinie 3132: "(Inductive Heating for Hot Forging)" Induktives Erwärmen für das Warmumformen, Düsseldorf, VDI-Verlag, 1953.
- 11.85 Geisel, H.: "Thermal Problems Encountered during Heating of Rolled Billets Using Direct Current" (*in German*), *Ind.-Anz.*, **80**, 1958, pp. 1260–1263.
- 11.86 Schmidt, Th.: "Scale-free Heating of Steel in Direct Fuel-Fired Furnaces" (*in German*), *Werkstattstechnik*, **53**, 1963, pp. 299–303.
- 11.87 Lange, K.: "Scale Formation and Decarburization as Undesirable Side Effects of Heating Forging Material" (*in German*), *Schmiedetech. Mitt.*, no. 3, 1953, pp. 3–16.
- 11.88 *Metals Handbook*, vol. 5, "Forging and Casting," Metals Park, OH, American Society for Metals, 1970.
- 11.89 Stodt, A.: *Open Die Forging* (*in German*), pt. II, 3d ed., Werkstattbücher no. XX (*in German*), Berlin/Göttingen/Heidelberg, Springer, 1950.
- 11.90 Nishihara, M., and Takeuchi, T.: "Forging of Large Crankshafts in Japan," in *Open-Die Forging* (Proceedings of the International Forging Conference, 1965), Düsseldorf, Verlag Stahleisen, 1966.
- 11.91 Javelle, J. F., and Ferry, R.: "Manufacture of Turbine Rotors for 600-MW Generators" (*in French*), in *Open-Die Forging* (Proceedings of the International Forging Conference, 1965), Düsseldorf, Verlag Stahleisen, 1966.
- 11.92 Blythe, A. J., and Gregson, W.: "An Integrated Forging Press and Manipulator," in *Open-Die Forging* (Proceedings of the International Forging Conference, 1965), Düsseldorf, Verlag Stahleisen, 1966.

## 11.128 BULK-METAL FORMING

- 11.93 "Closed-Die Forging I" (*in German*), Werkstattblatt 392, Group D, München, Hanser, 1966.
- 11.94 Kienzle, O., and Spies, K.: "The Design of Intermediate Shapes for Die-Forged Parts" (*in German*), *Werkstattstech. u. Maschinenbau*, 47, 1957, pp. 176–181.
- 11.95 Spies, K.: "Intermediate Shapes in Closed-Die Forging and Their Production by Means of Section Rolling" (*in German*), Dr.-Ing. thesis, Technische Universität Hannover, 1957.
- 11.96 Meyer, H.: "Mass Distribution in Forging Using Horizontal Forging Machines" (*in German*), *Werkstatttechnik*, 50, 1960, pp. 333–337.
- 11.97 Krausen, G.: "Forging Machines and Practical Examples of Their Use" (*in German*), *Werkstatttechnik*, 61, 1971, pp. 338–341.
- 11.98 Lange, K.: "The Role of Metal Deformation in Manufacture—Development Trends in Processes and Equipment" (*in German*), in *Conference Proceedings of the ICM '70*, Frankfurt, Verein Deutscher Werkzeugmaschinenfabriken, 1970; also Lange, K., and Geiger, M.: *Ind.-Anz.*, 93, 1971, pp. 22–26 and 185–189.
- 11.99 Peddinghaus, G., et al.: "Guidelines for the Design of Die forgings" (*in German*), *Konstruktion*, 21, 1969, pp. 130–137.
- 11.100 DIN 7523: "Schmiedestücke aus Stahl—Gestaltung von Gesenkschmiedestücken usw. (Forged Parts made of Steel—Design of Die-Forged Parts, etc.)," sheets 1–3, Aug. 1944.
- 11.101 DIN 1749: "Gesenkschmiedestücke aus Aluminium—Gestaltung (Die-Forged Parts Made of Aluminum—Design)," sheet 2, May 1963.
- 11.102 DIN 9005: "Gesenkschmiedestücke aus Magnesium—Gestaltung (Die-Forged Parts Made of Magnesium—Design)," sheet 2, May 1963.
- 11.103 DIN 17673: "Gesenkschmiedestücke aus Kupfer und Kupferlegierungen—Gestaltung (Die-Forged Parts Made of Copper and Copper Alloys—Design)," sheet 3, Mar. 1963.
- 11.104 *Aluminum-Forging Design Manual*, New York, Aluminum Association, 1967.
- 11.105 Lange, K., and Kemna, H.: "Problems Concerning the Preparation and Clamping of Die-Forged Parts for Machining" (*in German*), *Werkstattstech. u. Maschinenbau*, 46, 1956, pp. 434–442.
- 11.106 Eschelbach, R.: *Die Forming I* (*in German*), 4th ed., Werkstattbücher, no. 31, Berlin/Heidelberg/New York, Springer, 1970.
- 11.107 "Closed-Die Forging II" (*in German*), Werkstattblatt 393, Group D, München, Hanser, 1966.
- 11.108 Spies, K.: "Die Inserts" (*in German*), *Werkstattstech. u. Maschinenbau*, 44, 1954, pp. 643–647.
- 11.109 VDI-Richtlinie 3180: "Gesenk- und Gravureinsätze für Schmiedegesenke (Die and Impression Inserts for Forging Dies)," Düsseldorf, VDI-Verlag, 1956.
- 11.110 Zünkler, B.: "Guideways on Forging Dies" (*in German*), *Maschinenmarkt*, 74, 1968, pp. 1924–1928.
- 11.111 Watermann, D.: "The Fixing of Dies in Hammers Using New-Type Die Clamping Wedges" (*in German*), *Werkstatttechnik*, 52, 1962, pp. 563–566.
- 11.112 Ast: "Die Fixing Using Two-Part Die Clamping Wedges" (*in German*), *Werkstatttechnik*, 52, 1962, pp. 567–568.
- 11.113 VDI-Richtlinie 3183: "Befestigung von Schmiedewerkzeugen in Hämtern und Pressen (The Fixing of Forging Dies in Hammers and Presses)," Düsseldorf, VDI-Verlag, 1958.
- 11.114 Beck, G.: "On the Stressing of Forging Dies due to Heat" (*in German*), Dr.-Ing. thesis, Technische Universität, Hannover, 1957.
- 11.115 Stutzman, G. D.: "Use and Behavior of Cast Forging Dies" (*in German*), *Ind.-Anz.*, 88, 1966, pp. 1313–1315.
- 11.116 Jones, R. N.: "Cast dies and die inserts" (*in German*), *Ind.-Anz.*, 88, 1966, pp. 439–443.

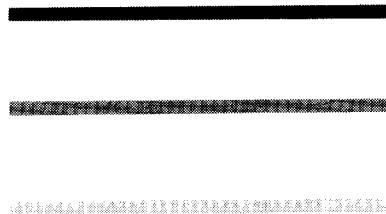
- 11.117 Kannappan, A.: "Wear in Forging Dies—A Review of World Experience," *Metal Forming*, 36, 1969, pp. 335–343; 37, 1970, pp. 6–14, 21.
- 11.118 Voss, H., Wetter, E., and Netthöfel, F.: "Wear Resistance of Heat-Treatable Die Steels" (in German), *Arch. Eisenhüttenwes.*, 1967, pp. 379–386.
- 11.119 Netthöfel, F.: "Wear Resistance of Die Steels" (in German), *Ind.-Anz.*, 91, 1969, pp. 914–915.
- 11.120 Salju, M. A.: "Work Hardening of Forging Dies by Boriding" (in Russian), *Kuzn.-Stamp. Proizvod.*, 10, 1968, pp. 47–48.
- 11.121 Rau, G.: "Die Forging Press with a New Type of Drive" (in German), *Ind.-Anz.*, 88, 1966, pp. 1841–1844.
- 11.122 Lange, K.: "The Horizontal Forging Machine in the Forge Shop" (in German), *Werkstattstechnik*, 49, 1959, pp. 461–468.
- 11.123 Rauhaus, H., and Grüner, P.: "Investigations into the Determination of Errors in Closed-Die Forging" (in German), *Stahl u. Eisen*, 70, 1950, pp. 253–264.
- 11.124 Nöthe: "Improved Productivity in the Manufacture of Closed-Die forgings through Elimination or Simplification of the Preform" (in German), *Schmiedetech. Mitt.*, 2, 1944, pp. 122–126.
- 11.125 Meyer-Nolkemper, H.: "On the Conditions Required for Higher-Accuracy Closed-Die Forging" (in German), *Ind.-Anz.*, 87, 1965, pp. 223–229, 397–404.
- 11.126 Sheridan, S. A.: *Forging Design Handbook*, Metals Park, OH, American Society for Metals, 1972.
- 11.127 Voigtländer, O.: "Limits of Closed-Die Forging—A Scientific Study" (in German), *Ind.-Anz.*, 96, 1974, pp. 2360–2363.
- 11.128 Voigtländer, O.: "The Manufacture of Turbine Blades" (in German), *Ind.-Anz.*, 91, 1969, pp. 908–913.
- 11.129 Buttstädt, K. H., and Theimert, P. H.: "Forging in Closed Dies" (in German), *Werkstatt u. Betr.*, 108, 1975, pp. 649–657.
- 11.130 Strugula, A.: "Development of a Mechanical Press for Ring-Shaped Parts with Automated Part Handling" (in German), *Werkstattstechnik*, 49, 1959, pp. 230–232.
- 11.131 Rötz, L., and Walter, M.: "Flashless Forging of Gear Blanks" (in German), *Fertigungstechn. u. Betr.*, 11, 1961, pp. 517–518.
- 11.132 Haller, K. W.: "Forgings with Optimal Shape and Finish" (in German), *Werkstatt u. Betr.*, 158, 1975, pp. 659–665.
- 11.133 Herrmann, K. H.: "Work Sequences Used in Hot Impact Extrusion" (in German), *Werkstattstechnik*, 71, 1981, pp. 603–606.
- 11.134 Lindner, H.: "Bulk Forging of Steel between 600 and 900°C" (in German), Dr.-Ing. thesis, Technische Universität, Hannover, 1965.
- 11.135 "Guidelines for Warm Working of Steels," ICFG Data Sheet 8/75, *Met. u. Met. Forming*, 1975, pp. 366–367.
- 11.136 Dannenmann, E., and Stefanakis, J.: "Demands on Lubricants Used in the Extrusion of Steel between Room Temperature and 1000 K" (in German), *Ind.-Anz.*, 97, 1975, pp. 1743–1746.
- 11.137 Saga, J., et al.: "Lubricants for Warm Forging of Steels," presented at the 5th International Cold Forging Conference, Brighton, 1975.
- 11.138 Haller, H.: *Forging Handbook* (in German), München, Hanser, 1971.
- 11.139 Huppmann, W., and Hirschvogel, M.: "Powder Forging," *Int. Met. Rev.*, 1978, pp. 233–239.
- 11.140 Huppmann, W., Dalal, K., and Zacharias, H.: "State of the Art and Uses of Powder-Metal Forging" (in German), *Werkstattstechnik*, 71, 1981, pp. 217–221.

## 11.130 BULK-METAL FORMING

- 11.141 Lange, K., and Hoang-Vu, Kh.: "Cold-Die Forging—An Alternative for Small, Precisely Shaped Parts" (*in German*), *Werkstattstechnik*, **70**, 1980, pp. 569–574.
- 11.142 Diether, U.: "Extrusion of Steel in the Temperature Range of 773–1073 K" (*in German*), Dr.-Ing. thesis, Universität Stuttgart, 1979.
- 11.143 Schröder, G.: "Isothermal and Superplastic Forging with Closed Dies" (*in German*), *Werkstatt u. Betr.*, **113**, 1980, pp. 765–770.
- 11.144 Lange, K., and Neitzert, Th., and Westheide, H.: "Possibilities Offered by Modern Forging Technology" (*in German*), in *Proceedings of the 5th Fertigungstechnisches Kolloquium* (Stuttgart, 1982).
- 11.145 Lange, K., Schaub, W., and Stilz, M.: "Special-Purpose Primary Forming and Forging Processes" (*in German*), *Werkstattstechnik*, **71**, 1981, pp. 197–205.
- 11.147 Schaub, W.: "Mechanical Properties of Warm Extruded Sinter Steels" (*in German*), *Werkstattstechnik*, **71**, 1981, pp. 223–227.

## CHAP. 12

### ROLLING



#### List of Special Symbols

---

$l$	deformed length
$n$	number of rotations of roll
$n_R$	number of rolling cycles
$p_R$	roll pressure
$r$	roll radius
$r_m$	equivalent roll radius
$s$	feed per revolution
$t$	rolling time
$x_N$	location of neutral plane from material entry
$x_R$	length of deformation or rolling zone
$\alpha_R$	roll bite angle
$\alpha_1$	angle of inclination of thread rolls
$\alpha_2$	pitch angle on thread rolls
$\alpha_W$	pitch angle of workpiece
$\gamma$	chamfer angle
$\Delta b$	spread
$\epsilon_h$	height reduction

The rolling process belongs to the compressive deformation processes, according to DIN 8583 [12.1], and has been classified based on kinematics, tool geometry, and workpiece geometry. A method of classifying the rolling process is shown in Fig. 12.1.

Rolling can be defined as a compressive deformation process in which there is either a continuous or a stepwise deformation with one or more rotary tools (rolls). Additional tools, such as

## 12.2 BULK-METAL FORMING

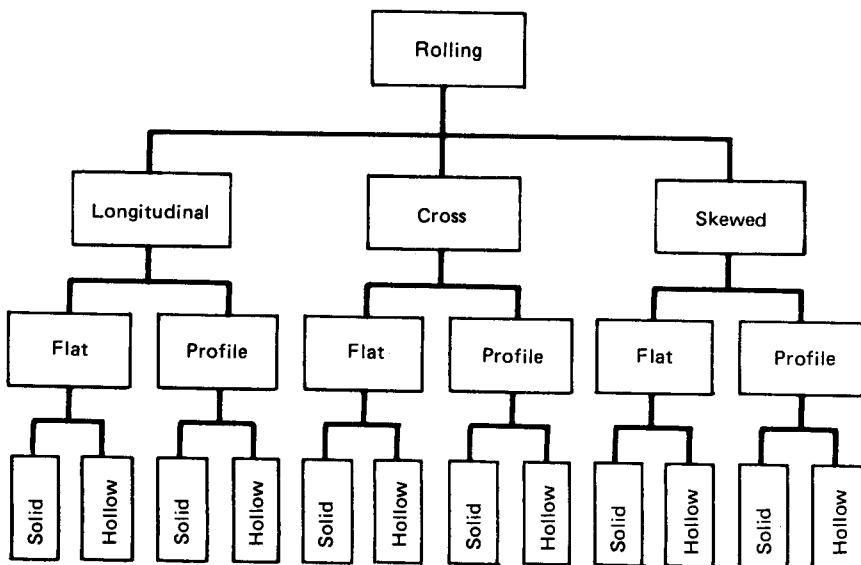


FIG. 12.1 Classification of rolling process. (After [12.1].)

mandrels, guide blocks, and support bars, may also be used in the rolling process. The force transmission is achieved either by power-driven rolls or by the workpiece transport.

Based on kinematics, the rolling process can be classified as follows: longitudinal, cross, and skewed (Fig. 12.2). In longitudinal rolling the rolled workpiece moves through the rolling gap perpendicular to the axis of the rolls, without rotation about the workpiece axis. Cross rolling is characterized by a rotary movement of the workpiece without translational motion. In skewed rolling a combination of both rotary and translational movements of the workpiece occurs.

The tool geometry is another characteristic that can be used to classify the rolling process. The process of rolling where the rolls have along their contact surfaces either a cylindrical or a conical form in the rolling gap is termed *flat-rolling*. If the contact surface of the rolls deviates from the cylindrical or conical form, the process is called *profile rolling*. The different rolls in a roll pass usually have the same section along the circumference. However, in reducer rolling operations the rolls may have variable sections along their circumference.

The rolling process can be further classified depending upon whether a solid or a hollow workpiece is rolled.

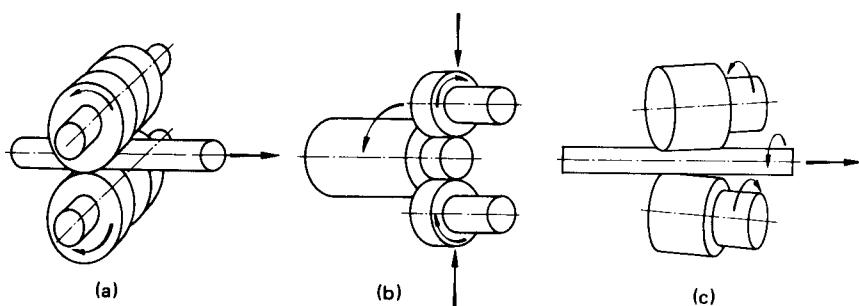


FIG. 12.2 Schematic representation of (a) longitudinal, (b) cross, and (c) skewed rolling.

The major emphasis in this chapter is not on the processes of semifinished product rolling, including tube rolling, which are very important in the iron and steel industries. The emphasis is mainly on sheet and strip rolling. The process of sheet rolling is convenient for defining the various basic parameters. Furthermore the sheet is the form of starting material that is used for many processes of tensile, compressive, and combination forming. The characteristics (dimensional accuracy, forming behavior, and surface quality) and thus the manufacturing conditions of the sheets are very important for their optimum use in the various deformation processes.

Processes used in the manufacture of typical workpieces by some of the rolling methods described above are dealt with in detail in this chapter. The very important industrial processes of flow turning, thread rolling, and surface rolling are also considered individually.

## 12.1 FUNDAMENTAL CONCEPTS

### 12.1.1 Definitions and Assumptions

During the rolling process, the rolls exert compressive stresses on some portion of the workpiece. These stresses in turn cause stresses in the workpiece, resulting in plastic flow. The interaction of these parameters will be analyzed for plate rolling without heating (Fig. 12.3).

The following geometrical relationship is valid for height reduction:

$$\Delta h = h_0 - h_1 = 2r(1 - \cos \alpha_R) \quad (12.1)$$

where  $\alpha_R$  is the roll bite angle. The strain is

$$\epsilon_h = \frac{\Delta h}{h_0} \quad (12.2)$$

The reduction in height results in both elongation and spreading. For  $b/x_R \geq 20$ , the spreading can be neglected because of large frictional resistance. Plane-strain conditions prevail in the deformation zone. From the continuity equation, the velocity of the workpiece in the  $x$ -direction (assuming no spread condition) is given by

$$v = \frac{v_0 h_0}{h} \quad (12.3)$$

The horizontal component of the circumferential roll velocity is (Fig. 12.4)

$$v_{R,x} = v_R \cos \alpha \quad (12.4)$$

The relative velocity between the workpiece and the roll is zero at the point  $x_N$  in the deformation zone. This section is called the neutral plane. The neutral plane divides the deformation zone into three areas:

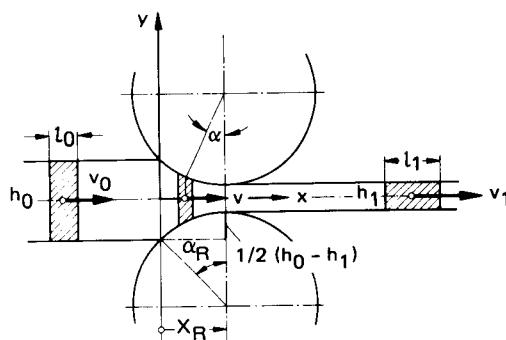


FIG. 12.3 Nomenclature in plate rolling.

- The entry zone ( $0 \leq x \leq x_N$ ), where the horizontal component of the roll circumferential velocity is greater than the velocity of the workpiece,

$$v - v_R \cos \alpha < 0 \quad (12.5)$$

- The neutral plane ( $x = x_N$ ), where the horizontal component of the roll circumferential velocity is equal to the workpiece velocity,

$$v - v_R \cos \alpha = 0 \quad (12.6)$$

- The exit zone ( $x_N \leq x \leq x_R$ ), where the horizontal component of the roll circumferential velocity is less than the workpiece velocity,

$$v - v_R \cos \alpha > 0 \quad (12.7)$$

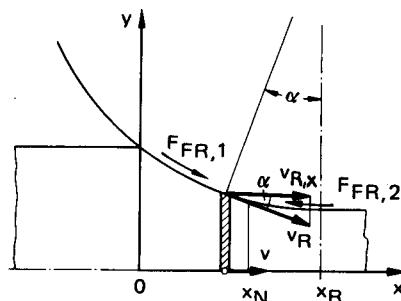


FIG. 12.4 Frictional forces and velocities in roll gap.

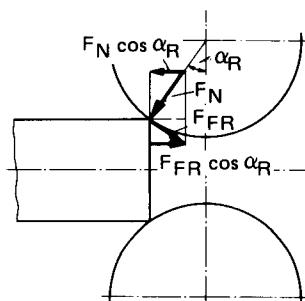


FIG. 12.5 Gripping condition for rolling.

### 12.1.2 Gripping Condition

For the rolling process to start, the forces exerted by the rolls should be sufficient to pull in the workpiece to be rolled. Assuming Coulomb's friction law to be valid, the friction force  $F_{FR}$  and the normal Force  $F_N$  are related by

$$F_{FR} = \mu F_N \quad (12.8)$$

Considering the various components of forces at the beginning of the deformation zone (Fig. 12.5), the following equation should be satisfied if the workpiece is to be pulled in:

$$F_N \sin \alpha_R \leq \mu F_{FR} \cos \alpha_R \quad (12.9)$$

With the assumption  $\tan \alpha_R \approx \hat{\alpha}_R$  (for small rolling angles  $\alpha_R$ ), the condition of rolling is given by

$$\hat{\alpha}_R \leq \mu \quad (12.10)$$

(For cold rolling of thin sheets,  $\alpha_R < 9^\circ$ .)

The following measures can be adopted to initiate the rolling process for large height reductions.

- Increasing the friction coefficient by roughing the roll surface. (In hot rolling with large height reductions, grooves are machined on the roll surface so that the gripping angle is around  $34^\circ$  [12.2].)
- Reduction of roll bite angle  $\alpha_R$  with large roll diameters
- Chamfering or pointing of the workpiece to be rolled
- Use of additional external forces (pushing, pulling)

### 12.1.3 Stresses in the Roll Gap

The plane-strain rolling of sheets can be analyzed by using simple mathematical techniques. With the slab method an equation has been derived based on equilibrium conditions (Eq. 5.55, Chap. 5). The same equation can be used for the exit zone in rolling. For the entry zone the same equation is also valid with a negative  $\rho$ . (The frictional forces change sign at the neutral zone.)

The common differential equation for the stress in the rolling gap can then be written as

$$\frac{d(\sigma_x h)}{dx} + 2\sigma_y \tan(\alpha \pm \rho) = 0 \quad (12.11)$$

The following simplifying assumptions will be made [12.3]:

$$\begin{aligned} \mu &= \tan \rho \approx \hat{\rho} \\ \tan(\alpha + \rho) &\approx \hat{\alpha} + \hat{\rho} \approx \hat{\alpha} \pm \mu \\ \hat{\alpha} &\approx \sin \alpha = \frac{x_N - x}{r} \end{aligned} \quad (12.12)$$

where the arc symbol ( $\curvearrowright$ ) denotes radians.

Hence

$$\tan(\alpha \pm \rho) = \left( \frac{x_N - x}{r} \pm \mu \right) \quad (12.13)$$

Assuming that no other longitudinal forces are applied on the workpiece, the longitudinal stress  $\sigma_x$  will be smaller than  $\sigma_y$ . Using the Tresca flow criterion ( $\sigma_x - \sigma_y = \sigma_f$ ),

$$\sigma_y \approx \sigma_f \quad (12.14)$$

Substituting Eqs. 12.13 and 12.14 in Eq. 12.11, the following differential equation must be solved to obtain the stresses:

$$\frac{d(\sigma_x h)}{dx} - 2\sigma_f \left( \frac{x_N - x}{r} \pm \mu \right) = 0 \quad (12.15)$$

Assuming an average flow stress  $\bar{\sigma}_f = (\sigma_{f,0} + \sigma_{f,1})/2$  for the deformation process, the integration of Eq. 12.15 gives the following equations:

entry zone ( $0 \leq x \leq x_N$ )

$$\sigma_{x,1} h = 2\bar{\sigma}_f \left( \frac{x_N x}{r} - \frac{x^2}{2r} - \mu x \right) + C_1 \quad (12.16)$$

exit zone ( $x_N \leq x \leq x_R$ )

$$\sigma_{x,2} h = 2\bar{\sigma}_f \left( \frac{x_N x}{r} - \frac{x^2}{2r} + \mu x \right) + C_2 \quad (12.17)$$

The constants of integration  $C_1$  and  $C_2$  are obtained by the boundary condition that  $\sigma_x = 0$  at  $x = 0$  and  $x = x_R$ ,

$$\begin{aligned} C_1 &= 0 \\ C_2 &= -2\bar{\sigma}_f \left( \frac{x_N^2}{2r} + \mu x_R \right) \end{aligned} \quad (12.18)$$

### 12.1.4 Neutral Plane, Continuous Rolling Condition

The magnitude  $\sigma_x h$  is the horizontal rolling force per unit width of the sheet. If this force does not have a singularity at the neutral plane, then it should be the same for both the entry and the exit zones at the neutral plane. For  $x = x_N$ ,

$$\sigma_{x,1} h = \sigma_{x,2} h \quad (12.19)$$

The position of the neutral plane can be obtained from the above equation as

$$x_N = \frac{x_R}{2} \left( 1 + \frac{x_R}{2\mu r} \right) \quad (12.20)$$

The workpiece should be rolled continuously once the rolling process is initiated. For this purpose the neutral plane should be in the deformation zone. Hence

$$x_N \leq x_R \quad (12.21)$$

The above equation is satisfied for the following two conditions:

$$x_R = 0 \quad \frac{x_R}{r} \leq 2\mu \quad (12.22)$$

The first condition is for no height reduction; hence the second condition is for continuous rolling.

Eq. 12.22 can be simplified with  $x_R/r = \sin \alpha_R \approx \hat{\alpha}_R$  to

$$\hat{\alpha}_R \leq 2\mu \quad (12.23)$$

Comparing the initial rolling condition (Eq. 12.10) with the continuous rolling condition (Eq. 12.23), it can be seen that once the rolling is initiated, the condition for continuous rolling is also automatically fulfilled.

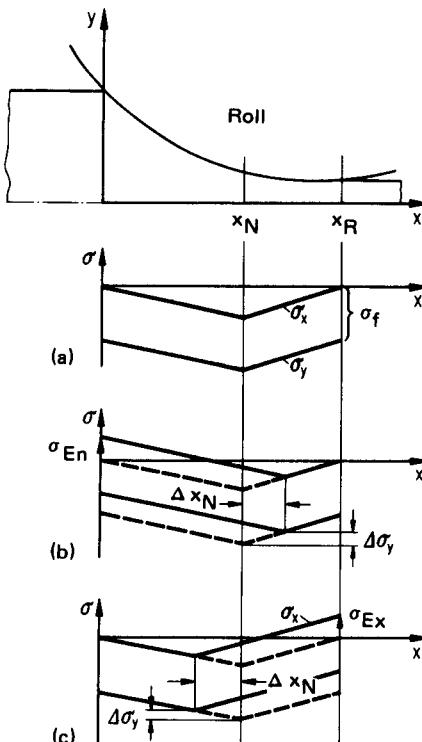


**FIG. 12.6** (a) Stress distribution without stress superimposition. (b) Stress distribution with superimposed tensile stress  $\sigma_{En}$  at entry. (c) Stress distribution with superimposed tensile stress  $\sigma_{Ex}$  at exit.

### 12.1.5 Back Tension and Front Tension

The stresses  $\sigma_x$  and  $\sigma_y$  in the rolling gap are shown schematically in Fig. 12.6a. The stresses have maximum values at the neutral plane,

$$\begin{aligned}\sigma_{x,\max} &= \sigma_x(x_N) \\ \sigma_{y,\max} &= \sigma_y(x_N)\end{aligned}\quad (12.24)$$

The magnitude of the stresses increases with increasing length  $x_N$  and increasing friction coefficient  $\mu$ .

The stresses on the rolls can be reduced by superimposed tensile stresses at the entry side (back tension) (Fig. 12.6b). However, the possible height reduction decreases in this case since it will be difficult to roll the workpiece continuously. When tensile stresses are superimposed on the exit side (front tension) (Fig. 12.6c), the maximum possible height reduction increases since the pulling force increases; the roll stresses are also lower in this case.

The lower roll stresses are especially important in the cold rolling of coils in order to ensure the dimensional control of the sheet strip over its width.

The stresses in the roll gap can be measured by pressure transducers inserted in the rolls [12.4]. Fig. 12.7a shows the stresses on the roll measured along the stressed length and width of the roll. The maximum roll stresses near the boundaries disappear in rolling with lubrication; in this case the maximum rolling stress is at the center of the roll. The effect of superimposed front tension on the shifting of the neutral plane toward the roll entry and a reduction in the roll stress can be seen from Fig. 12.7b. Correspondingly the maximum stresses at the roll boundaries are also reduced.

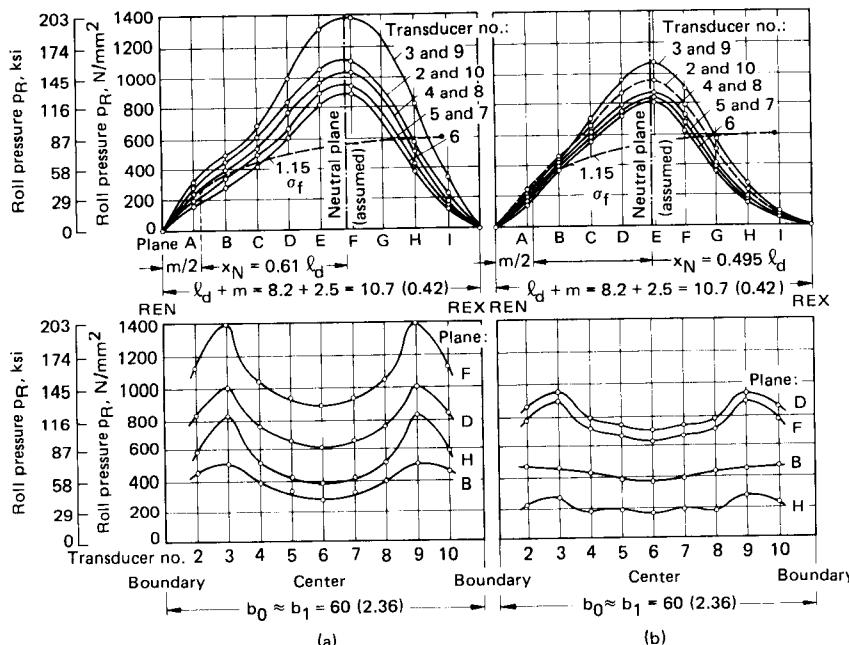


**FIG. 12.7** Variation of roll stress  $\sigma_R$  in cold rolling of sheets with a height reduction  $\epsilon_h = 0.2$  over the stressed length  $l_d$  and width  $b_0$ .  $m$  = transducer diameter. REN = Roll gap entry. REX = Roll gap exit. The transducers are arranged along the breadth of the roll with transducer 6 in the center. The planes are along the length of contact from the entry to the exit. (a) Without longitudinal stress. (b) With superimposed stress at the exit  $\sigma_{Ex} = 0.5 \sigma_f$ . Dimensions are in mm (in). (After [12.4].)

A superimposed front tension on the workpiece has less of an effect on the reduction of the roll stress than a superimposed back tension on the workpiece. Furthermore the reduction in the roll stress for combined superimposed front and back tensions is smaller than the sum of the reductions achieved by the individual stress applications.

It is not known how the frictional effects in the transducer movements affected the measured values in the above experiments. It can be opined that the errors in the measurements are larger, especially in the areas of roll entry and exit, because of inaccuracies inherent in the method of computing the roll stresses.

### 12.1.6 Rolling Force, Torque, and Power

The following equations can be used to compute the rolling force  $F$  (also referred to as the roll separating force), the rolling torque  $T_R$ , and the power  $P$  (Fig. 12.8):

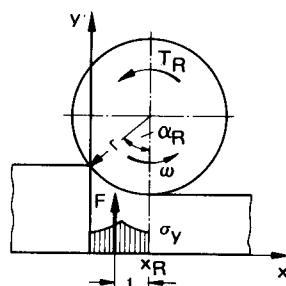


FIG. 12.8 Rolling force and torque.

$$F = b \int_0^{x_R} \sigma_y dx \quad (12.25)$$

$$T_R = b \int_0^{x_R} \sigma_y (x_R - x) dx = Fl \quad (12.26)$$

$$P = T_R \omega = \omega b \int_0^{x_R} \sigma_y (x_R - x) dx \quad (12.27)$$

Based on several theories of rolling (a summary can be found in [12.5]), the roll stresses can be calculated, and the values for  $F$ ,  $T_R$ , and  $P$  can be computed either numerically or graphically.

### 12.1.7 Correction Factors

#### *Spreading*

For values of  $b/x_R < 20$ , spreading cannot be neglected. The following formula can be used to obtain the amount of spread [12.6]:

$$\Delta b = \frac{\Delta h}{6} \sqrt{\frac{r}{h_0}} \quad (12.28)$$

#### *Sticking Zone*

For a friction coefficient  $\mu \leq 0.1$ , the neutral plane becomes a sticking zone [12.7]. The rolled material has a relative velocity  $v_{rel} = 0$  with respect to the roll surface in this zone. In such cases the entry and the exit zones do not meet at the same section. This also results in the measured stress distribution getting rounded off without exhibiting a peak [12.2].

#### *Elastic Deformation of the Rolls*

The rolls deform elastically under the effect of the rolling force. The flattening of the rolls under the rolling force will result in the plate not having a constant thickness over its width. The rolls may touch each other at their ends while rolling very thin sheets, limiting the minimum rollable thickness. The following compensations can be made in the rolls and the roll setup to obtain constant rolled thickness in spite of the elastic deformation:

- 1 The rolls are ground slightly convex (barrel-shaped).
- 2 The rolls and their stands are prestressed.
- 3 The working rolls are supported by supporting rolls.

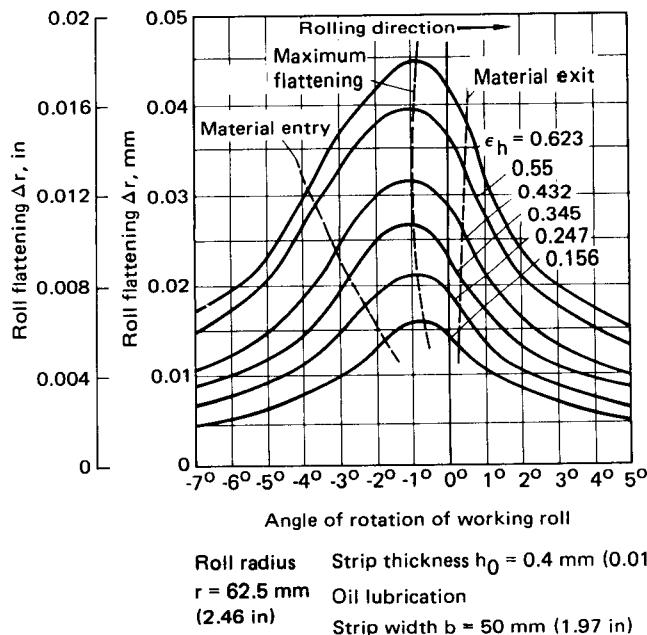


**FIG. 12.9** Roll flattening along the length of the roll gap for different height reductions in the rolling of steel. 0.05% C; 0.07% Si; 0.32% Mn; 0.12% P; 0.022% S; 0.033% Al. (After [12.9].)

The first compensation on the roll will increase the area of contact of the roll (increased arc of contact), thereby increasing the rolling force. For this reason roll stands with small working rolls supported by large back-up rolls have been developed.

Another possibility of reducing the effects of roll flattening is to compensate for the bending forces by exerting forces on the roll bearings by hydraulic cylinders [12.8]. A dynamic balancing of the bending moments is sought to compensate for different rolling conditions, especially in hot rolling.

A theoretical computation of roll flattening is extremely difficult because of the large number of factors that affect the bending process. However, measured values give some idea of the extent of roll flattening. Measurements were carried out by means of inductive transducers positioned in the working rolls of a four-roll-high rolling stand [12.9]. Roll flattening (decrease of the roll radius) is plotted in Fig. 12.9 against roll rotation for various height reductions.

The method suggested in 12.10 is the most widely used approach for the calculation of roll flattening. The deformed roll in the rolling zone is described by a circle of radius larger than the radius of the undeformed roll. Therefore rolled length increases under load. It has been shown that the values of rolled length under load calculated by this approach are on the high side [12.11]. This is especially true for thin sheets. For a reduction of height  $\epsilon_h = 0.4$  on a 0.2-mm (0.008-in) strip, the calculated value of length under load was 15% higher with the suggested approach. The deviations are smaller for thicker sheets [for a 0.6-mm (0.024-in) strip the deviation was 2.5%].

## 12.2 LUBRICATION

The temperature in the boundary areas between rolls and strip can be as high as 200°C (390°F) in the cold rolling of steel with the commonly used rolling speeds [12.12]. Hence the lubricants must not only lubricate but also cool the rolls. The use of natural oils, such as palm oils, is not very

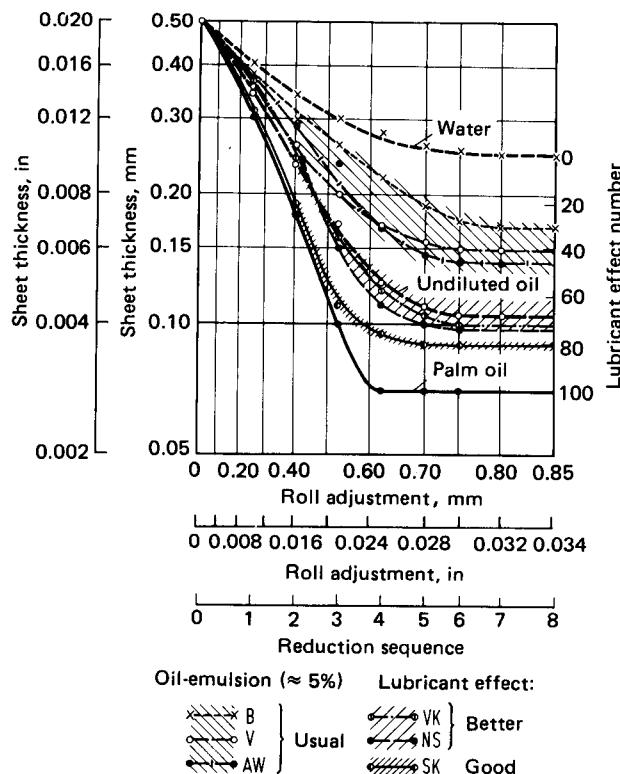


FIG. 12.10 Lubricant effect of various oil emulsions in comparison with water, undiluted oil (mineral oil), and palm oil in the rolling of steel. 0.05% C; 0.04% Mn; 0.045% P; 0.077% S. (After [12.12].)

effective at these temperatures. In undiluted form these oils produced residues on the rolls, thus affecting the surface quality of the strips. Special emulsions (made on the basis of natural fats, synthetic solids, and mineral oils) have been developed and used in concentrations of 2–15%. Mineral oil emulsions with additives (sulfur and phosphorous compounds) for withstanding large pressures have similar lubricating qualities as palm oils (Fig. 12.10). The lubricant quality is determined by the smallest achievable strip thickness and the number of passes necessary in a prefixed rolling mill arrangement.

No definite relation has been established so far between the dilution or mixing ratio and the lubricity [12.12]. The results have been erratic. However, the lubricity improves with an increasing proportion of lubricants in unsaturated fatty acids [12.13].

It should be pointed out that the relationship between the characteristic parameters of the emulsion and the quality of the rolled product is only valid for that particular rolling stand or rolling mill arrangement. The results thus obtained are not transferrable to other stands or mills.

In cold rolling aluminum, nonemulsifying oils were being used until recently. With such oils, the temperatures of the rolls could not be kept within reasonable limits, especially with increased rolling speeds. Lubricants with better cooling effects are needed. For lubricating with oils (nonemulsifying oil based on petroleum), the rolling speed limit is around 800 m/min (2625 ft/min) [12.14]. Emulsions must be used for higher rolling speeds.

### 12.3 MATERIAL CHARACTERISTICS

As in all other metal-forming processes, the rolling process also imparts a characteristic texture to the rolled workpiece. The texture can be classified into definite groups. All unalloyed face-centered cubic metals, with the exception of silver, exhibit a similar rolled texture [12.15]. The body-centered cubic metals also exhibit a rolled texture similar to that of face-centered cubic metals. However, hexagonal close-packed structure metals show three types of textures. The texture affecting the further forming characteristics of the workpiece can be controlled to a certain extent by proper combinations of rolling and heat treatment conditions.

### 12.4 LONGITUDINAL ROLLING

#### 12.4.1 Flat Rolling (Strips, Sheets, and Plates)

The simplest machine for rolling flats is the two-high mill stand. Both rolls can be driven either directly by an electric motor or through a gear drive (Fig. 12.11). The gear wheels have wide and strong teeth. They distribute the torque to both rolls. The three-high stand has an advantage over the two-high mill in that the rolling can be done in both directions without changing the direction of rotation of the rolls. A schematic representation of several types of rolling mill stands is given in Fig. 12.12.

In a typical rolling mill layout several individual stands are combined. Fig. 12.13 shows a schematic of a tandem cold rolling mill. Strip velocity, rolling force, strip thickness, and strip tension are generally measured and monitored continuously. The thickness variations are constantly compared with the required values, and the torques of the individual stands are changed to obtain the strip tension necessary for achieving the thickness tolerances [12.16].

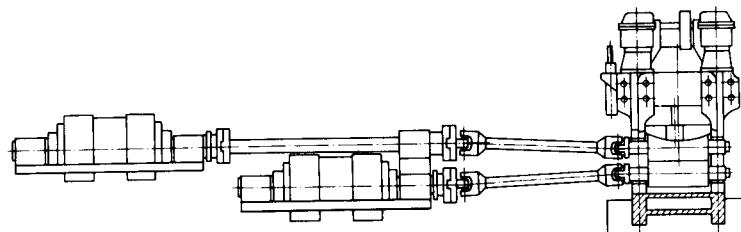


**FIG. 12.11** Individual drive of rolls for a two-high stand. (After [12.2].)

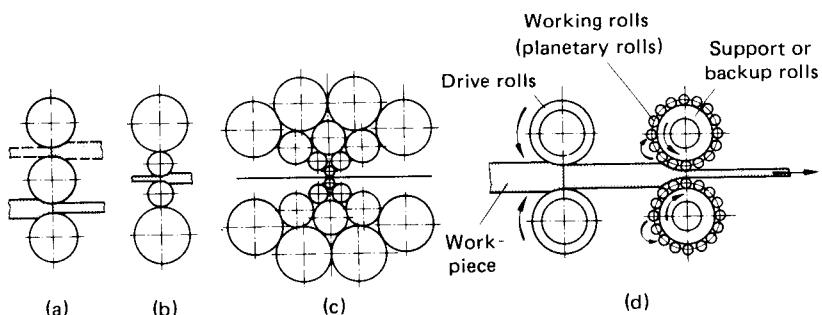


**FIG. 12.12** Schematic representation of several rolling mill stands. (a) Three high. (b) Four high. (c) Cluster (20 rolls). (d) Planetary.

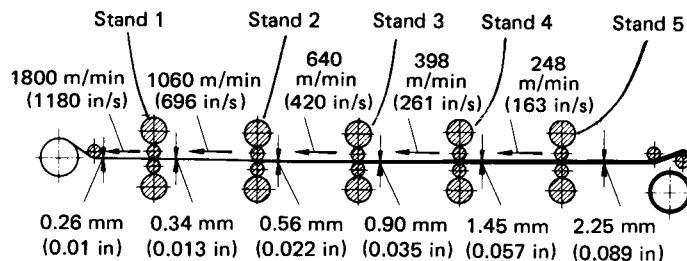


FIG. 12.13 Schematic of a tandem cold-rolling mill. (After [12.16].)

### 12.4.2 Profile Rolling (Shape)

#### *Constant Cross-Section in the Rolling Direction*

When hot rolling profiles, it is not usually possible to obtain the required shape from the ingot in a rolling stand. Roll-pass designs must be developed to obtain the required profile from a given starting ingot.

In the design of such roll passes two important factors must be considered:

- 1 If the height reductions in a section are large (and thus the elongations are also large), the workpieces may start to tear even at smaller reductions, resulting in improper fill.
- 2 For nonuniform height reductions over the cross section, the larger strain areas will be under compressive stress and the smaller strain areas under tensile stress. In such roll-pass designs large residual stresses will be present in the rolled workpieces.

Roll-pass design is mostly based on experience, and not many simple formulas are available. Several known patents exist on different roll-pass designs. Recently attempts have been made to apply advanced computer techniques to roll-pass designs [12.17] to [12.19].

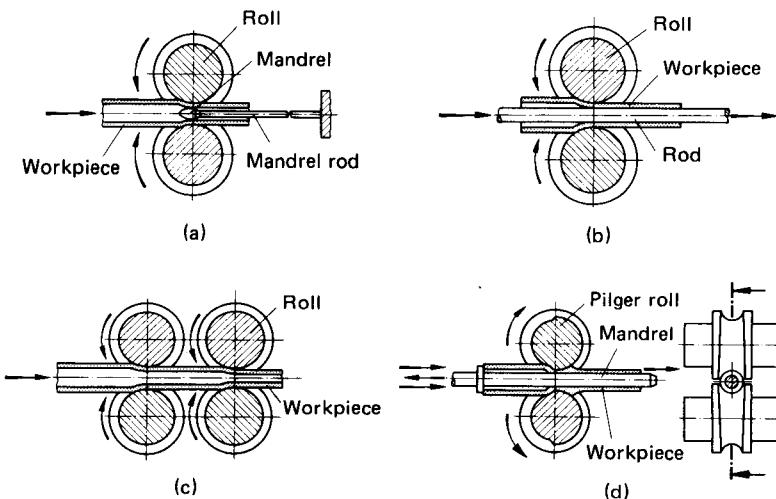


FIG. 12.14 Tube-rolling process. (After 12.11.) (a) Rolling with fixed mandrel in the rolling gap. (b) Rolling with moving rod or bar transported either by the rolls themselves or by the workpiece. (c) Rolling of tubes without using mandrels. (d) Pilger rolling over mandrel.

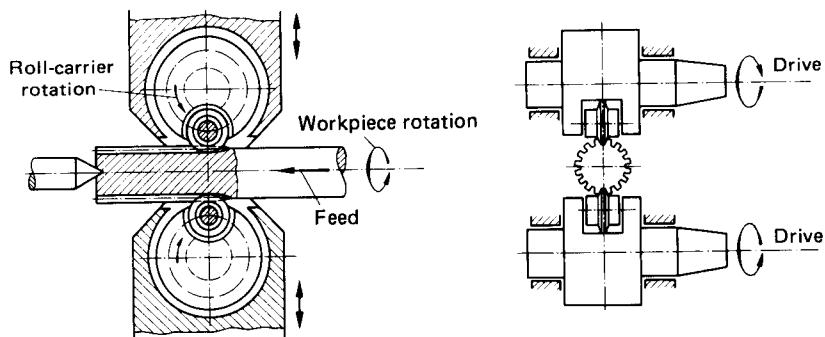


FIG. 12.15 Rolling of spline shafts with planetary rolls. (After [12.20].)

The most important profile rolling process for hollow workpieces is the tube rolling process (Fig. 12.14).

In cold rolling the trend has been to manufacture workpieces that may not have to be finish-machined. The important products in this category are spline shafts and workpieces with teeth. One well-known process has rolls mounted on the circumference of the workpiece to be rolled. The workpiece is fed in by hydraulic cylinders, and the flow of the material is in the axial direction [12.20]. The surface quality of the rolled profile (for example, gear teeth) shows an improvement over hobbed teeth, but the dimensional accuracy does not show any substantial improvement.

A modified version of the above process uses only two rolls. The roll carriers have one roll mounted planetarily [12.20]. In this method the deformation zone is therefore confined and the material flow is radial. The rolls move by superimposed vertical and rotary movements (Fig. 12.15). The workpiece is also rotated; the necessary angular adjustments necessary on the roll carriers can be made easily. Very accurate workpieces can be rolled by this process [dimensional and form accuracy within  $5 \mu\text{m}$  (200  $\mu\text{in}$ )]. Another widely used process of spline-shaft rolling is the Roto-Flo process [12.21]. In this process the spline shaft is rolled between two racks (Fig. 12.16), which are moved by hydraulic cylinders.

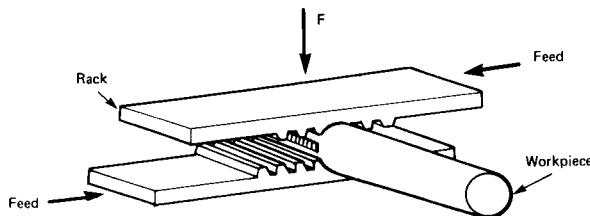
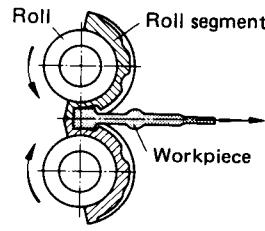


FIG. 12.16 Roto-Flo process of profile rolling. (After [12.21].)

#### *Change of Cross Section in Rolling Direction*

The most important process used for profiles with varying sections in the rolling direction is the reducer rolling process. This process is mostly used as an intermediate stage for forged workpieces and is carried out at warm or hot working temperatures. The roll forge machines are fitted with roll segments (Fig. 12.17). The cavities in the roll segments can be designed to obtain both a continuous and a sudden change of sections. The spreading factor must not be neglected in this process because of the small ratios of breadth to length. In order to reduce the effect of spreading, especially for large reductions in area, a roll-pass design schedule is used. Fig. 12.18 shows the



**FIG. 12.17** Reducer rolling process. (After [12.1].)

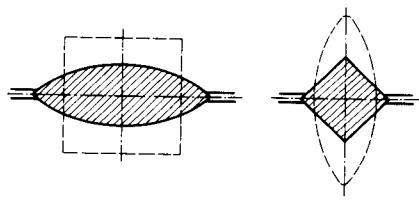


**FIG. 12.18** Roll-pass design: square-oval-square. (After [12.22].)

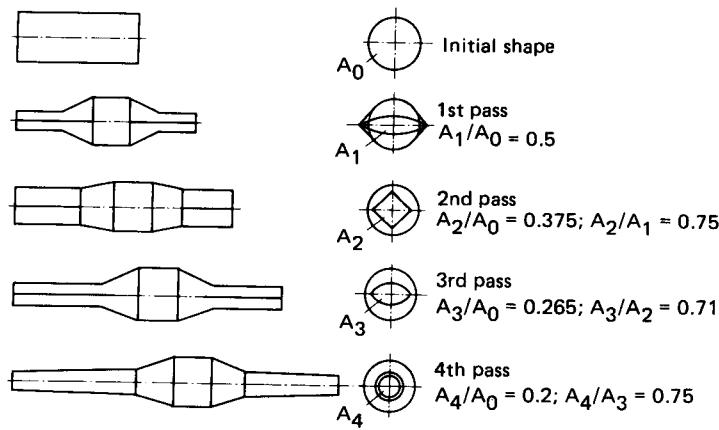
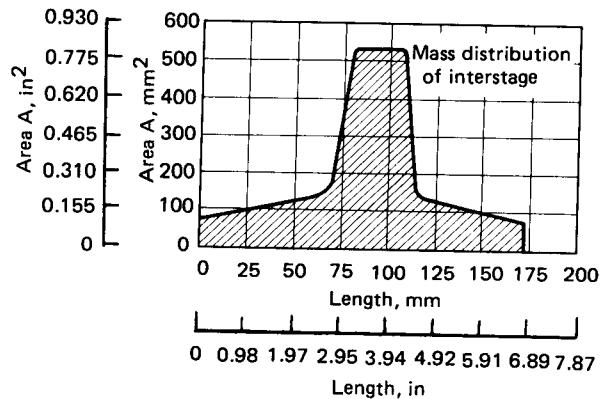


**FIG. 12.19** Development of roll-pass design for the interstage of a gear lever. (After [12.22].)

roll-pass design square–oval–square which is very common in industrial practice. A typical roll-pass design in reducer rolling of a gear lever interstage is shown in Fig. 12.19.

If the cross-sections change along the longitudinal (rolling) direction, roll-pass design becomes increasingly difficult. The velocity of the rolled product is greater at the exit section than the circumferential velocity of the roll, since the neutral plane does not generally coincide with the exit section. Hence the length of the rolled workpiece does not correspond to the developed length of the roll segment contour.

It is therefore necessary to determine the velocity increase of the rolled workpiece at every section so that the circular arc length on the roll segment can be reduced compared with the required length of the rolled workpiece. Another correction required on the roll-segment cavity is due to the cooling effect of the workpiece. The shrinkage allowance is of considerable magnitude [12.23]. The process parameters, especially the temperature, cannot be controlled very closely, and hence changes in the lengths cannot be eliminated completely. This is one of the main reasons why reducer rolls are not used for finish-forming processes.

For asymmetrical profiles, the effective working roll radius  $r_m$  should be designed to be of the same magnitude in both the normal and the tangential planes (Fig. 12.20).

The effective roll radius is the radius on which sticking friction prevails between the workpiece and the cavity. At all other radii there is a relative velocity between workpiece and cavity, since the circumferential velocity of the roll on the cavity bottom is smaller than that at the cavity flank. However, the workpiece moves with an average velocity since it is a continuum. If the

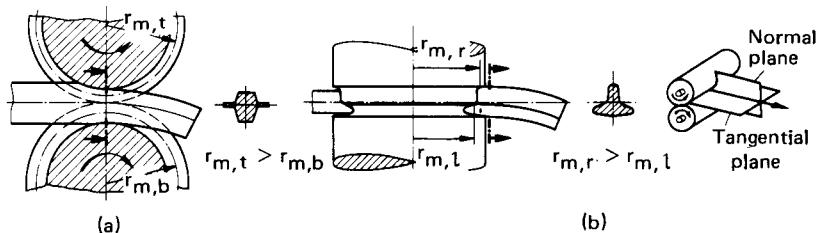


**FIG. 12.20** Curvatures on rolled profiles due to varying values of the effective roll radius  $r_m$ .  
(a) In top and bottom rolls. (b) In left and right cavity halves. (After [12.23].)

effective roll radius on the top roll  $r_{m,t}$  is greater than the effective roll radius on the bottom roll  $r_{m,b}$ , the rolled workpiece will bend (Fig. 12.20a). The neutral plane corresponding to the top region lies farther away from the exit section than the neutral plane of the lower roll, and thus the top portion of the workpiece (if the tangential plane can be thought of as being split) will try to move faster than the bottom half. Since the workpiece is a continuum, it will therefore bend. If the bending process cannot be avoided, reverse bending facilities must be used to correct the shape of the workpiece.

The process of reducer rolling is carried out in forging rolls. At the start of the operation the initial form can be pushed forward against a stopper in front of the first roll segment. After engaging the clutch to operate the rolling machine, it turns one rotation. The roll segment grips the initial portion and rolls the workpiece. The next rolling sequence starts when the interstage obtained after the first roll is in the second roll segment. The various interstages and the rolling machine are shown in Fig. 12.21. These forging rolls are equipped with automatic workpiece-handling systems for increased productivity.

## 12.5 CROSS ROLLING AND SKEWED ROLLING

A detailed classification of cross and skewed rolling processes is not attempted, since many important industrial processes are combinations of both.

Processes of piercing a tube by a combination of cross and skewed rolling with various roll



FIG. 12.21 Forge rolls. (Courtesy of EUMUCO.)

forms (barrel, cone, and disk) are shown in Fig. 12.22. Another interesting skewed rolling process is the manufacture of spherical balls [12.2]; balls up to a diameter of 20 mm (0.787 in) can be cold-rolled by this process (Fig. 12.23a). The spherical balls will be nearly red hot due to enormous frictional and deformation forces. Larger diameters are hot-rolled. The production rate is one ball per rotation of the roll ( $\approx 100 \text{ min}^{-1}$ ). The dimensional and form accuracies are comparable to those of forged spherical balls.

In the three-roll process (conical rolls) (Fig. 12.23b) an additional longitudinal tensile stress is used to prevent crack formation (porosity) along the axis. The porosity may be used advantageously for the tube-rolling process. The superimposed longitudinal tensile stress is also used in

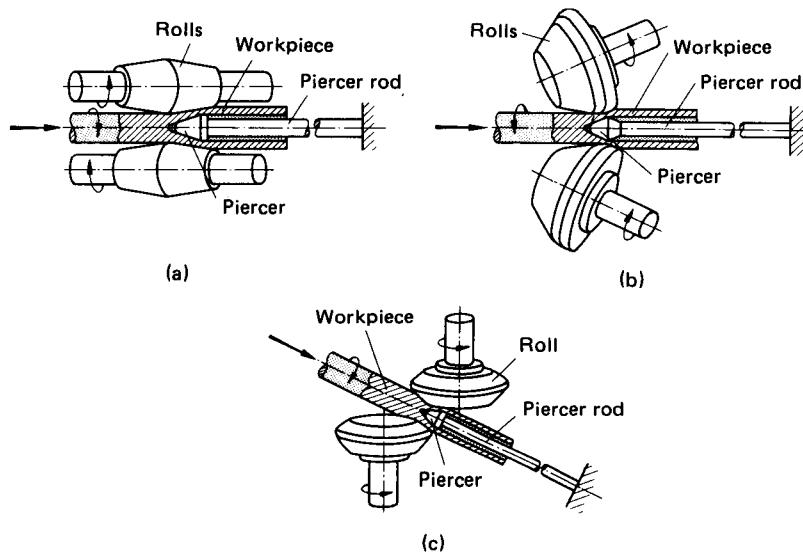
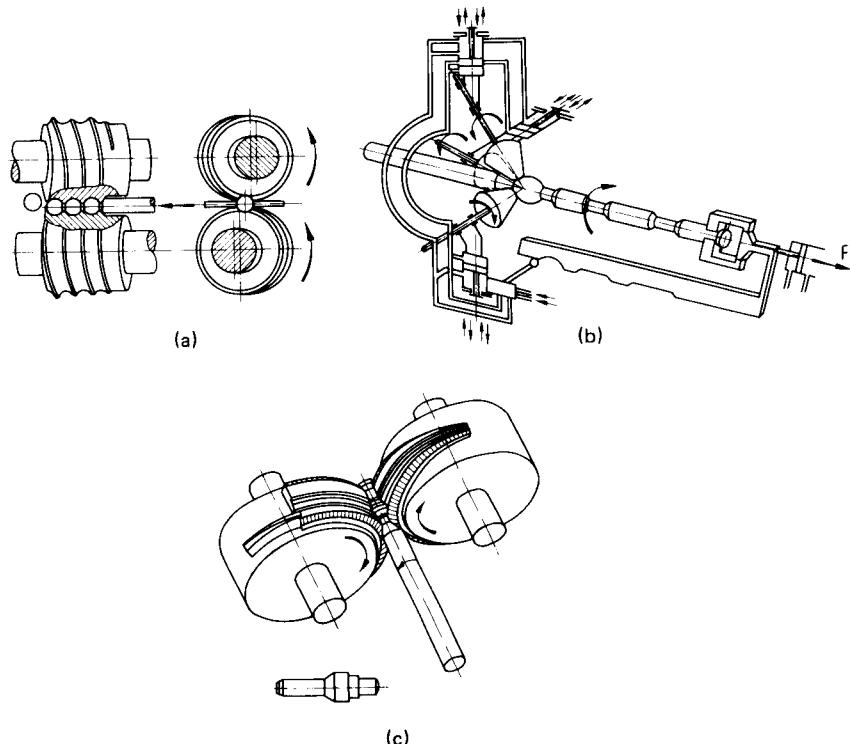


FIG. 12.22 Tube piercing processes by rolling. (a) Barrel-shaped rolls. (b) Conical rolls. (c) Disk rolls. (After [12.2].)



**FIG. 12.23** (a) Skewed rolling of spherical balls. (b) Three-roll process with conical rolls. (c) Cross rolling of stepped profiles. (After [12.24].)

cross-rolling processes to produce stepped profiles (Fig. 12.23c) [12.24]. The magnitude of tensile stress is a function of workpiece shape, workpiece material, and rolling temperature.

The profile (skewed) cold rolling of fin tubes from hollow preforms is among the most important industrial processes. The fin tubes (Fig. 12.24a) are used in heat exchangers. By relieving the rolls, as shown in Fig. 12.24b, the rolling forces and the roll torque can be reduced compared

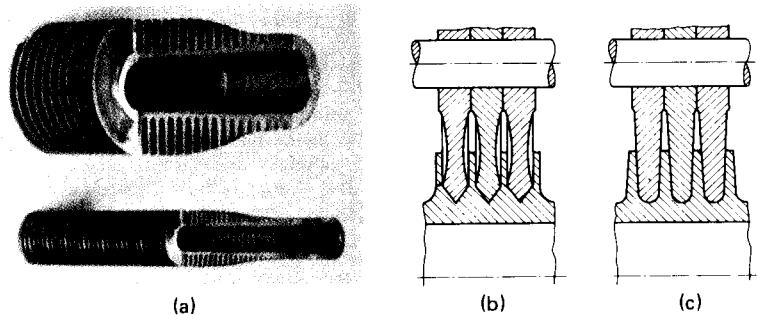


**FIG. 12.24** (a) Rolled fin tubes. (b) Relieved rolls. (c) Tapered rolls.

with the roll design illustrated in Fig. 12.24c. However, the achievable fin heights are also smaller. During rolling with relieved rolls, the material flows radially. The resultant circumferential tensile stresses will limit the fin heights that can be achieved before cracks occur. The tapered rolls impart additional hydrostatic pressure on the fin; hence larger fin heights are possible. At present fins have been achieved with heights of up to 12.5 mm (0.5 in) [root width = 1.3 mm (0.05 in) and top width = 0.4 mm (0.016 in)] on aluminum tubes of 38-mm (1.5-in) diameter, and with heights of 8.5 mm (0.335 in) [root width = 0.7 mm (0.028 in) and top width = 0.5 mm (0.02 in)] on copper tubes of 15.5-mm (0.61-in) diameter.

For more information on other cross and skewed rolling processes, the reader is referred to references for further reading quoted at the end of this chapter. We will briefly describe the processes of surface rolling, thread rolling, and flow forming (spinning) in the remainder of this chapter.

### 12.5.1 Surface Rolling

The surface quality, dimensional accuracy, and mechanical properties of workpieces can be improved by surface-rolling processes. The process of reducing the surface roughness of a workpiece is termed as *planishing*. This will lead to better wear behavior of sliding components (bearing race, valve rod, etc.). Sizing operations are those in which the dimensions are controlled within closer limits. The fatigue strength of workpieces can be increased with rolling processes by creating residual compressive stresses in the required areas (transient zone on piston rods, crank shafts, etc.).

The processes of surface rolling can also be classified based on kinematics: plunge rolling, through-feed rolling, and rolling with longitudinal feed. The longitudinal movement is achieved in the through-feed rolling process by positioning the roll slightly inclined to the workpiece. In rolling with longitudinal feed, the feed is achieved by longitudinal forces. In this case the workpieces should possess sufficient strength since the force and the torque are transmitted by the workpieces only.

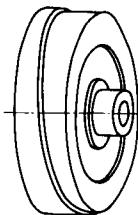


**FIG. 12.25** Roll with the planishing surface like a screw. (After [12.25].)

In plunge rolling, a roll with a rolling surface in the shape of a screw can be used (Fig. 12.25). The secondary rolling surfaces are positioned a few hundredths of a millimeter (a few thousandths of an inch) behind the actual rolling surface in the radial direction. The rolling forces are thereby reduced compared with those of cylindrical rolls [12.25].

#### Basic Principles and Process Limits

The surface-rolling process is used for machined workpieces. Considering the surface topography on a turned workpiece (Fig. 12.26a), one is likely to assume that the surface roughness peaks will be bent sideward during surface rolling. It can be seen that this is not likely to happen when the surface is observed with the same magnification for both axes (Fig. 12.26b). The material flow in surface rolling with feed is shown in Fig. 12.27. The flattening of the peaks has the effect of pushing the valleys up. The material flow in the circumferential direction is shown in Fig. 12.28a in the form of a welded seam running radially. The neutral plane will be assumed at N (Fig. 12.28b) for the explanation of tangential strains. The material velocity at E is larger than the roll velocity. The material builds up (upper bending of the seam), which will be seen as a bulge at the entry. The bulge does not increase in size during rolling because of material movement in the longitudinal direction.

The shear stress on the workpiece surface is zero at the neutral plane. It increases very rapidly to its maximum value and reduces slowly thereafter. This results in the plastic deformation in the internal area of the workpiece [12.27]. On the surface of the workpiece an elastic layer is present below which there are plastic zones. In this condition the workpiece gets rolled between the neutral plane N and the exit R. The workpiece diameter is reduced. The material is transported at a

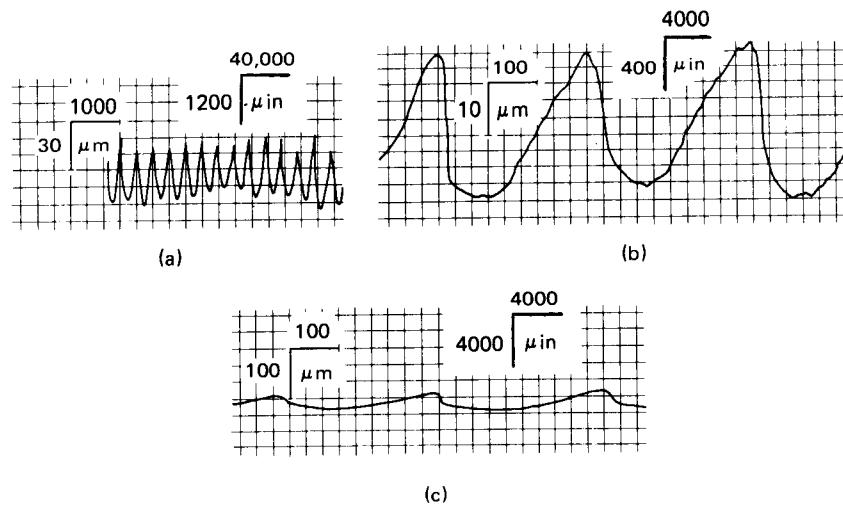


**FIG. 12.26** Surface roughness records of turned component.

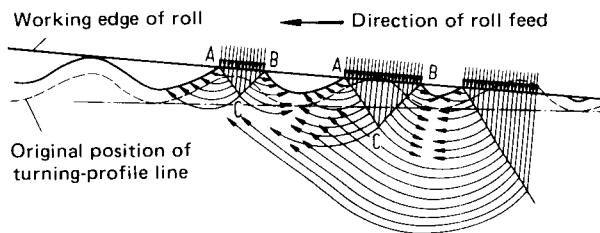


**FIG. 12.27** Streamlines of plastic movement of material in surface rolling with feed. (After [12.26].)

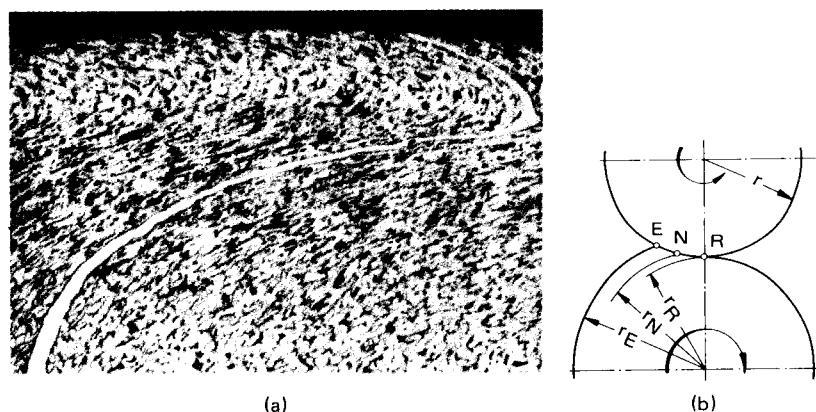


**FIG. 12.28** (a) Tangential strains on the surface layer of a cylindrical workpiece of 10-mm (0.4-in) diameter from AISI 1015. (After [12.27].) (b) Diameter change in the deformation zone in surface rolling.

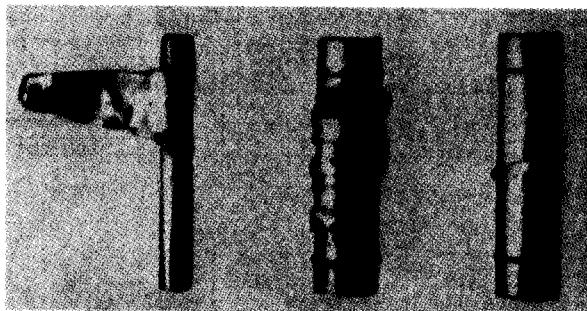


**FIG. 12.29** Peeled surface layers of workpieces after surface rolling.  
(After [12.27].)

greater velocity at the exit because of the higher roll velocity, thereby causing bending of the bulge.

The failure criterion in surface rolling is the peeling off of the surface layer of the workpiece (Fig. 12.29). This is due to very high rolling forces and the number of rolling cycles. The roll pressure is given by

$$p_R = \frac{F_r}{ld} \quad (12.29)$$

where  $F_r$  is the rolling force,  $l$  is the deformed length, and  $d$  is the equivalent diameter calculated from

$$\frac{1}{d} = \frac{1}{d_R} + \frac{1}{d_w} \quad (12.30)$$

The number of rolling cycles is the number of contacts of a point on the workpiece with the roll. For plunge rolling,

$$n_P = nt \quad (12.31)$$

and for through-feed rolling,

$$n_T = \frac{l}{s} \quad (12.32)$$

The number of rolling cycles has a more pronounced effect than larger roll forces on the peeling of the surface layer. An increase in the number of rolling cycles does not affect the depth of the deformation zone. However, it increases the tangential strains which cause peeling [12.27].

### Planishing

The surface roughness of the rolls is a very important parameter in planishing. The surface-rolled workpiece, however, exhibits a finer surface texture than the roll [12.28]. For smaller workpieces, the initial surface roughness  $R_t$  of the workpiece should not be greater than  $10 \mu\text{m}$  ( $400 \mu\text{in}$ ) to keep the rolling forces within limits and to prevent surface peeling.

The minimum achievable surface roughness  $R_t$  is between  $0.1$  and  $0.2 \mu\text{m}$  ( $4-8 \mu\text{in}$ ). Even with rolls of lower surface roughness and higher rolling forces it will be difficult to achieve better results. This limiting value is probably based on the crystal structure of the workpiece material [12.25]. Fig. 12.30 shows the waviness  $R_p$  as a function of roll pressure and the number of rolling cycles.

The surface quality (fineness) of the workpiece does not depend on the roll velocity. The lubri-

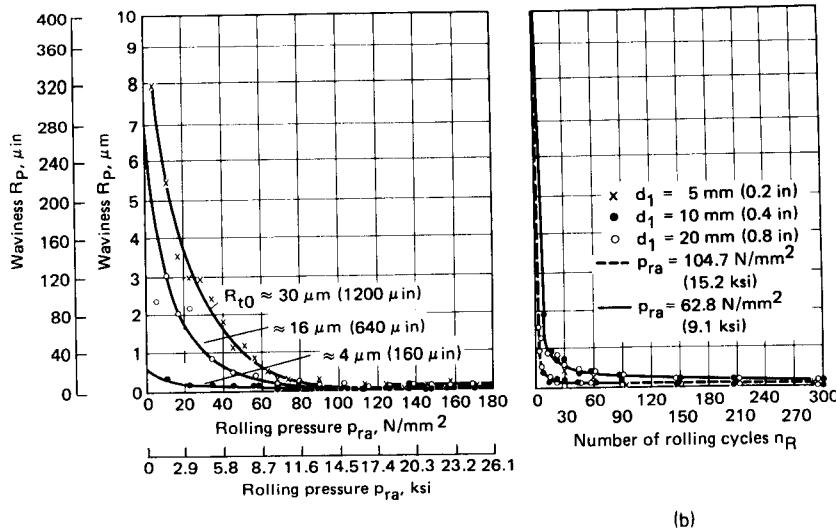


**FIG. 12.30** (a) Waviness  $R_p$  as a function of the rolling pressure  $p_{ra}$  for various surface roughness values  $R_{t0}$ . Number of rolling cycles  $n_R = 30$ . (b) Waviness  $R_p$  as a function of the number of rolling cycles  $n_R$  for various rolling pressures  $p_{ra}$ . Initial surface roughness  $R_{t0} \approx 30 \mu\text{m}$  (1200  $\mu\text{in}$ ); workpiece material—DIN X115CrV3K; workpiece diameter  $d_1 = 10 \text{ mm (0.4 in)}$ ; roll diameter  $d_2 = 75 \text{ mm (3 in)}$ ; roll width  $l = 30 \text{ mm (1.2 in)}$ . (After [12.25].)

cant also does not affect the fine texture of the surface. Efficient cleaning is a prerequisite for good surface finish since foreign particles must be washed out thoroughly to prevent scratching.

### Surface Rolling to Obtain Close Dimensional Tolerance

With smaller sizes [ $d < 20 \text{ mm (0.8 in)}$ ], surface rolling can be used to reduce the diameter [ $\Delta d \approx 0.1 \text{ mm (0.004 in)}$ ] [12.26] in order to obtain close dimensional tolerances. Workpieces with a diameter of 3 mm (0.12 in) can be surface-rolled to the tolerance quality level corresponding to IT 9. Of these workpieces 95% had actual tolerance levels corresponding to IT 5. The roundness values also improved after surface rolling. Typical values of roundness for a diameter range of 1.5–5 mm (0.06–0.2 in) are between 1 and 2  $\mu\text{m}$  (40–80  $\mu\text{in}$ ).

### Improvement of Mechanical Properties

Large residual stresses are present in the workpieces after surface rolling because of the combined effect of localized plastic deformation and the supporting elastic zones. The fatigue properties of the workpieces are considerably enhanced. To cite an example, the fatigue strength of a crank shaft in the bearing areas is improved 80% by surface rolling [12.29]. Another example is shown in Fig. 12.31, which illustrates the fatigue strength in bending tests of circular test pieces.

### Machinery and Accessories

Special machinery is available for surface-rolling processes depending upon individual requirements. In general the surface-rolling operations are built as part of a machine tool. The accessories for machine tools equipped for surface-rolling operations range from simple rolls to sophisticated hydraulic units [12.30].

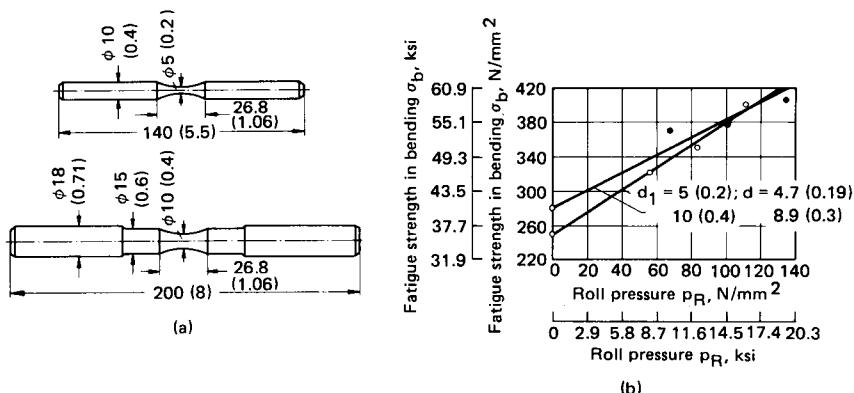


**FIG. 12.31** Change of fatigue strength due to surface rolling. (a) Testpieces. (b) Fatigue strength as a function of roll pressure  $p_R$ . Material—AISI 1045; initial roughness  $R_{t,0} = 2 \mu\text{m}$  ( $80 \mu\text{in}$ ); roll diameter—80 mm (3.15 in); roll width—26.8 mm (1.06 in); number of rolling cycles  $n_R = 30$ . Dimensions are in mm (in). (After [12.27].)

### 12.5.2 Thread Rolling

Apart from fastening threads, other thread types being rolled are trapezoidal, circular, saw tooth, and special threads. Either flat or round tools can be used for thread rolling. With circular tools, thread lengths that are longer than the width of the rolls can be rolled in the through-feed process.

During the rolling operation, the material flows along the flanks rather than at the center (Fig. 12.32). This can lead to folds, especially with very sharp threads. These folds can be found at about 20% of the tooth depth. Harder workpieces tend to form deeper folds than softer workpieces. The load-bearing capacity of the threads, however, is not reduced due to the formation of the folds. The sharp edges break very easily, and hence such threads cannot be used for the manufacture of thread chasers.

The hardness in the rolled thread increases because of strain hardening; it can reach up to twice the initial value (Fig. 12.33). When the deformation strain is computed from the localized elongation, values of  $\varphi_{\max}$  as high as 0.54 are found for M12 to M20 threads [12.33]. In the case of steel screws (M10) the load-bearing capacity due to strain hardening increases by between 6 and 12% as compared with that of machined screws. Strain hardening has a greater effect on the fatigue strength. Table 12.1 lists the fatigue strength in bending tests of various threaded bolts. If a heat-treatment operation is necessary because of functional requirements, then it is carried out before the thread-rolling operation. At the end of bolts, the outer layers of the deformation zone

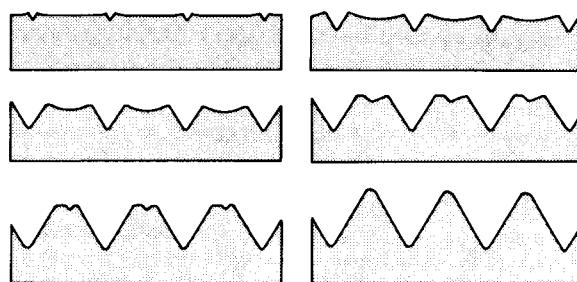


**FIG. 12.32** Material flow in thread rolling. (After [12.31].)

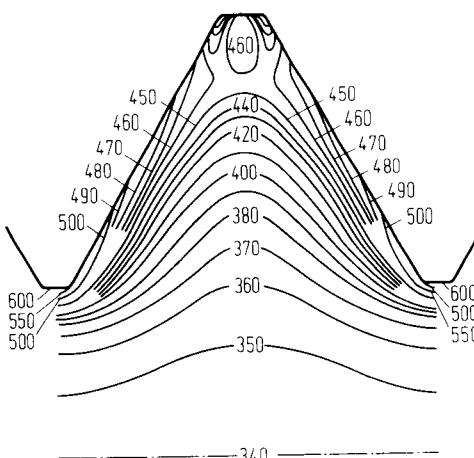


**FIG. 12.33** Hardness distribution in threads after thread rolling. Thread—M8; material—chrome-vanadium steel, hardened, core hardness HV 0.1 = 340. (After [12.32].)

elongate with respect to the core. This results in the formation of a concave surface. Bolts are generally pointed to overcome this phenomenon (Fig. 12.34a). Chamfering at the end is also necessary from the point of view of the tool life of the thread rolls since it reduces the possibility of unequal load on the threads (Fig. 12.34b). Chamfering also helps to lower gradually the axial pressure on the rolls (Fig. 12.34c). The chamfer angle  $\gamma$  is  $15^\circ$  for materials with tensile strength  $S_u < 1000 \text{ N/mm}^2$  ( $< 145 \text{ ksi}$ ) and  $20^\circ$  for materials with  $S_u > 1000 \text{ N/mm}^2$  ( $> 145 \text{ ksi}$ ). The tolerances required on the thread-rolling diameter for fine- and medium-quality threads can also be obtained by deformation processes such as extrusion (open-die or trapped). If the thread-rolling diameter is on the high side, shearing will occur on the thread surface [12.34].

#### Thread Rolling with Flat Dies

The threads are rolled between two flat dies, one of which is fixed. The second flat die moves relative to the fixed die. The drive is generally by a crank (Fig. 12.35a). The dies are so designed that the complete thread is formed in one forward stroke of the moving die. The dies have a length equal to 1.5 times the circumference of the thread on the bolt at the entry, and the threads are formed in this area. In the straight portion of the die (2–4 times the circumference of the bolt), the threads are sized and smoothened. The final path is relieved so that the finished threads are not damaged. The moving die is generally longer than the fixed die so that there is a positive release of the rolled bolt. If the threads are formed at a very fast speed at the entry portion of the

**Table 12.1** Comparison of Fatigue Strength in Bending Tests of Threaded Bolts

Condition 1	Condition 2	$\sigma_{b,1}/\sigma_{b,2}$
Rolled, hardened	Hardened, rolled	1–2
Hardened, machined	Hardened, rolled	1–3
Machined, hardened	Rolled, hardened	1–1

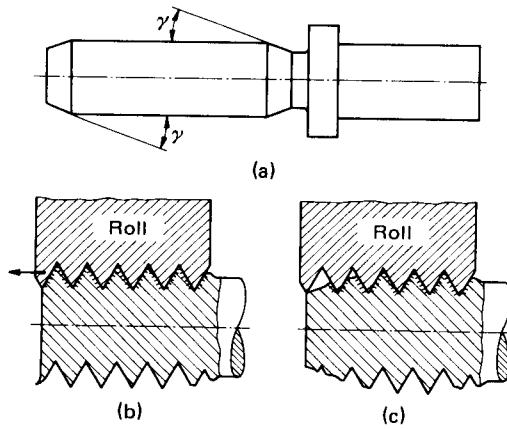


**FIG. 12.34** (a) Chamfered bolts. (b) Bolts without entry chamfer. (c) Bolts with correct entry chamfer.

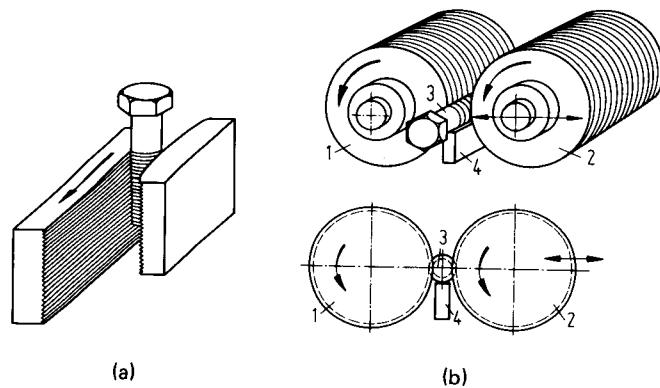


**FIG. 12.35** (a) Thread rolling with flat dies. (b) Thread rolling with round dies in single-feed process. 1—fixed roll; 2—adjustable roll; 3—workpiece; 4—workpiece support. (After [12.32].)

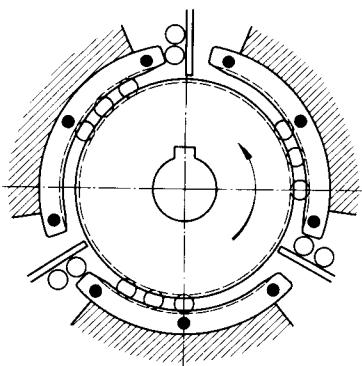


**FIG. 12.36** Segment rolls with fixed concave segments. (After [12.32].)

die, the bolt will not be round. Any large variation in roundness obtained in the entry zone cannot be rectified in the sizing area.

### Thread Rolling with Circular Dies

In the single-feed process two rolls are used which rotate in the same direction with the same speed (Fig. 12.35b). One roll is fixed, and the other roll is moved toward the fixed one hydraulically, in the radial direction. The workpiece is either held between centers or supported on the bottom. In the latter case, the setting up is done so as to have the workpiece axis slightly lower than the roll axes, thereby ensuring positive resting of the workpiece on the support.

The threads on the rolls should have the same pitch angle  $\alpha$  as those on the workpiece. Since the distances between the threads on the shell line must be equal to the pitch  $h$ , the threads on the rolls are of several leads. The number of times the thread is made on the roll is a function of the ratio of roll diameter to thread-roll diameter of the workpiece:

$$\frac{d_R}{d_w} = \frac{n_R}{n_w} \quad (12.33)$$

This means that regrinding of the rolls is possible only to a limited extent. As a guidance value, on a roll diameter of 140 mm (5.5 in) regrinding is possible up to 0.5 mm (0.02 in).

If the rolls are designed as segments for the single-feed process, the productivity can be increased (Fig. 12.36).

Three methods are used for the through-feed process (Fig. 12.37):

- 1 With rolls whose axes are parallel and whose profiles have pitch angles  $\alpha_2 > \alpha_w$  there is an axial feed of the workpiece. However, the difference between  $\alpha_2$  and  $\alpha_w$  should not be very large in order to avoid thread damage.
- 2 If the rolls do not have any pitch angle, they have to be tilted by an angle  $\alpha_1$  equal to the workpiece pitch angle  $\alpha_w$ . For larger pitches, the contact length between the workpiece and the die decreases, thereby setting limits for this process. The advantage is that the same set of rolls can be used for a wide range of pitch angles and diameters.
- 3 The third process is a combination of processes 1 and 2. The rolls are tilted by an angle  $\alpha_1$  and have a pitch angle of  $\alpha_2$  ( $\alpha_1 + \alpha_2 = \alpha_w$ ). This permits the thread rolling in the through-feed process for larger pitch angles with a high degree of accuracy.

The second process is used only in conjunction with thread rolling heads (Fig. 12.38). These heads can be used on turning lathes. Either two rolls [for  $d < 3$  mm (0.12 in)] or three rolls are used.

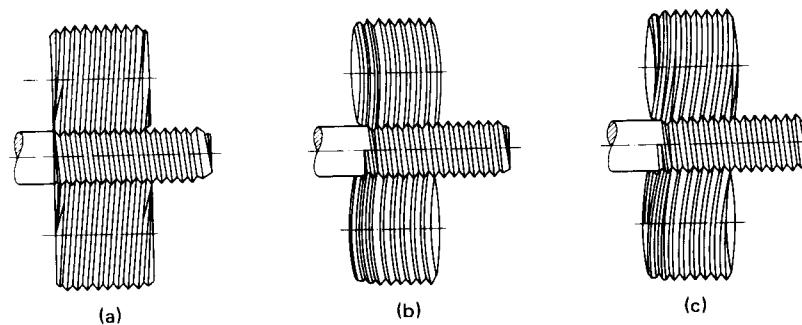


**FIG. 12.37** Thread rolling in through-feed process. (a) Rolls with their axes parallel; thread profile with pitch angle,  $\alpha_1 = 0$ ,  $\alpha_2 > \alpha_w$ . (b) Tilted rolls, thread profile without pitch angle,  $\alpha_1 = \alpha_w$ ,  $\alpha_2 = 0$ . (c) Tilted rolls; thread profile with pitch angle,  $\alpha_1 + \alpha_2 = \alpha_w$ .

### Accuracy

The tolerance levels obtainable in thread rolling can be found in [12.35]. Form errors on the initial workpiece (roundness, cylindricity) cannot be corrected or improved in the thread-rolling process. The tolerances on the thread-rolling diameter are reflected in the accuracy of the thread outer diameter. Variations on the thread outer diameter are around  $\Delta d \approx 0.05$  mm (0.002 in). The following values can be used as guidance for the dimensional tolerance and surface quality:

Tolerance on flank diameter	$\geq 0.02$ mm (0.001 in)
Pitch error	0.05–0.1 mm/100 mm (0.005–0.001 in/in)
Surface roughness on flank $R_t$	$\leq 5 \mu\text{m}$ (200 $\mu\text{in}$ )

If the number of roll cycles is very large, chip formation can occur, especially in the case of sharp contoured threads.

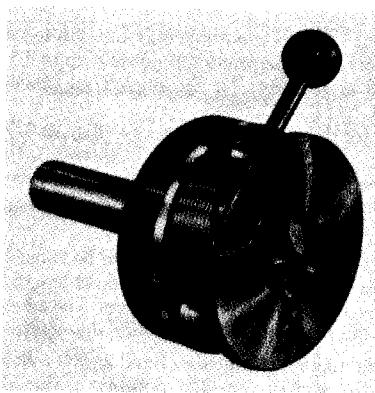


FIG. 12.38 Thread rolling head. (Courtesy of Fette.)

### 12.5.3 Flow Forming

Flow forming is the process of forming profiles by skewed rolling [12.1]. Contrary to metal spinning, where no reduction of wall thickness is attempted, the process of flow forming is used to obtain the desired wall thickness reductions. The process of metal spinning belongs to the category of sheet-metal forming and is dealt with in Chap. 21. A schematic representation of the flow-forming process is shown in Fig. 12.39.

The deformation zone in flow forming is confined to the area of the workpiece circumference in contact with the rolls. This phenomenon is different from the deformation zone in ironing, which is also used to reduce the thickness of walls on cylindrical components. The flow is also affected by the adjoining elastic zones in the workpiece. The hindered flow of material in flow forming results in an opening up of the component ahead of the roll (unrolled portion), which gets only partly corrected during further rolling (Fig. 12.40). For large reductions of wall thickness, both the opening up and bulge formation either cause overlapping or lead to cracking during the rolling of the already formed bulge, because the forming limits have already been reached. Another limiting criterion is the tearing of the workpiece for large deformation forces and torques. The thickness of the bulge depends on a number of factors. Fig. 12.41 shows a few results from experiments [12.37].

Several theoretical results have been reported concerning the determination of the force requirements in flow forming [12.36], [12.38] to [12.41]. However they are not very useful in industrial practice. This problem is basically due to the innumerable process parameters.

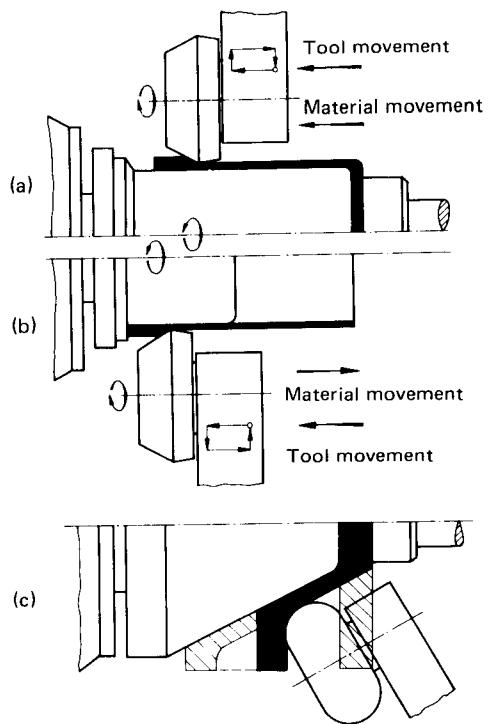


**FIG. 12.39** Schematic representation of the flow-forming process. (a) Hollow workpiece with cylindrical surface (forward flow). (b) Hollow workpiece with cylindrical surface (backward flow). (c) Hollow workpiece with conical surface.

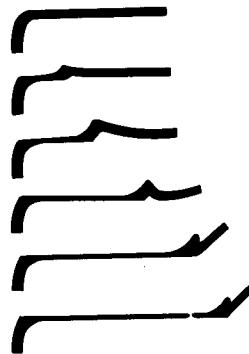


**FIG. 12.40** Bulge formation and opening up of unrolled portion in flow forming. (After [12.36].)

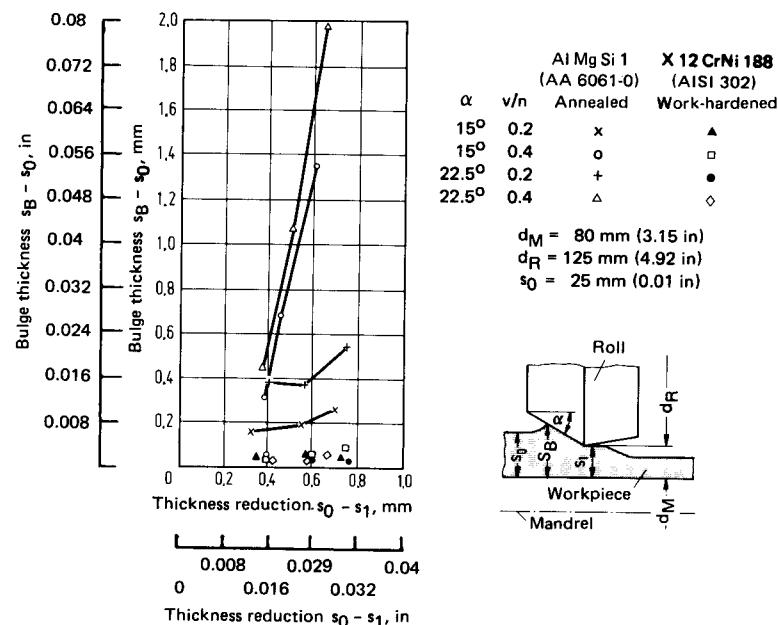


**FIG. 12.41** Bulge thickness as a function of thickness reduction in flow forming.  $\alpha$ —roll entry angle;  $v/n$ —relative feed (velocity per number of revolutions). Shown is a two-roll process. Material and roll move in the same direction. (After [12.37].)

### Hollow Workpieces with Cylindrical Shell Lines

The workpiece (drawn cups) are rolled generally from the bottom toward the top. The material flows in the direction of the feed (forward flow). In the case of workpieces without any bottom, the moment of the roll can be transferred to the workpiece by using a toothed mandrel. The workpiece is then pressed against this toothed mandrel by the axial component of the moment. The material flows opposite to the direction of feed (backward flow) (Fig. 12.39b).

The achievable reduction of thickness depends mainly on (1) the roll tip radius or the entry angle of the roll, (2) the feed per revolution, and (3) the setting angle of the roll (Figs. 12.42 and 12.43). The results shown, which were obtained for commercially pure aluminum, can also be used for low-carbon steels [12.38]. The bulge formation in the case of a low-carbon steel (AISI 1006) is smaller than that in commercially pure aluminum (refer to Fig. 12.41).

The dimensional accuracy obtainable in flow forming on a two-roll flow-forming machine has been reported in [12.42]. The tendency of the unrolled portion to open up results in large deviations in diameter tolerances. The results on the tolerances of the wall thicknesses are more favorable.

### Hollow Workpieces with Conical or Arbitrary Shell Lines

The starting piece is a round blank whose diameter is the same as the largest diameter on the workpiece to be produced. Depending on the shape of the finished component, the initial workpiece can also be a deep drawn or spun cup or a mechanically formed conical cup. The initial diameter of the blank does not change during the process. The material is pushed in the axial direction (Fig. 12.44). The following relationship holds for the change of wall thickness:

$$s_1 = s_0 \sin \alpha \quad (12.34)$$

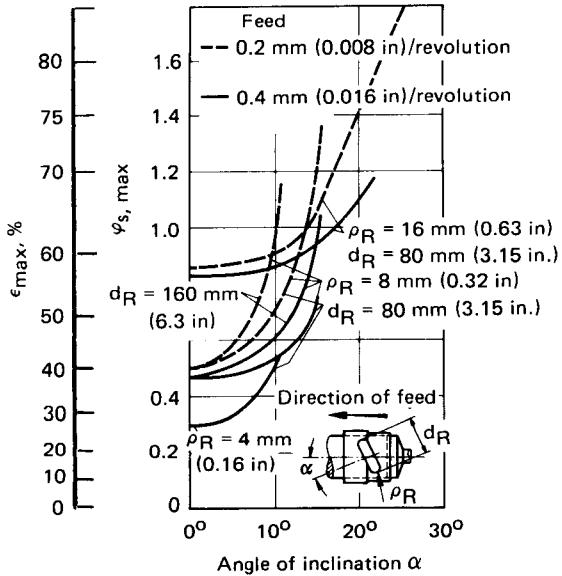


FIG. 12.42 Limits of forming for flow forming with inclined positioning of the roll. Material—AA 1050; initial wall thickness  $s_0 = 2 \text{ mm (0.08 in)}$ ; initial cup height  $h_0 = 40 \text{ mm (1.58 in)}$ ; cup diameter  $d = 100 \text{ mm (3.94 in)}$ ; roll diameter  $d_R = 80 \text{ mm (3.15 in)}$  and  $160 \text{ mm (6.3 in)}$ . (After [12.36].)

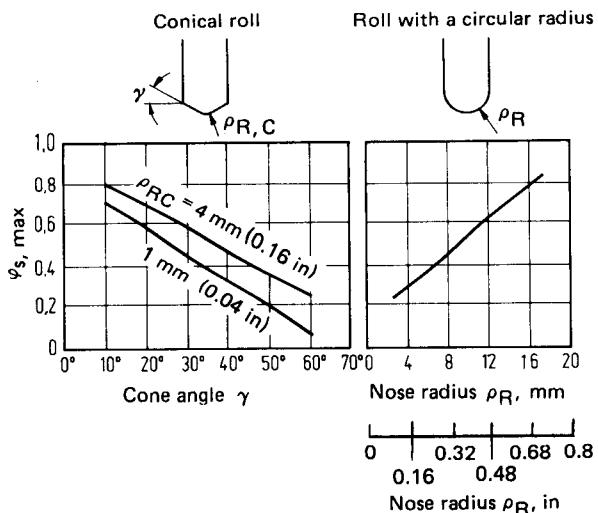
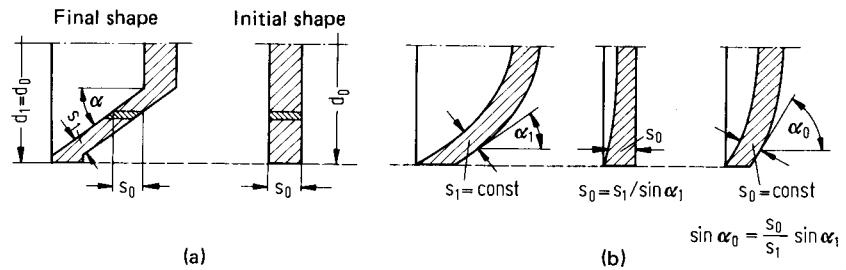
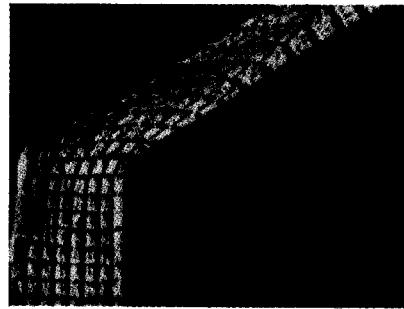


FIG. 12.43 Effect of roll shape on the forming limit in flow forming. Material—AA 1050; initial wall thickness  $s_0 = 2 \text{ mm (0.08 in)}$ ; initial height  $h_0 = 40 \text{ mm (1.58 in)}$ ; can diameter  $d = 100 \text{ mm (3.94 in)}$ ; roll diameter  $d_R = 80 \text{ mm (3.15 in)}$ . (After [12.36].)



**FIG. 12.44** (a) Geometry of initial and final shapes of a conical workpiece. (b) Initial and final shapes of a curved part.



**FIG. 12.45** Deformed grid lines in flow forming of a conical workpiece made from copper. (After [12.43].)

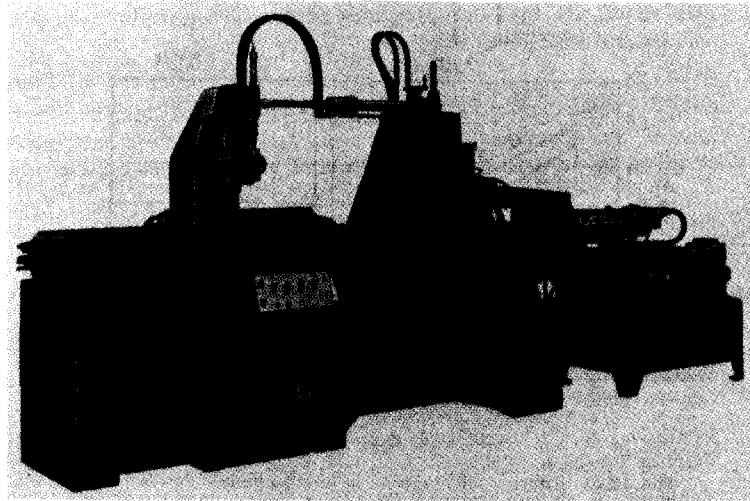


**FIG. 12.46** Flow-forming machine. (Courtesy of Bohner & Köhle.)

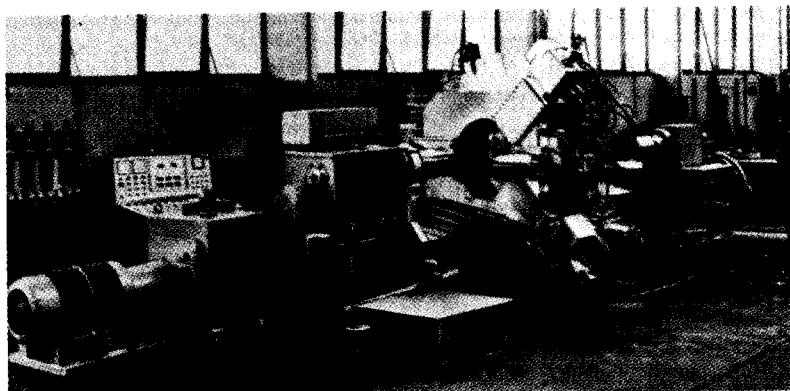


**FIG. 12.47** Flow-forming machine with samples. (Courtesy of Leifeld.)

If a constant wall thickness is desired, the initial blank should be of varying thickness, or it must have a curvature with constant thickness (Fig. 12.44b).

The analytical methods developed so far for the determination of forces are based on the mode of shearing [12.43]. It is assumed that the final shape is formed by the displacement of ring-type elements. This is valid only in part. Cut workpieces exhibit the shearing process only near the transition from the bottom to the wall. The deformation in the wall is a pure upsetting or rolling process (Fig. 12.45).

The maximum achievable deformation can be characterized by the smallest rollable angle of inclination of a conical cup. This depends, among other things, on the initial thickness of the blank, feed per unit revolution, and the roll geometry. The smallest inclination angle for AA 1050 is on the order of 9°; for AISI 1005 and AISI 304L, the angle is 11° [12.38]. These angles correspond to a wall thickness reduction of  $\epsilon_s \approx 0.81-0.84$ .

### Machines

The machines available in the market are used for both flow forming and metal spinning. Their appearance and construction are similar to that of lathes. For mass production, machines are used that have hydraulically actuated saddles with either semi- or fully automatic copying controls. In addition to single- and two-support machines, three-roll machines are also available (Figs. 12.46 and 12.47).

### REFERENCES

- 12.1 DIN 8583: "Fertigungsverfahren Druckumformen (Manufacturing Processes—Compressive Forming)," 1970.
- 12.2 Zelikow, A. J.: *Textbook of Roll Works (in German)*, Berlin, VEB Verlag Technik, 1957.
- 12.3 Hoff, H., and Dahl, T.: *Fundamentals of Rolling Processes (in German)*, Iron and Steel Books, vol. 9, Düsseldorf, Verlag Stahleisen, 1955.
- 12.4 Vater, M., Nebe, G., and Peterson, J.: "On the Pressure Distribution in the Roll Gap during Cold Rolling of Sheet Strips" (*in German*), *Stahl u. Eisen*, 86, 1966, pp. 710-720.
- 12.5 *Fundamentals of Forming (in German)*, Düsseldorf, Verlag Stahleisen, 1966.
- 12.6 Geleji, A.: *Forming of Metals (in German)*, Berlin, Akademie-Verlag, 1967.
- 12.7 Troost, A., and Hölling, K.: "Calculation of the Force Requirements in Rolling Thin Strips and the Determination of the Minimum Rollable Thickness" (*in German*), *Stahl u. Eisen*, 33, 1962, pp. 427-439.

## 12.32 BULK-METAL FORMING

- 12.8 Zelikow, A. J.: "Control of Thickness Variation along the Strip Width with Counterbending of Working Rolls" (*in German*), *Stahl*, 8, 1968, pp. 809–815.
- 12.9 Pawelski, O., and Schröder, H.: "Measurement of Roll Flattening in Cold Rolling in a Four-Roll-High Rolling Stand" (*in German*), *Arch. Eisenhüttenw.*, 39, 1968, pp. 747–754.
- 12.10 Hitchcock, J. H.: "Roll Neck Bearings," New York, American Society of Mechanical Engineers, 1935, pp. 33–41.
- 12.11 Pawelski, O., and Schröder, H.: "Effect of Roll Flattening in the Roll Gap Form and Pressure Distribution in Cold Forming" (*in German*), *Arch. Eisenhüttenw.*, 40, 1969, pp. 867–873.
- 12.12 Billigmann, J.: "Investigations on the Lubricant Effect of Oils, Especially Emulsions" (*in German*), *Stahl u. Eisen*, 75, 1955, pp. 1691–1701.
- 12.13 Lueg, W., and Funcke, P., Jr.: "Investigation on Oils and Emulsions in Cold Rolling Experiments" (*in German*), *Stahl u. Eisen*, 77, 1957, pp. 1817–1830; 78, 1958, pp. 333–343.
- 12.14 Hohmann, G.: "Rolling of Steel and Aluminum with Emulsions" (*in German*), *Mineralöletechnik*, 14, 1969, pp. 1–10.
- 12.15 Wasserman, G., and Grewen, J.: *Textures in Metallic Materials* (*in German*), 2d ed., Berlin/Göttingen/Heidelberg, Springer, 1962.
- 12.16 Hoff, H.: "Manufacture and Properties of Sheet Strip Steel" (*in German*), *Werkstattstechnik*, 53, 1960, pp. 351–357.
- 12.17 Akgermann, N., Lahoti, G. D., and Altan, T.: "Computer-Aided Roll Pass Design in Rolling of Airfoil Shapes," *J. Appl. Metalwork.*, 1, 1980, pp. 30–40.
- 12.18 Raghupathi, P. S., and Altan, T.: "Roll Pass Design in Shape Rolling" (A survey of German Technical Literature), unpublished rep., Columbus, OH, Battelle Memorial Institute, 1979.
- 12.19 Wilson, W. R. D., and Kennedy, K. F.: "An Analytical Model for Side Spread in Rolling of Flat Products," in *Proceedings of NAMRC-VI* (Gainesville, FL, May 1978), pp. 119–126.
- 12.20 Grob, E.: "Cold Rolling Machines for Spline Shafts and Gears" (*in German*), *Werkstattstechnik*, 50, 1960, pp. 351–357.
- 12.21 Krapfenbauer, H.: "Cold Rolling of Precision Profiles" (*in German*), in *Neuere Entwicklungen in der Massivumformung (New Developments in Bulk Forming)*, Seminar-Proceedings (Forschungsinstitut Umformtechnik der Ingest e. V. Stuttgart, Universität Stuttgart), June 1977, p. 24.
- 12.22 Spies, K.: "The Interstages in Die Forging and Their Manufacture by Rolling" (*in German*), *Forschungsberichte des Landes Nordrhein-Westfalen*, no. 728, Köln/Opladen, Westdeutscher Verlag, 1959.
- 12.23 Lange, K., and Meyer Nolkemper, H.: *Die Forging of Steel* (*in German*), 2d ed., Berlin/Heidelberg/New York, Springer, 1977.
- 12.24 Hašek, V.: *Fundamentals of Metal Forming* (*in Czech*), Prague, SNTL-Nakladatelství, 1969.
- 12.25 Pahlitzsch, G., and Krohn, P.: "On Planish Rolling of Cylindrical Workpieces with Diameters up to 20 mm" (*in German*), *Werkstattstechnik*, 53, 1963, pp. 447–453.
- 12.26 König, H.: "Planish Rolling" (*in German*), in *Das Industrieblatt, Schriftenreihe Feinbearbeitung* (Series on Fine Working), Stuttgart, Deutscher Fachzeitschriften- u. Fachbuchverlag, 1954.
- 12.27 Pahlitzsch, G., and Krohn, P.: "On Surface Rolling of Cylindrical Workpieces in Plunge Process" (*in German*), *Werkstattstechnik*, 56, 1966, pp. 2–12.
- 12.28 Pahlitzsch, G., and v. Eitzen, H. J.: "On Surface Rolling of Circular Parts with Diameters of 1.5 to 5 mm in Plunge Process" (*in German*), *Werkstattstech. u. Maschinenbau*, 47, 1957, pp. 589–597.
- 12.29 VDI-Richtlinie 3177: "Oberflächen-Feinwalzen (Surface Rolling)," March 1963.

- 12.30 Jäger, H.: "Surface Rolling on Automatic Lathes" (*in German*), *Werkstattstechnik*, **58**, 1968, pp. 570–573.
- 12.31 Apel, H.: *Thread Rolling (in German)*, München, Hanser, 1952.
- 12.32 VDI-Richtlinie 3174: "Rollen von Aussengewinden durch Kaltumformung (Rolling of External Threads by Cold Forming)," December 1958.
- 12.33 Richter, A., and Montag, G.: "Determination of the Maximum Torque in Thread Rolling with Three Rolls in Through-Feed Process" (*in German*), *Fertigungstech. u. Betr.*, **16**, 1966, pp. 45–47.
- 12.34 Reichel, W.: "Thread Rolling Process and Machines" (*in German*), *Draht*, **3**, 1952, pp. 226–238, 277–287, 316–329, 393–398.
- 12.35 DIN 13: "Metrisches ISO-Gewinde (Metric Screw Threads)," pt. 1, 1973.
- 12.36 Thamasett, E.: "Forces and Limit Strains in Flow Forming of Cylindrical Rotation-Symmetrical Hollow Workpieces of Aluminum" (*in German*), Dr.-Ing. thesis, Universität Stuttgart, 1961.
- 12.37 Dreikandt, H. J.: "Investigations on Flow Forming of Cylindrical Hollow Workpieces and Contribution to the Determination of the Deformed Area and Forces" (*in German*), *Berichte aus dem Institut für Umformtechnik, Universität Stuttgart*, no. 24, Essen, Girardet, 1973.
- 12.38 Sanner, P.: "Forces and Limit Strains in Profile Flow Forming of Conical Rotation-Symmetrical Hollow Workpieces" (*in German*), Dr.-Ing. thesis, Technische Universität, Berlin, 1963.
- 12.39 Avitzur, B., and Yang, C. T.: "Analysis of Power Spinning of Cones," *J. Eng. Ind.*, **82 B**, 1960, pp. 231–245.
- 12.40 Kobayashi, S., and Thomsen, E. G.: "Theory of Spin Forging," *CIRP Ann.*, **10**, 1961, pp. 114–123.
- 12.41 Hayama, M.: "Theoretical Study of Tube Spinning," *Bull. Faculty Eng. (Yokohama National University)*, **15**, 1966, pp. 33–48.
- 12.42 Schelosky, H., and Krämer, W.: "Comparative Investigations on Flow Forming and Ironing" (*in German*), *Ind.-Anz.*, **92**, 1970, pp. 1761–1722.
- 12.43 Kalpacioglu, S.: "On the Mechanics of Shear Spinning," *J. Eng. Ind.*, **83 B**, 1961, pp. 125–130.

## FURTHER READING

- Neumann, H.: *Roll Pass Design (in German)*, Leipzig, VEB Deutscher Verlag für Grundstoffindustrie, 1969.
- Tselikov, A. I., and Smirnov, V. V.: *Rolling Mills*, Pergamon, London, 1965.
- The Making, Shaping and Treating of Steel*, 9th ed., United States Steel, 1971.
- Wusatowski, Z.: *Fundamentals of Rolling*, Pergamon, London, 1969.
- Roll Pass Design*, British Steel Corp., Sheffield, England, 1979.



**FUNDAMENTALS OF  
EXTRUSION AND  
DRAWING****List of Special Symbols**

---

$F_B$ ( $W_B$ )	bending force (work)
$F_D$ ( $W_D$ )	force (work) in drawing over mandrel
$F_{FR}$ ( $W_{FR}$ )	friction force (work)
$F_{FR,M}$ ( $W_{FR,M}$ )	friction force (work) on mandrel
$F_{FR,S}$ ( $W_{FR,S}$ )	friction force (work) on die shoulder
$F_{FR,W}$ ( $W_{FR,W}$ )	friction force (work) on die wall
$F_{id}$ ( $W_{id}$ )	ideal deformation force (work); force (work) in homogenous deformation
$F_I$ ( $W_I$ )	force (work) in ironing
$F_P$	punch load
$F_{Sh}$ ( $W_{Sh}$ )	shearing force (work)
$F_T$ ( $W_T$ )	force (work) in tube drawing
$F_{tot}$ ( $W_{tot}$ )	total deformation force (work)
$\mu_M$	coefficient of friction on mandrel
$\mu_S$	coefficient of friction on die shoulder

The processes of extrusion and drawing make use of a tool in the form of a nozzle. The processes under this category are cold, warm, and hot extrusion; rod, tube, and profile drawing; and ironing. In all these processes the billet is either pushed (extrusion) or pulled (drawing) through a tool opening (die or orifice) (Fig. 13.1).

## 13.2 BULK-METAL FORMING

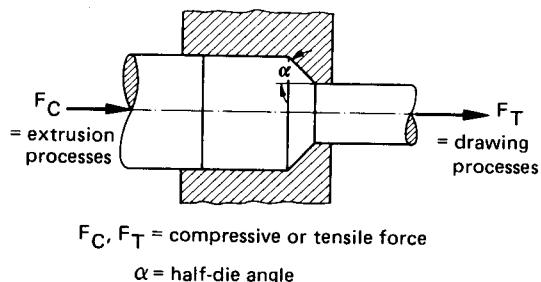


**FIG. 13.1** Schematic representation of drawing and extrusion processes.

The processes may also be classified as compressive forming (if the force is  $F_C$ ) [13.1] or tensile-compressive forming (if the force is  $F_T$ ) [13.2].

### 13.1 EXTRUSION PROCESSES

The processes of cold and hot extrusion are further classified depending upon the direction of material flow in relation to the tool movement direction. Another method of classifying these processes is by their geometry, namely, solid and hollow components. Some examples are hollow forward extrusion, solid backward extrusion, and hollow side extrusion. A system of classifying extrusion processes according to [13.1] is illustrated in Fig. 2.13. Figs. 13.2 and 13.3 show schematic sketches of the principal processes of hot and cold extrusion. The definitions of the process according to [13.1] are given below.

#### 13.1.1 Extrusion of Semifinished Products

Extrusion of semifinished products is the extrusion of a block enclosed by a container to produce basically sections (profiles) with a solid or hollow cross section. In the extrusion of semifinished products with rigid tools, the block is pushed through a die by a punch.

**Forward extrusion:** The flow of metal is in the same direction as the direction of action of the machine.

**Solid forward extrusion** (Fig. 13.2a): The final product is a solid workpiece with a profile. The shape of the die opening is determined by the die only.

**Hollow forward extrusion** (Fig. 13.2b): The final product is a hollow workpiece with a profile. The shape of the die opening is determined by both the die and the mandrel. The mandrel can be loose, fixed, clamped to the punch, or moved with the punch, or it can be designed as part of the die.

**Backward extrusion:** The flow of metal is opposite to the direction of action of the machine.

**Solid backward extrusion** (Fig. 13.2c): The final product is a solid workpiece with a profile. The shape of the die opening is determined by the die only.

**Hollow backward extrusion** (Fig. 13.2d): The final product is a hollow workpiece with a profile. The shape of the die opening is determined by both the die and the mandrel. The mandrel can be loose, fixed, or attached to the die.

**Lateral (side) extrusion:** The material flow is perpendicular or at an angle to the direction of action of the machine.

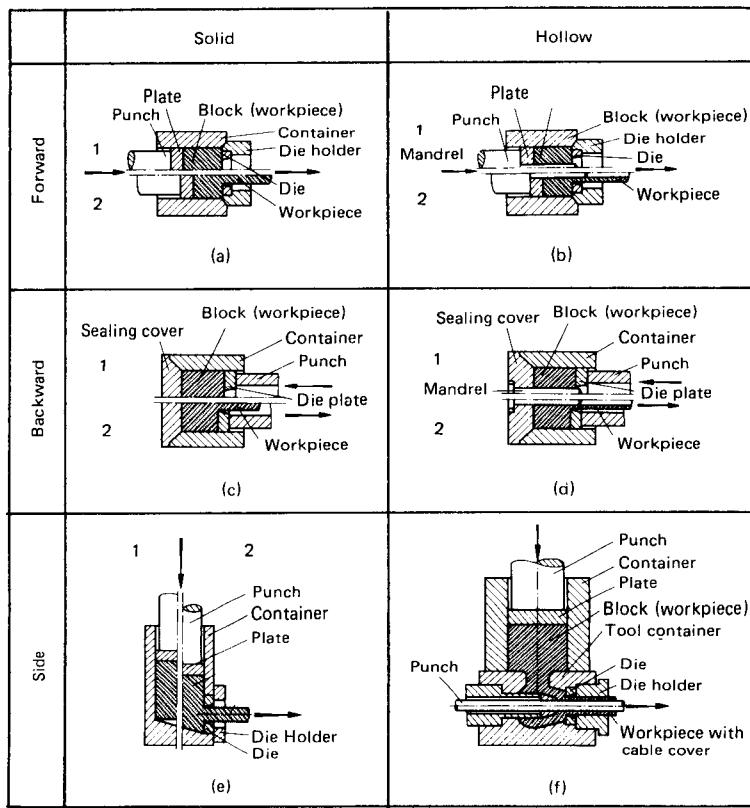


**FIG. 13.2** Schematic representation of extrusion processes for semifinished products. (a) Solid forward. (b) Hollow forward. (c) Solid backward. (d) Hollow backward. (e) Solid side. (f) Hollow side to make cable covers on workpiece. 1—initial shape of workpiece; 2—final shape of workpiece.

**Solid side extrusion** (Fig. 13.2e): The final product is a solid workpiece with a profile. The shape of the die opening is determined by the die opening only.

**Hollow side extrusion** (Fig. 13.2f): The final product is a hollow workpiece with a profile. The shape of the die opening is determined by both the die and the mandrel.

### 13.1.2 Extrusion of Components

Extrusion of components is the extrusion of a workpiece (rod or tube section, can)<sup>\*</sup> contained between tool parts to produce individual components. This process, which is generally conducted at room temperature, is also called *impact* extrusion. In contrast to open-die extrusion, higher strains are possible in cold (impact) extrusion.

\*Correspondingly processes are named using rod, tube, and can instead of solid and hollow (see Fig. 2.13).

### 13.4 BULK-METAL FORMING

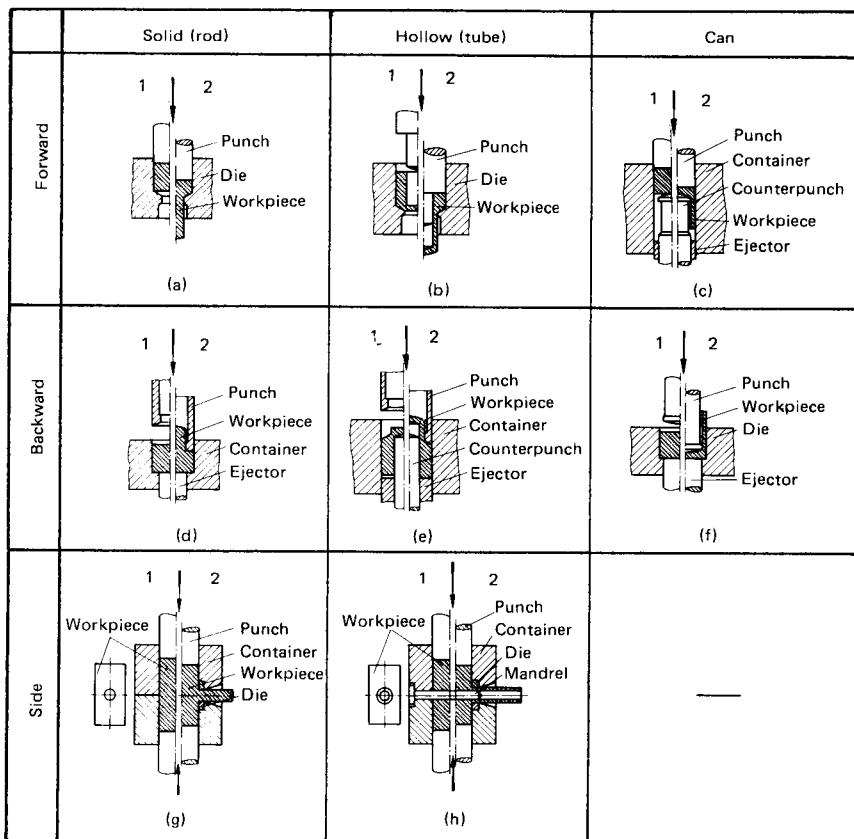


**FIG. 13.3** Schematic representation of extrusion processes for components. (a) Forward rod. (b) Forward tube. (c) Forward can. (d) Backward rod. (e) Backward tube. (f) Backward can. (g) Side rod. (h) Side tube. 1—initial shape of workpiece; 2—final shape of workpiece. (After [13.1].)

#### Extrusion of Components with Rigid Tools

The billet is pressed through a die by a punch.

**Forward extrusion:** The metal flow is in the direction of action of the machine motion.

**Rod forward** (Fig. 13.3a): A solid component of reduced cross section is produced from a solid component. The shape of the tool opening is determined by the die only.

**Tube forward extrusion** (Fig. 13.3b): A hollow cup or can of reduced wall thickness is produced from a hollow can or sleeve. The shape of the tool opening is determined by both the die and the punch. This process is also known as Hooker extrusion.

**Can forward extrusion** (Fig. 13.3c): A hollow cup, can, or sleeve is produced from a solid component. The shape of the tool opening is determined by the die and the counterpunch.

**Backward extrusion:** The metal flow is opposite to the direction of action of the machine.

**Rod backward extrusion** (Fig. 13.3d): A solid component with reduced cross section is produced from a solid component. The tool opening is determined by the punch only.

**Tube backward extrusion** (Fig. 13.3e): A sleeve or a can with reduced wall thickness is produced from a sleeve or a can. The tool opening is determined by the punch and the counterpunch.

**Can backward extrusion** (Fig. 13.3f): A thin-walled hollow body (can, sleeve, or cup) is extruded from a solid component. The tool opening is determined by both the die and the punch.

**Side extrusion:** The metal flow is either perpendicular or inclined at an angle to the direction of action of the machine.

**Rod side extrusion** (Fig. 13.3g): A solid body with a solid protrusion of any profile is extruded. The tool opening is determined by the split die only.

**Tube side extrusion** (Fig. 13.3h): A workpiece with a hollow protrusion of any profile is extruded. The tool opening is determined by the split die and the mandrel.

**Free extrusion:** The process of *free extrusion* or *open-die extrusion* (Fig. 13.4) also belongs to the category of extrusion processes. The strains are low in this case, and the process is generally used to manufacture individual components.

**Free die extrusion of solid bodies** (Fig. 13.4a): Reduction of the cross section of a solid body without supporting the undeformed portion of the component in any container. The unsupported portion should neither upset nor buckle during the process.

**Free extrusion of hollow bodies (also known as nosing)** (Fig. 13.4b and c): Nosing of a hollow body (can, sleeve, or tube) at its end. The requirement of a container at the end of the hollow body depends on its wall thickness.

In addition to deforming metals with rigid tools, it is also possible to work with some other medium. In such a case the billet is extruded through a tool opening by a working medium (high-pressure fluids). Processes of this nature are treated in Chap. 28.

The processes of extrusion can be carried out both at room temperature (cold extrusion) and at a definite working temperature (hot or warm extrusion). The extrusion process is generally hot or warm when the tools are heated, and the billet temperatures are generally higher than the recrystallization temperature of the material extruded. It is possible to reduce the flow stress of many materials by this method so that higher deformation strains can be obtained. The process of hot extrusion is suitable for manufacturing semifinished products (tubes, slabs, profiles), and

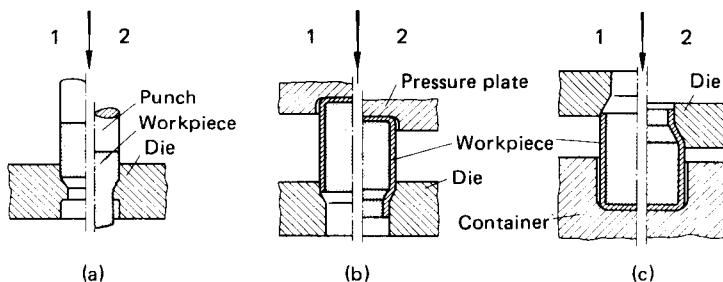


**FIG. 13.4** Schematic representation of free extrusion processes. (a) Of solid bodies. (b) Of hollow bodies (nosing). (c) Of hollow bodies (sinking) with container. 1—initial shape of workpiece; 2—final shape of workpiece. (After [13.1].)

**Table 13.1** Characteristics of Extrusion Processes for Components and Semifinished Products

	Components	Semifinished products
Process application	Mostly cold	Mostly hot
Product	Semifinished product → finished product	Wrought product → semifinished product

the process of cold extrusion is suitable for individual components (a small machining operation may be necessary). Table 13.1 gives the field of application of these two processes and the types of products.

## 13.2 Drawing Processes

The deformation force in the case of drawing processes is applied at the exit side of the tool as opposed to the extrusion processes where it is applied at the entry side. The stress condition in the deformation zone for the drawing processes is a combination of tensile and compressive stressing. The different drawing processes according to [13.2] are represented in Fig. 13.5. The definition of the processes is given below (Fig. 13.6).

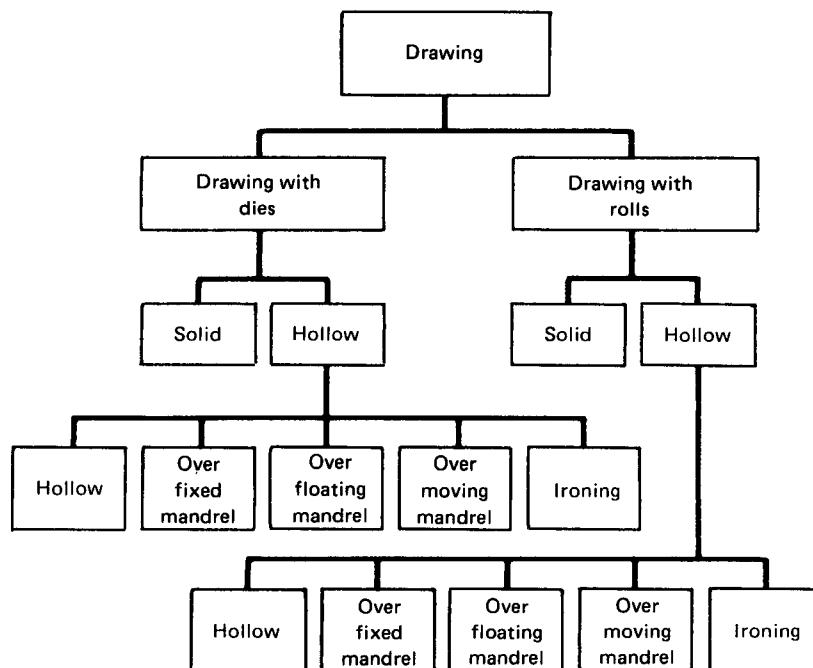


**FIG. 13.5** Classification of drawing processes. (After [13.2].)

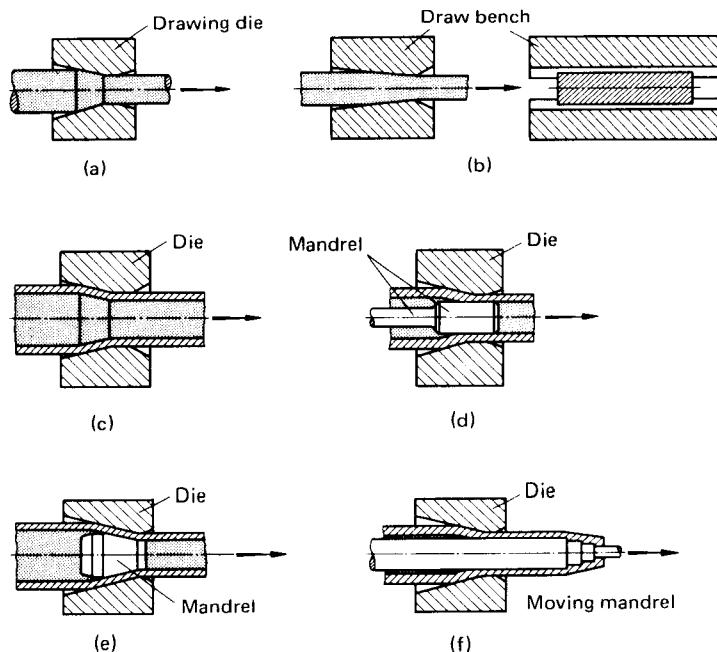


**FIG. 13.6** Schematic representation of drawing processes. (a) Drawing with dies of wire and bars. (b) Flat drawing. (c) Tube drawing with dies. (d) Drawing with dies over fixed mandrel. (e) Drawing with dies over floating mandrel. (f) Drawing with dies over moving mandrel. (After [13.2].)

### 13.2.1 Drawing

Drawing of a workpiece is drawing through tooling with reduced die opening.

### 13.2.2 Drawing through Dies

The drawing equipment is generally a fixed drawing die (draw, ring, or draw insert). The inner space of the tool is called the drawing zone.

**Drawing with dies of solid bodies:** In this case the workpiece is solid.

**Wire drawing** (Fig. 13.6a): Drawing of a wire of different shapes (round or profile) through a drawing die of either circular or other openings.

**Sheet drawing** (Fig. 13.6b): Drawing of a flat workpiece (sheet or strip) through a drawing bench with open dies.

**Drawing with dies of hollow bodies:** In this case the workpiece is hollow. The processes of drawing hollow bodies with dies are also known as *tube drawing* processes if the hollow bodies are tubes.

## 13.8 BULK-METAL FORMING

**Hollow drawing with dies** (Fig. 13.6c): This is a process of drawing hollow bodies without an inner tool in the drawing die.

**Hollow drawing over fixed mandrel** (Fig. 13.6d): This is drawing of hollow bodies over a fixed mandrel in the drawing die. The change of cross section in this case is a combination of diameter change (as in simple hollow drawing with die) and thickness reduction (as in ironing).

**Hollow drawing with dies over floating mandrel** (Fig. 13.6e): The drawing operation takes place over a floating mandrel. The floating mandrel is held in position by the equilibrium of forces in the backward direction due to the compressive forces and the frictional forces in the inner wall of the workpiece in the forward direction.

**Hollow drawing with dies over moving mandrel** (Fig. 13.6f): The mandrel moves along with the workpiece.

**Ironing** This is drawing of hollow bodies through an ironing ring, with an inner tool (mandrel or punch) pressing against the bottom of the workpiece, for example, to reduce the wall thickness of deep-drawn or cold-extruded cans or cups.

While all the processes illustrated in Fig. 13.6 are used to produce semifinished products, the process of ironing is used to produce individual workpieces. Thin-walled sleeves can be made advantageously by this process. The drawing processes are generally carried out at room temperature.

## 13.3 BASIC CONCEPTS

The common feature of the extrusion and drawing processes is that both have a die in the form of a nozzle through which the material is either pushed or pulled (Fig. 13.1). The nozzles or the openings are different for these two processes from the design point of view. Extrusion of components and a few processes of extrusion of semifinished products make use of dies whose inner contours are conical or described by a geometrical curve (exponential, for example). The drawing rings can also be designed with a conical inner contour. The die opening angle is, however, smaller for drawing rings than for extrusion dies. The dies for the extrusion of semifinished products of aluminum and its alloys are designed flat, that is, with a die opening angle  $2\alpha = 180^\circ$ . However, this is a special case.

The material behavior in both the extrusion of components and drawing is also similar since these processes are generally carried out at room temperature (the material work hardens). The work-hardening characteristic can be used to get workpieces whose mechanical properties are higher than for the initial material. The work-hardening behavior is also interesting from an economical viewpoint, since cheaper materials can be extruded or drawn to get the higher mechanical properties generally obtainable in higher-grade costlier materials. This aspect is all the more important in the case of certain materials (such as pure aluminum and pure copper) whose tensile strength cannot be increased except by work hardening.

The deformation process (for both drawing and extrusion) in the deformation zone is constrained, which means that there are no free surfaces, and therefore the achievable surface quality level is good.

The processes of extrusion and drawing are so very similar that they can be compared for material flow, stress condition, deformation forces, and the effect of tool geometry on the process.

### 13.3.1 Material Flow

Most of the extrusion and drawing processes are characterized by a quasi-stationary material flow. Therefore, the velocity field determined from the path of the material particles remains more or less unchanged throughout the deformation process. This is illustrated for an extruded workpiece

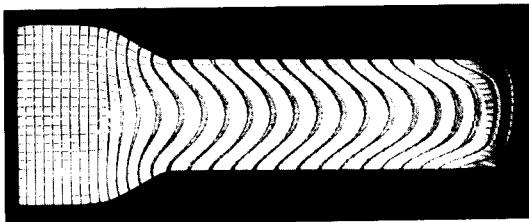


**FIG. 13.7** Grid lines after deformation in a cold-extruded workpiece. Material—63.1% Sn and 36.8% Pb; natural strain  $\varphi_{\max} = 0.88$ ;  $d_0 = 20.15$  mm (0.793 in); lubricant—MoS<sub>2</sub>.

in Fig. 13.7. The deformation process starts with a nonstationary zone in which the die cavity is filled with the material, and the material begins to flow out of the die. It is seen from the grid lines on the figure that the shape of the grid pattern does not change after the initial stages. A similar observation can be made on the partly deformed hot-extruded workpiece (Fig. 13.8). The main difference between the two processes, apart from the difference in the die shape, is in the frictional conditions along the die wall. In the case of cold extrusion, good lubrication conditions prevail; the grid lines in the head are not distorted. In the case of hot extrusion of aluminum, high shear stresses are present along the die wall, since the process is carried out mostly without lubricant. This results in very high distortions along the die wall. In spite of these distortions the velocity field in hot extrusion can be considered to be quasi-stationary. The near-ideal stationary velocity field is obtained in drawing. The length of the initial deformation zone is very small compared to the length of the drawn piece. The material enters the cylindrical portion of the drawing die without any friction, and the drawing velocity can be maintained constant. Fig. 13.9 shows the grid lines in the drawing process [13.3].

Comparing Figs. 13.7 to 13.9 which shows distorted grid lines, it can be seen that the tool geometry and the friction conditions must be analyzed to understand the metal flow. The effects of material and work hardening on the metal flow are not yet fully understood. Many authors suggest, however, that the effect of the above parameters on the metal flow is not as great as that of tool and friction conditions [13.4]–[13.6]. The metal flow is also not greatly affected by the punch velocity and the deformation temperature.

In addition to the transient deformation zone, a nonstationary deformation zone starts toward the end of the deformation process. This stage occurs at a particular rest billet height in the die assembly. The velocity field, and with that the plastic zone, will then not correspond to optimum flow conditions. The punch force starts to increase, and the velocity field changes with decreasing billet height in the die assembly. The result is the formation of a piping defect on the top surface of the billet. This defect is more prevalent in the extrusion of semifinished products and is discussed in Chap. 16.



**FIG. 13.8** Grid lines after hot extrusion. Material—AA 1050; natural strain  $\varphi_{\max} = 1.6$ ;  $d_0 = 71$  mm (2.8 in); without lubrication. (After [13.6].)



**FIG. 13.9** Grid lines after strip drawing. Material—AISI 1010; natural strain  $\varphi = 0.175$ ;  $d_0 = 44.0$  mm (1.73 in); lubricant—oil. (After 13.3].)

The quasi-stationary metal flow is not characteristic of all extrusion and drawing processes. The can extrusion process, used in many industrial applications, exhibits a nonstationary metal flow; the deformation zone changes throughout the deformation process. This process is discussed in detail in Chap. 15.

### 13.3.2 Stresses

The elementary plasticity theory developed by Sachs [13.7] and Siebel [13.8], also known as slab theory, will be used in this section to analyze the stresses in the deformation zone of extrusion and drawing processes. (Refer also to Chap. 5.) The tools are designed in the same manner for both extrusion and drawing processes (Fig. 13.10). The main differences between the processes (apart from the type of force application, namely, compressive and tensile) is that in the case of drawing, the tool (die) does not have a cylindrical portion (land); hence the frictional stresses for this portion are not present in the drawing processes. Hollow bodies can be manufactured by both drawing and extrusion without any inner tool.

It is assumed that the axial direction is the direction of maximum strain. Siebel uses the flow criterion of Tresca:

$$\sigma_1 - \sigma_3 = \sigma_f \quad \text{with } \sigma_1 > \sigma_2 > \sigma_3 \quad (13.1)$$

It is to be remembered that the elementary plasticity theory gives a qualitative idea of the stress condition in the deformation zone. Local stresses can be calculated only by using other methods. References of applicable methods are given at the appropriate places in the respective chapters.

A knowledge of the stress condition in the deformation zone contributes to the understanding of the deformation process. For axisymmetrical processes, three principal stresses are present: axial stress  $\sigma_z$ , radial stress  $\sigma_r$ , and tangential stress  $\sigma_t$ . The design of the die and an understanding of the metal flow will be simpler if the direction of action of the maximum principal stress is known.

A systematic procedure to analyze the process is highly recommended. First, the region of material undergoing plastic deformation is to be identified. This means that the boundary between the plastic and the elastic regions of the workpiece material must be determined.

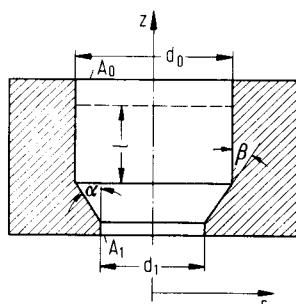


**FIG. 13.10** Tool (die) for extrusion and drawing.

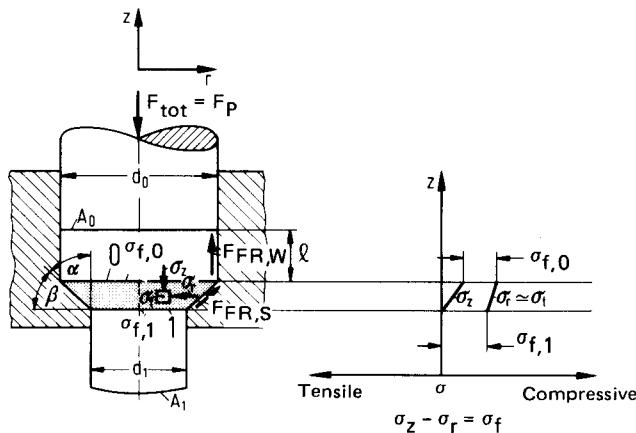


**FIG. 13.11** Stress condition and forces in solid forward extrusion.

The first question is therefore: *Where is the deformation zone?* The next question probes at the boundary conditions: *At what region in the deformation zone can the value of one of the three principal stresses be determined?*

In most cases it is easy to find certain points where a stress should be zero. It will therefore be necessary to determine the nature of this stress in the deformation zone (tensile or compressive).

Finally the maximum and minimum principal stresses must be ascertained: *Which are the maximum and minimum principal stresses?*

The last question is very important for the application of the Tresca flow criterion. This question is aimed at finding out whether the deformation process has more radial or more tangential movements.

With the above basic questions, the stress condition in the deformation zone of the drawing and the extrusion processes will be determined qualitatively.

### ***The Stress Condition in Solid Forward Extrusion of Components and Semifinished Products\****

The deformation force  $F_{tot}$  is applied on the punch. The material becomes plastic at cross section 0. The plastic zone extends up to cross section 1 (Fig. 13.11). The axial stress  $\sigma_z$  is zero at the exit of the die since the material can flow freely. The axial stress is compressive and increases in the deformation zone up to cross section 0. The stresses  $\sigma_r$  and  $\sigma_t$  are equal since, according to elementary plasticity theory, the strains are equal in both the radial and the circumferential directions. (See also Chap. 5.) The stress distribution in the deformation zone is related by

$$\sigma_z - \sigma_r = \sigma_f \quad (13.2)$$

since both the tangential and the radial stresses are compressive. The variations of  $\sigma_z$  and  $\sigma_r$  are not parallel. The increasing difference between these two stresses is due to the work-hardening effect of the workpiece material ( $\sigma_{f,1} > \sigma_{f,0}$ ).

### ***Stress Condition in Hollow Forward Extrusion***

The deformation zone is between cross section 0 and cross section 1 (Fig. 13.12). The stress condition in the deformation zone is similar to that in the case of solid forward extrusion. The max-

\*In the following only the terms solid and hollow extrusion will be used because the presentation applies both for semifinished products and for workpieces. See also footnote in Sec. 13.1.2.

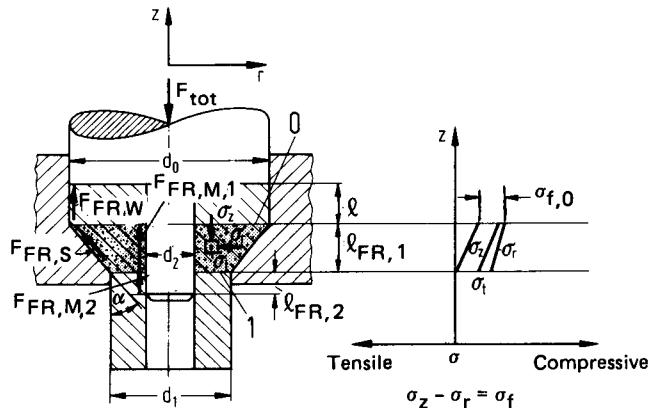


FIG. 13.12 Stress condition and forces in hollow forward extrusion.

imum axial stress  $\sigma_z$  occurs at cross section 0 and decreases to zero at cross section 1. The axial stress is compressive. The maximum compressive stress is the radial stress  $\sigma_r$ . The flow condition per Tresca in this case is again given by Eq. 13.2.

For thick-walled workpieces it can be assumed that the strains in both the radial and the circumferential directions are of the same magnitude. The tangential stresses will therefore be approximately equal to the radial stresses, as in solid forward extrusion. For thin-walled workpieces the circumferential strains are smaller than the radial strains. The tangential stress  $\sigma_t$  is given by (refer to Chap. 5)

$$\sigma_t = \frac{\sigma_z + \sigma_r}{2} \quad (13.3)$$

The stress condition shown in Fig. 13.12 considers a work-hardening material.

### Stress Condition in Drawing of Solid Bodies

The boundary of the deformation zone in the drawing of solid bodies is determined generally by the contact area of the tool with the workpiece (shaded region in Fig. 13.13). In solid forward extrusion, other areas of the workpiece also contact the tool. A characteristic difference between these processes is in the method of force application. In the case of drawing, the force is not applied by means of a punch, but by a drawing die on the material. This method of force application affects the stress condition in the deformation zone. The axial stresses  $\sigma_z$  are limited to the value of the tensile strength  $S_u$  at the exit cross section:

$$\sigma_{z,1} = \frac{F_z}{A_1} < S_u \quad (13.4)$$

The axial stress  $\sigma_z$  is a tensile stress which has its maximum at the exit of the tool and decreases to zero at cross section 0. The tangential and radial stresses are compressive and equal, as in solid forward extrusion. The flow condition is again given by Eq. 13.2. Fig. 13.13 shows the stress condition for a work-hardening material.

### Stress Condition in Drawing of Hollow Bodies

The maximum permissible tensile stress is also defined by Eq. 13.4, which is valid for solid bodies. At the exit the material is not to be subjected to a tensile stress higher than the tensile strength of the material. The axial stress  $\sigma_z$  is tensile and maximum at cross section 1, and decreases to zero

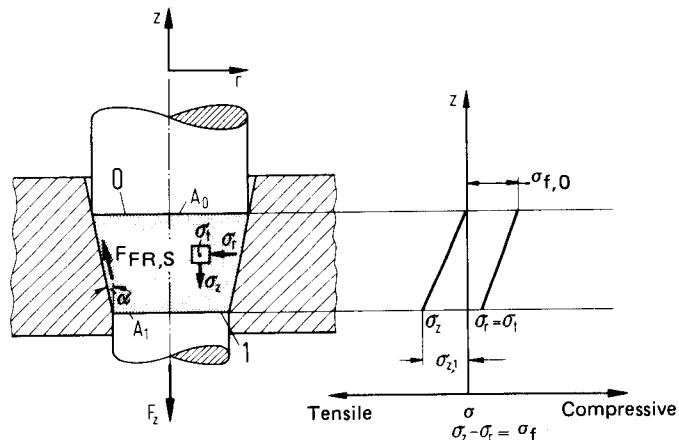


FIG. 13.13 Stress condition and forces in drawing of solid bodies.

at cross section 0 (Fig. 13.14). For drawing over a fixed mandrel without any change of the inner diameter (Fig. 13.14) and for ironing, the circumferential strains are smaller than the radial strains. The flow condition is again given by Eq. 13.2. The radial stress is compressive, and the tangential stress can be calculated from Eq. 13.3. The stress condition represented in Fig. 13.14 is for a work-hardening material.

For the drawing of hollow bodies with changing inner diameter (e.g., Fig. 13.6c), the circumferential strains are higher than radial strains. The flow condition in this case is given by

$$\sigma_z - \sigma_t = \sigma_f \quad (13.2')$$

This process will be described in more detail in Sec. 14.6.

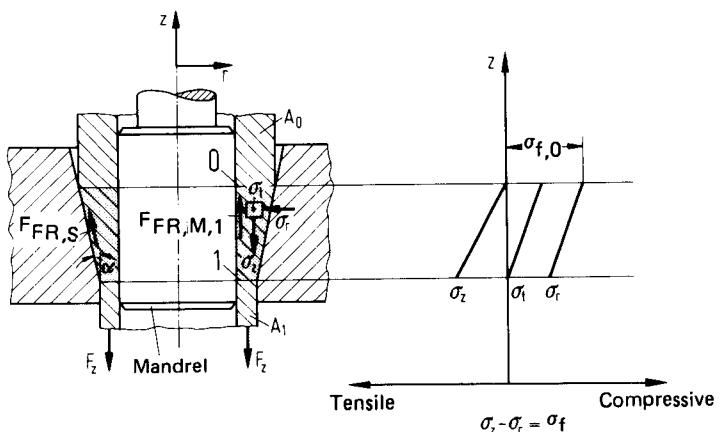


FIG. 13.14 Stress condition and forces in drawing of hollow bodies.

### 13.3.3 Deformation Work and Forces

A knowledge of stresses in the plastic zone of the workpiece is necessary for the design of the tooling. For the selection of a suitable forming machine tool, the deformation forces and the deformation work should be known. For industrial purposes, the force calculations based on elementary plasticity theory have been found to be sufficient. Siebel [13.8] and others calculate the deformation forces by deriving expressions for ideal, frictional, shearing, and bending work in deformation:

$$W_{\text{tot}} = W_{\text{id}} + W_{\text{FR}} + W_{\text{Sh}} + W_{\text{B}} \quad (13.5)$$

The total force  $F_{\text{tot}}$  can be calculated from  $W_{\text{tot}}$  as follows:

$$F_{\text{tot}} = F_{\text{id}} + F_{\text{FR}} + F_{\text{Sh}} + F_{\text{B}} \quad (13.6)$$

The expressions for  $F_{\text{FR}}$ ,  $F_{\text{Sh}}$ , and  $F_{\text{B}}$  in Eq. 13.6 may also contain a number of terms.

The expressions for solid forward extrusion will be derived. The expressions for other processes will be obtained from the expression for solid forward extrusion, indicating the deviations from the derived expressions. Table 13.2 gives the complete details of the force components for the drawing and extrusion processes.

#### **Deformation Work and Forces in Solid Forward Extrusion**

The ideal deformation work  $W_{\text{id}}$  in solid forward extrusion—friction and shearing are not considered—is calculated as follows (Fig. 13.15):

$$dW_{\text{id}} = \Delta z \, dA \, \sigma_r + A \, d\Delta z \, \sigma_z \quad (13.7)$$

From volume constancy,

$$\begin{aligned} \Delta V &= A \, \Delta z = \text{constant} \\ d\Delta V &= dA \, \Delta z + A \, d\Delta z = 0 \end{aligned} \quad (13.8)$$

$$\Delta z \, dA = -A \, d\Delta z = \Delta V \frac{dA}{A}$$

Eq. 13.7 changes to

$$dW_{\text{id}} = \Delta V \frac{dA}{A} (\sigma_r - \sigma_z) \quad (13.9)$$

Using the yield condition (Eq. 13.2) and integrating between areas  $A_0$  and  $A_1$ , the ideal deformation work becomes

$$W_{\text{id}} = V \int_{A_0}^{A_1} \sigma_f \frac{dA}{A}$$

If the integration is done for a work-hardening material, an average flow stress  $\sigma_{f,m}$  is used. This mean value  $\sigma_{f,m}$  is generally computed as the average value of the flow stress before and after deformation. If the flow stress can be expressed as a mathematical expression of the equivalent strain, the integration can in some cases be performed in a closed form. The exact value of  $\sigma_{f,m}$  is

$$\sigma_{f,m} = \frac{1}{\varphi} \int_{\varphi_0}^{\varphi_1} \sigma_f \, d\varphi$$

Then

$$W_{\text{id}} = V \sigma_{f,m} \varphi_{\text{max}} \quad (13.10)$$

with

$$\varphi_{\text{max}} = \ln \left( \frac{A_0}{A_1} \right) \quad (13.11)$$

The friction work  $W_{\text{FR}}$  for solid forward extrusion consists of two parts: (1) the frictional work  $W_{\text{FR},W}$  along the container or die wall and (2) the friction  $W_{\text{FR},S}$  on the shoulder of the container in the deformation zone:

**Table 13.2** Calculation of Force Components for Extrusion and Drawing Processes

Process	$F_{\text{id}}$	$F_{\text{Sh}}$	$F_{\text{FR,W}}$	$F_{\text{FR,S}}$	$F_{\text{FR,D,1}}$	$F_{\text{FR,D,2}}$
Solid forward extrusion	$A_0 \sigma_{f,m} \varphi_{\max}$	$\frac{2}{3} \alpha \sigma_{f,m} A_0;$	$\pi d_0 l \sigma_{f,0} \mu$	$\frac{2 \sigma_{f,m} \varphi_{\max} \mu A_0}{\sin 2\alpha};$ see note <i>a</i>		
Hollow forward extrusion	$A_0 \sigma_{f,m} \varphi_{\max}$	$\frac{1}{2} \alpha \sigma_{f,m} A_0;$	$\pi d_0 l \sigma_{f,0} \mu$	$\frac{2 \sigma_{f,m} \varphi_{\max} \mu A_0}{\sin 2\alpha};$ see note <i>a</i>	$\frac{\sigma_{f,m} \varphi_{\max} A_1 \mu}{\tan \alpha}$	$\pi d_2 l \mu p,$ see note <i>c</i>
Rod and bar drawing	$A_1 \sigma_{f,m} \varphi_{\max}$	$\frac{2}{3} \alpha \sigma_{f,m} A_1$				
Drawing over fixed mandrel ( <i>b</i> ) and ironing	$A_1 \sigma_{f,m} \varphi_{\max}$	$\frac{1}{2} \alpha \sigma_{f,m} A_1$		$\frac{2 \sigma_{f,m} \varphi_{\max} \mu A_1}{\sin 2\alpha}$	$\pm \frac{\sigma_{f,m} \varphi_{\max} \mu A_1}{\tan \alpha}$	see note <i>c</i>

*a*In hot extrusion with  $2\alpha = 180^\circ$ ,  $F_{\text{Sh}} \simeq F_{\text{id}}$  and  $F_{\text{FR,S}} = 0$ .

*b*Change of inner diameter neglected.

*c*Negative sign for ironing. Denotes the force on the bottom portion.

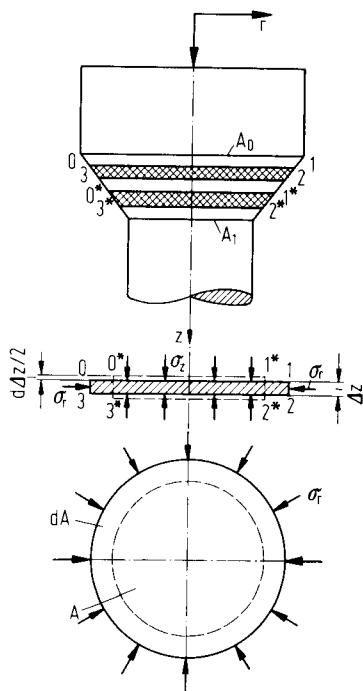


**FIG. 13.15** Derivation of ideal deformation work  $W_{id}$  in solid forward extrusion.

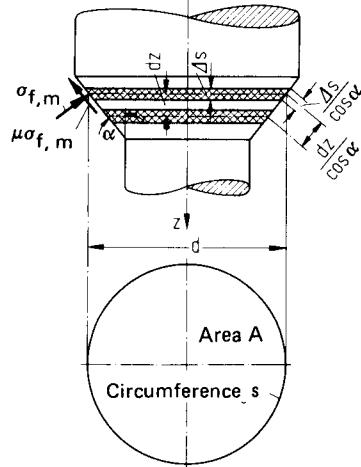


**FIG. 13.16** Derivation of frictional work  $W_{FR,S}$  on the shoulder of the extrusion die.

$$W_{FR} = W_{FR,W} + W_{FR,S} \quad (13.12)$$

It is difficult to make exact predictions of the pressure distribution along the container wall. The assumption is therefore made that the radial stress on the container wall is approximately of the same order of magnitude as the flow stress of the material of the workpiece, and thus that in the undeformed zone  $p = \sigma_{f,0}$  and in the shoulder zone  $p = \sigma_{f,m}$ .

Consider a disk-shaped volume element in the shoulder (Fig. 13.16) having cross section  $A$ , a mean circumference  $S = \pi d$ , and a disk thickness  $\Delta s$ . The disk is moved by  $\Delta z$  in the flow direction. The frictional force is given by

$$dW_{FR,S} = \mu \sigma_{f,m} \frac{\pi d \Delta s}{\cos \alpha} \frac{dz}{\cos \alpha} \quad (13.13)$$

Substituting

$$\pi d dz \tan \alpha = -dA \quad (13.14)$$

$$\Delta s = \frac{\Delta V}{A} \quad (13.15)$$

and integrating between the areas  $A_0$  and  $A_1$ , the total frictional work on the shoulder is given by

$$W_{FR,S} = V \sigma_{f,m} \varphi_{max} \frac{2\mu}{\sin 2\alpha} \quad (13.16)$$

For a die opening angle  $2\alpha = 90^\circ$ , the frictional work is a minimum for a given tool geometry and workpiece material.

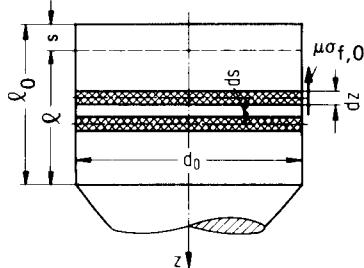


**FIG. 13.17** Derivation of frictional work  $W_{\text{FR},W}$  on the container wall in extrusion.

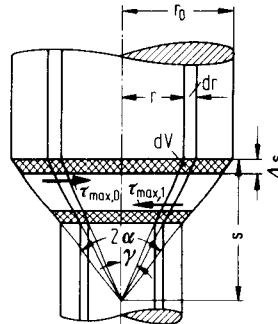


**FIG. 13.18** Derivation of shearing work  $W_{\text{Sh}}$  for solid forward extrusion.

The frictional work  $W_{\text{FR},W}$  on the die wall can be determined in a similar manner. If a disk with circumference  $S = \pi d_0$  and thickness  $ds$  is pushed by  $ds$  (Fig. 13.17), the frictional work for a frictional shear stress

$$\tau_{\text{FR},W} = \mu \sigma_{f,0} \quad (13.17)$$

is

$$dW_{\text{FR},W} = F_{\text{FR},W} ds \quad (13.18)$$

with

$$l = l_0 - s \quad \text{and} \quad dl = -ds \quad (13.19)$$

Eq. 13.18 becomes

$$W_{\text{FR},W} = \frac{1}{2} \pi d_0 \mu \sigma_{f,0} (l_0^2 - l^2) \quad (13.20)$$

The assumption of radial stresses as  $\sigma_{f,0}$  and  $\sigma_{f,m}$  for the different cases considered in the above derivations is a very rough approximation. Even the description of the frictional condition using Coulomb's friction law ( $\mu = \text{constant}$ ) does not represent the actual condition in the deformation zone.\*

The work required to bend and unbend a material particle in and out of the plastic zone will now be considered. The work required for shearing (also called *virtual work*) was first derived for rod and bar drawing [13.9]. The main assumption made is that the shearing is localized in the small zone of bending and unbending (Fig. 13.18).

The volume element  $dV$  is bent by an angle  $\gamma$  at the entrance of the deformation zone under the influence of the shear flow stress  $\tau_{\text{max},0} = \frac{1}{2} \sigma_{f,0}$ . The shearing work  $W_{\text{Sh},0}$  for small angles is given by

$$dW_{\text{Sh},0} = \frac{1}{2} \sigma_{f,0} \hat{\gamma} dV \quad (13.21)$$

with

$$\tan \gamma \approx \hat{\gamma} = \frac{r}{s} \quad (13.22)$$

The volume element  $dV$  can be calculated as  $dV = 2\pi r \Delta s dr$ . Eq. 13.21 then changes to

$$\Delta W_{\text{Sh},0} = \int_0^{r_0} \frac{1}{2} \sigma_{f,0} \frac{r}{s} 2\pi r \Delta s dr \quad (13.23)$$

\*See also the footnote in Sec. 15.1.4.

Integrating Eq. 13.23, we get the work per unit volume as

$$W_{Sh,0} = \frac{1}{3}\sigma_{f,0}\widehat{\alpha} \quad (13.24)$$

with  $\tan \alpha \simeq \widehat{\alpha} = \frac{r_0}{s}$ . Eq. 13.24 is not applicable for die opening angles  $2\alpha > 90^\circ$ . At the exit of the deformation zone, the shear flow stress is  $\frac{1}{2}\sigma_{f,1}$ . Similarly, the shearing work for unbending the fiber at the die exit is

$$\Delta W_{Sh,1} = \frac{1}{3}\sigma_{f,1}\widehat{\alpha} \quad (13.25)$$

The total shearing work is the sum of the work given by Eqs. 13.24 and 13.25,

$$\Delta W_{Sh,tot} = \frac{2}{3}\widehat{\alpha}\sigma_{f,m} \quad (13.26)$$

with

$$\sigma_{f,m} = \frac{1}{2}(\sigma_{f,0} + \sigma_{f,1}) \quad (13.27)$$

The total shearing work—every material fiber passes through this shearing zone—for the total deformed volume is

$$W_{Sh,tot} = \frac{2}{3}V\widehat{\alpha}\sigma_{f,m} \quad (13.28)$$

The shearing work  $W_{Sh,tot}$  is independent of  $\varphi_{max}$  for a non-work-hardening material.

The total work done in the solid forward extrusion process is given by Eq. 13.5 without bending

$$W_{tot} = W_{id} + W_{Sh} + W_{FR} \quad (13.5')$$

$$W_{tot} = V\sigma_{f,m} \left[ \frac{2}{3}\widehat{\alpha} + \left( 1 + \frac{2\mu}{\sin 2\alpha} \right) \varphi_{max} \right] + \frac{1}{2}\pi d_0 l \mu \sigma_{f,0} (l_0^2 - l^2) \quad (13.29)$$

For the quasi-stationary portion of the extrusion process in the deformation zone, with

$$\frac{W}{V} = \frac{F^*}{A_0} \quad (13.30)$$

the force  $F^*$  is given by

$$F^* = A_0\sigma_{f,m} \left[ \frac{2}{3}\widehat{\alpha} + \left( 1 + \frac{2\mu}{\sin 2\alpha} \right) \varphi_{max} \right] \quad (13.31)$$

The frictional force along the container wall should be added to  $F^*$ .  $F_{FR,W}$  is calculated from Eq. 13.18 as

$$F_{FR,W} = \pi d_0 l \mu \sigma_{f,0} \quad (13.32)$$

The total force (Fig. 13.11) is

$$F_{tot} = F^* + F_{FR,W} \quad (13.33)$$

The process of solid forward extrusion of semifinished components (as opposed to solid forward extrusion of components) is generally carried out with dies having angles  $2\alpha = 180^\circ$  (Fig. 13.19).

A “dead zone” forms in the tool corner (see also Chap. 16) at the boundaries of which very high shear stresses are present. This shear zone has a fictitious die opening angle  $2\alpha'$  instead of the actual angle  $2\alpha$ . The angle  $2\alpha'$  is generally assumed as  $90^\circ$ . The shear flow stress  $\tau_{max} = \frac{1}{2}\sigma_{f,m}$  is substituted in Eq. 13.16 for  $\tau_{FR,S} = \sigma_{f,m}\mu$ .

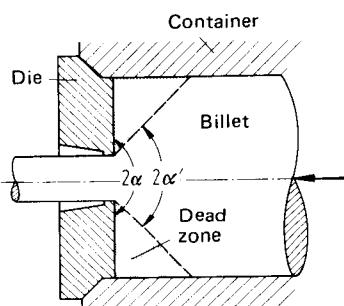


**FIG. 13.19** Derivation of shearing work  $W_{Sh}$  in solid forward extrusion of semifinished products.

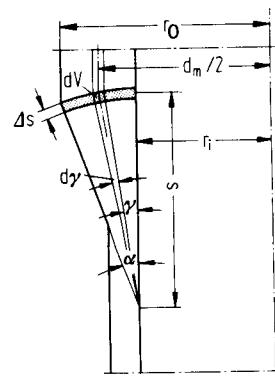


**FIG. 13.20** Derivation of shearing work  $W_{Sh}$  in hollow forward extrusion.

$$W_{FR,S} = V \sigma_{f,m} \varphi_{\max} \frac{1}{\sin 2\alpha'} \quad (13.34)$$

If  $\sin 2\alpha' \approx 1$ ,

$$\begin{aligned} W_{FR,S} &\approx W_{id} \\ F_{FR,S} &\approx F_{id} \end{aligned} \quad (13.35)$$

### Deformation Work and Force in Hollow Forward Extrusion

The conditions of friction and shearing are different in hollow forward extrusion compared to solid forward extrusion. Additional friction results on the mandrel. This frictional force is divided into two components (see Fig. 13.12). The frictional work  $W_{FR,M,1}$  in the deformation zone is calculated from the inner circumference  $S_i = \pi d_2$  and the friction length  $l_{FR,1}$ . A ring element with diameter  $d_2$  and thickness  $\Delta s$  is displaced by  $dz$ ,

$$dW_{FR,M,1} = \mu \sigma_{f,m} \pi d_2 \Delta s dz \quad (13.36)$$

With

$$dz = \frac{dA}{S_i \tan \alpha}$$

and integrating with

$$\Delta s = \frac{\Delta V}{A}$$

we have

$$W_{FR,M,1} = V \sigma_{f,m} \varphi_{\max} \frac{\mu}{\tan \alpha} \quad (13.37)$$

The frictional force in the deformation zone is

$$F_{FR,M,1} = A_1 \sigma_{f,m} \varphi_{\max} \frac{\mu}{\tan \alpha} \quad (13.38)$$

## 13.20 BULK-METAL FORMING

The frictional force at the exit is given by

$$F_{\text{FR},M,2} = \pi d_2 l_{\text{FR},2} \mu \bar{p}_r \quad (13.39)$$

where  $\bar{p}_r$  is the mean radial pressure acting on the mandrel.

The quantity  $\mu \bar{p}_r$  in Eq. 13.39 represents the frictional shear stress. According to [13.10],  $\mu \bar{p}_r$  has a value of 10–12 N/mm<sup>2</sup> (1450–1740 psi) in this zone (not plastic). The experimental values are for steels DIN Mbk 6 and DIN Cq 10 (AISI 1006 and 1010).

The Eqs. 13.37 and 13.39 are also valid for hollow forward extrusion of semifinished products. The frictional work  $W_{\text{FR},M,2}$  is obtained by integrating Eq. 13.39 over punch travel.

The redundant shear work is constrained to two small material strips at the material entry into and exit from the die (Fig. 13.20). For material entry into the die [13.9],

$$d\Delta W_{\text{Sh},0} = \tau_{\max,0} \widehat{\gamma} dV \quad (13.21')$$

With  $dV = \pi d_m \Delta s \, s \, d\gamma$ , where  $d_m$  is the average diameter, and integrating over the half-die angle, Eq. 13.21' becomes

$$\Delta W_{\text{Sh},0} = \frac{1}{2} \tau_{\max,0} \Delta V \widehat{\alpha} \quad (13.40)$$

with  $\Delta V \simeq d_m \Delta s \, s \, \widehat{\alpha}$ .

The shear work at the exit of the die is similarly obtained as

$$\Delta W_{\text{Sh},1} = \frac{1}{2} \tau_{\max,1} \Delta V \widehat{\alpha} \quad (13.41)$$

The total shear work, considering that the entire volume passes through this shear zone, is given by

$$W_{\text{Sh}} = W_{\text{Sh},0} + W_{\text{Sh},1} = \frac{1}{2} (\tau_{\max,0} + \tau_{\max,1}) V \widehat{\alpha} \quad (13.42)$$

and with Eq. 13.27 and  $\tau_{\max,m} = \frac{1}{2} \sigma_{f,m}$

$$W_{\text{Sh}} = \frac{1}{2} \sigma_{f,m} V \widehat{\alpha} \quad (13.43a)$$

The shear force is therefore calculated as

$$F_{\text{Sh}} = \frac{1}{2} A_0 \sigma_{f,m} \widehat{\alpha} \quad (13.43b)$$

### **Deformation Work and Forces in Bar and Wire Drawing**

Work and forces required for the drawing processes can also be calculated based on Siebel's method. The forces and the work terms refer in this case to the end cross section  $A_1$ . The equations for the drawing forces (bar and wire drawing) can be written similarly to those for solid forward extrusion. The friction conditions are represented in Fig. 13.13,

$$\begin{aligned} F_{\text{D,tot}} &= F_{\text{id}} + F_{\text{FR,S}} + F_{\text{Sh}} \\ F_{\text{D,tot}} &= \sigma_{z,1} A_1 = A_1 \sigma_{f,m} \left[ \left( 1 + \frac{2\mu}{\sin 2\alpha} \right) \varphi_{\max} + \frac{2}{3} \widehat{\alpha} \right] \end{aligned} \quad (13.44)$$

For small die opening angles  $2\alpha$ ,  $\sin 2\alpha \simeq 2\alpha$ . The frictional force on the die shoulder then becomes

$$F_{\text{FR,S}} = A_1 \sigma_{f,m} \varphi_{\max} \frac{\mu}{\alpha} \quad (13.45)$$

The total deformation work can be calculated from

$$W_{\text{D,tot}} = W_{\text{id}} + W_{\text{FR,S}} + W_{\text{Sh}}$$

### ***Deformation Work and Force in Drawing of Hollow Bodies (Tubes)***

In the case of drawing hollow bodies (tubes) with an inner mandrel, frictional stresses are present. There is, however, no friction before the material entry into the deformation zone. The forces are related to the final cross-sectional area  $A_1$ . The frictional force on the mandrel in *tube drawing* acts like an additional force in the final cross section in ironing [13.11]. Further, the force required in tube drawing is the force acting in the final cross section. The force required for *ironing*, however, is the sum of the force acting in the final cross section and the frictional force on the mandrel.

The processes of drawing over a fixed mandrel, with negligible change in the inner diameter, and of ironing will be dealt with in this chapter. Other processes of drawing will be described in Chap. 14.

The following equations are valid for drawing over a *fixed mandrel* with negligible change in the inner diameter:

$$\begin{aligned} W_{D,\text{tot}} &= W_{\text{id}} + W_{\text{FR,S}} + W_{\text{FR,M}} + W_{\text{Sh}} \\ F_{D,\text{tot}} &= F_{\text{id}} + F_{\text{FR,S}} + F_{\text{FR,M}} + F_{\text{Sh}} \\ \text{and } F_{D,\text{tot}} &= A_1 \sigma_{f,m} \left[ \left( 1 + \frac{2\mu_S}{\sin 2\alpha} + \frac{\mu_M}{\tan \alpha} \right) \varphi_{\max} + \frac{1}{2} \hat{\alpha} \right] \end{aligned} \quad (13.46a)$$

The force at the final cross section in *ironing* is

$$\begin{aligned} F_{I,\text{tot}} &= F_{\text{id}} + F_{\text{FR,S}} - F_{\text{FR,M}} + F_{\text{Sh}} \\ \text{and } F_{I,\text{tot}} &= A_1 \sigma_{f,m} \left[ \left( 1 + \frac{2\mu_S}{\sin 2\alpha} - \frac{\mu_M}{\tan \alpha} \right) \varphi_{\max} + \frac{1}{2} \hat{\alpha} \right] \end{aligned} \quad (13.46b)$$

Busch [13.11] has pointed out that the force on the bottom of the workpiece becomes smaller with smaller angle  $\alpha$ . (The frictional force on the mandrel increases.) This can also be seen from Eq. 13.46b if the values  $\mu_S = 0.024$  and  $\mu_M = 0.07$  are substituted [13.12]. Greater reductions in area are therefore possible due to lower axial stress  $\sigma_z$  [13.11]. The force and work required for ironing, that is, the force and work to be supplied by the machine, are given by

$$\begin{aligned} F_{\text{tot}} &= F_{I,\text{tot}} + F_{\text{FR,M}} = F_{\text{id}} + F_{\text{FR,S}} + F_{\text{Sh}} \\ W_{\text{tot}} &= W_{\text{id}} + W_{\text{FR,S}} + W_{\text{Sh}} \\ \text{and } F_{\text{tot}} &= A_1 \sigma_{f,m} \left[ \left( 1 + \frac{2\mu_S}{\sin 2\alpha} \right) \varphi_{\max} + \frac{1}{2} \hat{\alpha} \right] \end{aligned} \quad (13.46c)$$

### ***Summary of Equations***

Table 13.2 gives the different force components for drawing and extrusion processes. These expressions have been derived based on elementary plasticity theory. Calculation methods of other processes not contained in this table will be discussed in other chapters. Some processes have also been considered for special treatment with other well-known plasticity methods.

## **13.4 OTHER COMMON CHARACTERISTICS OF DRAWING AND EXTRUSION PROCESSES**

### **13.4.1 Friction Coefficient**

The formulas described earlier can be used to calculate the deformation work and force for drawing and extrusion processes if the flow curve of the deforming material and the geometry of the tooling are known. Various investigations have shown that the assumptions of a constant Coulomb's coefficient of friction and constant stress distribution are not generally valid. The coeffi-

**Table 13.3** Normal Friction Values for Drawing and Extrusion Processes

Process	Solid forward extrusion	Hollow forward extrusion	Drawing of bars and tubes	Ironing	Drawing of hollow bodies
Coefficient of friction $\mu$	0.04–0.08	0.1–0.125	0.02–0.05	0.02–0.07	0.08–0.02

cient of friction therefore represents an average empirical value used to predict the total force  $F_{\text{tot}}$  with reasonable accuracy for practical use. The friction values found accurate for the various processes are given in Table 13.3.

### 13.4.2 Deformation Efficiency

The deformation efficiency  $\eta_{\text{def}}$  is defined as the ratio of the theoretically required ideal work  $W_{\text{id}}$  and the actual work done  $W_{\text{eff}}$ :

In the case of quasi-stationary deformation processes, such as drawing and extrusion, the force is almost a constant throughout the deformation stroke (Fig. 13.21). The force can also be approximately calculated from the deformation efficiency  $\eta_{\text{def}}$  since the force–travel diagram has a trapezoidal shape:

$$\eta_{\text{def}} = \frac{W_{\text{id}}}{W_{\text{eff}}} \approx \frac{F_{\text{id}}}{F_{\text{eff}}} \quad (13.47)$$

(The figure represents an ideal case with a rectangular-shape force–travel diagram.)

The friction and shear losses are contained in the deformation efficiency. The deformation efficiency must be determined by conducting exhaustive experiments. It is an empirical value, with the coefficient of friction  $\mu$  contained implicitly in it.\*

$$F_{\text{eff}} = \frac{F_{\text{id}}}{\eta_{\text{def}}} = \frac{A \sigma_{f,m} \varphi_{\max}}{\eta_{\text{def}}} \quad (13.48)$$

Some factors that affect the deformation efficiency are workpiece material, deformation ratio, die opening angle, tool material, lubricant, and strain rate.

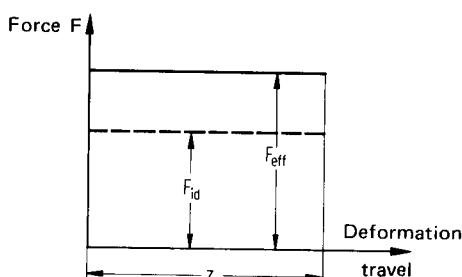


**FIG. 13.21** Derivation of the deformation efficiency from the force–travel diagram of quasi-stationary metal-forming processes.

\*Substitute  $A = A_0$  for extrusion processes and  $A = A_1$  for drawing processes.

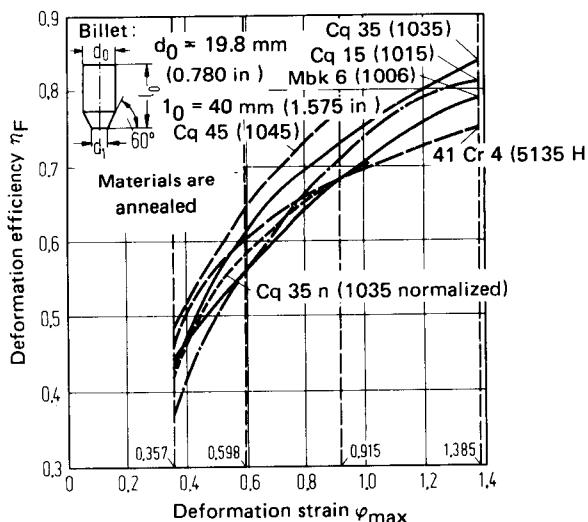


**FIG. 13.22** Deformation efficiency as a function of deformation strain with material as the parameter (After [13.13].)

Fig. 13.22 shows the effect of the deformation strain on the efficiency in rod forward extrusion, and Fig. 13.23 shows the effect of the die opening angle on the efficiency [13.13], [13.14]. The values of  $\eta_{\text{def}}$  given in Table 13.4 are to be considered as guidance values only. They can be used to calculate the deformation force as a first approximation.

#### 13.4.3 Optimum Die Angle

It can be seen from the various equations derived earlier for the deformation work and forces that the deformation work and force are dependent on the die opening angle  $2\alpha$ . In the case of rod forward extrusion of components, the friction force  $F_{\text{FR},S}$  on the die shoulder and the shear force  $F_{\text{Sh}}$  are functions of  $\alpha$  (from Eq. 13.29),

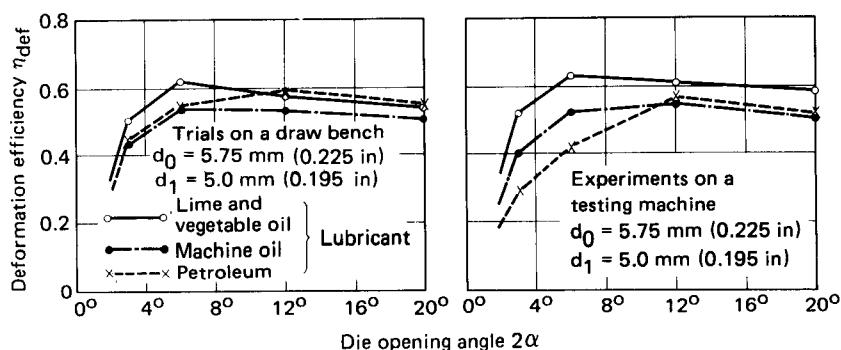


**FIG. 13.23** Deformation efficiency as a function of lubricant and die opening angle  $2\alpha$ . Material—steel with 0.02% C. (After [13.14].)

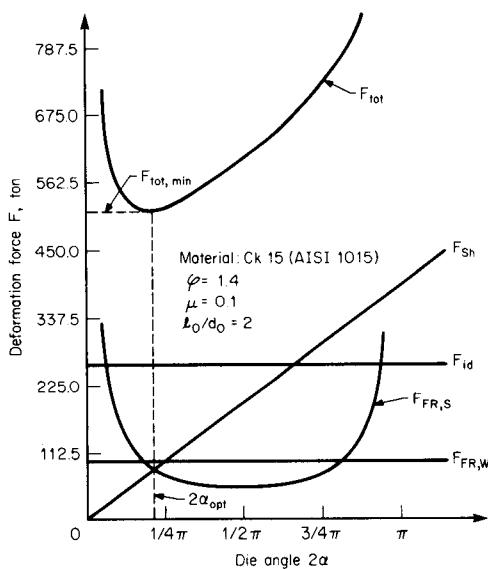
**Table 13.4** Deformation Efficiency for Drawing and Extrusion Processes

Solid forward extrusion of components	Solid forward extrusion or semi-finished products		Bar and wire drawing		Drawing of hollow bodies		Tube drawing	
	$\varphi_{\max}$	$\eta_{\text{def}}$	$\varphi_{\max}$	$\eta_{\text{def}}$	$\varphi_{\max}$	$\eta_{\text{def}}$	$\varphi_{\max}$	$\eta_{\text{def}}$
0.4	0.45	0.3–0.6	0.15	0.45–0.55	0.15	0.4–0.6	0.15	0.5
1.0	0.75		0.50	0.65–0.75	0.50	0.7–0.85	0.50	0.65–0.75
1.5	0.80							

$$F_{\text{FR},S} = A_0 \sigma_{f,m} \varphi_{\max} \frac{2\mu}{\sin 2\alpha}$$

$$F_{\text{sh}} = \frac{2}{3} A_0 \sigma_{f,m} \hat{\alpha}$$

The various components of forces for solid forward extrusion are plotted schematically as a function of the die opening angle  $2\alpha$  in Fig. 13.24. The force components that are independent of the die opening angle  $2\alpha$  are the ideal deformation force  $F_{\text{id}}$  and the friction  $F_{\text{FR},W}$  along the die wall. The shear force  $F_{\text{sh}}$  increases linearly with the die opening angle  $2\alpha$ , while the friction on the shoulder of the die is expressed through a trigonometric function in the force equation.

**FIG. 13.24** Determination of optimum die opening angle  $2\alpha$  from the individual force components.

**Table 13.5** Optimum Die Opening Angle (for the Deformation Force) for Drawing and Cold Extrusion Processes

Rod forward extrusion		Tube forward extrusion		Bar drawing		Ironing	
$\varphi_{\max}$	$2\alpha_{\text{opt}}$	$\varphi_{\max}$	$2\alpha_{\text{opt}}$	$\varphi_{\max}$	$2\alpha_{\text{opt}}$	$\varphi_{\max}$	$2\alpha_{\text{opt}}$
0.3	20°	0.3	40°	0.15	10°	0.15	10–12°
1.0	32°	1.33	70°	0.50	20°	0.50	20–24°

The total force  $F_{\text{tot}}$  is expressed as a function of the die opening angle  $2\alpha$ , and a minimum of the force is obtained by known mathematical methods. For solid forward extrusion we get

$$F_{\text{tot}} = A_0 \sigma_{f,m} \left[ \frac{2}{3} \hat{\alpha} + \left( 1 + \frac{2\mu}{\sin 2\alpha} \right) \varphi_{\max} \right] + \pi d_0 \sigma_{f,0} \mu l \quad (13.33')$$

for minimum force requirements

$$\frac{dF_{\text{tot}}}{d\alpha} = 0 \quad (13.49)$$

$$\cos 2\alpha_{\text{opt}} = -3\mu\varphi_{\max} \pm \sqrt{9\mu^2\varphi_{\max}^2 + 1} \quad (13.50)$$

The right-hand side of Eq. 13.50 should be less than or equal to 1 ( $\cos 2\alpha \leq 1$ ); hence only the positive sign before the square root is permissible. The optimum die opening angle  $2\alpha$  to minimize the total deformation force  $F_{\text{tot}}$  can therefore be obtained from Eq. 13.50. It can further be seen from Eq. 13.50 that the optimum die opening angle is also dependent on the coefficient of friction  $\mu$  and the natural strain  $\varphi_{\max}$ . The fact that the optimum die opening angle is independent of the material properties has been established in experimental investigations [13.10].

The optimum die opening angles for other drawing and extrusion processes can be determined in a similar manner. The friction and shear components of the forces assume different values depending on the process. The accuracy of  $\alpha_{\text{opt}}$  is, to a great degree, determined by the accuracy of determination of the coefficient of friction  $\mu$ .

The term *optimum* has been used in this context to denote an angle at which the deformation force is a minimum. This angle need not necessarily result in a very high tool life for which considerations of fatigue and other conditions of loading are necessary. The force peaks occurring at the beginning of the deformation process in the extrusion of components must also be reduced. This is generally achieved by choosing  $2\alpha > 2\alpha_{\text{opt}}$ . The total deformation force is higher for this chosen angle. However, this disadvantage is compensated by a higher tool life and the maintenance of measurements along the length of the extruded workpiece. The latter effect is caused by the constant elastic strains of the tooling due to reduced force peaks. Sieber [13.15] has indicated an optimum die opening angle  $2\alpha = 126^\circ$  for solid forward extrusion to achieve good tool life. Table 13.5 gives optimum values of die opening angles for various processes. These angles are valid for optimizing the total deformation force to a minimum and for conical shell line dies. It has to be pointed out that the optimum angle for ironing does not correspond to the workpiece loading condition.

#### 13.4.4 Process Limits

The process limits in drawing and extrusion processes are characterized by two criteria.

The extrusion processes are characterized by very high stresses. These high stresses cause, for example, failure of the die due to very high inner pressure, failure of the punch due to buckling, and so on. Although the processes can be operated with reinforced dies and short guided punches to increase the loading limit on the tooling, the limits on the processes are still the stresses that

**Table 13.6** Maximum Possible Natural Strains  $\varphi_{\max}$  in Drawing and Extrusion Processes

Forward extrusion of components (cold)	Forward extrusion of semifinished products (hot)	Drawing processes <sup>a</sup>
1.4–1.6	7.0	0.2–0.3 (0.5)

<sup>a</sup>Ironing not included.

can be transmitted through the tooling without tool failure. Based on the present knowledge, the maximum strain  $\varphi_{\max}$  in the case of cold forward extrusion of steels is 1.6 (Table 13.6).

The lower flow stresses at hot-working temperatures (hot extrusion of aluminum, for example) allow a greater amount of deformation ( $\varphi_{\max} \approx 7$ ).

The limits of drawing processes are characterized by the tensile strength of the final cross section. The maximum achievable natural strains  $\varphi_{\max}$  are between 0.25 and 0.3 for steels and nonferrous metals. The process of ironing must be considered separately since the final cross section is relieved of some load due to the frictional force on the mandrel. Hence larger amounts of deformation are achieved, especially with smaller die opening angles.

## REFERENCES

- 13.1 DIN 8583: "Fertigungsverfahren Druckumformen (Manufacturing Processes—Compressive Forming)," 1970.
- 13.2 DIN 8584: "Fertigungsverfahren Zugdruckumformen (Manufacturing Processes—Combined Tensile and Compressive Forming)," 1st ed., 1970.
- 13.3 Kopp, R.: "Investigations on the Temperature Distribution in Drawing of Rounds" (in German), Dr.-Ing. thesis, Technische Hochschule, Clausthal, 1968.
- 13.4 Frisch, J., and Thomsen, E. G.: "An Experimental Study of Metal Extrusions at Various Strain Rates," *Trans. ASME* 76, 1954, pp. 599–606.
- 13.5 Fister, W.: "Some Studies on Hot Extrusion Problems" (in German), Dr.-Ing. thesis, Technische Hochschule, Aachen, 1963.
- 13.6 Dahlheimer, R.: *Investigations on the Stresses, Strains, and Temperatures in Axisymmetric Hot Extrusion* (in German), Berichte aus dem Institut für Umformtechnik, Universität Stuttgart, no. 20, Essen, Girardet, 1970.
- 13.7 Sachs, G.: "On the Theory of the Drawing Process" (in German), *Z. angew. Math. u. Mech.*, 7, 1927, pp. 235–236.
- 13.8 Siebel, E.: *Metal Forming in Plastic Condition* (in German), Düsseldorf, Verlag Stahleisen, 1932.
- 13.9 Korber, G., and Eichinger, A.: "Fundamentals of Forming" (in German), *Stahl u. Eisen*, 60, 1940, pp. 829–832, 854–862, 882–887.
- 13.10 Schmoeckel, D.: *Investigations on the Tool Design for Forward Extrusion of Hollow Bodies of Steel and Nonferrous Metals* (in German), Berichte aus dem Institut für Umformtechnik, Technische Hochschule Stuttgart, no. 4, Essen, Girardet, 1966.
- 13.11 Busch, R. K.: *Investigation on Ironing of Hollow Bodies at Room Temperature* (in German), Berichte aus dem Institut für Umformtechnik, Universität Stuttgart, no. 10, Essen, Girardet, 1969.
- 13.12 Weiss, H.: "Investigations on Ironing" (in German), Dr.-Ing. thesis, Technische Hochschule, Stuttgart, 1964.

- 13.13 Kast, D.: *Investigations on the Force and Work Requirements and the Deformation Efficiency for Forward Extrusion of Hollow Bodies of Steel* (in German), *Berichte aus dem Institut für Umformtechnik, Technische Hochschule Stuttgart*, no. 3, Essen, Girardet, 1965.
- 13.14 Pomp, A. and Koch, A.: "On the Effect of Lubricants on the Force Requirements for Drawing of Wires with Krupp-Widia Dies" (in German), *Mitt. aus dem Kaiser-Wilhelm-Inst. Eisenforsch.*, 13, 1931, pp. 261-271.
- 13.15 Sieber, K.: "Special Tooling in Cold Forging Technology, Especially for Bulk Formings on Multistage Boltmaker" (in German), in *Kaltumformfibel*, vol. 2, Düsseldorf, Tritsch, 1962.



**DRAWING AND IRONING**

© 1992 Marcel Dekker, Inc. All Rights Reserved Worldwide

**List of Special Symbols**

---

$F_{FR,R}$ ( $W_{FR,R}$ )	friction force (work) on die radius
$W_B$	bending work
$k$	thermal conductivity
$l_C$	length of contact
$\mu_D$	coefficient of friction on die
$\mu_P$	coefficient of friction on punch
$\mu_T$	coefficient of friction in tube sinking
$\nu$	strain ratio
$\rho$	bending radius; density
$\sigma_{f,B}$	flow stress at bending radius

The processes of drawing were described briefly in Chap. 13. The methods of determining the stresses in the deformation zone, the deformation force, and the work for drawing processes were also dealt with in Chap. 13. Recent mathematical methods for analyzing the drawing processes, the effect of counterpull, and mandrel-less drawing are discussed in this chapter.

The drawing processes are not only important for wires and rods, but are increasingly applied for drawn profiles with asymmetrical sections. An important factor to be considered for these special profiles is the number of stages required to draw them. Round profile wires are supplied in coils. The larger sections that cannot be wound as coils are called bars. The deformation behavior of wires and rods is different only with regard to their geometries. Finally, the process of ironing is of great importance for the manufacture of thin-walled hollow bodies.

## 14.1 THEORETICAL BACKGROUND

The drawing process has been analyzed in Chap. 13 using elementary plasticity theory. It is, however, important to examine the validity of the various assumptions made in deriving the equations, since many numerical methods can now be used to solve plasticity problems.

### 14.1.1 Material Flow, Stresses, and Forces in Bars and Wire

The assumption made in the elementary analysis that the deformation is homogeneous is applicable only under favorable friction conditions and for small strains. Greater values of die-opening angle  $\alpha$  lead to an inhomogeneous strain distribution across the section. The deformation zone is also not bounded by straight lines and circles as assumed in the elementary analysis. In addition, the deformation zone extends further on the tool surface and occupies a small area in the vicinity of the workpiece axis. This shape of the deformation zone has been experimentally established by Wistreich [14.1] and Kopp [14.2], among others. The plastic zone can be made visible by etching (Fig. 14.1). The shape of the deformation zone shown in Fig. 14.1 is also confirmed by the slip-line theory. Although until now the slip-line theory has been applied to plane-strain problems only, useful information for the axisymmetric process can also be obtained from the slip-line method [14.3], [14.4]. Fig. 14.2 shows the deformation zone for strip drawing as obtained by slip-line fields. At the center of the strip, a point of singularity exists. At this point, based on the slip-line theory, the material velocity is increased from  $v_0$  to  $v_1$ . The stresses along the flow lines shown in Fig. 14.2 are plotted in Fig. 14.3; they apply for frictionless drawing. The axial stress  $\sigma_z$  increases from the entry to the deformation zone toward exit. The tensile stresses are higher for those flow lines that are nearer the workpiece axis. This pattern is also observed in the Mohr's stress circles plotted in Fig. 14.2. Pawelski and Lueg [14.3] have determined that in drawing with two flat tools all possible stress conditions exist in the deformation zone, from biaxial tension to biaxial compression. This is due to the interaction between the applied tensile force for the drawing process and the reactive compressive stresses on the tool surfaces. Some investigations by Adler [14.5], using approximate methods to solve three-dimensional plasticity equations, have shown that the slip-line method for plane-strain problems would be able to predict useful information for axisymmetric cases also. It is pointed out that the boundary of the plastic zone for all bar-drawing processes exhibits similar compressive forces very near the tool area and smaller elongations near the axis of the workpiece (Fig. 14.4). The axial stress  $\sigma_z$  has its maximum value at the entry on the drawing axis; it may become compressive near the tool surface. Experience has shown that such results are to be expected. When the die-opening angle  $\alpha$  increases and the reduction of area decreases, the material is upset near the tool surface; that is, at this point the axial

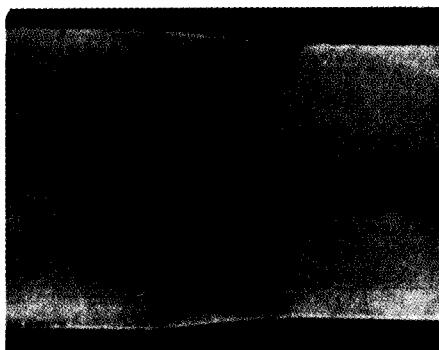


**FIG. 14.1** Plastic zone in annealed bars made visible by etching. Material—steel;  $d_0 = 44.0$  mm (1.74 in);  $d_1 = 40.4$  mm (1.59 in);  $2\alpha = 12^\circ$ . (After [14.2].)

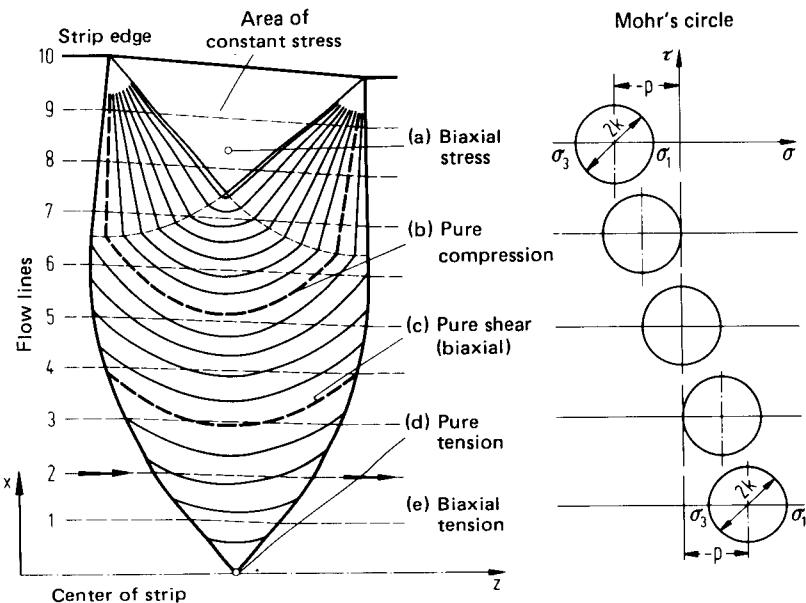


**FIG. 14.2** Deformation zone in plane-strain drawing represented by lines of equal average pressure (isobars).  $\epsilon = 0.051$ ;  $2\alpha = 12^\circ$ . (After [14.3].)

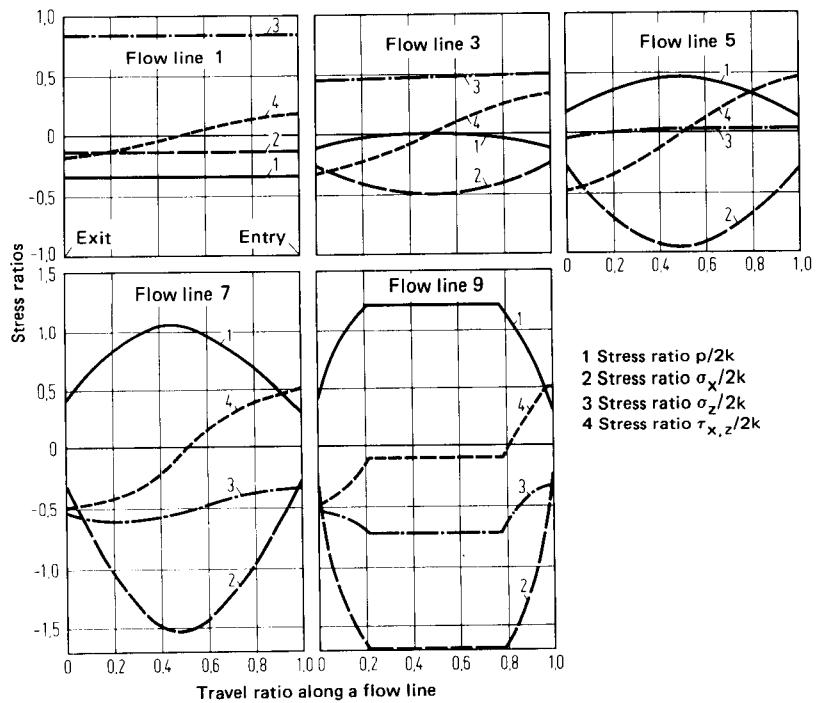


**FIG. 14.3** Stress distribution along a flow line in the deformation zone; plane-strain forming (refer to Fig. 14.2).  $\epsilon = 0.051$ ;  $2\alpha = 12^\circ$ . (After [14.3].)

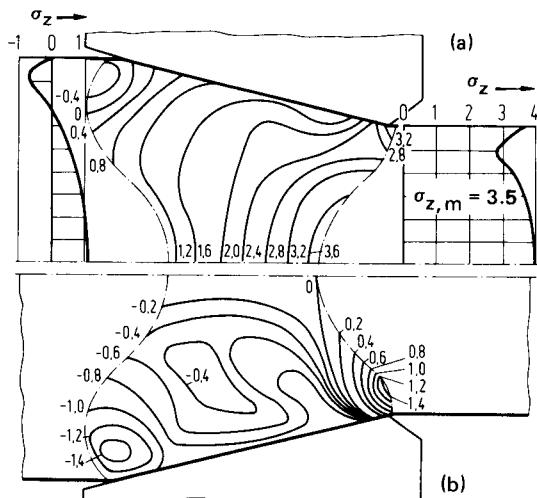


**FIG. 14.4** Strip drawing with work hardening,  $\mu = 0.05$ ;  $\varphi = 0.4$ . (a) Lines of constant axial stress  $\sigma_z/k$ ; distribution of axial stresses at the entry and exit. Dashed lines—boundary of deformation zone. (b) Lines of constant shear stress  $\sigma_{rz}/k$ . (After [14.5].)

stress  $\sigma_z < 0$ . The axial stress at the exit decreases with increasing radius; however, it increases near the boundary layers. It can be established easily from experience that the maximum values of axial stress  $\sigma_z$  occur near the axis. Cracks occur near the axis because of high axial tensile stresses. The radial stresses  $\sigma_r$  are highest near the tool surface at both the entry and the exit. The tangential stresses  $\sigma_t$  are of the same order of magnitude as the radial stresses (Fig. 14.5). This is also a result to be expected from elementary plasticity theory. Adler [14.5] has also investigated the strain rates, the strains, and the material flow in drawing. Three regions in the deformation zone exhibit especially high equivalent strain rates  $\dot{\epsilon}$ : (1) the surroundings near the  $z$ -axis, (2) the material entry near the tool surface, and (3) the material exit near the tool surface. The maximum strains occur along flow lines in these three regions. The lowest equivalent strains  $\bar{\epsilon}$  occur near the material axis (Fig. 14.6). The equivalent strain rate at these points represents the homogeneous deformation ratio. The equivalent strains increase toward the boundary. It is therefore to be expected that for a work-hardening material the hardness distribution along the section will show lower values near the axis and higher values near the strip end.

A change of the frictional conditions causes a movement of the deformation zone toward the material entry for increasing values of the coefficient of friction  $\mu$ . This result can also be expected from the predictions of the slip-line theory and has been established experimentally [14.2]. Similarly, the shear stresses  $\tau_{rz}$  increase near the tool surfaces for increasing values of the coefficient of friction  $\mu$  [14.5].

Force calculations sufficient for industrial use have already been derived in Chap. 13. Formulas derived on the basis of elementary plasticity theory can be found in [14.6], and others have been used in [14.7] to calculate the force values to be compared with measured values.

#### 14.1.2. Stresses and Strains In Tube Drawing

Apart from the processes of drawing hollow bodies discussed in Chap. 13, two processes of tube drawing, namely, tube sinking and tube drawing over fixed mandrels, are considered in this chapter.

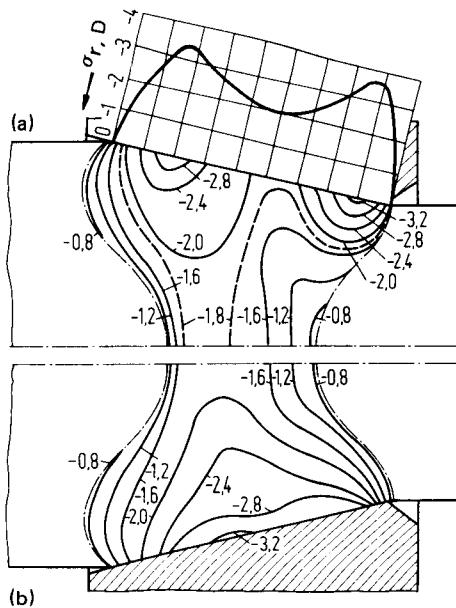


**FIG. 14.5** Strip drawing with work hardening.  $\mu = 0.05$ ;  $\varphi = 0.4$ . (a) Lines of constant radial stress  $\sigma_r/k$ ; distribution of normal stress  $\sigma_{r,D}/k$  perpendicular to die. (b) Lines of constant tangential stress  $\sigma_t/k$ . (After [14.5].)

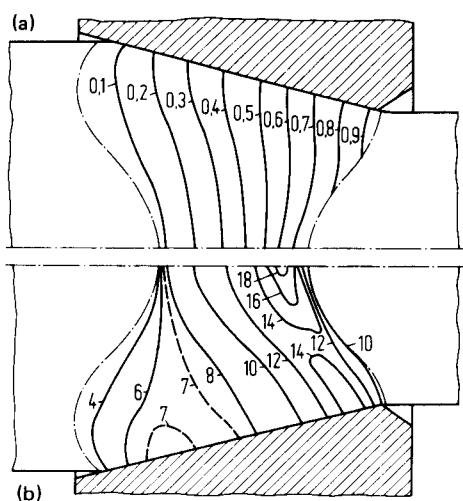


**FIG. 14.6** Strip drawing with work hardening.  $\mu = 0.05$ ;  $\varphi = 0.4$ . (a) Lines of constant equivalent strain  $\bar{\epsilon}$ . (b) Lines of constant equivalent strain rates  $\dot{\epsilon}$ . (After [14.5].)

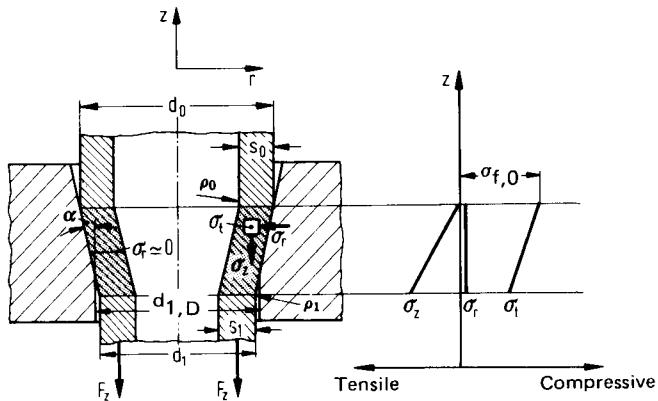


**FIG. 14.7** Stress condition in tube sinking.  $\rho_0, \rho_1$ —bending radii;  $d_{1,D}$ —die diameter at material exit.

Contrary to all processes using an orifice-shaped die, the tube-sinking process results in a free surface. On the inner surface of the tube no tool is used; the deformation can therefore take place without any constraint (Fig. 13.6c). The wall-thickness variations (decrease, increase, or no change) depend on the geometrical and technological parameters. The inner surface has a higher roughness than the outer surface because of the free deformation.

The force for tube sinking is applied directly on the workpiece material (Fig. 14.7). The deformation is caused by tangential compression and axial tension. The Tresca yield condition is therefore

$$\sigma_z - \sigma_t = \sigma_f \quad (14.1)$$

The axial stress increases from zero at the entry to a tensile stress at the exit. The tangential compressive stress  $\sigma_t$  varies throughout the deformation zone as defined by Eq. 14.1. The radial stress is zero at the inner diameter of the tube and has no significant value near the outer diameter since the tube can deform freely toward the inner diameter. The method suggested by Siebel is again used to calculate energy and force requirements for this process.

$$W_{\text{tot}} = W_{\text{id}} + W_{\text{FR}} + W_B$$

$$W_{\text{FR}} = W_{\text{FR,S}} + W_{\text{FR,R}} \quad (14.2)$$

$$W_B = W_{B,0} + W_{B,1}$$

The work due to bending at the entry and exit,  $W_{B,0}$  and  $W_{B,1}$ , is illustrated in Fig. 14.8. The frictional components to be considered are  $W_{\text{FR,S}}$  on the die shoulder and  $W_{\text{FR,R}}$  on the die radius.  $W_{\text{id}}$  can be determined from Eq. 13.10 and  $W_{\text{FR,S}}$  from Eq. 13.16. The frictional work  $W_{\text{FR,R}}$  can be calculated from the example of rope friction shown in Fig. 14.9:

$$dS = dF_{\text{FR}} = \mu dN \quad (14.3)$$

$$dN = 2S \frac{\sin d\alpha}{2} \simeq S d\alpha \quad (14.4)$$

Eqs. 14.3 and 14.4 can be combined as

$$S_1 = S_2 e^{\mu\alpha} \quad (14.5)$$

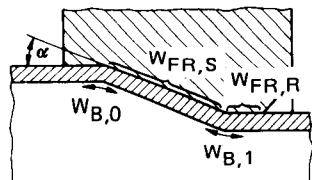


**FIG. 14.8** Work components in tube sinking.  $W_{B,0}$ —bending at entry;  $W_{B,1}$ —bending at exit;  $W_{\text{FR,S}}$ —frictional work on die shoulder;  $W_{\text{FR,R}}$ —frictional work on die radius.

$W_{\text{FR,S}}$  on the die shoulder and  $W_{\text{FR,R}}$  on the die radius.  $W_{\text{id}}$  can be determined from Eq. 13.10 and  $W_{\text{FR,S}}$  from Eq. 13.16. The frictional work  $W_{\text{FR,R}}$  can be calculated from the example of rope friction shown in Fig. 14.9:

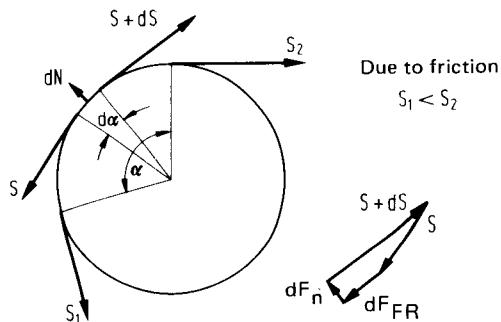


**FIG. 14.9** Derivation of frictional work  $W_{FR,R}$  on die radius.

The frictional work  $W_{FR,R}$  can be calculated as

$$W_{FR,R} = (W_{id} + W_{FR,S} + W_{B,0})(e^{\mu\alpha} - 1) \quad (14.6)$$

Bending of fibers into the deformation zone and unbending of fibers when they come out of the deformation zone require additional work. Fig. 14.10 illustrates this process. The length of the neutral layer is  $dl$ ,

$$dl = \beta \left( \rho + \frac{s}{2} \right) \quad (14.7)$$

The compression or tension  $dx_b$  on the center of the fiber [ $\frac{1}{2} dx_b = (\beta/2)(s/4)$ ] is given by

$$dx_b = \frac{dl s}{4(\rho + s/2)} \quad (14.8)$$

The deformation work is given by

$$\begin{aligned} \frac{dW_B}{2} &= A\sigma_{f,B} dl \frac{s}{4(\rho + s/2)} \\ W_B &= V\sigma_{f,B} \frac{s}{2(\rho + s/2)} \end{aligned} \quad (14.9)$$

where  $\sigma_{f,B}$  is the flow stress at the bending radius. Eq. 14.9 is a general equation for computing the bending work in the drawing of hollow bodies. For very sharp bending ( $\rho = 0$ ),  $W_B = V\sigma_{f,B}$ , and for very large radii,  $\rho \gg s$ ,  $W_B = V\sigma_{f,m}s/2\rho$  with  $\sigma_{f,B} \approx \sigma_{f,m}$  [14.8]. The total work in the drawing of hollow bodies (tube sinking), according to Fig. 14.7, is

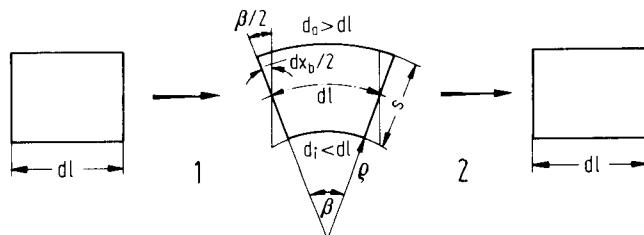


**FIG. 14.10** Derivation of bending work in drawing of hollow bodies.

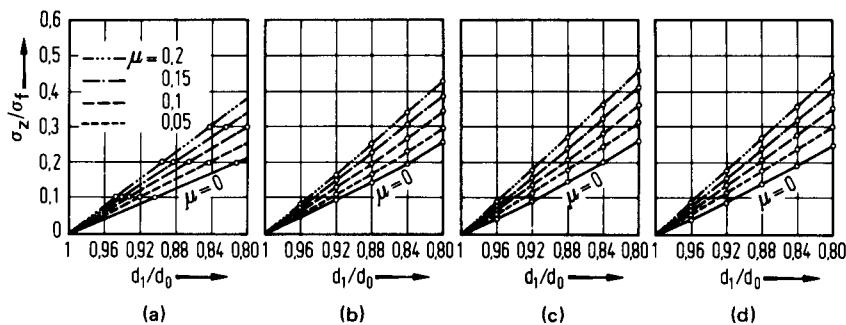


**FIG. 14.11** Comparison of ratio  $\sigma_z/\sigma_f$  in tube sinking for different coefficients of friction  $\mu$  and diameter ratios  $d_1/d_0$ . Calculated per: (a) Swift [14.10]; (b) Moore and Wallace [14.13]; (c) Woo [14.11]; (d) Schneider [14.12].

$$W_{T,\text{tot}} = V \sigma_{f,m} \varphi_{\max} e^{\mu \alpha} \left[ 1 + \frac{2\mu}{\sin 2\alpha} + \frac{\sigma_{f,B,0}}{\sigma_{f,m}} \frac{s_0}{2(\rho_0 + s_0/2)\varphi_{\max}} + \frac{\sigma_{f,B,1}}{\sigma_{f,m}} \frac{s_1}{2(\rho_1 + s_1/2)\varphi_{\max}} \right] \quad (14.10)$$

where  $\rho_0$  and  $\rho_1$  are the bending radii at the entry and exit, respectively (Fig. 14.7). (It is seen that the factor  $e^{\mu\alpha}$  has also been used for the bending work at the exit, but this is not quite correct since at least half of the bending work  $W_{B,1}$  takes place before the exit bending radius. However, the error is not very significant in the above formula.) The deformation force can be obtained from a consideration of the deformation work over travel. The quotient  $W_{\text{tot}}/V$  gives the drawing stress. As a first approximation,  $s_1$  can be substituted for  $s_0$  in Eq. 14.10. Several investigators, such as Geleji [14.9], Swift [14.10], Woo [14.11], Schneider [14.12], Moore and Wallace [14.13], and Chung and Swift [14.14], have contributed to a better understanding of the forces, stresses, and work aspects in the drawing of hollow bodies (Fig. 14.11).

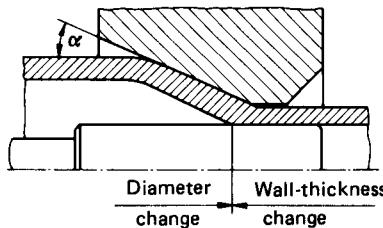


**FIG. 14.12** Tube drawing over fixed mandrel.

The equations of Siebel for deformation work give reasonably accurate results. Adler [14.5] has derived expressions for the deformation work by combining equations for drawing over fixed mandrel with negligible change in the inner diameter and equations for tube sinking (Eq. 14.2):

$$\begin{aligned} \text{Drawing } W_D &= W_{id,D} + W_{FR,S,D} + W_{FR,D} + W_{Sh} \\ \text{Tube sinking } W_{T,\text{tot}} &= W_{id,T} + W_{FR,S,D} + W_{FR,R} + W_{B,0} + W_{B,1} \end{aligned}$$

where the subscript D denotes drawing over fixed mandrel without wall-thickness reduction, and T denotes tube sinking. For a combination of these processes, the work components  $W_{FR,R}$  and the bending component  $W_{B,1}$  have to be deleted since they refer to components for wall-thickness reduction (Fig. 14.12). The total work for this widely used process combination is given by

$$W_{(D+T),\text{tot}} = V\sigma_{f,m,T}\varphi_{\max,T} \left[ 1 + \frac{2\mu_T}{\sin 2\alpha} + \frac{\sigma_{f,B,0}}{\sigma_{f,m,T}} \frac{s_0}{2(\rho_0 + s_0/2)\varphi_{\max,T}} \right] + V\sigma_{f,m,D}\varphi_{\max,D} \left[ 1 + \frac{2\mu_D}{\sin 2\alpha} + \frac{\mu_D}{\tan \alpha} + \frac{\hat{\alpha}}{2\varphi_{\max,D}} \right] \quad (14.11)$$

The deformation due to drawing (ironing) is difficult to determine. The approximate value of  $\varphi_{\max,D}$  can be calculated as  $\varphi_s = \ln(s_0/s_1)$ . The total natural strain expressed as ratios of  $\varphi_{\max}$  is

$$\frac{\varphi_{\max,D}}{\varphi_{\max}} \approx \frac{\varphi_s}{\varphi_{\max}} = \nu \quad (14.12)$$

The total deformation ratio comprises the deformation due to both diameter ( $\varphi_d$ ) and wall-thickness ( $\varphi_s$ ) change:

$$\begin{aligned} \varphi_{\max} &= \varphi_s + \varphi_d \\ \varphi_{\max,D} &\approx \varphi_s = \nu\varphi_{\max} \\ \varphi_{\max,T} &\approx \varphi_d = (1 - \nu)\varphi_{\max} \end{aligned} \quad (14.13)$$

The equation for total deformation work can be further simplified by substituting  $\sigma_{f,m,T} \approx \sigma_{f,m,D} \approx \sigma_{f,m}$

$$W_{(D+T),\text{tot}} = V\sigma_{f,m}\varphi_{\max} \left[ (1 - \nu) \left( 1 + \frac{2\mu_T}{\sin 2\alpha} \right) + \frac{\sigma_{f,B,0}}{\sigma_{f,m}} \frac{s_0}{2\varphi_{\max}(\rho_0 + s_0/2)} + \nu \left( 1 + \frac{2\mu_D}{\sin 2\alpha} + \frac{\mu_D}{\tan \alpha} + \frac{\hat{\alpha}}{2\nu\varphi_{\max}} \right) \right] \quad (14.14)$$

The load requirements can be calculated using Eqs. 14.11 and 14.14 by substituting the exit area  $A_1$  in place of  $V$ . The accuracy of this equation when compared with experimental results is satisfactory (Figs. 14.13 and 14.14).

#### 14.1.3 Effect of Back Tension in Drawing

If the axial stress  $\sigma_z$  at the material entry into the die is not zero but has a positive value (back tension), the stress condition in the deformation zone changes (Fig. 14.15). The drawing stress  $\sigma_{z,1}$  is increased by the back tension stress  $\sigma_{z,0}$ . The radial and tangential stresses  $\sigma_r$  and  $\sigma_t$  decrease

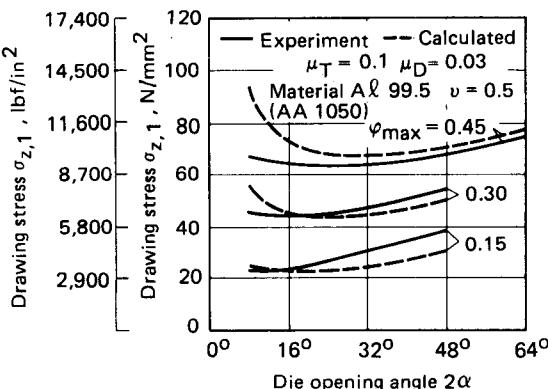


FIG. 14.13 Comparison of calculated and experimental results for drawing over fixed mandrel. Material—Al 99.5 (AA 1050). (After [14.5].)

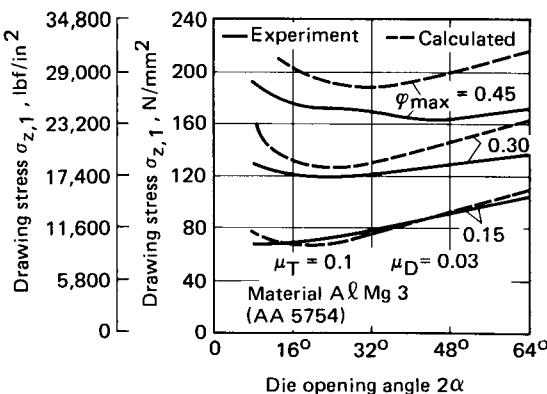


FIG. 14.14 Comparison of calculated and experimental results for drawing over fixed mandrel.

so that the total pressure on the tool is also reduced. This results in a workpiece drawn to close tolerance since the elastic strains on the tooling are smaller. As a result of decreased normal pressure on the tool, the frictional work (based on Coulomb's law) also decreases for the same value of the coefficient of friction  $\mu$ . On the boundary zones both the temperature peaks and the gradients are smaller [14.15]. These conclusions are a natural result of the mechanical conditions in the drawing process and are therefore not contested. However, there is no consensus on the influence of back tension on the die life. Lueg [14.16] suggests that the die wear is reduced in drawing with back tension, while the practical investigations by Wistreich [14.17] have not clearly proved the existence of such a direct relationship between back tension and die wear.

Energy saving is possible in drawing with back tension, since the friction work on the die shoulder is reduced. The reduction of the deformation work in drawing with back tension decreases with a decreasing coefficient of friction (for  $\mu = 0$ , reduction of work is also zero). Reduction of the deformation work is used only in cases where the work due to back tension can

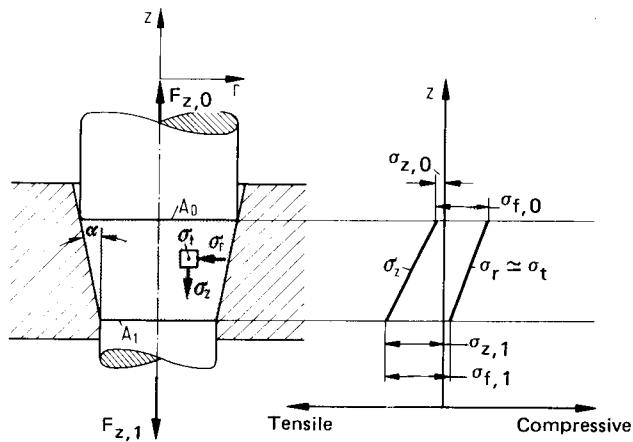


FIG. 14.15 Stresses in drawing with back tension.

be used. The work due to back tension cannot be used effectively without a major change in machine design. Additional features in the machine design also result in loss of useful work. Based on the above reasons, the back tension does not offer notable advantages [14.17], [14.18].

The maximum achievable natural strain per drawing stage decreases in the case of drawing with back tension, because the strain limits are lower in the tensile zone than in the compressive zone.

A common application of back tension is for wires whose straight entry into the die has to be guaranteed.

#### 14.1.4 Temperatures In Drawing

The drawing processes are generally carried out at room temperature. The velocities are higher for drawing than for other deformation processes. This results in the material entering the deformation zone filled with drawing lubricant at room temperature. A very high percentage of the deformation work and friction work is converted into heat energy. For materials deformed below the recrystallization temperature, the percentage of deformation work converted to heat energy is 85–95% [14.19]. Siebel and Kobitzsch [14.20] have proposed a simple equation to calculate the temperature increase  $\Delta T$  of a volume element in the wire assuming homogeneous deformation:

$$\Delta T = \sigma_{f,m} \ln \frac{A_0}{A_1} \left( \frac{1}{c\rho} \right) \quad (14.15)$$

where  $c$  is specific heat and  $\rho$  is density.

The temperature increase is dependent on the natural strain. The friction between the drawing lubricant and the wire surface area along the deformation zone contributes to a further increase in temperature in the boundary areas. Siebel and Kobitzsch have assumed in their investigations a parabolic temperature distribution in a boundary layer in the direction of the wire axis. An analysis of the heat flow will determine both the boundary-layer thickness and the temperature increase. An increase of the drawing velocity will result in less heat flow into the tools compared with the heat generated in the deformation zone.

An example based on elementary plasticity theory is presented in [14.18] (Fig. 14.16). It is seen from Fig. 14.16a that the surface temperature along the deformation zone increases with increasing drawing velocity. The friction heat is constant for all drawing velocities. The frictional work is, however, concentrated in a small layer (small volume) near the boundary for larger drawing

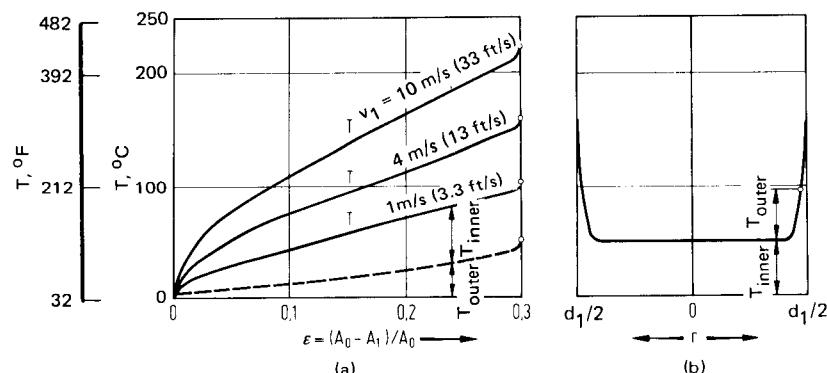
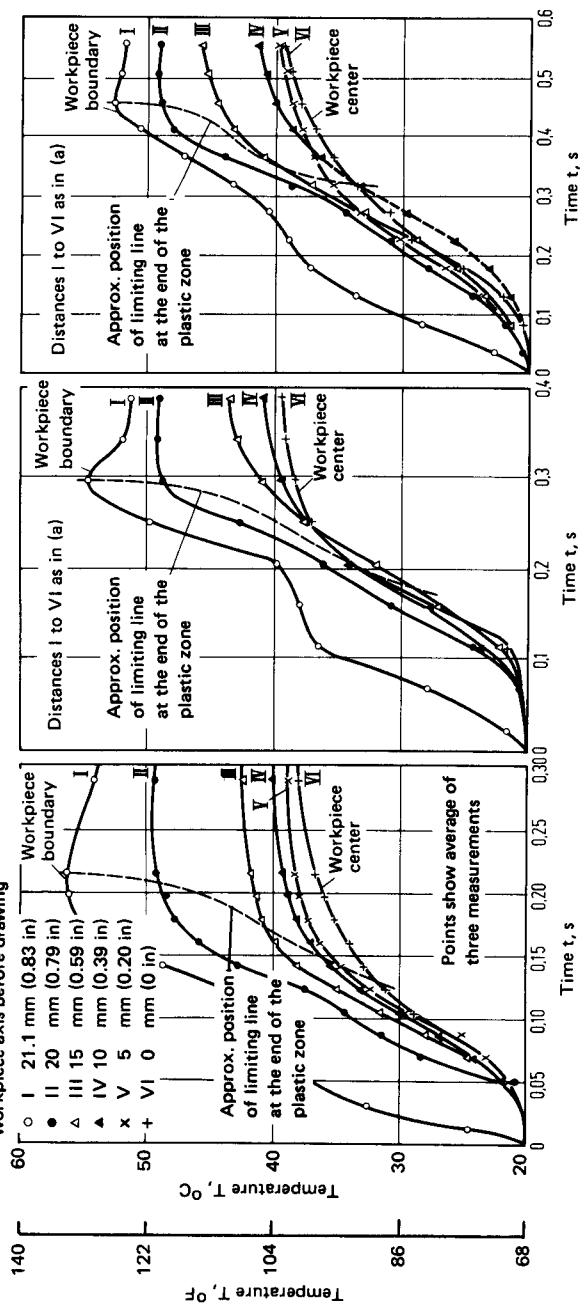
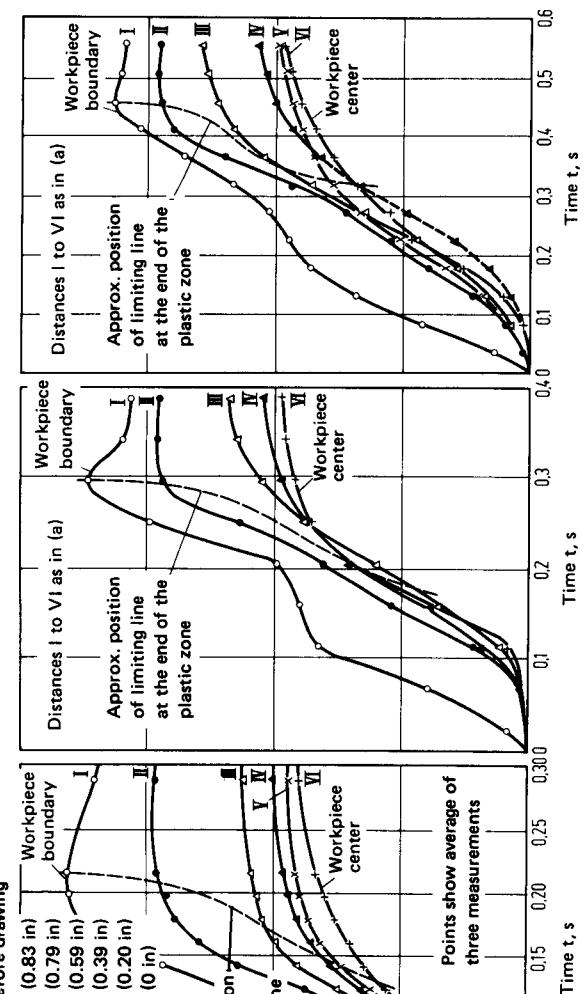


**FIG. 14.16** Temperature increase in drawing. Material—St37 (AISI 1015);  $\rho = 7860 \text{ kg/m}^3$  ( $491 \text{ lb/ft}^3$ );  $c = 483 \text{ J/kg} \cdot \text{K}$ ;  $k = 53.5 \text{ W/m} \cdot \text{K}$ ;  $2\alpha = 16^\circ$ ;  $\epsilon_{\text{tot}} = (A_0 - A_1)/A_0 = 0.3$ ;  $\mu = 0.05$ ;  $d_0 = 4 \text{ mm}$  (0.16 in.). (a) Surface temperature along deformation zone at different velocities. (b) Temperature profile at material exit.  $v_1 = 4 \text{ m/s}$  (13.1 ft/s). (After [14.18].)

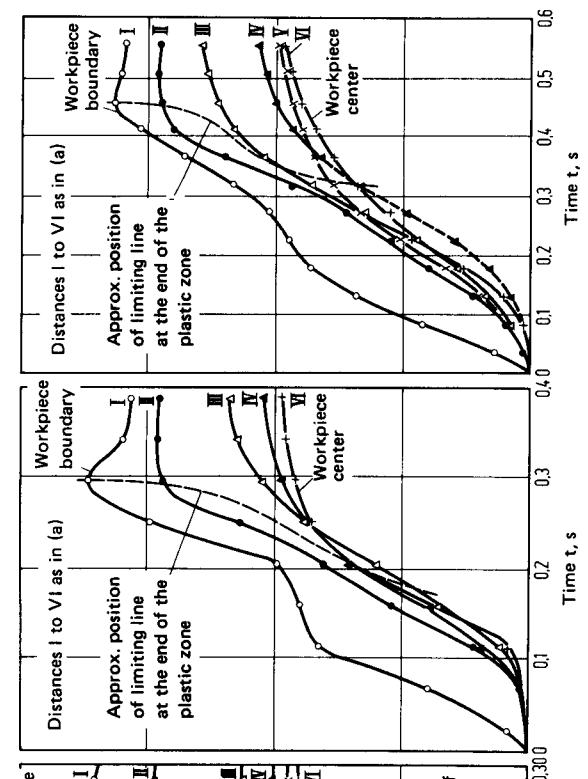
Distance of thermocouple from the workpiece axis before drawing



(a)



(b)



(c)

**FIG. 14.17** Temperature distribution as a function of time for bar and wire drawing. Material—Ck10 (AISI 1010); lubricant—oil;  $d_0/d_1 = 44.0$  mm (1.74 in/1.59 in);  $2\alpha = 12^\circ$ ; (a)  $v_1 = 6.7$  m/min (264 in/min), (b)  $v_1 = 4.9$  m/min (193 in/min). (c)  $v_1 = 3.2$  m/min (126 in/min). (After [14.2].)

velocities due to the time dependence of heat conduction. The temperature profile for an intermediate drawing velocity is shown in Fig. 14.16b.

The temperature gradients in the boundary layers lead to different expansions over the cross section as a whole. Residual stresses result. The mean adiabatic temperature rise due to pure deformation is independent of the drawing velocity (Eq. 14.15), assuming that the flow stress  $\sigma_f$  for cold forming is independent of velocity effects. The mean adiabatic increase for the case discussed in Fig. 14.16 is  $\Delta T_{\text{adiab}} = 62.5^\circ\text{C}$  ( $112.5^\circ\text{F}$ ).

The temperatures in the deformation zone in drawing have been investigated by considering localized velocity fields. The process of viscoplasticity (refer to Chaps. 5 and 7) is one such method. Analytical methods have also been proposed by Kopp [14.2] and Adler [14.5]. The temperature increase can be calculated from the local velocities  $v_i$  (or equivalent strain rates  $\dot{\epsilon}$ ) without considering the effect of friction,

$$\Delta T = \frac{1}{c\rho} \int_0^t \sigma_f \dot{\epsilon} dt \quad (14.16)$$

Some results of Kopp are shown in Figs. 14.17 to 14.19. At the material boundary the temperature increases steeply when the material enters the deformation zone. The temperature then flattens before increasing at the die exit. The temperature at the center of the bar does not vary very much with velocity; at the bar surface, however, it increases with increasing velocity (see also Fig. 14.16) [14.18]. The temperature as a function of the radius is shown in Fig. 14.18. The effect of lower velocity on the cooling of the die can also be seen from this figure.

The isotherms are plotted in Fig. 14.19. Temperature peaks occur only in a small region at the material exit on the workpiece surface. Attempts to cool the tool to achieve a homogeneous temperature field must therefore be concentrated in this small die zone.

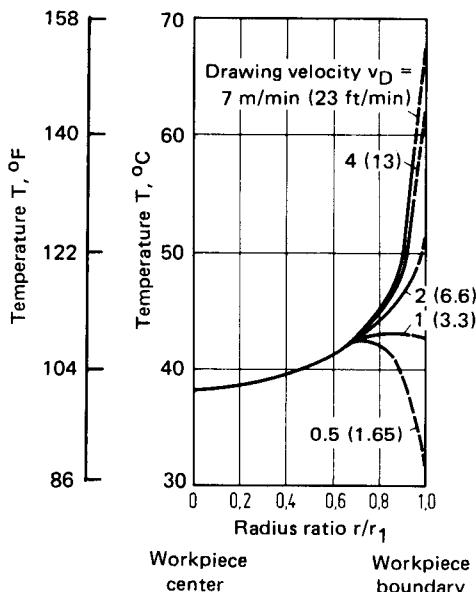
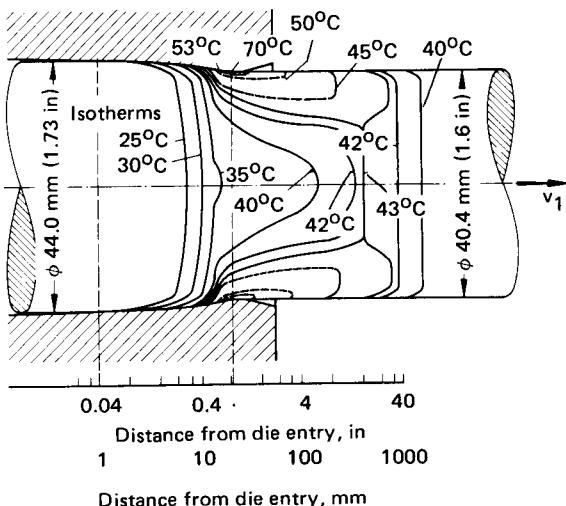


FIG. 14.18 Effect of drawing velocity on the temperature distribution over radius at the die exit. Test conditions as in Fig. 14.17. (After [14.2].)



**FIG. 14.19** Temperature field in drawing of a round bar.  $v_1 = 6.7$  m/min (264 in/min);  $T_0 = 20^\circ\text{C}$  ( $68^\circ\text{F}$ ). Test conditions as in Fig. 14.17; temperatures in  $^\circ\text{C}$ . (After [14.2].)

## 14.2 FRICTION AND LUBRICATION IN DRAWING

As for all other deformation processes, lubrication is very important for the drawing process. A good lubricant should have the following characteristics: a lower coefficient of friction, good separation characteristics on the tool-workpiece interface, be heat resistant, impart a good surface finish to the workpiece, and be clean. The lubricant should be easily applicable (spreading characteristic), be able to resist deformation pressure, and be easily removable. Another important characteristic of the lubricant to be considered is its mist and fume formation—it should not cause any health or other hazards.

The frictional conditions on the workpiece–tool interface are discussed in Chap. 6. Some special problems associated with the lubricant, especially in industrial production, are discussed here.

### 14.2.1 Lubricant Carriers

In drawing processes the surface areas do not increase as much during forming as in extrusion processes. Hence the problems of lubricant and lubricant carrier can be solved more easily for the drawing processes. The normal pressures on the tool surface which influence the deformation process are also relatively smaller.

The surface of the workpiece has to be cleaned before the lubricant carrier is applied. The scale in the case of steel can be removed by chemical pickling, by mechanical tumbling, or by shot blasting methods [14.21]. The lubricant carrier can then be applied on the workpiece surface. In the wire industry the process of applying lime is widely spread. The lime acts first as a neutralizer to remove the excess acid from the pickling treatment and then as a carrier for organic soaps used in drawing. Patented wires which are drawn through several dies are treated in the following manner before applying lime. After pickling and cleaning, the wires are either left in open air for 10–15 min or sprayed with some acidic water so that a light ferrohydroxide film forms on the workpiece surface. This process is also termed tanning because of the color of the workpiece surface [14.22].

Borax has replaced lime as the lubricant carrier in many steel-wire industries. It has better sticking properties than lime and improves the workpiece surface quality.

High-alloyed steels are coated with cooking salt with or without a lime carrier. Alkalies and soaps are also used as lubricant carriers [14.23].

Phosphating occupies a special position in the drawing of special wires. The phosphate coating is especially important for drawing with high velocities, high strains, and for steels with very high carbon content [14.24].

Stainless-steel wires are coated with oxalate for similar working conditions (see also Chap. 26 on surface treatment). Copper and aluminum alloys are generally drawn without special surface coatings.

#### 14.2.2 Lubricants

Four different types of lubricants are used in drawing processes—lubricated drawing, dry drawing, wet drawing, and shiny or white drawing [14.21].

**Lubricant drawing:** A container with lubricant is placed just before the entrance of the die, and the wire passes through this container. The workpiece is coated with the lubricant, some of which passes through the die, the remainder draining back to the container.

**Dry drawing:** The construction of the drawing fixture is the same as in the preceding case, except that the container has a solid dry lubricant such as soap in needle or powder form.

**Wet drawing:** The wires or bars are drawn wet (in a fluid medium). This method is used when the surface of the workpiece (steel) should retain its brightness (be shiny). The treatment of the wire has to be carried out in such a way that the wire is very clean before drawing and no decoloration occurs during the drawing process.

Chaps. 6 and 26 deal with the different interactions of lubricants and products.

The desirable lubrication condition in drawing is hydrodynamic lubrication. This condition can be achieved with soap after shorter initial lengths and then with wet lubricants. A hard soap gives better results than soft sodium soaps [14.25].

Table 14.1 gives an overview of the different lubricants used in drawing and their advantages [14.26]. The table is not necessarily complete since lubricants are being developed at a fast rate.

### 14.3 TOOLS FOR DRAWING

The tool is of paramount importance for drawing processes, although the failure criterion in drawing is the breaking of the drawn workpiece due to high tensile stresses. Several investigations on tool geometry, material, and wear have shown that the wire or bar quality and the economy of the process depend to a very great extent on the tools [14.27].

#### 14.3.1 Design

The drawing forces calculated in Chap. 13 assume a conical die. However, other shapes are also possible for drawing dies. Lippmann and Mahrenholtz [14.18] describe a curve-shaped die which requires lower drawing forces than conical dies. Computer models have been developed recently to design conical and streamlined dies for ironing processes [14.28]. The validity of these computer models was tested with ironing experiments conducted under regular production conditions. The models are capable of designing optimum ironing dies with both conical and streamlined profiles based on force requirements. The various stages during the ironing process are displayed and the force-displacement and wall stress-displacement diagrams are also displayed simultaneously (see Fig. 14.38). With these types of computer models a complete system for the ironing process can be designed. In spite of the above development, the conical shape is very widely used in industry since the inner conical shape can be more easily manufactured than other curved inner shapes. In addition, conical shapes are advantageous from the point of view of lubrication. The lubricant (especially soap and other dry lubricants) is trapped in the conical wedge formed by the workpiece and the die wall, and is drawn into the die along with the workpiece. The lubricant is

## 14.16 BULK-METAL FORMING

**Table 14.1.** Lubricants for Drawing Different Materials

Material	Lubricant	Remarks
<b>Wet</b>		
Aluminum	Petroleum with fatty oil; cylinder oil	Viscosity 20–40°E
Steel	Petroleum with flour for lime-coated wire (additions of graphite, zinc oxide, chalk); mineral oil	No high requirements on the surface
Steel (also platinum, gold, silver, copper, zinc)	Soap emulsions with fatty oils and water	Copper: 3% free fat Steel: 1.5% free fat, pH 9 Zinc: 2–3% free fat, pH 7
Austenitic steel, stainless steel	Sulfurized water-soluble oil with high-pressure additives ( $\text{MoS}_2$ , colloidal graphite)	
Zinc	3–5% soap–water solution	
Brass (also low-carbon steel wires)	Fermented solution of 20% bran and shredded grain in water	Unpleasant smell, but very inexpensive, characteristic flat and shiny surface (liquor finish)
<b>Dry</b>		
Aluminum, brass, noble metals	Powdered soap and beeswax	
Steel	Powdered soap with lime or oleate and tallow; mixtures of solid fat and lime	For lime-coated or similarly treated wires
Aluminum	Oleate and solid fat	Shiny, clean surfaces (also achievable with fatty oils, as in a mixture with calcium carbonate)
Steel	Metallic soaps (aluminum, calcium, and zinc stearate)	Surfaces are not pretreated; for higher requisites phosphating is necessary
Austenitic steel	Metallic soaps (aluminum, calcium stearate)	Oxalate lubricant carrier

Source: Compiled from [14.26].

pressed on the wire surface with high pressure [14.21]. Fig. 14.20 shows standard drawing dies made of carbides. The ratios of the dimensions can be obtained from [14.29].

A cylindrical land is generally used in the drawing dies immediately after the entry cone angle. Such a land has several advantages, including the reduction of total wear. This has been established by the extensive investigations of Wistreich [14.30] (Fig. 14.21). The die inner surface can be coated several times so that the nominal dimension does not change considerably [14.8]. The workpiece shows less springback effect than with drawing without land [14.31]. A disadvantage of drawing with land is that the drawing stress increases slightly, and therefore the limiting drawing strain decreases. However, this disadvantage is acceptable when compared with the numerous advantages of drawing with a die having a cylindrical land.

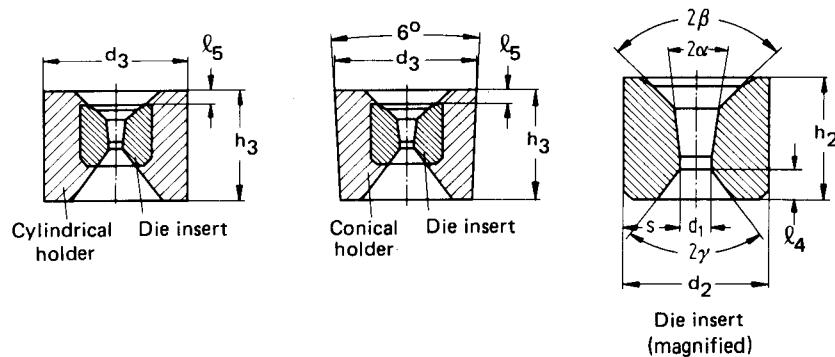


FIG. 14.20 Dies made from cemented carbides (After [14.29].)

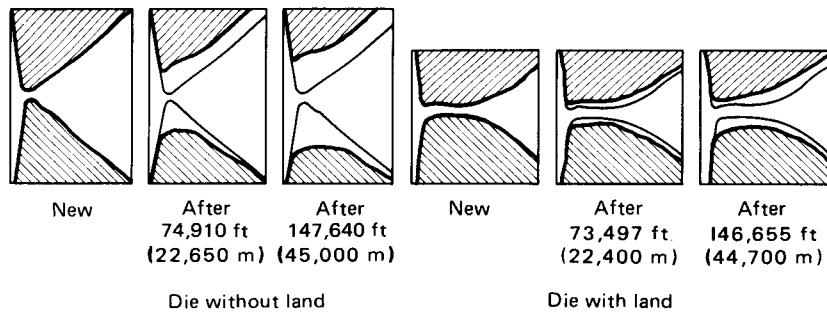


FIG. 14.21 Effect of drawn length on wear behavior of drawing die through dies with and without cylindrical land. (After [14.30].)

### 14.3.2 Material and Manufacture

The so-called drawing irons (English, German, and Viennese drawing irons), which in earlier days were used for drawing wire, are no longer widely utilized. These drawing tools are now used with oil- or air-hardening steels (Table 14.2, materials 7 and 8).

#### Steel Drawing Dies

Steel is a common die material for bar, rod, and profile drawing. The hardness of the steel should be between HRC 63 and 67. Since most of the steels are skin-hardening, the inner diameters of these steels reduce during the hardening process. The worn-out steel dies can be hardened again and ground for subsequent use. Table 14.2 gives the common steels used as die materials; their heat-treatment procedures are given in Table 14.3. Nitriding is done after hardening in some cases where a higher wear resistance is required [14.32].

Drawing dies for profiles either are single-piece tools or consist of several segments. The die segments are held together by a shrink ring. It is also possible to fit them into an adjustable tool head. In order to reduce excessive distortion of the profile drawing dies after heat treatment, forged drawing dies are frequently used. For profile drawing dies, high-alloyed chromium steels (no. 7 and 8 in Table 14.2) are preferred. Steels no. 3 and 4 are also used. For higher requirements, steels no. 9 and 10 are appropriate [14.32].

For tube drawing, the same steels are chosen as the die materials. The mandrels are generally made of steels no. 1 to 6 (Table 14.2).

If very high wear resistance is required, hard chromium plating of the die surface is recommended.

**Table 14.2.** Steel Tool Materials for Drawing Dies<sup>a</sup>

Steel type	Number	Designation	
		AISI	DIN 17006
Unalloyed steel	1	W1/1.0	C110W1
	2	W1/1.0	C125W1
Alloyed skin-hardening steels for water-jet hardening	3		145V12
	4		140CrV1
	5		X130W5
	6		145Cr6
	7	D3	X210Cr12
	8	D6	X210CrW12
Cast materials	9		G-X270CrV15
	10		G-X250CrV25
	11		G-X250CrWV15
	12		G-X250CrWV26
Mandrel material	13	6150	50CrV4
	14	6F3	56NiCrMoV7
	15	H11	X40CrMoV51

<sup>a</sup>See also App. A.

Source: Compiled from [14.32].

Cast-steel dies (no. 9 to 12 in Table 14.2) are used for hot drawing. They exhibit good wear resistance [14.32].

### Cemented Carbide Drawing Dies

Wires of small diameters are drawn using cemented carbides, which proved to be highly wear resistant. Table 14.4 lists the common cemented carbides used in the wire-drawing industries [14.33]. The cemented carbide drawing dies are sintered up to a die-opening diameter  $d_1 < 0.3$  mm (0.012 in). A small grinding allowance is generally given for these dies. Diamond powder and boron carbide are used for grinding and polishing cemented carbide drawing dies [14.21].

### Diamond Drawing Dies

Very-small-diameter wires, of 5  $\mu\text{m}$  to 1.5 mm (0.0002–0.06 in), are drawn using diamond dies. Diamond has the highest wear resistance. The major problem in the case of diamond drawing dies is their manufacture. The methods used nowadays are either chemical, electrical, or electrolytic processing. The various manufacturing steps are shown in Figs. 14.22 and 14.23 [14.34], [14.35]. The polishing effect, which is achieved by spark erosion (step 5 in Fig. 14.23) is sufficient to obtain a satisfactory wire surface and the necessary roundness on the drawn wire.

### 14.3.3 Selection Criteria for the Design of Floating Mandrels

Long tubes are not generally drawn over fixed mandrels, since the mandrel will have to be excessively long. In addition, very large drawing velocities cause resonance frequencies on long mandrels, which result in defective inner surfaces (scratch marks). Long tubes are therefore drawn over floating mandrels (Fig. 13.6e), and the danger of resonance frequency in the workpiece-die system is greatly reduced. The floating mandrel is held in equilibrium within the die by the opposing effect of the frictional forces acting in the drawing direction and the compressive forces acting

**Table 14.3.** Heat Treatment of Drawing Die Steels in Table 14.2<sup>a</sup>

Number	DIN specification	Rolling and forging, °C (°F)	Annealing temperature, °C (°F)	Hardness after annealing, HB <sub>max</sub>	Hardening	
					Temperature, °C (°F)	Medium
1	C110W1	1000–800 (1830–1470)	680–710 (1255–1310)	200	770–800 (1420–1470)	Water
2	C125W1	1000–800 (1830–1470)	680–710 (1255–1310)	210	760–790 (1400–1450)	Water
3	145V12	1000–800 (1830–1470)	710–750 (1310–1380)	230	800–830 (1470–1525)	Water
4	140CrV1	1000–800 (1830–1470)	710–750 (1310–1380)	230	770–800 (1420–1470)	Water
5	X130W5	1050–850 (1920–1560)	710–750 (1310–1380)	270	790–820 (1450–1510)	Water
6	145Cr6	1050–850 (1920–1560)	710–750 (1310–1380)	230	820–850 (1510–1560)	Water
7	X210Cr12	1050–850 (1920–1560)	800–840 (1470–1545)	250	930–960 (1705–1760)	Oil, warm bath
8	X210CrW12	1050–850 (1920–1560)	800–840 (1470–1545)	250	950–980 (1740–1800)	Air, oil, warm bath
9	G-X270CrV25	See note <i>b</i>	820–860 (1510–1580)	320	940–980 (1725–1800)	Air (oil)
10	G-X270CrV25	See note <i>b</i>	820–860 (1510–1580)	320	940–980 (1725–1800)	Air
11	G-X250CrWV15	See note <i>b</i>	820–860 (1510–1580)	340	940–980 (1725–1800)	Air (oil)
12	G-X250CrWV26	See note <i>b</i>	820–860 (1510–1580)	340	940–980 (1725–1800)	Air
13	50CrV4	1050–850 (1920–1560)	680–720 (1255–1330)	235	830–960 (1525–1760)	Oil
14	56NiCrMo7	1050–850 (1920–1560)	660–700 (1230–1290)	250	860–900 (1580–1650)	Air
15	X40CrMoV51	1100–850 (2010–1560)	800–820 (1470–1580)	240	1040–1090 (1905–1995)	Air

<sup>a</sup>Refer also to Table 14.2 and App. A.

<sup>b</sup>Very difficult to forge, generally cast.

Source: Combined from [14.32].

**Table 14.4.** Common Cemented Carbides and Their Composition<sup>a</sup>

Designation	Chemical composition of sintered carbides			Density, kg/m <sup>3</sup> (lb/in <sup>3</sup> )	Hardness HV 30	Bending strength, N/mm <sup>2</sup> (ksi)	Compressive strength, N/mm <sup>2</sup> (ksi)	Young's modulus, kN/mm <sup>2</sup> (10 <sup>3</sup> × ksi)	Coefficient of linear expansion, 10 <sup>-6</sup> × °C <sup>-1</sup> (10 <sup>-6</sup> × °F <sup>-1</sup> )	Heat conductivity, W/m.°C
	Co, %	TiC + TaC, %	WC, %							
G05	6	—	Remainder	14800 (0.535)	1600 (218)	1500 (218)	5700 (827)	630 (91)	5 (2.8)	4.5
G10	6	—	Remainder	14800 (0.535)	1550 (247)	1700 (247)	5400 (783)	620 (90)	5 (2.8)	4.5
G15	9	—	Remainder	14500 (0.524)	1450 (276)	1900 (276)	4500 (653)	580 (84)	5.5 (3.1)	4.0
G20	12	—	Remainder	14300 (0.517)	1300 (305)	2100 (305)	4500 (653)	580 (84)	5.5 (3.1)	3.8
G30	15	—	Remainder	14000 (0.506)	1200 (348)	2400 (348)	4100 (595)	540 (78)	6 (3.3)	4.0
G40	20	—	Remainder	13500 (0.488)	1100 (377)	2600 (377)	3800 (551)	500 (73)	6.5 (3.6)	3.8
G50	25	—	Remainder	13100 (0.473)	1000 (392)	2700 (392)	3300 (479)	470 (68)	7 (3.9)	4.0
G60	30	—	Remainder	12800 (0.462)	900 (406)	2800 (406)	3000 (435)	460 (67)	7.5 (4.2)	4.5

Source: Compiled from [14.33]. Refer also to [14.58].

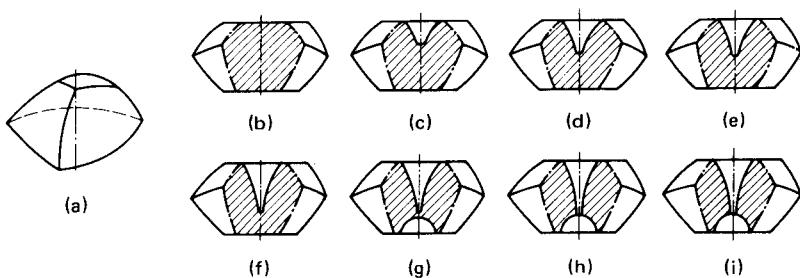


**FIG. 14.22** Manufacturing steps for diamond die. (a) Raw diamond. (b) Ground. (c) Pre-turned. (d) Rough-drilled. (e) Prebored. (f) Fine-bored. (g) Countermachined. (h) Through-bored. (i) Polished. (Courtesy of Joh. Urbanek and Co., Nürnberg.)

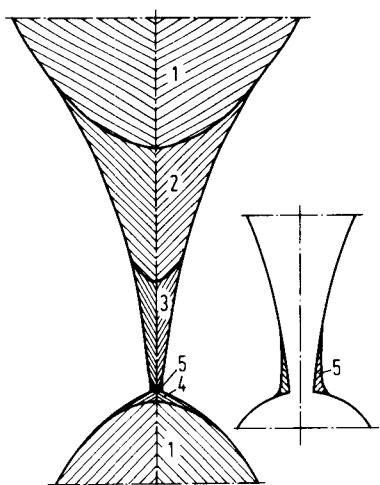


**FIG. 14.23** Manufacturing steps for diamond die by recent methods. 1—chemical burning with oxygen; 2—mechanolectric machining; 3—electrolytic machining; 4—mechanoelectric machining; 5—electroerosion. (After [14.34].)

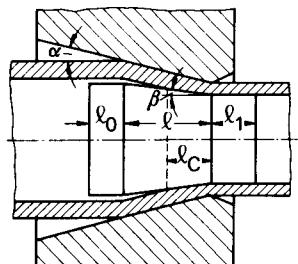


**FIG. 14.24** Schematic representation of various functional regions in a floating mandrel.

opposite to the drawing direction. The mandrel can be divided into three zones based on various functions (Fig. 14.24) [14.36]

- 1 The cylindrical portion with length  $l_0$  guides the tube. Its diameter should be slightly less than the inner diameter of the tube.
- 2 In the conical portion with length  $l$  the actual deformation takes place along the length  $l_C$ .
- 3 The cylindrical land  $l_1$  and the corresponding diameter serve to obtain the necessary wall thickness and the inner diameter of the tube.

The dimensions of the mandrel have to be designed in such a way as to (1) prevent it from drawing through the drawing die and (2) avoid any scratching defects on the workpiece if the mandrel

is pushed back. Investigations with steel-tube drawing [14.36] have suggested the following dimensions of the floating mandrel:

- 1 A reduction of the tube outer diameter of not very much less than 10%
- 2 A die-opening angle  $2\alpha$  of about  $10^\circ$
- 3 A difference between the die-opening angle  $2\alpha$  and the conical angle on the mandrel  $2\beta$  of more than  $4^\circ$

#### 14.3.4. Die Wear

The wear behavior of drawing dies is similar to that of other metal-forming tools. A new die wears very fast at the beginning. Then during the life cycle of the die wear is not that high, until the die finally fails (see also Chap. 9) [14.37]. The failure of the die is dependent on many factors, such as deformation strain, material, drawing velocity, pretreatment of the workpiece material, tool material, tool geometry, and lubricant. Other conditions remaining the same, friction and wear have a direct correspondence.

The wear does not follow a uniform pattern along the die wall. At the workpiece entry, a ring-shaped zone of considerable wear builds up in the die wall. Following this portion, there is less wear up to the material exit from the die, where the wear is again greater. This wear behavior is observed in almost all tool materials [14.21]. The wear pattern cannot be explained using elementary plasticity theory. Recent investigations [14.5] indicate that higher wear is found in regions of higher normal pressures on the die (Fig. 14.5a). Other measurements also confirm the normal stress distribution as in the previous case [14.36].

#### 14.3.5. Multistage Drawing

The multistage drawing process has been developed (1) to reduce the surface temperature of the wire and (2) to increase the total reduction of area. In this case the wire is passed through several dies, and a higher deformation ratio can be obtained by this method. The temperature gradients between the wire surface and the interior are reduced during the period when the wire is between two dies. Additional cooling can also be used.

The multiple stages can be designed either as an equal percentage reduction in area per stage, or as equal energy requirements per stage [14.38]. The formulas for single-stage drawing apply also for the design of multistage drawing. An example is worked out in [14.18].

#### 14.3.6. Profile Drawing

Profile drawing is mainly applicable for the precise drawing of steel and, sometimes, high-strength nonferrous alloys.

The deformation mechanism in profile drawing is not very different from that of flat or strip drawing. Profile drawing is, however, more complicated and very difficult to analyze mathematically because of the geometrical intricacies. The obtainable strains are small ( $\varphi_{\max} = 0.1\text{--}0.2$ ). In the case of steel it is necessary to anneal after every stage. The most important aspect for the economy of profile drawing is the correct design of the various drawing stages. For most of the profiles commonly available round or square slabs can be used as initial profiles. Special profiles should, however, be prerolled (Fig. 14.25) [14.39]. This incurs additional costs. Therefore, for special profiles, profile drawing may be economical for large batch sizes only.

The design of the intermediate stages requires a considerable amount of prior experience. Normally the final section is drawn, and the various intermediate stages are designed therefrom, making sure that the permissible reductions of the areas are not exceeded [14.10]. It is also necessary to consider the material flow and the neutral plane during the design. Examples of good and bad material additions and drawing stages are shown in Figs. 14.26 and 14.27 [14.20], [14.40].

The drawing allowances are so chosen as to have equal elongation in all zones of the cross

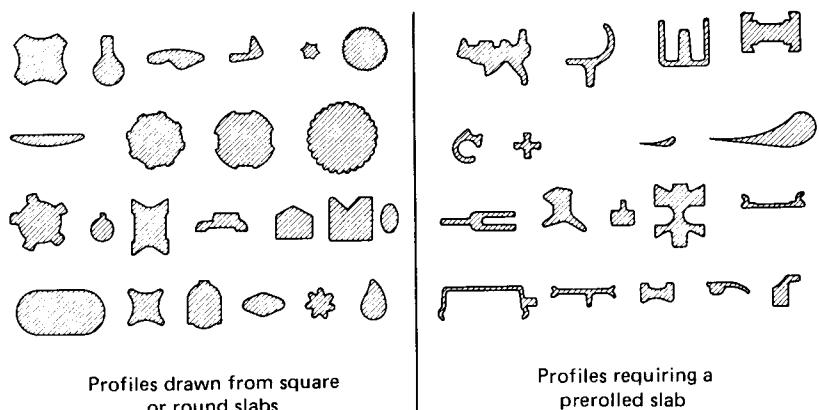


FIG. 14.25 Samples of drawn profiles. (After [14.39].)

section. Otherwise cracks may form, or the resulting residual stresses will cause bending and twisting of the drawn product. For a nonuniform cross section it is wrong to provide the same thickness allowance on all sides.

#### 14.4. Properties of Drawn Products

The customer generally makes some definite demands concerning the properties of drawn products. These can relate to the main geometry, tolerance, and form error limits, as well as to the mechanical properties. An overall survey of the various ASTM standards is given below:

A450-81	General Requirements for Carbon, Ferritic Alloy, and Austenitic Alloy Steel Tubes
A789-81	Seamless and Welded Ferritic/Austenitic Stainless Steel Tubing for General Service
A669-79a	Seamless Ferritic-Austenitic Alloy Steel Tubes
A493-80a	Stainless and Heat-Resisting Steel for Cold Heading and Cold Forging—Bar and Wire
A510-77	General Requirements for Wire Rods and Coarse Round Wire, Carbon Steel
A510M-77	As A510-77, but Metric
A752-77	General Requirements for Wire Rods and Coarse Round Wire, Alloy Steel
A581-80	Free-Machining Stainless and Heat-Resisting Steel Wire
A544-77	Steel Wire, Carbon, Scrapless Nut Quality
A545-77	Steel Wire, Carbon, Cold-Heading Quality for Machine Screws
A546-77	Steel Wire, Medium-High-Carbon, Cold-Heading Quality for Hexagon-Head Bolts
A547-77	Steel Wire, Alloy, Cold-Heading Quality for Hexagon-Head Bolts
A548-77	Steel Wire, Carbon, Cold-Heading Quality for Tapping or Sheet Metal Screws
A549-77	Steel Wire, Carbon, Cold-Heading Quality for Wood Screws
A276-81a	Stainless and Heat-Resisting Steel Bars and Shapes
A575-81	Steel Bars, Carbon, Merchant Quality, M-Grades

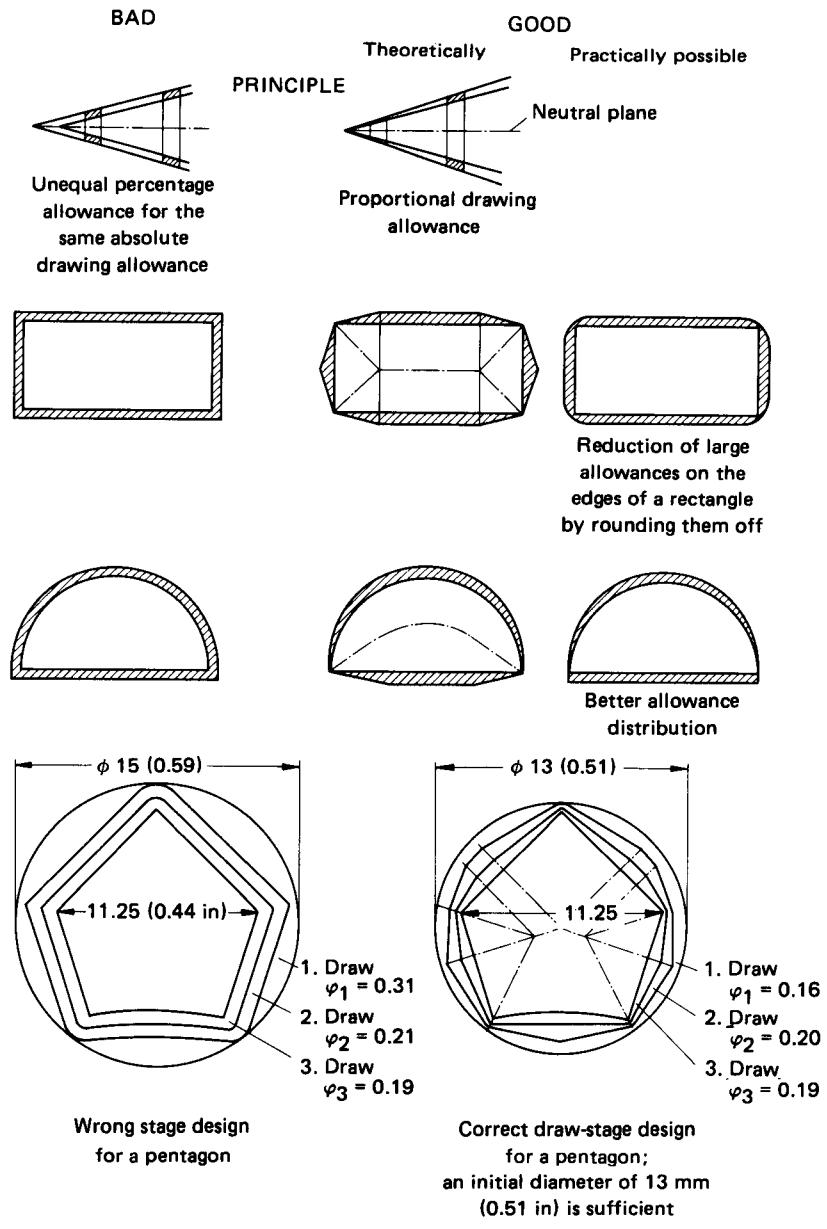


**FIG. 14.26** Example of determining drawing allowance in profile drawing. Dimensions are in mm (in). (After [14.41].)

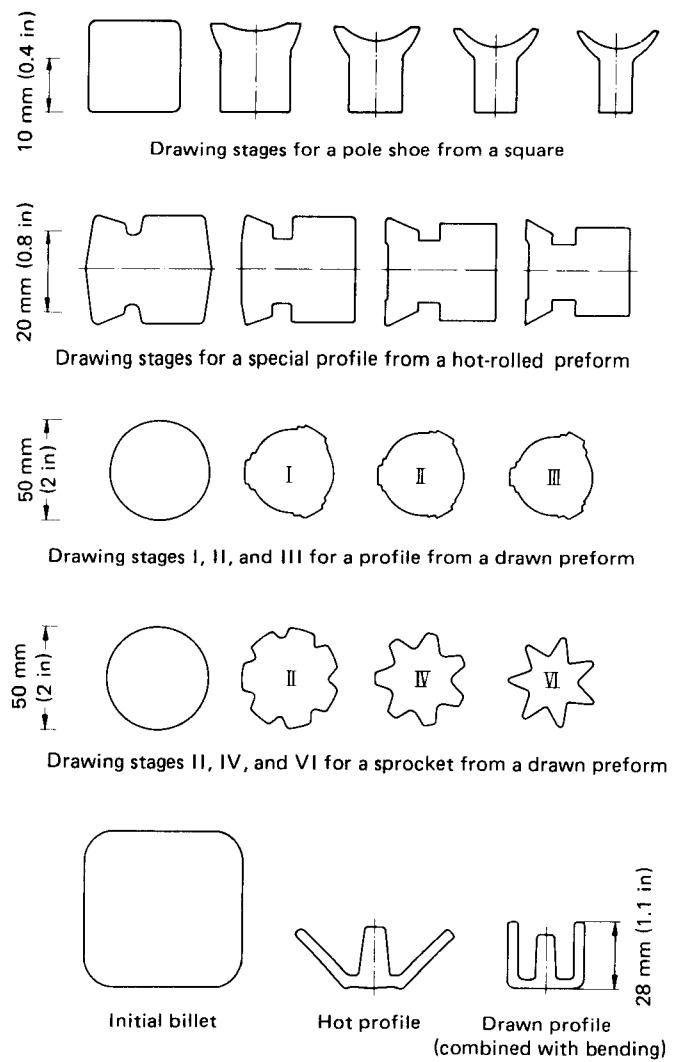


**FIG. 14.27** Drawing stages for various profiles. (After [14.39] to [14.42].)

A322-81	Steel Bars, Alloy, Standard Grades
A29-81	General Requirements for Steel Bars, Carbon and Alloy, Hot-Wrought and Cold-Finished
A108-81	Steel Bars, Carbon, Cold-Finished, Standard Quality
B1-70 (1976)	Hard-Drawn Copper Wire
B3-74 (1980)	Soft or Annealed Copper Wire
B133-81	Copper Rod, Bar, and Shapes

B133M-80	As B133-81, but Metric
B249-81	General Requirements for Wrought Copper and Copper-Alloy Rod, Bar, and Shapes
B249M-81	As B249-81, but Metric
B134-81	Brass Wire
B251-76	General Requirements for Wrought Seamless Copper and Copper-Alloy Tube
B251M-79	As B251-76, but Metric
B75-81	Seamless Copper Tube
B88-81	Seamless Copper Water Tube
B211-79a	Aluminum-Alloy Bar, Rod, and Wire
B211M-79	As B211-79a, but Metric
B210-80	Aluminum-Alloy Drawn Seamless Tubes
B210M-80	As B210-80, but Metric

#### 14.4.1. Residual Stresses

Residual stresses are stresses that exist in a body without the presence of external forces [14.43]. Nonuniform plastic strains in a cross section of a profile cause residual stresses in drawn workpieces. The temperature gradients between workpiece surface and core also cause residual stresses after cooling. Residual stresses can lead to tearing of the drawn workpiece and promote stress-crack corrosion. Cracks then open up during machining. A small reduction of area ( $<1\%$ ) leads to residual compressive stresses at the boundaries. With increasing deformation strain, tensile residual stresses are present in increasing quantities at the boundary zones. The tensile residual stresses reach a maximum for a natural strain  $\varphi_{\max} \approx 0.2$ . Other factors that influence the residual stresses are die geometry, friction, and workpiece material [14.44], [14.45].

The residual stresses can be reduced by the so-called “redrawing” process, which was developed by Bühler. A second drawing die is placed behind the main drawing die. The second die causes very little reduction on the product. During drawing through the first die, the material of the wire becomes entirely plastic. The elastic springback of the core is greater than that of the boundary zones, resulting in tensile stresses at the boundary zones and compressive stresses at the core. In the second die, only the boundary becomes plastic and the core remains elastic. The core cannot spring back completely so that tensile stresses are present in the core and compressive stresses develop in the boundary zones. Fig. 14.28 shows the opposing effects of these stresses [14.46]. For the above process Kreher [14.47] indicates a reduction of area with redrawing of 0.8% for wires and of 1.0% for hollow bodies.

#### 14.4.2. Surface Quality

Drawing is one of the metal-forming processes that could be used to obtain the best possible surface quality. Investigations on drawn bars have shown that for a natural strain  $\varphi_{\max} = 0.14$ , the average peak-to-valley roughness depth  $R_t$  of the original geometry decreased from  $\approx 45 \mu\text{m}$  to  $12 \mu\text{m}$  ( $0.002$  to  $0.0005$  in).

The surface roughness profile is smooth with hole-shaped troughs. During further drawing the profile becomes quite flat. Very favorable surfaces can be obtained if the deformation can be carried out in several stages, maintaining the same natural strain for every stage, instead of deforming the material in a single stage [14.48].

The optimum die opening for minimum force requirements also imparts good surface quality on the workpiece material. For hollow bodies the smallest die-opening angle gives the best surfaces [14.49].

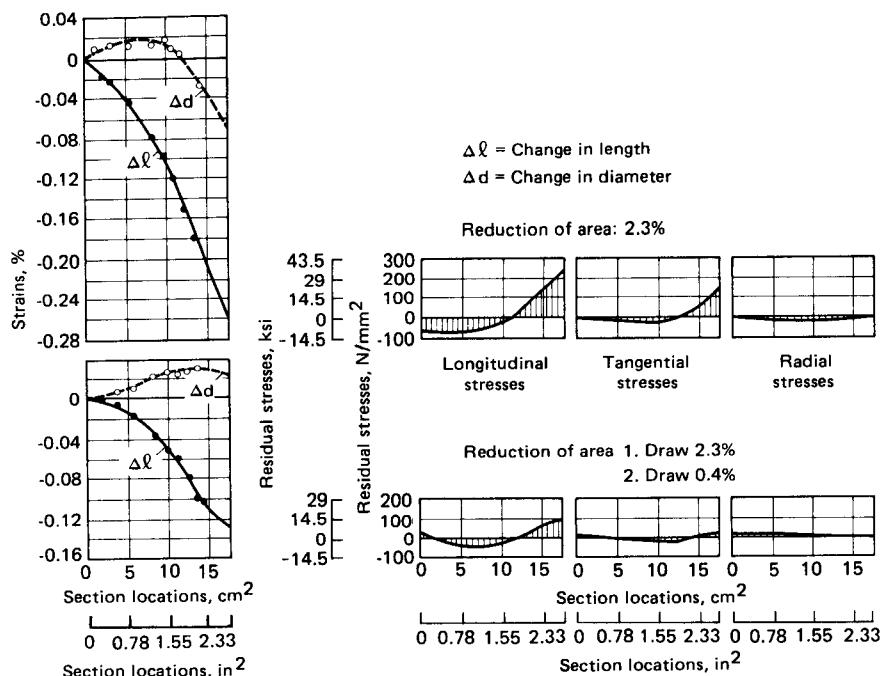


**FIG. 14.28** Reduction of residual stresses in cold-drawn brass bars by redrawing CuZn42 (UNS C28000).  $d_0 = 48.5$  mm (1.9 in). (After [14.46].)

#### 14.4.3. Mechanical Properties

Based on the relationship between strain and strain hardening in metallic materials, the hardness, strength, necking, and elongation for drawn bars and profiles exhibit the same trends as for other cold- or hot-formed products. The mechanical properties are dependent on the local strains in the cross section (see Sec. 14.4.1.). A knowledge of material flow is therefore necessary to predict the mechanical properties (refer also to Sec. 13.2.1 and Chap. 3).

### 14.5. MACHINE TOOLS FOR DRAWING

#### 14.5.1. Draw Benches

Thick bars and strips [ $(d_0 > 16$  mm (0.75 in)) as well as most tubes are drawn on draw benches. The principle of draw benches consists of a draw carriage that rolls on the draw-bench bed. One or several draw tongues are mounted on the draw carriage. The material to be drawn is held rigid by these tongues. The draw carriage is operated either mechanically or hydraulically to pull the material through the drawing die. The material can be either removed or passed through a series of draw benches. After every stroke, the draw carriage rolls back on the bed of the draw bench. The process is repeated. The classical draw bench is the chain draw bench, which is widely used in industry. Fig. 14.29 shows two types of draw benches with different drives [14.49].

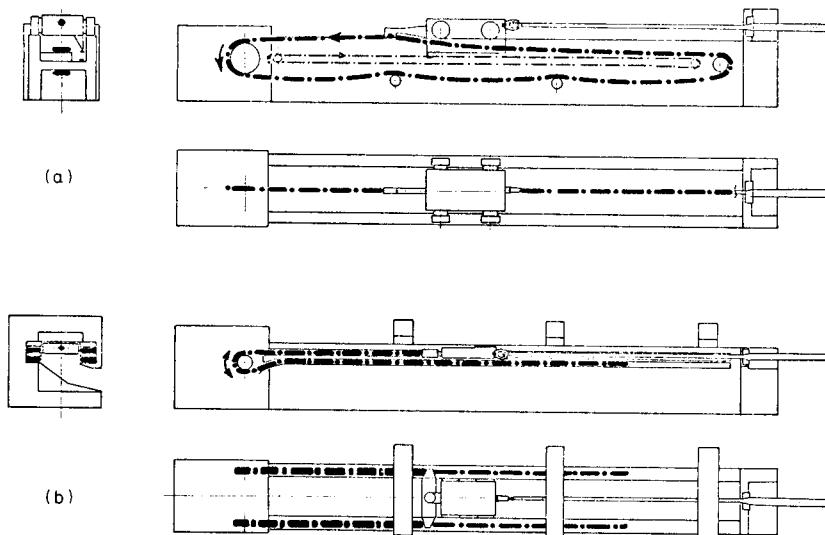


**FIG. 14.29** Types of draw benches. (a) With continuously rotating single chain (normal design). (b) With two reciprocating chains (special design). (After [14.49].)

Continuous operation is possible in a drawing plant with two draw carriages moving in opposite directions. They are controlled in such a way that when one grips the material, the second carriage is released from the material and returns. After the return stroke, the second draw carriage is accelerated in the drawing direction and holds the bar when the velocities of both the carriages are equal. The first draw carriage is then released and returns to the original position (Fig. 14.30). The productivity improves considerably in a multitonque operation.

#### 14.5.2. Wire-Drawing Machine

In the case of wire drawing, the wire is wound on a drum. If the wire is taken from the drum for subsequent use, the process is known as simple drawing. This process is used for rough and medium draws up to a diameter of  $d = 8 \text{ mm}$  ( $\frac{5}{16} \text{ in}$ ). For thinner wire the multistage drawing process is used, which offers many economic advantages, including saving of the work place and avoidance of winding after every single station. The wire passes through several drawing dies. The intermediate drums or discs rotate at velocities corresponding to the elongations of the wire. Multistage drawing machines are used for all wires with diameters  $d < 8 \text{ mm}$  ( $\frac{5}{16} \text{ in}$ ) [14.21].

Rough drawing	$d = 16\text{--}4.2 \text{ mm}$	( $\frac{5}{8}\text{--}\frac{1}{2} \text{ in}$ )
Middle drawing	$d = 4.2\text{--}1.6 \text{ mm}$	( $\frac{1}{2}\text{--}\frac{1}{32} \text{ in}$ )
Fine drawing	$d = 1.6\text{--}0.7 \text{ mm}$	( $\frac{1}{32}\text{--}0.0275 \text{ in}$ )
Superfine drawing	$d < 0.7 \text{ mm}$	(< 0.0275 in)

The drawing dies wear differently. This affects the drawing velocity in the different stages. The velocity change can be compensated by any of the following three methods: (1) regulating the drum speed, (2) slowing down the wire in the drum, (3) sliding the wire on the drawing discs [14.50].

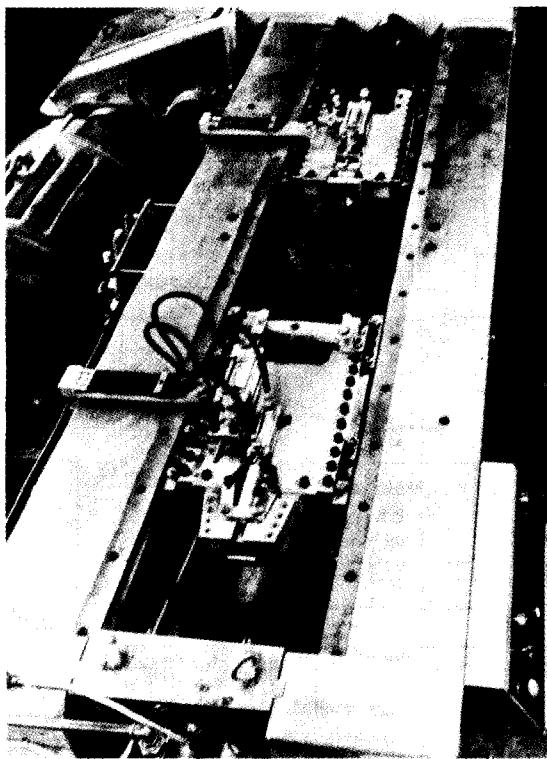


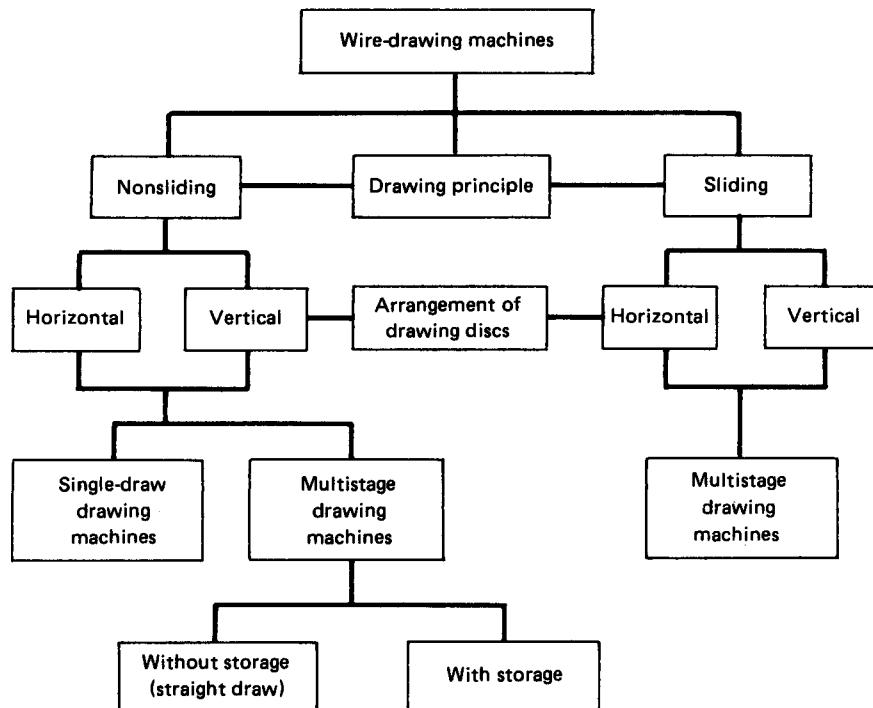
FIG. 14.30 Continuous drawing machine. (Courtesy of Schumag.)

Based on the above possibilities, there are two different drawing principles—sliding and nonsliding. Nonsliding drawing is used when there are no relative movements between the drum surface and the wire. In the case of sliding drawing, the circumferential velocity of the drawing drum is greater than that of the wire. It is also possible to slide-draw without storage on a drum. Fig. 14.31 gives a classification of the different types of drawing machines [14.50].

Single-stage drawing machines work on the nonsliding principle. These machines can also be arranged to be used for multistage operation (Fig. 14.32). This type of drawing results in a coil of wire. If the coil or twist of the wire is not desired, the straight-draw multistage drawing machine (nonsliding) can be used. The wire is led from one drawing die to the other without coil or twist (Figs. 14.33 and 14.34). Very-small-diameter wires are usually drawn in multistage drawing machines working on a sliding principle.

#### 14.5.3. Auxiliary Equipment

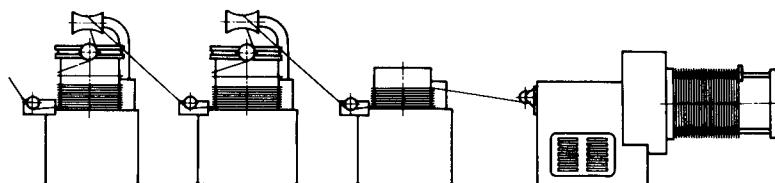
The wire end has to be chamfered in order to guide it into the drawing die. Special chamfering machines having either rolls or hammers are used for this purpose. Until recently chemical and electrical methods were used for chamfering. Detailed descriptions of other auxiliary drawing equipment, such as fixtures and winding equipment, can be found in [14.21], [14.27].

FIG. 14.31 Classification of drawing machines (*After [14.50].*)

#### 14.6. IRONING

The process of ironing deserves special consideration since it is frequently applied in the manufacture of components. This process, used for thin-walled hollow bodies, is especially important since these components are widely used as design elements. The competitive processes of ironing are flow forming and hollow forward extrusion (see Chaps. 12 and 15).

An important advantage of the ironing process as compared with the process of cold extrusion is that the deformation forces and the stresses on the tool are smaller. Other major advantages of ironing are better wall-thickness tolerance and surface finish. The preform for the ironing process is a drawn or extruded cup, which is pushed through one or more ironing rings (Fig. 14.35). The wall thickness is thereby reduced.

FIG. 14.32 Wire-drawing arrangement in multistage drawing with single-stage drawing machines. (*After [14.50].*)

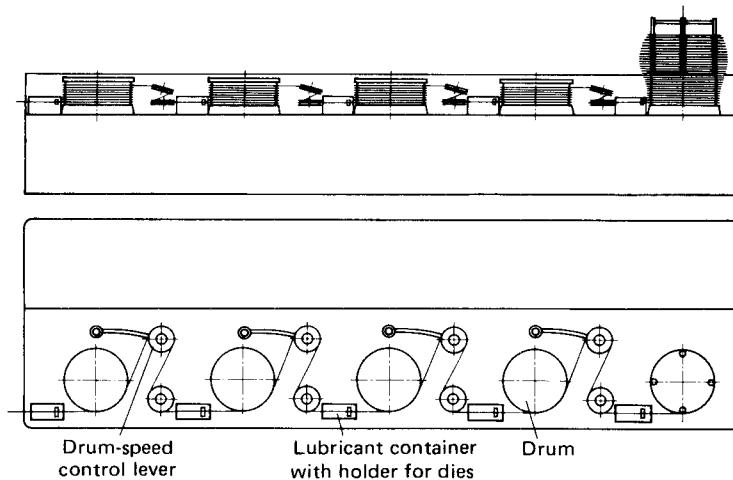


**FIG. 14.33** Principle of straight multistage wire-drawing machine. (*After [14.50].*)

#### 14.6.1. Forces and Stresses

Based on elementary plasticity theory, Eqs. 13.46a and 13.46c can be used to compute the forces. Other equations have been suggested by Weiss [14.52], Geleji [14.9], Thomsen and Kobayashi [14.53], and Busch [14.51].

From the point of view of economy it is generally attempted to obtain the maximum amount of deformation in a single pass. If the stress on the deformed wall increases more than the tensile strength of the material, failure occurs due to punch-through.

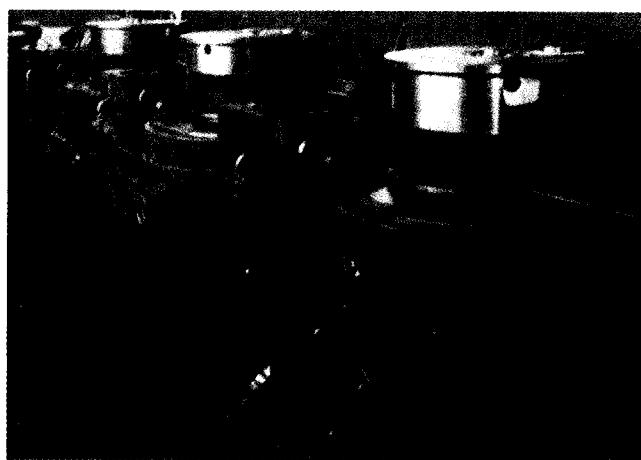


**FIG. 14.34** Straight multistage wire-drawing machine. (*Courtesy of Herborn.*)

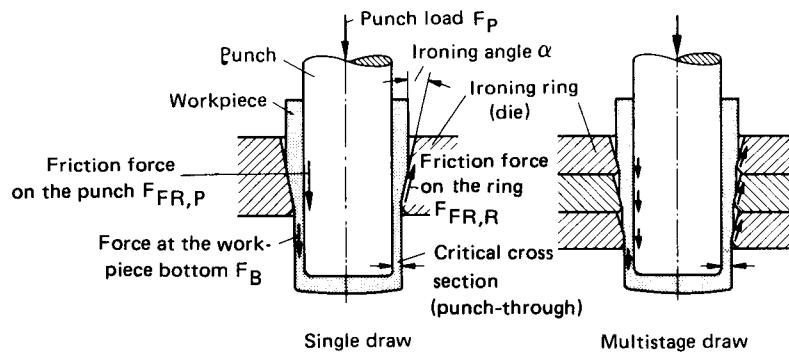


FIG. 14.35 Schematic representation of single- and multistage ironing. (After [14.51].)

The design of the tooling is changed to reduce the force requirements to a minimum since the stresses will also be reduced. Previous investigations had led to believe that the deformation force requirements in multistage ironing are smaller than those for single-stage ironing [14.54], [14.55]. However, recent investigations [14.51] indicate that single-stage ironing requires the least force. The force increases with the increasing number of ironing rings. The die-opening angle  $2\alpha$  affects the force on the bottom of the workpiece to a great extent. High forces on the bottom of the workpiece cause failure due to punch-through. The force acting on the workpiece bottom is

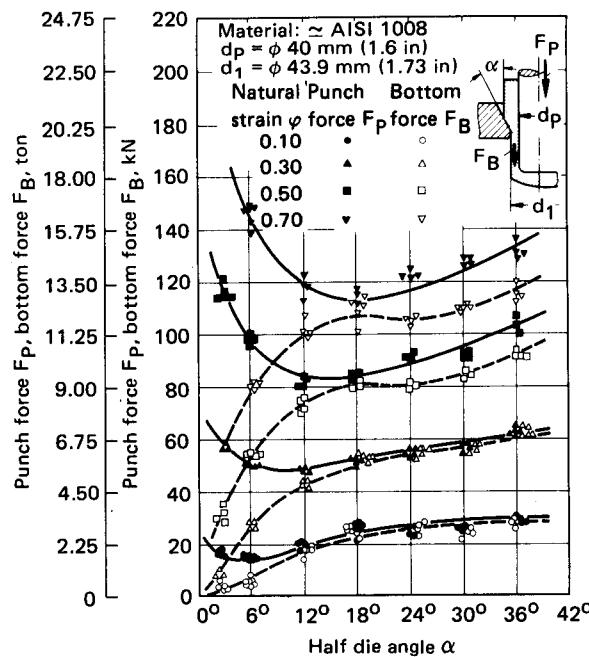
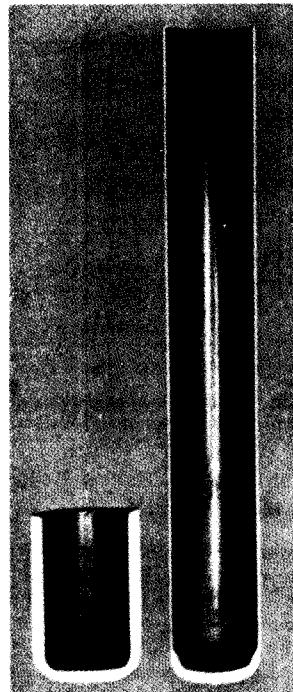


FIG. 14.36 Punch force and bottom force as a function of die half-angle. (After [14.51].)

reduced with decreasing ironing-ring angle. For a very small angle  $\alpha$ , the force on the bottom approaches zero (Fig. 14.36). The difference between the deformation force and the force on the bottom is the frictional force transferred onto the workpiece wall from the punch. For small angles the entire force is transmitted as frictional force [14.51], [14.28]. It must be remembered that  $\mu_p > \mu_s$  to achieve smaller forces at the bottom of the workpieces.

With decreasing die-opening angle the limiting natural strains can be increased. This is valid for both single-stage and multistage ironing. (A preform and the finished workpiece with high wall-thickness reduction are shown in Fig. 14.37.) The deformation force, however, increases with decreasing die-opening angle. This results in increased radial stresses, and therefore reinforced dies may be required. The design of such reinforced dies is described in Chap. 15. Recent mathematical modeling of the multi-stage ironing process simulates the operation by giving the following outputs: (1) process simulation, (2) the load-displacement diagram, and (3) the wall stress-displacement diagram [14.28], [14.56]. Fig. 14.38 shows a typical simulation on a computer terminal for a hot-ironing operation.

The die (ring) spacings, material data, forming temperature, and displacement steps desired for simulation are entered into the computer terminal. The forming process is then simulated by the computer for every displacement step. Position and shape of workpiece, ram load, and stresses acting on the ironed wall as a function of ram displacement are plotted simultaneously on the CRT screen. The undulations (peaks and troughs) in the force and stress plots are due to (1) material entering or exiting one or more rings, (2) material undergoing deformation in one or more rings, and (3) the number of elements assumed for mathematical simulation. The computer-aided design (CAD) system also delivers important messages concerning process limits, such as bottom punch-through if the wall stress exceeds the flow stress near the bottom zone. The CAD techniques, which are being developed for various forming processes, provide the designer with interactive capabilities.



**FIG. 14.37** Preform and finished workpiece.  $2\alpha = 4^\circ$ ;  $s_0 = 5 \text{ mm (0.2 in)}$ ;  $s_1 = 0.5 \text{ mm (0.02 in)}$ ;  $\epsilon = 0.90$ . (After [14.51].)

### 14.6.2 Workpiece Accuracy

Wall thickness differences present in the preform cannot be changed or corrected by ironing. Differences in wall thickness in the deep drawn cups due to anisotropy (e.g., earing; see Chaps. 18 and 20) also cannot be eliminated by ironing [14.51], [14.57]. The only way to overcome these defects is by machining.

It is frequently observed that the average inner diameter of an ironed workpiece is smaller than the outer diameter of the ironing punch. This point has to be considered in the design of the tooling [14.57].

The ironing process reduces the surface roughness of the workpiece compared with its preform. The workpiece surface becomes smoother and homogeneous with increasing reduction of area.

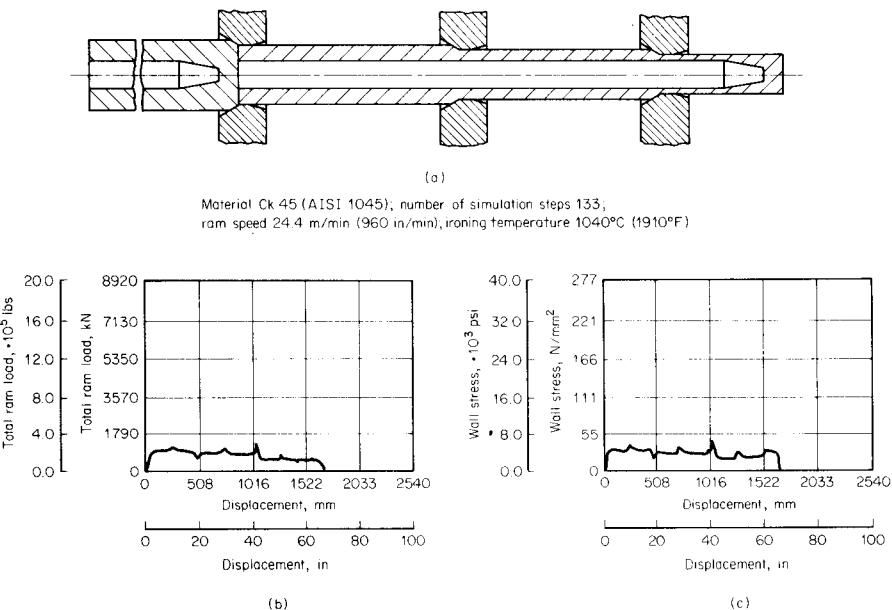


**FIG. 14.38** Mathematical model to simulate hot-ironing operation. (a) Simulation of process. (b) Load-displacement diagram. (c) Wall stress-displacement diagram. (After [14.28].)

### 14.6.3 Machine Tools

The presses used for ironing should have a large stroke since the finished workpieces are generally long. The stroke of the press must be at least twice the length of the ironed workpiece. Mechanical presses have to be so designed so that their minimum force equals the maximum ironing force. Only then is it possible to make use of the entire stroke of the press. Hydraulic presses are best suitable for ironing processes.

Special presses have been developed to keep the total stroke as small as possible. In these presses the total stroke is limited to the deformation travel only so that the free travel for feeding

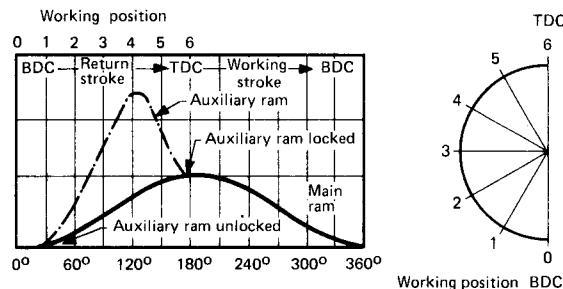


**FIG. 14.39** Motion sequence of crank press with auxiliary ram for ironing. TDC—top dead center; BDC—bottom dead center. (Courtesy of Maypres.)

in and for ejecting the workpiece must be obtained by other means. An example of a pneumatically operated auxiliary ram in the main crank drive is illustrated in Fig. 14.39. The auxiliary ram has a relative movement with respect to the main ram, especially during the return stroke of the main ram. The auxiliary ram rotates (moves up) faster than the main ram during the return stroke and releases the finished workpiece from the die. A new preform can then be placed in position. During the upward motion of the main ram, the auxiliary ram changes its direction of motion, picks up the new preform, and is locked in position with the main ram at the top dead center. The working stroke is then started.

## REFERENCES

- 14.1 Wistreich, J. G.: "The Fundamentals of Wire Drawing," *Metall. Rev.*, 3, 1958, pp. 97–142.
- 14.2 Kopp, R.: "Investigations on the Temperature Distribution in Drawing of Rounds" (*in German*), Dr.-Ing. thesis, Technische Hochschule, Clausthal, 1968.
- 14.3 Pawelski, O., and Lueg, W.: "The Stress Condition in Drawing and Nosing of Round Bars" (*in German*), *Untersuchungsberichte des Landes Nordrhein-Westfalen*, no. 1056, Köln/Opladen, Westdeutscher Verlag, 1962.
- 14.4 Hill, R., and Tupper, S. J.: "A New Theory of the Plastic Deformation in Wire Drawing," *J. Iron Steel Inst.*, 159, 1948, pp. 353–359.
- 14.5 Adler, G.: "A Process of Approximate Calculation of the Stress and Strain Condition for Flow of Rigid-Plastic Materials" (*in German*), *Berichte aus dem Institut für Umformtechnik, Universität Stuttgart*, no. 12, Essen, Girardet, 1969.
- 14.6 Pawelski, O.: "Fundamentals of Drawing and Nosing I" (*in German*), in *Fundamentals of Shaping*, Düsseldorf, Verlag Stahleisen, 1966.
- 14.7 Mahrenholz, O.: "On the Theory of Wire Drawing" (*in German*), *Drahtwelt*, 47, 1961, pp. 318–324, 413–418.
- 14.8 Eychmüller, W.: "Investigations on the Limiting Strains of Nonferrous Metals in Tube Drawing" (*in German*), Dr.-Ing. thesis, Technische Hochschule, Stuttgart, 1957.
- 14.9 Geleji, A.: *Shaping of Metals* (*in German*), Berlin, Akademie Verlag, 1967.
- 14.10 Swift, H. W.: "Stresses and Strains in Tube Drawing," *Philos. Mag.*, 11, 1949, pp. 883–902.
- 14.11 Woo, D. M.: "The Analysis of Axisymmetric Forming of Sheet Metal and the Hydrostatic Bulging Process," *Int. J. Mech. Sci.*, 6, 1974, pp. 303–317.
- 14.12 Schneider, M.: "Calculation of Forces in Tube Drawing," *Hutnik*, 28, 1960, pp. 79–84. Summarized by W. Dahl (*in German*), *Stahl u. Eisen*, 82, 1962, pp. 354–356.
- 14.13 Moore, G. G., and Wallace, J. F.: "Theoretical Study of Tube Sinking through Conical Dies," *J. Mech. Eng. Sci.*, 3, 1961, pp. 225–235.
- 14.14 Chung, S. Y., and Swift, H. W.: "A Theory of Tube Sinking," *J. Iron Steel Inst.*, 170, 1952, pp. 29–36.
- 14.15 Lueg, W., and Pomp, A.: "Effect of Back Tension in Drawing of Steel Wires" (*in German*), *Stahl u. Eisen*, 63, 1943, pp. 229–236.
- 14.16 Lueg, W. M.: "Drawing with Back Tension" (*in German*), *Stahl u. Eisen*, 62, 1942, pp. 432–439.
- 14.17 Wistreich, J. G.: "An Investigation of Back-Pull Wire Drawing as an Industrial Technique," *J. Iron Steel Inst.*, 163, 1949, pp. 316–330.
- 14.18 Lippmann, H., and Mahrenholz, O.: *Metal-Forming Plasticity for Metallic Materials* (*in German*), vol. 1, Berlin/Heidelberg/New York, Springer, 1967.
- 14.19 Farren, W. S., and Taylor, G. J.: "The Heat Developed during Plastic Extension of Metals," *Proc. R. Soc. London*, A107, 1925, pp. 422–451.
- 14.20 Siebel, E., and Kobitzsch, R.: "Heating of the Drawn Material in Drawing" (*in German*), *Stahl u. Eisen*, 63, 1943, pp. 110–113.

#### 14.36 BULK-METAL FORMING

- 14.21 Pomp, A.: *Steel Wire (in German)*, 2d ed., Düsseldorf, Verlag Stahleisen, 1952.
- 14.22 Lueg, W., and Treptow, K. H.: "The Lubricant Carrier for Drawing Steel Wires with Low and High Carbon Content" (*in German*), *Stahl u. Eisen*, **72**, 1952, pp. 1207–1212.
- 14.23 Lueg, W., and Treptow, K. H.: "Lubricant and Lubricant Carrier in Drawing of Steel Wires" (*in German*), *Stahl u. Eisen*, **72**, 1952, pp. 399–416.
- 14.24 Bader, G.: "Phosphating in Cold Forming in an Example of Steel Wire Manufacture" (*in German*), *Draht*, **18**, 1967, pp. 548–551.
- 14.25 Pawelski, O.: "Theoretical Considerations and Experiments to Obtain Thick Lubricant Film in Wire Drawing" (*in German*), *Stahl u. Eisen*, **85**, 1965, pp. 445–448.
- 14.26 Mohrnheim, A.: "Lubrication in Multistage Wire Drawing" (*in German*), *Draht*, **12**, 1961, pp. 431–434.
- 14.27 *Manufacture of Steel Wire (in German)*, pts. 1 and 2, Düsseldorf, Verlag Stahleisen, 1969.
- 14.28 Lahoti, G. D., Raghupathi, P. S., Subramanian, T. L., and Altan, T.: "Confirmation Tests of Hot and Cold Artillery Shell Drawing Operation," U.S. Army Armament Research and Development Command, Dover, NJ, Contract Rep. ARSCD-CR-79008, May 1979.
- 14.29 DIN 1547: "Hartmetall-Ziehsteine und -Ziehringe (Wire, Bar, and Tube Drawing Dies)," July 1969.
- 14.30 Wistreich, J. G.: "Wire Drawing Dies with and without Cylindrical Lead" (*in German*), *Stahl u. Eisen*, **70**, 1950, pp. 1178–1179.
- 14.31 Lueg, W., and Treptow, K. H.: "Recent Investigations on Drawing and Nosing of Bar Steel, Part 2" (*in German*), *Stahl u. Eisen*, **75**, 1955, pp. 769–776.
- 14.32 Hengler, E.: "Materials for Drawing Dies" (*in German*), in *Material Handbook, Steel and Iron*, 4th ed., Düsseldorf, Verlag Stahleisen, 1965.
- 14.33 Hinüber, J.: "Sinter Metal Alloys" (*in German*), in *Material Handbook, Steel and Iron*, 4th ed., Düsseldorf, Verlag Stahleisen, 1965.
- 14.34 Fritsch, O.: "The Manufacture of Diamond Drawing Dies by Old and New Methods" (*in German*), *Draht*, **15**, 1964, pp. 166–169.
- 14.35 Eschler, H.: "Diamond as a Fine Working Tool" (*in German*), *Draht*, **18**, 1967, pp. 213–218.
- 14.36 Pawelski, O., and Armstrong, O.: "Investigations on the Drawing of Steel Tubes with Floating Mandrel" (*in German*), *Stahl u. Eisen*, **88**, 1968, pp. 1348–1354.
- 14.37 Papsdorf, W.: "Friction, Wear, and Lubrication in Wire Drawing" (*in German*), *Stahl u. Eisen*, **72**, 1952, pp. 393–399.
- 14.38 Mohrnheim, A. F.: "Drawing Forces and Driving Power in Multistage Drawing Units" (*in German*), *Draht*, **12**, 1961, pp. 45–50.
- 14.39 Greulich, K.: "Drawing of Special Profiles in Steel" (*in German*), *Drahtwelt*, **47**, 1961, pp. 579–583.
- 14.40 Hahne, F. J., and Domalski, H. H.: "Drawn Profiles of Stainless Steel—Their Manufacture, Application, and Economy" (*in German*), *Blech*, **14**, suppl. "Rohre und Profile," 1967, pp. RP 4/2–4/12.
- 14.41 Preußler, H.: "Multi-Pass Design of Cold Drawn Profiles" (*in German*), *Stahl u. Eisen*, **69**, 1949, pp. 819–824.
- 14.42 Boehm, F.: "Deformation Process for the Manufacture of Precise Profiles of Steel" (*in German*), in "Application and Economy of Cold Forming in Manufacturing Technology," *VDI-Berichte*, no. 39, Düsseldorf, VDI-Verlag, 1959.
- 14.43 Bühler, H., and Peiter, A.: "Residual Stresses in Steel, A Survey for Practical Use" (*in German*), *Technische-Rundschau-Bericht*, no. 47, Bern, Hallwag, 1961.
- 14.44 Bühler, H., and Buchholtz, H.: "Effect of the Reduction of Cross Section in Cold Drawing on the Stresses in Round Bars" (*in German*), *Arch. Eisenhüttenwes.* **7**, 1933–34, pp. 427–434.

- 14.45 Linicus, W.: "Investigations on the Properties of Wires and the Force Requirements in Wire Drawing" (in German), Dr.-Ing. thesis, Technische Hochschule, Berlin, 1931.
- 14.46 Bühler, H., and Schultz, E. H.: "On the Reduction of Residual Stresses Developed in Cold Drawing of Metal Bars by Redrawing" (in German), *Metall*, **5**, 1951, pp. 195–198.
- 14.47 Kreher, P. J.: "Studies on the Problem of Residual Stresses in Cold Drawing of Wires and Tubes" (in German), Dr.-Ing. thesis, Technische Hochschule, Hannover, 1967.
- 14.48 Mietzner, K.: "Investigations on the Surface Quality of Drawn Steels" (in German), *Stahl u. Eisen*, **82**, 1962, pp. 1423–1432.
- 14.49 Mäkelt, H.: "Drawing of Bars and Tubes on Modern Draw Benches" (in German), *Z. Metallk.*, **52**, 1961, pp. 69–75.
- 14.50 Auerswald, H.: "Wire Drawing Machines" (in German), in *Engineer's Handbook*, vol. A, pt. 2, Leipzig, VFB Fachbuchverlag, 1965.
- 14.51 Busch, R. K.: "Investigation on Ironing of Hollow Cylindrical Bodies at Room Temperature" (in German), *Berichte aus dem Institut für Umformtechnik, Universität Stuttgart*, no. 10, Essen, Girardet, 1969.
- 14.52 Weiss, H.: "Investigations on Ironing" (in German), Dr.-Ing. thesis, Technische Hochschule, Stuttgart, 1964.
- 14.53 Thomsen, E. G., and Kobayashi, S.: "Methods of Solution of Metal-Forming Problems," in *Proceedings of the 9th Sagamore Army Metals Conference* (Syracuse, 1964), pp. 43–69.
- 14.54 Bauder, K.: "Derivations of Optimum Strain Values for Deep Drawing of Hollow Bodies from Thick Steel Plates" (in German), Dr.-Ing. thesis, Technische Hochschule, Stuttgart, 1949.
- 14.55 Kuhn, W.: "Investigations on Stretch Forming of Steel Housing with Several Die Rings" (in German), Dr.-Ing. thesis, Technische Hochschule, Zürich, 1959.
- 14.56 Fukui, S., and Hansson, A.: "Analytical Study of Wall Ironing, Considering Work Hardening," *Ann. CIRP*, **18**, 1970, pp. 593–599.
- 14.57 Schelosky, H., and Krämer, W.: "Comparative Investigations on Flow Turning and Ironing" (in German), *Ind.-Anz.*, **92**, 1970, pp. 1716–1722.
- 14.58 ICFG Document: "General Aspects of Tool Design and Tool Materials for Cold and Warm Forging," Document N. 4/82, International Cold Forging Group, Portcullis Press, Surrey, England.
- 14.59 *Steel Wire Handbook*, vols. I–III, Guilford, CT, Wire Association International, 1980.



## CHAP. 15

### COLD AND WARM EXTRUSION

#### List of Special Symbols

$a$	constant
$b$	bottom thickness
$C$	constant
$C_1$	carbon equivalent
$F$	force without friction component
$\bar{F}$	fictitious value of force
$F_B$	bottom tearing force
$F_{\text{def}}$	deformation force
$F_E$	ejector force
$F_{\text{eff}} (W_{\text{eff}})$	effective deformation force (work) due to friction and redundant work
$F_{\text{FR},B}$	friction force on counterpunch (ejector)
$F_{\text{av}}$	average force
$F_e$	deformation force at end of process
$F_N$	nominal force of press
$F_p$	punch force
$F_{\text{PB}}$	punch force, backward
$F_{\text{tot}}$	total force
$h$	billet height; product height
$h_N$	effective stroke of press
$K$	calculation factor
$m$	force correction factor; exponent for punch pressure equation

$n$	exponent for pressure equation
$p_B$	bottom pressure
$p_P$	punch pressure
$p_W$	wall pressure
$q$	correction factor
$Q$	diameter ratio
$r_D$	die entry radius
$R_t$	peak-to-valley-height, roughness
$v_p$	punch velocity
$z$	correction factor; interference
$\alpha$	die-opening half-angle
$\gamma$	punch nose angle
$\dot{\epsilon}_z$	strain rate
$\eta_{def}$	deformation efficiency
$\lambda$	scale factor
$\sigma_z$	axial stress

### 15.1 EXTRUDABLE SHAPES AND ADVANTAGES OF EXTRUSION PROCESSES

The basic processes of cold extrusion are solid and hollow extrusion (both forward and backward) (Fig. 13.3*a, b, d, e*) and solid and hollow side extrusion (Fig. 13.3*g, h*). The processes are in general carried out with rigid tools at room temperature and sometimes also at temperatures near the region of recovery and recrystallization (hot extrusion). In the case of hydrostatic extrusion, a working medium (hydraulic fluid) is used for transmitting the force to the workpiece.\* For smaller reductions of the cross section the process of open-die extrusion is used instead of solid forward extrusion, especially in fastener manufacture (Fig. 13.4*a*). Several combinations of extrusion processes are possible, for example, forward-forward extrusion. Industrially important combinations with can extrusion are discussed in Sec. 15.8. The processes of upsetting, heading, and coining can be combined with extrusion processes. Embossing and ironing operations are also used in combination with extrusion processes. Fig. 15.1 gives an overview of different combinations of extrusion processes with other processes to manufacture rotation-symmetric workpieces [15.2]. Apart from the shapes shown in Fig. 15.1, other shapes exhibiting axisymmetry can also be extruded [15.3]. Details of extrudable shape elements with examples showing transition areas are given in Fig. 15.2.

Material savings are higher in cold extrusion compared with machining and other metal-forming processes such as hot die forging. The productivity is also high for complicated workpieces. Other advantages are good dimensional and form error tolerance, good surface quality, and improved mechanical properties of the workpieces. The last advantage permits the use of steels of lower strength as machine and construction elements without need for further hardening.

The above-mentioned advantages in conjunction with the numerous possibilities of shapes that can be manufactured by extrusion have led to the increased use of cold extrusion of steel.

Based on the limitations with regard to load on the tooling and to the forming ability of the different materials, extrusion processes are also carried out above room temperature and below the hot-forging temperatures. These are called warm-extrusion processes. For low-carbon steels warm extrusion is used above 400°C (750°F) and below 800°C (1475°F) [15.5]. [Temperatures of 200–400°C (400–750°F) represent the blue brittleness range, while temperatures above 800°C (1475°F) cause excessive scale formation.] The tooling is similar to that of the cold-extrusion process. Lower flow stresses of steels at the warm-extrusion temperature allow for a larger reduction in area, thereby reducing in some cases the number of stages required to manufacture components. A combination of warm- and cold-extrusion processes can also be used for certain components.

\*Refer to Chap. 28 for more details.

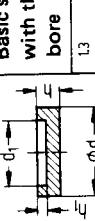
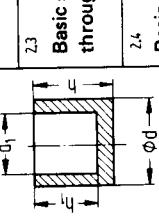
		Top surface		Without auxiliary shape		With cavity (hollow body)		With boss		With cavity and boss Double	
		Shell surface		Single	Double	Single	Double	Single	Double	Single	Double
<b>CLASS 1</b> Disc shape $d > h$ $d_1 > h_1$ 	1.1	1.1.1	—	1.1.2	—	1.1.3	1.1.4	1.1.5	1.1.6	1.1.7	1.1.8
	1.2	1.2.1	—	1.2.2	—	1.2.3	1.2.4	1.2.5	1.2.6	1.2.7	1.2.8
	1.3	1.3.1	Basic shape with through bore	1.3.2	Basic shape with curved, profiled, or conical shell lines	1.3.3	1.3.4	1.3.5	1.3.6	1.3.7	1.3.8
<b>CLASS 2</b> Dished shape $d \approx h$ $d_1 \approx h_1$ 	2.1	2.1.1	—	2.1.2	—	2.1.3	2.1.4	2.1.5	2.1.6	2.1.7	2.1.8
	2.2	2.2.1	Basic shape with boss or flange	2.2.2	—	2.2.3	2.2.4	2.2.5	2.2.6	2.2.7	2.2.8
	2.3	2.3.1	Basic shape with through bore	2.3.2	—	2.3.3	2.3.4	2.3.5	2.3.6	2.3.7	2.3.8
<b>2.4</b> Basic shape with curved, profiled, or conical shell lines	2.4.1	2.4.2	—	2.4.3	2.4.4	2.4.5	2.4.6	2.4.7	2.4.8	—	—

FIG. 15.1 Shape classification for rotation-symmetric workpieces. (After [15.1].)

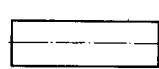
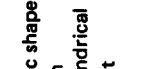
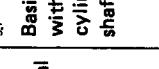
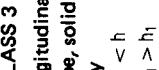
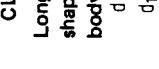
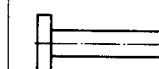
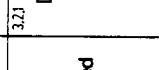
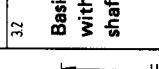
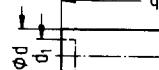
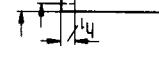
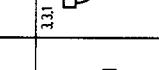
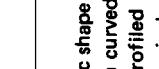
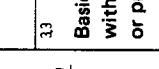
Top surface Shell surface	Without auxiliary shape		With cavity (hollow body) Double		With boss Double		With cavity and boss Double	
	Single	Double	Single	Double	Single	Double	Single	Double
CLASS 3 Longitudinal shape, solid body $d < h$ $d_1 > h_1$	3.1.1	3.1.2	3.1.3	3.1.4	3.1.5	3.1.6	3.1.7	3.1.8
3.1 Basic shape with cylindrical shaft								
3.2 Basic shape with stepped shaft								
3.3 Basic shape with curved or profiled or conical shell lines								

FIG. 15.1 (Continued)

		Without auxiliary shape		With cavity (hollow body)		With boss		With cavity and boss	
		Single	Double	Single	Double	Single	Double	Single	Double
	Top surface	Shell surface							
CLASS 4 Longitudinal shape, hollow body $d < h$ $d_1 < h_1$	4.1	4.1.1	4.1.2	4.1.3	4.1.4	4.1.5	4.1.6	4.1.7	4.1.8
	4.2	4.2.1	4.2.2	4.2.3	4.2.4	4.2.5	4.2.6	4.2.7	4.2.8
	4.3	4.3.1	4.3.2	4.3.3	4.3.4	4.3.5	4.3.6	4.3.7	4.3.8

The diagram illustrates the cross-sections of the components shown in the table. It features three main sections: 
 

- Shell Surface:** A vertical line with a stepped profile. The total height is labeled  $h$ . The top section has a diameter  $d$ , and the bottom section has a diameter  $\phi d$ .
- Top Surface:** A horizontal line with a stepped profile. The total width is labeled  $d_1$ . The top section has a height  $h_1$ , and the bottom section has a height  $h$ .
- Overall Dimensions:** The total length of the component is indicated by a dimension line above the shell surface.

 The cross-sections themselves are labeled with codes such as 4.1.1 through 4.3.8, corresponding to the entries in the table.

FIG. 15.1 (Continued)

	Top surface Shell surface	Without auxiliary shape Single	With cavity (hollow body) Single	With cavity (hollow body) Double	With boss Single	With boss Double	With cavity and boss Single	With cavity and boss Double
CLASS 4	4.4.1 Basic shape outer and inner stepped surfaces	4.4.2 4.4.3 4.4.4 4.4.5 4.4.6 4.4.7 4.4.8	4.4.3 4.4.4 4.4.5 4.4.6 4.4.7 4.4.8	4.4.4 4.4.5 4.4.6 4.4.7 4.4.8	4.4.6 4.4.7 4.4.8 4.5.6 4.5.7 4.6.7 4.6.8	4.4.6 4.4.7 4.4.8 4.5.6 4.5.7 4.6.7 4.6.8	4.4.7 4.4.8 4.5.7 4.6.6 4.6.7 4.6.8	4.4.8 4.5.8 4.6.8
	4.5 Basic shape with through bore	4.5.1 4.5.2 4.5.3 4.5.4 4.5.5 4.5.6 4.5.7 4.5.8	4.5.1 4.5.2 4.5.3 4.5.4 4.5.5 4.5.6 4.5.7 4.5.8	4.5.1 4.5.2 4.5.3 4.5.4 4.5.5 4.5.6 4.5.7 4.5.8	4.6.1 4.6.2 4.6.3 4.6.4 4.6.5 4.6.6 4.6.7 4.6.8	4.6.1 4.6.2 4.6.3 4.6.4 4.6.5 4.6.6 4.6.7 4.6.8	4.6.1 4.6.2 4.6.3 4.6.4 4.6.5 4.6.6 4.6.7 4.6.8	4.6.1 4.6.2 4.6.3 4.6.4 4.6.5 4.6.6 4.6.7 4.6.8
	4.6 Basic shape with curved, profiled, or conical shell lines	4.6.1 4.6.2 4.6.3 4.6.4 4.6.5 4.6.6 4.6.7 4.6.8						

FIG. 15.1 (Continued)

## 15.2 CHARACTERISTICS OF PROCESSES WITH STATIONARY MATERIAL FLOW

### 15.2.1 Material Flow

Figs. 15.3 to 15.5 show the metal flow in solid-rod and hollow-tube forward extrusion. The non-stationary metal flow in the extruded piece and the stationary or, more correctly, quasistationary regions of metal flow can be differentiated easily from the varying degrees of distortion of the grid patterns. The distortion of an individual element passing through the die opening in hollow forward extrusion (Fig. 15.4) can be explained as follows. At the beginning of the process (Fig. 15.4b, left) the element is extended radially and upset axially as a result of the curvature of the billet top surface and the positioning on the die shoulder. A radial upsetting follows. The element is pulled toward the outer surface during subsequent deformation due to the curvature on the top surface. The vertical grid lines in Figs. 15.3 and 15.4 clearly show the above phenomenon. After the initial nonstationary region, the deformation shows a uniform distortion pattern (Fig. 15.4b, right). For greater natural strains (reduction in area), the inner material flows faster than the outer material. The total deformation of an element in the stationary zone is smaller than in the non-stationary region, and the vertical grid lines remain parallel to the axis. The deformation zone near the die shoulder can be seen in Fig. 15.4a (dark area).

If the billets are chamfered to match the die-opening angle, the curvature on the top surface decreases with higher reductions ( $\varphi \gg 0.5$ ); the stationary region in the shaft does not change (Fig. 15.4). For small reductions ( $\varphi < 0.4$ ), a concave "negative" curvature on the top surface can occur in the case of solid shafts extruded from relatively hard materials, for example, C45 (AISI 1045). This can be explained by the fact that the core of the workpiece remains elastic while the outer layers deform plastically [15.8]. The metal flow in open-die extrusion is similar to that of solid forward extrusion with small reductions in area. The metal flow in hydrostatic cold and warm extrusion, for which very small die-opening angles ( $2\alpha < 45^\circ$ ) are used, exhibits very uniform element deformation similar to those shown in Figure 15.5. This is a result of tool geometry and frictional conditions and is not due to the hydraulic pressure (see also Chap. 28). It can generally be stated that tool geometry and friction conditions affect the metal flow most. A better understanding of these parameters will lead to an accurate determination of the velocity fields used to compute distortion, stresses, and forces.

### 15.2.2 Stresses

The material is under triaxial compressive stresses in the extrusion processes, the only exception being the free surfaces. The deformation zone according to elementary plasticity theory is the region between the material entry into and exit from the die. This, however, does not represent the real condition. Although elementary plasticity theory can predict the relation between  $\sigma_z$ ,  $\sigma_r$ , and  $\sigma_t$  for a given position of the principal axes, it is not possible to make predictions about the local stresses. Only the average stresses can be predicted, which can be used to compute forces and energy.

Even the variational methods (upper and lower bound) used to compute energy, work, and forces on the basis of the lowest deformation energy predict only the overall values.

For plane-strain deformation, the slip-line theory can be applied to obtain stress distribution in the material (refer also to Chap. 5). Fig. 15.6 shows lines of maximum shear stress  $\tau_{\max} = k$  assuming that there is no friction between the tool and the workpiece. Several such solutions have been proposed by various researchers for axisymmetric processes [15.10] to [15.12].

The method of viscoplasticity [15.13], [15.14] predicts useful results on the distortion and velocity. However, the stress distribution is not predicted (see Chaps. 5 and 7).

The method of weighted residuals (see Chap. 5) can be used to determine the stress distribution. The numerical method suggested by Steck [15.15] can be applied for both stationary and nonstationary processes, with or without considering the work hardening of the material. Fig. 15.7 shows the stress distribution in the deformation zone, calculated based on the above method, for solid forward extrusion with rounded die shoulder. Adler [15.16] has also proposed a solution for drawing processes based on the method of weighted residuals with and without material work

Plane		With elevations					
		Continuous	Single-step		Multistep		
		About workpiece axis			Nonsymmetrical	Symmetrical	Nonsymmetrical
Top surface	Continuous						
	Shell line cylindrical						
Outer form	Continuous				<b>Increase in one direction</b>		
	Single-step				<b>Multistep</b>		
Inner form	Continuous						
	Single-step						

FIG. 15.2 Form elements of cold-extruded workpieces. (After [15.4].)

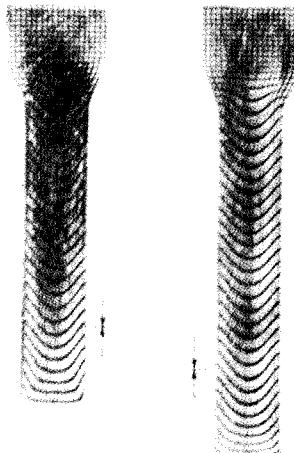


FIG. 15.3 Metal flow in solid forward extrusion.  
(a) Billet not chamfered. (b) Billet chamfered.  
(After [15.6].)

With grooves						With profile	
Continuous	Single-step		Multistep				
	About workpiece axis						
	Nonsymmetrical	Symmetrical	Nonsymmetrical	Symmetrical			
Increase in both directions						Profile section	
Continuous	Single-step		Multistep		Embossed	Recessed	

FIG. 15.2 (Continued)

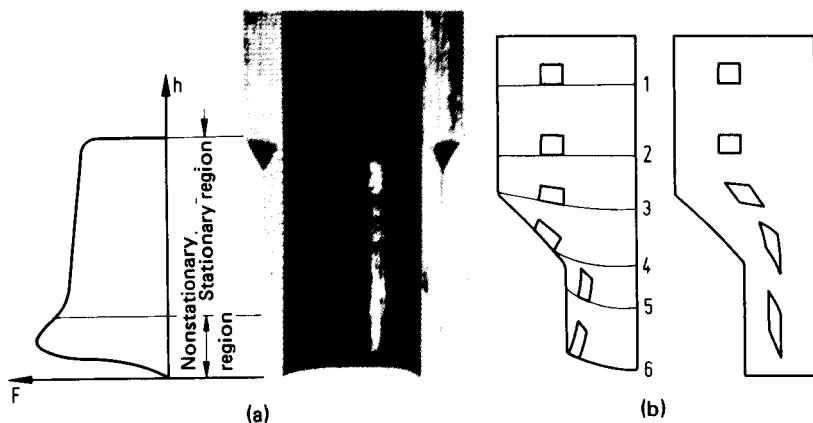
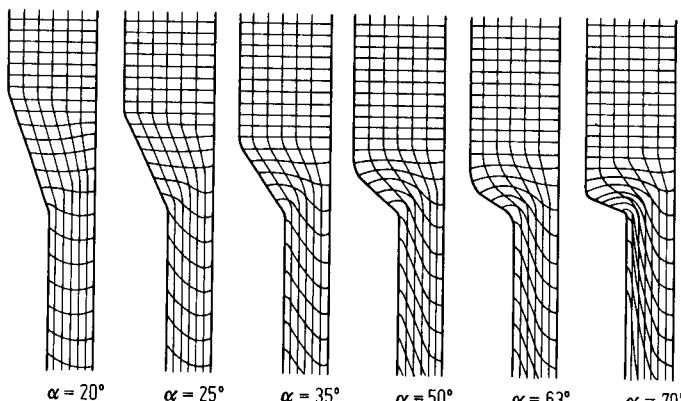


FIG. 15.4 Deformation of a workpiece element in hollow forward extrusion. (a) Nonstationary and stationary regions. (b) Deformation of an element in the nonstationary region (left) and stationary region (right). (After [15.7].)



**FIG. 15.5** Metal flow in hollow forward extrusion for different die-opening angles  $2\alpha$ . (After [15.7]).

hardening. These results have been extended to axisymmetric hot extrusion processes by Dahlheimer [15.17], who also calculates the temperature distribution in the deformation zone.

An exact determination of local stresses in cold extrusion is not necessary to analyze tool-material failure due to the presence of triaxial compressive stresses. However, from the point of view of tool loading the determination of average values of axial and radial stresses is necessary.

### 15.2.3 Forces and Energy

A typical force-travel diagram of a quasistationary cold-extrusion process is shown in Fig. 15.8. At the beginning the punch force (axial force) increases steeply, up to point 1, due to elastic deformations in the tool-workpiece system. This value is sufficient to deform the workpiece material plastically into the die opening. The force continues to increase up to point 2 during filling of the die shoulder with the material. This increase can be explained by means of the deformation behavior of the workpiece element (Fig. 15.4b) and the transition from sticking to sliding friction with low friction values on the die shoulder. During the subsequent process, the force drops down to point 3, which lies approximately on the straight line joining points 1 and 4, the end force. The monotonous decrease of the punch force from 3 to 4 is due to a reduction of the friction force in the container with decreasing length of the undeformed billet in the die. This force-travel diagram is valid for conical dies only. It is influenced by the following factors: (1) stiffness of the tool,

(2) workpiece material [ $E$  modulus, yield stress, and  $\sigma_y(\varphi)$ ], (3) die-opening angle  $2\alpha$ , (4) natural strain  $\varphi$ , (5) raw-material dimensions  $l_0/d_0$ , and (6) surface treatment and lubrication of the workpiece material (condition of friction).

The maximum force at point 2 increases with (1) a smaller die-opening angle  $2\alpha$ , (2) smaller initial billet hardness or yield stress, and (3) increasing natural strain. Fig. 15.9 shows examples of force-travel diagrams for solid and hollow forward extrusion. The effect of  $\varphi$ ,  $\sigma_f$  (material), and  $2\alpha$  can be seen in the figure. Fig. 15.10 gives the force-travel diagrams for hollow forward extrusion of aluminum Al99.5 (AA 1050) and Ck15 (AISI 1015)

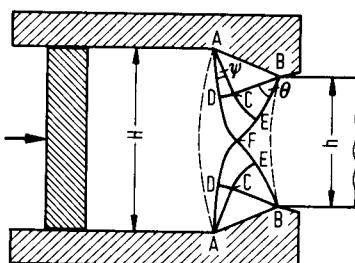


**FIG. 15.6** Slip-line field for plane solid forward extrusion. (After [15.9].)

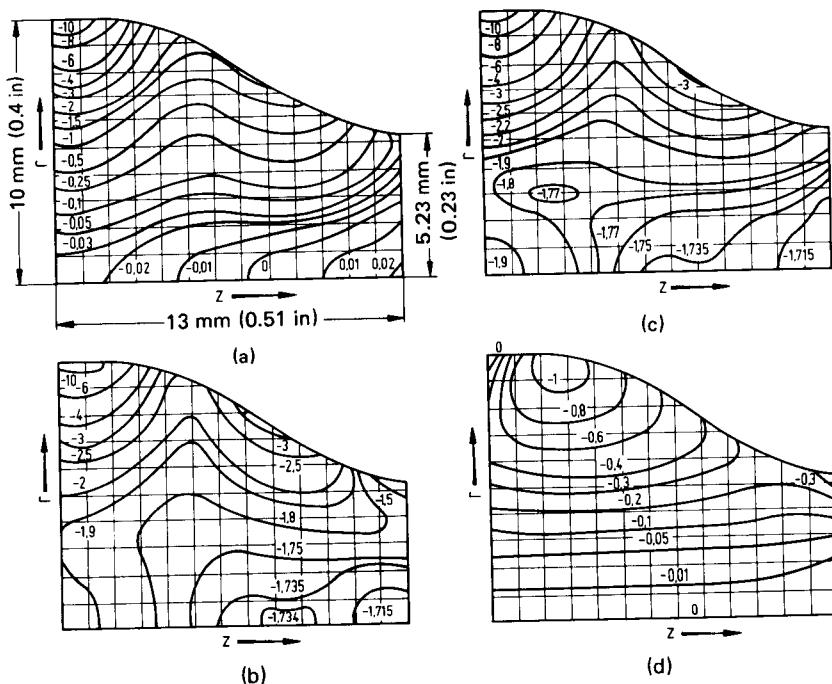


**FIG. 15.7** Stress distribution in the deformation zone for axisymmetric solid forward extrusion process. (a) Relative axial stress  $\sigma_z/k$ . (b) Relative radial stress  $\sigma_r/k$ . (c) Relative tangential stress  $\sigma_t/k$ . (d) Relative shear stress  $\tau_{rz}/k$ . (After [15.15].)

for  $2\alpha = 40$  and  $140^\circ$  [15.7] Table 15.1 on page 15.15 gives the values of the ratio  $F_{\max}/F_m \simeq F_{\max}/F_c$  for four different materials.<sup>\*</sup>

For practical use, the value of  $F_{\max}$  at point 2 is important. This force value is necessary for die design and the selection of the machine.  $F_{\max}$  can be calculated or estimated in different ways. For tool steel the upper limit for the maximum punch pressure (axial pressure =  $F_{\max}$ /area transmitting load) should be 2000–2500 N/mm<sup>2</sup> (290–350 ksi).

#### Calculation Using Deformation Efficiency $\eta_{def}$ and Force Correction Factor $m$

It has been pointed out in Chap. 13 that the total deformation force for the quasistationary process can also be calculated using the deformation efficiency, Eq. 13.48. The factors affecting the deformation efficiency were also mentioned there. Apart from the natural strain and the conditions of friction (lubricant, surface treatment), the deformation travel  $h$  has been found to affect the deformation efficiency [15.19]. However, a die-opening angle of between  $60$  and  $120^\circ$  does not affect the deformation efficiency [15.8]. For small strokes (relative to the billet diameter  $d_0$ ) the deformation efficiency can be greater than 1 ( $\eta_{def} > 1$ ) (Figs. 15.8 and 15.11), based on the definition  $\eta_{def} = W_{id}/W_{eff}$ . This is especially the case for billets with plane surface. For chamfered billets the relative stroke  $h_0/d_0$  does not have any appreciable effect. For most cases of punch travel with  $1 \leq h_0/d_0 \leq 1.5$ , the deformation efficiency  $\eta_{def}$  is between 0.7 and 0.8 for natural strains  $\varphi_{\max} \simeq 1.3$  and for steel Ck 15 (AISI 1015) (Fig. 15.11). The difference in deformation efficiency is due

\*  $F_m$  is the average of the forces corresponding to points 1 and 4 in Fig. 15.8. This force is not very different from  $F_3$ , and  $F_4 = F_e$  (refer to insert in Fig. 15.16).

to lubrication and billet surface quality (peeled, ground). Chamfering of the billet to the die-opening angle  $2\alpha$  has a negative effect on the deformation efficiency  $\eta_{def}$  (Fig. 15.12). A similar relation was found between  $\eta_{def}$  and  $\varphi_{max}$  for brass. However, for aluminum alloy Al Zn Mg Cu 1.5 (AA 7075) a different relationship was found in other investigations [15.20].

The deformation force  $F_{eff}$  calculated from Eq. 13.48 corresponds to the force  $\bar{F}$  in Fig. 15.8 and not to  $F_{max}$ . Dannenmann and Huber [15.21] have suggested a method for calculating the force correction factor  $m = \bar{F}/F_{max}$ . If the area  $W_{eff}$  under the force-travel curve in Fig. 15.8 is transformed into a rectangular area with the same punch travel  $h$ , then  $\bar{F} = W_{eff}/h$ . This force  $\bar{F}$  is related to the ideal force by

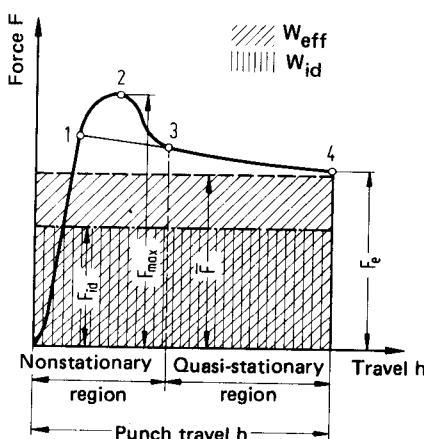


FIG. 15.8 Typical force-travel diagram for cold extrusion with quasistationary metal flow.  $W_{tot}$  corresponds to  $W_{eff}$  according to Eq. 13.47.

Nomograms to determine the forces in solid and backward can extrusion (see also Sec. 15.8) have been prepared [15.22], [15.23] for steels Ma 8 (AISI 1006), Ck15 (AISI 1015), 15 Cr 3 (AISI 5015), Ck 35 (AISI C1035), and 20 Mn Cr 5 (AISI 5120H). They can be used to calculate the maximum force  $F_{max}$  according to Eq. 13.48. The deformation efficiency  $\eta_{def}$  in the above equation contains a correction factor which considers the effects of billet length and die-opening angle. The value of punch pressure  $p_{p,max}$  as a function of the reduction of area  $\epsilon_A$  considers these effects. Similar curves for other materials—also non-ferrous metals—at temperatures other than room temperature can be obtained by conducting a series of experiments. The validity of the correction factor at higher temperatures has not yet been completely investigated.

### Calculation with Analytical Equations

Experimental investigations provide a basis for analytical equations involving the main variables used to calculate forces. Pugh [15.18] suggests an analytical expression for calculating the punch pressure as a function of the billet critical hardness  $H$  (HB, HV) and the natural strain  $\varphi_{max}$ ,

$$p_{p,max} = aH^m \left( \frac{A_0}{A_1} \right)^n \quad [\text{N/mm}^2] \quad (15.2)$$

The constants for steel with initial billet hardness between HB 80 and 240,  $A_0/A_1$  between 1.1 and 6.5, billet diameter between 10 and 75 mm (0.4 and 3 in) with  $l_0/d_0 = 1$ , die-opening angle

$$\bar{F} = \frac{F_{id}}{\eta_{def}}$$

(The value  $\bar{F}$  is a fictitious value.) The maximum force  $F_{max}$  is calculated from  $\bar{F}$  as

$$F_{max} = \frac{\bar{F}}{m} = \frac{F_{id}}{\eta_{def}m} \quad (15.1a)$$

$$= \frac{A_0 \varphi_{max} \sigma_{f,m}}{\eta_{def} m} \quad (15.1b)$$

The product of deformation efficiency and force correction factor is a measure to find the deviation of the actual deformation process from an ideal deformation process (no losses) with regard to force requirements. Fig. 15.13 shows the variations of  $\eta_{def}$ ,  $m$ , and  $\eta_{def}m$  for solid forward extrusion, and Fig. 15.14 shows the variation of  $m$  as a function of  $h/d_0$ . Fig. 15.15 illustrates the dependence of  $\eta_{def}m$  on the surface quality and lubrication. The results are all for Ck15 (AISI 1015).

The calculation of  $W_{eff}$  proceeds in a similar manner, starting from  $W_{id}$  and using the deformation efficiency  $\eta_{def}$  ( $\eta_{def} = W_{id}/W_{eff}$ ).

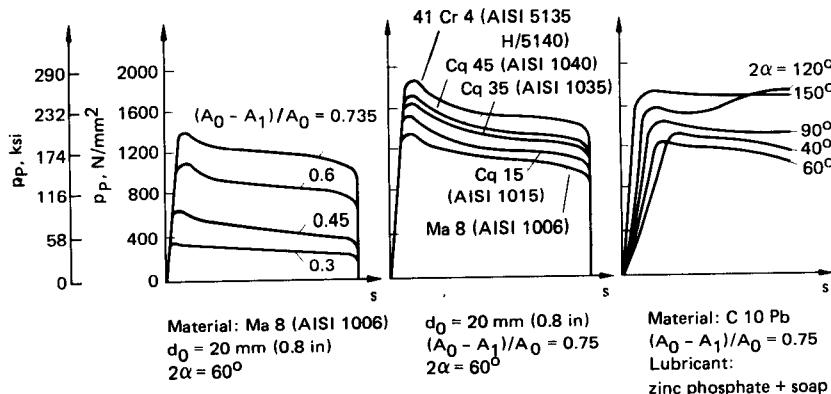
and hollow forward extrusion, open-die extrusion, and backward can extrusion (see also Sec. 15.8) have been prepared [15.22], [15.23] for steels Ma 8 (AISI 1006), Ck15 (AISI 1015), 15 Cr 3 (AISI 5015), Ck 35 (AISI C1035), and 20 Mn Cr 5 (AISI 5120H). They can be used to calculate the maximum force  $F_{max}$  according to Eq. 13.48. The deformation efficiency  $\eta_{def}$  in the above equation contains a correction factor which considers the effects of billet length and die-opening angle. The value of punch pressure  $p_{p,max}$  as a function of the reduction of area  $\epsilon_A$  considers these effects. Similar curves for other materials—also non-ferrous metals—at temperatures other than room temperature can be obtained by conducting a series of experiments. The validity of the correction factor at higher temperatures has not yet been completely investigated.

$2\alpha$  between 60 and 180°, and Bonderlube 235 as lubricant on a zinc phosphate coating are given as follows:

	<i>a</i>	<i>m</i>	<i>n</i>
Solid forward extrusion	47	0.75	0.8
Hollow forward extrusion	59.6	0.66	0.78 <sup>a</sup>

<sup>a</sup>Value not fully established.

The values of  $p_{P,\max}$  and  $F_{\max} = p_{P,\max}A_0$  are accurate to within  $\pm 10\%$ . Nomograms considering correction factors for other billet length-to-diameter ratios are available [15.23]. Eq. 15.2 is also found valid if  $S_u$  is used instead of hardness; however, the constants are different.



(a)

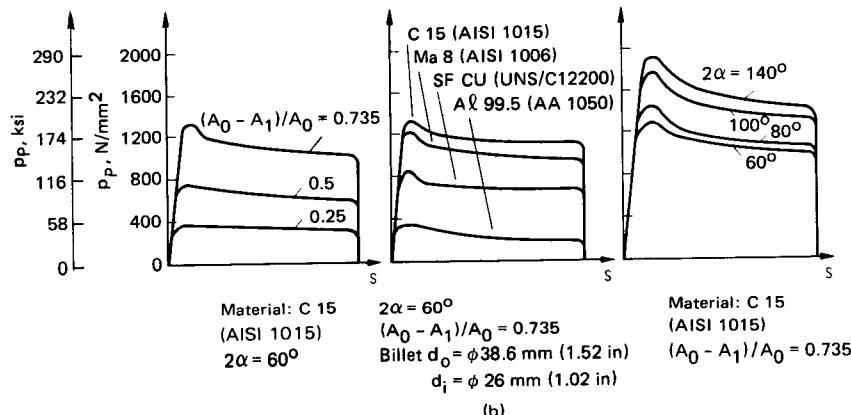
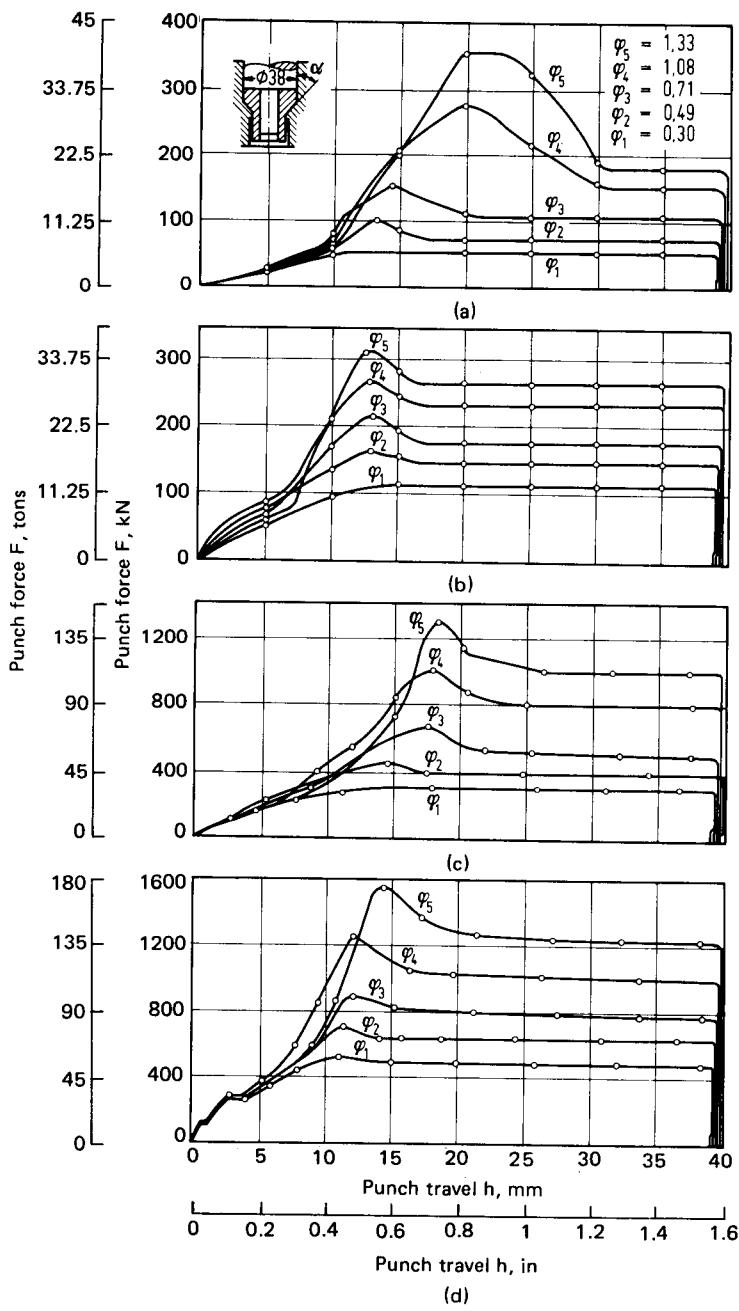


FIG. 15.9 Force-travel diagrams for forward extrusion. (a) Solid extrusion (rod extrusion). (b) Hollow extrusion (tube extrusion). (After [15.7], [15.8], [15.18].)



**FIG. 15.10** Force-travel diagrams for hollow forward extrusion. (a) Al 99.5 (AA 1050 O);  $2\alpha = 40^\circ$ . (b) Al 99.5 (AA 1050 O);  $2\alpha = 140^\circ$ . (c) C 15 (AISI 1015);  $2\alpha = 40^\circ$ . (d) C 15 (AISI 1015);  $2\alpha = 140^\circ$ . Lubricant—phosphating +  $\text{MoS}_2$  powder for C 15 (AISI 1015);  $\text{MoS}_2$  powder for Al 99.5 (AA 1050 O). (After [15.7].)

**Table 15.1** Ratio  $F_{\max}/F_m$  for Hollow Forward Extrusion<sup>a</sup>

Material designation		Die-opening angle $2\alpha$	$F_{\max}/F_m$		
DIN	U.S.		$\varphi = 0.4$	$\varphi = 0.8$	$\varphi = 1.2$
Al 99.5	AA 1050	40	1.20	1.53	1.77
		50	1.17	1.43	1.63
		60	1.16	1.36	1.50
		70	1.13	1.28	1.34
		80	1.10	1.18	1.22
		100	1.07	1.13	1.17
		140	1.04	1.10	1.15
SF Cu	UNS C12200	40	1.12	1.40	1.67
		50	1.10	1.30	1.46
		60	1.09	1.25	1.35
		70	1.08	1.23	1.33
		80	1.07	1.22	1.31
		100	1.06	1.21	1.29
		120	1.06	1.17	1.25
Ma 8	AISI 1006	140	1.05	1.13	1.21
		40	1.12	1.23	1.27
		60	1.11	1.22	1.26
		100	1.09	1.21	1.25
Ck 15	AISI 1015	140	1.07	1.18	1.21
		40	1.14	1.26	1.30
		50	1.12	1.23	1.27
		60	1.10	1.21	1.26
		80	1.09	1.20	1.25
		100	1.07	1.18	1.24
		120	1.06	1.15	1.22
		140	1.04	1.13	1.19

<sup>a</sup>Lubricants—steel: MoS<sub>2</sub> powder on ZnPO<sub>4</sub>; AA 1050-O: MoS<sub>2</sub> powder; C12200: mineral oil with additives.  
Source: Compiled from [15.7].

### Calculation Using Elementary Plasticity Theory

The force requirements for the quasistationary part of an extrusion process can be calculated as the sum of the ideal deformation force, the frictional force on shoulder and mandrel (hollow extrusion), the shearing force, and the frictional force on the die wall (the cylindrical portion of the die assembly) (Eqs. 13.31 to 13.33, 13.38, and 13.39). The factors affecting the force are workpiece dimensions, reduction of area (natural strain), die geometry (die-opening angle  $2\alpha$ ), and coefficient of friction (refer to Table 13.3). The total force  $F_{\text{tot}} = F^* + F_{\text{FR,W}}$ , calculated from Eq. 13.33, contains a force  $F^*$  which remains constant over the punch travel  $h$  and a force component  $F_{\text{FR,W}}$  which decreases with punch travel  $h$ .<sup>b</sup> (This is correct for solid forward extrusion only; for hollow extrusion it is only partly valid since the mandrel friction force decreases with increasing punch travel  $h$ .)  $F^*$  is normally smaller than  $F_e$ , which corresponds to point 4 in Fig. 15.8. If the billet length  $l_1$  in the container is small, then  $F^*$  will be almost equal to  $F_e$ .  $F^*$  is not identical with  $\bar{F}$ , although in many cases their values may be nearly the same. If  $F_{\text{FR,W}}$  is considered, the force at point 1 (Fig. 15.8) can be computed.  $F_{\text{tot}}$  approaches the force corresponding to point 2 ( $F_{\max}$ ) with increasing values of the  $l_0/d_0$  ratio of the billet.

<sup>b</sup>Refer also to Eqs. 13.31 and 13.32.

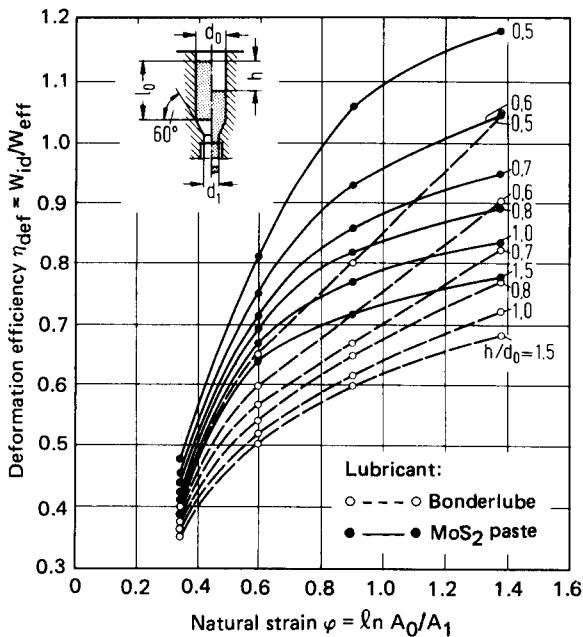


**FIG. 15.11** Deformation efficiency as a function of natural strain, punch travel, and lubricant. Material—C 15 (AISI 1015); annealed; peeled surface; plane billet surface. (After [15.19].)

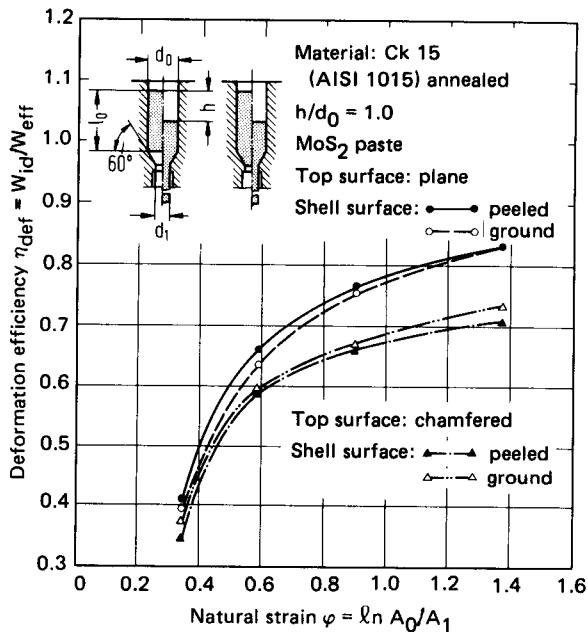


**FIG. 15.12** Deformation efficiency as a function of natural strain, billet shape, surface condition, and lubricant. (After [15.19].)

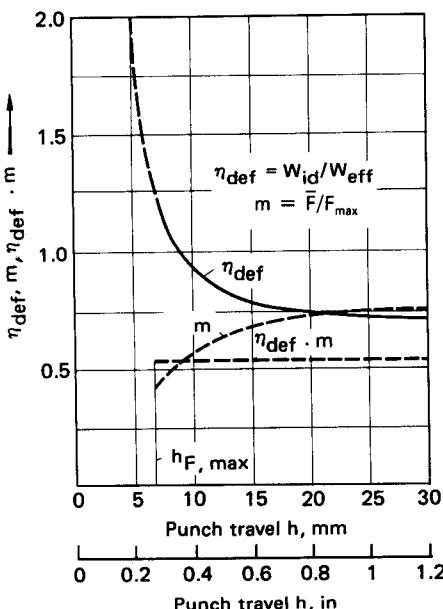


**FIG. 15.13** Deformation efficiency  $\eta_{\text{def}}$ , force correction factor  $m$ , and product  $\eta_{\text{def}}m$  as a function of punch travel for solid forward extrusion. Material—Ck 15 (AISI 1015); annealed; lubricant— $\text{MoS}_2$  paste;  $d_0 = 20 \text{ mm}$  (0.8 in);  $l_0 = 40 \text{ mm}$  (1.5 in);  $\varphi = 1.16$ ;  $2\alpha = 60^\circ$ . (After [15.21].)

The above analysis shows that by using elementary plasticity theory, the total force requirement can be calculated. The calculated value differs from  $F_{\text{max}}$ . It is therefore customary to use correction factors to obtain the maximum force requirement. The factors generally used are (1) the force correction factor  $m$  and (2) the ratio  $F_{\text{max}}/\bar{F}$ . We therefore have

$$F_{\text{max}} = \frac{\bar{F}}{m} = \frac{F^*}{m} \quad \bar{F} \approx F^* \quad (15.3)$$

If  $F_{\text{tot}} = F^* + F_{\text{FR},W}$  is substituted for  $F^*$  in Eq. 15.3, the  $F_{\text{max}}$  value so determined will be close to the actual value. In any case the values will be on the safe side. Experience has shown that the force values calculated using elementary plasticity theory are higher for higher natural strains.

#### Calculation Based on Methods of the Variational Principle

The upper-bound method (see Chap. 5) can be used to calculate the total force by the principle of minimum deformation energy,

$$F_{\text{tot}} = F_{\text{def}} + F_{\text{FR}} \quad (15.4)$$

where  $F_{\text{def}}$  is the deformation force and  $F_{\text{FR}}$  the friction force.

The force  $F_{\text{tot}}$  is (approximately) equal to  $\bar{F}$  (see insert in Fig. 15.16) and lies between  $F_1$  and  $F_4$  and close to  $F_3$  in Fig. 15.8 if  $l_0/d_0 < 1$ . The maximum force  $F_{\text{max}}$  has to be calculated using Eq. 15.3. Equations for hollow forward extrusion have been derived in [15.7] and [15.24]; other solutions are given in [15.25] to [15.27]. The computational time is higher for these methods, so that their applications are limited to systematic investigations only and not worthwhile for deter-

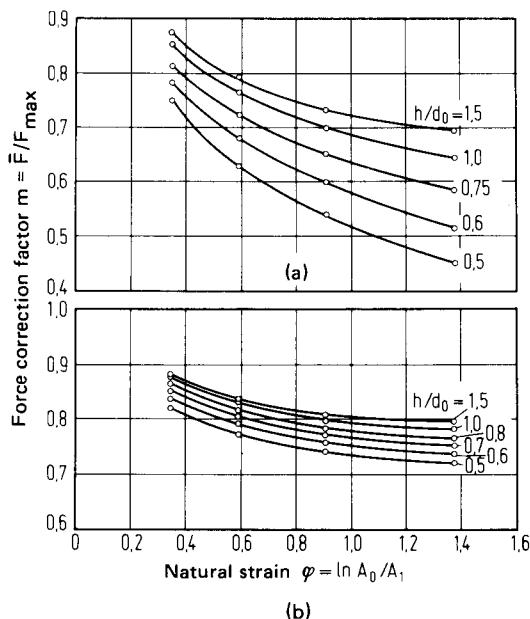


**FIG. 15.14** Force correction factor as a function of natural strain and relative deformation travel for solid forward extrusion. Material—Ck 15 (AISI 1015); annealed; lubricant—Bonderlube 235; surface ground. (a) Billet surface flat. (b) Billet chamfered. (After [15.21].)

mining the correction factor. On the other hand the variational methods have proved very useful in determining the optimum die-opening angle  $2\alpha$  (Fig. 15.16); this is discussed in Chap. 13.

#### Calculation Using Numerical Approximation Methods

The mathematical theory of plasticity mentioned in Chap. 15 and other methods can also be used for force computations. The computation of the average normal stress in the axial direction is

complicated and based on numerous assumptions and prerequisites. The force values computed are of the same order of magnitude as for the variational methods ( $\bar{F}$  or  $F_1$  in Fig. 15.8), so that a correction factor has to be used to compute  $F_{max}$ . Therefore the numerical methods are not very suitable for estimating force requirements in industrial practice. Their importance lies in their ability to compute strain, stress, and temperature distributions.

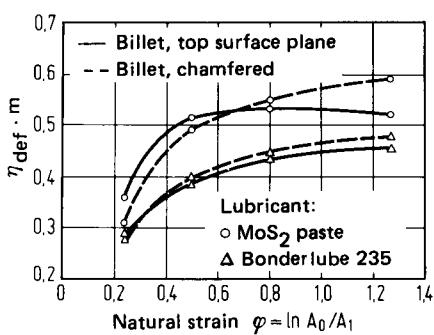


**FIG. 15.15** Product of deformation efficiency and force correction factor as a function of natural strain, lubricant, and shape. Material—Ck 15 (AISI 1015); annealed; surface peeled. (After [15.21].)

#### 15.2.4 Effect of Billet Dimensions on the Extrusion Force

In the preceding the effect of the billet length-to-diameter ratio on the extrusion force was mentioned briefly. Higher  $l_0/d_0$  ratios would increase the frictional component  $F_{FR,W}$  of the

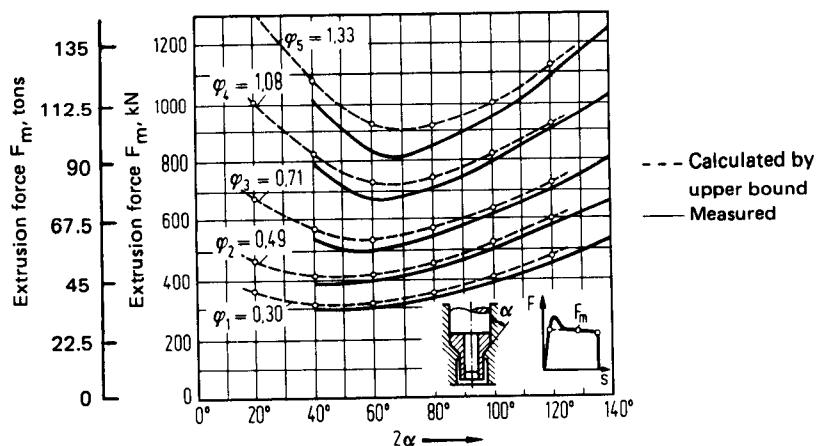


**FIG. 15.16** Extrusion force  $F_m$  as a function of die-opening angle  $2\alpha$  and natural strain. Material—Ck 15 (AISI 1015); lubricant— $\text{MoS}_2$  powder on zinc phosphate;  $\mu = 0.125$  assumed for computation. (After [15.7].)

total deformation force to such a level as to exceed the load limit on the tool. In such cases, namely, for  $l_0/d_0 > 6-8$ , the process of hydrostatic extrusion can be used. Here the value of  $F_{\text{FR},W}$  equals zero; however, the process is costly.

The friction force on the wall  $F_{\text{FR},W} = \pi d_0 l_0 \mu \sigma_{f,0}$  (Eq. 13.32) increases with increasing  $l_0/d_0$ . This has not been sufficiently established based on the work of Pugh [15.18]. The ratio of  $F_{\text{max}}$  (corresponding to a particular value of  $l_0/d_0 = x$ ) to  $F_{\text{max}}$  (corresponding to  $l_0/d_0 = 1$ ) shows an exponential increase according to the following equation (Fig. 15.17):

$$n = \frac{F_{\text{max}}(l_0/d_0=x)}{F_{\text{max}}(l_0/d_0=1)} = \exp \left[ 0.16 \left( \frac{l_0}{d_0} - 1 \right) \right] \quad (15.5)$$

The maximum error using the above equation is 7% for  $A_0/A_1 = 6.25$  ( $\varphi_{\text{max}} = 1.833$ ) [15.28].

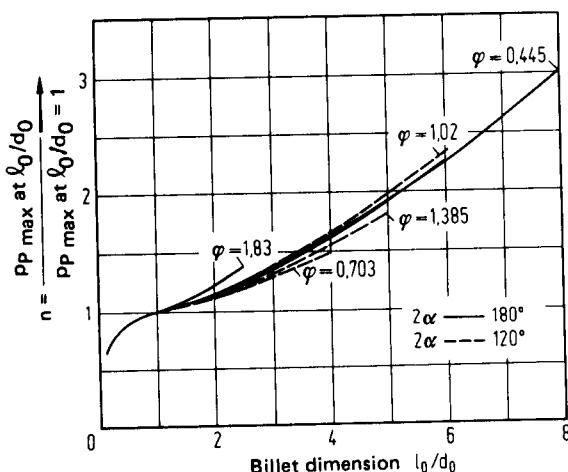


**FIG. 15.17** Effect of ratio  $l_0/d_0$  on maximum punch pressure in cold extrusion. Material—En 2A; lubricant—Bonderlube on zinc phosphate. (After [15.18].)

Assuming that the punch force transmitted to the deformation zone through the undeformed portion of the workpiece with length  $l$  (at the beginning  $l = l_0$ ) is always of the same magnitude, the application of the Tresca flow criterion gives

$$\sigma_r = \sigma_z - \sigma_f \quad (15.6)$$

and the frictional shear stress is

$$\tau_{FR} = \mu(\sigma_z - \sigma_f) \quad (15.7)$$

Substituting the appropriate value of  $\sigma_z$  for different values of maximum punch force, the component  $F_{FR,W}$  can be determined, and hence the value of  $\mu$ .

It can be seen from Eq. 15.7 that Eq. 13.32 is only approximate in determining  $F_{FR,W}$ . Even with Eq. 15.7, the computation of  $F_{FR,W}$  is questionable because of an absence of reliable information on the contact area and the coefficient of friction  $\mu$ .\*

A limiting case of solid forward extrusion—similar to that of hydrostatic extrusion with  $F_{FR,W} = 0$ —is the process of open-die extrusion (Fig. 13.4a). In this case the workpiece should not buckle before the die entry. The following equation holds:

$$p_{P,max,m} = \sigma_{f,m} \left[ \frac{2}{3} \alpha + \left( 1 + \frac{2\mu}{\sin 2\alpha} \right) \varphi_{max} \right] \leq S_y \quad (15.8)$$

[Recent investigations on open-die extrusion have led to the development of nomograms to calculate the punch pressure (Fig. 15.20) [15.31].

The maximum possible natural strain or the reduction of area depends on the die-opening angle  $2\alpha$  and the ratio  $\sigma_f/S_y$ . This means that the limiting strain is smaller for annealed workpieces and larger for preworked (work-hardened) material. In the case of fastener manufacture, the process of open-die extrusion is therefore used with wire pretension. Fig. 15.21 shows the maximum possible reductions of area for the coefficient of friction  $\mu = 0.05$  and  $0.15$  as a function of the die-opening angle. The maximum possible reductions of area for optimum die-opening angles are  $\epsilon_A = 30$  and  $25\%$  respectively for the assumed coefficients of friction [15.32]. Values limiting the buckling and upsetting of punches can be found in [15.31].

### 15.2.5 Optimum Die Shape

Generally a conically shaped die with rounded corners at the transition points is used in extrusion processes. The “optimum” die-opening angle  $2\alpha$  corresponds to minimum punch-force requirements (refer also to Fig. 15.16). It was pointed out in Sec. 15.2.3 that the difference between  $F_{max}$  and  $F_d$  (see Fig. 15.8) is greater for larger  $l_0/d_0$  billets, annealed (soft) materials, and larger natural strains. These variables lead to variations in radial stresses and hence in the elastic deformation of the dies and the workpiece during the forming process, which results in differences in diameter

\*In a recent publication Bay [15.29] presents a new result on the distribution of axial and radial stresses along the container wall using Avitzur's upper-bound solution [15.30]. The friction shear stress  $\tau_{FR}$  depends on normal (radial) pressure and the friction factor, while axial and radial stresses (pressures) depend on the friction shear stress, reduction in area, and the die-opening angle  $2\alpha$  for a given material over the relative billet contact length  $l_c/d_0$ . For  $l_c/d_0 \approx 4.2$  and a relative reduction in area  $\epsilon_A = 0.7$ , the following stresses are calculated:  $\sigma_z \approx 4\sigma_{f,0}$ ,  $\sigma_r \approx 3\sigma_{f,0}$  with a friction factor  $\tau_{FR}/k = 0.3$  (see Fig. 15.19). At the transition container-die the axial stress  $\sigma_z$  equals two times the initial flow stress  $\sigma_{f,0}$ . According to Tresca's law, the radial stress  $\sigma_r$  (or internal pressure  $p_i$ ) is obtained by  $|\sigma_r| = |\sigma_z| - |\sigma_{f,0}|$  and accordingly is equal to  $\sigma_{f,0}$  at the die entry. It can be seen that with the given parameters a punch pressure  $p_P \approx 4\sigma_{f,0}$  is required to initiate the plastic state in the deformation zone. Here, according to Fig. 13.11 and 13.12,  $|\sigma_r| = |\sigma_z| + |\sigma_{f,0}|$  is valid. Consequently  $\sigma_r$  must change discontinuously from  $\sigma_r = \sigma_{f,0}$  to  $\sigma_r = 3\sigma_{f,0}$  at the die entry. For other contact lengths and  $\epsilon_A = 0.7$  the required punch pressures may be taken directly from Fig. 15.18 in the form of  $\sigma_z$  as a function of  $l_c/d_0$ .

Siebel's assumption (Sec. 13.3.3), namely,  $\sigma_r = \sigma_z = p_P = \sigma_{f,0}$  (hydrostatic state), will lead with  $\sigma_r = \sigma_z = 2\sigma_{f,0}$  at the die entry to acceptable values for  $\sigma_r$  over  $l_c$  in the calculation of die loading, while with Eq. 15.6,  $|\sigma_r| = |\sigma_z| - |\sigma_{f,0}|$ , the average value over  $l_c$  obtained is too low. This equation may, however, be used if it is restricted to short billets. With smaller reductions in area, the value of  $\sigma_z$  at the die entry drops from  $2\sigma_{f,0}$  to  $\sigma_{f,0}$  (Fig. 15.20). In this case the die loading, the loss of punch pressure due to friction, and the die design are less critical.

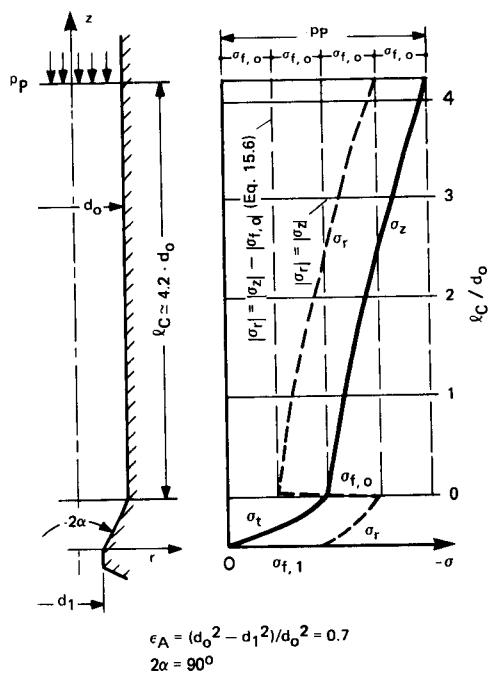


FIG. 15.18 Stress distribution in forward extrusion.  
(After [15.29].)

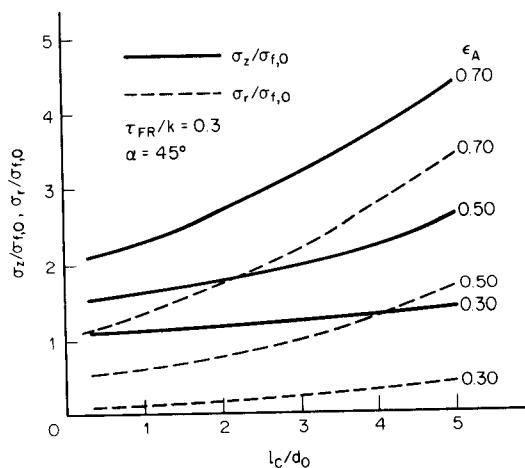
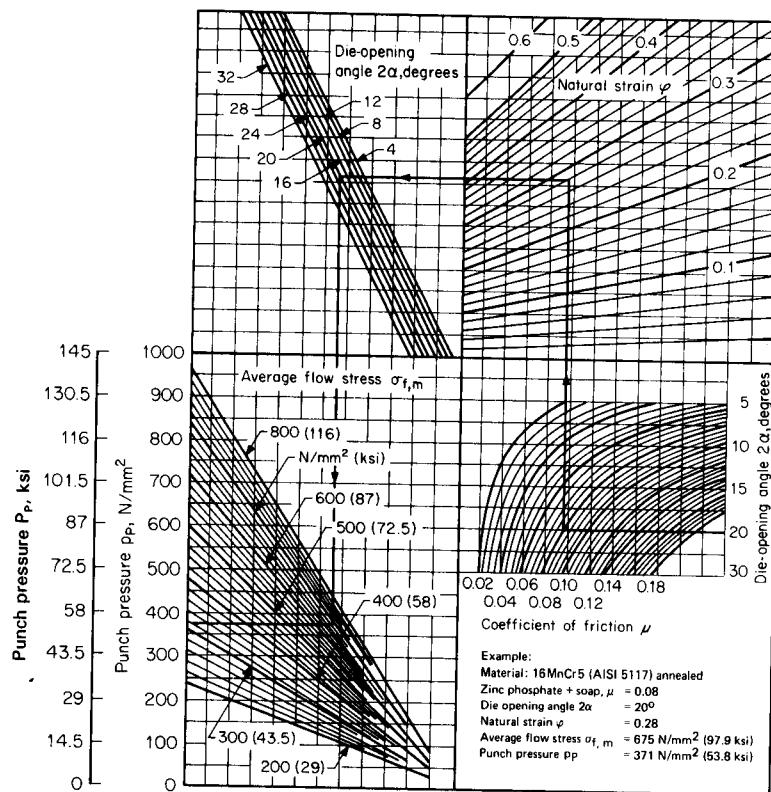


FIG. 15.19 Axial and radial stress distribution along the container wall in forward extrusion for phosphate-coated soap-lubricated aluminum specimens. (After [15.29].)



**FIG. 15.20** Nomogram to determine the average punch pressure in open-die extrusion based on upper-bound method. (Average flow stress  $\sigma_{f,m}$  to be determined for  $\varphi = \varphi_{\max}/2$ .) (After [15.31].)

on the extruded solid or hollow shaft. Investigations with other die forms for hollow forward extrusion have shown no significant changes in the punch-force requirements  $F_{\max}$  (Fig. 15.22). The force–travel diagram for concave die shapes does not deviate from the force–travel diagrams shown in Fig. 15.9. However, for the convex exponential form\* the difference between  $F_{\max}$  and  $\bar{F}$  was very small (Fig. 15.23); the force–travel diagram approaches an ideal trapezoidal curve. This may be useful for workpieces requiring very high accuracy along the length of the shaft. However, it requires higher forces than dies with optimum die angles.

#### 15.2.6 Friction, Lubrication, and Surface Treatment

The lubrication and surface treatment are very important in mass production using extrusion processes because of the enormous normal pressures. The requirements of a good lubricant are a

\*For this die form, the value  $\Delta r/(r - r_1)$  for a disk of thickness  $\Delta z$  is constant for every travel step. The equation of the curve defining the die shape is given by  $r - r_1 = Ae^{Cx}$ , where  $C$  is a given value and  $A$  is an integration constant which is obtained from the boundary conditions. The boundary conditions are obtained by considering a conical shape with an optimum die-opening angle of  $2\alpha = 70^\circ$ . Therefore the coordinates of the die at the entrance and exit are the same for both the conical shape and the exponential curve shape.

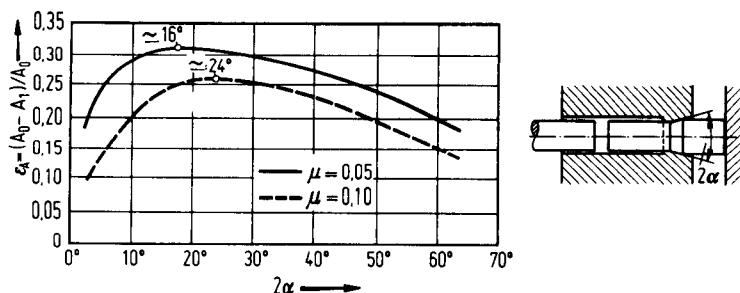


FIG. 15.21 Possible reduction of area in open-die extrusion. Material—C 15 (AISI 1015); annealed;  $S_y \approx 210 \text{ N/mm}^2$  (30.5 ksi). (After [15.32].)

small coefficient of friction (in some cases the frictional work can amount to as much as 50% of the total deformation work), enough resistance to high normal pressures, good surface sticking properties, adherence to the material surface for large surface-area increases, and prevention of cold welding. Lubricants which are very highly resistant to normal pressures can lead to a worsening of the surface quality due to the formation of lubrication pockets.

The above conditions are fulfilled for nonferrous metals by mineral oils, fats, and metallic stearates (soaps) and for steel by sodium-based soap, molybdenum disulfide, and graphite in conjunction with a phosphate coating. Stainless steels are oxalated instead of phosphated or plated with a metallic layer that has little cold-welding susceptibility with steel (copper, lead, tin, or zinc). Chap. 6 gives a detailed treatment of lubricants, while Chap. 26 deals with practical methods of surface treatment for cold extrusion. The effectiveness of the lubricant is also influenced by a uniform application of the correct lubricant quantity [15.33]. Table 13.3 gives the coefficients of friction for various lubricants.

Based on available experience and test results, a phosphate thickness of 1–30  $\mu\text{m}$  (40–1200  $\mu\text{in}$ ) [in production the values are  $\approx 5$ –10  $\mu\text{m}$  (200–400  $\mu\text{in}$ )] has no significant effect on the punch pressure. However, different lubricants can cause changes of about 20% in  $F_{\max}$  or  $p_{p,\max}$  [15.34]. The results were not reproducible since other factors, such as surface quality (rolled, peeled, machined, drawn), temperature, humidity, storing time after phosphating, and lubrication among others, also affect the punch force.

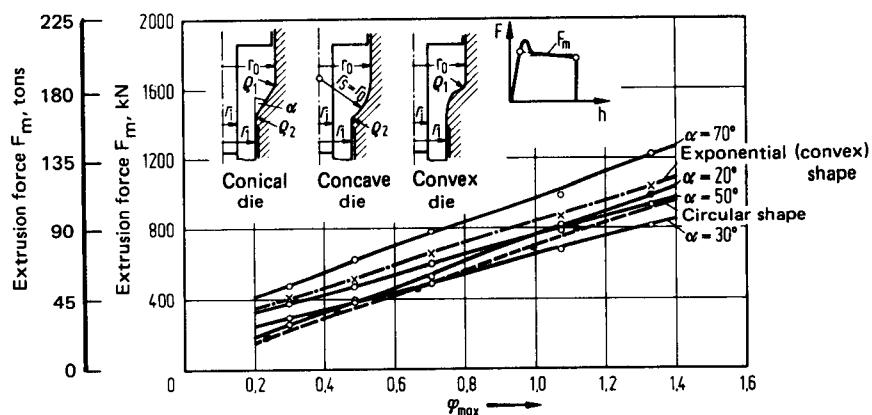


FIG. 15.22 Effect of die shape on the extrusion force  $F_m$  in hollow forward extrusion. Material—Ck 15 (AISI 1015); lubricant— $\text{MoS}_2$  powder on zinc phosphate. (After [15.7].)

### 15.2.7 Force Fluctuations in Mass Production

In mass production there will be variations in both force and energy requirements. They are due to:

- 1 Variations in the mechanical properties of the workpiece as a result of changes in chemical composition, microstructure (grain size), and unavoidable variations in heat treatment
- 2 Changes in friction conditions as a result of variations in surface condition, lubricant carrier, and lubricant
- 3 Variations in workpiece volume from the nominal value as a result of diameter changes of the bar and length variations in shearing

Measurements were made at room temperature on 15,000 steel workpieces (four different parts) with special equipment for continuous monitoring of  $F_{\max}$  and  $W_{\text{eff}}$ . The variations were measured for natural strains  $\varphi_{\max}$  between 0.6 and 1.4. The variations in force and energy requirements were between  $\pm 6$  and  $\pm 7\%$ ; at the beginning in cold tools they were  $\pm 2.5\%$ .

Higher variations were found for larger workpieces, with  $d_0 = 75 \text{ mm}$  (3 in) and with larger frictional surfaces (hollow extrusion), and lower variations were found for smaller workpieces, with  $d_0 = 20-26 \text{ mm}$  (0.787-1.023 in) and smaller frictional surfaces (solid extrusion). After a considerable number of pieces have been extruded, a constant working temperature of the tool is reached because of heat dissipation from the deformation energy due to forming. The increase in temperature on the working surface helps the lubricant and the lubricant carrier in reducing the friction and achieving a uniform working surface, which in turn results in smaller variations in the normal distribution of the process parameters. For larger workpieces there was a reduction of the extrusion force  $F_{\max}$  by about 4% and a reduction of the variations to between  $\pm 3.5$  and  $\pm 4\%$ .

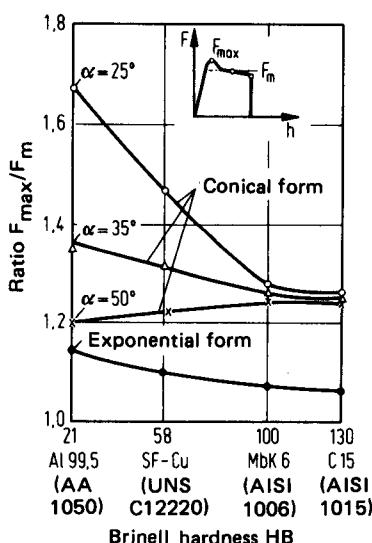
During experimental runs at different times the changes in  $F_{\max}$  were between 6 and 18%, all other conditions remaining the same [15.34], [15.35].

**FIG. 15.23** Ratio of  $F_{\max}/F_m$  for hollow forward extrusion with different die shapes as a function of material hardness. Natural strain  $\varphi_{\max} = 1.33$ . (After [15.22].)

It appears therefore that the conditions of friction have a considerable effect on the extrusion force. The systematic errors in extrusion force and energy requirements can be attributed to a very great extent to variations in the mechanical properties in a lot. Volume changes do not affect the force as long as the material can be formed without any restriction; however, they do affect the energy requirement. It can therefore be said that in the production of extruded workpieces with quasistationary material flow a slight heating of the workpiece to about  $\Delta T = 80-120^\circ\text{C}$  ( $145-215^\circ\text{F}$ ) above room temperature, or a corresponding preheating of the tools, helps the tool in attaining and maintaining the working temperature more quickly. In tool design and the selection of the machine it is safer to consider a variation of  $F_{\max}$  of up to about 20% (which is on the high side of the calculated value).

### 15.2.8 Extrusion at Warm-Working Temperatures

There is an increasing demand to cold-extrude unalloyed steels with larger carbon contents and alloyed carburizing and hardening steels to obtain higher dimensional accuracy and better surface



quality than by hot die forging. The formability of high-strength steel depends on (1) the maximum possible load on the tool, (2) the achievable deformation ratio in every stage (this is affected by the previous point), (3) the number of stages required to form the workpiece, (4) the fact that higher forces required for larger workpieces need higher-capacity presses, (5) a sufficient formability of certain materials, and (6) the changes in microstructure of metals during forming (e.g., austenitic stainless steels). Extrusion at higher temperatures up to  $700^{\circ}\text{C}$  ( $1300^{\circ}\text{F}$ ) [15.36] can solve some of the above-mentioned problems. Sometimes even higher temperatures, up to  $900^{\circ}\text{C}$  ( $1650^{\circ}\text{F}$ ), are used [15.37].

Warm extrusion between  $800$  and  $1250^{\circ}\text{C}$  ( $1475$  and  $2275^{\circ}\text{F}$ ) can be considered a special case of hot forging [15.38] (see also Chap. 11).

The flow stress<sup>\*</sup> of carbon steels and low-alloyed steels, such as 100 Cr 6 (AISI L3) and 20 Mn Cr 5 (AISI 5120),† decreases with rising temperature, first gradually and then steeply, and exhibits blue brittleness in between. The temperature range during which blue brittleness occurs depends more on the strain rate  $\dot{\phi}$  and less on the natural strain  $\varphi$ . The higher the value of  $\varphi$ , the more the blue-brittleness range shifts toward higher temperatures [15.39]. After a steep decrease, the flow stress beyond  $\approx 720^{\circ}\text{C}$  ( $1340^{\circ}\text{F}$ ) does not change appreciably for carbon steels with different carbon contents. Extrusion of steels with higher carbon contents seems to be advantageous at higher temperatures. High-alloyed steels, such as X 10 Cr 13 (AISI 410)† (ferritic stainless steel) and austenitic stainless steels, do not exhibit blue-brittleness maxima.

The forming limit, or the limiting natural strain  $\varphi_{\max}$ , has a minimum at  $\approx 525^{\circ}\text{C}$  ( $980^{\circ}\text{F}$ ) for carbon and low-alloyed steels exhibiting blue brittleness. The forming limit increases beyond  $\approx 525^{\circ}\text{C}$  ( $980^{\circ}\text{F}$ ) (red hotness range). The decrease in flow stress beyond  $T > 475^{\circ}\text{C}$  ( $890^{\circ}\text{F}$ ) is of no use in extrusion since the strength of the tool material also decreases at this temperature. Fig. 15.24 shows the variation of the ultimate tensile strength and flow stress of several tool and workpiece materials at different temperatures. In general the tool temperature is lower than the deformation temperature, which equals approximately the initial billet temperature. Based on Fig. 15.24, high-speed steel S 18-0-1† can be used as tool material for extruding 100 Cr 6 (AISI L3) steel at  $T \approx 325^{\circ}\text{C}$  ( $620^{\circ}\text{F}$ ) and austenitic stainless steel at  $T \approx 525^{\circ}\text{C}$  ( $980^{\circ}\text{F}$ ). Hot-working steel X 38 CrMoV 51 (AISI H11) cannot be used for both steels mentioned. However, it can be used for C 15 (AISI 1015) up to  $T \approx 475^{\circ}\text{C}$  ( $890^{\circ}\text{F}$ ) (It is not necessary to extrude AISI 1015 at higher temperatures since it has good extrudability at room temperature.)

The economy of extrusion at higher temperatures depends to a very great extent on the availability of a good lubricant. Coefficients of friction typical for various lubricants are given in Table 6.1 for a variety of workpiece materials. Another criterion to determine the suitability of a lubricant, namely, to accommodate large increases in surface, is dealt with later in this chapter. It has a special importance for backward can extrusion.

From experiments lubricants of colloidal graphite base have been found suitable for carbon steels because of their smaller friction values and their ability to withstand large increases in surface area. The deformation of austenitic stainless steel has more stringent requirements. For these and other alloyed steels extrusion at temperatures between  $525$  and  $625^{\circ}\text{C}$  ( $980$  and  $1150^{\circ}\text{F}$ ) offers many advantages.

Computation of the extrusion force at higher temperatures has not yet been completely resolved. Eq. 15.2 cannot be used to calculate the force since the hardness or the tensile strength at room temperature has no relationship with the flow stress at deformation temperatures. The other methods suggested in Sec. 15.2 can in principle be used. A thorough knowledge of  $\sigma_f = f(T, \varphi, \dot{\varphi})$  and of  $\eta_{\text{def}}$  and  $m$  as a function of  $T, \varphi, \dot{\varphi}$ , and frictional condition is necessary to compute the extrusion force. The main problem here is an exact substitution of the deformation temperature, which is very difficult to establish. It is also not known how the ratio  $l_0/d_0$  of the billet and the die-opening angle  $2\alpha$  affect the force. However, recent exhaustive investigations on the warm extrusion of steel between  $500$  and  $800^{\circ}\text{C}$  ( $930$  and  $1475^{\circ}\text{F}$ ) have thrown more light on the

\*The flow stress  $\sigma_f$  is greatly influenced by  $\dot{\varphi}$  at higher temperatures.  $\dot{\varphi}$  does not remain constant during the extrusion process. To determine  $\sigma_f$  for solid forward extrusion, an average strain rate  $\dot{\varphi} = v_p(r_0 + r_1)/r_1^2$  can be used, which is obtained from the punch velocity  $v_p$  and the die dimensions  $r_0$  (container radius) and  $r_1$  (die exit radius).

†For chemical composition see App. C.

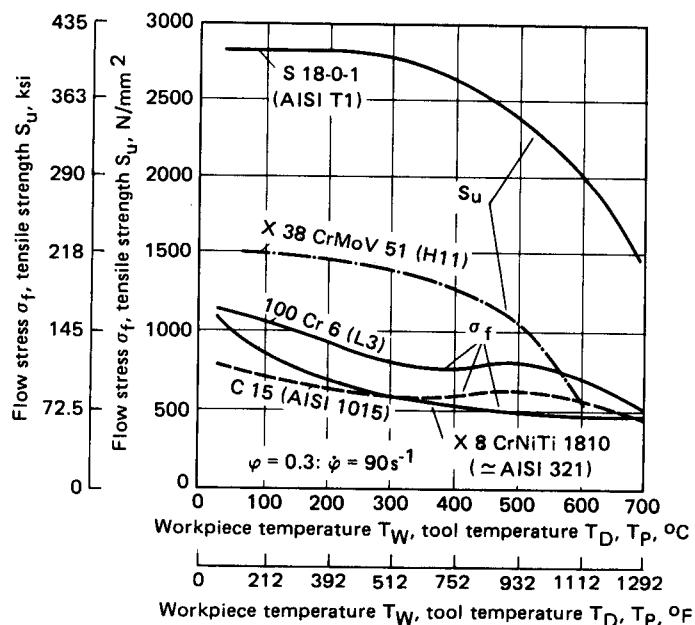


**FIG. 15.24** Tensile strength of high-speed and hot-working steels compared with flow stress for different steels. For high-speed steels, see App. A. (After [15.36].)

calculation of the force requirements, and a comparison of these values with experimentally measured values has been published [15.5]. Nomograms based on this investigation for computing the maximum punch pressure  $p_{p,\max}$  for forward and backward extrusion of various steels in the above range of warm-extrusion temperatures are shown in Figs. 15.25 and 15.26. Within the given range of parameters and materials, the accuracy of the computed values is better than  $\pm 10\%$  (see also [15.40]).

### 15.3 WORKPIECE MATERIALS

The following steps are usually considered before deciding on the suitability of materials for extrusion.

- 1 Summarize the necessary production steps (see Fig. 15.101).
- 2 Determine the materials with which the required mechanical properties can be obtained, taking the production sequence into consideration.
- 3 Decide on the production processes possible with the selected materials.

The final decision will in general be based on the economy of manufacture.

#### 15.3.1 Steels

Unalloyed and alloyed steels are best suited for cold forming. The main alloying elements are carbon (<0.5%), manganese (<2%), and chromium (<2%), as well as nickel, molybdenum and

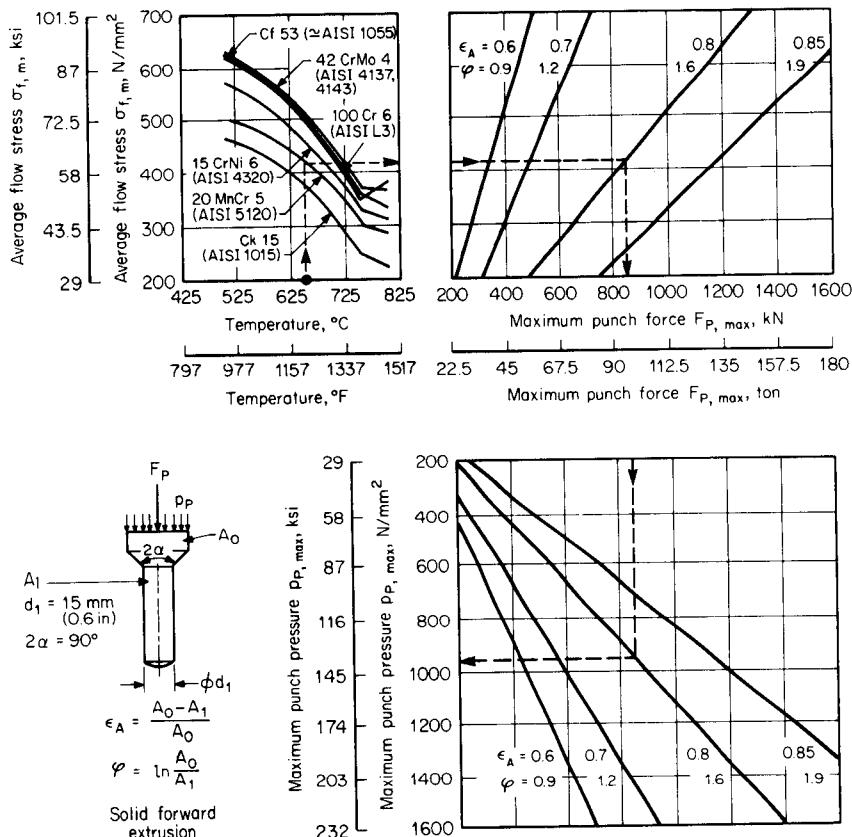


FIG. 15.25 Nomogram to determine the maximum punch force and pressure in warm solid forward extrusion. (After [15.5].)

vanadium. The alloying elements phosphorus, sulfur, and nitrogen make the steels brittle and reduce the forming limit; they have to be maintained at their lowest possible levels. The corresponding steel-refining processes have to be used (vacuum degassing, electro slag refining, and other methods depending upon requirements). For workpieces without special strength requirements [e.g.,  $S_u < 600 \text{ N/mm}^2$  (87 ksi)] the steels Ma 8 (AISI 1006) and Muk 7 (AISI 1008) can be used; they can be deformed easily at room temperature. The carbon steels C 10 (AISI 1010) and C 15 (AISI 1015) also belong to this category. If a complicated machining process is required, higher-sulfur-content low-carbon steels can be used.

For higher requirements, especially in automobiles, hardening steels (both case-hardening and through-hardening) which have good forming characteristics at room temperature are used. These steels are subjected to some sort of heat treatment to obtain the desired mechanical properties. If workpieces with hard surface and soft core are required (e.g., gears or shafts), case-hardening steels are used. Cold forming of corrosion-resistant steels pose difficulties. The ferritic chromium steels with 18–28% chromium and <0.12% carbon are only moderately corrosion-resistant. They have a body-centered cubic crystal structure and their work-hardening characteristics are similar to that of carbon steels; their cold-forming behavior is moderate. The martensitic chromium steels also have moderate corrosion resistance; however they can not be cold-formed easily. In addition to 18–28% chromium and 0.15–1.2% carbon, they have additions of cobalt, molybdenum, nickel,

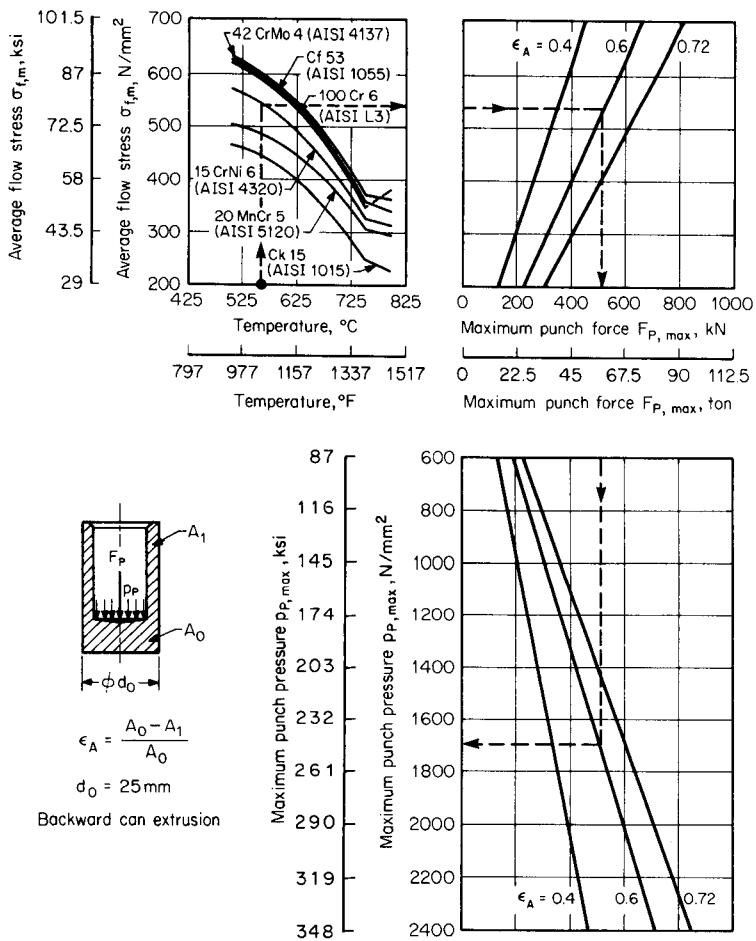


FIG. 15.26 Nomogram to determine the maximum punch force and pressure in warm backward can extrusion (After [15.5].)

and vanadium. The austenitic stainless steels with >16% chromium and  $\geq 8\%$  nickel have excellent corrosion and rust resistance. These face-centered cubic materials undergo a phase transformation during cold forming, resulting in very high strain hardening. Annealing operations are necessary after reductions of area of 35–40%. At temperatures of 200–300°C (385–570°F) the flow stresses of these steels decrease sharply. Heating the workpiece to those temperatures before forming allows higher reductions in area and increases the tool life. Table 15.2 shows the important steels for cold forming.

### 15.3.2 Nonferrous Metals

Aluminum and copper and their alloys are the major nonferrous metals used in cold forming. Other materials used to a lesser extent in cold forming are lead, zinc, and tin. Successful forming of titanium and zirconium has also been reported.

The nonferrous metals and alloys mentioned have good formability and machinability; mechanical working has therefore a number of advantages.

**Aluminum and its alloys:** These materials can be formed economically at room temperature because of their excellent cold-forming characteristics. The achievable reduction in area per stage and the tool life are very high; the force requirement is small. The selection of a suitable aluminum material is dependent on the requirements on the final product. Pure aluminum Al 99.5 (AA 1050) can be deformed easily. For higher requirements on the mechanical properties, alloys such as Al Mg 5 (AA 5056), which exhibits good cold-forming properties in the annealed condition only, and other precipitating hardenable aluminum alloys of Al Mg 5 or Al Cu Mg<sup>\*</sup> are used.

**Copper and its alloys:** Commercially pure copper has cold-forming properties similar to aluminum. The different processing conditions of copper (melting and pouring form) are used for cold forming of contact pieces, clamps, fasteners, and rivets. Among bronzes, tin bronze (up to 1–2 % tin) and silicon bronze are used to make clamping elements. Nickel ( $\leq 2\%$ )-silicon ( $\leq 0.7\%$ )-copper alloys can be precipitation-harden; they can also be formed in the hardened condition. The most important copper alloys are the brasses. For cold forming,  $\alpha$ -brasses (60–70% copper) are suitable. A higher zinc content ( $\beta$ -brass) makes the brass brittle, and therefore cold forming poses difficulties.

**Lead, zinc, and tin:** These can be cold-formed easily because of their low strength and high ductility. Applications are for thin-walled shells and cans.

**Titanium and its alloys:** Pure titanium can be cold-formed with reductions of up to 60% without intermediate annealing. Aluminum is an important alloying element in titanium alloys. Alloys having  $\beta$ -phase at room temperature are best suited for cold forming; the titanium alloys are, however, heated up before forming.

**Zirconium and its alloys:** Zirconium and some of its alloys are used as covering materials for atomic fuel and materials in the chemical industry since they are heat- and corrosion-resistant. These are difficult to form cold due to their high strength and low ductility.

Table 15.3 gives an overview of the important nonferrous metals for cold forming.

### 15.3.3 Properties before Extrusion

The initial state of material desirable for cold extrusion is a low flow stress and small work-hardening coefficient. This generally requires a heat-treatment operation. The principles of heat treatment are covered in Chap. 3. The practical methods of carrying out the heat-treatment operations and the equipment required for them are discussed in Chap. 26.

Steels are annealed to obtain spheroidal cementite. Fig. 15.27 on p. 15.34 shows the mechanical properties of carbon steels and low-alloy steels in the annealed condition and after deformation with  $\varphi_{\max} = 0.6$ –1.0. The carbon equivalent  $C_1$  is defined as

$$C_1 = \%C + \frac{\%Mn - 0.6}{4} + \frac{\%Cr + \%Ni}{20} [\%] \quad (15.9)$$

Details can be obtained from [15.41]. Only a general comment will be made here on the problems involved in the heat treatment of nonferrous metals and their alloys. It is necessary to obtain a fine-grain structure and uniform microstructure across any cross section. This is especially necessary for larger sections. In the case of titanium and zirconium a very close control of the temperature for heat treatment is important [600–700°C (1110–1300°F) for commercially pure titanium, 600–825°C (1110–1520°F) for titanium alloys,  $\leq 700^\circ\text{C}$  (1300°F) for zirconium alloys]. H<sub>2</sub> and O<sub>2</sub> should not be present in the alloys and metals; H<sub>2</sub> affects the mechanical properties considerably. These metals are therefore heat-treated in a protective gas atmosphere (argon) or in a vacuum. In [15.41] more details are given on the nonferrous metals—requirements, heat treatment, and properties.

\*See App. B.

**Table 15.2** Steels for Cold Bulk Forming<sup>a</sup>

Designation	AISI	Mechanical properties (minimum)						Application	
		Annealed			Cold-worked				
		S <sub>y</sub> , N/mm <sup>2</sup> (ksi)	S <sub>ut</sub> , N/mm <sup>2</sup> (ksi)	e <sub>5</sub> , %	S <sub>y</sub> , N/mm <sup>2</sup> (ksi)	S <sub>ut</sub> , N/mm <sup>2</sup> (ksi)	e <sub>5</sub> , %		
Carbon steels <sup>b</sup>									
QSt 32-3	1006	210 (30.4)	310 (44.9)	30	400 (58)	500 (72.5)	10	Bolts, screws	
UQSt 36-2	1008	230 (33.3)	340 (49.3)	30	400 (58)	500 (72.5)	10	Bolts, screws	
C10	1010	250 (36.2)	360-400 (52.2-58)	25	400 (58)	500-700 (72.5-101.5)	10	Small machine components <sup>c</sup>	
C15	1015	280 (40.6)	400-450 (58-65.2)	20	500 (72.5)	600-700 (87-101.5)	8	Levers, bosses, etc. <sup>c</sup>	
C22	1020	300 (43.5)	420-500 (60.9-72.5)	18	550 (79.7)	650-750 (94.2-108.9)	7	Shafts, bars <sup>d</sup>	
C35	1035	320 (46.4)	420-500 (60.9-72.5)	18	600 (87)	700-800 (101.5-116)	6	Bolts, nuts <sup>d</sup>	
C45	1043	340 (49.3)	500-600 (72.5-87)	16	650 (94.2)	750-800 (108.9-116)	6	Pressure rods <sup>d</sup>	
Alloyed steels									
16MnCr5	5117	300 (43.5)	400-500 (58-72.5)	18	500 (72.5)	600-700 (87-101.5)	8	Bolts, rolls <sup>c</sup>	
20MnCr5	5120 H	350 (50.7)	430-520 (62.3-75.4)	18	550 (79.7)	660-780 (95.7-113)	8	Medium/small gears <sup>c</sup>	
41Cr4	5135 H /5140	400 (58)	600-750 (87-108.9)	18	650 (94.2)	750-850 (108.9-123.2)	8	Gears, screws	

<b>40Mn4</b>	1039	350 (50.7)	600–750 (87–108.9)	16	550 (79.7)	700–800 (101.5–116)	8	Gears <sup>d</sup>
<b>34Cr4</b>	5130 H/ 5132	400 (58)	600–750 (87–108.9)	18	650 (94.2)	750–800 (108.9–116)	8	Piston rod, bolts, gears, lever <sup>d</sup>
<b>25CrMo4</b>	4130/ 4130H	450 (65.2)	600–750 (87–108.9)	14	600 (87)	700–800 (101.5–116)	10	Valves <sup>d</sup>
<b>49CrMo4</b>	4145	500 (72.5)	650–750 (94.2–108.9)	14	700 (101.5)	800–900 (116–130.5)	10	Piston rods <sup>d</sup>
<b>42CrMo4/ 34CrMo4</b>	4140 H/ 4137 H	500 (72.5)	650–750 (94.2–108.9)	14	750 (108.9)	900–1000 (130.5–145)	8	Connection lever <sup>d</sup>
<b>50CrMo4</b>	4147 H/ 4150 H	500 (72.5)	650–750 (94.2–108.9)	14	750 (108.9)	900–1000 (130.5–145)	8	Connection lever <sup>d</sup>
<b>50CrV4</b>	6150 H	450 (65.2)	700–800 (101.5–116)	14	650 (94.2)	800–900 (116–130.5)	8	Springs <sup>d</sup>
<b>100Cr6</b>	~L3	450 (65.2)	600–750 (87–108.9)	12	650 (94.2)	800–900 (116–130.5)	6	Wear parts <sup>d</sup>

#### High-alloyed steels

<b>X10Cr13</b>	410	450 (65.2)	600 (87)	18	600 (87)	750 (108.9)	10	Pieces used in wa- ter (screws, etc.)
<b>X20Cr13</b>	420	450 (65.2)	650 (94.2)	16	NA	NA	NA	Highly stressed parts in water
<b>X22CrNi17</b>	431	600 (87)	800 (116)	14	1000 (145)	NA	NA	Pump parts, valves,
<b>X35CrMo17</b>	440A	600 (87)	800 (116)	14	NA	NA	NA	Valves and shafts in organic fluids
<b>X5CrNi189</b>	304L	220 (31.9)	550–700 (79.7–101.5)	50	600 (87)	800–900 (116–130.5)	6	Corrosion-resistant parts, screws

<sup>a</sup>Equivalent American steels are given. The original table is based on DIN 17111, 17200, 17210, 1654, and VDI guidelines 3200, 3221.

<sup>b</sup>Some small alloying elements added to the above steels are used for gudgeon pins, spindles, drive components among others.

<sup>c</sup>Case-hardened.

<sup>d</sup>Tempered.

NA—flow curves not available.

**Table 15.3** Some Nonferrous Materials for Cold Bulk Forming

DIN	Designation	Mechanical properties				Application
		S <sub>y,0.2</sub> , N/mm <sup>2</sup> (ksi)	S <sub>b</sub> , N/mm <sup>2</sup> (ksi)	ε <sub>s</sub> , %	HB	
Aluminum and its alloys						
Al99.5, 5F10	AA 1050-H14	20 (2.9)	70 (10.2)	20	20	Pure aluminum for electrical parts
Al Mg5W	AA 5083-O	110 (15.9)	240 (34.8)	14	55	Vehicle parts
Al MgSi0.5	AA 6060	NA	150 (21.7)	14	35	Vehicle parts
—	AISI T4	270 (39.1)	400 (58)	8	100	Vehicle parts
Copper and its alloys						
E-CuF20	UNS C11000	100 (14.5)	200 (29)	30	50	Hot extruded parts
SnB22F26	—	NA	260 (37.7)	45	55	Screws, tubes
CuNi2SiF30	UNS C64700	NA	300 (43.5)	1	1	Screws, bolts, armature
CuZn37F30	UNS C27400/C27200	NA	300 (43.5)	45	70	Cold extruded parts
CuZn33F29	UNS C26800/C27000	NA	290 (42)	45	70	Higher cold formability
CuZn28F28	UNS C26000	NA	280 (40.6)	44	70	Excellent cold-forming property

Magnesium and its alloys						
Mg Mn 2 F 20	M1A-F	150 (21.7)	200 (29)	1.5	40	Low stress parts
Mg Al 3 Zn F 25	AZ31B-F	160 (23.2)	250 (36.2)	3	45	
Mg Al 6 Zn F 26	AZ61A-F	180 (26.1)	260 (37.7)	6	55	
Mg Al 8 Zn F 28	AZ80F	200 (29)	280 (40.6)	6	60	
Mg Zn 6 Zr F 29	ZK60A-F	180 (26.1)	260 (42)	7	60	High stress parts
Zinc and its alloys						
Zn 99.9	AISI B6	NA	120 (17.6)	NA	NA	Pure zinc parts
Zn 98.5	AISI B6	NA	NA	NA	NA	Commercial zinc
Zn Al 4 Cu 1	AC41A (UNS Z35530)	NA	300-350 (43.5-50.7)	5	80	Press parts, profile armatures
Zn Cu 4 Pb	AG40A (UNS Z33520)	NA	NA	5	70	Press parts, profile armatures
Titanium and its alloys						
Ti 99.2	Ti-6Al-4V	180 (26.1) 840 (121.8)	300-400 (43.5-58) 910 (131.9)	25	120	
Ti Al 6 Y 4 F 91	Ti-6Al-4V			10	NA	
Nickel and its alloys						
Ni 99.8	A-nickel	NA	NA	NA	NA	Chemical unit parts
NiMn1	D-nickel	NA	NA	NA	NA	
NiCu30Fe	67 Ni-30 Cu	NA	NA	NA	NA	
NiFe15Mo	—	NA	NA	NA	NA	

NA—Not available.

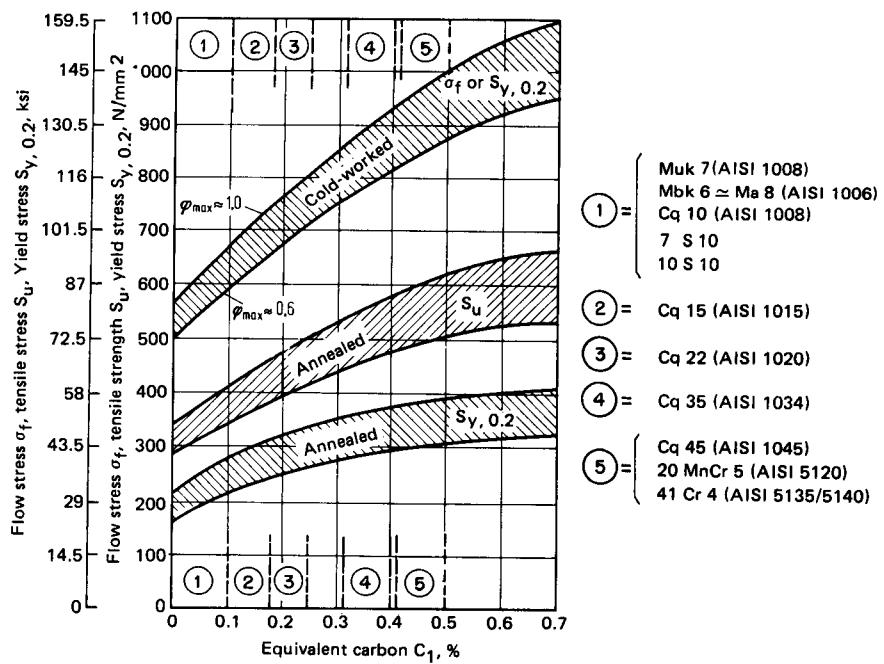


FIG. 15.27 Flow stress, ultimate tensile strength, and yield stress for annealed and cold-worked steels.  $\varphi_{\max} \approx 0.6-1.0$ ;  $\epsilon_A = 0.45-0.63$ ;  $\varphi \approx 1.0-10 \text{ s}^{-1}$ . (After [15.41].)

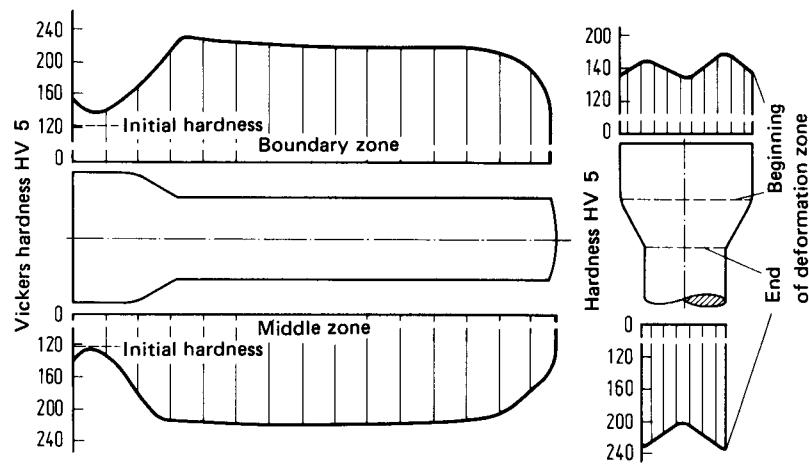
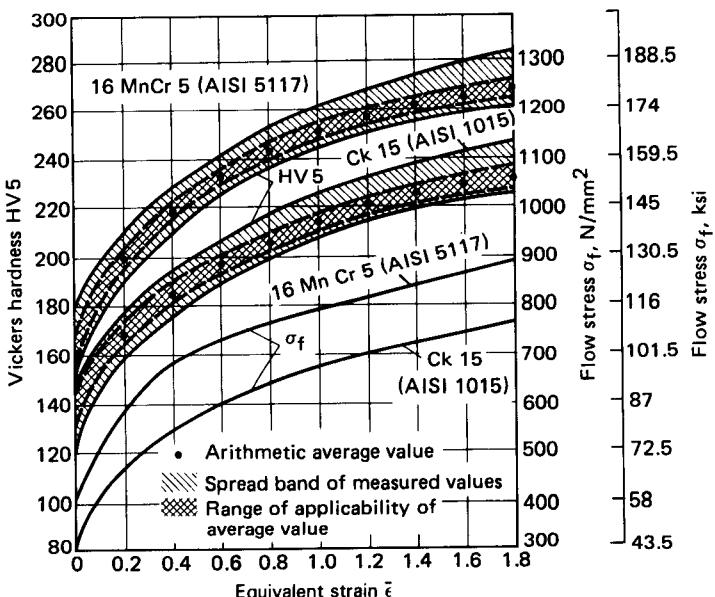


FIG. 15.28 Hardness distribution after solid forward extrusion. Material—Cq 15 (AISI 1015); annealed;  $\varphi_{\max} = 0.915$ ; billet end chamfered;  $d_0 = 20 \text{ mm (0.8 in)}$ ;  $l_0 = 40 \text{ mm (1.6 in)}$ . (After [15.8].)



**FIG. 15.29** Relationship between equivalent strain  $\bar{\epsilon}$ , Vickers hardness HV 5, and flow stress  $\sigma_f$  for steels. (After [15.42].)

#### 15.3.4 Properties after Extrusion

Working below the temperature range of recovery and recrystallization leads to work hardening of materials. The degree of work hardening depends on the equivalent strain  $\bar{\epsilon}$  of a particle in the material. The equivalent strain is not uniform over the cross section (Fig. 15.28). Wilhelm has established a relationship between hardness and the equivalent strain, and a similar relation exists between  $\bar{\epsilon}$  and  $\sigma_f$  (Fig. 15.29) [15.42]. It is therefore possible to estimate the local equivalent strain from hardness measurements if the corresponding curves are available.\*

It is also desirable to have a uniform work-hardening effect in the workpiece from the point of view of dynamic loading. This is true for pieces that are not heat-treated as well as for those that are heat treated (hardening, etc.). The results of the heat treatment will be better if the preconditions are uniform. In the case of cold extrusion it is possible to obtain uniform work hardening in the workpiece by a proper selection of billet dimensions and process sequence.

An example for the above possibility is the manufacture of fasteners by cold extrusion, open-die extrusion, and upsetting (see Chap. 10). Fig. 15.27 and Table 15.2 give the range of mechanical properties that can be obtained after cold forming of steels. More details about hardening can be obtained from [15.41].

Extruded workpieces have good fatigue strength. The fact that with increasing natural strain

\*These results are due to relations obtained by numerical approximation methods in the plasticity theory with the microhardness measuring technique. The equivalent strain of any element is

$$\bar{\epsilon} = \int_{t_0}^{t_1} \dot{\epsilon} dt \quad \text{where } \bar{\epsilon} = \sqrt{\frac{1}{3}(\dot{\epsilon}_x^2 + \dot{\epsilon}_y^2 + \dot{\epsilon}_z^2 + 2\dot{\epsilon}_{xy}^2 + 2\dot{\epsilon}_{xz}^2 + 2\dot{\epsilon}_{yz}^2)}$$

$\bar{\epsilon}$  is greater than  $\varphi_{max}$  along the boundary zones. This means that the value of equivalent strain along the boundary zones is many times greater than the natural strain  $\varphi_{max}$  determined from the change of dimension of the workpiece during deformation.

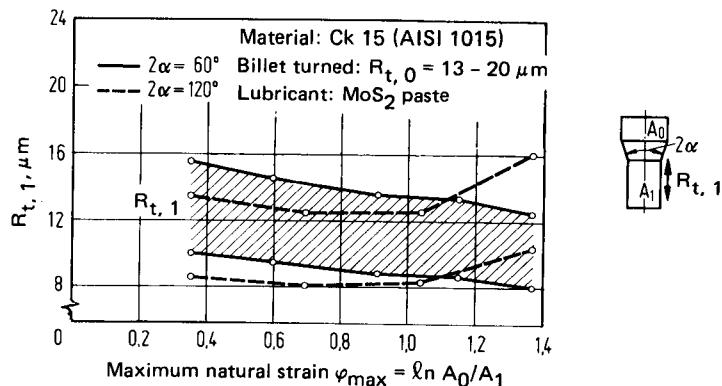


FIG. 15.30 Measured surface roughness values in solid forward extrusion of steel.  
(After [15.45].)

and aging time both tensile strength and yield strength increase and ductility and toughness decrease is well known [15.43]. Aging can occur within 2–3 s due to a temperature increase of the workpiece because of dissipation of the deformation work. This phenomenon can be observed in deformation on fast working presses (60 strokes per minute). For example the observed reduction of the work-hardening coefficient  $n$  by a maximum of 45% at  $T \approx 300^\circ\text{C}$  ( $570^\circ\text{F}$ ) for steels and at room temperature for Ma8 (AISI 1006) is important when use of multistage presses is considered [15.44].

Based on the dimensional accuracy achievable in extrusion, especially between IT 8 and IT 13 (sometimes even IT 7), little or no finish machining is necessary after extrusion. The economy of the process is based to a great extent on this factor. Good surface quality is ensured by almost all extrusion processes (including processes with nonstationary material flow). Fig. 15.30 shows the roughness depth  $R_t$  for a die-opening angle  $2\alpha = 60^\circ$ ; at  $2\alpha = 120^\circ$ ,  $R_t$  increases by 2–3  $\mu\text{m}$  (80–120  $\mu\text{in}$ ) for  $\varphi_{\max} \geq 1$ ; otherwise the trend in  $R_t$  for angles  $\alpha = 60$  and  $120^\circ$  is similar [15.45]. According to [15.2], the achievable surface quality decreases with increasing strength (or hardness) of the material. Values of  $R_t = 6-12 \mu\text{m}$  (240–480  $\mu\text{in}$ ) for lead, tin, and commercially pure aluminum, and of  $R_t = 12-22 \mu\text{m}$  (480–880  $\mu\text{in}$ ) for 100 Cr 6 (AISI L3) steels are the nominal values that can be obtained. It is, however, to be expected that differences in  $R_t$  values will be observed in the various zones and directions. This phenomenon has already been pointed out in various investigations [15.46], [15.47].

## 15.4 DESIGN AND PERMISSIBLE SIZE OF COLD-EXTRUDED COMPONENTS

### 15.4.1 Design

Optimum design of cold-extruded workpieces is a very important prerequisite for the economy of the extrusion processes. The product design should therefore be carried out with careful consideration of the production process. The various shapes that can be manufactured by solid and hollow forward extrusion, backward extrusion, and ironing were described in Figs. 15.1 and 15.2. Cold-extruded cans are preforms for hollow forward extrusion in which higher reductions in area can be obtained than with ironing. Ironing is used for reducing the wall thickness of extruded workpieces. In industry ironing is also used for reducing the wall thickness of deep-drawn cups.

Basically cold-extruded workpieces should be rotation-symmetric; one exception is axisymmetric workpieces (hexagon, square, etc.). For other sections the metal flow is difficult to control. Even the tools are subjected to nonuniform loading, which leads to lower tool life due to either cracking or other reasons (wear, etc.). Rotation-symmetric (if not axisymmetric) workpieces per-

mit the proper design of dies (mathematical methods); production of asymmetrical workpieces should be attempted by joining or separating symmetrical cold-extruded workpieces. Pieces with undercuts and inner and outer threads cannot be extruded. They will have to be machined or rolled after extrusion. Profiles, protrusions, and gears parallel to the axis and with some specific geometry can be extruded with limited accuracy.

Excessive material accumulation, large reductions in area (limits are given in Table 15.4), and sudden changes of sections (thick to thin) are to be avoided. The minimum thickness (wall) possible for steel is approximately 1 mm (0.04 in); for soft materials, such as commercially pure aluminum, up to 0.1 mm (0.004 in) is possible. The transition radius should be a minimum of 1 mm (0.04 in). A draft on the workpieces, as used in die-forged workpieces, makes extrusion difficult and is therefore to be avoided. This is also true for dead-end holes with very high  $h_i/d_i$  ratios. It is always necessary to provide for excess material flow in the design. This is important to compensate for billet weight variations. The excess material flow should be in those areas where larger tolerances can be permitted from the functional standpoint (such as length, flange, or diameter) where rougher surfaces are permitted, or where a machining operation may be necessary [15.2], [15.3].

#### 15.4.2 Maximum Reductions in Area and Wall Thickness

The maximum possible reductions in area and wall thickness in extrusion are dependent to a great extent on the maximum load-carrying capacity of the tool. The deformability of the workpiece plays a minor role due to the presence of a triaxial compressive stress condition in the deformation zone. It is therefore possible for a given load-carrying capacity to obtain higher strains for softer or less work-hardening materials than for harder or higher work-hardening materials. The general limiting values for reductions in area and wall thickness are given in Table 15.4.

For the three processes of solid and hollow forward extrusion and backward can extrusion, the absolute limits on the dimensions of the extruded pieces are also given in Table 15.4. The maximum available press capacity has been assumed as 25,000 kN (2800 ton). The maximum possible dimensions of the extruded pieces are also limited by the difficulties encountered in handling the workpiece. The use of higher-capacity presses is limited by the generally lower requirements of larger-size workpieces. The mass of commonly extruded workpieces varies between  $2 \text{ g} \leq m \leq 35 \text{ kg}$  (0.004–75 lb).

### 15.5 TOOLS

The tools used for extrusion play an important role for trouble-free operation of the process in mass production. Design of the tooling, optimum use of the tool materials in conjunction with good prestressing of the die, and accurate manufacture of the tooling are all important factors for tool performance. The very high loading stresses [up to  $2500 \text{ N/mm}^2$  (360 ksi) and higher in practice] have to be taken into account when designing the tool.

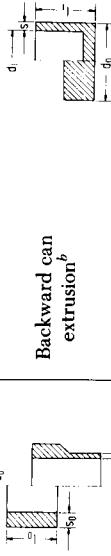
#### 15.5.1 Design, Load, and Material Selection

Fig. 15.31 shows a basic tool setup for solid forward extrusion. The design for hollow forward extrusion is similar except for the punch; a punch with mandrel is required. The different parts of the tooling are subjected to different loads. The design and material of specific parts of the tooling depend on the above factor. Design and material are interrelated by the fact that strength and hardness are not independent of the cross section.

The pressure plate and the intermediate plate support the punch, or the die, and distribute the pressure onto the base plate. The plates must be sufficiently thick, and their surfaces should be parallel within 0.02 mm (0.0008 in). Table 15.5 lists suitable materials for pressure plates and their characteristics.

The punch is a highly stressed tool part. It presses the material through the die opening in solid or hollow forward extrusion and forms the inner surface in backward can extrusion. In the

**Table 15.4** Guidance Values for Possible Workpiece Dimensions and Reductions of Area or Wall Thickness in Cold Extrusion

	Solid forward extrusion <sup>a</sup>			Hollow forward extrusion <sup>a</sup>			Backward can extrusion <sup>b</sup>						
	$d_0, \text{max}$ mm (in)	$\frac{A_0}{A_1, \text{max}}$	$\frac{l_0}{d_0, \text{max}}$	$d_0, \text{max}$ mm (in)	$\left(\frac{A_0}{A_1}\right)_{\text{max}}$	$\epsilon_{A, \text{max}}$	$\frac{s}{d_0}$	$\left(\frac{l_0}{d_0}\right)_{\text{max}}$	$d_0, \text{max}$ mm (in)	$\left(\frac{A_0}{A_1}\right)_{\text{max}}$	$\epsilon_{A, \text{max}}$	$\frac{s_{\min}}{d_0}$	$\left(\frac{l_1}{d_1}\right)_{\text{max}}$
Aluminum (AA 1050-O), lead, zinc	500–300 (20–12)	50	0.98	See note c	500–300 (20–12)	50	0.98 $\geq$ 0.05	See note c	500–300 (20–12)	50	0.98 $\geq$ 0.01 $\leq$ 0.4	5	
Copper (electrolyte)	350–200 (14–8)	5	0.80	See note c	350–200 (4–8)	5	0.80 $\geq$ 0.15	See note c	350–200 (14–8)	5	0.80 $\geq$ 0.03 $\leq$ 0.35	3.5	
Brass (Copper 63– 72%)	300–150 (12–6)	4	0.75	See note c	300–150 (12–6)	4	0.75 $\geq$ 0.20	See note c	300–150 (12–6)	3.3	0.70 $\geq$ 0.05 $\leq$ 0.3	2.5	
Steel— Good deformability (e.g., AISI 1008, 1010, 1015)	250–125 (10–5)	3.3	0.70	8–3	250–125 (10–5)	3.3	0.70 $\geq$ 0.20	8–3	250–125 (10–5)	2.9	0.65 $\geq$ 0.04 $\leq$ 0.3	2.5–2.5	
Medium deformability (e.g., AISI 5120 H, 1015)	220–110 (9–4.5)	2.2	0.55	6–2.5	220–110 (9–4.5)	2.2	0.55 $\geq$ 0.30	6–2.5	220–110 (9–4.5)	2.5	0.60 $\geq$ 0.07 $\leq$ 0.25	2	
Difficult to form (e.g., AISI 1045, 4145)	200–100 (8–4)	2.0	0.50	4–2	200–100 (8–4)	2.0	0.50 $\geq$ 0.40	4–2	200–100 (8–4)	2.2	0.55 $\geq$ 0.09 $\leq$ 0.22	1.5	

<sup>a</sup>From the smallest ( $\varphi \approx 0.4$ ) to the maximum permissible natural strains. The diameter  $d_0$  is based on a deformation force of 25,000 kN (2750 ton).

<sup>b</sup>From  $s/d_0 = 0.15$  to  $s_{\min}/d_0$ .

<sup>c</sup>Values not known.

Source: Compiled in part from [15.2], sheet 1.

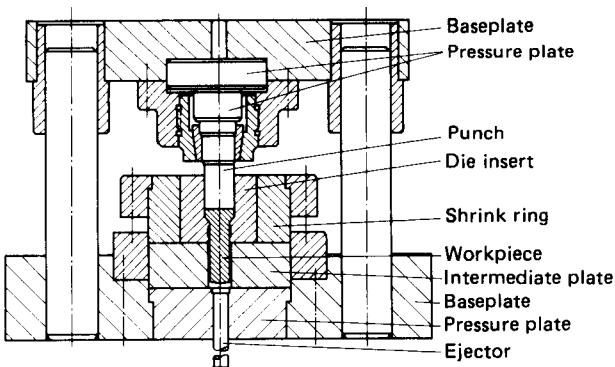


FIG. 15.31 Tooling for solid forward extrusion.

case of solid and hollow forward extrusion, the compressive strength of the punch is more important than its wear behavior. Table 15.6 lists some common materials used for punches.

The mandrel can be an integral part of the punch. It is used in hollow extrusion and forms the inner surface of the extruded piece. Mandrels are subjected to high tensile and friction loads. Table 15.7 lists typical materials used for mandrels. The die insert forms the outer surface of the workpiece. High fatigue strength and wear resistance are two important criteria for the selection of the die material (see Table 15.8). Sintered carbides are used especially for obtaining higher wear resistance.

The shrink ring forms the middle and outer parts of the die assembly and gives the required prestressing of the die. Table 15.9 lists suitable materials for shrink rings.

The counterpunch or the ejector forms the bottom face of the cup in backward can extrusion and serves to eject the workpieces. Combined counterpunch–ejection tooling is subjected to higher loads than a simple ejector system. Table 15.10 lists materials for ejectors and counterpunches.

Details on the chemical composition, heat treatment, mechanical properties, and working can also be found in [15.48] and [15.49].

**Table 15.5** Materials and Characteristics for Pressure Plates

Required yield strength $S_{y,0.2}$ , N/mm <sup>2</sup> (ksi)	Designation		Hardened to		
	DIN	AISI	HRC	HB	Remarks
1700 (245)	X 100 CrMoV51	A2	58–62		See note a
	X 165 CrMoV12	D2	58–62		
	X 210 CrV 12	D3	58–62		
	100MnCrW4	O1	58–61		
1400 (200)	X 40 CrMoV51	H13	50–54		
	100MnCrW 4	O1	50–54		
1100 (160)	X 37 CrMoW 51	A8	40–44		
	100MnCrW4	O1	40–44		
700 (100)	34 CrNiMo6	4340		270–330	
	42 CrMo4	4140		270–330	

<sup>a</sup>In special cases (backward extrusion), AISI M2 with a hardness of HRC 62–64 is used if the compressive yield strength is  $\geq 2000$  N/mm<sup>2</sup> (290 ksi).

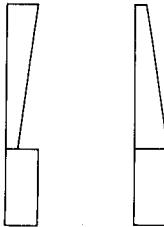
Source: Compiled from [15.48].

**Table 15.6** Materials and Characteristics for Punch, Forward Extrusion

Required yield strength $S_{y,0.2}$ , N/mm <sup>2</sup> (ksi)	Designation		Hardened to, HRC	Remarks
	DIN	AISI		
2100 (300)	S 6-5-2	M2	62–64	To be used where possible
2000 (90)	X 165 CrMoV 12	D2	60–62	
2000 (290)	105 WCr 6	O1	60–62	
1600 (230)	45 WCrV 7	S1	56–58	

Source: Compiled from [15.48].

**Table 15.7** Materials and Characteristics for Mandrels, Hollow Forward Extrusion

Schematic variation of properties		Designation		Hardened to, HRC	Remarks
Wear resistance	Ductility	DIN	AISI		
		S 6-5-3	M4	63–65	For highly stressed mandrels
		S 6-5-2	M2	62–64	
		X 165 CrMoV 12	D2	58–2	
		X 100 CrMoV 51	A2	58–62	
		X 40 CrMoV 51	H13	52–56	To be nitrided
				Nitrided surface has a hardness of DPN 1200	

Source: Compiled from [15.48].

### 15.5.2 Design of Punch and Mandrel

Fig. 15.32 shows some punches and mandrels used for solid and hollow forward extrusion. Punches for hollow forward extrusion cause generally no difficulties since the axial stress does not exceed 2000 N/mm<sup>2</sup> (290 ksi). They should, however, be made as short as possible, as is common with extrusion punches,<sup>\*</sup> and they should have no sudden variations in sections, but the transitions

\*For punches made from high-speed steel, the limit of axial stress (which equals the buckling stress) varies with the length-to-diameter ratio as follows [15.48]:

$l/d$	$p_{P,max}$ , N/mm <sup>2</sup> (ksi)
1	3000 (435)
2	2800 (405)
3	2400 (350)
4	1800 (260)
5	1300 (190)

Values are valid for rigidly fastened punches.

**Table 15.8** Materials and Characteristics for Die Inserts, Steels and Sintered Carbides

Schematic variation of properties		Steel		
Toughness	Wear behavior	Designation		Hardened to, HRC
		DIN	AISI	
		X165CrMoV12 S 6-5-2	D2 M2	60–62 60–64
Sintered carbide (tungsten carbide–cobalt combination)				
		Co, wt %	Density, g/cm <sup>3</sup>	Hardness, DPN
25–30	13.1–12.5	950– 750		
19–24	13.6–13.2	1050– 950		
15–18	14.0–13.7	1200–1100		

Source: Compiled from [15.48].

**Table 15.9** Materials and Characteristics for Shrink Rings

Required yield strength $S_{y,0.2}$ , N/mm <sup>2</sup> (ksi)	Designation		Hardened to, HB	Remarks
	DIN	AISI		
1400 (200)	X 40CrMoV51	H13	470–530	
1200 (175)	X 40CrMoV51	H13	440–510	To be used where possible
900 (130)	X 40CrMoV51	H13	330–390	
700 (100)	34 CrNiMo 6	4340	330–390	
	34 CrNiMo 6	4340	270–330	
	42 CrMo 4	4140	270–330	

Source: Compiled from [15.48].

**Table 15.10** Materials and Hardness Values for Counterpunch (*a*) and Ejector (*b*)

Schematic variation of properties		Designation		Hardened to, HRC	Remarks
Wear resistance	Ductility	DIN	AISI		
		S 6-5-2	M2	62–64	<i>a</i>
		X 165CrMoV12	D2	60–62	<i>a</i>
		X 100CrMoV51	A2	60–62	<i>a</i>
		105 WCr 6	O1	60–62	<i>a, b</i>
		45 WCrV7	S1	56–58	<i>b</i>

<sup>a</sup>Values for counterpunch.<sup>b</sup>Values for ejector.

Source: Compiled from [15.48].

nicely rounded and polished, or they should be ground along their entire lengths [ $R_t \leq 1 \mu\text{m}$  ( $40 \mu\text{in}$ )]. The diameter of the punch at the deformation zone should be chosen so that (1) there is sufficient entry clearance for the punch to enter the die cavity, (2) the clearance between the punch is not so large as to form a burr between the punch and the die, and (3) the clearance is not small enough to cause wear of the punch due to elastic deformation of the tooling (die and

punch would come into contact in this case).

A steel punch of 200-mm (8-in) length decreases in length by 1% [ $\approx 2 \text{ mm}$  ( $0.08 \text{ in}$ )] for every stroke, for a punch pressure  $p_{p,\max} = 2100 \text{ N/mm}^2$  (305 ksi). This results in an increase in diameter of  $0.15 \text{ mm}$  ( $0.0006 \text{ in}$ ) on a punch diameter  $d_p = 50 \text{ mm}$  (2 in), assuming a Poisson ratio of 0.3.

Punches for hollow forward extrusion can be in one of the versions shown in Fig. 15.32. The punch with integral mandrel (Fig. 15.32b) is used when the diameter difference between punch and mandrel is small, such as for extruding thin-walled workpieces and when the length-to-diameter ratio of the mandrel is  $< 1.5$ . The transition radius between punch and mandrel should be as large as possible to avoid stress concentration.

Punches with separate mandrels (Fig. 15.32b) are used in two versions: with fixed mandrel (Fig. 15.32c) and with movable mandrel (Fig. 15.32d). Design data for various dimensions are given in Table 15.11. The first design is used either to form a conical bore with a conical mandrel or to strip the workpiece from the punch. The diameters of punch and mandrel can vary considerably between each other; stress concentration will not be present. The floating or movable mandrel tends to move in the direction of metal flow due to the friction between mandrel and workpiece. This reduces the possibility of high tensile

**FIG. 15.32** Punches for solid and hollow forward extrusion. (a) Punch for solid forward extrusion. (b) Punch for hollow forward extrusion with integral mandrel. (c) Punch for hollow forward extrusion with separate fixed mandrel. (d) Punch for hollow forward extrusion with separate movable mandrel. 1—shaft; 2—head; 3—mandrel. (After [15.48].)

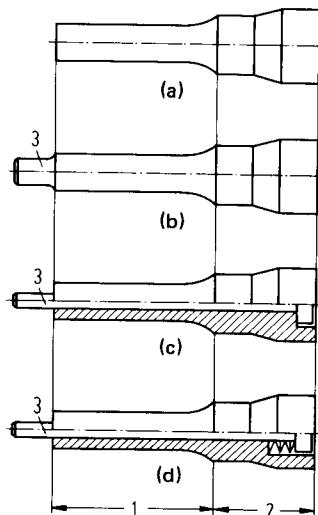
stresses on the mandrel. These tensile stresses can tear a mandrel of diameter  $\leq 10\text{--}12 \text{ mm}$  (0.4–0.5 in). If there is enough space behind the punch, Belleville washers are used to dampen the impact load on the mandrel at the beginning of the return stroke. It is also common to prestress the mandrel with springs up to  $0.8F_B$  (the bottom tearing force of the preform cup,  $F_B = \pi d_2^2 b_{\max} \tau_B$ ). This also ensures a geometrically defined ring gap in conjunction with the die insert and preformed cup (Fig. 15.34).

For extrusion punches, high-speed steels and 12% chromium steels have been found suitable materials. They are through hardenable in the range of dimensions used in industry and have very high compressive strength and wear resistance.

More details on material selection, manufacture, heat treatment, and finish machining of punches, maintenance in production, and causes for failure can be found in [15.48].

### 15.5.3 Design of Die Inserts

The die inserts are subjected to very high radial and tangential stresses. They have no known direct relationship with the maximum axial stress  $p_{p,\max}$ . For backward can extrusion the calculation is therefore made by assuming  $\sigma_r = p_i = p_p \epsilon_A = F_p / A_0$ , where  $A_0$  is being the cross section of the die. For the processes forward extrusion of rods, tube extrusion, and upsetting it is significant to subtract the flow stress  $\sigma_{f,0}$ :  $\sigma_r = p_i = p_p - \sigma_{f,0} = F_p / A_0 - \sigma_{f,0}$ ,  $A_0$  being the cross section of the punch. The die design is dependent on the loading, which is higher for solid extrusion than



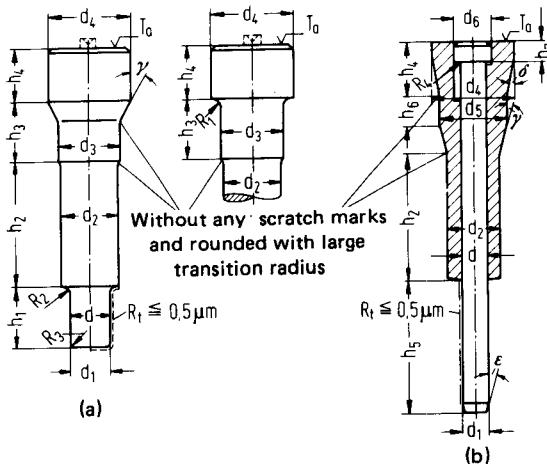


**FIG. 15.33** Design guidelines for punches and mandrels for hollow forward extrusion. (a) Punch with integral mandrel. (b) Punch with separate mandrel. (After [15.48].)

**Table 15.11** Design Data for Punches Shown in Fig. 15.33

Punch (a)	Punch (b)
$d_1, d_2$ according to preformed cup or tube	$d, d_1$ according to final shape of component
$d_{1,\max} = d - 0.01h_1$	$d_2$ according to die bore
$d_3 = d_2 + 0.5 \text{ mm}$	$d_3 \approx 1.3d$
$d_4 = 1.2\text{--}1.4d_2$	$d_4 \approx 1.3d_2$
$h_1 = 1.5d$	$d_5 \approx 1.6d_2$
$h_2 >$ penetration depth in die	$h_1$ depends on stroke, but $\leq 6d_2$
$h_3 = d_3$	$h_2 \approx d_4/2$
$h_4 \geq 0.5d_4$	$h_3 \geq d_5$
$R_1 = 0.3(d_4 - d_3)$	$h_4 \approx 0.7\text{--}1d_3$
$R_2 = 0.5(d_2 - d)$	$h_5 < 8d$
$R_3$ according to final shape	$\epsilon = 5\text{--}10^\circ$
$\gamma = 15^\circ$ to $30^\circ$	$\gamma = 15\text{--}30^\circ$
Eccentricity TIR $d, d_1, d_2$ to $d_3$ $< 0.01 \text{ mm}$	$\delta = 5\text{--}15^\circ$
	$R_1 \leq 0.3(d_3 - d)$

TIR—total indicator reading.

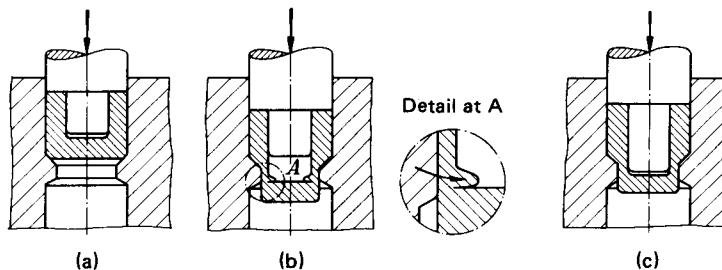


**FIG. 15.34** Effect of punch with fixed mandrel and preform on the material flow at the beginning of hollow forward extrusion. Punch position and workpiece (a) before and (b) after the beginning of metal flow. (c) Cup with preformed bottom.

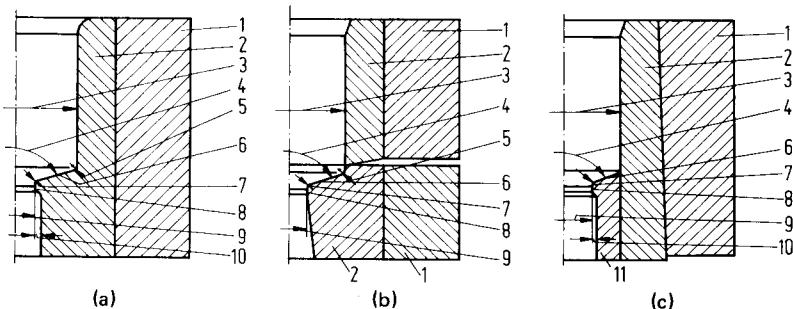


**FIG. 15.35** Die designs for solid and hollow forward extrusion. 1—shrink ring; 2—die insert; 3—die insert inner diameter; 4—die-opening angle  $2\alpha$ ; 5—shoulder entry radius; 6—shoulder; 7—shoulder exit radius; 8—die land; 9—exit diameter; 10—die relief; 11—die insert. (a) Unsplit. (b) Horizontally split. (c) Longitudinally split. (After [15.48].)

for hollow extrusion. Generally one or two shrink rings are used for prestressing the die insert. The inner dimension of such a shrink-fit assembly is limited by the workpiece geometry and the outer dimension depends on the available room in the press (Fig. 15.31).

For solid and hollow forward extrusion the three different designs shown in Fig. 15.35 are used. The single-piece die illustrated in Fig. 15.35a is not used for the very high punch pressures normally required for natural strains  $\varphi_{max} = 0.8-1.0$ . The horizontally split die in Fig. 15.35b is used for very high punch pressures ( $\varphi_{max} > 1$ ) or for extruding steels with very high flow stress. The longitudinally split die in Fig. 15.35c is used in cases where  $\varphi_{max} > 0.8$  and  $2\alpha > 90^\circ$ . The smaller die insert is shrunk in place with an interference of 0.2–0.4%. The following aspects have to be considered in the design of dies.

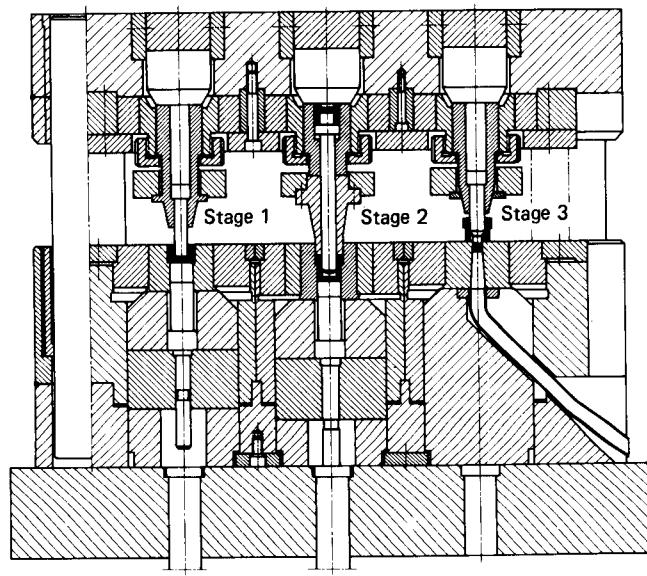
The transition radius between the shoulder of the die and the die entrance diameter should be as large as possible. The die-opening angle  $2\alpha$  is chosen to minimize  $p_{P,max}$ . (For steels it is between 40 and 130°, for light metals up to 180°.) The transition radius between the shoulder and the die land should be 0.2–1.5 mm (0.008–0.06 in) for steel, depending on the die diameter. The die land should be between 2 and 5 mm (0.08 and 0.2 in) for all metals and dimensions. The relief should be as small as possible [for steel 0.05–0.2 mm (0.002–0.008 in), for light metals 0.15 mm (0.006 in)] to ensure proper guiding of the extruded workpiece. Its dimension should, however, be greater than the wear allowance on the die land.

High-speed steels are suitable for both inserts and dies. Chromium steels and steels which can be surface-hardened are also sometimes used as tool material. Sintered carbides have very high wear resistance—the tool life is higher by 10–40 times. Shrink rings are made from cold-working steel if the shrinking is done cold, or from hot-working steel at warm shrink-fitting temperatures.

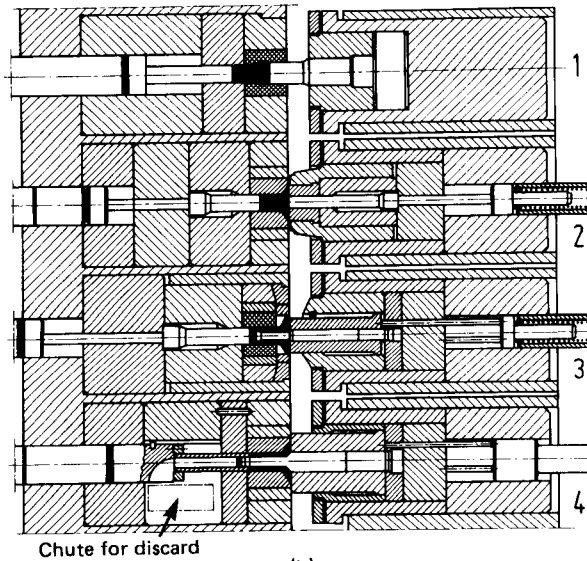
More details on material selection, manufacture, heat treatment, and shrink fitting can be obtained from [15.48]. The calculation of shrink fitting is treated in Sec. 15.10.4.

#### 15.5.4 Multistage Tooling

The design concepts for multistage tooling are the same as those described in the preceding section. The selection of tool material is also similar to the selection criteria mentioned in the last section; for high wear resistance, sintered carbides are preferred [15.50]. There are, however, certain aspects to be considered regarding the overall tool assembly. These are problems associated with space availability, that is, the space is limited by the machine and handling system (feeding, ejection, gripping, turning, transportation). The transportation plane for all tools should be the same as for sheet-metal working. The problem of removing the waste also has to be considered. The main consideration is that the work process should be interruption-free. The system design therefore calls for experience and special knowledge. Fig. 15.36a shows a three-stage cold-extrusion tooling on a vertical press. The stages are backward can extrusion, hollow backward extrusion, and piercing. Fig. 15.36b shows a four-stage cold-extrusion tooling on a horizontal press (solid forward extrusion, upsetting, backward can extrusion, and piercing) [15.48], [15.51], [15.52].



(a)



(b)

**FIG. 15.36** Multistage tooling for cold extrusion of steel. (a) Three-stage tooling for vertical press. (b) Four-stage tooling for horizontal press. (After [15.2].)

**Table 15.12** Materials and Tool Life for Punches

	Tool life, units	Material (workpiece)		Failure criterion
		DIN	AISI	
Solid forward extrusion	100,000	Ma8 to 41Cr 4	1006 5140	Fatigue
Hollow forward extrusion	100,000	Ma8	1006	
	50,000	16MnCr 5 Cq35 41Cr 4	5117 1035 5140	Fatigue and wear

**15.5.5 Tool Life**

The tool life—the number of good pieces produced by a tool before failure—depends on a number of factors: process, natural strain, lubrication, cooling, tool geometry, tool design, tool material, and dimensional tolerance of the extruded workpiece. In the case of steel, the main reason for tool failure is fatigue due to very high stressing; the second major failure is wear. In the case of light metals (aluminum), the reasons of failure are in reverse to those of steel. Cold extrusion of copper leads to tool life similar to that of aluminum; for brass the tool life is similar to that of steel. For forward extrusion of steel the punch life (punch material M2) has been found from experiments as shown in Table 15.12.

Table 15.12 shows clearly the effect of the process on tool life. The combination of punch and mandrel in hollow forward extrusion is subjected to less fatigue than the punch above in solid forward extrusion.

The tool life for dies is characterized by wear for lower stresses, by cross cracks (fatigue) for high stresses, and by longitudinal cracks for very high stresses. The design of dies as shown in Fig. 15.35 corresponds to designs suitable for the three loading conditions described above.

Fig. 15.37 shows the relationship between natural strain, tool material, and average tool life of radially prestressed dies used for extruding unalloyed and low-alloyed steels.

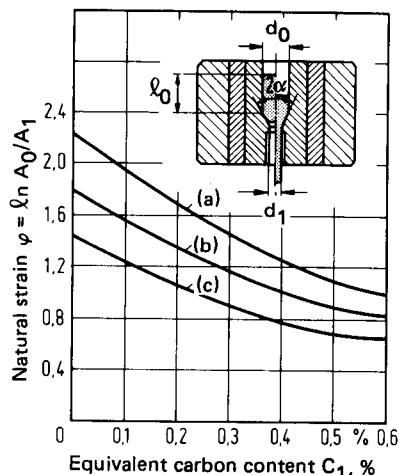


**FIG. 15.37** Tool life of radially prestressed dies for forward extrusion as a function of natural strain, workpiece material, and tool material. Workpiece material—annealed, pickled, phosphated, and lubricated;  $l_0/d_0 = 1.5-2$ ;  $2\alpha = 60^\circ$ ;  $\mu \approx 0.03-0.05$ ; equivalent carbon content  $C_1 = \%C + (\%Mn - 0.6)/4 + (\%Cr + \%Ni)/20$ . *a*—limit curve for tools made of steel; tool life 10,000 pieces (region above curve: cracks due to overloading; region below curve: failure due to fatigue); *b*—limit curve for sintered carbide die; tool life  $\approx 100,000$  pieces (region below curve: failure due to fatigue); *c*—same as *b*, tool life  $\approx 300,000$  pieces (region below curve: wear). (After [15.2].)

**15.6 MACHINE TOOLS**

For extrusion processes—including stationary, nonstationary, and process combinations—mechanical presses controlled by stroke (crank, eccentric, and knuckle joint) are used. There are horizontal and vertical versions, as well as single- and multistage variations and hydraulic presses. The various press types are described in detail in Chap. 8. The processes carried out in single-stage presses are characterized by (1) concentrated axial high loads, (2) proportionately long strokes (for solid and hollow forward extrusion much longer than for backward can

extrusion, especially for small deformation ratios), (3) high work capacity (or energy) requirements, and (4) sufficient forces for ejecting the workpiece. They require narrow longitudinally stiff columns with  $C_{\text{tot}} \geq 1000 \text{ kN/mm}$  (2875 ton/in), a bed and ram resistant to bending, long ram guides with little or no play (ram height  $\geq 1.5$  times ram width), availability of the nominal force at  $\alpha_N = 30^\circ$  (or better at  $45^\circ$ ), and an ejector with  $F_E \geq 0.2F_N$ . The presses should have a stepless ram adjustment, inching to set the press for the process, and overload safety or indication for both punch and ejector.

In the case of multistage presses, exact loading on the center of the press is not generally possible. Design of the press from the viewpoint of bearing damage due to offset loads is quite involved. For single-stage crank presses a two-point ram drive is recommended for the same reason, if the press design can accommodate this feature [as a rule above  $F_N \geq 5000 \text{ kN}$  (560 ton)].

The present maximum capacity of manufactured presses with crank drives is  $F_N = 25,000 \text{ kN}$  (2750 ton);  $31,500 \text{ kN}$  (3500 ton) for knuckle-joint presses (both as single-stage presses); and  $12,500 \text{ kN}$  (1400 ton) for other mechanical multistage presses. The limit for hydraulic presses is between  $25,000$  and  $40,000 \text{ kN}$  (2750 and 4500 ton). Higher capacities are technically possible, although not economical at this time. The general design ranges of these presses are shown in Fig. 15.38.

For crank presses, based on the above criteria, a useful stroke range of  $10$ – $80 \text{ mm}$  (0.4–3.15 in) for  $\alpha_N = 30$  or  $45^\circ$  and  $630 \text{ kN}$  (70 ton)  $< F_N < 20,000 \text{ kN}$  (4500 ton) are possible. These presses are used for (1) workpieces with large deformation ratios, (2) medium to large batch sizes, and (3) large stroke requirements. Fig. 15.39 shows a press with  $13,500 \text{ kN}$  (1500 ton) nominal force.

The work capacity of knuckle-joint presses is smaller than that of a crank press of the same nominal force since the effective available stroke of the knuckle-joint press is smaller. However, a higher number of strokes and larger production quantities with relatively smaller contact velocities can be obtained with knuckle-joint presses. The investment is also smaller because of the smaller weights of the press. The effective stroke is  $3 \text{ mm}$  (0.12 in)  $< h_N < 12 \text{ mm}$  (0.47 in). Knuckle-joint presses are used for processes with smaller deformation travel, such as coining, sizing, or upsetting of flanges. Among the extrusion process, knuckle-joint presses can be used for backward can extrusion. Horizontal knuckle-joint presses are used for the extrusion of thin-walled components from commercially pure aluminum, zinc, and other nonferrous metals with large numbers of strokes and production quantities for both medium and large batch sizes. An example of a horizontal knuckle-joint press is shown in Fig. 15.40.

Hydraulic presses are best suited, from the drive standpoint, for extrusion and ironing processes. Stroke and velocity can be chosen for individual requirements within given limits. The hydraulic presses cannot be overloaded. They have a rigid limit on the stroke. The elastic deflection under load will influence the dimensional accuracy of the workpiece in the direction of the force. The press frame deflection, on the other hand, does not affect the workpiece accuracy. The number of strokes of a hydraulic press is lower than that of a crank press of similar capacity (Fig. 15.38). However, unlike with crank presses, the force will be available during the entire stroke of a hydraulic press. The number of strokes can be increased (1) by limiting the stroke to the absolute requirement and (2) by fast approach and return travel (dashed line in Fig. 15.38b). For press capacities above  $5000$ – $6300 \text{ kN}$  (550–700 ton), hydraulic presses can generally compete with mechanical presses; above  $F_N = 10,000 \text{ kN}$  (1100 ton) the difference in production rates is negligible. An advantage of the hydraulic press is improved workpiece accuracy and tool life because of the central and axial positioning of the hydraulic unit (which increases the accuracy of the ram guidance). Hydraulic presses are used in the manufacture of workpieces with long deformation strokes as well as for small and medium batch sizes. Fig. 15.41 shows a modern hydraulic press with  $F_N = 4500 \text{ kN}$  (500 ton) and a maximum stroke  $h_{\max} = 1200 \text{ mm}$  (48 in).

Multistage presses are available operating either horizontally or vertically, with either mechanical or hydraulic drive. They are used for large batch sizes and workpiece masses between  $3 \text{ g}$  (0.1 oz) and  $3 \text{ kg}$  (6.8 lb). The material is fed either in the form of wire coil or in the form of rods or bars if its diameter is greater than  $30 \text{ mm}$  (1.2 in), and parting off is by shearing. An additional four to seven stages may be available in the press. Because of the number of stages the production of the component may be accomplished without intermediate treatments (such as annealing and surface treatment). A four-stage press is shown in Fig. 15.42 for workpieces such as drive shafts. Each stage can be individually loaded. Fig. 15.43 shows a heavy horizontal five-stage cold former with fully automated tool-changing system, and Fig. 15.44 a two-column two-

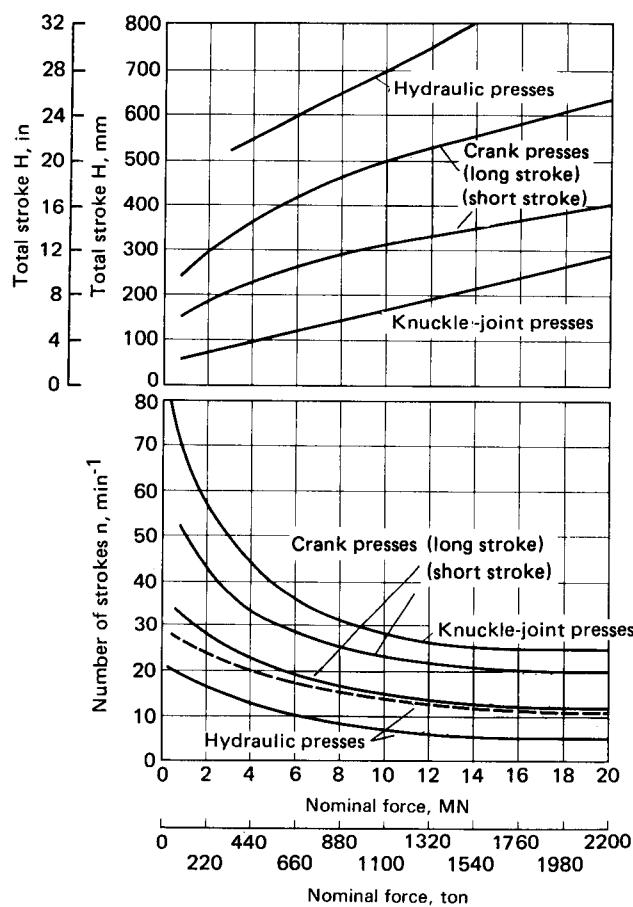


FIG. 15.38 Total stroke and number of strokes of mechanical and hydraulic presses for cold extrusion. (After [15.52].)

point eccentric press for multiple stages. Fig. 15.45 shows a view into the working area of a four-stage horizontal cold-extrusion press with vertical tool arrangement, and an example of a formed workpiece. More details on tool design, workpiece transportation, wire feeding, and control of ejectors for multistage cold-forming presses are given in Chap. 10.

## 15.7 SPECIAL PROCESSES

### 15.7.1 Process Combinations

In industry for cold bulk-forming processes, a combination of cold extrusion with other processes is widely used. The combined processes are generally carried out simultaneously in a single forming operation. Combinations of hollow and forward extrusion processes seldom are. A combination

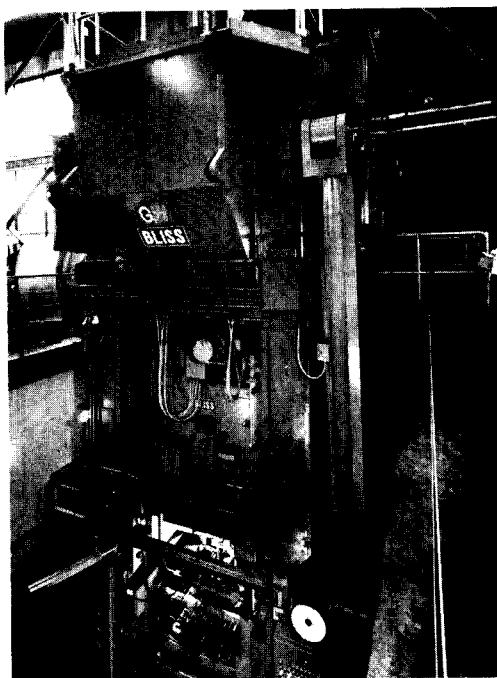


**FIG. 15.39** Two-column single-point cold-extrusion press.  $F_N = 13,500 \text{ kN}$  (1500 ton), with eccentric gear drive, mechanical lift, and press-driven transfer feed; stroke—460 mm (18 in); number of strokes— $10 \text{ min}^{-1}$ ; continuous. (Courtesy of Gulf and Western Manufacturing Co., E. W. Bliss Division, Salem, OH.)

of solid forward and solid backward processes is possible [15.18]. An example of a turbine-blade extrusion by the above combination is shown in Fig. 15.46. The material flow has to be effected properly by the control of either the counterpunch or the ejector. A technically interesting combination with unimpeded metal flow is the combination of solid backward extrusion and upsetting. This is widely used in the watch industry for manufacturing "tires" (plates of a desired shape with projections) and in the camera industry for making levers. It has been indicated that these processes have to be carried out in slow presses with accurate tools to obtain very accurate workpieces [15.53].\*

The above process can also be used for larger workpieces. An example of pressing a hollow punch on a thick plate is shown in Fig. 15.47. A portion of the material flows into the hollow punch (solid backward extrusion) and the remainder is upset radially or, in the case of very thick plates, in the vertical direction (fold formation). Higher extruded heights can be obtained by using a counterpunch and by roughening the upsetting portions of the tooling. This prevents the flow in the horizontal or lateral direction. The ratio of the flat punch surface to the bore area also plays an important role in the material flow. Fig. 15.48 shows the achievable extruded height for Ck35 (AISI 1035) for a plate thickness  $s_0 = 7 \text{ mm}$  (0.28 in) [15.54], [15.55]. For workpieces used in

\*The so-called *May* presses are built based on the same principle, namely, extended knuckle-joint and lower-drive presses (see also Chap. 8).

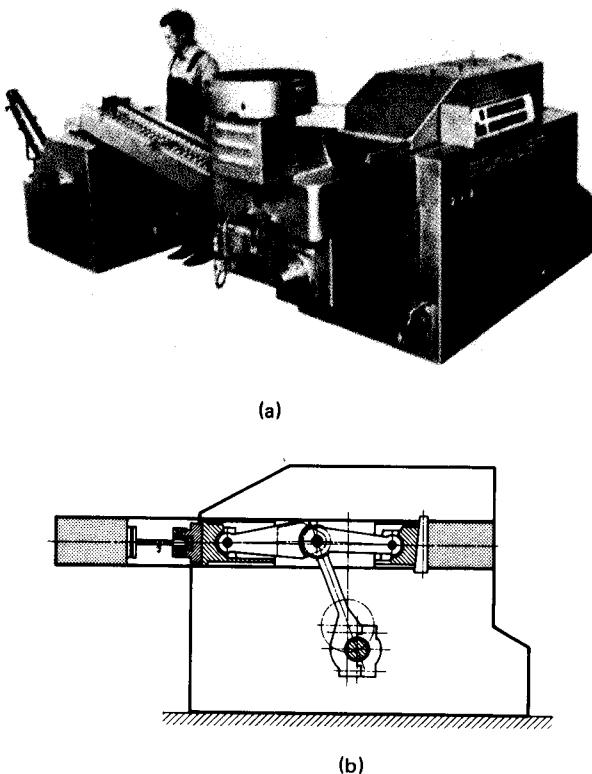


**FIG. 15.40** Horizontal knuckle-joint press for tube extrusion.  $F_N = 250\text{--}12,500 \text{ kN}$  (28–1400 t); number of strokes— $200\text{--}50 \text{ min}^{-1}$ ; maximum workpiece diameter  $20\text{--}150 \text{ mm}$  (0.8–6 in). (a) Complete view. (b) Principle of knuckle joint and method of extrusion. (Courtesy of Louis Schuler GmbH, Göppingen, Germany.)

watch industries, a tooling as shown in Fig. 15.49a is used; Fig. 15.49b shows the metal flow. Burgdorf [15.56], [15.57] has conducted extensive theoretical and experimental investigations on the above process. The effect of having a bore on one of the upsetting punches is twofold. First, the theoretical peak of the normal stress is rounded off; that is, there is relief of the peak stresses. Second, the neutral plane, from which the material flows outward and inward into the boss (Fig. 15.50), can be determined exactly by theoretical methods. The following values have been obtained from experiments. For rounds from aluminum Al 99.5 (AA 1050), with  $d_0 = 15 \text{ mm}$  (0.6 in) and  $s_0 = 20 \text{ mm}$  (0.8 in), a boss of 6-mm (0.24-in) length and 2-mm (0.08-in) diameter was obtained. For Ma 8 (AISI 1006) similar values were 3.5 mm (0.14 in) and 5 mm (0.2 in). The last value can also be obtained for a 0.5-mm diameter of boss. These results confirm the observations of other investigators regarding the effect of time and velocity on the material flow. For a transition from a drop hammer with  $v_{T,0} = 1.6 \text{ m/s}$  (5.3 ft/s) to an eccentric press with  $v_{T,0} = 0.016 \text{ m/s}$  (0.053 ft/s) and to a hydraulic press with  $v_{T,0} = 0.005 \text{ m/s}$  (0.0017 ft/s), the protrusion height increased, with the other conditions remaining the same. The increase can be as high as 80–100% for large upsetting forces. For smaller upsetting forces, the effect of the velocity on the height of the protrusion formed is not very remarkable. The bore in the punch reduces the normal stress peak (Fig. 15.50). This results in a smaller force for the above combined process than for

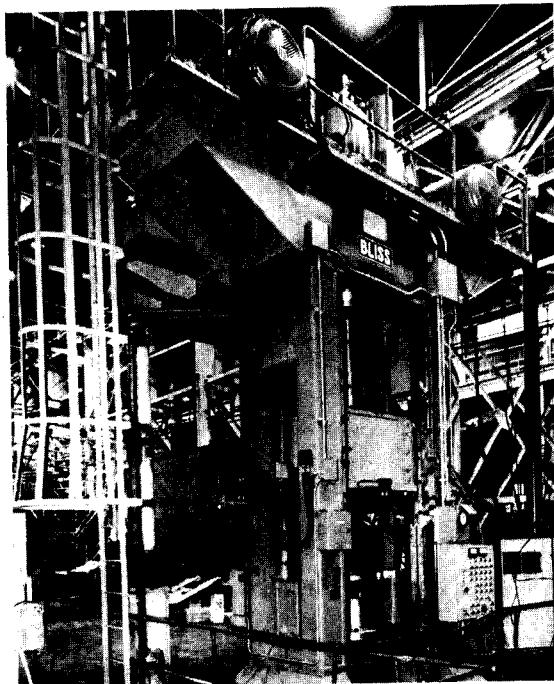


**FIG. 15.41** Hydraulic two-column cold- and warm-extrusion press.  $F_N = 4500 \text{ kN}$  (500 ton); stroke—1200 mm (48 in); rapid advance and return speed—0.33 m/s (780 in/min); press speed—0.07 m/s (170 in/min); power—150 kW (200 hp). (Courtesy of Gulf and Western Manufacturing Co., E. W. Bliss Division, Salem, OH.)

pure upsetting of a workpiece of the same material with the same dimensions (Fig. 15.51). The upsetting force is therefore an upper limit for the combined process. The principle of force-relieving bore, as established in the above case, can be used to advantage in other deformation processes in order to ease metal flow problems. Examples are coining and can extrusion. Cups or cans of large reductions of area with thin bottom thicknesses can be extruded easily with lesser punch forces if a small shaft (forward extrusion) is included in the process (Fig. 15.52). This idea has been used widely in cold-extrusion processes.

### 15.7.2 Special Applications

An increase in surface areas and high surface pressures cause cold welding between workpiece and tool if the surface treatment and the lubrication are bad. This negative aspect can be used deliberately, for example, to extrude a workpiece from two different materials by cold welding. The process is called cold press welding by extrusion. The surfaces to be welded should be technically pure and capable of undergoing large surface expansion. In the case of a bar-shaped copper-aluminum workpiece made by solid forward extrusion, aluminum deforms in the shape of a parabola into the copper, conforming to the distortion condition (Figs. 15.53 and 15.54), if the aluminum billet is placed inside the die on top of the copper billet. The oxide layers tear because of the extrusion loads, and cold welding takes place. However, no significant relative movement

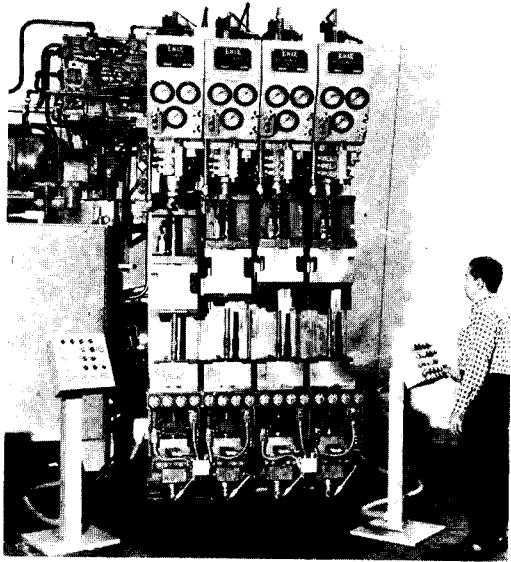


**FIG. 15.42** Four-station hydraulic c-frame cold-forming press.  $F_N = 675 \text{ kN}$  (75 ton) each; stroke—460 mm (18 in); main ram (double acting) 200 × 185 mm (8 × 7.5 in); drive—56 kW (75 hp); 400 parts/h. (*Courtesy of Erie Press Systems, Erie, PA.*)

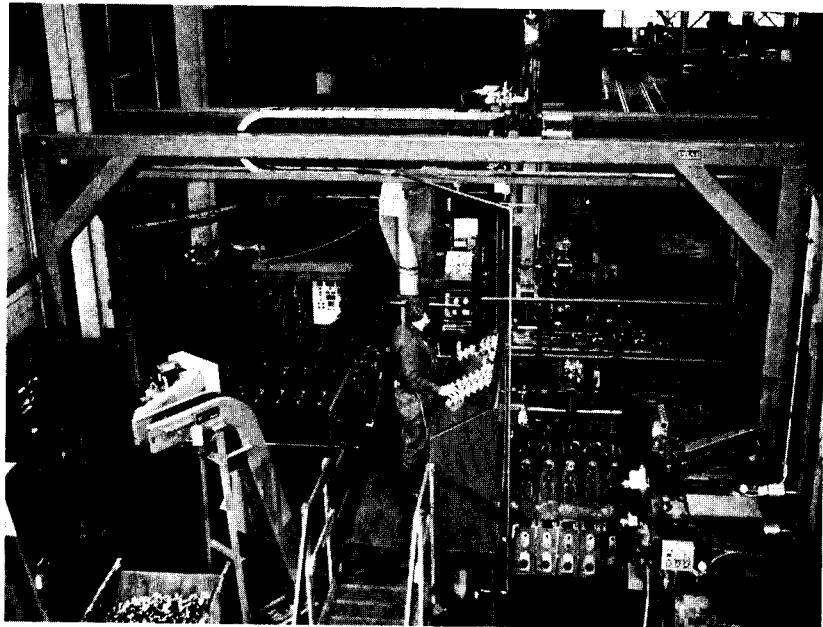


**FIG. 15.43** Horizontal five-stage cold former with automatic tool-changing system.  $F_N = 11,300 \text{ kN}$  (1250 ton); number of strokes— $60 \text{ min}^{-1}$  for 33-mm (1.3-in) wire diameter; changing time—entire tool set 17 min, single tool 3 min. (*Courtesy of National Machinery Co., Triflin, OH.*)

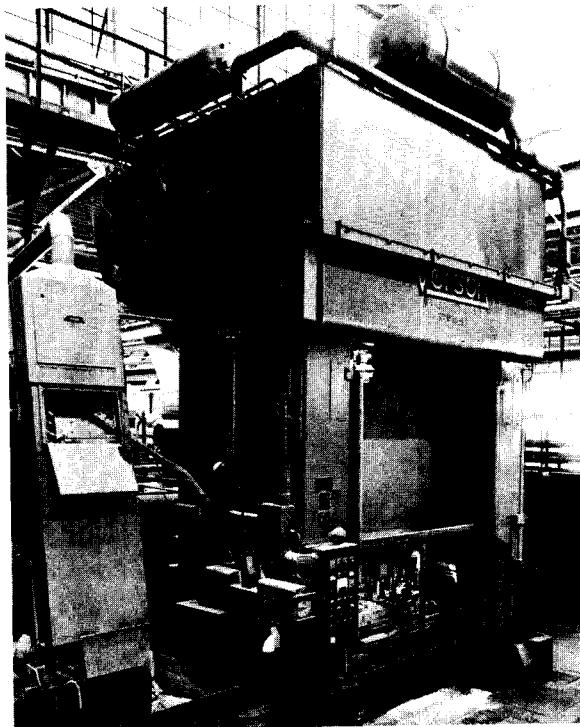
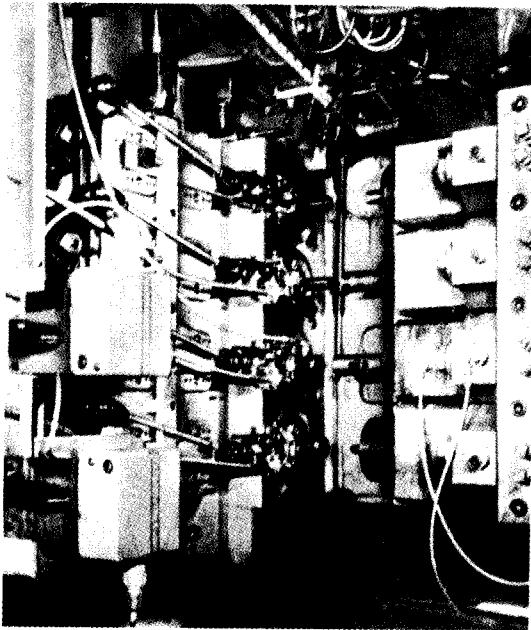


FIG. 15.44 Two-column two-point cold-forming press for multi-stage tooling. (Courtesy of Verson Allsteel Press Co., Chicago, IL.)

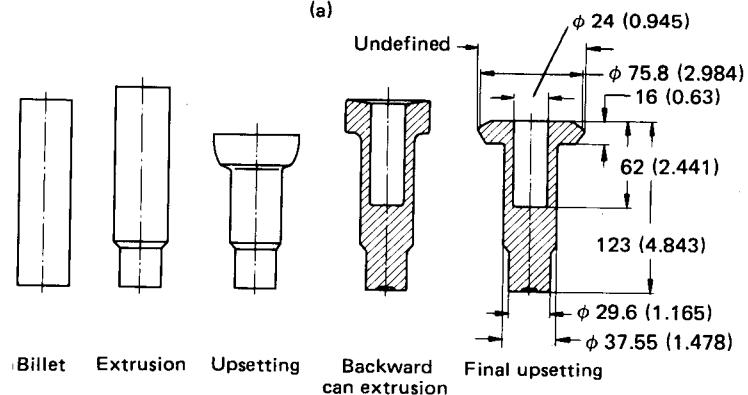
has been observed between the boundary layers of copper and aluminum. The tensile strength of such a cold-joined workpiece of copper and aluminum is on the order of that of cold-worked pure aluminum [15.58] to [15.60]. The weld surface between copper and aluminum can be affected by changing the deformation ratio and the percentage of copper by volume. The local tensile strength corresponds to the local increases in surface area—a linear relationship has been observed (Fig. 15.55). The formation of the weld surface is influenced by the angle of inclination  $\beta$  of the tube ends, the deformation ratio (reduction in area), and the die-opening angle  $2\alpha$ . Large angles of inclination and deformation ratios result in a long welded surface and high tensile strengths (up to  $140 \text{ N/mm}^2$  [20 ksi]). It is advantageous to press the harder material through the die first, since the longitudinal compressive stress  $\sigma_{z,m}$  will be higher and the values of  $\sigma_{r,m}$  and  $\sigma_{t,m}$  will be pushed further into the compression zone. The triaxial stress condition favors cold welding, since surface area increases on the order of 100% facilitate the cold-welding process [15.55]. Maximum surface area increases have been observed in backward can extrusion (Fig. 15.55). Here the weld is influenced also by the deformation ratio and the volume proportions of the individual elements.

It is possible to have a copper layer of 0.1-mm (0.004-in) thickness in the inner can surface (the increase in surface area is greatest at this point). The welding surface in the vicinity of the can wall is increased to up to 20 times the original area.

In a similar manner, material pairs of carbon steel–copper or carbon steel–nickel can also be welded by cold extrusion. In the case of a steel–copper workpiece made by solid forward extrusion, tensile strengths of up to  $400 \text{ N/mm}^2$  (58 ksi), that is, twice that of pure copper, are possible. For nickel–steel workpieces, values of  $600 \text{ N/mm}^2$  (87 ksi) can be obtained. In the case of backward can extrusion the shear strength is dependent on the localized increase in surface area. For



(a)



(b)

**FIG. 15.45** Horizontal four-stage cold-forming press with vertical tool arrangement.  $F_N = 12,500$  kN (1400 ton); total stroke—520 mm (20.5 in); number of strokes—25–35 min<sup>-1</sup>. (a) View of working area. (b) Bevel gear shaft billet made of 20 MnCr 5 (AISI 5120). (Courtesy of Louis Schuler GmbH, Göppingen, Germany.)

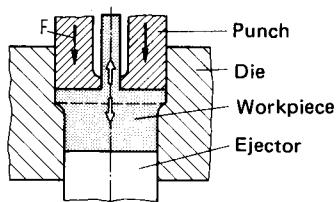


**FIG. 15.46** Example of a process combination: solid forward and solid backward extrusion. Process sequence (in a single stroke): (1) backward extrusion of blade with fixed ejector; (2) forward extrusion of blade with moving ejector.

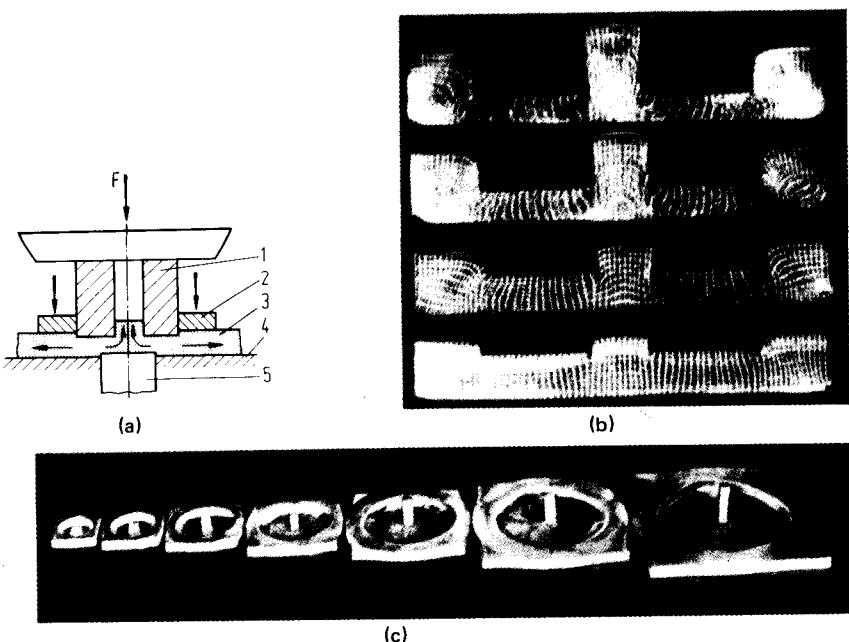


**FIG. 15.47** Solid backward extrusion and upsetting of plates. (a) Tooling. 1—punch; 2—blank holder; 3—plate; 4—support; 5—counterpunch. (b) Material flow. (c) Example. (After [15.54], [15.55].)

nickel–steel combinations with 20% nickel by volume, the shear strength obtained is  $400 \text{ N/mm}^2$  (58 ksi) for a reduction in area  $\epsilon_A = 0.75$ .

Future development of this technique will have to be extended to material pairs in which at least one partner is made from high-alloyed steel; an example is aluminum–austenitic chromium-nickel–steel [15.61].

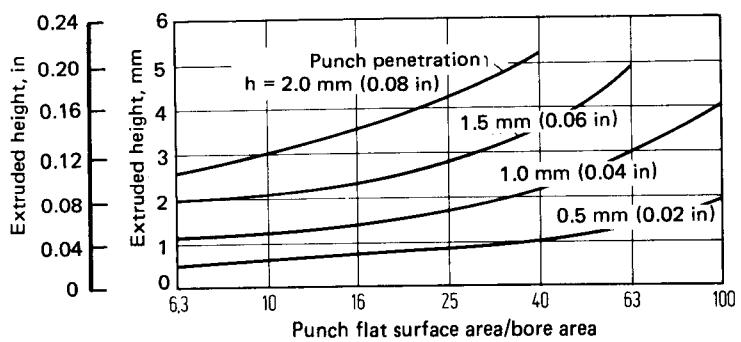


**FIG. 15.48** Relationship between the ratio of flat punch surface to bore area, punch penetration, and obtainable extruded height after Fig. 15.49. Material—AISI 1035;  $s_0 = 7 \text{ mm (0.28 in)}$ . (After [15.54].)

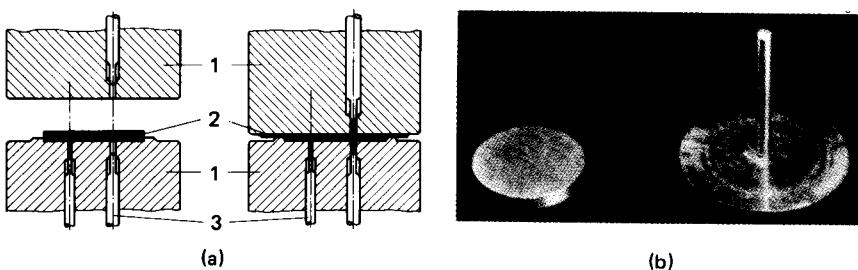


**FIG. 15.49** Process combination of upsetting and backward extrusion. (a) Tool design. 1—upsetting die with bores; 2—billet; 3—ejector. (b) Initial and final shapes (make in a similar tooling). (After [15.57].)

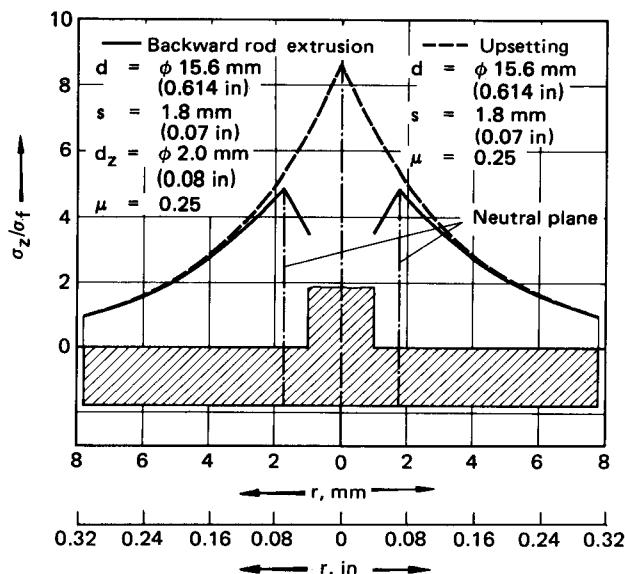


**FIG. 15.50** Normal stress distribution in upsetting and solid backward extrusion with neutral plane formation.  $d$ —billet diameter;  $s$ —plate thickness;  $d_z$ —bore diameter;  $d$ ,  $s$ , and  $r$ —instantaneous values. (After [15.56].)

## 15.8 EXTRUSION PROCESSES WITH NONSTATIONARY MATERIAL FLOW

The processes belonging to this group are the basic processes of can extrusion (both forward and backward) (refer to Fig. 13.3e and f) and bulk piercing.\* They differ from the processes mentioned earlier in this chapter on two scores: (1) the shape of the workpiece is formed by the gap between the die and the punch, and (2) the metal flow is nonstationary throughout the deforma-

\*Hot backward can extrusion of thick-walled hollow billets, which are further processed by hot extrusion, drawing, or ironing to obtain tubes with  $l \gg d$ . Hence the process of piercing (bulk) belongs to semifinished product manufacturing technology.

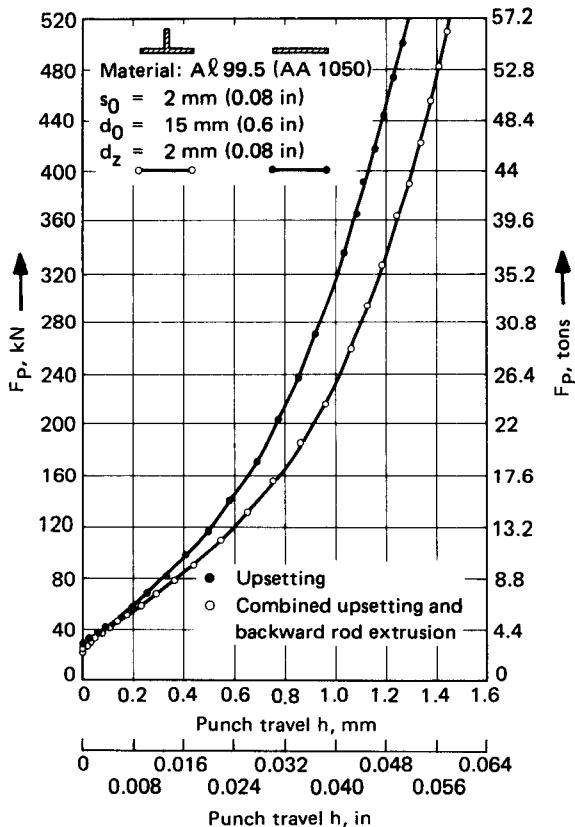


FIG. 15.51 Experimentally determined variation of punch force with punch travel for upsetting and a combination of upsetting and solid backward extrusion. (After [15.56].)

tion process. The most commonly used process in the industry is backward can extrusion. Its application ranges from thin-walled tubes of pure aluminum to thin-walled zinc containers for dry cells, to preforms of steel with medium wall thickness for the manufacture of hollow work-pieces by ironing or hollow forward extrusion, to heavy magnetic housings with square outer and circular inner forms, and to automotive and machine components with circular outer forms and various inner shapes (Fig. 15.56). In the fastener industry the backward extrusion process is used to extrude inner shapes. The can extrusion of soft materials like aluminum and tin belongs to the oldest applications of the process for mass production. It has been used since about 1880. Combinations of backward and forward can extrusion processes with other deformation processes are also widely used. They are dealt with later in this chapter. The

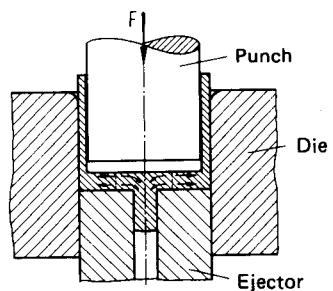
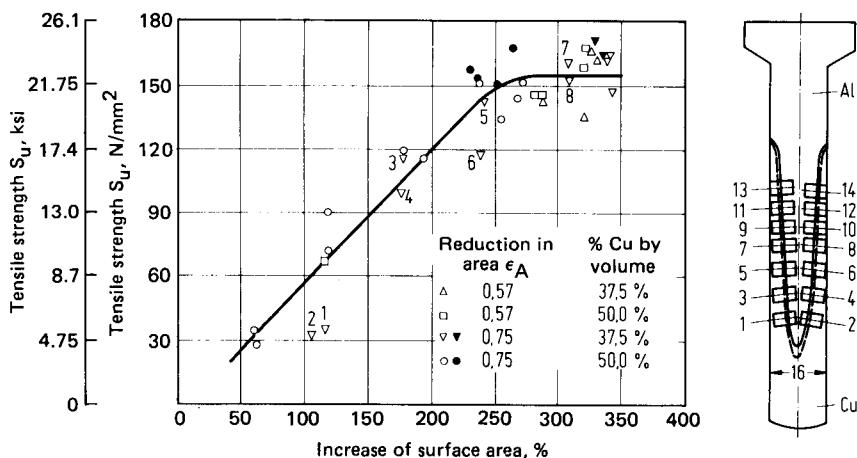


FIG. 15.52 Principle of force-relieving bore in backward can extrusion. (After [15.56].)



**FIG. 15.53** Tensile strength determined from small tensile test probes of copper-aluminum-welded workpiece as a function of the local increase in surface area of the weld. (After [15.58] to [15.60].)

important parameters in these processes are material selection, change of material properties, surface treatment and lubrication, selection of tool material, machines, and so on. These factors have already been analyzed in Secs. 15.2 to 15.4. The principles of die design are covered in Sec. 15.10.

### 15.8.1 Material Flow, Stresses, Forces, and Energy

#### Material Flow

The billet with diameter  $d_0$  and height  $l_0$  is slid into the die, using the small clearance between die and billet (Fig. 15.57). When the punch starts to penetrate into the billet, the material is axially upset and increases in diameter corresponding to the inner die diameter  $d_D$ . Once the conical face of the punch (most punch designs for backward can extrusion have this feature) is entirely inside

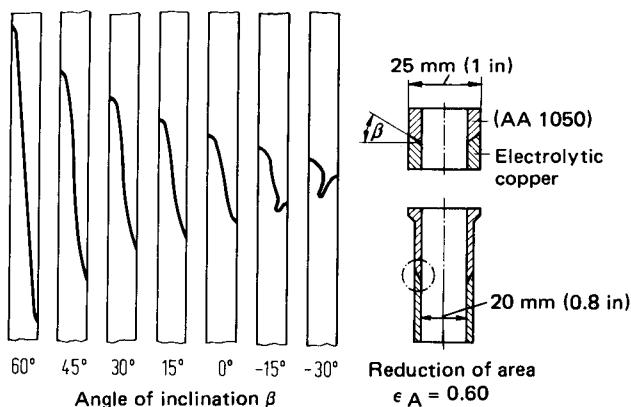


**FIG. 15.54** Formation of weld surface in cold welding of copper-aluminum tube welds by hollow forward extrusion. Parameters—angle of inclination of the workpiece; reduction of area  $\epsilon_A = 0.6$ . (After [15.58] to [15.60].)

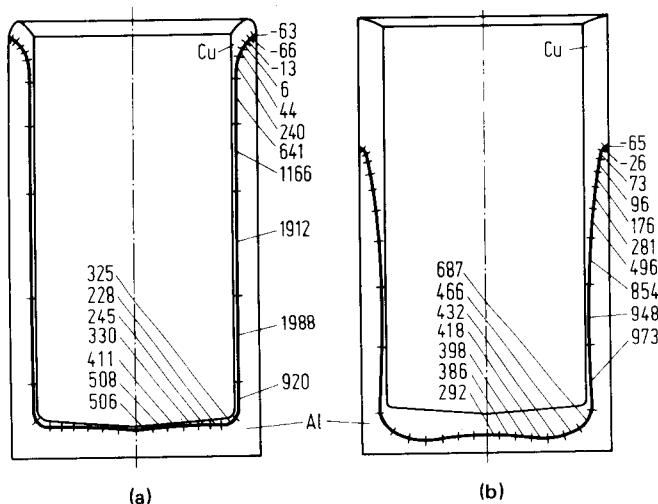


**FIG. 15.55** Longitudinally cut section of cold-welded copper-aluminum cup by backward can extrusion. Numbers give local increase in surface area in %.  $\epsilon_A = 0.64$ . (a) 10% copper. (b) 50% copper. (After [15.58] to [15.60].)

the billet, the material fills in the die cavity completely so that it has full contact with the tool surfaces (Fig. 15.58, stage 1). Further penetration of the punch into the billet forces the material to flow through the orifice formed by the die and the punch, in the opposite direction of the punch movement, first along the die wall and later outside of the die (Figs. 15.56a and 15.57).

The material coming through the orifice formed by the punch land and the die wall undergoes no strain after this point. The remaining volume between the punch and the die bottom (or the ejector) is only partly in the deformation zone. Depending upon the geometrical and the friction conditions, a dome-shaped rigid plastic zone is formed in this region (refer also to Fig. 15.73b). Among the factors affecting the above zone are the can bottom thickness  $b$  and the reduction in

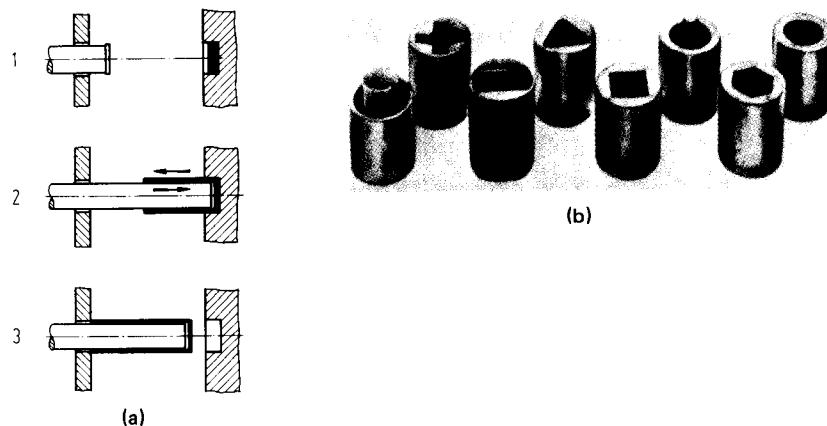


**FIG. 15.56** (a) Cold extrusion of thin-walled components from aluminum, zinc, and tin. (b) Backward extruded workpieces from steel with noncircular inner shapes. (After [15.6].)

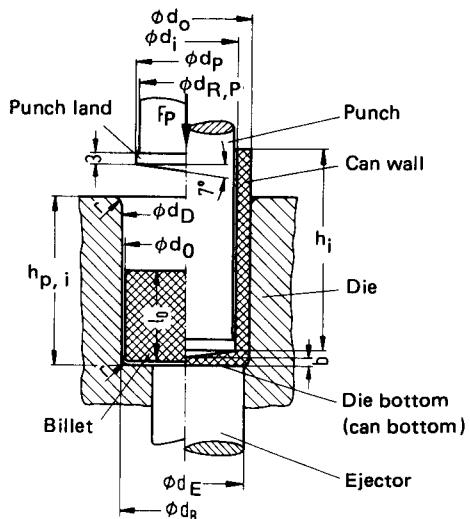
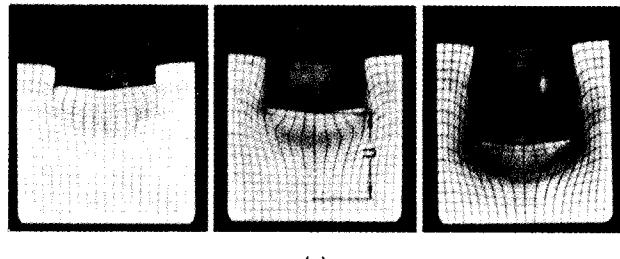
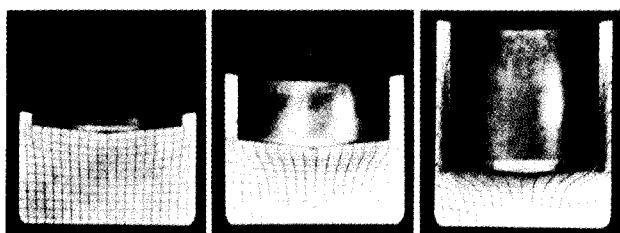


FIG. 15.57 Definitions of dimensions and other terms on the billet, can, and tool in backward can extrusion. (After [15.6].)



(a)



(b)

FIG. 15.58 Formation of deformation zone in backward can extrusion.  
 Material—Ma 8 (AISI 1006);  $d_0 = 56 \text{ mm}$  (2.2 in). (a)  $\epsilon_A = 0.316$ .  
 (b)  $\epsilon_A = 0.72$ . (After [15.6].)

area  $\epsilon_A = (A_0 - A_1)/A_0$ . Fig. 15.58 shows the deformation zone for Ma 8 (AISI 1006), for three separate punch positions. Kast [15.6] has shown for comparable cans that for all diameters the form of the deformation zone is similar and the material does not influence the shape of the deformation zone appreciably. The height  $u$  (see Fig. 15.58) of the deformation zone between the punch apex and the undistorted material portion is  $0.4 < u/d_0 < 0.5$  (and increases with decreasing  $\epsilon_A$ ). These values obtained for a punch with a cone angle of  $166^\circ$  agree very well with values for warm extrusion of steel [ $u/d_0 = 0.41$  (independent of  $\epsilon_A$ ) at a cone angle of  $150^\circ$ ] [15.38]. However, variations have been reported for cold extrusion of steel with a  $150^\circ$  cone angle—a value of  $u/d_0 = 0.64$  has been reported in [15.62]. Fig. 15.59 shows the path lines for steel Ma 8 (AISI 1006) with  $\epsilon_A = 0.5$  and  $l_0/d_0 = 1.07$ . They were obtained from the distorted grid pattern using viscoplasticity. A calculated streamline field is illustrated in Fig. 15.60 [15.62]. The streamlines and flow lines are not identical for nonstationary processes. (Streamlines are tangents at points on flow lines; they represent the direction of the stream direction at any instant of time.) The flow lines below the punch exhibit a curvature about the axis and the streamlines are curved toward the outside. Based on viscoplasticity experiments, it is possible to compute the local equivalent strains  $\epsilon$ . Fig. 15.61 shows the values of  $\epsilon$  computed by Schmitt [15.62] for the material region below the punch edge for a bottom thickness  $b/d_D = 0.2$ . This condition represents a fully plastic condition below the punch since  $u/d_0 < 0.5$ . The lowest equivalent strain occurs slightly outside the projection of the punch edges on the bottom surface; the maximum equivalent strain occurs on the press wall. The observed strains on the inner can wall (the increase in surface area is the highest in this case) have not yet been predicted satisfactorily by similar approaches (see Fig. 15.55a).

The deformation zone shown in Fig. 15.58 has also been observed in other investigations [15.63] at higher punch velocities [ $v_p$  up to  $500 \text{ m/s}$  ( $1640 \text{ ft/s}$ )]. Experiments on pure aluminum have shown that the value of  $u/d_0$  decreases with increasing punch velocity.

The so-called free cupping does not belong to the category of can extrusion processes, although for some particular conditions (material,  $\epsilon_A$ ,  $l_0/d_0$ ,  $b/d_0$ ) similar workpieces can be produced by free cupping. The process belongs to the category of indentation processes and is covered in Chap. 17.

### Stresses

Stresses can be determined from strain rates by approximate methods. However, these methods are complicated, using stepwise iterations from the displacement to reduce computational errors.

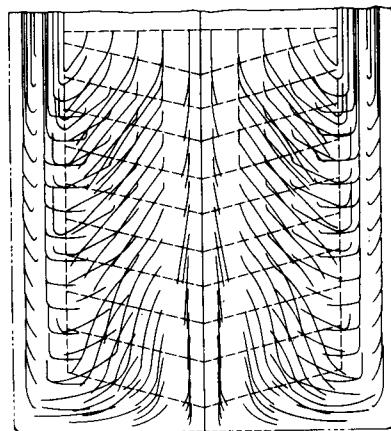


**FIG. 15.59** Flow lines of backward can extrusion. Material—AISI 1006;  $\epsilon_A = 0.5$ ;  $l_0/d_0 = 1.07$ . (After [15.62].)

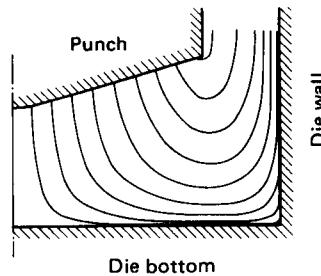


**FIG. 15.60** Calculated streamline field for backward can extrusion. Material—AISI 1015;  $\epsilon_A = 0.15$ ;  $l_0/d_0 = 0.47$ ;  $b/d_D = 0.33$ . (After [15.62].)

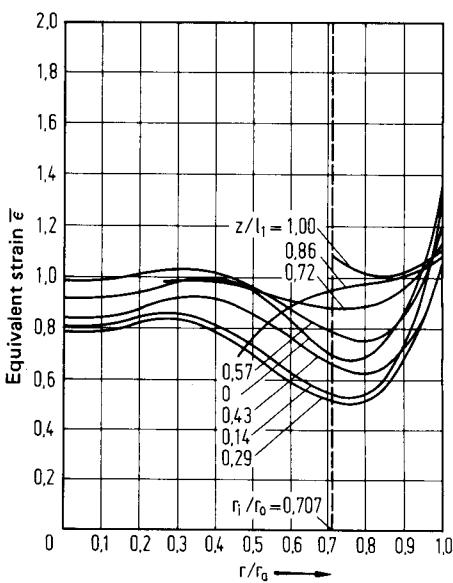


**FIG. 15.61** Calculated localized equivalent strains  $\bar{\epsilon}$  at end of backward can extrusion. Material—AISI 1015;  $\epsilon_A = 0.15$ ;  $l_0/d_0 = 0.47$ ;  $b/d_D = 0.2$ .

Solutions as suggested by Steck [15.15] are not available for many processes. For the case given in Fig. 15.60 Schmitt [15.62] has calculated the trajectory of the principal shear stress (slip-line field) for pieces with rotation symmetry and has shown that the axis of symmetry ( $z$ -axis) is intersected at an angle of  $45^\circ$  by the trajectories of the principal shear stresses. Based on this, the principal normal stress should act along the axis. In the imaginary vertical extension of the punch edge, the trajectory of the principal shear stresses is also vertical. Shearing takes place along this edge. This aspect is assumed in analyzing the backward can extrusion process for force calculations.

A thorough understanding of the stresses prevalent in the deformation zone of the workpiece is not very important from the point of view of formability because of the existence of triaxial compressive stress conditions in the deformation zone. On the other hand, high local stresses acting on the tooling should be known. The important values to be assessed are the punch pressure  $p_{p,\max}$ , the radial pressure acting on the die wall  $p_{W,\max}$ , and the relation between them.

#### Forces and Work Capacity

Fig. 15.62 shows the various forces acting in the backward can extrusion process. The punch force  $F_p$  and the force on the bottom  $F_B$  can be

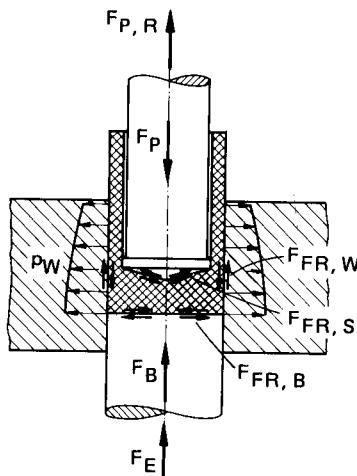


**FIG. 15.62** Forces on tool in backward can extrusion. (After [15.62].)

- A = Start of deformation  
 B = End of process and return of punch  
 C = Lifting of punch tip from the workpiece

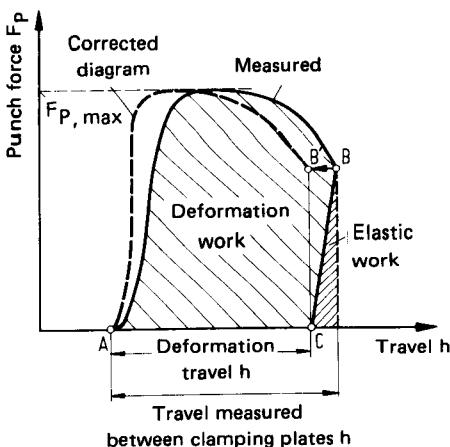


FIG. 15.63 Punch force-travel diagram for backward can extrusion. (After [15.6].)

measured easily. The variation of the punch force  $F_p$  as a function of the deformation travel is shown in Fig. 15.63. The force increases rapidly to its maximum and then reduces slowly to its final value.\* The first portion is characterized by the elastic deflection of the tooling-workpiece system and by the increasing influence of strain hardening, and the second is characterized by the decrease in volume of the material participating in the deformation process. The force variation is therefore different for different reductions of area  $\epsilon_A$ ; the force falls rapidly toward the end for larger values of  $\epsilon_A$  (Fig. 15.64). A force maximum is also observed due to the change in friction conditions from sticking to sliding.

For a very small bottom thickness  $b$ , the force increases again because of the increasing proportion of the axial upsetting force for larger values of  $d_i/b$ . [The variation of the force for  $b < 3$  mm (0.12 in) need not be the same for other billet and can dimensions and for other materials. For thicknesses  $b \geq 3$  mm (0.12 in) (for  $h_i/d_i = 2$  the value of  $l_0/d_0$  can be computed for a given reduction in area), the force-travel diagram can be considered as representative.] The maximum punch force  $F_{p,\max}$  increases with  $\sigma_f$ ,  $\epsilon_A$ , and  $d_0$  (Fig. 15.65). In addition,  $F_{p,\max}$  is dependent on  $l_0/d_0$  for  $0.15 < \epsilon_A < 0.6$  (Fig. 15.66). The punch pressure  $p_{p,\max}$  has minimum values for  $0.15 < \epsilon_A < 0.2$  with  $l_0/d_0 < 0.5$  and for  $0.4 < \epsilon_A < 0.5$  with  $l_0/d_0 > 0.8$ .

If the pressure acting on the can bottom is plotted against  $\epsilon_A$  (Fig. 15.67b), a trend of the punch pressure similar to that in hollow forward extrusion is observed (Fig. 15.67a), although the material flow is very different in these two processes. Neglecting wall friction, the valid equations are

$$F_{p,\max} = p_{p,\max}(A_0 - A_1) = p_{B,\max}A_0 \quad (15.10)$$

and

$$P_{B,\max} = \epsilon_A p_{p,\max} \quad (15.11)$$

From experiments it follows that for  $\epsilon_A \geq 0.45$  the following relationship is valid:

$$p_{W,\max} \approx p_{B,\max} \quad (15.12)$$

\*During its return stroke the punch is subjected to a tensile force due to the stripping action from the cup (or can) wall friction. This axial tensile force is not very important for the process itself and thus not generally determined during measurements.

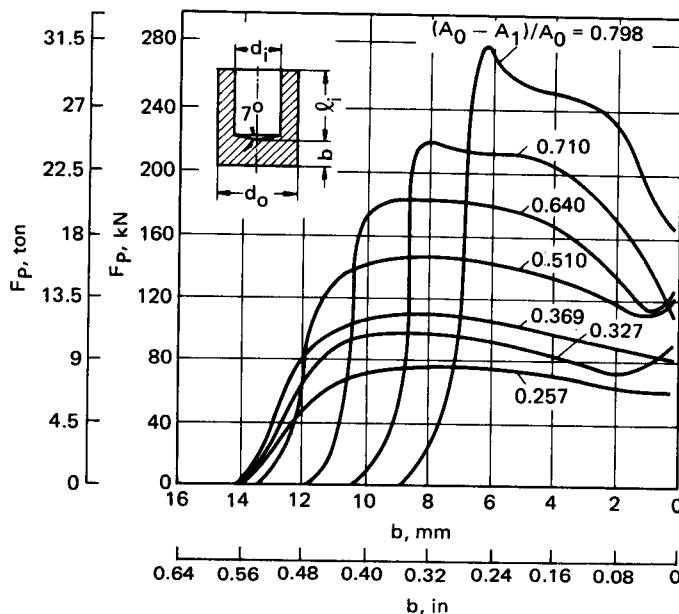


**FIG. 15.64** Measured punch force-travel diagrams for backward can extrusion as a function of reduction of area. Material—AISI 1006;  $d_0 = 14 \text{ mm}$  (0.55 in);  $l_i/d_i = 2$ ;  $b = 3 \text{ mm}$  (0.12 in). (After [15.64].)

The value of  $p_{W,\max}$  is the equivalent normal pressure on the die wall. Fig. 15.68 shows the relationship between  $p_{P,\max}$  and  $p_{W,\max}$  as a function of the reduction of area  $\epsilon_A$ .  $p_{W,\max}$  increases with  $\epsilon_A$ , but not proportionately. Here, for Ck15 (AISI 1015), when  $\epsilon_A = 0.2$ ,  $p_{W,\max} \approx 600 \text{ N/mm}^2$  (87 ksi), when  $\epsilon_A \approx 0.5$ ,  $p_{W,\max} \approx 1100 \text{ N/mm}^2$  (160 ksi), and when  $\epsilon_A = 0.8$ ,  $p_{W,\max} \approx 2000 \text{ N/mm}^2$  (290 ksi).

The friction force on the wall  $F_{FR,W}$  depends on the reduction of area and the billet dimensions. For the same  $d_0$ , larger values of  $l_0/d_0$  lead to higher values of  $F_{FR,W,\max}$ . For the same  $l_0/d_0$ ,  $F_{FR,W,\max}$  increases with increasing  $d_0$ . The maximum value occurs for  $\epsilon_A \approx 0.5$ . Plotting the ratio  $F_{FR,W,\max}/F_{P,\max}$  against  $\epsilon_A$  shows a degressive variation (Fig. 15.69). The curves shown for Ck15 (AISI 1015) in Fig. 15.69 are also reasonably accurate for 16MnCr5 (AISI 5117) and Ma8 (AISI 1006). For steels like Ck35 (AISI 1035) values are smaller for smaller  $\epsilon_A$ .

The axial force, which acts partly on the punch section and partly on the can bottom, can be computed by several methods.

**Calculation using deformation efficiency:** The force-travel diagram for backward can extrusion can be considered trapezoidal in shape except for cans with bottom thickness less than 3 mm (0.12 in) (Fig. 15.64). The variations between maximum and minimum force are also small. Similar to the method proposed in Sec. 15.2.3, the maximum force can be calculated if  $A_0$ ,  $\sigma_f$  or  $\sigma_{f,m}$ ,  $\eta_{def}$ , and  $\varphi_{\max}$  are known. As will be shown shortly, an exact determination of  $\varphi_{\max}$  and  $W_{id}$  is very difficult. This will also affect the exact determination of  $\eta_{def}$  and  $\sigma_f = f(\varphi)$ . Hence values of  $\eta_{def}$  for some ranges of  $\varphi_{\max}$  are given. This will help in determining the maximum punch force  $F_{P,\max}$ . For practical applications, a nomogram developed by Burgdorf and Müschenborn [15.22] can be used. (This nomogram is also included in [15.2].) Corrections for ratios of billet dimensions  $l_0/d_0$  and absolute outer diameters are also given.

**Calculation using analytical equations:** Eq. 15.2 can be used to calculate the forces in backward can extrusion. The following values have to be used for the constants:

Constant	<i>a</i>	<i>m</i>	<i>n</i>
Value	17.66	0.91	0.73

The equation calculates  $p_{B,\max}$ ;  $p_{P,\max}$  can then be found using Eq. 15.11. The equation is valid for steel with  $97 < HB < 153$  and extrusion ratios  $1.2 < A_0/A_1 < 6.5$  ( $0.16 < \epsilon_A < 0.83$ ), and for billet dimensions  $l_0/d_0 < 75$  mm (3 in) with  $0.5 < l_0/d_0 < 1.3$ . The effect of  $l_0/d_0$  on  $p_{B,\max}$  can be considered by applying a correction factor to the nomogram given in [15.23]. The values thus calculated are accurate to within  $\pm 10\%$  assuming that the billets are phosphated and lubricated with Bonderlube 235.

Another equation based on measured values has been suggested by Schmitt [15.65]:

$$p_{B,\max} = K \sqrt{\frac{A_0}{A_1} - 1} \quad (15.13)$$

The *K* factor, which has an accuracy of  $\pm 4.5\%$  (deviation between measured and functional values), is given by

$$K = 2.4S_u + 50 \quad [\text{N/mm}^2] \quad (15.14)$$

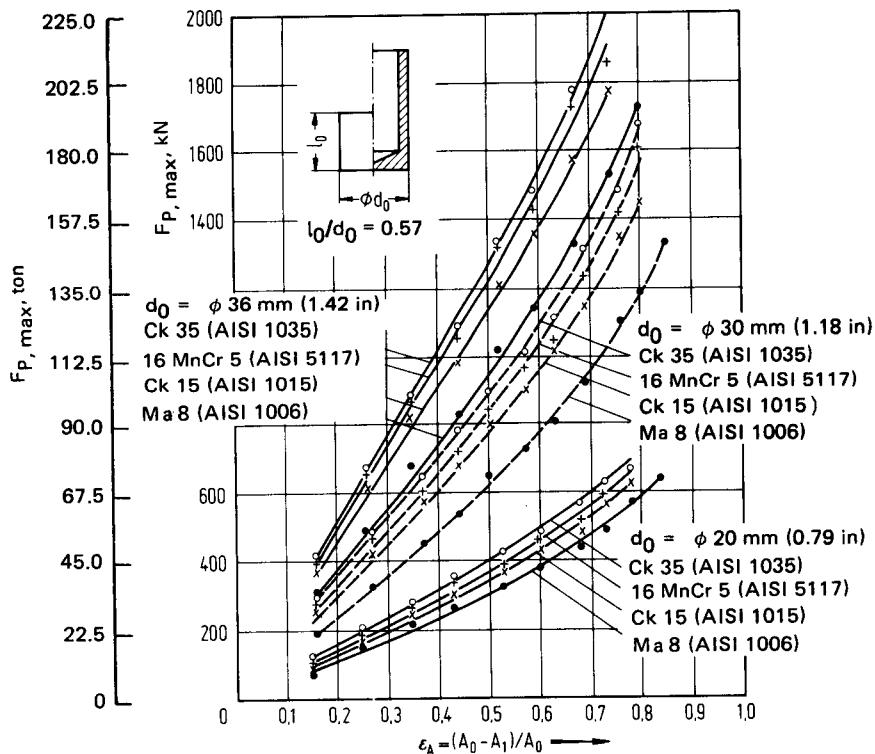


FIG. 15.65 Dependence of maximum punch force on reduction of area, material, and can diameter in backward can extrusion. (After [15.62].)

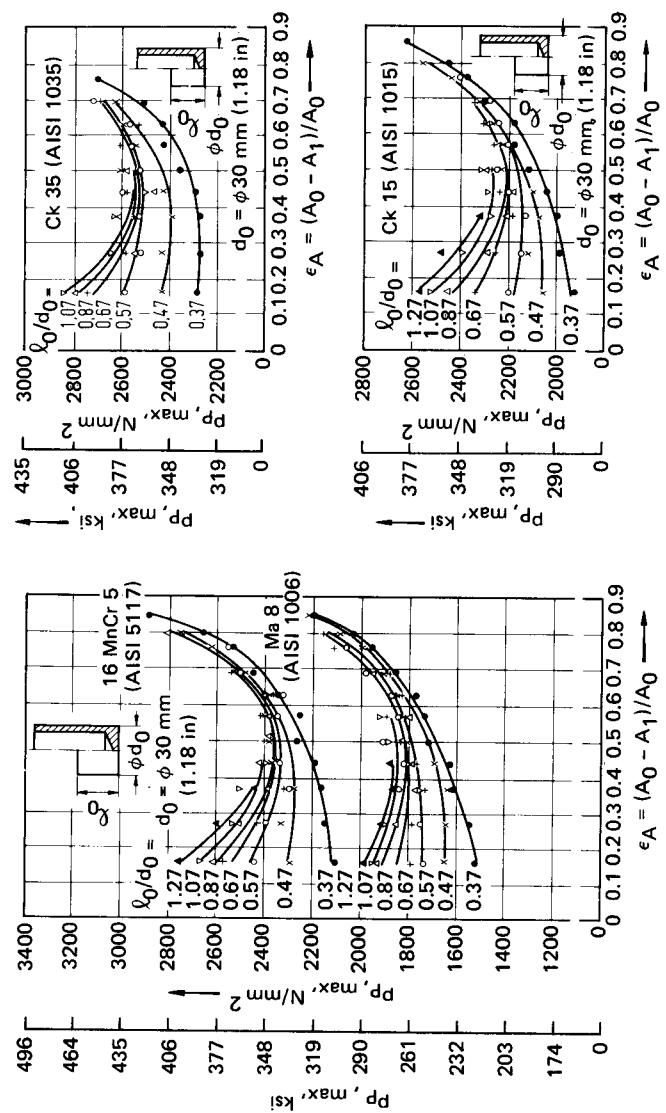


FIG. 15.66 Punch pressure versus reduction of area with material and  $l_0/d_0$  as parameters. (After [15.62].)

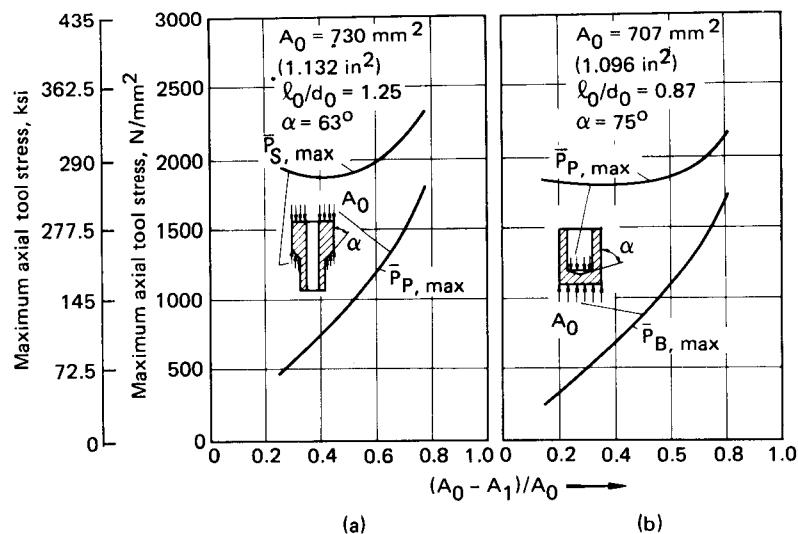


FIG. 15.67 Maximum axial stress. Material—Mbk 6 (AISI 1006);  $\bar{P}_{s,\max} = F/(\text{projected area of shoulder})$  represents pressure acting on shoulder area for hollow forward extrusion. (a) Hollow forward extrusion. (b) Backward can extrusion. (After [15.62].)

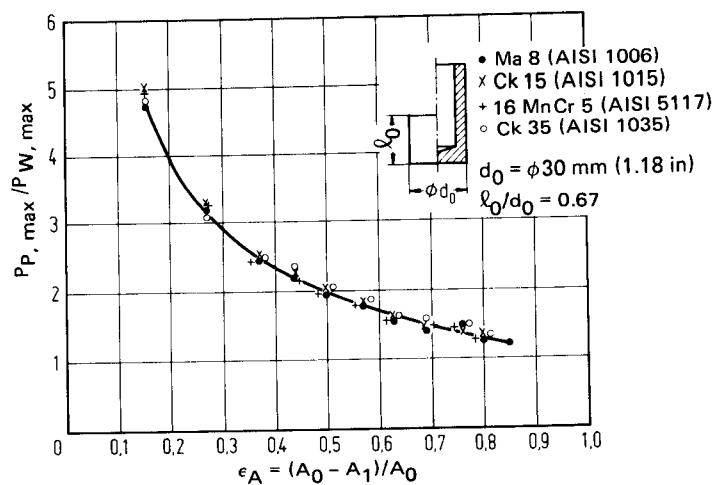


FIG. 15.68 Relationship between the ratio of punch force to equivalent normal pressure on die wall and reduction of area in backward can extrusion. (After [15.62].)

For annealed workpieces the following  $K$  values have been found for some common materials:

Material		
DIN	U.S.	$K$
Al 99.5	AA 1050	212
E Cu	Electrolyte copper	569
Ma 8	AISI 1006	869
Ck 15	AISI 1015	1071
16MnCr 5	AISI 5117	1136
Ck 35	AISI 1035	1230

The correction factor  $q$  (Fig. 15.70) takes into consideration the effect of the billet dimensions  $l_0/d_0$  on the punch force. No correction factor is considered for outer can diameter  $d_o$ . (The  $K$  values given above are based on measurements of cans with 30 and 36 mm (1.12 and 1.42 in) outer diameter.)

Using Eqs. 15.11, 15.13, and 15.14, the equation for the maximum punch pressure is

$$p_{P,\max} = q(2.4S_u + 50) \frac{A_0}{A_0 - A_1} \sqrt{\frac{A_0}{A_1} - 1} \quad [\text{N/mm}^2] \quad (15.15)$$

and the equivalent normal pressure on the die wall is

$$p_{W,\max} = zq(2.4S_u + 50) \sqrt{\frac{A_0}{A_1} - 1} \quad [\text{N/mm}^2] \quad (15.16)$$

where  $z$  is another correction factor given as follows:

$A_0 - A_1$	$z$
0.16	1.33
0.20	1.28
0.30	1.12
0.40	1.04
0.45 and larger	1.00

In the material range considered,  $z$  is independent of material.

**Calculation based on elementary plasticity theory:** The two methods suggested above permit calculating only  $F_{P,\max}$  or  $p_{P,\max}$ ; a method using elementary plasticity theory will be able to compute the force-travel variation. Dipper [15.66] considers the process of backward can extrusion as a double upsetting process (Fig. 15.71). The workpiece is upset first axially, between the punch and the die bottom (or the ejector), and later radially, between the workpiece portion below the punch and the die wall. The two deformation zones are the axial upsetting zone 1 and the radial upsetting zone 2. The material 3 squeezed into the ring zone between the punch and the die is considered rigid. Another assumption made is that thin-walled cans with  $\epsilon_A \geq 0.5-0.6$  are extruded. For zone 2 (radial upsetting), the coefficient of friction between zones 1 and 2, accord-

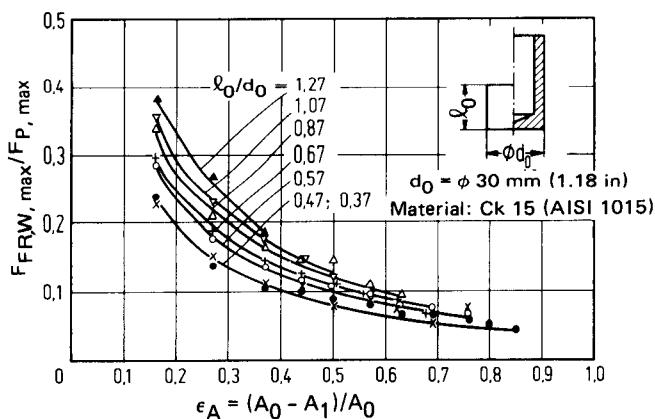


**FIG. 15.69** Plot of  $F_{FRW,\max}/F_{P,\max}$  versus reduction of area in backward can extrusion. (After 15.62].)

ing to Tresca, is  $\mu_2 = 0.5$  (the material undergoes shear here); on the press wall  $\mu = \mu_1$ . The following equation is used for computing the coefficient of friction:

$$\mu = \frac{1}{2}(\mu_1 + 0.5) \quad (15.17)$$

The frictional forces are calculated based on an average cylinder with radius  $(d_i + s)/2$ . The force equilibrium on a ring element in zone 2 gives:

$$[-\sigma_{z,2} + (\sigma_{z,2} + d\sigma_{z,2})] \frac{\pi}{4} (d_o^2 - d_i^2) = 2\mu\sigma_{f,2} dz \frac{d_i + s}{2} 2\pi$$

$$d\sigma_{z,2}s = 2\mu\sigma_{f,2} dz$$

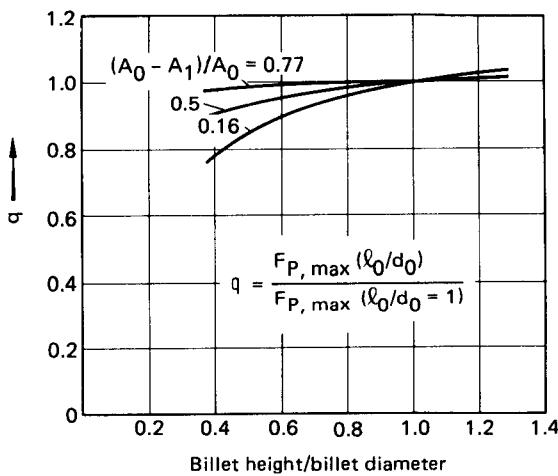


**FIG. 15.70** Correction factor  $q$  for taking billet dimensions into consideration. (After [15.65].)

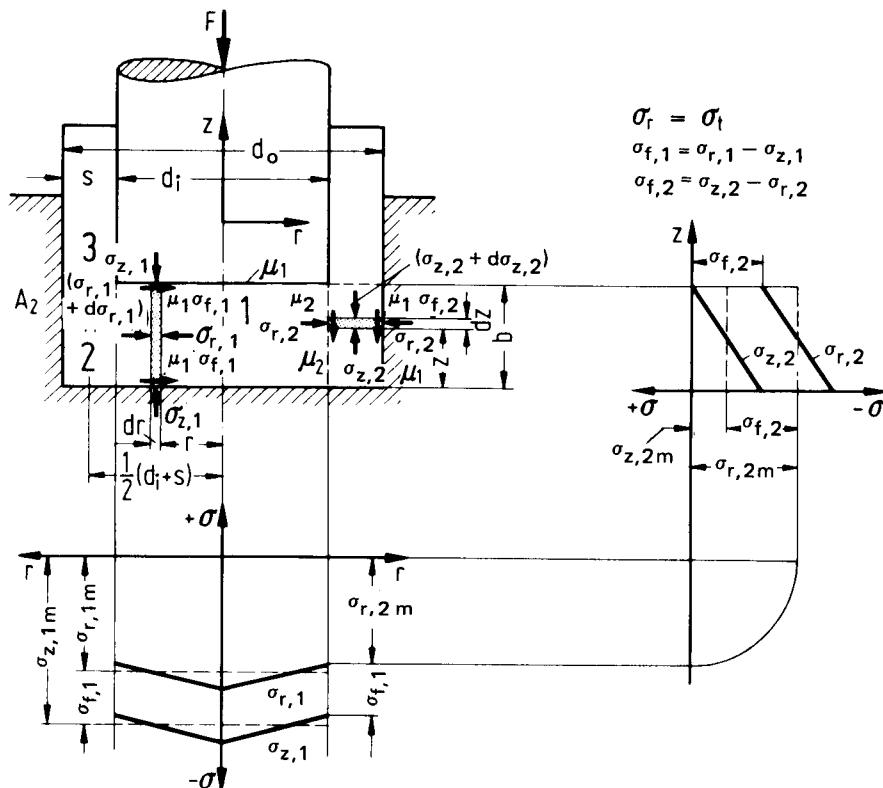


FIG. 15.71 Backward can extrusion as a double upsetting process. (After [15.66].)

Integrating with the boundary condition  $\sigma_{z,2} = 0$  at  $z = b$ , we have

$$\sigma_{z,2} = -\frac{2\mu\sigma_{f,2}}{s}(b - z) \quad (15.18)$$

The average normal stress can be calculated for the area  $A_2 = 2[(d_i + s)/2]\pi b$  as

$$\sigma_{z,2m} = -\mu\sigma_{f,2} \frac{b}{s} \quad (15.19)$$

According to the Tresca flow condition,

$$\sigma_{r,2m} = \sigma_{z,2m} - \sigma_{f,2} = -\sigma_{f,2} \left(1 + \mu \frac{b}{s}\right) \quad (15.20)$$

For zone 1—axial upsetting—the force equilibrium equation on the ring element is

$$\begin{aligned} [-\sigma_{r,1} + (\sigma_{r,1} + d\sigma_{r,1})]\pi rb &= 2\mu_1\sigma_{f,1}\pi r dr \\ d\sigma_{r,1}b &= 2\mu_1\sigma_{f,1} dr \end{aligned}$$

Using the boundary condition  $\sigma_{r,1} = \sigma_{r,2m}$  for  $r = d_i/2$  (transposition of the average radial pressure from zone 2 to zone 1), we have

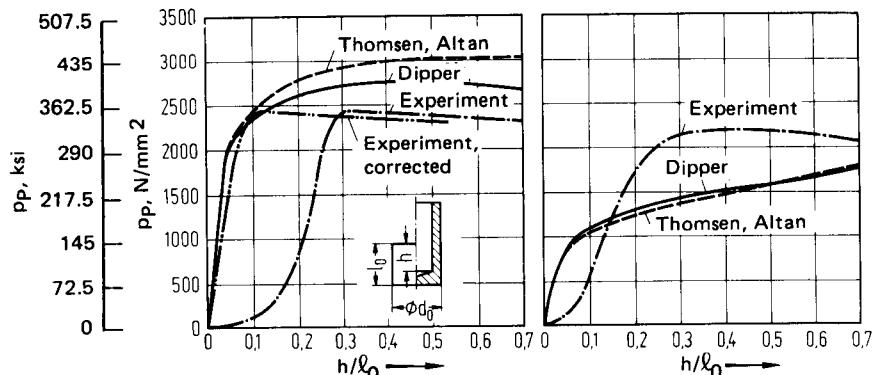


**FIG. 15.72** Comparison between calculated and measured force–travel diagrams of backward can extrusion. Material—AISI 1015;  $d_0 = 30 \text{ mm}$  (1.2 in);  $l_0/d_0 = 0.47$ ; coefficient of friction  $\mu = 0.04$ . (a)  $\epsilon_A = 0.08$  ( $A_0/A_1 = 5$ ). (b)  $\epsilon_A = 0.16$  ( $A_0/A_1 = 1.19$ ). (After [15.62].)

$$\sigma_{r,1} = -\frac{\mu_1 \sigma_{f,1}}{b} \left( \frac{d_i}{2} - r \right) + \sigma_{r,2,m} \quad (15.21)$$

The average radial stress over the area  $\pi d_i^2/4$  is given by

$$\sigma_{r,1,m} = -\frac{1}{3} \mu_1 \sigma_{f,1} \frac{d_i}{b} + \sigma_{r,2,m} \quad (15.22)$$

Substituting for  $\sigma_{r,2,m}$  from Eq. (15.20), we obtain the average radial stress as

$$\sigma_{r,m} = \sigma_{r,1,m} + \sigma_{r,2,m} = -\frac{1}{3} \mu_1 \sigma_{f,1} \frac{d_i}{b} - \sigma_{f,2} \left( 1 + \mu \frac{b}{s} \right) \quad (15.23)$$

Applying the Tresca flow condition, the axial stress on the punch is

$$\begin{aligned} \sigma_{z,m} &= \sigma_{r,m} - \sigma_{f,1} \\ &= -\sigma_{f,1} \left( 1 + \frac{1}{3} \mu_1 \frac{d_i}{b} \right) - \sigma_{f,2} \left( 1 + \mu \frac{b}{s} \right) = p_p \end{aligned} \quad (15.24)$$

The  $\sigma_f$  values are to be obtained from the flow curves,

$$\begin{aligned} \sigma_{f,1}: \varphi_1 &= \ln \left( \frac{l_0}{b} \right) \quad (l_0 \text{ being initial billet length}) \\ \sigma_{f,2}: \varphi_{tot} &= \varphi_1 + \varphi_2 = \varphi_1 \left( 1 + \frac{d_i}{8s} \right) \end{aligned} \quad (15.25)$$

Altan and Thomsen [15.67] have also considered the double upsetting process for computing the axial punch pressure. However, the normal stress is not taken as  $\sigma_f$  but as the unknown stresses  $\sigma_z$  and  $\sigma_r$ . A comparison of the two methods with experimentally measured values for a can having  $\epsilon_A = 0.8$  ( $A_0/A_1 = 5$ ) is shown in Fig. 15.72. The computed values are higher than the measured values. The results obtained with the method suggested by Dipper are closer to the measured values. Dipper's multiplication factor of  $(1 + d_i/8s)$  for  $\varphi_{tot}$  is lower than the factor  $(1 + d_i/2\sqrt{3}s)$  used by Altan and Thomsen. The force–travel diagrams computed according to both methods compare very well with that for the measured values if the experimental value is corrected for tool–workpiece clearance. Fig. 15.72b clearly shows that experiment and theory do not correlate very well for small reductions of area, that is, for thick-walled cans.\*

\*Selection of the coefficient of friction is a problem. The value of 0.04 used by Schmitt [15.62] was based on experiments. This value can be considered realistic for the above comparison.

Using the values of equivalent strains  $\bar{\epsilon}$  (see Fig. 15.61), Schmitt calculated the average equivalent strain  $\bar{\epsilon}_m$  for regions 1 and 2 for a given time at any punch travel as

$$\bar{\epsilon}_m = \frac{1}{V} \int_V \bar{\epsilon} dv \quad (15.26)$$

(Schmitt also equates  $\bar{\epsilon} = \varphi_m$ .) For region 1,  $\bar{\epsilon}_m$  is very nearly equal to  $\varphi_m = \ln(l/l_0)$ , or  $\varphi_1$ . For region 2, the value  $\bar{\epsilon}_m$  calculated by the above procedure results in smaller values than those calculated for  $\varphi_2$  by Altan and Thomsen and by Dipper. However, if one considers the average natural strain based on the equation

$$\varphi_m = \frac{\varphi_1 V_1 + \varphi_2 V_2}{V_1 + V_2} \quad (15.27)$$

then a very good agreement with the calculated value is obtained. This value is only slightly higher than  $\bar{\epsilon}_m$  using Dipper's equation, and the deviation of  $\varphi_m$  calculated using the equation of Altan and Thomsen is double that value ( $\approx 20\%$ , compared with 10% using Dipper's equation, for a punch travel corresponding to  $h/l_0 = 0.55$ ).

In all the above discussions, the deformation ratio or natural strain  $\varphi_m$  (which is obtained from the strain in the complete workpiece or in the larger region of the workpiece, assuming homogeneous deformation) is compared with the equivalent strain  $\bar{\epsilon}_m$  (calculated from the summation of strains experienced by a particle along a motion line). The comparison has therefore only limited validity.

Other methods of calculating the total deformation ratio have been suggested. The equation

$$\varphi_{tot} \approx \ln \frac{d_0}{d_0 - d_i} - 0.16 \quad (15.28)$$

proposed by Siebel and Fangmeier [15.68] gives a constant value over the entire length of the punch stroke. Plotted against  $\epsilon_A$ , the above value agrees very well, at  $\epsilon_A = 0.8$ , with  $\varphi_{tot}$  calculated according to Dipper for  $l_0/b = 1.6$ . (For higher values of  $l_0/b$  the agreement is not good);  $\varphi_{tot}$  is calculated in the above comparison by  $\varphi_{tot} = \varphi = \ln(A_0/A_1)$  [15.69]. The workpiece geometry thus has a considerable influence.

**Calculation using upper-bound method:** Among several solutions based on the upper-bound method, only those suggested by Steck [15.24], Tirosh [15.70], and Kudo and Johnson [15.71], [15.72] are reviewed here. These are based on the three velocity fields shown in Fig. 15.73: the parallel field, the spherical field, and the combined parallel and triangular field. A comparison of the results calculated from the above three velocity fields with experimental values, for Ma8 (AISI 1006), Ck15 (AISI 1015), and commercially pure aluminum [15.62], has shown that with the parallel and spherical velocity fields an upper-bound solution can be established for the pres-

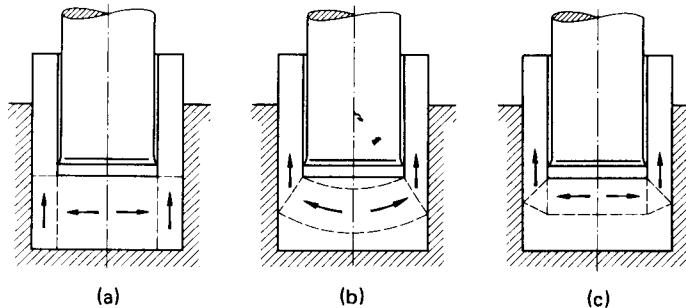


FIG. 15.73 Velocity field for force calculation by upper-bound method for backward can extrusion. (a) Parallel field. (After [15.24].) (b) Spherical field. (After [15.70].) (c) Combined field. (After [15.71], [15.72].)

sure variation  $p_{P,\max}$  with  $\epsilon_A$  or  $A_0/A_1$  [15.69]. The results obtained with  $\mu = 0.1\text{--}0.2$  for the parallel velocity field are somewhat closer to the measured values. Weber [15.69] has constructed a nomogram with this velocity field to calculate the punch pressure  $p_{P,\max}$ . The nomogram also considers the effect of the billet dimension  $l_0/d_0$  at  $\epsilon_A < 0.5$ . The average natural strain is calculated by using the model of the double upsetting process for the above nomogram:

$$\varphi_m = \varphi_1 \frac{d_i^2}{d_o^2} + \varphi_2 \frac{d_o^2 - d_i^2}{d_o^2} \quad (15.29)$$

Eq. 15.29 follows from volume constancy if the bottom thickness at the beginning of the process is  $b = 1$ . The upper-bound solution based on the spherical velocity field (this considers the rigid material under the punch very effectively) (Fig. 15.73b) leads to the following equation, neglecting the effect of the punch-head shape,

$$\frac{p_{P,\max}}{\sigma_f} = 2 \ln \frac{d_o}{d_i} + \frac{\sqrt{2}}{3} \sqrt{\ln \frac{d_o}{d_i} \left( 4 - \frac{1}{2} \ln \frac{d_o}{d_i} \right)} \quad (15.30)$$

Eq. 15.30 agrees well with experimental results (for copper and aluminum) in the region of  $0.2 < \epsilon_A < 0.95$ . The results also agree well with the solution in [15.71], [15.72] based on the combined velocity field (Fig. 15.73c).

For industrial practice it is recommended to use at least two or three of the above suggested methods.

### 15.8.2 Effect of Workpiece Dimensions on the Extrusion Force and Similarity Laws

The effect of the billet dimension ratio  $l_0/d_0$  on the axial force was discussed in the preceding section (Fig. 15.66). The minimum value of the maximum punch pressure  $p_{P,\max}$  as a function of the reduction in area  $\epsilon_A$  was also discussed together with the correction factor that considers the effect of the variable  $l_0/d_0$  ratio.

The absolute value of the outer diameter determines the size of an extruded can. If, for example, the diameter increases from 14 to 80 mm (0.55 to 3.15 in) (Fig. 15.74) [15.6], the ratio of the frictional area on the punch and due to the billet volume decreases hyperbolically. The punch force per unit volume decreases with increasing outer can diameter because of the high proportion of the frictional force in the total force. For some conditions the punch force per unit volume decreases also with increasing  $\epsilon_A$ . The flow stress  $\sigma_f$  also plays a role. For example, for Ck 15 (AISI 1015) and  $\epsilon_A = 0.8$ , the punch force per unit billet volume is  $320 \text{ N/mm}^2$  (46 ksi) for  $d_0 = 14 \text{ mm}$  (0.55 in), and  $80 \text{ N/mm}^2$  (14 ksi) for  $d_0 = 56 \text{ mm}$  (2.20 in). Kast [15.6], [15.73] has conducted extensive experimental investigations for six can diameters between 14 and 80 mm (0.55 and 3.15 in) with eight different reductions in area ( $\epsilon_A$  between 0.25 and 0.79) and for six different materials [aluminum Al 99.5 (AA 1050), Al Zn Mg Cu 1.5 (AA 7075), steel Ma 8 (AISI 1006), Ck 15 (AISI 1015), Ck 35 (AISI 1035), and 16 MnCr 5 (AISI 5117)] to determine similarities between comparable quantities: geometry of tool and workpiece, forces and work required for the process, and velocities as well as temperatures at the end of the deformation process due to the conversion of deformation work to heat energy. If the similarity conditions—geometry, time-dependent values, forces, and temperature scale of a mechanical system—are fulfilled, the punch pressure must be the same for all can diameters provided the material of the workpiece and the experimental conditions are the same. However, in the region of  $14 \text{ mm}$  (0.55 in)  $< d_0 < 80 \text{ mm}$  (3.15 in) the punch pressure  $p_{P,\max}$  decreases by 10% for all values of  $\epsilon_A$ . This is explained by the reduction of the friction component and the nonuniformity of the average can temperature. Smaller cans with higher frictional areas (higher contact areas) for heat conduction cool faster than larger cans with smaller frictional areas. This means that the temperature scale for similarity is not satisfied. The similarity law can be applied to approximate the punch forces from experiments conducted on softer-material and smaller-diameter cans:

$$F_{P,\max} = m F'_{P,\max} \frac{\sigma_{f,m}}{\sigma'_{f,m}} \frac{1}{\lambda^2} \quad (15.31)$$

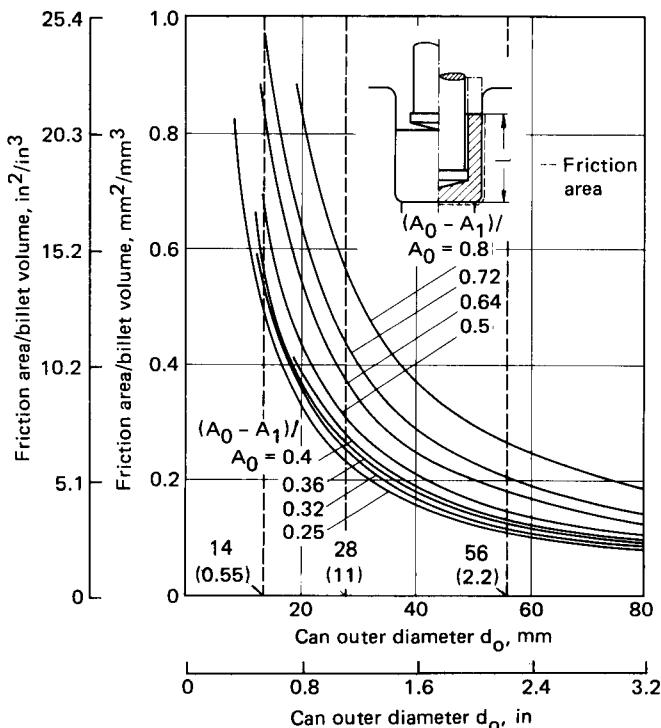


**FIG. 15.74** Ratio of friction area to billet volume at the instant of maximum punch pressure. (After [15.6].)

where  $F_{P,\max}$  = punch force for actual case

$F'_{P,\max}$  = punch force on model [a minimum diameter of the billet  $d_0 = 20$  mm (0.8 in) is recommended; smaller models are not suitable due to temperature variations between model and actual workpiece]

$m$  = correction factor

$\sigma_{f,m}$  = mean flow stress of actual workpiece

$\sigma'_{f,m}$  = mean flow stress for model workpiece

$\lambda$  = scale factor between model and actual workpiece,  $= d_0/d'_0$

$\sigma_{f,m}$  is calculated from the flow curve as  $(\sigma_{f,0} + \sigma_{f,1})/2$  with  $\sigma_{f,0} = S_y$  (yield strength) and  $\sigma_{f,1} = K\varphi_{tot}^n$ , using  $\varphi_{tot} = \ln(l_0/b)(1 + d_i/8s)$  based on Dipper [15.66]. The correction factor  $m$  is the ratio of calculated to measured punch force. For four material pairs (the softer material being used for the model)  $m$  can be determined from Fig. 15.75. The selected material pairs are materials that are used widely in industry. Linear interpolation to consider the effect of  $\epsilon_A$  is also possible.

### 15.8.3 Effect of Punch Shape on the Extrusion Force

#### *Effect of Punch-Face Shape*

The different punch-face shapes used for cold extrusion are shown in Fig. 15.76. Since the material glides along the face of the punch under enormous punch pressures, the punch-face shape has a great effect on the frictional force and hence the maximum punch force.

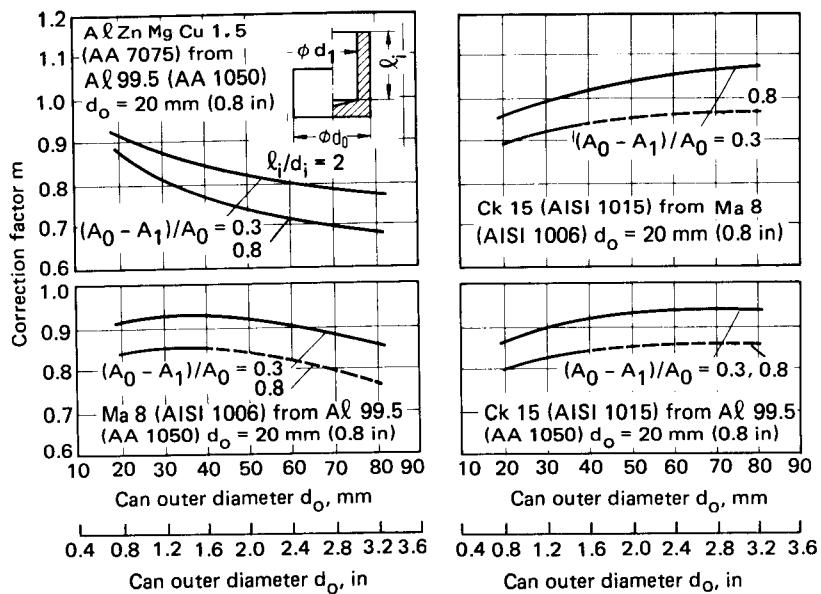


FIG. 15.75 Correction factor  $m$  for calculating the maximum punch force from model tests.  
(After [15.6], [15.73].)

Flat punches are very easy to manufacture. However, they require maximum punch pressures for a wide range of  $\epsilon_A$ . For geometry requirements, the flat punch is used for tubes, sleeves, and cups made from light metals. Punches with conical faces require lower punch pressures. The value of the punch pressure decreases with decreasing angle  $2\alpha$  (Fig. 15.77). Again based on geometrical considerations, a conical angle  $2\alpha$  between 160 and 170° is recommended for conical-faced punches. Punches with hemispherical faces require the least punch pressures [15.74], but the application of such a punch is very limited because of geometrical considerations of the work-piece. Punches with spherical faces are said to be optimum from the point of view of the smallest deformation work and punch force according to calculations of Tirosh [15.70] based on the spherical velocity field in Fig. 15.78b. The optimum angle  $\gamma$  (determined by  $r$ ) depends on  $\epsilon_A$ . It can be obtained from Fig. 15.78. For thin-walled cans, punches with flat faces are used; for thicker cans conical punches are used as an alternative to spherical shapes based on both theory and practice.

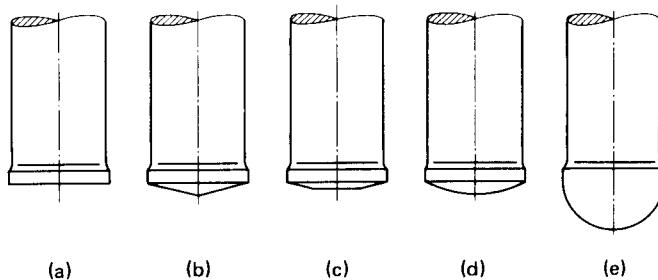


FIG. 15.76 Punch-face shapes for backward can extrusion. (a) Flat. (b) Conical. (c) Flat and conical. (d), and (e) Spherical.

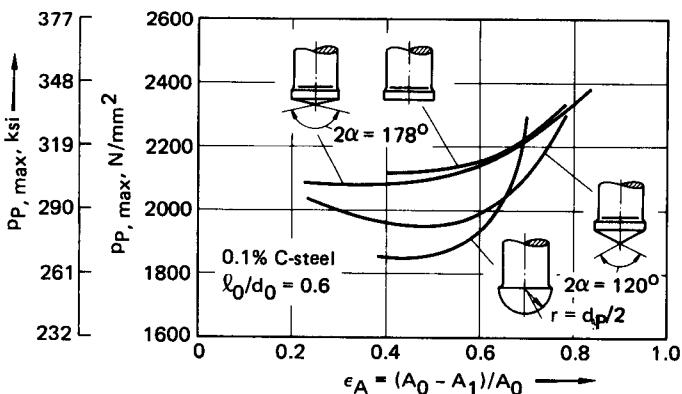


FIG. 15.77 Effect of punch-face shape on maximum punch pressure in backward can extrusion. (After [15.74].)

The effect of a combination of flat and conical punch faces on the punch pressure has not yet been thoroughly investigated. The curve for such a shape lies between those for flat and for spherical shapes. The advantage of this combination is that the lubricant carrier and the lubricant cannot be separated that easily or overextended locally as is the case with conical faces. This combination is therefore also recommended in [15.48]. The results discussed in the preceding sections were obtained using conical punches with  $150^\circ < 2\alpha < 176^\circ$ .

#### Effect of Punch Cross-Sectional Shape

There are two main factors which may affect the maximum punch pressure for different cross sections of a punch with cylindrical outer surfaces and constant reductions in area: (1) The circumference of the die land on the punch ( $\pi d_p$  for a circular punch) varies, and with it presumably the friction force in the region. (2) The material flow is no longer symmetrical; that is, the local distortions and the velocities associated with them are expected to differ. However, investigations by Kast [15.6] on cans with eight axisymmetric inner shapes showed that for all materials tested at the same  $\epsilon_A$ , seven inner shapes showed no variations in the maximum punch pressure. For the eighth shape higher values were recorded; here the local  $\epsilon_A$  was higher because of a larger circumferential area with smaller wall thickness. Thus even there the value of the total length of the punch land had no effect on  $p_{P,\text{max}}$  (Fig. 15.79).

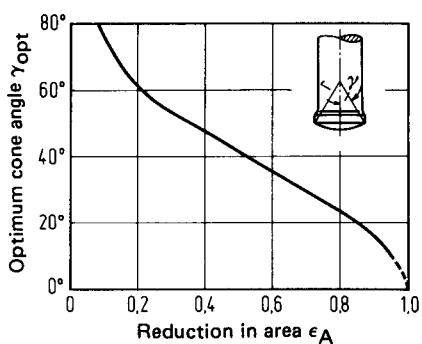


FIG. 15.78 Optimum angle  $\gamma$  for spherical punch face in backward can extrusion. (After [15.70].)

#### 15.8.4 Friction and Lubrication

The following forces act on the different portions of the tool and the workpiece during the deformation process: the punch force  $F_p$ , the force on the bottom  $F_B$  as a reaction to the punch force, the radial or normal pressure on the die wall  $p_w$ , and the frictional forces  $F_{FR,W}$  (on the wall),  $F_{FR,S}$  (on the punch), and  $F_{FR,B}$  (on the bottom) (Fig. 15.62). The ratio of the frictional force  $F_{FR,W}$  to the punch force  $F_p$  decreases with decreasing reduction of area  $\epsilon_A$  (Fig. 15.69). The ideal deformation force, however, increases correspondingly.

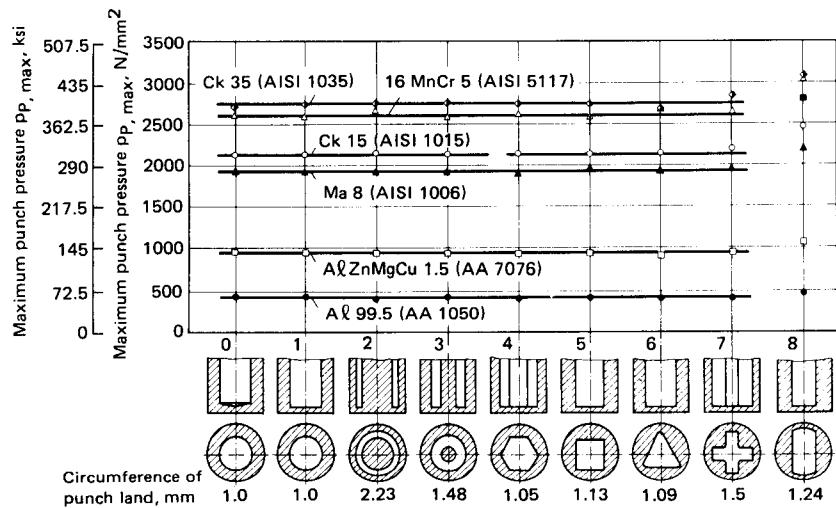


FIG. 15.79 Maximum punch pressure as a function of cross-sectional punch shape.  $d_0 = 40 \text{ mm}$  (1.67 in);  $\epsilon_A = 0.39$ . (After [15.6].)

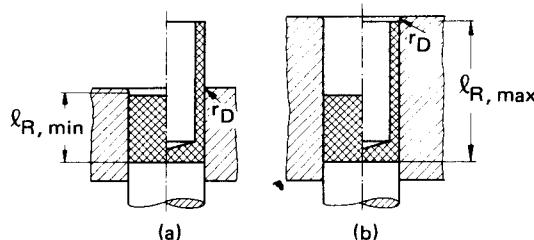
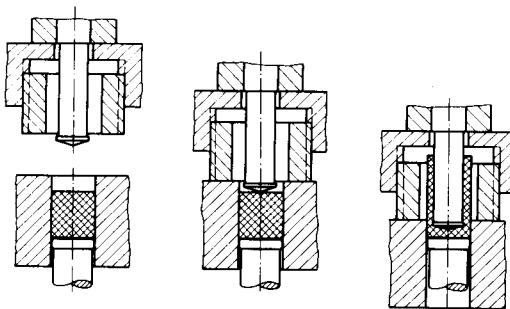


FIG. 15.80 Billet and die shape for backward can extrusion.  
(a) Billet not placed deep inside die. (b) Billet placed deep inside die. (After [15.62].)

During the return stroke of the punch or during ejection, axial forces caused by friction act on the punch ( $F_{\text{FR},P}$ ) and ejector ( $F_{\text{FR},E}$ ) (Fig. 15.62). These forces are affected by the material and the geometry (billet, can) of the workpiece, the process ( $\epsilon_A, l_i/d_i, b, \phi$ ), and the tool geometry. The force acting on the bottom  $F_B$  is smaller than the punch force  $F_P$  by the amount of friction force acting on the wall  $F_{\text{FR},W}$ , which can act in the direction of either  $F_P$  or  $F_B$ , depending upon the local radial pressure  $p_w$  and the relative movement between the workpiece and the tool. Placing the billet as shown in Fig. 15.80a reduces the punch force by a few percent; the major portion of the extruded workpiece has no contact with the die wall. Using a moving die (Fig. 15.81)—this can correspond to placing the billet as shown in Fig. 15.80a for the entire deformation process—will help in reducing the maximum punch force  $F_{P,\text{max}}$  for workpieces with large  $l_0/d_0$  ratios. The higher tooling costs for this design of die movement may not prove worthwhile, especially for cans with large heights.\*

\*Application of a moving die represents the transition to forward can extrusion—in this case the punch is fixed. Therefore the same advantage can be obtained more easily, with simpler tools, by using forward can extrusion.



**FIG. 15.81** Moving die in backward can extrusion. (After [15.62].)

The coefficient of friction  $\mu$  can be determined from a knowledge of frictional and normal forces. Experimentally determined values can also be used for this purpose. The average normal pressure  $p_w$  can be measured by strain measurements on the circumference of the die assembly after initial calibration with media simulating hydrostatic behavior. The coefficient of friction  $\mu$  determined from such experiments decreases with increasing  $p_w$ , as is to be expected from the definition of  $\mu$  itself (Fig. 15.82).

For a can with  $\epsilon_A = 0.5$  and  $l_0/d_0 = 0.67$ , from Fig. 15.66 the maximum punch pressure  $p_{P,\max}$  is  $\approx 2200 \text{ N/mm}^2$  (320 ksi), and from Fig. 15.68 the wall pressure  $p_{W,\max}$  is  $1100 \text{ N/mm}^2$  (160 ksi). From Fig. 15.82 the average coefficient of friction for this wall pressure is  $0.023 < \mu < 0.042$ . It is therefore recommended to use an average coefficient of friction  $\mu_m \approx 0.04$  for backward can extrusion of steel in the region  $0.4 < \epsilon_i < 0.6$ .

Lubricants should not only reduce the coefficient of friction from the point of view of reducing force and work requirements, but also separate the friction partners tool-workpiece to prevent cold welding. The inner surface of a backward extruded can is especially susceptible to cold welding because of very high surface-area increases<sup>\*</sup>—for example, for  $\epsilon_A = 0.8$  and  $l_i/d_i > 2.5$ , we have  $A_{i,1}/A_{i,0} = 9$  [15.36]. The suitability of a lubricant with regard to the achievable surface-area increase and a sufficient separation between friction partners so that no cold welding occurs can be judged from the maximum achievable ratio  $l_i/d_i$  without any cold welding [15.75]. For can extrusion at room temperature metal soaps are suitable for small reductions in area; MoS<sub>2</sub> and graphite in combination with a lubricant carrier are used for larger reductions in area. At higher temperatures, up to  $T \approx 675^\circ\text{C}$  (1250°F), graphite dispersions on a phosphate layer give satisfactory results [15.75].

A detailed description of the coefficient of friction for different lubricants in the temperature range of  $20^\circ\text{C}$  (70°F)  $< T < 770^\circ\text{C}$  (1420°F) is presented in Table 6.1. Other details given in Sec. 15.2 are also applicable for backward can extrusion at elevated temperatures.

### 15.8.5 Special Processes

The process shown in Fig. 15.34c is capable of extruding preforms for hollow forward extrusion or ironing by proper forming of the can bottom. However, these cans have proportionately smaller bottom thicknesses. Cans with large bottom thicknesses or sharp projections can be extruded by a process suggested by Kunogi [15.76], [15.77]. The process is a combination of forward can extrusion, expansion, and upsetting (Fig. 15.83). The dominant portion, as seen from the hardness distribution in the extruded component, is the forward can extrusion process. The maximum punch pressure has a minimum value at  $(d_o^2 - d_i^2)/d_o^2 = 0.5$  and is dependent on the ratio  $d_o/d_i$  in the region of  $0.8 < d_o/d_i < 1.0$ . The punch is located in the tooling so that its face is slightly lower

\*  $A_{i,1} \approx d_i \pi l_i$ ,  $A_{i,0} \approx \pi d_i^2/4$ . The increase in surface area is very localized and can be as high as 20-fold in the lower third of the can (Fig. 15.55a).

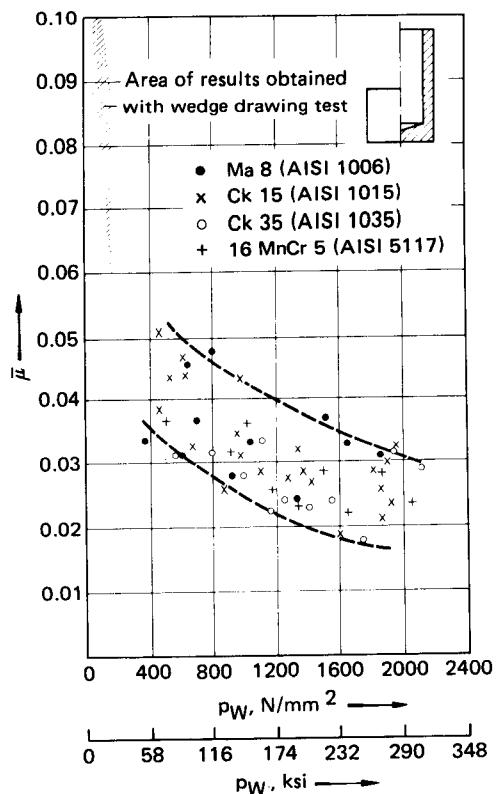


FIG. 15.82 Relationship between average coefficient of friction on die wall and average normal pressure. (After [15.62].)

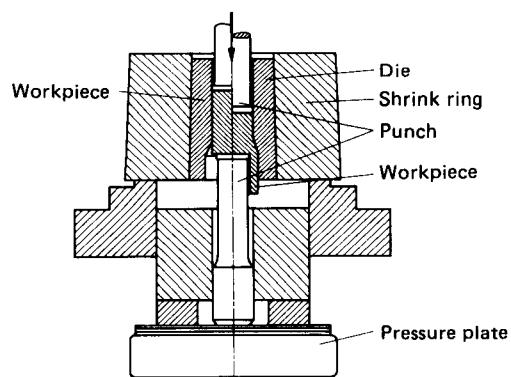


FIG. 15.83 Tooling for forward can extrusion. (After [15.76], [15.77].)

in the transition zone of the die between the conical and the cylindrical portions with  $d = d_D \approx d_o$ . The shape of the punch face does not affect the extrusion force appreciably. Conical punch faces with  $2\alpha \approx 150^\circ$  [15.76] or flat faces with small inclinations (included angle  $150\text{--}75^\circ$ ) are suitable for material flow, that is, to form perfect can shapes.

## 15.9 WORKPIECE DESIGN

Workpiece materials suitable for extrusion are discussed in Sec. 15.5. Fig. 15.1 (class 2) gives an overview of the basic extrudable can shapes. Details can be obtained from Fig. 15.2. Guidance values for achievable strains and dimensions of workpieces that can be manufactured economically are given in Table 15.4. The cans generally represent a prestige and should contain all shape elements which cannot be obtained subsequently by a wall-thickness-reduction process—for example, all bottom shapes. Apart from different bottom shapes, can walls having steps on the inside and on the outside can be manufactured [15.4]. Rotation symmetry or, at least, axisymmetry is desirable. Large localized reductions in area and small transient radii must be avoided. Based on the maximum possible loading on the punch, for cans made from steel a ratio of  $l_i/d_i = 3$  should not be exceeded.

## 15.10 TOOLS

Fig. 15.84 shows a schematic tool setup for backward can extrusion. Tool loads and the selection of tool materials are covered in Sec. 15.5.

### 15.10.1 Punch Design

The punch forms the inner surface of the workpiece in backward can extrusion and is subjected to very high compressive and bending loads. The permissible compressive stress dependent on the free buckling length can be obtained using the guidelines given in Sec. 15.5. The punch should be as short as possible without any large and sudden change of cross section, that is, with uniform and smooth transitions. Depending on the positioning of the workpiece stripper—either at the bottom or at the top of the tool—the punch length has to be short or long. Design details are given in Fig. 15.85. Material selection for punches is covered in Table 15.13; other details can be obtained from [15.48].

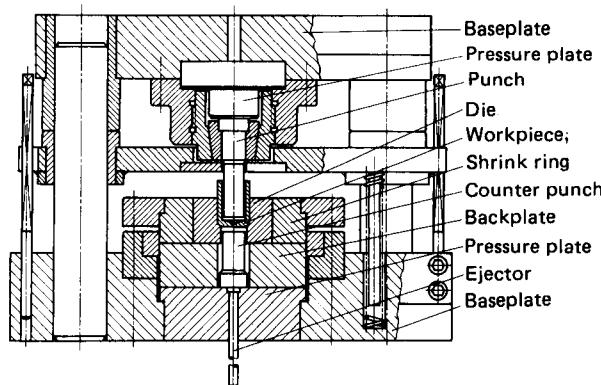
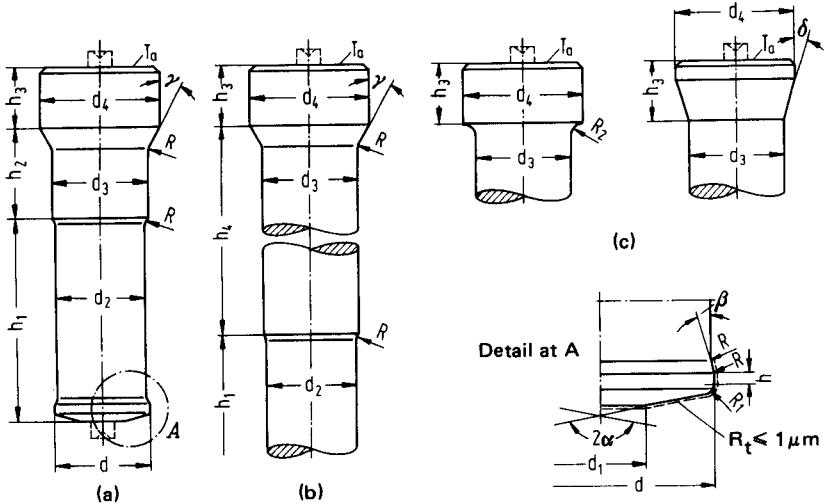


FIG. 15.84 Tooling for backward can extrusion.



$d$  based on inner diameter of workpiece  
 $d_1 = d - [2R_1 + (0.2...0.3)d]$   
 $d_2 = d - (0.1...0.2) \text{ [mm]}$   
 $d_3 \approx 1.3d$   
 $d_4 \approx (1.3...1.5)d$   
 $h = (0.3...0.7) \sqrt{d}$   
 $h_1 < 2.5d$   
 $h_2 \approx d_3$   
 $h_3 > 0.5d_4$   
 $h_4$  according to design of stripper sleeve

$R$  ground without scratches  
 $R_1 = (0.05...0.1)d$   
 $R_2 \approx 0.3(d_4 - d_3)$   
 $2\alpha = 170^\circ...160^\circ$   
 $\beta = 4^\circ...5^\circ$   
 $\gamma = 15^\circ...30^\circ$   
 $\delta = 5^\circ...15^\circ$   
 $T_a < 0.05 \text{ mm (axial runout)}$   
 $T_r \leq 0.01 \text{ for } d, d_1, d_2, d_3 \text{ (radial runout)}$

FIG. 15.85 Punch designs for backward can extrusion of steel. (a) Short. (b) Long. (c) Other punch-face shapes. (After [15.48].)

Table 15.13 Materials and Guidance Values for Backward Can Extrusion Punches

Required yield strength $S_{y,0.2}$ , N/mm <sup>2</sup> (ksi)	Steel designation		Hardened to, HRC	Remarks
	DIN	AISI		
2200 (320)	S6-5-3	M4 <sup>a</sup>	63-65 <sup>b</sup>	
2100 (300)	S6-5-2	M2	62-64	To be used where possible
2000 (290)	X165CrMoV12	D2	60-62	

<sup>a</sup>The material M42 is easy to grind and therefore to be used preferably.

<sup>b</sup>HRC 63 corresponds to 2200 N/mm<sup>2</sup> (320 ksi) and HRC 65 to 2500 N/mm<sup>2</sup> (360 ksi).

Source: Compiled from [15.48].

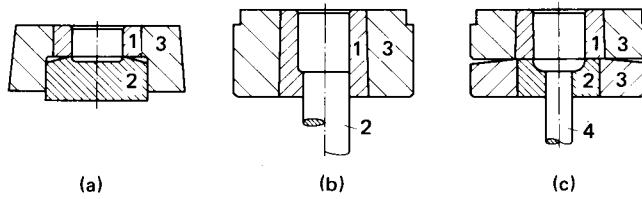


**FIG. 15.86** Die designs for backward can extrusion. 1, 2—die parts; 3—shrink ring; 4—ejector. (After [15.48].)

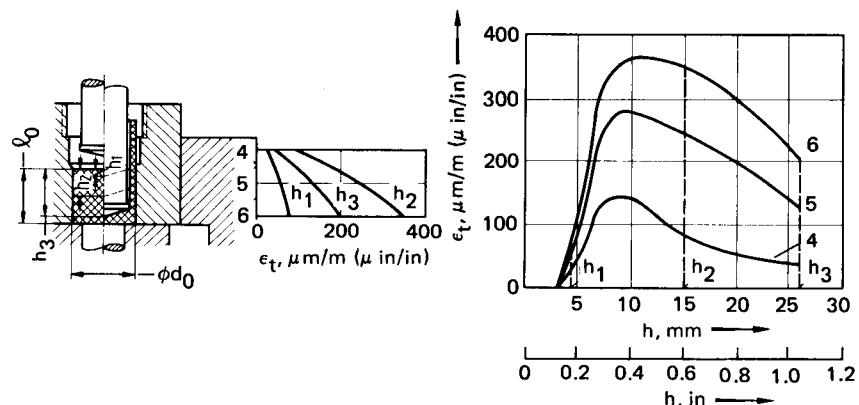
### 15.10.2 Die Design

Fig. 15.86 shows various die designs for backward can extrusion. The design in Fig. 15.86a is used for thin-walled workpieces of aluminum, tin, zinc, or other nonferrous metals with low flow stress. The workpiece generally sticks to the punch and is stripped from it by a stripper. The die consists of the prestressed die 1, the container 3, and the bottom piece 2. Die parts 1 and 2 have to be precisely centered and fixed in the axial direction.

For backward extrusion of steel and other difficult to extrude materials, the die wall is ground with a slight negative taper so that the can remains in the die during the return stroke of the punch. The workpiece is then ejected by the ejector 4 (designs in Fig. 15.86b and c). The ejector is loaded partially or fully with the bottom force  $F_B$  ( $d_E \leq d_D$ ), depending on the design. For design b the left and right portions correspond to partial and full ejector loading, respectively. This design is used for can bottoms that are flat with small radius or sharp edges. For designs b and c the dies or die parts have to be prestressed with shrink rings. Design c requires exact positioning of the tool parts with axial prestressing [15.48].

### 15.10.3 Die Loads

The dies for backward can extrusion as well as for solid and hollow forward extrusion are highly stressed by the radial inner pressure  $p_i$ , or  $p_r$ , which causes tangential hoop (tensile) stresses in the dies. The radial pressure  $p_r$  can be given only approximately and for the loaded region of the die



**FIG. 15.87** Variations of tangential strains on shrink ring during backward extrusion. Material—16 MnCr 5 (AISI 5150);  $d_0 = 30 \text{ mm}$  (1.2 in);  $l_0/d_0 = 0.87$ ;  $(A_0 - A_i)/A_0 = 0.63$ ;  $h_1, h_2, h_3$ —punch positions; 4, 5, 6—measuring points. (After [15.62].)

wall, or sometimes as an equivalent normal pressure  $\bar{p}_w$  acting on the die wall (see Fig. 15.68). Fig. 15.87 shows the variation of circumferential strains on the shrink ring during backward extrusion (the tangential strains  $\epsilon_t$  correspond to the ratio  $p_{w,\max}/p_{p,\max}$  in Fig. 15.68).

Similar results are not available for solid and hollow forward extrusion. Eq. 15.12 and Fig. 15.67 can be used to compute circumferential stresses for large reductions in area by using  $p_{w,\max} \approx p_{p,\max}$ . However, it should be remembered that the discontinuous change of direction of material flow in the transition from die shoulder to die land in conical dies causes changes in the wall pressure, as shown for strip drawing by Adler [15.16]. The remarks in the following paragraphs are therefore valid for dies subjected to partial loading only. Computation of the die loading is in general based on the assumption of a thick-walled infinite hollow cylinder under constant internal pressure  $p_i$ .

Applying the Tresca flow criterion and assuming static load with no residual stress on the die (Fig. 15.88), the variations of  $\sigma_r$ ,  $\sigma_t$ , and  $\bar{\sigma}$  can be obtained. The stresses  $\sigma_r$  and  $\sigma_t$  on the inner wall are approximately equal to  $p_i$ . Therefore since

$$\bar{\sigma} = |\sigma_r| + |\sigma_t| = 2p_i \quad (15.32)$$

the maximum allowable inner pressure can reach  $p_{i,\max} = S_y/2$  for  $\bar{\sigma} = S_y$  without causing failure of the die material. Thus if  $S_y = 2000$  N/mm<sup>2</sup> (290 ksi), a die without prestressing can be loaded to  $p_i = 1000$  N/mm<sup>2</sup> (145 ksi) before material failure occurs. However, very high inner pressures require reinforcement of the die with one or two shrink rings to compensate for the tangential tensile stresses. Fig. 15.89 shows the stresses in the shrink-ring assembly with and without inner pressure.

The stresses calculated for ring assemblies by the above method can be applied for extrusion to a limited extent only. This is due to the fact that (1) the radial pressure is not constant over the entire height of the die wall, (2) the die wall is not loaded along its entire height, and (3) the die wall is not infinitely long.

Stresses in dies of finite lengths, with limited areas of application of internal pressure, have been investigated [15.78], [15.79]. Fig. 15.90 shows the variations of tangential and equivalent stresses at the inner diameter of the inner ring as a function of the height ratio  $h_D/h_{tot}$  on which

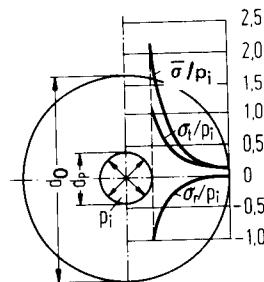


FIG. 15.88 Theoretical stress variations in thick-walled single-piece hollow cylinder under inner pressure.  $d_0/d_p = 4$ ;  $\bar{\sigma} = \sigma_{\max} - \sigma_{\min} = \sigma_t - \sigma_r$

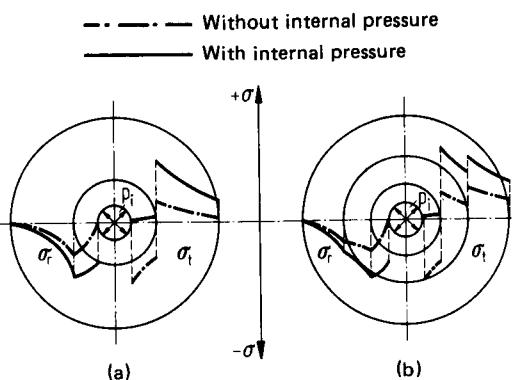


FIG. 15.89 Theoretical stress variations. (a) Two-piece die assembly. (b) Three-piece die assembly.

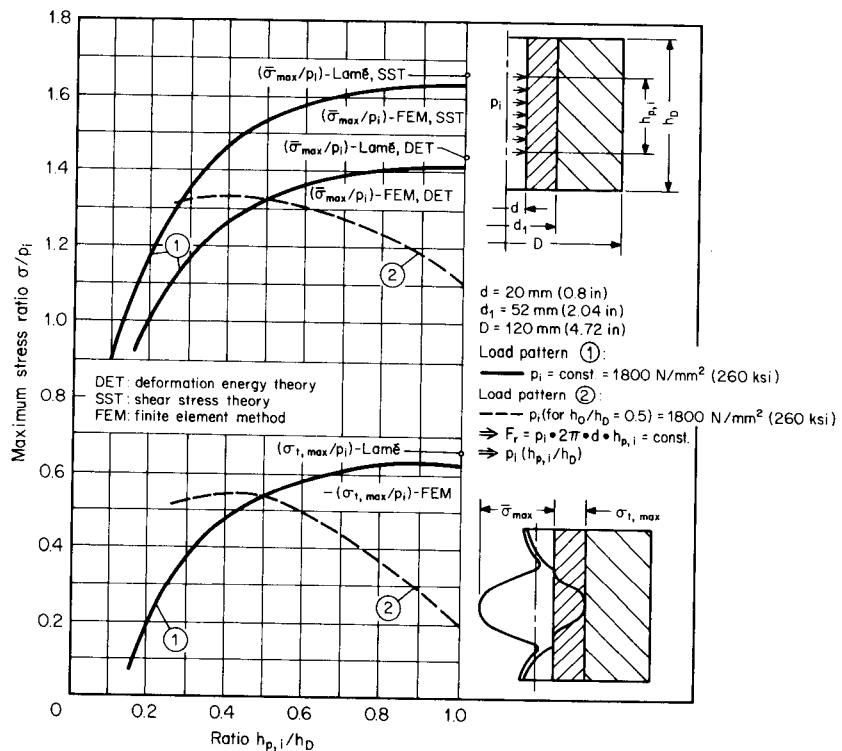


FIG. 15.90 Stresses in partially loaded die. (After [15.79].)

the inner pressure is applied [15.79]. Comparing the stress ratios  $\sigma_z/p_i$  (and  $\bar{\sigma}/p_i$ ) at  $h_D/h_{tot} = 1$  and at  $h_D/h_{tot} = 0.2$ , it can be seen that  $\sigma_z/p_i$  is reduced by 65% and  $\bar{\sigma}/p_i$  by 25% at  $h_D/h_{tot} = 0.2$ . Varying the type of loading on the insert (variation 2 in Fig. 15.90) leads to opposite results: smaller  $h_D/h_{tot}$  ratios result in larger  $\bar{\sigma}/p_i$  values. In this case the radial force is confined to a smaller area. The values of equivalent stress calculated by both the shear stress and the distortion energy criteria with Lamé's closed-form solution for thick cylinders have also been plotted in Fig. 15.90. Lamé's solution is 5% higher than the finite-element solution.

The axial stress ratio  $\sigma_z/p_i$  is plotted in Fig. 15.91 as a function of the ratio  $h_{p,i}/h_D$ . The two load variations do not affect the results appreciably. The axial stress increases in the middle region. It changes from positive (tensile) to negative (compressive) at the transition points of the load applications. The radial stress also changes sign at these points, which leads to cross cracking. This defect can be avoided by cross splitting the die (Figs. 15.35 and 15.86).

The normal and equivalent stresses in the shrink ring are shown in Fig. 15.92 as a function of the loaded length ratio of the die. The stress on the outer ring is not affected to the same extent as the axial stress on the inner ring if the relative loading length of the die is varied. In the design of partially loaded dies it is therefore important to consider the maximum permissible axial stress, especially on the inner diameter of the insert.

Fig. 15.93 shows the effect of different interference values on the stresses at the inner diameters of the insert and the shrink fit for a section of the middle region of the load. With decreasing interference values, the tangential stress, and thus the equivalent stress at the inner diameter of the insert, increases for the same internal pressure. This result is to be expected. In the case of the outer ring, the equivalent stress, and thus the tangential stress, increases with increasing interference values. The die-assembly design is therefore an optimum approach to minimizing the tan-

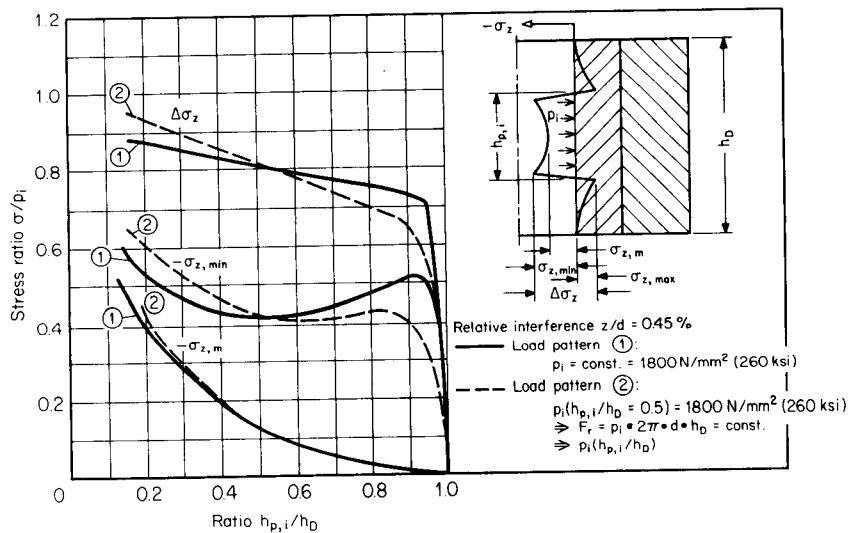


FIG. 15.91 Axial stresses in partially loaded die assemblies. (After [15.79].)

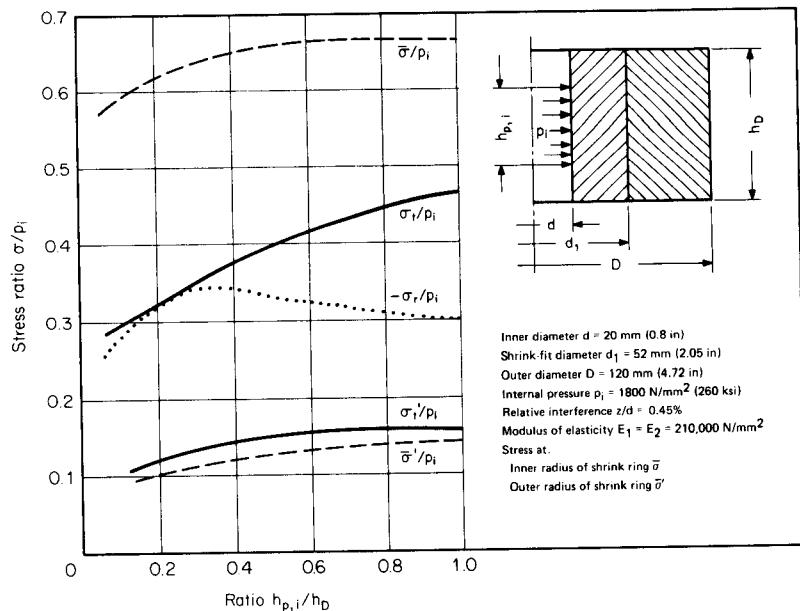
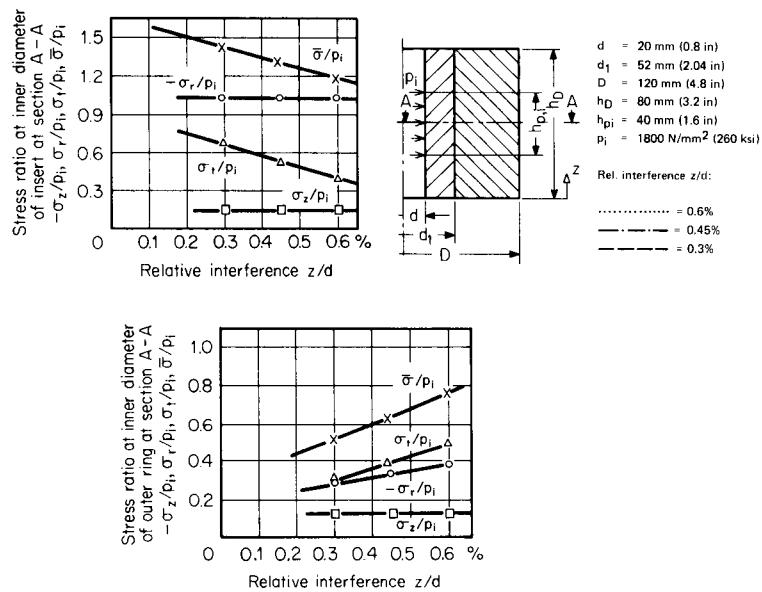


FIG. 15.92 Stresses  $\bar{\sigma}$ ,  $\sigma_r$ , and  $\sigma_t$  at outer ring for partial loading. (After [15.79].)



**FIG. 15.93** Effect of interference on stress values at inner diameters of insert and shrink ring. (After [15.79].)

gential stresses at the insert inner diameter and at the same time not exceeding the limits to which the inner diameter of the shrink ring can be subjected. Some design considerations for cold-extrusion tools are discussed in [15.80].

#### 15.10.4 Calculation of Die Assemblies

Computations of shrink-fit assemblies are still based on the theory of an infinitely long hollow cylinder, in spite of the various deviations of the stress conditions for finite die length and non-

**Table 15.14** Guidance Values for Load-Carrying Capacity and Dimensioning of Single-Piece Prestress Die

Inner pressure $p_i$ , N/mm $^2$ (ksi)	Number of shrink rings	Diameter ratio $d_0/d_1$	Approximate value for the interface diameter
To 1000 (to 145)	0	4–5	—
1000–1600 (145–230)	1	4–6	$d_1 \approx 0.9\sqrt{d_0 d_1}$
1600–2000 (230–290)	2	4–6	$d_1: d_2: d_o \approx 1: (1.6–1.8): (2.5–3.2): (4–6)$

Source: Compiled from [15.48].

uniform inner pressures in the  $z$ -direction. The above assumption has been used in industry with good success for the design of dies under high pressures. A simple guideline for die design is given in Table 15.14. An exact calculation is based on the various considerations given in the preceding section. Of the approaches suggested in the literature, one proven method is described briefly [15.81]. Recently a sophisticated method using finite-element techniques has been developed [15.79], [15.82]. The results have been published in the form of nomograms for easy use.

Fig. 15.94 shows a die with two shrink fits. A design procedure for this configuration is now presented.

The following values are given:

Inner pressure	$p_i$
Yield strength of die insert	$S_{y,1}$
Yield strength of inner shrink ring	$S_{y,2}$
Yield strength of outer shrink ring	$S_{y,3}$
Inner die diameter	$d_{D,i}$
Modulus of elasticity	$E$
Ratio of inner pressure to yield strength of die insert	$p' = p_i/S_{y,1}$
Ratios of yield strengths	$\kappa_1 = S_{y,1}/S_{y,2}$
	$\kappa_2 = S_{y,1}/S_{y,3}$

From the above values, determine the following:

Interface diameter between insert and inner shrink ring	$d_1$
Interface diameter between inner and outer shrink rings	$d_2$
Outer diameter of assembly	$d_o$
Absolute interference at $d_1$	$z_1$
Absolute interference at $d_2$	$z_2$

Based on the procedure suggested in [15.81], let us also assume that all the shrink rings are made of steel and hence have the same modulus of elasticity  $E$ . The calculation procedure differentiates between two cases—with and without allowable tangential tensile stress on the inner surface of the die insert. In the case of allowable tangential tensile stress the dimensions are calculated in such a way so that all parts under load are stressed up to their yield limits and the tool material is chosen corresponding to the load requirements.

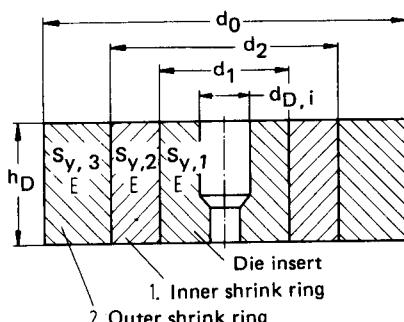


FIG. 15.94 Doubly shrunk die for extrusion.

**Shrink-ring assembly with permissible tangential tensile stress in the interior of the die insert:**

Single ring

$$d_1 = d_{D,i}/Q_1$$

$$d_o = d_{D,i}/Q$$

Double ring

$$d_1 = d_{D,i}/Q_1$$

$$d_2 = d_1/Q_2$$

$$d_o = d_{D,i}/Q$$

where

$$Q_1 = \sqrt{\frac{1}{2} \left( 1 + \frac{1}{\kappa_1} \right) - p'}$$

$$Q_2 = Q_1 \sqrt{\kappa_1}$$

$$Q = Q_1 Q_2$$

$$Q_1 = \sqrt{\frac{1}{3} \left( 1 + \frac{1}{\kappa_1} + \frac{1}{\kappa_2} - 2p' \right)}$$

$$Q_2 = Q_1 \sqrt{\kappa_1}$$

$$Q_3 = Q_1 \sqrt{\kappa_2}$$

$$Q = Q_1 Q_2 Q_3$$

The interference values are

$$z_1 = \frac{d_1 S_{y,1}}{E} \left( \frac{1}{\kappa_1} - Q_1^2 \right)$$

$$z_1 = \frac{d_{D,i} S_{y,1}}{E} \frac{2p' + Q^2 - 1}{1 - Q_2^2 Q_3^2}$$

$$z_2 = \frac{d_2 S_{y,1}}{E} \left( \frac{1}{\kappa_2} - Q_1^2 \right)$$

In the case of double-ring assemblies, when the die insert is overstressed because of shrinking only, and where no inner pressure is applied, the following conditions should be verified:  $0.95 < p' < 1.0$  and  $p' < 1 - Q^2$ .

If these conditions are not satisfied, the insert will be overstressed by tangential compressive stresses after shrink fitting. Then the calculation procedure has to be repeated with larger values of  $\kappa_1$  and/or  $\kappa_2$ . The values can also be obtained from the nomograms in Figs. 15.95 and 15.96.

**Shrink-ring assembly without tangential tensile stress in the interior of the die insert:**

Single ring

$$d_1 = d_{D,i}/Q_1$$

$$d_o = d_{D,i}/Q$$

Double ring

$$d_1 = d_{D,i}/Q_1$$

$$d_2 = d_1/Q_2$$

$$d_o = d_{D,i}/Q$$

where

$$Q_1 = \sqrt{\frac{1}{2} \left( \frac{1}{\kappa_1 p'} - 1 \right)}$$

$$Q = Q_1 Q_2$$

$$Q_2 = Q_1 \sqrt{\kappa_1 p'}$$

$$Q_1 = \sqrt{\frac{1}{3} \left( \frac{1/\kappa_1 + 1/\kappa_2}{p'} - 1 \right)}$$

$$Q_2 = Q_1 \sqrt{\kappa_1 p'}$$

$$Q_3 = Q_1 \sqrt{\kappa_2 p'}$$

$$Q = Q_1 Q_2 Q_3$$

The interference values are

$$z_1 = \frac{d_1 S_{y,1}}{E} \frac{1 + Q^2}{1 - Q_2^2} p'$$

$$z_1 = \frac{d_{D,i} S_{y,1}}{E} \frac{1 + Q^2}{1 - Q_2^2 Q_3^2} p'$$

$$z_2 = \frac{d_2 S_{y,1}}{E} \left( \frac{1}{\kappa_2} - p' Q_1^2 \right)$$

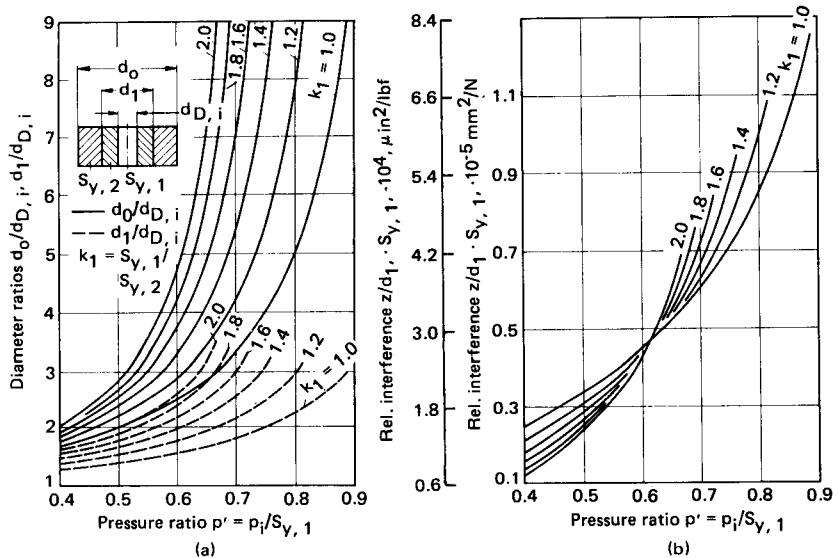


**FIG. 15.95** Nomograms to compute (a) dimensions and (b) interference of single-shrink-fit die assemblies. Tangential tensile stresses on inner diameter permissible.  $E = 210 \text{ kN/mm}^2$  (3000 ksi). (After [15.81].)

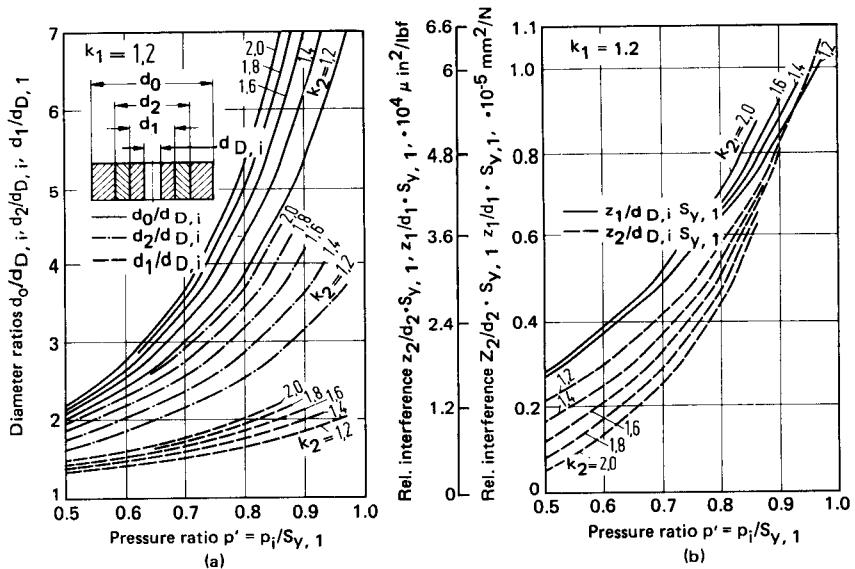


**FIG. 15.96** Nomograms to compute (a) dimensions and (b) interference of double-shrink-fit die assemblies. Tangential tensile stresses on inner diameter permissible.  $E = 210 \text{ kN/mm}^2$  (3000 ksi). (After [15.81].)

In this case the die insert can also be loaded by very high tangential compressive stresses due to shrinking. In addition to verifying that  $0.89 < p' < 1.0$ , it has to be ascertained that  $p' < (1 - Q^2)/(1 + Q^2)$ .

If these conditions are not satisfied, the calculations have to be repeated with larger values of  $\kappa_1$  and/or  $\kappa_2$ . Nomograms for these calculations are given in [15.48] and [15.81]. Other details for designing shrink-fit assemblies with different moduli of elasticity  $E$ , such as for tungsten carbide steel, can be obtained from [15.83] to [15.85] and [15.48].

The theoretical interference values  $z$  cannot be maintained exactly during actual manufacture. A loss of interference can reduce the permissible inner pressure  $p_i$  by up to 10% [15.48], [15.83]. An increase in interference can also cause overstressing of the various rings and the insert. The manufacturing tolerance should therefore be chosen no greater than IT 6, or smaller in critical cases.

Shrinking is carried out, for cylindrical mating surfaces with  $z/d < 0.4\%$ , by heating the outer ring and cooling after shrink fitting. The warm yield strength of the parts being shrunk should also be taken into consideration. For conical mating surfaces (taper 1:100) a hydraulic press is required. In this case no heating of the ring is required; however, the machining will be time-consuming. For values of  $z/d > 0.4\%$  a combination of conical taper and heating is necessary. The following procedure is recommended for shrink fitting to prevent overstressing of the inner die insert during shrinking:

- 1 Shrinking of the outer and inner rings
- 2 Grinding of the inner diameter of the inner ring to the computed value considering interference
- 3 Shrinking of both rings together with the insert

More details and information on material selection can be obtained from [15.48].

#### 15.10.4 Tool Life

The tool life of dies is greater for backward can extrusion than for solid forward extrusion for the same deformation ratio. The highly stressed punch made from high-alloyed high-speed steel with hardness between HRC 62 and 64 has a tool life of between 30,000 and 100,000 pieces for forming soft steels; for harder steels (carbon  $\geq 0.35\%$  or alloyed) the value is between 5000 and 20,000 pieces (the smaller value being for larger  $l_i/d_i$  ratios and the larger value for smaller  $l_i/d_i$  ratios) [15.48].

### 15.11 PROCESS COMBINATIONS

Possible process combinations are solid forward and backward can extrusion, forward and backward can extrusion, double backward can extrusion, and solid backward and backward can extrusion (Fig. 15.97). For all combinations where the flow takes place simultaneously without any hindrance, the force is either smaller than or equal to the force required for the process utilizing the smaller force. Correspondingly the portion of the process requiring the lesser force is executed easily. The material flow, however, is influenced by a number of factors. Process combinations are therefore developed empirically, by trial and error. Only a few systematic investigations have so far been carried out on combined extrusion processes. During simultaneous backward and forward can extrusion with the same reduction in area  $\epsilon_A$  for both processes, the depth of the can in the forward direction  $l_{i,F}$  is basically smaller than the depth of the can in the backward direction  $l_{i,B}$ , the difference being higher for larger  $l_0/d_0$  ratios (Fig. 15.98). This is due to the different friction conditions in the forward and backward directions. It is also reflected in the force requirements: The required force is higher for forward can extrusion than for backward can extrusion for the same reduction in area on both sides. The process takes place preferentially in the direction that requires the lesser force, which is generally the process with the smaller reduction in area (Fig.

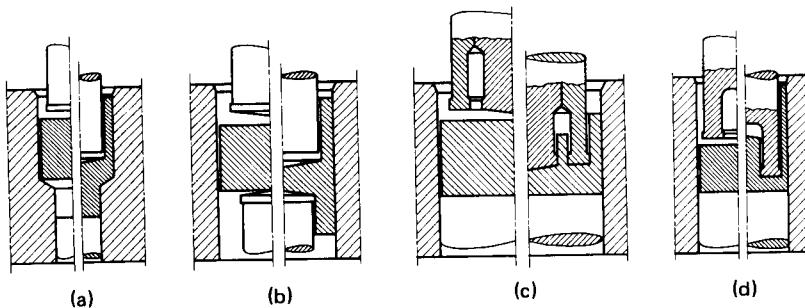


**FIG. 15.97** Process combinations with can extrusion. (a) Solid forward and backward can. (b) Forward and backward can. (c) Double backward can. (d) Solid backward and backward can.

15.99). The total force requirement follows the rule for process combinations as stated at the beginning of this section.

If a workpiece has to be manufactured with definite dimensions, the material flow must be controlled. Fig. 15.100 shows the variations of punch pressure as a function of punch travel for processes in which the material flow is controlled. The force-travel variations for the individual processes and unhindered material flow are also shown. At the beginning the combination of forward can and backward can processes determines the punch pressure until the process of forward can extrusion is stopped by tool design. The value of  $p_{P,\max}$  then follows the punch pressure required for backward can extrusion until this process ends. The final portion corresponds to solid forward extrusion only [15.28], [15.87].

## 15.12 ECONOMY

A minimum number of workpieces are required for the economic production by cold-extrusion methods because of heavy investments in tools, machines, auxiliary equipment, and development efforts. The economy has to be decided on an individual basis. The process is economical in the following cases:

- 1 Cold extrusion of sleeves instead of deep drawing in several stages. The greater bottom thickness required for the extrusion process does not affect the economy.
- 2 Manufacture of cans from bar crops instead of machining them from rods (material saving).
- 3 Manufacture of special sections.
- 4 Saving of machining instead of machining completely or finish-machining of forged workpieces. This is especially true for hollow parts and parts with steps or projections since rough machining can be completely eliminated and finish-machining can be decided upon depending on the accuracy required.
- 5 Saving of material compared to machining completely or from forged billets. The saving will be very high for hollow parts and parts with steps or projections.

The savings in material and time should as a general rule be larger than the total investment for cold extrusion. The material savings are smaller for smaller workpieces. Therefore, for smaller workpieces, machining on multispindle automatics may prove more economical than cold extrusion. A single-setting machining in multispindle automatics will also make cold extrusion uneconomical. Hence for small workpieces the trend is to form them in multistage presses (with up to seven stages) where a nearly finished workpiece can be produced. The number of workpieces, or batch size, should be very high ( $10^5$ – $10^6$ ) for this type of investment.

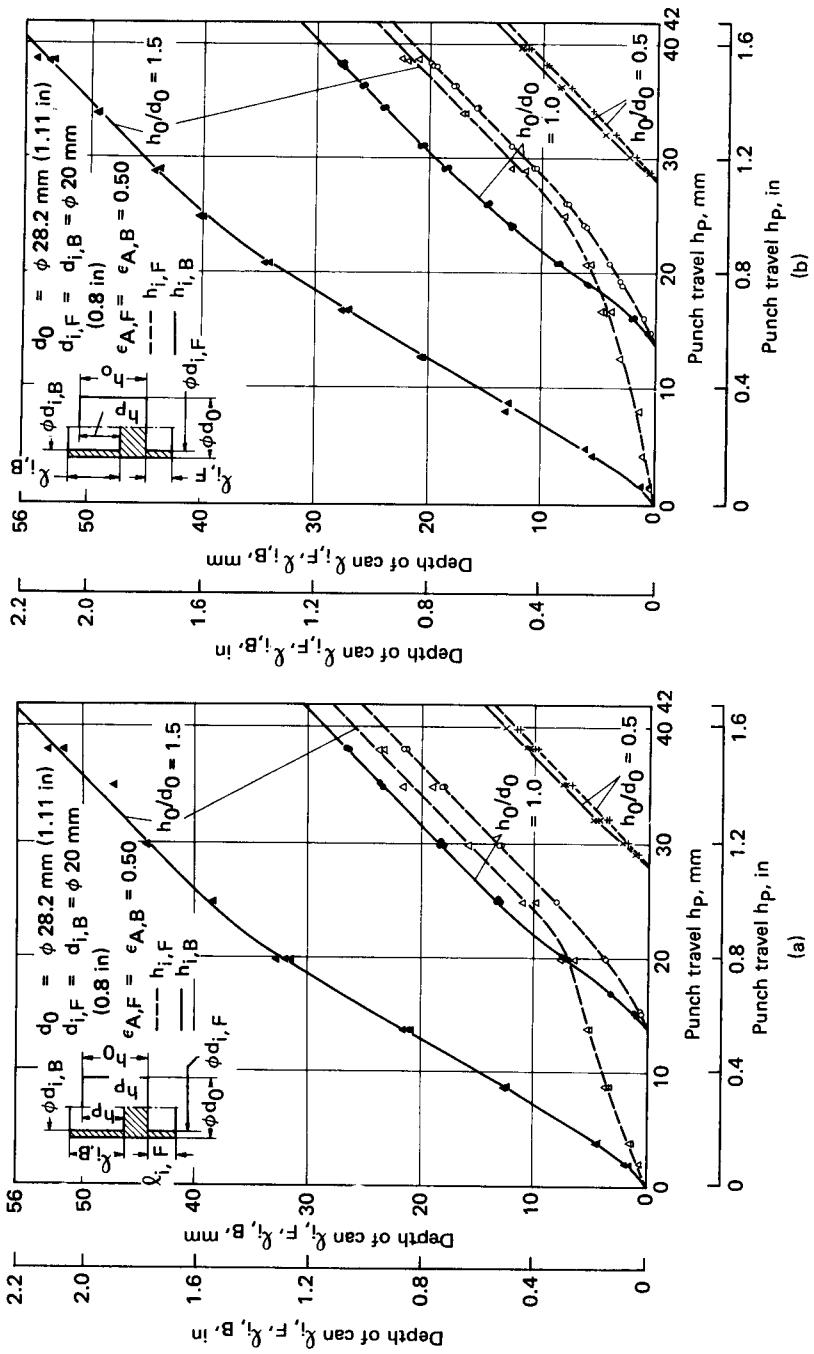


FIG. 15.98 Workpiece dimensions in process combination forward and backward can extrusion. (a) Material—Al-Zn-Mg-Cu 1.5 (AA 7075); phosphated + Bonderlube 234. (b) Material—Ma 8 (AISI 1006); phosphated + Bonderlube 234. (After [15.86].)

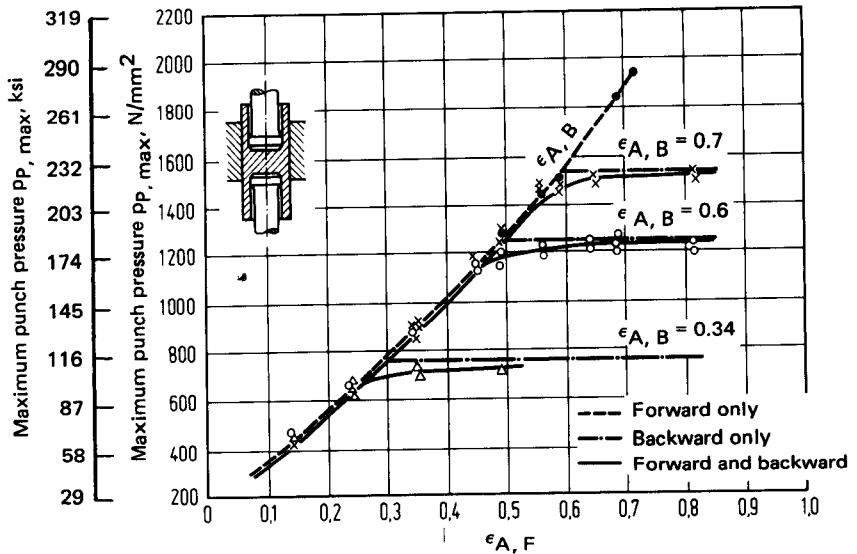


FIG. 15.99 Maximum punch pressure in process combination forward and backward can extrusion. Material—En 2E; lubricant—zinc phosphate + Bonderlube 235;  $l_0 = 38.1 \text{ mm (1.5 in)}$ ;  $d_0 = 25.4 \text{ mm (1 in)}$ . (After [15.18], [15.28], [15.87].)

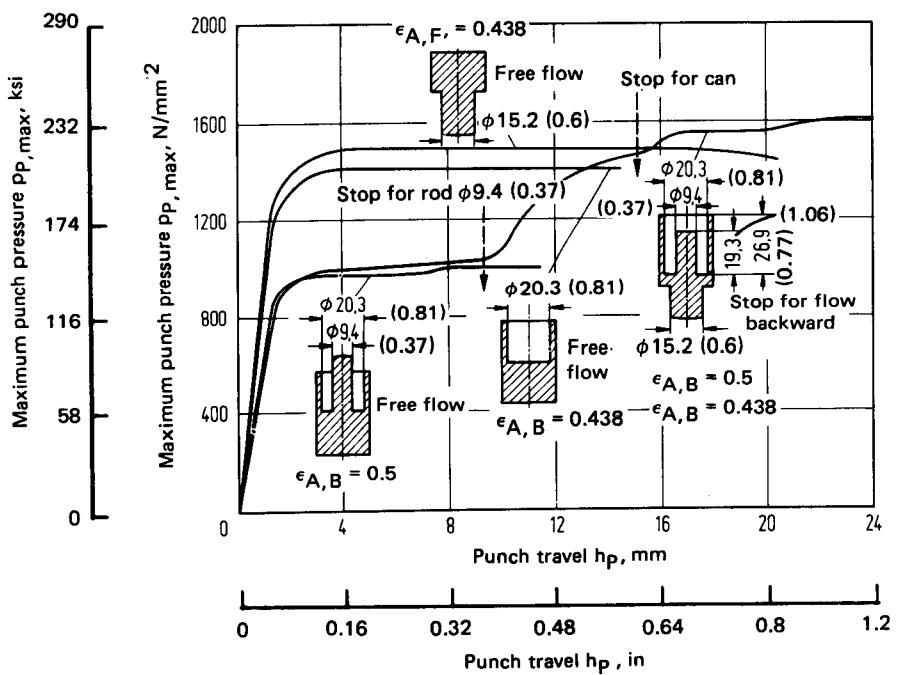


FIG. 15.100 Combination of solid backward and backward can with solid forward extrusion. Experimental conditions as in Fig. 15.99. Dimensions are in mm (in). (After [15.18], [15.28], [15.87].)

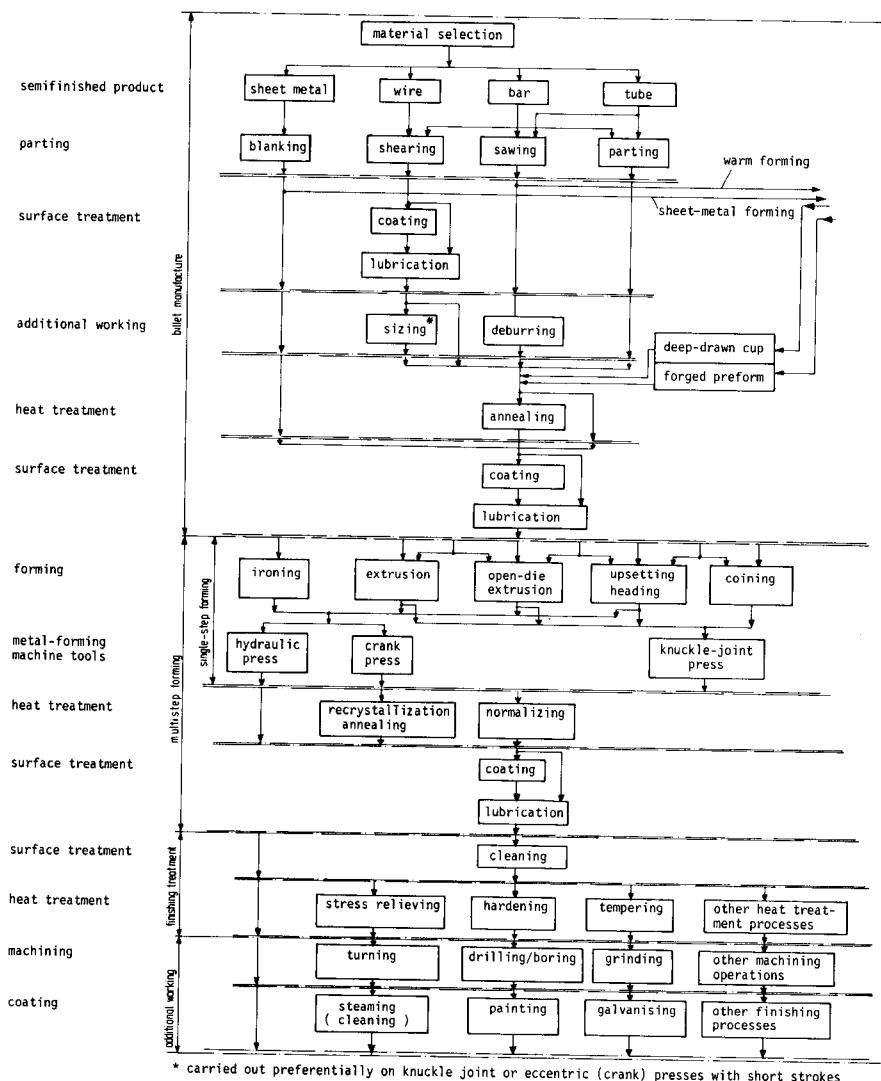


FIG. 15.101 Flow diagram of process sequence in cold bulk forming. (After [15.4].)

The economy for bigger workpieces depends on the efficient utilization of press strokes, mechanical feeding, and automation. More details and production examples can be found in [15.2] to [15.4]. Extra care has to be taken in designing the optimum production sequence because of the availability of a multitude of process combinations, presses, and heat and surface treatment operations. Computer-aided techniques have recently been used to determine process planning sequences and the costs involved for the various steps. A systematic investigation of the manufacture of solid and hollow bodies by cold extrusion and by a combination with other deformation

and machinery processes is presented in [15.4]. Fig. 15.101 shows a schematic representation of the process layout for cold bulk-forming processes. For individual cases the necessary decisions can be made using this flow diagram.

## REFERENCES

- 15.1 Wagener, H. W.: *Kabelmetal*, 1967.
- 15.2 VDI-Richtlinie 3138: "Kaltfließpressen von Stählen und NE-Metallen (Cold Extrusion of Steel and Nonferrous Metal)," Düsseldorf, VDI-Verlag, 1970.
- 15.3 Feldmann, H. D.: *Cold Extrusion of Steel (in German)*, Berlin/Göttingen/Heidelberg, Springer, 1959.
- 15.4 Noack, P.: "Computer Aided Process Planning and Cost Calculation for Cold Forging of Steel" (*in German*), *Berichte aus dem Institut für Umformtechnik, Universität Stuttgart*, no. 48, Essen, Girardet, 1979.
- 15.5 Diether, U.: "Extrusion of Steel in the Temperature Range of 500°C to 800°C" (*in German*), *Berichte aus dem Institut für Umformtechnik, Universität Stuttgart*, no. 54, Berlin/Heidelberg/New York, Springer, 1980.
- 15.6 Kast, D.: "Similarity Laws in Backward Extrusion of Geometrically Similar Cups" (*in German*), *Berichte aus dem Institut für Umformtechnik, Universität Stuttgart*, no. 7, Essen, Girardet, 1968.
- 15.7 Schmoekel, D.: "Investigations on the Tool Design for Hollow Forward Extrusion of Steel and Nonferrous Metals" (*in German*), *Berichte aus dem Institut für Umformtechnik, Universität Stuttgart*, no. 4, Essen, Girardet, 1966.
- 15.8 Kast, D.: "Investigation on the Force and Energy Requirements and the Deformation Efficiency in the Forward Extrusion of Steel" (*in German*), *Berichte aus dem Institut für Umformtechnik, Universität Stuttgart*, no. 3, Essen, Girardet, 1969.
- 15.9 Hill, R.: *The Mathematical Theory of Plasticity*, Oxford, Clarendon, 1950.
- 15.10 Besdo, D.: "Principal and Slip-Line Field Methods for Axisymmetric Rigid Plastic Deformation" (*in German*), Dr.-Ing. thesis, Technische Universität, Braunschweig, 1969.
- 15.11 Jordan, T.: "On a Method of Determining the Stress Relations in Stationary, Rotation-Symmetric Deformation Processes" (*in German*), Dr.-Ing. thesis, Technische Universität, Hanover, 1957.
- 15.12 Thomsen, E. G.: "Comparison of Slip-Line Solutions with Experiment," *Trans ASME, J. App. Mech.*, **23**, 1956, pp. 225–230.
- 15.13 Shabaik, A., Altan, T., and Thomsen, E. G.: "Visioplasticity," U.S. Navy, Bureau of Weapons, Contract N0W 65-0374-d, Final Rep., Feb. 1966.
- 15.14 Thomsen, E. G., Young, C. T., and Kobayashi, S.: *Mechanics of Plastic Deformation in Metal Processing*, New York, Macmillan, 1965.
- 15.15 Steck, E.: "Numerical Treatment of Deformation Processes" (*in German*), *Berichte aus dem Institut für Umformtechnik, Universität Stuttgart*, no. 22, Essen, Girardet, 1971.
- 15.16 Adler, G.: "A Method of Approximately Calculating the Stress and Strain Condition in the Flow of Rigid Plastic Workpieces" (*in German*), *Berichte aus dem Institut für Umformtechnik, Universität Stuttgart*, no. 12, Essen, Girardet, 1969.
- 15.17 Dalheimer, R.: "On the Question of Stresses, Strains, and Temperature in Axisymmetric Hot Extrusion" (*in German*), *Berichte aus dem Institut für Umformtechnik, Universität Stuttgart*, no. 20, Essen, Girardet, 1970.
- 15.18 Pugh, H. Ll. D.: "Recent Developments in Cold Forming," in *Bulleid Memorial Lectures, 1965*, vol. 3a, University of Nottingham, 1965.
- 15.19 Dannenmann, E., and Huber, J.: "Determination of Deformation Work and Force Using

- Deformation Efficiency in Solid Forward Extrusion" (*in German*), *Ind.-Anz.*, **90**, 1968, p. 1834–1837.
- 15.20 Huber, J.: Unpublished Results (*in German*), Institut für Umformtechnik, Universität Stuttgart, 1966.
- 15.21 Dannenmann, E., and Huber, J.: "The Value of Deformation Efficiency and the Force Correction Factor for Solid Forward Extrusion," (*in German*), *Ind.-Anz.*, **91**, 1969, pp. 1406–1410.
- 15.22 Burgdorf, N., and Müschenborn, R.: "Nomograms to Determine the Deformation Force in Cold Extrusion" (*in German*), *Werkstattstechnik*, **60**, 1970, pp. 503–506.
- 15.23 ICFG Data Sheets: "Calculation of Pressures for Cold Forward Extrusion of Steel Rods," no. 1/70; "Calculation of Pressures for Cold Forward Extrusion of Short Steel Tubes," no. 2/70; "Calculation of Pressures for Cold Forward Extrusion of Short Steel Tubes," no. 3/74, Surrey, ISME, 1970, 1974.
- 15.24 Steck, E.: "Force Calculation in Forming Processes with the Aid of the Upper-Bound Method" (*in German*), *Werkstattstechnik*, **57**, 1967, pp. 273–279.
- 15.25 Johnson, W.: "Estimation of Upper-Bound Loads for Extrusion and Coining Operations," *Proc. Inst. Mech. Eng., London*, **173**, 1957, pp. 61–72.
- 15.26 Kudo, H.: "An Upper Bound Approach to Plane Strain Forging and Extrusion," *Int. J. Mech. Sci.*, **1**, 1960, pp. 57–83, 229–252, 366–368.
- 15.27 Kobayashi, S., and Thomsen, E. G.: "Upper and Lower Bound Solutions to Axisymmetric Compression and Extrusion Problems," *Int. J. Mech. Sci.*, **7**, 1965, pp. 127–143.
- 15.28 Steck, E.: "English and Dutch Research Results in the Field of Cold Extrusion" (*in German*), *Ind.-Anz.*, **88**, 1966, pp. 772–777.
- 15.29 Bay, N.: "Friction and Pressure Distribution in Forward Extrusion," presented at the ICFG 14th Plenary Meeting, Birmingham, 1981.
- 15.30 Avitzur, B.: *Metal Forming Processes and Analysis*, New York, McGraw-Hill, 1968.
- 15.31 Binder, H., and Lange, K.: "Load Requirement and Process Limitations for Open Die Extrusion of Rod," in *Proceedings NAMRC*, vol. 7, 1979, pp. 114–121.
- 15.32 Sieber, K.: "Deformation and Tooling" (*in German*), *VDI-Berichte*, no. 39, 1959, pp. 49–55.
- 15.33 Dalheimer, R., and Kast, D.: "Cold Extrusion—A Process of Bulk Forming" (*in German*), *Werkstattstechnik*, **60**, 1970, pp. 498–502.
- 15.34 Witte, H. D.: "Investigations on the Spread Band for Forces and Work in Cold Extrusion in Regular Production and on the Effect of Phosphate Coating Thickness and Lubricant" (*in German*), *Berichte aus dem Institut für Umformtechnik, Universität Stuttgart*, no. 6, Essen, Girardet, 1967.
- 15.35 Witte, H. D.: "Variations in Forces and Work in Cold Extrusion in Regular Production" (*in German*), *Ind.-Anz.*, **90**, 1968, pp. 203–209.
- 15.36 Burgdorf, M.: "Cold Extrusion of Steel in the Temperature Range of 20°C to 700°C," in *Proceedings of the International Conference on Cold Forming* (Düsseldorf, 1970), Session 4, Düsseldorf, VDI-Verlag, 1970; also *Metal Forming*, **38**, 1971, pp. 76–79.
- 15.37 Lindner, H.: "Bulk Forming of Steel between 600°C and 900°C, Semihot Forging" (*in German*), *Fortschritts-Berichte, VDI-Z.*, ser. 2, no. 7, 1966.
- 15.38 Grotz, H.: "Warm Extrusion of Steel" (*in German*), Dr.-Ing. thesis, Technische Universität, Hannover, 1966.
- 15.39 Schack, J.: "The Behavior of Flow Stress of Iron–Magnesium–Carbon Alloys in the Region of Blue Brittleness" (*in German*), Dr.-Ing. thesis, Technische Universität, Hannover, 1965.
- 15.40 ICFG Data Sheets: "Determination of Pressures and Loads for Warm Extrusion of Steel," no. 9/79, Surrey, ISME, 1970.

- 15.41 VDI-Richtlinie 3143: "Werkstoffe für das Kaltfließpressen (Material for Cold Extrusion)," Düsseldorf, VDI-Verlag, 1976.
- 15.42 Wilhelm, H.: "Investigations on the Relation between Vickers Hardness and Equivalent Strain for Cold-Forming Processes" (in German), *Berichte aus dem Institut für Umformtechnik, Universität Stuttgart*, no. 9, Essen, Girardet, 1969.
- 15.43 Hasek, V.: "Effect of Aging on the Mechanical Properties of Steels for Cold Extrusion" (in German), *Berichte aus dem Institut für Umformtechnik, Universität Stuttgart*, no. 19, Essen, Girardet, 1970.
- 15.44 Munk, P. C. W.: "Investigations on the Aging Behavior of Steels in Multistage Forming" (in German), *VDI-Berichte*, no. 139, 1969, pp. 21–30.
- 15.45 Dannenmann, E.: "Investigations on the Surface Area Changes in Solid Forward Extrusion" (in German), *Ind.-Anz.*, 88, 1966, pp. 2156–2161.
- 15.46 Kienzle, O., and Mietzner, K.: *Fundamentals on the Typology of Deformed Metallic Surfaces* (in German), Berlin/Heidelberg/New York, Springer, 1965.
- 15.47 Kienzle, O., and Mietzner, K.: *Atlas of Deformed Metallic Surfaces* (in German), Berlin/Heidelberg/New York, Springer, 1967.
- 15.48 ICFG Data Sheets: "General Aspect of Tool Design and Tool Materials for Cold Forging of Steel," no. 4/70; "Punches and Mandrels for Cold Extrusion of Steel," no. 5/71; "Dies (Die Assemblies) for Cold Extrusion of Steel," no. 6/72, Surrey, ISME, 1970, 1971, 1972.
- 15.49 *Metals Handbook*, 9th ed., Metals Park, OH, American Society for Metals, 1978.
- 15.50 Kraft, W.: "Sintered Metal Tools for Cold Forming Steel and Nonferrous Metals" (in German), *VDI-Berichte*, no. 139, 1969, pp. 69–74.
- 15.51 Liekmeier, F.: "Introduction of Multistage Processes for Cold Massive Forming" (in German), *Draht*, 22, 1971, pp. 144–153.
- 15.52 Schmoeckel, D.: "Design and Development Guidelines for Cold Extrusion" (in German), Mekan Resultat 66003, Stockholm, Sveriges Mekanförbund, 1966, pp. 90–95.
- 15.53 May, O.: "Cold Pressing of Symmetrical and Asymmetrical Small Pieces" (in German), *VDI-Berichte*, no. 39, 1959, pp. 22–25.
- 15.54 Kienzle, O., and Rick, M.: "Machine Elements with Coined Projections" (in German), *Mitt. Forschungsges. Blechverarb.* 1965, pp. 275–279.
- 15.55 Rick, M.: "Generation of Working Surfaces on Sheet Metal Workpieces by Cold Forming" (in German), *Ann. CIRP*, 11, 1962/63, pp. 217–224.
- 15.56 Burgdorf, M.: "Investigations on Upsetting and Embossing" (in German), *Berichte aus dem Institut für Umformtechnik, Universität Stuttgart*, no. 5, Essen, Girardet, 1966.
- 15.57 Burgdorf, M.: "On the Theoretical Determination of Normal Stress Distribution and Press Forces in Coining (Embossing)" (in German), *Ind.-Anz.*, 89, 1967, pp. 1406–1411, 1558–1561.
- 15.58 Gumm, P.: "Combination of Deformation and Cold Welding by Cold Extrusion and Tube Drawing" (in German), Dr.-Ing. thesis, Technische Universität, Braunschweig, 1964.
- 15.59 Gumm, P., and Hoffman, W.: "Cold Welding in Cold Extrusion Processes" (in German), *Z. Metallk.*, 56, 1965, pp. 704–712.
- 15.60 Hoffman, W., and Gumm, P.: "Cold Welding in Cold Extrusion Processes" (in German), *Ann. CIRP*, 13, 1965/66, pp. 281–285.
- 15.61 Gumm, P., and Ruge, J.: "Cold Welding of Steel/Copper and Nickel/Steel Joined Workpieces by Cold Extrusion" (in German), *Werkstattstechnik*, 58, 1968, pp. 313–317, 468–471.
- 15.62 Schmitt, G.: "Investigations on Backward Can Extrusion of Steel at Room Temperature" (in German), *Berichte aus dem Institut für Umformtechnik, Universität Stuttgart*, no. 7, Essen, Girardet, 1968.

- 15.63 Farlik, A., and Ondracek, E.: *Theory of Dynamic Deformation (in Czech)*, Praha, SNTL-Nakladatelství Technické Literatury, 1968.
- 15.64 Kast, D., and Schuster, M.: "Investigations on Backward Can Extrusion" (in German), *Ind.-Anz.*, **89**, pp. 411-414.
- 15.65 Schmitt, G.: "Calculation of Tool Stressing in Cold Extrusion of Cans" (in German), *Ind.-Anz.*, **92**, 1970, pp. 438-439; also *HGF-Bericht*, no. 70/11, Essen, Girardet, 1970.
- 15.66 Dipper, M.: "Cold Extrusion of Sleeves in Both Theory and Experiment" (in German), Dr.-Ing. thesis, Technische Hochschule, Stuttgart, 1949; also *Arch. Eisenhüttenwes.*, **20**, 1949, pp. 275-286.
- 15.67 Altan, T., and Thomsen, E. G.: "Pressures Required for Backward Can Extrusion," *Ann. CIRP*, **13**, 1966, pp. 273-280.
- 15.68 Siebel, E., and Fangmeier, E.: "Investigations on Force Requirements in Pressing and Piercing" (in German), *Mitt. Kaiser-Wilhelm-Inst. Eisenforsch.*, **13**, 1931, no. 3, pp. 43-62.
- 15.69 Weber, W.: "Determination of Forming Pressure for Backward Can Extrusion" (in German), *Fertigungstechn. u. Betr.*, **21**, 1971, pp. 49-53.
- 15.70 Tirosh, J.: "Analysis of Tube Piercing," *Isr. J. Technol.*, **3**, 1965, pp. 198-202.
- 15.71 Kudo, H.: "Some Analytical and Experimental Studies of Axisymmetric Cold Forging and Extrusion I," *Int. J. Mech. Sci.*, **2**, 1966, pp. 102-127.
- 15.72 Johnson, W., and Kudo, H.: *The Mechanics of Metal Extrusion*, Manchester, University Press, 1962.
- 15.73 Kast, D.: "Similarity Laws in Backward Extrusion of Geometrically Similar Cans" (in German), *Ind.-Anz.*, **92**, 1970, pp. 1733-1734; also *HGF-Bericht*, no. 70/146, Essen, Girardet, 1970.
- 15.74 "Metal Forming, Cold Extrusion of Carbon Steels," PERA Rep. 102, Production Engineering Research Association, England.
- 15.75 Kaiser, H.: "Possibilities of Testing Lubricants for Cold and Warm Extrusion of Steel" (in German), *Ind.-Anz.*, **93**, 1971, pp. 2311-2313.
- 15.76 Kunogi, M.: "A New Method of Cold Extrusion," *J. Sci. Res. Inst. (Tokyo)*, **50**, 1956, pp. 215-246.
- 15.77 Watkins, M. T., McKenzie, J., and Whitfield, E.: "The Simultaneous Forward Extrusion and Upsetting of Cans," Rep. 33, East Kilbride, National Eng. Lab., 1967.
- 15.78 Kudo, H., and Matsubara, S.: "Analysis of Stresses in Cylindrical Tools with Finite Heights Subjected to Inner Pressures" (in German), *Ind.-Anz.*, **92**, 1970, pp. 631-636.
- 15.79 Krämer, G.: "Studies on the Optimum Design of Rotation-Symmetric Cold Extrusion Dies" (in German), *Berichte aus dem Institut für Umformtechnik, Universität Stuttgart*, no. 49, Essen, Girardet, 1979.
- 15.80 Sieber, K.: "Theoretical Principles and Practical Experience for the Design of Cold Extrusion Tools" (in German), in *Proceedings of the International Conference on Cold Forming* (Düsseldorf, 1970), Session 4, Düsseldorf, VDI-Verlag, 1970; also *Metal Forming*, **38**, 1971, pp. 101-105, 128-131.
- 15.81 Adler, G., and Walter, K.: "Calculations of Single and Multiple Shrink-Fit Assemblies" (in German), *Ind.-Anz.*, **89**, 1967, pp. 805-809, 967-971.
- 15.82 Neitzert, T.: "New Methods of Calculating Prestressed Cold Extrusion Dies," in Seminar Papers entitled *Neuere Entwicklungen in der Massivumformung*, Forschungsinstitut Umformtechnik der Ingest e.V. Stuttgart, June 1979.
- 15.83 Friedewald, H. J.: "Press Fits for Blanking and Forming Tools" (in German), *VDI-Forschungsheft*, no. 472, Düsseldorf, VDI-Verlag, 1959.
- 15.84 Becker, S. G., and Mollick, L.: "The Theory of the Ideal Design of a Compound Vessel," *Trans. ASME, J. Eng. Ind.*, **82**, 1960, pp. 136-142.

- 15.85 Schulz, E.: "Design of Prestressed Press Tools for Cold Forming of Steel" (*in German*), *Draht*, 16, 1965, pp. 546–557.
- 15.86 Geiger, R.: "Material Flow in Combined Can Extrusion" (*in German*), *Berichte aus dem Institut für Umformtechnik, Universität Stuttgart*, no. 36, Essen, Girardet, 1976.
- 15.87 Pugh, H. Ll. D., Watkins, M., and McKenzie, J.: "An Experimental Investigation into the Cold Extrusion of Steel," *Sheet Met. Ind.*, 38, 1961, pp. 253–279.



## CHAP. 16

### HOT EXTRUSION

#### List of Special Symbols

---

$A$ ,	temperature-independent material parameter
$A'$ , $A''$	temperature-dependent material parameters
$a$	temperature conductivity
$b$	heat diffusivity, $= \sqrt{k c_p \rho}$
$b_C$	heat diffusivity of container material
$c_p$	specific heat
$k$	thermal conductivity
$L_D$	length of friction surface or die land
$l_{per}$	length of periphery of an extruded section
$n$	temperature-independent material parameter
$R$	gas constant
$Q$	activation energy
$s$	punch travel
$T_B$	billet temperature
$T_C$	container temperature
$T_T$	tool temperature
$v_{ex}$	extrusion velocity (exit velocity of extruded product)
$v_P$	punch velocity
$z$	temperature-modified strain rate
$\alpha$	heat flux
$\bar{\alpha}$	temperature-independent material parameter
$\bar{\beta}$	temperature-independent material parameter
$\rho$	density

## 16.1 CLASSIFICATION OF HOT-EXTRUSION PROCESSES

The term hot extrusion is used to describe processes in which a billet, enclosed in a container, is pushed through a shaped opening (die, orifice) at an elevated temperature. As a result of the forming operation, the initial cross-sectional area of the workpiece is reduced and a bar of solid or hollow cross section is produced.

Hot extrusion is used primarily to manufacture semifinished products such as bars, tubes, or profile sections. The main advantage over other processes, such as rolling or bar drawing, is that practically any desired cross-sectional shape can be produced, that is, not only solid sections but also hollow sections with differently shaped inner and outer contours where required.

In contrast to cold extrusion, which is also a member of the compressive-forming group of processes, hot extrusion is, for the majority of metals, performed above the recrystallization temperature.

The most important parameters in hot extrusion are the material properties and the appropriate forming conditions, namely, the forming temperature  $T$ , the speed of the press  $v$ , and the ratio of the cross-sectional areas of billet and bar  $A_0/A_1$ , which may be expressed as the strain  $\varphi_{\max} = \ln(A_0/A_1)$ . The practicability of hot extrusion depends largely on the force available, on the forming plant, and on the cross-sectional area of the billet.

Classification of the various hot-extrusion processes, as with the cold-extrusion processes, is based on the direction of material flow with respect to the operating direction of the press and, thereafter, on whether a solid or a hollow product is to be produced. Accordingly, as already described in Sec. 13.1, a distinction can be made between the following hot-extrusion processes:

- 1 Solid forward extrusion (direct extrusion of solid sections)
- 2 Hollow forward extrusion (direct extrusion of hollow sections)
- 3 Solid backward extrusion (indirect extrusion of solid sections)
- 4 Hollow backward extrusion (indirect extrusion of hollow sections)
- 5 Solid side extrusion (side extrusion of solid sections)
- 6 Hollow side extrusion (side extrusion of hollow sections)

Sketches illustrating the operating principle of each of the different processes are shown in Fig. 13.2. In addition it should be mentioned that all the above processes are normally carried out using rigid tools, although in the case of solid forward hot extrusion, the forming operation may also be carried out using hydrostatic pressure. This so-called hydrostatic extrusion is described in Chap. 28.

For solid forward hot extrusion, dies with an opening angle of  $2\alpha = 180^\circ$  (flat dies) or  $2\alpha < 180^\circ$  (conical dies) are used. Light alloys are worked with  $2\alpha = 180^\circ$ , often without lubrication, with or without leaving a shell (skull). For other metals the die-opening angle is  $2\alpha < 180^\circ$  when lubrication is used and  $2\alpha = 180^\circ$  when extruding with a shell.

In the latter case a sharp-edged disk is placed in front of the punch, the disk diameter being somewhat smaller than the inner diameter of the container. In this way the core is sheared out of the billet, while a thin-walled layer, which may contain undesirable inclusions and other impurities, remains behind as a shell (skull) and can be removed after the extrusion operation proper has been completed. In the case of steels, titanium, and similar materials, dies with an opening angle  $2\alpha < 180^\circ$  are used together with suitable lubricants (e.g., powdered glass).

When hollow sections are to be produced by means of forward hot extrusion, either a (fixed or moving) mandrel or specially designed dies may be used (see Sec. 16.7). Such dies (bridge dies and porthole dies among others) are often used when tubes and especially hollow sections of complicated cross-sectional shapes (e.g., made of aluminum) are to be produced. As a rule, the billet is first split into several streams by applying a high pressure to the end face. The streams then flow over a short, exactly centered fixed mandrel and, behind this, weld together to form a hollow profile of the desired cross section.

Backward hot extrusion (often called indirect extrusion) differs from forward hot extrusion (also termed direct extrusion) above all in that the billet remains stationary with respect to the container. The punch used is of hollow construction and the extrusion die is attached to its front end. When the die moved in this way impinges on a billet placed in the container die, a bar is

extruded out through the hollow punch toward the back of the extrusion press. Since there is no relative motion between the billet and the container, no friction forces arise between these partners. The load required for forming is therefore lower than in other processes. This undeniable advantage, however, must be set against the fact that hollow punches are complicated in design and allow only lower mean extrusion pressures. Unless the press is specially designed, downtime for tool changing may be higher. Also, the ratio between the maximum profile diameter (see Sec. 16.7.1) and the inner diameter of the container is relatively small. For these reasons, backward hot extrusion—in particular extrusion of tubes—was up to the mid-seventies of only limited use. Since then, however, specially designed hydraulic presses, which overcome some of the above-mentioned disadvantages, have been introduced in the production process for the extrusion of aluminum alloys [16.1].

In side extrusion, the extruded material is forced out at a right angle to the direction of motion of the punch (Fig. 13.2e). In this way both solid and hollow sections can be produced. The main use of these processes is for cable sheathing in which, for example, a hollow aluminum profile is pressed onto a continually advancing cable acting as a mandrel (Fig. 13.2f).

## 16.2 MATERIALS USED IN HOT EXTRUSION

Hot extrusion may be used for forming all nonferrous alloys and nearly all alloy and carbon steels. A summary of the most common materials or groups of materials used in hot extrusion is given in Table 16.1. Information concerning further material data may be found in the bibliography compiled by Gentzsch [16.16].

The criterion that forms the basis of the classification in Table 16.1 is the degree of workability of the material. The upper temperature limit is usually the solidus temperature of the alloy. The information concerning the mean pressure  $p_m$  is based on experimental data obtained during extrusion operations at strains commonly occurring in practice. The load required for forward hot extrusion of bars (at the start of extrusion) is about 30% greater than that for backward hot extrusion [16.2]. The data for the maximum pressure  $p_{\max}$  concern values that may be reached in practice under acceptable loading of the extrusion dies [16.3].

## 16.3 PROCESS CHARACTERISTICS

Precise knowledge of the forming conditions under which a hot-extrusion operation should be carried out is a necessary precondition for the best use of existing equipment as well as for optimum design of new extrusion plant. Thus in order to calculate the force needed to initiate and maintain the extrusion operation, it is necessary to have the following information:

- 1 The strain  $\varphi$ , strain rate  $\dot{\varphi}$ , and extrusion temperature  $T$
- 2 The flow stress  $\sigma_f$  of the material to be extruded as a function of the strain, strain rate, and extrusion temperature

Further, a suitable basis for calculating the stresses, energy, and work requirements is needed. In the literature on hot extrusion there is, as yet, no comprehensive theoretical foundation which permits the optimum extrusion conditions to be specified in advance for a particular material on the basis of its material properties. In addition to the so-called elementary theory methods, there exist several exact solutions to the general equations of plasticity theory. However, these are only valid within certain limits. Furthermore there is a whole range of approximate formulas which the engineer may use to estimate the load requirements.

### 16.3.1 Material Flow

Experiments concerning material flow aim to permit the most accurate assessment possible of local deformation patterns in a particular workpiece. Thus they are an important instrument for determining the strains, forces, and work requirements at different stages of the extrusion process.

**Table 16.1** Extrusion Materials

DIN	U.S.	Material designation	Extrusion pressure				Maximum degree of deformation $\varphi_{\max} = \ln (A_0/A_1)$
			Extrusion temperature $T$ , °C (°F)	$p_m, 10^2 \times N/mm^2$ (ksi)	$f_{\max}, 10^2 \times N/mm^2$ (ksi)	Normal extrusion velocity $v_{ex}$ , m/s (ft/s)	
Easy to press							
Pure Al		360–500 (680–930)	3.5–5.0 (51–73)	8.0 (116)	0.3–2.0 (0.9–6.0)	6.9	
Pure Mg		250–300 (480–570)	3.0–4.5 (44–65)	8.0 (116)	0.03–0.2 (0.1–0.6)	5.3	
Pure Sn		120–200 (250–390)	1.0–2.0 (15–29)		0.03–0.2 (0.1–0.6)		
Pb, Pb alloys		120–180 (250–360)	0.5–1.5 (7–22)		0.15–1.0 (0.5–3.0)		
$\beta$ -brass (e.g., CuZn40Pb2)		500–750 (680–1380)	3.0–4.0 (44–58)	7.0 (102)	0.5–2.0 (1.5–6.0)	6.5	
Pressed without particular difficulties							
Pure Cu (FCu)	(UNS C11000) (UNS C28000)	800–900 (1470–1650) 700–800 (1290–1470)	3.0–4.5 (44–65) 3.0–4.5 (44–65)	8.0 (116) 7.0 (102)	0.6–2.0 (1.8–6.0) 0.5–2.0 (1.5–6.0)	5.7 6.4	
$\alpha$ -brass (CuZn37)	AA 6060	400–500 (750–930)	3.0–6.0 (44–87)	7.0 (102)	0.2–1.5 (0.6–4.5)	6.2	
AlMgSi0.5	AA 6082–O	400–500 (750–930)	3.0–6.0 (44–87)	8.0 (116)	0.1–0.4 (0.3–1.2)	5.5	
AlMgSi1w	AA 3108	400–500 (750–930)	3.0–5.0 (44–73)	8.0 (116)	0.2–1.0 (0.6–3.0)	6.0	
AlMn1	AA 5005A	380–450 (720–840)	3.0–5.0 (44–73)	8.0 (116)	0.1–0.2 (0.3–0.6)	4.6	
AlMg1	AA 5754	380–450 (720–840)	3.0–5.0 (44–73)	8.0 (116)	0.1–0.2 (0.3–0.6)	4.6	

		Difficult to press			
AlMg5	AA 5056A	380–420 (720–790)	6.0–8.0 (87–116)	10.0 (145)	0.05–0.1 (0.15–0.3)
AlCuMg1	AA 2017A	420–460 (720–860)	6.0–8.0 (87–116)	10.0 (145)	0.01–0.03 (0.03–0.09)
AlCuMg2	AA 2024	420–460 (720–860)	6.0–8.0 (87–116)	10.0 (145)	0.01–0.03 (0.03–0.09)
Al/ZnMgCu0.5	AA 7079	410–460 (770–860)	8.0–10.0 (116–145)		0.01–0.02 (0.03–0.06)
Al/ZnMgCu1.5	AA 7075	410–460 (770–860)	8.0–10.0 (116–145)		0.01–0.02 (0.03–0.06)
Cu-Ni alloys (e.g., Monel)	(e.g., Cu70–Ni30)	800–900 (1470–1650)	8.0–10.0 (116–145)		1.0–2.5 (3.0–7.5)
Al bronze (e.g., CuAl11Ni)	(e.g., UNS C63000)	800–900 (1470–1650)	7.0–9.0 (102–131)	10.0 (145)	0.1–0.12 (0.3–0.36)
Sn bronze		750–850 (1380–1560)	6.0–9.0 (87–131)	10.0 (145)	0.05–0.07 (0.15–0.21)
Zn-Al alloys (e.g., ZnAlCu1)	(e.g., UNS Z33530)	200–300 (390–570)	6.0–10.0 (87–145)	0.03–0.2 (0.09–0.6)	4.1
Very difficult to press					
Ti, Ti alloys		800–1000 (1470–1830)	10.0–12.0 (145–174)	0.5–4.0 (1.5–12.0)	4.6
P bronze (e.g., CuSn8)	(e.g., UNS C52100)	650–750 (1200–1380)	8.0–10.0 (116–145)	0.01–0.025 (0.03–0.08)	3.2
Zr, Zr alloys		800–1100 (1470–2010)		0.5–1.0 (1.5–3.0)	3.4
Be		890–960 (1634–1760)		1.0–2.3 (3.0–6.9)	3.7
Carbon steels		1100–1280 (2010–2340)	7.0–8.0 (102–116)	10.0 (145)	3.0–6.0 (9.0–18.0)
High-alloy steels		1150–1230 (2100–2250)	9.0–12.0 (131–174)	1.0–2.0 (3.0–6.0)	4.6

Source: Compiled from [16.2] to [16.15].

## 16.6 BULK-METAL FORMING

Furthermore it is possible to predict the likelihood of extrusion defects occurring, based on the type of material flow. The investigative methods may be grouped as follows:

- 1 Reduced-scale experiments using wax and plasticine bodies
- 2 Extrusion experiments carried out at room temperature or slightly above using easily deformable metals such as lead, tin, and bismuth
- 3 Laboratory experiments with actual extrusion materials
- 4 Extrusion experiments under actual factory conditions

Material movement is usually determined by measuring the distortion of individual volume elements. Methods of group 1 were mainly used at the beginning of the research into extrusion techniques. Easily deformed metals (group 2) are still sometimes used today for fundamental investigations. The knowledge gained from using methods 1 and 2 can, however, only be applied within limits to predict the flow characteristics of important extrusion materials since these often behave differently from the materials used in the experiments. Since the results of laboratory experiments carried out on small-scale presses can also be transferred only with difficulty to account for the conditions under which large presses are operated, it is of the greatest importance to perform tests and experiments under actual factory conditions in order to confirm the validity of the results [16.17].

Die geometry and punch velocity are important contributory factors in determining the extrusion velocity range and hence the strain rate, which, for a given temperature, determines the shear flow stress  $k$  in the work material. In addition, friction between the work material and the inner surface of the container, the die, and the pressure disk results in a friction shear stress  $\tau_{FR}$  which, depending on the type of extrusion process, may vary between  $\tau_{FR} = 0$  (hydrostatic extrusion) and  $\tau_{FR} = \tau_{FR,max} = k$  (direct extrusion with shell) according to Fig. 16.1 [16.18]. The relation  $\tau_{FR}/k$  dominates the material flow in extrusion, as has been shown by Schelosky for superplastic homogeneous, isotropic model material [16.19]. In addition, the anisotropy and inhomogeneity of plastic behavior across the billet cross section and length, caused by differences in concentration of the alloying elements, by the texture of the billet, and by local variations of temperature, may affect negatively the material flow during the forming operation.

The combined effects of these various influences permit identifying different types of material flow. In the case of solid forward hot extrusion using flat dies ( $2\alpha = 180^\circ$ ), these may be divided into four categories [16.20], [16.21] (Fig. 16.2):

**Flow type S** Occurs with homogeneous materials when friction is sufficiently low for a practically unimpeded flow of material to take place along all boundary surfaces

**Flow type A** Occurs with homogeneous materials when a certain amount of friction exists at the die end face

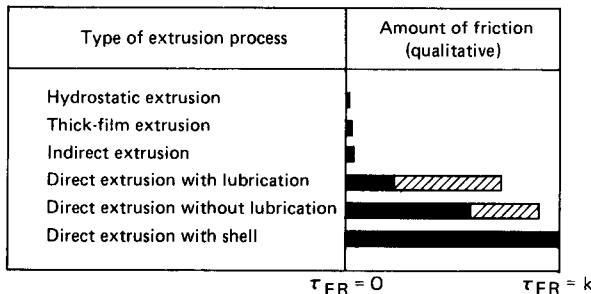


**FIG. 16.1** Amount of friction between billet and container wall for various hot-extrusion processes. (After [16.18].)

Type of flow				
Type of material	Homogeneous	Homogeneous	Homogeneous	Non-homogeneous
Material example	Theoretical	Pb, Al, Fe with lubrication	Cu, Al, Al alloys	Mg, $\alpha$ - and $\beta$ -brass
Friction	None	Low	High	High
Defects	None	None	Subsurface defect (rear portion of product)	Extrusion defects (rear portion of product)

**FIG. 16.2** Classification of different types of flow occurring in axisymmetric solid forward hot extrusion. (After [16.20], [16.21].)

Flow type **B** Occurs with homogeneous materials when considerable friction is present on all contact surfaces

Flow type **C** Is characteristic of billets with unevenly distributed plastic properties as a result of phase changes in the outer regions or variations in strength resulting from temperature differences; the occurrence of high levels of friction in the outer regions is a further typical characteristic

A suitable method for showing the effect of different factors on material flow has proved to be the visioplasticity method (see Chaps. 5 and 7). Here the billet to be extruded is first cut in half in the plane of symmetry and a network of lines is applied to one half. The two billet halves are then extruded together. A separating medium stops the two halves from welding together during the forming operation. The study of the distortion of the grid matrix after extrusion gives a good picture of the material movement during extrusion in general and of the degree of distortion of individual volume elements of the material in particular. Fig. 13.8 shows an example of flow type **B**, which is typical for the flow behavior of most technically significant materials.

It will be recognized that deformation begins already at a considerable distance from the die, especially along the billet centerline. In the corner of the die/container a "dead zone" develops where the material is considered rigid. Along the major part of the billet's boundary layer, a zone of high shear deformation exists. In front of the pressure disk follower block, at the end of the billet, the material tends to flow inward (piping effect).

Dalheimer [16.22] suggests dividing the billet into three zones to study the deformation process, as shown in Fig. 16.3. The same characteristics are found here as in Fig. 13.8, although it concerns a different material extruded under different conditions.

Zone I contains the real deformation zone in which the major shape changes take place. The

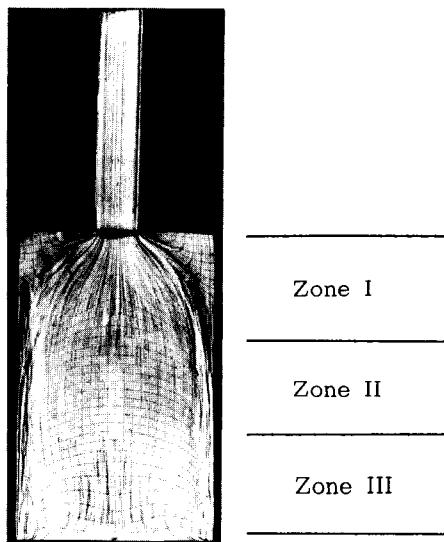


**FIG. 16.3** Material flow of AlMgSi1 (AA 6082). Axisymmetric solid forward hot extrusion; nonlubricated;  $d_0 = 71$  mm (2.8 in);  $\varphi = 3.0$ ;  $T_B = 450^\circ\text{C}$  ( $842^\circ\text{F}$ );  $T_T = 450^\circ\text{C}$  ( $842^\circ\text{F}$ );  $v_p = 8$  mm/s (0.3 in/s);  $s = 50$  mm (2 in);  $l_0 = 152$  mm (6 in). (After [16.22].)

occurrence of considerable radial velocities and axial accelerations may be surmised from the distortion of the grid lines. Particularly dramatic changes can be seen in the transition areas between the dead zone and the central deformation zone. Experiments have shown [16.22] that while the length of the dead zone on the inner wall of the container is affected only negligibly by the degree of deformation, the angle at which material approaches the die aperture increases with the degree of deformation.

Zone II is characterized by the fact that the material of the billet surface is slowed down or stopped by the friction between the material and the inner surface of the container, depending on whether extrusion takes place with or without lubrication. (Figs. 13.8 and 16.3 both show operations without lubrication.) Where no lubrication is provided, a shear zone forms between the outer layer and the main core of the billet. Different rates of flow prevail in the axial direction across the cross section, with the maximum velocity along the billet centerline; radial displacements are insignificant. In zone III the material in the outer surface layer is compressed by the pressure disk. It is forced inward, leading to an inward radial motion of the material already on the inside, with which it comes into contact. During extrusion, zone II is continually shortened until finally zone III and zone I are practically touching each other. As the deformation process continues, more and more material from the outer layer—often containing inclusions and other impurities—is forced toward the billet centerline. Finally internal material separation occurs, which can lead to a piping effect.

Hardly any literature exists which deals with solid forward hot extrusion of complicated profiles. The few papers that have been published concern only relatively simple cross-sectional shapes. They show that with profile extrusion, too, a dead zone is formed, although it may be of irregular shape. The flow rate distribution differs from that of the axisymmetric case: on crossing the die aperture, the material particles which are furthest away from the friction surfaces (i.e., the contact surfaces between extrusion material and die in the orifice) advance fastest.

This is, however, only true as long as the friction surfaces (die land) on the total circumference

of the die opening are equally long. In tool design it is thus common to adjust the length of the die land so that the material flow rate in a particular area may be influenced according to the shape of the cross section (see Sec. 16.7.1).

It should be pointed out here that the material flow may be improved by using conical dies ( $2\alpha < 180^\circ$ ) as compared with flat dies ( $2\alpha = 180^\circ$ ), which sometimes permits the extrusion of difficult materials. The advantage of easier material flow, however, must be weighed against the increased difficulty of finding a suitable lubricant. In addition, with extruded products, high demands are usually made on the quality of surface finish, and these can be satisfied far more easily when flat dies are used (where impurities and oxide layers are kept out of the region of material flow). Further, the butt (discard) is easier to remove from flat dies after extrusion is finished.

It is not the intention here to discuss further the material flow in hollow forward hot extrusion, backward hot extrusion, and side hot extrusion, nor to go into more detail on the subject of flow types S, A, and C. For this the interested reader is referred to the work of Dürrschnabel [16.20] and Laue and Stenger [16.23].

In addition to experimental studies, recent theoretical investigations are making use of computer models of extrusion processes for the optimization of material flow, aiming at homogeneous deformation combined with minimization of stresses and forces, even for noncircular axisymmetric sections. These CAD methods lead to streamlined die geometries (Fig. 16.4). The digital data describing the die configuration may be used for the generation of machine-tool control programs for die making (CAM) [16.24] to [16.26].

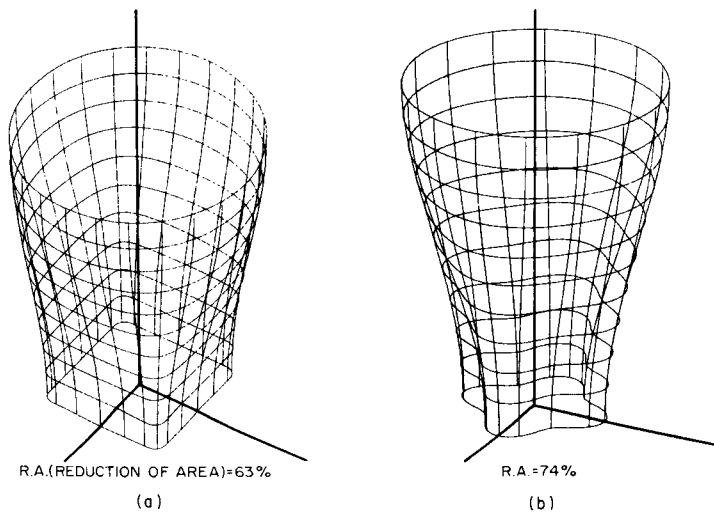


**FIG. 16.4** Three-dimensional die configuration for hydrofilm extrusion. Material—Ck 45(AISI 1015); lubricant—castor oil; initial billet radius—19.5 mm (0.77 in). (a) Square section. (b) Clover section.

### 16.3.2 Characteristic Microstructure

The microstructure resulting from a metal-forming process such as hot extrusion depends to a great extent on whether the material is subject to recovery (dislocation climb, cross slip, and polygonization; see Sec. 3.4) or to recrystallization (creation of new grains, movement of large-angle grain boundaries; see Sec. 3.6). The question is difficult to answer because microstructural investigations on hot-formed materials are only of limited use. A recrystallized structure may, even at

slow cooling rates, occur *after* the forming operation. If information is desired about the microstructure *during* the forming process, it is necessary to attempt interrupting the forming operation and bringing the material below the recrystallization temperature as quickly as possible. Only with materials that exhibit a deformed structure after forming can the idea of recrystallization as a softening mechanism be ruled out [16.27], [16.28].

A detailed overview of the numerous investigations into the problem of microstructure formation in hot forming—as yet without a clear general solution—is to be found in [16.29]. According to [16.28], agreement appears to exist that certain groups of metals, including aluminum, aluminum alloys, and  $\alpha$ -iron, are subject to recovery processes during hot forming; with other materials, such as copper, brass, and nickel, recrystallization during forming has been proven.

Besides the operations to inhibit work hardening, another important question is whether the breakdown and precipitation of intermetallic phases—above all in precipitation-hardening alloys—is influenced by the forming process. So far investigations have shown that the equilibria are more quickly reestablished during these forming operations [16.28].

### 16.3.3 Flow Stress $\sigma_f$

The flow stress  $\sigma_f$  is of great significance for quantifying forming operations. It gives an indication of the state of stresses that is required to make a specific material flow, that is, deform plastically.

Because the flow stress depends on many factors, there is a certain difficulty in using this parameter. While for many materials the relationship  $\sigma_f = \sigma_f(\varphi, \dot{\varphi}, T)$  is well known, as a rule the known stress-strain curves are normally not valid for strains larger than  $\varphi_{\max} = 1.0$  because of the experimental method used for their determination (e.g., cylindrical upsetting test). An extrapolation of these stress-strain curves to the very much larger strains occurring in hot extrusion (see Table 16.1) is highly questionable. While the stress-strain curves used in the calculation of cold-forming operations show a continuous increase due to the work hardening of the material, those related to hot forming may reach a constant level. After a starting-up phase a steady state is reached in the material in which the effects of work hardening and recovery are in dynamic equilibrium. Some stress-strain curves, however, pass through a maximum and then fall back to the steady-state value [16.28] or continue to decrease according to temperature and strain rate. Fig. 16.5 shows, for example, the stress-strain curves of AlMgSi1 (AA 6082) at 450°C (842°F) in which the flow stress  $\sigma_f$  at  $\varphi > 1$  falls back to a more or less constant value. Stress-strain curves at other temperatures show a similar behavior [16.30]. A carbon steel containing 0.25% carbon, for which the stress-strain curves at 1100°C (2012°F) are shown in Fig. 16.6, exhibits the described tendency even at low strains. The observation that at higher strains the flow stress is approximately constant is increasingly true at smaller strain rates  $\dot{\varphi}$ . The stress-strain curves shown in Figs. 16.5 and 16.6<sup>°</sup> were obtained in hot torsion experiments. While this method is based on simplifying assumptions [16.30] and therefore is somewhat controversial, it is a test method that can produce flow stress data up to high strains. It is, however, not yet exactly known under which conditions and with which accuracy such data may be applied to extrusion because of the completely different strain and stress states.

For the large strains typical in hot extrusion it is sufficient to determine the flow stress as a function of strain rate  $\dot{\varphi}$  and forming temperature  $T$ . Experimental values at low stresses may be described, according to [16.29], by

$$\dot{\varphi} = A' \sigma_f^n \quad (16.1)$$

On the other hand, for high stresses (or high strain rates) in the steady-state range, the following exponential function is valid [16.29]:

$$\dot{\varphi} = A'' e^{\bar{\beta} \sigma_f} \quad (16.2)$$

The variables  $n$  in Eq. 16.1 and  $\bar{\beta}$  in Eq. 16.2 are temperature-independent parameters. The temperature dependence of the flow stress is taken into account in the factors  $A'$  and  $A''$ .

<sup>°</sup>The mean strain rate  $\dot{\varphi}$  in hot extrusion may be estimated by the equation  $\dot{\varphi} = \varphi / \Delta t = 6\varphi v_p / d_0$  [16.30], [16.31].

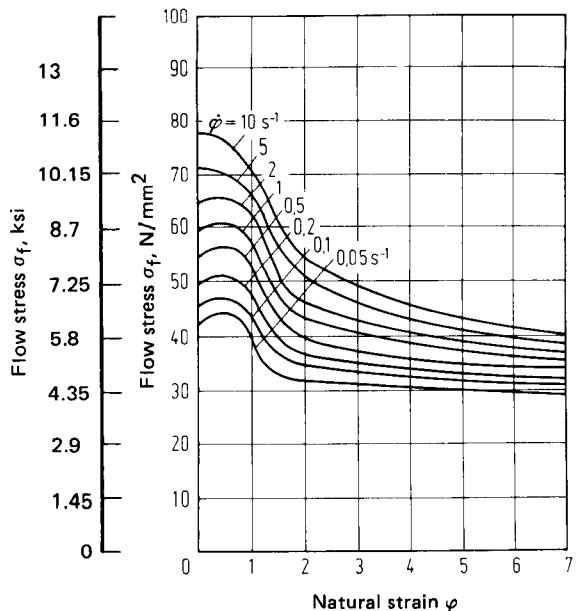


**FIG. 16.5** Flow-stress curves for AlMgSi1 (AA 6082) at 450°C (842°F). (After [16.30].)

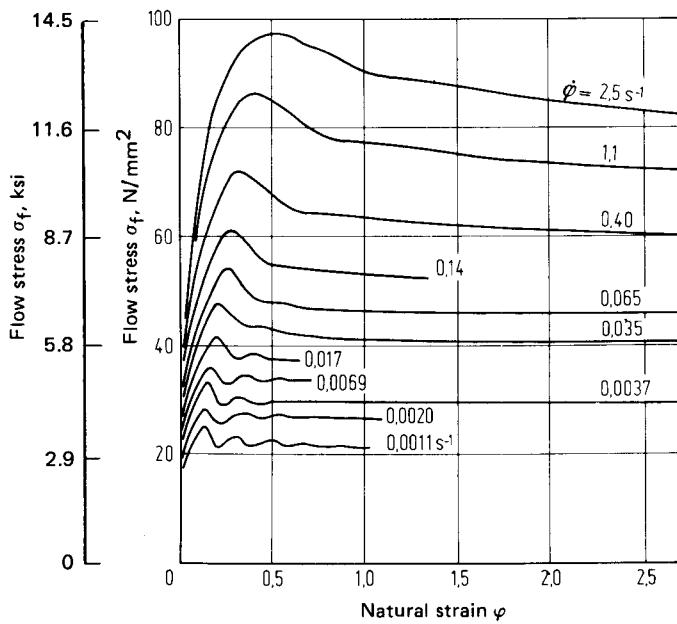


**FIG. 16.6** Flow-stress curves for carbon steel (0.25% carbon) at  $T = 1100^\circ\text{C}$  (2012°F). (After [16.29].)

## 16.12 BULK-METAL FORMING

Both equations have been known in this form or in a similar form for a long time. They are similar to the relationships used to describe creep. For a whole range of materials (e.g., aluminum and aluminum alloys, zinc, and  $\alpha$ -iron) similar microstructural changes occur during both creep and hot forming. It is thus convenient to apply a relationship well known in creep theory [16.32] in a modified form to hot forming:

$$\dot{\varphi} = Ae^{-Q/RT} [\sinh(\bar{\alpha}\sigma_f)]^n \quad (16.3)$$

$A$ ,  $\bar{\alpha}$ , and  $n$  are temperature-independent material parameters,  $Q$  is the activation energy, and  $R$  is the gas constant.\*

Using Eq. 16.3, a particular flow stress can be determined for a large range of metals and their alloys over a wide spectrum of strain rates and temperatures.

For low stresses ( $\sigma_f \ll 1/\bar{\alpha}$ ) it is possible to derive Eq. 16.1 from Eq. 16.3. For high stresses Eq. 16.3 leads to Eq. 16.2. Both approximations show good agreement with Eq. 16.3. Deviations of more than 10% occur only in the range of [16.29], [16.31]:

$$0.8 < \bar{\alpha}\sigma_f < 1.2$$

Since the constants  $\bar{\alpha}$ ,  $\bar{\beta}$ , and  $n$  are linked by the relationship

$$\bar{\beta} = n\bar{\alpha} \quad (16.4)$$

$n$  and  $\bar{\alpha}$  may be determined on the basis of available experimental data for low and high flow stresses.

When a range of measurements exists where different combinations of  $\dot{\varphi}$  and  $T$  lead to similar values of the flow stress  $\sigma_f$ , the activation energy may be determined on the basis of the rule [16.31]

$$Q = -R \left[ \frac{\partial \ln \dot{\varphi}}{\partial(1/T)} \right]_{\sigma_f} \quad (16.5)$$

Usually, however, such a range of measurements is not available, but rather the flow stress is measured as a function of strain at constant temperature or as a function of temperature at constant forming speed. In this case the following equation applies [16.31]:

$$Q = R \left[ \frac{\partial \ln \dot{\varphi}}{\partial \sigma_f} \right]_T \left[ \frac{\partial \sigma_f}{\partial(1/T)} \right]_{\dot{\varphi}} \quad (16.6)$$

The physical significance of the activation energy  $Q$  is discussed in [16.29]. Further detailed information on how to determine  $Q$  is given in [16.33].

Since an increase in temperature has the same effect on the flow stress as a reduction in strain rate, one aims to take both factors into account by introducing a temperature-modified strain rate  $z$  [16.29], [16.31]:

$$z = \dot{\varphi} e^{Q/RT} = A [\sinh(\bar{\alpha}\sigma_f)]^n \quad (16.7)$$

Introduction of the strain rate  $z$  makes it possible to determine the constants of Eq. 16.3 by graphic means and thus make a comparison with available measured values.

The diagram  $\log z = f(\log \sigma_f)$  represents a curve whose linear lower portion (small stresses) corresponds to Eq. 16.1; the slope of the line gives the constant  $n$ . On the other hand, the curve  $\log z = f(\sigma_f)$  in its upper portion (high stresses) merges into a straight line, that is, in the area of validity of Eq. 16.2. The slope of these lines is given by  $n\bar{\alpha}$ , thus permitting  $\bar{\alpha}$  to be determined. Subsequently the constant  $A$  may be read directly from the  $\log z/\log \sigma_f$  diagram:  $z = A$  for  $\sigma_f = 1/\bar{\alpha}$  [16.31].

Table 16.2 gives the values of the constants used in Eq. 16.3, determined as above for a range of materials.

Whether Eq. 16.7 or Eq. 16.3 is valid depends on the following criterion: when the activation energy of a material is the same in creep as in hot forming, both Eqs. 16.7 and 16.3 may be used without limitations. This is the case with aluminum and aluminum alloys, technically pure  $\alpha$ -iron, and ferritic alloys, among others. The activation energy differs only slightly from that measured

\*Gas constant  $R = 8.315 \text{ kJ/kmol} \cdot ^\circ\text{C}$ .

**Table 16.2** Constants of Eq. 16.3 for Different Materials

Material	$Q$ , kJ/mol	$n$	$1/\bar{\alpha}$ , N/mm <sup>2</sup> (ksi)	$A$ , s <sup>-1</sup>	Temperature range of measurements, °C (°F)
Aluminum, high purity	156	4.76	22.6 (3.3)	$1.4 \times 10^{12}$	300–600 (570–1110)
Aluminum, technical purity	156	4.1	22.6 (3.3)	$2.35 \times 10^{10}$	300–600 (570–1110)
Zinc	117	5.55	43.2 (6.3)	$5 \times 10^{10}$	110–320 (230–610)
$\beta$ -titanium	172	3.45	37.8 (5.5)	$3.8 \times 10^{10}$	900–1300 (1650–2370)
$\gamma$ -uranium	448	3.57	30.4 (4.4)	$10^{17}$	800–1000 (1470–1830)
$\alpha$ -zirconium	193	6.25	122.6 (17.8)	$3.7 \times 10^8$	600–850 (1110–1560)
$\beta$ -zirconium	264	3.03	81.4 (11.8)	$1.2 \times 10^{12}$	1000–1300 (1830–2370)
Armeo iron ( $\alpha$ ) (0.03% C)	276	4.55	58.8 (8.5)	$4.47 \times 10^{11}$	600–800 (1110–1470)
Silicon steel ( $\alpha$ ) (2.8% Si)	335	4.35	59.8 (8.7)	$6.03 \times 10^{13}$	650–1000 (1200–1830)
Carbon steel ( $\gamma$ ) (0.25% C)	306	4.55	63.8 (9.3)	$1.5 \times 10^{11}$	1100 (2010)

Source: Compiled from [16.31].

for self-diffusion, showing that the reduction in work hardening depends on recovery processes [16.29]. With materials such as copper and copper alloys, nickel and nickel alloys, and austenitic steels, where work hardening is removed in creep by recovery and in hot forming by recrystallization, the activation energies of creep and hot forming may differ considerably from each other. (A comparison is given in [16.29].) The parameter  $z$  and Eq. 16.3 thus correlate with the measured data only in a limited area. A fairly good agreement of activation energies is obtained with  $\gamma$ -iron, although it is classified into the second group of materials because of the development of its grain structure.

The validity of Eqs. 16.7 and 16.3 for aluminum is demonstrated in Fig. 16.7. The experimental results obtained by various authors in torsion, compression, creep, and extrusion experiments may be combined in a single diagram of  $\log(z/A)$  versus  $\log[\sinh(\bar{\alpha}\sigma_f)]$  for a wide range of values of  $z$  to form a substantially common line. In order to compensate for the differences in purity between the individual experimental materials, the parameter  $z$  is based in this diagram on the *structure factor A* [16.29], [16.31].

### 16.3.4 Calculation Methods

**Elementary plasticity theory:** The so-called elementary plasticity theory [16.34], [16.35] has already been used for the common fundamental discussion of pulling-through and pushing-through processes. The stress state in the deformation zone was discussed in detail in Sec. 13.3.2. Comments concerning the determination of work and forces required in forming and points to be taken into account during the calculation of hot-extrusion problems are discussed in Secs. 13.3 and 13.4.

**Empirical considerations:** A useful aid for the practical estimation of extrusion loads and forces is the deformation efficiency  $\eta_{def}$  (see Sec. 13.4.2 and Table 13.4). This empirical approach is based on the fact that extrusion, a steady-state forming operation like other pushing- and pulling-through processes, exhibits an approximately trapezoidal load-stroke curve. However, even with this method one cannot get around the fact that the flow stress  $\sigma_f$ , which depends on the parameters  $\varphi$ ,  $\dot{\varphi}$ , and  $T_B$ , must be either known or determined experimentally. Combinations of further empirical equations, in part developed especially to take account of extrusion conditions, are given in [16.20], [16.37].

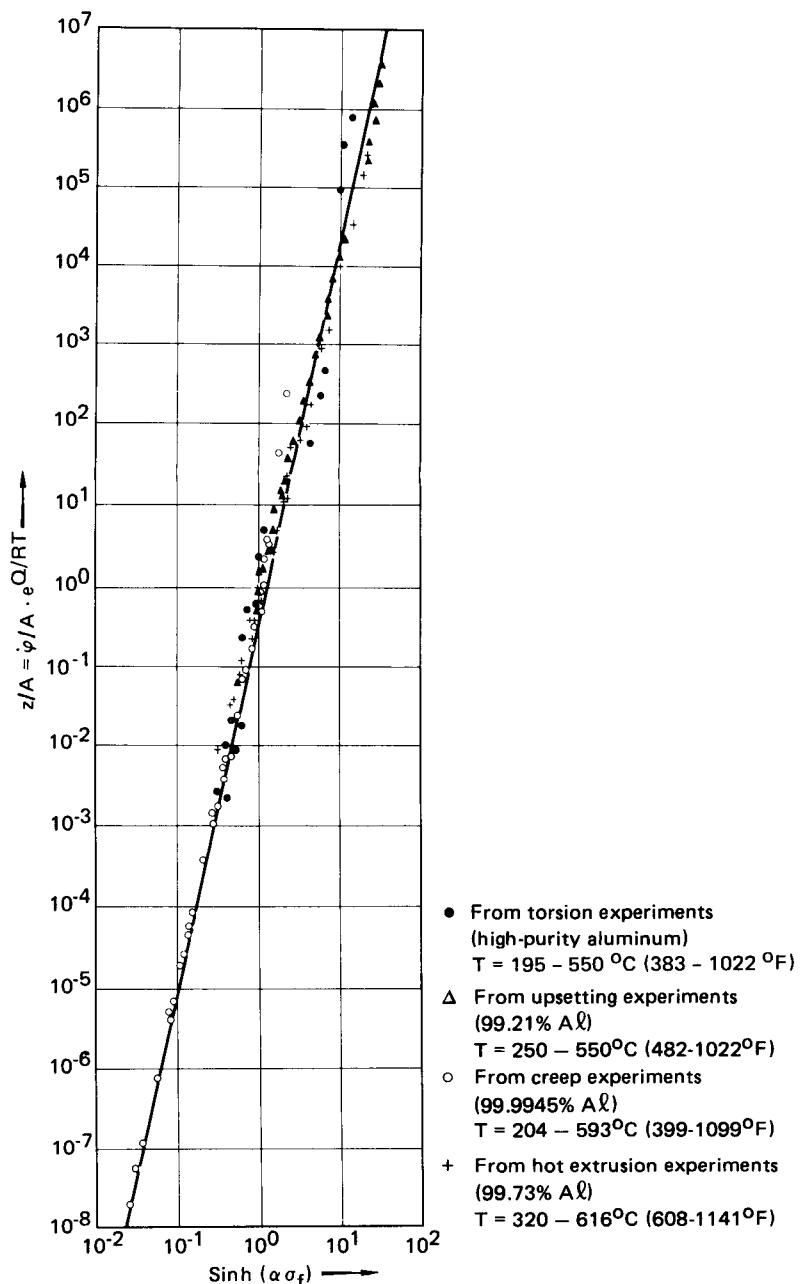


**FIG. 16.7** Linear relationship between  $\log(z/A)$  and  $\log[\sinh(\bar{\alpha}\sigma_f)]$  for aluminum (Eq. 16.7). (After [16.29].)

**Rigorous solutions to the basic equations of plasticity theory:** Elementary plasticity theory formulas for calculating forming loads often produce results which differ considerably from the forces that exist in practice. This is mainly due to the highly simplified assumptions concerning the state of motion. Therefore, attempts have been made to base the force calculations on conditions of motion which correspond better to the actual material flow. There exist several rigorous solutions to the general fundamental equations of plastic flow. However, they are only valid within certain specified limits.

Slip-line fields (for further detail see Sec. 5.4) are based on plane-state conditions. Fig. 16.8 shows an example of a slip-line field derived by Hill [16.38] for a plane hot-extrusion operation with lubrication. According to this solution, the material is subject to shear stresses along the line with lubrication. According to this solution, the material is subject to shear stresses along the line  $ABCD$ , while within the area  $BCD$  it is deformed continuously. A material particle transported from  $P$  to  $D$ , on the other hand, is subjected to no deformation.

For some time considerable efforts have been made to develop suitable calculation methods for axisymmetric forming as well. Few special solutions exist as yet [16.39]. Dalleheimer [16.22] has shown how a numerical approximation by finite difference methods [16.40], [16.41] may be successfully adapted to axisymmetric hot extrusion and how the local stresses, shape changes, and velocities may be determined with sufficient accuracy. With these methods, although the continuity equation and the equilibrium conditions at every point in the deformation zone are satisfied, the law of plastic flow is not fulfilled exactly but rather approximated by an error equation. An example of the computer results representing lines of equal axial stress and lines of equal deformation velocity is shown in Fig. 16.9. The axial stresses  $\sigma_z$  are mainly compressive. However, near the die opening, tensile stresses exist within the extruded bar.

The calculated axial stress distribution thus confirms suspicions that the cracks, which can often be found at the center of extruded bars, are due to tensile stresses in the deformation zone. Even piping in the later stages of the extrusion operation can thus be explained as the setting up of axial tensile stresses at the billet center. The distribution of strain-rate changes  $\dot{\epsilon}$  can also in part be explained in this way. Very large flow speeds occur in the deformation zone just in front of the die opening; particularly high stretching of the material occurs near the axis. The speeds of material flow there, however, are exceeded by those at the leading edge of the die opening. This fact explains in turn why, in adiabatic hot extrusion, the highest temperatures occur at the leading edge of the die or, correspondingly, at the surface of the extrusion passing through the orifice.

**Upper-bound solutions:** These provide a powerful tool for the theoretical calculation of deformation loads. The fundamentals of the upper-bound method are discussed in Sec. 5.4 (refer also to [15.25] to [15.30], [16.42]). The advantage of this method is that it may also be applied to axisymmetric forming operations and, moreover, requires a relatively modest amount of computation [16.39]. References to further reading are given in [16.16]. Critical treatments of the different approaches to the theoretical description of hot extrusion may be found in [16.43] and [16.44].

**Visioplasticity:** The visioplasticity method [16.45] has proved useful for making quantitative statements about the displacement of individual volume elements of the extrusion billet, for studying the transition stages during the extrusion process, and thus for determining the local material speeds. For further details, see Secs. 5.4 and 16.3.1.

### 16.3.5 Load as a Function of Stroke

The load requirements for forward and backward hot extrusion of bars are shown in Fig. 16.10 as a function of punch displacement.

In forward extrusion (curve  $a$ ) the load initially increases very fast from 0 to  $A$ . At this stage

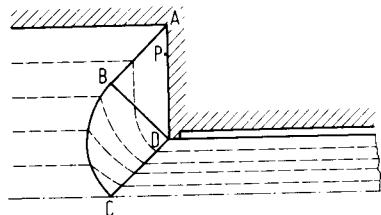


**FIG. 16.8** Slip-line field for plane-strain forward hot extrusion of a bar with lubrication. (After [16.38].)

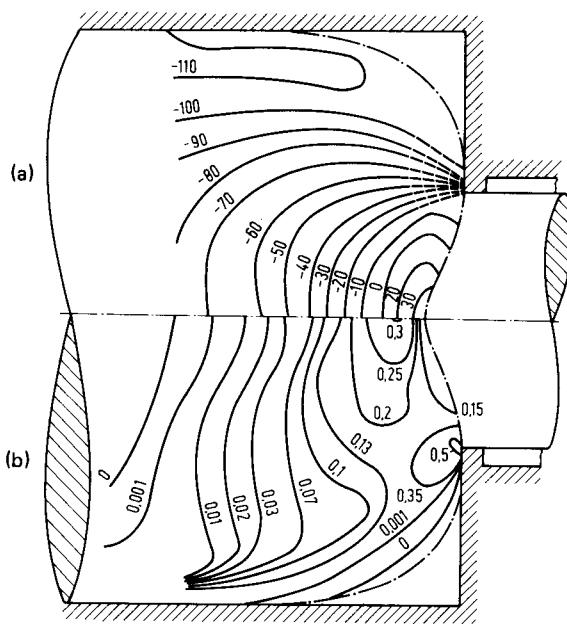


**FIG. 16.9** Forward hot extrusion of AlMgSi1 (AA 6082).  $d_0 = 71$  mm (2.8 in);  $\varphi = 1.6$ ;  $v_p = 1$  mm/s (0.04 in/s). (a) Lines of constant axial stress  $\sigma_z$  (N/mm<sup>2</sup>). (b) Lines of constant rate  $\dot{\epsilon}_r$  (s<sup>-1</sup>). (After [16.22].)

the billet, the outer diameter of which is slightly smaller than the diameter of the container, is upset such that its entire cylindrical surface is in intimate contact with the inner surface of the container. At the end of the non-steady-state starting-up process (curved bump at A) the load decreases continually until it reaches a minimum at B, whereafter it may again rise sharply.

The load increases at the end because when the material has been substantially extruded from the container, the punch is pressed into the deformation zone just in front of the die. It disrupts the material flow in that zone and subsequently initiates additional internal displacement, leading to increased load.

The reduction in load between A and B is a function of friction between the billet and the container, which depends linearly on the length of the billet. Thus its maximum value is reached at the beginning of the operation. Consequently the maximum load value, and thus the gradient of the curve between A and B, may be reduced by the use of suitable lubricants.

In backward hot extrusion (curve b in Fig. 16.10) the load increases initially in the same way until the billet has been upset in the container and the operation has commenced. Since there is relatively little movement between billet and container, flow is easier than in forward hot extrusion. This leads to lower initial values of the extrusion force. Furthermore, more or

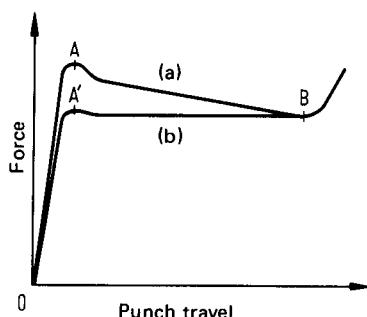


**FIG. 16.10** Load-stroke curve (qualitative). (a) Forward hot extrusion. (b) Backward hot extrusion.

less constant loading exists between  $A'$  and  $B$ , corresponding in value to the minimum force occurring in forward hot extrusion.

The hot-extrusion process is usually interrupted before the second force increase, that is, before the minimum extrusion force is reached, in order to avoid defects at the end of the bar; the butt or discard must then be parted off and removed using suitable equipment. The butt length depends on various factors, such as material, degree of deformation, forming temperature, and shape. In practice, in order to ensure good quality of the extrusion, it is between 10 and 25% (usually 15%) of the original billet length.

In [16.20] attention is drawn to the fact that load-stroke curves corresponding to Fig. 16.10 occur in practice only when no appreciable work hardening takes place. Otherwise, as in forward hot extrusion, the curves exhibit a less steep gradient at the beginning of the process, a more stretched out maximum load in the middle, and a considerably less pronounced minimum load at the end.

### 16.3.6 Significance of Temperature

Temperatures prevailing in hot extrusion have a decisive influence on the process and the properties of the extrusion. The relationships are shown clearly in Fig. 16.11 [16.46], in which the authors provide a qualitative definition of hot extrusion. Of the two shaded areas, one is characterized by insufficient force available to perform the extrusion operation, the other by the fact that excessively high billet temperatures lead to defects in the extruded bar (hot cracks, phase changes on reaching the solidus line). Thus only the nonshaded area of the diagram is suitable.

The difficulty that the extrusion load is insufficient for a given extrusion ratio  $A_0/A_1$  at a particular billet temperature may sometimes be overcome by increasing the initial temperature of the billet or the temperature of the container. However, care must be taken here that the right-hand boundary curve is not crossed due to excessive heat development during deformation. The closer the billet temperature is to the solidus temperature of the material at large extrusion ratios, the more one has to be concerned with the removal of heat generated by deformation and friction. Thus the extrusion velocity, which is a critical factor in heat generation, has its limits. This relationship has led to the development of hot-extrusion methods in which the exit temperature of the extrusion is held constant (isothermal extrusion) [16.47]. How this aim may be reached is described later. First, however, it is necessary to have an understanding of temperature changes in hot extrusion.

Recent literature refers to a range of methods which have been developed in order to describe

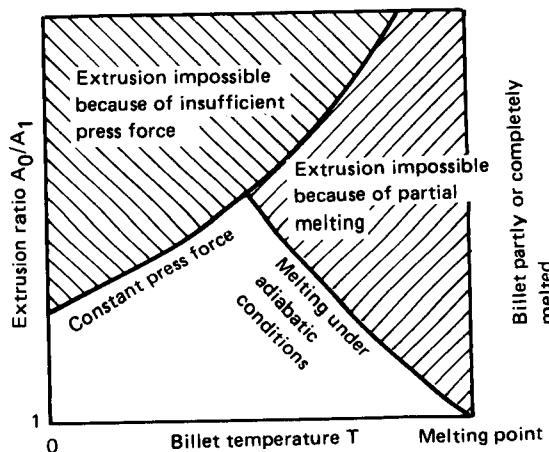


FIG. 16.11 Limiting curves for hot extrusion. (After [16.46].)

quantitatively the complicated heat-transfer processes [16.15], [16.22], [16.46], [16.48] to [16.60]. Detailed overviews are given in [16.22], [16.49].

All methods known up to now are based on a compromise between the number of factors not taken into consideration and the amount of calculation to be performed. According to [16.49], a satisfactory solution to the problem should take account of the following factors:

- Heat development in the deformation zone
- Heat development at the boundaries resulting from friction between billet and tools
- Distribution of the heat generated by deformation throughout the billet
- Removal of the frictional heat from billet and tools
- Heat exchange between billet and tools due to different temperatures
- Heat transfer as a result of the displacement of the billet during hot extrusion

The list of these factors shows the need for an analysis of the non-steady-state temperature field and the associated heat flow during hot extrusion in order to make quantitative statements about the relationships between the initial temperature distribution in the billet and in the tools, the work done, the extrusion speed, and the extrusion exit temperature. Under idealized initial and boundary conditions, this problem can be solved by integration of the heat-transfer equation for a particular volume element of the system. The interdependence of neighboring volume elements is not taken into account here. Numerical methods, on the other hand, allow a much better adaption to the specific conditions of a particular hot-extrusion operation [16.11]. For approximate solutions, in practice, consideration of the above-mentioned factors is often sufficient [16.59]. Examples of numerically calculated temperature curves are given in Figs. 16.12 and 16.13. They show clearly the influence of punch velocity and temperature distribution. In slower forming operations (Fig. 16.12) temperature differences in the billet and the extrusion are very quickly evened out because of the good thermal conductivity of the aluminum alloy [in this case AlMgSi1 (AA 6061)]. In addition, heat transfer from the workpiece to the tool helps to avoid pronounced temperature peaks. Interestingly, the cooling effect of the tools affects the temperature distribution across the cross section of the extrusion such that the core zones stay warmer than the surface zones.

With increasing punch velocity the situation is reversed. Considerable temperature differences occur often across the cross sections of both the billet and the extrusion. In the zones of small local deformation, the material remains relatively cool, while considerable temperature increases occur at the interface between the billet and the container and at the exit point (Fig. 16.13). Temper-

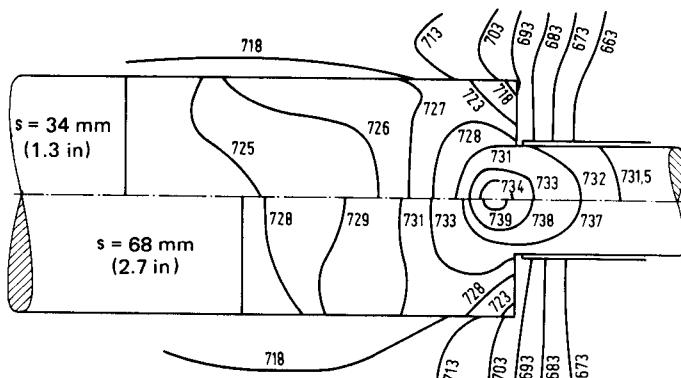


**FIG. 16.12** Isotherms during forward hot extrusion of AlMgSi1 (AA 6082).  $d_0 = 71 \text{ mm (2.8 in)}$ ;  $\varphi = 1.6$ ,  $T_B = T_T = 450^\circ\text{C}$  ( $842^\circ\text{F}$ );  $v_p = 2.5 \text{ mm/s (0.1 in/s)}$ ;  $l_0 = 152 \text{ mm (6 in)}$ ;  $\alpha = 4 \text{ kW/(m}^2 \cdot ^\circ\text{C)}$ . (After [16.22].)

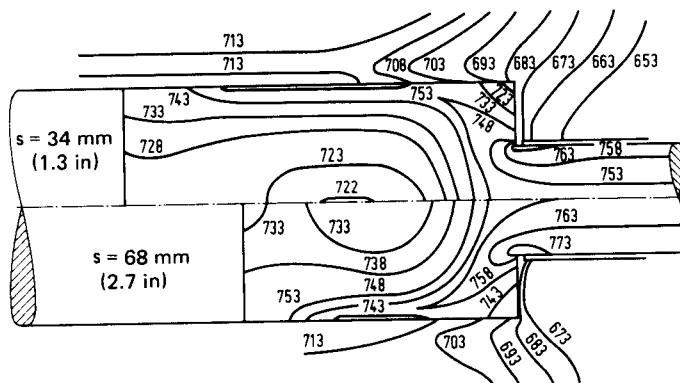


**FIG. 16.13** Isotherms during forward hot extrusion of AlMgSi1 (AA 6082).  $d_0 = 71$  mm (2.8 in);  $\varphi = 1.6$ ;  $T_B = T_T = 450^\circ\text{C}$  (842°F);  $v_p = 31.5$  mm/s (1.24 in/s);  $l_0 = 152$  mm (6 in);  $\alpha = 4 \text{ kW}/(\text{m}^2 \cdot ^\circ\text{C})$ . (After [16.22].)

ature differences become more pronounced with higher punch velocity, that is, the more one approaches the conditions of adiabatic deformation.

Since the surface of the extrusion must not heat beyond a certain material-related limit, it is important to know what kind of temperature increases are likely to occur during extrusion. Fig. 16.14 shows such temperature curves measured at the entry edge of a die opening as a function of punch travel, velocity, area reduction, and solid section geometry [16.60]. With very slow forming operations a more or less constant temperature is attained after an initial rapid temperature increase. Heating due to deformation, friction, and shearing in the boundary zone is in equilibrium with the amount of heat loss due to heat transfer between workpiece and tool.

With increasing punch velocity this equilibrium can no longer be sustained. Thus the temperature keeps rising, even at the end of deformation. With the relatively low strain of  $\varphi = 3$  for

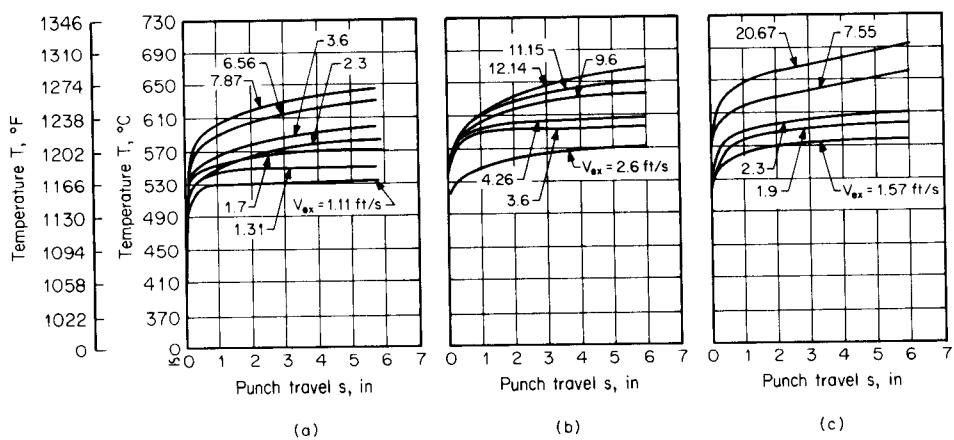


**FIG. 16.14** Forward hot extrusion of AlMgSi 0.5 (AA 6060). Surface temperature at the die entry edge. Unlabeled measurements are in inches; to convert to millimeters, multiply by 25.4. To convert ft/s into m/s, multiply by 0.3048.  $d_0 = 71$  mm (2.8 in);  $l_0 = 152$  mm (6 in);  $T_B = 450^\circ\text{C}$  (842°F). (a) Circular die opening,  $\varphi_{\max} = 3.0$ . (b) Circular die opening,  $\varphi_{\max} = 3.91$ . (c) Square die opening,  $\varphi_{\max} = 3.0$ . (After [16.60].)

## 16.20 BULK-METAL FORMING

AlMgSi 0.5 (AA 6060) it is already possible to reach the limit at which localized melting occurs at the extrusion surface [16.22]. Such temperature changes are typical also of other materials and strain rates.

The main reason for these temperature changes is that the time available for heat transfer is inversely proportional to the speed of the punch; that is, with increasing velocity an even smaller amount of heat is transferred to the tools. In the limiting case adiabatic conditions are attained. Furthermore the flow stress of the workpiece material increases with higher punch velocity and strain rate. Higher flow stresses cause the work of deformation to increase and thus lead to a greater temperature rise [16.57]. The direct effects of this on the temperature distribution in the workpiece are, however, comparatively small since for its part the flow stress decreases with increasing temperature.

The effect of the process conditions, above all the punch velocity, on the temperature field is of even greater significance when the shape of the extruded section is not axisymmetric. With angular profile sections, heat is likely to concentrate at the corners, leading to considerable temperature increases and thus endangering the extrusion surface. According to Lange and Stüwe [16.15] the temperature distribution in an extruded bar of square cross section caused by friction on the die land (see Fig. 16.27) can be calculated by the following equation with regard to the initial temperature of the extrusion:

$$\Delta T(x, y, z) = \frac{b_{ex}T_{FR}v_{ex}}{(b_D + b_{ex})k} \Phi\left(x, y, \frac{aL_D}{v_{ex}}, h\right) \quad (16.8)$$

where  $a$  = temperature conductivity

$b_{ex}$  = heat diffusivity of extruded material (see Table 16.3),  $= \sqrt{k_{ex}c_{p,ex}\rho_{ex}}$

$b_D$  = heat diffusivity of die material

$T_{FR}$  = friction shear stress,  $\leq T_{max} = \sigma_f/2$

$x, y$  = cross-section coordinates of coordinate system having its origin at the center of the square section

$2h$  = side length of square section

$k$  = thermal conductivity

$L_D$  = length of friction surface in die

According to [16.15] the function  $\Phi$  may be divided into three ranges. When profiles of cross-sectional areas that are not too small are extruded relatively fast,

$$\Phi(h, h) = 2.26 \sqrt{\frac{aL_D}{v_{ex}}} \quad (16.9)$$

is valid at the section corner ( $x = h, y = h$ ). Eq. 16.9 is valid for the range  $aL_D/h^2v_{ex} > 0.3$ , a condition that is usually fulfilled in hot extrusion. The section corner in this case heats up twice as much as the center of the side face:  $\Phi(h, h) = 2\Phi(h, 0)$ . The temperature at the interior of the extrusion remains substantially unchanged.

After a transition zone, a steady-state temperature drop occurs in the profile cross section at  $aL_D/h^2v_{ex} > 0.8$ . The condition at the section corner is then

$$\Phi(h, h) = \frac{2aL_D}{hv_{ex}} + \frac{2}{3}h \quad (16.10)$$

The difference in value of the functions between the section corner and the center of the side length as well as between the center of the side length and the interior is  $h/2$  in each case:

$$\Phi(0, 0) = \Phi(h, 0) - \frac{h}{2} = \Phi(h, h) - h \quad (16.11)$$

With longer heating times, the additional term in Eq. 16.10 is dropped. In hot extrusion, however, this is rarely the case [16.15].

According to [16.15], Eqs. 16.8 to 16.10 may also be used to estimate the temperature increase

**Table 16.3** Material Data for Use with Eqs. 16.8 to 16.13

Material	Extrusion temperature $T$ , °C (°F)	Temperature conductivity $a^a$ , $\text{m}^2/\text{s}$ ( $\text{ft}^2/\text{s}$ )	Thermal conductivity $k$ , $\text{W}/\text{m} \cdot ^\circ\text{C}$	Thermal diffusivity $b$ , $\text{kJ}/\text{m}^2 \cdot ^\circ\text{C}$	Shear flow stress $\tau_{\max}$ , $\text{N}/\text{mm}^2$ (ksi) <sup>b</sup>
Aluminum	450 (840)	$63 \times 10^6$ (567)	184	23.4	6.9 (1)
Aluminum alloys (containing copper)		$58 \times 10^6$ (522)	176	23.0	24.5 (3.6)
Copper	420 (790)				
	800–900 (1430–1650)	$77 \times 10^6$ (693)	322	36.4	9.8 (1.4)
Brass	650–850 (1200–1560)	$43 \times 10^6$ (387)	151	23.0	14.7 <sup>c</sup> (2.1) <sup>c</sup>
Die material X38CrMoV51 (AISI H11)		$8.2 \times 10^6$ (74)	39	13.8	
Die material X38CrMoV51 (AISI H11)	450 (840)				
		$5.3 \times 10^6$ (48)	26	11.3	
	800 (1470)				

<sup>a</sup> $a = kc_p\rho$ .<sup>b</sup>Figures in this column refer only to a temperature of 650°C (1200°F).<sup>c</sup>At 850°C (1560°F),  $\tau_{\max}$  for brass is 9.8 N/mm<sup>2</sup> (1.4 ksi).

Source: Compiled from [16.15].

on the surface of axisymmetric extrusions. It lies between the values calculated for the edges and the center of the sides of a square section of similar cross-sectional area, and shifts toward the value at the center of the side with larger extrusion diameters.

To illustrate the significance of material characteristics and extrusion velocity, Fig. 16.15 shows the temperature increases at the corners of a square section for different materials. The values were calculated with the aid of Eqs. 16.11 and 16.9 based on

$$\Delta T(h, h) = \frac{2.26 b_{ex} T_{FR}}{(b_D + b_{ex})k} \sqrt{a L_D v_{ex}} \quad (16.12)$$

When the thermal characteristics of the material differ from each other only slightly (e.g., as with two different kinds of brass), the friction will affect the temperature increases linearly according to material-dependent friction shear stress  $T_{FR}$  as long as the maximum value  $T_{FR,\max} = \sigma_f/2$  (Tresca's law) is not reached.

With low extrusion velocities and small cross sections the premises on which Eq. 16.9 is based are no longer valid, resulting in deviations from the square-root function (Eq. 16.12). This is of no significance for copper, brass, aluminum, and very many aluminum alloys since, as a rule, these materials are extruded at sufficiently high speeds. It is, however, important for some aluminum alloys which are difficult to extrude, such as AlZnMgCu 0.5 (AA 7022), in which case Eq. 16.8 should be used in conjunction with Eq. 16.10.

The interrelation between corner heating and the length of the friction surface is given in Fig. 16.16. This shows clearly why complicated extruded sections, especially those with large differences in wall thickness, need to be extruded much more slowly than shapes of simple cross section. To ensure that an extrusion of varying wall thickness leaves the die in a straight line, the material flow in the thick-walled zone has to be slowed down by means of long friction surfaces. In some cases these may be several times as long as the usual lengths of 3–6 mm (0.1–0.2 in), and they may even be as much as 30 mm (1.2 in). To avoid overheating at the guiding surfaces of the die, the extrusion velocity is decreased in inverse proportion to the length of the die land [16.59].

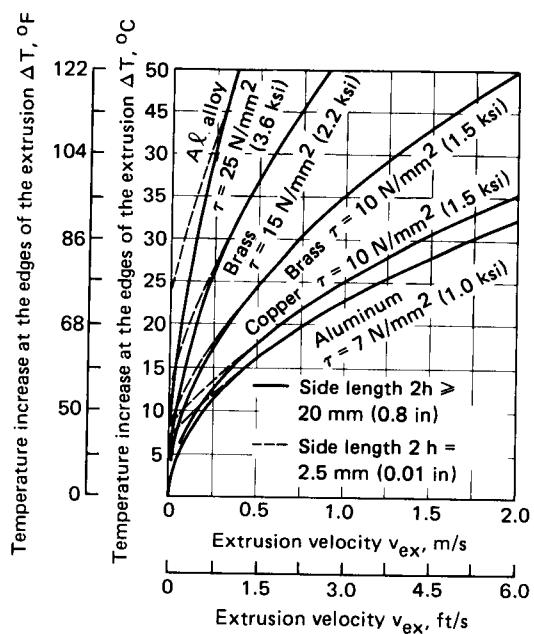


FIG. 16.15 Temperature increase at the edges of a hot-extruded square bar for different materials. (After [16.15].)

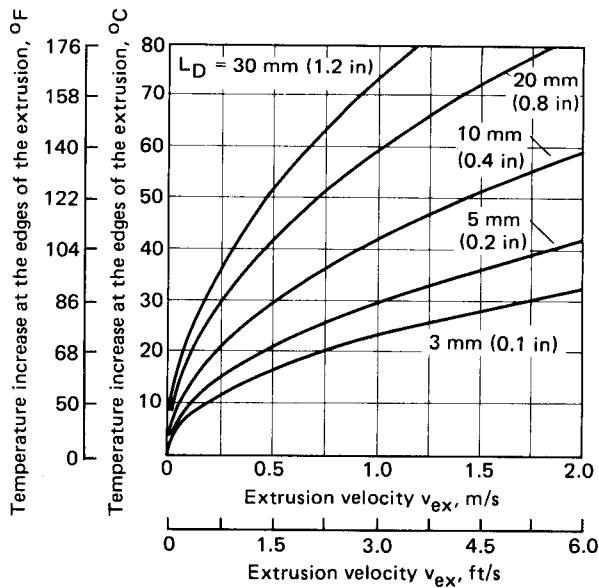


FIG. 16.16 Temperature increase at the edges of a square aluminum section [ $\tau_{\max} = 7 \text{ N/mm}^2 (1 \text{ ksi})$ ] of side length  $2h = 20 \text{ mm (0.8 in)}$  as a function of extrusion velocity  $v_{ex}$  and length of die-land surface  $L_D$ . (After [16.15].)

With the exception of those seldom used hot-extrusion processes which, because of small strains, simple cross-sectional shapes, and low billet temperatures (see Fig. 16.11), can be carried out under near adiabatic conditions, the usual aim is to maintain a constant exit temperature with regard to high productivity and consistent quality of the product. The generation of heat in the deformation zone is an inseparable part of the hot-extrusion process. On the other hand, steps can be taken to reduce the effect of heat generated through friction and shearing in the boundary zones. Here two main approaches to *isothermal extrusion* exist:

- 1 **Uneven heating of billet (so-called tapered heating):** The temperature profile is controlled in such a way that those parts which are subsequently subject to heat generation are initially colder.

A radial temperature gradient, which may be established by cooling the boundary zones, can be maintained only for a short time and does not take account of the fact that the individual cross sections of the billet are subject to different local deformations.

By means of a falling temperature gradient from the beginning to the end of the billet the extrusion exit temperature will be held constant through the contribution of heat generated during the extrusion process (Fig. 16.17). To avoid premature evening out of the temperature difference in the billet, this method is used most commonly in processes with high extrusion velocities. In practice, the desired temperature gradient is achieved by using a set of differently designed induction coils or by partial cooling with water after heating.

- 2 **Constant heating of the billet and control of the cooling rate and/or punch velocity:** Theoretically it would be possible to reduce the temperature of the container during the hot-extrusion operation in such a way that the heat removal rate remains constant, leading to a constant extrusion temperature. This aim, however, is difficult to achieve in practice. Recent development work has therefore tended to concentrate on adapting the punch velocity  $v_p$  to the heat-generation rate. The best solution to the problem is the continuous measurement of the extrusion exit temperature and closed-loop control of the punch velocity as a function of the difference between the measured temperature and the desired (constant) exit temperature.

According to Akeret [16.11], full use of the press capacity is possible only if the billet and

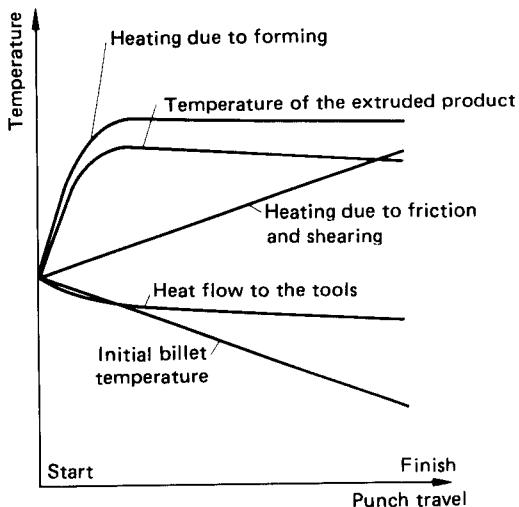


**FIG. 16.17** Extrusion exit temperature held constant by means of uneven (tapered) preheating of the billet. (After [16.57].)

container temperatures have been chosen correctly. Thus it is important, in the long term, to consider heating of the billet and control of the container temperature as integral parts of the overall system.

The considerable technical difficulties involved in controlling  $v_{ex} = f(T_{ex})$  may be avoided by trying to calculate in advance what deformation conditions one wishes to choose and how these are to vary during extrusion operation. According to Lange [16.49], the billet material must enter the forming zone at a constant temperature if one desires an extrusion to leave the die exit at a constant temperature. Both temperatures differ by an amount corresponding to the heat generated during forming. The frictional heat transferred to the billet should thus compensate for the losses due to thermal conduction. Furthermore it is assumed that no heat flows back into the billet from the forming zone.

These heat-flow considerations lead to the following relationship between punch velocity and extrusion time  $t$ :

$$v_p(t) = \frac{b_C(T_B - T_C)}{\sqrt{\pi} T_{FR}} \frac{1}{\sqrt{t}} \quad (16.13)$$

Integrating this equation with respect to time leads to an expression of punch velocity  $v_p$  as a function of punch travel  $s$  (the length of the extruded billet):

$$v_p(s) = \frac{2}{\pi} \left[ \frac{b_C(T_B - T_C)}{T_{FR}} \right]^2 \frac{1}{s} \quad (16.14)$$

The total extrusion time is given by

$$t_{tot} = \frac{\pi}{4} \left[ \frac{T_{FR}}{b_C(T_B - T_C)} \right]^2 l^2 \quad (16.15)$$

where  $b_C (\simeq b_D)$  = heat diffusivity of container (or die) (see Table 16.4)

$T_B - T_C$  = initial temperature difference between billet and container

$l$  = total extruded length of billet

Using Eqs. 16.13 and 16.14 it is possible to control the extrusion process (e.g., with a control curve) without having to measure the extrusion exit temperature [16.49]. Eq. 16.14 and Fig. 16.18 show that the mean punch velocity may be increased for shorter billets.

With longer billets it is advisable to work with a temperature gradient and, in addition, to control the punch speed in order to counteract the disadvantages of both methods. A given tem-

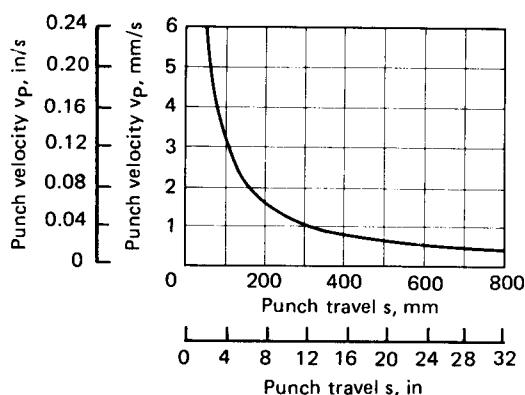


FIG. 16.18 Punch velocity  $v_p(s)$  during hot extrusion of AlZnMgCu0.5 (AA 7022) with constant extrusion exit temperature. (After [16.49].)

perature gradient alone would not lead to a sufficient temperature difference during deformation, while control of extrusion speed alone leads to uneconomical extrusion times [16.49].

The stipulation that no heat should be conducted from the forming zone to the billet is investigated theoretically in [16.49]. The calculation shows that heat flow occurs only in the vicinity of the die. Thus under steady-state conditions the given solutions are valid. The initial phase, before reaching the steady state, is completed fairly rapidly, provided the punch velocities are not too small.

For completeness, various other methods should be mentioned which have a role to play where temperature control is of prime importance [16.11]:

- 1 Lubrication of the interface between billet and tools:** This applies even for materials normally extruded without lubrication or extruded with a shell (especially aluminum alloys). The purpose of lubrication is to minimize the additional heat generated by friction or shearing. Well-known examples are (a) cold extrusion using solid, oily, or greasy lubricants; (b) hydrostatic cold extrusion (see Chap. 28); and (c) hot extrusion using glass-based viscous or solid lubricants similar to those used with high-melting-point metals (e.g., steel). These methods are particularly suitable where difficult alloys are to be extruded.
- 2 Backward hot extrusion (indirect extrusion):** Since with backward hot extrusion no relative motion occurs between billet and container, no frictional heat is generated by these partners [16.23], [16.61], [16.62].
- 3 Use of cooled dies:** Cooled dies are used to remove excess heat from the deformation zone. Using a suitable coolant, even materials normally difficult to form can be extruded successfully. This depends, however, on accurate metering of the coolant to prevent overcooling the material. This method is mostly used at lower speeds since in rapid extrusion processes the cooling effect is negligible.

## 16.4 FRICTION AND LUBRICATION

The effect of friction on material flow, and in particular the different types of flow that may occur, are discussed in Sec. 16.3.1. Section 13.2 shows the effect of friction conditions on the work done in deformation and on the forces required.

Friction itself depends on the finish of the contact surfaces (billet, container, die, pressure disk) and on lubrication where applicable. Light metals are often hot-extruded without lubrication, especially where an extrusion of high-quality surface finish is required. Elsewhere the main purpose of lubrication is to facilitate material flow and reduce the extrusion forces. The type of lubricant used depends on the material to be extruded. All high-pressure lubricants have in common an ability to provide an unbroken lubricating film and to stand up to the temperatures that arise.

For copper, brass, and bronze a lubricant made up of a mixture of oil, graphite, and other additives is generally used. The graphite content varies between 5 and 35%, and oil-soluble soap is used to bind the graphite better.

With aluminum and aluminum alloys, when lubrication is required, 10–15% colloidal graphite is mixed with light or heavy mineral oil. Beeswax is also sometimes used as a lubricant. With alloys which tend to weld together easily,  $\text{MoS}_2$  dispersions have proved useful, especially for mandrel lubrication.

Liquid and wax-type lubricants are generally put onto the contact surfaces, normally the tool surfaces, by brushing and spraying. Brushing may cause uneven film thicknesses, which can easily lead to variations in material flow.

In the extrusion of steel and other difficult materials, glass and glass-type lubricants are used (Ugine-Séjournet process [16.63]). Here the billet surface is coated by immersion or by rolling the hot billet on an inclined table covered with glass fiber or powder. In addition, a powder compact (of glass) is placed between the billet and the die. Thus a highly viscous layer is formed between the billet, the container, and the die, which subsequently becomes a thin glass coating on the emerging extrusion. Eutectic phosphor-based compounds have also been used as lubricants [16.64]. Graphite and (organic) oils and greases are used only for extruding relatively small steel parts on fast (mechanical) presses.

## 16.5 MATERIAL PROPERTIES PRIOR TO EXTRUSION

The basic requirement for achieving satisfactory extrusions is the use of suitable raw materials. Preparation of the billet material usually starts with casting from the melt. The bars formed in this way are cut to length by sawing or shearing, and the billets thus formed are heat-treated where necessary. In many cases heat treatment is performed immediately after casting.

Preparation of billets for hot extrusion depends on the following quality considerations:

- 1 The chemical composition must be within the specified tolerances.
- 2 The microstructure of the billet must be homogeneous and such as to assure consistent mechanical properties over the entire length and cross section of the billet.
- 3 The finish of the side and end faces of the billet, marked by impurities, scale, oxidation layers, cracks, and so on, must be inspected.

The methods of preparation and the necessary care in carrying them out depend to a large degree on the material to be extruded, on the conditions during extrusion, on the final use of the extruded product, and on the inspection facilities available. Billets made of materials subject to segregation are often heated to just below the solidus temperature after casting. The aim is to reduce stresses set up during casting which later could lead to cracking during sawing. Furthermore, structural changes occur: nonequilibrium eutectic particles at the grain boundaries dissolve, leading to an increase in the solidus temperature; easily dissolved alloying elements go into solution; elements which are difficult to dissolve are precipitated out of the saturated solution; and fine precipitates can become coarser [16.11].

The processes described, which can have a very significant effect on the subsequent extrusion process, depend in each case on the particular alloying elements, the annealing temperature and duration, and the cooling rate. The relationships between these factors are now outlined after [16.65], based on the aluminum-magnesium-silicon alloys which are of particular economic significance.

In this tertiary alloy system, a part of whose equilibrium diagram is shown in Fig. 16.19, silicon and magnesium form the intermetallic compound  $Mg_2Si$ . The magnesium silicide occurs in the cast microstructure at the grain boundaries in a eutectic form and is dissolved during the annealing process. As the quasibinary equilibrium diagram Al-Mg<sub>2</sub>Si in Fig. 16.20 shows, the solubility in the aluminum solid solution increases with temperature.

On rapid cooling, the  $Mg_2Si$  remains supersaturated in the solid solution. The more  $Mg_2Si$  there is available, the more it remains in solid solution, thus increasing the flow stress and reducing the mean extrusion exit velocity that can be obtained. With slow cooling, on the other hand, coarse

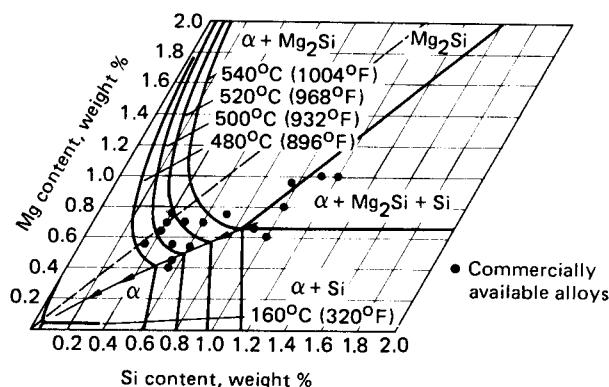


**FIG. 16.19** Equilibrium diagram (detail) for Al-Mg-Si alloys. (After [16.66].)

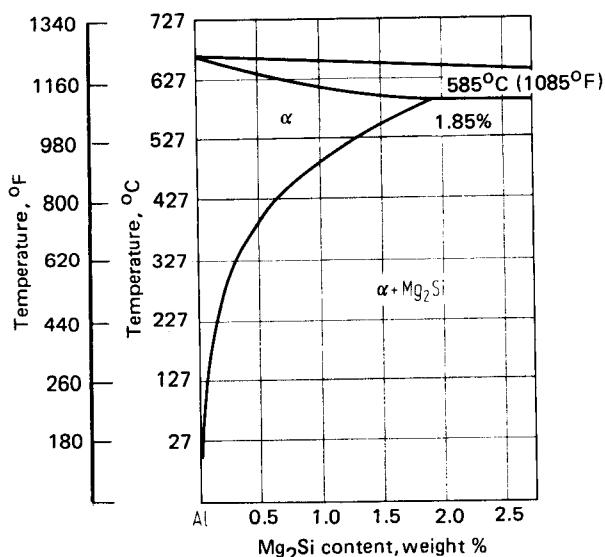


**FIG. 16.20** Pseudobinary equilibrium diagram for Al-Mg<sub>2</sub>Si. (After [16.66].)

secondary precipitation of Mg<sub>2</sub>Si results in the formation of round particles. As a result, the flow stress decreases and the permissible extrusion exit velocity increases. Since the coarse precipitated Mg<sub>2</sub>Si particles are only partly dissolved during subsequent hot extrusion (at usual forming temperatures), the finished extrusions are of lower strength and exhibit a less shiny surface finish after anodizing.

It is suspected that coarse precipitates accelerate the dissolution of a dense network of dislocations and facilitate the formation of secondary grain boundaries during forming. Fine precipitates, on the other hand, have an inhibiting effect on polygonization according to [16.67]. For AlMgSi0.5 (AA 6060) it is recommended to keep the size of the Mg<sub>2</sub>Si precipitates to about 0.5  $\mu\text{m}$  (20  $\mu\text{in}$ ) in order to achieve the best compromise between the demands of good extrudability (criteria are extrusion speed, mean extrusion pressure, and surface finish of the extruded product) and satisfactory strength and surface appearance after anodizing [16.68].

The cooling rate affects extrusion conditions considerably more than the annealing time [16.69].

The extrudability of high-alloy aluminum alloys containing manganese and chromium depends to a large extent on how high the annealing temperatures are (an exception is AlMn) [16.65]. Both alloying elements—but manganese in particular—delay the start of dynamic recovery during hot forming. This results in a pronounced maximum at the beginning of the stress-strain curve [16.70]. Coarse precipitation of manganese occurs at temperatures of around 500°C (930°F) and above (in the presence of iron and silicon), resulting in a considerable reduction of flow strength. When on the other hand fine precipitation of manganese occurs at or below 400°C (752°F), the pronounced maximum of the stress-strain curve remains unchanged or may even be increased [16.11], [16.65], [16.71]. Increasing the holding time improves extrudability just as an increase in temperature does [16.65]. However, the heat treatment that would lead to optimum extrudability cannot usually be performed since it leads to a substantially recrystallized microstructure and inadequate strength in the extruded product [16.71]. With manganese- and chromium-free alloys the influence of the annealing temperature is considerably reduced or even negligible [16.65].

Surface defects, impurities, oxide layers, and so on, of the billet surface may be removed by

an additional operation (e.g., turning). This operation is necessary in particular where high demands exist as to the strength and surface finish of the extruded product. However, it is usually omitted when extruding with a shell. Current developments in the field of casting technology aim at reducing the need for machining the billets to a minimum.

After the preparatory measures described, billets are heated to the required temperature in a furnace close to the extrusion press. The billet may be heated to the process temperature over its entire length, or a certain specified temperature gradient may be set up between the front and rear faces of the billet. It may also be heated to a temperature above the process temperature and then cooled (by water spraying) to the desired temperature just before pressing. The first method is the most common, the second makes it possible to maintain an approximately constant extrusion temperature, and the third produces a particularly suitable material structure [16.65].

With other materials, such as copper, some copper alloys, and steel, preparatory heat treatment plays a less important role than in the case of aluminum alloys. In general the main aim is to produce a homogenized structure. With copper alloys the way a billet is heated is of particular significance. Because of copper's tendency to oxidize, one tries to heat the billet in an inert gas, or at least in a reducing atmosphere. Since scale on the billet surface cannot be avoided entirely and the tendency to oxidation increases with temperature, copper alloys are usually worked at the lowest temperature possible. Moreover, extrusion with a shell should be used whenever possible.

Since steel, too, oxidizes on heating, it is advisable either to heat such billets as rapidly as possible or to provide for an inert gas atmosphere in the furnace. Where scale does exist, it first has to be removed in a descaling plant before the billet is transferred to the press.

Before heating, the rough outer skin of the cast or forged billet must be removed by turning or peeling since steel is pressed without a shell. When producing hollow billets, in order to obtain an inner surface free of defects, boring is preferred in most cases to piercing, especially where expensive or difficult to work steels are concerned. Austenitic alloys (chromium-nickel steels) are relatively insensitive to the heating process. As high demands are usually made on the quality of semifinished products made from these alloys, additional operations are often required before machining and again before heating. Suitable alloying additives and appropriate heat-treatment procedures are used to keep the ferrite content below 3% where possible. Carbide stabilization and deoxidation can have a positive effect on structural homogeneity. Furthermore the choice of casting technique (centrifugal casting, pressure die casting) also depends on the kind of billet required. In order to counteract inhomogeneity, to assure a more even distribution of deoxidation products, and to achieve a more consistent structure throughout the material, billets may be subjected to additional hot deformation (rolling, forging) before extrusion [16.72].

## 16.6 PRODUCT PROPERTIES AFTER EXTRUSION

### 16.6.1 Characteristics of Extruded Products

Extruded products are characterized by

Occurrence of residual stresses

Existence of particular structural features

Variations in the structure and—as a result—in the mechanical properties over the length and the cross section of the extrusion

Variations in the size of the cross section over the extruded length

Where the above characteristics represent shortcomings which can be influenced by appropriate preparation of the billet, by the tools, or by modification of the extrusion process, they are discussed in Sec. 16.6.3.

The residual stresses are primarily those internal stresses which are set up across the extrusion cross section as a result of material flow. Portions of the extrusion are more or less strongly deformed and twisted when they emerge from the die. In addition, internal stresses result from temperature differences across the cross section of the emerging product (cooling from different initial temperatures) and the uneven cooling rate over the cross section and length of the extrusion.

Owing to the fibrous structure developed in the extrusion direction, the mechanical properties of extruded products are directionally oriented (mechanical anisotropy). The anisotropy may be caused in different ways, such as a straight-line arrangement and linking of the heterogeneous structural elements in the extrusion direction (geometric anisotropy), banding of the structure, or the creation of preferential orientation in the crystals (texture). The practical consequence of mechanical anisotropy is generally a reduction in strength at a right angle to the extrusion direction, which, however, is unimportant in most cases [16.5].

Particularly pronounced differences in strength attributable to structural effects are observed in work-hardening aluminum alloys. They are characterized by high tensile strength and yield strength together with reduced elongation in the extrusion direction and comparatively low strength at a right angle to it. This so-called pressure effect, according to [16.73], occurs with alloys where the deformation texture remains in the extrusion as a result of inhibited recrystallization. Possible reasons for this are the existence of few soluble impurities or particular alloying additives, such as manganese and chromium, which have an inhibiting effect on recrystallization; and quenching of the extrusion immediately after it emerges from the die. In experiments on extruded aluminum-magnesium-silicon alloys it was possible, however, to show that the mechanical anisotropy also remains in the solution treated and in the cold-worked state. It decreases when the solution treatment is followed by hot quench-age hardening, which is accompanied by precipitation. A further decrease or even complete removal of the anisotropy may be achieved when the heat treatment is preceded by an additional cold-forming operation (e.g., drawing) which leads to random recrystallization during solution treatment [16.74], [16.75].

As already mentioned in Sec. 16.3.2, recrystallization plays an important part in determining the structure of extruded products, not only in materials that recrystallize during deformation (e.g., copper, brass), but also in those subject to dynamic recovery during extrusion (e.g., aluminum and aluminum alloys). Recrystallization may in part be superimposed on the recovery processes during extrusion. It may, on the other hand, only begin after deformation when the deformation rate is greater than the rate of the recovery and recrystallization processes, thus causing no major reduction in work hardening.

The grains formed by recrystallization may vary considerably in size, both in the direction of extrusion and at a right angle to it. The size depends on the type of material, the strain imparted, and the temperature. Large strains lead to a smaller grain size; high temperatures during deformation tend to increase grain size. This results in an irregular structure and thus variations in the mechanical properties. This takes the form of an increase in strength from the center to the edge of the cross section and from the beginning to end of the extrusion (assuming no subsequent heat treatment is performed). Variations in strength across the cross section can mostly be overcome by the use of larger strains [16.5].

Coarse grains may be found in the boundary layer of the extrusion when a critical value of residual stress still remains after recovery or recrystallization. Above all, this has often been observed in aluminum-copper-magnesium and aluminum-magnesium-silicon alloys after solution and heat treatment. The coarsely recrystallized layer is thinnest at the beginning of the extrusion and thickens toward the end. The material properties are very different in the coarse-grain zone from those in the extrusion core. Thus, for example, corrosion resistance is less, and the strength in the extrusion direction is also reduced. In contrast to the typical characteristics of extruded products (anisotropy), extrusions with coarse-grain zones may exhibit higher strength in the transverse direction than in the direction of extrusion, even though the structures in the coarse-grain zone may have grains parallel to the extrusion direction. Coarse-grain zones tend to cause surface roughening during subsequent forming operations and to lead to the formation of cracks during quenching [16.5].

### 16.6.2 Subsequent Treatment

The subsequent treatment of extruded products depends on the material and on the demands made on the product. The usual methods of treatment are described here for the example of aluminum alloys.

The treatment depends on whether one is dealing with precipitation-hardenable aluminum alloys (e.g., AlMgSi, AlCuMg, AlZnMgCu) or nonhardenable materials (pure aluminum, AlMg,

AlMn). Hardenability of an aluminum alloy depends on the presence of an alloying constituent (e.g., Mg<sub>2</sub>Si in AlMgSi) whose solubility in aluminum increases with temperature (Fig. 16.20). By quenching from above the solvus temperature, the enriched solid solution can be retained in the supersaturated state at room temperature.

If for hardening alloys the extrusion exit temperature is above the solvus temperature and highest possible strength is not of primary importance, the emerging extrusion may be quenched by a shower of water or cold air as soon as it comes out of the die. A separate solution heat treatment can thus be omitted. The coolant and the rate of cooling are chosen according to the type of material, section thickness, and strength requirements. Alloys of the type AlCuMg or AlZnMgCu require such high cooling rates that, as a rule, they have to be cooled with water. For alloys such as AlMgSi, air cooling is normally sufficient. Only very thick-walled sections require water cooling [16.76]. In the case of air cooling, the cooling speed or cooling time  $t$  required to cool a particular aluminum profile section to a particular temperature may be determined by the use of cooling curves (Fig. 16.21).

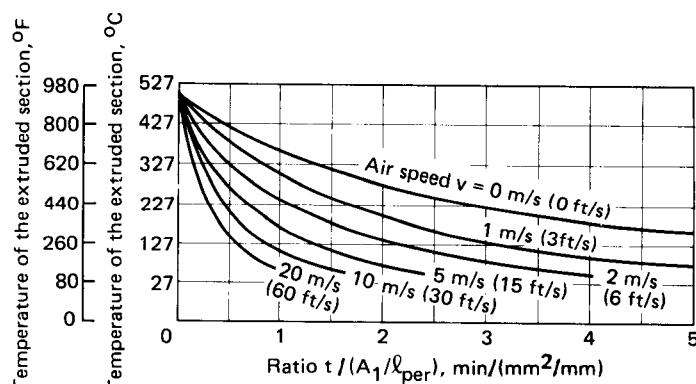


FIG. 16.21 Normalized cooling curves for aluminum for various air speeds at 20°C (68°F).  $t$ —cooling time,  $A_1$ —cross-sectional area of extruded section,  $l_{per}$ —peripheral length of extruded section. (After [16.76].)

A typical cooling path is shown in Fig. 16.22 for the aluminum alloy AlMgSi 0.5 (AA 6060) with an 0.8% Mg<sub>2</sub>Si content. In order to prevent precipitation of Mg<sub>2</sub>Si, the cooling rate has to be at least 60°C (108°F)/min. The effect of quenching increases with the concentration of dissolved Mg<sub>2</sub>Si.

Extruded products made of press-quenched as well as nonhardenable aluminum alloys are generally stretched following extrusion, that is, subjected to 0–2% plastic strain. With an increase in stretching strain, the 0.2% yield stress increases considerably, whereas the ultimate tensile strength is relatively little affected. After stretching, the extrusions are sawn to length and then straightened to within the required tolerances. Sections made of precipitation-hardening materials which cannot be quenched directly after extrusion are subjected to a three-stage treatment consisting of solution heat treatment, quenching, and aging. The effects on structure are similar to those shown in Fig. 16.22.

Solution heat treatment is generally performed in a salt bath or hot-air furnace at temperatures of 500°C (932°F) and above [for Al-Mg-Si alloys 510–540°C (950–1004°F)]. The holding time depends not only on the material but also on the wall thickness or cross-sectional area of the extrusion, the weight of the material, the type of stacking, and other factors specific to the annealing furnace.

After solution treatment the extruded sections are quenched by submerging them in cold water or sometimes by the use of water or air jets. Exceptions are, for example, thin-walled products which could warp on too rapid cooling. However, maximum hardness cannot be achieved in this way.

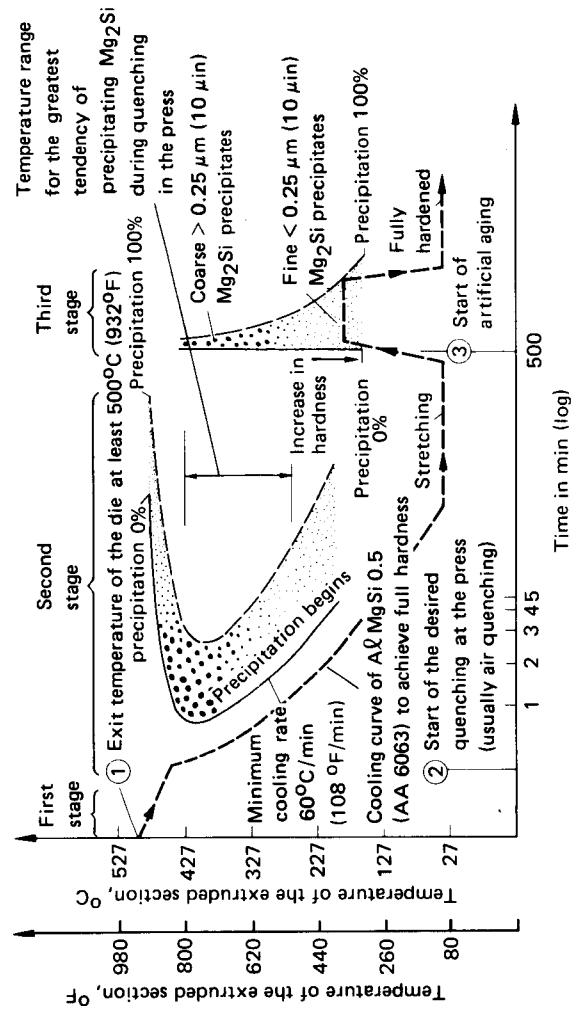


FIG. 16.22 Temperature-time curve for heat treatment of hot-extruded sections made of AlMgSi0.5 (AA 6060). (After [16.68].)

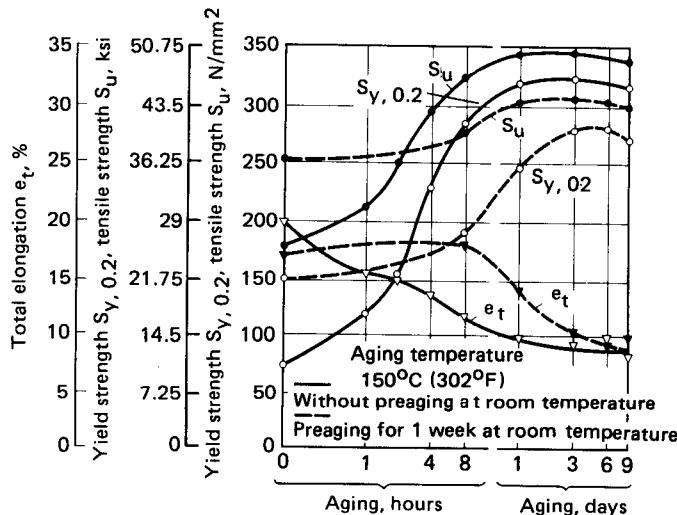


FIG. 16.23 Influence of artificial aging (with and without preaging) on mechanical properties of AlMgSi1 (AA 6082) (After [16.9].)

At this point the material is ductile and can be worked easily so that, if required, it can be stretched and straightened. Then the workpieces are aged at or slightly above room temperature (natural aging) or at temperatures between 120 and 180°C (248 and 356°F) (artificial aging). Natural aging usually takes 5–8 days; artificial aging depends on temperature and material and takes between 0.5 and 24 h. As a result the 0.2% yield stress, the tensile strength, and the hardness all increase while the elongation remains unchanged or is slightly reduced.

The strength increase due to natural aging is less than that due to artificial aging. However, the reduction in elongation is also less. Natural aging is characterized by the so-called incubation period of several hours during which the material remains ductile and can be worked easily.

With materials which can be either naturally or artificially aged, such as Al-Mg-Si alloys, artificial aging is usually preferred because of the higher strengths which may be obtained. The effectiveness can be further improved by increasing the speed with which the material is heated up to the aging temperature [16.65]. The cooling rate after aging is not considered critical [16.68].

Because of limited furnace capacity it is often impossible to avoid the storage of extrusions at room temperature prior to artificial hardening. Only when both the composition of the alloy and the length of the storage period are taken into account in the subsequent aging process is it possible to prevent room-temperature storage from having a negative effect on the strength of the product [16.77]. If these factors are not taken into account, the strength will still slowly increase, but it will not reach the value which would otherwise have been attained by direct artificial aging (see Fig. 16.23 for AlMgSi1 [AA 6082]). Also subsequent stretching is not fully effective in this case [16.9].

### 16.6.3 Defects

The quality of extruded product is a function of the following factors [16.4]:

- 1 Chemical composition
- 2 Geometric dimensions
- 3 Appearance and regularity of the microstructure

- 4 Variation of the mechanical properties over the length and cross section of the extrusion
- 5 Surface finish

The individual criteria are defined in hot-extrusion standards and in delivery specifications which are often based on internal work standards. Rejects, that is, unacceptable products which do not fulfill the specifications, may occur for any of the following reasons: defective billets, defective or unsuitable tooling, or defects arising during the extrusion process.

Rejects resulting from poor billets are caused by:

- 1 Major errors in the chemical composition
- 2 Inclusions of slag and other impurities
- 3 Scale, flakes, and segregations
- 4 Internal cracks
- 5 Undissolved oxides leading to phase rupture

In contrast to other forming processes, such as cold extrusion or die forging, no systematic studies have been done on geometric errors in hot extrusion as far as it is known.

The extrusion standards contain separate data concerning, among other things, permissible variations in cross-sectional dimensions (overall dimensions, wall thickness, radii), acceptable tolerances concerning straightness of the extrusion and flatness of its faces as well as permissible twist and angular deviations. Dimensional accuracy is affected by the accuracy obtained in tool making, the tool wear, and by the subsequent finishing of the extruded product. Over and above this the section dimensions are affected by the deformation and deflection of the dies under pressure and by the shrinkage of the extrusion after it has been formed.

Machining allowances are not common in the case of extruded products. Subsequent machining operations are expensive and may cause distortion. Where very high demands are made on the shape and dimensional tolerances, extruded profile sections undergo a subsequent cold-drawing operation, provided this can be justified economically. This calibrating operation rectifies any distortion of the cross section which may have occurred and reduces the tolerances to between a half and a fifth of the values for extrusion alone. [As a rough rule, wall-thickness tolerances of about 0.2–0.5 mm (0.01–0.02 in) and diameter tolerances for circular bars and tubes of about 0.3–2.0 mm (0.01–0.08 in), depending on an outer diameter of between 10 and 250 mm (0.4 and 10 in), are accepted.] Data concerning tolerances common in practice for the extrusion of steel can be found in [16.78], [16.5].

Besides its effect on dimensional accuracy, die quality is an important factor in achieving smooth, clean surfaces, especially in cases where the extruded sections are to be used for decorative purposes (anodizing quality). Scratches and ridges in the die land as well as inadequate cleaning out of the residual matter can affect the finish of the extrusion considerably.

The main defects as sources for rejection or errors connected with the extrusion process can be summarized as follows [16.4], [16.20], [16.79] to [16.81]:

- 1 Piping defects (coring) which occur during the final stages of extrusion of a billet through a die when the discard or butt is small
- 2 Extrusion defects (material separation in the extrusion core), caused by impurities from the billet surface flowing into the extrusion core toward the end of the extrusion operation
- 3 Formation of internal cracks and fibrous fractures as a result of an extrusion defect or insufficient heating of the billet core
- 4 Formation of shells or overlaps caused by impurities entering the surface of the product; these impurities may be either surface oxides or matter produced by the burning lubricant
- 5 Circumferential tearing of the extrusion as a result of hot shortness at forming speeds or temperatures that are too high
- 6 Blistering caused by localized melting at deformation speeds or temperatures that are too high

## 16.34 BULK-METAL FORMING

- 7 Longitudinal cracks in tubes caused by intense cooling of the outer skin of the extrusion while the inner surface is being forced over a fixed mandrel
- 8 Formation of pores and scoring caused by workpiece particles welding onto the tools
- 9 Surface defects caused by incorrect handling of the extrusion after it has left the die
- 10 Soiling of the extrusion surface caused by lubricants
- 11 Streaky structure caused by extruding at too low a temperature
- 12 Large variations in structure over the length of the extrusion due to excessive cooling of the billet during the extrusion operation (e.g., as a result of too long a billet or insufficient heating of the container)
- 13 Extreme variations in the mechanical properties, particularly over the length of the extrusion, due to temperature changes during extrusion
- 14 Growth of coarse-grain structure (see Sec. 16.6.1), combined with a reduction in static and dynamic strength values and a decrease of corrosion resistance; in subsequent forming operations this may lead to a rough surface finish and increased risk of cracks occurring during quenching

## 16.7 TOOLS FOR HOT EXTRUSION

Fig. 16.24 shows the design of a set of tools used in forward hot extrusion. This particular layout is used for extruding tubes and hollow sections over a fixed mandrel.

The following tool parts (shown shaded) are directly involved in the forming process:

Dies, backed up and held by the backer, die ring (holder) bolster, and tool carrier

Stem

Dummy block

Mandrel

As these components are subjected to high thermal stressing, especially in hot extrusion of copper-based nonferrous metals and steel, they have to be made of heat-resistant materials with good tempering properties. The most important steels for hot-extrusion tooling are given in Table 16.4. They are sufficient, under normal circumstances, to cover the entire range of economic hot-extrusion applications, provided, of course, that they are first suitably heat-treated. The latter operation improves the tempering properties and resistance to wear at high temperatures [16.72].

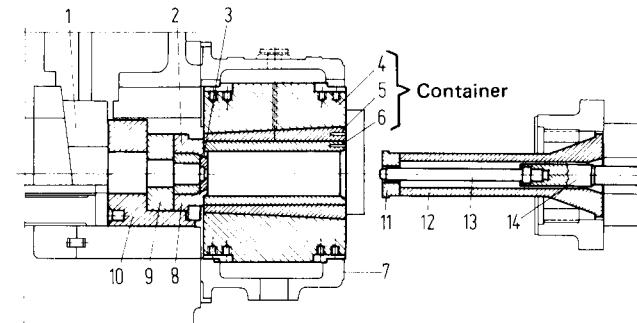


**FIG. 16.24** Tools for solid and hollow extrusion. 1—sealing wedge; 2—backer; 3—die; 4—jacket; 5—intermediate sleeve; 6—inner sleeve (liner); 7—container holder; 8—die holder; 9—bolster; 10—tool carrier; 11—dummy block; 12—stem; 13—mandrel; 14—mandrel holder. (After [16.8].)

**Table 16.4** Steels for Extrusion Dies

Designation		Compressive strength, N/mm <sup>2</sup> (ksi)
DIN	AISI	
X38CrMoV51	H11	1400–1800 (200–260)
X40CrMoV52	H14	1500–1800 (220–260)
X32CrMoV33	H10	1400–1700 (200–250)
X37CrMoV51	A8	1450–1600 (210–230)
X30WCrV53	H21	1400–1700 (200–250)
X30WCrV93	H21	1400–1700 (200–250)

Source: Compiled from [16.6], [16.82], [16.83].

### 16.7.1 Dies

The following demands are made on extrusion dies in order to ensure cost-effective production:

- 1 Dies should facilitate the manufacture of accurately shaped and dimensioned extrusions, requiring little or no subsequent straightening or calibrating.
- 2 They should permit high productivity, that is, high extrusion exit velocities and long strand lengths together with good tool life.
- 3 Their initial cost should be low.

These aims are achieved by the choice of suitable materials and by production-oriented tool design.

### Die Materials

The right choice of die material is particularly important since the die, as the shaping tool, is in direct contact with the hot extrusion material during the entire forming process, right up to the removal of the butt end. Thus it is not only subjected to high mechanical stresses but to high thermal stresses as well.

Fig. 16.25 shows the distribution of axial mechanical stresses over a 180° die entry surface which was obtained by pressure pins, while Figs. 16.26 and 16.27 represent the computed temperature field for the same die and the same process parameters as well as the computed temperature distribution in the die and the supporting tools. Fig. 16.28 on p. 16.38 illustrates the resulting axial and radial stresses computed for the same die and the same conditions by the finite-element method [16.60]. The temperature boundary conditions were determined with specially developed thermocouple elements [16.84].

Where the tool steels given in Table 16.4 are not sufficient (e.g., because of extreme thermal stressing), various special steels and specially developed materials are available, for instance, austenitic steels with 0.5% carbon, 13% chromium, 13% nickel, 0.5% vanadium, and 2.5% tungsten; or chromium-molybdenum-tungsten-cobalt steels with 0.2–0.3% carbon, 9–12% chromium, 1.0–2.5% molybdenum, 5–10% tungsten, and 1.0–10% cobalt; various high-grade nickel alloys (nimonic), and a range of cast and forged stellites. Among the special steels, high-temperature-resistant cobalt-based alloys are becoming increasingly important. The stellites are characterized by their hardness as well as their temperature and wear resistance. Thus they are very useful for large-batch profile extrusion dies. Because of their low toughness, dies made of stellite need to be backed by hot-forming-grade tool steel [16.82].

When using very high-alloy special materials, a certain impairing of the physical properties (stellite) must be expected. An exception here is the molybdenum alloy TZM (95.25% molybdenum, 0.5% zirconium, and 0.2% chromium), which is particularly well suited to the hot extrusion of steel and exhibits the following characteristics: very high heat resistance, high thermal conduc-

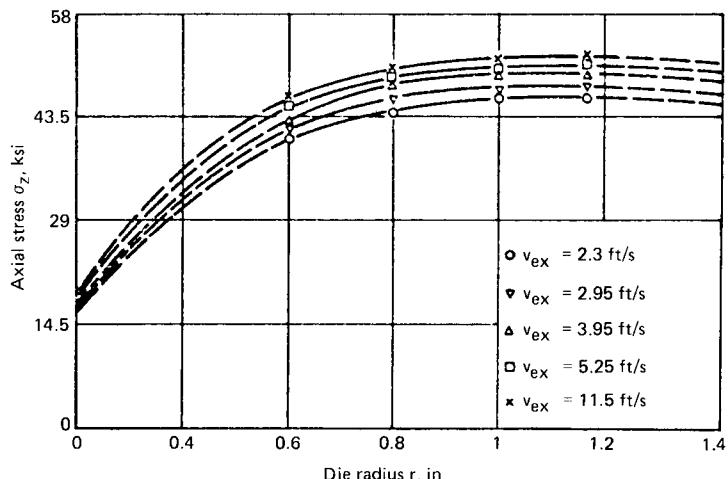


**FIG. 16.25** Axial (normal) stress distribution on entry surface of a flat extrusion die with circular orifice for different extrusion rates. To convert in to mm, multiply by 25.4; ksi to  $\text{mm}^2$ , multiply by 6.89655; ft/s to m/s, multiply by 0.3048. Billet diameter—71 mm (2.8 in); billet temperature— $450^\circ\text{C}$  ( $842^\circ\text{F}$ ); true strain  $\varphi_{\max} = 3.91$ ; material—AlMgSi0.5 (AA 6060). (After [16.60].)

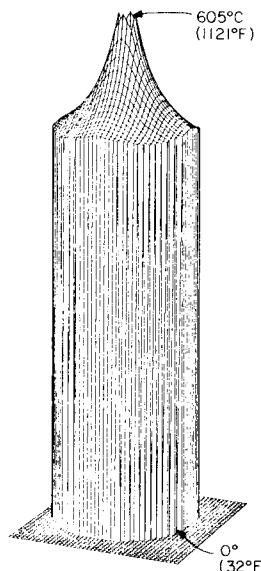


**FIG. 16.26** Temperature field (isotherms) on entry surface of flat extrusion die with square orifice. Valid for parameters of Fig. 16.25 with  $v_{ex} = 1.2 \text{ m/s}$  (3.95 ft/s). (After [16.60].)

tivity, very little thermal expansion, and good machinability [16.82].

Individual examples of the use of pure ceramic and metal ceramic materials (e.g., based on Mo-ZrO<sub>2</sub>) as well as cemented carbides as die liners can also be found [16.83].

#### Die Design

Attention has already been drawn to the difficulties involved in the theoretical analysis of the hot-extrusion process and the relation of the theoretical considerations to the practical situation since, as a rule, in order to simplify the analysis, a range of factors affecting the hot-extrusion process have to be neglected. Despite this, extensive knowledge concerning the most desirable extrusion conditions is now available, gained through numerous experimental investigations and from extensive production experience, thereby making it possible to produce a multitude of different profile shapes. Thus die design is based on guidelines resulting from years of practical experience.

The starting point for the design of each new die is always the cross-sectional shape. In addition, the following points must be clarified at the beginning:

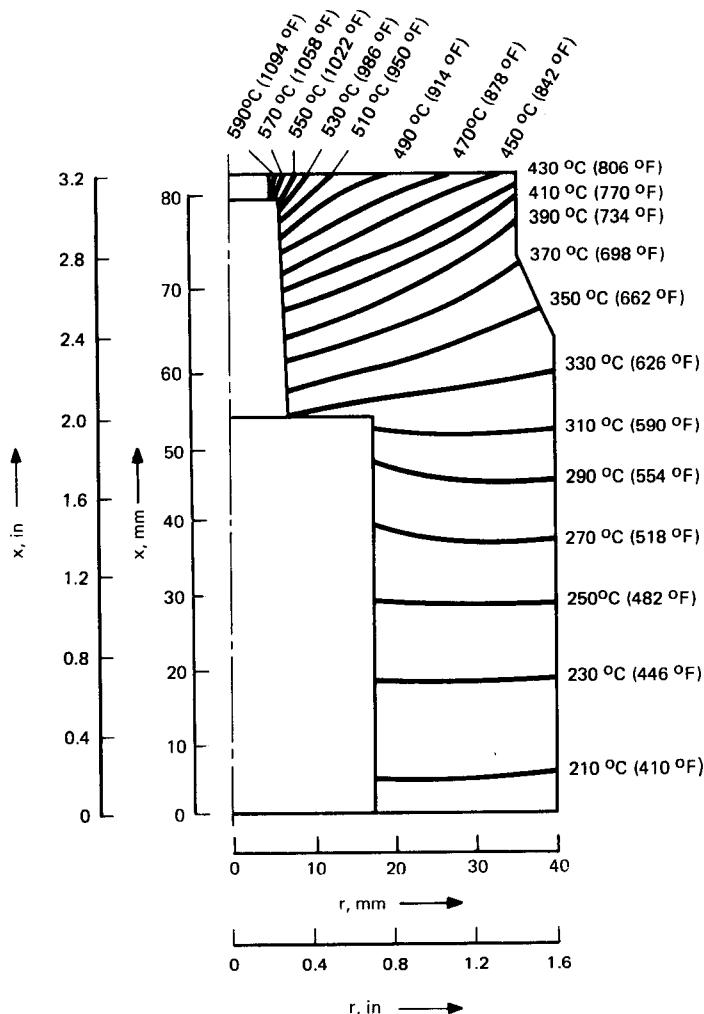
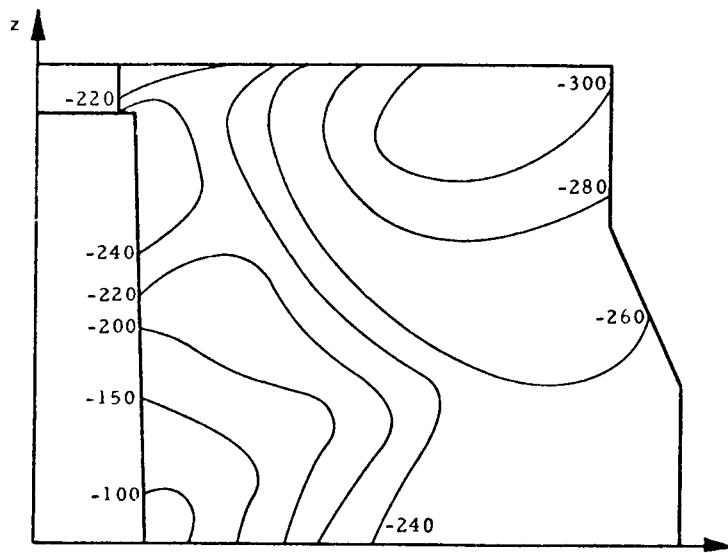


FIG. 16.27 Temperature field (isotherms) in extrusion die and backer with circular orifice. Valid for parameters of Fig. 16.25 with  $v_{ex} = 1.2 \text{ m/s}$  (3.95 ft/s). (After [16.60].)

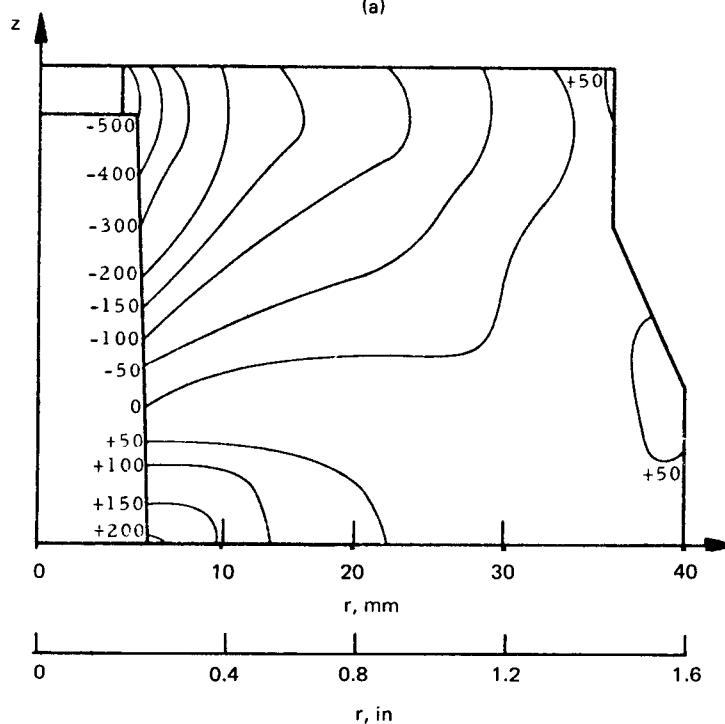
- 1 Choice of the most useful press and container for producing the hot extrusion from a particular material under optimum conditions (strain rate, extrusion and punch velocity, temperature, etc.). This leads to important information concerning load conditions.
- 2 Choice of the type of die that will lead to the most economical production conditions.

Besides the cross-sectional area of the extrusion, the individual dimensions of the cross section are important factors in determining the container diameter. Thus the maximum diameter of the circle surrounding the profile (Fig. 16.29) is given by [16.85]

$$0.8d_C \leq d_{u,\max} \leq 0.85d_C \quad (16.16)$$



(a)



(b)

**FIG. 16.28** Stresses in hot-extrusion die with circular orifice. Valid for parameters of Fig. 16.25 with  $v_{ex} = 1.2 \text{ m/s}$  (3.95 ft/s); radial displacement not restricted. Dimensions in  $\text{N/mm}^2$  ( $1 \text{ N/mm}^2 = 1 \text{ MPa} \approx 145 \text{ psi}$ ). (a) Lines of constant axial stresses  $\sigma_z$ . (b) Lines of constant tangential stresses  $\sigma_t$ . (After [16.60].)

where  $d_C$  is the internal diameter of the container. Typical values of the diameter surrounding the profile [16.80] are given by

$$0.5d_C \leq d_u \leq 0.6d_C \quad (16.17)$$

As a rule, related to the diameter  $d_{u,\max}$  is a particular die diameter  $d_D$  the size of which depends on the type of profile, its complexity, the material to be extruded, and the type of seal with the container. When the seal is between the container and the die holder (Fig. 16.30),

$$d_D = 0.8d_C \quad (16.18)$$

When there is a seal between the container and the die itself (Fig. 16.31), the die diameter in the limiting case,  $d_{u,\max}$ , for simple cross-sectional shapes must be in the following range:

$$1.0d_C \leq d_D \leq 1.23d_C \quad (16.19)$$

For difficult profiles, that is, those of thin wall thickness and sections to be made of materials which are difficult to extrude,  $d_D$  is increased to

$$1.16d_C \leq d_D \leq 1.36d_C \quad (16.20)$$

Of the various seals shown in Figs. 16.30 and 16.31 flat and cylindrical seals are those most commonly used in new extrusion presses. Both designs reduce the elastic deformation of the dies, which occurs in particular with conical seals because of the radial forces resulting from the extrusion pressure. These seals must be designed so that the supporting surface is large enough to withstand the forces which are applied and so that the resulting pressure guarantees a perfect seal. Flat seals require no particular size of die diameter. Application of Eqs. 16.18 and 16.20 is thus not mandatory. With cylindrical seals, dies are provided with a sufficiently large cone or flange to be capable of withstanding the withdrawal forces at the end of the hot-extrusion operation [16.85].

Detailed information concerning typical

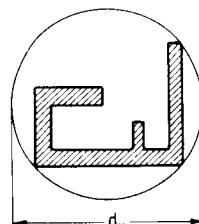


**FIG. 16.29** Diameter  $d_u$  of the smallest circle circumscribing the profile section. (After [16.85].)

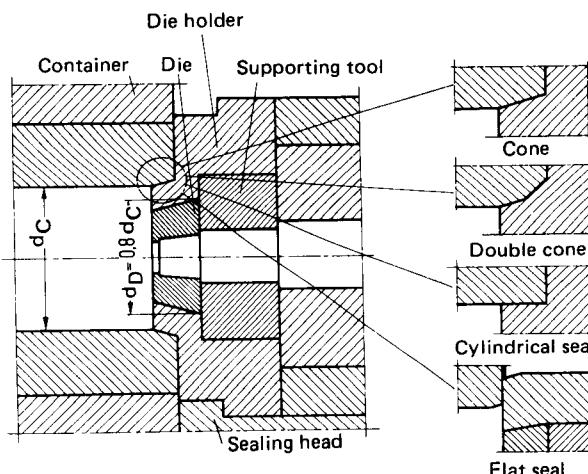


**FIG. 16.30** Type of seal between container and die holder. (After [16.85].)

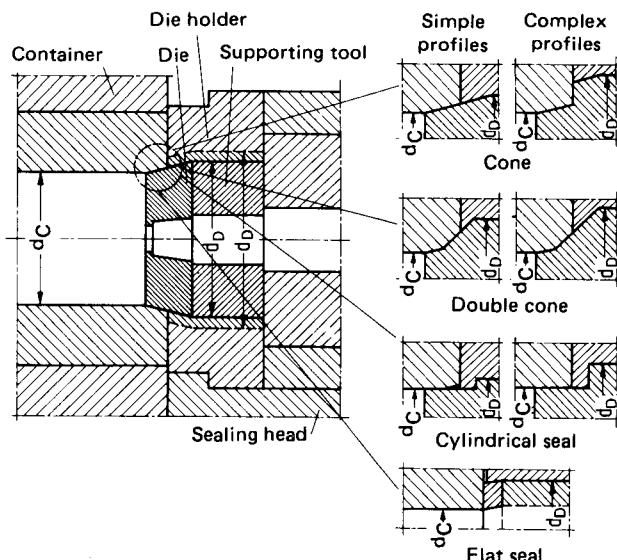


FIG. 16.31 Type of seal between container and die. (After [16.85].)

tool dimensions (diameters and thicknesses of dies and supporting tools) may be found in [16.85], [16.86] for hot extrusion of light alloys.

The diameter  $d_u$  of the circle surrounding the profile section is in practice usually less than the limiting value  $d_{u,\max}$  as determined by Eq. 16.16. For reasons of economy either the die diameter  $d_D$  is adapted to the particular value of  $d_u$  or several strands are pressed simultaneously to take full advantage of the die diameter. Multistrand pressing permits one to make full use of the available press capacity, which is particularly useful where there is a limited choice of equipment and containers, leading thus to increased productivity. Since the area of the cross section to be extruded is increased by a factor relating to the number of strands and since the strain rate is decreased accordingly, hot extrusion of the section on a particular press may be improved considerably. Indeed, this may be the only way of extruding a particular section under given conditions.

The individual die openings may be arranged in different ways. Horizontally and vertically symmetrical arrangements (Fig. 16.32a), chosen to assure smooth regular material flow, are the most common. Where this leads to difficulties in guiding the extruded sections after leaving the die, the openings may be arranged so that all the sections leave the die with the same orientation (Fig. 16.32b). Sections made of high-strength materials requiring fine-grained boundary zones are arranged in the die—where possible symmetrically—in such a way that the webs are pointing inward (Fig. 16.32c) [16.86]. As far as possible the following rule, which also applies to dies for single sections, should be respected: the die openings should be arranged so that the center of gravity of their area is at the center of the die.

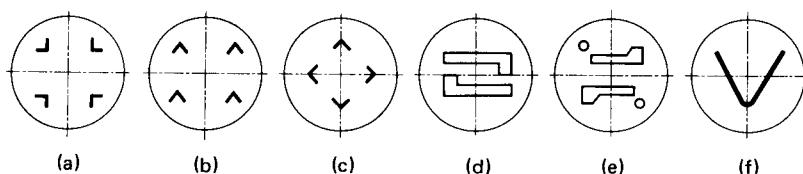


FIG. 16.32 Arrangement of die orifices. (After 16.2]; [16.86].)

This rule points to a further advantage of multistrand pressing since the requirement can be met more easily when several nonsymmetrical profile sections are pressed simultaneously (Fig. 16.32d). In other cases (usually circular) compensating extrusions may be pressed at the same time (Fig. 16.26e). The aim here is to obtain straight strands by controlling the material flow over the friction surfaces in the die openings without the need for extensive corrections.

Sections with very large surrounding circle diameters  $d_s$  can, through clever design of the die opening, be produced up to a certain point by using containers which would normally be considered too small. Thus, for example, flat sections (of large width and small thickness) may be extruded through a V-shaped die opening (Fig. 16.32f) and then pressed flat and straightened after extrusion. In extreme cases it is even possible to produce a tube, cut it open along one side, open it, and straighten it. In designing die openings, the following general rules apply.

With few exceptions, almost all die openings are designed cylindrically. In order to avoid changes in shape due to wear at the die inlet, which may result in dimensional variations in the extruded sections, the inlet edges are usually rounded off. This has the side effect of increasing the extrusion forces by up to 25%, which has to be accepted. The inlet radii depend on the material to be extruded; for example, for aluminum and aluminum alloys  $r = 0.5\text{--}1 \text{ mm}$  (0.02–0.04 in), for copper and brass  $r = 2\text{--}5 \text{ mm}$  (0.08–0.2 in), for copper-nickel alloys  $r = 4\text{--}8 \text{ mm}$  (0.16–0.3 in), and for Monel metal  $r = 10\text{--}15 \text{ mm}$  (0.4–0.6 in) [16.6].

On the outlet side the die openings are usually sharp-edged. After a recess [of about 0.5 mm (0.02 in)] they continue with a cone of about  $3\text{--}5^\circ$  (Fig. 16.33). The conical extension tends to increase the stability of the die land and gives the emerging extrusion a certain freedom of movement, thus reducing the likelihood of a strand getting stuck inside the die [16.86]. The ideal shape of the die land (Fig. 16.33) depends on the shape of the profile section. It has a determining effect on the material flow and thus on the correct extrusion of the section. Since the material flows faster at the center of the strand than at its edge, and, in the case of wall-thickness variations, it moves even faster the thicker the wall, it is necessary to modify the material flow rate by varying the length of the die land over the circumference. Thus with widely varying cross sections, the thin-walled parts are provided with shorter lengths of die land and the thick-walled sections with longer lengths (which has a braking effect). Precise quantitative results concerning variations in die-land dimensions as a function of the cross-sectional shape have not yet appeared in the literature. Industry thus has to rely on in-house experience charts derived by experiment. As a rule of thumb one may say that the die land should decrease by 1 mm (0.04 in) for every 20-mm (0.8-in) displacement from the center of the die, while it should be increased in proportion to the wall thickness [16.87]. The transition between the different friction lengths chosen on this basis should not be abrupt in order to avoid acceleration forces in the transition zones, which might damage the extrusion.

For simple profile sections made of easily extrudable materials, the die land may vary between 3 and 6 mm (0.12 and 0.24 in); for complicated sections made of alloys requiring slow extrusion, the die land may reach 30 mm (1.2 in). Lengths of 2.5–3 mm (0.10–0.12 in) may be considered minimum values. Below this limit, adjustment of the die land is generally not possible since the material is not in intimate contact with the die at the inlet edge itself, but 1–1.5 mm (0.04–0.06 in) beyond it [16.86]. When the die-land length needs shortening, this is usually performed on the outlet side, provided there is sufficient space. Otherwise the material flow may be varied by increasing the conical opening on the inlet side.

In addition to changes of the die land in order to modify the material flow, dimensional modifications of the dies are often necessary. These can, however, be kept to a minimum when the thermal expansion and the elastic deformation of the dies during hot extrusion are known as well as the contraction of the extrusion material after cooling, and are taken into account at the design stage.

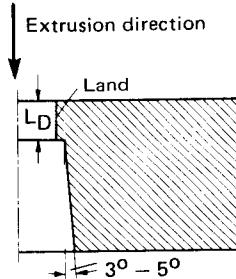
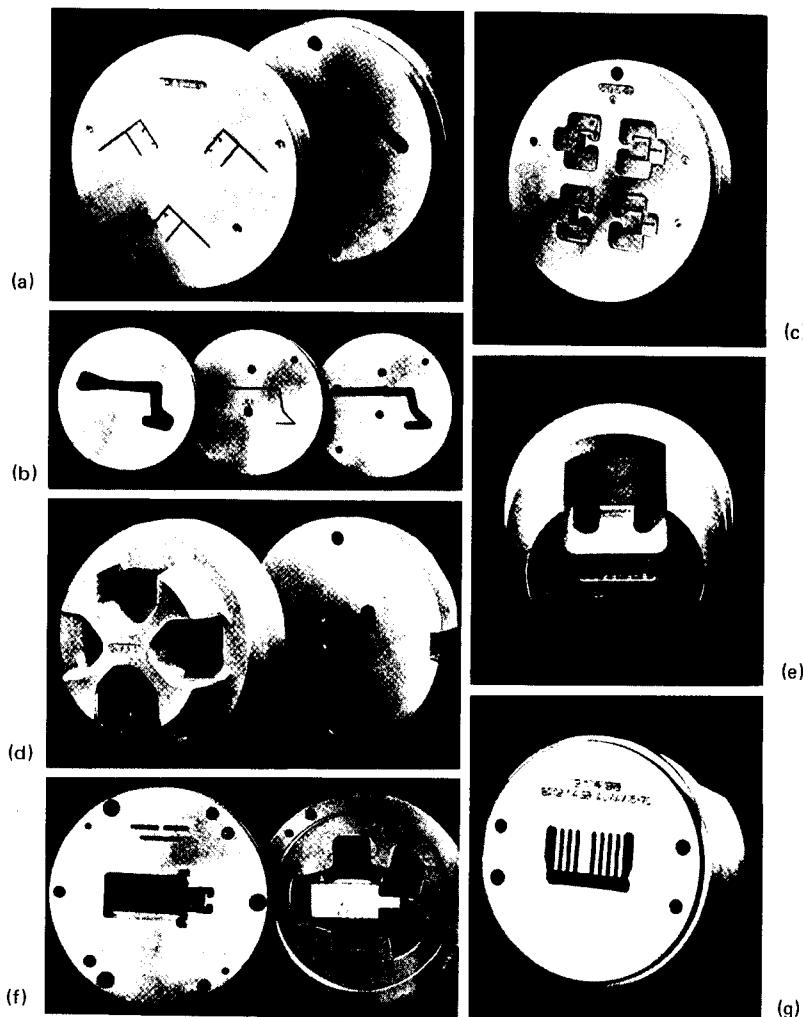


FIG. 16.33 Die outlet design. (After [16.86].)



**FIG. 16.34** Different types of die. (a) Flat die. (b) Die with feeder plate. (c) Prechamber die. (d) Bridge die. (e) Spider die. (f) Porthole die. (g) Solid bridge die. (After [16.88].)

#### *Types of Dies*

Depending on the extrusion material and the profile shape, one of the following die types may be chosen (Fig. 16.34) [16.88]:

- Flat dies
- Dies with feeder plate
- Prechamber dies
- Bridge dies

- Spider dies
- Porthole dies
- Solid bridge dies (one-piece hollow dies)

This list may be completed by including the conical dies ( $2\alpha < 180^\circ$ ) which are used for hot extrusion of steel and nonferrous copper-based metals with suitable lubricants.

Dies (flat dies) (Fig. 16.34a) with an opening angle of  $2\alpha = 180^\circ$  are the most common dies used for hot extrusion of sections. They usually consist of a circular disk which contains the shaping opening and which is backed up by supporting tools. With complicated light-alloy extrusions they often consist of several parts, one behind the other, in order to facilitate production. However, with materials which are difficult to extrude this is not possible because of the unacceptably high forces between individual parts. The superiority of flat dies when pressing light alloys is based on the fact that oxides and other impurities in the billet surface are kept separate from the extrusion. Furthermore, the butt or discard can be removed easily after the extrusion operation. In the case of copper-based metals, solid dies are used in hot extrusion in conjunction with shells.

Dies with feeder plates (Fig. 16.34b) are used for the following reasons: (1) they facilitate the control of material flow with sections made up from parts of different thicknesses; (2) they improve the possibility of pressing one billet after another; (3) they permit extruding certain sections with containers which, with regard to the diameter  $d_{u,\max}$  of the enclosing circle, would otherwise be considered too small; and (4) they reduce bending in the case of long thin sections.

Prechamber dies (Fig. 16.34c) are characterized by the fact that the die opening is set back by several millimeters with respect to the end face of the die. They are used mainly for small complicated U-shaped sections in order to protect the overall opening and, above all, the small tongues from bending and breaking.

Bridge dies, spider dies, porthole dies, and solid bridge dies, as already mentioned in Sec. 16.1, are special-purpose dies used in the manufacture of tubes and in particular for making hollow sections of complicated shapes in aluminum. In employing these dies one takes advantage of the tendency of aluminum materials to weld at high pressure. Compared with dies of simpler design, where material flow is only controlled by changing the design of the friction surfaces in the die opening, greater flexibility is given here for optimum design of the particular inlet openings and mandrel plates [16.88].

With the mostly two-part bridge dies (Fig. 16.34d) the billet material is first divided by the bridge, which also supports the mandrel. It flows past the bridge and enters the die opening where it welds together and then emerges as a tube or other hollow section. The main application is for thin-walled hollow sections. They require the lowest extrusion force compared with other hollow dies and permit the highest extrusion speed. They permit the use of extrusion lubricants and can be completely emptied and cleaned after each pressing, thus allowing corrections to be made to the friction surfaces in order to control flow behavior and reduce thermal loading. On the other hand, however, they are more expensive to make and the waste is higher (larger discard or butt because of the bridge). Furthermore, as a rule, only smaller sections can be pressed than is typical with other dies.

Spider dies (Fig. 16.34e) are used in conjunction with a special holder. Larger sections can be pressed than with bridge dies, the butt is smaller, and the production costs are lower. The dies cannot be emptied easily after each pressing but have to be scoured (in the case of aluminum, using sodium bicarbonate solution). Furthermore high extrusion forces are necessary. Exact centering of the die and holder is particularly important with this type of tool.

Porthole dies (Fig. 16.34f and Fig. 16.35) can be used to make almost all shapes of sections, even complicated shapes with very large apertures or several symmetrically or asymmetrically positioned holes. Their advantages and disadvantages are as with spider dies. Similar to these, they are usually designed with four inlet openings in order to facilitate flow control and correction. The extremely rigid construction permits good support of the mandrel. Of all the different types of hollow dies, porthole dies permit production of the largest sections on a given extrusion press.

Solid bridge dies (Fig. 16.34g) are used in particular to produce sections with very long ribs. Their design has a major disadvantage, however—the friction surfaces, which may have to be modified, are very inaccessible.

The dies discussed above are mainly produced by machining with conical milling cutters and

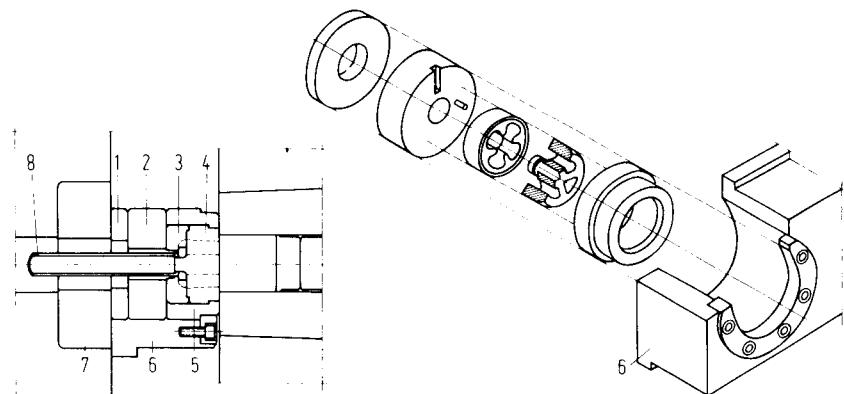


**FIG. 16.35** Exploded view of porthole die. 1—pressure ring; 2—support (bolster); 3—die cap; 4—mandrel; 5—die holder; 6—rotating or sliding tool carrier; 7—pressure-pad (platen); 8—extruded product. (After [16.8].)

increasingly by the use of EDM or spark-erosion machines using pulse generators (mostly with graphite and sometimes with copper electrodes). Other processes such as so-called liner milling and wire-EDM, are also being used increasingly [16.88].

The wear behavior of hot-extrusion tools in general and of dies in particular depends not only on the appropriate selection of the material and suitable design but also on correct treatment during manufacture and in use. The most important consideration here is the high thermal stress resulting from the heat flow cycle. The main considerations in heat-flow management are [16.89]:

- 1 Slow and regular warming up of the tools to the starting temperatures, which range between 300 and 500°C (572 and 932°F), depending on the extrusion temperature
- 2 Exactly controlled cooling of the tools during extrusion
- 3 Slow and regular cooling of the tools after use

Where heat management is not carefully considered, temperature differences may occur in different parts of the tools. The stresses which arise may lead to dimensional changes and cracks and thus to early failure of the tools. In addition, the following factors have an effect on tool life:

- 1 Correct forging of the tool material
- 2 Correct hardening and other surface treatment
- 3 Careful handling in the workshop, including avoidance of damage through dropping
- 4 Regular tool changing, cleaning, and inspection
- 5 Selection of and adherence to appropriate working conditions, in particular concerning the temperatures of the container, billet, and die
- 6 Type of extrusion material, particularly insofar as it affects the operation conditions
- 7 Cross-sectional shape of the extrusion
- 8 Required extrusion tolerances

Since certain light alloys have a tendency to localized welding to the tool surface, and since these particles may cause damage to the extrusion surface, the tool surfaces have to be polished or reground frequently, which will cause them to lose their dimensional accuracy. A suitable way of preventing the extrusion material from sticking or welding to the die (and thus of keeping mechanical wear within tolerable limits) is to nitride the tool surface, for example, by application

of the Tenifer process. An additional advantage here is that the nitrided surface also improves friction behavior.

### 16.7.2 Containers

The following demands are made on containers in hot extrusion:

- 1 Their inner surface must be capable of withstanding high pressures of up to approximately 1000 N/mm<sup>2</sup> (145 ksi) at high temperatures [e.g., up to approximately 1230°C (2230°F) for steel].
- 2 They must guarantee suitable forming temperatures.

In general a two- or three-part design—a container liner with two shrink rings—is employed similar to that used in cold extrusion (Fig. 16.24). The calculation of the prestressed assembly is performed in the same way. In this calculation, as well as considering the internal pressure and the initial load, it is also necessary to take thermal stresses into account [16.90].

In order to prevent the billet from cooling down—particularly in long extrusion operations—a suitable method of heating the container must be provided. Today this is usually an electrical method, such as induction or resistance heating, in place of the more primitive methods used previously (e.g., flame heating). Usually the heating elements are located in holes near the outer surface of the containers, parallel to its axis. The resulting stress peaks can be taken into account as so-called shape factors when calculating the assembly [16.90]. The inner liners of the containers are subject to wear despite careful selection of materials [16.91] and suitable heat treatment. Tool life for easily extruded materials is between 50,000 and 100,000 pressings; for difficult materials it may be between 15,000 and 20,000 pressings [16.6].

The container holder is in general insulated to prevent heat flow. In order to permit opening of the die–container seal between successive pressings, the container holder can usually be moved in the axial direction (with horizontal presses).

As a rule, containers used in hot extrusion have axisymmetric inner bores. Since for particular applications (construction and automobile manufacture) industry requires particular cross-sectional shapes, which are characterized by large widths, low heights, and thin wall thicknesses, these present considerable technical problems during extrusion. One thus tries to aid the flow behavior of the extrusion materials by using rectangular containers. This design, however, calls for specially constructed dies. For hollow sections, only bridge or porthole dies can be used.

### 16.7.3 Stems, Mandrels, Dummy Blocks and Scavenger Blocks

Pressure is applied to the billet by means of a cylindrical stem of circular or annular cross section (the latter being used for hollow forward hot extrusion over a mandrel and for backward hot extrusion). These components must be designed to withstand the pressures that arise and to prevent buckling. A suitable high-strength heat-resistant steel, for example, is X38CrMoV51 (AISI H11). The stem is fixed by a flange to the stem holder or fitted directly into the frame of the press.

In contrast to most other forming processes, the forming force in hot extrusion is, as a rule, not transmitted directly by the stem but via a dummy block. The dummy block, which is likewise made of heat-resistant steel, is applied to the front face of the stem and centered on the billet in solid extrusion and on the mandrel in hollow extrusion. The outer diameter of the dummy block is only slightly less than the diameter of the inner bore of the container. (In hot extrusion with shells the difference in diameter is greater and depends on the required shell thickness.) The purpose of the dummy block is to prevent the stem from coming into contact with the billet and possibly sticking to it. Since the dummy block is removed from the butt end of the billet outside the press, several dummy blocks may be used for a particular production run in order to reduce downtime between extrusion operations.

Tubes and simple hollow sections are extruded over a fixed or a moving (travelling) mandrel. In hot extrusion using a fixed mandrel, the mandrel tip is positioned in the die opening before

extrusion begins and locked in the so-called extrusion position. In this way a tool opening of constant cross section is created so that the wall thickness of the extruded tube or hollow section remains approximately constant. The mandrel is guided by a hollow stem and is connected via mandrel holder and mandrel bar to a special pressure cylinder. The mandrel is subjected to very high tensile stresses due to the frictional forces that occur.

A reduction in tensile loading can be achieved by allowing the mandrel to travel in the same direction as the motion of the stem. In this case, instead of fixing the mandrel to a special mandrel holder, it can also be fitted directly onto the stem. Such an arrangement, however, presupposes the use of pierced billets, since otherwise accurate centering of the mandrel cannot be guaranteed. In order to facilitate retraction of the mandrel after the extrusion operation has ended, the mandrel is given a slightly conical shape, which results in a gradual change in the wall thickness of the tubes or hollow sections.

Since the relative flow speed between extrusion material and mandrel is not identical to the stem velocity (nor to the extrusion exit velocity) and since it varies during the extrusion operation, modern extrusion presses are equipped with a device for varying the speed in order to take better account of the particular flow conditions.

Mandrels are subjected to particularly heavy wear when used as piercing mandrels, that is, when the extrusion press is equipped with a piercing attachment instead of working with pre-pierced billets. The right choice of material, optimum design, heat treatment during manufacture, and heat management during use are of cardinal importance here. Extremely high demands are made on the quality of the surface finish.

In order to keep thermal stressing of the mandrel within limits, it is possible to reduce the contact time between mandrel and material by increasing the extrusion speed or by reducing the length of the billet. Since, depending on the extrusion material, high extrusion speeds are not always possible, it has become increasingly common (mainly for economic reasons) to cool the mandrel internally.

In general, mandrels, mandrel holders, and mandrel bars are guided in the stem and stem holder and may be adjusted in both the axial and the radial directions. Axial adjustments can be achieved by using different kinds of mandrel displacing devices, driven by independent hydraulic units. Radial adjustment permits centering the mandrel in the die. It is usually performed by aligning the stem holder by means of positioning screws. In order to correct angular discrepancies between the mandrel and the die, it must be possible to rotate either the mandrel or the die. In most cases the extrusion press is equipped with a device for rotating the mandrel, activated via a worm gear.

Scavenger blocks serve to upset the remaining shell after extrusion. Their diameter is close to the inner diameter of the container. They are fixed onto the stem upon retraction after extrusion and fulfill their job during an additional stroke of the stem.

## 16.8 SUMMARY OF THE FACTORS INFLUENCING THE HOT-EXTRUSION PROCESS

The preceding sections have shown that the hot-extrusion process is affected by a range of factors, each of which in turn is dependent on the others. The main factors which influence the process are [16.4], [16.91]:

- 1 Stress distribution and loading
- 2 Temperature distribution
- 3 Composition and structure of the extrusion material together with its physical properties
- 4 Strain
- 5 Extrusion speed
- 6 Conditions of friction
- 7 Tools

Of these factors, which have already been discussed from various points of view, the loading conditions, for example, and their changes during the hot-extrusion operation depend for their part on the following:

- 1 The material properties under the particular extrusion conditions, that is,  $\sigma_f(\varphi, \dot{\varphi}, T)$
- 2 Strain
- 3 Size of the extrusion billet (cross section, initial billet length, butt)
- 4 Cross-sectional shape of the extrusion
- 5 Conditions of friction

The strain is in direct proportion to the force requirement, as is shown by the formulas of elementary plasticity theory (Sec. 13.3). It also has an indirect effect, together with temperature and extrusion speed, on the flow stress  $\sigma_f(\varphi, \dot{\varphi}, T)$ . The effect of block size is also given by the formulas of elementary plasticity theory. In addition, the influence of billet length is given by the load-stroke curve (Fig. 16.10).

Increasing complexity of the cross-sectional shape tends to increase the forming forces required. Vater and Heil [16.36] have shown a correlation between the circumferential length of the particular profile section and that of a circular section of equal area. They showed that the force requirement increases with increasing circumferential ratio, and the more so, the higher the strain and the lower the flow stress of the material. Different section shapes with similar circumferential ratios and the same section areas revealed no appreciable differences. According to Vater and Heil, the length of the die land has no appreciable effect on the extrusion force required.

The temperature distribution in hot extrusion has a direct effect on the flow stress of the material. Over and above this, in certain circumstances it may also affect the material properties when phase changes occur during the operation. Conversely, alloy composition and material structure can influence the temperature variation in hot extrusion.

According to [16.4], [16.20] both the way in which heat flows through the cross section and the length of the billet affect the material flow. Thus thermal conductivity itself is a temperature-dependent variable. In other investigations [16.45], [16.48], [16.54] these factors are not considered to be of much importance.

The composition and structure and thus the properties of the extrusion material call for particular process conditions within the limits of which the extrusion operation should be carried out [16.92]. In Sec. 16.6 more is said about the properties of the extrusion as a function of the process conditions.

The interdependence of strain and extrusion speed is clearly defined by the basic equations of plasticity theory. The physical state of the extrusion material during forming depends on the specified temperature conditions, the strain, the extrusion speed, and the conditions of friction.

The conditions of friction in particular affect the stress distribution and the material flow. They depend on the surface roughness of the contact surfaces, on the type of lubricant used for particular extrusion materials and operating conditions, and on the working conditions themselves, including the kind of extrusion process.

The influence of the dies on the extrusion force and the material flow depends on their type, the shape and location of the die openings, the size of the circle surrounding the profile section in comparison with the inner diameter of the container, the size of the die-opening angle, the behavior under load (bending, etc.), the surface structure, and the provision of cooling.

## 16.9 DESIGN OF EXTRUDED PRODUCTS

According to Kienzle [16.93], extruded sections may be divided into seven main groups and four subsidiary groups (Fig. 16.36). In general, extruded sections have (approximately) the same cross section over the entire length. Although tapered and stepped sections can be produced, they are limited to simple cross-sectional shapes and are relatively expensive.

Extruded products vary considerably in size to satisfy the requirements of very different branches of industry, ranging from precision engineering to ship building. The machine-tool,

Secondary categories 0 - 3	0 Basic shape	1 Modified basic shape (hollow section with concentric hole)	2 Symmetrical secondary shape elements (hollow section with concentric hole)	3 Nonsymmetrical secondary shape elements (hollow section with nonconcentric hole)	4 Example combining particular main and secondary categories 1)
Main categories 1 - 7					
1. Solid nearly circular section	10 ○	11 ○	12 ○	13 ○	10/30
2. Solid section with corners	20 □	21 □	22 □	23 □	20/42
3. Wide sections	30 └	31 └	32 └	33 └	33/53
4. Angular sections	40 ┌	41 ┌	42 ┌	43 ┌	42/10
5. Curved sections	50 ⌈	51 ⌈	52 ⌈	53 ⌈	52/10
6. Closed circular hollow sections	60 ○*	61 ○○	62 ○○	63 ○○○	60/33
7. Closed hollow sections with corners	70 ┌	71 ┌	72 ┌	73 ┌	70/43

1) First number concerns the main category, the second the secondary shape elements.

Hollow sections are always classified in the categories 6 and 7.

**FIG. 16.36** Shape classification system for steel and nonferrous extruded sections. (After [16.93].)

automobile, aerospace, construction, and furniture industries are the main users of extruded products.

The decisive factor in considering the suitability of hot extrusion is given by the maximum obtainable strain in conjunction with the characteristic properties of the particular material. Thus the material not only determines the strength of the desired profile section, but its deformability also has a decisive effect on the design of the section. Another criterion is the smallest wall thickness that can be achieved. This further narrows down the limit set by the largest permissible strain. The minimum wall thickness is dependent on the extrusion material, the type of section, and the diameter that can contain it. Approximate values of minimum wall thickness for aluminum and aluminum-alloy extruded sections are given in [16.23], [16.62].

Production difficulties tend to affect less the complicated asymmetric profile shapes than sections with large differences in wall thickness. With the latter, the strain rates vary across the cross section. When large differences in wall thickness cannot be avoided, one should at least try to assure gradual transition from one wall thickness dimension to the next. Hollow throats and edges are normally chamfered. Only easily extruded materials such as AlMgSi0.5 (AA 6060) may be used where sharp-edged extrusions are required. Exceptions to this rule are rare [16.94].

## 16.10 HOT-EXTRUSION EQUIPMENT

### 16.10.1 Drive Systems

In order to satisfy the increasingly high standards of the semifinished product industry and their customers, manufacturers of extrusion equipment have had to develop a wide range of different types of extrusion presses or plants. These differ primarily in the type of drive used and in their control systems, as well as in the operating direction of the equipment (horizontal or vertical, forward or backward), the design of the main body (two-, three-, or four-column or frame construction), and the layout for the production of particular extrusion products (strands, tubes, solid or hollow sections), or a combination of these. They further differ in design features relating to the kind of equipment provided (die-changing systems, tool and billet conveyors, loading equipment, parting-off devices, etc.) and in backup equipment (runout bays, stretching devices, product conveyors, etc.).

Today the large majority of extrusion materials are worked exclusively by using hydraulic presses. In the case of carbon and low-alloy steels, besides hydraulic presses, crank presses are also used, mainly for the mass production of smaller-size tubes (Sec. 16.10.4). The special features of hydraulic presses are discussed in Sec. 8.4.

For economic use of hydraulic presses, the following conditions must be satisfied: high productivity combined with adequate and consistent quality of the products, reliability of the press, low operating costs, and acceptable investment costs.

For a particular application and specific operating conditions, profitability depends largely on the correct choice of the type of drive. In general, the extrusion speed is the main factor which affects the productivity of a press, and which has a determining influence on the layout of the hydraulic circuitry [16.95].

The main drive types used are those with a storage vessel and direct-pump drives, although it is sometimes advantageous to employ a combination of these methods. Previously used steam or air hydraulic drives have proved to be uneconomic because of uneven fluid flow and low efficiency, and thus have been completely superseded by the other two types of drives mentioned [16.96]. Simplified schematic diagrams of both hydraulic systems are shown in Sec. 8.3 [16.97].

There is no general consensus as yet as to which of the two hydraulic systems is better from the economic and productivity points of view. However, agreement does exist that for a high-speed plant, where  $v_p = 150\text{--}500 \text{ mm/s}$  (6–20 in/s), only drives with storage vessels are suitable for the extrusion of steel and certain special metals. The use of a direct-pump drive here would require the installation of a very high pumping capacity [16.95]. For a low-speed plant, where  $v_p = 0.1\text{--}30 \text{ mm/s}$  (0.04–1.2 in/s), direct-pump drives are most suitable since they permit exact punch speeds to be set and maintained easily [16.8]. In the medium speed range the boundary is somewhat blurred; as a rule of thumb it may be taken as  $v_p = 50 \text{ mm/s}$  (2 in/s) [16.98].

As a result of improvements in pump design over the last few years, a further increase in the

use of direct drives may be expected. This development has already taken place as far as aluminum materials are concerned, so that today nearly all plants are based on hydraulic presses with direct drives—even those operating at high extrusion pressures [16.99].

The operating medium used in presses with storage vessels consists normally of water with a 1–2% anticorrosion oil additive. Using one or several pumps, this pressure liquid is pumped into one or a number of pressure vessels, from where it can be used as required. After use, the hydraulic medium usually flows from the press via a low-pressure vessel into a collecting reservoir, from where it is pumped back into the pressure vessel. The water contained in the low-pressure circuit can be used to carry out all operations where little pressure is required, that is, above all for displacements where the press is not under full load.

Three piston pumps are in general used for the high-pressure pumps since they assure relatively constant supply rates (at speeds in the range of 150–350 r/min).

The weight-loaded storage tanks common in the past have been replaced by vessels using compressed air. They consist of one or more water vessels connected to a battery of compressed-air vessels. With some small plants the compressed air and water may be contained in the same vessel. The ratio between the volume of water and the overall volume of the pressure vessel is usually 1–10. Compressed-air vessels require small foundations and are not sensitive to shock. However, one has to accept a pressure drop of about 10% of the operating pressure during the extrusion operation because of the expansion of the compressed air during the consumption of pressurized water.

In order to fill the vessels with compressed air and to counteract any pressure losses which may arise due to leaks and absorption, the storage vessels are equipped with multistage high-pressure compressors.

Occasionally oil is used as the working medium in drives with storage vessels. However, since the solubility of gases in oil increases with increasing pressure, the compressed air and oil have to be separated from each other by a piston or membrane. To remove any possibility of the oil catching fire, the compressed air is often replaced by compressed nitrogen.

Normal hydraulic oils are used as the operating media in direct-pump drives. Direct drives using water have not proved successful [16.98]. The operating medium is supplied to the press by means of axial or radial multipiston pumps (with or without equipment to regulate the supply rate; speeds up to about 1500 r/min). Gearing between drive motor and pump is usually not necessary. Since the pumps are installed directly next to the press, smaller units being integrated into the press itself, the resulting plant is usually compact and requires only short connecting pipes. In contrast to storage drives, where the storage vessels may be used to supply several presses and their supporting equipment, each directly driven press requires its own drive.

While pumps used to recharge pressure vessels work independently of the individual extrusion operations, and thus can be laid out for a lower power load, more powerful pumps have to be used for direct drives since here the desired stem velocity is related directly to the supply volume, and this must thus be capable of coping with the peak demands of the press. On the other hand, in the latter case the pressure fluctuations common to drives with storage vessels do not occur. It is only necessary to take account of losses due to leakage in the pumps and of pressure losses in the hydraulic circuit.

For particular applications it has proved advantageous to connect a direct-pump drive with a high-pressure vessel, which then permits high punch velocities to be maintained for short periods of time as, for example, in hot extrusion of copper [16.98].

Particular design features are associated with each type of press, depending on the type of drive and the hydraulic medium used. Thus, for example, extrusion presses supplied with water from storage vessels are equipped as a rule with plungers. The plunger then has to be drawn back using special retracting cylinders. In extrusion presses with direct oil pump drives preference is given to double-acting differential pistons so that retracting cylinders are not required.

The operating pressure (maximum pressure of the hydraulic medium) usually lies between 200 and 315 bar (2.8 and 4.5 ksi) for presses with water storage vessels. Lower values would lead to cross sections of the piston, connecting pipe, and control which are too large; higher values lead to too much wear of the control elements and seals. The pressures in the low-pressure reservoirs lie between 6 and 12 bar (85 and 170 psi). With direct-pump drives the operating pressures seldom surpass 315 bar (4.5 ksi), even though it is aimed at achieving the highest possible pressures in order to keep the piston supply pipe and control cross sections as well as the supply rates of the

**Table 16.5** Comparison of Two Types of Extrusion-Plant Drives

Type of drive	Direct-pump drive using oil	Accumulator drive using water
Type of pump	Multipiston pump	3-piston pump
Fluid medium	Hydraulic oil	Water with 1–2% anticorrosion oil
Gears	Not required	Required
Extension to several presses	Not possible	Possible
Flow losses	Less	Greater
Wear	Less	Greater
Cost of fluid medium	Greater	Less
Power of pumps	Greater	Less
Capital cost of drive	For low extrusion speeds, less For high extrusion speeds, greater	For low extrusion speeds, greater For high extrusion speeds, less

Source: Compiled from [16.98].

pumps as small as possible. Using variable-delivery pumps (where the supply rate is modified by variations in stroke), typical operating pressures are around 200 bar (2.8 ksi) in order to keep oil loss through leakage within acceptable limits. Valve-controlled pumps with constant supply rate, on the other hand, permit operating pressures of up to 400 bar (5.7 ksi).

The cross-sectional areas of the supply and control circuits also depend on the permissible flow rates. The maximum acceptable flow rate for water is 10 m/s (30 ft/s), and for oil it is 3–4 m/s (9–12 ft/s). Thus smaller cross sections are possible when water is used as the pressure medium than with oil.

Presses with storage vessels are operated with the aid of control valves, either with or without throttling. Direct-pump drives are in general used in conjunction with distributor valves and only occasionally with control valves.

Both types of drives are activated by hand using electrohydraulic or electric controls. Electrohydraulic controls mostly use solenoid-controlled stroke or rotary drives working with continuously controlled regulators. Electrical control of the drive motors is usually based on relay or solid-state technology, whereby the latter is likely to dominate in the future. Solid-state technology is particularly suitable for high-speed presses and for those with extensive supporting equipment.

In order to facilitate a comparison between drives with pressure vessels and direct-pump drives, the most important characteristics are summarized in Table 16.5. Further information may be found in [16.96].

### 16.10.2 Types of Extrusion Presses

The first distinction which can be made between different extrusion presses is whether they operate horizontally or vertically. The majority of presses—and almost all plants above 16 MN (1800 ton)—are of the horizontal type. Horizontal presses are easier to integrate with production lines and with the handling and additional equipment required. They thus represent a good starting point for automation of the production flow [16.95].

An example of a horizontal extrusion press of the four-column type is shown in Fig. 16.37. The cylinder crosshead, which supports the hydraulic cylinder, is fixed to the frame while the fixed crosshead (or counterplatens), which supports the tools, is linked to the cylinder crosshead by four solid or laminated columns (see Fig. 16.41). The container holder and the moving crosshead, to which the stem is fixed, travel on adjustable guideways in modern designs with x-guides [16.99].

The number of columns as a design feature has nothing to do with the method of operation of the press but rather depends on the forces and stresses liable to occur in practice. The four-column construction is being used increasingly because of the improved access it permits (from

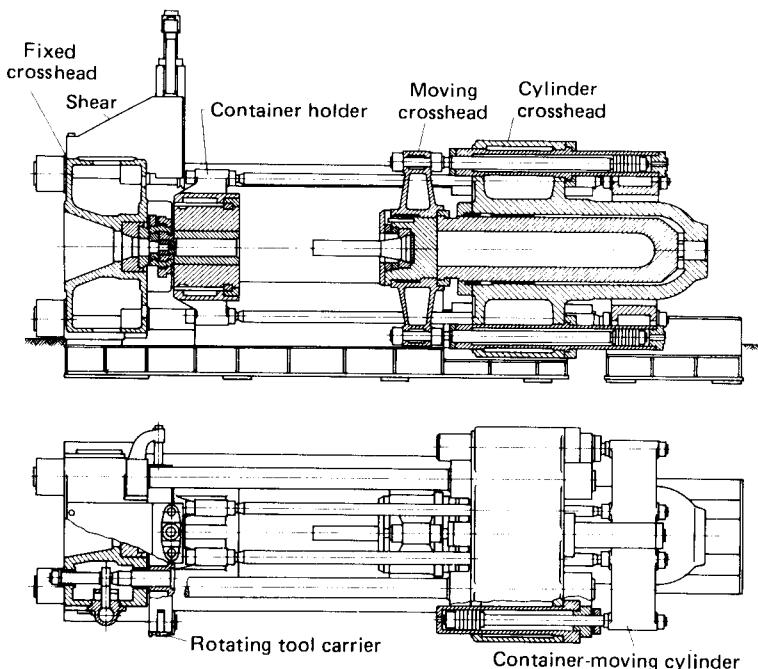


**FIG. 16.37** Horizontal hot-extrusion press (four-column type). (After [16.100].)

both above and below) as well as allowing convenient positioning of the shears or saws for parting off the butt or discard. On the other hand, the three-column type has the advantage of more even force distribution. Twin-column designs, used up to now for small horizontal presses, have now largely been superseded by the cheaper frame constructions. Typical of both are their good accessibility and, as a result, their short setting-up times.

Vertical presses, normally over 6–8 MN (675–900 ton), are mainly of the frame type. The advantage of the reduced space required must be set against the disadvantage that either a curved runout to a pit below the press must be accepted or the press itself has to stand on stilts high above the workshop floor. Since vertical pressing permits exact guiding of the moving parts of the equipment, thereby achieving tight wall thickness tolerances, such presses were in the past used frequently for the extrusion of pipes and thin-walled hollow sections.

Both vertical and horizontal presses for hollow forward hot extrusion are equipped with piercing devices, which operate independently of the main hydraulic cylinder, when tubes or other hollow sections are to be made from solid billets. However, when pre pierced billets are used, simpler mandrel positioning devices are all that is required since in this case displacement of the mandrel requires relatively little force. The piercing mandrel or the positioning devices may be positioned either within the press (centrally mounted in the moving crosshead) or external to it (behind the main cylinder or next to the moving crosshead) (Fig. 16.38). Internal piercing devices lead to a considerably reduced overall length of the press, resulting in a more economic use of floor space and reduced foundation costs [16.101].

Very few specially designed presses exist for backward hot extrusion. Rather, one resorts to presses which are suitable for both forward and backward hot extrusion. The tool-changing device (Sec. 16.10.3) is then modified to accept the hollow stem. The billet container, closed at the rear by a locking piece, is forced together with the billet via the hollow stem against the die (Fig. 16.39) [16.99]. Fig. 16.40 shows a specially designed indirect section and tube extrusion press with

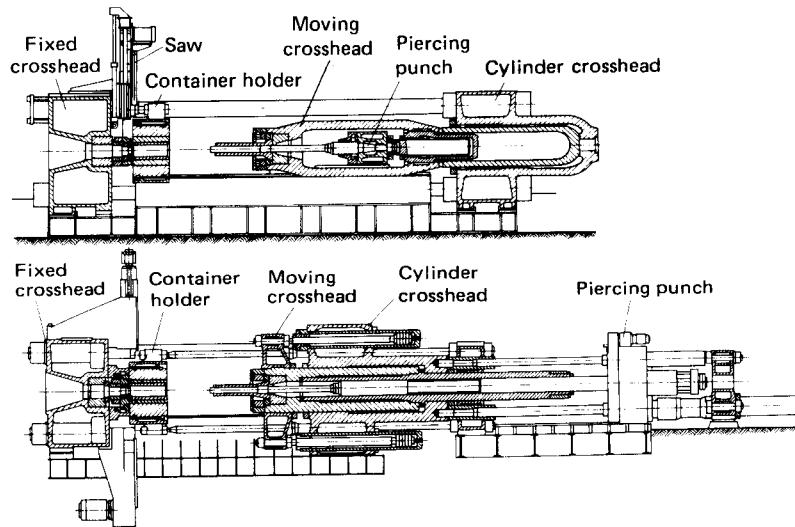


**FIG. 16.38** Horizontal solid and hollow extrusion presses with internal and external piercing devices. (After [16.98].)

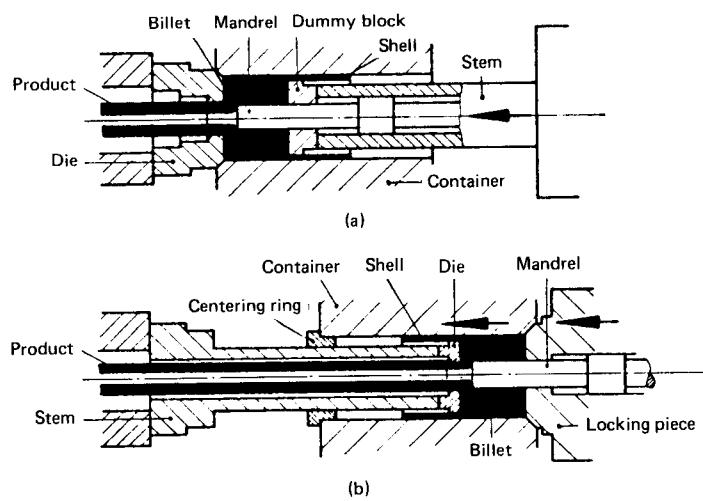


**FIG. 16.39** Extrusion of tubes with shell using a stationary mandrel (a) Forward (direct) extrusion. (b) Backward (indirect) extrusion. (After [16.99]; courtesy of Schloemann-Siemag AG, Düsseldorf.)

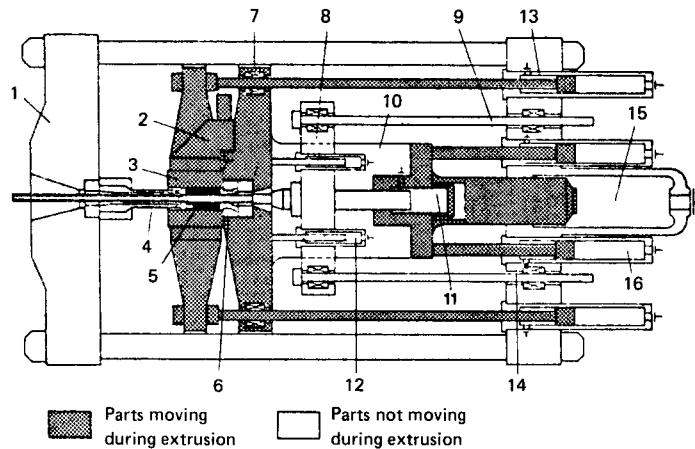


**FIG. 16.40** Indirect rod and tube extrusion press with internal piercer and stationary mandrel. 1—Fixed crosshead (counterplatzen); 2—shear; 3—container; 4—die stem; 5—mandrel; 6—locking piece; 7—coupling; 8—piercer crosshead; 9—mandrel stroke limiter; 10—moving crosshead; 11—piercing cylinder; 12—piercing pullback cylinder; 13—container shifting; 14—cylinder crosshead; 15—main cylinder; 16—advance and pullback cylinder. (*Courtesy of Schloemann-Siemag AG, Düsseldorf.*)

internal piercer and stationary mandrel. For further information on developments in the design and application of extrusion presses for metal processing see [16.1].

#### 16.10.3 Auxiliary Equipment

As a result of the increasing attention paid to the rationalization and automation of the production process, auxiliary equipment both surrounding the press and on the press itself is becoming more and more important and complex. The most important auxiliary equipment used in conjunction with extrusion presses concerns the tool (die) changing systems. Such systems are designed to keep setting time and downtime to a minimum. This aim increases in importance, the more the dies have to be cooled, inspected, and repaired, which in many cases may even be after each extrusion operation, especially during hot extrusion at high temperature and where extrusion times are long. Sliding tool carriers (Fig. 16.41) and rotating tool carriers (Fig. 16.42) have proved themselves for tool handling. With both systems the operating plane is at a right angle to the direction of pressing.

Tool-handling devices are usually equipped with two stations corresponding to the two possible working positions. There are two main types. With one type, one station is used for locating the die and die holder and the other for positioning the ejector tool; with the second type, both stations are designed to take dies so that during the extrusion operation dies can be changed, although from alternate sides of the press. This type necessitates the use of an additional butt- or discard-removing device. A further variant is the changing device with three stations: one ejector station in the middle and two die stations which likewise require access to the press from both sides [16.6], [16.102], [16.103].

Rotating tool carriers with two or more die stations have the advantage over sliding die carriers that cleaning, subsequent finishing, cooling, lubricating, or changing of the disengaged die can always be carried out on the same side of the press. They are usually built in two parts and consist of a platen arm and a die-rotating arm which can be swung either together or separately into the particular working position. When in addition the die-rotating arm can be moved in the pressing direction, the discard or butt can be parted from the extrusion behind the die [16.103]. A separate device is required, as with sliding tool carriers, for removing the discard [16.102]. In some

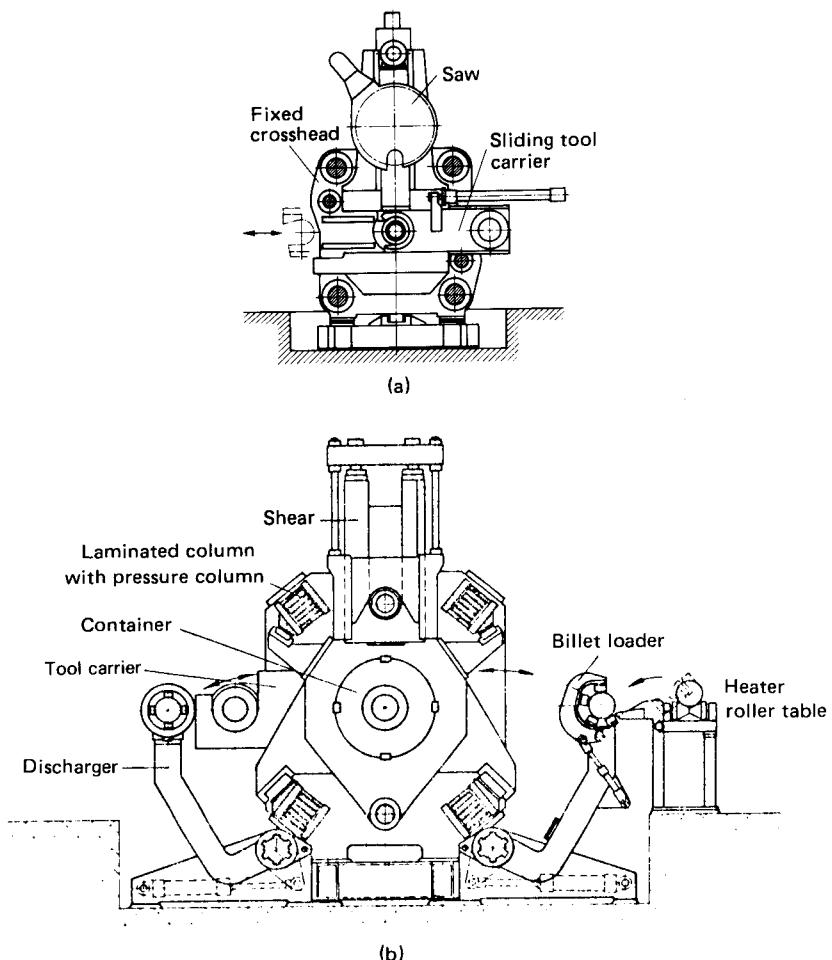


**FIG. 16.41** (a) Press with four solid columns and saw. (After [16.98].) (b) Press with four laminated columns and x-guide of movable parts. (After [16.99].)

instances, instead of rotating arms, heavy presses are equipped with rotating tables together with ejector devices.

The work flow in hot extrusion from raw material to finished product starts in the extrusion shop at the billet heating furnace or, more accurately, at the material store from which the billet is taken. The following features are expected of a high-performance billet furnace [16.104]: fast readiness for service, short heating time and even heating of the billet, accurate temperature control, fast changeover time, fully automatic operation, small space requirement, and easy servicing. These criteria are all fulfilled by induction furnaces. They are suitable for heating all billet materials and diameters that occur in hot extrusion. The criteria mentioned are also satisfied by modern gas-fired furnaces, although with the provision that they are only economical for light alloys and require a much longer time to heat up [16.104], [16.105].

The billets are transferred from the furnace to the loading device of the press by a suitable roller conveyor, a conveyer belt, or by means of a manipulator. Loading is either carried out by

linear-displacement charging and discharging machines or by swivelling devices which operate within the press or bring billets from outside into the work area. Such systems are usually operated hydraulically and sometimes pneumatically. Their function is to bring billets and dummy blocks or, after completion of an extrusion operation, the scavenger block to the container opening, from where they are moved into the container by the extrusion stem. Generally the two-part billet loader can be set to take a particular billet diameter. In the case of rectangular billets, the loader is equipped with special clamping jaws, permitting exact positioning of the billet in the direction of pressing. The dummy block or scavenger block is supplied to the billet loader from a storage magazine by a special block conveyor or, where the same block is continuously reused, by a cooling device which pushes the blocks onto the billet loader with the aid of a hydraulic ram.

In extrusion the following equipment is required for carrying out the actual work sequence: control of the press, including speed measurement and possibly associated control devices [16.106], [16.107]; stroke-monitoring device which, when coupled with limit switches, is capable of limiting and stopping the motions of the press; equipment for cooling, cleaning, and lubricating tools, as well as a centralized lubricating system.

With combined solid and hollow section extrusion presses and pure hollow section presses, piercers or mandrel-moving devices are required, as well as mandrel stroke setting devices for adapting the mandrel length to the length of the billet, mandrel stroke end stops for limiting the

mandrel stroke independently of the punch stroke, relative stroke devices (to counteract the tensile stresses caused by friction between the extrusion material and the moving mandrel), mandrel rotating devices for exact alignment of the mandrel profile with the die profiles, and equipment for internal cooling of the mandrel [16.106]. Where high demands are made on the accuracy of the extrusion, it is important to ensure that suitable measuring methods are available which permit monitoring the exact adjustment of individual parts of the tool assembly with respect to each other [16.108].

In automated presses roller conveyors, cranes, or similar equipment is used to supply the die changers with dies together with the associated dummy blocks or pressure plates straight from the die store or preheating furnaces. Control of such presses, including the indicated peripheral equipment for material and tool handling, is increasingly done by numerical control systems, preferably by programmable microprocessor control systems.

Upon completion of the actual hot-extrusion operation, the butt end or discard is separated from the extrusion proper by a saw or shearing blade mounted on the press. Saws are in general used for heavy metals and hollow sections made of light alloys. Presses intended for general use are often equipped with saws and shears. Cutting off usually takes place in front of the die and thus immediately in front of the container, leading to short easy to handle butts. Parting off behind the die, on the other hand, has the advantage that the extrusion product can be transported away immediately. With a sliding tool carrier it is sometimes possible to do without a separate shear. In this case, shearing off takes place between the pressure plates in the tool carrier and the die head using the sliding drive.

The most important equipment when trying to achieve shorter idle times are the devices for handling the butt and the dummy blocks. Butt-removal devices convey the butt and dummy block to a separator which normally acts automatically. After this separating operation, the dummy block and also the scavenger block are transported back to the billet loader by a conveyor while the butt is taken by conveyor belt or similar device to a scrap container [16.102], [16.103].

The extrusion sequence in solid forward hot extrusion with shells is divided into the following

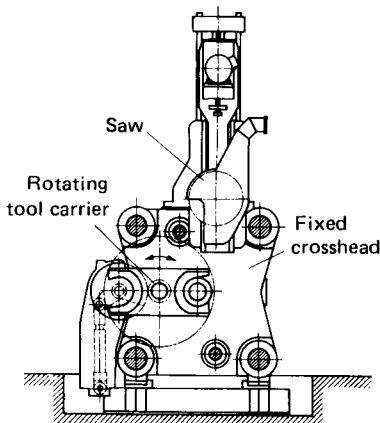


**FIG. 16.42** Press with rotating tool carrier.  
(After [16.98].)

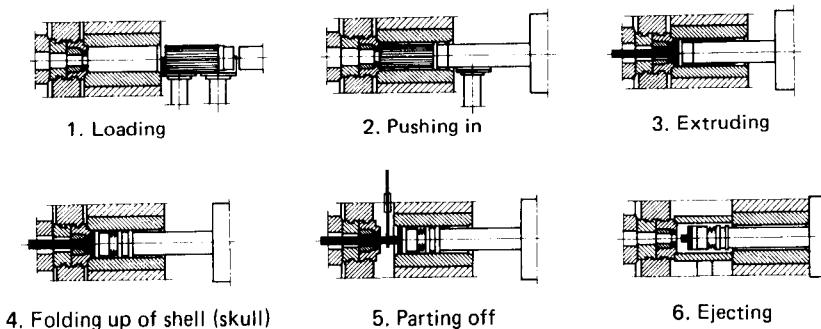


FIG. 16.43 Work sequence in forward hot extrusion with shell. (After [16.102].)

operations (Fig. 16.43): loading, pushing in (and upsetting) the billet, extrusion, upsetting the shell, parting off the butt, and ejecting.

In hollow forward hot extrusion using a mandrel, a piercing operation precedes extrusion except where preperforated or prebored billets are used. In hot extrusion without shells the fourth operation is left out.

The automatic hot-extrusion process is backed up by various auxiliary devices subsequent to the pressing operation. A number of different systems are used for discharging and cooling, the application of which depends on the particular extrusion product to be produced. An outline of the more common equipment used for hot extrusion of light metals, heavy metals, and steels is given in Table 16.6.

Table 16.6 shows that depending on the particular extrusion product and production conditions, different combinations of devices can be used. Only in the case of sections made of aluminum materials are the systems following pressing largely standardized. For the runout way, preference is given to graphite-coated driven roller conveyors with lifting devices for transfer to the walking beam conveyor, which then transports the extruded sections to the stretching machine. On emerging from the press, the sections are quenched with air or water and then cooled further by fans on the lateral transporter. Transport to the roller conveyor, which takes the extrusion to be cut to length, is by means of a walking beam conveyor or conveyor belts [16.99]. An overall view of a hot-extrusion plant for aluminum materials is shown in Fig. 16.44.

Large modern hot-extrusion plants are often equipped with an additional sawing station which removes the protruding front ends of the sections upon arrival at the walking beam conveyors so that all workpieces arriving at the stretching machine are of the same length. With smaller sec-

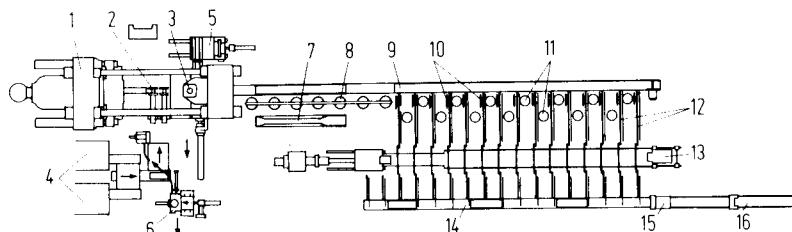


FIG. 16.44 Overall view of hot-extrusion plant for aluminum materials. 1—extrusion press; 2—double billet loader; 3—shears; 4—billet furnace; 5—die-changing and maintenance station; 6—butt parting-off device; 7—water quenching equipment; 8—spray cooling fan; 9—runout transport system; 10—transfer equipment; 11—cooling fan; 12—walking beam lateral conveyor; 13—stretching machine; 14—roller conveyor; 15—saw; 16—adjustment table. (After [16.111].)

**Table 16.6** Additional Equipment behind Press

Equipment	Function	Light metals	Heavy metals	Steel	Comments
Runout bay	Receives extrusion and transfers it to lateral conveyer	Runout table, beam surface, or roller surface	Runout table, plate surface, moving runout channel, or roller surface	Roller surface (tilting device possible)	Beam and plate surfaces as well as roller conveyers may be synchronized to work with press
Transfer device to runout table		Pushing-out or lifting devices	Pushing-out or lifting device or tilting runout channel	Lifting device or tilting roller conveyer	
Drawing device	Guides emerging extrusion	Drawing device for one or several strands	Drawing device for one or several strands		Movement synchronized with press
Lateral conveyer	Transports extrusion during air cooling to stretching machine or runout roller conveyer	Walking beam	Walking beam, chain shells, or chain conveyers (apron conveyers)	Chains, chain shells, or chain conveyers	Movement may be synchronized with press
Cooling and quenching device	Cools and quenches extrusion	Spraying or wave cooling (using water) following extrusion operation	Submerging in a cooling tank behind lateral conveyer		With light metals, additional air cooling in lateral and runout conveyers possible; with copper, extrusion in water tank possible

Equipment	Function	Light metals	Heavy metals	Steel	Comments
Runout roller conveyer	Brings extrusion to parting-off saw	Rollers combined with conveyer belt	Driven rollers	Driven rollers	Located between lateral conveyer and drawing machine or behind drawing machine
Stretching machine Saw	Straightens and stretches extrusion Parts off hot or cold extrusion	Frame or tension belt construction Pendulum, horizontal, or vertical saws	Frame or tension belt construction Pendulum, horizontal, or vertical saws	Frame or tension belt construction Pendulum, horizontal, or vertical saws	Feed rate with horizontal and vertical saws infinitely variable
Coiler	Rolls up wire or strip into coils	With wire: Vertical drum, lifting and removal device	With wire: Vertical drum, lifting and removal device	With strip: Horizontal drum	Wire coiler synchronized with press; air and water cooling possible
Coil conveyer	Transports coils to storage	Apron conveyer, coil-tilting device, coil collector or hook conveyor	Apron conveyer or rollers with transport chain, coil-tilting device, coil collector or hook conveyor	Horizontal drum	With heavy metals spray or bath cooling possible

Source: Compiled from [16,106].

tions (and smaller plant) the positioning head of the stretching machine is equipped with end shears [16.99].

#### 16.10.4 Special-Purpose Equipment

##### *Hydraulic Cable Presses*

Machines for sheathing cables work on the principle of hollow side hot extrusion. As sheathing material, aluminum (Al99.5 and aluminum of higher purity) is being used increasingly.

Hydraulic cable presses for aluminum are of the single- or of the double-punch design. With double-acting presses the two billet containers are each supplied with aluminum billets from two induction furnaces working in parallel. Subsequently both billets are pressed simultaneously into the extrusion chamber of the centrally located tool head. There they are extruded through the die and hollow mandrel to form a cable sheath completely surrounding the continuously advancing cable core (Fig. 16.45). Both halves of the sheath, formed from each of the two billets, weld together homogeneously under the extrusion pressure [16.108].

The use of double-acting presses naturally presupposes identical operating conditions on both sides of the press, that is, billets of similar chemical composition, dimensions, and temperatures, identical container temperatures, as well as similar friction and flow conditions. In this connection it is particularly important that the motion of both extrusion punches be synchronized exactly.

The advantage of this method of production compared to single-acting presses lies above all in the fact that the deformation resistance in the extrusion chamber can be reduced considerably by making use of the reaction forces. These have the effect not only of reducing the extrusion forces required, but also of lessening the load on the tool [16.109]. The use of double-acting presses is, however, not recommended when the press is to be used for sheathing cables with both aluminum and lead [16.6].

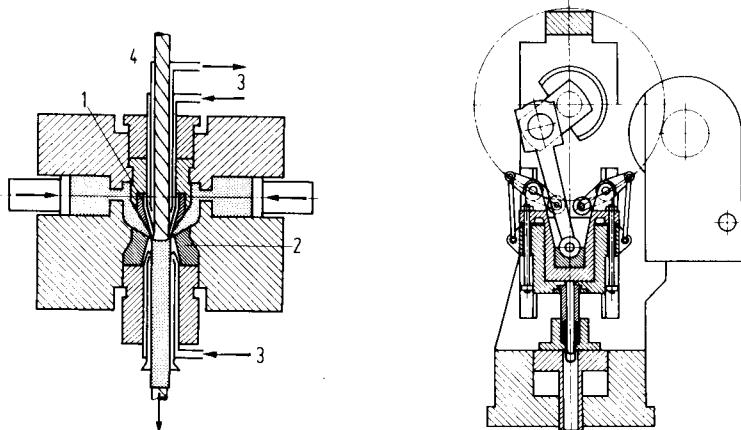


**FIG. 16.45** Tool head of double-acting aluminum cable extrusion press. 1—hollow mandrel, 2—die; 3—coolant; 4—cable. (After [16.109].)

**FIG. 16.46** Crank press for extrusion of steel tubes. (After [16.2].)

##### *Crank Extrusion Presses (Crank Tube Presses)*

Although hot-extrusion presses are almost all of the hydraulic type, in a few special cases mechanical presses are also used, such as for manufacturing steel valves, a combined extrusion and forging process. Since the development of heavy presses with suitable tools and auxiliaries, mechanical presses are also used increasingly for the production of small-sized mass-produced tubes made of carbon and low-alloy steels [16.5], [16.110].

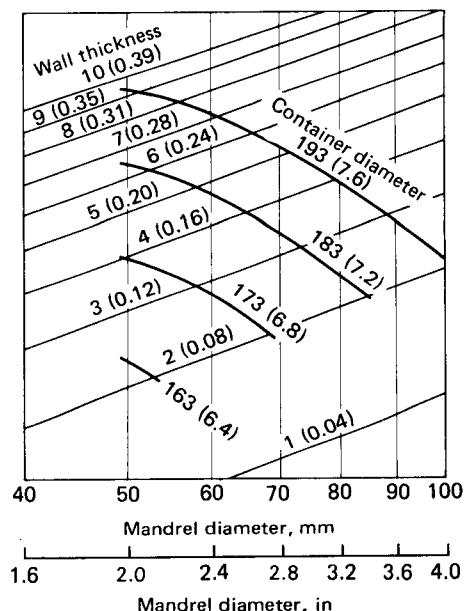


FIG. 16.47 Dimensions of steel tubes which can be produced with an extrusion force of 15 MN (1700 tonf) using a crank press. Dimensions in mm (in). (After [16.110].)

The disadvantages due to the lack of precise control systems in crank tube pressing (Fig. 16.46) are offset by the following economic advantages [16.110]: high productivity (cycle times of 20 s are obtainable), low energy consumption, easy adaptation to the desired production program by means of fast tool changing, and the manufacture of finished tubes in one heating.

The heated steel billet is transported to the press via a descaling plant and a calibrating mill. The lubricant is introduced at the same time as the billet and spreads out upon impact of the punch. Following this, the billet is pierced and the core material ejected downward. After extrusion the tube passes through a reducing mill to the cooling bay and then to the straightening device.

Fig. 16.47 shows the tube dimensions which can be produced on a 15-MN (1700-ton) mechanical press. The maximum tube length for this machine is given as 20 m (60 ft) and reaches 35 m (105 ft) after passing through the reduction mill. To obtain a good surface finish, the press is operated with billet temperatures between 1030 and 1130°C (1886 and 2066°F), that is, about 100°C (180°F) below the temperatures used in other processes for manufacturing steel tubes. The following factors have considerable effect on the economy of the process: tolerance requirements, material losses (size of butt and pierced core, waste occurring in the reduction mill) and the choice of lubricant (i.e., inexpensive oil-graphite-salt paste instead of glass) [16.110].

## REFERENCES

- 16.1 Chadwick, R.: "Developments in the Design and Application of Extrusion Presses for Metal Processing," *Int. Met. Rev.*, **25**, 1980, no. 3, pp. 94-136.
- 16.2 *Betriebshütte* (in German), vol. 1, "Manufacturing Processes," 6th ed., Berlin/München, Ernst, 1964.
- 16.3 Grüning, K.: *Metal Forming* (in German), Braunschweig, Vieweg, 1966.

## 16.62 BULK-METAL FORMING

- 16.4 Zolobov, V. V., and Zverev, G. J.: *The Hot Extrusion of Metals* (in German, translated from *Presovanie Metallov*, vol. 1, pts. 1–3, Moscow, 1969), Köln, Deutsche Gesellschaft für Metallkunde, 1967.
- 16.5 Pearson, C. E., and Parkins, R. E.: *The Extrusion of Metals*, London, Chapman and Hall, 1960.
- 16.6 Müller, E.: *Hydraulic Presses and Pressure Medium Equipment* (in German), vol. 3, Berlin/Göttingen/Heidelberg, Springer, 1959.
- 16.7 Krist, T.: *Chipless Machining* (in German), Darmstadt, Technik-Tabellen-Verlag, 1959.
- 16.8 Göner, H., and Marx, S.: *Aluminum Handbook* (in German), Berlin, VEB Verlag Technik, 1969.
- 16.9 *Aluminum Handbook* (in German), 12th ed., Düsseldorf, Aluminium Verlag, 1963.
- 16.10 Laue, K.: “Forming by Hot Extrusion” (in German), *Z. Metallkd.*, **58**, 1967, pp. 507–511.
- 16.11 Akeret, R.: “Productivity in Hot Extrusion of Aluminum Materials— Influence of Material and Process” (in German), *Z. Metallkd.*, **62**, 1971, pp. 451–456.
- 16.12 Kursetz, E.: “Hot Extrusion of High-Strength Aluminum Alloys and Aluminum Free-Cutting Alloys” (in German), *Draht*, **19**, 1968, pp. 770–775.
- 16.13 Dies, K.: *The Use of Copper and Copper Alloys in Technology* (in German), Berlin/Heidelberg/New York, Springer, 1967.
- 16.14 Kursetz, E.: “Hot Extrusion of Beryllium in American Semifinished Product Works” (in German), *Bänder, Bleche, Rohre*, **11**, 1970, pp. 228–232.
- 16.15 Lange, G., and Stüwe, H.-P.: “Heat Management in Hot Extrusion, Part 3” (in German), *Z. Metallkd.*, **62**, 1971, pp. 580–584.
- 16.16 Gentzsch, G.: *Hot Extrusion of Metals* (in German), Viersen, Dokumentationsstelle Umformtechnik, 1969.
- 16.17 Pawelski, O.: “Contribution to Similarity Theory of Metal Forming” (in German), *Arch. Eisenhüttenwes.*, **35**, 1964, pp. 27–34.
- 16.18 Lange, K., and Blaich, M.: “State and Development of Metal Processing by Extrusion” (in German), in *Berichte des Symposiums Strangpressen 1976*, Bad Nauheim, Deutsche Gesellschaft für Metallkunde, 1976.
- 16.19 Schelosky, H.: “Extrusion of Superplastic Materials” (in German), *Berichte aus dem Institut für Umformtechnik, Universität Stuttgart*, no. 43, Essen, Girardet, 1977.
- 16.20 Dürrschnabel, W.: “Material Flow in Hot Extrusion of Nonferrous Metals” (in German), *Metall*, **22**, 1968, pp. 426–437, 995–998, 1215–1219.
- 16.21 Tuschi, E.: “Differences in Flow Behavior during Hot Extrusion of Various Materials” (in German), *Z. Metallkd.*, **62**, 1971, pp. 513–516.
- 16.22 Dahlheimer, R.: “Investigations on the Stresses, Strains, and Temperatures in Axisymmetric Hot Extrusion” (in German), *Berichte aus dem Institut für Umformtechnik, Universität Stuttgart*, no. 20, Essen, Girardet, 1970.
- 16.23 Laue, K., and Stenger, H.: *Extrusion*, Metals Park, OH, American Society for Metals, 1981.
- 16.24 Nagpal, V., Altan, T., and Gagne, R.: “A Simplified Analysis of the Lubricated Shape Extrusion Process,” *Proc. NAMR-IV*, Society of Manufacturing Engineers, 1976, pp. 172–179.
- 16.25 Nagpal, V., and Altan, T.: “Analysis of the Three-Dimensional Metal Flow in the Extrusion of Shapes with the Use of Dual-Stream Functions,” *Proc. NAMRC-III*, Society of Manufacturing Engineers, 1975, pp. 26–31.
- 16.26 Yang, D. Y., and Lange, K.: “Analysis of Hydrofilm Extrusion of Three-Dimensional Shapes from Round Billets,” *Int. J. Mech. Sci.*, Vol. 26, 1984, pp. 1–19.
- 16.27 Stüwe, H. P., and Drube, B.: “Metallurgical Principles of Hot Forming” (in German), *Z. Metallkd.*, **58**, 1967, pp. 499–506.

- 16.28 Stüwe, H. P.: "Structure and Flow Stresses of Metals during Hot Extrusion" (*in German*), in *Hot Extrusion*, Stuttgart, Riederer, 1971.
- 16.29 Jonas, J. J., Sellars, C. M., and Tegart, W. J. McG.: "Strength and Structure under Hot-Working Conditions," *Met. Rev.*, **130**, 1969, pp. 1-24.
- 16.30 Akeret, R., and Künzli, A.: "Determination of the Yield Stress  $k_f$  of Aluminum Alloys by Means of Torsional Tests and Comparison of the Results with Those of Extrusion Experiments" (*in German*), *Z. Metallkd.*, **57**, 1966, pp. 789-792.
- 16.31 Stüwe, H. P.: "Flow Stress and Speed of Deformation in Hot Extrusion" (*in German*), *Z. Metallkd.*, **62**, 1971, pp. 697-701.
- 16.32 Böhm, H.: *Introduction to Physical Metallurgy* (*in German*), Mannheim/Wien/Zürich, Bibliographisches Institut, 1968.
- 16.33 Schindel, W.: "Raising the Yield Point of Aluminum Multiple Crystals" (*in German*), *Aluminium*, **47**, 1971, pp. 615-622.
- 16.34 Siebel, E.: "Forming in the Plastic State" (*in German*), Düsseldorf, Verlag Stahleisen, 1932.
- 16.35 Eisbein, W., and Sachs, G.: "Force Requirements and Flow Processes in Hot Extrusion" (*in German*), in *Chipless Forming of Metals*, Berlin, Springer, 1932.
- 16.36 Vater, M., and Heil, H. P.: "The Influence of Profile Shape on the Force Required in Hot Extrusion" (*in German*), *Aluminium*, **45**, 1969, pp. 141-149.
- 16.37 Boes, P. J. M., and Pouw, H. P.: "A Practical Calculation Method for Extrusion Pressures," *Sheet Met. Ind.*, **43**, 1966, pp. 377-390.
- 16.38 Hill, R.: "A Theoretical Analysis of the Stresses and Strains in Extrusion," *J. Iron Steel Inst.*, **158**, 1948, pp. 177-185.
- 16.39 Lippmann, H.: "The Mechanics of Hot Extrusion" (*in German*), *Z. Metallkd.*, **62**, 1971, pp. 85-86.
- 16.40 Pawelski, O.: "Principles of Drawing and Impacting" (*in German*), in *Principles of Plastic Deformation*, Düsseldorf, Verlag Stahleisen, 1966.
- 16.41 Steck, E., and Geiger, M.: "Approximation Calculation to Determine the Stress and Motion during Flow of a Difficult to Deform Material" (*in German*), *Ind.-Anz.*, **89**, 1967, pp. 1778-1781.
- 16.42 Prager, W., and Hodge, Jr., P. G.: *Theory of Ideal Plastic Solids*, Dover, New York, 1968.
- 16.43 Bishop, J. F. W.: "The Theory of Extrusion," *Met. Rev.*, **2**, 1957, pp. 361-390.
- 16.44 Lippmann, H.: "Theory of Indenting and Extruding Operations" (*in German*), *Bänder, Bleche, Rohre*, **5**, 1963, pp. 223-225.
- 16.45 Frisch, J., and Thomsen, E. G.: "An Experimental Study of Metal Extrusions at Various Strain Rates," *Trans. ASME*, **76**, 1954, pp. 599-606.
- 16.46 Hirst, S., and Ursell, D. H.: "Some Limiting Factors in Extrusion," *Met. Treat. Drop Forging*, **25**, 1958, pp. 409-413, 416.
- 16.47 Laue, K.: "Isothermal Hot Extrusion" (*in German*), *Z. Metallkd.*, **51**, 1960, pp. 491-495.
- 16.48 Fister, W.: "A Contribution to the Problem of Hot Extrusion" (*in German*), Dr.-Ing. thesis, Technical University, Aachen, 1963.
- 16.49 Lange, G.: "Heat Management in Hot Extrusion, Parts 1 and 2" (*in German*), *Z. Metallkd.*, **62**, 1971, pp. 571-579.
- 16.50 Bishop, J. F. W.: "An Approximate Method of Determining the Temperature in Steady-Motion Problems of Plane Plastic Strain," *Quart. J. Mech. Appl. Math.*, **9**, 1956, pp. 236-246.
- 16.51 Singer, A. R. E., and Coakham, J. W.: "Temperature Changes Occurring during the Extrusion of Aluminium, Tin, and Lead," *J. Inst. Met.*, **89**, 1960/61, pp. 177-182.
- 16.52 Singer, A. R. E., and Al-Sammurai, S.: "Temperature Changes Associated with Speed Variations during Extrusion," *J. Inst. Met.*, **89**, 1960/61, pp. 225-231.

## 16.64 BULK-METAL FORMING

- 16.53 Tanner, R. J., and Johnson, W.: "Temperature Distribution in Some Fast Metal-Working Processes," *Int. J. Mech. Sci.*, **1**, 1960, pp. 28–44.
- 16.54 Altan, T.: "Temperature Distribution in Axisymmetric Extrusion through Conical Dies," dissertation, University of California, Berkeley, 1966.
- 16.55 Altan, T., and Kobayashi, S.: "Numerical Method of Calculating Temperature Distribution in Dynamically Stationary Forming Operations" (*in German*), *Ind.-Anz.*, **89**, 1967, pp. 2223–2227.
- 16.56 Akeret, R.: "A Numerical Analysis of Temperature Distribution in Extrusion," *J. Inst. Met.*, **95**, 1967, pp. 204–211.
- 16.57 Akeret, R.: "Extrusion Experiments with Special Emphasis on Thermal Behavior" (*in German*), *Aluminium*, **44**, 1968, pp. 412–415.
- 16.58 Kemppinen, A.: "Computer Simulation of Temperature Rise during Extrusion," presented at the International Extrusion Technology Seminar, New Orleans, 1969.
- 16.59 Stüwe, H. P.: "Some Predictions Concerning Hot Extrusion" (*in German*), *Metall.*, **22**, 1968, pp. 1197–1200.
- 16.60 Gieselberg, K.: "Investigations about Hot-Extrusion Dies" (*in German*) *Berichte aus dem Institut für Umformtechnik, Universität Stuttgart*, no. 32, Essen, Girardet, 1975.
- 16.61 Ziegler, W., and Siegert, K.: "Indirect Hot Extrusion of Light Alloys" (*in German*), *Z. Metallkd.*, **64**, 1972, pp. 224–229.
- 16.62 *Aluminium Extrusion Die Design*, 2d ed., Oakland, CA, Kaiser Aluminum Co., 1977.
- 16.63 Séjournet, M.: "Lubrication of Steel Using Glass-Based Compounds (Ugine-Séjournet Process)" (*in French*), *Chim. et Ind. Gén. Chim.*, **97**, 1967, pp. 26–36.
- 16.64 Graue, G.: "High Temperature Lubrication in Chipless Metal Forming" (*in German*), *Mineralöltechnik*, **13**, 1968, pp. 1–12.
- 16.65 Achenbach, D.: "Hot Extrusion of Aluminum—Process Stages, Alloys, Variable Factors" (*in German*), *Aluminium*, **46**, 1970, pp. 607–613.
- 16.66 Altenpohl, D.: *Aluminum and Aluminum Alloys* (*in German*), Berlin/Göttingen/Heidelberg/New York, Springer, 1965.
- 16.67 Scharf, G., and Gruhl, W.: "Influence of Precipitates on Hot Strain and Recrystallization Behavior of Aluminum Alloys" (*in German*), *Aluminium*, **45**, 1969, pp. 150–155.
- 16.68 Lynch, C. V.: "The Effect of Production Conditions on the Quality of Profile Sections Made from the Alloy 6061 (AlMgSi0.5)" (*in German*), *Z. Metallkd.*, **62**, 1970, pp. 710–715.
- 16.69 Achenbach, D.: "Metal Forming Colloquium at the Institut für Bildsame Formgebung of the RWTH Aachen" (*in German*), *Draht*, **22**, 1971, pp. 23–24.
- 16.70 Akeret, R.: "Investigations into the Behavior of Aluminum Materials When Worked at Different Temperatures" (*in German*), *Z. Metallkd.*, **61**, 1970, pp. 3–10.
- 16.71 Scharf, G., and Achenbach, D.: "The Behavior of Non-Precipitation-Hardening Aluminum Alloys during Hot Forming" (*in German*), *Z. Metallkd.*, **60**, 1969, pp. 904–909.
- 16.72 Burggraf, J.: "Metal Forming Colloquium at the Institut für Bildsame Formgebung of the RWTH Aachen" (*in German*), *Draht*, **22**, 1971, pp. 20–21.
- 16.73 Lesbre, F.: "Study of the Effects of Pressure on Light Alloys" (*in French*), *Aluminium*, **38**, 1961, pp. 1147–1155.
- 16.74 Althoff, J., Drehfahl, K., and Wincierec, P.: "Characterization of the Mechanical Anisotropy of Hot-Extruded Precipitation-Hardening Aluminum Alloys by Means of Curves of the Start of Flow and of the *r*-Value" (*in German*), *Z. Metallkd.*, **62**, 1971, pp. 765–771.
- 16.75 Wincierec, P.: "Mechanical Anisotropy of Precipitation-Hardening Alloys Due to Pressure" (*in German*), in Grewen, J., and Wassermann, G.: *Textures in Research and Practice*, Berlin/Heidelberg/New York, Springer, 1969.

- 16.76 Beerens, H., and Feldmann, H.: "Heat Treating Hot-Extruded Aluminum Profile Sections Using Press Heat" (*in German*) *Aluminium*, **47**, 1971, pp. 545–549.
- 16.77 Hoffzimer, J.: "Heat Treatment and Mechanical Properties of Precipitation-Hardening Aluminum Alloys" (*in German*) *Aluminium*, **48**, 1972, pp. 248–257.
- 16.78 Elkan, R. M. L., and Schieren, K. H.: "Hot Extrusion of Steel Tubes" (*in German*) *Bänder, Bleche, Rohre*, 1964, 3, pp. 150–155.
- 16.79 Bryant, A. J.: "Metallurgical Investigation of Defects in Hot-Extruded Aluminum Alloys" (*in German*) *Z. Metallkd.*, **62**, 1971, pp. 701–705.
- 16.80 Bauser, M., and Fees, G.: "Surface Defects in Hot-Extruded Profile Sections Made of Al-Mg-Si Alloys" (*in German*) *Z. Metallkd.*, **62**, 1971, pp. 705–710.
- 16.81 Lotz, W., Steiner, U., Stiehler, H., and Schelzke, E.: "Defects Arising in the Hot Extrusion of Cu-Zn Alloys" (*in German*) *Z. Metallkd.*, **62**, 1971, pp. 186–190.
- 16.82 Laue, K.: "Experience Gained with Hot-Extrusion Dies" (*in German*) in *Hot Extrusion*, Stuttgart, Riederer, 1971.
- 16.83 Heinrich, E.: "Tool Steels" (*in German*), 2d ed., *Werkstattbücher*, no. 50, Berlin/Göttingen/Heidelberg, Springer, 1964.
- 16.84 Friedrich, K. H.: "Contribution to the Measurement of Strand Surface Temperatures during Extrusion" (*in German*) *Berichte aus dem Institut für Umformtechnik, Universität Stuttgart*, no. 32, Essen, Girardet, 1975.
- 16.85 Ames, A., Bielen, J., and Sauer, G.: "Suggestion for the Standardization of Tools for the Hot Extrusion of Light Metals Based on Extrusion Force" (*in German*) *Z. Metallkd.*, **62**, 1971, pp. 716–720.
- 16.86 Heinen, B.: "Manufacture and Treatment of Hot-Extrusion Tools. I—Observations on the Design and Dimensioning of Die Sets" (*in German*) *Z. Metallkd.*, **58**, 1967, pp. 215–217.
- 16.87 Möckli, F., and Lochner, H.: "State of the Art of Hot-Extrusion Die Design" (*in German*) *Aluminium*, **61**, 1965, pp. 629–633.
- 16.88 Aalberts, J.: "Manufacture and Design of Tools for the Hot Extrusion of Light-Alloy Profile Sections" (*in German*) *Z. Metallkd.*, **62**, 1971, pp. 191–196.
- 16.89 Kleinow, F.: "Manufacture and Treatment of Hot-Extrusion Tools. II—Treatment of Hot-Extrusion Tools in Practice" (*in German*) *Z. Metallkd.*, **58**, 1967, pp. 217–220.
- 16.90 Grüning, K.: "On the Stress Conditions in Hot-Extrusion Press Billet Containers" (*in German*) *Forschungsberichte des Landes Nordrhein-Westfalen*, no. 966, Köln/Opladen, Westdeutscher Verlag, 1961.
- 16.91 Laue, K.: "Hot Extrusion of Light Metals, Parts I and II" (*in German*) *Werkstattblätter*, no. 510 and 511, München, Hanser, 1972.
- 16.92 Roeder, E., and Troost, A.: "Effect of Material Behavior on Force Requirements and Extrusion Speeds in Hot Extrusion" (*in German*) *Z. Metallkd.*, **64**, 1973, pp. 230–235.
- 16.93 Kienzle, O.: "Documents of the Institut für Werkzeug Maschinen u. Umformtechnik, T. H. Hannover" (*in German*), 1960.
- 16.94 Geisel, G., Markworth, M., and Ribbecke, G.: "Characteristics of a Hot-Extruded Aluminum-Alloy Profile Section with Pronounced Variations in Wall Thickness" (*in German*) *Aluminium*, **49**, 1973, pp. 224–225.
- 16.95 Zymak, V.: "Hydraulic Circuits of Hot Extrusion Process" (*in German*) *Maschinenmarkt*, **75**, 1969, pp. 1451–1457.
- 16.96 Dohrn, W.: *Energy Loss in Hydraulic Presses* (*in German*), Düsseldorf, Schloemann, 1956.
- 16.97 Zymak, V.: "Simplified Type of Layout of Hydraulic Circuits for Forming Machines" (*in German*) *Ölhydraulik u. Pneuma.*, **12**, 1968, pp. 429–438.
- 16.98 Veltjens, D.: "Hot-Extrusion Plants with Auxiliary and Follow-on Equipment for the Extrusion of Copper-Based Materials" (*in German*) *Z. Metallkd.*, **62**, 1971, pp. 87–99.

## 16.66 BULK-METAL FORMING

- 16.99 Zilges, F. J.: "Indirect Extrusion of Aluminum and Copper Rich Tubes," *Metallurgia*, **48**, 5, 1981, pp. 219-228.
- 16.100 Kursetz, E.: "The Development of Tube and Strand Presses for the Extrusion of Aluminum" (in German), *Ind.-Anz.*, **86**, 1964, pp. 1721-1727.
- 16.101 Zilges, F. J.: "Solid and Hollow Extrusion Plants for Aluminum" (in German), *Aluminum*, **47**, 1967, pp. 213-220.
- 16.102 Zilges, F. J.: "Solid and Hollow Extrusion Plants for Heavy Metals" (in German), *Z. Metallkd.*, **60**, 1969, pp. 85-93.
- 16.103 Robra, H.: "Hot-Extrusion Plants for Aluminum" (in German), *Aluminium*, **43**, 1967, pp. 556-564.
- 16.104 Putz, J.: "Modern Billet-Heating Equipment" (in German), in *Hot Extrusion*, Stuttgart, Riederer, 1971.
- 16.105 Essmann, H.: "Development of Heating and Annealing Furnaces—Especially Electric Ones—in the Nonferrous Extrusion Plant" (in German), *Metall*, **18**, 1964, pp. 116-122.
- 16.106 *Horizontal Solid and Hollow Hot-Extrusion Presses* (in German), Düsseldorf, Schloemann, 1971.
- 16.107 Mosser, J.: "Device for Measuring the Extrusion Speed in Hot-Extrusion Plants" (in German), *Aluminium*, **68**, 1972, pp. 237-239.
- 16.108 Lardelli, A.: "Optical Methods of Measurement in Hot Extrusion" (in German), *Tech. Rundsch.*, **12**, 1973, pp. 33-35.
- 16.109 Steinmetz, A.: "Double-Acting Extrusion Presses for Sheathing Electric Wires with Aluminum" (in German), *Aluminium*, **46**, 1970, pp. 230-234.
- 16.110 Kolsch, A.: "Hot Extrusion of Steel Tubes Using Crank Presses" (in German), *Z. Metallkd.*, **62**, 1971, pp. 649-652.
- 16.111 Hertl, A., and Maier, H. D.: "State of the Art of Design of Hot Extrusion Plant for Aluminum-Based Materials" (in German), *Z. Metallkd.*, **62**, 1971, pp. 112-116.

### INDENTATION PROCESSES

According to the classification of the deformation processes introduced in Chap. 2, indenting is a subgroup of the category "compressive forming," along with rolling, free forming, die forming, and pushing through a die. DIN 8583 [17.1] defines indenting as compressive forming with a tool which penetrates a workpiece locally. Fig. 17.1 indicates that the kind of relative motion between tool and workpiece offers additional criteria for a subdivision of the individual processes. The associated concept definitions according to DIN 8583 are presented in detailed fashion in this chapter. They are supplemented by the sketches summarized in Fig. 17.2, illustrating the principles of operation.

#### *Indenting with Rectilinear Motion:*

Indenting with rectilinear motion is carried out with a tool oriented perpendicular, or almost perpendicular, to and moving in a straight line toward the workpiece surface.

**Indenting without sliding:** Rectilinear indenting without sliding designates a workpiece surface orientation perpendicular, or nearly perpendicular, to the direction of penetration and at rest.

- 1 **Marking** (Fig. 17.2a): A sharp, pointed tool is used to indent the workpiece surface, for example, to provide location or identification markings.
- 2 **Notching** (Fig. 17.2b): Notching involves indenting a wedge-shaped tool (notching punch) into the workpiece surface to generate depressions, such as file profiles.
- 3 **Punching** (Fig. 17.2c): An impression is made in the surface of a workpiece with a tool equipped with a symbol in its working face.
- 4 **Die hobbing** (Fig. 17.2d): Hobbing is indenting a forming tool (hob) into a workpiece to produce an exact cavity shape, such as a forming die.
- 5 **Piercing** (Fig. 17.2e, f): Piercing is indenting a workpiece with a rounded punch (mandrel) to create a cavity, for example, in cup piercing without restriction (Fig. 17.2e). By bringing two mandrels to bear from opposite directions a hole is generated without generation of waste, such as in ring forging.
- 6 **Opening out with mandrel** (Fig. 17.2g): This process involves indenting with a hollow, rounded punch to generate a through hole. Part of the work material is displaced into the cavity of the mandrel.

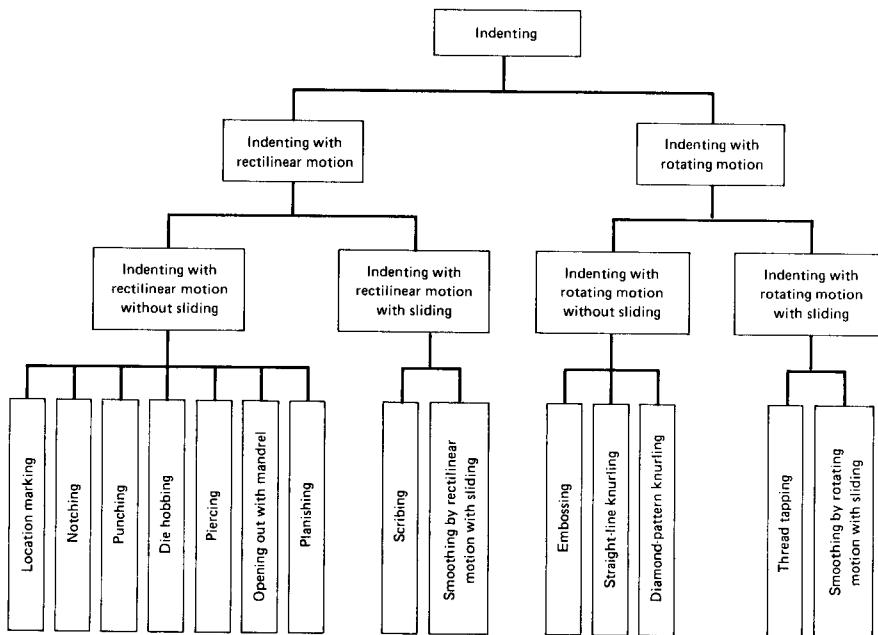


FIG. 17.1 Summary of indentation processes. (After [17.1].)

- 7 **Planishing** (Fig. 17.2*h*): In this process a tool with a raised, screenlike pattern is impressed into the surface of a thin workpiece for straightening.

**Indenting with sliding:** Rectilinear indenting with sliding designates tool motion relative to the workpiece.

- 1 **Groove forming** (Fig. 17.2*i*): A groove is created on a workpiece by sliding a pointed or wedge-shaped tool along its surface under pressure.
- 2 **Finish smoothing** (Fig. 17.2*k*): A rounded, polished tool is moved under pressure along straight paths over a workpiece to reduce its surface roughness.

#### **Indenting with Circumferential Motion**

Indenting with circumferential motion involves rotary contact between tool and workpiece.

**Indenting without sliding:** In this category of processes, the tool is passed over the workpiece in rolling motion.

- 1 **Embossing** (Fig. 17.2*l*): A tool with a symbol on its periphery (the coining roll) is pressed against the surface of the workpiece.
- 2 **Knurling** (Figs. 17.2*m, n*): Knurling is indenting the surface of a cylindrical workpiece with a tool having a continuous diamond-shaped or parallel-lined pattern on its periphery.

**Indenting with sliding:** In this category of processes, the tool is passed over the workpiece by sliding.

	Without sliding		With sliding
Indenting with rectilinear motion	(a) Marking	(b) Notching	(i) Groove forming, scratching
	(c) Punching	(d) Hobbing	(k) Finishing smoothing with rectilinear sliding motion
	(e) Piercing	(f) Piercing	
	(g) Opening out with mandrel	(h) Planishing	
	(j) Embossing	(l) Knurling	(o) Thread tapping
	(n) Knurling		
			(p) Finishing smoothing with circumferential sliding motion

FIG. 17.2 Pictorial representation of indentation processes. (After [17.1].)

## 17.4 BULK-METAL FORMING

- 1 **Thread tapping** (Fig. 17.2o): A threaded tool indents a thread into the sidewall of a hole.
- 2 **Finish smoothing** (Fig. 17.2p): A rounded, polished tool is pressed against a rotating work-piece in order to reduce its surface roughness.

The overwhelming number of processes defined above belong to the category of cold forming. In individual cases, such as die hobbing, forming is generally carried out cold, but under special circumstances the process can be hot.

Not all the indicated processes are described in detail; only the economically important ones are examined more closely.

### 17.1 FUNDAMENTALS OF INDENTATION PROCESSES

Establishing common theoretical fundamentals for indentation processes proves difficult, since these processes are too varied in geometrical shape and often occur as part of other forming processes. Studies of basic relationships between characteristic parameters are unavailable for the majority of the processes defined in this chapter. The formulas usually employed for determining forces and energy arise from the border regions of other processes and can therefore be applied here to a limited extent only.

In the following, known examples of the theoretical treatment of indentation processes are reviewed.

#### 17.1.1 State of Stress

Based on flow configurations, which form in soft steel under a penetrating prismatic body [17.2], [17.3], Prandtl [17.4] was the first to undertake the task of theoretically describing the indentation of a semi-infinite medium by a flat, rigid, frictionless punch using slip-line theory. Fig. 17.3 shows the slip-line field under a lubricated flat punch due to Hill as described in [17.5] (see Chap. 5).

The plastic zone, which forms on the left-hand side, is separated by the line  $CGFD$  from the workpiece region, which remains rigid. From the boundary conditions  $\sigma_y = \tau_{xy} = 0$  between points  $A$  and  $D$  (free surface) and  $\tau_{xy} = 0$  between  $A$  and  $C$  (frictionless interface), slip-line theory indicates that the family of first shear lines in regions  $ADF$  and  $ACG$  consists of straight lines which intersect the  $x$ -axis at  $45^\circ$ , that is, that throughout both regions the hydrostatic stress remains constant. A fan of first shear lines centered at point  $A$  provides the transition between both regions [17.5], [17.6]. As described in [17.5], other possibilities for describing the stress distribution under a flat frictionless punch exist, notably the one due to Prandtl. In either case, the solution for the punch pressure based on slip-line theory can be shown to be, for incipient plastic deformation,

$$\sigma_y = -(2 + \pi)k \quad (17.1)$$

The velocity field associated with the stress field of Fig. 17.3 satisfies all boundary conditions [17.6]. If the punch speed is taken as  $v_y = -1$  (unit speed) along  $AC$ , then the Geiringer equations (see Chap. 5) indicate the following about the velocity distribution.

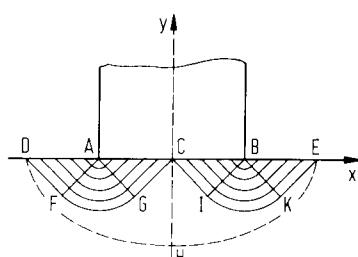


**FIG. 17.3** Slip-line field under lubricated flat punch. (After [17.5].)

In the entire plastic region the velocity component in the first shear direction vanishes. The second shear lines, parallel to line  $CGFD$ , which is itself a second shear line, are the streamlines of incipient plastic flow. Region  $ACG$  moves as a rigid body with velocity  $v = \sqrt{2}$  in the direction of  $CG$ . In the centered fan, the velocity has a constant value of  $\sqrt{2}$  along every circular second slip line. Region  $ADF$  moves as a rigid body with velocity  $v = \sqrt{2}$  in the direction of  $FD$ .

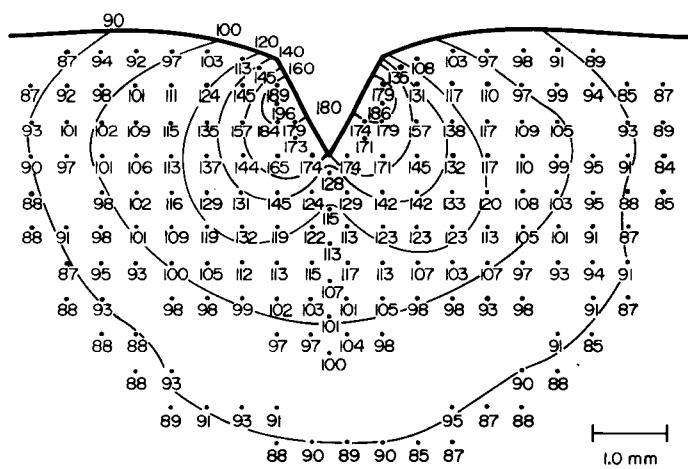
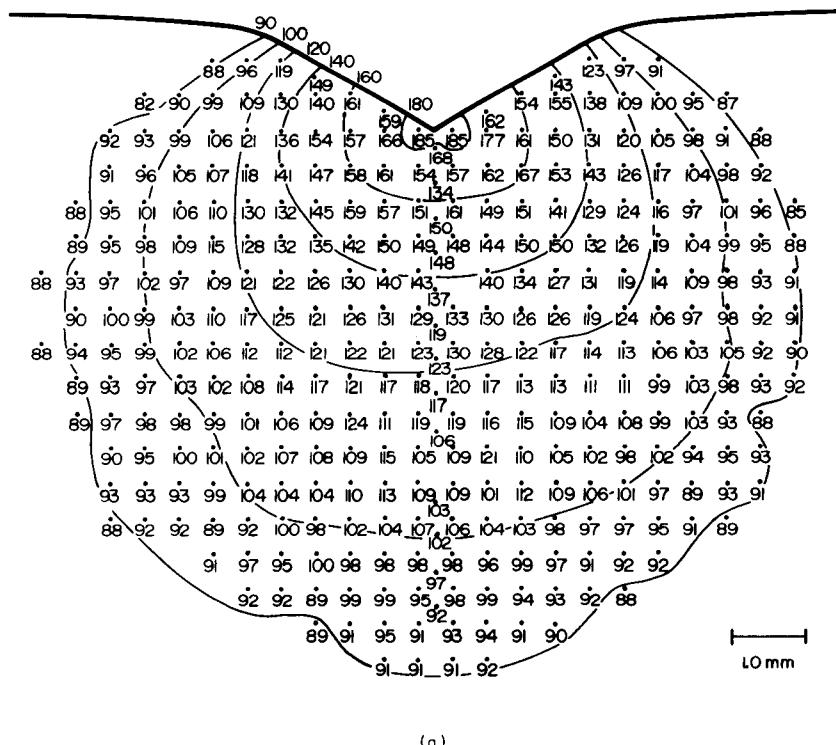


**FIG. 17.4** Hardness map and isoskleres. (a) 120° wedge indentation (plastic deformation due to an almost blunt indenter). (b) 60° wedge indentation. (After [17.8].)

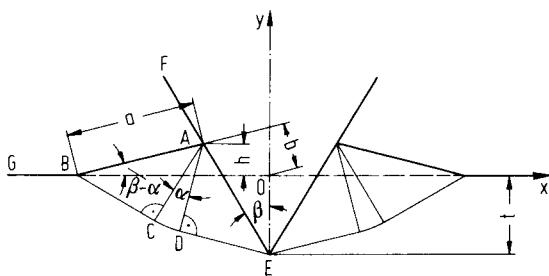


**FIG. 17.5** Slip-line field for penetration of lubricated wedge into semi-infinite body. (After [17.9], [17.5].)

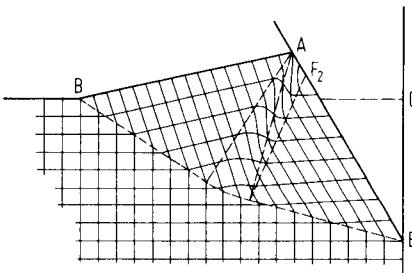


**FIG. 17.6** Deformed grid following penetration of lubricated wedge into semi-infinite body. (After [17.9], [17.5].)

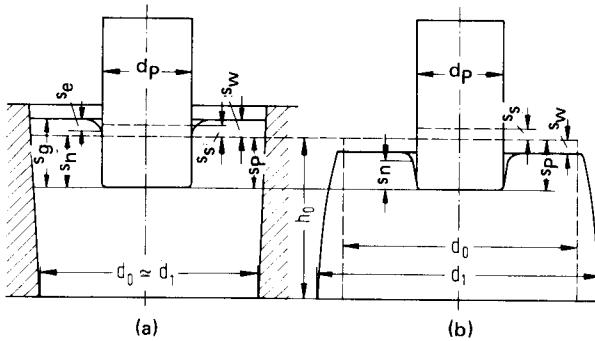


**FIG. 17.7** Cold hobbing (a) with and (b) without container ring, analogous to piercing with rising and lateral work-material displacement. (After [17.16].)

It is not implied that, in accordance with the described velocity field, the limitation of plastic flow to the region above  $DFGCIKE$  means that there is no plastic flow beneath this line, namely, that line  $DFGCIKE$  is the elastic-plastic boundary. It is to be assumed that the elastic-plastic boundary has the form of line  $DHE$ , that is, the work material between both lines remains at rest during initial plastic flow, although it experiences stress levels in the vicinity of the yield point. Subsequent work has removed many of the uncertainties surrounding the elastic-plastic boundary, however. Plastic flow beneath blunt indenters was analyzed based on the elastic-plastic nature of

the workpiece material, and it was shown that the elastic-plastic boundary extends into the workpiece in a near-circular fashion. This is due to the fact that the material can only be displaced into the workpiece and is accommodated there as a result of the volume change due to elastic deformation. Hence the size and shape of the plastic region underneath a flat punch or any other blunt indenter are subject to an elastic constraint rather than the velocity constraint of the slip-line field [17.7] (Fig. 17.4a).

The stress field for penetration of a semi-infinite body by a lubricated wedge can be described in a manner similar to that applied to the flat punch. Fig. 17.5 shows the slip-line field due to [17.9], [17.5]. Line *EF* is the left flank of the wedge with included angle of  $2\beta$ , *BG* is the still undeformed surface of the body, and *AB* is the lip which is raised due to wedge penetration. The isosceles right triangles *ABC* and *AED* represent regions of constant state of stress, and *ACD* is a centered fan of first shear lines. Fan angle  $\alpha$  is a direct function of wedge half-angle  $\beta$ :

$$\beta = \frac{1}{2} \left[ \alpha + \cos^{-1} \tan \left( \frac{\pi}{4} - \frac{\alpha}{2} \right) \right] \quad (17.2)$$

The velocity component in the first slip direction vanishes in the entire region *ABCDE*. Consequently the streamlines coincide with the second slip lines parallel to *BCDE*. Along each of these parallel slip lines the velocity must be of constant magnitude.

The force necessary to drive a wedge of unit depth into the plastic work material is given by [17.5] and [17.10] as

$$F = 4kt(1 + \alpha) \frac{\sin \beta}{\cos \beta - \sin(\beta - \alpha)} \quad (17.3)$$

An impression of the deformation occurring during punch indentation is to be conveyed by Fig. 17.6. It shows the calculated deformation of an originally square grid pattern [17.9].

The elastic constraint demonstrated in [17.7] affects the shape of the plastic region in wedge indentation as well. As the degree of bluntness decreases with closing wedge angle  $2\beta$ , the elastic constraint diminishes, and the plastic region begins to look similar to that shown in Fig. 17.6. This has been demonstrated repeatedly in experimental studies, as for example, in [17.8] (Fig. 17.4b).

### 17.1.2 Deformation Energy and Forces

Elementary calculations of deformation energy and forces are based on a formulation by Siebel [17.11] for the determination of the ideal deformation energy  $W_{id}$ :

$$W_{id} \approx V\sigma_{f,m} \varphi_{max} \quad (17.4)$$

where  $V$  = volume affected by deformation

$\sigma_{f,m}$  = mean flow stress

$\varphi_{max}$  = maximum strain

In the field of indentation processes, this expression was first applied to piercing [17.12]. In practice, a distinction is made between two methods: piercing with rising work-material displacement and piercing with lateral work-material displacement (Fig. 17.7). In the first case, the die-cavity cross section is completely filled by the workpiece. The process is thus similar to reverse cup extrusion in that the workpiece material is displaced in a direction opposite to the punch motion with a resulting increase in workpiece height. The second case occurs in unrestricted hobbing, for instance. The die, if present at all, permits lateral motion of the displaced material, so that the resulting part maintains approximately the height of the original workpiece, but will acquire a slightly larger outside diameter. To ensure minimum workpiece compression, the following area ratio should not be exceeded:

$$\frac{A_p}{A_1} = 0.3 \quad (17.5)$$

where  $A_p$  = cross-sectional area of punch

$A_1$  = cross-sectional area of workpiece

## 17.8 BULK-METAL FORMING

Indentation processes defined at the beginning of this chapter remain below this limit, that is, the force required for local penetration by the tool is exerted on a small area in relation to the workpiece dimensions.

During piercing, deformations of varying magnitudes occur in the different zones of the workpiece which are dependent upon the punch position. The energy of deformation must therefore be determined as the sum of the deformation energies of all individual volume elements, or approximated as the mean value of the largest strain to the entire volume affected by the deformation (Eq. 17.4). Since strain shows the largest value in the radial direction as long as no height reduction is involved [17.11], this value is to be used for the determination of the energy required for deformation. The mean value for the largest strain, in the radial direction, is given in [17.12] as

$$\varphi_{r,m} \approx \ln \frac{d_0}{d_1 - d_p} - C \quad (17.6)$$

where  $d_0$  = workpiece diameter

$d_1$  = outside diameter of finished part

$d_p$  = punch diameter

$C$  = empirical constant = 0.16

As an improvement of this approximate relationship, replacing the value for  $C$  of 0.16 by 0.19 has been suggested [17.13].

If in accordance with [17.12]  $\varphi_{\max}$  is replaced by  $\varphi_{r,m}$  in Eq. 17.4, one obtains

$$W_{id} \approx V \sigma_{f,m} \varphi_{r,m} \quad (17.7)$$

and the ideal force of deformation becomes

$$F_{id} \approx A_0 \sigma_{f,m} \varphi_{r,m} \quad (17.8)$$

where  $A_0$  is the original cross-sectional area of the workpiece.

To consider losses due to internal shear and tool friction, the ideal deformation energy  $W_{id}$  is divided by an experimentally determined deformation efficiency  $\eta_{def}$ , and the actual energy requirements are obtained. Accordingly, the actual mean forming force for the process becomes

$$F_m = A_0 \sigma_{f,m} \varphi_{r,m} \frac{1}{\eta_{def}} \quad (17.9)$$

Representative values for the forming efficiency  $\eta_{def}$  are:

- 0.4–0.5 Piercing with rising material displacement; in case of lateral displacement, use 10% less [17.11]
- 0.2–0.25 Hobbing in a container [17.14]
- 0.1–0.3 Hobbing without restriction [17.15]

## 17.2 HOBBLING

Forming by hobbing can be carried out cold (below the recrystallization temperature of the workpiece material) as well as hot (above the recrystallization temperature, usually at forging temperatures). Cold hobbing clearly outranks hot hobbing in industrial importance (see Sec. 17.2.6).

Cold hobbing distinguishes itself from other methods for the production of hollow shapes (chip removal, spark machining, and electrochemical methods) through the following advantages:

- Simple time- and material-saving production, also of complex hollow contours
- Cost savings, especially for the production of multipurpose tools (dies with several, usually similar hollow shapes)
- Great dimensional accuracy and uniformity of the manufactured hollow shapes

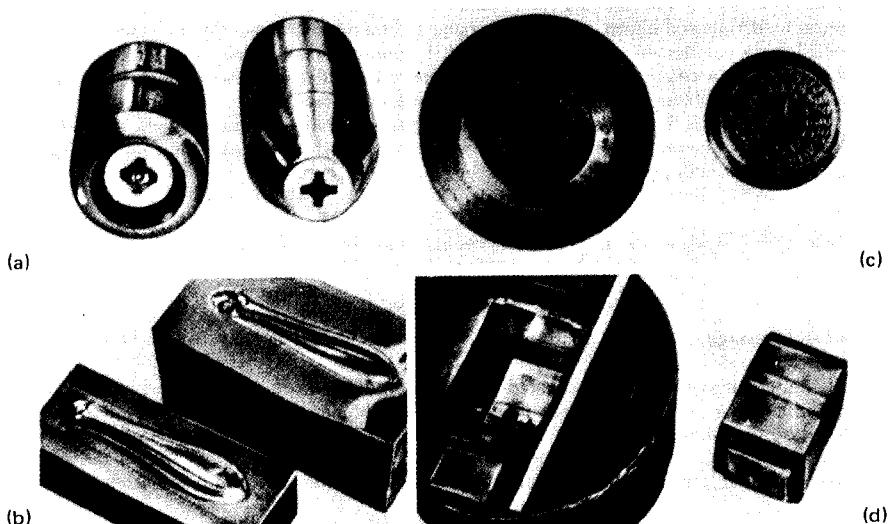


**FIG. 17.8** Examples of cold-hobbed unfinished tools. (a) Head punch for Phillips screws, made of S 6-5-2 (AISI M2) high-speed steel. (b) Coining die for table-wear handle, made of 55 NiCr10 steel. (c) Coining tool for coins, made of X 165 CrMoV12 (AISI D2) die steel. (d) Die-casting mold, made of X 6CrMo4 (AISI P4) steel (hobbed in three stages, two intermediate anneals). (After [17.17].)

#### Excellent surface finish

Long life of cold-hobbed tools due to surface finish and favorable fiber structure [17.16] to [17.18]

As a result of these advantages, cold hobbing is used in the production of the following workpieces (see Fig. 17.8 for examples):

Dies for forged and extruded parts

Tools for cold and hot forming of screws, nuts, rivets, and so on

Dies for coining coins, medals, jewelry, toys, and other metallic goods, such as table wear, armatures, watch parts, typewriter keys

Die- and chill-casting molds for brass, zinc, and light metals

Press, injection-molding, and blow dies for parts made of plastics, rubber, glass, ceramics

Trimming dies

Locating centers in workpieces, such as parts to be turned [17.17], [17.18]

Process limits are determined by formability, especially strain-hardening characteristics of the work material, shape and size of the indentations, loadability of the hobbing punch by which the attainable penetration depth is limited (see Eq. 17.10), and the forces available from hydraulic hobbing presses [17.19]. It is not economical to hob large tools due to the excessively large press forces required [17.18]. Added disadvantages are that no interior clearances in the hollow shapes are possible, and it is difficult to produce exact parallel walls, a situation which is complicated by the likelihood of dimensional distortions due to subsequent heat treatment [17.18].

Analogous to piercing with rising or lateral material displacement, cold hobbing can be carried out either with the workpiece placed in a container ring or without restriction (Fig. 17.7). Hob-

## 17.10 BULK-METAL FORMING

bing in a container requires higher forces than hobbing without restriction, but it permits greater penetration depths and higher forming accuracy, and therefore is generally preferred.

Shallow die cavities are produced successfully by unrestricted hobbing, however. Minor upsetting of the workpiece and possible shape deviations of the indentation become less significant as the area ratio of hobbing punch to original workpiece cross section  $A_p/A_0$  is reduced.

Hobbing depth is the path  $s_p$  which the working face of the punch traverses after penetrating the workpiece. It consists of press travel  $s_m$ , which is set on the press, and the combined spring components  $s_s$  of both press and tools:

$$s_p = s_m - s_s \quad (17.10)$$

The useful depth of the impression  $s_n$  results from components  $s_m$  and  $s_s$ , workpiece edge rounding  $s_e$ , and workpiece height change due to material flow  $s_w$ :

$$s_n = s_m - s_s - s_e \pm s_w \quad (17.11)$$

The height change  $s_w$  becomes positive for hobbing in a container and negative for hobbing without restriction, as illustrated in Fig. 17.7.

If the indentation depth  $s_p$  is related to the punch diameter  $d_p$ , the so-called hobbing ratio (reduced hobbing depth)  $s_p/d_p$  is obtained. For most hobbing shapes, the hobbing depth can be reduced by the diameter of an axisymmetric cylinder the cross section of which corresponds to the area of the impression. The diameter  $d_p$  of a circularly cylindrical punch of equal area can be approximated from an arbitrary punch area with help of the empirical relationship [17.17]

$$d_p = 1.13 \sqrt{A_p} \quad (17.12)$$

Since as a rule the magnitude of the cross-sectional area rather than the shape of the punch has the greatest effect on the required hobbing force, it is customary to divide the hobbing force  $F$  by the cross-sectional area of the punch  $A_p$  and to work with the hobbing pressure  $\bar{p}_p$ .

### 17.2.1 Workpiece Materials for Cold Hobbing

To judge the ability of a work material, for example, a tool steel, to be formed by cold hobbing, so-called hobbing curves are usually employed. Fig. 17.9 shows three scatter bands of hobbing curves which are divided into three groups (a, b, c) in accordance with the annealed hardness of the associated work materials. Table 17.1 provides a compilation of frequently used hobbing work materials with applications and association with one of the three scatter bands of Fig. 17.9. More complete tables and references regarding additional work materials are given in [17.14].

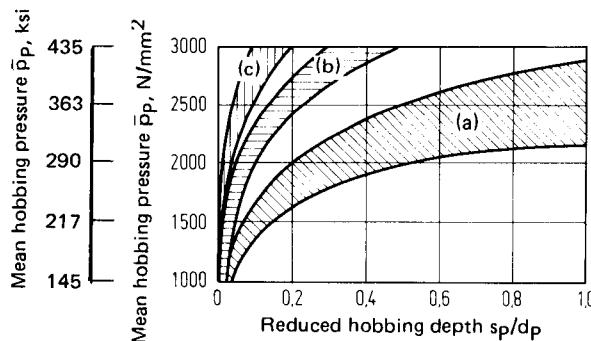


**FIG. 17.9** Hobbing curves of customary tool steels for cold hobbing with container ring and cylindrical punch.  $d_p = 30 \text{ mm (1.18 in)}$ ;  $d_0 = 67 \text{ mm (2.64 in)}$ ;  $h_0 = 60 \text{ mm (2.36 in)}$ ;  $v_p = 0.03 \text{ mm/s (0.07 in/min)}$ ; punch copper plated; lubrication with cylinder oil. (a) Steel with HB 100–140. (b) Steel with HB 170–210. (c) Steel with HB 210–250. (After [17.17].)

**Table 17.1** Workpiece Materials for Cold Hobbing<sup>a</sup>

Designation		Hardness after annealing, HB	Steel group after Fig. 17.8	Application
DIN	AISI			
<i>Case-Hardening Steels</i>				
C10WS	1010	110	<i>a</i>	
X6CrMo4	P4	110	<i>a</i>	
X8CrMoV5		140	<i>a</i>	
21MnCr5		175	<i>b</i>	
15CrNi6	3215	190	<i>b</i>	
<i>Cold-Working Steels</i>				
C100W1	W1/1.0	190	<i>b</i>	
95V4	W3/1.0 C-V-V	190	<i>b</i>	Heading punches and dies for bolt making
90Cr3		195	<i>b</i>	
X40Cr13	420	210	<i>c</i>	Coining punches Corrosion-resistant injection-molding dies
55NiCr10		215	<i>c</i>	
X45NiCrMo4		240	<i>c</i>	Coining tools for jewelry, etc.
X165CrMoV12	D2	240	<i>c</i>	Coin-embossing punches
<i>Hot-Working Steels</i>				
45CrMoV67	GG	175	<i>b</i>	
X32CrMoV33	H10	165	<i>b</i>	Die-casting molds, dies under presses
X38CrMoV51	H11	210	<i>c</i>	
45CrMoW58		220	<i>c</i>	
X30WCrV53	H21	220	<i>c</i>	Die-casting molds
55NiCrMoV6	6F2	220	<i>c</i>	
56NiCrMoV7	6F3	220	<i>c</i>	Dies under hammers
<i>High-Speed Steels</i>				
S3-2-2		240	<i>c</i>	
S2-9-1	(M1)	240	<i>c</i>	Glass jewelry dies Heading punches for Phillips screws

<sup>a</sup>For chemical composition see Appendix C.

Source: Compiled from [17.17]

The hardness of the fully annealed workpiece material has a deciding influence upon the pressure  $p_p$  necessary for cold hobbing and the achievable indentation depth, keeping in mind the load capacity of the hobbing punch. The higher the hardness, the smaller the indentation depth that can be obtained in a single hobbing stroke [17.17]. Annealed hardness is dependent upon the chemical composition of the work material, the heat treatment, and the microstructure obtained. The content of alloying elements dissolved in the ferrite, and the amount and distri-

bution of carbides influence the extent of the hardness of the workpiece steel. Spheroidal pearlite and low carbon and chromium contents provide the desirable low initial hardness, that is, hardness after annealing. For a number of work materials the hardness can be reduced by special annealing methods within the limits imposed by the alloying contents [17.17].

### 17.2.2 Description of the Cold-Hobbing Process

#### *Material Flow and Strain Hardening in Cold Hobbing*

Axisymmetric workpieces were employed to study material flow using the method of visioplasticity [17.15], [17.17]. Fig. 17.10 shows grid patterns which result from progressively increasing normalized hobbing depths  $s_p/d_p$  with punch and workpiece geometries held constant. It is evident that almost no material flow takes place directly under the punch in the vicinity of the axis of symmetry. Below this region axial distortions of varying intensities occur depending upon the magnitude of  $s_p/d_p$ . The ring region of the workpiece experiences radial upsetting locally, and increases in height as a result [17.17].

The most severe deformation takes place at the punch edge and along the wall of the impression. This fact can be further demonstrated by hardness scanning along the grid lines. The resulting lines of equal hardness (isosklers) are shown in Fig. 17.11. The greatest degree of cold work is clearly indicated for the regions of the most substantial material flow [17.16]. The extent of cold work is also shown to increase with deepening  $s_p/d_p$ , and with it both flow stress and hobbing force increase. The hardness increases and gradients can be eliminated by appropriate heat treatment (see Sec. 17.2.3).

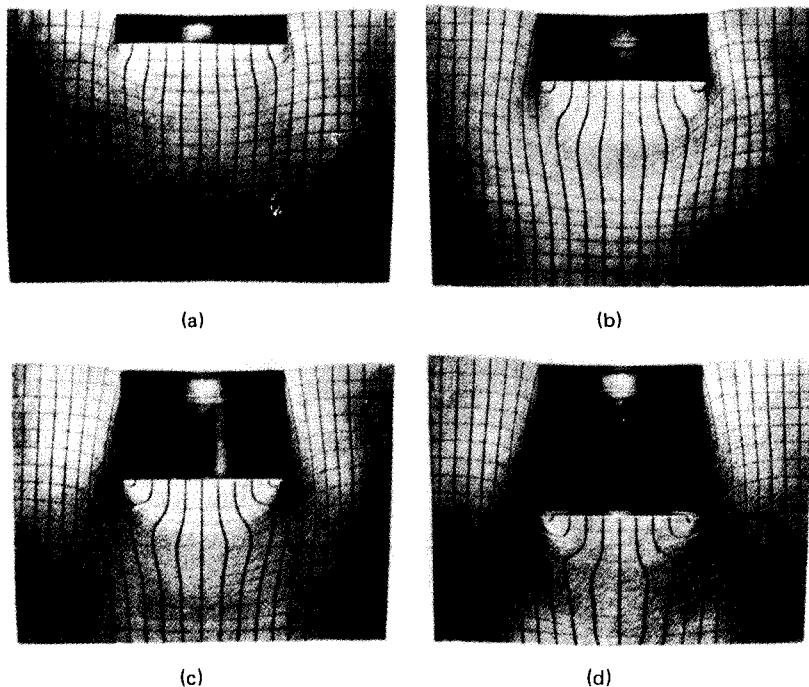


**FIG. 17.10** Grid-line patterns on meridional planes of workpieces with different reduced hobbing depths  $s_p/d_p$ .  $d_p = 40$  mm (1.57 in). (a)  $s_p/d_p = 0.2$ . (b)  $s_p/d_p = 0.4$ . (c)  $s_p/d_p = 0.6$ . (d)  $s_p/d_p = 0.8$ . (After [17.17].)

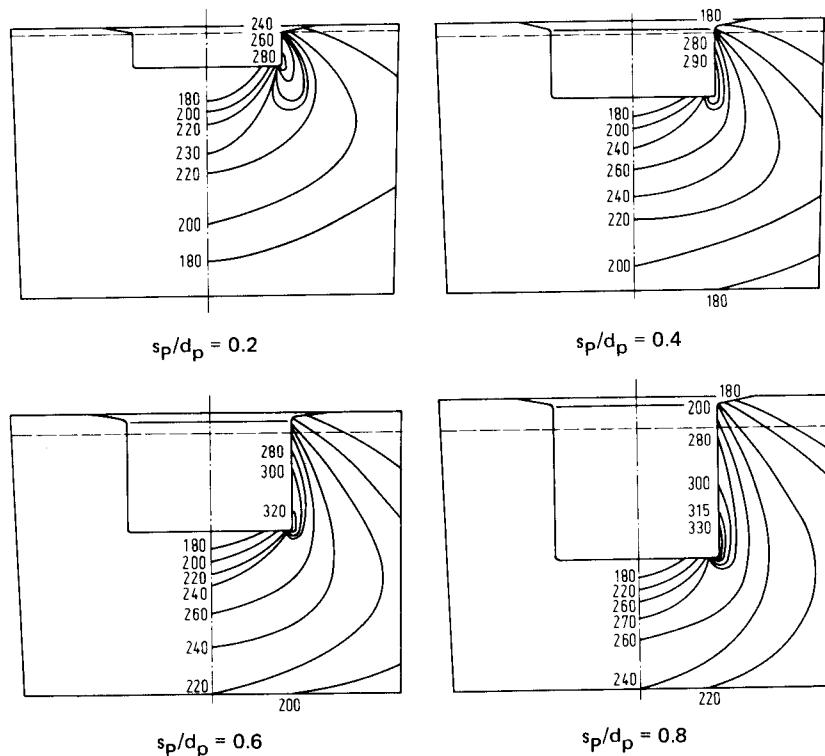


**FIG. 17.11** Lines of equal hardness (isoklkers HV 10) on meridional planes of workpieces with different reduced hobbing depths  $s_p/d_p$ . Workpiece material—X 32 CrMoV33 (AISI H10) steel; hardness after annealing HV 10 161. (After [17.16].)

### Calculation of and Parameters Affecting Forming Force and Penetration Depth in Cold Hobbing

In addition to the analytical considerations of Sec. 17.1.2, the cold-hobbing literature [17.14], [17.20] contains information about different empirical methods for estimating the hobbing force  $F$  or the mean hobbing pressure  $\bar{p}_p$  for simple, symmetric punches (excellent surface finish, good lubrication).

The simplest technique is the so-called  $\bar{p}_{p,\max}$  method: the maximum mean hobbing pressure is limited by the load capacity of the punch based on the punch material. These pressure values vary between 2200 and 3000 N/mm<sup>2</sup> (320 and 435 ksi), and are used in the expression for the maximum hobbing force:

$$F_{\max} = A_p \bar{p}_{p,\max} \quad (17.13)$$

The hobbing curves  $\bar{p}_p = \bar{p}_p(s_p/d_p)$  were measured for a number of hobbing-quality steels and related to the flow curves  $\sigma_f = \sigma_f(\varphi)$  of the materials, which had been established through compression tests [17.21]. Representation of the curves in the double-logarithmic coordinate system yielded the relationships

$$\bar{p}_p = C \sigma_f \quad (17.14)$$

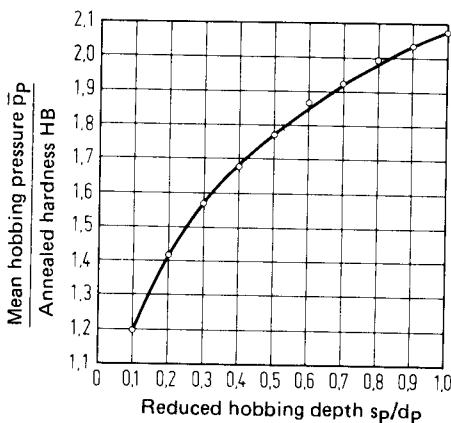


FIG. 17.12 Dependence of mean hobbing pressure  $\bar{p}_p$  (reduced by annealed hardness HB) upon reduced hobbing depth  $s_p/d_p$ . (After [17.20].)

and

$$\varphi = 0.33 \left( \frac{s_p}{d_p} \right) - 0.01 \quad (17.15)$$

within the limits  $0.1 < s_p/d_p < 1.0$ . Experimental comparisons provided a factor  $C = 4.5$  with which to multiply the flow stress  $\sigma_f$  in order to determine  $\bar{p}_p$  for a given hobbing depth  $s_p/d_p$ . With the help of this relationship the hobbing curves  $\bar{p}_p = \bar{p}_p(s_p/d_p)$  can be determined from the flow curves  $\sigma_f = \sigma_f(\varphi)$  with satisfactory accuracy ( $\pm 10\%$ ). The hobbing force  $F$  is obtained from the so-called  $4.5\sigma_f$  method,

$$F = 4.5\sigma_f A_p \quad (17.16)$$

Based on hardness measurements it was determined that the ratio of  $\bar{p}_p$  to Brinell hardness  $HB_{2.5}$  remains approximately the same for annealed tool steels at a constant  $s_p/d_p$  ratio [17.20]. This relationship, shown in Fig. 17.12, has found acceptance in the literature as the so-called HB method. It permits the determination of  $p_p$  with an accuracy of  $\pm 10\%$  from the Brinell hardness HB of the work material for a specified hobbing ratio  $s_p/d_p$ . Based on this information the hobbing force can be calculated, or from  $\bar{p}_p$  and HB the achievable penetration  $s_p/d_p$  can be ascertained.

Additional references regarding less known empirical techniques for the calculation of  $\bar{p}_p$  or the hobbing force are provided in [17.14]. Fig. 17.13 shows a nomogram with the help of which the required force for cold hobbing in a container can be estimated.

Useful empirical formulas for the calculation of the obtainable hobbing depth were developed from experimental data, which had been obtained by intensive testing of different hot-working steels of varying annealed hardnesses, different punch diameters [ $d_p = 3.5\text{--}30\text{ mm}$  (0.14–1.2 in)], and a hobbing speed  $v_p$  of 1 mm/min (0.04 in/min) [17.22]. The obtainable hobbing depth  $s_p$  is determined from the relationship

$$s_p = \frac{d_p}{13} \left( \frac{\bar{p}_p}{10 HB} \right)^3 \text{ [mm]} \quad (17.17)$$

when axisymmetric punches are used. For punches with rectangular cross section the expression becomes

$$s_p = 0.31 \frac{A_p}{U_p} \left( \frac{\bar{p}_p}{10 HB} \right)^3 \text{ [mm]} \quad (17.18)$$

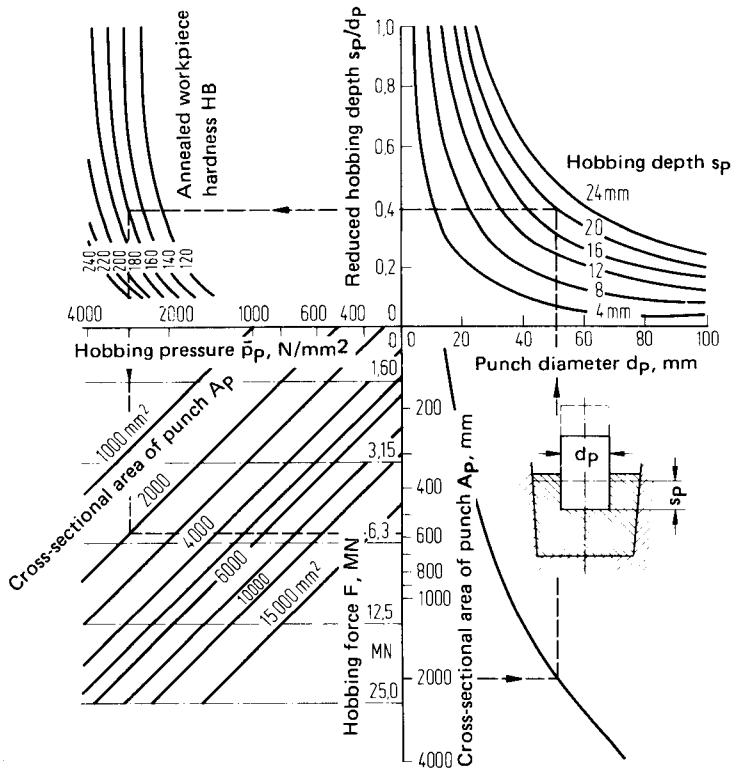


FIG. 17.13 Nomogram for the determination of hobbing force and other important parameters associated with cold hobbing in a container. For conversion of MN and N/mm<sup>2</sup> see Chap. 1, Table 1.3. (After [17.17].)

where  $d_p$  = punch diameter, mm

$A_p$  = punch cross-sectional area, mm<sup>2</sup>

$U_p$  = punch circumference, mm

$\bar{p}_p$  = mean hobbing pressure, N/mm<sup>2</sup>

HB = Brinell hardness of annealed workpiece material

Eqs. 17.17 and 17.18 are valid for cold hobbing in a container at a mean pressure  $\bar{p}_p$  of about 2500 N/mm<sup>2</sup> (360 ksi). An increase or decrease of  $\bar{p}_p$  by about 500 N/mm<sup>2</sup> (72 ksi) will result in a change of penetration depth of about 6%, according to [17.22]. Calculations using Eq. 17.17 show very good agreement with experimental values obtained in studies involving  $\bar{p}_p = 2500$  N/mm<sup>2</sup> (360 ksi) [17.20], [17.23].

The mean hobbing pressure and hobbing depth are dependent upon each other as well as upon the following factors:

- 1 The formability of the work material as affected by microstructure, hardness after annealing, temperature, strain-hardening characteristics, and so on
- 2 Possible prior work on the workpiece (such as reverse-side recesses for easier metal flow)
- 3 The shapes and sizes of workpiece and punch

## 17.16 BULK-METAL FORMING

- 4 The load capacity of the punch (see Sec. 17.2.4)
- 5 The type of process, that is, with or without a container
- 6 The hobbing speed
- 7 Friction and lubrication

The main influence upon the required hobbing forces or attainable depth emanates from the initial hardness of the workpiece material, as the empirical relationships presented in this chapter indicate (Sec. 17.2.1 and Fig. 17.9). The strain-hardening characteristics (Fig. 17.11) are generally independent of the alloying content of most of the common hobbing work materials. However, austenitic steels find limited use for cold hobbing because of their substantially stronger tendency to work-harden. Hobbing carried out perpendicular to the fiber structure of the workpiece requires considerably higher forming forces than when the fiber structure is oriented in the direction of punch motion.

Higher temperatures cause a reduction in both hardness and flow stress. It is therefore recommended [17.17] that workpieces of materials having higher hardness be heated to 200°C (392°F). As a result, the hobbing pressure is reduced by about 20% at a constant specific hobbing depth, while a substantial increase in penetration depth can be achieved with a constant hobbing force (Fig. 17.14). For materials of very high annealed hardness (HB 220 and more) warm hobbing at temperatures above 400–500°C (750–930°F) causes a substantial increase in penetration depth, in general by a factor of 2 [17.17]. Temperatures between 200 and 400°C (392 and 740°F) are eliminated because of blue brittleness.

An additional possibility for achieving greater penetration depths is offered by intermediate annealing (full annealing, possibly stress relief annealing). Residual stresses caused by previous forming and cold work in general can thus be eliminated. After intermediate annealing, hobbing can be continued until the limiting load capacity of the punch is reached.

Recesses in the workpiece are intended to facilitate material flow. Fig. 17.15 demonstrates the effect of different types of flow aids upon the attainable specific penetration depth at constant mean hobbing pressure, or upon pressure at constant depth of penetration.

For the dimensions of workpiece and punch an area ratio  $A_0/A_p$  of about 4 is considered favorable. Higher ratios result in an increase in the hobbing force [17.18]. The initial workpiece height  $h_0$  is to exceed the hobbing depth  $s_p$  by a factor of 2 or 3. Insufficient workpiece heights increase flow stress and hobbing force [17.18].

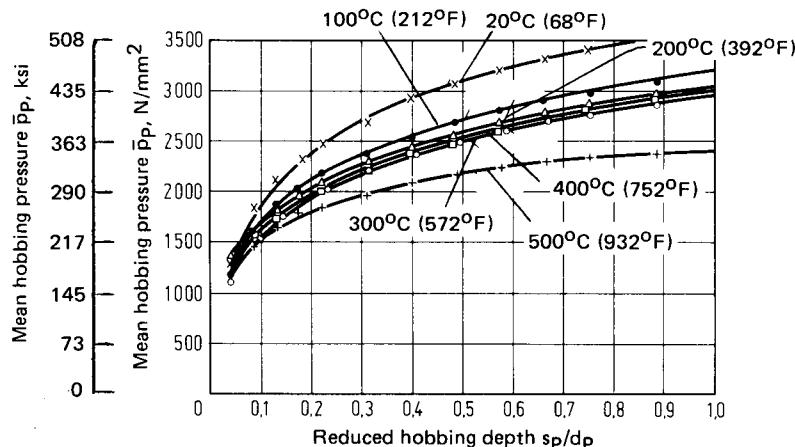
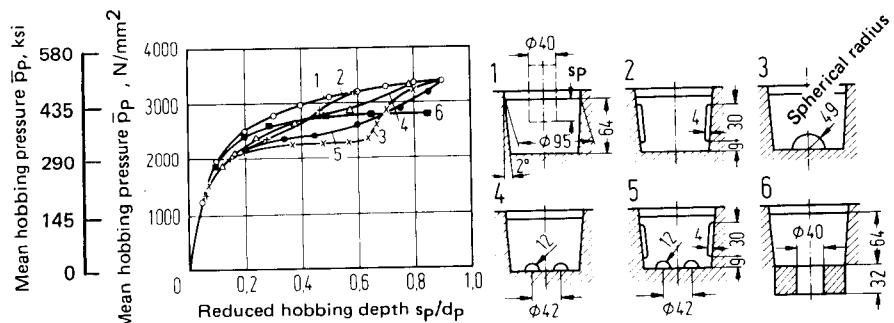


FIG. 17.14 Effect of temperature upon mean hobbing pressure  $p_p$  as a function of reduced hobbing depth  $s_p/d_p$ . Workpiece material—X 32 CrMoV33 (AISI H10) steel; hardness after annealing HB 161. (After [17.17].)



**FIG. 17.15** Effect of flow relief methods upon mean hobbing pressure  $\bar{P}_p$  as function of reduced hobbing depth  $s_p/d_p$ . Workpiece material—X 32 CrMoV33 (AISI H10); hardness after annealing HB 161;  $v_p = 0.03 \text{ mm/s}$  (0.07 in/min); punch copper plated; lubrication with MoS<sub>2</sub>. (After [17.17].)

Deviations from the axisymmetric punch shape impede material flow and increase the hobbing force whose magnitude depends on the complexity of the shape. Conical punches cause higher forces than cylindrical ones, the force increasing directly with the cone angle. Additional information about the effect of the shape of the punch nose are contained in [17.24] to [17.26].

The use of a container impedes material flow and increases friction between workpiece and tool. The forming forces are therefore higher than for the case of hobbing without restriction.

Hobbing velocities vary generally between 0.01 and 0.1 mm/s (0.025 and 0.25 in/min) depending on the workpiece material. Higher velocities [hobbing presses tend to have a top speed of 0.3 mm/s (0.75 in/min)] favor the rising of work material whenever elevations are to be produced inside impressions by hobbing. The effect of the hobbing speed on the force requirement is normally considered insignificant, although greater punch penetrations can be attained by slower speeds. Changes in speed in relation to the annealed strength of the workpieces are therefore of greater significance for the punch life than for the magnitude of the hobbing force.

### Friction and Lubrication

Since the surface roughness on the hobbing punch will imprint in the surface of the cavity, and will also influence friction during the forming process, it is essential to maintain an excellent surface finish. The surface finish of hobbing punches and workpieces is achieved by grinding and polishing. Together with suitable lubrication, the proper finish reduces friction shear stresses and hence the required forming forces. It also reduces or avoids notch stresses in the highly loaded punches, thus increasing their life, and creating surfaces free of grooves within the impressions. As a result, no additional finishing step is required. Only after heat treating, which can result in scale formation, a final polishing of the newly created die surfaces may be required.

In order to increase lubricity, the hobbing punches are usually copper-plated. Phosphate coatings as carriers of lubricant have also proven useful. Lubricants must hold up under pressure, and molybdenum disulfide (MoS<sub>2</sub>) is used as a rule. In addition, high-pressure oil, tallow, and castor oil mixed with colloidal graphite are mentioned as lubricants [17.18].

#### 17.2.3 Heat Treatment after Forming

Cold-hobbed die parts, such as forging die cavities, usually are subjected to heat treatment in order to eliminate residual stresses or work hardening caused by the forming process. The following treatments are under consideration:

- 1 Intermediate annealing (soft anneal, stress-relief anneal, recrystallization anneal)
- 2 Stress relief anneal with subsequent hardening

## 17.18 BULK-METAL FORMING

Intermediate annealing becomes necessary whenever the strain-hardening capacity of the work material is exhausted during cold hobbing before the desired penetration depth has been reached.

Dimensional and shape changes caused by thermal and transformation stresses during hardening generally are countered by prior stress relieving. This anneal takes place over a period of at least 2 hours at temperatures between 600 and 650°C (1100 and 1190°F) in an inert atmosphere with subsequent slow cooling in the furnace. Minor distortions after annealing can be eliminated by sizing. Hardening methods usually are through hardening, case hardening, or nitriding. The type of hardening treatment and its execution (temperature, duration, cooling rate, etc.) depend on the work material and the demands placed on the finished workpiece. A subsequent temper will reduce stress concentrations and increase toughness. The smallest stresses and hence the smallest distortions are obtained by martempering.

Although currently much emphasis is placed on stress relieving before hardening for the purpose of maintaining the dimensions of die impressions, more recent studies [17.27] seem to indicate the value of this treatment to be minor. Instead, dimensional deviations of cold-hobbed cavities after heat treatment are claimed to depend primarily upon hobbing ratio and initial hardness of the workpiece material. In most cases, stress relieving can thus be eliminated as an additional work step, provided the austenitizing temperature is reached during hardening, and time at this temperature is sufficiently long [17.27]. Stress relieving will still be necessary for especially complex parts in which extreme stress concentrations occur, a condition which could lead to crack formation during rapid heating.

### 17.2.4 Cold Hobbing Tooling

The setup of a tool and die assembly for hobbing in a container is shown in Fig. 17.16. For the feasibility of a hobbing process and the economy of the process, the quality of the punch is of decisive significance. The punch is subject to wear by friction, and in the flow of force of the process, it represents the element exposed to the most severe pressure, which can reach 3000 N/mm<sup>2</sup> (435 ksi) according to [17.19], or even 3500 N/mm<sup>2</sup> (500 ksi) according to [17.18]. The selection of suitable work materials, the shaping of a functional punch that can also be produced economically, and its careful heat treatment must therefore receive considerable attention.

Selection of the punch material depends upon punch shape and dimensions, the kind of impression, and the magnitude of the expected hobbing force. A number of customary tool steels are listed in Table 17.2. Additional tool steels can be found in [17.14] and [17.29].

For simple punch shapes, 12% chrome steels such as X165CrV12 (AISI D2) are generally preferred due to their resistance to pressure and wear. For more complicated shapes, the lower-alloy cold-form steel 76CrMoNiW67 has proved useful. It has the same compressive strength, but displays a significantly higher toughness. Tough chrome-nickel steels, like 50NiCr13, are preferred for shapes with large dimensions and significant changes in cross section. Plain carbon

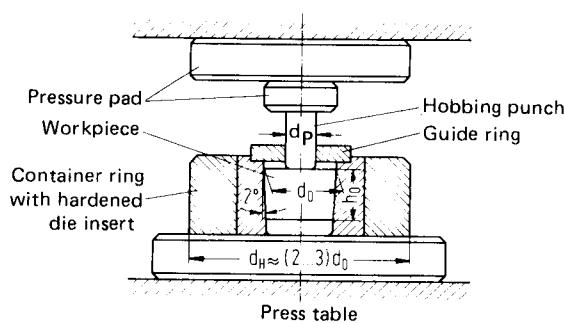


FIG. 17.16 Tooling for cold hobbing in a container. (After [17.28].)

**Table 17.2** Tool Steels for Hobbing Punches<sup>a</sup>

DIN	Designation	AISI	Working hardness, HRC	Maximum pressure capacity, N/mm <sup>2</sup> (ksi)
C110W1		W1/1.1	63–65	2200 (319)
X210Cr12		D3	60–65	3000 (435)
X165CrV12			58–64	3000 (435)
X155CrVMo121			60–62	3000 (435)
X165CrMoV12		D2	60–63	3000 (435)
55NiCr10			52–57	2200 (319)
50NiCr13			53–58	2300 (334)
75CrMoNiW67			57–61	2800 (406)
S 6-5-2		M2	65–68	3200 (464)

<sup>a</sup>For chemical composition see Appendix C.

Source: Compiled from [17.14], [17.17], [17.18], [17.28].

steels, like AISI W1/1.1, are useful for simple, symmetric shapes of small size, for which hardening is not expected to create difficulties.

Hardness, ability to absorb energy, and other parameters (yield point, fracture strength, etc.) of the punch materials can be influenced significantly by heat treatment. In the interest of maintaining hardness, decarburization of the punch material during hardening must be avoided. Additional references regarding guidelines of heat treatment are found in the literature [17.29], [17.30]. The significance of correct heat treatment is illustrated by the following example [17.17], [17.31].

High-speed steels, such as S6-5-2 (AISI M2), are known for their ability to withstand high loading as well as impact. They have proved especially successful for hobbing at temperatures between 100 and 500°C (212 and 900°F) since their compressive strength and wear resistance do not decrease until a temperature of 600°C (1100°F) is exceeded. For hobbing tooling, sufficient toughness is required, which is achieved by hardening at temperatures customary for high-speed steels, namely, about 1200°C (2200°F). It has proved favorable to set hardening temperatures about 50°C (90°F) lower than recommended and to increase the holding time at that temperature correspondingly. This measure results in a significantly higher toughness and hence the ability to absorb energy without sacrificing hardness and fracture strength noticeably.

The strength of hobbing punches is strongly influenced by their design. The shank is designed without (Fig. 17.17a) or with (Fig. 17.17b) cross-sectional transitions to the punch stem, or as press fit (Fig. 17.17c), which is convenient for punches of circular cross section. The enlarged shank (Fig. 17.17b), which is the design used most frequently, provides the punch with greater stiffness, reduces pressure on the back-up plate, and facilitates the withdrawal of the punch from the workpiece after deep indentations [17.28]. Favorable flow of force and hardness considerations require that significant differences in cross section be avoided. Stress concentrations are reduced by large

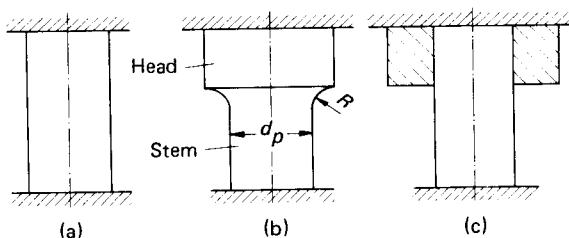


**FIG. 17.17** Different shank designs for hobbing punches. (After [17.28].)

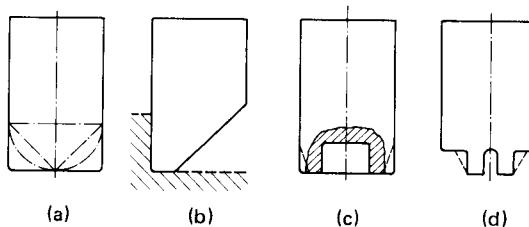


FIG. 17.18 Basic shapes of punch noses. (After [17.28].)

fillet radii, rounding of sharp corners and edges, and an excellent surface finish in the transition zone [17.31], [17.32].

The noses of hobbing punches can be reduced to four basic shapes [17.17], [17.28] (Fig. 17.18):

- 1 Full punches with symmetric noses
- 2 Full punches with nonsymmetric noses
- 3 Punches with cavities in the noses
- 4 Punches with rib- and fork-shaped noses

Often the nose of a punch is composed of several of these basic elements. Difficulties are to be expected whenever deviations from shape 1 are involved.

Nonsymmetric punch noses, especially unilaterally inclined planes, superimpose unbalanced force components on the compressive axial forces, thus reducing the strength of the punch significantly. If such lateral forces cannot be avoided by design, they can be supported by suitable backing surfaces on the workpiece, which are removed after completion of the hobbing operation.

Cavities in the punch face lead to the superposition of radial stresses, which tend to rupture the punch. This effect can be minimized or balanced with a conical exterior punch shape. For rib-shaped faces, stress conditions similar to those occurring in punches with cavities are encountered [17.17], [17.28].

The punch shaft is generally kept as short as possible in order to maintain resistance to buckling; 5–8 mm (0.2–0.3 in) above penetration depth is considered satisfactory [17.33]. Occasionally it is recommended to shape the punch shaft slightly conically (cone angle at least  $0.5^\circ$ ) to facilitate withdrawal of the punch from the workpiece after hobbing [17.33]. It must be kept in mind, however, that the hobbing force can increase significantly with increasing cone angle, as does the tendency to gall. In any case, cavities and notches in nose, stem, and shank should be avoided, and an excellent surface finish should be applied through grinding and polishing in order to eliminate notch stresses.

The container ring, which is used in most cold-hobbing applications, affects material flow of the workpiece and prevents bulging and tearing of its outside surface. It is subjected to high radial compressive stresses, and is therefore designed as press fit assembly (Fig. 17.16). The diameter  $d_H$  of the outer ring should be 2.5–3 times  $d_0$ , while diameter  $d_0 \approx 2d_P$  (i.e.,  $A_0/A_P \approx 4$ ). The height of the container ring depends upon the initial height of the workpiece, which in turn should be greater than 2–3 times  $s_P$ . The interior surface of the inner ring is provided with draft (recommended angle  $2\text{--}3^\circ$ ) for easier ejection of the workpiece, which has its own conical preform matching the die.

Backing plates, punch holders, and die blocks serve to reduce pressures on the ram and upper press pressure plate. Suitable materials for these components and the container ring are recommended in VDI guideline 3170 [17.34]. They are tool steels that can be hardened and tempered to high toughness and strength. According to [17.17], the inner container ring and the smaller upper and lower pressure plates are produced from X45NiCrMo4 steel, for example, which after hardening is tempered to a tensile strength of 1600–1800 N/mm<sup>2</sup> (230–260 ksi). As material for the outer ring and the large upper and lower pressure plates 55NiCrMoV6 (AISI 6F2) steel is mentioned, which is tempered to about 1200 N/mm<sup>2</sup> (170 ksi) tensile strength. The guide ring serves to center and guide the punch during the forming process [17.17].

### 17.2.5 Cold-Hobbing Machine Tools

For cold hobbing special hydraulic presses are available, with capacities ranging from 1.6 to 32 MN (180 to 3600 ton). Hobbing speeds can be varied infinitely from 0 to 0.3 mm/s (0 to 0.7 in/min) on these machines for optimal adaptation to the properties of a specific work material [17.17]. Switching from the higher closing speed to the slow, precision-controlled hobbing speed takes place automatically (when a given pressure is reached after contact between punch and workpiece has been established) and can be varied between certain limits in order to extend the range of application of the press.

The desired hobbing depth can be selected with the aid of a displacement transducer, and the peak hobbing force with a pressure transducer. After reaching preselected values, the hobbing process is terminated automatically by the press. In view of the high precision requirements, the presses are equipped with especially rigid frames. Closed-frame designs, like the 12.5-MN (1400-ton) press with lower piston drive shown in Fig. 17.19, have therefore gained a preeminent role. Special attention is directed to the exact guidance of the ram and hence the parallelism of the work surfaces in order to lessen the danger of punch fracture [17.17], [17.18].

### 17.2.6 Hot Hobbing

Hot hobbing, in practice for many centuries, has been largely superseded by cold hobbing, which results in superior precision and surface finish and is also more economical. Nonetheless, the process limitations of cold hobbing (shape and size of impressions, maximum depth of penetration, load-carrying capacity of the punch, force capacity of specialized hydraulic presses) can in part be exceeded substantially by hot hobbing. As Fig. 17.14 shows, the hobbing force, referred to the hobbing area, can be lowered considerably for the same specific hobbing depth through high forming temperatures. Thus hot hobbing permits either greater hobbing areas or greater hobbing depths for equal forming-force magnitudes. Furthermore, punch speeds are substantially higher with  $v_p = 0.15\text{--}2.5 \text{ mm/s}$  (0.35–5.9 in/min) so that the process can be carried out with customary forging presses or hammers instead of with the slow, precision-controlled specialized presses described earlier. The main application of hot hobbing is in the fabrication of forging dies [17.19], [17.35], [17.36].

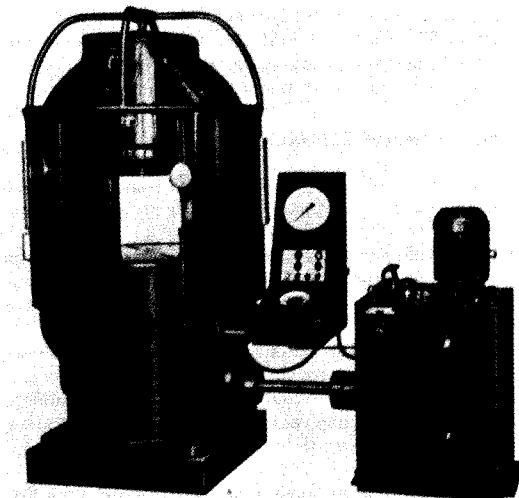


**FIG. 17.19** Hydraulic 12.5-MN (1400-ton) hobbing press.  
(Courtesy of Sack and Kiesslbach.)

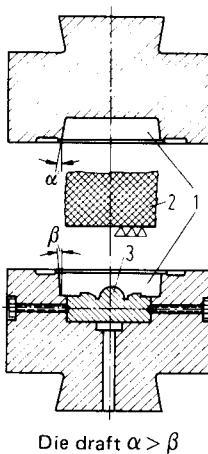


**FIG. 17.20** Device for hot hobbing of forging cavities. 1—recesses for master punch and die slug; 2—die slug; 3—master punch. (After [17.35].)

prevent both scale formation and shape distortion due to nonuniform cooling. After cooling the die block is trimmed, then annealed, its outside is machined, and finally it is hardened to  $S_u \approx 1500\text{--}1600 \text{ N/mm}^2$  (220–230 ksi) [17.35], [17.36].

The dimensioning of the master punches, which have the shape of the forgings, must reflect thermal shrinkage. Punches must therefore account for twice the degree of shrinkage of the forgings. For large forging production rates requiring a considerable number of dies, it may be economically advantageous to produce the master punch through forging with a primary die instead of by machining. When machining primary dies, three times the degree of shrinkage must now be accounted for [17.35].

Work materials for primary dies, master punches, and working dies are the usual hardenable hot-working steels, such as 56NiCrMoV7 (AISI 6F3). About 300 master punches can be forged with one primary die, and roughly 300 working dies can be hobbed with one master punch. The life of hot-hobbed dies is 1.5–3 times better than the life of machined dies.

### 17.3 CUP PIERCING WITHOUT RESTRICTION

Cup forming without container, a cold-forming process, corresponds to piercing with lateral work material displacement. It is closely related to hobbing without restriction, but differs from reverse cup extrusion (Fig. 17.21). For small area ratios  $A_p/A_0$  (e.g.,  $A_p/A_0 = 0.1$ ) the cup height  $h_1$  remains nearly equal to the billet height  $h_0$ . The greater  $A_p/A_0$ , that is, the thinner the wall thickness of the cup, the more the workpieces are compressed and expanded accordingly. The deeper the punch penetrates into the workpiece and reduces the bottom thickness, the more the cup bulges, while the bottom turns up toward the edge (Fig. 17.21) [17.15].

Cup piercing without restriction can be of use when for small cross-sectional ratios  $A_p/A_0$  certain preforms are required which approach the final shape of cold-forged parts (e.g., of bevel gears). Of course, the process is limited to materials with great formability, that is, nonferrous metals and carbon steels with low carbon content. Steels with higher carbon content like Ck15 (AISI 1015) can suffer axial cracks along the internal cup wall due to tangential tensile stresses [17.15].

Based on Eq. 17.9, the mean forming force  $\bar{F}$  can be estimated using Eq. 17.6:

$$\bar{F} = \frac{h_0}{s} A_0 \sigma_{f,m} \varphi_{r,m} \frac{1}{\eta_{def}} \quad (17.19)$$

Forging die impressions are hot hobbed with the aid of convex-shaped master punches. It is desirable to produce entire dies or die inserts, including flash lands, on one press or one hammer such that no additional finishing work is necessary. Experience has shown that hot hobbing a die or die insert with flash land requires about three times the forging energy necessary for the production of the actual forging part [17.36].

The success of the process depends upon a flawless surface finish of the hot-hobbed cavity. The surface of the workpiece into which the die cavity is to be pressed or struck is therefore ground flat and covered with a ground protective plate during heating to forging temperature in order to prevent scale formation and decarburization. The heated workpiece is usually placed into the upper holder of the hobbing device, and the highly polished master punch is placed in the lower holder (Fig. 17.20). Hobbing must be carried out within the briefest time possible to prevent scale formation. The finished die block is packed in cast iron chips or old cementing powder, again to

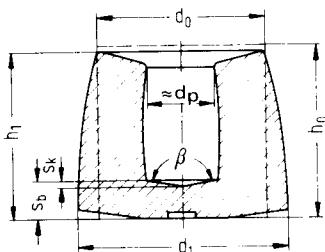


**FIG. 17.21** Cup piercing without restriction. Dimensional notations for slug and cup. (After [17.15].)

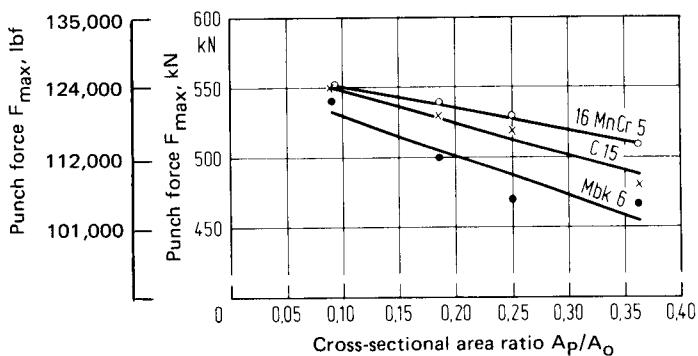


**FIG. 17.22** Dependence of maximum punch force upon cross-sectional ratio  $A_p/A_0$  for cup piercing without restriction.  $h_0/d_0 \approx 0.8$ ;  $s_b = 8.4$  mm (0.33 in);  $d_p = 15$  mm (0.59 in); cone angle of punch  $\beta = 120^\circ$ . (After [17.15].)

The factor  $\frac{h_0}{s}$  (where  $s = h_0 - s_b - s_k$ ; Fig. 17.21) takes into account the fact that the workpieces are not pierced completely, but a finite residual bottom thickness remains. Values for efficiency of deformation are about  $\eta_{def} = 0.1-0.3$ .  $\eta_{def}$  increases with rising strain of deformation  $\varphi_{r,m}$  and flow stress  $\sigma_{f,m}$  and decreases with growing ratio  $h_0/d_0$  [17.15]. The dependence of the experimental maximum punch force upon the area ratio  $A_p/A_0$  is represented in Fig. 17.22 for three different cup materials and constant ratio  $h_0/d_0$ . The trend of the curves shown can be explained as follows. As a result of the absence of a die, the lateral forces that have to be overcome during cup formation, and hence the required punch forces, decrease with the wall thickness of the cup [17.15].

## REFERENCES

- 17.1 DIN 8583: "Fertigungsverfahren Druckumformen (Manufacturing Processes—Press Forming)," sheet 5, May 1970.
- 17.2 Mesmer, G.: "Comparative Photoelastic Studies and Flow Tests under Concentrated Pressure" (in German), *Tech. Mech. Thermodyn.*, 1, 1930, pp. 85-100, 106-112.
- 17.3 Sachs, G.: *Metal Forming, Residual Stresses in Metals* (in German), Leipzig; Akademische Verlagsgesellschaft, 1937.

## 17.24 BULK-METAL FORMING

- 17.4 Prandtl, L.: "On the Hardness of Plastic Bodies" (*in German*), *Gött. Nachr., Math.-Phys. Kl.*, 1920, pp. 74–85.
- 17.5 Prager, W., and Hodge, P. G.: *Theory of Perfectly Plastic Solids*, New York, Dover, 1968.
- 17.6 Hill, R.: "The Plastic Yielding of Notched Bars under Tension," *Quart. J. Mech. Appl. Math.*, **2**, 1949, pp. 40–52.
- 17.7 Shaw, M. C., and DeSalvo, G. J.: "A New Approach to Plasticity and Its Application to Blunt Two-Dimensional Indenters," *Trans. ASME, J. Eng. Ind.*, **92**, 1970, pp. 469–479.
- 17.8 Weinmann, K. J.: "On Wedge Indentation and Its Relationship with Incipient Plastic Deformation in Metal Cutting," *Trans. ASME, J. Eng. Ind.*, **99**, 1977, pp. 702–707.
- 17.9 Hill, R., Lee, E. H., and Tupper, S. J.: "The Theory of Wedge Indentation of Ductile Materials," *Proc. R. Soc. London (A)*, **188**, 1947, pp. 273–289.
- 17.10 Johnson, W., and Mellor, P. B.: *Plasticity for Mechanical Engineers*, London/Toronto/New York/Princeton, van Nostrand, 1962.
- 17.11 Siebel, E.: *Forming in the Plastic State (in German)*, Düsseldorf, Verlag Stahleisen, 1932.
- 17.12 Siebel, E., and Fangmeier, E.: "Investigation of the Force Requirement in Forging and Piercing" (*in German*), *Mitt. Kaiser Wilhelm Inst. Eisenforsch.*, **13**, 1931, pp. 29–41.
- 17.13 Kühne, H. J.: *The Force Requirement in Extrusion of Cylindrical Hollow Parts (in German)*, Halle (Saale), 1951.
- 17.14 Gentzsch, G.: *Cold Upsetting, Extrusion, Massive Coining (in German)*, Düsseldorf, VDI-Verlag, 1968.
- 17.15 Schmitt, G.: "Investigation of Cup Piercing without Restriction" (*in German*), *Berichte aus dem Institut für Umformtechnik, Universität Stuttgart*, no 2/3, Essen, Girardet, 1965.
- 17.16 Hoischen, H.: "Cold Hobbing of Impressions for Forging Dies" (*in German*), *Ind.-Anz.*, **89**, 1967, pp. 1255–1261.
- 17.17 Hoischen, H.: "Tool Forming by Cold Hobbing" (*in German*), *Werkstatt u. Betr.*, **104**, 1971, pp. 275–282.
- 17.18 Liegel, L.: "Cold Hobbing" (*in German*), pts. I and II, *Werkstattblätter*, no. 438 and 439, München, Hanser, 1968.
- 17.19 Lange, K.: "Concave Forming Tools for Primary Forming and Deformation Processes" (*in German*), *VDI-Berichte*, no. 166, 1971, pp. 83–95.
- 17.20 Belser, P.: "Investigation of Cold Hobbing" (*in German*), Dr.-Ing. thesis, Technical University, Stuttgart, 1956.
- 17.21 VDI-Richtlinie 3200: "Fließkurven (Flow Curves)" pt. 1: "General," pt. 2: "Ferrous Metals," pt. 3: "Nonferrous Metals," Düsseldorf, VDI-Verlag, 1979–1981.
- 17.22 Thelning, K. E.: "Cold and Hot Hobbing of Hot Working Steel" (*in German*), *Schweiz. Arch.*, **27**, 1961, pp. 503–510.
- 17.23 Haufe, W.: "On the Properties of Work Materials in Cold Hobbing of Tools" (*in German*), *Werkstatttech. u. Maschinenbau*, **46**, 1956, pp. 163–168.
- 17.24 Huber, H.: "Large Radii—Inexpensive Tools" (*in German*), *Maschinenmarkt*, **78**, 1972, pp. 720–723.
- 17.25 Huber, H.: "Flow Processes in Cold Hobbing" (*in German*), *Ind.-Anz.*, **94**, 1972, pp. 1397–1398.
- 17.26 Huber, H.: "Dimensional Discrepancies between Punch and Trimming Die in Cold Hobbing" (*in German*), *Maschinenmarkt*, **79**, 1973, pp. 796–799.
- 17.27 Barz, W., and Dingel, W.: "Effect of Heat Treatment on Concave Shapes" (*in German*), *Maschinenmarkt*, **76**, 1970, pp. 2177–2181, 2376–2381.
- 17.28 Hoischen, H.: "Load Capacity of Punches in Cold Hobbing" (*in German*), *Ind.-Anz.*, **91**, 1969, pp. 1087–1082.

- 17.29 Füssl, A.: "Work Materials and Their Heat Treatment for Hobbing Tools" (in German), *Z. Prakt. Metallbearb.*, **61**, 1966, pp. 7/8.
- 17.30 Treml, F. A.: "Tool Steels for Cold Hobbing and Extrusion" (in German), *Tech. Rundsch.*, **52**, 1960, pp. 17, 19, 21, 23.
- 17.31 Hoischen, H.: "Load Capacity and Shape Accuracy of Punches in Cold Hobbing" (in German), *Forschungsberichte des Landes Nordrhein-Westfalen*, no. 1625, Köln/Opladen, Westdeutscher Verlag, 1966.
- 17.32 Schimz, K.: *Cold Hobbing of Tools* (in German), VDI-Bildungswerk.
- 17.33 Hinze, G.: "Production of Impressions by Cold Hobbing" (in German), *Fertigungstech. u. Betr.*, **19**, 1969, pp. 30–33.
- 17.34 VDI-Richtlinie 3170: "Kalteinsenken von Werkzeugen (Cold Hobbing Tools)," Düsseldorf, VDI-Verlag.
- 17.35 Schultz-Balluff, M.: "Hot Hobbing of Forging Die Cavities" (in German), *Werkstattstech. u. Maschinenbau*, **45**, 1955, pp. 677–680.
- 17.36 Lange, K.: *Die Forging of Steel* (in German), Berlin/Göttingen/Heidelberg, Springer, 1958; 2d ed., with H. Meyer-Nolkemper, 1977.
- 17.37 Matthée, G.: "Encyclopedia of Manufacturing and Machine Tools" (in German), vol. 9 of *Lueger Lexikon der Technik*, Stuttgart, Deutsche Verlags-Anstalt, 1968.



**3**

**SHEET-METAL FORMING**

THE SHEET-METAL FORMING SECTION OF THE BOOK



## **SHEET-METAL PROPERTIES AND TESTING METHODS**

---

---

© 1990 by John Wiley & Sons, Inc.

For a proper selection of the workpiece material from both manufacturing and functional viewpoints and to ensure smooth production flow in industry with optimum material utilization, a thorough knowledge of the material behavior is necessary. Optimum selection is achieved by choosing materials with the required properties and designing special test procedures for determining the suitability of the material for the forming operation. In this chapter a few well-known material properties and the test methods commonly used in practice are discussed. These material characteristics and test methods determine the behavior of steel and nonferrous metals with regard to their suitability for the deformation process. Some important sheet-metal forming processes are bending, deep drawing, and stretch forming. Several combinations of the processes are possible, for example, in automobile panel forming. A number of testing methods have been developed depending on the type of deformation process [18.1] to [18.7].

### **18.1 MATERIAL CHARACTERISTICS FOR THE DETERMINATION OF FORMABILITY**

#### **18.1.1 General Tensile Data**

The material properties generally determined from tension tests, such as tensile strength  $S_u$ , yield strength  $S_y$ , percentage elongation after fracture  $e_t$ , and uniform elongation  $e_u$ , are not sufficient to describe the sheet behavior for deformation processing. These characteristics are, however, important to sort out unsuitable sheet materials. Although  $e_t$  and  $e_u$  describe the material suitability for forming operation approximately, these values determined from tension tests (uniaxial loading) may not be sufficient to determine the suitability of a sheet metal for deformation processing since the stress condition may be very different.

The value of the work-hardening coefficient  $n$  and the anisotropy factor  $r$  also determined from tension tests permit predicting approximately the maximum possible strain achievable in deep-drawing and stretch-forming operations.

### 18.1.2 Strain-Hardening Exponent

Flow curves of unalloyed and low-alloyed steels and a few known nonferrous metals can be described by the following equation (under definite conditions) with the help of parameters obtained in tension tests:

$$\sigma_f = C\varphi^n \quad (18.1)$$

Eq. 18.1 is not valid for high-alloyed steels and copper because of a different strain-hardening behavior of these materials. The flow curve of these materials can be described by the following equation [18.8]:

$$\sigma_f = \frac{S_u e_u n}{(1 - e^{-n})^{e_u}} (1 - e^{-\varphi})^{e_u} \quad (18.2)$$

The constant  $n$  is given by [18.8] to [18.11]

$$n = \varphi_u = \ln(1 + e_u) \quad (18.3)$$

This constant is equal to the natural strain  $\varphi_u$  corresponding to the uniform elongation  $e_u$  determined from tensile tests.

If there is no thermally activated action, such as recrystallization or recovery, during the deformation process, the exponent  $n$  is a measure of the work hardening observed in all metallic materials. This represents the increase of the flow stress  $\sigma_f$  with increasing natural strain  $\varphi$ . Based on this phenomenon, the work-hardening coefficient  $n$  is a measure of achievable maximum formability for different materials during forming with the same external restraints. For example, larger strains can be achieved in stretch forming for higher values of the work-hardening coefficient  $n$ . A higher work-hardening coefficient means a higher uniform elongation value, thereby reducing the tendency for local necking in the material (see Chap. 23). For deep drawing the limiting drawing ratio increases marginally for larger work-hardening coefficients since at the beginning of drawing, the process is not just deep drawing but a combination of deep drawing and radial drawing (stretch forming).

### 18.1.3 Anisotropy Factor

Anisotropy of plastic properties of multicrystalline metallic materials is caused by the anisotropy of the crystal structure of the material. In the case of multicrystalline materials, the structural anisotropy is more pronounced when the orientation of the crystals (grains) exhibits preferred orientation (textures) as opposed to statistically random distribution of their orientation. Textures (orientations) are formed during the working of multigrain materials due to the existence of definite casting, deformation, and heat treatment conditions. If the textures are very pronounced, the mechanical properties exhibit anisotropy (direction dependence of their material properties).

A measure for anisotropy of the plastic characteristics of sheet-metal materials is the  $r$ -value. This is obtained in tension tests as the ratio between the width strain and the thickness strain [18.2] to [18.18]:

$$r = \frac{\varphi_b}{\varphi_s} = \frac{\ln(b_0/b)}{\ln(s_0/s)} \quad (18.4)$$

where  $b_0, s_0$  = initial width and thickness

$b, s$  = width and thickness of the tensile test specimen at any point in time

The value of  $r$  (normal anisotropy) is not generally constant in the sheet plane but changes with inclination from the rolling direction. A measure for the change of anisotropy (planar anisotropy), that is, the change of  $r$ -value in the sheet plane, is  $\Delta r$ . The value  $\Delta r$  is calculated from different  $r$ -values in the sheet plane. The test pieces for determining the  $\Delta r$  values are cut from the sheet at different angles ( $0^\circ, 45^\circ, 90^\circ$ ) to the rolling direction (Fig. 18.1):

$$\Delta r = \frac{1}{2} (r_0 + r_{90} - 2r_{45}) \quad (18.5)$$

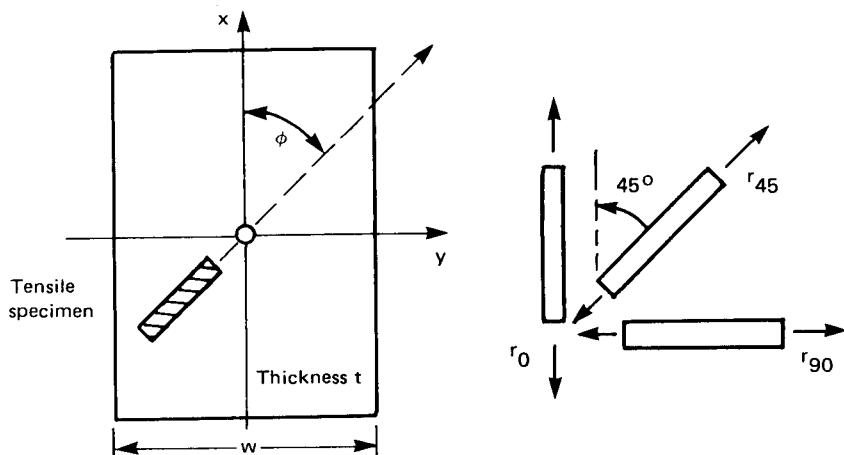


**FIG. 18.1** Rolled sheet and location of tensile specimens to obtain anisotropy factors.  $x$ —rolling direction;  $y$ —transverse direction;  $\phi$ —angle of inclination with reference to rolling direction.

An average value of normal anisotropy  $\bar{r}$  is also calculated using the  $r$ -values determined for different directions as follows:

$$\bar{r} = \frac{1}{4} (r_0 + r_{90} + 2r_{45}) \quad (18.6)$$

This value of  $\bar{r}$  can be used to predict the behavior of sheet metal for deep drawing.

In addition to the work-hardening coefficient  $n$ , the anisotropy factor  $r$  (or  $\bar{r}$ ) affects the magnitude of the limiting drawing ratio  $\beta_{\max}$ . With increasing values of  $r$  (or  $\bar{r}$ ) the value of  $\beta_{\max}$  also increases since (1) the force required for tearing the bottom of the deep-drawn cup also increases with  $r$  (or  $\bar{r}$ ) and (2) the total draw force required decreases. Well-known effects of anisotropic behavior of material in sheet metals are, for example, earing and its effects and the wall-thickness variations in deep drawing. Sheet metal with good deep-drawing characteristics should have a high  $r$  (or  $\bar{r}$ ) and a small planar anisotropy  $\Delta r$  (see Chap. 20).

Sheet metal for combined forming by deep drawing and stretch forming should have both a very high average normal anisotropy value  $\bar{r}$  and a high work-hardening coefficient  $n$ . The bottom tearing force in deep-drawn cups (affected by  $\bar{r}$ ) is also affected by the work-hardening coefficient  $n$ . A larger value of work hardening results in an increase in the transferable load on the deep-drawn workpiece; a higher work-hardening coefficient also means higher strain before necking. Depending on which of the processes (deep drawing or stretch forming) plays the major role during forming, the average normal anisotropy  $\bar{r}$  or the work-hardening coefficient  $n$  will have a decisive role in determining the material behavior.

## 18.2 PROCESS SIMULATING TESTING METHODS

The different testing methods used to determine the suitability of sheet metals for forming processes do not completely represent the various sheet-forming processes. Hence they have limited use in predicting the behavior of sheet metal for a specific deformation process. This factor is made evident by the fact that there are a large number of testing methods. All the processes acknowledge that the results obtained in actual deformation are not exactly the same as those obtained in the testing methods, but deviate from them. Hence it is not possible to make generally valid conclusions and extract comparable characteristic values from any of the testing methods for predicting the behavior of sheet metal during forming. Consequently several tests must be done with slight changes to obtain a good correlation between test and forming results.

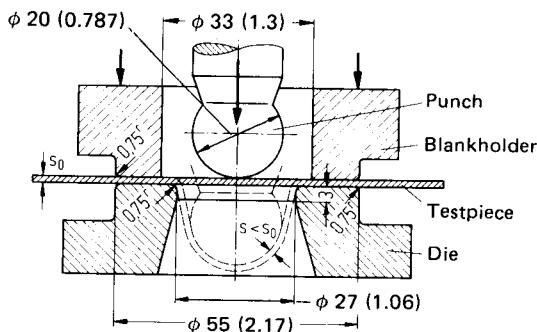


**FIG. 18.2** Tooling for Erichsen cupping test. Application range for sheets and strips [width  $\geq 90$  mm (3.5 in)] with a thickness of 0.2–2 mm (0.08–0.8 in). Dimensions inside the figure are in mm (in). (After [18.19].)

### 18.2.1 Stretch-Forming Tests

#### Erichsen Cupping Test

This test consists of stretching a rigidly held sheet strip or piece to a cup until a crack appears (Fig. 18.2). The characteristic parameter from this test is the depth of the cup as the first crack appears. Standards have been published on the minimum cupping depth as a function of sheet or strip thickness for sheets and strips of unalloyed steels.

Since the cupping depth is determined under biaxial tensile stress conditions, it is a measure of the formability of sheets by stretch forming. Correspondingly a definite relation exists between the cupping depth and the value of the work-hardening coefficient  $n$ . However, there is no relation between the cupping depth and the limiting drawing ratio  $\beta_{\max}$  in deep drawing. The cupping takes place at the expense of the sheet thickness, which influences the cupping depth considerably. Hence apart from a change in the lubrication conditions, the variations in sheet thickness are sources of errors. The band spread of cupping depths due to the above error can be as large as the difference between the various sheet-metal qualities [18.1], [18.20].

#### Hydraulic Bulge Test

This method, like the Erichsen cupping test, is also used to check the suitability of thin sheets for stretch forming. A rigidly fixed sheet is loaded under oil pressure until the cracks appear (Fig. 18.3). The results of this test are not normally transferable to sheet-forming processes because of the absence of friction in testing. However, the suitability of sheets for deep drawing with working media limited by force can be judged by the hydraulic bulge test [18.3].

Other technical characteristics and errors in deep drawing sheets, such as flow figures, folds, inclusions, and porosity, can be determined with the help of the above process.

The hydraulic bulge test is especially suitable for the determination of flow curves of sheets.

#### Expansion-Draw Test

In this method a cylindrical cup is drawn from a rigidly clamped round sheet-metal blank with a hole in its center (Fig. 18.4). The hole is expanded during the test. The cracks appearing on the outer edge of the hole after expansion are a measure of the deformability of the sheets. The expansion ratio  $d_m/d_0$  is the limiting factor at the base of crack formation, where  $d_0$  is the initial hole diameter and  $d_m = (d_{\max} + d_{\min})/2$  the mean diameter of the hole after deformation [18.1].

Based on the prevalent stress and strain conditions in the testing method, this method is suitable only for processes with similar conditions, for example, flange drawing and automobile panel drawing.

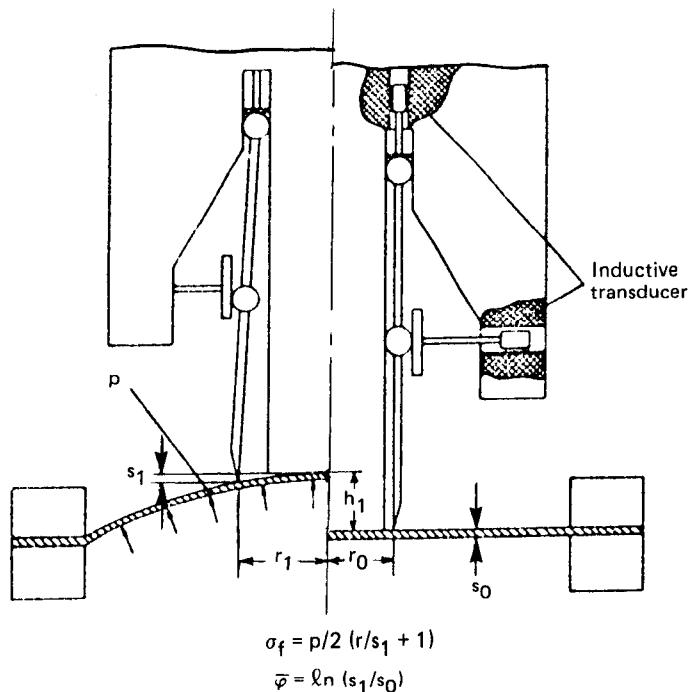


**FIG. 18.3** Tooling for hydraulic bulge test.  $p$ —hydraulic pressure;  $h_1$ —bulge height;  $s_1$ —sheet thickness of cup;  $r_0$ —initial radius of gauge circle;  $r_1$ —final radius of gauge circle;  $s_0$ —initial sheet thickness. (After [18.2], [18. 22].)

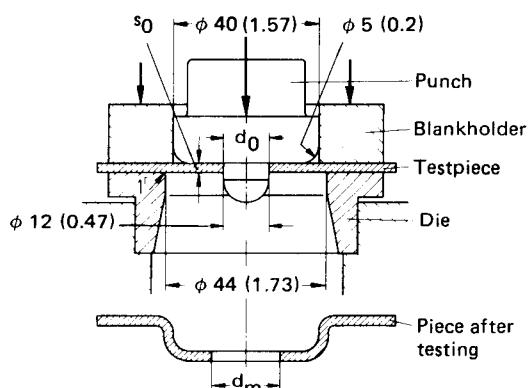


**FIG. 18.4** Tool for deep-draw-expansion test. Dimensions are in mm (in).

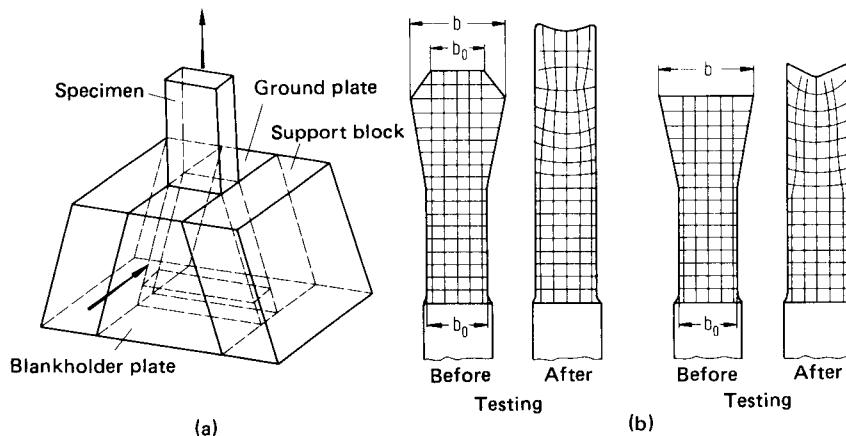


**FIG. 18.5** Wedge-drawing test (after Sachs). (a) Tooling for wedge-drawing test. (b) Effect of specimen shape on strain.

### 18.2.2 Deep-Drawing Tests

#### *Wedge-Drawing Test after Sachs*

In the wedge-drawing test the plane tensile-compressive stress condition in the flange of a deep-drawn cup is simulated. A wedge-shaped sheet strip is drawn through a wedge-shaped tool opening under constant blank holder force (Fig. 18.5). The characteristic value is  $b_{\max}/b_0$ , which is the ratio of maximum drawable width  $b_{\max}$  to test piece width  $b_0$ . The required drawing force for drawing standardized specimens is also measured. The width  $b_{\max}$  is estimated in such a way that the width  $b$  is increased until the plate cracks when pulled through a die with the same wedge angle. Since the shape and dimensions of the specimen have a great effect on the results, they are important for comparing results [18.20].

This testing method simulates closely the stress condition in deep drawing (radial tensile stresses, tangential compressive stresses). However, the results are largely affected by the friction condition on the wedge walls. In comparison with cup-drawing tests, the drawing ratios obtained by this method are smaller, although in this test the effects of bending and friction on the die entrance radius, as in cup-drawing tests, are not considered [18.1]. Hence the results of the wedge-drawing process have only limited applicability in predicting the deep-drawability of sheet metal.

#### *Cup-Drawing Test after Swift (IDDRG)*

This method is very widely used to test the suitability of sheets for deep drawing. The International Deep Drawing Research Group (IDDRG) has issued a standardized procedure to conduct the cup-drawing test [18.23].

Circular blanks with stepwise increasing diameters are deep-drawn to cups with a flat bottom with a punch of fixed diameter. The limit of deep-drawability of the sheet is judged by the deep-drawing ratio at which there is still no bottom punch-through (Fig. 18.6). The characteristic value of the cupping test used to characterize the deep-drawing process is the limiting drawing ratio  $\beta_{\max}$ .

The major disadvantage of this method is that it requires extensive investigations to determine the limiting drawing ratio with sufficient accuracy. In addition, the limiting drawing ratios determined for different sheet qualities differ from each other only slightly. The total results are within a working spread for experimental results [18.24].

The experimental results vary considerably if hemispherical punches are used. This test method is suitable for stretch forming only and not for deep drawing since the nature of the stresses on the punch surface are similar to those in stretch forming [18.1], [18.2].

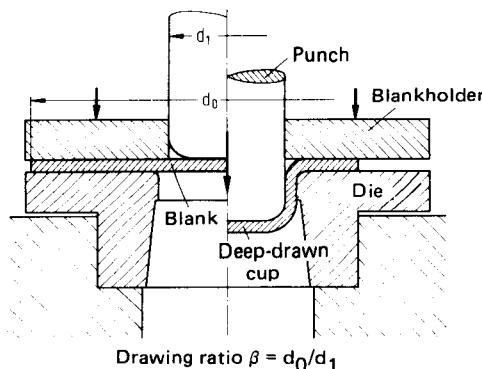


FIG. 18.6 Cup-drawing test (After Swift).

The results of this test cannot be transferred unconditionally to deep drawing of sheets with large tools since friction conditions affect the process considerably [18.2] to [18.4]. The limiting drawing ratio obtained in the cupping test is generally higher than that in the actual deep-drawing operation since it decreases with increasing ratio of punch diameter to sheet thickness. The reduction in the limiting drawing ratio for larger ratios of punch diameter to sheet thickness is due to increased friction in the region of the blank holder.

#### Cup-Drawing Test after Fukui

In this testing method a circular blank is drawn through a conical die without a blank holder by a cylindrical punch until crack formation starts (Fig. 18.7). The dimensions of the blank and tool required for the test method are chosen depending on the sheet-metal thickness.

The characteristic value describing the deep-drawability is obtained as the ratio of the minimum diameter  $d$  at which the crack formation has not yet started to the blank diameter  $d_0$ . A smaller drawing ratio therefore represents better deep-drawability [18.25].

The above characteristic value can be determined from conducting only one test. The initial blank diameter  $d_0$  is chosen to be slightly greater than  $d_{0,\max}$ , the diameter with which the cup can be drawn without bottom punch-tear. This would mean that with the chosen diameter  $d_0$ , a bottom punch-tear can definitely be obtained.

This simple testing method also does not provide appreciably different results for different sheet-metal qualities [18.1]. However, the use of a semispherical punch instead of a flat punch will indicate the suitability of the sheet metal for stretch forming and deep drawing [18.25].

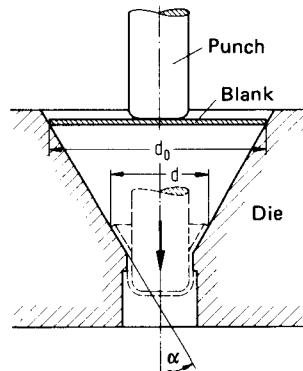


FIG. 18.7 Cup-drawing test (After Fukui).

#### 18.2.3 Bending Tests

During bending along an axis without additional tensile or compressive loading, the outer fibers are subjected to tensile stresses and the inner fibers to compressive stresses. The failure criterion is the rupture of the blank because the strain limit on the outer fiber is exceeded. The fracture

## 18.10 SHEET-METAL FORMING

occurs at a higher strain (elongation) than in tensile tests, since the outer fibers are protected by the fibers behind them as a result of nonuniform stress and strain distribution.

A discontinuous yielding of the sheet metal is disadvantageous since it will not be possible to obtain well-rounded bent specimens (radii). If the ratio of yield strength to tensile strength is small, the springback of the bending specimen after deformation will be very high because the percentage of plastic deformation in the total deformation is less [18.3].

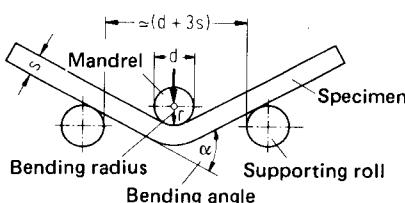


**FIG. 18.8** Fold test. (After [18.26].)

either cracking or fracture sets in. The number of bendings to  $90^\circ$  and back until the initiation of cracks or fracture is used as a measure to determine the bendability of the material. The result depends, among other factors, on the width of the test piece and the angle of inclination of the test piece location to the rolling direction.

The other most commonly used bending tests for sheet-metal strips are also suitable for determining the material quality. However, comparison with actual industrial results depends on the design of the testing apparatus [18.28] and the method of conducting the test. In order to obtain reproducible, comparable, and operator-independent results, it is desirable to use a single apparatus suitable for both fold and to and fro bending tests [18.29].

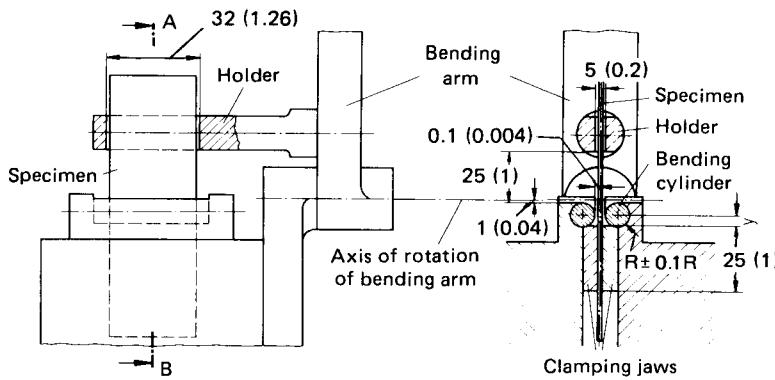
To determine the bendability of sheets in general, the folding test after [18.26] is used (Fig. 18.8). For sheets under 3-mm (0.12-in) thickness the to and fro bending test after [18.27] is used (Fig. 18.9). In the case of the fold test, the bending angle for a given radius at which cracks are not yet initiated on the tensile side of the specimen is a measure of the bendability of the sheet material. In the case of the to and fro bending test, the specimen is first bent  $90^\circ$  to one side and bent back to its initial position, and then it is bent  $90^\circ$  to the other side and back. The process is repeated until

either cracking or fracture sets in. The number of bendings to  $90^\circ$  and back until the initiation of cracks or fracture is used as a measure to determine the bendability of the material. The result depends, among other factors, on the width of the test piece and the angle of inclination of the test piece location to the rolling direction.

## 18.3 STRAIN ANALYSIS AND FORMING LIMITS

### 18.3.1 Methods

The complex deformation process of drawing large nonuniform sheet-metal workpieces can be analyzed by a circular grid pattern engraved by some method on the surface of the sheet. This



For  $R = 2.5 \text{ mm (0.1 in)}$ :  $y = 3 \text{ mm (0.12 in)}$   
 $R < 2.5 \text{ mm (0.1 in)}$ :  $y = 1.5 \text{ mm (0.06 in)}$

**FIG. 18.9** To and fro bend testing apparatus. Dimensions are in mm (in). (After [18.27].)

will permit analyzing the distribution, value, and direction of strains on the sheet metal [18.6], [18.30] to [18.39]. The forming process can be carried out in stages, analyzing the grid pattern at each stage. This will help in locating critical areas on the drawn workpiece so that improvements on the draw bead design, lubrication, or the process sequence can be made at the tryout stage itself. An analysis of the strain distribution on the drawn workpiece helps in solving the critical problems faster so that regular tooling can be used in production without major problems. In addition, the method helps in selecting the right sheet-metal material and allows a simple control over changes in the tool during mass production due to wear and changes in lubrication, sheet-metal quality, and press setting.

The grid pattern consists generally of a system of circles. The advantage of using circular grids is that they change to ellipses during deformation and whole axes represent the direction of principal strains. This is true if the direction of the principal strains does not change during deformation. If this condition is not satisfied, then the circles deform to irregular curves and figures. If the ellipses have the same surface areas as the corresponding original circles, then the deformation in the zone considered has taken place without any change in blank thickness.

Grid patterns also help in judging the suitability of sheets for deformation under biaxial stress conditions. If the strain measured in a few critical areas of a drawn workpiece are compared with strains measured in experiments, the tendency of the tested sheet metal to fracture or necking can be determined approximately. The strains chosen for comparison are determined from test pieces formed to failure (fracture) under biaxial stress conditions.

### 18.3.2 Forming-Limit Diagram

Circular grid patterns deform differently based on the type of loading. There exists a relationship between the distortion of the circle and the type of stressing (Fig. 18.10). By conducting a series of experiments it will be possible to find combinations of maximum strain (corresponding to the major axis of the ellipse) and minimum strain (perpendicular to the major strain and corresponding to the minor axis of the ellipse) for which neither necking nor fracture occurs. These data can be plotted in the shape of a diagram, known as the forming-limit diagram (FLD) (Fig. 18.11) [18.30] to [18.32]. These diagrams are valid for a definite sheet-metal quality and define two zones—fracture and beginning of necking. The strains plotted are at the critical points, that is, the points where cracks are likely to form. Between the two zones of “good” and “failure” there is a zone of critical deformation. The zone between these boundaries denotes areas of instability.

Forming-limit diagrams can be obtained by conducting experiments for the different zones. The most widely used method of obtaining the forming-limit diagram is by means of drawing tests with strips and a hemispherical punch. The different stress conditions are simulated by

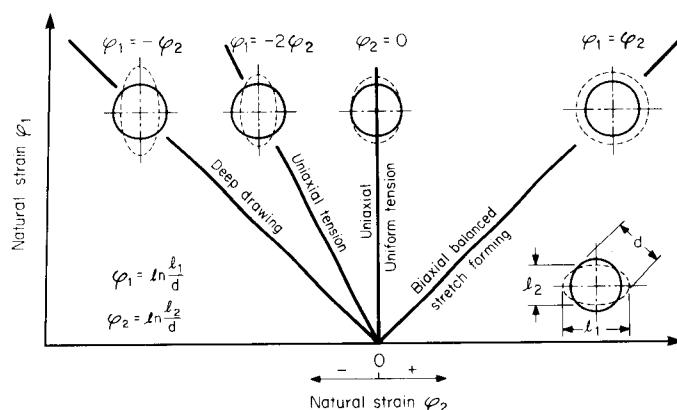


FIG. 18.10 Strains in circular grid elements. (After [18.39].)

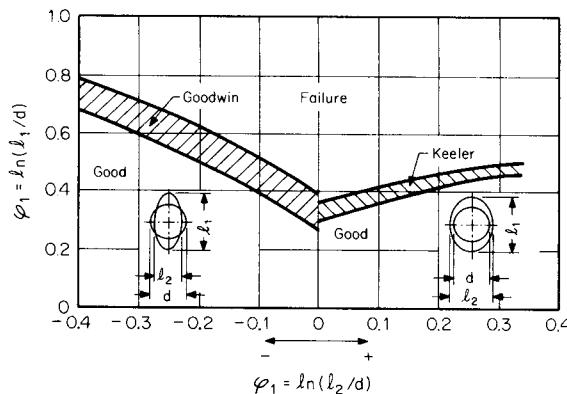


FIG. 18.11 Forming-limit diagram. (After [18.30] to [18.32].)

changing the width of the strips. Improvements on these testing methods have been made by using circular-shaped strips with material removed on the side (Fig. 18.12) [18.39]. The strips are drawn until cracks occur. With details from these tests, the forming-limit diagram can be obtained for strain paths ranging from biaxial tension (stretch forming) to equal tension and compression (deep drawing). The diagram must be determined for each particular sheet material. The forming-limit diagram is also influenced by the diameter of the circular grids, the relative position of the strip with respect to the rolling direction, the lubricant, the sheet thickness, the deformation (strain) history, and the strain rate.

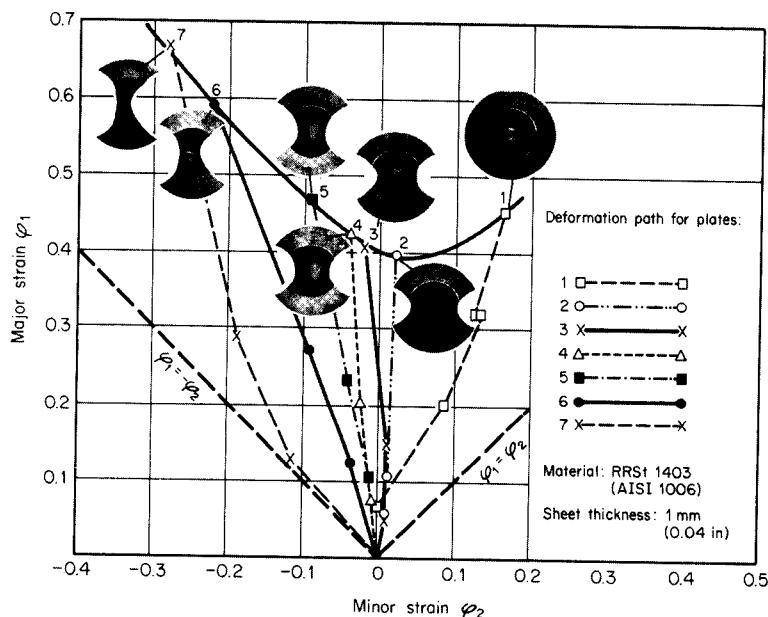
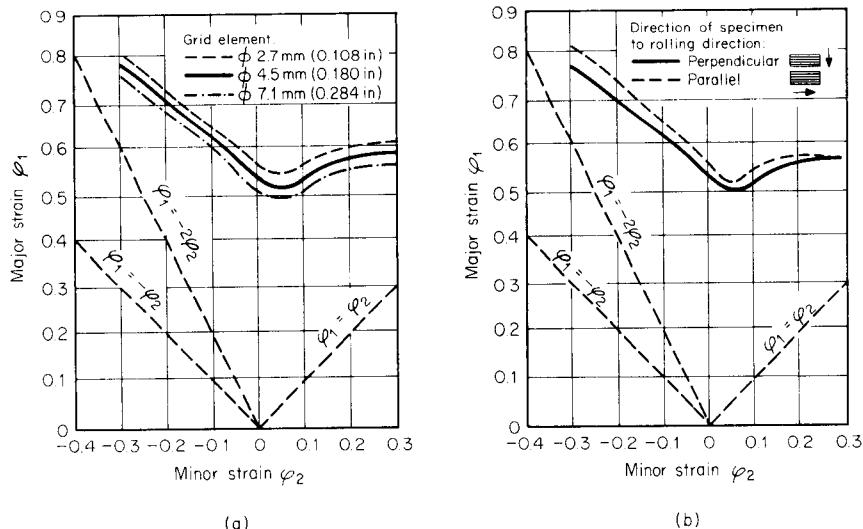
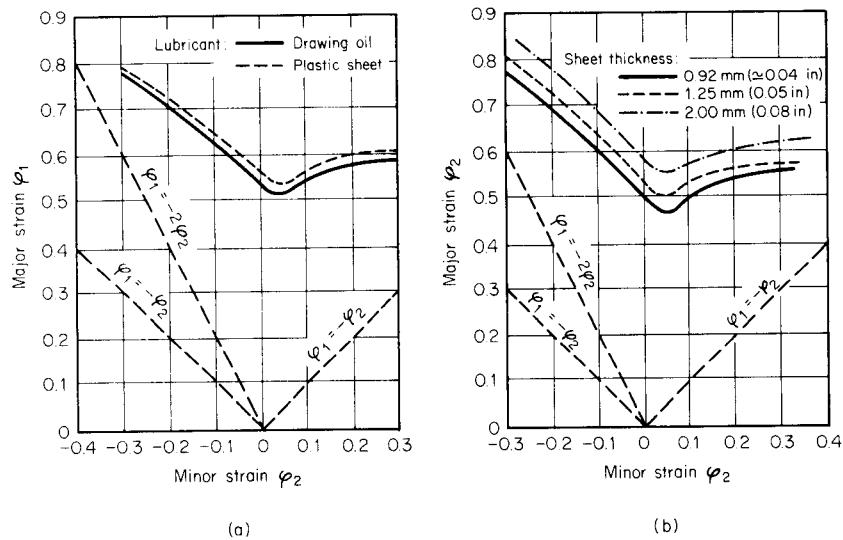


FIG. 18.12 Forming-limit diagram obtained from drawing tests with specially shaped blank. (After [18.39].)



**FIG. 18.13** Influence of (a) grid size and (b) planar anisotropy on forming-limit curve. Material—RRSt1403 (AISI 1006); sheet thickness—0.92 mm (0.036 in). (After [18.39].)

As shown in Fig. 18.13a, the forming-limit curve is shifted to slightly lower strain values with increasing grid-circle diameter since the location of cracks or zones of necking can be determined more accurately with narrower grids. The influence of the direction of the test specimen to the strip-rolling direction, that is, the influence of planar anisotropy, is small but significant for steel sheet RRSt1403 (AISI 1006) according to Fig. 18.13b. The influence of lubrication can be seen in Fig. 18.14a: with improving lubrication (plastic sheet compared with drawing oil) the forming-



**FIG. 18.14** Influence of (a) lubrication and (b) sheet thickness on forming-limit curve. Material—RRSt1403 (AISI 1006); sheet thickness—0.92 mm (0.036 in). (After [18.39].)

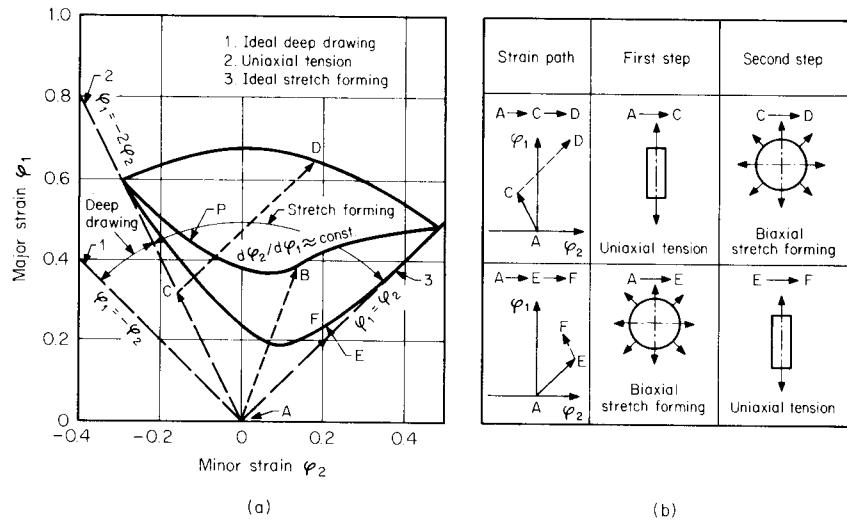


**FIG. 18.15** Strain history and forming-limit diagram structure. (a) Influence of strain history on location of forming-limit curve. (b) Schematic presentation of various strain paths. (After [18.39].)

limit curve is shifted to slightly higher strain values. The same holds true and is even more obvious for increasing sheet thickness according to Fig. 18.14b. The influence of the strain rate, however, was found to be very small and practically negligible for the strain rates and velocities that occur normally in deep drawing under industrial conditions.

More recently the deformation or strain history has been taken into consideration by Hašek [18.38], Makazima et al. [18.40], Müschenborn and Sonne [18.41], Matsuoka and Sudo [18.42], and others. It could be shown that the forming-limit diagram as presented in Fig. 18.11 is only valid for a constant strain ratio ( $d\varphi_2/d\varphi_1 \approx \text{constant}$ ) over the entire deformation process. This is, however, not true in many cases, because the strain ratios governing plane stress states may change significantly. Consequently, according to Fig. 18.15, the forming-limit diagram is influenced considerably. If, for instance, uniaxial stretching ( $\varphi_1 = -\varphi_2$ ) is followed by ideal biaxial stretch forming ( $\varphi_1 = \varphi_2$ )—line ACD—the forming-limit curve is shifted to higher strain values compared with a constant proportional strain path P—line AB. On the other hand, uniaxial stretching ( $\varphi_1 = -\varphi_2$ ) following ideal biaxial stretch forming ( $\varphi_1 = \varphi_2$ )—line AEF—will lead to significantly lower forming-limit strains. Under production conditions the strain path may be heavily influenced by various parameters, such as blank holder force and geometry, punch geometry, die radius, lubrication, blank size and thickness, anisotropy, and the mechanical properties of the sheet.

### 18.3.3 Applications and Limitations

A major advantage of the strain analysis with either simple experiments or theoretical methods is the determination of critical areas in a particular drawn component. Any changes required in the tooling or the process can then be made, based on the above analysis, without excessive trials. The analysis also helps in the selection of the optimum-quality sheet, avoiding the use of the best and the most expensive material. In the case of mass production, cracks may appear suddenly during smoothly running production. The strain analysis helps here to determine the causes of material failure, such as (1) wear of tool, (2) changes in lubricant, (3) sheet quality, (4) press setting, and (5) other causes. The strain analysis will be transferable to a production problem only when the test conditions during determination of the forming-limit diagram are comparable to the actual conditions during production.

For this reason a realistic strain analysis (see Sec. 20.3.4) requires exact knowledge of the specific forming-limit diagram and all conditions mentioned in Sec. 18.3.2. For the part of the process to be analyzed all details influencing the strain path or history must be known in order to draw realistic conclusions. Generally speaking, today the forming-limit diagram is a suitable tool for process design in sheet-metal forming. However, its successful application requires expert knowledge and experience in the laboratory and at the shop level.

## REFERENCES

- 18.1 Adler, G., and Noack, P.: "Process and Possibilities to Estimate Deep-Drawability of Sheets" (*in German*), *Ind.-Anz.*, **87**, 1965, pp. 2002–2009.
- 18.2 Beisswanger, H., and Günther, H.: "On the Testing for Deep-Drawability of Sheets" (*in German*), *Werkstatt u. Betr.*, **99**, 1966, pp. 693–701.
- 18.3 Ebertshäuser, H.: *Technology of Sheet-Metal Working* (*in German*), Düsseldorf, Michael Tritsch Verlag, 1967.
- 18.4 Mäde, W.: "Technical Tests for Deep-Drawability and Bulging" (*in German*), *Fert. u. Betr.*, **17**, 1967, pp. 36–41.
- 18.5 Mäde, W.: "New Results in Deep-Draw Test and the Results Leading to Procure Technically Sound Sheets and Strips" (*in German*), *Neue Hütte*, **14**, 1969, pp. 365–370, 434–438.
- 18.6 Keeler, S. P.: "Understanding Sheet-Metal Formability," *Sheet Met. Ind.*, **48**, 1971, pp. 357–361, 364, 440–442, 447–449, 511–517, 589–593, 618, 687–691, 699, 739, 742–745.
- 18.7 Ziegler, W.: "Limits of Formability in Sheet-Metal Working" (*in German*), *Blech*, 1972, pp. 235–243.
- 18.8 Panknin, W., and Shawki, G.: "Relation between Flow Curve and Material Properties of Formable Material" (*in German*), *Z. Metallk.*, **52**, 1961, pp. 455–461.
- 18.9 Laska, R.: "Work Hardening and Work-Hardening Coefficient of Unalloyed Low-Carbon Steels" (*in German*), *Werkstatt u. Betr.*, **104**, 1971, pp. 533–540.
- 18.10 Grusch, J.: "Work-Hardening Behavior and Material Characteristics of Sheets of Unkilled Steels" (*in German*), *Werkstofftechnik*, **61**, 1971, pp. 352–358.
- 18.11 Küpper, H.: "Investigation on Uniform Elongation  $\varphi_u$  and  $n$  Factor for Different Deep-Drawing Materials" (*in German*), *Fert. u. Betr.*, **21**, 1971, pp. 749–753.
- 18.12 Wilken, D.: "Process for Measuring the Anisotropy and Work-Hardening Coefficients—Effect of a Few Factors" (*in German*), *Ind.-Anz.*, **89**, 1967, pp. 1788–1789.
- 18.13 Mäde, W., Kreissig, R., and Bensch, V.: "Methods to Determine the  $r$ - and  $n$ -Values and Comparison of these Values with the Stretch Forming Limit and the Fracture Elongation" (*in German*), *Wiss. Z. TH Otto Von Guericke, Magdeburg*, **12**, 1968, pp. 557–565.
- 18.14 Grewen, J., and Wassermann, G.: "Textures as Causes for Anisotropic Behavior during Forming" (*in German*), in *Mechanische Umformtechnik*, O. Kienzle, Ed., Berlin Heidelberg New York, Springer, 1968.
- 18.15 Shawki, G.: "Plastic Anisotropy as an Important Criterion to Determine the Deep-Drawability of Steel Sheet" (*in German*), *Blech*, **16**, 1969, pp. 547–555.
- 18.16 Laska, R.: "Plastic Anisotropy of Sheets and Strips of Killed and Unkilled Deep-Drawing Steels" (*in German*), *Werkstatt u. Betr.*, **103**, 1970, pp. 557–566.
- 18.17 Deh, R.: "Determination of Material Characteristics  $r$  and  $n$  Necessary for Quality of Fine Sheets" (*in German*), *Fert. u. Betr.*, **20**, 1970, pp. 288–292.
- 18.18 Lafferty, S. P., Schmidt, G. E., and Lawley, A.: "In-Situ Determination of the  $r$ -Value in Sheet Tensile Testing," *Sheet Met. Ind.*, **48**, 1971, pp. 185–188.
- 18.19 DIN 50101: "Prüfung metallischer Werkstoffe—Tiefungsversuch nach Erichsen (Testing of Metals—Cupping Test for Sheet and Strip after Erichsen)," Sept. 1979.

## 18.16 SHEET-METAL FORMING

- 18.20 Beisswanger, H.: "The Cupping Process to Determine the Deep-Drawing Characteristics of Sheets and Strips" (*in German*), in *Deep Drawing*, Siebel, E. and Beisswanger, H., Eds., München, Hanser, 1955.
- 18.21 Gologranc, F.: "The Determination of Flow Curves by Continuous Hydraulic Bulge Test" (*in German*), *Berichte aus dem Institut für Umformtechnik, Universität Stuttgart*, no. 31, Essen, Girardet, 1975.
- 18.22 Gologranc, F.: "Automatic Determination of Stress-Strain Curves by Continuous Hydraulic Bulge Test," *Strojnicki Vestn. Mech. Eng. J.* **26**, 1980, no. 7-8.
- 18.23 Ziegler, W.: "The Cup-Drawing Test after Swift" (*in German*), *Ind.-Anz.*, **91**, 1969, pp. 2250-2252.
- 18.24 Panknin, W.: "Fundamentals of Deep Drawing Considering the Testing Methods" (*in German*), *Bänder Bleche Rohre*, **2**, 1961, pp. 133-143, 201-211, 264-271.
- 18.25 Kirsch, A.: "The Conical Cupping Test after S. Fukui" (*in German*), *Stahl u. Eisen*, **83**, 1963, pp. 1128-1130.
- 18.26 DIN 1605: "Werkstoffprüfung; mechanische Prüfung der Metalle, Allgemeines und Abnahme (Material Testing: Mechanical Testing of Metals; General and Acceptance)," Feb. 1936.
- 18.27 DIN 50153: "Prüfung metallischer Werkstoffe; Hin- und Herbiegenversuch an Blechen, Bändern, oder Streifen mit einer Dicke unter 3 mm (Testing of Metals; Reverse Bend Testing of Sheets or Strips less than 3 mm thick)," Aug. 1979.
- 18.28 Oehler, G.: *Sheet Metal and Its Testing* (*in German*), Berlin/Göttingen/Heidelberg, Springer, 1953.
- 18.29 Dewsnap, R. F., and Oxley, D. C.: "New Strip Bend Testing Machine," *Sheet Met. Ind.*, **46**, 1969, pp. 858-861.
- 18.30 Keeler, St. P.: "Determination of Forming Limits in Automotive Stamping," *Sheet Met. Ind.*, **42**, 1965, pp. 683-691.
- 18.31 Goodwin, G. M.: "Application of Strain Analysis to Sheet-Metal-Forming Problems in the Press Shop," *La Metall. Ital.*, **60**, 1968, pp. 767-776.
- 18.32 Keeler, St. P.: "Circular Grid System—A Valuable Aid for Evaluating Sheet-Metal Formability," *Sheet Met. Ind.*, **45**, 1968, pp. 644-634, 636-641.
- 18.33 Veerman, C. Chr., Hartman, L., Peels, J. J., and Neve, P. F.: "Determination of Appearing and Admissible Strains in Cold-Reduced Sheets," *Sheet Met. Ind.* **48**, 1971, pp. 678-680, 692-694.
- 18.34 Hasek, V.: "Analysis of Grid Pattern in Drawing of Large Irregular Sheet-Metal Workpieces" (*in German*), *Ind.-Anz.*, **93**, 1971, pp. 403-405.
- 18.35 Müschenborn, W., Sonne, H. M., and Meyer, L.: "Manufacturing-Process-Dependent Material Characteristic of Cold-Rolled Sheets from the Point of View of Cold Formability" (*in German*), *Thyssenforschung*, **4**, 1972, no. 1 and 2, pp. 43-55.
- 18.36 Drewes, E. J., Henning, H., Pape, R., and Wrede, W.: "Near Practice Investigations to Characterize the Formability of Deep-Drawing Steels" (*in German*), *Hoesch-Reports on Research and Development*, **7**, 1972, no. 1, pp. 26-36.
- 18.37 Funke, P., Korri, E., Piorko, J., and Pavlidis, Chr.: "A Simple Process to Determine the Forming-Limit Curve" (*in German*), DFBO-Mitt., **24**, 1973, pp. 126-130.
- 18.38 Hasek, V.: "On the Strain and Stress Condition in Drawing Large Irregular Workpieces" (*in German*), *Berichte aus dem Institut für Umformtechnik, Universität Stuttgart*, no. 25, Essen, Girardet, 1973.
- 18.39 Hasek, V., and Lange, K.: "Forming-Limit Diagram and Its Applications in Deep-Drawing and Stretch-Forming Processes" (*in German*), *Wirtsch. Z. Ind. Fertig.*, **70**, 1980, pp. 575-580.

- 18.40 Makazima, K., Kikuma, T., and Hasuko, K.: "Study of the Formability of Steel Sheets," *Yawata Tech. Rep.*, no. 284, 1968, pp. 140-141.
- 18.41 Müschenborn, W., and Sonne, H. M.: "Influence of Strain Path on the Forming-Limit Diagram of Sheet Metal" (*in German*), *Arch. Eisenhüttenwes.*, **46**, 1975, pp. 597-602.
- 18.42 Matsuoka, T., and Sudo, C.: "The Effect of the Strain Path on the Fracture Strain of Steel Sheets," *Sumitomo Res.*, **1**, 1969, pp. 71-80.

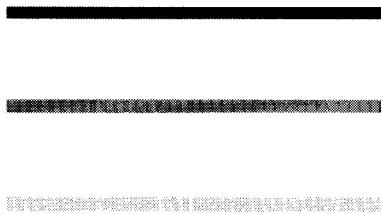
#### FURTHER READING

- Doege, E., Fetzer, H., Kellenbenz, R., and Bergmann, E.: "Deep Drawing on Single-Acting- and Double-Acting-Body Drawing Presses Considering the Knuckle Drive" (*in German*), *Werkstatt u. Betr.*, **104**, 1971, pp. 737-747.
- Panknin, W., and Eychmüller, W.: "Investigations on the Applicability or Transferability of Results from Cup-Drawing Tests to Large Tools for Deep Drawing Cylindrical Round Work-pieces" (*in German*), *Mitt. Dtsch. Forschungsges. Blechverarb.*, **6**, 1955, pp. 205-209.
- Sawada, T.: "Error Estimates during Stress-Strain Diagram Measured with Hydraulic Bulge Test," Department of Mechanical Engineering, Tokyo University of Agriculture and Technology, Japan.



## CHAP. 19

### BENDING



#### List of Special Symbols

---

$\alpha$	bend angle
$\alpha_D$	die angle in V-die bending
$\alpha_r$	bend angle after springback
$\beta$	friction angle
$\epsilon_{o,b}$	limiting strain in outer fiber
$\epsilon_Y$	yield strain
$\epsilon_z$	circumferential or bending strain
$\epsilon_x^*$	fictitious bending strain
$\epsilon_{x,i}$	bending strain of inner fiber
$\epsilon_{x,o}$	bending strain of outer fiber
$\epsilon_{x,r}$	residual bending strain after springback
$\varphi$	true strain
$\mu$	coefficient of friction
$\rho$	springback angle
$\sigma_z$	circumferential or bending stress
$\sigma_x^*$	fictitious bending stress
$\sigma_{x,i}$	bending stress of inner fiber
$\sigma_{x,o}$	bending stress of outer fiber
$\sigma_{x,r}$	residual bending stress

## 19.2 SHEET-METAL FORMING

$\sigma_y$	radial stress
$\sigma_z$	longitudinal stress
$a$	length of leg of bent part
$A_r$	reduction in area
$b$	workpiece length as measured along bend axis
$g$	slope of plastic part of stress-strain curve
$h$	punch displacement
$K$	springback ratio
$l_0$	original length of fiber
$M$	bending moment
$m$	unit moment
$r_D$	die-shoulder radius
$r_i$	radius of inner fiber
$r_j$	radius of strain boundary fiber
$r_m$	radius of middle fiber
$r_o$	radius of outer fiber
$r_p$	punch radius
$r_r$	radius after springback
$r_s$	radius of stressfree fiber
$r_u$	radius of unstretched or neutral fiber
$s$	instantaneous sheet thickness
$s_0$	original sheet thickness
$\sigma_B$	bending stress
$u$	tool clearance in U-die bending
$w$	die width
$W$	bending work

Bending belongs to the most widely applied types of sheet-metal forming. It extends from the mass production of minute workpieces to the fabrication of single parts in ship building and the construction of large machinery. In addition to sheet material, pipe, strip, wire, and bar stock of varied cross-sectional shapes is formed by bending in a multitude of processes. In the majority of cases bending is carried out at room temperature. However, for large cross sections or very small bend radii forming at elevated temperatures is preferred in order to limit forming forces and to avoid embrittlement by work hardening.

This chapter deals with bending around straight axes. Bending involving curved axes is treated in the next chapter. A classification of the bending processes was presented in Chap. 2. The basic bending process is studied here in some detail, and the most important processes are treated subsequently. The emphasis is on sheet bending.

### 19.1 THEORY OF PURE-MOMENT BENDING OF SHEET

Bending of sheet has been investigated thoroughly, and will be discussed in depth. It will also serve as basis for explaining phenomena that occur during bending in general. Parameters associated with a part undergoing bending are indicated in Fig. 19.1. In pure-moment bending a constant bending moment is assumed to act along the bending arc. Calculations based on this assumption can be checked easily by experiments.

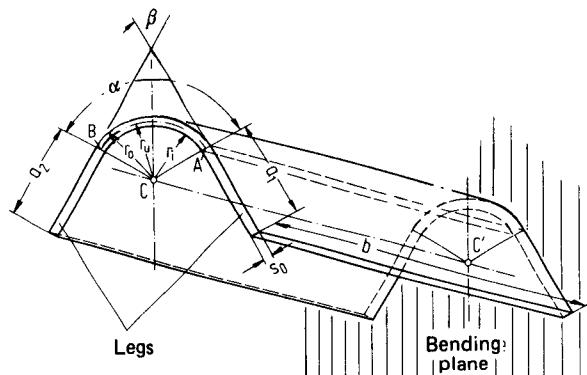


**FIG. 19.1** Terms describing geometry of bent sheet. The bending plane corresponds to the plane in which any point in the sheet moves during the bending process.  $AB$ —bending arc;  $CC'$ —bend axis;  $\alpha$ —bend angle;  $r_i$ —inner bend radius;  $r_o$ —outer bend radius;  $r_u$ —bend radius of unlengthened fiber;  $s_0$ —original sheet thickness;  $b$ —sheet length;  $a_1, a_2$ —length of legs of bent sheet. (After [19.1].)

#### 19.1.1 Basic Analysis of Sheet Bending

The bending process was first subjected to a thorough theoretical investigation by Ludwik [19.2]. Assumptions made by him and adopted later by other authors (e.g., [19.3] to [19.6]) are the following:

- 1 The uniformly thick and uniformly wide sheet is bent by a pure moment; the bending line is therefore a circular arc (Fig. 19.2).

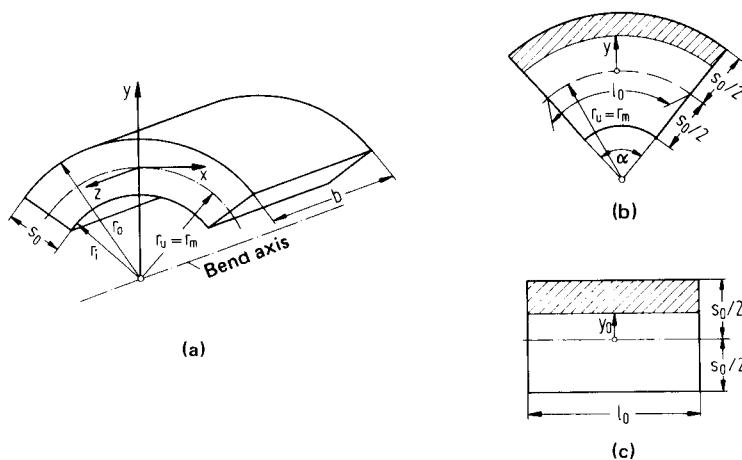


**FIG. 19.2** Terminology describing bending arc. (a) General view. (b) Section normal to bend axis. (c) Longitudinal section (plane of section contains bend axis).

#### 19.4 SHEET-METAL FORMING

- 2 The sheet is infinitely wide in relation to its thickness, so that edge deformations (see Sec. 19.3.1) do not occur and a plane state of strain exists (no deformations normal to the bending plane).
- 3 The work material is homogeneous and isotropic; there are no residual stresses prior to bending.
- 4 Plane sections normal to the sheet surface and parallel to the bend axis remain plane.
- 5 The sheet consists of many thin layers independent of one another. Existing compressive stresses perpendicular to the sheet surface, which are necessary for the creation of curvature, are neglected. Stresses parallel to the bend axis are neglected as well.
- 6 The stress-strain curves of the workpiece in the tensile and compressive regions are symmetric with respect to the origin.
- 7 Sheet thickness remains constant during the bending process. This follows from volume constancy when assumptions 1 to 6 are satisfied.

Under these simplifying conditions it is easy to analyze strains and stresses in the bending plane, as well as bending moment and bending work. Assumptions 1 to 4 require that strains and stresses in the direction of the bend axis and along the bending arc do not change, while those normal to the sheet surface do. It therefore suffices to consider only one cross section parallel to the bending plane (e.g., the  $xy$ -plane, Fig. 19.2), and in it only one straight line intersecting the bend axis (e.g., the  $y$ -axis).

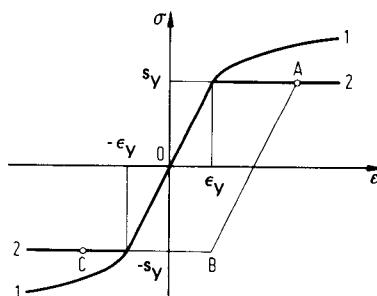


**FIG. 19.3** Symmetric stress-strain curves. 1—elastic-plastic work material; 2—elastic-ideal plastic work material.

to the yield point ( $s_y, \epsilon_y$ ) followed by flow with increasing stress (plastic with strain hardening). The stress-strain curve is symmetric about the origin, that is,  $\sigma(\epsilon) = -\sigma(-\epsilon)$ , where  $\sigma$  is always the true stress, and  $\epsilon$  is always the change in length referred to the original length (engineering strain). The concept of "flow curve" does not apply at this point, since it involves true strain and the neglect of elastic deformation.

Based on these assumptions, the central fiber of a cross section also becomes the stressfree as well as the nonlengthened fiber (see Sec. 19.1.4). Hence the stress-strain distribution is symmetric about a point on the centerline of the cross section.

From Fig. 19.2 the longitudinal strain  $\epsilon_x$  of a fiber with distance  $y$  from the center, having bend radius  $r_u$  and bend angle  $\alpha$ , is

$$\epsilon_x = \frac{\Delta l}{l_0} = \frac{(r_u + y) \bar{\alpha} - l_0}{l_0}$$

where

$$\bar{\alpha} = \frac{l_0}{r_u} \quad (19.1)$$

$$\epsilon_x = \frac{y}{r_u} \quad (19.2)$$

For edge strains ( $y = s_0/2$  and  $y = -s_0/2$ ) one obtains

$$\epsilon_{x,o} = \frac{s_0}{2r_u} \quad (19.3)$$

$$\epsilon_{x,i} = -\epsilon_{x,o} \quad (19.4)$$

For purely elastic bending, that is,  $\epsilon_{x,o} \leq \epsilon_Y$ ,

$$\sigma_{x,el} = E\epsilon_x \quad (19.5)$$

applies for the stress distribution, and for the bending moment

$$M_{el} = 2 \int_{y=0}^{s_0/2} \sigma_{x,el} b y \, dy \quad (19.6)$$

With Eqs. 19.5 and 19.2 the integration results in

$$M_{el} = \frac{Ebs_0^3}{12r_u} = \frac{1}{6} S_Y b s_0^2 \frac{\epsilon_{x,o}}{\epsilon_Y} \quad (19.7)$$

if  $E = S_Y/\epsilon_Y$  and Eq. 19.3 are applied. If the bending moment is reduced by sheet width  $b$  and sheet thickness  $s_0$ , the so-called unit moment is obtained. Thus Eq. 19.7 becomes

$$m_{el} = \frac{M_{el}}{bs_0^2} = \frac{Es_0}{12r_u} = \frac{1}{6} S_Y \frac{\epsilon_{x,o}}{\epsilon_Y} \quad (19.8)$$

At incipience of plastic flow ( $\epsilon_{x,o} = \epsilon_Y$ ),  $\sigma_{x,o} = S_Y$  and the bending moment becomes

$$M_Y = \frac{1}{6} S_Y b s_0^2 \quad \text{or} \quad m_Y = \frac{1}{6} S_Y \quad (19.9)$$

If  $\epsilon_{x,o} > \epsilon_Y$  with progressing curvature, regions of plastically deformed work material spread from the edges toward the middle (partially plastic state, see Fig. 19.4a). The boundaries between the elastic regions and the plastic regions ( $y = \pm y_Y$ ;  $\epsilon_x = \pm \epsilon_Y$ ) are

$$y_Y = \epsilon_Y r_u \quad (19.10)$$

from Eq. 19.2. Eq. 19.5 continues to apply to the remaining elastic region ( $-y_Y \leq y \leq y_Y$ ). In the plastic regions ( $y_Y \leq y \leq s_0/2$  and  $-s_0/2 \leq y \leq -y_Y$ ) stress is governed by the stress-strain curve (Fig. 19.3, curve 1). If  $\sigma = \sigma(\epsilon)$  is defined by an analytic function, the bending moment

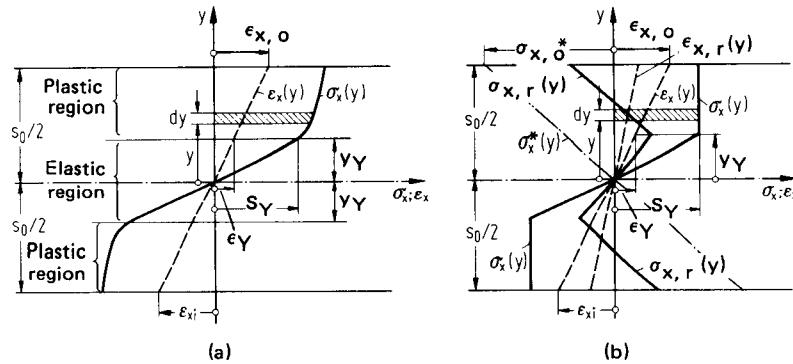


**FIG. 19.4** Stress-strain distributions in cross section during bending. (a) Actual plastic work material. (b) Ideal plastic work material. Stress and strain conditions after springback are also represented.

## 19.6 SHEET-METAL FORMING

can be calculated for the partial plastic state. In general,

$$M = \int_{y=-s_0/2}^{y=s_0/2} \sigma_s(y)by dy \quad (19.11)$$

and for symmetric stress-strain curves,

$$M = 2 \int_{y=0}^{s_0/2} \sigma_s(y)by dy \quad (19.12)$$

This bending moment consists of parts for the elastic and plastic regions:

$$\begin{aligned} M &= M_{el} + M_{pl} \\ &= 2 \int_{y=0}^{y_Y} \sigma_{x,el} by dy + 2 \int_{y=y_Y}^{s_0/2} \sigma(\epsilon) by dy \end{aligned} \quad (19.13)$$

If  $\sigma(\epsilon)$  is known, Eqs. 19.5 and 19.2 can be substituted and the integrations performed. For an elastic-ideal plastic work material, for instance,  $\sigma(\epsilon) = S_Y = \text{constant}$  (Fig. 19.3, curve 2; Fig. 19.4b), and Eq. 19.13 yields

$$M_{el} = \frac{2}{3} S_Y b s_0^2 \quad (19.14)$$

$$M_{pl} = S_Y b \left( \frac{s_0^2}{4} - y_Y^2 \right) \quad (19.15)$$

$$M = \frac{1}{4} S_Y b s_0^2 \left[ 1 - \frac{4}{3} \left( \frac{y_Y}{s_0} \right)^2 \right] \quad (19.16)$$

$$m = \frac{1}{4} S_Y \left[ 1 - \frac{4}{3} \left( \frac{\epsilon_Y r_u}{s_0} \right)^2 \right] = \frac{1}{4} S_Y \left[ 1 - \frac{1}{3} \left( \frac{\epsilon_Y}{\epsilon_{x,0}} \right)^2 \right] \quad (19.17)$$

For the limit of purely elastic bending ( $y_Y = s_0/2$ ) Eq. 19.9 is again obtained. Fig. 19.5 shows the change of the unit moment as a function of edge strain according to Eqs. 19.14, 19.15, and 19.17.

If the plastic regions were to extend to the middle ( $y_Y \rightarrow 0$ ), the fully plastic moment would be obtained:

$$M_{fpl} = \frac{1}{4} S_Y b s_0^2 \quad \text{or} \quad m_{fpl} = \frac{1}{4} S_Y \quad (19.18)$$

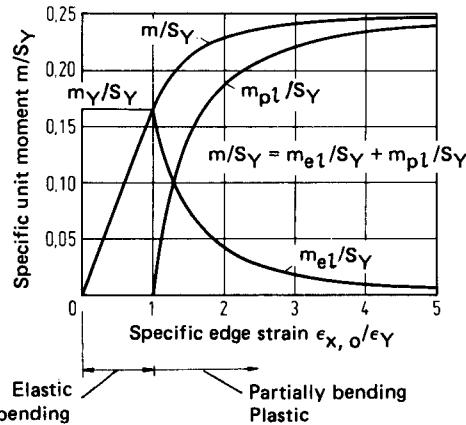


FIG. 19.5 Behavior of unit moment for small boundary strains, elastic-ideal plastic work material.

and

$$M_{\text{fpl}} = 1.5M_Y \quad \text{or} \quad m_{\text{fpl}} = 1.5m_Y \quad (19.19)$$

This mathematical borderline case cannot be attained, however, as  $\epsilon_{x,0}$  would have to become infinitely large or the bend radius  $r_u$  would have to approach zero. The smallest reasonable value for  $r_u$  is  $s_0/2$ , for which  $y_Y$  becomes so small that the state of deformation can be considered fully plastic for all practical purposes.

The required bending work  $W$  can be determined from both bending moment and bend angle:

$$W = \int_{\alpha=0}^{\bar{\alpha}_{\max}} M d\bar{\alpha} = W_1 + W_2 \quad (19.20)$$

where

$$W_1 = \int_{\alpha=\bar{\alpha}_Y}^{\bar{\alpha}_Y} M_{\text{el}} d\bar{\alpha} \quad (19.21)$$

is the bending work up to incipient plastic flow at the edge, and

$$W_2 = \int_{\alpha=\bar{\alpha}_Y}^{\bar{\alpha}_{\max}} M d\bar{\alpha} \quad (19.22)$$

the bending work required between  $\bar{\alpha}_Y$  and  $\bar{\alpha}_{\max}$ . For evaluation of the integrals the bending moment according to Eq. 19.7 or 19.17 is substituted into Eqs. 19.21 and 19.22, and  $r_u$  is replaced by  $l_0/\alpha$  according to Eq. 19.1.  $\bar{\alpha}_Y$  results from Eqs. 19.1 and 19.3 by letting  $\epsilon_{x,0} = \epsilon_Y$ .

### 19.1.2 Springback after Bending

A purely elastically bent sheet will return to its original configuration upon removal of the bending moment. After partially plastic bending, permanent deformation and residual stresses remain after unloading. The following analysis assumes—not always correctly—that springback is purely elastic; that is, no additional plastic deformation is induced, and that the work material is elastic-ideal plastic (Fig. 19.3, curve 2).

A bending process with the unloading moment  $-M$  is superimposed on the sheet which is being bent by the loading moment  $M$ . The opposite bending process causes a fictitious stress distribution according to Eq. 19.5:

$$\sigma_x^* = E\epsilon_x^* = 2\sigma_{x,0}^* \left( \frac{y}{s_0} \right) \quad (19.23)$$

with edge stress

$$\sigma_{x,0}^* = \frac{-M}{W_b} \quad (19.24)$$

where  $W_b = bs_0^2/6$  is the resisting moment of the sheet against bending (Fig. 19.4b). From Eq. 19.16,

$$\sigma_{x,0}^* = -\frac{3}{2}S_Y \left[ 1 - \frac{4}{3} \left( \frac{y_Y}{s_0} \right)^2 \right] \quad (19.25)$$

is obtained. Since the sum of loading moment and unloading moment equals zero, the residual stress distribution is the sum of the stress distribution during bending and the fictitious stress distribution:

$$\sigma_{x,r} = \sigma_x + \sigma_x^* \quad (19.26)$$

Once  $\sigma_{x,0}^*$  has been calculated with Eq. 19.24, the residual stress distribution is easily determined by graphic means using Eq. 19.26 (Fig. 19.4b). A radiographically measured stress and residual stress distribution is shown in Fig. 19.6.

## 19.8 SHEET-METAL FORMING

Since the strain distribution remains linear during bending and springback, and Hooke's law applies in the cross-sectional region, the residual strain distribution can be obtained from the residual stress distribution:

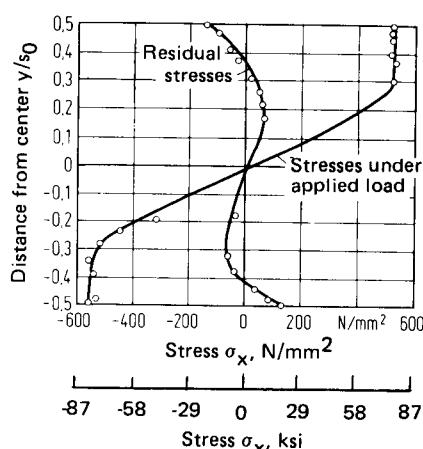


**FIG. 19.6** Stress distribution during bending and after springback, measured by radiography.

$$\epsilon_{x,r} = \frac{\sigma_{x,r,el}}{E} \quad (19.27)$$

The elastic residual stress  $\sigma_{x,r,el}$  is determined from Eq. 19.26 under utilization of Eqs. 19.25, 19.23, 19.5, and 19.2. The bend radius after springback is

$$r_{u,r} = \frac{s_0}{2\epsilon_{x,o,r}} \quad (19.28)$$

The expression

$$K = \frac{r_u}{r_{u,r}} = \frac{r_i + s_0/2}{r_{i,r} + s_0/2} \quad (19.29)$$

or

$$K = \frac{\alpha_r}{\alpha} \quad (19.30)$$

is called the springback ratio. If  $K$  is known from experiment (Fig. 19.7), the springback angle is easily determined to be

$$\rho = \alpha - \alpha_r = \left( \frac{1}{K} - 1 \right) \alpha_r \quad (19.31)$$

It should be emphasized that Eqs. 19.30 and 19.31 apply only to pure moment bending. Conditions are much more complicated for different bending processes (see Sec. 19.3.1).

### 19.1.3 Unit-Moment Curves

Eq. 19.11 for the bending moment can be rewritten as

$$M = b r_u^2 \int_{\epsilon_x=\epsilon_{x,i}}^{\epsilon_{x,o}} \sigma_x(\epsilon_x) \epsilon_x d\epsilon_x \quad (19.32)$$

by substituting  $y = \epsilon_x r_u$ . For  $\epsilon_x = \epsilon$  the unit moment becomes

$$m = \left( \frac{r_u}{s_0} \right)^2 \int_{\epsilon_x=\epsilon_{x,i}}^{\epsilon_{x,o}} \sigma(\epsilon) \epsilon d\epsilon \quad (19.33)$$

The integral is merely a function of the stress-strain curve  $\sigma(\epsilon)$  of the work material, and can be evaluated if the assumption is made that the stress-strain curves are equal in tension and compression so that  $\epsilon_{x,o} = -\epsilon_{x,i}$ . Unit-moment curves have been determined for various metallic materials [19.7] to [19.9]. Fig. 19.8 shows a number of examples for different types of steel sheet. If  $s$ ,  $b$ , and  $r_u$  are known, the bending moment can now be determined easily:

$$M = m b s_0^2 \quad (19.34)$$

### 19.1.4 Relative Displacement of Fibers

It has been demonstrated [19.10] to [19.12] that the concept of one neutral layer or fiber is no longer valid for partially plastic bending, particularly when small bend radii are involved. All work material fibers in the bending arc traverse stress and strain states that change continually

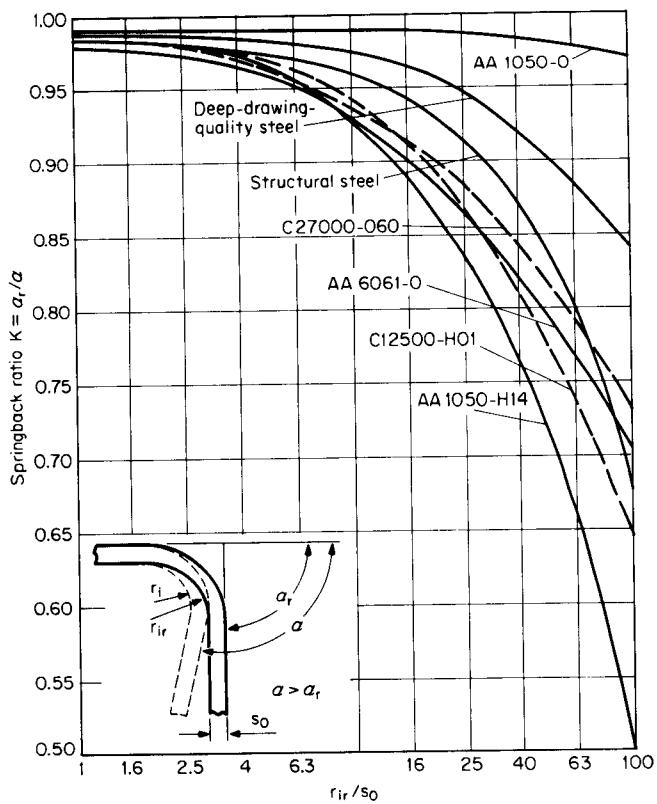


FIG. 19.7 Springback ratio of different work materials as a function of bend radius. (After [19.7].)

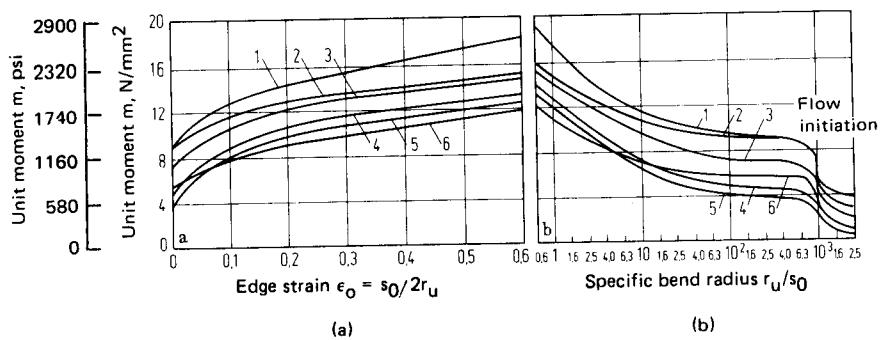
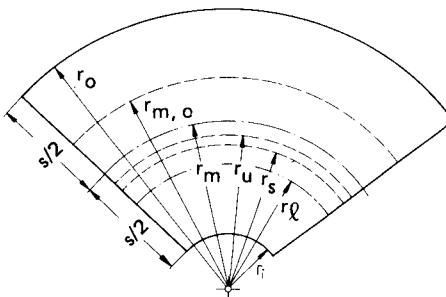


FIG. 19.8 Unit-moment curves for various carbon steel sheets. 1— $S_u = 520 \text{ N/mm}^2$  (74 ksi) normalized; 2— $S_u = 520 \text{ N/mm}^2$  (74 ksi) spheroidized; 3— $S_u = 420 \text{ N/mm}^2$  (61 ksi); 4— $S_u = 370 \text{ N/mm}^2$  (54 ksi); 5, 6— $S_u = 340 \text{ N/mm}^2$  (50 ksi). (a) Small bend radii. (b) Large bend radii. (After [19.7].)

## 19.10 SHEET-METAL FORMING

during the bending process. No fiber is ever free of strain, none ever free of stress. The strainfree fiber coincides with the stressfree fiber at the beginning of the bending process only.

In bending, distinction must be made between the following fibers in the bending arc, starting with the outer surface (Fig. 19.9): outer fiber  $r_o$ , originally middle fiber  $r_{m,0}$ , middle fiber  $r_m$ ,



**FIG. 19.9** Location of important fibers in bending arc.

unlengthened fiber  $r_u$ , stressfree fiber  $r_s$ , fiber at the boundary of compressive strain  $r_\ell$ , and inner fiber  $r_i$ .

All fibers from  $r_o$  to  $r_{m,0}$  are only stretched during bending; those between  $r_{m,0}$  and  $r_u$  are first compressed and then stretched more than they are compressed originally. For  $r_u$  the extension equals the compression; fibers between  $r_u$  and  $r_\ell$  are first compressed and subsequently stretched less than they were compressed originally. At  $r_\ell$  compression has just been completed, but an extension has not yet taken place. Fibers between  $r_\ell$  and  $r_i$  are compressed only.

With the assumption that sheet thickness remains constant and hence the middle fiber is always the unlengthened fiber, the shifts of the fibers in the cross section and their strains can be analyzed. For a fiber originally located at a distance  $y_1$  from the middle fiber, distance  $y$  after bending can be shown to be

$$y = -\frac{s_0}{2\epsilon_{x,0}} + \sqrt{\left(\frac{1}{\epsilon_{x,0}}\right)^2 + 1 + \frac{4}{\epsilon_{x,0}} \frac{y_1}{s_0}} \quad (19.35)$$

using constancy of volume (Fig. 19.2). This displacement of fibers is depicted in Fig. 19.10. The strains of the migrating fibers can be followed with

$$\epsilon_x = -1 + \sqrt{1 + \epsilon_{x,0}^2 + 4\epsilon_{x,0} \frac{y_1}{s_0}} \quad (19.36)$$

which is obtained by using Eqs. 19.1, 19.3, and 19.35. Fig. 19.11 reveals that the fibers on the compression side ( $y_1/s < 0$ ) are first compressed and subsequently stretched again in accordance with the magnitude of edge strain  $\epsilon_{x,0}$ . Compression stops at the instant when

$$\frac{d\epsilon_x}{d\epsilon_{x,0}} = 0 \quad (19.37)$$

The locus of all these points is a circle ( $\epsilon_\ell$ ) which is indicated in the figure. Its intersections with the strain lines determine the respective fiber at the boundary of compressive strain. The fact that unlengthened fiber, stressfree fiber, and fiber at the boundary of compressive strain do not coincide is easily demonstrated with the stress-strain diagram (Fig. 19.12). A fiber with  $r < r_m$  before bending is compressed at first, and originating at 0, reaches point C where a strain reversal takes place. The stress decreases parallel to the elastic curve to zero (point F). From there, stress increases to point G on the stress axis where the fiber has regained its original length (unleng-

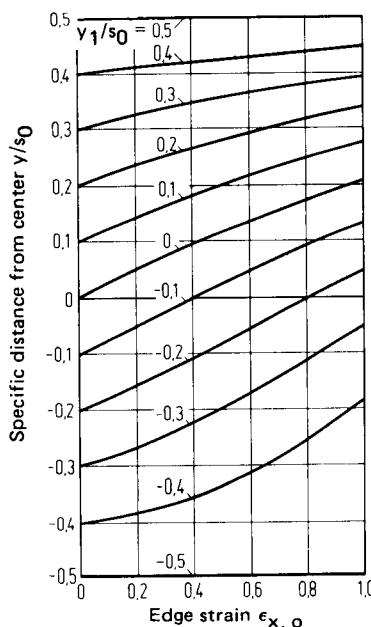


**FIG. 19.10** Shift of individual fibers in cross section with increasing boundary strain. (After [19.12].)

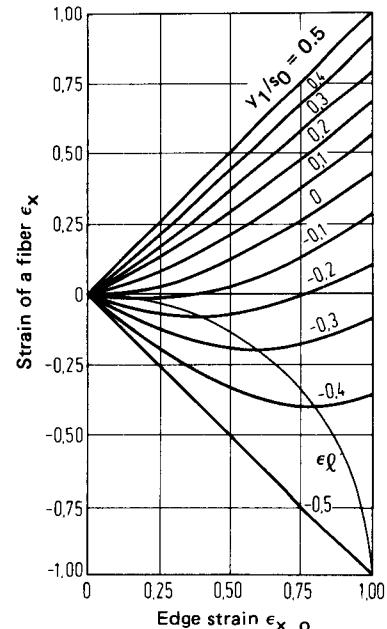


**FIG. 19.11** Strain of individual fibers with increasing boundary strain. (After [19.10].)

thened fiber) but is subjected to tension. A more interior fiber will be compressed to point *B* and stretched again to point *H*. Although stressfree, it has not yet regained its original length. At the time when the two fibers just described are nonlengthened and stressfree, respectively, another even more interior fiber has reached the state corresponding to point *D*: compression is completed and extension has not yet begun (strain reversal, fiber at the boundary of compressive strain).

The locations of unlengthened, stressfree, and strain-boundary fibers relative to one another are dependent upon the shape of the stress-strain curve in the compressive region [19.12].

The described shift of fibers is only possible when a single bending moment is acting along the entire bending arc. A pure moment can only be applied by clamping both straight ends of the sheet. Consequently a transition state between the fibers in the bent and the unbent portions of the sheet must exist at the clamping locations. An inclination of cross sections in the bending arc far into the legs is the result: on the tension side material flows from the legs into the arc, while the opposite is the case on the compression side (Fig. 19.13).

The question arises to what extent the shift-

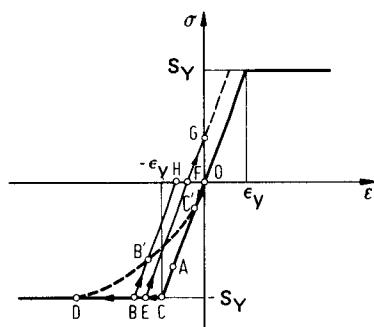


**FIG. 19.12** Stress-strain behavior of specific fibers in compressive region. Final conditions: *C*—fiber with incipient flow; *G*—nonlengthened fiber; *H*—stressfree fiber; *D*—strain-boundary fiber.

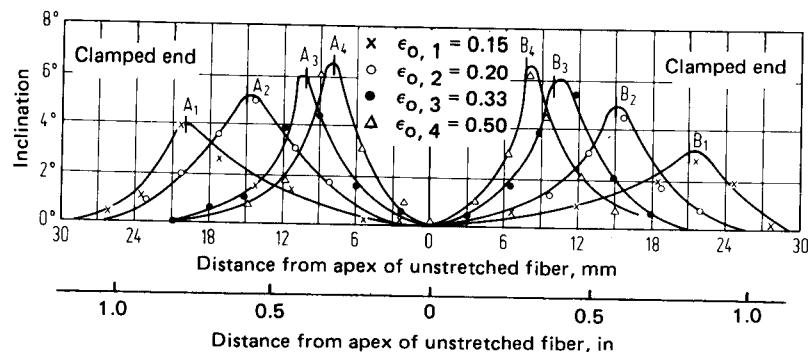


**FIG. 19.13** Inclination of cross sections in pure moment bending. Material—commercial-purity aluminum, half-hard;  $b/s_0 = 6.2$ ;  $\alpha = 90^\circ$ ; points A and B identify limit of corresponding bending arc. (After [19.13].)

ing of fibers must be taken into account. If  $|\epsilon_x| \leq \epsilon_y$ , the stress-strain state of all fibers lies on the original stress-strain curve. For this to be the case it is necessary that (from Eqs. 19.36, 19.37, and 19.3),

$$\epsilon_{x,0} \leq + \sqrt{1 - (1 - \epsilon_y)^2} \quad (19.38)$$

or

$$r_u \geq \frac{s_0}{2\sqrt{1 - (1 - \epsilon_y)^2}} \quad (19.39)$$

[e.g.,  $\epsilon_y = 0.002$ ,  $s_0 = 1 \text{ mm (0.04 in)}$ , and  $r_u = 7.9 \text{ mm (0.3 in)}$ ]. For bend radii based on Eq. 19.39 the shift of fibers can be neglected. As the bend radius decreases, all fibers, which now become fibers at the boundary of compressive strains, will be loaded beyond the compressive yield strength, with their state as described previously. Since their reverse extension varies in magnitude, the stress distribution in this region follows a curve (Fig. 19.12, curve DB'C') for which an approximate equation has been established [19.12].

Fig. 19.12 shows that between originally middle fiber and strain-boundary fiber stresses are not simply the result of the stress-strain curve based on strains according to Fig. 19.11. Instead, they are based upon so-called active strains, that is, strains which cause stress. Their magnitude depends upon the compressive stress-strain curve. Fig. 19.14 shows their qualitative behavior for an elastic-ideal plastic work material. Fibers of strain-hardening work materials, which have experienced plastic deformation in the compressive region but are not becoming plastic in the tensile region, are subject to the Bauschinger effect [19.14] with a concomitant effect of the stress distribution in the cross section [19.15].

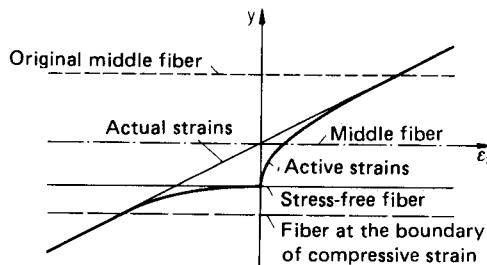


**FIG. 19.14** Active strains in centrally located region of cross section. (After [19.12].)

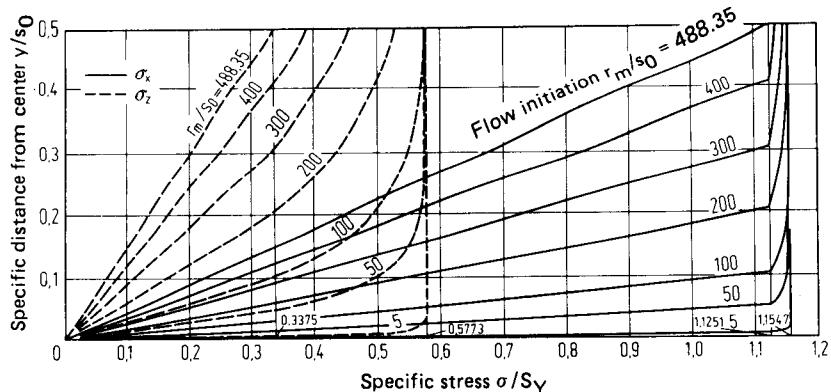


**FIG. 19.15** Distribution of stresses  $\sigma_x$  and  $\sigma_z$ . Analysis after [19.11] using Prandtl-Reuss relations and von Mises yield criterion ( $\sigma_y = 0$ ).

Analysis of springback by taking into account the shifting of fibers has been reported in [19.12]. For a known unit-moment curve  $m = m(r_u/s_0)$ , the springback ratio  $K$  can be determined according to

$$K = 1 - m \frac{12r_u}{E\delta_0} \quad (19.40)$$

### 19.1.5 Application of Plasticity Theory to Sheet Bending

If the stresses  $\sigma_y$  and  $\sigma_z$  are to be taken into account in addition to  $\sigma_x$ , the stress distribution in the plastic region must be determined by involving a yield condition (according to Tresca or von Mises). This permits different possibilities for taking into account the multiaxial stress state in bending. The choice of the work material characterization plays an important part: For very small bend radii the elastic portion of deformation can be neglected; that is, a rigid-plastic work material is assumed. Also, the analysis can be carried out with or without strain hardening.

The simplest approach involves taking into account stresses  $\sigma_x$  and  $\sigma_z$  (the stress in the direction of the bend axis) and incorporating assumptions 1 to 7 (see Sec. 19.1.1). The solution for an elastic-ideal plastic work material is outlined by Hill [19.11] (see also [19.16]). Stresses  $\sigma_x$  and  $\sigma_z$  are calculated based on Hooke's law for the elastic region, the Prandtl-Reuss relations [19.11], and the von Mises yield condition for the plastic region (Fig. 19.15).

A general solution for plastic bending of a rigid-ideal plastic material in plane strain is also due to Hill [19.11], and is valid for arbitrarily small bend radii. Using the equilibrium condition

$$\frac{d\sigma_y}{dy} = \frac{\sigma_x - \sigma_y}{y} \quad (19.41)$$

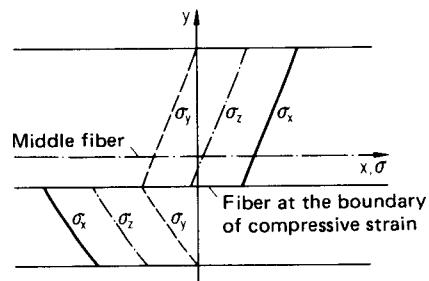


**FIG. 19.16** Stress distribution, assuming rigid-ideal plastic work material. (After [19.11].)

and the von Mises yield condition, longitudinal stress  $\sigma_x$  and radial stress  $\sigma_y$  are obtained:

$$\left. \begin{array}{l} \sigma_x = 2k[1 - \ln\left(\frac{r_o}{r}\right)] \\ \sigma_y = -2k \ln\left(\frac{r_o}{r}\right) \end{array} \right\} \quad r_i < r \leq r_o \quad (19.42)$$

$$\left. \begin{array}{l} \sigma_x = -2k[1 + \ln\left(\frac{r}{r_i}\right)] \\ \sigma_y = -2k \ln\left(\frac{r}{r_i}\right) \end{array} \right\} \quad r_i \leq r \leq r_l \quad (19.43)$$

The stress in the direction of the bend axis is

$$\sigma_z = \frac{\sigma_x + \sigma_y}{2} \quad (19.44)$$

In these relations  $k = S_y/\sqrt{3}$  (von Mises). Strain reversal is just taking place in the fiber at the boundary of compressive strain ( $r_f = \sqrt{r_i r_o}$ ). Due to the assumption of a rigid-ideal plastic material,  $\sigma_x$  changes instantaneously (Fig. 19.16). The sheet thickness  $s$  remains constant as does the bending moment,

$$M = \frac{k}{2} b s_0^2 \quad (19.45)$$

A refinement of Hill's solution was provided by accounting for strain hardening with the relationship

$$\sigma = \pm S_y + g\varphi \quad (19.46)$$

to describe the flow curve of the work material [19.17]. This flow characteristic is applied to the plane state of deformation by the yield criterion

$$\sigma_x - \sigma_y = \pm 2k + 2k_v \varphi_z \quad (19.47)$$

where

$$k = \frac{S_y}{\sqrt{3}} \quad \text{and} \quad k_v = \frac{2}{3}g \quad (\text{von Mises}) \quad (19.48)$$

$$k = \frac{S_y}{2} \quad \text{and} \quad k_v = \frac{1}{\sqrt{3}}g \quad (\text{Tresca}) \quad (19.49)$$

Incorporation of equilibrium condition 19.41 results in

$$\sigma_y = -2k \ln\left(\frac{r_o}{r}\right) - k_v \left\{ \left[ \ln\left(\frac{r_o}{r_u}\right) \right]^2 - \left[ \ln\left(\frac{r}{r_u}\right) \right]^2 \right\} \quad (19.50)$$

for  $r_i < r \leq r_o$  and

$$\sigma_y = -2k \ln\left(\frac{r}{r_i}\right) + k_v \left\{ \left[ \ln\left(\frac{r}{r_u}\right) \right]^2 - \left[ \ln\left(\frac{r_i}{r_u}\right) \right]^2 \right\} \quad (19.51)$$

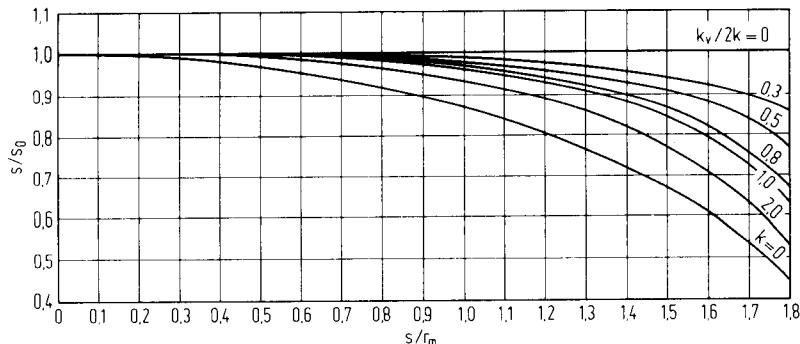
for  $r_i \leq r < r_l$ .

Further analysis shows a decrease in sheet thickness during bending. The decrease in thickness becomes more pronounced with increasing strain hardening (Fig. 19.17).

The longitudinal stresses are

$$\sigma_x = 2k + \sigma_y + 2k_v \ln\left(\frac{r}{r_u}\right) \quad r_f < r \leq r_o \quad (19.52)$$

$$\sigma_x = -2k + \sigma_y + 2k_v \ln\left(\frac{r}{r_u}\right) \quad r_i \leq r < r_f \quad (19.53)$$



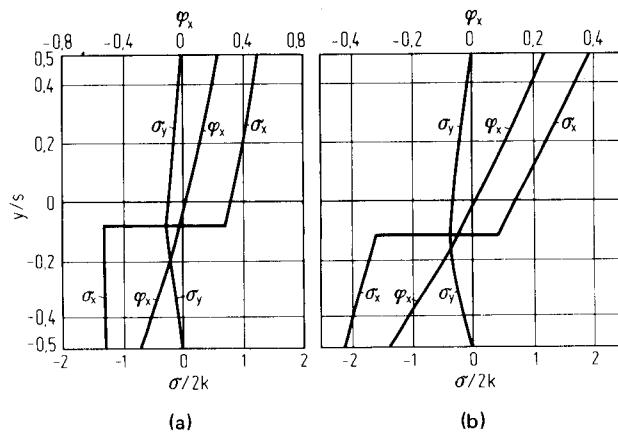
**FIG. 19.17** Reduction of sheet thickness with increasing boundary strain for varying strain-hardening levels. (After [19.17].)

Fig. 19.18 shows the distribution of stresses and strains for one bend radius and two different strain-hardening levels. The resulting bending moment is not constant, but initially increases with tightening curvature and directly with increasing strain hardening. Since sheet thickness decreases, however, the bending moment will reach a maximum followed by a decrease in magnitude.

Relatively recent theoretical work considers the effect of elastic deformation upon stress and strain [19.18] to [19.21]. However, the analysis is only valid for relatively large bend radii, that is, as long as none of the plastic fibers located in the compression region are unloaded again (see Sec. 19.1.4).

### 19.1.6 Comparison with Experimental Results

Ludwik [19.2] attempted to verify his calculations with different steel sheets on a three-roll bending machine. His assumption of a symmetric stress-strain curve with strain hardening is believed to be the reason for his values falling short of experiment by about 10%.



**FIG. 19.18** Stress distribution for rigid-plastic work material for  $r_m/s = 2$ . (a) Low strain-hardening level ( $k_v/2k = 0.5$ ). (b) High strain-hardening level ( $k_v/2k = 2$ ). (After [19.17].)

## 19.16 SHEET-METAL FORMING

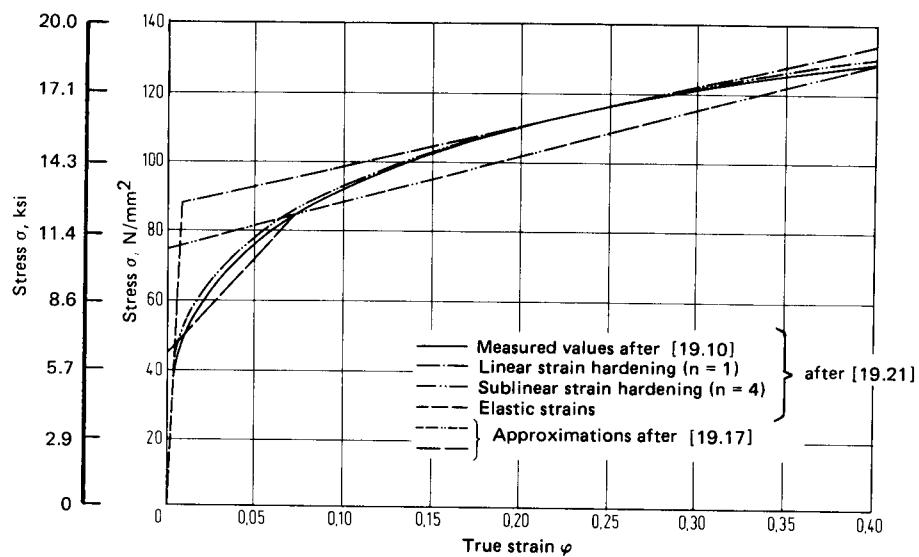


**FIG. 19.19** Experimental and approximated flow curves for commercial-purity aluminum. (After [19.10], [19.17], [19.21].)

Tests conducted with commercial-purity aluminum strips on a device for pure-moment bending resulted in good agreement with unit moments determined from Eq. 19.33 [19.10]. Figure 19.19 shows the measured flow curve of 99.5% pure aluminum and approximations made to this curve by others [19.17], [19.21]. The unit moment based on different calculations is shown in Fig. 19.20. Deviations of experimental values from the calculated curve for small  $r_u$  are believed to be

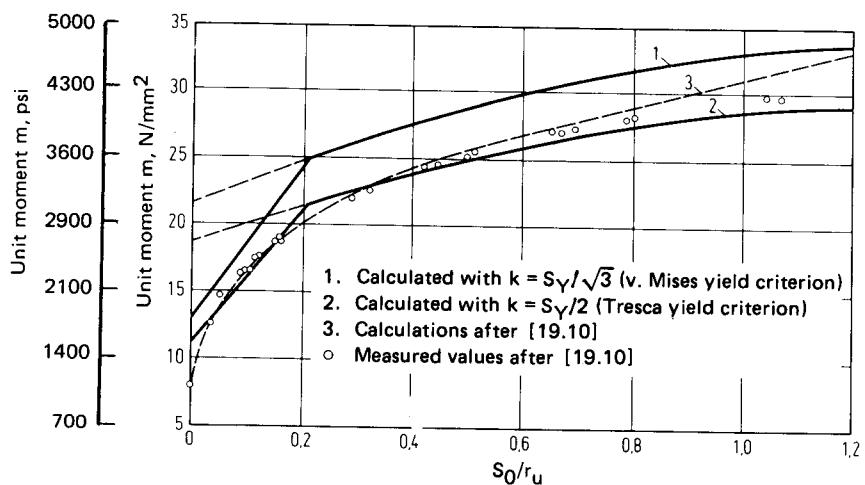


**FIG. 19.20** Unit moment for commercial-purity aluminum, experimental and calculated. (After [19.17], [19.10].)

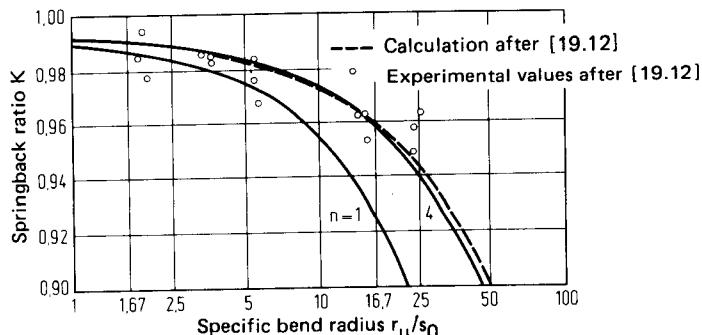


FIG. 19.21 Springback ratio for commercial-purity aluminum, experimental and calculated.  $n$  according to Fig. 19.19. (After [19.21], [19.12].)

due to the edge distortion of the test samples (anticlastic bending). Experimental and analytical results of springback are shown in Fig. 19.21. The measured values display considerable scatter so that a meaningful comparison can only be made based on a bandwidth.

The usually good agreement between analysis and experiment for bending moment and springback does not allow the conclusion that the assumptions made earlier are satisfied with near exactness. It has been shown [19.13] that the width of the bent strip has considerable influence on both unit moment and springback due to edge deformation, and that cross sections will become inclined during pure-moment bending.

## 19.2 THE MOST SIGNIFICANT SHEET-BENDING PROCESSES

In this section the most important sheet-bending processes as well as some methods for calculating bending line and bending force are introduced. Both air- and die-bending processes are examined in some depth, while folding, roll bending, section rolling, and bending with pliable tools are discussed only briefly. Workpiece properties, tooling, and machines are considered in Secs. 19.3 to 19.5.

### 19.2.1 Air Bending

In air bending the function of the tools is merely to transmit forces and moments to the workpiece. The shape of the workpiece is generally not a function of the geometry of the individual tool components, but rather depends upon the relative position of the tool components to one another, the flow curve of the work material, and the thickness of the sheet.

Pure-moment bending, which is discussed in Chap. 19.1, belongs into the category of air bending. It has no commercial significance, however, and its usefulness is restricted to experimental studies. Levelling and straightening are discussed in Chap. 19.7. This leaves two air-bending processes for discussion: (1) three-point bending, in which a sheet, supported by two shoulders on opposite sides, is deformed by a punch which engages the sheet at midspan (Fig. 19.22a); and (2) a sheet, clamped along one edge, is deformed by a punch engaging the sheet along the free edge (Fig. 19.22b). In either case air bending takes place as long as the smallest inner bend radius is larger than the punch radius (case 1) or larger than the clamping die radius (case 2). A variant of case 2, in which the punch moves in an arc instead of along a straight line, is known as free folding. It is treated in Sec. 19.2.3.

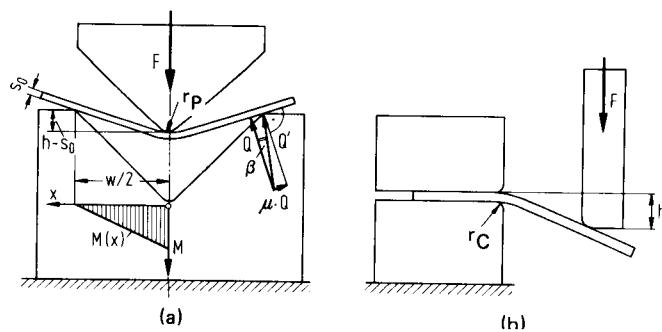


**FIG. 19.22** Air bending.  $F$ —bending force;  $h$ —punch travel;  $r_p$ —punch radius;  $r_C$ —clamping die-shoulder radius;  $w$ —die width;  $Q$ —lateral force;  $\beta$ —friction angle;  $\mu$ —coefficient of friction;  $M$ —bending moment. (a) Early stages of die bending. (b) Sheet with one end clamped.

### Workpiece Shape during Air Bending

Forces acting on the sheet for a given punch displacement  $h$  are shown in Fig. 19.22a. Initially bending is elastic. Plastic deformation sets in when the stresses in the outer fibers of the sheet exceed the elastic limit. Permanent deformation starts directly underneath the punch where the bending moment is the greatest, then propagates outward toward the die shoulders. As the process continues, the sheet moves into the die opening, causing a change of the effective die width. Stress and strain distributions in the sheet change continually from midspan to die shoulder. As the strain is greatest at the punch nose, the mean radius of curvature is smallest there, but increases toward the die shoulder. The radius of curvature of the sheet is independent of the punch radius. Instead, it is a function of bending moment, die width, sheet thickness, and the flow curve of the sheet material. A bending operation involving a punch with a radius equal to the thickness of the sheet tends to result in an inner part radius larger than the punch radius. However, when the punch radius becomes sufficiently large, an inner part radius smaller than the punch radius may be produced (see Fig. 19.27). Two points of contact between punch and sheet are the result, and the length of the bending moment arm is greatly reduced.

A graphic technique enables the determination of the bending line based on bending moment and unit-moment curve of the material [19.10]. Fig. 19.23 illustrates two results for  $\alpha = 90^\circ$ , for which friction at the die shoulders was neglected.

Based on the pure bending theory described earlier [19.17], a numerical approach was developed to analyze bending of the sheet under a varying moment [19.22]. The sheet was divided into small elements, and each element was subjected to the constant bending moment corresponding to its location in the sheet. Pure bending analysis was applied to each element. With computer programs based on this approach, the entire bending process was simulated. The deformation of the sheet itself can be displayed on a graphic terminal display screen (Fig. 19.24).

A highly accurate although time-consuming analysis of the air-bending process of sheet is provided by the finite-element method [19.23]. The deformation of the sheet can be described completely by this technique. Both elasto-plastic and rigid-plastic analysis formulations were used to examine the process for a fixed set of tool dimensions, one sheet thickness, and one sheet material. Friction between sheet and die shoulders was neglected. Both formulations were shown to yield results in close agreement with each other.

### Bending Moment and Bending Force in Air Bending

The transverse force bending of sheet including friction at the die supports was analyzed [19.24] based on the theory developed in [19.17]. Comparison with experiments showed the bending moment based on the plane-strain analysis of pure-moment bending of a rigid-plastic material to agree well with results of plane-strain, transverse force bending tests for operations involving die widths very much greater than the sheet thickness, and punch radii on the order of the sheet

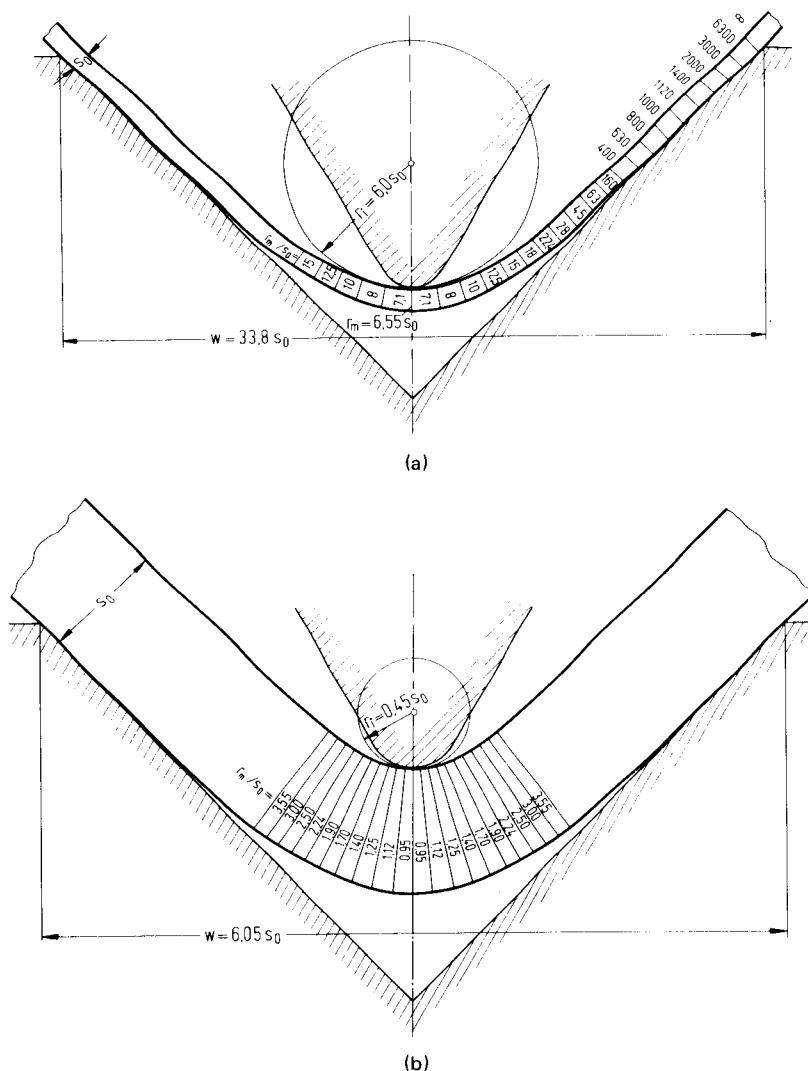


**FIG. 19.23** Bending curvatures during air-bending stage of  $90^\circ$  V-die bending. Work material—commercial-purity aluminum. (a) Die width  $w = 33.8s_0$ . (b) Die width  $w = 6.05s_0$ . (After [19.10].)

thickness. An independent concurrent analysis of transverse force bending [19.25] assumed simplified elastic-plastic work material behavior and no changes in cross section. The bending force in air bending was derived based upon plastic deformation of a cantilever beam. Bending conditions were restricted to large die-width-to-plate-thickness ratios and small punch radii. The resulting bending force is

$$F = \frac{g}{3\lambda} \left( \cos \frac{\alpha}{2} + \mu \sin \frac{\alpha}{2} \right) \frac{bs_0^2}{w} \left[ 3 \frac{S_Y}{g} + \frac{\alpha s_0}{\lambda w} + \sqrt{\frac{6\alpha S_Y s_0}{\lambda w g} + \left( \frac{\alpha s_0}{\lambda w} \right)^2} \right] \quad (19.54)$$

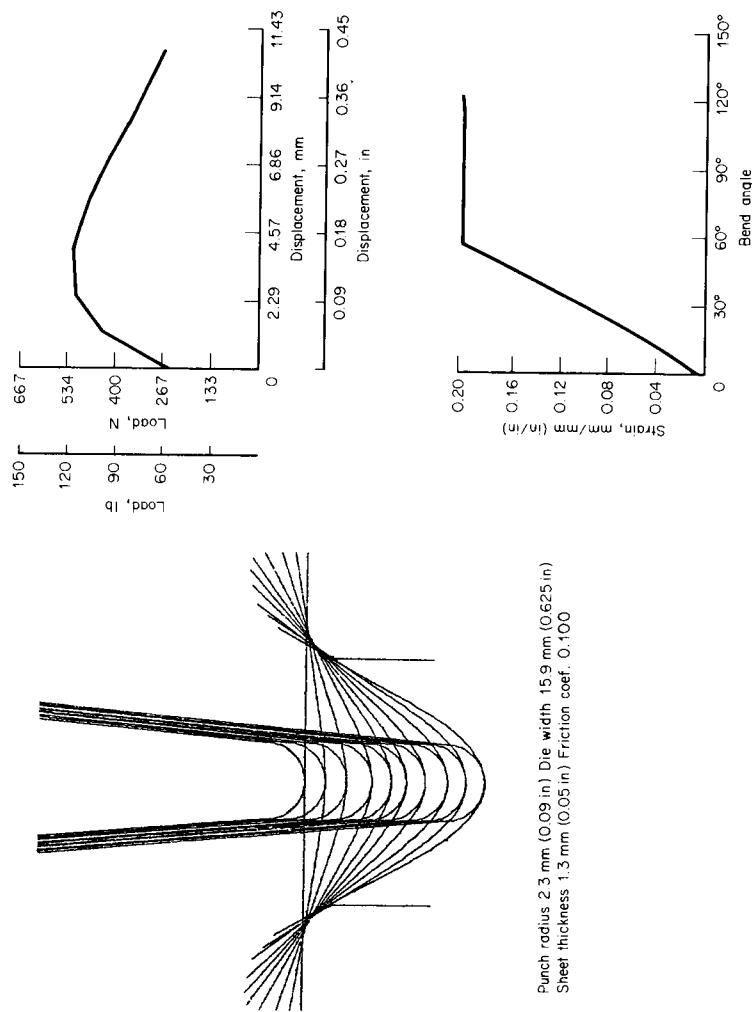


**FIG. 19.24** Brake-bending simulation as seen on graphic terminal. (After [19,22].)

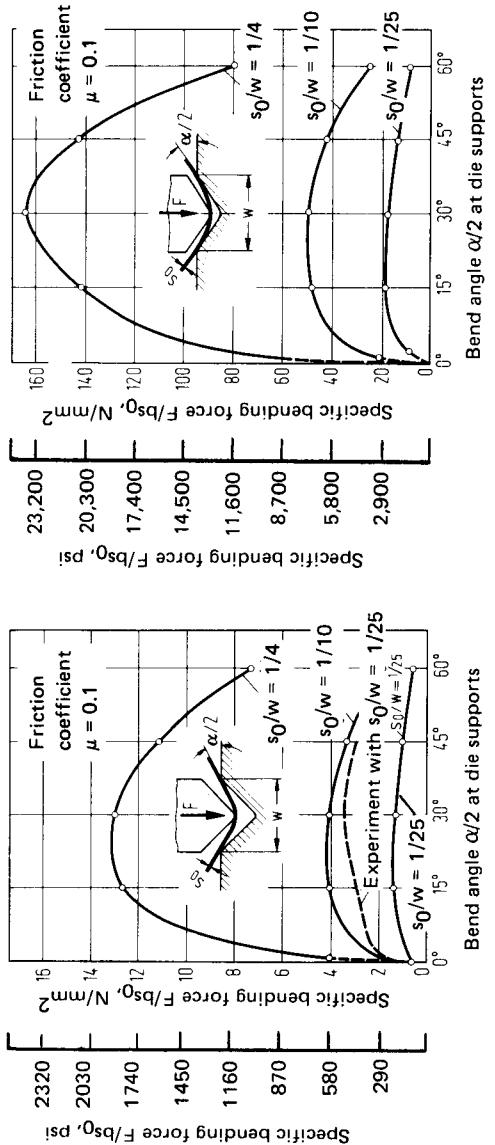


**FIG. 19.25** Specific bending force in air bending for different die widths. (a) Commercial-purity aluminum. (b) AISI 1035 steel, normalized. (After [19.25].)

## 19.22 SHEET-METAL FORMING

where  $g$  is the slope of the plastic portion of the stress-strain curve and  $\lambda$  is a correction factor for bending length dependent on  $w$ . For  $w/s_0 = 10$ , for example,  $\lambda$  for bend angles  $\alpha = 30, 60, 90$ , and  $120^\circ$  is 1.01, 1.05, 1.15, and 1.50, respectively. The resulting bending force is shown in Fig. 19.25 for two work materials. It is noteworthy that Eq. 19.54 does not contain the punch radius as a parameter. The main geometric parameter is the ratio of plate thickness to die width.

The importance of the punch radius in the bending process was demonstrated in two independent studies. Examination of the effect of the punch radius on the air-bending force based on a semiempirical analysis revealed that omission of the punch radius in calculating the maximum air-bending force is justified only if the die width is at least 5–8 times the punch radius [19.26]. This is due to the fact that the force maximum shifts toward larger punch displacements as the punch radius increases (see Fig. 19.28). A significant increase in the maximum air-bending force is associated with this shift as well. An increase in die shoulder friction is shown both to increase the air-bending force and to shift the air-bending force maximum to larger punch displacements.

A simple equilibrium model was used to analyze forces in the bending of heavy plate under plane-strain conditions [19.27]. The resulting bending force equation accounts for plate thickness as well as for punch radius:

$$F = \frac{\sigma_B b s_0^2 \cos(\alpha/2) [\cos(\alpha/2) + \mu \sin(\alpha/2)]}{w - 2(r_p + s_0) \sin(\alpha/2)} \quad (19.55)$$

where  $\sigma_B$  is the bending stress, and is defined by flow stress  $S_Y$  for a rigid, perfectly plastic material in accordance with Eq. 19.18. The aspect ratio

$$Z = \frac{w}{r_p + s_0} \quad (19.56)$$

was defined and used to study the effect of  $\alpha$  on the maximum air-bending force. A decrease in  $Z$  was shown to lead to an increase in the value of  $\alpha$  for which  $F$  is maximum. A limit to the air-bending process is indicated when  $Z < 1$ . A refined version of Eq. 19.55 showing better agreement with experiment [19.28] is

$$F = \frac{\sigma_f b s_0^2 \cos(\alpha/2) [\cos(\alpha/2) + \mu \sin(\alpha/2)]}{w - 2(r_p + s_0) \sin(\alpha/2) + \mu s_0 \cos(\alpha/2)} \quad (19.57)$$

The evaluation of the flow stress  $\sigma_f$  is based on the assumption that  $\sigma_f$  corresponds to the highest tangential stress, that is, the stress in the outer fiber, and that Hill's analysis of the radius of the stress free fiber [19.11] applies. If the flow curve has the form  $\sigma = C\epsilon^n$ , then

$$\sigma_f = C \left( \ln \sqrt{1 + \frac{s_0}{r_p}} \right)^n \quad (19.58)$$

The numerical approach of [19.22] (Fig. 19.24) and the finite-element method [19.23] predict the air-bending force as a function of punch travel with a high degree of accuracy.

The maximum in the air-bending curve (Figs. 19.24 and 19.25) is caused by three effects. The internal bending moment in the sheet increases with growing bend angle. As the sheet slides past the die supports, the effective bending length increases, and the direction of the support forces deviates more and more from the direction of the punch force. While the rise in bending moment predominates at first, the influence of geometric changes becomes more significant in the later stages of the process.

### 19.2.2 V- and U-Die Bending

Die bending involves bending of the sheet between punch and die until the workpiece contacts the sides of the die. Bottoming or coining, that is, pressing the sheet flat against the die sides, can follow as part of the same process [19.29]. The most important die-bending process, bending in a V-shaped die, is now described in some detail. A discussion of bending in a U-shaped die will follow.

### V-Die Bending

The process of V-die bending consists of two distinct parts [19.30]:

**Air bending** (see Sec. 19.2.1): Air bending starts at the moment the punch establishes contact with the sheet, and is completed either when the legs of the workpiece become tangent to the die faces (i.e.,  $\alpha = \alpha_D$ , Fig. 19.26b) or when the smallest internal radius of the workpiece becomes

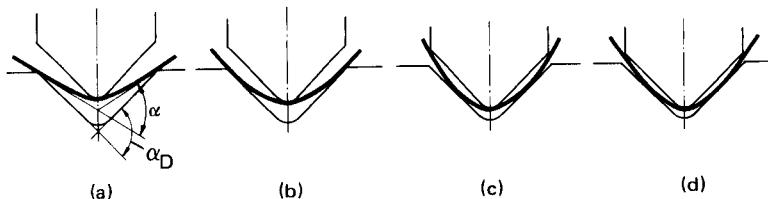


FIG. 19.26 90° V-die bending with small punch radius. (a) Air bending. (b) End of air bending. (c) End of overbending. (d) Re-forward bending. (After [19.26].)

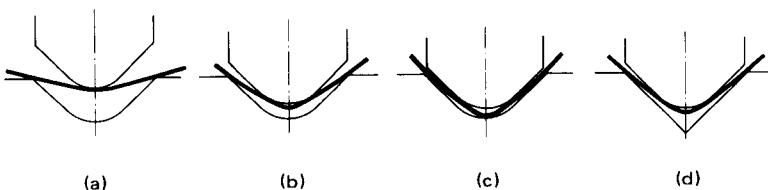


FIG. 19.27 90° V-die bending with large punch radius. (a) Air bending. (b) Continued air bending with two-point contact at punch curvature. (c) Start of coining. (d) Semiclosed-die bending. (After [19.30].)

smaller than the radius of the punch (Fig. 19.27b). In both cases the tool geometry affects the subsequent deformation of the sheet. At the end of air bending, the shape of the curved portion of the plate is undefined.

**Coining:** Coining has the purpose of removing the undefined geometry of the sheet curvature by forcing the sheet to conform to the shape of the punch-die system. The shape assumed by the part during coining is determined to a considerable extent by the inner curvature of the apex of the part (i.e., directly underneath the punch) at the end of air bending in relation to the punch curvature.

After completion of air bending, load application occurs at three points: by the punch and by the two faces of the die. The external bend angle is the same as the die angle. With continued downward motion by the punch, the plate-die contact points are shifted toward the die centerline, and the plate tends to close around the punch until its legs establish contact with it (Fig. 19.26). The workpiece is overbent, and the external bend angle exceeds the die angle. As the punch proceeds further, the plate is opened up again by the outside corners of the punch, and the bend angle approaches the die angle. Also, the inner radius of curvature of the plate decreases as it is forced to conform to the punch. The described phenomena apply to operations with small and large punch radii alike. For the case when the inner part radius is smaller than the punch radius after air bending, the discrepancy between the two is so small that the coining operation generally does not effect any changes in the radius of the part (Fig. 19.27). It is noteworthy that the inner part radius is approximately equal to the punch radius at the end of air bending for a  $w/r_p$  ratio of 5–8.

V-die bending can be carried out by closed dies; that is, the bottom of the die has a radius equal to the sum of punch radius plus plate thickness, or by a semiclosed die, in which the bottom

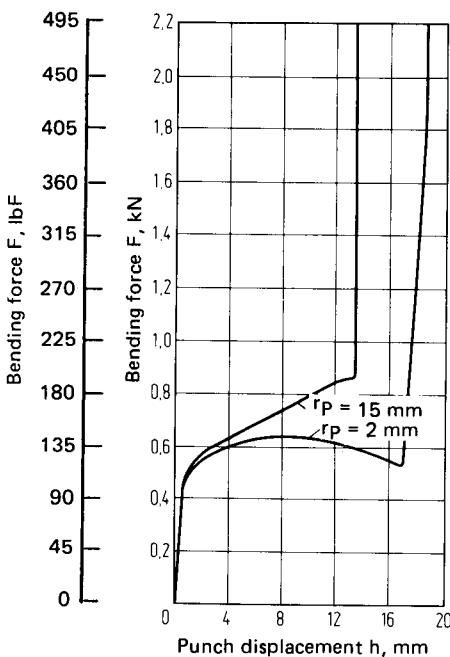


**FIG. 19.28** Punch-force-punch-path curves for 90° V-die bending for small and large punch radii.  $w = 42 \text{ mm (1.65 in)}$ ;  $s_0 = 2 \text{ mm (0.079 in)}$ .

of the die has a radius smaller than punch radius plus plate thickness (typically the die has the shape of a sharp V). For the case that the internal curvature of the part is smaller than the curvature of the punch, the semiclosed die is not able to cause the inner curvature of the plate to conform to the punch by coining.

During the air-bending stage, the bending force changes with punch displacement as described in Sec. 19.2.1. As soon as the workpiece begins to contact the sides of the die, however, force progresses subject to the constraints imposed by the die. As the points of contact between die and sheet move toward the bottom of the die, the effective-moment arm is reduced and causes the force to rise rapidly (Fig. 19.28). As the sheet is pressed against the die in coining, the force increases at an even much steeper rate and becomes open-ended, much like in forging. For sufficiently small punch-radius-to-die-width ratios, a peak is reached in the air-bending force. As the punch radius increases, and the force peak in air bending is raised to higher magnitudes and shifted to higher punch displacements (see Sec. 19.2.1), the force maximum in the air-bending stage of V-die bending will eventually become lost. This is caused by the termination of air bending before the force peak can be reached.

The magnitude of the bending force applied during coining is dependent upon the accuracy required of the finished part (i.e., radius and angle). This aspect is treated in Sec. 19.3.1.

### ***U-Die Bending***

U-die bending is the bending of a U-shaped part in a single die. Parts are composed of two legs, or walls, usually parallel, connected by a web (Fig. 19.29). A distinction is made between two processes:

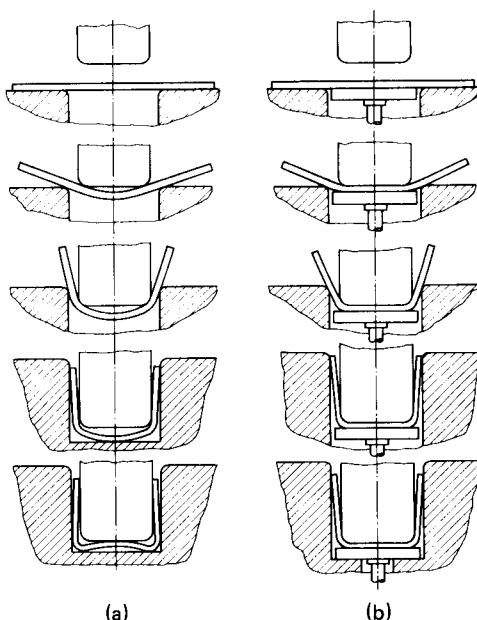


**FIG. 19.29** U-die bending. (a) Without pressure pad.  
(b) With pressure pad. (After [19.7].)

**U-die bending without pressure pad** (Fig. 19.29a): As in V-die bending, the process is characterized by different stages of deformation. The punch establishes contact with the sheet and effects elastic bending, which produces a circular arc in the domain of the web due to the constant moment distribution. The legs of the workpiece fold upward, close to the punch, as it moves into the die, and the curvature of the web is increased. No significant deformation takes place from this point on until the web touches the bottom of the die and coining begins. During coining, the curvature of the web changes from convex to concave. Eventually the web is flattened, causing the walls to close tightly against the punch. It should be noted that the displacement of workpiece material from the web into the corners can easily lead to embrittlement there during cold bending.

**U-die bending with pressure pad** (Fig. 19.29b): The pressure pad is intended to keep the web from bending by pressing it against the bottom of the punch throughout the entire bending process. Coining becomes superfluous as a result. Except for this difference, the bending process is identical to bending without a pressure pad.

Studies with steel sheet [19.31], [19.32] show that a pressure pad force having a magnitude of only 0.3 times the force needed to push the workpiece into the die (insertion force) is required if the web is to remain flat. By contrast, 3 times the insertion force is required for coining when no pressure pad is used. These figures apply to steel sheet at room temperature. Although the smaller force requirements favor bending with a pressure pad, there are serious disadvantages. Equipment is expensive, and in general the process is limited to small bending lengths.

The shape of the force-deformation curve in U-die bending depends initially upon the die radius  $r_D$  and subsequently on the die depth  $h_D$  and the tool clearance  $u$  (Fig. 19.30). For larger  $r_D$  the insertion force is lowered and the force peak occurs later. For a tractrix-shaped die profile the insertion force is reduced significantly. After the workpiece has been pushed into the die, the force drops and may remain constant for a while, depending on the depth of the die. When no

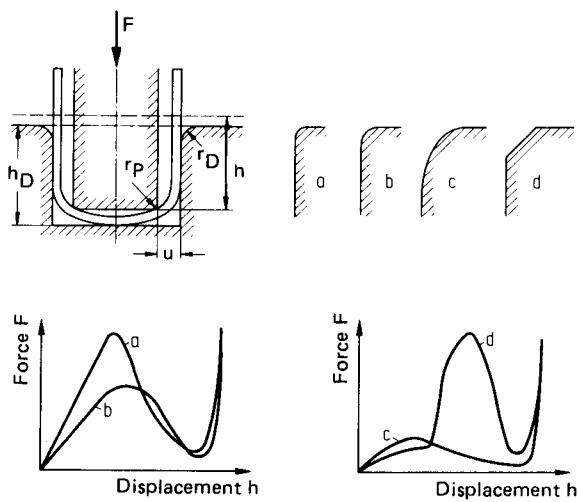


**FIG. 19.30** Force-path curves in U-die bending for different die-shoulder curvatures. (After [19.1].)

pressure pad is used, the force will rise sharply during coining of the web. For calculation of the insertion force see [19.7], [19.33].

### 19.2.3 Folding

In folding, one leg of the workpiece is clamped and the other leg is bent by a rotating wing (Fig. 19.31). As long as the smallest bend radius is larger than the radius of the folding leaf, the process is one of air bending [19.10]. In [19.34] folding is treated for the case when both radii are equal.

A major advantage of folding over die bending is its ability to bend substantially smaller leg lengths. The minimum clamping length is dependent upon the cross-sectional design of the clamping elements, the clamping force, and the bend angle. An insufficient clamping length may lead to slipping of the sheet from between jaw and folding leaf [19.7] (see Fig. 19.44). When lot sizes are large, folding is economical only for substantial bending lengths.

### 19.2.4 Roll Bending

Roll bending is used primarily in the production of cylindrical and conical parts for containers and vessels. It is essentially an air-bending process except for the bending of the ends of the sheet. However, due to the rotation of the rolls the constant bending moment continually migrates in the direction of the legs. As a result, every section experiences the same deformation during the course of the process, and a workpiece with circular cross section is obtained. Fig. 19.32 indicates the individual stages of the roll-bending process on a three-roll bending roll. Bending of the ends of the sheet need not be part of the roll-bending process, however. It can be postponed until after the process is completed. The ends can then be bent in a die. Care must be taken to ensure the proper radius of the ends. This is particularly true for the production of pressure vessels, where incorrect bend radii can create a notch effect along the welding seam (Fig. 19.33).

Roll bending of conical parts on machines with cylindrical rolls causes some difficulties due to different surface speeds at the large and small ends of the workpiece. Although the lower rolls are inclined to achieve the different diameters, considerable effort must be expended in controlling the friction conditions [19.35], [19.36]. The determination of force, torque, and power for the roll-bending process is addressed in [19.37].

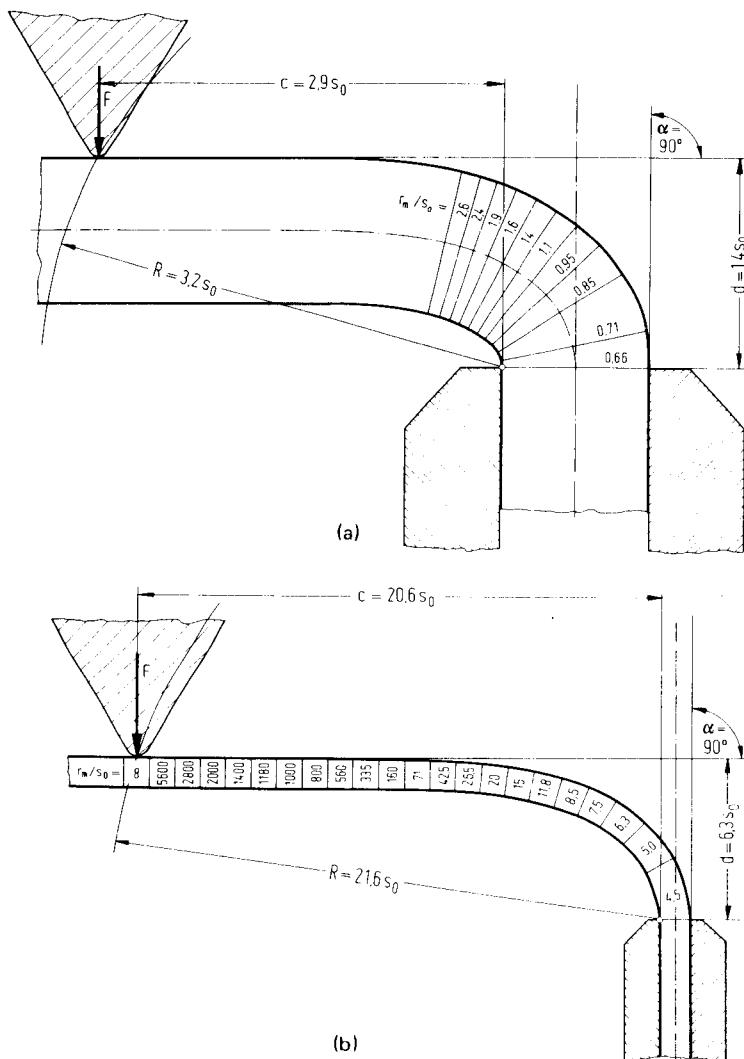


FIG. 19.31 Wiper bending of commercial-purity aluminum. (a) Wiping radius  $R = 3.2s_0$ . (b) Wiping radius  $R = 21.6s_0$ . (After [19.10].)

### 19.2.5 Roll Forming

Long components of various cross sections are formed by passing sheet metal through a succession of progressively shaped power-driven contoured rolls. From stand to stand, the gap between upper and lower rolls changes from the shape of the sheet to the shape of the finished section. The process permits the economical production of both simple and complex cross sections of almost arbitrary length of strips up to 2000 mm (80 in) wide and 0.2–20 mm (0.008–0.8 in) thick at speeds in excess of 100 m/min (330 ft/min). It competes with brake bending, extrusion, and hot rolling of

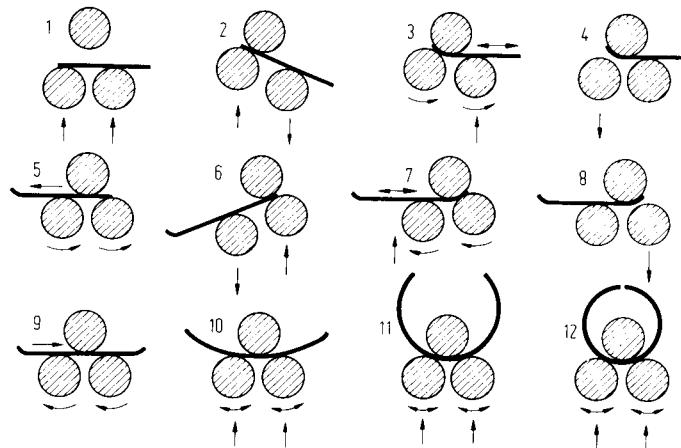


FIG. 19.32 Working stages in roll bending.

sections [19.38]. Fig. 19.34 illustrates the fabrication of a door frame section by brake bending, folding, and roll forming.

Complications arise in roll forming as a result of warping, which can be caused by corner strains. These strains are greater than the strains in the remaining section, since bending does not take place simultaneously over the entire sheet width. Warping is avoided by various means:

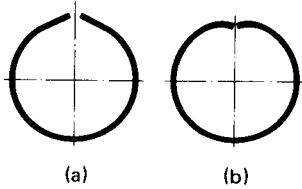


FIG. 19.33 Flaws in roll bending. (a) Leading and trailing edges not bent. (b) Leading and trailing edges overbent.

strength by rolling with increasing velocity. From stage to stage forming takes place with the same angular velocity, but increasing roll diameters. Severe wear of the rolls and scratching of the workpiece are the drawbacks of this technique.

- 4 Curved sections can be straightened continually by passing them through a straightening die or the rolls of a leveller. They can also be bent straight in the last stand of the roll former [19.38].

More details on strains, stresses, forces, and torques are available in the literature [19.39] to [19.49].

#### 19.2.6 Bending with Pliable Tools

In this variant of brake bending one half of the forming tool, usually the die, consists of a pliable pad. The material for this pad generally is polyurethane with a hardness of 70-98 Shore A. For small production runs this process is preferable to conventional brake bending since only one rigid tool need be supplied, while the inexpensive and versatile rubber pad takes the place of the other

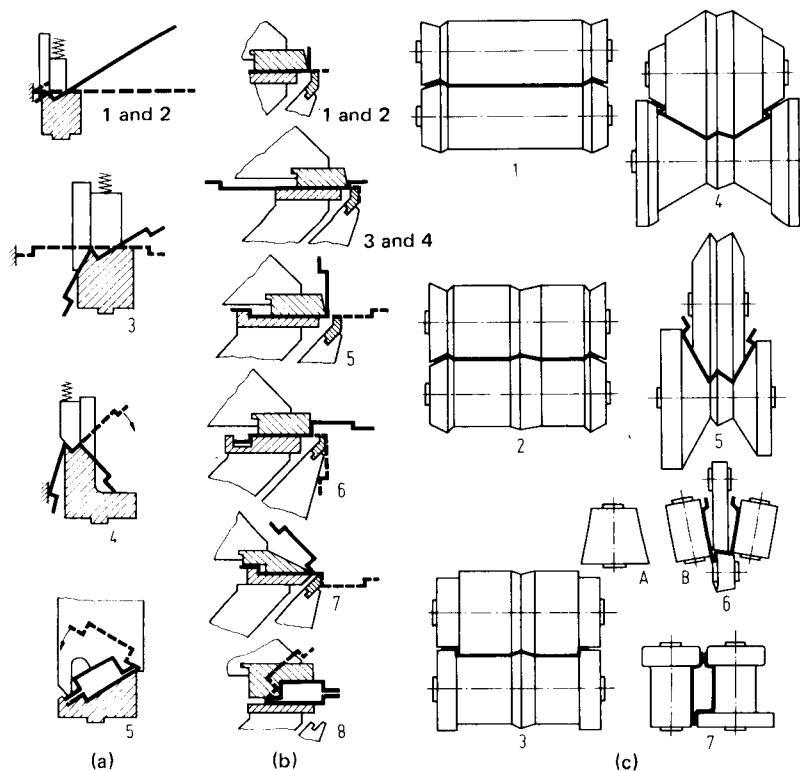


**FIG. 19.34** Manufacture of door-frame cross section. (a) Die bending. (b) Folding. (c) Contour roll forming. (After [19.7].)

tool component. Setup time is low, and the workpiece surface on the side of the pad will remain undamaged by imprints of dust and metal particles. This is important for sheet metal coated with plastic on one side.

For 90° V bending with rigid punch and rubber pad the relationships between pad hardness, pad dimension, punch radius, bending force, and springback were studied [19.50] (Fig. 19.35). The punch force is considerably higher than in a comparable air-bending process, since about 50–90% of the energy expended by the punch is required for deformation of the pad. Since deformation will cause the pad to heat up, operations must be controlled to keep the temperature of the pad below 77°C (170°F).

#### 19.2.7 Determination of Workpiece Length

This topic is restricted to brake bending, folding, and roll bending. It is assumed that the shape of the tool is transferred accurately to the workpiece, and the cross section consists of pieces bounded by straight lines and circular arcs.

Even if these conditions are met, an exact determination of the size to which the blank must be cut is made difficult by the internal displacements of work material in the bending arc. Different approaches to analysis are indicated in the literature [19.7]. An empirical method is presented here which is useful in industrial practice. In the following equation for blank length the

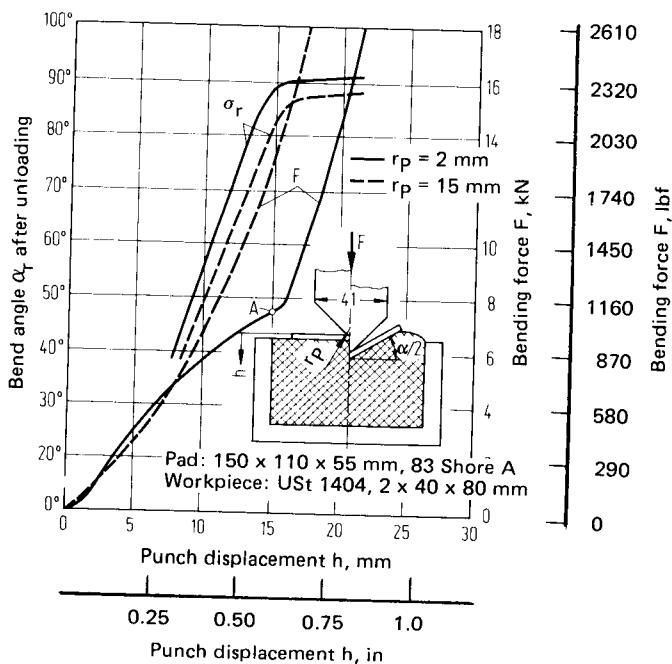


**FIG. 10.35** Bending force and bend angle (after unloading) in bending with pliable tools. (After [19.50].)

difference between unlengthened and mean fiber is taken into account by means of a correction factor:

$$l = a_1 + \frac{\alpha\pi}{180} \left( r_i + \frac{s_0}{2} \xi \right) + a_2 \quad (19.59)$$

where  $\alpha$  is in degrees, and the correction factor  $\xi$  is taken from Fig. 19.36 for different bend radii  $r_m$  and bend angles  $\alpha$ .

### 19.3 PROPERTIES OF BENT SHEET PARTS

With V-die bending as an example, the following workpiece properties are considered: mechanical properties, surface quality, geometric accuracy after bending, springback, and edge deformation.

#### 19.3.1 Springback, Bending Accuracy, and Edge Deformation

The forming process for which springback is most significant and most in need of control is bending. The mechanism characteristic for pure bending (see Sec. 19.1.2) is fundamentally the same for all bending processes. Control of springback for the bending processes applied in practice is difficult for a number of reasons, especially in mass production.

Fig. 19.7 illustrates the dependence of the springback ratio  $K$  (see Eqs. 19.29 and 19.40) upon work material and the ratio of inner bend radius after springback to sheet thickness. Evidently variations in sheet thickness (15–20% for thin sheets according to DIN 1543 and 1544) affect  $K$  more significantly as the desired bend radius increases. The same holds for variations in work

material properties. Therefore processes such as air bending and roll bending are prone to considerable scatter in springback if unfavorable conditions cause the two effects to overlap. In single-unit production these discrepancies (i.e., in bend angle) can be corrected easily. In automatic mass production special measures must be taken to keep the scatter within specified limits. This can be achieved simply by restricting sheet thickness tolerances. A more advanced approach to the control of springback error is indicated by the process model for air bending described in [19.22] (see Sec. 19.2.1). The computer model calculates springback for a set of given bending parameters and material properties, and the overbend (i.e., punch travel) necessary to minimize the error. A prototype adaptive sheet-bending system automatically compensating for springback was developed [19.51], in which an error signal based on an angular transducer output is used to control punch position. The design angle is approached iteratively: the sheet is bent in a number of loading-unloading cycles by a microcomputer system. During each cycle the sheet is bent to a certain angle, unloaded, the point of unloading automatically detected, springback measured, and a new bend angle determined. Convergence to a small fraction of a degree is obtained in a few cycles. This approach is insensitive to variations in material properties and sheet geometry.

If such measures are insufficient, die bending with coining must be applied. The shape of punch and die can be transferred accurately to the workpiece. However, new problems arise caused by the peculiarities of die bending (see Sec. 19.2.2) [19.28], [19.30].

During coining, the bend angle is no longer determined by die angle and elastic springback alone. The loaded bend angle can differ considerably from the die angle due to overbending and re-forward bending (see Fig. 19.26) as a consequence of local coining phenomena. Under otherwise equal conditions, the effects of the resulting deformation become dependent upon the applied coining load. Thus the degree of accuracy of the bend angle achieved with coining is affected by the magnitude of the coining force.

The amount of elastic springback and the effects of overbending, re-forward bending, and local coining phenomena are dependent upon tool geometry, the stress-strain relationship of the work material, and the geometry of the workpiece, notably its thickness. The following should be observed if precisely dimensioned parts are to be produced by V-die bending.

If a premium is placed on precision of both bend angle and the inner curvature of the apex of the bent part, the use of a closed punch and die system is required. The punch radius must equal the desired inner radius of curvature of the workpiece. During bending, punch and die must approach each other until the punch radius has been transferred completely to the workpiece. Subsequently the bend angle must be corrected subject to the remaining angular error.

This procedure requires considerable effort with regard to both tooling and especially the machine tool. This effort can be reduced considerably, whenever demands for dimensional accuracy of the workpiece can be relaxed. Semiclosed-die bending or possibly even open-die (air) bending may then be sufficient.

### 19.3.2 Formability in Bending

The mechanical properties of a part produced by bending are primarily determined by the material properties on one hand and the magnitude of the bend radius in relation to the smallest bend

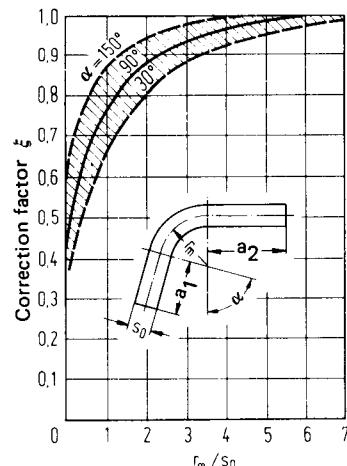
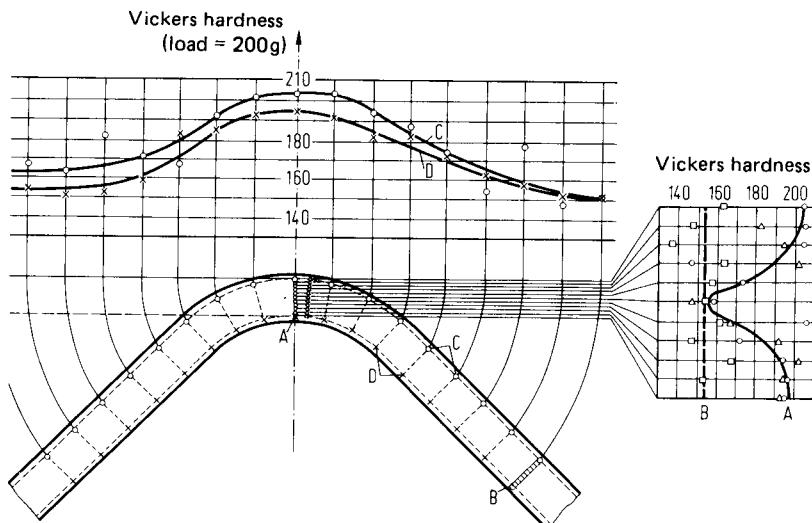


FIG. 19.36 Correction factor  $\xi$  for determining straight length of bent parts (After [19.7].)



**FIG. 19.37** Hardness variation in bent steel sheet resulting from pure-moment bending. (After [19.1].)

radius achievable without the occurrence of cracks in the domain of the bending arc on the other. As a result of the increase in strain toward the inner and outer surfaces in the bending arc, the outer layers harden, as can be verified by hardness scanning (Fig. 19.37). Although the hardness drops off along the arc from the apex toward the leg, hardening does extend a considerable distance into the leg. This is a direct consequence of the inclination of longitudinal cross sections discussed in Sec. 19.1.4.

While the bending arc is strengthened by strain hardening, the danger of fracture increases with rising bending strain when the part is under load. This danger is in part caused by the biaxial stress state at the outer bend radius which is weaker for narrow parts, where edge deformation is less restricted, but more significant for longer parts, where conditions of plane strain exist. Fig. 19.38 illustrates the dependence of the limiting strain in outer fiber  $\epsilon_{o,b}$  (from Eq. 19.3) upon the ratio  $b/s_0$  for steel sheet. The relationship between the smallest bend radius possible and outer strain  $\epsilon_{o,b}$ , based upon Eq. 19.3, is

$$r_{i,\min} = \frac{s_0}{2} \left( \frac{1}{\epsilon_{o,b}} - 1 \right) = c s_0 \quad (19.60)$$

Some values for curvature factor  $c$  for various sheet materials are given elsewhere [19.7].

Bendability of a wide range of materials was successfully related to their percent area reduction  $A_r$  obtained in uniaxial tension

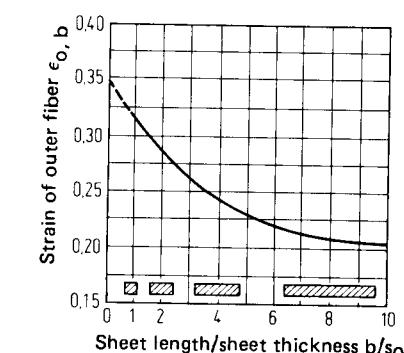


**FIG. 19.38** Largest strain of outer-boundary fiber as a function of sheet length. (After [19.52].)

[19.53]. For pure-moment bending of sheet in plane strain, the true strain in the outside fiber was equated to the true fracture strain in simple tension. For the case when the neutral fiber is assumed to coincide with the middle fiber, the limiting ratio of internal bend radius to sheet thickness is

$$\frac{r_i}{s_0} = \frac{50}{A_r} - 1 \quad (19.61)$$

This relationship tends to be valid for  $A_r \leq 20\%$ . When the neutral fiber is displaced from the center of the sheet, the following relationship is shown to hold:

$$\frac{r_i}{s_0} = \frac{(100 - A_r)^2}{200A_r - A_r^2} \quad (19.62)$$

The orientation of the bend axis with respect to the rolling direction of the sheet has a considerable influence on the magnitude of  $\epsilon_{ab}$ . Smaller bending strains may lead to failure when these directions coincide. According to DIN 6935 [54], values for  $r_{i,\min}$  tend to be higher by  $0.50s_0$  in this case than when bending at a right angle to the rolling direction.

While the control of scatter in springback necessitates small bend radii (see Fig. 19.7), large bend radii are preferable in view of the mechanical properties of bent parts. Compromises are necessary as a result. If bending to a radius below  $r_{i,\min}$  is required for design purposes, the work-piece must be heated prior to forming.

### 19.3.3 Defects in Bending

As a result of the triaxial stress state in bending—the tangential, tensile, and compressive stresses cause stresses directed along the bend axis—anticlastic bending occurs. Sections taken parallel to the bend axis in the region of high deformation, such as directly underneath the punch, for example, do not remain plane along the entire depth of the bent part (Fig. 19.39). The nature of the deformation near the edges of the plate is such that the plate bends away from the punch. Thus the plate is not in contact with the punch over its entire length, and localized coining is necessary to establish complete contact. Clearly closed-die bending is required to correct for this phenomenon during coining, although semiclosed-die bending could also tend to minimize this flaw. A considerable effort in force must be expended to eliminate the effects of antilastic bending by closed-die bending. To illustrate, coining forces up to 100 times the peak air-bending force were

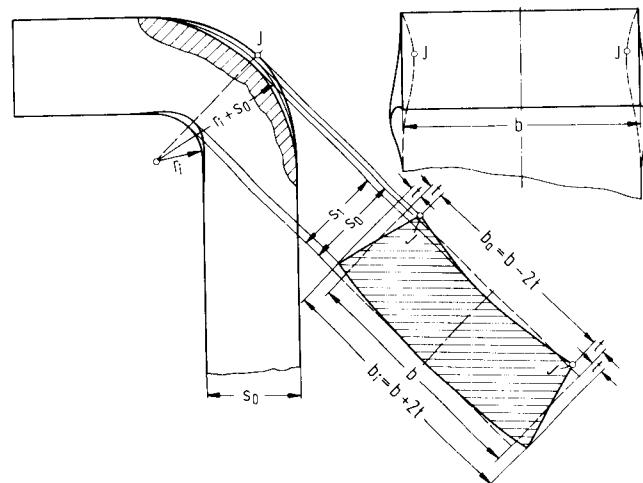
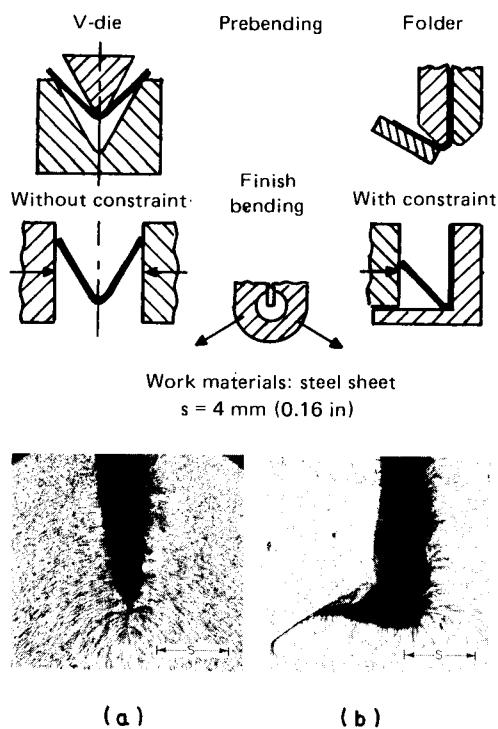


FIG. 19.39 Edge deformations in bending. (After [19.7].)

found to be required for this effort when  $w/r_p = w/s_0 = 21$  [19.30]. At times localized coining can also be exerted by the punch nose, particularly when nose radii are small.

Workpieces are most frequently cut to size by shearing (see Chap. 24). The sheared edge has poor surface quality and is greatly strain-hardened, particularly in the vicinity of the burr. If the sum of the maximum effective shearing strain and the maximum bending strain exceeds the fracture strain of the work material, cracking will occur along the outer edge of the bending arc. If such cracks cannot be tolerated, the strain-hardened portion of the edge can be removed prior to bending, preferably by milling. It has been shown that elimination of strain hardening by annealing will remove the danger of edge cracking as well [19.55]. In some applications small edge cracks are acceptable, especially if the edge is joined to another part by welding. In this case the size of the cracks should be kept small by observing proper shearing practice, that is, avoiding shearing with dull blades, and maintaining the optimum gap between the shearing blades.

Sheet metal is often bent to form seams and hems. In these operations bending is carried out through  $180^\circ$ ; that is, the final angle formed by the legs of the part is  $0^\circ$ . Seaming, which joins two sheets end to end by interlocking their ends, always involves finite internal bend radii. Hemming, on the other hand, represents the most severe case of  $180^\circ$  bending, since the sheet is flattened onto itself so that the internal bend radius approaches zero. The first stage is a prebending operation involving a punch-type tool with finite nose radius. Typical prebending processes are V-die and air bending or folding (Fig. 19.40). During the final stage the two legs of the V-shaped workpiece are squeezed together without constraints at the inside of the bending arc. The inside surface assumes a roughness the configuration of which is a function of strain and grain size [19.56]. As the inside radius approaches zero, the wrinkles tend to form cracks and folds. Fig.



**FIG. 19.40** Formation of (a) cracks and (b) folds in 180° bending. (After [19.56].)

19.40 shows the development of cracks or folds to depend upon the bending technique employed. Since such defects are likely to lead to failure in cyclic load applications, it is preferable to avoid sharp bends and to retain a sufficiently large inside radius instead by open or teardrop hemming.

#### 19.4 TOOLING AND MACHINE TOOLS FOR THE BENDING OF SHEET AND PLATE

Bending tools and machine tools for bending differ greatly in shape in accordance with the multitude of bending processes (see Chap. 2). A primary distinction can be made:

- 1 Tools for processes involving small workpieces, such as air bending, die bending, and edge rolling, which are carried out on machine tools with rectilinear tool motion
- 2 Tools for processes as in 1, except for large workpieces which require specialized bending machines
- 3 Tools for processes with rotating tool motion, which are carried out on specialized bending machines without exception, that is, roll bending, roll forming, roller levelling, folding

Some fundamental concepts for the design of tooling and the construction of the machine tools are now presented. Details of the design of tooling for category 1 are described in [19.57] to [19.59] with numerous practical examples. Fundamentals of stroke-, load-, and energy-restricted presses are discussed in Chap. 8.

##### 19.4.1 Bending with Rectilinear Tool Motion

###### *Tools for C-Type and Straight-Side Frame Presses*

Tools are designed similar to those for blanking or deep drawing, except that the blanking die or drawing die is replaced by the bending punch. Depending upon accuracy requirements, the upper tool is either unguided, guided along the punch, or guided by special columns.

When tooling is simple, punch and die are attached directly to the ram and the bed of the press. More complex tooling is usually affixed to standardized die sets. Once it is guided, the tool can then be installed outside the press. Important additional components are ejector or stripper as well as stops in the form of strips or pins for locating the workpiece. A simple bending tool with punch guide is shown in Fig. 19.41.

Bending with such tools has the advantage that several bends can be performed in the same operation by using wedge slide feeders, for example, and that bending at separate workpiece locations can be combined with simple shearing and deep-drawing work (in one operation or in progressive tools).

Plain carbon steels and possibly low-alloy steels serve as tool materials for punches and dies. For larger tools, less expensive construction steel or grey cast iron are also used. However, edges prone to wear are made of higher-quality steel, and even of carbide for large production runs.

###### *Press Brake Bending*

Bending with rectilinear tool motion is primarily performed on press brakes whenever the bending length exceeds a specified amount, or production runs are so small that making a tool for a conventional press is uneconomical. A large portion of workpieces processed on press brakes consists of sheet sections which can also be made on folders and roll formers (see Fig. 19.34).

Press brakes are generally hydraulic, that is, load-restricted C-type frame presses with double-column construction (Fig. 19.42) for bending lengths of about 2–6 m (6–20 ft), in special cases up to 10 m (33 ft). Bed and ram consist of trapezoidal plates to which the upper and lower tools are attached. Steps in the production of a section are illustrated in Fig. 19.43. The die can be shifted on the table for positioning of the various die shapes underneath the punch. On some machine tools several punches can be affixed to the ram so that they remain movable for efficient tool

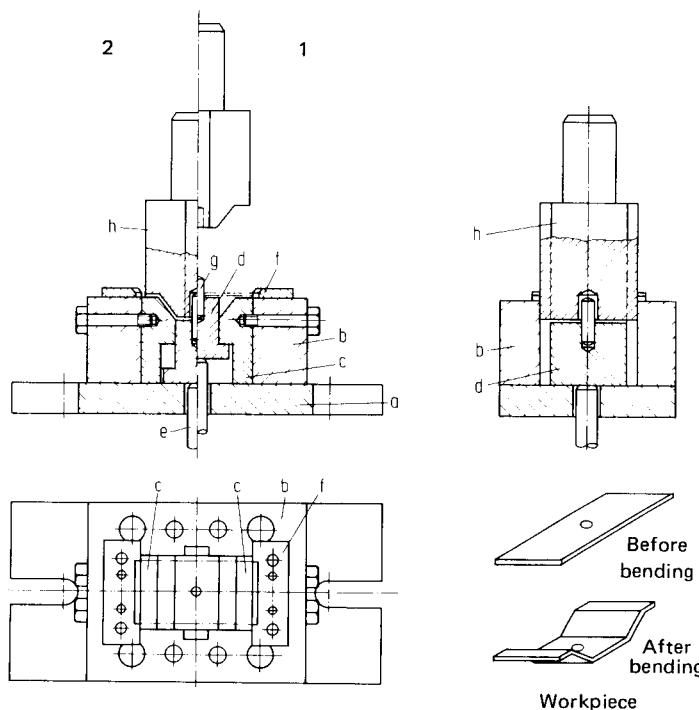


**FIG. 19.41** Bending tooling with punch guide. *a*—Baseplate; *b*—take-up frame for bending die inserts; *c*—two bending-die inserts; *d*—ejector; *e*—pressure pin; *f*—two-sheet positioning guides; *g*—locating pin; *h*—punch with machined spigot; 1—configuration during loading of sheet; 2—configuration after bending. (*After* [19.59].)

changing. For average production runs, numerical control systems are installed for such movements as well as for punch stroke movements to minimize production time per piece.

#### 19.4.2 Bending with Rotating Tool Motion

##### *Folders*

Folders are used for the same jobs as press brakes. Bending on the folder takes longer, however, since the workpiece must first be clamped between folding leaf and jaw. But folders are generally less expensive, and shorter legs can be bent (see Sec. 19.2.3). They are therefore preferred in job-shop operations. The basic design of folders is shown in Fig. 19.44. Folding leaf, jaw, and wing are arranged between two columns. They can be adjusted in height or distance to the folding axis to fit the geometry of the workpiece. This is done by hand or mostly by motor through lead screws. The folding motion takes place mechanically by transmission or hydraulically. Numerical control is used for these machines as well for clamping, folding, and return stroke movements. As for tooling, a bending die insert of the appropriate geometry is attached to the folding leaf (Fig. 19.45).

##### *Roll Formers*

Machine tools of this type (Fig. 19.46) are built mostly with interchangeable parts. Systems of different sizes can be assembled from units with one or two roll pairs. They may involve a few

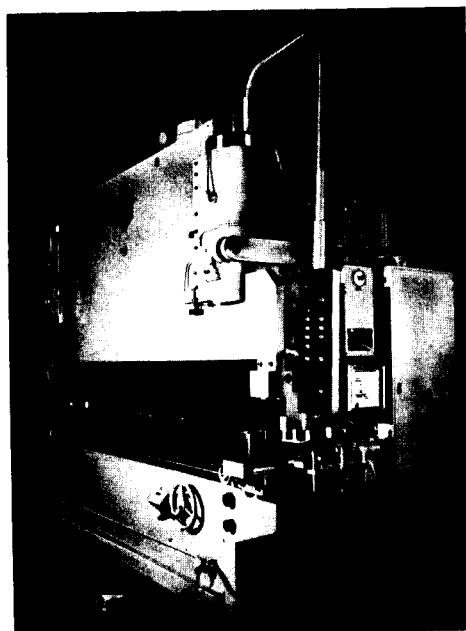


**FIG. 19.42** Program-controlled press brake. (*Courtesy of Hässler.*)

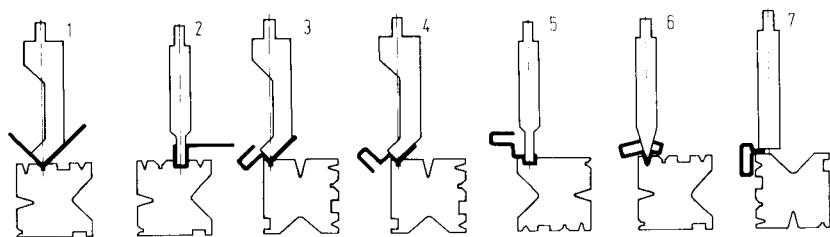


**FIG. 19.43** Stages in the production of a sheet section by die bending.

stages for simple sections, or 15 stages, for example, for very complex sections. The use of roll formers becomes economical whenever sections, which otherwise could be produced on press brakes or folders, are of extensive length, and production quantity is large. They are fed from coil stock, and can be fitted out with straightening and cut-off equipment. They are designed so that rolls can be replaced quickly for easy changeover to the production of a different section. The upper rolls are adjustable in height to accommodate sheet thickness and roll diameter. Considerations of springback and smallest bend radius are important in the shaping of the rolls and the sections to be produced.

#### ***Roll Benders***

Roll benders for sheet are usually equipped with three or, more rarely, with four rolls (Fig. 19.47). Great varieties in drive and roll adjustment systems exist: powered upper roll or powered lower rolls which are mostly arranged symmetrically; vertical adjustment of the upper roll or the lower

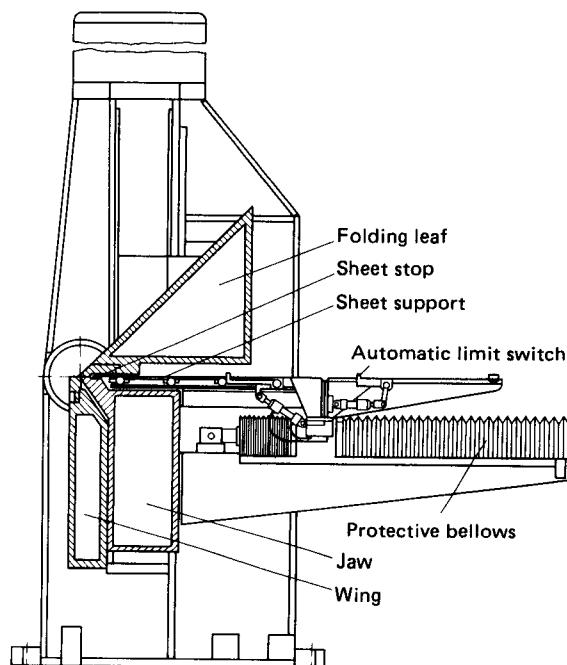


FIG. 19.44 Cross-section of a folder. (Courtesy of Reinhardt.)

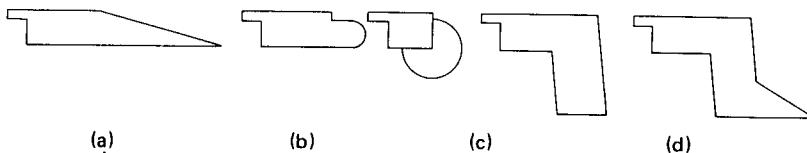


FIG. 19.45 Die inserts for folding. (a) Simple insert with sharp edge. (b) Rounded insert. (c) Gooseneck insert. (d) Z-shaped insert with sharp edge. (After [19.7].)

rolls, or skew adjustment of the lower rolls. In most cases the lower rolls are driven and adjusted for workpiece curvature. To be able to remove a circularly bent sheet from the bender, the bearing of the upper roll opposite the driven side can be swung open, and the roll easily tilted up. On larger benders—the bending length may reach 10 m (33 ft)—the lower rolls are protected against extensive deflection by support rolls. The upper roll can have a crown, and can be supported further by being extended beyond the bearing.

The rolls are driven by reversing transmissions, reversing motors, or individual motor drive for both rolling directions, since the sheet must traverse the rolls several times (see Fig. 19.32). The intermediate positioning of the lower rolls is done with motors over suitable worm gears and lead screws. The rolls are forged from plain carbon steel, and from low-alloy steels for hot roll bending. Rolls with larger diameter are made hollow.

## 19.5 Bending of Rectangular and Round Bars

Bending of bars belongs to the category of massive forming, although no workpiece material is displaced as in forging or rolling, and no change in cross section is intended. Areas of application

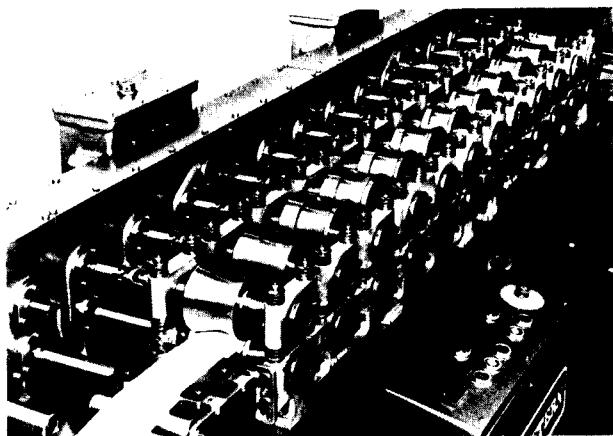


**FIG. 19.46** Roll former, quick-change construction. (*Courtesy of Dreistern.*)

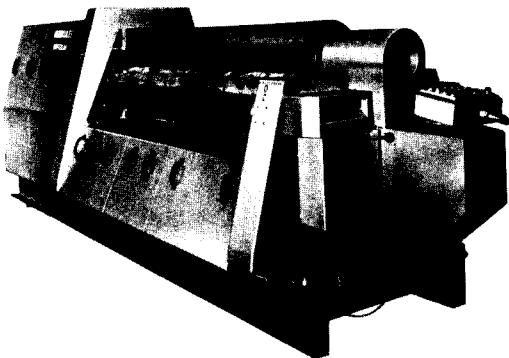


**FIG. 19.47** Roll bender with four rolls. (*Courtesy of Herkules.*)

are steel construction and container and vehicle manufacture, including the production of helical springs of all types. In contrast to sheet bending, rectangular bars are understood to have a length (parallel to the bend axis) no larger than the thickness (normal to the bend axis).

Bending of round bars has so far been analyzed utilizing the assumptions of elementary bending theory and neglecting the shifting of fibers (see Sec. 19.1) [19.60], [19.61]. Almost complete solutions based on advanced theory exist for rectangular bars [19.62], [19.63]. Internal stresses were determined from strains measured on the surface [19.64]. Cross-sectional changes were investigated for a variety of bending processes [19.65], [19.66]. Deformed cross sections of the apex of air-bent bars with different ratios  $b/s_0$  and equal ratios  $r_m/s_0$  are shown in Fig. 19.48.

In addition to the bending methods applied to sheet bending, wiper bending is used for bars. (For bend angles larger than  $360^\circ$ , the process becomes coiling, such as coiling of helical springs.) In this process one end of the bar is clamped to the periphery of a rotating disk or roll, while the remaining straight portion is held against a stop, which often is in the form of a roll. A wiper is shown in Fig. 19.49. If rectangular cross sections with small  $b/s_0$  ratios are bent, dies or rolls must be designed such that the section does not tip over, or no folds can occur on the compression side by buckling (Fig. 19.50).

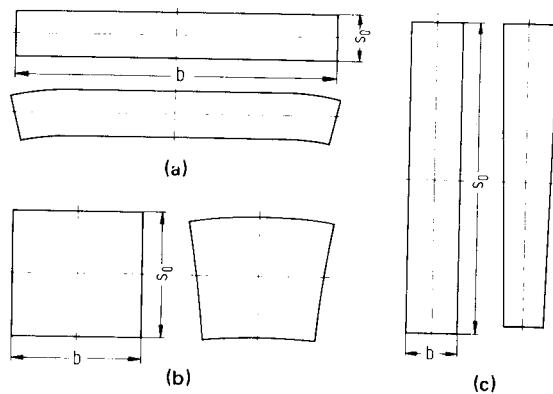


**FIG. 19.48** Deformation of different cross sections of  $r_m/s_0 = 2$ .  
 (a)  $b/s_0 = 6.66$ . (b)  $b/s_0 = 1$ . (c)  $b/s_0 = 0.15$ .

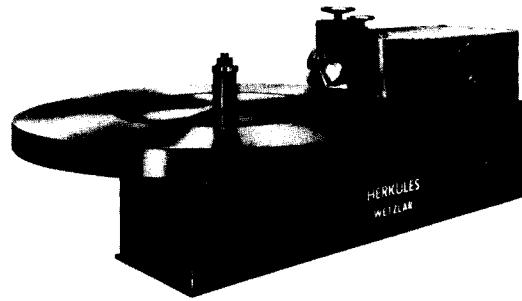


**FIG. 19.49** Wiper bender. (*Courtesy of Herkules.*)

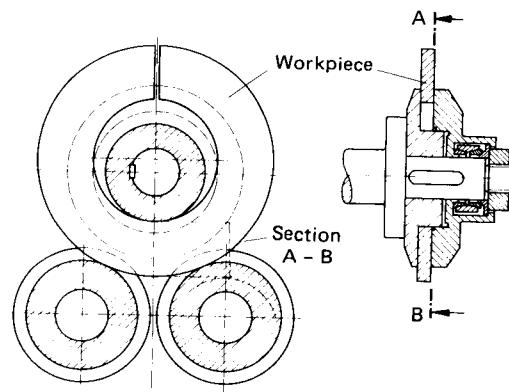


**FIG. 19.50** Circular spring-loaded rolls of roll bender for bending of narrow beams. (*After [19.66].*)

## 19.6 BENDING OF TUBES AND BEAMS

Bending of tubes with circular cross section is of considerable importance in the manufacture of boilers and the construction of pipelines. All bending methods according to DIN 8586 [19.29] (except die beading, die flanging, bending by buckling, roll forming, and roll and draw bending) are applied with numerous variants, for which a process classification has been established [19.67]. In the application of these processes an internal bending arc surface free from folds and wrinkles is generally considered important.

Selection of a process for a specific case is influenced by economic considerations as well as the mechanical properties of the workpiece material, tube or pipe dimensions, and specified bend radius. The most frequent methods are tube bending with a mandrel (wiper bending, Fig. 19.51) and tube bending without mandrel (folding, Fig. 19.52). In addition to the application of the

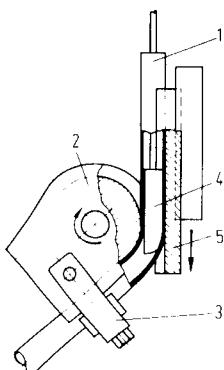


**FIG. 19.51** Pipe bending with support mandrel. 1—pipe; 2—bending die; 3—clamping bracket; 4—support mandrel; 5—bending bar. (After [19.67].)

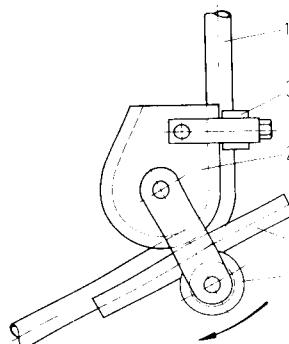


**FIG. 19.52** Pipe bending without mandrel. 1—pipe; 2—bending die; 3—clamping bracket; 4—roll; 5—bending bar. (After [19.67].)

bending force, the bending tools have the task of preventing undesirable forming defects such as wrinkling in the compressive region, flattening of the ring cross section, and weakening of the wall in the tensile region. All of them reduce the strength of the tube in the region of the elbow during mechanical loading, which usually means internal pressure. Tube bending with a mandrel is primarily justified for thin-walled tubes with a wall-thickness-to-outside diameter ratio  $\leq 0.06$ . An example of such a bender, equipped with numerical control for pipe feed and bend angles in two planes, is shown in Fig. 19.53.

Both processes cause a reduction in wall thickness in the tensile domain. This can be prevented by so-called pressure bending, in which compressive stresses are superimposed on the bending stresses in the longitudinal direction. Although the wall thickness is increased considerably on the inside, the thickness of the outer wall can be kept constant.

During bending of thin-walled semihollow or hollow sections (Fig. 19.54) it is also important to avoid wrinkling or fold formation and cross-sectional changes, especially the collapse of the cross-sectional components lying in the bending plane. The processes described for tube bending are frequently joined by stretch forming (see Chap. 23). The machine tool shown in Fig. 19.55 applies longitudinal pull, but also lateral force by means of a forming shoe. Such machines also enable the bending of sections with variable cross section as they occur in aircraft construction. Additional possibilities for the support of sections are offered by the insertion of steel chain links, flexible plastic strips, and the filling of hollow sections with low-melting-point alloys, such as lead [19.69].

Such measures are unnecessary for bending thick-walled sections, such as channels, T-beams, and I-beams. They are usually bent on roll benders (Fig. 19.56) or on wiper benders (Fig. 19.49).

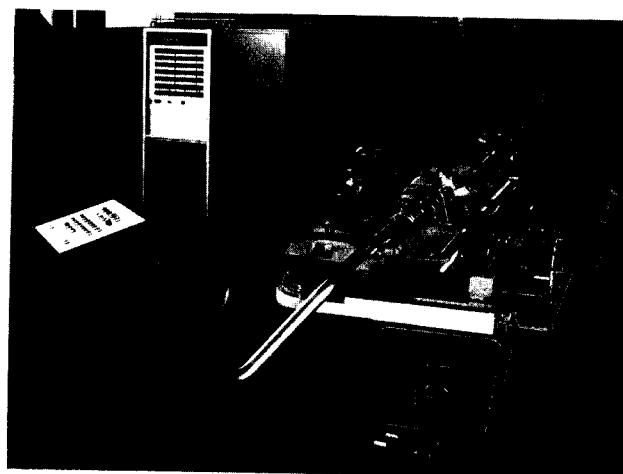


**FIG. 19.53** Numerically controlled pipe bender. (*Courtesy of Banning.*)

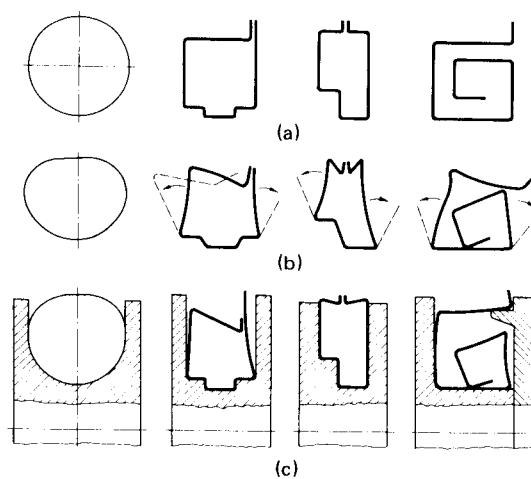


**FIG. 19.54** Alternate shapes of sections bent without mandrel. (a) Straight cross sections. (b) Bent without support. (c) Bent with support roll. (*After [19.68].*)

## 19.7 LEVELLING AND STRAIGHTENING BY BENDING

All bending processes discussed so far are intended to impart a specific permanent curvature to a plane or straight workpiece by bending. Straightening processes have the opposite task: they are to remove unwanted curvature that may be present in workpieces. Such curvature, which is significantly smaller than that induced by bending processes, is caused by unsymmetric residual stress formation during forming, differential cooling after forming, release of residual stresses by machining, and so on.

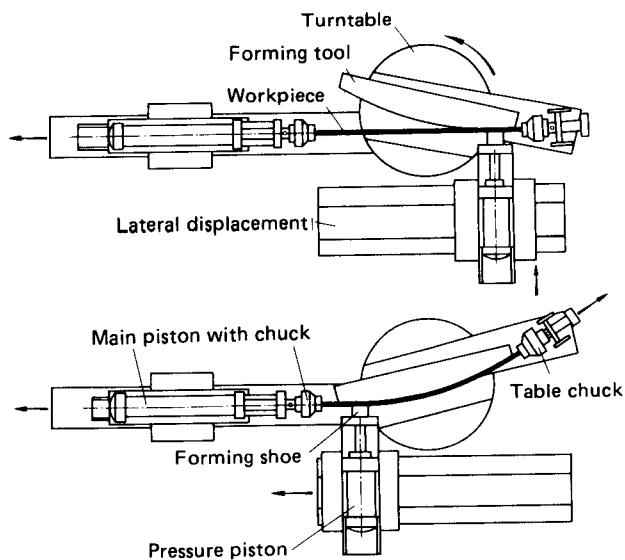


FIG. 19.55 Schematic of combined stretch bending with auxiliary tooling. (After [19.69].)

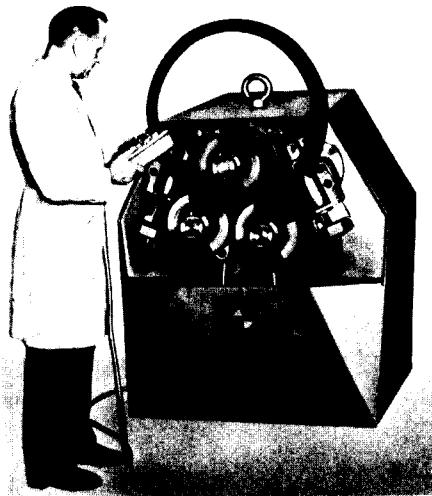
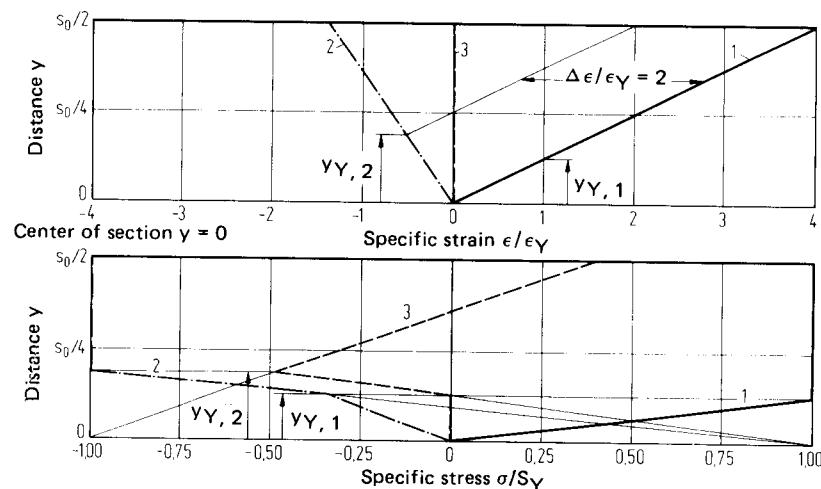


FIG. 19.56 Roll bender for sections. (Courtesy of Pullmax.)



**FIG. 19.57** Strain and stress distribution. (1, 2) twofold bending, (3) unloading. (After [19.16].)

The principle of straightening by bending can be illustrated with the example of a straight, residual stressfree sheet, which is first bent, then straightened. The elementary theory presented in Sec. 19.1 is applied for this purpose [19.70], [19.71]. The sheet bent by partially plastic deformation (Eqs. 19.1 to 19.22) and subsequent springback (Eqs. 19.23 to 19.31) must be subjected to a second bending process—with reversed sign—such that it ends up straight after it springs back. In the example of Fig. 19.57 the sheet is bent with an outer fiber strain  $\epsilon_{o,1} = 4\epsilon_Y$  (line 1), then bent back to  $\epsilon_{o,2} = -1.37\epsilon_Y$  (line 2); the residual stress distribution (line 3) after unloading satisfies the condition that the resulting moment and the residual strain  $\epsilon_{o,3}$  vanish.  $\epsilon_{o,2}$  can be determined analytically [19.72] or graphically [19.16].

### 19.7.1 Straightening by Air Bending

This process is primarily intended for short bars, stepped shafts, crank shafts, and so on, which have suffered distortions due to heat treatment and chip removal. They must be straightened prior to the final grinding operation. This is done on hydraulic-stroke-controlled straightening presses, which are equipped with fixtures for mounting workpieces of different shapes. Special presses are used when production runs are large. Straightening presses are usually operated by hand. There are presses, however, which are equipped with electronic controls for fully automatic straightening.

### 19.7.2 Roller Levelling of Sheet

Plates up to 50 mm (2 in) thick and sheet strip down to the thinnest foils are straightened on roller levellers before subsequent processing. The sheet is subjected to multiple back-and-forth bending with decreasing curvature between a number of staggered rolls (Fig. 19.58). The number of rolls (5–30) depends upon thickness, yield stress, and modulus of elasticity of the sheet. Thin sheets with high yield stress and small modulus of elasticity are the most difficult to straighten and require as many rolls as possible. Five rolls suffice for the straightening of residual-stress-free sheet with bending curvature in the longitudinal direction only [19.72]. This induces a twofold bending

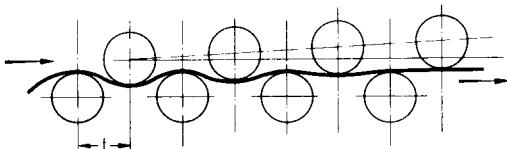


**FIG. 19.58** Principle of roller straightening.

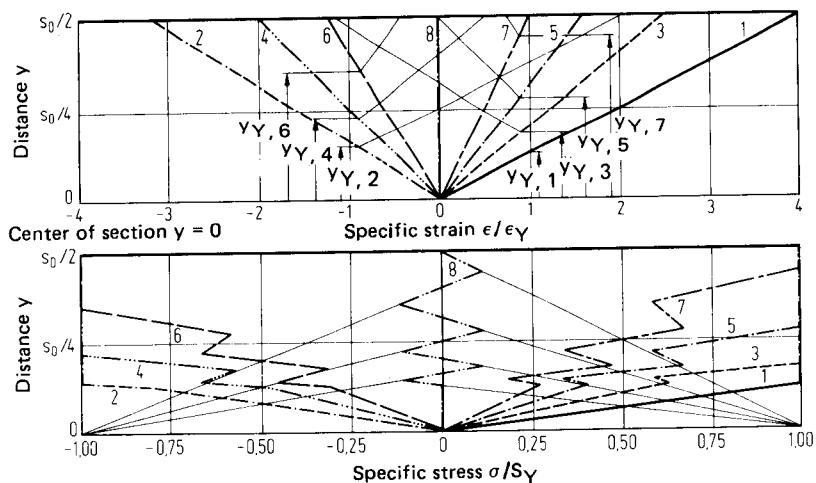


**FIG. 19.59** Strain and stress distribution in eightfold bending (1 to 8). Elastic-ideal plastic work material, elementary theory. (After [19.16].)



**FIG. 19.60** Roller straightener for plate stock. (Courtesy of Siemag.)

process in case of symmetrically adjusted rolls. Since the remaining residual stresses are relatively high, the back-and-forth bending process is repeated several times with decreasing surface strains.

With this approach the residual stresses can be reduced arbitrarily [19.71]. The stress distributions for an eightfold bending process are shown in Fig. 19.59.

Roller levellers generally have constant roll spacing and equal roll diameters. The lower rolls are usually fixed and the upper rolls adjustable (depth and angle). The angle adjustment causes the decreasing curvature in the sheet as it travels from roll to roll. Levellers for large sheet widths require support rolls to prevent sagging of the straightening rolls. A roller leveller for heavy sheet is shown in Fig. 19.60.

In roller levelling of sheet tension can be superimposed on the alternating bending action (straightening by stretch bending). This improves the straightening results [19.73], [19.74].

### 19.7.3 Roller Straightening of Round Bars and Tubes

In contrast to sheets, which are generally bent and straightened in two planes, round bars, pipes, and all other sections can be bent arbitrarily in many planes and must be straightened accordingly. Cornered sections are straightened like sheets, except that rolls must be of the appropriate shape and bending takes place in two mutually perpendicular planes. Round bars and pipes are mostly straightened in two- or three-roll straighteners in which the rolls are inclined to the bar axis. By this arrangement rotary motion is superimposed on the longitudinal motion of the bar which provides back-and-forth bending in all planes.

In two-roll units (Fig. 19.61a) one roll is a hyperboloid of revolution, the other a circular cylinder. Lateral guide rails are required to hold the straightening stock between the rolls. By the inclination of both rolls, the straightening gap can be adjusted either to create three-point support, or to cause the straightening

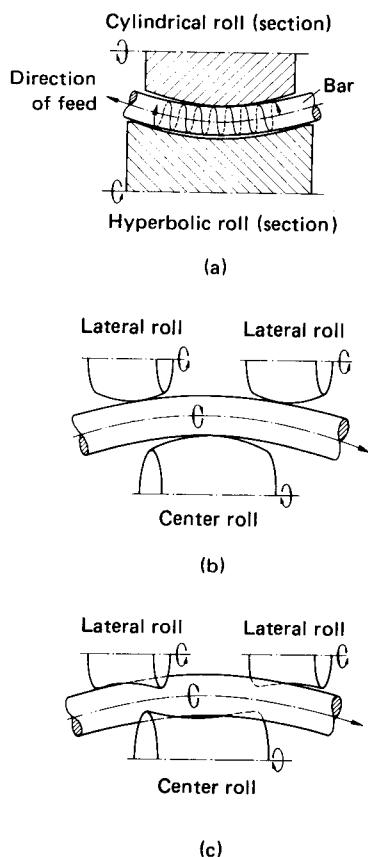


**FIG. 19.61** Roller straightening of round bars.  
(a) With two rolls. (b) With three convex rolls.  
(c) With three hyperbolic rolls.

stock to be in contact along the entire length of the hyperbolic roll. In the latter case additional lateral pressure can be applied to smooth out the surface [19.75].

The three-roll principle utilizes either convex (Fig. 19.61b) or hyperbolic rolls (Fig. 19.61c). Again, the convex rolls require guide rails. A noteworthy feature of this principle is a slight increase in bar diameter of up to 1%. It is also noticeable in the two-roll operation when no additional lateral pressure is applied. This phenomenon is traced back to friction stresses acting between workpiece and rolls and residual stresses present in the workpiece, which are superimposed on the bending stresses [19.75], [19.76]. A complete explanation of the phenomenon is not available, however. Fig. 19.62 shows a nine-roll straightener for straightening of round bars or pipes.

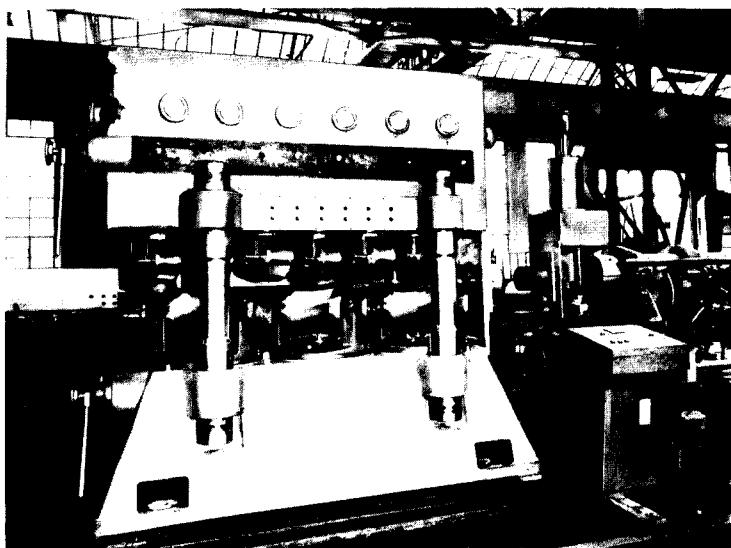


**FIG. 19.62** Roller straightener for pipes or bars, with nine rolls. (Courtesy of Kieserling.)

## REFERENCES

- 19.1 Kienzle, O.: "Investigations of Bending" (in German), *Mitt. Dtsch. Forschungsges., Blechverarb. u. Oberflächenbehand.*, 1952, pp. 57-65.
- 19.2 Ludwik, P.: "Engineering Study of Sheet Bending" (in German), *Technische Blätter*, no. 35, Prag, Verlag des Deutschen Polytechnischen Vereins in Böhmen, 1903, pp. 133-159.
- 19.3 Bach, C.: *Elasticity and Strength* (in German), Berlin, Springer, 1924.
- 19.4 Nadai, A.: *Plasticity of Materials* (in German), Berlin, Springer, 1927.
- 19.5 Poóczka, A.: "Bending of Sheet with Nonlinear Stress-Strain Behavior" (in German), *Blech*, 12, 1965, pp. 64-67.
- 19.6 Zünkler, B.: "Investigation of Elastic-Plastic Bending Based on a Simple Approach" (in German), *Bänder Bleche Rohre*, 6, 1965, pp. 503-508.
- 19.7 Oehler, G.: *Bending* (in German), München, Hanser, 1963.
- 19.8 Oehler, G.: "Unit-Moment Curves" (in German), *Werkstatt u. Betr.*, 93, 1960, pp. 497-503.
- 19.9 Oehler, G.: "New Unit-Moment Curves" (in German), *Werkstatt u. Betr.*, 102, 1969, p. 169.
- 19.10 Wolter, K. H.: "Air Bending of Sheet" (in German), *VDI-Forschungsheft*, no. 435, Düsseldorf, VDI-Verlag, 1952.
- 19.11 Hill, R.: *The Mathematical Theory of Plasticity*, Oxford, Clarendon Press, 1950.
- 19.12 Schwark, H. F.: "Springback of Plastically Bent Sheet" (in German), Dr.-Ing. thesis, Technische Universität, Hannover, 1952.
- 19.13 Reehlin, B.: "Comparative Studies of Different Cold-Bending Processes for Sheets" (in German), *Prog. Rep. VDI-Z.*, ser. 2, no. 18, Düsseldorf, VDI-Verlag, 1967.

- 19.14 Panknin, W., and Fritz, H.: "The Effect of Reversal of the Deformation Direction on the Flow Stress of Metallic Work Materials" (*in German*), *Draht*, **18**, 1967, pp. 1–6.
- 19.15 Krisch, A., and Gramberg, U.: "On the Origin of the Bauschinger Effect in Plastic Bending" (*in German*), *Arch. Eisenhüttenwes.*, **43**, 1972, pp. 753–755.
- 19.16 Höness, H.: "Systematic Analysis of Stresses and Strains in Back-and-Forth Bending of Sheet, Accounting for Springback," unpublished, Institut für Umformtechnik, Universität Stuttgart, 1969.
- 19.17 Proksa, F.: "On the Theory of Plastic Bending of Sheet" (*in German*), Dr.-Ing. thesis, Technische Universität, Hannover, 1958; abstracted in *Stahlbau*, **28**, 1959, pp. 29–36.
- 19.18 De Boer, R.: "Elastic-Plastic Finite-Strain Bending of a Plate Strip of Incompressible Material" (*in German*), *Ing. Arch.*, **36**, 1967, pp. 145–154.
- 19.19 De Boer, R., and Bruhns, O.: "On the Analysis of Residual Stresses in an Incompressible Plate Strip Formed by Finite Bending" (*in German*), *Acta Mech.*, **8**, 1969, pp. 146–159.
- 19.20 Bruhns, O., and Thermann, K.: "Elastic-Plastic Bending of a Plate Strip in Finite Bending" (*in German*), *Ing.-Arch.*, **38**, 1969, pp. 141–152.
- 19.21 Bruhns, O.: "Consideration of Isotropic Strain Hardening in Elastic-Plastic Sheet Bending with Finite Strains" (*in German*), *Ing.-Arch.*, **39**, 1970, pp. 63–72.
- 19.22 Nagpal, V., Billhardt, C. F., Raghupathi, P. S., and Subramanian, T.: "Development of a Process Model for Press Brake Bending," presented at the ASM Conference on Process Modelling, Chicago, 1979.
- 19.23 Oh, S. I., and Kobayashi, S.: "Finite-Element Analysis of Plane-Strain Sheet Bending," *Int. J. Mech. Sci.*, **22**, 1980, pp. 583–594.
- 19.24 Martin, G., and Tsang, S.: "The Plastic Bending of Beams Considering Die Friction Effects," *Trans ASME, J. Eng. Ind.*, **88B**, 1966, pp. 237–250.
- 19.25 Zünkler, B.: "Analytical Description of Processes in V-Die Bending" (*in German*), *Ind.-Anz.*, **88**, 1966, pp. 1601–1605.
- 19.26 Dannenmann, E.: "Tool Geometry and Punch Force in V-Die Bending" (*in German*), *Werkstattstechnik*, **64**, 1974, pp. 527–531.
- 19.27 Pawalkat, H.: "Bending Plate with Large Radii: On the Determination of Bending Forces" (*in German*), *Bänder Bleche Rohre*, **16**, 1975, pp. 373–381.
- 19.28 Weinmann, K. J., and Shippell, R. J.: "Effect of Tool and Workpiece Geometries upon Bending Forces and Springback in 90° V-Die Bending of HSLA Steel Plate," *Proceedings of the 6th North American Metal Working Research Conference* (Gainesville, FL, 1978), pp. 220–227.
- 19.29 DIN 8586: "Fertigungsverfahren Biegeumformen" (Manufacturing Processes—Forming by Bending) April 1971.
- 19.30 Dannenmann, E.: "Shape Accuracy of the Workpiece in 90° V-Die Bending and Coining" (*in German*), *Berichte aus dem Institut für Umformtechnik, Universität Stuttgart*, no. 8, Essen, Girardet, 1969.
- 19.31 Vater, M., and Stapper, H.: "On Cold and Hot Bending of Plate" (*in German*), *Mitt. Dtsch. Forschungsges. Blechverarb. u. Oberflächenbehandl.*, **18**, 1967, pp. 272–290.
- 19.32 Vater, M., and Stapper, H.: "U-Shape Bending of Plate with Pressure Pad" (*in German*), *Mitt. Dtsch. Forschungsges. Blechverarb. u. Oberflächenbehandl.*, **21**, 1970, pp. 153–155.
- 19.33 Zünkler, B.: "Theoretical Determination of Punch Force in U-Die Bending of Sheet" (*in German*), *Bänder Bleche Rohre*, **7**, 1966, pp. 829–832.
- 19.34 Draeger, E.: "Round Bending Work on Folding Machines" (*in German*), *Ind.-Anz.*, **86**, 1964, pp. 918–921.
- 19.35 Oehler, G.: "Friction Conditions in Conical Bending on Roll Bending Machines" (*in German*), *Mitt. Dtsch. Forschungsges. Blechverarb. u. Oberflächenbehandl.*, **21**, 1970, pp. 229–237.

- 19.36 Draeger, E.: "Roll Bending of Thin and Medium Thickness Sheet" (*in German*), *Blech*, **14**, 1967, pp. 160–168.
- 19.37 Oehler, G.: "Force and Power Determination on Roll Bending Machines" (*in German*), *Forschungsberichte des Landes Nordrhein-Westfalen*, no. 1614, Köln/Opladen, Westdeutscher Verlag, 1966.
- 19.38 Weimar, G.: "Measurement and Control of Corner Strains in Roll Forming" (*in German*), *Ind.-Anz.*, **90**, 1968, pp. 2012–2013.
- 19.39 Ditges, G.: "On the Determination of Geometry and Deformation Energy in Tube Roll Forming" (*in German*), Dr.-Ing. thesis, Technische Universität, Aachen, 1966.
- 19.40 Ditges, G.: "Tube Roll Forming and Experimental Determination of Edge Loading" (*in German*), *Bänder Bleche Rohre*, **8**, 1967, pp. 213–223.
- 19.41 Ditges, G.: "Basic Equations of Bending and Tube Roll Forming Deformation" (*in German*), *Bänder Bleche Rohre*, **8**, 1967, pp. 380–390.
- 19.42 Weimar, G.: "Longitudinal Strains and Warping in Sheet Section Rolling (Roll Forming)" (*in German*), Dr.-Ing. thesis, Technische Universität, Hannover, 1966.
- 19.43 Weimar, G.: "Longitudinal Strains and Warping in Roll Forming of Steel Sheet" (*in German*), *Arch. Eisenhüttenwes.*, **39**, 1968, pp. 37–44.
- 19.44 Biswas, A. K.: "On Sheet Bending of Tubes and Sections" (*in German*), Dr.-Ing. thesis, Universität Saarbrücken, 1967.
- 19.45 Neubauer, A.: "Investigation of Torques and Material Flow in Roll Forming of Steel Sheet" (*in German*), Dr.-Ing. thesis, Technische Universität Otto von Guericke, Magdeburg, 1967.
- 19.46 Neubauer, A.: "Springback in Roll Forming and Bending" (*in German*), *Fertigungstech. u. Betr.*, **17**, 1967, pp. 495–499, 503.
- 19.47 Neubauer, A.: "Investigation of Residual Stresses of the First Kind in Roll Forming" (*in German*), *Fertigungstech. u. Betr.*, **17**, 1967, pp. 673–678.
- 19.48 Pawalkat, H.: "Comparison of Processes and Fundamentals of Analysis for the Production of Cold Sections" (*in German*), *Mitt. Dtsch. Forschungsges. Blechverarb. u. Oberflächenbehandl.*, **21**, 1970, pp. 194–201.
- 19.49 Toelke, K. D.: "Undesired Deformations and Section Distortions in Roll Forming" (*in German*), Dr.-Ing. thesis, Technische Universität, Hannover, 1970.
- 19.50 Wilhelm, H.: "V-Die Bending of Sheet with Pliable Tools" (*in German*), *Ind.-Anz.*, **92**, 1970, pp. 1743–1744.
- 19.51 Gossard, D. C., and Allison, B. T.: "Adaptive Brake Forming," *Proceedings of the 8th North American Manufacturing Research Conference* (Rolla, Mo., 1980), pp. 252–256.
- 19.52 Sangdahl, G. S., Aul, E. L., and Sachs, G.: "An Investigation of the Stress and Strain States in Bending Rectangular Bars," *Proc. Soc. Exp. Stress Anal.*, **6**, 1948, pp. 1–18.
- 19.53 Datsko, J., and Yang, C. T., "Correlation of Bendability of Materials with Their Tensile Properties," *Trans. ASME, J. Eng. Ind.*, **82B**, 1960, pp. 309–314.
- 19.54 DIN 6935: "Kaltbiegen von Flacherzeugnissen aus Stahl" (Cold Bending of Flat Rolled Steel), October 1975.
- 19.55 Weaver, H. P.: "A Study of Properties of Sheared Steel Plate Edges," M. S. thesis, Michigan Technological University, Houghton, 1980.
- 19.56 Schaub, W.: "A Study of Process Limits in 180° Bending of Thin and Medium Thickness Sheets" (*in German*), *Berichte aus dem Institut für Umformtechnik, Universität Stuttgart*, no. 52, Berlin-Heidelberg-New York, Springer, 1980.
- 19.57 Oehler, G., and Kaiser, F.: *Cutting, Stamping, and Drawing Tools* (*in German*), Berlin-Göttingen-Heidelberg, Springer, 1962.
- 19.58 Romanowski, W. P.: *Handbook of Stamping* (*in German*), Berlin, VEB Verlag Technik, 1965.

## 19.50 SHEET-METAL FORMING

- 19.59 Hilbert, H. L.: *Stamping (in German)*, vol. 2, "Forming Tools," München, Hanser, 1970.
- 19.60 Pawelski, O., and Lueg, W.: "Elastic-Plastic Bending of Round Bars and Its Application to the Straightening Process in Three-Roller Straighteners" (*in German*), *Stahl u. Eisen*, **79**, 1959, pp. 1852–1861.
- 19.61 Geleji, A.: "Elastic-Plastic Bending of Round Bars," *Ann. CIRP*, **12**, 1964, pp. 165–169.
- 19.62 Gaydon, F. A.: "An Analysis of the Plastic Bending of a Thin Strip in Its Plane," *J. Mech. Phys. Solids*, **1**, 1952, pp. 103–112.
- 19.63 Lippmann, H.: "Plane Bending of a Narrow Beam with Strain Hardening" (*in German*), *Ing.-Arch.*, **27**, 1959, pp. 153–168.
- 19.64 Gramberg, U.: "Stresses and Strains in Plastic Bending of Bars with Rectangular Cross Section" (*in German*), Dr.-Ing. thesis, Technische Universität Clausthal, 1971; abstracted in *Arch. Eisenhüttenwes.*, **43**, 1972, pp. 667–674.
- 19.65 Oehler, G.: "Cold Narrow-Beam Bending" (*in German*), *Werkstatt u. Betr.*, **102**, 1969, pp. 37–41.
- 19.66 Oehler, G.: "Narrow-Beam Bending of Sheet" (*in German*), *Forschungsberichte des Landes Nordrhein-Westfalen*, no. 1879, Köln/Opladen, Westdeutscher Verlag, 1967.
- 19.67 Franz, W.-D.: *Cold Bending of Tubes (in German)*, Berlin-Göttingen-Heidelberg, Springer, 1961.
- 19.68 Oehler, G.: "On the Error Geometry of Bent Tube Cross Sections" (*in German*), *Werkstatt u. Betr.*, **100**, 1967, pp. 335–341.
- 19.69 Kursetz, E.: "Machine Tools for Cold Bending and Stretch Forming of Tubes and Sections of Aluminum Work Materials" (*in German*), *Bänder Bleche Rohre*, **11**, 1970, pp. 447–454.
- 19.70 Hayashi, T.: "On the Theory of Roll Levelling of Sheet Bars," *J. Faculty Eng., Univ. Tokyo*, no. 2, 1954, pp. 45–61.
- 19.71 Witte, H. D.: "Theoretical Stress Distributions in Roller Levelling of Sheet Metal" (*in German*), *Ind.-Anz.*, **92**, 1970, pp. 1097–1100.
- 19.72 Witte, H. D.: "Studies of Roller Levelling of Metal Strips with Symmetrically Arranged Five-Roller Leveller" (*in German*), *Berichte aus dem Institut für Umformtechnik, Universität Stuttgart*, no. 16, Essen, Girardet, 1970.
- 19.73 Noé, O.: "Effect of Continuous Stretch-Bend Straightening on Sheet Properties" (*in German*), *Stahl u. Eisen*, **91**, 1971, pp. 916–924.
- 19.74 Funke, P., Kottmann, K., and Piorko, I.: "Continuous Processes for the Improvement of the Flatness of Strips" (*in German*), *Stahl u. Eisen*, **91**, 1971, pp. 929–931.
- 19.75 Pawelski, O., and Fangmeier, R.: "Diameter Change, Surface Quality, and Strain Hardening of Cold-Rolled Steel during Straightening in Two-Roller Straighteners" (*in German*), *Stahl u. Eisen*, **88**, 1968, pp. 1027–1036.
- 19.76 Pawelski, O.: "Straightening Force and Change in Bar Diameter during Straightening of Cold-Rolled Steel in Three-Roller Straighteners" (*in German*), *Stahl u. Eisen*, **82**, 1962, pp. 836–846.
- 19.77 Böklen, R.: "Some Observations on Steel during Pure, Static Bending" (*in German*), *Z. Metallk.*, **42**, 1951, pp. 170–174.

## FURTHER READING

1. Dadras, P., and Majlessi, S. A.: "Plastic Bending of Work Hardening Materials," *Trans. ASME, J. Eng. Ind.*, **104B**, 1982, pp. 224–230.
2. Stelson, K. A., and Gossard, D. C.: "An Adaptive Pressbrake Control Using an Elastic-Plastic Material Model," *Trans. ASME, J. Eng. Ind.*, **104B**, 1982, pp. 389–393.
3. Stelson, K. A.: "Real Time Identification of Workpiece Material Characteristics from Measurements during Brakeforming," *Trans. ASME, J. Eng. Ind.*, **105B**, 1983, pp. 45–53.

4. Raghupathi, P. S., Karima, M., Akgerman, N., and Altan, T.: "A Simplified Approach to Calculate Springback in Brake Bending," *Proceedings of the 11th North American Manufacturing Research Conference*, Madison, Wisconsin, 1983, pp. 265-270.
5. DeVries, W. R., and Lauderbaugh, L. K.: "A Model for Bending Bimetallic Strip," *Trans. ASME, J. Eng. Ind.*, **106B**, 1984, pp. 62-69.



## CHAP. 20

### DEEP DRAWING

#### List of Special Symbols

---

$A_{BH}$	effective contact area between blankholder and flange
$d_0$	blank diameter
$d'_0$	equivalent blank diameter
$d_{1,2}$	intermediate flange diameter during drawing
$d_D$	die diameter
$d_p$	punch diameter
$F_{BH}$	force produced by blankholder
$F_{cr}$	bottom cracking load
$F_d$	drawing load
$h_c$	cup height
$h_s$	length of rolled-out side walls
$h_u$	usable cup height
$p_{BH}$	blankholder pressure
$r_B$	radius between bottom and side walls
$r_C$	corner radius
$r_D$	die radius
$r_p$	punch radius
$s$	sheet thickness
$u_D$	die clearance
$\alpha_N$	effective crank angle for mechanical presses
$\beta$	drawing ratio
$\epsilon_c$	relative wall thickness change
$\varphi_s$	thickness strain

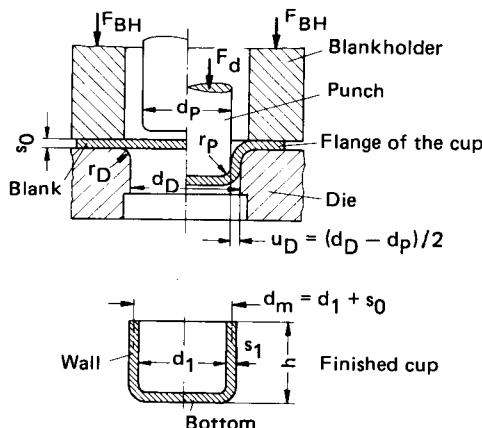


**FIG. 20.3** Deep drawing—tool and technology for the first draw.

finally reaches position III in the cup wall. During this move the element experiences tensile stresses in the radial direction and compressive stresses in the circumferential direction. Correspondingly the element is radially stretched and tangentially compressed. In addition, bending takes place as the element moves from the flange over the rounded edge of the die into the cup wall.

Neglecting friction, the equilibrium condition in the radial direction can be written as

$$(\sigma_r + d\sigma_r)(r + dr) d\alpha s_0 - \sigma_r d\alpha s_0 + 2|\sigma_t| s_0 dr \sin\left(\frac{d\alpha}{2}\right) = 0 \quad (20.1)$$

Replacing  $\sin(d\alpha/2)$  by  $d\alpha/2$  and neglecting products of differential terms simplifies Eq. 20.1 to

$$d\sigma_r = -(\sigma_r + |\sigma_t|) \frac{dr}{r} \quad (20.2)$$

The Tresca yield criterion states that

$$\sigma_1 - \sigma_3 = \sigma_f \quad (20.3)$$

at the onset of plastic flow. Substituting  $\sigma_1 = \sigma_r$  and  $\sigma_3 = -\sigma_t$ , Eq. 20.3 becomes

$$\sigma_r + |\sigma_t| = \sigma_f \quad (20.4)$$

Frequently the von Mises yield criterion is used in place of the Tresca criterion. The former is more accurate and predicts higher shear stresses than are determined using the maximum shear stress hypothesis (see Chap. 5).

During deep drawing both criteria agree only at one location, which is the point where the mean normal stress  $\sigma_m$  is equal to the median principal stress  $\sigma_2$ . At all other points the Tresca criterion predicts values which on the average are about 10% too small. In order to still be able to use the simpler Tresca equation, a correction factor is introduced:

$$\sigma_r + |\sigma_t| = 1.1\sigma_f \quad (20.5)$$

From Eqs. 20.2 and 20.5,

$$d\sigma_r = -1.1\sigma_f \frac{dr}{r} \quad (20.6)$$

The radial stresses are obtained by integration of Eq. 20.6 from the outside radius of the flange to the interior:

$$\int_{\sigma_r=0}^{\sigma_r} d\sigma_r = -1.1 \int_{r=R}^r \sigma_f \frac{dr}{r} \quad (20.7)$$

$$\sigma_r(r) = 1.1 \sigma_{f,m,I} \ln \left( \frac{R}{r} \right) \quad (20.8)$$

In Eq. 20.8  $\sigma_{f,m,I}$  is the mean flow stress in the flange between points 1 and 2 and  $R$  is the instantaneous outside radius of the flange. In [20.2] Geleji has determined that the error is less than 3% if the arithmetic mean of the values of  $\sigma_f$  at points 1 and 2 is used for  $\sigma_{f,m,I}$ :

$$\sigma_{f,m,I} = 0.5(\sigma_{f,1} + \sigma_{f,2}) \quad (20.9)$$

A more accurate mean value is obtained from Eq. 20.10:

$$\sigma_{f,m,I} = \frac{1}{\varphi_2 - \varphi_1} \int_{\varphi_1}^{\varphi_2} \sigma_f(\varphi) d\varphi \quad (20.10)$$

where  $\varphi_1$  and  $\varphi_2$  are the tangential strains at points 1 and 2, respectively.

In order to avoid wrinkle formation in the flange area, a blankholder is commonly used (Fig. 20.3). In this situation the median principal stress is compressive:

$$\sigma_2 = \sigma_z < 0 \quad (20.11)$$

Without a blankholder

$$\sigma_2 = \sigma_z = 0 \quad (20.12)$$

In the above discussion, friction between die and flange and between blankholder and flange has been ignored. If friction is included in the analysis, the radial stresses are increased by a friction term which is proportional to the blankholder pressure  $p_{BH}$  and the coefficient of friction  $\mu$ , and is inversely proportional to the workpiece thickness  $s$ :

$$\begin{aligned} \sigma_r(r) = 1.1 \sigma_{f,m,I} \ln \left( \frac{R}{r} \right) \\ + 2\mu(R - r) \frac{p_{BH}}{s} \quad (20.13) \end{aligned}$$

Using typical values in Eq. 20.13 one can show that friction increases the radial stresses only slightly as long as  $p_{BH}$  does not exceed a practical maximum value of  $p_{BH} = 10 \text{ N/mm}^2$  (1450 psi).

If friction and bending at the die radius are neglected, the axial stress  $\sigma_z$  in the wall of the cup equals the radial stress in the flange at point 2 (Fig. 20.4). However, stress components due to friction and bending increase the axial stress in the cup wall significantly.

Considering only the friction at the die radius (Fig. 20.5), the equilibrium condition in the radial direction for the indicated element is

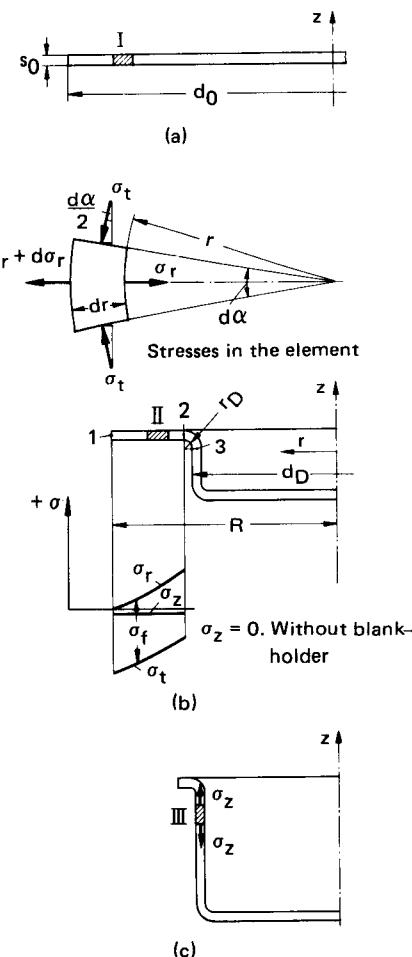


**FIG. 20.4** Draw stages and stresses in deep drawing. (a) Initial state. (b) Intermediate state. (c) Almost completed cup.

## 20.6 SHEET-METAL FORMING

$$dN - F \sin\left(\frac{d\alpha}{2}\right) - (F + dF) \sin\left(\frac{d\alpha}{2}\right) = 0 \quad (20.14)$$

where  $N$  is the normal force between the sheet and the die radius and  $F$  is the radial tension force in the sheet.

Approximating  $\sin(d\alpha/2)$  by  $d\alpha/2$ , Eq. 20.14 can be written as

$$dN - F d\alpha = 0 \quad (20.15)$$

The equilibrium condition in the tangential direction is

$$dF = dR = \mu dN \quad (20.16)$$

from which follows

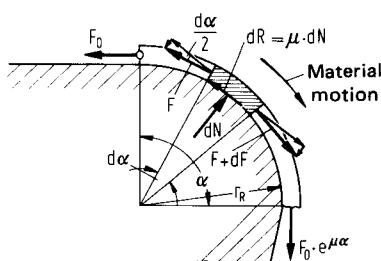
$$\frac{dF}{F} = \mu d\alpha$$

and after integration,

$$\ln\left(\frac{F_2}{F_1}\right) = \mu\alpha$$

or

$$F_2 = F_1 e^{\mu\alpha} \quad (20.17)$$



Since the die radius  $r_D$  is very small compared with the diameter of the cup, the stress components due to friction for  $\alpha = 90^\circ$  can be calculated from

$$\sigma_z = \sigma_r e^{\mu\pi/2} \quad (20.18)$$

where  $\sigma_r$  is the radial stress in the flange at the die entrance and  $\sigma_z$  is the axial stress at the die exit. However, Eq. 20.18 does not include stresses due to bending.

In the region of the die radius the sheet metal undergoes twofold bending. The central fiber is bent to a radius  $(r_D + s/2)$  at the die entrance and is unbent again at the exit.

**FIG. 20.5** Friction conditions at the die radius. (After [20.2].)

In [20.2] Geleji calculates the required force for bending as follows (Fig. 20.6). At the entrance of the die radius (section 1) an element of thickness  $s$  and width  $b$  is bent over the die radius  $r_D$ . The required work  $W$  equals the product of the bending moment  $M_b$  times the angle of bending  $\alpha$ :

$$W = M_b \alpha = F_1 r_D \alpha$$

or

$$F_1 = \frac{M_b}{r_D} \quad (20.19)$$

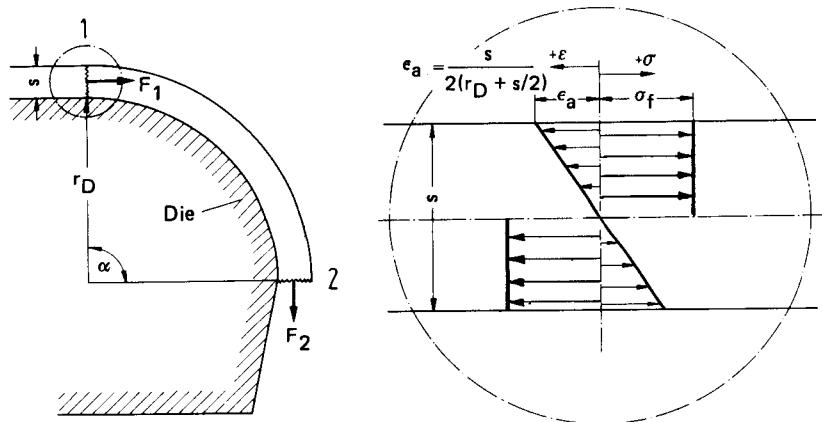
During bending the individual fibers are stretched or compressed until the internal moment in the cross section is equal to the externally applied bending moment. The internal moment can be calculated based on the assumption that the material is fully plastic and the magnitude of the bending stress equals the flow stress  $\sigma_f$ :

$$M_b = \frac{\sigma_f b s^2}{4} \quad (20.20)$$

Combining Eqs. 20.19 and 20.20 yields

$$F_1 = \frac{\sigma_f b s^2}{4 r_D}$$

\*Refer to Chap. 19.



Stress and strain distribution in cross section 1

FIG. 20.6 Geometric relationships for bending and unbending at the die radius. (After [20.2].)

At the exit of the die (section 2) the sheet is straightened again. Since this restores the original state, the same amount of work is necessary as in section 1, assuming that the material does not work harden. The total force required for bending, which must be transmitted in section 2, is therefore

$$F_b = 2F_1 = \frac{\sigma_f b s^2}{2r_D}$$

For circular deep-drawing tools the width  $b$  is given by

$$b = \pi d_m$$

where  $d_m$  is the mean diameter of the cup wall, and the bending force in section 2 is given by

$$F_b = \frac{\pi \sigma_f d_m s^2}{2r_D} \quad (20.21)$$

### 20.1.2 Strains

Strains are evaluated without considering bending over the die radius. The directions of the principal stresses coincide with the strains in the radial, circumferential, and normal directions. The finished cup shows the following strains, where  $s_1$  is the instantaneous wall thickness and  $d'$  is the original diameter of the ring element under consideration:

$$\varphi_t = \ln \left( \frac{d_1}{d'} \right)$$

$$\varphi_z = \ln \left( \frac{s_1}{s_0} \right) \quad (20.22)$$

$$\varphi_r = \ln \left( \frac{s_0 d'}{s_1 d_1} \right)$$

Which of the two strains  $\varphi_z$  and  $\varphi_t$  is the smaller one depends on the position of the ring element (Fig. 20.7). The volume continuity condition requires that  $\varphi_r + \varphi_t + \varphi_z = 0$ .

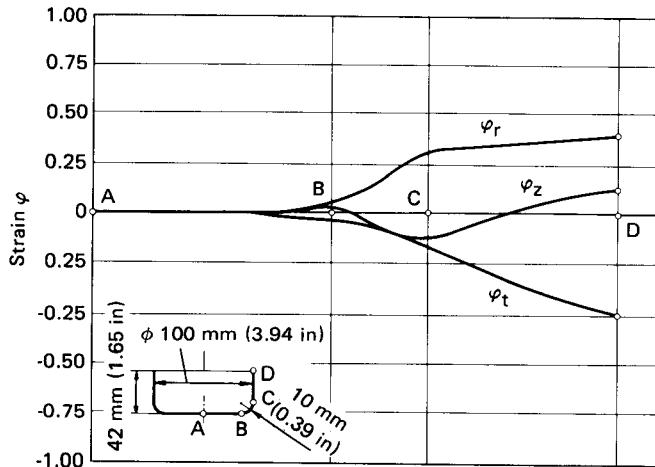


**FIG. 20.7** Distribution of local strains along the development of the drawn component. ( $\varphi_z$  corresponds to thickness strain  $\varphi_s$ .) (After [20.3].)

The magnitude of the deformation of a deep-drawn part is usually characterized by the drawing ratio  $\beta$ , which is defined as the ratio of the initial blank diameter  $d_0$  to the inside diameter of the finished cup  $d_1$ :

$$\beta = \frac{d_0}{d_1} \quad (20.23)$$

Immediately after contact between the punch and the blank, deformation is limited to the area under the punch. As the punch progresses, the material in this region is stretch-formed with superimposed bending over the rounded edges of the punch and the die [20.4]. This description explains why the strains in the bottom of the cup (A-B) are not zero everywhere, as shown in Fig. 20.7.  $\varphi_r$  increases continuously between A and C, while  $\varphi_t$  decreases.

The numerically largest strain  $\varphi_{\max}$  occurs at the top edge of the cup at point D:

$$\varphi_{\max} = |\varphi_t| \quad (20.24)$$

The normal strain  $\varphi_z$  in the thickness direction is always negative in the bottom of the cup; that is, the sheet is thinned here. In the cup wall the normal strain increases continuously such that the wall thickness at the top edge is generally greater than the initial sheet thickness  $s_0$ . The wall-thickness distribution throughout the cup wall depends among other parameters on the drawing ratio, the tool geometry, the blankholder pressure, and the properties of the sheet material (anisotropy).

Experimentally, local deformations are often measured using grids inscribed or photochemically etched [20.5] onto the undeformed blank.

With the assumptions that the principal strain directions and the ratios of the incremental strains  $d\varphi_1:d\varphi_2:d\varphi_3$  remain constant, an equivalent uniaxial strain can be computed:

$$|\bar{\varphi}| = \sqrt{\%(\varphi_1^2 + \varphi_2^2 + \varphi_3^2)} \quad (20.25)$$

In deep drawing the first condition is satisfied but not the second one (Fig. 20.7). Nevertheless Eq. 20.25 can be used with satisfactory accuracy. The calculated value of  $|\bar{\varphi}|$  is then used to determine the strength of the sheet at a particular point from its stress-strain curve.

### 20.1.3 Forces, Efficiency of Deformation

#### Drawing Load

The required drawing loads and their variations along the punch stroke can be determined in two ways, either from theoretical equations based on plasticity theory, or by using empirical equations. The following equation for calculating the maximum drawing load  $F_{d,\max}$ , which is based on the elementary theory by Siebel, [20.6], has been used successfully in practice:

$$F_{d,\max} = \pi d_m s_0 \left[ \underbrace{e^{\mu\pi/2}}_C \underbrace{1.1\sigma_{f,m,I} \ln \frac{d_{F,\max}}{d_m}}_A + \underbrace{\frac{2\mu F_N}{\pi d_{F,\max} s_0}}_B + \underbrace{\sigma_{f,m,II} \frac{s_0}{2r_D}}_D \right] \quad (20.26)$$

In this equation term  $A$  represents the ideal deformation load, term  $B$  is the load component produced by friction between die and flange and also between flange and blankholder, term  $C$  describes the load increase due to friction at the die radius, and term  $D$  is the load necessary for bending the sheet around the die radius.  $d_m = d_1 + s_0$  is the mean wall diameter and  $d_{F,\max}$  is the outside diameter of the flange when the drawing load is a maximum.

Siebel and Beisswanger [20.6] have suggested that the maximum drawing load is almost independent of the workpiece material and the drawing ratio and occurs when  $d_{F,\max} \approx 0.77 d_0$ . According to Zunkler in [20.7], however, strain hardening behavior has a significant influence on the occurrence of the load maximum. (See Sec. 20.1.4.)

In Eq. 20.26  $\sigma_{f,m,I}$  is the mean value of the flow stress in the flange between the outside edge (point 1) and the entrance to the die radius (point 2), and  $\sigma_{f,m,II}$  is the average value of  $\sigma_f$  in the region of the die radius between points 2 and 3 (Fig. 20.4).

In order to determine the strains at points 1, 2, and 3 the initial location of these points in the undeformed blank must be ascertained. Point 1 was at the outside edge of the blank of radius  $d_0$ . Therefore

$$\varphi_{\max,1} = |\varphi_{t,1}| = -\ln \left( \frac{d_{F,\max}}{d_0} \right) \quad (20.27)$$

The material in the annulus between points 1 and 2 formed an annulus with outside diameter  $d_0$  and unknown inside diameter  $d_i$  in the blank. Assuming constant sheet thickness, the unknown diameter  $d_i$  can be calculated from the condition that the volume remains constant:

$$\frac{\pi(d_0^2 - d_i^2)}{4} = \frac{\pi(d_{F,\max}^2 - (d_D + 2r_D)^2)}{4}$$

or

$$d_i = \sqrt{d_0^2 + (d_D + 2r_D)^2 - d_{F,\max}^2} \quad (20.28)$$

The strain  $\varphi_{\max,2}$  at point 2 when the load is a maximum is given by

$$\begin{aligned} \varphi_{\max,2} &= |\varphi_{t,2}| = \ln d_i - \ln (d_D + 2r_D) \\ &= \ln \frac{\sqrt{d_0^2 + (d_D + 2r_D)^2 - d_{F,\max}^2}}{d_D + 2r_D} \end{aligned} \quad (20.29)$$

Adding the strain due to bending to the strain at point 3 yields the strain at point 2. Since the die radius is generally large compared to the thickness  $s_0$ , bending may be considered gentle without causing further strain hardening. For  $r_D/s_0 > 10$  one can therefore assume that  $\sigma_{f,m,II}$  is equal to  $\sigma_f$  at point 2:

$$\sigma_{f,m,II} \approx \sigma_{f,2} \quad (20.30)$$

If the ratio  $r_D/s_0 < 10$ , then the increase of  $\sigma_f$  due to bending should be taken into account for highly strain-hardening materials.

In bending, the incremental strain  $\epsilon_s$  of the outside fibers can be determined from the radius of the curvature  $r_m$  of the neutral fiber and the sheet thickness  $s$ :

$$\epsilon_s = \frac{s}{2r_m}$$

Applying this relationship to the die radius yields

$$\epsilon_s = \frac{s}{2r_D + s}$$

Since the strain distribution is linear across the sheet thickness, the mean bending strain  $\bar{\epsilon}$  in the cross section is given by

$$\bar{\epsilon} = \frac{\epsilon_s}{2}$$

The workpiece undergoes twofold bending in the region of the die radius so that the total mean bending strain after unbending is

$$\bar{\epsilon}_{\text{tot}} = 2\bar{\epsilon} = \epsilon_s \quad (20.31)$$

The corresponding natural strain  $\varphi_{\text{tot}}$  is given by

$$\varphi_{\text{tot}} = \ln(1 + \bar{\epsilon}_{\text{tot}}) \quad (20.32)$$

Using this result, the strain at point 3 for maximum load can now be determined if  $\varphi_{\text{max},2}$  is known:

$$\varphi_{\text{max},3} = \varphi_{\text{tot}} + \varphi_{\text{max},2} \quad (20.33)$$

The flow stresses  $\sigma_{f,1}$ ,  $\sigma_{f,2}$ , and  $\sigma_{f,3}$  at points 1, 2, and 3 are obtained from the stress-strain curve. The mean value  $\sigma_{f,m,1}$  in the flange is determined from Eq. 20.9 or Eq. 20.10. The mean value  $\sigma_{f,m,II}$  in the region of the die radius is given by Eq. 20.30 for  $r_D/s_0 > 10$ , and for smaller values of  $r_D/s_0$  it is calculated as the arithmetic mean of the flow stresses at points 2 and 3:

$$\sigma_{f,m,II} = 0.5(\sigma_{f,2} + \sigma_{f,3}) \quad (20.34)$$

The value of the coefficient of friction  $\mu$  has been determined in investigations by Siebel and Beisswanger [20.6] and in experiments by Reihle [20.8] to range from 0.10 to 0.15.

Several simplified equations have been proposed for the calculation of the maximum value of the drawing load. In an equation suggested by Siebel and Beisswanger [20.6], the maximum load can be determined from the efficiency of deformation  $\eta_{\text{def}}$ :

$$F_{d,\text{max}} = \pi d_m s_0 \left[ 1.1 \frac{\sigma_{f,m,I}}{\eta_{\text{def}}} \left( \ln \frac{d_0}{d_1} - 0.25 \right) \right] \quad (20.35)$$

The efficiency of deformation was determined in [20.6] to be in the range of  $\eta_{\text{def}} = 0.5\text{--}0.7$ . The mean flow stress in the flange  $\sigma_{f,m,I}$  can be determined approximately from the ultimate tensile strength  $S_u$ :

$$\sigma_{f,m,I} \approx 1.3S_u \quad (20.36)$$

Romanowski [20.9] suggests another equation to calculate the maximum drawing load:

$$F_{d,\text{max}} = \pi d_1 s_0 S_u k \quad (20.37)$$

where  $k$  is a correction factor which was tabulated as a function of the drawing ratio and the relative sheet thickness.

Of the three equations 20.26, 20.35, and 20.37, the first is the best for calculating the drawing load. It considers the most important influence parameters in a clear manner and makes it possible to calculate the drawing load at every stage. One only has to replace  $d_{F,\text{max}}$  by the instantaneous flange diameter  $d$ . Eqs. 20.35 and 20.37 have the disadvantage that they start with the ideal deformation load, and all other load components are considered only through correction factors, either the efficiency of deformation  $\eta_{\text{def}}$  or the  $k$ -factor.

### Blankholder Pressure

In the flange there are tangential compressive stresses. They can cause wrinkles due to buckling. Wrinkles can be avoided through the use of a blankholder (Fig. 20.3), which is pressed with a

pressure  $p_{BH}$  against the flange of the drawn component. If the contact area is  $A_{BH}$ , then the load applied by the blankholder is

$$F_{BH} = A_{BH}p_{BH} \quad (20.38)$$

The pressure necessary to avoid wrinkling depends on the sheet material, the relative sheet thickness, and the drawing ratio. Investigations by Siebel and Beisswanger [20.6] show that the required blankholder pressure can be estimated from

$$p_{BH} = 10^3 c \left[ (\beta - 1)^3 + \frac{0.005d_0}{s_0} \right] S_u \quad (20.39)$$

where the factor  $c$  ranges from 2 to 3. In Fig. 20.8 the pressures calculated from Eq. 20.39 for a drawing ratio  $\beta = 2.0$  and materials with ultimate tensile strengths  $S_u = 100, 200, 400, 600$  N/mm<sup>2</sup> (14.5, 29, 58, and 87 ksi) are plotted as functions of the relative sheet thickness  $s_0/d_0$ .

### Cracking Load

The largest allowable drawing load is limited by the load that can be transmitted by the sheet in the region of the punch radius or at the transition from cup wall to bottom radius. This load is called the cracking load. It must always be larger than the maximum drawing load. The cracking load can be determined approximately by the equation

$$F_{cr} = \pi d_m s_0 S_u \quad (20.40)$$

At the transition from the bottom to the wall of the cup there exists a multidimensional state of stress which is not completely known. There may be local strains which are larger than the uniform strain in a uniaxial tensile test. Strictly speaking, the ultimate tensile strength should not be used to determine the strength of the sheet in this region; rather the yield stress corresponding to the local equivalent strain at the time of the maximum drawing load should be used. This value is as unpredictable as is the local sheet thickness at this instant. However, since on the one hand  $s$  will be less than  $s_0$ , and on the other hand the yield stress  $S_y$  will be larger than the engineering

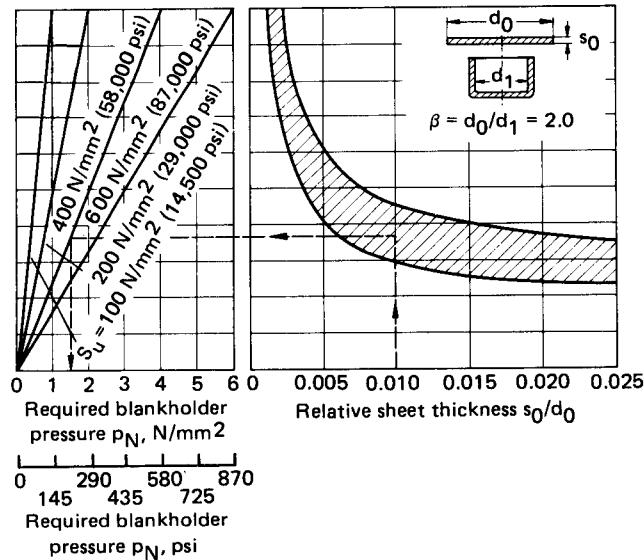


FIG. 20.8 Required blankholder pressure for the first draw. (After [20.6].)

stress  $S_u$ , with the latter effect being the dominant one, a conservative estimate is obtained from Eq. 20.40.

### Load-Stroke Diagram and Drawing Work

A typical load-stroke diagram for deep drawing is shown in Fig. 20.9. If the clearance between the punch and the die is too small (curve B), then the wall thickness which initially was increased by compressive tangential stresses in the flange will be reduced again (ironing). This causes the maximum drawing load to occur after a longer punch travel than in the case without wall thinning.

In order to explain the diagram qualitatively, the ideal drawing load will be considered:

$$F_{d,id} = \pi d_m s_0 \sigma_{f,m} \ln \left( \frac{d}{d_m} \right) \quad (20.41)$$

In this equation  $d$  is the outside flange diameter at any instant. As indicated in Fig. 20.9, the flow stress increases continuously with progressing deformation because of strain hardening, while the flange diameter becomes smaller and smaller such that  $\ln(d/d_m)$  decreases continuously until it reaches zero at the end of the draw. The product of these two quantities shows a distinct maximum which is reached when the ratio of flange diameter to blank diameter is about  $d_{f,max}/d_0 \approx 0.77$ .

The required work  $W_d$  for deep drawing a cup is given by the area under the load-stroke diagram. One can estimate the work from the maximum drawing load using a correction factor  $\kappa$  [20.10]:

$$W_d = \kappa F_{d,max} h_c \quad (20.42)$$

The height of the drawn component is  $h_c$  and  $\kappa$  is a correction factor with a value between 0.65 and 0.77. The larger values apply to softer materials, larger drawing ratios, and those components which are not fully drawn such that a small flange remains. The smaller values refer to small drawing ratios and sheet materials of higher ultimate tensile strengths.

### Efficiency of Deformation

The efficiency of deformation is defined as the ratio of the ideal deformation work  $W_{id}$  to the actually used work  $W_{tot}$ :

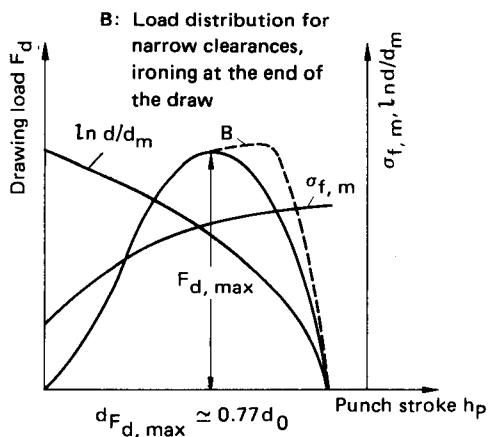


FIG. 20.9 Load-stroke diagram for a first draw.

$$\eta_{\text{def}} = \frac{W_{\text{id}}}{W_{\text{tot}}} \quad (20.43)$$

The deformation efficiency can be approximated by the ratio of the maximum loads:

$$\eta_{\text{def}} \approx \frac{F_{\text{d,id}}}{F_{\text{d,tot}}}$$

where  $F_{\text{d,id}}$  is the load for ideal deformation and  $F_{\text{d,tot}}$  is the actually required load.

The efficiency of deformation  $\eta_{\text{def}}$  for deep drawing ranges from 0.5 to 0.7 [20.6]. The smaller values apply to thin-walled cups and the higher values to thick-walled components. Friction at the die radius dissipates 10–20% of the total applied work, friction at the flange requires 1–10%, and bending over the die radius consumes another 5–25%.

#### 20.1.4 Cracking and Limiting Drawing Ratio

The larger the chosen drawing ratio  $\beta = d_0/d_1$ , the larger will be the maximum drawing load under otherwise constant conditions. This load must be transmitted by the wall of the drawn component. Therefore the drawing ratio must not exceed a maximum value, the limiting drawing ratio  $\beta_{\text{max}}$ , in order to prevent cracks at the bottom of the cup. Doege [20.11] has conducted intensive investigations on this subject. Cracking can occur during and after the formation of the cup bottom. The first failure mode is called a premature crack, and the other mode is called a proper crack. Premature cracks always happen in the region of the bottom radius, while proper cracks can occur in the bottom radius as well as in the transition from the bottom radius to the cup wall. The latter failure mode is often called an optimal crack since in this case the largest possible load has been transmitted to the deformation zone.

The cracking load is given in [20.11] by

$$F_{\text{cr}} = S_u \pi d_m s_0 a_{\text{cr}} \quad (20.44)$$

where  $a_{\text{cr}}$  is the cracking factor. It is the ratio of the measured cracking stress  $\sigma_{\text{cr}} = F_{\text{cr}} / (\pi d_m s_0)$  to the ultimate tensile strength  $S_u$ . Eq. 20.44 follows from Eq. 20.40 when the right-hand side is multiplied by  $a_{\text{cr}}$ . Since the measured cracking load is larger than the value calculated from Eq. 20.40, the cracking factor must be greater than unity if  $F_{\text{cr}}$  as calculated from Eq. 20.44 is to agree with the measured load. Doege has found that the largest load which can be transmitted from the bottom radius to the cup wall increases with increasing friction between the blank and the punch, and consequently the cracking factor also increases. It increases further as the ratio of punch radius  $r_p$  to punch diameter  $d_p$  increases. There also exists a strong influence of the sheet material. The cracking load and, therefore, the cracking factor as well as the limiting drawing ratio become larger as the strain-hardening coefficient  $n$  or the  $r$ -value increases. The effect of these parameters is discussed later in this chapter. For a few sheet materials the cracking factor is given below:

Material	$a_{\text{cr}}$
Deep-drawing steel sheet, RSt 14 (SAE 1006)	1.05–1.55
Austenitic steel sheet, X 5 Cr Ni 18 9 (AISI 304)	0.95–1.30
Brass, Cu Zn 37 (UNS C27000)	0.92–1.27
Pure aluminum, Al 99.7 w (AA 1050-O)	0.99–1.22

To calculate the limiting drawing ratio  $\beta_{\text{max}}$ , Siebel and Beisswanger [20.6] equate the largest drawing stress  $\sigma_{z,\text{max}}$  to the cracking stress  $\sigma_{\text{cr}}$ , which is assumed to be approximately equal to the ultimate tensile strength of the sheet. The drawing stress  $\sigma_{z,\text{max}}$  is given by the term in square brackets in Eq. 20.35. It follows:

$$\sigma_{z,\max} = \frac{1.1\sigma_{f,m,I}}{\eta_{\text{def}}} \left[ \ln \left( \frac{d_0}{d_1} \right) - 0.25 \right] = S_u \quad (20.45)$$

The mean flow stress is given by Eq. 20.36, and the efficiency of deformation can be assumed to be  $\eta_{\text{def}} = 0.7$ . From Eq. 20.45 one obtains

$$\ln \left( \frac{d_0}{d_1} \right)_{\max} = 0.74$$

or

$$\beta_{\max} = \left( \frac{d_0}{d_1} \right)_{\max} = 2.1 \quad (20.46)$$

$\beta_{\max}$  is called the limiting drawing ratio. The value  $\beta_{\max} = 2.1$  should only be used for sheet steel as a first guess. This value is influenced by several parameters. Approximate values of  $\beta_{\max}$  for a few materials and a diameter-to-thickness ratio  $d_0/s_0 = 50$  are given below:

Material	$\beta_{\max}$
Steel sheet, depending on quality	1.8–2.2
Aluminum, copper, Al Cu Mg sheets	2.1
Brass sheet, depending on prestrain	1.7–2.2

According to Panknin and Grosch [20.12], when isotropic materials and tools of fixed dimensions are used,  $\beta_{\max}$  depends mainly on the friction conditions at the punch and the die. The smaller the friction at the die and the blankholder and the larger the coefficient of friction  $\mu$  at the punch, the larger are the achievable limiting drawing ratios. The sheet thickness and the punch diameter also influence  $\beta_{\max}$ . Kotthaus [20.13] has determined that  $\beta_{\max}$  decreases as the relative sheet thickness  $s_0/d_0$  decreases or the relative punch diameter  $d_p/s_0$  increases (Fig. 20.10).

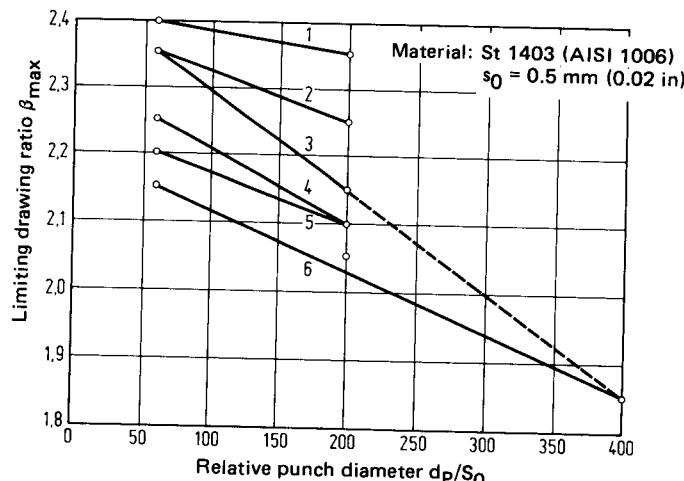


FIG. 20.10 Limiting drawing ratio  $\beta_{\max}$  as a function of the relative punch diameter  $d_p/s_0$ . 1—lubricating film with grease; 2—deep-draw coating with grease; 3—deep-draw coating without grease; 4—tinned sheet without grease; 5—copper-coated sheet with grease; 6—sheet without surface treatment with grease.

The explanation for this behavior can be found in the friction conditions. The smaller the relative sheet thickness, the larger are the frictional losses, and the limiting drawing ratio is lower. Friction does not only depend on lubrication, but also on the material combination of the tool and the blank, their surface conditions, and on the blankholder pressure [20.14].

Oehler [20.15] gives an approximate equation from which the limiting drawing ratio  $\beta_{\max}$  can be calculated for any ratio  $d_0/s_0$  if the limiting drawing ratio  $\beta_{\max,100}$  for  $d_0/s_0 = 100$  is known:

$$\beta_{\max} = (\beta_{\max,100} + f) - \frac{fd_0}{100s_0} \quad (20.47)$$

The correction factor  $f$  depends on the ductility of the material, its surface roughness, and the lubrication conditions. Values of  $f$  range from 0.05 to 0.15. The smaller values apply to materials with good ductility and smooth surfaces while the larger values are for sheets with low ductility and rough surfaces. The limiting drawing ratio increases with increasing  $r$ -values of the normal anisotropy of the material (see Sec. 20.1.5).

The effect of the strain-hardening exponent  $n$  on the limiting drawing ratio is not yet clearly determined. Although some investigators believe that  $n$  does not influence  $\beta_{\max}$ , since both the drawing load and the cracking load are higher for materials with higher values of  $n$ , there is without doubt an effect of  $n$  on the limiting drawing ratio [20.16], [20.17]. This is true especially at the beginning of the draw where the process is not exclusively deep drawing but a combination of deep drawing and stretch drawing [20.4]. Stretch drawing is clearly aided by a high strain-hardening coefficient. Therefore in order to achieve high limiting drawing ratios,  $n$  should be high.\*

In order to take into account the effects of both the normal anisotropy and the strain-hardening coefficient, Mäde and Deh [20.18] have proposed the use of the product  $rn$  for the characterization of the deep-drawing behavior of sheets. The larger the product, the better is the drawing behavior.

The yield stress ratio  $S_y/S_u$  appears to have minimal effect on the limiting drawing ratio. Koelzer [20.19] has found that cylindrical components can be deep-drawn better if the yield stress ratio is lower.

The effect of the rate of drawing on the limiting drawing ratio was investigated by Panknin [20.20]. He found that the main reason for a rate effect is friction, which in general, depending on the lubricating medium, is lower at higher rates. When forming cylindrical components, no negative effects need to be expected from higher drawing rates. Different conditions are encountered in the production of automobile body parts and in stretch drawing. Based on shop experiences and results, the limiting drawing ratio appears to decrease with increasing impact velocity of the punch in cases of modified deep drawing. It is assumed that the load buildup time is responsible for these observations. This time is larger with hydraulic presses than with mechanical ones, and in practice the larger limiting drawing ratios are achieved on hydraulic presses. In order to produce cups having a total drawing ratio larger than the limiting drawing ratio several draws are required.

Table 20.1 lists the most important deep-drawing sheet materials together with drawing ratios used in industry for the first draw and for redraws, with and without intermediate annealing. These values are in part lower than the ones mentioned above, which were obtained under laboratory conditions. In industry safety is most important. Rather than risk cracking because of too large a drawing ratio, an additional redraw step is used.

\*Zünker [20.7] has shown analytically and experimentally that the limiting drawing ratio is influenced by the strain-hardening coefficient. From Eq. 20.35 and a stress-strain relationship of the form  $\sigma = c\varphi^n$  it follows, after some manipulation,

$$\ln \beta_{\max} = \left( \frac{\eta_{\text{def}}}{1.1} \right)^{1/(n+1)} (n + 1)$$

This equation clearly shows an influence on the strain-hardening coefficient on the limiting drawing ratio. This result has also been verified in about 400 experiments. For a drawing ratio  $\beta = 2.0$  with  $n = 0.1$ , the load maximum occurs when  $d_{F,\max} = 0.94 d_0$ , and with  $n = 0.5$  the maximum is reached when  $d_{F,\max} = 0.79d_0$ .

**Table 20.1** Selection of the Most Important Workpiece Materials for Deep Drawing

DIN	Designation	Minimum $S_{u0.2}$ , N/mm <sup>2</sup> (ksi)	Minimum fracture strain, $\delta_5$ , % (Specimen: $l_0 = 80$ mm, $b_0 = 20$ mm) <sup>a</sup>	Achievable drawing ratio $\beta$			Remarks
				First draw	First redraw without annealing	First redraw with annealing	
				Lubrication			
<i>Mild steel</i>							
US12 <sup>a</sup>	AISI 1008	≤280 (40.6)	270–410 (39.15–59.45)	28	1.8	1.2	1.6
US13	AISI 1008	≤250 (36.25)	59.45	32	1.9	1.25	1.65
RHS14	SAE 1006	≤220 (31.9)	270–370 (39.15–53.65)	36	2.0	1.3	1.7
			270–350 (39.15–50.75)				
<i>Stainless steel</i>							
<i>Ferritic</i> X8Cr17 <i>Austenitic</i> X5CrNi18-9	AISI 430	270 (39.15)	450–600 (65.25–87) 500–700 (72.5–101.5)	20 l, 15 p <sup>c</sup> 50 l, 37 p <sup>c</sup>	1.55	—	1.25
	AISI 304	185 (26.8)			2.0	1.2	1.8
<i>Heat-resistant steel</i>							
<i>Ferritic</i> X10CrAl13 <i>Austenitic</i> X15CrNi25-20	ASTM type 405	285 (42.8)	500–650 (72.5–94.25) 500–740 (85.55–107.3)	15	1.7	1.2	1.6
	AISI 314	295 (42.8)		40	2.0	1.2	1.8

<sup>a</sup> Specimen:  $l_0 = 80$  mm,  $b_0 = 20$  mm;  $s_0 \leq 5$  mm<sup>b</sup>

<sup>b</sup> Specimen:  $l_0 = 80$  mm,  $b_0 = 20$  mm<sup>a</sup>

<sup>c</sup> Specimen:  $l_0 = 80$  mm,  $b_0 = 20$  mm<sup>a</sup>

<sup>d</sup> Specimen:  $l_0 = 80$  mm,  $b_0 = 20$  mm<sup>a</sup>

<sup>e</sup> Specimen:  $l_0 = 80$  mm,  $b_0 = 20$  mm<sup>a</sup>

<sup>f</sup> Specimen:  $l_0 = 80$  mm,  $b_0 = 20$  mm<sup>a</sup>

<sup>g</sup> Specimen:  $l_0 = 80$  mm,  $b_0 = 20$  mm<sup>a</sup>

<sup>h</sup> Specimen:  $l_0 = 80$  mm,  $b_0 = 20$  mm<sup>a</sup>

<sup>i</sup> Specimen:  $l_0 = 80$  mm,  $b_0 = 20$  mm<sup>a</sup>

<sup>j</sup> Specimen:  $l_0 = 80$  mm,  $b_0 = 20$  mm<sup>a</sup>

<sup>k</sup> Specimen:  $l_0 = 80$  mm,  $b_0 = 20$  mm<sup>a</sup>

<sup>l</sup> Specimen:  $l_0 = 80$  mm,  $b_0 = 20$  mm<sup>a</sup>

<sup>m</sup> Specimen:  $l_0 = 80$  mm,  $b_0 = 20$  mm<sup>a</sup>

<sup>n</sup> Specimen:  $l_0 = 80$  mm,  $b_0 = 20$  mm<sup>a</sup>

<sup>o</sup> Specimen:  $l_0 = 80$  mm,  $b_0 = 20$  mm<sup>a</sup>

<sup>p</sup> Specimen:  $l_0 = 80$  mm,  $b_0 = 20$  mm<sup>a</sup>

<sup>q</sup> Specimen:  $l_0 = 80$  mm,  $b_0 = 20$  mm<sup>a</sup>

<sup>r</sup> Specimen:  $l_0 = 80$  mm,  $b_0 = 20$  mm<sup>a</sup>

<sup>s</sup> Specimen:  $l_0 = 80$  mm,  $b_0 = 20$  mm<sup>a</sup>

<sup>t</sup> Specimen:  $l_0 = 80$  mm,  $b_0 = 20$  mm<sup>a</sup>

<sup>u</sup> Specimen:  $l_0 = 80$  mm,  $b_0 = 20$  mm<sup>a</sup>

<sup>v</sup> Specimen:  $l_0 = 80$  mm,  $b_0 = 20$  mm<sup>a</sup>

<sup>w</sup> Specimen:  $l_0 = 80$  mm,  $b_0 = 20$  mm<sup>a</sup>

<sup>x</sup> Specimen:  $l_0 = 80$  mm,  $b_0 = 20$  mm<sup>a</sup>

<sup>y</sup> Specimen:  $l_0 = 80$  mm,  $b_0 = 20$  mm<sup>a</sup>

<sup>z</sup> Specimen:  $l_0 = 80$  mm,  $b_0 = 20$  mm<sup>a</sup>

<sup>aa</sup> Specimen:  $l_0 = 80$  mm,  $b_0 = 20$  mm<sup>a</sup>

<sup>bb</sup> Specimen:  $l_0 = 80$  mm,  $b_0 = 20$  mm<sup>a</sup>

<sup>cc</sup> Specimen:  $l_0 = 80$  mm,  $b_0 = 20$  mm<sup>a</sup>

<sup>dd</sup> Specimen:  $l_0 = 80$  mm,  $b_0 = 20$  mm<sup>a</sup>

<sup>ee</sup> Specimen:  $l_0 = 80$  mm,  $b_0 = 20$  mm<sup>a</sup>

<sup>ff</sup> Specimen:  $l_0 = 80$  mm,  $b_0 = 20$  mm<sup>a</sup>

<sup>gg</sup> Specimen:  $l_0 = 80$  mm,  $b_0 = 20$  mm<sup>a</sup>

<sup>hh</sup> Specimen:  $l_0 = 80$  mm,  $b_0 = 20$  mm<sup>a</sup>

<sup>ii</sup> Specimen:  $l_0 = 80$  mm,  $b_0 = 20$  mm<sup>a</sup>

<sup>jj</sup> Specimen:  $l_0 = 80$  mm,  $b_0 = 20$  mm<sup>a</sup>

<sup>kk</sup> Specimen:  $l_0 = 80$  mm,  $b_0 = 20$  mm<sup>a</sup>

<sup>ll</sup> Specimen:  $l_0 = 80$  mm,  $b_0 = 20$  mm<sup>a</sup>

<sup>mm</sup> Specimen:  $l_0 = 80$  mm,  $b_0 = 20$  mm<sup>a</sup>

<sup>nn</sup> Specimen:  $l_0 = 80$  mm,  $b_0 = 20$  mm<sup>a</sup>

<sup>oo</sup> Specimen:  $l_0 = 80$  mm,  $b_0 = 20$  mm<sup>a</sup>

<sup>pp</sup> Specimen:  $l_0 = 80$  mm,  $b_0 = 20$  mm<sup>a</sup>

<sup>qq</sup> Specimen:  $l_0 = 80$  mm,  $b_0 = 20$  mm<sup>a</sup>

<sup>rr</sup> Specimen:  $l_0 = 80$  mm,  $b_0 = 20$  mm<sup>a</sup>

<sup>ss</sup> Specimen:  $l_0 = 80$  mm,  $b_0 = 20$  mm<sup>a</sup>

<sup>tt</sup> Specimen:  $l_0 = 80$  mm,  $b_0 = 20$  mm<sup>a</sup>

<sup>uu</sup> Specimen:  $l_0 = 80$  mm,  $b_0 = 20$  mm<sup>a</sup>

<sup>vv</sup> Specimen:  $l_0 = 80$  mm,  $b_0 = 20$  mm<sup>a</sup>

<sup>ww</sup> Specimen:  $l_0 = 80$  mm,  $b_0 = 20$  mm<sup>a</sup>

<sup>xx</sup> Specimen:  $l_0 = 80$  mm,  $b_0 = 20$  mm<sup>a</sup>

<sup>yy</sup> Specimen:  $l_0 = 80$  mm,  $b_0 = 20$  mm<sup>a</sup>

<sup>zz</sup> Specimen:  $l_0 = 80$  mm,  $b_0 = 20$  mm<sup>a</sup>

<sup>aa</sup> Specimen:  $l_0 = 80$  mm,  $b_0 = 20$  mm<sup>a</sup>

<sup>bb</sup> Specimen:  $l_0 = 80$  mm,  $b_0 = 20$  mm<sup>a</sup>

<sup>cc</sup> Specimen:  $l_0 = 80$  mm,  $b_0 = 20$  mm<sup>a</sup>

<sup>dd</sup> Specimen:  $l_0 = 80$  mm,  $b_0 = 20$  mm<sup>a</sup>

<sup>ee</sup> Specimen:  $l_0 = 80$  mm,  $b_0 = 20$  mm<sup>a</sup>

<sup>ff</sup> Specimen:  $l_0 = 80$  mm,  $b_0 = 20$  mm<sup>a</sup>

<sup>gg</sup> Specimen:  $l_0 = 80$  mm,  $b_0 = 20$  mm<sup>a</sup>

<sup>hh</sup> Specimen:  $l_0 = 80$  mm,  $b_0 = 20$  mm<sup>a</sup>

<sup>ii</sup> Specimen:  $l_0 = 80$  mm,  $b_0 = 20$  mm<sup>a</sup>

<sup>jj</sup> Specimen:  $l_0 = 80$  mm,  $b_0 = 20$  mm<sup>a</sup>

<sup>kk</sup> Specimen:  $l_0 = 80$  mm,  $b_0 = 20$  mm<sup>a</sup>

<sup>ll</sup> Specimen:  $l_0 = 80$  mm,  $b_0 = 20$  mm<sup>a</sup>

<sup>mm</sup> Specimen:  $l_0 = 80$  mm,  $b_0 = 20$  mm<sup>a</sup>

<sup>nn</sup> Specimen:  $l_0 = 80$  mm,  $b_0 = 20$  mm<sup>a</sup>

<sup>oo</sup> Specimen:  $l_0 = 80$  mm,  $b_0 = 20$  mm<sup>a</sup>

<sup>pp</sup> Specimen:  $l_0 = 80$  mm,  $b_0 = 20$  mm<sup>a</sup>

<sup>qq</sup> Specimen:  $l_0 = 80$  mm,  $b_0 = 20$  mm<sup>a</sup>

<sup>rr</sup> Specimen:  $l_0 = 80$  mm,  $b_0 = 20$  mm<sup>a</sup>

<sup>ss</sup> Specimen:  $l_0 = 80$  mm,  $b_0 = 20$  mm<sup>a</sup>

<sup>tt</sup> Specimen:  $l_0 = 80$  mm,  $b_0 = 20$  mm<sup>a</sup>

<sup>uu</sup> Specimen:  $l_0 = 80$  mm,  $b_0 = 20$  mm<sup>a</sup>

<sup>vv</sup> Specimen:  $l_0 = 80$  mm,  $b_0 = 20$  mm<sup>a</sup>

<sup>ww</sup> Specimen:  $l_0 = 80$  mm,  $b_0 = 20$  mm<sup>a</sup>

<sup>xx</sup> Specimen:  $l_0 = 80$  mm,  $b_0 = 20$  mm<sup>a</sup>

<sup>yy</sup> Specimen:  $l_0 = 80$  mm,  $b_0 = 20$  mm<sup>a</sup>

<sup>zz</sup> Specimen:  $l_0 = 80$  mm,  $b_0 = 20$  mm<sup>a</sup>

<sup>aa</sup> Specimen:  $l_0 = 80$  mm,  $b_0 = 20$  mm<sup>a</sup>

<sup>bb</sup> Specimen:  $l_0 = 80$  mm,  $b_0 = 20$  mm<sup>a</sup>

<sup>cc</sup> Specimen:  $l_0 = 80$  mm,  $b_0 = 20$  mm<sup>a</sup>

<sup>dd</sup> Specimen:  $l_0 = 80$  mm,  $b_0 = 20$  mm<sup>a</sup>

<sup>ee</sup> Specimen:  $l_0 = 80$  mm,  $b_0 = 20$  mm<sup>a</sup>

<sup>ff</sup> Specimen:  $l_0 = 80$  mm,  $b_0 = 20$  mm<sup>a</sup>

<sup>gg</sup> Specimen:  $l_0 = 80$  mm,  $b_0 = 20$  mm<sup>a</sup>

<sup>hh</sup> Specimen:  $l_0 = 80$  mm,  $b_0 = 20$  mm<sup>a</sup>

<sup>ii</sup> Specimen:  $l_0 = 80$  mm,  $b_0 = 20$  mm<sup>a</sup>

<sup>jj</sup> Specimen:  $l_0 = 80$  mm,  $b_0 = 20$  mm<sup>a</sup>

<sup>kk</sup> Specimen:  $l_0 = 80$  mm,  $b_0 = 20$  mm<sup>a</sup>

<sup>ll</sup> Specimen:  $l_0 = 80$  mm,  $b_0 = 20$  mm<sup>a</sup>

<sup>mm</sup> Specimen:  $l_0 = 80$  mm,  $b_0 = 20$  mm<sup>a</sup>

<sup>nn</sup> Specimen:  $l_0 = 80$  mm,  $b_0 = 20$  mm<sup>a</sup>

<sup>oo</sup> Specimen:  $l_0 = 80$  mm,  $b_0 = 20$  mm<sup>a</sup>

<sup>pp</sup> Specimen:  $l_0 = 80$  mm,  $b_0 = 20$  mm<sup>a</sup>

<sup>qq</sup> Specimen:  $l_0 = 80$  mm,  $b_0 = 20$  mm<sup>a</sup>

<sup>rr</sup> Specimen:  $l_0 = 80$  mm,  $b_0 = 20$  mm<sup>a</sup>

<sup>ss</sup> Specimen:  $l_0 = 80$  mm,  $b_0 = 20$  mm<sup>a</sup>

<sup>tt</sup> Specimen:  $l_0 = 80$  mm,  $b_0 = 20$  mm<sup>a</sup>

<sup>uu</sup> Specimen:  $l_0 = 80$  mm,  $b_0 = 20$  mm<sup>a</sup>

<sup>vv</sup> Specimen:  $l_0 = 80$  mm,  $b_0 = 20$  mm<sup>a</sup>

<sup>ww</sup> Specimen:  $l_0 = 80$  mm,  $b_0 = 20$  mm<sup>a</sup>

<sup>xx</sup> Specimen:  $l_0 = 80$  mm,  $b_0 = 20$  mm<sup>a</sup>

<sup>yy</sup> Specimen:  $l_0 = 80$  mm,  $b_0 = 20$  mm<sup>a</sup>

<sup>zz</sup> Specimen:  $l_0 = 80$  mm,  $b_0 = 20$  mm<sup>a</sup>

<sup>aa</sup> Specimen:  $l_0 = 80$  mm,  $b_0 = 20$  mm<sup>a</sup>

<sup>bb</sup> Specimen:  $l_0 = 80$  mm,  $b_0 = 20$  mm<sup>a</sup>

<sup>cc</sup> Specimen:  $l_0 = 80$  mm,  $b_0 = 20$  mm<sup>a</sup>

<sup>dd</sup> Specimen:  $l_0 = 80$  mm,  $b_0 = 20$  mm<sup>a</sup>

<sup>ee</sup> Specimen:  $l_0 = 80$  mm,  $b_0 = 20$  mm<sup>a</sup>

<sup>ff</sup> Specimen:  $l_0 = 80$  mm,  $b_0 = 20$  mm<sup>a</sup>

<sup>gg</sup> Specimen:  $l_0 = 80$  mm,  $b_0 = 20$  mm<sup>a</sup>

<sup>hh</sup> Specimen:  $l_0 = 80$  mm,  $b_0 = 20$  mm<sup>a</sup>

<sup>ii</sup> Specimen:  $l_0 = 80$  mm,  $b_0 = 20$  mm<sup>a</sup>

<sup>jj</sup> Specimen:  $l_0 = 80$  mm,  $b_0 = 20$  mm<sup>a</sup>

<sup>kk</sup> Specimen:  $l_0 = 80$  mm,  $b_0 = 20$  mm<sup>a</sup>

<sup>ll</sup> Specimen:  $l_0 = 80$  mm,  $b_0 = 20$  mm<sup>a</sup>

<sup>mm</sup> Specimen:  $l_0 = 80$  mm,  $b_0 = 20$  mm<sup>a</sup>

<sup>nn</sup> Specimen:  $l_0 = 80$  mm,  $b_0 = 20$  mm<sup>a</sup>

<sup>oo</sup> Specimen:  $l_0 = 80$  mm,  $b_0 = 20$  mm<sup>a</sup>

<sup>pp</sup> Specimen:  $l_0 = 80$  mm,  $b_0 = 20$  mm<sup>a</sup>

<sup>qq</sup> Specimen:  $l_0 = 80$  mm,  $b_0 = 20$  mm<sup>a</sup>

<sup>rr</sup> Specimen:  $l_0 = 80$  mm,  $b_0 = 20$  mm<sup>a</sup>

<sup>ss</sup> Specimen:  $l_0 = 80$  mm,  $b_0 = 20$  mm<sup>a</sup>

<sup>tt</sup> Specimen:  $l_0 = 80$  mm,  $b_0 = 20$  mm<sup>a</sup>

<sup>uu</sup> Specimen:  $l_0 = 80$  mm,  $b_0 = 20$  mm<sup>a</sup>

<sup>vv</sup> Specimen:  $l_0 = 80$  mm,  $b_0 = 20$  mm<sup>a</sup>

<sup>ww</sup> Specimen:  $l_0 = 80$  mm,  $b_0 = 20$  mm<sup>a</sup>

<sup>xx</sup> Specimen:  $l_0 = 80$  mm,  $b_0 = 20$  mm<sup>a</sup>

<sup>yy</sup> Specimen:  $l_0 = 80$  mm,  $b_0 = 20$  mm<sup>a</sup>

<sup>zz</sup> Specimen:  $l_0 = 80$  mm,  $b_0 = 20$  mm<sup>a</sup>

<sup>aa</sup> Specimen:  $l_0 = 80$  mm,  $b_0 = 20$  mm<sup>a</sup>

<sup>bb</sup> Specimen:  $l_0 = 80$  mm,  $b_0 = 20$  mm<sup>a</sup>

<sup>cc</sup> Specimen:  $l_0 = 80$  mm,  $b_0 = 20$  mm<sup>a</sup>

<sup>dd</sup> Specimen:  $l_0 = 80$  mm,  $b_0 = 20$  mm<sup>a</sup></p

<i>Copper</i>							
FCu	UNS C25000	<140 (20.3)	215-255 (31.2-37)	>45	2.1	1.3	1.9
<i>Copper-zinc alloys (brass)</i>							
CuZn37F30	UNS C27400	<195 (28.3)	295-370 (42.8-53.65)	50	2.1	1.4	2.0
CuZn28F28	UNS C26000	<155 (22.5)	275-350 (39.9-50.75*)	50	2.2	1.4	2.0
CuZn10F24	UNS C32000	<135 (19.6)	295-295 (34.1-42.8)	42	2.2	1.3	1.9
CuNi12Zn24F35	UNS C75700	<295 (42.8)	340-410 (49.3-59.45)	45	1.9	1.3	1.8
CuNi20FeF30	UNS 71000 [Monel]	110 (15.95)	295 (42.8)	35	1.9	1.3	1.8
<i>Aluminum</i>							
Al99.5w	AA 1050-A	<59 (8.6)	69 (10)	35	2.1	1.6	2.0
	AA 1050-H14	68 (9.9)	90 (14.5)	6	1.9	1.4	1.8
Al99.5F10	AA 1200-O	<88 (9.9)	79 (11.5)	30	2.05	1.6	1.95
Al99w	AA 1200-H14	79 (11.5)	108 (15.7)	5	1.9	1.4	1.8
Al99F11	AA 6082	145 (21)	145 (21)	18	2.05	1.4	1.9
AlMg51w							
<i>Titanium</i>							
Ti99.7	ASTM B265 gr 2	250 (36.25)	395-540 (57.3-78.3)	22	1.9	—	1.7

\*80 mm = 3.15 in; 20 min = 0.79 in.

 $t_2$  mm = 0.2 in. $t_1$  = longitudinal direction;  $\perp$  = perpendicular direction.

Source: Compiled from [20,3].

Drawing is often carried out at elevated temperatures of 77-327°C (170-620°F).

For specific purposes high limiting drawing ratios may be desired. Investigations have been conducted to find out how  $\beta_{\max}$  can be increased above the generally known values. In principle the limiting drawing ratio is increased if one can manage to reduce the flow stress in the flange or to increase the strength of the sheet in the transition region from the bottom of the cup to the wall. Several measures have been tried, such as localized heating of the blank in the region of the flange, the use of cooled punches with heated blanks, or the use of blanks which have been pre-stressed under the punch.\* Because of the required high effort none of these measures has found wide industrial application.

### 20.1.5 Effect of Anisotropy on Deep Drawing

Deep drawing is the forming process which shows anisotropic material behavior most clearly and for which the effect of anisotropy has been known for the longest time. It was mentioned above that the limiting drawing ratio increases with increasing  $r$ -value, as shown in Fig. 20.11 [20.12]. This has been confirmed in several other investigations [20.21] to [20.24]. The use of sheet material with a large  $r$ -value not only produces less wall thinning in the transition region from the cup bottom to the wall but also reduces the drawing load.

Consider a plane state of stress with principal stresses  $\sigma_x$  and  $\sigma_y$ , as it exists during deep drawing in the flange area. (The relatively small blankholder pressure will be neglected.) The von Mises yield criterion for such a state of stress for homogeneous, isotropic materials is

$$\sigma_f = \sqrt{\sigma_x^2 + \sigma_y^2 - \sigma_x \sigma_y} \quad (20.48)$$

Hill [20.25] has applied the von Mises criterion to anisotropic materials. Hosford and Backofen [20.26] to [20.28] simplified Hill's theory by assuming a constant  $r$ -value across the thickness of the sheet. This results in the following yield criterion:

$$\sigma_f = \sqrt{\sigma_x^2 + \sigma_y^2 - \sigma_x \sigma_y \frac{2r}{r+1}} \quad (20.49)$$

In Fig. 20.12 the relationship described by Eq. 20.49 is represented graphically. For  $r = 1$  isotropic material behavior results as stated by Eq. 20.48. During deep drawing of a component (Fig. 20.13) there exists a tension-compression state of stress in the flange. The radial stress  $\sigma_r$  corresponds to  $\sigma_x$  and is positive, and the tangential stress  $\sigma_t$  corresponds to  $\sigma_y$  and is negative, such that the state of stress lies in the second quadrant of the coordinate system of Fig. 20.12. It follows that the absolute values of the stresses required to cause yielding are smaller as  $r$  increases. This causes a lowering of the drawing load.

In the wall of the drawn part no deformation takes place in the tangential or  $y$ -direction. The material element shown in Fig. 20.13 carries axial tensile stresses  $\sigma_z$ , which attempt to reduce the sheet dimensions in the  $y$ - and  $z$ - (thickness) directions. Prevention of deformation in the  $y$ -direction by the rigid punch produces tensile stresses in the same  $y$ -direction. Fig. 20.12 shows that in the first quadrant larger tensile stresses can be sustained without yielding as the  $r$ -value increases. Increasing the  $r$ -value, therefore, strengthens the cup wall while it reduces the flow stresses in the flange. This explains the increased limiting drawing ratio  $\beta_{\max}$  for increasing values of the normal anisotropy  $r$ .

In general the  $r$ -value is not constant in the plane of the sheet but shows a distribution, as indicated in Fig. 20.14. Many sheet materials exhibit four maxima for a rotation through  $360^\circ$  when the  $r$ -value is plotted as a function of the angle from the rolling direction. These maxima are equally spaced every  $90^\circ$ , but need not be positioned at  $0^\circ$ ,  $90^\circ$ ,  $180^\circ$ , and  $270^\circ$  with respect to the rolling direction. Rather, their orientation depends on the material (microstructure), the production process, and the heat treatment. Their relative magnitudes can also be variable. This material property is called planar anisotropy  $\Delta r$  and is commonly defined as

$$\Delta r = r_{\max} - r_{\min}$$

\*This is done by cold rolling the blank and subsequent annealing of the flange area.

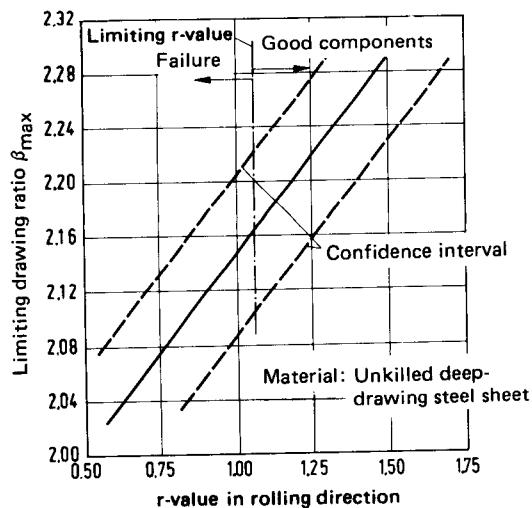


FIG. 20.11 Effect of normal anisotropy on the limiting drawing ratio. (After [20.12].)

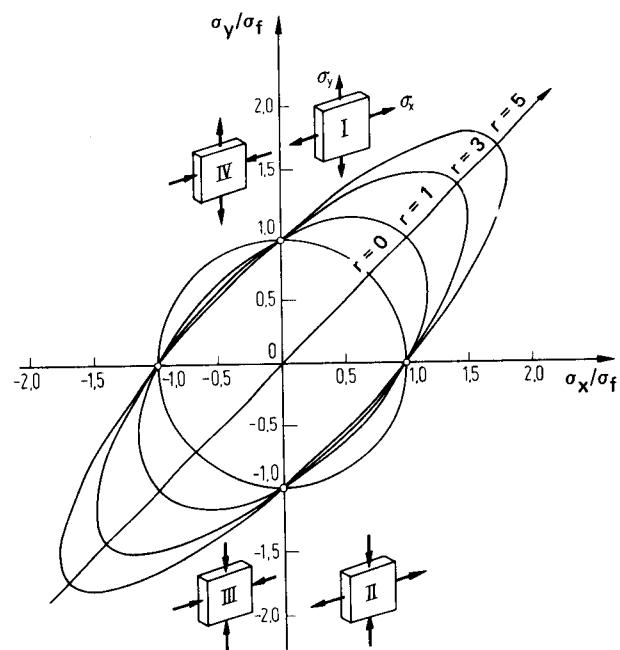
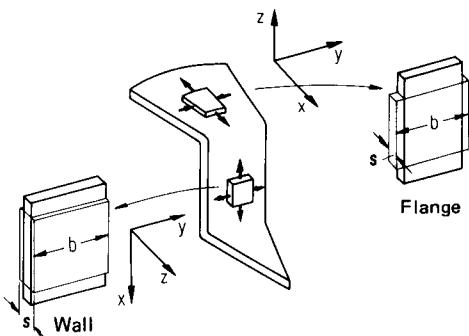
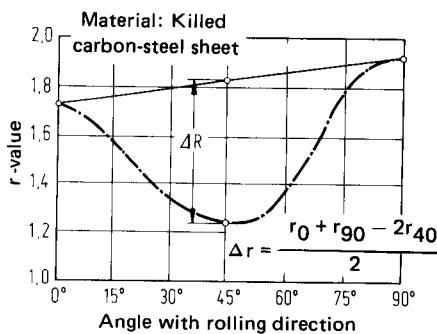


FIG. 20.12 Flow stress locus for plane stress ( $\sigma_z = 0$ ) as a function of normal anisotropy assuming zero planar anisotropy. (After [20.28].)



**FIG. 20.13** Schematic diagram of the state of stress during deep drawing. Thin lines—element before deformation; thick lines—element after deformation. (After [20.28].)



**FIG. 20.14** Distribution of  $r$ -value of the normal anisotropy as a function of orientation to the rolling direction.

Planar anisotropy causes uneven edges of the deep-drawn components, as illustrated in Fig. 20.15. The effect is known as earing. It is undesirable since it requires an additional processing step and leads to wall-thickness variations.

To date it has not been possible to correlate earing with the variation of the mechanical properties in the plane of the sheet. In a rough simplification of the true behavior it may be assumed that the sheet poses a heavy resistance to changes in its thickness in those directions along which  $r$  is large. Consequently upsetting in these directions will not be as large as in directions of low  $r$ -values, but ears will be formed to accommodate the displaced material. The height of the ears will increase as the planar anisotropy  $\Delta r$  increases (Fig. 20.14). The height of the ears (peak to valley) can be as large as 15–20% of the height of the cup. In [20.29] it is stated that there exists an approximate proportionality between  $\Delta r$  and the height of the ears. Blade and Pearson [20.30], Wright [20.31], and Buschmann [20.32] describe a number of influence factors on ear-

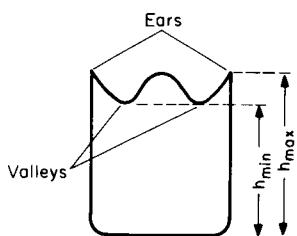


**FIG. 20.15** Deep-drawn component with ears due to planar anisotropy.

ing in general, on the height of the ears, and on the average useful height of the cup when drawing aluminum sheet in the first draw. The influence factors are related to tool geometry, such as die clearance and punch radius, and to the drawing process, such as drawing ratio, sheet thickness, punch diameter, and blankholder force.

To estimate the deep-drawing behavior of sheets one commonly uses a mean  $r$ -value  $\bar{r}$ , which is calculated from the  $r$ -values measured at angles of  $0^\circ$ ,  $45^\circ$ , and  $90^\circ$  to the rolling direction:

$$\bar{r} = 0.25(r_0 + 2r_{45} + r_{90}) \quad (20.50)$$

More accurate predictions of the drawing behavior would probably result if the minimum value  $r_{\min}$  were used rather than the mean value  $\bar{r}$  since failure already occurs if  $r_{\min}$  falls below a lower limit.

It is desirable that  $r$  should be as large as possible in deep drawing and constant in the plane of the sheet ( $\Delta r = 0$ ), or earing will take place. For components of noncylindrical shape the drawing process is not pure drawing but a combination of drawing and stretching. Sheets for these parts should have a large mean  $r$ -value  $\bar{r}$ , and the direction with the largest  $r$ -value  $r_{\max}$  should be placed in the direction of the largest strain.

Jakovlev and Sevelev [20.33] have proposed that earing can be reduced by using "predrawn" blanks, that is, noncircular blanks for circular parts if the distribution of the  $r$ -values in the plane of the sheet is known. The cup will then no longer show distinct earing, but wall-thickness variations due to the varying  $r$ -values will remain. Similar results have been reported by Galinowski [20.34], [20.35]. He used square blanks with the diagonals oriented at a predetermined angle to the rolling direction to deep draw circular cups. Some earing was observed in these tests, but he obtained larger useful cup heights than when starting with circular blanks of diameters equal to the sides of the square. It was concluded that this method is more economical in use.

### 20.1.6 Wrinkle Formation during Deep Drawing

It was already mentioned in this chapter that the flange has a tendency to buckle under the influence of the tangential compressive stresses. The resulting folds are called wrinkles, in contrast to pockers which are observed in noncylindrical components. Wrinkle formation can be prevented by pressing a blankholder with sufficient pressure  $p_{BH}$  against the workpiece.

As long as the blank is clamped rigidly between blankholder and die, as is the case at the beginning of the draw, buckling cannot occur. During deformation the thickness does not remain constant but increases toward the outside edge of the flange while the center portion near the die radius becomes thinner than the initial thickness  $s_0$  in the early stages of the draw. Since the distance between blankholder and die is determined by the greatest flange thickness, there will be a small gap between blankholder and sheet at places of smaller thickness. This gap offers an opportunity for the initiation of wrinkles. Investigations by Siebel and Beisswanger [20.6] have shown that the thickness variations can amount to over 10% of the initial sheet thickness for a drawing ratio  $\beta = 2.0$ . Thin sheets ( $d_0/s_0 > 25-40$ ) are especially sensitive to wrinkle formation because their moment of inertia in buckling is small. They require larger blankholder pressures than thick sheets. This is clearly demonstrated in Fig. 20.8, which shows the blankholder pressure as a function of the relative sheet thickness. Thick sheets with  $d_0/s_0 < 25$  in general do not tend to form wrinkles because they have a large moment of inertia and thus sufficient resistance against buckling. They can be drawn without a blankholder.

In [20.36] anisotropy is shown to have some effect on wrinkle formation and thereby on the blankholder pressure necessary to avoid wrinkles. Material with a small  $r$ -value requires relatively large pressures. In addition  $p_{BH}$  must be increased as the planar anisotropy  $\Delta r$  increases.

## 20.2 FUNDAMENTALS OF DEEP DRAWING—REDRAW

### 20.2.1 General Remarks, Stresses

There are many deep-drawing sheet materials which allow drawing ratios of  $\beta_{\max} = 2.0$  for the first draw. Such a ratio makes it possible, for example, to draw a blank of diameter  $d_0 = 200$  mm

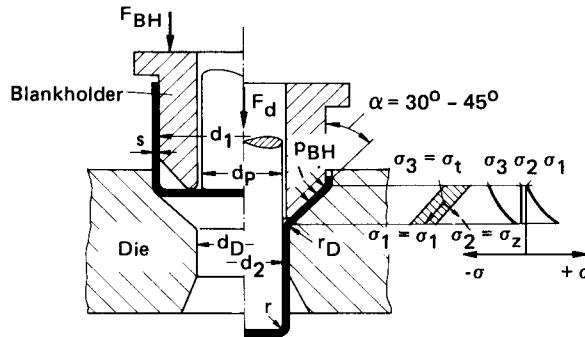


FIG. 20.16 Tool for redrawing.

(8 in) into a cup of diameter  $d_1 = 100$  mm (4 in) and a cup height  $h_c = 75$  mm (3 in). In order to produce a cup with a larger ratio of height to diameter one or more redraws are required.

Figure 20.16 shows a schematic diagram of a deep-drawing tool for redrawing. The distributions of the stresses  $\sigma_z$  and  $\sigma_t$  in the deformation zone are qualitatively equal to those occurring during the first draw. Because of the generally conical shape of the die entrance an additional normal pressure  $p_n$  acts even in the absence of a blankholder, which presses the cup against the die. This normal pressure is caused by the tangential compressive stress  $\sigma_t$  and can be calculated from the equation

$$p_n = \frac{2s\sigma_t}{d} \cos \alpha$$

where  $s$  is the sheet thickness and  $d$  is the selected diameter [20.6]. The tendency to form wrinkles is much smaller for a redraw than it is for the first draw since the drawing ratios are generally smaller for redraws. It is possible to work without a blankholder [20.6] if the initial sheet thickness is  $s_0 > 0.011d_{p,n}\beta_n$ . In this inequality  $d_{p,n}$  is the punch diameter and  $\beta_n$  the drawing ratio for the  $n$ th redraw.

If a blankholder is used, lower blankholder pressures  $p_{BH}$  in the range of 0.6–1.2 N/mm<sup>2</sup> (90–175 psi) are sufficient. The larger values apply to thin sheets and large drawing ratios.

The purpose of the blankholder during a redraw is not so much to exert pressure, but rather to give support. In the beginning of the redraw the bottom of the cup does not yet rest against the conical die entrance (Fig. 20.16). Because of the tangential compressive stresses puckers can occasionally appear in thin sheets in this region during the early stages of the redraw. If they occur, puckers are formed in the region between the die and the punch where the workpiece does not contact either the die or the punch but is simply clamped.

If wrinkles are formed as drawing continues, they appear mostly toward the end of the process when the upper edge of the component has already been drawn over the die radius. The choice of the cone angle of the die greatly influences the buckling behavior. For small angles  $\alpha$  the tendency to form wrinkles is reduced, while the tendency to form puckers is increased. In most cases angles between 30 and 45° are chosen.

### 20.2.2 Forces during Redrawing

Analogous to the first draw, the largest drawing load must be less than the cracking load  $F_{cr}$ , which can be calculated from Eq. 20.40. Siebel and Beisswanger [20.6] derived the following equation for the largest drawing load  $F_{d,max}$ :

$$F_{d,max} = \pi d_m s \sigma_{f,m} \left[ \underbrace{\frac{2e^{\mu\alpha}}{d_1 + d_m} 1.1}_B + \underbrace{\frac{\mu}{\tan \alpha}}_C + \underbrace{\frac{s}{2r_D}}_D \right] \quad (20.51)$$

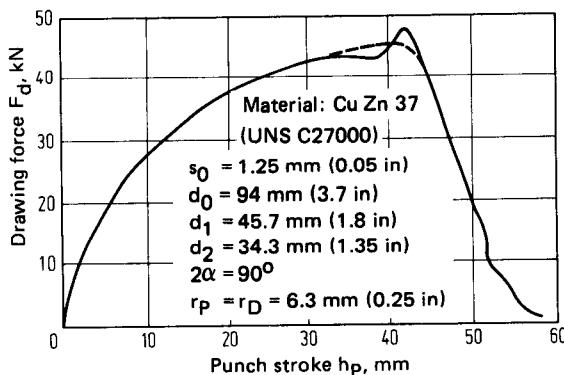


FIG. 20.17 Force–stroke diagram for a redraw.

In this equation  $d_m = d_1 + s$  is the mean diameter of the redrawn cup and  $\sigma_{f,m}$  is the mean flow stress in the conical deformation zone. When determining  $\sigma_{f,m}$ , the strain hardening due to all prior draws must be taken into account if no intermediate annealing took place.

Term A describes the ideal deformation load. The factor 1.1 results from the flow criterion which was already applied to the first draw (Eq. 20.5). Term B accounts for the friction at the two radii at the entrance and exit of the deformation zone, term C accounts for the friction at the conical shoulder, and term D represents the bending load.

The load–stroke diagram for a redraw is shown in Fig. 20.17. During the first draw the material strain hardens with increasing intensity toward the outside edge of the cup and the sheet thickness increases. During the redraw without prior annealing the drawing load must therefore increase as the punch proceeds since both the wall thickness and the mean flow stress increase. All other parameters remain constant. Only when the upper edge of the drawn component has made contact with the conical shoulder does the drawing load decrease again.

The shape of the die barely affects the maximum drawing load. However, experiments conducted by Siebel and Beisswanger [20.6] showed that higher limiting drawing ratios are obtainable with small die half-angles ( $\alpha = 22.5^\circ$ ) than with large die half-angles ( $\alpha = 45^\circ$ ).

### 20.2.3 Drawing Ratios and Drawing Increments for Redraws

When selecting the drawing ratio one must distinguish between redraws with and without intermediate annealing. If the material is not annealed between draws, successively smaller drawing ratios must be used because of the prior strain hardening.

For redraws with intermediate annealing larger drawing ratios are permissible than without the heat treatment. Because of the wall thickening in the upper portion of the cup wall, the drawing ratio must not be chosen as large as for the first draw, or cracking may result. For components having a large height-to-diameter ratio the desired cup height may not be obtainable with one redraw. Several redraws are then carried out successively. The total drawing ratio  $\beta_{tot}$  is equal to the product of the drawing ratios of all draws. A large total drawing ratio is obtained by choosing the drawing ratio for the first draw as large as possible. For deep drawing steel without annealing total drawing ratios of  $\beta_{tot} \approx 6.5$  are obtainable without failures. Under these circumstances wall-thickness ratios of about 1:2 result from the thinning at the punch radius and the thickening at the upper edge of the cups. Experiments [20.6] have shown that it is possible to use small die clearances of  $u_D \approx 1.1s_0$ , at least during the first draw and the first redraw, without having to reduce the drawing ratios. Small die clearances produce an ironing effect toward the end of the drawing steps. The resulting wall thinning partly cancels the incurred wall thickening. Table 20.1 lists the achievable drawing ratios with and without annealing for the most important deep-drawing materials.

**Table 20.2** Suggested Drawing Ratios  $\beta$  for Deep Drawing of Cylindrical Components without Intermediate Annealing<sup>a</sup>

Number of draws	Relative sheet thickness $s_0/d_0 \times 10^{-2}$					
	1.5–2.0	1.0–1.5	0.6–1.0	0.3–0.6	0.15–0.3	0.08–0.15
1	2.00–2.08	1.87–2.00	1.82–1.87	1.72–1.82	1.67–1.72	1.59–1.67
2	1.33–1.37	1.32–1.33	1.28–1.32	1.26–1.28	1.25–1.26	1.22–1.25
3	1.28–1.32	1.26–1.28	1.25–1.26	1.23–1.25	1.22–1.23	1.19–1.22
4	1.25–1.28	1.23–1.25	1.22–1.23	1.20–1.22	1.18–1.20	1.16–1.18
5	1.22–1.25	1.19–1.22	1.18–1.19	1.16–1.18	1.15–1.16	1.14–1.15

<sup>a</sup>Workpiece material—RSt 14 (SAE 1006).

Source: Compiled from [20.9].

Romanowski [20.9] suggests the drawing increments given in Table 20.2 for drawing steel and brass sheets with and without intermediate heat treatment. The larger values are for first draws with large punch and die radii. Materials with lower drawing ability such as hard aluminum and brass must be drawn using smaller drawing ratios. On the other hand, the drawing ratios may be increased for materials such as St13 (AISI 1006) and St14 (SAE 1005), which have good drawing characteristics.

Choosing the proper drawing increments for noncylindrical or even square components is much more difficult. The interested reader is directed to the specialized literature, for example, [20.3], [20.4].

When very large quantities of a component requiring several redraws are needed, the part is most often drawn on high-production transfer presses. Drawing without intermediate annealing is preferred since heat treatment is expensive and cannot be done in the press. Rather, one more redrawing step is added. Also, the least expensive material is selected since the material costs constitute a higher portion of the total cost than do the tool costs, which are shared among many components in large-batch production.

The order of the cost factors is reversed for small batch sizes. Because tool costs are shared among few components, one tries to minimize the number of draws by utilizing higher-quality drawing sheets and by using intermediate annealing steps.

Thin sheets must be heat treated in inert atmospheres or even in vacuum in order to avoid oxidation. Even heating up and cooling down must be done in an inert atmosphere. Annealing should therefore be avoided, especially for thin sheets.

#### 20.2.4 Redrawing with Wall Thinning

Redrawing with wall thinning, in practice generally called ironing, belongs to the bulk-deformation processes and was treated in depth in Chap. 14. It is mentioned here solely because it is very often carried out following the first draw or the first redraw, using the same tools and presses as ordinary deep drawing.

Ironing is used for those cylindrical components whose wall thickness should be less than or at most equal to the initial sheet thickness  $s_0$ . For load calculation the formulas for ironing given in Chap. 14 have to be taken into consideration.

### 20.3 DRAWING OF NONCYLINDRICAL COMPONENTS AND SPECIAL DRAWING PROCESSES

#### 20.3.1 Drawing of Conical, Parabolic, and Spherical Parts

Drawing of these components presents considerably more difficulties than the deep drawing of cylindrical parts. There are two main reasons for this fact:

- 1 The drawing loads must be transmitted by a small cross section of the sheet since the circumference of the line of contact between the punch and the component is small. This is especially true for spherical components at the beginning of the draw. For this reason the danger of cracking is high, even for small drawing ratios.
- 2 Deformation takes place not only in the flange, but also in the zone between the die and the punch where the workpiece is unsupported (Fig. 20.18, region A-B'). In this region there also exist tangential compressive stresses which can cause pockers.

Puckering must be avoided since pockers cannot be removed. Investigations by Beisswanger [20.37] have shown that pockers formed in the early stages of the draw in thick sheets can be reduced during continuing deformation, but pockers in thin sheets always tend to grow.

All actions to prevent pockers try to influence the state of stress in the deformation zone in such a way as to eliminate tangential compressive stresses. This is accomplished by:

- 1 Increasing the blankholder pressure  $p_{BH}$ . This increases the frictional stresses in the flange and thereby the radial tensile stresses  $\sigma_r$  in the free zone between the die and the punch. According to the flow criterion the tangential compressive stresses  $\sigma_t$  are reduced and pockers are avoided.
- 2 Increasing the blank diameter  $d_0$ . This action also has the effect of increasing the radial stresses in the free zone since the radial stresses increase from the outside edge of the flange toward the punch. The larger the blank diameter  $d_0$ , the larger will be the radial tensile stresses  $\sigma_r$ , and the smaller the tangential compressive stresses  $\sigma_t$ . It is even possible for the tangential stresses to change sign in the free zone and to become tensile near the punch.
- 3 Use of a draw bead (Fig. 20.19). The clearance between the draw bead and the blankholder is a little smaller than the sheet thickness  $s_0$ . Therefore the material is slightly upset as it passes through the gap and is cold-worked. The upsetting and bending around the bead increase the radial tensile stresses, and the tendency to form pockers is reduced. Drawing beads have been standardized in Germany [20.38]. When shallow cones with cone angles greater than  $65^\circ$  are produced from thin sheets, springback makes the production of workpieces of high accuracy very difficult. In order to reduce elastic recovery, high stresses are again superimposed with the aid of draw beads.

Occasionally one or several concentric bevelled blankholders are used in the manufacture of shallow workpieces (Fig. 20.20). These blankholders also produce a drawing action and form part of the conical cup even before the punch contacts the die.

Flat cones made from thick sheets undergo only little upsetting during drawing and can be drawn without pockers in the absence of a blankholder.

Because of the large radial tensile stresses, small drawing ratios per draw must be used when making conical components. Also, the relative sheet thickness  $s_0/d_0$  influences the limiting drawing ratio to a greater extent than when drawing cylindrical parts. The limiting drawing ratio in addition depends on the cone angle and the ratio of the largest to the smallest cone diameter. Schmidt [20.39] has produced a nomogram which can be used to determine the limiting drawing ratio as a function of these parameters. Typical values for the drawing increments for conical

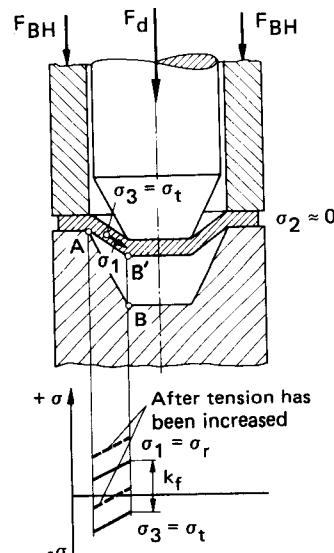
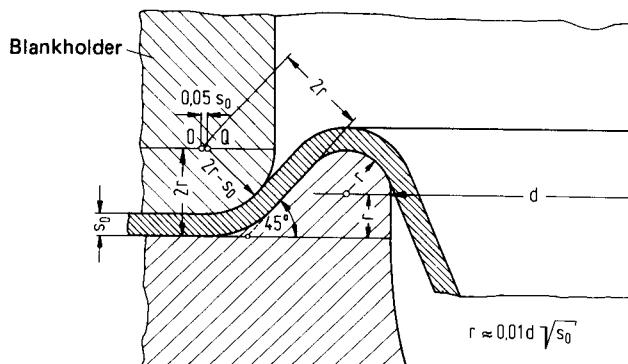


FIG. 20.18 Schematic diagram of drawing of conical components.



**FIG. 20.19** Draw bead for deep drawing of noncylindrical components.  
(After [20.38].)

components are best obtained from the appropriate handbooks [20.3], [20.9]. If the cone angle is less than 20°, the tool design can proceed analogous to that for cylindrical draws.

Whenever possible, cylindrical preforms are used, which require only simple tooling, and the final conical shape is produced in the last step (Fig. 20.21). Several successive redraws are carried out which are not quite completed. The last redraw is often replaced by closed-die calibrating in a drop hammer or in a screw press. All components which have been produced with cylindrical preforms show local wall-thickness variations, because the material is restricted from flowing into the deformation zone and additional thinning must take place during the draw. The steplike shoulders cannot be removed completely because of the elastic recovery of the material. Often the impressions made by the edges of the drawing punches also remain in the finished component so that its surface is wavy and irregular. For these reasons workpieces of high accuracy and surface quality, such as reflectors for headlights, cannot be produced using this method.

In contrast to cylindrical parts, the drawing load constantly increases when drawing noncylindrical components and reaches its maximum at the end of the draw. Simple equations to predict the drawing load, similar to those developed by Siebel for cylindrical components [20.6], do not exist to date.

The problems encountered when deep drawing hemispherical and parabolic shapes are very similar to those found in drawing conical parts. Here, too, the main problem is to avoid the formation of puckers. The difficulty arises because the drawing load is applied to a very small contact area in the center of the punch. There exists a large unsupported area which tends to form puckers easily. In addition, the material is highly stretched because of the large tensile stresses so that even more redraws are necessary than for conical components.

In the production of conical, parabolic, and spherical components drawing processes which utilize fluids to apply the drawing load instead of a rigid punch are often used. They offer the advantage that the workpiece is completely supported during the draw such that puckers are prevented.

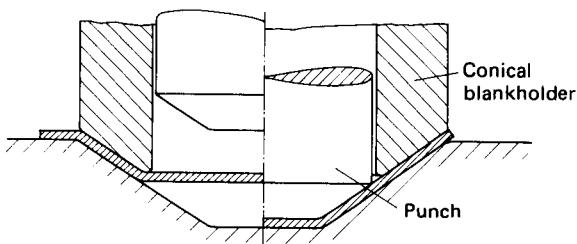


**FIG. 20.20** Drawing with conical blankholder.

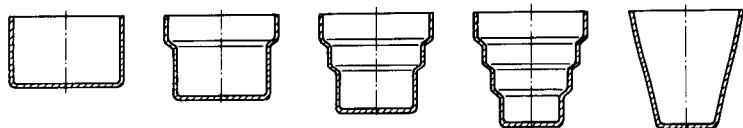


FIG. 20.21 Drawing of conical component from cylindrical preforms.

### 20.3.2 Reverse Drawing

Reverse drawing is defined in [20.1] as a redraw in which the punch travels in the opposite direction, relative to the component, to that used for the previous draw. Therefore the direction of motion of the material is reversed and the cup is turned inside out, as illustrated in Fig. 20.22.

This process is preferred for the production of conical, hemispherical, and sometimes even cylindrical workpieces. Reverse drawing is often used to accumulate material in certain locations in order to aid the subsequent drawing of noncylindrical shapes or to produce workpieces having special shapes, such as cups with large flanges. The first of these two applications is illustrated in Fig. 20.23. A workpiece with a small cup of height  $h > 0.35 h_{c,\text{theor}}$  and a very large flange is to be produced (Fig. 20.23c). If this shape were drawn in a single draw, the required drawing load would immediately exceed the cracking load because of the very high drawing ratio

$$\beta = \frac{d_0}{d_2} \gg \beta_{\max}$$

In order to reduce the drawing ratio, the preform shown in Fig. 20.23b is produced first from the blank (Fig. 20.23a), and the final shape is generated in a reverse draw. The design of the preform is such that

$$\beta_1 = \frac{d_0}{d'_2} < \beta_{\max} \quad \text{first draw}$$

$$\beta_2 = \frac{d_1}{d_2} < \beta_{\max} \quad \text{reverse draw}$$

The punch diameter for the first draw is given approximately by

$$d'_2 \approx d_2 + 2h$$

Generally the first draw and the reverse draw are executed in the same operation. The punch for the first draw is hollow and also forms the die for the reverse redraw (Fig. 20.22). The effect of

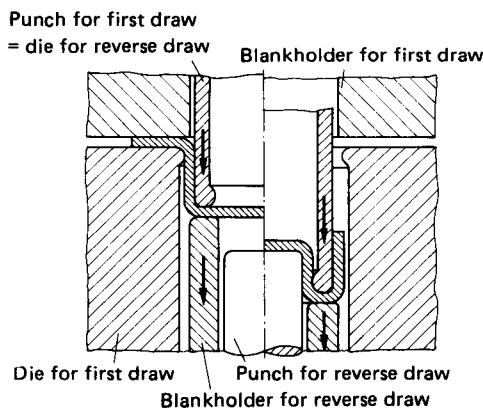
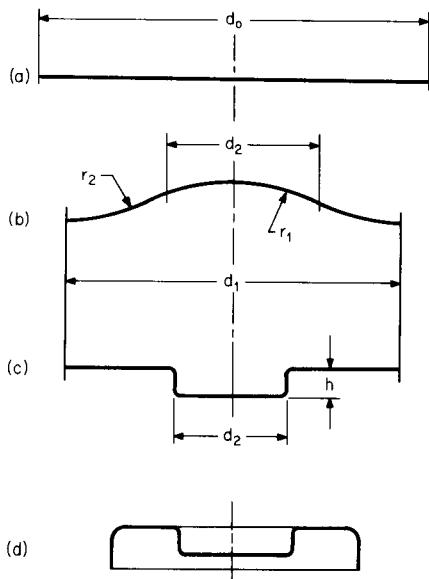
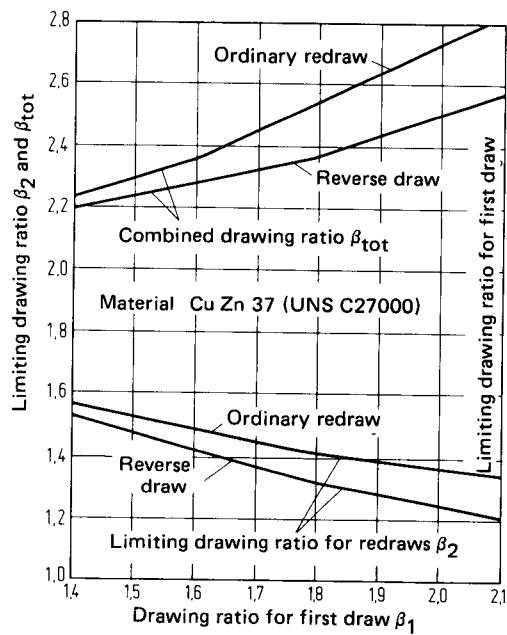


FIG. 20.22 Principle of reverse drawing.



**FIG. 20.23** Using reverse drawing to produce components with large flanges. (a) Blank. (b) First draw. (c) Reverse draw. (d) Final draw.



**FIG. 20.24** Comparison of the limiting drawing ratios for a reverse draw and an ordinary redraw. (After [20.6].)

this tool arrangement closely corresponds to that of a drawing bead and is very well suited to prevent puckering. The efficiency of the reverse draw is smaller than that of a "normal" redraw because of the large amount of bending and the increased friction such that the diameter reduction possible in a single drawing step is reduced, as shown in Fig. 20.24 [20.6]. Radtke [20.40] determined that in contrast to a "normal" draw the drawing ratio for a reverse draw does not only have an upper limit but a lower limit as well. If the drawing ratio is too small, then the reversing die must have a small radius, causing large bending stresses, which can lead to fractures.

Reverse drawing should be carried out with a blankholder since the sheet is bent through 180° around the reversing die. This can easily cause wrinkles. The preformed cup tries to expand toward the end of the reverse draw because of the bending stiffness of the cup wall, and it is possible for the edge of the cup to lift the blankholder. It is therefore recommended to combine the first draw with a slight ironing to reduce the wall thickness.

Calculation of the drawing load proceeds analogous to that for a "normal" redraw [20.6]. The advantages of reverse drawing are mainly that two draws can be combined into a single tool in a simple manner. However, this process requires material with high drawing ability and triple-action presses with long strokes.

### 20.3.3 Deep Drawing of Square and Oval Components

While the deformation occurs evenly along the circumference of the blank when deep drawing circular components, deep drawing of noncircular parts induces the highest strains and stresses at the corners, and lower stresses and strains are acting in the sidewalls. The distribution of the stresses and the strains depends on the ratio of the length of the edges to the corner radius and also on the height of the wall. The sidewalls are not only bent but experience radial tensile and tangential compressive stresses.

Investigations by Panknin and Dutschke [20.41] show that the often used drawing factor  $q$ , that is, the ratio of the corner radius of the punch to the blank radius, is not suited to characterize the limiting drawing ratio. Rather, it is possible to apply the rules for drawing circular components to the drawing of noncircular parts by replacing the punch and the blank areas by circles of equal size and calculating their respective equivalent diameters  $d'_p$  and  $d'_0$ :

$$d'_p = 2 \sqrt{\frac{A_p}{\pi}}$$

$$d'_0 = 2 \sqrt{\frac{A_0}{\pi}}$$

The drawing ratio  $\beta$  can then be calculated as for circular components:

$$\beta = \frac{d'_0}{d'_p}$$

This method is applicable for components with small and also with large corner radii  $r_C$ . Dutschke [20.42] has conducted experiments in which the ratio of the length of the edges  $l$  to the corner radius  $r_C$  was no larger than  $l/r_C = 64$  for quadratic parts and  $l/r_C = 89$  for other rectangular components and could detect no influence of the corner radius on the limiting drawing ratio. The limiting drawing ratio follows the same trend found in drawing circular parts and increases with increasing relative sheet thickness. Fig. 20.25 shows that for square components almost the same limiting drawing ratios can be achieved as for circular parts. The equivalent diameters can also be used to determine the drawing loads for square components [20.42]. To form square parts of great heights suitable drawing increments must be chosen. For quadratic components cylindrical preforms are normally used, and the quadratic shape is produced only during the last redraw. If the corner radius is very small, a noncylindrical shape is already used in the second to last redraw. For rectangular components, and especially for narrow rectangles such as lighter cases, oval preforms are used with a smooth transition to the rectangular shape.

Öettinger [20.43] has shown that the equivalent diameters may also be used for elliptical components to calculate the limiting drawing ratios, the drawing loads, and the stresses for these parts in a manner similar to the calculations for cylindrical components.

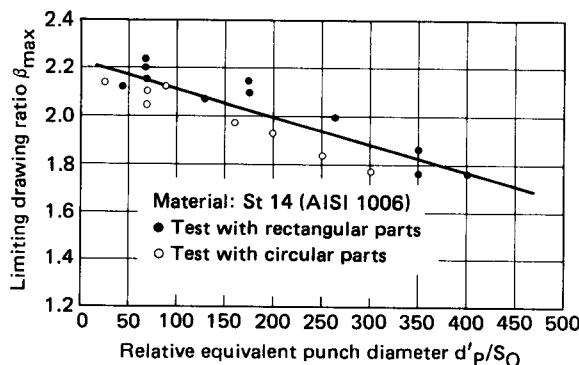


FIG. 20.25 Limiting drawing ratios for circular and rectangular components as a function of the equivalent punch diameter. (After [20.42].)

#### 20.3.4 Drawing of Automobile Body Parts and Other Irregular Components

Drawing of irregular shallow components, as are found frequently on automobile bodies, is only loosely related to deep drawing and contains elements of stretch forming and bending. The design principle of the tools consisting of punch, die, and blankholder is the same as in deep drawing. The condition that the drawing load be less than the cracking load must also be satisfied, but up to now it has been extremely difficult to treat the problem theoretically because of the complicated workpiece geometry.

Experimental investigations of the strains [20.5] in these components with the aid of electrochemically etched grids have shown that a relatively large fraction of the material necessary to form the recessed portion of the component is obtained through a reduction of the sheet thickness while only little material flows from the flange. The local stresses can be in the tension-compression region or in the region of biaxial tension, or they can be zero. To this day it is a matter of experience to estimate the required drawing loads and drawing limits, to design the tools, and to select the proper sheet quality.

One of the most powerful tools for analyzing the stresses and strains in irregularly shaped deep-drawn components is the grid method mentioned above. It allows the process engineer to study the flow of the material into the die and to evaluate improvements and trade-offs in tool design and material selection. A factor of safety against cracking of the sheet can be obtained from a forming-limit diagram (FLD) (see Sec. 18.3.2). The forming-limit diagram is a plot of the principal strains in the plane of the sheet and defines regions of safety, uncertainty, and failure as a function of the local strain combination, the strain-hardening exponent, the anisotropy, and the strain path. The use of these tools is illustrated briefly in the following. More information can be found in [20.44] to [20.46].

Fig. 20.26 shows a deep-drawn automobile body part with an imprinted grid pattern. The evaluation of the deformed grid is illustrated in Fig. 20.27. The three principal strains  $\varphi_1$ ,  $\varphi_2$ , and  $\varphi_3$  can be computed from the diameter  $d$  of the undeformed circular grid and from the major and minor axes ( $a$  and  $b$ , respectively) of the ellipse resulting from the deformation of the sheet. Fig. 20.28 defines three sections through the deformed part along which the strains have been evaluated. Fig. 20.29 summarizes these results in plots of the three principal strains and the equivalent strain  $\bar{\varphi}$ , which is computed using the von Mises criterion:

$$\bar{\varphi} = \frac{2}{\sqrt{3}} \sqrt{\varphi_1^2 + \varphi_1\varphi_2 + \varphi_2^2}$$

The strain distribution in section A-A is rather constant between points  $d$  and  $e$ , and there are only slight maxima at points  $b$  and  $g$ . Larger strains are observed in sections B-B and C-C, which

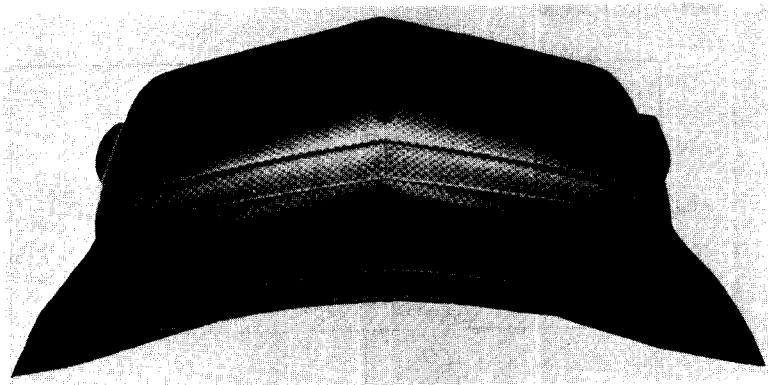
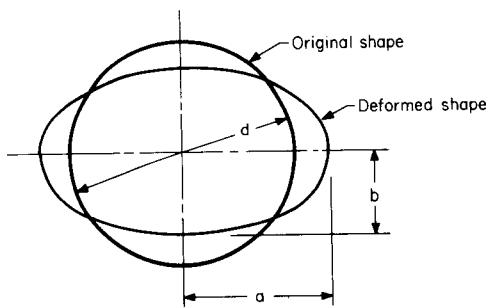


FIG. 20.26 Irregular drawn component, automobile radiator cover.



$$\varphi_1 = \ln \frac{2a}{d} \quad \varphi_2 = \ln \frac{2b}{d} \quad \varphi_3 = \ln \frac{s_1}{s_0}$$

FIG. 20.27 Strain measurements using circular grids.

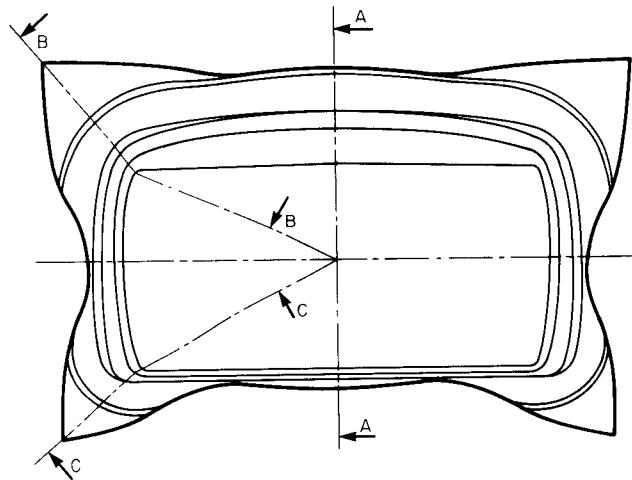
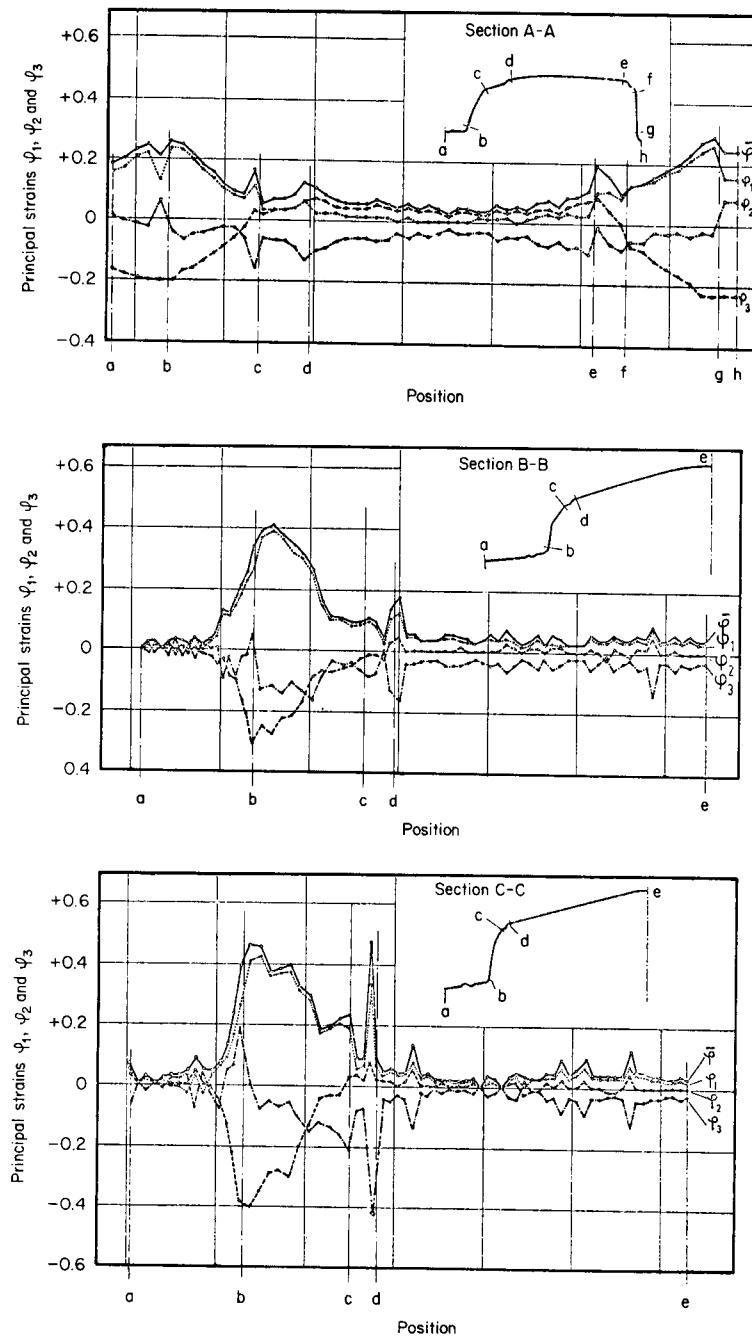
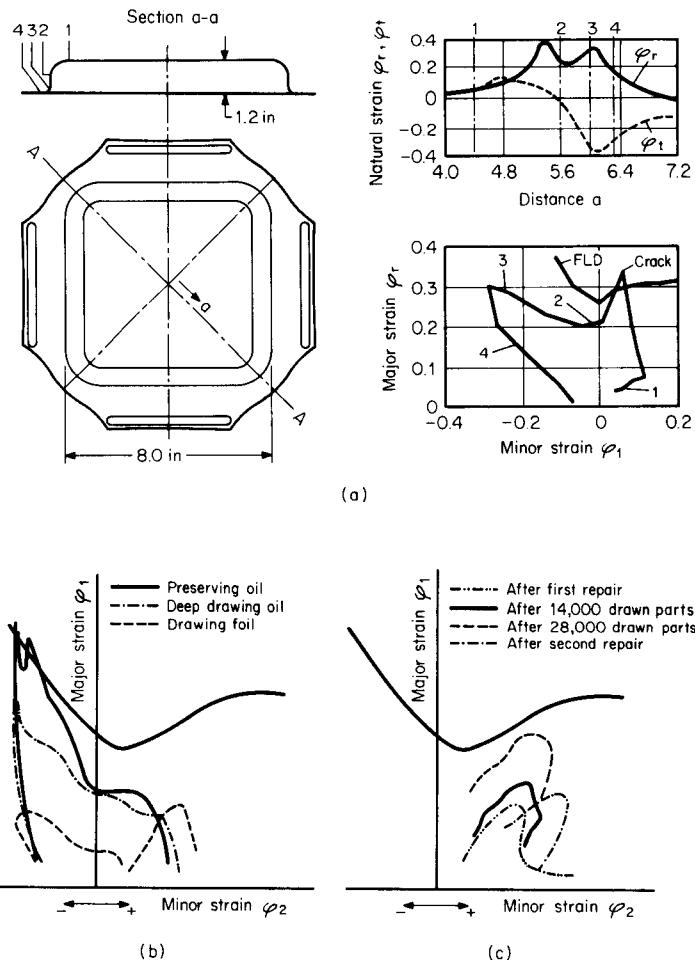


FIG. 20.28 Defining the sections for strain measurement.

**20.32 SHEET-METAL FORMING**



**FIG. 20.29** Principal strains in deep-drawn automobile radiator cover.



**FIG. 20.30** Examples for strain analysis in sheet drawing. (a) Drawn square component and strain distribution. (b) Influence of lubricant on strain distribution. (c) Influence of tool wear and maintenance on strain distribution. (After [20.44], [20.47], [20.48].)

are caused by a localized stretch drawing in the corners of the component. The strains in the flange and the flat center portion are very small.

When using this grid method to measure the strains in the sheet, two points must be kept in mind. First, since the area of the grid circles is finite, only average strain values can be determined. The real strains could be significantly higher than the measured values if the strains are highly localized. Therefore the diameter of the circles must be carefully chosen in a trade-off between accuracy and the amount of effort involved. Second, only strains at the end of the draw can be observed from the grid measurements. If the component is very irregular, it is possible that the state of stress will change during the draw, for example, from tension-compression to biaxial tension. This change leads to erroneous conclusions about the formability of the sheet material since the forming-limit diagram also depends on the loading history (strain path, see Sec. 18.3.2).

The strain analysis method as described above is used increasingly to determine the margin of safety against cracking in a deep-drawing operation at the press shop level. The grid is applied only to critical zones of the drawn component, that is, where heavy necking or cracking occurs or may be expected from experience. The strains measured at the critical points of the irregular component are plotted in the forming-limit diagram, as shown in Fig. 20.30. Fig. 20.30a presents the distribution of measured strains along the diagonal of a square component of Al Mg 5 (AA 5056) and in the forming-limit diagram of that material and sheet thickness. A crack was observed where the measured strain combination exceeds the values given in the forming-limit diagram. In Fig. 20.30b the influence of lubrication on the distribution of strains in these critical regions of a steel-sheet part is proven to be significant, while Fig. 20.30c shows the shifting of the strain distribution according to tool wear and maintenance or repair during production for another steel-sheet component. Detailed information is given in [20.44], [20.47] to [20.49].

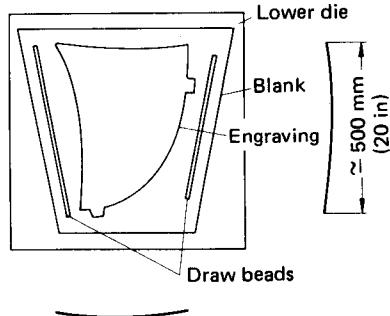


**FIG. 20.31** Drawing of a shallow Ti-6Al-4V aircraft component at elevated temperature with draw beads.

15% in order to limit the surface roughness to levels acceptable for painting without additional surface preparation. This limits the draw depth. Surface-quality requirements also make it generally impossible to anneal or to draw in several stages. Significant difficulties are encountered when drawing large, relatively shallow components, such as car hoods and roofs, because of the large amount of elastic springback. In such cases the portion of stretch forming in the drawing process must be increased, such as by applying drawbeads. According to the impediment of the material flow into the die the stress state is converted from tensile-compressive into mostly tensile, and the component is more or less stretch-formed. Fig. 20.31 shows an example from the aerospace industry.

The uneven material flow caused by a multitude of shapes (see Fig. 20.37) and the irregularities of the components often require the use of draw beads and holes for stress relief in addition to increased blankholder pressure.

Along extended, little curved edges there are generally no tangential compressive stresses. The material can therefore be easily drawn into recesses, while the material flow is impeded in corners and sharply curved edges. Consequently large axial stresses can develop in the border of the component, which may exceed the fracture limit. To achieve more even material flow without wrinkles, draw beads are applied in areas of straight edges to impede the material flow.

Furthermore, in order to reduce the tendency to cracking or to direct the crack to noncritical areas, stress-relieving holes are cut into those areas of the workpiece which subsequently will be eliminated anyway, such as openings for windows. These holes make it possible for the material to flow more freely into the corners without causing cracks. If cracks still appear, they start at the stress-relief hole and are cut out later on. Fig. 20.32 shows an automobile body part and the drawing tool with draw beads and holes for stress relief. Draw beads should not go beyond a distance of  $10^\circ$  from the center of the corner radius in order to avoid penetration into the zone of stress concentration and hence possible cracking.

The effectiveness of draw beads depends on their size (height and width) and on their position within the tool-die set (Fig. 20.33) [20.50]. Experiments have shown that properly designed draw beads produce sufficient restraining forces in the plane of the sheet but at the same time increase the punch load by only an insignificant amount. Fig. 20.34a illustrates the various draw-bead orientations that have been investigated, and Fig. 20.34b shows typical results of the measured drawing load and the restraining force as a function of the draw-bead width. The experimental parts (see Figs. 20.30a and 20.33) were drawn from steel sheet RRSt1403 (AISI 1006) of 1-mm

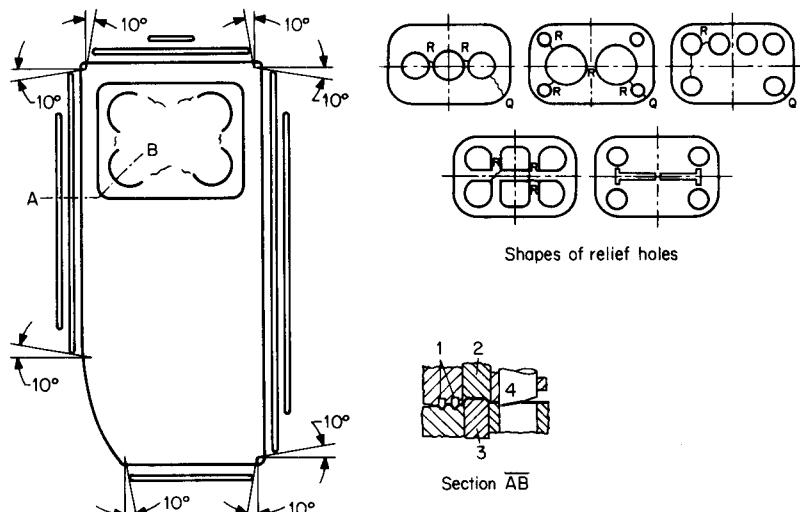


**FIG. 20.32** Car body door tool layout with draw beads and stress-relief holes. 1—draw beads in die; 2—counterpunch; 3—drawing punch; 4—shearing punch. R = crack between stress-relief holes (acceptable); Q = crack between stress-relief hole and contour (not acceptable). (After [20.3].)

(0.04-in) thickness using circular blanks with 390-mm (15.35-in) diameter [20.50]. The experimental tool set with a typical arrangement is shown in Fig. 20.35a, while Fig. 20.35b illustrates a modern industrial tool set featuring the above-mentioned design principles together with a workpiece.

While the material flow may be restrained by draw beads or increased blankholder pressure (as discussed earlier in this chapter), a certain more limited restraining can be obtained by chang-

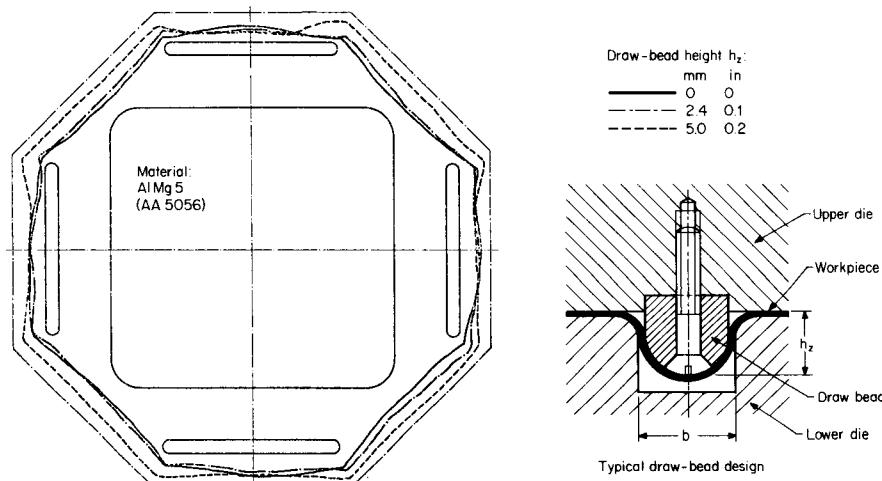
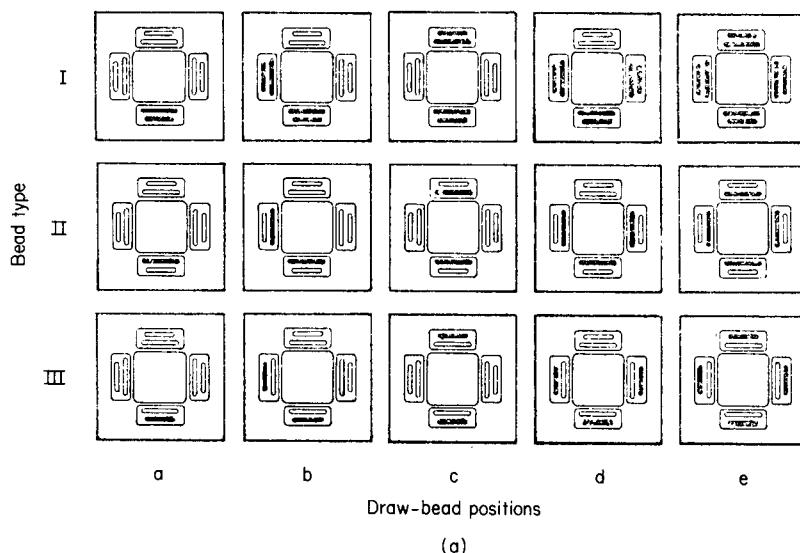
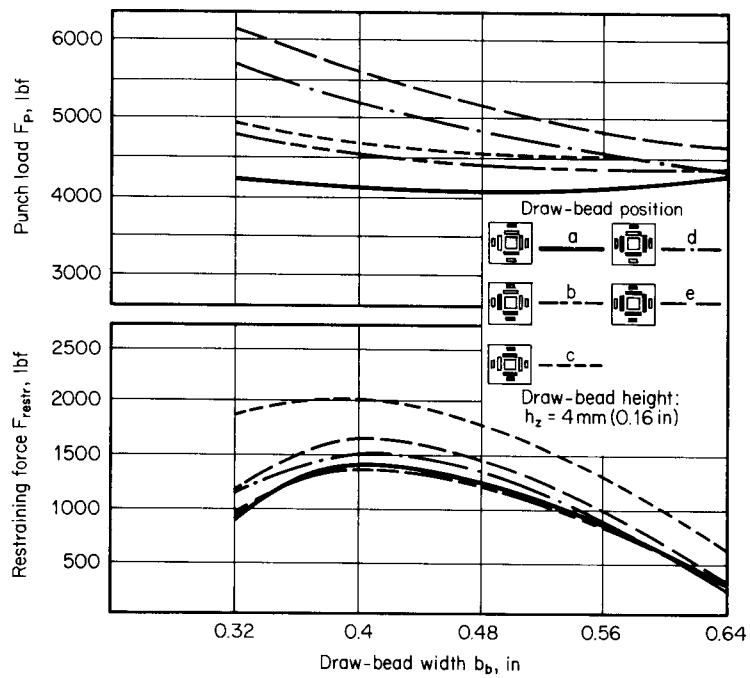


**FIG. 20.33** Influence of draw-bead height on material flow in drawing a square component as demonstrated by the outer contour of the flange.



(a)



(b)

**FIG. 20.34** Application of draw beads. (a) Possible orientation in test die set (see Fig. 20.35a). (b) Drawing load and restraining force as a function of draw-bead size and orientation.

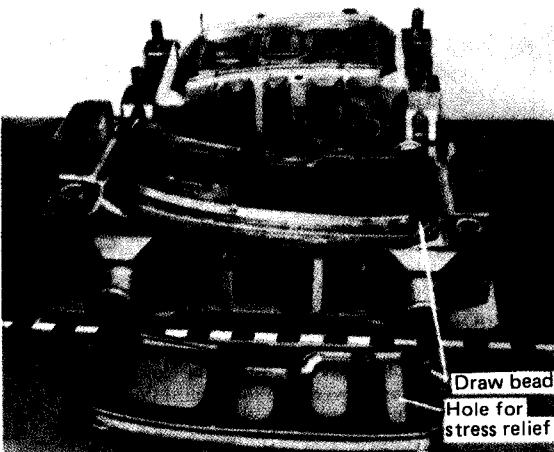
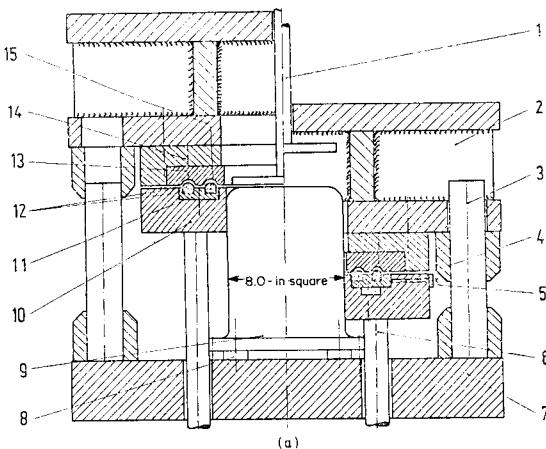


**FIG. 20.35** Die sets for irregularly shaped drawn sheet components. (a) Experimental die set for square sheet parts. (After [20.50].) (b) Die set showing draw beads and stress-relief holes with drawn automobile body part. (Courtesy of L. Schuler.)

ing the blank diameter or geometry. The larger the blank diameter, the higher are the tangential and radial stresses and hence the restraining forces. This is generally also true for noncircular parts, as may be seen in Fig. 20.36 for a square component drawn with draw beads; the influence on the region of wrinkle formation is small but visible.

Many automobile parts are asymmetrical. In order to achieve balanced symmetrical loading of the sheet and the press, two or sometimes four tools are mounted as mirror images in a combination tool so that the process is again symmetrical.

In the automobile, aircraft, and spacecraft industries a large number of asymmetrical, difficult to produce sheet-metal components are required. A shape classification of these parts according to Sachs [20.51] is given in Fig. 20.37. Production of these components requires a combination of bending, deep-drawing, and stretch-forming processes. For details see [20.3], [20.9], [20.51].

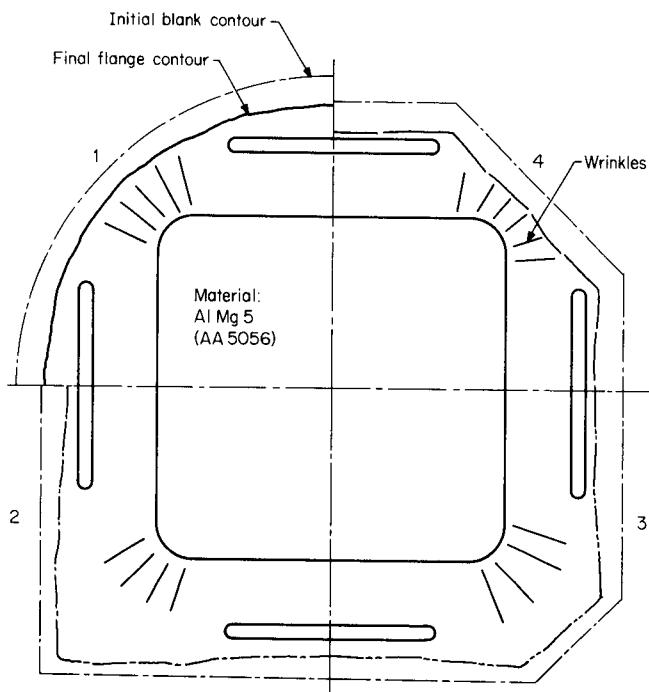


**FIG. 20.36** Influence of blank geometry on flange contour and wrinkle area.

### 20.3.5 Deep Drawing with Elastic Tools

Deep-drawing processes with pliable tools or with working fluids and other special drawing processes have been developed in order to overcome the limits inherent in deep drawing with rigid tools. In particular it is aimed at eliminating the following disadvantages:

- 1 Large tensile stresses in the wall
- 2 Local wall-thickness variations
- 3 Wrinkle and pucker formation
- 4 High tooling cost, especially for irregularly shaped components
- 5 Limited drawing ratio

These special processes use only one rigid tool half for either the punch or the die, which corresponds to the desired workpiece shape, while the other half is replaced by a universal rubber pad. This pad is often made from several layers of a very flexible artificial rubber compound. The top layer wears very rapidly and must be replaced after 100–10,000 strokes, depending on the workpiece. Compressive stresses act in the contact area between the tool and the workpiece. These are very advantageous for the formability of the workpiece and make higher drawing ratios possible. A disadvantage of the method is that it requires very high punch loads.

The most important processes are presented schematically in Fig. 20.38. Additional information can be found in [20.52].

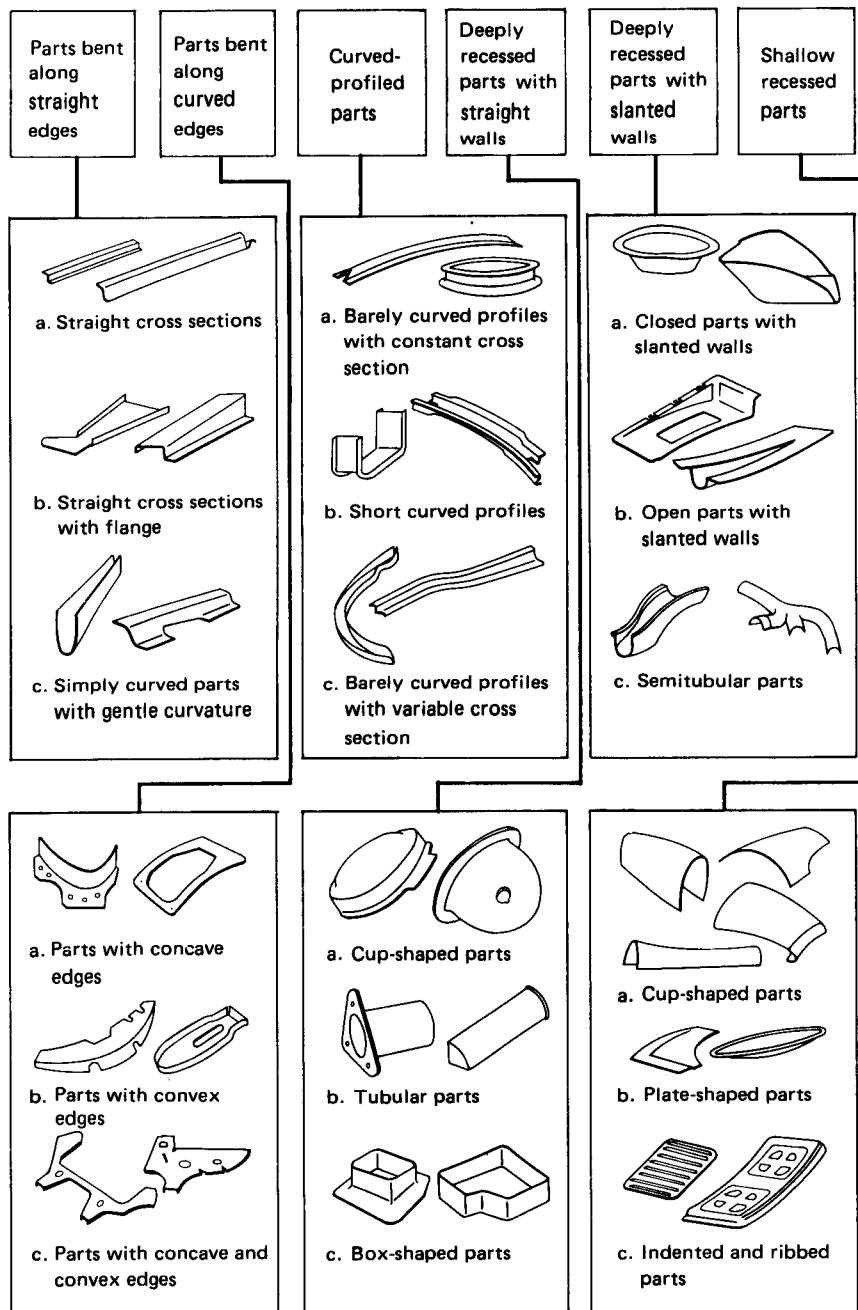


FIG. 20.37 Shape classification for irregularly shaped sheet-metal components. (After [20.51].)

	Container or case	During deformation			
		Rubber curtain or bag	Punch or die	Table or baseplate	
Initial blank shape Deep drawing with flexible cushion (Marform process)	Pad holder Rubber pad Part piece Punch Blankholder	Movable	Movable	Fixed	Movable
Deep drawing with water bag	Die Workpiece Water bag Blankholder	—	Fixed	Movable	Movable
Deep drawing with membrane	Connection for pressure control valve Fluid containers Fluid Membrane Blankholder Workpiece Punch	Fixed	Fixed	Movable	Fixed
Deep drawing with two-sided fluid pressure	Connection for pressure-regulating valve for $P_2$ Die Workpiece Seal Fluid Connection for pressure-regulating valve for $P_1$ Fluid container	Fixed	—	Fixed	Fixed
Deep drawing with single-sided fluid pressure (hydroforming)	Punch Blankholder Seal Fluid container Workpiece Fluid Connection for pressure control valve	Fixed	—	Movable	Fixed
Deep drawing with explosive charge	Upper tool Explosive charge Fluid medium Workpiece Die (lower tool) Vacuum	Fixed	—	Fixed	—

FIG. 20.38 Special deep-drawing processes.

### 20.3.6 Deep Drawing with Working Media or Activated Energy

This group of processes is characterized by the working media or by the activated energy which pushes the blank or other preforms into a rigid die or pulls the workpieces over a rigid punch. Liquids and gases are used as working media. They only serve to transmit the deformation energy

from its source (such as punch, hydraulic pump, spark chamber, or explosive charge) to the workpiece. The only activated energy is magnetic energy, which acts directly upon the workpiece without the need for a working medium.

Some of the processes used in industry are shown in Fig. 20.38. In the hydraulic drawing processes the elastic pad has been replaced by a pressurized liquid which often is closed off from the blank by a rubber membrane. These processes are used in the production of conical, parabolical, and hemispherical components. It is thus possible to draw components in a single step which with rigid tooling would require several increments. These components also satisfy very high accuracy and surface-finish requirements so that they can be used without further finishing operation, for example, reflectors for headlights.

Extensive investigations of these important processes have been conducted by Beisswanger [20.37], Schmidt [20.39], Pichel [20.53], Panknin [20.54], Lawrenz [20.55], Herold [20.56], and others.

### 20.3.7 Deep Drawing at Hot Forming Temperatures

Sheets of materials which are difficult to form, such as titanium alloys and some light metals, are sometimes drawn at elevated temperatures in order to increase their ductility. Prior to forming, the workpiece is heated either completely or partially, that is, with the exception of the area of the bottom of the cup. The die is heated electrically. Occasionally the punch is cooled such that the drawn component is as strong as possible in the transition region from the bottom to the wall of the cup and can transmit high drawing loads. With these measures, drawing ratios for the first draw of aluminum-magnesium alloys of  $\beta_{\max} \approx 2.8-3.0$  can be obtained [20.15], and for brass sheet Cu Zn 37 (UNS C27000) the limiting drawing ratio is increased from  $\beta_{\max} = 2.2$  without heating to  $\beta_{\max} \approx 3$ .

Because of the considerable effort necessary for tooling and heating chambers with inert atmospheres to avoid oxidation, deep drawing at elevated temperatures is generally not used in the mass production of steel-sheet components. It is used mainly for the manufacture of components from nonferrous metals.

### 20.3.8 Processes for the Production of Small Parts

Small cases and cups with diameters of up to 5 mm (0.2 in) are often produced using the so-called Oeillet process. Its characteristic is that the workpieces are not drawn from individual blanks but directly from a strip. The final shape is generally obtained after many preform steps (sometimes more than ten). The achievable total drawing ratio is about twice as large as the drawing ratio for a "normal" first draw. Only at the very end is the workpiece cut from the strip, on which several components may be arranged side by side. Material flow from the strip into the component is hardly possible such that most of the material forming the component is taken from the sheet thickness. Therefore this process more closely resembles stretch drawing than deep drawing.

For larger components of up to 30 mm (1.2 in) in diameter a modified Oeillet process is used; curved slots are punched into the strip. The material between the slots forms blanks connected by webs from which the components are drawn. The slots allow the material to flow from the flange into the cup during drawing. Details of this process can be found in [20.3].

## 20.4 TOOL DESIGN

### 20.4.1 Die Clearance

In practice the dimensions of the die clearance are often determined from the empirical equations suggested by Oehler and Kaiser [20.3]. These equations are valid only for deep drawing of circular components without ironing:

$$\begin{aligned} u_D &= s_0 + 0.07\sqrt{10s_0} && \text{for steel sheet} \\ u_D &= s_0 + 0.02\sqrt{10s_0} && \text{for aluminum sheet} \\ u_D &= s_0 + 0.04\sqrt{10s_0} && \text{for other nonferrous metals} \\ u_D &= s_0 + 0.20\sqrt{10s_0} && \text{for high-temperature alloys} \end{aligned}$$

If the die clearance  $u_D$  is too large, the component does not form a true cylinder, but the upper edge of the cup remains expanded. If the die clearance is too small, ironing can take place, which increases the drawing load and increases the danger of cracking. Furthermore cold welding between the die and the workpiece is possible.

A significant problem for the selection of the die clearance is caused by unavoidable sheet-thickness variations due to relatively large thickness tolerances. It is possible that some components crack while others wrinkle when drawing with a die clearance properly dimensioned for the nominal sheet thickness. If the sheet thickness approaches the upper tolerance limit, the die clearance is too small and ironing occurs, which increases the possibility of cracking. If the sheet thickness is close to the lower tolerance limit, the die clearance is too large and pockers can be formed.

When square workpieces are produced, larger die clearances than for the sidewalls are used at the corners where material flow is restricted. For deep drawing with wall-thickness reduction (ironing) die clearances are used which are smaller than the initial sheet thickness.

#### 20.4.2 Die and Punch Radii

The die radius  $r_D$  (Fig. 20.3) depends on the size of the workpiece and its thickness. In order to lower the drawing load and to increase the limiting drawing ratio, large die radii are desired. Large radii, however, reduce the contact area between the blankholder and the flange and increase the tendency to form wrinkles in the region of the die radius. Conversely, the possibility of wrinkle formation is reduced if the die radius is made small.

Oehler and Kaiser [20.3] have developed the following empirical equation for the die radius:

$$r_D = 0.035[50 + (d_0 - d_1)]\sqrt{s_0} \quad (20.52)$$

Koelzer [20.19] has found that the factor 0.035 in Eq. 20.52 can be increased to 0.08. Romanowski [20.9] suggests the values given in Table 20.3 for sizing the die radius.

The die radius should be reduced for each subsequent redraw. It has been found to be good practice to reduce the die radius by a factor of 0.6 to 0.8 from one draw to the next.

Sellin [20.57] has found that the die radius should be related to the sheet thickness by the following expression:

$$r_D = (5-10) \times s_0 \quad (20.53)$$

The punch radius  $r_P$  (Fig. 20.3) should be larger than the die radius by a factor of 3–5.  $r_P$  must never be smaller than  $r_D$  or the punch might pierce the material. For small components of large sheet thickness it is advisable to use a gentle transition (for example, parabolic) from the punch radius to the cylindrical portion of the punch in order to avoid wall thickness reductions in the transition zone from the bottom of the cup to the wall.

Suction between the component and the punch can be eliminated by providing a vent in the punch.

**Table 20.3** Suggested Die Retail  $r_D$  for the First Draw as a Function of the Relative Sheet Thickness

Type of part	Relative sheet thickness $s_0/d_0$		
	0.001–0.003	0.003–0.01	0.01–0.02
Without flange	$(15-10) \times s_0$	$(10-8) \times s_0$	$(8-6) \times s_0$
With flange	$(30-20) \times s_0$	$(20-15) \times s_0$	$(15-10) \times s_0$

Source: Compiled from [20.9].

### 20.4.3 Tool Design for the First Draw without Blankholder

Cups can be drawn from a blank without a blankholder and without wrinkling if the buckling stiffness of the sheet against tangential compressive stresses is high enough. This is generally true if the ratio of blank diameter to sheet thickness  $d_0/s_0$  is less than 25–40. The smaller values apply to large drawing ratios.

Drawing without a blankholder has the advantage that the tools are simple to construct. Because there is no friction at the blankholder, the drawing load is reduced and the limiting drawing ratio might be increased. In addition only a single-action press is necessary.

When drawing without a blankholder, the die is given a special geometric shape. The simplest possibility is to increase the die radius  $r_D$ . This die shape is easy to produce, but only small drawing ratios can be achieved before the edge of the blank will lift off the die, which encourages wrinkle formation.

Investigations by Shawki [20.58] have proven that conical and tractrix dies are very effective. For conical dies the cone half-angle  $\alpha$  should be small ( $\alpha = 15^\circ$ ) when drawing thicker sheets [ $s_0 > 2.5 \text{ mm (0.1 in)}$ ] and larger ( $\alpha = 45^\circ$ ) when drawing thin sheets [ $s_0 < 1 \text{ mm (0.04 in)}$ ].

The optimal die shape with respect to drawing load and limiting drawing ratio is the tractrix shape shown in Fig. 20.39, which was suggested by May [20.59]. The tractrix die has the advantage that the maximum leverage is used for bending throughout the entire draw. As a consequence the punch load is reduced significantly compared to the load for ordinary die shapes. This has special advantages for mechanical presses since the lower peak load allows working far in advance of bottom dead center. The elimination of blankholder friction, the reduced friction at the die radius, and the reduced bending load (only simple bending occurs, not bending and unbending) all combine to lower the drawing load, raise the drawing efficiency, and increase the limiting drawing ratio. A limiting drawing ratio of about  $\beta_{\max} = 2.8$  can be achieved for the first draw of steel sheet with a tractrix die.

A disadvantage of both the conical and the tractrix dies is their greater height, which requires presses with a longer stroke. The tractrix shape is difficult to manufacture and is often replaced by an approximate tractrix shape, which is also shown in Fig. 20.39.

### 20.4.4 Blankholder Design

The purpose of a blankholder is to maintain an approximately constant gap between itself and the die during the draw. In so doing the blankholder exerts pressure on the flange of the drawn component and thereby prevents wrinkling. During the remainder of the stroke this gap must be

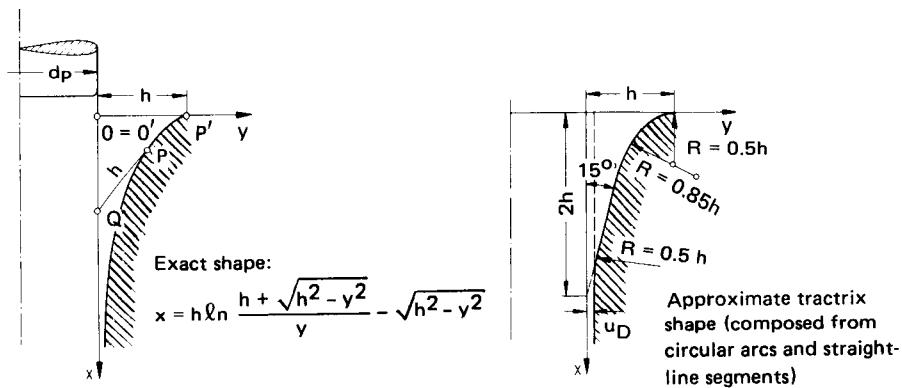
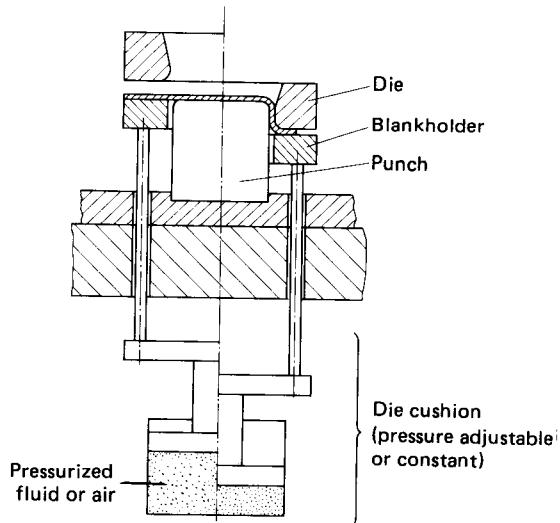


FIG. 20.39 Drawing die with precise and approximated tractrix shape. (After [20.59].)



**FIG. 20.40** Tool arrangement for deep drawing. The blankholder is actuated by a die cushion.

opened up for loading and unloading of the workpiece. There are two basic possibilities to achieve this:

- 1 The blankholder is indirectly driven by the ram of the press and the blankholder load is produced by a pneumatic or hydraulic die cushion. It is customary to arrange the tool with a fixed punch and a movable die, as shown in Fig. 20.40. The die cushion is most often placed under the press table. The disadvantage of this method is that the constantly acting blankholder load increases the load on the ram.
- 2 The blankholder is driven directly by the press. Mechanical presses often actuate the blankholder with knuckle levers or with cams in such a way that the blankholder remains at bottom dead center throughout the draw. This arrangement offers the advantage that the energy

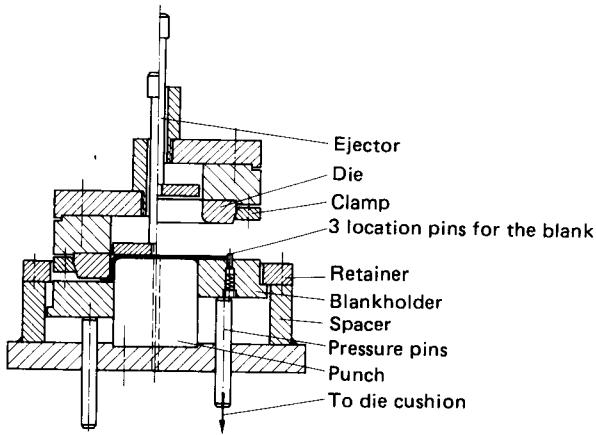


**FIG. 20.41** Tooling for first draw.

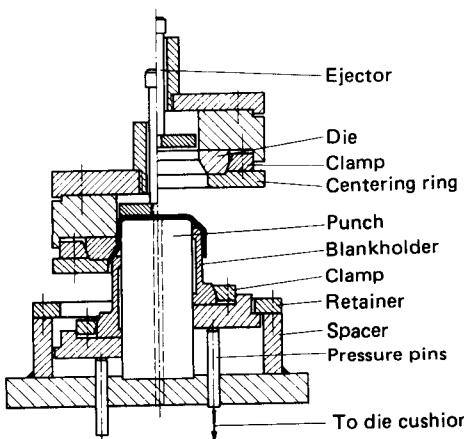


**FIG. 20.42** Tooling for redraw.

requirement for the blankholder drive is low, but has the disadvantage that the press design is more complex.

Examples of drawing tools for the first draw and for redraws are presented in Figs. 20.41 and 20.42.

#### 20.4.5 Tool Materials

Materials for deep-drawing tools are mostly cast iron, cast steel, cast-zinc alloys, carbon steels, unalloyed and alloyed tool steels, carbides, and aluminum-bronze alloys. In special cases plastics and hard woods are used.

Tool material selection depends mainly on the size, number, and material of the components to be drawn. For example, small tools for large batch sizes will be made from wear-resistant expensive tool steels. In contrast large tools for prototypes often consist of cast-iron frames in which the workpiece form is cast in synthetic resin. Only the highly stressed die radii are reinforced with steel.

The die radii are often chrome-plated in order to increase their wear resistance and to reduce the tendency to cold welding. For very large batch sizes carbide inserts are used.

Table 20.4 contains a selection of the most important tool materials. More comprehensive lists can be found in the appropriate handbooks [20.3, 20.9].

### 20.5 WORKPIECE MATERIALS AND LUBRICANTS FOR DEEP DRAWING

#### 20.5.1 Workpiece Materials

Table 20.1 on p. 20.16 gives a selection of the most important materials for deep-drawn components. The drawing ratios given for the first draw and for redraws and the lubricants suggested are only to be used as typical parameters which can be modified by a large number of factors. Some of the variables which have significant influence on the limiting drawing ratio are the tool geometry, the punch velocity, the relative sheet thickness, the lubricant, and the combination of tool and workpiece materials.

**Table 20.4** Selection of the Most Important Materials for Deep-Drawing Tools

Designation		
DIN	US	Application
Cast iron		
GG18	$\approx$ UNS F10004	Low-stressed large tools, draw punches, upper parts, base plates
GG22, GG26	$\approx$ UNS F10005	Drawing tools with high wear resistance; base plates and upper parts of high strength and large lot sizes but simple shapes; edges may be reinforced with steel
Plain carbon steels		
St37	$\approx$ AISI 1015	Low-stressed tool parts, base plates, strippers
St50 <sup>a</sup>		Wear parts, such as ejector plates, locating pins
St70 <sup>a</sup>		Small highly stressed parts (punch, die); used mostly hardened
Unalloyed tool steel		
C100W1, C110W1 <sup>a</sup> C85W1	$\approx$ AISI 1095 $\approx$ AISI 1086	Larger drawing tools (punch, die) with higher stresses; also armatures
Alloyed tool steels		
210 Cr W46 90 Cr 3	$\approx$ AISI D3 $\approx$ UNS E51100	Dies with highest wear resistance
Aluminum-bronze alloys		
AMPCO metal		Dies with low tendency toward fretting; used with stainless-steel sheets

<sup>a</sup>See Appendix C.

### 20.5.2 Lubricants

The selection of the proper lubricant depends on the workpiece material, its surface condition, and also on the tool material and its surface. The main lubricants for deep drawing are given in Table 20.5.

Additives such as graphite, zinc sulfide, lime, chalk, and halogen and phosphorus compounds or white lead oxide are often added to mineral oils in order to increase their stability under high pressure. Some of these compounds are poisonous, and their use is regulated by OSHA or other agencies.

Solid lubricants, mostly metal soaps, molybdenum disulfide, and colloidal graphite, are also used in deep drawing. They are capable of preventing direct contact between the die and the blank. Investigations by Wiegand and Kloos [20.60] and Krämer [20.61] have shown that metal soaps have significantly better lubricating properties than lubrication oils. Krämer found a reduction of 8% in the drawing load when a deep-drawing sheet St1302 (AISI 1008) is drawn in a tool-steel die with cadmium stearate rather than with machine oil. The austenitic material

**Table 20.5** Lubricants for Deep Drawing

	Animal	Vegetable	Mineral
Oils <sup>a</sup>	Whale oil	Rape oil Linseed oil Castor oil	Cylinder oil Kerosene Carbide oil
Greases	Stearin Wool grease		Lubrication grease Vaseline

<sup>a</sup>Used either straight or in water-based emulsions.

X 5 CrNi 18 9 (AISI 304 SS) could be deep-drawn without scoring in a die made from 210 Cr 46 ( $\approx$  AISI D3) tool steel using only metal soap. Surface-finish measurements proved that the microtexture at the surface of cups drawn with cadmium stearate corresponds to the texture of the blank, indicating no direct contact between the blank and the die.

The disadvantage of solid lubricants lies in the difficulty of applying and removing them. Table 20.1 on p. 20.16 lists some suitable lubricants for the most important deep-drawing materials. This list is not complete because of the large number of available products. This is true in particular for the lubricants for deep drawing stainless steel [20.62].

When drawing materials which are difficult to deform, it may be necessary for draws of square shapes or deep cylindrical shapes to apply a lubricant carrier (phosphate coating) in addition to the lubricant itself in order to prevent fretting.

Drawn components with a large bottom radius require that the lubricant be applied with uniform thickness. Otherwise it is possible that the workpiece will be drawn unevenly.

Drawing foils made from plastics (PVC, PTFE) have been successful in the production of simply shaped components of ductile materials. Occasionally even stainless-steel sheets are coated with plastic films, which must be applied by dipping or spraying.

Large limiting drawing ratios are obtained if the coefficient of friction between the punch radius and the blank is high (roughen the punch, no lubrication in this area) and friction between the blank and the die is as low as possible.

## 20.6 SIZING THE BLANK

It is very important to determine the size of the blank necessary for drawing the component accurately. First, because of economic reasons it is desirable to cut the blank as small as possible. Second, an unnecessarily large blank diameter increases the drawing ratio and can cause cracking.

The size of the blank is determined from the condition that the volume of the blank must equal the volume of the drawn component. In most calculations the simplifying assumption will be made that the sheet thickness remains constant during the draw, and the volume constancy condition is satisfied when the surface areas of the blank and the component are equal. This assumption is correct for simple parts with rotational symmetry since both wall thickening and wall thinning occur in these components such that the mean value of the wall thickness remains approximately constant. When deep drawing components of complex shapes, however, stretch drawing may take place in localized areas, which reduces the wall thickness and increases the surface area of the material. The changes in wall thickness cannot be determined from calculations. Rather, it is first assumed that the wall thickness remains constant and the blank size is determined accordingly. Next the size and shape of the blank are improved in experiments.

For parts of rotational symmetry the surface area of the blank is equated to the surface area of the drawn component. For workpieces composed of several geometric elements the surface area is the sum of the areas  $A_i$  of the individual elements. The blank diameter is then obtained from the equation

$$d_0 = \sqrt{\frac{4}{\pi} \sum_{i=1}^n A_i} \quad (20.54)$$

Table 20.6 lists the blank diameters determined from Eq. 20.54 for some of the more frequently drawn component shapes. If the surface of the part is composed of many separate elements, then a calculation of the partial areas becomes very tedious. For these cases graphic methods are suggested, which can be found in the appropriate handbooks [20.9], [20.10].

Determination of the blank size and shape for square components is explained using Fig. 20.43

**Table 20.6** Formulas to Determine the Blank Size for Deep-Drawn Components with Rotational Symmetry

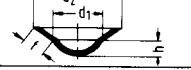
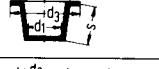
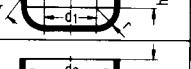
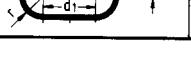
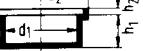
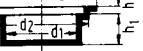
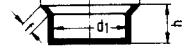
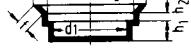
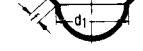
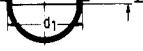
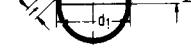
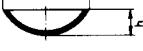
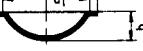
Workpiece shape	Blank diameter $d_0$
	$\sqrt{d_2^2 + 4(h_1^2 + d_1 h_2)}$
	$\sqrt{d^2 + 4(h_1^2 + dh_2)}$
	$\sqrt{d_1^2 + 4h^2 + 2f(d_1 + d_2)}$
	$\sqrt{d_1^2 + 4(h_1^2 + d_1 h_2 + f/2(d_1 + d_2))}$
	$\sqrt{d_1^2 + 2s(d_1 + d_2)}$
	$\sqrt{d_1^2 + 2s(d_1 + d_2) + d_3^2 - d_2^2}$
	$\sqrt{d_1^2 + 2(s(d_1 + d_2) + 2d_2 h)}$
	$\sqrt{d_1^2 + 6.28rd_1 + 8r^2}$ or $\sqrt{d_2^2 + 2.28rd_2 - 0.56r^2}$
	$\sqrt{d_1^2 + 6.28rd_1 + 8r^2 + d_3^2 - d_2^2}$ or $\sqrt{d_3^2 + 2.28rd_2 - 0.56r^2}$
	$\sqrt{d_1^2 + 6.28rd_1 + 8r^2 + 4d_2 h + d_3^2 - d_2^2}$ or $\sqrt{d_3^2 + 4d_2(0.57r + h) - 0.56r^2}$
	$\sqrt{d_1^2 + 6.28rd_1 + 8r^2 + 2f(d_2 + d_3)}$ or $\sqrt{d_2^2 + 2.28rd_2 + 2f(d_2 + d_3) - 0.56r^2}$
	$\sqrt{d_1^2 + 6.28rd_1 + 8r^2 + 4d_2 h + 2f(d_2 + d_3)}$ or $\sqrt{d_2^2 + 4d_2(0.57r + h + f/2) + 2d_3 f - 0.56r^2}$
	$\sqrt{d_1^2 + 4(1.57rd_1 + 2r^2 + hd_2)}$ or $\sqrt{d_2^2 + 4d_2(h + 0.57r) - 0.56r^2}$

Table 20.6 (Continued)

Workpiece shape	Blank diameter $d_0$
	$\sqrt{d^2 + 4dh}$
	$\sqrt{d_2^2 + 4d_1h}$
	$\sqrt{d_2^2 + 4(d_1h_1 + d_2h_2)}$
	$\sqrt{d_3^2 + 4(d_1h_1 + d_2h_2)}$
	$\sqrt{d_1^2 + 4d_1h + 2f(d_1 + d_2)}$
	$\sqrt{d_2^2 + 4(d_1h_1 + d_2h_2) + 2f(d_2 + d_3)}$
	$\sqrt{2d^2} = 1.414d$
	$\sqrt{d_1^2 + d_2^2}$
	$1.414 \sqrt{d_1^2 + f(d_1 + d_2)}$
	$1.414 \sqrt{d^2 + 2dh}$
	$\sqrt{d_1^2 + d_2^2 + 4d_1h}$
	$1.414 \sqrt{d_1^2 + 2d_1h + f(d_1 + d_2)}$
	$\sqrt{d^2 + 4h^2}$
	$\sqrt{d_2^2 + 4h^2}$

Source: Compiled from [20.10].

[20.63]. The straight sidewalls are developed into the plane of the bottom. In order to find the shape of the corners of the blank, the four corners of the component are assembled into a cylindrical cup of diameter  $d = 2r_C$ , where  $r_C$  is the corner radius of the square component. The blank diameter for this cup is given by

$$2r = \sqrt{0.253d^2 + d(h_s + 0.506r_b)} \quad (20.55)$$

The height of the developed sidewalls is:

$$h_s = 0.57r_b + h + r_C \quad (20.56)$$

In Eqs. 20.55 and 20.56  $r_b$  is the radius between the bottom of the cup and the sidewalls.

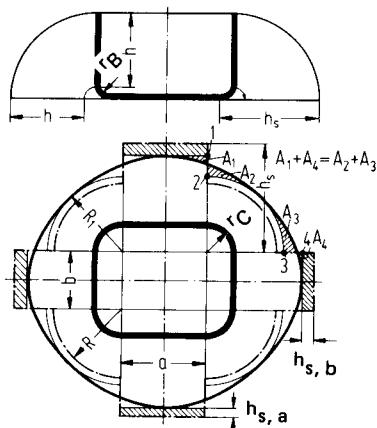


**FIG. 20.43** Determining blank size and shape for rectangular deep-drawn components. (After [20.63].)

The development of the component is given by the dash-dotted line in Fig. 20.43. In practice, however, the material at the corners is constrained since the tangential compression is not limited to the corners but extends to parts of the sidewalls. For this reason the sidewalls grow too high and the corners remain too low when drawn from the above development. In order to account for this constraint, the blank diameter of the cylindrical cup  $2r$  is increased by a correction factor  $\kappa$  such that

$$r' = \kappa r \quad (20.57)$$

with

$$\kappa = 0.074 \left( \frac{r}{2r_C} \right)^2 + 0.982 \quad (20.58)$$

The resulting increase in area must be compensated for by a reduction in height  $h_s$  of the developed sidewalls. This is achieved by removing strips of equal total area of height  $h_{s,a}$  and  $h_{s,b}$  and width  $a$  and  $b$ , respectively:

$$h_{s,a} = \frac{y r^2}{a} \quad (20.59)$$

$$h_{s,b} = \frac{y r^2}{b} \quad (20.60)$$

with

$$y = \frac{\pi(\kappa^2 - 1)}{4} \quad (20.61)$$

The basic blank size and shape are now determined. In general the contour of the blank is smoothed such that the final blank shape marked by the heavy line results.

The blank geometry for irregularly shaped components, such as automobile body parts, cannot be calculated and must be determined from experience. As a first approximation one also tries to develop the blank as shown above, taking local material stretch into account. This rough blank is then refined in experiments until a shape is found which satisfies all requirements.

## 20.7 Workpiece Accuracy and Properties after Drawing

During cold working the flow stress  $\delta_f$  increases with increasing strain. The local strains in the region of the bottom are small. Wall thinning (stretching) has occurred in the transition radius to the wall. In the wall itself the strains and the thickness generally increase toward the upper edge. The distribution of the wall-thickness variations along the cup height depends on the drawing ratio and the tool geometry, especially the relative die clearance  $u_D/s_o$  (Fig. 20.44). The stiffness of the cup causes it to contact not the punch but the die while it is drawn through the die.

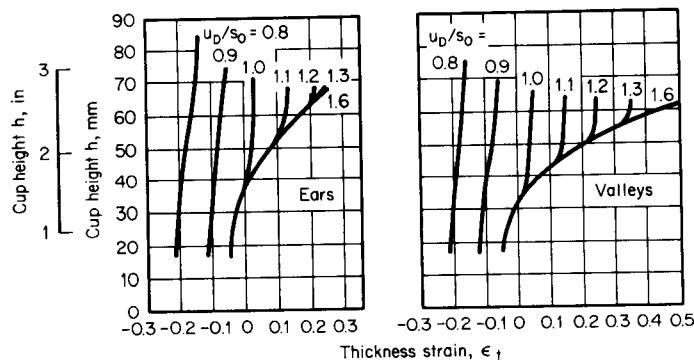


**FIG. 20.44** Effect of relative die clearance  $u_D/s_0$  on relative wall-thickness changes,  $\epsilon_s$ . Material—RRSt1403 (AISI 1006);  $d_p = 80 \text{ mm (3.15 in)}$ ;  $s_0 = 1 \text{ mm (0.039 in)}$ ;  $r_p = 10 \text{ mm (0.393 in)}$ ;  $\beta = 2$ . (After [20.64].)

Because of the increase in wall thickness and variable amounts of springback due to varying residual stresses the cups are not perfectly cylindrical.

Planar anisotropy causes earing of the components. The wall thickness is smaller in regions with ears than in regions between ears. Depending on the tool geometry it is possible that the inside diameter of a cup with planar anisotropy increases along the height of the cup in the area of the ears, as indicated in Fig. 20.45. A very troublesome consequence of planar anisotropy is that the cups are no longer circular and the usable cup height  $h_U$  is reduced.

The usable heights of cups drawn from three different materials having varying degrees of planar anisotropy under identical conditions are illustrated in Fig. 20.46. Particularly when using large drawing ratios, the material with the lowest planar anisotropy [copper alloy Cu Zn 36, i.e., Cu 64%, Zn 36% (=UNS C27000),  $\Delta r = 0.19$ ] allows significantly larger cup heights than the material with the largest planar anisotropy [RRSt 14 (AISI 1006),  $\Delta r = 0.74$ ] [20.64].

Ironing (Chap. 14) can reduce the diameter variations along the cup height and produce a more even wall thickness. The out-of-roundness due to planar anisotropy, however, cannot be eliminated completely. The workpiece tolerances which can be achieved with ironing are IT 6–9 for the diameter and IT 11–12 for the wall thickness. (See Chap. 1 for a brief explanation of the ISO standard for tolerances.)

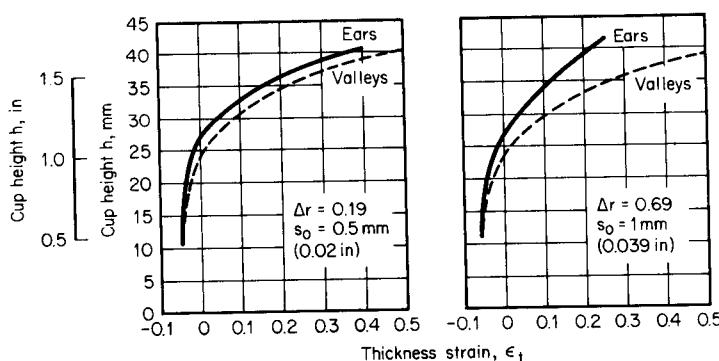


**FIG. 20.45** Effect of sheet thickness  $s_0$  and planar anisotropy  $\Delta r$  on relative wall-thickness change  $\epsilon_s$ . Material—RRSt1403 (AISI 1006);  $d_p = 50 \text{ mm (1.97 in)}$ ;  $r_p = 6.3 \text{ mm (0.248 in)}$ ;  $\beta = 2$ ;  $u_D/s_0 = 1.6$ . (After [20.64].)

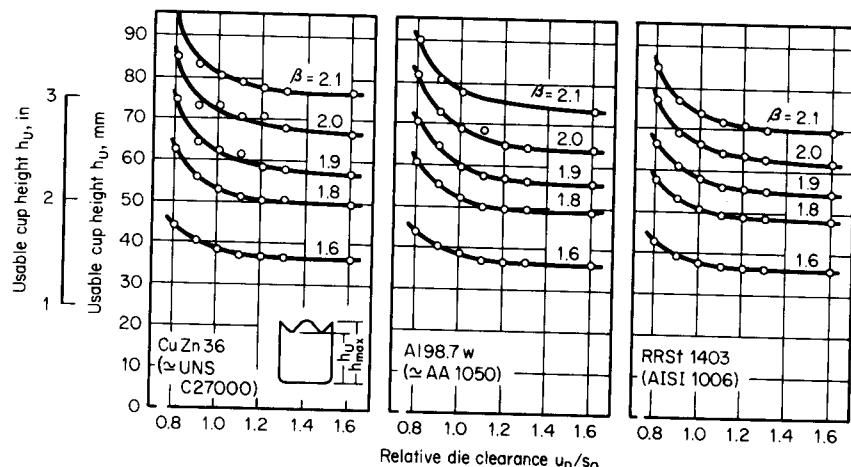


FIG. 20.46 Effect of relative die clearance  $u_D/s_0$  on useful cup height  $h_U$ .  $d_p = 80$  mm (3.15 in);  $s_0 = 1$  mm (0.039 in);  $r_p = 10$  mm (0.393 in). (After [20.64].)

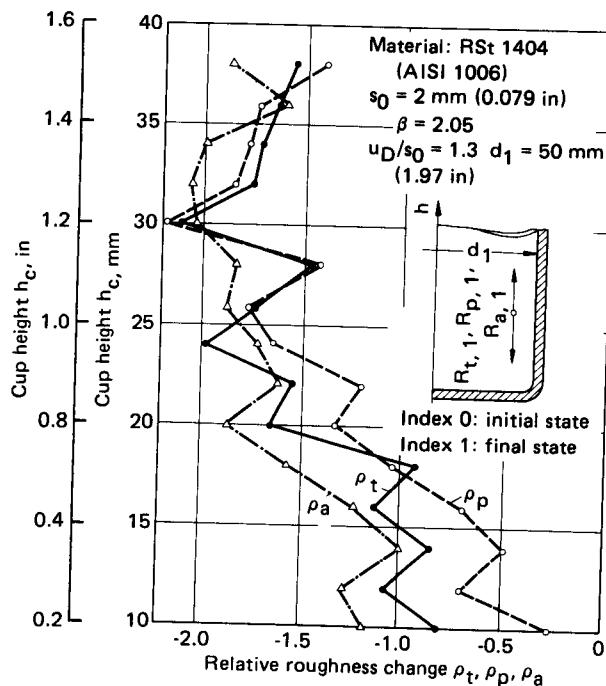
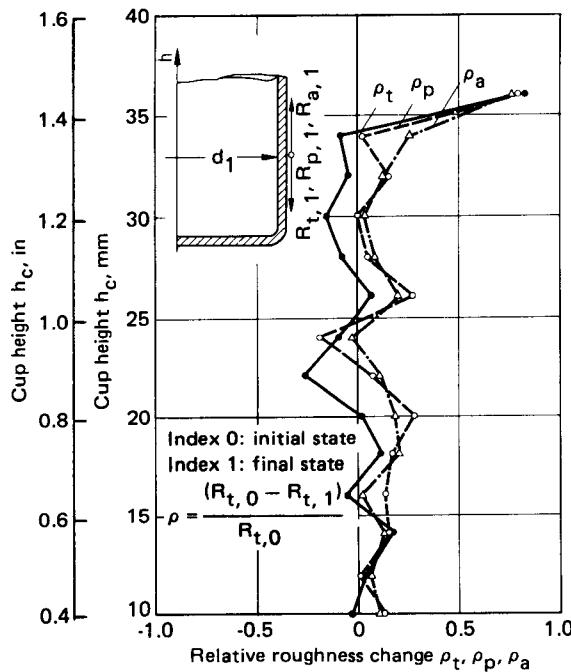


FIG. 20.47 Relative change in surface roughness on the inside cup wall. Material—RSt 1404 (AISI 1006);  $s_0 = 2$  mm (0.079 in);  $\beta = 2.05$ ;  $u_D/s_0 = 1.3$ ;  $d_1 = 50$  mm (1.97 in); lubrication—mineral oil with EP additives. (After [20.65].)



**FIG. 20.48** Relative change in surface roughness on the outside cup wall. Material—RSt1404 (AISI 1006);  $s_0 = 2$  mm (0.079 in);  $\beta = 2.05$ ;  $u_D/s_0 = 1.3$ ;  $d_1 = 50$  mm (1.97 in); lubrication—mineral oil with EP additives. (After [20.65].)

For some applications the surface condition of the drawn cup is of importance. The results of experiments by Dannenmann [20.65] with deep-drawn cups are presented in Figs. 20.47 and 20.48. The surface of the bottom of the cup has not been changed noticeably from that of the blank.

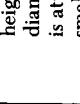
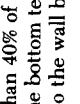
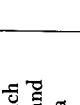
Changes in the surface condition on the inside of the cup can be related to observations of free deformation. This means that the surface roughness on the inside of the wall is greater than the initial roughness of the blank and that the roughness increases in the direction of increasing local strain, that is, toward the upper edge of the cup (Fig. 20.47). In contrast to the inside, the outside of the cup does not appear to have experienced any change in surface finish (Fig. 20.48). However, since the outside surface, too, has undergone free deformation in the flange, it must be assumed that the resulting rougher surface has been smoothed again when it passed over the die radius and through the die clearance.

## 20.8 DEFECTS IN DEEP DRAWING

A large number of defects and failure modes are encountered in deep drawing. Hornauer [20.66] has grouped most defects into three main classes:

- 1 Shape and dimensional errors
- 2 Defects in the workpiece or on its surface
- 3 Unsatisfactory properties

**Table 20.7** Selection of the Most Important Deep-Drawing Failures

Exterior appearance and failure	Failure cause	Methods to eliminate failure
 Bottom cracks <ul style="list-style-type: none"> <li>a After forming a shallow cup with a height less than 40% of the punch diameter, the bottom tears off and is attached to the wall by only a small web</li> </ul>	Drawing ratio too large with respect to workpiece material and tool geometry	Reduce drawing ratio
 <ul style="list-style-type: none"> <li>b Very shallow cup; flange very wide on one side and narrow on the opposing side</li> </ul>	Eccentric loading of blank	Install locating pins or centering rings
 <ul style="list-style-type: none"> <li>c Very shallow cup; flange wider on two opposing sides than elsewhere</li> </ul>	Uneven sheet thickness	Reduce sheet thickness tolerance
 <ul style="list-style-type: none"> <li>d Almost completed draw with heavy wrinkles in flange</li> <li>e Very shallow cup; heavy pressure marks on inside of wall in the region of the crack</li> </ul>	<ul style="list-style-type: none"> <li>a Blankholder pressure too low</li> <li>b Die clearance too small</li> <li>c Die radius too large</li> </ul> <ul style="list-style-type: none"> <li>a Blankholder pressure too low</li> <li>b Die clearance too small</li> <li>c Die radius too large</li> </ul>	<ul style="list-style-type: none"> <li>a Increase blankholder pressure</li> <li>b Increase die clearance</li> <li>c Reduce die radius</li> </ul> <ul style="list-style-type: none"> <li>a Increase blankholder pressure</li> <li>b Increase die clearance</li> <li>c Reduce die radius</li> </ul>
 Bottom is torn off all around the punch; no cup is formed	Punch not centered in die <ul style="list-style-type: none"> <li>a Die radius too small</li> <li>b Die clearance too small</li> <li>c Punch velocity too high</li> <li>d Blankholder pressure too high</li> </ul>	Change tool adjustment; use guided die sets <ul style="list-style-type: none"> <li>a Die radius too small</li> <li>b Die clearance too small</li> <li>c Punch velocity too high</li> <li>d Blankholder pressure too high</li> </ul>
 Uneven cup edge with vertical wrinkles in otherwise completed cup	<ul style="list-style-type: none"> <li>a Die clearance too wide</li> <li>b Die radius too large</li> <li>c Blankholder pressure too low</li> </ul>	Select proper die and punch radii, die clearance, punch velocity, blankholder pressure, and drawing increments

	Ears formed at cup edge or in flange (for incomplete draws)	Unavoidable in all sheets with planar anisotropy	If possible, use sheet with lower planar anisotropy
	Cup wall bulges out and lips are formed at edge of cup (shown highly exaggerated)	Die clearance too wide	Replace punch or die to reduce die clearance
	Puckers are formed in wall of conical, spherical, or parabolic drawn components	Tangential compressive stresses in "free" area between punch and die	<p>Improve state of stress by increasing radial tensile stresses by:</p> <ul style="list-style-type: none"> <li>a Increasing blankholder pressure</li> <li>b Increasing blank diameter</li> <li>c Using draw beads</li> <li>d Using special drawing process</li> </ul>
	In rectangular shapes: a Cracks in middle of the wall b Vertical crack in a corner initiated at edge c Almost horizontal crack in a corner	<p>For rectangular or other parts without rotational symmetry repeated failures can result from improper shapes of the blank</p> <p>For <b>b</b>, insufficient material; for <b>c</b>, too much material; less common causes for <b>b</b> and <b>c</b>:</p> <ol style="list-style-type: none"> <li>1 Eccentric blank positioning</li> <li>2 Uneven sheet thickness</li> <li>3 Unsuitable lubrication</li> <li>4 Wear of punch and die radii at corners</li> <li>5 Die clearance too small</li> </ol>	<p>Increase die clearance at corners of rectangular draws; punch must be cleaned here of all leftover lubrication media</p> <p>For <b>c</b>, change blank geometry at corners</p>
	Slip bands (Lüders' lines) appear mostly after mild deformation at high stresses, as found in the bottom but seldom in the wall of a cup; they are objectionable, in particular in shallow parts of large areas, such as automobile body parts which will be painted	Crystal texture; slip lines appear mainly in age-sensitive materials with well-defined yield points at low plastic strains and disappears at higher strains	If possible increase strain in the "critical" zone; store material at low temperatures and use quickly to reduce aging

Sources of defects can be:

- 1 Defective blank material
- 2 Faulty design of the workpiece
- 3 Defective processing (machine, tooling, fixtures, process)

In the preceding sections possible drawing defects have been pointed out several times, for example, cracking, wrinkling, and earing. Table 20.7 lists the most important drawing defects, their external appearances, their causes, and methods of prevention.

## 20.9 MACHINE TOOLS FOR DEEP DRAWING

For deep drawing and stretch drawing both hydraulic and mechanical presses with controlled displacement are used. Mechanical energy-controlled presses such as hammers and screw presses are seldom used, except perhaps in the production of shallow components (dishing) from thick sheets or for finishing cylindrical preforms into parabolic or conical components. These machines are considered here.

The theoretical foundations for the design of hydraulic and mechanical presses with controlled paths are covered in Chap. 8. The following discussions concentrate on the requirements on the presses generated by the drawing processes. Design possibilities to meet these requirements are also pointed out.

### 20.9.1 Mechanical Presses with Controlled Paths

Crank and eccentric presses as well as knuckle-joint presses, multicrank presses, and cam-operated presses are used for deep drawing. Since long strokes are required to produce deep cups, customary press designs with an effective crank angle of  $\alpha_N = 30^\circ$  would require very long strokes. The greatest force is not required at the end but toward the middle of the stroke. Therefore mechanical presses with an effective crank angle of over  $70^\circ$  have been built for deep drawing. If the deep-drawing process begins far in advance of bottom dead center of the press, then the punch hits the blank with high velocity. This is undesirable. In order to avoid high contact velocities, large crank presses for automobile body parts are operated at a maximum of 10–14 strokes per minute. Faster operation of 16–20 strokes per minute is achieved with presses with modified kinematic arrangement, for example, compound crank presses. The ram velocity of these presses during the effective stroke is only about half as large as that for ordinary crank presses. Ram advance and return are performed at increased velocities.

Because of the parabolic load–stroke relationship in deep drawing, the nominal load  $F_{\max}$  cannot be fully utilized in general if the press is operated continuously at full power capacity.

The elastic spring energy absorbed in deforming the frame and the tooling is recovered in deep drawing in all cases, even though the presses are characterized by a limited degree of stiffness.

#### *Drive Types and Designs for Mechanical Presses*

The most frequently used drive types for drawing presses of small and medium size are crank and knuckle-joint drives, which are discussed in Chap. 8. In addition to these drives many others are utilized, such as toggle-lever and cam-operated drives. Of these the most important ones are treated here briefly.

**Rockerarm:** Fig. 20.49 illustrates the principle of a rockerarm, a drive type that is common in the United States. It is a drive with an oscillating lever whose ram velocity lies between those of a crank and of a knuckle-joint drive.

**Two-crank drive (compound crank drive):** This drive type is shown schematically in Fig. 20.50. It has the advantage of a longer effective stroke (effective crank angle  $\alpha_N$ ) and an almost constant ram velocity in the effective range. After the lower bottom dead center is reached, the greatly accelerated return stroke begins whose speed can be two to three times the pressing speed.

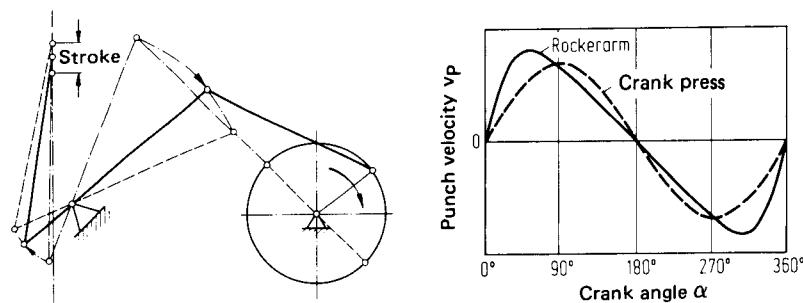


FIG. 20.49 Kinematics of a rockerarm drive.

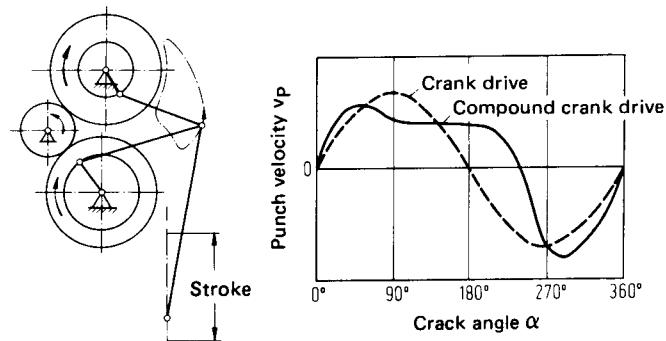


FIG. 20.50 Kinematics of a two-crank drive.

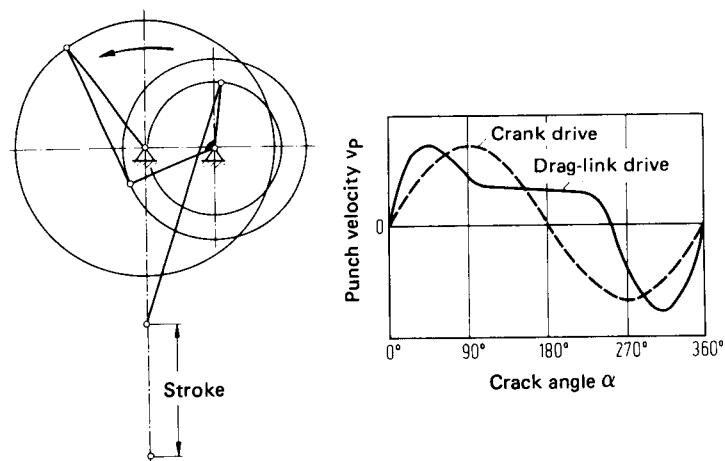


FIG. 20.51 Kinematics of a drag-link drive.

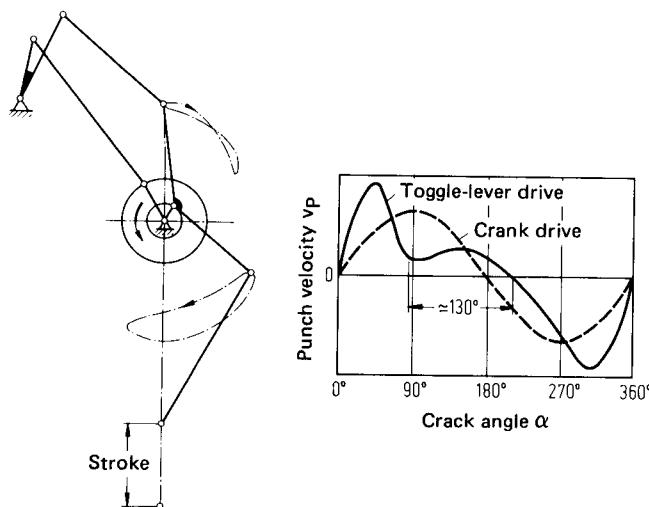


FIG. 20.52 Kinematics of a toggle-lever drive.

**Drag-link drive:** The drag-link drive shown in Fig. 20.51 exhibits similar operating characteristics as the two-crank drive. Here, too, the effective stroke covers a crank angle of more than  $110^\circ$ . Its maximum speed ranges from 12 to 14 strokes per minute.

**Toggle-lever drive:** This drive (Fig. 20.52) has operating properties which are rather similar to the two previous drives, but it has an even larger effective stroke of about  $130^\circ$  crank angle. In addition, the punch contacts the workpiece with a very low velocity, then accelerates briefly, and finally approaches lower bottom dead center very slowly. The highest ram velocity outside the effective range is four times the mean pressing speed. The large velocity changes cause significant acceleration forces which limit the drive to speeds of 14–18 strokes per minute.

A distinguishing feature of mechanical presses is the position of the drive shaft with respect to the front of the machine. In machines with longitudinal drive the crankshaft is parallel to the front, and in machines with transverse drive the crankshaft is perpendicular to the front of the machine. Both designs are used for drawing presses. Presses with wide frame widths, such as transfer presses and large presses for automobile body parts, are preferred with transverse drive. This arrangement allows short crankshafts of great bending stiffness. However, because of the width of the ram two crankshafts must be used in most cases. In order to avoid thrust forces, the rotations of the crankshafts are opposed to each other. If the press is very large, two connecting

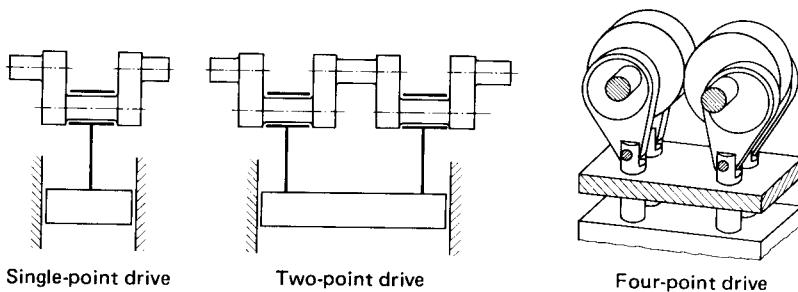


FIG. 20.53 Schematic representations of a one-, two-, and four-point drive.

rods are used per crankshaft. Depending on the number of connecting rods, one distinguishes between one-, two-, and four-point drives (Fig. 20.53).

### Control of Blankholder

Most deep-drawing and combined stretching-drawing processes require a blankholder. This blankholder is driven either mechanically, pneumatically, or hydraulically. The blankholder must contact the blank before drawing begins and must retract only after drawing is completed.

Fig. 20.54 shows the stroke of the ram and the blankholder as a function of the crank angle.

### Die Cushion

In order to be able to draw with a blankholder on single-acting presses these machines must be equipped with an additional fixture which performs the function of a blankholder ram. This fixture is a mechanical, pneumatic, or hydraulic die cushion and is located in most designs in the bed of the press. This then requires a different arrangement of the tooling in the machine than is customary in double-acting presses. The die is connected to the ram, and the punch and the blankholder are attached to the bed. The connection between blankholder and die cushion is achieved with compression pins fed through the bed (Figs. 20.41 and 20.42).

Fig. 20.55 shows a spring-actuated die cushion. These die cushions are suitable for small components only, or they can be used as ejectors. The spring column is attached to a container, which hangs in a cutout of the bed. Inside this container there is a pressure plate which is connected with pins to the movable spring plate. The disadvantage of this design is that the force increases in accordance with the spring characteristic as the draw progresses.

A pneumatically operated die cushion is shown in Fig. 20.56. Pneumatic die cushions are preferred over spring-actuated die cushions because they can be controlled more easily. The blankholder force is generated with compressed air and in general does not change as much during the drawing stroke as is the case with spring-actuated cushions.

Die cushions can be used with or without control. If no control is used, the blankholder remains in contact with the flange of the component or of the die from the beginning to the end of the draw.

For certain processes, such as deep drawing and shaving, however, a blankholder is required which retracts only after some time delay with respect to the ram.

The drawing fixture shown in Fig. 20.57 can be used with or without control. When operated without control, the pressure chamber of the fixture is connected with  $\frac{3}{4}$  directional control valves to the compressed air accumulator as indicated. The increase in pressure during the draw is less than 10% of the initial pressure. The effective blankholder force can be regulated with a pressure-

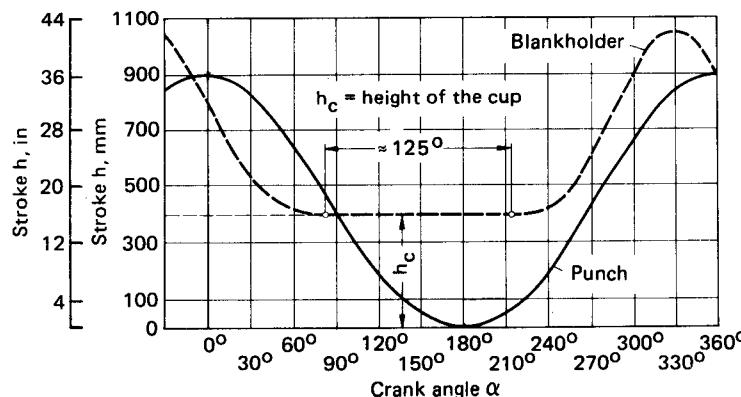


FIG. 20.54 Motions of ram and blankholder as a function of crank angle.

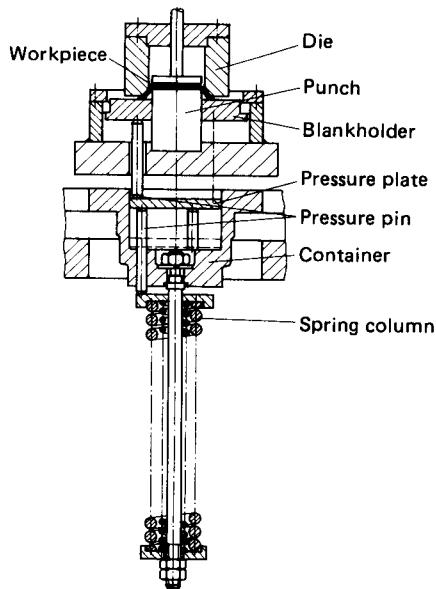


FIG. 20.55 Spring-operated draw cushion.

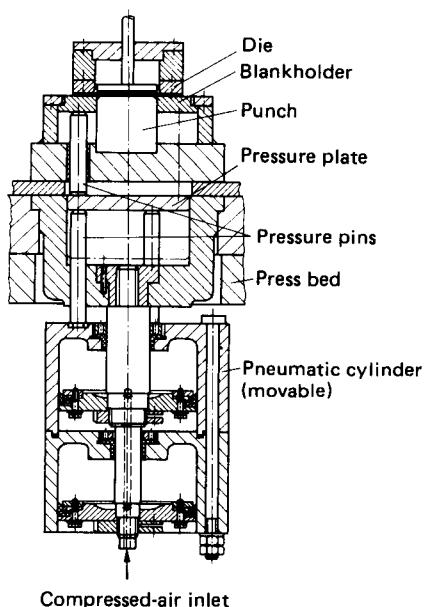
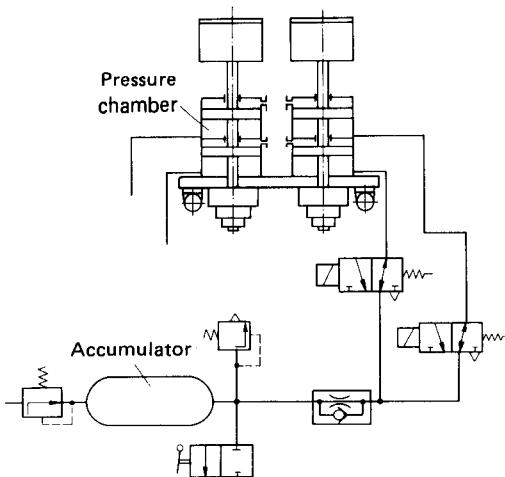


FIG. 20.56 Pneumatic draw cushion.



**FIG. 20.57** Schematic diagram of the control for a pneumatic draw cushion.

reducing valve to accommodate any drawing process. In order to prevent jerky liftoff of the blankholder when the punch returns, a throttle valve is mounted between the accumulator and the pressure chamber.

When the drawing fixture is used as an ejector with gravity return, then the pressure chamber is without pressure during the draw. After the draw is completed compressed air from the accumulator is allowed in the pressure chamber and the drawn component is ejected. When the ram has returned to the upper dead center, compressed air in the pressure chamber is allowed to escape through the  $\frac{3}{8}$  directional valves. Piston, piston rod, and pressure chamber drop down under their own weight. In this mode of operation the air in the pressure chamber and in the lines from the directional valves is lost at every stroke—the apparatus works uneconomically. However, with special expedients the compressed air losses can be reduced considerably.

Another possibility to actuate the blankholder is through the use of cams. Their application is restricted to small- and medium-size presses since no high blankholder force can be generated because of the line contact between the cam and the follower roll. Fig. 20.58 shows a schematic view of a cam-controlled blankholder. The punch is guided in the blankholder. The cam is connected rigidly with the crankshaft. Two follower rolls, which are mounted in a frame attached to the blankholder, run on the cam.

Larger mechanical presses often have a blankholder which is actuated by the crankshaft through levers. Fig. 20.59 shows a sketch of the principle of such a drive and the corresponding motions of the blankholder and ram as a function of the crank angle.

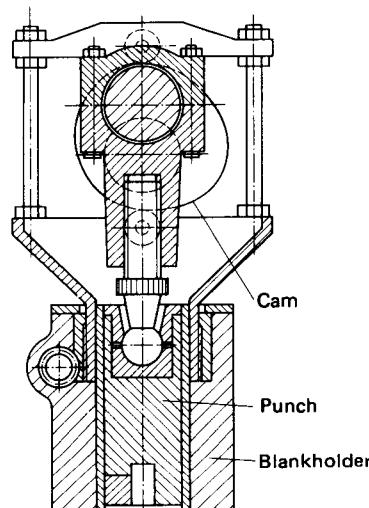


**FIG. 20.58** Cam-operated blankholder. (Courtesy of Kieserling.)

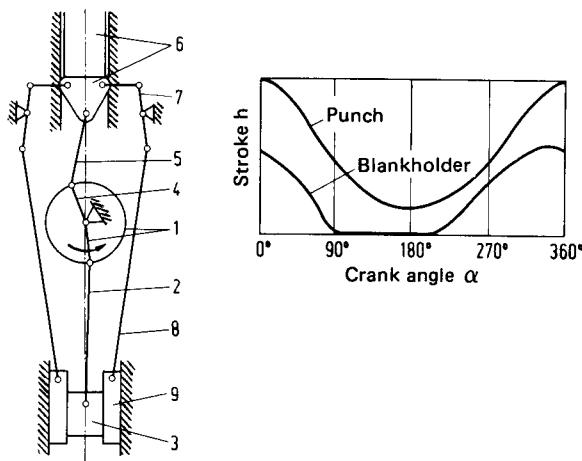


**FIG. 20.59** Drive of a double-acting press. The blankholder is driven by a toggle-lever drive. 1—crankshaft; 2—connecting rod; 3—ram; 4—crank for knee-lever drive; 5—auxiliary connecting rod; 6—slider; 7—toggle lever; 8—rod; 9—blankholder ram. (Courtesy of Bliss.)

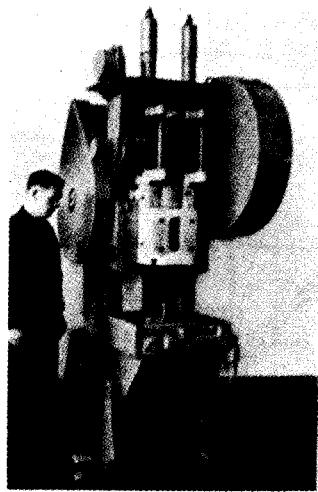


**FIG. 20.60** Crank press (C-frame) with cam-operated blankholder. Maximum drawing force—160 kN (17.9 ton); blankholder force—180 kN (20.2 ton);  $n_{\max} = 40 \text{ min}^{-1}$ . (Courtesy of L. Schuler.)

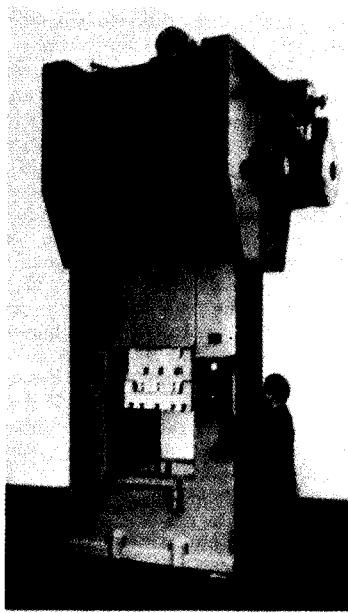


**FIG. 20.61** Double-frame crank press with longitudinal drive shaft. Maximum drawing force—2500 kN (280 ton);  $n_{\max} = 24 \text{ min}^{-1}$ . (Courtesy of L. Schuler.)

**Examples of Mechanical Presses with Controlled Ram Paths**

The following examples of mechanical presses with controlled displacement are intended as a short overview of the most important types of presses, without claim of completeness. The latter is impossible because of the great number of design variations.

Fig. 20.60 illustrates a double-acting crank press [ $F_{\max} = 160 \text{ kN}$  (17.9 ton)] with longitudinal drive shaft and with cam-controlled blankholder ram. In these very small and simple drawing presses the blankholder is actuated by two cams attached to the crankshaft. The body of the press is constructed as a C-shaped double frame and can be inclined to facilitate gravity feeding and ejection.

Larger presses are usually designed with O-frames. Fig. 20.61 shows a typical example. It is a crank press with a double frame and upper longitudinal drive shaft and has a capacity of  $F_{\max} = 2500 \text{ kN}$  (280 ton). A pneumatic drawing fixture may be mounted in the bed.

Fig. 20.62 shows a large double-acting press for forming automobile body parts. The maximum load of the ram, which is driven by a lever, is  $12,000 \text{ kN}$  (1350 ton). The blankholder is actuated by a knuckle lever and can produce  $6000 \text{ kN}$  (675 ton). The machine is driven by two transverse drive shafts and has an open-frame width of  $4.5 \text{ m}$  (180 in).

For special applications drawing presses with frame widths of over  $8 \text{ m}$  (315 in) have been built.

To increase the productivity when drawing components in several increments, transfer presses are often used. These are machines in which several forming tools are mounted side by side such that with every stroke a corresponding number of steps is executed. The transport of the work-

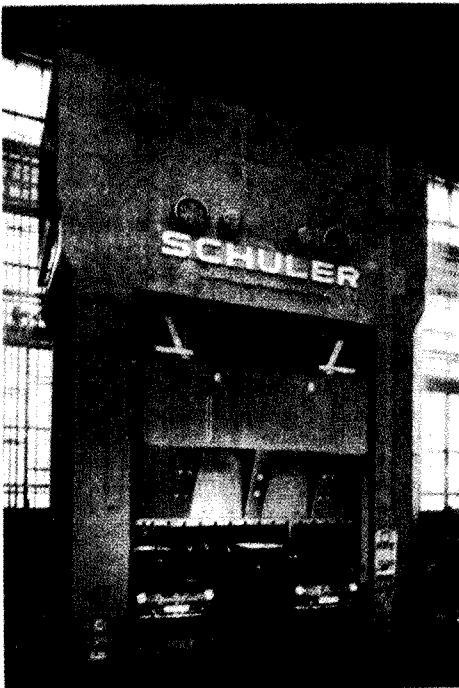


**FIG. 20.62** Double-acting draw press. Maximum drawing force— $12,000 \text{ kN}$  (1350 ton); blankholder force— $6000 \text{ kN}$  (675 ton); frame width— $4.5 \text{ m}$  (180 in). (Courtesy of L. Schuler.)

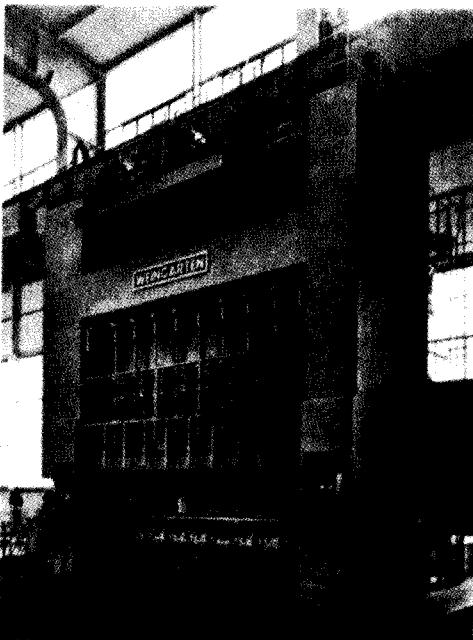


**FIG. 20.63** Transfer press with eight stages having a maximum ram force of 20,000 kN (2240 ton) and an additional blanking stage with 2500-kN (280-ton) blanking force. (*Courtesy of Müller-Weingarten*).

pieces from one tool to the next is accomplished with gripper tracks. Fig. 20.63 shows a transfer press with eight forming tools and one additional blanking stage.

Generally automobile body parts cannot be produced in transfer presses because of their size. They are most often produced in press lines. These lines consist of several presses arranged one after the other where every press carries out one processing step. Feeding, unloading, and transporting the workpieces from one machine to the next either is done manually or, more often, is partially or fully automatic with steel arms (tongues) or with gripper tracks as described for transfer presses. Fig. 20.64 shows a press line consisting of six machines.

To reduce the unproductive times of the presses, sliding tables are used more and more frequently. Every machine has two sliding tables. The first one carries the tooling which currently is in production and the second one is pulled from the machine and receives the next set of tooling. Tables and die sets have quick disconnects such that the idle time for changing tools is only a few minutes.

### 20.9.2 Hydraulic Presses

In addition to the mechanical presses discussed, hydraulic presses are used frequently for deep drawing and for drawing automobile body parts. The purchase prices of hydraulic presses are usually higher than those of mechanical ones. Hydraulic presses generally are slower (fewer strokes per minute) than mechanical presses. Because of the increased electrical power input, the hydraulic leakage losses, and the necessity to change the hydraulic fluid at regular intervals the operating costs for hydraulic presses are also relatively high. Further, automation and linking of

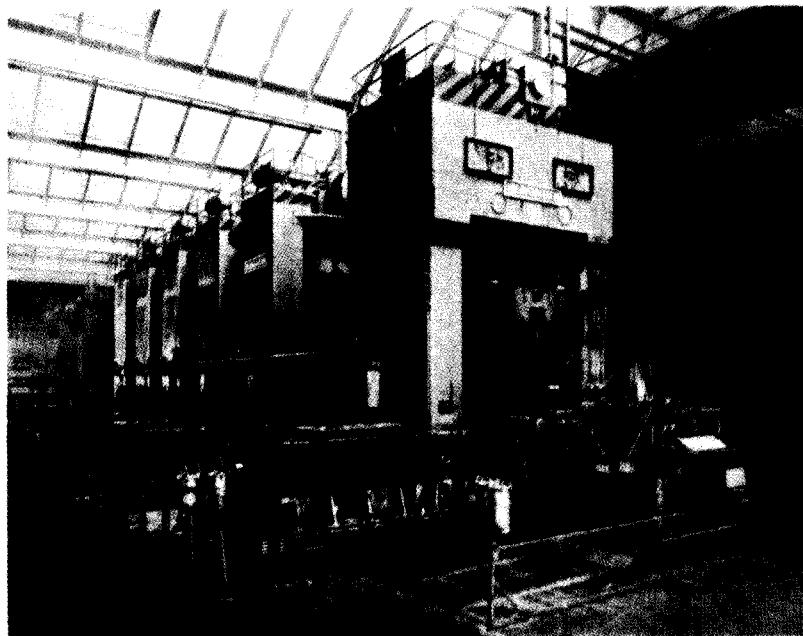


**FIG. 20.64** Press line consisting of six mechanically driven presses. First press has a maximum drawing force of 8000 kN (900 ton) and a blankholder force of 4000 kN (450 ton); the remaining presses have a drawing force of 8000 kN (900 ton) and no blankholder. All machines have sliding tables. (*Courtesy of Müller-Weingarten.*)

several presses in a press line is not as easy with hydraulic presses as it is with mechanical ones, but these problems are overcome by modern numerical control systems with wearfree reliable sensors.

These disadvantages are contrasted with significant advantages. The main advantage of a hydraulic press is that the press load and the ram velocity can be tailored to the requirements of the deformation process much better than is possible with mechanical presses since the hydraulic press does not have a kinematic linkage. There is no difficulty in controlling the hydraulic press in such a way that it rapidly approaches the blank, slows down, makes slow contact, and continues drawing at a slow punch speed. It is possible to stop the press at any position in order to allow the material time to flow. After the working stroke is completed the ram is rapidly returned to its initial position. In order to achieve such a sequence of motions elaborate linkages would be necessary for mechanical presses. Another big advantage of the hydraulic press over the mechanical one is the fact that a hydraulic press is overload safe. If two blanks were loaded by mistake, a mechanical press with controlled stroke could be overloaded and damaged, which cannot happen with a hydraulic press.

Equally simple as the control of the ram of a hydraulic press is the control of its blankholder, which requires considerable effort with mechanical presses. Hydraulic presses are used mostly with hydraulic die cushions since the pressurized fluid is available in the machine in any case. Hydraulic die cushions can be controlled to suit the drawing process. Control is ram-stroke dependent. For example, the blankholder load is controlled by the ram via a template such that the load is reduced in proportion to the decreasing flange area in order to maintain constant pressure on the flange.

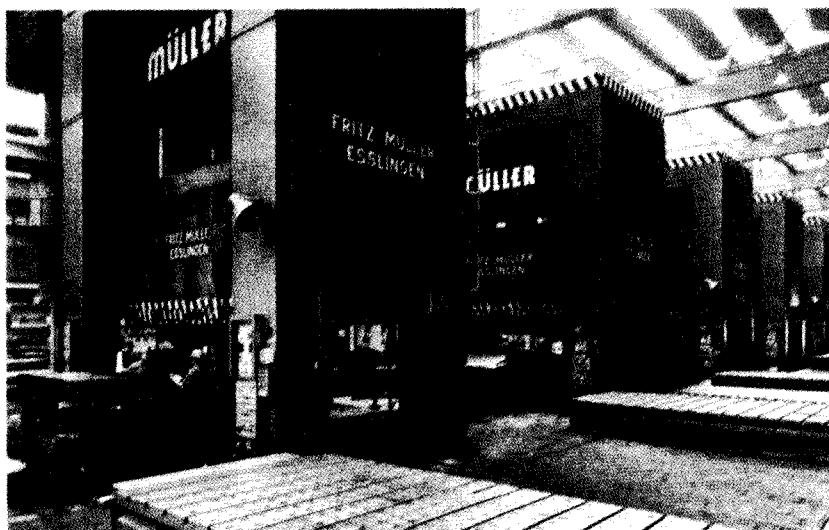


**FIG. 20.65** Press line consisting of five hydraulic presses. First press has a maximum drawing force of 20,000 kN (2,250 ton); the remaining presses have a drawing force of 13,000 kN (1460 ton). All machines have sliding tables. (Courtesy of Müller-Weingarten.)

#### *Examples of Hydraulic Drawing Presses*

Analogous to mechanical presses with controlled stroke, small components are drawn on single-frame hydraulic draw presses which are built similar to small eccentric presses with C-frames. The bed can accommodate a die cushion.

Larger hydraulic presses are designed mostly with O-frames. They may be single- or double-acting. These presses are regularly built with capacities of over 20,000 kN (2250 ton) and frame widths of about 5 m (200 in). Fig. 20.65 shows a press line consisting of several such presses for the production of large components.

#### REFERENCES

- 20.1 DIN 8584: "Fertigungsverfahren Zugdruckumformen (Manufacturing Process—Tension-Compression Forming)," sheet 3, Apr. 1971.
- 20.2 Geleji, A.: *Plastic Forming of Metals (in German)*, Berlin, Akademie-Verlag, 1967.
- 20.3 Oehler, G., and Kaiser, F.: *Blanking, Punching, and Drawing Tools (in German)*, 6th ed., Berlin/Heidelberg/New York, Springer, 1973.
- 20.4 Romanowski, W.: "The Initial Stage in Deep Drawing" (*in German*), Fertigungstech. u. Betr., 17, 1967, pp. 611–613.
- 20.5 Müschenborn, W.: "Investigation of the Deformation of Two Drawing Halves with Photochemically Applied Grids" (*in German*), Thyssenforschung, 1, 1969, pp. 109–115.
- 20.6 Siebel, E., and Beisswanger, H.: *Deep Drawing (in German)*, München, Carl Hanser, 1955.
- 20.7 Zünkler, X.: "Workhardening Influence on Drawing Force and Limit-Drawing Ratio during Deep Drawing" (*in German*), Blech Rohre Profile, 20, 1973, pp. 343–346.
- 20.8 Reihle, M.: "Determination of the Sliding Friction Coefficient for Deep Drawing Sheets under High Pressures" (*in German*), Dr. -Ing thesis, Technische Hochschule, Stuttgart, 1959.

- 20.9 Romanowski, E.: *Handbook of Blanking Technology (in German)*, Berlin, VEB Verlag Technik, 1959.
- 20.10 *Handbook of Chipless Forming (in German)*, 4th ed., Göppingen, L. Schuler, 1964.
- 20.11 Doege, E.: "Investigations of the Maximum Transmittable Load in Deep Drawing of Circular Cylindrical Components" (in German), Dr.-Ing. thesis, Technische Universität, Berlin, 1963.
- 20.12 Panknin, W., and Grosch, J.: "The Effect of Workpiece Material on Cracks in Deep Drawing of Unkilled Steels" (in German), *Bänder Bleche Röhre*, **10**, 1969, pp. 339–348.
- 20.13 Kotthaus, H.: "An Investigation of the Transportability of Test Results from Models to Full-Scale Tooling for Deep Drawing of Round Cylindrical Components" (in German), Dr.-Ing. thesis, Technische Hochschule, Stuttgart, 1955.
- 20.14 Siebel, E., and Panknin, W.: "The First Draw in Deep Drawing," (in German), *Werkstattstech. u. Maschinenbau*, **46**, 1956, pp. 321–326.
- 20.15 Oehler, G.: "Design of Drawn Sheet-Metal Components" (in German), *Konstruktionsbücher*, no. 11, Berlin/Göttingen/Heidelberg, Springer, 1966.
- 20.16 Arbel, C.: "Relationship between the Deep-Drawing Properties of Metals and the Results of a Tensile Test" (in German), *Stahl u. Eisen*, **70**, 1950, pp. 1118–1119.
- 20.17 Ziegler, W.: The Importance of the Material for the Limiting Drawing Ratio in Deep Drawing of Metals" (in German), Dr.-Ing. thesis, Technische Universität, Berlin, 1966.
- 20.18 Mäde, W., and Deh, R.: "Deep-Drawing Tests and Failure of Soft, Unalloyed Steels" (in German), *Fertigungstech. u. Betr.*, **17**, 1967, pp. 665–672.
- 20.19 Koelzer, H.: "The Behavior of Deep-Drawing Sheets as a Function of the Testing Method" (in German), Dr.-Ing. thesis, Technische Hochschule, Braunschweig, 1949.
- 20.20 Panknin, W.: "Effect of the Drawing Rate in Deep Drawing" (in German), *Blech*, **6**, 1959, pp. 391–396.
- 20.21 Lankford, W., Snyder, S., and Bauscher, J.: "New Criteria in Predicting the Press Performance of Deep-Drawing Sheets," *Trans. ASM*, **42**, 1950, pp. 1197–1232.
- 20.22 Whitely, R., Wise, D., and Blickwede, D.: "Anisotropy as an Asset for Good Drawability," *Sheet Met. Ind.*, **38**, 1961, pp. 349–358, 358.
- 20.23 Pomey, G., and Grumbach, M.: "The Effects of Anisotropy and the Strain-Hardening Coefficient in Deep Drawing" (in French), *Rev. Metall.*, **61**, 1964, pp. 885–900.
- 20.24 Lilet, L., and Wybo, M.: "An Investigation into the Effect of Plastic Anisotropy and Rate of Work Hardening in Deep Drawing," *Sheet Met. Ind.*, **41**, 1964, pp. 783–803, 815.
- 20.25 Hill, R.: *The Mathematical Theory of Plasticity*, London, Oxford University Press, 1950.
- 20.26 Backofen, W., Hosford, W., and Burke, J.: "Texture Hardening," *Trans. ASM*, **55**, 1962, pp. 264–267.
- 20.27 Hosford, W., and Backofen, W.: "Strength and Plasticity of Textured Metals," in *Fundamentals of Deformation Processing, Proceedings of the 9th Sagamore Army Materials Research Conference (AMRA)*, Syracuse, Syracuse University Press, 1964, pp. 259–291.
- 20.28 Hosford, W.: "Texture Strengthening," *Met. Eng. Quart.*, *ASM*, 1966, pp. 18–19.
- 20.29 Baldwin, W., Howald, T., and Ross, A.: "Relative Triaxial Deformation Rates," *Trans. AIME*, **186**, 1946, pp. 86–113.
- 20.30 Blade, J. C., and Pearson, W. K. J.: "The Requirements for a Standard Earing Test," *J. Inst. Met.*, **93**, 1962/3, pp. 10–18.
- 20.31 Wright, J. C.: "Influence of Deep-Drawing Conditions on the Earing of Aluminum Sheet," *J. Inst. Met.*, **93**, 1965/6, pp. 289–297.
- 20.32 Buschmann, E. F.: "Testing for Earing in Practice," *Z. Metallk.*, **57**, 1966, pp. 337–344.
- 20.33 Jakovlev, S. P., and Sevelev, V. V.: "On the Possibility to Eliminate Earing in Deep Draw-

- ing of Anisotropic Materials," *Umformtechnik*, **3**, 1969, pp. 43–47; publ. by Zentralinstitut für Fertigungstechnik, Zwickau; transl. from Russian to German.
- 20.34 Galinowski, J.: "Using Planar Anisotropy in Sheet Metal to Facilitate the Production of Deep-Drawn Cups," *Sheet Met. Ind.*, **52**, 1975, pp. 79–87, 132–137, 185–189.
- 20.35 Galinowski, J.: "Metal Forming Analysis of Cylindrical Cups Drawn from Square Blanks with Anisotropy," *Fertigungstech. u. Betr.*, **23**, 1973, pp. 669–674.
- 20.36 Naziri, H., and Pearce, R.: "The Effect of Plastic Anisotropy on Flange-Wrinkling Behavior during Sheet-Metal Forming," *Int. J. Mech. Sci.*, **10**, 1968, pp. 681–694.
- 20.37 Beisswanger, H.: "Deep Drawing of Thin Sheets with Special Tools" (*in German*), Dr.-Ing. thesis, Technische Hochschule, Stuttgart, 1947.
- 20.38 VDI-Arbeitsblatt 3141: "Ziehen über Wülste (Drawing with Draw Beads)," Düsseldorf, VDI-Verlag, June 1965.
- 20.39 Schmidt, E.: "Deep Drawing of Conical Components" (*in German*), Dr.-Ing. thesis, Technische Hochschule, Stuttgart, 1953.
- 20.40 Radke, H.: "Technology of Reverse Drawing" (*in German*), *Bänder Bleche Röhre*, **12**, 1971, pp. 17–23.
- 20.41 Panknin, W., and Dutschke, W.: "The Rules of Deep Drawing of Circular, Quadratic, and Elliptical Components in the First Draw" (*in German*), *Mitt. Forschungsges. Blechverarb.*, **2/3**, 1959, pp. 13–23.
- 20.42 Dutschke, W.: "The Basics of Deep Drawing of Noncircular Prismatic Components" (*in German*), Dr.-Ing. thesis, Technische Hochschule, Stuttgart 1958.
- 20.43 Oettinger, H.: "Investigations of Deep Drawing of Elliptical Components in the First Draw" (*in German*), Dr.-Ing. thesis, Technische Hochschule, Stuttgart, 1953.
- 20.44 Hasek, V. V.: "On the States of Strain and Stress in Drawing Irregular Sheet-Metal Components" (*in German*) *Berichte aus dem Institut für Umformtechnik, Universität Stuttgart*, no. 25, Essen, Girardet, 1973.
- 20.45 Hasek, V. V.: "Influence of Various Factors on the Shape and Size of Forming-Limit Diagrams," *Proceedings of the First North American Metalworking Research Conference* (Hamilton, 1973), pp. 35–48.
- 20.46 Hasek, V. V.: "Investigation and Theoretical Description of the Important Factors Affecting the Forming-Limit Diagram" (*in German*), *Blech, Rohre, Profile*, **25**, 1978, pp. 213–223, 285–292, 493–499, 619–627.
- 20.47 Lange, K., and Blaich, M.: "Forming of Aluminum Alloys for Autobody Components," *Mém. Sci. Rev. Metall.*, **77**, 1980, pp. 373–381.
- 20.48 Suy, J.: "Deep Drawing of Irregularly Shaped Sheet Components" (*in German*), *Ind.-Anz.*, **99**, 1977, pp. 174–176.
- 20.49 Lange, K., and Blaich, M.: "Process Optimization in Sheet Metal Forming of Aluminum Alloys," in *Proceedings of the 9th NAMRC 1981, SME Trans.*, 1981, pp. 145–152.
- 20.50 Hasek, V. V., and Lange, K. L.: "Effects of Tool and Process Parameters on the Deep Drawing of Irregular Components" (*in German*), *Wt-Z. Ind. Fertigung*, **68**, 1978, pp. 545–553.
- 20.51 Sachs, G.: *Principles and Methods of Sheet Metal Fabricating*, New York, Reinhold, 1958.
- 20.52 Ebertshäuser, H.: *Technology of Sheet-Metal Working* (*in German*), Düsseldorf, Michael Triltsch, 1967.
- 20.53 Pichel, H.: "Hydroforming" (*in German*), *Mitt. Dtsch. Forschungsges. Blechverarb. u. Oberflächenbehandl.*, **21**, 1970, pp. 15–19.
- 20.54 Panknin, W.: "Basic Concepts of Hydraulic Deep Drawing (Hydroform) and Hydraulic Deep-Drawing Equipment" (*in German*), *Werkstattstech. u. Maschinenbau*, **47**, 1957, pp. 295–303.

- 20.55 Lawrenz, K. J.: "Investigations about the Drawability of Organic Coated Steel Sheet and Testing of This Composite Material" (*in German*), Dr.-Ing. thesis, Universität Dortmund, 1978.
- 20.56 Herold, U.: "Hydromechanic Deep Drawing Permits the Optimization of Dimensions, Shapes, and Tolerances" (*in German*), *Maschinenmarkt*, **87**, 1981, pp. 920–923.
- 20.57 Sellin, W.: *Handbook of Drawing Technology* (*in German*), Berlin, Springer, 1931.
- 20.58 Shawki, G.: "Deep Drawing without Blankolder in Dies Having Various Throat Geometries" (*in German*), *Bänder Bleche Röhre*, **10**, 1969, pp. 597–601.
- 20.59 May, O.: "The Tractrix Curve, a Die with Helical Shoulder and the Ironing in Several Dies" (*in German*), *Werkstattstechnik*, **51**, 1961, pp. 476–479
- 20.60 Wiegand, H., and Kloos, K.: "Friction and Lubrication in Cold Working" (*in German*), *Werkstatt u. Betr.*, **93**, 1960, pp. 181–187
- 20.61 Krämer, W.: "An Investigation of Lubricants for Deep Drawing" (*in German*), *Ind. Anz.*, **86**, 1964, pp. 2167–2170.
- 20.62 Schulz, D.: "The Usefulness of Various Lubricants in Deep Drawing of Stainless Steels with Dies of Tool Steel and Bronze" (*in German*), *Blech*, **18**, 1971, pp. 135–140.
- 20.63 AWF Blatt 5791: "Zuschmittsermittlung für rechteckige Hohlteile (Sizing the Blank for Square Hollow Components)," Ausschuss für Wirtschaftliche Fertigung.
- 20.64 Schlosser, D.: "Geometric Properties of Deep-Drawn Cups" (*in German*), *Blech, Rohre, Profile*, **25**, 1978, pp. 566–574.
- 20.65 Dannemann, E.: "Change of the Surface Condition during Deep Drawing of Cups" (*in German*), *Ind.-Anz.*, **91**, 1969, pp. 2253–2254.
- 20.66 Hornauer, H.: "Defects in Producing Components by Forming and Cutting" (*in German*), *Blech*, **6**, 1959, pp. 107–120.



## CHAP. 21

### METAL SPINNING

© 1984 by Prentice-Hall, Inc., Englewood Cliffs, NJ 07632

#### List of Special Symbols

---

$d_0$	blank diameter
$d_1$	diameter of finished component
$d_{ch}$	chuck diameter
$d_R$	roller diameter
$r_R$	roller radius
$s_0$	initial sheet thickness
$\beta$	spinning ratio

Spinning is a forming process for producing from sheet metal hollow parts with rotational symmetry in which the sheet thickness remains essentially unchanged. The initial workpiece shape is either a flat blank or a preformed hollow component. It is a characteristic of this process that the deformation does not occur in an annular zone around the axis of rotation but that the tools act upon a very localized area in which plastic flow takes place. During spinning the tools are moved relative to the rotating workpiece.

Spinning belongs to the tension-compression forming processes since tangential compressive and radial tensile stresses are generated in the deformation zone just as in deep drawing. In contrast, flow turning (spinning with wall-thickness reduction) is a compressive forming process like rolling and is treated in that connection (Chap. 12).

#### 21.1 DEFORMATION PROCESS

Fig. 21.1 shows a schematic sketch of the spinning process for the production of a conical component. A flat blank is clamped with the follower against the face of a chuck which has been preformed to the desired shape of the component.

## 21.2 SHEET-METAL FORMING

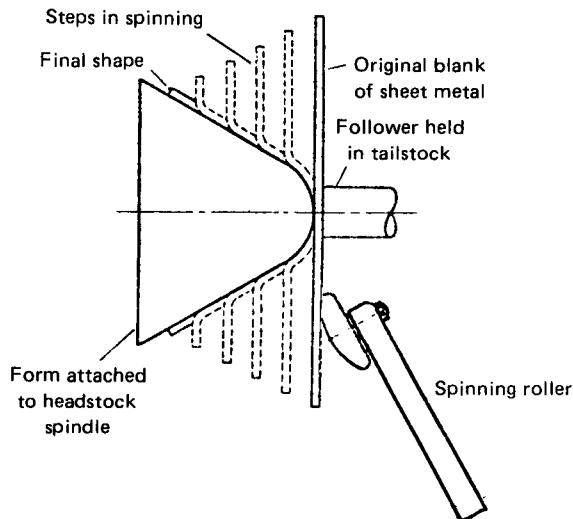


**FIG. 21.1** Progressive stages in forming of sheet metal by spinning.

Chuck and workpiece are rotating. The workpiece is shaped with a roller in several increments (for example, five increments in Fig. 21.1) until the final shape is achieved. For smaller workpieces it is possible to use a forming bar in place of the roller.

The forming process can also be carried out in a single step, as shown in Fig. 21.2. In this situation the process is very similar to deep drawing. However, forming does not take place along the entire circumference at once, but is limited to the small region near the roller.

A material element in the deformation zone is loaded by radial tensile and tangential compressive stresses. The Tresca flow criterion is

$$\sigma_1 - \sigma_3 = \sigma_f$$

With  $\sigma_1 = \sigma_r$  and  $\sigma_3 = -|\sigma_t|$ ,

$$\sigma_r + |\sigma_t| = \sigma_f$$

In the wall of the workpiece there are axial tensile stresses. Analogous to the drawing ratio the ratio of initial to final diameter is called the spinning ratio  $\beta$ .

The largest spinning ratio  $\beta_{\max}$  that can be achieved in a single step is limited by three failure modes (Fig. 21.3):

- 1 Because of the compressive tangential stresses the flange tries to buckle. During spinning the flange is supported only in the region of the tool and is free over the remainder of the circumference. Thus the tendency to buckle and to form wrinkles is greater here than it is in deep drawing. The limiting spinning ratio is reached when the waves (wrinkles) in the flange become so large that they cannot be removed by subsequent passes of the tool.
- 2 If the spinning ratio is very large or if the edge radius of the roller is small ( $r_R < 3s_0$ ), then the axial thrust force of the roller can generate very high tensile stresses in the wall which cannot be transmitted by the corresponding portion of the cup cross section. In this case tangential cracks will appear in the transition from the flange to the wall.
- 3 Radial cracks can form in the outermost portion of the flange at the end of the process when wrinkles are removed by continued spinning. The resulting alternating bending stresses can cause cracks.

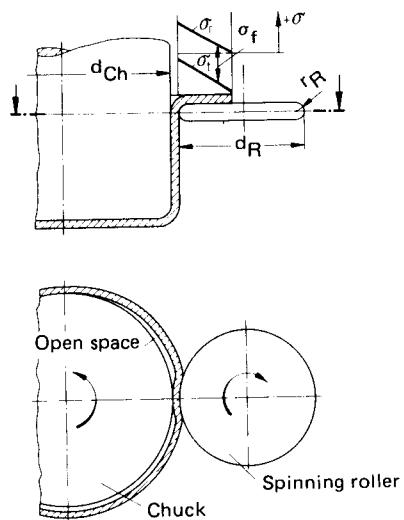


FIG. 21.2 Stresses and deformations in spinning.

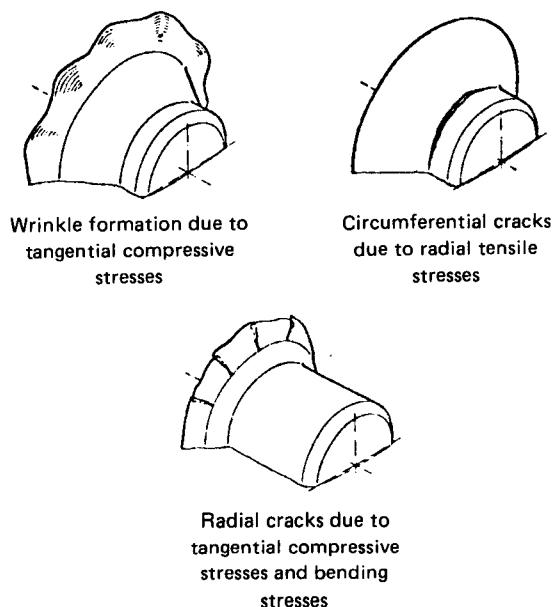


FIG. 21.3 Failure modes of spun components. (After [21.1].)

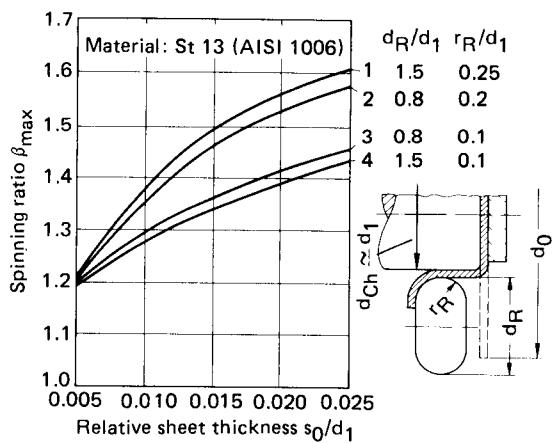


FIG. 21.4 Maximum values for spinning ratio  $\beta_{\max}$ . (After [21.2].)

Fig. 21.4 shows the main influence parameters on the limiting spinning ratio  $\beta_{\max}$  as determined by Dröge [21.2]. As the relative sheet thickness  $s_0/d_1$  increases,  $\beta_{\max}$  also increases, since the resistance against buckling increases with increasing sheet thickness. The ratio of roller diameter to inside diameter of the cup has practically no effect, while  $\beta_{\max}$  increases significantly for larger edge radii of the roller.

The roller exerts a force on the workpiece with components in the radial, axial, and tangential directions. The tangential force component is generally small and can be neglected. Dröge has investigated these forces and their influence parameters. He found that in addition to the relative sheet thickness, the roller radius  $r_R$  has an especially great effect on the force, particularly on the axial component (Fig. 21.5). Calculations of the forces based on plasticity theory have been attempted [21.2] to [21.5], but have not yet brought satisfactory results.

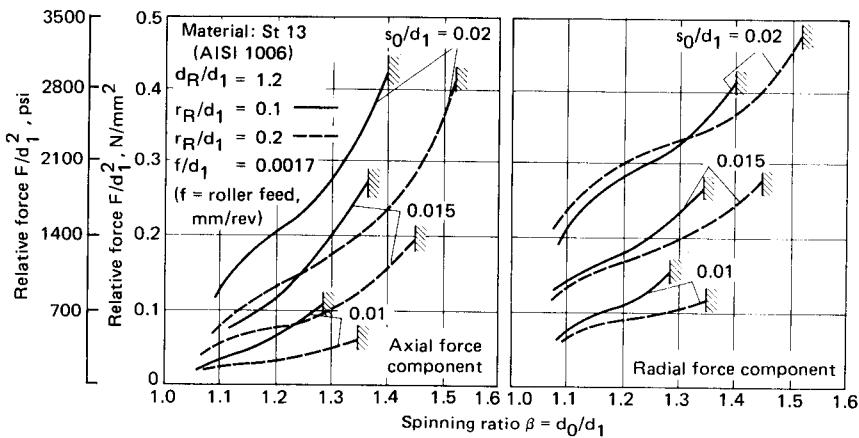


FIG. 21.5 Axial and radial force components developed in spinning. (After [21.2].)

## 21.2 APPLICATIONS

Spinning can produce workpieces with rotational symmetry of almost any shape. Fig. 21.6 shows a few sample components formed by spinning. With the aid of special equipment it is also possible to produce elliptical and oval components on a spinning lathe (Fig. 21.7). Bulges and necks are both possible (for examples, see Fig. 21.8). To produce bulges or necks, split chucks with several segments are used. Workpieces of several meters in diameter can be spun. Typical examples of such parts are bowls, container ends, and reflectors for radar installations.

When deforming thin sheets of large dimensions, the tendency to form wrinkles is great. In these cases hollow chucks are used in which the blank is clamped along the outside edge, as shown in Fig. 21.9. The resulting deformation process resembles stretching, that is, drawing with the state of stress of biaxial tension. This eliminates the possibility of wrinkle formation.

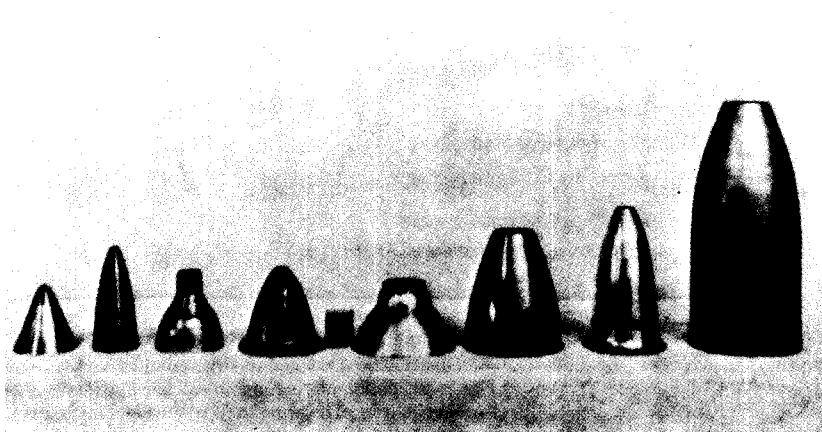


FIG. 21.6 Examples of components produced by manual spinning. (After [21.6].)

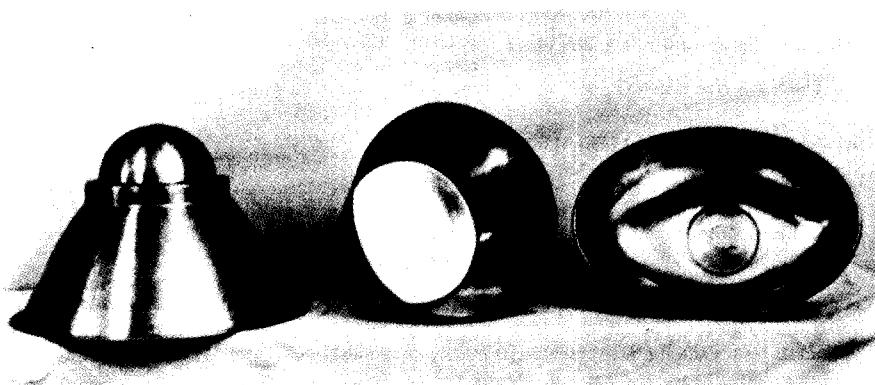
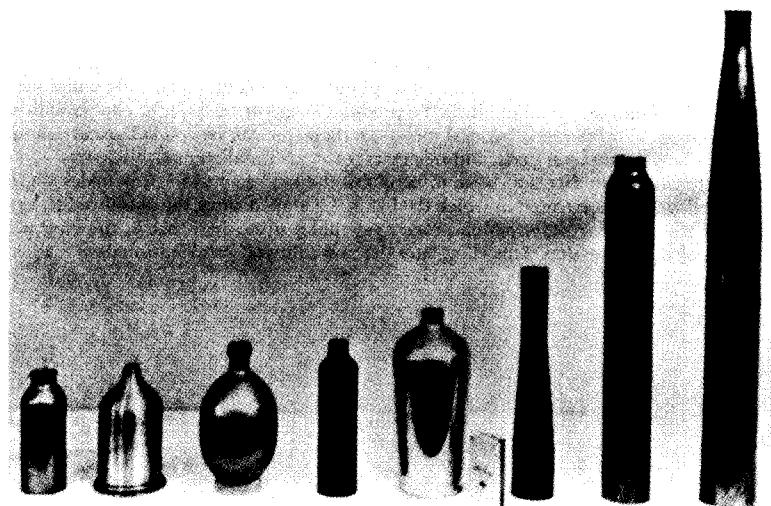
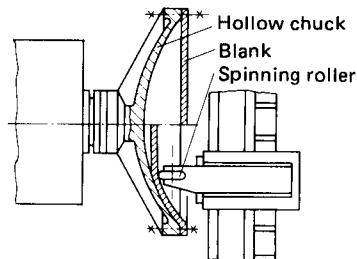


FIG. 21.7 Examples of spun reflectors. Largest diameter of reflector on the left—600 mm (23.6 in). (After [21.7].)



**FIG. 21.8** Examples of necked workpieces. (After [21.6].)



**FIG. 21.9** Spinning with a hollow chuck.

Spinning of cylindrical workpieces is in direct competition with deep drawing. For small components to be produced in large quantities deep drawing is generally more economical because of its shorter cycle times. The opposite is true when large cups, such as drums for commercial washing machines or cook pots for large kitchens, must be produced. These components could possibly be made on deep-drawing presses, but the tooling and machine cost would be very high. These parts are therefore rather made by spinning. For even larger components, such as radar reflectors, there are no forming processes which can compete with spinning.

The blank size is determined by assuming constant sheet thickness, as for deep drawing.

### 21.3 WORKPIECE MATERIALS

All metallic workpiece materials which are available in sheet form can be spun. The most important of these are mild steel, high-temperature steels, stainless steels, nonferrous heavy metals, and light metals. Most of these are spun at room temperature. However, some aluminum-magnesium alloys are heated to about 347°C (657°F) in order to achieve the necessary formability.

Tungsten, titanium, molybdenum, and zirconium alloys are used for rocket and aircraft components as well as for containers for chemical and nuclear industries. They are processed at elevated temperatures. The required temperatures are in the range of the generally used forming temperatures for these metals. Heating is mostly done locally with torches during spinning.

### 21.4 TOOLS FOR SPINNING

Spinning is carried out with either bars or rollers. Bars are made from hard woods, bronze, or hardened tool steel. Depending on the application, the shapes of the bars or the rollers can vary

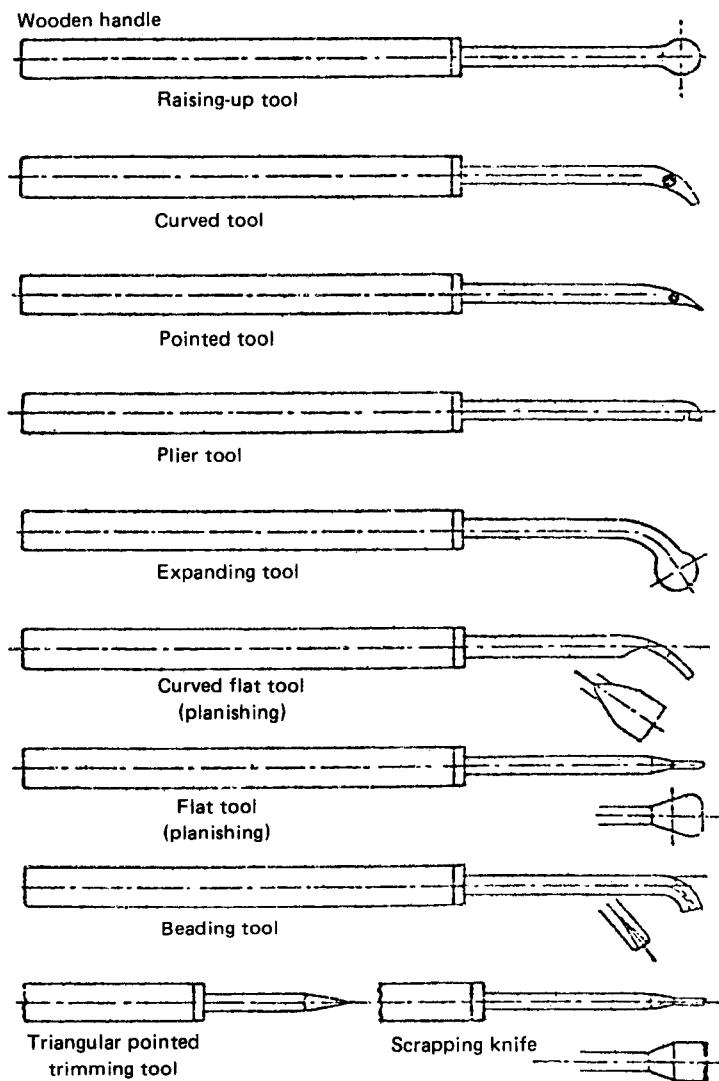


FIG. 21.10 Various types of tools used for hand spinning. (After [21.6].)

widely. Figs. 21.10 and 21.11 show some typical bar and roller tools. Spinning rollers, which are used almost always for large components, have ball bearings and are made mostly from hardened tool steel. Sometimes rollers made from plastics are used, for example, to spin pure aluminum and copper parts or to smooth the surface of steel components.

The outside shape of the chuck determines the inside shape of the components, but the reverse is true when using a hollow chuck, as is the case when producing bulges. For prototype work and for small lots chucks are made from wood, for medium-size lots cast iron or steel is used, and for large lots alloyed tool steel is preferred. Some typical chuck configurations are shown in Fig. 21.12.

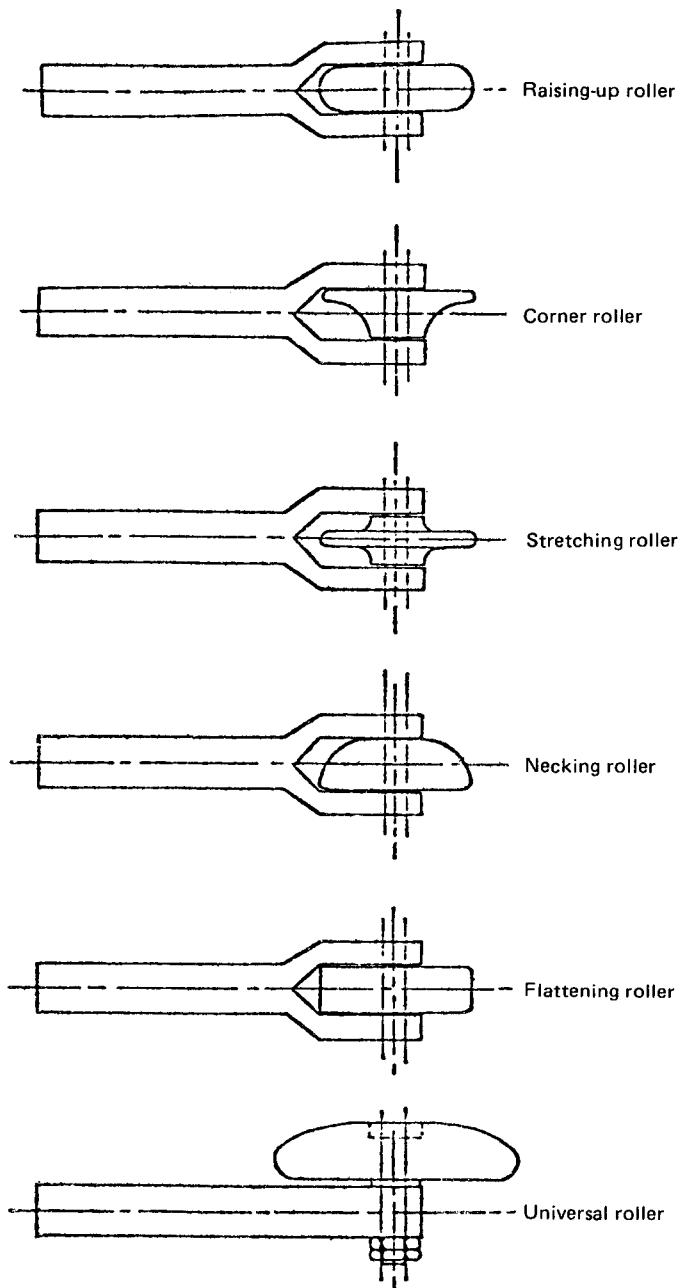


FIG. 21.11 Various types of roller tools. (After [21.6].)

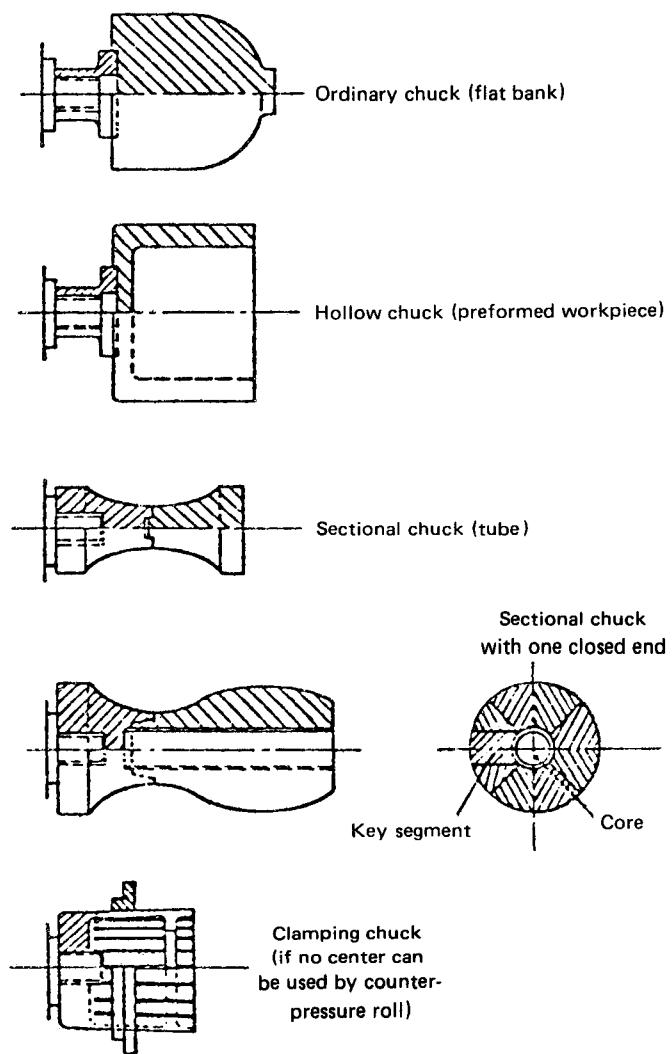


FIG. 21.12 Spinning chucks. (After [21.6].)

Very large components from titanium alloys and similar materials, which must be formed at elevated temperatures, would require very expensive chucks because of the required heat-resistant tool material. In these situations one frequently works without chucks and uses a supporting back-up roller instead, as illustrated in Fig. 21.13.

To produce components with diameter reductions (necks), sectional chucks must be used. They are made from cast iron or steel.

## 21.5 MACHINE TOOLS FOR SPINNING

Spinning machines are built similar to lathes. Fig. 21.14 shows the work space of a single-roller spinning machine. Larger machines often have two or three rollers mounted in equal intervals around the circumference of the chuck.

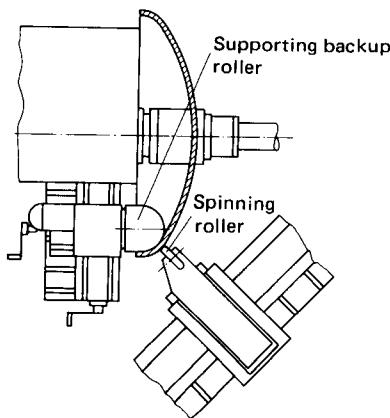


**FIG. 21.13** Spinning a large component without preformed chuck.

When spinning using hand-held tools, the tool rests on a support which carries a number of adjustable stops. Fig. 21.15 illustrates the principle. The forces necessary for deforming the blank are produced using lever advantage.

Simple mechanical spinning machines use manually operated threaded spindles to position the roller in the axial and radial directions (Fig. 21.16). For large-lot productions of spun components machines with hydraulically operated slides are used. These machines can operate semiautomatically or fully automatically.

Semiautomatic spinning lathes generally utilize templates to guide the tool in a series of steps such that the sheet is laid down in gentle strokes until it conforms to the size and shape of the chuck [21.6], [21.7]. To produce the successive spinning stages, two template arrangements are used: the parallel stack of templates where each template guides the roller during one increment and the single pivoting template whose position is adjusted from step to step. These two tracing methods are shown in Fig. 21.17.

When automatic blank loading and clamping devices and automatic unloading devices are added to a hydraulic spinning lathe, its operation can become fully automatic, requiring only one operator for every two or three machines. Because of the large effort involved in setting up a tracer-controlled spinning lathe and in designing and cutting the appropriate templates, their application has been limited to large-lot production.

In recent years efforts have begun to automate not only the mechanics of the spinning operation, but also to determine the intermediate workpiece contours for each stage automatically and to eliminate the need for templates [21.1], [21.8] to [21.10]. These efforts have led to the introduction of numerically controlled spinning lathes. In these machines the templates, and in many

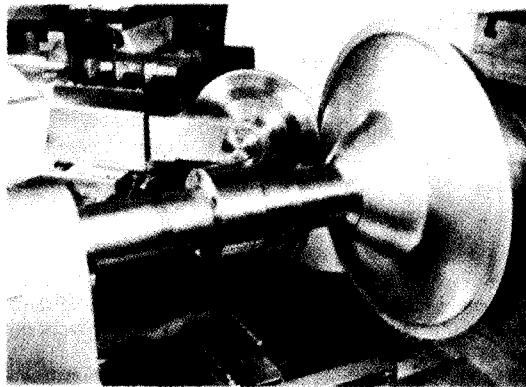


**FIG. 21.14** Work space of single-roller spinning machine.  
(Courtesy of Bohner and Köhle.)

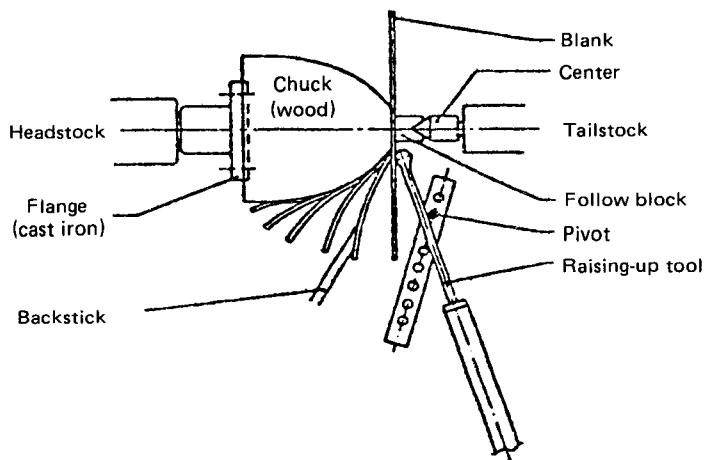


**FIG. 21.15** Sequence of operations for hand spinning. (After [21.6].)

instances the preformed chuck as well, have been replaced by numeric instructions to the machine-tool controller. Since many workpiece geometries can be produced with only a few roller shapes, changeover to a new workpiece geometry and other setup times are reduced drastically. Fig. 21.18 shows a typical arrangement with a forming roller and a supporting backup roller which are both numerically controlled.

To minimize the possibilities of workpiece failure (Fig. 21.3) the behavior of the workpiece during spinning must be better understood. In [21.8] an algorithm for determining the paths of the forming roller and of the supporting roller is mentioned which takes into account the maximum radial tensile stresses and the maximum tangential compressive stresses. In addition, the algorithm considers springback of the workpieces, which increases as spinning progresses and the work material strain hardens.

Programming of the numerically controlled spinning lathe is done off-line, especially for complex workpieces and for machines which combine spinning with metal-cutting operations such as

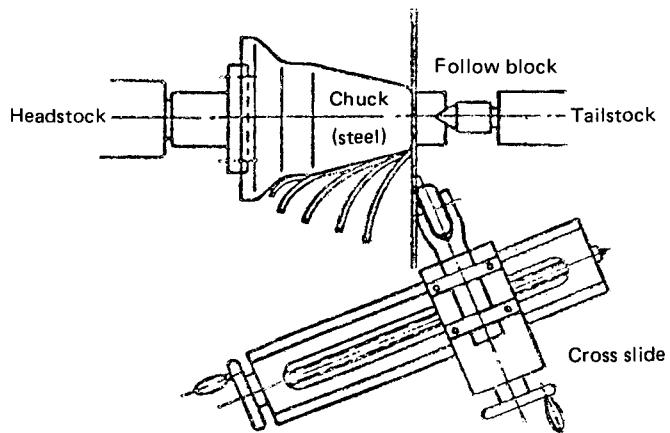


**FIG. 21.16** Schematic diagram of spinning setup using a cross slide. (After [21.6].)

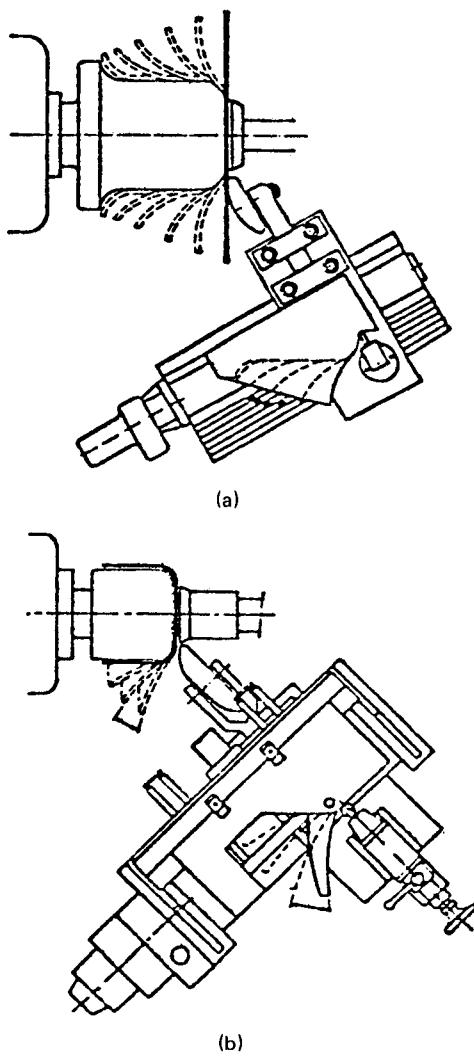


**FIG. 21.17** Schematic diagrams of tracer-controlled spinning machines. (a) Parallel stack. (b) Pivoted template. (After [21.6].)

turning, drilling, and even milling. These machining centers finish the workpiece completely in one setup.

Very large components are manufactured on spinning machines with a vertical axis, which makes loading and unloading easier. Fig. 21.19 shows a machine of this type.

## 21.6 MANUFACTURING TOLERANCES

The workpiece tolerances of the interior diameter which can be achieved with spinning depend mainly on the size of the component and the type of the spinning process itself. Spinning with

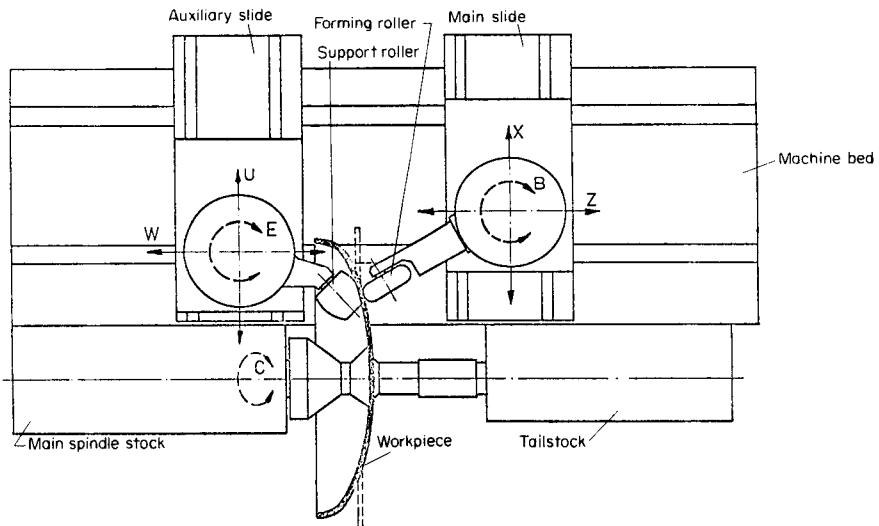


**FIG. 21.18** Numerically controlled spinning machine. (After [21.9].)

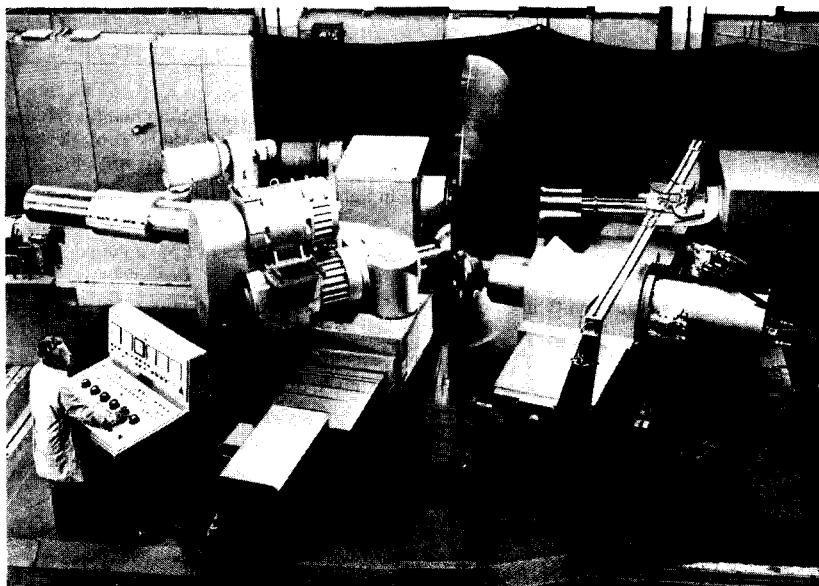


**FIG. 21.19** Large hydraulic spinning machine type BOD 47/BOD 75. Maximum workpiece diameter—4.7–7.5 m (185–295 in). (Courtesy of Leifeld.)

manual roller feed control yields lower accuracies than when automatic roller feed control is used, for example, in the form of a template follower. The achievable diameter tolerances are given in Table 21.1.

The surface condition depends heavily on the number of passes of the forming roller and on the roller radius. When the roller radius is large, the surface roughness of the worked surface may be smaller than the roughness of the blank.

**Table 21.1** Manufacturing Tolerances in Spinning

Workpiece diameter, mm (in)	Tolerance, mm (in)
Spinning without tracer control	
<600 (23.6)	0.8–1.6 (0.0315–0.063)
600–1200 (23.6–47.2)	1.6–3.2 (0.063–0.126)
1200–3000 (47.2–118.1)	3.2–6.4 (0.126–0.252)
Spinning with tracer control	
<500 (19.7)	±0.2 (0.008)
>500 (19.7)	±0.4 (0.0157)

The wall-thickness variations of a spun component are similar to those of a deep-drawn component; that is, the thickness is reduced in the transition region between the bottom and the wall and it is increased at the upper edge of the cup.

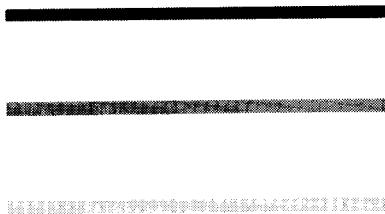
In addition, the workpiece tolerances are affected by the properties of the workpiece material, in particular its tendency to strain harden (spring back) and its planar anisotropy (wall-thickness variations around the circumference). As was mentioned in the previous section, numerically controlled spinning can offer the capability of reducing workpiece tolerances by taking these work material related effects into account. However, we are only at the beginning of these developments, and a lot of research is still required to completely understand the technology of metal spinning.

## REFERENCES

- 21.1 Younger, A., and Brown, C. C.: "A Copying System for Low Batch Quantity Hydraulic Metal Spinning," in *Proceedings of the 20th International Machine Tool Design and Research Conference* (Birmingham University, Birmingham, 1980), pp. 485–492.
- 21.2 Dröge, K. H.: "Forces and Material Flow in Spinning" (*in German*), Dr.-Ing. thesis, Universität Stuttgart, 1954.
- 21.3 Sortais, H. C., Kobayashi, S., and Thomsen, E. G.: "Mechanics of Conventional Spinning," *Trans. ASME*, **85B**, 1963, pp. 346–350.
- 21.4 Kobayashi, S.: "Instability in Conventional Spinning of Cones," *Trans. ASME*, **85B**, 1963, pp. 44–48.
- 21.5 Hayama, M., and Murota, T.: "On the Study of Metal Spinning," *Bulletin of the Faculty of Engineering*, no. 12, Yokohama National University, 1963.
- 21.6 "A Practical Look at Spinning and Flow Turning," *Sheet Met. Ind.*, **52**, Jan. 1975, pp. 7–11; Feb. 1975, pp. 72–89.
- 21.7 Sligte, J. G.: *Spinning and Flow Turning of Steel* (*in Dutch*), Amsterdam, Staalcentrum Nederland, Publ. 301, 1978.
- 21.8 Finkenstein, E. von, and Kohne, R.: "On the Technology of NC Spinning" (*in German*), *Wt.-Z. Ind. Fertigung*, **71**, 1981, pp. 231–235.
- 21.9 Frisch, J., and Achmad, M.: "An Experimental Study of Computer Controlled Shear Spinning," in *Proceedings of the 20th International Machine Tool Design and Research Conference* (Birmingham University, Birmingham, 1980), pp. 25–28.
- 21.10 Massberg, W.: "The Use of Computers in Metal Forming" (*in German*), *Z. Wirtsch. Fertigung*, **75**, 1980, pp. 12–19.

## CHAP. 22

### COLLAR DRAWING



#### List of Special Symbols

---

$d_0$	diameter of hole in blank
$d_1$	inside diameter of collar
$d_C$	outside diameter of collar
$d_D$	diameter of collar drawing die
$d_m$	mean diameter of collar
$F_b$	punch load due to bending of sheet material
$F_C$	contact force
$F_e$	punch load due to expansion of collar diameter
$F_{\max}$	maximum value of punch load
$F_p$	punch load; axial thrust
$h$	height of collar
$h_{th}$	theoretical height of collar
$r_C$	transition radius of collar
$r_D$	die radius
$u_D$	die clearance
$z_C, z_S$	number of thread cycles over height of collar, over sheet thickness

#### 22.1 BASIC PRINCIPLES AND GEOMETRIC RELATIONSHIPS

The purpose of drawing collars in sheet metal is to escape from the plane of the sheet into the third dimension (Fig. 22.1). Collars are used to provide material for thread cutting and to provide additional support for press fits for bolts or for making solder connections with tubes.

A collar is formed when a punch enters the precut hole and expands it. During this operation the material deforms out of the plane of the sheet. The greatest strains are encountered in the tangential and radial directions. This means that the major deformations act to increase the hole

diameter (from  $d_0$  to  $d_C$ ) while the wall thickness is reduced at the same time. The strains in the direction of the axis of the punch are small by comparison. There are compressive stresses in the radial and axial directions and tensile stresses in the circumferential direction.

The height  $h$  of the collar can be estimated quite accurately using Eq. 22.1 if its relative diameter is large ( $d_1 > 5s_0$ ), the die clearance is narrow ( $u_D \leq s_0$ ), and the die radius is very small:

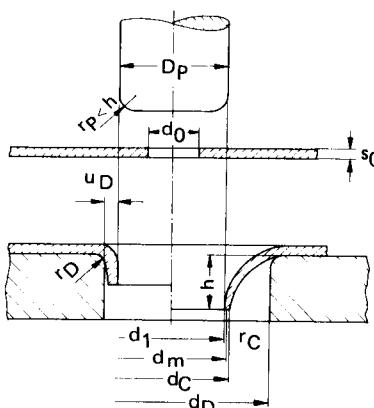


FIG. 22.1 Schematic diagram of collar drawing.

The actual collar height is larger than the computed theoretical value by a correction factor  $c$ :

$$h = ch_{th} \quad (22.4)$$

where  $c$  ranges from 1 to 1.6. The correction factor  $c$  can be estimated from the relationship

$$c = 1 + \frac{1}{10} \left[ 2.5 \left( 2.5 - \frac{2s_0}{d_C - d_1} \right)^2 + \left( 2.5 - \frac{2s_0}{d_C - d_1} \right) \right] \quad (22.5)$$

Eq. 22.5 resulted from experiments using sheets of St13 (AISI 1006) steel having a thickness of 1–2 mm (0.04–0.08 in). The value of  $c$  should be selected somewhat larger for soft sheet metals and slightly smaller for hard materials (maximum  $\pm 20\%$ ).

When using small die clearances ( $u_D < s_0$ ), greater collar heights can be achieved by wall-thickness reduction due to ironing. If  $u_D < 0.65s_0$ , even the outside wall surface becomes cylindrical and  $h$  is approximately equal to  $h_{th}$ . Care must be exercised in this case not to reduce the wall thickness too much, which could increase the punch load to the point where the collar is torn off [22.2].

## 22.2 COLLAR DRAWING RATIO

The achievable collar drawing ratio  $d_1/d_0$  is limited by the state of stress in the sheet metal, which depends on the relative diameter  $d_0/s_0$  of the precut hole [22.3]. Fig. 22.2 shows test results obtained by Wilken [22.4, 22.5], which apply to collars of large diameters.

In order to obtain a collar without cracks, the precut hole must have a surface that is as smooth as possible. Experiments with pointed punches which first pierce the sheet and then draw a collar produced cracked, unusable collars. The condition of the precut hole is of great importance for large collar drawing ratios and, therefore, for collars of large heights. Punched holes are significantly poorer than drilled holes. Burrs and the final fracture surface tend to initiate cracks. The shape of the punch, on the other hand, has only a small effect on the achievable collar drawing ratio.

However, if the die radius or the die clearance is large, this fact must be considered when computing the height of the collar. Investigations by Romanowski resulted in the following equation [22.1]:

$$h = \frac{d_D - d_0}{2} + 0.43r_D + 0.72s_0 \quad (22.2)$$

Eq. 22.2 applies for collars with large die radii. For collars with large clearance the same formula applies with  $r_C$  instead of  $r_D$  (Fig. 22.1). These equations do not apply to collars of relatively small diameters ( $d_1 < 5s_0$ ). In these situations the theoretical height of the collar  $h_{th}$  can be computed assuming constant volume:

$$h_{th} = s_0 \frac{d_C^2 - d_0^2}{d_C^2 - d_1^2} \quad (22.3)$$

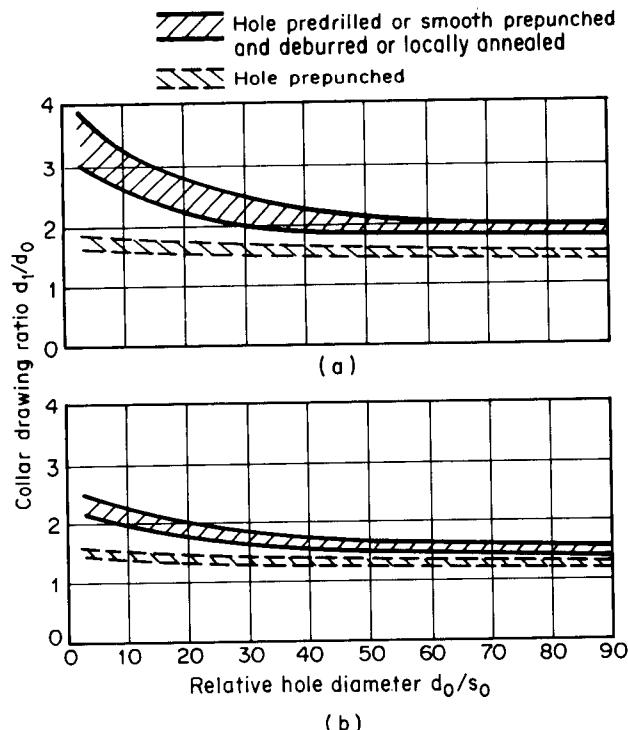


**FIG. 22.2** Maximum collar drawing ratio  $\beta_{\max}$  as a function of relative hole diameter. (a) Material—St14 (AISI 1005); lubrication—machine oil. (b) Material—Al 99.5w (AA 1050-O). (After [22.3].)

The values for the limiting collar drawing ratio given in Table 22.1 apply to narrow collars of small diameters ( $d_1 < 5s_0$ ) [22.2].

### 22.3 PUNCH LOAD

Collar drawing is a nonstationary process. For this reason it has not been possible to compute the punch load satisfactorily based on plasticity theory. The maximum punch load  $F_{\max}$  is composed

**Table 22.1** Maximum Collar Drawing Ratio  $d_1/d_0$  in Drawing of Small-Diameter Collars

Designation		Collar without cracks	Collar with slight cracks
DIN	US		
St 14	AISI 1005	<2.5	<3.9
St 13	AISI 1006	<2.4	<3.7
CuZn37F30	UNS C27400	<2.3	<3.9
Al 99.5w	AA 1050-O	<3.4	<3.9
Al 99.5h	AA 1050-H	<2.3	<3.4
Zn 99.99	—	<2.4	<3.4

Source: Compiled from [22.1].

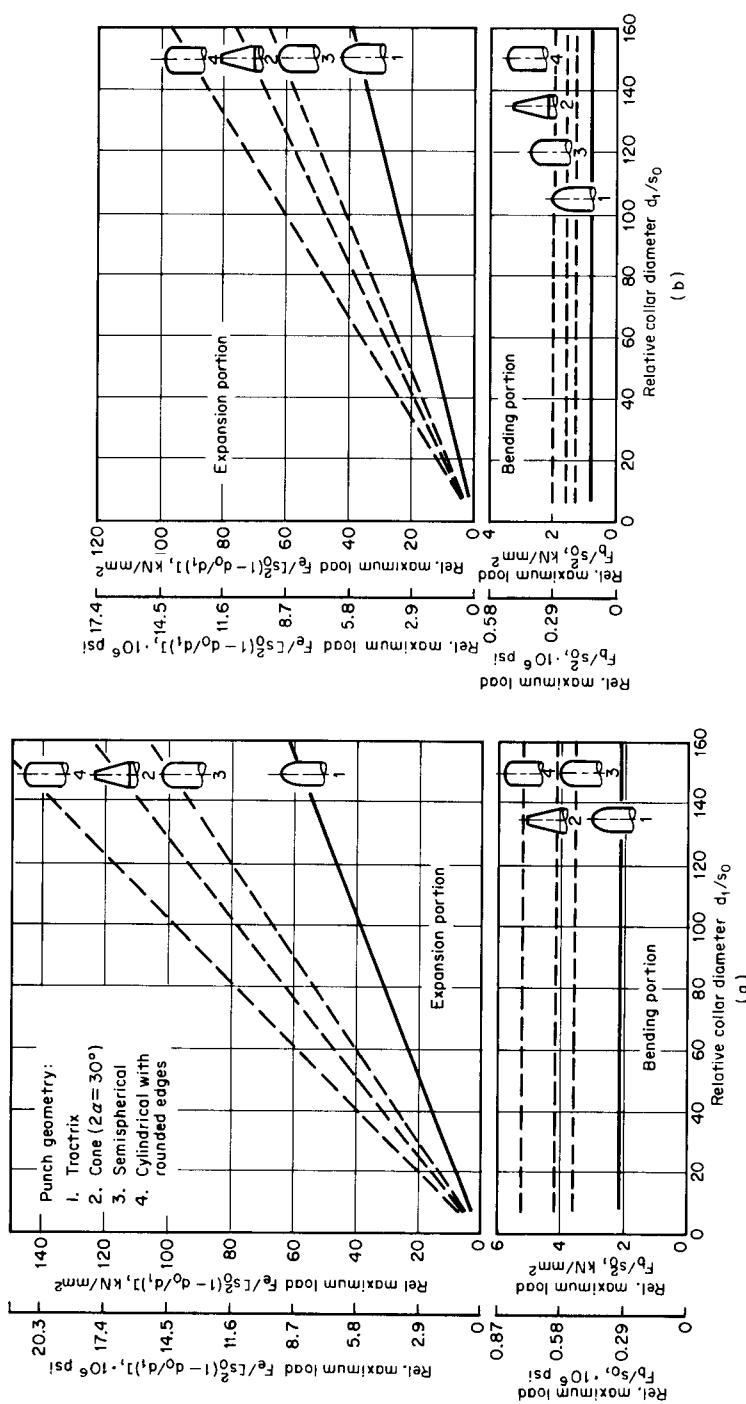


**FIG. 22.3** Expansion and bending load components in collar drawing with narrow die clearance,  $w_D = s_0$ . When working with large die clearances ( $w_D > 10s_0$ ), the bending component is reduced by  $\approx 30\%$  from the given values. (a) Material—St14 (AISI 1005); lubrication—machine oil. (b) Material—Al99.5 w (AA 1050-O). (After [22,3].)

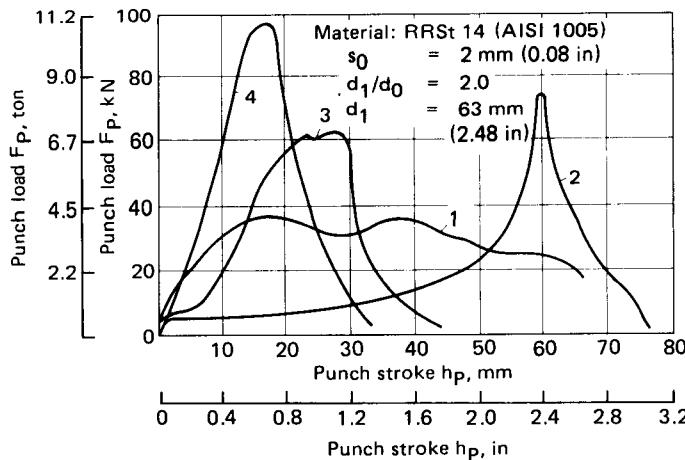


FIG. 22.4 Load-stroke diagram in collar drawing. Punch shapes are explained in Fig. 22.3. (After [22.4].)

of a bending component  $F_b$  and an expansion component  $F_e$ . Wilken has determined both components experimentally for various punch shapes. His results are shown in Fig. 22.3. For punch-load estimation both  $F_e$  and  $F_b$  must be calculated from Fig. 22.3 according to the actual sheet thickness  $s_0$  and the relation  $d_0/d_1$ .<sup>6</sup>

It is clear that the tractrix-shaped punch† always requires the lowest loads, since the collar is formed using the largest possible leverage. In addition, the formed collar is very nearly cylindrical. The disadvantages of this shape are the difficulty of machining it and the long required punch stroke. Semispherical or conical punches are easier to produce. The forming loads are higher, however, and the resulting collar may become cracked and noncylindrical, especially with conical punches. Shape 4 requires the largest loads since the sheet is bent twice, first around the punch radius and then around the die radius. Its stroke is the shortest of all punches investigated, and it is used in combination punches which produce the hole and the collar with one stroke. For hole punching a flat punch face is needed.

The die radii  $r_D$  for these punches are designed with the following guidelines [22.2]:

$$\begin{aligned} r_D &= 4-6s_0 && \text{for } s_0 \leq 2 \text{ mm (0.08 in)} \\ r_D &= 2-3s_0 && \text{for } s_0 > 2 \text{ mm (0.08 in)} \\ r_D &= 0.1d_C && \text{for small-diameter collars } (d_1 < 5s_0) \end{aligned}$$

The relationships between punch load and punch stroke are shown in Fig. 22.4 as functions of the punch shape. As expected, the load for the tractrix shape is approximately constant during the entire duration of the long stroke. The punch with only a rounded edge has a high load peak while its stroke is very short.

## 22.4 SMALL-DIAMETER COLLARS WITH THREAD

Collars with small diameters are frequently used with thread if nuts are not applicable and the loading of the fit corresponds to the strength of the thread. For a thread according to Fig. 22.5,

<sup>6</sup>Example: For steel sheet RRSt 14 (AISI 1005)  $s_0 = 2 \text{ mm (0.08 in)}$ ,  $d_0 = 40 \text{ mm (1.6 in)}$ ,  $d_1 = 80 \text{ mm (3.2 in)}$ , and punch type 3, one obtains  $F_h/s_0^2 = 3.7 \text{ kN/mm}^2 (536.13 \text{ ksi})$  and  $F_b = 14.8 \text{ kN (3300 lbf)}$ ,  $F_e/[s_0(1 - d_0/d_1)] = 27 \text{ kN/mm}^2 (3912.3 \text{ ksi})$ , and  $F_r = 54 \text{ kN (12,150 lbf)}$ . Then  $F_e + F_b = 68.8 \text{ kN (15,480 lbf)}$ .

†For details on tractrix see Sec. 20.4.3.

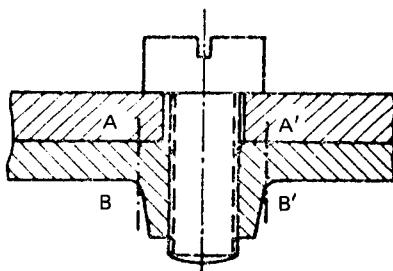


FIG. 22.5 Narrow collar with thread. (After [22.2].)

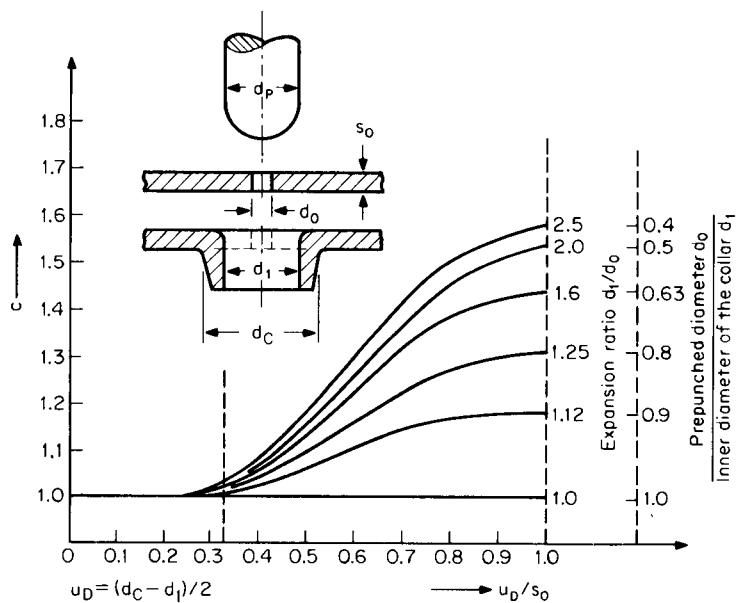


FIG. 22.6 Correction factor  $c$  for effective collar height. (After [22.2].)

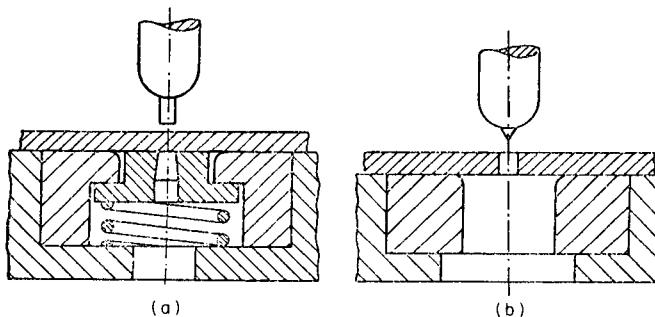


FIG. 22.7 Tools for collar drawing. (a) With spring-supported punching die. (b) For prepunched sheet. (After [22.2].)

**Table 22.2** Dimensions, in Millimeters, of Metric Threads in Drawn Narrow Collars<sup>a</sup>

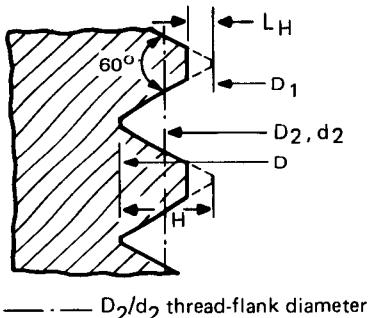
Standard-pitch thread										
	M2	M2.3	M2.6	M3	M3.5	M4	M5	M6	M8	M10
D	2.036	2.336	2.642	3.044	3.554	4.062	5.072	6.090	8.112	10.136
D <sub>1</sub>	1.480	1.780	2.016	2.350	2.720	3.090	3.960	4.700	6.376	8.052
d <sub>1</sub> > D <sub>1</sub>	1.65	1.95	2.2	2.5	2.95	3.4	4.3	5.1	6.8	8.6
p	0.4	0.4	0.45	0.5	0.6	0.7	0.8	1.0	1.25	1.5

Fine-pitch thread						
	M5	M6	M8	M10	M12	M14
D	5.044	6.068	8.068	10.090	12.136	14.136
D <sub>1</sub>	4.350	5.026	7.026	8.760	10.052	12.052
d <sub>1</sub> > D <sub>1</sub>	4.5	5.3	7.25	9.0	10.6	12.6
p	0.5	0.75	0.75	1	1.5	1.5

<sup>a</sup>Thread dimensions: D—major diameter; D<sub>1</sub>—minor diameter; p—pitch; d<sub>1</sub>—internal diameter of collar.

Source: Compiled from [22.2].



**FIG. 22.8** Thread geometry in drawn collar.  
D<sub>1</sub>—minor diameter; D—major diameter; H—  
height of thread; L<sub>H</sub> ≈  $\frac{1}{3}H$ —loss of thread height  
according to drawing process. (After [22.2].)

with 8-mm ( $\approx 0.3$ -in) diameter and 0.75-mm ( $\approx 0.03$ -in) pitch in 2.5-mm (0.1-in) steel sheet, an axial fracture strength of 16 kN (3550 lbf), which equals 65% of the shear strength along lines AB, A'B' in Fig. 22.5, will be achieved. Such collars aiming at maximum heights must be produced with a die clearance  $u_D/s_0 \leq 1$ . The height may be calculated from Eq. 22.4 with correction factor *c* according Fig. 22.6. The sheet should be prepunched in a separate tool, but a spring-loaded combined prepunching and drawing tool will also give good results (Fig. 22.7). The recommended die-entry radius is  $0.05\text{--}0.1d_D$ . Using the data given in Table 22.2, threads according to Fig. 22.8 with a minimum number of threads  $z_C \geq 1.5z_s$  can be obtained for sheet thicknesses of 0.05–4.5 mm (0.02–0.18 in) with major thread diameters of 2–10 mm (0.08–0.4 in) for standard-pitch threads and of 5–14 mm (0.2–0.55 in) for fine-pitch threads. For detailed information see [22.1, 22.3, 22.6].

## 22.5 FORMING OF SMALL-DIAMETER COLLARS WITH ROTATING PUNCH

This process, which had already been known in the United States in the 1920s, was redeveloped and improved by van Geffen during 1972–1977. According to Fig. 22.9, a rotating tapered punch

**22.8 SHEET-METAL FORMING**

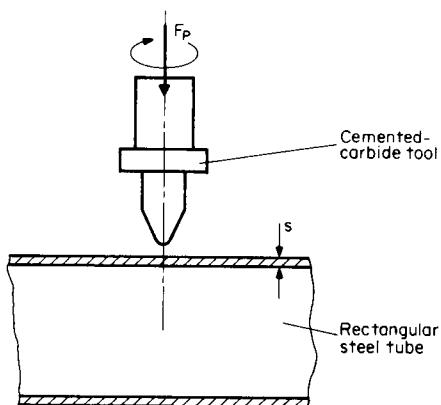


**FIG. 22.9** Rotating tool for collar forming. (After [22.7].)

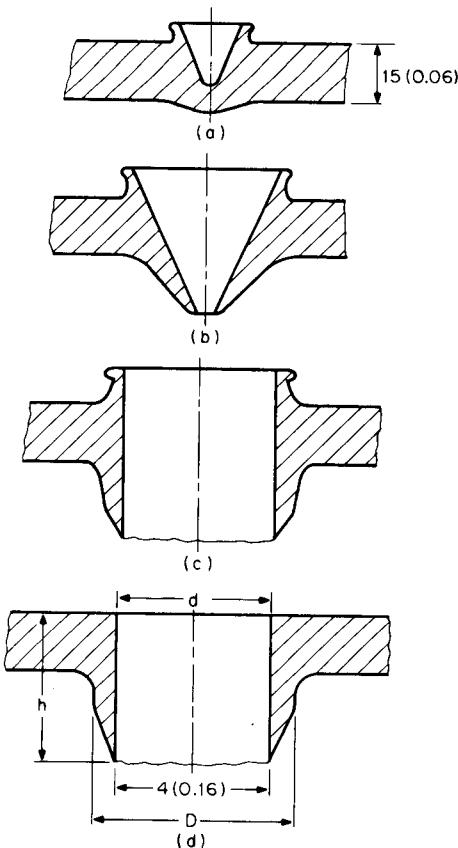


**FIG. 22.10** Steps in collar forming with rotating punch. Dimensions are in mm (in). (After [22.7].)

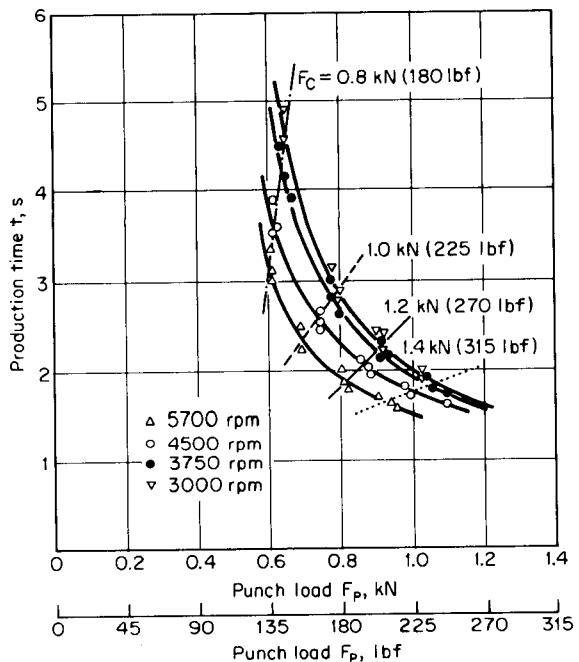


**FIG. 22.11** Production time as a function of normal force  $F_n$  for  $s = 1.8 \text{ mm (0.07 in)}$  and  $d = 4.2 \text{ mm (0.165 in)}$ . Parameters—punch load (axial thrust) and number of revolutions per minute of tool. (After [22.7].)

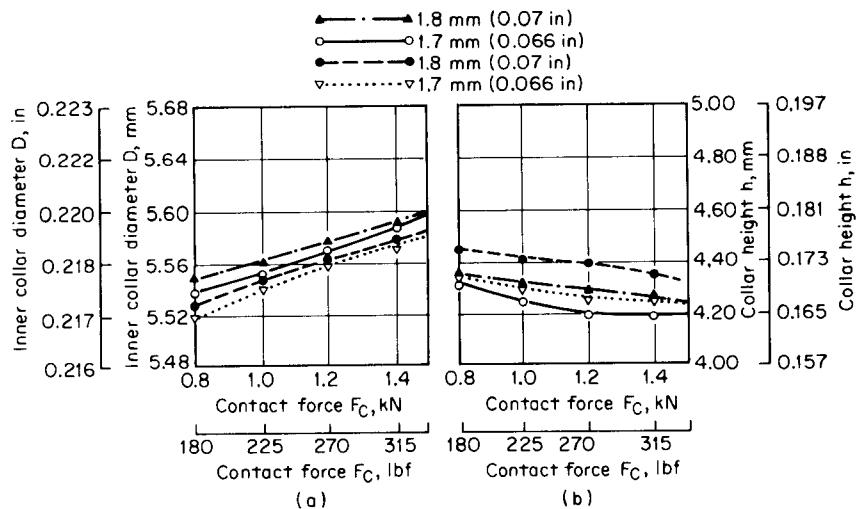


**FIG. 22.12** Dimensions of collar and influencing parameters for  $a = 4.2 \text{ mm (0.17 in)}$ . Parameters—sheet thickness and number of revolutions per minute. (a) Inner diameter of collar as a function of contact force. (b) Collar height as a function of contact force. (After [22.7].)

## 22.10 SHEET-METAL FORMING

made from cemented carbide penetrates the sheet or tube wall and forms a collar. During the continuous process several intermediate stages occur (Fig. 22.10). The last stage, stage *d*, follows metal removal on the punch side by an integrated milling tool element. The process has the advantage that collars suitable for various purposes, such as for welded or soldered joints, bearings, or threads, can be produced without die, even at inaccessible locations [22.7, 22.8].

During the process the rotating tool may reach temperatures of more than 600°C (1112°F) if collars are formed within 1.5–5 s. Productivity depends on the forming time, which may be decreased by increasing the punch load  $F_P$  (which is closely connected with the contact force  $F_C$ ) and the number of revolutions per minute (Fig. 22.11). The required power increases nearly linearly with the torque, which increases with axial thrust and decreases with increasing number of revolutions per minute (ranging between 3000 and 5700). The dimensional accuracy of the hole depends only on the tool dimension, while the collar height is influenced by the punch load and the number of revolutions per minute (Fig. 22.12).

### REFERENCES

- 22.1 Romanowski, E.: *Handbook of Blanking Technology (in German)*, Berlin, VEB Verlag Technik, 1959.
- 22.2 Kienzle, O., and Timmerbeil, H.: "Design and Production of Narrow Collar in Thin Sheet Metal" (*in German*), *Mitt. Forschungsges. Blechverarb.*, 1953, pp. 250–252, 1954, pp. 2–9, 41–43, 66–70.
- 22.3 VDI-Richtlinie, 3359: "Blechdurchzüge (Collars in Sheet Metal)," Düsseldorf, VDI-Verlag, Aug. 1961.
- 22.4 Wilken, R.: "Drawing of Collars with Punches" (*in German*), *Forschungsberichte des Landes Nordrhein-Westfalen*, no. 794, Köln/Opladen; Westdeutscher Verlag, 1959.
- 22.5 Wilken, R.: "Drawing of Collars with Punches" (*in German*), *Mitt. Forschungsges. Blechverarb.*, 1958, pp. 56–63.
- 22.6 DIN 7952: "Blechdurchzüge mit Gewinde (Collars in Sheet Metal with Thread)," Köln, Beuth-Verlag, 1972.
- 22.7 Kretschmer, G.: "Forming of Small-Diameter Collars in Sheet Components" (*in German*), *Wt. Z. Ind. Fertigung*, 67, 1977, pp. 667–669.
- 22.8 Kretschmer, G.: "Contribution to Forming of Small-Diameter Collars in Sheets" (*in German*), Dr.-Ing. thesis, Universität Siegen, 1980.

## CHAP. 23

# STRETCH FORMING, EXPANDING, AND OTHER TENSILE FORMING PROCESSES

### List of Special Symbols

$a_o$	width of die
$F_G$	gripper load
$F_p$	stretch-forming load
$r_e$	entrance radius
$r_p$	punch radius
$s_0$	initial sheet thickness
$t$	depth of embossed bead

Metal-forming processes in which the desired workpiece contour is produced mainly by tensile forces are called tensile forming processes. They were classified and defined as such in [23.1]. Fig. 23.1 shows a classification of these processes depending on the major type of deformation encountered by the workpiece and the types of tooling used. In all these processes the workpiece surface area will be increased while its thickness is reduced.

Using the definitions provided in [23.1], the different tensile forming processes are presented briefly:

- 1 **Tensile forming:** The deformation of a solid body in which the plastic state is created mainly through the application of tensile forces in one or more directions.

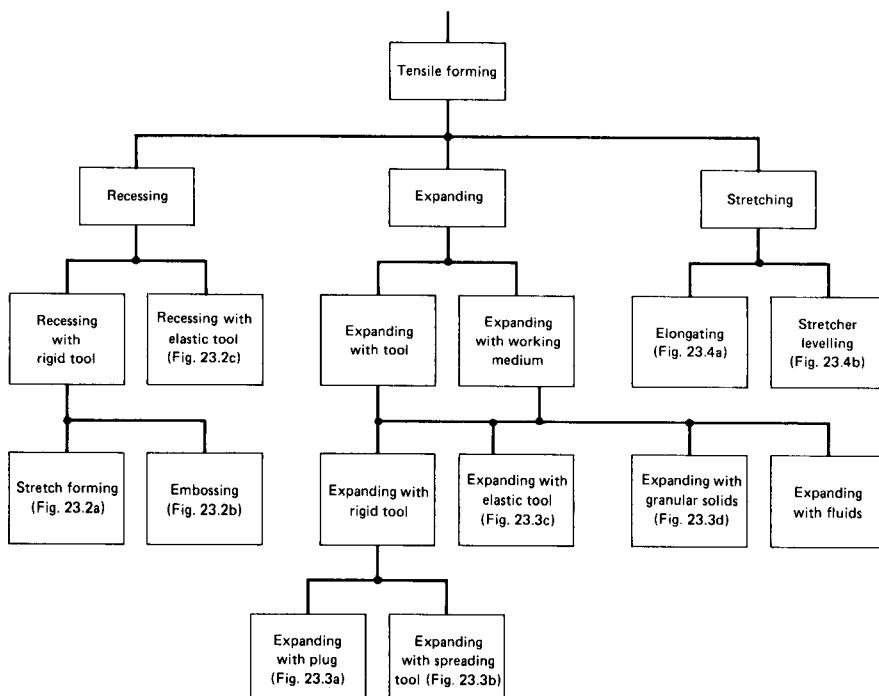


**FIG. 23.1** Classification of tensile forming processes. (After [23.1].)

**2 Recessing:** A tensile forming process which produces recesses in flat or bent sheet-metal workpieces. The surface area of the workpieces is increased through a reduction in sheet thickness.

**Recessing with rigid tooling:** A recessing process in which a rigid punch exerts pressure on the workpiece. Frequently a rigid die is also used in order to define the workpiece shape precisely.

**Stretch forming:** A recessing process in which the edge of the workpiece is clamped rigidly. A rigid punch is used to apply the load. The workpiece can be clamped either between rigid sections of the tool or with special clamps (Fig. 23.2a).

**Embossing:** A recessing process which uses a rigid punch to pull the workpiece into a rigid die. The depth of the recess is small compared to the workpiece dimensions (Fig. 23.2b).

**Recessing with elastic tools:** A recessing process in which the load is applied with an elastic cushion (Fig. 23.2c).

**3 Expanding:** A tensile forming process to increase the diameter of a hollow workpiece.

**Expanding with tools:** An expansion process in which a tool is used to apply pressure to the inside of the workpiece. Usually a female die is used on the outside to control the shape of the workpiece accurately.

**Expanding with rigid tools:** An expansion process in which a rigid tool is used to apply pressure to the inside of the workpiece.

**Expanding with plug:** An expansion process in which a plug is pushed into or pulled through the workpiece (Fig. 23.3a).

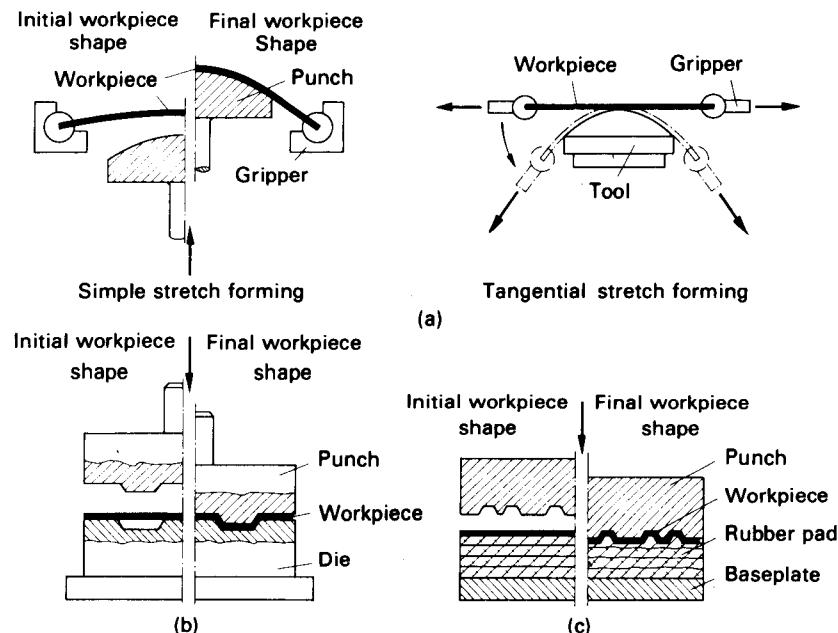


**FIG. 23.2** Processes to produce recesses. (a) Stretch forming without die. (b) Embossing. (c) Coining with rubber pad. (After [23.1].)

**Expanding with spreading tools:** A bulging process in which a sectioned tool is actuated by a conical or wedge-shaped punch (Fig. 23.3b).

**Expanding with elastic tools:** A bulging process in which the load is applied to the workpiece by an elastic interior tool (Fig. 23.3c).

**Expanding with working medium:** An expansion process which uses a medium to apply interior pressure to the workpiece. In most cases a female die is used on the outside to control the workpiece geometry. The medium serves to transmit static forces and may be in direct contact with the workpiece, or it may be contained by a gasket or pliable bag.

**Expanding with granular solids:** An expanding process in which a granular solid medium is used to transmit the forming load (Fig. 23.3d).

**Expanding with fluids:** An expanding process in which the working medium is a fluid (Fig. 23.3e).

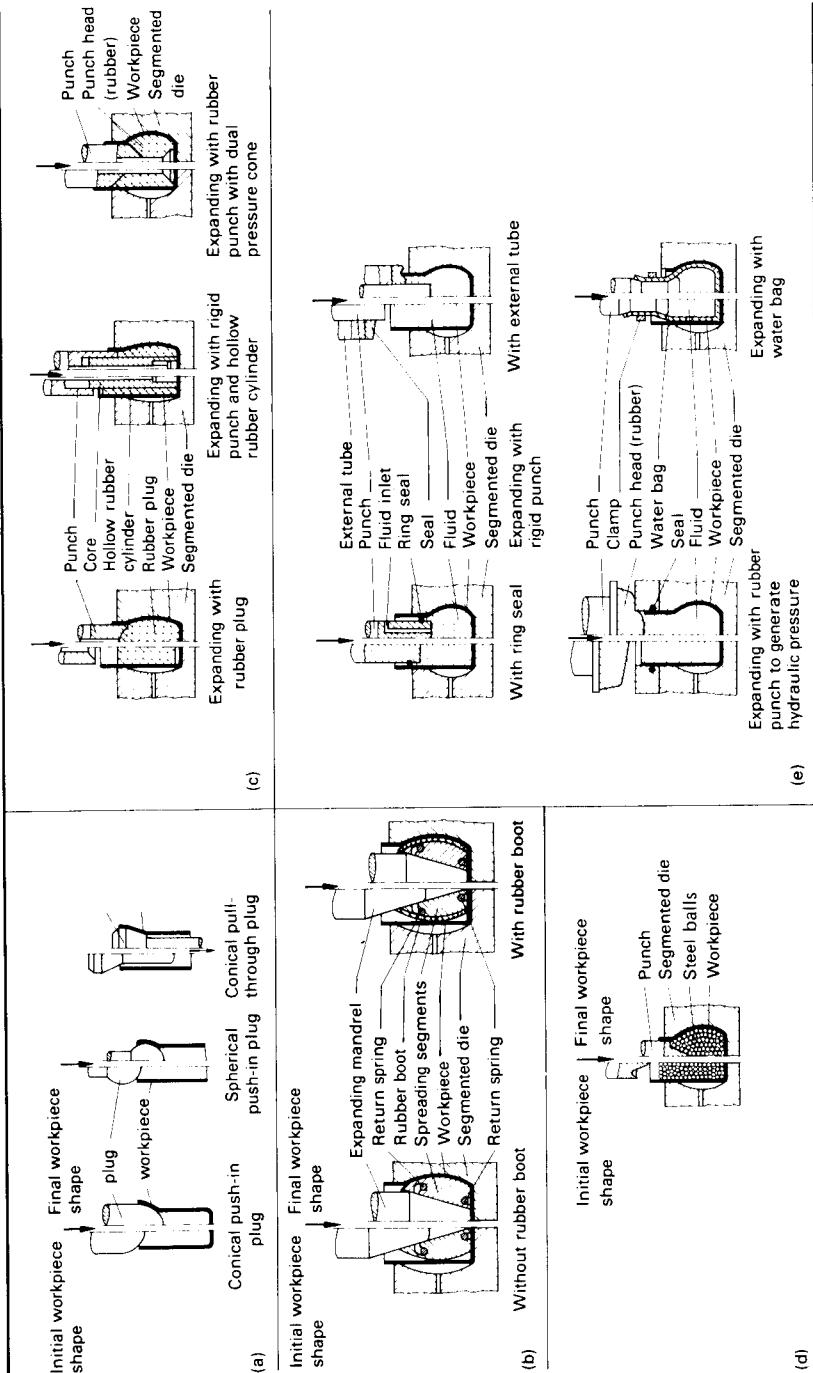
- 4 **Stretching:** A tensile forming process in which the applied tensile force acts in the direction of the workpiece axis.

**Elongating:** A stretching process to increase the size of the workpiece in the direction of the applied force (Fig. 23.4a).

**Stretcher levelling:** A stretching process whose purpose it is to remove bends from rods and tubes as well as to eliminate dents from sheet metal (Fig. 23.4b).

### 23.1 STRETCH FORMING

Stretch forming is used in particular for forming body panels, such as doors, roofs, or fenders for trucks, buses, and special vehicles and in the aircraft industry (Fig. 23.5). In these applications



23.4

**FIG. 23.3** Expansion processes. (a) Expanding with plug. (b) Expanding with spreading tool. (c) Expanding with elastic tool. (d) Expanding with steel spheres. (e) Expanding with fluids. (After [23.1], [23.2].)

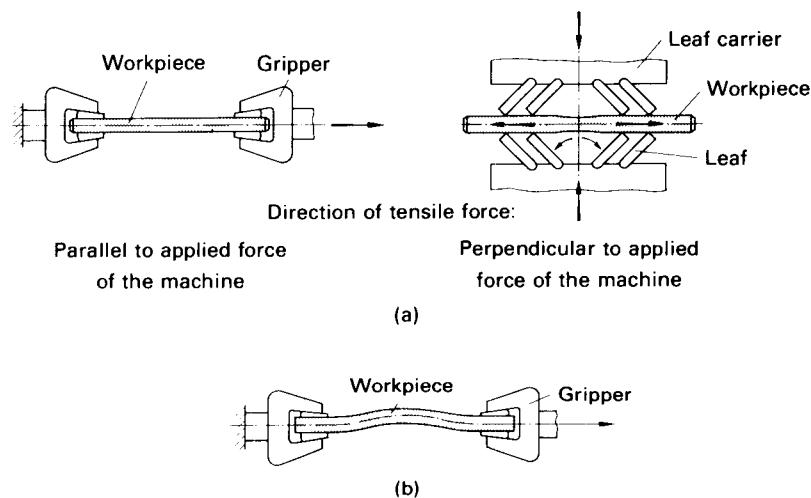


**FIG. 23.4** Stretching processes. (a) Elongating. (b) Stretcher levelling. (*After [23.1].*)

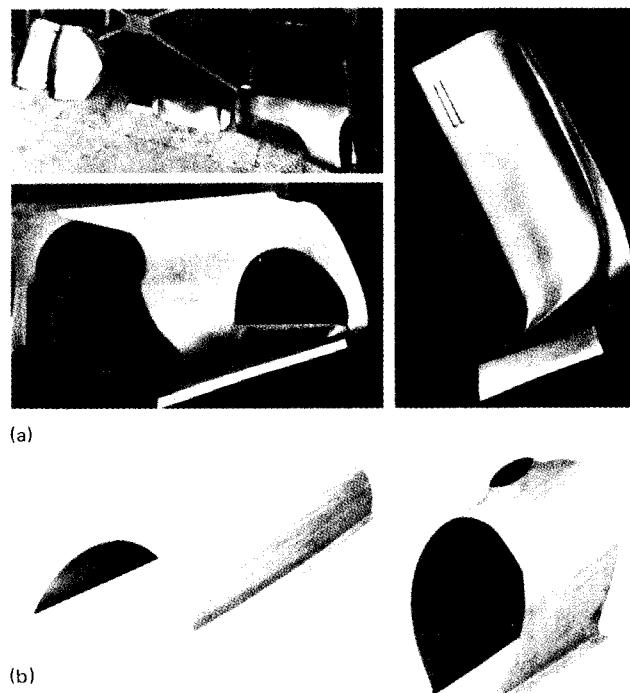


**FIG. 23.5** Stretch-formed workpieces. (a) Automobile components. (b) Aircraft components. (*Courtesy of Ateliers et Chantiers de Bretagne.*)

formed sheet-metal components with surface areas of more than  $50 \text{ m}^2$  ( $540 \text{ ft}^2$ ) are sometimes needed for which conventional forming processes cannot be used because of the necessary machine size.

The required components are usually more or less curved over the entire extent of the part, and sometimes compound curvatures are also needed. The components are generally produced from flat sheets. The blanks are rectangular in most cases, but sometimes trapezoidal blanks are used. In exceptional cases circular, oval, or kidney-shaped blanks are used.

There are two stretch-forming processes, simple stretch forming and tangential stretch forming.

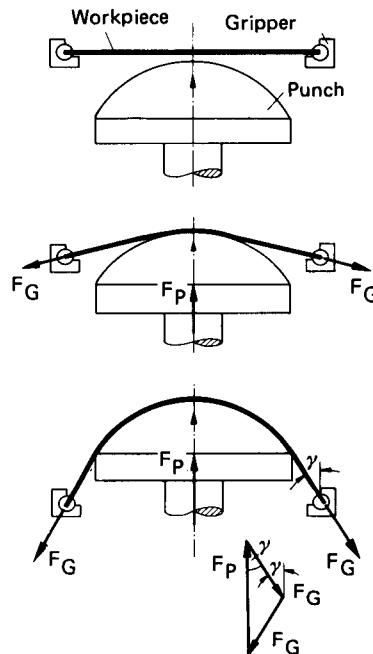


**FIG. 23.6** Deformation during simple stretch forming.

In order to form components which require larger strains than the uniform strain limit of a particular workpiece material, either one must choose a different material with a larger uniform strain limit, or the blank must be gripped at all sides. In the latter case the state of strain and stress in the component is such that larger deformations are possible before necking occurs (see Chaps. 18 and 20).

Fig. 23.7 shows the stress distribution in the cross section of a component during stretch forming. In the beginning the material is only bent and stretched elastically; then plastically deformed zones appear at both surfaces of the sheet metal. At the end of the deformation process stretching dominates bending, and the stress in the cross section is uniform and equal to the yield or flow stress. If the material work hardens, then the tensile stresses at the outside surface are slightly higher than those at the inside surface.

For components of arbitrary shapes the precise stress and strain distributions are not known, but the required stretch-forming load  $F_P$  for forming a sheet of 1-mm (0.04-in) thickness can be estimated using Eq. 23.1 [23.2], [23.4]:

$$F_P = \frac{A_1}{\eta_{def}} \sigma_{f,m} \ln \frac{A_0}{A_1} \quad (23.1)$$

### 23.1.1 Simple Stretch Forming

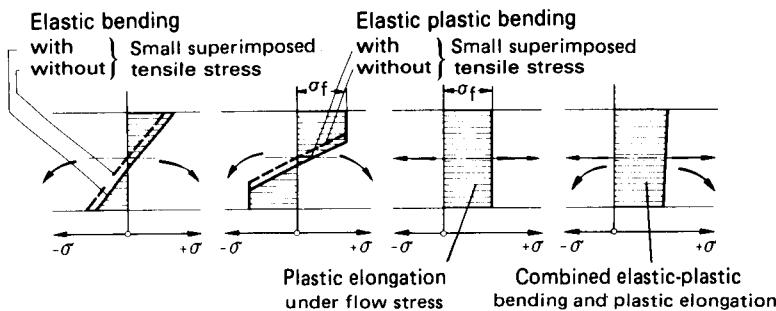
#### Process Description

Fig. 23.6 illustrates the forming process in simple stretch forming. The sheet metal is usually gripped at two opposing sides, less often at all sides. The grippers can rotate in their mounts.

The tensile stresses required to cause deformation are applied directly with a punch, called a former, which has been given the desired interior shape of the component. First, the sheet metal contacts the top of the former, and then it begins to stretch as the former's stroke proceeds. The sheet metal conforms more and more to the shape of the tool and reaches its final shape at the dead point of the stroke [23.2], [23.3].

#### Strains, Stresses, and Forces

It is a general rule in stretch forming that the mean strain in the total deformed region must be kept below the uniform strain limit  $\epsilon_u$  of the material, which is determined in a tensile test. Since the uniform strain limit ranges from 5% for titanium alloys at room temperature to 35% for steel sheet of deep-drawing quality, only relatively shallow components can be produced by stretch drawing [23.3].



**FIG. 23.7** Stress distribution during simple stretch forming.

where  $A_0$  = initial surface area of sheet metal

$A_1$  = surface area of finished stretch-formed component

$\sigma_{f,m}$  = mean flow stress

The efficiency of deformation,  $\eta_{def}$  ranges from 0.5 to 0.7. If the strains are uniform over the area, the larger efficiency value may be used. For unevenly distributed strains the lower value applies. It has not yet been determined what modifications of Eq. 23.1 are necessary to predict the forming load for sheets of arbitrary thickness.

The upper limit of the stretch-forming load is determined by the maximum tensile load that can be transmitted by the workpiece material and the angle  $\gamma$  between the sheet metal at the grippers and the direction of travel of the punch. The maximum transmitted tensile load  $F_{G,max}$  is obtained from the ultimate stress of the material  $S_u$ , the total width of the clamped sheet  $b$ , and the sheet thickness  $s$  [23.2]:

$$F_{G,max} = bsS_u \quad (23.2)$$

Neglecting frictional loads caused by the deformation, the punch load and the tensile load at the clamps are related as illustrated in Fig. 23.6:

$$F_p = 2F_s \cos \gamma \quad (23.3)$$

Frictional effects can be considered using a correction factor  $c = 1.2$ . The upper limit of the punch load can then be obtained by combining Eqs. 23.2 and 23.3:

$$F_{p,max} = 2cbsS_u \cos \gamma > F_p \quad (23.4)$$

The actual stress and strain distributions in simple stretch-formed components with rotational symmetry have been predicted theoretically by Woo [23.5] and Chakrabarty [23.6]. Good correlations with experiments using several different workpiece materials have been obtained. However, these results cannot be applied to components of irregular shapes.

### 23.1.2 Tangential Stretch Forming

In tangential stretch forming the deformation occurs in two distinct stages [23.7] to [23.10]:

- 1 The material is stretched up to its yield point in order to achieve uniform strains. If the sheet metal is not uniform, some portions of the sheet will start to yield before others. Plastic flow of the material in these areas will cause a strengthening due to work hardening until the whole blank is loaded into the plastic range, typically exceeding the yield strain independent of the material by 2–4% [23.10] to [23.12], sometimes even by 6% [23.13].
- 2 The loaded prestretched workpiece is brought tangentially into contact with the tool in such a way that there is no relative motion between the workpiece and the tool. The stretch-forming load is always tangential to the contour of the tool.

The stretch-forming load depends on the yield stress of the material and its thickness, the required strains, and the depth of the component. The applied force must therefore be controlled as a function of the angle of the clamping fixture in order to maintain a constant stress in the material. This is especially important for high-alloyed steels, which have a high yield strength ratio, in order to avoid overloads [23.12], [23.14] to [23.16]. After the workpiece has been brought into complete contact with the tool, the stretch-forming load is increased briefly to reduce spring-back.

### 23.1.3 Workpiece Materials

In addition to aluminum, magnesium, and their alloys, all ductile materials can be stretch-formed, ranging from carbon steels to high-alloyed steels, to acid- and temperature-resistant materials, such as titanium and its alloys, to special metals, such as niobium and beryllium [23.6], [23.13], [23.14].

The formability of a material in stretch forming is judged mainly based on the results of tensile tests (uniform elongation limit and fracture strain) and the Erichsen cupping test and on the strain-hardening exponent  $n$ . The higher the numerical values of these measurements, the better the material is suited for stretch forming. The test procedures have already been described in Chap. 18.

A summary of the tensile test results for several materials used for stretch forming is given in Table 23.1. Most of the materials can be formed at room temperature, but titanium and its alloys

**Table 23.1** Elongation at Fracture and Uniform Elongation of Some Materials Used for Stretch Forming

Material	Uniform elongation $e_{ub}$ , %	Elongation at fracture $e_t$ , %
Steel sheet, deep-drawing quality	25–35	50–60
Carbon steel, austenitic steel	50–60	70–80
Brass		
Soft	45–50	55–70
Hard		10–18
Aluminum		
Soft	25–30	30–50
Hard		5–10
Aluminum alloy		
Soft	10–30	10–40
Hard		5
Titanium, room temperature	10–20	40–50
Titanium alloy		
Room temperature	5–8	15–25
410 °C (756°F)	5–8	15–25
610°C (1125°F)		60
Magnesium		5–10
Magnesium alloy		5–10
Beryllium		
Soft		35–50
Hard		2–6
Fully hardened		1–15
Copper		
Soft		38
Hard		5–6
Copper alloy		
Soft		40–60
Hard		3–5

require elevated temperatures for forming. With the exception of pure titanium, which at room temperature behaves like a low-alloyed carbon steel, the formability of these materials at room temperature is too low.

The larger its uniform elongation is, the smaller is a material's tendency toward necking; that is, the larger is the deformation that can be obtained with stretch forming. If local necking can be tolerated in some components, then the fracture strain is also of importance in determining the formability.

The depth of the cup produced in an Erichsen test in which the flow of the material into the cup is prevented is a measure for the limiting strain in a biaxial state of stress. This value is directly applicable to the simple stretch-forming process. It is also comparable to the fracture strain in a simple tensile test. The greatest achievable depth in the Erichsen test depends on the condition of the material, the friction conditions, the surface finish, the sheet thickness, and the geometry. For this reason the sample size and the test conditions are standardized.

The work-hardening coefficient  $n$  is a measure of the increase of the plastic flow stress as the deformation process proceeds. The larger the  $n$ -value, the greater is the increase in flow stress and the smaller is the tendency toward necking. This means that a sheet-metal material having a large  $n$ -value is well suited for stretch forming.

#### 23.1.4 Workpiece Properties after Stretch Forming

Stretch forming causes an increase in strength due to work hardening of the material [23.11], [23.14]—the yield strength of automobile body parts increases up to 10% and their hardness increases up to 2% [23.12]. Compared to drawn components, stretch-formed components can withstand up to 30% higher loads applied normal to their surface [23.10].

There are no compressive stresses generated in stretch forming which could cause wrinkles. Stretching also reduces residual stresses which could cause local springback [23.11], [23.14]. The tensile loads eliminate springback by eliminating residual stresses of opposing directions which are frequently generated by other forming processes, such as bending. The stretch-formed component will not deform during trimming or welding. This effect is also utilized in stretcher levelling of extruded profiles (see Chap. 16).

Components produced by simple stretch forming are dimensionally less accurate than those produced by tangential stretch forming, in which process tight tolerances can be maintained. The reason for this fact is that in simple stretch forming the flow of the material is restricted by friction between workpiece and tool so that the stress distribution is not as uniform in the cross section [23.3], [23.14]. Components which are to be produced by stretch forming should not have protruding form elements since these require larger strains than the remainder of the workpiece.

#### 23.1.5 Friction and Lubrication

Friction forces are generated during simple stretch forming between the tool and the contacting workpiece. These friction forces reduce the strain of the workpiece in the direction of the applied load. The type of lubrication, or rather the magnitude of the coefficient of friction, influences the shear stresses at the interface between workpiece and tool, the tensile stresses in the plane of the sheet, and the local strains. Variations of the coefficient of friction can cause nonuniform stress distributions and, therefore, nonuniform local strain distributions. Sufficient uniform lubrication is essential for achieving maximum strains [23.3], [23.17].

There is no relative motion between the contacting tool and the workpiece in tangential stretch forming, and hence no frictional shear stresses are generated. Cracking of the sheet metal during the second phase of stretch forming is thus eliminated. However, any initially present cracks or flaws will become more obvious during stretching so that a quality-control check is already possible at this time [23.9].

Usually one uses the same lubricants in stretch forming as in deep drawing (see Chap. 20). For certain tool and workpiece material combinations other lubricants or procedures may be applicable: Stretch-forming tools made from wood can be covered with sheet metal in order to reduce the coefficient of friction [23.8]. Films of ice of 1.5–2-mm (0.06–0.08-in) thickness can give very low coefficients of friction ( $\mu = 0.015$ ) when used at temperatures of  $-2$  to  $-5^\circ\text{C}$  (30–

(23°F). Tools coated with special polymer films (such as PTFE) have very uniform friction conditions and allow more uniform sliding of the workpiece as compared with wooden or metallic tools. Stretch forming of workpieces of titanium or titanium alloys requires drawing oils with special additives because otherwise very large coefficients of friction are encountered [23.17].

### 23.1.6 Failure Modes

The amount of deformation that can be achieved in stretch forming is limited by necking and fracture of the workpiece material. Necking in simple stretch forming has been investigated by Keeler [23.18], Marciniak and Kuczyński [23.19], and others using rigidly clamped workpieces and various lubricants.

If the material necks or if it fractures before the desired workpiece geometry has been reached, then the uniform strain limit is too low relative to the required strain, or the frictional forces developed during deformation are too large. Three failure modes that can be distinguished are illustrated in Fig. 23.8 [23.20].

Cracks in the regions close to the grippers and other areas not yet in contact with the tool can result from excessive applied loads. These cracks occur only in materials with good formability. In addition, stress concentrations are present due to the action of the grippers, which can cause cracking of the material near or within the jaws. Since these cracks usually appear only toward the end of the stretch-forming process, the component may still be usable.

The other two failure modes occur in the region of the apex of the stretch-forming punch. Brittle materials fail because of brittle fracture since they conform only poorly to the shape of the tool. Ductile materials fail later because of necking in the apex region. Since necking is considered a failure in most components, only forming-limit diagrams are applicable, which are based on the strain at the beginning of necking (see Chap. 18).

If the required strains are small, visible slip bands may appear (see Chap. 20) since the material yields only in localized areas which are surrounded by areas loaded in the elastic range. These slip bands, often called Lüders' lines or stretcher's strain, occur only in materials having a very distinctive yield point [23.21].

Heat-treated aluminum sheet especially shows slip bands at very low strains (5%), which appear at an angle of 120° to each other (Fig. 23.9).

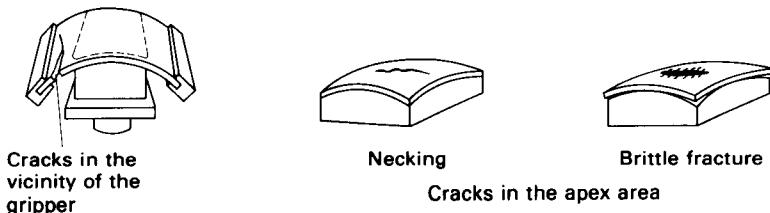


**FIG. 23.8** Failure modes in stretch forming. (After [23.20].)

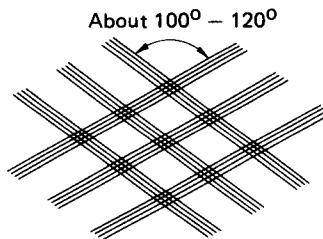


**FIG. 23.9** Slip bands due to stretch forming of heat-treated aluminum sheet metal.

### 23.1.7 Tooling for Stretch Forming

The choice of the tool materials depends on the geometry, the material, and the number of components to be produced. When stretch forming a small number of components from light metal alloys, the tools are often made from hardwoods—sometimes the tool is composed of individual wooden spars—and higher-stressed regions are reinforced with steel [23.2], [23.4].

Other workpiece materials can be stretch-formed using a wide variety of tool materials. For light work, tools made from wood, plastic wood, plastic-coated wood [23.22], concrete, plastics, or low-melting alloys, such as zinc alloys [23.4], [23.9], [23.11], [23.15], can be used. For heavier work and large numbers of components, tools are made from cast iron [23.6].

Stretch-forming of titanium and its alloys requires tools made from steel or ceramics [23.17]. Large tools for forming titanium parts, especially in the aircraft industry, are often heated with gas burners, while smaller tools are heated electrically with induction coils or conductively [23.9]. Steel tools are heated up to maximum temperatures of 550–650°C (1017–1197°F), while ceramic tools are heated to just below the transition temperature of the workpiece material [pure titanium 880°C (1611°F), titanium alloys 980–1030°C (1791–1881°F)] in order to achieve isothermal forming. The temperature of the workpiece is slightly higher than that of the tool.

When stretch-forming saddle-shaped components, wrinkles are often formed in the valley. In order to avoid such wrinkles, the tool is made much larger than the finished component [23.23]. Fig. 23.10 shows a typical example. The dashed line indicates the finished component. The blank [406 mm (16 in)] is wider than the tool [330 mm (13 in)] and is placed into the gripper jaws in such a manner that it extends beyond the tool on both sides. During stretch forming the blank contacts the tool first at the locations marked X. As the forming process continues, the extended portions of the blank acts to restrain the sheet metal from flowing freely into the saddle area. The effect of this arrangement is similar to the action of draw beads when drawing body panels for automobiles or parabolic and conical components.

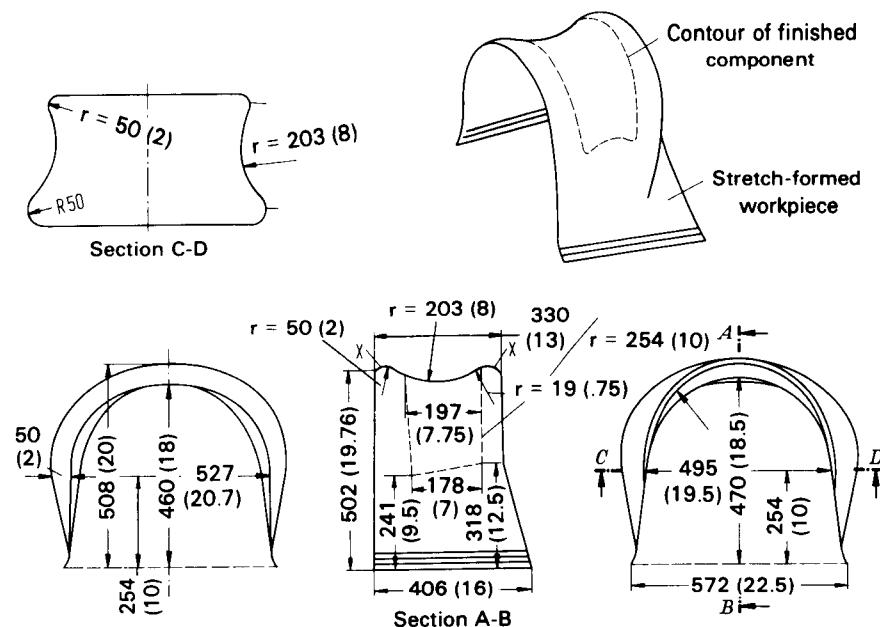


**FIG. 23.10** Stretch forming of a saddle-shaped component made from steel X10CrNiNb189 ( $\approx$  AISI 347). Dimensions are in mm (in). (After [23.23].)

### 23.1.8 Equipment

#### Machines for Simple Stretch Forming

Machines for simple stretch forming usually are special-purpose presses. The tool is mounted on the bed which can be lifted hydraulically by an electrically driven hydraulic pump. It is also possible to actuate the hydraulic bed with water pressure. The grippers are mounted on guided slides such that they can also rotate. On larger machines the grippers are divided into several individually movable jaws. All of the jaws can therefore adjust independently to the motions of the punch and the workpiece.

The distance between the opposing jaws is at least 1–1.5 m (39.4–59.1 in), but it may also be considerably larger, up to 5 m (197 in). The widths of the blank sheets are between 1 and 4 m (39.4 and 157.5 in).

Much larger sheets of the type used in the aircraft industry can be stretch-formed when several presses are placed side by side and operated hydraulically in unison. The working width can thereby be increased severalfold.

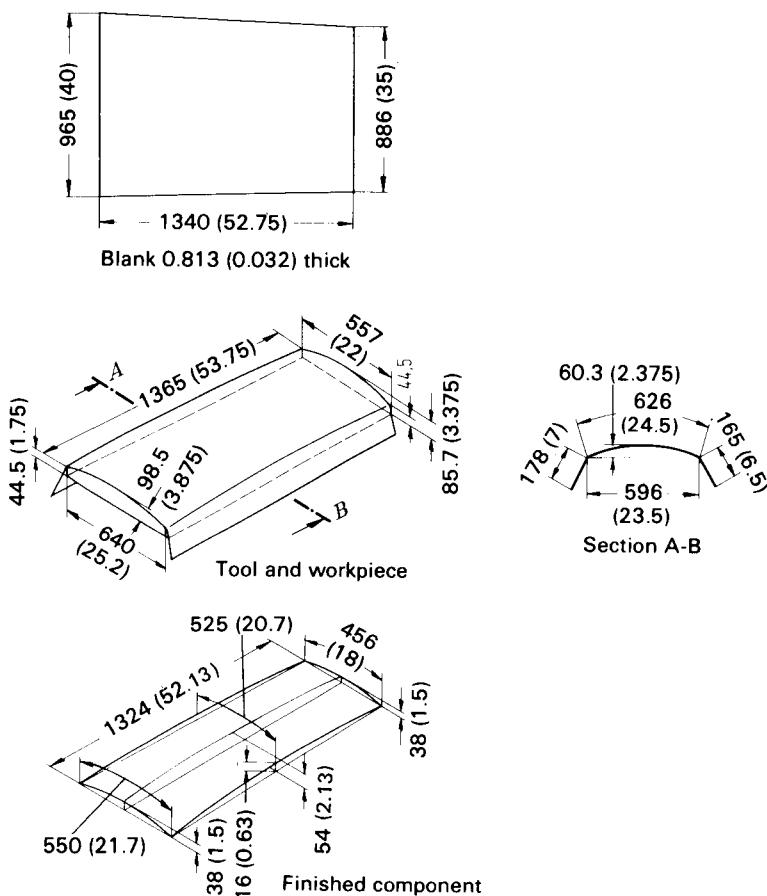


FIG. 23.11 Component made from aluminum alloy AlCuMg2 (AA 2024) by simple stretch forming. Dimensions are in mm (in). (After [23.23].)

Fig. 23.11 shows a workpiece made from aluminum alloy Al Cu Mg 2 (AA 2024), which was produced by simple stretch forming [23.23]. The component has little curvature and was formed from a trapezoidal blank which was gripped along the nonparallel sides. The figure shows the blank, the tool with the workpiece after forming, and the finished, trimmed component.

In order to produce components with compound curvature, that is, for components which require forming in the opposite direction from the curvature of the punch, an external die or a dual-acting press is necessary [23.4], [23.15].

### Machines for Tangential Stretch Forming

Sheet metal of up 15 m (590 in) in length and 9 m (354 in) in width can be processed by tangential stretch forming with a maximum applied force of 5000 kN (561 ton) [23.9], [23.24].

Presses for tangential stretch forming are either single-acting mechanical and hydraulic presses with the clamping fixtures mounted on the bed [23.10], [23.11], [23.16] or, especially for large sheets, specially designed presses. These machines have a hydraulic drive such that the forming process can be adjusted continuously to optimal values. The clamping force and the stretching force can be continuously controlled with hydraulic valves. The magnitude of the setting force can also be controlled [23.11]. The stretching force is controlled as a function of the position and orientation of the grippers. In order to maintain a desired amount of strain in the workpiece, presses with controlled stroke are preferred over machines with controlled force.

Tangential stretch forming of components with compound curvatures is frequently necessary in the automobile industry. Fig. 23.12 shows an example. First the sheet is stretched at least 2% by moving the grippers toward the outside (Fig. 23.12a), and then the workpiece is brought tan-

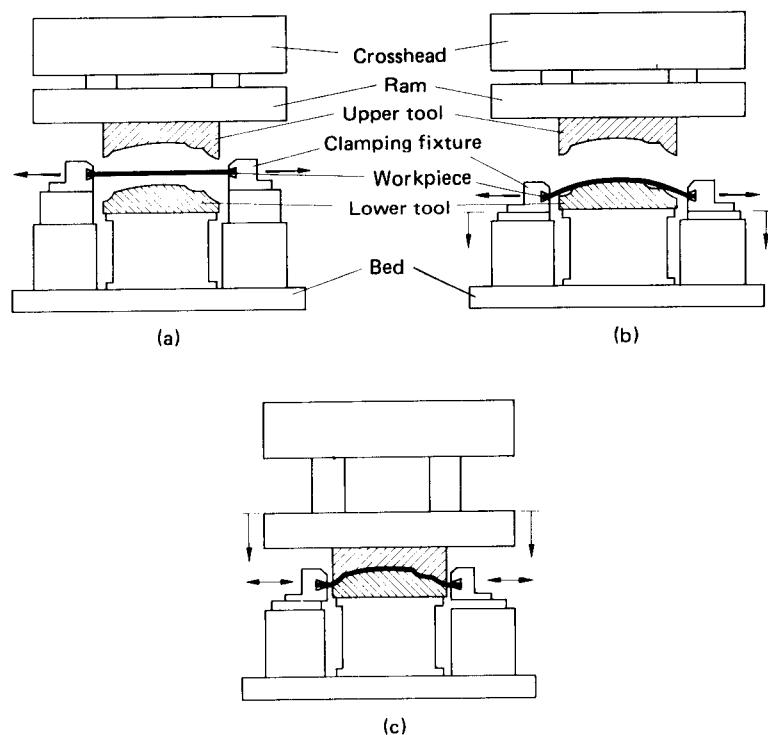
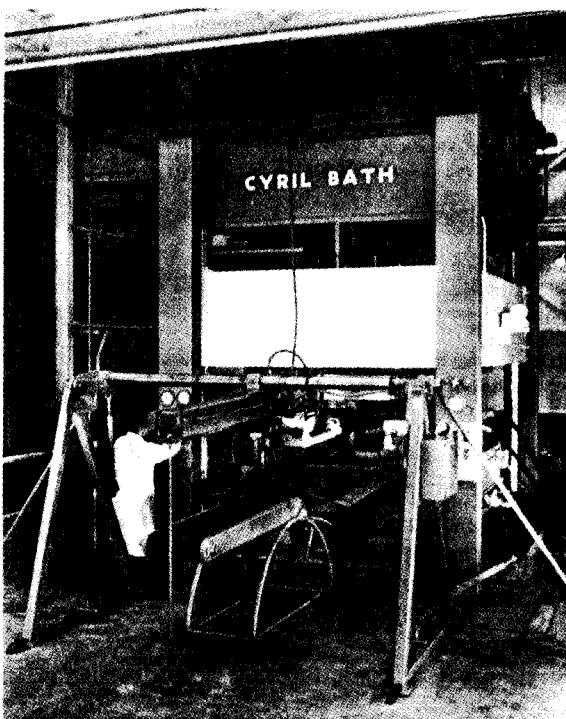
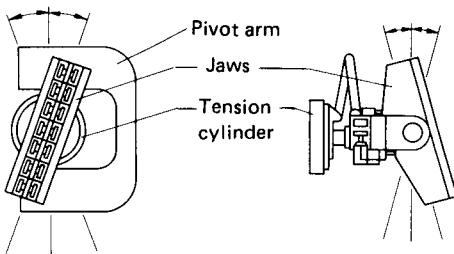


FIG. 23.12 Stages in tangential stretch forming with die, system Cyril Bath.



**FIG. 23.13** Stretch-forming press, system Cyril Bath. Maximum ram force—2250 kN (250 ton). (*Courtesy of Cyril Bath Company.*)

gentially into contact with the lower tool by simultaneously lowering the grippers (Fig. 23.12b). Because of the required complexity of the finished part, the sheet does not contact the tool everywhere and an upper tool (die) is required. The motion of this upper tool (Fig. 23.12c) must be closely correlated with the lowering of the grippers in order to avoid excessive local strains. As the upper tool lifts off again, the grippers also rise to their initial position, thus lifting the workpiece from the lower tool [23.25]. Fig. 23.13 shows a stretch-forming press which uses this principle. The press has a maximum punch load of 2250 kN (250 ton) and a clamping force of 770



**FIG. 23.14** Degrees of freedom of a gripper. (*After [23.26].*)

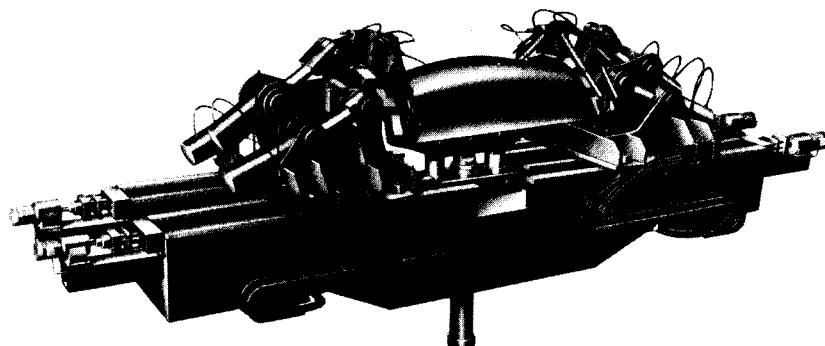


**FIG. 23.15** Hydraulic stretch-forming press, type Loire. (Courtesy of Ateliers et Chantiers de Bretagne.)

kN (86 ton) with a stroke of 60 mm (2.4 in) per cylinder. The press is designed with four columns for better access to the tooling.

In contrast to the stretch-forming press just described, the grippers for specially designed machines for tangential stretch forming can both rotate and swivel in order to accommodate any tool shape. Fig. 23.14 shows the degrees of freedom of these clamps [23.26]. Special presses for tangential stretch forming clamp the sheet in either a vertical or a horizontal position; other machines use special procedures.

Presses with horizontal sheet-metal clamping carry the tool mounted on the bed which can be tilted up to  $15^\circ$  in each direction. Fig. 23.15 shows such a hydraulic press for tangential stretch forming with horizontal sheet-metal clamping, which can handle sheets with lengths of up to 9 mm (354 in) and widths of up to 2.5 m (98 in). Using a tensile force of 1350 kN (150 ton) for each clamping arm, the total load on the bed is 2700 kN (300 ton). The maximum stroke of each clamping arm is 1830 mm (72 in).

Tangential stretch-forming presses with vertical sheet-metal clamping are used to produce either long and narrow or short and wide components. Fig. 23.16 and 23.17 illustrate the principle of such a machine. The machine bed (1 in Fig. 23.16) carries the pivoted arms (2) on which the adjustable clamping devices (4) are mounted. The arms are actuated by hydraulic cylinders (3) and can rotate independently through more than  $90^\circ$ , as indicated in Fig. 23.17. Incorporated into the clamping devices are the hydraulic cylinders used to stretch the sheet. The cylinders can pivot with respect to the centerline of the arms by  $25\text{--}30^\circ$  (Fig. 23.16). The position of the clamping devices along the rotating arms can be varied to give a maximum distance of over 6 m (236

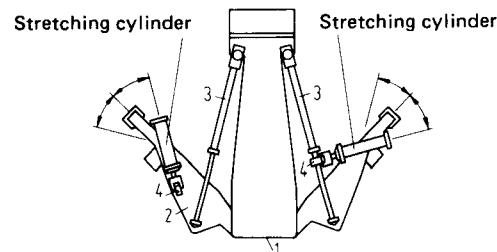


**FIG. 23.16** Pivoting arrangement of stretching cylinders. 1—bed; 2—pivoted arms; 3—hydraulic cylinder; 4—clamping devices. (After [23.26].)

in) between grippers in the largest machines built to date. Blanks of up to 1.2 m (47 in) in width can be accommodated [23.15], [23.26].

Fig. 23.18 shows a tangential stretch-forming machine with vertical sheet-metal clamping. It has independent motion of the two arms and can exert a maximum tensile force of 550 kN (61.7 ton) over a stroke of 760 mm (30 in) per cylinder. The largest width of the blank is 765 mm (30.1 in), and the maximum distance between grippers is 6.1 m (240 in).

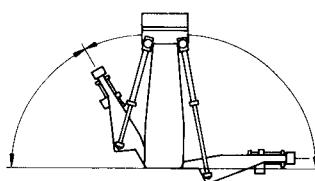


**FIG. 23.17** Independent rotation of swivel arms. (After [23.26].)

of sufficient magnitude to exceed the yield strength of the material. Because of the mobile mounting of the grippers, the tensile force is always applied in a tangential direction to the tool. Deformation takes place continuously [23.14].

Using a reversible table with several tools that can be moved during the stretch-forming process, S- and W-shaped workpieces can be produced. Examples are shown in Fig. 23.20. Frequently, profiled blanks are used for these components. The forming process for the workpiece in Fig. 23.20a is shown in Fig. 23.21. The straight blank is clamped between the grippers and then stretched. As the table is turned, the workpiece contacts tool 1. Tool 2 is now advanced until it makes contact with the workpiece. The table rotation is then reversed, and the first arc is formed. The second arc is formed similarly.

Stretch-forming machines with revolving tools are also made with horizontal sheet-metal clamping (Fig. 23.22). These machines are suited for sheet metal with a width of more than 3.5 m (138 in) and can produce large and small curvatures alike. The tensile force can reach 20,000 kN (2240 ton).

The tool of the stretch-forming machines discussed up to this point has been mounted in a fixed position on the bed. Fig. 23.19 shows a machine that employs a different principle: the tool revolves along the workpiece. The workpiece is held at its ends by grippers and passes through the hydraulic stretch-forming unit. The tool is mounted on a slide on a turntable. The slide also carries one of the grippers. As the table is turned, the tool moves against the workpiece. At the same time a tensile load is maintained with the second gripper, which is

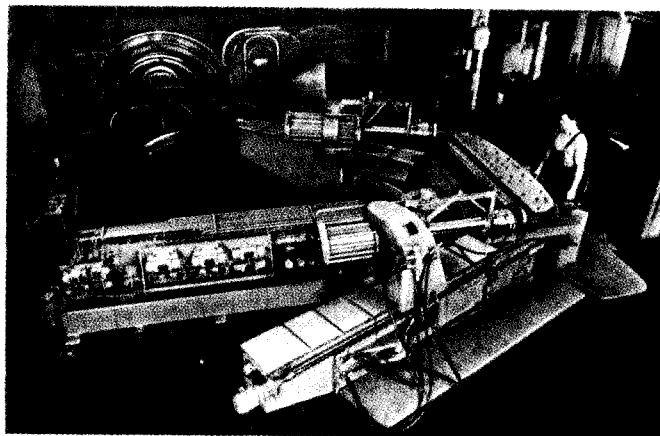


**FIG. 23.18** Press for tangential stretch forming, system Schuler-Hufford. With vertical sheet-metal clamping and a maximum force of 550 kN (61.7 ton) per stretching cylinder. (Courtesy of L. Schuler.)

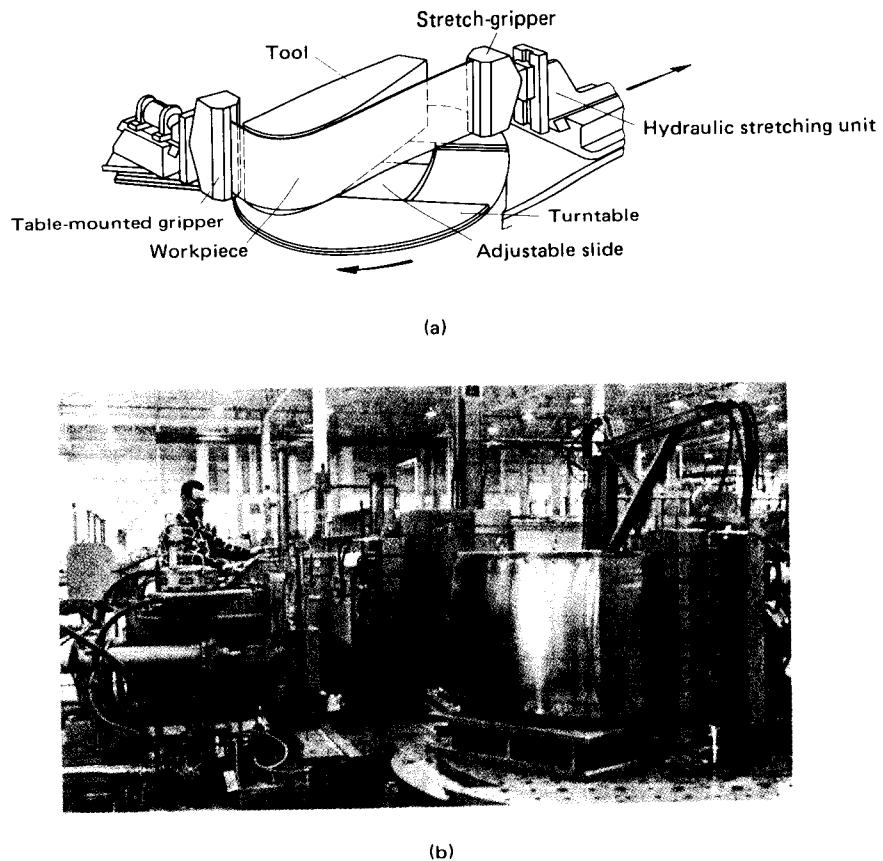


**FIG. 23.19** Hydraulic stretch-forming machine, system Cyril Bath. With revolving tool and vertical sheet-metal clamping. (a) Schematic arrangement. (b) Machine with maximum force of 450 kN (50 ton) per stretching cylinder. (Courtesy of Cyril Bath Company.)

### Clamping Devices

Clamping devices are preferred which increase the clamping force automatically as the tensile force increases. The grippers should hold the workpiece without producing additional stress concentrations, they should be adjustable over a wide range, and they should be able to rotate to maintain alignment with the workpiece. If profiled blanks are formed, grippers with profiled jaws are used [23.2], [23.9], [23.13].

To reduce the stress-concentration factor when forming titanium parts, the workpiece is coated with aluminum where it is placed into the jaws [23.17]. Possible clamping techniques include (Fig. 23.23):

- Clamping roller with wedge
- Eccentric lever
- Conical yaws which are closed mechanically or by a hydraulic cylinder
- Special designs [23.2], [23.12], [23.13]

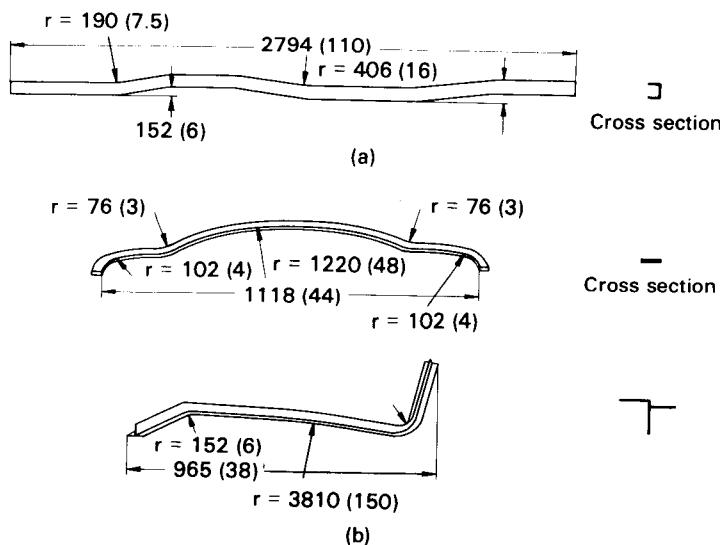


**FIG. 23.20** Components formed by stretch forming. (a) Automobile frame. (b) Aircraft components.

Dual eccentric grippers guarantee proper clamping independent of the thickness of the sheet metal. In mass production hydraulically operated wedge-shaped yaws are frequently used.

In place of few large grippers, several smaller ones are sometimes used which are tied together through joints. Each element contacts only a small part of the total clamping length. The element can therefore conform to the shape of the tool and can adjust to the shape of the workpiece [23.4], [23.9], [23.13].

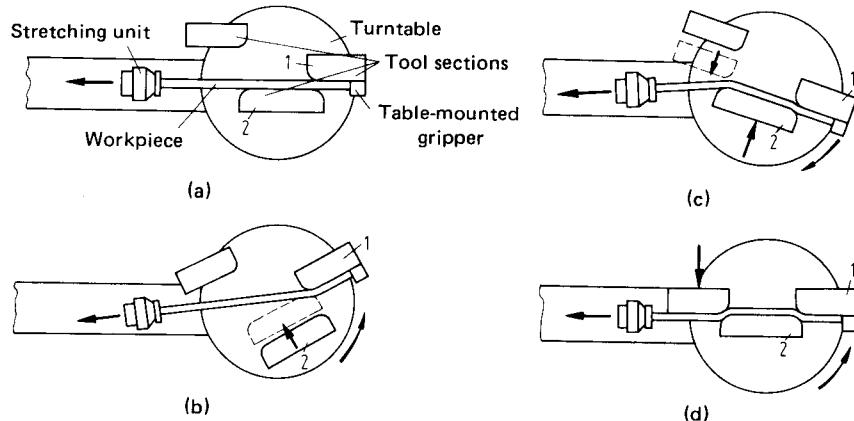


**FIG. 23.21** Manufacture of S- and W-shaped workpieces by tangential stretch forming.

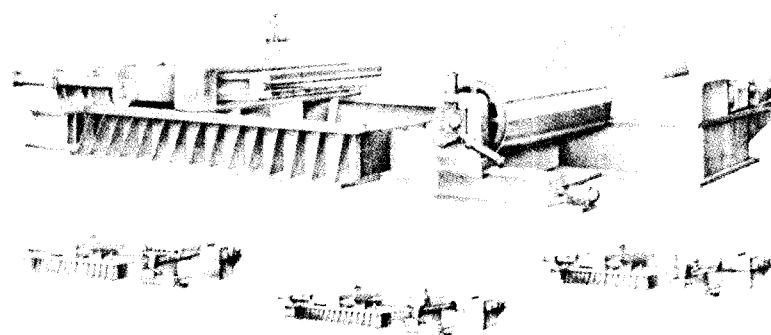


**FIG. 23.22** Hydraulic stretch-forming machine, system Cyril Bath. With revolving tool and horizontal sheet-metal clamping. (*Courtesy of Cyril Bath Company.*)

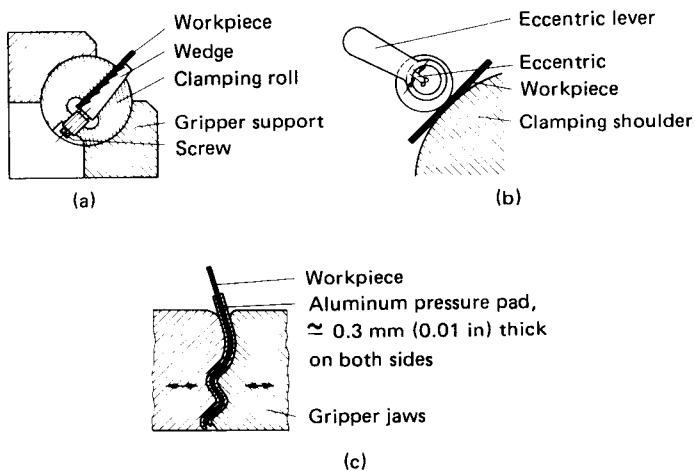


**FIG. 23.23** Gripper designs. (a) Clamping roller with wedge. (b) Eccentric lever. (c) Special design. (*After [23.2], [23.17].*)

## 23.2 EMBOSsing

Embossing is a recessing process which uses rigid tools (Fig. 23.2b). It has the characteristic that for every recess on one side of the sheet there is a corresponding rise on the other side. The size of the recess is small compared to the dimensions of the workpiece.

The most frequently used embossing process is the embossing of beads. The beads

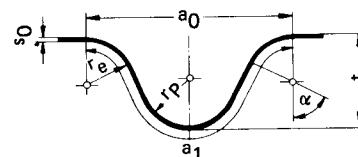


**FIG. 23.24** Geometric relationships for semicircular beads. (*After [23.27].*)

## 23.20 SHEET-METAL FORMING

increase the strength of the workpiece with respect to elastic and plastic deformations due to bending or torsional loads by increasing the moment of inertia of the cross section. For a given bead shape and fixed sheet thickness, the magnitude of the strength increase depends only on the depth of the bead.

For semicircular beads the following geometric inequality must be satisfied (Fig. 23.24):

$$a_0 - 2r_e > 2(r_p + s_0) \quad (23.5)$$

where  $a_0$  = width of die

$r_e$  = entrance radius

$r_p$  = punch radius

$s_0$  = initial sheet thickness

Only the material within the width of the die  $a_0$ , takes part in the deformation process since the flow of material from the sides is restricted. The larger the entrance radius is made, the more uniform will be the wall-thickness reduction in the cross section of the bead. This means that a larger mean tangential strain  $\epsilon_t = \ln(a_0/a_1)$  and therefore a greater depth can be achieved. The tangential strain is not constant over the cross section of the bead [23.27].

The greatest depth of the bead can be determined from Fig. 23.25 or from the equation [23.27]

$$t_{\max} = cna_0$$

where  $n$  is the strain-hardening exponent and  $c = 1.5$  for steel and 1.1 for copper and aluminum.

Since the tools used for embossing use only a single stroke, only single-acting presses are needed. In most applications single-acting mechanical presses are utilized, but hydraulic presses are also used. In addition, drop hammers and their associated tools are sometimes used to form beads [23.7].

## 23.3 EXPANDING AND BULGING

Expanding is a forming process which is used mainly to produce containers, skirts, drums, automobile body parts, and so on. Circular or oval components can be formed as well as polygonal hollow components. The preforms to be expanded are formed partly by other forming processes, such as deep drawing, or are manufactured from sheet metal by bending into cylinders, cones, or prisms and by welding of the seams [23.28], [23.29]. If the second method is used to produce the preform, it is important that the seam be placed into the expanding tool in a fixed orientation in order not to damage the tool and to produce flawless components.

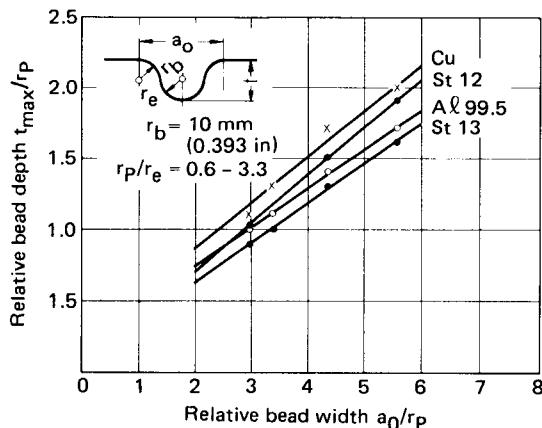


FIG. 23.25 Relationship between relative bead width  $a_0/r_p$  and relative bead depth  $t_{\max}/r_p$ . (After [23.27].)

### 23.3.1 Expanding with Rigid Tools

#### *Expanding with Plug*

Expanding a preform with a plug causes the workpiece to expand at its ends or along its full length. It is not possible to expand only the center portion of the blank. The plug has a conical or spherical shape (Fig. 23.3a). The preform is a hollow workpiece which may or may not be closed at one end. If the plug is pulled through the part (Fig. 23.3a, right), then both ends of the part must be open. If the plug is pushed into the part, the workpiece may be open at both ends (Fig. 23.3a, center), or it may be closed at one end (Fig. 23.3a, left).

#### *Expanding with Spreading Tool*

In contrast to the expanding process with a plug, expanding with a spreading tool can produce workpieces with expanded center portion only. Preforms with or without a bottom may be used. The segmented parts of the tool are pushed toward the outside by a wedge or a cone (Fig. 23.3b) and generate the workpiece shape by pressing the workpiece into a die [23.7], [23.28] to [23.30].

Parts with rotational symmetry require that the external die be split in halves, while components of arbitrary shape require a die having several sections. The segments of the tool are returned to their initial position by springs, such that the tool can be retracted easily from the finished workpiece.

The quality of the formed components can be improved by covering the tool segments with a rubber boot (Fig. 23.3b, right). The rubber boot serves to transmit the pressure more evenly and prevents imprints by the edges of the segments [23.2].

Typical strains encountered in expanding are about 15% [23.28], [23.31]. During expanding, the pressure is applied evenly over the circumference such that the wall-thickness reduction is uniform and a shape tolerance of 0.2–0.3% of the diameter can be achieved [23.7]. With special care it is possible to reduce the diameter tolerance, including all shape tolerances, to 0.05 mm (0.002 in) [23.28].

Expanding with spreading tools is used in the United States to produce complete containers, skirts, and so on, for food-processing machines, stoves, and refrigeration units. The preform is produced mainly by bending and welding of a cylinder. It is also possible to use closed cylindrical or polygonal hollow preforms which can be expanded in such a manner that several components of equal or differing shapes are produced simultaneously. Examples of the latter are automobile body parts [23.28] to [23.31].

Fig. 23.26 illustrates as an example the expanding of a ring made from X10CrNiTi189 ( $\approx$  AISI 321/321H) [23.23]. The ring was manufactured by bending and welding. The tool consists of four segments which are held together by springs. The die is split into two halves which are held in the open position by compression springs. During the stroke of the machine, a slider first closes the die, then the wedge spreads the tool and presses the ring into the external die. The resulting workpiece is not completely circular since it is only stretched between the segments of the tool. The process is therefore repeated after the workpiece has been rotated 45°. This second stage produces a workpiece which is uniformly circular and ready for use.

Special machines are frequently used for the mass production of components expanded with spreading tools [23.28], [23.29], [23.31]. Fig. 23.27 shows the schematic diagram of such a machine with a maximum tensile force of 15,000 kN (1680 ton) acting on the wedge [23.7]. The preform is slipped over the contracted segments of the inner tool with as little clearance as possible. Radially distributed around the inner tool there are typically four exterior radial slides to guide external die segments which match the inner tool. The outer die segments are closed and locked and form a continuous surface enclosing the workpiece. A hydraulic cylinder pulls the wedge down, which pushes the inner tool segments radially out. The workpiece is stretched and formed between the inner tool and the outer die. Then the inner tool segments are retracted by releasing the wedge and the outer die segments are opened to release the workpiece.

If several components are produced from a single preform, then the formed workpiece can be slit vertically following the deformation process by slitting knives embedded into the outer die segments. Suction cups, also embedded into the die segments, hold the workpiece sections in place and release them only after the die has been opened completely. There are openings in the machine bed through which the sections can slide out of the machine to the next work stations.

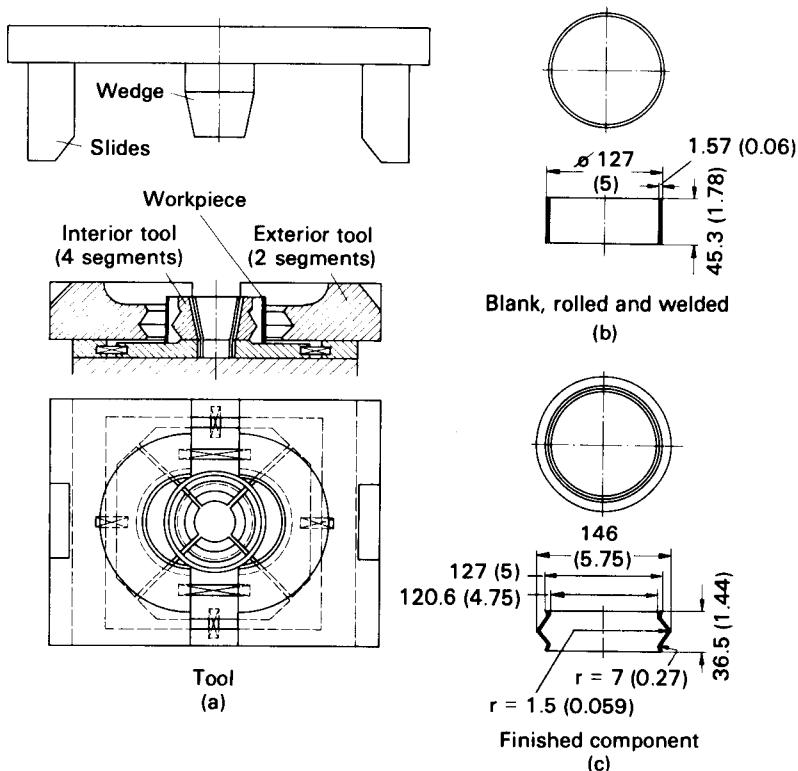


**FIG. 23.26** Tooling to expand a ring made from X10CrNiTi189 ( $\approx$  AISI 321/321H). (a) Tool. (b) Preform, rolled and welded. (c) Finished component. Dimensions are in mm (in). (After [23.23].)

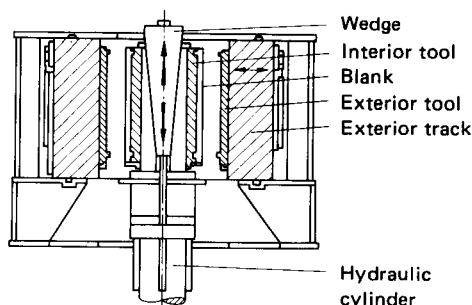


**FIG. 23.27** Schematic diagram of expanding machine. (After [23.29].)

The arrangement of the hydraulic cylinder below the tooling has the advantage of easing the loading of the preforms into the machine. Since the preform has been manufactured by bending and welding, it can easily be fed to the expanding machine by automatic feeding devices.

### **23.3.2 Expanding with Elastic Tools**

Expanding with elastic tools can be grouped together with expanding with rigid tools as a dry bulging process. The pressure necessary to cause workpiece deformation is transmitted by a compliant medium, such as uncured and cured rubber or cork. These materials have been quite successful in spite of their high wear rate and cost. Fig. 23.3c, left, shows a rubber pad which is compressed by a recessed punch and causes bulging without the sharp edges of a segmented tool.

The wear of the rubber can be reduced by using the arrangement shown in Fig. 23.3c, center. The punch presses on a thick-walled hollow rubber cylinder which can move over a core. The core is guided in the punch. If both the punch and the core have conical faces (Fig. 23.3c, right), bulging with a conforming rubber ring is improved [23.2], [23.23].

Rubber punches can be used economically only for small workpieces up to 100 mm (3.94 in) in diameter. Friction between the rubber punch and the workpiece increases the required forces [23.7]. Friction also causes the workpiece to flow axially into the die. This causes a shortening of the workpiece whose magnitude depends on the workpiece material. Soft stainless steel contracts the most (12% for cylindrical components) and brass the least (2%).

The greatest possible circumferential strain, that is, the strain at which cracks begin to appear at the bulge, depends on the yield strength of the material at the start of expanding, on its strain-hardening exponent, and on the amount of friction between the rubber and the workpiece. Soft stainless steel allows the greatest strains of up to 66%. The values are smaller for aluminum (12%) since aluminum shortens by only 4% in the axial direction compared to 12% for steel because of different friction conditions.

### **23.3.3 Bulging with Working Medium**

#### **Bulging Using Granular Solids as Working Medium**

In these processes steel or rubber spheres or sand are used as the working medium. A rounded punch pushes the spheres toward the outside and thus bulges the workpiece (Fig. 23.3d). The use of rubber spheres has not been successful since the heat generated by friction tends to destroy the rubber spheres very quickly. Additives to reduce friction, such as talcum powder, are not effective. Since the rubber spheres also tend to stick together, they cannot be removed easily from the finished part and they are almost useless for the next workpiece. Steel shot generally leaves imprints which are sometimes even desired, such as for household and decorative items.

Filling the working medium into the workpiece and removing it is time-consuming and makes these processes awkward to use, and therefore they are only applicable for very small production lots.

#### **Bulging Using Fluids as Working Medium**

In addition to the granular solids, fluids can be used as working medium for bulge forming. Possible fluids are oil, water, and others.

The pressure is generated by pushing the punch into the fluid. The workpiece is placed in a sectioned die and then either it is filled with the fluid or the fluid is fed through the punch (Fig. 23.3e, upper left). The ring seal on the moving punch is subject to substantial wear and is frequently replaced by an external tube (Fig. 23.3e, upper right) which is guided by the punch. The additional pressure on the rim of the workpiece aids the bulging process. The rim should be flanged in order to prevent cutting the seal. Fig. 23.3e, lower left, shows a rubber punch which simultaneously acts as a seal and generates the forming pressure. The reciprocating punch continuously pumps small amounts of fluid into the increasing cavity until the final workpiece geometry is reached.

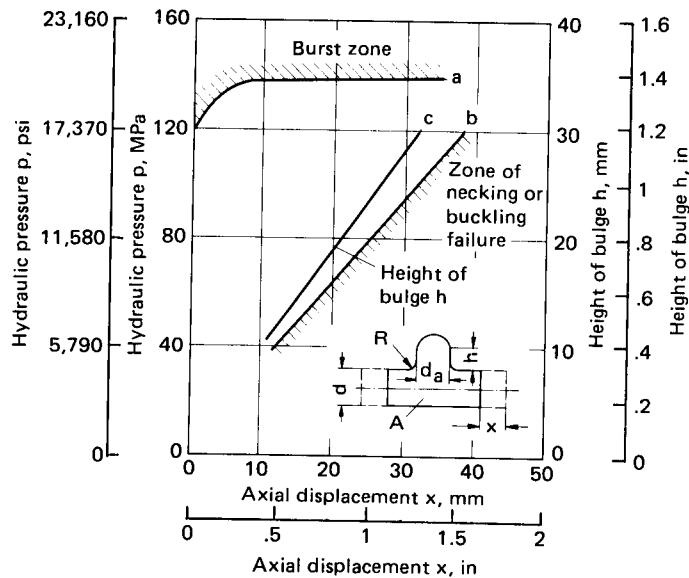


**FIG. 23.28** Forming diagram of asymmetrical bulging. Material—C 22 (AISI 1020); tube diameter  $d = 40$  mm (1.6 in), wall thickness  $s_0 = 2$  mm (0.078 in), diameter of branch  $d_b = 30$  mm (1.2 in). (After [23.34].)

Because of the uniform pressure distribution, the workpiece material begins to flow first in places where the wall thickness and the material strength are lowest. A local bulge frequently results, which greatly increases the danger of forming a crack. The processes shown in Fig. 23.3e, upper and lower left, are therefore used only to form small bulges. The use of a water bag (Fig. 23.3e lower right) reduces the danger of forming a local bulge because of variations in wall thickness and material strength [23.2], [23.26], [23.32].

Hydraulic bulging in which the hydraulic pressure is generated by a pump and a pressure intensifier is used industrially to form bulge fittings with one, two, or more branches in arbitrary directions [23.33], [23.34]. In most cases, the hydraulic pressure is augmented by a mechanically applied axial force on the workpiece. The axial force pushes the workpiece material into the deformation zone such that larger strains can be achieved. Fig. 23.28 shows the relationship between the axial distance  $x$ , the hydraulic pressure  $p$ , and the height of the bulge. The hydraulic pressure must be between curves  $a$  and  $b$ . If the pressure exceeds curve  $a$ , the bulge will crack. Pressures below curve  $b$  cause necking or buckling. Whether the workpiece necks or buckles depends on the shape of the workpiece and on its material. The height of the bulge is roughly proportional to the axial distance  $x$ . The slope of curve  $c$  depends on the diameter  $d$ , the length, and the material of the tube [23.34].

### 23.3.4 Equipment

Most bulging processes require only single-acting presses. Only the process shown in Fig. 23.3e, upper right, requires a double-acting press or a special fixture. In general both mechanical and hydraulic presses can be used. However, bulging with a water bag (Fig. 23.3e, lower right) and bulging with granular solids (Fig. 23.3d) are performed only on hydraulic presses [23.35].

Special machines are needed for liquid bulge forming [23.34]. Fig. 23.29 illustrates their schematic design. The die cavity is closed by a maximum load of 13,000 kN (145 ton). The pressurized fluid is fed into the workpiece through the hollow punch from a pressure intensifier. The pressure

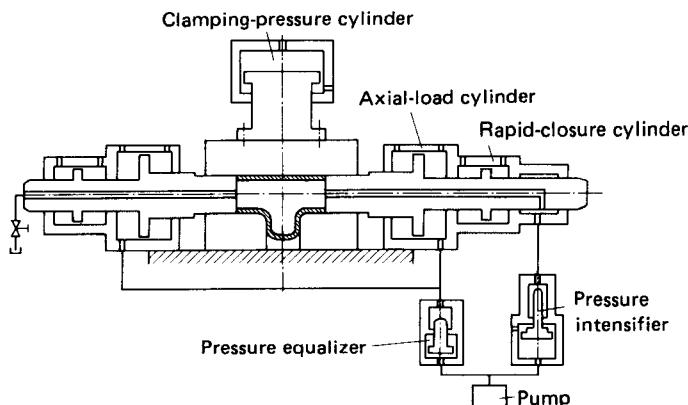


**FIG. 23.29** Schematic diagram of liquid bulge-forming press with direct pressure application to workpiece. (After [23.34].)

in the interior of the workpiece reaches  $100\text{--}300 \text{ N/mm}^2$  (14.5–43.5 ksi). Two differential axial pistons, which are connected via a pressure equalizer, deliver an axial force of 7000 kN (785 ton) to the workpiece. These pistons must be accelerated rapidly in order to maintain the axial seal at both ends of the tube.

### 23.3.5 Comparison of Bulging Processes

Reduction of the axial length of the workpiece is relatively small for the wet bulging processes shown in Fig. 23.3e. There is no relative motion between the fluid and the workpiece, and therefore there are no frictional forces generated which could feed additional material into the deformation zone. The processes using elastic tools (Fig. 23.3c) or granular solids (Fig. 23.3d) produce greater reductions in the workpiece caused by the friction between the punch and the workpiece. Because of the additional material in the deformation zone, the achievable circumferential strains are larger for the latter processes [23.35] than for the wet bulging processes.

The disadvantages of the expanding process with spreading tools (Fig. 23.3b), namely, a shape which is not precisely circular and the imprints of the sharp edges of the tool segments, are balanced by the disadvantages of the other processes, namely, wear of the seals and the rubber pads.

## 23.4 STRETCHING

### Elongating

Elongating is a stretching process to increase the length of the workpiece in the direction of the applied force (Fig. 23.4a, left). The direction of the applied force in the workpiece does not necessarily coincide with the direction of the force generated by the machine (Fig. 23.4a, right). Elongating can occur uniaxially and for sheet metal also biaxially. This process is commonly used to achieve prescribed workpiece dimensions.

### Stretcher Levelling

Stretcher levelling is used to eliminate bends in rods, profiles, and tubes as well as wrinkles in sheet metal (Fig. 23.4b). The workpiece is gripped by jaws and stretched usually by means of hydraulic cylinders.

The tensile force first acts on the locally shortened areas and causes material flow locally before

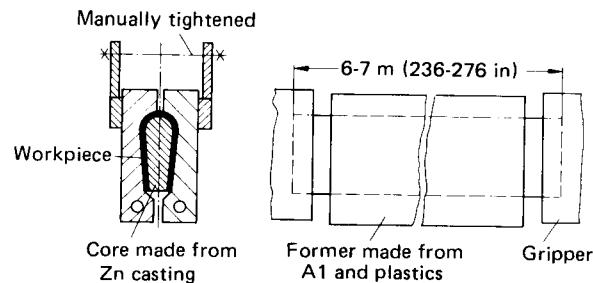


**FIG. 23.30** Stretcher levelling of covers for stabilizers made from AlCuMg 2 (AA 2024).

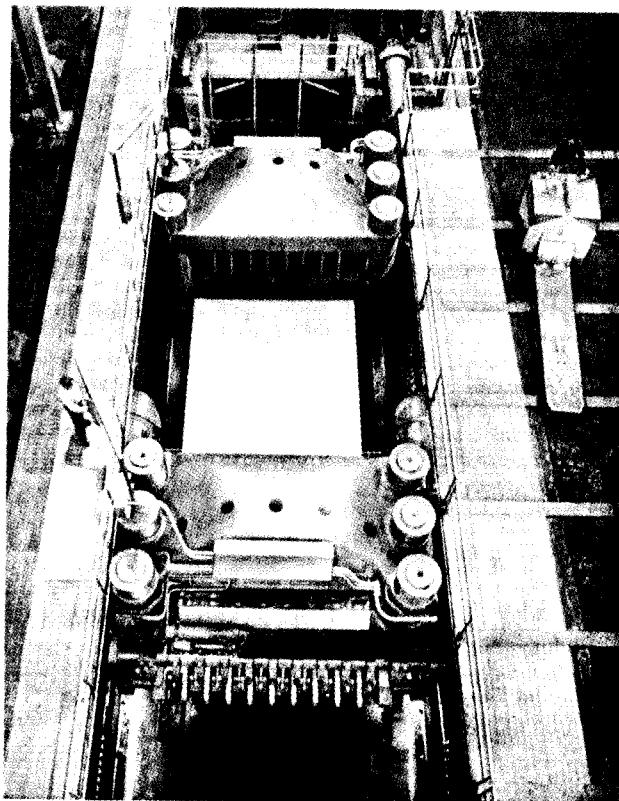


**FIG. 23.31** Sheet- and plate-stretching machine with maximum force of 136,000 kN (15,250 ton). Maximum sheet length—18.3 m (720 in); maximum sheet width—4 m (157 in); maximum sheet thickness—152 mm (6 in). (Courtesy of Hydraulic GmbH.)

the full tensile force has been applied. Because of the material flow, the material is strengthened locally. The applied force is increased until the complete cross section has yielded. A plastic strain of 1–2% is generally quite sufficient for stretcher levelling.

Fig. 23.30 shows an example of stretcher levelling for the reduction of residual stresses. The preformed parts with a length of 6–7 m (236–276 in) are made from AlCuMg 2 (AA 2024). They are placed over a core made from a precision zinc-alloy casting and into a bending fixture made from light metal coated with a polymer. The bending fixture is closed and tightened by hand. The bent profile is then elongated by 3% such that the profile sets permanently.

### Machines

Machines for stretching generally use mechanically or hydraulically activated gripper jaws mounted horizontally and pivoting. The maximum length between grippers is about 20 m (787 in). For stretcher levelling of profiles most machines are equipped with an antitwist device.

Stretching machines for sheet metal can produce up to 136,000 kN (15,250 ton) (Fig. 23.31). This force is sufficient to stretch sheets having a maximum cross-sectional area of 413,000 mm<sup>2</sup> (640 in<sup>2</sup>). The largest sheet thickness is 152 mm (6 in). The stroke of the machines is such that workpieces of maximum length can be elongated by 7% [23.36].

### REFERENCES

- 23.1 DIN 8585: "Fertigungsverfahren Zugumformen (Manufacturing Process—Tensile Forming)," 1970.
- 23.2 Oehler, G., and Kaiser, F.: *Shearing, Blanking, and Drawing Tools (in German)*, 4th ed. Berlin/Göttingen/Heidelberg, Springer, 1962, pp. 467–487.
- 23.3 Panknin, W.: "Special Methods for Deep Drawing," in *Basic Principles of Plastic Deformation of Metals (in German)*, Düsseldorf, Verlag Stahleisen, 1966, pp. 489–503.
- 23.4 VDI Richtlinie 3140: "Streckziehen auf Streckziehpressen (Stretch Forming with Stretch-Forming Presses)," Düsseldorf, VDI-Verlag, 1954.
- 23.5 Woo, D. M.: "The Sheet Forming Test," *The Engineer*, **222**, 1965, pp. 876–880.
- 23.6 Chakrabarty, J.: "A Theory of Stretch Forming over Hemispherical Punch Heads," *Int. J. Mech. Sci.*, **12**, 1970, pp. 315–325.
- 23.7 Ebertshäuser, H.: *Technology of Sheet-Metal Working (in German)*, Düsseldorf; Michael Trötsch Verlag, 1967, pp. 24–28.
- 23.8 Möhrlin, W.: "The Basic Deep-Drawing Methods." (in German), *Ind. Anz.*, **84**, 1962, pp. 1901–1903.
- 23.9 Kursetz, E.: "Forming of Sheet Metal and Profiles on Stretch-Forming Machines" (in German), *Maschinenmarkt*, **71**, 1965, pp. 21–24.
- 23.10 Kursetz, E.: "Combined Stretch Forming and Deep Drawing" (in German), *Maschinenmarkt*, **75**, 1968, pp. 1368–1370.
- 23.11 Bath, C.: "Stretch Forming of Automobile Body Parts" (in German), *Werkstatt u. Betr.*, **98**, 1965, pp. 143–144.
- 23.12 Wick, C.: "Stretch Forming. Better Parts, Lower Costs," *Machinery*, **75**, 1968, pp. 96–99.
- 23.13 Sanson, M.: "Sheet-Metal Working with Stretch-Forming" (in German), *TZ Prakt. Metallbearb.*, **61**, 1967, pp. 147–149.
- 23.14 Krauss, W.: "New Methods for Forming Sheet Metal and Profiles from the United States" (in German), *Bänder Bleche Rohre*, **7**, 1966, pp. 403–406.
- 23.15 Hoffmann, R.: "Modern Design of Stretch-Forming Presses" (in German), *Industriekurier, Techn. u. Forsch.*, **18**, 1965, pp. 893–894.
- 23.16 Mote, H.: "Stretch Forming of Auto Panels," *Am. Machinist*, **111**, Apr. 10, 1967, pp. 154–155.

## 23.28 SHEET-METAL FORMING

- 23.17 Hauber, D.: "Use of Titanium in the Manufacture of Aircraft" (*in German*), *Blech*, **14**, 1967, pp. 448–454.
- 23.18 Keeler, S. P.: "Determination of Forming Limits in Automotive Stampings," *Sheet Met. Ind.*, **42**, 1965, pp. 683–691.
- 23.19 Marciniak, J., and Kuczyński, K.: "Limit Strains in the Processes of Stretch Forming Sheet Metal," *Int. J. Mech. Sci.*, **9**, 1967, pp. 609–620.
- 23.20 Adler, G.: "Forming of Sheet Metal at Room Temperature" (*in German*), *Ind. Anz.*, **88**, pp. 1608–1612, pp. 1823–1833.
- 23.21 Panknin, W.: "The Importance of the Material Properties during Sheet-Metal Forming," in *Basic Principles of Plastic Deformation of Metals* (*in German*), Düsseldorf, Verlag Stahleisen, 1966, pp. 364–383.
- 23.22 Young, A. W.: "Pushbutton Stretch Former Uses Arched, Rotated Jaws," *Iron Age*, **199**, 1967, pp. 64–65.
- 23.23 Sachs, G.: *Principles and Methods of Sheet Metal Fabricating*, 4th ed., New York, Reinhold, 1958, pp. 456–475.
- 23.24 DeGroat, G.: "Stretch Forming in a Big Way," *Am. Machinist*, **112**, 1968, pp. 85–87.
- 23.25 Law, L. W.: "Stretch Draw Forming," *Sheet Met. Ind.*, **43**, 1966, pp. 748–760.
- 23.26 Schuler, L., Ed.: *Handbook of Metal Forming* (*in German*), 4th ed., Stuttgart, Ernst Klett, 1964.
- 23.27 Petzold, W.: "Determination of the Greatest Bead Depth for Embossing" (*in German*), *Fertigungstechn. u. Betr.* **20**, 1970, pp. 427–430.
- 23.28 Spizig, J. S.: "Expanding and Reducing Hollow Workpieces" (*in German*), *VDI-Nachr.* **24**, 1970, pp. 28–29.
- 23.29 Roper, R. E.: "Expanding of Metals" (*in German*), *Ind. Anz.*, **91**, 1969, pp. 2007–2009.
- 23.30 "New Methods, New Markets Expand Range of Stretch Forming," *Steel*, **156**, 1965, pp. 102–105.
- 23.31 Spizig, J. S.: "Stretch Forming of Sheet-Metal Cylinders" (*in German*), *Werkstattstechnik*, **55**, 1965, pp. 560–562.
- 23.32 Hofner, K. H.: *Methods of Forming* (*in German*), München, Carl Hanser, 1970.
- 23.33 Kursetz, E.: "Fluids Form Tubes" (*in German*), *Maschinenmarkt*, **76**, 1970, pp. 270–271.
- 23.34 Ogura, T., Ueda, T., and Takagi, R.: "On the Application of a Hydraulic Bulging Process" (*in German*), *Ind. Anz.*, **88**, 1966, pp. 769–772, 1001–1004.
- 23.35 Al-Qureshi, H. A.: "Comparison between the Bulging of Thin-Walled Tubes Using Rubber Forming Technique and Hydraulic Forming Process," *Sheet Met. Ind.* **47**, 1970, pp. 607–612.
- 23.36 Hertl, A.: "Design of Machines to Stretch Sheet Metal and Plate" (*in German*), *Z. Metallk.*, **51**, 1960, pp. 555–560.

**4**

**BLANKING, PIERCING, SLUG PRODUCTION**



© 2002-2003 The McGraw-Hill Companies, Inc. All Rights Reserved.



## CHAP. 24

### BLANKING AND PIERCING

#### List of Special Symbols

$a_R$	ring-indenter distance
$d_D$	diameter of die
$d_{\min}$	smaller diameter of sheared blank or pierced hole
$d_{\max}$	larger diameter of sheared blank or pierced hole
$d_P$	diameter of punch
$F_{BH}$	blankholder force
$F_H, F'_H$	horizontal forces
$F_E$	ejector force
$F_R$	ring-indenter force
$F_S$	shearing force
$F_V, F'_V$	vertical forces
$F_{WF}$	punch withdrawal force
$h_b$	burr height
$h_R$	ring-indenter height
$k_s$	shearing resistance
$l_R$	ring-indenter length
$l_s$	length of sheared line
$p_{BH}$	blankholder pressure
$s$	sheet thickness
$s_e$	edge draw-in
$t_c$	depth of crack penetration
$u$	clearance
$u/s$	relative clearance

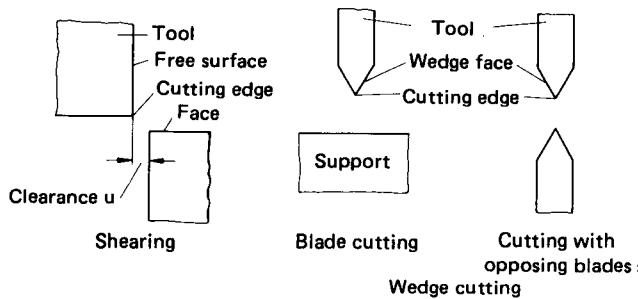


FIG. 24.1 Shear and wedge cutting.

Blanking is one of the most frequently used processes in sheet-metal working. For all the workpieces made of sheet metal, either the blank is made by punching or the final workpiece is separated by trimming after forming. Both processes, blanking and trimming as well as piercing, are shearing processes. Shearing as a group of processes belongs to the third main group, separating processes (see Chap. 2), and hence in the strictest sense is not a deformation process, but it is always accompanied by a small plastic deformation.

Fig. 24.1 shows the processes of parting off workpieces by shearing and wedge cutting, together with the tool definitions. Among the two processes, the process of shearing (blanking, piercing, and trimming) is mainly used in sheet-metal working. The process of wedge cutting is sometimes used for trimming or cutting the discard after drawing operations. It is not dealt with here in great detail because of its limited applicability and importance. The process of shearing for bulk-forming processes is dealt with in detail in Chap. 25.

Depending on the position of the sheared surface with respect to the workpiece coordinates, various processes of shearing are used, such as blanking, piercing, notching, cutting off, lancing, and trimming. Blanking and piercing (Fig. 24.2) are shearing processes with completely enclosed cutting lines. With blanking, the entire outer surface of the workpiece is obtained in one working stroke. Usually after blanking the strip would have a grid-shaped discard; blanking processes are always accompanied by scrap. With piercing, the inner form of a workpiece is obtained; the pierced piece is generally scrap. Cutting off or cropping is shearing of a portion of either a blank—sheet strip or sheared strip—or a semifinished product or workpiece (Fig. 24.3). The shearing contour is open; that is, it crosses the workpiece boundary. In general there is no scrap in cutting off.

Notching is shearing either an inner or an outer notch in a flat piece (Fig. 24.4). The shearing contour is open. When a workpiece has to be cut out, notching is used in cases where it is difficult

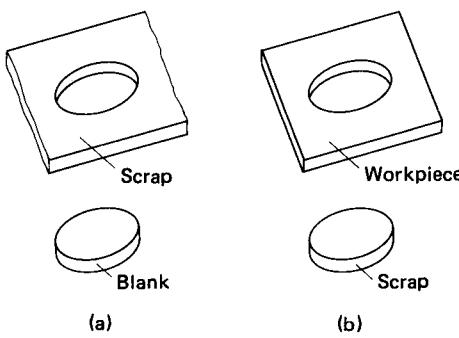
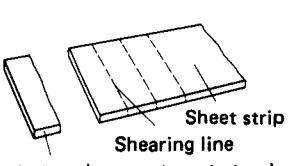
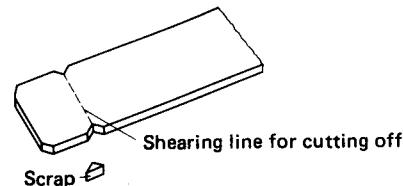


FIG. 24.2 (a) Blanking. (b) Piercing.



**FIG. 24.3** Manufacture of workpieces by cutting off.



**FIG. 24.4** Manufacture of an outer contour by notching.

to apply another shearing process. Notching is also used to prepare blanks of a required shape for production (Fig. 24.5).

Lancing (Fig. 24.6) is partly shearing a portion of the workpiece without complete separation, generally in preparation for further deformation processing. The shearing contour is not completely closed in this case.

Trimming (Fig. 24.7) is shearing from a workpiece a particular portion which is not required on the final product. The shearing contour can be either open or completely closed.

## 24.1 SHEARING

### 24.1.1 Force Components In Shearing Operations

The forces  $F_V$  and  $F'_V$  acting a small distance from the cutting edges are caused by nonuniformly distributed compressive stresses along a small length near the cutting edge. The distance  $l$ , resulting from the action of forces, causes a moment which either bends or tilts the workpiece (Fig. 24.8). The reaction moment causes a counterclocking moment, which results from bending and horizontal normal stresses on the workpiece and tool. The horizontal normal stresses can be represented by the resultants  $F_H$  and  $F'_H$ . Additional horizontal forces will be present when the tools do not have an edge angle of  $90^\circ$  or when the workpiece surface is not perpendicular to the direction of the sheet plane.

In addition to the above forces, frictional forces also act on the tooling. The horizontal forces  $F_H$  and  $F'_H$  cause frictional forces on the side surfaces of the tooling, namely,  $\mu F_H$  and  $\mu F'_H$ . The shearing force, which is due to the sliding of the material on the tool faces, causes frictional forces  $\mu F_V$  and  $\mu F'_V$ .

Investigations conducted so far have shown no conclusive evidence with regard to the distribution of the forces in the horizontal and vertical directions. It is only known that the forces  $F_H$  and  $F_V$  are affected by various parameters in the shearing process.

### 24.1.2 Shearing Mechanism and Stresses

The process of shearing and the structure of the sheared surface are influenced by both the tool geometry and the properties of the workpiece material. The characteristics of the tooling that are

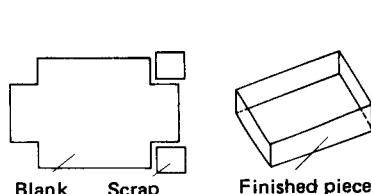


**FIG. 24.5** Blank manufacture by notching.

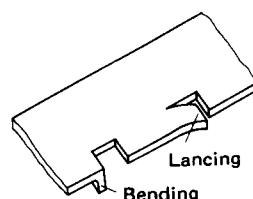


**FIG. 24.6** Lancing operation.

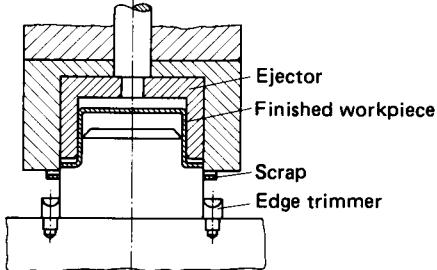


FIG. 24.7 Manufacture by trimming.

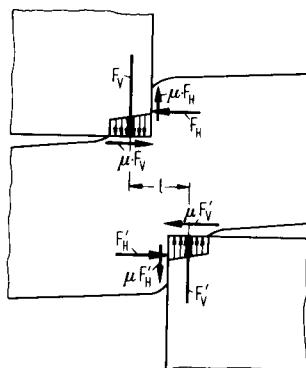
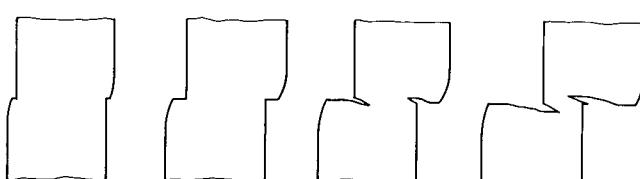
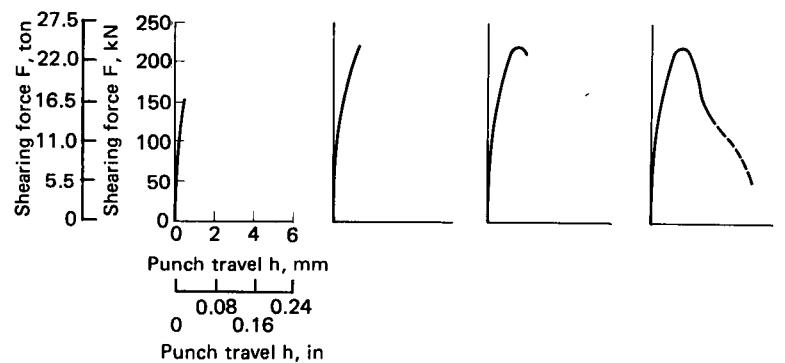


FIG. 24.8 Force components in shearing.

important are the shearing clearance  $u = (d_D - d_T)/2$ , the rounding off of the cutting edge, and the wear of the cutting edge. Other factors affecting the process to a lesser extent are the shape of the cutting edge and the tool velocity. Material characteristics important for the process are blank thickness, mechanical properties, chemical composition, microstructure, and grain size.

Fig. 24.9 illustrates the various sequences involved during the blanking process of steel with a small clearance  $u = 0.01s$  as well as the force-travel diagrams for the respective sequences. At the beginning of the process the sheet is bent, first elastically and then plastically. This bending can be seen in a permanent curving of the blank surface. Further penetration of the punch into



Formation of sheared surfaces

FIG. 24.9 Various stages in blanking. Material—C 10 (AISI 1010);  $s = 5 \text{ mm (0.2 in)}$ ;  $S_u = 37.2 \text{ N/mm}^2 (5.4 \text{ ksi})$ ;  $u/s = 0.0095$ ; blanked diameter—40 mm (1.6 in).

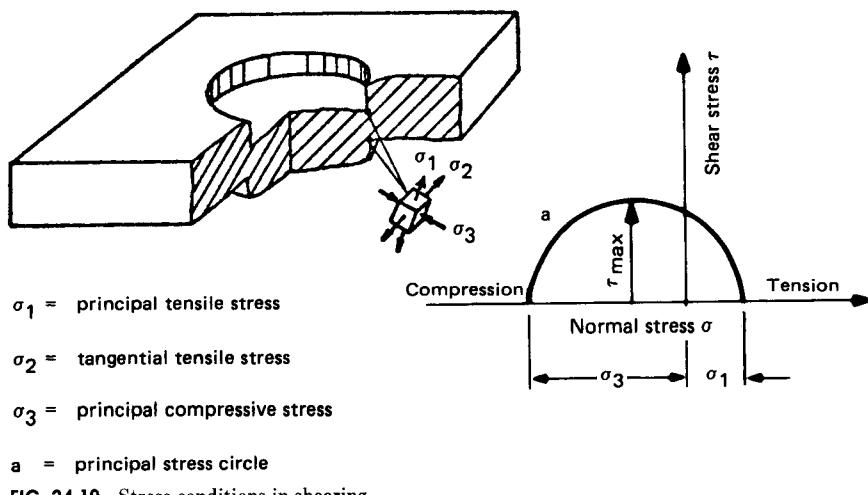


FIG. 24.10 Stress conditions in shearing.

the sheet causes a little curvature or draw-in (up to a stroke corresponding to 0.2s) on the remaining strip as well as on the blank. Thereafter the actual shearing takes place along the cutting edges of the tooling, producing a smooth sheared surface. At a particular depth of punch penetration (this value depends on the workpiece material and the tool geometry), cracks will start forming from the cutting edges inward. In general crack formation starts at the cutting edge of the die when shearing with closed cutting lines, and only thereafter at the cutting edge of the punch [24.1]. With increasing punch penetration, new partial shearing can take place in spite of the cracks already formed. This causes the typical blanking ear for small shearing clearances.

In the shearing zone the stress condition during crack formation is triaxial (Fig. 24.10). According to Tresca, the flow criterion is

$$\tau_{\max} = \frac{\sigma_1 - \sigma_3}{2} = \frac{\sigma_f}{2} \quad (24.1)$$

The stress condition changes throughout the deformation process. At the initiation of the crack,  $\tau_{\max}$  reaches the fracture limit before the yielding limit (Fig. 24.11). The cracks are propagated

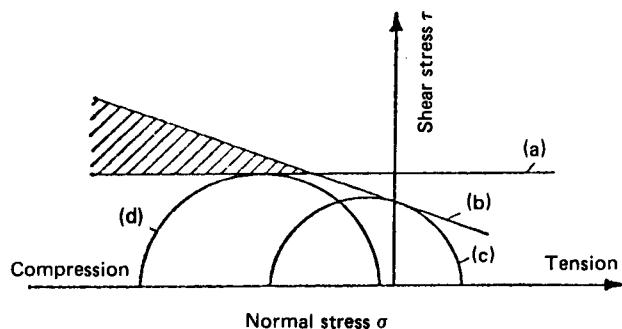


FIG. 24.11 Stress conditions at the shearing edge in blanking and fine blanking. (a) Shear yield limit. (b) Shear fracture limit. (c) Blanking. (d) Fine blanking.

in the direction of maximum shear stresses. Various investigators have experimented in an effort to understand the stress condition in the workpiece. Bach [24.2] tried to obtain an analytical solution for the stress condition, assuming different normal stress distributions under the blanking punch. However, the solution of Bach is valid only for an elastic stress-distortion condition. The conditions of the theory of plasticity were not used for the analysis. Hence the analysis is very approximate for determining the actual stress condition in the deformation zone during blanking.

Photoelasticity methods were used by different researchers to analyze stresses [24.1], [24.3], [24.4]. Fig. 24.12 shows typical isochromes for the loading of a beam model by a blanking punch and die as well as the resulting stresses in the different cutting planes. Up to now these studies have been performed in the elastic range of the model only because of the nonavailability of a suitable model material for the plastic range. The stress conditions obtained by this method are thus only applicable for the onset of plastic flow. The method is not suitable for a complete description of the process, including any indication concerning crack formation and the structure of the sheared surfaces.

The various stages in a shearing process can be recognized easily from its force-travel diagram (Fig. 24.9). Initially the force increases steeply with increasing punch travel. The first rupture or crack corresponds to the maximum force. Formation of a crack is accompanied by a sudden drop in the force. Any burr or ear formation will be observed as a step in the force-travel diagram.

#### 24.1.3 Effect of Tool Geometry

It has been pointed out in the preceding section that in the blanking process the clearance and the shape of the shearing edge are important parameters of the tooling. Fig. 24.13 shows for different materials the formation of the sheared surfaces when sharply ground blanking tools are used with various clearances  $u$  as well as the force-travel diagrams for these cases (see also Fig. 25.19).

Materials with high ductility in tensile tests, such as Al 99.5 (AA 1050A) in Fig. 24.13, have a nearly smooth sheared surface for small clearance. With increasing clearance, the smooth portion of the total sheared surface decreases while the fractured portion increases. Formation of burr or secondary shear is in general not found in such materials (see also Fig. 24.27).

Materials with greater strength properties and lower ductility, such as the steel workpiece in Fig. 24.13, show similar trends as softer materials for smaller sheet thicknesses; they also do not have a tendency to form burrs or secondary shears. The proportion of the fractured area increases with increasing clearance.

For larger sheet thicknesses [ $s \geq 2.5$  mm (0.1 in)] one or more secondary shears form during the blanking of steel; they even form for a clearance of  $u = 0.1s$ . Other investigations show that secondary shear formation is no longer present in the clearance range of  $u = 0.08\text{--}0.1s$  [24.1]. Investigations of Eickhoff [24.5] on the piercing of sheets [Ck 35 (AISI 1035)], 8 mm (0.32 in) thick, with a hole of 15-mm (0.6-in) diameter, showed that the punched piece was free from secondary shear for a clearance of  $u = 0.06s$ ; the work metal also showed no secondary shear in this case. A comparison of the various investigations shows that in addition to the clearance, the form of the shearing line and other conditions, such as the condition of the cutting edges and the use of a blankholder, are important factors to be considered when examining the blanking process. Increased strength of the material increases the proportion of the fractured surface on the blanked workpiece and reduces the possibility of secondary shear formation for smaller clearances.

Proper selection of the clearance will ensure that the cracks originating from the punch and the die meet each other, thus avoiding secondary shear formation. An increased clearance will increase the dimensional tolerance obtainable on the sheared surface.

The force-travel diagrams in Fig. 24.13 show that the maximum shearing force decreases with increasing clearance. The maximum deviation of the punch force, based on the maximum punch force is here 14%. The requirement in blanking is more affected by the change in shape of the force-travel diagram than by the blanking force. In the examples shown in Fig. 24.13 the difference in work requirements for small and large clearances is 39%.

Because of the relative movement between tool and workpiece, wear on the cutting tool ele-

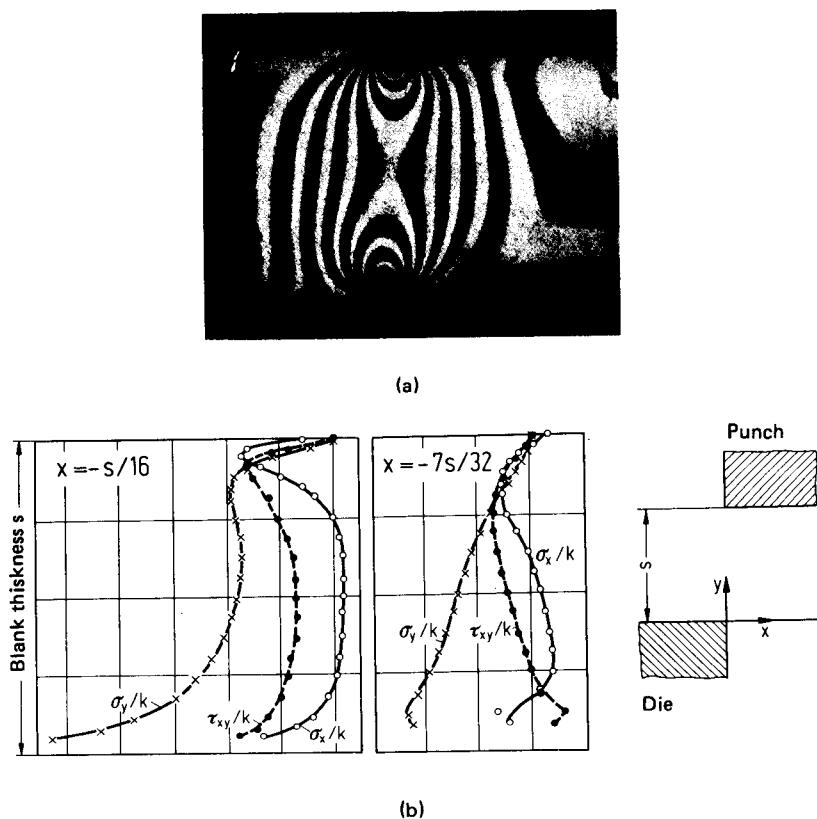
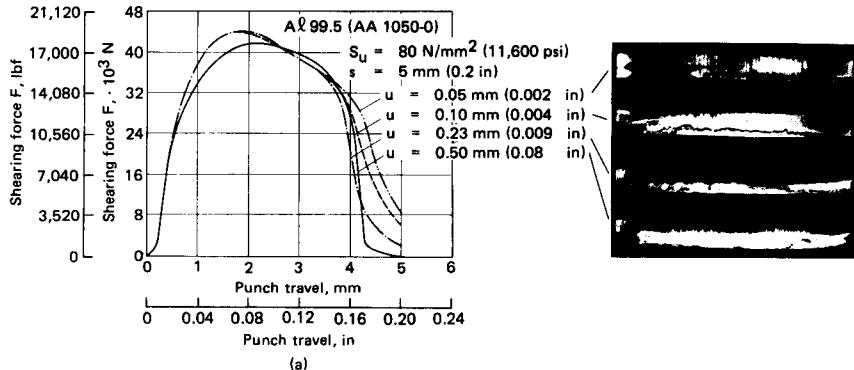


**FIG. 24.12** (a) Isochromes. (b) Stress distribution determined from isochromes. (After [24.4].)

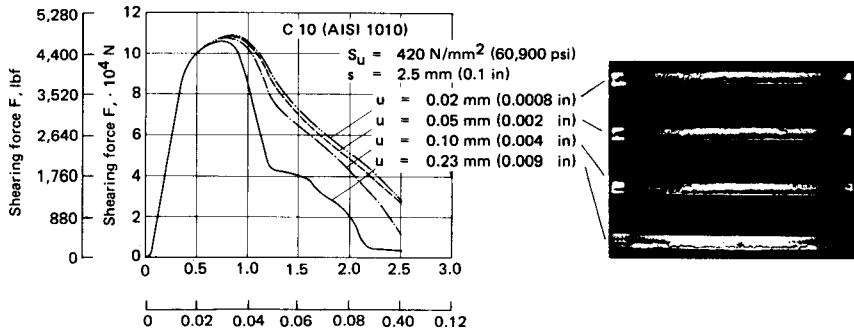
ments is unavoidable. Wear takes place on the face of the cutting blade and on its free surface (Fig. 24.14). It causes the cutting edges to be rounded. Increasing wear increases the penetration depth of the punch needed for cracks to form [24.7]. The proportion of the smooth sheared surface also increases. Because of the greater punch penetration at the start of cutting, the ratio of the clearance to the area to be sheared increases, thus causing crack formation. The cracks then move toward each other, thereby reducing the chance of burr formation, which may occur with sharp cutting edges.

Based on the investigations presented in [24.7] to [24.10], with worn-out tools the cracks do not emanate from the blanking edge but from the relieved (free) surface. This change in crack propagation leads to burr formation, which increases as the number of pieces made with a single tooling increases (Fig. 24.15). The size of the burr is dependent on the wear and the material, whereby the wear in turn is dependent on the workpiece and tool materials. The relationships are complicated, and based on [24.8] to [24.10], they cannot be represented in a generalized form.

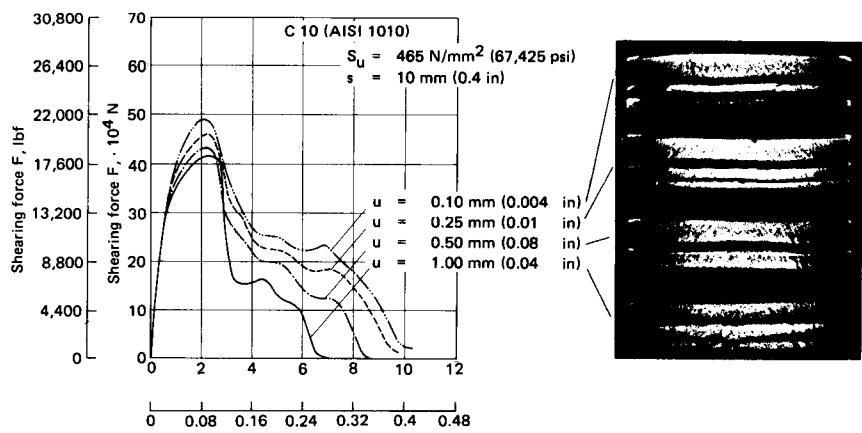
Wear increases the blanking force and hence the blanking work required [24.7]. Buchmann [24.8] has found an erratic behavior of the blanking force as a function of wear. Wear increases by 60% and sometimes decreases by about 20% in blanking with sharp-edged blanking tools. The blanking work increases with increasing wear as a result of increased punch penetration until rupture is obtained.



(a)



(b)



(c)

**FIG. 24.13** Surface formation and force-travel diagrams in blanking of various materials with different clearances. (After [24.6].)

## 24.2 FORCES AND DEFORMATION WORK

### 24.2.1 Force Requirement

The effects of clearance and tool wear on the force variation were discussed in Sec. 24.1.3. For blanking processes the maximum blanking force  $F_{B,\max}$  is important for the selection of a suitable press. A parameter called the shearing resistance  $k_s$  is calculated from the maximum shearing force as follows:

$$k_s = F_{S,\max}/A_S \quad (24.2)$$

where  $A_S$  is an area calculated from the sheet thickness  $s$  and the length of the shearing line  $l_s$  as

$$A_S = sl_s \quad (24.3)$$

The shearing resistance  $k_s$  is a parameter that considers the effects of clearance, tool wear, influencing parameters of material properties, sheet thickness, and blank contour.

The shearing resistance  $k_s$  decreases with increasing clearance  $u$  (Fig. 24.16). Within a clearance of range  $u = 0.01\text{--}0.1s$ , the decrease is approximately 14% of the maximum value of  $u$ . The values given in Fig. 24.16 are for sharp-edged tools. The shearing resistance is also related to tool wear in a similar manner as the blanking force. Depending on the type of workpiece material and the number of workpieces to be produced, the shearing resistance  $k_s$  increases to up to 1.6 times its value for sharp-edged tools.

Based on investigations in [24.1] and [24.11], the shearing resistance  $k_s$  is also affected by the diameter of the hole to be blanked or pierced. All other blanking conditions remaining the same, the shearing resistance decreases with increasing blanking punch diameter (Fig. 24.17). Similar results have been reported in [24.5] for piercing thick sheets and in [24.12] for piercing austenitic sheets with hole diameters of 0.9–6 mm (0.035–0.24 in).

The shearing resistance is also dependent on the curvature of the cutting contour. The stress on the tooling will be higher for pieces with a large curvature of the blanking contour (the extreme being sharp corners) than for pieces with smaller curvature of the blanking contour. This explains why in blanking operations sharp corners are susceptible to breakage.

As explained in Sec. 24.1.1 the shearing process is a deformation process until the maximum blanking force is reached. Hence to determine the shearing force, the flow curve of the workpiece material should be known. The effect of increased work hardening of austenitic stainless steels on the shearing resistance has been investigated [24.12]. For the same initial strength of workpieces, the shearing resistance is higher for austenitic stainless steels than for ferritic stainless steels. However, the tensile strength  $S_u$  is used to characterize the material properties, and hence the shearing resistance is related to the tensile strength. Fig. 24.18 shows that the ratio of shearing resistance

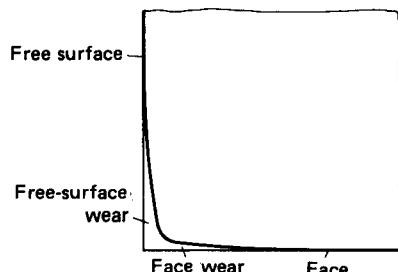


FIG. 24.14 Wear on blanking tools.

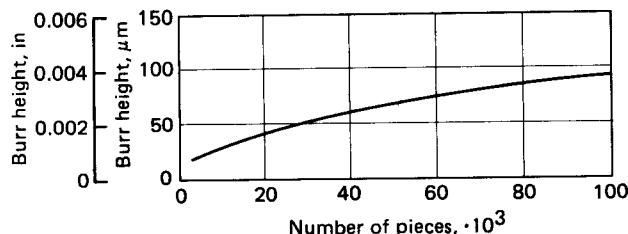
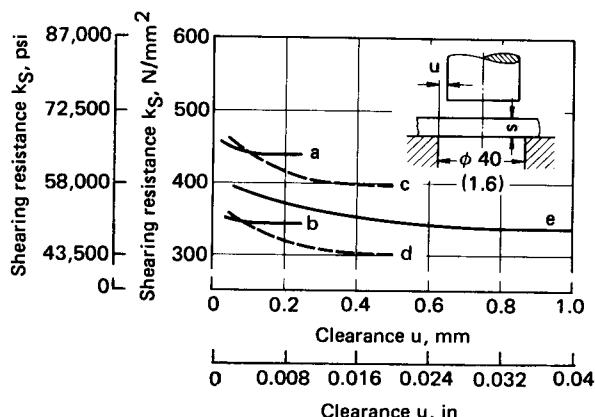


FIG. 24.15 Burr height on blanked workpieces. (After [24.10].)



**FIG. 24.16** Blanking pressure as a function of clearance  $u$  [after 24.6]. (a) For C 35 (AISI 1035),  $S_u = 610 \text{ N/mm}^2$  (88.45 ksi),  $s = 2.5 \text{ mm}$  (0.1 in). (b) For C 10 (AISI 1010),  $S_u = 420 \text{ N/mm}^2$  (60.9 ksi),  $s = 2.5 \text{ mm}$  (0.1 in). (c) For C 35 (AISI 1035),  $S_u = 630 \text{ N/mm}^2$  (91.35 ksi),  $s = 5 \text{ mm}$  (0.2 in). (d) For C 10 (AISI 1010),  $S_u = 450 \text{ N/mm}^2$  (65.25 ksi),  $s = 5 \text{ mm}$  (0.2 in). (e) For C 15 (AISI 1015),  $S_u = 460 \text{ N/mm}^2$  (66.7 ksi),  $s = 10 \text{ mm}$  (0.4 in).

to tensile strength decreases with increasing tensile strength of the workpiece material. The spread of values in Fig. 24.18 shows the effect of various sheet thicknesses on the result [24.6].

Various investigations have shown that the sheet thickness also affects the shearing resistance [24.4], [24.6], [24.12]; the shearing resistance decreases with increasing sheet thickness (Fig. 24.19).

Various methods of calculating the shearing forces have been proposed in [24.13] to [24.15] by different researchers. For these calculations the shearing process is assumed to be a deformation process throughout the punch stroke. This permits the calculation of the shearing force-travel

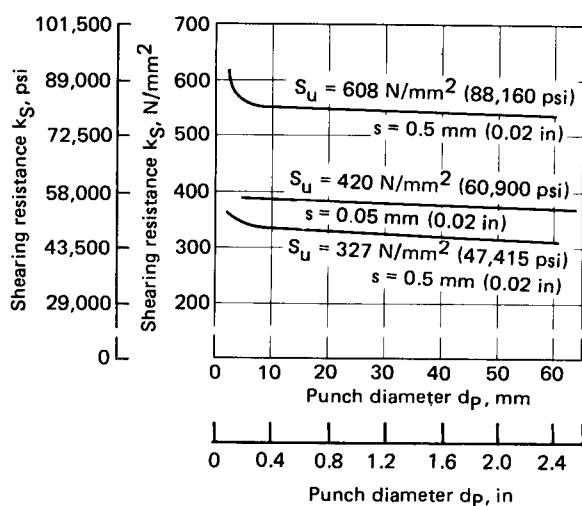


**FIG. 24.17** Effect of punch diameter  $d_p$  on blanking resistance. (After [24.1], [24.11].)

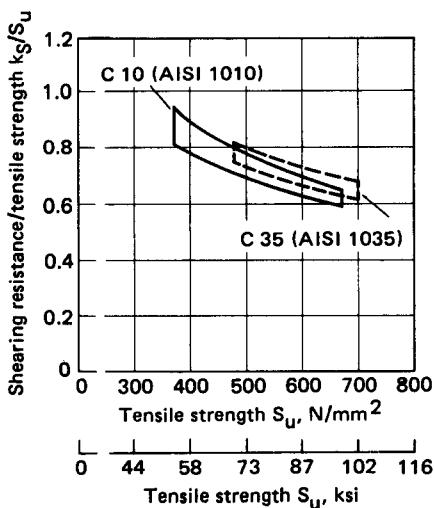


FIG. 24.18 Ratio  $k_s/S_u$  as a function of tensile strength  $S_u$  for steel sheets. Punch diameter—40 mm (1.6 in),  $u/s = 0.1$ ;  $s = 1$ –10 mm (0.04–0.4 in).

curve using established mathematical equations from the theory of plasticity. The method used in [24.18] is described briefly.

The shearing force–travel curve is obtained by using the upper-bound method for the deformation work or energy. It is assumed that the plastic strains and distortions take place in a localized region in the shape of a parabola. This assumption is based on the experimental results that grid patterns on the split blank distort only within a lens-shaped region (Fig. 24.20). The boundary

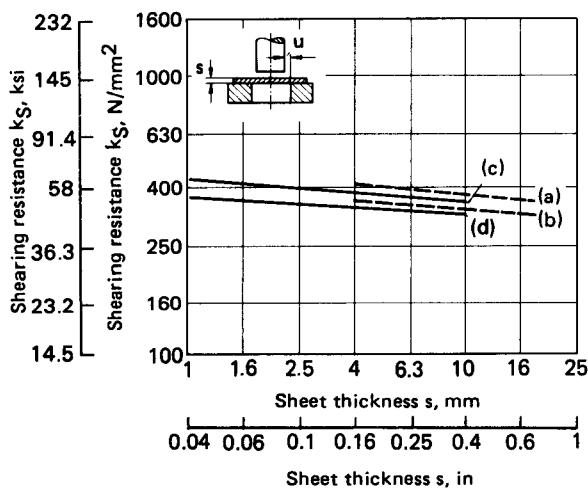


FIG. 24.19 Shearing resistance  $k_s$  as a function of sheet thickness  $s$ .  $u = 0.1s$ .  $a$ — $S_u = 500 \text{ N/mm}^2$  (72.5 ksi). (After [24.5].)  $b$ — $S_u = 395 \text{ N/mm}^2$  (57.3 ksi). (After [24.5].)  $c$ — $S_u = 500 \text{ N/mm}^2$  (72.5 ksi). (After [24.6].)  $d$ — $S_u = 445 \text{ N/mm}^2$  (64.5 ksi). (After [24.6].)

## 24.14 BLANKING, PIERCING, SLUG PRODUCTION

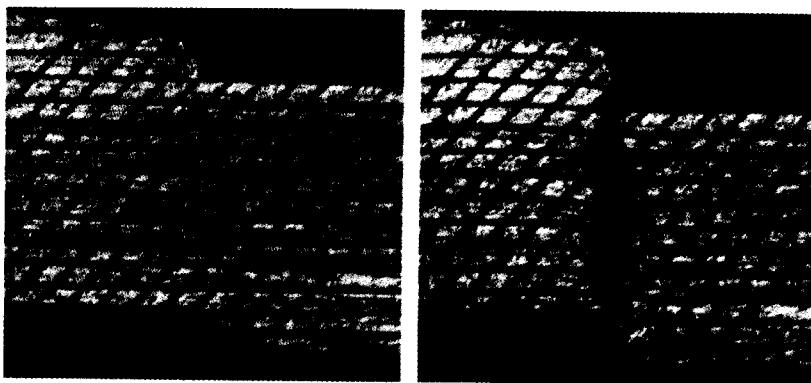


FIG. 24.20 Distortion of grid patterns in blanking.

lines pass through the cutting edges of the tools, and the boundary conditions for the mathematical analysis can be obtained from Fig. 24.21. The velocity of the material along the boundaries in the direction of tool movement should be continuous and also within the deformation zone; the velocity should be continuous at all points. Details of the computation method may be obtained from [24.13].

The above method was used for computing the force of plane-strain blanking. A similar approach is possible for axisymmetric blanking also. Results of such computations for axisymmetric blanking and a comparison of results with experimentally measured values for aluminum Al 99.5 (AA 1050) are plotted in Fig. 24.22. Similar calculations were also done for steel sheets. The computations show that it is possible to determine the shearing force–travel diagram accurately by this method if the coefficient of friction is assumed between 0.025 and 0.05.

The above process is not suitable for estimating loads for industrial use because of the requirement of a computer. For industrial practice the shearing force is estimated with good accuracy using the following formula:

$$F_s = l_{ss} k_s \quad (24.4)$$

The value of  $k_s$  is either obtained from tables or calculated from the tensile strength as

$$k_s \approx 0.8 S_u \quad (24.5)$$

The factor of 0.8 has been suggested by Bach [24.16]. The deviation of the actual shearing force from the approximate value from Eqs. 24.4 and 24.5 is  $\pm 20\%$ .

The increase of the shearing force due to wear can be considered by using a correction factor of 1.6 in Eq. 24.4:

$$F_s = 1.6 l_{ss} k_s \quad (24.6)$$

The shearing force can be reduced by reducing the effective shearing line length  $l_{ss}$ . This can be achieved for piercing or blanking by machining a taper either on the die or on the punch. If several pieces of different circumferential shapes are blanked or pierced in a single stroke of the press, the force can be reduced by piercing or blanking at different time intervals. Fig. 24.23 shows both possibilities. The height  $h$  for the taper can be up to 1–1.5s [24.17]. For sharp-edge tooling the maximum blanking force is

$$F_s = 0.67 l_{ss} k_s \quad (24.7)$$

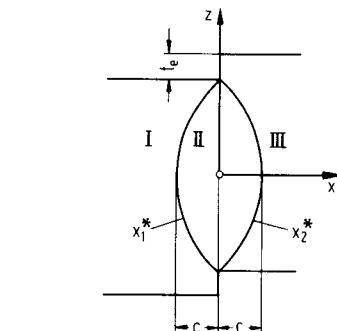
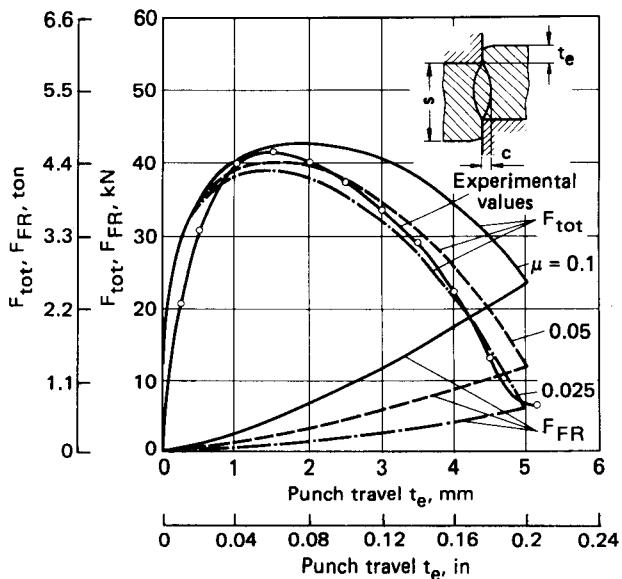


FIG. 24.21 Coordinate system and designation for plane-strain distortion condition.



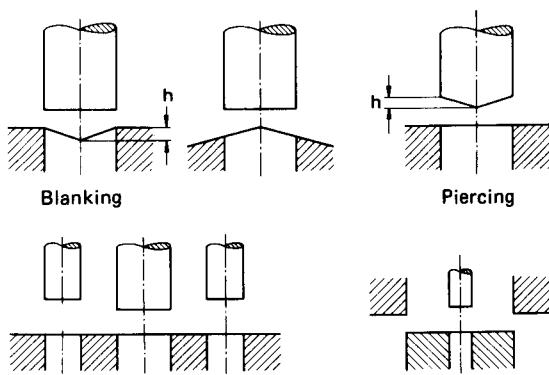
**FIG. 24.22** Calculated and measured force–travel diagrams for Al 99.5 (AA 1050A). (After [24.13].)

Irrespective of the method of manufacture, whether piercing or blanking with tapered tools and/or at different time intervals, the useful stroke of the press should not be exceeded.

#### 24.2.2 Side Thrust

During the blanking process forces perpendicular to the blanking direction (side thrust) develop due to the effect of bending moments and frictional forces. This side thrust must be considered during tool design:

In [24.18], [24.19] it is pointed out that the side thrust during the length of blanking travel has a similar trend as the blanking force. Kienzle and Jordan [24.20] found a different trend, however.



Blanking and piercing carried out at different time intervals

**FIG. 24.23** Methods of reducing blanking or piercing force.

**Table 24.1** Ratio of Withdrawal Force to Shearing Force

Material designation <sup>a</sup>		Yield strength or tensile strength, N/mm <sup>2</sup> (ksi)	Thickness, mm (in)	Punch diameter, mm (in)	Clearance to thickness ratio $u/s$	$\frac{F_{WF}}{F_s}$	Reference
DIN	US						
St37	$\approx$ AISI 1010	$S_u = 376$ (54.5)	8 (0.315)	15 (0.6)	0.005 0.1	0.39 0.08	[24.5]
X5CrNi 189	AISI 304 L	$S_y = 300$ (43.5)	2.5 (0.1) 2.0 (0.08) 2.0 (0.08)	5 (0.2) 2 (0.08) 4 (0.16)	0.01 0.05 0.05	0.29 0.01 0.1	[24.12]
A199.5	AA 1050A	$S_u = 83$ (12)	2.5 (0.1)	40 (1.6)	0.01	0.06	[24.6]
C10	AISI 1010	$S_u = 400$ (58)	2.5 (0.1)	40 (1.6)	0.05 0.01	0.02 0.03	
		$S_u = 600$ (87)	2.5 (0.1)	40 (1.6)	0.1	0.03	
C35	AISI 1035	$S_u = 505$ (73.2)	10 (0.4)	40 (1.6)	0.01 0.05	0.07 0.03 0.05 0.015	

<sup>a</sup>See Apps. C and D.

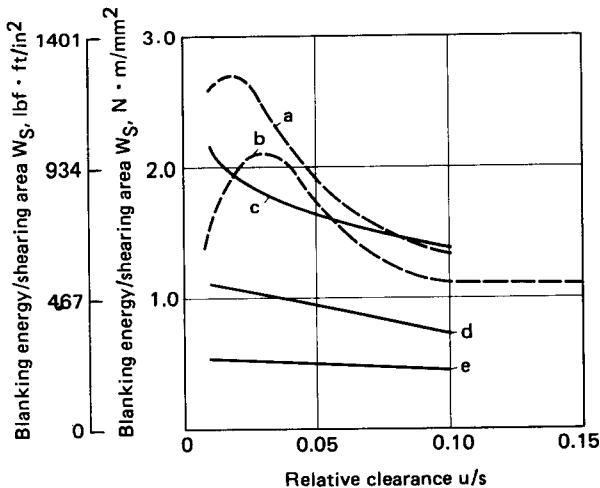
The values given for the ratio of side thrust to blanking force range from 0.02 and 0.2. Definitive conclusions on the dependence of sheet thickness, material strength, and clearance on the side thrust cannot be drawn because of the lack of sufficient information.

### 24.2.3 Withdrawal and Ejection Force

The strains in the workpiece during blanking cause radial stresses between punch and sheet strip and between blanked workpiece and die, even after termination of the process. As a result, frictional forces are present during the return stroke of the punch from the surrounding strip and during ejection of the blank; they are designated withdrawal and ejection forces, respectively.

The magnitude of the withdrawal forces is dependent on clearance, punch dimension, sheet thickness, and strength properties [24.5], [24.6], [24.12], [24.21], [24.22]. The important parameters are the clearance and punch dimensions. Table 24.1 gives an overview of various ratios of withdrawal force to shearing force found in the literature. The ratio varies between 0.01 and 0.06 in most cases; the withdrawal force decreases with increasing clearance and punch diameter.

The ejection forces are smaller than the withdrawal forces. Measurements [24.6] have shown a maximum value of  $F_E/F_S = 0.005$ . These values were measured for a clearance of  $u = 0.001s$  for a 1-mm (0.04-in) thick sheet. There is no clearly demonstrated relationship between ejection force and punch diameter. For additional information see Secs. 24.3.2 and 24.3.3. (See also [24.23].)



Curve	Material		$S_u$ N/mm <sup>2</sup> ( $\times 10^3$ psi)	$s_r$ mm (in)	$d_p$ , mm (in)
	DIN	AISI			
a	St37	AISI 1010	387 (56.1)	18 (0.71)	15 (0.6)
b	St37	AISI 1010	376 (54.5)	8 (0.32)	15 (0.6)
c	C 15	AISI 1015	464 (67.3)	10 (0.4)	40 (1.6)
d	C 10	AISI 1010	377 (54.7)	5 (0.2)	40 (1.6)
e	C 10	AISI 1010	397 (57.6)	2.5 (0.1)	40 (1.6)

FIG. 24.24 Blanking energy per unit area as a function of  $u/s$ .

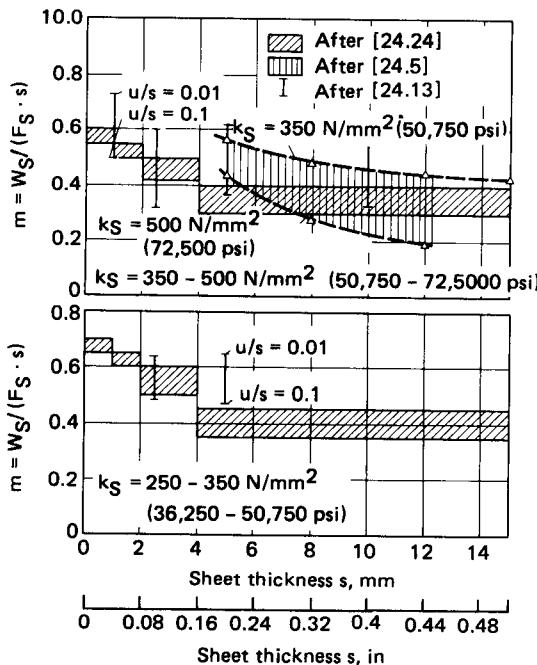


**FIG. 24.25** Factor  $m = \text{shearing work}/(\text{shearing force} \times \text{blank thickness})$ .

#### 24.2.4 Energy

The energy requirement in blanking is influenced by the tool geometry and the material properties. It is affected by the above parameters to a greater extent than the blanking force. Fig. 24.24 shows that the blanking energy decreases with increasing clearance-to-sheet-thickness ratio  $u/s$  and increases with increasing sheet thickness. A generalized statement on the effect of the material characteristics on the blanking energy is not possible due to the simultaneous combined effect of material properties, sheet thickness, and clearance on the force-travel diagram.

The work consumed in blanking is calculated as

$$W_s = m F_{ss} \quad (24.8)$$

The correction factor  $m$  is used to take into account the effect of various parameters described above on the energy requirement.

In [24.5] the material strength and the sheet thickness are considered and the factor  $m$  is determined from a nomogram. In [24.24] the correction factor  $m$  is given in tabular form as a function of strength and sheet thickness. The results proposed in [24.5], [24.24] are valid for normal clearance. Guidi [24.25] also considers the effect of the ratio of yield strength to tensile strength and the ratio  $u/s$  and not the effect of the sheet thickness in determining the correction factor  $m$ . Fig. 24.25 gives a comparison of the results presented in [24.5], [24.6], [24.24]. For the purpose of comparison the value  $k_s$  given in [24.24] is calculated from the tensile strength using

$$k_s = 0.86 S_u \quad (24.9)$$

whereas the values from [24.5], [24.6] were determined from measured values. The comparison clearly shows a very important difference between calculated and measured values. A factor  $m = 0.6$  gives larger values of actual blanking energy and is hence safe to use.

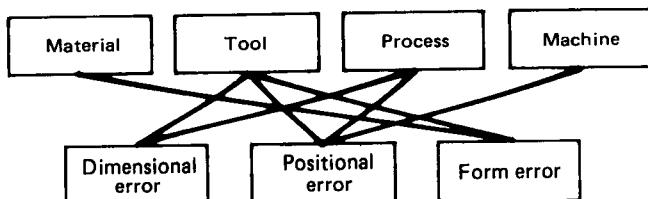


FIG. 24.26 Factors affecting errors on sheared workpieces.

## 24.3 WORKPIECE PROPERTIES

### 24.3.1 Accuracy

The accuracy of workpieces can be characterized by the following errors: dimensional error, positional error, form error, and surface error. The first three errors in blanking are described here.

The errors on blanks are influenced by the material, the tooling, process variations, and the machine (Fig. 24.26). The following form errors can be found on the blanked surface: plastic deformation or edge draw-in  $s_e$ , depth of crack penetration  $t_c$ , and burr height  $h_b$  (Fig. 24.27). In addition deviation of the blank from a flat surface can also occur. In the case of blanks with relatively small ratios of outer diameter to thickness, bulges can occur. In blanking of straightened strips (by multibending), residual stresses could be released, causing deviations from the plane surface.

The plastic deformation or edge draw-in  $s_e$  is affected by the material, the blanking clearance, and the shape of the blank contour. The information given in Fig. 24.28 can be used as a guide for the edge draw-in  $s_e$ . The edge draw-in is constant for circular sections and varies for other sections. It increases with increasing curvature. The edge draw-in will be negligibly small on small pierced surfaces and on steps or projections on surfaces with small radii. On outer surfaces with small radii the edge draw-in can be up to 30% of the sheet thickness [24.25].

The penetration depth of cracks depends on the material and the blanking clearance if there is burr or secondary shear formation during blanking. If the burr or secondary shear can be avoided by proper selection of the blanking clearance, the penetration depth of the crack will be approximately equal to the blanking clearance. Fig. 24.29 gives some guidance values for the penetration depth of cracks. The upper limit of the hatched zone is valid for thick sheets with higher strength properties of the materials blanked, and the lower limit is valid for thin sheets with smaller strength properties. More details on the penetration depth of cracks are given in Sec. 24.5.1. One possibility of reducing the penetration depth of cracks is by counterblanking [24.26] to [24.28] (see Sec. 24.5.3). Details on the height of burr can be obtained from Fig. 24.15 and [24.10], [24.12].

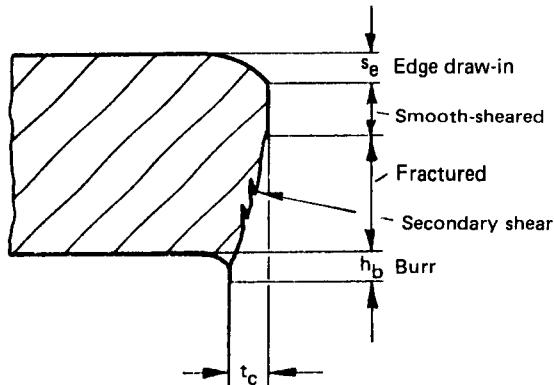


FIG. 24.27 Form errors on sheared workpieces.

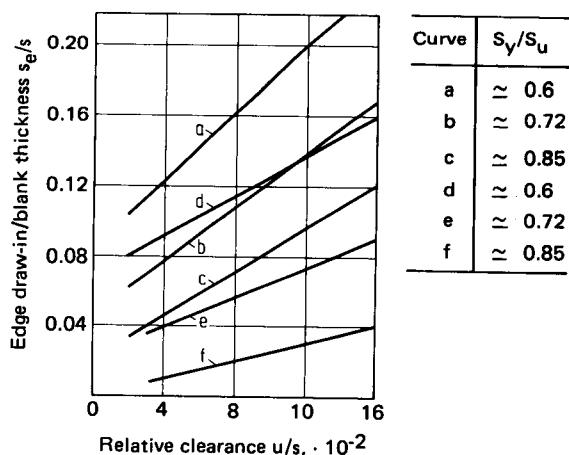


FIG. 24.28 Edge draw-in in sheared surfaces. Blank diameter—30 mm (1.2 in); pierced-hole diameter—30 mm (1.2 in). (After [24.25].)

The dimensions on the burnished blanked surface are determined by the tool dimensions. The die size determines the outer surface dimension and the punch dimension that of the sheared surface. Inaccuracies in the tooling will cause errors in the workpieces. Unavoidable small irregularities of the feed in transfer tooling will also cause dimensional errors. The elastic deformation of the tooling and the elastic-plastic straining of the workpiece also cause dimensional errors on the workpieces. The dimensions of hole and blank in piercing and blanking, respectively, are a function of the dimension of the tooling according to [24.29] (Fig. 24.30). Based on these investigations, the hole can be smaller than the punch dimension. If the clearance is chosen as  $u < 0.05s$ , the dimension of the hole is always greater than the dimension of the punch. Neglecting the form errors in Fig. 24.30 due to the formation of cracks, the deviations of dimensions from the actual values can be up to  $-0.07 \text{ mm} (-0.003 \text{ in})$  for the blank and to  $+0.04 \text{ mm} (+0.002 \text{ in})$  for the hole.

Positional errors in blanked pieces are generally parallel offsets of the cracks from one another and with respect to the outer surface. These defects are due either to defective positioning of the blanking tools with respect to one another or to inaccuracy of the tools, defects in press guides, or

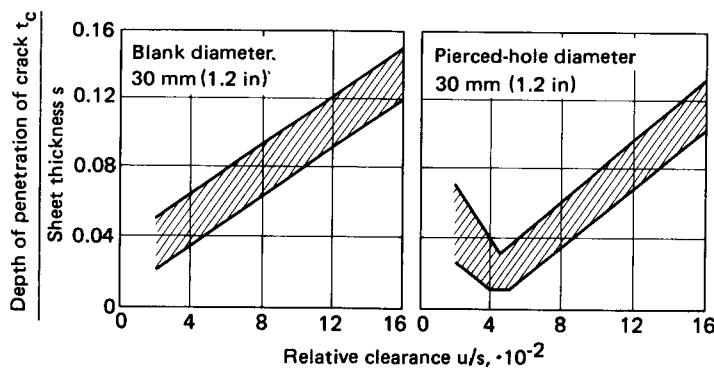
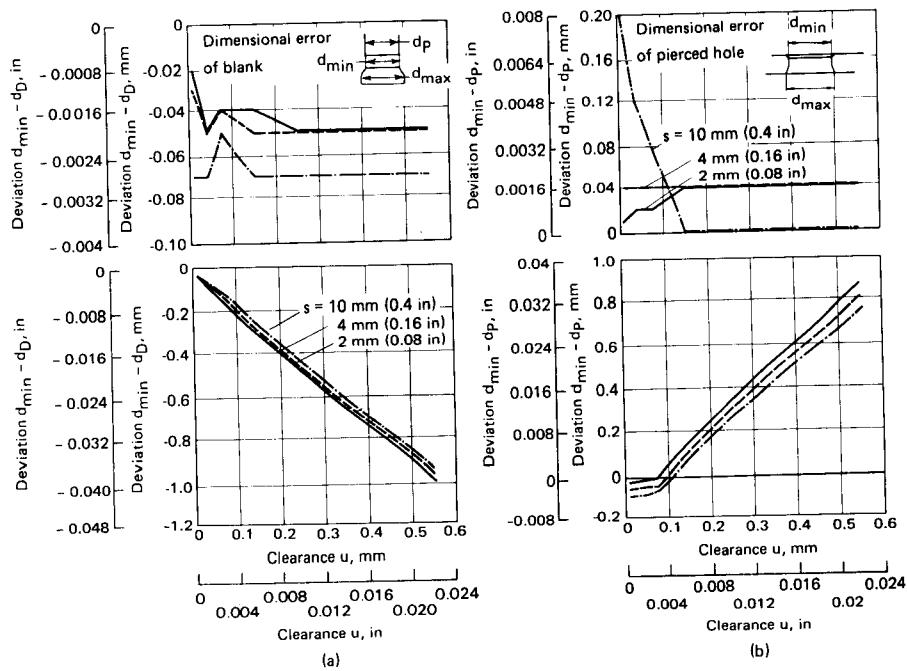


FIG. 24.29 Depth of penetration of cracks on sheared surfaces in blanking and piercing. (After [24.25].)



**FIG. 24.30** Diameter variations of scrap from standard values for blanked and pierced workpieces.  
(After [24.29].)

feed errors in transfer tooling. Deviations in the perpendicularity of the sheared contour surfaces can be caused by the angular deflection of C-type presses.

The inaccuracies of blanked pieces are also caused by inaccuracies in the tooling used. Table 24.2 shows examples of inaccuracies in blanking and piercing which are made from toolings manufactured differently. Tables 24.3 and 24.4 contain values for tolerances in blanking and piercing [24.24].

### 24.3.2 Strength and Hardness

Blanking and piercing are accompanied by the plastic deformation of the workpiece. A result of this plastic deformation is the work hardening of the material. The effect of this work hardening

**Table 24.2** Inaccuracies in Piercing

Manufacture of locating holes for the tooling parts	Method of finishing (for cutting elements)	Tolerance of distances between holes, mm (in)	Tolerance of shearing, mm (in)
Drilling, boring	Grinding	0.25 (0.01)	0.125 (0.005)
Jig boring and grinding	Grinding	0.1 (0.004)	0.125 (0.005)
Jig boring and grinding	Grinding with higher accuracy	0.05 (0.002)	0.025 (0.001)

Source: Compiled from [24.30].

**Table 24.3** Tolerances for Blanking

Sheet thickness, mm (in)	Workpiece dimension, mm (in)			
	<10 (<0.4)	>10 to <50 (>0.4 to <2.0)	>50 to <150 (>2.0 to <6.0)	>150 to <300 (>6.0 to <12.0)
Achievable accuracy without special measures, mm (in)				
0.2–0.5 (0.008–0.02)	0.08 (0.003)	0.1 (0.004)	0.14 (0.006)	0.20 (0.008)
0.5–1.0 (0.02–0.04)	0.12 (0.0047)	0.16 (0.006)	0.22 (0.009)	0.30 (0.012)
1.0–2.0 (0.04–0.08)	0.18 (0.007)	0.22 (0.009)	0.30 (0.012)	0.50 (0.02)
2.0–4.0 (0.08–0.16)	0.24 (0.009)	0.28 (0.011)	0.40 (0.016)	0.70 (0.028)
4.0–6.0 (0.16–0.24)	0.30 (0.012)	0.35 (0.014)	0.50 (0.02)	1.00 (0.04)
Achievable accuracy with special measures, mm (in)				
0.2–0.5 (0.008–0.02)	0.025 (0.001)	0.03 (0.0011)	0.05 (0.002)	0.08 (0.003)
0.5–1.0 (0.02–0.04)	0.03 (0.0012)	0.04 (0.0016)	0.06 (0.0024)	0.10 (0.004)
1.0–2.0 (0.04–0.08)	0.04 (0.0016)	0.06 (0.024)	0.08 (0.003)	0.12 (0.0047)
2.0–4.0 (0.08–0.16)	0.06 (0.024)	0.08 (0.003)	0.10 (0.004)	0.15 (0.006)
4.0–6.0 (0.16–0.24)	0.10 (0.004)	0.12 (0.0047)	0.15 (0.006)	0.20 (0.008)

Source: Compiled from [24.24].

**Table 24.4** Tolerances for Piercing

Sheet thickness, mm (in)	Hole dimension, mm (in)		
	<10 (<0.4)	>10 to <50 (>0.4 to <2.0)	>50 to <150 (>2.0 to <6.0)
Achievable accuracy without special measures, mm (in)			
0.2–1.0 (0.008–0.04)	0.05 (0.002)	0.08 (0.003)	0.12 (0.0047)
1.0–2.0 (0.04–0.08)	0.06 (0.0024)	0.10 (0.004)	0.16 (0.006)
2.0–4.0 (0.08–0.16)	0.08 (0.003)	0.12 (0.0047)	0.20 (0.008)
4.0–6.0 (0.16–0.24)	0.10 (0.004)	0.15 (0.006)	0.25 (0.001)
Achievable accuracy with special measures, mm (in)			
0.2–1.0 (0.008–0.04)	0.02 (0.0008)	0.04 (0.0016)	0.08 (0.003)
1.0–2.0 (0.04–0.08)	0.03 (0.0012)	0.06 (0.0024)	0.10 (0.004)
2.0–4.0 (0.08–0.16)	0.04 (0.0016)	0.08 (0.003)	0.12 (0.0047)
4.0–6.0 (0.16–0.24)	0.06 (0.0024)	0.10 (0.004)	0.15 (0.006)

Source: Compiled from [24.24].

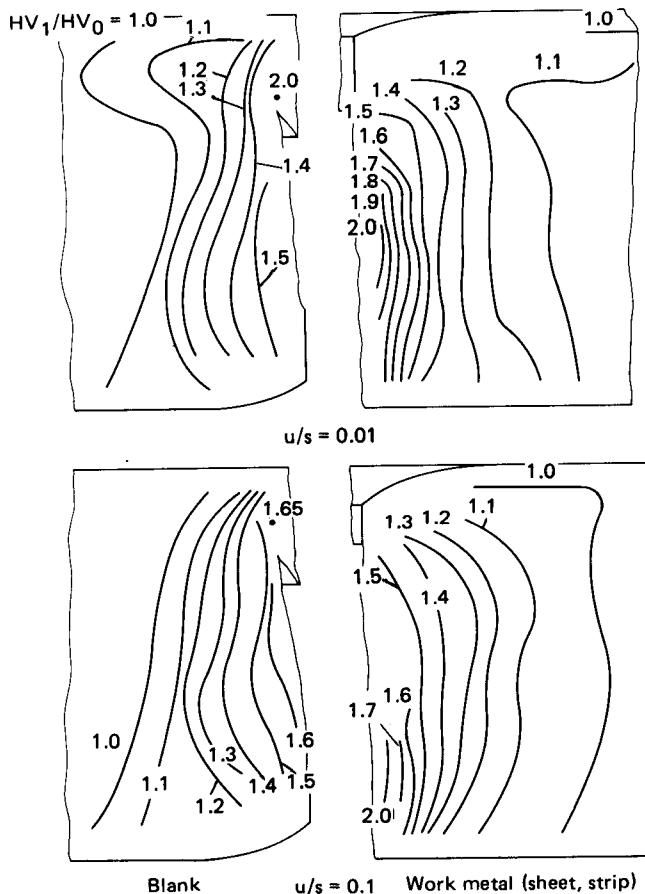


**FIG. 24.31** Changes in hardness in blanked workpieces. Material—C 10 (AISI 1010);  $HV_0 = 117$ ,  $s = 5 \text{ mm (0.2 in)}$ .

can be measured only in the change of hardness since the plastic deformation is confined to a very small zone near the surface (range approximately equal to sheet thickness).

The hardness variations can be significant (Fig. 24.31). The clearance does not have much effect on the work hardening and the region of work hardening. The flow curve of the material, however, plays a major role. The hardness itself as well as the zone of hardening increase with the work-hardening coefficient  $n$  of the workpiece material. Based on various investigations, an increase in hardness of between 2 and 2.2 times the initial hardness is possible for soft steel sheets [24.5], [24.31]. Increased hardness was found up to depths of 0.3–0.58 $s$ .

## 24.4 TOOLING

### 24.4.1 Types

Depending on the type of guidance for the shearing elements with respect to one another, the tools are divided into free, plate-guided, and pillar-guided blanking tooling.

The structure of a free blanking tool is similar to the one shown in Fig. 24.32. The shearing elements of the tooling are not guided with respect to one another; the guidance of the tooling is

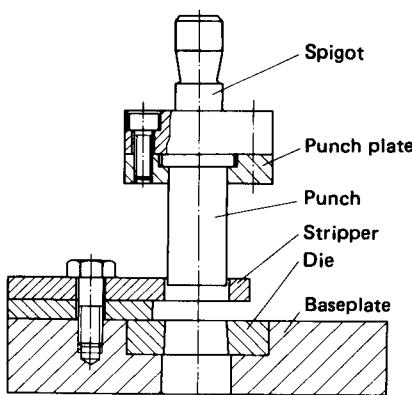


FIG. 24.32 Free blanking tool setup.

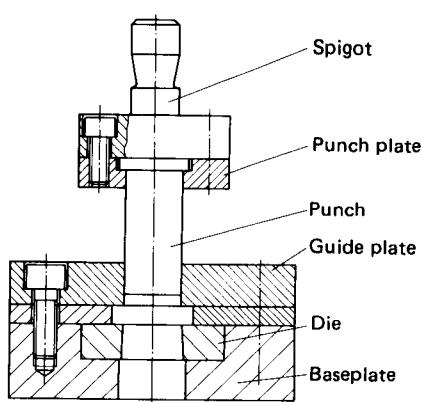


FIG. 24.33 Plate-guided blanking tool setup.

generally controlled by the press ram guides. For a good-quality press and its ram guides, the tools can be expected to be well guided under load.

The free blanking tool is the cheapest type of blanking tooling based on the simplicity of design. It is therefore used for smaller batch sizes. It is difficult to adjust the clearance all around uniformly at the time of initial setup of the tooling. This can lead to larger wear, especially for small thickness as  $s \leq 1 \text{ mm}$  (0.04 in), when the clearance can be as small as 0.01 mm (0.0004 in).

In the case of a plate-guided tool setup (Fig. 24.33) the blanking punch is guided by the guide plate. In setting up the tooling a positional error can thus be avoided. The effects of poor guidance of the press guides due to bearing clearances and the angular deflection of C-frame presses are reduced by guiding the punch. Another advantage of punch guidance is the resistance of long punches to buckling. The guide plate is also used as a stripper.

The use of a blanking element as a guiding element may pose some disadvantages. If proper measures are not taken, the material particles sticking to the punch or to the punch shoulder will cause a faster wear of the guide plate. Also, the manufacture of large accurate guidance holes for large complicated tooling is difficult and expensive.

In the case of pillar-guided blanking tooling (Fig. 24.34) the functions of guidance and shear-

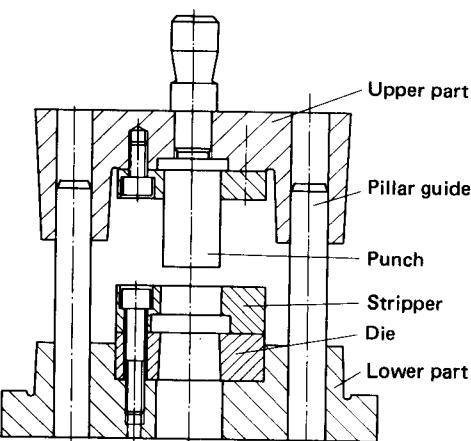
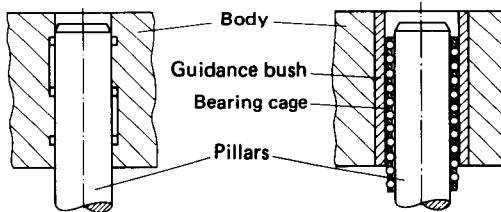


FIG. 24.34 Pillar-guided blanking tool setup.



**FIG. 24.35** Types of guidance for pillar guides.

ing are separated from each other. The pillar guides make this tooling accurate, with the corresponding design of the other elements reducing the tool wear. The errors in bearing clearances of the press need not be taken care of during setting up because of the excellent accuracy of guidance by the pillar die set. Setting the tooling is simple and less time-consuming.

The pillar-guided tooling, like the plate-guided tooling, can contribute to the reduction of defects due to bearing clearance and angular deflection of the press on load. Basically the pillar guides are to be viewed as tools to help in setting up and manufacturing accurate tools. Normally used pillar guides are not stiff enough to take the strong side thrusts caused by noncentral loading on the tools and the tilting movement in C-type presses without allowing large displacements. Hence the pillar guides are not substitutes for inaccurate press guides and less rigid presses.

There are different types of pillar guides. Guidance can be accomplished with either bushings or ball bearings (Fig. 24.35). Guides with ball bearings are very rigid under load [24.32]. They have little friction, and are hence used in fast-stroking presses or in cases where sufficient lubrication is not possible.

Pillar-guided tooling can also be equipped with movable guidance plates for the punch. The guidance plates are mounted on the pillar-guided tooling body and are in general supported by springs on the upper portion of the tool. This design is generally used for blanking thin sheets to ensure the flatness of blanked sheets. The punch can be guided until it touches the sheet. This calls for very precise manufacture of the guidance hole in the plate since there is double guidance, namely, guidance of the punch in the pillar-guided tooling and in the guidance plate. Double guidance is always costly to manufacture.

#### 24.4.2 Basic Design

Workpieces with inner and outer contours can be manufactured in a single- or a multistage tooling. If the workpiece with different inner and outer forms can be made in one stroke, the tooling is called single-stage tooling. If the various processes are carried out in different working strokes, the tooling is called transfer tooling. Both designs are shown in Fig. 24.36.

In single-stage tooling the positional errors of the outer shapes with respect to the holes or openings in the workpiece are determined entirely by the accuracy of manufacture of the tooling. In the case of transfer tooling, in addition to the above, inaccuracies in strip or tool feed also play a part. For the same accuracy of tooling, there will be greater inaccuracies in workpieces made from transfer tooling than in those made from single-stage tooling.

In single-stage tooling the blanked or pierced pieces (and in special cases the scrap also) should be either ejected out of the die or pushed through the die opening. In the case of transfer tooling the pieces and the scrap can be discarded through the holes in the die. Transfer toolings are complicated and costlier because of the necessity of ejection and removal of pieces of complicated shape. Removal of the workpiece must be either automatic or watched and controlled carefully to avoid tool damage or breakage due to pieces remaining in the tooling.

The tools have to be positioned in a press in such a way that the resultant of individual forces passes both through the center of the press bed and the ram area. If this is not the case, eccentric loading causes a tilting moment, which leads to displacement (feeding) and angular (positional) errors. This in turn causes relative maladjustment of tool positions, which results in increased tool wear and inaccuracies of blanked or punched pieces.

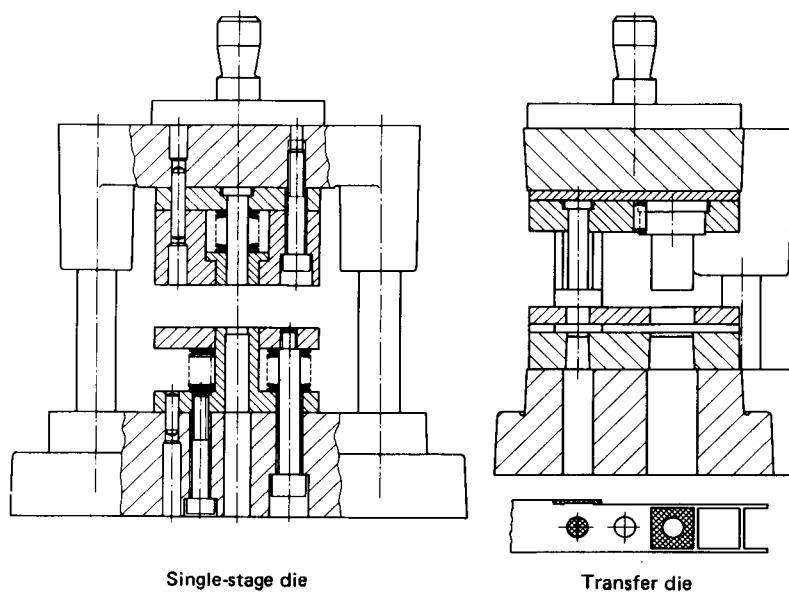


**FIG. 24.36** Tooling for single-stage and transfer blanking and piercing.

The resultant of forces in blanking can be assumed to coincide with the center of gravity of the various blanking lines. Care must therefore be taken during tool design that the center of gravity of the blanking contour coincides with the ram center.

#### 25.4.3 Die Clearance

The clearance between the die and the punch affects the blanked or pierced surfaces and the force-travel diagram. There is no general rule for selecting the clearance value since the parameters are many. The blanking or piercing clearance can be selected based on the appearance of the blanked or pierced surface, inaccuracies, further operations, and functional aspects. If no special conditions are placed on the blanked surfaces, the blanking clearance is generally chosen to result in minimum force requirements.

Guidance values for clearance to produce a burr-free sheared surface are available in the literature. Table 24.5 gives values based on [24.24] and [24.33]. In [24.33] only the strength of the material is considered. Romanowski [24.24] also considers the sheet thickness. Other literature sources [24.30] give different values for a few materials and deviate from the values given in Table 24.5. However, the basic trend is confirmed in all the literature cited.

#### 24.4.4 Die and Punch Shapes

Blanking or piercing punches are generally cylindrical in shape. Punches with a back relief are used for piercing thick sheets [24.34].

Punches, especially for piercing, should be designed for both compressive strength and buckling. To avoid buckling, either stepped punches or punches guided in bushes are used (Fig. 24.37). For piercing smaller holes of  $d < 2$  mm (0.08 in) or holes with a ratio of  $d/s < 0.5$ , punches mounted with spring-loaded guide plates are used, which rest on the sheet during piercing.

Holes or openings in dies are designed as shown in Fig. 24.38. The die with a cylindrical hole over the entire die plate is used if the cut pieces are to be ejected out of the die opposite to the

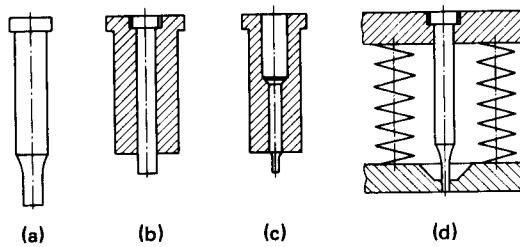
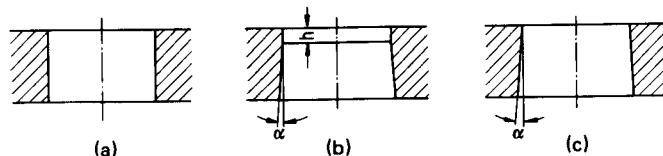
**Table 24.5** Guidance Values for Clearance-to-Thickness Ratio  $u/s$ 

Sheet thickness, mm (in)	Tensile strength of material, N/mm <sup>2</sup> (ksi)				Reference
	<250 (<36.3)	250–400 (36.3–58)	400–600 (58–87)	>600 (>87)	
Irrespective of thickness	0.03	0.04	0.05	0.06	[24.33]
<1 (<0.04)	0.025	0.025	0.03	0.035	[24.24]
1–2 (0.04–0.08)	0.03	0.03	0.035	0.04	
2–3 (0.08–0.12)	0.035	0.035	0.04	0.045	
3–5 (0.12–0.2)	0.04	0.04	0.045	0.05	
5–7 (0.2–0.28)	0.045	0.045	0.05	0.055	
7–10 (0.28–0.4)	0.05	0.05	0.055	0.06	

direction of working, or when the relief on the hole is technically very difficult to achieve because of the composition of the die; for example, stator and rotor sheets are punched with sintered carbide dies made from several plates joined together.

The relief angle in the openings of shapes *b* and *c* in Fig. 24.38 reduces the friction between the cut piece and the die and facilitates pushing the cut piece through the die opening. Guidelines concerning the height (or thickness) of the cylindrical piece and the relief angle to be selected vary considerably. Table 24.6 gives some values for these parameters. If the die plate is machined conically, the dimensions of both the opening and the clearance change with regrinding.

Punches and die plates are made in one piece when it is feasible from both the economical and the manufacturing standpoints. Split tooling is used for pieces with larger dimensions. In this case the various tool elements are made separately and screwed or piloted onto the supporting plate. Split tooling is also used in cases where a grinding operation is required for the tooling and the operation cannot be carried out in the unsplit condition. An example of the tooling used for the blanking of stator and rotor sheets is shown in Fig. 24.39. In this case the punch and the die plate are made from separate pieces and joined together.

**FIG. 24.37** Designs of stepped punches and punch guides.**FIG. 24.38** Opening or hole designs in die plate.

## 24.28 BLANKING, PIERCING, SLUG PRODUCTION

**Table 24.6** Guidance Values for the Design of Openings in Die Plates (Shown in Fig. 24.38)

Sheet thickness $s$ , mm (in)	Opening (conical) $\alpha$	Opening (cylindrical) $h$ mm (in)	$\alpha$	Reference
Irrespective of sheet thickness	5'-10' 1°	4 (0.16) $\leq 2$ ( $\leq 0.08$ )	15'-30' 2°	[24.35] [24.84]
<0.5 (<0.02)	10'-15'	3-5 (0.12-0.2)	3°-5°	[24.24]
0.5-1 (0.02-0.04)	15'-20'	5-10 (0.2-0.4)	3°-5°	
1-2 (0.04-0.08)	20'-30'	5-10 (0.2-0.4)	3°-5°	
2-4 (0.08-0.16)	30'-45'	5-10 (0.2-0.4)	3°-5°	
4-6 (0.16-0.24)	45'-1°	5-10 (0.2-0.4)	3°-5°	
5-10 (0.2-0.4)		10-15 (0.4-0.6)	3°-5°	

### 24.4.5 Feed Stops

Feed stops are used to interrupt the feed of the strip and position it in the tool for processing. In the case of single-stage tooling, the feed stops help reduce scrap; in transfer tooling feed stops help in aligning the strip for the respective stations.

Either pilots or side stops are used as feed stops. Pilots represent the simplest form of feed stop; they are used only when the sheet is moved manually. Fig. 24.40 shows several designs of pilots. Other designs and applications can be obtained from [24.36].

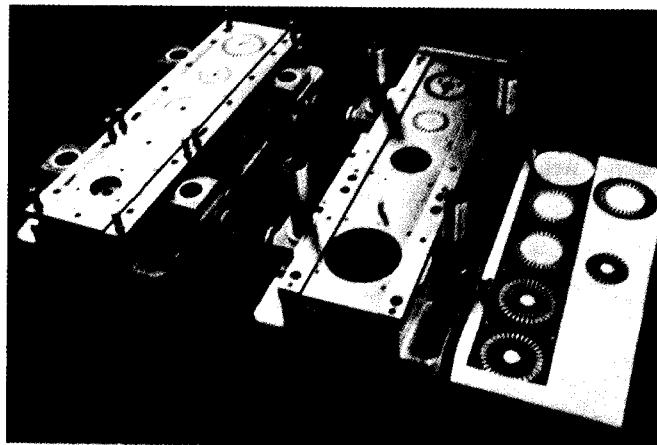


**FIG. 24.39** Sheet utilization in blanking various pieces for stator and rotor.  
(Courtesy of Maschinenfabrik Weingarten.)

Side punches are used to limit the feed for both hand and mechanical feeding operations. They permit more accurate feeding than the pilots. The various designs of side punches have been standardized. A few typical designs are shown in Fig. 24.41. Some side stops are designed to produce the desired contour on the workpiece.

The length of the side punch corresponds to the feed length. The minimum sheet thickness is 0.1 mm (0.004 in) when side punches and stops are used because of the stiffness of the strip. The upper limit is 3 mm (0.16 in). With side stops the blanking contour becomes open, causing side thrusts on the strip and side punch. To counteract these side thrusts, the side punches are guided on their back sides in the die plate.

In addition to the above methods of limiting the feed, locating or holding pins are used which grip either the scrap portion or the portion to be blanked or pierced. Locating pins have an initial conical location portion and a cylindrical guidance portion. They can only be used for sheet thicknesses above 0.2 mm (0.008 in) [24.35]. For smaller sheet thicknesses the strip may bend under the action of the holding pins. The design of round holding pins has also been standardized.

The strip must have a tolerance both in the guide and in the direction of material flow so that the holding pins can correct the position of the material with respect to the cutting direction. The feed is selected to be 0.1–0.2 mm (0.004–0.008 in) greater than the actual feed if holding pins are used. The positional correction always occurs in the direction opposite to the material feed.

Modern fast-stroking presses with a large number of strokes per minute require also a fast feed rate of the material. Average feed velocities of up to 20 m/min (66 ft/min) are possible, with maxima of around 40 m/min (131 ft/min). At these high feed rates it is not possible to limit the feed position by means of side stops because of the high inertia forces. The feeding equipment for the above feed rates, including roll feed arrangements with special drives, must have a feeding accuracy in the range of 0.01 mm (0.0004 in).

#### 24.4.6 Materials

The selection of material for punches and die plates is generally based on economical considerations and hence on various factors. The important factors are wear resistance, stresses acting on the tooling, and workability of the tool material.

The wear resistance of tool steels is dependent on the type, quantity (amount), and distribution of carbides [24.10]. It increases mainly with increasing amounts of carbide and, also, with hardness once a minimum hardness is exceeded [24.8]. This means that to satisfy higher requirements with regard to wear resistance, steels with higher carbon and carbide-builder contents should be chosen.

It is possible to increase the wear resistance of a tool by substituting sintered carbides for steels. When shearing silicon-alloyed sheets of 0.5-mm (0.02-in) thickness, a tool life of  $1.4 \times 10^5$  pieces was obtained for steel tools and a tool life of  $1.4 \times 10^6$  pieces for sintered carbide tooling.

In addition to wear due to friction, the cutting tool elements can also become chipped at their

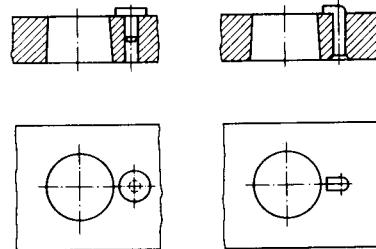


FIG. 24.40 Pilots used in tooling.

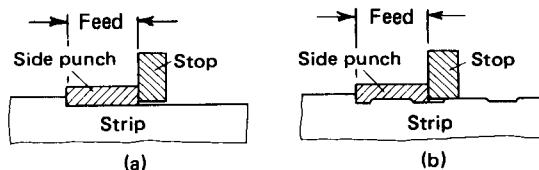


FIG. 24.41 Side punches and side stops.

**Table 24.7** Common Tool Materials for Blanking and Piercing

Material designation <sup>a</sup>		Hardness, HRC	Application		Remarks
DIN	AISI		Sheet thickness, mm (in)	Lot size	
Cemented carbides	—	—	≤1 ( $\leq 0.04$ )	$10^6$	Wear-resistant and brittle
S 3-3-2	—	62-64	<2 ( $< 0.08$ )	$>10^4$	Punches for piercing and fast-stroking tooling
X210Cr12 X210CrW12 X165CrMoV12	D3 D6 D2	60-64	≤4 ( $\leq 0.16$ )	$>10^3$	Wear-resistant, less distortion
90 MnV 8 105 WCr 6	O2 O1	60-64	4-6 (0.16-0.24)	All	Less distortion average toughness
60WCrV7 X45NiCrMo4	T6 —	56-61 48-54	>6 ( $> 0.24$ )	All	Tough
C85W2 C100W1	—	54-62	<4 (0.16)	$<10^4$	Case hardening, core is tough; simple tools and small lot sizes

<sup>a</sup>See App. C.

Source: Compiled from [24.37], [24.38].

edges during the cutting operation. Chipping is usually increased with increasing load, especially when blanking thicker sheets. The danger of edge chipping can be prevented by selecting tool materials with higher toughness. Because of their lack of toughness sintered carbides are not used for sheets more than 1 mm (0.04 in) thick. For thicker sheets, steels with higher toughness are used. Greater toughness can be achieved either by tempering at higher temperatures (there are, however, limitations for high-alloyed steels), by using steels with smaller amounts of carbon and alloying elements [24.37], or by using alloying elements which increase the toughness of steels. An increase of the toughness of steels is generally accompanied by lower wear resistance due to decrease of the amount of carbides following a reduction of the contents of alloying elements.

The above comments permit giving only very general guidelines for the selection of tool materials. Table 24.7 lists frequently used materials for different cutting elements of blanking and piercing tools with their areas of application [24.37], [24.38].

Die plates and punches made from steel are generally hardened if more than a few pieces are to be produced. Every hardening operation causes dimensional changes of the tool. These dimensional changes do not follow any regular pattern, especially in steels not hardened. Some steels hardened by oil and air quenching produce small and uniform changes in the tool. Very small or negligible dimensional changes occur in ledeburitic chromium steels with 12% chromium. In these steels the dimensional changes, though small, are greatest in the direction of the carbide cells, that is, in the longitudinal direction of the bar from which the tool is made.

The nonhardened steels have to be finish-machined to obtain the required dimensions, unless there are no dimensional requirements or the clearances have been selected sufficiently large at the outset to compensate for heat-treatment distortions. Tools made from hardened steels are often finish-machined before hardening.

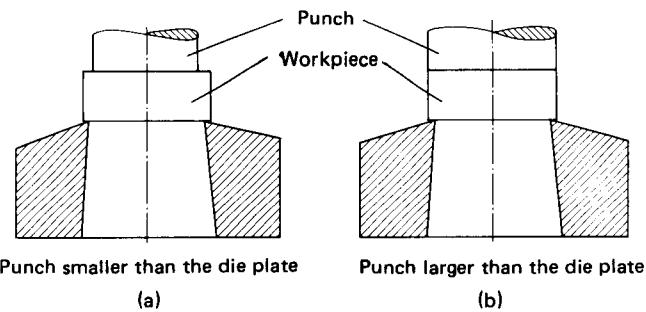


**FIG. 24.42** Shaving of stamped workpieces. (After [24.25].)

## 24.5 SPECIAL PROCESSES

The structure of the sheared surface and its dependence on the tool geometry and material were discussed in Sec. 24.3.1. Plane, smooth sheared surfaces without cracks, with good tolerances perpendicular to the sheet surface, are required if these surfaces are used to transmit forces or motions or if they are used as fitting surfaces. These conditions are not satisfied by common shearing operations. Blanked pieces either have to be shaved or must be made by a special process to achieve the above stringent requirements. Some of the processes used to obtain these surfaces are discussed here.

### 24.5.1 SHAVING

Shaving is a kind of machining operation for finishing the sheared surfaces. In general the material is shaved from the sheared surface in a single working stroke. Fig. 24.42 illustrates the principle of the process. The material to be shaved is pressed through the opening of a die plate by a punch. The die opening is smaller than the workpiece by twice the thickness of the material to be shaved. In general the die plate is manufactured with a conical angle of 10–16°. In this case (Fig. 24.42a) the punch can be smaller than the die plate opening. The workpiece will be fully pressed into the die plate by the punch. A clearance of 0.05 mm (0.002 in) was chosen [24.25]. This design is very commonly used. The punch can also be chosen larger than the die opening. Since the workpiece cannot be pushed completely into the die opening by the punch, successive pieces are pushed one over the other (Fig. 24.42 b).

Fig. 24.43 gives the shaving allowance for various materials and thicknesses to obtain a smooth crack-free sheared surface. The depth to which the crack has propagated can be obtained from Fig. 24.29. The thickness of the layer that can be shaved is limited by the formation of the cracks and will be between 0.1 and 0.5 mm (0.004 and 0.02 in).

According to [24.1], [24.25], the direction in which stamped workpieces are pushed through the die plate should be the same as the direction of blanking. If the operation is done in reverse, cracks may form at the end of the shaving operation due to an increase in thickness of the layer and due to edge draw-in, which prevent support of the punch.

All commonly available presses can be used for the shaving operation. A special shaving process uses a press in which a vibratory movement is superimposed on a normal ram movement. The movements are synchronized in such a way that the working stroke is distributed in small strokes of approximately 0.05–0.1 mm (0.002–0.004 in). With this process it is possible to shave materials of thicknesses greater than 15 mm (0.6 in).

### 24.5.2 Fine Blanking

Fine-blanking processes cover all blanking processes which satisfy the requirements of blanked surfaces discussed in Sec. 24.3.1. Of the various fine-blanking processes known so far [24.34], only

### 24.32 BLANKING, PIERCING, SLUG PRODUCTION

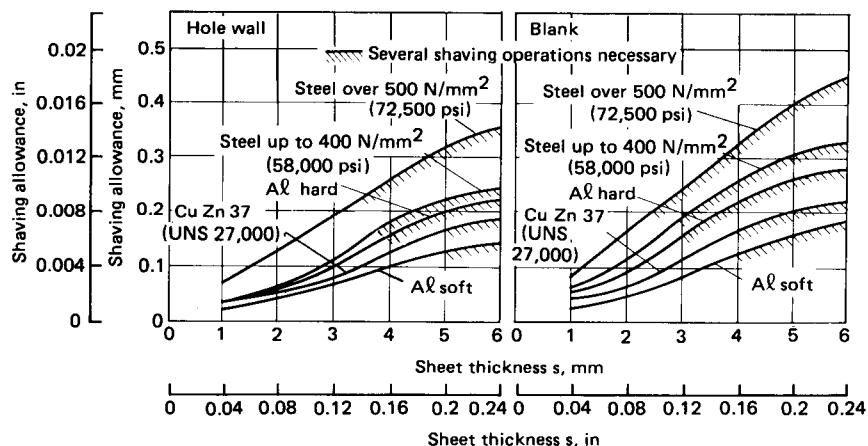
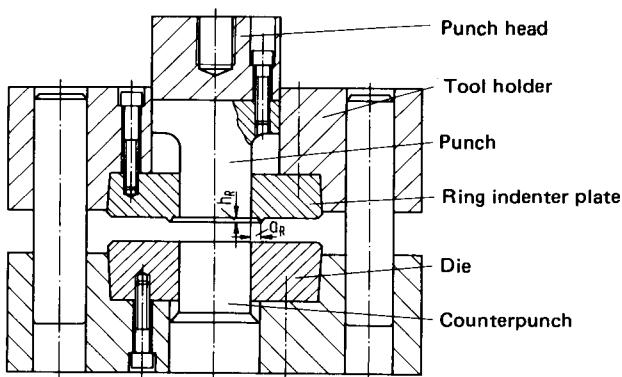


**FIG. 24.43** Shaving allowances and number of shaving operations needed. (After [24.1].)

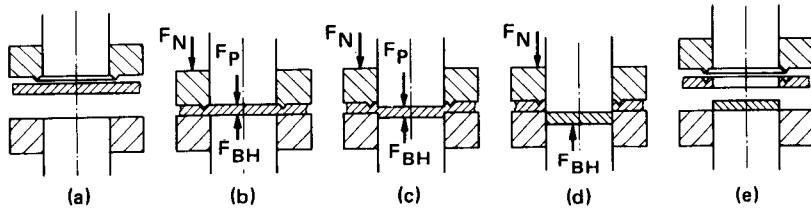
a process developed in Switzerland is widely used in production [24.39]. In this process a ring indenter is pressed onto the sheet to be blanked outside the blanking contour before the process is started. The purpose of using the ring indenter is to superimpose compressive stresses during blanking. Based on Siebel [24.40] the shear fracture stress will become larger than the shear flow stress for a sufficiently high superimposed compressive stress, thereby reducing the chances of crack formation.

Bridgeman [24.41] has shown that by superimposing a pure hydrostatic compressive stress a fully smooth sheared surface can be obtained.

A schematic representation of tooling used for fine blanking is shown in Fig. 24.44. For a sheet thickness of up to 4–5 mm (0.16–0.2 in) only one ring indenter is pressed onto the sheet on the punch side; for greater thicknesses an additional ring indenter is used. Irrespective of the number of ring indenters, they are pressed onto the sheet prior to the blanking operation. In all cases the piece to be blanked is pressed by a counterpunch against the punch. The counterpunch is also used to eject the piece after the blanking operation.



**FIG. 24.44** Fine-blanking tooling.



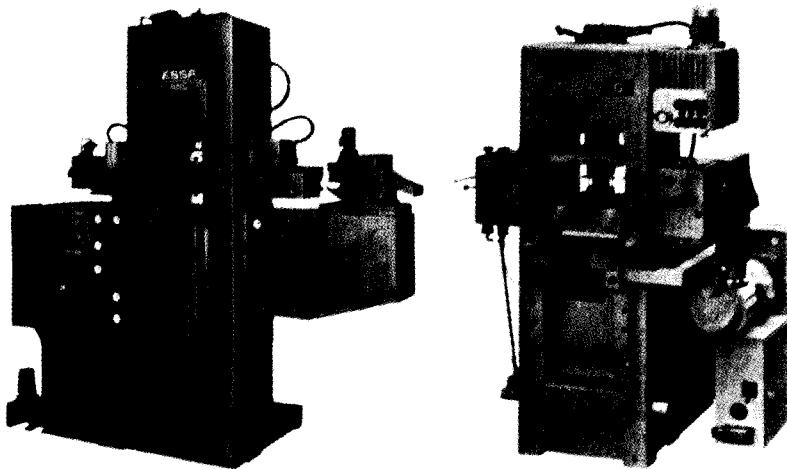
**FIG. 24.45** Different stages of fine-blanking process. (a) Initial position. (b) Pressing in of ring indenter. (c) Blanking against blankholder pressure. (d) End of blanking process. (e) Sheet stripping and ejection of blanked workpiece. (After [24.25].)

Fig. 24.45 shows the various stages of operation of a fine-blanking process. Before the actual blanking process the ring indenter is pressed onto the sheet along the blanking contour. During the blanking operation the counterpunch force holds the workpiece flat by acting in the opposite direction of the punch movement. After the blanking operation the ring indenter and the blanking punch retract to their original positions. The sheet is stripped from the punch by the ring indenter, and the counterpunch is used as the ejector. The counterpunch does not press the blanked piece onto the sheet again but follows the punch and the ring indenter with a time delay, thereby ejecting the workpiece.

The process of fine blanking must be done on triple-action presses since in addition to the blanking force two additional forces, one for the ring indenter and the other for the counterpunch, should be available for the process. In general triple-action hydraulic presses or knuckle-joint presses with hydraulic equipment for triple action are used for fine blanking (Fig. 24.46).

For the successful operation of the fine-blanking process the tool geometry and the additional forces required play an important role. The important tool geometry characteristics are clearance, form or shape of the ring indenter, distance between ring indenter and blanking contour, height of the ring indenter, and die-edge radius.

The clearance for fine-blanking tools is given as  $u \leq 0.01 \text{ mm (0.0004 in)}$  [24.25], [24.42]; for other thicknesses the clearance has been found to be material-dependent. Another important fac-



**FIG. 24.46** Fine-blanking presses. (a) Hydraulic press. (Courtesy of Essa.) (b) Mechanical press. (Courtesy of Feintool-Osterwalder.)

## 24.34 BLANKING, PIERCING, SLUG PRODUCTION

tor to be considered in selecting the blanking clearance is the fact that for larger clearances higher ring-indenter forces are required to obtain a crack-free blanked surface.

Investigations of Krämer [24.13] and Maeda and Nakagawa [24.43] have established a relationship between the ring-indenter distance  $a_R$  and the ring-indenter force required for fine blanking; the ring-indenter force decreases with increasing  $a_R$ .

Any abnormal increase of the ring-indenter distance beyond the optimum required for fine blanking increases the material requirement. For this reason, in industry the ring-indenter distance  $a_R$  is chosen as 0.6–0.75s, and in some cases, where ring indenters are used from both sides, the ring-indenter distances chosen are even smaller [24.44]. The height of ring indenters  $h_R$  is chosen as 0.17–0.33s; the lower values are used for materials with less formability [24.25]. If the ring indenters are used on both sides, the values given here apply for the sum of the height of both ring indenters.

A special feature of the tool geometry is the rounding of the cutting edges of the die plate and the punch. Investigations [24.43] have indicated that a small rounding of about 0.06 mm (0.002 in) in the die plate reduced the proportion of fractured surface on the total surface from 25% to zero, while rounding on the blanking punch increased the proportion of fractured surface on the total sheared surface. Such results have also been established qualitatively for normal blanking [24.7]. In regular production, the cutting edges of the tools are rounded off with oilstone after sharp grinding of the edges. Details on the optimum values of the roundings are not yet well established. The rounding-off radius can be chosen as  $r \leq 0.05$  mm (0.002 in). Differences have been observed with regard to the values of the rounding radius and other parameters, such as the ring-indenter force and distance, between actual production [24.25], [24.45] and other investigations [24.13].

In addition to the blanking force, optimum ring-indenter and counterpunch forces are necessary for a successful operation of the fine-blanking process. The counterpunch holds the sheet plane and flat during blanking, thereby preventing bending of the sheet [24.13]. A direct effect of these parameters on the formation of the sheared surfaces can only be observed for thicknesses above 1 mm. The counterpunch forces required for 40-mm (1.6-in) blanks are one-third the shearing force [24.13]. The counterpunch pressure  $p_{BH}$  calculated for these orders of magnitude of forces agrees very well with the information in [24.25], which gives the permissible variation of the counterpunch pressure as 20–70 N/mm<sup>2</sup> (2900–10,150 psi). The required ring-indenter force can be approximately calculated as [24.25]

$$F_R = 4S_u l_R h_R \quad (24.10)$$

where  $l_R$  is the length and  $h_R$  the height of the ring indenter, which is chosen between 0.17s and 0.33s. The ring-indenter forces can also be obtained from experimentally determined values [24.13]. Haack [24.45] gives the value of the ratio of ring-indenter force to punch force as between 0.3 and 1. The indicated range of the suggested value is due to the possible differences in the position of the ring indenter from the blanking contour.

Smooth crack-free sheared surfaces can be obtained for nearly all materials. Most important for the workability for fine blanking are not so much the mechanical properties of the material as the chemical composition and the microstructure due to heat treatment and chemical composition [24.13]. The following materials are suitable for fine blanking: aluminum and aluminum alloys, copper and brass with copper content  $\geq 63\%$ , unalloyed steels with carbon content  $\leq 1\%$ , case hardening steels, low-alloyed heat-treatable steels, and ferritic and austenitic stainless steels [24.39], [24.46]. The accuracy of fine-blanked workpieces as measured on the blanked surfaces lie between IT7 and IT8 [24.13], [24.25].

A variation of fine blanking has been developed by Kienzle and Meyer [24.3]. The basic difference between this process and the standard fine-blanking process is that instead of a ring indenter, a blankholder with an inclination of 0.75° is used. The clearance is chosen as about 0.05 mm (0.002 in) to produce smooth sheared surfaces on both the blank and the strip. The rounding radius on the shearing edges must be 0.01 mm (0.0004 in). The blankholder forces required must be around 1000 N (5600 lbf) per millimeter (inch) length of the blanking contour for materials with a tensile strength of 200 N/mm<sup>2</sup> (29 ksi) and 2000 N (11,320 lbf) per millimeter (inch) length for materials with a tensile strength of 700 N/mm<sup>2</sup> (101.5 ksi). The required counterpunch pressure lies between 100 and 230 N/mm<sup>2</sup> (14.5 and 33.5 ksi). Any application of this process in industrial production is not yet known.

### 24.5.3 Counterblanking

Another special blanking process developed in recent years is counterblanking [24.27], [24.28]. In this process the blanking action is done in three stages (Fig. 24.47). During the first stage the punch penetrates into the sheet only slightly. In the second stage counterblanking takes place—the bottom punch comes into action. Finally the top punch pushes the blank through the die cavity. This is done in a transfer tooling with three sets of punches, and the clearances are matched for every stage. It is not possible to achieve smooth sheared surfaces by this process, but sheared surfaces completely free from burrs, with an increased smooth portion, can be obtained. Details on the clearance and punch-penetration values and the application of the process can be obtained from the literature cited.

### 24.5.4 Flow Piercing

The surface quality of the pierced hole can be influenced by influencing the stress condition in the deformation zone (see Sec. 24.5.2). Investigations [24.31] have shown that changes in piercing (or blanking) clearance and geometry of the tools have very little influence on the direction of the maximum shear stress.

Another method of piercing is to prevent the formation of cracks (if possible) so that the shear flow stress is reached before the shear strength (see also Fig. 24.11). The location of the shear yield

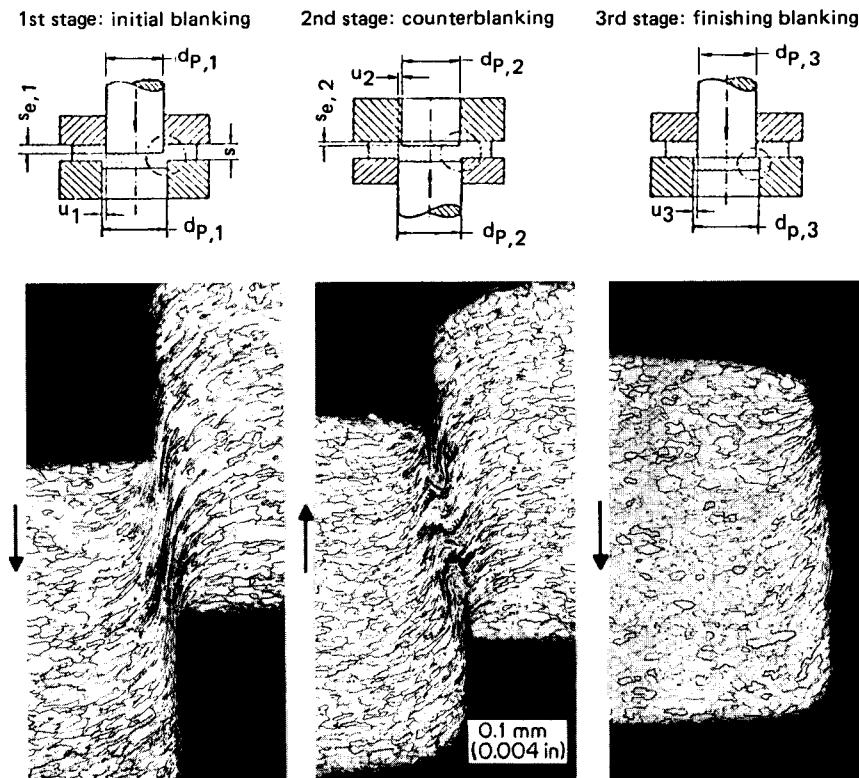


FIG. 24.47 Stages and micrographs of counterblanking process.

point is affected to a large extent by the deformation strain. It should therefore be attempted to achieve plastic deformation in the hatched zone in Fig. 24.11. This can be done by superimposing hydrostatic stress in the deformation zone by which the principal stress circle is pushed into the compressive zone.

A method using the above principle has been described in [24.31]. In this method the shape of the piercing punch is changed (Fig. 24.48). The face diameter of the punch is smaller than the step diameter of the punch, resulting in different piercing clearances. The two diameters are joined by a conical shell line.

The piercing operation takes place in one stroke without the need for special arrangements on the press. The punch face diameter pierces a smaller hole with a relatively larger clearance. At the end of this stage the pierced hole has a small ductile and a large brittle fracture. The conical portion of the punch acts more or less like a cylindrical punch.

During the second stage of operation a process similar to that of forward extrusion takes place. A trapezoidally shaped ring is pushed out as scrap by the shoulder punch diameter. This scrap is removed by the next piercing operation. Fig. 24.49 illustrates the process of flow piercing. The various stages of the process are shown in Fig. 24.50.

The accuracy of the holes manufactured is around 0.3 mm (0.01 in) for sheets with a thickness of 8–15 mm (0.3–0.6 in) and a hole diameter of 20 mm (0.8 in).

## 24.6 INTERACTION BETWEEN MACHINE, TOOLING, AND PROCESS

Every deformation process requires a machine capable of delivering the required force at all punch positions. The forces are transmitted from the machine tool through the tooling onto the workpiece. In addition, the machine, sometimes together with the tooling, should guide the blanking tools with respect to each other. Alignment or positional errors are to a great extent responsible for inaccuracies in the stamped workpiece and for excessive tool wear. Common errors are parallelism, offset, runout, and errors in height (see Chap. 8). Depending upon the time sequence of the operations, two major sources of errors in stamping operations are contact errors during blanking and errors during ejection [24.47], [24.48]. These defects are also included in the major defect categories mentioned earlier. An offset of the blanking contour of the outer or inner form affects the parallelism, the central offset, and the runout. Defects in height, that is, errors in the travel of the tooling, do not cause any major defects in the workpiece.

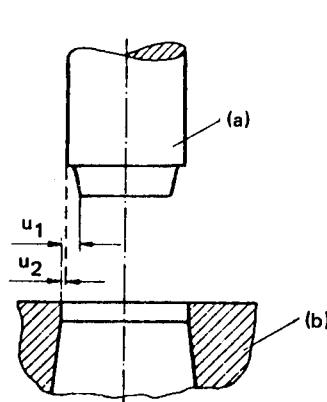


**FIG. 24.48** Tooling for flow piercing. *a*—punch; *b*—die;  $u_1$ ,  $u_2$ —piercing clearances. (After [24.31].)

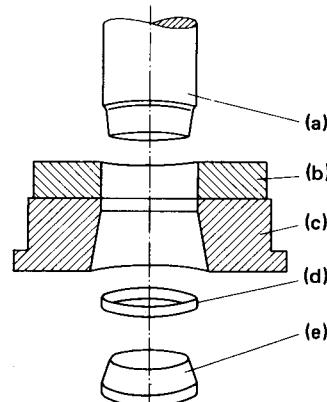


**FIG. 24.49** Flow piercing: tooling end product. *(a)* Punch. *(b)* Finished hole. *(c)* Die. *(d)* Trapezoidal ring. *(e)* Discard. (After [24.31].)

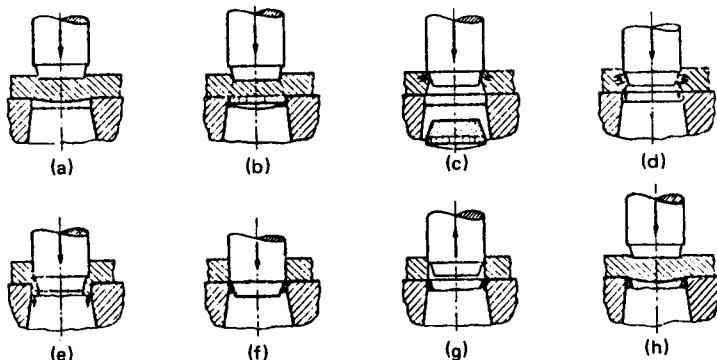


**FIG. 24.50** Stage sketches in flow piercing. (a) Preforming. (b) Crack initiation. (c) Application of compressive stress condition in preformed hole. (d), (e) Flow process. (f) Position at bottom dead center of press. (g) Return stroke. (h) Same as (a) with pushing out trapezoidal ring still in the die. (After [24.31].)

Wear on the tools is caused by, among other factors, errors in displacement (feed) and position (height) [24.47]. Increased displacement errors cause increased wear of the cutting edges. Breakage occurs when at one point the two cutting edges hit against each other. This occurs mostly during and after loading, due to vibrations. Any punch penetration in the die plate, that is, an error in height, increases the wear of the punch shell.

For the errors in displacement and height to remain as small as possible, the tolerance in the guides and the drives of the press must be small and the stiffness of the press and the tool must be large [24.47], [24.48]. There are, however, limitations to increasing the stiffness of the press and tooling beyond a particular limit.

Based on the type of press design, the stiffness and the angular deflection vary. A classification based on the stiffness in the transverse direction and on the angular deflection and the resulting displacement of the tools with respect to one another ranks the presses as follows [24.47, 24.48]: four-column press (Fig. 24.51), two-column press (Fig. 24.52), and C-frame press with and without tension bar (Figs. 24.53 and 24.54). The four-column press is considered best for the purpose of blanking. It should, however, be remembered that even with four-column presses, due to defects in parallelism, offset loading can occur.

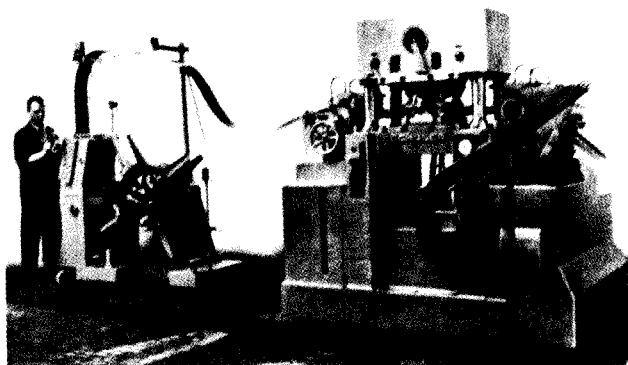


**FIG. 24.51** Four-column fast-stroking blanking press. (Courtesy of L. Schuler.)

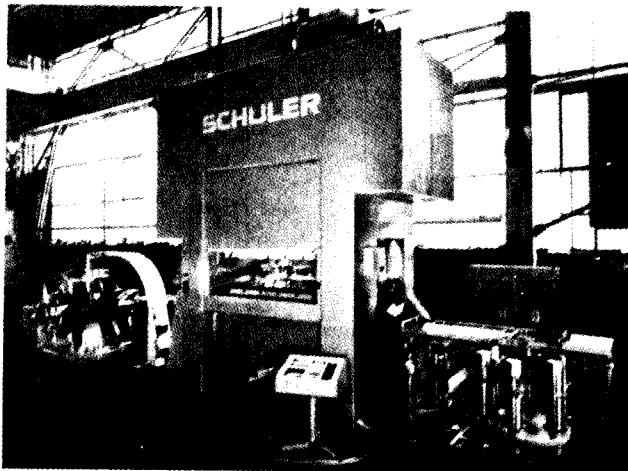


FIG. 24.52 Two-column blanking press. (*Courtesy of L. Schuler.*)

In order to keep the effects of play and friction in the ram guides small, ball-bearing pillar guides are used for tooling. In addition any displacement defect can be completely eliminated for central loading by eliminating the play required in the ram guides [24.49].

The use of pillar-guided tooling in less rigid presses is no substitute for stiffer presses with small ram play. However, the displacement errors or defects are affected by the type of tool guide and the clamping of the tool on the machine. Comparative investigations on free-blanking tools (without any tool guidance) and on pillar-guided toolings (with both two and four columns and/or ball-bearing-guided) for blanking on C-frame presses have indicated that the pillar guides reduce the displacement of the blanking tool elements with respect to one another [24.32]. Four-column-guided tooling did, however, have no advantage over two-column-guided tooling in

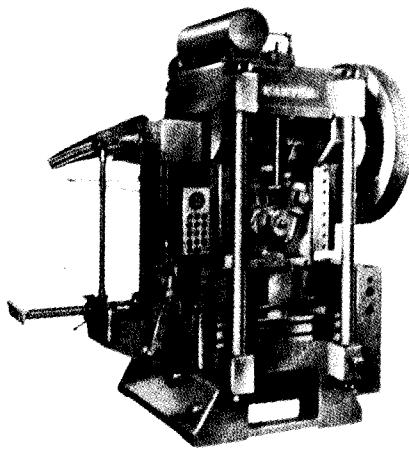


FIG. 24.53 C-frame press with tension rod. (*Courtesy of H. Raster.*)

reducing the displacement defects. The use of sliding guides is preferable to the use of ball-bearing-guided toolings. The type of connection or clamping between the upper portion of the tooling and the press ram affects the displacement of the tools relative to one another considerably. Floating or movable clamping leads to smaller displacements than rigid clamping [24.47]. For blanking processes the best combination with C-frame presses is to use a four-column slide-guided tooling with movable or floating clamping between the upper tooling and the ram.

According to the foregoing, when the blanking clearance and a suitable press are to be selected, the blanking clearance should be large for a press with lesser stiffness to achieve less tool displacement on the stamping plane. If a smaller clearance is required (such as for thinner sheets), then a stiffer press must be chosen.

#### 24.7 ECONOMICAL CONSIDERATIONS AND MATERIAL UTILIZATION

The maximum utilization of a material when blanking from a sheet is a problem of geometry. Scrap-free blanking can be done for geometrically matching shapes, such as triangles, rectangles, and hexagons. The rules for matching shape geometry are given in [24.50]. A few examples of scrap-free blanking are given in Fig. 24.55.

Scrap-free blanking is only possible in some special cases. Therefore a change of the geometry of the workpieces should be attempted in order to approach scrap-free blanking. For workpieces whose geometry cannot be changed to scrap-free blanking, the pieces have to be arranged on the sheet or strip to be blanked in such a way that the material utilization can be improved. A classic example is the blanking of round plates. For single-row blanking the material utilization is around 60%, for two rows it is 67%, and for six-row blanking it is 72% with a web clearance of 0.1 times the blank diameter.

In many cases it may be possible to use the scrap for some other pieces. For this to be economical and feasible, the thickness of the pieces to be made from the scrap should be the same as that of the scrap. The sequence of operations should also permit the parts from sheet and scrap to be made in quick succession without having to store the scrap. The manufacture of stator and rotor sheets for the electrical industry is an example (Fig. 24.39) of excellent material utilization. In this case a transfer tooling is used to blank or pierce out all the required pieces from the same sheet. The beginning and end pieces of strips result in additional scrap. For reasons of economy, it may

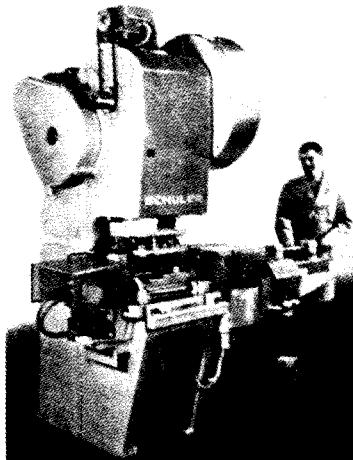


**FIG. 24.54** C-frame press. (*Courtesy of L. Schuler.*)

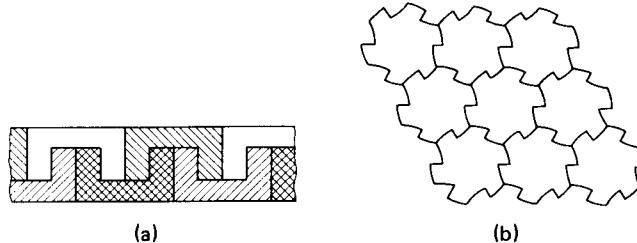


**FIG. 24.55** Scrap-free blanking shapes. (a) Transformer blanks. (b) Sprockets. (*After [24.38].*)

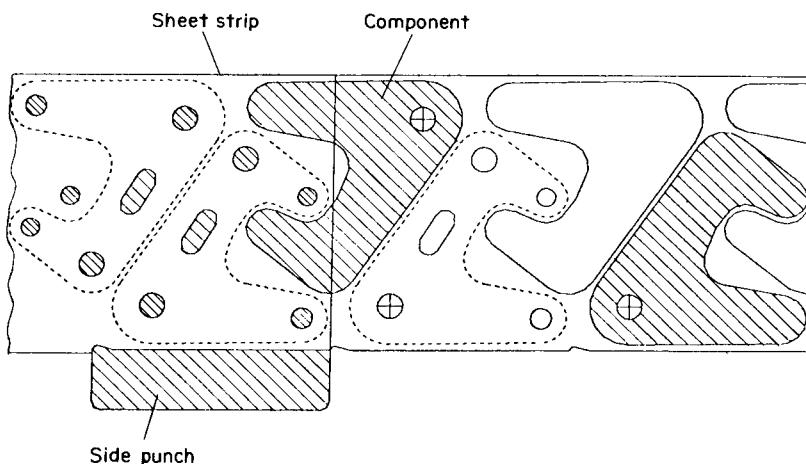


**FIG. 24.56** Computer-aided design and drafting of nesting in blanking processes. (After [24.51].)

be preferable not to use sheet plates or strips in blanking tooling, but to feed directly from coils, which reduces scrap at the beginning and end pieces substantially. The additional effort of feeding in separate strips can also be avoided in this case.

Recently several researchers have investigated nesting of blanks on strips for minimum loss of material as scrap [24.51]. Computer-aided methods are used to lay out the blanking operations. The computer is used to make the necessary drawings and to indicate the position of the side stops and the processing sequence. Fig. 24.56 shows the computer-developed nesting of a lever part. In the future, computer-aided design methods will find increasing application for this purpose.

## REFERENCES

- 24.1 Timmerbeil, F. W.: "Investigation on the Blanking Process of Sheet, Especially with Closed Cutting Edge" (*in German*), *Werkstattstech. u. Maschinenbau*, **47**, 1957, pp. 231–239, 350–356.
- 24.2 Bach, E. L.: "Stresses under a Circular Punch" (*in German*), Dr.-Ing. thesis, Technische Hochschule, Karlsruhe, 1923.
- 24.3 Kienzle, O., and Meyer, M.: "Process to Obtain Smooth Blanked Surfaces in Full-Length Blanking of Sheets" (*in German*), *Forschungsberichte des Landes Nordrhein-Westfalen*, no. 1162, Köln/Opladen, Westdeutscher Verlag, 1963.
- 24.4 Hojo, H.: "On the Shearing Mechanism of Phenolic Paper Base Laminated Sheets," *Ann. CIRP*, **14**, 1966/1967, pp. 409–428.
- 24.5 Eickhoff, W.: "On Punching of Thick Plates" (*in German*), Dr.-Ing. thesis, Technische Hochschule, Darmstadt, 1961.
- 24.6 Krämer, W.: "Contribution to the Determination of Force and Deformation Work in Sheet Blanking" (*in German*), *Ind.-Anz.*, **90**, 1968, pp. 361–365.
- 24.7 Timmerbeil, F. W.: "Effect of Blank Edge Wear on the Blanking Process of Sheet" (*in German*), *Werkstattstech. u. Maschinenbau*, **46**, 1956, pp. 58–66.
- 24.8 Buchmann, K.: "On Wear and Its Effects on Blanking of Steel Sheets" (*in German*), *Werkstattstechnik*, **53**, 1963, pp. 128–134.

- 24.9 Bühler, H., Pollmar, F., and Rose, A.: "Effect of Tool Material and Its Heat Treatment on the Shearing of Sheets" (*in German*), *Arch. Eisenhüttenwes.*, **41**, 1970, pp. 989–996.
- 24.10 Sondershaus, E.: "Wear Studies on Blanking Tools" (*in German*), *Mitt. Dtsch. Forschungsges. Blechverarb. u. Oberflächenbehand.*, **19**, 1968, pp. 142–156.
- 24.11 Peter, H.: "Blanking Clearance in Tools" (*in German*), *Werkstatttech. u. Maschinenbau*, **46**, 1956, pp. 53–58.
- 24.12 Stromberger, C., and Pfaff, K. O.: "Punching of Austenitic Stainless-Steel Sheets with Small Punch Diameters" (*in German*), *Werkstatt u. Betr.*, **103**, 1970, pp. 135–140.
- 24.13 Krämer, W.: "Investigations on Fine Blanking of Steel and Nonferrous Metals" (*in German*), *Berichte aus dem Institut für Umformtechnik, Universität Stuttgart*, no. 14, Essen, Girardet, 1969.
- 24.14 Masuda, M., and Jimma, T.: "Theoretical Research on the Blanking of Sheet Metal," *Ann. CIRP*, **11**, 1962/1963, pp. 224–228.
- 24.15 Zünkler, B.: "Studies on the Geometry of Blanking Tools and the Mechanics of the Blanking Process" (*in German*), *Bänder Bleche Rohre*, 1963, pp. 344–350.
- 24.16 Bach, C. von: *Elasticity and Strength (in German)*, Berlin, Springer, 1971.
- 24.17 "Blanking Technology" (*in German*), in *Betriebshütte Akademischer Verein Hütte e.V.* (ed.), vol. 1, 6th ed., Berlin/München, Ernst und Sohn, 1964.
- 24.18 Ballhausen, C., and Moers, P.: "Investigations on Side Thrust in Blanking of Thin Sheets" (*in German*), *Werkstatttech. u. Maschinenbau*, **46**, 1956, pp. 410–412.
- 24.19 Kondo, K.: "Mechanism of Shearing Process of Double Sheet Metals," *Bull. Jpn. Soc. Prec. Eng.*, **2**, 1967, pp. 89–94.
- 24.20 Kienzle, O., and Jordan, T.: "Measurements of Side Thrust in Punching of Sheets" (*in German*), *Mitt. Forschungsges. Blechverarb.*, 1954, pp. 217–219.
- 24.21 Timmerbeil, F. W.: "Effects of Back Force on Punching of Sheets" (*in German*), *Mitt. Forschungsges. Blechverarb.*, 1953, pp. 77–92.
- 24.22 Stromberger, C., and Dies, R.: "Investigations on the Force, Temperature, Friction, and Wear Conditions in Punching of Sheets with Circular Punches" (*in German*), *Mitt. Forschungsges. Blechverarb.*, 1955, pp. 415–451.
- 24.23 Matuszewsky, H.: "Investigations on Shearing and Withdrawal Forces as a Function of Various Parameters in the Piercing of Sheets" (*in German*), *Forschungsberichte des Landes Nordrhein-Westfalen*, no. 2994, Köln/Opladen, Westdeutscher Verlag, 1980.
- 24.24 Romanowski, W. P.: *Handbook of Punching Technology (in German)*, Berlin, VEB-Verlag Technik, 1959.
- 24.25 Guidi, A.: *Shaving and Fine Blanking (in German)*, München, Hanser, 1965.
- 24.26 Brockhaus, J., and Singer, H.: "Counterblanking of Steel Strip—Its Characteristic Properties" (*in German*), *Mitt. Dtsch. Forschungsges. Blechverarb. u. Oberflächenbehand.*, **23**, 1972, pp. 73–81.
- 24.27 Lange, K., and Liebing, H.: "Blanking and Piercing without Any Burr" (*in German*), *Ann. CIRP*, **27**, 1978, pp. 177–181.
- 24.28 Liebing, H.: "Counterblanking—A Shearing Process for Producing Blanks without Any Burr," *Int. MTDR*, 1978, pp. 369–375.
- 24.29 Keller, F.: "Effect of Blanking Clearance in Punching of Steel Sheets on the Dimensions of the Hole and the Blank" (*in German*), *Werkstatt u. Betr.*, **84**, 1951, pp. 479–482.
- 24.30 *Metals Handbook*, vol. 4, "Forming," 8th ed., Metals Park, OH, American Society for Metals, 1969.
- 24.31 Thomsen, T.: "Smooth Hole Surfaces in Punching of Sheets" (*in German*), Dr.-Ing. thesis, Technische Hochschule, Darmstadt, 1966.

## 24.42 BLANKING, PIERCING, SLUG PRODUCTION

- 24.32 Mikkers, J. C.: "Investigations on the Punch Offset in Blanking" (*in German*), *Bänder Bleche Rohre*, **11**, 1970, pp. 223–228.
- 24.33 VDI-Richtlinie 3368: "Schneidspalt, Schneidstempel und Schnittplattenmaß für Schnittwerkzeuge (Blanking Clearance, Blanking Punch, and Die Dimension for Blanking Tools)," Düsseldorf, VDI-Verlag, 1965.
- 24.34 Oehler, G., and Kaiser, F.: *Cutting, Stamping, and Drawing Tools* (*in German*), 5th ed., Berlin/Heidelberg/New York, Springer, 1966.
- 24.35 Hilbert, H.: *Stamping Technology* (*in German*), vol. 1, "Cutting Tools," 5th ed., München, Hanser, 1954.
- 24.36 VDI-Richtlinie 3358: "Vorschubbegrenzungen an Stanzwerkzeugen (Feed Stops in Stamping Tools)," Düsseldorf, VDI-Verlag, 1961.
- 24.37 "Steels for Stamping Tools" (*in German*), Bull. 1122/10, Deutsche Edelstahlwerke, Krefeld, 1964.
- 24.38 Verein Deutscher Eisenhüttenleute: *Material Handbook Steel and Iron* (*in German*), 4th ed., Düsseldorf, Verlag Stahleisen, 1965.
- 24.39 Lange, K.: "The Potential of the Fine-Blanking Technique," *Information, Fine-Blanking Technical Review*, ed. A., no. 20, Lyss, Switzerland, Feintoil AG, 1978, pp. 1–6.
- 24.40 Siebel, E.: *Forming in Plastic Condition* (*in German*), Düsseldorf, Verlag Stahleisen, 1932.
- 24.41 Bridgeman, P. W.: *Studies in Large Plastic Flow and Fracture*, New York/Toronto/London, McGraw-Hill, 1952.
- 24.42 Schmidt, W.: "Practical Applications of Fine-Blanking Technology" (*in German*), *Tech. Rundsch.*, **5**, 1967, no. 38, pp. 5–6.
- 24.43 Maeda, T., and Nakagawa, T.: "Experimental Investigation on Blanking," *Scientific Papers of the Institute of Physical and Chemical Research*, no. 62, 1968, pp. 65–86.
- 24.44 "The HSR-Fine Blanking and Its Applications" (*in German*), pamphlet, Rapperswil, Switzerland, Heinrich Schmid.
- 24.45 Haack, J.: "A Few Specialties of Fine Blanking" (*in German*), *Werkstatt u. Betr.*, **101**, 1968, pp. 425–429.
- 24.46 Beck, G.: "Importance of Workpiece Materials in Fine Blanking, parts I and II" (*in German*), *Bänder Bleche Rohre*, **14**, 1973, pp. 339–344, 373–377.
- 24.47 Seidenberg, H.: "Press Effects on Tool Wear and Burr Height in Blanking of Thin Sheets with Closed Blanking Line" (*in German*), Dr.-Ing. thesis, Technische Universität, Hannover, 1965.
- 24.48 Juesten, V. "Investigations on the Important Press Factors on Blanking" (*in German*), Dr.-Ing. thesis, Technische Universität, Hannover, 1969.
- 24.49 Doege, E., Dangelmaier, K., and Hoffmann, H.: "Requirements on Fast-Stroking Presses Using Cemented Carbide Tooling" (*in German*), *Werkstattstechnik*, **60**, 1970, pp. 423–428.
- 24.50 Heesch, H., and Kienzle, O.: *Scrap-Free Blanking, Geometrical Rules for Blanking Flat Pieces* (*in German*), Berlin/Göttingen/Heidelberg, Springer, 1963.
- 24.51 Cornely, H., and Guldin, W.: "Computer-Aided Design of Transfer Tooling" (*in German*), *Ind.-Anz.*, **96**, 1974, pp. 611–614.

## **SLUG PRODUCTION**

In general slug production consists of the following tasks:

- 1 Selection of the semifinished product from which the slug is to be made
- 2 Cutting into lengths or blanks
- 3 Heat treatment
- 4 Surface treatment

The sequence of operations after the semifinished product has been selected may vary. While the first two operations as well as the surface treatment occur almost always, the third, namely, heat treatment to obtain a soft and homogeneous material structure, is not always necessary. Depending on the particular forging conditions, it is sometimes possible to leave out the surface treatment. Further information is given in Sec. 25.3.2.

### **25.1 MATERIAL FOR SLUGS AND BLANKS**

The following semifinished products are used to make slugs and blanks:

- Sheets (slabs or strip), for both sheet and bulk forming
- Billets, for forging processes
- Rods or coils, for bulk forming
- Bars, for bulk forming
- Tubes, for sheet and bulk forming

In many cases the choice of the semifinished product is based solely on the mechanical characteristics required of the component. Possible changes in mechanical properties during forming may also have to be taken into account. An example is sheet forming. The usual starting materials

are rolled sheet strip or, increasingly, continuously cast ingots. However, an exception is the zinc sheet bar, used in the extrusion of cups, which is cut off from or out of continuously cast strip. The scrap resulting from the cutting process is returned to the melt.

For bulk forming of steel the choice of the semifinished product is less critical than in sheet forming. Usually it is sufficient to specify the material to be used and the dimensions required.

Economic manufacture by means of cold bulk forming is often decisively influenced by the slug production costs. Thus special care must be taken in the choice of semifinished product, given the numerous possibilities offered.

Cutting circular blanks from sheet strip is accompanied by relatively large amounts of scrap, possibly up to 30% of the original material. For this reason circular blanks are cut from sheet only for can extrusion of nonferrous metals because of their relatively high scrap value.

Rods (coils) and bars are the semifinished products most commonly used because in most cases slugs of the required lengths can be cut from them without resulting scrap. Without exception, nonferrous metals are formed in an extruded or drawn state. Steel bars "as hot rolled" are the cheapest raw material and are used where there are no special demands on the quality of surface finish and decarburization. The fine surface cracks which may occur with rolled bars are also found in the resulting workpieces.

Drawn rod or bar steel is most suitable for components requiring a good surface finish; peeled materials may be used when no decarburization is permitted because the workpiece is to be hardened after forming or where higher demands are placed on the quality of surface finish of the part. In the latter case, peeling prior to forming is often cheaper than extensive machining of the part after the forming process. The decision which of the three initial states to choose depends on the requirements on the finished component.

## 25.2 PRODUCTION OF SLUGS AND BLANKS

Slugs and blanks can be produced from semifinished products using parting-off processes (see Chap. 24) and chip-forming machining processes. On the basis of the classification given in Chap. 2, these processes all belong to the main group "separating processes." Since the components to be produced are completely parted off from the semifinished product, the term parting off will be used hereafter.

Furthermore only those parting-off processes are discussed which are of particular significance to slug and blank production for sheet and bulk forming (Fig. 25.1). Reference will be made in passing to parting processes of minor importance, such as friction cutting [25.1], [25.2], abrasive cutting [25.3], [25.4], and flame cutting [25.5] to [25.7].

### 25.2.1 Shearing (Cropping)

Shearing of slugs from bar stock is generally called cropping. This section discusses bar cropping at room temperature. Hot cropping, as used mainly in forges for parting off large cross sections, and where the parting operation results in a larger portion of smooth-sheared (burnished) surface than in cold shearing, is discussed in [25.8] and [25.9]. The sizing of cropped slugs is discussed in Sec. 25.3.1.

#### *Definition*

Cropping is the complete parting off of a slug or billet from the semifinished product (rod, bar, billet) along an open cutting line (Fig. 25.2).

#### *Application*

Cropping permits almost scrap-free parting off of slugs and billets from rods and bars. Only the bar ends are lost as scrap. In general, only closed solid sections, that is, circular and multifaceted cross sections, are parted off by cropping. Parting-off processes are usually automatic in order to achieve high-volume throughput. For example, parting off 100-mm (4-in) thick billets can lead to a throughput 17.5 times higher than that obtained by sawing [25.10]. The practical limit of cropping is given by the length-to-diameter ratio  $l/d$  of the slugs concerned and is approximately  $0.5 \leq l/d < 0.6$ . However, lower values may be obtained by adding axial compressive load [25.11].

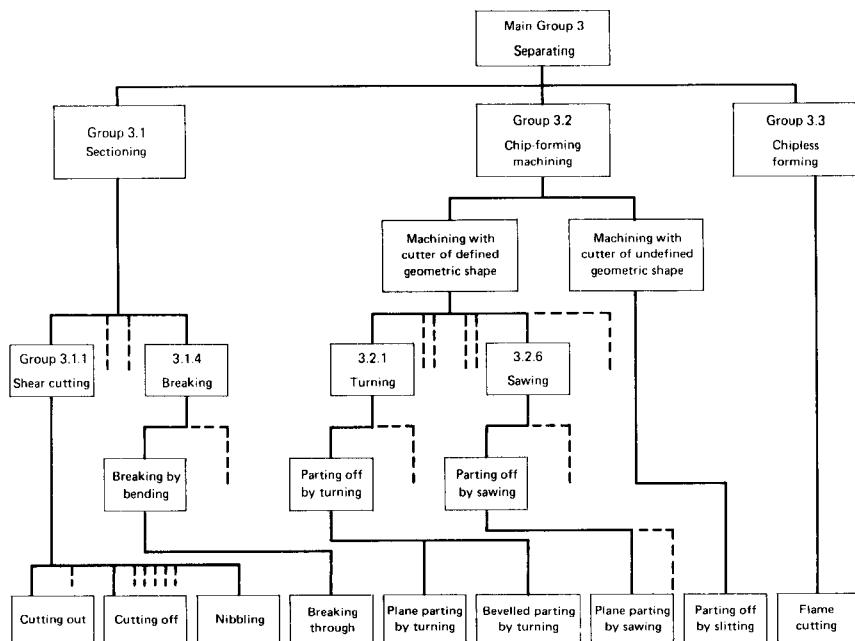


**FIG. 25.1** Classification of separating processes. (After DIN 8580.)

### Procedure

The cropping operation may be carried out in different ways. Important distinguishing characteristics are:

1. Kinematics of tool motion
  - a Shearing tool performs a linear motion
  - b Shearing tool performs a nonlinear motion
2. Stress condition in shearing zone
  - a Shearing without the influence of additional external forces
  - b Shearing under axial compressive stress
3. Tool
  - a Open or closed shearing blade
  - b Single-cut or multiple-cut tool (i.e., one or several slugs per stroke)
  - c Tool without bar and slug holder (free shearing)
  - d Tool with bar holder and with or without slug holder
4. Shearing speed
  - a low,  $v < 0.5 \text{ m/s}$  ( $1.5 \text{ ft/s}$ )
  - b high,  $v > 1.0 \text{ m/s}$  ( $3 \text{ ft/s}$ )

In addition, the effect of the workpiece temperature must be taken into account. Thus a distinction may be made between cold and hot shearing, depending on whether the workpiece is at room or at a higher temperature.

## 25.4 BLANKING, SLUGGING, PIERCING

The shearing operation proceeds as follows. The workpiece material is subjected to plastic deformation, caused by the shearing blade, until its deformability is finally exhausted. At this point shearing cracks occur, which lead to fracture (see also Fig. 24.9). In this case the slug shows a smooth (sheared) and a rough (fractured) surface portion. Whereas the quality of the sheared surface generally satisfies the given requirements, the fractured surface is often not satisfactory. For this reason, efforts are often made to increase the size of the smooth sheared zone at the expense of the fractured zone. This may be achieved by superimposing external compressive stresses [25.12], [25.13].

The most common way of creating such compressive stresses is to subject the bar to an axial compressive load. Extensive experimental findings are available on the effects of axial compressive stress on shearing [25.11]. The results obtained represent a significant improvement compared to conventional cropping. However, these methods have not found considerable industrial application because of the practical difficulties involved, such as substantial pickup and lubrication problems.

### *Shearing Processes*

The most widely used shearing method is the conventional shearing process shown in Fig. 25.2. The shearing blade performs a linear motion, usually perpendicular to the centerline of the bar. In general such shearing tools are mounted in an eccentric press. The shearing speed is normally less than 1 m/s (3 ft/s).

Other shearing processes aim at higher shearing speeds and/or at influencing the stress condition in the shearing zone by means of superimposed axial compressive stresses. For example, a rotary process has been developed which is capable of shearing speeds  $v > 1 \text{ m/s}$  (3 ft/s) and which can be reset quickly to a different shearing speed [25.14]. A process which differs fundamentally from conventional shearing is that of translational shearing [25.15], where the moving part of the tool performs a spiral motion. The desired aim (in this case) is for the shearing force acting in a radial direction to be applied gradually on the entire circumference. The process is said to be suitable for the production of solid and hollow closed sections as well as for all types of open sections.

Furthermore, since the liability of metals to brittle fracture is related to temperature, this liability can be reduced by cooling or warming the material concerned. For example, with carbon and low-alloyed steels, the area of so-called blue brittleness lies between approximately 200 and 500°C (440 and 980°F), depending on the shearing velocities.

### *Clearance*

The shearing clearance has a considerable influence on the quality of the sheared surface. When the clearance is set correctly, the cracks emanating from both sides progress more or less straight toward each other. As a general rule, the clearance should decrease with increasing hardness of the material.

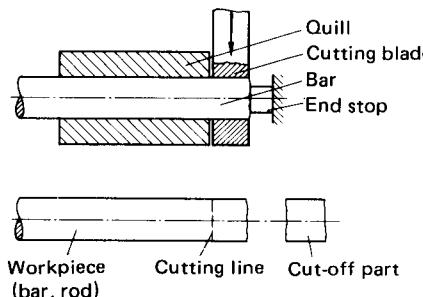
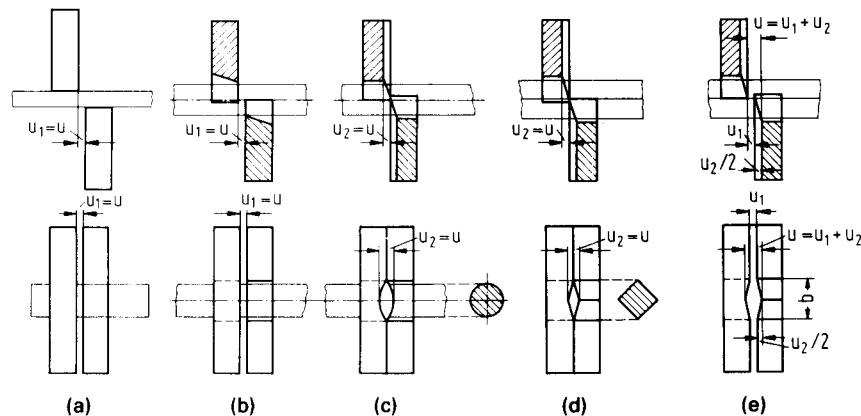


FIG. 25.2 Bar cropping.



**FIG. 25.3** Shearing gap shape.  $u$ —clearance. (a) Flat blade. (b) Semicircular/diamond blade without relief. (c) Semicircular blade with relief. (d) Diamond blade with relief. (e) Combination of (b) and (d). (After [25.17].)

Exceptions to this rule are aluminum and lead, which require a small clearance [25.16]. Fig. 25.3 shows a number of different shapes of shearing gaps in order to ensure a more or less uniform clearance over the cross section. Typical clearance values as a percentage of material thickness may be given as follows [25.17]:

Soft steels	5–10%
Tough, hard steels	3–5%
Brittle steels	1–3%

The effects of different clearance values on the shearing surface were investigated in [25.16]. Rough fractured surfaces, breakouts, and burrs indicate too large a gap, while lateral fracture planes and tongues occur when the clearance is too narrow (Fig. 25.4).

Lateral protrusions may occur at the edge of the sheared surface with a shearing gap of constant clearance along the entire length of the blade. In [25.16] the author suggests designing the shearing gap such that for each cutting element the ratio of the shearing gap at a particular point to the thickness of the material to be parted off by the cutting element is approximately equal. The shearing plane of a round bar then lies at a right angle to the centerline of the bar. Square bars cut with a pointed blade (as is usual) need a slightly larger gap than is required for round bars. Fig. 25.5 shows clearance ranges for shearing using flat-edged blades at low speeds. Suitable clearance widths are given as the side length for square bars and 0.8 of the diameter for round bars.

### Quality of Cropped Slugs

Common shortcomings of cropped slugs and billets, which often make their use difficult or even impossible are as follows (see also Fig. 25.4):

- 1 Defective smooth sheared surface (burrs, cracks, too rough)
- 2 Defective fractured surface (shape, breakouts, tongues, lateral fracture planes, protrusions, bosses, burrs, cracks, too rough)
- 3 Sheared and fractured surfaces not at right angle to the centerline of the bar and/or not plane parallel

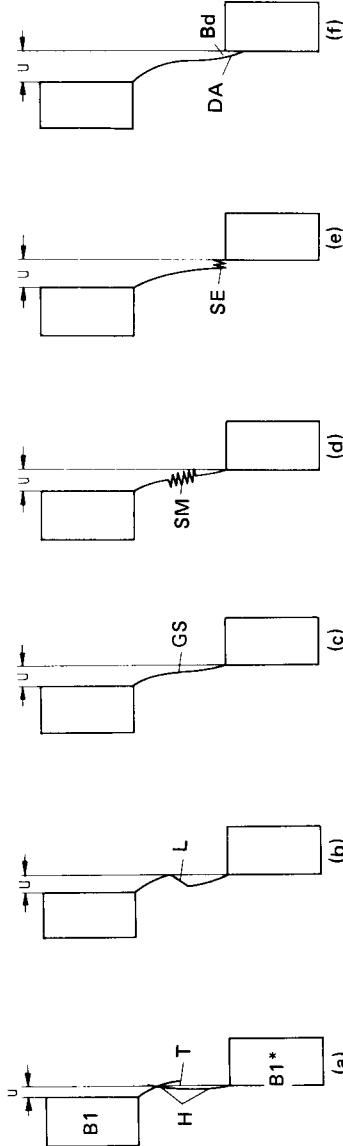
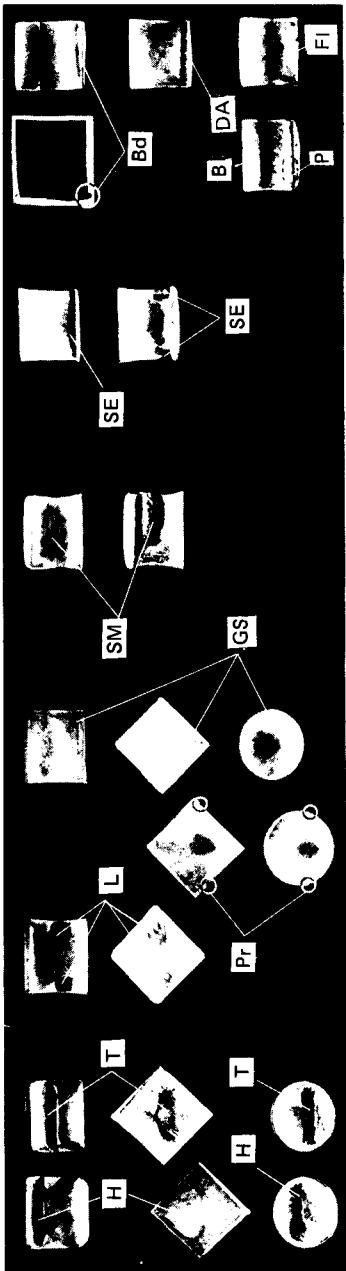


**FIG. 25.4** Relationship between shearing gap, crack propagation, and quality of the sheared surface. **B**—burr; **Bd**—beard; **B1,  $B1^*$** —bar-side blade, slug-side blade; **DA**—ductile fracture absent; **Fl**—flash; **GS**—good shear face; **H**—hollows; **L**—lateral fracture planes; **P**—plastic zones; **Pr**—protrusions; **SE**—spalling at the edge of the fractured surface; **SM**—spalling in the middle of the fractured surface; **T**—tongues. (a)–(f) Appearance of sheared surfaces with increasing clearance  $u$ . (After [25.16].)

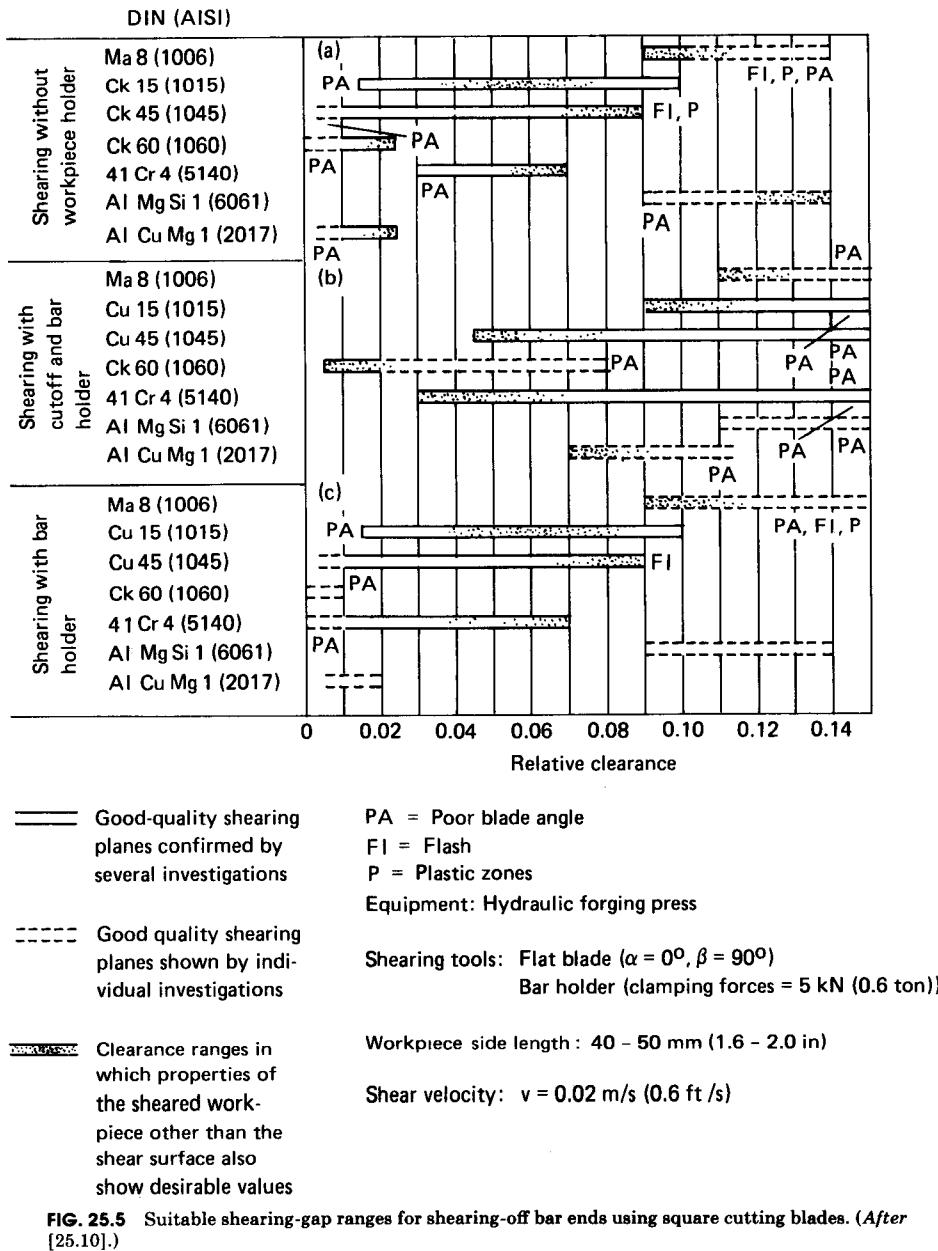
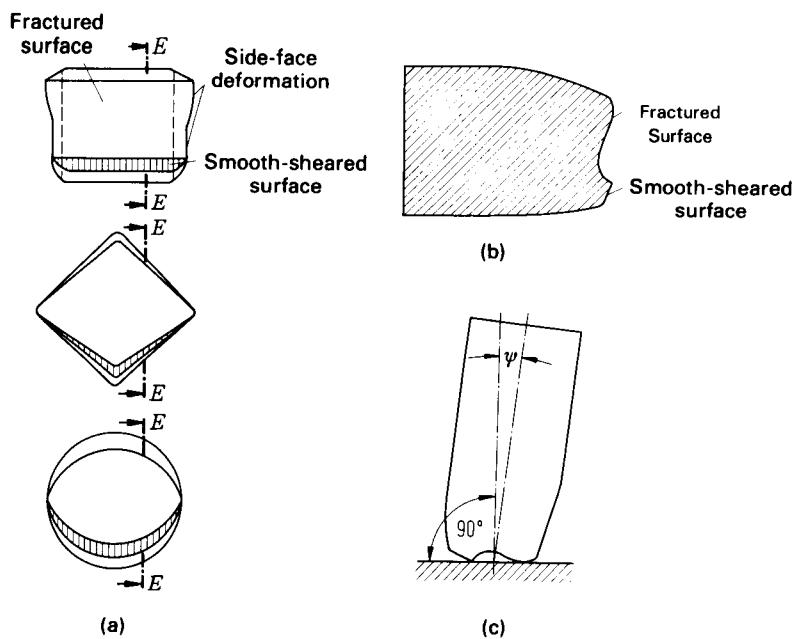


FIG. 25.5 Suitable shearing-gap ranges for shearing-off bar ends using square cutting blades. (After [25.10].)



**FIG. 25.6** Deformation of a slug due to shearing. (a) Cross-sectional deformation. (b) View E-E, cut and parting contour. (c) Workpiece inclination angle. (After [25.16].)

- 4 Deformed cross section
- 5 Length or dimensional variations too large
- 6 Material hardening in the sheared zone

The main factors affecting the quality of the cropped part are the workpiece material (analysis of the melt, initial treatment, temperature), the workpiece geometry (shape, dimensions, tolerances), the shearing tool (material, shape, state of the blade, type and effect of the clamping elements), and the machine used (stiffness, shearing speed).

The cross section is deformed by the action of the blade. Fig. 25.6 shows the deformation of a slug. Because of poor clamping, short slugs are deformed considerably during shearing without axial compressive loading. With longer slugs the cross-sectional deformation is less. Reduced cross-sectional deformation may be achieved by the use of semicircular or diamond blades together with bar and slug holders [25.18].

The quality of the sheared surface is largely a function of the shearing clearance. Surface roughnesses in the range of  $R_t = 4\text{--}16 \mu\text{m}$  (0.16–0.63 mil) have been recorded [25.11]. Further information is given in [25.19].

For shearing with an open blade, angles of inclination of the shearing face with respect to the slug axis ranging from  $+8^\circ$  to  $-8^\circ$  are recommended [25.10]. In addition, possible ways of reducing the angle of inclination have been put forward. In [25.11] the author reports on the dependence of the angle of inclination on the clearance (positive proportional), on the wedge angle of the blade (negative proportional for wedge angles  $> 90^\circ$ ) and on the workpiece material (see also [25.20]).

The length tolerances obtainable depend largely on the diameter of the material to be parted off. The following typical values are given for conventionally sheared hot-rolled steel bars [25.10]:

Bar diameter		Length tolerance	
mm	(in)	mm	(in)
≤10	(≤0.4)	±0.1	(±0.004)
>10–20	(>0.4–0.8)	±0.15	(±0.006)
>20–50	(>0.8–2.0)	±0.2	(±0.008)
>50	(>2.0)	±0.3	(±0.012)

In industrial production, length tolerances of  $\pm 1\%$  are common practice. Where drawn materials are concerned, length tolerances given by the machine-tool manufacturers (for multistage cold presses) are often in the range of  $\pm 0.5\%$ .

### Material Hardening

In cropping, work hardening occurs in the shearing zone and affects the subsequent forming operation unfavorably. The amount of hardening varies across the sheared zone; it is less when slug and bar holders are used than with free shearing. Minimum values are obtained when sharp blades are used; maximum values occur with square blades. In the case of steel, with increasing initial tensile strength of the material a reduction in the amount of work hardening and in the size of the hardened area is found [e.g., with Ck 15 (AISI 1015) the hardness may be doubled in cropping; with Ck 60 (AISI 1060) it may rise only to 1.3 times the initial hardness] [25.10]. The situation is the opposite with aluminum alloys. Generally the greatest amount of work hardening occurs in the regions of highest cross-sectional deformation, that is, in the region of the fracture surface nearest the shearing blade (see also Fig. 24.31).

### Shearing Velocity

Numerous investigations have been carried out to determine the effect of the shearing velocity on the resulting sheared surface [25.10], [25.11], [25.14], [25.17], [25.18]. Low shearing speeds lead to higher deformation. During the deformation of larger volumes of material, compressive stresses set up in the shearing zone may cause cracks to appear in the shearing plane [25.11]. With increasing shearing velocities the affected area becomes smaller, the hardening is more evenly distributed, and the increase in hardness is less; that is, the material is more brittle. (Exceptions are austenitic chrome nickel and chrome manganese steels [25.10]). The percentage of the fractured surface in comparison to the total sheared surface increases with the shearing velocity.

The quality of the sheared surface may be improved by higher shearing speeds [25.10], [25.11], [25.14], [25.17], [25.18]. Investigations have been carried out at speeds of  $v > 1 \text{ m/s}$  ( $> 3 \text{ ft/s}$ ) [25.14],  $v = 3\text{--}4 \text{ m/s}$  (9–12 ft/s) [25.11], and  $v = 4\text{--}20 \text{ m/s}$  (12–60 ft/s) [25.18]. All the authors come to the conclusion that higher shearing velocities result in increased dimensional accuracy, elimination of cracks in the shearing surface, and lower cross-sectional deformation. The minimum desirable velocity for good-quality slugs is given as  $v = 3 \text{ m/s}$  (9 ft/s) [25.17]. A further increase of the shearing velocity to  $v = 6 \text{ m/s}$  (18 ft/s) and even higher, as obtained when using explosives, does not lead to any further significant improvement. Finally, in experiments carried out at  $v = 3 \text{ m/s}$  (9 ft/s) on different steels with  $S_u < 900 \text{ N/mm}^2$  (130 ksi) it was found that material selection significantly affects the quality of the sheared surface obtained [25.17].

### Superimposed Compressive Stress

The stress distribution in the shearing zone may be altered by superimposing a compressive load, thereby improving the deformability of the material to be sheared. The axial load largely prevents any increase in blank length during the shearing operation. Extensive investigations to determine the effects of superimposed axial stresses on the sheared surface are contained in [25.11]. The dimensional accuracy of the blank increases linearly with the superimposed compressive stress

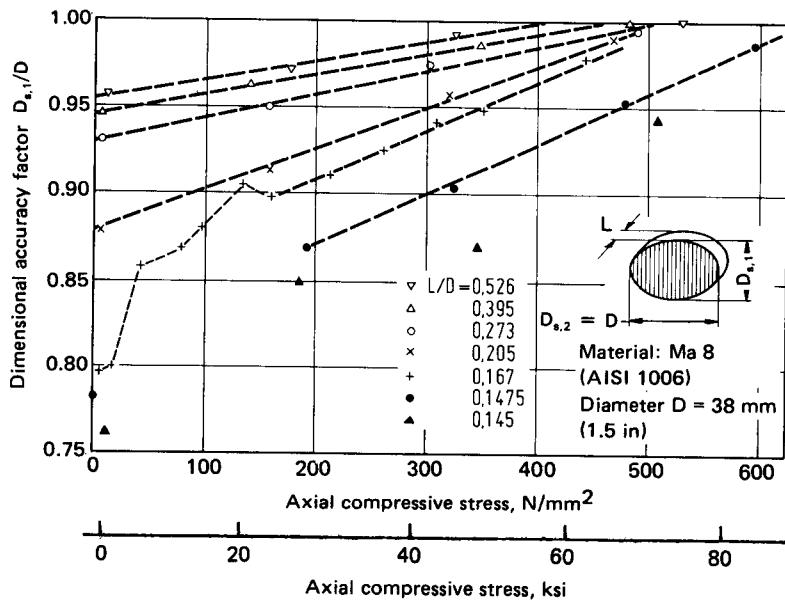


**FIG. 25.7** Dimensional accuracy during shearing under axial compressive load as a function of the sheared-off length. (After [25.11].)

where  $L/D > 0.2$  (Fig. 25.7); the size of the bar diameter is of no direct importance. The size of the deformation zone decreases with increasing axial pressure. The shearing force and the hardness of the material in the immediate vicinity of the shearing zone remain unaffected by the additional compressive stresses. Only at greater distances from the shearing plane, for example,  $> 1.5 \text{ mm (0.06 in)}$  [25.11], is the hardening more evenly distributed and the increase in hardness noticeably less than in cropping without superimposed axial compressive stress. The shearing force required is not measurably affected by the altered stress condition [25.11].

#### Force and Work Requirement

The force requirement is made up on the one hand of the force needed to part off the material and on the other hand of the force needed to overcome the friction between the moving tool and both the fixed and the cropped sections of the bar. An analysis of force requirements is given in [25.10], [25.11]. An approximate formula for selecting the most suitable shearing machine is

$$F_s = A_s k_s \quad (25.1)$$

where  $F_s$  = shearing force

$A_s$  = cross-sectional area of shearing plane

$k_s$  = shearing resistance

Approximate values of the shearing resistance  $k_s$  are given in Table 25.1. Additional data may be found in [25.12].

The work required is given approximately by

$$W_s = \gamma F_s s_{sm} \quad (25.2)$$

where  $s_{sm}$  is the cutting blade path during indentation and smooth shearing; it varies between  $\approx 20\%$  (for hard, brittle materials) and  $40\%$  (for soft, tough materials) of the largest dimension of the shearing cross section in the direction of force. The correction factor  $\gamma$  is formulated for the

**Table 25.1** Shear Resistance  $k_s$  of Certain Materials in the Annealed State

Material	Shear resistance $k_s$ N/mm <sup>2</sup> (ksi)	
Steel with		
0.1% carbon	260	(38)
0.2% carbon	320	(46)
0.3% carbon	360	(52)
0.4% carbon	450	(65)
0.6% carbon	560	(81)
0.8% carbon	720	(104)
Stainless steel	520	(75)
Brass	250	(36)
Copper	200	(29)
Aluminum	220	(32)
AlCuMg	220	(32)
Zinc	120	(17)
Lead	20-30	(2-4)
Tin	30-40	(4-6)

Source: Compiled from [25.21].

force-travel curve to approximate a rectangle (Fig. 25.8). It depends primarily on the material concerned and varies from about 0.7 to 0.8.

### Tooling

The most important components used in cropping are the tool blades and the clamping elements. The blades may have either an open or a closed contour (Fig. 25.9). Open blades are cheaper, closed blades generally produce a better cut. Moreover, where closed blades are used, no slug holder is required. The shape of the blade should be adapted to the shape of the cross section to be cropped in order to keep cross-sectional deformation to a minimum. Fig. 25.10 gives an outline of possible blade shapes.

According to [25.22] the following materials are recommended for cutting blades:

Tool steels	X165CrMoV12 (AISI D2) X210CrW12 (AISI D6) X210Cr12 (AISI D3)
High-speed steels	S 6-5-2 (AISI M2)
Cemented carbides	G40, G50, G60 (refer to Table 14.4)

The tool life of cutting blades used for bar cropping is shown in Fig. 25.11 on p. 25.14. (For details of the equipment used see the following subsection.) Blade wear may be reduced by lubricating the free surface and the face, for example, with a mixture of oil and MoS<sub>2</sub> powder additives [25.17].

A distinction can be made between single-cut and multiple-cut tools, depending on the location of the blankholder and the shearing blade (Fig. 25.12).

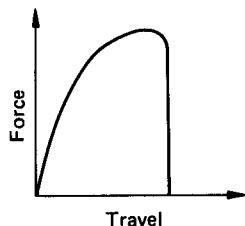
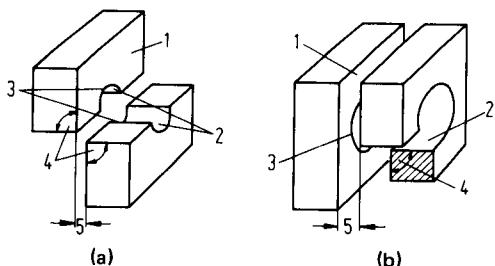


FIG. 25.8 Force-displacement curve during shearing.



**FIG. 25.9** Open and closed blades. 1—free surface; 2—pressure surface; 3—cutting edge; 4—wedge angle; 5—shear clearance. (a) Open blade (b) Closed blade. (After [25.17].)

Holders are used to prevent axial displacement of the bar or slug during shearing. The basic options with regard to the use of bar and slug holders are shown in Fig. 25.13.

### Machine Tools

High throughput and sufficient stiffness are the major requisites of shearing machines. In general no emphasis is placed on the possible use of the machine for operations other than cropping.

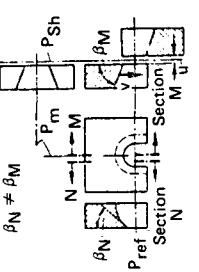
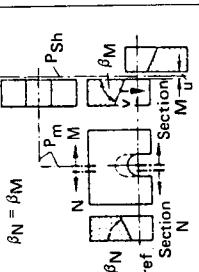
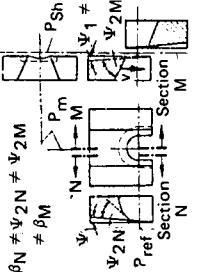
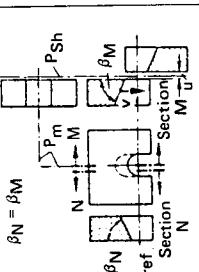
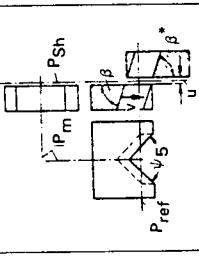
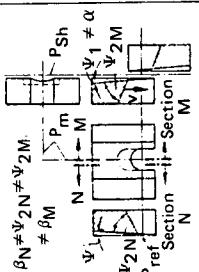
Large sections, such as those used in forging, are usually cropped using billet shears. Both mechanical and hydraulic drives are used, the latter mainly for very large cross sections. For cropping square cross sections, a V-shaped indentation is usually made in the upper and lower blades in such a way that the outer surface of the bar is enclosed during shearing. This often permits cropping without the use of a blankholder. Fig. 25.14 shows a billet shear with hydro-mechanical drive.

To produce rod and bar slugs for further working by means of compressive forming (e.g., by extrusion, swaging, upsetting) the machines used are mainly high-speed eccentric presses and occasionally crank presses. These machines are usually equipped with one or two sets of shearing tools consisting of blades, magazine with automatic bar-feeding device or coiler and straightening rolls, and, where desired, with automatic sorting devices for sorting out the ends of the rod or bar. Throughput per tool is in the region of 150 parts per minute; it is limited mainly by the length of the slug and the cycle time of the feed unit.

With slug or billet shears all these functions are integrated in a single unit. These devices are usually equipped with a crank or cam drive and have approximately the same performance as crank and eccentric presses equipped with shearing tools. Fig. 25.15 shows a shear which operates at shearing speeds of 1 m/s (3 ft/s). A further development is fully automatic high-performance units for shearing and sizing. Moreover, multistage presses working with rod and wire have a shearing stage prior to the forming operation.

In addition to these shears, which usually operate at speeds of less than 1 m/s (3 ft/s), pneumatic shears have more recently become available. They permit a sudden release of large amounts of energy, thus attaining shearing speeds of up to 10 m/s (30 ft/s) [25.24].

When rolled steel is cropped, a frequent problem is large variations in diameter which lead to differences of about  $\pm 2\%$  in cross-sectional areas. Sorting each charge of the semifinished product according to diameter and setting shears appropriately can reduce the overall variations in slug size. More automated still is a shearing device which determines the diameter using isotopes. A computer determines the required slug length, and the stop is set accordingly [25.25]. It is also possible to weigh the blanks after cropping by means of a fast weighing device and to sort them into different categories in order to protect the tools and the equipment during the sizing operation (see Sec. 25.3.1).

FLAT BLADE	DIAMOND BLADE Face: 2 roof-like planes (often with rounded fillet)	SEMICIRCULAR BLADE Face: Conical
 <p>Face: Flat</p>	 <p>Face: Cylindrical</p>	 <p>Face: Conical</p>
 <p><math>P_{Sh}</math></p> <p><math>P_m</math></p> <p><math>\beta</math></p> <p><math>\beta^*</math></p> <p><math>P_{ref}</math></p> <p><math>\beta_N = \beta_M</math></p> <p><math>\beta_N \neq \beta_M</math></p> <p><math>P_{ref}</math></p> <p><math>P_m</math></p> <p><math>\beta_N</math></p> <p><math>\beta_M</math></p> <p><math>P_{ref}</math></p> <p><math>P_m</math></p> <p><math>\beta_N \neq \beta_M</math></p>	 <p><math>P_{Sh}</math></p> <p><math>P_m</math></p> <p><math>\beta</math></p> <p><math>\beta^*</math></p> <p><math>P_{ref}</math></p> <p><math>\beta_N = \beta_M</math></p> <p><math>\beta_N \neq \beta_M</math></p> <p><math>P_{ref}</math></p> <p><math>P_m</math></p> <p><math>\beta_N</math></p> <p><math>\beta_M</math></p> <p><math>P_{ref}</math></p> <p><math>P_m</math></p> <p><math>\beta_N \neq \beta_M</math></p>	 <p><math>P_{Sh}</math></p> <p><math>P_m</math></p> <p><math>\beta</math></p> <p><math>\beta^*</math></p> <p><math>P_{ref}</math></p> <p><math>\beta_N = \beta_M</math></p> <p><math>\beta_N \neq \beta_M</math></p> <p><math>P_{ref}</math></p> <p><math>P_m</math></p> <p><math>\beta_N</math></p> <p><math>\beta_M</math></p> <p><math>P_{ref}</math></p> <p><math>P_m</math></p> <p><math>\beta_N \neq \beta_M</math></p>
 <p><math>P_{Sh}</math></p> <p><math>P_m</math></p> <p><math>\beta</math></p> <p><math>\beta^*</math></p> <p><math>P_{ref}</math></p> <p><math>\beta_N \neq \beta_M</math></p>	 <p><math>P_{Sh}</math></p> <p><math>P_m</math></p> <p><math>\beta</math></p> <p><math>\beta^*</math></p> <p><math>P_{ref}</math></p> <p><math>\beta_N \neq \beta_M</math></p>	 <p><math>P_{Sh}</math></p> <p><math>P_m</math></p> <p><math>\beta</math></p> <p><math>\beta^*</math></p> <p><math>P_{ref}</math></p> <p><math>\beta_N \neq \beta_M</math></p>
<p>Free surfaces</p> <p>Flat free surfaces inclined at an angle <math>\psi_1</math> to the direction of the shear velocity <math>v</math> parallel to the direction of the shear velocity <math>v</math></p>	<p>Free surfaces</p> <p>Flat free surfaces inclined at an angle <math>\psi_1</math> to the direction of the shear velocity <math>v</math> parallel to the direction of the shear velocity <math>v</math></p>	<p>Free surfaces</p> <p>Flat free surfaces inclined at an angle <math>\psi_1</math> to the direction of the shear velocity <math>v</math> parallel to the direction of the shear velocity <math>v</math></p>

$\alpha$  = clearance angle,  $\beta$  = wedge,  $\psi_1 - \psi_5$  = auxiliary angles,  $u$  = clearance,  $v$  = shear velocity,  $P_{ref}$  = reference plane,  $P_m$  = mean plane,  $P_{Sh}$  = shearing plane

FIG. 25.10 Possible blade shapes. (After [25.10].)

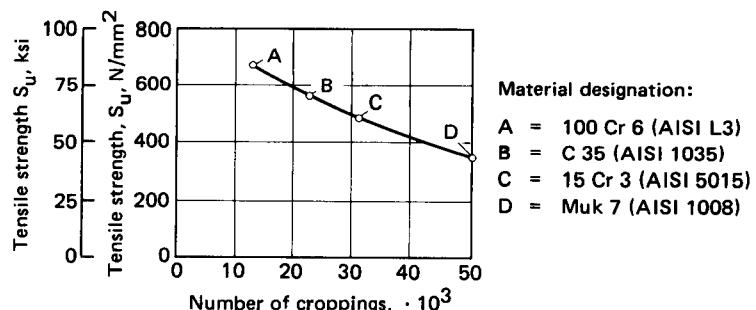


FIG. 25.11 Tool life of quill and blade during shearing off with a cropping shear.  
(After [25.22].)

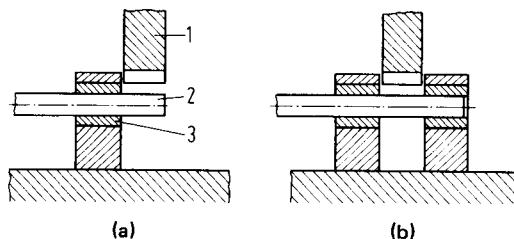


FIG. 25.12 Single- and double-cut cropping tools. 1—shear blade; 2—bar; 3—bar holder. (a) Singlecut (b) Doublecut.

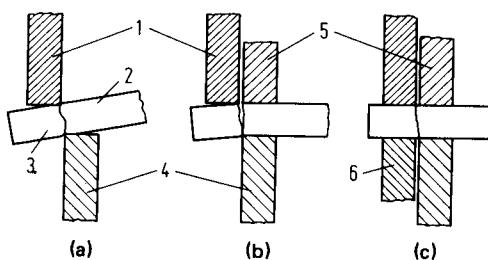


FIG. 25.13 Diagram showing the use of holder elements. 1—moving blade; 2—bar; 3—slug; 4—fixed blade; 5—bar holder; 6—slug holder. (a) Shearing without holder. (b) Shearing with bar holder. (c) Shearing with bar and slug holders. (After [25.17].)

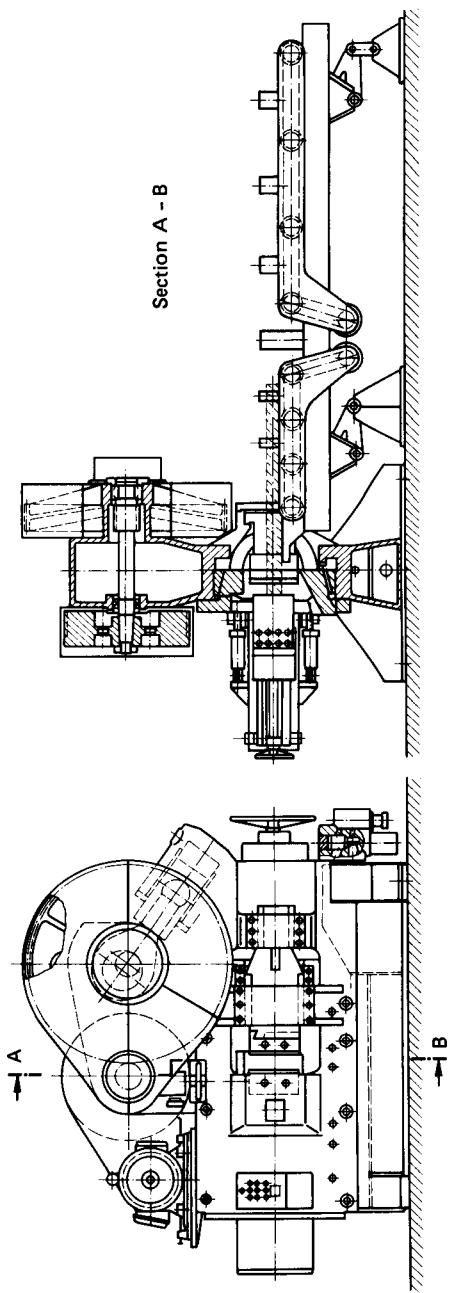
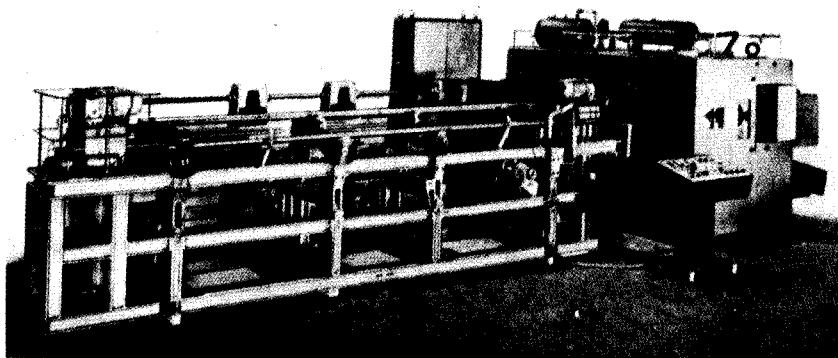


FIG. 25.14 Billet shears. (Courtesy of Eumuco. After [25.23].)



**FIG. 25.15** Blank shears MSR 115 for bars of 16–51-mm (0.6–2.0-in) diameter. (Courtesy of Maypres.)

### 25.2.2 Breaking

With breaking, a bar is loaded beyond its ultimate tensile strength by applying either an external bending load (breaking by bending) or an external torque (torque bending).

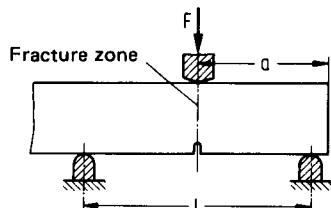


**FIG. 25.16** Billet breaking. F—breaking force; a—cut-off length; l—distance between supports. (After [25.26].)

grinding, or flame cutting) can reduce the breaking force considerably—according to [25.26] to between one-fifth and one-tenth of the value for an unnotched cross section—and will improve the quality of the fractured surface.

The deformation of the slug at the support locations is insignificant, and hardly any work hardening occurs at the fracture surface. The dimensional accuracy is given as  $\pm 1\text{--}2\%$ . The devices described are called block breakers; they are robust force- or path-controlled special-purpose machines.

### 25.2.3 Sawing

Sawing [25.27] is machining by means of a circular or linear motion using a multitoothed tool of narrow width for the parting off or slotting of workpieces. The sawing processes considered here are for plane sawing, that is, for parting off workpieces with a flat parting plane. The following section concerns the sawing of cold materials.

#### Cold Sawing

In cold sawing the material to be parted is at room temperature. The main use of cold sawing in the field of metal forming is to produce slugs or billets for bulk forming. Furthermore thick sheets,

semifinished products of large cross-sectional areas, which are used in hot bulk forming, are parted by breaking. Breaking through is the most common method used (Fig. 25.16). A condition for the successful use of this method of parting for billet production is that the material is relatively brittle. Carbon steels need to have a tensile strength of at least  $550 \text{ N/mm}^2$  (79 ksi), while the values for alloyed steels must be even higher [25.26]. The minimum slug or billet length is given as 1.1–1.3 times the diameter or face length of the bar [25.22]. A notch about 2 mm (0.08 in) deep on the side of the bar facing the point of application of the breaking tool (made by shaping, grinding, or flame cutting) can reduce the breaking force considerably—according to [25.26] to between one-fifth and one-tenth of the value for an unnotched cross section—and will improve the quality of the fractured surface.

such as produced by rolling mills, are cut to size by cold sawing before delivery to the customer for further working.

Because of the considerably greater output of the shearing processes, cold sawing is generally restricted to small batches and bar diameters of less than 50 mm (2 in). Furthermore sawing is used where flat slugs are required, which would be distorted too much during shearing (the limit is about  $l/d < 0.5\text{--}0.7$ ), and where very tough or very hard materials are required or particularly high demands are made on the dimensional accuracy of the slug or billet.

Sawn cross sections are characterized by very good dimensional accuracy [length tolerance  $< \pm 0.2$  mm (0.008 in)] and by cut surfaces of high quality exhibiting practically no change in material structure. An additional advantage of cold sawing lies in the short setting-up time of about 10–15 min. The main disadvantages are material waste (Table 25.2), low output, and the formation of burrs. Where the workpieces on both sides of the saw blade are clamped firmly, parting off may be performed almost without burrs. When this is not the case, some material may be left at the edge of the cut surface and has to be removed by deburring.

Slugs are usually cut to length on cold circular saws with semiautomatic (material being fed into the machine by hand) or fully automatic drive. Diameters of up to about 500 mm (20 in) can be sawn in this way. Large diameters are more commonly cut using band saws since tool costs are less. A cost comparison of different sawing methods [25.22] is shown in Fig. 25.17.

The tools most commonly used for sawing workpieces up to 500 mm (20 in) in diameter are circular saw blades (usually made of high-speed steel or cemented carbide) and sectional saw blades, especially for large cross sections. The relationship between the size of the circular saw blade and the workpiece to be sawn is presented in Table 25.2.

Typical values for particular sawing operations are given in [25.28]. The cutting performance achieved in cold sawing of steel and certain nonferrous metals is given in Table 25.3.

Modern sawing machines (e.g., cold automatic circular saws) are controlled in such a way that in equal periods of time equal volumes of material can be sawn. Cooling lubricants, such as oil emulsions or cutting oils, improve surface finish, increase tool and machine life (through chatter-free cutting), and reduce cutting time [25.29]. This is especially true in the case of materials which tend to form built-up edges due to insufficient lubrication, such as aluminum and aluminum alloys.

### Deburring

Sawn-off workpieces generally require deburring. On small and medium-sized parts deburring is performed most economically by means of vibratory grinding, using grinding media in vibrators or slowly rotating drums which, in addition, may also perform an oscillating motion. Where no

**Table 25.2** Circular Saw-Blade Sizes with Respect to Billet Cross Section on Cold Sawing

Saw-blade diameter mm (in)	Saw-blade thickness mm (in)	Tooth pitch mm (in)	Cutting range,	
			mm (in)	mm (in)
250 (9.8)	4 (0.16)	5.5–22 (0.22–0.87)	90 (3.5)	80 (3.1)
315 (12.4)	4.5 (0.12)	6.0–23 (0.24–0.91)	112 (4.4)	100 (3.5)
400 (15.7)	5 (0.20)	6.5–26 (0.26–1.02)	140 (5.5)	125 (4.5)
500 (19.7)	5.6 (0.22)	7.5–29 (0.30–1.14)	180 (7.1)	160 (6.3)
630 (24.8)	6 (0.24)	8.5–33 (0.33–1.30)	224 (8.8)	200 (7.5)
800 (31.5)	6.5 (0.26)	8.5–35 (0.33–1.38)	280 (11.0)	250 (9.8)
1000 (35.4)	7.5 (0.30)	8.5–35 (0.33–1.38)	355 (14.0)	315 (12.4)
1250 (49.2)	9 (0.35)	9.0–36.5 (0.35–1.44)	450 (17.7)	400 (15.7)
1600 (63.0)	12.5 (0.50)	10.5–42 (0.41–1.65)	560 (22.0)	500 (19.7)

Source: Compiled from [25.30].

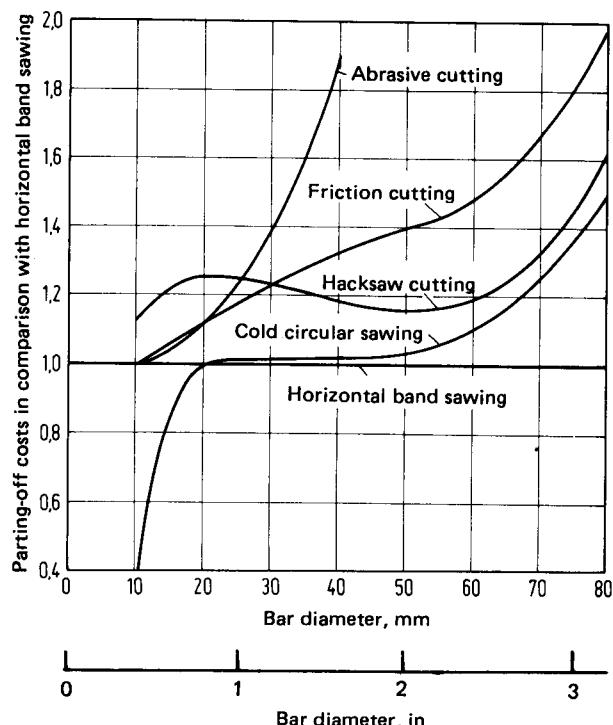


FIG. 25.17 Relative parting-off costs for 100Cr6 (AISI L3). (After [25.1].)

specific requirements exist concerning surface finish, and in the case of small steel components which only slightly impinge upon each other, grinding may be performed without the addition of a grinding medium. The use of a soft filling agent reduces workpiece damage. For example, sawdust is used as a filling agent in the deburring of aluminum bars. In deburring steel components, natural materials, such as feldspar, and artificial abrasives, such as ceramic, organic, or resin-bonded corundum, silicon carbide, boron carbide, and others, have proved their worth. Besides these, metal objects such as steel shot are also used. The size, shape, and composition of the grinding medium, including any necessary additives, are chosen in each case according to the particular application.

Following deburring, the workpiece and the grinding medium are separated by sieving or using magnetic separators. The particles which remain on the surface of the workpiece are removed by washing.

Machines for wet or dry vibratory grinding are either drum-shaped or in the form of rotary or linear vibrators. Semiautomatic or nonautomatic models are most economical for small batches, while for continuous operation with large throughput, fully automatic plant is preferable.

Deburring by vibratory grinding is both fast and cheap. A side effect, however, which cannot be overcome fully, is that some particles of the abrasive medium may be pressed into the workpiece surface, leading to increased tool wear during the forging process.

Large circular workpieces may be deburred on boring or turning machines using tools such as rotary blades, milling cutters, and turning tools. Such methods turn out excellent slugs; however, they are expensive and productivity is low.

Beside these methods, deburring may be performed by grinding. The machines used are equipped with either abrasive belts or disks.

**Table 25.3** Productivity in Sawing with Cold Automatic Circular Saws

Type	Material designation		Tensile strength		Cutting speed		Capacity	
	DIN	AISI	N/mm <sup>2</sup>	(ksi)	m/min	(ft/min)	cm <sup>2</sup> /min	(in <sup>2</sup> /min)
<b>Construction steels</b>								
Nonalloyed	St 34	—	340–450	(49–65)	22–28	(66–24)	120–230	(19–36)
	St 42, C 22	1043, 1020	420–500	(61–72)	20–24	(60–72)	110–170	(17–26)
	St 50, C 35	1043, 1035	500–600	(72–87)	15–20	(45–60)	100–150	(16–23)
	St 60, C 45	1043, 1045	600–720	(87–104)	13–17	(39–51)	80–140	(12–22)
	St 70, C 60	1043, 1060	700–850	(102–123)	12–15	(36–45)	60–120	(9–19)
Alloyed	16 MnCr 5	5117	500–700	(72–102)	13–17	(39–51)	70–120	(11–19)
	20 MnCr 5	5120	600–750	(87–109)	13–17	(39–51)	70–120	(11–19)
	42 MnV 7	1541	650–800	(94–116)	12–15	(36–45)	60–100	(9–16)
	50 CrMo 4	4147	700–800	(102–116)	10–15	(30–45)	40–90	(6–14)
	50 CrV 4	6150	700–800	(102–116)	10–15	(30–45)	40–90	(6–14)
	15 Cr 3	5015	800–900	(116–131)	10–15	(30–45)	30–60	(5–9)
<b>Stainless steels</b>								
High-speed steels		500–900	(72–131)	6–15	(18–45)	15–90	(2–14)	
Tool steels		1000–1400	(145–203)	6–10	(18–30)	10–60	(2–9)	
		800–900	(116–131)	9–12	(27–36)	15–40	(2–6)	
Light alloys				400–1250	(1200–3750)	1000–2000	(155–310)	
Brass				200–600	(600–1800)	500–2000	(78–310)	
Copper				100–600	(300–1800)	300–2000	(47–310)	
Bronze				40–120	(120–360)	150–500	(23–78)	

Source: Courtesy of Hans Kaltenbach Maschinenfabrik KG.

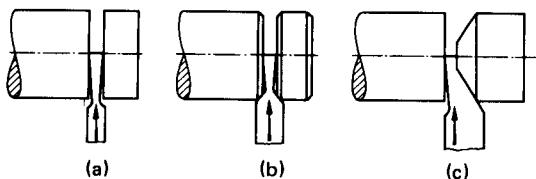


FIG. 25.18 Parting off by turning. (a), (b) Plane. (c) Bevelled.

#### 25.2.4 Turning

In parting off by turning, lengths are cut from a rod, bar, tube, or wire by means of a narrow square-nosed cutting tool which moves at a right angle to the workpiece axis (Fig. 25.18).

Parting or turning off is mainly used for cutting thin-walled tubes to length. A further application is for cutting lengths from mostly small-diameter rods.

The main advantages of this method are high dimensional accuracy, length tolerances of  $\leq \pm 0.1$  mm (0.004 in), and a very clean parting surface which requires no further operation. Changes in material structure are negligible in practice. The disadvantages are low throughput, high material waste, and high costs.

The machines used for parting off by turning are general-purpose machines, such as simple and automatic lathes, as well as special-purpose parting-off lathes, the latter being more economical when a considerable amount of parting off is carried out. Such machines may function either with rotating material and fixed tools (suitable for thick-walled tubes [25.28]) or with fixed material and rotating tools (suitable for thin-walled tubes and long bars [25.28]). The rotating cutting heads in general contain several parting-off tools, which are staggered with respect to each other, and a chamfering tool. Clamping and ejector devices assure high-quality parts.

The tool material is normally high-speed steel or, less commonly, cemented carbide. Optimal cutting speeds and feed rates depend largely on the material to be parted off, its cross-sectional area, the tool material, and the distance between cutters. Table 25.4 shows some typical values. For further information the reader is referred to [25.30].

Table 25.4 Cutting Speeds and Feed Rates Used in Parting Off by Turning

Material	Cutting speed, m/min (ft/min)	Feed rate, mm/rev (in/rev)
Steel	50–100 (150–300)	0.05–0.20 (0.002–0.008)
Light alloy	150–200 (450–600)	0.12–0.25 (0.005–0.01)
Brass	100–150 (300–450)	0.15–0.30 (0.006–0.012)

#### 25.2.5 Blanking

Blanking and piercing as shearing processes are discussed in general in Chap. 24. Blanking processes are mainly used for the parting of sheet metal. The blanks thus produced are normally further deformed using another sheet-metal working process (e.g., cupping or deep drawing). When the blanks are to be used for cold bulk forming, crack- and protrusion-free smooth sheared surfaces are necessary.

Sheared blanks exhibit the following main characteristics:

1. The sheared surface is divided into a smooth shear zone and a fracture zone (Fig. 25.19). The sheared zone is work-hardened at temperatures below the recrystallization temperature while the fracture zone is not.
2. Shear surfaces show no microstructural changes.

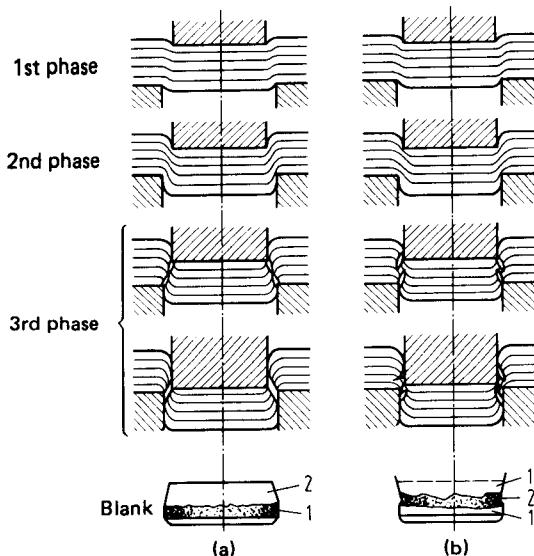


**FIG. 25.19** Deformation and fracture zones due to shearing.  
1—deformation zone; 2—fracture zone. (a) With correct clearance. (b) With insufficient clearance. (After [25.21].)

3. Both material and clearance strongly affect the shape of the sheared surfaces (Fig. 25.20).
4. Blanks exhibit a burr on the punch side and edge draw-in on the die side. The degree to which these occur depends on the condition of the tools (see Fig. 24.27).

The following section concerns only the production of circular blanks. Reference is made to parting off by shearing to produce square or rectangular blanks. In one-off and small-batch production, extensive use is made of nibbling. With thin sheets, hand shears may also be used.

#### **Production of Circular Blanks**

Blanking involves cutting along a closed-contour shearing line which forms the outer circumference of the workpiece (Fig. 25.21).

Blanks made of thin sheet or sheet strip are produced almost without exception by this method. As far as economically justified, use may be made of suitable presses and special blanking tools. The main advantage here is the high output rate of up to 600 parts per minute per tool for small parts, which is only limited by the speed of the feeding device of up to 30–35 m/min (90–105 ft/min). The presses used—mainly high-speed, short-stroke eccentric presses—are normally equipped with one, and seldom with more than two cutting tools. The uncoiled sheet may be flattened beforehand where necessary (roll straightening; see Chap. 19).

The production of blanks for cold bulk forming is also of great importance. Flat blanks ( $l/d < 0.25\text{--}0.3$ ), for which the desired quality cannot be obtained by cropping (see Sec. 25.2.1) or cropping and sizing (see Sec. 25.3.1), may be cut more cheaply from sheet metal than they can be produced by sawing from a bar. This concerns mostly aluminum materials which are subsequently worked by backward can extrusion to produce thin-walled tubes or cans of all kinds. Furthermore the smooth, crack-free surface of the cold-rolled sheet causes less difficulties than a sheared-off, sized surface, where the occurrence of overlapping, burrs, and cracks cannot be excluded. The large amount of material discarded in blanking is of less importance with nonferrous metals than with steel because of their comparatively high scrap value. Thus in the area of bulk forming, blanking is used almost exclusively to produce blanks made of nonferrous metals.

Type of material	Sheet thickness	Relative clearance	
		Small $u/s = 0.02 \text{ to } 0.03$	Large $u/s = 0.08 \text{ to } 0.10$
Very soft materials such as Al 99.5 w (1050-0)	Up to 3, max 4 mm (0.1, max 0.15 in)	Sheet Blank	Sheet Fracture or tear Blank
	Over 4 mm (0.15 in)		
Soft materials of up to 400 N/mm <sup>2</sup> (58 ksi) tensile strength	Up to 3, max 4 mm (0.2, max 1.5 in)	Sheet Indentation	
	Over 4 mm (0.15 in)		
Hard, brittle materials of over 500 N/mm <sup>2</sup> (73 ksi) tensile strength	Up to 3, max 4 mm (0.1, max 1.5 in)	Sheet Blank	Sheet Tear
	Over 4 mm (0.15 in)		

FIG. 25.20 Shape of cut formed by blanking as a function of material and clearance. (After [25.31].)

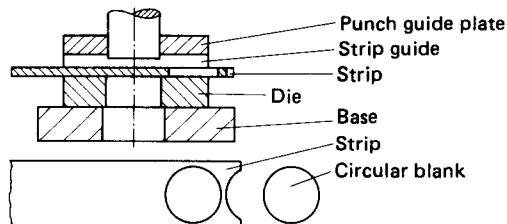


FIG. 25.21 Blanking of circular blanks.

Finally, as a guideline to the useful limit of blanking, the sheet thickness may be given as at most 15–20 mm (0.6–0.8 in) and  $s/d < 0.5$ . The use of blanking beyond this point often leads to poor-quality cuts.

### 25.3 SUBSEQUENT TREATMENT OF SLUGS

#### 25.3.1 Sizing and Calibrating

Sizing is the pressing into shape of cropped slugs without flash, in order to produce flat end faces which are parallel to each other (Fig. 25.22). During the process the slug length is reduced. At the same time it is possible to press centers and other marks (e.g., trademarks) into the end faces as well as to produce short shanks (Fig. 25.23). Sizing is a very commonly used forming process in slug production for cold bulk forming.

The deficiencies in sheared-off slugs mentioned in Sec. 25.2.1 can be overcome to a large extent by upsetting in a closed die, although in general this is not carried through to the end. Further advantages of sizing are:

- 1 Reduction of the diameter tolerances, thereby reducing the clearance required for the subsequent forging operation to  $\leq 0.2$  mm (0.008 in)
- 2 Improved roundness
- 3 Simplified stock keeping (only frequently required diameters need to be held in stock)

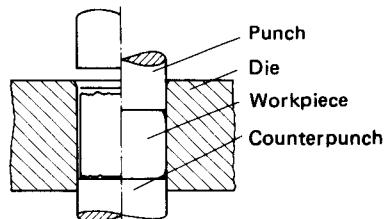


FIG. 25.22 Sizing of cropped slugs.

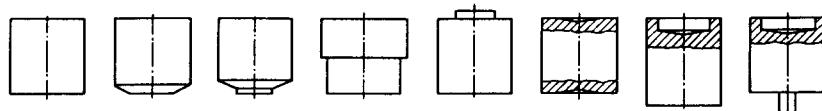


FIG. 25.23 Selection of simple workpiece shapes produced by sizing.

The sized slug has the shape of a thick blank. Slugs which are to be worked by cold backward can extrusion should always be sized first. Only with short extrusion punches guided in the die insert is it sometimes possible to omit sizing. When solid bodies are to be produced, sizing of the cropped slugs may not be necessary when the latter are only slightly deformed.

Usually it is sufficient to grease or oil the slugs before sizing. However, where sharp-edged slugs made of high-strength materials, such as steel, are to be produced, they need to be coated with a lubricant-carrying layer prior to lubrication (see Secs. 6.4 and 26.2).

The sizing tools consist of a short punch, a counterpunch (also used as ejector), and a die which is generally reinforced with a single ring. The machines used are typically high-speed eccentric, toggle, and crank presses.

#### 25.3.2 Heat and Surface Treatment

Heat treatment has the function of producing the material structure required for the subsequent forming operation. With slugs and blanks for cold forming of steel, the aim is to achieve a soft structure condition, and this is best done by spheroidizing; occasionally subcritical annealing is sufficient (see Sec. 26.1).

The decision as to whether annealing is required depends on the method of parting used, the forming operation, and the demands made on the finished workpiece, and, finally, it is also a question of cost. Thus, for example, thin cut-out blanks need not be annealed before deep drawing since the relatively small deformation zone leads to no appreciable disadvantages during the subsequent sheet-forming operation. It is far more common to order annealed semifinished products from the rolling mill. On the other hand bar and wire slugs and blanks used in cold bulk forming, such as in cold extrusion on single-stage presses, are very often annealed (usually spheroidized) in order to ensure the most suitable homogeneous material properties for all parts. Some advantages of these measures are more consistent workpieces, lower load and work requirements, closer workpiece tolerances for a particular machine, longer tool life, and fewer interruptions of the production. On the other hand, multistage presses are used with one shearing and several forming stages, and hence heat treatment after shearing is normally omitted. Here the work sequence has to be designed in such a way that acceptable tool lives are obtained. Where it is not possible to achieve this, excessively work-hardened zones may have to be heated inductively during the work sequence.

Generally applicable rules concerning the need for heat treatment cannot be laid down. The main purpose of annealing is to assure the disturbance-free running of a particular process. On the other hand the cost saving resulting from each reduction in the total number of operations must be kept in mind. Further details concerning heat treatment are given in Sec. 26.1.

Surface treatment aims at achieving an effective separating layer between workpiece and tool material. It is discussed in detail in other sections. For instance, in Chap. 6 the fundamentals of friction and lubrication are dealt with. The chapter also goes into the details of some important practical applications, such as in cold bulk forming. Moreover the appropriate chapters report on the very extensive experience which has been gained with lubricants and lubricant carriers used in particular processes. The techniques of applying lubricants and lubricant carriers as well as the equipment used are described in Sec. 26.2.

#### **25.4 SINTERED SLUGS**

Conventionally produced metals, which prove difficult to forge, often exhibit considerably improved formability as sintered metals. Examples are alloyed and high-alloyed steels, tungsten, molybdenum, tantalum, and their alloys, and alloys of titanium. Where shaping is to be carried out by means of forming, sintered slugs are produced and forged to give the desired workpieces.

Sintering is only seldom used for slug production. In [25.32] the authors report on sintered cups used for cold forging 0.5-in cartridge cases by means of a five-stage ironing process. Prior to the process the cups were copper-plated and greased. Some recent investigations show that by appropriate selection of metal powder, compacting, and sintering, mechanical properties can be obtained after cold and warm extrusion which are comparable with those for conventional steel extrusions [25.33] to [25.35].

Other authors have described the use of sintered slugs for hot forging [25.36], [25.37], noting the following advantages:

- 1 Consistently accurate quantity of material, leading to less material waste
- 2 Fewer forming stages, leading to savings in investment and personnel
- 3 Reduced power requirements, resulting in smaller forging plants and less die wear
- 4 Fewer subsequent finishing operations

A particularly economic way of working is to dispense with the cooling phase after sintering and forge straight from the sintering temperature, thereby increasing the strength of the workpiece. Where this is not desirable, the material is cooled to the prescribed forging temperature and then forged.

The very much shorter throughput times achieved with sintering, which are especially advantageous in cold bulk forming, must be emphasized. Whether sintering of slugs is economical must be judged on the basis of each individual case.

## REFERENCES

- 25.1 Bunge, G.: "Possibilities of Material Savings with Chip-Forming Parting Processes" (*in German*), *Fertigungstech. u. Betr.*, **19**, 1969, pp. 155–159.
- 25.2 Barz, E., and Oberwinter, K.: "On Operations in Friction Cutting" (*in German*), *Werkstattstechnik*, **56**, 1966, pp. 13–21.
- 25.3 Bunge, G.: "Surface Quality in Abrasive Cutting" (*in German*), *Fertigungstech. u. Betr.*, **16**, 1966, pp. 568–572.
- 25.4 Cornelissen, T. J. A.: "News about Abrasive Cutting" (*in Dutch*), *Metaalbewerking*, **25**, 1960, pp. 279–284.
- 25.5 Bialecki, H.: "Use of Flame Cutting in Forging Works" (*in German*), *Fertigungstech. u. Betr.*, **15**, 1965, pp. 80–84.
- 25.6 Christoph, H., and Herzfeld, W.: "Economic Flame Cutting and Desirable Accuracies" (*in German*), *Ind.-Anz.*, **80**, 1958, pp. 286–292.
- 25.7 Christoph, H., and Herzfeld, W.: "Flame Cutting—An Economic Method of Sheet-Metal Working" (*in German*) *Blech*, **5**, 1958, pp. 36–44.
- 25.8 Pechau, G.: "Influence of the Shear Parameter on the Characteristics of the Hot Shearing Operation" (*in German*), *Neue Hütte*, **14**, 1969, pp. 153–157.
- 25.9 Wever, F., Lueg, W., and Müller, H. G.: "Force and Work Requirements in Hot Shearing of Steel as a Function of Temperature and Cutting Speed" (*in German*), *Forschungsberichte des Wirtschafts- und Verkehrsministeriums Nordrhein-Westfalen*, no. 408, Köln/Opladen, Westdeutscher Verlag, 1957.
- 25.10 Kienzle, O., and Zabel, H.: "Sectioning of Metal Bars by Cropping" (*in German*), *Forschungsberichte des Landes Nordrhein-Westfalen*, no. 1462, Köln/Opladen, Westdeutscher Verlag, 1965.
- 25.11 Herbst, U.: "Precision Shearing of Materials for Extrusion" (*in German*), Dr.-Ing. thesis, Technische Universität, Hannover, 1967.
- 25.12 Cotrell, A. H.: "Theory of Brittle Fracture in Steel and Similar Metals," *Trans. Metall. Soc. of AIME*, 1958, pp. 192–203.
- 25.13 Stüwe, H. P.: "Mechanisms of Deformation and Brittle Fracture" (*in German*), *Arch. Eisenhüttenwes.*, **4**, 1963, pp. 633–640.
- 25.14 Bräunlich, B., Keller, F., Kunath, G., and Östreicher, K.: "Development of a High-Productivity Cutting Process for the Production of Bar Sections" (*in German*), *Fertigungstech. u. Betr.*, **14**, 1964, pp. 621–624.
- 25.15 Kessler, K., Keller, F., Renatus, R., and Gross, H.: "Cutting Off of Bar Stock by Lateral Cutting" (*in German*), *Fertigungstech. u. Betr.*, **15**, 1965, pp. 663–666.
- 25.16 Zabel, H.: "The Parting Surface of Sheared-Off Bar Sections" (*in German*), *Werkstatstechnik*, **54**, 1964, pp. 530–538.
- 25.17 Kessler, K., and Keller, F.: "Cutting of Profile Sections—Current State of the Art" (*in German*), *Fertigungstech. u. Betr.*, **16**, 1966, pp. 532–537.
- 25.18 Organ, A. J., and Mellor, P. B.: "The Preparation of Metal Billets by Bar Cropping," *Iron and Steel*, **39**, 1966, pp. 481–487.
- 25.19 ICFG Data Sheet 7/72: "Bar Cropping Billet Defects," Redhill, Surrey, Institute of Sheet Metal Engineering, 1972.
- 25.20 ICFG Data Sheet 3/82: "Cropping of Steel Bar—Its Mechanism and Practice," Redhill, Surrey, Institute of Sheet Metal Engineering, 1982.
- 25.21 Romanowski, W. P.: *Stamping Technology Handbook* (*in German*), 4th ed., Berlin, VEB Berlag Technik, 1965.
- 25.22 VDI Richtlinie 3144: "Rohteilherstellung für das Kaltumformen (Slug Preparation for Cold Forging)," Berlin/Köln, Beuth, 1982.

- 25.23 Fritzsche, E.: "Billet Shear with Hydromechanical Drive" (*in German*), *Werkstatt u. Betr.*, **103**, 1970, pp. 767–770.
- 25.24 Liebmann, W.: "Parting, Too, Is Racing Ahead" (*in German*), *Maschinenmarkt*, **77**, 1971, p. 449.
- 25.25 Meščerin, V. T.: "Use of Isotopes for Inspection Operations in Bar Cropping" *Ind.-Anz.*, **92**, 1970, pp. 2425–2433.
- 25.26 Lange, K.: *Die Forging of Steel* (*in German*), Berlin/Göttingen/Heidelberg, Springer, 1958.
- 25.27 DIN 8589: "Fertigungsverfahren Spanen (Manufacturing Process: Chip-Removal Machining Methods)," part 6, 1st ed., 1982.
- 25.28 Hake, O.: "Modern Separating Processes" (*in German*), *Ind.-Anz.*, **80**, 1958, pp. 151–160.
- 25.29 Conrad, H.: "Rationalization in Cutting Techniques through the Use of New Types of Coolants" (*in German*), *Z. Wirtsch. Fertigung*, **64**, 1969, pp. 123–125.
- 25.30 Degner, W., Lutze, H., and Smejkal, E.: *Machining* (*in German*), Berlin, VEB Verlag Technik, 1968.
- 25.31 Timmerbeil, F. W.: "Investigations into Sheet-Metal Cutting, Part 2" (*in German*), *Werkstatttech. u. Maschinenbau*, **47**, 1957, pp. 350–356.
- 25.32 Steinitz, R., Scanlan, J. P., and Zaleski, F. I.: "Drawn Shapes from Metal Powder Now Possible," *Materials and Methods*, **40**, 1954, pp. 101–103.
- 25.33 Schacher, H. D.: "Cold Forming of PM Preforms" (*in German*), *Berichte aus dem Institut für Umformtechnik, Universität Stuttgart*, no. 47, Essen, Girardet, 1978.
- 25.34 Stilz, M.: "Deformation of Alloyed Iron Powder Preforms" (*in German*), *Berichte aus dem Institut für Umformtechnik, Universität Stuttgart*, no. 59, Berlin/Heidelberg/New York, Springer, 1981.
- 25.35 Schaub, W.: "Warm Extrusion of PM Preforms in the Temperature Range between 600 and 900°C" (*in German*), *Berichte aus dem Institut für Umformtechnik, Universität Stuttgart*, no. 63, Berlin/Heidelberg/New York, Springer, 1982.
- 25.36 Hirschhorn, J. S., and Bargainier, R. B.: "The Forging of Powder Metallurgy Preforms," *Met. Form.*, **37**, 1970, pp. 320–327.
- 25.37 Brown, G. T., and Jones, G. K.: "Experimental and Practical Aspects of the Powder Forging Process," *Int. J. Powder Metall.*, **6**, 1970, pp. 29–42.

## **HEAT AND SURFACE TREATMENT**

---

---

The practicability of many processes used in forming semifinished and finished workpieces depends on the precise use of heat- and surface-treatment methods. Because of the often considerable costs incurred by these auxiliary processes—in particular soft annealing, descaling, phosphating, and greasing of workpieces produced by cold extrusion—they should be used as sparingly as possible. In this chapter the processes concerned are described as well as their purpose and the procedures to be followed in carrying them out, and mention is made of their most appropriate areas of application. Because heat- and surface-treatment operations are often carried out one after the other, they are dealt with in the same chapter.

### **26.1 HEAT TREATMENT**

Heat treatment permits the modification of the mechanical properties of metals within certain limits in order to create suitable conditions for subsequent manufacturing operations and for the final use of the component. This section discusses the heat-treatment processes used directly in conjunction with cold-forming processes.

For ease of comprehension, special emphasis has been placed on the connection between existing heat-treatment processes and their main areas of application as well as on the equipment used and the types of components treated.

Information concerning the practical procedure used in individual annealing processes is discussed in connection with well-known steels only. Data relating to nonferrous metals are given in Tables 26.1 and 26.2. In order to avoid misunderstandings, reference should be made to the manufacturer's heat-treatment standards wherever possible.

Annealing processes used to facilitate the subsequent manufacture of forged workpieces, such as coarse-grain annealing to improve machinability, hardening, or hardening plus tempering, are not considered here.

Heat treatment as a preparation to hot forming as well as the method of heating itself are likewise not discussed in this chapter since this information is contained in the appropriate process

**Table 26.1** Outline of the Most Important Heat-Treatment Processes with Data Concerning the Appropriate Temperature Ranges for Different Groups of Nonferrous Metals

Material group	Soft annealing, °C (°F)		Stress relieving, °C (°F)		Recrystallization annealing, °C (°F)		Solution annealing, °C (°F)	
	°C	°F	°C	°F	°C	°F	°C	°F
UNS C10100–13000	450–650	(840–1200)	200–250	(390–480)	200–400	(390–750)	—	—
UNS C22000–24000	500–600	(930–1100)	200–250	(390–480)	300–500	(570–930)	—	—
UNS C26000–27000	450–550	(840–1020)	200–250	(390–480)	200–400	(390–750)	—	—
Titanium	650–750	(1200–1380)	450–700	(840–1280)	—	—	—	—
Titanium alloys	650–880	(1200–1610)	260–280	(500–530)	—	—	760–980	(1400–1790)
Magnesium alloys	250–300	(480–570)	—	—	—	—	—	—

Source: Compiled from [26.1] to [26.4].

**Table 26.2** Guidelines for the Heat Treatment of Aluminum and Aluminum Alloys (Forgeable Materials)<sup>a</sup>

Material designation	Soft annealing temperature <sup>b,c</sup> , °C (°F)			Remarks	Solution annealing temperature <sup>b</sup> , °C (°F)	Annealing time <sup>d</sup> , min	Aging temperature <sup>b,e</sup> , °C (°F)	Aging time, h
	DIN	US	°C (°F)					
Al99.9 + Al99.98	AA 1050	290–310	(554–590)	—	—	—	—	—
Al99.7 + Al99.8	AA 1050	320–350	(608–662)	—	—	—	—	—
Al99 + Al99.5	AA 1050	340–380	(644–716)	—	—	—	—	—
AlMg1–3	AA 5005	340–380	(644–716)	—	—	—	—	—
AlMg5	AA 5056	320–360	(608–680)	Cool slowly	—	—	—	—
AlMg3Si	—	350–380	(662–716)	Cool slowly	—	—	—	—
AlMgMn	AA 5754	360–400	(680–752)	—	—	—	—	—
AlMn	AA 3103	360–400 <sup>f</sup>	(680–752) <sup>f</sup>	Heat quickly	—	—	—	—
E-AlMgSi	AA 6082	300–330	(542–590)	Cool slowly	500–580 (932–956)	20–60 (281–299)	155–165 (281–299)	6–18
AlMgSi0.5	AA 6060	330–360	(596–680)	Cool slowly	510–540 (950–974)	10–30 (272–347)	150–175 (272–347)	4–16
AlMgSi1	AA 6061	340–380	(644–716)	Cool slowly	510–540 (950–974)	10–30 (272–347)	150–175 (272–347)	4–16
AlCuMg0.5	—	350–380	(662–716)	—	495–505 (893–911)	—	Room temperature	5 days
AlCuMg1	AA 2017	360–400	(680–752)	Cool slowly	495–510 (893–950)	8–30	Room temperature	5 days
AlCuMg2	AA 2024	360–400	(680–752)	Cool slowly	450–500 (884–932)	5–30	Room temperature	5 days
AlZnMg1 <sup>g</sup>	AA 7020	380–430	(716–806)	20°C/h up to 220°C (36°F/h up to 400°F)	450–480 (812–866)	10–60	120–140 (218–284)	16–48
AlZnMg3	—	400–450	(752–842)	Cool slowly	460–485 (830–875)	10–30	Room temperature	90 days
AlZnMgCu0.5	AA 7079	420–450	(788–842)	Cool slowly	460–485 (830–875)	10–30	120–150 (218–272)	8–48
AlZnMgCu1.5	AA 7075	420–450	(788–842)	Cool slowly	455–475 (821–857)	10–20	120–150 (218–272)	8–48

<sup>a</sup>The values should be considered as approximate; it is advisable to obtain the supplier's own heat-treatment specifications.  
<sup>b</sup>Metal temperature.

<sup>c</sup>Soft annealing takes approximately 30 min, depending on workpiece thickness and heating-up speed.

<sup>d</sup>Usually followed immediately by quenching in water.

<sup>e</sup>Air cooling.

<sup>f</sup>Or 500–550°C (932–1,022°F) in the case of rapid heating. This depends on the initial condition, which should therefore be ascertained from the supplier.

<sup>g</sup>Standard in preparation.

Source: Compiled from [26.2].

## 26.4 BLANKING, PIERCING, SLUG PRODUCTION

chapters; for example, in Sec. 11.4 for free forging and die forging and in Sec. 16.4 for hot extrusion.

Thermomechanical treatment—a group of methods to improve the mechanical properties of medium- and high-alloyed construction and tool steels using a combination of heat-treatment and forming methods—is discussed in Sec. 30.2.

### 26.1.1 Main Heat-Treatment Processes for Steel

Fig. 26.1 aims at clarifying some of the terms used in this section. It represents a detail from the iron-carbon diagram and shows the typical temperature ranges of the most important heat-treatment processes as well as the changes in structure which arise. The literature relating to the heat treatment of steel [26.3] to [26.12] is mentioned here globally rather than making reference individually to specific texts.

#### Stress Relieving

**Purpose:** Stress relieving is used to compensate for and reduce internal stresses in workpieces caused by locally differing forming conditions and by the effects of uneven heat distribution. These internal or residual stresses lie in the elastic range. In the case of superposition of similarly oriented stresses, the elastic limit may be surpassed, thus leading to early failure of the component. This is sometimes brought about by temperature fluctuations or vibration during transport. The situation is made worse by the fact that the extent and distribution of internal stresses cannot be determined exactly in advance, and the investigation of such stresses is complicated.

Where stress relieving is required, it is usually carried out after the last forming operation and thus may be termed after-treatment.

**Procedure:** The annealing operation is carried out at temperatures which produce a notable reduction in the yield strength without causing any change in the material structure. Where heating is too rapid, there is a danger that stress peaks may be set up and the workpieces crack—in the case of insufficiently thorough heating—as a result of insufficient plastic deformability. For the same reason care should be taken to ensure slow rates of cooling.

In the case of steels, a temperature range of 500–650°C (930–1200°F) should be aimed at. Higher temperatures should be avoided in order to prevent or minimize the formation of scale.

The duration of the heat-treatment operation depends on the temperature chosen and is shorter for higher temperatures than for lower ones. Cooling to temperatures of around 250–300°C (480–570°F) is best performed in the furnace; thereafter air cooling is sufficient.

The temperature-time curve of a stress-relieving operation is shown schematically in Fig. 26.2.

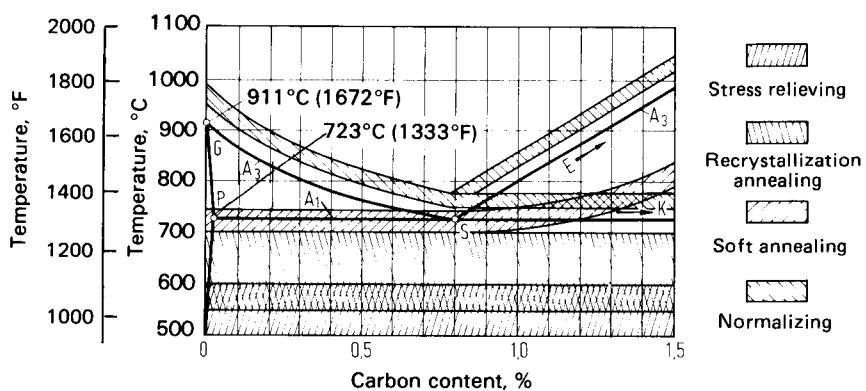
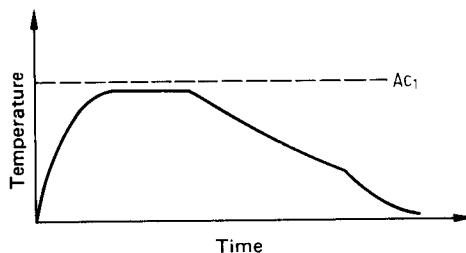


FIG. 26.1 Detail from the iron-carbon diagram showing annealing temperatures.



**FIG. 26.2** Schematic temperature-time curve for stress relieving of steel. (After [26.5].)

### Recrystallization Annealing

**Purpose:** In recrystallization annealing a new grain structure is created. This counteracts the work hardening of the material and increases its formability so that further forming operations can be performed.

The newly created structure should be fine-grained so as to improve the mechanical properties and forming conditions. Coarse-grained structures exhibit reduced stress and strain values and are unsuitable for forming operations. They are particularly troublesome in sheet-metal forming. In deep-drawing, stretch-forming, bending, and drawing-out operations the coarse surface finish resulting from the large average grain size of the initial material often leads to the workpiece being unusable. In cold metal forming, recrystallization annealing performs an important role as an intermediate treatment. Nevertheless here, too, in zones of small local deformations, such as in the deformation zone in the case of cold extrusion, coarse grain structure may occur. Where this cannot be tolerated, normalizing should be carried out instead of recrystallization annealing (see subsection on normalizing).

The recrystallization diagram shown in Fig. 26.3 illustrates the relationships which are fundamental to recrystallization (see also Sec. 3.6).

**Procedure:** In determining the temperature and duration of the annealing operation, the factors mentioned above must be taken into account. Additional factors of importance are the rate of heating and the holding time. Rapid heating reduces the danger of coarse-grain formation.

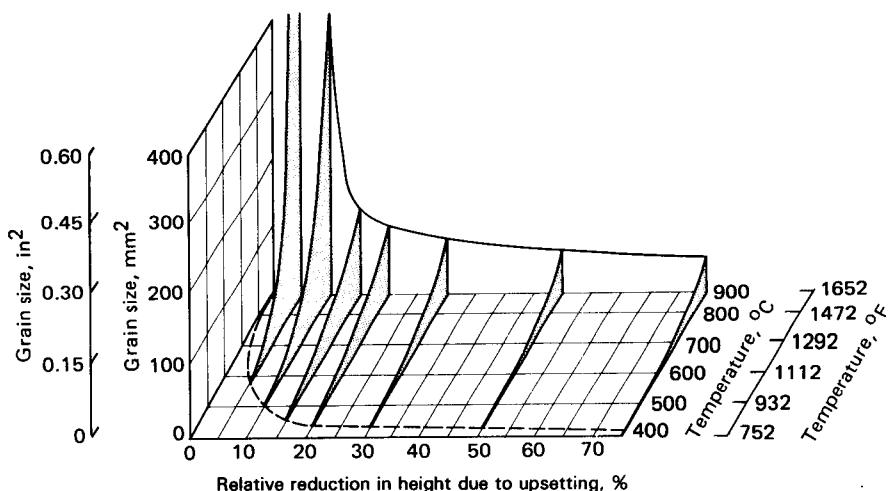


**FIG. 26.3** Recrystallization diagram of electrolytic iron according to Oberhoffer and Oertel. (After [26.13].)

## 26.6 BLANKING, PIERCING, SLUG PRODUCTION

The recrystallization temperature depends on the material properties and on the degree of deformation. In general it lies in the range of 600–700°C (1110–1290°F). More exact values may be obtained from the appropriate recrystallization diagram.

With hypereutectoid steels, the temperature must lie below the transformation line  $A_{C_1}$ . When the  $A_{C_1}$  line is crossed, pearlite dissolution takes place, leading to a brittle cementite structure [26.6].

This danger does not exist in the case of hypoeutectoid steels because of the low pearlite content so that here the annealing time can be reduced by increasing the annealing temperature. The specified recrystallization time must be respected exactly. Exceeding the specified time leads to coarse-grain formation.

The area of critical deformation of the structure, which includes structural changes up to approximately  $\epsilon \leq 0.10$ , should be considered in more detail because of the coarse-grain formation at the recrystallization temperature. Often critical deformation, as occurs for example in bending, cannot be avoided. In such cases, by using prestrained materials it is possible to ensure that the critical deformation limit is exceeded over the entire workpiece. A further possibility is to replace recrystallization annealing by normalizing or recovery annealing.

Where recrystallization takes place during the forming operation, as is the case in hot rolling, work hardening of the material does not occur. This depends not only on recrystallization but also on crystal recovery (see also Sec. 3.6).

### Soft Annealing, Spheroidizing

**Purpose:** In soft annealing the aim is to transform the lamellar pearlite into globular pearlite (Fig. 26.4). During the forming operation the soft ferrite is transformed into pearlite grains while the hard cementite remains unchanged. In the lamellar state the possibility of ferrite slipping is severely limited. On the other hand, in globular pearlite the spheroidized cementite offers much less resistance to ferrite slipping, thus facilitating the forming operation.

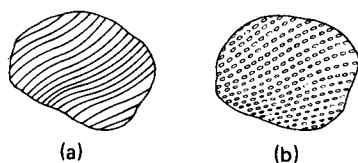


**FIG. 26.4** Schematic illustration of (a) lamellar and (b) globular pearlite.

Soft annealing is performed as a pretreatment prior to the forming operation. The aim is to achieve low flow stress and high ductility values.

Particularly in cold bulk forming, soft annealing of coils and slugs is an important part of the raw-material preparation.

**Procedure:** In the case of steel two types of annealing operation are widely used:

- 1 **Annealing at temperatures just below  $A_1$ :** The temperature is chosen near to  $A_{C_1}$ , that is,  $\approx 680\text{--}720^\circ\text{C}$  (1250–1325°F). In this case the strength of the cementite is reduced so far that the lamellar structure breaks down. Complete dissolution takes place after 3–5 h. This is followed in all soft-annealing processes by slow cooling in the furnace.
- 2 **Pulse or cycle annealing about  $A_1$ :** Increasing the temperature in the area of  $\gamma$ -transformation leads to a faster breakdown of the cementite laminae. Heat cycling about  $A_1$  shortens the annealing time. Guidelines for the upper temperature value, which should be maintained for about 15 min, are given as follows as a function of the carbon content:

Carbon content, %	Approximate temperature, °C (°F)
< 0.9	730 (1340)
0.9–1.2	750 (1380)
1.2–1.5	770 (1415)

The lower temperature value is about 650°C (1200°F) with a holding time of approximately 30 min.

Apart from the two methods already mentioned, there are two further soft-annealing processes one of which should be mentioned in particular because it reduces the annealing time considerably. The material to be annealed is brought to a temperature just above  $Ac_3$ , held there for a short time, quenched, and then tempered for a longer period of time just below  $Ac_1$ .

The time curves of different soft-annealing processes are shown schematically in Fig. 26.5.

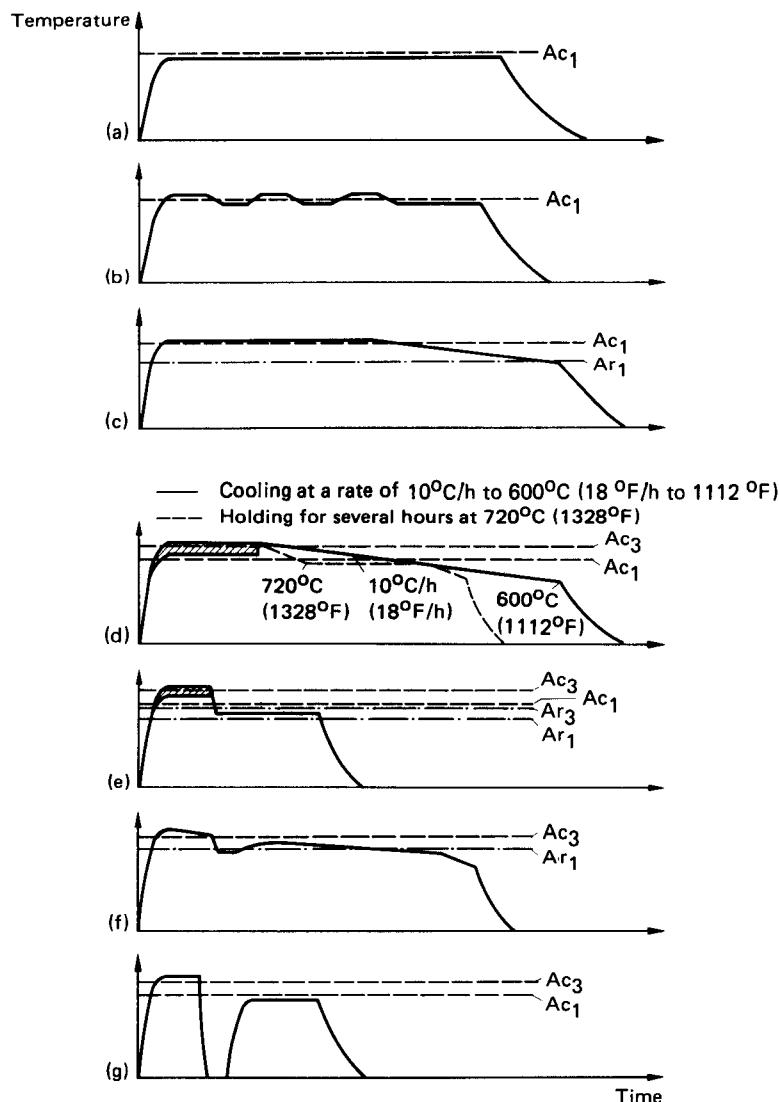


FIG. 26.5 Schematic temperature-time curves for soft annealing of steel. (a) Long annealing time just below  $Ac_1$ . (b) Temperature oscillation about  $Ac_1$ . (c) Long annealing time  $10\text{--}20^{\circ}\text{C}$  ( $18\text{--}36^{\circ}\text{F}$ ) above  $Ac_1$  followed by gradual cooling to below  $Ar_1$ . (d) Annealing in a temperature range from above  $Ac_1$  to just above  $Ac_3$ . (e) Annealing around  $Ac_3$  followed by controlled cooling to below  $Ar_1$ . (f) Hardening with subsequent long-time tempering at a temperature just below  $Ac_1$ . (After [26.5].)

### Normalizing

**Purpose:** The main aim of normalizing is to transform the material structure. In this way structural differences resulting from the preceding heat-treatment and forming operations are overcome together with the removal of any coarse grain structure. Work hardening is largely removed by reducing the dislocation concentration so that following the heat treatment further forming operations may be carried out. As in soft annealing, the aim is to achieve a basic pearlite structure enclosing spheroidized cementite.

Normalizing is necessary in very many different cases. Thus, for example, cold-extruded and subsequently quenched shells tend to crack in the transition zone between the cup bottom and the walls; this can be avoided by normalizing. In hot forging pronounced structural differences may occur due to differing forming and cooling conditions, and these must be removed. Highly stressed die forgings must therefore be normalized.

Furthermore the so-called secondary band structure, consisting of ferrite lines interspersed with pearlite, leading to reduced mechanical properties lateral to the rolling direction, may be overcome by normalizing followed by rapid cooling.

In practice, normalizing is often used instead of recrystallization annealing, particularly where the latter process leads to localized formation of coarse grain structure.

**Procedure:** In normalizing steel, the aim is often to create a secondary structure suitable to a particular application. The approach adopted in practice depends largely on the chemical composition of the material concerned.

For hypoeutectoid steel ( $C < 0.8\%$ ) the most suitable temperature is about  $30\text{--}50^\circ\text{C}$  ( $85\text{--}120^\circ\text{F}$ ) above the G-S ( $\text{Ac}_3$ ) line, whereby the lower temperature should be chosen in conjunction with low-carbon steels (see Fig. 26.1). Higher temperatures should be avoided, since besides encouraging growth in the grain size, they also cause increasing segregation of ferrite at the grain boundaries. With hypereutectoid steels ( $C > 0.8\%$ ) two different annealing processes are used. When normalization is carried out in a temperature range just above the S-K ( $\text{Ac}_1$ ) line [26.4], [26.6], that is, at  $\approx 750\text{--}780^\circ\text{C}$  ( $1380\text{--}1430^\circ\text{F}$ ), only the basic pearlite structure is modified, while the secondary cementite remains largely unaffected [26.7]. Where, on the other hand, annealing takes place at temperatures of  $\approx 30\text{--}50^\circ\text{C}$  ( $85\text{--}120^\circ\text{F}$ ) above the S-E ( $\text{Ac}_3$ ) line followed by rapid cooling, the segregation of the secondary cementite can be suppressed. A homogeneous fine lamellar pearlite structure results which is tough and which may be easily soft-annealed to form globular cementite [26.7].

The annealing time depends on the carbon content, its distribution, and on the cross section of the workpiece. Basically, heating to just below  $\text{Ac}_1$  or  $\text{Ac}_3$  may be carried out slowly (e.g., in a continuous annealing furnace) or rapidly (e.g., in a chamber or batch furnace). In the case of rapid heating small mixed  $\gamma$ -crystals are produced, and under similar cooling conditions, the finer  $\gamma$ -crystals lead to a fine-grained secondary microstructure. On the other hand, rapid heating leads to the danger of setting up internal stresses. In both cases uniform thorough heating is of prime importance. Thereafter it is important to reach the specified temperature as fast as possible. The holding time should be long enough to permit the complete transformation of the structure (e.g., the time for hypoeutectoid steels to become completely austenitized). As a rule of thumb, the following relationship can be applied:

$$20 + \frac{d [\text{mm}]}{2} = \text{holding time} [\text{min}]$$

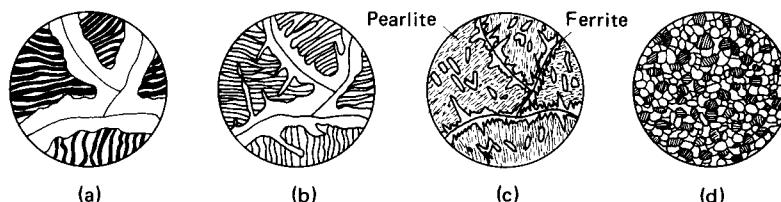


**FIG. 26.6** Schematic illustration of the structural changes arising due to increasingly fast rates of cooling of a hypoeutectoid normalized steel. (After [26.4].)

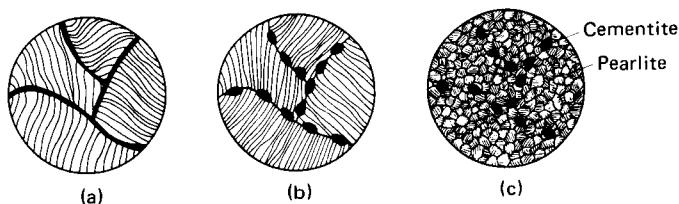


**FIG. 26.7** Schematic illustration of the structural changes occurring during normalizing of hypereutectoid steels. (a) Before annealing. (b) After annealing followed by slow cooling. (c) After annealing followed by rapid cooling. (After [26.4].)

where  $d$  is the maximum diameter of the workpiece [26.8]. Cooling is best carried out in still air. Where the resulting structure is not fine-grained enough, an air current can be used as the cooling medium. Care should be taken to ensure that all workpieces are separated from each other by an air gap. Only in this way can consistent cooling be achieved.

Structural changes obtained after cooling are shown schematically in Figs. 26.6 and 26.7.

### 26.1.2 Additional Heat-Treatment Processes for Steel

#### Bright Annealing

**Purpose:** Production of a clean scale-free surface. Any oxide layer which may be present can be removed in this way. Bright annealing may be performed in conjunction with a number of heat-treatment processes described in Sec. 26.1.1. Both semifinished (coils, bars, sheet, strip) and finished products may be bright-annealed.

**Procedure:** During the heating period in the furnace, a neutral or mildly reductive atmosphere is required. Oxidation occurs during the cooling phase. For this reason the material to be annealed must be protected from contact with oxygen during cooling, for example, by using a protective gas (as in the Siemens-Prüfert and Vitry bright-annealing processes) or by airtight containers (as in the Grünwald process). Protective or inert gases envelope the work surfaces in a neutral atmosphere. Information concerning the inert gases most often used (endothermic, exothermic, and monogases), their production, method of action, and use in the heat treatment of cold-formed semifinished and finished workpieces is given in [26.14] to [26.16].

#### Patenting

**Purpose:** The drawing of steel wires and coils may be performed best when the initial material structure is of fine lamellar pearlite, known as sorbite. This structure is achieved by means of suitable heat treatment. The process is used to produce the initial material for high-strength wire, for example, for springs, wire ropes, and piano wires.

**Procedure:** The material is heated to the austenitizing temperature and rapidly cooled to a temperature in the region of the lower pearlite point. Quenching may be performed in a lead or salt bath or alternatively in air. Lead patenting may either be carried out as bath patenting, where the coils to be annealed are submerged in a bath, or as continuous patenting.

The following sections concentrate on the most important annealing processes used for the most commonly formed nonferrous metals and their alloys. Further information may be obtained in condensed form from Table 26.1. In case of the annealing processes already mentioned in Sec. 26.1.1, only the procedure used will be discussed. Beside the references mentioned specifically in the text, further information is given in [26.1], [26.3], [26.4], and [26.17].

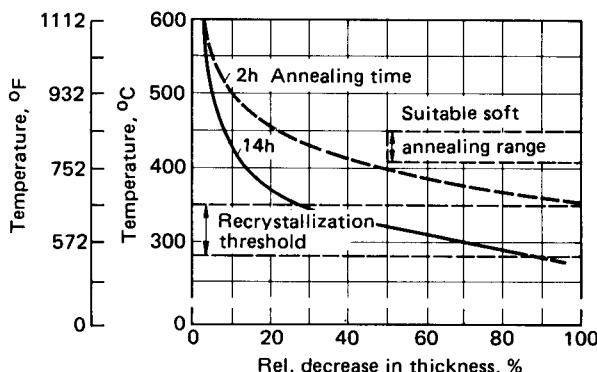


**FIG. 26.8** Lowest recrystallization temperatures of cold-rolled aluminum (so-called recrystallization threshold). (After [26.2].)

### 26.1.3 Heat-Treatment Processes for Aluminum and Aluminum Alloys

#### Recovery Annealing

**Purpose:** This annealing process is mainly used to produce so-called semihard products (mainly semifinished products). With this aim in mind an operation with severe work hardening is followed by annealing. Compared with less work-hardened material without subsequent annealing—for equal strength—higher strain values can be achieved [26.2]. Furthermore, recovery annealing reduces work hardening.

**Procedure:** The temperature range must lie below the recrystallization threshold (Fig. 26.8). A long annealing time followed by slow cooling guarantees uniform results.

#### Stress Relieving

The aim already described in Sec. 26.1.1 can be achieved at temperatures similar to those used for recovery annealing.

Further information on stress relieving, such as on solution annealing used to reduce the internal stresses set up in hot-extruded bars and sections, can be found in Sec. 16.5.2. Guidelines on the procedure to be followed in solution annealing are given in Table 26.2.

#### Recrystallization Annealing

The recrystallization effect, the creation of new grains by means of suitable heat treatment following work hardening due to cold working (see subsection on recrystallization annealing in Sec. 26.1.1), depends to a large extent on the influence of the particular degree of deformation, the annealing temperature, and the annealing time on the grain size of the material to be annealed. These relationships are illustrated in Figs. 26.8, 26.9, and 26.10. Fig. 26.8 shows typical values for the heat-treatment process as a function of the degree of cold forming which has already taken place. The recrystallization temperature decreases with the degree of deformation. Fig. 26.9 shows the well-known influence of cold forming on the grain size during recrystallization. The recrystallization diagram in Fig. 26.10 illustrates the areas of growth of coarse grain structure. In this connection reference is made to the process of secondary recrystallization, which in the case of highly deformed grains and unnecessarily high temperature (see Fig. 26.8) leads to the formation of extremely coarse grain.

#### Soft Annealing

The most suitable structure for cold forming with the lowest strength and the highest ductility values is achieved by soft annealing performed under the condition outlined in Table 26.2. The

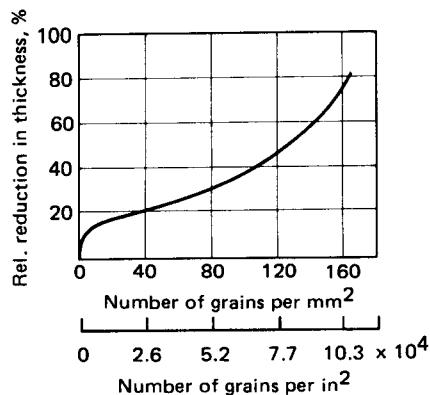


**FIG. 26.9** Grain size of cold-rolled recrystallized pure aluminum Al99.5 (AA 1050 A). (After [26.2].)

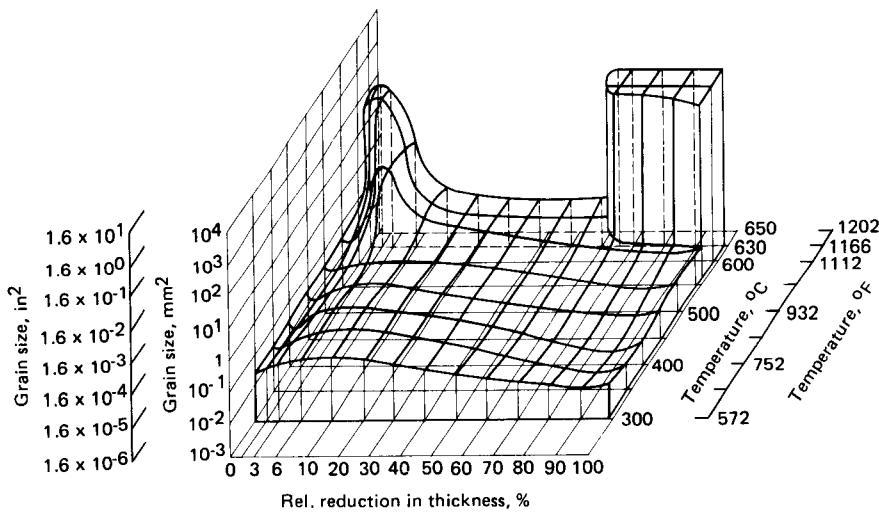
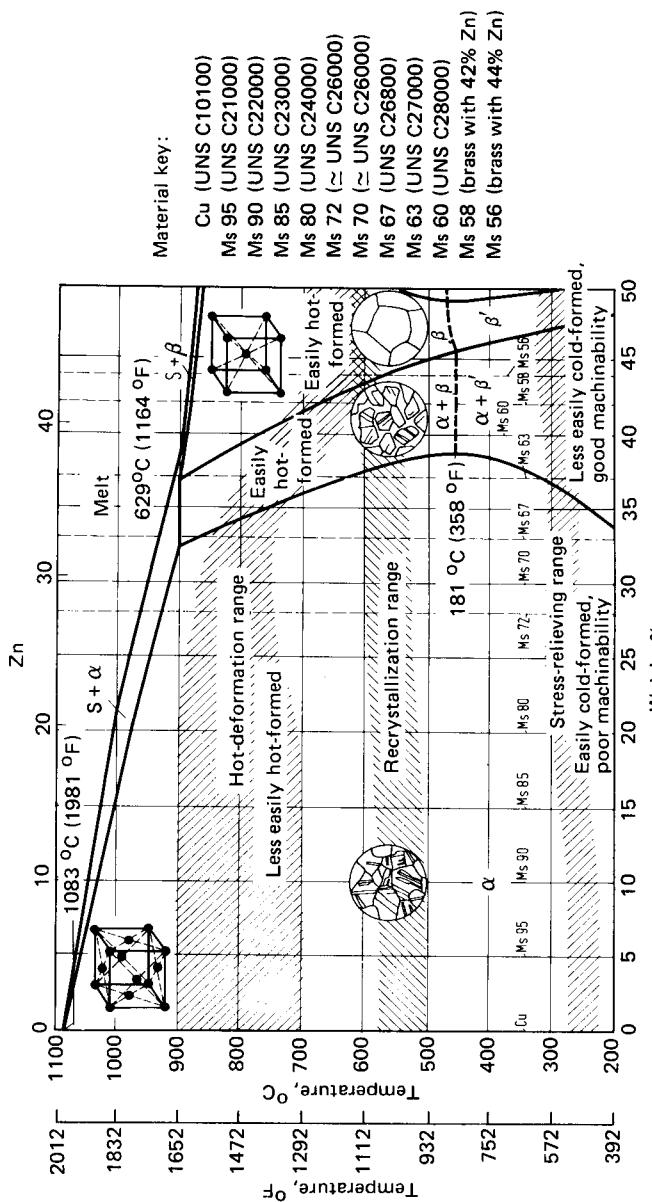


**FIG. 26.10** Recrystallization diagram of pure aluminum Al 99.6. (After [26.2].)

furnace must have reached the annealing temperature at the start of the annealing operation. The annealing time depends on the size of cross section to be treated. Cooling is carried out slowly. With cold-drawn semifinished material there is an onset of recrystallization during the soft-annealing process.

It is important to ensure that the alloying elements, which in the case of aluminum alloys go into solution, are precipitated out during cooling so that no further precipitation hardening can occur during longer periods of storage.



26.12

FIG. 26.11 Detail from the copper-zinc equilibrium diagram showing temperature ranges for the heat treatment of cast and forgeable alloys. (After Kopp and Kummerle.)

#### 26.1.4 Heat-Treatment Processes for Copper and Copper Alloys

Because of the considerable importance attached to the use of brass in metal-forming operations this section concentrates mainly on this material. Further information is given in [26.18], Fig. 26.11, and Table 26.1; refer also to [26.17].

##### **Stress Relieving**

Drawn hollow bodies, such as deep-drawn cups or drawn tubes made of brass, exhibit locally very different internal stresses as a result of cold work hardening. Such workpieces tend to exhibit stress cracks initiated by external stresses or by corrosion. The stress sensitivity of brass increases with the zinc content. Such internal stresses and the danger of cracking can largely be removed by annealing below the recrystallization threshold, that is, in a temperature range of 200–280°C (390–530°F) with an annealing time of up to 1 h.

A typical example of the need for this kind of heat treatment is given in Fig. 26.12, which shows a cracked tea-glass holder formed from a deep-drawn brass cup.

##### **Recrystallization Annealing**

Information concerning the relationship between the degree of deformation, the annealing temperature, and the Brinell hardness as well as rough values relating to the average obtainable grain diameters as a result of recrystallization annealing (see also Sec. 26.1.1) are given in [26.18]. The rate of heating is also of importance; increasing values lead to increasingly fine grains. Particularly fine grains are achieved by annealing in the lower temperature range suitable for soft annealing, that is, at about 450°C (840°F).

Typical average grain diameters are 30–40  $\mu\text{m}$  (1.2–1.6  $\mu\text{in}$ ). For grain sizes starting at about 50  $\mu\text{m}$  (2.0  $\mu\text{in}$ ) the well-known “orange-skin” effect begins to appear during deformation.

##### **Soft Annealing**

The most suitable temperature range for soft annealing may be considered to be 450–700°C (840–1290°F) [26.18]. With the exception of  $\alpha$ - $\beta$  alloys, the rate of heating and cooling has little significant effect on the heat-treatment result [26.3]. More important, on the other hand, are the heat source, type of furnace, and furnace atmosphere as well as the shape of the material to be annealed.

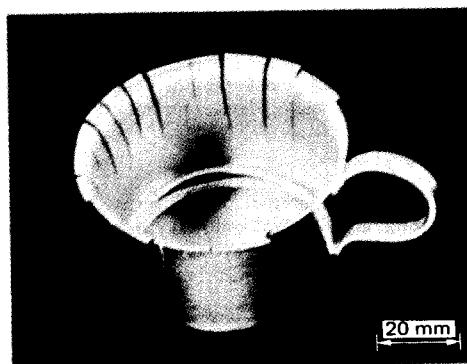


**FIG. 26.12** Stress cracks in a tea-glass holder made of (silver-plated) brass which was not stress-relieved after cupping. (Courtesy of Staatliche Materialprüfungsanstalt Stuttgart.)

### ***Homogenizing***

Phosphor bronzes with a high zinc content ( $> 8\%$ ) tend to exhibit block segregation. In order to achieve a homogeneous structure before deformation (e.g., hot or cold rolling), the cast slabs are annealed at high temperatures,  $730\text{--}780^\circ\text{C}$  ( $1340\text{--}1430^\circ\text{F}$ ), and long holding times. Before annealing, a solid solution of high zinc concentration exists in the slab core. The equalization of the differences in concentration takes place during annealing by means of a relatively slow diffusion process (see Sec. 3.6).

#### **26.1.5 Defects Caused by Improper Heat Treatment**

The major problems caused by incorrect heat treatment prior to the forming operation are:

- Formation of coarse grain
- Surface decarburization
- Surface burning

Coarse grains are caused by overheating or by holding for too long a time at the annealing temperature. They can be completely removed by normalizing, in some cases after several successive treatments.

Surface or skin decarburization may occur in steels as a result of the diffusion of carbon into the atmosphere due to excessively long annealing times. In this way the surface layer is decarburized; as a result this layer exhibits poorer mechanical properties than those of the core. Where the surface layer is not to be removed by a subsequent machining operation, the defect can be overcome by recarburization. To this end, the workpieces are exposed to a carburizing atmosphere from which the surface layer reabsorbs carbon.

A burnt structure is a defect which cannot be overcome. Heat treatment carried out at too high a temperature leads to an irreversible oxidation of the grain boundaries. This weakens the material cohesion at the grain boundaries; the strength decreases, rendering the material unusable.

#### **26.1.6 Equipment**

The multitude of heat-treatment processes require a wide range of equipment in order to cope with the variety of workpieces which are to be annealed under controlled conditions. Since the emphasis in this *Handbook* is on manufacturing and auxiliary processes only, the most important types of equipment in use for the heat treatment of semifinished and finished workpieces in the area of metal forming are discussed here. More detailed information can be found in [26.19] and [26.20].

Heating equipment for heating workpieces up to the temperatures required for forging processes is described in Sec. 11.4, while heating devices for hot extrusion are outlined in Sec. 16.4.

### ***Heating Media***

The media used for heating the many different kinds of furnaces include gas (town gas, grid gas, natural gas, and generator gas), oil (both light and heavy mineral oil), and electric energy. Heat transmission to the material to be annealed may be either direct by means of convection and radiation, as with gas- and oil-fired furnaces, or, principally by radiation, as in the case of most electrically heated furnaces.

Gas- and oil-fired furnaces generally heat up faster and are often cheaper than electrically heated furnaces. Energy consumption may be reduced by preheating the combustion air by heat exchange with the waste gases, thereby improving the efficiency of the equipment. Electric energy offers the advantages of freedom from soot and operational dangers as well as more exact temperature control. Heating elements are either coiled resistance wire or bands up to  $1000^\circ\text{C}$  ( $1830^\circ\text{F}$ ) or ceramic rods up to temperatures of about  $1300^\circ\text{C}$  ( $2370^\circ\text{F}$ ) under continuous operation. Because of the absence of turbulence in the furnace—set up naturally in the case of oil and

gas burners by the exhaust gases—undesirable temperature distribution may occur in the furnace, which has to be overcome by the provision of fans. The possibilities of heating workpieces by means of induction heating or conductive heating are described in Sec. 11.4.

### Annealing Furnaces

An outline of the most important types of furnaces and of the main categories of materials to be annealed is given in Table 26.3. A classification based on the method of heating is no longer applicable since any given annealing furnace can now be equipped to operate with any desired heating medium. Furthermore, annealing processes themselves offer no differentiating criteria since the attainable temperatures depend on the layout and the capacities of the individual heating devices, which in turn depend on the particular application.

The heat treatment of wire calls for long annealing times—here one is principally concerned with soft annealing—for which pot annealing furnaces (Fig. 26.13) and bell annealing furnaces (Fig. 26.14) are most suitable. Pot annealing furnaces are still widely used in Europe, while in the United States they have largely been replaced by multiple-stack bell furnaces [26.19]. Alloy steels may also be annealed in salt bath or roller-hearth continuous annealing furnaces, whereas in connection with galvanizing plants conveyer furnaces are used almost exclusively [26.18].

**Table 26.3** Main Types of Furnaces Used for Heat Treatment in Metal-Forming Processes

Annealing furnaces	Material					Comments
	Bars, rods, tubes	Wire bundles	Coils	Massive parts (bar and wire sections, slugs, formed parts)	Sheet-metal parts (blanks, formed parts)	
<i>Batch furnaces</i>				x	x	For small batches and in the laboratory
	Chamber furnace <sup>a</sup>					
	Shaft furnace, pot furnace	x	x	x	x	
	Bell-type furnace <sup>a</sup>	x	x	x	x	
<i>Increasing quantities</i>	Bogie hearth furnace	x	x			
	<i>Throughput furnaces<sup>b</sup></i>			x		Only for small parts Also with con- veyer chains
	Spiral furnace			x		
	Conveyer-belt furnace			x	x	
<i>Increasing quantities</i>	Grate continuous- discharge furnace	o	o	x	x	
	Roller hearth furnace	x	x	x	o	

<sup>a</sup> Without or with retort.

<sup>b</sup> The types of furnaces listed represent a selection of the numerous existing furnaces, which differ mainly in the way the workpieces are transported.

x—frequent; o—seldom

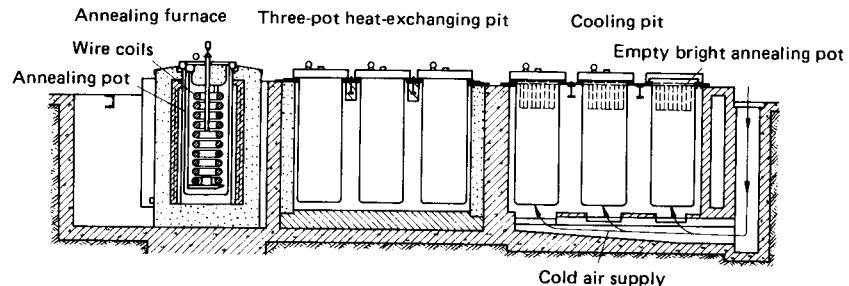


**FIG. 26.13** Electrically heated postannealing furnace, as built by BCC and Grünwald. (*After [26.19].*)

The most common furnaces used for the heat treatment of wide cold-rolled strip are bell and conveyer furnaces. Bell and pot furnaces (Fig. 26.15) as well as roller-hearth continuous furnaces are used for heat treating coils of medium and small widths [26.20]. With conveyer furnaces the strip is unrolled prior to annealing. It passes rapidly in succession through the heating, holding, and cooling zones and is then recoiled, in contrast to the other types of furnaces mentioned where the coils themselves are annealed. Pot and bell furnaces sometimes give rather inconsistent annealing results. They are, however, more economical than fully automated continuous furnaces which give more consistent results.

For small batches the heat treatment of particular components is carried out in chamber furnaces (Fig. 26.16). For medium-batch sizes pot and bell furnaces are most commonly used. Large batches are generally annealed in continuous-throughput furnaces (Fig. 26.17).

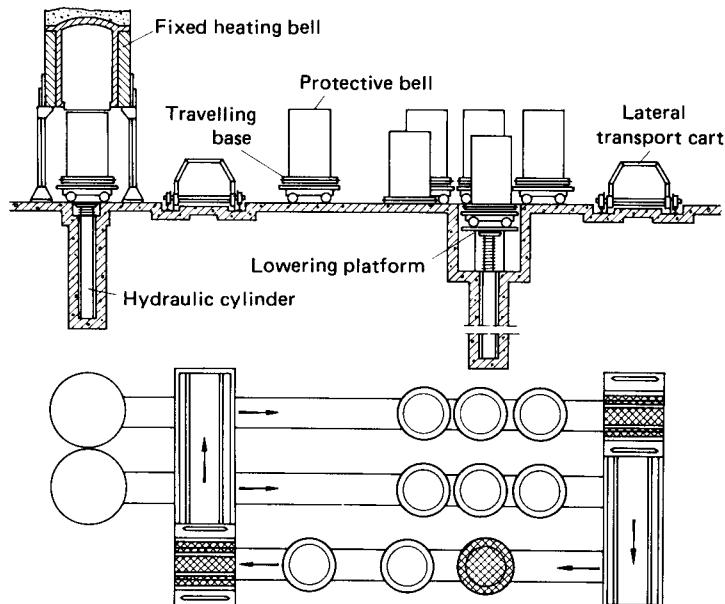


**FIG. 26.14** Hood or bell-type annealing furnace with fixed heating bell, as built by Fritz. (*After [26.19].*)

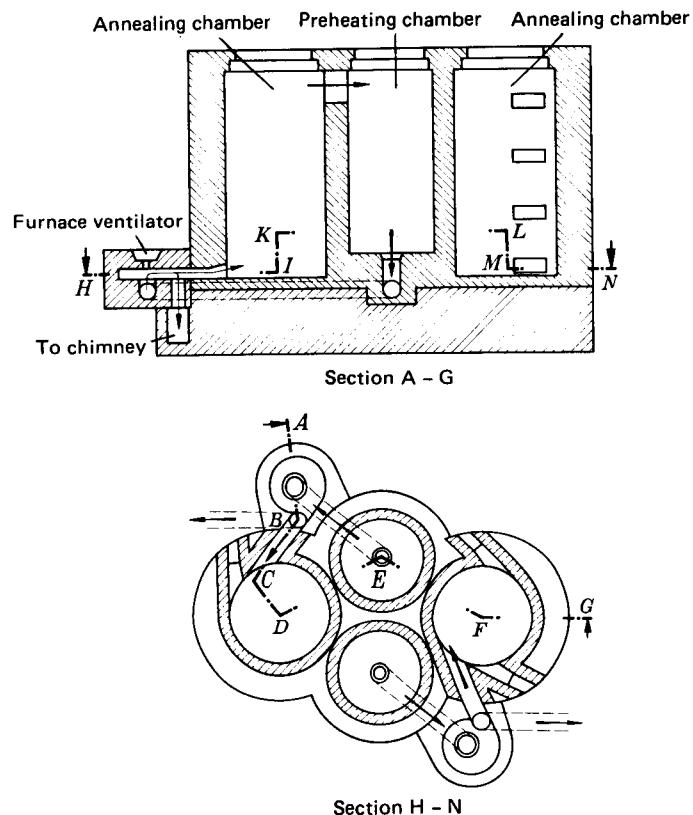


**FIG. 26.15** Four-chamber pot annealing furnace, after J. G. Brockhaus, R. Horst, and A. Lüth. (After [26.20].)

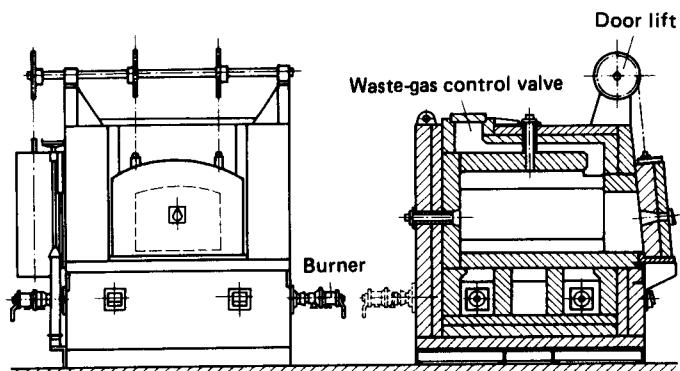


**FIG. 26.16** Single-chamber furnace with gas or oil burners, as built by Aichelin.

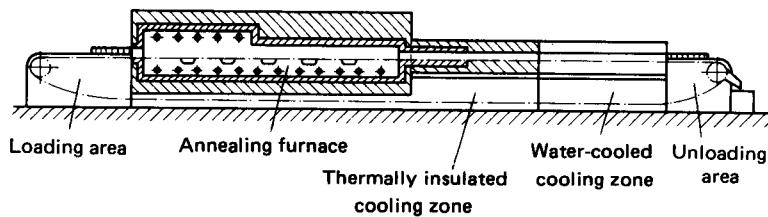


**FIG. 26.17** Schematic diagram of a conveyer-type continuous annealing furnace, as built by Aichelin.

## 26.2 SURFACE TREATMENT

The significance of surface treatment as a way of preparing workpieces for metal-forming operations was discussed in detail in Chap. 6. Information on specific methods of surface treatment, such as descaling [26.21], [26.22], cleaning [26.23], application of lubricant carriers [26.24] to [26.26], and lubricants [26.27], [26.28] is given in the references quoted. Since lubricant carriers and lubricants themselves are discussed in the relevant chapters, it is sufficient to concentrate here on the techniques of applying these layers and on the equipment used to do so. Only a brief outline is given of the lubricants themselves.

Only very few forming processes can be carried out without recourse to surface treatment of the workpiece. Examples of these are free-forming processes, such as swaging, spreading, fullering, expanding, and hammering, as well as some bending processes and hot extrusion of easily extrudable materials. In other cases effective lubrication is carried out by the pressure medium itself so that additional treatment of the surface is not required; an example of this is hydrostatic extrusion. In die forging, the material to be forged generally requires no specific surface treatment. Instead, graphite-based lubricants are applied to the working surfaces of the dies with the aim of providing a separating layer between tool and workpiece at the same time as reducing the rate of die wear. Separation alone is often achieved by covering the die in a thin layer of sawdust. When the sawdust ignites, the combustion gases force the workpiece out of the die. By contrast, in precision forging, the workpiece itself is often coated with a lubricant in order to increase the tool life of the closely tolerated dies.

Besides this heterogeneous variety of measures to avoid a special surface treatment of materials and workpieces, numerous metal-forming processes require a similar approach to surface treatment, for example, in the case of large increases in surface area combined with high normal stresses.

In deep drawing of sheet metal, a film of lubricant is usually sufficient to prevent contact between the workpiece and die materials. Oil and grease are the most common lubricants used here. For light drawing operations emulsions may be sufficient, while in cases of higher surface pressures, oils with high-pressure additives or containing solid lubricants may be used. On the other hand coated sheet metal can also be deep-drawn. A distinction can be made here between the forming of composite materials (e.g., plastic-coated steel sheet or strip) and the specific application of coatings to facilitate the forming operation. The latter is sometimes carried out in conjunction with the deep drawing of some stainless steels in cases where grease and oil have proved unsuccessful. The sheets in this case are covered with a self-adhesive plastic coating (e.g., polyvinylchloride) or painted with a drawing paint. These coatings may easily be removed after the forming operation has been completed. They act as a protective foil during transport, storage, and cutting; during the drawing process they form a first-class separating and lubricating layer.

Still higher compressive stresses in the deformation zone occur during pushing-through and pulling-through processes. With easily deformed nonferrous metals a lubricating layer is often sufficient to avoid metallic contact between the workpiece and the die. In steel this function is performed by a pressure-resistant lubricant-carrier layer in conjunction with an appropriate lubricant. This section deals mainly with the surface treatment of steel, which in general causes more difficulties than is the case with nonferrous metals. It is not possible to take account here of all metal-forming processes. Further information should therefore be sought in the chapters relevant to the particular processes.

Finally reference should be made in passing to several specialized topics not mentioned later in the text. Information on lubricants for cold rolling of steel is given in [26.29]; lubricants for hot and cold rolling of aluminum are discussed in [26.30]. In cold rolling of aluminum, low-viscosity mineral oils at 20°C (68°F) with fatty oil additives are employed with rolling speeds of up to 800 m/min (2400 ft/min). Above this speed, emulsions are more suitable because of their better cooling effect and reduced amounts of deposit. The lubricants most commonly used for rod and wire drawing of nonferrous metals (copper, brass, aluminum) are discussed in [26.28] (see also Table 14.1). The same authors also describe lubricants used for tube drawing. A lubricant for hot drawing of titanium is described in [26.31].

### 26.2.1 Rod and Wire Drawing

Rolled steel wire requires extensive surface treatment before drawing, consisting mainly of descaling, application of a lubricant-carrier layer (this may sometimes be dispensed with when the reduction in cross-sectional area is small [26.32]), and application of a lubricant layer (see also Sec. 14.2). The process is interspersed with numerous washing operations; subsequent drying is carried out either in air or in the furnace. Surface treatment in connection with the drawing of steel rod and bars is carried out in much the same way.

#### *Mechanical Descaling*

In descaling by bending the wire is usually drawn through either two or four rolls. The layer of scale cracks at about 3–5% strain, at 8–9% strain the scale falls off partly, and at 12% strain it falls off completely [26.32]. This is generally followed by mechanical cleaning (brushing or rubbing off).

In abrasive descaling the abrasive—usually particles of steel wire of 0.4–0.5 mm (0.016–0.020 in) diameter—are accelerated by means of centrifugal wheels [26.33], either in a continuous-throughput plant (for uncoiled wire) or in a circular plant [for loose coils, mainly of wire diameter < 7.5 mm (0.3 in)] [26.34]. This is usually followed by a rapid pickling operation as an integral part of a subsequent surface-treatment procedure.

The costs of mechanical descaling lie between approximately 60 and 70% of those incurred during pickling [26.32], [26.33].

#### *Chemical Descaling (Pickling)*

Unalloyed steels can be descaled by means of sulfuric-acid or hydrochloric-acid pickling. In the case of alloy steel, mixed pickling baths have proved valuable, which in addition to sulfuric acid also contain hydrochloric acid or nitric acid, or both [26.35]. Pickling plants with multiple dipping baths mostly arranged in a line, but sometimes also in a circle, are widely used for pickling wire coils, whereas continuous-throughput pickling plants, in which uncoiled wire is drawn through the baths in several strands at a time (Fig. 26.18), is usually economical only in conjunction with heating and other surface-treatment operations [26.37]. The pickling time can be reduced by vibrating the wire coils or by inducing ultrasonic waves through the baths.

#### *Application of Lubricant Carriers*

After descaling, lubricant carriers are applied by dipping the material in hot solutions or slurries. This is followed by the application of the lubricants themselves.

**Lime:** This is the cheapest and most commonly used lubricant carrier. It is used where the degree of deformation during forming is small. It neutralizes the remains of the pickling acid and saponifies organic fats during drawing. The procedure used is to immerse the wire, usually several times, in milk of lime containing between 3 and 30 g Ca (OH)<sub>2</sub> per liter at a temperature of 90°C (194°F) [26.38].

**Ironhydroxide:** This is a product formed on the surface when wire left moist from spraying comes in contact with oxygen in the air (so-called bluing) [26.35]. After subsequent treatment with lime it forms a strongly adhesive lubricant carrier for natron soap. It is used in the drawing of patented wire and where forming is carried out in several draws.

## 26.20 BLANKING, PIERCING, SLUG PRODUCTION

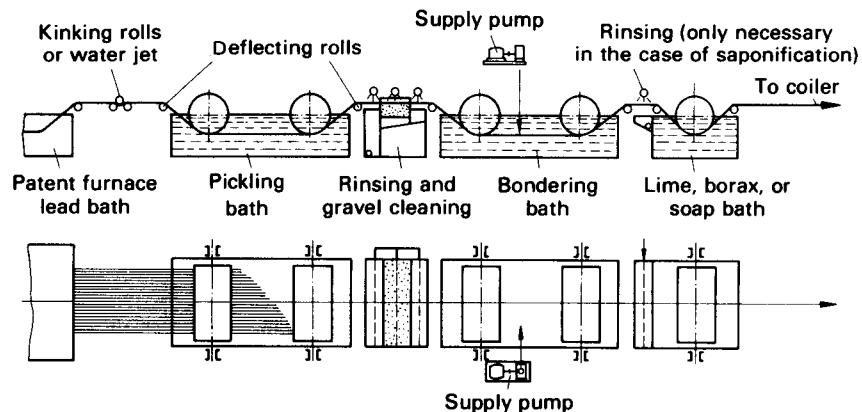


**FIG. 26.18** Schematic illustration of continuous pickling plant for steel wire. (After [26.36].)

**Phosphate coatings:** These are most suitable for difficult drawing operations. The lubricant-carrier layers are of zinc or iron phosphate [26.36], [26.39] formed by chemical reactions between the phosphate solution and the surface of the steel. The pressure resistance, wear resistance, and adhesion are far better than with other common lubricant carriers. Phosphate layers are therefore used where the degree of deformation is high, for high drawing speeds, and for drawing high-strength steels. Their main disadvantage is the relatively high cost.

The phosphating operation is normally integrated into the work sequence of the pickling department. It requires three baths: a preheating bath (also used for rinsing) operating at 80–90°C (176–194°F), a phosphating bath operating at temperatures of about 70–75°C (128–137°F), and a bath of cold water for rinsing after phosphating. The phosphating operation itself is carried out either by submerging the rolled-up coil of wire for 5–15 min in the phosphating bath or, in the continuous-throughput process, by unwinding the wire coils and passing 20–40 strands simultaneously for 30–60 s through the bath, the latter producing the more consistent results.

**Further lubricant layers:** Besides lime, borax is also used in continuous plant. Wet bright drawn wire with a shiny surface may be copper-plated [26.32]. With alloy steels specially pressure-resistant carrier layers are required. Besides phosphate layers, oxalate (used with stainless steel) and chromate layers, which are likewise water soluble, are also used. Treatment is carried out by submersion in baths containing oxalic or chromic acid. High-strength steel wires are also sometimes covered with a coating of sodium salt with or without a lime base (see also Sec. 14.2).

### *Application of Lubricants*

For further details see Sec. 14.2 and [26.35], [26.40].

## 26.2.2 Sheet-Metal Forming

With sheet-metal forming a lubricant alone is usually sufficient to avoid local wear of workpiece and die (see Secs. 6.4, and 20.5). However, in the case of drawing with decreasing wall thickness, as in ironing of steel, a lubricant carrier layer is usually required [26.36]. The same authors also quote the use of very thin phosphate coatings—with layer thicknesses of 1–3 µm (40–120 µin)—for special cupping operations without change in wall thickness.

Sheet strip is generally delivered already lightly oiled (as a protection against corrosion). The anticorrosion oil is often left on the strip or just wiped off with a cloth. It must, however, be removed where drawing paints or oils are to be applied.

### *Application of Lubricants*

The method of application depends on the properties of the lubricant concerned. With liquid media submersion is possible, but this is little used because of the high consumption involved. The application of both thin and thick fluid as well as pasty lubricants by hand, for example, using cloths or brushes, permits locally different lubrication according to requirement, but does not lead to consistent results, and the amounts of lubricant used are also high. These methods are thus only used for small batches. For large batches mechanical application is most suitable. The application of lubricants to strip metal is relatively easy; the strip passes over felt strips or rolls covered with felt soaked in lubricant. Thin lubricant can also be sprayed from nozzles, whose working cycles are coupled with that of the press, or sprayed by hand using a spray gun. The advantage of the latter method is that locally differing layer thicknesses can be achieved. The lubrication of blanks and formed parts is carried out by means of spraying or sprinkling, either in the press tool or beforehand. The former method is sometimes used in multistage presses. The thin lubricants are dispensed by ring or drip lines integrated in the tooling.

### *Degreasing*

Before galvanizing, enamelling, or painting operations the metal surface must be completely clean. The change in lubricant as a result of the forming operation (e.g., the formation of metal soap due to the reaction between fatty acids and the metal surface) makes this more difficult. Aggressive high-pressure additives containing chlorine and sulfur compounds, acidic lubricants, and metal soaps tend to corrode the metal surface. When stored for a longer period of time, unsaturated fatty acids and fat may lead to oxidation.

Most degreasing plants have a number of warm baths—at approximately 90°C (194°F) [26.41]—containing alkaline cleaners which, either partially or completely, convert the fats to soap. Both submersion and continuous-throughput plant with spray nozzles are found. Where the workpiece is connected to a dc supply, cleaning is intensified due to electrolysis. Any small contamination which may remain can be removed by the use of emulsifiers containing organic grease solvents. More important contamination can be treated with organic solvents, such as tri- or perchloroethylene followed by subsequent alkaline cleaning. If the methods mentioned so far do not prove sufficient, the anneal-scale degreasing process may be followed in which the workpiece is dipped in hydrochloric acid, allowed to rust in air, furnace-heated to the scale formation temperature, and then hot-pickled [26.41].

#### **26.2.3 Cold Bulk Forming**

High local surface pressures often occur where workpieces are produced by cold extrusion (see Chap. 15), drawing (see Chap. 14), and upsetting (see Chap. 10). In addition, in the first two processes this is accompanied by a considerable increase in surface area, which places very high demands on the surface layer between the workpiece and the tool.

In cold forming, most nonferrous metals can do without lubricant-carrying layers. Surface treatment in this case consists of cleaning and lubricating. In some cases no lubrication at all is required (e.g., when upsetting copper with a low degree of deformation). In cold upsetting of soft steels and sizing of sheared-off lengths, a lubricant layer alone is very often sufficient.

On the other hand for cold extrusion, including free extrusion (nosing) or ironing of steel, a lubricant-carrying layer is essential. With large batch production, surface treatment is mostly carried out using semiautomatic or fully automatic equipment. With small batches and in the case of bulky workpieces, separate plant is often used for cleaning and degreasing (immersion baths and spraying equipment, solvent/steam degreasing plant, cleaning equipment such as rotary drums and vibrators), pickling and phosphating or oxalating, as well as baths for intermediate and subsequent rinsing in order to prepare the workpiece surface for cold bulk forming [26.42]. The layout of an immersion bath for cleaning is shown in Fig. 26.19; that of a steam-heated phosphate bath is shown in Fig. 26.20.

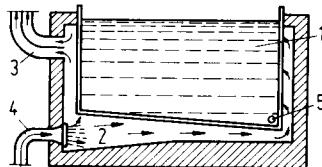


**FIG. 26.19** Immersion bath for cleaning and degreasing. 1—scalding tank; 2—heating jacket; 3—waste-gas pipe; 4—gas burner; 5—draining valve. (After [26.23].)

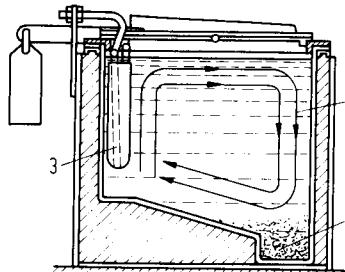


**FIG. 26.20** Steam-heated phosphating bath. 1—liquid circulation; 2—sediment; 3—heating element.

### *Application of Lubricant Carriers*

Phosphating is carried out almost exclusively using zinc phosphate. The typical work sequence is shown in Fig. 26.21. Oxalic layers [iron oxalate  $\text{Fe}(\text{COO})_2 \cdot \text{H}_2\text{O}$ ] are being used as lubricant carriers when forming stainless steel; they are also applied as above. These types of lubricant carriers are described in detail in [26.36].

Where there is a lot of scale, the sequence of operations as shown in Fig. 26.21 may be preceded by descaling, for example, by blasting with steel shot [ $d = 0.2\text{--}0.3\text{ mm (0.008--0.012 in)}$ ] or with particles made of steel wire [ $d \leq 2\text{ mm (0.08 in)}$ ], or by tumbling in a rotating drum containing a granular grinding medium such as sand [26.22].

Phosphating and oxalic-acid treatment is usually carried out as a semiautomatic or fully automatic continuous process. Only loading, unloading, and sometimes transfer from one bath to another are carried out by hand. In this way consistent results can be obtained, which are so important in cold bulk forming. In rotary drum plants the drums in which the workpieces are placed rotate at very low speeds. The progress of the workpieces through the bath is assured, for example, by means of screw conveyors; conveyor belts and vibrating conveyors are also found [26.27]. Baths are in very widespread use, ranging in size from very small to very large. Wire baskets containing the parts are moved from one bath to the next, in the case of fully automatic plants in a fixed cycle time. Transfer of the baskets is by means of special lifting devices. Where throughput is low, tilting buckets are sometimes used. Here the workpieces are held in the buckets during treatment (one bucket per bath).

During cold bulk forming on multistage presses working with wire coils or rods, the starting material has usually been completely surface-treated by the manufacturer. This method has

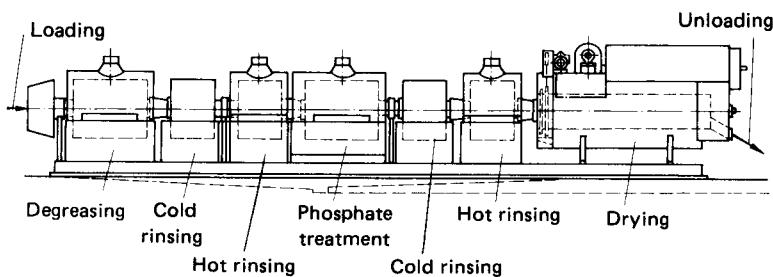


**FIG. 26.21** Drum-type plant for phosphate coating of small parts.

proved to be the most economical. However, in mass production, for example, in screw factories which buy rolled wire and draw it themselves down to the required diameter, the wire coils are surface-treated by the part manufacturer (see also Sec. 26.2.1).

Lengths of slugs which require surface treatment after parting off from a coil or rod, as is common during forming on single-stage presses, are coated with a lubricant-carrier layer over the entire surface. By contrast, with multistage presses working from rods or coils of wire, the sheared surfaces have no lubricant-carrier layer. This is a considerable disadvantage, for example, in the cold extrusion of cans, leading to reduced can depth and higher tool wear.

### *Application of Lubricants*

A distinction must be made here as to whether single- or multistage presses are to be used for forming. Single-stage presses permit optimal heat and surface treatment to be carried out for a particular operation, while with multistage presses in general the same lubricant has to be used in the same way at all stages of the process (central lubrication).

Care must be taken that the lubricant is distributed evenly and economically. Besides the obvious benefits of the savings achieved, the danger of clogging up the dies, which may lead to incompletely formed workpieces or to tool breakage, is best avoided in this way.

Aluminum and aluminum alloys are mainly lubricated using zinc stearate powder applied either by rotating in a drum or by dipping the workpieces into a bath containing the powder in suspension in a highly volatile solution such as trichlorethylene. Fats such as wool fat in solution may also be used.

For small degrees of deformation of copper and copper alloys the most commonly used lubricant is wool grease, with which the wire or rod is lubricated by passing through a fat-soaked cloth, for example, at the entrance of multistage presses. In other cases wool grease is dissolved in organic solvents and applied to the workpiece by plunging it into the solution. Where higher degrees of deformation are required, oils containing fatty additives and fat are most common.

Workpieces made of steel are first coated with a phosphate or oxalic-acid layer. Where forming is to take place on multistage presses, oil with high-pressure additives is used for lubrication. In the case of single-stage presses the lubricant to be used can be chosen to suit the particular operation. For cold extrusion, molybdenum disulfide ( $\text{MoS}_2$ ) and metal soaps (in the case of inert metals) or fatty acids (which under pressure form metal soaps with the base metal) have proved particularly useful.

The cheapest method of applying  $\text{MoS}_2$  is to use a rotating drum.  $\text{MoS}_2$  powder and the workpieces concerned are placed in the slowly rotating drum for about 1–2 min (batch process). The method is only suitable for solid bodies (e.g., for bolts). Uneven application and damage of the lubricant-carrying layer have a negative effect on the process. Dipping into a suspended solution of the powder is also often used. In this case either  $\text{MoS}_2$  paste (powder plus binder) dissolved in warm water at about  $70^\circ\text{C}$  ( $158^\circ\text{F}$ ) or  $\text{MoS}_2$  powder together with a bonding agent is poured into an organic solvent such as trichlorethylene [26.43]. (The disadvantages here are mainly the escaping vapors, which may be harmful to health, and the permanently varying concentration of the bath.) In order to keep the lubricant particles in suspension, stable suspensions have to be used which do not tend too much toward sedimentation, and the bath must be stirred from time to time. A significant advantage of dip-type application of lubricants is that it permits uninterrupted operation in continuous processes, for example, for the lubrication of workpieces still warm from phosphating [bath temperature  $90$ – $98^\circ\text{C}$  ( $194$ – $208^\circ\text{F}$ )] without intermediate reheating. Factories are often equipped with plant for both batch operation and continuous operation. Particularly advantageous are processes where dipping is followed by a short period of drum rotation [26.43]. With the dip method alone it is not possible to avoid uneven layer thickness. Subsequent drum rotating assures more even layer thickness and has the further advantage that excess lubricant can be reclaimed.

Occasionally  $\text{MoS}_2$  is also sprayed, coating either the workpiece (more common in cold forming) or the tool (as used in hot forming) with a lubricant film. Workpieces are saponified by dipping them into an approximately  $70^\circ\text{C}$  ( $158^\circ\text{F}$ ) soap solution consisting of water and soap powder (mainly with additives) or dissolved fatty acids. The workpieces are placed in a drum which is then submerged in the bath and rotated intermittently. The typical immersion time is about 5–10 min.

## 26.24 BLANKING, PIERCING, SLUG PRODUCTION

### REFERENCES

- 26.1 *Materials Handbook: Nonferrous Metals (in German)*, Düsseldorf, VDI-Verlag, 1960.
- 26.2 Aluminium Zentrale e.V., Düsseldorf: *Aluminum Handbook (in German)*, 12th ed., Düsseldorf, Aluminium Verlag, 1963.
- 26.3 Lymann, T., et al.: *Metals Handbook*, vol. 2, "Heat Treating, Cleaning and Finishing," 8th ed., Metals Park, OH, American Society for Metals, 1964.
- 26.4 Stüdemann, H.: *Heat Treatment of Steel, Cast Iron, and Nonferrous Metals (in German)*, 2d ed., München; Hanser, 1967.
- 26.5 Fischer, O.: *Practical Heat Treatment (in German)*, Verband Deutscher Gesenkschmiede, 1967.
- 26.6 Kauczor, E.: *Metals under the Microscope (in German)*, 2d ed., Workshop Books, no. 121, Berlin/Göttingen/Heidelberg, Springer, 1964.
- 26.7 Schumann, H.: *Metallography (in German)*, Leipzig, VEB Verlag für Grundstoffindustrie, 1969.
- 26.8 Ruhfus, H.: *Heat Treatment of Ferrous Metals (in German)*, Düsseldorf, Verlag Stahleisen, 1958.
- 26.9 Verein Deutscher Eisenhüttenleute: *Materials Handbook: Steel and Iron (in German)*, 4th ed., Düsseldorf, Verlag Stahleisen, 1965.
- 26.10 *Steel Heat Treatment Atlas (in German)*, Düsseldorf, Verlag Stahleisen, 1954.
- 26.11 *The Iron-Carbon Diagram and the Principles of Heat Treatment of Iron-Carbon Alloys (in German)*, Düsseldorf, Verlag Stahleisen, 1961.
- 26.12 *Betriebshütte (in German)*, 6th ed., vol. 1, "Manufacturing Processes," Berlin/München, Ernst, 1964.
- 26.13 Ahlborn, H.: "The Technological Use of Recrystallization" (in German), *Maschinenmarkt*, 72, 1966, pp. 67–73.
- 26.14 VDI Richtlinie 3163: "Schutz- und Reaktionsgase für die Wärmebehandlung von Kaltformteilen (Protective and Reactive Gases for the Heat Treatment of Cold-Formed Workpieces)," Düsseldorf, VDI-Verlag, 1963.
- 26.15 Schmidt, T., and Wünning, J.: "On the Possible Interaction between the Furnace Atmosphere and the Workpieces Being Treated during Annealing of Cold-Formed Steels in a Protective Atmosphere" (in German), *Stahl u. Eisen*, 81, 1961, pp. 361–366.
- 26.16 Schimz, K.: *Cold Forming Primer II (in German)*, Düsseldorf, Tritsch, 1962.
- 26.17 *Metals Handbook*, 9th ed., vol. 2, "Properties and Selection: Nonferrous Alloys and Pure Metals," Metals Park, OH, American Society for Metals, 1979.
- 26.18 Deutsches Kupfer-Institut e.V., Berlin: *Brass (in German)*, Berlin, Elsnerdruck, 1956.
- 26.19 Verein Deutscher Eisenhüttenleute: *Manufacture of Steel Wire, Part 2 (in German)*, Düsseldorf, Verlag Stahleisen, 1969.
- 26.20 Verein Deutscher Eisenhüttenleute: *Manufacture of Cold-Rolled Strip, Part 2 (in German)*, Düsseldorf, Verlag Stahleisen, 1970.
- 26.21 Straschill, M.: *Modern Methods of Metal Pickling (in German)*, Galvanizing Technology Series, vol. 8, Saulgau, Leuze, 1962.
- 26.22 VDI Richtlinie 3162: "Entzündern vor der Kaltformung (Descaling prior to Cold Forming)," Düsseldorf, VDI-Verlag, 1963.
- 26.23 VDI Richtlinie 3161: "Reinigen und Entfetten metallischer Oberflächen (Cleaning and Degreasing of Metal Surfaces)," Düsseldorf, VDI-Verlag, 1963.
- 26.24 VDI Richtlinie 3164: "Phosphatieren zum Erleichtern der Kaltformung (Phosphate Coating to Facilitate Cold Forming)," Düsseldorf, VDI-Verlag, 1963.
- 26.25 Machu, W.: *Phosphate Coating (in German)*, Weinheim, Verlag Chemie, 1950.

- 26.26 Mang, T., and Neumann, W.: "Choose First, Then Lubricate" (*in German*), *Maschinenmarkt*, 77, 1971, pp. 405–408.
- 26.27 VDI Richtlinie 3165: "Schmierstoffe der Kaltformung (Lubricating Materials Used in Cold Forming)," Düsseldorf, VDI-Verlag, 1963.
- 26.28 Mang, T., and Neumann, W.: "First Lubricate, Then Form" (*in German*), *Maschinenmarkt*, 77, 1971, pp. 445–448.
- 26.29 Billigmann, J., and Fichtel, W.: "Studies Concerning the Characteristics and Behavior of New Roll-Oil Emulsions" (*in German*), *Stahl u. Eisen*, 78, 1958, pp. 344–357.
- 26.30 Hohmann, G.: "Rolling of Steel and Aluminum Using Emulsion." (*in German*), *Mineralöltechnik*, 14, 1969, pp. 1–10.
- 26.31 "Hot-Forming Lubricants for Titanium" (*in German*), *Maschinenmarkt*, 77, 1971, p. 448.
- 26.32 Verein Deutscher Eisenhüttenleute: *Manufacture of Steel Wire, Part 1* (*in German*), Düsseldorf, Verlag Stahleisen, 1970.
- 26.33 Zieler, W., and Lepand, H.: (*Shot and Sand*) *Blasting and Blasting Abrasives* (*in German*), München, Hanser, 1964.
- 26.34 Martin, M.: "Influences of Heat Treatment on the Descaling of Rolled Wire by (Sand) Blasting" (*in German*), *Stahl u. Eisen*, 88, 1968, pp. 285–286.
- 26.35 Pomp, A.: *Steel Wire* (*in German*), 2d ed., Düsseldorf, Verlag Stahleisen, 1952.
- 26.36 Schwarz, G. K.: "Phosphate Coating in Cold Forming with Special Reference to Wire Drawing" (*in German*), *Draht*, 18, 1967, pp. 7–17.
- 26.37 Doty, D. L.: "Continuous-Process Pickling and Sheathing of Steel Wire" (*in German*), *Stahl u. Eisen*, 70, 1950, pp. 1174–1176.
- 26.38 Stenzhorn, R.: "Lime" (*in German*), *Draht*, 11, 1960, pp. 147–150.
- 26.39 Bader, G.: "Phosphate Coating in Cold Forming Based on the Example of Steel-Wire Manufacture" (*in German*), *Draht*, 18, 1967, pp. 548–551.
- 26.40 *Steel Wire Handbook*, vols. 1 to 3, Guilford, CT, Wire Association International, 1980.
- 26.41 Groebler, H.: "Greasing and Degreasing of Sheet Metal in Swarfless Metal Forming" (*in German*), *Blech*, 16, 1966, no. 6, C-22, C-24, C-26.
- 26.42 VDI Richtlinie 3160: "Oberflächenbehandlung vor der Kaltformung—Allgemeines (Surface Treatment Used in Cold Forming—General)," Düsseldorf, VDI-Verlag, 1963.
- 26.43 Lüders, R., Münster, A., and Wild, H.: "New Method of Lubrication for Use in Metal Forming" (*in German*), *Z. Wirtsch. Fertigung*, 65, 1970, pp. 172–174.



**5**

**METAL FORMING UNDER  
SPECIAL CONDITIONS**

---

---

© 1998-2000 KENNAMONTI GROUP INC.



**HIGH-ENERGY-RATE  
FORMING**

**List of Special Symbols**

---

$A_{sw}$	amplitude of shock wave
$B$	magnetic induction
$C$	capacity
$e$	specific potential (inner) energy
$E_{def}$	deformation energy
$E_L$	charging energy
$i$	instantaneous current
$I$	effective current; polar moment of inertia
$l^*$	relative shear length
$p'$	form stability factor
$s$	workpiece thickness
$t$	time instant
$U$	direct voltage
$v_{pt}$	velocity of particle
$v_{sw}$	velocity of shock wave
$\mu$	relative permeability; coefficient of friction
$\mu_0$	constant of magnetic field
$\rho$	density
$\omega$	angular velocity

## 27.4 METAL FORMING UNDER SPECIAL CONDITIONS

In the following chapters several new forming processes are introduced which function under working conditions that are different from those of the conventional processes. The affected working conditions are state of stress, period of operation (operating speed), state of friction, and temperature. The chief aim of these new processes is to use to advantage the particular behavior of a workpiece material, to increase the limit strain, to ease the material flow, and to increase the product accuracy, which in turn will lead to savings due to a reduction in the number of required operations and in the tool costs. The skillful utilization of given preconditions will make it possible, to a certain extent, to form workpieces to certain geometric shapes, which would not be achievable otherwise or only with extensive technical efforts.

The processes described in this chapter make use of solid masses accelerated to high speeds, employing either certain pressure media or some activating energy. Chapter 28 includes the processes which utilize hydrostatic pressure for deformation or change the stress state in such a manner that tensile stresses are avoided but the average pressure increases. The processes described in Chap. 30 either require a particular state of the workpiece material, as in superplastic forming, or change certain characteristics of the processed material, as in thermomechanical treatment. In Chap. 29 a short survey is given on the superposition of mechanical vibrations in metal-forming processes. Such new processes offer the possibility to solve a number of special problems which arise in certain branches of forming technology. Because of inherent difficulties and disadvantages, especially in view of their economy, these processes may even in the distant future not entirely replace their conventional counterparts, but may complement them effectively.

### 27.1 TERMINOLOGY AND HISTORIC DEVELOPMENT

Fig. 27.1 lists the high-energy and high-energy-rate metal-forming processes. The following are dealt with in the present chapter:

Processes using solid masses accelerated to high speeds

Processes using pressure media which impart either a static or a dynamic action

Processes utilizing activating energies

The field of high-energy-rate forming includes all those processes in which the forming energy is applied to a workpiece during a very short time period so that a high instantaneous strain is achieved. If in such a case a high amount of energy is also expended, then this high-energy-rate forming can also be termed high-energy forming:

High-energy forming → W very high  
High-energy-rate forming →  $dW/dt$  very high

The same process, namely, building up a magnetic field by induction and using it as activating energy, can, depending on the duration of the forming operation, be termed either high-energy or high-energy-rate forming.

Table 27.1 compares the characteristics of the most important high-energy-rate forming processes with those of the conventional processes [27.1]. The period of operation, operating speed, power rating, and achievable pressure are compared for both process types. The data show that, for example, the capacity of these special processes is not much higher than that of conventional hammer forging. In this respect the term high-energy-rate forming is misleading. Notwithstanding, since these falsely termed high-energy-rate processes have different operating speeds and periods of operation from those of the conventional processes, it is suggested to use the term high-speed forming for the new processes. According to Fig. 27.2, the high-speed processes are used not only for forming, but also in other main branches of manufacturing technology, as mentioned in Chap. 2: forming, separating, joining, changing certain material properties, and so on [27.2].

Even today the above-mentioned processes are identified as new. This is due to their historic development. High-speed forming has already been known since 1888, when C. E. Munroe discovered a possibility of impressing figures into iron plates by using explosives. The first patents for explosive forming were awarded in the United Kingdom in 1897 and in the United States in 1901. For many years this development had hardly any significance because of a lack of economic

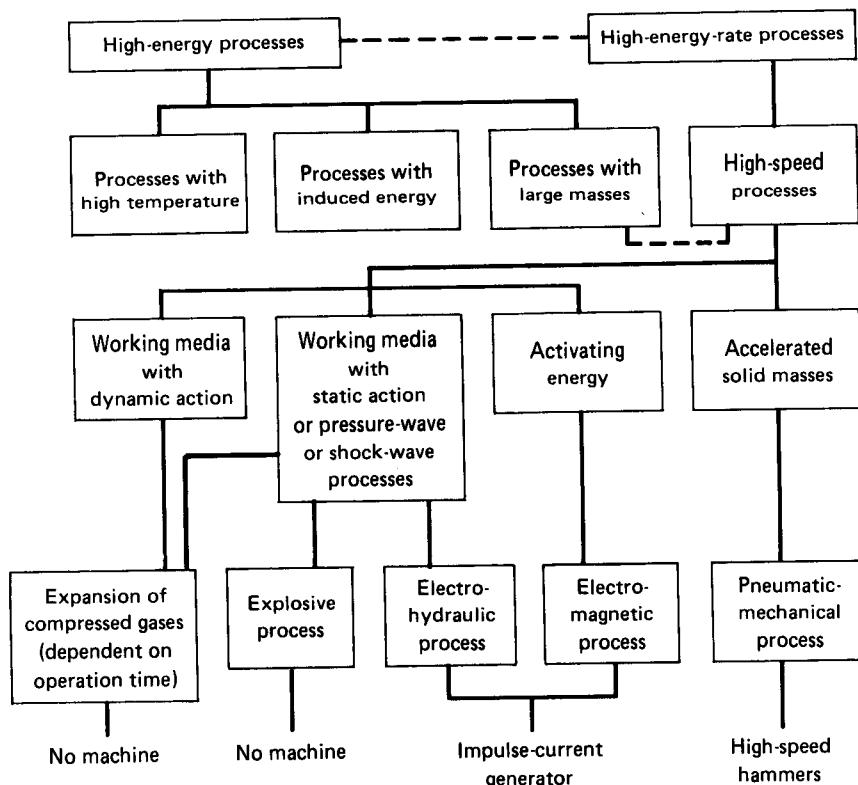


FIG. 27.1 Survey of high-energy and high-energy-rate metal-forming processes.

advantages and since no technological need for such process arose. Only in the late 1950s, during the progressive development of aviation and rocket technology, such processes aroused interest. For small-scale production they facilitated the integration of subsections of axially symmetric workpieces made of materials that were either difficult or impossible to be worked in conventional forming processes. During this period of "rediscovering" these processes their possibilities of application and their advantages, in particular with respect to the behavior of work material during processing, were optimistically overestimated, which led to many inevitable disappointments. Basic research during recent years has finally produced an overview of their realistic possibilities for industrial application.

## 27.2 PROCESSES USING HIGH-SPEED HAMMERS

In industry high-speed hammer forging is the process used almost exclusively under this category. Furthermore, as shown in Fig. 27.3, the acceleration of solid masses, such as a forging or a blanking die, is possible by means of explosive detonation without any need for a suitable special machine.

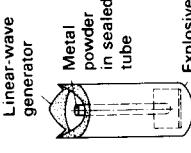
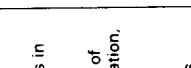
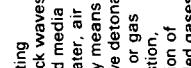
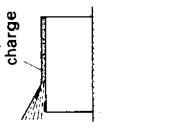
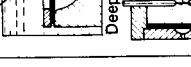
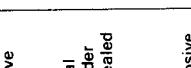
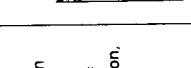
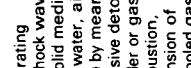
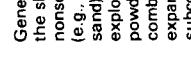
In forming technology the processes with solid masses accelerated to high speeds are applied preferably in hot and cold bulk forming (forging, upset forging, upsetting, extrusion), in processes of separating, such as to shear small metal slugs, and finally in master forming for powder compacting.

**Table 27.1** Characteristics of the Most Significant High-Energy-Rate Metal-Forming Processes

Process or machine	Operating speed <sup>a</sup> m/s (ft/s)	Duration of operation for small deformation (typical), s	kW	Power rating, (hp)	Achievable pressure (typical), MPa (ksi)
Forging hammer Pneumatic-mechanical process	5 20 $\leq$ 300	(16.4) (66) $10^{-2}$ (984)	$10^{-2}$ – $10^{-2}$ $10^{-2}$ – $10^{-3}$ $10^{-4}$	$10^4$ $10^5$ $10^4$ – $10^5$	$(1.325 \times 10^4)$ $(1.325 \times 10^5)$ $(1.325 \times 10^4$ – $10^5)$
Electromagnetic process	$\leq$ 300	$10^{-3}$ (984)	$10^4$	$(1.325 \times 10^4)$	$10^3$ (142)
Electrohydraulic process	$\leq$ 300	$10^{-3}$ (984)	$10^4$	$(1.325 \times 10^4)$	$10^3$ (42.6–71)
Explosive forming under water	$\leq$ 300	$10^{-3}$ (984)	$10^6$	$(1.325 \times 10^6)$	$6 \times 10^3$ (852)

<sup>a</sup>Operating speed for mechanical and pneumatic-mechanical processes is the tool speed or die speed. The operating speed for the shock-wave process is that speed with which the workpiece moves relative to and onto the die impression.

Source: Compiled from [27.1].

	Primary forming	Deformation	Separating	Joining	Changing the material properties
		Bulk	Sheet-metal		
<b>Shock waves</b>					
Generating the shock waves in nonsolid media (e.g., water, air sand) by means of explosive detonation, powder or gas combustion, expansion of subcooled gasses, spark discharge, or wire explosion.	Linear-wave generator  Metal powder in sealed tube  Explosive charge 	1. Metal forming with pressure waves  Explosive charge  Explosive charge igniter  Deep drawing  Spark gap  Bulging 	Explosive charge  Explosive charge igniter  Shearing 	Welding and cold-weld plating  Joining 	Hardening
<b>Magnetic fields</b>					
Magnetic field is produced in the workpiece by impulse induction			Hollow embossing 	Joining 	
<b>Solid dies</b>					
Solid dies are accelerated (by using powder, explosive charge, or highly compressed gases, for example)	Explosive charge  Igniter  Punch  Powder compacting 	3. Metal forming with impact of solid masses at high speed 	Explosive charge  Igniter  Punch  Die forging  Deep drawing 	Shearing  Hollow embossing  Joining 	Wood wedge  Linear-wave generator  Plate-shaped explosive  Glass  Main charge  Metal plate  Hardening

**FIG. 27.2** Examples of industrial application of high-speed processes in manufacturing technology.  
(After [27,21].)

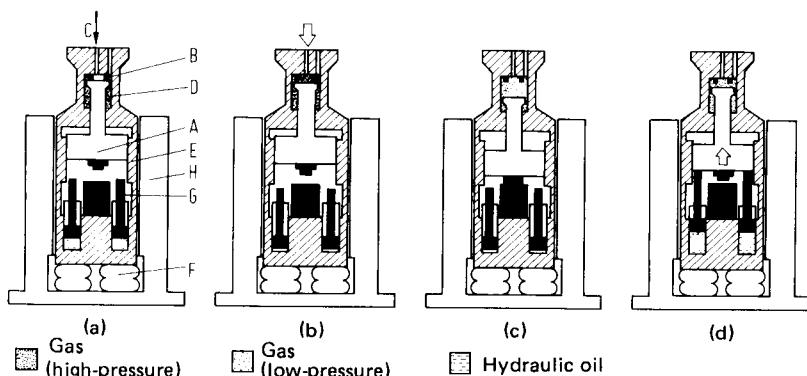


**FIG. 27.3** Operating principle of Dynapak high-speed hammer. (a) Starting position. (b) Beginning of working stroke. (c) Beginning of deforming operation. (d) Reverse stroke. (After [27.3].)

### 27.2.1 Design Principles and Characteristics of High-Speed Hammers

In the mid 1950s the first high-speed forging hammers came on the market in the United States. The following considerations led to their development. The amount of kinetic energy needed for a particular process can be produced by using a large solid mass that moves at relatively low speed. The same amount of energy can also be produced by means of a small solid mass moving at a very high speed. For the same work capacity a high-speed forging hammer is considerably smaller in size and lighter in weight, thus requiring a smaller capital investment for its construction than is needed in conventional hammer forging. A short stroke is sufficient for a high-speed hammer, since the large accelerating force permits to achieve very high speeds, on the order of  $\gg 8 \text{ m/s}$  ( $26 \text{ ft/s}$ ) within a period of  $20\text{--}30 \text{ ms}$ , this time interval being only a fraction of 1% of the total operating period. Because of this situation it would be quite uneconomical to keep the full work capacity and the total accelerating force at the disposal during the entire cycle of operation. Hence a comparatively small drive mechanism is chosen, which builds the necessary energy reserves during the long ancillary period (long when compared with the actual accelerating period) of the operating cycle. All the machines used, whether in industrial production or in research laboratories, function on the principle of either sudden release or instantaneous conversion of the energy conserved in a medium. In essence three different working principles are employed:

- 1 Compressed gas serves as the source of potential energy. Sudden expansion of this gas accelerates a solid mass.
- 2 Chemical energy is conserved in the form of volatile hydrocarbons (e.g., gasoline, kerosene), which are mostly employed for this principle. By burning the hydrocarbon-air mixture in a closed chamber, analogous to a combustion engine, the machine ram is accelerated.
- 3 In a linear induction motor electric energy is converted into kinetic energy, and the machine ram is accelerated by the gliding core of the linear motor.

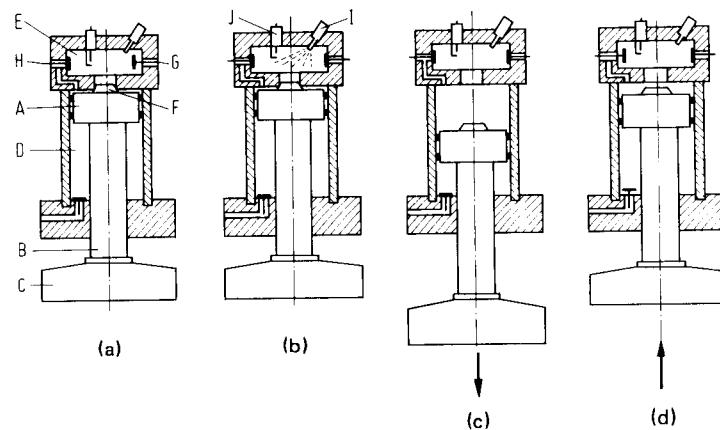
So far only principles 1 and 2 have been used in industry, with principle 1 receiving greater attention. A machine working on this principle is described in the following example. The first high-speed forging hammer for industrial use was a machine operated with compressed gas. The machine was developed in the United States by the Convair Division of the General Dynamics Corporation and is called Dynapak high-speed forging hammer. Its operating principle is represented in Fig. 27.3.

Fig. 27.3a shows the machine in the starting position. Ram A is pressed against seal B, which is fitted in the framing E. A pressure of about 20 MPa (2.84 ksi) is built up in chamber D and acts upward on the piston shoulder. Nitrogen gas or air (any such medium must be free of oil traces) can be used as the pressure gas. The chamber, whose boundaries are formed by the inner diameter of the seal, the piston surface, and the framing, is connected in this instance to the outer atmosphere by means of valve C. A static equilibrium in the system is maintained due to the counteraction of the downward force of the weight and the gas pressure acting upward against the piston shoulder. The ram moves down when, within the inner area of the seal, the piston surface is given a pushing stroke through valve C. This stroke causes a loss of equilibrium of the system, and the piston or ram A is lifted from the seal (Fig. 27.3b). The pressure medium in chamber D can now escape upward through the ring-shaped crevice between piston A and framing E, and the pressure now acts on the entire piston surface. Since the final resultant force acts downward, the ram is rapidly accelerated down until it impacts on the workpiece (Fig. 27.3c). Framing E rests on the air cushion F. This framing is also guided in casing H [27.3]. Through the combined effect of action and reaction, framing E is accelerated upward due to a similar acceleration of ram A. Since the mass of the framing is quite large compared to that of the ram, both the path and the speed of the framing are considerably smaller than those of the ram. At the instant when the tool impacts on the workpiece, 70% of the pressure energy is converted into kinetic energy. On completion of the forming operation framing E slides down to its starting position due to its own weight. Application of the counterstroke principle and resting the framing on an air cushion ensure that the machine foundation receives only slight jerks. The two auxiliary hydraulic pistons G bring the ram back to its starting position (Fig. 27.3d), and the machine is again ready for the next working stroke.

Similar machines, which are used on a more or less large scale, are manufactured by U.S. Industries, Inc. [27.3] and Weingarten [27.4].

Principle 2 is represented by a machine that was developed in the United Kingdom by the Department of Mechanical Engineering at the University of Birmingham and which is called Petro-Forge hammer. Fig. 27.4 shows the operating principle.

In Fig. 27.4a piston A is situated in its upper position under the effect of a pressure of 2-5 MPa (0.284-0.71 ksi) acting in chamber D. This piston is fitted rigidly with ram C and closes combustion chamber E at seal F. In this loading position the combustion chamber is filled with air compressed at 3-15 MPa (0.426-2.13 ksi) through entry valve G. The piston is now subjected to the forces from two sides, one side on the choke at seal F and on the other side on its shoulder in pressure chamber D. When a particular value is reached of either the ratio of the surface areas



**FIG. 27.4** Operating principle of Petro-Forge hammer. (a) Loading position. (b) Injection and ignition of fuel. (c) Working stroke. (d) Reverse stroke. (After [27.3].)

**Table 27.2** Characteristics of High-Speed Hammers

Machine type	Work capacity, kN · m (lbf · ft)	Impact velocity of ram, m/s (ft/s)	Stroke index, strokes/min
Dynapak	10 (7376)	≈20 (≈66)	20
U.S. Industries, Inc.	300 (211,280)	≈20 (≈66)	7
	70 (51,632)	≈20 (≈66)	>8
	200 (147,520)	≈20 (≈66)	8
	400 (295,040)	≈20 (≈66)	<8
Petro-Forge	20 (14,752)	≈18 (≈59)	60
Linear induction motor	1 (737.6)	≈15 (≈49)	>60

or the ratio of two different pressures, a final resultant force acts upward. Fig. 27.4b shows the start of combustion. This operation is initiated by injecting the fuel through nozzle *I*. The spark plug *J* then ignites the compressed gas-air mixture. The ignited mixture tries to expand in the closed spacing, thus raising the initial pressure to 5–7 times its value. At this instant the resultant force accelerates piston *A* downward, lifting it from the seal, so that now the entire piston surface is pushed with the total pressure. This causes ram *C* to move down rapidly with increasing speed until it impacts on the workpiece. At the end of the work stroke exhaust valve *H* is opened and the assembly piston–ram is brought back to its loading position due to pressure acting now in the pressure chamber, as shown in Fig. 27.4d [27.3].

The linear induction motor, which works according to principle 3, is still in its developing stage. Basically the motor is constructed like a conventional asynchronous motor, but with the usual short-circuit squirrel-cage rotor replaced by a flat plate which serves as the gliding core and is made of a conductive material, preferably aluminum or copper. The commonly used ring-shaped stator of the asynchronous motor is converted into a primary flat coil, and one such coil is fitted on each of the two sides of the flat plate rotor which is now called gliding core.

The important characteristics of the high-speed forging hammer are the work capacity *E*, the impact velocity *v<sub>i</sub>*, and the stroke rate *n* (Table 27.2). The data in this table show that with increasing work capacity, the stroke-rate values remain quite low when compared with their counterparts of conventional hammers, which precludes an economic operation of these new machines. Hence in industry their application is only justified if by employing the high-speed process, certain significant improvements are obtained, such as raising the maximum achievable strain or ductility, improving other material properties, or preventing rapid cooling of very narrow cross sections. This will facilitate the forging of extremely thin-walled workpieces from materials having high flow stress (see Chap. 11).

### 27.2.2 Hot Forging

Since the high-speed forming processes were first developed, they have aroused the greatest interest in the hot forging of steel and other special metals. The main advantage of high-speed forging is supposed to be that the required deformation of the workpiece can be completed in a single forging stroke, while the conventional process requires a great number of strokes. This remark is based on the fact that due to very high ram speeds, the forging operation is completed within a very brief period ( $t \approx 1$  ms). This results in less heat loss of the workpiece during its short exposure on the forging machine and in less heat radiation to the environment, but comparatively more heat is lost by conduction into the tool. The amount of heat generated during the rapid forging operation can more than outweigh the above-mentioned heat losses. Thus compared with conventional forging at the same initial temperature of the workpiece, the processed workpiece attains a higher temperature with high-speed forging. Because of this phenomenon alone the workpiece

**Table 27.3** Comparison of the Achievable Web Thickness in Hot-Die Forging of a Low-Carbon Steel with Conventional and High-Speed Processes

Machine	Number of strokes	Energy per stroke, kJ (ft·lbf)	Total energy, kJ (ft·lbf)	Web thickness, mm (in)
$E_N \approx 5 \text{ kJ}$ , drop hammer	1	4 (2948)	4 (2948)	2.54 (0.100)
	2	4 (2948)	8 (5896)	1.68 (0.066)
	4	4 (2948)	16 (11792)	1.52 (0.060)
$E_N \approx 10 \text{ kJ}$ , drop hammer	1	11.4 (8402)	11.4 (8402)	1.37 (0.054)
	2	11.4 (8402)	22.8 (16804)	1.25 (0.049)
	3	11.4 (8402)	34.2 (25206)	1.22 (0.048)
High-speed hammer	1	11.3 (8328)	11.3 (8328)	0.96 (0.038)

Source: Compiled from [27.5].

can be formed with higher strain. Initiating a second stroke or a series of strokes is inappropriate for high-speed forging since the hammer, which works according to principle 1, has a lower stroke rate. Thus completion of the forging operation with a single stroke becomes the obvious option offered on these forging hammers.

Fig. 27.5 shows a workpiece shape with extreme differences in its cross-sectional areas, which is typical for high-speed forging. A comparison of conventional and high-speed forging processes with respect to the minimum achievable web thickness of this workpiece (Table 27.3) showed that with conventional hammers a web thickness of 0.96 mm (0.0378 in) could not be achieved [27.5], even when three times as much energy was expended (forging with three consecutive strokes).

The precondition for optimum operation of the high-speed forging hammer working on principle 1, namely, that the forging be completed in a single stroke, becomes a disadvantage in the case of asymmetrically shaped workpieces. In conventional forging with several strokes, the first strokes are used to obtain optimum material distribution since these strokes help increase the material flow within the forging die. Thus in individual cases of critical workpiece shapes, one can best try to determine a particularly favorable shape of the workpiece so that optimum material flow is obtained within the die while forging the workpiece with a single stroke. Another problem arises in the hot forging of those metals which acquire appropriate ductility only within a short temperature range. In such a case it should be attempted to determine the temperature rise of the metal during the few milliseconds when the work of forging is converted into heat.

In certain investigations, such as in [27.6], it is reported that by means of high-speed forging very narrow dimensional tolerances are achieved in the stroke direction, for example, 0.1 mm (0.004 in). However, it is not yet definitely proved that such narrow tolerances are made possible by the high-speed forging itself. The tolerances may be achieved, more possibly, because the forging machines used are able to carry out an exact amount of work in each repetition of the operating cycle and due to precisely guided motion of the ram. In the same way certain improvements of the surface finish of the workpieces are achieved since the coefficient of friction is to some extent reduced because of the high speed of material flow within the die.

In the following paragraphs certain individual problems of high-speed forging are discussed.

### Lubricants

According to Crawley and Wills [27.7], a dispersion of flake graphite in water has proved to be the best lubricant for compressing cylinders, and it serves simultaneously as a good coolant. In the case of lubricants based on mineral oils, the Diesel effect (self-ignition due to compression of a trapped quantity of oil) is observed in certain cases.

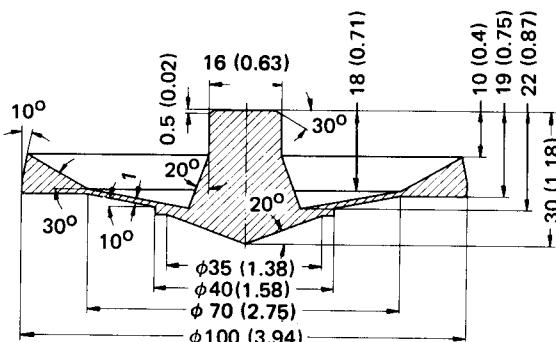


**FIG. 27.5** Typical workpiece to be processed with high-speed forging; extreme differences in cross-sectional areas. Dimensions are in mm (in). (After [27.5].)

### *Service Life of the Forging Die*

No definitely determined results are available regarding the service life of forging dies, the results known up to now are contradictory. In general there are three main causes for the failure of forging dies: thermal fatigue, mechanical fatigue, and frictional wear (see Chap. 11). Thermal fatigue and frictional wear are caused by frequent alternating heating and cooling of the die surface. These phenomena cause changes in surface tensions which lead to an extensive network of fine cracks. Since the high-speed forging operation is completed within a very short period as compared with the conventional processes, during this operation a smaller amount of heat is transmitted to the die so that—in fact—the magnitude of alternating thermal stress should remain low. But another consideration reveals a major disadvantage of high-speed deformation, especially in machines working with compressed gas. Such machines require a longer time before initiating the reverse motion of the ram, bringing the ram back to its starting position. This causes a longer contact period between the ram and the forged workpiece. The danger of mechanical fatigue due to high pressure that exists within the die impression is greater in the case of high-speed forging than for the conventional process. But this danger can be mitigated to some extent by a particularly skillful design of the dies. The frictional wear depends on the effect of friction and the relative motion between die and workpiece, hence—to a large extent—on the product of the coefficient of friction and the contact pressure between the material partners of the friction system. In high-speed forging the coefficient of friction is smaller because of the influence of high speed, but on the other hand the pressure in the die impression is much greater so that the resultant frictional forces may be almost the same in both processes. The combined effect of all three causes of material fatigue leads to rapid die failure in high-speed forging. Hence a shorter service life of such dies must be expected as compared with that of dies for conventional forging processes.

### *Die Design*

In addition to the common rules for designing drop forging dies (see Chap. 11), certain peculiarities must be kept in mind. In conventional forging the flash takes up extra metal. Because of its own higher resistance to material flow, it also guarantees that the impression in the forging die will be filled completely (Fig. 27.6a). This increased resistance is created by the friction in the very narrow flash gap and is also due to rapid cooling of the material present within the flash. When the same workpiece is forged by the high-speed process, the material flows more easily in the radial direction into the flash than it is able to be "raised" against the ram motion because of the inertia forces resulting from different accelerations. Thus in high-speed forging the resistance to material flow into the flash is quite small; that is, too big a flash is formed. This phenomenon

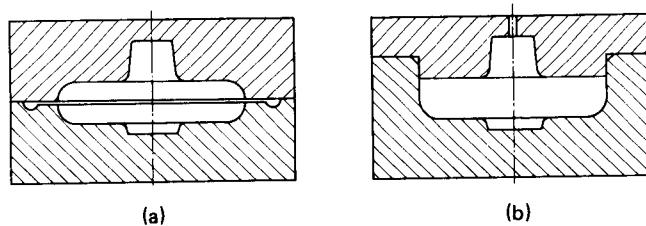


**FIG. 27.6** Die design. (a) With flash gap for conventional forging. (b) Closed (without gap) for high-speed forging. (After [27.3].)

prevents a complete filling of the impression in the forging die. Therefore in such a case flashless forging in a closed die is used (Fig. 27.6b), where the extra material must flow upward so that complete filling of the impression is ensured. Due to these facts, except in the case of very simple workpiece shapes, closed dies should always be preferred for high-speed forging. Furthermore good evacuation of such a die must be ensured since otherwise the material flow in the die could be hampered.

#### Die Material

Very strong strokes during high-speed forging require a very tough material for the forging dies. Moreover, as in conventional drop forging, the die material should also be wear-resistant, high-temperature-resistant, and should not form heat cracks. However, the toughness of the die material as well as its wear resistance are mutually contradictory demands. As a good compromise, an optimum die material is considered to consist of 1.3% nickel or tungsten, 0.4% carbon, 5% chromium, and 1–2% molybdenum. Such a die material is hardened up to HRC 46 and then draw-tempered [27.3].

#### 27.2.3 Cold Forging

Similar to the conventional cold extrusion process (see Chap. 15), its high-speed counterpart also comprises forward rod extrusion and backward can extrusion as well as several combinations of the two. For this type of forging the machines described in Sec. 27.2.1 are mostly employed. In manufacturing axially symmetric workpieces, the ram impact speed is chosen as 10–25 m/s (33–82 ft/s), depending on the type of workpiece material. Moreover, in certain experiments very high speeds, up to a few hundred meters per second (approximately 330–1000 ft/s), are applied. According to the test results obtained so far, the following effects of the impact speed on the characteristics of the workpieces are found.

##### *Effect on the Surface Structure*

In general, compared with the conventional processes, an improved surface structure of the workpiece is obtained by employing the high-speed process [27.8]. In this case it is assumed that due to higher speed, a different friction state prevails, a state of friction that is favorable to improved surface structure. This friction state leads also to an improved material flow at the die entrance in forward rod extrusion. With a die-opening angle of  $2\alpha = 180^\circ$  the so-called dead zone is very small.

##### *Effect on the Straightness of Extruded Shafts*

The workpiece material flows already at high speed prior to entering the die. Once the extrusion operation is completed, this speed is decreased rapidly, and due to mass inertia the so-called self-adjustment effect occurs.

### *Effect on the Dimensional Tolerances of Extruded Shafts*

Due to this self-adjustment effect there results, in principle, a slightly increasing reduction of the cross-sectional area of the workpiece in the direction toward the die outlet.

### *Limitations of the Process*

The process is limited in two respects, mechanically and thermally. The mechanical limitation is determined by the inertia forces acting on the extruded shaft. The self-adjustment effect could become so strong that local shrinkage or breaking may occur on the workpiece. The thermal limitation of the process is due to the great amount of heat generated during the forming operation, which restricts its application to certain areas of extrusion.

### *Design of Extrusion Dies*

Since in high-speed extrusion the dies are stressed instantaneously, it is necessary to keep the notch effect as low as possible. In general this is achieved by keeping the transition radii larger. Since the punch is the weakest member of the extrusion tool assembly, the ratio of punch length to punch diameter should not exceed 3. In order to avoid even micronotches (scratches), good polishing of the inner surface of the die is recommended, with a surface roughness of  $0.1\text{-}\mu\text{m}$  ( $3.987\text{-}\mu\text{in}$ ) peak-to-valley height or less.

Because of a lack of economic advantages and a rather negligible superiority in technical aspects when compared with the conventional processes, this process of high-speed extrusion may find industrial implementation only to a limited extent.

#### **27.2.4 Shearing**

Conventional shearing processes, for example, shearing of slugs having different cross-sectional areas, in cold and hot bulk forming have advantages such as shorter operating cycles and no material waste, but they also have the disadvantages of severely distorting the workpieces and of poor structure of the sheared surfaces. These disadvantages can be greatly diminished by taking various countermeasures, such as using high shearing speeds so that the slugs can be deformed without additional preparatory metal-working steps such as sizing. Extensive development in this relatively new field of metal deformation was undertaken with the Petro-Forge hammer. By mechanizing the workpiece handling, the duration of the complete operating cycle was reduced to 1 s. Comparative investigations of conventional shearing and its high-speed counterpart found that with high-speed shearing the distortion of the workpiece is minimal, while at the same time

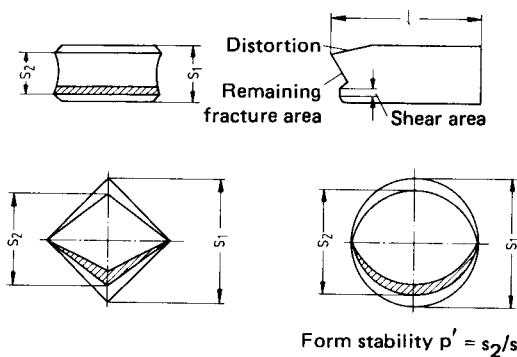


**FIG. 27.7** Determination of form stability factor  $p'$  for different cross sections. (After [27.9].)

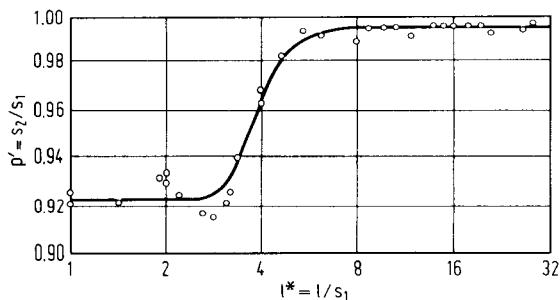


FIG. 27.8 Correlation of form stability factor  $p'$  with relative shear length  $l^*$ . (After [27.9].)

a greatly improved structure of the sheared surface is obtained [27.9]. A useful criterion for judging the quality of the shearing operation is the form stability factor  $p' = s_2/s_1$  as defined in Fig. 27.7. For a given workpiece material this factor depends on the length to be sheared and the shearing speed. At a ratio of the length to be sheared to the thickness  $l^* = l/s_1 < 1$ , one cannot achieve a distortion-free workpiece having a good sheared surface structure, even with high-speed shearing. Only beyond the ratio  $l^* > 1$  can the surface structure be improved with high-speed shearing. Fig. 27.8 shows a correlation between the formability and the relative shear length  $l^*$ , according to which there exists a critical relative shear length beyond which the quality of the sheared surface of the slug is greatly improved. This critical value depends on the shearing speed [27.3].

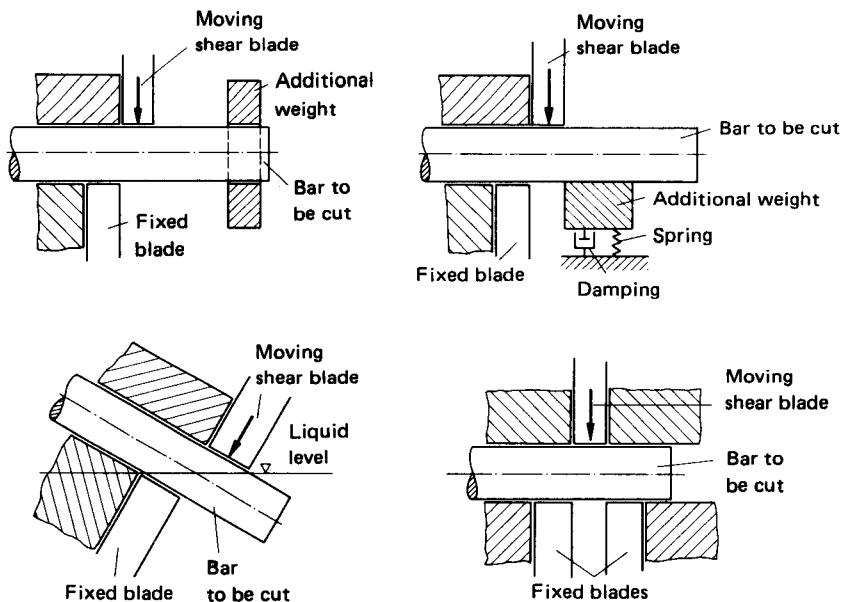


FIG. 27.9 Reducing the critical shear length by preventing the bar to be cut from turning due to the moment of inertia. (After [27.9].)

## 27.16 METAL FORMING UNDER SPECIAL CONDITIONS

An evenly sheared surface, perpendicular to the bar axis, is obtained, as proved by high-speed photography, because mass inertia prevents an otherwise observed rotation of the workpiece during the shearing operation. This rotation occurs just before fracture of the remaining portion of the slug. Though the critical length could be reduced substantially by taking countermeasures, as represented in Fig. 27.9, the expenditure on tools is increased greatly, and handling of both the machine and the workpiece becomes increasingly difficult.

In the design of the shearing tool its rigidity should be given particular attention because of the high bending forces that act during the shearing operation. Moreover, dissipation of the kinetic energy that still remains in the tool after completion of the shearing operation is an undesirable problem which has not yet been solved. Materials suitable for the tools are high-carbon steels containing 1–2% carbon, 5–12% chromium, and approximately 1% molybdenum.

## 27.3 METAL-FORMING PROCESSES UTILIZING WORKING MEDIA

These processes are very commonly applied for deep drawing, expanding, and stretch drawing, whereby transmitting media such as fluids and gases are used. Although these processes do not in fact belong to the categories of high-energy-rate and high-speed forming, they are nevertheless included in the high-speed category since a large amount of energy is consumed in them and they can thus be classified primarily as high-energy processes. Accordingly they are discussed in the chapters on stretch drawing (see Chap. 20), stretch forming (see Chap. 23), and sheet-metal testing methods (see Chap. 18). These processes are once again mentioned here because they are at the beginning of a logical chain which leads to the processes using various media with dynamic action.

Within the structure of this logical chain of high-speed forming processes we find the so-called hydro-punch process, a typical transition process, also termed hydraulic bulging process [27.10]. The machine used for this operation consists of four main mechanisms:

- 1 Compressed air equipment (air compressor, pressure vessel, etc.)
- 2 Vertically driven piston
- 3 Pressure hammer
- 4 Tool assembly

A pressure of 1 MPa (0.142 ksi), built up by the compressed-air equipment, accelerates the piston downward. This impacts with a velocity of approximately 30 m/s (100 ft/s) on the water stored in the pressure vessel, thereby exerting a pressure of 300 MPa (42.6 ksi) maximum. This pressure is transmitted to the die assembly, which executes metal deformation. The die assembly itself consists of inserts and a pressure casing generally made of many sections. To ensure an afterflow of the work material in the axial direction as the tube section widens, so that the local variations in wall thickness can be kept at a minimum, another pressure in the axial direction is built up by two auxiliary pistons acting face to face. The motion of these two pistons is exactly synchronized with that of the main piston. (The tools construction is similar to that used for the expanding process with hydraulic pressure, as described in Chap. 23; see Fig. 23.29.)

### 27.3.1 Processes Utilizing Pressure Media with Dynamic Action

These processes are generally known as shock-wave forming processes. They also include explosive forming and electrohydraulic (hydrospark) forming.

#### *The Shock Wave and Its Characteristics*

In both the explosive and the electrohydraulic processes described below, the pressure is built up steadily but irregularly and is transmitted as either a pressure wave or a shock wave. Fig. 27.10a represents a shock wave propagating toward the right. This figure shows various instantaneous characteristics of the pressure medium, where  $p$  is the pressure,  $\rho$  the density,  $e$  the specific inner

energy, and  $v_{pt}$  the particle velocity. These characteristics are followed by the subscript 0 when the medium has not yet been reached by the shock wave, whereas the subscript 1 denotes the corresponding characteristics of the medium once the shock wave has reached it.

To determine the above-mentioned instantaneous characteristics, the following conditions must be fulfilled:

- 1 For the steady but irregular increase in pressure and density of the shock wave  $d(p, \rho)/dt \rightarrow \infty$  must be fulfilled.
- 2 The shock wavefront can have any random dimensional form and the wave can also take any random turn in space, as shown in Fig. 27.10b. Each instant of time ( $t_1, t_2, t_3$ ) is denoted by the corresponding instantaneous characteristics.
- 3 The instants  $t_2$  and  $t_3$  should be considered to be so near to each other (Fig. 27.10b) that at this juncture the tiny segment of the shock wave front has only negligible curvature and the areas  $A_2$  and  $A_3$  perpendicular to this segment are considered to be sufficiently plane and

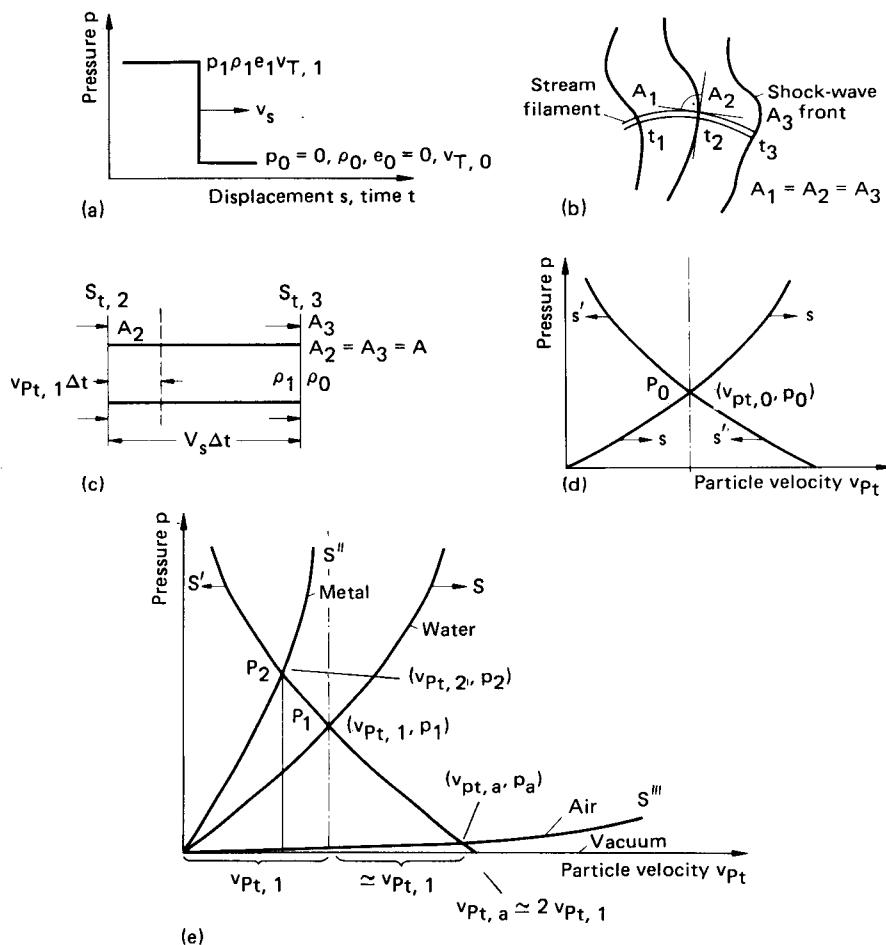


FIG. 27.10 Characteristics of a shock wave. (After [27.11].)

## 27.18 METAL FORMING UNDER SPECIAL CONDITIONS

parallel to each other. The closest possible setting of these two surfaces is feasible because the precondition  $dp/dt \rightarrow \infty$  must be valid.

Under such preconditions the following basic physical principles are derived [27.11–27.13]:

- 1 Conservation of mass  $m_0 = m_1$  (Fig. 27.10c):** During the time interval  $\Delta t$  the shock wave propagates from point  $S_{t,2}$  to  $S_{t,3}$ . The mass affected by the shock wave, before the wave passes through its neutral axis, is  $m_0 = v_{SW} \Delta t A \rho_0$ . After the shock wave has passed beyond its neutral axis, the mass is compressed; thus it acquires a high density. At the same time it is accelerated to a higher velocity,  $m_1 = (v_{SW} - v_{Pt,1}) \Delta t A \rho_1$ . For  $m_0 = m_1$  the density becomes

$$\rho_1 = \frac{\rho_0 v_{SW}}{v_{SW} - v_{Pt,1}} \quad (27.1)$$

- 2 Instantaneous force = impulse:**

$$A(p_1 - p_0) \Delta t = m_0 v_{Pt,1}$$

For  $p_0 = 0$ ,

$$p_1 = \rho_0 v_{SW} v_{Pt,1} \quad (27.2)$$

- 3 Conservation of energy:** The work done by the pressure difference between  $p_1$  and  $p_0$  and due to the motion of mass  $m$  corresponds to the increase in the kinetic and potential (inner) energies:

$$(p_1 - p_0) v_{Pt,1} A \Delta t = \frac{1}{2} \rho_0 v_{SW} \Delta t A v_{Pt,1}^2 + (e_1 - e_0) v_{SW} \Delta t A \rho_0$$

Work      =      kinetic energy + potential energy

For  $e_0 = 0$  and  $p_0 = 0$  we obtain, from Eqs. 27.1 and 27.2,

$$e_1 = \frac{p_1}{2} \left( \frac{1}{\rho_0} - \frac{1}{\rho_1} \right) \quad (27.3)$$

If the shock wave propagates into the mass which moves with velocity  $v_{Pt,0}$ , whereby the pressure  $p_0$  prevailing here must be taken into consideration, the superposition of Eqs. 27.1 and 27.2 gives

$$\rho_0(v_{SW} - v_{Pt,0}) = \rho_1(v_{SW} - v_{Pt,1}) \quad (27.4)$$

and

$$(p_1 - p_0) = \rho_0(v_{SW} - v_{Pt,0})(v_{Pt,1} - v_{Pt,0}) \quad (27.5)$$

Eqs. 27.4 and 27.5 give

$$(v_{Pt,1} - v_{Pt,0}) = \pm \sqrt{(p_1 - p_0) \left( \frac{1}{\rho_0} - \frac{1}{\rho_1} \right)}$$

or, in general,

$$v_{Pt} = v_{Pt,0} \pm \sqrt{(p - p_0) \left( \frac{1}{\rho_0} - \frac{1}{\rho_1} \right)} \quad (27.6)$$

In Eq. 27.6, represented in Fig. 27.10d, the term with the positive root is valid for the portion of the curve at the right of point  $P_0$ . The equation term with negative root is valid for the portion of the curve at the left of point  $P_0$ . Curve  $S$  contains all the instantaneous characteristics of the (original) shock wave propagating to the right, curve  $S'$  contains all the instantaneous characteristics of the shock wave (reflected) to the left. These curves are named after Rankine and Hugoniot who introduced them for the first time. Each curve is characteristic of a particular material. The

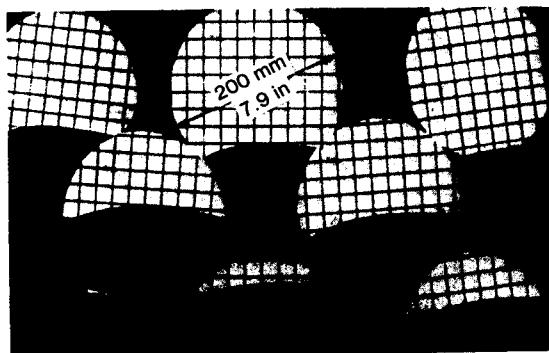


**FIG. 27.11** Propagation of a shock wave. Instantaneous shapes of the wave propagation are arranged in a sequence moving from right to left for each row, starting at the top. Sequence of exposures— $t = 18 \mu\text{s}$  per instantaneous shape. 200 mm = 7.9 in. (After [27.11].)

slopes of the Rankine–Hugoniot curves are greater for metals than for water, but the slope of the curve for water is again greater than are the slopes of curves for gases.

At the shock-wave transition front, if two materials are not expected to separate from each other, then the pressures and the particle velocities must be the same for both materials.

Fig. 27.10e shows a characteristic curve for the shock wave and the media pair metal–air. First the shock wave propagating through water should have its instantaneous characteristics as  $p_1$  and  $v_{p1,1}$ . Now if the shock wave reaches the metal, the wave divides into two branches, one propagating in metal and the other through the water. The new state having instantaneous characteristics  $p_2$ ,  $v_{p2,2}$  can lie only on the branch  $s''$  for the metal and on the reflected curve branch  $S'$  for the water. Curve branch  $S'''$  is valid for air, the curve deviating somewhat from the characteristic curve for the vacuum. For reasons of symmetry, the particle velocity in vacuum is given by the relation  $v_{p1,s} = 2v_{p1,1}$ .

Since the Rankine–Hugoniot curves are known for most metals, the particle velocity or deformation speed and the pressure values can be determined quite easily.

Fig. 27.11 shows the propagation of shock waves through water. The bright–dark limiting front shows the shock wavefront.

### Transmission of the Shock-Wave Impulse to the Workpiece

When a shock wave propagating through water reaches a metal, then two waves are spread from the transition front water–metal, one propagating through the metal and the other reflected back through the water (Fig. 27.10e). If both materials are not separated, then pressure  $p$  and particle velocity  $v_p$  at the transition front remain the same. At this front the sudden pressure increase to double its initial value is due to a different mechanical impedance.

Fig. 27.12 shows the conditions for pressure transmission for a shock wave with idealized pressure profile having certain temporal behavior. These periodic pressure profiles (hatched surfaces in Fig. 27.12) are obtained by overlapping the oncoming waves and the reflected waves. If the transition front metal–air is approximated to the metal–vacuum front, the pressure diminishes completely at each given instant; that is, the oncoming pressure wave runs back against a “tension” wave. For the wave propagating back from metal into water, the pressure has only half its initial value due to impedance.

The vertical front of the returning shock wave running toward the left in water is obtained only on a theoretical basis. Actually its curve is formed in the shape of the dashed line in Fig. 27.12e.

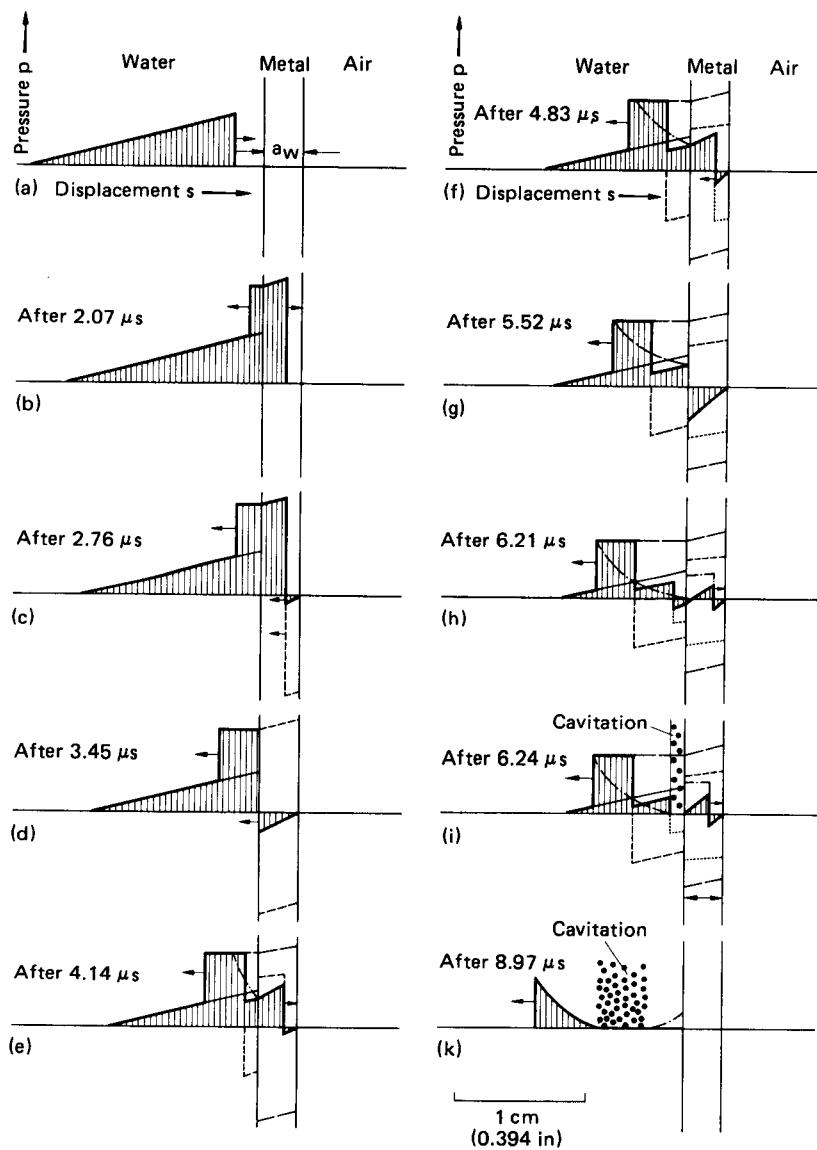


FIG. 27.12 Pressure transmission of shock waves. (After [27.11].)

The situation illustrated in Fig. 27.12*h* can occur only if the transition front as well as the transmitting medium can transmit stresses on the left side of the front. Water can transmit only negligibly small tensile stresses. This transmission phenomenon causes lifting and cavitation, which are indicated in Fig. 27.12*i* by means of gas bubbles.

The pressure profiles, which follow each other at precise time intervals as shown in Fig. 27.12*a* to *k*, are a function of the periodic pressure profile of the oncoming shock wave, of the shock-

wave velocity  $v_{sw}$  in the corresponding media, and of the thickness  $s$  of the material to be deformed. (In the present case  $s$  is the sheet-metal thickness.)

### *Effect of the Shock Wave on the Deformation of the Workpiece*

On the path segment which the shock wave has described up to a given instant in time, the kinetic energy of a particle of the transmitting medium (generally water) is transferred to the next particle by the mode of impulse transmission. As the shock wave reaches the workpiece surface, that part of the kinetic energy which is not lost in reflection of the wave is transferred over. During this phenomenon the workpiece is accelerated to a higher velocity [on the order of 50 m/s (165 ft/s) for steel and 100 m/s (330 ft/s) for aluminum]. The data are given for electrohydraulic forming according to [27.14]. If the workpiece happens to be sheet metal rigidly clamped by fixtures, then its velocity is reduced to a standstill because of stresses produced in the workpiece. During this retardation the workpiece is bulged by "free" deformation.

An "implemented" deformation occurs when the workpiece is moved until it touches the tool surface and receives the corresponding shape of the die impression.

In most cases the spacing between the die and the workpiece has to be evacuated because the air located there cannot escape completely during the forming operation. Otherwise the highly compressed air quantity would create undesirable bulges on the workpiece, and the die (e.g., punch) surface would even melt locally because of the intense heat generated by compression of the trapped air.

### **27.3.2 Explosive Forming—Equipment and Application**

In this process either a high pressure or a certain amount of kinetic energy is generated by converting the chemical energy available in the explosives. The explosive compounds (used in the form of balls, bars, or strands) serve as energy-transmitting media when they are ignited under water to explode, and they produce a large quantity of gaseous products from the chemical reaction. This energy release serves the purpose of metal deformation. Such energy conversions occur at very high speeds of as much as 8000 m/s (26,250 ft/s). Due to the very short period available, the mass inertia of the water hardly allows an increase in volume enlargement. Thus the pressure built up by the explosion propagates in the form of a shock wave [27.15].

The explosive compounds used may be classified into two groups: low-pressure explosives (firing materials) and high-pressure explosives (detonating materials). Fig. 27.13 shows their pressure-time behavior. In the explosive forming process, detonating materials are preferred. The most widely known detonating materials are trinitrotoluene (TNT), cyclotrimethylenetrinitramine (RDX), pentaerythriol tetranitrate (PETN), and their mixtures. Fig. 27.14 shows Rankine-Hugoniot curves for water and certain metals as well as the pressures achieved with particular explosives [27.14]. The explosive materials are given suitable shapes, depending on the desired form of the finished workpiece. For drawing metal plates, ball-shaped explosives are chosen. Strands of explosives are chosen for expanding tubes, whereas foil-shaped explosives are selected for cutting, hollow embossing, and plating. There are two basic possibilities to arrange an explosive charge of a given shape with regard to the raw workpiece: balls and strands are arranged at regular spacings near the workpiece, whereas foil-shaped explosives are laid on the workpiece. The process is then carried out by immersing the die together with the explosive charge under water in a tank.

The limitation of the workpiece size is mainly imposed by the economics of construction of the water tank and not by the nature of

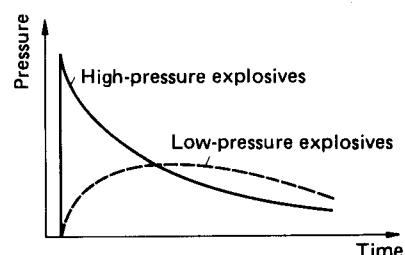


**FIG. 27.13** Pressure-time behavior of high-pressure and low-pressure explosives.

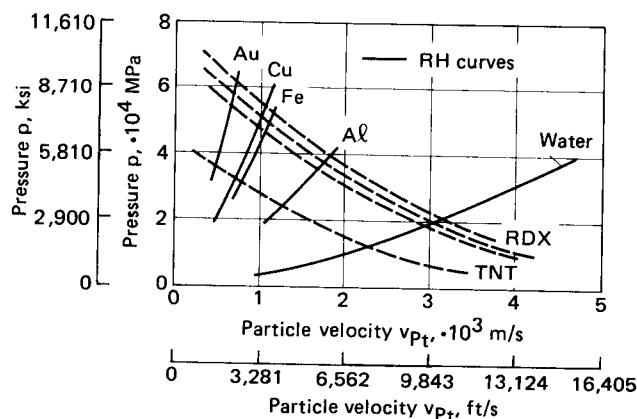


FIG. 27.14 Rankine-Hugoniot curves for water and certain metals together with pressures and speeds achieved with RDX and TNT. (After [27.13].)

the process. Fig. 27.15 illustrates the construction scheme of such a tank. In order to suppress any further propagation of the shock wave into the bottom of the tank, air-filled tubes are placed under the die at the tank bottom. Air, which is blown through the tubes, bubbles along the tank walls, thereby preparing an air layer which prevents direct action of the shock wave on the walls, thus protecting them. Fig. 27.16 shows the principle of construction of a die to draw metal plates [27.3].

Matching the appropriate quantity of explosive charge to be used with the given workpiece size as well as the proper arrangement of this charge with respect to the workpiece need extensive experience and the corresponding preliminary tests. Since many different parameters are involved in the process, it is hardly possible to give information that will be generally applicable for different cases. To improve the process efficiency, which may be as low as 2–6%, either the propagation of the shock wave can be steered in a suitable direction by means of guiding reflectors, or closed dies are used for workpieces of small and medium sizes.

#### Dies and Other Tool Equipment

Various types of materials are used for dies of the explosive forming process. They range from forged steel, casting steel, and concrete to synthetic polymers and even ice (in special cases even a mixture of water and paper). Selection of the die material depends on many factors, such as the number of workpieces to be processed, the mechanical stress on the machine, and the type of work material and impression in the die. Very strict safety regulations with respect to storage and handling of the explosive materials are imposed on industrial management. As a consequence, the frequently used equipment shown in Fig. 27.16, which is of the semiopen type and has the die immersed in a water bath, cannot be placed in a normal factory building and operated there. In order to facilitate the operation of an explosive forming machine on an industrial shop floor, different types of non-dangerous machines have been constructed. Such machines essentially function with a closed die. Two of these are introduced here, a machine using explosive cartridges and an inertia-locked machine of the type Hertel/Ruppin [27.16]. Objects having surface areas of

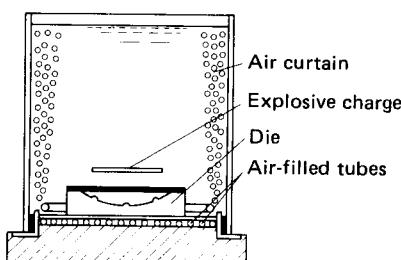
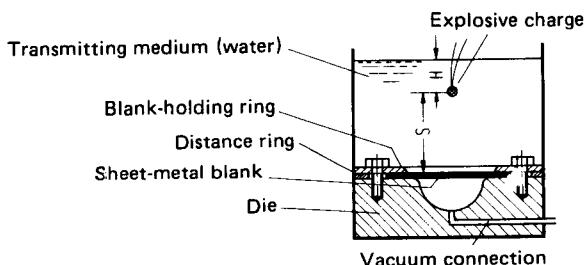


FIG. 27.15 Water tank for explosive metal-forming process. (After [27.3].)



**FIG. 27.16** Schematic design of semiopen die for the explosive metal-forming process.

a few square meters can be worked with such machines installed on a normal shop floor (e.g., making copper electrodes to be used on a spark-erosion machine).

#### *Possibilities of Industrial Application*

Explosive forming is interesting in many respects as far as its industrial application is concerned, first for workpieces having large surface areas for which nominal forming forces of the conventional machines do not suffice, and second for workpieces of complicated shapes and made from materials which cannot be formed easily. The third area of application is the small-scale production and manufacture of prototypes.

The workpieces produced by the explosive forming process can be classified in three groups: drawn objects, flat embossed workpieces, and cylindrical hollow pieces. The first two groups may have a diameter range of 30 mm to 5 m (1.2 in to 16.4 ft) and a sheet-metal thickness range of 0.5–30 mm (0.02–1.2 in). In the case of relatively small workpieces, the cutting operation could also be coupled with explosive forming. By suitable division of the die it is easy to produce a back taper which would be very difficult to obtain when forming with a conventional process. Last but not least, it must be emphasized here that the embossing accuracy achieved by the new process is superior to that of conventional processes.

#### *Advantages and Disadvantages*

The main advantage of explosive forming are its manyfold applications. The economy of its industrial application has to be determined for every individual case. Compared with many metal-working processes, machines used in explosive forming require little investment, consume less energy, and their die costs are low. Unlike with the conventional machines, the number of operations necessary to complete the same job can be reduced. Moreover, another technological advantage is secured in terms of narrower dimensional tolerances. The disadvantages are a very long preparatory period and strict safety regulations, although the latter could be overcome by using the safe machines mentioned.

### **27.3.3 Electrohydraulic Forming (Hydrospark Forming)**

#### *Equipment and Industrial Application*

In this process electric energy is stored in the capacitors and suddenly discharged over a spark gap placed under water. Due to ionization and steam produced during the discharge, a high pressure is built up. Connecting the spark gap with a wire piece also creates a high pressure during the electric discharge. As in explosive forming, the pressure then acts in the mode of a propagating shock wave.

#### *Impulse-Current Generator*

The electric equipment for carrying out the electrohydraulic process consists of three functional groups of components (Fig. 27.17):

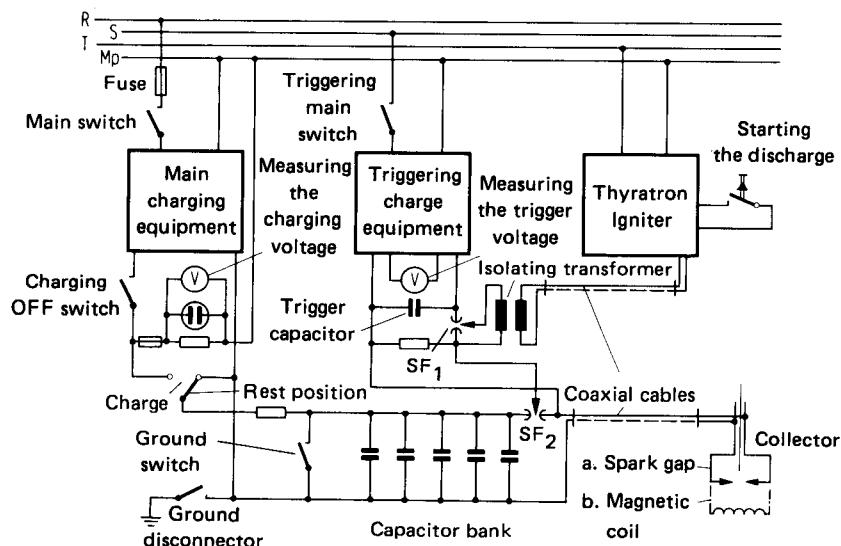


**FIG. 27.17** Simplified circuit diagram of an impulse-current generator for electrohydraulic and electromagnetic metal-forming processes. (After [27.11].)

- 1 Charging equipment with transformer, rectifier, and charging resistances
- 2 Parallel connected capacitors for capacitive energy storage; discharging unit equipped with spark gaps
- 3 Coaxial cables and spark heads

The simplified circuit diagram of Fig. 27.17 helps to understand how the electric equipment works. Over a range of safety devices, electric power is tapped from a 220/380-V three-phase supply. The capacitors are supplied from the main charging unit by means of a transformer, a high-voltage rectifier, and charging resistors. When a switch button is pressed, an electric discharge is started over a Thyatron spark unit. Following the discharge over the transformer, the spark unit ionizes switching spark gap SF<sub>1</sub>. From here the trigger capacitor is discharged over switching spark gap SF<sub>2</sub>, which becomes ionized, and subsequently the capacitor bank is also discharged. This complicated discharging sequence is necessary since only a sufficiently strong ionization guarantees a disturbance-free electric discharge [27.11].

Two types of switching spark gaps are usually employed. The relatively cheap and simple air gap has two electrodes with their tips arranged opposite to each other. Its disadvantage is that while functioning it makes a loud noise and has very heavy electrode wear. Also its deionization period is very long. The second type is the Ignitron, an electron tube having three electrodes. It does not have the above-mentioned disadvantages, but again it is very costly and operates well only with limited (relatively low) current strength.

For the machines used in industry the service life of the capacitors is very important. It depends on the ratio of operating voltage to supply voltage, the discharge frequency, the suppression (dampening) of the discharge shock wave, as well as on the type of capacitor oil (Fig. 27.18).

Analogous to explosive forming, the process of electrohydraulic forming also offers two possibilities of die construction, an open die immersed in a water tank and a closed die built within the machine. Since only the latter type of die can be considered for industrial application of the electrohydraulic process, our further considerations do not deal with the open die. In the case of a load spark gap immersed under water, two different arrangements of the electrodes are possible:

- 1 Two electrodes arranged opposite each other
- 2 A coaxial electrode

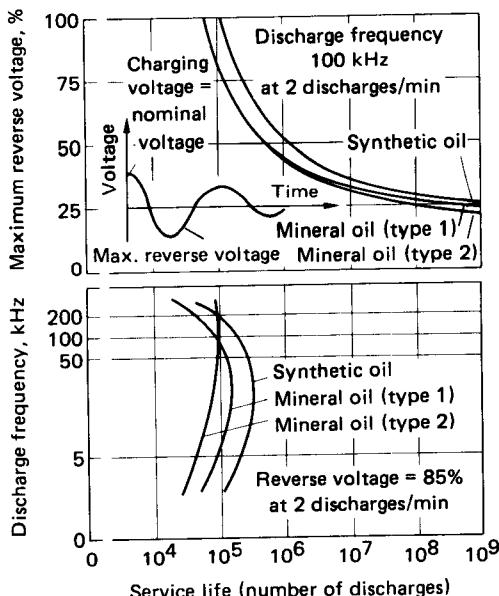


**FIG. 27.18** Service life of electric capacitors in correlation with maximum reverse voltage and resonance frequency. (After [27.14].)

Both types are suitable for industrial electrohydraulic forming of flat and hollow workpieces. Fig. 27.19a and b shows such electrodes used to deform flat workpieces. In the present case the coaxial arrangement is advantageous in view of superior machine construction, and it also permits keeping the inductance low, while in the case of electrodes arranged opposite to each other, electrical insulation becomes simpler.

Under certain conditions the electrodes may penetrate the hollow spacing of a workpiece. Fig. 27.19c shows the electrodes arranged opposite to each other. The grade of metal forming in this case is particularly high. The length and the diameter of the electrodes depend on the dimensions of the finished object. Obviously a narrow tube diameter permits only thin electrodes, which reduces their strength and service life. With regard to the smaller-diameter electrodes used for narrower hollow workpieces, still greater difficulties must be confronted when coaxial electrodes are used because they need a larger space in the radial direction.

Fig. 27.19d and e shows the basic arrangement of electrodes for shaping tubes of smaller diameters. In such a case the original pressure waves are guided in the required direction by means of reflectors, while energy losses that occur due to guiding the pressure wave in another direction are also taken into account.

Stainless steel is the appropriate material for electrodes because their wear can be kept within acceptable limits. An elastic type of polyurethane is employed in insulating the coaxial electrode.

Since it has to be replaced after every spark discharge, a connecting wire piece that bridges the spark gap between the electrodes is seldom used.

#### Machines

The development of machines for electrohydraulic forming is well advanced, so that a number of different types are available on the market. The charging-energy capacity varies from 6 kJ (4426 lbf·ft) to 150 kJ (110,640 lbf·ft). The machines permit an automatic sequence of the following operations: safety locking of the die, checking and governing the functions of all safety

## 27.26 METAL FORMING UNDER SPECIAL CONDITIONS

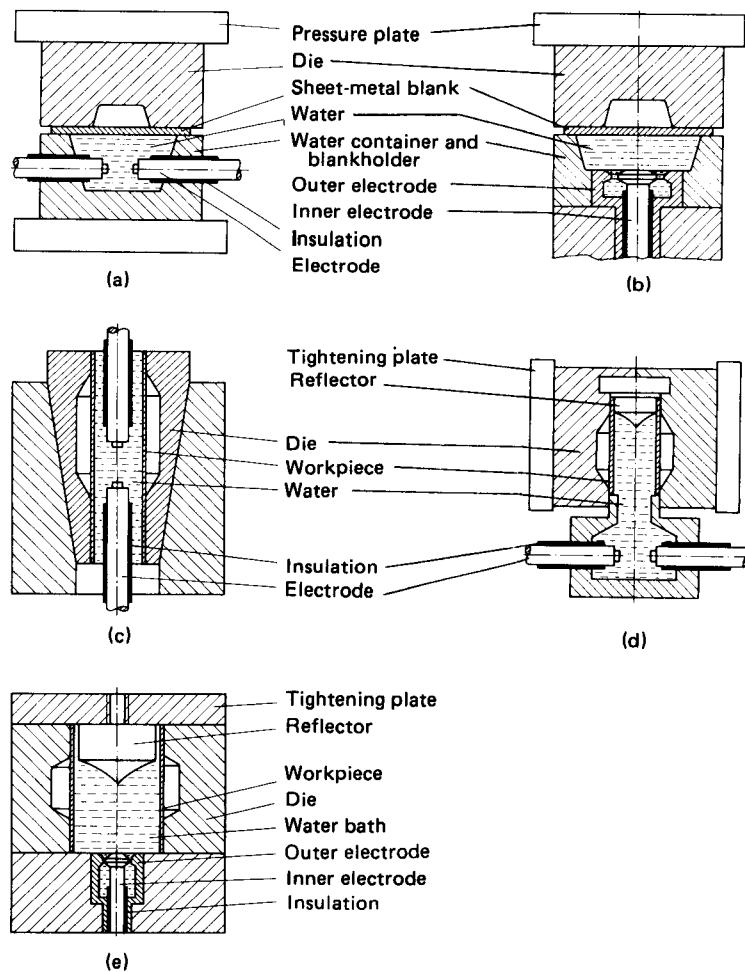


**FIG. 27.19** Different arrangements of electrodes. Dies *c*, *d*, and *e* are split longitudinally.

devices, maintaining the level in the water tank, evacuating the die impression, charging the capacitors up to a given voltage, and discharging and grounding the capacitors. The machine operator must do only the following work: arrange the workpiece in the machine, start the controlling and operating sequence, and remove the formed workpiece. Fig. 27.20 shows an example of such a machine working with 150 kJ charging energy. The base area measures 1600 by 1600 mm (5.25 by 5.25 ft), the machine height is 1000 mm (3.28 ft), the stroke length 750 mm (29.53 in), and the closing pressure 1000 kN (112.5 ton). In approximately 15 s the capacitors are charged to 18 kV. The machine is equipped with an evacuating device.

Fig. 27.21 shows the principle of a machine using a coaxial electrode. The equipment was developed and tested at the Institut für Umformtechnik in Stuttgart, West Germany. The high-voltage unit (capacitor bank) for this machine is kept in a separate room. The superiority of this equipment was achieved by means of simple mechanisms and cost-saving construction.

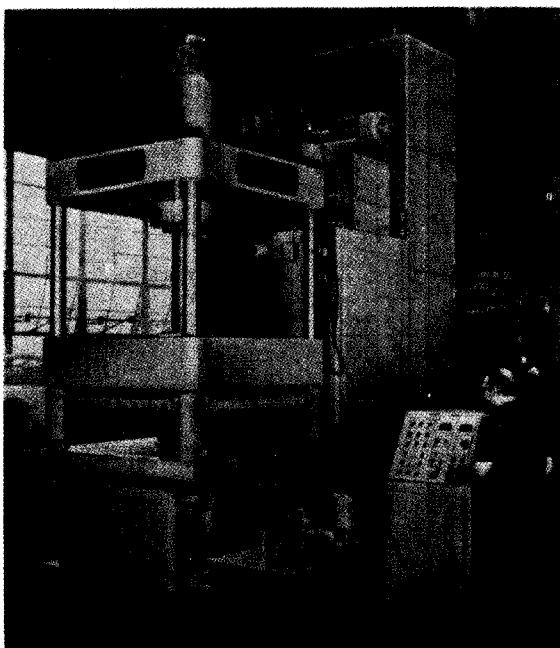


**FIG. 27.20** Electrohydraulic metal-forming machine with horizontal work table. Charging energy—150 kW·s; charging voltage—18 kV. (Courtesy of Cincinnati/Milacron.)

### Dies

As mentioned above, closed dies are used almost exclusively on such machines in industrial production. Compared to open dies immersed in a water tank, closed dies have the following advantages:

- 1 Their simplified handling shortens the complete operating cycle considerably.
- 2 By skillful exploitation of the physical laws, the volume of the water bath can be reduced in such a manner that the pressure wave can be better utilized (improving the machine efficiency).
- 3 Because of space saving, increased safety, and low noise, the machine can be operated on a shop floor with acceptable working conditions; moreover, a machine with a closed die and rigid interlocking arrangement operates more smoothly and is practically free from vibration.

As in the explosive forming process, similar considerations lead to the choice of suitable die materials. Due to the very good embossing accuracy that can be achieved, the impression surface in the die must be at least as smooth as the desired surface finish of the processed product.

As in explosive forming, the air trapped in the gap between die and workpiece must also be removed in this process. According to [27.17], optimum pressure values during the forming operation are considered to lie in the range of 100–2500 Pa (0.014–0.356 psi), depending on the workpiece shape and the material flow within the die. They are supposed to be optimum because any pressure higher than 2500 Pa (0.356 psi) causes undesired bulging in the workpiece, while with lower pressures [less than 100 Pa (0.014 psi)] the impulse exchange between workpiece and die is not suppressed sufficiently, which causes springback of the workpiece. Regarding the place of origin of the shock wave relative to the die impression and in relation to the amount of energy

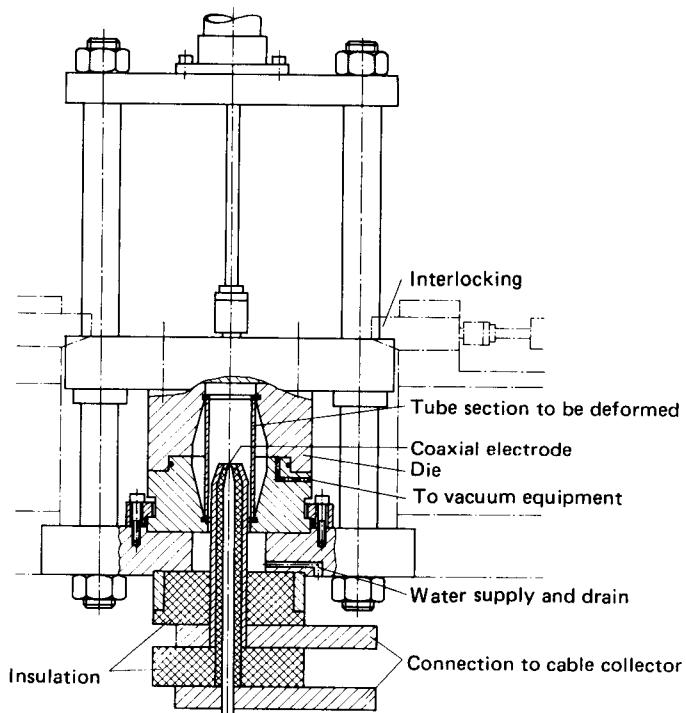


**FIG. 27.21** Schematic design of electrohydraulic metal-forming machine with coaxial electrode. Charging energy—50 kW·s; charging voltage—18 kV. (Courtesy of Institut für Umformtechnik, University of Stuttgart.)

needed, specifications that are generally applicable in different situations cannot be offered. Especially in the closed-die machine, shock-wave reflections can be arranged in many different ways, which change the state of pressure decisively. On the other hand, such reflections can be exploited skillfully in order to process workpieces of complicated shapes.

Thus Fig. 27.22 shows expanding of a tube having an extremely low  $d/l$  ratio, where  $d$  is the tube diameter and  $l$  the tube length. Fig. 27.23 shows forming of a tube with an extremely high ratio of  $d/l = 7$  achieved by skillful deviation of the pressure waves. When choosing the dimensions of the water bath, special attention must be given to the deviation of pressure waves, which should be avoided as far as possible because every such deviation is accompanied by energy loss and an additional stress on the die. An unsuitable shape of the water bath can interfere with the operation so much that due to frequent subsequent reflections of the pressure wave hardly any energy reaches the workpiece. The path of propagation of a small segment of the pressure wave-front indicates such a situation, as shown in Fig. 27.23 [27.14].

While determining and producing the required amount of energy, attention should be given that the workpiece does not impact the die impression at a very high speed. Such a strong collision would cause mechanical fatigue of the die, whereby the notch effect, if present, intensifies the extent of such damage.

#### *Possibilities of Industrial Application*

The electrohydraulic process is mainly applied for expanding tube sections, to draw sheet-metal parts, for hollow impressing, to calibrate profile sections, and for cutting as well as joining. In

general these operations can also be carried out on conventional machines, but they would require very costly dies in such special cases, so that conventional processes become unsuitable for small-scale production when compared with the electrohydraulic process, which offers a superior alternative because it also delivers workpieces of better quality.

The type of workpiece which can be suitably formed with electrohydraulic operation is decided on the basis of the amount of forming energy needed. Limitations to the application of the process are imposed by economical considerations concerning the required equipment and ancillary machines. In general the capacitor banks are equipped with a capacity of up to 150 kJ (110,640 lbf·ft). Since the overall efficiency of such equipment amounts to only  $\eta \leq 0.1$ , workpieces requiring about 15 kJ (11,062 lbf·ft) of forming energy can be worked on such machines. The diameters of finished objects range from 30 mm to a few hundred millimeters (1.2 in to about 1 ft), and even larger. The wall thickness ranges from 0.5 to 3 mm (0.02–0.12 in); some special materials are also used in addition to aluminum and steel which are chosen extensively as work materials (Fig. 27.24).

Figs. 27.25 and 27.26 show several workpiece shapes which could be worked advantageously on an electrohydraulic machine. Mostly two or more parts of a tube section are formed simultaneously during one discharge. Cutting can also be done favorably at those places where material flow attains a high speed. An expansion, bulging, and the cut edge need not be axially symmetric.

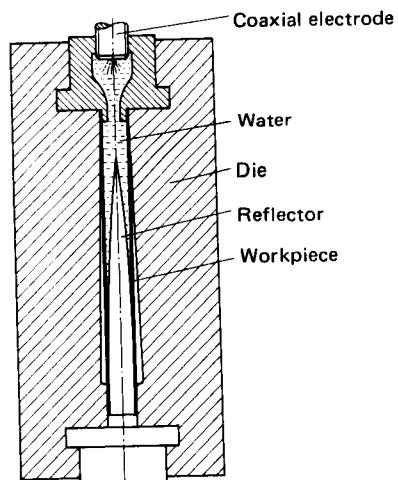


**FIG. 27.22** An example of industrial manufacture: tube with extremely small ratio of tube diameter to tube length; longitudinally split die. (After [27.14].)

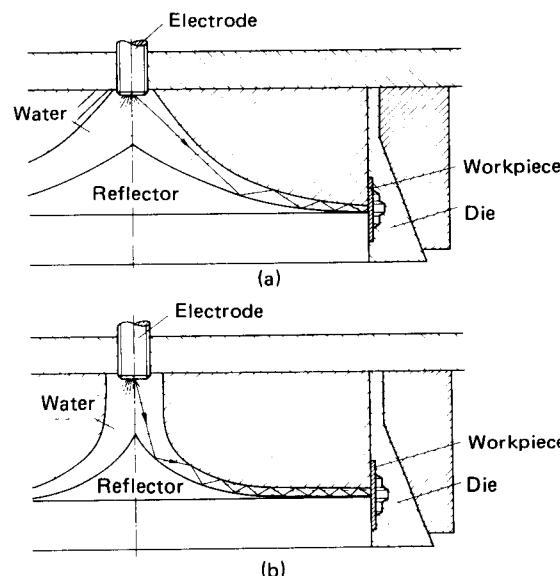


**FIG. 27.23** Example of industrial manufacture: tube with extremely large ratio of tube diameter to tube length. (a) Suitable shape of pressure cavity. (b) Too many reflections of shock wave. (After [27.14].)



**FIG. 27.24** Examples of industrial manufacture: products at right—made by electrohydraulic process; products at left—made by electromagnetic process.

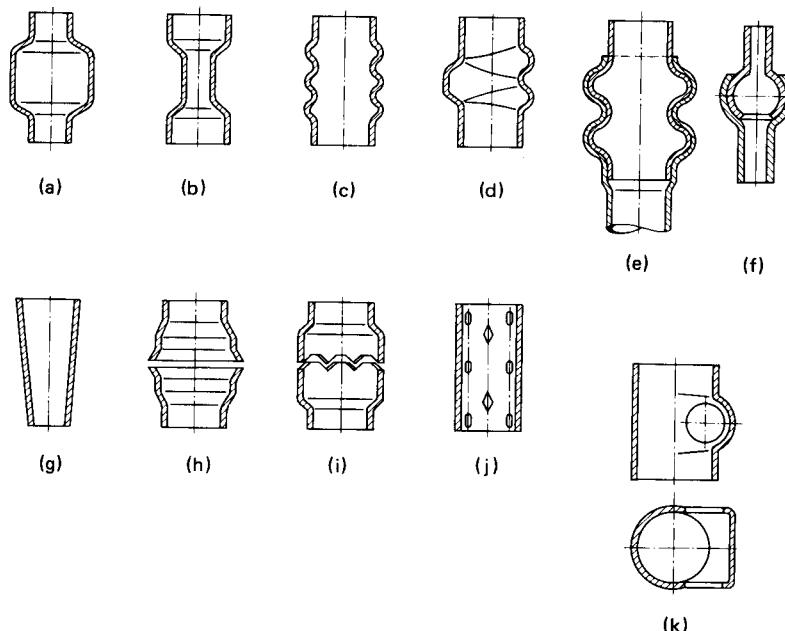


**FIG. 27.25** Examples of industrial manufacture starting with tube sections. (a)–(d) Bulging. (e), (f) Fixed and movable connections. (g)–(j) Bulging and shearing. (k) One-sided exaggerated bulging. (l) Embossing and bulging. (m) Embossing. (n), (o) Embossing and shearing. (After [27.18].)

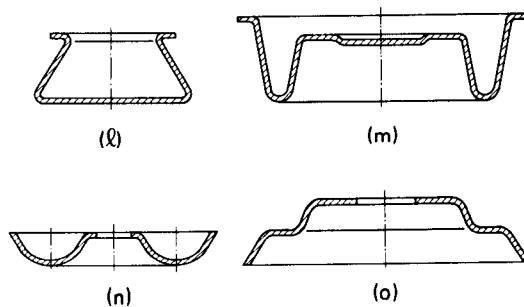


**FIG. 27.26** Examples of industrial manufacture starting with sheet-metal blanks. (After [27.18].)

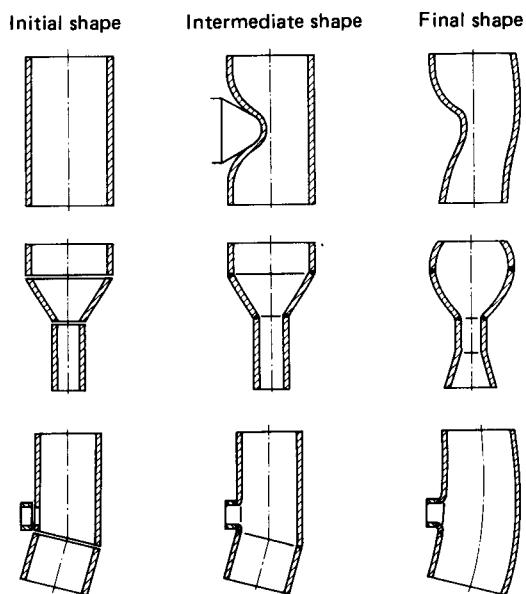


**FIG. 27.27** Sequence of shape changes for different workpieces. (After [27.18].)

Certain workpieces must have an appropriate preliminary shape so that they can be placed easily within the die. Such a preliminary shape is given mostly by means of conventional forming processes (pressing, drawing, etc.). Other categories of similarly complicated workpieces are prepared by welding different parts together, especially when the formability of the work material is known definitely. Then by means of one or more energy discharges or shots the desired shape of the workpiece can be achieved with the electrohydraulic forming process (Fig. 27.27).

### *Advantages and Disadvantages*

This process has the advantage of versatility. The machines can be operated like other production machines, and despite their high-voltage units, they can be safely installed on a normal shop floor. Workpieces which would need many operations with conventional processes can now be formed in a single operation. The die costs are low, and different metal-forming operations (such as expanding combined with cutting) can be done simultaneously. The complicated shapes processed by electrohydraulic forming often cannot be achieved by conventional production methods. This advantage permits combining different parts of an object which may eventually complicate its geometry, but on the other hand such preintegration requires only few forming operations at subsequent stages. Moreover the simplified construction without many attachments leads to an easy assembly of such products.

High investment and operating costs are the disadvantages of the process, which also result in limiting the maximum amount of available deformation energy. Also, compared with conventional processes, the operating cycle is still comparatively long.

## 27.4 PROCESSES UTILIZING ACTIVATING ENERGIES

### 27.4.1 Electromagnetic Forming

#### *Operating Principle, Equipment, and Applications*

In this process electric energy stored in capacitors is discharged into an electromagnetic coil. When a current having a suppressed wave profile flows in the coil, the magnitude of this discharge current amounts to  $i = i_0 \exp(-t/t_p) \sin \omega t$ . It induces a magnetic field having induction  $B = B_0 \exp(-t/t_p) \sin \omega t$  (e.g., 100,000 Gauss), which again produces in the workpiece a countercurrent  $i'$  (Fig. 27.28).

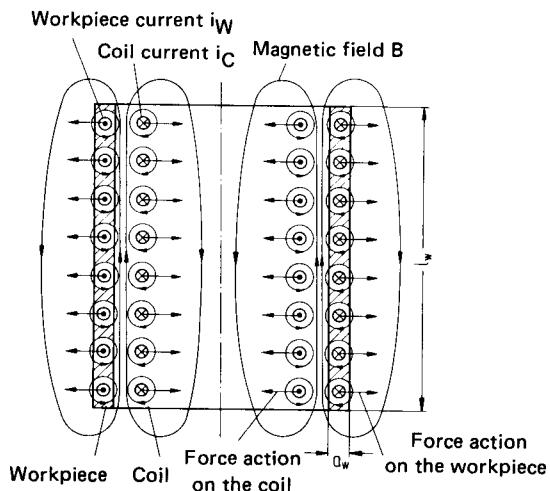
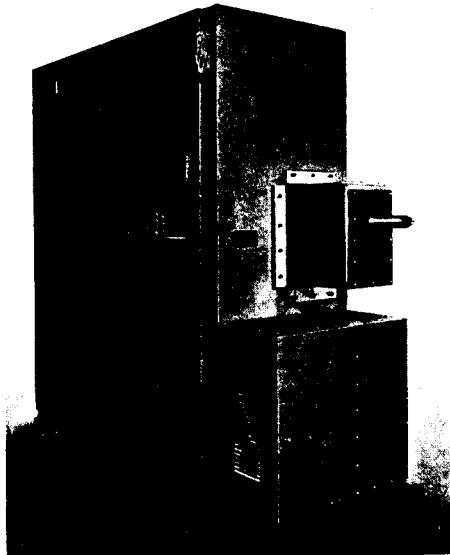


FIG. 27.28 Operating principle of electromagnetic metal-forming process.



**FIG. 27.29** Example of an electromagnetic metal-forming machine. (*Courtesy of Magneform.*)

According to Lorentz this axially directed magnetic field imparts an outward-directed radial force  $\mathbf{F} = \mathbf{i} \times \mathbf{B}$  on each volume element (right-hand rule). By mathematical integration in the radial direction the force applied per unit surface area of the workpiece can be calculated. The behavior of this magnetic pressure, also termed Maxwell pressure, is expressed by the equation  $p_M = B_0^2/2\mu \exp(-2t/t_p) \sin^2 \omega t$ . This force per unit surface area accelerates the material until it impacts on die impression or on another die-half, as in the case of a joining operation [27.11], [27.19], [27.20].

A magnetic field of negligible strength acts within the coil and outside the die.

The low deformation efficiency  $\eta_{def} = E_{def}/E_L \approx 0.1$  (charging energy  $E_L = CU^2/2$  and forming energy  $E_{def} = B^2/2\mu_0 As$ ) can be explained as the result of Joule's heat loss, the loss occurring during field penetration, and the residual field loss [27.11].

### Machines

Basically the machines of the electrohydraulic process can also be used for electromagnetic deformation. Instead of discharging the load over an air gap, an induction coil is used in the electromagnetic process. Due to its flexible behavior with respect to time, the inductance of the equipment must be kept as low as possible. On the other hand, the inductance can always be increased by external means if needed. Basically the time behavior of the current can be suitably matched with the nature of the forming operation. Frequently several machines, each having a capacity of 6 kJ (4426 lbf·ft) of forming energy, are combined as needed to obtain the required energy storage capacity. Fig. 27.29 shows a machine with 12 kJ (8852 lbf·ft) of energy storage capacity. This machine can produce 600 pieces per hour.

### Field Coils

The windings of an induction coil are arranged either spirally to make a flat coil or helically in a hollow cylindrical coil. The latter type has again two variations, the inner and the outer coils, depending on the position of the coil with respect to the tube-shaped workpiece. The inner coil is used for inward flanging or shrink fitting of tubes. Both coil types are also called expansion or compression coils, according to their mode of operation [27.18]. For a given number of windings, a high pressure can only be achieved by increased current strength, which in turn causes undesirable heat generation and heat stress resulting from temperature gradients. To keep such heat stresses as low as possible, only copper or copper alloys are considered appropriate coil materials.

It is important that in the design of a field coil the breaking strength at mechanical fatigue be considered as well as the dynamic behavior of the workpiece material. Hence short preliminary performance tests deliver only misleading hints. For a coil whose service life must generally last for periods on the order of  $10^8$  time units, such a service life is obtained with beryllium copper, which performs up to pressures of 180 MPa (25.56 ksi). With coils made from molybdenum copper alloy working pressures of up to 400 MPa (56.8 ksi) can be used.

According to the experience of a coil manufacturer, it should be kept in mind that the magnetic field strength  $B$ , and thus the pressure  $p$ , depend on the current strength per unit length  $i/l_0$  of the coil, that is,  $\sqrt{p} \sim B \sim i/l_0$ . Thus the specific current strength  $i/l_0$  necessary for the required pressure depends on the coil diameter.

The necessary voltage  $U$  is proportional to the magnetic induction  $B$  and the circular cross-sectional area between coil and workpiece, that is,  $U \sim BA$ , where  $A = 2\pi d_m b$ , with  $d_m = (d_C + d_W)/2$  and  $b = d_C - d_W$ ,  $d_m$  being the mean gap diameter,  $d_C$  the coil diameter,  $d_W$  the workpiece diameter, and  $b$  the gap width.

For a given coil type, a desired pressure and the matching voltage for a given workpiece material can be increased by enlarging the coil diameter and widening the spacing between coil and workpiece. The necessary current strength is reduced with increasing coil length. Consequently, the required amount of deformation energy is limited by the achievable pressure and the volume of the gap between coil and workpiece.

### Inner Coils

Inner coils must be arranged in the inner spacing of the hollow workpiece to be formed. At small diameters it is difficult to provide electric insulation. The conducting wire must be supported by the insulating inner core. The maximum possible pressure depends on the strength of this inner core.

### Outer Coils

In industry the outer coils are used more frequently than the inner coils. When the inner part of a workpiece is either a solid bar or a shaft or when the workpiece has a very narrow bore, joining of two coaxial workpieces can only be achieved from the outside. Thus in recent years more attention was paid to outer coils. However, as compared with inner coils, the outer coil is subjected to higher tensile stress and hence to greater danger of breaking.

Fig. 27.30 shows the basic construction scheme of an outer coil with field former. For the reasons given below, the majority of outer coils are equipped with field formers.

- 1 The field former relieves the coil windings from the effect of very high working pressures. It has a large mass and hence is mechanically robust. Undesirable heat generation, which causes overheating of the equipment, can be dissipated easily by cooling the field former with air or water.
- 2 With simple means the field former permits obtaining the required pressure distribution over the workpiece surface. Moreover, the field former is easily replaceable.

The field former operates on the following principle. The primary current  $I_1$  in the coil windings generates a secondary current  $I_2$  in the surface opposite to the field former. By partitioning the field former, the current flow is influenced as shown in Fig. 27.30. Again current  $I_2$  induces a

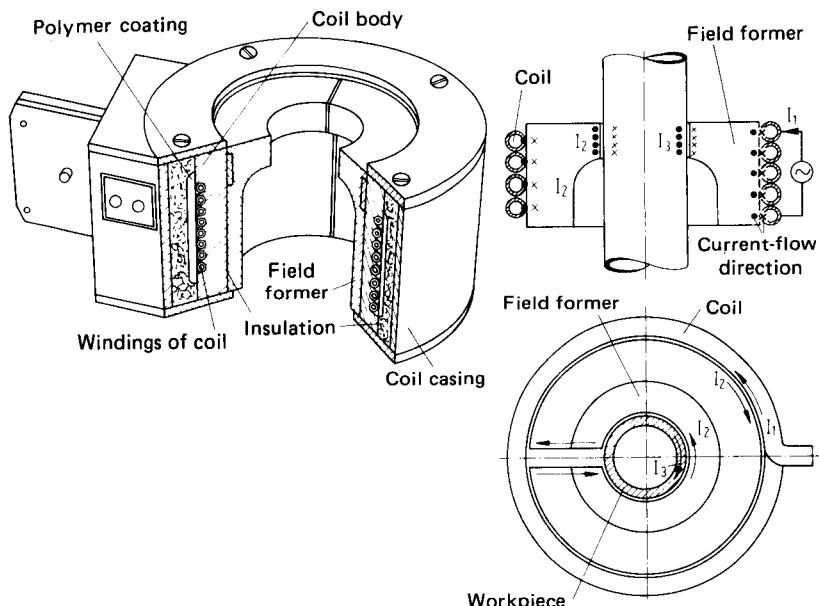


FIG. 27.30 Construction scheme and operating principle of outer coil. (After [27.18].)

countercurrent  $I_3$  on the surface area of the workpiece. The magnetic fields of these two currents  $I_2$  and  $I_3$  repel each other. This sudden repulsion brings about the deformation of the metal.

The coil type called wafer (Fig. 27.31) consists of two flat coils whose windings are on both sides of a disk-shaped field former. This former is made of two massive plates screwed together by strong bolts so that the plates can withstand very great forces. The primary current  $I_1$  induces the secondary current  $I_2$ , which flows on the surface opposite to the flat coil, up to the insulated separating slit, and then returns via the outer surface and, mainly, the inner surface (facing the workpiece) of the field former.

The advantages of this coil type equipped with a field former include its longer service life and higher loading capacity. Moreover, the pair of bolted plates can be mounted as a movable assembly, so that they can be separated if any parts in front of them have to be dismounted or changed (Fig. 27.32).

### Flat Coils

Flat coils having spiral windings are used preferably for light jobs such as repairs of damaged workpieces. They are not used extensively in the manufacture of small workpieces. These coils are nicknamed electromagnetic hammers. Undesired bends or bulges and uneven shapes caused by welding can be removed in this simple manner.

### Possibilities of Application

The main area of industrial application of the electromagnetic forming process is the joining by bending or folding. Fig. 27.33 shows examples of joining workpiece parts. In this process the joint is sealed by pressing the relatively thin-walled part onto the rigid second part, whereby the weaker (thinner) piece is either expanded or shrunk. In such operations the residual elastic stress remains within the workpiece. Similar to conventional sealing, the high compression between the joined surfaces is achieved by either folding or grooving.

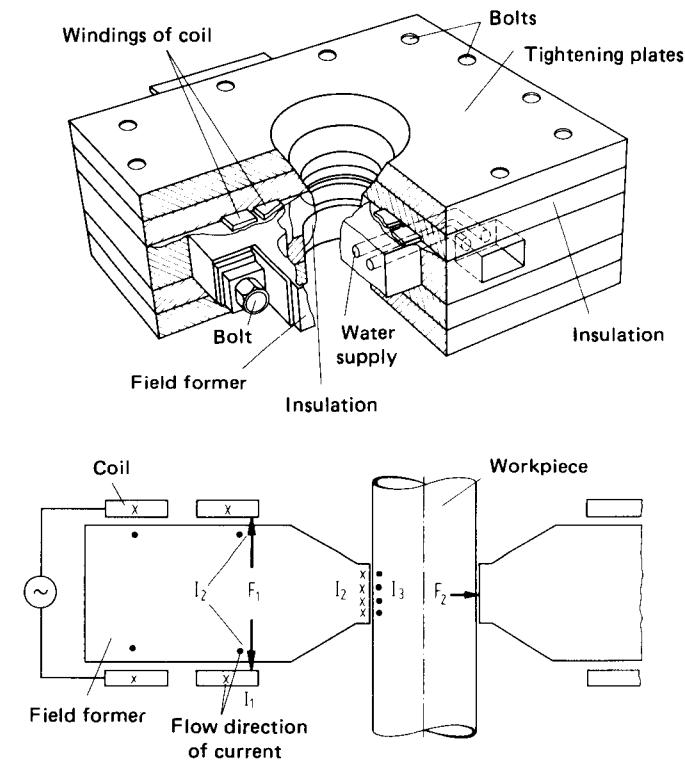


**FIG. 27.31** Construction scheme and operating principle of wafer coil.  
(After [27.18].)

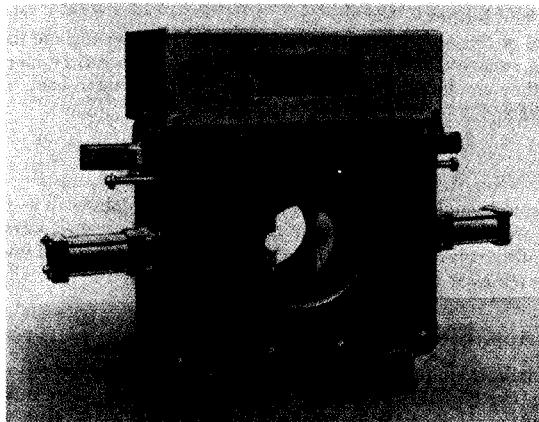


**FIG. 27.32** Actual construction of a coil of which both halves are movable to ease assembly operations. (Courtesy of Magneform.)

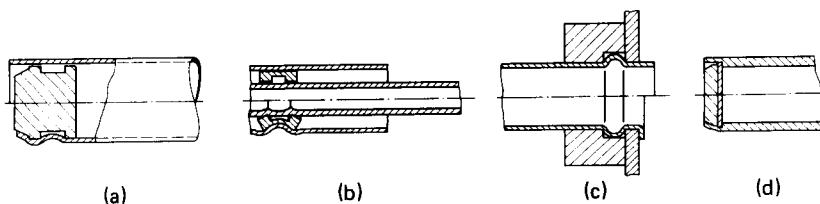


**FIG. 27.33** Examples of industrial manufacture: sealing of tube ends. (After [27.18].)

Further examples are shown in Fig. 27.34. In Fig. 27.34a two tubes are joined by using a lining to obtain an airtight seal. In Fig. 27.34b a turbine rotor is fitted onto its shaft. The intermediate sleeve has two inner grooves, which are bulged inward by shrinking the concentric copper bands. The grip of these grooves on the shaft gives a rigid joint.

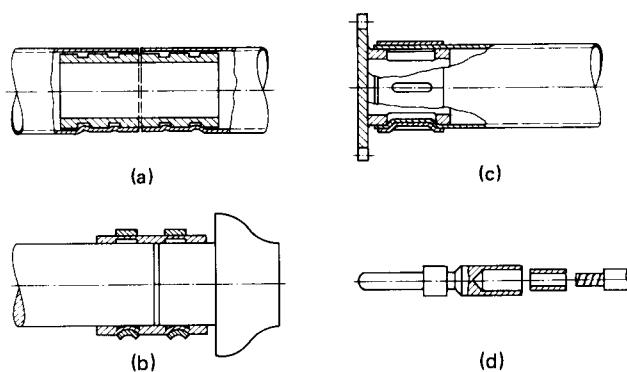
The type of joint shown in Fig. 27.34c can transmit a relatively high torque. The hub of the gear wheel has oblong holes. Both gear wheel and hub are made of alloyed steel having low conductivity. Therefore a highly conducting "driver sleeve" made from copper must be used to make a rigid joint. An electric conductor usually requires pressing a clamp on the wire end. If the conductor consists of a number of thin wires, it is advantageous to fit a narrow copper sleeve on the wire bundle so that good conductivity and sufficient mechanical strength of the connection are assured (Fig. 27.34d).

Fig. 27.35 shows a fan rotor assembled by the electromagnetic process.

In addition to such joining and forming operations, industrial applications of the electromagnetic forming process also include drawing, embossing (Fig. 27.36), and calibration.

### *Advantages of the Process*

- 1 Since the machines used for this process have no moving parts, their operating, maintenance, and repair costs are low.
- 2 No energy-transmitting medium is needed.
- 3 The process can be employed in conveyer-belt production.



**FIG. 27.34** Examples of industrial manufacture: joining of workpieces. (After [27.18].)

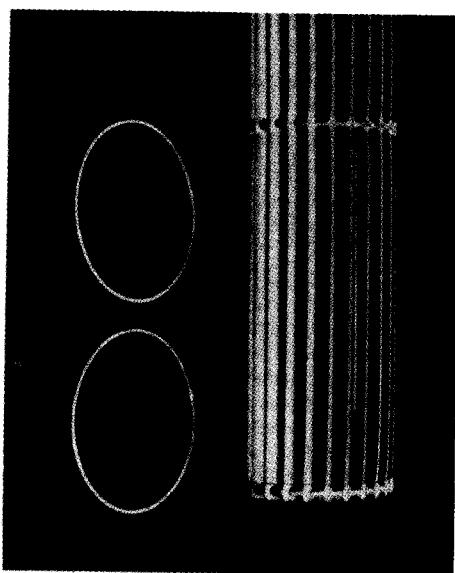


**FIG. 27.35** Assembly of fan rotor. (Courtesy of Magneform.)

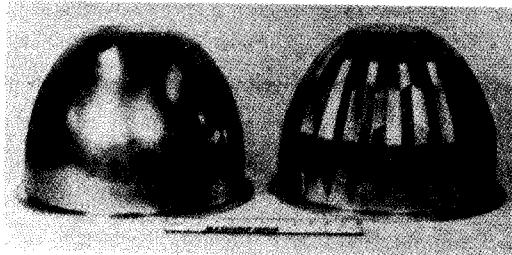


**FIG. 27.36** Electromagnetic embossing of parabolic reticotor. (Courtesy of Magneform.)

#### *Disadvantages of the Process*

- 1 Only work materials having good conductivity and low yield stress can be processed advantageously. Thus aluminum is found to be an appropriate work material.
- 2 Since from an economical point of view the equipment is limited to an energy storage capacity of 150 kJ (110,640 lbf·ft) and the machine efficiency is quite low ( $\eta \leq 0.1$ ), the required deformation energy should not exceed the limit of 15 kJ (11,064 lbf·ft).

#### **REFERENCES**

- 27.1 Opitz, H.: "Achievements in and Significance of the Technology of Manufacturing Processes" (in German), *Ind.-Anz.*, 84, 1962, pp. 1709-1720.

- 27.2 Burckhardt, A.: "High-Energy-Rate Processes for Metal Working" (*in German*), *Feinwerktech. u. Micronic*, **76**, 1972, pp. 93–101.
- 27.3 Davies, R., and Austin, E. R.: *Developments in High Speed Metal Forming*, London, Machinery Publishing, 1970.
- 27.4 Knauss, P., and Schneider, M.: "Machines for Forging Turbine Blades" (*in German*), *Werkstattstechnik*, **61**, 1971, pp. 333–337.
- 27.5 Dean, T. A.: "A Comparison of High Rate and Conventional Forging Machines," in *Proceeding of the 7th Machine Tool Design and Research Conference* (Birmingham), London, Pergamon, 1966, p. 25.
- 27.6 Mang, W. G.: "Dynapak—A New Dimension in High Energy Rate Forming," *Sheet Met. Ind.*, **39**, 1962, p. 541.
- 27.7 Crawley, J., and Wills, G.: "Production Forging by High Energy Rate," in *Proceedings of the 7th Machine Tool Design and Research Conference* (Birmingham), London, Pergamon, 1966, p. 5.
- 27.8 Davies, R.: "Some Effects of Very High Speeds in Impact Extrusion," in *Proceedings of the 5th International Machine Tool Design and Research Conference* (Birmingham), London, Pergamon, 1964, p. 253.
- 27.9 Organ, A. J., and Mellor, P. B.: "The Preparation of Billets by Bar Cropping," *Iron and Steel*, **39**, 1966, pp. 481, 534.
- 27.10 Ratjen, R., and Takamatsu, M.: "High-Energy Forming Process: Hydropunch" (*in German*), *Werkstatt u. Betr.*, **104**, 1971, pp. 41–44.
- 27.11 Müller, H.: "Operations during Electrohydraulic and Electromagnetic Forming of Metallic Workpieces" (*in German*), *Berichte aus dem Institut für Umformtechnik, Universität Stuttgart*, no. 11, Essen, Girardet, 1969.
- 27.12 Cole, R. H.: *Underwater Explosions*, Princeton, N.J., Princeton University Press, 1948.
- 27.13 Duvall, G.: *Response of Metals to High Velocity Deformation*, New York, Interscience, 1960, pp. 165–200.
- 27.14 Müller, H.: "Electrohydraulic and Electromagnetic Forming Processes in Manufacturing Technology" (*in German*), *Ind.-Anz.*, **92**, 1970, pp. 844–848.
- 27.15 Rinehart, J. S., and Pearson, J.: *Explosive Working of Metals*, New York, Pergamon, 1963.
- 27.16 Hertel, H., Ruppin, D., and Rodenberg, G.: "High-Speed Forming Machines (Systems Hertel/Ruppin)" (*in German*), *Werkstattstechnik*, **59**, 1969, pp. 565–568.
- 27.17 Zeller, R.: "Results of Tests on the Precision Achieved in Duplication Using Electrohydraulic Forming" (*in German*), *Ind.-Anz.*, **94**, 1972, pp. 20–24.
- 27.18 Müller, H.: "Electrohydraulic and Electromagnetic Forming Processes in Manufacturing Technology" (*in German*), *Ind.-Anz.*, **92**, 1970, pp. 1100–1103.
- 27.19 Bauer, D.: "Expanding Cylindrical Workpieces by Rapidly Changing Magnetic Fields" (*in German*), Dr.-Ing thesis, Technische Universität, Hannover, 1967.
- 27.20 Dietz, H., Lippmann, H. J., and Schenk, H.: "Theory of Magnetic Forming Process" (*in German*), in "Movement of the Workpiece," *Elektrotech. Z. A*, **89**, 1968, pp. 273–278.
- 27.21 Ecker, W., and Müller-Axt, F.: "High Energy Rate Forming—Deformation of Sheet by Shock Waves" (*in German*), *Werkstatt u. Betr.*, **96**, 1963, pp. 163–177.



**FORMING UNDER  
HYDROSTATIC PRESSURE****List of Special Symbols**

---

$F_{\text{buck}}$	critical buckling load
$F_p$	punch load
$F_{\text{tot}}$	total load
$p_c$	counterpressure
$p_p$	punch pressure
$p_{\text{hydr}}$	hydraulic pressure
$p_{\text{hyd}}$	hydrostatic pressure
$\beta_{\max}$	maximum drawing ratio
$\varphi_{\text{fract}}$	strain at fracture
$\varphi_{\text{lim}}$	limit strain
$\varphi_{\text{rest}}$	remaining strain (formability)
$\varphi_{\text{tot}}$	total strain (formability)
$\sigma_m$	mean stress (hydrostatic pressure)

This chapter introduces some of the modern metal-forming processes known as high-pressure forming, in which hydrostatic pressure is applied. These processes are classified into two groups according to their different ways of pressure application:

- 1 Processes in which high-pressure media are used to replace rigid tools, for example, hydro-

## 28.2 METAL FORMING UNDER SPECIAL CONDITIONS

static (hot and cold) extrusion processes. In these processes the necessary hydraulic pressure is as high as the relative punch pressures of the process using rigid tools.

- 2 Processes in which a counter or transverse pressure is superimposed on the normal pressure on the workpiece with the aim of increasing the formability of the product material.

### 28.1 HYDROSTATIC EXTRUSION PROCESSES

These are hot and cold processes utilizing working media. They belong to the manufacturing processes in the category of compressive forming, subgroup pushing-through processes (see Chap. 2) [28.1]. They are bulk deformation processes.

The basic principle of such a process is that the extrusion force is applied mainly by a fluid pressure medium kept under high pressure, and not by a rigid punch as in the conventional processes (Fig. 28.1). This principle was already established in 1893 in a British patent [28.2]. Initially the required high hydraulic pressure—up to 3000 MPa (435 ksi)—precluded any technical exploitation of such an idea due to problems encountered in sealing. Only starting in 1950 modern developments in machine design and construction technology as well as a simultaneous increasing demand for processes to deform “nonconventional” light and heavy metals—especially in aviation and space technology and atomic-reactor construction—have triggered the search, and this process caught the attention of the scientific and technical communities [28.3] to [28.5]. Hydrostatic extrusion processes are only at the beginning of their development. Hence a difference between hot and cold processes is rarely made in practice. Also in the following such a difference is mentioned only when it is absolutely necessary; otherwise the technique is termed generally as extrusion process.

#### 28.1.1 Principles of Hydrostatic Extrusion

At present the very well tested and the most extensively applied hydrostatic extrusion process is the forward rod extrusion (Fig. 28.1). In addition to that, the forward tube-extrusion process is also used (see Fig. 28.18).

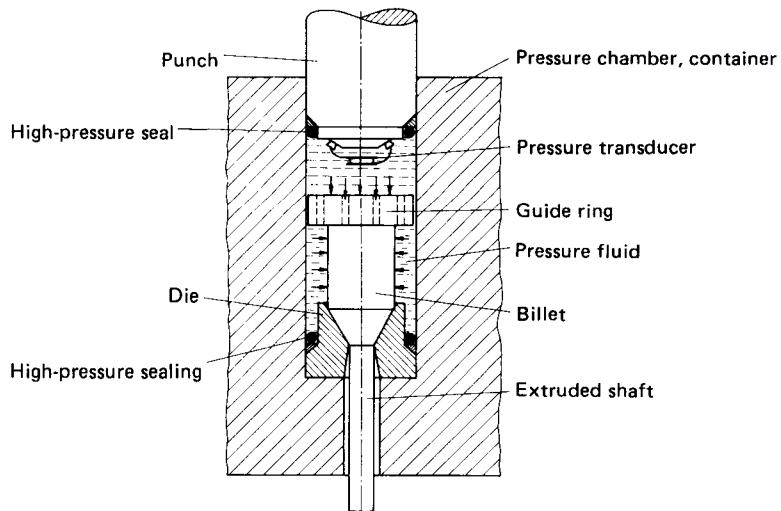
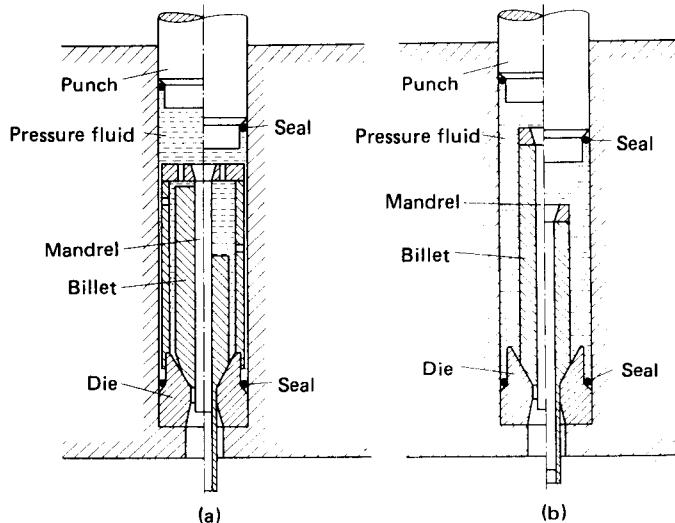


FIG. 28.1 Experimental apparatus for hydrostatic rod-extrusion process. (After [28.7].)



**FIG. 28.2** Hydrostatic tube extrusion (a) With stationary mandrel. (b) With jointly moving mandrel. (After [28.10].)

For hydrostatic tube extrusion either a fixed or a jointly moving mandrel is used, just as in the conventional processes [28.10], [28.26] to [28.28]. The mandrel is inserted into the bore of the hollow billet and thus seals it against eventual leakage due to high hydraulic pressure built up in the container, which also serves the purpose of a pressure chamber (Fig. 28.2). Good lubrication between mandrel and workpiece material is mandatory.

According to the principle of hydrostatic forward tube extrusion with jointly moving mandrel, cold weld platings and coated products (cables) can also be manufactured.

In augmented hydrostatic extrusion (see Sec. 28.1.6) hydraulic pressure in the chamber is superimposed with a mechanical pressure or tension which acts on either the undeformed workpiece or a particular undeformed section of the partly deformed workpiece. In this way better control of the extrusion operation is achieved and any eventual stick-slip phenomena can be suppressed (see Sec. 28.1.3).

To deform brittle and critically deformable materials, such as cast iron, molybdenum, magnesium, and beryllium, hydrostatic extrusion with counterpressure can be employed successfully (see Sec. 28.2.2). In such a case the counterpressure acts on the cross-sectional area of the rod as it extrudes from the die. Under this effect, the longitudinal stress at the die outlet is shifted more into the pressure region, and thus the hydrostatic pressure  $\sigma_m = (\sigma_1 + \sigma_2 + \sigma_3)/3$  is increased so that the formability of the workpiece material is also improved.

Hydrostatic extrusion is carried out mostly at room temperature, although hot extrusion may also be performed with the help of suitable pressure media [28.25], [28.29], [28.30].

Several modifications of individual processes have been developed in view of building up the hydraulic pressure independent of the direction of deformation [28.24]. Also, instead of feeding short billets, it is partly aimed at feeding long billets continuously or intermittently into the pressure chamber [28.31].

### 28.1.2 Process Description

Fig. 28.1 shows an experimental apparatus for hydraulic forward rod extrusion. The billet with tapered end is inserted into the die, touching neither the walls of the pressure chamber nor the

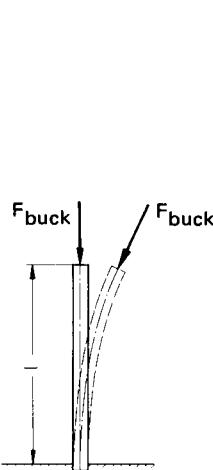


**FIG. 28.3** Buckling bar under the action of a follow-up force.

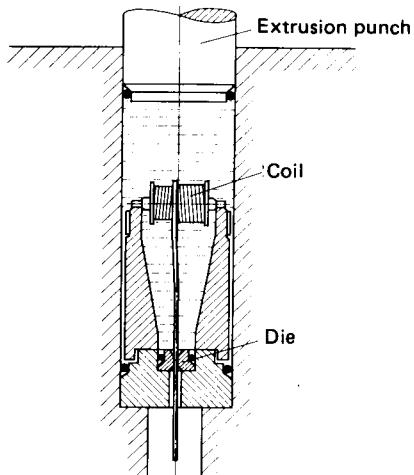


**FIG. 28.4** Hydrostatic wire extrusion. (After [28.16].)

extrusion punch. The guide ring at the upper end of the billet should prevent tilting of the billets, which may happen in particular in the case of large die-opening angles. High-pressure seals between die and pressure chamber at the height of the die neck permit utilizing the hydraulic pressure to support the die. This arrangement helps avoid the need for costly prestressing of the die and permits even the use of thin-walled dies.

The operational sequence in hydrostatic extrusion is as follows:

- 1 Put billet in container (pressure chamber)
- 2 Fill up with pressure medium
- 3 Raise pressure and apply it to billet
- 4 Extrude workpiece
- 5 Remove extruded product and remaining material from die [28.32]

The billet must be tapered in order to match the die-opening angle exactly. Otherwise sealing of the pressure chamber against the hydraulic pressure cannot be achieved. Except for this matching, the billet shape and the chamber geometry are to a great extent independent from each other. The billet diameter can be smaller than the chamber diameter, and yet there is no danger of the workpiece being compressed or buckled in the chamber while the billet is extruded through the die opening (Beck's stability problem<sup>\*</sup>).

\*Comparing with Euler's buckling, Beck's stability problem involves the phenomenon of "buckling with a follow-up force;" that is, the direction of the force always follows the deviation of the rod axis, and the force acts always in the direction of the momentary rod axis (Fig. 28.3). For this kind of buckling, according to the method of energy derivation, there exists a critical load

$$F_{\text{buck}} \approx 20.05 \frac{EJ}{l^2}$$

where  $E$  is the modulus of elasticity,  $J$  the polar moment of inertia, and  $l$  the rod length. However, in case I of Euler's buckling the critical load is given by the relation [28.33]

$$F_{\text{buck}} = \frac{\pi^2}{4} \frac{EJ}{l^2}$$

Thus a rod under normal pressure with a following force can be subjected to a load eight times the buckling load of a corresponding rod having constant direction of action before it buckles.

It is not necessary that the billet be straight or cylindrical, and it need not have a constant cross-sectional area along its entire length. Thus, for example, spirally bent billets [28.6] or even a coiled wire (Fig. 28.4) [28.13], [28.14] or multisteped workpiece (see Fig. 28.12) can be extruded. Since there is no friction in the billet chamber, the billet length is dependent only on the dimensions of the pressure chamber. Thus in hydrostatic wire extrusion a wire coil placed in the pressure chamber can be extruded up to a ratio of raw-wire length to raw-wire diameter on the order of  $10^5$ .

Once the billet has been placed in the container, the pressure medium is added. The fluids chosen as pressure media (e.g., water, oils) also serve simultaneously as lubricants for gliding surfaces between workpiece and die. Such fluids may also be enriched with lubricating additives. In certain cases the billets themselves are covered with a coating layer of lubricant (fat) [28.16]. Paraffin-type solid materials [28.34] or easily deformable metals (soft metals) may be used as pressure media in special cases [28.6], [28.16], [28.35], [28.36].

The pressure rise in the medium and the extrusion operation are largely independent of one another. Usually the pressure is applied by means of a punch entering into the pressure chamber (Fig. 28.1). But pressure can also be built up in a pressure chamber separated from the billet chamber (container) or by means of a high-pressure pump [28.24]. The latter possibility is cheaper but limited to lower pressures only [ $< 1500$  MPa (213 ksi)], especially if no hydraulic pressure amplifier is used as an aid.

Near the end of the hydrostatic extrusion operation, as a result of the stick-slip phenomena, there exists the danger of the extrusion of the entire billet happening too early and with unexpected speed. Here the workpiece and the pressure medium escape suddenly from the die and at that instant possess great kinetic energy. Steps should be undertaken to forestall such accidents (mechanical braking of the punch or piston motion; see Sec. 28.1.6).

### 28.1.3 Material Flow and Extrusion Pressure

#### *Material Flow*

Phenomena of unsteady start, as observed in conventional forward rod extrusion as well as in tube extrusion during filling of the die cavity (see Chap. 15), do not occur in hydrostatic extrusion, the main reason being that only billets with tapered ends are used, which properly match die-opening angle.

As a rule, small die-opening angles ( $2\alpha = 45^\circ$ ) are used in the hydrostatic extrusion process. Yet due to favorable friction conditions in the die cavity, frictional losses are low. At small die-opening angles even the shear losses remain low, and the material flow approaches the ideal conditions of deformation, whereby it is assumed that the plane layers of material entering into the die opening remain plane during their passage through the die and get only radially compressed (Fig. 28.5).

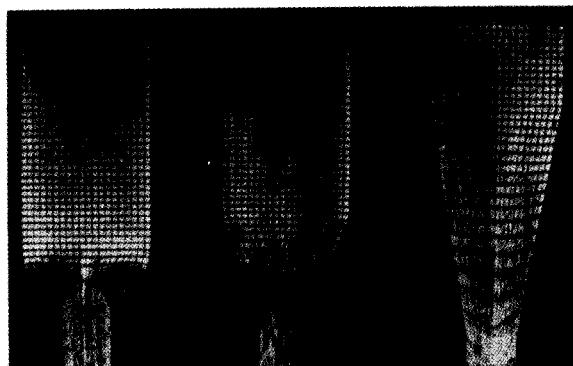


**FIG. 28.5** Distortion of a grid by hydrostatic cold rod extrusion of aluminum (99.5% purity). Die-opening angle  $2\alpha = 20^\circ, 45^\circ$ , and  $90^\circ$ . (After [28.7].)

According to visioplastic tests (see Chap. 7), uniform deformation occurs at an optimum die-opening angle [28.10], [28.37]. If the die-opening angle differs from this optimum value, the material flow becomes inhomogeneous. In the case of smaller angles this happens due to higher frictional losses, whereas with larger die-opening angles it is due to greater shear losses (redundant work). These conditions are valid for all extrusion processes, that is, also for conventional cold extrusion [28.37], [28.38], the only difference being that, compared with hydrostatic extrusion, in the conventional process far greater frictional losses occur because usually larger die-opening angles are used in the process.

### ***Required Extrusion Pressure***

The required pressure (continuous pressure) in hydrostatic forward rod extrusion is up to 40% lower than its conventional counterpart because of smaller frictional and shear losses. The pressure in conventional forward rod extrusion carried out with rigid tools is the relative deformation force [28.20].

For extruding noncylindrical profiles somewhat higher pressures are necessary than for round cross-sectional areas. The pressure magnitude is also dependent on the absolute dimensions of the billet and of the workpiece—for the same strain a smaller cross section requires somewhat higher pressure than a larger cross section [28.39].

Since the frictional losses in hydrostatic extrusion are usually smaller, the pressure medium and the lubricating materials ( $\text{MoS}_2$ ,  $\text{PbO}$ , graphite, etc.) mostly mixed with it have no significant effect on the magnitude of the extrusion pressure. But this situation changes if, during the extrusion operation, the lubricating film fails in its function, and as a result instantaneous pressure peaks or stick-slip phenomena occur. Then in exceptional cases the pressure may increase up to 2–4 times the pressure under undisturbed lubricating conditions [28.23], [28.40]. Usually it hardly matters which lubricants are used as long as they are compatible with the fluid used as pressure medium [28.41].

### ***Instantaneous Pressure Peaks and Stick-Slip Phenomena***

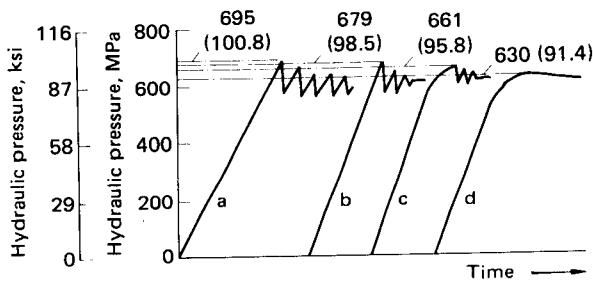
Hydrostatic forward rod extrusion is a quasi-stationary deformation process, yet the pressure-displacement as well as the pressure-time behavior frequently show two peculiarities: an instantaneous pressure peak at the beginning of the extrusion operation and subsequently the stick-slip phenomena during the extrusion operation (Fig. 28.6).

The pressure peak is the result of a changeover from static friction to dynamic friction on the punch shoulder. According to the nature of the phenomenon, the tendency to build pressure peaks is dependent on the friction conditions. It increases with strain, with the hardness of the workpiece material, and with the die-opening angle. When the friction conditions are improved, for example, either by applying in addition a coating layer of fat on the billet, by adding lubricant to the pressure medium, or preferably by using sand-blasted billets instead of polished billets having smooth surfaces [28.16] (the sand-blasted billet surfaces can store a certain amount of oil in their rough structures), the pressure peaks can be reduced and in some cases even totally eliminated. Moreover the viscosity of the pressure media can also influence the occurrence and formation of pressure peaks [28.42].

The pressure-time behavior shown in Fig. 28.6 is caused by a stick-slip phenomenon which is initiated mainly by a local break in the lubricating film of the fluid. As a result the workpiece material gets cold-welded at some contact places with the die material, thus blocking the workpiece movement. The motion is restarted when the hydraulic pressure is raised again so high that the workpiece material at cold-welded bridges is sheared off. Since by now the dynamic friction conditions prevail in the die, though only for a short duration, further extrusion needs only a lower extrusion pressure. Such irregularities in pressure and extrusion speed can repeat themselves many times during the extrusion operation [28.10].

The stick-slip motion can be initiated by pressure variations in the hydraulic system, where these variations are started by a sudden pressure reduction at the beginning of the extrusion operation.

Thus stick-slip phenomena are usually in causal relationship with unsteady friction conditions. Therefore these phenomena are frequently encountered in those operations which involve high loads on the lubricating film in the die: in extruding high-strength materials, at high strains, and



Curve	Oil volume	Billet pretreatment
a	329 cm <sup>3</sup> (20.08 in <sup>3</sup> )	—
b	115 cm <sup>3</sup> ( 7.02 in <sup>3</sup> )	—
c	115 cm <sup>3</sup> ( 7.02 in <sup>3</sup> )	Sandblasted
d	115 cm <sup>3</sup> ( 7.02 in <sup>3</sup> )	Sandblasted, rounded edges

**FIG. 28.6** Influence of fluid volume, billet surface area, and shape of billet front surface area on the occurrence of stick-slip phenomena. Workpiece material—aluminum alloy HE30 (AA 6061-O);  $A_0/A_1 = 4$ ;  $2\alpha = 45^\circ$ ; pressure fluid—mixture of glycerin and glycol; lubricant—MoS<sub>2</sub> in graphite paste. (After [28.17].)

for large die-opening angles [28.7], [28.10], [28.42]. The pressure medium, its viscosity, as well as its quantity together with added lubricants can influence the tendency of stick-slip movements [28.6], [28.17], [28.23], [28.40], [28.41], [28.43].

Initial pressure peaks and stick-slip amplitudes become smaller if billets are tapered to an angle 1–2° smaller than the die-opening angle [28.10]. Also with increasing extrusion speed the tendency to pressure peaks and stick-slip phenomena is reduced [28.10], [28.18], [28.29], [28.41].

### Optimum Die-Opening Angle

According to elementary plasticity theory, in forward rod extrusion the necessary deforming force or the corresponding hydraulic pressure consists of three parts: the force needed for ideal deformation, the shearing force, and the friction (Fig. 28.7). While the ideal deformation force is independent of the die-opening angle, the shear loss increases with reduced die-opening angles due to an enlarged friction surface. Thus as a rule there exists a die-opening angle for which the hydraulic pressure necessary for the deformation is reduced to a minimum value (see Chap. 18).

The magnitude of the optimum die-opening angle is dependent on the deformation conditions, where larger optimum die-opening angles are generally observed to be accompanied by increasing deformation forces or pressure. Here it hardly makes a difference whether, for example, a harder workpiece material (Fig. 28.8a) or a higher strain (Fig. 28.8b) is responsible [28.5], [28.10]. The decisive factor is that with increasing normal stress on die surfaces the load on the lubricant film increases and the frictional losses increase also. The optimum die-opening angle also changes if the friction conditions are changed by choosing other media and lubricants.

### Possibilities of a Computed Derivation of the Extrusion Pressure

For a rough calculation of the required extrusion pressure it is advisable to use a simple empirical equation. For an interrelation between hydraulic pressure (continuous pressure)  $p$  and strain  $\varphi =$

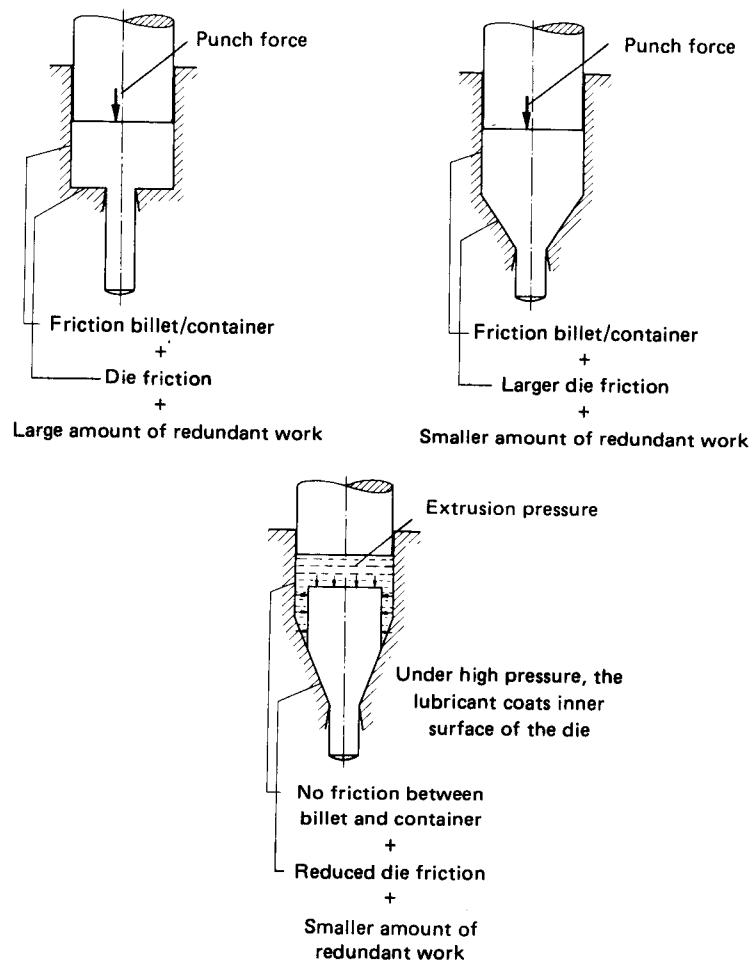


**FIG. 28.7** Schematic presentation of conventional and hydrostatic rod extrusion.  
(After [28.7].)

$\ln(A_0/A_1)$  in hydrostatic forward rod extrusion there exists a relation according to Pugh [28.10], [28.16]:

$$p = \varphi(5.79H + 61.7) \text{ [MPa]} \quad (28.1)$$

where  $p$  = extrusion pressure (continuous pressure)

$H$  = initial billet hardness (Vickers hardness)

$\varphi$  = strain =  $\ln(A_0/A_1)$

$A_0$  = billet cross-sectional area

$A_1$  = workpiece cross-sectional area after deformation

In Fig. 28.9 experimentally found values of the ratio  $p/\varphi$  are plotted for a number of materials against billet hardness  $H$ . There is good agreement between measured values and results calcu-

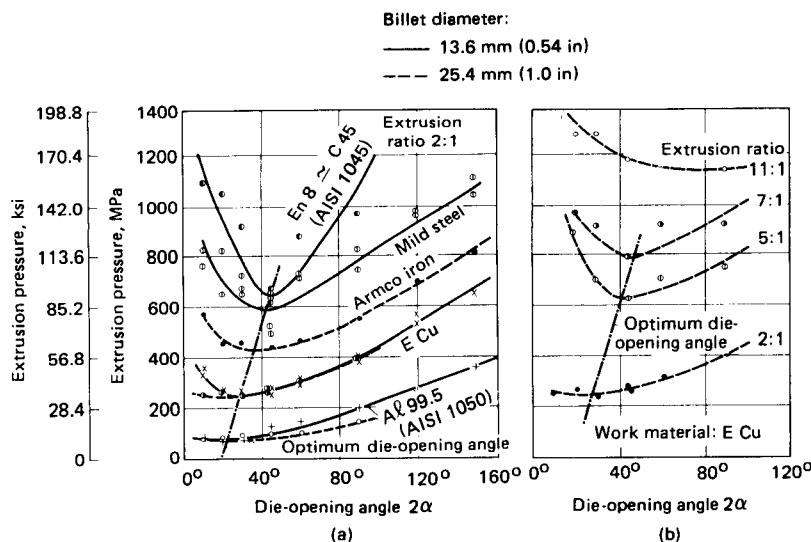


**FIG. 28.8** Dependence of extrusion pressure on die-opening angle  $2\alpha$  and (a) workpiece material and (b) extrusion ratio  $A_0/A_1$ . Billet length—50.8 mm (2.0 in) plus billet tip; pressure fluid—mineral oil SAE 30 with a 10% MoS<sub>2</sub> dispersion; lubricant mix—graphogen fat. (After [28.10].)

lated with Eq. 28.1a or 28.1b, so that the necessary extrusion pressure can be estimated to an accuracy of  $\pm 25\%$ .

The calculated pressure is lower than the pressure peak at the beginning of the extrusion operation, which is decisive in loading of the pressure chamber and the extrusion press. Thus if needed, corrections must be made similar to those given for conventional extrusion operations (see Chap. 15). As a rule even for extrusion pressures calculated by any other method only limited accuracy can be achieved.

In the following only a short survey is given of other possible calculating methods because, as described in Chaps. 13 to 16, the methods mentioned for pushing-through and drawing processes can similarly be applied here (see Chaps. 2 and 13).

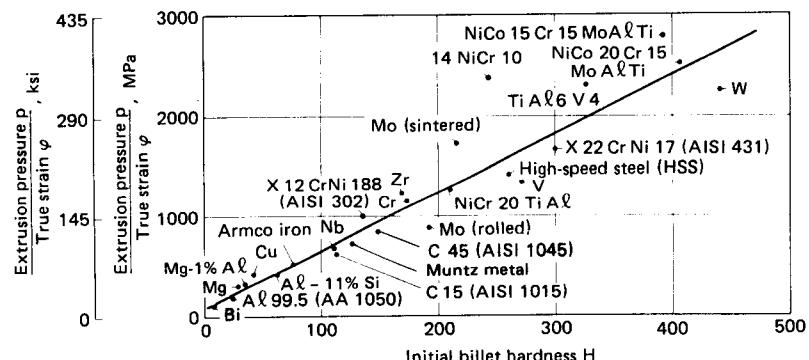


**FIG. 28.9** Correlation between extrusion pressure  $p$ , limit strain  $\varphi$ , and initial billet hardness  $H$  for different work materials. (After [28.10], [28.16].)

The calculation according to elementary plasticity theory is carried out as for conventional extrusion (see Chap. 13). Initial parameters are workpiece dimensions, strain, workpiece geometry, die-opening angle  $2\alpha$ , and coefficient of friction  $\mu$ , whereby it should be noted that for hydrostatic extrusion small die-opening angles are usually chosen since no friction occurs in the pressure chamber, and the frictional losses in the die are as a rule very low. (If they do occur, the coefficient of friction is lower than 0.05.) Detailed calculating steps of such methods are outlined in Chaps. 15 and 16.

A better approximation of the calculated values is obtained by means of limiting methods and especially by the upper-bound method (see Chap. 5). The upper-bound method for axially symmetric pushing-through and drawing operations is described in [28.44] to [28.48]. Pugh [28.19] and Avitzur [28.49] give interesting solutions, especially for hydrostatic forward rod extrusion. The initial derivation step of Avitzur was further developed in [28.50] under special consideration of hydrodynamic friction conditions.

Advanced methods were devised in recent years with the help of the mathematical plasticity theory and constructed on the basis of viscoplasticity. These methods for deriving local stress and strain distributions (see Chap. 5) are applied to calculate the temporal and local temperature distribution in hydrostatic extrusion. The buildup of the deformation zone, the pressure-displacement behavior, and the stress and strain distributions are derived in [28.51] according to the method of finite elements.

These methods involve extensive calculating operations. Since they are very complicated and time-consuming, they are unsuitable for application for individual special cases.

#### 28.1.4 Applications

##### *Work Materials and Achieved Strains*

Whether the hydrostatic process or the conventional process, that is, with rigid tools, has to be applied depends less on the material than on the shape and dimensions of the extruded workpiece. Basically in both cases the same workpiece materials can be deformed. (Further details on workpiece materials are given in Chaps. 15 and 16.) In special cases, such as for high-strength work materials, hydrostatic extrusion can be advantageous. Here in general a more uniform deformation can be achieved, and no excessive shear occurs in the boundary zones, as observed in particular in conventional extrusion with large die-opening angles, which may lead to tangential surface cracks.

In certain cases very large changes in cross-sectional areas can be achieved with pressures of 1500–2000 MPa (213–284 ksi) commonly applied in the hydrostatic process. As Fig. 28.10a shows, with a pressure of only 1600 MPa (227 ksi) at room temperature, the following ratios of cross-sectional areas (extrusion ratios) could be achieved:  $A_0/A_1 \approx 15,000$  for pure aluminum (99.5% purity),  $A_0/A_1 = 80$  for copper (99.9% purity), and  $A_0/A_1 = 3.5$  for high-speed forming steel [28.52] to [28.54]. For molybdenum, tungsten, and high-temperature nickel alloys the corresponding values lie between 3 and 5 [28.10]. Higher pressures and temperatures (Fig. 28.10b) allow even greater reductions in cross-sectional areas.

The achievable strain values depend on the yield stress of extruded workpiece material and on its formability. It should be kept in mind, however, that with extrusion ratios  $A_0/A_1$  of 15,000:1, achieved in wire extrusion of aluminum (99.5% purity), the winding of the wire coming out of the die at very high speed presents great difficulty. Thus higher temperatures and pressures are meaningful only if for high-strength work materials greater changes in cross-sectional areas must be achieved.

##### *Feasible Workpiece Shapes for Extrusion*

In industry the rod-extrusion process offers the following technical possibilities. The production of wire at very high speed with a very large extrusion ratio can be achieved in a single deformation step, such as in multiple-wire extrusion presses (Fig. 28.11) [28.10], [28.55]. Furthermore for wires of high-strength work materials at corresponding small extrusion ratios the hydrostatic process opens new vistas of industrial production (extruding instead of drawing).

The production of very thin-walled tubes out of 99.5% pure aluminum, with a wall thickness  $s = 0.15$  mm (0.006 in) and an outer diameter  $d_o = 10$  mm (0.4 in) [28.53], can be achieved by

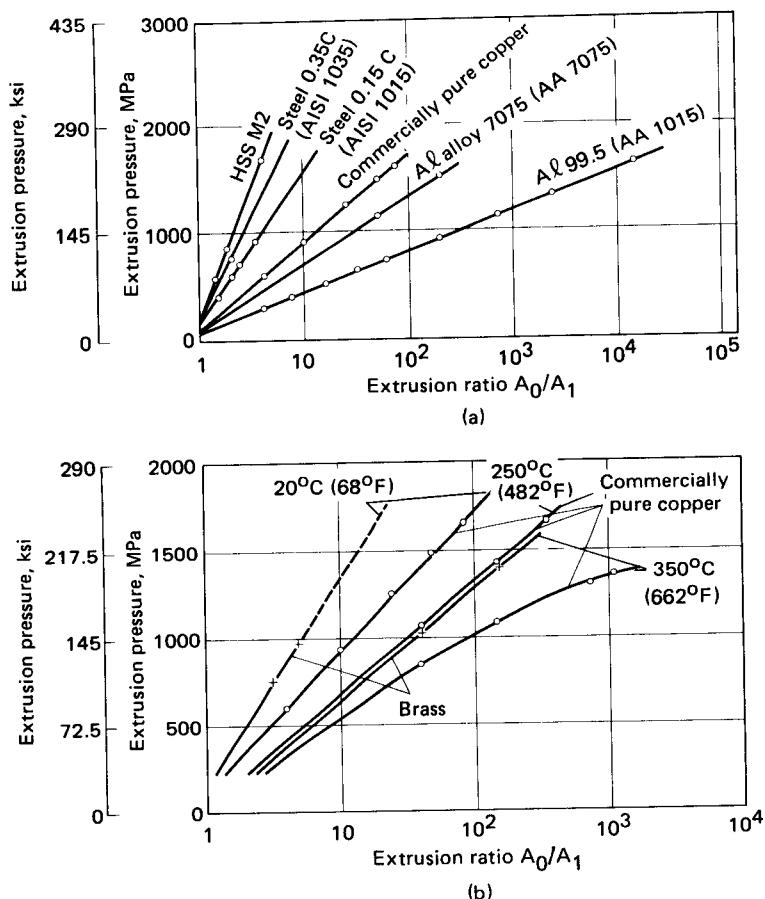


**FIG. 28.10** Dependence of extrusion pressure on (a) extrusion ratio  $A_0/A_1$  and (b) billet temperature for different work materials. (After [28.54].)

hydrostatic extrusion. On the other hand very thick-walled tubes, with  $s = 0.9$  mm (0.035 in) at  $d_o = 2$  mm (0.08 in), can also be manufactured. Hence the process will attain significant importance in the future.

In addition to wires and tubes, special profiles having greater section lengths can also be produced by the hydrostatic process (Fig. 28.12), but cannot be manufactured with any other process. When steel is extruded with the hydrostatic process, many operational steps can be saved in certain cases without disadvantage, steps that would be indispensable with the technology commonly employed today, that is, hot extrusion followed by multistep cold drawing of the workpiece.

Since the billet shape and the workpiece geometry are almost independent of one another, the immediately following shaft section can be extruded with a section differing greatly from the beginning section of the extruded workpiece. The shaft can have any desired cross-sectional area and contour (Fig. 28.12). Due to the absence of friction in the container, it is also possible to use very long billets and extrude them at low hydraulic pressures. As occasionally mentioned in the references, extruding shafts in two directions and in two extrusion operations for the same workpiece can also be performed with conventional cold extrusion using rigid tools provided that the punch has a corresponding shape.

### *Workpiece Properties after Hydrostatic Extrusion*

As a result of almost homogeneous deformation, the hydrostatically extruded products possess almost constant values of their mechanical and metallurgical properties over their entire cross sections [28.10], [28.16]. Such constancy of properties is especially desired when in its practical service life the product is put under dynamic loading.

As was shown with the help of microhardness measurements on hydrostatically and conventionally extruded products [28.37], similarly constant material properties can also be obtained by

extruding with rigid tools when the same small die-opening angles are used as in the hydrostatic process and when the extrusion is carried out in accordance with other deformation parameters, such as strain and friction (Fig. 28.13). The validity of such findings is corroborated by other investigators [28.24], [28.56].

In hydrostatic extrusion, as in any operation of cold bulk deformation, the material is first reinforced; that is, its strength values are raised with a simultaneous reduction in ductility. However, at large strains and high deformation speeds, the temperatures are in certain cases raised so high that softening phenomena (recovery, recrystallization—see Chap. 3) occur, and they can get superimposed on the reinforcement process of the material.

In hydrostatic extrusion the dimensional accuracy of the extruded product is achieved in the tolerance range of IT 8-9 [28.52], [28.54]. Because of the favorable friction conditions that prevail in the extrusion die, products have no surface defects caused by local cold welding between workpiece surface and die surface. Hence the surfaces of these products can be directly employed for functional purposes. In the hydrostatic extrusion of tubes the inner surfaces of these tubes are in general not as good as the outer ones. This may be explained by the fact that the lubricating con-

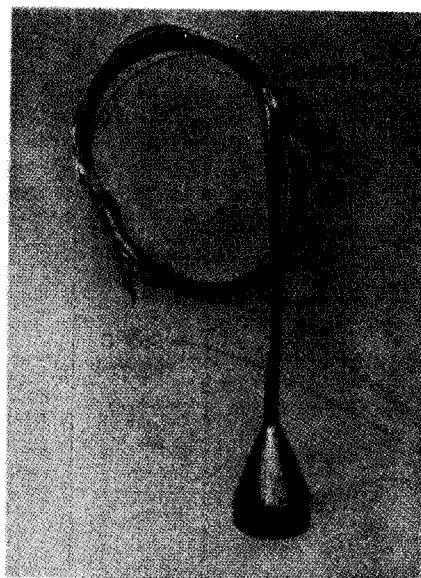


**FIG. 28.11** Multiple-wire extrusion of aluminum wires for cable. (Courtesy of ASEA.)

ditions between mandrel and workpiece are not as good as those between the die and the outer surface of the workpiece (tube).

#### **28.1.5 Equipment**

##### *Dies*

As in the conventional processes, the tool assembly of the new processes consists of billet chamber (container), die, and punch. Depending on where the pressure builds up, the punch can either be arranged to function in a pressure chamber separated from the actual tool assembly (Fig. 28.14) or it can be fitted in a hydraulic pressure amplifier. At comparable deformations the hydrostatic pressure in forward rod extrusion is up to 40% lower than the inner pressure built up in the pressure chamber of a press with rigid tools. Thus the same tool materials can be used in both conventional and hydrostatic rod extrusion (see Chaps. 15 and 16). A special problem, which does not arise in the conventional process, is that of sealing against high hydraulic pressures.

Nowadays an industrial hydrostatic extrusion press is expected to build up pressures of 1500–2000 MPa (213–284 ksi). Further development of such machines leads to still higher hydraulic pressures. Considering the available tools and the present state of the art of the sealing technology, pressures beyond 3000 MPa (435 ksi) cannot be applied economically.

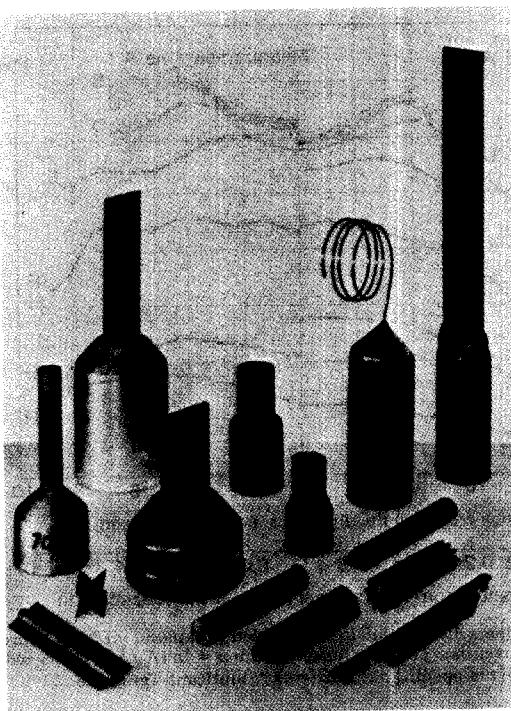


**FIG. 28.12** Workpieces manufactured by hydrostatic extrusion. (Courtesy of ASEA.)

Developments in the design of pressure vessels have led toward permitting load cycles of very high magnitudes ( $>10^6$ – $10^7$ ). Here reinforcing layers are combined, whereby each layer may be made of rings of different materials, and is shrunk on the layer previously shrunk on the outer surface of the vessel wall. Such coatings may consist of as many as seven different layers. This arrangement is, however, challenged by another structure which consists of pressure vessels reinforced with outer layers of sheet strip or wire coils (Fig. 28.15) [28.39]. These pressure chambers consist of an inner cylinder made of high alloyed steel. Around the outer surface of this cylinder wall a very strong steel wire having a rectangular cross section is wound under high tension. If needed, two or more thin-walled cylindrical sheaths are shrink-fitted within the cylindrical pressure vessel. In view of the strict safety requirements, these pressure vessels offer the certainty that any cracks will be prevented from running through the wire layers thanks to the layered structure of the reinforcement coating.

Detailed guidelines for the calculation of the parameters of such wire-wound high-pressure vessels are given in [28.57]. Other possible methods to calculate multiple-armored pressure vessels are outlined in [28.58] to [28.63].

Since the high hydraulic pressures can also be used to support the die in the container, costly prestressing of the die is no longer necessary. Thin-walled dies can also be used here. In most cases a die-opening angle  $2\alpha = 45^\circ$  is chosen. This value is not much different from the optimum die-opening angles (see Sec. 28.1.2), and costs for tapering the billets are kept within tolerable limits. The dies can be replaced easily after every extrusion operation because they are not rigidly fitted in the container but merely set in the chamber. Suitable die materials are chromium-alloyed steels, high-speed steels, or even cemented carbides [28.64].

For a long time the most difficult problem was sealing off against high hydraulic pressures.

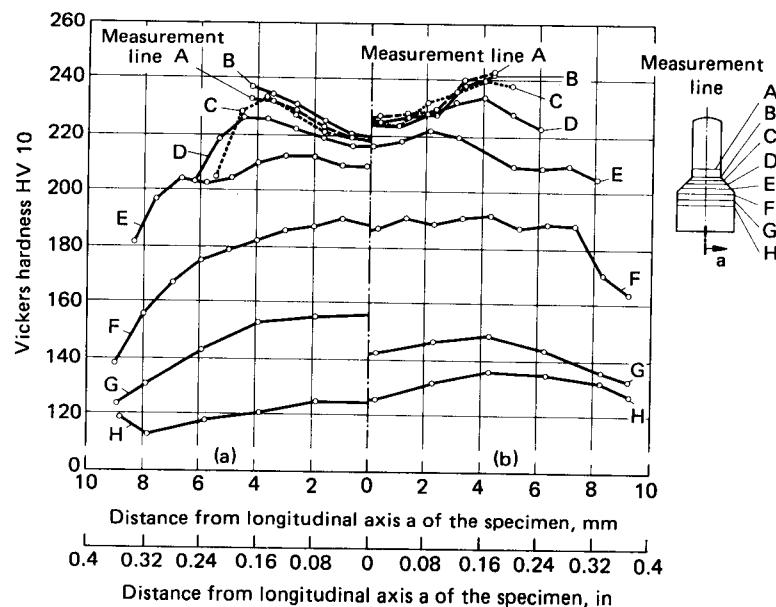


**FIG. 28.13** Hardness distribution in an extruded workpiece. (a) After hydrostatic extrusion. (b) After conventional cold extrusion. Strain  $\varphi = \ln(A_0/A_1) = 1.39$ ; work material—Ck15 (AISI 1015); die-opening angle  $2\alpha = 90^\circ$ ; lubricant—graphite.

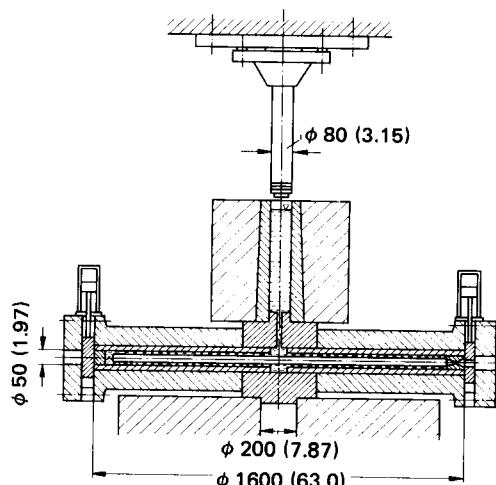


**FIG. 28.14** Tool assembly for hydrostatic rod extrusion with a separate chamber to build up hydraulic pressure. Dimensions are in mm (in). (According to Krhánek.)

However, at present pressures of up to 3000 MPa (426 ksi) can be controlled safely by using O-rings which function as stationary or movable seals [28.10], [28.63], [28.65]. Successfully employed sealing materials are polytetrafluoroethylene (PTFE) and synthetic rubber.

### Machines

The machines developed for industrial production are designed for the rod-extrusion process only. These machines were constructed partly in the laboratory (e.g., National Engineering Laboratory, East Kilbride, Scotland) and partly in the industrial sector [28.64]. From the start preference was given to machines carrying out fully automatic operations. Extrusion presses are now available which operate in either the horizontal or the vertical direction.

Fig. 28.16 shows a horizontal hydrostatic extrusion press with extrusion forces of 12–63 MN (1350–7087.5 ton) on which blocks of up to 1200-mm (47.24-in) length and up to 300-mm (12-in) diameter can be extruded. The frame and the pressure chamber are reinforced with wire layers. In its operational sequence this 63-MN (7087.5-ton) machine hardly differs from the equipment used commonly for conventional hot rod extrusion (see Chap. 16). The following additional operations are provided in the extrusion cycle: insertion of the billet into the die cavity, centering the billet in the pressure chamber, which is then shifted above the die, and refilling the hydraulic fluid which serves as the pressure medium. Fig. 28.17 illustrates the sequence of an extrusion cycle. The production capacity of such a press lies within the range of commonly used conventional hot-extrusion presses.

#### 28.1.6 Augmented Hydrostatic Extrusion

In the hydrostatic extrusion process, difficulties are still encountered in controlling, with sufficient accuracy, the material flow through the die with changing friction conditions (intermittent operation, stick-slip phenomena—see Sec. 28.1.3). This precludes extensive industrial application of this process and has led to a search for solutions to this problem. Two possible solutions have been

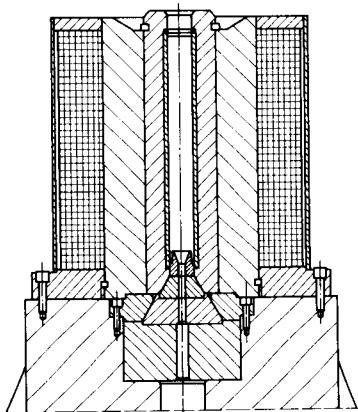


**FIG. 28.15** Assembly of tools for hydrostatic extrusion using a wire-wound pressure vessel. (Courtesy of ASEA; after [28.52].)

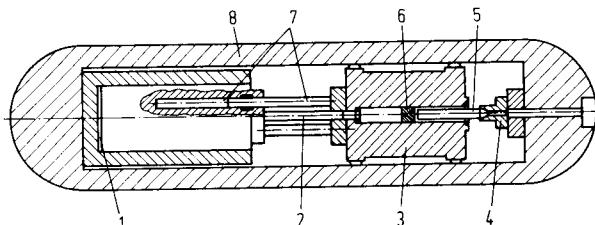


**FIG. 28.16** Basic construction scheme for horizontal hydraulic extrusion press of 12–63-MN (1350–7087.5-ton) extrusion force. 1—main cylinder; 2—piston; 3—container (pressure chamber); 4—die; 5—billet; 6—guide ring; 7—expanding and damping system; 8—framing of extrusion press (wire-wound construction). (Courtesy of ASEA.)

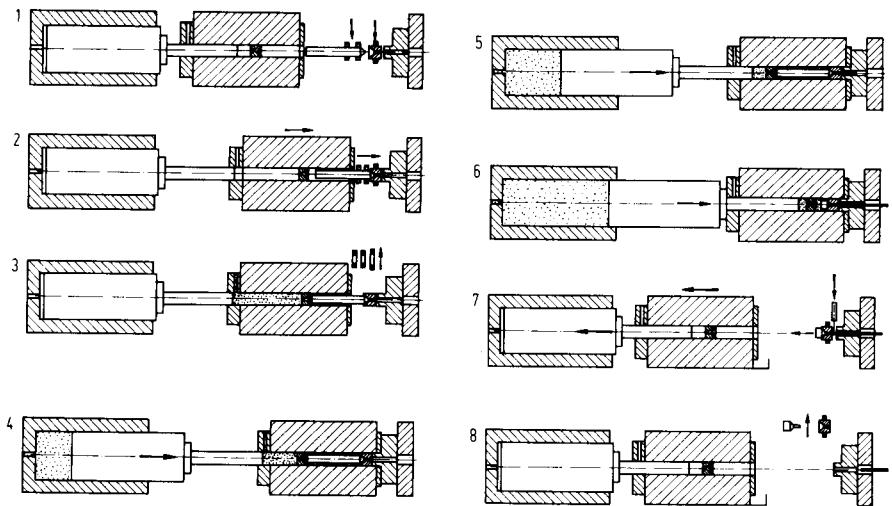


**FIG. 28.17** Schematic representation of the sequence of operation in hydrostatic extrusion process executed on a horizontal hydraulic extrusion press. 1—Insertion of die and billet. 2—Die and billet are kept in position for extrusion and container is brought into position to fill its cavity with pressure fluid. 3—Filling of pressure fluid; billet holder and die holder recede. 4—Container is slid onto die with increasing punch pressure; pressure fluid flows through a valve positioned in guide ring and surrounds the billet. 5—Punch seals pressure chamber and extrusion begins. 6—Workpiece is extruded. 7—Punch and container recede to their initial positions. 8—Residual work material is discarded and die is brought back to its initial position. Individual parts of mechanism are indicated as shown in Fig. 28.16. (Courtesy of ASEA.)

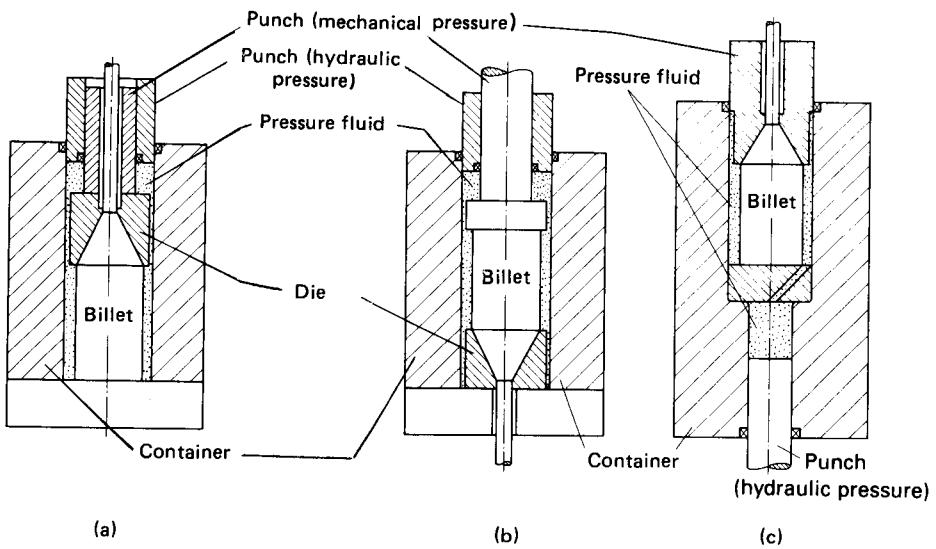


**FIG. 28.18** Augmented extrusion with additional mechanical pressure. (a) Hydrostatic backward rod extrusion. (b) Hydrostatic forward rod extrusion. (c) Extrusion with hydraulic container. (After [28.26].)

investigated: using viscous damping materials and combining the process with conventional cold extrusion or with wire or bar drawing [28.10], [28.16], [28.26]. The dampers function according to the principle of hydraulic braking. The pressure medium surrounding the billet is arranged to flow through the braking channels with narrow cross sections. These channels may be so adjusted that sudden changes in the extrusion speed of the workpiece, as occur due to stick-slip phenomena, are prevented.

In such process combinations (Fig. 28.18) the hydraulic pressure in the pressure chamber is purposely kept lower than it would be necessary to extrude the billet material through the die. As a compensation, mechanical pressure or tension is ultimately superimposed on the workpiece.

If part of the deformation force is exercised by means of a rigid punch and the remaining part is imparted by the pressure medium, then the total force, as shown in Fig. 28.19, has the components

$$F_{\text{tot}} = F_p + p_{\text{hydr}}A \quad (28.2)$$

where  $A$  is the cross-sectional area of the annular ring. If on the rigid punch, which imparts the mechanical pressure, a hydraulic pressure is also superimposed, to a certain extent, then the corresponding surface area should be given a negative sign in Eq. 28.2 (Fig. 28.18b).

In the limiting situation, where  $A = 0$ , the process becomes a conventional cold or hot extrusion with hydraulic container (Fig. 28.18c).

The difference between mechanically imparted pressure and hydraulic pressure should not be very large in order to prevent plastic deformation or buckling of the billet in the pressure chamber. On the other hand mechanical pressure must be high enough (generally 10–20% higher than the required mechanical pressure) so that the punch is constantly in touch with the back of the billet, which allows full control of the advancing speed of the billet and hence of the extrusion speed of the work material. This also means that the process is less suitable to deform soft work materials at higher strain or to extrude long billets.

### 28.1.7 Thick-Film Hydrostatic Extrusion

A special development toward process combination is thick-film hydrostatic extrusion, or hydrofilm extrusion (Fig. 28.20). The concentric narrow gap between the billet and the cylindrical wall of the pressure chamber has a width not greater than 0.25 mm (0.01 in). This gap is filled with the pressure medium [28.66], [28.67], which consists of wax-type or paraffin-type materials, fats, or liquids. The billet can also be coated with a lubricant film by immersing it into a liquid bath. The thick-film technique eliminates the operational step of filling the medium into the pressure chamber. Thus shorter operating periods, similar to those in the conventional automated cold impact extrusion process, can be achieved, such as 40 strokes/min for shorter workpieces. Because of these advantages the process is especially attractive for cold extrusion. In the process combination of hydrostatic extrusion with wire or bar drawing (hydrostatic extrusion drawing, or Hydraw process), reduced hydraulic pressures are applied in the pressure chamber. The required additional force is superimposed by mechanical tension acting on the extruded bar or wire. The tension  $\sigma_z$  and the hydraulic pressure  $p_{\text{hydr}}$  are added together to give the total stress necessary for the required deformation:

$$p_{\text{tot}} = p_{\text{hydr}} + \sigma_z \quad (28.3)$$

The material flow is fully controlled. The process is also applicable for the drawing of tubes and the coating of wires [28.10].

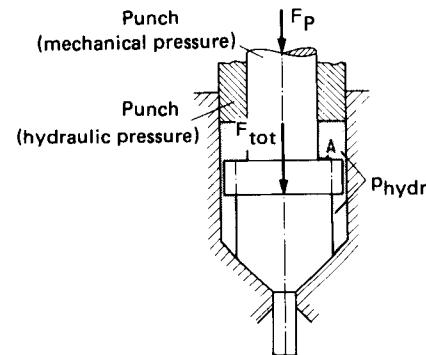


**FIG. 28.19** Balance of forces in augmented hydrostatic extrusion.

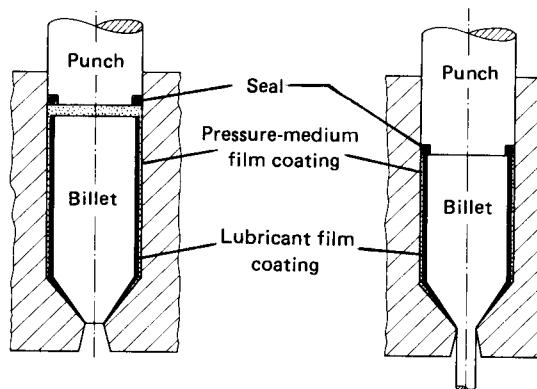


**FIG. 28.20** Thick-film hydrostatic extrusion. (After [28.66], [28.67].)

## 28.2 DEFORMATION WITH SUPERIMPOSED HYDROSTATIC COMPRESSIVE STRESSES

The deformability of metallic work materials (see Chap. 5) is dependent on the material characteristics and the deformation conditions. Besides the temperature level and the deformation speed, the stress condition is another decisive factor in determining the formability (Fig. 5.11). It is mainly a question of the deformation conditions, whether the material behaves as a ductile or as a brittle substance. After all, there exists neither a completely brittle nor a totally ductile material, but only corresponding material states. This knowledge has been increasingly applied in the production processes of metal-forming technology.

### 28.2.1 Effect of Stress State on Formability

All the deformation processes, although they may differ from each other in many respects, differ basically with respect to the stress state. In none of the processes is the stress state completely homogeneous, and so different stress magnitudes and stress-state distributions are observed at different points in the deformation zone. Thus in the initial stage the formability is fully achieved at those points where the most unfavorable stress states exist [28.68]. The parameter for measuring the magnitude of formability is the achievable strain at fracture  $\varphi_{\text{fract}}$ . If, for example, the following interrelationship, valid for a particular stress state, is obtained from the experimental tests:

$$\varphi_{\text{fract}} = \varphi_{\text{fract}}(\sigma_1, \sigma_2, \sigma_3) \quad (28.4)$$

then it can be applied to estimate the effective or useful formability in all deformation processes. The limit strain  $\varphi_{\text{lim}}$  achievable in a particular process can be limited by the type of work material and in addition also by the die or by particular demands put on the deformation process, so that for the same operational conditions (work material, temperature, speed, and stress state), the following relation is valid:

$$\varphi_{\text{lim}} = \varphi_{\text{fract}} \quad (28.5)$$

A phenomenological description of the correlation between formability and stress state is given in Kármán [28.69], [28.70] who was successful in achieving plastic deformation of a solid material (marble) which behaves as a totally brittle material under normal conditions of loading. This was obtained by superimposing on the stone an additional hydraulic pressure on the longitudinal load (Fig. 28.21).

In the same way the extent of deformation of metallic work material can also be influenced

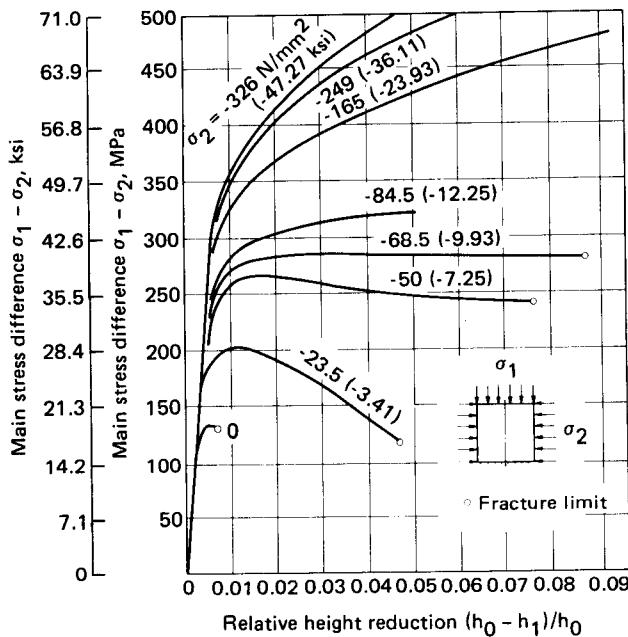


**FIG. 28.21** Compression tests with transverse pressure on marble.  
(After [28.69], [28.71].)

by superimposing a transverse stress [28.68] to [28.74]. In such an attempt the stress state can be represented by the average stress or the hydrostatic stress component  $\sigma_m$  (mean stress) of the main stress system  $(\sigma_1, \sigma_2, \sigma_3)$ , which is defined as the arithmetic average value of the three main stresses  $\sigma_1$ ,  $\sigma_2$ , and  $\sigma_3$ :

$$\sigma_m = \frac{\sigma_1 + \sigma_2 + \sigma_3}{3} \quad (28.6)$$

Negative values of  $\sigma_m$  indicate a stress state where the pressures are higher than the tensions, whereas positive  $\sigma_m$  values are the result of greater tensions. With decreasing  $\sigma_m$ , that is, with increasing pressures, the extent of deformation of a work material increases.

However, more recent investigations [28.68], [28.71] show that the formability of metallic work materials does not solely depend on the average stress value  $\sigma_m$ , but for the same value of  $\sigma_m$ , it also changes with the magnitude of the middle principal stress  $\sigma_2$ .

If the strain at fracture  $\varphi_{fract}$  is calculated not on the basis of the mean stress  $\sigma_m$ , but on the basis of the ratio  $\sigma_m/\sigma_f$ ,

$$\frac{\sigma_m}{\sigma_f} = \frac{(\sigma_1 + \sigma_2 + \sigma_3)/3}{\sigma_f} \quad (28.7)$$

then the correlation represented in Fig. 28.22 is obtained. As shown, the effect of the stress state on the formability of a definite material is not given by only one curve, but is represented by a group of curves having similar curvatures, where the distance between the boundary curves is determined by the magnitude of the middle main stress  $\sigma_2$ . The two boundary curves represent the states  $\sigma_1 > \sigma_2 = \sigma_3$  and  $\sigma_1 = \sigma_2 > \sigma_3$ , respectively; all other states  $\sigma_1 > \sigma_2 > \sigma_3$  lie within the range described by those two curves which form the boundaries of the area. Viewing the phenomenon by considering Mohr's principle, the influence of the middle main stress  $\sigma_2$  can be

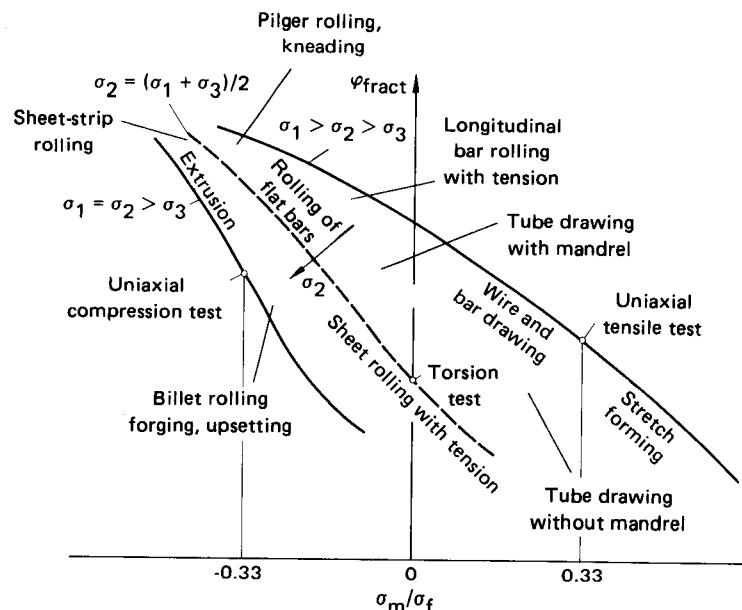


**FIG. 28.22** Schematic representation of the dependence of the extent of deformation on the relative mean stress. (After [28.68], [28.71].)

explained by the fact that different shear strengths exist for different work materials according to their individual  $\sigma_2$  values. To a particular  $\sigma_2$  value corresponds in turn a particular strain at fracture according to the stress-strain curve of the material.

Fig. 28.22 shows again that when there are excessive pressure components (negative value of  $\sigma_m/\sigma_f$ ), the formability is greater than in the loading state when there are multiaxial tensions (large positive values of  $\sigma_m/\sigma_f$ ). However, in certain situations more extensive deformation may be available in tension tests with superimposed additional transverse pressure than in single-axis compression tests.

For deformation processes commonly used today, the relative average stress  $\sigma_m/\sigma_f$  lies between +0.5 (for multiaxial tension load) and -2.0 (for multiaxial compressive load) [28.68], [28.71]. Fig. 28.22 illustrates some deformation processes with respect to the achievable stress states. The conclusion becomes obvious, namely, that it is advantageous to produce deformation under multiaxial compressive loading as far as possible so that the material formability can be utilized to the greatest possible extent. This can be achieved in hot and cold extrusion by simultaneously applying a counterpressure on the workpiece as it exits from the die (Sec. 28.2.2).

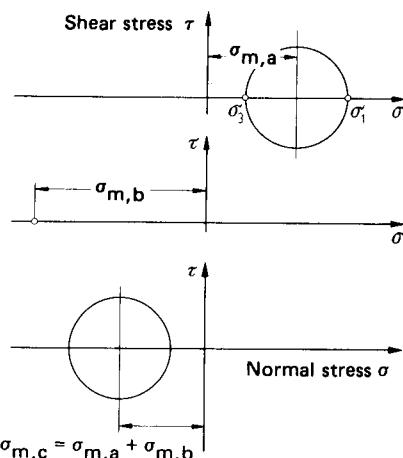


**FIG. 28.23** Superposition of a tension loading state ( $\sigma_{m,a}$ ) and a hydrostatic pressure ( $\sigma_{m,b}$ ) to a compressive loading state ( $\sigma_{m,c}$ ).

The increased formability of metallic work materials with increasing average pressure seems to be due to the phenomenon that superposition of a hydrostatic pressure prevents the occurrence and spreading of microgaps and microcracks in the work material, which would otherwise build up in the deformation zone as a result of tensions (see Chap. 3). By superimposing hydrostatic pressure, the system of main stresses acting in the deformation zone is shifted more in the direction of the pressures (Fig. 28.23), so that the tensions are reduced below their critical values at which the microcracks would spread further.

Since the microstructure of the work material is less damaged during deformation with hydrostatic pressure, the loss of ductility in a workpiece material processed by cold extrusion is small compared with the increase in strength by work hardening. During the operation, with increasing hydrostatic pressure, the achievable deformation at fracture increases in magnitude; furthermore there remains also a residual formability which permits carrying out subsequently additional deformation under atmospheric pressure.

For example, Pugh [28.9] upset test specimens of an aluminum-silicon alloy (11% Si) in castor oil, which served as the pressure medium. He then immediately deformed the specimens under normal uniaxial pressure loading until the first crack appeared on the specimen. Under uniaxial pressure loading this aluminum-silicon alloy withstood a strain  $\varphi_{\max} = \ln(h_0/h_1) = 0.6$  [the relative height reduction  $(h_0/h_1)/h_0$  was 0.43] until appearance of the first crack. After a prior deformation of the specimen under a hydrostatic pressure of 1120 MPa (162.4 ksi) a total strain  $\varphi_{\text{tot}} = \ln(h_0/h_1) = 2.28$  was achieved (the relative height reduction was 0.9), which consisted of two components. One was the prior deformation under a hydrostatic pressure of  $\varphi_{\text{hyd}} = \ln(h_0/h_1) \approx 2.1$ , and the second was the immediately following additional deformation under atmospheric pressure of  $\varphi_{\text{rest}} = \ln(h_1/h_2) \approx 0.18$  (uniaxial upsetting test, Fig. 28.24).

Clearly an improvement of the remaining formability by deformation under the effect of hydrostatic pressure is realized only for those materials which are characteristically difficult to deform under normal conditions. Well-deformable materials, such as the metals copper, niobium, and zinc, show no such improvement. To the contrary, in the case of copper specimens, which were cold-extruded under hydrostatic pressure, the remaining formability was found to be lower than that of copper specimens that were cold-extruded without counterpressure [28.10].

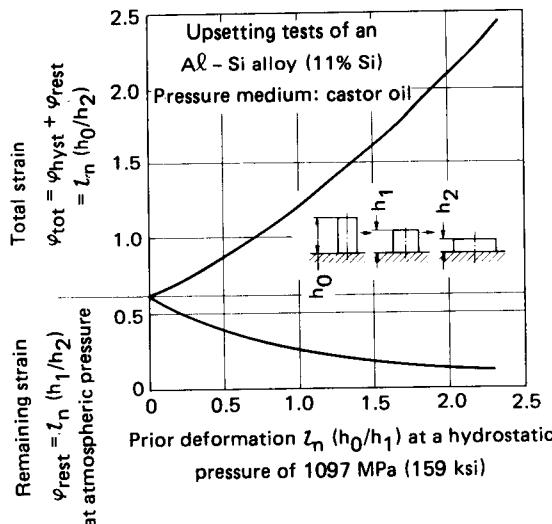


FIG. 28.24 Remaining formability of an aluminum-silicon alloy after deformation by upsetting under a hydrostatic pressure of 1120 MPa (162.4 ksi). (After [28.9].)

### 28.2.2 Typical Processes Utilizing Superimposed Hydrostatic Compressive Stresses

As mentioned in the previous section, the formability of metallic work materials can to a certain extent be considerably improved by superimposing a hydrostatic pressure during their deformation. In this manner even those materials can be deformed which would otherwise behave as totally brittle substances, or which are hardly or not at all deformable, such as cast iron, magnesium, beryllium, tungsten, or alloys of magnesium, zirconium, nickel, vanadium, chromium, or tantalum. Such possibilities can only be exploited in those deformation processes in which the limit strain that is achievable in a particular process is dependent on the formability of the work material. These processes are in particular the deformation processes with either direct pressure or tension loading, such as compressing and bending, and in certain cases also the processes with indirect pressure loading, such as hot and cold extrusion of brittle work materials.

The above-mentioned possibilities cannot be used to advantage in the following situations:

- 1 In deformation processes with indirect tension or pressure loading in which the deformation force acts on an already or not yet deformed section of the workpiece, for example, in bar, wire, and tube drawing, deep drawing, stretch forming, and nosing. In these cases the achievable limit strain is determined, as a rule, by the loading capacity of the workpiece cross section on which the deformation force acts. Such a loading capacity may be limited as the cross-sectional area begins to contract under tension loading. The start of this contraction cannot be influenced favorably by the superposition of hydrostatic pressure (Fig. 28.25) [28.8]. Here extremely brittle materials, such as cast iron, are an exception, although even in their case the achievable limit strain still depends on the formability of the work material.
- 2 If the loading capacity of the tool or the machine determines the limit strain, then in the case of conventional cold extrusion of ductile materials the limit strain is generally determined by the loading capacity of the tools used in the process.

If no correlation exists between useful limit strain and formability of the workpiece material, then no further increase in limit strain can be achieved, even by superimposing a hydrostatic

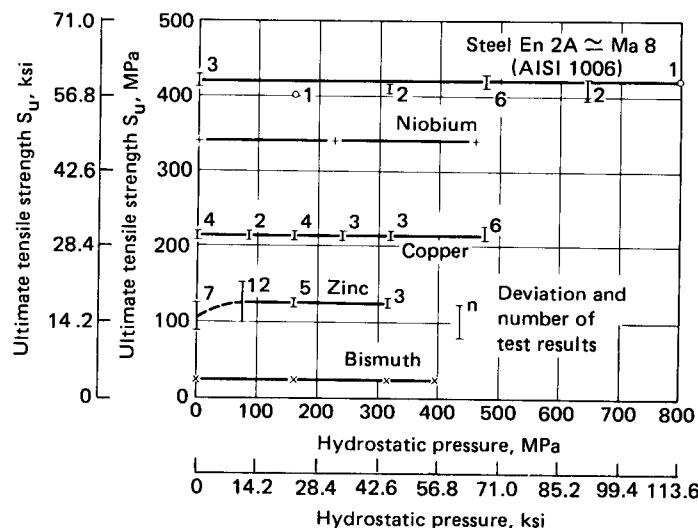


FIG. 28.25 Influence of hydrostatic pressure on tensile strength of different metals. (After [28.8].)

pressure, until the conditions of the initiation of the force action are changed by such a superposition of pressure. Notwithstanding, as shown in some of the following examples, even in such cases, hydrostatic pressure can offer certain advantages.

In the following an attempt is made to explain with the help of a few examples the practical application of a superimposed pressure loading. These examples represent only a narrow range of several possibilities. Those cases in which the hydraulic pressure is applied only to replace the rigid tools, as is the case for many sheet-metal forming operations, are not dealt with here. A comprehensive description of test results obtained so far is given in [28.10].

### *Operations of Deformation Limited by the Formability of Work Material*

**Extrusion with Counterpressure:** In both conventional and hydrostatic cold extrusion with counterpressure this additional pressure is applied in such a manner that the deformed workpiece enters into a chamber where a required hydraulic pressure is maintained and this pressure can be changed in a desired manner during the operation. Practically the same effect can also be achieved with a rigid counterpunch which functions mechanically (e.g., by means of a spring), or which is imparted with hydraulic or pneumatic pressure. However, here the rigidity of the workpiece to buckling limits use of this alternative method. In this respect, use of a pressure chamber is advantageous in the case of longer bars and for higher pressures.

Application of a counterpressure (Fig. 28.26) does not influence the magnitude of the ideal deformation force. This force is dependent only on the difference between the main stresses. Accordingly, to calculate the force the same conditions are valid as described in Chap. 13 for conventional cold extrusion and in Sec. 28.1.2 for hydrostatic cold extrusion. Fig. 28.9, for example, also gives the test results of hydrostatic cold extrusion with counterpressure, where the extrusion pressure is computed as the difference between the pressures in the pressure chambers situated in front of and behind the die. On the other hand, with regard to the loading of the tool assembly and the extrusion press, the pressure in the pressure chamber is the decisive factor, which is computed as the sum of extrusion pressure and counterpressure.

**Conventional Extrusion with Counterpressure:** In the mid-1950s Kienzle, Lange, and Meyer [28.75], [28.76] already investigated—on the basis of theoretical considerations by Schlegel [28.77]—the hot extrusion of cast iron in different compositions by applying axial counterpressure on rigid tools at temperatures ranging from 793 to 1077°C (1459 to 1971°F). Here low counterpressures of merely 20–60 MPa (2.9–8.7 ksi) were sufficient to avoid transverse cracks totally (Fig. 28.27).

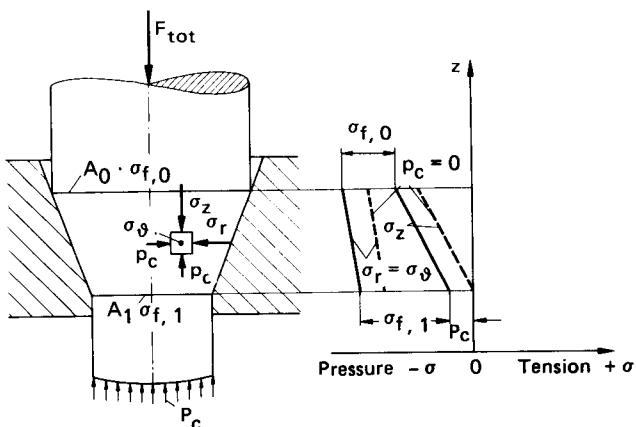


FIG. 28.26 Stress distribution in cold extrusion with counterpressure.

According to investigations made in [28.78], in conventional rod and tube extrusion of bismuth, magnesium, and brass with hydraulic counterpressure, the magnitude of the critical hydraulic pressure, beyond which no cracks were observed, is dependent on the workpiece material and strain.



FIG. 28.27 Crack formation in forward rod extrusion of spheroidal graphite iron. Die-opening angle  $2\alpha = 180^\circ$ . (After [28.76].)

The hydrostatic counterpressure necessary to prevent crack formation in extruded work material is of the same magnitude as in conventional cold extrusion with counterpressure. Moreover it is dependent on the type of work material and the strain. Also, in this case the maximum counterpressure is reached at the extrusion ratio of  $A_0/A_1 = 2.5$  [28.10].

Hydrostatic cold extrusion with counterpressure has been used successfully under laboratory conditions to extrude, among other materials, cast iron, magnesium and magnesium alloys, beryllium, molybdenum, tungsten, chromium, and a niobium-zirconium alloy [28.6], [28.10], [28.13].

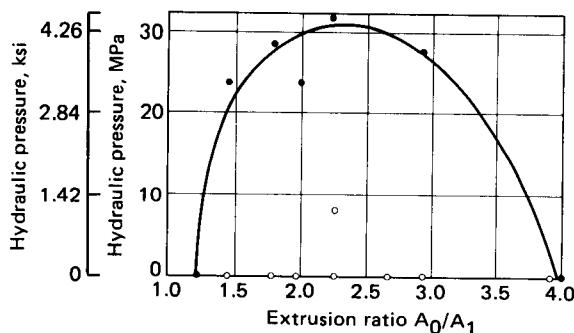
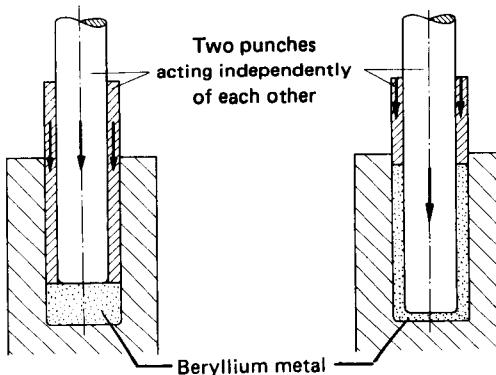


FIG. 28.28 Dependence of "critical" fluid pressure on extrusion ratio in forward rod extrusion of magnesium. Die-opening angle  $2\alpha = 180^\circ$ . (After [28.78].)

Fig. 28.28 shows that for magnesium the required hydraulic pressure reaches a maximum at an extrusion ratio of  $A_0/A_1 = 2.5$  and decreases with both greater and smaller ratios. The maximum counterpressure correlates with the minimum pressure built up in the deformation zone [28.61]. At  $A_0/A_1 > 4$  no counterpressure is needed. Most probably the pressures, which built up while the workpiece was pushed through the die, are themselves large enough to prevent crack formation.

The principle is applied in industry to deform beryllium by means of backward can extrusion with counterpressure (Fig. 28.29) [28.79]. In this case the can height is limited because otherwise the punch may buckle.

**Hydrostatic Cold Extrusion with Counterpressure:** In this process only hydraulic pressures are used since the conditions for building up hydrostatic pressure according to the principle of the hydrostatic extrusion process (pressure chamber, hydraulic fluid as pressure medium) are already fulfilled. The tools hardly differ from those used in hydrostatic cold extrusion, with the exception that here the workpiece exiting the die enters into a pressure chamber (Fig. 28.30).



**FIG. 28.29** Backward can extrusion with counterpressure. Work material—beryllium. (After [28.79].)

Table 28.1 shows the maximum achievable extrusion ratios. The process offers advantageous possibilities to extrude, for example, thin and very thin wires of high-strength materials that are difficult to deform, such as tungsten.

**Compressing, Forging, and Upsetting:** To build up hydrostatic pressure, hydraulic fluids were used by Kármán [28.69], [28.70] and Pugh [28.9] (see Sec. 28.2.1), and even soft solids can be used, such as paraffin-type materials or easily deformable metals [28.35], [28.79], [28.80].

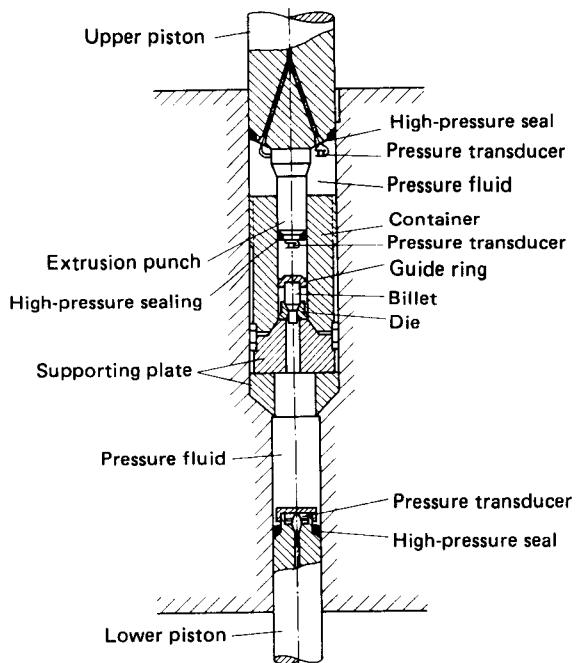


**FIG. 28.30** Mechanism for hydrostatic cold extrusion with counterpressure (After [28.10].)

**Table 28.1** Extrusion Ratios Achieved with Hydraulic Counterpressure in Cold-Extrusion Process

Work material	Extrusion ratio $A_0/A_1$
Cast iron	3
Magnesium and magnesium alloys	1.2–12
Beryllium	1.2–1.5
Molybdenum	1.05–5
Tungsten	1.2–2
Chromium	3, 4
Niobium with 2% zirconium	1.5, 2

Source: Compiled from [28.10], [28.13].

Fig. 28.31 shows a mechanism in which cylindrical test specimens of materials that are difficult to deform are inserted into the bore of a ring-shaped receptor made of either lead or aluminum; then both the specimen and the receptor are compressed together [28.35].

In this process the softer material is first extruded through a bore of the holed plate until the punch touches the oncoming surface of the inner specimen. Then, simultaneously with further extrusion of the receptor material, the cylindrical inner specimen is compressed. At this instant a hydrostatic pressure starts acting. Its magnitude depends on the type of receptor material and on the number and the diameter of the bores in the holed plate. With this very simple mechanism test specimens of hardened and nontempered steel [25 CrMo4 (AISI 4130)] and of cast iron of different compositions were compressed, and relative height reductions  $(h_0 - h_1)/h_0$  of magnitudes greater than 0.5 were achieved, without having completely expended the achievable limit strain, while in compressing without counterpressure the test specimens broke already at very low values of relative height reduction (Fig. 28.32).

A process to forge beryllium in closed dies is shown in Fig. 28.33. Here the hydrostatic pressure is applied by a spring-loaded auxiliary punch.

Fig. 28.34 shows how a hydrostatic pressure can be applied in upsetting bars and tubes. Either fluids [28.32] or soft metals, such as a bismuth-lead alloy [28.80], [28.81], are used as filling materials for the space between the workpiece and the forging die. During flange pressing the filling material is pressed out of the side openings of the die. This material then imparts a hydrostatic pressure on the flange being formed.

Fig. 28.35 shows another mechanism, which can be used to upset tube sections of any desired

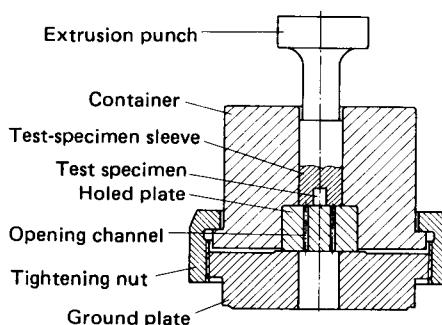


**FIG. 28.31** Mechanism for hydrostatic upsetting.  
(After [28.35].)

length on either one or both ends. The chosen pressure medium is polytetrafluoroethylene (PTFE). The filled quantity is subjected to a pressure of 1500–2200 MPa (213–312 ksi) by means of a punch cylinder. This pressure is then transmitted to the tube section put in the pressure vessel. At a downward movement of the mandrel, the tube, which is supported by friction on the contact surface of the mandrel, is pressed through the pressure chamber into the forging-die space closed by the counterpart and fills up this die space under the effect of the pressure transmitted by the counterpart. With this equipment flange thicknesses of up to eight times the wall thickness of the tube can be achieved, while with commonly used bulging-out and upsetting processes the maximum possible flanging thickness is only as large as the initial wall thickness of the tube used as the workpiece [28.83], [28.84].

**Rolling:** Starting from the basic principle of superimposing a pressure and thereby increasing the achievable strain, Schey developed an experimental rolling mill for spreadless rolling of brittle materials such as titanium alloys and high-temperature alloys based on nickel (Fig. 28.36). The pressing rolls each have a diameter of approximately 350 mm (13.8 in) and a width of approximately 200 mm (7.9 in). Two guiding rails, running in the guiding grooves of both rolls, exercise a transverse pressure on the material to be rolled because they prevent spreading of the rolling work material.

**Bending:** At present very few investigations are known about the influence of hydrostatic pressure on bending [28.85] to [28.87]. In practice it is possible to achieve a greater strain by superimposing pressures while bending the brittle work materials, because bending is a deformation process with a directly acting force. Fig. 28.37 shows typical results of V-bending tests on sheets made of tungsten and beryllium [28.85]. At a maximum hydrostatic pressure of 2840 MPa (403 ksi) both materials could be bent to very large angles without crack formation.

**Fine Blanking and Precision Shearing:** These processes are not deformation processes (see Chap. 2). They are auxiliary processes which can be employed in combination with different deformation processes, for example, to manufacture billets (see Chap. 25). In recent years partic-

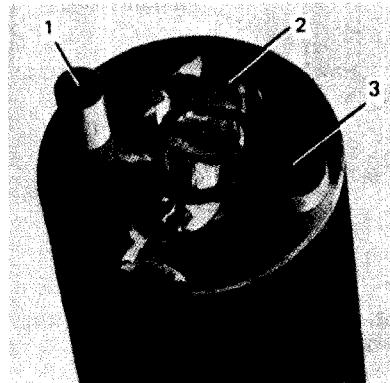


**FIG. 28.32** Extent of deformation of a cylindrical test specimen (1) by means of free upsetting (2) and by hydrostatic upsetting within a lead sleeve (3). Relative height reduction in case of (3) = 0.5. Work material—25CrMo4 (AISI 4130) hardened to martensitic state; initial hardness value before deformation—55 HRC. (After [28.35].)

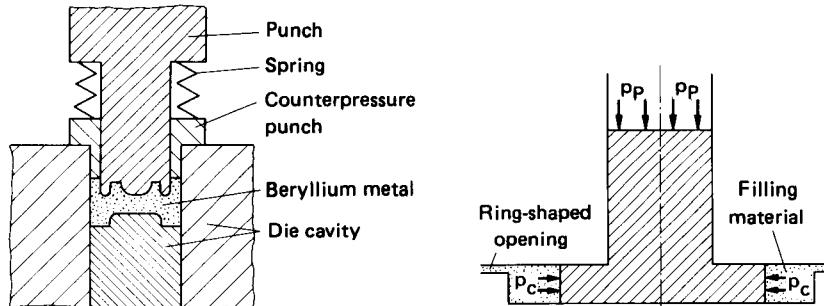


**FIG. 28.33** Forging of beryllium with spring-loaded auxiliary punch. (After [28.79].)

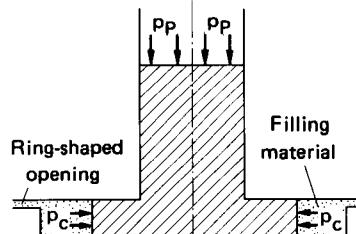


**FIG. 28.34** Radial extrusion of bars against hydrostatic pressure. (After [28.80].)

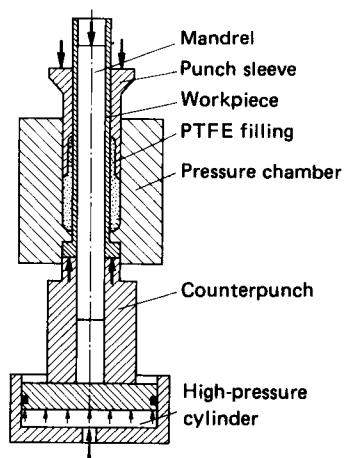


**FIG. 28.35** Tool assembly for upsetting of flanges at tube ends. (After [28.83].)

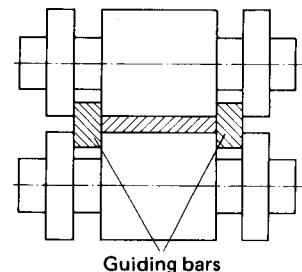


**FIG. 28.36** Spreadless rolling (according to Schey).

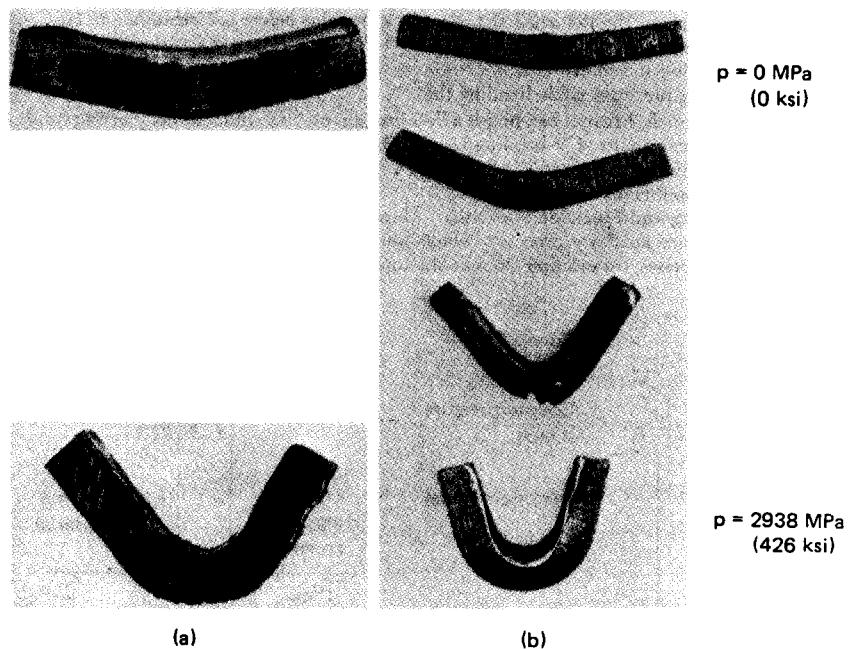


**FIG. 28.37** Increase in bending angle during bending of sheet metals with increasing hydrostatic pressure. (a) Tungsten. (b) Beryllium. (After [28.85].)

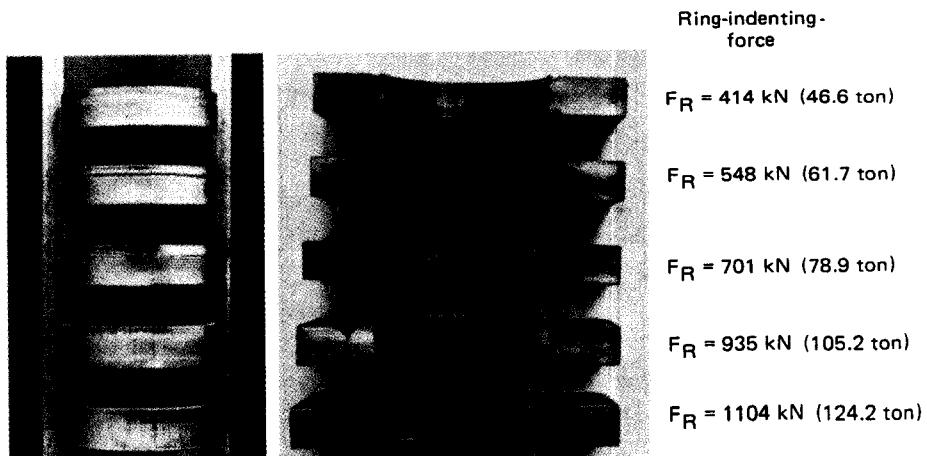


**FIG. 28.38** Formation of sheared surfaces with different ring indenters and ring-indenting forces. Work material—C10 (AISI 1010) forged. (After [28.88].)

ular attention has been given to the fine-blanking process because of the improvement achieved in the structure of sheared surfaces and because of the precision obtained in the dimensions and shapes of the workpieces. Under normal operating conditions in both the blanking and the shearing processes, a mixed surface structure usually results, which is partly sheared and partly fractured. The portion of the sheared surface (shift fracture) is normally smaller than the fractured portion (separation fracture). For practical purposes it is sometimes desired to get a surface with a uniform smooth structure. This can be achieved by increasing the hydrostatic pressure in the shearing zone by forcing a ring indenter into the workpiece surface around the punch contour (see Figs. 24.44 and 24.45). As a result of superimposing the hydrostatic pressure, Mohr's circle is shifted more into the pressure region, as shown in Fig. 24.11, thus allowing the shear yield stress of the work material to be reached prior to the fracture stress. For the quality of the sheared surface, the shape and the arrangement of the ring indenters as well as the magnitude of the indenting pressure are the determining factors (Fig. 28.38) [28.88]. This process has been employed industrially since the 1920s; corresponding detailed technical information is given in Chap. 24.

For the shearing of bar sections the application of an axial counterpressure has proved advantageous, especially when sheared cross sections are needed which are exactly perpendicular to the axis, with minimum distortion and good surface structure or smoothness [28.89], [28.90].

#### *Operations of Deformation Limited by the Loading Capacity*

**Drawing and Deep Drawing:** Both processes belong to the category of tension-compression deformation (see Chap. 2) [28.91] with a directly acting force. The case of functional failure is therefore determined by the loading capacity of the cross-sectional area where the action of the deforming force is initiated.

Yet even in these situations the application of high pressures can be meaningful because it has the following advantages.

First, the material still possesses a higher remaining formability after deformation under hydrostatic pressure, so that, if desired, a higher total strain can be achieved without annealing the workpiece.

Second, the working medium kept under high pressure also acts simultaneously as the lubricating fluid, and in certain cases this fluid medium may be enriched with lubricant additives. This combination greatly improves the lubricating conditions compared with those of the conventional processes, so that, for example, in wire drawing, where even hydrodynamic friction conditions

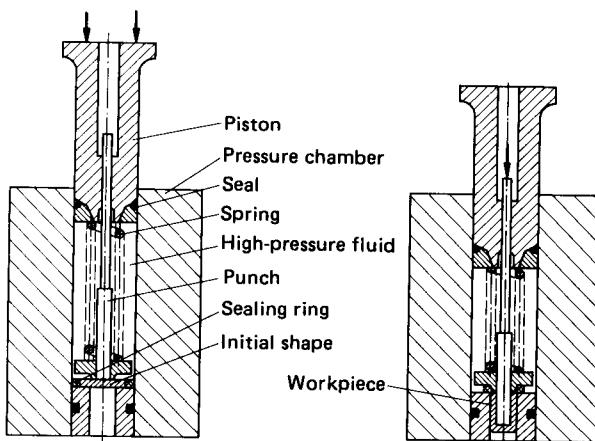


**FIG. 28.39** Deep drawing with hydrostatic pressure. (After [28.83], [28.84].)

may be obtained [28.92], very low drawing forces are needed. The tool wear is also reduced so that it is possible to achieve the same reduction in cross-sectional area with fewer drawing passes. Thus, for example, a piano bar wire of  $d_0 = 1.9\text{-mm}$  (0.075-in) initial diameter [tensile strength  $S_u = 2320 \text{ N/mm}^2$  (336.4 ksi)] with a hydrostatic pressure of 1156 MPa (164 ksi) was drawn in six passes, without annealing, to a final diameter of  $d_1 = 0.65 \text{ mm}$  (0.026 in), while with a conventional wire-drawing process 15 passes would have been necessary to achieve the same total strain. With the conventional process there was no remaining strain (remaining formability), whereas with the hydrostatic process this value amounted to  $\varphi_{\text{rest}} = 0.29$  [28.3].

Finally, with the help of a hydrostatic pressure it is possible to change certain drawing passes in such a manner that either the area-contracting conditions are no longer created (by reducing the drawing force, etc.) or the danger of area contraction is entirely removed, since the drawing operations are converted into extrusion operations. Because of the phenomenon of area contraction of the cross section this would not be possible with conventional processes. One example of such a modification is wire extrusion (see Fig. 28.4). In a similar manner, the usual deep-drawing process can be converted into quasi-radial cold extrusion of sheet metal [28.83], [28.84], [28.93], [28.94]. While with normal deep drawing of ductile materials maximum drawing ratios of  $\beta_{\text{max}} = d_0/d_1 = 2.2$  can be achieved in a single draw (see Table 20.1), with hydrostatic pressure (Fig. 28.39) the drawing ratio achieved for copper in a single draw was 4 [28.83], [28.84]. The required hydrostatic pressure amounted to approximately 685 MPa (97 ksi).

## REFERENCES

- 28.1 DIN 8583: "Fertigungsverfahren Druckumformen. Durchdrücken." (Manufacturing Process Compressive Forming. Pushing Through), sheet 6, 1st ed., 1969.
- 28.2 Robertson, J.: British patent 19356, Jan. 1894.
- 28.3 Bridgman, P. W.: "Large Plastic Flow and Fracture," in *Metallurgy and Metallurgical Engineering* ser., New York, McGraw-Hill, 1952.
- 28.4 Bridgman, P. W.: "Physics of High Pressure," in *International Text Books of Exact Science*, London, Bell and Sons, 1949.
- 28.5 Pugh, H. Ll. D.: "Ramless Extrusion," British Patent 20500, 1961.
- 28.6 Pugh, H. Ll. D.: "Recent Developments in Cold Forming," in *Bulleid Memorial Lectures*, vol. 3B, University of Nottingham, England, 1965.

- 28.7 Pugh, H. Ll. D., and Ashcroft, K.: "The Hydrostatic Hot and Cold Extrusion of Metals" (*in German*), *Ind.-Anz.*, **86**, 1964, pp. 605–612.
- 28.8 Pugh, H. Ll. D.: "Application of High Pressures in Tensile Deformation" (*in German*), *Ind.-Anz.*, **90**, 1968, pp. 970–973.
- 28.9 Pugh, H. Ll. D.: "Application of Hydrostatic Pressure in the Deformation of Metals" (*in German*), *Ind.-Anz.*, **90**, 1968, pp. 1403–1407.
- 28.10 Pugh, H. Ll. D.: *The Mechanical Behaviour of Materials under Pressure*, Amsterdam/London/New York, Elsevier, 1970.
- 28.11 Pugh, H. Ll. D., and Green, D.: "Progress Report on the Behaviour of Metals under High Hydrostatic Pressure," in MERL Plasticity Report 103, East Kilbride, Glasgow, National Engineering Laboratory, 1954.
- 28.12 Pugh, H. Ll. D., and Green, D.: "The Behaviour of Metals under High Hydrostatic Pressure, II: Tensile and Torsion Tests," in MERL Plasticity Report 128, East Kilbride, Glasgow, National Engineering Laboratory, 1956.
- 28.13 Pugh, H. Ll. D., and Low, A. H.: "The Hydrostatic Extrusion of Difficult Metals," *J. Inst. Met.*, **93**, 1964/65, pp. 201–217.
- 28.14 Green, D.: "An Experimental High-Speed Machine for the Practical Exploitation of Hydrostatic Extrusion," *J. Inst. Met.*, **93**, 1964/65, pp. 65–70.
- 28.15 Pugh, H. Ll. D.: "New Trends in Cold Forming" (*in Swedish*), in *Kallsmidning—En mass-produktions-metod på frammarsch*, MEKAN-Resultat, no. 66003, Stockholm, Jan. 1966.
- 28.16 Pugh, H. Ll. D.: "Hydrostatic Extrusion," presented at the 9th Commonwealth Mining and Metallurgical Congress (London, 1969), Paper 18.
- 28.17 Low, A. H., Donaldson, C. J., and Wilkinson, P. T.: "Developments in Hydrostatic Extrusion at the National Engineering Laboratory," in *High Pressure Engineering*, London, The Institution of Mechanical Engineers, 1968, pp. 188–196.
- 28.18 Low, A. H.: Report 358, East Kilbride, Glasgow, National Engineering Laboratory, 1968.
- 28.19 Pugh, H. Ll. D.: "Redundant Work and Friction in the Hydrostatic Extrusion of Pure Aluminum and an Aluminum Alloy," *J. Mech. Eng. Sci.*, **6**, 1964, pp. 362–370.
- 28.20 Low, A. H.: "Extrusion with Hydraulic Pressure" (*in German*), *Technica*, 1967, pp. 745–749.
- 28.21 Beresnev, B. I., Vereščagin, L. F., and Rjabinin, Ju. N.: "Peculiarities in the Rheological Behavior of Metals during Extrusion with Hydraulic Fluids" (*in Russian*), *Izv. Akad. Nauk SSSR, Ot. Teh. Nauk*, **5**, 1957, pp. 48–55.
- 28.22 Beresnev, B. I., Vereščagin, L. F., and Rjabinin, Ju. N.: "Extrusion of Metals with Fluids under High Pressure" (*in Russian*), *Fiz. Met. Metalloved.*, **7**, 1959, pp. 128–132.
- 28.23 Beresnev, B. I., Vereščagin, L. F., and Rjabinin, Ju. N.: "Preconditions for the Extrusion and Change of Mechanical Properties of Metals by Extrusion with High-Pressure Fluids" (*in Russian*), *Inž.-Fiz. Ž.*, **3**, 1960, pp. 43–48.
- 28.24 Beresnev, B. I., Vereščagin, L. F., Rjabinin, Ju. N., and Vivšic, L. D.: *Some Problems of Large Plastic Deformation of Metals at High Pressures*, London, Pergamon, 1963.
- 28.25 Beresnev, B. I., Bulychev, D. K., and Rodionov, K. P.: "Peculiarities in the Extrusion of Metals with Highly Stressed Fluids at High Temperatures" (*in Russian*), *Fiz. Met. Metalloved.*, **11**, 1961, pp. 115–121.
- 28.26 Alexander, J. M.: "Hydrostatic Extrusion," BISRA-Inter-Group Laboratories of the British Steel Corporation, Report MW/FRB/2/69, London, 1969.
- 28.27 Thompson, P. J.: "Hydrostatic Extrusion of Steel," in *Proceedings of the 9th Machine Tool Design and Research Conference (Birmingham)*, London, Pergamon, 1968.
- 28.28 Fiorentino, R. J., Richardson, B. D., Sabroff, A. M., and Boulger, F. W.: "New Developments in Hydrostatic Extrusion," in *Proceedings of the International Conference on Manufacturing Technology* (Ann Arbor, MI, 1967), pp. 941–954.

## 28.32 METAL FORMING UNDER SPECIAL CONDITIONS

- 28.29 Randall, R. N., Davies, D. M., Siergiej, J. M., and Lowenstein, P.: "For Refractory Metals—Experimental Hydrostatic Extrusions Point to New Production Techniques," *Mod. Met.*, **18**, 1962, pp. 68–72.
- 28.30 Sauve, C.: "Lubrication Problems in the Extrusion Process," *J. Inst. Met.*, **93**, 1965, p. 553.
- 28.31 Alexander, J. M., and Lengyel, B.: British Complete Specifications no. 12326/65, 56241/66, and 41249/67.
- 28.32 Grünert, P.: "Hydrostatic Extrusion—A New Deformation Process" (*in German*), *Fertigungstechn. u. Betr.*, **16**, 1966, pp. 546–551.
- 28.33 Bolotin, V. V.: *Nonconservative Problems on the Theory of Elastic Stability*, Oxford, Pergamon, 1963.
- 28.34 Ondraček, E., and Pelar, E.: "Deformation under Hydrostatic Pressure" (*in Czech*), *Strojírenství*, **15**, 1965, pp. 270–277.
- 28.35 Pawelski, O.: "Hydrostatic Upsetting" (*in German*), *Ind. Kur., Tech. u. Forsch.*, **20**, 1967, pp. 682, 684, 686.
- 28.36 Discussion: "Extrusion under High Pressure," *J. Inst. Met.*, **93**, 1964/65, pp. 581–582.
- 28.37 Geiger, R.: "Material Flow and Distribution of Strength in Workpieces Treated by the Conventional and the Forward Rod-Extrusion Processes" (*in German*), *Ind.-Anz.*, **94**, 1972, pp. 1579–1582.
- 28.38 Wilhelm, H.: "Investigation on Correlation between Vickers Hardness and Comparative Deformation in Cold Deformation Processes" (*in German*), *Berichte aus dem Institut für Umformtechnik, Universität Stuttgart*, no. 9, Essen, Girardet, 1969.
- 28.39 Johnson, S.: "Advances in Hydrostatic Extrusion" (*in German*), *Draht-Welt*, **54**, 1968, pp. 209–213.
- 28.40 Bobrowsky, A., and Stack, E. A.: "An Investigation of Fluid Extrusion of Metals," Report NASA-CR-63789, Feb. 1965.
- 28.41 Fiorentino, R. J., Sabroff, A. M., and Boulger, F. W.: "Investigation of Hydrostatic Extrusion," in Final Technical Documentary Report AFML-TD-64-372, Contract AF 33 (600)-43328, Columbus, OH, Battelle Memorial Institute, Jan., 1965.
- 28.42 Fiorentino, R. J., Sabroff, A. M., and Boulger, F. W.: "Hydrostatic Extrusion at Battelle," *Mach. Lloyd (European ed.)*, **35**, 1963, pp. 18–23.
- 28.43 Fiorentino, R. J., Richardson, B. D., Sabroff, A. M., and Boulger, F. W.: "Development of the Manufacturing Capabilities of Hydrostatic Extrusion Process," in Interim Engineering Progress Report IR-8-198 (VIII), Contract AF 33 (615)-1390, Columbus, OH, Battelle Memorial Institute, Dec. 1966.
- 28.44 Steck, E.: "Calculation of the Force in Deformation Processes by Means of the Upper-Bound Method" (*in German*), *Werkstatttechnik*, **57**, 1967, pp. 273–279.
- 28.45 Kobayashi, S.: "Upper-Bound Solutions of Axisymmetric Forming Problems, Parts I and II," *Trans. ASME, J. Eng. Ind.*, **86B**, 1964, pp. 122–126, 326–332.
- 28.46 Kobayashi, S., and Thomsen, E. G.: "Upper- and Lower-Bound Solutions to Axisymmetric Compression and Extrusion Problems," *Int. J. Mech. Sci.*, **7**, 1965, pp. 127–143.
- 28.47 Johnson, W., and Kudo, H.: *The Mechanics of Metal Extrusion*, Manchester, England, University Press, 1962.
- 28.48 Lambert, E. R., and Kobayashi, S.: "A Theory of the Mechanics of Axisymmetric Extrusion through Conical Dies," *J. Mech. Eng. Sci.*, **10**, 1968, p. 367.
- 28.49 Avitzur, B.: "Hydrostatic Extrusion," *Trans. ASME J. Eng. Ind.*, **87B**, 1965, pp. 487–494.
- 28.50 Hillier, M. J.: "A Hydrodynamic Model of Hydrostatic Extrusion," *Int. J. Prod. Res.*, **5**, 1966, pp. 171–181.
- 28.51 Iwata, K., Osakada, K., and Fujino, S.: "Analysis of Hydrostatic Extrusion by the Finite-Element Method," *Trans. ASME, J. Eng. Ind.*, **94B**, 1972, pp. 697–703.

- 28.52 Hornmark, N., Nilsson, J. O. H., and Mills, C. P.: "QUINTUS Hydrostatic Extrusion," *Met. Form.*, 37, 1970, pp. 227–233.
- 28.53 Larker, H.: "Hydrostatic Extrusion at ASEA," presented at the 1st Czechoslovakian Conference on Forming by High Pressure and High-Energy-Rate Forming, Jihlava, Apr. 1969.
- 28.54 Erbe, R.: "Hydrostatic Extrusion—A New High-Pressure Process of Metal Deformation" (*in German*), *Klepzig Fachber.*, 79, 1971, pp. 258–261.
- 28.55 Samanta, S. K.: "Hydrostatic Extrusion" (*in Swedish*), *av tråd. Jernkontorets Annaler*, 152, 1968, pp. 29–34.
- 28.56 Lengyel, B., and Culver, L. E.: "Properties of Materials Extruded by Orthodox Hydrostatic Extrusion," *J. Inst. Met.*, 97, 1969, pp. 97–103.
- 28.57 Lengyel, B.: "Design of Experimental and Production Equipment: Pressure Vessels, Lectures 3 and 4," in Post-Experience Course—Hydrostatic Extrusion, Imperial College of Science and Technology, London, July 1969.
- 28.58 Adler, G., and Walter, K.: "Calculation of Tolerances for Single and Multiple Shrink Fits" (*in German*), *Ind.-Anz.*, 89, 1967, pp. 805–809.
- 28.59 Friedewald, H. J.: "Tolerance for Shrink Fits of Shear and Deformation Tools" (*in German*), *VDI-Forschungsheft*, no. 472, Düsseldorf, VDI-Verlag, 1959.
- 28.60 Becker, S. G., and Mollick, L.: "The Theory of the Ideal Design of a Compound Vessel," *Trans. ASME, J. Eng. Ind.*, 82B, 1960, pp. 136–142.
- 28.61 Schulz, E.: "Calculation of Prestressed Extrusion Dies for Cold Deformation of Steel" (*in German*), *Draht*, 16, 1965, pp. 546–557.
- 28.62 VDI-Richtlinie 3176: "Vorgespannte Presswerkzeuge für das Kaltumformen (Prestressed Extrusion Dies for Cold Forging)," Düsseldorf, VDI-Verlag, 1964.
- 28.63 Davidson, T. E., and Kendall, D. P.: "The Design of High-Pressure Containers and Associated Equipment," in *Mechanical Behaviour of Materials under Pressure*, Pugh, H. L. D., Ed., Amsterdam/London/New York, Elsevier, 1970.
- 28.64 Feldmann, H. D.: "Consideration of Hot and Cold Hydrostatic Extrusion of Metals, Pts. I and II" (*in German*), *TZ f. prakt. Metallbearb.*, 63, 1969, pp. 116–119, 426–443.
- 28.65 Lengyel, B.: "Design of Experimental and Production Equipment: Static and Dynamic Seals," Lecture 8 in Post-Experience Course—Hydrostatic Extrusion, Imperial College of Science and Technology, London, July 1969.
- 28.66 Fiorentino, R. J., Meyer, G. E., and Byrer, T. G.: "The Thickfilm Hydrostatic Extrusion Process," Society of Manufacturing Engineers, Technical Paper MF 71-103, 1971.
- 28.67 Fiorentino, R. J.: "Comparison of Cold, Warm, and Hot Extrusion by Conventional and Hydrostatic Methods," Society of Manufacturing Engineers, Technical Paper, 1972.
- 28.68 Stenger, H.: "Importance of Formability in Deformation" (*in German*), *Bänder Bleche Röhre*, 8, 1967, pp. 599–605.
- 28.69 Kármán, Th. v.: "Strength Tests under Hydrostatic Pressure" (*in German*), *VDI-Z.*, 55, 1911, pp. 1749–1757.
- 28.70 Kármán, Th. v.: "Strength Tests under Hydrostatic Pressure" (*in German*), *VDI-Forschungsheft*, no. 118, Berlin, 1912, pp. 37–68.
- 28.71 Stenger, H.: "On the Dependence of the Formability of Metallic Work Materials on the Stress State" (*in German*), Dr.-Ing. thesis, Technische Universität, Aachen, 1965.
- 28.72 Maier, A. F.: "Influence of the Stress State on the Formability of Metallic Work Materials" (*in German*), Dr.-Ing. thesis, Technische Universität, Stuttgart, 1934.
- 28.73 Scheele, H.: "Tension Tests under Slip Prevention" (*in German*), *Arch. Eisenhüttenwes.*, 14, 1940/41, pp. 505–511.
- 28.74 Siebel, E.: "Basic Principles and Terminology of Plastic Deformation" (*in German*), *Werkstattstech. u. Maschinenbau*, 40, 1950, pp. 373–380.

## 28.34 METAL FORMING UNDER SPECIAL CONDITIONS

- 28.75 Meyer, H.: "Possibilities and Limitations in the Hot Deformation of Cast Iron in Die Cavities" (*in German*), Dr.-Ing. thesis, Technische Universität, Hannover, 1960.
- 28.76 Kienzle, O., Lange, K., and Meyer, H.: "Hot Extrusion of Cast Iron with Counterpressure" (*in German*), Institut für Werkzeugmaschinen und Umformtechnik, Technische Universität, Hannover, Interner Bericht, 1957.
- 28.77 Schlegel, F. W.: "Plastic Deformation of Cast Iron Alloys in Closed-Gap Dies" (*in German*), Dr.-Ing. thesis, Technische Universität, Aachen, 1952.
- 28.78 Pugh, H. Ll. D., and Gunn, D. A.: "Cold Extrusion with Hydrostatic Counterpressure of Work Materials Difficult to Deform" (*in German*), *Ind.-Anz.*, 86, 1964, pp. 1732-1735.
- 28.79 Hayes, A. F., and Yoblin, J. A.: "New Concepts for Fabricating Beryllium by Advanced Forging and Powder Metallurgy Techniques," presented at the Institute of Metals Conference on Metallurgy of Beryllium, London, 1961.
- 28.80 Cogan, R. M.: "Hydrodynamic Forming," *Trans. ASME, J. Eng. Ind.*, 87B, 1965, pp. 105-109; *Machinery*, 1964, pp. 1147-1151.
- 28.81 Cogan, R. M.: "Forging against Back Pressure," *Am. Machinist*, 107, no. 21, Oct. 14, 1963, pp. 105-107.
- 28.82 Alexander, J. M., and Lengyel, B.: "On the Cold Extrusion of Flanges against High Hydrostatic Pressures," *J. Inst. Met.*, 93, 1964/65, pp. 137-144.
- 28.83 Fuchs, Jr., F. J.: "Hydrostatic Pressure—Its Role in Metal Forming," *Mech. Eng.*, 88, no. 4, 1966, pp. 36-40.
- 28.84 Fuchs, Jr., F. J.: "Production Metal Forming with Hydrostatic Pressure," presented at the ASME Metals Engineering and Production Engineering Conference, Berkeley, CA, 1965, Paper 65-Prod-17.
- 28.85 Bobrowsky, A., Stack, E. A., and Austen, A.: "Extrusion and Drawing Using High-Pressure Hydraulics," presented at the ASTME Conference, Nov. 1964, Paper SP 65-33.
- 28.86 Galli, J. R., and Gibbs, P.: "The Effect of Hydrostatic Pressure on the Ductile-Brittle Transition in Molybdenum," *Acta Metall.*, 12, 1964, pp. 775-778.
- 28.87 Meyer, G. E., Love, K. L., and Fiorentino, R. J.: "Bending Titanium and Beryllium Sheet in Pressurized Fluid," *Trans. ASME, J. Basic Eng.*, 94D, 1972, pp. 589-594.
- 28.88 Krämer, W.: "Investigations of Precision Shearing of Steel and Nonferrous Metals" (*in German*), *Berichte aus dem Institut für Umformtechnik, Universität Stuttgart*, no. 14, Essen, Girardet, 1969.
- 28.89 Herbst, U.: "The Precision Shearing of Work Materials for Cold Forging" (*in German*), Dr.-Ing. thesis, Technische Universität, Hannover, 1967.
- 28.90 Maeda, T., and Nakagawa, T.: "Experimental Investigations on Blanking," *Scientific Papers of the Institute of Physical and Chemical Research* (Osaka Pref.), 62, 1968, pp. 65-68.
- 28.91 DIN 8584: "Fertigungsverfahren Zugdruckumformen. Durchziehen und Tiefziehen" (Manufacturing Process Pressure-Tension Deformation. Drawing through and Deep Drawing), sheets 2 and 3, Apr. 1971.
- 28.92 Christopherson, D. G., and Naylor, H.: "The Promotion of Fluid Lubrication in Wire Drawing," *Proc. Inst. Mech. Eng.*, 169, 1955, p. 643.
- 28.93 Maslenikov, N. A.: "Deep Drawing of Sheet Metal by Friction Forces" (*in Russian*), transl. in *The Engineers Digest*, 17, no. 9, 1965.
- 28.94 Sizov, E. S., Antonov, E. A., and Petrov, S. A.: "Deep Drawing of Workpieces with Fluid Support" (*in Russian*), *Kuznecčno-štamp. proizv.*, no. 4, 1970, pp. 23-25; (*German transl.*), *Umformtechnik*, 4, 1970, pp. 36-40.
- 28.95 Schröder, G., and Kammerer, M.: "Effect of Temperature on Quality and Force Requirement in the Shearing of Steel with Low Carbon Content" (*in German*), HGF-Bericht no. 72/1, *Ind.-Anz.*, 94, 1972, pp. 32-33.

**FORMING WITH  
SUPERIMPOSED  
VIBRATIONS**



**List of Special Symbols**

---

$A_s$	amplitude of sonic wave
$d_1$	inner diameter of blank
$d_0$	diameter of disk
$t_{\text{per}}$	period of oscillation
$u$	deflection
$v_s$	velocity of sonic wave
$\delta_s$	amplitude of sonic velocity
$\alpha$	half die-opening angle
$\hat{\epsilon}_s$	amplitude of strain induced by sonic wave
$\lambda$	wavelength
$\sigma_s$	sonic vibrating stress
$\hat{\sigma}_s$	amplitude of sonic vibrating stress
$\omega$	angular velocity

The application of vibrations in metal-forming processes is not widely practiced. Notwithstanding as a special branch in the field of forming, this method is included in this publication to complete the presentation of the entire range of metal-forming processes.

If mechanical vibrations, for example, in the ultrasonic range, are superimposed on the external forming forces acting on the tools, then the magnitudes of these external forces needed for

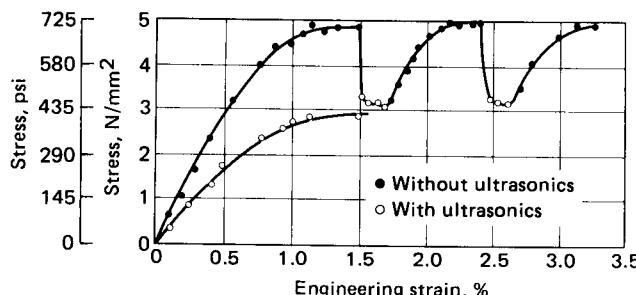


FIG. 29.1 Beginning portions of stress-strain curves. (After [29.1].)

the desired deformation can be reduced. The first basic tests of this phenomenon were carried out by Blaha and Langenecker [29.1]. They showed that there occurs a distinct reduction in magnitude of the stress on metal crystals when a particular mechanical vibration is superimposed on the static load during the tension test (Fig. 29.1). The stress is reduced considerably if during the tension test an ultrasonic field is superimposed at the stage when the apparent limit of elasticity (yield point) of the test material has been exceeded. If the ultrasonic field is then removed and the test continued further, the stress increases again to its original magnitude. When the experiment with such superimposed mechanical vibration is carried out right from the beginning, the stress-strain diagram of the tension test shows a considerably flatter shape than that of the metal crystal.

It has been the aim of several patents and tests to make use of such a stress reduction in the metal-forming processes. In most attempts ultrasonic vibrations having frequencies higher than 16 kHz are used.

To impart ultrasonic vibration on solid bodies, magnetostrictive vibrators are used extensively. These vibrators make use of the phenomenon in which a ferromagnetic bar, when placed in the magnetic field of a coil, is imparted a mechanical vibration in the axial direction. For this purpose, however, the frequency of the coil field must be almost the same as the resonant frequency of the bar. The magnetostrictive vibrators are suitable up to about 200 kHz. If mechanical frequencies higher than 200 kHz are needed, piezoelectric material is suitable for the purpose.

## 29.1 BASIC PRINCIPLES

As already indicated, the superposition of ultrasonic vibration on a metal crystal during tension tests apparently reduces the yield stress as compared with the magnitude attained during static tensile loading. For this phenomenon the following theoretical model is presented in [29.2].

The dislocations, forming a distributed network of linear defects in metal crystals, are considered the main cause of plastic deformation of a metal crystal (see Chap. 3). These dislocations are distributed in "potential wells." A static load imparted on the metal causes its potential wells to deform asymmetrically, whereby the dislocations remain within the wells. When an ultrasonic vibrating stress is superimposed on this existing static load, the dislocations become capable of leaving the potential wells, and such motion contributes to plastic deformation of the metal crystal.

In [29.3] this theoretical model is referred to with the following remarks: "If this atomistic model is correct, then the same behavior of the stress, showing a statistical average value of all microscopic stresses, should occur in the test specimen also at the macroscopic level. To check the occurrence of such a macroscopic phenomenon, the magnitude of the vibrating stress due to such a superposition on the workpiece should first be determined. In addition, it should also be investigated how this stress, which fluctuates between its positive and negative maxima, influences in a particular range the stress-strain behavior of the workpiece."

The behavior of a bar-shaped test specimen, its static load in the tension test being superim-

posed with an axial vibration, can be derived as follows. From the equation of motion for the vibrating bar,

$$u = A_s \sin\left(\frac{2\pi}{\lambda} x - \omega t\right) \quad (29.1)$$

where  $u$  is the deflection at point  $x$  at time  $t$ ,  $A_s$  is the sonic-wave amplitude,  $\lambda$  the wavelength of vibration imparted to the test specimen,  $f$  the frequency of the imparted vibration, and  $\omega = 2\pi f$ , the angular velocity. The strain value in the bar is derived as

$$\frac{du}{dx} = \frac{2\pi}{\lambda} A_s \cos\left(\frac{2\pi}{\lambda} x - \omega t\right) \quad (29.2)$$

By means of Eqs. 29.1 and 29.2 the ultrasonic vibrating stress, according to the definition in Hook's law, can be derived as

$$\sigma_s = \frac{du}{dx} E \quad (29.3)$$

where  $E$  is the modulus of elasticity of the test material.

From Eqs. 29.2 and 29.3 the ultrasonic vibrating stress is found:

$$\sigma_s = \frac{2\pi}{\lambda} A_s E \cos\left(\frac{2\pi}{\lambda} x - \omega t\right) \quad (29.4)$$

and  $\hat{\sigma}_s = \frac{2\pi}{\lambda} A_s E$  (29.5)

$\hat{\sigma}_s$  being the amplitude of the ultrasonic vibrating stress [29.3].

Now this vibrating stress should be superimposed on the static tensile stress. Two cases can be distinguished:

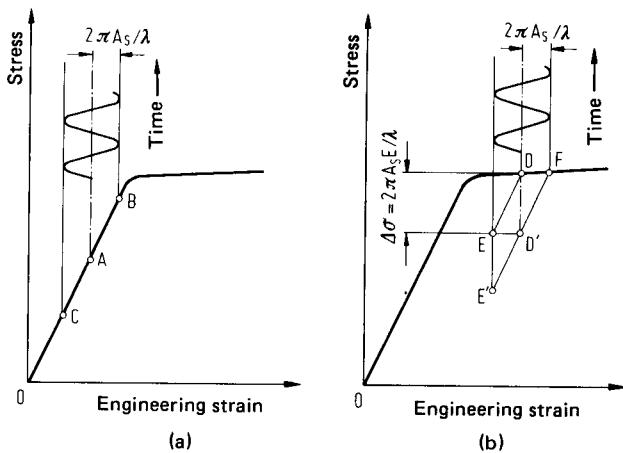
- 1 The vibrating stress is superimposed only within the range of elastic deformation (elasticity range).
- 2 The vibrating stress is superimposed only within the range of plastic deformation.

Fig. 29.2 shows both cases by means of an idealized stress-strain diagram in which an additional time coordinate is used to show the superposition of a vibrating stress having the strain amplitude  $\dot{\epsilon}_s = (2\pi/\lambda) A_s$  (see Eq. 29.2).

The test specimen is considered to be strained within the elastic range only up to point  $A$ , which lies quite below the yield limit (Fig. 29.2a). The specimen deforms up to point  $B$  due to the additional vibrating stress acting on it during the first half-period of the imparted vibration, whereby point  $B$  still remains within the elastic range of the stress-strain diagram. In this manner the curve of imparted stress sets forth periodically within the limiting points  $B$  and  $C$ . However, at the center of the vibration period the magnitude of the static stress remains the same as at point  $A$  so that externally no reduction in total stress is registered.

In the second case, however (Fig. 29.2b), the specimen is subjected to plastic deformation and elongated up to point  $D$ , which lies beyond the elastic range. The superimposed vibration at this stage reduces the stress on the specimen up to point  $E$ , from where the plastic deformation of the specimen proceeds beyond point  $D$  up to point  $F$ . During the following periods of vibration the stress varies between points  $E'$  and  $F$ , this deformation being of purely elastic nature only. Due to this phenomenon, the static stress is reduced from  $D$  to  $D'$  in the center of the period of vibration, the amount of stress reduction depending on the strain amplitude of the imparted vibration as well as on the modulus of elasticity of the test material. This difference in stress  $\Delta\sigma = 2\pi A_s E / \lambda$  is identical to the amplitude of the ultrasonic vibrating stress  $\hat{\sigma}_s$  in Eq. 29.5 (see [29.3]).

According to the above derivation, the experiment must also show a reduction in the static stress amounting to the amplitude of the ultrasonic vibrating stress if the test material is in the totally plastic state. Actually this fact was proved in tension, upsetting, bending, and shear tests.



**FIG. 29.2** Stress-strain diagrams with superimposed vibrations. (a) In range of elastic recovery. (b) In range of plastic deformation. (After [29.3].)

The statement in [29.3], that an “apparent” reduction of the yield stress due to superimposed ultrasonic vibration could be explained as a result of the resultant effect of the static and dynamic stresses and that this reduction has a magnitude equal to the amplitude of the ultrasonic vibrating stress, has been confirmed by several authors. For example, in [29.4] to [29.6] a linear correlation is reported between force reduction and sonic amplitude.

Most metal-forming processes are accompanied by energy losses due to external friction, which could be influenced favorably by superimposed vibration. In [29.3] it was established by means of a model test that under the influence of ultrasonic vibration and at different relative velocities of the tool with regard to the workpiece, the conditions of friction, as compared with those found in similar tests without ultrasonic vibration, could be influenced considerably by the resultant effect of the individual directions of motion. If the direction of vibration is perpendicular to both the direction and the surface of friction, hardly any noticeable reduction in frictional force could be achieved. When the direction of vibration is parallel to the surface as well as the direction of friction, the achievable reduction in frictional force is greatest at small velocities of friction between the members of the friction system. But such a reduction in frictional force diminishes to almost zero when the relative velocity is increased substantially. Again, if the direction of vibration is perpendicular to the direction of friction but parallel to the surface of friction, then the work of friction is also reduced considerably. In this case the relative velocity barely affects the frictional force.

## 29.2 APPLICATIONS

As stated at the beginning of this chapter, the application of ultrasonics in metal-forming processes is not widely used. The greatest efforts made to introduce superimposed vibrations in industrial production are known in wire- and tube-drawing processes. Certain application tests are also carried out for cold upsetting, forging, rolling, and in the case of sheet-metal forming.

### 29.2.1 Wire and Tube Drawing

#### Wire Drawing

In wire drawing it is easier to impart vibrations to the drawing die. Several possibilities are shown schematically in Fig. 29.3, where the different types of vibration of the drawing die are indicated

by their corresponding amplitudes of wave motion. In Fig. 29.3a the die, fitted at a distance  $\lambda/2$  at the right end of a  $\lambda/2$  transformer, is situated in the trough portion of a wave motion of this transformer, which vibrates at point  $N_1$  in a direction parallel to the direction of drawing. In this arrangement both the  $\lambda/2$  transformer and the sonic transmitter must have an identical end-to-end bore so that the drawn wire can be passed through. In the arrangement shown in Fig. 29.3b the die is placed at a node of the wave-motion path of the transformer. However, the direction of the imparted vibration and that of the drawing are perpendicular to each other. Finally for the arrangement shown in Fig. 29.3c the direction of the imparted vibration is again perpendicular to that of the drawing, but the die is situated in the trough portion of the wave-motion path of the transformer with length  $\lambda$ .

#### Drawing Die Is Excited along Its Axial Plane (Axially Excited)

In the case of drawing with a superimposed ultrasonic field, when the drawing force is plotted graphically against the drawn wire length, the curve indicates a periodic variation in magnitude of the drawing force. Fig. 29.4 shows such a diagram plotted for a copper wire. Its relative change in wire cross section amounted to  $\epsilon_A = 0.18$  at an initial wire diameter of  $d_0 = 2.27$  mm (0.089 in) and for an opening angle of the drawing die of  $2\alpha = 12^\circ$ . It could be determined that the drawing force had minimum values at regular intervals of half the wavelength of the axial vibration imparted to the wire. In other words, the maximum reduction in magnitude of the drawing force could be achieved only when the drawn wire had a resonant length, that is, a length equal to half the wavelength of the superimposed vibration, or a submultiple of  $\lambda/2$ . Such variations in the drawing force can be suppressed if a second drawing die is arranged at a suitable distance from the first one. This second die serves to match the wire length with the imparted wavelength and simultaneously permits a further reduction in the wire cross section by means of a second drawing pass. Besides, as other experiments have demonstrated, it is not sufficient to use a guide pulley as an alternative to the second drawing die since in such a case the wire length could not be matched properly [29.3], [29.4].

Extensive tests in the drawing of wire by means of several drawing dies in tandem have been reported in [29.7]. It should be kept in mind, however, that the wire could be imparted not only an axial but also a bending vibration, which permits a reduction in magnitude of the drawing force needed.

#### Drawing Die Is Excited in the Plane Perpendicular to Its Axis (Vertically Excited)

As shown in Fig. 29.3b, in this case the vibrating die is situated in the node of the wave-motion path of the vibrating transformer. At this point the strain  $du/dx$  has a maximum value in the direction of vibration according to Eq. 29.4, since the trough portion of the stress curve joins here. Hence in the direction parallel to that of the superimposed vibration, the die is periodically expanded and compacted, giving it a slightly elliptical shape. There are reports that a considerable

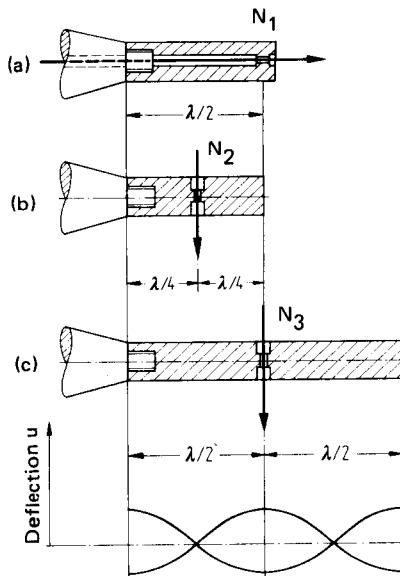


**FIG. 29.3** Different methods of vibrating the drawing die. (a) Vibrator bar length  $\lambda/2$ , axially vibrated die. (b) Vibrator bar length  $\lambda/2$ , vertically vibrated die. (c) Vibrator bar length  $\lambda$ , vertically vibrated die. (After [29.3].)

## 29.6 METAL FORMING UNDER SPECIAL CONDITIONS

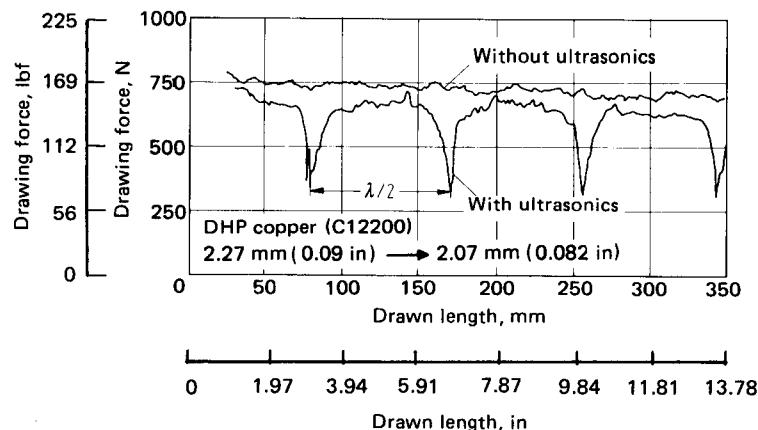


**FIG. 29.4** Measurement of drawing force in wire-drawing process with axially vibrated drawing die, as shown in Fig. 29.3a. (After [29.3].)

reduction in stress has been achieved in drawing a copper wire [29.3], [29.8]. Fig. 29.5 shows a linear correlation between the drawing stress and the amplitude of the imparted vibration. Since no axial vibrations are produced in this arrangement of exciting the drawing die, the drawn wire length has virtually no influence on the drawing force. In cases where a similar die was vibrated in the direction perpendicular to its own axis, reductions in drawing force of up to 48% have been achieved for steel wires and of up to 37% for aluminum wires [29.9].

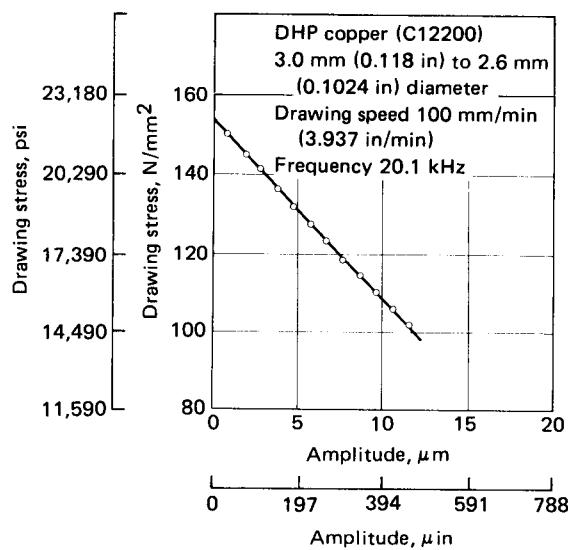


**FIG. 29.5** Graphic presentation of correlation between drawing stress and amplitude of superimposed vibration in wire drawing with vertically vibrated drawing die, as shown in Fig. 29.3b. (After [29.3].)

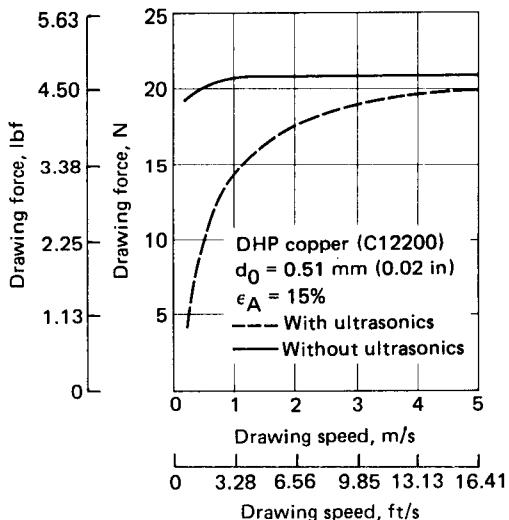


FIG. 29.6 Influence of drawing speed on drawing force in wire drawing with ultrasonic superimposed vibration of 300-W (0.4-hp) capacity. (After [29.10].)

In the case of a vertically vibrated die, as shown in Fig. 29.3c, similar problems arise in matching the drawn wire length as in the case of the axially vibrated die shown in Fig. 29.3a. The drawing die vibrates in a direction perpendicular to the direction of wire drawing and imparts bending vibrations to the drawn wire. If the drawn wire length is matched correctly to the wavelength of imparted vibration, the drawing force could be reduced by up to 25%.

In all methods of wire drawing described, a disadvantage common to all of them should not be forgotten, especially if one intends to superimpose mechanical vibration: an optimum reduction in the drawing stress is possible only at small drawing speeds. It was found that in wire drawing for a speed of 0.5 m/s (19.68 in/s), a reduction in drawing force of 53% could be observed, as compared with that in drawing without superimposed ultrasonic vibration, whereas for a drawing speed of 5 m/s (16.4 ft/s) a relative reduction in the drawing force of only 4% could be achieved [29.10] (Fig. 29.6).

It appears that the ratio of drawing speed to sonic velocity of the vibrating die has a decisive effect on the drawing process with superimposed vibration [29.7], [29.8]. The sonic velocity  $v_s$  is the velocity with which the die vibrates around its stationary position. A reduction in drawing stress can only be expected if the amplitude of the sonic velocity is greater than the drawing speed. The magnitude of  $v_s$  can be derived from Eq. 29.1:

$$v_s = \frac{du}{dt} = -\omega A_s \cos\left(\frac{2\pi}{\lambda} x - \omega t\right) \quad (29.6)$$

$$\text{where } \dot{v}_s = \omega A_s \quad (29.7)$$

$\dot{v}_s$  being the amplitude of the sonic velocity.

### Wire Drawing with Ultrasonically Agitated Lubricants

In addition to vibrating a metal-forming tool directly, there exists the possibility of agitating the drawing lubricant with ultrasonics in the case of wet drawing. The advantages of wet drawing of fine wires as compared with fine-wire drawing without ultrasonic superposition are reported in

[29.11]. In drawing a copper wire of initial diameter  $d_0 = 0.381$  mm (15 mil) to a final diameter  $d_1 = 0.071$  mm (2.8 mil) at a drawing speed of 5 m/s (16.4 ft/s), five drawing passes could be spared out of a total of 14 passes needed with the conventional method. Thus when drawing with ultrasonic superposition the same result was achieved with only nine passes. The authors of the report mentioned the further advantage that the wire-drawing die was free from disturbing depositions due to the cleaning effect of the ultrasonically agitated lubrication bath. This phenomenon produces a better wire surface and less wear of the drawing die. Even the uniformity of the dimensional tolerances was excellent in the tests reported in [29.11]. For example, in the case of a 300-m (984-ft) long aluminum wire of final diameter  $d_1 = 0.071$  mm (2795  $\mu$ in) the maximum deviation from the desired measurement was only 0.2%. Possibly the cleaning effect of ultrasonic vibration was not alone responsible for the test results described in [29.11]. Since the lubricant fluid was agitated ultrasonically, an almost ideal hydrodynamic lubrication may have been achieved in the drawing die as well as ideal lubrication of the drawing system, which permitted adequate slipping of the drawn wire on the drawing rolls. This latter consideration is significant in estimating the feasibility of the drawing method described in [29.11]. Because five drawing passes are spared out of 14, the wire would be subjected to such a drastic rise in the drawing stress and to an even more drastic reduction in the wire cross-section during these passes, that in the case of conventional drawing without ultrasonically agitated lubricant, the wire would break [29.12] (refer also to Chap. 14).

### **Tube Drawing**

The possibilities of using ultrasonically agitated drawing dies for the tube drawing are basically similar as in the case of wire drawing. Moreover, if drawing over a stationary mandrel is necessary (see Chap. 14), the mandrel could also be imparted vibration. Several U.S. firms are applying the method of tube drawing with ultrasonic superposition for industrial manufacture. Reductions in drawing force of up to 68% are reported in [29.13] to [29.16]. Compared to the conventional drawing method, drawing with ultrasonics offers considerable advantages, especially for thin-walled tubes of large diameters. Exact calibration of streamlined section tubes is achieved more easily when drawing with ultrasonic superimposed vibration.

#### **29.2.2 Upsetting and Forging**

Little is known about the application of mechanical vibrations in upsetting and forging. Some basic investigations reported in [29.17], [29.18] showed that a considerable reduction in the drawing stress was achieved in some cases where different materials were upset with ultrasonics as compared with "static" upsetting tests. Fig. 29.7 shows upsetting curves for three different materials. These curves clearly demonstrate that the reduction in the force needed for upsetting is mainly dependent on the amplitude of the imparted vibration.

Upsetting a material with superimposed ultrasonic vibration leads to less bulging of the test specimen than when upsetting without ultrasonics. This indicates a lower coefficient of friction between workpiece and platen, so that metal forming is more homogeneous. This assumption is verified by the experience that upsetting a workpiece with ultrasonic vibration gives a uniform microstructure of the metal and a balanced distribution of the hardness values in the workpiece.

More upsetting tests with ultrasonic vibrations are reported in [29.3]. Compared to static upsetting, a resultant effect of the static and dynamic stresses occurs in upsetting with ultrasonic vibration, which causes a reduction in the resultant stress value. This is explained as a possible reason for the lower upsetting force needed when compared with static upsetting tests (see Sec. 29.1).

However, besides ultrasonic vibrations, the sounds of lower frequencies can also influence metal-forming processes. Thus [29.19] reports on a static-dynamic press which permits more effective filling of the forging die in comparison with the conventional forging method. Fig. 29.8 shows the load-displacement characteristic of forging operation on such a press. The machine is a combination of a hydraulic press and a mechanical hammer which permits a hydraulic superposition of the vibration on the load-displacement characteristics of a conventional forging operation.

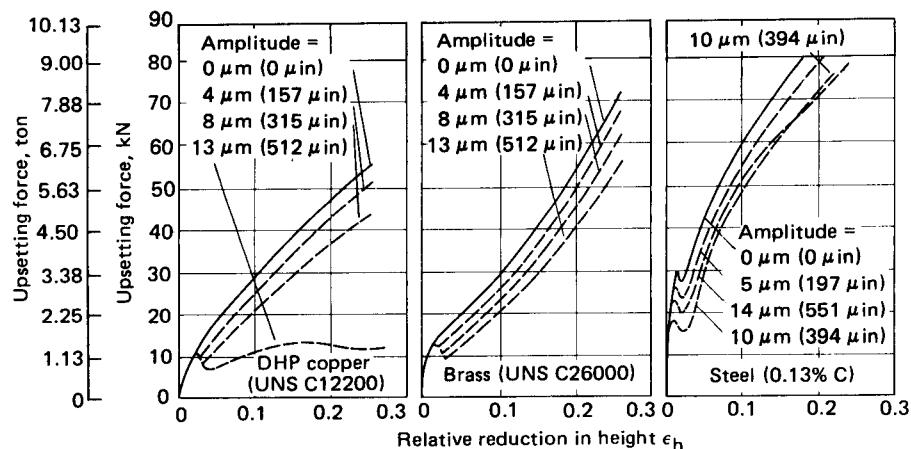


**FIG. 29.7** Influence of amplitude of superimposed vibration on behavior of upsetting force in process of upsetting with ultrasonic superimposed vibration (22 kHz). (After [29.18].)

### 29.2.3 Other Processes of Bulk-Metal Forming

Except for the processes of bulk-metal forming described above, very little is known about other methods using superimposed vibrations. For example, it is possible to impart vibrations to both the punch and the forging die in the cases of punching and extrusion. Reductions in the extrusion force of up to 15–25% were achieved for aluminum, as reported in [29.14].

Similarly it is quite logical to achieve reductions in the forming forces in rolling with superimposed vibrations. Thus, eventually either the rolls can receive the vibrations or the withdrawing section can transmit such vibrations to the rolled material [29.12], [29.20].

### 29.2.4 Sheet-Metal Forming

Besides giving a literature survey on the use of superimposed vibrations in metal-forming processes [29.12], Hansen and Treis also report that sheet-metal forming with superimposed vibrations can be advantageous in all those cases where high external friction has to be overcome. Such a situation occurs, for example, in the stretch forming of metal sheets over draw punches. Tests have shown [29.21], [29.22] that a reduction in friction leads to a uniform material yield along the tool surface and that the depth of draw can be increased. To this end either the sheet or the draw punch, or both, can be imparted mechanical vibrations. The investigations described in [29.14] mention a low punching force required and an increase of up to 37% in the achievable drawing ratio in the deep-drawing process. In Fig. 29.9 the reduction in the deep-drawing force, achieved for two different frequencies of mechanical vibration imparted to the punch, is plotted against the deep-drawing force needed in the method

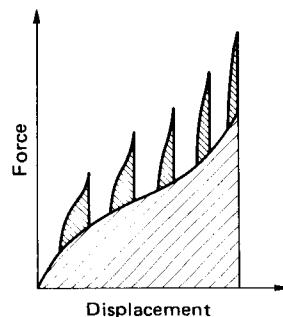


**FIG. 29.8** Basic load-displacement characteristic of a static-dynamic forging process. (After [29.19].)

without ultrasonics. In [29.3] it is found that the reduction in the deep-drawing force is mainly the result of a reduction in friction between tool and workpiece and, only to a lesser extent, due to the resultant effect of static and dynamic stresses (see Sec. 29.1).

Even in the case of cutting, vibrations superimposed on the motion of the cutting tools can influence the cutting force and the quality of the cut surface favorably. Thus compared with "conventional" cutting, the cutting force can be reduced by up to 30%, and a smoother cut surface is obtained because the cutting tool that is subjected to vibrations acts as a smoothing agent for the surface while cutting it.

### 29.2.5 Economic Expectations

It can be concluded from the above considerations that metal forming with superimposed vibrations permits lowering the magnitude of force and work, narrowing the dimensional tolerance ranges, improving the quality of the worked surfaces, as well as achieving a longer service life of the tools. In this manner, some working steps may be spared, the metal-forming rate can be increased (e.g., in wet drawing), the weight of the machines can be reduced, and their capacity can be increased. Against the above advantages, however, the following factors must be weighted. Higher investment costs for sonic devices and high sonic power consumption become inevitable. Not only are such devices costly, but they should also be operated by specially trained personnel. The sonic power capacity of such devices depends on specific conditions of metal forming. It is known that a higher capacity is needed, but exact requirements of machine capacity and sonic power for a particular metal-forming process have not yet been determined accurately [29.12].

In addition to the economic considerations, it should also be remembered that the problems arising in the industrial application of metal forming with superimposed vibration have not yet been completely solved. To the question, which metal-forming process with superimposed vibration brings advantages, only a general answer can be given: advantages are achieved wherever an "apparent" reduction of stress (refer also to Sec. 29.1) makes an otherwise nonfeasible metal-forming process possible, or when quite high components of external friction can be overcome which generally make the metal forming critical. It should be remembered in any case that on the one hand the metal-forming work can be reduced, while on the other hand sonic power consumption, which is accompanied by high energy losses, increases the power consumption as a whole [29.5]. Detailed data on the calculation of the resultant efficiency are given in [29.8]. In [29.24] an example shows that in spite of a 50% reduction in the mechanical power needed for

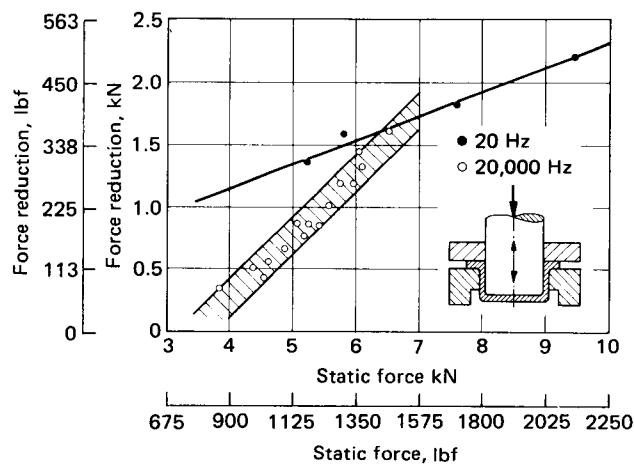


FIG. 29.9 Reduction of drawing force in deep drawing of annealed steel sheet AISI 4130 (After [29.23].)

metal forming, the resultant efficiency sank to  $\eta_{\text{eff}} = 0.082\%$  due to the great amount of sonic power consumed in the process.

## REFERENCES

- 29.1 Blaha, F., and Langenecker, B.: "Strain of Zinc Monocrystals under the Effect of Ultrasonic Vibrations" (*in German*), *Naturwissenschaften*, **42**, 1955, p. 556.
- 29.2 Blaha, F., and Langenecker, B.: "Plasticity Tests of Metal Crystals in the Ultrasonic Field" (*in German*), *Acta Metall.*, **7**, 1959, pp. 93–97.
- 29.3 Lehfeldt, E.: "Influencing the Friction between Metals with Ultrasonics in the Frequency Range around 20 kHz" (*in German*), Dr.-Ing. thesis, Technische Universität, Aachen, 1968.
- 29.4 Winsper, C. E., and Sansome, D. H.: "A Study of the Mechanics of Wire Drawing with Superimposed Ultrasonic Stress," in *Advances in Machine Tool Design and Research*, pt. 2, Oxford/London/New York, Pergamon, 1970.
- 29.5 Winsper, C. E., and Sansome, D. H.: "Application of Ultrasonic Vibrations to the Plug Drawing of Tubes," *Met. Form.*, **38**, 1971, pp. 71–75.
- 29.6 Friedrich, R., Kaiser, G., and Pechhold, W.: "Influence of Mechanical Vibrations on the Plasticity Behavior of Metals" (*in German*), *Z. Metall.*, **60**, 1969, pp. 390–398.
- 29.7 Sämann, K. H.: "On Influencing Deformation Processes of Metals with Mechanical Vibrations in the Ranges of 20 kHz and 40 kHz, Shown with an Example of the Wire Drawing Process" (*in German*), Dr.-Ing. thesis, Technische Universität, Aachen, 1970.
- 29.8 Naujoks, B.: "Investigations on the Influence of Ultrasonics in the Wire-Drawing Process" (*in German*), Dr.-Ing. thesis, Technische Universität, Berlin, 1970.
- 29.9 Oelschlägel, D., and Weiss, B.: "Improved Efficiency in Wire Drawing with Ultrasound," *Trans. ASM*, **59**, 1966, pp. 685–693.
- 29.10 Maropis, N., and Clement, J. C.: "Transition between Theory and Practice in Ultrasonic Metal Deformation Processing," American Society for Metals, Technical Report C6-26.3.
- 29.11 Olsen, K. M., Jack, R. F., and Fuchs, E. O.: "Wire Drawing in Ultrasonically Agitated Lubricants," *Wire W. Prod.*, **40**, 1965, pp. 1563, 1566, 1637–1638.
- 29.12 Hansen, N., and Treis, H.: "Metal Forming with Vibrations" (*in German*), *Bänder Bleche Röhre*, **9**, 1968, pp. 573–583.
- 29.13 "Sonic Forging Press Is a Possibility," *Metalwork. Prod.*, **109**, no. 11, 1965, pp. 52–53.
- 29.14 Young, A. W.: "Metals Gain New Formability with Ultrasonic Boost," *Iron Age*, **195**, no. 12, 1965, pp. 73–76.
- 29.15 "Tube Drawing with Ultrasonics," *Steel*, **159**, no. 20, 1966, p. 38.
- 29.16 Kearns, T. F.: "MPEP—The Metalworking Processes and Equipment Program," *Met. Eng. Quart.*, **4**, no. 2, 1964, pp. 1–11.
- 29.17 Izumi, O., Oyama, K., and Suzuki, Y.: "On the Superposition of Ultrasonic Vibration during the Compressive Deformation of Metals," *Trans. Jpn. Inst. Met.*, **7**, 1966, pp. 158–162.
- 29.18 Izumi, O., Oyama, K., and Suzuki, Y.: "Effects of Superimposed Ultrasonic Vibration on the Compressive Deformation of Metals," *Trans. Jpn. Inst. Met.*, **7**, 1966, pp. 162–167.
- 29.19 Stankowic, P.: "Static-Dynamic Forging Principles and Some Characteristics," *Met. Treat. and Drop Forg.*, **159**, 1958, pp. 489–494.
- 29.20 Gentzsch, G.: "Application of Ultrasonic Vibrations in Metal-Forming Processes" (*in German*), *Draht-Welt*, **55**, 1969, pp. 22–28.
- 29.21 German patent 729429: Alois Riedl, Augsburg, Messerschmidt AG, "Stretch Forming Process for Sheet Metal" (*in German*), Deutsches Reichspatent 19, Nov. 1942.
- 29.22 Sorokin, J. N.: "Some Problems of Metal Sheet Deformation in Stretch Forming with Vibration" (*in Russian*), *Kuznečno-stamp. protiv.*, **8**, no. 4, 1966, pp. 23–24.

## **29.12 METAL FORMING UNDER SPECIAL CONDITIONS**

- 29.23 Kristoffy, J.: "Metal Forming with Vibrated Tools," *Trans. ASME, J. Eng. Ind.*, **91B**, 1969, pp. 1168-1174.
- 29.24 Panknin, W., Naujoks, B., and Siegert, K.: "Influence of Longitudinal Ultrasonic Vibrations on the Metal-Forming Process with Particular Consideration of Efficiency" (*in German*), *Z. Metall.*, **64**, 1973, pp. 145-151.
- 29.25 Langenecker, B., Fountain, C. W., and Jones, W. O.: "Ultrasonics—An Aid to Metals Forming?" *Met. Prog.*, **85**, 1964, pp. 97-101.
- 29.26 Schmid, E., and Lintner, K.: "The Significance of Ultrasound for Plastic Deformation Behavior of Metals" (*in German*), *Phys. Bl.*, **22**, 1966, pp. 454-462.

**FORMING BY  
EXPLOITING SPECIAL  
MATERIAL PROPERTIES**

---

---

**30.1 FORMING OF SUPERPLASTIC MATERIAL**

**30.1.1 Definition of Superplastic Behavior**

Most metallic work materials have a relatively high flow stress and limited capacity for strain during deformation. By contrast, numerous alloys display superplastic behavior when deformed at low strain rates and high deformation temperatures. A finely grained microstructure is required, which is achieved by special treatment prior to deformation (micrograin superplasticity). When compared with the flow stress of conventional metals subjected to hot forming, the flow stress in superplastic deformation is quite small.

Superplastic alloys, such as tin-lead, zinc-aluminum, aluminum-copper, and some alloys of the iron-nickel-chromium system, can develop extraordinarily large strains without visible evidence of necking during uniaxial tension tests. An elongation of 4850% has been reported for a tin-lead alloy [30.1]. The initiation of necking is prevented by an especially high strain-rate dependence of the flow stress [30.2].

Both the high strains and the low flow stresses associated with superplasticity are of great interest for possible applications in metal forming. Since the behavior of metallic work materials in the superplastic state corresponds roughly to that of hot glass or heated polymers, manufacturing techniques employed for these substances can, in principle, be applied to forming of superplastic metals as well. Favorable properties of superplastic work materials during deformation are not sufficient for engineering applications, however. The required technology, production cost, and properties of the finished parts are just as important.

**30.1.2 Conditions Required for Superplasticity**

Although extraordinarily large strains are a fundamental characteristic of superplastic materials, they alone cannot be used in many cases to distinguish the typical superplastic behavior from

## 30.2 METAL FORMING UNDER SPECIAL CONDITIONS

ordinary plastic behavior as in hot forming, for instance. Therefore the strong dependence of the flow stress on strain rate and the resulting resistance to necking are taken as distinguishing features of superplasticity.

The main conditions for the occurrence of superplasticity are:

- 1 A very finely grained microstructure with grain sizes of a few micrometers, often on the order of  $1\text{--}5 \mu\text{m}$ , which is maintained during deformation
  - 2 A deformation temperature  $T_{\text{def}}$  greater than half the absolute melting temperature  $T_m$ ,
- $$T_{\text{def}} > \frac{1}{2} T_m \quad [\text{K}]$$
- 3 Relatively small strain rates

The requirement for a very finely grained microstructure implies that superplasticity is limited to selected metals and alloys. In addition, special techniques are necessary for the production of the work material itself. Another problem regarding engineering applications of superplastic materials rests in the need to eliminate the superplastic properties once the forming process is completed. Otherwise there may be a strong tendency for the material to creep during use.

Relative to the superplastic behavior of certain steels, distinction is made between micrograin or isothermal superplasticity and transformation superplasticity. Transformation superplasticity is based on the fact that plastic strains can result from small stresses during the course of phase transformations of steel ( $\alpha/\gamma$  transformation). A test sample is subjected to specific temperature cycling under constant stress such that a phase transformation takes place each time the sample is heated or cooled. These transformations are accompanied by a limited plastic strain. By repeated phase transformations a large cumulative strain consisting of the sum of the small individual strains can be achieved. In contrast to superplastic materials in which the entire microstructure deforms simultaneously at constant temperature, the individual strains are limited to the locations in the microstructure where the transformations take place. The characteristic dependence of flow stress upon strain rate does not exist with these materials, however [30.3].

### 30.1.3 Continuum-Mechanical Formulation of Superplasticity

A sample of a metal with normal plastic behavior subjected to uniaxial tension will exhibit a neck following uniform deformation. Additional plastic deformation will concentrate in the necked region. The cross-sectional area of the neck decreases until the fracture strength is reached and the sample breaks.

A condition for the prevention of further area reduction in an existing neck can be established [30.4], [30.5]. For uniaxial deformation

$$d\varphi = \frac{dl}{l}$$

and hence

$$\dot{\varphi} = \frac{d\varphi}{dt} = \frac{1}{l} \frac{dl}{dt} = \frac{v}{l} \quad (30.1)$$

where  $\varphi$  = strain

$\dot{\varphi}$  = strain rate

$l$  = gauge length

$v$  = crosshead speed

$t$  = time

Under tensile loading a local area reduction leads to elongation of the test sample. If cross-sectional area  $A$  is reduced by  $dA$  over a length  $l$ , then from volume constancy

$$V = lA = \text{constant} \quad (30.2)$$

and

$$dV = A \, dl + l \, dA = 0 \quad (30.3)$$

Substitution into Eq. 30.1 yields

$$d\varphi = - \frac{dA}{A} \quad (30.4)$$

A local reduction in area will not increase with additional plastic deformation only if the area reduction  $dA$  is offset by an increase in strength  $d\sigma_f$ :

$$(A + dA)(\sigma_f + d\sigma_f) > \sigma_f A \quad (30.5)$$

With  $dA/d\sigma_f \ll \sigma_f/dA$ , and Eq. 30.4

$$\frac{d\sigma_f}{d\varphi} > \sigma_f \quad (30.6)$$

is obtained. A tensile specimen with an existing local area reduction will stabilize without additional necking only if this condition is satisfied. To prevent necking entirely,  $d\sigma_f/d\varphi$  must in general be positive and as large as possible.

Flow stress  $\sigma_f$  is now a function of several variables:

$$\sigma_f = f(\varphi, \dot{\varphi}, T_{\text{def}}, \dots) \quad (30.7)$$

If it is assumed that deformation takes place at constant temperature and the microstructure of the work material does not undergo changes,  $\sigma_f$  can be expressed as a function of  $\varphi$  and  $\dot{\varphi}$ . Thus differentiation of Eq. 30.7 results in

$$\frac{d\sigma_f}{d\varphi} = \left( \frac{\partial \sigma_f}{\partial \varphi} \right) + \left( \frac{\partial \sigma_f}{\partial \dot{\varphi}} \right) \frac{d\dot{\varphi}}{d\varphi} \quad (30.8)$$

For plastic extension without necking Eq. 30.6 must be satisfied. Two possibilities exist according to Eq. 30.8:

- 1 Hardening due to plastic deformation. Customary metallic materials strain harden, but  $\partial\sigma_f/\partial\varphi$ , the slope of the stress-strain curve, decreases rapidly with increasing strain. As a result, uniform deformation of over 50% is seldom achieved in uniaxial tension with these materials. Instead, beyond uniform deformation a neck forms and intensifies until fracture. The second term in Eq. 30.8 usually is small, since dependence of  $\sigma_f$  upon  $\dot{\varphi}$  is not significant.
- 2 Increase of flow stress with rising strain rate:  $\partial\sigma_f/\partial\dot{\varphi} \gg 0$ . This applies especially to the superplastic state of metals and alloys. Considerable sensitivity of flow stress to changes in the speed of deformation is considered the characteristic continuum-mechanical property of superplastic work materials.

When a tension sample begins to neck locally, plastic deformation is concentrated in the necked-down region. This leads to a reduction in length of the region undergoing plastic deformation and an increase in strain rate for constant crosshead speed (see Eq. 30.1). This means that  $d\dot{\varphi}/d\varphi > 0$ .

Since  $\partial\sigma_f/\partial\dot{\varphi} > 0$  for superplastic materials (Fig. 30.1),  $d\sigma_f/d\dot{\varphi}$  can become so large according to Eq. 30.8 that Eq. 30.6 is satisfied and necking will not take place. On the other hand, flow stress is only slightly dependent upon strain in the superplastic state:  $\partial\sigma_f/\partial\varphi \approx 0$ .

In contrast to strain hardening, the stabilizing effect of  $\partial\sigma_f/\partial\dot{\varphi}$  is maintained for very large strains. A superplastic material can therefore be extended uniformly without fracture occurring by flow localization.

Fig. 30.1 shows the relationship between  $\sigma_f$  and  $\dot{\varphi}$  for tin, lead, and tin-lead alloys [30.6]. Based upon the fundamentally similar behavior of other materials, a mathematical relationship between  $\dot{\varphi}$  and  $\sigma_f$  was formulated [30.7] which can describe experimental curves in certain regions:

$$\sigma_f = C\dot{\varphi}^m \quad (30.9)$$

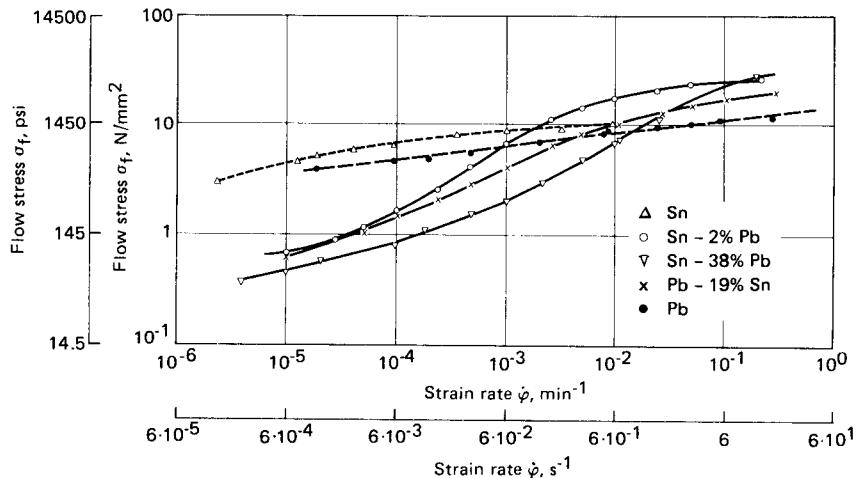


**FIG. 30.1** Dependence of flow stress  $\sigma_f$  upon strain rate  $\dot{\phi}$  in the domain of steady plastic flow based on tension tests at 20°C (68°F). Tin-lead alloys of different compositions, extruded. (After [30.6].)

where  $m$  is known as the strain-rate sensitivity index. It is generally defined as

$$m = \frac{\partial (\log \sigma_f)}{\partial (\log \dot{\phi})} \quad (30.10)$$

and is determined from the slope of a  $\log \sigma_f$  versus  $\log \dot{\phi}$  plot (Fig. 30.1).

If a bar of superplastic material with cross-sectional area  $A$  is considered which is loaded by a tensile load  $P$ , then

$$\sigma = \frac{P}{A} = C\dot{\phi}^m$$

Then

$$\dot{\phi} = \left( \frac{P}{C} \right)^{1/m} \left( \frac{1}{A} \right)^{1/m} \quad (30.11)$$

From Eqs. 30.1 and 30.3

$$\dot{\phi} = \frac{1}{l} \frac{dl}{dt} = - \frac{1}{A} \frac{dA}{dt} \quad (30.12)$$

Combining Eqs. 30.11 and 30.12 yields

$$-\frac{dA}{dt} = \left( \frac{P}{C} \right)^{1/m} \frac{1}{A^{(1-m)/m}} \quad (30.13)$$

Eq. 30.13 indicates that the rate of area reduction  $-dA/dt$  is inversely related to the cross-sectional area and is sensitive to  $m$  at the same time. For  $m < 1$  the area is reduced more quickly as the cross-sectional area becomes smaller. As  $m \rightarrow 1$  the rate of neck initiation is sharply reduced. When  $m = 1$ , deformation is Newtonian viscous and  $dA/dt$  is independent on  $A$ . This means that no necking can occur. Should any incipient neck be present, it will simply be preserved, but will not grow during the stretching process [30.8].

For nonsuperplastic work materials  $m$ -values range from 0.02 to 0.25, even at temperatures up to  $0.9T_m$ . For heated polymers  $m$  ranges from 0.3 to 1.0. For hot glass  $m = 1$ . For metallic

materials clear indications of superplastic behavior exist when  $T_{\text{def}} > 0.5 T_m$  and  $m \geq 0.3$ . Thus  $m$  is the dominating parameter determining superplasticity.

### 30.1.4 Metallurgical Processes in Superplasticity

Superplastic behavior of metallic materials requires that  $m \geq 0.3$ . The relationship between  $m$  and fracture strain has been demonstrated with tests of titanium, zirconium, and tin-lead alloys [30.9], [30.10] (Fig. 30.2). Fig. 30.3 shows the dependence of  $m$  upon grain size or the metallographic mean free path in the microstructure. The curves  $m = f(\phi)$  of most superplastic materials display a distinct maximum for strain rates between  $10^{-5}$  and  $10^{-2} \text{ s}^{-1}$ . This limited  $\phi$ -range, where  $m$  is sufficiently high for superplastic deformation, is known as stage 2. Fig. 30.3 also underscores the fact that the high  $m$ -values required for superplasticity are obtained only with fine-grained microstructures. As the grain size decreases,  $m$  increases, and the maximum is shifted to higher strain rates. A fine-grained microstructure is especially easily obtained and maintained with eutectic and eutectoid alloys. For these materials different phases form simultaneously at subeutectic or subeutectoid temperatures and then precipitate in a very fine dispersion. It was demonstrated, however, that superplasticity is not restricted to two-phase structures [30.11], but can occur in fine-grained pure metals as well. A condition for high  $m$ -values is that  $T_{\text{def}}/T_m \geq 0.5$ . Only then is the microstructure nearly independent of the preceding deformation, and the flow stress is a function only of the initial microstructure, of  $\phi$ , and of  $T_{\text{def}}$  as a first approximation. Frequently maxima of the  $m$ -value and of the fracture strain were detected near the eutectoid temperature (Fig. 30.4). For the eutectic aluminum-copper alloy of fixed microstructure, larger  $m$ -values are observed for higher temperatures, and the maximum of the curves  $m = f(\phi)$  is shifted to higher strain rates [30.12].

A characteristic feature of superplastic deformation is that large macroscopic elongations are possible with virtually no elongation of individual grains [30.1]. A number of studies have indeed revealed that for many superplastic alloys grain-boundary sliding constitutes the greatest contribution to strain in the superplastic region [30.13], [30.14]. A number of different models exist to

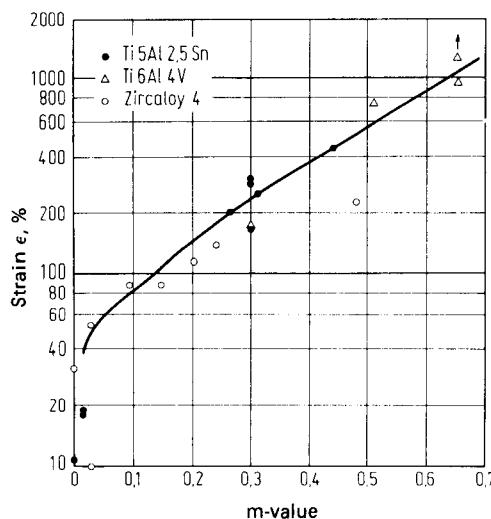
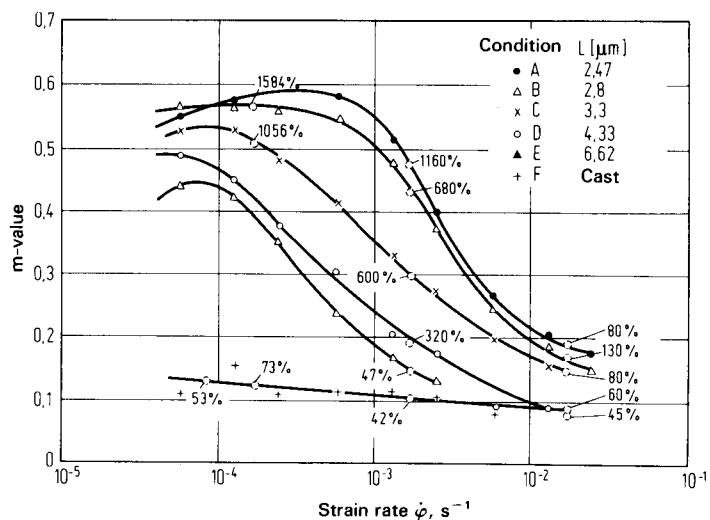
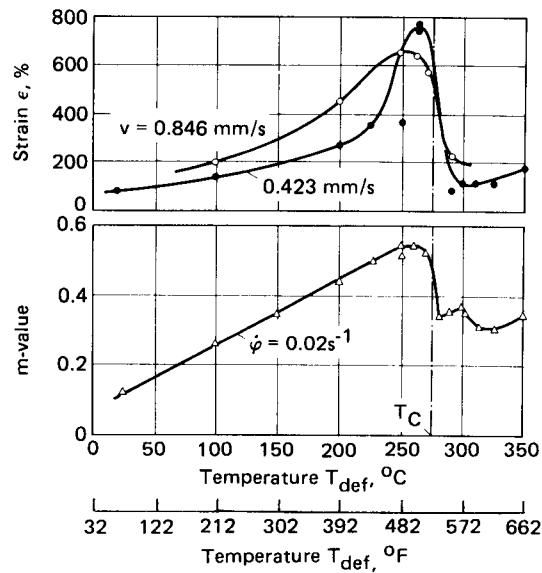


FIG. 30.2 Relationship between  $m$ -value and fracture strain obtained in uniaxial tension testing of titanium and zirconium alloys. Temperature range—20–1000°C (68–1832°F). (After [30.9].)

### METAL FORMING UNDER SPECIAL CONDITIONS



**FIG. 30.3** Dependence of *m*-value upon strain rate  $\dot{\phi}$  and grain size  $L$  (metallographic mean free path), obtained from uniaxial tension tests at  $20^\circ\text{C}$  ( $68^\circ\text{F}$ ) of a eutectic tin-lead alloy, extruded, and subjected to different heat treatments. Fracture strains based on constant starting strain rates  $\dot{\phi}$  are indicated on curves. (After [30.10].)



**FIG. 30.4** Temperature dependence of fracture strain and *m*-value in uniaxial tension of a nearly eutectoid ZnAl<sub>20</sub> alloy.  $T_C$ —eutectoid temperature;  $v$ —constant crosshead speed. (After [30.7].)

describe the grain-boundary sliding mechanism [30.14], but none seems to be preeminent. Diffusional creep mechanisms of the Nabarro-Herring type [30.15], [30.16] and the Coble type [30.17] as well as intragranular dislocation movement [30.1] appear to be involved in the accommodation of interfacial sliding. Joint action of grain-boundary sliding and dislocation slip within the grains are believed to be made possible by recovery processes between grain boundaries and dislocations (slip-recovery cycle) [30.13].

### 30.1.5 Superplastic Alloys and Their Properties

A number of surveys of presently known superplastic work materials have been conducted [30.1], [30.2], [30.4], [30.18], [30.19]. Table 30.1 lists a number of superplastic alloys and some of their properties.

Several methods for obtaining a fine-grained superplastic microstructure for tin-lead, zinc-aluminum, and iron-nickel-chromium alloys have been described [30.20]. The respective microstructures are achieved by hot forming alone for tin-lead alloys, by special heat treatment for zinc-aluminum alloys, and by a combination of hot or cold forming and special heat treatment for iron-nickel-chromium alloys.

A superplastic microstructure was obtained for a manganese steel through cold forming followed by repeated cyclic heat treatment [30.21]. A suitable microstructure can also be achieved by electrolytic segregation. Electrodeposited composites of copper-nickel were shown to have limited elongation in spite of high  $m$ -values, however [30.22]. This was shown to be due to intercrystalline void formation. Another effective method of obtaining a fine superplastic structure is by powder metallurgy, such as extrusion or rolling [30.7].

### 30.1.6 Applications

The first successful application of superplasticity was reported in 1949 [30.23]. Gaskets produced of "highly ductile" aluminum-zirconium alloys had proved very successful. The possibilities for superplastic sheet-metal forming were introduced when a balloon was formed from a nearly eutectoid aluminum-zirconium alloy rolled into sheet [30.7]. Sheet-metal parts of complicated shape geometry were produced from a eutectoid aluminum-zirconium alloy by evacuation in a die heated to 280°C (530°F) [30.24]. This demonstrated the ability of a superplastic material to reproduce the most detailed contours of a die. The production of automobile body parts (Fig. 30.5) and refrigerator doors from a eutectoid aluminum-zirconium alloy with superplastic prop-

**Table 30.1** Superplastic Alloys.

Material	Grain size $L$ (metallographic mean free path), $\mu\text{m}$ ( $\mu\text{in}$ )	Deformation temperature $T_{\text{def}}$ , $^{\circ}\text{C}$ ( $^{\circ}\text{F}$ )	Strain rate $\dot{\phi}$ , $\text{s}^{-1}$	Maximum $m$ -value <sup>a</sup>	Flow stress $\sigma_f$ , $\text{N/mm}^2$ ( $\text{psi}$ )
62Sn-38Pb	2.5 (98)	20 (67)	$3 \times 10^{-4}$	0.6	10 (1450)
78Zn-22Al	1.8 (71)	250 (480)	$1 \times 10^{-4}$	0.5	8.5 (1230)
67Mg-33Al	2.2 (87)	350 (750)	$3 \times 10^{-2}$	0.9	28 (4000)
67Al-33Cu	5 (197)	520 (970)	$4 \times 10^{-4}$	0.8	4 (580)
0.42C-1.87Mn					
0.24Si-0.02P	1.4 (55)	730 (1340)	$3 \times 10^{-5}$	0.7	21 (3000)
0.02S					
Ti-6Al-4V	7 (276)	950 (1740)	$1.5 \times 10^{-4}$	0.8	3.5 (510)
Ti-5Al-2.5Sn	20 (787)	1010 (1850)	$6 \times 10^{-4}$	0.7	4 (580)

<sup>a</sup>Grain size  $L$ , deformation temperature  $T_{\text{def}}$ , strain rate  $\dot{\phi}$ , and flow stress  $\sigma_f$  represent the values for which  $m$  is maximum.

Source: Compiled from [30.4].



**FIG. 30.5** Automobile door made from a superplastic ZnAl20 alloy at 250°C (482°F) in a die of heat-resistant concrete. (After [30.25].)

erties was attempted in England [30.25]. The deformation of a sheet of a eutectoid superplastic aluminum-zirconium alloy was investigated by performing the process in two parts [30.26]. First the forming of the sheet into the basic shape of the die (macroforming) was studied. This was followed by a study of the shaping of the fine details of the die (microforming). The production of round and rectangular cups with corrugated bottoms (Fig. 30.6) as well as hemispherical cups from different alloys with superplastic properties was also investigated [30.27]. One study dealt with the effects of pressure and deformation time on superplastic aluminum-zirconium sheet during 90° V-die bending [30.28], while another shed light on bending of Ti 6 Al 4 V sheet at temperatures of 600–900°C (1110–1650°F) [30.29]. Pipe sections of a eutectic superplastic lead-tin alloy were deformed by internal pressure (Fig. 30.7), and other intricately shaped parts as well as shells were produced from sheet blanks by a process illustrated in Fig. 30.8 [30.30]. Various investigations involving deformation of a eutectoid superplastic aluminum-zirconium alloy were reported in [30.31] (Fig. 30.9).

These sheet-metal deformation studies were carried out with processes basically identical to those used in the production of thermoplastics, such as vacuum forming (Fig. 30.10).

In an extrusion study a eutectic lead-tin alloy with superplastic properties was compared with pure lead under excellent lubrication conditions [30.32]. For widely different extrusion speeds the flow behavior of the two metals was found to be quite similar. This led to the conclusion that this

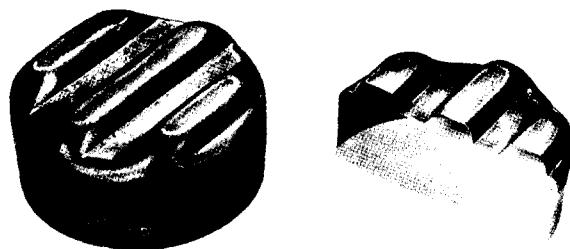


**FIG. 30.6** Cups with corrugated bottoms and different heights made of a superplastic Ti6Al4V at 925°C (1697°F). (After [30.27]; reprinted with permission of Pergamon Press, Ltd.)

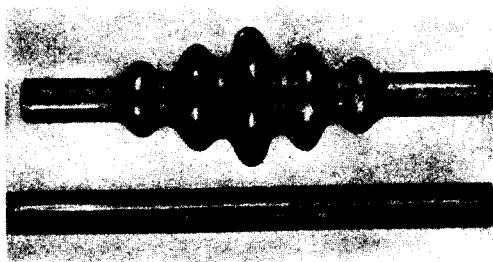


**FIG. 30.7** Segment of pipe of a eutectic superplastic lead-tin alloy expanded in a die by internal pressure at room temperature. (After [30.30]; reprinted with permission of Pergamon Press, Ltd.)

particular superplastic lead-tin alloy is suitable as model material for studying the flow behavior of ordinary metals in the plastic state. However, a subsequent study of direct forward extrusion of a eutectic superplastic lead-tin alloy indicated clearly that a change in strain rate and particularly in friction conditions can lead to considerable alterations in the flow behavior of such materials [30.33]. A process for the production of superplastic wires without die is described in [30.19]. Area reduction is achieved by passing an induction coil along a bar which is under tension, and creating a localized deformation zone by raising the metal to the required deformation temperature.

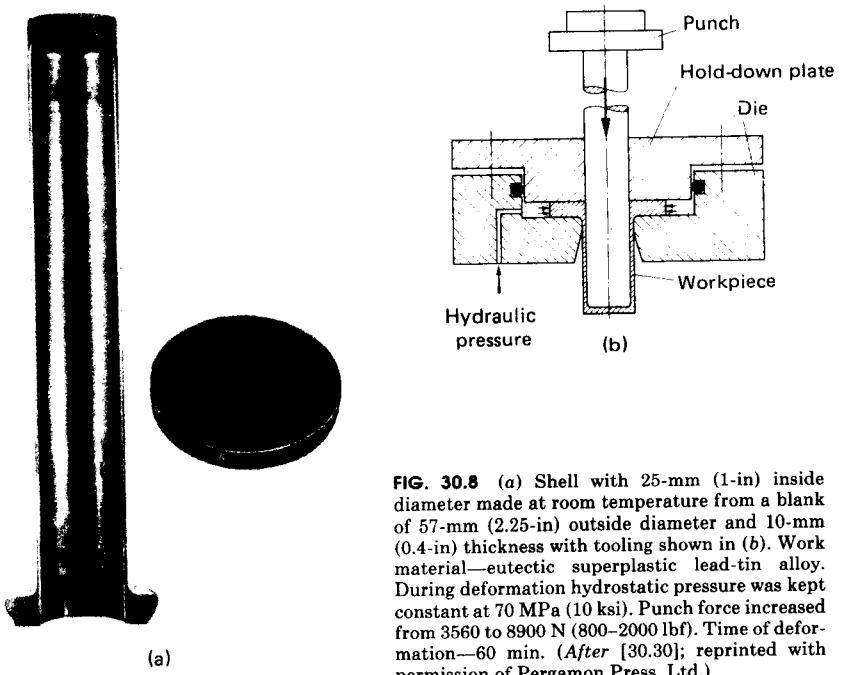


**FIG. 30.8** (a) Shell with 25-mm (1-in) inside diameter made at room temperature from a blank of 57-mm (2.25-in) outside diameter and 10-mm (0.4-in) thickness with tooling shown in (b). Work material—eutectic superplastic lead-tin alloy. During deformation hydrostatic pressure was kept constant at 70 MPa (10 ksi). Punch force increased from 3560 to 8900 N (800–2000 lbf). Time of deformation—60 min. (After [30.30]; reprinted with permission of Pergamon Press, Ltd.)

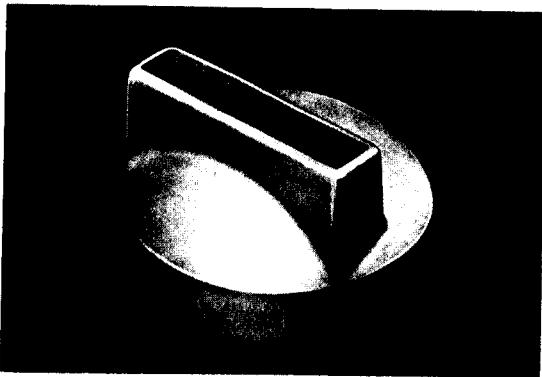


**FIG. 30.9** Housing part produced from eutectoid superplastic ZnAl12 alloy at about 250°C (482°F). (After 30.31); reprinted with permission of Pergamon Press, Ltd.)

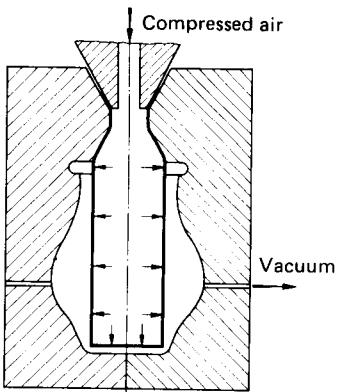


**FIG. 30.10** Schematic representation of superplastic forming of a cylindrical hollow container in heated, vertically split die. Forming with vacuum and pressure. (After [30.26].)

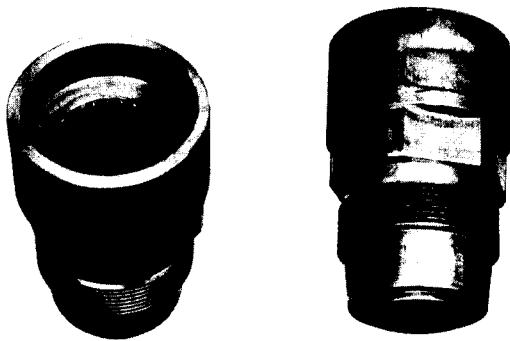


**FIG. 30.11** Prototype of a part produced from eutectic superplastic lead-tin alloy in a single operation at room temperature. (Courtesy of Holmes, Institut für Umformtechnik, Stuttgart University.)

Their excellent ability to fill dies and reproduce shapes make superplastic work materials suitable for other massive forming processes as well, such as indenting, coining, and impression die forging.

The possibilities of superplastic massive forming are demonstrated with the sample part shown in Fig. 30.11. The part was shaped from a eutectic lead-tin alloy with fine-grained superplastic microstructure at room temperature in a longitudinally split die in a single operation.

The superplastic state of the work material has advantages and disadvantages which are significant for production [30.34]. Both the low flow stresses and the high strains which can be achieved without necking represent a distinct advantage of superplastic materials for metal forming applications. For example, low flow stresses make possible the use of simpler tooling designed for lower loads. The high strains achievable without intermediate annealing and without necking make superplastic materials suitable for forming processes involving primarily tensile stresses in the deformation zone, such as sheet-metal forming processes. For these processes the dependence of flow stress upon strain rate is an advantage as thickness distribution is more uniform than in conventional forming.

The main disadvantages of superplastic work materials are the long time periods required for deformation, which may be as much as a thousand times higher than for conventional forming, and the requirement to form at temperatures  $T_{\text{def}} > 0.5T_m$ . It is expected, however, that a considerably finer microstructure will be achieved for many superplastic work materials in the future so that the strain rate could be increased for constant  $m$ -values. The need for new processes and increased expense in the production of superplastic work materials is an added disadvantage. Finally the creep tendency of superplastic materials must be eliminated after forming by special heat treatment.

All disadvantages associated with the manufacture of work materials with superplastic properties will diminish in significance as increased application and concomitant increased demand cause a reduction in the cost of work-material production. It is also expected that greater demand of superplastic work materials will spur the development of more economical methods for achieving fine-grained superplastic microstructures.

## 30.2 THERMOMECHANICAL TREATMENT

### 30.2.1 Survey of Processes and Terms

The entire spectrum of methods encompassing mechanical and thermal processes during forming has frequently been designated by the term thermomechanical treatment [30.35] to [30.40]. In view of the application to high-strength structural steels this term, abbreviated TM treatment, currently signifies a process characterized by specific criteria.

Thermomechanical treatment can be represented schematically as shown in Fig. 30.12. In simplified form the numerous combinations of mechanical and thermal treatments of steel, which are described in the literature and are frequently applied on a large-scale basis, are subdivided

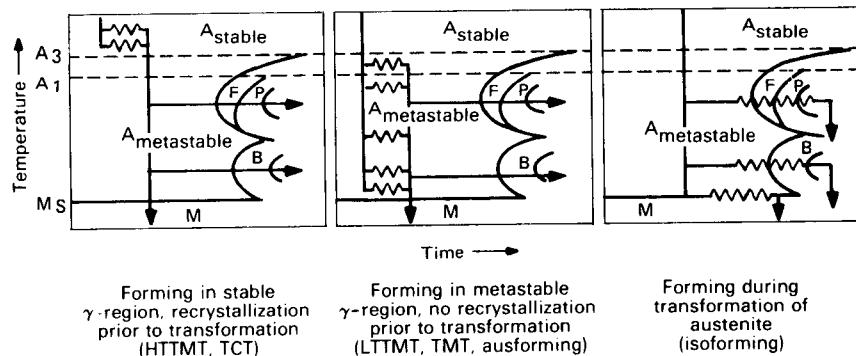


FIG. 30.12 Classification of thermomechanical treatments of steel. (After [30.36].)

## 30.12 METAL FORMING UNDER SPECIAL CONDITIONS

into three groups. The schematic time-temperature-transformation (TTT) diagrams illustrate the essential role of both deformation and  $\gamma/\alpha$  transformation on one hand and recrystallization on the other. The serrated line usually indicates the final stage of the transformation.

**High-temperature thermomechanical and temperature-controlled treatments:** If forming of steel occurs at relatively high temperature, where austenite is the stable form, recrystallization generally takes place prior to transformation. This process, known as high-temperature thermomechanical treatment, has been applied to common construction steels for many years. In this treatment, transformation takes place in the ferrite-pearlite stage following fine-grained recrystallization. The resulting microstructure and its mechanical properties correspond to those of the normalized state. Due to the necessity to carry out the last phase of the deformation in a specified temperature range, the term temperature-controlled rolling was introduced in Germany. Independent of this process and its equivalence to normalizing, the customary hot forming of bar stock, wire, and forgings belongs into the category of the treatments illustrated by the left diagram of Fig. 30.12.

**Low-temperature thermomechanical and thermomechanical treatments:** Whenever forming is carried out in the temperature range of metastable austenite, partial or complete recrystallization does not take place in many steels prior to transformation (Fig. 30.12 center). Instead, the transformation reaction precedes any recrystallization process. Thermomechanical treatment of structural steels falls into this category of processes in a narrower sense. This process is referred to as low-temperature thermomechanical treatment. In microalloyed steels, recrystallization is delayed significantly by deformation-induced precipitation. Because of very high dislocation densities, very small grain size, and extremely fine precipitates, the resulting ferritic and bainitic microstructure has mechanical properties which can be altered significantly by subsequent heat treatment.

Classical hot forming is not used whenever forming of metastable austenite takes place at temperatures at which the austenite decomposition product has a high hardness. This process, known as ausforming [30.41] to [30.43], requires a relatively high alloy content. This is necessary in order to maintain a field of austenite metastability sufficiently broad for deformation.

**Isoforming:** In principle deformation can be carried out during the  $\gamma/\alpha$  transformation (Fig. 30.12 right). This is known as isoforming. In eutectoid steels this leads to an unusual transformation which results in finely dispersed cementite instead of lamellar pearlite. A special case is represented by forming in the martensite formation temperature region, where martensite formation is accelerated by the deformed structure of the austenite.

A widespread concept in thermomechanical treatment should be mentioned, namely, controlled rolling of structural steel. This term should no longer be used, since it provides no unique definition, and hence cannot be categorized clearly. The designation TG (temperature-controlled treatment) or, more generally, thermomechanical treatment should be used instead.

### 30.2.2 Processes Caused by Thermal and Mechanical Treatments

Thermal processes preceding deformation are illustrated in Fig. 30.13. Austenitizing requires a definite time, which is dependent upon heating rate and holding temperature [30.44]. This must be taken into account, especially in cases of rapid heating as, for example, in inductive heating. Inhomogeneities in the austenite, caused by the dissolution of cementite and other phases, as well as by partitioning of carbon and other elements in two-phase alloys, are removed by diffusion processes. Complete elimination of all concentration variations is, however, unlikely.

For numerous structural steels containing carbonitride-forming elements the solution of finely dispersed precipitates plays an important role (Fig. 30.13 center). The state of partial or complete solution of the carbonitrides resulting from heating has a considerable effect upon the subsequent processes of microstructural change and renewed precipitation, during which the dissolved alloy [Me], and the remaining larger carbonitride particles play different roles.

Austenite grain growth is strongly impeded by particles of a definite size dispersion (Fig. 30.13 right). If the fine-particle density drops below the minimum number per unit volume required to restrict grain growth, accelerated grain growth ensues. This secondary recrystallization results in medium austenite grain sizes, which can be larger than those in steels without precipitate-forming elements.

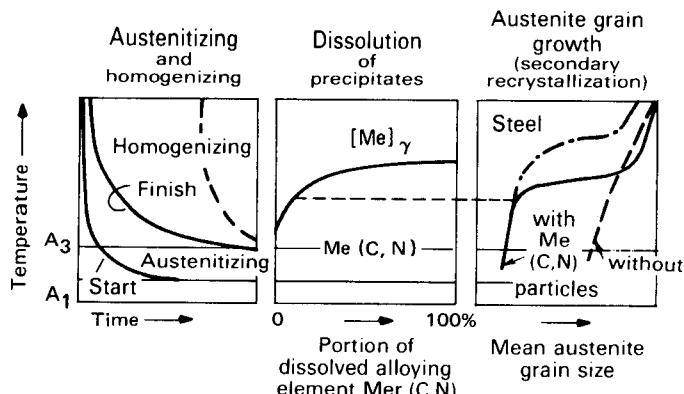


FIG. 30.13 Thermal processes prior to forming.

In recent years alloying systems have been studied which demonstrate significant resistance to dissolution and particle coarsening provided certain concentrations of the precipitate are present. These alloys, consequently, have a resulting small austenite grain size even when austenitizing temperatures are high. Especially TiN is a particularly effective precipitate in this regard.

For the utilization of precipitation processes during and after forming, carbonitride formers which dissolve readily prior to deformation are preferred. For high-strength structural steels with the customary carbon and nitrogen contents NbC, TiC, and VN are therefore important [30.45]. While the particles dissolve during holding at 1200°C (2190°F), significant supersaturation sets in at final rolling temperatures and during further cooling, and this leads to subsequent reprecipitation. For steels with higher carbon content the solubility of these alloys is too minimal at the heating temperatures prior to deformation. A comparable solubility state and subsequent precipitation hardening can be achieved with the more soluble VC. In practice, both temperature and time at temperature in the heating stage are important in affecting the structure of the austenite prior to deformation. During further forming and subsequent cooling, various interactions between hardening, recrystallization, transformation, and precipitation take place. Acceleration or retardation of the basic processes are the result. These interactions should be resolved into single steps to enhance understanding. For the description of the fundamental relationships schematic representations are usually selected, although a multitude of data for these problems are available in the literature [30.46] to [30.51].

### 30.2.3 Influencing the $\gamma/\alpha$ Transformation

#### *Initial State of the Austenite*

Transformation of a steel, which can be represented in the time-temperature domain, is not characterized solely by the cooling rate, but depends to a great extent upon the initial state of the austenite (Fig. 30.14). Starting from the time-temperature-transformation diagram of a structural steel after the customary austenitizing, an acceleration of the transformation is observed in certain cases. Ferrite or bainite formation begins at a higher temperature or after a shorter time period when incoherent, as yet undissolved particles become active as nuclei in the austenite (Fig. 30.14 center). On the other hand, a noticeably delayed transformation and increased hardening tendency are achieved when a very coarse austenite grain size is produced as a result of a high austenitizing temperature, and the austenite is alloyed by solution of MeX particles of metals like niobium or vanadium. The different effects of a carbonitride former can be demonstrated with niobium-alloyed steels (Fig. 30.15). Depending on the austenitizing temperature, the critical cooling period for the start of the ferrite-pearlite transformation is changed by more than an order of magnitude.

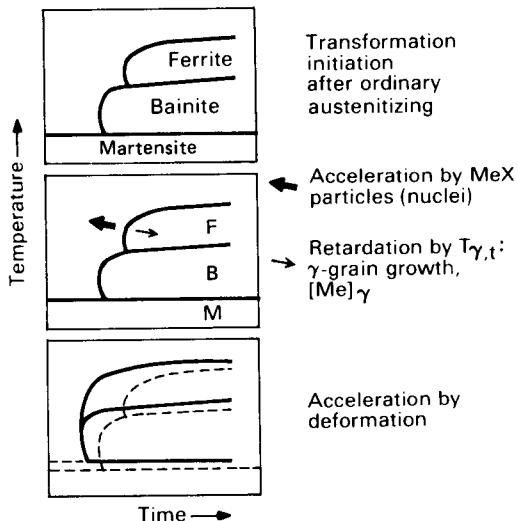


FIG. 30.14 Schematic diagram of  $\gamma/\alpha$  transformation as affected by initial state or austenite deformation.

### Preforming

The driving force for austenite transformation is increased by any stored energy of cold work which is manifested in the form of lattice defects such as dislocations. Such defects frequently serve as nucleation sites for the transformation as well. In the time-temperature-transformation diagram, prior deformation therefore manifests itself in a shift of the transformation curve toward

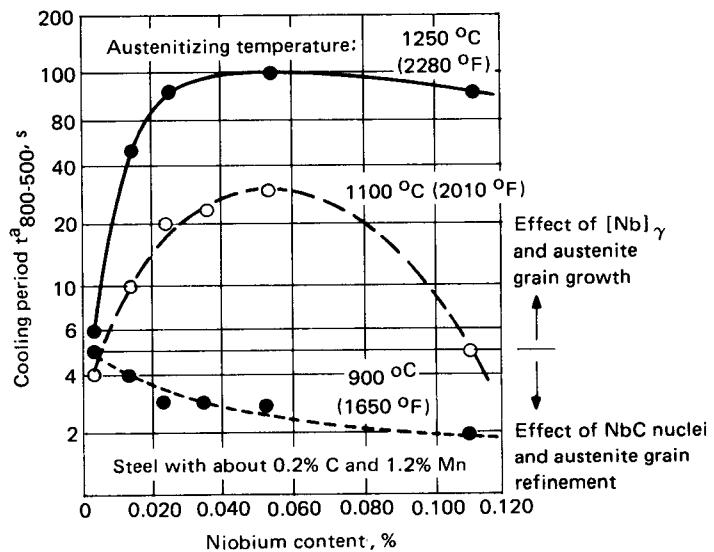


FIG. 30.15 Cooling periods for the initiation of ferrite-pearlite formation of niobium steels following austenitizing at different temperatures.

shorter times or higher temperatures (Fig. 30.14 bottom). The ferrite nose experiences the greatest shift [30.52]. For example, deformation caused an increase in the  $A_{rs}$  temperature of  $50^{\circ}\text{C}$  ( $120^{\circ}\text{F}$ ) in a low-carbon steel with fine austenite grains, while the deformation-dependent increase of the transformation temperatures corresponding to the maximum rate in a coarse-grained austenite was as high as  $150^{\circ}\text{C}$  ( $300^{\circ}\text{F}$ ) [30.53].

A characteristic of the austenite transformation of microalloyed steels is that the substructure of the resulting ferrite is frequently heavily or moderately dislocated. In these steels deformation-induced precipitation in effect prevents recrystallization from occurring in the austenite. This retardation can be passed on to the ferrite structure during transformation. Such a substructure not only stabilizes precipitation but contributes significantly to strengthening of the ferrite as well.

### 30.2.4 Deformation and Recrystallization

#### *Dynamic Recrystallization*

At first, deformation at high and at low temperatures leads to an increase in strength due to dislocation multiplication and entanglement. When deformation reaches an amount sufficient to induce spontaneous or dynamic recrystallization, considerable softening sets in. A maximum in the flow curve is the result (Fig. 30.16).

A microalloyed steel differs from a plain carbon steel in that its flow stress rises and the critical deformation  $\epsilon_c$  required for triggering dynamic recrystallization increases significantly. The cause for the delayed dynamic recovery and recrystallization lies in the fact that the motion of dislocations and subgrain boundaries is slowed down considerably by the presence of solute atoms and freshly formed precipitates. Therefore the tendency for microalloyed steels to soften by recrystallization during rolling is substantially reduced.

An additional consequence of the newly formed precipitates is the fine-grained recrystallization microstructure which is maintained, as mentioned previously, by retardation of grain growth.

#### *Static Recrystallization*

When deformation is interrupted before reaching the critical strain, and the test sample is unloaded but held at temperature, static recrystallization can take place. In the recent past, several careful investigations have been conducted involving different testing methods such as hot torsion, hot upsetting, hot tension, and hot rolling, all of which yield a logical interpretation of the recrystallization processes in steels with alloying elements capable of precipitation. The results can be presented schematically in time-temperature diagrams (Fig. 30.17).

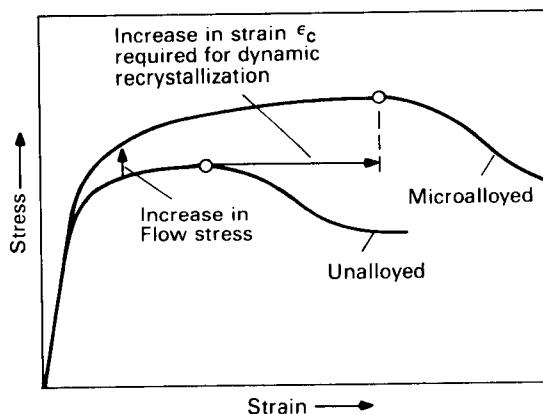
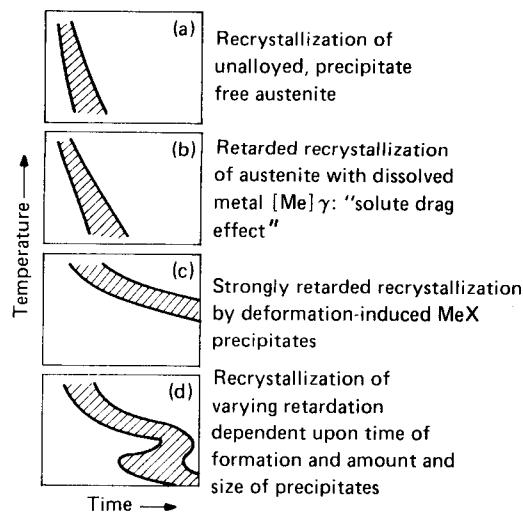


FIG. 30.16 Hot-flow curves of unalloyed and microalloyed structural steels.



1. Dissolution of Me (C, N) in austenite:  $\text{Me} (\text{C}, \text{N}) \longrightarrow [\text{Me}]_\gamma + [\text{C}, \text{N}]_\gamma$
2. Forming below recrystallization temperature  $T_\epsilon < T_R$
3. Recrystallization retardation by Me (C, N) precipitation due to sufficient supersaturation of the deformed austenite

$$S = \frac{[\text{Me}] [\text{C} + 12/14\text{N}] \text{ actual at } T_\epsilon}{[\text{Me}] [\text{C} + 12/14\text{N}] \text{ equilb. at } T_\epsilon}$$

4. Transformation of the unrecrystallized austenite:  $\gamma_\epsilon \longrightarrow \alpha$
5. Controlled cooling

**FIG. 30.17** Schematic diagram of the influence of dissolved or precipitating alloy metals on static recrystallization after hot forming.

In plain carbon steel, static recrystallization is slowed down with decreasing temperature, yet it takes place within a few seconds (Fig. 30.17a). However, if the austenite contains alloying elements in solid solution, which exhibit a strong solute drag effect, recrystallization is retarded (Fig. 30.17b). In addition to the effect of dissolved microalloying elements, a weak effect is discernible for other solid solution formers such as molybdenum, manganese, chrome, and nickel. In a recent study [30.54] a doubling of the time for 50% recrystallization at 900°C (1650°F) was observed when 0.02% vanadium, 0.2% chromium, or 0.2% nickel were added to the comparison steel. The addition of 0.2% molybdenum delayed recrystallization by a factor of 10 in the time scale.

#### ***Deformation-Induced Precipitates***

Recrystallization is decisively retarded when carbonitride formers, which are originally in solution in the austenite, precipitate rapidly in a fine dispersion in the deformed microstructure (Fig. 30.17c). The causes for this deformation-induced precipitation are favorable conditions for nucleation and accelerated diffusion of the affected atoms. In the lower range of the customary hot-forming temperatures, the deformed substructure can be stabilized by minute precipitates in such a way that recrystallization cannot be completed and effectively comes to a halt. The most effective particle diameter appears to be on the order of 5 nm.

Studies conducted with low-carbon steels containing niobium or titanium [30.55] allow a comparison between these microalloying elements, which are important for thermomechanically treated steels (Fig. 30.18). With equal alloy content, niobium displays an increasingly strong effect on recrystallization with decreasing temperatures. At 850°C (1560°F) it delays the time for soft-

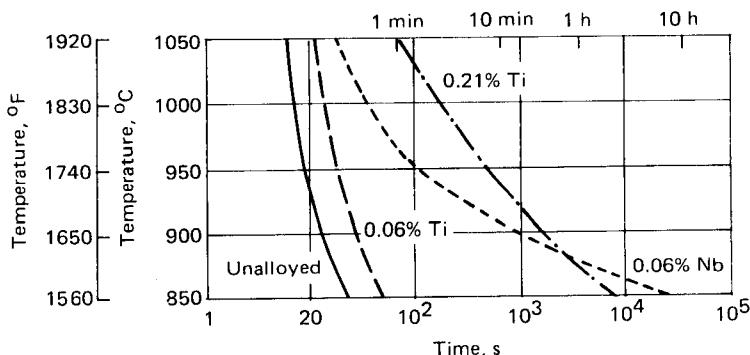


**FIG. 30.18** Static recrystallization. Holding time for 90% softening in niobium- or titanium-alloyed steels containing 0.05% carbon and 0.60% manganese. (After [30.55].)

engineering by three orders of magnitude. Higher titanium contents, as they are customary in microalloyed steels, have a similarly strong retarding effect. Compared to these elements, vanadium effects a one hundred times smaller recrystallization retardation.

It is clear that the effects of the precipitates on the mobility of subgrain and grain boundaries depends upon the number and size of the precipitates (Fig. 30.17d). At relatively low temperatures precipitation is increasingly impeded by slower diffusion of the alloy atoms. Thus an overall S-shaped recrystallization diagram can result.

#### **Recrystallization Process in the Rolling Mill**

Static recrystallization is important for the understanding of softening and the nucleation of recrystallized grains between two deformation steps, such as between rolling reductions during rolling of plate stock. For forming steps occurring in rapid succession, as in the finishing stage of hot rolling of sheet, where the rolling temperatures correspond to the lower temperature limits for austenite stability, static recrystallization apparently no longer occurs according to available data, at least not in microalloyed steels. At best only dynamic recrystallization can take place under these circumstances.

Based on temperature and forming conditions prevalent for the finishing process of a hot-rolling mill for sheet, a comparison was made of the actual deformation—the total deformation summed from stand to stand—with the critical deformation required for dynamic recrystallization for 8-mm (0.32-in) thick steel sheet with different niobium and titanium contents (Fig. 30.19). Recrystallization becomes possible whenever the total deformation exceeds the critical deformation. Figure 30.19a indicates that this condition is satisfied in the second rolling stand for the plain carbon steel and the steel containing 0.06% titanium. By contrast, the critical deformation curve for the steel containing 0.06% niobium lies far above the total deformation curve. Conditions for dynamic recrystallization do not exist during finish rolling of steels with typical microalloying content (Fig. 30.19b). In both steels noted deformation accumulates with concomitant hardening until the rolling process is complete. Since no static recrystallization can take place subsequently, the  $\gamma/\alpha$  transformation emanates from a heavily deformed austenite.

#### **30.2.5 Influencing Precipitation**

##### **Precipitation Kinetics**

While thermodynamical data concerning the solubility of carbonitride-forming alloying elements provide the framework for the precipitation behavior, the kinetics are determined by the condi-

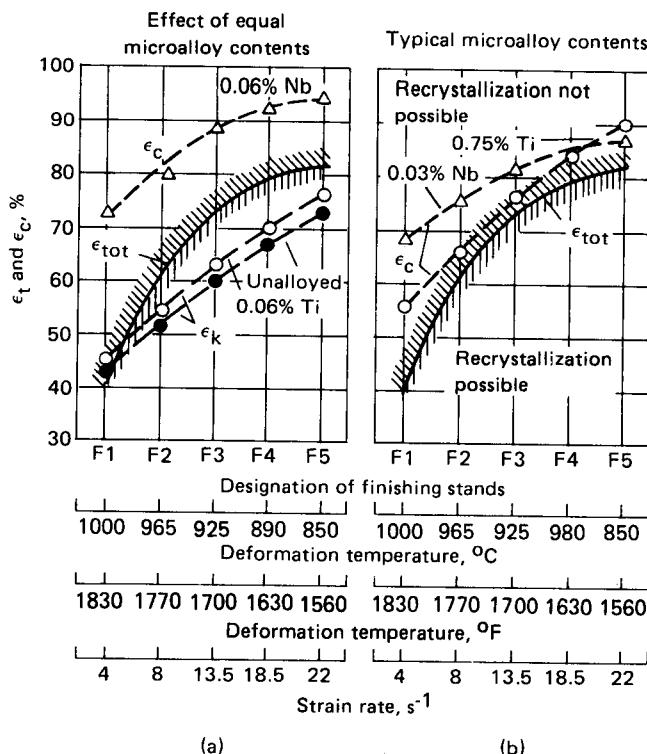


FIG. 30.19 Comparison of critical deformation  $\epsilon_c$  for dynamic recrystallization with total deformation  $\epsilon_{tot}$  of rolling sequence of a hot-rolling finishing mill for niobium- or titanium-alloyed steel sheet. (After [30.55].)

tions of nucleation and growth. As growth of precipitates is significantly impeded with decreasing temperature, an increasingly severe retardation of the transformation occurs at lower temperatures in spite of increasing supersaturation of the solid solution. As a result, precipitation curves in the time-temperature domain display a characteristic C-shape (Fig. 30.20).

If nucleation of particles and the diffusion of alloy atoms are significantly facilitated by deformation of the supersaturated austenite, precipitation occurs considerably more rapidly. Whether deformation is already completed when precipitation begins, or dynamic precipitation during slow deformation is involved, as in the present example [30.56], is of minor importance. In the lower temperature region of the austenite, precipitation kinetics are accelerated by two or three orders of magnitude. Under conditions typical for engineering deformations, an increase of strain and strain rate intensifies the acceleration of the subsequent precipitation.

#### Precipitation–Recrystallization Interdependence

The relationship between precipitation and recrystallization described earlier can be characterized as one of interdependence [30.56], [30.57] (Fig. 30.21). While recrystallization and precipitation of MeX particles occur in sequence independently of one another at high temperatures, a marked acceleration of precipitation is observed for sufficient supersaturation of the deformed solid solution below a critical temperature (arrow P). Substructure and grain-boundary mobilities are reduced simultaneously because of the rapidly nucleating particles (arrows R).

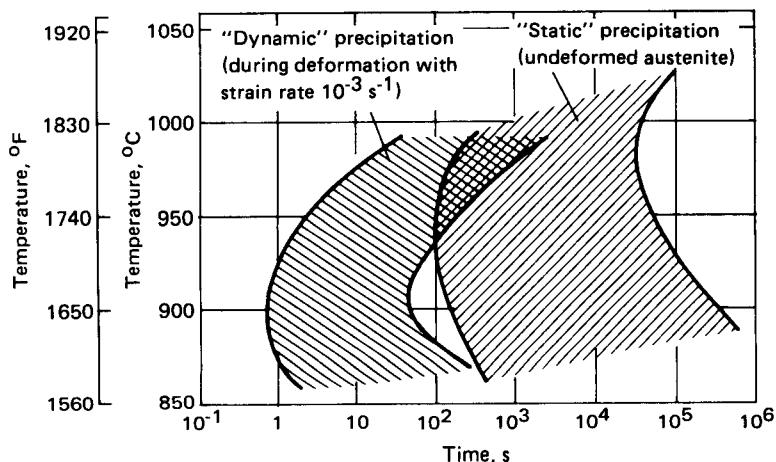


**FIG. 30.20** Precipitation of Nb(C,N) in undeformed austenite or during slow deformation. Steel containing 0.05% carbon and 0.035% niobium. (After [30.56].)

To apply the principle of recrystallization retardation during the thermomechanical treatment of structural steel, it is desirable to know accurately the critical temperature below which the thermomechanical effect can be utilized. At this point only data regarding supersaturation of the MeX precipitation are available.

If supersaturation is defined as the ratio of the product of the reaction components actually in solution and the product of the components in equilibrium solution, a minimum of a fivefold supersaturation is required for deformation-induced precipitation [30.58]. Of course, precipitation kinetics depend also upon strain and strain rate.

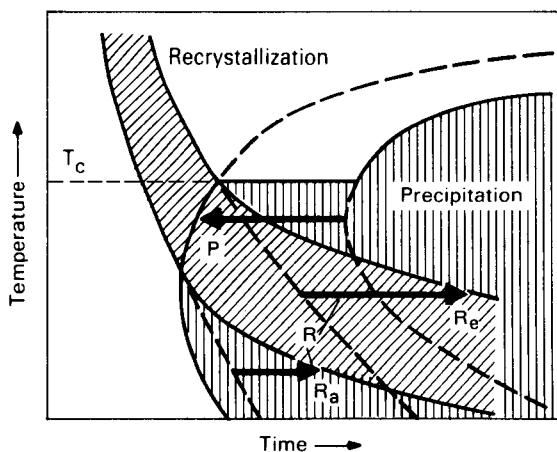


**FIG. 30.21** Schematic diagram of interdependence of recrystallization  $R$  and precipitation  $P$ . Retardation of  $R$ , acceleration of  $P$ .

### 30.2.6 Thermomechanical Treatment of Microalloyed Structural Steels

#### *Hot-Rolled Sheet*

An especially effective link between thermal and mechanical processes during forming can be demonstrated with thermomechanical treatment of sheet or strip of microalloyed structural steels as an example. The individual steps described above are part of an entire process sequence (Fig. 30.17). During heating of the workpiece material, at least a partial solution of carbonitrides must occur. In addition, a reduction in initial grain size can be achieved by reduction of the furnace temperature which is usually kept at 1250°C (2280°F). Total deformation is adjusted so that a larger amount of deformation remains to be applied only when no additional recrystallization will ensue. For sufficient supersaturation of the solid solution with alloy metal, carbon, and nitrogen, recrystallization is delayed by deformation-induced precipitation to such an extent that transformation and recrystallization occur concurrently. The result is a structure with favorable mechanical properties.

#### *Microstructural Characteristics*

The ferrite structure is characterized by a very fine ferrite grain size and extremely fine precipitates. These structural characteristics stabilize the ferrite against recovery and recrystallization effects. Since the austenite exhibits a deformation texture prior to transformation, the ferrite transformation product does also; the orientation relationship is that of Kurdjumov-Sachs. During rolling of flat stock a texture develops with concentration about the {112}〈110〉 orientation.

A peculiarity of the ferrite resulting from thermomechanical treatment is its tendency to form cracks. This becomes apparent after considerable cold forming [30.57]. Under special loading conditions, test samples or structural parts show cracks in the rolling direction.

#### *Mechanical Properties*

The characteristics of the ferrite structure of thermomechanically treated structural steels described above determine the macroscopic mechanical properties of the rolled product. The most important property, and the one affected the most, is the flow strength. Almost all structural characteristics described above contribute to its increase. This structural strengthening permits a reduction of conventional solute-strengthening elements in the composition of steel, particularly carbon. The simultaneous lowering of the ductile-to-brittle transition temperature is the result of the dominating influence of grain refinement. A reduction in toughness as an indication of reduced ductility is a consequence of the higher strength level and a certain longitudinal orientation of the microstructure. The texture-dependent anisotropy in the rolling direction increases with increasing intensity of the thermomechanical treatment.

Application of the thermomechanical treatment is explained briefly with hot-rolled sheet or plate as an example. It should be noted that the principle of thermomechanical treatment can also be utilized for structural shapes.

### 30.2.7 Recent Developments in Flat Steel

#### *Rolling in the Two-Phase Region*

An obvious extension of the classical thermomechanical treatment consists in shifting the final rolling step into the  $(\gamma + \alpha)$  two-phase region. Large increases in dislocation density, formation of subgrains, and promotion of precipitation in ferrite collectively result in considerable strengthening. With an increasing proportion of ferrite in the deformed microstructure the {100} component in the texture, which promotes brittle fracture, increases. When the increased occurrence of subcritical microcracks (which are beneficial since they reduce the triaxiality of stresses) cannot compensate for the detrimental effect of dislocation density, precipitation hardening, and texture, intensified deformation in the two-phase region can lead to an increase in the brittle-fracture temperature. Tension testing at room temperature no longer shows a distinct yield point for steel rolled in the two-phase region, since ferrite has been deformed in the rolling sequence.

### ***Direct Quenching and Tempering***

There is a special incentive to combine forming and heat treatment through direct quenching and tempering [30.59], [30.60]. Currently technical problems stand in the way of a broader application of direct quenching and tempering.

### ***Cooling***

If the temperature obtained via accelerated cooling after forming does not reach the martensite start temperature, a microstructure consisting of bainite and ferrite with high dislocation density can result. Its tensile strength is determined to a great extent by the bainite content and its yield strength by the grain and bainite needle size [30.61]. If rapid cooling is intercepted above the age-hardening temperature region, precipitation hardening can take place as well.

### ***SHT Process***

A combination of sheet rolling and normalizing has been developed in Japan during which a cooling and reaustenitizing step is inserted prior to final rolling. This method, known as the SHT process, results in an especially fine-grained, uniform microstructure. It also requires considerable adaptation to be applied commercially [30.62].

### ***Dual-Phase Microstructure***

A mixed microstructure consisting primarily of ferrite with embedded martensite has proven especially useful for thin- and medium-gauge sheet, which is expected to possess high tensile strength and good cold formability [30.63]. Steel strip with such a dual-phase microstructure can be produced by annealing in the  $(\gamma + \alpha)$  two-phase region with subsequent accelerated cooling. If suitable continuous heat-treating furnaces are not available, hot rolling must be combined with cooling, which is controlled in such a way that a dual-phase microstructure is formed without additional heat treatment. For existing hot strip rolling mills, a method must be determined to influence appropriately the transformation behavior as it is related to the chemical composition of the steel [30.64], [30.65].

## **REFERENCES**

- 30.1 Taplin, D. M. R., Dunlap, G. L., and Langdon, T. G.: "Flow and Failure of Superplastic Materials," *Ann. Rev. Mater. Sci.*, **9**, 1979, pp. 151–189.
- 30.2 Stüwe, H. P.: "Superplasticity" (*in German*), *Z. Metallk.*, **61**, 1970, pp. 704–710.
- 30.3 Weiss, V.: "Superplasticity" (*in German*), *Metall*, **23**, 1969, pp. 1264–1269.
- 30.4 Schröder, G., and Winter, K.: "Superplastic Materials—A Survey" (*in German*), *Ind.-Anz.* **92**, 1970, pp. 425–430.
- 30.5 Backofen, W. A., Azzarto, F. J., Murty, G. S., and Zehr, St. W.: "Superplasticity," in *Ductility*, Metals Park, OH, American Society for Metals, 1968.
- 30.6 Cline, H. E., and Alden, T. H.: "Rate-Sensitive Deformation in Tin-Lead Alloys," *Trans. AIME*, **239**, 1967, pp. 710–714.
- 30.7 Backofen, W. A., Turner, I. R., and Avery, D. H.: "Superplasticity in an Al-Zn Alloy," *Trans. ASM*, **57**, 1964, pp. 980–990.
- 30.8 Dieter, G. E.: *Mechanical Metallurgy*, 2d ed., McGraw-Hill, New York, 1976, pp. 352–353.
- 30.9 Lee, D., and Backofen, W. A.: "Superplasticity in Some Ti and Zr Alloys," *Trans. AIME*, **239**, 1967, pp. 1034–1040.
- 30.10 Avery, D. H., and Backofen, W. A.: "A Structural Basis for Superplasticity," *Trans. ASM*, **58**, 1965, pp. 551–562.

### 30.22 METAL FORMING UNDER SPECIAL CONDITIONS

- 30.11 Floreen, S.: "Superplasticity in Pure Nickel," *Scripta Metall.*, **1**, 1967, pp. 19-23.
- 30.12 Holt, D. L., and Backofen, W. A.: "Superplasticity in the Al-Cu Eutectic Alloy," *Trans. ASM*, **59**, 1966, pp. 755-768.
- 30.13 Lee, D.: "The Nature of Superplastic Deformation in the Mg-Al Eutectic," *Acta Metall.*, **17**, 1969, pp. 1057-1069.
- 30.14 Langdon, T. G.: "The Significance of Grain Boundary Sliding in Creep and Superplasticity," *Met. Forum*, **4**, 1981, pp. 14-23.
- 30.15 Nabarro, F. R. N.: "Report of the Conference on Strength of Solids," London, The Physical Society, 1948, p. 75.
- 30.16 Herring, C.: "Diffusional Viscosity of a Polycrystalline Solid," *J. Appl. Phys.*, **21**, 1950, pp. 437-445.
- 30.17 Coble, R. L.: "A Model for Boundary Diffusion Controlled Creep in Polycrystalline Materials," *J. Appl. Phys.*, **34**, 1963, pp. 1679-1682.
- 30.18 Johnson, R. H.: "Superplasticity. Metals and Materials," *Metal. Rev.*, **146**, no. 4, 1970, pp. 115-134.
- 30.19 Pearce, R., and Swanson, C. J.: "Superplasticity and Metal Forming," *Sheet Met. Ind.*, **47**, 1970, pp. 599-604.
- 30.20 Hayden, H. W., Gibson, R. C., and Brophy, J. H.: "Superplastic Metals," *Sci. Am.*, **220**, 1969, pp. 28-35.
- 30.21 Schadler, H. W.: "The Stress-Strain Rate Behavior of a Manganese Steel in the Temperature Range of the Ferrite-Austenite Transformation," *Trans. AIME*, **242**, 1968, pp. 1281-1287.
- 30.22 Holmes, B. B.: "Mechanical Behavior of Electrodeposited Composites of Copper-Nickel," Cambridge, M.I.T., MA, 1969.
- 30.23 Sauerwald, F.: "On the Highly Ductile State of Al-Zn Alloys" (in German), *Arch. Metallk.*, **5**, 1949, pp. 165-173.
- 30.24 Fields, D. S.: "Sheet Thermoforming of a Superplastic Alloy," *IBM J. Res. Develop.*, **9**, 1965, pp. 134-136.
- 30.25 "A New Work Material for Automobile Bodies" (in German), *Ind.-Anz.*, **91**, 1969, pp. 1101-1102.
- 30.26 Thomsen, T. H., Holt, D. L., and Backofen, W. A.: "The Forming of Superplastic Sheet Metal in Bulging Dies," in Final Report, "Deformation Processing of Anisotropic Metals," July 1, 1968, through June 30, 1969, Cambridge, MA, M.I.T., 1969.
- 30.27 Cornfield, G. C., and Johnson, R. H.: "The Forming of Superplastic Sheet Metal," *Int. J. Mech. Sci.*, **12**, 1970, pp. 479-490.
- 30.28 Holt, D. L.: "An Analysis of the Bulging of a Superplastic Sheet by Lateral Pressure," *Int. J. Mech. Sci.*, **12**, 1970, pp. 491-497.
- 30.29 Wilkening, W. W., and Backofen, W. A.: "Hot Bending of Ti-6Al-4V," in Final Report, "Deformation Processing of Anisotropic Metals," July 1, 1968, through June 30, 1969, Cambridge, MA, M.I.T., 1969.
- 30.30 Al-Naib, T. Y. M., and Duncan, J. L.: "Superplastic Metal Forming," *Int. J. Mech. Sci.*, **12**, 1970, pp. 463-477.
- 30.31 Fields, D. S., and Stewart, T. J.: "Strain Effects in the Superplastic Deformation of 78Zn-22Al," *Int. J. Mech. Sci.*, **13**, 1971, pp. 63-75.
- 30.32 Jovane, F., Shabaik, A. H., and Thomsen, E. G.: "Some Extrusion Studies of the Eutectic Alloy of Pb and Sn," *Trans. ASME, J. Eng. Ind.*, **91B**, 1969, pp. 680-686.
- 30.33 Schelosky, H., Schröder, G., and Winter, K.: "Investigation of the Superplastic Behavior of an Extruded Eutectic Pb-Sn Alloy" (in German), *Ind.-Anz.*, **94**, 1972, pp. 1045-1048.
- 30.34 Naziri, H., and Pearce, R.: "A Guide to Superplasticity," *Sheet Met. Ind.*, **46**, 1969, pp. 11-14.

- 30.35 Meyer, L.: "Fundamentals of Work Material Development by Combining Thermal and Mechanical Processes during Preforming" (*in German*), *Stahl u. Eisen*, **101**, 1981, pp. 483–491.
- 30.36 Lepot, L., Greday, T., and Habraken, L.: "Thermomechanical Treatment of Steel" (*in French*), Report MPS 76, Centre National de Recherches Metallurgiques (CNRM), Liège, Belgium, 1968.
- 30.37 Schmidtmann, E.: "Effect of a Thermomechanical Treatment on the Recrystallization and Transformation Behavior of Steels" (*in German*), in Dahl, W., Ed.: *Grundlagen des Festigkeits- und Bruchverhaltens (Fundamentals of Strength and Fracture Behavior)*, Düsseldorf, Verlag Stahleisen, 1974, pp. 232–238.
- 30.38 Rassmann, G., and Müller, P.: "On the Interpretation of the Strengthening of Steels by Thermomechanical Treatment" (*in German*), *Neue Hütte*, **17**, 1972, pp. 2–7.
- 30.39 Delaey, L.: "Thermomechanical Treatment of Alloys" (*in German*), *Z. Metallk.*, **63**, 1972, pp. 531–541.
- 30.40 Zackay, V. F.: "Thermomechanical Processing," *Mater. Sci. Eng.*, **25**, 1976, pp. 247–261.
- 30.41 Burmester, J.: "Material Behavior and Residual Stress State after Ausforming" (*in German*), Dr.-Ing. thesis, Technische Universität, Hannover, 1968.
- 30.42 Möller, J.: "On the Effect of Several Alloying Elements on the Strengthening of Steels by Ausforming" (*in German*), Dr.-Ing. thesis, Technische Universität, München, 1969.
- 30.43 Bühler, H., and Liebig, H. P.: "Basic Difficulties during the Production of Ausformed Forgings and Methods to Overcome Them" (*in German*), *Stahl u. Eisen*, **92**, 1972, pp. 209–211.
- 30.44 Ohrlich, J., Rose, A., and Wiest, P.: "Time-Temperature Austenitizing Diagrams" (*in German*), in *Atlas zur Wärmebehandlung*, vol. 3, Düsseldorf, Max-Planck-Institut für Eisenforschung, 1973.
- 30.45 Irvine, K. J., Pickering, F. B., and Gladman, T.: "Grain-Refined C-Mn Steels," *J. Iron Steel Inst.*, **205**, 1967, pp. 161–182.
- 30.46 "The Hot Deformation of Austenite," in Ballance, J. B., Ed.: *Proceedings of the TMS-AIME Fall Meeting* (Cincinnati, OH, Nov. 11–13, 1975), New York, AIME, 1977.
- 30.47 Pritsch, W., Ed.: "Fundamentals of Heat Treatment of Steel (Transformation, Precipitation, Recrystallization)," Düsseldorf, Verlag Stahleisen, 1976.
- 30.48 "Microalloying, 75," in *Proceedings of the International Symposium on High-Strength, Low-Alloy Steels* (Washington, DC, Oct. 1–3, 1975), New York, Union Carbide Corporation, Metals Division, 1977.
- 30.49 Le Bon, A., Rofes-Vernis, J., and Rossard, C.: "Recrystallization and Precipitation Caused by Hot Forming of Weldable Structural Steels Microalloyed with Niobium" (*in French*), in *Traitements thermomécaniques des aciers*, EGKS-Report EUR 6131, Europäische Gemeinschaft für Kohle und Stahl, 1978, pp. 221–275.
- 30.50 Abrams, H., et al., Ed.: *Optimization of Processing, Properties, and Service Performance through Microstructural Control*, Philadelphia, PA, H. Abrams, 1979.
- 30.51 Hertel, J.: "A Model of Dynamic Recovery of Steels during Hot Forming" (*in German*), Dr.-Ing. thesis, Technische Universität, Aachen, 1979.
- 30.52 Desalos, Y., Laurent, R., and Le Bon, A.: "Influence of Austenite Work Hardening on the Transformation Behavior of Low- and Medium-Alloy Steels" (*in French*), *Mém. Sci. Rev. Metall.*, **76**, 1979, pp. 377–396.
- 30.53 Tanaka, T., and Tabata, N.: "Measurement of Austenite-to-Ferrite Transformation Temperatures in Niobium-Bearing Steels during Controlled Rolling" (*in Japanese*), *Tetsu to Hagané*, **64**, 1978, pp. 1353–1362.
- 30.54 Kunitake, T., Fujino, N., and Maehara, Y.: "Investigation of Recrystallization Behavior of Austenite by a Double-Tension Method," *Trans. Iron Steel Inst. Jpn.*, **20**, 1980, p. B-1405.
- 30.55 Robiller, G., and Meyer, L.: "Work Hardening and Softening Behaviour of Ti- and Nb-

- Alloyed Steels during Hot Deformation," in *Recrystallization and Grain Growth of Multi-Phase and Particle Containing Materials* (1st Ris International Symposium on Metallurgy and Materials Science, 1980), pp. 311-316.
- 30.56 Weiss, I., and Jonas, J. J.: "Interaction between Recrystallization and Precipitation during High Temperature Deformation of HSLA Steels," *Metal. Trans.*, **10A**, 1979, pp. 831-840.
- 30.57 Köster, U., and Hornbogen, E.: "Electronmicroscopic Study of the Precipitation of Copper and the Recovery Processes in Deformed Aluminum-Copper Solid Solutions" (in German), *Z. Metallk.*, **59**, 1968, pp. 792-799.
- 30.58 Hansen, S. S., Van der Sande, J. B., and Cohen, M.: "Niobium Carbonitride Precipitation and Austenite Recrystallization in Hot Rolled Micro-Alloyed Steels," *Metal. Trans.*, **11A**, 1980, pp. 387-402.
- 30.59 Beck, H.: "Effect of Heat Treatment from Rolling Heat upon Material Properties of Rolled Steel Wire and Bar Stock" (in German), *Stahl u. Eisen*, **101**, 1981, pp. 541-550.
- 30.60 Fascher, P., Klemz, R., Hüskes, H.-R., Schmidt, R., and Bender, W.: "Simplified Heat Treatment" (in German), *VDI-Z.* **122**, 1980, pp. 939-949.
- 30.61 Ouchi, C., et al.: in *Optimization of Processing, Properties, and Service Performance through Microstructural Control*, Philadelphia, PA, H. Abrams, 1979, pp. 105-125.
- 30.62 *The Development of a New Process for Production of High-Toughness Steel by Special Thermomechanical Treatment*, Sumitomo Metal Industries Ltd., twenty-fifth grand production prize, Japan. See also Tanaka, T., Nozaki, N., Bessyo, K., Fukuda, M., and Hashimoto, T.: Sumitomo Research, no. 19, 1978, pp. 47-61.
- 30.63 Becker, J., et al.: "Dual-Phase Microstructures" (in German), *Z. Metallkd.*, **7**, 1980, pp. 27-  
*Z. Metallk.*, **7**, 1980, pp. 27-31.
- 30.64 Coldren, A. P., and Eldris, G. T.: "Using CCT Diagrams to Optimize the Composition of an As-Rolled Dual-Phase Steel," *J. Met.*, **32**, 1980, pp. 41-48.
- 30.65 Kunishige, K., Takahashi, M., Sugisawa, S., and Mazui, Y.: "As-Rolled Dual-Phase Steel with Good Ductility and High Strength" (in Japanese), *Tetsu to Hagané*, **65**, 1979, pp. 1916-1925.

6

## **TOOLS FOR METAL FORMING**

多謝你，我會仔細閱讀你的意見，並考慮如何改善。



**DIES FOR METAL  
FORMING, SEPARATING  
AND JOINING  
PROCESSES**

• PAPER RECYCLED IN U.S.A. • 100% POSTCONSUMER

In manufacturing, dies are used in the application of primary forming, deforming, separating, and joining. Among the important deforming processes are die forging of steels and nonferrous metals, cold bulk-forming processes, such as extrusion, upsetting, and coining, as well as deep drawing, recessing, bending of sheet-metal components, and numerous other processes and process combinations. Dies are used in the separating processes, such as blanking, piercing, clipping, and trimming. In joining processes, dies are used, for example, when two hollow bodies are joined by explosive forming or riveting.

Die working surfaces may vary in size from a few square millimeters up to several square meters. The masses involved vary from less than 0.1 kg (0.2 lb) to about 50 t (55 tons).

**31.1 BASIC FEATURES OF A DIE**

**31.1.1 Definition and Function**

Dies, in the sense of the introductory remarks, are all tools which completely or in part contain the negative contour of the workpiece and either transmit this to the workpiece, the latter thus being deformed in the dies [31.1], or contact an already preformed workpiece so that the latter can be further processed. The first application is typical of deformation processes, for example, forging dies and tools for electrohydraulic stretch forming. The second is typical of separating and joining processes, for example, clipping and trimming dies for sheet-metal components (Fig. 31.1).

The stresses exerted on the dies vary. In deformation processes they are caused by forces, heat, and material movement (resulting in frictional wear and surface erosion); in separating processes they are mainly caused by linear forces acting at the cutting edges; in joining processes, by deformation due to applied forces.

### 31.4 TOOLS FOR METAL FORMING

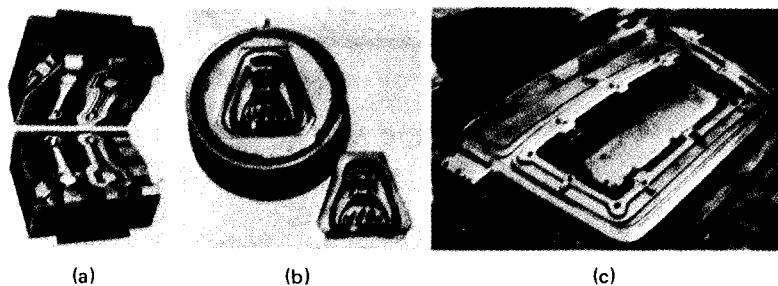


**FIG. 31.1** Dies used in metal forming. (a) Die forging. (Courtesy of Drop Forging Association.) (b) Electrohydraulic deepening. (Courtesy of WMF.) (c) Deep drawing and trimming. (Courtesy of L. Schuler.)

Key No. 1	Parting line	1-piece die = 0 2-piece die = 1 3-piece die = 2 4- or more-piece die = 3 Others = 9		
Key No. 2	Location of the working surface	In the plane of the parting line = 0  Recessed; flat parting line = 1  Raised; flat parting line = 2  Recessed and raised; flat parting line = 3  Raised; broken parting line = 6  Recessed and raised; broken parting line = 7 	Recessed; flat parting line = 1  In the plane of the broken parting line = 4  Recessed; broken parting line = 5  Others = 9	Raised; flat parting line = 2  Recessed; broken parting line = 5  Others = 9
Key No. 3	Direction of the geometrical axis of the cavity	Random = 0  Perpendicular to parting line = 1  Parallel to parting line = 2 Others = 9 	Perpendicular to parting line = 1  Parallel to parting line = 2 Others = 9 	Parallel to parting line = 2 Others = 9 
Key No. 4	Basic shape of the working surface	Plane = 0  Sphere = 4  Severely curved irregular surfaces or surfaces with abrupt changes of curvature = 7 	Cylinder = 1  Surface formed by rotation of a random line = 5  Spiral surfaces = 8 	Cone = 2  Pyramid, wedge = 3  Mildly curved irregular surfaces or cones composed of regular surface elements = 6 

**FIG. 31.2** Die classification.

### 31.1.2 Die Geometry

Dies are usually in at least two parts, with three-part and multipart dies being used where recesses or cavities occur in the workpiece. In certain processes, however, only one die either raised (male) or recessed (female) is necessary, such as in explosive forming.

In general with pairs of dies, one may distinguish between the upper and the lower die or the male and the female die. Cavities may be open, as in blanking or piercing, or closed, as is usual in die forging. The surfaces of the dies which are in contact with the workpiece are referred to as the working surfaces. These may be classified as shown in Fig. 31.2 [31.2] by nine key numbers.

#### Key No. 1—Parting Line

This may be single or split into two or more parts. Where there is only one die, no parting line is present.

Key No. 5	Main subsidiary shape of the working surface	None = 0 cylinder = 1 	Cone = 2 	Sphere = 3 	Web, rib = 4 
		Lug = 5 	Slit = 6 	Depression = 7 	Spiral = 8 
		Others = 9			
Key No. 6	Macrogeometry of the working surface	Smooth = 0 	Grained = 1 	Pitted = 2 	Wavy = 3 
		Corrugated = 4 	Engraved = 5 	Others = 9 	
Key No. 7	Microgeometry of the working surface	Without special requirements: Milled/turned = 1 Ground = 2      Mech. polished = 3			
		Chem. or electrochem. polished = 4    Lapped = 5    Shotblasted = 6			
		Embossed = 7      Eroded = 8      Others = 9			
Key No. 8	Area of the working surface	<10 mm <sup>2</sup> = 0 (<0.015 in <sup>2</sup> = 0)	<10 <sup>2</sup> mm <sup>2</sup> = 1 (<0.155 in <sup>2</sup> = 1)	<10 <sup>3</sup> mm <sup>2</sup> = 2 (1.55 in <sup>2</sup> = 2)	<10 <sup>4</sup> mm <sup>2</sup> = 3 (15.5 in <sup>2</sup> = 3)
		<10 <sup>5</sup> mm <sup>2</sup> = 4 (<155 in <sup>2</sup> = 4)	<1 m <sup>2</sup> = 5 (<10.8 ft <sup>2</sup> = 5)	<10 m <sup>2</sup> = 6 (<108 ft <sup>2</sup> = 6)	>10 m <sup>2</sup> = 7 (>108 ft <sup>2</sup> = 7)
Key No. 9	Die material	Zn = 0      Al and Mg alloys = 1 Cast iron = 3      Carbon steels = 4      Low-grade alloy steels = 5 High-grade alloy steels = 6      Ni and Mo special alloys etc. = 7 Carbide = 8      Others = 9			

FIG. 31.2 Die classification (cont.).

***Key No. 2—Location of Working Surface***

This group refers to the location of the working surfaces with respect to the parting line (flat, recessed, raised) as well as to the shape of the parting plane (flat, broken).

***Key No. 3—Direction of Geometrical Axis of Cavity***

This group specifies whether the geometrical axis of the cavity is perpendicular, parallel, or randomly inclined with respect to the parting line.

***Key No. 4—Basic Shape of Working Surface***

The working surface of a die may be defined by geometric shapes, such as cylinders, cones, pyramids, wedges, and spheres; rotational surfaces made up of flat or regularly curved elements; helicoid surfaces and irregularly or regularly curved elements; helicoid surfaces and irregularly shaped surfaces. The latter cannot easily be described analytically, which, in some cases, is also true of rotational surfaces with random line generators. Most other surfaces, on the other hand, can be exactly described analytically. Working surfaces made up of several individual types of surfaces may have edges where the boundary is discontinuous. With continuous boundaries the transition is referred to as smooth in the mathematical sense.

***Key No. 5—Main Subsidiary Shape of Working Surface***

The subsidiary shape elements together with the basic shape determine the geometry of the working surface. They are either simple geometric shapes, such as cylinders, cones, pyramids, spheres, ribs, ridges, and slits, or irregular shapes, such as lugs or protrusions.

***Key No. 6—Macrogeometry***

This describes the shape elements of an order of magnitude smaller than the main subsidiary shape elements describing the geometry of the working surface. A surface may be smooth in the macrogeometric sense, or it may be grained, pitted, wavy, corrugated, or engraved.

***Key No. 7—Microgeometry of Working Surface***

This group describes the microgeometry of the surface based on the quality of machining, such as milled, turned, ground (mechanically, chemically, or electrochemically), polished, lapped, shot-blasted, coined, embossed, or eroded.

***Key No. 8—Surface Area of Working Surface***

Here the absolute size of the working surface is given in terms of one of eight categories ranging from less than  $10 \text{ mm}^2$  ( $0.01 \text{ in}^2$ ) to more than  $10 \text{ m}^2$  ( $100 \text{ ft}^2$ ).

***Key No. 9—Die Material***

This group classifies the dies with respect to the material which ranges from zinc, aluminum and magnesium alloys, cast iron, steel (carbon to high-alloy), up to high-temperature-resistant alloys and carbides.

These nine groups form a classification system for dies. While groups 2 to 6 are important to die design, groups 1 and 7 to 9 contain important information relevant to die manufacture.

This system of classification can be used for grouping dies into families (group technology) and—what is more important—as a basis for producing programs for numerically controlled machining [31.2] to [31.6].

The chapters which follow discuss the important characteristics of die manufacture for some deformation and separation processes, as well as the means available today for economic production of such dies. The external machining of die blocks, although very important, is not considered here.

## 31.2 PROCESS CHARACTERISTICS AFFECTING DIE REQUIREMENTS

Hot and cold bulk (massive) forming, sheet forming, and the separation processes include many methods of manufacturing workpieces of particular basic shapes, sizes, and weights, made from a wide range of materials. It is these particular characteristics which directly influence the type of dies required.

### 31.2.1 Hot Bulk Forming (Die Forging)

The geometry of die-forged workpieces—with weights varying from a few grams to more than a ton—is characterized by sharply varying cross sections, as shown in the shape classification system according to Spies [31.7] (see Fig. 11.70). The more twisted the workpiece geometry and the lower the formability of the material, the larger is the number of intermediate steps which are required for redistributing the mass, for bending, and for preforming the required cross section—that is, the more dies, or die impressions, are necessary (see Chap. 11).

The elements of the workpiece must conform to particular design rules which, above all, are a function of the workpiece material, the material flow, and the die loading (see Chap. 11). They concern fillet and corner radii, minimum wall thicknesses, and draft on the sides of the die (see Table 11.12) [31.4], [31.8], [31.9].

The die geometry is characterized by division of the die into usually two, but sometimes three or more, parts, for example, for forging in horizontal forging machines (see Fig. 11.79). Here the parts of the die, which determine the external shape of the workpiece, usually have recessed working surfaces and are thus genuine impression dies. The die loading, and thus also the choice of die material and assembly, depend on the workpiece materials and their forming characteristics. Table 31.1 shows values concerning the degree of mechanical and thermal loading of forging dies for different workpiece materials, based on the assumption that steel is mainly forged using hammers and mechanical presses, brass using mechanical presses, and light alloys using mechanical and hydraulic presses.

The thermal loading of forging dies not only depends on the workpiece material and the equipment used, but also on the die temperature. With light alloys this may be near the forging temperature of 330–530°C (626–986°F) as a result of continuous heating (gas, induction). The thermal stress is low since no significant thermal stresses are present between the surface and the core of the die. In the case of steel, the situation is quite different. The dies, heated only intermittently, rise to a temperature of around 80–180°C (176–356°F) in drop forging and to around 600°C (1112°F) in press forging as a result of contact with the workpiece. The high temperature increase at the die surface during the short contact period leads to the presence of alternating thermal stresses. This may lead at times to exceeding the heat-fatigue resistance of the die material. The generation of surface heat cracks may be the result (see Fig. 11.91) [31.10], [31.11].

Frictional wear, that is, erosion on the die surface, is a function of the interaction between workpiece and die materials, the interface layer, the pressure at the interface, and the relative sliding motion at the die–material interface. The high relative interface velocity is typical of hammer forging of steel and it results, as a rule, in greater frictional wear, whereby the damage to the surface of the die increases with the appearance of heat cracks [31.10], [31.12].

It is possible to set up a list of requirements on the die material based on the die loading (Fig. 31.3). Steel-forging dies have the highest requirements as far as strength and resistance to thermal stresses are concerned. The thermal conductivity of the die material should be high enough to reduce quickly the temperature differences between the surface and the core of the die without, however, taking too much heat from the workpiece, because cooling of the workpiece leads to increased resistance to flow and to higher mechanical stresses. The requirements concerning thermal conductivity and wear resistance are somewhat less critical in the forging of brass and light alloys.

### 31.2.2 Cold Bulk Forming (Extrusion)

Extruded components, weighing from 2 g to 35 kg (0.004–77 lb), are usually rotationally or axially symmetric in shape due to considerations of material flow, die technology, and cost. The variations

**Table 31.1** Die Loading

Process	Compressive stress $p$ , N/mm <sup>2</sup> (ksi)			Dwell time, ms			Die temperature, °C (°F)		
	Light alloy	Brass	Steel	Light alloy	Brass	Steel <sup>a</sup>	Light alloy	Brass	Steel <sup>b</sup>
Die forging	800–1500 (120–220)	600–1000 (90–150)	800–2000 (120–290)	250–600 × 10 <sup>3</sup>	100–500	5–250	300–500 (620–980)	100 > 500 (260 > 980)	30–80H, 300 > 600P (80–170H, 620 > 1070P)
Extrusion	800–1500 (120–220)	800–1700 (120–250)	1200–2400 (180–350)		50–500		30–80 (80–170)	30–80 (80–170)	30–80 (80–170)
Coining	900–1600 (130–230)	1000–1800 (150–260)	1200–3500 (180–510)		20–>500				
Deep drawing: Blankholder	0.5–8 (0.1–1.2)	0.5–10 (0.1–1.4)	0.5–10 (0.1–1.4)		200–>500				
Die entry radius	5–100 (0.7–15)	10–150 (1.4–22)	30–250 (4–36)						
Trimming <sup>c</sup>	100–500, ex > 500 (1.4–70, ex > 70)	300–1200, ex > 1200 (40–170, ex > 170)	300–1800, ex > 1800 (40–260, ex > 260)		10–300				

<sup>a</sup>The smallest dwell time occurs with hammers, the largest with hydraulic presses; in between these are crank presses and eccentric presses.

<sup>b</sup>H—hammer; P—press.

<sup>c</sup>ex—exceptionally.

Process \ Requirements		Heat resistance	Tempering properties	Fatigue resistance	Hot crack resistance	Thermal conductivity	Wear resistance
Process	Requirements						
Die forging	Steel	•	• • •	• • •	• • •	•	• • •
	Brass	•	• •	• • •	• •	•	• • •
	Light alloy	• • •	•	• •	•	•	• •
Extrusion	Steel	—	•	• • •	—	—	• • •
	Brass	—	•	• •	—	—	• • •
	Light alloy	—	•	• •	—	—	• •
Deep drawing	Steel	—	—	• •	—	—	• •
	Brass	—	—	• •	—	—	• •
	Light alloy	—	—	•	—	—	• •
Trimming	Steel	—	—	• •	—	—	• •
	Brass	—	—	•	—	—	• •
	Light alloy	—	—	•	—	—	•

FIG. 31.3 Requirements on materials of metal-forming dies.

in shape (see Fig. 15.1) range from simple flat disks to parts with longitudinal internal or external hollow or solid profiled sections. The number of forming stages, and thus the complexity of the dies, is a function of the geometric shape of the workpiece and of the material properties; that is, highly profiled workpieces from materials that are difficult to form require a large number of dies.

The layout of the dies and the rules governing the design of individual die elements such as pressure plates, punches, mandrels, and blankholders, are described in detail in Chap. 15. The material flow, deformation force, and die wear are influenced by friction, particularly in portions of the workpiece where the ratio of surface to volume is large. For this reason, the surface roughness of the die elements must be kept to a minimum, namely, with  $R_t < 1 \mu\text{m}$  (3.9 mil) peak-to-valley height.

While the die or punch stresses may be as high as  $2500 \text{ N/mm}^2$  (360 ksi) when forming steel, the average die temperature is usually not much above room temperature (see Table 31.1). When selecting the die material (see Tables 15.5 to 15.10, 15.12) the requirements concerning strength (fatigue strength) and wear resistance are very high, while the resistance to thermal stress is of less importance (Fig. 31.3).

### 31.2.3 Sheet Forming

Symmetrical or nonsymmetrical parts formed from sheet metal, weighing from 10 g to approximately 50 kg (0.2–110 lb), exhibit changes in cross section and wall thickness to a much lesser degree than bulk-formed parts. The variation in geometry is clearly expressed by the Sachs shape classification system (see Fig. 20.37) [31.13]. The geometry of sculptured nonsymmetrical sheet-metal components shows that, in the manufacture of such workpieces, it is necessary to use a combination of various sheet-formed processes, such as deep drawing, stretch forming, and bending. The cost of the tooling required is correspondingly high—often higher, in fact, than for forging or extrusion dies.

The rules governing the design of sheet-metal components consider above all the dimensioning of radii (see Chap. 20). These radii determine the material flow, the load exerted on the sheet during deformation, and the die life. Material movement and stresses can be determined with the aid of a grid of lines applied to the workpiece surface by a chemical, photochemical, or similar process [31.14]. They permit sources of failure during deformation to be located and subsequently to be eliminated by correcting the shape of the workpiece and die, the friction, and the forces applied to the blankholder. The more complex the component, the more intermediate stages (passes) or dies are required in order to form the part without failure.

Dies for sheet-metal working are usually in two or more parts (see Fig. 33.7). In general the working surfaces of the male and the female dies match, being only separated by the sheet thickness, except in areas of the dies where irregular material movement is present. The latter case may be accounted for in different ways, such as by incorporating drawing beads or modifying the drawing gap (see Chap. 20). Die life depends on the male and the female dies maintaining a constant drawing gap. However, the machine guides alone do not always assure exact alignment of the tools. Therefore large dies are equipped with pin or plate-type guides made of cast iron, hardened steel, bronze, or plastic plates for assuring the centering of the male die with respect to the blankholder and of the blankholder with respect to the female die [31.15]. Where tools are used for drawing and trimming, the cutting edges of the tools are, in addition, aligned with each other by means of guide pins. Thus locating lugs assure rough alignment, and the guide pins provide precise alignment.

Compared to other metal-forming processes, the die loads are relatively low since the blankholder pressure is only  $0.5\text{--}10 \text{ N/mm}^2$  ( $0.07\text{--}1.45 \text{ ksi}$ ) and the normal stress near the die radius is approximately  $5\text{--}250 \text{ N/mm}^2$  ( $0.73\text{--}36.2 \text{ ksi}$ ), depending on the workpiece material (see Table 31.1). Consequently die materials of low strength may be used, such as cast iron or steel, carbon or low-alloy steels (see Table 20.4) [31.16], [31.17]. Especially subject to wear are the guides, drawing die radii, blankholder faces, and—where they exist—protrusions in the die, that is, all the parts of the tool along which material moves during the forming operation. The punch or male die is less affected since the sheet metal rests against the die surface. For production these requirements on the workpiece material (Fig. 31.3) must be just as much taken into account as the final shape of the workpiece and the lot size. Because of the generally sudden stressing of the tools, the die and blankholder should be designed to a high degree of stiffness by providing adequate wall thickness and stiffening members. Thus resistance to fatigue failure is increased.

#### 31.2.4 Separating (Blanking and Piercing)

The geometric shape of the workpieces formed by blanking and piercing—measuring  $2 \text{ mm}^2$  ( $0.003 \text{ in}^2$ ) to  $2 \text{ m}^2$  ( $22 \text{ ft}^2$ )—is usually flat when the workpiece is cut out of sheet metal (see the Sachs classification of sheet-metal parts [31.13], Fig. 20.37). When the workpiece is blanked or pierced, following a deformation operation (see the Spies' classification of forged workpieces [31.7], Fig. 11.70), then the part geometry is usually complex. The complexity of design and manufacture of the cutting tool is similar to that of the workpiece. Flat components require simple tools, basically a die whose opening corresponds to the workpiece contour and a punch with the same contour but smaller by an amount corresponding to the die clearance. Preformed components, especially those made of sheet metal, on the other hand, must be placed in the die and located positively before shearing; that is, the die, the blankholder, and possibly the punch have working surfaces which conform to the shape of the workpiece (Fig. 31.1).

The total shearing load can be determined accurately. However, the local stresses in the tools can only be estimated approximately (Table 31.1). Depending on the material to be cut and the speed of the cutting operation itself, local normal stress peaks may occur which are well above the values shown in Table 31.1. Critical parts of the tool must therefore be fully supported. Further details concerning tool design and materials are given in Chap. 24.

#### REFERENCES

- 31.1 Dolezalek, C. M.: "The Engineer's View of Industrial Production" (in German), *Tech. Rundsch.*, 35, 1965.

- 31.2 Lange, K.: "Dies for Primary Formation and Deformation Processes" (*in German*), VDI Berichte, no. 166, 1971, pp. 83–96.
- 31.3 "Use of Dies in Metal Forming," *Met. Form.*, 38, 1971, pp. 3–5.
- 31.4 *Metals Handbook*, vol. 5, "Forging and Casting," Metals Park, OH, American Society for Metals, 1970.
- 31.5 Akgerman, N., and Altan, T.: "Recent Developments in Computer-Aided Design of Forging Process," Technical Paper MF 72-110, Dearborn, MI, Society of Manufacturing Engineers, 1972.
- 31.6 Legner, H.: "Numerical Control in the Automobile Body Shop" (*in German*), *Werkstatt u. Betr.*, 105, 1972, pp. 565–632.
- 31.7 Spies, K.: "Shape Classification for Forged Parts" (*in German*), *Werkstattstech. u. Maschinenbau*, 47, 1957, pp. 201–205.
- 31.8 Jenson, J. E.: *Forging Industry Handbook*, Cleveland, OH, Forging Industry Association, 1966.
- 31.9 DIN 7523: "Gestaltung von Gesenkschmiedestücken (Design of Components for Forging)," 1st ed., 1970.
- 31.10 Lange, K.: *Die Forging of Steel* (*in German*), Berlin/Göttingen/Heidelberg, Springer, 1958.
- 31.11 Beck, G.: "Thermal Loading of Forging Dies" (*in German*), Dr.-Ing. thesis, Technische Hochschule, Hannover, 1957.
- 31.12 Kienzle, O., Lange, K., and Meinert, H.: "The Effect of Surface Finish on Wear in Forging Dies" (*in German*), *Forschungsberichte des Wirtschafts- und Verkehrsministeriums Nordrhein-Westfalen*, no. 285, Köln Opladen, Westdeutscher Verlag, 1956.
- 31.13 Sachs, G.: *Principles and Methods of Sheet Metal Fabrication*, New York, Reinhold, 1958.
- 31.14 Müschenborn, W.: "Investigation of the Deformation of Two Drawn Components by Means of a Photoelectrically Applied Line Matrix" (*in German*), Thyssen Research Report, no. 1, 1969, pp. 109–115.
- 31.15 VDI-Richtlinie 3357: "Ecken- und Stollenführungen mit und ohne Führungssäulen (Corner and Post Guides with and without Guide Columns)," Düsseldorf, VDI-Verlag, 1961.
- 31.16 Hilbert, H. L.: *Stamping Technology* (*in German*), vol. 2, "Forging Tools," München, Carl Hanser, 1970.
- 31.17 Oehler, G., and Kaiser, F.: *Cutting, Stamping, and Drawing Tools* (*in German*), Berlin/Heidelberg/New York, Springer, 1966.



**DIE MANUFACTURE**

The manufacture of metal-forming dies is based on single-piece or small-batch manufacturing methods [32.1], while the dies themselves are used for mass production [32.2], [32.3].

In die manufacture—here only the die cavity is considered—there are three main objectives:

- 1 Generation of the working surfaces of a die as quickly as possible
- 2 Generation of a die surface with the required macro- and microgeometry
- 3 Manufacture of the die to specified dimensional and shape tolerances

Overriding all three points is the need to achieve the most economic production method or the lowest overall costs. However, not all the objectives can be satisfied simultaneously by one particular die-manufacturing process. A compromise between several processes must be made with regard to geometry, material, surface quality, and accuracy requirements. Concerning dimensional accuracy, die tolerances need to be about one to three IT grades tighter than the tolerances of the components to be produced by these dies. The higher die tolerances apply where high rates of die wear are likely to occur. The ability to satisfy these requirements depends, among other things, on the size of the die.

The typical definition of small, medium, and large dies varies according to the process and the application concerned. In general working surfaces  $>1 \text{ m}^2$  ( $9 \text{ ft}^2$ ) are considered large dies, while small dies have working areas  $<10^3\text{--}10^4 \text{ mm}^2$  ( $1.5\text{--}15 \text{ in}^2$ ).

**32.1 VOLUME TO BE REMOVED FOR INTERNAL AND EXTERNAL SHAPES**

Recessed working surfaces require internal machining. Raised working surfaces require external machining, which permits higher material removal rates.

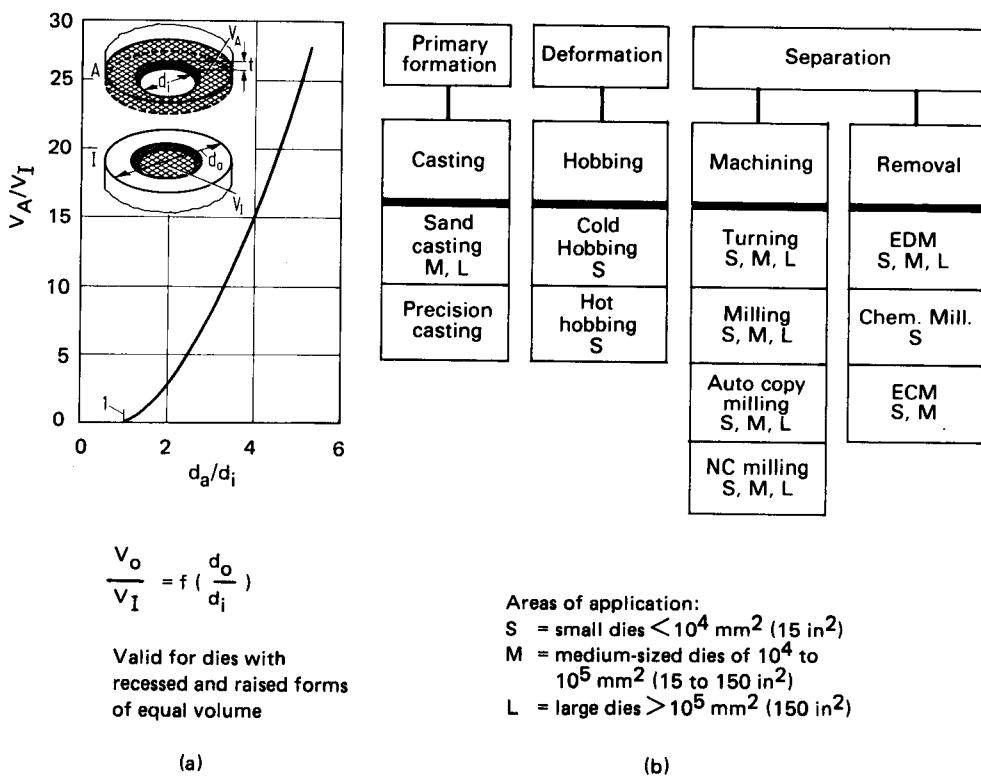


FIG. 32.1 Manufacture of metal-forming dies. (a) Volume to be removed. (b) Manufacturing methods.

Fig. 32.1a shows that for generating recessed and raised shapes of equal volume, it is necessary to remove different volumes of material,  $V_A$  (raised) and  $V_I$  (recessed). The volume to be removed to produce the raised shape ( $V_A$ ), plotted against the ratio of outer diameter to inner diameter  $d_o/d_i$ , is a parabolic function. This function is independent of the depth  $t$ . In the typical case of  $d_o/d_i = 2$ ,  $V_A/V_I = 3$ . For higher values of  $d_o/d_i$ , mandrels are often used so as to reduce the amount of material removed and the required machining time.

## 32.2 PROCESSES FOR GENERATING BASIC AND SUBSIDIARY WORKING SURFACES

The processes used in die manufacturing are selected from those which represent the main manufacturing process groups: primary forming, deformation, and separation (Fig. 32.1b). The main characteristics of the more important processes are shown in Table 32.1.

### 32.2.1 Casting

Casting represents the shortest path from raw material to the finished shape of the die. For small, medium, and large dies there are a wide range of processes, which permit the manufacture of dies for steel and nonferrous metal working, such as drawing, forging, or extrusion dies [32.4] to

**Table 32.1** Characteristic Data for Different Die-Manufacturing Methods

Process	Suitable materials	Metal removal rate V, $\text{cm}^3/\text{min}$	Tolerance $\mu\text{m} (\times 10^{-3} \text{ in})$	Surface finish $R_a, \mu\text{m} (\times 10^{-3} \text{ in})$	Necessary equipment	Capital investment	Additional Aids			Degree of automation	Basic shapes	Subsidiary shapes	Application for group according to Fig. 31-2
							Type	Material	Complexity				
Sand casting	Cast iron, steel, light alloy	—	$>2000$ ( $>80$ )	$>100$ ( $>4$ )	Foundry	●●●●	Pattern	Wood, polystyrene	●●	○	All	0-5, 7, 8	
Precision casting	Light alloy, cast iron	—	$<100-1000$ ( $<4-40$ )	$>20$ ( $>0.8$ )	Foundry	●●●●	Pattern	Plastic, metal, wax	●●	○	All	0-5, 7, 8	
Electrolytic depositing	Copper, nickel	—	$>5$ ( $>0.2$ )	$>2$ ( $>0.08$ )	Depositing plant	●●●●	Pattern	Plastic	●●●	○	All	0-5, 7, 8	
Cold hobbing	Steel (A)	$>10$ ( $>0.6$ )	$>5$ ( $>0.2$ )	$>5$ ( $>0.2$ )	Hydraulic hobbing press	●●●	Hobbing punch	Tool steel	●●●●	●	All	0-5, 7	
Hot hobbing	Steel	$>50$ ( $>3$ )	$>50$ ( $>2$ )	$>15$ ( $>0.6$ )	Hydraulic hobbing press, hammer	●●●	Hobbing punch	Tool steel	●●●●	●P+H	All	0-5, 7	
Turning	All metals <sup>a</sup> (HT, A)	16-500 (1-30)	$\approx 10$ ( $\approx 0.4$ )	$>2$ ( $>0.08$ )	Lathe	●●●(●)	Templates	●(●)	●(●)	0, 1, 2, 4, 5	0-3		
Milling	All metals <sup>a</sup> (HT, A)	1-400 (0.06-25)	$>100$ ( $>4$ )	$>15, SH > 200$ ( $>0.6, SH > 8$ )	Milling machine	●●●(●)	Templates	●●(●)	○	All	0-5, 7		

**Table 32.1 (Continued)**

Process	Suitable materials	Metal removal rate $V, \text{cm}^3/\text{min}$ ( $\text{in}^3/\text{min}$ )	Tolerance $\mu\text{m}$ ( $\times 10^{-3}$ in)	Surface finish $R_a, \mu\text{m}$ ( $\times 10^{-3}$ in)	Necessary equipment	Capital investment	Additional Aids			Application for group according to Fig. 31.2
							Type	Material	Complexity	
Automatic copy milling	All metals <sup>a</sup> (HT, A)	1-180 (0.06-50)	>100 (>4)	>15; SH >200 (>0.6; SH >8)	Copy-milling machine	●●●●	Master templates	●●●(●)	●●●	All 0-5, 7
Numerically controlled milling	All metals <sup>a</sup> (HT, A)	1-180 (0.06-50)	>80 (>3)	>15; SH >180 (>0.6; SH >7)	Milling machine with numerical control	●●●●●	Program	●●●●●	●●●●●	All All
Etching	Steel (HT)	<1 (<0.06)	<5 (<0.2)	>2 (>0.08)	Hydraulic press, chemical equipment	●●(●)	Etching tool	●●●	○	All All
Electric-discharge machining	Conductive metals incl. carbide (HT, A)	1.5/100 A (0.09/100 A)	>10 (>0.4)	>4 (>0.16)	Erosion plant	●●●(●)	Electrodes Graphite, copper	●●●	●●●	All All
Electrochemical machining	Steel, cast steel (HT, A)	2/1000 (0.12/1000 A)	>100 (>4)	>2 (>0.08)	Electrochemical plant	●●●	Electrode Copper	●●●●●	●●●	All All

<sup>a</sup> Up to 1300 N/mm<sup>2</sup> (190 ksi).

HT—heat treated; A—annealed; H—hammer; P—press; SH—scalloped height.

**Table 32.2** Typical Materials and Molding Processes for Making Cast Dies

Typical pattern material	Molding process	Costs	Accuracy of cast workpiece		
			Contour definition	Surface quality	Dimensional accuracy
Polystyrene	Molding by hand, using fire clay, silica sand, chrome ore sand, zirconium sand, with oil, water glass, or resin as bonding agents	Low pattern costs, varying material costs (increasing in the order listed under processes)	•	$R_t = 100 \mu\text{m}$ (3.9 mil)	•
Wood		Average pattern costs (see above)	••	$R_t = 100-60 \mu\text{m}$ (3.9-2.4 mil)	••
Epoxy resin	Molding by hand, using fine-grained mullite, zirconium, or sillimanite, with resin (e.g., ethyl silicate) as bonding agent (shell molding).	High pattern costs, high material costs	•••	••• $R_t = 60-30 \mu\text{m}$ (2.4-1.2 mil)	•••
Metal		Highest pattern costs, high material costs	••••	•••• $R_t = 30-20 \mu\text{m}$ (1.2-0.8 mil)	••••

Source: Compiled from [32.7].

[32.8]. The methods used to produce the cast shapes and the quality of the pattern used for casting as well as the properties of the material used to make the die affect the accuracy, the clarity of definition, and the surface finish of the cast die (Table 32.2).

The molds for large workpieces of between 0.5 and 30 t (0.55-33 ton), as used for large deep-drawing dies, are produced by hand using chamotte or sand as the mold material. They require a machining allowance of 3-20 mm (0.1-1 in) on each surface. Dies of up to 0.2 t (0.22 ton) can be made using resins (e.g., ethyl silicate) with such accurate working surfaces that very little subsequent finishing is required (shell molding). Between these two extremes, specific areas of application exist for casting materials consisting of quartz, zirconium, or chromium ore sand, mixed with binding materials based on water, glass, oils, and resins.

In casting, the part responsible for determining the geometry of the die is called the pattern. With workpieces where the surface finish requirements are not too strict and where a large machining allowance is permissible, expanded polystyrene is a suitable pattern material. The patterns, which are relatively easy to make with this material, may either be left in the mold, where they are consumed during the casting process, or they may be destroyed when the casting is removed from the mold. By comparison, wooden patterns have the advantage of being reusable, but they may distort when stored for long periods of time. The highest degree of accuracy is obtained when patterns made of either epoxy resins or metal are used. When dimensioning patterns, besides taking the machining allowances into account, one must also allow for shrinkage of the molten material upon solidification.

The structure of cast workpieces after solidification is very different from that of both forged and rolled steel. On a macroscopic scale, cast workpieces exhibit different primary grain sizes in the surface and core zones. The primary precipitation phases formed at the grain boundaries may be removed by subsequent heat treatment. For this reason, in the manufacture of cast dies pref-

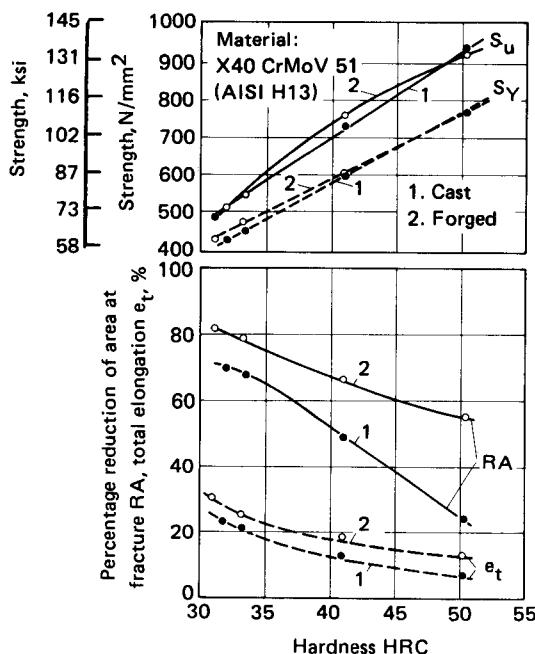


FIG. 32.2 Mechanical properties of cast and forged test workpieces at 700°C (1292°F). (After [32.9].)

erence is given to steels which, due to their alloy composition, show little tendency toward the formation of large crystals and segregation.

Fig. 32.2 shows the results of comparative investigations into the behavior of cast and rolled test specimens made of H13 steel [32.9]. The tensile strengths and the yield points of both specimens are about equal. The cast specimen, however, has a lower notch toughness, total elongation, and reduction in area after fracture. In practice, according to [32.10], the useful life of cast dies should be at least equal to that of forged dies, in some cases even 10–15% higher because the mechanical properties of castings are not directionally oriented, that is, they have no preferential direction of deformation as is the case with rolled steel. In casting, dimensional inaccuracies may be reduced by modifying the pattern after the initial test casting. Fig. 32.3 shows the upper and lower halves of a cast die.

### 32.2.2 Deformation Processes (Cold and Hot Hobbing)

The technology, areas of application, and limits of the cold and hot hobbing processes are described in detail in Chap. 17.

### 32.2.3 Mechanical Machining Processes

The methods most commonly used for manufacturing dies are the mechanical machining processes such as turning, milling, and grinding. Turning, which is used for the rough and finish machining of rotary working surfaces, and grinding, which is mainly used for finishing both symmetrical and nonsymmetrical surfaces, are so well known that it is unnecessary to describe them here in detail.

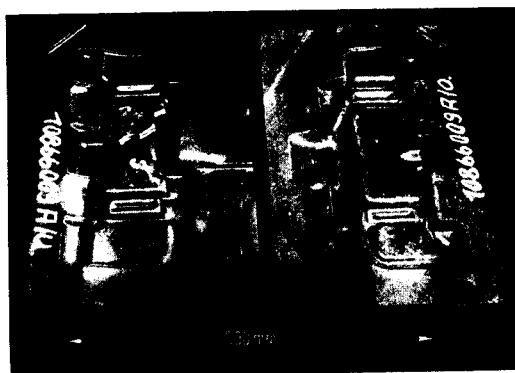


**FIG. 32.3** Cast forging dies for manufacturing chain links [32.7]. Mass—290 kg (640 lb); material—X37CrMoW51 (A8); machining allowance—impression 0.3 mm (0.01 in), parting faces 2 mm (0.08 in).

The complete machining of dies with cavities or working surfaces of any given geometry is only possible by means of milling (Fig. 32.4). All basic shapes of the working surface can be machined by this method, either by manual sinking after layout and/or by copy milling using templates or patterns. Until recently copy milling was almost the only automatic milling method in use. Numerically controlled milling, however, may be used as an alternative to copy milling in cases where an appropriate mathematical description of the die geometry is available.

Necessary motions	Shape of cross section		
	Trapezoid		Multiform
	Simple	Multiple	
A single motion in the horizontal plane			
Two simultaneous motions in the horizontal plane			
Two simultaneous motions in the vertical plane			
Three simultaneous motions			

**FIG. 32.4** Types of milling occurring in die sinking. (After [32.11].)

### 32.8 TOOLS FOR METAL FORMING

In copy milling the following processes are distinguished:

- 1 Manual copy milling, where the feed of the spindle is controlled by hand
- 2 Semiautomatic copy milling, where the feed in the longitudinal and lateral axes is automated and the vertical movement is controlled by hand
- 3 Automatic copy milling, where the movement of the cutting tool is controlled automatically by the movement of a sensor over the surface of a three-dimensional pattern

Of these methods, automatic copy milling, because of its high quality and its capability to produce sculptured surfaces economically, is the most significant for the manufacture of both small and large dies.

The amount of material to be removed depends principally on the die geometry, the geometry of the cutting tool (flat end, ball-end mill, etc.), and the depth and width of cut [32.11] to [32.13]. While large volumes can be roughed out most efficiently using strong rigid tools capable of high removal rates, surfaces with small radii or with rapid changes in geometry can only be machined using long and thin cutters, leading to correspondingly low rates of metal removal. By dividing the machining up into linear paths, the milling cutter is moved along a line by varying two coordinates (Fig. 32.5a). In general on reaching the end of a line, the sensor and the cutter are lifted, moved a short distance at a right angle to the cutting direction, and then moved back in the opposite direction (zigzag milling). In these milling methods, machining is usually performed using a reverse cut with a rising axial feed component because this is more desirable from the machining point of view than the falling axial feed, which corresponds to the plunge cut (Fig. 32.5c). The latter has the disadvantage that the part of the milling cutter actually machining during the plunge cut operates at reduced cutting speed, thus resulting in pressure being exerted on the tool. For this reason the depth of cut has to be kept small.

Rough machining is performed using a different method of path milling, namely, reciprocal milling (Fig. 32.5a). In this method the cutting tool moves with a rising axial component on all the cutting paths. On completing one line, the tool is withdrawn from the workpiece and moved in rapid approach to the start of the next line. In contour milling, the tool is usually moved in just one plane normal to its axis along the outline of a template or pattern. Both internal and external shapes can be produced in this way (Fig. 32.5b). Since the cutting edges on the circumference of the tool are used for the machining, good cutting conditions and smooth surface finishes can be obtained.

A special type of contour milling is the so-called three-dimensional copy milling. In this method the tool is moved along a contour, and in addition the tool position is controlled in the tool-axis direction (Fig. 32.5b). Complex surfaces may be machined by three-dimensional milling, using the appropriate machining strategy (Fig. 32.6).

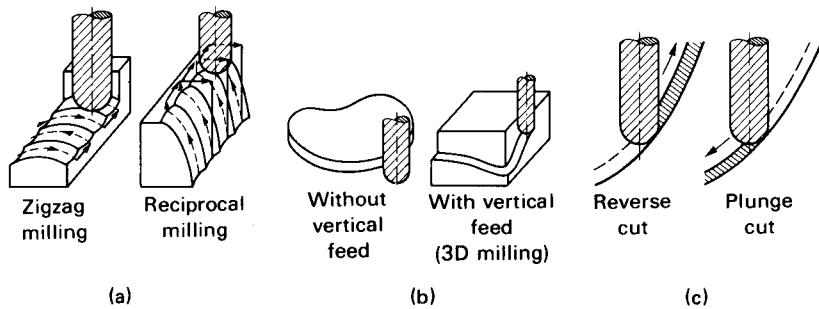


**FIG. 32.5** Methods and types of cuts used in copy milling. (a) Straight line milling. (b) Contour milling. (c) Types of cut.

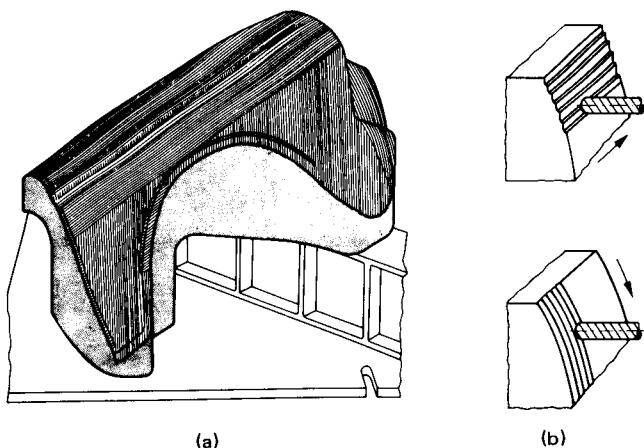


**FIG. 32.6** (a) Subdivision of surface to be machined. (b) Surface profile resulting from milling. (After [32.12].)

Basically the same rules apply to copy and numerically controlled milling as to other milling processes. The limits to copy milling are not only set by the relationship between the shape to be machined and the cutting tool as well as by the tolerance requirements. They are also set by the fact that the shaft diameter and the tip radius of the sensor following the pattern cannot be infinitely small because of the probing forces involved. Therefore die cavities with sharp small corner radii cannot be machined easily by milling. A critical limit for the use of numerically controlled and copy milling, given by the loading of the cutting tool, is reached when materials with a strength of  $> 1300 \text{ N/mm}^2$  (188 ksi) are machined.

The machining of dies in the annealed state, where the material strength is  $700\text{--}800 \text{ N/mm}^2$  (100–115 ksi), raises the performance of these milling methods considerably [32.13] and should be preferred.

Advances in the development of continuous path control have opened up new horizons in numerically controlled die machining. However, the application of this technology depends on the availability of a numerical description of the die geometry and on the development of suitable programs for aiding the preparation of the punched tapes [32.14], [32.15].

For machining surfaces of relatively simple analytical description, such as spheres, cylinders, cones, and second-order surfaces, problem-oriented programming languages such as APT<sup>\*</sup> and EXAPT† have been developed. These permit programming the cutter paths required to machine the entire surface by means of a few appropriate instructions. The instructions are processed with the aid of processing programs (processor and postprocessor) using a suitable computer (Fig. 32.7a).

Surfaces which cannot be easily described analytically may be described using suitable mathematical surface models generated directly by computer-aided design (e.g., with the help of Coons or Bezier algorithms [32.16], [32.17]) or indirectly by digitizing from technical drawings or from measurements made on three-dimensional models (as shown in Fig. 32.7b, based on the example of part of an automobile body [32.16]).

Whenever a sculptured surface of given curvature is machined with an unsuitable cutting tool, tool marks corresponding to the tool geometry are left on the die surface, that is, a certain amount of material remains between adjacent cutter paths. All milled surfaces are thus characterized by milling marks or scallops (Fig. 32.6b). With medium and large dies the scallop height lies in the range of 0.2–0.5 mm (0.01–0.02 in) [32.12].

\*APT—automatic programmed tools.

†EXAPT—extension of APT.

### 32.10 TOOLS FOR METAL FORMING

#### Programming of:

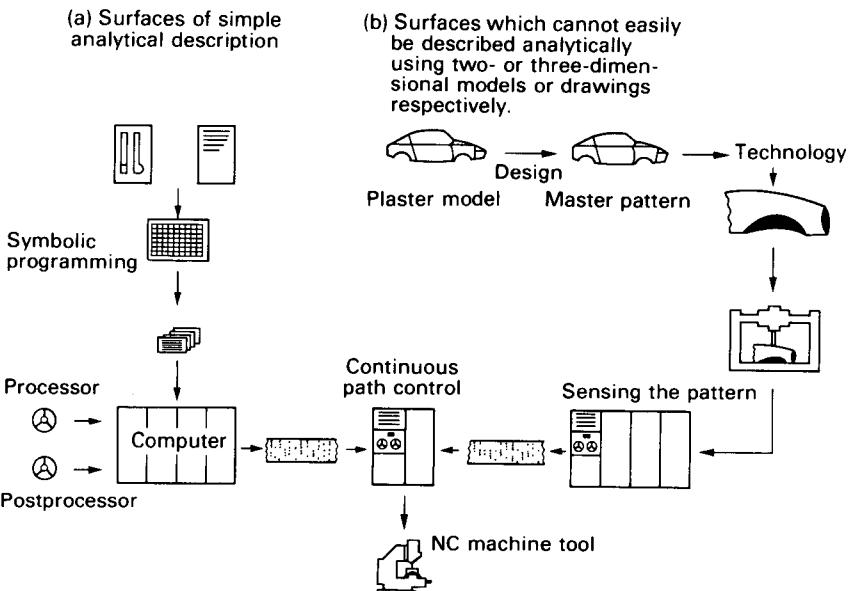


FIG. 32.7 Preparation of control tapes for numerically controlled milling. (After [32.14].)

As a result of improved properties of the cutting tool materials and increased cutting speeds, the performance of chip-forming processes is being improved continually (Table 32.1).

In copy milling the dimensional accuracy is determined by the size and geometry of the die, the characteristics of the sensing device (deflection, response), the pattern (accuracy), the tool (size, stability, wear), and the material to be machined (composition, strength). Since in numerically controlled milling the geometric data do not come from a pattern but from a punched tape, the dimensional errors can be limited in certain cases to 0.08 mm (0.003 in). The machining of dies with a given sculptured surface by means of copying requires the copying of the corresponding analog information in the form of templates or patterns.

Patterns can be made of metal (aluminum alloy), nonwarping well-seasoned wood (ash, elm), gypsum, and above all epoxy resin because of its ease of handling, minimal shrinkage, and water resistance. Epoxy resin can be fixed or hardened using a hardener of the amine type. Its strength can be increased by the addition of metallic or mineral fillers in either powder or fiber form (Table 32.3) [32.18], [32.19]. Which method is most appropriate for producing a template or pattern depends on the size and geometry of the particular application as well as on the material of the pattern.

The most important processes for cast materials, the solid-casting and the laminating methods, are shown in Fig. 32.8. Because of the speed of casting and also the high proportion of material costs, solid casting is mainly used to make small and medium-sized patterns, while the laminating method is preferred for large components. To facilitate the separation of model and cast, the surface is treated with a substance which can be polished, such as silicon wax, thereby producing a good surface finish. With the laminating method the shell must have a stable shape and good resistance to distortion. For this reason it is supported by a structure consisting of steel, aluminum, or epoxy-resin tubes. Further information concerning the number of masters—positive (male) or negative (female)—needed for die manufacture is contained in Chap. 33 (Figs. 33.6 and 33.7).

Machines for copy milling are available in various designs and sizes with one or more horizontal or vertical spindles, copying ranges of up to  $2500 \times 5000$  mm ( $8 \times 16$  ft), and using one

**Table 32.3** Properties of Cold-Hardening Casting Resins

Properties	Unfilled	Filling material		Laminates	Pastes
		Mineral powder	Metal powder		
Density, g/cm <sup>3</sup> (lb/in <sup>3</sup> )	1.2–1.4 (0.04–0.05)	1.4–1.8 (0.05–0.07)	1.7–2.2 (0.06–0.08)	1.5–1.7 (0.05–0.06)	1.4–1.6 (0.05–0.06)
Hardness HB 10, N/mm <sup>2</sup> (ksi)	120–140 (17–20)	160–240 (23–35)	220–260 (32–38)	120–160 (17–23)	160–190 (23–28)
Tensile strength $S_u$ , N/mm <sup>2</sup> (ksi)	15–25 (2–4)	20–30 (3–4)	20–60 (3–9)	190–220 (28–32)	10–30 (1–4)
Compressive strength $S_c$ , N/mm <sup>2</sup> (ksi)	70–80 (10–12)	90–130 (13–19)	80–130 (12–19)	230–250 (33–36)	80–100 (12–15)
Bending strength $S_b$ , N/mm <sup>2</sup> (ksi)	30–50 (4–7)	60–90 (9–13)	60–80 (9–12)	180–190 (26–28)	40–50 (6–7)
Modulus of elasticity $E$ , N/mm <sup>2</sup> ( $10^6$ lbf/in <sup>2</sup> )	5000–7000 (0.7–1.0)	5500–10,000 (0.8–1.4)	5000–12,000 (0.7–1.7)	10,000–12,000 (1.4–1.7)	6000–9000 (0.9–1.3)
Coefficient of linear expansion $\alpha$ , $10^{-5}$ mm/mm·°C ( $10^{-5}$ in/in·°F)	63–68 (35–38)	30–50 (17–28)	45–65 (25–36)	20–35 (11–19)	40–75 (22–42)
Linear contraction, %	0.05–0.15	0.03–0.12	0.01–0.1	0.01–0.07	0.01–0.1

Source: Compiled from [32.19].

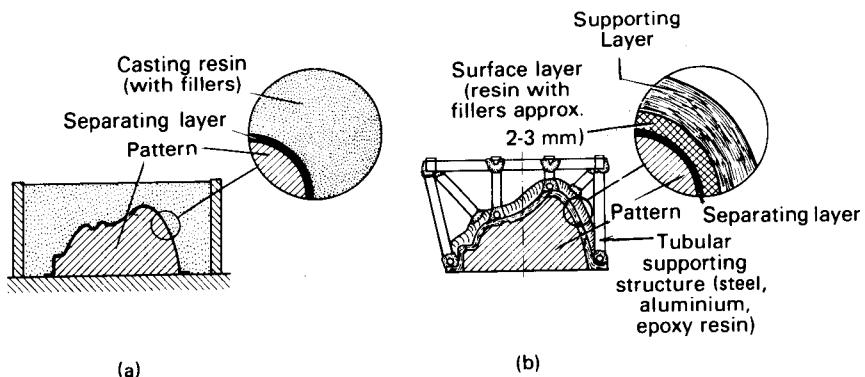


**FIG. 32.8** Methods of making copying templates and patterns. (a) Solid-casting method. (b) Laminating method.

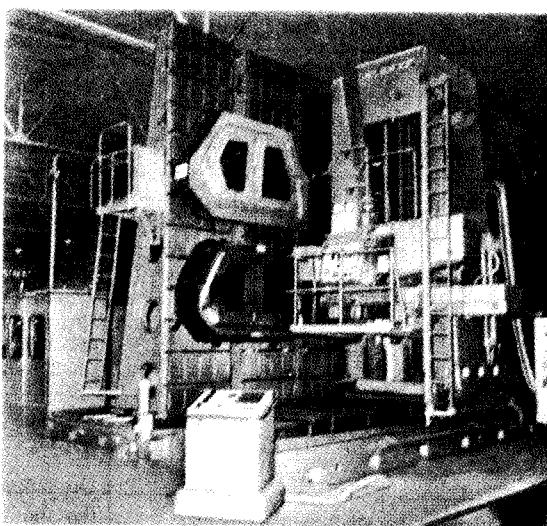


**FIG. 32.9** Copy milling machine with horizontal spindle (*courtesy of Heyligenstaedt*) with continuous path control (*courtesy of Bendix*).

of a number of different copying systems. Their feed rates go up to approximately 1500 mm/min (60 in/min).

In the case of machines with horizontal spindles, the workpiece and the copying pattern are positioned one above the other (Fig. 32.9). This means that the floor space required when producing large dies is kept to a minimum and that good conditions exist for removing the chips. It has the disadvantage, however, that the setup time required for clamping and adjusting the workpiece and the pattern can be considerable. For this reason not only small and medium-sized dies (Fig. 32.10) but also increasingly large dies are being machined on machines with horizontal beds and vertical spindles.

Multispindle machines permit not only the simultaneous machining of several identical dies but also, with suitable equipment, the simultaneous machining of both the upper and lower dies, that is, mirror images of each other, starting from just one pattern [32.20]. Optical setting devices and digital displays assist the machine operator in the exact positioning of both pattern and workpiece prior to milling.

There are many different copying systems. They have been developed to replace the discontinuous elements (contact sensor, clutch drive) by continuous ones (inductive sensors, hydraulic drives, or continuously variable drives), whereby the magnitude of the feed speed remains constant [32.21].

#### 32.2.4 Electroremoval Processes

Common to all electroremoval processes is that die material particles are vaporized, melted, or dissolved by means of thermal, electrochemical, or chemical energy conversion at a rate which is independent of the mechanical strength of the material being machined. Thus these processes are particularly well suited to machining the hardened, tempered, high-temperature-resistant materials used in die making [32.22] to [32.26].

**Electroerosion (Spark Erosion) Processes:** The most important of the electroremoval processes is electric-discharge machining (EDM), which is used for manufacturing both dies with working surfaces of just a few square millimeters, common in precision engineering, and dies of

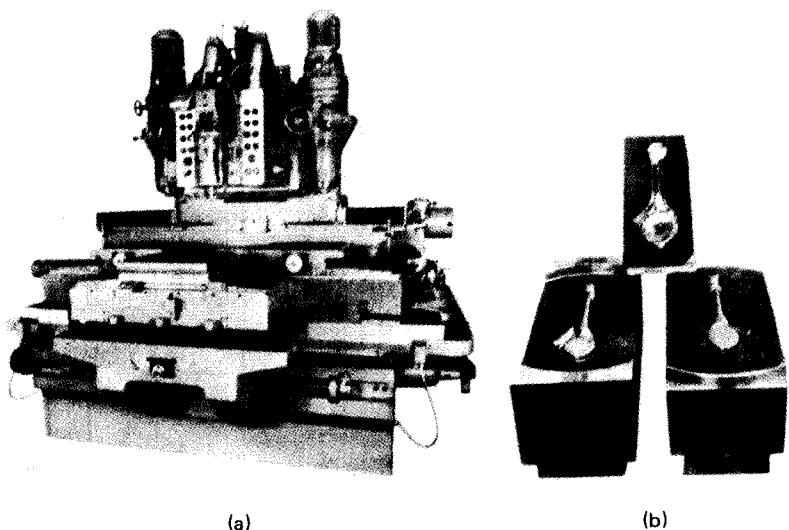


**FIG. 32.10** Copy milling. (a) Machine with two vertical spindles. (Courtesy of Nassovia). (b) Simultaneously machined connecting-rod dies with mirror-image shapes.

several square meters of working surface, such as those required for sheet-metal working in the automobile industry.

The material removal is based on the erosive effect of electric discharges between the electrode and the workpiece by means of which material is melted—in some cases vaporized—and removed by the simultaneous action of electrical and mechanical forces [32.22], [32.23], [32.27]. The abrasion of the workpiece and tool is of different magnitudes, and appears in the form of flat craters which, as a result of numerous repeated attacks, lead to the formation of the required workpiece surface. The process itself is performed in a dielectric medium which has the effect of increasing the energy density through insulation of the discharge channel. This medium also cools both the tool and the workpiece and carries away the abrasive and discharge particles from the machining gap (Fig. 32.11). The die geometry is obtained from the shape of the tool electrode or, as in the

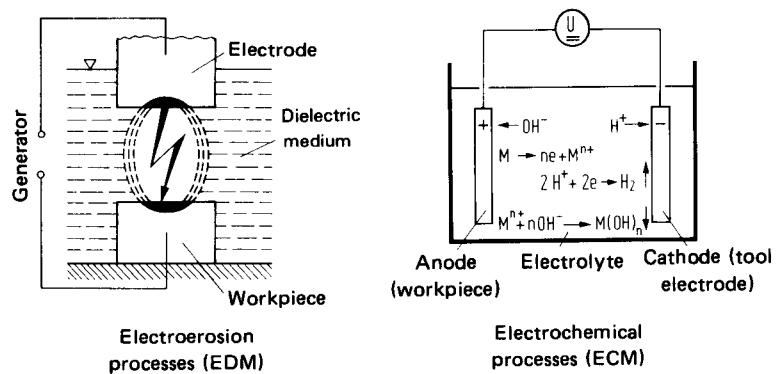


**FIG. 32.11** Principles of electroerosion (spark-erosion) and electrochemical machining processes. (After [32.23].)

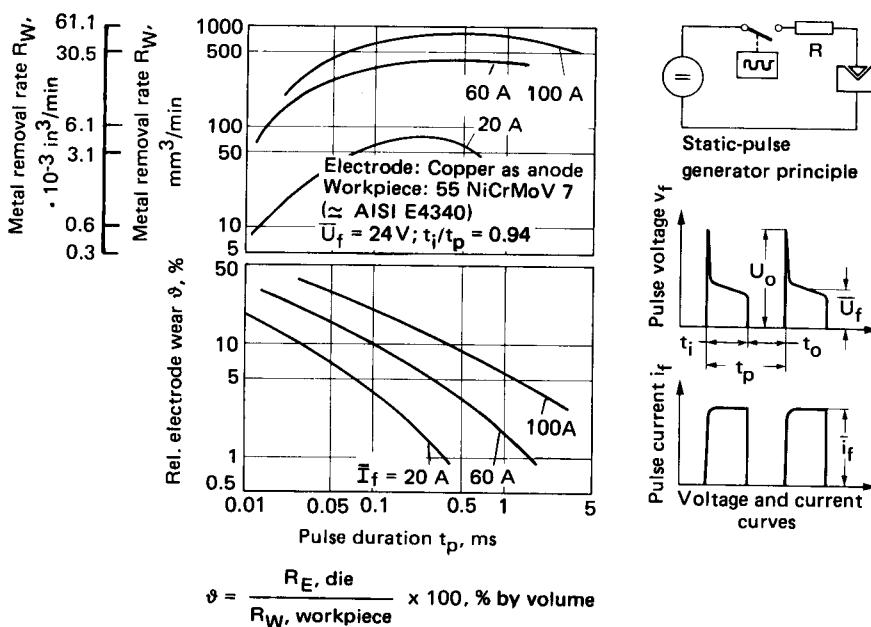


**FIG. 32.12** Removal rate and tool wear during electroerosion. (After [32.26].)

case of a particular spark-erosive cutting process, by means of a numerically controlled wire electrode (see Fig. 32.18) [32.26].

The rates of metal removal and electrode wear are principally influenced by the parameters pulse voltage, pulse current, and pulse duration. A typical relationship between metal removal and electrode wear using static pulse generators is shown in Fig. 32.12. The current density should not exceed  $12 \text{ A/cm}^2$  ( $77 \text{ A/in}^2$ ) at the face of the electrodes, since otherwise the removal of the abrasion products from the machining gap and the deionization of the discharge channel may no longer be assured.

With high removal rates, electrode wear and dimensional variations are high. In addition the surface finish is poor. In general the machining of three-dimensional shapes is carried out, as in conventional machining, in several stages of roughing and finishing. In the roughing stage the main goal is to achieve a high removal rate without particular attention to surface quality. In the finishing stage the equipment is set so as to achieve the required surface finish and dimensional accuracy.

In order to generate large surface areas or multiple impressions in one die block (automobile body dies, multiple dies, multistage dies) the technique of multichannel machining may be employed in order to increase the effective rate of metal removal, thereby shortening the erosion time [32.28].

All materials which conduct electricity can be machined by spark or electroerosion, irrespective of their mechanical properties; that is, these methods can also be used where conventional methods are not suitable either because the strength of the material is too high (as with carbides) or because the die geometry is difficult to machine by milling (narrow openings in cutting dies, Fig. 31.2, group 6). The time necessary for electroerosion is determined largely by the physical properties of the material (materials with low melting points can be machined more easily) and by the geometry, accuracy, and surface finish required.

The material of the electrodes and the methods used to produce them (Table 32.4) are important factors in determining the profitability of electroerosive machining.

Electrode materials must have as high a melting point as possible in order to minimize wear and exhibit good thermal conductivity. In practice, copper and graphite have been proven to be particularly successful. Copper has the advantage of high fracture resistance. Also it can be worked easily using chip forming or deformation methods and is ideally suited for producing very fine surface finishes with  $R_t \approx 4 \mu\text{m}$  (150  $\mu\text{in}$ ). Electrodes made of graphite, on the other hand, show very little wear (<0.1% by volume) [32.27], [32.29].

Depending on the volume to be removed and the required accuracy, a number of similar electrodes are used for sinking one single die. The tolerance, of at least the finishing electrodes, should be one ISO quality category better than that required of the parts to be made using dies produced by electric-discharge machining.

Chip-forming machining methods are usually used for the production of small and medium-sized electrodes because of their high accuracy and their universal application for all main and secondary shape elements (Fig. 32.13). In a special abrading process, used for making graphite electrodes, the graphite blank is pressed against a die made of a hard material with a rough surface and machined by means of small rotary movements of just a few tenths of a millimeter [32.26].

In addition to mechanical machining methods, small and medium-sized copper electrodes are extensively formed by forging or hot pressing (Fig. 32.14), especially where suitable equipment is readily available. Electrodes for electroerosion of large dies (e.g., automobile body dies) are produced for economic reasons by deforming 1–2-mm (0.04–0.08-in) thick copper sheet or using electroplating techniques. High-energy-rate forming processes are particularly suited to the deformation of copper sheet, that is, explosive forming and electrohydraulic processes (Chap. 27, Figs. 27.1 and 27.2). For this purpose it is possible to use a female die made from fiberglass-reinforced cast resin (Fig. 27.16). With electroplating methods the electrode is formed by depositing a 3–6-mm (0.1–0.2-in) layer of copper onto the epoxy-resin cast of the original model of the surface, which has been coated with an electrically conducting paint (Fig. 32.15a) [32.30], [32.31]. The reinforcements needed to support the electrode shell in each case are similar to those used for supporting copy milling patterns and are normally made of tubular steel and laminated epoxy resin.

For rough machining small and medium-sized workpieces, simple general-purpose rod electrodes are most suitable (Fig. 32.15b) [32.26]. A matrix, usually of circular rods made of copper or copper alloys, is placed on a model of the die in such a way that the initially fixed rods take on the shape of the die. The rods are then locked in place by tightening the clamping frame which surrounds them. Electrode wear, which may occur at steeply sloping areas, may be counteracted by readjusting the length of the rods.

Even the brief outline given here of just a few processes shows that up to now no single method exists which is equally suitable for all machining applications and electrode materials. The most important criteria for deciding which process to use will always be the cost factor.

With high-energy roughing the metal removal rate may reach  $1.5 \text{ cm}^3/\text{min} \cdot 100 \text{ A}$  ( $0.1 \text{ in}^3/\text{min} \cdot 100 \text{ A}$ ), surface quality  $R_t > 40 \mu\text{m}$  (0.0015 in), and dimensional tolerance  $T > 500 \mu\text{m}$  (0.02 in). The corresponding values for finishing operations (using lower energy rates) are  $0.01 \text{ cm}^3/\text{min} \cdot 10 \text{ A}$  ( $0.001 \text{ in}^3/\text{min} \cdot 10 \text{ A}$ ),  $R_t = 4\text{--}20 \mu\text{m}$  (0.16–0.8 mil) and  $T > 10 \mu\text{m}$  (0.4 mil) (Table 32.1), respectively.

Increasing energy concentration, however, also has an increasing effect on the microstructure of the generated die surface (hardness, cementite and martensite formation), which in roughing may extend to a depth of 0.08–0.3 mm (0.003–0.01 in), while in finishing it lies under 8  $\mu\text{m}$  (0.32 mil). In subsequent use of the die, the remaining cementite or martensite layer may increase the useful life of the eroded dies [32.32]. Where the desired surface finish does not satisfy the given requirements, it is possible to smooth the die surface by hand grinding, lapping, or even electrochemical polishing. Thus the surface roughness can be reduced by about 10–30%.

Important advantages of electroerosion, compared with more conventional die manufacturing processes, are:

- 1 The toughness and hardness of the die material do not affect the removal rate or electrode wear; that is, dies can be machined after heat treatment, thus avoiding distortion or heat cracks in critical areas.

**Table 32.4** Methods of Making Electrodes for Electroerosion

Process	Area of application	Advantages	Disadvantages
Copy milling, numerically controlled milling	Mainly used for the production of noncircular dies, large or small, using single- or multitool milling machines	May be used for all machinable materials, high accuracy, small or large batches; tolerances to $< \pm 0.04$ mm ( $< \pm 0.001$ in)	
Turning, copy turning	Symmetrical shapes of small or medium dimensions		
Shaping on a shaping machine	Electrodes for making holes		Templates sometimes required, labor-intensive
Abrading [32.26]	Graphite electrodes, suitable for all shapes of small and medium size	Method used for making graphite electrodes in larger batches	Only suitable for graphite; tolerances $> \pm 0.1$ mm ( $> \pm 0.004$ in)
Forging or hot pressing and sizing (Fig. 32.14)	All shapes of small or medium dimensions, frequently used as alternative to machining	Economical methods for making small and medium batches, compact structure, good current distribution, little material waste, tolerances $\pm 0.08$ mm ( $\pm 0.003$ in)	
Extrusion	Electrodes for making small holes in large batches	Compact structure, little waste	Not suitable for graphite, only suitable for large batches of similar electrodes
Coining forming	Small precision electrodes, usually of copper	Inaccuracy $< 50 \mu\text{m}$ ( $< 2$ mil), good-quality surface	Limited to small flat shapes, accurate coining dies required

Primary forming		Secondary forming	
Deep drawing (or special process, see Chap. 20)	Mainly electrodes made of sheet copper, 1–1.5 mm (0.04–0.06 in) thick, small to medium dimensions, small batches	Little material waste	Electrode support required
High-speed forming (electromagnetic, electrohydraulic, and explosive forming, see Chap. 27)	Electrodes made of sheet copper, 1–1.5 mm (0.04–0.06 in) thick, small and large batches	Little material waste, simplified tooling, suitable for large sizes	
Metal spraying	Practically all shapes of small and medium dimensions, small and large batches, mainly for copper electrodes	Simple, universal, inexpensive	Varying density, high electrode wear, high internal stresses
Casting	Low-precision electrodes, making preforms, e.g., for subsequent forging	Cheap, simple	Usually inaccurate $> \pm 0.1\text{--}0.2$ mm ( $> \pm 0.004\text{--}0.008$ in), high electrode wear
Electrolyte depositing	Small to medium-sized copper electrodes, layer thickness 3–6 mm (0.1–0.2 in), mainly used for making large dies for sheet-metal working	Highly accurate copy of pattern with good surface finish, even with complicated shapes, dimensional accuracy of pattern electrode 0.1–0.25 mm (0.004–0.01 in), depending on size [3900 × 1600 mm (118 × 63 in) and more]	Large baths of electrolyte required
Sintering	Usually for small-sized graphite electrodes, medium and large batches	Little material waste	Uneven electrode wear as a result of uneven density, costly equipment and materials required
Numerically controlled wire electroerosion	Small to medium-sized dies with holes, punches	Complex contouring, high precision	Special machine and programming required

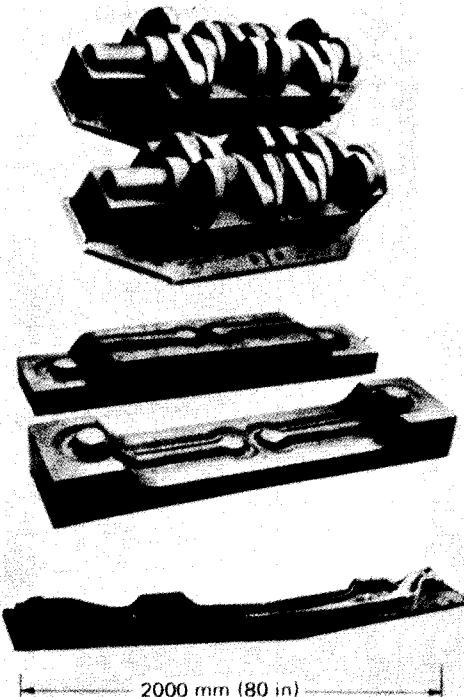


**FIG. 32.13 Manufacture of electrodes for electroerosion:**  
Copy-milled graphite electrodes for automobile crankshafts, bicycle cranks, and truck axles. (*Courtesy of Le Carbone-Lorraine.*)

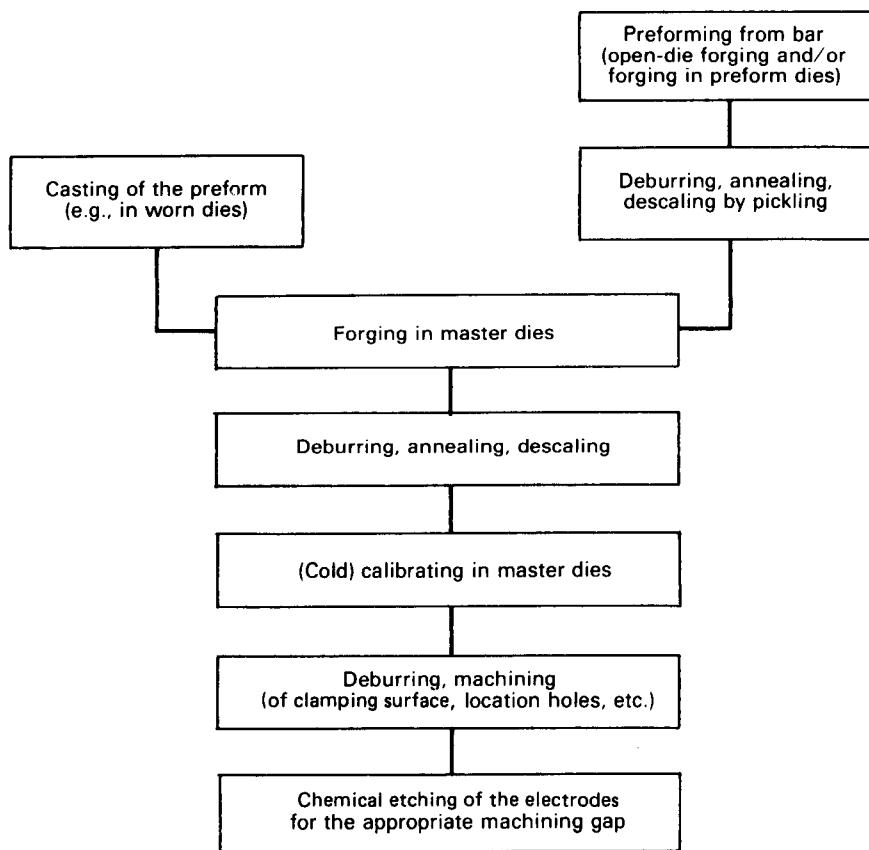
- 2 The conventional machining of complex internal shapes is replaced by the easier machining of external shapes made from materials such as copper and graphite.
- 3 A large portion of the typical hand-finishing operations, such as hand grinding, are no longer necessary.

However, there are also the following disadvantages:

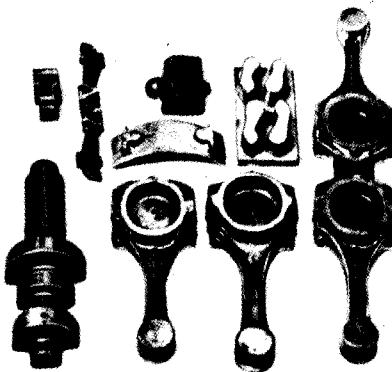
- 1 Because of electrode wear, separate electrodes are required for roughing and finishing, or alternatively the die cavity must be premachined using a chip-forming process.
- 2 The finishing electrode must be made to closer tolerances than those required of the die itself.

The equipment used in electroerosion consists of a machine tool, a generator, and a dielectric-medium supply. Sometimes because of the considerable weights of the electrode and the die and the effect of the sensitive hydraulic or electrohydraulic feed controls on the final result, the machine tool must exhibit a high degree of stiffness and good accuracy in the moving axes in order to assure the required repeatability. Small and medium-sized electroerosion machines are usually designed as universal machines of the single-column type with a tank for the dielectric medium, which can be lowered or removed for ease of access (Fig. 32.16).

The work head contains the feed mechanism, permitting the advance movement of the electrode toward the workpiece or die. For dies with working surfaces of several square meters (e.g.,



(a)



(b)

**FIG. 32.14** Manufacture of electrodes for electroerosion: Forged tool electrodes. (a) Work sequence.  
(b) Electrode shapes.

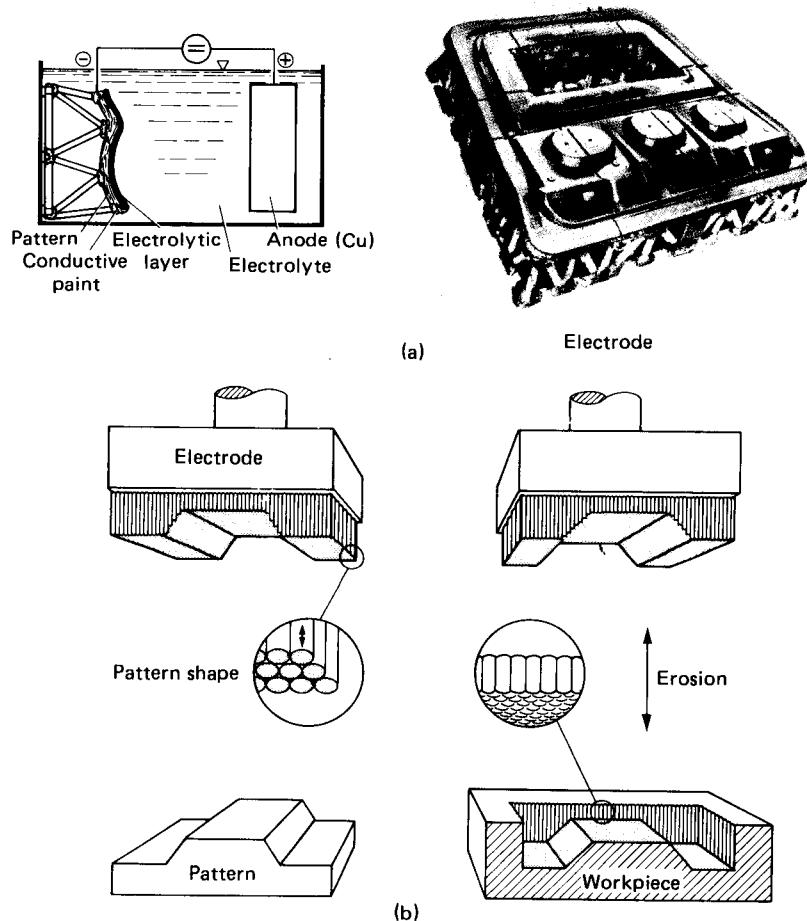
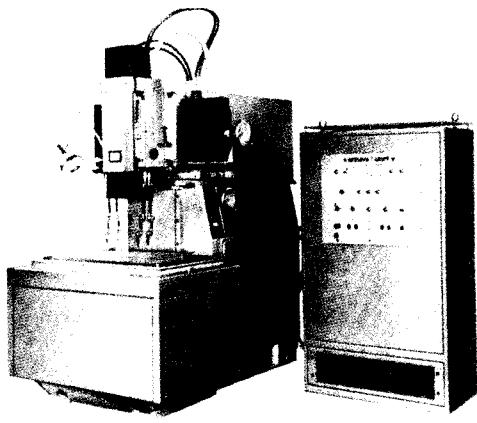


**FIG. 32.15** Manufacture of electrodes for electroerosion: (a) Principle of electrolytic deposition. (b) Composite electrode for rough machining. (Courtesy of AGIE.)

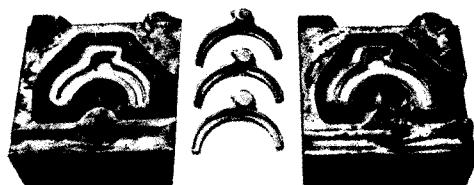
dies for sheet-metal working) large twin-column machines are on the market. These machines, even under the difficult conditions caused by the large electrode and die, satisfy the high requirements of rigidity. To facilitate machine loading, either the machine table or the columns may be moved (Fig. 32.17).

As a result of developments in the field of semiconductors, the controlled static pulse generator is the one most commonly used today. It provides high removal rates, low electrode wear, as well as permitting the use of the same material for both electrodes, for example, steel to steel, which is particularly important for electroerosive finishing [32.26], [32.33], [32.34].

A special application of electric-discharge machining is its combination with numerical path control (Fig. 32.18). A continuously moving wire is used as the electrode and produces a cut equivalent to that produced by a band saw. In this way dies with any type of opening can be machined. The process is thus suitable for machining jig, blanking tools, and orifices. The necessary programs can be produced easily with the aid of a small computer, using the lines and circles which define the contour to be machined.



(a)



(b)

**FIG. 32.16** Electroerosion (spark-erosion): (a) Program-controlled spark-erosion equipment. Work area— $1120 \times 800$  mm (44  $\times$  32 in). (*Courtesy of Nassovia.*) (b) Spark eroded dies for gearshift forks. (*Courtesy of AEG.*)

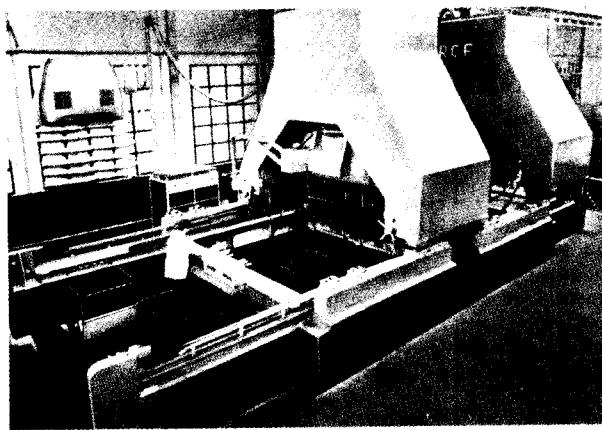


**FIG. 32.17** Electroerosion equipment for machining dies up to  $5500 \times 2800 \times 1800$  mm (217  $\times$  110  $\times$  71 in). (*Courtesy of RCF.*)

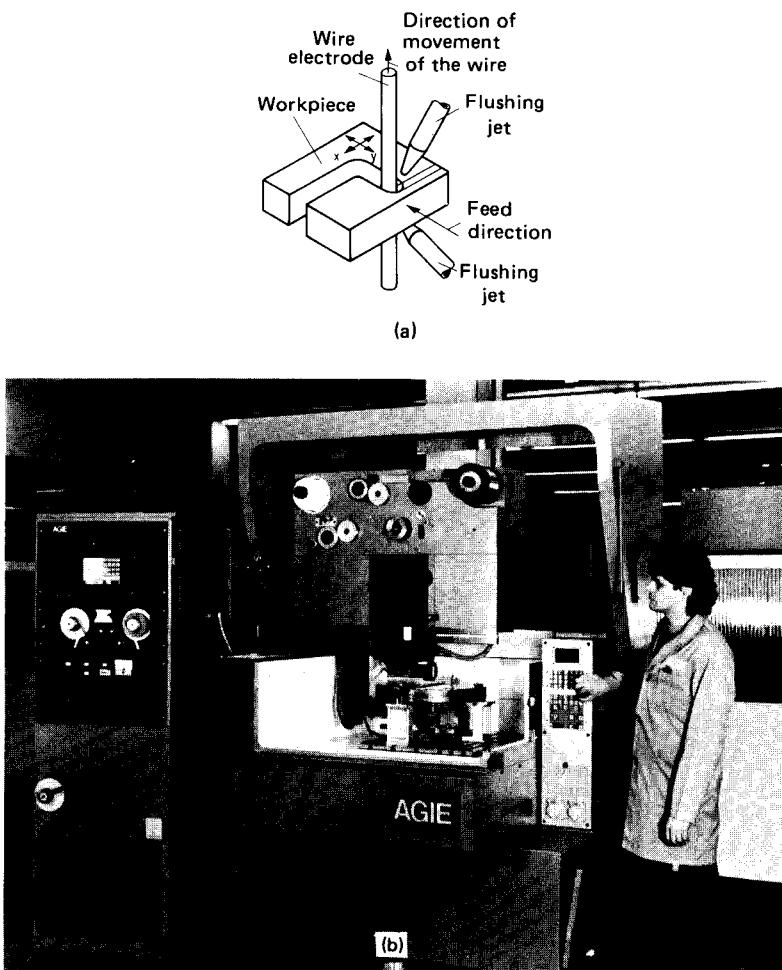


**FIG. 32.18** Electroerosion using a wire electrode. (a) Sketch of fundamental principle. (b) Manufacturing equipment (Courtesy of AGIE.)

Since in electroerosion the optimal machining conditions vary, the application of adaptive control techniques for the optimization of the erosion process and for improving the loading of the equipment is gaining in economic significance [32.33].

**Electrochemical processes:** Of the electrochemical processes, it is electrochemical sinking which is of greatest significance for die production. Following its initial introduction in the 1950s in aerospace technology, it is widely used today as a way of machining tough high-temperature-resistant materials, such as chromium-nickel alloys and titanium. Since the late 1960s the process has been used for manufacturing dies with working surfaces up to approximately  $250 \text{ cm}^2$  ( $40 \text{ in}^2$ ) [32.24], [32.33].

All electrochemical processes are based on the principle of anodic dissolution of metal (Fig. 32.11). Under the influence of the direct current supplied to the electrodes, the anode material dissolves, giving up a number of electrons proportional to its valency and combining with OH

molecules contained in the electrolyte to form metal hydroxide, which is precipitated out. Hydrogen ions contained in the solution are given off at the cathode. As with electroerosion, the desired geometry is imparted to the die through the shape of the electrode which, however, in this case is not subject to wear.

Faraday's and Ohm's laws are the basis for determining the parameters and relationships governing the process [32.23], [32.35]. According to these, the electrochemical abrasion at the anode (workpiece) is directly proportional to the charge flowing through the electrolyte. The rate of advance or the rate at which the machining gap increases depends on the anode material (atomic weight, valence, specific gravity), the supply voltage, and the specific conductivity of the electrolyte. In practice a constant voltage of between 5 and 20 V and a tool electrode feed rate of 0.2–2.5 mm/min (0.008–0.1 in/min) are usually maintained, leading to a constant gap of 0.05–1 mm (0.002–0.04 in) and to a feed rate directly proportional to the current density of  $<2 \text{ A/mm}^2$  (1300 A/in<sup>2</sup>).

In electrochemical die sinking the electrode and the die surfaces are not usually parallel to each other since the gap width largely depends on the shape to be produced. The gap increases with the taper of the die contour, resulting in changes in the machining conditions [32.35], [32.36]. For this reason the geometry of the electrodes is corrected [32.37], or passivating electrolytes such as NaNO<sub>3</sub> are used under special conditions [32.33], [32.36].

A factor which greatly contributes to the success of electrochemical die sinking is the design of the high-precision tool electrode usually machined from copper, brass, or graphite, depending on the shape of the impression to be produced and on the passage of electrolyte through the machining gap [32.23]. The supply of electrolyte must be such that the electrolyte flows via the shortest route at a high constant speed over the entire working surface without interruptions in flow, thereby removing both the heat and the waste products.

The main factor influencing the accuracy in electrochemical die sinking is the machining gap [32.35] to [32.37]. It becomes smaller—and thus the accuracy is increased—when the electrode feed rate, supply voltage, and conductivity are reduced. However, the danger of short circuits is also increased thereby. Recommendations on how to achieve a constant machining gap are given in Fig. 32.19.

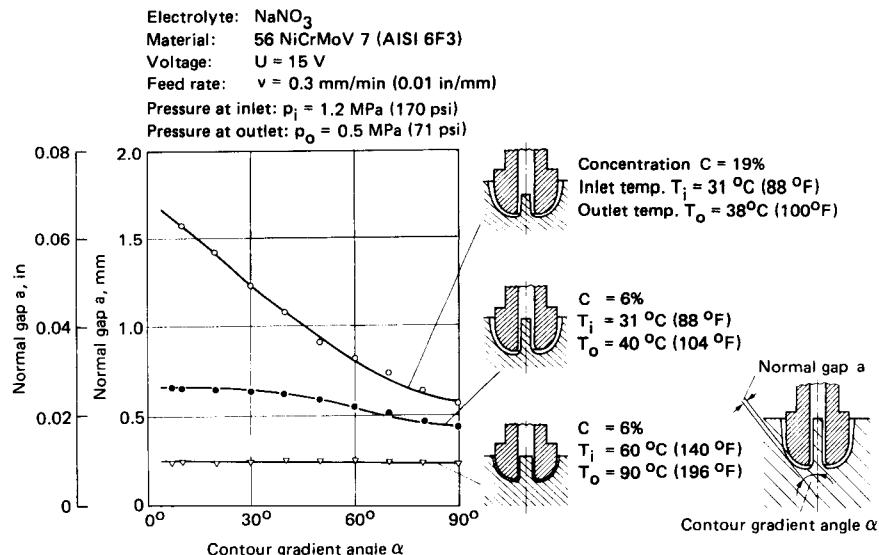
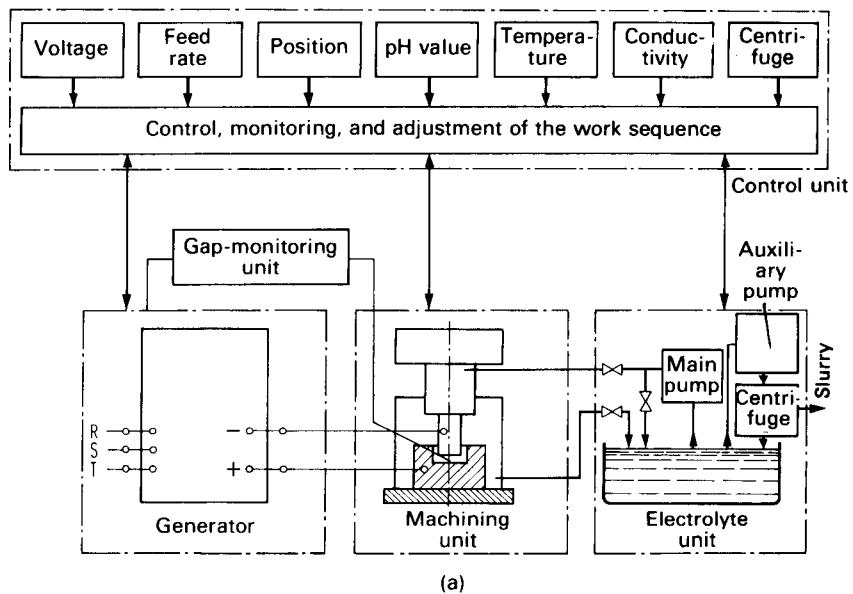
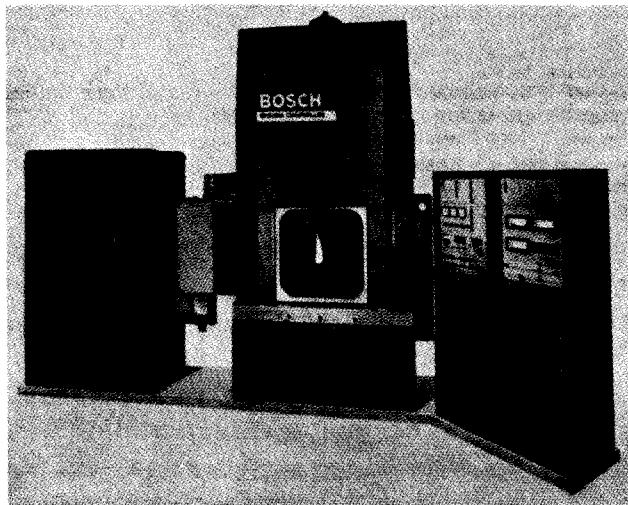


FIG. 32.19 Electrochemical die sinking. Gap widths for different machining conditions. (After [32.36].)



(a)



**FIG. 32.20** (a) General principle of electrochemical machining installation. (After [32.33].) (b) Example of a plant with 5–20-V, 10,000-A generator. (Charmilles system, courtesy of Bosch.)

At the present state of the art, tolerances of  $\pm 0.05$  mm (0.002 in) may be achieved in the manufacture of shallow-cavity dies and  $\pm 0.07$  mm (0.003 in) with deeper-cavity dies under appropriate conditions [32.36].

The quality of electrochemically machined surfaces (peak-to-valley height  $R_z$ ) depends on the microstructure and the composition of the die materials. With steels, for example, nickel and ferrite are preferable, while carbide dissolves little or not at all. With gray cast iron the graphite lamellae are not susceptible to chemical attack; steadite (2.4% carbon, 6.89% phosphorus), too, cannot be removed in this way. This explains why cast iron is unsuitable for electrochemical machining. On the other hand the surface quality improves with increasing current density, since the current density is proportional to the feed rate of the electrode, with increasing removal rates up to  $40 \text{ cm}^3/\text{min} \cdot 2000 \text{ A}$  ( $2.4 \text{ in}^3/\text{min} \cdot 2000 \text{ A}$ ). As a result the process is not divided into roughing and finishing operations as in electroerosion. Further, no thermal or mechanical influences affect the surface structure of the workpiece. In order to achieve a good surface finish, the material to be machined should be of a fine-grained homogeneous structure.

Experiments have shown that, depending on the exact die geometry, electrochemically machined forging dies may have a higher die life than conventionally machined dies due to the nonmechanical removal process and the resulting improved fatigue resistance [32.38].

The advantages of electrochemical processes compared to spark erosion are:

- 1 No separate roughing and finishing operations but just a single machining operation is required to produce a good surface finish.
- 2 The electrode, as cathode, is not subject to wear.
- 3 The workpiece structure is not affected by thermal or mechanical stresses.
- 4 High removal rates may be achieved.

The disadvantages are:

- 1 Complex electrodes are required.
- 2 Higher disparity exists between electrode and impression (Fig. 32.2).
- 3 Higher investment is required for electrochemical equipment.
- 4 Machining of surfaces larger than  $250 \text{ cm}^2$  (40 in $^2$ ) is uneconomical.

The equipment required for electrochemical die sinking consists of a machine tool, a generator, a control system, and an electrolyte supply unit (Fig. 32.20). The machines are usually designed with a twin-column welded construction in order to cope with the high stresses which arise due to electrolyte pressures of up to 25 bar (356 psi) without reducing the feed rate of the electrode. The elastic behavior of the machine frame and the electromechanical or electrohydraulic feed drive is compensated by special design and control features which maintain a constant feed rate even under full load and assure that the slide movement is free of play or "stick slip." In the generator (voltages of 5–20 V, currents up to 20,000 A) rectification is performed using power thyristors, which also permit easy control of the working voltage. Electrical monitoring of current and voltage variations can detect disturbances (short circuits) in the machining gap and stop the process within a few milliseconds before serious damage occurs to the electrode or workpiece. In the electrolyte unit the temperature, conductivity, and pH value of the electrolyte are continuously monitored and adjusted, and precipitated metal hydroxides are removed by means of centrifuges or filters.

## REFERENCES

- 32.1 Opitz, H.: *Part Systems and Part Family Manufacture (in German)*, Essen, Girardet, 1963–1967.
- 32.2 Lange, K.: "Development Trends in the Field of Metal Forming" (in German), *Ind.-Anz.*, 87, 1965, pp. 1843–1847.

### 32.26 TOOLS FOR METAL FORMING

- 32.3 Lange, K.: "Concerning the 9th European Machine Tool Exhibition in Brussels" (*in German*), *Ind.-Anz.*, 87, 1965, p. 1567.
- 32.4 Jones, R. N.: "Cast Dies and Die Linings" (*in German*), *Ind.-Anz.*, 88, 1966, pp. 58–63.
- 32.5 Roll, F.: *Handbook of Casting Technology* (*in German*), Berlin/Göttingen/Heidelberg, Springer, 1959–1970.
- 32.6 "Mold Making and Developments," *Plastics*, 1969, pp. 511–514.
- 32.7 Zeuner, H., and Menzel, A.: "Manufacture and Use of Cast Dies" (*in German*), *Rheinstahl-Tech.*, 1971, pp. 91–97.
- 32.8 Verderber, W.: "A New Method of Die Making: Casting" (*in German*), *Ing. Dig.*, 7, 1968, pp. 54–68.
- 32.9 Stutzman, G. D.: "Use and Behavior of Cast Forging Dies" (*in German*), *Ind.-Anz.*, 88, 1966, pp. 1313–1315.
- 32.10 "Use of Dies in Metal Forming," *Met. Form.*, 38, 1971, pp. 3–5.
- 32.11 Vogt, H. T.: "Economic Milling of Die Contours" (*in German*), *Mitt. Dtsch. Forschungsges. Blechverarb. u. Oberflächenbehand.*, 7, 1956, pp. 266–274.
- 32.12 Hilbert, H. L.: "Copy Milling of Large Dies" (*in German*), *Werkstatt u. Betr.*, 99, 1966, pp. 391–397.
- 32.13 Hegewald, H., and Thurm, M.: "Use of Copy Milling for the Manufacture of Die Contours in Forging" (*in German*), *Fertigungstechn. u. Betr.*, 19, 1969, pp. 360–362.
- 32.14 Henning, H., and Schwegler, H.: "Significance of NC Milling for the Machining of Complex Shapes" (*in German*), *Steuerungstechnik*, 4, 1971, pp. 208–215.
- 32.15 Schwegler, H.: "Contribution to the Description and Programming of Surfaces and the Manufacture Using Numerically Controlled Machines" (*in German*), Dr.-Ing. thesis, Universität Stuttgart, 1972.
- 32.16 König, W., Lange, K., Rüdt, W., and Schacher, H. D.: "Study of the Design and Manufacture of Forging Dies Based on Systems Analysis" (*in German*), *Ind.-Anz.*, 96, 1974, pp. 177–183.
- 32.17 Wilfert, H. G.: "Problems Concerning Computer-Aided Design and Manufacture in the Body Shop" (*in German*), *Ind.-Anz.*, 96, 1974, pp. 453–456.
- 32.18 Schieber, H.: "Plastics Shape Sheet Metal" (*in German*), *Maschinenmarkt*, 77, 1971, pp. 2252–2253.
- 32.19 Wissler, K.: "Use of Resins in Die Making" (*in German*), *Maschinenmarkt*, 76, 1970, pp. 1360–1365.
- 32.20 Pond, J. B.: "Copy Milling Machine Doubles Die Making Productivity," *Machinery*, 117, 1969, pp. 71–73.
- 32.21 Augsten, G.: "Investigation of a Continuous Biaxial Copying Device" (*in German*), Dr.-Ing. thesis, Universität Stuttgart, 1972.
- 32.22 VDI-Richtlinie 3400: "Elektroerosive Bearbeitung (Electroerosive Machining)," Düsseldorf, VDI-Verlag, 1970.
- 32.23 VDI-Richtlinie 3401: "Elektrochemische Bearbeitung (Electrochemical Machining)," Düsseldorf, VDI-Verlag, 1970.
- 32.24 Visser, A.: "The Significance of Chipless Machining Processes in Modern Technology" (*in German*), *CIRP Ann.*, 18, 1970, pp. 49–56.
- 32.25 Winkelmann, A.: "Electroerosive and Electrochemical Machining Processes" (*in German*), *Werkstattberichte*, 27, 1969, pp. 53–68.
- 32.26 "Spark Erosive and Electrochemical Machining" (*in German*), *VDI-Berichte*, no. 159, Düsseldorf, VDI-Verlag, 1970.
- 32.27 Zolotych, B. N.: "Theory and Characteristics of Spark Erosion" (*in German*), *Tech. Rundsch., Fertigung*, 2, 1971, pp. 185–192.

- 32.28 Kracht, E.: "Fundamentals of Spark-Erosive Multichannel Machining" (*in German*), Dr.-Ing. thesis, Technische Hochschule, Aachen, 1970.
- 32.29 Petitembert, J.: "The Image of the Stamping Die by Electroerosion: The Electrode Tool" (*in French*), *Formage et Traitements des Métaux*, **28**, 1971, pp. 33–37.
- 32.30 Haas, E.: "A Comparison of Copy Milling and Spark Erosion" (*in German*), *Werkstatt u. Betr.*, **103**, 1970, pp. 859–864.
- 32.31 Hilbert, H. L.: "Erosion" (*in German*), *Werkstatt u. Betr.*, **105**, 1972, pp. 163–178.
- 32.32 Weiss, H.: "Recent Applications of Spark Erosion for Machining Sculptured Surfaces" (*in German*), *Ind.-Anz.*, **89**, 1967, pp. 1839–1843.
- 32.33 König, W.: "Increasing the Productivity of Chip-Forming and Chipless Machining Processes" (*in German*), *Girardet-Taschenbücher Technik*, vol. 6, Essen, Girardet, 1971.
- 32.34 Schumacher, B.: "The Performance and Tool Wear in Spark-Erosive Machining of Steel with Storage and Impulse Generators" (*in German*), Dr.-Ing. thesis, Technische Hochschule, Aachen, 1966.
- 32.35 Kubeth, H.: "The Removal Operation between Electrode and Workpiece in Electrochemical Machining" (*in German*), Dr.-Ing. thesis, Technische Hochschule, Aachen, 1965.
- 32.36 Pahl, D.: "Concerning the Removal Accuracy in Electrochemical Machining" (*in German*), Dr.-Ing. thesis, Technische Hochschule, Aachen, 1969.
- 32.37 Heitmann, H.: "The Determination of Optimal Machining Conditions in Electrochemical Machining" (*in German*), Dr.-Ing. thesis, Technische Hochschule, Aachen 1966.
- 32.38 Atrošenko, A. P., and Davydon, A. P.: "Influence of Mechanical and Electromechanical Machining Processes on the Useful Life of Forging Dies" (*transl. into German*), *Kuznečno-stampovočnoe proizvod.*, **15**, no. 9, 1973.



**PROCESS  
COMBINATIONS  
FOR DIE MANUFACTURE  
AND DIE-  
MANUFACTURING COSTS**

---

---

Die geometry (see Sec. 31.1.2), process characteristics (see Sec. 31.2), and various technological options available for die manufacture (see Chap. 32 and Fig. 31.2) have led in practice to a variety of process combinations for die manufacture. The most important of these are shown in Fig. 33.1. This figure provides the basis for a systematic consideration of die-manufacturing methods, including the various ways of preparing technical drawings and reducing die-making costs.

In addition to established processes, such as casting, hobbing, conventional and copy milling, and electroerosion, new developments such as numerically controlled milling and electrochemical die sinking are also considered. It is natural that particular processes should each have areas of application for which they are best suited. For dies, heat-treated to obtain a particular strength or surface hardness, the choice of the machining process depends on whether the heat treatment is performed before or after machining. Even more important considerations are what equipment (machines) and additional aids (patterns, electrodes, etc.) are required (see Table 32.1) and what equipment is already available. The choice of which method to use is based primarily on the manufacturing costs involved, and these for their part are a function of many different factors (Fig. 33.2).

### **33.1 MANUFACTURE OF DIES FOR HOT BULK FORMING**

Of all the different sizes and shapes of dies employed in hot bulk forming, 90% are machined using chip-forming methods, mainly by automatic copy milling with the aid of a master model. Following heat treatment, the scallops left by the milling cutter are removed by hand grinding. The danger of distortion of the nearly finished impression, of formation of cracks due to hardening, and of decarburization is nearly eliminated in electroerosive machining by using a heat-treated die block. More important, however, is that hand-finishing time, as compared to copy milling, can be reduced by about 70%. Preferably, forged electrodes made of copper or copy-

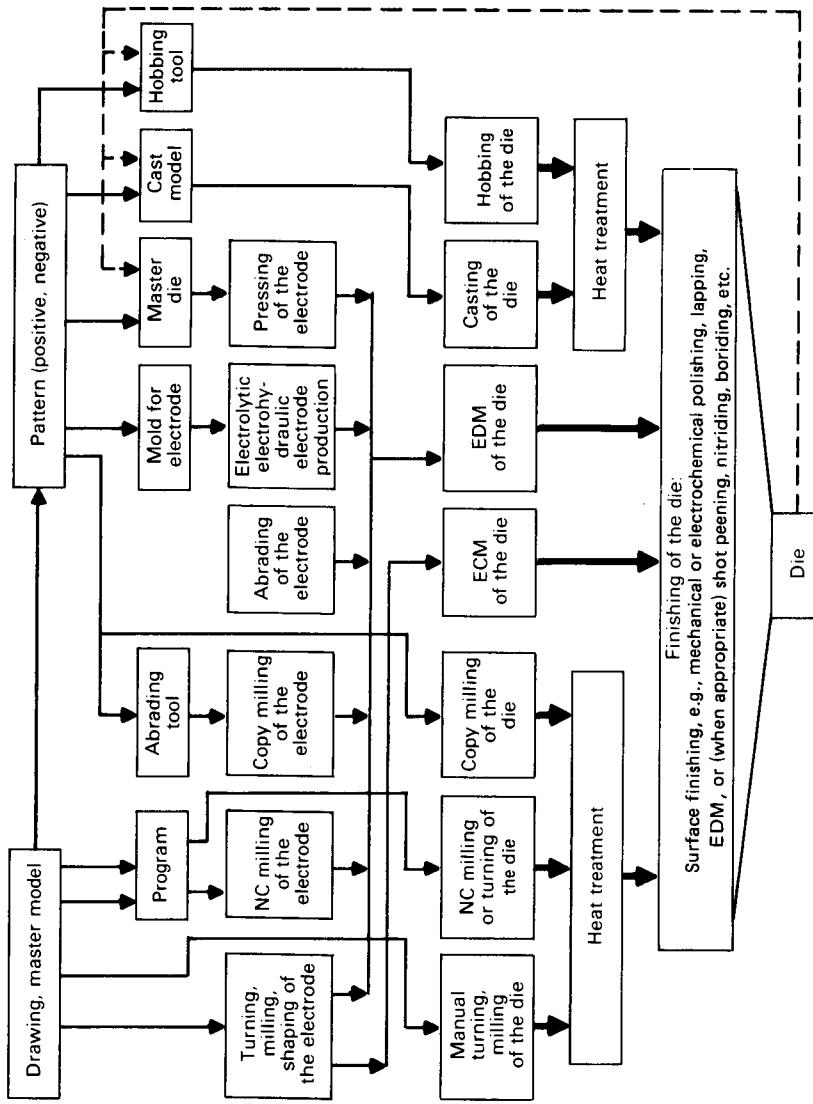


**FIG. 33.1** Routes to machining of the working surfaces of dies.

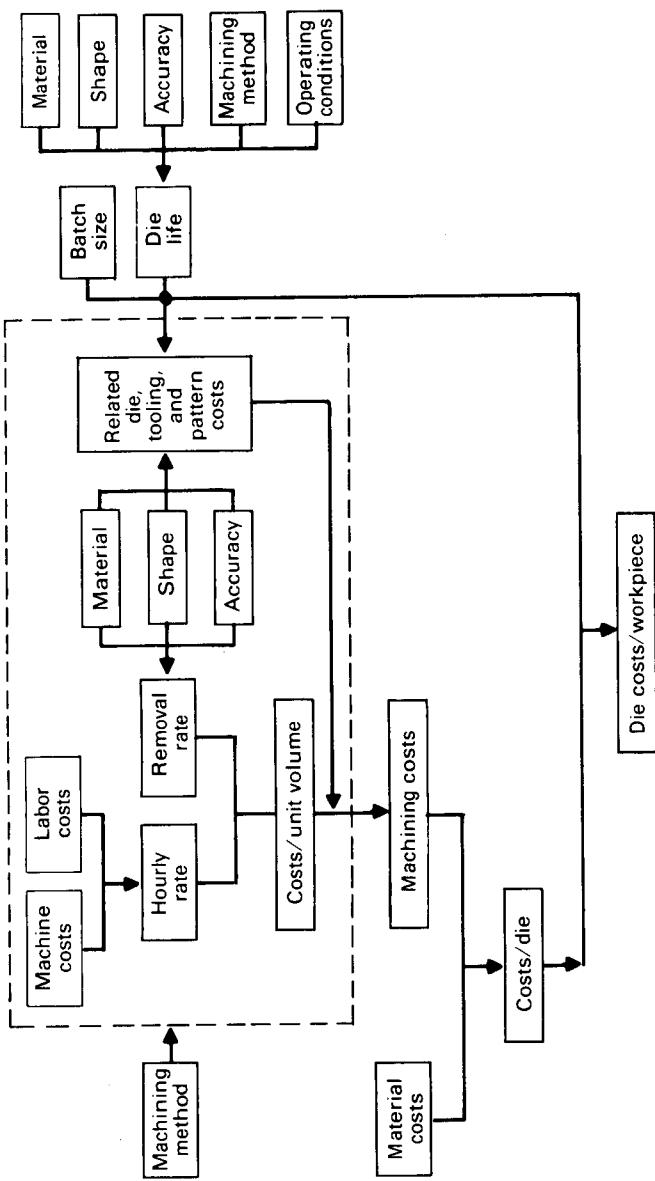


**FIG. 33.2** Die manufacturing costs. (After [33.1].)

### 33.4 TOOLS FOR METAL FORMING

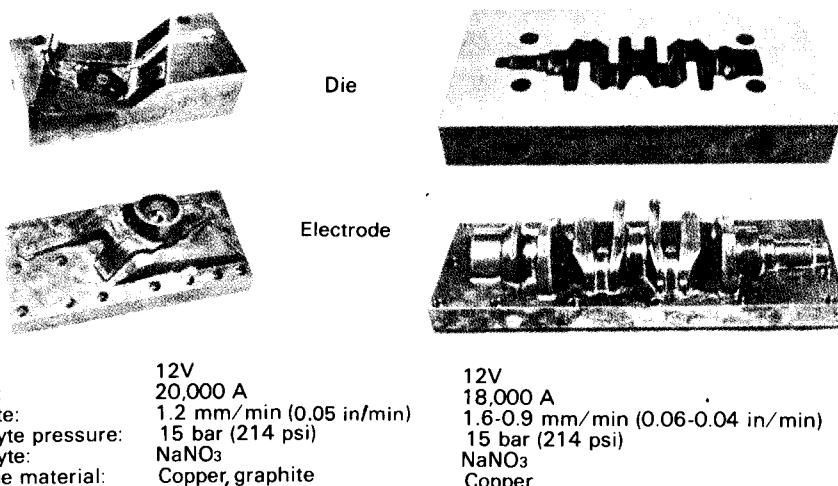


**FIG. 33.3** Electrochemical die sinking. Axle and crankshaft die. (Charmilles system, Courtesy of Bosch.)

milled graphite electrodes are used for electroerosion [32.26]. For the reasons mentioned above, electroerosive machining is used extensively in the manufacture of new dies and in resinking of worn-out hardened dies. This is valid in particular for dies of complex shape.

On the other hand, much work is currently being carried out on electrochemical die sinking (Fig. 33.3). Important advances in electrochemical machining have been made toward automatic batch production of even complex forging dies with tolerances of about  $\pm 0.1$  mm ( $\pm 0.004$  in). The reduction in time required to machine a die impression electrochemically may be as high as 70–80% compared with the time needed for electroerosion [31.3]. While the hand finishing required by both methods is about the same, more time is needed to produce and test the electrode in the case of electrochemical machining. The number of similar dies to be produced using the electrode is a critical factor in determining the electrode costs per die. The die-related costs can also be reduced in electrochemical machining if the electrolyte is not supplied through the die, but is fed directly into the pressure chamber. Thus the process-development costs can be limited to the manufacture of the electrodes [32.26].

Hot-forging dies may be cast where large tolerances are acceptable, where a large number of similar dies are required, or where the dies are to be finished using electroerosion or traditional machining methods. One of the main difficulties in manufacturing cast dies is obtaining the required dimensional accuracy and controlling the shrinkage variation from one die to the next, that is, the difficulty of achieving reproducibility in casting without affecting the material structure.

Cold and hot hobbing are—within the limits of available press capacity for hobbing—particularly well suited to the manufacture of a number of similar small cavities (multiple dies), such as dies for double-ended spanners or pliers (Fig. 33.4). In contrast to the electroremoval processes, in hobbing the accuracy initially achieved may be affected by subsequent heat treatment. Fig. 33.4 compares the use of milling, electroerosion, and cold-hobbing to produce a double-ended spanner die [33.1].

Since the macrogeometry of the die surface largely determines the surface finish of the forged parts and the die life, the working surfaces of the dies are finish-machined using mechanical, chemical, or electrochemical processes [31.9, 31.11, 33.2, 33.3].

In die forging the cost of the dies accounts for about 8% of the total forging costs. Typically the cost of the die material and the cost of making the impression account for about 4% each. The

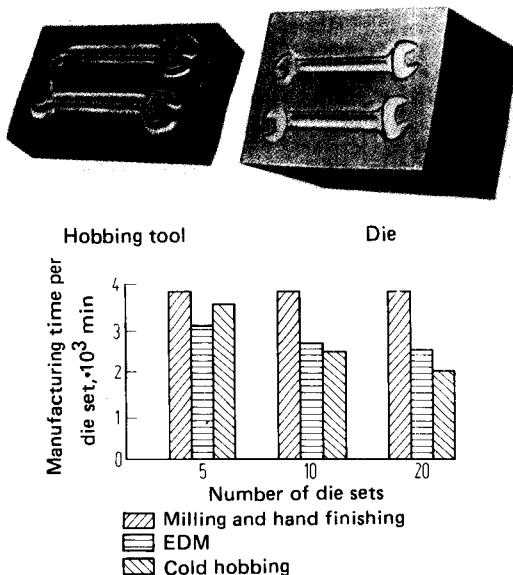


**FIG. 33.4** Cold hobbing of spanner dies. Comparison of time required for milling, EDM (electroerosion), and hobbing (After [32.37].)

latter depends above all on the number of similar dies to be manufactured (Figs. 33.2 and 33.4) [33.4].

The comparison of the manufacturing costs of a universal-joint fork cavity, shown in Fig. 33.5, is based on the long-term study of over 100 pairs of dies. According to this, the unit costs—in this case for the development of the complicated electrode necessary for electrochemical die sinking—is small and full advantage can be taken of the low machining time of the electrochemical process

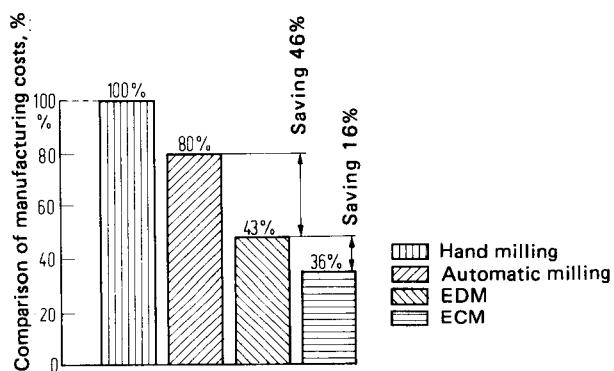


**FIG. 33.5** Cost comparison of different machining methods used to make a double-impression die. Universal joint die. EDM—electroerosion; ECM—electrochemical machining.

### 33.6 TOOLS FOR METAL FORMING

and the insignificant electrode wear compared with electroerosion. Where a smaller number of dies are required, the advantage shifts to the more widely used electroerosion process, copy milling, or—especially with simpler, for example, flat shapes—to forging methods.

A further important factor affecting die costs is the workload of the die shop concerned. The higher the investment costs (Table 32.1), the more use must be made of the die-shop facilities, for example, by shift working, which will lead to higher personnel requirements and additional organizational complications, which should not be underestimated. In practice electroerosion and chip-forming methods are in many areas today the most economical ways of manufacturing dies for hot bulk forming.

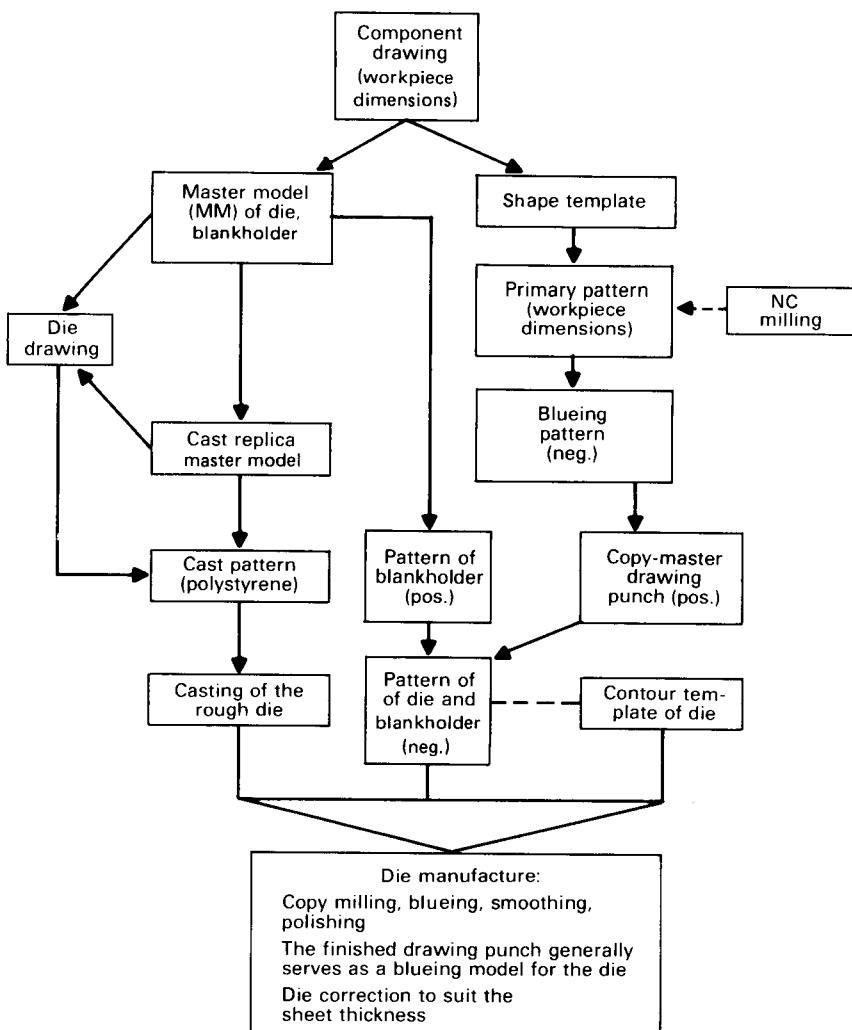


**FIG. 33.6** Manufacture of large deep-drawing die. Schematic outline of the production sequence for patterns and other aids.

### 33.2 MANUFACTURE OF DIES FOR COLD BULK FORMING

Cavities in dies used in cold bulk forming are mainly machined using the well-known chip-forming processes, especially when they are cylindrical in shape. Nonsymmetrical shapes or those where access is difficult, however, can often be machined more easily by electroerosion, thereby avoiding the necessity for using split dies [33.2]. The same is true when particular requirements exist concerning the macrogeometries of the working surface (Fig. 31.2, criterion 6), as, for example, in the case of coining dies [33.10] or when particular materials (e.g., carbide) have to be machined. The finish machining of the die surface is best performed after heat treatment, without affecting the material structure, by grinding, polishing, or lapping, or in certain cases using electrochemical polishing [32.23].

### 33.3 MANUFACTURE OF DIES FOR SHEET-METAL WORKING

The single or double convex or concave working surfaces of sheet-metal-working dies are largely machined using copy milling or electroerosion. In the case of medium- and large-sized dies, the die block is generally cast with a 10–25-mm (0.4–1-in) machining allowance. The choice of one of two process combinations is based primarily on the complexity of master models and electrodes and on the amount of hand finishing required in the form of spot grinding, lapping, polishing, and so on (about 60–80% of the overall machining time [32.30], [32.31]).

Figs. 33.6 and 33.7 show the principal factors involved in conventional manufacture using copy milling. Individual dies, such as deep-drawing dies, are first rough- and finish-milled following a master pattern. After initial grinding to smooth down the milling scallops, the surface is

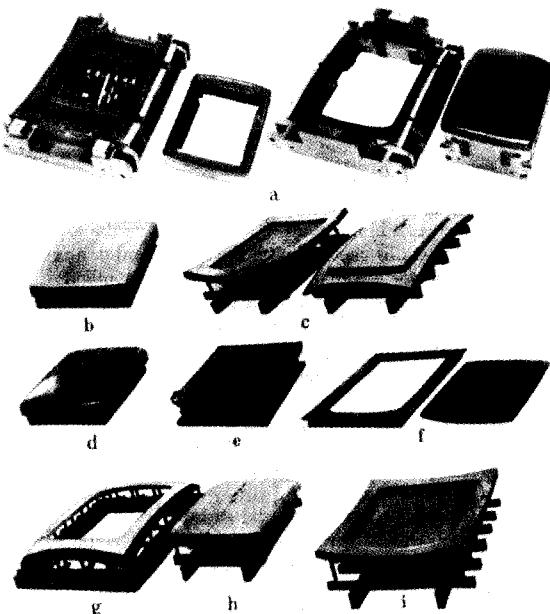


**FIG. 33.7** Manufacture of deep-drawing die set: tools, patterns, and other aids. (a) Die set. (b) Master model. (c) Plaster cast of master model. (d) Primary pattern. (e) Blueing pattern. (f) Contour template. (g) Copy pattern of blankholder. (h) Copy pattern of drawing punch. (i) Copy pattern of drawing die. (*Courtesy of Läpple.*)

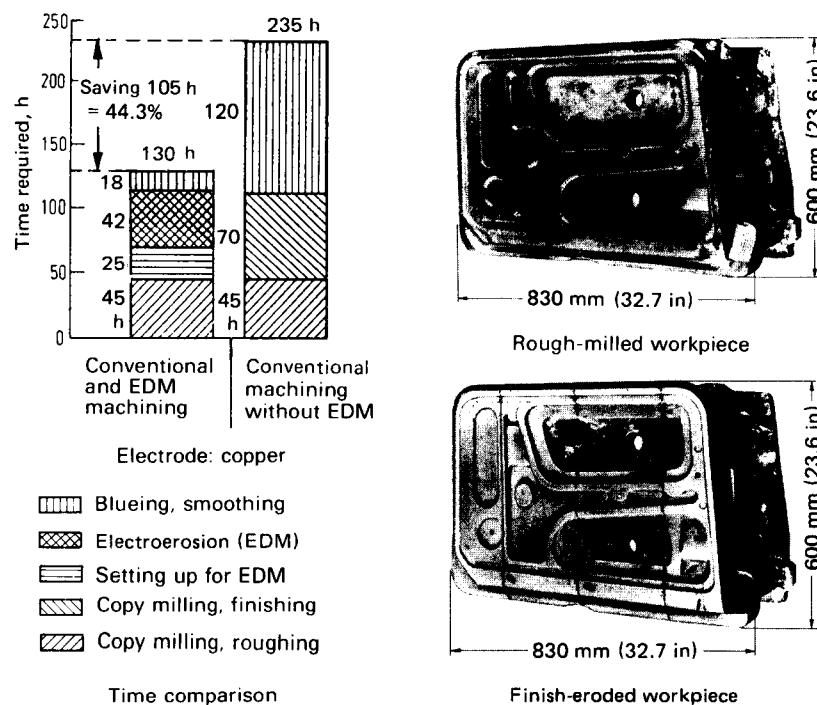


FIG. 33.8 Manufacture of deep-drawing die for inner portion of an automobile door by means of copy milling and EDM (electroerosion).

spot-ground using a blueing model, smoothed, and then polished. With complex die shapes the finished male die may be used as a blueing aid in finish-grinding the lower die. The desired gap width required for the sheet metal is checked with the aid of lead or aluminum wire.

Electroerosion is best suited for finishing premachined (copy-milled) dies to a high standard of accuracy and surface finish. The machining allowance may vary between 0.2 and 3 mm (0.008 and 0.12 in). The overall machining time may be reduced by 20–50%, and, depending on the die geometry, the time required for manual finishing by 40–90% (Fig. 33.8) [32.26], [32.31].

This implies a reduction in the throughput time required for die manufacture. Finish electric-discharge machining of a die block made by precision casting using just one electrode is difficult to achieve due to the size of the dies involved and the requirement in casting tolerances of  $\pm 1\text{--}2 \text{ mm}$  (0.04–0.08 in). Therefore die blocks made by the less precise sand-casting method are first contour-milled (since electroerosion of perpendicular surfaces is time-consuming and causes high electrode wear), and then the remaining working surfaces are rough-machined using copy milling. About 0.2–3 mm (0.008–0.12 in) is left on the die surface and machined by electroerosion to tolerances of 0.1–0.3 mm (0.004–0.012 in) and a surface finish of  $R_t = 10\text{--}30 \mu\text{m}$  (400–1200  $\mu\text{in}$ ). The final manual finishing consists of grinding the projections left opposite the electrolyte supply channels as well as the scallops formed between neighboring elements in the case of multiple electrodes. This is best done by using a blueing model. In addition, minor shape corrections may be made where the electrodes are worn out and the drawing radii may be smoothed out and polished.

Dies of large working surface areas and gradually changing curvatures, such as dies for automobile body parts (doors, roof panels, etc.), are mainly machined by copy or numerically controlled milling and require little subsequent hand finishing. With large body panels perfect

streamlining is essential. This requires special precision machining. Heavily ribbed and ridged deep-drawing dies may be machined advantageously using electroerosion (Fig. 33.8). When improved methods of electrode manufacture become available, significant time savings and a reduction in the amount of manual finishing may be expected.

The overall costs of sheet-metal-working dies are made up of about 15% material costs and 85% machining costs. In addition to the high cost of manual operations, the cost of jigs is also appreciable since dies of similar geometry are seldom required more than once. With electroerosion the cost savings are not extensive because of the cost of making the electrodes. Under optimal conditions, savings of 2–10% may be achieved. Any cost comparison, however, must take into account the latest data on electrode-manufacturing methods.

### 33.4 MANUFACTURE OF BLANKING AND TRIMMING DIES

The manufacture of dies for blanking, piercing, and trimming involves processes and process combinations by means of which the die opening and the punches may be manufactured economically [33.5]. Consequently among mechanical machining processes, in addition to the more common methods of milling, turning, and grinding, processes such as sawing, shaping, and planing are also employed. With electroerosion processes, besides die sinking, cutting may also be performed using a numerically controlled wire electrode (see Fig. 32.18). The size of the workpiece, the desired contour, the die material, and the required accuracy all influence the choice of the machining process. Deep or narrow openings, for example, often require the splitting up of a die into separate parts when using mechanical methods or machining by electroerosion. Cutting edges are usually machined conventionally to required tolerances in the case of simple contours, such as those with cylindrical openings. More complicated contours are usually machined by conventional or wire electroerosion.

To achieve the quality required (constant cutting clearance, no hardness cracks, etc.) it is sometimes advantageous, with both multistage and progressive dies, to erode a number of openings simultaneously with one set of electrodes. By choosing appropriate methods (vacuum flushing, electrode design, etc.) the taper of the eroded opening can be reduced to less than 0.01 mm/20 mm (0.0005 in/in).

With precision blanking dies the high requirements of precision (see Chap. 24) have usually been satisfied up to now by conventional die-manufacturing techniques [33.6]. Electroerosion die sinking and cutting, using a wire electrode, has led to improvements in quality (elimination of distortion and improved strength) and to considerable cost and time savings (Fig. 33.9) [32.26, 33.7].

As a result of developments in the computer-aided design of cutting tools, the data describing the contour of the cutting edge can be stored in such a way that the preparation of tapes for numerically controlled machining of both punch and die can be performed easily [33.8].

Additional heat treatment of the die surface, such as nitriding, depositing of a layer of tungsten carbide, or ion implantation, leads to a significant reduction in the wear of the cutting edge [33.9].

In manufacturing blanking dies, economy is achieved by optimal die design and by making full use of the advantages offered by the electroerosion process (e.g., machining hardened tools by electroerosion). Thus with complicated cutting-edge contours, the use of electroerosion leads to significant cost savings. For example, with dies made of tungsten carbide, savings of 30–50% may be achieved [32.30]. This is in general above the corresponding values for the manufacture of large drawing dies.

### 33.5 DEVELOPMENT TRENDS

The numerous factors affecting die manufacture, such as die geometry, material, accuracy, size, and number of dies required, together with company-related considerations, make it impossible to provide precise guidelines for choosing the most economical and optimal method of die manufacture. However, there should be no doubt that the electroremoval processes (electroerosion and electrochemical machining) offer advantages when compared with conventional processes. For

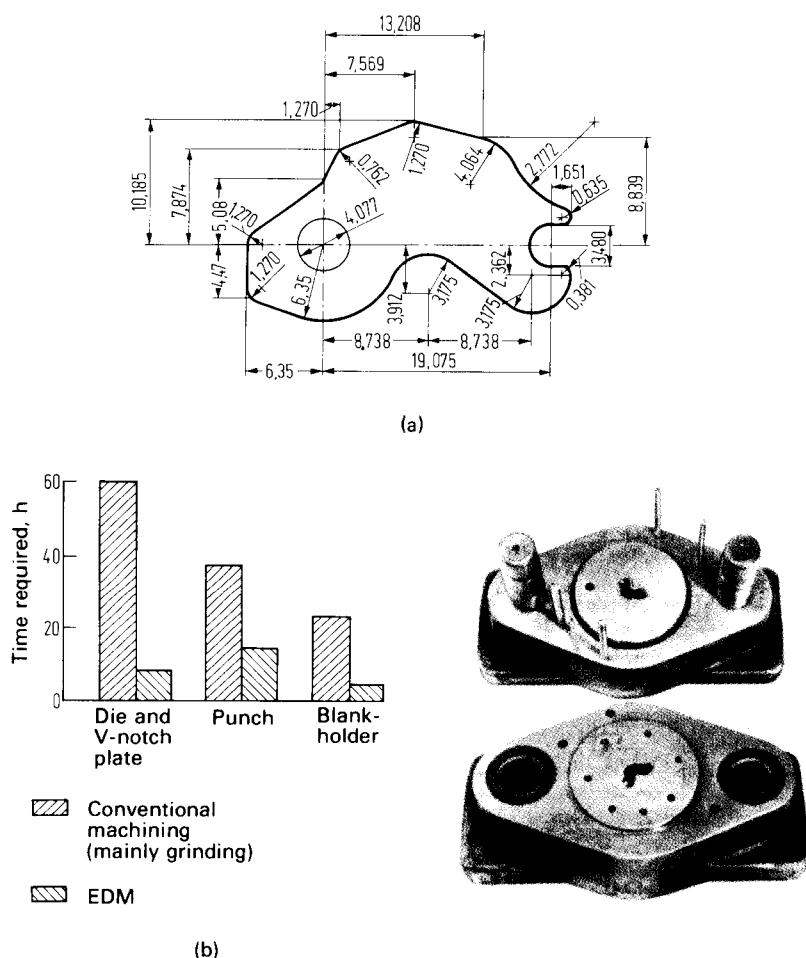


**FIG. 33.9** Machining of die set for fine blanking by means of wire EDM (electroerosion). (a) Workpiece contour. (b) Cost comparison. (c) Die set. (Courtesy of AGIE.)

For example, materials of any given strength may be machined to such high surface quality that hand finishing is minimized. Therefore it is certain that their use will increase in the future.

The specific energy necessary for material removal ( $\text{kWh/mm}^3$  or  $\text{ft}\cdot\text{lbf/in}^3$ ) in mechanical processes is about 100–1000 times smaller than in electroerosion (100) and electrochemical (1000) processes. Therefore the mechanical processes are more economical for dies of strengths less than  $1300 \text{ N/mm}^2$  (188 ksi) and for high removal rates, such as those occurring in rough machining. The answer to the question whether in the future milling will increasingly be performed by copy or numerically controlled milling methods depends on the development of suitable programs for complex shape descriptions [32.14]. In the United States and Europe the large aerospace and automobile companies are developing improved ways of describing the part geometry by means of digitizing the master models and by designing the dies using computer-aided design techniques. In addition, they are also using numerically controlled milling for making the die impressions, the patterns necessary for copy milling, or the electrodes for electroerosion [31.5], [31.6], [32.15],

[32.16], [33.8]. The optimal utilization of the capabilities offered on the one hand by the use of computers and on the other hand by the application of new machining technologies calls for fundamental changes in the die shop, that is, die manufacture will increasingly be carried out in modern well-equipped production units, using computer-aided manufacturing techniques [33.10].

With good reason one may speak today of die technology as a subject in its own right, especially when referring to the large volume of literature now available. Today's die technology already includes elements of physics (physical metallurgy, thermodynamics, theory of elasticity), chemistry (metallurgy, material science), tribology, process technology, manufacturing technology, design theory, and systems analysis (optimization, decision theory).

## REFERENCES

- 33.1 Hoischen, H.: "Die Sinking by Hobbing" (*in German*), *Werkstatt u. Betr.*, **104**, 1971, pp. 275–282.
- 33.2 "Surface Treatment of Forging Dies" (*in German*), VDI-Arbeitsblatt 5.3181, Düsseldorf, VDI-Verlag, 1957.
- 33.3 Lange, K., and Meinert, H.: "Wear of Chrome-Plated Forging Dies" (*in German*), *Forschungsberichte des Wirtschafts- und Verkehrsministeriums Nordrhein-Westfalen*, no. 286, Köln Opladen, Westdeutscher Verlag, 1956.
- 33.4 Opitz, H.: "Comparative Costs of Different Methods of Machining Forging Dies" (*in German*), *Ind.-Anz.*, **88**, 1966, pp. 608–610.
- 33.5 Hilbert, H. L.: *Stamping Technology* (*in German*), vol. 1, "Cutting Tools," München, Carl Hanser, 1972.
- 33.6 Guidi, A.: *Sharpening and Fine Cutting* (*in German*), München, Carl Hanser, 1965.
- 33.7 Hughes, D. G.: "Developments in Die-Making Techniques" (*in German*), *Information* (Fachzeitschrift über Feinstanztechnik der Firma Feintool AG, Lyss), no. 14.
- 33.8 Cornely, H., and Guldin, W.: "Display-Aided Layout of Successive-Cut Tools" (*in German*), *Ind.-Anz.*, **96**, 1974, pp. 611–614.
- 33.9 "Stamping Technology" (*in German*), VDI-Berichte, no. 114 and 148, Düsseldorf, VDI-Verlag, 1966 and 1969.
- 33.10 Lange, K.: "Metal Forming on the Threshold of the Seventies" (*in German*), *Ind.-Anz.*, **91**, 1969, pp. 2419–2424.
- 33.11 Lange, K.: "A System for the Investigation of Metal Forming Processes," in *Proceedings of the 10th International MTDR Conference*, Oxford, Pergamon, 1970.



**APP. A**

**COMPARATIVE  
DESIGNATIONS FOR  
STEELS**



.....

**Table A-1** Construction Steels

Designation DIN 17006	Material no. DIN 17007	AISI (and other)	UNS
C 10	1.0301	1010	G10100
Ck 10	1.1121	1010	G10100
C 15	1.0401	1015	G10150
Ck 15	1.1141	1015	G10150
Cq 15	1.1132	1015	G10150
C 22	1.0402	1020	G10200
Ck 22	1.1151	1020	G10230
Cq 22	1.1152	1020	G10220
C 35	1.0501	1035	G10350
Ck 35	1.1181	1035	G10340
Cq 35	1.1172	1035	G10350
C 45	1.0503	1045	G10450
Ck 45	1.1191	1045	G10450
Cq 45	1.1192	1045	G10450
C 60	1.0601	1060	G10600
C 67 (C 67 W 3)	1.1744	1065	G10650
C 70 W 2	1.1620	1070	G10700
C 85 W 2	1.1630	1086	G10860
C 100 W 1	1.1540	1095	G10950
USt 12	1.0330	1006/1008	C10060
USt 13	1.0333	1006/1008	C10060
RRSt 14	1.0338	1005/1006	C10050
QSt 32-3, Ma 8	1.0303	1006	G10060
St 34	1.0100	1010	G10100
UQSt 36-2 <sup>a</sup>	1.0204	1008	G10080
St 37	1.0100	1015	
RPSt 37-2	1.0172	(SAE C1015)	G10150
UPSt 37-2	1.0160	(SAE C1015)	G10150
St 42	1.0130	1020	
St 50		(ASTM A572-575, grade 55)	
PSt 50-2	1.0530	(SAE C1031) (ASTM A572-575, grade 65)	G10310
St 60	1.0540		
15 Cr 3	1.7015	5015	G50150
34 Cr 4	1.7033	5132	G51320
41 Cr 4	1.7035	5140	G51400
100 Cr 6	1.2067	(ASTM A295-70)	52100
15 CrNi 6	1.5919	4320	G43200
25 CrMo 4	1.7218	4130	G41300
34 CrMo 4	1.7220	4137	G41370
42 CrMo 4	1.7225	4140(H)	G41400(H)
50 CrMo 4	1.7228	4147	G41470
50 CrV 4	1.8159	6150(H)	G61500
24 CrMoV 55	1.7733	(AMS 6385C)	
34 CrNiMo 6	1.6582	4340	G43400
16 MnCr 5	1.7131	5117	G51170
20 MnCr 5	1.7147	5120	G51200
40 Mn 4	1.5038	1039	G10390
42 MnV 7	1.5223	1541	G15410
90 MnV 8	1.2842	02	T31502

<sup>a</sup>Muk 7.

**Table A-2** Medium-Alloyed Cold-Working Steels

Designation	Material no.	AISI	UNS
90 Cr 3	1.2056	E51100	G51986
145 Cr 6	1.2063	E52100	G52986
200 Cr 50	1.2080	≈D3	T30403
21 MnCr 5	1.2162	≈5120	G51200
30 NiCrMoV 16	—	P21	T51621
55 NiCrMoV 6	1.2713	≈E4340	G43400
45 WCrV 7	1.2542	S4	T41901
105 WCr 6	1.2419	O1	T31501

**Table A-3** High-Alloyed Steels

Designation DIN 17006	Material no. DIN 17007	AISI	UNS
X 8 Cr 17	1.4016	430	S43000
X 10 Cr 13	1.4006	410	S41000
X 15 Cr 13	1.4024	410	S41000
X 20 Cr 13	1.4021	420	S42000
X 210 Cr 12	1.2080	≈D3	T30403
X 10 CrAl 13	1.4724	405	S40500
X 6 CrMo 4	1.2341	≈P4	T51604
X 8 CrMoV 5	1.2342	≈F5	A336
X 32 CrMoV 33	1.2365	H10	T20810
X 35 CrMo 17	1.4122	440 A	S44002
X 37 CrMoV 51	1.2345	H12	T20812
X 38 CrMoV 51	1.2343	H11	T20811
X 40 CrMoV 51	1.2344	H13	T20813
X 40 CrMoV 52	1.2344	H14	T20814
X 165 CrMoV 12	1.2601	D2	T30402
X 37 CrMoW 51	1.2606	H12	T20812
X 5 CrNi 18 9	1.4301	304 L	S30403
X 12 CrNi 18 8	1.4300	302	S30200
X 10 CrNiMo 17 12	—	316	T631600
(X 5 CrNiMo 18 10)	1.4401		
X 15 CrNiSi 25 20	1.4841	314	S31400
X 45 CrSr 9	1.4718	HNV3	SAE 775a-69
X 155 CrVMo 121	1.2379	D2	T30402
X 210 CrW 12	1.2436	D6	T30406
X 22 CrNi 17	1.4057	431	S43100
X 130 W 5	1.2453	≈F3	T60603
X 30 WCrV 53	1.2567	H21	T20821
X 30 WCrV 93	1.2581	H21	T20821

**Table A-4** High-Speed Steels

Designation DIN 17006	Material no. DIN 17007	AISI	UNS
S 2-9-1	1.3346	M1	T11301
S 6-5-2	1.3343	M2	T11302
S 6-5-3	1.3344	M3-2	T11323
S 18-0-1	1.3355	T1	T12001



**APP. B**

**COMPARATIVE  
DESIGNATIONS FOR  
NONFERROUS METALS**



## 8.2 APPENDIX B

**Table B-1** Aluminum and Aluminum Alloys

German designation	German material no.	DIN		AA designation <sup>a</sup>	
		Standard	Part	Traditional	Revised <sup>b</sup>
Al 99.5	3.0255	1712	3	1050A	
Al 99.5 w	3.0255.10	1745	1	1050A-O	
Al 99.5 F 10	3.0255.26	1745	1	1050A-H14	
Al 99 w	3.0205.10	1745	1	1100-O	
Al 99 F 12	3.0200.26	1745	1	1100-H14	
Al Mg 1	3.3315	1725	1	5005A	
Al Mg 3	3.3535	1725	1	5754	
Al Mg 4 Mn	3.3545	1725	1	5086	
Al Mg 5	3.3555	1725	1	5056A	
Al Mg 5 w	3.3555.10	1725	1	5056A-O	
Al Mg Si 0.5	3.3206	1725	1	6063	6060
Al Mg Si 1 w	3.2315.10	1745	1	6061	6082-O
Al Mn 1	3.0515	1725	1	3103	
Al Cu Mg 1	3.1325	1725	1	2017A	
Al Cu Mg 2	3.1355	1725	1	2024	
Al Cu Si Mn	3.1255	1725	1	2014	
Al Zn Mg 1	3.4335	1725	1	7005	
Al Zn Mg Cu 0.5	3.4345	1725	1	7079	7022
Al Zn Mg Cu 1.5	3.4385	1725	1	7075	

<sup>a</sup>While this book was in press, some of the AA designations were revised. Both old and new forms are found in the text. Refer to this table for their equivalents.

<sup>b</sup>Alloy designation taken from "Registration Record of International Alloy Designation and Chemical Composition Limits for Wrought Aluminum Alloys." Temper designation taken from "Aluminum Standards and Data." Editor: Aluminum Association, Washington, D.C. 20006.

**Table B-2** Copper and Copper Alloys

German designation	German material no.	DIN standard	U.S. designation	UNS
F Cu	2.0080.10	1787	FR copper	C12500
E Cu F 20	2.0060	1787	ETP 99.95 Cu - 0.04O	C11000
SF Cu	2.0090	1787	DHP copper	C12200
Cu Zn 10	2.0230.10	17660	Commercial bronze	C22000
Cu Zn 28	2.0261.10	17660	Cartridge brass 70%	C26000
Cu Zn 33	2.0280	17660	Yellow brass 66%	C26800
Cu Zn 37	2.0321.10	17660	Yellow brass 65%	C27000
Cu Zn 40	2.0360	17660	Muntz metal	C28000
Cu Ni 2 Si	2.0855	17666	Silicon bronze	C64700
Cu Ni 12 Zn 24	2.0730.10	17663	65 Ni - 12 Ag	C75700
Cu Ni 20 Fe	2.0878.10	17664	Cu - 20 Ni	C71000
Cu Al 11 Ni	2.0978	17665	Aluminum bronze	C63200
Cu Sn 2	2.1010	17662	Phosphor bronze	C50500

**Table B-3** Magnesium and Magnesium Alloys

German designation	German material no.	DIN standard	U.S. designation	UNS
Mg Mn 2	3.5200	1729	M1A F	M15110
Mg Al 3 Zn	3.5312	1729	AZ31 B	M11311
Mg Al 6 Zn	3.5612	1729	AZ61 A	M11610
Mg Al 8 Zn	3.5812	1729	AZ80 A	M11800
Mg Zn 6 Zr	3.5161	1729	ZK60 A	M16600

**Table B-4** Nickel and Nickel Alloys

German designation	German material no.	DIN standard	U.S. designation
Ni 99.8	2.4050	17740	A-nickel 99.4 Ni - Co
Ni 99.2	2.4066	17740	A-nickel 99.4 Ni - Co
Ni Mn 1	2.4106	17741	D-nickel 95 Ni - 2.0 Mn
Ni Cu 30 Fe	2.4360	17743	Monel 67 Ni - 30 Cu
Ni Cu 30 Al	2.4375	17743	K-Monel 66 Ni - 29 Cu - 3 Al

**Table B-5** Titanium and Titanium Alloys

German designation	German material no.	DIN standard	U.S. designation
Ti 99.7	3.7035.10	17850	Grade 4, titanium
Ti 99.2	3.7025.10	17850	Grade 1, unalloyed titanium
Ti Al 5 Sn 2	3.7115	17851	Ti - 5 Al - 2.5 Sn
Ti Al 6 V 4 F 91	3.7165.10	17851	Ti - 6 Al - 4 V
Ti Al 6 V 6 Sn 2		17862	Ti - 6 Al - 6 V - 2 Sn
Ti Al 6 Mo 1 V 1		17862	Ti - 8 Al - 1 Mo - 1 V
Ti Al 6 Zr 4 Mo 2 Sn 2		17862	Ti - 6 Al - 2 Sn - 4 Zr - 2 Mo
Ti V 3 Cr 11 Al 3		17862	Ti - 13 V - 11 Cr - 3 Al

**Table B-6** Zinc and Zinc Alloys

German designation	German material no.	DIN standard	U.S. designation	UNS
Zn 99.99	2.2040	1706	Pure zinc	
F Zn	2.2201.38		Commercial rolled zinc (0.08% Pb)	
Zn 98.5	2.2085	1706	Commercial rolled zinc (0.06 Pb - 0.06 Cd)	
Zn Al 4 Cu 1	2.2141	1743	AC41 A 4 Al - 1 Cu - 0.04 Mg	Z35530
Zn Cu 4	2.2140	(1743)	Zamak 5 AC40 A 4 Al - 0.04 Mg	Z33520
			Zamak 3	

**APP. C**

**CHEMICAL  
COMPOSITION OF STEELS**

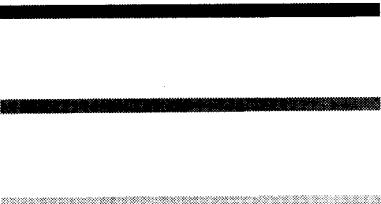


**Table C-1** Construction Steels

Designation DIN 17006	Material no. DIN 17007	C	Si	Mn	P	S	Cu	Cr	Ni	Mo	V	W	Co
C 10	1.0301	0.07 0.13	0.15 0.35	0.30 0.60	0.045	0.045							(Pb = 0.15-0.3)
Ck 10	1.1121	0.07 0.18	0.15 0.35	0.30 0.60	0.035	≤0.035							
C 10 WS	1.1805	0.10	0.30	0.40									
C 15	1.0401	0.12 0.18	0.15 0.35	0.25 0.50	0.045	0.045							
Ck 15	1.1141	0.12 0.18	0.15 0.35	0.25 0.50	0.035	0.035							
Cq 15	1.1132	0.12 0.18	0.15 0.35	0.25 0.50	0.035	0.035							
C 22	1.0402	0.18 0.25	0.15 0.35	0.30 0.60	0.045	0.045							
Ck 22	1.1151	0.18 0.25	≤0.35	0.30 0.60	0.035	≤0.035							
Cq 22	1.1152	0.18 0.24	0.15 0.35	0.30 0.60	0.035	≤0.035							(Pb = 0.15-0.3)
C 35	1.0501	0.32 0.40	0.15 0.35	0.40 0.70	0.045	0.045							
Ck 35	1.1181	0.32 0.40	0.15 0.35	0.40 0.70	0.035	0.035							

Cq 35	1.1172	0.32 0.39	0.15 0.40	0.50 0.80	0.035	$\leq 0.035$
C 45	1.0503	0.42 0.50	0.15 0.35	0.50 0.80	0.045	0.045
Ck 45	1.1191	0.42 0.50	0.15 0.35	0.50 0.80	$\leq 0.035$	
Cq 45	1.1192	0.42 0.50	0.15 0.35	0.50 0.80	0.035	$\leq 0.035$
C 60	1.0601	0.57 0.65	0.15 0.35	0.60 0.90	$\leq 0.045$	$\leq 0.045$
C 67 (C 67 W 3)	1.1744	0.64 0.72	0.15 0.40	0.60 0.80	$\leq 0.035$	$\leq 0.035$
C 70 W 2	1.1620	0.65 0.74	0.10 0.30	0.10 0.35	0.030	0.030
C 85 W 2	1.1630	0.80 0.90	0.10 0.30	0.10 0.35	0.030	0.030
C 100 W 1	1.1540	1.00	0.20	0.20		
C 110 W 1	1.1550	1.10	0.25	0.25		
C 125 W 1	1.1560	1.25	0.20	0.20		
USt 12	1.0330	$\leq 0.10$		0.20 0.45	0.035	$0.035$ (N $\leq 0.007$ )
USt 13	1.0333	$\leq 0.10$		0.20 0.40	0.025	$0.025$ (N $\leq 0.007$ )

**Table C-1** Construction Steels (*Continued*)

Designation DIN 17006	Material no. DIN 17007	C	Si	Mn	P	S	Cu	Cr	Ni	Mo	V	W	Co
(Al $\leq$ 0.02 and N $\leq$ 0.007)													
RSt 14	1.0338	$\leq$ 0.08	0.08 0.10	$\leq$ 0.04	0.025	0.025							
CSt 32-3 Ma 8	1.0303	$\leq$ 0.06	$\leq$ 0.10	0.20 0.40	0.04	0.04							
St 34	1.0100	$\leq$ 0.17		(0.20 0.50)	0.080	0.050							
UQSt 36-2	1.0204	0.08 0.13		0.25 0.45	0.04	0.04							
St 37	1.0110	$\leq$ 0.2		0.2 0.5	0.08	0.050							
RPS 37-2	1.0172	0.19			0.055	0.055							
UPSt 37-2	1.0160	0.22			0.063	0.063							
St 42	1.0130	$\leq$ 0.25		(0.20 0.50)	0.080	0.050							
St 50	1.0530	0.25	0.03 0.30	0.20 0.50	0.080	0.050							
PSt 50-2		0.30		0.20 0.50	0.055	0.055							
St 60	1.0540	0.35	0.03 0.30	0.30 0.50	0.080	0.050							

								(N = 0.007)
St 70	1.0632	0.50	(≤0.30)	(≤0.50)	0.050	0.050		
15 Cr 3	1.7015	0.12 0.18	0.15 0.35	0.40 0.60	0.035	0.035	0.50 0.80	
25 Cr 60		0.26	0.37	0.35			15.80	
34 Cr 4	1.7033	0.30 0.37	0.15 0.35	0.50 0.80	0.035	0.035	0.90 1.20	
41 Cr 4	1.7035	0.38 0.45	0.15 0.40	0.50 0.80	0.035	0.035	0.90 1.29	
100 Cr 6	1.2067	0.95 1.10	0.15 0.35	0.25 0.45	0.030	0.030	1.35 1.65	
15 CrNi 6	1.5919	0.12 0.17	0.15 0.35	0.40 0.60	0.035	0.035	1.40 1.70	1.40 1.70
25 CrMo 4	1.7218	0.22 0.29	0.15 0.40	0.50 0.80	0.035	0.035	0.90 1.20	0.15 0.30
34 CrMo 4	1.7220	0.30 0.37	0.15 0.40	0.50 0.80	0.035	0.035	0.90 1.20	≤0.60 0.30
42 CrMo 4	1.7225	0.38 0.45	0.15 0.35	0.50 0.80	0.035	0.035	0.90 1.20	0.15 0.25
50 CrMo 4	1.7228	0.46 0.54	0.15 0.40	0.50 0.80	0.035	0.035	0.90 1.20	≤0.60 0.30
24 CrMoV 55	1.7733	0.20 0.28	0.15 0.35	0.30 0.60	0.035	0.035	1.20 1.50	≤0.60 0.60
50 CrV 4	1.8159	0.47 0.55	0.15 0.40	0.70 1.10	0.035	0.035	0.90 1.50	0.10 0.20

**Table C-1** Construction Steels (*Continued*)

Designation DIN 17006	Material no. DIN 17007	C	Si	Mn	P	S	Cu	Cr	Ni	Mo	V	W	Co
34 CrNiMo 6	1.6582	0.30 0.38	0.15 0.35	0.40 0.70	0.035	0.035		1.40 1.70	1.40 1.70	0.15 0.25			
16 MnCr 5	1.7131	0.14 0.19	0.15 0.35	1.00 1.30	0.035	0.035		0.80 1.10					
20 MnCr 5	1.7147	0.17 0.22	0.15 0.40	1.10 1.40	0.035	0.035		1.00 1.30					
40 Mn 4	1.5038	0.36 0.44	≤0.50	≤1.10	0.035	≤0.035							
42 MnV 7	1.5223	0.38 0.45	0.15 0.35	1.60 1.90	0.035	0.035					0.07 0.12		
90 MnV 8	1.2842	0.85 0.95	0.10 0.40	1.90 2.10	0.030	0.030		0.20 0.50			0.05 0.15		

**Table C-2** Medium-Alloyed Cold-Working and Hot-Working Steels, Mostly for Oil Hardening

Designation DIN 17006	Material no. DIN 17007	C	Si	Mn	P	S	Cu	Cr	Ni	Mo	V	W
90 Cr 3	1.2056	0.90	0.20	0.30				0.80				
145 Cr 6	1.2063	1.45	0.20	0.60				1.40				(0.10)
40 CrMnMo 7	1.2331	0.35 0.45	0.20 0.40	1.30 1.60	0.035	0.035		1.80 2.10		0.15 0.25		
45 CrMoW 58	1.2603	0.45	0.60	0.40	'			2.00		0.50	0.80	0.50
75 CrMnNiW 67	1.2762	0.75	0.20	0.25				1.50	0.50	0.70	0.30	
140 CrV 1	1.2206	1.40	0.30	0.30				0.30			0.10	
200 Cr 50	1.2080	2.00	0.70	0.32				12.60				
210 CrW 46	DDR	2.00 2.25	0.20 0.40	0.20 0.40	<0.030	<0.030		11.0 12.0				0.60- 0.80
21 MnCr 5	1.2162	0.21	0.30	1.20				1.00				
60 MnSi 4	1.2826	0.58 0.65	0.80 1.00	0.80 1.20	0.035	0.035						
30 NiCrMoV 16		0.34	0.36	0.47				1.49	4.29	0.38	0.16	
35 NiCrMo 16	1.2766	0.32 0.38	0.15 0.30	0.40 0.60	0.035	0.035		1.20 1.50	3.80 4.30	0.20 0.40		
50 NiCr 13	1.2721	0.50	0.25	0.50				1.00	3.50			

**Table C-2** Medium-Alloyed Cold-Working and Hot-Working Steels, Mostly for Oil Hardening (*Continued*)

Designation DIN 17006	Material no. DIN 17007	C	Si	Mn	P	S	Cu	Cr	Ni	Mo	V	W
55 NiCr 10	1.2718	0.55	0.20	0.40				0.60	2.70			
55 NiCrMoV 6	1.2713	0.55	0.20	0.60				0.70	1.70	0.20	0.10	
56 NiCrMoV 7	1.2714	0.55	0.30	0.70				1.00	1.70	0.50	0.10	
57 NiCrMoV 77	1.2744	0.50	0.15	0.60	0.035	0.035		0.90	1.50	0.70	0.07	
		0.60	0.35	0.80				1.20	1.80	0.90	0.12	
95 V 4	1.2835	0.95	0.30	0.40							0.40	
145 V 12	1.2203	1.45	0.30	0.30				0.20			1.20	
45 WCrV 7	1.2542	0.40	0.80	0.20	0.035	0.035		0.90	1.20			
		0.50	1.10	0.40							0.15	1.80
											0.20	2.10
60 WCrV 7	1.2550	0.55	0.50	0.15	0.030	0.030		0.90	1.20		0.10	1.80
		0.65	0.70	0.45							0.20	2.10
105 WCr 6	1.2419	1.00	0.10	0.80	0.030	0.030		0.90	1.10		1.00	
		1.10	0.40	1.10							1.30	

**Table C-3** High-Alloyed Steels

Designation DIN 17006	Material no. DIN 17007	C	Si	Mn	P	S	Cu	Cr	Ni	Mo	V	W	Co
X 8 Cr 17	1.4016	0.07	0.65	0.32				17.50					
X 10 Cr 13	1.4006	0.08 0.12	≤1.00 ≤1.00	0.045 0.030				12.00 14.00					
X 15 Cr 13	1.4024	0.12 0.17	≤1.00 ≤1.00	≤0.045 ≤0.030				12.00 14.00					
X 20 Cr 13	1.4021	0.17 0.22	≤1.00 ≤1.00	0.045 0.030				12.00 14.00					
X 40 Cr	1.4034	0.4	0.4	0.3				13.00					
X 210 Cr 12	1.2080	2.10	0.30	0.30				12.00					
X 10 Cr Al 13	1.4724	≤0.12	1.20	0.60				13.00					
X 6 CrMo 4	1.2341	≤0.07	≤0.20	≤0.20	0.03	0.03		3.58 4.00	0.3 0.6				
X 8 CrMoV 5	1.2342	0.08	0.2	0.3				5.00		0.7	0.3		
X 32 CrMoV 33	1.2365	0.28 0.35	0.10 0.40	0.15 0.45	0.030	0.030		2.70 3.20		2.60 3.00	0.40 0.70		
X 35 CrMo 17	1.4122	0.33 0.43	≤1.00	≤1.00	0.045	0.030		15.5 17.5	≤1.00 1.30	0.90 1.30			
X 37 CrMoV 51	1.2345	0.37	0.90	0.60				4.80		1.50	0.20	1.4	

**Table C-3** High-Alloyed Steels (*Continued*)

Designation DIN 17006	Material no. DIN 17007	C	Si	Mn	P	S	Cu	Cr	Ni	Mo	V	W	Co
X 38 CrMoV 51	1.2343	0.36 0.42	0.90 1.20	0.30 0.50	0.030	0.030		4.80 5.50		1.10 1.40	0.25 0.50		
X 40 CrMoV 51	1.2344	0.40	1.00	0.40				5.30		1.40	1.00		
X 40 CrMoV 52	1.2344	0.40	1.00	0.40				5.00		1.30	1.00		
X 165 CrMoV 12	1.2601	1.65	0.30	0.30				12.0		0.60	0.10	0.50	
X 37 CrMoW 51	1.2606	0.32 0.40	0.90 1.20	0.30 0.60	0.035	0.035		5.00 5.60		1.30 1.60	0.15 0.40	1.20 1.40	
X 5 CrNi 189	1.4301	≤0.07	≤1.00	≤2.00	0.045	0.030		17.0 20.0	8.5 10.5				
X 12 CrNi 188	1.4300	≤0.12	1.00	2.00				17.0 19.0	8.0 10.0				
X 10 CrNiMo 228		0.12	0.62					21.7	8.05	3.20			
X 10 CrNiMo 1712 (X 5 CrNiMo 1810)	1.4401	0.12 0.07	0.78 1.00	2.00				16.9 16.5- 18.5	12.6 10.5- 13.5	2.90 2.50 3.50			

X 15 CrNiSi 25 20	1.4841	$\leq 0.20$	1.50 2.50	$\leq 2.00$	0.045	0.030	24.0 26.0	19.0 21.0		
X 45 CrSi 9	1.4718	0.45	3.00	0.45	0.030	0.030	9.0			
X 165 CrV 12	1.2201	1.65	0.30	0.30			12.0		0.10	
X 155 CrVMo 121	1.2379	1.55	0.30	0.30			12.0		0.70	1.00
X 210 CrW 12	1.2436	2.00	0.30	0.30			12.0			0.70
X 110 Mn 14	1.3402	1.09		13.70						
X 22 CrNi 17	1.4057	0.15 0.23	$\leq 1.00$	0.045	0.030		16.00 18.00	1.50 2.50		
X 45 NiCrMo 4	1.2767	0.45	0.25	0.50			1.30	4.0	0.20	0.50
X 45 SiCr 4	1.4704	0.45	4.00	0.45	0.030	0.030	2.65			
X 130 W 5	1.2453	1.30	0.20	0.30			0.10			5.00
X 30 WCrV 53	1.2567	0.25 0.35	0.15 0.30	0.20 0.40	0.035	0.035	2.20 2.50		0.50 0.70	4.00 4.50
X 30 WCrV 93	1.2581	0.25 0.35	0.15 0.30	0.20 0.40	0.035	0.035	2.50 2.80		0.30 0.40	8.00 9.00

**Table C-4** High-Speed Steels

Designation DIN 17006	Material no. DIN 17007	C	Si	Mn	P	S	Cu	Cr	Ni	Mo	V	W
S 2-9-1	1.3346	0.78 0.86	0.45	0.30	0.030	0.030	3.50 4.20	8.00 9.21	1.00 1.30	1.50 2.00		
S 3-3-2	1.33333	0.95 1.03	$\leq 0.45$	$\leq 0.40$	0.030	0.030	3.80 4.50	2.50 2.80	2.20 2.50	2.70 3.00		
S 6-5-2	1.3343	0.84 0.92	$\leq 0.45$	$\leq 0.40$	0.030	0.030	3.80 4.50	4.70 5.20	1.70 2.00	6.00 6.70		
S 6-5-3	1.3344	1.17 1.27	$\leq 0.45$	$\leq 0.40$	0.030	0.030	3.80 4.50	4.70 5.20	2.70 3.20	6.00 6.70		
S 18-0-1	1.3355	0.70 0.78	$\leq 0.45$	$\leq 0.40$	0.030	0.030	3.80 4.50		1.00 1.20	17.50 18.50		

**APP. D**

**CHEMICAL  
COMPOSITION OF  
NONFERROUS METALS**

---

---

---

**Table D-1** Aluminum and Aluminum Alloys

Designation	Material no.	DIN standard	Si	Fe	Cu	Mn	Mg	Cr	Zn	Ti	Other
Al 99.5	3.0255	1712 sheet3	0.25	0.40	0.05				0.07	0.05	0.5
Al 99	3.0205	1712 sheet3	0.50	0.60	0.07				0.08	0.05	1.0
Al 99.9 Mg 0.5	3.3308	1725 sheet1	0.05	0.04	0.01	0.03	0.40 0.60	0.03	0.05	0.006	0.1
Al Mg 1	3.3315	1725 sheet1	0.30	0.40	0.05	0.20	0.80 1.20	0.10	0.20	0.10	0.15
Al Mg 3	3.3535	1725 sheet1	0.40	0.40	0.05	0	2.60 3.40	0	0.20	0.10	0.15
Al Mg 4 Mn	3.3545	1725 sheet1	0.40	0.50	0.10	0.20 0.70	3.50 4.50	0.05 0.25	0.25	0.15	0.15
Al Mg 5	3.3555	1725 sheet1	0.40	0.40	0.05	0	4.30 5.50	0	0.20	0.10	0.15
Al Mg Si 0.5	3.3206	1725 sheet1	0.35 0.70	0.30	0.05	0.10	0.40 0.80	0.05	0.20	0.10	0.15

Al Mg Si 1	3.2315	1725 sheet1	0.75 1.30	0.50 0.10	0.40 1.00	0.60 1.20	0 0.30	0.20 0.05	0.10 0.20	0.10 0.15
Al Mn	3.0515	1725 sheet1	0.50	0.60	0.10	0.90 1.40	0 0.30	0.05 0.10	0.10 0.20	0.10 0.15
Al Cu Mg 1	3.1325	1725 sheet1	0.60	0.50	3.50 4.50	0.30 1.00	0.40 1.20	0.10 0.10	0.50 0.50	0.20 0.20
Al Cu Mg 2	3.1355	1725 sheet1	0.40	0.40	4.00 4.80	0.30 0.90	1.20 1.80	0.10 0.10	0.25 0.25	0.20 0.20
Al Cu Si Mn	3.1255	1725 sheet1	0.50 1.20	0.70 5.00	3.90 5.00	0.40 1.20	0.20 0.80	0.10 0.10	0.25 0.25	0.15 0.15
Al Zn Mg 1	3.4335	1725 sheet1	0.50	0.50	0.10 0.50	0.10 0.50	1.00 1.40	0.10 0.25	4.00 5.00	0.01 0.20
Al Zn Mg Cu 0.5	3.4345	1725 sheet1	0.50	0.50	0.50 1.00	0.20 0.40	2.60 3.60	0.10 0.30	4.30 5.20	0.20 0.20
Al Zn Mg Cu 1.5	3.4365	1725 sheet1	0.40	0.50	1.20 2.00	0.30 0.30	2.10 2.90	0.18 0.40	5.10 6.10	0.20 (+Zr)

**Table D-2** Copper and Copper Alloys

Designation	Material no.	DIN standard	Cu	P	Pb	Zn	Ni	O	Sn	Mn	Fe	Other
FCu	2.0080.10	1787	≥99.9									≤0.1 rem.
FCu F 20	2.0060	1787	≥99.9									
SFCu	2.0090.10	1787	≥99.9	0.015 0.040								
Cu Zn 10	2.0230.10	17660	90			10						
Cu Zn 28	2.0261.10	17660	72			28						
Cu Zn 33	2.0280	17660	67			33						
Cu Zn 37	2.0321.10	17660	63			37						
Cu Zn 40	2.0360	17660	61		0.2	38.8						

Cu Zn 40 Ni	2.0571	17660 / 1	56.0 58.0	39.0 42.5	1.0 2.0		0.5 1.0
Cu Ni 2 Si	2.0855	17666	97.2 97.5		2.0		Si 0.5 Si 0.8
Cu Ni 12 Zn 24	2.0730.10	17663	64	24	12.0		
Cu Ni 20 Fe	2.0878.10	17664	75.5 79.0	20.0 22.0		0.5 1.5	0.5 1.0
Cu Al 9 Mn	2.0960	17665	86.5 90.0			1.5 3.0	Al 7.7 9.7
Cu Al 11 Ni	2.0978	17665	74.0 78.5	5.0 7.5			4.8 7.3
Cu Sn 2	2.1010	17662	97.5 99.0		1.0 2.5		Al 10.5 Al 12.5

**Table D-3** Titanium and Titanium Alloys

Designation	Material no.	DIN standard	Ti	Fe	O	N	C	H	Al	V	Sn	Other
Ti 99.7	3.7035.10	17850	Rem.	0.25	0.20	0.06	0.08	0.013				
Ti 99.2	3.7025.10	17850	Rem.	0.20	0.10	0.05	0.08	0.013				
Ti Al 5 Sn 2	3.7115	17851	90 <sub>94</sub>	0.50	0.20	0.05	0.08	0.020	4.00 6.00	4.00 6.00	2.0 3.0	
Ti Al 6 V 4 F 91	3.7165.10	17851	88.0 90.4	0.30	0.20	0.05	0.08	0.015	5.50 6.75	3.5 4.5		
Ti Al 6 V 6 Sn 2		17862	Rem.	0.35	0.20	0.04	0.05	0.015	5.0 6.0	5.0 6.0	2.5 1.5	Cu 0.35
Ti Al 8 Mo 1 V 1		17862	Rem.	0.30	0.12	0.05	0.08	0.015	7.5 8.5	0.75 1.25		Mo 0.75 Mo 1.25
Ti Al 6 Zr 4 Mo 2 Sn 2		17862	Rem.	0.25	0.12	0.05	0.05	0.015	5.5 6.5		1.8	Mo 1.8, Zr 3.6 Mo 2.2, Zr 4.4
Ti V 13 Cr 11 Al 3		17862	Rem.	0.30	0.20	0.05	0.05	0.020	2.5 4.0	12.5 14.5	Cr 10 Cr 12	

**Table D-4** Magnesium and Magnesium Alloys

Designation	Material no.	DIN standard	Mg	Mn	Al	Zn	Zr
Mg Mn 2 F 20	3.5200	1729	98.0	2.00			
Mg Al 3 Zn	3.5312	1729	94.6 95.0	0.15 0.40	3	0.5 1.5	
Mg Al 6 Zn	3.5612	1729	92.1 93.35	0.15 0.40	6	0.5 1.5	
Mg Al 8 Zn	3.5812	1729	90.9 91.7	0.12 0.30	8	0.2 0.8	
Mg Zn 6 Zr	3.5161	1729	93.2 95.5			6.0	0.45 0.80

**Table D-5** Zinc and Zinc Alloys

Designation	Material no.	DIN standard	Zn	Al	Cu	Mg	Other
Zn 99.99	2.2040	1706	≥99.99				≤0.01
F-Zn	2.2201.38		≥99.975				≤0.025
Zn 98.5	2.2085	1706	≥98.5				≤1.5
Zn Al 4 Cu 1	2.2141	1743	94.39 95.83	3.5 4.3	0.75 1.25	0.02 0.06	
Zn Cu 4	2.2140	(1743)	96.0		4.00		

**Table D-6** Nickel and Nickel Alloys

Designation	Material no.	DIN standard	Ni	Mn	Fe	Cu	Mo	Ti	Al	Other
Ni 99.8	2.4050	17740	≥99.8							≤0.2
Ni 99.2	2.4066	17740	≥99.2							≤0.8
Ni Mn 1	2.4106	17741	≥98	≤2						
Ni Cu 30 Fe	2.4360	17743	63		1.0 2.5	34.5 36.0				
Ni Cu 20 Ti	2.4630	17743	78			20.0		2.0		
Ni Cu 30 Al	2.4375	17743	63		0.5 2.0	30.0 34.2		0.3 1.0	2.0 4.0	
Ni Fe 15 Mo	2.4540	17745	78.5		16.5 18.5		3.0 5.0			
Ni Cr 20 Ti Al	2.4932	17742	65	≤1.0	≤1.5	≤0.2		1.8	1.0	Cr 18-21 Si 1.0 C 0.04-0.10 B 0.008
Ni Co 15 Cr 15 Al Mo Ti	—	—	57					2.7	1.8	
Ni Co 20 Cr 15 Mo Al Ti	—	—	54				3.5	4.0	5.0	Cr 15 Co 15 C 0.15
Ni Cr 20 Ti	2.4630	17742	Rem.	≤1.0	≤5.0	C=0.08 to 0.15	P≤ 0.03 S≤ 0.02	0.2-0 0.6 0.02	≤0.5	Cr 18-21 Co 5.0 Si 1.0

## APP. E

### GENERAL REFERENCES

#### STEEL

- Handbook of Comparative World Steel Standards*, International Technical Information Institute, Tokyo, Japan, 1980.
- Jenson, J.: *Forging Industry Handbook*, Forging Industry Association, Cleveland, OH, 1966.
- Kyle, P. E.: *The Closed Die Forging Process*, Macmillan, New York, 1954.
- Unterwieser, P. M.: *ASM Engineering Handbook, Worldwide Guide to Equivalent Irons and Steels*, American Society for Metals, Metals Park, OH, 1979.
- Wegst Stahlschlüssel 1980*, Verlag Stahlschlüssel Wegst, Marbach.
- Wellinger, et al.: *Werkstoff-Tabellen der Metalle*, Alfred Körner Verlag, Stuttgart, 1972.
- Metals Handbook*, vol. 1-3, 9th ed., American Society for Metals, Metals Park, OH, 1978.

#### NONFERROUS METALS

- Aluminum Standards and Data*, 2d ed., Aluminum Association, New York, 1969.
- Dies, K.: *Kupfer und Kupferlegierungen in der Technik*, Springer, Berlin Heidelberg New York, 1967.
- DIN Taschenbuch 27, Nichteisenmetalle*, 3d ed., Deutsches Institut für Normung, Beuth Verlag, Berlin Köln, 1977.
- Hufnagel, W.: *Key to Aluminium Alloys: Standard Designations, Compositions, Trade Names of Aluminium Materials*, Aluminium Zentrale, Aluminium Verlag, Düsseldorf, 1982.
- Metals Handbook*, vols. 1-3, 9th ed., American Society for Metals, Metals Park, OH, 1978.
- Titanium Alloys Handbook*, MCIC-HB-02, Metals and Ceramics Information Center, Battelle Columbus Laboratories, Columbus, OH, 1972.
- Vergleich US-Amerikanischer, Britischer und Deutscher Normen auf dem Gebiet der Kupferarten*, Deutsches Kupfer-Institut, Berlin, 1962.
- Zwicker, V.: *Titan und Titanlegierungen*, Springer, Berlin / Heidelberg / New York, 1974.

**NEW BOOKS ON TECHNIQUES AND PROCESSES**

Altan, T., Oh, S., and Gegel, H.: *Metal Forming: Fundamentals and Applications*, Metals Park, Ohio, American Society for Metals, 1983.

Avitzur, B.: *Handbook of Metal Forming Processes*, New York, Wiley, 1983.

Krauss, G., ed.: *Deformation, Processing and Structure*, Metals Park, Ohio, American Society for Metals, 1984.

Wilhelm, D. F., ed.: *Understanding Presses and Press Operations*, Dearborn, Michigan, Society of Manufacturing Engineers, 1981.

## APP. F

### ABBREVIATIONS USED IN THIS BOOK

---

---

AA	Aluminum Association
AIME	American Institute of Mining, Metallurgical, and Petroleum Engineers
AISI	American Iron and Steel Institute
ASLE	American Society of Lubricating Engineers
ASM	American Society for Metals
ASME	American Society of Mechanical Engineers
ASTM	American Society for Testing and Materials
CDA	Copper Development Association
CIRP	International Institution for Production Engineering Research (Collège International pour l'Etude Scientifique des Techniques de Production Mécanique)
DGM	Deutsche Gesellschaft für Metallkunde
DIN	Deutsches Institut für Normung
ICFG	International Cold Forging Group
IDDRG	International Deep Drawing Research Group
ISME	Institute of Sheet Metal Engineering
ISO	International Standards Organization
MCIC	Metals and Ceramics Information Center
MTDR	Machine Tool Design and Research Conference
SAE	Society of Automotive Engineers
SME	Society of Manufacturing Engineers
UNS	Unified numbering system for metals and alloys
USCS	U.S. customary system of units



# INDEX

- Accuracy, 9.4 to 9.17, 24.19 to 24.21  
blanking, 9.16, 24.19 to 24.21  
coining, 9.12 to 9.15  
cold extrusion, 9.15  
cold forming, 9.6, 9.11  
cross rolling, 12.26  
deep drawing, 20.50 to 20.53  
factors in, 9.4 to 9.11  
layout, 9.10  
machine tools, 8.11, 9.8 to 9.10  
elastic deformation, 9.9  
guidance, 9.8  
work capacity, 9.10  
material, 9.6  
process design, 9.10  
tools, 9.6  
hot-die forging, 9.4  
hot forming, 9.6, 9.11  
ironing, 14.33  
shearing, 9.16  
sheet bending, 19.30  
sizing, 9.12 to 9.15  
(*See also* Dimensional tolerances; Errors; Surface quality)  
Air bending (*see* Sheet bending, air)
- Anisotropy, 3.23, 3.29  
crystal, 3.24 to 3.26  
elastic, 3.26 to 3.29  
plastic, 3.26 to 3.29  
structure, 3.24 to 3.26  
texture, 3.26
- Anvil hammers, 8.15 to 8.18  
Ausforming, 30.12
- Austenite, 30.13  
Austenitizing, 30.12  
Automobile body parts, drawing of, 20.30 to 20.37
- Axisymmetric extrusion, 5.19
- Back tension, 12.7  
Backward extrusion, 5.24, 13.2, 13.4
- Bar bending, 19.38  
Bauschinger effect, 19.12  
Beam bending, 19.41  
Beck's stability problem, 28.4  
Bending, 11.7, 19.2 to 19.46  
bar, 19.38  
beam, 19.41  
levelling by, 19.42 to 19.46  
with linear tool motion, 2.18

- Bending (*Cont.*):  
     with rotary tool motion, 2.18  
     sheet (*see* Sheet bending)  
     straightening by, 19.42 to 19.46  
     tube, 19.41
- Blanking, 17.1, 24.4 to 24.40  
     accuracy, 9.16, 24.19 to 24.21  
     counterblanking, 24.35  
     die manufacture for, 33.9  
     dies, 31.10  
     errors, 24.36  
     fine, 24.31 to 24.34  
     flow piercing, 24.35  
     forces, 24.5, 24.11 to 24.18  
         deformation work, 24.18  
         ejection, 24.17  
         requirement, 24.11 to 24.15  
         side thrust, 24.15 to 24.17  
         withdrawal, 24.17  
     material utilization, 24.39  
     shaving, 24.31  
     shearing, 24.5 to 24.10, 25.20  
         stresses, 24.5 to 24.8  
         tool geometry, 24.8 to 24.10  
     tooling, 24.23 to 24.30  
         design, 24.25  
         die and punch shapes, 24.26 to 24.28  
         die clearance, 24.26  
         feed stops, 24.28  
         materials, 24.29  
         types, 24.23 to 24.25  
     workpiece properties, 24.19 to 24.23  
         accuracy, 24.19 to 24.21  
         hardness, 24.21 to 24.23  
         strength, 24.21 to 24.23  
     (*See also* Slug production)
- Blue brittleness, 3.14
- Boundary area, 2.21
- Boundary friction, 9.25
- Bridge dies, 16.43
- Bulging, 20.23 to 20.25
- Bulk forming, 2.19
- Bulk piercing, 15.56 to 15.80
- Burgers circuit, 3.8
- Burgers vector, 3.8
- Can backward extrusion, 13.5
- Can extrusion, 15.56 to 15.80  
     (*See also* Cold extrusion)
- Can forward extrusion, 13.4
- Center line, 9.20
- Center line average, 6.11
- Characteristic values (*see* Process parameters, measurement of)
- Closed-die forging, 11.12, 11.20 to 11.45  
     equipment, 11.97 to 11.103  
         finish-forging, 11.97 to 11.100  
         preforming, 11.97 to 11.99, 11.101 to 11.103
- with flash: deformation, 11.23 to 11.25  
     forces, 11.30 to 11.45  
     material flow, 11.23 to 11.25  
     stresses, 11.30 to 11.45
- without flash: deformation, 11.20 to 11.25  
     forces, 11.25 to 11.30  
     material flow, 11.20 to 11.25  
     precision, 11.109 to 11.114  
     stresses, 11.25 to 11.30
- lubrication, 11.45 to 11.48
- sequencing, 11.71 to 11.78
- surface finish, 11.45 to 11.48
- tools, 11.84 to 11.89  
     dies, 11.84 to 11.88  
     trimming, 11.88
- Coining, 19.23  
     accuracy, 9.12 to 9.15  
     upsetting, 10.18
- Cold die forging, 2.6
- Cold extrusion, 15.2 to 15.24, 15.26 to 15.95  
     accuracy, 9.15  
     advantages, 15.2 to 15.6  
     component design, 15.36  
     component size, 15.36  
     economic production, 15.91 to 15.95  
     machine tools, 15.46 to 15.48  
     nonstationary material flow, 15.56 to 15.80  
         effect of punch shape, 15.74 to 15.76  
         effect of workpiece dimensions, 15.73  
         extrusion force, 15.73 to 15.76  
         forces and energy, 15.62 to 15.73  
             analytical equations, 15.64  
             deformation efficiency, 15.64  
             elementary plasticity theory, 15.68  
                 upper-bound method, 15.72  
             friction, 15.76 to 15.78  
             lubrication, 15.76 to 15.78  
             similarity laws, 15.73  
             stresses, 15.61

- Cold extrusion (*Cont.*):  
 process combinations, 15.48, 15.90  
 shapes, 15.2 to 15.6  
 stationary material flow, 15.7 to 15.26  
   effect of billet dimensions, 15.18 to 15.20  
   extrusion force, 15.18 to 15.20  
   force change in mass production, 15.24  
   forces and energy, 15.10 to 15.18  
     analytical equations, 15.12  
     deformation efficiency, 15.11  
     elementary plasticity theory, 15.15  
   force correction factor, 15.11  
   numerical approximation methods, 15.18  
     variational principle, 15.17  
   friction, 15.22  
   lubrication, 15.22  
   optimum die shape, 15.20 to 15.22  
   stresses, 15.7 to 15.10  
   surface treatment, 15.22  
   warm extrusion, 15.24 to 15.26  
 tools, 15.37 to 15.46, 15.80 to 15.90  
   design and setup, 15.37 to 15.40, 15.80  
   die assembly calculation, 15.86 to 15.90  
   die design, 15.82  
   die inserts, 15.42 to 15.44  
   die loads, 15.82 to 15.86  
   life of, 15.46, 15.90  
   mandrels, 15.40 to 15.42  
   multistage tooling, 15.44  
   punch design, 15.80  
   punches, 15.40 to 15.42  
 workpiece design, 15.80  
 workpiece materials, 15.26 to 15.36  
   nonferrous metals, 15.28  
   postextrusion properties, 15.35  
   preextrusion properties, 15.29 to 15.35  
   steels, 15.26 to 15.28  
 Cold forging, 2.6  
 Cold press welding, 15.51  
 Collar drawing, 22.1 to 22.10  
   drawing ratio, 22.2  
   geometric principles, 22.1  
   punch load, 22.3 to 22.5  
 Collar drawing (*Cont.*):  
   small-diameter collars, 22.5 to 22.10  
     forming of, with rotating punch, 22.7 to 22.10  
     threaded, 22.5 to 22.7  
 Compressive forming, 2.5 to 2.11  
 Constrained displacement, 11.12  
 Constrained surfaces, deformation of, 6.13  
 Copy milling, 32.7 to 32.12  
 Counterblanking, 24.35  
 Counterblow hammers, 8.17, 8.18  
 Cracking, 20.13  
 Cracking factor, 20.13  
 Cracking load, 20.11, 20.13  
 Crank extrusion presses, 16.60  
 Cross rolling, 12.15 to 12.26  
   surface, 12.18 to 12.22  
   thread, 12.22 to 12.26  
     accuracy, 12.26  
     circular dies, 12.25  
     flat dies, 12.23 to 12.25  
   (See also Skewed rolling)  
 Crystal deformation, 3.5 to 3.7  
   elastic, 3.5  
   plastic, 3.5  
 Crystal lattice, 3.3  
 Crystal structure of metals, 3.3  
 Crystallites, 3.3  
 Cup-draw test, 18.8, 18.9  
 Cylindrical piece upsetting test, 4.6 to 4.8  
 Deep drawing, 2.11, 20.3 to 20.66  
   automobile body parts, 20.30 to 20.37  
   blank sizing, 20.47 to 20.50  
   classification, 20.3  
   defects, 20.53 to 20.56  
   definition, 20.3  
   first (see First draw)  
   irregular components, 20.30 to 20.37  
   lubricants, 20.46  
   machine tools, 20.56 to 20.66  
     hydraulic presses, 20.64 to 20.66  
     mechanical presses, 20.56 to 20.64  
       blankholder control, 20.59  
       die cushion, 20.59  
       drive systems, 20.56  
   noncylindrical components, 20.24 to 20.29  
   postdrawing materials properties, 20.50 to 20.53

- Deep drawing (*Cont.*):**
- redraw (*see Redraw*)
  - special processes, 20.38 to 20.41
    - elastic tools, 20.38
    - hot forming temperatures, 20.41
    - small parts, 20.41
    - working media, 20.40
  - tool design, 20.41 to 20.45
    - blankholder, 20.43
    - die and punch radii, 20.42
    - die clearance, 20.41
    - first draw without blankholder, 20.43
    - materials, 20.45
  - workpiece accuracy, 20.50 to 20.53
  - workpiece materials, 20.45
- Deformation, crystal**, 3.5 to 3.7
- elastic, 3.5
  - plastic, 3.5
- Deformation efficiency**, 13.22, 15.11, 15.64, 16.13, 20.12
- Deformation-induced precipitates**, 30.16
- Deformation methods**, 2.4 to 2.22
- bending, 2.18
  - classification, 2.4, 2.7, 2.10, 2.17, 2.21
  - combined tensile and compressive forming, 2.11 to 2.15
  - compressive forming, 2.5 to 2.11
  - shearing, 2.19
  - tensile forming, 2.15 to 2.18
- Deformation parameters** (*see Process parameters, measurement of*)
- Deformation work**, 5.11
- blanking, 24.18
  - drawing (*see Drawing, deformation work and forces*)
  - extrusion (*see Extrusion, deformation work and forces*)
- Degreasing**, 26.21
- Descaling**, 26.19
- Die forming**, 2.15
- Die hobbing**, 17.1
- Die manufacture**, 32.1 to 32.25, 33.1 to 33.11
- for blanking, 33.9
  - casting, 32.2 to 32.6
  - for cold bulk forming, 33.7
  - copy milling, 32.7 to 32.12
  - electrochemical, 32.22 to 32.25
  - electroerosion, 32.12 to 32.22, 33.4
  - for hot bulk forming, 33.1 to 33.6
  - machining, 32.1, 32.6 to 32.12
- Die manufacture (*Cont.*):**
- for sheet-metal working, 33.7
  - for trimming, 33.9
- Dies**, 31.3 to 31.10
- characteristics, 31.3
  - classification, 31.5
  - geometry, 31.5
  - manufacture of (*see Die manufacture*)
  - requirements, 31.7 to 31.10
    - blanking, 31.10
    - cold bulk forming, 31.7
    - hot bulk forming, 31.7
    - sheet forming, 31.9
- Dimensional errors**, 9.3
- Dimensional tolerances**, 9.17
- Dishing**, 2.11
- Disk theory**, 5.16
- Dislocations**, 3.10 to 3.13
- movement of, 3.10
  - sources of, 3.11
  - strain hardening, 3.12
- Displacement**, 5.2
- Drag-link drive**, 20.58
- Drawing**, 13.6 to 13.26, 14.1 to 14.30
- back tension effect in, 14.9 to 14.11
  - bars and wire, 14.2 to 14.4
  - classification, 13.6
  - collar (*see Collar drawing*)
  - deep (*see Deep drawing*)
  - deformation efficiency, 13.22
  - deformation work and forces, 13.14 to 13.21
    - bar and wire, 13.20
    - hollow forward extrusion, 13.19
    - hollow tube, 13.21
    - solid forward extrusion, 13.14 to 13.19
  - friction in, 14.14
  - friction coefficient, 13.21
  - lubrication in, 14.14
  - machine tools, 14.27 to 14.30
    - auxiliary equipment, 14.29
    - draw benches, 14.27
    - wire-drawing, 14.28
  - material flow, 13.8 to 13.10, 14.2 to 14.4
  - optimum die angle, 13.23 to 13.25
  - process limits, 13.25
  - product properties, 14.23 to 14.26
    - mechanical, 14.27
    - residual stresses, 14.26

- Drawing, product properties (*Cont.*):  
     surface quality, 14.26  
     stresses, 13.10 to 13.13, 14.2 to 14.9  
     temperatures in, 14.11 to 14.13  
     through dies, 13.7  
     tools for, 14.15 to 14.23  
         design, 14.15  
         die wear, 14.22  
         drawing dies, 14.17  
         floating mandrels, 14.18 to 14.22  
         multistage drawing, 14.22  
         profile drawing, 14.22  
     tube, 14.4 to 14.9  
     (*See also* Extrusion; Ironing)
- Drawing load, 20.9
- Drawing ratio, 20.13 to 20.18, 20.23, 22.2
- Drawing work, 20.12
- Drop hammers, 8.15 to 8.18
- Dry drawing, 14.15
- Dry friction, 9.25
- Dummy blocks, 16.45, 16.56
- Dynamic recovery, 3.20
- Dynamic recrystallization, 3.22, 30.15
- Earing, 20.20, 20.51
- Effective length, 4.11
- Elastic–perfectly plastic models, 5.22
- Elastic range, 3.3
- Elastoplastic range, 3.3
- Electrochemical sinking, 32.22 to 32.25, 33.4
- Electroerosion, 32.12 to 32.22, 33.4
- Elongating, 23.25
- Embossing, 2.15, 17.2, 23.19
- Energy of distortion, 5.8
- Equivalent strain, 5.11
- Erichsen cupping test, 18.6
- Errors, 9.2 to 9.4  
     blanking, 24.36  
     random, 9.2  
     systematic, 9.2  
     workpiece, 9.3  
     (*See also* Accuracy; Dimensional tolerances; Surface quality)
- Expanding, 2.15, 23.20 to 23.23  
     with elastic tools, 23.23  
     with plug, 23.21  
     with spreading tool, 23.21
- Expansion-draw test, 18.6
- Extrusion, 13.2 to 13.6, 13.8 to 13.26  
     cold (*see* Cold extrusion)
- Extrusion (*Cont.*):  
     of components, 13.3 to 13.6  
     deformation efficiency, 13.22  
     deformation work and forces, 13.14 to 13.21  
         hollow forward extrusion, 13.19  
         solid forward extrusion, 13.14 to 13.19  
     friction coefficient, 13.21  
     hot (*see* Hot extrusion)  
     material flow, 13.8 to 13.10  
     optimum die angle, 13.23 to 13.25  
     process limits, 13.25  
     semifinished products, 13.2  
     stresses, 13.10 to 13.13  
     warm, 15.24 to 15.26  
     (*See also* Drawing; Ironing)
- Extrusion force, 15.18 to 15.20
- Feeder plate dies, 16.43
- Fine blanking, 24.31 to 24.34, 28.27
- Finish smoothing, 17.2, 17.4
- Finite-element methods, 5.29 to 5.32
- First draw, 2.11, 20.3 to 20.21  
     anisotropy, 20.18 to 20.21  
     cracking, 20.13  
     deformation efficiency, 20.12  
     forces, 20.9 to 20.13  
         blankholder pressure, 20.10  
         cracking load, 20.11, 20.13  
         drawing load, 20.9  
         drawing work, 20.12  
         load-stroke diagram, 20.12  
     limiting drawing ratio, 20.13 to 20.18  
     strains, 20.7  
     stresses, 20.3 to 20.7  
     wrinkle formation, 20.21
- Flange forming, 2.15
- Flanging, 2.11
- Flat dies, 16.43
- Flat rolling, 12.2
- Flow curve determination, 4.5 to 4.11  
     tensile test, 4.5  
     torsion test, 4.9 to 4.11  
     upsetting test, 4.6 to 4.9
- Flow curves, 4.1 to 4.5  
     determination (*see* Flow curve determination)  
     of metals, selected, 4.11 to 4.15  
     thin-sheet testing, 4.11

## I.6 INDEX

- Flow lines, 5.2  
Flow piercing, 24.35  
Flow rule, 5.9  
Flow stress, 4.3, 4.5, 4.6  
(*See also* Flow curves)  
Force correction factor, 15.11  
Force-travel diagram, 7.2  
Forging, 11.1 to 11.123  
    bending, 11.7  
    cavity formation, 11.8  
    closed-die (*see* Closed-die forging)  
    cross-section alteration, 11.3 to 11.7  
    defects, 11.103  
    design of die forgings, 11.78 to 11.84  
        die layout, 11.78 to 11.83  
        dimensional accuracy, 11.83  
        machining ease, 11.84  
        material flow, 11.78 to 11.83  
    equipment, 11.89 to 11.95  
        (*See also* Closed-die forging, equipment; Open-die forging, equipment)  
    heating, 11.60 to 11.65  
        conduction, 11.64  
        furnace, 11.62  
        induction, 11.63  
    hot-die, 11.121  
    hot-impact extrusion, 11.114  
    isothermal, 11.122  
joining, 11.12  
materials for, 11.48 to 11.60  
open-die (*see* Open-die forging)  
parting, 11.9 to 11.11  
powder-metal preforms, 11.118 to 11.121  
    powder-metal components, 11.119 to 11.121  
    tool design, 11.119  
precision, 11.105 to 11.109  
process sequence, 11.65 to 11.69, 11.71 to 11.78  
shear-forming, 11.7  
superplastic, 11.123  
warm, 11.115 to 11.118  
Form errors, 9.3  
Forming limit, 5.10  
Forming tool, 2.21  
Forward extrusion, 13.2, 13.4  
Frank-Read mechanism, 3.11  
Free extrusion, 13.5  
Free surfaces, deformation of, 6.13  
Friction, 4.5 to 4.8, 6.3 to 6.5, 9.25  
    adhesion, 6.5  
    die-workpiece interface, 6.3  
    mathematical representation of, 6.4  
    measurement, 6.18 to 6.25  
        in metalworking, 6.24  
        simulation, 6.22 to 6.24  
    shear factor, 6.5  
    (*See also* Lubricants; Lubrication)  
Friction coefficient, 4.6, 6.4, 13.21  
Friction polymer, 6.8  
Front tension, 12.7
- Geiringer equations, 5.24  
Grain boundaries, 3.9, 3.10  
Grain growth, 3.19  
Groove forming, 17.2
- Hall-Petch equation, 4.2  
Hammers, 8.13 to 8.24  
    blow efficiency, 8.23  
    characteristic values, 8.18 to 8.21  
    classification, 8.13 to 8.18  
    operating efficiency, 8.21 to 8.24  
    (*See also* Presses)  
Heat lines, 11.16  
Heat treatment, 26.1 to 26.17  
    bright annealing, steel, 26.9  
    equipment, 26.14 to 26.17  
        annealing furnaces, 26.15  
        heating media, 26.14  
    homogenizing, copper, 26.14  
    incorrect, 26.14  
    normalizing, steel, 26.8  
    patenting, steel, 26.9  
    recovery annealing, aluminum, 26.10  
    recrystallization annealing: aluminum, 26.10  
        copper, 26.13  
        steel, 26.5  
    soft annealing: aluminum, 26.10  
        copper, 26.13  
        steel, 26.6  
    stress relieving: aluminum, 26.10  
        copper, 26.13  
        steel, 26.4
- Hencky equations, 5.24

- High-energy-rate forming, 27.4 to 27.38  
 electromagnetic forming, 27.32 to 27.38  
 coils, 27.34  
 machines, 27.33  
 principles, 27.32  
 explosive forming, 27.21 to 27.23  
 high-speed hammers, 27.5 to 27.15  
 cold forging, 27.13  
 design principles, 27.8 to 27.10  
 hot forging, 27.10 to 27.13  
 die design, 27.12  
 die life, 27.12  
 die material, 27.13  
 lubrication, 27.11  
 shearing, 27.14  
 hydrospark forming, 27.23 to 27.32  
 dies, 27.27  
 impulse-current generator, 27.23  
 machines, 27.25  
 shock-wave forming, 27.16 to 27.21  
 characteristics, 27.16 to 27.19  
 impulse transmission, 27.19 to 27.21  
 workpiece deformation, 27.21  
 terminology, 27.4
- Hobbing, 17.8 to 17.22  
 cold, 17.8, 17.10 to 17.21  
 forming force, 17.13 to 17.17  
 friction, 17.17  
 lubrication, 17.17  
 machine tools, 17.21  
 material flow, 17.12  
 penetration depth, 17.13 to 17.17  
 postforming heat treatment, 17.17  
 strain hardening, 17.12  
 tooling, 17.18 to 17.20  
 workpiece materials, 17.10 to 17.12  
 hot, 17.21
- Hollow backward extrusion, 13.2
- Hollow drawing, 13.8, 13.21
- Hollow forward extrusion, 13.2, 13.11, 13.19
- Hollow lateral extrusion, 13.3
- Hollow workpieces, 12.28
- Hot-die forging, 9.4, 11.121
- Hot extrusion, 16.2 to 16.61  
 classification, 16.2  
 equipment, 16.49 to 16.61  
 auxiliary, 16.54 to 16.60  
 drive systems, 16.49 to 16.51  
 presses, 16.51 to 16.54, 16.60
- Hot extrusion, equipment (*Cont.*):  
 special-purpose, 16.60  
 flow stress, 16.10 to 16.13  
 forces, 16.13 to 16.15  
 deformation efficiency, 16.13  
 elementary plasticity theory, 16.13, 16.15  
 upper-bound methods, 16.15  
 viscoplasticity method, 16.15  
 friction, 16.25  
 load-stroke curve, 16.15 to 16.17  
 lubrication, 16.25  
 material flow, 16.3 to 16.9  
 materials, 16.3  
 microstructure formation, 16.9  
 postextrusion materials properties, 16.28 to 16.34  
 defects, 16.32 to 16.34  
 subsequent treatment, 16.29 to 16.32  
 preextrusion materials properties, 16.26 to 16.28  
 product design, 16.47 to 16.49  
 temperature, 16.17 to 16.25  
 billet heating, 16.23  
 material characteristics and, 16.21  
 punch velocity and, 16.18 to 16.20  
 tools, 16.34 to 16.46  
 blocks, 16.45  
 containers, 16.45  
 dies, 16.35 to 16.45  
 design, 16.36 to 16.41  
 materials, 16.35  
 types, 16.42 to 16.45  
 mandrels, 16.45  
 stems, 16.45
- Hot forming, 3.15 to 3.23  
 accuracy, 9.6, 9.11  
 dynamic structural changes, 3.19 to 3.23  
 recovery, 3.16, 3.20  
 recrystallization, 3.18, 3.22  
 static structural changes, 3.19 to 3.23
- Hot-impact extrusion, 11.114
- Hydraulic bulge test, 18.6
- Hydraulic presses, 8.7, 8.34 to 8.41, 20.64 to 20.66  
 cable, 16.60  
 characteristics, 8.40  
 designs, 8.40  
 drive systems, 8.38 to 8.41  
 accumulator, 8.39

- Hydraulic presses, drive systems (*Cont.*):  
     applications, 8.39  
     direct pump, 8.38  
     fluids, 8.35 to 8.38  
         characteristics, 8.35 to 8.37  
         fire-resistant, 8.37  
         functions, 8.35
- Hydrodynamic friction, 9.25
- Hydrostatic compressive stress, superimposed, 28.18 to 28.30  
     compressing, 28.25  
     drawing, 28.29  
     extrusion with counterpressure, 28.23  
     fine blanking, 28.27  
     forging, 28.25  
     hydrostatic cold extrusion with counterpressure, 28.24  
     precision shearing, 28.27  
     rolling, 28.27  
     stress state and formability, 28.18 to 28.21  
     upsetting, 28.25
- Hydrostatic extrusion, 28.2 to 28.18  
     augmented, 28.15 to 28.17  
     dies, 28.12 to 28.15  
     extrusion pressure, 28.6 to 28.10  
     machines, 28.15  
     material flow, 28.5  
     optimum die-opening angle, 28.7  
     postextrusion materials properties, 28.12  
     principles, 28.2 to 28.5  
     strains, 28.10  
     thick-film, 28.17  
     work materials, 28.10  
     workpiece shapes, 28.10
- Hydrostatic pressure, 5.8
- Impact extrusion, 13.3
- Indentation, 2.5, 17.1 to 17.23  
     with circumferential motion, 17.2  
     cup piercing, unrestricted, 17.22  
     deformation energy and forces, 17.7  
     hobbing (*see Hobbing*)  
     with rectilinear motion, 17.1  
     stresses, 17.4 to 17.7
- Initial flow stress, 5.2
- Ironing, 13.8, 14.30 to 14.35  
     forces, 14.31 to 14.33  
     machine tools, 14.34
- Ironing (*Cont.*):  
     stresses, 14.31 to 14.33  
     workpiece accuracy, 14.33  
     (*See also Drawing; Extrusion*)
- Isoforming, 30.12
- Isothermal extrusion, 16.23
- Isothermal forging, 11.122
- Joggling, 2.19
- Knurling, 17.2
- Lancing, 24.5
- Lateral extrusion, 13.2, 13.5
- Lattice defects, 3.7 to 3.10  
     dislocations, 3.8  
     two-dimensional, 3.9  
     zero-dimensional, 3.9
- Levy-von Mises equations, 5.23
- Limiting drawing ratio, 20.13 to 20.18
- Limiting spinning ratio, 21.4
- Limiting upset ratio, 10.10 to 10.12
- Load-bearing area, 6.11
- Load-stroke curve, 16.15 to 16.17
- Load-stroke diagram, 20.12
- Longitudinal rolling, 12.11 to 12.15  
     flat, 12.11  
     profile, 12.12 to 12.15
- Lower-bound theorem, 5.25
- Lower yield point, 3.13
- Lubricant drawing, 14.15
- Lubricants, 6.15 to 6.18  
     application, 6.18  
     aqueous, 6.17  
     attributes, 6.16  
     boundary, 6.8  
     carriers, 6.18, 26.19, 26.22  
     conversion coatings, 6.18  
     greases, 6.17  
     oil-base, 6.16  
     soaps, 6.17  
     solid-film, 6.17  
     (*See also Friction; Lubrication*)
- Lubrication, 6.5 to 6.15  
     boundary, 6.8  
     dry interfaces, 6.6  
     extreme-pressure, 6.8  
     hydrodynamic, 6.8

- Lubrication (*Cont.*):  
 mixed-film, 6.9  
 solid-film, 6.6 to 6.8  
 surface-roughness, 6.10 to 6.15  
   constrained surface deformation, 6.13  
   die surface, 6.14  
   free surface deformation, 6.13  
   measurement, 6.10 to 6.13  
   workpiece, 6.14  
 (*See also* Friction; Lubricants)
- Lüders' lines, 3.13
- Ludwik equation, 4.5, 4.11
- Machine tools, 8.1 to 8.69  
 accuracy, 8.11  
 (*See also* Accuracy, factors in, machine tools)  
 characteristic values: energy, 8.2 to 8.8  
   force, 8.2 to 8.8  
   time-related, 8.8  
 classification, 8.2  
 cold extrusion, 15.46 to 15.48  
 deep drawing (*see* Deep drawing, machine tools)  
 drawing (*see* Drawing, machine tools)  
 hammers (*see* Hammers)  
 hobbing, 17.21  
 ironing, 14.34  
 presses (*see* Presses)  
 slug production, 25.12 to 25.15  
 spinning, 21.10 to 21.12  
 upsetting (*see* Upsetting, machine tools)  
 velocity, 8.8
- Marking, 17.1
- Material flow:  
 closed-die forging, 11.20 to 11.25  
 drawing, 13.8 to 13.10, 14.2 to 14.4  
 extrusion, 13.8 to 13.10  
 forging, 11.78 to 11.83  
 hobbing, 17.12  
 hot extrusion, 16.3 to 16.9  
 hydrostatic extrusion, 28.5  
 nonstationary, cold extrusion (*see* Cold extrusion, nonstationary material flow)  
 open-die forging, 11.13 to 11.16  
 stationary, cold extrusion (*see* Cold extrusion, stationary material flow)  
 upsetting, 10.3
- Material properties errors, 9.3  
 Maximum shear-stress criterion, 5.7  
 Mean coefficient of linear thermal expansion, 9.7  
 Mechanical presses, 8.41 to 8.65, 20.56 to 20.64  
   accuracy, 8.56 to 8.60  
   loaded, 8.56  
   unloaded, 8.57  
 blankholder control, 20.59  
 classification, 8.41  
 die cushion, 20.59  
 drives, 8.64, 20.56  
 frames, 8.60 to 8.64  
 kinetics and kinematics of, 8.43 to 8.56  
   direct-crank drive, 8.43 to 8.52  
   forces and moments, 8.43 to 8.51  
   ram velocity, 8.51  
   eccentric, 8.52 to 8.54  
 knuckle-joint, 8.54 to 8.56  
   design, 8.54  
   ram force, 8.55  
   ram velocity, 8.56  
   stroke adjustment, 8.52  
 safety, 8.66 to 8.68  
   entire stroke range, 8.68  
   useful stroke region, 8.66 to 8.68
- Metal-forming methods (*see* Deformation methods)
- Miller indexes, 3.24
- Mixed friction, 9.25
- Mohr's circle, 5.7
- Natural strain, 4.2, 5.6
- Necking, 4.5, 23.10
- Non-steady-state displacement, 5.2
- Normal anisotropic materials, 3.26
- Normal strain, 5.3
- Nosing, 13.5
- Notching, 17.1, 24.4
- Oillet process, 20.41
- Open-die extrusion, 13.5
- Open-die forging, 11.13 to 11.20  
   deformation, 11.13 to 11.16  
   equipment, 11.95 to 11.97  
   forces, 11.16  
   material flow, 11.13 to 11.16  
   sequencing, 11.65 to 11.69  
   stresses, 11.16

- Optimum die angle, 13.23 to 13.25  
 Optimum die-opening angle, 28.7  
 Orthotropic materials, 3.26
- Parameters, deformation (*see* Process parameters, measurement of)  
 Path lines, 5.2  
 Pencil glide, 3.28  
 Phase boundaries, 3.9, 3.10  
 Phase transformation, 3.4  
 Pickling, 26.19  
 Piercing (*see* Blanking)  
 Plane strain upsetting test, 4.8  
 Planishing, 12.18, 12.20, 17.2  
 Plastic zone, 2.21  
 Plasticity theory, 5.1 to 5.32  
     applications, 5.17 to 5.21  
     fundamentals, 5.1 to 5.12  
         displacement, 5.2  
         equivalent strain, 5.11  
         forming limit, 5.10  
         homogeneous deformation, 5.5, 5.10  
         natural strain, 5.6  
         power and work, 5.10  
         strain, 5.3 to 5.5  
         strain hardening, 5.2  
         strain rate, 5.3 to 5.5, 5.11  
         stress-strain relations, 5.7 to 5.9  
         yield criteria, 5.7 to 5.9  
         yield strength, 5.2  
 Prandtl-Reuss, 5.22  
 solution methods, 5.12 to 5.21  
     axisymmetric forming, 5.16  
     strip theory, 5.12 to 5.16  
 von Mises (*see* von Mises plasticity theory)  
 Pole figure, 3.26  
 Porthole dies, 16.43  
 Positional errors, 8.11, 9.3  
 Prandtl-Reuss plasticity theory, 5.22  
     (*See also* von Mises plasticity theory)  
 Prechamber dies, 16.43  
 Precipitation kinetics, 30.17  
 Precipitation-recrystallization interdependence, 30.18  
 Presses, 8.6 to 8.8  
     energy-controlled, 8.6  
     force-controlled, 8.7  
     hydraulic (*see* Hydraulic presses)  
     mechanical (*see* Mechanical presses)
- Presses (*Cont.*):  
     screw (*see* Screw presses)  
     stroke-controlled, 8.7  
     (*See also* Hammers)  
 Pressure peaks, 28.6  
 Primary recrystallization, 3.18  
 Principal stresses, 5.7  
 Process parameters, measurement of, 7.1 to 7.8  
     deformation, 7.4 to 7.8  
         local stresses, 7.6  
         model technique, 7.7  
         visioplasticity, 7.4 to 7.6  
     force, 7.1  
     methods, 7.3  
     travel, 7.2  
 Profile rolling, 12.2, 12.17  
 Proof stress, 3.3  
 Pulling through a die, 2.11  
 Punching, 17.1
- Rastegaev test, 4.7  
 Real crystals, 3.7  
 Recessing, 2.15, 23.2  
 Recrystallization, 3.18 to 3.19, 3.22, 16.9, 30.15, 30.17, 30.18  
 Redraw, 2.11, 20.21 to 20.24  
     draw increments, 20.23  
     drawing ratios, 20.23  
     forces, 20.22  
     reverse drawing, 20.27  
     stresses, 20.21  
         with wall thinning, 20.24  
 Reverse drawing, 2.11, 20.27  
 Rigid-perfectly plastic models, 5.22  
 Rockerarm drive, 20.56  
 Rod backward extrusion, 13.5  
 Rod forward extrusion, 13.4  
 Rod lateral extrusion, 13.5  
 Roll bending, 2.18  
 Roll deformation, 12.8  
 Rolling, 12.1 to 12.31  
     back tension, 12.7  
     classification, 12.2  
     correction factors, 12.8  
     cross (*see* Cross rolling)  
     definition, 12.1  
     front tension, 12.7  
     gripping condition, 12.4  
     longitudinal (*see* Longitudinal rolling)

- Rolling (Cont.):**  
 lubrication, 12.9  
 neutral plane, continuous rolling condition, 12.5  
 parameters, 12.3  
 power, 12.8  
 roll gap stresses, 12.5  
 rolling force, 12.8  
 rolling torque, 12.8  
 skewed (*see* Skewed rolling)  
**Roughness, 9.20**
- Sachs wedge-drawing test, 18.8**  
**Sawing, 25.16 to 25.19**  
 cold, 25.16  
 deburring, 25.17  
**Scavenger blocks, 16.45, 16.56**  
**Schmid's law, 3.7**  
**Screw dislocation, 3.8**  
**Screw presses, 8.24 to 8.34**  
 applications, 8.33  
 capacities, 8.33  
 classification, 8.26  
 controls, 8.33  
 drives, 8.26 to 8.30  
 efficiency, 8.30 to 8.32  
 energy conversion, 8.30 to 8.32  
 ram travel characteristics, 8.26 to 8.30  
 safety, 8.69  
**Secondary recrystallization, 3.19**  
**Shear factor, 6.5**  
**Shear-pressure zone, 11.45**  
**Shear strain, 4.9, 5.4**  
**Shear stress, 4.9**  
**Shearing, 2.19, 24.5 to 24.10, 25.20**  
 accuracy, 9.16  
 force, 24.14  
 resistance, 24.11  
 stresses, 24.5 to 24.8  
 tool geometry, 24.8 to 24.10  
**Sheet bending, 19.2 to 19.38**  
 accuracy, 19.30  
 air, 19.17 to 19.22  
 bending moment and force, 19.18 to 19.22  
 straightening by, 19.44  
 workpiece shape, 19.18  
 defects, 19.33 to 19.35  
 edge deformation, 19.30  
 empirical comparisons, 19.15 to 19.17
- Sheet bending (Cont.):**  
 fiber displacement, 19.8 to 19.13  
 folding, 19.26  
 formability, 19.31 to 19.33  
 plasticity theory and, 19.13 to 19.15  
 pliable tool, 19.28  
 roll, 19.26 to 19.28  
 springback, 19.7, 19.13, 19.30  
 theoretical considerations, 19.3 to 19.7  
 tools, 19.35 to 19.38  
 folders, 19.36  
 frame presses, 19.35  
 press brakes, 19.35  
 roll benders, 19.37  
 roll formers, 19.36  
**U-die, 19.24**  
**unit-moment curves, 19.8**  
**V-die, 19.23**  
 workpiece length, 19.29  
**Sheet drawing, 13.7**  
**Sheet forming, 2.19**  
**Sheet metal, 18.3 to 18.15**  
 formability, 18.3 to 18.5  
 anisotropy factor, 18.4  
 strain hardening exponent, 18.4  
 tensile data, 18.3  
 forming limits, 18.11 to 18.14  
 strain analysis, 18.10 to 18.15  
 test methods, simulating, 18.5 to 18.10  
 bending, 18.9  
 deep-drawing, 18.8  
 stretch-forming, 18.6  
**Shell lines, 12.28**  
**SHT process, 30.21**  
**Similarity laws, 15.73**  
**Sintering, 25.24**  
**Sizing, 9.12 to 9.15, 25.23**  
**Skewed rolling, 12.15 to 12.18, 12.26 to 12.31**  
 flow forming, 12.26 to 12.31  
*(See also Cross rolling)*  
**Slab theory, 5.12 to 5.16, 13.10 to 13.13**  
**Sliding friction zone, 11.45**  
**Slip-line theory, 5.24**  
**Slug production, 25.1 to 25.24**  
 breaking, 25.16  
 cropping, 25.2 to 25.15  
 application, 25.2  
 clearance, 25.4  
 definition, 25.2  
 force requirement, 25.10

- Slug Production, cropping (*Cont.*):  
     hardening, 25.9  
     machine tools, 25.12 to 25.15  
     procedures, 25.3  
     slug quality, 25.5 to 25.9  
     superimposed compressive stress, 25.9  
     tooling, 25.11  
     velocity, 25.9  
     work requirement, 25.10  
 heat treatment, 25.23  
 materials, 25.1  
 sawing, 25.16 to 25.19  
     cold, 25.16  
     deburring, 25.17  
 sintering, 25.24  
 sizing, 25.23  
 turning, 25.20  
 (*See also* Blanking)  
 Solid backward extrusion, 13.2  
 Solid bridge dies, 16.43  
 Solid forward extrusion, 13.2, 13.11, 13.14 to 13.19  
 Solid lateral extrusion, 13.3  
 Spark erosion, 32.12 to 32.22  
 Spider dies, 16.43  
 Spinning, 2.13, 21.1 to 21.14  
     applications, 21.5  
     deformation, 21.1 to 21.4  
     machine tools, 21.10 to 21.12  
     manufacturing tolerances, 21.12 to 21.14  
     tools, 21.6 to 21.9  
     workpiece materials, 21.6  
 Spinning ratio, 21.2, 21.4  
 Spreading, 12.8, 23.21  
 Springback, 19.7, 19.13, 19.30  
 Static recrystallization, 30.15  
 Steady-state displacement, 5.2  
 Step dislocation, 3.8  
 Stepping, 11.11  
 Stick-slip phenomena, 28.6  
 Sticking friction, 6.4  
 Sticking friction zone, 11.45  
 Sticking zone, 12.8  
 Strain, 3.2, 5.3 to 5.5  
 Strain aging, 3.14  
 Strain hardening, 3.12, 5.2, 17.12, 18.4  
 Strain rate, 4.4, 5.3 to 5.5, 5.11  
 Strains:  
     first draw, 20.7
- Strains (*Cont.*):  
     hydrostatic extrusion, 20.10  
     stretch forming, 23.6  
     (*See also* Stresses)  
 Streamlines, 5.2  
 Stress, 3.2  
 Stresses:  
     closed-die forging, 11.25 to 11.45  
     cold extrusion, 15.7 to 15.10, 15.61  
     drawing, 13.10 to 13.13, 14.2 to 14.9, 14.26  
     extrusion, 13.10 to 13.13  
     first draw, 20.3 to 20.7  
     indentation, 17.4 to 17.7  
     ironing, 14.31 to 14.33  
     open-die forging, 11.16  
     redraw, 20.21  
     rolling, 12.5  
     shearing, 24.5 to 24.8  
     stretch forming, 23.6  
     upsetting, 10.12  
     (*See also* Strains)  
 Stretch drawing, 2.15  
 Stretch forming, 23.3 to 23.19  
     equipment, 23.12 to 23.19  
     clamping, 23.17 to 23.19  
     tangential stretch forming, 23.13 to 23.17  
     failure modes, 23.10  
     forces, 23.6  
     friction, 23.9  
     lubrication, 23.9  
     poststretch forming properties, 23.9  
     strains, 23.6  
     stresses, 23.6  
     tangential, 23.7  
     tools, 23.11  
     workpiece materials, 23.8  
 Stretcher levelling, 23.25  
 Stretching, 2.15, 23.25 to 23.27  
 Strip theory, 5.12 to 5.16, 13.10 to 13.13  
 Structure factor, 16.13  
 Superimposed hydrostatic compressive stress (*see* Hydrostatic compressive stress, superimposed)  
 Superimposed vibration forming, 29.1 to 29.10  
     forging, 29.8  
     principles, 29.2 to 29.4  
     sheet-metal forming, 29.9  
     tube drawing, 29.8

- Superimposed vibration forming (*Cont.*):  
 upsetting, 29.8  
 wire drawing, 29.4 to 29.8  
   axial excitation of die, 29.5  
   ultrasonically agitated lubrication,  
     29.7  
   vertical excitation of die, 29.5
- Superplasticity, 30.1 to 30.11  
 alloy properties, 30.7  
 applications, 30.7 to 30.11  
 conditions for, 30.1  
 continuum-mechanical formulation of,  
   30.2 to 30.5  
 metallurgical processes in, 30.5 to 30.7
- Surface errors, 9.3
- Surface quality, 9.18 to 9.26  
 burnishing, 9.25  
 cold forming, 9.21  
 constrained forming, 9.22 to 9.25  
 free forming, 9.22  
 hot forming, 9.21  
 parameters, 9.20  
*(See also Accuracy; Dimensional tolerances; Errors)*
- Surface reactions, 2.21
- Surface treatment, 26.18 to 26.23  
 cold bulk forming, 26.21 to 26.23  
 lubrication, 26.19, 26.21 to 26.23  
 rod and wire drawing, 26.19  
 sheet-metal forming, 26.20
- Tapered heating, 16.23
- Technical elastic limit, 3.3
- Tensile forming processes (*see* Bulging;  
 Embossing; Expanding; Stretch forming; Stretching)
- Tensile test, 4.5
- Texture of metals, 3.3
- Thermomechanical treatment, 30.11 to  
 30.21  
 austenitizing, 30.12  
 concepts, 30.11  
 deformation, 30.16  
 of flat steel, 30.20  
 homogenizing, 30.12  
 influencing the  $\gamma/\alpha$  transformation,  
   30.13 to 30.15  
 of microalloyed structural steels, 30.20  
 precipitation, 30.17 to 30.19  
 recrystallization, 30.15, 30.17, 30.18
- Thread tapping, 17.4
- Time strain, 4.2
- Toggle-lever drive, 20.58
- Tolerances, dimensional, 9.17
- Torsion test, 4.9 to 4.11
- Tresca criterion, 4.11, 5.9, 13.10, 20.4,  
   21.2, 24.7
- Tribology (*see* Friction; Lubricants; Lubrication)
- Trimming, 24.5  
 die manufacture for, 33.9
- Tube backward extrusion, 13.5
- Tube bending, 19.41
- Tube drawing, 13.7, 13.21, 14.4 to 14.9
- Tube forward extrusion, 13.4
- Tube lateral extrusion, 13.5
- Tube sinking, 14.4 to 14.9
- Twin boundaries, 3.10
- Twin plane, 3.7
- Twisting, 2.19
- Two-crank drive, 20.56
- Uniform elongation, 4.5
- Unit-moment curves, 19.8
- Upper bound method, 15.17, 15.72, 16.15
- Upper-bound theorem, 5.25
- Upper yield point, 3.13
- Upset bulging, 2.15
- Upset ratio, 10.10 to 10.12
- Upsetting, 10.3 to 10.27  
 characteristic parameters, 10.9 to 10.13  
 coining, 10.18  
 cold, 10.11  
 cold heading, 10.15 to 10.18  
 fundamentals, 10.3 to 10.7  
 deformation, 10.7  
 elementary plasticity theory, 10.4 to  
   10.7  
 friction, 10.3  
 lubrication, 10.3  
 material flow, 10.3  
 stress states, 10.7  
 hot, 10.11  
 hot heading, 10.18  
 machine tools, 10.19 to 10.24  
   cold heading, 10.19 to 10.23  
   hot upsetting, 10.24  
 preform header, 10.13 to 10.15  
   solid, 10.13  
   spring-loaded, 10.14

- Upsetting (*Cont.*):  
process limits, **10.9** to **10.13**  
    forming, **10.9**  
    limiting upset ratio, **10.10** to **10.12**  
    tool stresses, **10.12**  
test, **4.6** to **4.9**  
tool design, **10.24** to **10.27**
- Variational principle, **15.17**  
Velocity field, **5.2**  
Vibration forming, superimposed (*see*  
    Superimposed vibration forming)  
Visioplasticity, **5.28**, **7.4** to **7.6**  
Visioplasticity method, **16.15**  
von Mises criterion, **4.11**, **5.8**, **20.18**,  
    **20.30**  
von Mises plasticity theory, **5.21** to  
    **5.32**  
    equations, **5.22** to **5.24**  
    material models, **5.22**  
    solution methods, **5.24** to **5.32**  
        bound theorems, **5.25**  
        exact, **5.24**  
        finite-element, **5.29** to **5.32**  
        slip-line theory, **5.24**
- von Mises plasticity theory, solution  
methods (*Cont.*):  
    visioplasticity, **5.28**  
    weighted residuals, **5.26** to **5.28**
- Warm extrusion, **15.24** to **15.26**  
Warm forging, **11.115** to **11.118**  
Waviness, **9.20**  
Wear, **6.15**  
Wedge-drawing test, **18.8**  
Wet drawing, **14.15**  
Wiper bending, **2.18**  
Wire drawing, **13.7**, **13.20**  
Workpiece characteristics, **2.21**  
Workpiece materials:  
    cold extrusion (*see* Cold extrusion,  
        workpiece materials)  
    deep drawing, **20.45**  
    hobbing, **17.10** to **17.12**  
    hydrostatic extrusion, **28.10**  
    spinning, **21.6**  
    stretch forming, **23.8**
- Yield criteria, **5.7** to **5.9**  
Yield points, **3.13**  
Yield strength, **5.2**

صنایع و پژوهشکده شهید باکری  
کتابخانه تخصصی و مرکز اسناد